VOLUME 1

Advanced Testing and Characterisation of Bituminous Materials

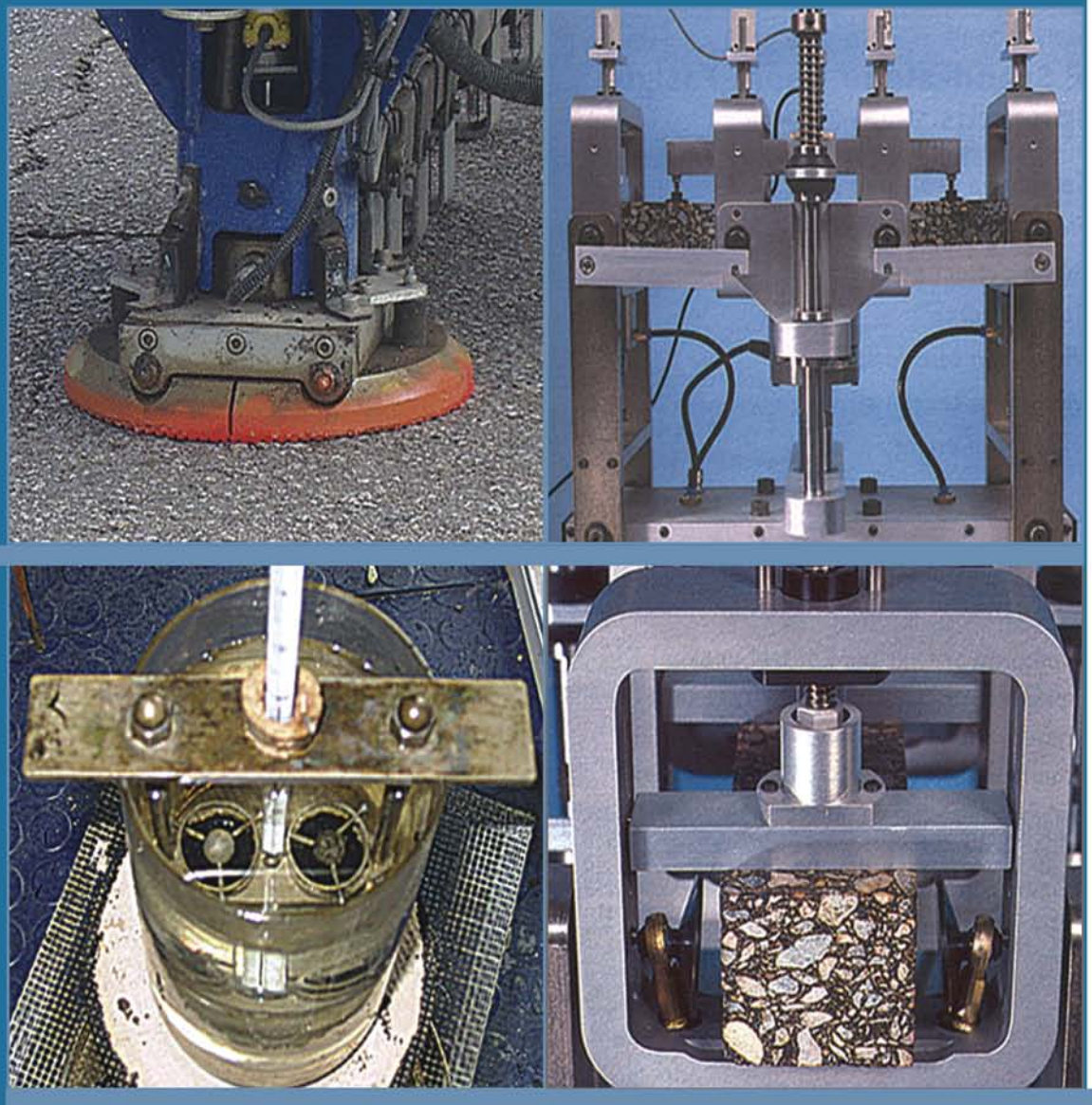

EDITORS:
ANDREAS LOIZOS, MANFRED PARTL, TOM SCARPAS & IMAD AL-QADI

CRC Press
Taylor & Francis Group
A BALKEMA BOOK

ADVANCED TESTING AND CHARACTERIZATION OF BITUMINOUS MATERIALS

PROCEEDINGS OF THE 7TH INTERNATIONAL RILEM SYMPOSIUM ATCBM09 ON ADVANCED TESTING AND CHARACTERIZATION OF BITUMINOUS MATERIALS, RHODES, GREECE, 27–29 MAY 2009

Advanced Testing and Characterization of Bituminous Materials

Editors

Andreas Loizos
National Technical University of Athens, Athens, Greece

Manfred N. Partl
EMPA, Chair of RILEM TC 206-ATB, Switzerland

Tom Scarpas
Delft University of Technology, Delft, The Netherlands

Imad L. Al-Qadi
University of Illinois at Urbana Champaign, Urbana, Illinois, USA

VOLUME I

CRC Press
Taylor & Francis Group
Boca Raton London New York Leiden

CRC Press is an imprint of the
Taylor & Francis Group, an **informa** business

A BALKEMA BOOK

CRC Press/Balkema is an imprint of the Taylor & Francis Group, an informa business

© 2009 Taylor & Francis Group, London, UK

Typeset by Vikatan Publishing Solutions (P) Ltd., Chennai, India
Printed and bound in Great Britain by Antony Rowe (A CPI-group Company), Chippenham, Wiltshire

All rights reserved. No part of this publication or the information contained herein may be reproduced, stored in a retrieval system, or transmitted in any form or by any means, electronic, mechanical, by photocopying, recording or otherwise, without written prior permission from the publisher.

Although all care is taken to ensure integrity and the quality of this publication and the information herein, no responsibility is assumed by the publishers nor the author for any damage to the property or persons as a result of operation or use of this publication and/or the information contained herein.

Published by: CRC Press/Balkema
P.O. Box 447, 2300 AK Leiden, The Netherlands
e-mail: Pub.NL@taylorandfrancis.com
www.crcpress.com – www.taylorandfrancis.co.uk – www.balkema.nl

ISBN: 978-0-415-55854-9 (set of 2 volumes + CD-ROM)
ISBN: 978-0-415-55856-3 (vol 1)
ISBN: 978-0-415-55857-0 (vol 2)
ISBN: 978-0-203-8674-88 (e-book)

Advanced Testing and Characterization of Bituminous Materials – Loizos, Partl, Scarpas & Al-Qadi (eds)
© 2009 Taylor & Francis Group, London, ISBN 978-0-415-55854-9

Table of contents

Preface XIII

Organization XV

VOLUME I

1. Evaluation of binder properties

Laboratory study on interlayer bonding using cationic tack coats 3
C. Raab & M.N. Partl

Factors affecting recovered asphalt binder properties: A theoretical and experimental study 13
F.G. Praticò & V. Dattola

Influence of low temperature behaviour of PmB on life cycle 23
M. Hase & C. Oelkers

Influence of granular polymer additives on the asphalt quality 33
P. Sivapatham, H.J. Beckedahl & S. Janssen

Phase angle determination and interrelationships within bituminous materials 43
G. Rowe

Evaluation of initial road performance correlating with different tests of binders 53
G. Malkoç

Laboratory study of environmental performance of binders by headspace gas chromatography 61
J.E. Poirier, C. Gueit, L. Fanouillet & G. Durand

New fatigue test on bituminous binders and mastics using an annular shear rheometer prototype and waves propagation 69
J. Van Rompu, H. Di Benedetto, G. Gauthier & T. Gallet

Functional forms for master curve analysis of bituminous materials 81
G. Rowe, G. Baumgardner & M. Sharrock

Linear viscoelastic spectra of asphalt binders from DSR and BBR 93
I.B. Kazatchkov, P. Michalica, J. Stastna & L. Zanzotto

Principal component analysis of rheological and hardening data from bituminous binders 99
E. Nielsen

Rheological and functional evaluation of the interactions between bitumen and rubber 109
E.J. Peralta, H.M.R.D. Silva, J.C. Pais & A.V. Machado

A thermodynamic approach to healing in bitumen 123
N. Kringos, A. Scarpas, T. Pauli & R. Robertson

Nanoclay for binder modification of asphalt mixtures 133
M.F.C. van de Ven , A.A.A. Molenaar & J. Besamusca

First-principles investigation of the multiple phases in bituminous materials: The case of asphaltene stacking 143
A.J.M. Schmets, N. Kringos, A. Scarpas, C.P. Duif, G. Schitter & T. Pauli

The morphology of SBS modified bitumen in binders and in asphalt mix 151
H. Soenen, X. Lu & P. Redelius

2. Testing and modeling the influence of climate and ageing effects

Developing a test method for the accelerated ageing of bituminous mixtures in the laboratory 163
N. Piérard & A. Vanelstraete

Chemical characterization of laboratory and field bitumen aging in Porous Asphalt Concrete 173
E.T. Hagos, A.A.A. Molenaar & M.F.C. van de Ven

Influence of temperature and aging on laboratory fatigue performance of asphalt mixtures 185
I. Artamendi, B. Allen & P. Phillips

Aging of SBS polymer in hot and cold bituminous coatings. Relationship between microstructure and performances: Low temperature and cohesion properties 195
C. Gueit, M. Robert & G. Durand

Impact of freeze-thaw cycles on the performance of asphalt mixture based permeability 205
J. Yi, D. Feng & D. Wang

Formulation of authoritative temperature gradients for an analytical design process of flexible pavements using statistical techniques 215
S. Kayser & F. Wellner

Performance evaluation of prepared gelled hot sealant in cold climates 227
AI A1-Hadidy & Yi-qiu Tan

Age hardening behaviour of bituminous stabilized materials 239
M.E. Twagira & K.J. Jenkins

Investigation of friction properties of various road surfaces affecting road safety 251
T. Pellinen, M. Currie & J. Valtonen

Combined experimental and numerical analysis of moisture infiltration in the modified Lottman test 261
N. Kringos, A. Scarpas & H. Azari

Assessment of moisture effect on open graded mixes using water sensitivity and Cántabro after immersion tests 271
B. Rubio, R. Jiménez, F. Pérez & A. Martínez

Moisture damage on bituminous stabilized materials using a MIST device 283
M.E. Twagira & K.J. Jenkins

Determination of gradual reduction of the flexible pavement bearing capacity 295
G. Fodor, C. Capitanu & T.C. Damian

Testing of low temperature behaviour of asphalt mixtures in bending creep test 303
M. Pszczoła & J. Judycki

Effect of beam size on the creep stiffness of asphalt mixtures at low temperatures 313
R. Velásquez, M. Marasteanu, M. Turos & J. Labuz

Assessment of water sensitivity of asphalt rubber mixtures for wearing course 323
F.A. Batista, M.L. Antunes & P. Fonseca

Development of a laboratory bituminous mixtures ageing protocol 331
C. de la Roche, M. Van de Ven, W. Van den bergh, T. Gabet, V. Dubois, J. Grenfell & L. Porot

3. *Hot bituminous mixtures characterization and design*

Optimum loading speed for deformation strength test of bitumen mixtures 349
S.H. Baek, J.C. Kim, Y.S. Doh & K.W. Kim

Enhanced algorithms for the derivation of material parameters from triaxial cyclic compression tests on asphalt specimen 357
K. Kappl & R. Blab

Reliability and suitability for standardization of methods for HMA density measurements: Experimental investigation on transverse vs longitudinal variations 367
F.G. Praticò, R. Ammendola & A. Moro

Research on coordinating deformation between Fiber Bragg Grating strain sensor and asphalt mixture 377
D. Zejiao, T. Gengliang & T. Yiqiu

Influence of treatments on the surface characteristics of aggregate 387
D.Q. van Lent, A.A.A. Molenaar & M.F.C. van de Ven

Mix design of grouted porous asphalt concrete for wearing course layers 399
M. la Agostinacchio, D. Ciampa & S. Olita

"Liquefaction" of asphalt caused by cyclic loading, as a potential reason of extreme rutting 409
G. György, F. Wellner & I. Herle

Experimental investigation on the dynamic properties of asphalt concrete using filler with waste hydrated lime 423
M. Arabani, H.R. Joodi & V. Shakeri

Monitoring and designing of wearing courses for orthotropic steel decks throughout the five-point bending test 433
A. Houel, T.L. N'Guyen & L. Arnaud

Evaluation of modified bitumen, High Modulus Asphalt Concrete and steel mesh as materials for road upgrading 443
M. Tušar, M. Ravnikar Turk, W. Bańkowski, L.G. Wiman & B. Kalman

Theoretical investigation of the stress distribution in a Bimodular IDT specimen 453
S. Katicha & G. Flintsch

Investigation of Alkali-Silica Reaction in asphalt mixtures exposed to potassium acetate deicing solution 463
A.K. Apeagyei, L.J. Struble & W.G. Buttlar

Laboratory tests used in Cuba as low financial resources country for the evaluation of the mechanical properties of the asphalt mix 477
R. Herrera de la Rosa

Polypropylene fiber modification of asphalt by using mechanical and optical means 487
S. Tapkın, Ş. Özcan, M. Tuncan & A. Tuncan

Evaluation of Petroleum-Contaminated Soil effect on the properties of hot-mix asphalt concrete using dynamic modulus |E*| and indirect tensile tests 497
H.F. Hassan

Overview of the LOT meso mechanical research into porous asphalt raveling 507
M. Huurman, L. Mo, M.F. Woldekidan, R.N. Khedoe & J. Moraal

Monitoring the introduction of Enrobé à Module Élevé class 2 onto UK roads 519
R.C. Elliott, R. Perera, A. Hunter, J.C. Nicholls, N.B. Meite & D. James

On the fracture properties of epoxy asphalt mixture with SCB test 531
X. Chen, H. Li & Z. Qian

Viscoelastic response of asphalt-aggregate mixes to transient confining conditions 541
E. Levenberg & J. Uzan

Evaluation of creep compliance of rubberized asphalt in compare with conventional hot mix asphalt 551
M. Arabani & S.M. Mirabdolazimi

Characterizing volumetric deformation behavior of naturally occurring bituminous sand materials 559
J.K. Anochie-Boateng & E. Tutumluer

Alternative materials for asphalt mixture—steel slags 569
E. Diaconu & Ş.M. Lazăr

Evaluation on the shear performance of asphalt mixture through triaxial shear test 575
J. Yang, H. Zhu & Z. Chen

Development of a Dog-Bone Direct Tension Test (DBDT) for asphalt concrete 585
C. Koh, G. Lopp & R. Roque

Evaluation of performance grading parameters for crumb rubber modified asphalt binders and mixtures 597
N. Tabatabaee, H.A. Tabatabaee, M.R. Sabouri & P. Teymourpour

4. Warm and cold bituminous mixtures characterization

Design method for cold and warm emulsion mixtures based on links between laboratory and field 609
J.P. Serfass, X. Carbonneau, B. Eckmann & J.P. Triquigneaux

Fundamental property evaluation of styrene monomer modified warm-mix asphalt concrete 619
I. La, M.Y. Ryu, H.H. Kim, K. Ahn, Y.S. Doh & K.W. Kim

An evaluation of use of synthetic waxes in warm mix asphalt 627
F. Cardone, V. Pannunzio, A. Virgili & S. Barbati

Study of the mechanical behaviour of gravel-emulsions using triaxial tests 639
P. Hornych, V. Gaudefroy, J.L. Geffard & S. Goyer

Laboratory performance-based assessment of half-warm mix asphalts with high recycling rate by means of the factorial experiment design approach 651
F. Olard, E. Beduneau, N. Seignez, S. Dupriet & D. Bonneau

Evaluation of the rheological behaviour of Warm Mix Asphalt (WMA) modified binders 661
H.M.R.D. Silva, J.R.M. Oliveira, E.J. Peralta & C.I.G. Ferreira

Author index 675

VOLUME II

5. Cracking in bituminous pavement materials

Modeling of Top-Down Cracking (TDC) propagation in asphalt concrete pavements using fracture mechanics theory 681
M. Fakhri, M. Farokhi & P.T. Kheiry

The cracking device with temperature control for the laboratory identification of the road material performance 693
M. Dicu & M. Lobază

Mode II cracking in asphalt concrete 699
A. Braham & W. Buttlar

Experimental study on resistance to cracking of bituminous mixtures using the Fénix test 707
F. Pérez, R. Botella & G. Valdés

Fatigue effects in uniaxial cyclic tensile stress test: The link between stiffness decrease and accumulation of irreversible strain 715
K. Mollenhauer & M. Wistuba

Experimental study of the waveform shape effect on asphalt mixes fatigue 725
D. Bodin, J.-M. Balay, M. Merbouh, D. Breysse & L. Moriceau

Experimental investigation of crack propagation in asphalt concrete 735
R.A. Tarefder & E.M. Kias

Theoretical analysis of the 4 point bending test 749
M. Huurman & A.C. Pronk

Investigation of the PH model as a prediction tool in fatigue bending tests with rest periods 761
A.C. Pronk & A. Cocurullo

Fatigue behaviour of bitumen in tension-compression loading mode: Rheological analysis and comparison with mix fatigue 773
E. Chailleux, D. Bodin, C. de La Roche, M. Leguern & N. Vignard

Mixed-mode cracking in asphalt concrete 785
A. Braham, C. Peterson & W. Buttlar

Fatigue lines for asphalt mixtures used in wearing course 795
C. Răcănel, C. Romanescu, M. Dicu, A. Burlacu & C. Surlea

Mechanism of fatigue crack growth and fracture behavior in bituminous roads 807
R. Lugmayr, M. Jamek & E.K. Tschegg

Simplified fatigue performance modeling of ALF pavements using VECD+3-D Finite Element Modeling 817
B.S. Underwood, Y.R. Kim, S. Savadatti, S. Thirunavukkarasu & M.N. Guddati

Size effect investigation on fracturing of asphalt concrete using the cohesive softening Discrete Element Model 827
H. Kim, M.N. Partl, M.P. Wagoner & W.G. Buttlar

6. Fundamental laboratory test methods and models

On the importance of performing accurate material characterization tests for bituminous materials 839
N. Kringos & A. Scarpas

Prediction of rutting risk of bituminous concrete using complex modulus 849
K. Ait Mokhtar, E. Ghorbel, S. Saoula & S. Haddadi

Application of simplified VECD modeling to the fatigue life prediction of asphalt concrete mixtures 859
B.S. Underwood, E.T. Hou & Y.R. Kim

Experimental observation of asphalt mix characteristics in the range of low temperatures 869
P. Mondschein & J. Valentin

Calibration and validation of a visco-elasto-plastic constitutive model for bituminous conglomerates 879
N. Baldo, M. Pasetto, N. Kringos, C. Kasbergen & A. Scarpas

Modulus measurement: European standardisation possibilities 889
X. Carbonneau, Y. Legal & S. Quigniot

The influence of the specimen shape on the results of the uniaxial tensile test 899
C. Weise & A. Blasl

Experience with triaxial loading systems for the testing of road construction materials 909
P. Hyzl, D. Stehlik, M. Varaus & P. Zdralek

The estimation of the dynamic modulus of asphalt mixture from creep test results 917
F. Martinez & S. Angelone

Application of a balanced mix-design concept to thin asphalt overlay mixes: Minimizing rutting and reflective-cracking 927
L.F. Walubita & T. Scullion

3D finite element modeling of polymer modified asphalt base course mixes 939
X. Liu & A. Scarpas

Neural networks in rheology: Theory and application 949
M. Oeser & S. Freitag

7. Test methods and models for permanent deformation

Permanent deformation behaviour of bituminous mixtures containing incinerator bottom ash aggregates under uniaxial testing conditions 961
M.M. Hassan & H.A. Khalid

A new performance related test method for rutting prediction: MSCRT 971
S. Dreessen, J.P. Planche & V. Gardel

Effect of binder type on the permanent deformation resistance of asphalt mix at different temperatures 981
M. Smiljanic, I. Pap & U. Tatic

Rutting evaluation of asphalt binders and mixes 989
T.L.J. Wasage, I.B. Kazatchkov, J. Stastna & L. Zanzotto

An integrated approach to modeling rutting of flexible pavements 999
V.T. Thushara & J. Murali Krishnan

Equiviscous temperature based on Low Shear Viscosity: Evaluation as binder indicator for rutting and critical discussion of the test procedure 1009
J. De Visscher & A. Vanelstraete

The effect of volumetric properties of asphalt concrete mixture to wheel track rutting with respect to EN and BS rutting test methods 1019
A. Nikolaides & E. Manthos

Rutting resistance of SMA determined with triaxial and wheel-tracking tests 1029
J.L.M. Voskuilen & M.F.C. van de Ven

Rut resistance of asphalt concretes of different aggregate gradation 1039
K. Zhdanyuk, O. Volovyk, V. Zhdanyuk & Y. Prusenko

8. Field methods for structural behavior assessment

Damage identification in flexible pavements using FWD technique 1049
A. El Ayadi, B. Picoux & C. Petit

Dynamic approach for the evaluation of the load carrying capacity and stability of flexible pavements with the Falling Weight Deflectometer 1059
S. Riedl

Behavior of asphalt pavements subjected to non-standard heavy vehicles 1071
P.E. Sebaaly & R.V. Siddharthan

Field behavior of foamed bitumen pavement material 1081
V. Papavasiliou & A. Loizos

Evaluation of cracking in overlays in Quebec: A case study 1091
A. Carter, D. Perraton, M. Meunier & M. Paradis

9. Recycling of bituminous pavement materials

Utilization of aggregate production waste filler in cold recycling mix optimization 1101
J. Valentin & P. Mondschein

Rehabilitation of an Italian highway by Cold In-Place Recycling techniques 1113
F.A. Santagata, M. Bocci, A. Grilli & F. Cardone

Fracture energy evaluation of Cold In-Place Recycling mixtures 1123
S. Charmot & P. Romero

The use of marginal materials in road constructions: Proposal of an eco-compatible section 1131
M. Agostinacchio, M. Diomedi & S. Olita

Influence of active filler, curing time, and moisture content on the strength properties of emulsion and foamed bitumen stabilized mix 1143
S. Zulakmal, A.A. Nafisah, M. Mohd Yazip & H. Mat Zin

An experimental study on the recycling of powder extinguishers into bituminous mixtures 1151
F.G. Praticò, A. Moro & R. Ammendola

Key characteristics of materials stabilised with foamed bitumen 1161
D.C. Collings & K.J. Jenkins

In-plant asphalt cold recycling in rehabilitation of Babaei expressway project 1169
V. Ayan, A. Khavandi, A. Nikzad Gharehaghaji

10. Synthesis of international coordinated research initiatives

RILEM interlaboratory test on interlayer bonding of asphalt pavements 1181
H. Piber, F. Canestrari, G. Ferrotti, X. Lu, A. Millien, M.N. Partl, C. Petit, A. Phelipot-Mardelé & C. Raab

RILEM interlaboratory test on pavement performance prediction and evaluation 1191
H. Piber, M.N. Partl & C. Raab

New tests for polymer-modified binders: Results of a Belgian round robin test 1201
J. De Visscher, S. Vansteenkiste, A. Leuridan, N. Piérard, E. Schelkens & Ph. du Bus de Warnaffe

Comparative test on indirect tension modulus test 1211
X. Carbonneau & Y. Le Gal

Binder fatigue properties and the results of the Rilem Round Robin Test 1221
D. Sybilski, M. Gajewski, W. Bańkowski, H. Soenen, E. Chailleux & G. Gauthier

11. Other topics

Skid-resistance capability of two newly resurfaced runways in Israel 1235
M. Livneh

Chemical spill tolerance of hot mix asphalts: New research and gaps identification 1247
F.G. Praticò, R. Ammendola & A. Moro

Result of numerical analysis of efficacy geogrids on reinforced pavements' vertical and horizontal deformations 1257
F. Saleh, Gh. Shafabakhsh & Ah. Hadad

Life cycle costs of typical asphalt pavement rehabilitation techniques in Colorado USA 1265
S. Shuler, C. Schmidt & J. Goldbaum

Performance oriented payment adjustment for flexible pavements 1269
P. Sivapatham & H.J. Beckedahl

Performance of hot mix asphalt surface under high tire pressure aircraft landing gear configuration at the FAA National Airport Pavement Test Facility 1279
N. Garg, T. Bennert & H. Brar

Quantification of the highway costs as a function of the road traffic and speed 1289
A.C. Valle de Souza & D. Cardoso de Lima

Author index 1299

Advanced Testing and Characterization of Bituminous Materials –
Loizos, Partl, Scarpas & Al-Qadi (eds)
© 2009 Taylor & Francis Group, London, ISBN 978-0-415-55854-9

Preface

Bituminous materials are used to build durable roads that sustain diverse environmental conditions. However, due to their complexity and a global shortage of these materials, the design and technical development of bituminous materials has become challenging. The *International Union for Testing and Research Laboratories for Materials and Structures* RILEM has contributed to this challenging task for the past several years through Technical Committees that focus on the characterization and performance of bituminous binders and mixtures. These Committees provide a platform for researchers from all over the world to share their expertise, develop recommendations on testing and evaluation approaches and publish state-of-the-art reports and papers in the RILEM *Journal of Materials and Structures* as well as other journals and conferences.

The *7th International RILEM Symposium on Advanced Testing and Characterization of Bituminous Materials* ATCBM09 is under the auspices of the RILEM TC 206-ATB. The ATCBM09 RILEM Symposium aims to provide an international forum for the exchange of ideas, information, and knowledge amongst experts involved in the development and implementation of specifications for the experimental characterization, design, utilization and evaluation of binders and bituminous mixes.

Currently, the committee, chaired by Manfred N. Partl of EMPA, Switzerland, comprises 50 experts from 20 countries. The committee focuses on fundamental and performance testing of binders and asphaltic mixtures. The committee is composed of five Task Groups:

- *TG 1 Binders* (Convener: Dariusz Sybilski, IBDiM, Poland): Focused on evaluating *bin*der properties with respect to durability relevant distress accumulation, *performance*, and application.
- *TG 2 Mixture design and compaction* (Convener: Hussain Bahia, University of Wisconsin, USA): Focused on the evaluation of laboratory compaction methods and models with respect to field compaction.
- *TG 3 Mechanical testing of mixtures* (Convener: H. Di Benedetto, ENTPE, France): Focused on the evaluation of existing test methods and models for different types of mixtures considering topics such as permanent deformation, micromechanics, and size effects.
- *TG 4 Pavement performance prediction evaluation* (Convener: Herald Piber, Bautechnik Carinthia, Austria, followed by Francesco Canestrari, Univ delle Marche, Italy): Focused on the evaluation of test methods to assess structural behavior such as interlayer bond and pavement performance prediction evaluation.
- *TG 5 Recycling* (Convener: Chantal De La Roche, LCPC, France): Focused on the evaluation of reclaimed asphalt pavements and hot-mix recycling.

This Symposium represents the seventh in a series of RILEM Symposia on characterization, performance testing, and evaluation of bituminous binders and mixtures. In chronological order, the previous symposia convened at the following locations: 1st 1968 Dresden, 2nd 1975 Budapest, 3rd 1983 Belgrade, 4th 1990 Budapest, 5th 1997 Lyon, 6th 2003 Zürich, 7th 2009 Rhodes.

All submitted contributions were subjected to an exhaustive refereed peer review procedure by at least three reviewers and the Editors. On the basis of their recommendations, the papers that contributed to the symposium subject and met the goals and the objectives of the Symposium were selected for inclusion in the Proceedings.

The accepted contributions indicate that many researchers from the academia, industry, and governmental agencies are currently utilizing advanced experimental and computational techniques to better understand the behavior of binders and bituminous mixtures and their role in the design and performance of complex pavement systems. The Proceedings clearly show that modern experimental material characterization techniques, sophisticated constitutive modeling, and innovative design provide the appropriate tools for pavement performance prediction. This ultimately would lead to the development and implementation of truly "mechanistic" pavement design methodologies.

The Editors would like to thank the reviewers and the Scientific Committee for their thorough and timely review of the papers. Special thanks also are extended to the Organizing Committee for their management of the Symposium.

The Editors

Andreas Loizos
Manfred Partl
Tom Scarpas
Imad Al-Qadi

Rhodes, May 2009

Advanced Testing and Characterization of Bituminous Materials – Loizos, Partl, Scarpas & Al-Qadi (eds)
© 2009 Taylor & Francis Group, London, ISBN 978-0-415-55854-9

Organization

Chairmen

Andreas Loizos	National Technical University of Athens, Greece
Manfred Partl	EMPA, Chair of RILEM TC 206-ATB, Switzerland
Tom Scarpas	Delft University of Technology, The Netherlands
Imad Al-Qadi	University of Illinois at Urbana-Champaign, USA

Scientific Committee

Chairmen: A. Loizos, M. Partl

G. Airey, UK
M. Ayala Canales, Spain
H. Azari,USA
H. U. Bahia, USA
W. Bankowski, Poland
R. Blab, Austria
D. Bodin, France
W. Buttlar, USA
F. Canestrari, Italy
C. Celauro, Italy
A. Chabot, France
E. Chailleux, France
J.S. Chen, Taiwan
A. Collop, UK
J. D'Angelo, USA
M. Darter, USA
C. De la Roche, France
H. Di Benedetto, France
B.J. Dongo-Engeland, Norway
R. Dongre, USA
G. Doré, Canada
B. Eckmann, Belgium
S. Erkens, The Netherlands
A.C. Freire, Portugal
G. Gauthier, France
M. Greenfield, USA
R. Gubler, Switzerland
T. Harman, USA
J. Harvey, USA
G. Huber, USA
M. Hugener, Switzerland
U. Isacsson, Sweden
I. Ishai, Israel
K. Jenkins, South Africa
K. Kaloush, USA
H.A. Khalid, UK
R. Kim, USA
G. King, USA
B. Koenders, France
N. Kringos, The Netherlands
D. Little, USA
H. Litzka, Austria
X. Lu, Sweden
B. Lytton, USA
J. Maeck, Belgium
M. Marasteanu, USA
E. Masad, USA
L. Mohammed, USA
A.A. Molenaar, The Netherlands
J. Nodes, USA
M. Oeser, Australia
J.C. Pais, Portugal
T. Pauli, USA;
D. Perraton, Canada
K. Petros, USA
H. Piber, Austria
J.P. Planche, France
J.E. Poirier, France
L. Porot, France
C. Raab, Switzerland
R. Robertson, USA
R. Roque, USA
G.M. Rowe, USA
S. Said, Sweden
M. Saleh, New Zealand
E. Santagata, Italy
C. Schwartz, USA
P. Sebaaly, USA

M. Smiljanic, Serbia
H. Soenen, Belgium
J.M.B. Sou sa, Portugal
D. Sybilski, Poland
G. Tebaldi, Italy
S. Toth, Hungary
M. Van de Ven, The Netherlands
A. Vanelstraete, Belgium
H. Von Quintus, USA
L.B. Wang, USA
M.W. Witczak, USA
J. Youtcheff, USA
M. Zaman, USA
L. Zanzotto, Canada

1. Evaluation of binder properties

Advanced Testing and Characterization of Bituminous Materials –
Loizos, Partl, Scarpas & Al-Qadi (eds)
© 2009 Taylor & Francis Group, London, ISBN 978-0-415-55854-9

Laboratory study on interlayer bonding using cationic tack coats

C. Raab & M.N. Partl
Department of Road Engineering and Sealing Components, Empa, Duebendorf, Switzerland

ABSTRACT: The paper summarizes the results of a laboratory study in which a cationic tack coat was used between two layered specimens. The specimens were produced with a roller compactor and the adhesion of cores taken from the specimens was evaluated by means of direct shear testing according to Leutner. To evaluate the limits of the application of tack coats dirt and moisture was applied between the two layers before and after the application of a tack coat. In addition, the influence of tack coats on fine milled surfaces and the influence of curing time on the bonding properties were investigated. It could be shown that especially in the case of dirt and moisture—common phenomena on construction sites-tack coats have a great potential to secure and improve adhesion properties. Contrary to the benefit of tack coats on dirty and wet surfaces the advantage of tack coats on fine milled surfaces is doubtable.

1 INTRODUCTION

Tack coats have been used in road construction for many years to improve the bond between the different pavement layers. Although the benefit of using a tack coats is not debated (Uzan et al. 1978), (Recasens et al. 2003), (Canestrari et al. 2005) it is not clear how much tack coats effectively contribute to the bonding properties. In most cases tack coats are applied empirically based on the practical experience of contractors and consultants. Parameters, such as surface characteristics, cleanness of the underlying base course surface and the age of the underlying layer play an important role, although their influence is often neglected in reality.

In order to provide for these deficiencies a laboratory study (Raab & Partl, 2007) was conducted in which a cationic tack coat was used between two layered specimens. The specimens were produced with a roller compactor and the adhesion of cores taken from the slabs was evaluated by means of direct shear testing according to Leutner (Leutner, 1979). Different parameters such as surface characteristics and the influence of curing time were investigated and their influence on the bond between the layers was determined. To evaluate the limits of the application of tack coats dirt and moisture was applied between the two layers before and after the application of a tack coat.

2 OBJECTIVE

Although the results from laboratory studies are different to the in situ behaviour of asphalt pavements, such studies provide a good opportunity to look at specific parameters and to determine their influence on certain material and construction properties.

The objective of this laboratory study was the evaluation of the interaction of different surface characteristics of the underlying layer, such as cleanness, dryness, roughness and age, with a cationic tack coat as well as the determination of the influence on bonding properties.

3 SPECIMEN PREPARATION

3.1 *Slab construction*

Although the investigation was a laboratory study, the slab construction should be as close to reality as possible. After trials with other laboratory compactors the MLS roller compactor constructed at the University of Stellenbosch, South Africa was used.

The compactor (Figure 1) consists of a steel roller with a width of about 91 cm and a diameter of about 35 cm and a metal frame with a rail on which the steel roller can be displaced horizontally. In the vertical direction a winder enables the steel roller to be moved; furthermore an automatic vibration system can be applied. During compaction the steel roller is spayed with water and prior to compaction it is heated with a heater reflector. The steel roller is pushed manually back and forth in the longitudinal direction of the slab. A piece of concrete within the metal frame builds the base for compaction.

For the construction of the asphalt slabs a wooden frame with the dimension of 0.95 on 1.08 m was applied and the hot mixture was filled into it and compacted. The slabs were constructed in two layers. The base layer which consisted of asphalt concrete 22 (AC T 22) and had a thickness of 6 cm, while the surface layer consisting of asphalt concrete 11 (AC11) was 4 cm thick. The asphalt concrete mixes had been taken in 25 kg batches from the asphalt plant and wee mixed again in a 120 kg laboratory mixer for the individual slabs.

The mixtures followed the European standard 13108-1 (EN 13108-1 Bituminous mixtures, 2008). Both mixtures consisted of an unmodified penetration grade binder 50/70. The slabs had a dimension of 0.99 m × 0.86 m. After the construction of the base layer 200 g/m^2 of tack coat were sprayed on the surface on one side of the slab using a spray gun and the surface layer was applied after the emulsion had broken. The time between bottom layer and surface layer compactions was in all cases 20 to 24 h. The tack coat was an unmodified bituminous cationic emulsion C 50 with a nominal bitumen content of 50% according to the European standard, EN 13808 (European Standard EN 13808, 2005). For the investigation of the influence of polymer modified tack coats in one case the tack coat C 60 P with a nominal bitumen content of 60% and a polymer modification was used. Here, according to manufacture's specifications the total application rate the was also 200 g/m^2. The tack coat was weighted on a scale and evenly distributed over the surface using a spray gun.

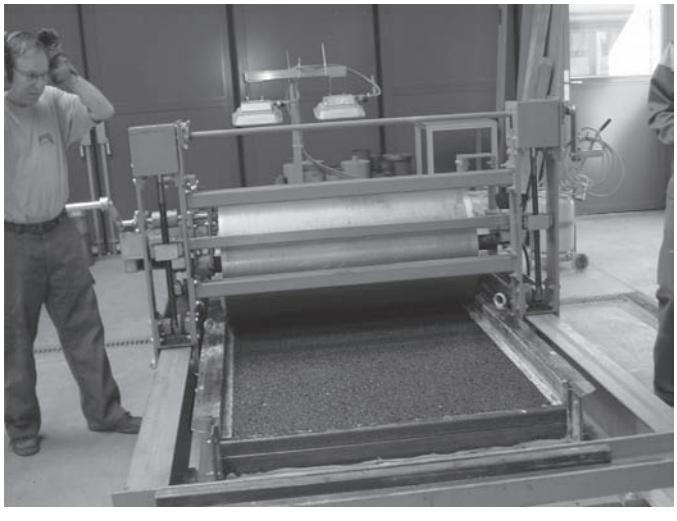

Figure 1. Laboratory steel roller compactor.

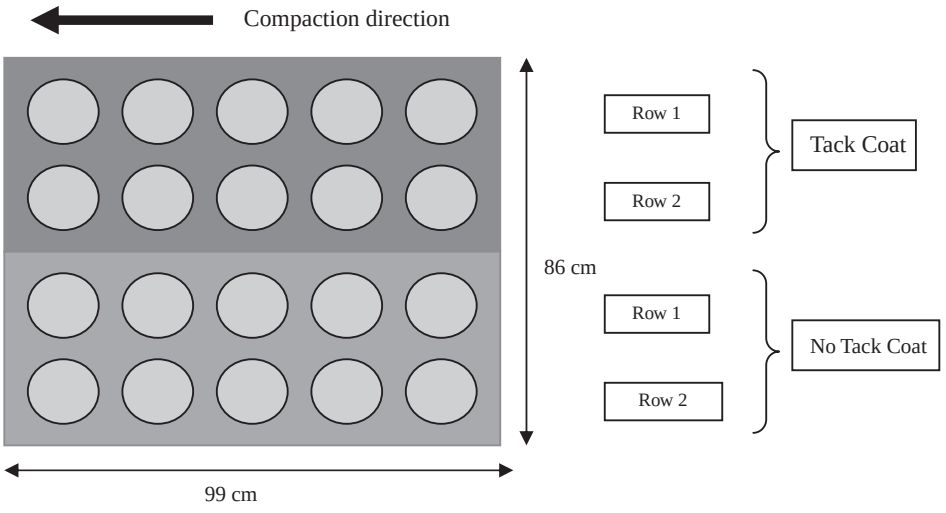

Figure 2. Slab with coring pattern.

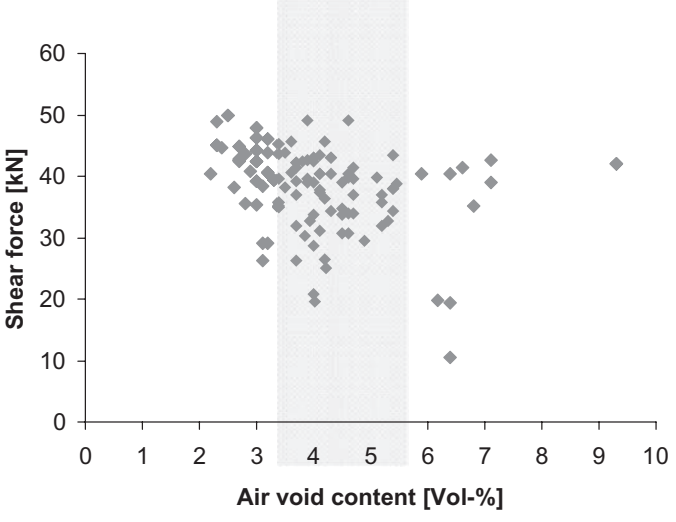

Figure 3. Air void content of the surface layer AC 11 and shear force.

3.2 *Coring*

Two days after construction 12 cores were taken on either side of the slab (with and without tack coat). Figure 2 shows a schematic of coring for one slab:

3.3 *Air void content*

Although the construction with the MLS roller compactor proved to be more close to the compaction on a real construction site, there were still some difficulties regarding the air void content of the surface layer. The air void content was measured according to the European standard EN 12697-6 using the saturated dry surface bulk density. While the air void content of the base layer with 5 to 7 Vol-% was quite evenly distributed over the slab, considerable differences from 2 to 10 Vol-% could be found for the air void content of the surface layer. That there is no correlation between the shear force and the air void content can be illustrated by Figure 3, although a slight trend of low air void contents towards high shear forces and

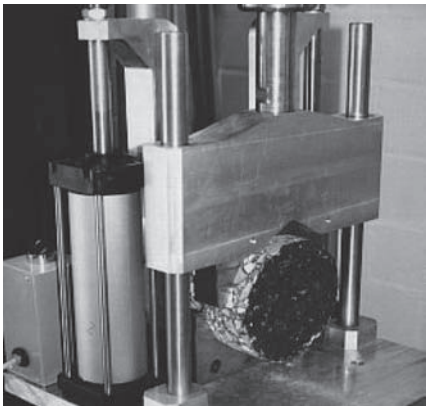

Figure 4. Layer Parallel Direct Shear Test Device (LPDS).

vice versa cannot be neglected. In this Figure shear forces and air void content of cores from different slabs (with and without tack coat, but only for untreated slabs, e.g. slabs without water, dirt or milling) are depicted.

To minimize the influence of the air void content on the bond between the layers, slabs with air void contents of more than 8 Vol-% were rejected and replaced. The majority of tested cores had an air void content of the surface layer between 3 and 5 Vol-% and in this region not even a tendency between high air void content towards low shear forces and vice versa is visible.

4 BOND TESTING

The Layer-Parallel Direct Shear (LPDS) test device is an EMPA modified version of equipment developed in Germany by Leutner (Leutner, 1979). The modified LPDS test device fits into an ordinary servo-hydraulic Marshall testing machine and allows testing of cores with a diameter of about 150 mm; (Raab & Partl, 1999), (Partl & Raab, 1999). One part of the core (up to the shear plane to be tested) is laid on a circular u-bearing and held with a well defined pressure by a semicircular pneumatic clamp. The other part, the core head, remains unsuspended. Shear load is induced to the core head by a semi-circular shear yoke with a deformation rate of 50 mm/min, thus producing fracture within the pre-defined shear plane of 2 mm width.

The cores were conditioned in a climate chamber for 8 hours and all tests were conducted at a temperature of 20°C (Swiss Standard SN 671961, 2000).

5 TEST PROGRAM

The test program is depicted in Table 1.

Slab 1, Original state: In order to have a slab, which could be used for comparative purposes, the first slab was untreated. On one half of the slab the cationic tack coat C 50 was applied, while the other had no tack coat.

Slab 2, Polymer modified tack coat: The second slab also had no special treatment, but this time one side of the slab was sprayed with a polymer modified tack cot C 60 P.

Slabs 3 and 4, Surface roughness: Slabs 3 and 4 were constructed to determine the influence of the surface roughness. Both slabs were fine milled. This was done using a small milling machine as depicted in Figure 4, left. After the milling, which removed up to 5 mm of

Table 1. Test program.

Slab no.	Parameters	Tack coat	Treatment of base layer surface and other remarks
1	Original state	C 50	No treatment
2	Polymer modified tack coat	C 60 P	No treatment
3	Surface roughness	None	Fine milling of base layer surface
4	Surface roughness	C 50	Fine milling of base layer surface
5	Cleanness	C 50	Dirt (filler) was applied *before* tack coat application
6	Cleanness	C 50	Dirt (filler) was applied *after* tack coat application
7	Cleanness and dryness	C 50	Wet dirt (filler) was applied *before* tack coat application
8	Cleanness and dryness	C 50	Wet dirt (filler) was applied *after* tack coat application
9	Curing time and age	C 50	Slab was stored outside for 2 months (summer conditions) before testing
10	Curing time and age (comparison)	C 50	Slab was cored and directly tested after construction

Figure 4. Left: Fine milling device, Right: Surface of base layer after fine milling.

the existing surface (see Figure 4, right), a tack coat was applied on slab 4, while slab 3 had no further treatment.

Slab 5, Cleanness: The purpose of the treatment was the simulation of a dirty road surface before the application of tack coat. Fine filler, representing dirt on the road during construction, was put on the surface of the lower layer, before the application of tack coat on one half of slab 5. This procedure was done with the help of a sieve, the application rate was 360 g/m^2.

Slab 6, Cleanness: The purpose of the treatment was the simulation of a dirty road surface *after* the application of tack coat. For slab 6 the same procedure as for slab 5 was used, the only difference was, that one half of the slab had been sprayed with tack coat before the filler (dirt) was applied.

Slab 7, Cleanness and dryness: The purpose of the treatment was the simulation of a dirty and wet road surface before the application of tack coat. Fine filler was mixed

with water with a relationship of 2.5:1 and brushed n the surface of the lower layer, before the application of tack coat on one half of slab 7. The application rate was about 1000 g/m^2.

Slab 8, Cleanness and dryness: The purpose of the treatment was the simulation of a dirty and wet road surface after the application of tack coat. For slab 8 the same procedure as for slab 7 was used, the only difference was, that one half of the slab had been sprayed with tack coat before the wet filler (dirt and moisture) was applied.

Slabs 9 and 10, Curing time and age: Slabs 9 and 10 were constructed to evaluate the effect of curing time and aging. Slab 9 was constructed (applying tack coat on one half of the slab) and stored outside for 2 months before coring and testing. Slab 10 was cored and tested directly after construction similar to all other slabs.

6 RESULTS OF BOND TESTING

The test results are given in Table 2:

Table 2 lists the test results for all slabs, giving the minimum and the maximum shear force, the mean value of the shear force and the standard deviation for each slab. From all slabs 12 cores with and 12 cores without tack coat were tested. In case of slabs 3 and 4 the investigation was based on 24 cores each.

6.1 *Influence of unmodified tack coat*

The comparison of slab 1 and slab 10, which were prepared and tested the same way, showed that the application of tack coat in the laboratory can have a positive result on the bonding of the layers; although in the lab a tack coat seems not to be absolutely necessary. For the first slab a mean value of 34 kN without tack coat and a mean value of 40 kN with tack coat was determined, while slab 10 received a mean value of 35 kN with no tack coat and 33 kN when a tack coat was used.

6.2 *Influence of polymer modified tack coat*

The application of a polymer modified tack coat as opposed to a non modified one did not seem to have a positive influence on the adhesion between the two layers: In case of the polymer modified tack coat a mean value of 40 kN was measured, while the mean value for the cores without tack coat came up to 44 kN.

Table 2. Test results.

	Shear force with tack coat				Shear force without tack coat			
	kN				kN			
Slab no.	min	max	mean	stdev	min	max	mean	stdev
1	31.0	49.0	40.3	4.7	20.9	46.3	34.0	8.3
2	35.0	45.3	40.0	3.8	39.3	49.9	44.0	3.3
3	–	–	–	–	1.9	36.3	26.0	4.1
4	3.0	24.7	12.6	6.9	–	–	–	–
5	10.7	32.7	24.6	7.8	0.7	19.4	8.4	5.2
6	3.4	20.4	10.2	5.2	0 (broken)	8.1	2.8	3.1
7	1.9	11.1	7.5	3.9	0 (broken)	11.1	2.9	3.9
8	0 (broken)	6.9	5.1	2.7	0 (broken)	5.7	1.0	1.9
9	37.9	49.1	42.1	3.8	26.2	43.5	34.9	5.2
10	23.9	40.3	33.5	4.3	27.7	43.9	35.4	5.4

6.3 *Influence of surface roughness*

When comparing the fine milled slabs with and without cationic tack coat, in case of tack coat, the mean value was dramatically lower (12.6 kN) than for no tack coat, where the mean value achieved 26 kN.

6.4 *Influence of cleanness before tack coat application*

In order to simulate the cleanness of the base layer surface, before the application of a tack coat about 360 g/m^2 of fine corundum was put on this surface and distributed evenly. Then the cationic unmodified tack coat was sprayed and the surface layer was applied.

Here, the results clearly revealed the potential of a tack coat to ensure the bonding properties even in a critical situation: When the mean value for the non treated cores came up to only 8.4 kN, when usinga tack coat the mean value reached nearly 25 kN.

6.5 *Influence of cleanness after tack coat application*

The importance of cleanness after the application of a tack coat was demonstrated by the results of the LPDS testing. Even in this situation the use of tack coats could prevent the worst: When no tack coat was applied most cores were already destroyed by coring and the mean value only reached 2.8 kN, whereas in case of tack coat all cores were still intact and the mean value was measured with 10 kN.

6.6 *Influence of cleanness and moisture before tack coat application*

In order to simulate an unclean and wet base layer surface, fine corundum was mixed with water and brushed on the base layer before a tack coat was sprayed.

This experiment showed that the presence of water on an unclean base layer surface was even more critical, than when no water was present. In this case the two layers were very weakly bonded when no tack coat was applied. LPDS tests determined a mean value of 2.9 kN, while many cores were already broken before testing. When using a tack coat the mean value of LPDS testing achieved 7.5 kN.

6.7 *Influence of cleanness and moisture after tack coat application*

The combination of dirt and water when the tack coat was already applied proved to be the most critical case. For the situation of an untreated surface similar results as shown above (mean value of 2 kN, with many of the cores already destroyed by coring) were achieved. But even when a tack coat was applied on the dirt and wet surface the adhesion properties were extremely weak. The mean value only came up to 5 kN, while many of the cores already lost their bond during coring.

6.8 *Influence of curing time and age*

In order to simulate the influence of curing time and age, slab 9 was constructed, but left for 2 months outside before the cores were taken and the testing effectuated. Since the whole experiment took place during summer time (June to August), the temperatures were between 11°C and 35°C and occasionally heavy rain fall occurred.

When looking at the comparison of the mean values with and without the application of a tack coat it seemed clear that curing and aging had a positive effect on the bonding properties. When the mean value without tack coat was determined to be 35 kN, the mean value in the case of cationic tack coat received a value of 42 kN.

6.9 *Comparison of results*

Figure 5 shows a summary and a comparison for all tested slabs. The Figure depicts the mean force values for the LPDS testing of 12 cores and also depicts the standard deviation. In case of slabs 3 and 4 (influence of surface characteristics) the mean value was calculated from 24 cores.

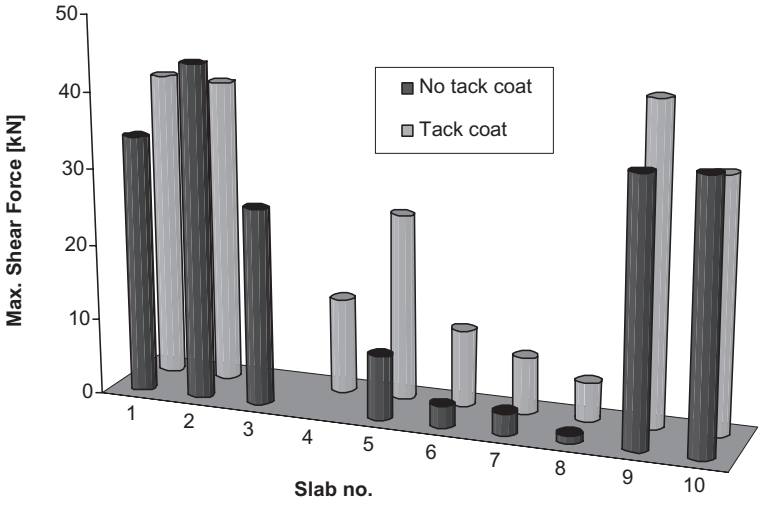

Figure 5. Mean force values from LPDS testing for all slabs.

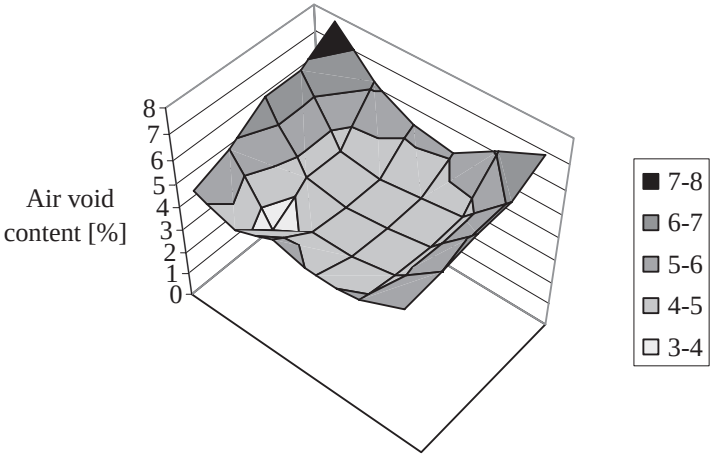

Figure 6. Air void distribution of the surface layer over the surface of the specimen.

7 SUMMARY AND DISCUSSION

7.1 *General remarks*

The research summarized in this paper aimed at the investigation of tack coats and their influence on the bond between asphalt pavements. Although it was a laboratory study the construction of the slabs (asphalt laying and compacting) tried to simulate the construction on the road as good as possible.

That the situations in the lab and on the road all the same show severe differences cannot be neglected. The laboratory steel roller compactor did not lead to a uniform compaction and revealed considerable differences in the compaction over the slab surface, as shown by the contribution air void content of the surface layer over the slab surface in Figure 6.

Nevertheless, laboratory studies provide a good opportunity to look at specific parameters and to determine their influence on certain properties.

7.2 *Influence of polymer modified tack coat*

As shown by the results of this research using a polymer modified tack coat does not seem to have an advantage compared to the use of an unmodified one. Although one has to keep in mind that the asphalt mixture which was used in these experiments consisted of unmodified bitumen. The reason for the stated fact could also be found in a different bonding mechanism of polymer modified tack coats, which according to their chemical structure need a longer curing time, before the bond is totally developed.

7.3 *Influence of surface characteristics*

That fine milling does not necessarily have a positive effect on the adhesion properties determined by LPDS testing had already been shown in other publications (Raab & Partl, 2006). Furthermore, the application of tack coat on fine milled asphalt concrete surfaces seems even to have a negative influence on the determined adhesion values, resulting in considerable lower shear forces when compared to slabs where no tack coat was applied.

Here again, the mechanism of bonding could be different. Since fine milling removes the binder on the asphalt concrete surface, the time needed for bonding is considered to be longer than on a non milled surface. Furthermore, the amount of tack coat in case of a milled surface should be increased in order to fill the holes.

7.4 *Influence of cleanness*

In case of a dirty base layer surface the advantage of the application of a tack coat is clearly revealed. Especially, when the tack coat is applied on a dirty surface its potential to restore the bond between the layers and to lead to acceptable adhesion force values becomes clear. When applying the tack coat before the pollution takes place, its potential is limited, but still the advantaged when compared to the situation without tack coat is obvious.

7.5 *Influence of cleanness and water*

Also in case of the presence of wet dirt the use of tack coats proves to be favorable regarding the adhesion properties of asphalt pavements. Although, the potential of tack coats is smaller than in case of dry dirt, still a rest bond can be achieved, when without tack coat in extreme cases wet dirt might cause total separation between the layers. As shown above, the potential of tack coats to ensure the bond between layers is greater if tack coat was applied before the pavement was polluted.

7.6 *Influence of curing time and age*

The curing time and the age have as shown by the high adhesion values a positive effect on the bonding properties of asphalt pavements when tack coats were applied. When the curing and aging is done according to the procedure described earlier (in moderate to hot climate) the adhesion values for the coated slabs increase by about 10 kN.

8 CONCLUSIONS

In this laboratory study the effect of different surface characteristics of the underlying layer, such as cleanness, dryness, roughness and age, on bonding properties, were evaluated with a cationic tack coat.

It could be shown that especially in the case of dirt and moisture—common phenomena on construction sites—tack coats have a great potential to secure and improve adhesion properties. When—in case of "no tack coat"—the cores already broke during coring, the cores with tack coat achieved shear forces up to 10 kN. Although, there is a difference if the tack coat is applied before or after the dirt/moisture treatment, the use of tack coats is still beneficial.

Curing time and age are also important factors for the improvement of bonding on coated surfaces.

As opposed to the benefit of tack coats on dirty and wet surfaces as well as in case of longer curing times, the advantage of tack coats on fine milled surfaces is doubtable. Also, the use of polymer modified tack coats seems not to be beneficial when the pavement is constructed using ordinary e.g. non polymer modified binders. In both latter cases the different bonding mechanism might be responsible for the stated behaviour and lead to a different testing regime in these cases. So, adhesion testing not directly after construction but after some time might lead to different (higher) adhesion values.

Again, it is important to mention that a laboratory study might give first hints, but that the situation in the lab is not totally comparable to the situation on a construction site. Even if, parameters such as cleanness or moisture influence might be simulated in laboratory tests, the compaction itself and its differences from in situ compaction seem to be important factors.

Therefore, it is recommended that some of the parameters and their influences should be looked at in 1:1 field tests. Especially since in the framework of the research project many of the investigated aspects (fine milling, aging, polymer modified tack coats) were only touched on very briefly and therefore require a broader inspection.

REFERENCES

Canestrari, F., Ferrotti, G., Partl, M.N. & Santagata, F. 2005. Advanced Testing and Characterization of Interlayer Shear Resistance. CD Proceedings of the 84th TRB Annual Meeting, Washington DC, USA.

European Standard EN 12697-6 2003. Bituminous mixtures—Test methods for hot mix asphalt—Part 6: Determination of bulk density of bituminous specimens.

European Standard EN 13808 2005. Bitumen and bituminous binders—Framework for specifying bituminous cationic emulsions European Committee for Standardisation, Brussels or Schweizer Norm SN 670205 NA, 2007. Bitumen und bitumenhaltige Bindemittel Rahmenwerk für die Spezifizierung kationischer bitumenhaltiger Emulsionen, Schweizerischer Verband der Straßen-und Verkehrsfachleute VSS, Zürich, (in German and French).

European Standard EN 13108-1 2008. Bituminous mixtures, European Committee for Standardisation, Brussels or Schweizer Norm EN SN 640431-1b NA Asphaltmischgut. Schweizerischer Verband der Straßen- und Verkehrsfachleute VSS, Zürich, (in German and French).

Leutner, R. 1979. Untersuchungen des Schichtenverbunds beim bituminösen Oberbau. Bitumen. *Journal No:3:* 84–91, (in German).

Partl, M.N. & Raab, C. 1999. Shear Adhesion between Top Layers of Fresh Asphalt Pavements in Switzerland. Proceedings of 7th CAPSA Conference on Asphalt Pavements for Southern Africa. Victory Falls, Zimbabwe, Victory Falls, Zimbabwe, 5.130–5.137.

Raab, C. & Partl, M.N. 1999. Methoden zur Beurteilung des Schichtenverbunds von Asphaltbelägen. ASTRA-Project VSS 12/94, Report No. 442, (in German).

Raab C. & Partl, M.N. 2006. Adhesion Testing of Rehabilitated Concrete Pavements. 10th International Conference on Asphalt Pavements, Paper Nr. 79, Quebec, Canada.

Raab, C. & Partl, M.N. 2007. Prüfung von Haftklebern (Testing of Tack Coats), ASTRA-Project VSS 1999/277 Report No 1196 (in German).

Recasens, M., Jiménez P., Gonzalez B. & Manuel J. 2003. Evaluation of the effect of tack coats. LCB shear test, 6th RILEM Symposium PTEBM'03, Zurich, Switzerland.

Swiss Standard SN 671961 2000. Bituminöses Mischgut, Bestimmung des Schichtenverbunds (nach Leutner), Schweizerischer Verband der Straßen-und Verkehrsfachleute VSS, Zürich, (in German and French).

Uzan, J., Livneh, M. & Eshed, Y. 1978. Investigation of adhesion properties between asphaltic-concrete layers, Asphalt Paving Technology 47.

Advanced Testing and Characterization of Bituminous Materials –
Loizos, Partl, Scarpas & Al-Qadi (eds)
© 2009 Taylor & Francis Group, London, ISBN 978-0-415-55854-9

Factors affecting recovered asphalt binder properties: A theoretical and experimental study

F.G. Praticò & V. Dattola
DIMET Department, Mediterranea University, Reggio Calabria, Italy

ABSTRACT: As is well-known, as far as high RAP (Reclaimed Asphalt Pavement) contents are involved, the performance of the recycled bituminous mixture will depend on the real properties of the asphalt binder contained in RAP and therefore on the possibility to carry out asphalt binder extraction and recovery, through one of the existing methods.

In the light of the above-mentioned facts the main goal of the paper has been confined into the analysis of factors affecting recovered asphalt binder properties.

The obtained results have contributed to assess the effective importance of the main parameters of procedures in order to improve the extraction and recovery process, to stimulate to use of RAP in the normal practice pavement design, and to guarantee the good performance of asphalt binder.

The pavement information developed is going to be used by DIMET Department to monitor performance trends of various lots of pavements.

1 PROBLEM STATEMENT

The asphalt extraction and recovery procedure is a vital part of the quality control and assurance of asphalt pavement recycling projects.

Extractions can be carried out through hot solvents, by using cold solvents without vacuum, or, finally, through "disruption" methods.

Asphalt binder recovery can be carried out thorough the Abson method or by using the Rotary Evaporator, or through the Fractionating column.

On the other hand, it is important to remark that age hardening and test procedures interact in determining the properties of the recovered asphalt binder.

It is well known that age hardening is a result of a number of factors, among which there are oxidation, volatilization, polymerization, thixotropy, syneresis, separation (Vallerga et al. 1957, Finn 1967 as referenced by Roberts et al. 1996). Attempts to correlate asphalt chemical properties with performance have not been very successful, but of course it is chemical composition that actually determines physical properties. In particular, the hardening of asphalt due to oxidation is almost entirely caused by the increase in asphaltene content (Lin et al. 1995a, Lin et al. 1995b) and it is primarily the result of the oxidation of polar aromatics, while the presence of original asphaltenes accelerates the process.

As for test procedures, solvent properties, time, temperature, use of carbon dioxide (CO_2), rotation speed, can affect the effective final properties.

As a consequence, many issues still call for further investigation in this research field and the sensitivity of asphalt binder properties to changes of each of the main parameters of recovery procedures still needs to be investigated.

In the light of the above-mentioned facts, the main goal of the paper has been confined into the analysis of process sensitivity to the following main parameters:

- Solvent action;
- Aging;
- Carbon dioxide flow.

The next section deals with the design of experiments and the analysis of the obtained results, while the conclusions are drawn in the last section.

2 EXPERIMENTS AND DISCUSSION

In order to pursue the above-mentioned objectives and scopes an experimental plan has been designed. Figures 1 and 2 and table 1 refer to the design of experiments, while figures 3 to 10 show the used devices.

2.1 *Experimental plan*

Figure 1 summarizes the experimental plan which has been focused on the comparison among the main characteristics of asphalt binder before (path, P1), after mixing with solvent and re-covering (path P2), and after production (of DGFC), extraction and recovering (path P3).

Note that two standard methods for the recovery of asphalt binder from the solution using a rotary evaporator have been considered:

– ASTM D 5404-02;
– EN 12697-03.

It is important to point out that 36 theoretical combinations of the four considered parameters (S_i, t_s, Q_k and C_r) have been considered. Table 1 summarizes some of the monitored characteristics. In practice, the main problems have been the following (see also figure 2):

- Type of solvent (S_i);
- Time of rotation (t_s);
- Quantity of asphalt binder in the rotating flask (Q_k);
- Flow of CO_2 into the rotating flask (C_r).

Figures 3 to 7 show the some of the devices used in the experiments. Note that a rotary evaporator with others equipments has been employed for all the recovery procedures (see figures 3 to 6).

As is well-known the rotary evaporator is one of the devices used for the efficient and gentle removal of solvents from the asphalt binders samples by evaporation.

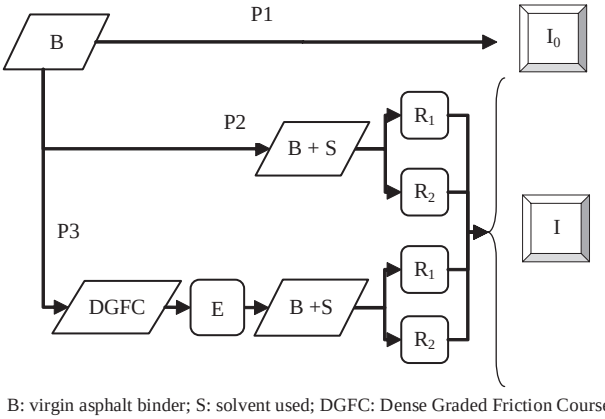

B: virgin asphalt binder; S: solvent used; DGFC: Dense Graded Friction Courses; E: extraction method; R_k: k-th recovery method; I_0: indicator related to the virgin asphalt binder; I = I (I_0, M&L, E, R): indicator related to the asphalt binder mixed with the solvent, M: mixing; L: laying and compaction of the mix, S_i: type of solvent, t_s: flask rotation time, Q_k: initial quantity of asphalt binder in the rotating flask (see table 3), C_r: flow of CO_2

Figure 1. Experimental plan.

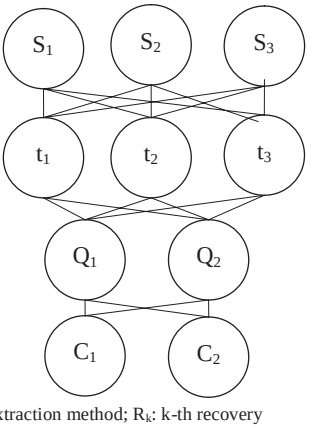

Figure 2. Theoretical combinations of the variables *S*, *t*, *Q* and *C*.

Table 1. Recovery tests (see figures 1 and 2).

Sample	Path	Test	Standard	Solution	Q (ml)	C
2	P2	(14/05/08)	EN 12697-3	Virgin bit. + Trichlorethylene/ *propanol*	400	No
3	P2	(15/05/08)	EN 12697-3	Virgin bit. + Trichlorethylene/ *propanol*	400	No
4	P3	(16/05/08)	EN 12697-3	Extracted bit. + Trichlorethylene/ *propanol*	400	No
5	P2	(19/05/08)	EN 12697-3	Virgin bit. + Trichlorethylene/ *propanol* (known quantity)	400	No
6	P2	(20/05/08)	EN 12697-3	Virgin bit. + Tetracloroethylene (known quantity)	400	No
7	P2	(27/05/08)	EN 12697-3	Virgin bit. + Dichloromethane (known quantity)	400	No
8	P2	(28/05/08)	ASTM D5404	Virgin bit. + Dichloromethane (known quantity)	0 (gradual)	Yes
9	P3	(04/06/08)	ASTM D5404	Extracted bit. + Dichloromethane (known quantity)	0 (gradual)	Yes

Note: $t_i \approx$ costant.

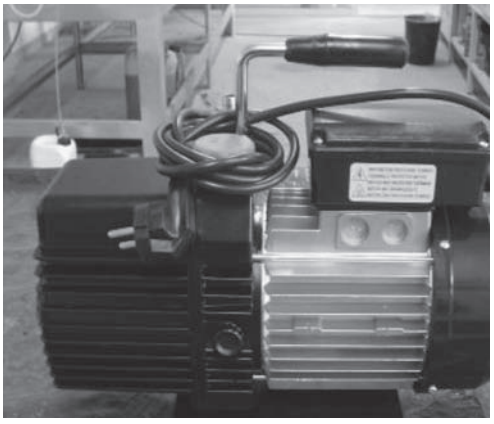

Figure 3. Vacuum pump.

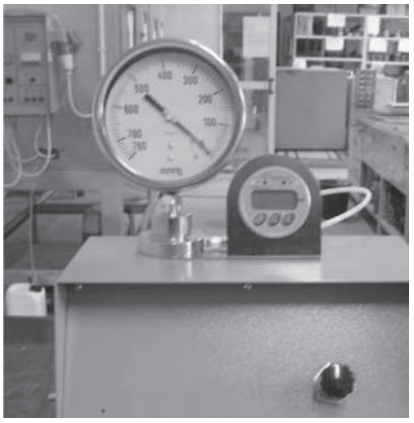

Figure 4. Pressure control unit.

Figure 5. System of CO_2 input tube.

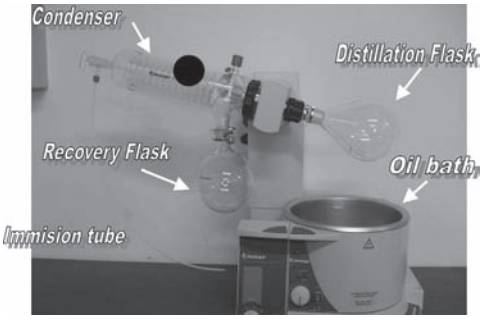

Figure 6. Rotary evaporator.

The following main lines/paths can be pointed out (see figures 3 to 6):

- Line of the solution (from the glass container to the distillation flask through a straw);
- Path of the solvent (from the distillation flask to the recovery flask, through the condenser);
- Line of the CO_2 (from the CO_2 cylinder to the distillation flask, through the pressure meter and the straw);
- Line of the air/vacuum pump (from the distillation flask/condenser to the vacuum pump, through the pressure control unit);
- Line of the water (from the water stopcock to the sink, through the condenser).

The major components of the rotary evaporator are below specified:

a. a vacuum system (see figures 3 and 4), to substantially reduce the pressure within the evaporator system. The vacuum system used with rotary evaporators can be as simple as a water aspirator with a trap immersed in a cold bath (for non-toxic solvents), or as complex on as a regulated mechanical vacuum pump with refrigerated trap (see figure 3). Modern equipments often adds features such as digital control of vacuum, see figure 4, digital display of temperature and rotational speed, see figure 6;
b. a motor unit which rotates the evaporation flask containing the sample (see figure 6);
c. a vapor duct which acts both as the axis for sample rotation, and as vacuum-tight conduit for the vapor being drawn off of the sample (see figure 6);
d. a heated oil bath, to heat the sample being evaporated (see figure 6);
e. a condenser with within a coil through which coolant passes, cold water (see figure 6);
f. a condensate collecting flask o recovery flask at the bottom of the condenser, to catch the distilling solvent after it re-condenses (see figure 6);
g. a mechanical mechanism to quickly lift the evaporation flask from the heating bath (see figure 6).

After the recovery the following tests have been carried out:

– Penetration test, through a penetrometer, according to the standards C.N.R. B.U. n° 24–29/12/71 and UNI EN 1426.
– Softening point – Ring & Ball tests, through a R & B device, according to the standards C.N.R. B.U. n° 35 – 22/11/73 and UNI EN 1427;
– Dynamic viscosity tests, through a Brookfield viscosimeter (see figure 7), according to the standard ASTM D 4402 – 06.

Figure 7. Brookfield viscosimeter.

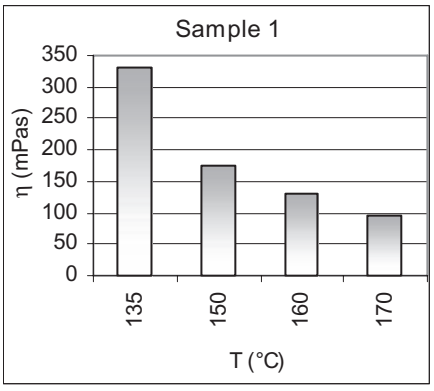

Figure 8. Unaged bitumen viscosity.

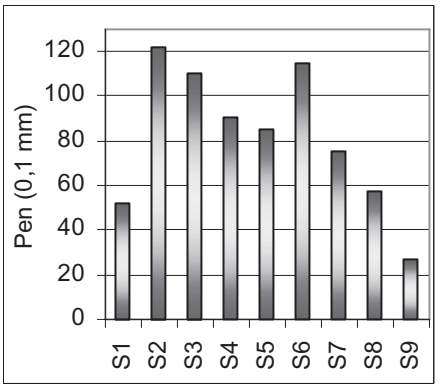

Figure 9. Results of penetration tests.

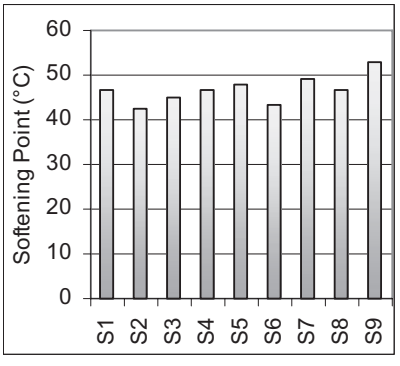

Figure 10. Softening Point (°C).

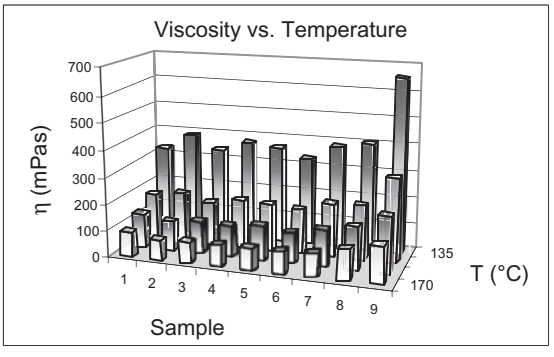

Figure 11. Viscosities.

2.2 *Results and analysis*

Figures 8 to 17 and table 2 summarize the obtained results.

Table 2 refers to the obtained results in terms of Penetration (*pen*), Softening Point (*SP*) and viscosity at four different temperatures.

Figure 8 details the reference in terms of viscosity (unaged bitumen), while in figures 9 to 11 all the obtained results are compared.

The results of penetration test show that the asphalt binder recovered after extraction is harder than the unaged asphalt binder. Penetration decreases of about 50% (see table 2 and figure 9) when CO_2 is used.

This phenomenon is confirmed also in terms of Softening Point (figure 10), where the temperature increases of about 7°C.

The results obtained by a Brookfield Viscometer show that the sample 9 (the short-aged asphalt binder) results more viscous than the unaged asphalt binder.

This fact could be due to a different degree of oxidation due to construction, laying, extraction and recovery.

Figures 12 to 17 show the comparison between literature and obtained results. Three main issues are addressed:

a. *SP* (softening point) *vs*. *pen* (penetration at 25°C). In this case the behaviour of *SP* for low penetrations results quite different from literature references (see figure 12 and 13).
b. Viscosity *vs*. *pen* (see figures 14 and 15). In this case a direct comparison was not possible due to the different temperatures. Importantly, the slope of the viscosity

appears lower for the obtained data (135 to 170°C) than for the literature references (25 to 60°C).

c. Viscosity (η) *vs.* temperature (see figures 16 and 17). In this case it is possible to point out that there is a good agreement between literature references (MEPDG, 2008) and experimental data.

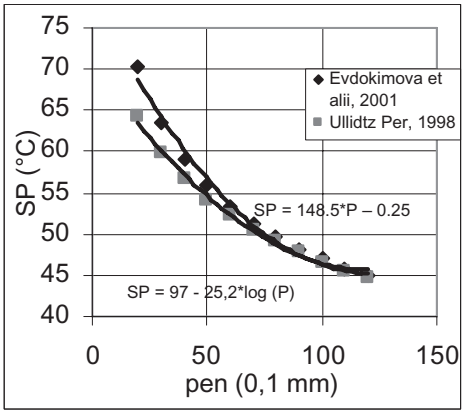

Figure 12. *SP vs. pen* (literature).

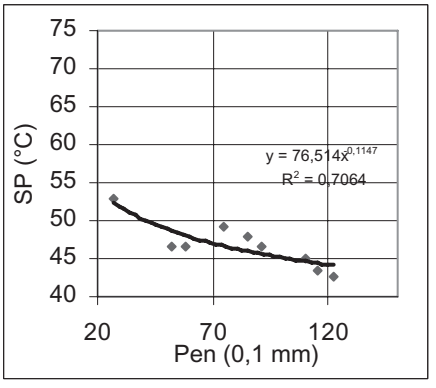

Figure 13. *SP vs. pen* (results).

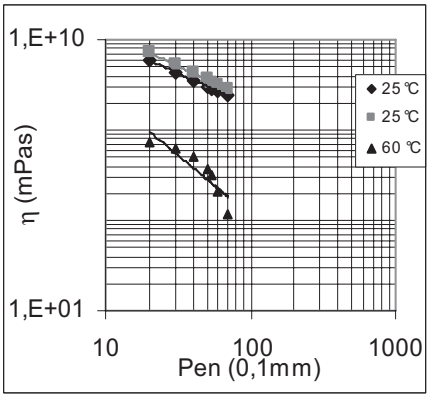

Figure 14. Viscosity *vs. pen* (literature).

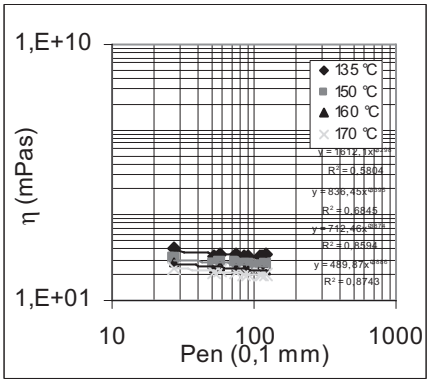

Figure 15. Viscosity *vs. pen* (results).

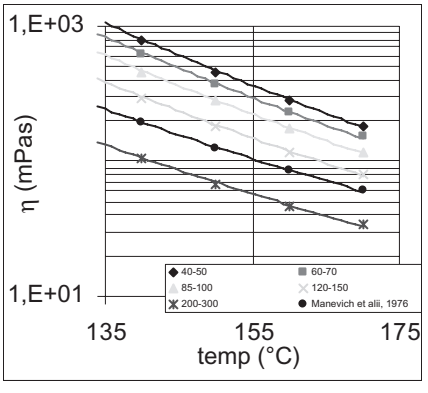

Figure 16. Viscosity *vs.* temp (literature).

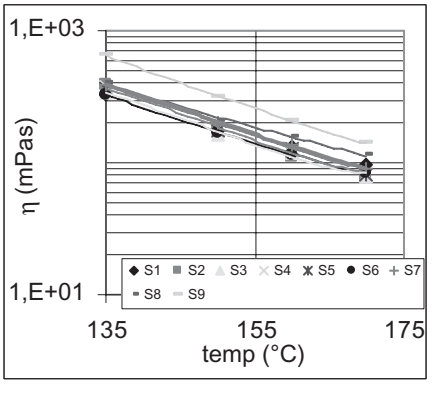

Figure 17. Viscosity *vs.* temperature (results).

Table 2. Results of penetration test, Softening Point and viscosity (see table 1).

			Test					
			Pen	SP	Viscosity			
			25°C		135°C	150°C	160°C	170°C
Sample	E	R	0.1 mm	°C		mPa.s		
1 B			51,7	46,5	330	175	130	95
2 B + S		EN 12697-03	122	42,6	390	190	112	77
3 B + S		EN12697-03	110	45,0	339	162	121	79
4 DGFC	n. 2-EN 12697-1	EN 12697-03	91	46,5	376	183	117	82
5 B + S		EN 12697-03	85	47,9	365	177	129	81
6 B + S		EN 12697-03	115	43,4	331	168	113	83
7 B + S		EN 12697-03	75	49,3	385	200	138	89
8 B + S		ASTM D-5404	57,7	46,5	405	205	160	115
9 DGFC	n. 2-EN 12697-1	ASTM D-5404	27,0	53,0	655	315	210	140

(Symbols: E: extraction method; R: recovery method; Pen: penetration; SP: softening point; B: bitumen; S: solvent; DGFC: dense graded friction courses).

The relationships η *vs*. temperature agreed with literature (Manevich & Rozental 1976, Rochester & Spikes 1992, Alabama DoT 1997, Andreozzi 2006, MEPDG 2008). Similarly, the relationships η *vs*. *pen* showed to be consistent with literature (Hardin 1993, TxDOT, 1999, NCHRP 2001, Bosma & Patience 2005), and relationships of the type η *vs*. softening point (Ullidtz 1998, Evdokimova et al. 2001).

3 MAIN FINDINGS

Figures 18 to 20 and table 3 summarize the main outputs obtained and provide an interpretation on the basis of the number and of the type of the involved processes.

Processes (*i.e.* causes) are analyzed on the x-axis, while the y-axis refers to each of the three parameters, *i.e. pen*, *SP* and viscosity. Similarly, in table 3, for each indicator, the per cent variation is derived ($100 * (I_2–I_1)/I_1$), where *I* stands for *pen*, *SP*, or viscosity.

More research is needed in order to carry on the experimental plan and improve the reliability of the obtained results. Though this, the experiments carried out permit to draw the following preliminary conclusions, based on the above-mentioned plots.

The transition from the virgin bitumen state (S1) to the recovered bitumen state, following a simple series mixing & recovering (S2, S3, S5, S6 and S7) has caused an increase in penetration (and, usually, a decrease of viscosity and softening point) probably due to a residual content of solvent (see the paths $RS_{3/4}$ and RS_2, where RS_2 stands for recovery by type-two solvent, *i.e.* dichloromethane). The dependence on the type of solvent could be due to the different boiling point (87°C *c.a*, for trichlorethylene –3– or 121°C *c.a*, for tetracloroethylene –4– *vs.* 40°C *c.a* for the dichloromethane –2–) and/or to the different solving power.

On the contrary, the transition from the EN to the ASTM standard and above all the introduction of a CO_2 flow originated a decrease in penetration of 23% *c.a* (see the sample S8; path CO_2) and a corresponding increase of viscosity, remaining quite unintelligible the variation of softening point.

On the other hand, the Short Term Aging (path STA), during the production, was the cause for another decrease in penetration (of 34% *c.a*), as in (Ullidtz, 1998) and a corresponding increase in viscosity and softening point.

In the light of the above facts it is possible to conclude that short term aging plays an easy-detectable role in changing bitumen properties and the relative effects seem to overcome

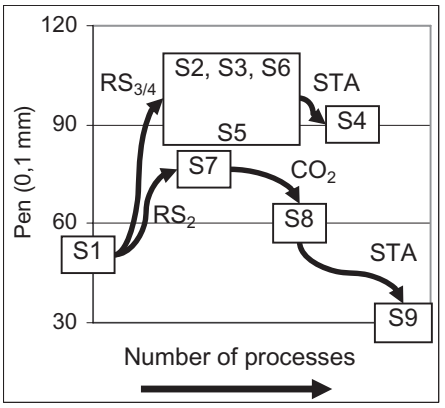

Figure 18. Summary of Penetration tests.

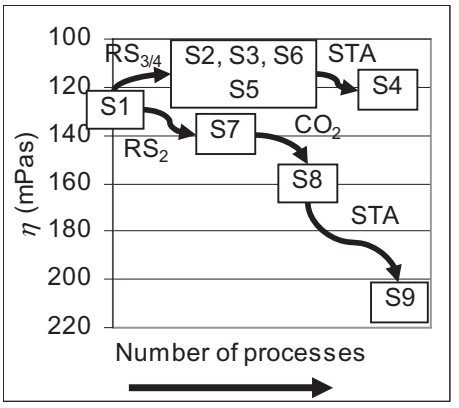

Figure 19. Summary of viscosity tests (t = 160°C).

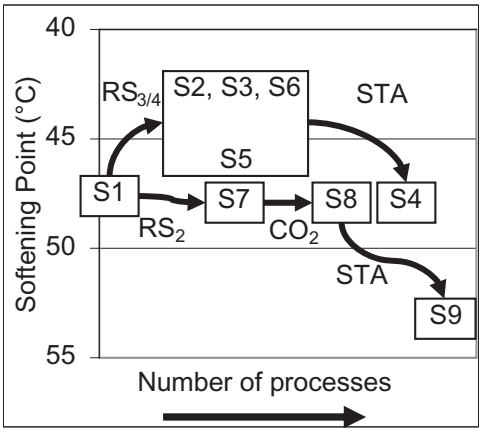

Figure 20. Summary of softening point test.

Table 3. Variation of analyzed parameters (*).

Cause	ΔPen (%)	ΔSP (%)	$\Delta\eta_{160°C}$ (%)
$RS_{3/4}$, RS_2 (**)	96	–2	–6
STA (**)	–34	6	25
CO_2	–23	–6	16

*values rounded to the nearest integer.
**average value.
$RS_{3/4}$: recovery by trichloroethylene/tetracloroethylene; RS_2: recovery by dichloromethane; STA: Short Term Aging; CO_2: carbon dioxide; pen: penetration; SP: softening point; η: viscosity.

recovery process and typology influence. The effect of CO_2 (and therefore of the used standard) appears more evident in terms of penetration and/or viscosity.

Except that for the softening point (whose behaviour calls for further research) the only action of recovery (with solvent but without CO_2) seems to cause a softening, due to the practical prevalence of residual solvent effects on hardening effects due to thermodynamic issues.

Information gained is going to be used by the DIMET laboratory at the *Mediterranea* University to monitor performance trends of various lots of pavement.

Further research will aim to gain a better and more reliable understanding of factors influence through more and more robust experimental plans.

ACKNOWLEDGEMENTS

The authors would like to acknowledge Eng. Casciano and Eng. Tramontana for the assistance provided during the tests.

REFERENCES

Alabama Department of Transportation. 1997. ALDOT-344-83, Design method for selecting the grade of recycling agent and optimum Asphalt cement content of hot-mix recycle bituminous mixtures. *Bureau of Materials and Tests, Testing Manual, ALDOT Procedures.*

Andreozzi, L. 2006. Lezione: Laboratorio di Fisica Generale I. Università di Pisa.

ASTM D 4402–06. Standard Test Method for Viscosity Determination of Asphalt at Elevated Temperatures Using a Rotational Viscometer.

ASTM D5404–02. Standard Practice For Recovery Of Asphalt Using Rotary.

Bosma, G.M. & Patience, R. 2005. Techinical Note: Penetration and viscosity grading of bitumen. Roading New Zealand.

C.N.R. B.U. n° 35–22/11/73. Norme per l'accettazione dei bitumi per usi stradali. Metodi di prova: punto di rammollimento (Metodo palla e anello).

C.N.R. B.U. n° 24–29/12/71. Norme per l'accettazione dei bitumi per usi stradali. Metodi di prova: penetrazione.

Evdokimova, N.G., Murtazin, F.R. & Tselishchev, I.V. 2001. Regression Analysis Of Operation Of A Modified Paving Asphalt Production Plant. *Chemistry and Technology of Fuels and Oils* 37(3).

Finn, Fred N. 1967. Factors Involved in the Design of Asphaltic Pavement Surfaces. *HRB, NCHRP Report 39.*

Hardin, John, C. 1993. Physical Properties of Asphalt Cement Binders. *ASTM Committee D–4 on Road and Paving Materials—Foreword.*

Lin, M.S., Glover, C.J., Davison, R.R. & Bullin, J.A.. 1995a. The Effects of Asphaltenes on Asphalt Recycling and Aging. *Transp. Res. Rec.* 1507:86–95.

Lin, M.S., Lunsford, K.M., Glover, C.J., Davison, R.R. & Bullin, J.A.. 1995b. The Effects of Asphaltenes on the Chemical and Physical Characteristics of Asphalts. In *Asphaltenes: Fundamentals and Applications*, E.Y. Sheu and O.C. Mullins (Eds.), Plenum Press, New York, NY: 155–176.

Manevich, R.M. & Rozental', D.A. 1976. Viscosity-temperature relationships of asphalts. *Chemistry and Technology of Fuels and Oils.*

MEPDG. 2008. Mechanistic-Empirical Pavement Design Guide. Mechanistic-Empirical Pavement Design Guide, Interim Edition: A Manual of Practice, ISBN Number: 1-56051-423-7.

NCHRP. 2001. Guide for Mechanistic-Empirical Design of new and rehabilitated pavement structures. final document, appendix cc-1: correlation of CBR values with soil index properties, ARA, Inc., ERES Division, Illinois.

Roberts, F. L., Kandhal, P.S., Brown, E.R., Lee, D.Y. & Kennedy, T.W. 1996. Hot mix asphalt materials, mixture design and construction. *2nd ed. Lanham, MD: NAPA Research and Education Foundation.*

Rochester, U.K. & Spikes, H. 1992. Development of a portable, automatic, microprocessor-controlled viscometer. *3rd year project by Flags Summer Department of Physics, Imperial College of Science, Tecnology and Medicine*.

TxDOT. 1999. Test Procedure for Calculating Viscosity From Penetration. TxDOT Designation: Tex-535-C.

Ullidtz, P. 1998. Modelling Flexible Pavement Response and Performance. ISBN: 8750208055.

UNI EN 1426. Determinazione della profondità di penetrazione di un bitume.

UNI EN 1427. Determinazione del punto di rammollimento (metodo palla ed anello).

UNI EN 12697-3. Bituminous Mixtures—Test Methods For Hot Mix Asphalt—Part 3: Bitumen Recovery: Rotary Evaporator.

Vallerga, B.A., Monismith, C.L. & Granthem K. 1957. A Study of Some Factors Influencing the Weathering of Paving Asphalts. *Proceedings AAPT.* 26, 1957.

http://en.wikipedia.org/wiki/Rotovap

http://training.ce.washington.edu/WSDOT/Modules/09_pavement_evaluation/09-7_body.htm#bleeding

Advanced Testing and Characterization of Bituminous Materials – Loizos, Partl, Scarpas & Al-Qadi (eds)
© 2009 Taylor & Francis Group, London, ISBN 978-0-415-55854-9

Influence of low temperature behaviour of PmB on life cycle

M. Hase & C. Oelkers
NORDLABOR GmbH für bautechnische Prüfungen, Pinneberg, Germany

ABSTRACT: The low temperature behaviour of bituminous binders can be characterised by tests with the Bending Beam Rheometer, that of asphalt by uniaxial tension tests and cooling tests. A study in cooperation with the German BP corporation tested various binders in the BBR at different temperatures. Furthermore two kinds of bituminous mixtures, each with various binders, were tested on their low temperature behaviour. The correlation between the stiffness of the binders and the low temperature behaviour of the asphalts is presented. For the evaluation a special software for the design of asphalt traffic areas was used that calculated the influence of the cryogenic tensile stress on the life cycle of different asphalt constructions. The found correlation between binder and asphalt properties raises the question whether the knowledge of the low temperature behaviour of the binder alone allows the estimation of its influence on the life cycle of asphalt traffic areas.

1 INTRODUCTION

The life cycle of asphalt areas is highly dependent on the mechanical properties of the used asphalt. Those however are strongly influenced by the temperature dependent rheological behaviour of the used binder. The much higher viscosity of binders at low temperatures leads to the appearance of cooling down induced tensile stress, so called cryogenic stress, additional to the traffic induced tensile stress. The superposition of those stresses can lead to fractures and eventually to the failure of the whole construction. The ongoing development of software that can calculate the life cycle of asphalt areas shows that the simultaneous consideration of the temperature dependent tensile strength and the cooling down induced tensile stress makes the life cycle assessment much more realistic. As the testing of the asphalt takes a relatively long time and is rather expensive, the question occurs whether the results of relatively simple binder tests allow the prognosis of the behaviour of asphalt under certain loads.

2 EXPERIMENTAL

2.1 *Binder tests*

In this research twelve binders of different kind and provenance were investigated regarding their low temperature behaviour. For this purpose specimen were tested in the Bending Beam Rheometer according to DIN EN 14771 [1] at three different temperatures T_i (–10°C, –16°C and –25°C). They were loaded with a constant load of 980 mN, the resulting deformation was measured. From this data the temperature dependent stiffness S_i as well as the m-value that allows the evaluation of the relaxation-capability were calculated. Table 1 shows the results for the Stiffness S and the m-value after 60s for the respective temperatures.

2.2 *Asphalt tests*

The mechanical properties of the asphalt at low temperatures were determined on a Stone mastic asphalt 0/8S (SMA) and a Binder course asphalt 0/16S (BCA). The composition of each asphalt mix was constant, only the used binders were varied. In order to minimise the influence of the void content on the results its amount was tried to hold constant for the respective mixes.

The low-temperature performance of prismatic asphalt specimens can be tested by uniaxial tension tests and cooling tests (see figure 1a) with standardised testing procedures [2].

In the uniaxial tension test, a specimen is pulled with a constant strain rate of 1mm/min at constant temperature until failure. Results are the maximum stress (tensile strength) $\beta_t(T)$ and the corresponding tensile failure strain $\varepsilon_{failure}(T)$ at the test temperature T.

Table 1. Low temperature behaviour of the tested binders (mean values).

Binder (and anon. provenance)	Stiffness S [MPa]			m-value [–]		
	–10°C	–16°C	–25°C	–10°C	–16°C	–25°C
30/45	73,18	160,98	366,55	0,429	0,370	0,244
PmB 25 A (1)	124,00	247,32	701,08	0,368	0,321	0,193
PmB 25 A (2)	93,68	147,42	442,42	0,386	0,330	0,218
PmB 45 A (1)	85,11	224,34	660,09	0,463	0,379	0,240
PmB 45 A (2)	99,23	217,85	670,42	0,439	0,347	0,217
PmB 45 A (3)	71,67	146,78	437,92	0,454	0,377	0,250
PmB H (1)	68,47	120,18	288,20	0,383	0,346	0,254
PmB H (2)	28,68*	73,58	303,38	0,485**	0,413	0,308
PmB H (3)	31,61*	97,18	293,80	0,516**	0,399	0,289
PmB H (4)	66,06	133,27	335,85	0,402	0,345	0,264
PmB NV 25	112,26	207,02	554,22	0,346	0,277	0,191
PmB NV 45	90,21	206,02	494,60	0,433	0,361	0,277

*calculated from the data after 8, 15, 30 seconds with potential extrapolation.
**at a temperature of T = –10°C the testing range was exceeded so no data were measured; the presented value was calculated by linear extrapolation from the m-value of 0,437 resp. 0,438 at –14°C.

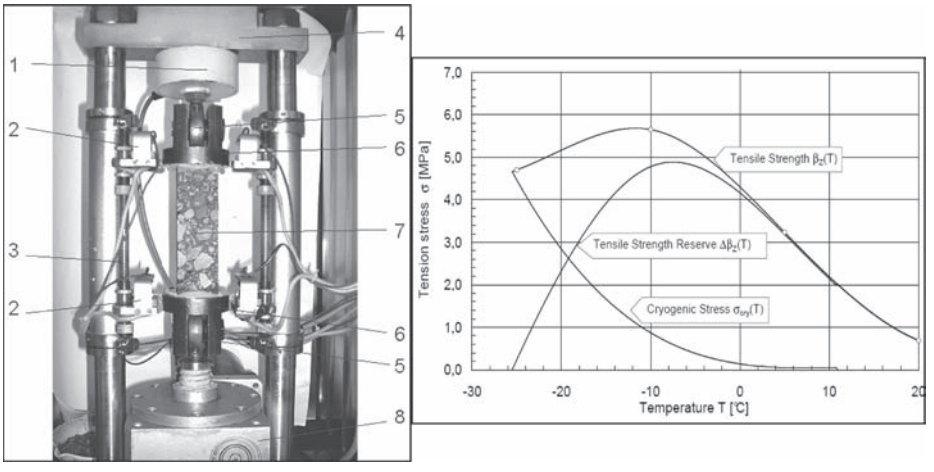

Figure 1. a) Example for a test device for Uniaxial tension tests at low temperatures and Cooling tests Key: 1 Load Cell, 2 Displacement Transducer, 3 Thermal Indifferent Measurement Base, 4 Crossbeam, 5 Gimbal suspension, 6 Adapter, 7 Specimen, 8 Gear box with stepping motor b) Principle of evaluating the tensile strength reserve from the test graphs of the tension tests and the cooling test in the temperature-stress diagram.

In the cooling test, a specimen which length is held constant, is subjected to a temperature decrease with a constant temperature rate of –10 K/h. Due to the prohibited thermal shrinkage cryogenic stress is built up in the specimen until failure. As results, the progression of the cryogenic stress over the temperature $\sigma_{cry}(T)$ is charted and the failure stress $\sigma_{cry,\,failure}$ at the failure temperature $T_{failure}$ are registered.

To calculate and visualise the tensile strength reserve the results of uniaxial tension tests are plotted in a temperature-tensile strength diagram (see figure 1b).

The measured tensile strengths are linked with a cubic spline function. The course of cryogenic stress measured in the cooling tests is plotted into the same temperature-stress diagram. The tensile strength reserve is the difference between the tensile strength and the cryogenic stress at the same temperature T:

$$\Delta\beta_t(T) = \beta_t(T) - \sigma_{cry}(T) \tag{1}$$

Results for the SMA 0/8 S are listed in table 2, for the BCA 0/16 S in table 3.

Table 2. Low temperature behaviour of Stone mastic asphalt 0/8 S with variation of binder (means).

Binder (and anon. provenance)	Failure tensile stress $\sigma_{cry,\,failure}$	Failure temperature $T_{failure}$	Maximum tensile strength reserve $\Delta\beta_t$		Cryogenic tensile stress σ_{cry} [N/mm²] at a temperature of T =		
	[N/mm²]	[°C]	[MPa]	[°C]	–10°C	–16°C	–25°C
PmB 45 A (1)	4,147	–26,9	4,59	–8,7	0,6507	1,4791	3,6669
PmB 45 A (2)	3,618	–25,5	3,67	–7,4	0,6737	1,4982	3,5006
PmB 45 A (3)	3,212	–31,6	3,66	–11,2	0,3429	0,7665	2,0048
PmB H (1)	3,547	–34,0	3,94	–11,5	0,3376	0,6827	1,8522
PmB H (2)	4,462	–31,3	5,68	–11,9	0,3716	0,9218	2,7239
PmB H (3)	4,203	–32,4	4,91	–12,2	0,3111	0,7612	2,2470
PmB H (4)	3,871	–33,2	3,94	–10,3	0,3090	0,7814	2,1282
PmB NV 25	4,352	–30,1	5,06	–9,6	0,7649	1,4552	3,1911
PmB NV 45	4,654	–32,2	5,92	–10,9	0,4903	1,0616	2,7807

Table 3. Low temperature behaviour of Binder course asphalt 0/16 S with variation of binder (means).

Binder (and anon. provenance)	Failure tensile stress $\sigma_{cry,\,failure}$	Failure temperature $T_{failure}$	Maximum tensile strength reserve $\Delta\beta_t$		Cryogenic tensile stress σ_{cry} [N/mm²] at a temperature of T =		
	[N/mm²]	[°C]	[MPa]	[°C]	–10°C	–16°C	–25°C
30/45	2,137	–26,5	2,24	–7,8	0,2734	0,6640	1,9057
PmB 25 A (1)	3,850	–22,5	4,25	–1,9	1,3410	2,3750	3,850*
PmB 25 A (2)	2,811	–28,8	2,92	–6,6	0,3635	0,8545	2,1484
PmB 45 A (1)	4,076	–26,2	4,34	–4,4	0,7550	1,6030	3,8050
PmB 45 A (2)	3,852	–26,4	4,69	–6,3	0,7220	1,5290	3,6250
PmB 45 A (3)	3,387	–30,5	3,11	–9,0	0,2909	0,7445	2,2254
PmB H (1)	3,378	–35.5	3,57	–13,5	0,2265	0,5052	1,4028
PmB H (2)	4,463	–29,0	4,87	–10,0	0,5290	1,2250	3,1210
PmB NV 25	4,516	–28,8	5,00	–8,8	0,8995	1,6384	3,4632
PmB NV 45	4,924	–30,4	5,21	–10,9	0,6119	1,2843	3,1296

*The presented value is identical with the measured failure tensile stress, as the specimen failed at a mean temperature of T = –22,5°C. Thus a tensile strength at T = –25°C can not be specified. In the regression analysis the stated value was taken into consideration.

3 CORRELATION OF LOW TEMPERATURE PROPERTIES OF BINDER AND ASPHALT

3.1 *General*

The binder data gained in the tests with the Bending Beam Rheometer were compared with the data of the asphalt tests by means of single and multiple regression analysis.

For the m-value that was determined at $T_1 = -10°C$, $T_2 = -16°C$ and $T_3 = -25°C$ there could not be found any satisfying result regarding all asphalt properties at low temperatures (cryogenic tensile stress σ_{cry}, failure temperature $T_{failure}$, failure tensile stress $\sigma_{cry, failure}$, maximum tensile strength reserve $\Delta\beta_t$ and corresponding temperature T). This is valid for the Stone mastic asphalt 0/8 S as well as the Binder course asphalt 0/16 S. The calculated coefficients of determination are too low and therefore not presented here.

The stiffness S at $T_1 = -10°C$, $T_2 = -16°C$ and $T_3 = -25°C$ shows no correlation regarding the asphalt properties failure tensile stress $\sigma_{cry, failure}$ and maximum tensile strength reserve $\Delta\beta_t$, neither for the Stone mastic asphalt 0/8 S nor for the Binder course asphalt 0/16 S. As the coefficients of determination are very low the results are not presented.

The results are very different though if the stiffness S of the binder is used to describe the following low temperature properties of the asphalt:

1) cryogenic tensile stress σ_{cry}
2) failure temperature $T_{failure}$ and
3) temperature T at maximum tensile strength reserve $\Delta\beta_t$.

The identified functional correlations will be described in the following for both asphalt mixes. At this point it should be mentioned that all found coefficients of determination have been identified as statistically significant.

3.2 *Correlation between low temperature properties of binder and stone mastic asphalt 0/8 S*

Between the Stiffness S and the cryogenic tensile stress σ_{cry} the following correlation was found with single regression analysis:

$$y(T) = 0{,}0053 * x(T) + 0{,}1873 \qquad (R^2 = 0{,}9307) \qquad (2)$$

with $y(T)$ = cryogenic tensile stress σ_{cry} [MPa] of SMA 0/8 S at the temperature T_i
$x(T)$ = stiffness S [MPa] of the binder used in the SMA 0/8 S at the temperature T_i

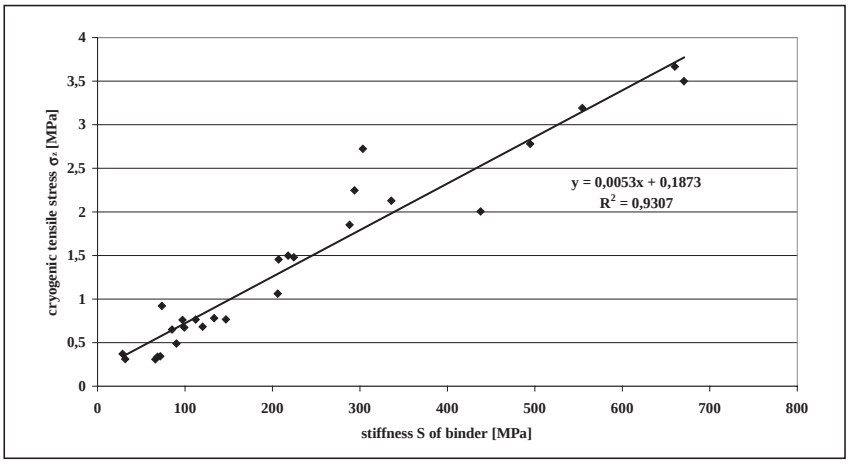

Figure 2. Correlation between stiffness S of binder and cryogenic tensile stress σ_{cry} of SMA 0/8 S; results of single linear regression analysis.

From equation (2) the conclusion can be drawn that the knowledge of the stiffness S of a binder, gained in the BBR-test at a certain temperature after 60s, allows the calculation of the cryogenic tensile stress at the same temperature of a Stone mastic asphalt 0/8 S, made with that binder, with a very high coefficient of determination. Figure 2 illustrates this correlation.

The failure temperature $T_{failure}$ can be estimated by equation (3) found by multiple linear regression analysis regarding the stiffness S at T = –25°C and T = –16°C:

$$y = -37{,}8565 - 0{,}0597 * x_1 + 0{,}0368 * x_2 \qquad (R^2 = 0{,}9646) \qquad (3)$$

with y = failure temperature $T_{failure}$ of SMA 0/8 S [°C]
x_1= stiffness S [MPa] at T = –16°C (BBR) of the binder used in the SMA
x_2= stiffness S [MPa] at T = –25°C (BBR) of the binder used in the SMA

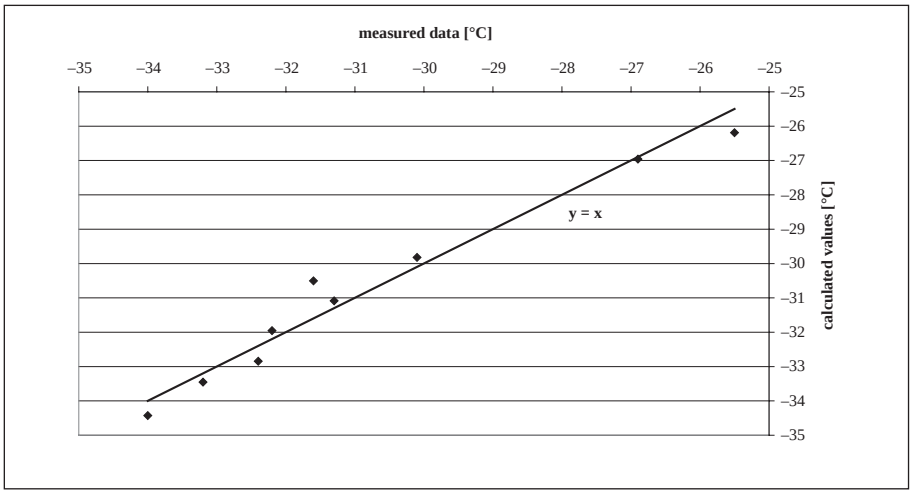

Figure 3. Measured data and values calculated by equation (4) of failure temperature $T_{failure}$ [°C] of SMA 0/8 S.

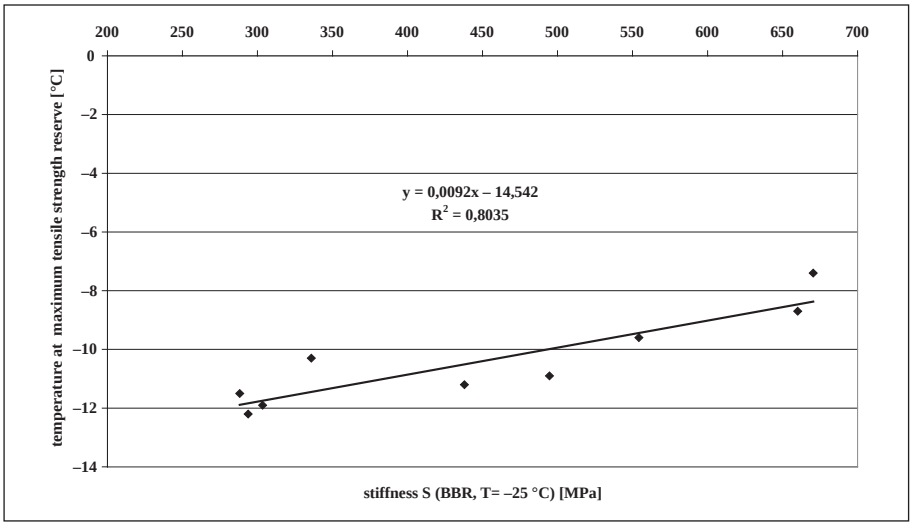

Figure 4. Correlation between stiffness S of the binder and temperature T at the maximum tensile strength reserve $\Delta\beta_t$ of SMA 0/8 S; result of single linear regression analysis.

Using equation (3) the values of the failure temperature $T_{failure}$ were calculated and compared with the measured data. As the pairs of variates only scatter very little from the straight line y = x the quality of equation (3) becomes clear (see figure 3).

The Stiffness S and the temperature T at maximum tensile strength reserve $\Delta\beta_t$ showed the following correlation by simple linear regression analysis (see figure 4):

$$y = 0{,}0092 * x - 14{,}542 \qquad (R^2 = 0{,}8035) \qquad (4)$$

with y = temperature T at maximum tensile strength reserve $\Delta\beta_t$ of SMA 0/8 S [°C]
x = stiffness S at T = –25°C [MPa] of the binder used in the SMA 0/8 S

3.3 *Correlation of the low temperature behaviour of binder and binder course asphalt 0/16 S*

The calculated coefficients of determination that were found for the Binder course asphalt 0/16 S in multiple linear regression analysis do not differ significantly from those found in

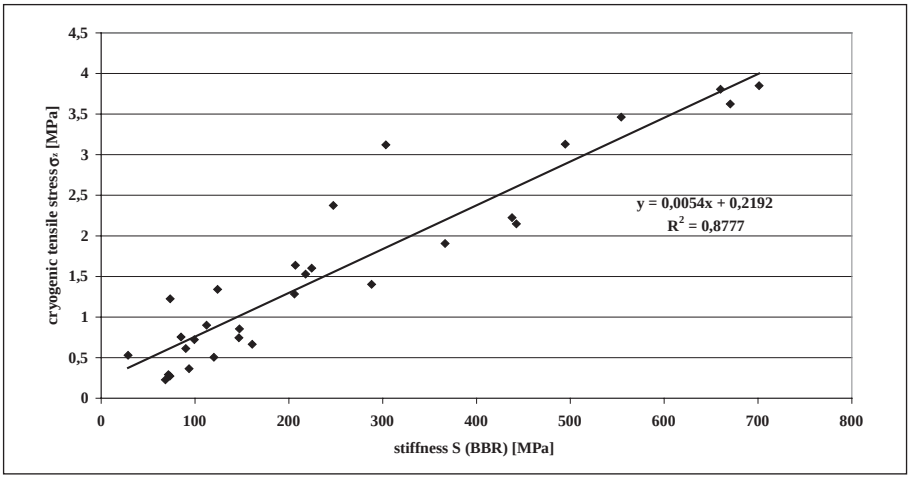

Figure 5. Correlation between stiffness S of Binder and cryogenic tensile stress σ_{cry} of Binder course asphalt 0/16 S; results of single linear regression analysis.

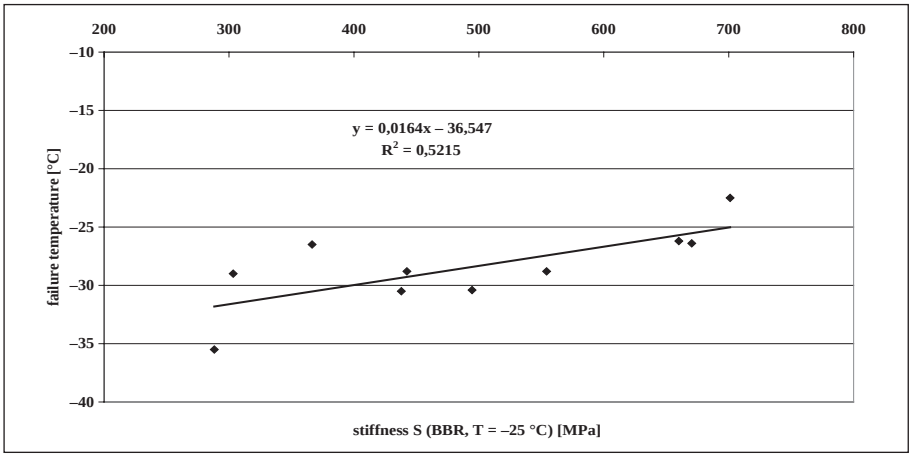

Figure 6. Correlation between stiffness S of Binder at a temperature of T = –25°C (BBR-test) and failure temperature $T_{failure}$ of Binder course asphalt 0/16 S; results of single linear regression analysis.

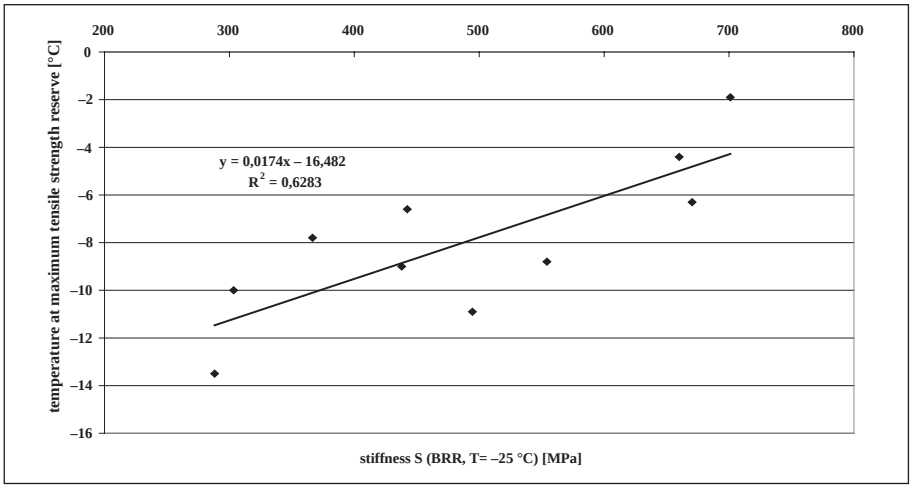

Figure 7. Correlation between stiffness S of the binder and temperature T at the maximum tensile strength reserve $\Delta\beta_t$ of Binder course asphalt 0/16 S; result of single linear regression analysis.

single linear regression analysis. Therefore only the results of latter will be presented for the correlation between the binder stiffness S at $T_1 = -10°C$, $T_2 = -16°C$ and $T_3 = -25°C$ and the three asphalt properties cryogenic tensile stress σ_{cry}, failure temperature $T_{failure}$ and temperature T at maximum tensile strength reserve $\Delta\beta_t$. Figures 5, 6 and 7 illustrate the results.

4 LIFE CYCLE PROGNOSIS OF ASPHALT TRAFFIC AREAS IN CONSIDERATION OF THEIR LOW TEMPERATURE BEHAVIOUR

For the evaluation of the data determined in the cooling tests the software PaDesTo [3] for the design of asphalt traffic areas was used.

4.1 *Software*

The applied design method allows the calculation of the necessary thickness of an asphalt construction for a given traffic load. The calculation considers the influences of the different layers and their building material as well as the environmental conditions.

Starting from the layer sequence that is chosen by the user the stress in the asphalt is calculated for the decisive spots within the construction. Using a fatigue function the bearable number of axle loads for the different layers is calculated and compared with the existent or prognosed number of axle loads.

The number of axle loads are distributed by percentage to according classes of axle loads. The calculation of the stress is carried out for the respective given surface temperatures and the consequential temperatures within the asphalt layers for each class of axle loads. By this all decisive combinations of temperature and load, whose single results are combined by the hypothesis of MINER, can be regarded for the calculation.

Result of the calculation is the percentage of used resistance against fatigue cracking at the undersurface of the asphalt construction. A value of 100% or more means that the construction will not be able to bear the traffic load, a value significantly lower than 100% may allow to chose a thinner asphalt construction.

By varying the thickness of the asphalt layers the software makes the adjustment of the construction on the given loads possible and even allows the evaluation of the application of alternative materials.

4.2 *Results*

Traffic loads were assumed to be 32 * 10^6 equivalent 10-t-axle loads with a prognosed yearly 2% – increase of heavy traffic. The environmental conditions follow a software given frequency distribution for Germany. The following parameters for the layer sequences were chosen:

Frost save thickness of 90 cm
Frost blanket course with E_{V2} = 120 N/mm²
Formation level with E_{V2} = 45 N/mm².

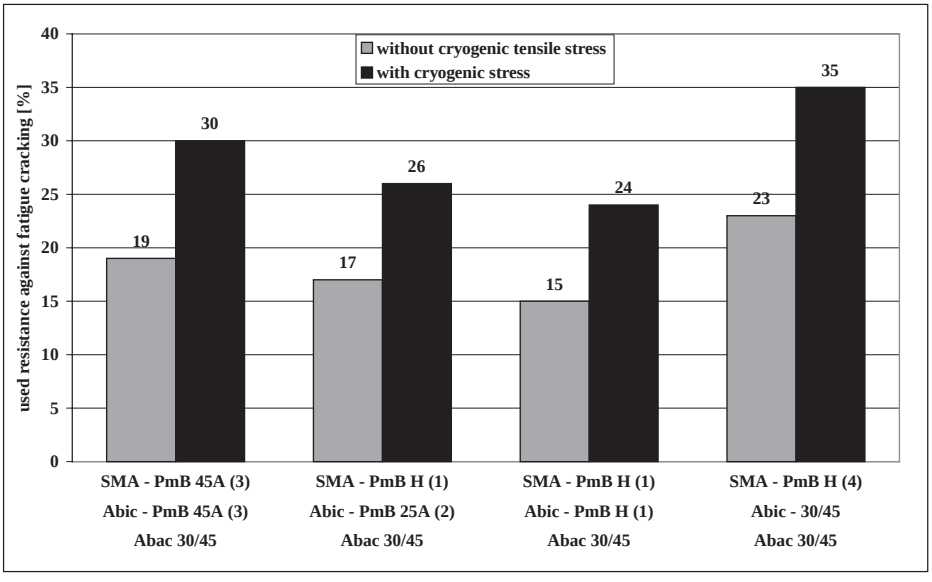

Figure 8. Exemplary percentage of used resistance against fatigue cracking with and without regard of cryogenic tensile stress under variation of the binder.

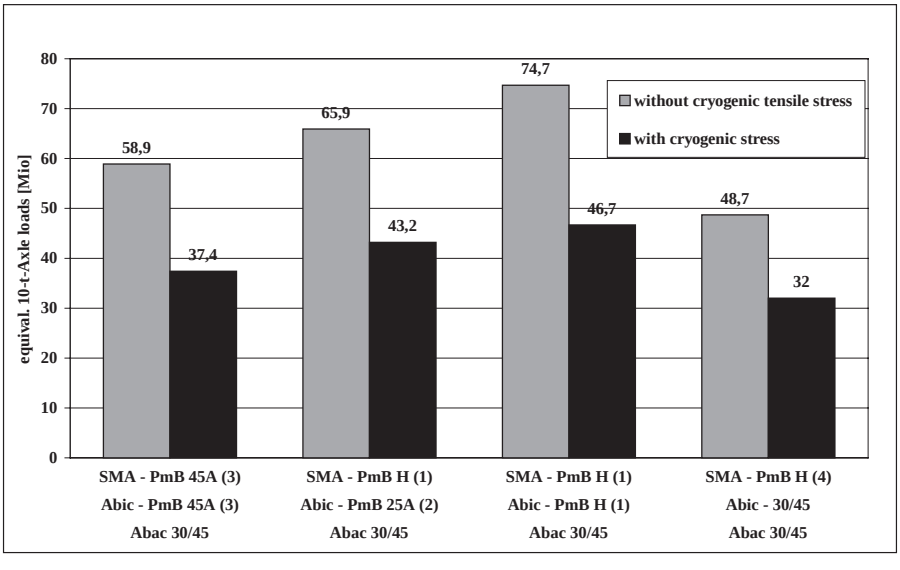

Figure 9. Exemplary equivalent 10-t-axle loads within life cycle of 30 years without and with consideration of cryogenic tensile stress under variation of binder.

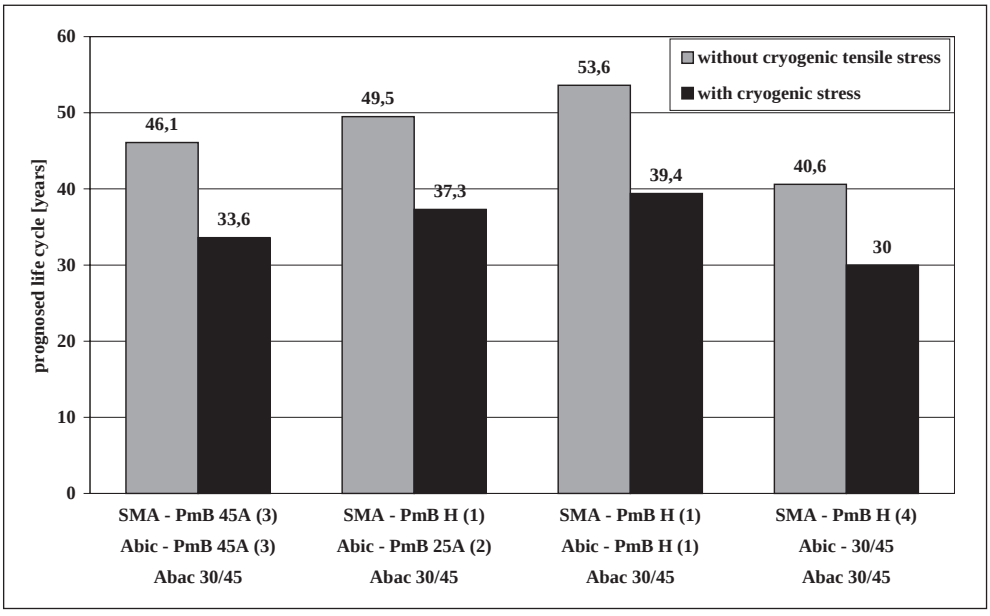

Figure 10. Exemplary prognosed life cycle without and with consideration of cryogenic tensile stress under variation of the binder.

The asphalt construction on the frost blanket course was chosen according to RStO 01, BK SV, for heavy traffic:

4,0 cm Stone mastic asphalt 0/8 S. (SMA 0/8 S)
8,0 cm Asphalt binder course 0/16 S. (Abic 0/16 S)
22,0 cm Asphalt base course CS 0/32. (Abac 0/32)

The asphalt construction was varied only in the used binders of the respective asphalts. Material parameters for the calculations were the respective resilient modulus E and the functions for the cryogenic tensile stress σ_{cry} determined in the cooling tests.

The calculation of the percentage of used resistance against fatigue cracking was carried out without as well as with the influence of the cryogenic stress in order to emphasise on its strong influence on the prognosis of the life cycle of asphalt constructions. Figure 8 exemplary shows this as well as the influence of the used binder on fatigue cracking.

In order to allow the relative comparison for the prognosed life cycle between the variants it was assumed that the variant with the highest percentage of used resistance against fatigue cracking under consideration of the cryogenic tensile stress was just able to bear 32×10^6 equivalent 10-t-axle loads within a life cycle of 30 years (see figure 9).

The method 1(iteration) for the prognosis of life cycles that is listed in the annex 1 of the RstO 01 was applied to the determined values to calculate the life cycle with and without consideration of the cryogenic tensile stresses (see figure 10).

5 SUMMARY

Asphalt areas are subjected to manifold stresses that are for instance induced by traffic or the environment. In this work a Stone mastic asphalt 0/8 S and a Binder course asphalt 0/16 S under variation of the binder were tested on their low temperature behaviour with cooling tests and uniaxial tension tests. Also the used binders were tested on their properties in the Bending-Beam-Rheometer.

The data gained on the asphalt was used for the calculation of life cycle prognosis. It was shown that the found life cycles of asphalt constructions are strongly influenced by the

cryogenic tensile stress of the asphalt. By disregarding of the (in reality occurring!) cryogenic tensile stress the prognosed life cycle is much longer than by taking into account the tensile stress that develops by restraining the cooling down shrinking. This has a great influence on feasibility studies.

An important question of this work was whether "simple" binder tests can give information on the low temperature behaviour of asphalt. It was shown that the appraisement of the cryogenic tensile stress in the asphalt is possible by using the stiffness S of the used binder determined in the Bending-Beam-Rheometer. Furthermore correlations between the stiffness S and the asphalt properties failure temperature $T_{failure}$ and temperature T at maximum tensile strength reserve $\Delta\beta_t$ were verified.

REFERENCES

1. DIN EN 14771: "Bitumen und bitumenhaltige Bindemittel—Bestimmung der Biegesteifigkeit—Biegebalkenrheometer (BBR)" according EN 14771: "Bitumen and bituminous binders—Determination of the flexural creep stiffness—Bending Beam Rheometer (BBR)".
2. Technische Prüfvorschrift Verhalten von Asphalten bei tiefen Temperaturen, Ausgabe 1994, Forschungsgesellschaft für Straßen- und Verkehrswesen, Köln according work item XX: „Bituminous Mixtures—test methods for hot mix asphalt—low temperature cracking and properties by uniaxial tension tests".
3. PaDesTo 2006, „Dimensionierung von Asphaltbefestigungen für Verkehrsflächen", A. Kiehne, primia—Ingenieursoftware.

Advanced Testing and Characterization of Bituminous Materials –
Loizos, Partl, Scarpas & Al-Qadi (eds)
© 2009 Taylor & Francis Group, London, ISBN 978-0-415-55854-9

Influence of granular polymer additives on the asphalt quality

P. Sivapatham, H.J. Beckedahl & S. Janssen
Pavement Research Centre, University of Wuppertal, NRW, Germany

ABSTRACT: To find out the influence of the gravimetric content of polymers in asphalt mixtures, conventional asphalt mixtures were modified with different polymer additives and gravimetric polymer content. They have been tested and compared to asphalt mixes which were produced with different ready mixed PmB. The quality of asphalt mixtures were characterized by means of the rutting resistance and mechanical characteristics, the resilient modulus. Conventional asphalt mixtures modified with granular polymers show a similar asphalt quality compared to PmB 45A if a gravimetric content of about 4% with respect to the mass of the base bitumen is chosen. Conventional asphalt with a gravimetric polymer content of 10% with respect to the mass of the base bitumen provides a similar or better asphalt quality compared to a special bitumen PmB 25H. These results confirm that high quality asphalt can be produced by modifying conventional asphalt mixtures with granular polymer additives in a dry process.

1 INTRODUCTION

Asphalt modifications are done to improve the performance quality of asphalt mixtures. There are two different production processes to provide polymer modified asphalt. The first method is the use of ready mixed polymer modified bitumen and the second one is to add granular polymers to aggregates and bitumen during the mixing process. The effect of polymers varies with the polymer used and with the polymer content. Thus, polymers, polymer content and base bitumen should be selected with respect to the application and the requirements. In general, the polymer modified asphalt can increase resistance against rutting, thermal cracking, and/or fatigue cracking. To point out the influence of polymer type and content in corresponding asphalt mixtures, it is necessary to investigate mechanical as well as performance properties of different asphalt mixtures.

Pavements with longer lifetime, less maintenance and lower life cycle costs should be realized by means of using polymer modified asphalt. In this study eighteen different polymer modified asphalt mixes with four different polymers have been investigated in the laboratory BESTLAB of the University Wuppertal with respect to mechanical properties and resistance against rutting. Therefore nine stone mastic asphalt (SMA 0/11 S) and nine asphalt binder mixtures (ABi 0/16 S) with different binders have been produced.

2 MODIFICATION OF ASPHALT

Normally ready mix polymer modified bitumen will be preferred because polymers are much more homogeneous distributed than in case of dry polymer modification process. For this paper asphalt mixtures were prepared using both methods and four different polymers. An elastomer modified bitumen PmB 45A (denotation according to EN: 25/55-55 A) and a high polymer modified special bitumen PmB 25H (denotation according to EN: 10/40-85 A) as ready mix binders have been used. The high polymer modified bitumen PmB 25H is a special bitumen with a higher content of polymers compared to conventional polymer modified bitumen. The authors are unaware of the exact composition and the polymers used. Normally polymer modified bitumen PmB 45A contain about 3% to 5% polymers by mass

whereas high polymer modified bitumen contain about 6% to 10% polymers by mass. For the binder content both, bitumen and polymer content has to be taken into account. The special bitumen PmB 25H contains a viscosity-modifying additive which reduces the viscosity of the bitumen at mixing and laying temperatures. This provides better workability and compaction of the asphalt mixtures.

For the production of polymer modified asphalt (PmA) two different granular polymers have been used by means of dry process. One of the polymer additive used is a grained thermoplastic synthetic material. It is a mixture of premium polyethylene copolymer and a special type of bitumen (ECB) and is provided as a granular material (additive 1). Additive 1 melts completely and can easily mixed with bitumen, increases consequently softening point ring and ball, decreases penetration value and improves Fraaß breaking point of the resulting binder. Because these additives completely melt with binder, the bitumen content can be reduced as to the percent by weight of the additive. The producer of additive 1 recommends the dry blending of a 30/45 pen bitumen with additive 1 to get an asphalt mixture with high resistance against rutting.

The second polymer additive (additive 2) used is of dark lentil formed pellets made from industrial polymer waste. It consists of 95% polyolefin and 5% fillers. This additive has been blended into conventional asphalt mixtures with 50/70 pen bitumen. It does not melt completely and cannot modify the bitumen so that in consequence the properties of a "resulting" binder are not affected. Additive 2 has a point bonding effect between aggregate grains. That is the reason why adding this polymer does not replace any amount of binder. Table 1 shows the additive content by mass based on the percentage of bitumen. There are different data for each asphalt mixture listed because of the different binder contents of stone mastic asphalt and asphalt binder.

Different polymer contents (three for additive 1 and four for additive 2) have been systematically selected to find out the improvement of asphalt quality. By means of these test results optimum polymer content can be determined for any application. Furthermore the polymer content which will lead to similar qualities of asphalt mixes with PmB 45A and/or PmB 25H can be also determined.

In total nine different polymer modified asphalt variants for each asphalt mixture type have been designed (table 1). The polymer additives used in this study increase the viscosity of modified asphalt, so the processing temperature and blending duration have to be raised. The blending duration can be extended between 10 an 15 seconds with respect to polymer additive content and mixture composition. The increase of mixing and compaction temperature depends on the bitumen type and on the polymer content. The different temperatures are listed in table 2.

Table 1. Production of nine different polymer modified asphalts.

	Abbreviation	Base binder with grade	Additive content by mass based on the percentage of bitumen SMA/ABi [%]
Polymer modified binder PmB 45A	PmB 45A	[–]	[–]
High polymer modified binder PmB 25H	PmB 25H	[–]	[–]
Base binder and lowest additive 1 content	PmA 1.1	30/45	4.0
Base binder and medium additive 1 content	PmA 1.2	30/45	7.0
Base binder and highest additive 1 content	PmA 1.3	30/45	10.0
Base binder and lowest additive 2 content	PmA 2.1	50/70	2.9/4.0
Base binder and medium additive 2 content	PmA 2.2	50/70	4.3/6.0
Base binder and high additive 2 content	PmA 2.3	50/70	5.8/8.0
Base binder and highest additive 2 content	PmA 2.4	50/70	8.2/11.9

[–] not known.

Table 2. Processing temperature of used asphalt components and the blending.

	Temperature [°C]			
Type of Asphalt	Bitumen	Aggregate	Blending	Compaction temperature SMA/ABi
PmB 45A	145	145	145	145/145
PmB 25H	180	170	170	155/155
PmA 1.1	170	190	180	165/145
PmA 1.2	170	190	180	175/145
PmA 1.3	170	190	180	185/170
PmA 2.1, 2.2, 2.3, 2.4	140	170	160	150/150

3 LABORATORY TEST PROGRAMME

In order to quantify the effect of modification type on mechanical properties of flexible pavements resilient modulus and temperature sensitivity as well as resistance against permanent deformation have been tested. To carry out the asphalt tests, specimens were prepared with asphalt mixtures for surface and binder course. Marshall Specimens, laboratory roller compacted slabs and cores drilled out of the slabs were prepared as test specimens. Resistance against permanent deformation was determined by means of wheel tracking tests and the temperature sensitivity by means of resilient modulus tests at different temperatures by indirect tensile tests.

In total eighteen different asphalt mixtures with nine different binders and two different asphalt mixture types were produced. The type of aggregate as well as the gradation was kept constant for each asphalt mix type. Following types of aggregate were used:

- limestone filler (0/0.09 mm),
- high quality diabase sand (0/2 mm) and
- high quality diabase chippings (2/5, 5/8, 8/11, and 11/16 mm).

Following asphalt mixture-types were selected according to German Standards (ZTV Asphalt-StB 2001) which were valid at time of research:

- Stone mastic asphalt, surface course (SMA 0/11 S, comparable to SMA 11 S) and
- Asphalt concrete binder course (ABi 0/16 S, comparable to AC 16 B S).

The grading curves of stone mastic asphalt and asphalt concrete range between the border lines of the German Standards (ZTV Asphalt-StB 2001) which were valid at time of research.

To characterise the four different binders the following binder tests were carried out:

- Softening point Ring & Ball (SP R&B),
- Needle penetration and
- Elastic recovery test.

4 ANALYSING OF TEST RESULTS

4.1 *Binder properties*

The test results of the binder properties are listed in table 3 and are averages of four single measurements. The properties of the first three binders range between the target values (European Standard EN 12591 and German Standards TL PmB respectively which were valid at time of research). The properties of high polymer modified special binder PmB 25H do not meat the properties of PmB 25A or PmB H after German technical specifications TL PmB. Therefore the binder PmB 25H shall be classified as special bitumen. PmB 25H is a hard binder with a penetration value of 22 dmm and a softening point R&B of 91.3°C.

Table 3. Binder properties.

	SP R&B [°C]	Needle penetration [dmm]	Elastic recovery [%]
50/70	49.4	54	11
30/45	53.9	34	14
PmB 45A	57.9	56	77
PmB 25H	91.3	22	86

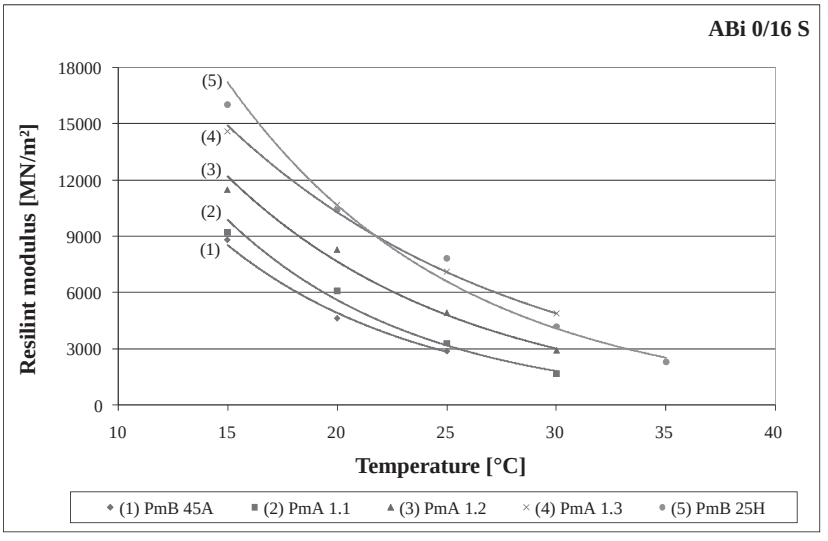

Figure 1. Mastercurve for ABi (additive 1, PmB 45A and PmB 25H).

A high softening point R&B indicates a good performance against permanent deformation. Asphalt mixtures with soft binder will cause a relatively high rutting compared to asphalt mixtures with stiff binder if all other parameters are kept constant.

4.2 *Resilient modulus*

The temperature dependent resilient modules were tested by means of the dynamic indirect tensile test according to the European Standard EN 12697-26. The resilient modulus characterizes the stiffness of asphalt mixtures and indirectly also performance properties. To characterize temperature sensitivity of asphalt mixtures resilient modules were determined at different temperatures. Furthermore the bearing capacity of asphalt layers increase with increasing resilient modules. Consequently the thicknesses of asphalt pavement constructions with high resilient modules can be reduced compared to asphalt pavement constructions with lower resilient modules. However, in this paper the design of asphalt pavement construction will not be discussed.

Figures 1, 2, 4 and 5 show the resilient modules for each tested asphalt mixture with respect to temperature. As expected, resilient modules decrease with increasing temperature for all tested asphalt mixtures and increase with increasing polymer content. Clear correlations between resilient modulus and polymer content are computed. Depending on the content of granular polymers resilient modules corresponding to PmB 45A and PmB 25H asphalt mix variants can be exceeded, see figure 3 and 6. Clearly less than 4% polymer content is sufficient to reach resilient modules similar to SMA and ABi mixes with PmB 45A. Appropriate 8% of additive 1 as well as additive 2 is required to get resilient modules similar to SMA mixes with PmB 25H. About 10% additive 1 or additive 2 are needed to reach resilient modules similar

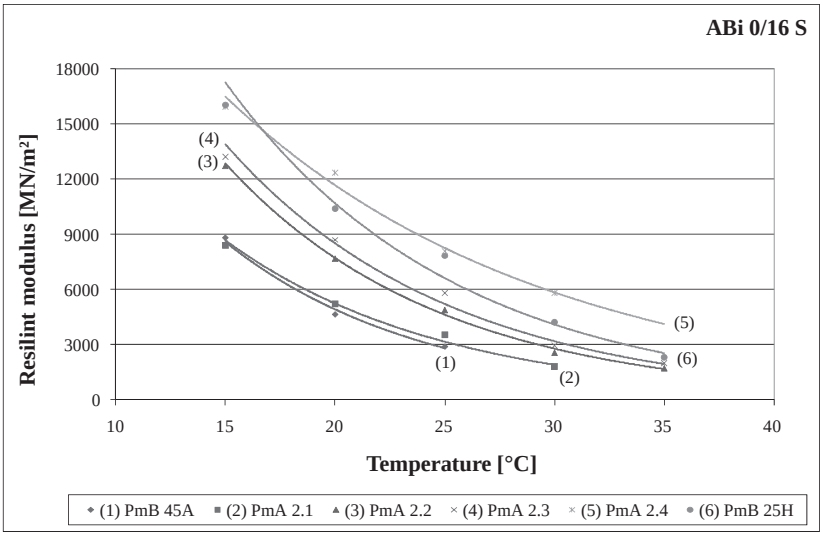

Figure 2. Mastercurve ABi (additive 2, PmB 45A and PmB 25H).

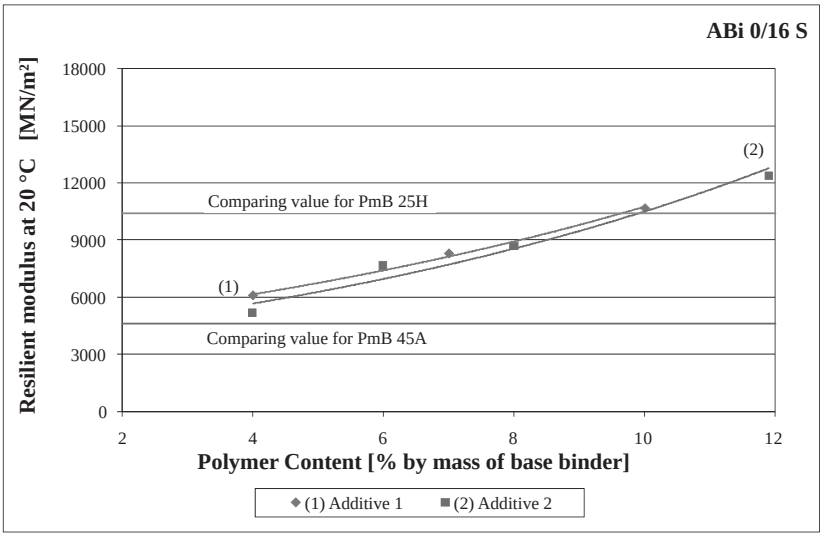

Figure 3. Resilient modulus with respect to polymer content at 20°C (ABi).

to ABi mixed with PmB 25H. It has to be mentioned that resilient modules of asphalt mixtures with PmB of different PmB blenders show a big range with respect to the PmB blend used. Thus the presented data of PmB mixed asphalt can not be generalized.

4.3 *Wheel Tracking Test (WTT)*

One of the most important deterioration of flexible pavements is rutting. Rutting is mostly formed within surface and binder courses. Thus, permanent deformation tests were done on specimens made of SMA and ABi mixes. Worldwide there exist numerous test methods and mixture response parameters to characterize rutting. One of widely adapted test methods to characterize resistance against permanent deformation is the wheel tracking test (WTT). In this study WTT have been conducted after the European Standard EN 12697-22

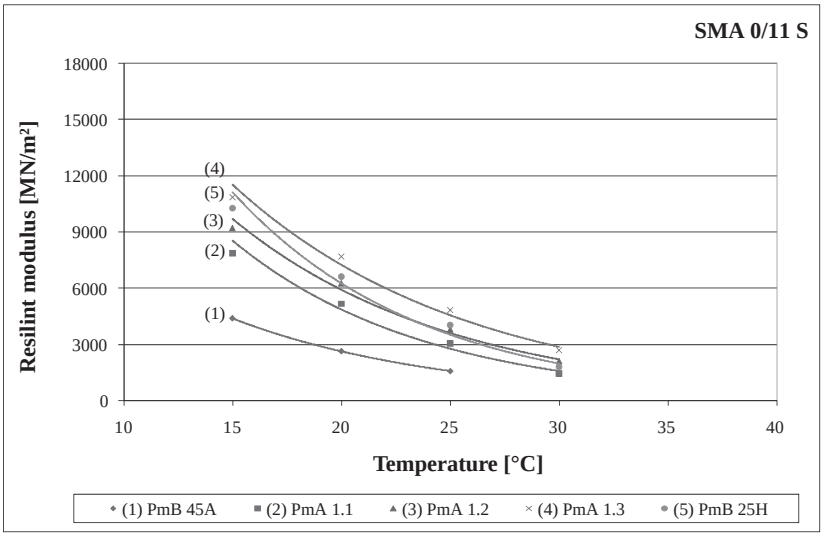

Figure 4. Mastercurve SMA (additive 1, PmB 45A and PmB 25H).

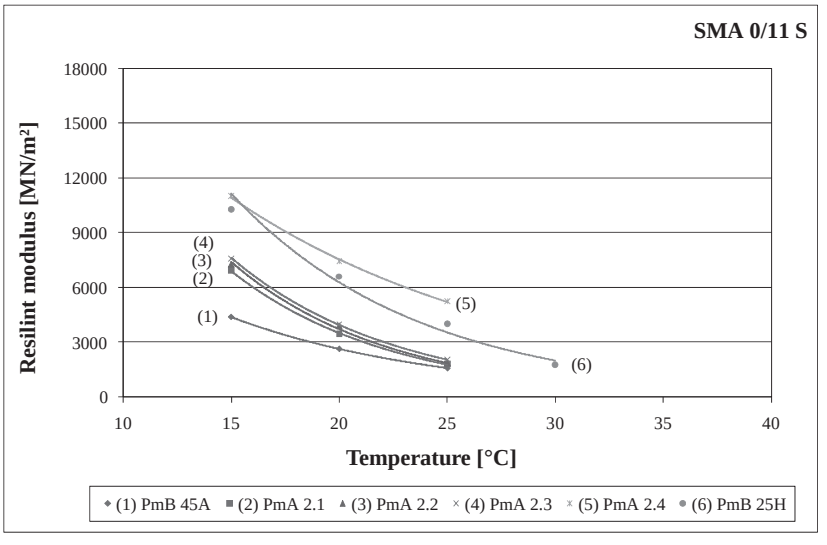

Figure 5. Mastercurve SMA (additive 2, PmB 45A and PmB 25H).

in an air temperature controlled device at 60°C using a rubber wheel as well as after German Standards TP A-StB SBV in water temperature controlled device at 50°C. The variants with additive 1 have been tested after European and the variants with additive 2 after German Standards. The reference values for variants PmB 45A and PmB 25H have been tested after both Standards. The results gained in water and in air can not be compared with each other, because the test methods differ in temperature control medium, test temperature and wheel construction. Therefore comparison is done with correspondence to test results which were determined under same test conditions.

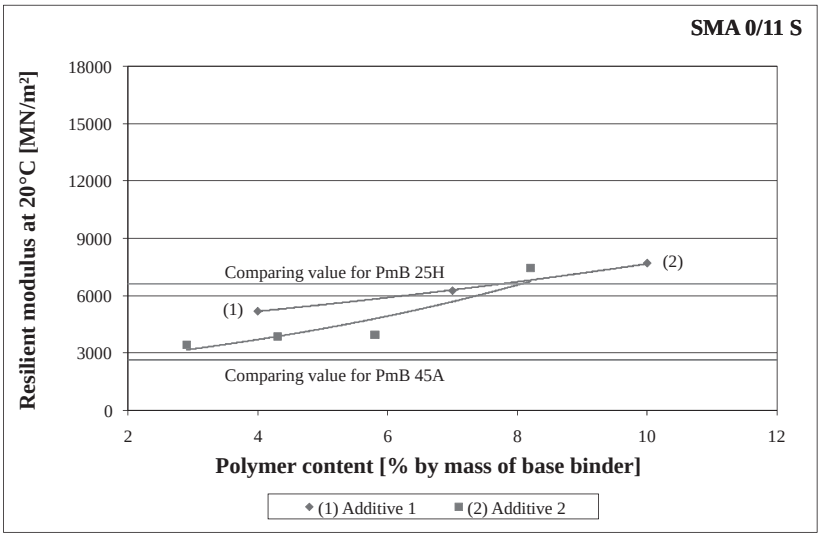

Figure 6. Resilient modulus with respect to polymer content (SMA).

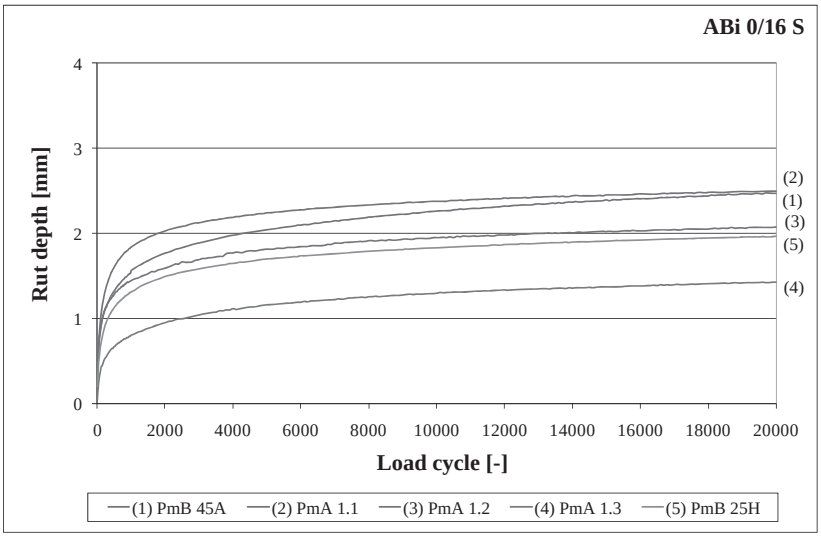

Figure 7. Wheel tracking test result of variants with additive 1, PmB 45A and PmB 25H (ABi, rubber wheel, 60°C, temperature controlled by air).

The specimens are loaded for 20,000 passes and the rut depth is the result of two simultaneously tested slabs. The results of the WTT are displayed in figures 7 to 10. The progression of rut depth clearly shows the influence of the binder used as well as the influence of the polymer content. In most cases variants with PmB 45A have the highest rut depth and highest progression. The rutting of variants with additives decrease with increasing additive content as it was expected from the asphalt stiffness results. The variants with high polymer modified special binder PmB 25H show very low rut depth compared to polymer modified binder PmB 45A but test results also show, that the conventional asphalt in combination with high polymer additive content can show better resistance against rutting than the variant PmB 25H.

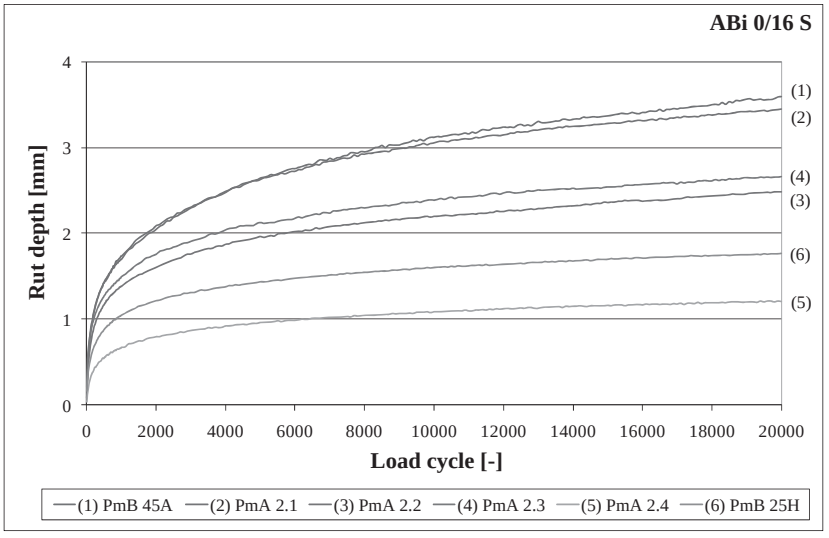

Figure 8. Wheel tracking test result of variants with additive 2, PmB 45A and PmB 25H (ABi, steel wheel, 50°C, temperature controlled by water).

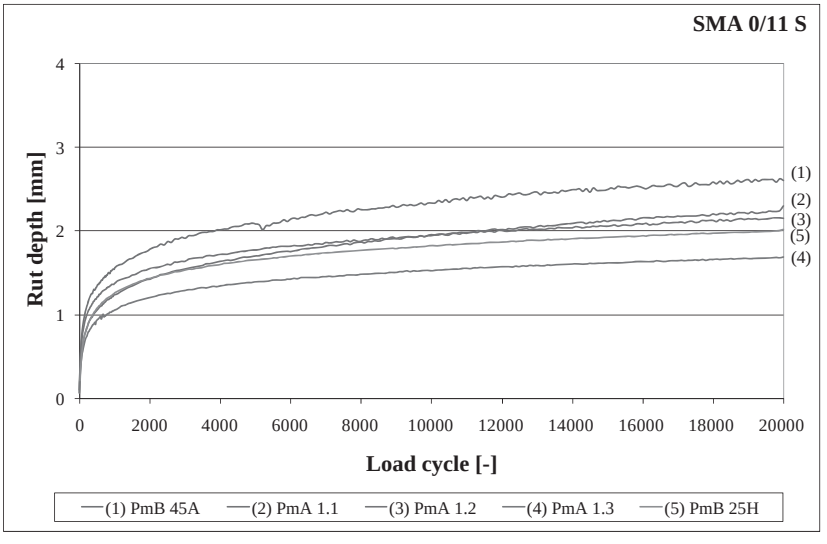

Figure 9. Wheel tracking test result of variants with additive 1, PmB 45A and PmB 25H (SMA, rubber wheel, 60°C, temperature controlled by air).

Correlations between rut depth development and polymer content are clearly shown in figures 11 to 12. Conventional ABi mixtures modified with about 4 up to 4.5% of additive 1 or additive 2 provide similar rut depths as asphalt mixtures with ready mixed polymer modified bitumen PmB 45A. For SMA mixtures clearly less than 4% of additive 1 and circa 4% of additive 2 are necessary to get values equivalent to PmB 45A variants. Nearly 7% of additive 1 and approximately 10% of additive 2 is required to get ABi mixtures with such low rut depths as with PmB 25H mixed ABi. Conventional SMA mixtures modified with about 7.5 up to 8% of additive 1 or additive 2 can achieve rut depths similar to SMA mixed with PmB 25H.

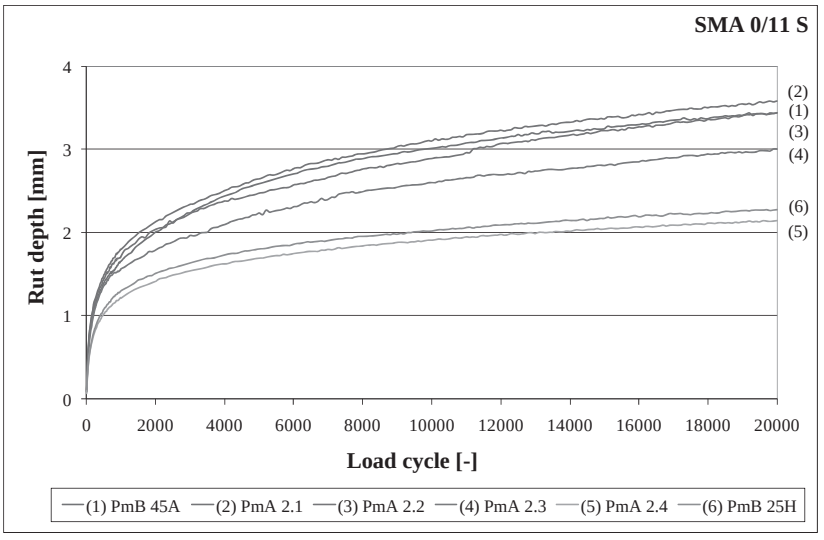

Figure 10. Wheel tracking test result of variants with additive 2, PmB 45A and PmB 25H (SMA, steel wheel, 50°C, temperature controlled by water).

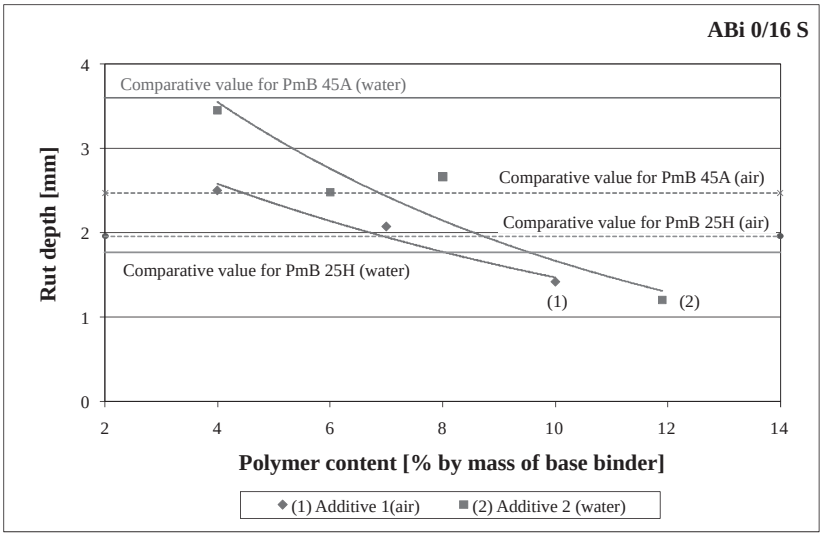

Figure 11. Development of rut depth with respect to polymer content (ABi).

The test results (resilient modulus, WTT) show that the quality of conventional asphalt mixtures modified with granular polymer additives in dry process provide similar high performance qualities of asphalt mixtures with ready mixed polymer modified bitumen PmB 45A and/or PmB 25H. Equivalent or better results than asphalt mixtures with PmB 45A are gained by adding about 4% granular additive. Adding about 8% granular polymers to SMA respectively 10% to ABi similar or better rutting resistance and stiffness can be achieved than equivalent asphalt mixtures with high polymer modified special bitumen PmB 25H.

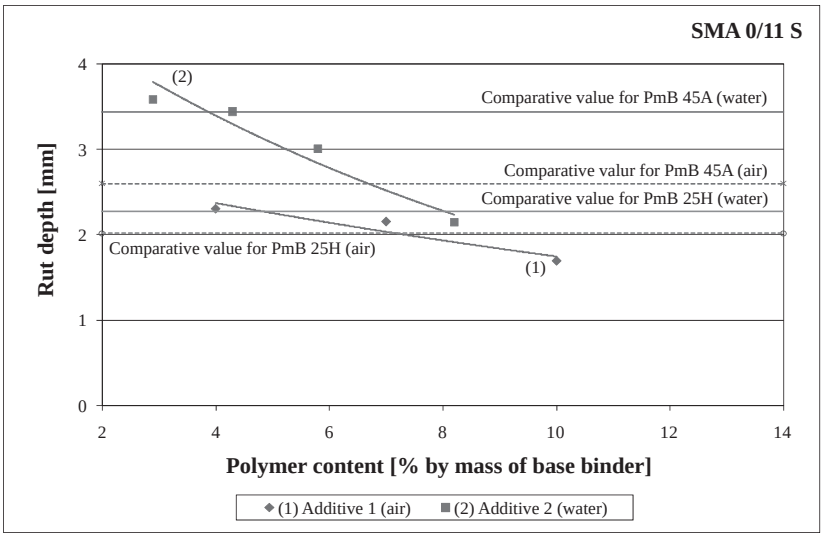

Figure 12. Development of rut depth with respect to polymer content (SMA).

5 SUMMARY

The modification of asphalt proceeds to improve the performance quality of asphalt mixtures. The production of modified asphalt mixtures takes place in two different ways. The first method is the use of ready mixed polymer modified bitumen and the second one is to add granular polymers during the asphalt mixing procedure. This paper focuses on stone mastic asphalt mix (SMA 0/11 S) and asphalt binder course mix (ABi 0/16 S) which have been prepared in both methods with four different polymers. A polymer modified bitumen PmB 45A, a special high polymer modified bitumen PmB 25H and two conventional bituminous binders in combination with two different granular polymer additives have been used. Polymer content has been systematically varied to rank the improvement of asphalt quality with respect to the granular polymer content. Asphalt mixtures modified with granular polymer additives shall provide similar quality as asphalt mixes with ready mixed polymer modified bitumen PmB 45A and/or PmB 25H. The qualities of asphalt mixtures were determined by means of resilient modulus tests and wheel tracking tests. The gained test results lead to comparable asphalt qualities no matter whether granular polymer modified asphalt mixes or asphalt mixes with ready mixed PmB are considered.

REFERENCES

EN 12591: Bitumen and bituminous binders—Specification for paving grade bitumen, Beuth Verlag, Berlin, Germany, 2000.

EN 12697-22: Test methods for hot mix asphalt—Part 22: Wheel tracking, Beuth Verlag, Berlin, Germany, 2004.

EN 12697-26: Test methods for hot mix asphalt—Part 26: Stiffness, Beuth Verlag, Berlin, Germany, 2004.

TP A-StB SBV: Technische Prüfvorschriften für Asphalt im Straßenbau, Teil: Spurbildungsversuch - Bestimmung der Spurrinnentiefe im Wasserbad, FGSV-Verlag, Cologne, Germany, 1999 [Specifications for testing asphalt mixes, part: wheel tracking test carried out in water with steel wheels].

TL PmB: Technische Lieferbedingungen für gebrauchsfertige polymermodifizierte Bitumen, FGSV-Verlag, Cologne, Germany, 2001 [Technical delivery conditions for ready mix polymer modified bitumen].

ZTV Asphalt-StB: Zusätzliche Technische Vertragsbedingungen und Richtlinien für den Bau von Fahrbahndecken aus Asphalt, FGSV-Verlag, Cologne, Germany, 2001 [Additional terms of contract and guidelines for asphalt pavement construction].

Advanced Testing and Characterization of Bituminous Materials –
Loizos, Partl, Scarpas & Al-Qadi (eds)
© 2009 Taylor & Francis Group, London, ISBN 978-0-415-55854-9

Phase angle determination and interrelationships within bituminous materials

G. Rowe
Abatech, Blooming Glen, Pennsylvania, USA

ABSTRACT: The phase angle of bituminous materials is often required when in-sufficient data exists to define this with a high degree of accuracy. In addition, the measurement of phase angle has a higher variability than that associated with the complex modulus (G^* or E^*). Often historical data consists only as complex modulus versus frequency with no phase angle information. To enable use of these data sets in current analysis procedures requires the use of the phase angle information that has to be obtained from mathematical and/or predictive methods. Phase angle can be calculated from the retardation and relation spectra. This approach is contrasted to the method developed from the relationship found between the log-log gradient of complex modulus versus frequency and phase angle. Data is presented for a range of materials that includes non-bituminous products. It is concluded it would be reasonable to analyze complex modulus vs. frequency and estimate the phase angle from numerical procedures.

1 INTRODUCTION

1.1 *Background*

The phase angle of bituminous material is a parameter that has been growing in importance in specifications in the USA since the early 1990's following the Strategic Highway Research Program (SHRP). Since that time a phase angle measurement has been a feature of the binder specification described in the AASHTO specification M320. In addition, some states (for example Georgia) specify a minimum phase angle as an additional requirement. In asphalt mixtures the phase angle is routinely measured and reported using the latest testing methods as being considered as part of the Mechanistic-Empirical Pavement Design Guide (ARA, Inc., 2004). In addition, a large volume of data exists in the industry for complex dynamic modulus, either in extension/compression (E^*) or shear (G^*) for which no phase angle is reported. To obtain phase angle information from these data sets using simple methods would advantageous and increase the utility of the data. Currently, methods exist where Prony series or relaxation/retardation spectra can be fitted to the data with the phase angle then calculated from the resulting spectra fits. However, this fitting process is relatively complex requiring specialized software and can be numerically confounded depending upon the amount and quality of data available.

Dickersen and Witt (1974) presented a relationship that linked the phase angle of bitumen to a relationship between G^* and frequency. Christensen and Anderson (1992) further developed this relationship idea by presenting a relationship between phase angle with frequency and binder parameters, as follows:

$$\delta(\omega) = \frac{90}{\left[1+\left(\frac{\omega}{\omega_0}\right)^{\sqrt{(\log 2/R)}}\right]} \tag{1}$$

where $\delta(\omega)$ is the phase angle at a frequency (expressed as radians/second, ω), ω_0 is the crossover frequency and R is the rheological index. This equation for phase angle is based upon the parameters determined from the Christensen-Anderson (CA) stiffness equation which works well for unmodified binders.

For asphalt mixtures several researchers have developed relationships between phase angle and modulus. Bonnaure et al. (1977) developed a relationship that was limited to binder stiffness (S_b) values greater than 5 MPa and less than 2 GPa (when S_b is greater than 2 GPa the mixture phase angle (ϕ_m) is taken to be zero). The relationship used the volume of binder (V_b) in the prediction and is as follows:

$$\phi_m = 16.36 \times V_b^{0.352} \exp\left[\frac{\log_{10} S_b - \log_{10} 5 \times 10^6}{\log_{10} S_b - \log_{10} 2 \times 10^9} \times 0.974\, V_b^{-0.} \right. \tag{2}$$

During the SHRP project Tayebali et al. (1994) developed a relationship linking the phase angle to the mix stiffness as follows:

$$\phi_0 = 260.096 - 17.172 Ln(S_0) \tag{3}$$

where ϕ_0 is the mixture phase angle and S_0 is the mixture stiffness. This relationship was developed from a study of fatigue properties. The subscript to the parameters denotes that the initial condition is used. Christensen et al. (2003) published a relationship developed from the Hirsch model. This relationship links the phase angle to binder properties and mixture volumetrics, as follows:

$$\phi_0 = -21(\log Pc)^2 - 55 \log Pc \tag{4}$$

where

$$Pc = \frac{\left(20 + \frac{VFA \times 3G_b^*}{VMA} \right)^{0.58}}{650 + \left(\frac{VFA \times 3G_b^*}{VMA} \right)} \tag{5}$$

with VFA being the voids filled with asphalt, G_b^* being the complex shear modulus of the binder and VMA being the percent voids in the mineral aggregate. All of the described relationships for bituminous mixtures are empirical in nature with derived constants from regression analysis of materials.

1.2 *Log-log relationships*

In Dickerson and Witt's paper the relationship developed made use of the slope (or derivative) of the log-log relationship between the G^* and frequency to estimate the phase angle. Christensen and Anderson (1992) further developed this idea and presented a relationship between the phase angle and stiffness which can be shown to be the derivative of CA stiffness equation, as follows:

$$G^*(\omega) = G_0 \left[1 + \left(\frac{\lambda}{\omega} \right)^{\beta} \right]^{-1/\beta} \tag{6}$$

then

$$\delta(\omega) = 90 \left[1 + \left(\frac{\omega}{\lambda} \right)^{\beta} \right]^{-1} = 90 \times \frac{d \log G^*}{d \log \omega} \tag{7}$$

where $G^*(\omega)$ and $\delta(\omega)$ are the complex shear modulus and phase angle at a frequency ω. The parameters λ and β are used to define the shape of the master curve in the same manner as the crossover frequency and rheological index in equation 1. The implication of this relationship is that it implies two approaches for obtaining an estimation of the phase angle being 1) use of model parameters directly with equation 1 or 5, or 2) using an alternate numerical procedure to obtain the slope of the log G* versus log frequency relationship. Conceptually, this relationship should not be limited to one case being unmodified binders but rather it should be universal in application.

The use of log-log relationships are investigated for a number of materials using numerical differentiation. In addition, the use of model differential schemes are applied to asphalt mixtures and compared to differentials of other fitting functions such as high-order polynomials.

2 MATERIALS

2.1 *Material types and analysis methods*

Analysis is applied to a standard asphalt binder; a SBS modified resin binder; polystyrene; a roofing product (high content of SBS with modified filled binder), and various hot mix asphalt samples. Several analysis methods are applied to the data sets, as follows:

- A polynomial (order 3 or 4) fit has been applied to many of the master curves and the differentiated with respect to frequency in an attempt to obtain a good estimation of the slope of master curves.
- An approximation of the slope at a given point is estimated from consideration of data points either sides.
- A fit of the discrete spectra as determined using the method defined by Baumgaertel and Winter (1989).
- By the differential of an equation considered to describe the shape of the master curve.

The equations used to describe the shape of the master curve the CA method as defined in equation 6 and 7. The standard logistic (Verhulst, 1838) initially adopted by the Asphalt Institute (1982) and subsequently further developed for use in the AASHTO Mechanistic-Empirical Pavement Design Guide (MEPDG) (ARE, Inc., 2004) and the generalized logistic (Richards, 1959), expressed in a form to be used with the E* definition of hot mix asphalt, have the functional forms and differentials used to compute the phase angles as follows:

$$\text{Standard logistic} - \log E^* = \delta + \frac{\alpha}{1 + e^{[\beta + \gamma(\log \omega)]}} \tag{8}$$

$$\text{Standard logistic} - \delta(\omega) = 90 \times \frac{d \log E^*}{d \log \omega} = -90 \alpha \gamma \frac{e^{[\beta + \gamma(\log \omega)]}}{\left[1 + e^{[\beta + \gamma(\log \omega)]}\right]^2} \tag{9}$$

$$\text{Generalized logistic} - \log E^* = \delta + \frac{\alpha}{\left[1 + \lambda e^{[\beta + \gamma(\log \omega)]}\right]^{1/\lambda}} \tag{10}$$

$$\text{Generalized logistic} - \delta(\omega) = 90 \times \frac{d \log E^*}{d \log \omega} = -90 \alpha \gamma \frac{e^{[\beta + \gamma(\log \omega)]}}{\left[1 + \lambda e^{[\beta + \gamma(\log \omega)]}\right]^{(1+1/\lambda)}} \tag{11}$$

2.2 *Analysis of various materials*

A sample was taken from the data base developed during the SHRP program. With this material testing has been conducted using the torsion bar (TB) and dynamic shear rheometer

(DSR) tests. The master curve for this material using data collected between –23.5 and 63.2°C. The resin modified binder is a clear resin modified by SBS with testing conducted between –5 and 60°C. Both these data sets are shifted to a reference temperature of 50°C as illustrated in Figure 1. The conventional (straight run asphalt) binder conforms to the CA model whereas the SBS resin binder clearly does not conform to the CA model. The analysis of these binders with various methods is illustrated in Figure 2 which shows fits of the various methods. The conventional binder has a good fit with all methods but some increased scatter is apparent in the data at the low G^*/high δ end of the range when the approx slope method is used due to inherent variability in the data sets. With the resin modified binder, two methods (standard logistic and 4th order polynomial) result in a poor estimation at the low frequency/high temperature end of the data sets where the phase angle turns upwards. The slope estimated from the discrete spectra fit which results in over 20 fitting parameters for the curves produces a good estimation of the phase angle in both cases.

A polystyrene material has a complex stiffness and phase angle relationship. The master curve of this material using isotherms collected between 132 and 269°C is presented in Figure 3 along with that of a high polymer content roofing material (Rowe and Baumgardner, 2007). For the polystyrene two methods of estimating the log-log slope were used; 1) differential of the Prony series determined from a discrete spectra analysis, and 2) and approximation of the slope. No functional form models were attempted with this material since it was obvious these would not apply to the shape of the master curve. For the roofing

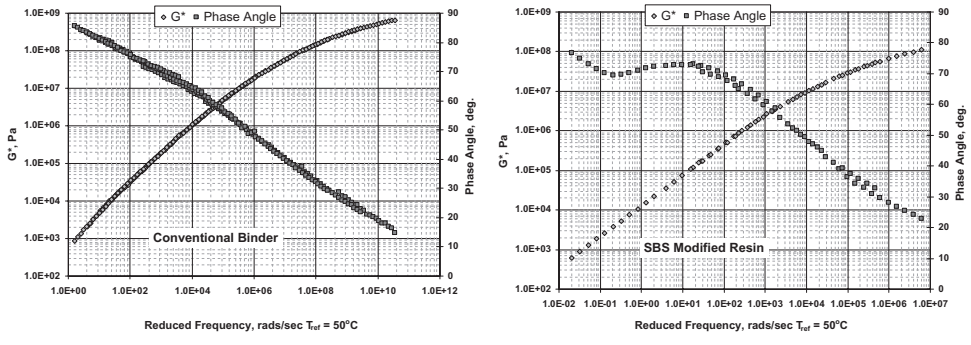

Figure 1. Master curves for conventional and SBS resin binders, T_{ref} = 50°C.

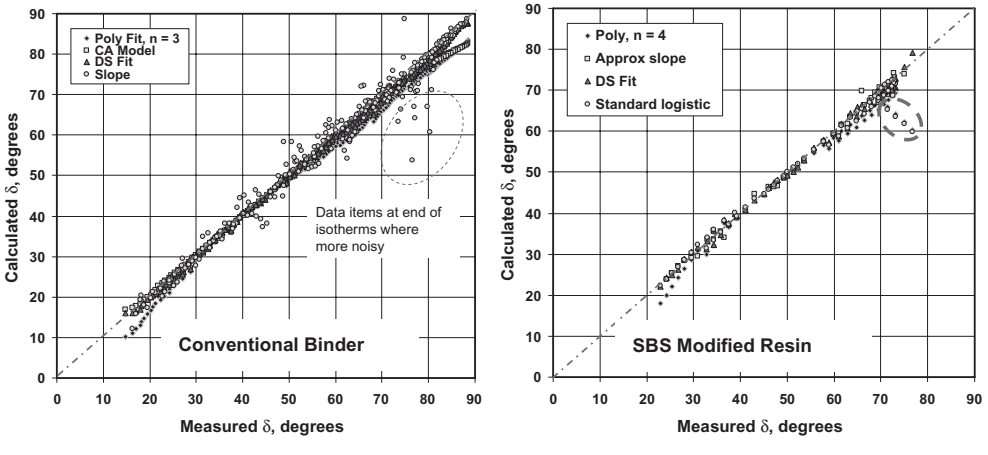

Figure 2. Measured versus calculated phase angles for conventional (straight run) and SBS resin modified binders.

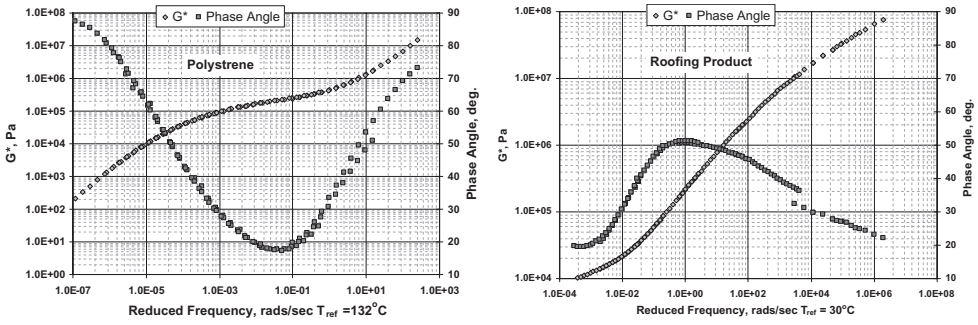

Figure 3. Master curves for polystyrene and roofing product.

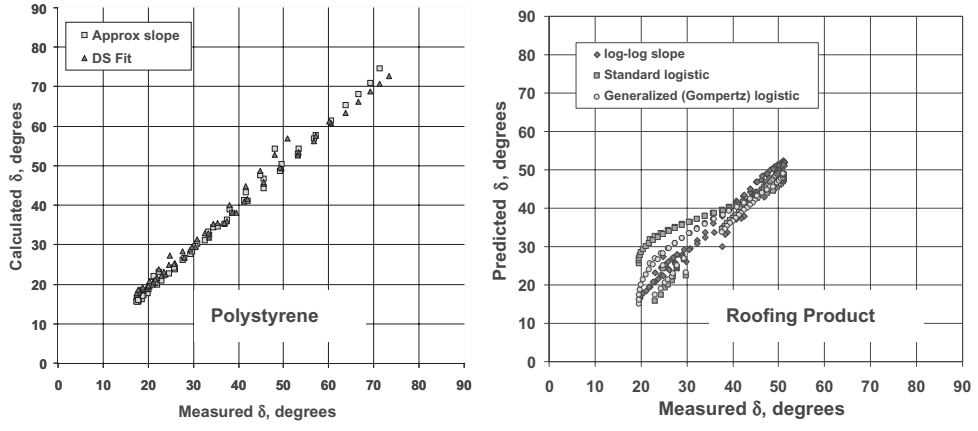

Figure 4. Measured versus calculated phase angles for polystyrene and roofing product.

product two functional forms were applied, the standard logistic and the generalized logistic functional forms. The generalized logistic analysis resulted in the limiting Gompertz (1825) case of the Richards curve. The results from the phase angle estimation are presented in Figure 4 which demonstrates that both methods provide very good estimations of the phase angle. The discrete spectra fit and the approximate slope methods provide the best estimations. With the roofing material the two logistic models are evaluated. From the results of the analysis it is clear that the use of the generalized logistic provides a better fit that the standard logistic since it more accurately captures the shape of the master curve.

The key aspect of obtaining a good fit of the measured phase angle data is that the curve adopted to describe the master curve (or part of the master curve being considered) must be a good representation of the shape. The models that more accurately define the shape of the master curve are the generalized logistic function or discrete spectra fits.

2.3 *Hot mix asphalt*

The analysis has been applied to several HMA material data sets. For example the Center of Advanced Infrastructure Testing (CAIT) produced data on a series of mixtures representing modified and unmodified materials. The fit obtained from analysis of the standard logistic function is given in Figure 5 which shows a reasonable correspondence with the measured data.

Use of this same method has been applied to data taken from frequency sweep tests conducted in shear developed as part of the SHRP test program. Data from this test is presented

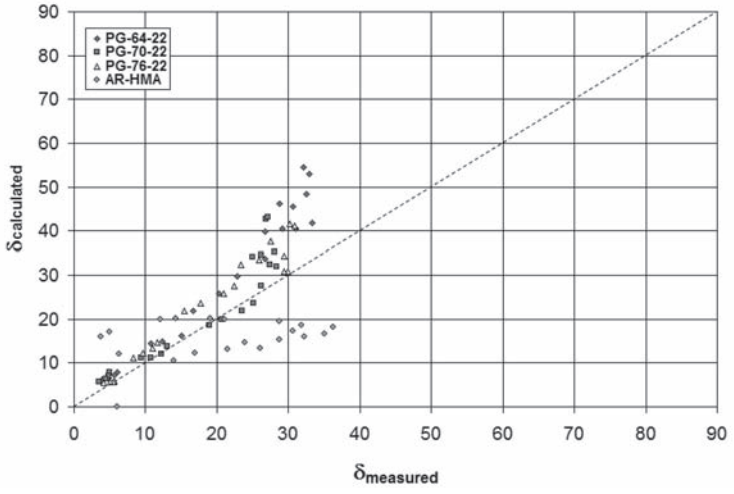

Mixtures are made with PG grades are in accordance with AASHTO M320 specifications except the AR-HMA which is a crumb rubber (20%) modified PG64-22. Mix details are given in Bennert et al, 2004.

Figure 5. Phase angle calculated using standard logistic curve (equation 9) vs. measured for four HMA mixtures containing conventional and modified binders (E^* and δ data obtained from Bennert et al., 2004).

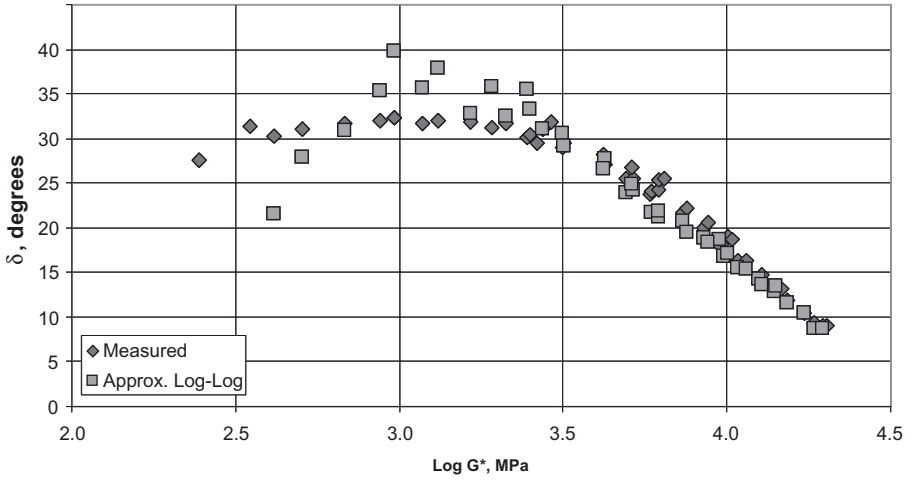

Figure 6. Mixture complex modulus and phase angle measured in shear with the calculated phase from the approximation of the logG^* vs. logω slope.

in Figure 6 on a plot of G^* versus δ, commonly referenced as a Black Space Plot. The differences observed in predicted from measured results occurs at the lower end of the stiffness range as the complex modulus G^* reduces below 1,000 MPa. It should be noted as the stiffness reduces the accuracy of measurements is often questionable and certainly the problem of fitting data at the extremes of the data ranges is often problematic.

In a study conducted with the Asphalt Institute (Hakimzadeh-Khoee, 2009) it was observed that at the highest test temperature some densification of the specimens was taking place. The results obtained from the E^* and δ test for one of the specimens is illustrated in Figures 7 and 8. Figure 8 also shows how the predictive relationship from the differential of the standard logistic equation compares over a much wider range of stiffnesses. It was concluded from

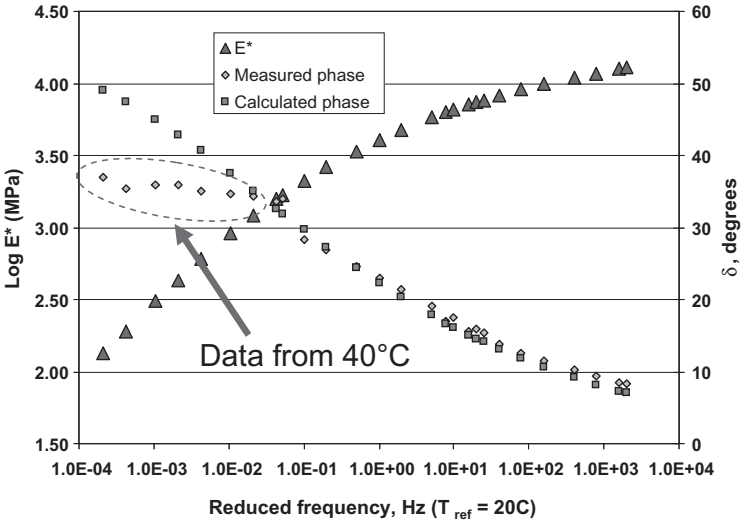

Figure 7. Mixture complex modulus and phase angle measured in shear with the calculated phase from the approximation of the logG^* vs. logω slope.

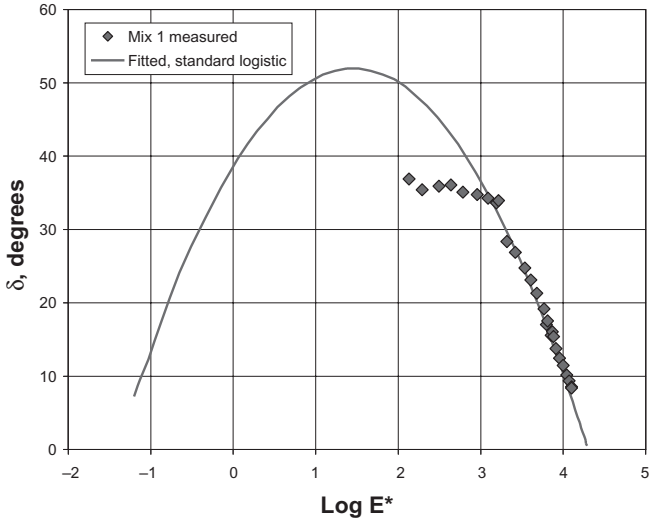

Figure 8. Mixture complex modulus and phase angle measured in shear with the calculated phase (standard logistic, equation 9) from the approximation of the logG^* vs. log ω slope.

this data that the secondary compaction of the material during the testing was affecting the phase angle result which can be clearly observed by inspecting the calculated versus measured phase angle relationships.

The concept of using differential of the complex modulus vs. frequency relationship appears to be sound for mixtures and it has functionality in that it shows where mixture data has poor phase angle measurement.

3 DISCUSSION

The discrete spectra analysis (Baumgaertel and Winter, 1989) is more commonly applied to visco-elastic data when both modulus and phase angle are available and the elastic and

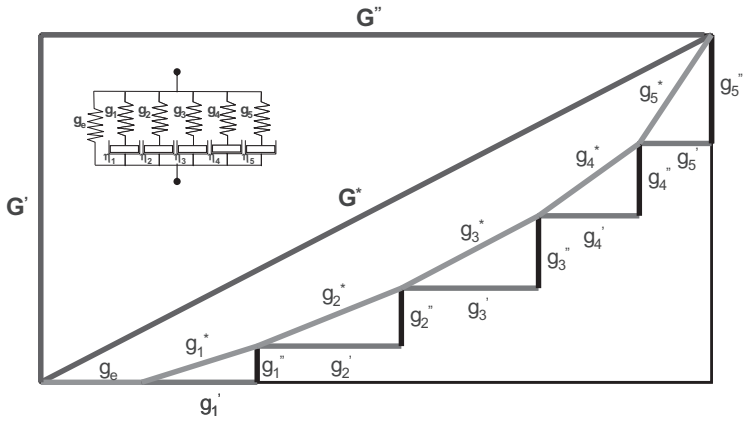

Figure 9. Representation of G^* made up from relaxation spectra components.

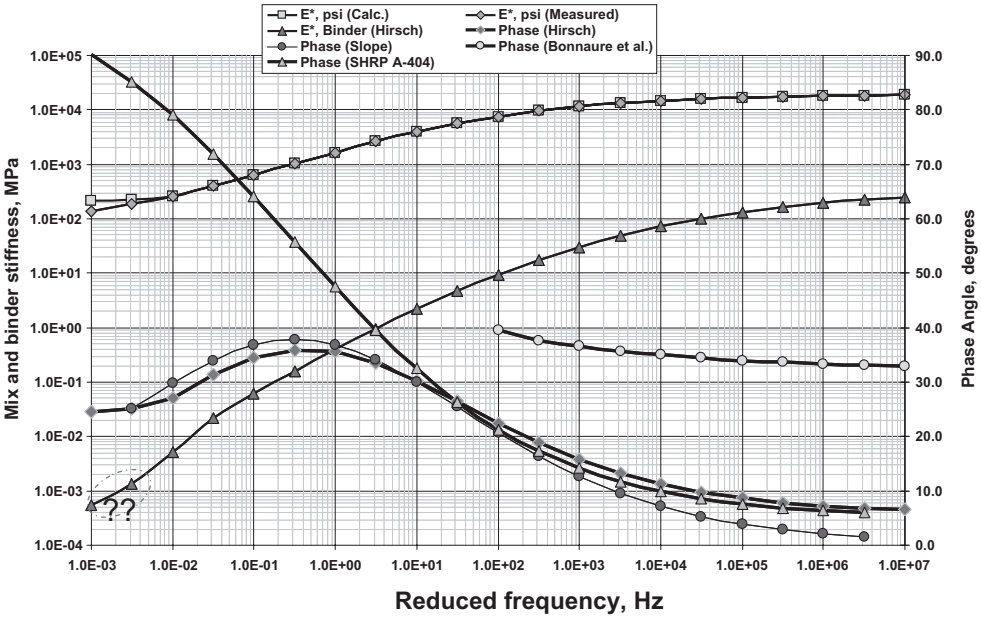

Figure 10. Mix and binder complex modulus and various estimations of mixture phase angle.

viscous parts of the complex modulus are used. A representation of how visco-elastic components—expressed as loss and storage modulus in shear (g' and g" respectively) are considered as spectra components to produce the calculation of phase of total G^*, G' and G'' is illustrated in Figure 9. While this figure shows the shear (G^*) version of the graph it should be noted that this also applies equally to the use of the extensional form, E^*. A fit of the discrete spectra can be applied when any visco-elastic parameter is described as a function of frequency or loading time (e.g. G^*, E^*, $E(t)$, $G(t)$, $S(t)$ etc.). Thus if only G^* or E^* data exists, such as that found in many older references, it is still possible to determine phase angle information from an analysis of the spectra information or from fitting the master curve the log-log slope information from the master curve.

Recent discussion between Daniel and Rowe (2008) have suggested the utility of this approach. It is possible to determine the phase angle information for both binder and mixture, and the complex shear modulus of the binder given just the complex dynamic modulus

master of a mixture. An example of an analysis conducted using mixture properties is given in Figure 10. The mixture stiffness is shown and compared to the Hirsch predictive equation. This data shows close agreement. In addition, the graph shows the mixture phase angle deduced from the Hirsch model along with that determined from the $d\log E^*/d\log\omega$ relationship. These two curves are in very good agreement and contrast to the poor fits of phase angle obtained from the method developed by Bonnaure et al. (1977) and the SHRP-A-404 method (Tayebali et al., 1994). In addition, the binder E* curve is also shown. The two lowest points on this curve were estimations since they were beyond the limit of the Hirsch model for back-calculation. Regardless of this, using the remainder of the data it is still possible to fit the binder stiffness curve to a CA model (Christensen and Anderson, 1992) and use this with equation 7 to obtain the phase angle information. This type of analysis could be applied to any type of mix where the effective binder properties is required, for example a blend of virgin mix with recycled asphalt pavement.

Traditionally phase angle of binder and mixtures has presented a complex verification of properties. Only recently an article in the Society of Rheology commented on the difficulty that occurs due to a lack of calibration standards for phase angle measurement (Velankar and Giles, 2007). However, accepting the relationships that exist and using these to verify and check the adequacy of phase angle measurements will assist in this aspect of lack of calibration.

4 CONCLUSIONS

The analyses of experimental data obtained from testing various materials have been conducted. These materials have been very wide ranging, covering asphalt binders; polymer modified binders; roofing compounds; polymers (such as polystyrene); hot mix asphalt, and many other materials.

The use of interrelationships between the stiffness and frequency dependency allows the use of two methods for obtaining the phase angle information using a fundamental analysis approach. The first of these is to fit discrete spectra to the complex modulus master curve whereas the second makes use of the log-log relationship between the complex stiffness modulus and frequency and shows how this relates to phase angle. The spectrum fit involves sophisticated software in the implementation of analysis methods (Baumgaertel and Winter, 1989). While these have been implemented in a number of software packages the use of $d\log G^*/d\log\omega$ (or $d\log E^*/d\log\omega$) provides a simple rapid method for obtaining the phase angle information.

The experimentation with many materials has confirmed this validity of this approach which is essentially similar to that originally suggested by Christen and Anderson (1992) in the analysis of binder with their differential analysis of the CA equation for binder master curves. For mixtures a differential form of the generalized logistic sigmoid as proposed by Rowe et al., (2009) provides a reliable means of estimation of phase angle for many filled materials.

REFERENCES

ARE, Inc. 2004. Guide for Mechanistic-Empirical Design of New and Rehabilitated Pavement Structures, Final Report, Part 2. Design Inputs, Chapter 2 Material Characterization. *National Cooperative Highway Research Program, Transportation Research Board, National Research Council*.

Baumgaertel, M. and Winter, H.H. 1989. Determination of discrete relaxation and retardation time spectra from dynamic mechanical data. *Rheol Acta* 28. pp. 511–519.

Bennert, T., Maher, A. and Smith, J. 2004. Evaluation of Crumb Rubber in Hot Mix Asphalt. *Center for Advanced Infrastructure and Transportation (CAIT), Rutgers Asphalt/Pavement Laboratory (RAPL)*, Rutgers University, Department of Civil and Environmental Engineering, 623 Bowser Road, Piscataway, NJ 08854.

Bonnaure, F., Gest, G., Gravois, A. and Uge, P. 1977. A New Method of Predicting the Stiffness of Asphalt Paving Mixtures. *Proceedings, Association of Asphalt Paving Technologists*.

Christensen, D.W. and Anderson, D.A. 1992. Interpretation of Dynamic mechanical Test Data for Paving Grade Asphalt Cements. *Journal, Association of Asphalt Paving Technologists*, Volume 61, pp. 67–116.

Christensen, D.A., Pellinen, T. and Bonaquist, R.F. 2003. Hirsch Model for Estimating the Modulus of Asphalt Concrete. *Journal of Asphalt Technologists*, Volume 72. pp. 97–121.

Dainel, J. and Rowe, G.M. 2008. Discussions on Phase Angle Relationships, FHWA Asphalt Fundamental Properties and Advanced Modeling Expert Task Group, minutes on web - www.asphaltmodelsetg.org/Tampa%20Models%20ETG%20Minutes%20Feb%202008.pdf

Dickinson, E.J. and Witt, H.P. 1974. The Dynamic Shear Modulus of Paving Asphalts as a Function of Frequency. *Transactions of the Society of Rheology* 18:4, 591–606.

Gompertz, B. 1825. On the Nature of the Function Expressive of the Law of Human Mortality, and on a New Mode of Determining the Value of Life Contingencies. *Phil. Trans. Roy. Soc*. London, Vol. 115, pp. 513–585.

Hakimzadeh-Khoee, S., Rowe, G.M. and Blankenship, P. 2009. Evaluation of Aspects of E* Test with using HMA Specimens with Varying Void Contents. *Paper submitted to Transportation Research Board Annual Meeting*.

Richards, F.J. 1959. A Flexible Growth Function for Empirical Use. *Journal of Experimental Botany*, Vol. 10, No 29, pp. 290–300.

Rowe, G.M. and Baumgardner, G. 2007 Evaluation of the Rheological Properties and Master Curve Development for Bituminous Binders Used in Roofing. *Journal of ASTM International*, Vol. 4, No. 9.

Rowe, G.M., Baumgardner, G. and Sharrock, M.J. 2009. Functional forms for master curve analysis of bituminous materials. *Paper submitted to the 7th International Symposium on Advanced Testing and Characterization of Bituminous Materials Organized by RILEM TC 206 ATB, Rhodes, Greece.*

Tayebali, A.A., Deacon, J.A., Coplantz, J.S., Finn, F.N. and Monismith, C.L. 1994. Fatigue Response of Asphalt-Aggregate Mixes, Part II Extended Test Program. *Strategic Highway Research Program, National Research Council, Washington DC.* Report SHRP-A-404.

The Asphalt Institute. 1982. Research and Development of the Asphalt Institute Thickness Design Manual (MS-1) Ninth Edition. *The Asphalt Institute, RR-82-2*.

Velanker, S.S. and Giles, D. 2007. How do I know if my phase angles are correct? *Rheology Bulletin, 76(2), July, pp. 8–20*.

Verhulst, P.F. 1838. Notice sur la loi que la population poursuit dans son accroissement. *Correspondance mathématique et physique* 10: pp. 113–121.

Advanced Testing and Characterization of Bituminous Materials –
Loizos, Partl, Scarpas & Al-Qadi (eds)
© 2009 Taylor & Francis Group, London, ISBN 978-0-415-55854-9

Evaluation of initial road performance correlating with different tests of binders

G. Malkoç
Turkish Asphalt Contractors Association, Ankara, Turkey

ABSTRACT: The highway, in southern part of Turkey, where has quite heavy load traffic (more then 42%) and steep gradient (till to 8%) together with very hot weather conditions (reaching 48°C in the summer), was constructed with Hot Mix Asphalt (HMA). In this application the binder was used as PmB (Polymer Modified Binder) with SBS (5%).

In this study, it is aimed to evaluate the initial road performance correlating with original and PmB binders' tests, that are chemical, conventional & performance based. (Such as Iatroscan test, Size Exclusion Chromatography (SEC), paraffin content, microscopic observations of PmB, Thermal Fracture Toughness & Fracture Energy test, Zero Shear Viscosity tests). Besides, the properties of the mix, aggregate and PmB production high shear mill (grinder to distribute to polymer in bitumen) were also observed. Then, the test results were evaluated and correlated with initial road performance.

1 INTRODUCTION

During road construction some factors, such as heavy volume of traffic, extreme climatic conditions, ageing of binder and/or the steep gradient require specific hot mixes. In those cases, the binder is preferred as PmB to prevent road deformations, such as rutting. The highway, in South East Turkey, the wearing course where has the steep gradient up to 8%, volume of heavy traffic 42% at minimum, and up to 48°C in summer, was constructed HMA. Since it is expected that the rutting would be occur in that road because of the mentioned factors, the binder was used as PmB. In this paper, it is aimed to perform the chemical, conventional & performance tests of the binders (both original and PmB) and to evaluate them with initial road performance.

2 THE ENVIRONMENTAL CONDITIONS OF THE HIGHWAY

2.1 *The local climatic properties*

The monthly minimum, mean and maximum temperature averages of the cities Şanlıurfa and Birecik, where the highway was constructed, presented by the Turkish State Meteorological Service (2005) can be viewed in Table 1A and Table 1B.

2.2 *Road traffic values*

The average daily traffic values during 2002–2003 of the Section of the Highway are shown in Table 2. The info is taken from Turkish General Directorate of Highways, Traffic and Access Information (2003, 2004).

In regard to the data given above there has been an increase in the ratio of heavy vehicles like trucks and trailers in 2003 according to 2002 by 16.5% in section 1 and 14.7% in section 2 (an average of 15.6%). The heavy vehicle traffic ratio was much higher than the above mentioned 41–42%.

Table 1A. Monthly minimum, mean and maximum temperatures in Şanlıurfa.

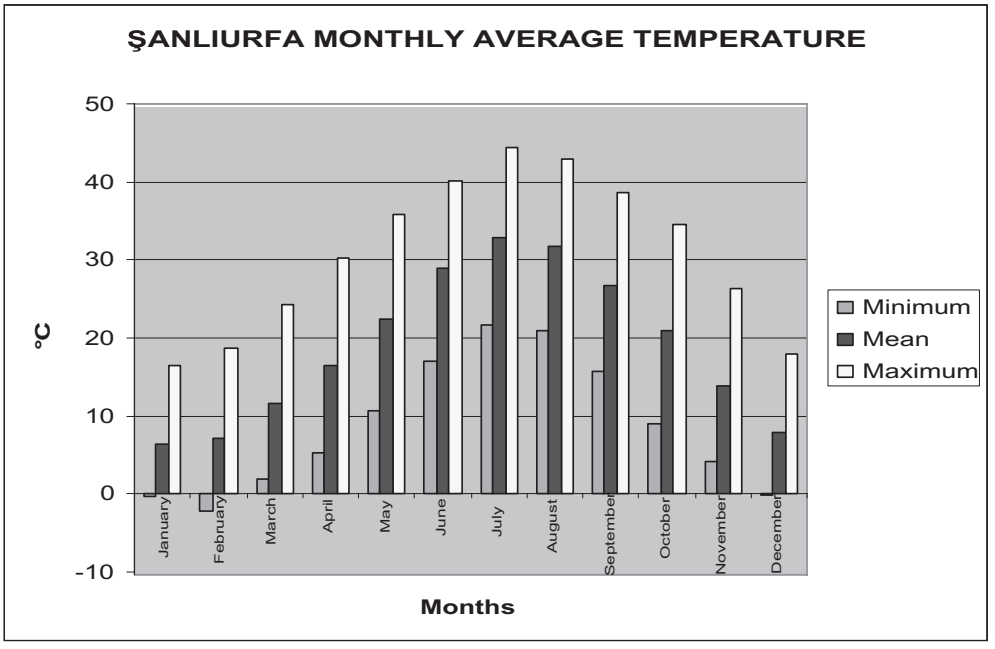

Table 1B. Monthly minimum, mean and maximum temperatures in Birecik.

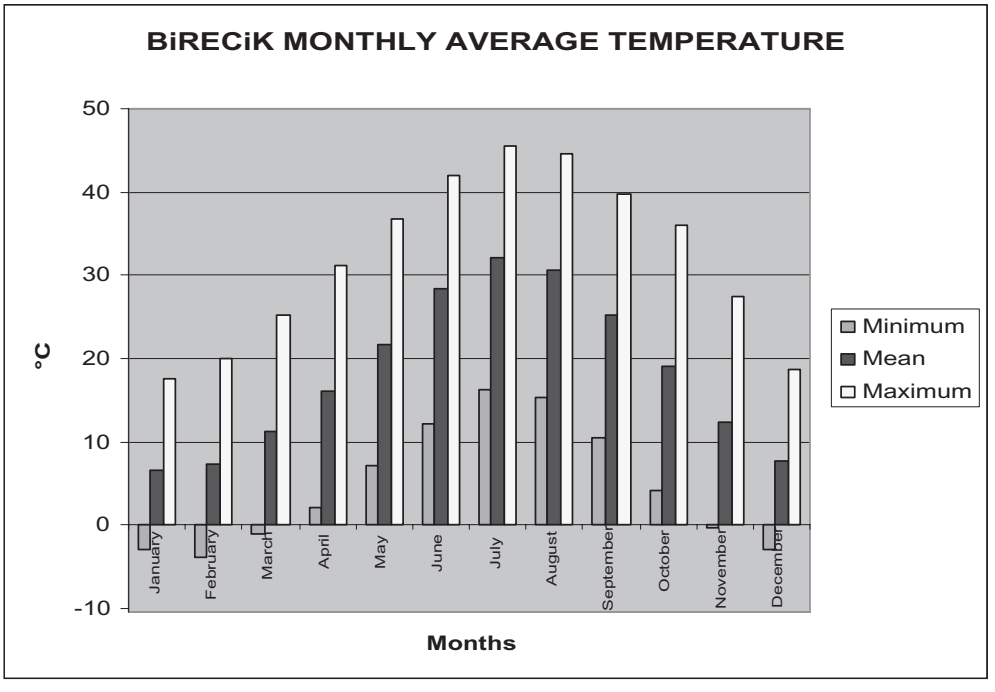

Table 2. Traffic values for 2002 and 2003.

Control section		Section No	Km	Car	Bus	Truck	Trailer	Total vehicle	Trailer %	Heavy vehicle %
2002	400-24	1	2	4463	289	3200	262	8314	3	42
	400-24	2	43	4378	386	3120	243	8127	3	41
2003	400-24	1	2	5313	312	3605	430	9660	4	42
	400-24	2	43	5212	304	3515	344	9435	4	41

Table 3. The gradient distribution ratio of the road.

Gradient intervals	Highways total gradient ratio, %	Highway length (m)
Gradient between 0% & 1%	35.70	15,285.80
Gradient between 1% & 2%	19.08	8171.68
Gradient between 2% & 3%	13.31	5699.25
Gradient between 3% & 4%	11.13	4766.47
Gradient between 4% & 5%	8.40	3598.57
Gradient between 5% & 6%	4.71	2018.81
Gradient between 6% & 7%	4.13	1766.63
Gradient between 7% & 8%	3.32	1421.27
Gradient between 8% & 9%	0.21	90.06
TOTAL	100.00	42,818.54

2.3 *The gradient distribution ratio of highway*

The road of gradient distribution ratios have been given in Table 3 taken from Construction Project Measurements.

2.4 *The design of the road is as follows*

Plant-Mix base course: 100 mm
Bituminous base course: 120 mm
Binder course: 70 mm
Wearing course: 50 mm

Wearing course is constructed with using polymer Modified binder.

3 PmB PRODUCTION PRINCIPLE IN GENERAL

The parameters such as polymer and bitumen properties and production process together with mill properties effect on PmB production. The PmB production principle generally depends on the fact of milling the polymer and bitumen pre-mixture through a high-shear mill in a specified cycle-number. The polymer becomes micron size by milling. During this process the rising temperature solutes the polymer in the bitumen. Afterwards there is needed for maturing period. The successful distribution of polymer in the bitumen affects PmB's properties.

4 PmB PRODUCTION ON SITE

In construction site, PmB was produced on the site by using high shear mill. The high-shear homogenizing-mill also had the mechanical seal type cooling system. In order to be able to fix the cycling-number and ratio of SBS, different PmB's was produced by adding different (4.5%, 5.0%, 5.5%) ratios of Kraton D 1101. The original bitumen was heated to temperatures between 180–185°C. Then several cycles were performed while preparing the PmB. After each cycle, microscopic

observations of PmB were carried out up to 7 cycles. Since after 3 cycles there weren't any differences during the, microscopic observations, the cycle number was specified as 3, by using %5 SBS.

5 TESTS OF MATERIAL USED IN HMA APPLICATION WITH PMB

5.1 *Original bitumen and PmB tests results*

The bitumen used in PmB production is a bitumen 50/70. The PmB (with 5% SBS) and the bitumen tests carried out in a laboratory on site is given in Table 4.

Table 4. Original bitumen and modified bitumen properties.

No	Tests	50/70	PmB
1	Penetration (25°C,100 g, 5 sec.) 0.1 mm, in	70	43
2	Ductility at 25°C, (5 cm/min) cm, min.	100	82
3	Softening point (r/b) °C, min.	49	75
4	Fraass breaking point, °C, max.		–15
5	Elastic recovery (25°C), %, min.		98

5.2 *Polymer type—modifier*

Table 5. Polymer properties.

Density	0.94
Melting point (°C)	180
Particle size (mm)	Granule
SBS	Kraton D 1101 Cs

5.3 *Aggregate (basalt) tests*

Table 6. Aggregate properties.

Los Angeles (%)	12.1
Nicholson	60–65 (no additive), 80–85 (with additive)
Polishing Value	0.53
Flakiness Index	18

Table 7. Specific gravity and absorption values of aggregates.

Materials	Bulk specific gravity, t/m³	Apparent specific gravity, t/m³	Abs. (%)
Coarse	2.832	2.986	1.8
Fine	2.815	2.969	1.9
Filler	–	2.900	–

5.4 *Mixture specifications*

Table 8. Mixture gradation & specification limits.

Sieve		Passing %	
Iinch	mm	Mixture gradation	Specification limits
3/4″	19.1	100	100
1/2″	12.7	88.7	83–100
3/8″	9.5	80.7	70–90
No. 4	4.75	49.1	40–55
No. 10	2.00	27.7	25–38
No. 40	0.42	13.3	10–20
No. 80	0.177	9.0	6–15
No. 200	0.075	6.8	4–10

5.5 *Design values*

Table 9. Design values.

Bitumen %	5.98
Bulk Specific Gravity, t/m³	2.829
Theoretical Specific Gravity, t/m³	2.626
Void (%)	4.45
VMA (Void in Mineral Aggregates) (%)	15.95
Voids filled with Asphalt (%)	71.3

6 PmB APPLICATION VS CONVENTIONAL ONES

The most important differences between conventional and PmB wearing coarse applications are mentioned as below:

- When 50/70 is used in conventional applications, the temperature of the mixture discharged from the plant is between 140–155°C, and is then laid out in required area. After the necessary processes have been carried out, the first compaction can start between the temperatures 130–135°C and finished at 80–90°C by using steel wheel roller. With most mixtures (except special conditions), 5 passes (the one going back and forth movement of the roller is accepted as one passing) is usually enough. After compaction is completed, one passing without vibration is applied. During operation, sometimes local segregations, small local leveling problems can be removed quite easily with good workmanship.
- However, the hot mix application with PmB was different than conventional one mentioned above. The most important subjects when preparing a mixture with PmB are; temperature of mixture, the starting and ending temperature of compaction process and the number of rolling passes. The mixtures temperature at plant discharge changed from 185–190°C (while preparing PmB the temperature was between the temperatures 180–185°C).
- In this hot mix application with %5 SBS PmB, after transporting and laying the mixture, the compaction was started by using only steel wheel rollers. The compaction was started when the mixtures temperature was between 170–175°C and finished at 140–145°C. Three passes were generally enough. The first pass was carried out without vibration and the other two passes were carried out with vibration. At the end of the compaction, one pass without vibration was applied. (The hot mix application with PmB, it is very difficult to mend small local errors because of the characteristic of PmB.) Below 140°C, the workability of the mixtures was decreasing.

7 THE OTHER RESEARCH STUDIES

In this part, some additional tests such as Iatroscan Analysis, Paraffin (Wax) Content, and Size Exclusion Chromatography (SEC) Analysis (Raymond, 1991) separating the bitumen molecules based on molecular size of conventional bitumen, performance tests of original and PmB binders and microscopic observations of PmB's according to manufacturing phases are performed to be able to correlate their test results with the (initial) road performance. The test are performed in Turkish Petroleum Cooperation's Laboratory and presented as follows:

7.1 *Original bitumen chemical test results*

Table 10. Iatroscan analysis results.

	Asfalten %	Saturated %	Aromatic %	Polar %
Original 50/70	21.91	9.28	55.60	13.21

Table 11. Paraffin (Wax) content.

	Parafin, %
Original 50/70	6.44

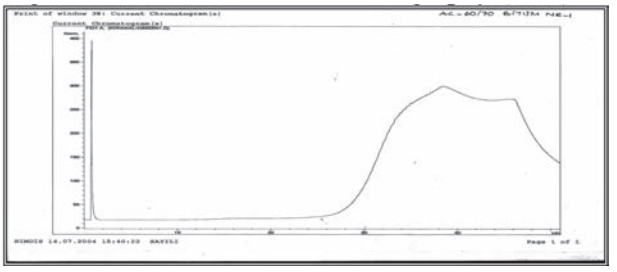

Figure 1. Size Exclusion Chromatography (SEC) analysis of original binder.

7.2 *Microscope observations, conventional and performance test results*

PmB Ultraviolet Microscope Observations are performed in KRATON Polymers Research Laboratory Results, B.V Amsterdam. To observe the polymer distribution during production and the effect of high shear mill properties to production, samples were taken during PmB production after 1, 2 and 3 cycles (1 cycles means: polymer and bitumen goes together into the shearing mill at the same time for distributing polymer in bitumen) and after a three hour maturing period of the bitumen- polymer mixture, their ultraviolet microscopic photographs were taken. The pictures of the polymer distribution in PmB and phase systems are shown in pictures 1, 2, 3 and 4.

Pictures 1, 2, 3, 4: Microscopic observations of the samples taken from at different cycles during PmB manufacturing.

After 3rd cycling, on the samples there were not observed any significant difference on the microscopic observation of PmB. Therefore, after 3rd cycling and after 3 hour maturing period, the samples were taken to carry out conventional and performance tests. Conventional tests are already mentioned in 5.1.

7.3 *Performance based new binder tests*

In Table12, the performance tests of the binders for cold and hot weather conditions, discussing in CEN-TC 336 European Standardization Committee-TC 336 Working Group-1 are shown.

Resistance to hot weather conditions:

An indicator for permanent deformation of mixture is wheel tracking test. However, for bitumen the tests related with rutting are; ZSV, Softening Point and SHRP T ($G^*/\sin\delta$). The results of correlation coefficients (presenting road performance by tests in the laboratory) are given below:

For the Zero Shear Viscosity : 0.91
For the Softening Point (R&B) : 0.84
For the SHRP T($G^*/\sin\delta$) : 0.77

Based on the results above, although the ZSV test is quite new, it is the most proper one for correlating with the performance of the road for predicting hot weather conditions .The test is performed on 40°C and 50°C to stimulate the asphalt surface-temperature, in KRATON Polymers Research Laboratory Results, B.V Amsterdam. The test results of ZSV for PmB and 50/70 can be seen in Table 13.

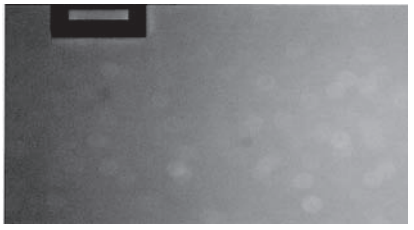

Picture-1 After 1st cycles

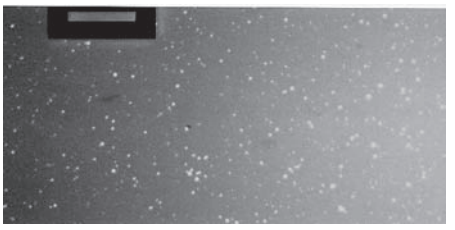

Picture-2 After 2nd cycles

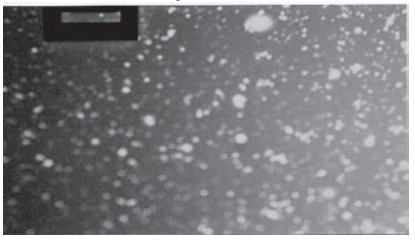

Picture-3 After 3rd cycles

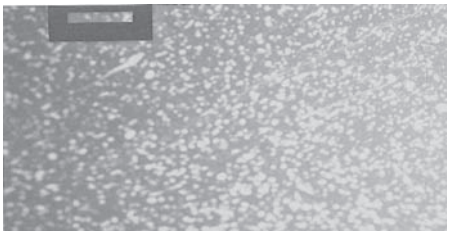

Picture-4 After 3rd cycles + 3 hour maturing period

Experiments based on cold weather conditions:

The results of the "Fracture Energy" & "Fracture Toughness" tests are shown in Table 14. and those tests are performed in KRATON Polymers Research Laboratory Results, B.V Amsterdam.

8 DISCUSSIONS

1. Based on the chemical tests of original bitumen; SARA test where asphaltene content was approximately 22%, and SAC test where the ratio of heavy molecules was quite high, it is obvious that the original bitumen was quite hard structure in its composition. This situation affected the bitumen—polymer system. Therefore, in microscopic observations, it is observed a polymer rich-two-phase system, even after PmB maturing period (Picture 4).

Table 12. Different test methods for binders in cold and hot weather conditions.

CEN TC 336 WG-1	– BBR, Bending Beam Rheometer
Performance Based Tests	– DDT, Direct Tension Test
	– Fracture toughness test
	– Complex Modulus (DSR)
	– Dynamic viscosity—Cone & Plate
	– Dynamic viscosity—Coaxial
	– Zero Shear Viscosity (ZSV)

Table 13. ZSV results for original and polymer modified bitumen.

ZSV	40°C	50°C
Original bitumen (Pa.s)	7800	820
PmB (Pa.s)	1,300,000	60,000

Table 14. Original and polymer modified bitumen resistance test results.

	50/70 Bitumen	PmB
Fracture toughness, kN/m^3 –20°C	98.3	153.1
Fracture energy, kN/m^3 –20°C	43.3	104.9
Fraass °C		–17

2. The hard structure of original bitumen could effect on production of PmB, as follows:
   – Considering resistance to hot weather conditions, based on ZSV value, the PmB at 50°C's according to original bitumen is quite high (almost shows 10/15 penetration grade bitumen properties whose ZSV value is approximately 40.000 Pa.s at 50°C). So, PmB was expected to be more resistant to permanent deformation by having that high ZSV value.
   – Considering resistance to cold weather conditions, based on thermal fractures with Fracture Toughness and Fracture Energy results, PmB shows minimum 50% better performance then original 50/70.
   – High asphaltene ratio and high heavy molecules in original binder may affect the homogeneity of PmB, so if the storage would be required, mixing/heating in appropriate conditions would be necessary for PmB.
3. Differences in samples taken from high shear mill interval cycles and after maturing period were observed microscopically and in experimental results, the required PmB experimental results were only reached after the maturing period after 3 cycles in the mill. To obtain the "proper PmB" for the highway construction according to its conditions/properties, it is important to perform some tests in advance on original bitumen to check its compatibility with polymer.

9 CONCLUSION

1. When the highway was observed after one year later, app 25–30 mm. deep rutting is observed only at the climbing lane with steep gradients (over 5.5–6%.) However, the downward and upward lanes of those sections (up to 5.5–6% gradient) did not show the same sensitivity/problem. When the cores were taken from the wearing course and tested, the results were found within the limits of the design values. On the other hand, both northern part and the southern part of the road had so hot climatic weather conditions that there is no any thermal cracking was observed on that road. So, it could be concluded that if a highway with quite steep gradient and heavy traffic load, (as mentioned in that paper having the steep gradient up to 8%, the weather reaches 48°C in summer, and the heavy volume of traffic is 42% at minimum,) the usage of %5 SBS modified bitumen in hot mix asphalt couldn't be enough to prevent rutting over the gradient 5.5–6% at the climbing lane with conventional Hot Mix Asphalt on wearing course.
2. Based on the results in this study, both conventional, chemical and performance tests of bitumen and PmB's; it is wiser to start producing PmB with softer original bitumen, instead of 50–70 penetration, whose asphaltene and heavy molecule content less (then at least %22) that will allow to use more SBS content in the bitumen. In that way, PmB in hot mix may be able to prevent rutting over the gradient %5.5–6 on the highways whose conditions mentioned above.
3. It is important to evaluate the chemical properties of original bitumen together with its compatibility with polymer be used before producing PmB to be able to determine the amount of SBS added. Besides, the mill properties and the cycling numbers are important.

REFERENCE

Raymond, E.R. 1991. SHRP Report.

Advanced Testing and Characterization of Bituminous Materials – Loizos, Partl, Scarpas & Al-Qadi (eds)
© 2009 Taylor & Francis Group, London, ISBN 978-0-415-55854-9

Laboratory study of environmental performance of binders by headspace gas chromatography

J.E. Poirier, C. Gueit, L. Fanouillet & G. Durand
COLAS S.A, Campus Scientifique et Technique, Magny les Hameaux, France

ABSTRACT: Minimizing fumes and emissions has become one of the main goals during the laying of bituminous coatings. The first priority is of course to avoid overheating the binders during storage and laying. Warm mix processes have also been developed in many countries in order to lower laying temperatures. However, the question that arises is how would it be possible to predict the environmental impact from laboratory experiments? This study uses headspace gas chromatography to characterise the propensity of bitumens to emit volatile compounds. The target substances were Volatile Organic Compounds (VOC) and Polycyclic Aromatic Hydrocarbons (PAH). This technique involves heating a sample in a sealed vial, which causes the volatile compounds to diffuse into the gaseous phase, or headspace, above the sample. At steady state, a gaseous phase aliquot taken using a specific type of syringe is injected, with a carrier gas, into the separation column where the different molecules are separated from each another. On exiting the column, these molecules enter the mass spectrometer detector. Each signal is shown as a peak on the resulting chromatogram. The chromatogram plots the intensity of the emitted signal (μV) against the retention time (min). The chemical composition for each peak is easily identified from the mass spectrum profile. Quantification is also possible. Experiments have been carried out on a wide variety of pure bitumens with several penetration grades and various origins. The technique was used to analyze different types of fluxes, fluxed bitumens, as well as synthetic and vegetable binders. The samples were incubated at different temperatures up to 180–200°C. The conclusions concerning environmental performance include the following:

- Incubation temperature has a very major impact on VOC emissions.
- The origin of the bitumen may be responsible for major differences.
- There is a clear benefit to using lower mixing temperatures.

1 INTRODUCTION

Bitumen products other than emulsions are generally laid at high temperatures to ensure the material has sufficient workability and laying of the surfacing can be performed satisfactorily.

In recent years, however, there have been attempts to decrease the laying temperature to reduce energy consumption and emissions of fumes and greenhouse gases. This process is for improved safety and for environment and sustainable development.

Some of the molecules likely to be present in bitumen fumes at high temperature merit particular attention:

– Polycyclic aromatic hydrocarbons (PAHs), which are the most toxic component of the fumes. High temperatures promote emissions of penta- and hexa-cyclical PAHs. PAHs are already present in bitumen in variable proportions, generally very low, and their release depends on the actual laying temperature.
– Saturated, unsaturated and aromatic light hydrocarbons: toluene, xylene, benzene, and particularly naphthalene, which is considered to be the lightest PAH and the heaviest VOC.
– Various added products or components are present in bitumen. One example is sulphurated compounds.

The concentration of these compounds in the fumes depends on the origin of the crude, the bitumen manufacturing method and the laying temperature and technique. In the case of mastic asphalt the laying temperature may exceed 200°C.

New procedures have been developed which enable the surface laying temperature to be reduced by several degrees which leads to a reduction of fumes that is visible to the naked eye. This reduction can be measured by collecting gas samples in-situ and analyzing them. It is however difficult to completely eliminate interference from the construction works in order to compare several processes. Furthermore, the test trials are somewhat complex. This explains why we have used a laboratory method to assess the propensity of a given bitumen to emit volatile compounds into its environment. It would appear possible to correlate the results from this method with those from in-situ analysis (Stroup et al. 2005). The method presented in this article permits the identification and relative quantification of the various substances emitted by binders.

2 THE BINDERS STUDIED

Table 1 shows the characteristics of the binders used in the study. They are produced from different sources.

Table 1. Characteristics of binders used in the study.

	160/220 pen A	160/220 pen B	50/70 pen B	Light-coloured binder 1	Light-coloured binder 2
Penetration at 25°C (1/10 mm)	169	170	56	15	15
R&B temperature (°C)	38.8	40.2	48.4	94.0	96.6
Penetration index	–1.6	–0.7	–1.1	3.3	3.6

3 THE METHOD

3.1 *Headspace gas chromatography*

3.1.1 *Principle*

The bitumens were characterised with regard to their propensity to release volatile compounds. The target compounds sought were Volatile Organic Compounds (VOC) and Polycyclic Aromatic Hydrocarbons (PAH).

The volatile compounds contained in a sample in a 20 ml sealed heated vial diffuse into the headspace (gaseous phase) until they reach steady state with the sample, which is governed by their partition coefficient.

A gaseous phase aliquot taken using a specific type of syringe is injected, with a carrier gas, into the separation column where the different compounds are separated from each another. Headspace GC allows us to analyze the volatile compounds in a complex matrix with no prior preparation.

3.1.2 *Equipment*

- CP 3800 gas chromatograph (Varian) equipped with a flame ionization detector.
- VF 624-ms capillary column (60 m × 0.32 mm; DF 1.8 µm, Varian). Its stationary phase is apolar to slightly polar. This column is specific to VOCs. Another column may be used to analyse PAHs.
- Combi-Pal Multi-function Autosampler (CTC Analytics) which comprises, among other things, a syringe for Headspace injections, an incubation/mixing oven which may be heated to 200°C as well as a sample changer.

3.1.3 *Test procedures/methodology*

The parameters used for the chromatographic analysis of the various bitumens are detailed in Table 2. The incubation time is selected in order for the liquid phase and the gaseous phase to reach steady state.

Repeatability was assessed on 10 samples of the same bitumen analyzed under the same conditions. The variation coefficient for the peak area was less than 5%.

3.2 *Mass spectrometry coupling*

3.2.1 *Principle*

Although gas phase chromatography is suitable for complex and varied mixtures, certain compounds have the same affinity with the stationary phase. This means the retention time on the chromatogram is the same and precise identification is impossible.

In order to overcome this problem, coupling with a mass spectrometer was chosen. First, GC-MS is used to separate molecules on the basis of their retention time (by GC), second, concise identification of molecules according to their molecular weight is performed (by MS).

Mass spectrometry is based on the ionization (by electron impact in this case) of molecules in gaseous phase. The fragments obtained are then sorted according to their mass-to-charge ratio (m/z).

The mass spectrometer comprises four compartments: An ionization source and an analyser (in high vacuum), a detector and a computerized processing system (see Figures 1 and 2).

A computerized system continuously records a mass spectrum that shows signal intensity (%) against mass-to-charge ration (m/z). The charge z is generally equal to 1. The IUPAC considers

Table 2. Test conditions for gas chromatography.

Parameters	Conditions
Temperature of headspace syringe	85°C.
Carrier gas	Helium
Temperature of oven	40°C for 2 mins 10°C/min up to 260°C 260°C for 6 mins (total duration: 30 mins)
Nature of stationary phase	6% of cyanopropylphenyl, 94% PDMS
Test sample	3 g.
Conditioning time in temperature	30 minutes (the temperature depends on the bitumen category = usual temperature of use; for example 140°C for 160/220 grade bitumens)
Volume injected	1 ml of the gaseous phase

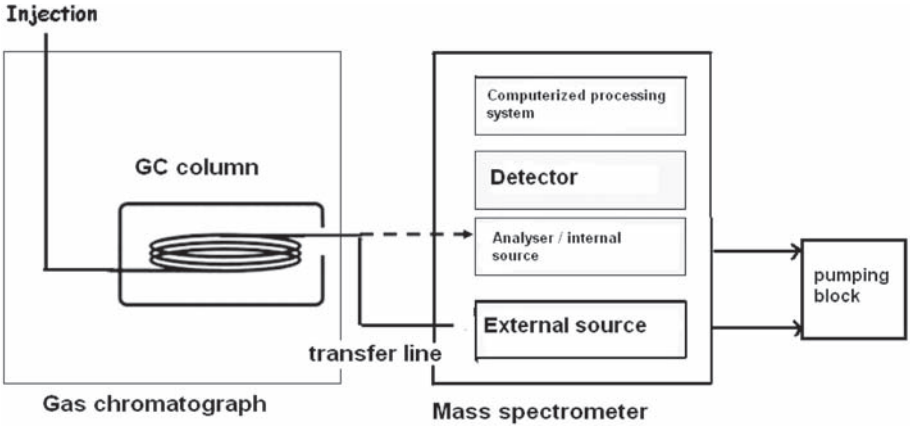

Figure 1. GC/MS coupling diagram. The four compartments are common to all mass spectrometers.

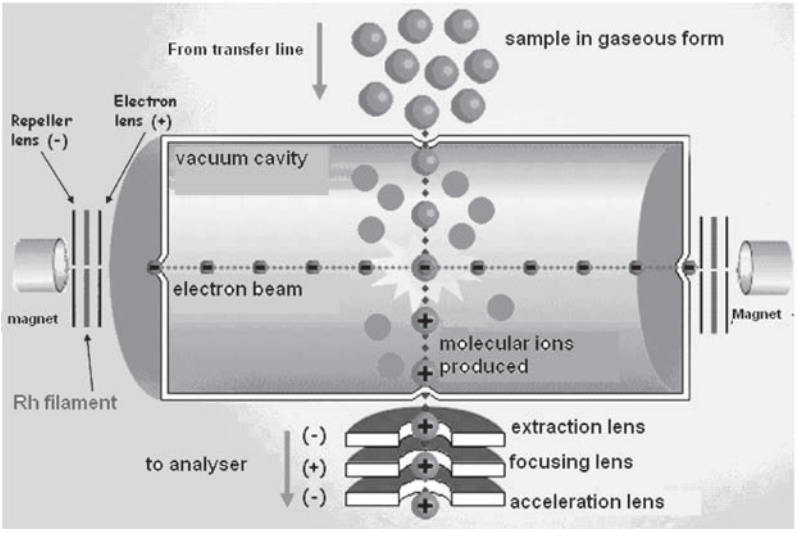

Figure 2. Diagram of the external source diagram. Electron impact ionization ($M + e^- \rightarrow M^+ + 2e^-$).

that the m/z ratio is nondimensional but it is generally expressed in atomic mass units (amu). The range extends from 50 to 1,000 amu.

At the end of the analysis, the computer system sums all the mass spectra to arrive at a mass chromatogram that plots the Total Ionization Current (TIC) against the retention time. A 3D spectrum is obtained as shown in Figure 3:

3.2.2 *Equipment*

- VARIAN MS4000 Mass spectrometer (see Figure 4)
- TURBO V301 Turbo-molecular pump

3.2.3 *BTEX calibration*

The calibration mixture consisted of a BTEX mixture (Benzene, Toluene, Ethylbenzene, (o,m)-Xylene, 1,2,4 and 1,3,5 Trimethylbenzene and Naphthalene).

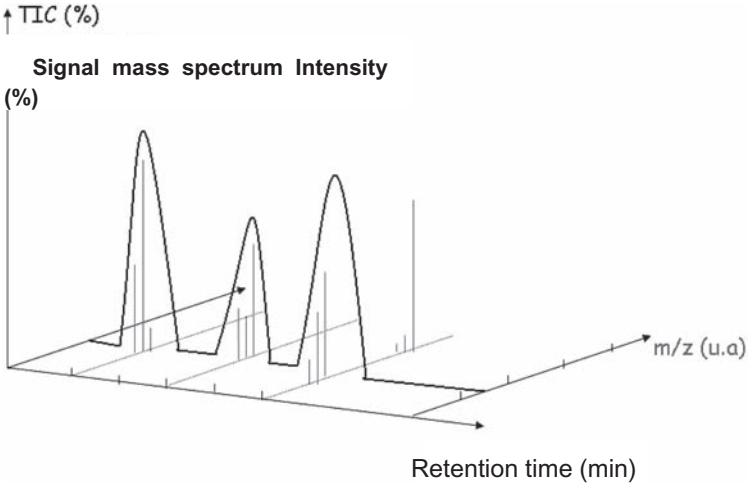

Figure 3. Diagram of a mass spectrum plot from a GC-MS analysis.

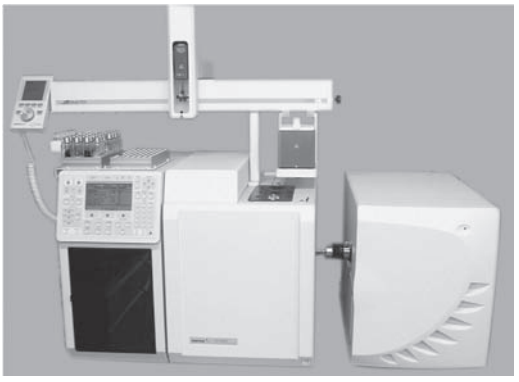

Figure 4. Gas chromatograph/mass spectrometer coupling.

3.2.4 *Methodology*

The parameters to be fixed for the MS were the Total Ionization Current (TIC), which is proportional to the number of species entering the ion trap (between 10,000 and 50,000 counts), and the Ionization Time (IT) of the gaseous molecules in the source (25,000 and 65,000 µs).

These parameters were optimized on the basis of their impact on the signal/noise ratio.

Thus, for synthetic binders and bitumen we obtained the parameters given in Table 3.

Table 3. Results of optimisation of mass spectrometers.

	Optimum TIC targets (Counts)	Optimum $_{\text{theoretical}}$IT (µs)
Bitumen	15,000	25,000
Synthetic binder	20,000	25,000

4 ANALYSIS OF BITUMEN, EXPERIMENTAL DETERMINATION OF VOC'S BY HEADSPACE GC/MS (IDENTIFICATION, QUANTIFICATION APPROACH)

For each bitumen analysed by headspace GC/MS, a mass chromatogram was obtained covering a range from 50 to 1,000 amu.

An initial analysis of the form of chromatograms enabled us to differentiate between the analyzed bitumens in qualitative terms. Significant differences were found between the 160/220 pen bitumens from different refineries (Poirier et al. 2008).

The peaks in a chromatogram are identified in two ways depending on whether or not we know the mass of a given ion.

4.1 *1st case: Unknown compound*

The 160/220 pen bitumen A is distinguished by the presence of a majority peak at a retention time of 15.37 minutes (Figure 5 (a)).

The mass spectrum was used to obtain the m/z ratio of the fragment in question, which was 95.1 amu. (Figure 5 (b)). A library search enabled us to identify the compound on the basis its retention time and m/z ratio: the substance in question was furfural, a solvent used in oil refining and in this case for extracting aromatic compounds from de-asphaltened oils.

In this case, therefore, the headspace GC/MS analysis reveals the role of the bitumen production process.

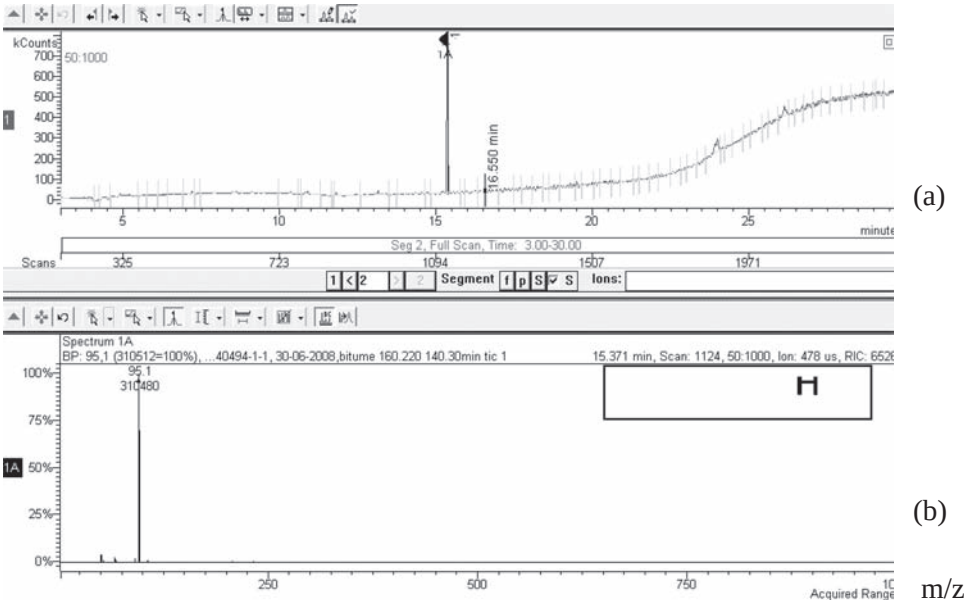

Figure 5. Mass chromatogram of 160/220 pen bitumen A (a). Mass spectrum of the compound at 15.37 min (b).

4.2 *2nd case: Search for a known compound*

In the case where we wish to find a compound with a known m/z ratio, we can extract this species from the total mass chromatogram (Figure 6a).

For example, if we know the m/z ratio of the alkanes (m/z = 57, 85 and 71 amu) and the naphthalene (m/z = 128 amu) contained in the bitumen, a chromatogram can be obtained just for the desired compound (Figure 6b and 6c).

Since the peak area is proportional to the number of ions analyzed, by integrating the chromatograms of extracted ions and comparing it with that for total chromatogram, we can obt estimate the relative proportion of the different VOCs in bitumen emissions subjected to the selected heating protocol.

Initially, our VOC search focused on 3 families: Alkanes, Monocycloparaffins and Alkylbenzenes. The m/z ratios of fragments belonging to these 3 families are shown in Table 4 (Kriech et al. 2002).

4.3 *3rd case: Relative quantification of the different VOC's emitted according to the conditions, in particular an incubation temperature that simulates the coating temperature*

The 50/70 pen bitumen B was processed at different temperatures. It can be seen in Figure 7, which shows the intensity of the peaks of 7 of the bitumen VOCs between 100 and 180°C, that the quantity of VOC drops by a factor of almost 10 when the temperature is lowered from 160°C, which is the usual coating temperature, to 120°C, which is the coating temperature for warm mixes. This confirms the absence of visible fumes at the lower temperature.

5 ANALYSIS OF LIGHT-COLOURED SYNTHETIC BINDERS FOR MASTIC ASPHALT: IMPACT OF LAYING TEMPERATURE

The purpose of this study was to analyse the main VOCs emitted at 170°C and 190°C in the case of two light-coloured binders for mastic asphalt (1 and 2) formulated to be laid at a lower temperature than usual (170°C instead of 220°C), to ensure the fumes contained no toxic compounds. The laying temperature was 170°C, and the maximum temperature reached was 190°C.

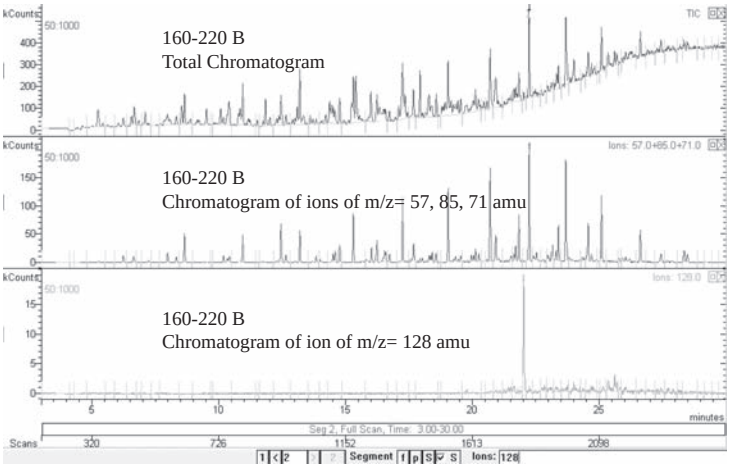

Figure 6. (a) Total mass chromatogram of bitumen 160/220 B.
(b) Mass chromatogram of ions with an m/z = 57, 85, 71 amu (Alkanes) contained in the total chromatogram (a).
(c) Mass chromatogram of the ion with an m/z = 128 amu (Naphthalene) contained in the total chromatogram (a).

Table 4. m/z ratios of relevant fragments for the 3 families of VOC sought: Alkanes, Monocycloparaffins and Alkyl-benzenes

	m/z (amu)
Alkanes	57 + 85 + 71
Monocycloparaffins	67 + 68 + 69 81 + 82 + 83 96 + 97
Alkyl-benzenes	91 + 92 105 + 106 119 + 120 133 + 134 147 + 148

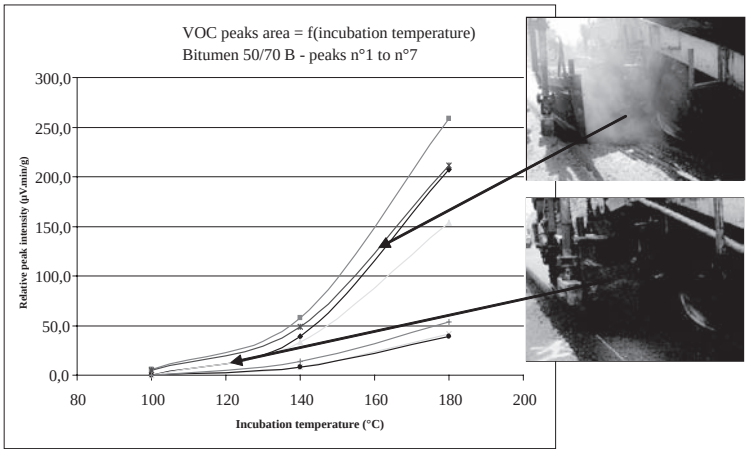

Figure 7: Influence of temperature on peaks area.

Table 5 shows the compounds that account for more than 5% of the fumes emitted at 170°C by the two binders.

Table 5. The compounds that account for more than 5% of the fumes emitted at 170°C by light-coloured binders 1 and 2.

Name of compound	RT (min)	Clear binder 1	Clear biner 2	Toxicity
Isopropylbenzene	16,473	5,82	13,34	R10-R37-R51-R53-R65
Methylstyrene	17,655	6,37	8,45	not classified
1-propenylbenzene	18,003	8,10	5,26	not classified
Indene (C_9H_8)	19,253	10,18	12,00	not classified
Naphtalene	21,966	8,96	<5%	R22-R40-R50/53
Not identified	26,125	<5%	9,76	?

The identified compounds such as isopropyl benzene, methylstyrene, propenylbenzene and indene as well as those found in lower proportions such as cyclopentadiene or furfural are monomers and reagents used for manufacturing resins.

Benzene (R45) was not detected.

Naphthalene (R40) was detected at a concentration of almost 9% in light-coloured binder 1. Light-coloured binder 2 is therefore to be preferred.

At 190°C, as at 170°C, the two products had similar profiles. The relative proportions of the different VOCs remained almost the same but the percentages were higher than at 170°C.

Benzene (R45) emissions, which were zero at 170°C, becomes noticeable at 190°C (0.3% of total emissions).

In quantitative terms, a comparison of the peak area at these 2 temperatures showed that VOC emissions were halved when temperature was reduced from 190°C to 170°C.

6 CONCLUSION

This project was concerned with the study of emissions from road binders at their laying temperature using the Headspace GC/MS technique.

After fine-tuning the methodology to suit road binders (bitumen, light-coloured synthetic binders), in the first phase of the study we were able to identify the main VOCs emitted.

For bitumens, the VOC search focused in particular on 3 families: Alkanes, Monocycloparaffins and Alkyl-benzenes. Each family was characterised by relevant fragments with known m/z ratios. The emission profile differed according to the type of bitumen and its method of production.

For synthetic binders, the analyses showed the presence of monomers used during the manufacture of resins and higher naphthalene emissions from one such binder.

The second phase showed the beneficial impact of a temperature reduction on VOC emissions, and hence the benefits of "low temperature" processes.

Ongoing projects, which are not detailed in this article, also seem to show the benefits of bio-products compared with oil-based products.

REFERENCES

Kriech, A.J, Kurek, J.T, Wissel, H.L, Osborn, L.V & Blackburn, G.R. 2002. *AIHA Journal* 63:628–635.

Poirier, J.E, Gueit, C. & Durand, G. 2008. Chromatographic and thermogravimetric analyses of bituminous binders (E&E Congress).

Stroup-Gardiner & Lange, C.R. 2005. *The international journal of Pavement Engineering* déc2005 6 (4): 257–263.

Advanced Testing and Characterization of Bituminous Materials – Loizos, Partl, Scarpas & Al-Qadi (eds)
© 2009 Taylor & Francis Group, London, ISBN 978-0-415-55854-9

New fatigue test on bituminous binders and mastics using an annular shear rheometer prototype and waves propagation

J. Van Rompu
Département Génie Civil et Bâtiment, Université de Lyon—ENTPE, France & Total France

H. Di Benedetto
Département Génie Civil et Bâtiment, Université de Lyon—ENTPE, France

G. Gauthier & T. Gallet
Total France—CReS, France

ABSTRACT: The annular shear rheometer (ASR), an experimental device initially developed at the ENTPE/DGCB laboratory to study linear viscoelastic (LVE) properties of bituminous binders and mastics, was recently adapted to the evaluation of fatigue properties of these materials. An experimental campaign has been performed, using a new and innovative protocol. Two parameters are measured during the tests:

1. During fatigue periods, the non linear shear complex modulus G_e^* (modulus and phase lag) is measured continuously, using a sinusoidal shear loading at 10 Hz and 10°C.
2. The LVE shear complex modulus G^* is measured punctually (every 20000 cycles) at low strain levels and at 6 frequencies (from 0.03 Hz to 10 Hz).

At constant strain amplitude, obtained results are qualitatively similar for bitumen and mastic. Three phases are identified during the tests. In the first phase, measured LVE G^* complex moduli remains very close to the G^* (LVE) master curve of the undamaged material. It indicates that, in this phase, the decrease of G^* could be explained only by an "equivalent" heating. Yet, the increase of temperature of the material, which is measured by an inner sensor, cannot explain entirely the decrease of G^*. Another phenomenon, such as thixotropy, should occur. During the second phase, the decrease of G^* does not remain on master curve. This decrease is probably due to micro-cracking damaging. It corresponds to a phase with rather stable temperature. At the beginning of the third phase, macro cracks appear and develop in the sample. As the sample is no more homogeneous, this phase cannot be easily interpretable.

It is also observed that there is a link between the evolution of both moduli (G_e^* and G^*). The interest of the proposed approach is to allow a rational modeling of the evolution of G^*, which is a parameter describing the linear behavior of the material.

Another system was also used on recent tests. It is based on waves propagation travel time measurements, which allow to obtain G^* complex modulus at high frequency (100 KHz) using back analysis continuously during the fatigue test.

1 INTRODUCTION

Fatigue is one of the main failure mode in pavement structures for bituminous materials. Repeated applications of loading cycles damage the mate`rials until macro-cracking appears. It seems that binder plays an important role in bituminous mixture failure mechanism

induced by fatigue (Bahia et al. 1999). Then, the fatigue properties of bituminous binders have been evaluated by different authors, using DSR (Dynamic Shear Rheometer) cyclic loading (Anderson et al. 2001, Soenen et al. 2003, Bodin et al. 2004, Planche et al. 2004, Soenen et al. 2004, Bocci et al. 2006). The correlation between fatigue behaviour of binder and the one of bituminous mixtures was also studied in previous works (Baaj 2002, Soenen et al. 2003, Soenen et al. 2004). It is widely admitted that mastic, the indivisible phase composed of bitumen and filler, is the "real" binder of bituminous mixture. It plays an important role in the performance of bituminous mixtures. Consequently, studies on mastics, rather than on pure bitumen, may be more appropriate to investigate correlations between fatigue behaviour of binders and asphalt mixtures. Recent studies showed that there is a significant quantitative difference between the fatigue results on pure bitumen and associated mastics. Fatigue life was significantly affected by the filler concentration (Airey et al. 2006, Thom et al. 2006).

A general research topic aimed at analyzing and modelling fatigue behaviour of mastics, for different types of fillers and bitumen, is currently being conducted at the ENTPE/DGCB laboratory in cooperation with Total Company. The chosen fatigue study approach, which is introduced in this paper, presents two interests. On the one hand, the experimental device (the annular shear rheometer (ASR)) allows performing homogeneous tests, which is generally not the case for classical apparatuses (Di Benedetto et al. 2004). On the other hand, the linear viscoelastic properties are measured punctually in the small strain domain, at different frequencies (from 0.03 Hz to 10 Hz) during fatigue test. Results allow analyzing the change of the "true" LVE (linear viscoelastic) complex modulus (G^*) during fatigue test.

Furthermore, a new system, using shear waves propagation in the sample, allows to study the evolution of $|G^*|$ at about 100 KHz continuously during the fatigue test.

In this paper, the experimental campaign is first presented. It includes the description of the annular shear rheometer, the wave propagation system, the loading protocols and the tested material. Then, some typical results are detailed by plotting different measured parameters as a function of cycle number, such as complex modulus during fatigue (G_e^*), phase lag, temperature and linear viscoelastic modulus G^*. Interpretation of the parameters evolution is also proposed. The results obtained using the wave propagation system are also presented and compared to the one given by the modelling of G^* evolution with 2S2P1D model (Olard & Di Benedetto 2003, Di Benedetto et al. 2004, Di Benedetto et al. 2007, Di Benedetto et al. 2007).

2 EXPERIMENTAL CAMPAIGN

2.1 *Presentation of the annular shear rheometer*

The principle of the annular shear rheometer (ASR) consists in applying sinusoidal shear stress or sinusoidal shear strain (distortion) on a hollow cylinder of bitumen or mastic, at different temperatures and frequencies. The hollow cylinder has a rather large size: 5 mm thickness, 105 mm outer diameter and 40 mm height. With these geometrical features, the test is homogenous as a first approximation even with aggregate sizes up to 1 millimetre. As ASR is very stiff, it also allows covering a wider frequency/temperature range than classic rheometer. A schematic view of the apparatus is presented in Figure 1 (Delaporte et al. 2005, Delaporte et al. 2007).

A sinusoidal cyclic excitation is applied in stress or strain mode using the control system of a 50 kN capacity hydraulic press on which the ASR cell is fixed. Three displacement transducers placed at 120° around the sample measure strain. The control strain is made with the mean value of the three displacement measurements. The transducers measure the displacement between outer lateral surface and inner lateral surface of the bituminous hollow cylinder. The outer surface sticks to the aluminium hollow cylinder linked to the mobile piston of the press. The inner surface of the sample adheres to the aluminium core, which is linked to the load cell.

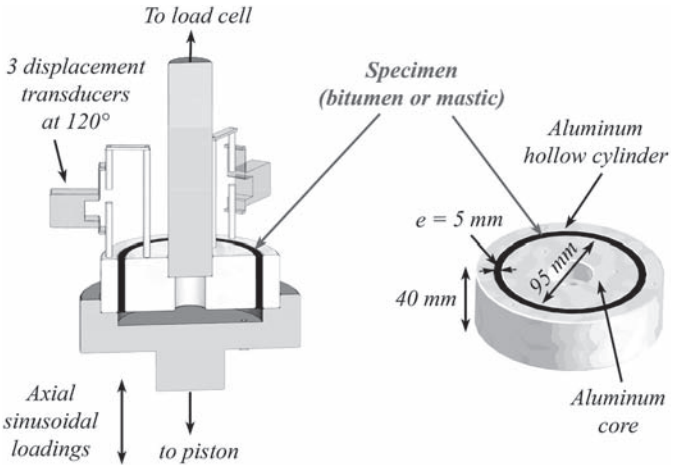

Figure 1. Schematic view of the annular shear rheometer (ASR) for bitumen and mastic, which is placed in a thermal chamber (not represented).

The complex shear modulus (G^*) of the material can be obtained from the data. Expression of the complex shear modulus G^* is given in equation (1):

$$G^* = |G^*| e^{i\phi} = G_1 + iG_2 \tag{1}$$

$|G^*|$ is the norm of the complex shear modulus, ϕ is the phase angle, G_1 is the storage modulus and G_2 is the loss modulus. G^* can be measured at different temperatures from about –25°C to 80°C and different frequencies (f_r) from 0.03 Hz to 10 Hz. $|G^*|$ is the ratio between the amplitude of distortion γ_A with $\gamma(t) = \gamma_A \sin(\omega t - \phi)$, and the amplitude of shear stress τ_A with $\tau(t) = \tau_A \sin(\omega t)$, where $\omega = 2\pi f_r$. Phase angle ϕ is calculated by measuring the phase lag between load and displacement signals.

As the material is non linear, G^* is a function of strain amplitude. It is noted G_e^*, "e" standing for "equivalent". In the small strain domain, the behaviour becomes linear viscoelastic (LVE) and the constant value of G^* (independent of strain amplitude) is noted G^* (Olard et al. 2003, Airey & Behzad 2004, Delaporte 2007).

Two sensors are used for the temperature measurements. One is fixed in the thermal chamber. The second one is an inner sensor, plunged in the middle of the sample (Figure 2).

2.2 *Waves propagation system*

The waves propagation system is used to measure propagation rate of shear waves in the bitumen or mastic sample. The propagation speed C_S of a shear wave at a given frequency $f = \omega/2\pi$ in a LVE medium at a temperature T is a function of the value of the LVE complex modulus $G^*(\omega,T)$ and ρ, the density of the material (equation 2). Measuring the speed of a wave allows to get the value of $|G^*(\omega,T)|$ at the wave frequency ($f = \omega/2\pi$) if the phase lag at this frequency is known. An interest of such a device is to allow obtaining complex modulus at high frequencies, which is unreachable with classic rheometers. The system was recently used to measure the stiffness of bituminous mixtures samples (Sohm 2007, Savary 2008) and bituminous mastics (Flohart, 2008). It gave interesting results on both kinds of materials.

$$C_s = \frac{1}{\cos\left(\dfrac{\phi(\omega,T)}{2}\right)} \sqrt{\frac{|G^*(\omega,T)|}{P}} \tag{2}$$

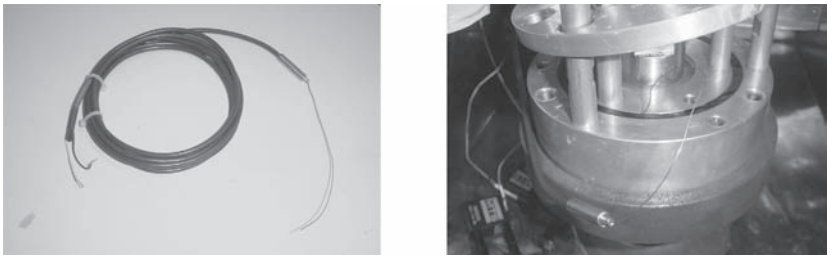

Figure 2. Pictures of the temperature sensor (left) and sample with this sensor plunged in the middle (right).

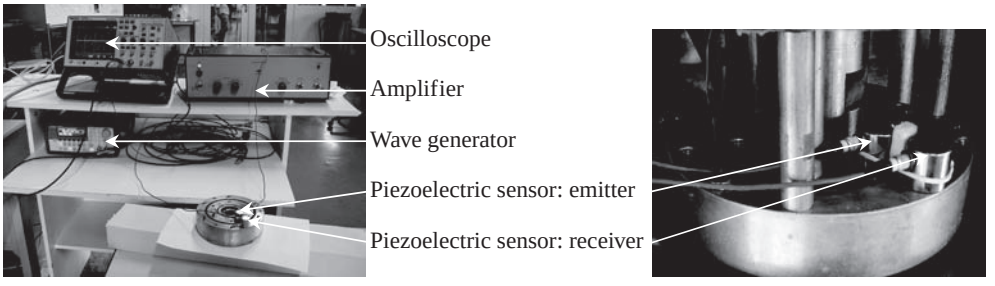

Figure 3. Pictures of the waves propagation system, general view (left), ASR cell equipped with the piezoelectric sensors (right).

Figure 3 shows pictures of the developed waves propagation system. Two piezoelectric sensors are used. The first one is an emitter, fixed on the inner mold. An electric sinusoidal signal, produced by a wave generator and then amplified, is applied to this sensor, which makes it vibrates. An excitation frequency of 100 KHz close to the resonance of the sensor is used, to obtain the best signals. A mechanical shear wave is emitted at a frequency close to 100 KHz, and propagates through the sample. When this wave touches the second sensor, that acts as receiver, it makes it vibrates (Figure 4, scheme a). The electric signal is then recorded with the oscilloscope, which allows obtaining the flying time of the wave in the sample.

Because of the lower speed of shear waves compared to compression waves (Di Benedetto 2006), the arrival of the shear wave propagating through the material is detected when the received signal reaches it first local minimum (Figure 4, graph b). All the process has been carefully evaluated and analyzed in an other study, which gave convincing results (Flohart 2008).

To find the "real" travel time, it is necessary to subtract the time lag induced by the electronic system. This time lag has been measured on the ASR mold without sample. The shear wave propagation rate C_S is equal to $\Delta t/e$, where Δt is the real travel time and e is the thickness of the sample, which is equal to 5 mm.

The value of C_S leads to the determination of $|G^*|_{100\ \mathrm{KHz}}$ by applying equation (3):

$$|G^*|_{100\ \mathrm{KHz}} = P\left(C_S \cos\left(\frac{\phi_{100\ \mathrm{KHz}}}{2}\right)\right)^2 \tag{3}$$

2.3 *Testing procedures*

Fatigue tests consist in applying cyclic shear strain at a frequency of 10 Hz and a temperature of 10°C. The presented results concerns a mastic composed of a 50/70 penetration grade pure bitumen associated to a silicate fumes filler proportioned at 30% in volume ($V_{filler}/(V_{bitumen}/ + V_{filler}) = 30\%$). The

mastic is called "B5070S30(2)". Two fatigue tests in strain control mode, at a strain level $\varepsilon_{tz} = \gamma/2$ of 0.18%, are presented. This strain level is not within the small strain domain (linear domain). Then, the complex modulus measured during the fatigue test G_e^* is a non-linear complex modulus.

Two kinds of testing protocols were applied.

The first protocol is currently used in the study on the fatigue behavior of bituminous mastics led at the ENTPE/DGCB laboratory (Delaporte et al. 2008). The general testing protocol is presented Figure 5. The great originality and improvement of the test is that, at chosen intervals, complex modulus measurements in the linear domain are inserted during fatigue test. The specimen is then punctually loaded at lower strain levels. These measurements are performed for 6 frequencies, from 0.03 Hz to 10 Hz (0.03, 0.1, 0.3, 1, 3 and 10 Hz) after each block of 20000 fatigue cycles. Additional measurements are performed before starting the fatigue cycles and 10000 cycles after the test has started. It has to be underlined that G^* measurements period (about 218 seconds or 3.6 minutes) is "short" in comparison to fatigue period (about 33 minutes for 20000 cycles). For the material, this period can probably be considered as a quasi rest period. Transition between, i) fatigue loading and G^* measurements, as well as, ii) G^* measurements and fatigue loading is instantaneous. The interest of this protocol is to allow analysing the G^* change during fatigue test. The use of different frequencies allows characterizing the LVE properties not only at 10 Hz (frequency of the fatigue test) but on a range of frequencies.

The second protocol is associated with the waves propagation system. It is presented figure 6. A continuous 10 Hz fatigue loading is applied. $|G^*|_{100\,KHz}$ measurements are done, using the waves propagation system, every 3 minutes. One measure consists in recording the average signal of

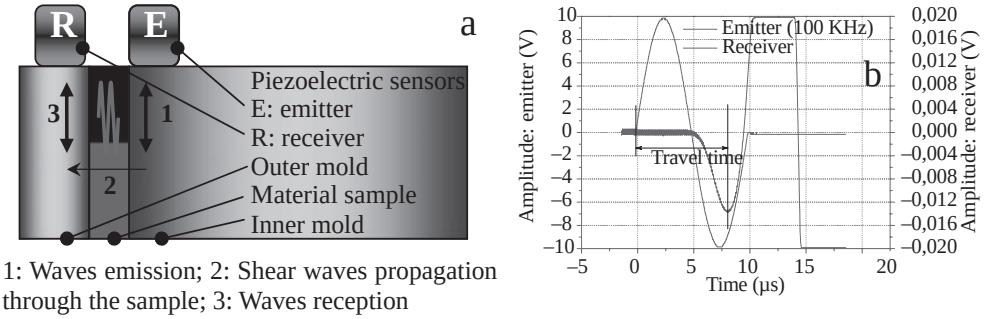

Figure 4. Schematic representation of the ASR cell during a wave propagations test (a), emitted and received wave signal during test B5070S30(2)D1800W (b).

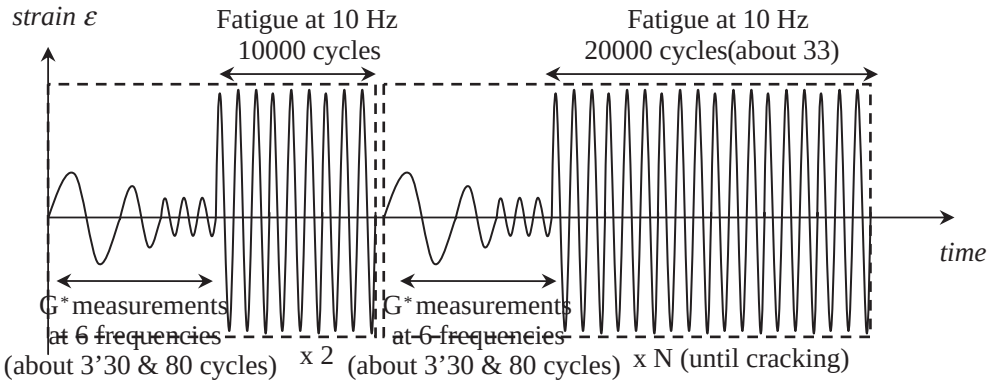

Figure 5. Fatigue testing protocol in strain control: G^* is measured from 0.03 to 10 Hz.

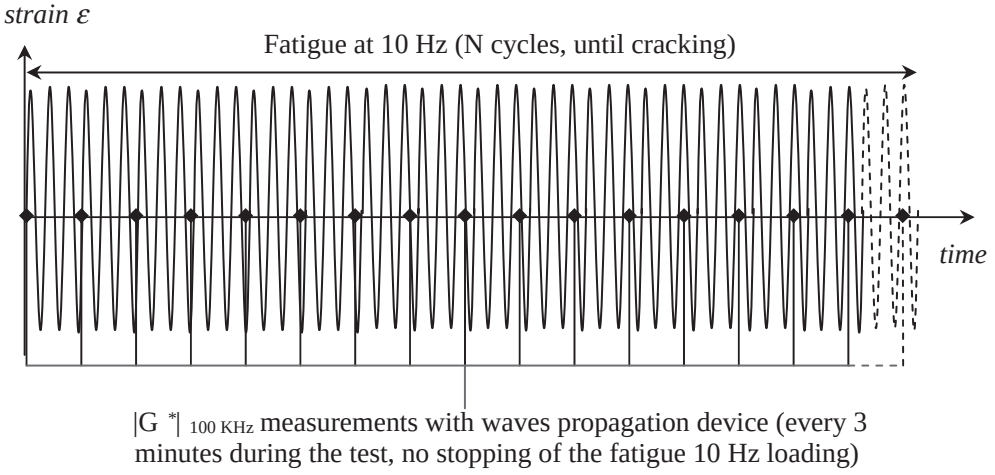

Figure 6. Fatigue testing protocol in strain control with the waves propagation device.

Table 1. Characteristics of the fatigue tests.

Test name	Control mode	Strain amplitude $\varepsilon_{rz} = \gamma_A/2$ (%)	Initial stress amplitude τ_{Ai} (kPa)	Test type
B5070S30(2)D1800	Strain	0.18	920	Fatigue test with LVE G^* punctual measurements
B5070S30(2)D1800W	Strain	0.18	919	Fatigue test with $\|G^*\|_{100\ KHz}$ continuous measurements (waves propagation device)

256 waves emitted, in order to suppress the data noise. The main interest of this protocol is that the fatigue loading is not stopped during $|G^*|_{100\ KHz}$ measurements, contrary to the first protocol, which needs some short periods for G^* measurements.

Table 1 summarizes characteristics of the two presented tests.

3 RESULTS

3.1 *Equivalent complex modulus* (G_e^*)

Results obtained on G_e^* during the two fatigue tests B5070S30(2)D1800 and B5070S30(2)D1800W are both presented figure 7. The modulus $|G_e^*|$ and the phase lag ϕ_e are plotted as a function of the number of cycles respectively on graphs *a* et *b*. The evolution of G_e^* in Black space ($|G_e^*|$ vs. ϕ_e) is plotted on graph *c*. As previously underlined by some authors (Di Benedetto & Ashayer Soltani 1996, Baaj 2002, Di Benedetto et al. 2004, Baaj et al. 2005), three phases, appearing successively during a fatigue test on bituminous materials, can be identified.

– Phase I (or adaptation phase) characterized by a rapid decrease of the modulus $|G_e^t|$. The decrease is not only explained by fatigue damage. Heating and a third phenomenon such as thixotropy probably play important role.

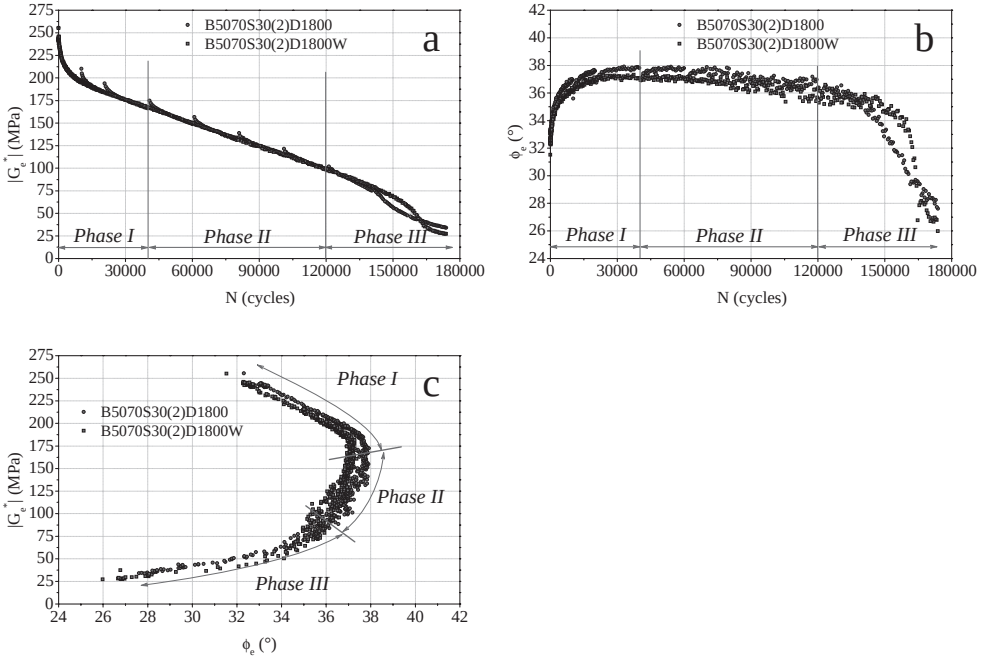

Figure 7. Equivalent complex modulus $|G_e^*|$ (a) and phase lag ϕ_e (b) as a function of the number of cycles and representation of G_e^* in Black space (c). Tests B5070S30(2)D1800 and B5070S30(2)D1800W.

– Phase II (or quasi-stationary phase) where $|G_e^*|$ decrease is quasi-linear as a function of the number of cycles. In this phase, the role of fatigue by micro-cracks development is predominant. Phase II begins when $|G_e^*|$ decrease becomes quasi-linear and when the phase angle is maximum.
– Phase III (or failure phase), which corresponds to the macro crack-propagation, where the test is not interpretable, as it cannot be considered as homogenous anymore.

Discontinuities can be seen every 20000 cycles, on the results of test B5070S30(2)D1800,. They are due to the G^* measurement periods, which correspond to quasi-rest periods for the material. The fatigue loading is stopped during those periods, and the material is loaded at low strain levels. So, a "healing" process, which can be explained by a cooling of the material (see section 3.2), may occur: $|G_e^*|$ slightly increases and ϕ_e decreases. This phenomenon seems reversible. Indeed, it can be observed that, after several fatigue cycles following the G^* measurements periods, the measurements points reach a unique curve. During the test B5070S30(2)D1800, no G^* measurements were done, the resulting curves are continuous. It can be noticed that both tests give very closed results (except at the end of the test, during the failure phase where the test is not valid anymore), which seems indicate that G^* measurements periods have no influence on the progress of the fatigue process. The good repetability of the test can also be underlined.

3.2 *Heating*

The temperature evolution obtained from the probe plunged in the middle of the sample during the 2 fatigue tests are represented Figure 8. As can be shown, heating due to viscous dissipation is important (more than 1°C). Temperature increases rapidly at the beginning of the test. The temperature of the material reaches its maximum value within 30000 cycles (test B5070S30(2)D1800W) and 50000 cycles (test B5070S30(2)D1800). It roughly corresponds

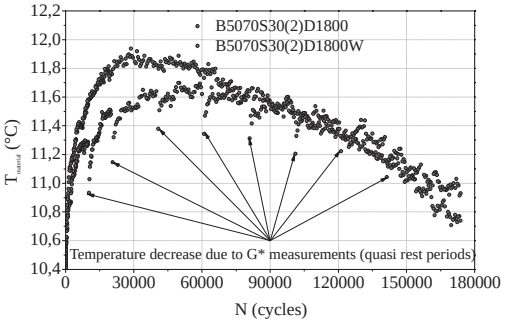

Figure 8. Temperature of the material as a function of the number of cycles. Tests B5070S30(2)D1800 and B5070S30(2)D1800W.

to the phase I/phase II boundary. Then, temperature slowly decreases. During this phase of relative temperature stabilization, it can be considered that heating plays a small role in the evolution of G_e^*, compared to fatigue damage.

Figure 8 also reveals that, during G^* measurement periods, temperature slightly decreases (about 0.3°C). It partially explains the G_e^* recovery observed figure 7: as the material is cooling, it's becoming stiffer ($|G_e^*|$ increasing) and "less viscous" (ϕ_e decreasing). It can be noticed that the temperature curve of the test B5070S30(2)D1800W reaches a 0.3°C higher maximum value than test B5070S30(2)D1800. This might be a consequence of the quasi rest periods induced by G^* measurements (where sample does not dissipate energy in heat), but it has very low influence on the modulus evolution, as shown on figure 7.

3.3 *LVE Complex modulus* (G^*)

As explained in section 2.3, LVE complex modulus G^* is measured at 6 frequencies at the beginning of the test, and then every 20000 fatigue cycles until the end of the test, plus an additional measurement after 10000 cycles. No G^* measurements were done during the test B5070S30(2)D1800W, they were replaced by continuous $|G^*|$ measurements at 100 KHz with the waves propagation system.

The evolution of G^*, at each frequency, is qualitatively the same than G_e^* (Figure 9). The 3 phases of the test can also be observed: $|G^*|$ quickly decreases and ϕ increases at the beginning of the test (phase I), then the modulus decreases almost linearly and the phase lag is quasi stable (phase II). In the failure phase (phase III), both values quickly decrease.

In Black space (Figure 9, graph c), the points corresponding to measurements performed during phase I are a little above but remains very closed to the LVE master curve of the undamaged material. During phase II, the points do not lay on the master curve because both modulus and phase lag decrease. The following interpretation is proposed to explain the observed phenomena:

- During phase I, the LVE properties of the material are few affected by fatigue damage. $|G^*|$ decreasing and ϕ increasing, quite along the non damaged master curve, can be explained by heating and probably another phenomenon such as thixotropy. The fact that the points remain above the master curve is maybe due to another phenomenon, whose introduction is out of the scope of this paper and that will be discussed in future publication.
- Then, in phase II, G^* values do not remain on the master curve of the undamaged material. The LVE properties become gradually different, which can be explained by damage evolution caused by cyclic loading: micro cracking is the predominant phenomenon in phase II.

The main interest of the G^* measurements during fatigue tests is to allow a modeling of the LVE behavior during fatigue process. An analogical model, called 2S2P1D (Olard & Di

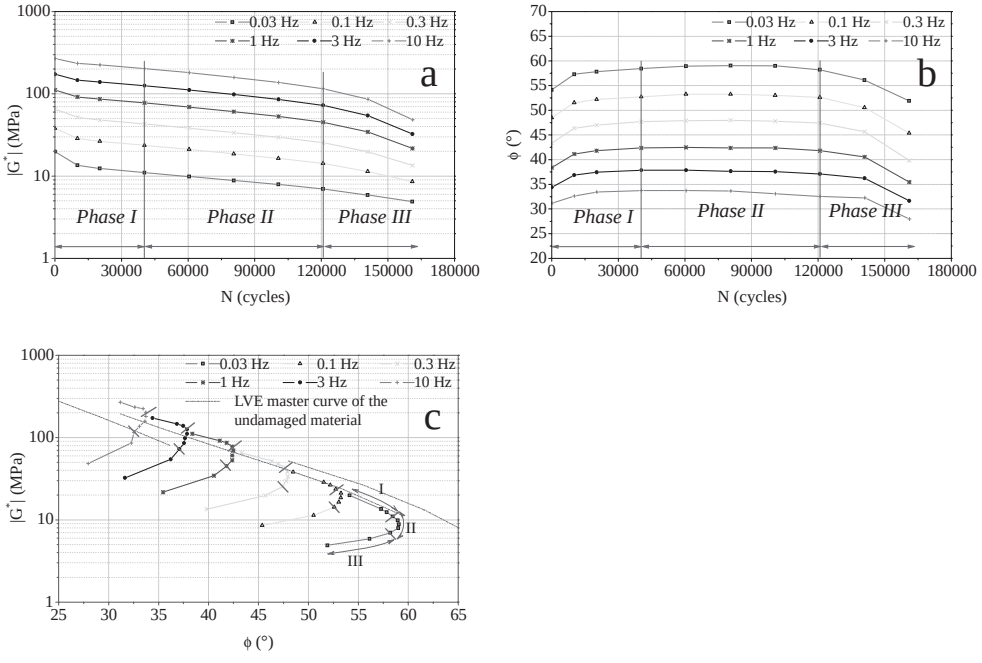

Figure 9. LVE complex modulus G^*, $|G^*|$ (a) and phase lag ϕ (b) as a function of the number of cycles and representation of G^* in Black space (c). Test B5070S30(2)D1800.

Benedetto 2003, Di Benedetto et al. 2004, Di Benedetto et al. 2007, Di Benedetto et al. 2007), developed at the ENTPE/DGCB laboratory to model the LVE behavior of bitumen, mastics and asphalt mixes, is used. Due to a lack of space, this modeling is not developed in this paper.

4 WAVES PROPAGATIONS

As explained in section 2.2, the waves propagation system allows to get the value of $|G^*|$ at 100 KHz. A special protocol, presented in section 2.3, was used during the test B5070S30(2)D1800W: $|G^*|_{100\ KHZ}$ measurements were done continuously with an interval of 3 minutes. The value of the density ρ of the mastic is determined considering the density and concentration (30% in volume) of the filler and the density of the bitumen. Modeling back analysis shows that, at 100 KHz, the value of the phase lag ϕ doesn't vary too much during the fatigue test. So it is considered equal to its initial modeled value of 10° during all the test.

To verify the efficiency of the waves propagation system, results obtained during both tests are compared. G^* measurements, at 6 frequencies, done during the test B5070S30(2)D1800 are used to obtain by optimization the constants of the 2S2P1D model. Using the model, it is then possible to plot the whole $|G^*|$ master curve (for all frequencies) for each cycle where G^* measurements is done. The calculated $|G^*|_{100\ KHz}$, is compared with the $|G^*|_{100\ KHz}$ value obtained with the waves propagation system at the same fatigue cycle in Figure 10.

It can be noticed (Figure 11) that $|G^*|_{100\ KHz}$ obtained with the waves propagation system (test B5070S30(2)D1800W) is rather dispersed at the beginning of the test, but the values are close to the values given by the model (test B5070S30(2)D1800). During phase II, the difference between the two procedures is bigger, but both give a linear variation of $|G^*|_{100\ KHz}$. Furthermore, the 2 slopes are very close. This encouraging comparison validates the waves propagation system which have the big advantage of being performed without stopping the fatigue test.

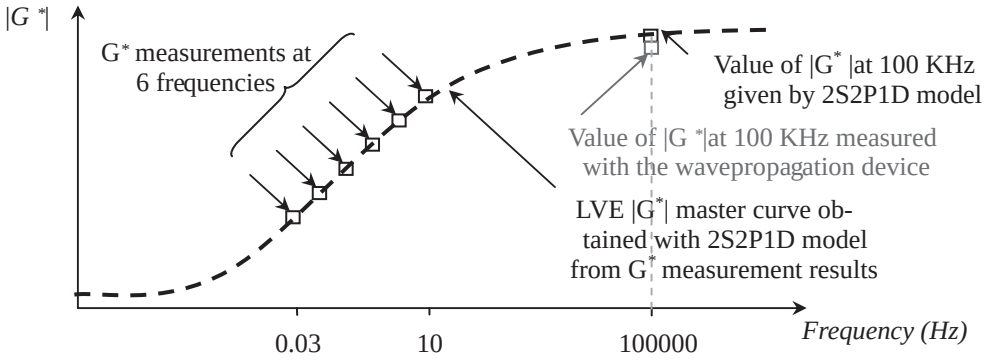

Figure 10. Schematic $|G^*|$ master curve at a given cycle N during the fatigue test, and $|G^*|$ at 100 KHz values obtained, i) from 2S2P1D model and, ii) waves propagation back analysis. T is fixed at 10°C.

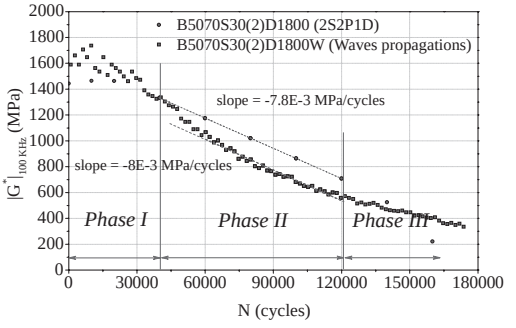

Figure 11. $|G^*|$ at 100 KHz as a function of the number of cycles. Tests B5070S30(2)D1800 (2S2P1D modelling) and B5070S30(2)D1800W (waves propagation back analysis).

5 CONCLUSION

Two procedures developed at the ENTPE/DGCB laboratory to study fatigue of bitumen and bituminous mastics give new perspectives to understand the phenomenon. The ASR intrinsic qualities (size of the sample, homogeneity) and the originality of the test protocols (measurement of the LVE properties evolution during the fatigue test using two different procedures: G^* measurements at 6 frequencies and $|G^*|_{100\ KHz}$ measurements using waves propagation system) can be underlined. It must be noticed that these two procedures give coherent results.

Thanks to the modeling process, which will be presented more in detail in a next publication, the fatigue damage, as well as the other phenomena occurring during the fatigue tests, can be identified and analyzed. The respective influence of each of them can be estimated, allowing formulate an intrinsic damage law.

REFERENCES

Airey, G.D. & Behzad R. 2004. Combined bituminous binder and mixture linear rheological properties. Construction and Building Materials 18: 535–548.

Airey, G.D., M.-C. Liao & Thom N. H. 2006. Fatigue Behaviour of Bitumen-Filler Mastics. ISAP 2006 - 10th International Conference on Asphalt Pavements, Québec.

Anderson, D.A., Le Hir, Y.M., Marasteanu, M.O., Planche J.-P., Martin D. & Gauthier, G. 2001. Evaluation of fatigue criteria for asphalt binders. *Transportation Resarch Record* No. 1766, Asphalt Binders 2001: 48–56.

Baaj, H. 2002. Comportement des matériaux granulaires traités aux liants hydrocarbonés. Mecanique, Energétique, Acoustique et Génie Civil. PhD ENTPE—INSA Lyon. p. 247 [French].

Baaj, H., Di Benedetto, H. & Chaverot P. 2005. Effect of Binder Characteristics on Fatigue of Asphalt Pavement Using an Intrinsic Damage Approach 6 (2): 147–174.
Bahia, H.U., Zhai, H., Bonetti K. & Kose S. 1999. Non-Linear Viscoelastic and Fatigue Properties of Asphalt Binders. Association of Aspahlt Pavement Technology (75th) 68: 1–35.
Bocci, M., Cerni, G & Santagata, E. 2006. Rheological Characterization of the Fatigue Resistance of Asphalt Binders. ISAP 2006 - 10th International Conference on Asphalt Pavements, Québec.
Bodin, D., Soenen, H. & De La Roche C. 2004. Temperature Effetcs in Binder Fatigue and Healing Tests. 3nd Euraspahlt & Eurobitume Congress, Vienna.
Delaporte, B. 2007. Etude de la rhéologie des mastics bitumineux à l'aide d'un rhéomètre à cisaillement annulaire. Mecanique, Energétique, Acoustique et Génie Civil. PhD ENTPE—INSA Lyon. p. 248 [in french].
Delaporte, B., Di Benedetto H., Chaverot P. & Gauthier G. 2007. Linear Viscoelastic Properties of Bituminous Materials: from Binders to Mastics. *Journal of the Association of Asphalt Paving Technologists* Vol. 76.
Delaporte, B., Di Benedetto, H., Sauzéat C. & Chaverot P. 2005. Linear viscoelastic properties of mastics: results from a new annular shear rheometer, and modelling. Bearing Capacity of Roads, Railways and Airfileds (CD-Rom), Trondheim.
Delaporte, B., Van Rompu J., Di Benedetto H., Gauthier G. & Chaverot P. 2008. New procedure to evaluate fatigue of bituminous mastics using an annular shear rheometer prototype. 6th RILEM International Conference on Cracking in Pavement, Chicago.
Di Benedetto, H. 2006. Small strain behaviour and viscous effects on sands and sand-clay mixtures. *Soil Stress-Strain Behavior: Measurement, Modeling and Analysis*. Springer, Solid Mechanics and its Applications. 146: 159–190.
Di Benedetto, H. & Ashayer Soltani M.A. 1996. Fatigue damage for bituminous mixtures: a pertinent approach. *Journal of the Association of Asphalt Paving Technologists* Vol. 65.
Di Benedetto, H., Neifar, M., Sauzéat C. & Olard F. 2007. Three-dimensional thermo-viscoplastic behaviour of bituminous materials: the DBN model. Road Materials and Pavement Design 8 (2): 285–315.
Di Benedetto, H., De La Roche, C., Baaj, H., Pronk A. & Lundström R. 2004. Fatigue of bituminous mixtures. Materials and Structures 37: 202–216.
Di Benedetto, H., Delaporte, B. & Sauzéat C. 2007. Three-dimensional behavior of bituminous materials: experiments and modeling. I*nternational Journal of Geomechanics (ASCE)* 7: 149–157.
Di Benedetto, H., Olard F., Sauzéat C. & Delaporte B. 2004. Linear viscoelastic behaviour of bituminous materials: from binders to mixes. Road Materials and Pavement Design 5 (Special Issue EATA): 163–202.
Flohart, L. 2008. Comportement à la fatigue des bitumes et mastics bitumineux (mémoire de Master Recherche). DGCB. ENTPE—Université de Lyon. p. 158 [French].
Olard, F. & Di Benedetto H. 2003. General "2S2P1D" model and relation between the linear viscoelastic behaviors of bituminous binders and mixes. Road Materials and Pavement Design Vol. 4 (Issue 2).
Olard, F., Di Benedetto, H., Eckmann B. & Triquigneaux J.-P. 2003. Linear viscoelastic properties of bituminous binders and mixtures at low and intermediate temperatures. Road Materials and Pavement Design 4 (2): 185–224.
Planche, J.-P., Anderson D.A., Gauthier, G., Le Hir Y.M. & Martin D. 2004. Evaluation of fatigue properties of bituminous binders. *Materials and Structures* 37 (269): 356–359.
Savary, M. (2008). Propagation d'ondes dans les enrobés bitumineux (mémoire de Master Recherche). DGCB. ENTPE—Université de Lyon. p. 159 [French].
Soenen, H., De La Roche, C. & Redelius P. 2003. Fatigue Behaviour of Bituminous Materials: From Binders to Mixes. Road Materials and Pavement Design 4(1): 7–27.
Soenen, H., De La Roche, C. & Redelius P. 2004. Predict Mix Fatigue Tests from Binder Fatigue Properties, measured with DSR. 3nd Euraspahlt & Eurobitume Congress, Vienna.
Sohm, J. 2007. Etudes de la propagation des ondes dans les enrobés bitumineux (mémoire de Master Recherche). DGCB. ENTPE—Université de Lyon. p. 104 [French].
Thom, N.H., Osman, S., Collop, A.C. & Airey G.D. 2006. Fracture and Fatigue of Binder and Binder/filler Mortar. ISAP 2006—10th International Conference on Asphalt Pavements, Québec.

Advanced Testing and Characterization of Bituminous Materials – Loizos, Partl, Scarpas & Al-Qadi (eds)
© 2009 Taylor & Francis Group, London, ISBN 978-0-415-55854-9

Functional forms for master curve analysis of bituminous materials

G. Rowe
Abatech, Blooming Glen, Pennsylvania, USA

G. Baumgardner
Paragon Technical Services, Jackson, Mississippi, USA

M. Sharrock
Abatech, Winchester, UK

ABSTRACT: The modeling of asphalt materials to produce master curves is becoming more important in the development of pavement design methods. However, the current method being applied in the USA in the Mechanistic-Empirical Pavement Design Guide (MEPDG) uses a symmetrical sigmoidal model. This model can clearly be shown not to apply to many types of asphalt materials. This paper presents several additional approaches with different sigmoidal models which can be assessed within a mechanistic-empirical framework. This analysis is anticipated to be important as materials containing more modifiers are used and/or the greater use of materials not typical of those used to develop the original sigmoidal model adopted by many researchers. The generalized logistic sigmoid known as a Richards curve is a widely-used and flexible sigmoidal. Various forms of this generalized model are assessed and discussion is presented with relation to using this curve to describe the shape of a mastercurve of complex dynamic stiffness modulus of bituminous materials. The analysis shows that for the materials evaluated a generalized model format works very well. In addition, the data shows that the resulting master curves are non-symmetrical about a point of maximum gradient.

1 INTRODUCTION

1.1 *Background*

A study of several unusual binders was conducted (Rowe and Baumgardner, 2007) and these where used as trial binders in a procedure to determine damping properties as part of other experimental work being conducted. It was initially suggested that a procedure could be adopted were a master curve was fitted with sigmoid properties and then used in the determination of various functions via a shift relationship. It was initially envisaged that a standard logistic sigmoid (Verhulst, 1838), adopted as part of the American Association of State Highway Transportation Officials (AASHTO) Mechanistic Empirical Pavement Design Guide (MEPDG) (ARA, Inc., 2004), could be employed. However, some problems were immediately apparent when this was evaluated in trials with roofing compounds, mastics and other materials. It was observed that these materials did not exhibit symmetric sigmoid properties as required by this method. Further work with mixtures suggested that many mixtures also did not have the expected sigmoid behavior. Consequently, alternative sigmoid formats were investigated to explore which methods would have a better universal fit to bituminous materials. As part of this process several methods were investigated, including Weibull (1951), Gompertz (1825) and Richards (1959) sigmoid formats.

Weibull (1951) presented a non-symmetric sigmoid format that was developed as a statistical distribution with wide functionality. His work has been extensively applied to the study

of fracture and the probability of survival. Gompertz (1825) worked as a mathematician developing methods for assessing the probability of human survival for insurance companies in the early 1800's. His work on mathematical formulations has been widely used in various industries, particularly insurance. Richards (1959) presented a generalized logistic curve as a development of the standard logistic curve developed by Verhulst (1838). Richards curve allows a non-symmetric form of the relationship whereas the standard logistic curve is entirely symmetric.

The mathematical solutions were applied to various asphalt binders, mastics and mixtures. Experimentation includes testing with binders and mastics with dynamic shear rheometer (DSR), torsion bar, bending beam rheometer (BBR) and a direct tension test (DTT). In addition, data sets of dynamic complex modulus (E^*) were obtained for asphalt mixes. Data was reduced to complex modulus for binders, mastics and where necessary the relaxation modulus E(t) and bending stiffness S(t) results are converted to complex shear modulus via fundamental interconversions. The results are combined to produce master curves which are compared to analysis with consideration of the symmetrical sigmoidal function used within the AASHTO MEPDG method. Results are produced for filled and non-filled materials which include blown and elastomeric modified binders, jointing compounds, and asphalt mixtures.

1.2 *Functional forms*

The standard logistic sigmoid is symmetric in shape around a mid-point. For work with asphalt mixtures, constants are added which represent the lower and upper asymptotes of the data; using these in the typical format presented by other workers the standard sigmoid equation is represented as:

$$\log E^* = \delta + \frac{\alpha}{1 + e^{\beta + \gamma(\log \omega)}} \tag{1}$$

where E^* = complex dynamic modulus, δ is lower asymptote, α is the difference between the values of upper and lower asymptote, β and γ define the shape between the asymptotes and the location of the inflection point (inflection point obtained from $10^{(\beta/\gamma)}$).

The parameters of the model have been used in predictive relationships for pavement design since the early 1980's (The Asphalt Institute, 1982) with δ and α being a function of the mixture volumetrics and gradation parameters, whereas, the viscosity temperature susceptibility parameter is used to estimate β. The final parameter γ is taken as a constant value. It should be noted that in recent forms of the predictive equation a loading time is substituted for a frequency (ARE, Inc., 2004) which is not correct since all complex dynamic properties should be expressed in the frequency domain consistent with the test methods used to develop the data.

From this analysis we deduce that the upper and lower asymptotes do not relate to any binder property but rather reflect only aggregate properties. The shape of the master curve between these two asymptotes is dependent upon binder properties but with only a single parameter describing the shape. It should be noted that a further constant describes the temperature susceptibility which is built into the shift factor relationship. Consequently, a total of five parameters are determined from the mixture testing and viscosity testing of the component materials to describe the master curve. An example of a fitted sigmoid function of this form is illustrated in Figure 1.

Weibull's equations have been used in the representation of sigmoid functions and the equation evaluated in this work was:

$$\log(E^*) = A + B\left[C - e^{-\left(\frac{x+D}{E}\right)^F}\right] \tag{2}$$

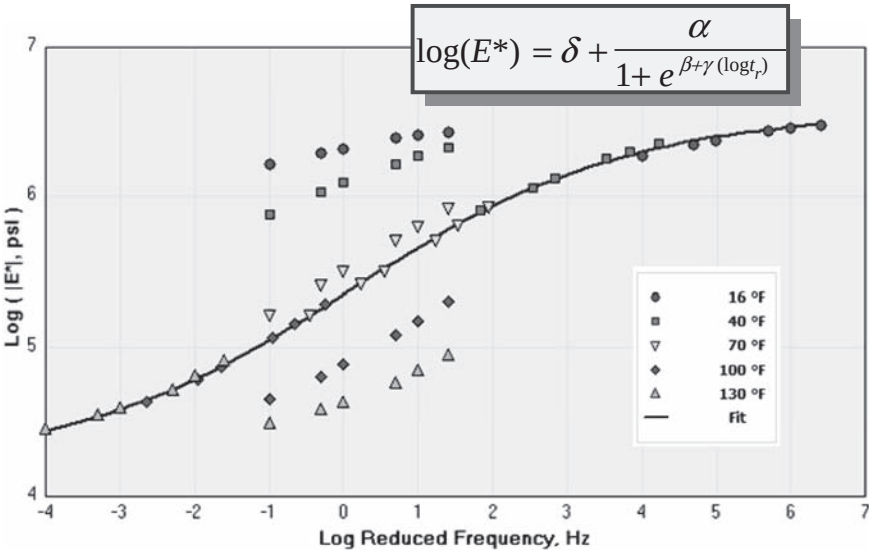

Figure 1. MEPDG master curve fitted to example data set.

where E^* = complex dynamic modulus, A is lower asymptote and B, C, D and F define the upper asymptote, the shape between the asymptotes and the location of the inflection point. This equation uses additional parameters to describe the non-symmetric format of the curve. Again it should be noted that an additional parameter (or parameters, will be needed) to describe the shift factor relationship as with all the relationships discussed below.

The Gompertz (1825) equation was developed in the early 1800's and is represented as:

$$y(t) = ae^{be^{ct}} + d \tag{3}$$

where a, b, c and d are constant values that define the shape of the sigmoid. The constant d allows the representation of a lower asymptote in a similar manner to the δ term in the standard logistic form.

Richards (1959) developed a generalized relationship of a sigmoid and this is presented in a format similar to the method developed with the standard sigmoid. The representation is defined as:

$$\log E^* = \delta + \frac{\alpha}{\left[1+\lambda e^{(\beta+\gamma(\log\omega))}\right]^{1/\lambda}} \tag{4}$$

where E^* = complex dynamic modulus, δ is the lower asymptote, α is the difference between the values of upper and lower asymptote, λ, β and γ define the shape between the asymptotes and the location of the inflection point. The difference between equation 1 and 4 is the introduction of the lambda parameter, λ, which allows the curve to take a non-symmetric shape. The value of the inflection point has a minimum limit of 36.8% of the relative difference between the upper and lower asymptotes. At this condition the equation produced is consistent with the Gompertz equation with lambda approaching zero. When lambda is equal to unity the equation reduces to the standard sigmoid format as represented by equation 1. The variation in sigmoid shape with different values of lambda (λ) is illustrated in Figure 2, which includes two special cases; Gompertz and Standard Logistic curves. In addition, a curve is shown when λ becomes negative with an inflection point below 36.8% but with a shape not consistent with sigmoid type behavior.

The sigmoid format provides a powerful function in analysis of pavements since, when combined with time-temperature shift factors, it enables the determination of complex dynamic stiffness at any time of loading and temperature. This type of information is currently being implemented in pavement design methods in the USA, MEPDG (ARE, Inc., 2004). The format currently implemented is the standard logistic sigmoid which has a symmetrical shape. However, other functional forms discussed above might offer a better characterization of the physical behavior of asphalt materials.

2 ANALYSIS OF MATERIALS

2.1 *Specialized materials*

Three specialized materials were considered in the analysis; a roofing product (Rowe and Baumgardner, 2007) and two compound materials used for repairing concrete roads. All of these materials contained a significant amount of polymer modifications and could be considered filled polymer mastics materials.

The analysis of these materials was initially attempted using a standard logistic curve. However, it was observed that the standard logistic curve did not fit the modified mastic type materials. Master curves were created using a software implementation of the shifting techniques described by Gordon and Shaw (1994). In this method algorithms are applied to successive pairs of isotherms to develop a shift factor which is independent of any underlying model constraints. The resulting master curves were then fitted to the various functional forms to assess which described more closely the results of the shifting. An example of the analysis obtained is presented in Figure 3. This figure is represented in both logarithmic and semi-logarithmic format to show the fit at the extremes of the fitted master curve. For this instance, it is observed that the Gompertz case of the logistic curve provides the best fit to the data set; demonstrating that this material clearly behaves in a non-symmetric sigmoid fashion. This analysis was extended to several other specialized

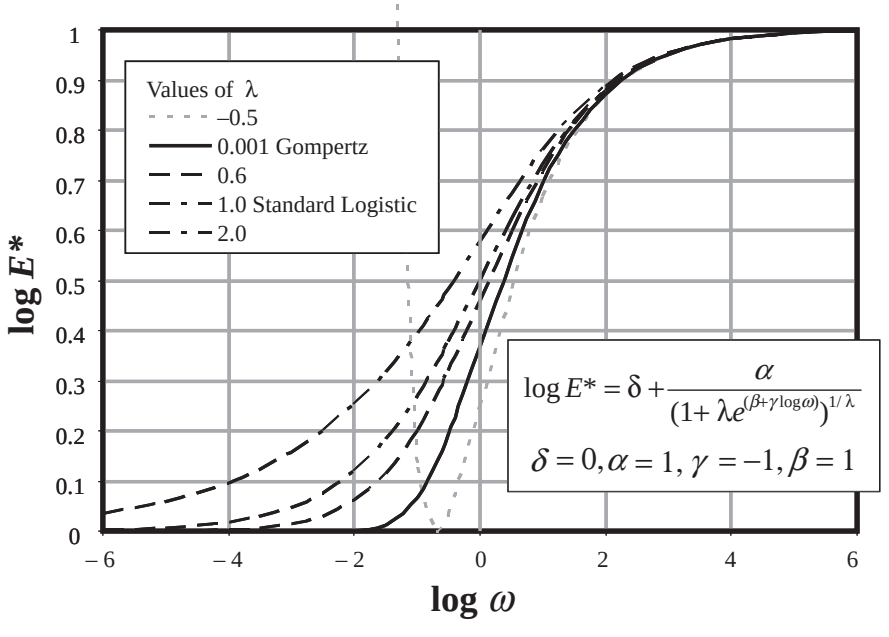

Figure 2. Richards curves with different values of lambda (λ) showing two special cases, Gompertz and Standard Logistic.

materials, the conclusion being, from the methods investigated; that the Richards equation provides a better fit compared to the Weibull method; although, in many cases the final Richards equation adopted was the special case with Gompertz type behavior. In cases analyzed the Weibull function generally had a significant error in predicting the shape of the master curve towards the asymptotes. Consequently, this method was dropped from further consideration.

2.2 *ALF study materials*

The Accelerated Load Facility (ALF) is an experimental pavement test facility operated by Federal Highway Administration at the Turner-Fairbank Research Center in Virginia, USA. A series of pavements had been built at this facility in the summer of 2002 and the data from these experiments have been made available for analysis. Isotherms of stiffness have been collected at temperatures of –9, 4.4, 21.1, 37.8 and 54.4°C. It should be noted that this data set was collected at significantly fewer frequencies than that recommended in the Gordon and Shaw (1994) and this resulted in a more difficult data analysis.

The mixtures used in these pavements contain conventional and polymer modified asphalt covering the range of materials found in road construction. Each of these materials has been analyzed to determine fitting model parameters using the Richards equation with non-functional form shifting using the Gordon and Shaw method. The results obtained for the λ parameter which determines the inflection point of the sigmoid along with a description of the materials are presented in Table 1. It can be seen that in one instance the data analysis produced a fit close to the standard logistic curve (section 1). In three of the eleven cases the solution adopted was when λ tended to zero (sections 2, 9 and 11). In two cases the inflection point was above the mid point whereas in the remaining cases the analysis had inflection points below the mid point of the two asymptotes.

The consequence of this analysis is that is demonstrates that the standard logistic sigmoid only closely fits the measured data in one case when the shift factors are not controlled by the need to fit to the sigmoid shape. Additional work is needed to fully understand the various material parameters that affect the parameters determining the shape parameters of the sigmoid.

Table 1. Lambda results for analysis of ALF test sections.

ALF section	Binder system	λ	Note
1	AZCR 70-22	0.962	
2	PG 70-22	0.001	Gompertz
3	Air Blown	3.464	
4	SBS LG	0.180	
5	CR-TB	0.156	
7	PG 70-22 + Fibers	0.012	
8	PG 70-22	1.421	
9	SBS 64-40	0.001	Gompertz
10	Air Blown	0.260	
11	SBS LG	0.001	Gompertz
12	TP	0.088	

CR-AZ = Crumb rubber asphalt binder, Arizona Department of Transportation (DOT) wet process.
PG 70-22 = Unmodified asphalt binder control.
Air Blown = Air-Blown asphalt binder.
SBS LG = Styrene-Butadiene-Styrene modified asphalt binder with linear grafting.
CR-TB = Crumb rubber asphalt binder, Terminal Blend.
Fiber = Unmodified PG 70-22 asphalt binder with 0.2 percent polyester fiber by mass of the aggregate.
SBS 64-40 = Styrene-Butadiene-Styrene modified asphalt binder graded PG 64-40.
TP = Terpolymer, Ethylene Terpolymer modified asphalt binder.

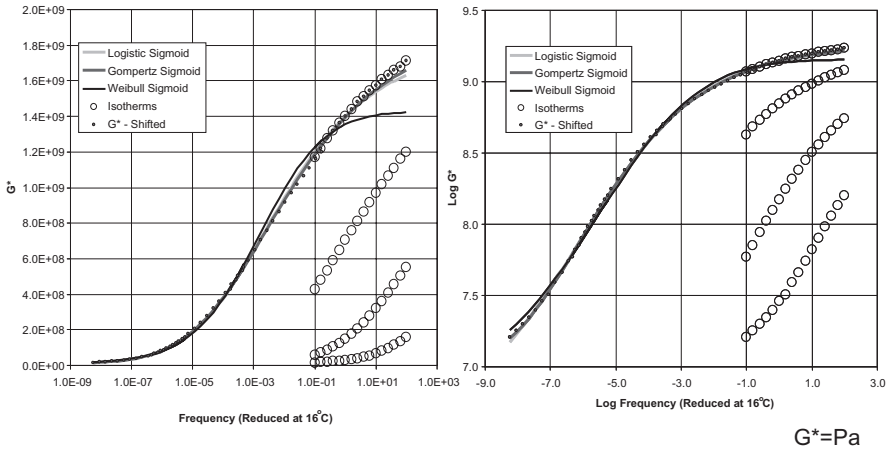

Figure 3. Sigmoid analysis of material used for thin surfacing of bridge decks (Reese, 2008).

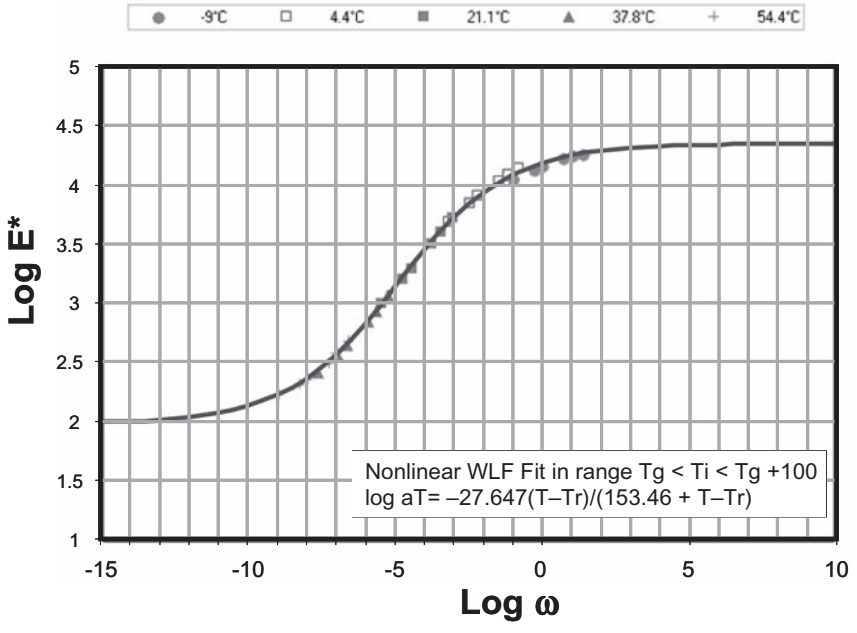

Figure 4. Example of data analysis ALF Section 1, Crumb rubber asphalt binder, Arizona Department of Transportation (DOT) wet process 70-22 with standard logistic fit showing.

2.3 *Data base of materials used for MEPDG analysis*

An extensive database of E^* results has been made available with information pertaining to the MEPDG (ARE Inc., 2004). Various materials from this data set have been analyzed using the Gordon and Shaw (1994) shifting techniques and generalized logistic sigmoid model. An example of a typical result, with AC-20 and Trinidad Lake Asphalt (TLA) mixtures supplied to the Port of Baltimore, are in Figure 5. All the mixtures in the database can be analyzed with the generalized logistic sigmoid model and the fit produced with this model is equal or better than that obtained with the standard logistic since an extra parameter is used to describe the fit.

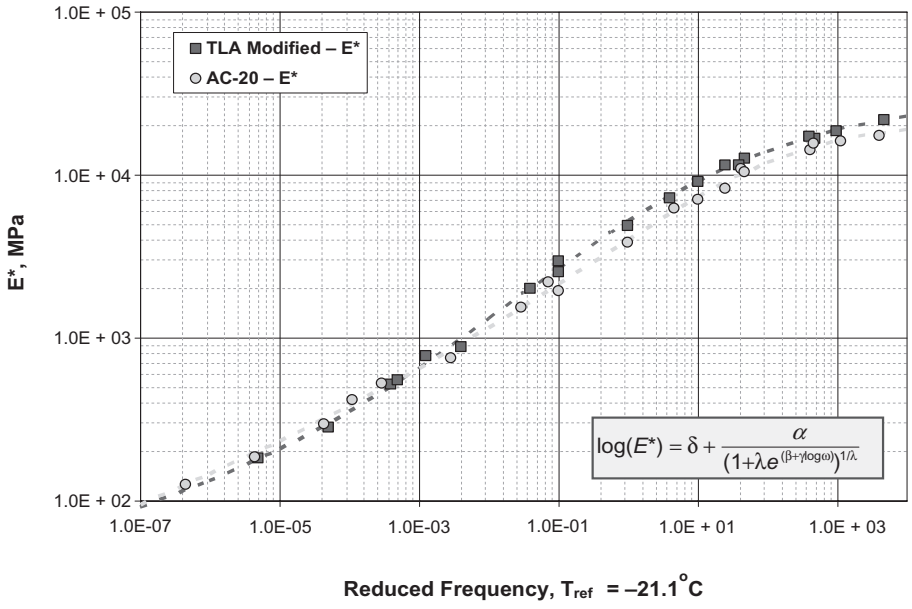

Figure 5. Example of data analysis with TLA modified binder and AC-20 generalized logistic fit.

In the analysis it was observed that the shift factors that occur when applying Gordon and Shaw procedure could not be adequately modeled by Arrhenius of Williams-Landel-Ferry (WLF) procedures. These two methods are considered satisfactory for most applications with Arrhenius typically used at the colder temperatures and WLF format above glass transition temperature (T_g). In early work Witczak made use of a polynomial relationship to analyses shift factors from mixture data; however, a fundamental problem exists with all these formats. Clearly a polynomial relationship will have the potential for unstable extrapolation. The Arrhenius and WLF equations both have a hyperbolic form, with the values at lower temperatures increasing. In the analysis, both of these relationships do not describe the shift factors well. An alternate method evaluated is to use the modification to the WLF relationship proposed by Kaelble (1985) which results in a shift relationship which is sigmoidal in shape, as follows:

$$\log a_T = -\frac{C_1(T - T_g)}{C_2 + |T - T_g|} \tag{5}$$

where a_T is the shift factor, C_1 and C_2 are constants, T_g is the glass transition temperature (Kelvin) and T is the temperature (Kelvin) of interest.

Figure 6 shows the extension of shift factors to lower temperatures using the Arrhenius, WLF and Kaelble methods. It can be clearly observed that both the Arrhenius and WLF have relationships that tend to high values as the temperature drops with the WLF producing the highest values. This is consistent with the claims of the WLF method which notes that it best suits data between the glass transition temperature and $T_g + 100^o$. The Kaelble method shows a sigmoid type behavior which does not result in excessively high values as the temperature drops.

The Kaelble modification is applied to the mix example with the TLA binder from the MEPDG database (Figure 7) and it can be observed that the fit is very good. The relationship was attempted with various materials from this database and similar results were obtained in all cases. In some of the data sets it was observed that a high vale of T_g was required to produce a good fit of the shift parameters and consequently it may be better to consider this

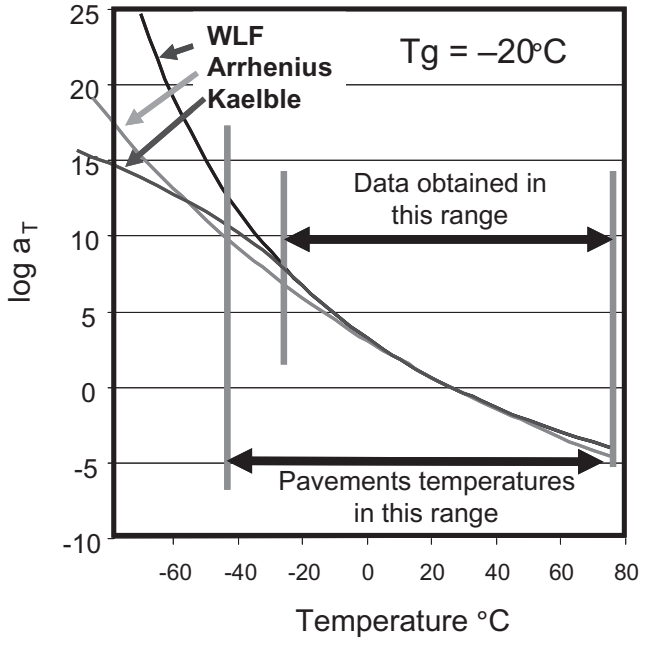

Figure 6. Shift parameters calculated using different algorithms with cold temperature extensions.

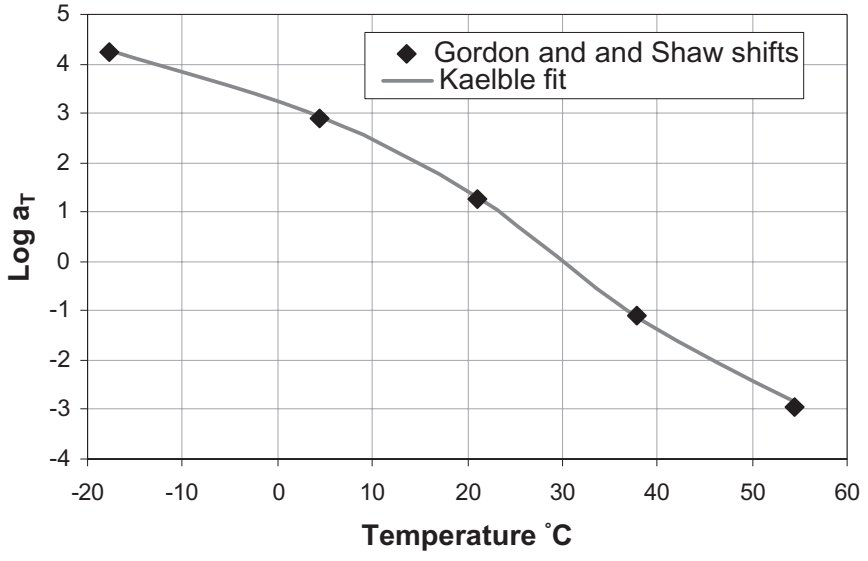

Figure 7. Kaelble fit applied to mixture data set with TLA binder.

as defining temperature rather than a glass transition temperature. This point would then effectively control the inflection point of the sigmoid of shift factors described by the Kaelble function. For example, if Figure 7 is studied, it can be observed that this inflection appears to occur at around 25 to 30°C and below this temperature both WLF and Arrhenius fits do not provide a good description of the shift factor. This could be due to the effect of the aggregate skeleton that occurs in bituminous mixes influencing the shift factors. However, it must be noted that the Kaelble shift factor has the ability to better describe the properties of the

material in the lower range of temperatures. Further study of this method is recommended since is provides a better shift factor to describe the data.

3 DISCUSSION

The type of shifting adopted in the analysis is important. In this work we have allowed the isotherms of successive pairs to be shifted without any underlying assumptions with regard to the fit model of the shift factors. This is in contrast to the methods used in the MEPDG which use shift factors derived from viscosity functions and forces the fit of the master curve to a standard logistic sigmoid curve. The adoption of restrictive shifting methods prevents adjacent isotherms from shifting in a manner that may best describe the time-temperature behavior of the material. It would appear that the main limitations in shifting used within the MEPDG method result from the need to apply viscosity aging models to account for material hardening over time; however, using the Hirsh model developed by Christensen et al. (2003) it is possible to back calculate the binder stiffness properties (Rowe, 2008) and this approach might be preferable to establish the effective binder properties which could then be used in an aging analysis with a Mechanistic-Empirical pavement design method.

The analysis of materials in this study clearly shows that the sigmoid shape is non-symmetric for asphalt mixtures with conventional and polymer modified binders. The data analysis of mixtures from the ALF sections and the data base used to develop the modified MEPDG predictive equation confirm this aspect. It is of interest to note that, in the development of binder models during the Strategic Highway Research Program (SHRP), Christensen et al. (2003) adopted a model that could consider a skewed logistic functional. If we consider that the main effect of loading time and temperature are those associated with binder stiffness it makes sense that the functional form for mixtures should also have a skewed logistic format. This skewed form is provided by the generalized logistic equation whereas it is not provided by the standard logistic equation used currently.

In the shifting scheme adopted, problems existed in some of the data sets due to limited data. Gordon and Shaw's method follows a stepped procedure. Initially estimates of the shift factors are made using WLF parameters and standard constants (17.44 and 51.6). The fit is then refined using a pairwise shifting technique and straight lines representing each data set. These shifts are then further refined using pairwise shifting with a polynomial function representing the data being shifted with the order of the polynomial being related to the number of data points and the decades of time per frequency covered by the isotherm pair. This gives shift factors for each successive pair, which is summed from zero at the lowest temperature to obtain a distribution of shifts with temperature above the lowest. The shift at the reference temperature is interpolated and subtracted from the shift factor at every temperature, causing reference temperature to become the origin of the shift factors. An example of the pairwise shifting, E' in this case, is illustrated in Figure 8.

The shifting scheme relies on sufficient data points to represent each isotherm to ensure that the fitted polynomial is sound. In addition, the data points should be uniformly distributed as a function of the logarithm of frequency. Experience with this method suggests that a good number of data points to collect per decade of frequency would be five which should be equally log-spaced throughout the test frequency range. This is in contrast to the data collected as part of the MEPDG procedure which has two data points per decade with non-equal spacing on the logarithmic scale—see example in Figure 9. To improve the understanding of material behavior it is recommended that additional test points are captured during the frequency sweep testing at a single temperature.

4 CONCLUSIONS

The analysis of master curves from various materials has demonstrated that a non-symmetric sigmoid format is required for accurate modeling of the shape of the master curve. The analysis conducted suggests that the generalized sigmoid format provides an excellent approach.

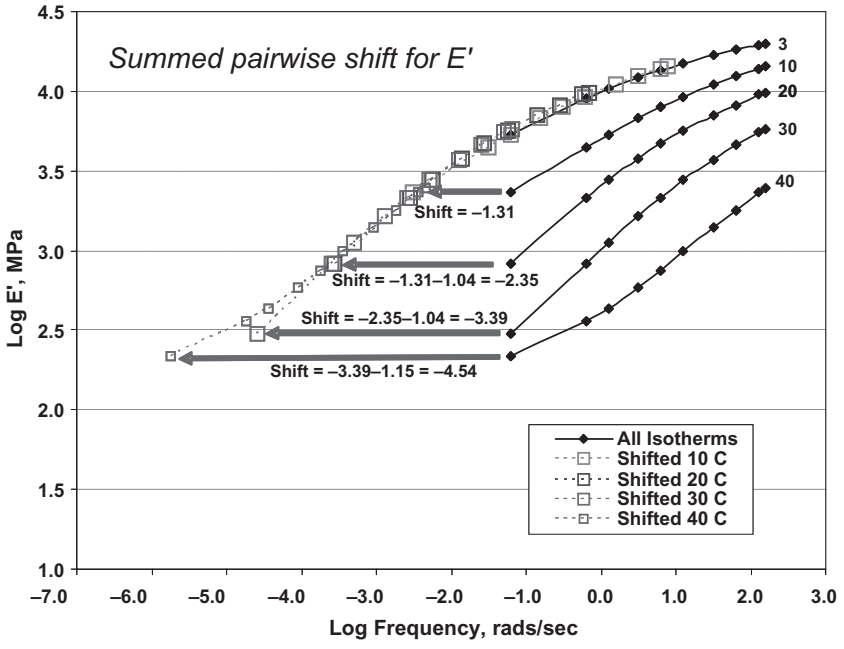

Figure 8. Example pairwise shift for hot mix asphalt sample.

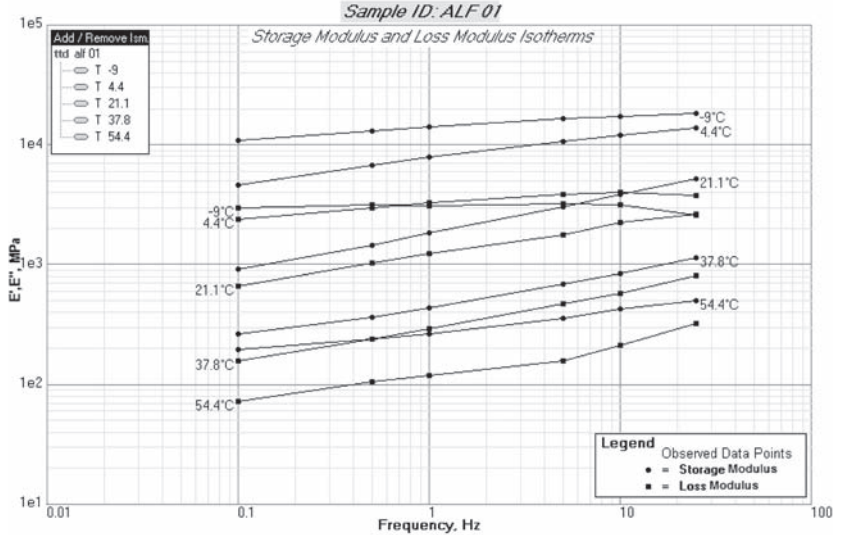

Figure 9. Example of isotherms of stiffness (E' and E") collected using MEPDG procedures.

This equation has special cases of the standard sigmoid (as currently used) and the Gompertz equation. The form of Richards equation used is re-stated to present a similar functional form to that used in the MEPDG with the definition of one additional parameter to describe the non-symmetric shape of the sigmoid function. The lambda parameter must be constrained to be >0 and a lower bound value of 0.001 has been used in our work, which can be considered to represent the Gompertz case.

The analysis of mixture data collected with the sampling scheme adopted by MEPDG is complex due to the poor definition of data. Better data sets could be produced for shifting if additional data points were collected in each isotherm. It is recommended that a minimum of five data points are collected per decade of frequencies considered and that these be spaced at equal intervals considering a logarithmic scale.

Shifting of data sets with materials behaving as visco-elastic solids with bituminous binders suggest that neither Arrhenius of WLF relationships describe the shift factors adequately. Preliminary analysis of several mixture data sets suggests that the modification to the WLF relationship proposed by Kaelble resulting in a sigmoidal format for the shift factor produces a much better fit when unrestrained shifting using Gordon and Shaw's procedures is allowed.

REFERENCES

ARE, Inc. 2004. Guide for Mechanistic-Empirical Design of New and Rehabilitated Pavement Structures, Final Report, Part 2. Design Inputs, Chapter 2 Material Characterization. *National Cooperative Highway Research Program, Transportation Research Board, National Research Council*.

Christensen, D.A., Pellinen, T. and Bonaquist, R.F., 2003. Hirsch Model for Estimating the Modulus of Asphalt Concrete. *Journal of Asphalt Technologists*, Volume 72. pp. 97–121.

Gompertz, B., 1825. On the Nature of the Function Expressive of the Law of Human Mortality, and on a New Mode of Determining the Value of Life Contingencies. *Phil. Trans. Roy. Soc*. London, Vol. 115, pp. 513–585.

Kaelble, D.H., 1985. Computer-Aided Design of Polymers and Composites. *Marcel Dekker*, New York, pp. 145–147.

Richards, F.J., 1959. A Flexible Growth Function for Empirical Use. *Journal of Experimental Botany*, Vol. 10, No 29, pp. 290–300.

Rowe, G.M., and Baumgardner, G., 2007. Evaluation of the Rheological Properties and Master Curve Development for Bituminous Binders Used in Roofing. *Journal of ASTM International*, Vol. 4, No. 9.

Rowe, G.M., 2008. Phase Angle Determination and Interrelationships within Bituminous Materials. 45th Petersen Asphalt Research Conference, University of Wyoming, Laramie, Wyoming,

The Asphalt Institute. 1982. Research and Development of the Asphalt Institute Thickness Design Manual (MS-1) Ninth Edition. *The Asphalt Institute, RR-82-2*.

Verhulst, P.F., 1838. Notice sur la loi que la population poursuit dans son accroissement. *Correspondance mathématique et physique* 10: pp. 113–121.

Weibull, W., 1951. A Statistical Distribution Function of Wide Applicability, *ASME Journal Of Applied Mechanics Paper*. pp. 293–297.

Advanced Testing and Characterization of Bituminous Materials –
Loizos, Partl, Scarpas & Al-Qadi (eds)
© 2009 Taylor & Francis Group, London, ISBN 978-0-415-55854-9

Linear viscoelastic spectra of asphalt binders from DSR and BBR

I.B. Kazatchkov, P. Michalica, J. Stastna & L. Zanzotto
Bituminous Materials Chair, Schulich School of Engineering, University of Calgary, Canada

ABSTRACT: Viscoelastic properties of asphalt binders strongly influence the performance of asphalt pavements. These properties can be described in terms of relaxation and retardation spectra. The spectra contain sufficient information from which the mechanical properties of binders can be determined. The range of frequencies or times over which the various experimental data were obtained, has a significant effect on the quality of the spectra. Different techniques can be employed to expand the range of relaxation and retardation times, these involve the combination of different types of tests. In the case of the asphalt binders studied, the creep experiments at lower temperatures (BBR) were coupled with the small amplitude oscillations (DSR) at higher temperatures. To combine the spectra obtained from these two types of tests, we used a numerical technique which was applied for two conventional asphalt binders of different origin. A practical example of predicting the response of asphalt binders in multiple creep and recovery tests is also demonstrated.

1 INTRODUCTION

Asphalts are viscoelastic materials which are used in the construction of roads and highways and are designed to serve in a broad range of temperatures, e.g. from –40 to 70°C (Barth, 1962). Therefore their rheological characterization is important at both low and high temperatures. Two commonly used tests are creep at low temperatures, using a bending beam rheometer, and dynamic shear tests at higher temperatures.

Relaxation and retardation spectra are often used to describe the linear viscoelastic properties of viscoelastic materials, since other linear material functions can be easily calculated from them. The applicability of these functions strongly depends on the range of frequencies or relaxation times over which the experimental data were obtained.

The creep recovery time can be chosen such that it exceeds the initial creep time several times, and thereby allows accessing the long-time behavior. He (2004) applied this technique for branched polypropylenes and illustrated that the retardation spectra inferred from the creep recovery data extended into the terminal zone, and that could not be accessed by means of the frequency sweeps only.

On the other hand, the higher end of the frequency range of the oscillatory tests, as our data indicate, does not always yield valid data points for various reasons. Of course, the overall range of relaxation times can be expanded by means of the time-temperature superposition. We have found that the dynamic shear rheometer measurements, both from the oscillatory shear and creep/recovery tests, can be supplemented by the data obtained from a bending beam rheometer. This rheometer is widely used to obtain stiffness data of asphalts at low temperatures, and can be adapted to run long-time creep recovery tests to further broaden the range of relaxation times. The next step is to combine the data from these three types of tests, i.e. oscillatory shear, creep/recovery in shear and creep/recovery in bending beam geometries. In this report we demonstrate our technique of obtaining the retardation spectra over a broad range of retardation times for an asphalt sample.

2 EXPERIMENTAL

The asphalt sample chosen for the purpose of this study originated from the Cold Lake region (Alberta, Canada), having a penetration of 260 dmm (at 25°C, 100 g, 5 s) and a softening point of 37°C.

A bending beam rheometer (BBR, Cannon Instrument) with an extended version of software which allows for much longer testing times compared to a conventional BBR test, was used to conduct the low-temperature creep and recovery tests. Rectangular beams of asphalt (125 × 12.5 × 6.25 mm) were conditioned in an isopropanol cooling bath at testing temperatures (from –10 to –34°C) for 1 hour prior the test. The loads used during the creep part of the test varied from 350 to 1500 mN and the loading times from 240 to 720 seconds, depending on the temperature. The deformation was kept small enough (deflections of less than 1.5 mm) to be within a linear region. After removal of the load the samples were left to freely recover for a sufficient time (up to 2 hours).

A stress-controlled Bohlin C-VOR-200 dynamic shear rheometer (DSR) was used with 25 mm parallel plates at temperatures from 10 to 40°C, and with 8 mm serrated parallel plates at lower temperatures (down to –10°C) for the dynamic and creep measurements. The applied stress levels were chosen so that the total strain was sufficiently small to avoid slip and to remain within a linear region. Depending on the temperature, the creep part of the test lasted from 1 to 12 minutes, while the recovery data points were collected for much longer periods, up to 1.5 hours. This rheometer was also used for performing frequency sweeps at the same temperature range (10 to 40°C), with the angular frequencies ranging from 0.02 to 200 rad/s.

The creep and recovery experiments with viscoelastic fluids can be described by a discrete retardation spectrum, and the shear compliance for the creep part is given by Ferry (1980):

$$J(t) = J_g + \sum J_i(1 - e^{-t/\lambda_i}) + \frac{t}{\eta_0} \tag{1}$$

and for the creep recovery part (started at time t'):

$$J(t) - J(t - t') = \sum J_i \left(e^{-(t-t')/\lambda_i} - e^{-t'/\lambda_i} \right) + \frac{t'}{\eta_0} \tag{2}$$

where J_g is the glassy compliance, λ_i are retardation times, J_i are the weights of individual retardation modes, and η_0 is the zero-shear viscosity. The experimental data were fitted by using a custom software package based on a Fortran code developed by Zhu (1994), in an unconstrained optimization mode.

The BBR data, representing a tensile creep compliance, $D(t)$, was converted into the shear compliance $J(t)$, assuming that the contribution of the bulk compliance can be neglected (Ferry, 1980):

$$J(t) = 3D(t) \tag{3}$$

The zero-shear viscosities, obtained by fitting the creep and recovery data, are shown in Figure 1. The smooth transition from the BBR data (–10°C and below) to the DSR data (–10°C and above) indicates the validity of the assumption, Equation 3.

The obtained retardation spectra for the range of temperatures from –34 to 40°C, are shown in Figure 2 for $T_{ref} = 0$°C, together with the points obtained from the frequency sweep. It can be seen that the spectrum from the DSR tests has been expanded at both ends with the spectra calculated from the extended creep and recovery tests. The combined spectrum, in the form shown in Figure 2, however, cannot be used for any further analysis, since it contains too many extra points resulting from the application of the time-temperature shifts.

There are several techniques of combining spectra (see for example [3]). Some of them involve a transformation of a discreet spectrum into a continuous one. The problem is in the choice of a material function that contains information from several data sets. In our study,

we used a numerical technique, which briefly can be described as follows (Fig. 3): use the optimization software with bounds set at both ends of the spectra, while leaving the remainder of the domain to unconstrained optimization. Thus the overall function for optimization includes the frequency sweep data and the two end points coming from the BBR creep/recovery data. The result is a spectrum which contains information collected from both types of experiments.

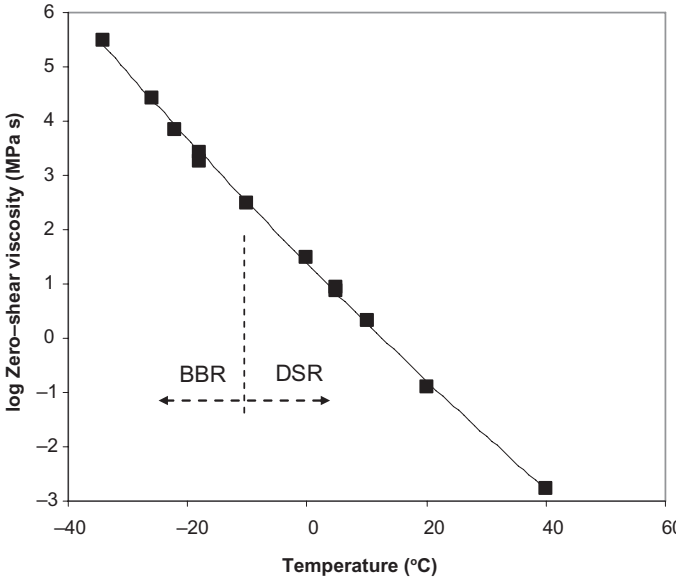

Figure 1. Zero-shear viscosity for the full range of temperatures obtained in BBR and DSR tests.

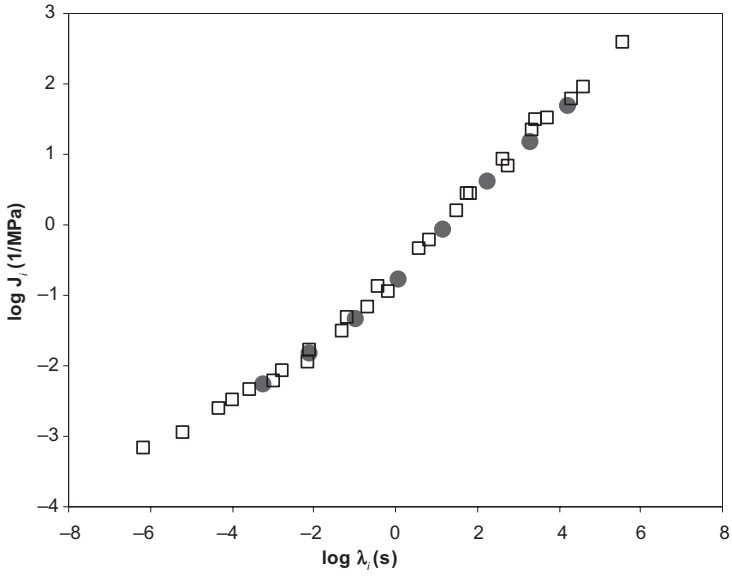

Figure 2. Retardation spectrum, time-temperature superposition of all data sets at T_{ref} = 0°C (squares: BBR data, circles: from DSR frequency sweep).

This spectrum now can be used to calculate other material functions. For example, we illustrate the application of this expanded retardation spectrum to predict the response of same sample of asphalt to a repeated creep/recovery test. This test is used in testing the rutting potential of asphalts and typically involves 100 cycles, with 1 second of creep and 9 seconds of recovery. The comparison of the calculated and experimental data sets is shown in Figure 4.

In this figure the repeated creep and recovery test for a conventional Cold Lake asphalt is described via using Equations 1 and 2 with the retardation spectrum obtained by the method

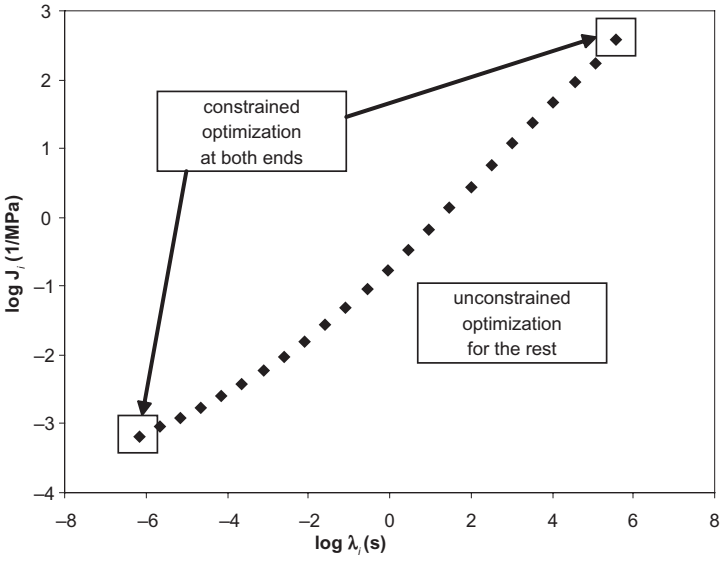

Figure 3. Schematic illustration of the proposed technique of combining sets of spectra.

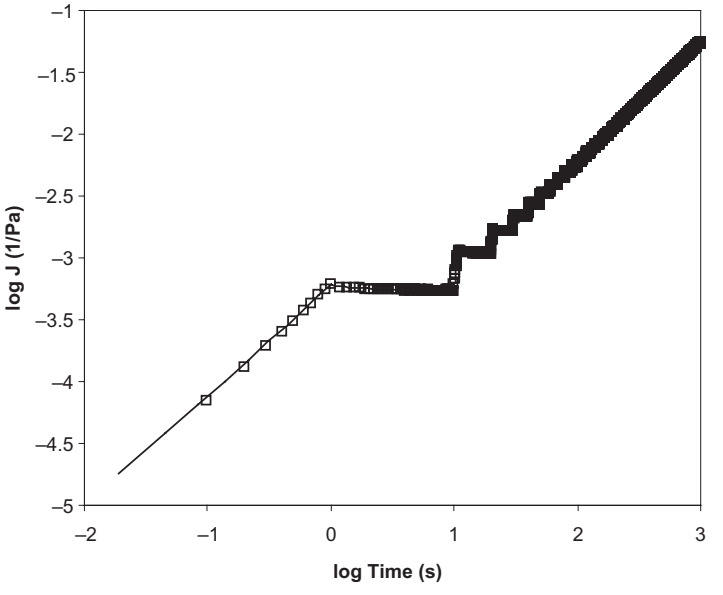

Figure 4. Predicted response of the asphalt sample based on the retardation spectrum (solid line: calculated, squares: experimental data).

outlined in Figure 3. The Bohlin DSR was used with 25 mm parallel plates, the testing temperature was 20°C, and the shear stress applied in each cycle was 100 Pa.

3 CONCLUSIONS

By combining the information from frequency sweeps and the BBR data and using the outlined numerical method the extended retardation spectrum of a conventional bitumen was obtained. It was shown that this spectrum completely characterizes the studied material. This can be seen from the excellent fit of the repeated creep and recovery data taken at an arbitrary temperature, with the shear stress within the linear region. The linear viscoelastic model of the studied bitumen allows the prediction of accumulated strain response to any number of cycles of the repeated creep and recovery test.

The basic assumption of the presented method is that the studied material behaves as a linear viscoelastic fluid. The future work in the proposed direction will deal with the behavior of polymer modified asphalts, which exhibit much larger recovery than that observed in conventional asphalts. Another possible application of this technique would be to model the rutting behavior of asphalt mixes.

ACKNOWLEDGMENTS

The authors express their gratitude to the Natural Sciences and Engineering Research Council of Canada and to Husky Energy Inc. for their financial support of this work.

REFERENCES

Barth E.J. 1962. Asphalt: Science and Technology. Gordon and Breach, NY.

Ferry J.D. 1980. Viscoelastic properties of polymers, 3rd ed. John Wiley and Sons.

He C., Wood-Adams P. & Dealy J.M. 2004. Broad frequency range characterization of molten polymers, J. Rheol. 48(4), 711–724.

Zhu C., Byrd R.H., Lu P. & Nocedal J. 1994. L-BFGS-B: A limited memory FORTRAN code for solving bound constrained optimization problems, Tech. Report, EECS Department, Northwestern University.

Advanced Testing and Characterization of Bituminous Materials – Loizos, Partl, Scarpas & Al-Qadi (eds)
© 2009 Taylor & Francis Group, London, ISBN 978-0-415-55854-9

Principal component analysis of rheological and hardening data from bituminous binders

E. Nielsen
Danish Road Directorate, Danish Road Institute

ABSTRACT: Modern measuring equipments like Dynamic Shear Rheometer (DSR) and infrared spectroscopy (IR) have the advantage (but also disadvantage) to produce a lot of data when applied to various types of bituminous binders (fresh or aged, modified or unmodified samples). The question is: Which pieces of information are relevant or the most important?

Danish Road Institute has started a project where rheological profiles of bituminous binders (in three stages: original, RTFOT and PAV material) are measured by DSR in the temperature range of 30–100°C. Traditional binder tests are also collected. To evaluate the hardening behaviour and/or addition of different modifications, infrared spectroscopy (IR-spectra) is used on the same samples to deliver a "chemical" profile.

Principal Component Analysis (PCA) or Chemometrics will be applied, when sufficient data are collected. The objective is to "extract"—if possible—structures in the multi-variant data set in order to describe the material behaviour.

1 INTRODUCTION

1.1 *Background on bituminous binders*

Many of the "old" and traditional test methods on bituminous binders (e.g. penetration) described to some extent the consistency of the bituminous binder by a single value. By combination of a few of these tests (penetration, softening point ring & ball and breaking point Fraass) straight run paving grade bitumens and their temperature susceptibility could be described in the 1950s and 1960s because the fresh bituminous binders were relatively rheologically simple as demonstrated by W. Heukelom (Heukelom 1969) with the Bitumen Test Data Chart. A reasonably good predictive model for translation into viscosity over a wider temperature range was at hand, if a few consistency tests were performed.

Unfortunately, not all binders were "simple". Aged binder recovered from old (or even new) pavements showed different levels of rheological complexity. This was also the case when laboratory sample were aged in either short term aging (TFOT, RTFOT or RFT) or long term aging (PAV or RCAT). In the refineries some of the early processes (oxidation, semi-blowing) could be used to alter the behaviour of the fresh binder as well as deviations from "normal" behaviour (increased temperature susceptibility) were detected, when some natural waxes were present which could be traced back to the origin of the crude oil.

Increasing traffic intensity and loads brought forward the risk of permanent deformation and binder improvements to deal with this. For common road applications, polymer modified bitumens were introduced where the broad range of different elastomers and plastomers offered almost infinite possibilities to introduce complexity in the binders and improved performance against permanent deformation. In joint seals and roofing felts—due to the small volume and high demand of the material characteristics—heavy modification was used. Even though it sounds like a contradiction, special waxes were also introduced to minimize the rutting potential of an asphalt mix. Recently modifiers are introduced to lower viscosity at mixing temperature without endangering the rutting resistance in order to save energy at production.

Sustainability, recycling of reclaimed asphalt, long life pavement and Life Cycle Assessment approaches also stress the need for characterisation of bituminous binders—not only the first time the binder enters the cycle, but also the second and the third and… .

The bottom line is that our bituminous binders are becoming more complex and perhaps even tailor-made which means that the old traditional consistency tests are not sufficient any more. This fact has been recognised several years ago, but development of new tests is slow and it takes time for them to be generally introduced for instance in the European binder specifications.

Another development is also causing problems for the characterization of bituminous binders. Many of the new modifiers can be introduced directly into the asphalt mixer or just before entering the mixer which makes them extremely versatile for the asphalt contractors due to ease of operation and savings on binder storage capacity. The researchers are forced to use model-blends in the laboratory to mimic the binder in the finished mix and then introduce short and long term aging procedures to predict the changes in binder characteristics over time. Characterization of modified asphalt/modified binder by solvent extraction and binder recovery is often questionable with the available methods at present. This is due to the ability of the operation to recreate the binder from the road material in the same rheological and chemical form as it existed in the bituminous mortar in the mix.

1.2 *Possibilities in binder characterization*

The complexity of modern bituminous binders in the high service temperature area (roughly 25–80°C) was in need of new analytical tools that also would enable results in real engineering terms than the former more consistency oriented data. One of such tools—the Dynamic Shear Rheometer (DSR)—was developed and adapted for bituminous binders during the SHRP programme. It provides rheological information on the material behaviour in real engineering terms through stress-strain relationships in the frequency domain over a large temperature range. Like many new techniques, DSR has the advantage (but also disadvantage) to produce a lot of data.

The disadvantage is that instead of having too little information we have plenty and the problem is to find the important part of it for a focused but yet sufficient characterisation of the rheological properties of the binder. The need for an interpretation and data-reduction is both highlighted and challenged by the numerous modifications that are available. If specification limits are set according to certain test conditions without really understanding the mechanisms bituminous binders can unintended be excluded that have some potential role to play. A knowledge gathering phase will provide information that will facilitate the contractor to make the optimum choice of bituminous binder for a certain application and for the standardisation community to make good and valid (meaningful) specifications.

2 THE PROJECT ON RHEOLOGY AND HARDENING

Danish Road Institute has started a project that focuses on the rheology and hardening potential of bituminous binders with respect to short and long term aging in the high service temperature range. The plan is that the main bulk of the samples shall be tested in three stages: as original, RTFOT and PAV material by measurement by DSR in the temperature range of 30–100°C. When PAV—Pressure Aging Vessel—hardened material is mentioned in this paper, it will always represent material PAV-hardened at 100°C that initially has been subjected to RTFOT-hardening.

Traditional binder tests (penetration, softening point ring & ball and dynamic viscosity at 60°C) are also collected. To evaluate the hardening behaviour and/or addition of different modifications, infrared spectroscopy (IR-spectra) is used on the same samples to deliver a "chemical" profile.

The main objectives are

- to obtain knowledge on better rheological characterisation of bituminous binders
- to find indicators for undesired premature aging properties in the binders by combination of several parameters
- to support identification of unknown binders.

The samples for the project will be an anonymous collection of

- samples from bitumen surveys in Denmark representing all bitumen suppliers
- binders and additives used in demonstration project where Danish Road Institute (DRI) is involved
- samples from the annual Round Robin tests on bituminous binders coordinated by DRI
- special binders—like oxidised bitumens and hard industrial bitumens—in order to provide "limiting examples" of the population of bituminous binders
- other samples that could contribute to the data collection without adding much work load to the laboratory.

Apart from the main objectives additional spin-off benefits are anticipated to appear when special groups of samples are entered for the data collection. A special spin-off related to the knowledge on the rheological/chemical behaviour of blends of bitumens will enable the laboratory to verify the mix ratio of two binders or between a binder and a modifier. It will be an important tool if the used ratio can be verified with a certain documented level of confidence through a fixed procedure. The tradition in Denmark is that the contractors mix intermediate grades from a hard and a soft grade of bituminous binder and it is not possible to sample the combined binder at the asphalt plant.

Even though a somewhat negative remark was made on testing recovered binder, it might be possible in the future to establish a link between the field application and laboratory aging procedure in order to improve on the predictability of hardening and recyclable potential of bituminous binders.

3 STATISTICAL ANALYSIS AND CHEMOMETRICS

In traditional statistical analysis hypothesises are tested for the existence of a possible correlation between one dependent parameter against one or a few independent variables and the number of involved samples will by far exceed the number of parameters and variables. This gives sufficient degrees of freedom for a valid statistical regression analysis.

Traditional statistics can with surplus of degrees of freedom handle if an occasional data point for one variable is missing due to the surplus of other data points. But what if lumps of data is missing? Can valid information still be extracted out of the rest? This is a situation which many researchers have faced when some part of an experimental design failed to give all the results expected and with traditional statistics it is a problem.

But what if the situation is the other way around? Even though a large number of samples exists but it is by far exceeded by the number of variables. This cannot be treated by traditional statistical regression analysis. This scenario is a daily occurrence for researchers in analytical chemistry and food technology working with ultraviolet or infrared spectra of their compounds or samples (Nørgaard 2008a). A Fourier Transform infrared spectrum consists typically of the absorbance determined for every second reciprocal centimetre (cm^{-1}) between 4000 cm^{-1} and 400 cm^{-1}. That means 1800 variables! Chemical interesting in food science is often especially the part called near infrared (NIR) which is between either 1500 cm^{-1} or 1800 cm^{-1} and down to 400 cm^{-1} but nevertheless 550 or 700 is still a lot of variables.

The question in sensory analysis could on 20 samples of cheese in dairy production for development of a new and quick test method be: which part of the NIR spectra can be used as an indicator for undesired fungal growth on surface of cheese to avoid the use of expensive sensory panels? To analyse this and similar scenarios, a statistical approach called Principal

Component Analysis (PCA) can be applied. The term Chemometrics is often used when the technique is applied in chemistry and food technology.

It is difficult to explain the technique and a pure mathematical explanation is also difficult for most people to comprehend. A simple description of the technique is if the population of data can be visualised as data points plotted against n axes in a n-th dimensional space. This "cloud" of data looks like an ellipsoidal figure in this n-th dimensional space. Try to use n = 3 for a start.

The first Principal Component (PC1) is the longest "distance" that can be made up by a linear combination of n variables by applying different weights to them. This means that PC1 contains the linear combinations of variables responsible for the largest variation in the data material where the variables with the highest weights have the largest impact (either positive or negative). Perpendicular to the first Principal Component the second Principal component is determined as the longest "distance" in this direction by a new linear combination of the n variables with a new set of weights describing the next part of the variation. This gives PC2. Perpendicular to both PC1 and PC2 the next Principal Component is then determined in a similar way. It is seldom necessary to determine more than 5–8 PCs because they will normally together describe the dominant part of the variation in the "cloud" of data.

In special Score- and Scatter-plots two selected PCs and the weights of the variables associated to them are plotted against each other. By identifying the different variables analysis can "reveal" structures/relations in the data where certain variables either group together or are in opposite corners of the plot which will give information about the relationship between them.

A description of the technique applied on a study of bituminous binders can be found in (Pieri 1996 and Ballié 2008). The calculations are complex, but commercial software packages (e.g. Unscrambler®, Umetrics®) are available to take care of that part.

A remarkable thing about this technique is that grouping of variables and other relevant information can be detected even if large parts of the data are missing. But at some point it is of course a trade off between how much information/relations are hidden in the data and how much data have been provided.

In the rheology project Danish Road Institute aimed from the start to use this technique. This approach had been applied successfully on smaller projects earlier and our data was of a spectral nature. The infrared information was directly spectral and that analogy could also be used for the rheological information as will be explained later.

4 THE POPULATION OF DATA

4.1 *Considerations for traditional binder data*

In order to fit in with the present specification for bituminous binders the project has tried to focus on a limited core number of tests that the laboratory on the other hand would try to have filled out completely. The tests are

EN 1426 Penetration @ 25°C (and perhaps @ 15°C for the soft grades)
EN 1427 Softening point ring & ball
EN 12596 Dynamic viscosity @ 60°C
EN 12595 Kinematic viscosity @ 135°C

EN 12607-1 Rolling Thin Film Oven Test (RTFOT)—short term aging
EN 1426 Penetration @ 25°C
EN 1427 Softening point ring & ball
EN 12596 Dynamic viscosity @ 60°C

EN 14769 Pressure Aging Vessel (PAV)—long term aging @ 100°C on RTFOT material
EN 1426 Penetration @ 25°C
EN 1427 Softening point ring & ball
EN 12596 Dynamic viscosity @ 60°C

The project concerns especially hardening potential and high service temperatures, so breaking point Fraass has been left out for this reason and for the relatively poor precision of the test method particularly for polymer modified binders.

4.2 *Considerations for rheological data*

Through a fruitful cooperation with Petri Uhlbäck, Nynas Sweden, Danish Road Institute was able to set up a procedure with conditions for temperatures and frequencies and selected stress levels that would ensure that measurements would be inside the linear visco-elastic domain for nearly all type of bituminous binder samples. The procedure consists of a logarithmic frequency sweep between 0.01 Hz and up to 10 Hz (11 values) for eight temperatures from 100°C down to 30°C for every 10°C giving a total of 88 sets of data of phase angle and complex shear modulus, G*.

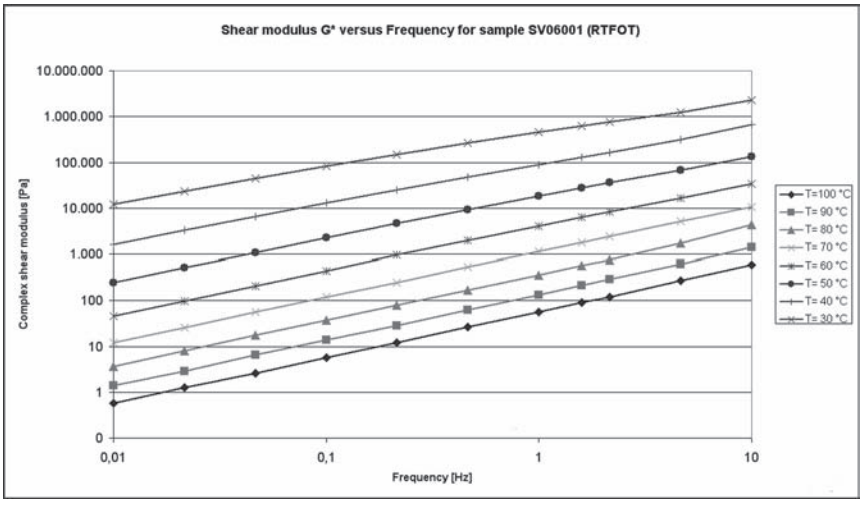

Figure 4.1. Sample SV06001 RTFOT—Complex shear modulus versus frequency.

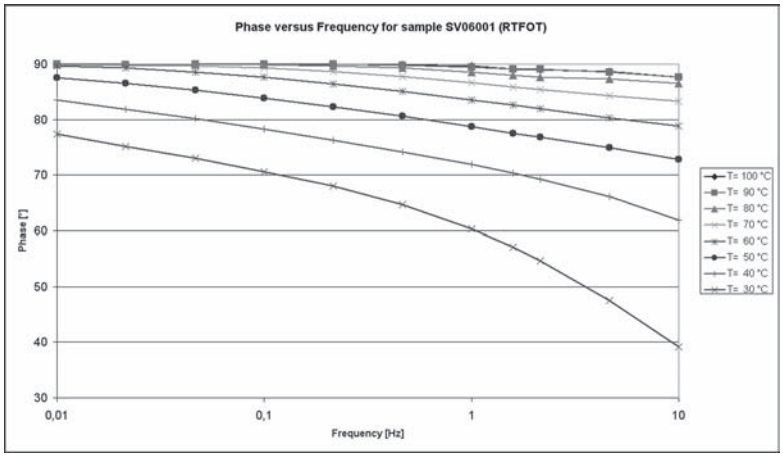

Figure 4.2. Sample SV06001 RTFOT—Phase angle versus frequency.

This would produce a "rheological profile" of the sample in the temperature range of interest with a redundant amount of information to produce mastercurves for model fitting. Through the extended overlap between the measurements at different temperatures it was also possible to evaluate if some data points could be erroneous. Due to the robustness of Chemometrics we could remove erroneous values if we found measurements outside the compliance of the equipment (likely to happen for the softest grades at high temperatures) or if special samples indicated that they were outside the linear visco-elastic domain. These verified profiles could then be used as input as "spectral" data in the Principal Component Analysis.

4.3 *Considerations for infrared data*

Even though the inspiration partly came from NIR measurements in the food industry (example in Nørgaard 2008b) Danish Road Institute at the moment intends to use the whole infrared spectrum between 4000 cm^{-1} and 400 cm^{-1}. It is evident that plenty of information exists in that range if the samples contain what in chemical terms is called "functional groups". On the other hand fresh bituminous binders have a limited number of functional groups which is linked to the amount of hetero atoms like oxygen, nitrogen, sulphur etc. These groups become more pronounced in hardened or oxidised samples. Furthermore Danish Road Institute would like to detect additions of SBS polymer which also have no functional groups but have certain bands outside the NIR range.

Principal Component Analysis and IR (NIR) have successfully been combined before in several cases on bituminous binders. Pieri 1996 demonstrates correlations between chemical composition (among other through selected peak areas under the IR absorbance curve) and physical characteristics by applying PCA. Lima 2004 applies the methodology to predict properties of bitumen blends in a delivery situation following in-line blending of hard and soft grades at the refinery—an interesting perspective that could fit well with the Danish tradition of in-line blending.

4.4 *Preprocessing of data*

When the data from the different types of variables are collected it is advantageous to perform some preprocessing of the data. In the initial step variables like penetration, dynamic viscosity at 60°C and complex shear modulus is transformed using the logarithm function, while variables like softening point ring and ball, phase angle from the rheologi and the absolute peak areas (according to Pieri 1996) remain unchanged.

The second step involves a transformation for all variables apart from data from the Infrared spectra which go through a special preparation. The transformation is given in (1).

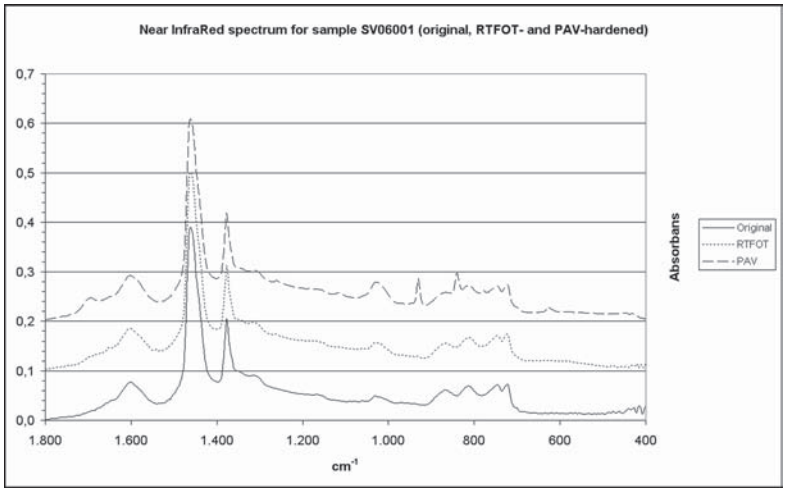

Figure 4.3. Sample SV06001—NIR spectra (original, RTFOT & PAV; with vertical shifts).

$$x_{i,\,\text{normalised}} = \frac{x_i - x_{\text{mean}}}{\sigma} \tag{1}$$

where x_i = original data point value for the individual variable; x_{mean} and σ = mean value and standard deviation respectively for the corresponding variable; $x_{i,\,\text{normalised}}$ = result for the individual data point of the transformation.

The effect of the transformation is that variation of the n-th dimensional "cloud" mentioned earlier will

- contain the same information on variation as the original data
- have values roughly between –3 and +3 with few data points outside this range
- have no off set from the centre of the "cloud".

The effect on data from different variables is shown in Figure 4.4 and Figure 4.5 for traditional binder data and rheological data respectively.

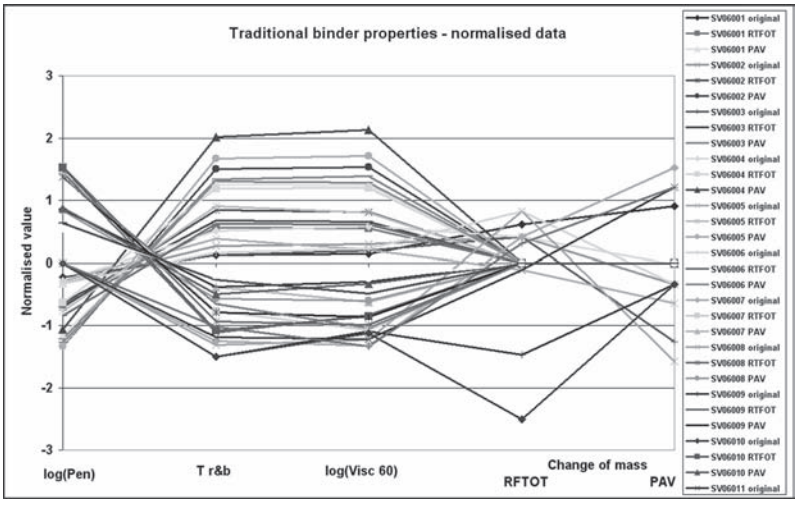

Figure 4.4. Traditional binder data after normalisation.

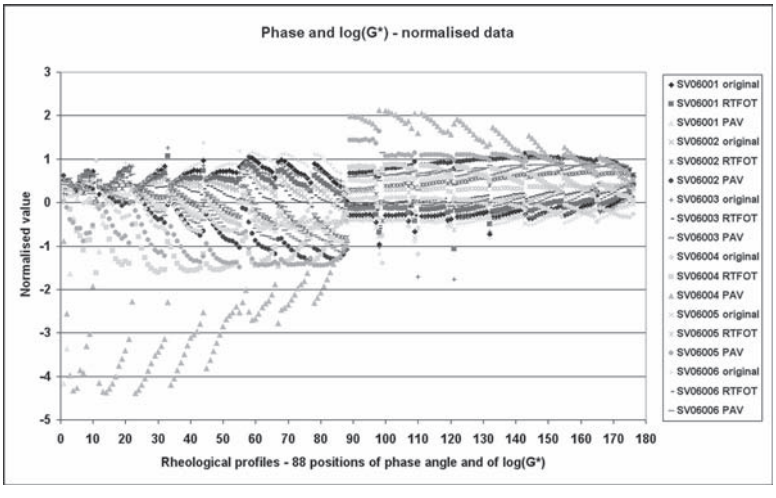

Figure 4.5. Rheological data (phase angle and log(G*)) after normalization.

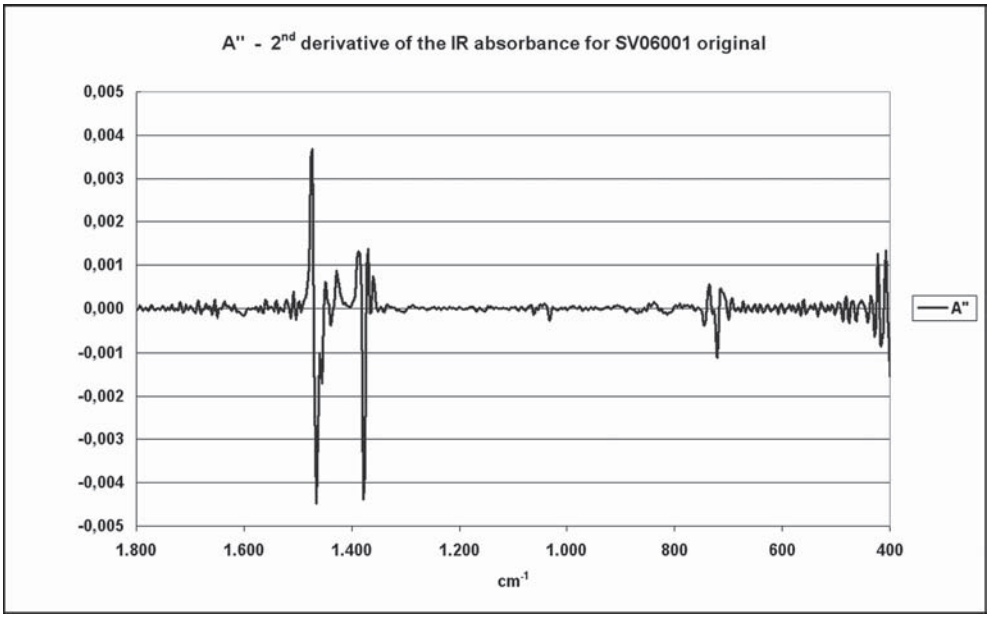

Figure 4.6. Example of 2nd derivative of IR spectrum of original sample SV06001 (see Figure 4.3).

The absorbance curves from the Infrared spectra are taken through another transformation which has almost similar effect as the normalisation. The IR spectra can be bias by an off-set (e.g. due to concentration of the individual spectre) or a drift of the absorbance as a function of the wave number (cm^{-1}) (due to imperfections in the equipment etc.). By taking the second derivative of the absorbance with respect to wave number all relative information is intact, but the mentioned bias is removed. It remains to be seen whether or not normalisation will be necessary on the second derivative of the IR spectra.

4.5 *PCA—initial calculation*

The data population is still small, but a PCA has been performed on a part of the population to give an example on the type of response. It illustrates also the graphical nature of the interpretation of specialised plots in PCA.

Analysis of an extract from the data population for selected variables consisting of traditional and DSR data is shown in Figure 4.7 in form of a loadings or weights plot of the first and second Principal Component, PC1 and PC2. The data set consists of 12 bitumen samples (in original, RTFOT and PAV state) and 38 variables, but the data matrix is not complete. From the DSR measurements variables are selected with two frequencies (0.01 Hz and 1 Hz) at each of the eight temperatures from 100°C stepwise down to 30°C. The phase angle and log complex shear modulus are named Fx and Gx where x refers to the number of measuring sequence of 88 values (See Figure 4.5). Low number means high temperature and vice versa. Variables with $\Delta x = 6$ means variables at same temperature two decades of frequency apart while $\Delta x = 11$ means same frequency 10°C apart.

Five PC's are necessary to describe the variation in the data set. PC1 explains 65% and PC2 21%, so Figure 4.7 covers 86% of the variability. The position of a variable relative to the centre depicts its influence (weight). Variables with positions close together have same influence on the variability and suggest that a correlation may exist between them.

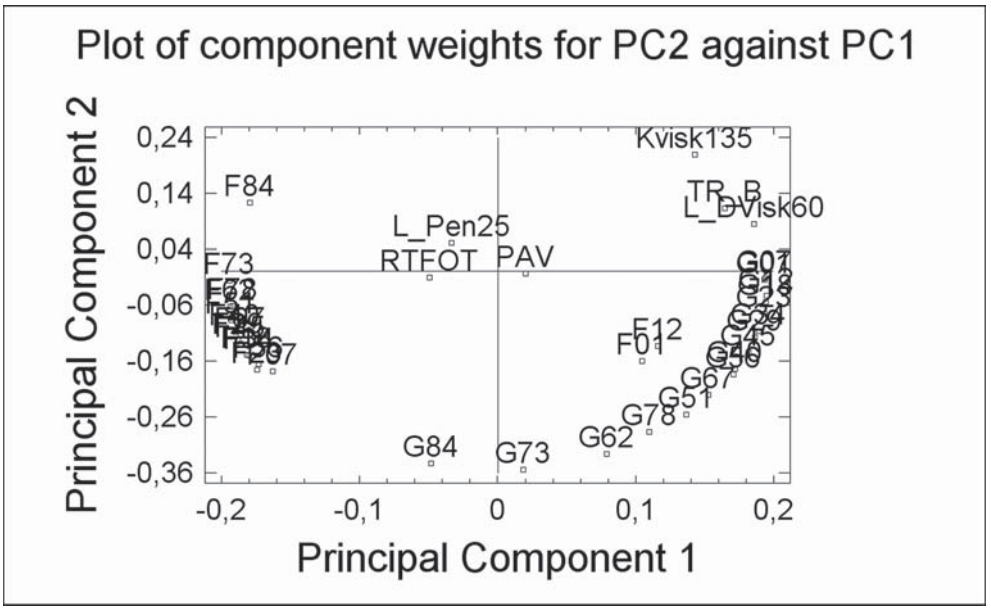

Figure 4.7. Loadings/weights for PC1 and PC2 for selected variables (trad. data and rheology).

Examples of interpretation from Figure 4.7 which can be starting point for a more in depth analysis:

- Softening point ring and ball (TR_B) has more influence on sample variation than the logarithm of the penetration at 25°C (L_Pen25).
- Softening point ring and ball (TR_B) shows almost same influence as the logarithm of the dynamic viscosity at 60°C (L_DVisk60).
- Change of mass by ageing/hardening following RTFOT and PAV has opposite influence on sample variation.
- Complex shear modulus at high temperature (low G numbers) tends to have a negative correlation with the phase angle (low P numbers) but the correlation seems to become poorer at lower temperatures (high G and P numbers).
- Complex shear modulus at high temperature (low G numbers) follow roughly same variability with respect to PC1 as dynamic viscosity at 60°C (L_DVisk60) and kinematic viscosity at 135°C (KVisk135).
- Penetration (L_Pen25) and G62 (complex shear modulus at 50°C and 1 Hz) lie on a straight line through the centre. This suggests that a negative correlation might exist between these two variables.

5 THE NEXT STEPS

In the autumn of 2008 several samples have been run in triplicate in order to assess the internal repeatability of the rheological and "chemical" profiles. This background information is important in the future when differences between samples and/or between hardening stages shall be evaluated whether or not they are significant.

At the moment (January 2009) the population of test samples contains twenty two samples of bituminous binders (predominantly of normal paving grade origin) and four recovered binders from Danish trial sections.

Danish Road Institute is presently optimising automatic process and transfer of data from initial determination to dedicated software for performing the Principal Component

Analysis. Parallel to this, Danish Road Institute will slowly gather test results to expand the amount and diversity of the population of samples. Focus in 2009 will be on samples with "in-situ" modifications with wax or polymer and on polymer modified binders according to EN 14023.

6 CONCLUSION

Danish Road Institute has started a long term project focusing on hardening potential of bituminous binders (in three stages: original, RTFOT and PAV material). Information of rheological profiles measured by DSR in the temperature range of 30–100°C will be gathered together with traditional binder tests. The hardening behaviour and/or addition of different modifications will be determined by the use of infrared spectroscopy (IR-spectra) to deliver a "chemical" profile on the same samples.

Principal Component Analysis (PCA) or Chemometrics will be applied on the data in order to achieve the objectives

- better description of hardening potential of bituminous binders,
- identify relevant/important "structures" in the data population,
- obtain data reduction of advanced device outputs like DSR and IR,
- identification of unknown samples.

REFERENCES

Ballié, M., Chailleux, E., Dumas, P., Eckmann, B., Leroux, C., Lombardi, B., Planche, J-P., Such C. & Vaniscote, J-C. 2008: Characteristics of Bituminous Binders and Their Consequences on The Mechanical Performance of Asphalts, Paper 402-108, E&E Conference Copenhagen, May 2008.

Heukelom, W. 1969: A Bitumen test Data Chart for Showing the Effect of Temperature on the Mechanical Behaviour of Asphaltic Bitumens, Journal of The Institute of Petroleum, November 1969, pp. 404–417.

Lima, F.S.G. & Leite, L.F.M. 2004: Determination of Asphalt cement Properties by Near Infrared Spectroscopy and Chemometrics, Petroleum Science and technology, Vol.22, No. 5–6, pp. 589–600, 2004.

Nørgaard, L., Balling Engelsen, S. & Bro, R. 2008a: Principal Component Analysis of Near infrared spectral data (in Danish), dansk kemi, Vol. 89, No 2, pp. 30–32, 2008.

Nørgaard, L., Bro, R. & Balling Engelsen, S. 2008b: Extract in beer determined by Principal Component Regression (in Danish), dansk kemi, Vol. 89, No 8, pp. 34–36, 2008.

Pieri, N., Planche, J.-P., Martin, D., Germanaud, L. & Kister, J. 1996: A new approach to predict rheological properties of bitumens from their chemical composition determined by FTIR and synchronous U.V. fluorescence, Paper 5.120, E&E Congress Strassbourg, France, 1996.

Advanced Testing and Characterization of Bituminous Materials –
Loizos, Partl, Scarpas & Al-Qadi (eds)
© 2009 Taylor & Francis Group, London, ISBN 978-0-415-55854-9

Rheological and functional evaluation of the interactions between bitumen and rubber

E.J. Peralta, H.M.R.D. Silva & J.C. Pais
Department of Civil Engineering, University of Minho, Guimarães, Portugal

A.V. Machado
IPC-Institute of Polymers and Composites, University of Minho, Guimarães, Portugal

ABSTRACT: It is estimated that about ten kilograms of tires are discarded per inhabitant annually. The negative impact of this residue can be reduced, since rubber can be reused as a constituent of asphalt rubber (AR) binder in road pavements. However, the materials which constitute the AR binders and their interaction are not sufficiently characterized. In this work several base bitumens interacted with crumb rubber, in order to produce AR binders, which were subsequently separated, by using a modified "Basket drainage method" to recover the residual bitumen and rubber. EN 12591 or 14023 standards tests and the Dynamic Shear Rheometer (DSR) were used to evaluate the changes in the properties of the binders during AR production. The swelling and depolymerisation changes in the rubber were evaluated through microscopic tests. It was observed that the characteristics of the base bitumen significantly affect the rubber and the AR binder properties (mainly for interactions with softer bitumens).

1 INTRODUCTION

The introduction of crumb rubber in the production of Asphalt Rubber (AR) mixtures for road pavements should be considered as a sustainable technology which transforms an unwanted residue into a new bituminous mixture highly resistant to fatigue and fracture. However, the addition of rubber into a bituminous mixture increases its complexity. Hence, it is essential to carry out a study to understand the interaction between its constituents, in order to optimize the performance of AR mixtures.

The main objective of this study is to evaluate the properties of the AR binder components (base bitumen and rubber) and their influence in the functional and rheological properties of the AR modified binder. Another objective of this research is to assess the changes that occur in the base bitumen and in the rubber after their reciprocal interaction in the process of the AR binder production. Finally, this work also aims to establish the relationship between the rheological and functional properties of AR binders.

2 LITERATURE REVIEW ON BITUMEN AND RUBBER INTERACTION

At present the pavement technology and the evaluation of bituminous mixtures are essentially based on empirical-mechanist studies. Frequently, the materials that constitute asphalt pavements are not sufficiently characterized, more specifically concerning their physicochemical constitution, their rheological properties and their mutual interaction at a microscopic scale.

Therefore, it is essential to develop the knowledge about the interaction between the constituents of bituminous materials used in flexible pavements by carrying out their characterization at a microscopic level, so as to understand their macroscopic structural and functional behaviour. This additional study becomes more significant for modified or unconventional mixtures due to their complexity (e.g. Asphalt Rubber). Actually, beyond the traditional constituents

of the bituminous layers of the pavements, the use of crumb rubber (recycled from used tires) should be studied as a form of environmental protection and as a pavement performance enhancer.

When crumb rubber is blended at high temperatures with bitumen to produce a modified binder (i.e. wet process), the two materials interact once bitumen components migrate into the rubber causing it to swell (Bahia and Davies, 1994). Initially, the interaction between crumb rubber and bitumen is a non-chemical reaction, where the rubber particles are swollen by the absorption of the aromatic oils of bitumen (Heitzman, 1992).

Absorption of bitumen components by the rubber inevitably depletes the bitumen of the absorbed components and, consequently, modifies its properties, by making it stiffer and more brittle (Singleton et al. 2000, Artamendi et al. 2002, Airey et al. 2003). Furthermore, the rubber particles may also suffer some form of degradation (mainly devulcanization and depolymerisation) when they are mixed with bitumen at high temperatures for prolonged periods of time (Billiter et al. 1997a, Billiter et al. 1997b, Zanzotto et al. 1996). The extent of swelling and degradation depends on the nature of the rubbers, the chemical composition of bitumen and the mixing conditions of time, temperature and degree of agitation. In addition, these processes will determine the mechanical properties of the crumb rubber modified binders (Abdelrahman & Carpenter, 1999). The asphalt rubber binders are very asphalt dependent: lower saturates and asphaltenes contents improve the asphalt capacity to dissolve rubber (Billiter et al. 1996).

Blending crumb rubber into asphalt is believed to improve its elastic and energy absorption properties, which are directly related to the resistance of the binder to cracking and rutting failures (Gopal et al. 2002). Bahia & Davis (1995) concluded that the impact of crumb rubber content (2–20%) on the reduction of stiffness at low temperature (–20 to 0°C) is a linear function of the rubber content and independent of the rubber source and that the lower the stiffness of the asphalt, the less significant the effect of the rubber. The addition of crumb rubber improves the resistance of asphalt binders to low temperature cracking. Optimum crumb rubber contents must be determined for each crumb rubber size and asphalt binder (Gopal et al. 2002).

The use of low penetration grade bitumens in asphalt-rubber mixtures reduces the rate and the amount of swelling of the crumb rubber particles. However, any changes in the rheological properties of the binder following rubber-bitumen interaction could result in the binder becoming embrittled (losing flexibility and capacity to resist cracking and fretting). The use of high penetration grade bitumen will increase the rate and the amount of rubber swelling and therefore the shape and rigidity of the rubber. However, the binder should still have sufficient flexibility following the rubber–bitumen interaction to resist cracking and fretting (Airey et al. 2003). The basket drainage bitumen absorption method was found to be a simple and effective way to monitor rubber-bitumen interaction. The crumb rubber particles absorb bitumen and swell when added together at mixing temperatures. The rate and amount of absorption is mainly dependent on the test temperature and complex chemical nature of bitumen, but only marginally dependent on the bitumen type and grade. In addition to normal oxidation, the residual bitumen experienced further changes in mechanical and rheological properties in terms of increase in stiffness, elasticity, viscosity and reduction in penetration (Rahman, 2004).

Rheology is the science that deals with the deformation and flow of matter. The rheological characteristics of bitumen at a particular temperature are determined by the constitution (chemical composition) and the structure (physical arrangement) of the molecules. Any changes in the constitution, structure or both will result in changes in the rheology. Thus, to understand changes in bitumen rheology, it is essential to understand how the structure and constitution of bitumen interact to influence its rheology (Read & Whiteoak, 2003).

Asphalt rubber (wet method) is a very special binder if compared to others. Extremely low phase angles at high temperatures/low frequencies and relatively high phase angles and low stiffness at very low temperatures/high frequencies make it a very interesting binder

(van de Ven & Jenkins, 2003). The addition of crumb rubber to bitumen decreases the elastic and viscous moduli at low temperatures and, therefore, it causes an increase in binder flexibility. On the contrary, at high temperatures a significant increase in both moduli and a notable drop in the loss tangent values result in a more elastic binder. Furthermore, it can be deduced that the thermal susceptibility of the binder is clearly reduced as a consequence of rubber addition. Consequently, enhanced resistance to permanent deformation, low-temperature and fatigue cracking should be expected in the resulting asphalt rubber mixtures (Navarro et al. 2005).

3 ASPHALT RUBBER PRODUCTION, SEPARATION AND CHARACTERISATION

3.1 *Bitumen selection, sample preparation and crumb rubber selection*

A single source of petroleum was used in the experimental work with the aim of reducing the number of factors that can influence the analysis of the results. Four types of bitumens, with penetrations varying between 10 and 200 dmm, were collected from the same distillation column, intentionally selected to represent the usual commercial bitumens (pen grades 10/20, 40/50, 60/70 and 150/200). These bitumens were combined in different proportions, as indicated in Table 1, in order to obtain sixteen different samples of bitumen for characterisation.

According to the supplier (RECIPAV), the crumb rubber used in this work was obtained by the cryogenic process and was grinded from 30% of truck tires and 70% of car tires. The supplied rubber was sieved in laboratory, in order to obtain and use only the fraction of rubber that went through the sieve ASTM #20 (0.850 mm) and retained in the sieve ASTM #40 (0.425 mm).

Table 1. Proportions of commercial bitumen used to obtain the sixteen samples of bitumen.

Bitumen Sample	Commercial bitumen used to produce the samples (%)			
	10/20	40/50	60/70	150/200
A	100	0	0	0
B	75	25	0	0
D	25	75	0	0
E	0	100	0	0
F	0	75	0	25
G	0	50	0	50
H	0	25	0	75
I	0	0	100	0
J	25	0	75	0
K	50	0	50	0
L	75	0	25	0
M	0	0	0	100
N	0	0	25	75
O	0	0	50	50
P	0	0	75	25

3.2 *Production and separation of the asphalt-rubber binder*

The asphalt-rubber binder production facility consisted of an electric heating device in which the aluminium containers with the bitumen were placed. A wire basket (# 0.420 mm) was also placed inside the container in order to allow the final separation between rubber and bitumen constituents (rubber particles were retained in the basket). The procedures for the production of the asphalt rubber binder and for the separation of its constituents were the following:

- Heating of 1 kg of each base bitumen at 180°C and collecting of a sample (BASE);
- Introduction of 17.5% of crumb rubber (CR) by mass of asphalt rubber;
- Continuous heating of the asphalt rubber binder at 180°C for 60 minutes (digestion time) while stirring the binder at a velocity of 230 rot/min (Fig. 1);
- After finishing the production period, a sample of asphalt rubber (AR) were collected;
- Suspension of the wire basket with the AR binder in an oven at 180°C for 15 min, so as to separate its constituents, and collection of a sample of the dry recovered rubber (RR) and of the residual bitumen (RES) (Fig. 2);
- The recovered rubber was washed with toluene for further analysis;
- The residual bitumen was dissolved in toluene and filtered to reclaim some residual rubber particles (FR) eventually suspended in the residual bitumen.

3.3 *Analytical determinations*

The characteristics of the materials involved in the production of AR, crumb rubber and bitumen, were assessed in this work by using several test methods carried out on the samples of binder (BASE, AR, RES) and rubber (CR, RR, FR) collected during the previous procedures.

Following the EN 12591 and 14023 standards, the characteristics of the different samples of binder (BASE, AR, RES) evaluated in this work were the penetration (PEN) at 25°C

Figure 1. Production of the asphalt-rubber binder.

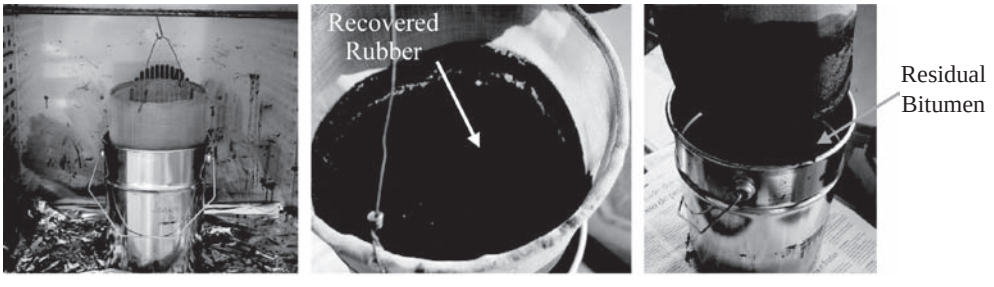

Figure 2. Separation of the AR binder in its constituents (residual bitumen and recovered rubber).

(following the EN 1426 standard), the softening point, also known as ring and ball (RB) temperature (following the EN 1427 standard) and the dynamic viscosity (DV) at 180°C, by using a rotating spindle apparatus (following the EN 13302 standard). The elastic recovery (ER) was also assessed in accordance with the ASTM D5329 standard, but only for the AR modified binder. In order to determine the behaviour of all the binders (BASE, AR, RES) at different temperatures (operating, application and mixing temperatures) and frequencies, they were tested in a Dynamic Shear Rheometer (DSR) capable of measuring their rheological properties (in accordance with the EN 14770 standard).

The characteristics of the different samples of rubber (CR, RR and FR) were evaluated by carrying out solubility and microscopic (MIC) tests in the rubber particles before and after the interaction with the bitumen (to study the changes occurred in the production of the AR).

The analytical research performed in this work is systematized in Table 2.

The rheological properties of the binders were measured in a rotational DSR with parallel plate sample geometries of 40 mm and 1 mm gap. The rheometer was set up to test in an oscillatory mode to guarantee a dynamic response from the specimen, ensuring that the specimen was tested in the linear region over the temperature (25 to 180°C) and frequency range chosen (0.1 to 10 Hz). Preliminary tests were carried out at different temperatures and frequencies, in order to select stress values at which the binders are in the linear range. The stress values selected to carry out the DSR tests varied between 1000 Pa at 25°C and 3 Pa at 180°C.

The DSR tests began at the lowest selected temperature and frequency and continued to the highest. During the test, the selected oscillatory shear stress was applied to the specimen and the torque (ι) and angular rotation (θ) values were measured, as well as the resulting shear strain.

The final results of the test involved the determination of the standard of the complex shear modulus (|G*|—ratio between peak stress and peak strain), the phase angle (δ - phase difference between stress and strain), the viscosity and the G*/sen(δ) (equivalent to |G*|/sen(δ))

Table 2. Analytical determinations carried out in this work.

	Analytical determinations			
Sample	PEN, RB and DV tests	ER tests	MIC tests	DSR tests
Rubber			CR	
A	BASE, AR, RES	AR	RR, FR	BASE, AR, RES
B	BASE, AR, RES	AR		BASE, AR, RES
C	BASE, AR, RES	AR		
D	BASE, AR, RES	AR		
E	BASE, AR, RES	AR	RR, FR	BASE, AR, RES
F	BASE, AR, RES	AR		
G	BASE, AR, RES	AR		
H	BASE, AR, RES	AR		
I	BASE, AR, RES	AR	RR, FR	BASE, AR, RES
J	BASE, AR, RES	AR		BASE, AR, RES
K	BASE, AR, RES	AR		
L	BASE, AR, RES	AR		
M	BASE, AR, RES	AR	RR, FR	BASE, AR, RES
N	BASE, AR, RES	AR		
O	BASE, AR, RES	AR		BASE, AR, RES
P	BASE, AR, RES	AR		BASE, AR, RES

values of the binders over a range of test frequencies and test temperatures. Other results of this test presented in this work were G′ (storage modulus), the real part of the complex shear modulus |G*| associated with the elastic part of the material behaviour, and G″ (loss modulus), the imaginary part of the complex shear modulus associated with the viscous part of the material behaviour.

4 RESULTS AND DISCUSSION

4.1 *Rubber characteristics and changes observed during the AR production*

Initially, the crumb rubber solubility was assessed according to ASTM D 6814-02 standard, in order to indirectly evaluate the depolymerisation potential of the studied rubber after interacting with bitumen. Two solvents were used in this test, toluene and cyclehexane, being the crumb rubber mass loss equal to 10.9% and 10.7% respectively (low depolymerisation potential).

The crumb rubber particles collected during the AR production, before (CR) and after (RR and FR) interacting with different types of bitumen, were cleaned with toluene and analysed by microscopic methods. The results of the microscopic analysis of the rubber that have interacted with the four commercial bitumens used in this work (A, E, I and M) are presented in Figure 3.

The differences between the initial crumb rubber particles and the recovered rubber are evident for all the AR binders produced with the four commercial bitumens. The recovered rubber particles vary in shape and size, whereas the initial crumb rubber particles are clearly more homogeneous. These changes in the crumb rubber morphology cannot result simply from its solubility in the solvent constituents of the bitumen, since the observed changes are visibly superior to 11% (depolymerisation and devulcanization changes may be occurring).

Comparing the recovered rubber particles from ARs produced with different bitumens, it was possible to observe that the interaction with softer bitumens (M) resulted in a greater variability in the shape and size of the rubber particles than the in harder bitumens (A),

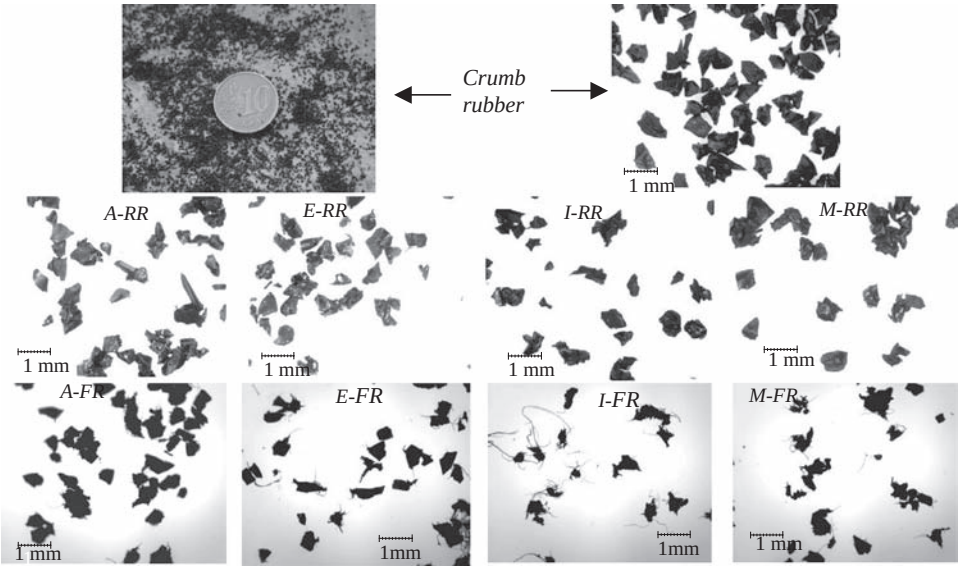

Figure 3. Microscopic photographs of crumb rubber before and after interacting with four base bitumens.

suggesting that the bitumen constitution has a significant influence in its interaction with the crumb rubber.

The clear evidence of the changes in the rubber particles properties during the AR production can be observed in the microscopic photos of the rubber particles filtered (FR) from the residual bitumen. In fact the size of the crumb rubber particles has inevitably changed during the AR production, since the residual bitumens present some residual rubber particles in its constitution although the initial rubber particles cannot pass through the wire basket.

In conclusion the crumb rubber particles interact with the bitumen in the AR production, and the changes in the shape and size of the rubber particles are more evident in softer bitumens.

4.2 *Functional characterization of the studied binders*

Traditionally, bitumen is the binding material used in flexible pavements. The evolution of technology brought new bituminous materials by using modified binders with more complex behaviour, namely asphalt rubber mixtures modified with crumb rubber.

The functional characteristics of the different samples of binder (base bitumen—BASE; final asphalt rubber binder—AR; residual bitumen removed from the AR—RES) collected throughout the AR production were assessed in this part of the work, in order to evaluate the changes in the binder properties caused by the addition of rubber to the bitumen. Thus, the functional characteristics (penetration, R&B and Viscosity) of the sixteen (A to P) different base or BASE bitumens used in this study are presented in Figure 4, as well as the properties of the corresponding AR and RES binders. The elastic recovery property is also presented for AR binders.

The results of the different tests were very consistent with the proportions of the commercial bitumen used to produce the sixteen base bitumens. Actually, the changes in the constitution of the samples (from harder to softer bitumens) originated an ordered sequence for the evaluated functional properties, represented by a trend line in Figure 4.

For every functional property evaluated, the AR binder results presented the greatest dispersion, mainly due to the heterogeneity of this material.

As expected, the AR binder presented much lower penetration values and higher R&B temperatures and dynamic viscosities than the corresponding base bitumen. However, it was noticed that the residual bitumens (RES) had penetration values similar to the AR binders,

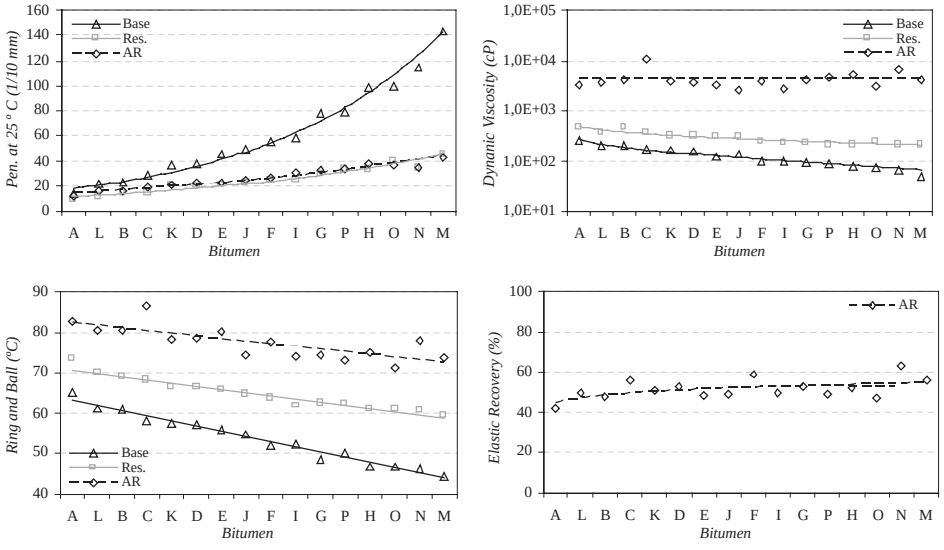

Figure 4. Functional characterization of the different binders (BASE, AR and RES).

although the R&B temperature and the dynamic viscosity of these two materials were very different. Thus, the decrease of the AR binder penetration is greatly influenced by the hardening of the base bitumen during the AR production, while the behaviour of the AR binder at higher temperatures (R&B and dynamic viscosity temperatures) is more influenced by the crumb rubber particles.

The R&B test is the most effective to find variations in the behaviour of the different materials, given that it distinguish very well the several base bitumens (A to P) and the different types of binder (BASE, AR, RES). The greatest variation of all the functional characteristics, between the sixteen bitumens, was observed for the base bitumens (BASE). In opposition, the functional characteristics of the AR binders produced with the different bitumens are very similar, mainly the dynamic viscosity and the elastic recovery which hardly vary.

The analysis of the residual bitumen (RES) characteristics demonstrated that significant changes in the base bitumen characteristics are induced by the rubber during the AR production, since the residual bitumen became harder and the remaining functional characteristic were clearly different from the ones of the base bitumen (BASE).

The comparison between the several types of bitumen used to produce AR showed that the highest variations in the functional characteristics of the binder (AR and RES binders compared with the BASE bitumen) are obtained by softer bitumens. This result is consistent with the microscopic evaluation of the most significant changes in the morphology of rubber particles when softer bitumens are used to produce AR binders. Thus, even if the 150/200 bitumen (M) was not generally used to produce asphalt rubber or hot asphalt mixtures, the experimental results showed that it presents the greatest interaction with the crumb rubber, thus being a very good alternative to produce AR binders with final properties similar to those of ARs made with 60/70 bitumens.

4.3 *Rheological characterization of the studied binders*

One of the most significant values normally used to describe the bitumen rheology is G*/sen(δ), specially in the Superpave method developed in the context of SHRP program. Figure 5 shows the isochronal plots of G*/sen(δ) of the BASE bitumen and of the resultant AR and RES binders at a frequency of 1.0 Hz and temperatures between 25 and 180°C for eight bitumens selected to carry out the rheological tests (A, B, E, I, J, M, O and P). A comparative plot of the three materials (BASE, AR and RES) is also presented for the commercial base bitumens (A, E, I and M).

The isochronal plot of the rheology of the BASE bitumens illustrates the variation of their stiffness and viscoelastic nature with the temperature and type of bitumen evaluated. The lines representing the rheological properties of the different BASE bitumens are in conformity with the previous functional characterisation, i.e. the harder bitumens with lower penetrations and higher R&B temperature and dynamic viscosity also present the highest values of G*/sen(δ) in the rheology tests for every tested temperature. The change in the gradient of the rheology lines demonstrates a variation in the nature of the bitumen. It is mostly a viscoelastic semisolid material below 100°C (when the quick reduction of stiffness results mainly from the loss of the elastic component), becoming a viscous liquid at higher temperatures (when the stiffness decrease is a consequence of the reduction of viscosity). At approximately 180°C the bitumen behaviour is almost independent of the bitumen type, trending for a constant and very low value of G*/sen(δ).

The isochronal plot of the rheology of the residual bitumen (RES) is very similar to one of the new bitumen. However, the RES bitumen is stiffer (higher values of G*/sen(δ), mainly below 100°C) and the lines representing the rheology of the different RES bitumens are closer to each other (small differences between the rheology of the several types of RES bitumen, since the interaction with the crumb rubber has hardened the softest bitumens). The inflexion of the rheology curves at 100°C is less pronounced than for new bitumens, because the transition between the semisolid and the liquid phases is not so sudden and some elasticity is maintained.

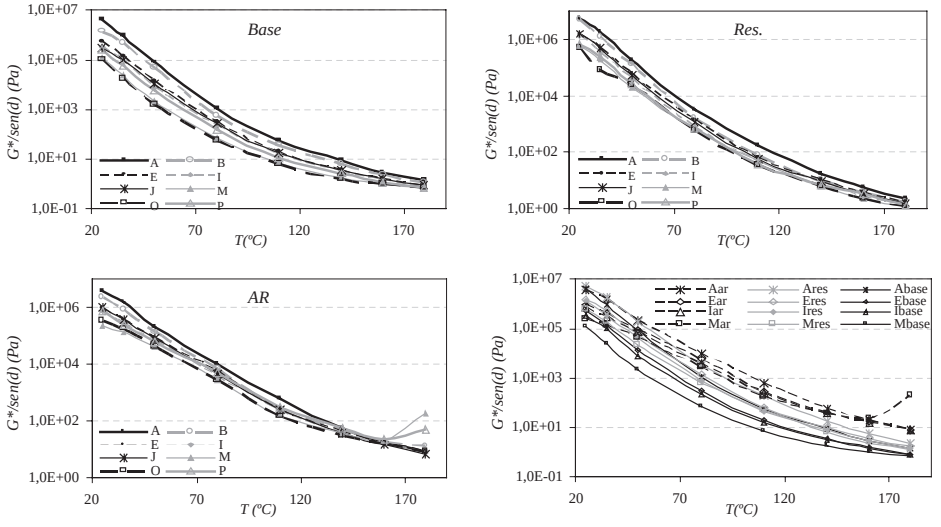

Figure 5. Isochronal plots of G*/sen(δ) rheological characteristic of the studied binders at 1.0 Hz.

The analysis of the rheology of the AR binder showed that it is the stiffest material, being the less susceptible to the change of the base bitumen type (plots are very similar) and to the variation of temperature. In fact, the high increase in the elasticity of the AR binder at all the studied temperatures, caused by the presence of rubber particles, totally changes the rheology of the binder, by reducing the influence of the temperature in the nature of the binder behaviour, mainly for temperatures above 100°C (the AR does not totally become a viscous liquid).

Asphalt binders must have a set of characteristics, in order to allow its adequate use in road pavement construction at different temperatures. Binders should not be very rigid at low and medium operating temperatures (to avoid cracking distresses), but they should be sufficiently stiff at high operating temperatures to improve their resistance to permanent deformation. The AR binders fulfil these demands for every base bitumen used, even for the softer bitumen 150/200 (M), since the G*/sen(δ) values at 25–35°C are similar to the BASE bitumens, being much higher at 60–80°C. However, the several AR binders present elevated viscosities at high temperatures, making the mixing and application of AR mixtures difficult.

In pavements, bituminous mixtures performance depends on the weather conditions, as well as on the load and speed of the heavy vehicles. The influence of these parameters in the behaviour of the asphalt binders were evaluated by carrying out rheology tests at different frequencies and temperatures, the results of which are presented in Figure 6 for the commercial bitumen I.

Figure 6 exemplifies, only for one of the tested bitumens (60/70 or I), the typical variation of the rheological behaviour (G*/sen(δ) value) of the different types of binder evaluated (BASE bitumen, AR binder and RES binder). The left side illustrates the isochronal plots (for frequencies between 0.1 and 10 Hz) of the binders from 25 to 180°C, while the right side illustrates the isothermal plots (for temperatures between 25 and 180°C) of the same binders from 0.1 to 10 Hz.

At 25–35°C the rheology of the different materials (BASE, AR and RES) is less influenced by the frequency than at higher temperatures (superior to 100°C).

The rheological behaviour of the BASE and RES bitumens is similar, especially at higher temperatures (near 180°C), although the RES bitumen has higher values of G*/sen(δ) for all frequencies at 25°C. The comparison of these two materials with the AR binder showed that, if the temperature increases, the rheology of the BASE and RES bitumens evolves differently from the AR binder (which is clearly stiffer).

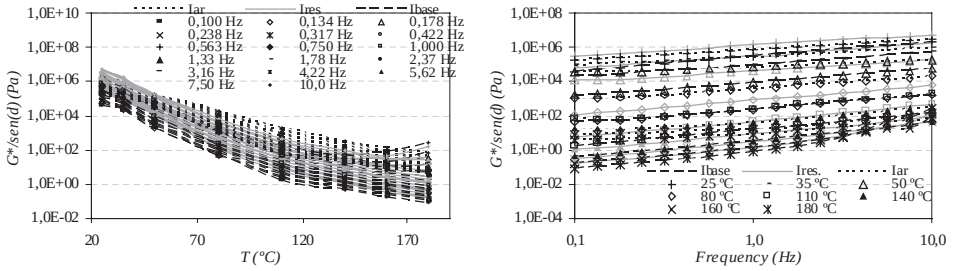

Figure 6. Variation of G*/sen(δ) with temperature and frequency for one binder (BASE, AR and RES).

By observing the isochronal and isothermal plots of the AR binder, it is noticeable that its rheological behaviour is analogous to that of the BASE and RES bitumens for temperatures inferior to 100°C at all frequencies. However, for temperatures above 100°C the behaviour of the AR binder almost becomes independent of the frequency, trending for a single value of G*/sen(δ) clearly superior to the ones of the BASE and RES bitumens (except for frequencies near 10 Hz).

Finally, by analysing the effect of the frequency in the rheology of the binders for the different isothermal curves, it is possible to observe that all curves have the same shape (being almost parallel), for all the materials, for temperatures below 100°C, presenting higher values of G*/sen(δ) as the temperature reduces and the frequency increases. The influence of the frequency is still the same for the AR binder at higher temperatures and frequencies, but for the BASE and RES bitumens the influence of the frequency in the rheology increases substantially for temperatures above 150°C and frequencies superior to 3.0 Hz.

4.4 *Comparison between the rheological and functional properties of binders*

During the pavement life cycle, the asphalt binders used in bituminous materials should always present the adequate characteristics, initially during the mixing and application phases at elevated temperatures (Fig. 7), then during the operating phase, in order to resist to the weather and traffic actions at low and medium temperatures (Figs 8, 9) and, finally, in the removal and recycling of the distressed mixtures (this last phase was not studied in this work).

The results of the two different approaches used to assess the binder behaviour (functional and rheological for a reference frequency of 1 Hz) will be compared next for the eight BASE, AR and RES binders (A, B, E, I, J, M, O and P) evaluated in this study.

At mixing and application temperatures, the functional parameter measured in this work was the dynamic viscosity at 180°C. Figure 7 compares the dynamic viscosity at 180°C with two rheological properties measured at 180°C, the complex viscosity (η^*) and the complex shear modulus (G*). The values of G* are approximately the same of G*/sen(δ) at this temperature (180°C), because the phase angle (δ) is nearly 90°. In fact, at this temperature the binders behave as a viscous liquid with an insignificant elastic component.

The relations between the functional and rheological properties at 180°C represented in the graphics of Figure 7 are nearly linear, with a similar positive slope for the BASE, AR and RES binders. The AR binder is clearly more viscous than the BASE and RES bitumens, being the viscosity of the AR binder less dependent on the base bitumen characteristics. The comparison between the dynamic viscosity (functional) and the complex viscosity (rheology) presented the best relation, being the slope nearly equal to 1 (since 1 Pa.s = 1000 cP).

At high operating temperatures causing rutting distresses, the functional parameter measured in this work was the R&B softening temperature. Figure 8 compares the R&B temperature with two rheological properties measured at 50 and 80°C, the η* and the shear modulus (G*).

The set of lines presented in Figure 8 show an exponential relation between the R&B functional properties of all the binders and the corresponding rheological parameters (η* and G*)

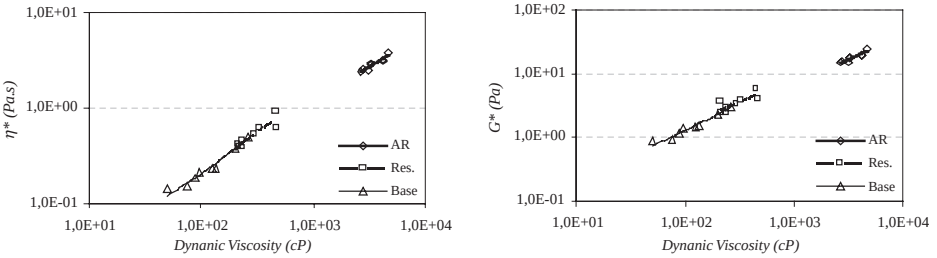

Figure 7. Rheological vs. functional properties at production and application temperatures.

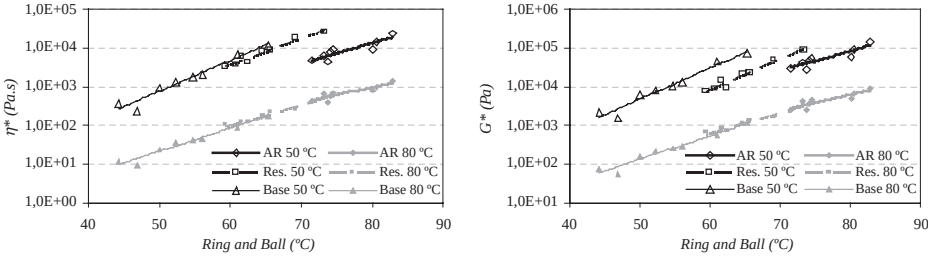

Figure 8. Rheological vs. functional properties at high operating temperatures cause rutting.

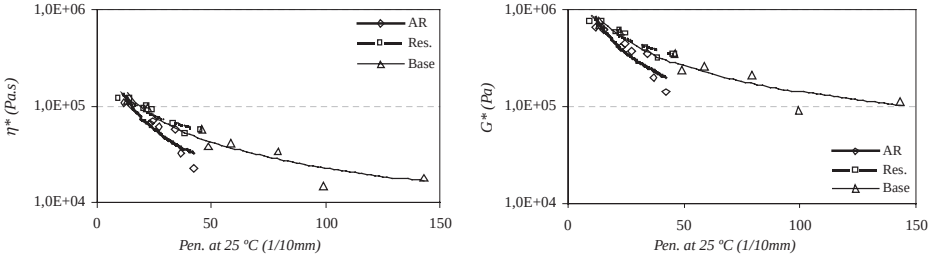

Figure 9. Rheological vs. functional properties at operating temperatures cause fatigue cracking.

measured at 50°C and 80°C. The range of values of the R&B results is visibly inferior to the rheological classification, and thus the rheology axis is presented in a logarithmic scale.

At 50°C the differences between the different binders (BASE, AR and RES) are clear, since the lines relating the functional and rheological properties of those binders are visibly disconnected. This occurs because the softening temperature of several binders is superior to 50°C, mainly the AR binders that only melt above 70°C. At 80°C the relation between the functional and rheological properties can be drawn by a continuous line adjusted to all binders. Thus, the R&B temperature has a very good correspondence to the rheological properties at 80°C. Figure 8 also confirms the previous observations that the softer AR binder is stiffer than all the BASE bitumens, especially if this comparison is made at 80°C.

At medium operating temperatures causing fatigue cracking distresses, the functional parameter measured in this work was penetration at 25°C. Thus, Figure 9 relates the penetration value of the several binders to two rheological properties measured at 25°C, namely the complex viscosity (η*) and the complex shear modulus (G*).

The potential trending lines shown in Figure 9 presented the best fit to the relation between the functional and rheological properties measured at 25°C. Apparently the relation between

both properties is not so good at this temperature, since the dispersion of the several points has increased (probably due to the type of rheometer used in this work). Furthermore, the relation between the functional and rheological properties of the different types of binder (BASE, AR and RES) cannot be adjusted by a single trending line, in opposition to the previous relations.

The range of values of the penetration results is visibly inferior to the rheological classification, especially for the RES and AR binders, and thus the rheology axis is presented in a logarithmic scale. Actually, the penetration values of the RES and AR binders show little variation, being always inferior to 50 dmm. It is worth to mention that, by analysing the rheology of the different binders for the same penetration value, the RES bitumen is the stiffest material, followed by the BASE bitumen, being the AR binder the softest material (this result is consistent with the best fatigue cracking resistance of this material).

5 CONCLUSIONS

The main conclusions that can be drawn from the results of this work are the following:

- during the AR binder production, the interaction of the crumb rubber particles with softer bitumens is clearly superior than with harder bitumens, and thus the morphology of the rubber particles is clearly more influenced by softer bitumens (apparently the rubber particles in contact with softer bitumens swell much more, splitting and releasing a great amount of very small elements recovered in the residual bitumen);
- the functional characterization of binders is more effective for bitumens than for AR modified binders, because the AR functional properties are poorly influenced by the type of base bitumen used (especially at higher temperatures); the AR binder results present greater dispersions, mainly because of the heterogeneity of this material;
- the 150/200 bitumen is rarely used to produce asphalt rubber, but it greatly interacts with crumb rubber, being a very good alternative to produce AR binders with very good characteristics (similar to those obtained with 60/70 bitumens) during the life cycle of the pavement;
- the rheology of AR binders at higher temperatures (160 to 180°C) is independent from the type of base bitumen used (trending for the same value of $G^*/\text{sen}(\delta)$), although being clearly stiffer than the BASE and RES bitumens at these temperatures (the high stiffness of the AR binder at those temperatures makes difficult its mixing and application; the increase of temperature beyond 160°C almost does not affect the AR rheological characteristics);
- the lowest values of $G^*/\text{sen}(\delta)$ for AR binders at application temperatures were obtained for lower frequencies (apparently the compaction of AR mixtures should be carried out at low speeds), in opposition to the softening effect of frequency for the BASE and RES bitumens;
- the relation between functional and rheological properties of binders depends on the test temperature, being this relation very good for all the studied binders (BASE, AR and RES) at higher temperatures (dynamic viscosity and R&B temperature), but not so good at medium operating temperatures (penetration).

ACKNOWLEDGEMENTS

The materials used in this work were kindly supplied by CEPSA and by RECIPAV to which the authors want to especially thank for their support and for the supply of bitumen and crumb rubber, respectively.

REFERENCES

Abdelrahman, M.A. & Carpenter, S.H. 1999. Mechanism of interaction of asphalt cement with crumb rubber modifier. *Transportation Research Record* 1661: 106–113.

Airey, G.D., Rahman, M.M. & Collop, A.C. 2003. Absorption of bitumen into crumb rubber using the basket drainage method. *International Journal of Pavement Engineering* 4 (2): 105–119.

Artamendi, I., Eastmond, G.C. & Khalid, H. 2002. Influence of crumb rubber modifier (CRM) from tyre waste on the rheological properties of bituminous binders. *Proc. 3rd Int. Conf. Bituminous Mixtures and Pavements, Vol. 1, Thessaloniki, 21–22 November*.

Bahia, H.U. & Davies, R. 1994. Effect of crumb rubber modifiers (CRM) on performance-related properties of asphalt binders. *Journal of the Association of Asphalt Paving Technologists* 63: 414–449.

Bahia, H. & Davies, R. 1995. Role of Crumb Rubber Content and Type in Changing Critical Properties of Asphalt Binders. *Journal of the Association of Asphalt Paving Technologists* 64: 130–162.

Billiter, T.C., Chun, J.S., Davison, R.R., Glover, C.J. & Bullin, J.A. 1997a. Investigation of the curing variables of asphalt-rubber binder. *Petroleum Science and Technology* 15 (4–5): 445–469.

Billiter, T.C., Chun, J.S., Davison, R.R., Glover, C.J. & Bullin, J.A. 1996. Investigation of the curing variables of asphalt-rubber binder. *American Chemical Society, Division of Fuel Chemistry 41(4)*.

Billiter, T.C., Davison, R.R., Glover, C.J. & Bullin, J.A. 1997b. Production of asphalt-rubber binders by high-cure conditions. *Transportation Research Record* 1586: 50–56.

Gopal, V.T., Sebaaly, P.E. & Epps, J. 2002. Effect of Crumb Rubber Particle Size and Content on the Low Temperature Rheological Properties of Binders. *Transportation Research Board Annual Meeting, Washington D.C., 13–17 January*.

Heitzman, M. 1992. *State of the Practice—Design and Construction of Asphalt Paving Materials with Crumb Rubber Additive. Report No. FHWA-SA-92-022*. Federal Highway Administration.

Navarro, F.J., Partal, P., Martínez-Boza, F. & Gallegos, C. 2005. Influence of crumb rubber concentration on the rheological behaviour of a crumb rubber modified bitumen. *Energy and Fuels* 19: 1984–1990.

Rahman, M.M. 2004. *Characterisation of Dry Process Crumb Rubber Modified Asphalt Mixtures. Thesis submitted to the University of Nottingham for the degree of Doctor of Philosophy*. Nottingham, University of Nottingham.

Read, J., Whiteoak, C.D., 2003. The Shell Bitumen Handbook. *Shell Bitumen UK, Thomas Telford Publishing, 5th edition, London.*

Singleton, T.M., Airey, G.D. & Collop, A.C. 2000. Effect of rubber-bitumen interaction on the mechanical durability of impact absorbing asphalt. *Proc. 2nd Eurasphalt & Eurobitume Congress, Vol. 1, Barcelona, 20–22 September*.

van de Ven, M. & Jenkins, K. 2003. Rheological characterization of some (polymer modified) bitumen and bitumen-filler system at compaction and in service temperatures. *6th RILEM Symposium on Performance Testing and Evaluation of Bituminous Materials (PTEBM 2003), Zurich, 14–16 April.*

Zanzotto, L. & Kennepohl, G.J. 1996. Development of rubber and asphalt binders by depolymerization and devulcanization of scrap tires in asphalt. *Transportation Research Record* 1530: 51–58.

Advanced Testing and Characterization of Bituminous Materials –
Loizos, Partl, Scarpas & Al-Qadi (eds)
© 2009 Taylor & Francis Group, London, ISBN 978-0-415-55854-9

A thermodynamic approach to healing in bitumen

N. Kringos & A. Scarpas
Delft University of Technology, Delft, The Netherlands

T. Pauli & R. Robertson
Western Research Institute, Wyoming, USA

ABSTRACT: The self-restoring or healing capacity of bitumen has been known for quite some time. Yet, to this date, there is no consensus of the fundamental mechanism underlying this phenomenon. In this paper a new finite element based model is presented which focuses on the healing phenomenon from a thermodynamic point of view. In the model, healing of bituminous material is simulated via a phase field model, utilizing a modified version of the Cahn Hilliard and Flory-Huggins equations. The paper presents the developed hypothesis and summarizes the theory behind it. The model has been implemented in the 3D finite element system CAPA-3D and preliminary results are shown.

1 INTRODUCTION

1.1 *Recognized healing capacity of bitumen*

Over the last two decades various laboratory experiments have shown clear evidence of the beneficial effects of rest periods in restoring the stiffness and strength characteristics of asphaltic samples subjected to fatigue loading (Jones and Kennedy 1991, Little and Bhasin 2007). There is consensus among researchers that cracking failure prediction models grossly underestimate asphalt concrete pavements field life and it is accepted that the reason for this discrepancy is largely the exclusion of healing effects from design calculations.

Over the years, researchers have tried to understand the healing in bituminous materials from a purely mechanical point of view. Unfortunately, this approach has not resulted into a consistent picture for the healing behavior nor has it had a significant impact on production and design. So far, the fundamental mechanisms of the chemical and physical interactions within asphaltic concrete responsible for healing at crack faces are merely speculations rather than based on thorough scientific analysis. Moreover, the majority of speculated healing mechanisms all exploit the comparison with high molecular weight polymer systems, whereas asphalt has a more complex composition, and consists of thousands of very different organic molecules, allowing for a very rich variety of interactions.

Considering the importance and uniqueness of the healing phenomenon in bitumen, an international research consortium was set-up to investigate the fundamental mechanisms and develop a model which enables the accurate prediction. In this paper an overview of the developed model within the framework of this research project and its theoretical and experimental background is given.

1.2 *Postulated healing mechanism*

From extensive Atomic Force Microscopy (AFM) studies performed at the Western Research Institute (Pauli et al. 2001), it has become clear that bitumen has the tendency to phase separate under certain kinetic conditions. From these AFM scans it can be seen that this separation leads to a predominant clustering of two types of phases, α and β, Figure 1.

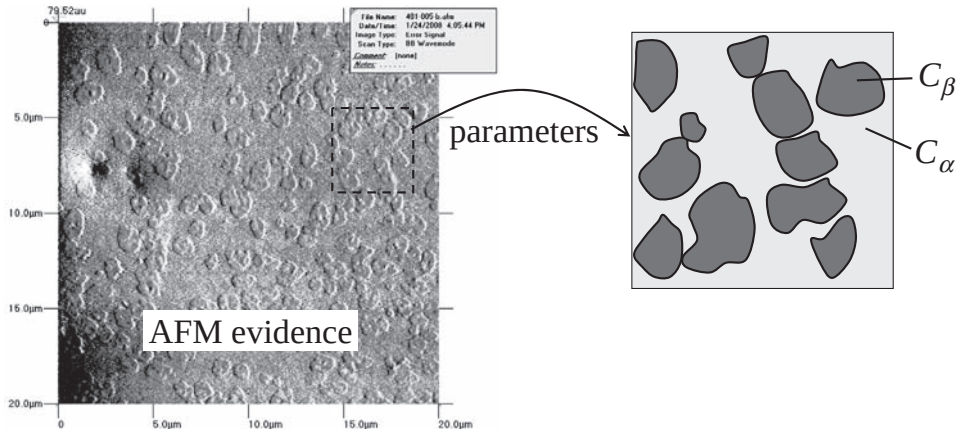

Figure 1. AFM evidence of phase-separation in bitumen (Pauli et al. 2001).

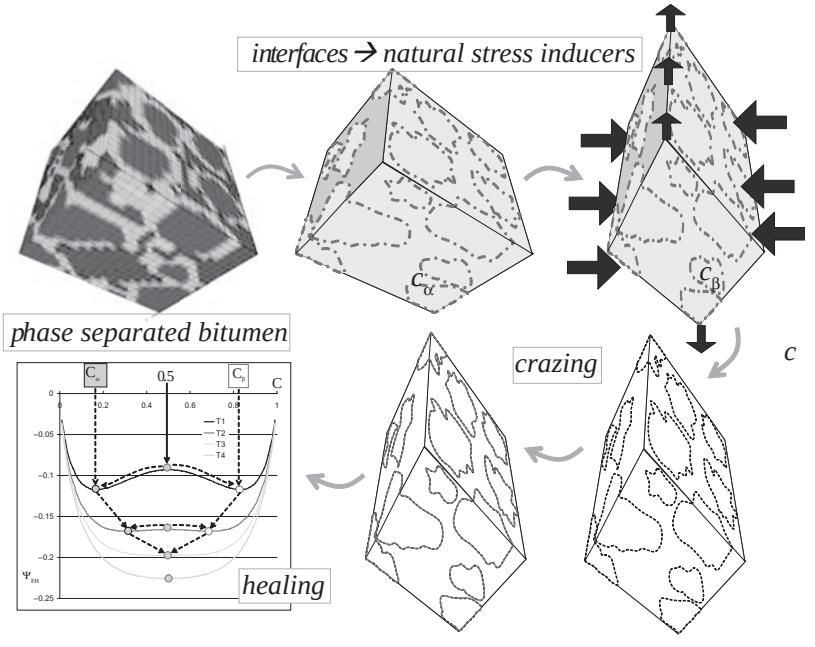

Figure 2. Delft healing model development.

From mechanical considerations it is known that the interfaces between two materials with different stiffness properties serve as natural stress inducers. This means that when the material is exposed to mechanical and or environmental loading, these interfaces will attract high stresses and are prone to cracking. On this scale, this would result into a crazing pattern which can be detected on a macro-scale by a degradation of the mechanical properties of the material. If this process would continue, these micro-cracks (crazes) would continue developing, start merging and finally form macro-cracks.

At the stage of micro-crack development, however, the degraded material properties could be reversed by diminishing and/or totally removing the crazes from the materials. This, in fact, is what could happen by changing the kinetics of the material (e.g. by increasing the temperature). The phases would re-arrange themselves in either a new configuration or mix themselves into a more homogeneous state, giving the appearance of the existence of

a single phase. The material would thus have lost its memory of the micro-cracks, and this will result into a recovery or healing of the mechanical properties. This re-arrangement of the phases is modeled with a so-called phase field theory and serves as a basis of the finite element based healing model for bitumen, Figure 2. The driving force for the rearrangement of the phases upon a changed thermodynamic state is explained in the following.

2 KINETICS OF PHASE SEPARATION

The choice of the appropriate scale to describe a material depends on the type of information required about the system under consideration. Macroscopic quantities, which reflect the physico-chemical properties of the studied material are closely connected with the characteristics of single particles (i.e. atoms, molecules or phases). So, for instance, the temperature is connected with the mean energy of the thermal motion of the particles, the mass density straightforwardly depends on the mean number of particles in unit volume, etc. Thus, the description of the system at the macroscopic level reflects its microscopic characteristics.

To study the properties of phase separating material, a certain number of its macroscopic characteristics, i.e. state variables, must be identified. The set of independent macroscopic parameters then represents the state of the system under consideration. The thermodynamic state of the system is given by the complex of all the external conditions acting on the system and also by the set of the independent properties of the system. If all macroscopic parts of the given system exist in the same state when the system as a whole is in the equilibrium state, the system is called homogeneous.

In the classical thermodynamic description of a system in chemical equilibrium the given phase areas in the phase diagrams represent zones of minima of the Gibbs energy, whereas the phase coexistence is given by the Gibbs phase rule. To construct such a phase diagram requires the mapping of all available phases and locating their phase boundaries which, unfortunately, is not possible by mere direct measurements of temperature or concentration dependences of the change of the Gibbs potential.

Equilibrium phase diagrams, however, cannot say anything about the reaction which transforms one phase to another, nor about the composition or the structure of phases occurring under conditions different from those that make equilibrium possible.

Under conditions of phase equilibrium, when the chemical potential of the phase α, ${}_{\alpha}\mu$ is equal to that of phase β, ${}_{\beta}\mu$, stable coexistence of both phases occurs. For a real material, however, the system temperature deviates from the equilibrium one for which the equality of chemical potentials is violated, producing thus a driving force of the phase separation. The measure of this force is the chemical potential difference

$$\Delta\mu = {}_{\alpha}\mu - {}_{\beta}\mu \tag{1}$$

In other words, for $\Delta\mu < 0$ the phase β fraction, ${}_{\beta}C$, will diminish and the fraction of phase α, ${}_{\alpha}c$, will increase. For $\Delta\mu < 0$ the reverse will happen. The phase fractions can therefore only be changed under non-equilibrium conditions of a definite driving force.

There are cases where the slowness of phase transformation can considerably affect the equilibrium. For instance, in an under-cooled liquid the meta-stable phases can be frozen and if the viscosity rapidly increases with decreasing temperature the vitreous state can freeze-in, resulting in an unstable solid state called glass transition. The time dependence of phase transition is therefore important for a better understanding of the relevant transformation kinetics locating at the same time the actual phase boundary between the two phases investigated.

The main processes that take place during phase separation and which influence the results of the whole process are the conditions (e.g. pressure or temperature) under which the new phase arises in the system and the structure of its composition; the nucleation of the new phase, first they arise and then they grow (i.e. the kinetics of the phase transformation) and the transport of energy and mass in the system.

The total Gibbs energy of a biphasic system is

$$G = N\left[{}_1c\,{}_1\mu + \left(1-{}_1c\right){}_2\mu + k_B T\left\{ {}_1c\ln {}_1c + \left(1-{}_1c\right)\ln\left(1-{}_1c\right) + H\left({}_1c, {}_2c, T\right)\right\}\right]$$
$$\text{with } {}_1c + {}_2c = 1.0 \tag{2}$$

where ${}_{\alpha}c$ is the concentration of component α in the system, N is the total number of molecules, ${}_{\alpha}\mu$ are the chemical potentials per atom of the component α, $k_B = R/N$ is the Boltzman constant, relating energy at the molecule level with temperature T observed at the bulk level, and H is the Gibbs mixing energy per molecule.

From Eq. (2), the Gibbs energy, otherwise known as the configurational free energy Ψ_0, can also be can written as

$$\Psi_0 = {}_1c\,{}_1g + \left(1-{}_1c\right){}_2g + RT\left\{ {}_1c\ln {}_1c + \left(1-{}_1c\right)\ln\left(1-{}_1c\right) + H\right\} \tag{3}$$

In equilibrium conditions it must hold that

$$\frac{\partial \Psi_0}{\partial \underset{\sim}{c}} = 0;\ \frac{\partial \Psi_0}{\partial N} = 0 \tag{4}$$

An example of two equilibrium phase transformations is shown in Figure 3.

It is possible that for kinetic reasons (e.g. very fast cooling, slow nucleation or growth etc.) the first phase transformation is not realized and the phase transitions that correspond to the lower temperature assert themselves. This would result in a change of the phase diagram and a new equilibrium or meta-stable state will form, Figure 4.

On the basis of the construction of the common tangent, the concentrations of the equilibrium or meta-stable phases which fulfill Eq. (4) can be found. Cahn and Hilliard [1958] formulated the continual theory of phase transition based on the change of the free energy during the phase transformation in the form:

$$\Delta F = \int_V \left[\Delta f' + k_{CH}\left(\nabla C\right)^2 \right] dV \tag{5}$$

where V is the volume of the new phase and

$$\Delta f' = f'(C) - f'(C_0) - \left(C - C_0\right)\left.\frac{\partial f'}{\partial C}\right|_{c=\bar{c}} \tag{6}$$

where $f'(C)$ is the free energy per unit volume of the homogeneous system with the concentration C, $\bar{C}$ is the mean value of the concentration in the system and k_{CH} is a constant.

The dynamics of the 1st order phase transformation under non-equilibrium conditions at a given constant temperature can proceed essentially via two mechanisms: in the nucleation and the following growth of overcritical nuclei or in the spinodal decomposition. The spinodal decomposition appears in systems that are rapidly cooled to unstable states delimited by a curve—the spinodal. The nucleation occurs in the meta-stable region between the bimodal (corresponding to the equilibrium coexistence of phases) and the spinodal, Figure 5.

The spinodal corresponds to the inflection point on the curve $\Psi_0({}_{\alpha}c)$ at the temperature T. On the spinodal the following equation holds:

$$\frac{\partial \Psi_0}{\partial \underset{\sim}{c}^2} = 0 \tag{7}$$

For thermodynamic reasons a composition barrier exists in the meta-stable region, meaning that the system is unstable only regarding large changes of composition and it is stable regarding small fluctuations for which the free energy of the system increases. This barrier

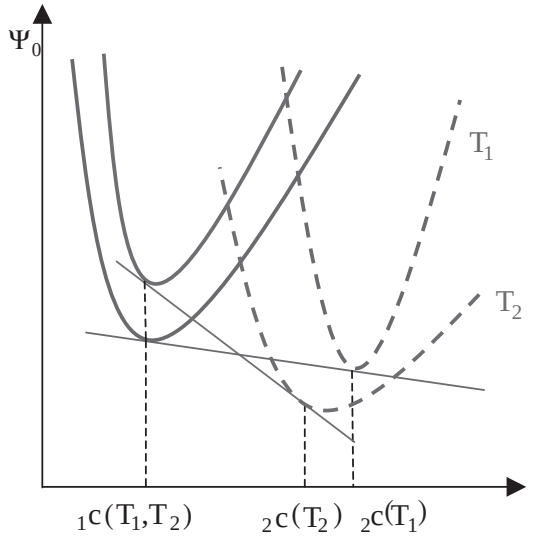

Figure 3. Equilibrium coexistence of two phases at temperature T_1 and T_2, $T_1 > T_2$.

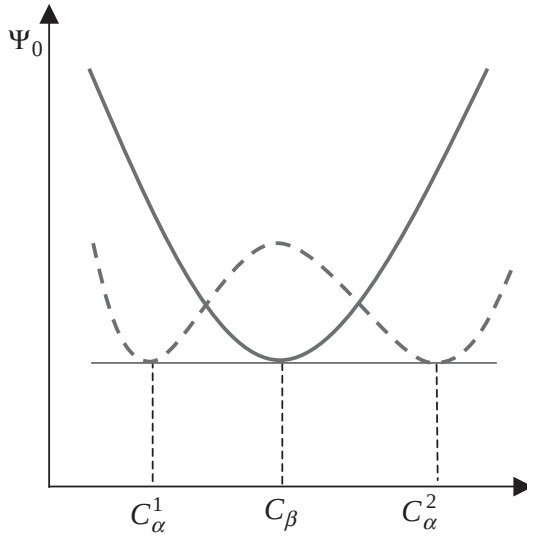

Figure 4. A possible dependence of Ψ_0 on the concentration C at equilibrium temperature T_E.

results in a relatively long-term stability of meta-stable states. Thus, in the meta-stable region the phase change proceeds by the nucleation mechanism, when only the overcritical nuclei grow with the critical composition.

Another situation is under the spinodal in the unstable region. In this region the composition barrier does not exist and the system is unstable even regarding small fluctuations of composition, which results in a decrease of the total energy of the system. The morphology is thus different in meta-stable and unstable regions.

Above the spinodal large changes of composition with a sharp phase interface are necessary for the phase transformation. Under the spinodal, however, every small change of the composition steadily increases to attain the difference of composition between the two

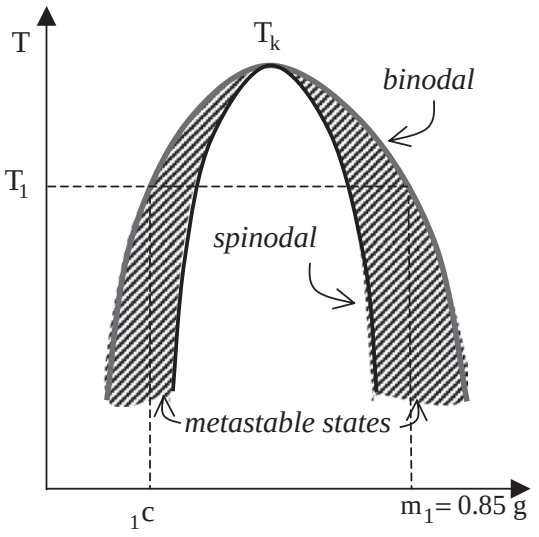

Figure 5. Coexistence of two phases at T_1.

phases given by the equilibrium phase diagram. At the beginning the differences between the phases are not sharp and a periodic shape of composition appears.

These mechanisms of phase transformation describe the evolution of the system at constant temperature and they do not answer the question, when and what metastable state is formed during rapid changes in temperature.

It is important to make sure that the observed material behavior is not merely an artifact of the test method. For instance, liquid flow originating from the gradient of surface tension along the free surface due to temperature or concentration inhomogeneity (i.e. Marangoni flow) and/or to different curvature. This effect is weak under normal conditions and becomes more important in microgravity experiments with a free surface formed in space or in melt spinning techniques when thin films are formed. For this reason, in addition to AFM tests, an extensive experiment on the Spin Echo Small Angle Neutron Scattering spectrometer at the Reactor Institute Delft has been set up. This unique facility allows for the 'in bulk' determination of the particle (size)—particle (size) correlation function. More details on this work are described in an accompanying paper.

To enable the three-dimensional simulation of phase separation in bitumen, in the following the governing equations are derived.

3 GOVERNING EQUATIONS

To develop the governing equations for the phase-separation model, the general mass conservation for phase α can be found as

$$\rho \frac{\partial_\alpha c}{\partial t} = -\nabla \cdot \left({}_\alpha \rho \left({}_\alpha \underset{\sim}{v} - \underset{\sim}{v} \right) \right) = -\nabla \cdot {}_\alpha \underset{\sim}{j} \tag{8}$$

In this, the term ${}_\alpha \underset{\sim}{v} - \underset{\sim}{v}$ is the diffusion velocity and the term ${}_\alpha \rho \left({}_\alpha \underset{\sim}{v} - \underset{\sim}{v} \right)$ is the momentum of phase, which can be represented by the mass diffusion flux ${}_\alpha \underset{\sim}{j}$.

This mass diffusion flux can also be expressed in terms of the gradient of the functional derivative of the free energy function Ψ

$$
\begin{aligned}
{}_{\alpha}\underset{\sim}{j} &= -\rho_{\alpha}\underset{\approx}{M}\cdot\nabla\left(\frac{\delta\Psi}{\delta_{\alpha}c}\right) \\
&= -\rho_{\alpha}\underset{\approx}{M}\cdot\nabla\left({}_{\alpha}\mu\right)
\end{aligned}
\tag{9}
$$

in which ${}_{\alpha}\mu$ is the chemical potential of phase α and ${}_{\alpha}\underset{\approx}{M}$ is the diffusional mobility tensor of phase α in the material.

Replacing Eq. (9) into Eq. (8) gives the governing transport equation

$$
\rho\frac{\partial_{\alpha}c}{\partial t} - div\left(\rho_{\alpha}\underset{\approx}{M}\cdot\nabla_{\alpha}\mu\right) = 0 \tag{10}
$$

This formulation is also known as the Cahn Hilliard equation. In Cahn–Hilliard-based models, sharp interfaces are replaced by narrow transition layers (diffuse interfaces) that result from a competition between the different terms in the energy density.

The chemical potential μ_{α} can be written as the functional derivative of the free energy Ψ

$$
{}_{\alpha}\mu = \frac{\delta\Psi}{\delta_{\alpha}c} \tag{11}
$$

The free energy is composed of three terms

$$
\Psi = \Psi_0 + \Psi_{\gamma} + \Psi_{\varepsilon} \tag{12}
$$

where Ψ_0 is the configurational free energy, Ψ_{γ} is the surface free energy and Ψ_{ε} is the strain energy.

Substituting Eq. (12) into Eq. (11) gives

$$
{}_{\alpha}\mu = \frac{\delta\Psi}{\delta_{\alpha}c} = \frac{\delta\Psi_0}{\delta_{\alpha}c} + \frac{\delta\Psi_{\gamma}}{\delta_{\alpha}c} + \frac{\delta\Psi_{\varepsilon}}{\delta_{\alpha}c} \tag{13}
$$

Using Eq. (3), the configurational free energy Ψ_0 can be expressed as

$$
\psi_0\left({}_{\alpha}c,{}_{\beta}c,T\right) = \sum_{\alpha=1}^{n}\left({}_{\alpha}c\,{}_{\alpha}g + RT_{\alpha}c\ln({}_{\alpha}c)\right) + RT\sum_{\alpha=1}^{n}\sum_{\beta>\alpha}^{n}{}_{\alpha}c\,{}_{\beta}cX^{\alpha\beta} \tag{14}
$$

with the mixing energy expressed as

$$
H\left(\underset{\sim}{c}\right) = \sum_{\alpha=1}^{n}\sum_{\beta>\alpha}^{n}{}_{\alpha}c\,{}_{\beta}c\,X^{\alpha\beta} \tag{15}
$$

in which $X^{\alpha\beta}$ is the Flory Huggins interaction parameter between the phases and can be found from the solubility parameters of the phases α and β as:

$$
X^{\alpha\beta} = \frac{{}_{\alpha}V}{RT}\left({}_{\beta}\delta - {}_{\alpha}\delta\right)^2 \tag{16}
$$

in which ${}_{\alpha}V$ is the molar volume of fraction ${}_{\alpha}C$ and ${}_{\alpha}\delta$ and ${}_{\beta}\delta$ are the solubility parameters of the two fractions. The term ${}_{\alpha}\delta^2$ is also known as the cohesive energy of fraction α.

For a biphasic material, Eq. (14) can be written as

$$
\begin{aligned}
\psi_0\left({}_1c,T\right) = {} & \left({}_1c\,{}_1g + \left(1-{}_1c\right){}_2g\right) \\
& + \left(RT_1c\ln\left({}_1c\right) + RT\left(1-{}_1c\right)\ln\left(1-{}_1c\right) + RT\,{}_1c\left(1-{}_1c\right)X^{12}\right)
\end{aligned}
\tag{17}
$$

In which the second part of the free energy is often referred to as the chemical free energy or as the Flory Huggins free energy:

$$\psi_{FH}({}_1c,T) = RT_1c\ln({}_1c) + RT(1-{}_1c)\ln(1-{}_1c) + RT\,{}_1c(1-{}_1c)X^{12} \tag{18}$$

The Flory Huggins interaction parameter X^{12} is controlling the shape of the chemical free energy. For $X^{12} \leq 2$ it has a single well and results in a single phase. In the case of $X^{12} > 2$ it is non-convex and has two wells, driving thus the phase separation into two binodal points, Figure 6.

The surface free energy Ψ_γ was formulated by Cahn and Hilliard as

$$\Psi_\gamma = \kappa_1\nabla^2{}_\alpha c + \kappa_2\nabla{}_\alpha c\cdot\nabla{}_\alpha c \tag{19}$$

in which κ_1 and κ_2 are constants associated with gradients of compositions.

The Ψ_ε is the Helmholz free energy associated with the deformation of the material and is elaborately described in many publications (e.g. Holzaphel 2001, Scarpas 2005, Kringos et al. 2007).

4 SIMULATION OF HEALING IN BITUMEN

The equations described in the previous section have been implemented for a bi-phasic mixture within the framework of the CAPA-3D software platform (Scarpas 2001). Choosing the solubility parameters and temperature such that a natural phase separation in the bitumen will occur, the model is capable of simulating the formation of distinct clusters within the initially homogeneous bitumen, Figure 7.

The resulting inhomogeneous pattern can be easily brought back to its original, more homogeneous, structure by changing the temperature back to a convex situation, such as illustrated in Figure 6.

In the model, there are several parameters which need to be calibrated such as, for instance, the parameter λ which is introduced into the model to avoid the use of higher order elements. This parameter is controlling the thickness of the interfaces between the phases and is therefore an important parameter in the resulting crazing and healing cycle, Figure 8.

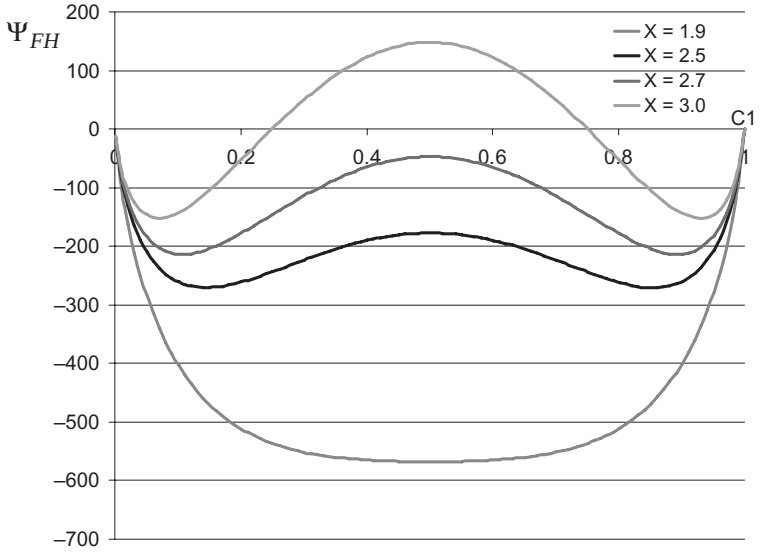

Figure 6. Convex and non-convex shape of Ψ_{FH} depending on X^{12}.

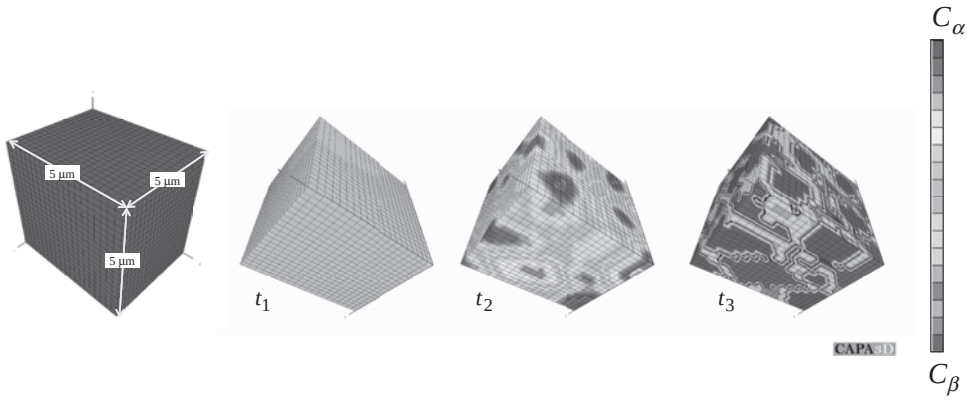

Figure 7. CAPA-3D simulation of phase separation.

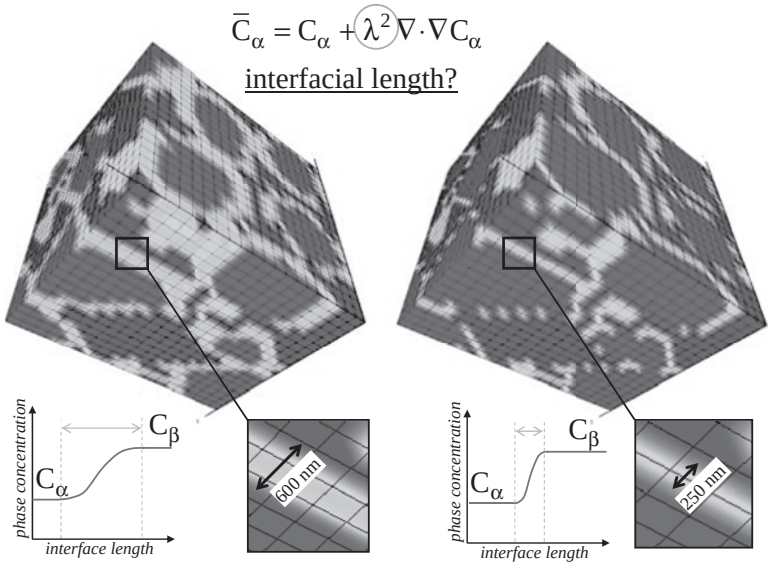

Figure 8. The thickness of the interface is controlled by the model parameter λ.

Considering the nanometer scale of the interfaces, this is in fact a parameter which can only be found from an interactive procedure between the computational model and the available experimental characterization techniques. This is one of the parameters which will be investigated in the coming years.

5 CONCLUSIONS

In this paper the development of a new model for simulating the mechanism of healing in bituminous materials has been discussed. The paper has given an overview of the theory behind the developed model and has shown some of the governing equations. The necessary experimental parameters for the calibration of the model are currently being determined.

The main objective of the final model will be to enable a more accurate prediction of the healing capacity of bitumen, based on the physico-chemical parameters which can be

determined in the lab. This will assist bitumen manufacturers as well as pavement engineers to make a better choice for their bitumen blends to ensure better long-term performance of the asphaltic mixes.

ACKNOWLEDGEMENTS

The research described in this paper has been performed in the context of the 'Delft Healing Consortium'. In this context, the authors gratefully acknowledge the support of Shell Global Solutions, Nynas AB, the Dutch Ministry of Public Works, Ooms Nederland Holding bv, the Delft Centre for Materials Research, the Western Research Institute and the US Federal Highway Administration.

REFERENCES

Cahn J.W. & Hilliard J.E. 1958. "*Free energy of a nonuniform system. I. Interfacial energy,*" J. Chem. Phys 28, 258.

Jones, D.R. & Kennedy, T.W. 1991. '*Asphalt Chemistry and its Effects on Roadway Surface Conditions*'.

Holzaphel G. 2001. *Nonlinear Solid Mechanics: A Continuum Approach for Engineering*, John Wiley & Sons.

Kringos N., Scarpas A. & Kasbergen C. 2007. *Three Dimensional Elasto-Visco-Plastic Finite Element model for Combined Physical-Mechanical Moisture Induced Damage in Asphaltic Materials*, Journal of the Association of Asphalt Paving Technologists, Vol. 76.

Little, D.N. & Bashin, A. 2007. '*Exploring Mechanisms of Healing in Asphalt Mixtures and Quantifying Its Impact*', in Self Healing Mateterials: an alternative approach to 20 centuries of materials science, Springer Series in Materials Science 100.

Pauli A.T., Branthaver J.F. Robertson R.E., Grimes & W., Eggleston C.M. 2001. "Atomic Force Microscopy Investigation of SHRP Asphalts", *American Chemical Society, Division of Petroleum Chemistry*, 46(2), 104–110.

Scarpas A. 2001. *CAPA-3D Finite Element System User Manual*, Delft University of Technology Publication.

Scarpas A. 2005. *A Mechanics based Computational Platform for Pavement Engineering*, Delft press.

Advanced Testing and Characterization of Bituminous Materials –
Loizos, Partl, Scarpas & Al-Qadi (eds)
© 2009 Taylor & Francis Group, London, ISBN 978-0-415-55854-9

Nanoclay for binder modification of asphalt mixtures

M.F.C. van de Ven & A.A.A. Molenaar
Delft University of Technology, Delft, The Netherlands

Jeroen Besamusca
Bitumen Department, Kuwait Petroleum Research & Technology

ABSTRACT: Based on the positive experience with polymers nanoclay modification of bitumen was introduced. Nanoclay modification can influence properties like stiffness, fatigue resistance, strength, resistance to ageing and thermal stability.

In this paper the potential of modifying bitumen with nanoclay is investigated. In all research a reference was compared to the modified material. Test results are reported for binders and asphalt mixtures containing standard and nanoclay modified bitumen. Influence of the nanoclay on ageing and rheology of the binder and influence on the performance of asphalt mixtures is discussed. The influence of nanoclay modifiers on fresh (unaged) and aged bitumen was measured with dynamic shear rheometer (DSR) and empirical tests like penetration and softening point. The effect of a nanoclay modified binder on an asphalt mixture was researched with the indirect tensile strength-, fatigue-, resilient modulus test at lower temperatures and dynamic creep test at high temperatures.

The Cloisite nanoclay modifications increased the stiffness, the indirect tensile strength and the rutting resistance of a mix with standard 40/60 Pen bitumen. The Nanofill modification improved the ageing resistance of a 70/100 Pen bitumen in the short term ageing test strongly and good in the long term ageing test.

The first conclusion is that nanoclay modifications can improve characteristics of asphalt binders and asphalt mixtures like ageing resistance and mechanical properties. Improvements are not yet such to justify application at large scale. Further studies on the chemistry of the nanoclay and bitumen are recommended to utilize the full potential of the nanoclay modifications.

1 INTRODUCTION

1.1 *General*

A number of physical properties of polymers can be successfully improved when a polymer is modified with small amounts of nanoclay under the condition that the clay is dispersed at nanoscopic level (Pinnavaia et al. 2000, www.iprime.umn.edu, Krishnamoorti et al. 2001, Ke et al. 2005, Al-Malaika et al. 2001). Based on the same principle, nanoclay modification of bitumen was introduced in the Netherlands by research institute TNO (Bos et al. 2004). Two types of nanoclay modifications were suggested: Nanofill and Cloisite. The expectation with the nanoclay modification is that it can influence properties like stiffness, fatigue resistance, strength, resistance to ageing and thermal stability. The purpose of this research was to test the potential of nanoclay modification of bitumen in relation to two important actual problems. In the Netherlands raveling of Porous Asphalt (PA) is a major durability problem that is strongly associated to the aging of the binder. If nanoclay could strongly reduce ageing during service life, this would be a very important contribution to tackle the raveling problem. The second special application includes the design of asphalt mixtures for heavily loaded airport pavement. In this paper the contribution to reduction of aging and mechanical properties are taken as leading subjects to research the potential of nanoclay modified

bitumen. The influence of nanoclay modifiers on binder characteristics was determined with rheological studies of fresh and aged bitumen with dynamic shear rheometer (DSR) and empirical tests like penetration and softening points. The effect of a nanoclay modified binder on the mechanical properties of an asphalt mixture designed for heavy loading situations (airport) was determined with the indirect tensile strength test, fatigue test, resilient modulus test and dynamic creep test. A short introduction will be given in nanoclay modification. The testing program will be discussed in general terms as it is impossible to describe all details (Ghile 2006). Some important test results will be given and discussed. The paper closes with conclusions.

1.2 *Nanoclay*

Hardly any published information concerning nanoclay modified bitumen is available. However, a large number of studies were done and are still underway on nanoclay modified polymers (Pinnavaia et al. 2000, www.iprime.umn.edu, Krishnamoorti et al. 2001, Ke et al. 2005, Al-Malaika et al. 2001). This study focuses on nanoclay modified bitumen, but understanding of nanoclay modified polymers is of significance since both modifications can be based on similar principles. The term nanocomposite is in the broadest sense referring to every type of material with fillers in the nanometer size range at least in one dimension. A number of physical properties are successfully enhanced when a polymer is modified with a relatively small amount of nanoclay on the condition that the clay is dispersed at nanoscopic level. Material variables which can be controlled and which can have a profound influence on the nature and properties of the final nanocomposite include the type of clay, the choice of clay pre-treatment, the selection of polymer component and the way in which the nanocomposite is incorporated into the polymer. Separation of the clay discs from each other will result in a nanoclay with an enormous large active surface area (it can be as high as 700 to 800 m^2 per gram). This makes an intensive interaction between the nanoclay and its environment possible (bitumen in our case). The process to realize the separation (surface treatment) is dependent on the type of material to be mixed, which can be explained as follows. Clay discs are negatively charged, but stay together in a clay particle because of the positive ions between the clay discs. In this way the clay particle as a whole is neutral. In addition, unmodified montmorillonite clays are generally highly hydrophilic species and therefore naturally incompatible with a wide range of polymer types. A necessary prerequisite for successful formation of polymer-clay nanocomposites is therefore alteration of the clay polarity to make the clay 'organophilic'. Dutch national research institute TNO has developed some nanoclay modifications that can be well mixed with polymers or bitumen (6). Bentonite and montmorillonite are the clays selected for this purpose. The developed nanoclay which is called organoclay can be processed to fit the binder. If the modifier is fully compatible with the binder, it is possible to get a homogeneous distribution of the clay at nano scale within the binder by intensive mixing.

However, there is a difference in the structure of bitumen and most polymers. Bitumen has a very complex molecular composition. The structure of polymers is mostly well defined and it can be altered and tailored to meet the demands much more easily. The complex and highly variable nature of bitumen could probably be a drawback to the success of the interaction between bitumen and the clay. It could demand a special approach to get interaction between clay and bitumen. TNO has selected two different nanoclays specially for bitumen. The treatment of the clay modifications was done by TNO (Bos et al. 2004). Based on the TNO research a Nanofill and a Cloisite were selected for use in bitumen. No detailed information on the nanoclays was made available from the supplier.

2 EXPERIMENTAL PROGRAM

2.1 *Overview testing program*

The testing program was designed first to give an indication if modification with nanoclay considerably reduce the aging of the binder: this question is of special importance for

mixes with high void content (>15%) like porous asphalt. Secondly it was questioned if modification with nanoclay can improve mechanical properties like stiffness, strength and fatigue and permanent deformation: this question is of special importance for heavy loaded airport pavements.

As it is clear that these two different requirements could ask for different nanoclays, some pre-investigation was done on the two nanoclays selected for the research. The outcome of the binder testing of these two modifications resulted in a decision to select one modification for improved aging resistance (nanofill) and one for improved mechanical properties (cloisite). The testing program is summarized in table 1.

The rheological properties of the modified binder were determined and compared to the standard binder. The binders considered for the test were a Penetration 40/60 bitumen for dense asphalt concrete and Penetration 70/100 bitumen for porous asphalt (10). The quantities of modifications used were 3% and 6% cloisite and 6% nanofill by weight of bitumen. The 6% cloisite modified DAC was compared with the standard DAC.

2.2 *Binder testing programme*

The rheological tests were divided in empirical tests (penetration, softening point as used in Europe (EN-NEN 12591 2004) and fundamental tests with the DSR. For the ageing of the binder special attention was given to the possible influence on ageing of mixing in the nanoclay after 1 hour of high shear mixing. In principle the Rotating Cylindrical Ageing Tester RCAT (EN-NEN 15323 2005) was used for short term and long term aging. However, in the RCAT the binder is continuously moved during the ageing process. This is a reasonable assumption during production, but does not simulate the service life period very well. Because of the possible negative influence of the movements in the RCAT test on the effectiveness of the nanoclay against oxidation, it was decided to compare also with the pressure ageing vessel PAV (EN-NEN 14769 2005).

2.3 *Dense mix testing program*

The nanoclay is separately mixed in the bitumen and seen as part of the bitumen.

A dense mixture used at Amsterdam airport was taken as reference. Test specimens were compacted according to the Marshall compaction method with 2 ∗ 75 blows. The average thickness of the test specimen was between 60 and 65 mm. The aggregate used in the preparation of specimens is Norwegian granite and the composition of the dense mixture is given in table 2.

The tensile strength, resilient modulus and fatigue resistance were determined with the Indirect Tensile test set up according to European specifications (EN-NEN 12697-23 2004, EN-NEN 12697-24 2004, EN-NEN 12697-26). The permanent deformation with dynamic creep (EN-NEN 12697-25 2004). For details of the test parameters see (Ghile 2006). No statistical analysis was done due to the low number of repetitions for most tests. For each

Table 1. Overview of testing program.

Group	Materials	Testing programme
Rheology binders (fresh and aged)	Bitumen 70/100, 70/100 nanofill Bitumen 40/60, 40/60 cloisite	Fresh, short term aged, long term aged Empirical: penetration, softening point Fundamental: DSR master curves
Mechanical properties dense mixture	Dense Asphalt Concrete (DAC) DAC cloisite modified binder	Indirect tensile strength, resilient modulus, Fatigue (all ITT) Perm. Deform. (uni-axial cyclic compression)

Table 2. Composition of dense mixture.

Component type	% [weight/(total weight of aggregates)]	% of components	weight of components
22.4–16	0,0%	0,0%	0,0
16–11.2	11,5%	10,8%	132,3
11.2–8	10,5%	9,9%	120,8
8–5.6	11,5%	10,8%	132,3
5.6–2	20,8%	19,6%	239,2
Crushed sand	39,0%	36,8%	448,5
Wigro filler	6,7%	6,3%	77,1
*Binder	6,0%	5,7%	69,0
	106,0%	100,0%	1219,0

*Binder = 40/60 for standard mixture and binder = 40/60 + 6% cloisite for modified dense mixture.

material one batch was produced, one batch was aged, etcetera. Penetration and softening point were just determined for the material used. One frequency sweep was done for each binder type. One Indirect tensile strength was done per temperature. Resilient modulus ITT was done 3 times, fatigue line determined on 8 samples per temperature, for the creep test three repetitions/temperature/loading condition were done.

3 TEST RESULTS

The test results are discussed according to the general testing program given in table 1. A summary of the rheological test results will be given first and after that the mechanical test results of the mix will be summarized. No statistical analysis is added, just an indication of what could be possible can be seen from the results.

3.1 *Rheological test results on the (modified) bitumen*

Empirical rheological tests including the penetration and softening point test (because they are still leading tests in Europe) and fundamental rheological tests including master curves with the DSR were done.

The penetration and softening point tests were performed on fresh (un-aged), short term and long term aged samples of standard and modified binders. Figure 1 shows that the modification improves the resistance to ageing of the 70/100 binder both for the retained penetration and the increment in softening point. Especially the PAV results look promising. From the PAV analysis it can be observed that there is some improvement in the resistance to ageing in the long term with the Nanofill modification.

The results for Cloisite are given in Figure 2. From this figure it can be seen that the improvement is marginal, especially compared to the short term ageing results. In addition the modified 40/60 material has a higher viscosity than the regular 40/60 and therefore probably suffers less contact with hot air or hot oxygen. Hence, the small improvement can also be due to the influence of the viscosity instead of the influence of the modification.

With the DSR test results it was possible to compare the master curves of the stiffness and the phase angle of the modified and unmodified binders and to analyze the change in ageing effect of the binder due to the modification and the rutting and fatigue resistance parameters for the modified and unmodified binders.

Frequency sweep results can be used in the construction of master curves. All master curves in this project were composed at the reference temperature of 20°C. A typical example of master curves of the stiffness is given in Figure 3. All master curves for stiffness and phase angle are reported in (Ghile 2006). To get an indication of the effect of the nanoclay types is summarized with two parameters as developed in SUPERPAVE (NCHRP report 459 2001, NCHRP report 465 2002) for fatigue resistance and permanent deformation, with the assumption that RTFOT

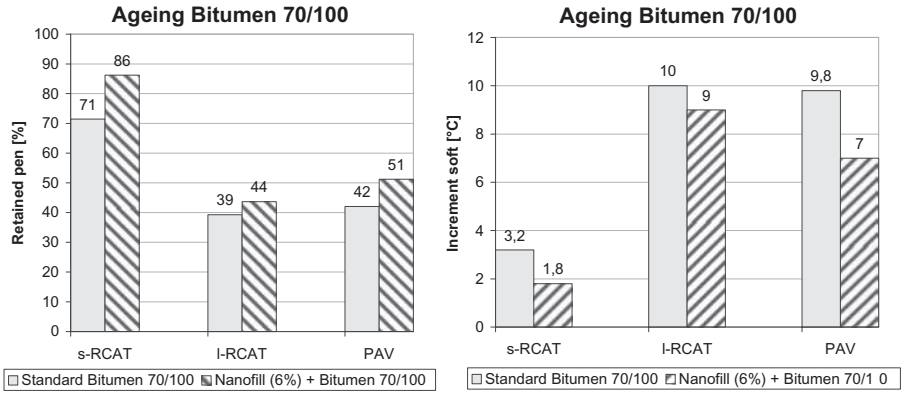

Figure 1. Retained penetration and increment in softening point for standard and modified 70/100 binder (s-RCAT = short term aged in RCAT, l-RCAT = long term aged in RCAT).

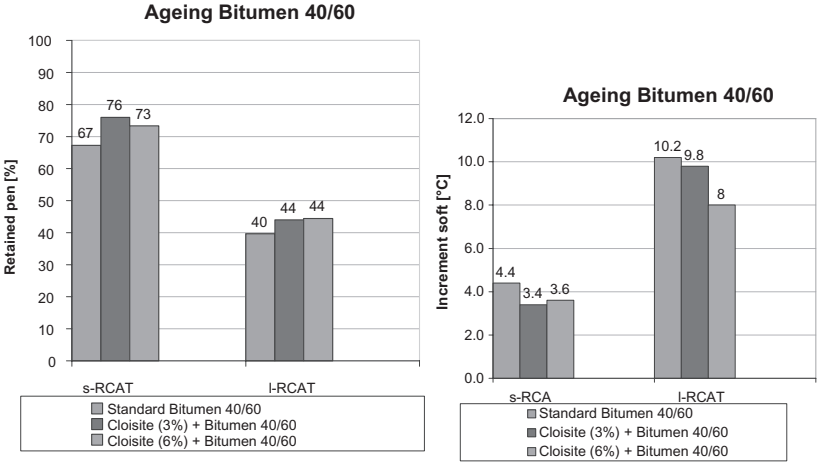

Figure 2. Retained penetration and increment in softening point for standard (left column) and modified 40/60 binder (s-RCAT = short term aged by RCAT, l-RCAT = long term aged by RCAT).

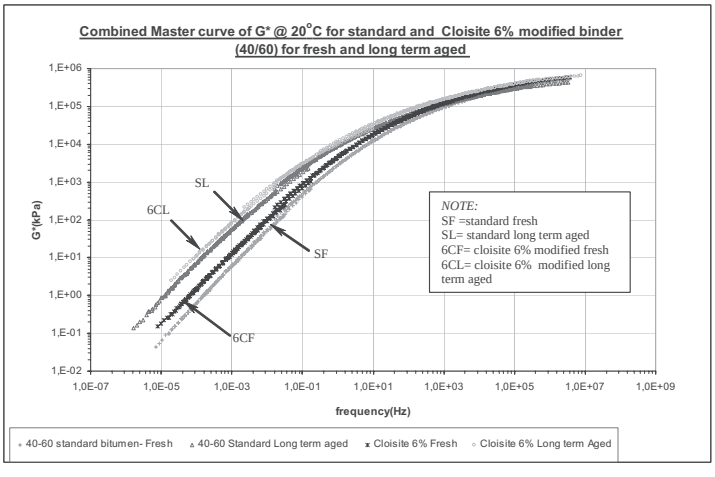

Figure 3. Master curves at 20ºC of stiffness of Cloisite 6% modified 40/60 binder and unmodified 40/60 binders (fresh and RCAT long term aged).

Table 3. Temperature values at minimum limits from RCAT of G*/sinδ.

Binders	Temperature (°C)	
	Unaged-G*/sinδ = 1 kPa	Short aged- G*/sinδ = 2.2 kPa
Standard 70–100	65.0	63.4
6% Nanofill	65.2	62.8
Standard 40–60	69.0	68.4
3% Cloisite	73.8	69.5
6% Cloisite	76.8	74.4

Table 4. Temperature values at minimum limits from RCAT of G*/sinδ.

Binders	Temperature (°C)
	long aged-G*/sinδ = 5000 kPa
Standard 70–100 (RCAT)	19,2
6% Nanofill (PAV)	20.0
6% Nanofill (RCAT)	19,8
6% Nanofill (PAV)	19.2
Standard 40–60	22.1
3% Cloisite	24.0
6% Cloisite	25.2

and PAV give similar results compared to s-RCAT and l-RCAT. The rutting parameter (G*/sinδ) is calculated at 10 rad/s (1.6 Hz) from the master curves. According to SUPERPAVE (NCHRP report 459 2001, NCHRP report 465 2002) the minimum limit of G*/sinδ is 1.0 kPa for unaged binder and 2.2 kPa for RTOFT aged binders and the limiting temperature corresponds to the highest temperature in which the binder is actually expected to serve. The maximum temperature values at which the minimum limit of G*/sinδ is still satisfied both for unaged and short term aged binder is given in table 3. The results of Table 3 show that the 6% Cloisite modified binder shows significant better rutting resistance than the standard and the 3% Cloisite modified 40–60 binders. This is not the case for the 6% Nanofill.

To improve the fatigue life the work dissipated during each loading cycle should be minimized (NCHRP report 459 2001, NCHRP report 465 2002, EN-NEN 12591 2004). Limiting the G*/sinδ parameter, decreasing G* and/or sinδ will result in better fatigue behavior. A summary for all binders of the minimum temperature values at which the maximum limit of G*/sinδ is satisfied is given in Table 4.

The results of Table 4 indicate that the Cloisite modified 40/60 binder has a higher fatigue temperature than the standard 40/60 binder, whereas the Nanofill modified binder shows more or less the same fatigue temperature as the standard 70/100 binder in the long term aged samples.

3.2 *Mechanical properties of the dense asphalt concrete*

Indirect tensile strength, resilient modulus, dynamic creep and fatigue results are reported in this section.

3.2.1 *Tensile strength*

Tensile strength was determined with the indirect tensile test (EN-NEN 12697-23 2004). A comparison of ITS values of the modified and unmodified dense specimens is summarized in Figure 4.

A comparison of the ITS results of the modified and unmodified dense mixtures show that the ITS results of the modified specimens is higher than the ITS of standard mixtures at all test temperatures, a percentage increment in ITS values due to the modification varies from 8% to 40% and the percentage of increment is higher for the higher testing temperature,

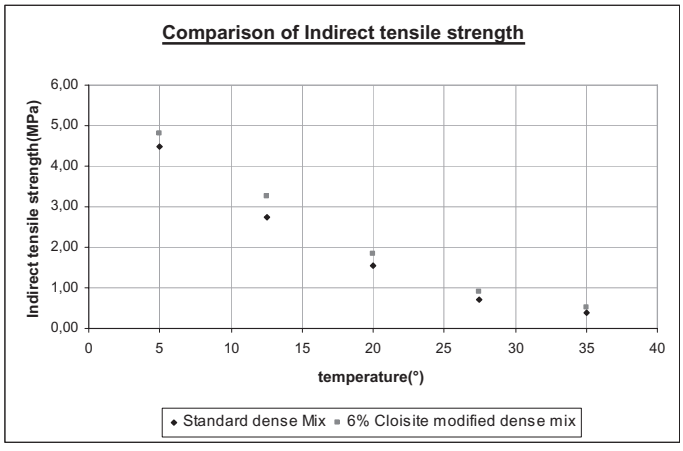

Figure 4. Comparison of ITS (in MPa) of modified and unmodified dense mixes.

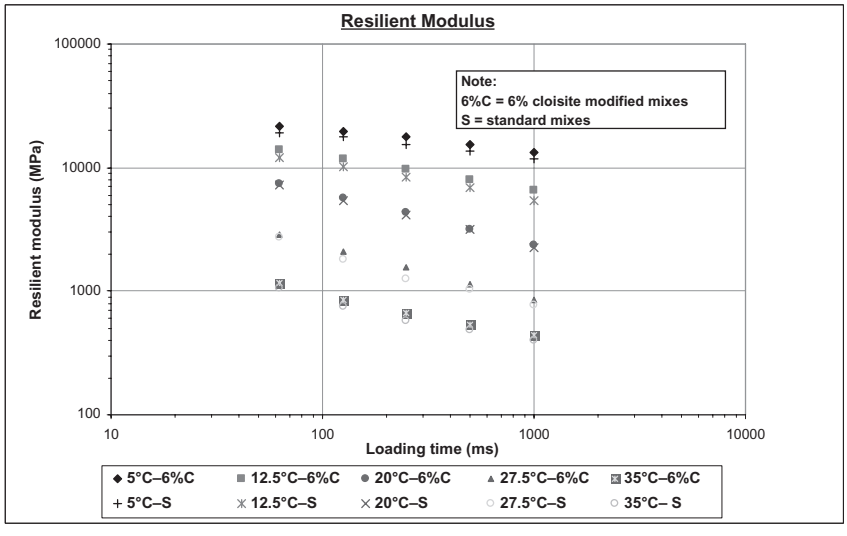

Figure 5. Comparison of resilient modulus (MPa) of standard and 6% Cloisite modified dense mixes.

at 35°C the specimen of the modified mixture fails due to pure crack where as the specimen of the standard mixture fails due to crack and deformation.

Also fracture energy was determined from the load-displacement curves in the ITS. In all cases the Cloisite modified mixture showed increased fracture energy compared to the reference mixture (Ghile 2006).

3.2.2 *Resilient modulus results*

A comparison of the average resilient modulus between the mixture modified with 6% cloisite and the standard mixture is given in Figure 5. It shows that the dense mixture modified with 6% cloisite has a higher stiffness than the standard dense mixture at all test temperatures; tthe 6% cloisite modification increases the stiffness between 3% to 17%. An average 12% increase in stiffness is obtained with 6% cloisite modification for the frequencies and testing temperatures considered.

3.2.3 *Dynamic uni-axial creep test results.*

The dynamic creep test was carried out at three temperatures and at different stress levels, according to (EN-NEN 12697-25 2004). An example of typical creep test results at a

temperature of 40ºC is given in Figure 6. From the creep curves the mean rate of permanent deformation in the secondary stage (K) and the flow number (the number of cycles where the tertiary creep stage starts), are the two parameters recommended as rutting resistance indicators (Ghile 2006, NCHRP report 465 2002). In this paper K is summarized in figure 7 for all mixtures and test conditions. All rutting resistance indicators show that the dense mixture modified with 6% Cloisite results in better rutting resistance compared to the standard dense mixture. This is in line with the indications from the rutting analysis of the binders.

3.2.4 *Fatigue results*

The indirect tensile test (EN-NEN 12697-24 2004) was used to compare the fatigue resistance of the standard and modified dense mixtures. In this test, a constant repetitive haversine compressive load is applied and the resulting vertical deflection is measured in

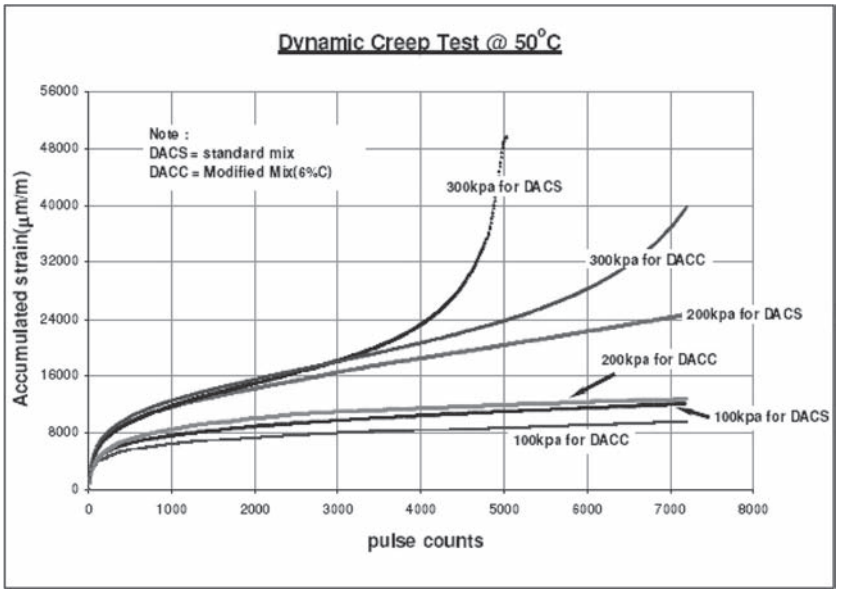

Figure 6. Dynamic creep test results at 50°C.

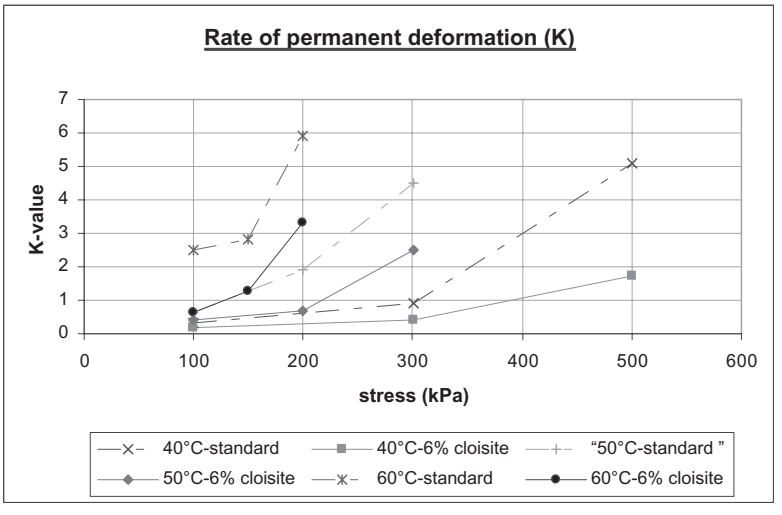

Figure 7. Rate of permanent deformation (K) in relation to the vertical stress level (in kPa).

Table 5. k and R-square values at 5°C and 20°C test temperature for $N = k_1 \cdot \sigma^{-k_2}$.

Temp	Mixture type	k_1	k_2	R^2
5°C	Standard dense mix	$1{,}549 \times 10^{17}$	4,1077	0,9964
	6% cloisite modified dense mix	$7{,}568 \times 10^{17}$	4,362	0,9995
20°C	Standard dense mix	2.716×10^{12}	3.3249	0,9964
	6% cloisite modified dense mix	4.467×10^{13}	3.748	0,9995

relation to time (pulse counts). The fatigue life of a specimen was defined as the number of load repetitions at which specimen failure takes place. Here it is reported as stress versus fatigue life. Fatigue tests were done at 5°C and 20°C with the ITT test set up. The relationship between σ and Nf at 5°C was determined by means of linear regression analysis at log scale of the formula: $N = k_1 \cdot \sigma^{-k_2}$. The k values and R-square values are summarized in Table 5.

As can be seen from the results at 5°C the standard dense mixture performs better in fatigue than the 6% cloisite modified dense mixture, whereas at 20°C the dense mixture modified with 6% cloisite performs better than the standard dense mixture. The comparison of the fatigue parameter, G*/sinδ, of the standard 40/60 binder and 6% cloisite modified 40/60 binders at 20°C shows that the fatigue life of the standard binder is better than that of the 6% cloisite modified 40/60 binder. At 20°C, G*/sinδ of the 6% cloisite modified 40/60 binder is about 1.4 times that of the standard 40/60 binder and this could result in a reduction in fatigue life due to the modification. This is not in line with the conclusion drawn from the fatigue performance of the modified and unmodified dense mixtures in table 5. A physical explanation could be that at 20ºC the test set up is more vulnerable to creep and the modified mix performs better in creep.

4 CONCLUSIONS

The conclusions should be seen as indications from a preliminary test programme in which no statistical analysis could be done for most of the parameters due to low number of test repetitions. It was not possible to design this test programme statistical, due to the limited possibilities. Also the decision to use the Superpave parameter values for RCAT aged material is questionable and is only done for comparison (ranking) indication.

4.1 *Rheological test results on binders*

The Cloisite (3 and 6%) modification increases the stiffness of the bitumen considerably. Nanofill hardly changes the stiffness.

The nanofill (6%) modification improves the ageing resistance of the 70/100 binder in the short term and long term too.

Both the empirical tests (Pen SP) and fundamental tests (DSR) show the same trend for Cloisite and Nanofill.

Permanent deformation prediction based on stiffness and phase angle (G*/sinδ) show strong improvement with cloisite and no improvement with Nanofill. Fatigue prediction (G*/sinδ) shows higher temperature for Cloisite and same temperature for Nanofill.

4.2 *Mechanical properties of dense asphalt mixture*

Cloisite modification (6%) increased the strength, stiffness, and strongly improved the rutting resistance of mixtures with the standard 40/60 binder. Fatigue resistance performance of mixtures with 6% Cloisite modification is not improved at low test temperatures.

4.3 *General*

The improvements observed with the nanoclay modification are not at a level yet to justify application at large scale. Assuming that the improvement is related to the chemical additive that opens up the clay structure and is responsible for the interaction of the clay mineral with the bitumen, further studies on the chemistry of the nanoclay and bitumen and further development of the nanoclay technology is necessary to utilize the full potential of the nanoclay modification. Also storage stability in bulk applications should be investigated especially with nanoclay percentages above 3%.

REFERENCES

Al-malaika, Golovoy A. & Wilkie C.A. 2001, Specialty polymer additives principles and applications, Blackwell science Ltd, London.

Bos B., Fischer H.R. & Timmer K. 2004, Possibilities to improve the wear properties of bituminous anti-skid with nano composite technology (in Dutch). Report DMP-RRT-04-071, TNO-TPD, The Netherlands.

Ghile D.B. 2006, Effects of nanoclay modification on the rheology of bitumen and performance of asphalt mixtures. MSc thesis Delft University of Technology.

Ke Y.C. and Stroeve P. 2005, Polymer–layered silicate and silica nanocomposites, Elsevier science publishers B.V., Amsterdam.

Krishnamoorti R. and Vaia R.A. 2001, Polymer nanocomposites, Oxford University Press, Washington.

Pinnavaia T.J. and Beall G.W. 2000, Polymer–clay nanocomposites, John Wiley and Sons Ltd, England.

EN-NEN 15323, 2005, Accelerated long-term ageing conditioning by rotating cylinder method (RCAT), European standard.

EN-NEN 14769, 2005, Accelerated long-term ageing conditioning by pressure ageing vessel (PAV), European standard.

EN-NEN 12591, 2004, Bitumen and bituminous binders-Specification for Paving Grade bitumen

NCHRP report 459, 2001, Characterization of modified asphalt binders in superpave mix design, Washington D.C.

NCHRP report 465, 2002, Simple performance test for superpave mix design, Washington D.C.

EN-NEN 12697-23, 2004, Determination of the indirect tensile strength of bituminous specimens, European standard.

EN-NEN 12697-24, 2004, Resistance to fatigue of bituminous mixtures, European standard.

EN-NEN 12697-26, 2004, Bituminous mixtures – test methods for hot mix asphalt –part 26 – stiffness, European standard.

EN-NEN 12697-25, 2004, Bituminous mixtures – test methods for hot mix asphalt –part 25 – cyclic compression test, European standard.

http://www.iprime.umn.edu/pdfs/NanoWorkshop/Hunter1.I'MPnano050310.pdf, Nanocomposite Organoclays.

Advanced Testing and Characterization of Bituminous Materials – Loizos, Partl, Scarpas & Al-Qadi (eds)
© 2009 Taylor & Francis Group, London, ISBN 978-0-415-55854-9

First-principles investigation of the multiple phases in bituminous materials: The case of asphaltene stacking

A.J.M. Schmets, N. Kringos & A. Scarpas
Faculty of Civil Engineering and Geosciences, Delft University of Technology, Delft, The Netherlands

C.P. Duif
Faculty of Applied Sciences, Delft University of Technology, Delft, The Netherlands

G. Schitter
Faculty of Mechanical, Maritime and Materials Engineering, Delft University of Technology, Delft, The Netherlands

T. Pauli
Western Research Institute, Wyoming, USA

ABSTRACT: The existence of a microstructure in bituminous materials can explain this materials tendency to self heal. By means of atomic force microscopy and small angle neutron scattering the existence of the microstructure is demonstrated once again. Then it is suggested that the observed microstructure may very well be a consequence of the aggregation of asphaltenic molecules (providing internal volumes with a low H/C-ratio). This is a rather unadventurous suggestion, because flocculation of asphaltenes costs the global oil industry millions of dollars per day. A model asphaltene (a coronene-like molecule) has been selected for calculating semi-empirically the tendency to form stacks. It was found that there is some tendency to cluster, but the effect is not strong enough to be responsible for the observed microstructure.

1 INTRODUCTION

1.1 *Multiple phases and a healing mechanism for bitumen*

It has been known for long that materials which can autonomously mitigate the initial stages of damage due to fatigue or impact loading exhibit a dramatic improvement of service life. Better service life characteristics automatically imply a more sustainable and more efficient utilization of the raw materials. In the composite material that is commonly used in road pavements it is the bituminous binder that will become a rare material eventually. Moreover, it is this component, which amounts for 5 to 8 weight percent of the pavement structure, where damage in the form of cracks will occur first, deteriorating the performance of the pavement as a whole. And finally, it has been known for long that it is this component of the asphalt system that has the ability to mitigate damage partially, i.e. it exhibits the property of self healing (Little and Bhasin 2007). Thus we motivate that a better understanding of the healing behavior of pavement materials should start from the level of the binder.

If the bituminous binder were a perfect homogeneous material, the existence of cracks and damage would occur because of yielding and traditional fracture mechanics applies. However, it has been demonstrated (Pauli 2001), and we'll provide here some evidence from additional experiments, that bitumen at ambient temperatures are far away from being an homogeneous material. In contrary, it appears that bitumen exhibits a very rich microstructure, whose exact appearance depends on the type and composition of the bitumen and the thermal history of

the material. Speculating that the various phases in the bitumen possess a different stiffness, means that under loading conditions cracks may be expected to form preferentially at the interfaces between the phases, i.e. at those locations in the material where there is a significant gradient in stiffness.

In another contribution to this volume by Kringos et al. a model is presented that utilizes the existence of multiple phases in the bitumen to explain the observed self healing behavior. The authors formulate a theory that explains how the phases can reversibly appear and disappear by thermodynamically driven spinodal decomposition. The reversible formation and disappearance of the microstructure in the bitumen is then believed to be the major reason for the longer than expected service life time observed in these materials.

In this paper we show additional evidence of the rich microstructure in bitumen, and we'll test the hypothesis that the phases are formed by stacked asphaltene molecules.

1.2 *Experimental signature of multi-phase behaviour*

Extensive Atomic Force Microscopy (AFM) studies performed at the Western Research Institute (Pauli 2001) have shown that bituminous materials appear to possess a rich microstructure. Similar experiments have been performed at TU Delft on 70–100 pen-grade bitumen, a grade that is typically used in Dutch road constructions (Schitter et al 2008, Schmets & Schitter 2009). Also these experiments showed conclusively, as can be seen in Figure 1, that the material possesses a very rich and complex microstructure. The typical bee-structures, also observed by Pauli, are clearly visible. The bee-structures (coined 'Marangoni bees') have the shape of jagged ellipsoids (the envelope is an ellipsoid), with long axes that measure typically about 10 μm.

Although the evidence provided by the AFM experiment does very decisively proof that bituminous materials possess multiple phases, it should be noted that the AFM technique does essentially probe the surface of the material under investigation. The observed phase behavior might then be only a surface effect, rather than a pattern that is present throughout the bulk of the material. For this reason other experimental techniques had to be called in for exploring the existence of the multiple phases throughout the bulk of the material. The technique of choice would be a small angle neutron scattering technique, because of the ability of

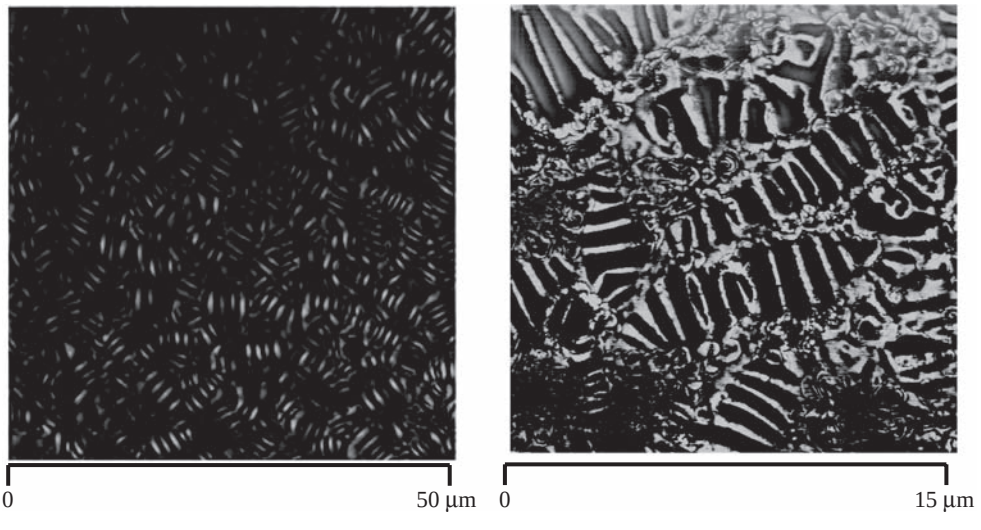

Figure 1. Microstructure of 70–100 pen-grade bitumen observed with a Vyco AFM. Clearly visible are the 'Marangoni bees'. The right image is a detail of the left image, and reveals more details of the complex beauty of this microstructure.

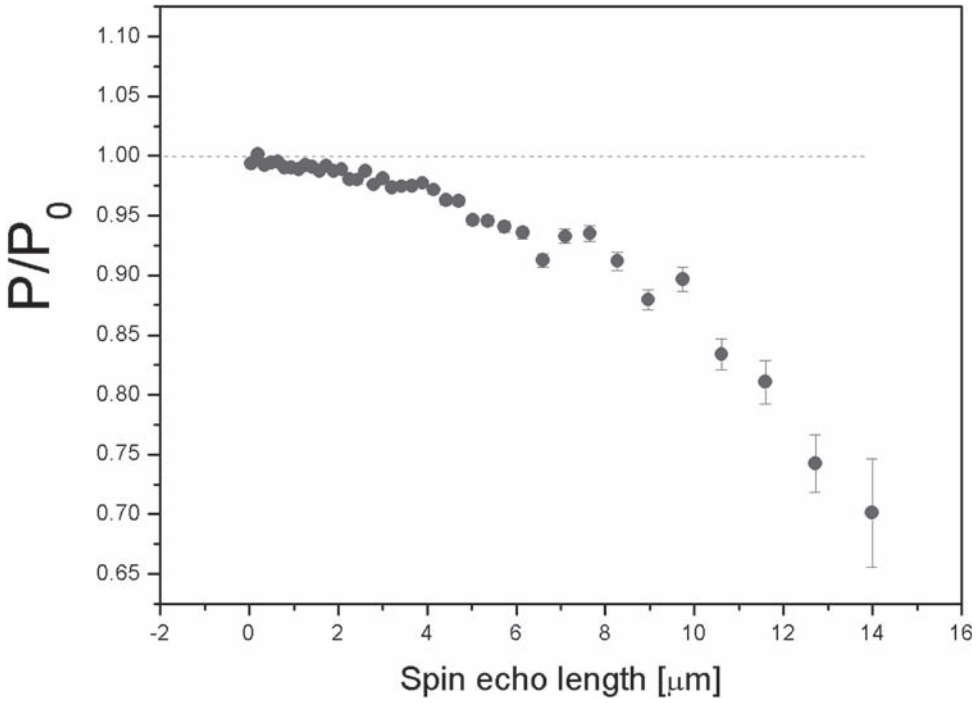

Figure 2. SESANS response to the 70–100 pen-grade bitumen. The dotted red line would be the response if there were no microstructure present in the sample (with features between 20 nm and 20 micrometer).

neutrons to 'look inside materials' and the accessibility of the observed length scales of the microstructure by small angle techniques.

The 70–100 pen grade bitumen that was studied with atomic force microscopy has been subjected to small angle neutron scattering experiments. The bitumen has been dispersed on a 1 mm thick aluminum plate of 3 cm by 5 cm, and was mounted in the Spin Echo Small Angle Neutrons Scattering instrument (SESANS) in the TU Delft research reactor. SESANS (Rekveldt 1996) is a small angle instrument that produces real-space data, in contrast to traditional small-angle scattering instruments. First results as depicted in Figure 2, suggest that there are patterns present in the material with a typical spatial dimension of about 5 to 10 μm, very similar as was observed with the AFM (Schmets & Bouwman 2009). The observation of a microstructure in the material with SESANS is only possible if there is some sort of a 'contrast' present in the sample.

In the case of SESANS this would be a contrast in scattering length density. Given the composition of bitumen that consists mainly out of carbon and hydrogen atoms the contrast in scattering length density is most likely caused by a spatial variation of the hydrogen to carbon ratio (H/C-ratio) in the bitumen. Thus we may conclude from Figure 2 that the bitumen under scrutiny is a non-homogeneous material with respect of H/C-ratio.

2 COLUMNAR PHASES OF STACKED ASPHALTENES

Although the existence of the microstructure in bitumen has been confirmed, the exact composition of the observed phases is still heavily debated. One scenario would be that one of the phases consists of stacked asphaltene molecules (Bergman et al. 2003, Groenzin et al. 2000), because these molecules (essentially sheets of graphite dressed with aliphatic ligands and hetero atoms) have a very different number of hydrogen atoms per carbon compared

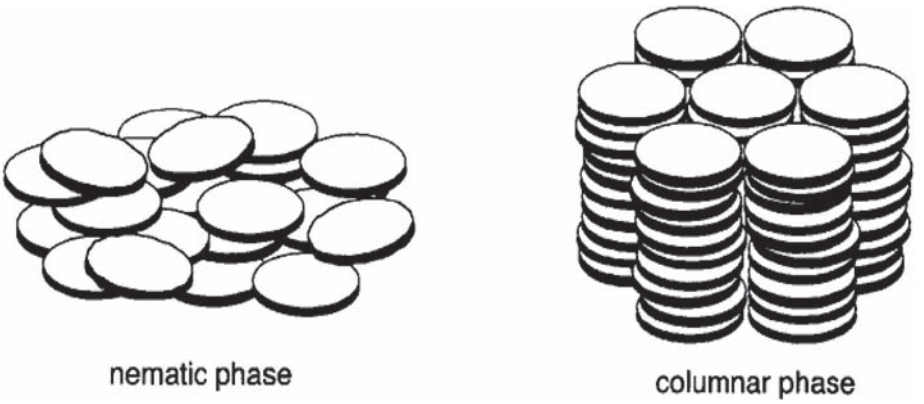

Figure 3. Nematic and columnar ordering of the disk-like ('asphaltenic') molecules.

to more aliphatic components in the bitumen. This is due to the pericondensed aromatic rings that constitute the backbone of the group of molecular species that have been called asphaltenes (formally asphaltenes are defined as the fraction that is separated out of bitumen by n-heptane). Typically asphaltene molecules have an H/C-ratio of 1.1, where the bitumen as a whole will have an H/C-ratio close to 1.5.

Coagulation or stacking of the asphaltenes would produce volumes of realy distinct H/C-ratios, and could hence be the observed feature in the SESANS experiment. It is also well known that flat and rigid structures of aromatic macrocycles possess extensive molecular π-orbitals in which the electrons are delocalized on both sides of the core plane. The π-orbitals of different (asphaltene) molecules tend to interact with each other, giving rise to various ordered, liquid crystalline, structures as shown in Figure 3. This type of structures (discotics) are widely studied (e.g. (Piris 2004)), and are known to be very common for porphyrin-like molecules (another component of every bitumen, though occurring in very small concentrations therein).

The stacks of asphaltene molecules might very well represent one of the phases that are observed. And even if the stacks of asphaltene molecules do not constitute the main ingredient of one of the phases observed, their stacking behavior can be at the onset of the formation of the microstructure, i.e. associations of asphaltene molecules catalyze the formation of microstructure. It should also be noted that the mutual attraction of asphaltene molecules is a well known problem in the oil industry. Pipelines get blocked by hard and glassy material. It is a known fact that this material are just precipitated asphaltenes; so, at least in the presence of many light fractions, asphaltenes like to stick together and form a insoluble phase, causing blockage of oil pipelines.

The remainder of this text will deal with the formation of stacks of model asphaltene molecules.

3 CALCULATION OF ASPHALTENE-ASPHALTENE INTERACTION

3.1 *A model asphaltene molecule for molecular simulation*

Over the years the understanding of the exact nature of asphaltene molecules has changed significantly. Initially it was believed that asphaltene are very large (M_w > 10000 amu's) molecules. Over time it was found that this high molecular weight picture of asphaltenes could be an artifact of the π–π interaction of the rings, i.e. asphaltene molecules were always observed as stacked clusters instead as an isolated molecule.

It was through the work of Mullins and co-workers that the exact nature of the asphaltene component of crudes and bitumen was finally elucidated (Bergman 2003, Groenzin & Mullins 2000) that (petroleum derived) asphaltenes consist on average out of 4–10 fused rings, and

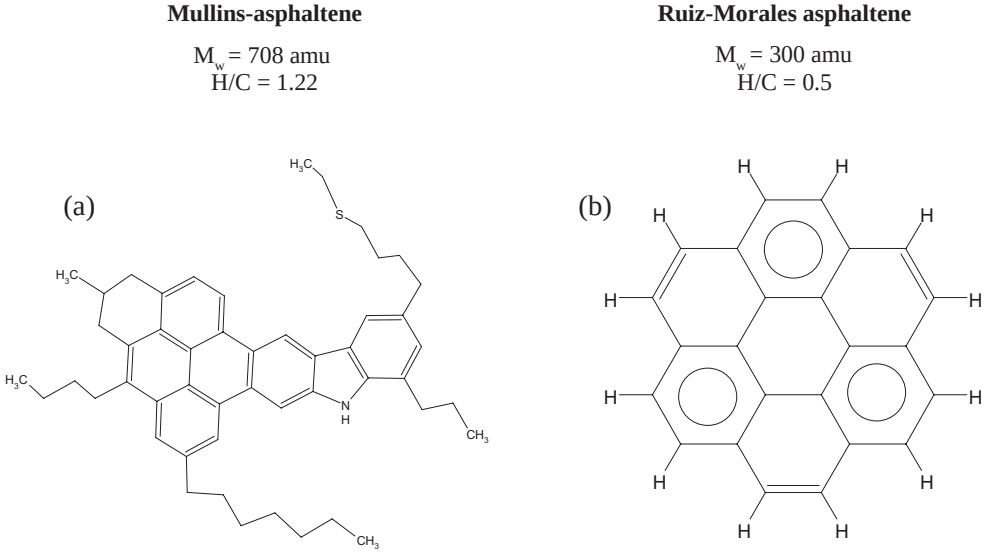

Figure 4. (a) Average structure of a petroleum derived asphaltene (Groenzin & Mullins 2000) and (b) the 'coronene'-like model system used in our simulation of the stacking behaviour of asphaltenic molecules.

that their molecular weight averages between 500 and 800 atomic mass units. They suggest the structure depicted in Figure 4a as a kind of average asphaltene molecule.

For the context of this research, the asphaltene model molecule as presented by Mullins is far too complex to start with. For reasons of computational efficiency, one would like to have a molecule that shares the polycyclic nature of a true asphaltene, though a high degree of symmetry would speedup calculations, and would also lead to non-tilted, i.e. parallel, association of the asphaltenes. Therefore we remove the ligands of the asphaltene and find a suitable ring structure. Consequently we have come to a coronene-like molecule, a choice that was also suggested by the work of Ruiz-Morales (Ruiz-Morales 2007). The molecular structures discussed in the text are displayed in Figure 4.

3.2 *Semiemperical methods*

The calculations of the interaction between our asphaltene representing molecules were performed using the computer code VAMP (Clark 2002). This programme is a semi-empirical molecular orbital package that has been optimized to be numerically stable and fast. It includes routines implementing the natural atomic orbital/point charge model for molecular electrostatic properties, which guarantees accurate calculation of dipoles and quadrupoles, and high quality molecular electrostatic potentials. Moreover, the VAMP code outputs a number of molecular properties, for example ionization potentials, multipole moments, molecular polarizabilities and potential-derived charges. The programme is especially useful for geometry optimization and as such it is a very useful tool to prepare large scale complex molecular dynamics simulations involving many different molecular types (a task that the authors are currently undertaking).

Semi-empirical techniques use the same Linear Combination of Atomic Orbitals-Self Consistent Field theory as true ab initio (i.e. only the type of atoms and their initial positions are required) codes. The main difference is that many of the more complex integrals are removed or replaced by simple approximations. Empirical parameters and functions are used to repair for the errors that occur in the result by removing those integrals. These empirical parameters are fitted to reproduce experimental data.

The molecular wave function, Ψ, is built up by a Slater-determinant consisting of molecular spin orbitals, Ψ_i. These are described by the usual LCAO method, in which the molecular orbitals are obtained as a linear combination of the atomic orbitals,

$$\Psi_i = \sum_{\alpha} c_{\alpha i} \Phi_{\alpha} \tag{1}$$

Molecular orbitals can then be built up by an iterative procedure that optimizes the coefficients $c_{\alpha i}$. Once the molecular wave function has been found, VAMP uses it to evaluate the energy of the molecule, the atomic forces, and many other electronic properties. The energy and the atomic forces are used to optimize the geometry of the molecule to a stationary point at which the atomic forces are ideally all zero.

Semi-empirical programs are used for molecules that are too large for geometry optimization by true ab initio methods like the Hartree-Fock method. At present (March 2008) semi-empirical codes like the one we utilized in the current context are used for molecules comprising 50 to 400 atoms. The asphaltene representing molecule, $C_{24}H_{12}$, which we consider in this contribution, consists of 36 atoms. So for calculating their mutual interactions semi-empirical methods are currently indispensible.

3.3 *Structural optimization of a single molecule*

Before the association behavior of our model-asphaltene molecules can be studied, the geometry of an individual molecule should first be optimized, using the same semi-empirical method as will be used for the remainder of the calculations.

For the geometry optimization we utilized the 'neglect of diatomic differential overlap' (NDDO) approximation with the PM3 hamiltonian and the electron spin was treated in a restricted Hartree-Fock manner. The structure was considered 'optimized' when the energy was converged to between two subsequent self consistent steps to -5×10^{-7} eV atom^{-1}. The resulting optimized structure, together with the calculated bond lengths, is given in Figure 5 below.

The calculated values for the various bond lengths in the molecule are in good agreement with spectroscopic data of similar molecular systems. This gives confidence for the accurateness of the computational method that was selected in this research effort.

3.4 *Do the asphaltene molecules stack?*

Because of symmetry considerations it is clear that the parallel arrangement of two of the 'asphaltenes' must be the energetically most favorable. Therefore only single point energy

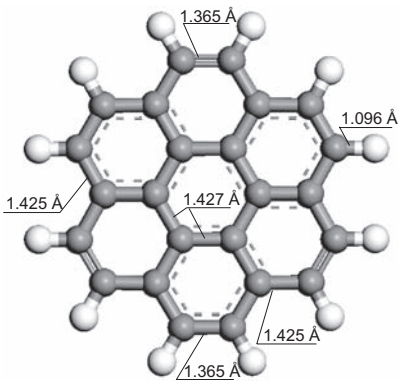

Figure 5. Optimized structure of our 'model' asphaltene.

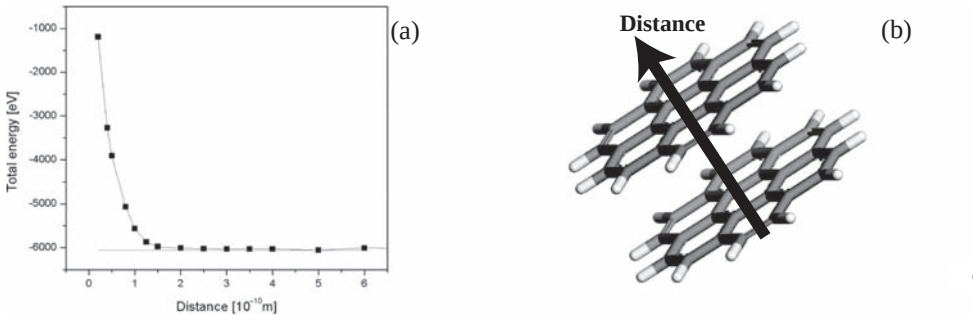

Figure 6. (a) Calculated energy of the two molecule system. (b) Trajectory taken for single point energy calculations.

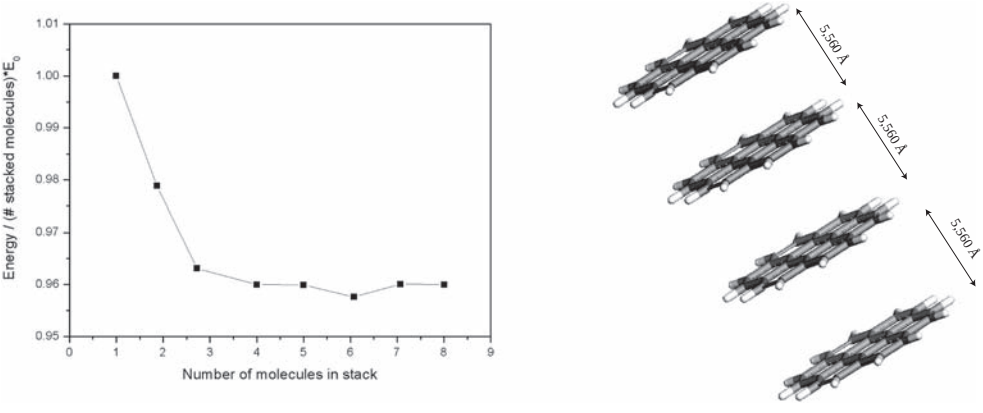

Figure 7. (a) Energy per molecule as function of the number of molecules that participate in a stack and (b) a typical result for a stack of 4 model asphaltenes.

calculations have been performed as a function of the asphaltene-asphaltene distance, see Figure 6b. Remarkably, we do not find a clear energy minimum (Figure 6a), only a clear repulsive part up to 2 Å and a very shallow minimum at about 6 Å . This suggests that there is no bonding between the two π-systems, at least not due to polarization effects of the fused ring systems. A subsequent geometry optimization of the system, where the forces on both molecules were minimized, gave a rather large equilibrium distance between both molecules of 6.41 Å.

Then an equivalent procedure has been repeated for stacks of 3–8 molecules. Surprisingly enough, there is a much more distinguished minimum in the total energy of the 3 molecule system, with an equilibrium inter-molecular distance of 5.55 Å . Adding more molecules to the stack does not change anything, what leads to the conclusion that these type of systems will most likely occur in nature as stacks of 3 molecules. All this is clearly demonstrated in Figure 7a, where the energy per 'asphaltene' molecule is given as function of number of atoms that participate in the stack, i.e. the calculated total energy of the system is divided by N (number of molecules in the stack) times the energy of a free single molecule. When this number deviates from unity there is an energy advantage to form a stack. It is clear that the stack of 3 atoms is energetically favorable over a single molecule or a stack of 2 molecules. Figure 7b shows how the minimum energy structure of a stack of molecules would look like. Obviously, these are not the structures we are after, because they are significantly smaller than the detection limit of the experimental techniques that we have used for studying the microstructure in the bituminous material.

4 CONCLUSIONS

It has been demonstrated by various means that bituminous materials possess a very rich microstructure, depending on the molecular make-up of the bitumen as well as its thermodynamic history. The micro-structural features can be distinguished by their C/H-ratio as SESANS results suggest.

A candidate with a distinct enough H/C-ratio, namely stacks of asphaltenes have been considered. By means of semi-empirical methods it was found that a selected model-asphaltene prefers to stack in clusters of 3 molecules. This can not give rise to the observed microstructural pattern. We dare to conclude that it is quite unlikely that the observed microstructural features consist of aggregates of asphaltenes; even not if more realistic models are to be selected to represented the fraction of asphaltenes.

ACKNOWLEDGEMENTS

The research described in this paper has been performed in the context of the 'Delft Healing Consortium'. In this context, the authors gratefully acknowledge the support of Shell Global Solutions, Nynas AB, the Dutch Ministry of Public Works, Ooms Nederland Holding bv, Delft Centre for Materials, the Western Research Institute and the US Federal Highway Administration.

The authors thank the Reactor Institute Delft and Dr Wim Bouwman for allowing the use of the unique SESANS setup and the Delft Centre for Systems and Controls for allowing the use of their state-of-the-art AFM equipment. Finally, Robijn Niemeijer is thanked for other kinds of support.

REFERENCES

Bergmann, U., Groenzin, H., Mullins, O.C., Glatzel, P., Fetzer, J., & Cramer, S.P., 2003. Chem Phys. Lett. 369, 184.

Clark, T., Alex, A., Beck, B., Burkhardt, F., Chandrasekhar, J., Gedeck, P., Horn, A.H.C., Hutter, M.2002. Martin, B., Rauhut, G., Sauer, W., Schindler, T., & Steinke, T., Vamp 8.1, Erlangen.

Groenzin H., Mullins O.C. 2000. "Asphaltene molecular size and structure", *Journal of Physical Chemistry, A* 103, pp. 11237–11245.

Little, D.N., & Bashin, A. 2007. 'Exploring Mechanisms of Healing in Asphalt Mixtures and Quantifying Its Impact', in Self Healing Materials: an alternative approach to 20 centuries of materials science, Springer Series in Materials Science 100.

Pauli, A.T., Branthaver, J.F., Robertson, R.E., Grimes, W., & Eggleston, C.M. 2001. "Atomic Force Microscopy Investigation of SHRP Asphalts", *American Chemical Society, Division of Petroleum Chemistry*, 46(2), 104–110.

Piris, J., 2004. Optoelectronic Properties of Discotic Materials for Device Applications, Delft University Press.

Rekveldt M.Th. 1996. Nucl. Instr. & Methods in Phys. Res. B 114 366.

Ruiz-Morales, Y., Molecular orbital calculations and optical transitions of PAHs and asphaltenes, in 'Asphaltenes, Heavy Oils, and Petroleomics', Mullins, O.C., et al. (editor), Springer, 2007.

Schitter, G., & Rost M.J. 2008. Scanning probe microscopy at video-rate, Materials Today, Volume 11, Supplement 1, Pages 40–48.

Schmets, A.J.M., & Bouwman, W.G. et al. 2009. 'Small angle neutron scattering on bituminous materials with various wax contents', to be published.

Schmets, A.J.M., & Schitter, G. et al. 2009. 'Temperature and cooling rate dependence of the microstructural features present in waxy crudes', to be published.

Advanced Testing and Characterization of Bituminous Materials –
Loizos, Partl, Scarpas & Al-Qadi (eds)
© 2009 Taylor & Francis Group, London, ISBN 978-0-415-55854-9

The morphology of SBS modified bitumen in binders and in asphalt mix

H. Soenen
Nynas N.V., Antwerp, Belgium

X. Lu, & P. Redelius
Nynas AB, Nynäshamn, Sweden

ABSTRACT: The morphologies of SBS modified binders and their asphalt mixes were studied using fluorescence microscopy. In a first part, the morphology of an SBS polymer in different bituminous binders was investigated as a function of the preparation method, in particular as a function of the cooling rate and isothermal annealing periods. Storage stable and unstable SBS-bitumens, as defined by the tube test after 3-day at 180°C, were selected. The microscopic observations showed that the morphology strongly depends on the thermal history of the respective samples. These microscopic observations are supported by the differences seen in the rheological properties and in the force ductility curves of the respective binders.

In a second step, the morphology of the SBS binders was investigated directly in the corresponding asphalt mix. The morphology was studied in compacted specimens as well as in the loose mix using several preparation procedures. Asphalt specimens were sliced in plane or alternatively in thin sections according to the methods developed by the Danish Road Institute. Also cold fractured asphalt surfaces were investigated. The analysis of the asphalt surfaces showed clearly that the morphology in the asphalt mix was very similar for all the binders tested, and was in most cases rather different from the morphology observed in the binder specimens. In the asphalt mix, the SBS phase is located in separate and distinct domains; this was observed for all the mixes tested. The observations suggest that the differences in PMB morphologies between compacted asphalt and binders is an important factor that should be considered when investigating the properties of polymer modified binders, and especially when searching for performance related binder tests.

1 INTRODUCTION

It is quite well known that most polymers commercially used like SBS and EVA, are only partially miscible with bitumen (Kraus, 1982). It has been demonstrated that phase separation occurs upon cooling the binder from the high production temperatures (180°C–200°C). Even at these high production temperatures some polymer modified bitumen (PmBs) may already show phase separation. The extend of this phase separation is dependent on the bitumen type, the concentration of polymer, and the characteristics of the polymers, for which the polymer molecular weight is certainly an important one. Some literature reports have indicated that the morphology in PmB binders is dependent on the thermal history of the binders, like the cooling conditions. It is also known that the morphology can have an influence on some physical properties of PmBs, properties like the rheological behavior and the force ductility. (Brûlé et al. 1988, Dony & Durrieu 1990, Pasquier et al. 1997, Mouillet et al. 2004, Soenen et al. 2008)

The purpose of this paper is to demonstrate how the morphology of PmBs depends on the sample preparation method, how this can be investigated, and to show how large these effects can become. Furthermore, this study also shows how the morphology obtained in a

small binder sample can differ from the morphology of the same binder when it is embedded in a (necessarily larger) asphalt mixture structure. This observation is important, since physical properties of polymer modified binders, like the softening point or the rheological behavior, are dependent upon the morphology of the phase structure. And as many performance indicator tests for binders are studied on small sample volumes, for example in a plate-plate rheometer, the morphology in these small samples can be very different from the morphology that is finally obtained in the asphalt mix. This observation can be an explanation why binder performance indicators that often work well for unmodified binders only partially work for PmBs.

2 EXPERIMENTAL

2.1 *Fluorescence microscopy*

The morphology was studied with an epi fluorescence microscope. This microscope was a Carl Zeiss Axioskop 40Fl, equipped with a digital camera, deltapix DP200. The exposure time of the camera can be changed from a few ms up to 6s, due to slight variations in this exposure time, the colors in the graphs can slightly vary as well. The UV light source comes from a high pressure mercury arc lamp HBO50. The microscope uses a three filter system; an excitation filter, a beam splitter and an emission filter. From the light source, the light first goes through the excitation filter which transmit light with a wavelength between 450 to 490 nm. Light of this wavelength hits the surface of the specimen, part of this incident light is reflected and a part is emitted by the sample. The emitted light has a longer wavelength than the incident light. Reflected and emitted light will hit the beam splitter, where only wavelengths longer than 510 nm are transmitted. Finally this transmitted light hits a third filter which has a high transmission for wavelengths longer than 515 nm.

Magnifications levels of 50x, 100x and 200x are available. The microscope is also equipped with a Mettler hot stage, which allows to investigate samples at elevated temperatures, or during controlled heating and cooling.

2.2 *Samples*

Four PmBs were used, referred to as PmB1 to PmB4, and the base binders were derived from different crude origins. All base bitumen were of the 70/100 type. A linear SBS triblock copolymer was used in the preparation of the PmBs. The SBS had a weight average molecular weight of 189000, the fraction of tri- versus diblock copolymer was 0.8, and the styrene content was about 30%. The polymer was supplied by Kraton Polymers, type name Kraton D-1101CU. CU refers to the fact that in this polymer silica powder was not added, this powder also gave a signal in the fluorescence microscope. PmBs were made in 5% SBS concentrations, conventional properties of the blends and also results of the storage stability tests are summarized in table 1. The storage stability test refers to the tube test, (EN 13399) in which a tube of PmB is stored in an oven at 180°C for 3 days, afterwards the softening points of the top and bottom fractions are investigated. Blends were prepared by mixing polymer and bitumen at 180°C, stirring was continued for 3 hours at a speed of about 500 rpm.

Table 1. Overview of the PmBs used.

			Tube test-3 days at 180°C		
	Pen 25°C	R&B	Top-R&B	Bottom-R&B	Δ R&B
PmB	dmm	°C	°C	°C	°C
PmB1	57	76.0	94.5	69.0	25.5
PmB2	52	85.0	86.5	86.5	0
PmB3	56	77.8	54.6	55.6	–1.0
PmB4	52	65.0	84.2	52.2	32.0

2.3 *Asphalt mix type*

The asphalt mixture was a dense graded asphalt concrete (Swedish standard ABT 11) with a maximum aggregate size of 11 mm. A crushed granite material was used, the nominal binder content was 6.5% by weight, and the void content was about 3%. Asphalt specimens were compacted using the gyratory compactor, to the desired density, which means gyrations vary slightly from specimen to specimen. The mixes are referred to as M1 to M4. Different methods were used to visualize the morphology of the PmB in the asphalt mix. These methods will be discussed in section 4.

3 MICROSCOPIC OBSERVATIONS IN THE BINDERS SAMPLES

3.1 *Drop method*

In this procedure, samples for the microscope were prepared by taking a small drop from a (hot) can, and by letting this drop fall on a cold glass plate. After cooling to room temperature, which only took a few seconds, the samples were viewed through the bottom plate. This procedure is often used in literature, since it is very simple.

In this procedure the sample is necessarily cooled very quickly to room temperature, because the volume of the drop is very small, and the glass plate is at ambient temperature. So one can assume that the morphology obtained in this way is similar to the morphology present at the moment the sample is taken. Photographs of morphologies are shown in figure 1. In this figure, the temperature refers to the temperature in the can, at the moment the drops are taken out. This temperature was varied from 200°C to 120°C, as follows: A can was first heated to 200°C, and after 10 minutes a drop was taken. Afterwards, the same can was cooled to 180°C, and again after 10 minutes a drop was taken. This procedure was

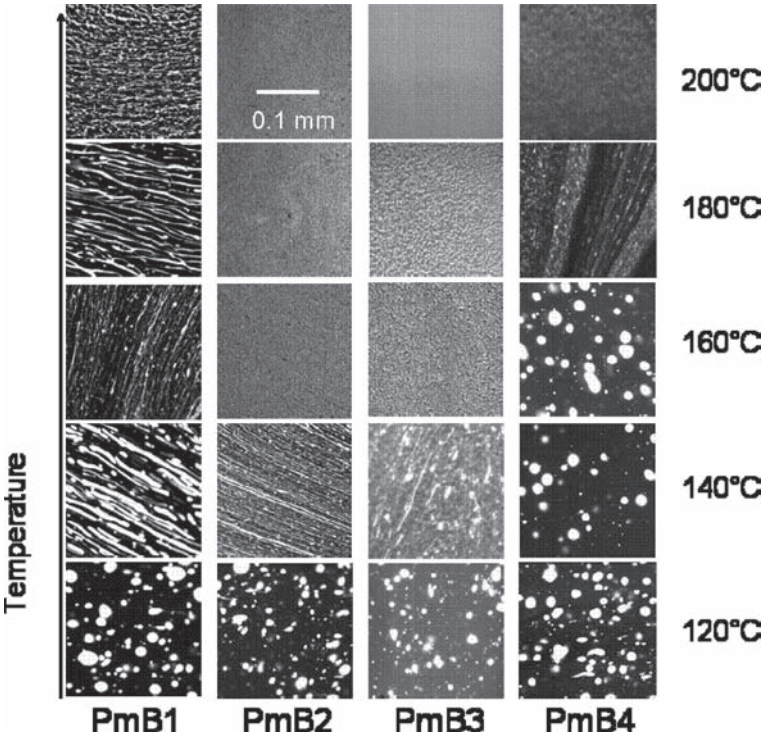

Figure 1. Morphologies of drops of samples, the temperature of the can when the drops were taken is indicated, as well as the PmB type (magnification = 200x).

repeated until 120°C. Below 120°C it became difficult to take a drop of sample. During the procedure, the can was continuously stirred by a mechanical stirrer, and therefore, sometimes orientation effects are obvious.

From figure 1 it is quite clear that all the Pmbs show a less distinct polymer phases when the temperature is higher. This corresponds to the general knowledge that SBS type of polymers become more compatible when temperature is higher. At high temperatures differences depending on the type of base binder are clear, some already have a homogeneous appearance when the temperature is at 160°C, while others are even at 180°C not fully homogeneous. However at lower temperatures, 120°C, the binders all have a phase separated structure even though the samples were stirred, and all have a very similar appearance.

In this respect it needs to be noted that homogeneous refers to the resolution of the microscope, which is for this particular magnification limited to about 2 micrometer. With this resolution, it is not possible to observe a phase separation between the styrene and the butadiene blocks of the SBS copolymer, since this occurs on a smaller length scale.

3.2 *Thin film method*

If the drops of PmB, taken on a cold glass plate, are reheated, they start to flow and form a thin film. An example of such an experiment is shown in figure 2. In figure 2, a drop of PmB2 was taken from a can at 200°C, and was afterwards reheated to 140°C. It is quite clear that at this temperature the mobility is high enough to start a phase separation. With time the phase separation continues, smaller polymer phases coagulate and become larger, and more distinct. This experiment was repeated for all the binders, at various temperatures. In figure 3 the morphology after isothermal annealing for 1 hour at the indicated temperatures is shown. Again clear differences at higher temperatures are obvious, some binders still have a homogeneous appearance at 160°C, while others do not. At lower temperatures (120°C), all the morphologies after 1 hour annealing, show distinct polymer-rich and bitumen-rich phases, and the bitumen forms the continuous phase. At ambient temperature, and slightly higher, tested up to 60°C, the morphology remained constant and did not change isothermally.

3.3 *Freeze fractured samples*

The PmBs were also investigated using the freeze fracture method, which is described in EN 13632. According to the norm, specimens have to be prepared by pouring an amount of sample in an aluminum mould which is completely surrounded by a sand bath. The mold, the sand bath and the binder have to be at a high temperature. After filling, mold and sand bath, should be left to cool to ambient. In this way a controlled (and because of the large volume a rather slow) cooling of the sample is obtained. Afterwards the mold is cooled to a low temperature (a temperature where brittle fracture is obtained), and after fracturing, the fractured surface is investigated. This method gives a picture of the undisturbed bulk structure.

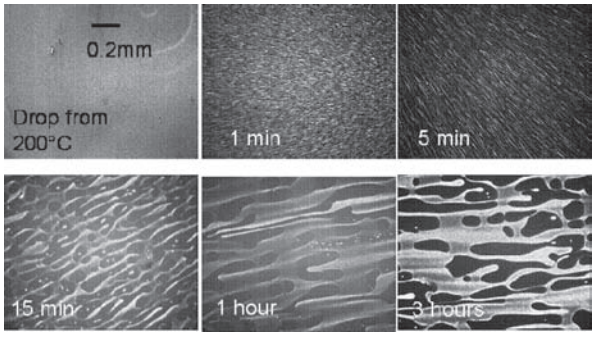

Figure 2. Morphology of PmB2 after isothermal annealing at 140°C. The annealing time is indicated. The starting sample was taken at 200°C (time = 0) (magnification = 200x).

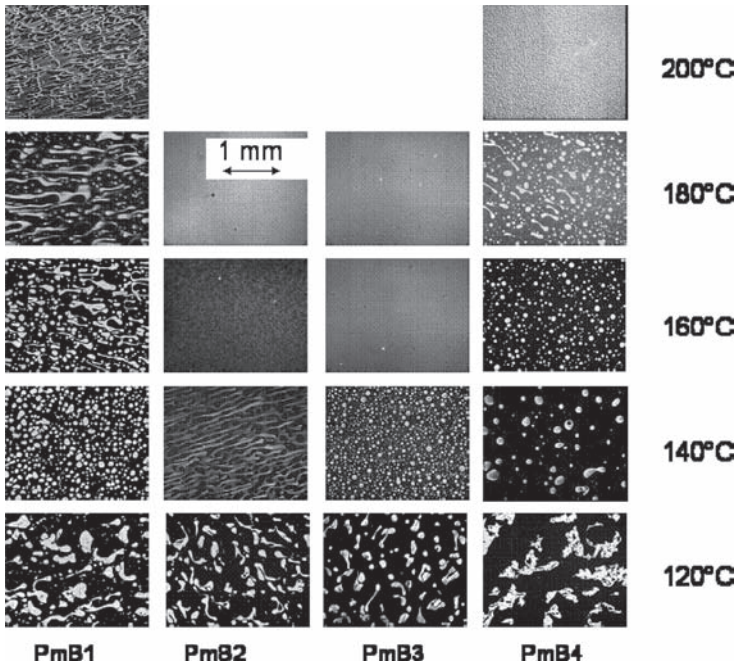

Figure 3. Morphologies after 1 hour isothermal annealing. The annealing temperature and the binder type are indicated. The starting sample was each time taken at 200°C (magnification = 50x).

In this paper, this procedure was not exactly followed, since silicon molds were used with a diameter of 2.5 cm. These molds were in fact the same as the ones used to make samples for testing in a rheometer, with the 25 mm plates. Different cooling rates were obtained: first by just leaving the mold after filling to cool to ambient, secondly by leaving the molds for an hour at 120°C, and finally by leaving the molds in an oven with a controlled cooling rate of 2°C/min. In figure 4A, the freeze fractured morphologies obtained after different cooling procedures of the molds are shown. In these experiments, the PmB was taken form a hot can (200°C) and was manually stirred.

3.4 *Rheology and force ductility of the binders*

In this section, it is investigated if the different polymer structures have an influence on the mechanical properties of the binders. Two tests were evaluated, rheological measurements and force ductility tests. Black curves are shown in figure 5 for two of the PmB samples, after several preparation procedures. In this respect the procedure denoted as standard refers to the conditions normally used when preparing samples for the DSR rheometer: a cold silicon mold is filled with hot binder (in this case taken at 200°C) and is left to cool to ambient. The rheological test after annealing at 120°C are different and may be related to the differerent morphologies. Especially for PmB2, the effects are large, and the effects are also larger in the lower modulus region or at higher temperatures (50°C–80°C). For PmB2, the specimen prepared according to the standard procedure has a rather homogeneous morphology and the polymer forms an entangled network throughout the sample (in figure 4, the freeze fracture after quick cool). The presence of this network gives a rubbery-like behavior. For a dry polymer this rubbery-like behavior (entanglement region) is around modulus levels of 10^6 Pa. In this case, as the rubbery phase is swollen with components from the base binder, the modulus level is reduced to around 10^4, 10^3 Pa, what also corresponds to a phase angle of 40–60°. After leaving the binder for some time at 120°C however, the polymer is concentrated in

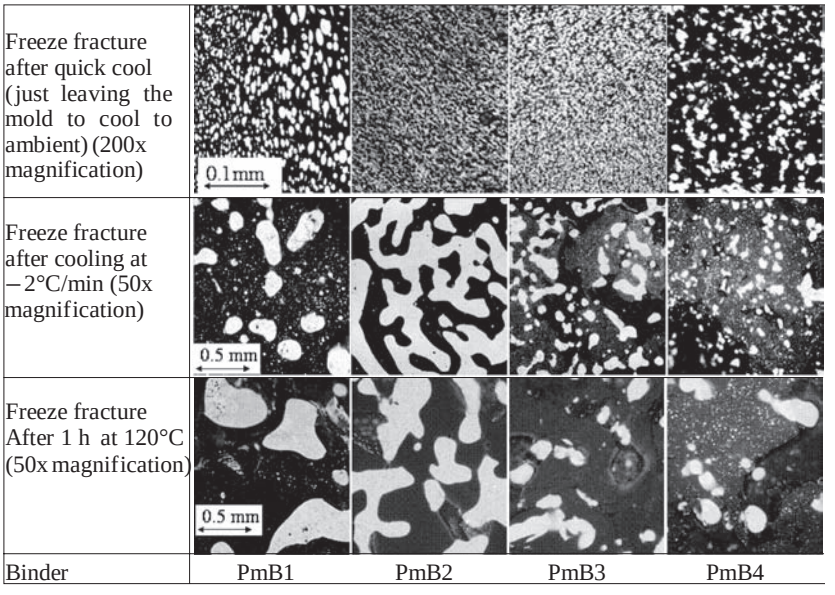

Figure 4. Morphologies obtained after freeze fracture. The thermal history of the PmBs and the type of sample are indicated.

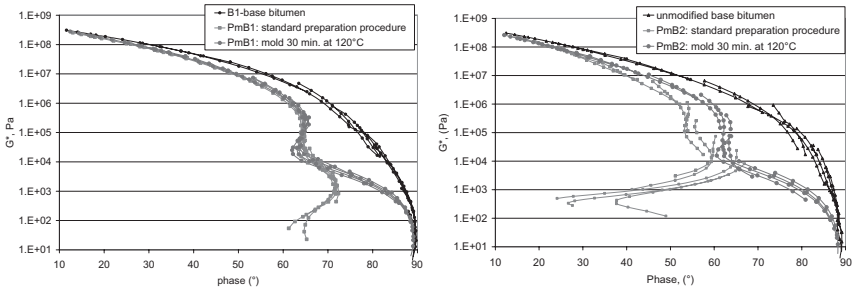

Figure 5. Black curves of two PmBs as a function of thermal history of the specimen. Standard procedure indicates filling a cold silicon mold with hot binder and leaving it to cool to room temperature.

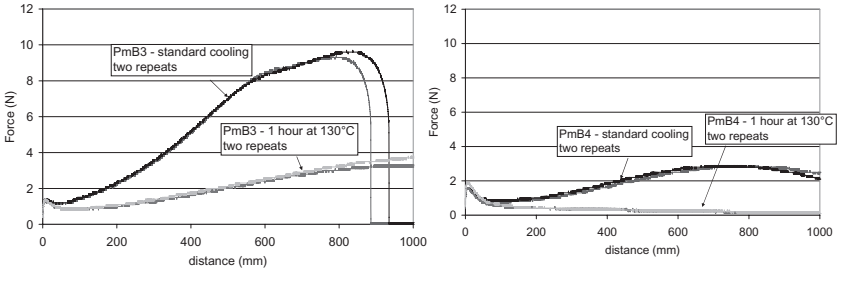

Figure 6. Force ductility curves for two of PmBs, after different preparation conditions.

separated domains and the entanglements are now only in the separate droplets, surrounded by a bitumen-rich continuous phase. In this morphology they cannot provide a large elastic effect. For PmB1, the morphology after quickly cooling the binder was already somewhat disperse (figure 4), showing very small polymer-rich droplets so in this case even after quickly cooling the specimen there is already less effect of the polymer network.

In figure 6, force ductility curves for two PmBs are shown, and the differences due to the preparation methods become obvious at long elongations.

After standard cooling, the morphology of PmB4 is already phase separated, figure 4, so the starting elasticity for this PmB is lower compared to PmB3, which has, after standard cooling a rather homogeneous appearance. When the binders are stored at 120°C, phase separation starts (PmB3) or continues (PmB4), and ductility levels decrease. So in conclusion, the differences observed in the morphology of the PmBs and the influences due to cooling rate and isothermal annealing are confirmed in the mechanical properties of these binders.

4 MICROSCOPIC OBSERVATIONS OF THE PMB IN AN ASPHALT MIX

4.1 *Morphologies of plane and thin sections*

Initially, in this project, we tried to observe the polymer phase in a relatively thin, 1 cm, standard sawed asphalt slice. However, it was not possible to investigate the binder morphology in such a specimen, since there was too much fluorescence from the stone surfaces and from other stone material. And since the surface was not flat enough, it was impossible to have a larger part of the structure in focus.

In 1999, the Danish Road Institute published a report on the morphologies of PmBs in binder and in mixture tests (Wegan, 1999). They also developed a method to prepare plane and thin asphalt slices. The preparation method is described in (Wegan, 1999), but a short summary of preparing a thin slice is given below. The asphalt mixture is first cut with a diamond saw (3.3 mm blade thickness) from an asphalt core. A smaller asphalt specimen is cut, approximately 30 × 45 mm and 10–20 mm in thickness, by means of a thinner saw (1.3 mm blade thickness). The specimen is then glued onto a plane glass slide, which helps to attach the specimen. The specimen is then impregnated under vacuum with a colorless epoxy resin, which after curing helps to stabilize the specimen during further preparation procedure. The surface is sawed further, ground to levelness by diamond coated rollers. An object glass is glued to the surface of the specimen, which is the first finished side of the thin section. The specimen is further cut, ground and polished to a final thickness of 20 μm. Throughout the preparation procedures the specimen and equipment is constantly cooled to approximately –5°C to avoid smearing of the polymer phase. The Danish Road Institute agreed to prepare thin slices from the asphalt cores containing the four PmBs selected for this study. In figure 7, photographs from these thin slices are shown. In addition to the four PmB mixes, an unmodified mix is added as a reference.

From figure 7, the areas with large fluorescence are due to the stone surface, and they are of little interest, and are mostly outside the image. But the mastic phase in between the stones, shows small spots which are probably polymer rich phases, these are not present in the reference mix. From figure 7, we can observe that for the 4 PmB mixes, the polymer phase is for all samples in separate domains, and the bitumen-rich phase is the continuous one.

4.2 *Other methods*

Other ways of investigating the morphology in the asphalt mixture were tried. For example, we also looked at the morphology of a piece of mix that was freeze fractured, in a similar way as the binder samples. The advantage of this method is that there is no or only very limited interference from stone surfaces. Since at least for this type of mixtures, the fracture was within the mastic phase. Results are shown in figure 8. Again we can observe the polymer-rich phases as distinct droplets. The result is very similar to what was observed for the thin sections. But as is also obvious from figure 8, there are area's out of focus, since the surface after fracture is uneven, and in this case we did not apply any method to flatten it.

Finally, we also looked at the surface of the loose mix as such, and also in this case there is no interference from the stone material (except if the coating would not be good). The results are also presented in figure 8, and we see again that the polymer phase is present in distinct domains. But, in this case the domains seem to be somewhat larger compared to those in the

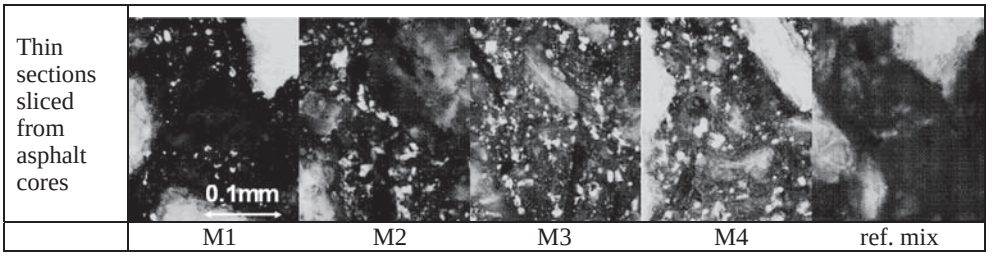

Figure 7. Microscopic observations in thin asphalt sections, prepared by the Danish Road Institute (magnification is 200x).

compacted asphalt cores. The reason for this is due to the larger sample amount in the loose mix, when it was prepared and the consequently slower cooling rate.

Finally in figure 9, a comparison is made between the morphology of the mix after a normal cooling of the loose mix, and after storing this mix for 4 hours at 135°C. These conditions were chosen since they are sometimes used to simulate a short term aging of the mix. It can be observed that also in the mixtures, the phase separated domains increase after isothermal annealing. So some care is needed when applying isothermal procedures to PmB mixes.

5 DISCUSSION

In this study, three methods to test the morphology of bituminous binders were used and compared. Each method has its advantages and limitations. It was also shown that the morphology observed in binder specimen, after different thermal treatments, was in agreement with the results of rheological and force ductility tests.

Methods to measure the morphology in the asphalt mix have been presented; It seems from these investigations that studying thin asphalt mix specimens gives a similar result to measurements on the fractured asphalt mix. Even loose mix can be used, although the morphology can be different if the thermal treatment of the mix is different. In the thin sections, the whole surface can be brought in focus, but there is also interfering fluorescence from stone material and it is not 100% sure that the sample treatment did not influence the morphology. When looking at fractured surfaces the surface is not flat, so there are areas in the photographs that are not in focus, but all fluorescence observed comes from the polymer phases. And one can also assume that disturbances in the morphology due to fracturing the samples are limited.

In this study all the binders finally showed a phase separated structure in the asphalt mix, independent of the base binder used. Even for PmB2 and PmB3, which were storage stable, the morphology in the mix was phase separated. The storage stability has certainly an effect on the morphology at high temperatures and also after quickly cooling a small specimen. The two storage stable PmBs (PmB2 and PmB3) were in the drop method and the thin film morphology compatible to lower temperatures than PmB1 and PmB4. But in the final mix morphology the differences between these four binders were very limited. It should be noted that the morphology also depends on the polymer concentration, the polymer molecular weight and structure, and these parameters were not varied in this study.

In this paper, we showed that the cooling rate, and by this the sample volume of a specimen can play a role in the morphology, when working with SBS modified binders. And the morphology can in turn also influence the mechanical properties. In tests, using small specimens the chance of having a more homogenous morphology is larger, and in those tests the mechanical behavior can be different than in tests using large specimens, where the bulk sample is cooled slowly. In the European norm for the visualization of polymer dispersions (EN 13632) a slow cooling rate is obtained. Since, the sample has to be poured in an aluminum mold, which is in turn surrounded by a sand bath of about 600 ml content. The mold and the sand bath have at the time the sample is prepared, the same temperature as the binder. And according to the

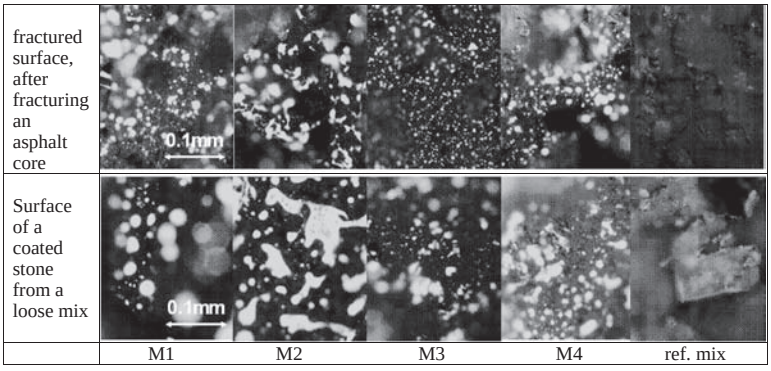

Figure 8. Microscopic observations from fractured compacted mix samples, and from loose mix samples (magnification is 200x).

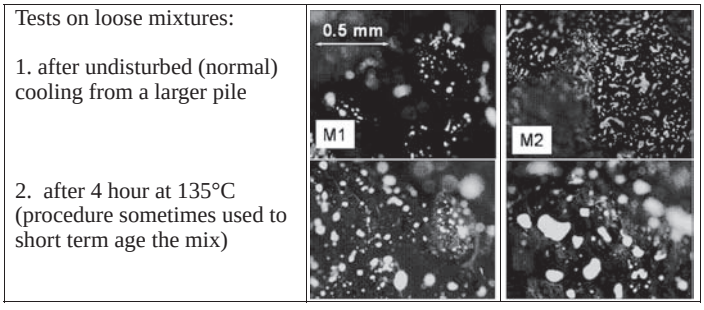

Figure 9. Microscopic observations from loose mix samples (magnification = 100x).

norm on sample preparations (EN 12594), for a PmB this temperature needs to be between 180°C and 200°C. The reason for this rather complicated procedure is to obtain a thermal trajectory in the binder that is close to what is obtained in an asphalt core. If this slower cooling is needed to investigate the morphology, it should also be interesting to apply this preparation method when testing mechanical properties on SBS modified PmBs. There are a lot of test methods where small and even very small sample specimens are used: for example the specimens in rheological testing, in the Fraass breaking point, in the ring and ball softening point can be considered as very small and also the samples for force ductility and the bending beam rheometer can still be considered as small, compared to an asphalt mix.

This paper wants to encourage investigations on morphology, especially when they can be carried out directly in the asphalt mix, since there is a need to have more insight in the phase morphology of mixes as they are placed on the road These investigations can also help in revealing possibly new mechanisms by which the addition of polymers can influence asphalt performance. At this stage little is known how a distinct polymer phase, located in separate domains can play a role in for example crack initiation, or in crack growth. Knowledge of these aspects can help to optimize PmB formulations with respect to performance.

6 CONCLUSIONS

In this paper, the morphology of four SBS modified binders and their corresponding mixes, was investigated, and the main findings are summarized below. It was shown that:

– the morphology of the binders depends on the thermal treatment of the samples, cooling rate, isothermal annealing, and even stirring can have an effect.

– At lower temperatures, below 60°C, the morphology in binder samples is not changing anymore with time.
– the morphology in the drop method relates to the morphology at the time the sample is taken, because of its very small volume and correspondingly high cooling rate.
– the freeze fracture method can be used to investigate the morphology in larger binder samples, different cooling rates or isothermal annealing can be applied by modifying the procedure.
– the morphology in a binder sample, obtained by changing the thermal history of the binders also has a clear influence on the mechanical properties measured by force ductility and by rheology.
–the morphology in the asphalt mix can be investigated by either preparing thin sections, or simply by investigating the fractured surface of a broken mix. This conclusion is at this moment still preliminary since it was only tested on these four mixes.
– As the morphology depends on the cooling rate, it will also depend on the size or volume of the investigated specimen. Since asphalt cores are often much larger than binder samples, the cooling rates in an asphalt mix sample are very often slower compared to cooling rates in a binder sample. The difference in cooling rate between binder specimen and asphalt mix cores can have a strong influence on the phase morphology. As morphology influences the mechanical properties, this conclusion can have important consequences for the relation between binder and mixture properties. If in both tests (binder versus mix tests) the morphology of the PmB is different, it would be rather surprising to find a good correlation between these tests.
– For all four mixes investigated, the morphology in the mix is observed as a phase separated structure with distinct polymer phases in a continuous bitumen-rich matrix. The question if a binder is storage stable at high temperatures, does not seem to have an influence on the final morphology in the mix.
– In mix tests, the morphology is also dependent on the thermal treatment of the mixtures. This should be taken into account when performing for example mix aging tests at 135°C on loose or on compacted mixtures.

REFERENCES

Brûlé B., Brion Y., Tanguy A. 1988. Paving asphalt polymer blends: relationship between composition, structure and properties. *AAPT* 57: 41–64.

Dony A. & Durrieu F. 1990. Influence de la nature du bitume sur les propriétes et la stabilité des liants bitumes-polymères, *Bull. liaison Labo. P. et Ch.* 168: 57–63.

EN 13632: 2003. Bitumen and bituminous binders-determination of polymer dispersion in polymer modified bitumen-prepared by Technical Committee CEN/TC 336 « bituminous binders ».

Kraus G. 1982. Modification of asphalt by block polymers of butadiene and styrene, *Rubber Chemistry and Technology* 55: 1389–1402.

Pasquier M., Antoine J.P., Dumont A.G., Pittet M. 1997. Quantification de la microstructure des bitumes modifiés par microscopie optique à épifluorescence. In Di Benedetto & Francken (eds) *Mechanical Tests for bituminous materials*: 61–65. Rotterdam: Balkema.

Mouillet V., Lapalu L., Planche J.P., Durrieu F. 2004. Rheological analysis of bitumens by Dynamic Shear Rheometer: effect of the thermal history on the results. *Euroasphalt & Eurobitume Congress* paper 91.

Soenen H., Lu X., Redelius P. 2008. The morphology of Bitumen-SBS blends by UV microscopy: An evaluation of preparation methods. *RMPD* 9 (1): 97–110.

Wegan V. & Brûlé B. 1999. The structure of polymer modified binders and corresponding asphalt mixtures. *AAPT* 68: 64–88.

2. Testing and modeling the influence of climate and ageing effects

Advanced Testing and Characterization of Bituminous Materials – Loizos, Partl, Scarpas & Al-Qadi (eds)
© 2009 Taylor & Francis Group, London, ISBN 978-0-415-55854-9

Developing a test method for the accelerated ageing of bituminous mixtures in the laboratory

N. Piérard & A. Vanelstraete
Belgian Road Research Centre, Brussels, Belgium

ABSTRACT: Various standardized test methods for binders are available to simulate in the laboratory both the ageing of bituminous binders during mix manufacture and laying and their ageing on site in a bituminous mixture in service. However, there is currently no standardized test method for the laboratory ageing of an entire bituminous mixture. Research was, therefore, undertaken to develop a test method for the reproducible laboratory ageing of bituminous mixtures in a relatively short time. Materials (mixture, binder, aggregate) were sampled on site during the laying of new surface courses, and ageing tests were performed at 60°C on mixtures in bulk. This contribution will describe the development of the new method and its potentialities. The new method is also compared with the RCAT (Rotating Cylinder Ageing Test, EN 15323) ageing method for binders.

1 INTRODUCTION

To simulate the ageing of bituminous mixtures, many tests have been developed on their binders. Some of them make it possible to simulate the ageing process of the binder during mix manufacture and laying (RTFOT, TFOT, …), while others rather simulate binder ageing once the mixture has been laid on site (RCAT, PAV). All these tests have been standardized. However, they have the disadvantage of not investigating the ageing of the entire mixture. There is currently no common test method standardized at the European level to simulate mix ageing. Nevertheless, the working groups of CEN TC 227 and 336 have pointed out the need for conditioning methods in assessing the durability of asphalt mixtures. Several laboratories are engaged in developing an adequate test, such as the Porot & Bobrisow protocol for recycled asphalt pavement production in the laboratory [Porot et al. 2008].

In this context, BRRC has been interested in one particular aspect of the ageing of a bituminous mixture, viz. the effect of oxidation. This phenomenon makes the binder harder and more brittle, and modifies the interface between binder and aggregate. This contribution invites you to discover the method which was developed to simulate in the laboratory the ageing process of a mixture in a road pavement in service. The method is based on the accelerated ageing of bulk mixtures in an oven at 60°C while monitoring the development of binder characteristics in this process. In a second part, the new method is compared with the RCAT (Rotating Cylinder Ageing Test) ageing method for binders.

2 EXPERIMENTAL SETUP

2.1 *Development of the ageing method on bulk material*

To develop this new method, we looked for a test meeting the following criteria:

- easy to perform (no exacting equipment required);
- not too time-consuming;
- no binder flow during testing, i.e., the test temperature had to be lower than the softening temperature of the mastic.

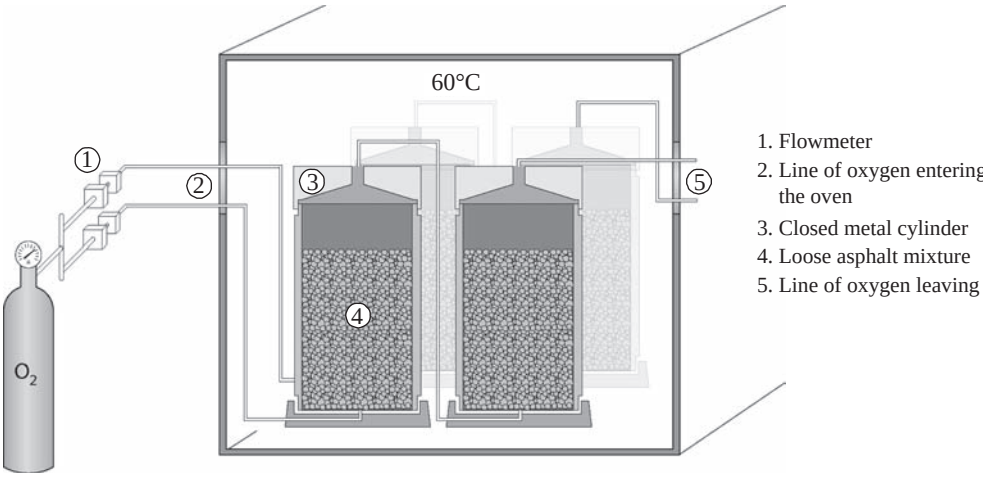

Figure 1. Device used for ageing bulk mixtures at 60°C under a flow of oxygen.

Table 1. Compositions of the mixtures laid on the sites at Ohain and in Ghent.

AC14 (type 1)—Ohain			AC10 (type 4)—Ghent		
Aggregate	Type	Content	Aggregate	Type	Content
7/14	Sandstone from Lustin	35.07%	6/10	Porphyry	10.0%
2/7	Porphyry from Bierges	19.76%	4/6	Porphyry	48.0%
0/2	Sand from Chaumont	18.76%	0/2	Porphyry	21.8%
0/2	Sand from Beez	18.76%	0/1	Fine sand	13.0%
Filler	IIa	7.65%	Filler	IIa	7.2%
Binder	Bitumen 50/70	5.9%	Binder	Bitumen 50/70	6.0%

To avoid binder flow, the test temperature was set at 60°C.

To shorten the duration of the test, oxygen was used at first. In view of the reasonable duration of the test under oxygen—as we shall see in Section 3.1.1—and of the markedly easier and safer performance of the test, we then investigated the possibility to conduct mix ageing tests under open air conditions.

Ageing tests under oxygen require the use of hermetically sealed cylinders (Fig. 1) through which a flow of oxygen is passed (from bottom to top; flow rate = 15 ml/min). In practice, four cylinders (H = 23 cm and ϕ = 11 cm) are filled with approximately 1.6 kg of bulk mixture and placed in an oven at 60°C. The cylinders are grouped into two separate circuits (circuit 1: Cyl1 and Cyl2; circuit 2: Cyl3 and Cyl4) connected to a feed of oxygen.

Ageing tests in open air are performed with the mixture under test spread in cake pans. About 1.2 kg of bulk mixture is spread in each pan (ϕ = 25 cm), to a thickness of 2 to 3 cm. Each pan is then placed in an open air-ventilated oven maintaining a temperature of 60°C throughout the test.

2.2 *Bituminous mixtures and binders*

The samples tested came from two work sites in Belgium: one at Ohain, the other (a private site) in Ghent. The mixtures sampled were of types AC14 (type 1) and AC10 (type 4). They were used in surface courses. Their compositions are given in the table below.

After compaction on site, the voids contents of these mixtures were 3.8 ± 1.3% for the AC14 (type 1) and 3.5 ± 0.9% for the AC10 (type 4). They were close-graded mixtures.

The binders used were pure bitumens, not polymer-modified bitumens.

Various samples (bulk material, binders, aggregates) were taken during laying:

- loose asphalt mixture: to develop the test method for ageing;
- aggregates and binder: to be able to prepare a bulk mixture equivalent to that laid on site, if necessary;
- binder: to compare the ageing of binders recovered from the laboratory-aged mixture to that of the same binder aged by the RCAT method.

In addition, core samples were taken at regular intervals on both sites with a view to the later validation of the ageing method developed on the bulk mixture.

2.3 *Ageing methods for binders*

To allow comparison of the binders extracted from the aged mixtures with the binder aged in the RCAT, the binders were aged by the RCAT procedure described in standard EN 15323. Each binder (500 g) was first aged at 163°C (RCAT163, 4.0 l/min air, 235 min, 5 revs/min) to simulate the ageing that occurs during the production and laying of an asphalt mixture (also called short-term ageing, STA). After that, it was aged for 140 h at 90°C (RCAT90, 1 rev/min) under a flow of oxygen (4.5 l/h O_2), to simulate ageing in a pavement in service (also called long-term ageing, LTA).

2.4 *Methods of analysis*

The binders extracted from the laboratory-aged mixtures and the binders aged in the RCAT were characterized. Their technological and rheological properties were evaluated from measurements of:

- needle penetration at 25°C (Pen) according to NBN EN 1426;
- ring-and-ball softening temperature (TR&B) according to NBN EN 1427;
- viscosity at 60°C, using the plane-plane method;
- the complex modulus and the phase angle at 52°C and at the frequencies of 1.6 and 10 Hz, according to EN 14770. The measurements were made during a frequency sweep.

The rheological measurements were carried out on a Bohling CVO 120 DSR device.

The chemical characteristics (extent of oxidation) were determined with an IR spectrometer (Perkin Elmer Spectrum One). The binders were dissolved to a concentration of 75 g of binder/l of CCl_4. Each spectrum was normalized (correction of the base line between 1,885 and 459 cm^{-1} and absorbance coefficient of a standard bitumen peak situated between 1,400 and 1,500 cm^{-1} brought to 1.2). The peak surface areas investigated were:

- A1700 (area comprised between 1,530 and 1,770 cm^{-1}) indicating the presence of carbonyl functions (ketones, esters, carboxylic acids);
- A1030 (area comprised between 1,000 and 1,105.3 cm^{-1}) indicating the presence of sulfoxides;
- Atot summing all modifications recorded between 946 and 1,885 cm^{-1}.

For the bulk mixtures, the binder characteristics were determined on the binder extracted and recovered by the procedures described in NBN EN standards 12697-1 (part B2, continuous flow centrifuge) and 12697-3. Only the dissolution method differed from that specified in the standard: the loose mixture was dissolved in toluene for one night, under light stirring.

3 RESULTS AND DISCUSSION

3.1 *Ageing tests on bulk mixtures*

3.1.1 *Tests under oxygen*

An ageing test on the AC14 (type 1) mixture in bulk was performed at 60°C under oxygen flow, by the procedure described in Section 2.1. The test lasted 78 days. Coarse aggregate was

Table 2. Technological and rheological characteristics of the binder extracted from the AC14 (type 1) mixture in bulk aged at 60°C under oxygen for 36 and 78 days.

			36 d.		78 d.	
		0 d.	Circuit 1 (Cyl2)	Circuit 2 (Cyl3)	Circuit 1 (Cyl1)	Circuit 2 (Cyl4)
Pen	(1/10 mm)	47	18	20	18	18
TR&B	(°C)	53.1	64	63.3	66.4	65.8
Viscosity 60°C	(Pa.s)	532	2,683	2,594	4,253	3,803
$G^*_{1.6\ Hz}$ 52°C	(kPa)	15.7	62.4	62.0	96.3	83.3
$G^*_{10\ Hz}$ 52°C	(kPa)	70.6	362.0	310.0	352.1	326.2
$\delta_{1.6\ Hz}$ 52°C	(°)	79.7	70.8	71.6	68.7	69.1
$\delta_{10\ Hz}$ 52°C	(°)	76.0	67.1	67.0	63.0	63.6

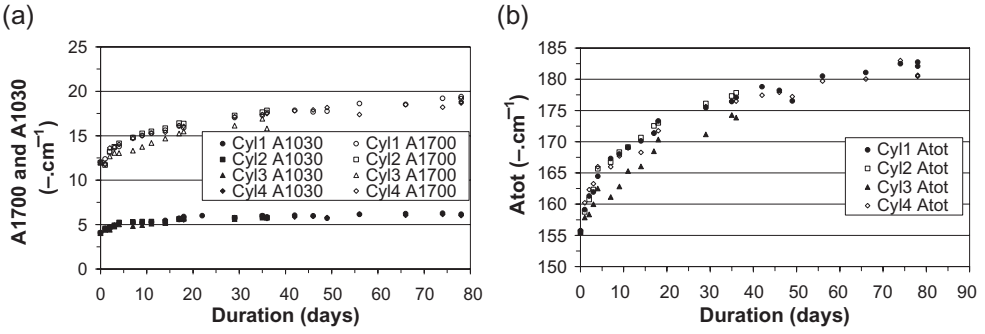

Figure 2. Ageing of the AC14 (type 1) mixture in bulk at 60°C under oxygen: development (a) of the carbonyl functions (A1700) and the sulfoxide functions (A1030) and (b) of the total area (Atot) measured in infrared spectrometry on coarse aggregate samples from the various cylinders.

sampled very regularly to monitor ageing by infrared analysis. The binder was extracted from the loose mixture and characterized at the beginning of the test and after 36 (Cyl2 and Cyl3) and 78 days (Cyl1 and Cyl4). The values measured are presented in Table 2. The development of the infrared results is shown in Figures 2a and 2b.

From Table 2 and Figures 2a and 2b it appears that:

- the binder extracted from the mixture aged severely during the test. It became harder, as shown by the decrease in penetration and the phase angle of the rigidity modulus and by the increase in ring-and-ball softening temperature, viscosity, rigidity modulus and oxidation peaks (A1700, A1030 and Atot);
- The characteristics of the binder extracted after 36 days of ageing already indicate an advanced stage of binder ageing, but the binder has not yet reached its final state: its characteristics are still evolving. However, for what concerns the simulation of field ageing, the duration of the test can be shortened. Indeed, Choquet F.C. characterized the binders extracted from the top half centimetre slice of asphalt surface courses[1] after 6 to 19 years of service [Choquet 1991]. Their needle penetration averaged 23 dmm (with individual values ranging between 14 and 37 dmm). This value is of the same order of magnitude as the 18–20 dmm measured in our test after 36 days of ageing. Futhermore, the chemical characteristics of the binder provide information on the test duration to be specified. The oxidation of the binder (carbonyl functions: A1700 and Atot) progresses very rapidly in the first 15 days and then tends to stabilize at a certain level. For the sulfoxide functions the development is faster (5–10 days), but smaller in amplitude. Since the chemical

[1] Voids content lower than 5%, road bitumen of penetration grade 50/70.

characteristics are correlated to the technological characteristics, the duration of the test can be shortened and reduced to about two weeks, for practical reasons;
- the ageing can be considered as reproducible. The IR characteristics are very similar, whichever the cylinder from which samples were taken after a given time (Figs 2a–2b).

In view of the reasonable duration of the test (about two weeks), we tried to develop it for open-air conditions rather than under oxygen. This would simplify the test procedure (no more need to work with hermetically sealed cylinders) and benefit safety.

3.1.2 *Tests under air*

Further ageing tests at 60°C on the mixtures in bulk were undertaken, this time in ambient air. A first test was performed on a bulk mixture prepared in the laboratory with the composition of the AC14 (type 1), using the mixing procedure described in standard NBN EN12697-35. The same materials were used in the same mix proportions, except for the filler which was slightly different. A second test was carried out on the AC10 (type 4) mixture sampled on the site in Ghent.

In both cases[2], the bulk mixture spread in several pans was aged in an open air-ventilated oven set at 60°C, by the procedure described in Section 2.1. During the test, the pans were removed one after the other from the oven. The binder contained in the aged bulk mixture was then extracted and recovered for a full determination of its technological, (rheological) and chemical (IR) characteristics. The results are presented in Tables 3 and 4.

In both cases, the binder contained in the mixtures aged at 60°C in open air aged rapidly: within 5 days, the penetration of the binder from the AC14 (type 1) mixture decreased by 20 dmm, while that of the binder from the AC10 (type 4) decreased by 16 and 20 dmm after

Table 3. Development of the technological and IR (oxidation peak) characteristics of the binder extracted from the AC14 (type 1) mixture in bulk aged at 60°C in open air.

Duration (d.)	Pen (1/10 mm)	TR&B (°C)	A1700 (–.cm^{-1})	A1030 (–.cm^{-1})	Atot (–.cm^{-1})
0	47	53.0	12.3	4.0	155.2
1.0	36	55.7	14.7	4.4	162.9
4.2	29	58.6	16.5	4.7	170.0
5.0	27	58.7	16.9	4.7	171.1

Table 4. Development of the technological, chemical, and rheological characteristics of the binders extracted from the AC10 (type 4) mixture in bulk aged at 60°C in open air.

							52°C			
Duration (d.)	Pen (1/10 mm)	TR&B (°C)	A1700 (–.cm^{-1})	A1030 (–.cm^{-1})	Atot (–.cm^{-1})	Visco 60°C (Pa.s)	$G^*_{1,6Hz}$ (kPa)	$G^*_{10\ Hz}$ (kPa)	$\delta_{1,6\ Hz}$ (°)	$\delta_{10\ Hz}$ (°)
0	40	54.5	12.6	3.9	157.7	711	18.4	85.3	78	75
1.1	34	56.5	13.4	4.2	160.8	968	24.5	110.1	77	74
3.1	27	59.2	15.4	4.5	167.8	1,412	34.7	146.9	75	71
8.1	24	61.4	16.7	4.8	172.2	2,066	48.2	203.5	73	69
16.1	20	64.2	18.7	5.4	180.3	3,159	69.2	275.1	71	66

[2] Prior to the test on the loose mixture prepared in the laboratory a treatment was necessary, as the freshly manufactured mixture did not exhibit a sufficient extent of ageing comparable to that of the bulk mixture sampled on site. The procedure used for this treatment was based on AASHTO procedure R30-1. It consisted in placing several pans containing the bulk mixture spread to a thickness of 2 to 3 cm in an oven at 135°C, to simulate short-term ageing. The duration of this treatment was limited to 75 minutes (instead of the planned 4 hours), since by that time the binder had reached the IR characteristics of the bulk mixture sampled on site. After this prior ageing, the various pans were aged in open air in an oven at 60°C.

8 and 16 days, respectively. This decrease was invariably attended by an increase in ring-and-ball softening temperature and in the intensity of the oxidation peaks (A1700, A1030 and Atot). The developments of the rigidity modulus and the phase angle corroborated this ageing.

When comparing the technological and chemical characteristics of the two mixtures aged at 60°C in open air, it can be seen that:

- five days of testing are not enough to reach the stage where the ageing kinetics slows down considerably. It is more advisable to extend the duration of the test to 10 days or even two weeks to have an overall idea of the ageing process of the mixture;
- ageing seems to be slower for the AC10 (type 4) mixture in bulk than for the AC14 (type 1) mixture. This suggests that the method is capable of revealing composition and materials-related differences in ageing behaviour between mixtures.

The results of these two open-air ageing tests show that it is possible to age a bulk bituminous mixture in the laboratory so as to simulate the ageing of this mixture in a road pavement in service. The test developed is not too time-consuming, does not require a costly investment and produces considerable quantities of aged mixture. Compared to the method discussed in 3.1.1, it can be shown that this method in air leads to a faster ageing of the bituminous mixture. However, it is premature to draw conclusions about this. The fillers used in AC14 mixture (that was studied according the both methods) were slightly different. This could have influenced the results.

3.2 *Comparison of the open-air ageing test at 60°C for mixtures with the RCAT for binders*

It is interesting to compare this ageing test for mixtures in bulk with a standardized ageing test for binders, such as the RCAT (EN 15323). The binders of the two mixtures investigated above were, therefore, aged by the RCAT procedure—first at 163°C and then at 90°C, to simulate short-term and long-term ageing. Samples of the binder taken during the test made it possible to monitor the progress of binder ageing for the technological, (rheological) and IR characteristics. Figure 4 shows comparative plots of the characteristics of the binders extracted and recovered from the loose mixture aged at 60°C in open air and those of the corresponding binders aged at 90°C in the RCAT (LTA).

It can be seen that:

- during the first days of testing (3 to 5 days, depending on the mixture) the technological characteristics and the sulfoxide functions of the binders extracted from the mixtures in bulk (AC14 and AC10) developed in a similar way as for the same binders aged at 90°C in the RCAT. Note that for the AC10 (type 4) mixture a shift is

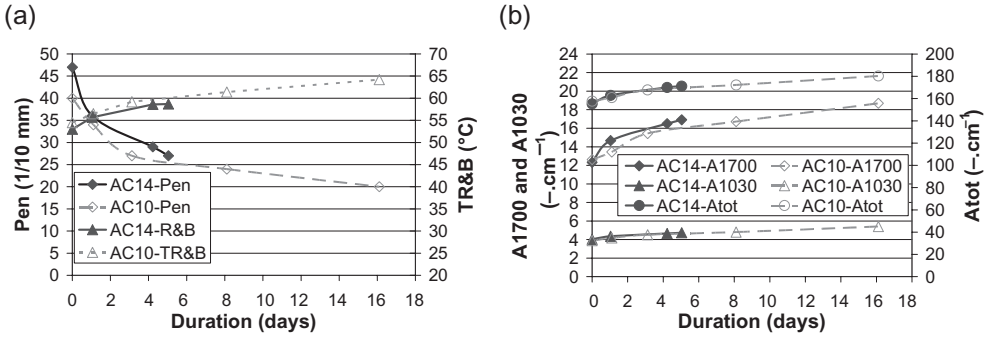

Figure 3. Comparison of the development of the (a) technological and (b) IR characteristics of the AC14 (type 1) and AC10 (type 4) mixtures in bulk aged in open air in an oven at 60°C.

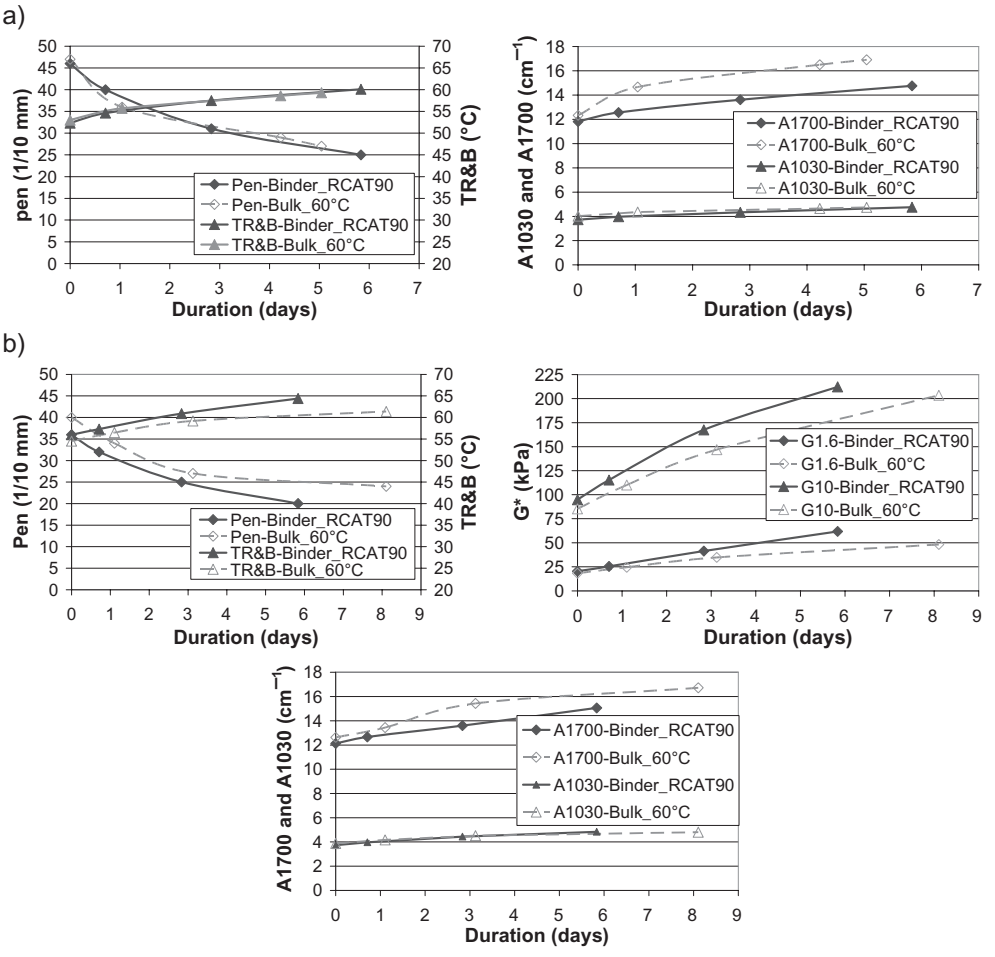

Figure 4. Development of the technologica, (rheological)l and IR (oxidation peak) characteristics of the binder aged at 90°C in the RCAT and of the binder extracted from the loose mixture aged at 60°C in open air: a) AC14 (type 1), b) AC10 (type 4).

observed (on the y axis) between the initial characteristics of the extracted binder and the binder aged at 163°C in the RCAT. This is due to the ageing of the bulk material sampled on site being less advanced than that obtained by RCAT163 (STA) on the corresponding binder. However, when looking at the shapes of the curves it remains possible to compare the ageing tests on the mixture and the binder, like in the case of the AC14 (type 1) mixture;

- in the longer run, the technological and rheological characteristics of the binders extracted from the aged AC10 mixtures in bulk developed slower than those of the same binder aged at 90°C in the RCAT;
- the carbonyl functions (A1700) of the binders extracted from the aged mixtures (AC10 and AC14) increased faster than those of the binder aged at 90°C in the RCAT. This different behaviour may be explained by the role of the filler in the ageing of a bituminous mixture. There is, indeed, a similarity between the development of the carbonyl functions of the mastic and those of the bulk material aged under the same conditions, while no major change is observed in the sulfoxide functions (Fig. 5). This means that the filler plays a predominant part in the development of the carbonyl functions during the ageing of a bituminous mixture;

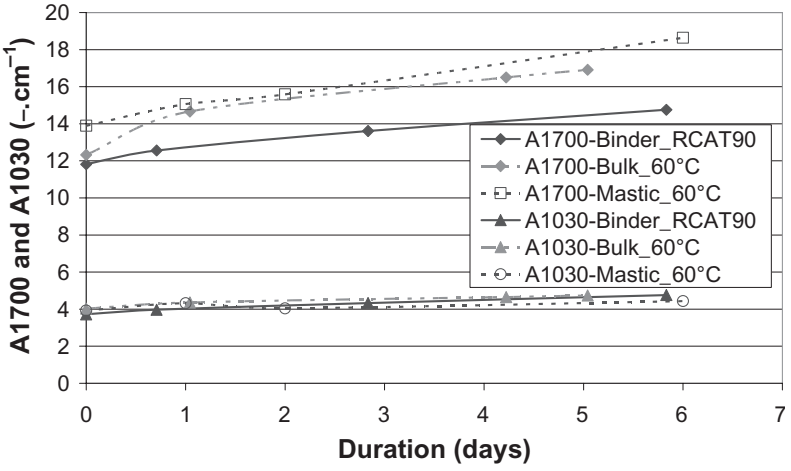

Figure 5. Development of the carbonyl (A1700) and sulfoxide (A1030) functions during RCAT90 ageing of the binder and during the ageing of the mastic[3] in cupels[4] and of the mixture (AC14 (type 1)) in bulk, both at 60°C in open air for several days.

- the ageing tests on the loose mixture in a ventilated oven at 60°C and on the binder in the RCAT at 90°C were relatively similar in duration. However, some "exhaustion" is observed for the ageing process of the binder contained in the mixture when comparing with the binder aged by the RCAT method. The ageing of the mixture is also less advanced than that of the binder in the RCAT. This seems logical: on the one hand, the ageing temperature of the mixture is lower and, on the other, mix ageing at 60°C in open air is a static test—as opposed to the RCAT, which is dynamic. As a result, the film of binder is not constantly renewed and the ageing process is saturated sooner.

4 CONCLUSION

This research project has shown that it is possible to age a bulk bituminous mixture in a laboratory test which is easy to perform and is not too time-consuming. The method developed consists in spreading the mixture in bulk to a thickness of 2 tot 3 cm in a cake pan and placing it in an open-air ventilated oven at 60°C for about two weeks.

A method to age bulk asphalt under oxygen flow was also investigated, but is not to be recommended as it is more difficult to implement (because of the need to have hermetically sealed cylinders) and less safe (owing to the use of oxygen). After two weeks of testing, it produces ageing comparable to that observed in surface courses after 8 to 22 years of service.

Comparison of the characteristics of the binders extracted from the mixtures aged at 60°C in open air with those of the corresponding binder aged at 90°C in the RCAT has shown that the ageing of the binder in the mixture is very similar to that of the binder in the RCAT during the first days of testing, but that the ageing process of the binder in the RCAT is faster in the long run.

For the future, BRRC is monitoring the ageing on site of the two mixtures on which the ageing test for mixtures was developed. This will permit more accurate comparison of the

[3] Prepared with the filler and binder used for this mixture.

[4] 3 grammes of mastic (aged at 163°C in the RCAT to simulate short-term ageing) were poured in each of a number of metal cupels to form a film a few millimetres thick. The cupels were placed in a ventilated oven at 60°C. After 1, 2, 3 and 6 jours, one cupel was removed from the oven and the mastic was dissolved in CCl_4 for an IR analysis of the binder (before the spectrum was taken, the solution was filtered to remove the filler).

characteristics determined on the laboratory-aged mixtures in bulk with those of the binders extracted from these mixtures in service, and allow further validation of this new test.

ACKNOWLEDGEMENTS

The authors gratefully acknowledge the federal government for the financial support of this project under contract number CC-CCN 357. In addition the authors wish to thank P. Crabbé and C. Motte for their technical support.

REFERENCES

AASHTO R30-1:2006, Standard method of test for Mixture Conditionning of Hot-Mix Asphalt.

Choquet F.C. 1991, The search for an ageing test based on changes in the generic composition of bitumens, *Proc. Inter. Symp. Chemistry of Bitumens, 5–8 June 1991, Rome, Italy*: 788–812.

EN 14770:2005, Bitumen and bituminous binders: determination of complex shear modulus and phase angle: dynamic shear rheometer (DSR).

EN 15323:2007, Bitumen and bituminous binders—Accelerated long-term ageing/conditioning by the rotating cylinder method (RCAT).

NBN EN 1426:2007, Bitumen and bituminous binders: determination of needle penetration.

NBN EN 1427:2007, Bitumen and bituminous binders: determination of softening point: ring and Ball method.

NBN EN 12697-1:2006, Bituminous mixtures—Test methods for hot mix asphalt—Part 1: soluble binder content.

NBN EN 12697-3:2005, Bituminous mixtures—Test methods for hot mix asphalt—Part 3: Bitumen recovery: Rotary evaporator.

NBN EN12697-35:2004/A1:2007, Bituminous mixtures—Test methods for hot mix asphalt—Part 35: Laboratory mixing.

Porot, L. & Bobrisow, L. 2008, Laboratory mixture ageing protocol for RAP production, *Proc. Eurobitume & Eurasphalt congress, Copenhaguen*, paper 403-006.

Advanced Testing and Characterization of Bituminous Materials –
Loizos, Partl, Scarpas & Al-Qadi (eds)
© 2009 Taylor & Francis Group, London, ISBN 978-0-415-55854-9

Chemical characterization of laboratory and field bitumen aging in Porous Asphalt Concrete

E.T. Hagos, A.A.A. Molenaar & M.F.C. van de Ven
Delft University of Technology, Faculty of Civil Engineering and Geosciences, Road and Railway Engineering, The Netherlands

ABSTRACT: This paper deals with the chemical characterization of bitumen which was part of the rheological and chemical investigations into the effect of aging on the binder properties of Porous Asphalt Concrete (PAC). Analytical methods such as Infrared spectroscopy (FTIR) and Gel-permeation chromatography (GPC) are effective tools to assess the chemical changes in bitumen. These methods were adopted to investigate the effect of bitumen aging on the molecular structure (Molecular Weight distribution, MWD) and the functional groups responsible for oxidation/aging of laboratory aged and field binders. The test results show that aging increases the large molecular seize portion in the binder molecular distribution due to the formation of oxidation products—Ketones (C=O) and sulphoxides (S=O). Laboratory aging of bitumen using a standard aging method and PAC mixture aging under a proposed new aging protocol that combines temperature, UV light, and humidity were employed to simulate the field aging of PAC. Prediction based on the kinetic approach with the use of the characteristic peak areas of oxidation products in the IR spectrum shows that the field aging of PA is much more severe than the lab bitumen aging. The standard long term lab bitumen aging was found to be not satisfactory in predicting field aging of PAC. Although only 2.1 years of field aging could be predicted, the proposed lab mixture aging protocol showed similar aging behaviour as the field aging. An improved mixture aging protocol is suggested in order to better simulate the binder aging in reality.

Keywords: Aging, Porous Asphalt (PA), IR spectrum, GPC, Kinetic approach

1 INTRODUCTION

Porous Asphalt Concrete (PAC) surfacing layer is a cheaper solution to reduce traffic induced noise compared to other noise reducing measures such as noise barriers. PAC is being used in combination with noise barriers to protect inhabitants living close to the motorway from noise pollution. Currently, about 70% of the major roads in the Netherlands are surfaced with Single Layer Porous Asphalt SLPA. Two Layer Porous Asphalt (TLPA) is also being researched to further minimize noise. In comparison to the reference Dutch Dense Asphalt Concrete (DAC) surface layer, a noise reduction of 4 dB (A) with the SLPA and 6 dB (A) with the TLPA can be attained (IPG 2002, Hofman et al. 2005).

However, ravelling or loss of aggregates from the pavement surface is not only a major durability problem of PAC resulting in relatively low service life compared to DAC, but also reduces noise absorption. The causes of raveling in PAC can be cohesive or adhesive failure, or a combination of the two. Aging strongly influences the cohesive characteristics of the bituminous mortar. Because of high voids content of PAC, the binder is exposed to environmental influences which accelerate aging. Interaction with the environment causes oxidation to take place that results in a change in the bitumen properties with time. This paper focuses on the effect of weathering actions on the chemical characteristics of the binder.

Laboratory aging methods to simulate binder aging during the construction phase (short term aging) and service period of the pavement (long term aging) are available. However, the

standard/conventional test methods of binder aging focus primarily on oxidation and results are mostly calibrated for dense mixes. As a result, the oxidation technique does not seem to simulate accurately the complex nature of field aging of PAC due to the influence of environmental factors involving the combined effects of temperature, UV light, and moisture. The change in the rheological and chemical properties of the binding material is usually used as indicators to investigate the effects of aging. The change in the viscoelastic behaviour, cohesive strength, adhesion and other characteristics of the bitumen are dependant on the chemical changes occurring in the material (Ishai 1996, Peterson 2000). This implies that realistic simulation of weathering actions is essential to characterize the performance of the binder similar to field conditions. For this reason, an aging method that combines the effects of temperature, UV light and moisture is considered important.

2 THE RESEARCH PLAN

In Figure 1, the research plan that has been adopted to compare field aging of PAC with laboratory aging is shown. Accordingly, PAC specimens from new construction and road sections after service periods of 1, 3, 7, and 12 years were sampled from the field. The binder from these samples was recovered for chemical analysis. Similarly, the recovery of binder from laboratory prepared PAC mixtures was conducted after aging in a weatherometer. Furthermore, the aging of virgin 70/100 penetration grade bitumen was conducted using the standard aging methods in the laboratory. The laboratory aging protocols for the mixture and bitumen are presented in section 3.2.

The field specimens were cored from the emergency lane (EL) and the slow lane (SL) in order to take the influence of heavy traffic into consideration. In addition, the condition of the road was taken into account for 7 and 12 years field specimens because of a large variability in their pavement condition.

The top and bottom parts of all asphalt mixture specimens were recovered separately to carry out independent investigations. Even though the aging of PAC occurs over the entire thickness, differences in aging between the top and bottom part is expected due to the non-uniform influence of environmental factors (temperature, UV light, and moisture/humidity) along the pavement thickness. Moreover, possible differences in the binder content or binder film thickness in the upper and bottom parts of the layer as a result of binder/mortar drainage during the paving operations are expected to have an impact on the aging behaviour of the binder in the two zones.

Polymer Modified Bitumen (PMB) is intended for use in two layer PAC (TLPAC) in the Netherlands. For this purpose research is being carried out on test sections. It is believed that the proposed mixture testing protocol for single layer PAC is also applicable for the TLPAC since the surfacing layer will be subjected to the same weather conditions. In terms of long term aging behaviour of the unmodified and modified binders, the two binders will experience differences in chemical and rheological properties (Oliver and Tredrea 1997).

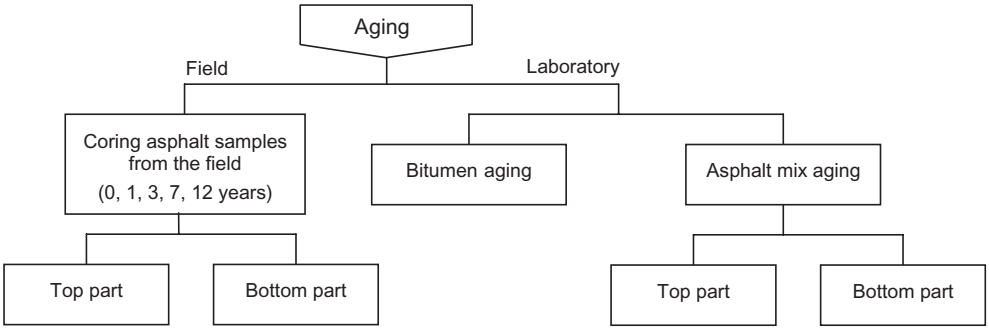

Figure 1. Schematic outline of the research plan.

3 MATERIALS AND TESTING PROGRAM

The materials used for conducting chemical investigations were taken from laboratory aging protocols and field aged specimens.

- Laboratory aging protocols
  - Conventional aging method:
    Short term (RTFOT/RCAT) and long term (RCAT) aging.
  - Porous asphalt mixture (PAC) aging:
    Weatherometer aging of PAC Marshall tablets and PAC beams under the combined influence of temperature, UV light, and humidity.
- Field materials—Core specimens taken from the road with service periods of 0, 1, 3, 7, and 12 years.

3.1 *Porous asphalt concrete*

The Dutch PAC design was used to produce the laboratory mixtures following the standard procedure RAW 2005. The specification for the mixture design with maximum 0/16 aggregate size is given in Table 1.

PAC mixtures produced for aging in the laboratory include:

1. Marshall tablets (dia. 100 mm), and
2. Beams sawn from porous asphalt slab produced in the lab.

The Marshall tablets were produced using the Marshall Compaction method with 50 blows on both sides of the specimen. The Marshal tablets have a diameter of 100 mm and a variable thickness (40–43 mm). Also produced in the lab was a slab with a size of $700 \times 700 \times 80$ mm. Beam sizes of 300×100 mm were sawn from the slab for aging in a weatherometer. The mean voids content of the PAC specimens were 17.5% for the Marshall tablets, 23.1% for the beams sawn from the slab, and 22.9% for the field specimens.

The materials used in the aging program of bitumen and asphalt mixtures are presented below.

- Aggregate: quarry material, sand stone (size: 2 mm–16 mm).
  – average density 2770 kg/m^3.
- Sand: crushed sand (size: 0.063 mm–2 mm)
- Filler: Wigro 60 K limestone filler with 25% hydrated lime.
  (size: <0.125 mm (90% <0.063 mm), Bitumen Number BN53/62, Voids 46%)
- Bitumen: 70/100 pen, 4.5% by wt. of 100% aggregate. (Pen = 90.7 dmm, $T_{R\&B} = 45.4^{\circ}C$)

Table 1. Single layer 0/16 PAC mixture design according to the Dutch standard RAW 2005.

Sieve size	Dutch Standard PAC (Aggregate size: 0/16)			
C 16	0.0–7.0	*Requirements:*		
C 11.2	15.0–30.0	Bitumen: 70/100 pen	4.5% by wt. of 100% aggregates	
C 8	50.0–65.0		(≈8% by vol.)	
C 5.6	70.0–85.0	Aggregates:	≈95.7% by wt. of total mix	
2 mm	85.0		(≤68% by vol.)	
63 mm	95.5	– Aggregate: ≥2 mm sieve		85.0% by wt.
Bitumen	4.5% by weight	– Sand: <2 mm and ≥0.063 mm		10.5% by wt.
Fibre	–	– Filler: <0.063 mm		4.5% by wt.
Layer thickness	50 mm	**middle sort filler with 25% hydrated lime (*KA*25, bitumen number BN54/60)		
		– Voids:		≥20%

3.2 *Aging procedures*

Laboratory aging of bitumen samples was performed on bulk bitumen and lab produced asphalt mixtures. The specimen categories and the corresponding aging procedures adopted are presented in Table 2 and Table 3.

3.2.1 *Aging of bitumen*

Short Term Aging (STA): the Rotating Thin Film Oven Test (RTFOT, EN 12607-1) was adopted to simulate the loss of volatiles and oxidation reaction that takes place during the production (mixing and transportation), laying and compaction stage of the asphalt mixture.

Long Term Aging (LTA): the Rotating Cylinder Aging Test (RCAT) was used in accordance with the recommended European procedure NEN-EN 15323. The long-term aging simulates the aging of dense asphalt mixtures for a period of at least 10 years. The RCAT aging is a dynamic aging test and it can be used to combine the short term and long term aging. RCAT140 and RCAT185 represent the number of aging hours in RCAT, i.e. 140 and 185 hrs respectively.

3.2.2 *Aging of Porous Asphalt concrete samples*

Three aging protocols were used for laboratory aging of asphalt mixtures (Hagos 2008):

- Protocol 1: aging under the influence of temperature,
- Protocol 2: aging under the combined effects of temperature and UV light, and
- Protocol 3: aging under the combined effects of temperature, UV light, and humidity.

Table 2. Aging tests for bitumen and asphalt mix specimens.

Aging and testing methods for bitumen and asphalt mixture specimens		
Specimens	Aging	Chemical test
Bitumen	STA: RTFOT LTA: (RTFOT) + RCAT	IR*, GPC** Vanadium content
Lab PAC mixture	Aging protocol 1 (weatherometer) Aging protocol 2 (weatherometer) Aging protocol 3 (weatherometer)	IR, GPC
Field cores	Field aging Age: 0, 1, 3, 7, 12 yrs	IR, GPC Vanadium content
	**IR = Infra red,* ***GPC = Gel Permeation Chromatography also known as Seize Exclusion Chromatography or SEC.*	

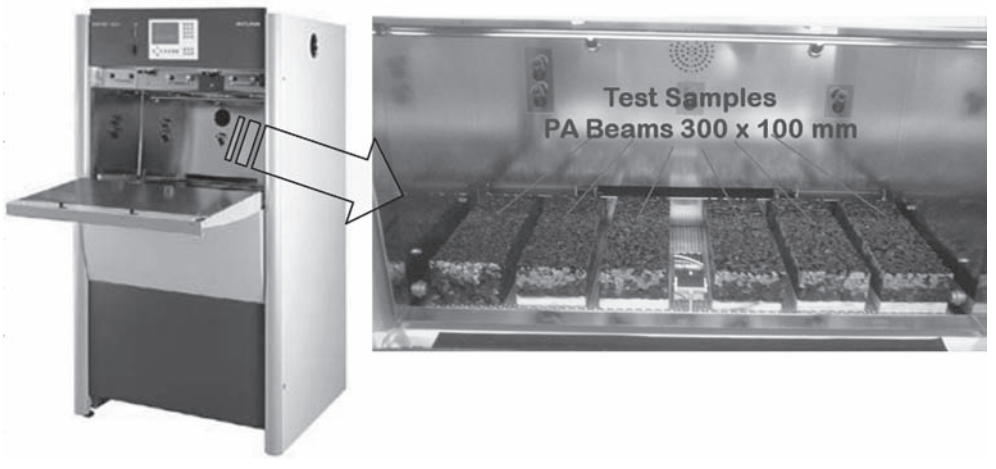

Figure 2. Weatherometer (SUNTEST XXL+) used for aging of asphalt mixtures.

Table 3. Aging procedures for laboratory produced porous asphalt mixtures.

Laboratory aging protocols for lab PAC (mixture)			
Marshall tablets (ϕ = 100 mm)	Reference samples	Temperature aging (*Aging protocol 1*)	Temperature + UV (*Aging protocol 2*)
No. of core samples	8	8	8
Avg. Voids Content [%]	18.2	16.2	17.8
Aging Temperature	Unaged	60°C	60°C
Time of aging	–	1000 Hrs	1000 Hrs
UV exposure (300–400 nm)	–	–	60 W/m^2
Beams from PAC slab		Temperature + UV light + humidity (*Aging protocol 3, AP3*)*	
Size: 300 × 100 mm	No. of beams	5	
	Avg. Voids Content (%)	23.1	
	Aging Temperature	60°C	
	Time of aging	1000 Hrs	
	UV exposure (300–400 nm)	60 W/m^2	
	Humidity (RH)	70%	

*NB: Aging protocol AP3 was developed based on the analysis of weather conditions data in the Netherlands between 1981–2001. In addition, experiences in aging methods of other materials in the weatherometer were considered in designing the protocol (ATLAS 2001, CIE 1989, Hagos 2008).

In Table 3, the test conditions for the three aging protocols are shown. Chemical tests were performed on the recovered bitumen to characterize the chemical properties of the binders after aging in the weatherometer.

The weatherometer used for aging porous asphalt mixture beams is shown in Figure 2.

3.3 *Binder recovery*

Recovery of the binder from the field cores and lab produced PAC mixtures was performed according to the European standard EN 12697-3 and NEN3971, which entails:

1. Extraction of the binder from the mixture: separation of the aggregates, sand, and filler from the binder using Dichloromethane (Methylene Chloride, CH_2Cl_2) solvent.
   a. Binder extraction by dissolving the asphalt mix in cold solvent (Dichloromethane, CH_2Cl_2).
   b. Separation of mineral matter from the binder solution (centrifuge extraction method).
2. Recovery of the binder from the solution (EN 12697-3): recovery of the bitumen from the solvent using the rotary evaporation method.

As explained before, the recovery of binder for the top 25 mm of the PAC cores (Upper Zone, UZ) and the bottom 25 mm (Lower Zone, LZ) was performed separately. The focus was on the binder characteristics of the top part since the ravelling of porous asphalt occurs at the surface.

The reader is referred to Hagos (2008) for more details on the adopted research methodology and the rheological and chemical test results.

4 TEST RESULTS & DISCUSSION

Three tests were conducted to investigate the chemical characteristics of binders from the field and lab aging. These are:

1. Vanadium content determination—to verify whether the field and lab binders are from the same source/origin.

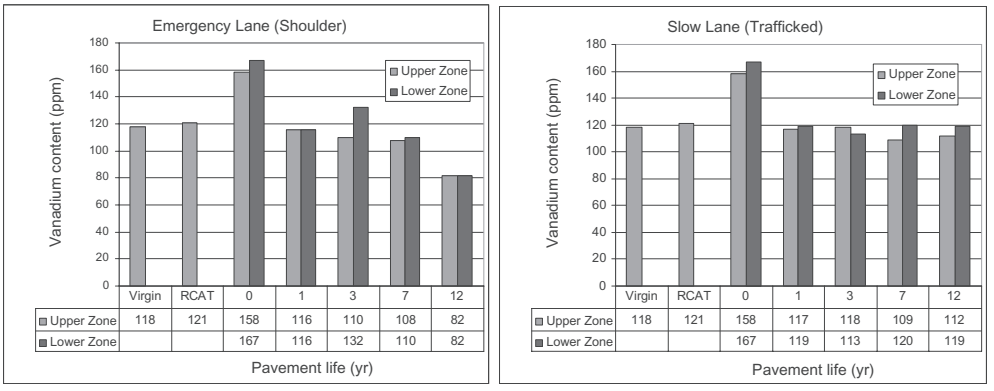

Figure 3. Vanadium content of laboratory and field binders.

2. Attenuated total refraction Fourier transform infrared spectroscopy (ATR/FTIR)—to investigate the development of the functional groups responsible for aging.
3. Gel-permeation chromatography (GPC)—to determine the Molecular Weight Distribution (MWD).

4.1 *Vanadium content*

The determination of vanadium content of the binders was conducted using the x-ray spectrometry method following the standard procedure DIN 51790-7. The results are shown in Figure 3.

The determination of vanadium content was carried out in order to verify whether the field binders and the binder used for lab aging belong to the same source/origin. This was important because no information was available about the field binders. Since binders from different sources have different proportions of the so called "hetro-atoms", this will have an influence on the aging characteristics of the binders. The aging of the binder during the service period of the pavement is believed to have no influence on the vanadium content of the bitumen.

Based on the results shown in Figure 3, the vanadium content, in general, ranges between 100–120 ppm. Exceptions that fall out of this range are the 12 year old field specimen with 82 ppm (lowest) and the bitumen recovered from section G (after construction) with 167 ppm (highest). Nevertheless, it seems that the difference in the vanadium content is small considering the expected difference among different sources as reported in the Shell Bitumen Handbook (Reed and Whiteoak 2003). The slight differences in the vanadium content of the samples recovered from the top and bottom part of the pavement layer is regarded negligible.

4.2 *Infra-red spectroscopy*

The apparatus used to conduct the IR test was a Galaxy Series FTIR 3000. The scanning was performed in the Middle Infrared Region (MIR, 400–4000 cm^{-1}). A computer software program "*WinFirst*" was used to process the Attenuated Total Refraction (ATR) interferogram into an absorption diagram (spectrum) through Fourier Transformation function, thus the name ATR/FTIR.

Figure 4 shows the IR spectrum of lab aged bitumens (RCAT185), 12 year old field specimen (UZ), and binders recovered from weatherometer aging (AP3). As it can be observed in Figure 4, the materials from the 12 yr old pavement and the 1000 hr weatherometer aging have comparable peaks at the S=O bond and seem to have relatively higher peaks at the C=O

bond. The LTA binder (conventional long term aging using RCAT) does not seem to have significant effect on the C=O bond at 1700 cm^{-1} and has the lowest peak in the S=O band at 1030 cm^{-1} next to the virgin bitumen. The recovered bitumen from the lab mixture aging test (AP2: temp. + UV aging) has the highest peak at the sulfoxide band (S=O) while showing a small increment at the ketones band (C=O). This indicates that the effect of temperature and UV light on the aging process seem to be reflected in the development of the sulfoxide peak. The combined effect of the UV light and temperature has a greater effect on binder aging than the protocol with only temperature. The effect of the UV light on the aging process can also be seen at the C–C bond (1600 cm^{-1}). The combination of the three aging effects, i.e. temperature, UV light, and humidity (RH), is resulting in the development of the two major oxidation products (C=O and S=O), which is consistent with the characteristic of the field aged binders. In summary, the combined effect of temperature, UV exposure and humidity/moisture seems to result in the formation of both the ketones and sulfoxides similar to the field aging whereas the conventional aging results in S=O formation with minimum effect on C=O development. This supports the assertion that the conventional binder aging method does not simulate field aging.

The kinetic approach was used to fit the development of the oxidation products (C=O and S=O) of the EL (emergency lane) and SL (slow lane) field binders. This approach was used by Verhasselt (1997) to predict the aging rate of field and lab binders based on the development of the asphaltene content with aging time. The approach is briefly described below.

The kinetic approach is a method used to predict the rate of change of binder properties due to accelerated aging in the laboratory or the aging of the binder in asphalt pavements. With this approach, developments in binder characteristics such as penetration, ring and ball temperature (T_{RB}), viscosity, and asphaltenes content can be described effectively.

A one-dimensional diffusion model resulted in best fits for reaction indicators such as asphaltene content (AS), and softening point (T_{RB}) for tests performed below 100°C. Equation 1 is the corresponding equation (Verhasselt & Choquet 1997, Verhasselt 2002):

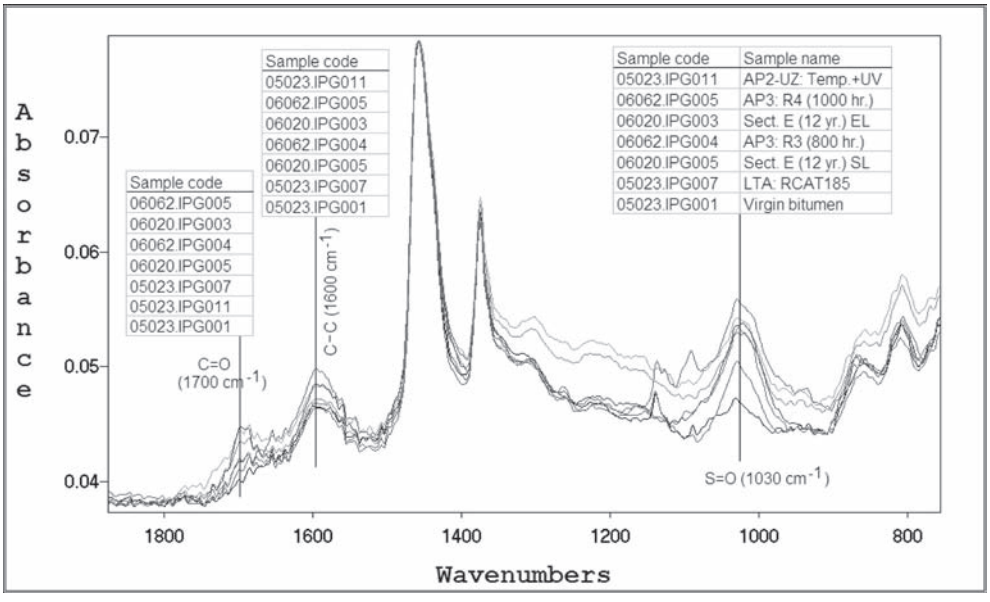

Figure 4. IR spectra of lab aged and field aged bitumens recovered from the upper part (UZ) of the cores.

$$\alpha^n = \left[\frac{S_t - S_0}{S_f - S_0} \right]^n = \left(\frac{dS_t}{dS_\infty} \right)^n = k \times t \tag{1}$$

where:
α = the extent of reaction.
S_0 = values of the signal or indicator S at times $t = 0$,
S_t = values of the signal or indicator S at times $t = t$,
S_f = values of the signal or indicator S at the end of the reaction,
k = the reaction constant,
n = aging coefficient, $n = 2$ for tests performed below 100°C and $n \approx 3/2$ for tests performed above 100°C.

Equation 1 can be reduced to a more practical equation (equation 2):

$$S_t = S_0 + (K^r \times t^r) \tag{2}$$

where:
K = overall reaction constant,
r = $1/n$.

when K results from an aging test performed at a given temperature T, it may be recommended to specify it with an index, K_T. When overall reaction constants, K_T, are known for different test temperatures, the activation energy (E) can be calculated from these values by applying the Arrhenius equation (equation 3):

$$K_T = A \times e^{-E/RT} \tag{3}$$

where:
K_T = overall reaction constant of aging at temperature T,
A = a constant (frequency factor),
E = activation energy. E ranges between 68,500 and 86,400 KJ.°K/mole,

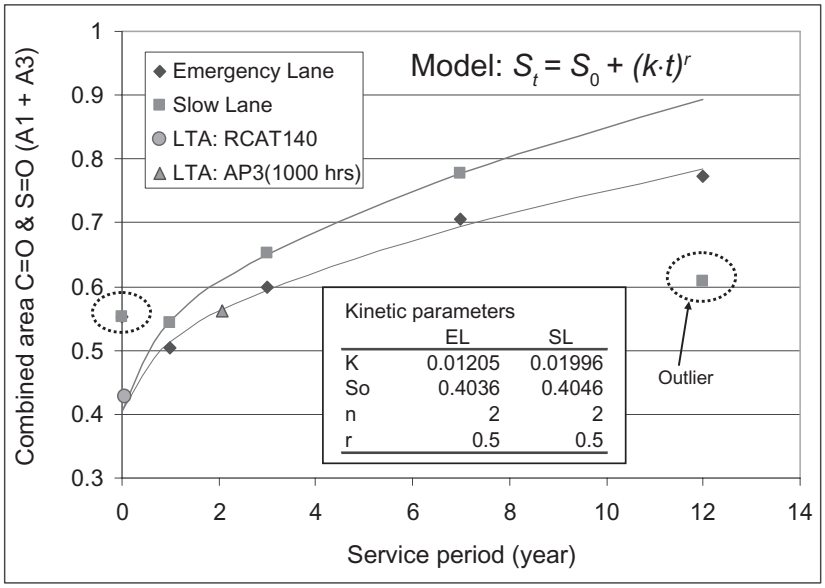

Figure 5. Development of oxidation products of field materials retrieved from the upper part.

R = perfect gas constant (8.314 J·K^{-1}mol^{-1}),
T = absolute temperature (°K).

Because of the activation energy, equal time of aging at various temperatures will contribute in different ways to the aging of the binder. As a result of temperature variations in the field, the total in-service aging will be the sum of a series of partial aging processes in which the contribution of a particular temperature will depend on the time of exposure. The sum of the partial aging is equivalent to an identical aging obtained at a certain constant temperature, T_k, called "*annual kinetic mean temperature*" (Verhasselt 2002). Note that higher temperatures contribute most to binder aging, which implies that most of the aging can be assumed to happen during summer periods.

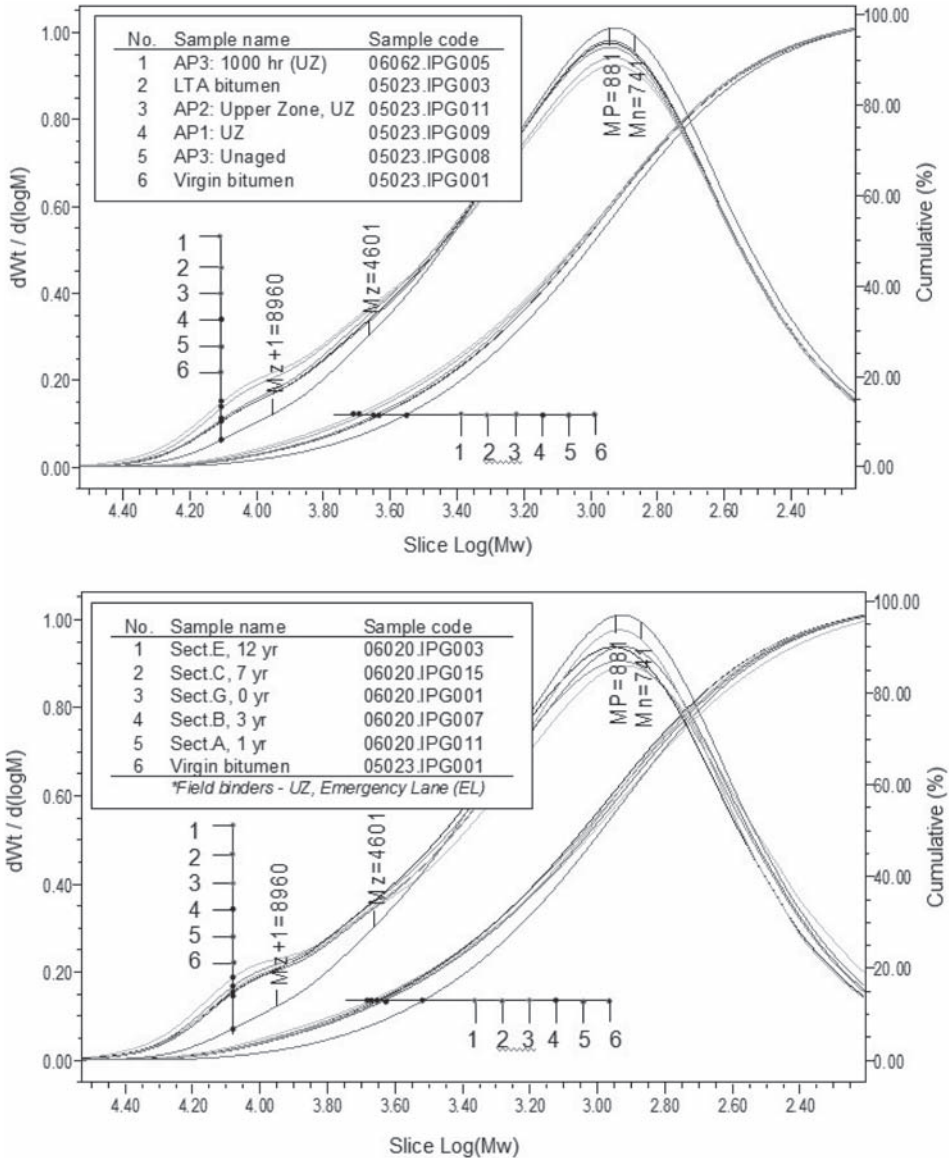

Figure 6. Molecular weight distribution of lab aged binders (top) and field binders from EL, UZ (bottom).

In Figure 5, the aging curve was determined based on the sum of the characteristic peak areas for oxidation at C=O and S=O. Accordingly, the most aged binders in the lab using the standard and weatherometer aging have less area than the 1 year old pavement binders. The LTA bitumen using RCAT predicted 0.43 year and the binder aged for 1000 hrs in the weatherometer predicted 2.1 years of field aging using the EL model. Hence, it was practically not possible to correlate the lab and field aging of binders.

The aging rate of the trafficked lane (SL) binder is higher than the lane with no traffic (EL). One logical explanation for this could be as follows: The damaging effect of traffic loading especially at lower temperatures results in micro-cracks. Micro-cracks create new surfaces to be exposed to the influence of the environmental factors promoting aging to take place.

The two outliers that are indicated in the figure might be related to the fact that the vanadium content of the bitumen recovered from these sections was outside the 100–120 range that was observed for the bitumen recovered from the other sections and the bitumen used in the laboratory.

It can be concluded that the aging protocols and procedures used in the laboratory are not able to simulate the aging that is observed in the field.

4.3 *Gel-permeation chromatography*

Gel-Permeation Chromatography (GPC), also known as Size Exclusion Chromatography (SEC), is a chromatographic method in which particles are separated based on their molecular size, or in more technical terms, their hydrodynamic volume. GPC or SEC is a technique used to analyze the Molecular Weight Distribution (MWD) of materials soluble in organic solvent. The method is a powerful tool to study the effects of bitumen modification and age hardening in bitumen related researches (Molenaar et al. 2004).

In Figure 6, results of a GPC test for lab aged binders and field binders are shown. The corresponding parameters that describe the MWD curves of the binders are shown in Table 4.

Table 4. MWD distribution parameters for lab and field aged binders.

	Bitumen type	Sample code	M_n	M_w	M_p	M_z	M_{z+1}	PDI
Lab	Virgin	05023.IPG001	741	1765	881	4601	8960	2.382562
	LTA bitumen	05023.IPG003	792	2199	894	6175	11077	2.777947
	AP3 (Unaged)	05023.IPG008	780	2028	908	5620	10542	2.599246
	AP1 (UZ)	05023.IPG009	781	2037	909	5645	10623	2.607673
	AP2 (UZ)	05023.IPG011	792	2082	913	5737	10680	2.627882
	AP3 (UZ)	06062.IPG005	797	2297	887	6660	12023	2.881359
Field	Sect.G (new)	06020.IPG001	807	2238	894	6455	11685	2.773153
	Sect.A (1 yr)	06020.IPG011	778	2186	877	6321	11457	2.809592
	Sect.B (3 yr)	06020.IPG007	815	2272	937	6493	11894	2.786442
	Sect.C (7 yr)	06020.IPG015	792	2293	901	6639	11890	2.894708
	Sect.E (12 yr)	06020.IPG003	758	2356	866	7241	12837	3.110002

M_n = number-average molecular weight [g/mol, daltons],
M_w = weight-average molecular weight [g/mol],
M_p = peak molecular weight [g/mol],
M_z = z-average molecular weight [g/mol],
M_{z+1} = (z + 1)–average molecular weight [g/mol],
$PDI = M_w/M_n$ = Polydispersity Index—relative spread in molecular weights [–].

Based on Table 4, the following evaluations are made:

– Comparison based on the M_z and M_{z+1} parameter shows that aging increases the large molecular size. These parameters are related to the asphaltenes content in the binder.
– Aging simulation using AP1 and AP2 protocols did not result in equivalent aging as long term field aging. Similar degree of aging was achieved using the AP3 and LTA aging protocols, but comparison with long term field aging appears not straight forward.
– Parameter M_p shows a decrease with aging which signifies that medium molecular sizes (MMS) are transformed to large molecular sizes (LMS) as a result of oxidation. The aging process is resulting in a spread of the MWD curve as indicated by an increase in the polydispersity index (PDI).
– According to the PDI results, the LTA bitumen compares well with the 3 year field binder and the AP3 is simulating the 7 year field binder. It is noted that the PDI of the 1 year old field binder behaves exceptionally.

5 CONCLUSIONS

Based on the results obtained in this research, the following conclusions are drawn.

a. Aging is a very complex process that is influenced by many factors.
b. Because of the large number of factors involved, it seems difficult to simulate precisely in the laboratory the aging that will occur in the field.
c. The existing laboratory aging protocols might be good enough to simulate the aging of dense asphalt mixtures in the field but they are certainly insufficient to simulate long term field aging of PAC. It is suggested that a lower humidity level during AP3 weatherometer aging combined with a gradual increase in aging temperature as the aging progresses will result in a better simulation of field aging.
d. Comparison of the results of the different aging tests as performed in the laboratory with the amount of aging that is determined from field samples, shows that subjecting lab specimens to a combined effect of moisture, temperature and UV radiation is necessary to obtain changes in chemical composition that are comparable to what happens in practice.
e. The RTFOT + RCAT aging of laboratory samples results in a different chemical composition than aging by means of a weatherometer using temperature, oxygen and UV radiation.
f. From the results obtained from the field samples it is concluded that not only environmental influences are causing aging. Also traffic has an indirect influence that cannot be neglected.

REFERENCES

ATLAS materials (2001). Weathering testing guidebook. *Rep. no. 2062/098/200/AA/03/01*, ATLAS materials testing solutions.

CIE (1989). "Solar Spectral Irradiance." *Rep. No. CIE 85*, CIE International Commission on Illumination.

Hagos, E.T. 2008. *The Effect of Aging on Binder Properties of Porous Asphalt Concrete.* PhD thesis, Delft University of Technology. Delft.

Hofman, R., J.B.M., van Wieringen, And J.C. Visser, 2005. Noise Innovation Programme, IPG (NIP): Two Layer Porous Asphalt for use on the Dutch Main. In *Rio Inter Noise 2005: Congress and Exposition Noise Control Engineering*. Rio de Janiero, Brazil.

IPG, 2002. Noise Innovation Programme (NIP) for Road and Rail Traffic. Ministry of Transport, Public Works, and Water Management (V&W).

Ishai, I. (1996). "The Effects of Asphalt Composition on its Physical and durability Characteristics." *Transportation Research Record*, (Transport Research Board 75th annual meeting).

Molenaar, J.M.M., Hagos, E.T., Ven, M.F.C. v. d., and Hofman, R. (2004). "An investigation into the analysis of polymer modified bitumen (PMB)." *3rd Eurasphalt & Eurobitume Congress*. Vienna, Austria.

NEN-EN 12607-1. 2007. Bitumen and bituminous binders—Determination of the resistance to hardening under the influence of hear and air—Part1: RTFOT method. *European standard (norm)*.
NEN-EN 15323. 2007. Bitumen and bituminous binders—Accelerated long-term aging conditioning by the Rotating Cylinder Method (RCAT). *European standard (norm)*.
Oliver, J.W.H., and Tredrea, P.F. (1997). "The change in properties of polymer modified binders with simulated field exposure." *Association of Asphalt Paving Technologists (AAPT)*, Vol. 66.
Peterson, J.C. (2000). "Chemical composition of asphalt as related to asphalt durability." In *Asphaltenes and Asphalts, 2. Developments in Petroleum Science, 40B*. 1st edition, Elsevier Science BV.
Raw 2005. RAW Bepalingen (Dutch standard specification).
Reed, J., and Whiteoak, D. (2003). "The shell bitumen handbook." Thomas Telford, London.
Verhasselt, A.F., Choquet, F.S. 1997. Field Aging of Bituminous Binders: Simulation and Kinetic Approach. In *Proceedings 5th RILEM Symposium on Mechanical Test Methods for Bituminous Material.*
Verhasselt. A.F. 2002. Long Term Aging—Simulation by RCAT Aging Test. In *Proceedings 9th International Conference of Asphalt Pavements*. Copenhagen.

Advanced Testing and Characterization of Bituminous Materials –
Loizos, Partl, Scarpas & Al-Qadi (eds)
© 2009 Taylor & Francis Group, London, ISBN 978-0-415-55854-9

Influence of temperature and aging on laboratory fatigue performance of asphalt mixtures

I. Artamendi, B. Allen & P. Phillips
Technical and Development Department, Aggregate Industries, Ashbourne, UK

ABSTRACT: This paper presents a laboratory study into fatigue characteristics of bituminous mixtures using the indirect tensile test. Three different asphalt concrete dense binder course materials were used in the study. These include an AC 20 designed with a 40/60 pen bitumen and two AC 14 designed with a 10/20 pen bitumen and a polymer modified binder, respectively. Controlled stress fatigue tests were carried out at two temperatures, namely 20 and 10ºC, on both unaged and aged cylindrical specimens. As the stiffness values of the materials were significantly high, reduced specimen thicknesses of 25 mm were employed to generate the required horizontal stresses. These specimens were obtained by sawing in half 50 mm thick specimens cored from roller compacted slabs. Furthermore, comparisons were made between the stiffness values of the core specimens and their respective halves. As regards fatigue performance, it was found that as the temperature decreased the fatigue life of the AC 20 material decreased, whereas those of the AC 14s, increased. Aged materials also showed shorter lives than the unaged ones but this reduction was more severe for the AC 20 mixture.

1 INTRODUCTION

Fatigue cracking is one of the major distresses experienced in asphalt pavements and occurs when a bituminous asphalt layer is subjected to repeated loading under the passing traffic. Load-induced fatigue cracking could lead to significant damage and consequent failure of flexible pavements. It is, therefore, necessary to characterise the fatigue behaviour of bituminous mixtures both in the laboratory and on site.

In the laboratory, there are many techniques to depict fatigue behaviour, including bending tests, direct and indirect tensile tests. Furthermore, different approaches have been used to define failure due to fatigue (Artamendi & Khalid, 2005). In Europe, the methods for characterising fatigue are specified in EN 12697-24. In the UK, on the other hand, the Indirect Tensile Fatigue Test (ITFT) has been the preferred method to assess fatigue resistance of asphalt mixtures. In this test, a cylindrical specimen is subjected to a repeated pulse load across its vertical axis until it cracks (Brown, 1995).

The resistance of a bituminous material to fatigue cracking is affected by many factors which can be broadly classified as material and environmental factors. Material factors include the volumetric composition of the mixture; in particular, binder content and air void content, and the rheological properties of the binder. Environmental factors include among others the ambient temperature and the age of the material (SHRP, 1994).

The aim of this study was to investigate the fatigue performance of various asphalt mixtures by means of the Indirect Tensile Fatigue Test. The materials used were produced with two penetration grade binders and a polymer modified binder. Fatigue tests were carried out at 20 and 10ºC to investigate the effect of temperature on fatigue life. The effect of aging on fatigue performance was also investigated.

2 MATERIALS AND SPECIMEN PREPARATION

Three dense binder course asphalt concrete (AC) mixtures were designed in the laboratory and used in the study. These include an AC 20 designed with a 40/60 pen bitumen and two AC 14 designed with a 10/20 pen bitumen and a polymer modified binder (PMB), respectively. The AC 20 material was designed at 4.1% binder content. The two AC 14s were designed at the same binder content, thus, 5.3%. Particle size distribution for these materials is presented in Figure 1. Mixture composition is presented in Table 1.

Porphyritic andesite aggregates and limestone filler were used in the study. Proportioned aggregate blends were heated at the selected temperatures, i.e. 170ºC for the AC 20 and 180ºC for the AC 14s, and mixed with the binders also heated at the same temperatures. The mixtures were then compacted to 305 × 305 × 50 mm^3 slabs using a laboratory roller compactor in accordance with EN 12697-33. Compaction temperature was 160 and 170ºC for the AC 20 and AC 14 respectively. Target air void content for compacted mixtures was 4%. Six slabs were made per material. Four specimens, 100 mm diameter, were then cored from each slab which gave a total of 24 cores per material. These specimens were used to determine bulk densities and air void contents as per EN 12697-6 Proc. C-sealed and EN 12697-8, as shown in Table 2 (average values). The maximum density of the mixtures was determined as per EN 12697-5.

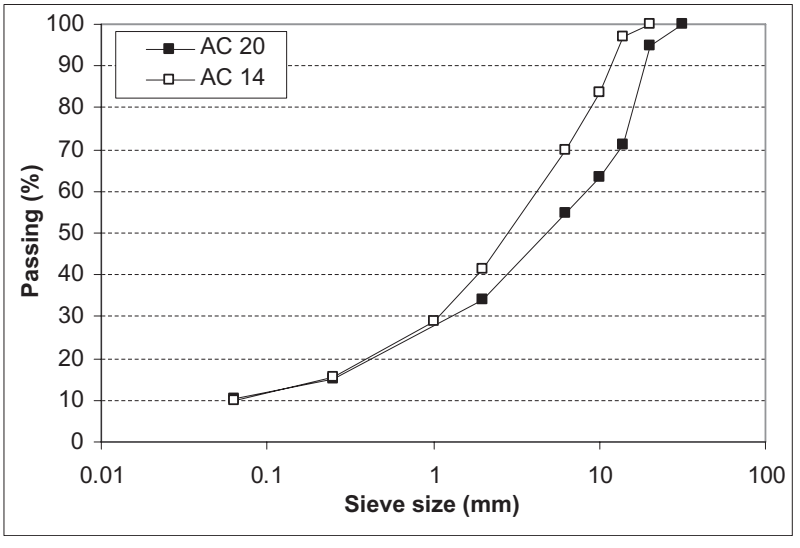

Figure 1. Particle size distribution.

Table 1. Composition of AC mixtures.

	AC 20 40/60 Pen	AC 14 10/20 Pen	AC 14 PMB
Component	% by mass	% by mass	% by mass
20 mm	28.8	–	–
14 mm	8.6	22.7	22.7
10 mm	8.6	10.4	10.4
6 mm	8.6	10.4	10.4
Dust	33.6	45.5	45.5
Limestone filler	7.7	5.7	5.7
Binder	4.1	5.3	5.3

Table 2. Density and voids of AC mixtures.

Material	Maximum density (kg/m³)	Bulk density (sealed) (kg/m³)	Voids (%)
AC 20 40/60 Pen	2564	2471	3.6
AC 14 10/20 Pen	2537	2446	3.6
AC 14 PMB	2534	2438	3.8

3 EXPERIMENTAL

The Indirect Tensile Stiffness Modulus (ITSM) test was used to determine the stiffness of the materials (BS DD 213: 1993). In this test a cylindrical specimen is subjected to a load pulse across its vertical diametral axis and the resultant deformation along the horizontal diametral axis is measured by two Linear Variable Differential transducers (LVDTs). The stiffness modulus is then calculated as follows:

$$E = \frac{P}{\Delta h \times t} \times (0.273 + v) \tag{1}$$

where E = stiffness modulus (MPa); P = peak vertical load (N): Δh = peak deformation along the horizontal diametral axis (mm); t = specimen thickness (mm): and v = Poisson's ratio (assumed to be 0.35). Furthermore, standard "target deformation", i.e. horizontal deformation produced by the peak load, of 0.005% of the specimen diameter (controlled deformation stiffness test) was used.

The fatigue characteristics of the different mixtures were determined by means of the Indirect Tensile Fatigue Test (ITFT) (BS DD AFB: 2002). In this test, a cylindrical specimen is subjected to a repeated compressive pulse load across its vertical diametral axis. This load originates a relatively uniform constant tensile stress at the centre of the specimen. The repeated application of the load causes the specimen to crack along the vertical diameter. The maximum tensile stress at the centre of the specimen is given by:

$$\sigma_0 = \frac{2P}{\pi \times d \times t} \tag{2}$$

where σ_0 = maximum tensile stress at the centre of the specimen (kPa); d = specimen diameter (mm); and P and t are defined as before. Furthermore, during the test the applied stress and the vertical permanent deformation of the specimen, measured with two LVDTs, are recorded at selected intervals. The fatigue life (N_f) is defined as the number of load applications that causes complete fracture of the specimen. When the specimen does not fracture completely, the number of cycles corresponding to a vertical displacement of 9 mm is used. The test set-up is presented in Figure 2.

Moreover, for the indirect tensile test the initial tensile strain, ε_0, at the centre of the specimen can be obtained as follows:

$$\varepsilon_0 = \frac{\sigma_0 \times (1 + 3v)}{E_0} \times 1000 \tag{3}$$

where E_0 is the stiffness modulus at the corresponding tensile stress σ_0. Thus, to determine the initial strain a stiffness test was first carried out at the selected tensile stress (controlled-stress stiffness test). Then, the same specimen was used for fatigue testing at that tensile stress.

As regards the tests conditions, controlled deformation stiffness tests were carried out on 50 mm thick cylindrical specimens at a temperature of 20ºC. For controlled stress stiffness tests and fatigue tests, however, 25 mm thick specimens were used. These specimens were obtained

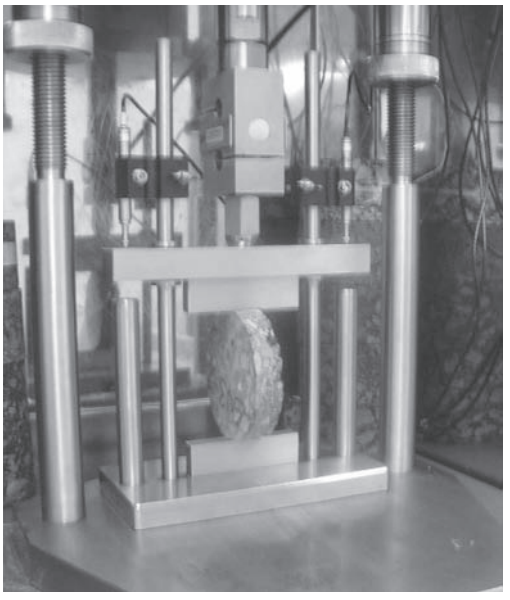

Figure 2. Indirect tensile fatigue test set-up.

by cutting in half 50 mm thick specimens cored from the slabs. This specimen thickness was used to generate the required level of tensile stresses for the materials and test conditions selected with the equipment available. Fatigue test were then performed at 20 and 10ºC. Also, aged specimens were used in the study. The aging protocol consisted of conditioning 25 mm thick specimens at 85ºC for 5 days in a fun-assisted oven (Harrigan et al. 1994). Fatigue tests on aged specimens were then carried out at 20ºC. A minimum of 10 specimens were tested per material and test condition.

4 RESULTS AND DISCUSSIONS

4.1 *Stiffness*

Controlled deformation stiffness tests test at 20ºC on 50 mm thick specimens at a target deformation of 5 μm were first performed and the results are presented in Table 3. These values represent average values from 24 specimens per mixture. Data showed that the mixture with the harder bitumen, i.e. AC 14 10/20 pen, was the stiffer followed by the polymer modified mixture, i.e. AC 14 PMB, and the conventional mixture, i.e. AC 20 40/60 pen.

For fatigue testing, the stiffness of the specimens at the required stress levels was first determined. Figure 3 shows the result obtained at 20ºC for 25 mm thick unaged specimens. Results indicated that for AC 20 40/60 pen and AC 14 PMB the stiffness values were independent of the applied stress indicating linear viscoelastic behaviour for the range of stresses selected, i.e. from 400 to 800 kPa approximately. For AC 14 10/20 pen, however, the stiffness values tended to decrease at high stress levels suggesting non-linear behaviour as these levels, as seen in Figure 3.

Average stiffness values and standard deviations from tests at different stress levels are presented in Table 3. The table also includes average stiffness values from controlled deformation stiffness test. Results indicated that, at 20ºC, the average stiffness values obtained from controlled stress stiffness tests were lower than those determined from controlled deformation stiffness test. The largest difference was found for the AC 20 40/60 pen (28% lower), followed by the AC 14 PMB (19% lower) and the AC 10/20 pen (4% lower). These differences were attributed to specimen thickness, i.e. 50 and 25 mm, and applied loads (stresses) that were

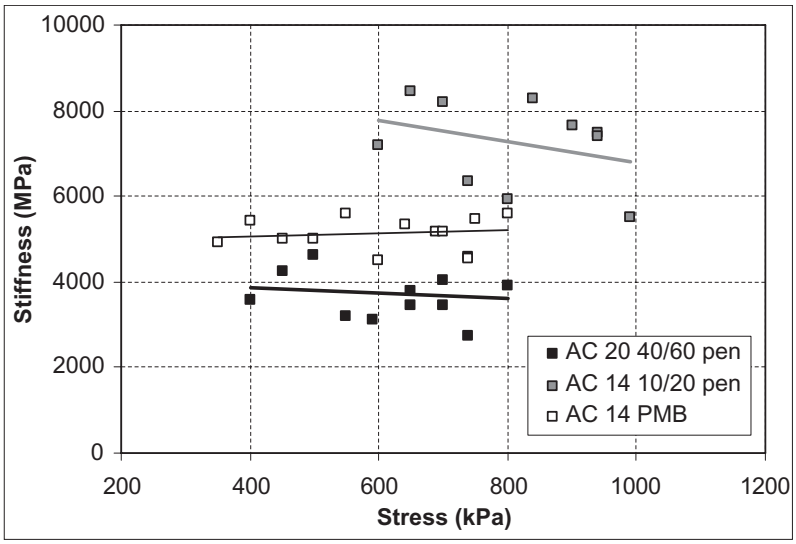

Figure 3. Relationship between stiffness and applied stress.

Table 3. Average stiffness values and standard deviations.

	E (MPa)	E_0 (MPa)		
Material	T = 20ºC	T = 20ºC	T = 10ºC	T = 20ºC - Aged
AC 20 40/60 pen	5141 (327)	3724 (583)	11653 (1555)	7398 (1317)
AC 14 10/20 pen	7532 (1082)	7239 (1018)	13327 (2796)	9451 (890)
AC 14 PMB	6364 (552)	5141 (375)	14549 (1862)	7434 (739)

E = Stiffness from controlled deformation tests.
E_0 = Stiffness from controlled stress tests.

much higher for the constants stress stiffness tests. It can also be seen that for a mixture with a 20 mm maximum aggregate size, testing specimens 25 mm thick leads to significant lower stiffness values and larger variability.

Table 3 also shows average stiffness values from controlled stress test carried out at 10ºC. Results showed that as the temperature decreased the stiffness modulus increased as a result of the viscoelastic character of the binders. Furthermore, data also showed higher temperature susceptibility of the AC 20 mixture than the AC 14s mixtures, with the AC 14 10/20 pen being the least temperature susceptible of all.

As regards aging, it can be seen that aged specimens had higher stiffness than those unaged due to hardening of the binder by oxidation. Furthermore, data presented in Table 3 suggested higher oxidation rate of the soft binder compare to the PMB and the hard bitumen which aged relatively the least.

4.2 *Fatigue*

Fatigue data have been used to derive a relationship between the initial tensile strain, ε_0, and fatigue life, N_f, as follows (Monismith & Deacon, 1969):

$$N_f = A\left(\frac{1}{\varepsilon_0}\right)^m \tag{4}$$

Table 4. Materials constants and fatigue failure results.

Material	Temperature (ºC)	A	m	R^2	ε_6 (μm/m)	N_{200} (Cycles)
AC 20 40/60 pen	20	3.80×10^{15}	4.83	0.86	115	29229
	10	9.26×10^{18}	6.62	0.81	108	5417
	20 (aged)	7.93×10^{15}	5.44	0.81	80	2408
AC 14 10/20 pen	20	3.40×10^{15}	4.87	0.95	95	21157
	10	9.52×10^{14}	4.55	0.79	112	32281
	20 (aged)	6.56×10^{15}	5.13	0.89	90	10295
AC 14 PMB	20	1.36×10^{12}	3.53	0.87	66	10254
	10	1.73×10^{13}	3.47	0.87	71	17926
	20 (aged)	1.84×10^{14}	4.52	0.91	75	7314

where A and m are regression constants that depend on both the material and the test conditions.

Figure 4 shows the fatigue lives against the initial strain for the materials and conditions investigated. It can be seen that when the temperature decreased the fatigue life of the AC 20 material also decreased. For the AC 14 materials, on the other hand, the opposite effect was observed; thus, as the temperature decreased the fatigue live increased. This behaviour has been mainly attributed to differences in binder content and, consequently, to binder film thickness between mixtures. For the AC 20 designed at 4.1% binder content the relatively thinner binder film surrounding the aggregates stiffened as the temperature decreased. As a result, the mixture became more brittle. For the AC 14s designed at 5.3% binder, however, thicker and stiffer binder films around the aggregates increased the overall resistance to fatigue.

The effect of ageing on laboratory fatigue performance can also be seen in Figure 4. Data shows the detrimental effect of aging on fatigue life. Aging of the binder due to oxidation leads to loss of volatile components of the bitumen resulting in lack of ductility and adhesion (Karlsson & Isacsson, 2006). Furthermore, the decrease in fatigue life as a result of aging was more severe for the AC 20 which could be attributed to higher oxidation rates of the thinner binder films surrounding the aggregates.

Regression constants, A and m, and regression coefficients, R^2, for the fatigue relationships given by equation 4 are presented in Table 4. The constant m (slope) gives and indication of the susceptibility of the material to applied strain. Results showed that the PMB material was the least susceptible of all, as seen by the values of the constant m. Also, the susceptibility of the mixtures to the applied strain increased with aging. Furthermore, R^2 values for the AC 20 were lower than those for the AC 14s. These differences were attributed to size effects.

Two criteria, one based on the microstrain at 10^6 loading cycles (ε_6) and the other based on the number of loading cycles at 200 microstrain (N_{200}), have also been used to evaluate, in a simply way, the effect of material type, temperature and age on fatigue performance. Calculated ε_6 and N_{200} values are presented in Table 4. It can be seen that in general the two criteria agreed relatively well.

4.3 *Suitability of the ITFT*

During this study some concerns have arisen regarding the suitability of the UKs ITFT to adequately depict fatigue characteristics of asphalt mixtures. Some of these concerns are outlined below.

The ITFT is typically carried out at 20ºC. At this temperature, however, fatigue cracking is rarely observed. Moreover, laboratory fatigue testing is normally performed at lower temperatures, typically 10ºC (Di Benedetto et al. 2003).

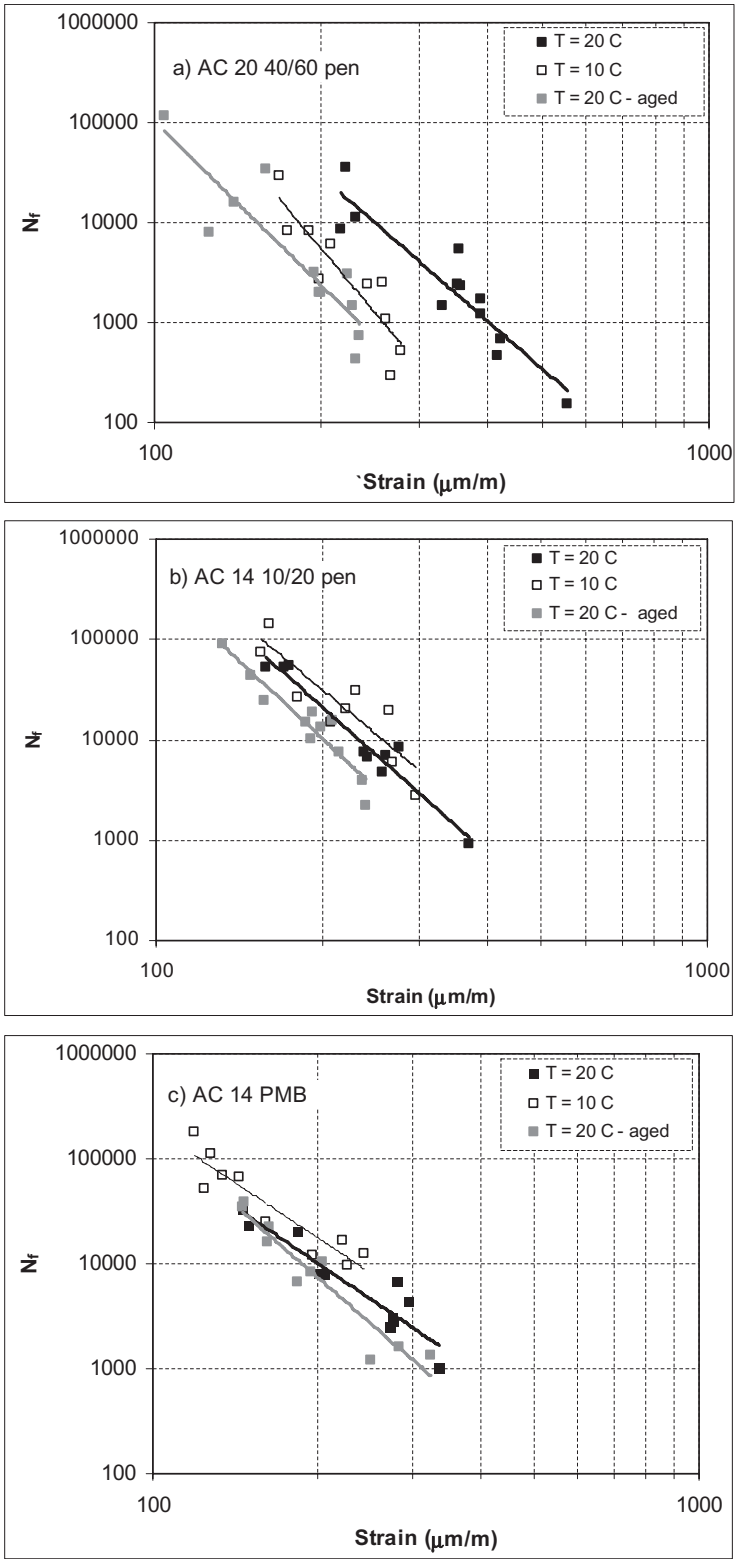

Figure 4. Relationships between fatigue life and initial strain.

Different modes of failure have also been observed for ITFT, as shown in Figure 5. In the majority of the cases the specimens fractured completely or a visible fatigue crack was clearly present (see Fig 5a). Sometimes, however, the specimen did not fracture and there were not any visible cracks. In these cases the failure was attributed to the accumulation of permanent vertical deformation (see Fig 5b). Finally, a reduced number of specimens failed due to indentation of the loading strip into the specimen (see Fig 5c).

The ITFT is a controlled stress mode of loading test and it is, therefore, more applicable to thick asphalt pavements where high stiffness is the fundamental parameter that underpins fatigue life. Controlled strain fatigue tests, on the other hand, have been associated with thin conventional flexible pavements, where the elastic recovery properties of the material have a fundamental effect on fatigue life (Khalid, 2000). Furthermore, controlled strain mode of loading is the method generally adopted for pavement design purposes (Delorme et al. 2007 and AASHTO, 1994).

Moreover, the control of the load (stress) during the test is sometimes poor. This generally occurs when the applied stress selected is high (>1000 kPa) and the stiffness is also high. High stiffness could be due to material composition and/or test conditions (low temperature and/or aged material). Figure 6 shows fatigue data, vertical deformation and applied tensile stresses, for an AC 10/20 pen specimen tested at 10ºC. The initial stiffness of the specimen at this temperature was 13228 MPa and the target tensile stress was 1000 kPa. The figure shows that although the average tensile stress for the whole duration of the test was 1018 kPa, which

Figure 5. Failure modes for ITFT specimens.

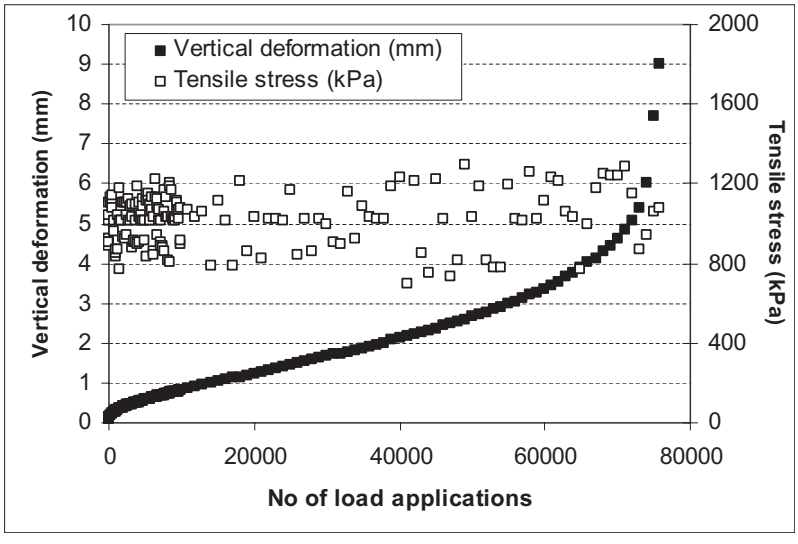

Figure 6. Vertical deformation and tensile stress for a test a 10ºC.

was close to the target of 1000 kPa, the variability of the tensile stress during the test was significant.

Finally, in the ITFT the maximum horizontal strain is determined by performing a controlled stress stiffness test at the corresponding stress level. The calculated stiffness and stress are then used to determine the strain using equation 3. This strain is then assumed to be the initial strain for the fatigue test. In the Indirect Tensile Test on cylindrical shaped specimens (ITT-CY) as per EN12697-24 Annex E, however, the horizontal deformation is measured continuously by means of transducers. The initial strain is then measured at the 100th load application once the deformation has become stable. It should be noted that although this is an improvement with respect to the ITFT, the strain measured during ITT-CY is the permanent strain and not the resilient, i.e. recoverable one (Said & Wahlström, 2000). Consequently, the evolution of the stiffness during the test can not be computed as both stress and resilient strain are required.

5 CONCLUSIONS

From the laboratory work carried out in this study the following conclusion can be drawn:

- Average stiffness values obtained from controlled stress stiffness tests were lower than those determined from controlled deformation stiffness test. These differences were attributed to specimen thickness, i.e. 50 and 25 mm, and applied stress that was much higher for constant stress stiffness tests.
- It was found that as the temperature decreased the fatigue life of the AC 20 material decreased, whereas those of the AC 14s, increased This behaviour was attributed to differences in binder content and, consequently, to binder film thickness, between mixtures.
- Aging due to binder oxidation had a detrimental effect on fatigue life. Furthermore, the decrease in fatigue life as a result of aging was more severe for the AC 20 which could be attributed to higher oxidation rates of the thinner binder films surrounding the aggregates.
- The polymer modified material was less susceptible to the applied strain that the materials produced with the straight run binders, as seen by the values of the constant *m* on the fatigue life vs strain relationship.
- During this study some concerns were arisen regarding the suitability of the UKs ITFT to adequately depict fatigue characteristics of asphalt mixtures. These included poor control of the stress during the test at high stress levels (>1000 kPa), indirect determination of the initial strain by means of a stiffness tests and the different nature of the failure modes observed (fatigue, permanent deformation and indentation).

REFERENCES

AASHTO, 1994. Standard test method for determining the fatigue life of compacted hot mix asphalt (HMA) subjected to repeated flexural bending, American Association of State Highways and Transportation Officials, AASHTO Designation TP8-94.

Artamendi, I. & Khalid, H. 2005. Characterization of fatigue damage for paving asphaltic materials. *Int. Jl. Fatigue and Fracture of Engineering Materials and Structures* 28(12): 1113–1118.

Brown, S.F. 1995. Practical test procedures for mechanical properties of bituminous materials. *Transport*, ICE, 111: 289–297.

BSI, 1993. British Standard Draft for Development DD 213—Method for the determination of the indirect tensile stiffness modulus. British Standard Institution, London.

BSI, 2002. British Standard Draft for Development DD AFB—Method for the determination of the fatigue characteristics of bituminous mixtures using indirect tensile fatigue. British Standard Institution, London.

CEN, 2002. European Standard EN 12697-5, Bituminous mixtures—Test methods for hot mix asphalt—Part 5: Determination of the maximum density. Comité Européen de Normalisation, Brussels.

CEN, 2003. European Standard EN 12697-6, Bituminous mixtures—Test methods for hot mix asphalt—Part 6: Determination of bulk density of bituminous specimens. Comité Européen de Normalisation, Brussels.
CEN, 2003. European Standard EN 12697-8, Bituminous mixtures—Test methods for hot mix asphalt—Part 8: Determination of void characteristics of bituminous specimens. Comité Européen de Normalisation, Brussels.
CEN, 2004. European Standard EN 12697-24, Bituminous mixtures—Test methods for hot mix asphalt—Part 24: Resistance to fatigue. Comité Européen de Normalisation, Brussels.
CEN, 2003. European Standard EN 12697-33, Bituminous mixtures—Test methods for hot mix asphalt—Part 24: Specimen prepared by roller compactor. Comité Européen de Normalisation, Brussels.
Delorme, J-.L., de la Roche, C. & Wendling, L. 2007. *LPC Bituminous Mixtures Design Guide*. The RST Working Group Design of Bituminous Mixtures. Laboratoire Central des Ponts et Chaussées, Paris.
Di Benedetto, H., de La Roche, C., Baaj, H., Pronk, A. & Lundstron, R. 2003. Fatigue of bituminous mixtures: different approaches and RILEM group contribution. *Proceedings of the 6th International RILEM Symposium, Performance Testing and Evaluation of Bituminous Materials*, Zurich, 15–38.
Harrigan, E.T., Leahy, R.B. & Youtcheftf, J.S. 1994. The superpave mix design system: manual of specifications, test methods and practices. SHRP-A-379, *Strategic Highway Research Program*, National Research Council, Washington, D.C.
Karlsson, R. & Isacsson, U. 2006. Material-related aspects of asphalt recycling—State of the art. *Journal of Materials in Civil Engineering* 18(1): 81–92.
Khalid, H.A. 2000. A comparison between bending and diametral fatigue tests for bituminous materials. *Materials and Structures* 33: 457–465.
Monismith, C.L. & Deacon, J.A. 1969. Fatigue of asphalt paving mixtures. *ASCE Transportation Engineering Journal* 95(2): 317–346.
Said, S.F. & Wahlström, J. 2000. Validation of indirect tensile method for fatigue characteristics of bituminous mixes. *2nd Euroasphalt & Eurobitume Congress*, Barcelona, I: 772–778.
SHRP, 1994. Fatigue response of asphalt-aggregate mixes. *Strategic Highway Research Program*, Report SHRP-A-404, National Research Council, Washington, D.C.

Advanced Testing and Characterization of Bituminous Materials –
Loizos, Partl, Scarpas & Al-Qadi (eds)
© 2009 Taylor & Francis Group, London, ISBN 978-0-415-55854-9

Aging of SBS polymer in hot and cold bituminous coatings. Relationship between microstructure and performances: Low temperature and cohesion properties

C. Gueit, M. Robert & G. Durand
COLAS S.A, Campus Scientifique et technique, Magny les Hameaux, France

ABSTRACT: It is well known that SBS polymer modified bitumens (PMB) exhibit better performances than pure bitumens. But to what extent are these performances remaining after long term aging on site, as well for hot asphalt mixes as for thin layer coatings?

In order to answer to this question, a laboratory study has been performed on several PMB on the one hand and on different types of recovered binders from modified (PMB or latex) emulsions on the other hand: we focused respectively on low temperature properties measured by BBR (Bending Beam Rheometer) and DTT (Direct tensile strength Test) methods, and on cohesion and elastic recovery tests.

Long term aging is simulated by using RTFOT (Rolling Thin Film Oven Test) followed by PAV (Pressure aging vessel).

Simultaneously, we monitored the evolution of polymer characteristics from the initial stage to the aged stage in term of microstructure and more especially in terms of intrinsic molecular weight properties. For this assessment we carried out GPC (Gel Permeation Chromatography) experiments that consist in separating molecules according to their size on a porous matrix.

The conclusions of the study are the following ones:

– SBS is still present and active after aging: only a moderate evolution in polymer molecular size occurs after long term aging.
– These observations can be correlated with a small decrease in low temperature and cohesion performances for the aged binders compared to initial ones. Elastic recovery is not relevant in the context of strongly aged binders.
– Performances remain far better than without SBS. This confirms the observations on site too.

1 INTRODUCTION

Due to its characteristics, a bituminous binder guarantees the longevity of road paving. It is therefore chosen or formulated according to its ability to withstand various types of stresses on the road. Replacement of pure bitumen by a polymer-modified binder, particularly using SBS, allows its scope of application to be extended (Corté et al. 1999).

In the case of asphalt mix, the thickness of the surface layer may be reduced: Thin asphaltic overlay, usually 3 to 4 cm thick, may be replaced by Very thin asphaltic overlay (2 to 3 cm) or even Ultra-thin asphaltic overlay (1 to 2 cm). Furthermore, the field of application for Thin asphaltic overlay (3 to 4 cm) may be extended to damaged or deformed surfaces.

In addition, use of modified bitumen is vital in the case of porous asphalt, where contact surfaces between aggregates are reduced.

In surface coatings, in the form of anhydrous or emulsion binders, the presence of a polymer in the binder allows them to be applied on high-traffic road surfaces with many curves.

Lastly, used as an emulsion, a modified binder improves the effectiveness of a bonding layer.

In all cases, the longevity of the surface depends on the resistance of the binder, which undergoes two types of aging: rapid "construction" aging (transit via the coating plant, application), and slow "service" aging in the following years, during which the surface will be exposed to the climatic conditions of the region. These two types of change can be simulated

in a laboratory environment; the variations observed on the characteristics of bitumen constitute a valuable indicator of their durability.

This process is particularly interesting when assessing the benefit achieved by addition of a polymer: the study involves comparing the results obtained on pure bitumen on the one hand and on several modified bitumens on the other, thus eliminating uncertainty as to how far the aging simulated in the laboratory represents actual conditions.

The evaporation of the lightest fractions of the bitumen, the chemical change of species present by condensation polymerisation and oxidation on contact with the air and the deterioration by ultra-violet rays are all factors that accelerate aging of a binder. Inclusion of a polymer in the bitumen increases its durability and limits or delays the consequences of these phenomena. This improvement can be shown by a wise choice of methods for characterising the bituminous binder, taking into account the presence of the polymer. In certain cases, the polymer can be analysed independently of the bitumen.

In order to reveal the benefit contributed by the polymer, two comparative studies were conducted, one on anhydrous binders for use in surfacing, the other on emulsions for use in spraying. In both cases, the binders were characterised after simulation of aging in several stages.

2 SIMULATION OF AGING

Two protocols are applicable for simulating aging of the binder, one for surfacing binders and the other for bitumen emulsions.

In the first case, the hardening resulting from processing in the coating plant is simulated by the RTFOT test (Rolling Thin Film Oven Test; EN 12607-1), which involves exposing the binder, in a thin film in cylindrical vials, to a temperature of 163°C for 1 hour 15 minutes. During the test, the binder film is constantly renewed by rotating the vial and blowing hot air into the vials accelerates the oxidation process.

The binder produced in this step can then be used for an aging test through PAV or Pressure Aging Vessel (EN 14769), which simulates effect of several years in situ. The binder is exposed for a minimum of 20 hours to a pressure of 2.1 MPa, in an oven at a chosen temperature, between 80°C and 115°C.

In the second case, simulation of aging involves first stoving of the bituminous emulsion in a thin film, for 24 hours at ambient temperature then 24 hours at 50°C, with the thickness of the residual binder film at 1 mm (EN 14895). The binder is then in "recovered" state (simulation of short-term aging: a few days after application in situ). The test may also be extended to 24 hours at 85°C, and the binder is then in "stabilised" state (simulation of medium-term aging: 6 months to 1 year in situ). The binder produced by this operation may then be used for aging by PAV (EN 14769) according to the same conditions as for bitumen for surfacing (simulation of long-term aging—several years in situ).

At each stage, the binder is sampled and characterised; the change in its characteristics in relation to those of the fresh binder gives us information on its conservation properties.

3 CHARACTERISATION OF BINDERS AND POLYMER

In addition to the values for penetration (EN 1426) and the softening point (EN 1427), other properties of binders were monitored during this study.

3.1 *Analyses to assess the binder's performance*

Elastic recovery (EN 13398) characterises the binder's ability to return to its original shape after being deformed; this property tells us about its self-healing capacity and about its fatigue resistance.

Pendulum cohesion (EN 13588), suitable particularly for spraying binders, gives information on the shearing and stripping resistance of aggregates.

Characterisation tests according to the Superpave reference system (Asphalt Institute, 1995) were also performed.

BBR (Bending Beam Rheometer) according to AASHTO T313/EN 14771 is used for characterisation of performance at low temperature. The test involves exposing a beam of bitumen to three-point bending and determining the influence of temperature on the resulting deflection and the rigidity of the bitumen.

This test determines two critical temperatures below which there is risk of cracking for an asphalt mix.

The first is the equimodule temperature (temperature at which the bitumen has a stiffness modulus of S = 300 MPa): when the modulus becomes too high, the binder becomes fragile and is likely to crack.

The second is the temperature at which the modulus variation gradient according to the load time (m) is 0.300: a higher gradient is needed to relax the stresses inside the material and reduce the risk of cracking.

DTT (Direct Tensile Strength) AASHTO T314: this test characterises the binder's behaviour when subjected to stretching at low temperature: it involves determining the temperature at which, during stretching at constant rate, the elongation at break reaches 1%.

The suitability of Superpave tests for PMB characterisation has been studied previously (Lecomte et al. 2000, Chappat et al. 2000).

3.2 *Analyses for checking the state of the SBS polymer*

Infrared absorption spectroscopy helps identify the chemical functions present in a sample. In fact, the links between atoms making up a molecule may be considered to be "springs" with specific vibration frequencies and absorb the electromagnetic rays of the corresponding energy.

When the molecule is exposed to infrared rays, it absorbs at various frequencies, with each frequency characteristic of a chemical function. In particular, in the case of SBS-modified bitumen, two characteristic peaks are clearly visible: a peak at 966 cm^{-1} (C-H bond connected to C=C function from the butadiene) and a peak at 700 cm^{-1} (aromatic C-H bond of the styrene).

These two peaks are usually observed to check the presence of SBS in a modified binder and may also in certain conditions be used for quantity dosing.

Epi-fluorescent microscopy is carried out as follows: a sample subjected to ultraviolet excitation (365 nm) emits radiation in the visible spectrum, when it contains aromatic molecules. Given the differences between bitumen and polymer in terms of distribution of the aromatic functions, this is clearly distinct from the bitumen matrix. This technique may therefore be used to observe the morphology of the SBS in a modified binder and check the compatibility of the bitumen and the polymer.

Gel permeation chromatography (GPC), also known as Steric exclusion chromatography (SEC), is a technique allowing separation of molecules according to their size. This technique, applied to analysis of polymers in a bitumen matrix, will be described in greater detail in a subsequent paragraph.

4 RESULTS

4.1 *Study on anhydrous binders*

The study on bitumen for hot mixes was conducted on different modified bitumens. A pure bitumen with the same penetration has been taken as a point of comparison.

The choice to give all binders in this study equal penetrability (55–60 1/10 mm) eliminates uncertainties due to different hardness of bitumens: difference in rheological behaviour between hard bitumen and soft bitumen.

The improvement of properties of bitumen binders by adding polymer is already widely aknowledged: it reduces thermal susceptibility, increases the plasticity range and cohesion, and gives a considerable elongation capacity.

Generally speaking, long-term aging results in deterioration and transformation which cause the binder to become fragile, which may lead to thermal cracking in the bitumen mix.

Table 1. Characteristics of fresh binders.

		Pure bitumen	C2.5	C5	C7.5
Penetration at 25°C	1/10 mm	53	56	60	60
R&B temperature	°C	50,2	51,8	81,0	84,5
Fraass temperature	°C	–16,7	–17,1	–19,1	–20,1
BBR					
T at m = 0.300	°C	–18,2	–18,4	–18,6	–21
T at S = 300 MPa	°C	–18,6	–18,8	–19,3	–23,6
m at T(S = 300 MPa)		0,295	0,293	0,289	0,267
DTT					
T at 1% elongation	°C	–16,7	–19,4	–22,5	–25,4

Table 2. Characteristics of aged binders.

		Pure bitumen	C2.5	C5	C7.5
Penetration at 25°C	1/10 mm	20	24	28	38
R&B temperature	°C	63,2	66,3	73,1	81,5
Fraass temperature	°C	–13,2	–14,1	–16,1	–18,2
BBR					
T at m = 0.300	°C	–12,5	–12,8	–12,5	–15
T at S = 300 MPa	°C	–15	–15,2	–17,3	–19,1
m at S = 300 MPa		0,275	0,275	0,258	0,250
DTT					
T at 1% elongation	°C	–15,6	–16	–20,7	–21,3

This study was focused on the cold behaviour of binders and the change in this behaviour during long-term aging. The properties at low temperature of the binders analysed are characterised by the Fraass breaking-point tests and behaviour is characterised by the bending beam rheometer (BBR) and in direct tensile strength testing (DTT).

These various tests were performed on three modified bitumens with different SBS contents (2.5%, 5% and 7.5%), which we will call C2.5, C5 and C7.5, as well as on a benchmark bitumen (pure bitumen grade 50/70). The characteristics of "fresh" binders are shown in table 1.

Note the slight influence of the change on the critical temperatures determined on the bending beam rheometer. This observation turns out consistent with the results obtained from studies performed previously: indeed, the binder's behaviour is improved only with SBS contents higher than 5% (Corté et al. 1999, Asphalt Institute 1995).

Afterwards, these binders undergo two successive aging processes: RTFOT (Rolling Thin Film Oven Test - EN 12607-1) and PAV (Pressure Aging Vessel - EN 14769). Following these two aging processes, the binders are characterised again: table 2 shows the results obtained.

After RTFOT + PAV aging, the following graphs (figures 1 to 3) show that the improvement of the properties of modified binders due to addition of an SBS-type polymer is still significant.

Indeed, the Fraass breaking temperature as well as the critical equimodule temperature decrease constantly as the polymer rate increases, which is a sign of improved behaviour of bitumen binders at low temperature.

The temperature at 1% elongation decreases significantly as the SBS content increases.

We find that the temperature at m = 0.300, conveying the ability to relax stresses, is constant up to a polymer content of 5%.

In conclusion, although we find a slight reduction in the properties at low temperature of modified binders following RTFOT + PAV aging, modification of bitumen binders by SBS-type elastomers helps preserve binders whose characteristics after aging are better than those of pure bitumen.

4.2 *Study on binders recovered from emulsions*

Various methods are available, in order to recover the binder from an emulsion. According to the technique chosen, the binder properties and rheological behaviour can be noticeably affected (Salomon et al. 2008). Indeed, some techniques are designed for simulation of short-term aging, other ones for medium- or long-term aging. One technique of each kind has been used for this 2nd part of the study, which was conducted on two 160/220 bitumen-based emulsions: a pure 160/220 bitumen emulsion and a 160/220 bitumen emulsion modified with 2.5% SBS (the polymer is incorporated into the bitumen before emulsification). Table 3 shows the characteristics of binders before emulsification.

The first stage involves tracking the change in these characteristics after emulsification of the binders, then simulating aging in successive stages: short term (recovered binder), medium term (stabilised binder) and long term (binder aged by PAV). Note that during this study,

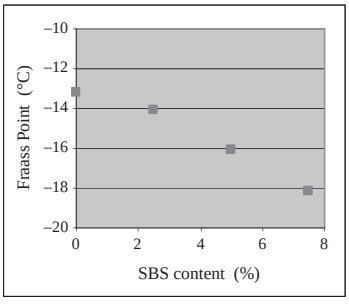

Figure 1. Change in the Fraass point of aged binders as a function of the polymer content.

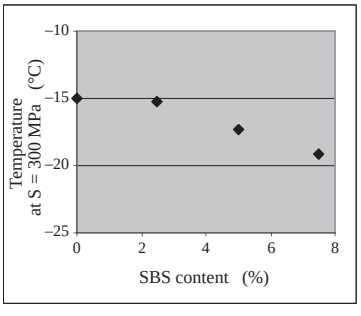

Figure 2. BBR tests: Change in the critical equimodule temperature as a function of the polymer content—aged binders.

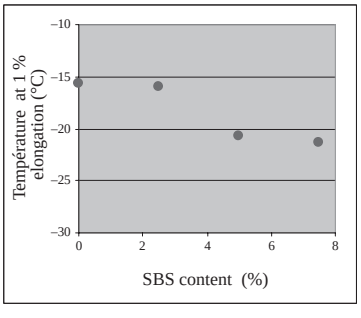

Figure 3. DTT tests: Change in the temperature at 1% of elongation at break as a function of the polymer content—aged binders.

Table 3. Initial characteristics of binders.

	160/220 pure	160/220 + SBS
Penetration at 25°C in 1/10 mm (EN 1426)	187	137
Softening point R&B in °C (EN 1427)	39.0	41.8

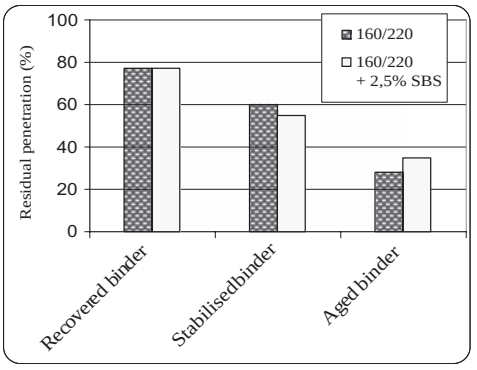

Figure 4. Change in penetration of binders during aging, as a %age of initial penetration.

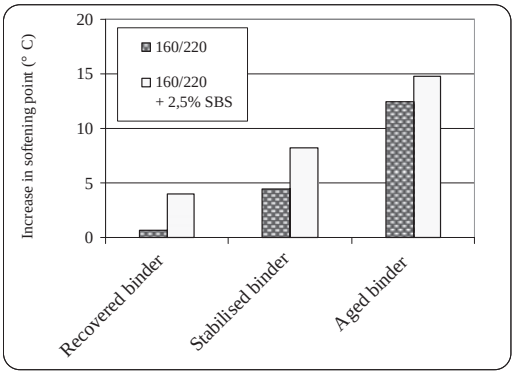

Figure 5. Change in the softening point during aging, in °C compared with the initial value.

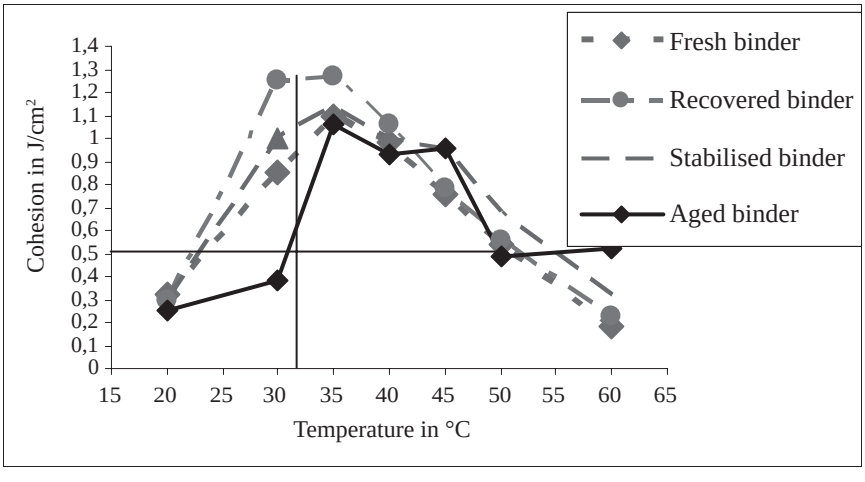

Figure 6. Variation in the cohesion of the SBS-modified binder, as a function of temperature: change in the curves during aging of the binder.

Table 4. Temperature interval for which cohesion of the SBS-modified binder is greater than 0.5 J/cm² —evolution during aging.

	Temperature interval C > 0.5 J/cm²	Range
Initial binder	23–51	28°C
Recovered binder	22–52	30°C
Stabilised binder	23–55	32°C
Binder aged by PAV	31–50	19°C

other aging methods were used to complete the assessment, and other types of emulsions were also considered. The results were published elsewhere (Gueit et al. 2008).

The graphs in figures 4 and 5 show the percentage of residual penetrability compared with the initial value and the assessment of the R&B softening points, during aging.

It appears that these two tests are not sufficient for checking the maintenance of the modified binder's performance or for differentiating it from pure bitumen. The SBS-modified binder was thus put through additional tests more suited to its specificity.

Elastic recovery was determined at 10°C according to the EN 13398 standard. The value obtained on the initial binder was 61%. Following the recovery stage, elastic recovery reached 76%, and this value was maintained during the stabilisation stage.

Following aging by PAV, elasticity could no longer be determined since the specimens broke during stretching, due to the hardening of the binder.

Pendulum cohesion was determined for the 4 binders according to the EN 13588 standard. In addition to the graphs in figure 6, showing the variation in cohesion as a function of temperature for each binder, a comparison was made based on the temperature interval on which the binder cohesion was greater than 0.5 J/cm². The results are given in table 4. By way of comparison, cohesion of the binder recovered from pure bitumen emulsion does not exceed 0.8 J/cm².

The results obtained show that the binder maintains is cohesion properties after short-term (recovery) or medium-term (stabilisation) aging. Following the long-term aging simulation stage, the binder maintains its performance in terms of cohesion for temperatures of 35°C and higher. For temperatures below 35°C, the cohesion value decreases sharply due to hardening of the binder; remember that at this degree of aging, elasticity is also affected by hardening of the binder.

The conjunction of the results obtained by these two tests therefore calls for further investigation, in the form of tests that produce a more accurate characterisation of the polymer itself.

The binders were thus observed via epi-fluorescent UV microscopy. The photos in figure 7 show the structure of the bitumen + polymer mix.

The morphology of the polymer did not change significantly during aging, which confirms that the polymer was still present in the binder following the aging by PAV stage. This quality result was combined with a quantity test.

In this aim, the infrared spectrum was conducted on the binders at successive stages in aging to check whether the reduced performance, initially attributed to hardening of the bitumen, was also connected to a change in the level of the polymer itself. An example of infrared spectrum is given in figure 8.

Since the intensity of peaks at 966 cm^{-1} and 700 cm^{-1} was in proportion to the binder's polymer content, it was determined for the different binders considered. It appears that it changes little during aging, and that finally, the binder aged by PAV (simulation of long-term aging) has an infrared spectrum that is almost identical to that of the initial binder, although the elasticity and pendulum cohesion characteristics show a change in the performance of the binder, suggesting possible deterioration of the polymer.

In short, the tests for characterising the binder's performance reveal the strong impact of the PAV stage (simulation of long-term aging). However, the two tests performed to try to explain this trend by analysing the polymer do not show any significant change. The following theory

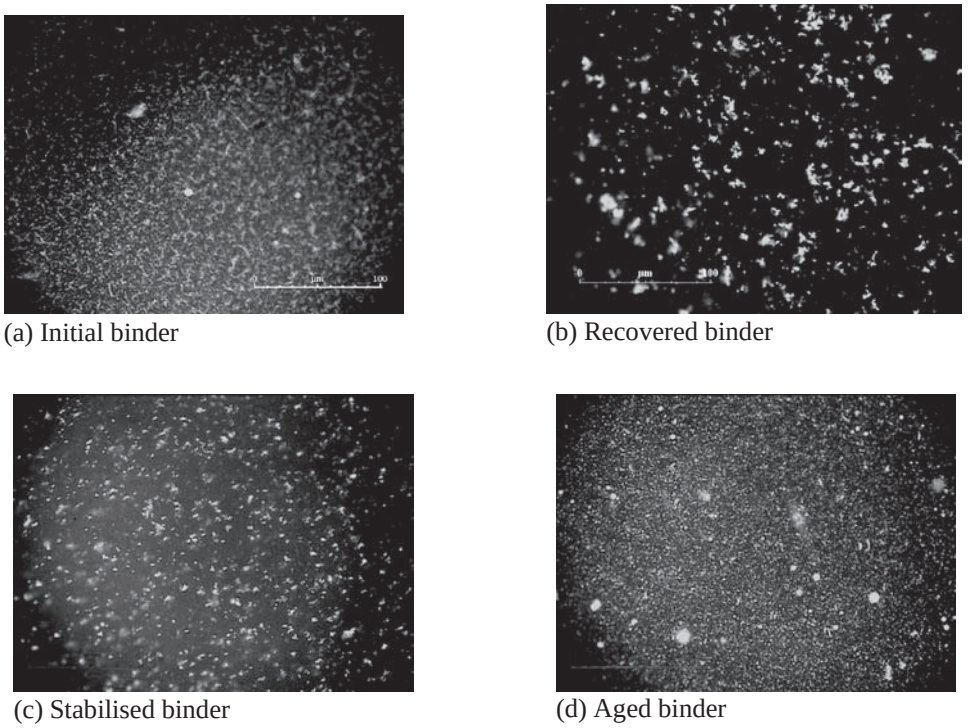

Figure 7. Epi-fluorescent microscopy—Observation of SBS-modified bitumen at different stages in the aging process.

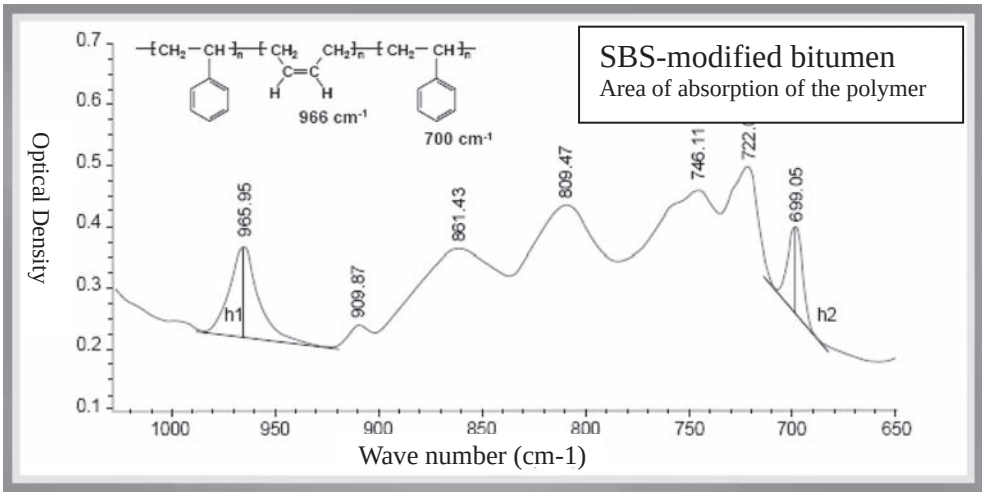

Figure 8. Detection of presence of SBS in a binder modified by infrared spectrometry—characteristic peaks at 966 cm^{-1} and 700 cm^{-1}.

may be put forward to explain this phenomenon: deterioration of the SBS occurs by segmentation of macro-molecules, but not by their complete destruction. The elementary chemical functions are therefore still detected by infrared absorption spectroscopy, and the length of the molecules remains sufficient for them to be revealed by epi-fluorescent microscopy. In short,

these two analytical techniques allowed us to check that the polymer was still present in the binder following aging by PAV, but did not give indications as to its state of conservation.

To better understand the change in SBS during aging of the binder, it is therefore necessary to refine the study using a technique for separating molecules according to their size. gel permeation chromatography.

This technique can be used for all types of polymer-modified binders, whether they are anhydrous binders for surfacing or binders recovered from emulsion.

4.3 *Characterisation by gel permeation chromatography*

GPC, also named "steric exclusion chromatography", is a technique which consists of separating molecules according to their size, by injecting a solution of the sample through a porous matrix. Largest molecules are not retained and flow freely in the column at the same speed as the solvent (here, tetrahydrofurane), whereas the smallest molecules are retained in the matrix pores. Retention time is inversely proportional to the logarithm of molecular weight. This kind of technique has been previously used for the analysis of pure bitumens (Brûlé & Migliori 1983, Brûlé et al. 1987) and polymer modified binders (Kraus 1981, Xiaohu & Ulf 2000).

Typically, the chromatogram for a PMB comprises two peaks: one for the polymer (high molecular weights) and the second for the bitumen (average and low molecular weights). To understand why there are two peaks that correspond to the bitumen and the polymer, we can give a few orders of magnitude: SBS has an average molecular weight of about 160,000 daltons, whereas that of bitumen is under 1000 daltons. The maximum molecular weight of asphaltenes, the heaviest molecules in bitumen, is around 10,000 daltons.

In order to produce a more marked SBS peak to provide a better understanding of how the polymer changes, the results shown here are for a PMB containing 5% polymer instead of 2.5%. Figure (9) displays the results obtained for a PMB at three stages: fresh binder, binder after a "low ageing" thin film method and binder after Pressure Ageing Vessel ("high aging method").

During the aging process, especially in the PAV, the polymer peak corresponding to the highest molecular weights (a) decreases slightly. This tends to confirm that one part of the polymer undergoes a change. Fragmentation of molecules leads to a broadening of the right side of the polymer peak in the area corresponding to medium molecular weight (b). Furthermore, the left side of the bitumen peak (c) is also higher after the ageing process. This is usually

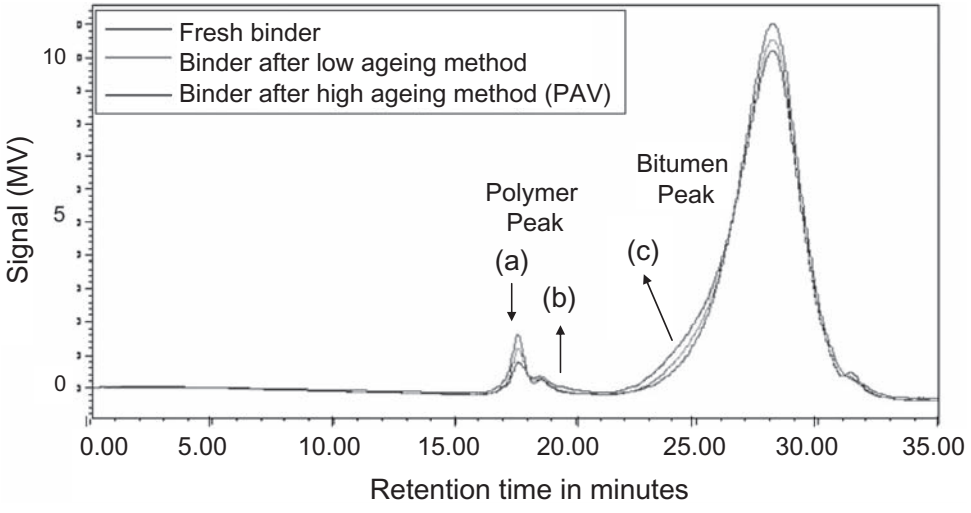

Figure 9. Gel permeation chromatography of Polymer Modified Binder.
Solvent: tetrahydrofurane.
Detection by refractometer.
Signal intensity as a function of retention time in minutes.

explained by an increase in asphaltene content (the heaviest molecules in bitumen), but may also be partly due to the presence of polymer fragments with a molecular mass similar to that of asphaltenes. However, the evolution of the shape of the peak corresponding to SBS throughout binder aging shows that the main part of the polymer remains intact.

5 CONCLUSION

These different studies have proven the utility of modifying a bitumen using SBS. We observe improvements in the binder's performance in many aspects, which can be measured in a laboratory and are tangible on the ground: improvement in mechanical behaviour at low temperature, increase of the softening temperature, addition of elasticity, increase in cohesion on broad temperature range.

The addition of polymer also has a positive impact on the binder's durability. This was assessed initially by characterising several binders following their manufacture, then by tracking the change in their characteristics during successive aging stages (short term, medium term, long term) simulated in the laboratory.

Laboratory assessment of the evolution of polymer efficiency during aging was affected by the hardening of the bitumen: this caused the binder to become rigid at low temperature, leading to decreased performance in terms of elasticity and cohesion. This phenomenon could also be attributed firstly to deterioration of the SBS; to eliminate any uncertainty, additional tests were conducted to assess its state of conservation. The objective was to characterise the SBS itself, using a technique to separate it from the bitumen. The gel permeation chromatography analyses showed that most of the polymer had retained its original characteristics, particularly in terms of the size of molecules, a property that determines the polymer's effectiveness in the mix.

In conclusion, we have been able to show that incorporating a polymer into bitumen improved its mechanical performance in a sustained manner.

REFERENCES

Asphalt Institute (USA) 1995, Performance Graded asphalt—Binder specification an testing, *Asphalt Institute Superpave Series n°1.*

Brûlé, B. & Migliori, F. 1983, Application de la chromatographie sur gel perméable (GPC) à la caractérisation de bitumes routiers et de leur susceptibilité au vieillissement artificiel, *Bulletin de liaison du laboratoire des Ponts et Chaussées,* 128, ref 2868. LCPC, France.

Brûlé, B., Ramond, G. & Such, C. 1987, Relations composition—structure—propriétés des bitumes routiers - Etat des recherches au LCPC, *Bulletin de liaison du laboratoire des Ponts et Chaussées,* 148, ref 3179. LCPC, France.

Chappat, M., Poirier, J.E., Robert, M. & Durand, G. 2000. Appréciation à partir des essais SUPERPAVE et de traction sur liants de l'impact du vieillissement de liants modifiés vis à vis du comportement à froid, *RGRA* n° 787. Colas, France.

Corté, J.F. et al. 1999. World Road Association (PIARC), Committee 8—Flexible roads, 1999, Use of modified bituminous binders, special bitumens and bitumens with additives in road pavements, *LCPC Technical guide*, n° 502 714. LCPC, France.

Gueit, C., Robert, M. & Durand, G. 2008. Characterisation of the different phases in the life cycle of the binder in a bitumen emulsion: recovery methods. *Eurasphalt Congress,* publication n° 405–004. Colas, France.

Kraus, G. (Phillips Petroleum Company, USA), 1981. Modification of bitumen by butadiene—styrene block polymers.

Lecomte, M.J. (Shell Global Solutions, France), Durand, G., Robert, M. (Colas) & Phillips, M.C. (Consultant) 2000. Examination of the capability of Superpave tests to predict the low-temperature performance of polymer-modified binders. *Eurasphalt Congress*, Proc. 0094.

Salomon, D. (Pavement preservation systems, USA), Thompson, M. (Midland Asphalt, Colas Inc., USA) & Durand, G. et al. (Colas, France) 2008. Comparison of rheological properties for recovered residue from emulsified asphalt obtained by three recovery procedures. *ISAET Meeting.*

Xiaohu, L. & Ulf, I. 2000, Artificial aging of polymer modified bitumens, *Journal of Applied Polymer Science* 76: 1811–1824.

Advanced Testing and Characterization of Bituminous Materials – Loizos, Partl, Scarpas & Al-Qadi (eds)
© 2009 Taylor & Francis Group, London, ISBN 978-0-415-55854-9

Impact of freeze-thaw cycles on the performance of asphalt mixture based permeability

Junyan Yi, Decheng Feng & Dongsheng Wang
Harbin Institute of Technology, Harbin, China

ABSTRACT: Raveling caused by water under freeze-thaw cycles is the main distress in highway of Chinese seasonal frozen region. Through the studies on permeability of AC-16 mixtures, the quantity of water infiltrating mixtures could be controlled. Experiments of freeze-thaw cycles based on permeability were performed to investigate the strength variation of asphalt mixtures. Other parameters investigated in freeze-thaw cycles were percent air voids, relative volume, water absorptivity and height of mixtures. Results from the experiments indicate that the strength damage of mixture can consist of three successive phases, which can be validated from the variation of other parameters. The study can interpret the damage process under freeze-thaw cycles and have guidance effects to the construction of asphalt mixtures.

1 INTRODUCTION

Performance after freeze-thaw cycles is important for asphalt mixtures in seasonal frozen region. As we know, water and its change of phase state have been the main factors of influencing the pavement performance. The bad effects of water lie in the displacement of asphalt film (Höbeda 1998, Kettil et al. 2005) and causing structure damage through the volume expansion when temperature decreases. For the asphalt mixtures in some moisture areas, the infiltration of water is unavoidable. The main problem is the quantity. Recent study have indicated that if the asphalt mixtures had the enough voids (>9%) to accommodate the expanding of water after decrease of temperature, the frozen effects would have less influence on asphalt mixtures (Pan et al. 2003). However, the dense mixtures used in China usually have percent air voids of 3~6%. Once excess water infiltrating mixtures, they will have performance degradation in a short time when temperature changes.

For the serious effects of freeze-thaw, there had been some studies on the impacts of it on the asphalt mixtures performance recently (Pan et al. 2003, Cao et al. 2004, Hou et al. 2006, Li & Li 2005). And some researches on the change of chemical composition in the asphalt-aggregate interfacial region during repeated freeze-thaw cycles had also been conducted (Huang et al. 2005). The environmental scanning electron microscope was already used to study water stripping (Williams & Miknis 1998). As to micromechanics and numerical model describing the materials behavior in freeze-thaw process, the studies nowadays mainly concern the soil (Talamucci 2003) and cement concrete (Zhou & Hirozo 2008). But for the asphalt mixtures, most of previous studies only tried to find the relationships between some mixtures macro-characteristics (strength, fatigue lifetime, etc.) and freeze-thaw cycles. How to reduce the mixtures damage after freeze-thaw cycles remains a problem. Furthermore the change laws of volume and strength properties of mixtures in freeze-thaw cycles also do not have accepted conclusions, which need to be studied. The objective of this paper is to propose the measures of reducing the effects of freeze-thaw cycles on mixtures and demonstrate the variation laws of mixtures characteristics in freeze-thaw cycles.

Because water can influence the damage extent of mixtures caused by freeze-thaw, reasonable measures of reducing the quantity of water in mixture should be considered firstly

to improve the freeze-thaw durability of mixtures. Thus a laboratory permeability test has been selected to find the permeability of mixture. Then criteria of air voids based on permeability can be proposed to control the infiltration of water. Some similar theoretical and experimental approaches on the flow of water in asphalt mixtures had been conducted in previous studies (Cooley & Ray 2001, Mallick et al. 2003, Praticò & Moro 2008). But these studies mainly concerned the field permeability of mixtures and did not combine it with the performance.

Based on the proposed criteria, this paper had carried out the experiments of freeze-thaw cycles to study the variation laws of mixtures performance including indirect tensile strength, relative volume, percent air voids, water absorptivity and height of mixtures. Another type of mixtures which had bigger air voids had been used to validate the rationality of proposed criteria and analyze the damage phase of mixtures in freeze-thaw cycles.

2 MATERIALS CHARACTERIZATION AND MIXTURES DESIGN

2.1 *Materials characterization*

Aggregate samples were obtained from materials used in the construction of an expressway in China. All aggregates were crushed limestone. The specific gravity and absorption for the different sizes of aggregates are shown in Table 1.

The used binder was penetration grade 80–100 asphalt cement. The properties of the binders are shown in Table 2.

Table 1. Aggregate specific gravity and absorption.

	Properties		
Aggregate size	Bulk specific gravity	Apparent specific gravity	Percent absorption (%)
19 mm	2.649	2.697	0.7
16 mm	2.655	2.701	0.6
13.2 mm	2.645	2.703	0.8
9.5 mm	2.645	2.707	0.9
4.75 mm	2.629	2.711	1.1
2.36 mm	—	2.664	—
1.18 mm	—	2.656	—
0.6 mm	—	2.654	—
0.3 mm	—	2.649	—
0.15 mm	—	2.625	—
0.075 mm	—	2.561	—
Filler	—	2.832	—

Table 2. Properties of binders.

Test	Binder properties	Specification in China
Penetration at 25°C/0.1 mm	93.7	80 ~ 100
Penetration index	–2.1	–1.5 ~ +1.0
Softening point/°C	45.9	>44.0
Ductility at 15°C/cm, 5 cm/min	>150	>100
Retained penetration after RTFOT/%	60	>57
Retained ductility at 15°C after RTFOT/cm, 5 cm/min	149	—

2.2 *Mixtures design*

The mixture used in the experiments is the AC-16, whose maximum grain size is 19 mm. Mixtures design was performed according to the design procedure of Marshall Mixture Design Method. The mixtures design involves selecting a mixture gradation and optimum asphalt content. The mixed specimens were evaluated for percent air voids, marshall stability, flow value, percent voids in mineral aggregate (VMA) and density. Finally the optimum asphalt content could be selected based on the limits proposed by Specifications for Design of Highway Asphalt Pavement (SDHAP) in China (Yang et al. 2006).

The mixture gradations used in the freeze-thaw cycles test is the medium of gradation range also proposed by SDHAP, which can be shown in Table 3. In experiments of permeability, to evaluate the effects of gradation variation on the permeability of mixtures in construction, three other gradations are considered (Table 3). Therefore only the optimum asphalt content for the medium of gradation range had been selected and the asphalt content for other gradations were same to the medium. What need to be noticed is that the S gradation in Table 3 is defined to be the mixture which has dense-framework structure.

For the bad moisture resistance of mixtures in practical test, hydrated lime had been added to all mixtures. The content of hydrated lime is 40% weight of filler. Finally, the optimum asphalt content for the medium could be selected at 5.2% by total weight of the mixtures.

In the permeability experiments, the different percent air voids for every type of mixtures was controlled by different blows on each side using the Marshall hammer. And the specimens used in experiments of freeze-thaw cycles were prepared using a gyratory compactor.

3 *Laboratory permeability experiment*

3.1 *Laboratory permeability device*

The permeability device in the laboratory can be used to test the permeability of cylindrical specimens (101.6 mm diameter by 63.5 mm high) (Figure 1).

3.2 *Results and discussion*

Figure 2 is the plot of permeability for the four types of mixtures. It can be seen that the gradations have important influences on the permeability of mixture. The coarse mixture would be more permeable than other mixtures at the same percent air voids.

Table 3. Mixture gradations selected.

	Percent passing				
Sieve size (mm)	Gradation range in SDHAP	Coarse	Medium	Fine	S
19	100	98	100	100	100
16	90–100	93	95	95	95
13.2	76–92	81	84	88	88
9.5	60–80	61	70	75	75
4.75	34–62	40	48	55	55
2.36	20–48	30	34	40	30
1.18	13–36	22	25	28	20
0.6	9–26	16	18	20	15
0.3	7–18	12	13	15	11
0.15	5–14	8	10	10	8
0.075	4–8	4	6	6	6

Figure 1. Laboratory permeability device.

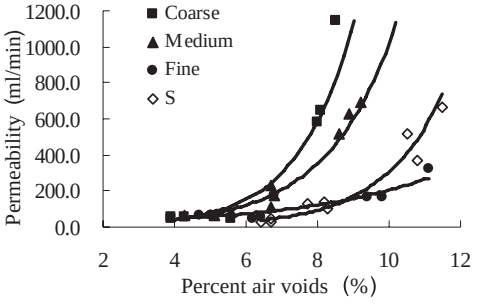

Figure 2. Plot of permeability versus air voids — four types of mixtures.

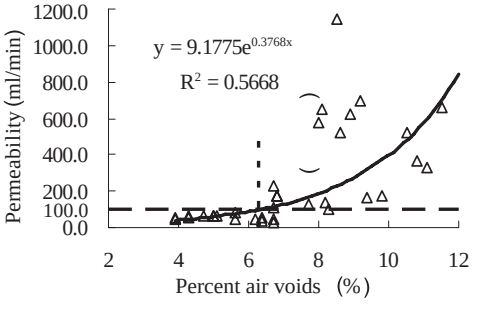

Figure 3. Plot of permeability versus air voids — all mixtures.

Integrate the all data of permeability in Figure 3. Nowadays the permeability criterion in China for all dense mixture is 120 ml/min. To control the infiltration of water more strictly, this paper propose the criteria of 100 ml/min. Through the plot of permeability versus air voids, the critical percent air voids versus permeability criteria can be got. Figure 3 shows the results that the 6.3% percent air voids can assure the less infiltration of water into mixtures. Finally to simplify the control criteria, the critical percent air voids was determined as 6% for AC-16 mixtures. Through the control of air voids, the quantity of water infiltrating mixtures can be cut down, consequently there should be less damage caused by water under freeze-thaw cycles.

To validate the rationality of critical percent air voids proposed, the experiments of freeze-thaw cycles would be carried out for mixtures which have the critical and bigger percent air voids.

4 EXPERIMENT OF FREEZE-THAW CYCLES

The experimental mixture used in freeze-thaw cycles is the medium gradation mixture of AC-16. All specimens (including 100 mm diameter by 63.5 mm high and 100 mm diameter by 100 mm high), whose air voids was controlled to be approximately 6 ± 1%, were molded using gyratory compacter by diminishing the rotation amount. In order to contrast the effects of critical air voids, specimens with approximately 8 ± 1% air voids (only 63.5 mm high) were prepared to carry on the experiments of freeze-thaw cycles.

For each of the mixtures, freeze-thaw cycles up to 25 cycles were conducted. Each cycle consisted of freezing for 9 h at −18°C ± (–0.4°F) followed by soaking for 3 h at 25°C (77°F) (Yi 2006). Several parameters including indirect tensile strength (ITS) at 25°C, tensile strength ratio (TSR), percent air voids (PAV), relative volumes, water absorptivity (WA) and height (only for mixtures with critical air voids) were determined at 0, 5, 10, 15, 20 and 25 cycles. And all specimens were water conditioned by vacuum saturation for 15 min with distilled water before experiments of freeze-thaw cycles.

There were totally 18 specimens (3 duplicates × 6) with 63.5 mm high and 3 specimens with 100 mm high for mixtures with critical percent air voids and 18 specimens with 63.5 mm high for mixtures with 8 ± 1% air voids. In the experiments for mixtures with critical percent air voids, the specimens with 63.5 mm high were used to determine the indirect tensile strength at 25°C and tensile strength ratio; comparably specimens with 100 mm high, which did not destroy in cycles, could determine the variation laws of other parameters for these mixtures had the same gradation and structure. Using the same specimens can diminish the effects caused by individual difference and reflect the real variation for mixtures in freeze-thaw cycles. For the mixtures with 8 ± 1% air voids, the strength variation was the primary research object. Thus the volume properties of mixtures in the cycles of freeze-thaw were directly tested through the specimens with 63.5 mm high before strength test. And the variation laws in the cycles were only the rough trend.

4.1 *Mixtures with critical percent air voids*

4.1.1 *Effects of freeze-thaw cycles on strength*

Figure 4 shows the variation of indirect tensile strength and tensile strength ratio for mixtures with critical percent air voids by repeated freeze-thaw cycles. The values in the plot are the average of three duplicates. Generally, the decrease of ITS can be divided into two phase along with the cycles increase: decreased rapidly in 0–15 cycles and slowly in last cycles.

In fact, the damage in the first 15 cycles was mainly caused by the expansion of water in the mixtures under the change of temperature, which could be supported through the variation of water absorptivity. Figure 5 shows that the water absorptivity of three specimens with 100 mm high which are listed as 1 to 3 has changed rapidly from 0 to 15 cycles, and gradually stay in steady state in the last cycles. Because the inner structure and materials are similar, the variation of mixture characteristics for the two mixtures with different height can be interchangeable. The water absorptivity is defined as the percentage of water volume the mixtures absorbed accounting for total volume of mixtures, actually representing the quantities of connected voids in the mixtures. Therefore the performance variation of mixtures can be analyzed according to the Figure 4 and Figure 5.

In the beginning of freeze-thaw cycles, the volume of water saturating in the mixtures had increased when placing into the circumstance of –18°C, which brought the extending of connected voids in the asphalt mixture. Subsequently there would appear more macroscopic

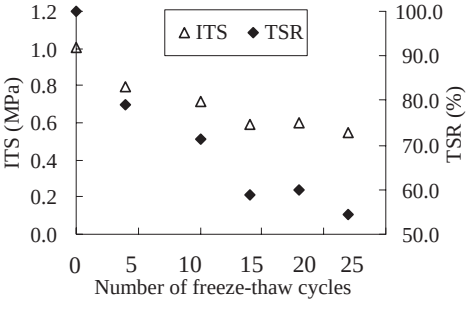

Figure 4. Impact of freeze-thaw cycles on ITS and TSR.

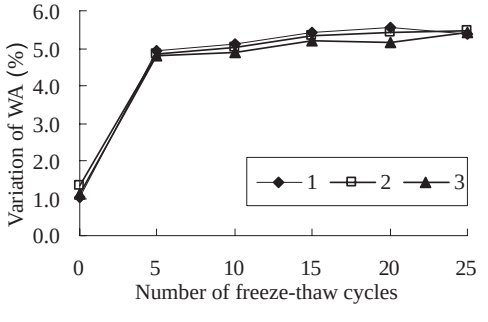

Figure 5. Impact of freeze-thaw cycles on water absorptivity—mixtures with 100 mm height.

cracks for mixtures, and make more water infiltrating mixtures at next freeze-thaw cycle. Consequently the water absorptivity and connected voids all had a continuing increase. Because the added connected voids were mostly the macroscopic cracks which would be the weak parts of mixtures structure for the stress concentration beside the cracks, the ITS and TSR had decreased sharply. This can be defined as the macroscopic effects of freeze-thaw cycles on the strength of asphalt mixtures.

When the connected voids were increased to certain extent, parts of water could flow freely out of mixtures along with the large connected voids under the effects of temperature gradient. Therefore the damage caused by expansion of water could be reduced. The data in Figure 4 clearly demonstrate the assumption. From the previous experience we can suppose that the state is only temporary, and there will be a new damage phase in some periods in which damage characteristic is the absorption loss of asphalt-aggregate interface. To validate the hypothesis and rationality of critical percent air voids, mixtures with larger air voids will be conducted to experiments of freeze-thaw cycles.

4.1.2 *Effects of freeze-thaw cycles on volume properties*

The volume properties including percent air voids, relative volumes and height of asphalt mixtures with 100 mm high in cycles of freeze-thaw were also determined (Figs 6, 7 and 8). The relative volume in Figure 7 is the difference between the mass of the specimen in saturated surface-dry condition and the mass of the specimen submerged in water.

The variation of volume properties indicates that the percent air voids and relative volume have nearly a continual linear increase in the freeze-thaw cycles, which have important influence on the performance of mixtures. In fact, there are also complex relationships between

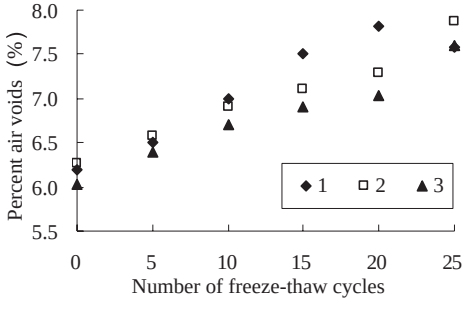

Figure 6. Impact of freeze-thaw cycles on PAV—mixtures with 100 mm height.

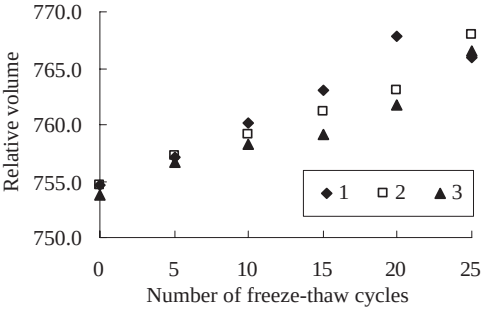

Figure 7. Impact of freeze-thaw cycles on relative volume—mixtures with 100 mm height.

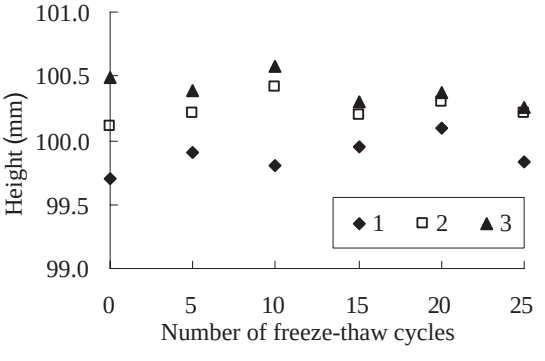

Figure 8. Impact of freeze-thaw cycles on height mixtures with 100 mm height.

the percent air voids and relative volume. The expansion of relative volume mainly caused by frozen water would result in the appearance of inner cracks. This is probably the reason of increasing for percent air voids. And similarly the increase of percent air voids may cause to the expansion of relative volume.

Figure 8 demonstrates that there is little variation for height in cycles of freeze-thaw, and the biggest variation of which is only approximately 0.5 mm. This small change contributes a little to the variation of relative volume. Therefore the expansion along the radial direction should be the main reason to volume variation. This can be explained by the material characteristic of asphalt mixtures. As a typical viscoelastic material, the asphalt mixtures have a self-healing performance. After the expansion of volume, the height variation along with the vertical direction could recover gradually for the effects of gravity. Contrarily, the expansion along the radial direction is not easy to recover.

4.1.3 *Summary*

The experimental results above for mixtures with critical air voids mainly indicate the performance variation of asphalt mixtures in cycles of freeze-thaw. On the whole, the decrease of ITS and TSR can be divided into two phase: phase of reducing sharply and of keeping steady. To validate the rationality of critical air voids and the hypothesis that there will be a new reducing phase in some periods, the experiments of freeze-thaw cycles for asphalt mixtures with 8 ± 1% air voids were conducted.

4.2 *Mixtures with bigger percent air voids*

In this test, parameters including ITS and TSR were mainly determined for specimens at 0, 5, 10, 15, 20, and 25 cycles. Before the test of indirect tensile strength, other indexes such as water absorptivity, relative volume and percent air voids were obtained for the mixtures with 63.5 mm high which would be destroyed. And the line in Figures was the average value of three specimens. Thus the variations of these parameters were only the total tendency for mixtures.

4.2.1 *Effects of freeze-thaw cycles on strength*

Figure 9 indicates that the indirect tensile strength of mixtures with 8 ± 1% air voids are obviously smaller comparing with mixtures with critical air voids at every five cycles. And the decrease extent of TSR is similar to mixtures with critical air voids in the 0–20 cycles. At the last five cycles, the mixtures with 8 ± 1% air voids have showed the different performance.

Like the mixtures with critical air voids, the specimens with bigger air voids also have a steady phase of strength from 15 to 20 cycles. However, there appears obvious decrease after 20 cycles for the relatively worse structure defects. This can be demonstrated by the reducing of TSR. Figure 9 shows that there are obviously stepwise decrease for TSR and ITS. And it was found that the mixtures had surface loosening in the last cycles. Thus the test results

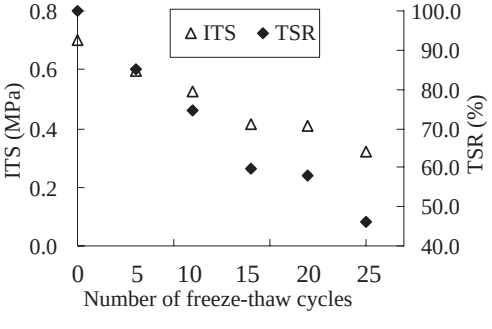

Figure 9. Impact of freeze-thaw cycles on ITS and TSR.

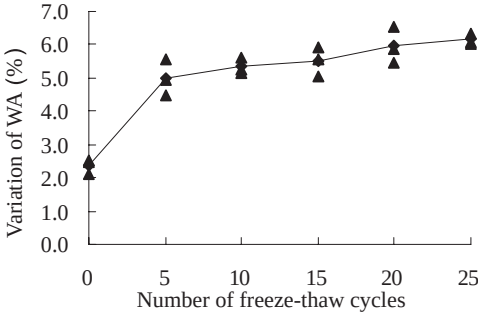

Figure 10. Impact of freeze-thaw cycles on water absorptivity—mixtures with 63.5 mm height.

demonstrate the hypotheses on the damage process of asphalt mixtures in freeze-thaw cycles, which are that the damage process consists of three phases: (1) the phase of connected voids extending and macroscopical cracks increasing caused by frozen water; (2) the phase of performance stabilizes; (3) the phase of the absorption of asphalt-aggregate interface losing.

Comparing the Figure 9 with Figure 4, the TSR in the second phase of damage is similar, which is 50~60%. This shows that the difference of structure has less impact on the TSR but important on the ITS for the initial cycles. Thus the value of ITS is also very important index besides the TSR for evaluating the performance of asphalt mixtures in cycles of freeze-thaw.

Figure 10 indicates the variation of water absorptivity in freeze-thaw cycles for mixtures with 8 ± 1% air voids, which also demonstrates the change laws of strength for mixtures as mentioned before. At the third phase of damage, because the damage of mixtures was the absorption losing of asphalt-aggregate interface, the water absorptivity did not changed rapidly.

4.2.2 *Effects of freeze-thaw cycles on volume properties*

Figure 11 and Figure 12 show that the percent air voids and relative volume are continually increasing in the initial 15 cycles and staying at a steady state gradually in the remaining cycles. This is probably because that the air voids were big enough for the free flow of water after 15 cycles and there should be not obvious change for these indexes anymore.

4.2.3 *Summary*

From the test results of mixtures with 8 ± 1% air voids, the rationality of critical air voids can be validated. Mixtures having bigger air voids have a worse performance in cycles of freeze-thaw. And the strength of mixtures will decrease more rapidly than specimens with critical air voids.

5 CONCLUSIONS AND RECOMMENDATIONS

The study in this paper has proposed the measures of decreasing the damage and provided new information regarding damage phase of asphalt mixtures under freeze-thaw cycles. Specifically, the following conclusions are proposed.

1. Controlling of percent air voids can have the advantages of improving the performance of asphalt mixtures under freeze-thaw cycles.
2. The strength damage of mixtures under freeze-thaw cycles can be divided into three phase. Firstly, the volume of water in the connected air voids are expanded when the temperature decrease, which result in the increase of connected air voids. Then the structures of mixtures are destroyed and the strength reduces to 50~60% of initial mixtures rapidly. Secondly, when the connected air voids are big enough for the free flow of water in mixtures and simultaneously the asphalt have not been displaced by water at asphalt-aggregate

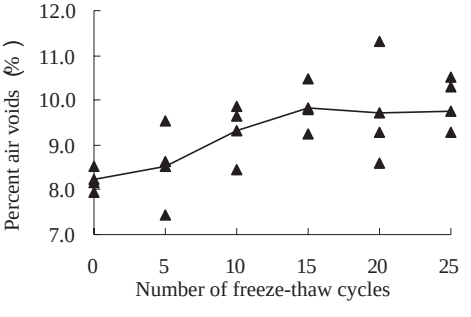

Figure 11. Impact of freeze-thaw cycles on PAV—mixtures with 63.5 mm height.

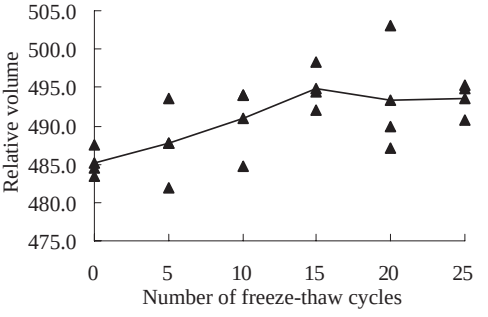

Figure 12. Impact of freeze-thaw cycles on relative volume—mixtures with 63.5 mm height.

interface, the performance of mixtures will keep steady. And the periods of steady state are different for mixtures with different material characteristics. Lastly, the water infiltrates the asphalt-aggregate interface, which results in the absorption losing of asphalt-aggregate interface. Therefore the strength of asphalt mixtures under cycles of freeze-thaw has reduced rapidly again.

3. The percent air voids, relative volume and water absorptivity of mixtures have increased gradually at the first and second damage phases under freeze-thaw cycles, and stayed steadily after that.

ACKNOWLEDGEMENT

The authors are grateful to the reviewers for their comments and advices on this paper. And the financial support by Ministry of Transport of the People's Republic of China is gratefully acknowledged.

REFERENCES

Cao Xiao-yan, Chen Yong-xing & Bao Fu-tang. 2004. Research of freeze-resistance performance of asphalt mixtures. *Journal of Heilongjiang institute of technology* 18(2):36–38.

Cooley, Allen L. & Ray Brown, E. 2001. Development of Critical Field Permeability and Pavement Density Values for Coarse-Graded Superpave Pavements. Transportation Research Board 0344.

Höbeda, P. 1998. Water sensitivity of asphalt pavements. Swedish National Road and Transport Research Institute (VTI) VTI note 35.

Hou Shu-guang, Wang Hong-chang, Huang Xiao-ming & Zhi-dong Li 2006. Analysis of Freez-thaw Fatigue Performance for Asphalt Mixture in Low Temperature Zone. Journal of Highway and Transportation Research and Development 23(4):7–10.

Huang, Shin-che, Raymond Robertson, E., Jan Branthavr, F., et al. 2005. Impact of Lime Modification of Asphalt and Freeze–Thaw Cycles on the Asphalt–Aggregate Interaction and Moisture Resistance to Moisture Damage. Journal of Materials in Civil Engineering, ASCE, 17(6): 711–718.

Kettil, P., Engström, G. & Wiberg, N.-E. 2005. Coupled hydro-mechanical wave propagation in road structures. Computers and Structures, 83:1719–1729.

Mallick, Rajib B., Cooley, Allen L. & Teto. Matthew R. 2003. An Evaluation of Factors Affecting Permeability of Superpave Designed Pavements. NCAT Report 03-02.

Pan Bao-feng, Wang Zhe-ren & Chen Jing-yun. 2003. Test and study of the alternate freezing and thawing capability of the bituminous mixture. China Journal of Highway and Transport 16(2):1–4.

Praticò, F. G. & Moro A. 2008. Flow of water in rigid solids: Development and experimental validation of models for tests on asphalts. Computers and Mathematics with Applications, 55:235–244.

Talamucci, F. 2003. Freezing Processes in Porous Media: Formation of Ice Lenses, Swelling of the Soil. Mathematical and Computer Modelling, 37:595–602.

Williams, Theresa M. & .Miknis, Francis P. 1998. Use of Environmental SEM to Study Asphalt-Water Interactions. Journal of Materials in Civil Engineering, ASCE, 10(2):121–124.

Yang Meng-yu, Feng De-cheng, et al. 2006. Specifications for Design of Highway Asphalt Pavement. Ministry of Transport of the People's Republic of China.

Yi Jun-yan. 2006. Research on Freezing-Thawing Performance and Permeability of Asphalt Mixture. Thesis for Master's Degree of Harbin Institute of Technology, China.

Zhe, Li & Zhi-dong, Li 2005. The Evaluation of Fatigue Feature of Cycle of Freezing and Thawing for Bitumen Mixture Based on Energy Method. Shanxi Science and Technology of Communications (1):26–28.

Zhou, Zhi-Yun & Hirozo Mihashi. 2008. Micromechanics Model to Describe Strain Behavior of Concrete in Freezing Process. Journal of Materials in Civil Engineering, ASCE, 20(1):46–53.

Advanced Testing and Characterization of Bituminous Materials – Loizos, Partl, Scarpas & Al-Qadi (eds)
© 2009 Taylor & Francis Group, London, ISBN 978-0-415-55854-9

Formulation of authoritative temperature gradients for an analytical design process of flexible pavements using statistical techniques

S. Kayser & F. Wellner
Chair of Pavement Engineering, Dresden University of Technology, Germany

ABSTRACT: Within an analytical design process of flexible pavements various input parameter are required. Beside the material properties the climatic conditions as well as the traffic load will play an important role within the design process. These properties have an important influence on the flexible pavement design. It can be concluded that the temperature dependant behavior of the flexible pavements should be taken into account in the design process as accurate as possible. The time dependant temperature stages within the asphalt layers that are based on the climatic conditions can be modeled by numerical simulations. For the mechanistic design procedure of asphalt pavements all relevant temperature gradients within the asphalt layer should be considered. Within the research presented in this paper, twelve standardized characteristic temperature profiles could be determined for Germany. However, the general procedure to determine relevant temperature functions is universally valid.

1 INTRODUCTION

The analytical pavement design processes are based on MINERS law. That means, a material is fatigued if the sum of all individual damages, which result from all stress conditions, is greater than 1. The number of these conditions results from the number of the temperature stress conditions in combination with the predicted traffic load conditions. The number of possible combinations depends on the time slice and can theoretically be infinite. If a time slice of one hour is assumed, you must consider approximately 8,760 temperature stress conditions per year and more than 262,000 temperature stress conditions for a service life of 30 years. Here it becomes obvious that it is necessary to minimize the enormous number of temperature stress conditions and the time required for the analytical design process of flexible pavements. Currently, 13 temperature functions have been implemented in the German pavement design tool PADESTO (Kiehne, unpublished) to consider the influence of temperature within the analytical pavement design process. Each of these temperature functions describes a vertical temperature profile along the thickness of the asphalt layers and represents a specific range of asphalt surface temperatures. These temperature regions range from smaller than –10°C to more than +45°C and have a range size of 5 K. Each of these temperature classes is represented by its mean. The 13 temperature stress conditions result from these 13 temperature functions. The stress conditions are weighted by applying the frequencies of occurrence. The 13 temperature ranges for the pavement design process in Germany were reviewed and modified.

2 OBJECTIVES

It is generally agreed that complete temperature responses and temperature profiles, which depend on the time slice, should be used. Although the accuracy of the pavement design results improves with a decreasing time slice, the calculating effort increases disproportionately above all concerning the optimization of the pavement designs. If you choose a time slice of one hour, it is necessary to consider more than 262,000 temperature profiles for the pavement

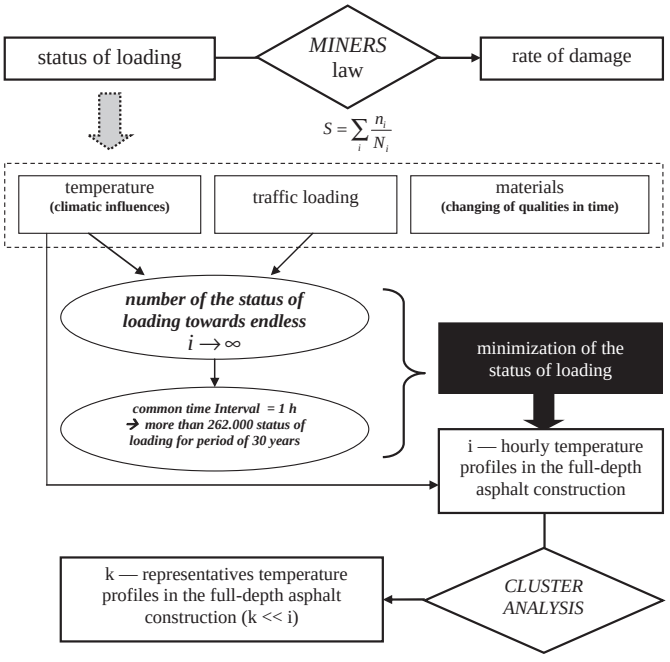

Figure 1. Structure chart demonstrating the necessity to prepare authoritative vertical temperature functions for the flexible pavement design process.

design on the basis of a service life of 30 years. It was the aim of this research to work out authoritative temperature functions for the German analytical pavement design tool PADESTO. The range of the temperature profiles that are represented by the authoritative temperature functions should be as wide as possible, while the number of the authoritative temperature functions should be as small as possible to optimize the calculation time.

3 APPROACH

The authoritative temperature functions for the analytical pavement design process were formulated in two major steps. First, the vertical hourly temperature profiles were numerically calculated on the basis of measured surface temperatures. The results were implemented in a database.

At the same time, extensive sensitivity calculations were performed within this process. These calculations helped assess the influence of the factors listed below on the vertical temperature profiles:

- material parameters
- thickness of the full depth asphalt pavements.

In the second step, the simulated vertical temperature profiles were arranged according to their similarity with each other using the statistical tool 'cluster analysis'. For each of these groups, characteristic features were found which form the basis for the selection.

4 NUMERICAL CALCULATION OF TEMPERATURE PROFILES

The calculation of the vertical hourly temperature profiles, which were grouped later, was done using the differential method for one-dimensional unsteady thermal conduction.

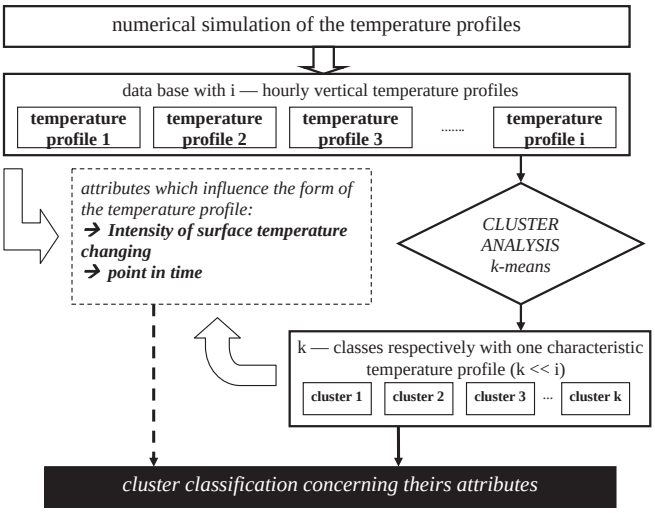

Figure 2. Simplified schematic to explain the approach to formulating the authoritative temperature functions for the flexible pavement design process.

Calculation of the time-variable temperature profile:

$$\frac{\partial T}{\partial t} = a_T . \frac{\partial^2 T}{\partial x^2} \tag{1}$$

where T = temperature; t = time; a_T = diffusivity and x = thickness of the asphalt structure.

It is necessary to know various boundary conditions for the numerical calculations of the temperature profiles (along the thickness of the asphalt structure).

- temperature profile at the beginning of the calculations
- temperature response on the underside of the considered system (underside temperature)
- temperature response on the upper surface of the considered system (surface temperature).

The vertical temperature gradient at the beginning of the temperature simulation was determined by iteratively solving the calculation algorithm. The difference of two consecutive iteration steps should be smaller than 0.01 K for each layer temperature of the chosen system.

The temperature response on the underside of the considered system corresponded to the temperature response of the soil at a depth of 2.5 m under the surface. Hence the thickness of the complete system is 2.50 cm. The temperature of underside layer is defined by a seasonal temperature cycle (Pohlmann 1989). Table 1 shows the monthly underground temperatures.

The most essential of the three boundary conditions is the surface temperature. Extensive measured data of surface temperatures were available. The temperature data were measured by the Road Condition and Weather Information System (SWIS). A total of 74 measuring

Table 1. Seasonal cycle of the soil temperature at a depth of 2.5 meters under the surface.

Month	Jan.	Feb.	Mar.	Apr.	May	Jun.	Jul.	Aug.	Sep.	Oct.	Nov.	Dec.
Temperature*	5.8	4.9	4.2	4.5	6.2	8.6	11.2	12.8	13.0	11.9	9.8	7.8

*Underground temperature in a depth of 2.5 meters under the surface [°C].

points in Germany were chosen whose measured data were used for the numerical calculation of the vertical temperature profiles.

The period of data collection underlying the calculation was from 2002 to 2005. Altogether, a total of 450,000 hourly vertical temperature profiles were calculated, analyzed and evaluated.

In addition to the three boundary conditions for the numerical calculations of the vertical temperature profiles, other parameters also influence the calculation results. These are:

– thermal conductivity
– density
– specific thermal capacity.

These three material-specific parameters can be summarized as the thermal diffusivity. Calculation of the thermal diffusivity:

$$a_T = \frac{\lambda_W}{\rho \cdot c_p} \tag{2}$$

where λ_ω = thermal conductivity; ρ = density and c_p = specific thermal capacity.

Because the thermal diffusivity is also a material-specific parameter, structural parameters of the pavement (material components, thickness of the asphalt) may also have effects on the temperature calculations. For example in (Kayser 2007b) and (Kayser 2008), extensive calculations are performed to assess the influence of different materials on the results of the temperature calculations. Both bound and unbound materials and their different material parameters are assessed.

4.1 *Material properties*

The different thermal diffusivities are decisive in how the different materials influence the results of the thermal simulation. It is a general rule that the lower a layer is found under the surface, for which layer the thermodynamic parameters are changed, the smaller the influence on the temperature profile of the upper layers in the system. The variation range of the thermal diffusivities of the several layers was chosen this wide in order to include the thermal diffusivities of the most different materials. As the maximum temperature differences concerning the reference value were between –1.0 K and +1.5 K, the influence of the different materials, which are normally used in road constructions, on the numerical temperature simulations can absolutely be neglected.

4.2 *Asphalt layers*

Normal, full depth asphalt pavements consist of three different asphalt layers for which different asphalt materials are used depending on their different requirements. In (Pohlmann 1989) you can find that the relative differences between the thermal diffusivities of the top course, grade course, and subgrade course average about 10%. As noted in different literature (e.g. (Krebs 1981) (Wistuba 2001) and (Wistuba 2004)), it is not necessary to differentiate between the three asphalt layers in temperature calculations. Hence the different thermal diffusivities can be neglected. Instead, it is practicable to use only one average thermal diffusivity for the full depth asphalt pavement. These statements conform the results obtained in (Kayser 2007b) and (Kayser 2008).

4.3 *Thickness of the full-depth asphalt pavement*

Given the climatic factors and their influence on the temperature-dependent attributes of asphalt, the pavement design engineer currently assumes that the characteristic temperature profile of a surface temperature class can be described with one specifically defined temperature function. The temperature functions are independent of the thickness of the full-depth asphalt pavement and one can use this function for all possible thicknesses. Regardless of the fact

whether this function is really representative, it should be examined if the temperature function is actually significant independent of the thickness of the full-depth asphalt pavement. The thickness of the full-depth asphalt pavement was varied between 15 and 35 cm with an increment of 5 cm. In accordance with the specific variants, the frost blanket course was changed such that the total thickness of the frost-proof pavement superstructure was always 85 cm.

With a frequency of more than 90% for maximum absolute temperature differences of ≤0.5 K, it can be assumed that the thickness of the asphalt layer is not decisive for the definition of relevant characteristic temperature functions.

5 CLUSTER ANALYSIS METHOD

Cluster analysis aims to allocate similar objects (here hourly vertical temperature profiles) into groups (clusters) on the basis of their similarity. The individual objects are combined in clusters such that the formed cluster is as homogenous as possible and that the clusters are as heterogeneous as possible when compared with each other.

Cluster analysis uses different techniques. Depending on the classification principle, cluster analysis comprises incomplete, deterministic and probabilistic approaches (Bacher 1996). Whereas the incomplete cluster analysis approach describes the classification objects spatially, the deterministic cluster analysis method assigns the objects to one or more clusters with a probability of 0 or 1. In contrast, probabilistic clustering groups objects into clusters with a probability between 0 and 1 (Bacher 1996). Within these clustering approaches, which are summarized depending on their classification principle, there are further different sub-methods (see Table 2).

5.1 *Partitioning method k-means*

Using the cluster analysis method k-means, the clusters were determined iteratively through the definition of the number of clusters at the beginning of the calculations. First, each cluster was assigned with a randomly chosen cluster center (here this was a random temperature profile). Subsequently, the remaining objects (temperature profiles) were assigned to the cluster that was closest to them and a new arithmetic mean (*k-means*) was calculated (representation temperature profile) for each cluster. This procedure was iterated until the grouping of the objects did not change anymore and the mean square deviation in the clusters became minimum.

The mean square deviation or mean square error describes the variance of objects which cannot be explained by the cluster. It is defined like this (Bacher 1996):

$$F(C_i) = \sum_{C_i} \sum_{T \in C_i} D_{T,C_i}{}^2 \rightarrow \min \tag{3}$$

where F = mean square error; C_i = cluster i; T = temperature profiles of a cluster and $D_{T,Ci}$ = Euclidean distance between temperature profile T and the center of cluster C_i.

Table 2. Choice of cluster analysis methods according to the classification principle employed (Bacher 1996).

Classification principles	Incomplete	Deterministic	Probabilistic
Cluster	multiple correspondence analysis	next–neighbor–method	latent profile analysis
Analysis	non-metric multidimensional scaling	representatives–method	analysis of latent classes for nominal scaled variables
Methods*	nominal factor analysis of McDonald	hierarchical methods for the construction of cluster centers	analysis of latent classes for ordinal scaled variables
	bivariate correspondence analysis	k–means–method	analysis of latent classes for mixed variables

*The partitioning of the temperature profiles was performed using the k-means method.

The measure of distance used here is the Euclidean distance. It can be calculated using the following equation

$$D_{T,C_i} = \sqrt{\sum_x (T_x - T_{ix})^2} \tag{4}$$

where x = variable of the object (in this case: depth position under the pavement surface); T_i = arithmetic mean of cluster C_i.

With a partition algorithm, the cluster was determined using the k-means method. The necessary steps are described below.

Initialization: random choice of the cluster.

Attribution: Each object was assigned to the cluster whose cluster center was the nearest to the object.

New calculation: The new cluster center (arithmetic mean of all objects of the cluster) was calculated for each cluster.

Iteration: If the assignment was different, go to step *Attribution* (iteration until the mean square error stops decreasing).

5.2 *Definition of classification criteria*

The groups formed by the cluster analysis may have quite specific attributes. These cluster attributes were passed on by the objects of the cluster to the relevant class. Thus these object and cluster attributes constituted the classification criteria and finally allowed the definition of class limits. The form of the vertical temperature profiles also depends on the intensity of a time-variable surface temperature. According to this, time and amplitude of the daily surface temperature changes were used as classification criteria.

5.3 *Scaling of temperature profiles*

In order to make the vertical temperature profiles comparable with each other, they must be scaled. Scaling allows the presentation and analysis of qualitative and quantitative temperature profile independent of absolute temperatures. Scaling makes the absolute temperature changes visible and comparable depending on the depth beneath the pavement surface. Using the scaling direction, the authoritative normalized characteristic temperature function could be derived for each class (defined amplitude and time range). The transfer to absolute temperature functions was made by addition of the surface temperatures or the temperature that was representative of a certain surface temperature class.

5.4 *Specifying the number of classes and class limits*

It is essential to specify the number and thus the limits of the classes for the classification criteria obtained for the determination of the authoritative characteristic temperature functions regarding the actual class width. The number and the limits of the classes and the resulting characteristic temperature functions were determined and specified in accordance with the procedure illustrated in Figure 3. The definition of the class limits of both classification criteria required to perform the cluster analysis twice. Since the amplitude criterion is a measure of the quantitative changes of a normalized temperature profile and the time criterion defines the qualitative temperature profile, it is recommended to define the limits of the amplitude classes during the first cluster analysis and then define the necessary time ranges (time classes) for each amplitude class.

5.5 *Determination of necessary amplitude classes*

For the formulation of the necessary amplitude classes and their class limits, respectively, all calculated temperature profiles (~450,000) were arranged in accordance with the time (hour

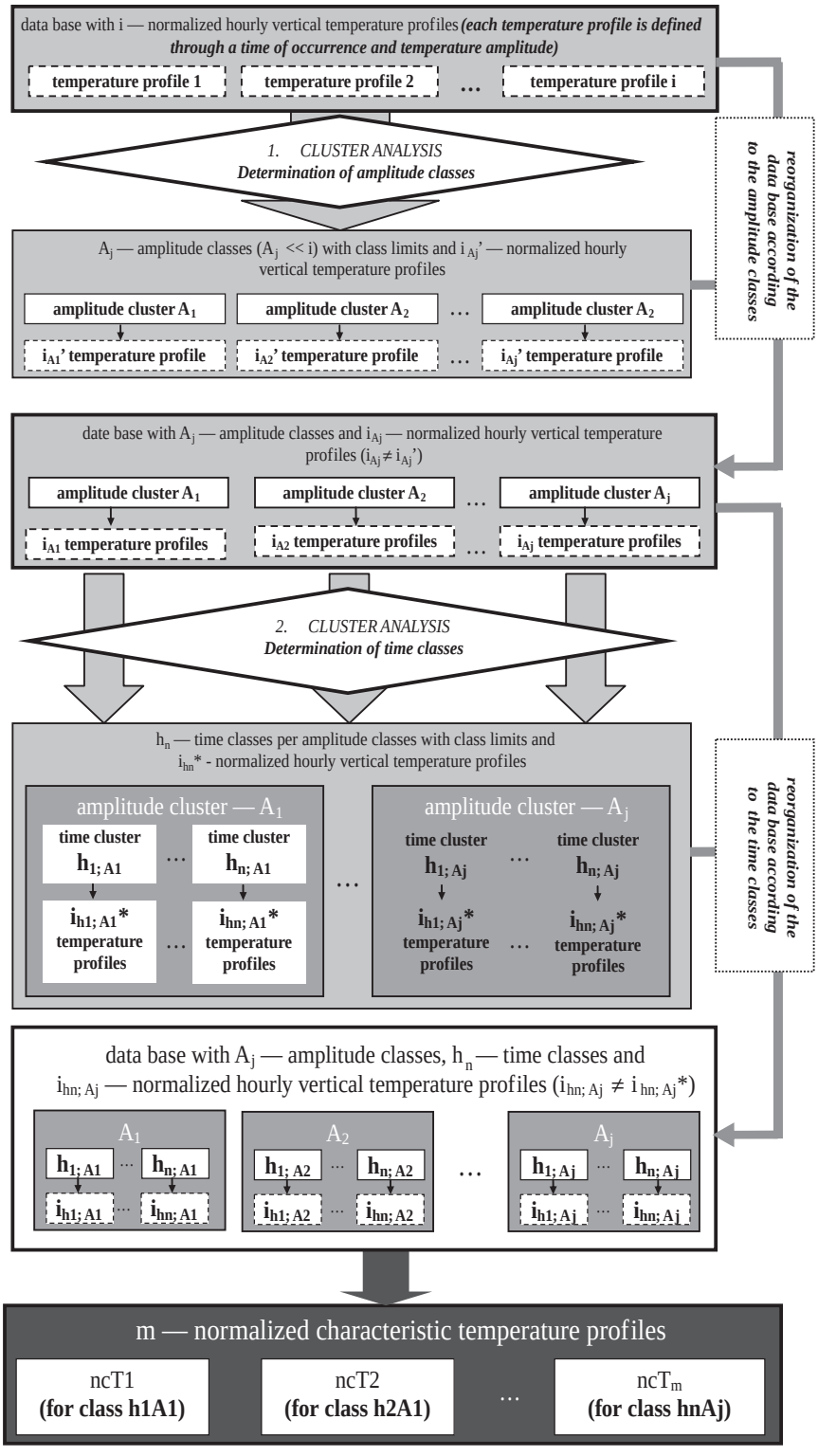

Figure 3. Schematic view of the procedure to define the necessary amplitude and time classes including the representative temperature functions.

of the day) for which they were calculated. For each of these 24 hour groups (each group with the same number of vertical temperature profiles) the cluster analysis was performed four times to define the limits of the amplitude classes. In the first analysis, the number of clusters, which requires setting before the analysis starts, was defined to be two. For each of the following cluster analyses, this number was increased by one cluster per analysis and was five at the end. Each cluster was checked for its amplitude significance after each of the four cluster analyses. Each temperature profile could be assigned a certain amplitude value independent of the cluster assigned. The cluster significance test was based on a frequency analysis of these amplitude data. This algorithm was applied to all 24 hour classes. Subsequently, the absolute amplitude frequencies for each cluster were added for all hour classes, separately for all four cluster analyses. Figure 4 shows an example of the absolute amplitude frequency distribution.

To avoid interpretation mistakes, which may result from the unequal distribution of the temperature amplitudes, the absolute frequency distributions of the clusters were also standardized. In other words, the absolute amplitude frequency per cluster was no longer accumulated over all hour ranges, instead one authoritative cluster was determined for each time and amplitude range. Afterwards, all time ranges of one amplitude range were added for each cluster. These were the time ranges for which this cluster is decisive.

For the following cluster analysis, the overall amplitude range was divided into three amplitude classes to define the hour classes and their class limits. The relevant limits of the three amplitude classes were obtained from the amplitude ranges for which one cluster showed the maximum frequency compared with the two other clusters.

Small amplitude: $\Delta A_T < 6.5°C$

Medium amplitude: $6.5°C <= \Delta A_T < 11.5°C$

Large amplitude: $\Delta A_T >= 11.5°C$

If the number of amplitude classes is reduced from 22 to 3 and if 24 hour ranges are considered, the total of all classes (amplitude classes × hour classes) decreases from 528 to 72. Assuming that for each class the total surface temperature range is decisive, the number of absolute characteristic temperature functions is reduced from 6,864 to 936. This latter number can be reduced even further by decreasing the hour classes.

5.6 *Determination of necessary time classes*

For each of these three amplitude classes, the relevant time classes (hour classes) must be defined. These classes were established in the same way like the amplitude classes. For this

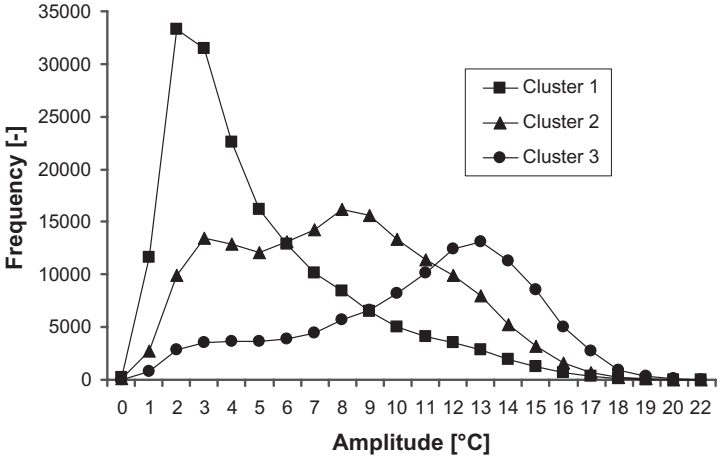

Figure 4. Cluster-related absolute frequency distribution depending on the amplitude and with three clusters predefined. (Kayser 2007a).

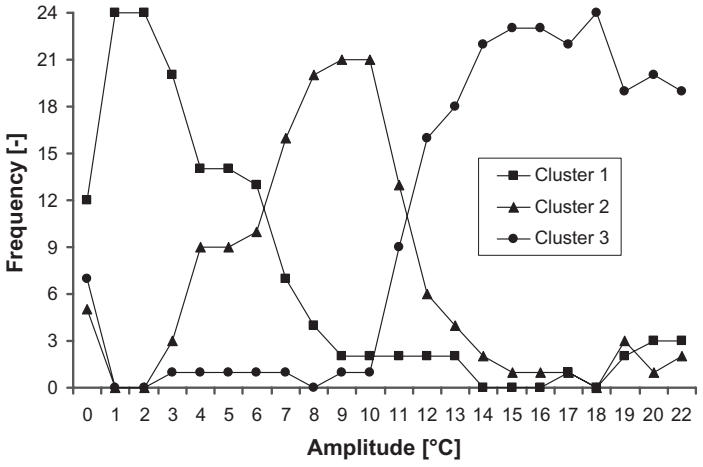

Figure 5. Cluster-related standardized absolute frequency distribution depending on the amplitude and with three clusters predefined. (Kayser 2007a).

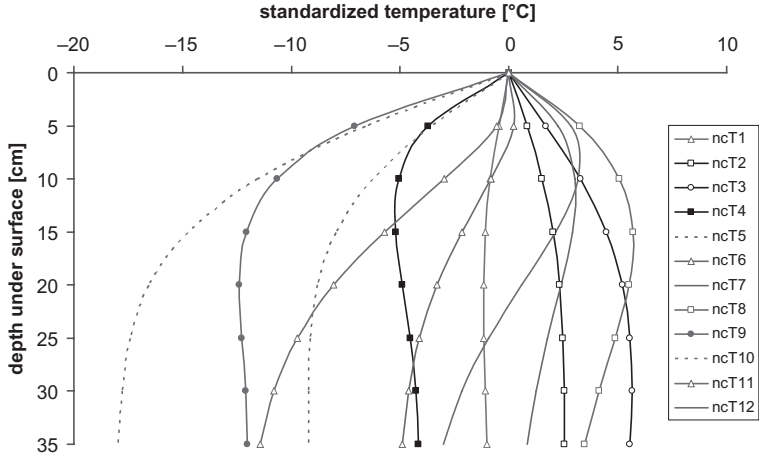

Figure 6. Normalized characteristic temperature profiles. (Kayser 2007a).

purpose, all vertical temperature profiles, which were calculated from pavement surface temperatures using the difference method, were assigned to the three amplitude classes in accordance with the relevant amplitude. For each of these groups, several cluster analyses were performed again with different numbers of clusters given. For each cluster analysis, the clusters formed were checked for their significant time range (hour range) for which each cluster is decisive. In constrast to the amplitude classes, scaling of the absolute frequencies was not necessary since the 24 hour classes of one day were uniformly distributed within one amplitude class. Table 3 gives an overview of the time classes (hour classes) that were essential for the three amplitude classes.

On the basis of the fact that the total range of the daily surface temperature became narrower if the daily amplitude was smaller, the number of necessary time (hour) classes must also decrease. The authoritative time (hour) ranges and also their class limits were again obtained from the frequency distributions depending on the hour of the day of each cluster formulated.

Table 3. Number of the necessary time (hour) classes depending on the three amplitude classes. (Kayser 2007a).

Amplitude range	Number of necessary time (hour) classes
Small amplitudes	2
Medium amplitudes	7
Large amplitudes	8

5.7 *Supplementary combination of individual clusters*

All numerically simulated vertical temperature profiles were classified in accordance with the classification criteria to determine the actual representative temperature profiles of each of the 17 clusters. Afterwards, the average temperature profiles were calculated for each cluster. The temperature profiles within each amplitude class were rather different. On the other hand, it was observed that some of the resulting temperature profiles from different amplitude classes were very similar. This was caused by the two-phase partitioning (first phase: determination of the amplitude classes; second phase: determination of the time classes).

5.8 *Standardized characteristic temperature profiles*

Finally, 12 standardized characteristic temperature profiles were formulated. Each of these temperature profiles has two defined classification criteria (amplitude and time classes) and can be approximated by a polynomial.

$$T(x) = k_5 \cdot |x|^5 + k_4 \cdot |x|^4 + \cdots + k_1 \cdot |x| \tag{5}$$

where $T(x)$ = temperature; k = coefficients and x = depth under the surface.

5.9 *Absolute characteristic temperature profiles*

For the analytical design processes of flexible pavements it is necessary to consider absolute temperature profiles as an input parameter. Using equation (5) in conjunction with the coefficients from Table 5 it is possible to calculate the standardized characteristic temperature profiles. The latter were transferred into absolute characteristic temperature profiles due to the overlap with the surface temperatures. Equation (5) was extended by an absolute member that represents the surface temperature.

Table 4. Authoritative time (hour) ranges (Kayser 2007a).

Normalized characteristic temperature profile	$k_5 * 10^{-8}$	$k_4 * 10^{-5}$	$k_3 * 10^{-4}$	$k_2 * 10^{-4}$	$k_1 * 10^{-4}$
ncT1	0	–0.15	0.74	13.80	–1046.64
ncT2	0	0.20	–1.08	–16.73	1772.06
ncT3	0	0.58	–3.88	10.90	3484.09
ncT4	0	1.87	–19.36	711.20	–10,444.00
ncT5	0	0	–2.78	270.69	–8695.52
ncT6	37.00	–4.99	25.42	–552.20	2614.52
ncT7	0	–0.88	10.47	–435.71	6431,31
ncT8	0	–0.18	5.65	–386.43	8379.71
ncT9	0	2.18	–24.49	1033.69	–18,776.82
ncT10	0	0	–4.72	468.62	–15,753.32
ncT11	63.00	–8.31	41.56	–864.89	2282.53
ncT12	0	–1.88	20.71	–778.89	9081.79

Table 5. Authoritative amplitude and time (hour) ranges for each normalized characteristic temperature profile (Kayser 2007a).

Normalized characteristic temperature profile	Amplitude range	Time range
ncT1	$\Delta A_T < 6.5°C$	10 am to 7 pm
ncT2	ΔA_T Δ 6.5°C	20 pm to 9 am
	$6.5°C <= \Delta A_T < 11.5°C$	10 pm to 1 am and 7 am to 8 am
ncT3	$6.5°C <= \Delta A_T < 11.5°C$	2 am to 6 am
	$\Delta A_T >= 11.5°C$	2 am to 7 am
ncT4	$6.5°C <= \Delta A_T < 11.5°C$	9 am to 11 am
	$\Delta A_T >= 11.5°C$	8 am 9 am
ncT5	$6.5°C <= \Delta A_T < 11.5°C$	12 am 3 pm
ncT6	$6.5°C <= \Delta A_T < 11.5°C$	4 pm to 6 pm
ncT7	$6.5°C <= \Delta A_T < 11.5°C$	7 pm to 9 pm
ncT8	$\Delta A_T >= 11.5°C$	9 pm to 1 am
ncT9	$\Delta A_T >= 11.5°C$	10 am to 11 am
ncT10	$\Delta A_T >= 11.5°C$	12 am to 3 pm
ncT11	$\Delta A_T >= 11.5°C$	4 pm to 6 pm
ncT12	$\Delta A_T >= 11.5°C$	7 pm to 8 pm

$$T(x) = k_5 \cdot x^5 + k_4 \cdot x^4 + \cdots + k_1 \cdot x + T_O \tag{6}$$

where T_O = surface temperature.

6 SUMMARY

As a result of the research presented in this paper it was found that a direct relation between the temperature gradient and the temperature range does not exist. In fact, by the means of thermodynamic principles a more practicable criterion than the asphalt surface temperature was defined. Based on the time of day and the daily intensity of the asphalt surface temperature variation the arrangement of the temperature profil was determined. Using these values and the deterministic partitioning method k-means decisive temperature profiles were defined. The investigation was based on the statistical analysis of calculated temperature profiles due to measured pavement surface temperatures. Because the surface temperature is not relevant for the classification of the temperature profiles, the results of the partitioning process are standardized. The standardized temperature profiles can be calculated and represented by using polynomial fifth grade. By adding an absolute element to this polynomial the standardized temperature profiles can be transferred into absolute temperature profiles. As a result, the number of the characteristic temperature profiles that are required for the design process could be reduced significantly. The frequency of occurrence of these characteristic temperature profiles is influenced by the asphalt surface temperature.

BIBLIOGRAPHY

Bachner, J. 1996. *Clusteranalyse—Anwendungsorientierte Einführung*. München/Wien: Oldenbourg Verlag.

Kayser, S. 2007a. Grundlagen zur Erfassung klimatischer Einflüsse für Dimensionierungsrechnungen von Asphaltbefestigungen. *PhD Thesis*. Dresden.

Kayser, S. 2007b. Weiterentwicklung der Bemessungsmethoden für Verkehrsflächen—Teil Betonstraßen. *Forschung Straßenbau und Straßenverkehrstechnik* (976). Bonn: Bundesministerium für Verkehr, Bau und Stadtentwicklung.

Kayser, S. 2008. Grundlagen zur Erfassung der Temperaturbedingungen für eine analytische Bemessung von Asphaltbefestigungen. *Forschung Straßenbau und Straßenverkehrstechnik* (996). Bonn: Bundesministerium für Verkehr, Bau und Stadtentwicklung.

Kiehne, A. Rechnerische Dimensionierung von Verkehrsflächen in Asphaltbauweise—Entwicklung und Umsetzung eines Verfahrens. *PhD Thesis*. Dresden: unpuplished.
Krebs, H.G. & Böllinger, G. 1981. Temperaturberechnungen am bituminösen Straßenkörper—Abschätzung der monatlichen Fahrleistungen mit aggressiven Reifen und normalen Reifen. *Forschung Straßenbau und Straßenverkehrstechnik* (347). Bonn: Bundesministerium für Verkehr.
Pohlmann, P. 1989. Simulation von Temperaturverteilungen und thermisch induzierten Zugspannungen in Asphaltstraßen. *Schriftenreihe des Instituts für Straßenwesen* (15). Braunschweig.
Wistuba, M. 2001. Klimakenngrößen für den Straßenoberbau in Österreich. *Straßenforschung* (507). Wien: Bundesministerium für Verkehr, Innovation und Technologie.
Wistuba, M. 2004. Oberbauverstärkungen von Asphaltstraßen. *Straßenforschung* (546). Wien: Bundesministerium für Verkehr, Innovation und Technologie.

Advanced Testing and Characterization of Bituminous Materials –
Loizos, Partl, Scarpas & Al-Qadi (eds)
© 2009 Taylor & Francis Group, London, ISBN 978-0-415-55854-9

Performance evaluation of prepared gelled hot sealant in cold climates

AI Al-Hadidy & Yi-qiu Tan
School of Transportation Science and Engineering,
Harbin Institute of Technology, Harbin, Heilongjiang, China

ABSTRACT: In this study, three types of gelled hot applied joint sealants are produced. A series of different tests have been used in the asphalt industry according to the ASTM procedures, to characterize the behavior of joint sealants. In addition, the field evaluation was performed on these sealants after 12 months and 18 months of it application in three selected sites in Heilongjiang Province located in the northern part of China. Results indicated that joint sealant complied with the requirements of ASTM D1191, D6690-06a, and D3405. The field evaluation observations revealed that starch joint sealant type 2 is a reliable material for crack treatment. The results also revealed that this sealant reduced the safe heating and application temperature by 12% and 12.5%, respectively, when compared with hot rubber asphalt crack sealant, as well as it shows resistant to fuels, most common chemicals and solvents.

1 OVERVIEW

Concrete pavement joints are cracks intentionally formed in the pavement to accommodate expansion and contraction due to temperature changes. Today, 98% of the agencies building and maintaining concrete roadways, and 100% of the agencies building and maintaining concrete airport pavements in the United States require the sealing of these joints for new pavements. There are two major reasons for sealing rigid pavement joints. The first is to reduce the amount of water infiltrating the pavement structure, which results in slab erosion and loss of support. The second reason is to minimize the entry of incompressible materials into the joint reservoir, resulting in point loading when slabs expand under hot temperatures and subsequent joint spalling damage. Another reason for sealing rigid pavement joints is to reduce the potential for dowel bar corrosion by reducing entrance of de-icing chemicals (Soliman et al., 2008; Brigitte & Nii, 2006; Donald et al., 2004; Morian & Stoffels, 1998; Lynch, 1996). The proper sealing and maintenance of concrete pavement joints thus seems to be essential for the overall performance of the rigid concrete pavement.

On the other hand, the spillage of petroleum based materials on HMA pavements will soften and leach away the asphalt binder. The damaged pavement will eventually require repair or replacement. HMA pavements are susceptible to damage from petroleum products because the asphalt cement binder in the pavement is derived from the same petroleum material. These petroleum products include hydraulic fluid, motor oils, diesel, and gasoline. Spillage occurs most often in parking, maintenance, and refueling areas. Coal-tar emulsions have been historically used as a fuel resistant binder material for sealers and in some cases for the pavement itself. The major limitation in the use of coal-tar sealers has been their lack of durability. Cracking of the coal-tar sealer often occurs within a year or two after placement. These cracks eventually increase in number and size until a new sealer or other pavement rehabilitation is required. The normal useful life of a coal-tar sealer generally varies from about 2 to 5 years (James & Tere, 2007).

In recent years polymer additives have been introduced as a way to improve the performance of the sealers. However, in many instances these additives have not provided a significant increase in durability and more expensive. Therefore, it is important to find a way to

select the most appropriate sealant from the host of available sealants or to prepare the cost-effectiveness and performance crack sealant for any given transverse joint system usable by any province in any climatic region including Heilongjiang especially, and at the same time must have properties that will withstand jet blast, jet fuel, hydraulic fluid, and to fuel spillage or jet blast but will be in the other fluids as required. This would help prevent/ minimize premature sealant failures. Understanding the factors, and in what way these factors lead to sealant failures, is therefore essential for the preservation of pavement life. The results of a study reported herein provide some of this type of information for the prepared gelled hot applied sealers.

However, substantial quantities of starch are potentially available widely in the world. Starch is a fine white powder mainly composed of two carbohydrate polymers, ammylose and amylopection. It characterized with low weight and is generally much cheaper (0.8 $/kg) than other conventional polymers such as polyethylene, styrene-butadiene-styrene, and polypropylene. Starch granule size varies from (1–100) microns in diameter and shape (James, 1980).

Starch represents an ideal material for inclusion as an asphalt modifier for a number of reasons. Firstly, it exists as microscopic white grains that are insoluble in alcohol, ether, and cold water. Secondly, it is a highly organized mixture of two carbohydrate polymers, ammylose and amylopection. Thirdly, substantial quantities of starch are potentially available widely in the world at low cost. Finally, unlike many other materials such as used tires, starch comes from its source as a fine, free-flowing powder, which obviates any need for preprocessing the starch before mixing it into the asphalt. On the other hand, beta-hydroxytrioarboxylic (citric) acid is a fine white powder with an average particle size of 100 mesh. Citric acid is a very useful and effective preservative, obtained from naturally occurring organic acids and is much cheaper than polymers such as styrene, butadiene-styrene, SBS… etc. It consists of 10 ppm heavy metal, 150 ppm sulphate, not more than 0.1 percent sulphated ash, 0.2 ppm aluminum, less than 3 ppm ash, and 350 ppm oxalate (James, 1980). These characteristics make citric acid and starch especially desirable to develop low cost-effective waterproofing materials.

As a result of binder modification with starch and citric acid, the physical and chemical properties of the binder are improved. This improvement takes place because of the change in the chemical properties of the binder.

There is one approach for producing starch modified asphalt. That is by blending starch into the asphalt using hot water (60 ± 1ºC). Starch granules when heated in water gradually absorb water and swell in size, causing the mixture to thicken. With continued heating however, the swollen granule fragments become less thick, and amylose and amylopectin become soluble in the hot mixture. This process of granule swelling and fragmenting is called "gelatinization". Because of the larger size of the swollen granules compared to the size of amylose and amylopection. The viscosity of the swollen granules mixture is much higher than the viscosity of the amylose/amylopection mixtures.

In this research, it is intended to prepare the cost-effectiveness and performance hot pour gelled-asphalt crack sealant by blending starch into 20% citric acid modified asphalt with the use of a liquid blending agent. The blending is carried out with slow-speed drill and at temperature above about 160ºC. A series of different tests according to the ASTM (2000) procedures have been used in the asphalt industry to characterize the behavior of joint sealant. In addition, we conducted the field study in Heilongjiang Province located in the northern part of China to evaluate the field performance of joint and crack sealants.

2 EXPERIMENTS

2.1 *Material selection*

70–100 asphalt binder was selected for the present study. The physical properties of asphalt cement as per ASTM (2000) are penetration: 78 dmm, and softening point: 42ºC. Calcium carbonate ($CaCO_3$) finer than 200 sieve and had specific gravity of 2.73 was used as mineral filler. Starch included in this study has a chemical formula $[C_6H_{10}O_5]_{n=100\text{-}1000,}$ purity of 99.2% and contains 27.49% Amylose. It was obtained from one market in China. Citric acid is a

white powder material with an average particle size of 100 mesh and purity of 99.98% was used as a modifier for asphalt cement.

2.2 *Preparation of starch joint sealant samples*

Citric acid was mixed with asphalt at 20 weight percentage for 7 minutes at a temperature of 160 ± 5ºC to produce an economically asphalt cement that comply with the requirements of asphalt mastic ASTM (2000). Its characteristic properties according to ASTM (2000) are: penetration at 25 and 4ºC: 39 and 8 dmm, respectively, ductility: 18.181, softening point: 64ºC, and solubility: 99.184%.

The starch joint sealant (SJS) samples were prepared in the following procedure: 20% citric acids modified asphalt that comply with the physical requirements of asphalt mastic ASTM (2000) was heated to the desired temperature in a three-neck flask provided with stirrer and contact thermometer. The temperature was held constant by an automatic control system while stirring intensively. The starch was dispersed into the citric acid modified asphalt by using hot water (60 ± 1ºC). The resultant asphalt was then combined with filler. The citric acid modified asphalt was treated with different percentages of starch (10, 30, and 50 wt% of virgin asphalt) and one percentage of calcium carbonate filler (125 wt% of virgin asphalt). The best results were achieved when the blending temperature was maintained above about 160ºC.

2.3 *Tests of samples*

A series of tests were carried out in the asphalt industry on SJS samples according to ASTM (2000). These tests include: Penetration before and after aging, D-5; Softening point, D-36; Flow, D-1191; Recovery before and after aging, D-5329; Flexibility, D-5329; Compatibility, D-5329; Density, D-70; Tensile adhesion, D-412 Die C; Chemical resistance, D-147 and Fuel resistance, D-3569. Descriptions of some of these tests were in the following paragraphs:

2.3.1 *Tensile adhesion to concrete*

Nine specimens of each mixture were prepared to determine the tensile properties using Materials Testing System (MTS-810). Specimens were divided into three groups. The first group placed in water bath at 25ºC, and then loaded at a ratio of 12.7 mm/minutes. The second group was cured in a cooling room maintaining a temperature of –19ºC for more than 3 h, and then loaded at a ratio of 0.05 mm/minutes. The third group was immersed in benzene solvent for 4 h, and then loaded at a ratio of 12.7 mm/minutes, and the stress and elongation values were obtained.

2.3.2 *Chemical (Alkali and acid) resistance test*

Two groups of starch joint sealant samples were subjected to alkali and acid resistance test in accordance with ASTM D147.The first group was placed in 40 percent NaOH at 21ºC solution for 1000 h. The second group was immersed in 95 percent Hcl at 21ºC solution for 1000 h. After that the samples were brought to weight loss determination as designated as alkali and acid-resisting.

2.3.3 *Fuel resistance test*

Three groups of starch joint sealant samples were tested for fuel resistance in accordance with ASTM D5329. The first group was immersed in JP-4 fuel bath at 40 ± 1ºC for 24 h. The second group was placed in hydraulic bath at 25 ± 1ºC for 7-days. The third group was immersed in glycol/water (50/50) bath at 25 ± 1ºC for 168 h. The samples were then brought to weight loss determination as designated as fuel-resisting.

2.4 *Field installation sections and evaluation procedures*

We conducted the field study in Heilongjiang Province located in the north part of China to evaluate the field performance of joint and crack sealants. The test sections were located in an

asphalt concrete (AC) and Portland cement concrete (PCC) roadways. The pavement in the test section No.1 consists of a 200 mm thick, fourteen-year old PCC on cement treated base. This section is subjected to high traffic volumes of passenger cars and buses. The pavement in the test sections 2 and 3 consists of a 100 mm thick, twelve-year old wearing AC placed over a 50 mm binder AC pavement on granular base. These sections are subjected to medium traffic volumes of passenger cars and buses. The total pavement width for sections 1, 2 and 3 are 15, 9.20 and 7.20 m, respectively. Figures 1–3, show the sketches of these sections.

The pavement in the test locations is subject to severe temperature changes. The high and low pavement design temperatures were found to be +40 and –27°C, respectively. The laboratory performance of the sealants used in this study should be evaluated at these temperatures, since they represent the extreme temperatures that a sealant experiences during the year.

Sealants were applied to transverse cracks of the test sections in 2007. Sealants were inspected in 2008 after 12 months, and 18 months. Inspections of transverse sealed cracks

Figure 1. Joint sealant installation section at parking lot in Harbin airport; SJS3 type.

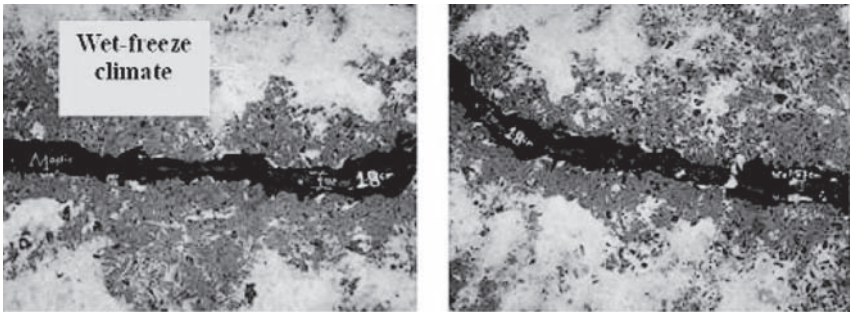

Figure 2. Joint sealant installation section at irregular crack of a roadway in HIT campus; SJS2 type.

Figure 3. Joint sealant installation section at regular crack of a roadway in HIT campus; SJS2 type.

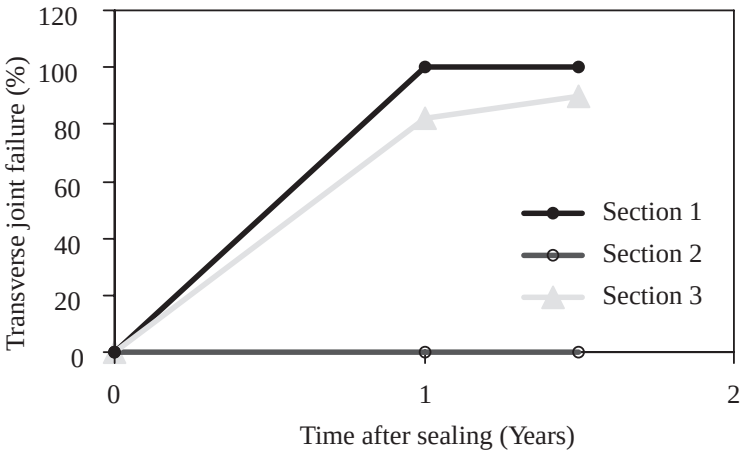

Figure 4. Transverse joint failures from field evaluation results.

were made in early spring when adhesion failures can be visually observed. Figure 4 shows the failure rates of transverse sealed joints. In addition, the following observations were made based on procedures detailed in SHRP (1999).

2.4.1 *Sealant condition number*

A "Sealant Condition Number" (SCN) was assigned to the sealant once a year. The SCN was based upon two distress types: water infiltration and debris retention. Each distress type was rated as having no distress or low, medium or high severity distress (described below). The results of two distress ratings were inserted into the Equation 1 to provide the SCN.

$$SCN = 1(L) + 2(M) + 3(H) \quad (1)$$

where SCN = sealant condition number; L = the number of low severity sealant conditions; M = the number of medium severity sealant conditions; and H = the number of high severity sealant conditions.

If the sealant material has no defects, then the SCN is defined as 0, the best possible rating. A SCN of 6, the worst possible rating, is obtained when both the debris retention and water infiltration are rated as high severity. The results of this observation were summarized in Table 1.

2.4.2 *Water infiltration*

Water infiltration was measured as a percentage of the overall crack length where water can bypass the sealant and enter the crack either through complete adhesion or cohesion failure. Adhesion and cohesion failures were determined through the visual inspection method. The visual cracks, splits or openings in the sealant or between the sealant and asphalt or concrete were examined and the depth of the opening was determined using a thin blade spatula. The percentage of cracks that allows water infiltration was determined by the Equation 2.

$$\%L = (Lf \,/\, Ltot.) * 100 \quad (2)$$

where $\%L$ = percent length of the crack allowing water infiltration; Lf = total length of the crack sealant field evaluation section allowing the infiltration of water (m); and $Ltot.$ = total length of the crack sealant field evaluation section (m).

If $0 < \%L \leq 1$ no water infiltration; $1 < \%L \leq 10$ low severity water infiltration; $10 < \%L \leq 30$ medium severity water infiltration; $\%L > 30\%$ high severity water infiltration.

The results of this observation were summarized in Table 1.

Table 1. Field observation results.

Adhesion/Cohesion/Infiltration

Section	Date of test	L_f	$L_{tot.}$	%L	Severity	SCN component
1	2008	6.4	6.4	100	High	3.0*(1)
2	2008	0.03	3.0	0.01	No	0.01
3	2008	4.3	4.4	98	High	3.0*(1)

Stone/Debris retention

Section	Date of test	Severity	SCN component	Section	SCN	Comments and failure reason(s)
1	2008	High	3.0*(1)	6.0	1	Cohesion failure, already this sealant type (SJS_3) does not comply with the requirements and the laboratory tests confirm that
2	2008	No	0.0	0.01	2	Comply with the requirements and the laboratory tests confirm that
3	2008	High	3.0*(1)	6.0	3	Adhesion failure. This sealant was installed at temperature below 23°C

2.4.3 *Debris or stone retention*

Stone or debris retention was rated as follows:

No Debris Retention: No stones or debris are stuck to the top of the sealant or embedded on the surface of the sealant /hot mix asphalt (HMA) interface.

Low Severity**:** Occasional stones and /or debris are stuck to the top of the sealant, or debris embedded on the surface of the sealant/HMA interface.

Medium Severity: Stones or debris are stuck to the sealant and some debris is deeply embedded in the sealant or material embedded between the sealant and the crack face but not entering the crack below the sealant.

High Severity: A large amount of stones and debris is stuck to and deeply embedded in the sealant or filling the crack, or a considerable amount of debris is embedded between the sealant and the crack face and entering the crack below the sealant. The results of this observation are summarized in Table 1. It can be seen that section 1 has sustained the continental climate (i.e. a wide temperature difference between summer and winter) and passed the requirements for field observation evaluation (i.e. SCN = 0.01, %L = 0.01, and No debris retention). Whether sections 2 and 3 failed SCN test and the reasons for failure were mentioned in Table 1.

2.4.4 *Example SCN calculation*

Section 3 was inspected and it was noted that there was a considerable amount of debris embedded between the sealant and the crack face. Some was entering the crack below the sealant and approximately 4.3 m exhibited adhesion failure that would allow water infiltration through the crack. From this information, one would calculate the total percentage of water infiltration from $\%L = (L_f/L_{tot}) * 100$ or $\%L = (4.3/4.4) * 100 = 98\%$. Therefore, this section would have the SCN equal to 6, which represents the worst possible rating.

3 RESULTS AND DISCUSSION

The effect of ST contents on the physiochemical and mechanical properties of the ST joint sealant is shown in Table 2 and Figure 5. To investigate the novel improvement of the properties of the SJS, the results were compared with (ASTM, 2000; SHRP, 1999; Maine, 2006; Joint sealing, 2005; Pacific, 2005).

3.1 *Physiochemical properties*

Examining Table 2 indicates that sample SJS_2 of joint sealant complies with ASTM D1191, D6690-06a, and D3405 requirements of hot applied joint sealant, for Portland cement concrete and asphalt concrete pavements. However, this joint sealant sample is resistant to water, fuel, oil and most other liquids and chemicals in a range of conditions and provides a high level of sealing properties for extended periods of time. In addition, the field evaluation observations also revealed that this sealant is a reliable material for crack treatment, which is one of the most common maintenance activities performed on pavements (See Table 1). It is therefore recommended for sealing horizontal and inclined joints on highways, airport runways, bridges, driveways, and for interior uses including sealing joints in industrial floors, garage floors, and airplane hangar floor without using primer for installation. The results also revealed that SJS_2 reduced the safe heating and application temperature by 12% and 12.5%, respectively, when compared with hot rubber asphalt crack sealant (see Table 3).

3.2 *Uniaxial tension test*

Tensile strength is important for joint sealants, in that greater strengths would enable the sealants to resist the thermal stresses and movements that cause cracking. Increased tensile strength is only a part of preventing this cracking; sealants that allow an increased amount of deformation before the maximum tensile strength is obtained (reduced stiffness) will also help prevent cracking from occurring.

The laboratory-cured samples of each sealant were evaluated with three specimens of each type in the uniaxial test. Difficulties encountered during specimen preparation and in setting up and testing. Table 2 shows the maximum tensile strength (stress), and deformation that were achieved during the uniaxial test for three percentages of ST-joint sealant. Table 2 includes data for each sealant evaluated, at 25ºC and –19ºC at 0.22 and 8.33E-04 mm/s displacement rate. Load versus deformation tests, when run at a constant displacement rate, provide an indication of the relative stiffness of the sealer mixtures. Mixtures that achieve their maximum tensile strength (stress) with the least amount of deformation (steeper slope) are relatively stiffer mixtures. One method of quantifying the type tensile failure that the mixtures exhibit is to determine a secant modulus for each sealant at the point of maximum strength, using Equation 3.

$$St = T/D \tag{3}$$

where St = stiffness at time t (kPa); T = maximum tensile strength (maximum stress) (kPa); and D = deformation at maximum stress (mm).

The lower the secant modulus, the lower the stiffness of the sealant as shown in Figure 5. From this Figure, it can be observed that the tensile strength and secant modulus for SJS_2 sealant sample at 25ºC (water immersion) and –19ºC are 152.1 kPa and 2.6174 kPa, and 70.689 kPa and 12.763 kPa, respectively.

3.3 *Field performance*

Sealants with good field performance should maintain adequate adhesion strength with pavement and have sufficient strength to resist the penetration of incompressible materials. The most severe conditions that may cause adhesion failure to sealants exist in winter at low temperatures, where sealants are subjected to high tensile stresses. On the other hand, the most severe conditions that may cause infiltration of incompressible materials to sealants exist in summer at high temperatures, where sealants become softer with warmer temperatures.

Manitoba Infrastructure and Transportation (MIT) requires that the failure rate of crack sealant does not exceed 7% after one year of sealant application, and 10% after two years (Soliman et al, 2008). Sealants can be classified into three groups according to their failure rates in the field, shown in Figure 4, after one and half year:

Table 2. Test results of gelled joint sealant samples.

Property	Sealer type SJS_1	SJS_2	SJS_3	Specifications
	Cone penetration at: Before aging			
0°C	8.0	16	14	≥15
25°C	44	53	41	≤90 or ≤70
	After aging (168 h, 70°C)			
0°C	3.0	10	7.5	
25°C	17	37	27	
Softening point, °C	63	90	98	≥76.6 or ≥65.5
	Flow, 5 hrs, 75 ± 1°, mm at:			
60°C	43.0	0.0	0.0	≤5 mm
72°C	N/A	0.621	0.0	≤5 mm
	Recovery, 25°C, %			
Before aging	28	44	38	≥30
After aging (168 h, 70°C)	3.8	11	8	–
	Initial ball pentretion, 25°C			
Before aging	5.0	10	6	≥5
After aging(168 h, 70°C)	0.5	5.3	3.0	–
Flexibility	pass	pass	pass	Pass
Compatibility	Comp.	Incom.	Incom.	incompatible
Density, gm/cm^3	1.7640	1.7003	1.4490	
	Tensile adhesion to concrete			
Stress, kPa, 25°C, water immersion, 12.7 mm/minutes	92.413	152.1	132.759	100–300
Elongation, %, 25°C	227	581.1	423.0	≥500
Stress, kPa, –19°C 19°C, 0.05 mm/min.	N/A	70.689	48.966	
Elongation, %, –19°C,	N/A	55.385	25.576	
Stress, kPa, 25°C, 4 h, Fuel (Benzene) immerssion, 12.7 mm/minutes	N/A	3.897	0.6897	–
Elongation, %, 25°C, 4 h Fuel (Benzene) immersion	N/A	17.954	6.303	–
	Chemical resistant, % loss			
HCL, 1000 h	N/A	0.857	1.023	≤5
NaOH, 1000 h	N/A	0.410	0.609	–
	Fuel resistant, %loss			
24 hrs, Jp-4 immersion	0.6525	0.6554	0.7059	≤5
Hydrulic, 168 h immersion	0.503	0.411	0.382	–
Glycol/water (50/50), 168 h immersion	0	0	0	–
Safe Heating temperature, °C	175	184	210	–
Recommended pouring temperature, °C	168	175	198	–
Recommended extended heating	5 h ± 20 minutes	–		

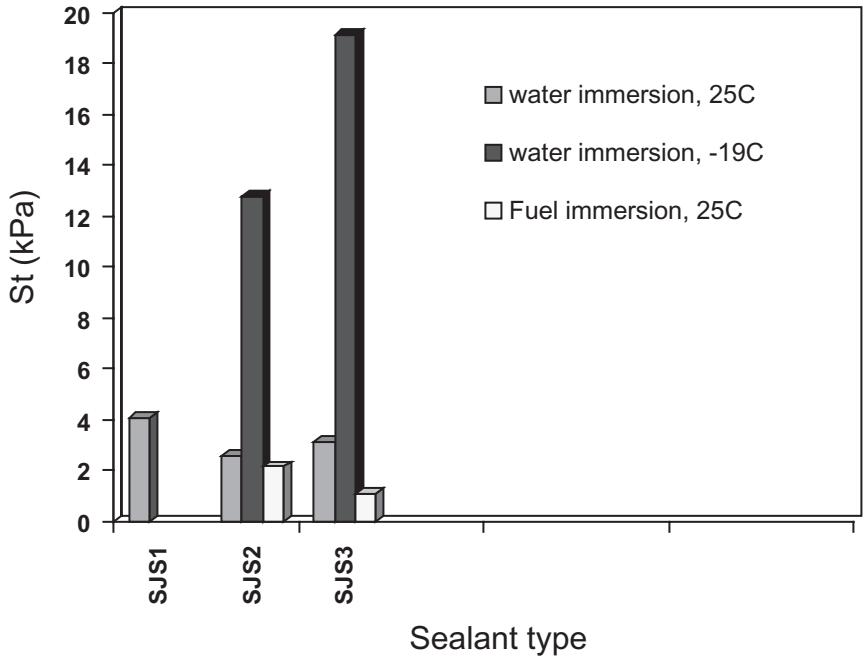

Figure 5. Secant modulus of sealer.

Table 3. Starch joint sealant benefits summary.

Property	SJS_2	Hot rubber sealant	Benefit (% reduction)
Safe heating temperature (°C)	184	206–212	12
Recommended application temperature (°C)	175	195–200*	12.5

*Recommended for cold climate.

- Group 1: good performance, percent transverse failure after one and half year less than 10%;
- Group 2: satisfactory performance, percent transverse failure after one and half year from 10% to 35%; and
- Group 3: poor performance, percent transverse failure after one and half year greater than 35%.

A rating system was developed in SHRP project H-106 SHRP (1991) to rank sealants according to the percent of sealant failures. In this rating system, sealants were classified into five groups (from excellent to very poor performance), and a 35% failure rate was the boundary between fair and poor performance. The 35% failure rate was adopted in this study to distinguish between satisfactory and poor performance based on the SHRP rating system. From Figure 4, it can be seen that percent transverse failure after one and half year for sections 2 (SJS_2 type) and 3 (SJS_3 type) is 0% and 87%, respectively.

4 CONCLUSIONS AND RECOMMENDATION

A laboratory evaluation of prepared joint and crack sealants in cold climates is performed according to ASTM test methods, which are commonly used for characterizing joint sealants. The results of a limited study and a field evaluation conducted in a cold climatic zone led to the following findings:

1. Penetration, softening point, percentage recovery, flexibility, compatibility and flow properties are within the ASTM D1191, D6690-06a, and D3405 specification limits when using starch as a modifier in the manufacture of gelled hot applied sealant.
2. Uniaxial tension testing showed that increasing the amount of starch in a mixture up to 30%, resulted in an increase in maximum tensile stress; decrease in secant modulus, and less brittle tensile failure. Decreased temperature resulted in decreased maximum tensile stress and increase in secant modulus for all mixtures.
3. Penetration and flow test results indicated that the starch joint sealant provides a firm, smooth, non-tracking surface in summer and retains flexibility in winter.
4. The chemical and fuel laboratory test results showed that SJS_2 and SJS_3 conforming to the limits of Pacific Polymers International sealant commission specifications. Therefore it can be used in special paving construction such as fuel station.
5. Form field study, it was found that the percent length of the crack, sealant condition number and the percent transverse failure after one and half year for section 2 (SJS_2 type) are 0.01%, 0.01 and 0%, respectively. Based on SHRP rating system, it is clear that this sealant in a good performance.
6. The field observations indicated that SJS_2 should not be installed when temperature is below 23ºC.
7. It was found in this research that 30% starch is a good content to produce gelled hot applied sealant, which is used to seal and fill cracks and joints in both asphalt and Portland cement concrete pavements in moderate to cold climates, and the field observations insure this result.
8. Based on the laboratory tests and the field evaluation observations, SJS_2 sealant type is a reliable material for crack treatment. It is therefore, recommended for sealing horizontal and inclined joints on highways, airport runways, bridges , driveways, and for interior uses including sealing joints in industrial floors, garage floors, airplane hangar floor without using primer for installation.
9. SJS requires no caulking gun or special metering equipment, and blends with a slow-speed drill, and
10. SJS_2 reduced the safe heating and application temperature by 12% and 12.5%, respectively, when compared with hot rubber asphalt crack sealant.

ACKNOWLEDGMENTS

The authors would like to extend their appreciation to the Bituminous Laboratory/School of Transportation Science and Engineering/Harbin Institute of Technology, National Natural Science Foundation (NSFC) and the Research Fund for the Doctoral Program of Higher Education (RFDP) of China for technical assistance and the various companies that provided materials used in this study. Special thanks go to Dr.Wu Si-gang and Jasim A.A without whom this study would not have been completed.

REFERENCES

Annual Book of ASTM Standards. 2000, Section 4, Vol. 04–03.

Brigitte, O. & Nii, A. 2006. Sealing system selection for jointed concrete pavements—A review. *Construction and Building Materials* (20): 591–602.

Donald, et al. 2004. *Standard practice for sealing joints and cracks in rigid and flexible pavements*. Unified facilities criteria (UFC), UFC 3-250-08FA.

James, E. & Tere, A. 2007. Material Properties of Coal-Tar Emulsion Sealers. *Mater Civil Eng*. 19(4): 305–312.
James, M. 1980. The albumen and salted paper book; Published by Light Impressions Corporation.
Joint Sealing-Asphalt to concrete. 2005. *Standard Specification of asphalt/rubber joint sealant*. Section 508.
Lynch, L.1996.Rheological analysis of silicone pavement joint sealants. Technical rep.No. GL-96-4, U.S. Army Corps of Engineers, Waterways Experiment Station, Vicksburg, Miss.
Morian, D. & Stoffels, S. 1998. Joint seal practices in the United States. *Transportation Research Record No. 1627*. Pavement and Winter Maintenance: 7–12.
Maine Department of Transportation. 2006. Longitudinal joint treatment. *Transportation research division*, technical report 00–18.
Pacific Polymers International. 2005. Jet Fuel Resistant Joint Sealant, Elasto—Thane 200. Inc.12271 Monarch St.Garden Grove, CA92841, Technical Data, USA.
SHRP. 1999. *Materials and procedures for sealing and filling cracks in asphalt-surfaced pavements-manual of practice*. Strategic Highway research program (SHRP). *FHWA. Report* No.FHWA-RD-99-147.
Soliman, et al. 2008. Performance evaluation of joint and crack sealants in cold climates using DSR and BBR tests. *Mater Civil Eng.* 20(7): 470–477.
SHRP. 1991. *Transverse joint resealing in concrete pavements: Evaluation and analysis plan*. Strategic Highway Research Program (SHRP), National Research Council: Washington, D.C.

Advanced Testing and Characterization of Bituminous Materials –
Loizos, Partl, Scarpas & Al-Qadi (eds)
© 2009 Taylor & Francis Group, London, ISBN 978-0-415-55854-9

Age hardening behaviour of bituminous stabilized materials

M.E. Twagira & K.J. Jenkins
University of Stellenbosch, South Africa

ABSTRACT: In recent times, fundamental durability properties of bitumen stabilized materials (BSMs), in-terms of age hardening and moisture damage, have been a concern for practitioners. It is known from hot-mix asphalt (HMA) that age hardening occurs during in-plant mixing, construction and long-term in-service conditions in the pavement. The same principle has been used to investigate the age hardening behaviour of BSMs, but looking at in-plant production and in-service condition, which are critical for BSMs. This paper discusses the results on the behaviour of bitumen age hardening in the foamed bitumen and bitumen emulsion mixes. The study shows that short term age hardening can occur in foamed bitumen due to long hours of circulation of the binder at high temperature (between 170° to 180ºC) before mixing. However, it has been shown that the foaming process itself does not alter the physical properties of the bitumen significantly. For bitumen emulsion, the rheological properties (penetration, viscosity, and softening point) of residual emulsified bitumen after evaporation of the water found to be consistent with the base bitumen. During long-term in-service conditions, however, foamed bitumen and bitumen emulsion mixes yield significant age hardening of the binders. At the same time, age hardening behaviour differs for the foamed bitumen and bitumen emulsion, with the formed bitumen having higher age hardening potential.

1 INTRODUCTION

The durability properties in terms of resistance to ageing of the bitumen binder, is the key factor for the binder characterization in asphaltic mixes, and hence pavement performance. The limited research done in the past has indicated that BSMs can age significantly during in-service pavement life (Jenkins et al. 2000, Overby et al. 2004, Gueit et al. 2007, Serfass et al. 2008). Jenkins' research on foamed bitumen mastic indicated that the thin film binder thickness and high surface area of bitumen in BSM-foam can render it susceptible to premature ageing if not properly compacted or sealed on surface. Overby et al's investigation of the field performance of foamed bitumen, indicated that bitumen properties reduced from 80/100 penetration to approximately 10 dmm penetration after 10 years of pavement life. Guites et al. recognized the need for investigating age hardening behaviour of bitumen emulsion. However their emphasis was on finding the appropriate method for binder extraction. Serfass et al investigated age hardening behaviour of emulsion mixes in the laboratory prepared samples and field constructed sections. Their results found that bitumen penetration decreases from 88 dmm to 42 dmm in 90 days under accelerated curing at 35°C and 20% relative humidity, and field age hardening from 82 dmm penetration to 7 dmm for unsealed and 14 dmm for sealed sections. For these reasons binder ageing of BSMs has been of concern to practitioners globally, hence the need for further investigation of this behaviour.

Short term age hardening of the original bitumen in HMA is different from that of BSMs. The variables that can cause age hardening of the HMA are high aggregate and bitumen temperatures, thin binder films and presence of air during in-plant mixing, and mixing time on construction. These phenomena do not occur during the BSM mixing process because field or in-plant mixing and construction are done at ambient temperature of the aggregate. Some researchers have indicated concern at the high bitumen temperature required during

foaming process, i.e. where bitumen is heated at 170°C to 180°C and combined with moisture. The physiochemical change of bitumen which might be influenced by these factors needs to be investigated. For bitumen emulsion, elevated temperature is not an issue for both mixing and construction. Therefore, short term hardening due to high temperature will not play a key role. However, influence of chemical reaction of bitumen with emulsifying agent and high shearing process during production of emulsion requires investigation.

During the long-term in-service conditions of an asphalt pavement the bitumen can undergo age hardening, depending on mixture characteristics and environmental conditions. The rate of age hardening process will be dictated by factors such as the severity of the temperature, time of exposure, ultraviolet light, access of air and water into the mix, and the intrinsic reactivity of the bitumen. Unlike HMA, which is exposed directly to environmental conditions (at the surface of the pavement structure), access of oxygen into thin films of binder in BSM base layers is linked to high air void content, presence of moisture in the mix, and inadequate compaction or sealing on the surface. The high surface area of bitumen droplets and non-continuous nature of the dispersed bitumen, particularly on the mortar fractions, could influence the rate of age hardening of BSMs.

Tuffour & Ishai (1990) expressed the dependency of binder age hardening in terms of the variation in value of physical or rheological properties with time, as illustrated in Equation 1:

$$P(t) = f(T, t, l, K) \quad (1)$$

where P(t) = physical or rheological properties of bitumen; T = environmental temperature; t = time of exposure; l = length of diffusion path; and K = intrinsic reactivity of bitumen. Parameter P(t) measures resistance to detrimental effects of the oxidation process, where durable bitumen would reflect little change in P(t). Modelling of age hardening is not an objective of this paper, hence the age hardening function is not discussed further.

In this study the short-term ageing to simulate in-plant production, was first investigated using different types of bitumen from different refineries. The base and foamed bitumen were tested for its rheological properties i.e. viscosity, penetration and softening point with respect to time after circulation of bitumen in the laboratory foam plant (WBL10). The same rheological properties were determined for the residual of bitumen emulsion after evaporation of moisture.

Secondly, medium term age hardening was investigated from laboratory prepared specimens of foamed bitumen or bitumen emulsion mixes. BSMs produced from different aggregate types were mixed in the laboratory (compacted and cured). The bitumen was then extracted and rheological properties of recovered bitumen were tested. Thirdly, the long-term age hardening was investigated on cores extracted from pavements that had been in-service for five to ten years. In this way, the differential ageing (if any) of the foamed bitumen and bitumen emulsion was investigated for purpose of guiding the mix design process for BSMs. The extraction and recovery of bitumen from the field cores and compacted specimens for both foamed bitumen and bitumen emulsion binders was carried out using a cold centrifuge with minimum force of 3000 times gravity the Abson method. The Abson method was performed in accordance to ASTM D1856-95a immediately after cold centrifuge.

2 EXPERIMENTAL PROGRAM

2.1 *Materials*

Four types of straight run bitumen (penetration grade) from two different refineries and slow setting emulsion were procured for the laboratory investigation on this study. Two penetration grade binders i.e. 80/100 and 60/70 were sourced from NATREF in Gauteng Province, and two binders i.e. 80/100 and 60/70 were sourced from CALTEX in Western Cape Province. These bitumen types are commonly used for the foaming process in South Africa. Therefore, the selection was made to compare age hardening behaviour of bitumen of different grade and from different source of refineries. The slow setting emulsion (ANi B SS-60) commonly used for recycling process was also procured from COLAS-SA in Western Cape Province.

Table 1. List of pavement section selected for field ageing studies.

Bitumen emulsion	Foamed bitumen
N7 TR 11/1, near Cape Town Grassy park, Cape Town	P243/1, near Vereeniging N7 TR11/1, near Cape Town Grassy Park, Cape Town Shedgum road, Saudi Arabia

Table 2. Summary of cores sourced for investigating BSMs field age hardening behaviour.

Pavement section	Mix type	Cores number	Location of cores	Remark
Grassy Park				
– at the robot	Foam	4	OWP, BWP	Binder
– Straight section	Foam	6	OWP, BWP, YL	extracted
– Straight section	Emulsion	6	IWP, BWP, YL	and tested
N7 TR11/1, near Cape Town				
– Straight section	Foam	6	OWP, BWP, YL	On going
– Straight section	Emulsion	6	OWP, BWP, YL	
P243/1, near Vereeniging				
– Straight section	Foam	18	OWP, BWP, YL	On going
– Straight section	Emulsion	18	OWP, BWP, YL	
Shedgum road, in Saudi Arabia				Binder
– Straight section	Foam	6	OWP, IWP, BWP	extracted and tested

Note: OWP = outer wheel pass, BWP = between wheel pass, IWP = inner wheel pass, YL = yellow line.

Pavement sections constructed with either foamed bitumen or bitumen emulsion were listed for the field age hardening experimental investigation. To be able to compare the effect of different environmental conditions, 28 cores were sourced from Western Cape Province, and 36 cores from Gauteng Province. An additional 6 cores were sourced from Saudi Arabia. The list of pavement sections included in this study is indicated in Table 1 above.

Table 2 is a summary of the source of cores and pavement sections, mix type, cores number, and location of extractions in pavement.

2.2 *Method of binder extraction and recovery*

The conventional methods for qualitative extraction and recovery of asphalt from paving mixture are done either by centrifuge, vacuum, or reflux extraction (ASTM, 2003). Different common solvents have been used in the binder extraction and recovery procedures, e.g. trichloroethylene (TCE), methylene chloride, benzene, 1-trichloroethane (TCA).

The extraction and recovery of bitumen has an important influence on the binder characteristics. Many studies have been performed to define the most suitable extraction method and solvent, sometimes with contradictory conclusions with no consensus (Okan & Mang 2003). To date there are several extraction-recovery methods and solvent choices for both binder content determination and binder performance characterization. However, the consensus in Europe for the removal of solvent is by using rotavapour distillation, with an alternative of

using the Abson method (ASTM, 2003). The studies have indicated that the standard Abson recovery method may leave a residual amount of solvent in the recovered binder or could over heat the bitumen, if not done with care, which might result in change of viscosity properties (Burr et al. 1990, SABS 307 1993, Peterson et al. 2000, National Highway Cooperative Research Program 2000).

In this study, the extraction and recovery of the bitumen from the extracted field cores was done using standard Abson method according to ASTM D 1856-95a. The process consists of cold centrifuge with minimum force of 3000 times gravity. Centrifuge cups were used to collect filler. Trichloroethylene solvent was used to separate binder from aggregates. It was observed during extraction that the first application of the centrifuge process is unable to capture all fillers. Therefore, the centrifuge processes was repeated three to four times. The tendency of foamed bitumen or emulsion binders to adhere to the filler particles on the mix created challenges for total separation of binder-aggregate using the cold centrifuge process. This resulted in some super fines (significantly smaller than 0.075 mm i.e. about 0.002 mm) being recovered with bitumen.

The recovery of bitumen from the aqueous phase in bitumen emulsion was achieved through evaporation method in accordance to ASTM 244-A. 200 g of ANi B SS-60 was poured into a container placed on a burner with a controlled flame using a thermometer, and stirred continuously until no remaining moisture was observed. Check on complete evaporation of water from emulsion was done by placing clear glass on top of the container to check any trace of water vapour.

2.3 *Determination of rheological properties*

Physical or rheological properties of recovered bitumen were determined by carrying out penetration, viscosity and softening point tests. The penetration test was performed at 25°C with 100 g of loading weight and needle penetrating bitumen for 5 seconds in accordance to ASTM D5-IP49. The softening point test was done in accordance to ASTM D36. The viscosity test was done in accordance to ASTM D4402 using a Brookfield Model DV-I viscometer with thermocel temperature control system. The applied spindle was SC-29 at the 60°C and SC-21 at 135°C. These temperature ranges are standard for determining viscosity behaviour of bitumen at field condition and in plant mixing condition respectively. The results that were obtained could be compared with the South African SABS 307 specification.

The SABS 307 standard specification for the penetration, softening point and viscosity are indicated in Table 3 below.

2.4 *Characterisation of age hardening of BSMs*

2.4.1 *Temperature susceptibility*

The approach used for characterisation of temperature susceptibility of the bitumen of different grade from different refineries was Penetration Index (PI). The PI of bitumen is calculated from the relationship between bitumen penetration value on a log scale and the corresponding temperature (softening point) as indicated in Equation 2 below (Shell Bitumen, 2003):

Table 3. Specification for road bitumen in South Africa, SABS 307.

Properties	Penetrati on grade			Test method
	40/50	60/70	80/100	
Penetration at 25°C, 1/10 mm [dmm],	40–50	60–70	80–100	ASTM D5-IP49
Softening point, [°C],	49–59	46–56	42–51	ASTM D36
Viscosity at 60°C, [Pa.s],	220–400	120–250	75–150	ASTM D4402
Viscosity at 135°C, [Pa.s]	0.27–0.65	0.22–0.45	0.15–0.4	ASTM D4402

$$PI = \frac{1952 - 500 \cdot \log Pen - 20SP}{50 \log Pen - SP - 120} \quad (2)$$

where SP = Softening point (°C); Pen = Penetration at 25°C (dmm).

2.4.2 *Ageing index*

The factors influencing age hardening on BSMs have been stated above. Shell Bitumen (2003) indicated that the effect on change of bitumen viscosity due to thin film binder dispersed in the mix can be measured by the Ageing Index (AI). AI is determined by the ratio of the viscosity of the aged bitumen (η_a) to the viscosity of the original base bitumen (η_o) both measured at the same temperature.

3 ANALYSIS AND DISCUSSION OF RESULTS

3.1 *Short-term age-hardening behaviour of BSMs*

The consistency of foamed bitumen during in plant circulation (i.e. 1 hr, 4 hrs, and 8 hrs) was measured to investigate a short term age hardening of foamed bitumen during production (mixing) process. The initial rheological properties of the grades of bitumen obtained from NATREF and CALTEX refineries, both 80/100 and 60/70 were tested and the results are indicated in Table 4.

The total circulation time in the plant was 8 hours. Rheological properties were measured on samples taken at intervals of 1 hr, 4 hrs, and 8 hrs from the base bitumen (before foaming) and from the foamed bitumen. The 8 hours of circulation is considered minimum applicable for in plant and field construction. The decline in penetration values shown in Figure 1 indicates that 80/100 base bitumen from both NATREF and CALTEX refineries undergoes age hardening of approximately 30% in short term, when circulated at a temperature between 170°C to 180°C. The circulation temperature between 170°C to 180°C is considered suitable for producing best foam properties in the mix (Jenkins et al. 2000). Similar trends of age hardening occurred for the foamed bitumen that was tested after collapse. The comparison between the two refineries indicates that the higher the penetration of the base bitumen (e.g. initial 96 penetration vs. 84 penetration) the lower the age hardening effect.

Figure 2 shows the ageing behaviour of the base bitumen versus foamed bitumen made from 60/70 penetration binder circulated at a temperature of between 170°C and 180°C. Both base bitumen and foamed bitumen show no signs of significant ageing in the first four hours. However after eight hours of age hardening, a drop in penetration of 17% for the NATREF and 12% for the CALTEX was realized. It can be seen from the results that initial penetration value for CALTEX 60/70 base bitumen did not comply with SABS 307 specification, with a

Table 4. Initial rheological properties of NATREF and CALTEX pen-grade bitumen.

	NATREF bitumen		CALTEX bitumen	
	Penetration grade			
Properties	80/100	60/70	80/100	60/70
Penetration at 25C/100 g/5 s, 1/10 mm,	96	65	84	73
Softening Point, [°C],	47	50	47	50
Viscosity at 60°C, [Pa.s],	132.0	220.2	134.0	202.0
Viscosity at 135°C, [Pa.s]	0.306	0.370	0.342	0.361
Penetration Index, (PI)	–0.324	–0.574	–0.721	–0.284

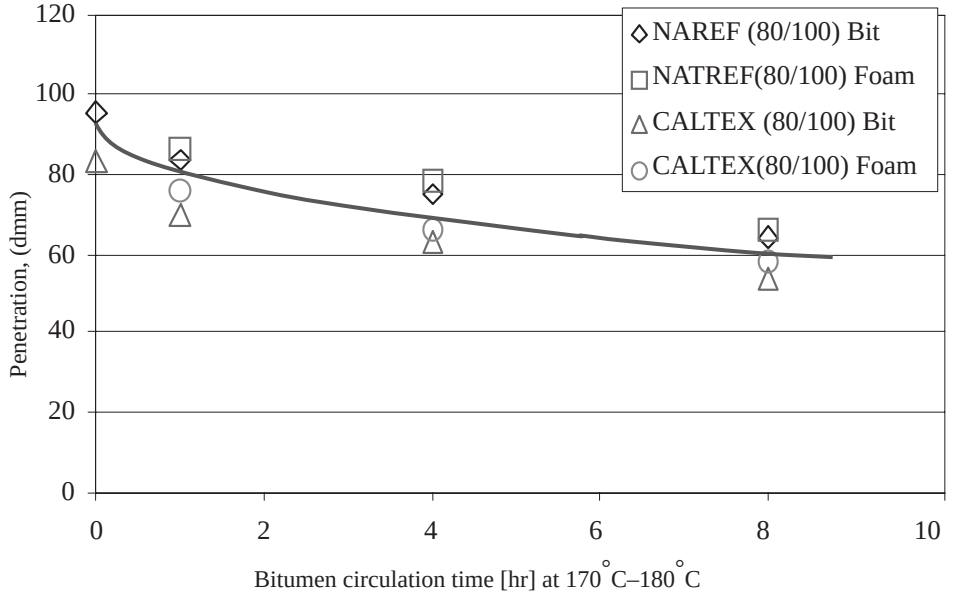

Figure 1. Penetration versus ageing time [hr] of base bitumen and foamed bitumen (80/100 penetration) circulated at temperature between 170°C–180°C.

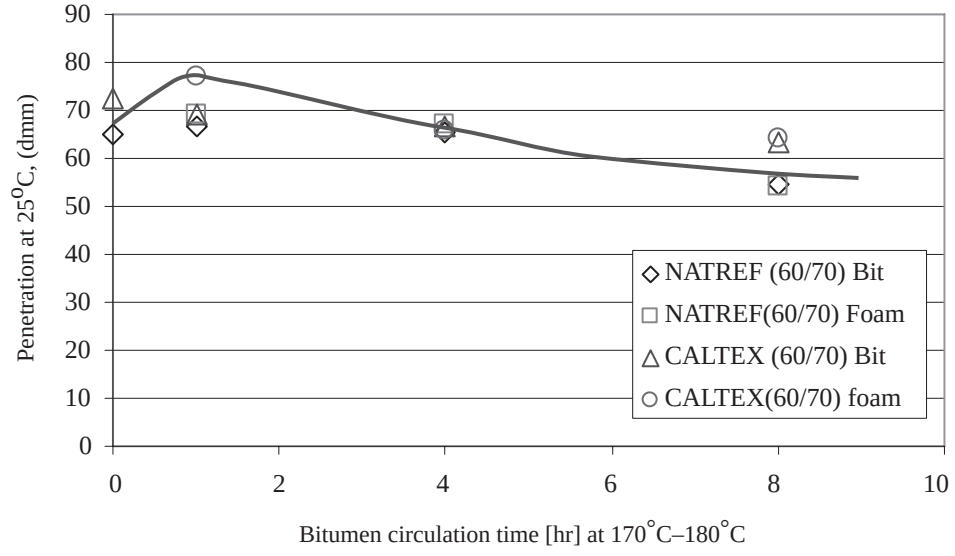

Figure 2. Penetration versus ageing time [hr] of base bitumen and foamed bitumen (60/70 penetration) circulated at temperature between 170°C–180°C.

result of 73 dmm maximum penetration as opposed to 70 maximum specified. The penetration of residual foamed bitumen circulated for one hour is higher than the base bitumen.

The relationship between penetration and softening point of 80/100 penetration grade from NATREF and CALTEX is shown in Figure 3. The relationship reveals an increase in binder hardness over the short term. This behaviour gives an insight into the behaviour of BSM-foam. Foam bitumen is recognised as having a high affinity for the fine aggregate

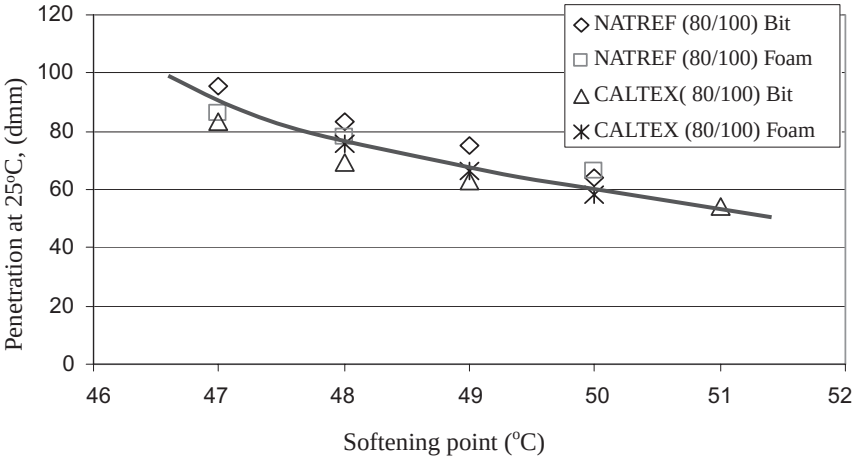

Figure 3. Penetration versus softening point of 80/100 base bitumen and foamed bitumen

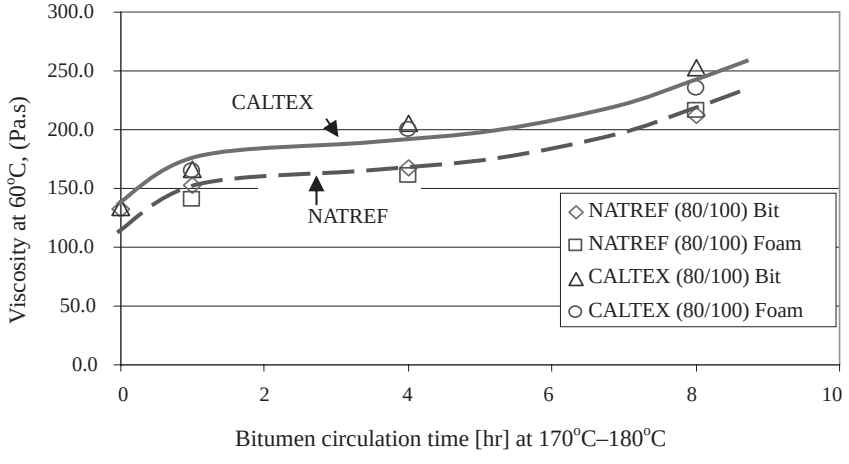

Figure 4. Viscosity versus Circulation time [hr] of 80/100 base bitumen and foamed bitumen at temperature between 170°C–180°C.

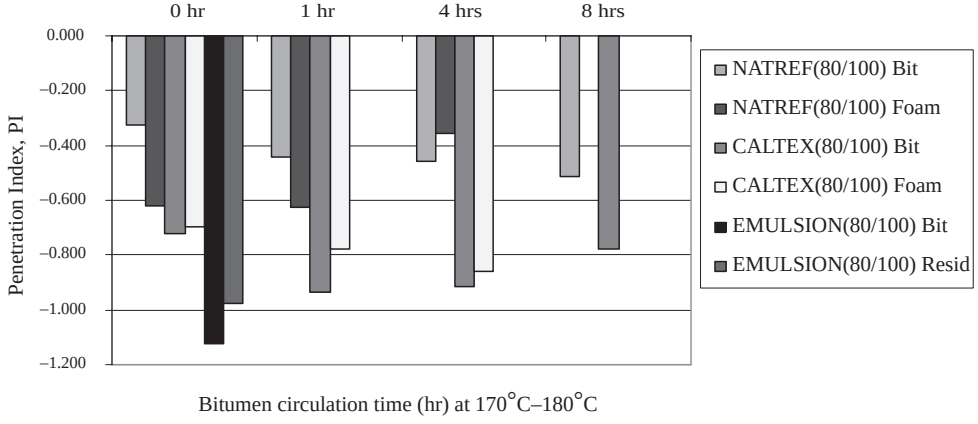

Figure 5. Penetration Index, (PI) of the base bitumen versus foamed bitumen for 80/100 penetration bitumen.

particles with high surface area to mass ratio. The effect on age hardening of foamed bitumen could influence cohesive behaviour of foam mastic both positively and negatively. The positive effect would be increase in stiffness of the mix, while the negative effect is the influence on moisture damage (Jenkins et al. 2008). In addition, it should also be noted that the foamed bitumen is dispersed in a non-continuous form in the mixture, which means age hardening could significantly influence long term durability behaviour of the BSM-foam.

Figure 4 above shows viscosity behaviour of 80/100 base bitumen and foamed bitumen at 60°C. It is evident from the trend line that viscosity increases as the bitumen hardens. CALTEX bitumen shows higher rate of change of viscosity with time than NATREF bitumen. However, the behaviour of NATREF bitumen and foamed bitumen show minimal thermal susceptibility during the first 4 hours, with a sharp increase at 8 hours of thermal ageing. It can be concluded from this behaviour that foamed bitumen mixes produced with binder that has been circulated at high temperatures for extended periods (>8 hours) may compromise the mix performance. In addition, it is apparent that age hardening differs, depending on the binder source and refining process. The bitumen age hardening characteristics should therefore be considered during mix design. Although not presented, 60/70 penetration grade provided similar results.

3.2 *Effect on bitumen grade and source on temperature susceptibility*

Figure 5 shows the relationship between PI and bitumen circulation time, for 80/100 penetration grade binder at a temperatures range between 170°C–180°C. The calculated PI values for base bitumen and foamed bitumen ranges between –0.32 to –1.13. According to Shell Bitumen (2003), most good paving binder has PI values ranging between +1 to –1. This reveals the age hardening effects and temperature susceptibility of the bitumen types that have been tested. It is evident from Figure 5 that bitumen emulsion has higher thermal susceptibility than foamed bitumen. Foamed bitumen and base bitumen from NATREF lie within the limits while CALTEX base bitumen and foamed bitumen shows relatively high temperature susceptibility compared to NATREF.

3.3 *Field age hardening behaviour of BSMs*

The recovered bitumen from the laboratory prepared specimens and field cores were tested for rheological properties. At present, the results of BSM-emulsion from laboratory specimens and two pavement sections from field cores are available and only these will be presented. The testing program is on-going to accomplish the list indicated in Table 2 above. The rheological properties results of laboratory prepared specimens (Hornfels aggregates stabilized with emulsion at 0% (H + 0CE) or 1% (H + 1CE) cement) and field cores (sourced from Shedgum and Grass park road sections) are summarized in Table 5 below.

Figure 6 shows ageing behaviour of foamed bitumen and bitumen emulsion with respect to laboratory accelerated cure and position of extracted cores in the pavement. It can be seen from the graph that the age hardening effects of the bitumen are more prevalent in trafficked position (OWP and IWP) compared to un-trafficked position (YL and BWP) and laboratory. The age hardening behaviour of foamed bitumen and bitumen emulsion mixes in the field cannot be distinguished easily from the results in Figure 6. However, it is evident from the figure that foamed bitumen mixes experience more age hardening effects than bitumen emulsion mixes, whilst accelerated curing in the laboratory results in age hardening behaviour similar to the field IWP. It can be concluded that the expected age hardened penetration values of the foamed bitumen and bitumen emulsion in trafficked pavement sections lies between 10 dmm and 20 dmm and on the un-trafficked sections it lies between 30 dmm to 50 dmm. This behaviour however contradicts other studies on HMA which indicated that age hardening is more prevalent in un-trafficked sections due to higher void contents. Therefore further investigation on BSMs behaviour is needed to verify these effects.

Table 5. Recovered bitumen rheological properties for different location on pavement.

Road name	Properties	BSM-foam				BSM-emulsion			
		BWP	OWP	IWP	YL	Lab	BWP	IWP	YL
H + 0CE	Penetration, 25°C [dmm]					17			
	Softening point, [°C]					78			
H + 1CE	Penetration, 25°C [dmm]					25			
	Softening point, [°C]					61			
Shedgum	Penetration, 25°C [dmm]	22	17	11					
	Softening point, [°C]	67	74	81					
Grassy park	Penetration, 25°C [dmm]	49	15		37		40	22	39
	Softening point, [°C]	56	80		51		54	63	56

Note: BWP = between wheel path, OWP = on-wheel path, IWP = inner wheel path, YL = yellow line.

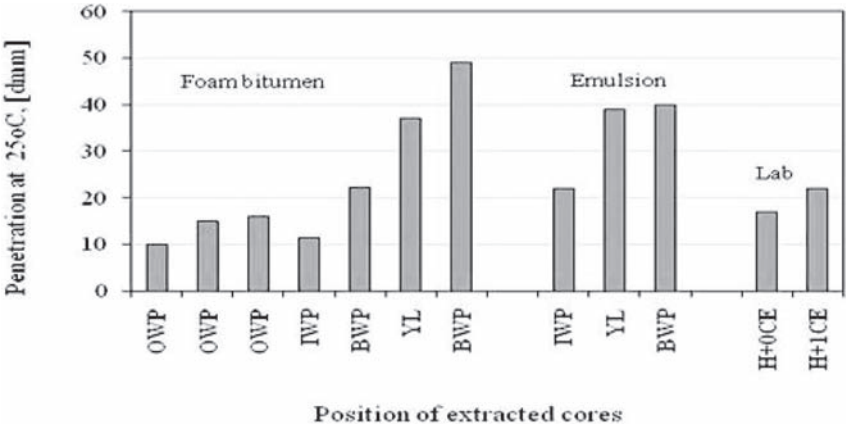

Figure 6. Field ageing behaviour in respect to coring position of foamed bitumen versus bitumen emulsion.

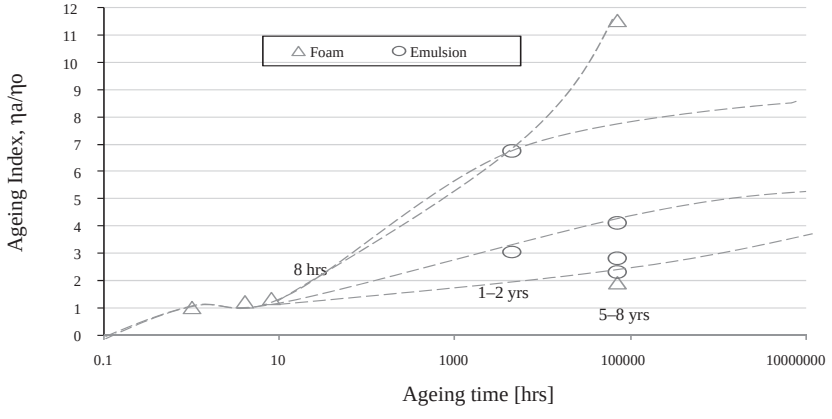

Figure 7. Age hardening behaviour, short term medium term & long term of BSMs combined.

3.4 *Age hardening effect on viscosity behaviour of BSMs*

The access of oxygen into the thin film of binder in foamed or emulsion mixes is linked to the air-void content in the mixture. The high surface area of bitumen in foamed mixes and uneven distribution of the bitumen over the different granular fractions, coupled with ageing during mixing is likely to influence the viscosity behaviour of BSMs. Indeed, as the bitumen disperses selectively into the mortar fraction, the binder is distributed discretely (in droplets) on the larger aggregates. The droplets of bitumen have high surface area and could have a tendency to age more rapidly during long term in-service pavement. The probable difference of the binder hardening between the course and filler fractions of BSMs should be further investigated. At the same time, the non-continuous nature further complicates the condition of the binder.

The use of the AI method can distinguish the ageing hardening behaviour of foamed bitumen and bitumen emulsion (see Figure 7). This principle can be applied to determine the relationship of the age hardening behaviour during in plant or field mixing (short term) and in-service condition (long term). The viscosity at 135°C was used in calculating the AI of BSMs. The use of viscosity at 60°C was inappropriate because most of bitumen had no flow properties at 60°C. Figure 7 shows the age hardening behaviour of BSMs in the short term (hours), medium term (1–2 years) and long term (5–8 years) combined, with medium term considered as age period during laboratory accelerated curing. However, from the graph it can be seen that there is no clear distinction in the trend of age hardening behaviour of foamed bitumen with bitumen emulsion mixes. This could result from variability introduced due to the recover methods. The presence of super fines in the recovered bitumen would influence variability in the viscosity test results. Therefore, the extent of the age hardening of BSM-foam or BSM-emulsion has not been clearly defined, making the limits of mix design properties difficult to establish. The study is ongoing, with a strategy to acquire sufficient data for a better understanding durability behaviour in terms of age hardening on BSMs.

4 SUMMARY AND CONCLUSIONS

The age hardening of BSMs and fundamental characteristics of BSMs associated with short term and long term age hardening have been investigated through laboratory testing. Based on the data of the study, the following conclusions are drawn:

- The time bitumen is kept in circulation in the laboratory plant at elevated temperatures before producing of BSM-foam, contributes to the age hardening of the binder, especially after 8 hours. The effects of age hardening are more notable for softer bitumen (80/100) than hard bitumen 60/70.
- It is apparent from the study that some short term age hardening of foamed bitumen during mixing occurs. However, the trend follows that of the age hardening of the base bitumen. Nevertheless, the foaming process in itself does not appear to alter the bitumen properties. For the bitumen emulsion, negligible age hardening occurs in short term because no elevated temperature is used in the mixing process.
- The study has also shown that bitumen from different refinery sources, ages at different rates. This is consistent with other studies, as the compositional balance and chemistry of the binders varies even if they comply with the same classification requirements.
- Age hardening behaviour of the foamed bitumen and bitumen emulsion has proved to be a point of considerations during mix design and long term performance. The drop of penetration to an estimated average of 30% of the original value, in short term i.e. 10 to 20 dmm for the trafficked section, and an increase in viscosity at 60°C to a stiffness that resists flow is a major concern. The impact of these changes in the binder on the mix durability behaviour remains to be investigated.
- Presently, the Ageing Index has shown no clear distinction on the trend of age hardening of BSMs, due to variability in the measured viscosity of the recovered bitumen. This emphasises the need to acquire more data to be able to determine the boundaries for age hardening, and thereafter proposing parameters for mix design considerations.

– The studies have also indicated that age hardening of the foamed bitumen and bitumen emulsion mixes is dependent on the effects of traffic. Ageing occurs differently in trafficked versus un-trafficked locations in the pavement. The trafficked position (OWP and IWP) have higher ageing influences than un-trafficked locations (YL and BWP). This tendency is contrary to previous studies on HMA, where lower air voids in the wheel paths reduced rutting. These factors require further investigation.
– The extreme values measured for penetration of binders exposed to field ageing are questionable, raising the concern that total separation of filler with bitumen during extraction is very difficult. The centrifuge extraction might not be able to capture all filler (super fines) which is a key component on the mix design of the BSMs. The Abson method of recovery can also cause variability of the results by leaving some solvent in the residual and or over-heating the bitumen.

ACKNOWLEDGMENTS

The authors wish to acknowledge SABITA and Gauteng Department of Transport and Public Works, South Africa for sponsoring this research work.

REFERENCES

American Standard Test Method 2003. Standard test for recovery of asphalt from solution by Abson method. ASTM Designation D 1856–95a.

Burr B.L., Davidson R.R., Glover C.J. & Bullin J.A., 1990. Solvent removal from asphalt. Transport Research records TRR, 1269. Washington DC.

Gueit C., Robert M. & Durand G., 2007. Characterization of different phases in the life cycle of the binder in bitumen emulsion. Recovery method. Transport research circular E-C122. ISSN0097–8515.

Jenkins, K.J., 2000. Mix design consideration for cold and half-warm bituminous mixes with emphasis on formed bitumen. PhD dissertation. University of Stellenbosch, South Africa.

Jenkins, K.J. Ebels, LJ., Twagira, M.E., Kelfkens, R.W.C. Moloto, P.K. & Mulusa, W.K., 2008. Updating bituminous stabilized materials guideline. Research report, SABITA, South Africa.

National Cooperative Highway Research Program, 2000. Recommended use of reclaimed asphalt pavement in the superpave mix design method. NHC Final Report D9–12, USA.

Okan S. & Mang T., 2003. Investigation of problem in binder extraction from conventional and rubber modified asphalt mixture. 6th Rilem Symposium, Zurich, Pg. 212–219.

Overby, C., Johanson, R. & Mataka, M., 2004. Bitumen foaming: An innovative technique used on a large scale for pavement rehabilitation in Africa. Case study: Same-Himo monitored pilot project. Proceedings of the 8th Conference on Asphalt Pavements for Southern Africa (CAPSA'04). Sun City, South Africa.

Peterson G.D., Soleymani H.R., Anderson R.M. & McDaniel R.S., 2000. Recovery and testing of RAP binder from recycled asphalt pavement. *Proceedings of the Association of Asphalt Pavement Technologisst*.

SABS 307. 1993. Standard specification for the bitumen rheological properties for road construction. South Africa.

Serfass, J.P., Carbonneau X., Delfosse F., Triquigneaux J.P. & Verhee F., 2008. Mix design method and field performance of emulsion cold mixes. 4th Eurobitume and Eurasphalt Congress, Copenhagen.

Shell Bitumen, 2003. Shell bitumen handbook. Shell bitumen UK.

Tuffour Y.A. & Ishai I., 1990. The Diffusion Model and Asphalt Age-Hardening. Proceedings of Association of Asphalt Paving Technologist: 73–92.

Advanced Testing and Characterization of Bituminous Materials – Loizos, Partl, Scarpas & Al-Qadi (eds)
© 2009 Taylor & Francis Group, London, ISBN 978-0-415-55854-9

Investigation of friction properties of various road surfaces affecting road safety

T. Pellinen
Helsinki University of Technology, Finland

M. Currie
University of Strathclyde, Scotland

J. Valtonen
Helsinki University of Technology, Finland

ABSTRACT: In this study, three different pavement surfaces were investigated to assess their friction properties in terms of traffic safety. The study was initiated after a fatal traffic accident that occurred when a motorcyclist was changing lanes in a motorway in rainy weather. The studied circumstances included longitudinal joint patching with fine asphalt mastics with and without chippings, random pavement patches, and road markings. Measurements were done using the pendulum test (PVT) and using the Portable Friction Tester (PFT). Friction was measured by obtaining the dry and wet surface friction values and a reference friction value from intact pavement adjacent to the patched areas. The study findings generally confirmed the visual assessment of surface slipperiness; and the friction values were generally lower for the wet surfaces than for the dry surfaces. In addition, the longitudinal joint strips without chippings had lower friction values compared to the sanded strips. Due to the lack of proper criteria, it was not possible to judge if the measured friction values were acceptable. However, this preliminary study is the first step in the development of friction criteria for pavement rehabilitation work to ensure the safety of road users.

1 INTRODUCTION

In this study, different pavement surfaces were investigated to assess their friction properties in terms of road safety. This study was initiated after a fatal traffic accident in Finland where a motorcyclist was killed when changing lanes in a motorway at high speed (120 km/h) in wet conditions. The longitudinal joint between the two lanes had been patched by applying a 330 mm wide strip of fine asphalt mixture. However, chippings or sand were not applied to the hot-laid material to form a skid-resistant surface. To investigate this matter, the Finnish Road Administration requested Helsinki University of Technology to measure the friction properties of the various materials used in road rehabilitation work. The targets were selected based on their visual appearance of slipperiness. The investigation took place in the Helsinki metropolitan area and the central Uusimaa in summer 2007. The aim of the survey was to identify the slipperiness and friction of various road materials/surfaces during wet and dry conditions. This information would then be used to develop guidelines or criteria for the assessment of rehabilitation work in terms of road safety.

Three cases, with different materials/surfaces and work methods, were studied, and included the patching work of the longitudinal joints with and without application of chippings or sand (Case-I), random pavement patches with various sizes (Case-II), and road markings (Case-III). Friction was measured for three different conditions, obtaining dry surface, wet surface, and reference surface friction values. The reference value was obtained from the intact pavement adjacent of the patched area studied.

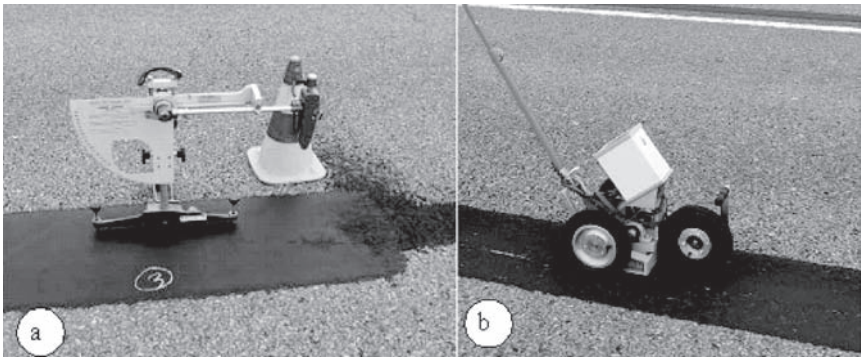

Figure 1. Test equipments (a) Pendulum tester (PTV) and (b) Portable Friction tester (PFT).

Measurements were done using two devices and methods, the European standard EN 13036-4 method (EN, 2003) for measurement of slip/skid resistance of a surface, the pendulum test, and using the Portable Friction Tester (PFT) developed by VTI, Swedish National Road and Transport Research Institute (Bengstöm et al. 2003, Wallman & Åström, 2001). The skid resistance tester (PTV) device or pendulum is shown in Figure 1a. The use of the pendulum tester is time consuming as each measurement must be conducted separately. The PFT, shown in Figure 1b, is a friction measuring device for continuous measurements at walking speed designed for measurements on road markings. It is easy to operate and calibrate in the field.

The PFT measurements are based on the fact that the front wheel spins at a different speed than that of the pushed rear wheels. The friction is calculated by the machine by using the different speeds at which the front and rear wheels turn (front wheel ratio). The PFT uses fixed longitudinal slip (21%) with a friction number defined as the friction force/test wheel load. In this study, the device measured friction at intervals of 26 mm and was able to store 50 meters of measured friction values. The wheel used on the device was at atmospheric pressure. Measurement errors due to the tire pressure were negligible. The device was pushed with a speed of 0.5 m/s, a slow speed due to it been pushed by hand. Both the PFT and the PTV devices produce their own friction values and they do not directly measure the physical friction coefficient. Therefore, the test results are relative and not directly comparable to criteria for skid resistance for asphalt pavements by the Finnish Pavement Technology Advisory Council (PANK, 2000).

For measuring the friction of the longitudinal joints, five-meter long test strips were used; and for the patching and road markings, two-meter long test strips were used. The Pendulum tests and the PFT runs were repeated several times in each test location. In addition, continuous profile measurements were undertaken at some of the test sites using the PTF apparatus. The purpose of these repetitive measurements was to investigate if the apparatus was able to distinguish surfaces that were visibly different in appearance.

2 TESTED SURFACES

2.1 *Longitudinal joint patching (Case-I)*

Longitudinal joint patches are a common rehabilitation procedure when the joints between the two adjacent traffic lanes are deteriorating. This is primarily caused by frost action and water damage, with poor quality paving work contributing to the problem.

Joint patching of the arterial motorway Vt4 in the Lahti—Järvenpää road section north of Helsinki was completed in spring 2007. Patching was laid in the joint between the two adjacent traffic lanes. The material used was a fine mastic asphalt (MA) mixture with a maximum aggregate size of 6 mm. A total of four test locations were selected that were 1.2 km south of the Mäntsälä interchange, north of Helsinki (see Table 1). Measurement

Table 1. Test conditions and locations for longitudinal joint patches at the time of testing.

Road no.	Air/Surface temp. (°C) /weather	Mix type	Test locations	Joint patch width (mm)	Age of patch
motorway Vt4	18/24 overcast but dry	MA6	1	250	<6 mo
			2	250	<6 mo
			3	550	<6 mo
			4	550	<6 mo
motorway Vt3	18/21 overcast but dry	mastics with chippings	1	330	<6 mo
			2a	330	<6 mo
			2b	330	<6 mo
45	22/30–35 sunshine	mastics	1	330	1 yr
			2	330	1 yr

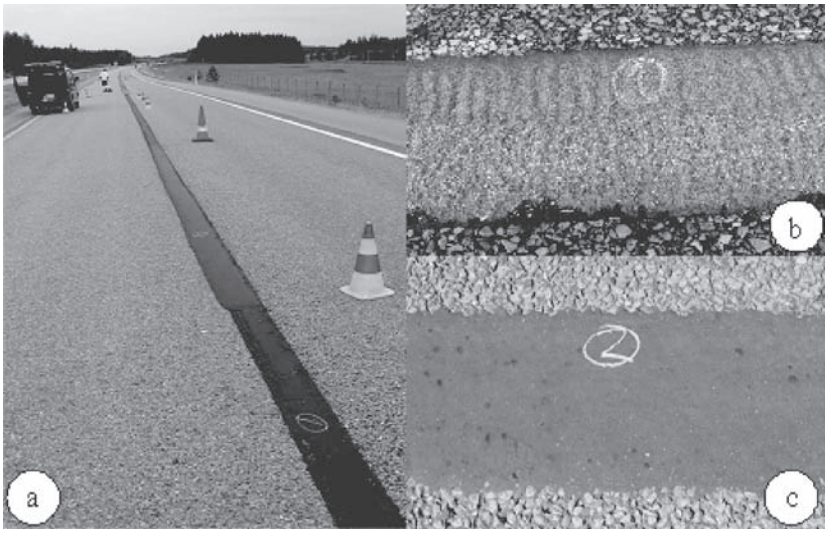

Figure 2. Test sites for joint patches, (a) Vt4/1 & 2, (b) Vt3/1, (c) Road 45/2.

points were selected in such a way that a single pass with each measuring device was sufficient for each surface. Figure 2a shows the joint patch and measurement arrangements.

On motorway Vt3 from Helsinki to Tampere, the joint rehabilitation work was conducted in spring 2007. The material used was fine mastics. The applied joint patch was approximately 4–5 mm higher than the surrounding pavement surface. Later on, the joint patching was found to be very slippery when it rained, and it was decided to roughen the surface by adding chips and pressing strips to the surface, as shown in Figure 2b. In addition, some roughening touch up work was carried out later. Joint patching of road 45 in Tuusula was completed during the summer of 2006. The edges of the patch joints were at level with the pavement surface. Material used was fine mastics, as shown in Figure 2c.

2.2 *Gussasphalt patches (Case-II)*

Another common method of road rehabilitation is the use of gussasphalt in various distresses, such as filling rutted wheel paths and sealing the openings of joints between the travel lane and the shoulder. Gussasphalt is a type of fine mastics asphalt, which has certain composition specified by PANK (PANK, 2000). As gussasphalt looks visibly very slippery, it

Table 2. Test conditions and locations for gussasphalt patching.

Road no.	Air/Surface temp. (°C)/weather	Mix type	Test locations	Description of patch	Age of patch	Notes
140	–/36 overcast but dry	guss-asphalt	1	rut	>1 yr	variable types
			2	rut	>1 yr	
			3	edge repair	>1 yr	
			4	rut	>1 yr	
152	18/– sunshine	guss-asphalt	5	rut, 500 mm	>1 yr	wheel path patching

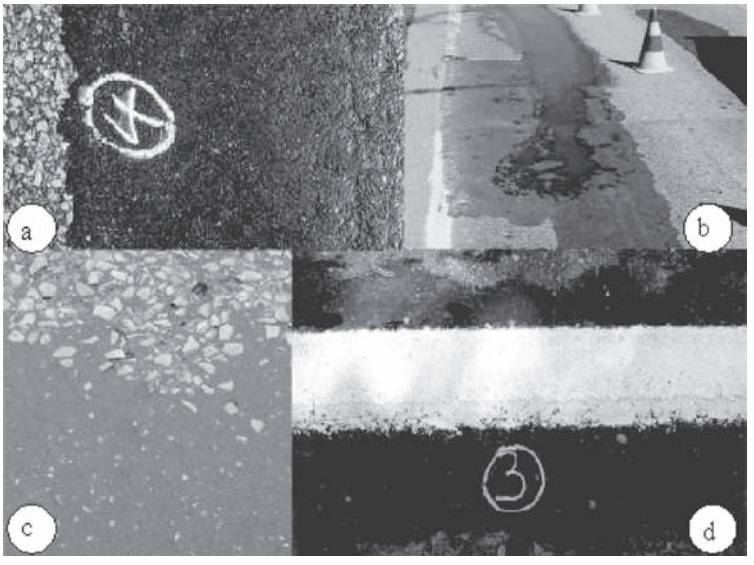

Figure 3. Test sites for gussasphalt patches; (a) on road 140/4, (b) on road 152, (c) on road 140/2 and (d) on road 140/3.

was decided to measure some of these patches for reference purposes. Table 2 shows the test conditions for measurements at two locations on roads 140 and 152.

At Road 140 in Jokivarsi, four locations were measured, including patching of ruts on wheel paths (Figures 3a and c) and edge repair (Figure 3d). Figure 3b shows 500 mm wide rut repair on Road 152. All patches were more than one year old. As a close-up picture of the pavement patches show, the surface texture is quite different in different materials.

2.3 *Road markings (Case-III)*

Similarly, the road markings were studied at two locations to obtain some reference information about the friction of these types of surfaces. The materials used for road markings can be thermoplastics or paint. Table 3 gives the test conditions and locations. On Road 140 there were three locations for pedestrian crossing, see Figure 4, and one sideline measurement. On Vt3 and Road 45, the thermoplastic side lines with different ages were measured.

3 TEST RESULTS

3.1 *Average friction values at each test location*

Tables 4 and 5 show the number of replicates/runs, average test results, and standard deviations for all locations for the PTV and PFT measurements, respectively. The Pendulum results

Table 3. Test conditions and locations for road markings.

Road no.	Air/Surface temp. (°C)	Mix type	Test locations	Description of patch	Age of patch	Notes
140	–/22	thermoplastic	1	pedestrian crossing	>1 yr	pedestrian crossing
			2	pedestrian crossing	>1 yr	
			3	pedestrian crossing	<6 mo	
			4	side line	<6 mo	
Vt3	–/–	thermoplastic	5	side line	<6 mo	new/old sideline
			6	side line	>1 yr	
45	–/–	thermoplastic	7	side line	1 yr	sideline

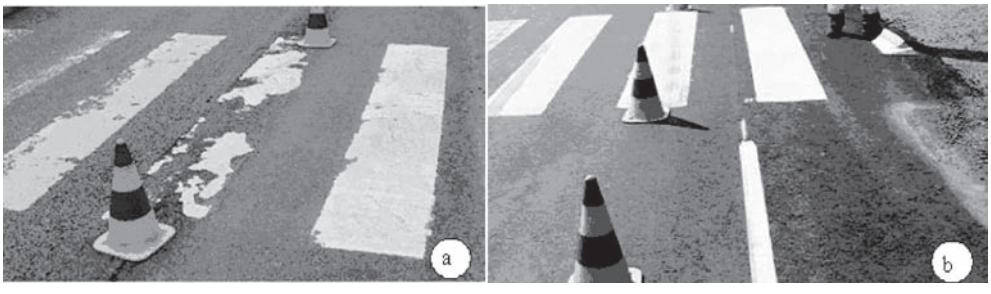

Figure 4. Test sites for road markings, (a) Road 140/1, (b) Road 140/3.

were rounded up or down to the nearest ten. The temperature of the rubber foot used in the measurements was approximately 20°C. A correction due to temperature was therefore not necessary as described in the standard (EN, 2003).

Tables 4 and 5 show that the lowest wet friction values were measured, by both devices, on Vt4 (Case-I) for locations 2 and 3 and on road 140 (Case-II) at location 3. These locations also appeared to be more slippery during the initial visual inspections. Vt3 was the road where the motorcyclist had run off the road after running over the fresh joint rehabilitation. The joint patches on Road 3 were roughened after the accident and the measurements presented here were taken from the roughened surfaces.

On Vt3 (Case-I) the measurement points were chosen to highlight areas where the roughening might have been poor. As Table 4 shows, there were no differences for the dry measurements but wet surface 3/2b, which received poor sanding, had lower wet friction values. However, these results were not confirmed by the PTV results shown in Table 5. The measurements of dry surfaces are logical, but the measurements for the wet surfaces are controversial; the poorly roughened surface had a higher friction value than the properly treated surface. The PFT was however not suited for measuring small areas of poorly sanded patches compared to the pendulum. The PFT is meant to be used for continuous measurements for longer areas while the PTV is better suited for discrete locations.

3.2 *Continuous friction profile measurements by PFT tester*

Figures 5 and 6 show the continuous profile measurements for the longitudinal joint patching (Case I) for sites Vt4 and road 45. Figure 5 shows that on Vt4, about five meters from the start of measurements, the PFT values of the dry surface fell sharply. This is the area that also visually appeared to be slippery (location 2). The wet PFT value, however, did not decrease as

Table 4. Pendulum test values (PTV) averaged over replicate measurements (n).

	Dry						Wet					
	Tested surfaces			Adjacent surface			Tested surfaces			Adjacent surfaces		
Road/Loc.	n	Avg.	St.De	n	Avg.	St.De	n	Avg.	St.De	n	Avg.	St.De
C-I												
Vt4/1	5	110	1.8	6	120	3.4	5	70	0.5	7	80	1.1
Vt4/2	5	120	2.7				10	40	2.7			
Vt4/3	4	130	2.2				8	50	1.4			
Vt4/4	5	110	2.1	2	120	0.7	9	80	1.4	6	90	3.8
Vt3/1	8	130	0.7	8	120	2.5	8	110	2	8	80	0.7
Vt3/2a	4	120	1.3				3	90	1.7			
Vt3/2b	4	120	2.8				5	70	2.5			
45/1	8	110	5.8				7	90	1.8			
45/2	3	110	6.5				8	100	3.2			
Mean	46	118	2.9	16	120	2.2	63	78	1.9	21	83	1.9
C-II												
140/1							5	70	1.3			
140/2							5	70	1.8			
140/3							6	40	1.1			
C-III												
140/1	5	110	1.9	5	110	1.5	5	70	1.8	5	80	1.8
140/2	4	120	2.4									
140/3	6	100	8.8				6	70	3.3	6	70	3.1
140/4							1	60	3.2			
Vt3/5							1	60	0			
Vt3/6							1	90	0			

much as the PTV values shown in Table 4 would suggest. The slippery surface continued over a 10 m length, after which the friction value slowly increased. The friction value decreased again when the next patch (location 3) began at about 50 m.

For road 45, the results contradict each other as the dry friction is higher for the Pendulum test, as expected, but for the PFT test the wet friction is higher. The most likely source of this anomaly is the surface temperature difference. The wet surface was about five degrees cooler than the dry surface and this may have affected the readings taken by the PFT. The sunny weather during the measurements made the joint patches quite soft, which consequently affected the measurements.

4 ANALYSIS AND DISCUSSION

It was not feasible to analyze the variance of the data as the testing was not systematic (i.e., some areas were tested with one but not both equipment). Others were tested in the dry, but not in the wet, conditions. Therefore, error bars were used to indicate the statistical significance of test results. Figures 7 and 8 show the average test values for Case I for each test location with error bars. Error bars were calculated using the variation of two times the standard deviation. The figures show that the PTV measurements seem to be less variable compared to the PFT measurements. As the error bars do not overlap for the PTV values, the wet and dry measurements also are statistically significantly different. Lower variation is confirmed by the coefficient of variation (CV), which was calculated for both sets of measurements. The average CV for the PTV value for dry and wet surfaces was 2.51% and 2.71%, respectively, and for the PFT 4.80% and 5.44%.

Table 5. Portable friction tester (PFT) test results averaged over repeated runs (n).

	Dry						Wet					
	Tested surfaces			Adjacent surfaces			Tested surfaces			Adjacent surfaces		
Road/Loc.	n	Avg,	St.De	n	Avg.	St.De	n	Avg.	St.De	n	Avg.	St.De
C-I												
Vt4/1	2	1.05	0.05	2	1.08	0.08	3	0.80	0.05			
Vt4/2	2	0.95	0.04	2	1.03	0.03	3	0.69	0.05	4	0.71	0.05
Vt4/3	3	0.85	0.04				4	0.75	0.05			
Vt4/4	3	1.04	0.04	1	1.04	0.04	3	0.80	0.04	7	0.70	0.05
Vt3/1	3	1.09	0.05	3	1.06	0.06	6	0.99	0.05			
Vt3/2a	2	1.06	0.09				2	0.86	0.04			
Vt3/2b	3	0.91	0.06				3	0.95	0.05			
45/1	4	0.85	0.02	3	1.05	0.06	6	0.91	0.04	2	0.60	0.04
45/2	6	0.82	0.03	2	0.89	0.04	2	0.90	0.04	2	0.63	0.04
C-II												
140/1	7	1.01	0.04	3	1.13	0.06	2	0.87	0.03	2	0.81	0.05
140/2	3	1.04	0.03				2	0.85	0.03			
140/3	2	0.66	0.05				2	0.49	0.04			
140/4	2	1.17	0.04				2	0.85	0.04			
152/5	4	0.62	0.06	1	0.81	0.04	3	0.76	0.04	2	0.55	0.03
C-III												
140/1	4	0.91	0.06	4	1.03	0.05	4	0.78	0.12	4	0.84	0.04
140/2	2	0.94	0.03	3	0.99	0.07	4	0.88	0.04	2	0.82	0.03
140/3	5	1.14	0.04	4	1.07	0.03	2	0.75	0.03	2	0.80	0.03
140/4	7	0.92	0.04	2	0.62	0.03						
Vt3/5							1	0.61	0			
Vt3/6							1	0.87	0			
45/7							1	0.70	0			

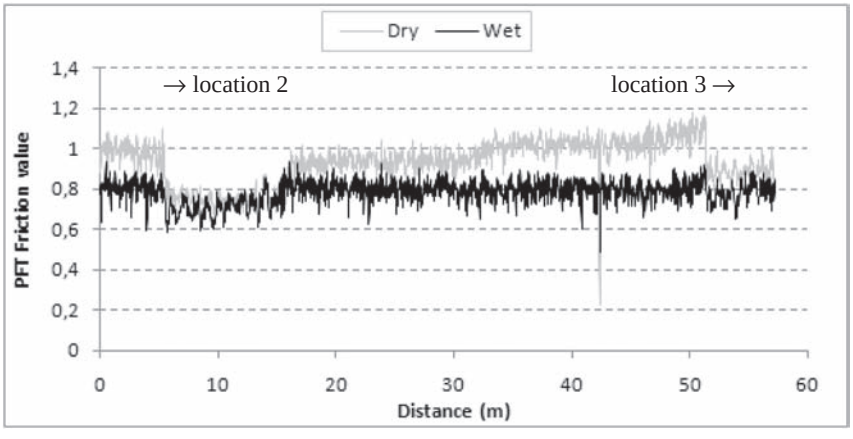

Figure 5. Friction profile on motorway Vt4, picture of test site is shown in Figure 1a.

Figure 9 shows the wet/dry ratios for both measurements. The two bars rising above a ratio of one demonstrate poor results where the friction was greater for the wetted surface. Instances of this only occurred with the PFT.

A recent study was undertaken in Sweden by Bergström et al. (2003) to measure friction on cycleway surfaces using PFT equipment. When compared to values from Bergström et al.

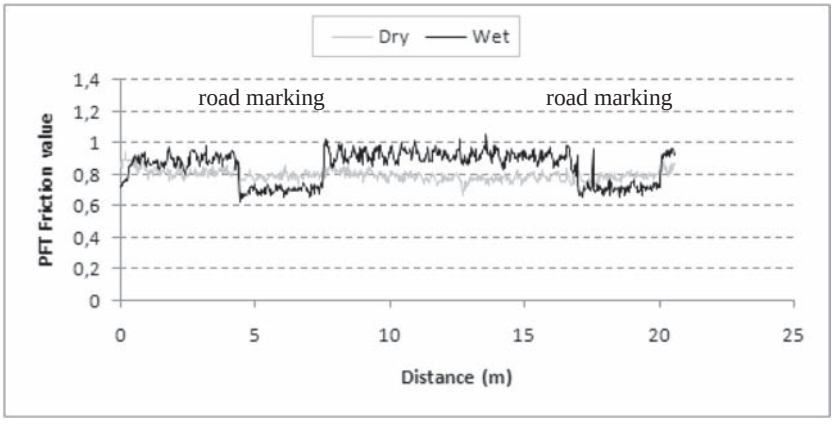

Figure 6. Friction profile on road 45; photo of test site is shown in Figure 2c.

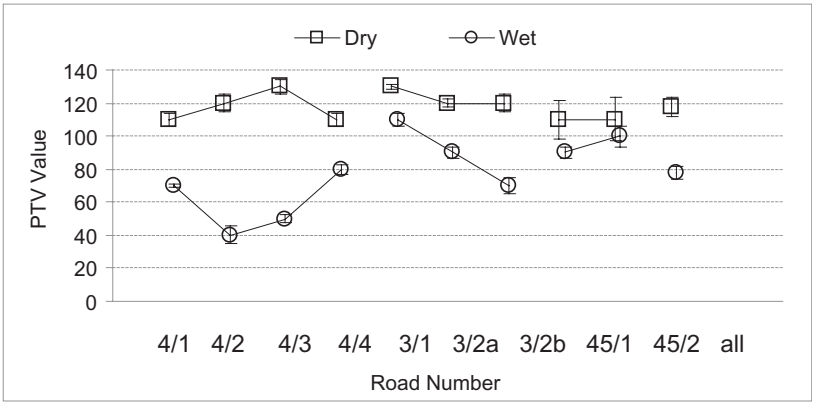

Figure 7. Average PTV values and error bars for longitudinal joint patching (Case-I).

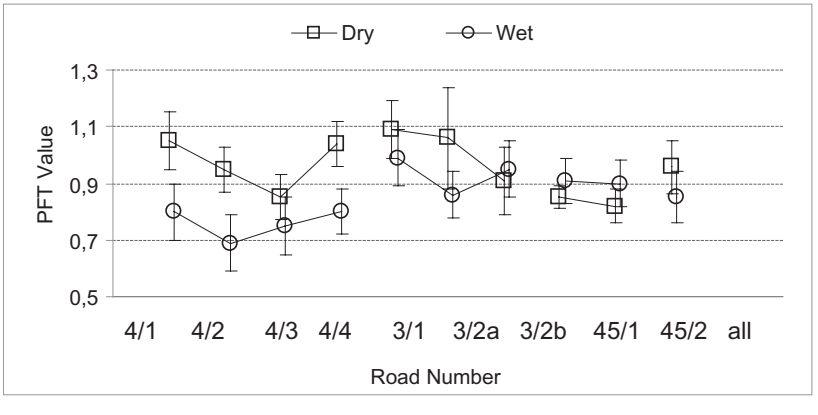

Figure 8. Average PFT values and error bars for longitudinal joint patching (Case-I).

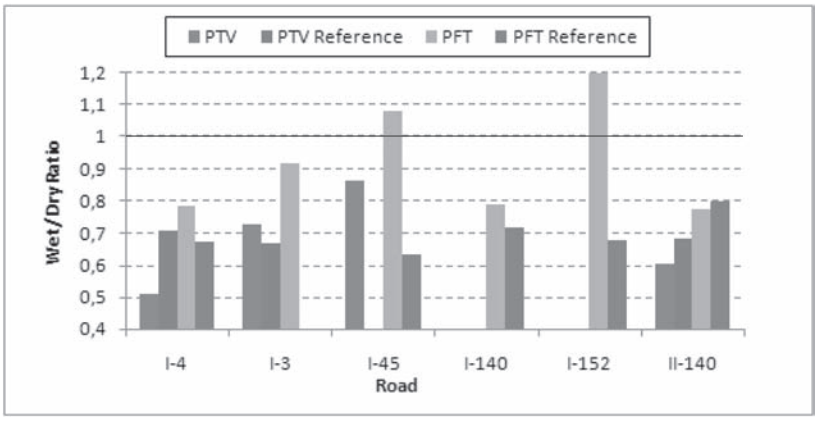

Figure 9. Ratio of wet and dry measurements.

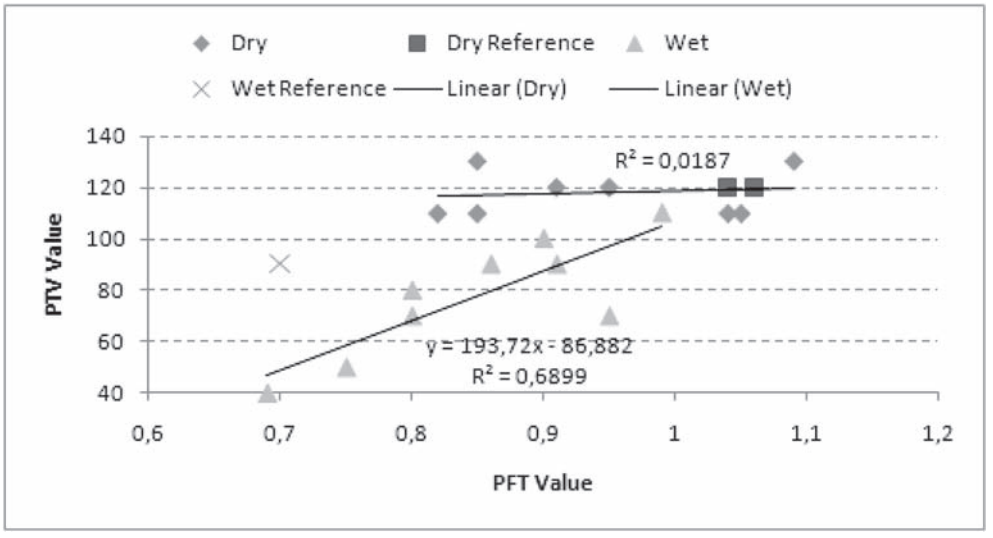

Figure 10. Correlation between the PTV and PFT measurements for Case-I.

obtained from wetted bare cycleway surfaces, the PFT measured values were comparable. The EN 1436 standard states that the lowest acceptable friction PTV value for road marking material is 45. Another study by Wallman and Åström (2001) correlated the PFT and PTV measurements in such a way that a PVT value of 45 would correspond to a PFT value of 0,60. Comparing the two types of equipment in Figure 10 shows that the wet measurements are more related than the dry measurements, which is shown by the greater R^2 value. However, the linear regression line between the PVT and PFT values for the asphalt patches deviates from that developed for the road marking materials in terms of bias and steepness of the regression slope (PANK 2000, Bengström et al. 2001). The PFT value for mastics patches corresponding to the PFT value of 0,60 for road marking materials is approximately 0,68 based on the regression line shown in Figure 10.

The value of slip is difficult to define. For example, on the wet reference surfaces, the value of friction is quite small for the PFT device. This is due to the fact that the device measures friction over the smooth surface of polished aggregate particles, which are, of course, slippery. The spacing between aggregate particles and the size also may have some effect on friction values.

During the investigation, the equipment operators felt that surface temperature could have an impact on measurements. They claimed that the most suitable climatic conditions for obtaining friction values were dry and cloudy and at a temperature of approximately 15–20 °C. The PFT operated best in dry, clear weather, and the operators felt that use of the PFT device should not be recommended during periods of rain.

5 CONCLUDING REMARKS

After concluding friction measurements for this study, all slippery patches on motorways were roughened to improve traffic safety. Generally, all the points which visually appeared slippery were proven to be slippery by the PFT and PTV tests. During the investigation, the lowest friction values were measured on road 140 at Jokivarsi for the edge repairs where gussasphalt was used. When assessing measurements with the help of the criteria developed for road marking materials, it appears that both devices were able to identify the inferior surfaces, although overall the PFT measurements showed more variation and some anomalies in the results that could not be explained. Although traffic control was needed to safely operate both devices, the use of PTF device was slightly handier than the use of PTV device.

When measuring friction using the PFT machine, it may be necessary to undertake further investigation into the effects of temperature on the friction values. Certain surfaces displayed higher friction values in the wet, which is highly unlikely. The surface temperatures could also be the cause of the anomalies in the data. It is important to push the handle of the PFT at the correct angle or the wheel otherwise has a tendency to lift. It would be recommended that a modification to the PFT device would ease this problem. The advantage of the PFT device is that its use is faster and simpler than the PTV device. Rough surfaces also proved difficult to measure effectively using the PTV device.

Although there were problems associated with the PFT device, it could be used as a quick tool to identify the problem areas to ensure the safety of road users. Ultimately, having clear criteria for acceptable road surface friction would facilitate the use and development of portable and easy to use devices for quality control and quality assurance work.

ACKNOWLEDGEMENTS

The authors wish to thank the Finnish National Road Administration for the financial support. Also, the authors wish to thank Master's student Sauli Sainio from Helsinki University of Technology and M.Sc. student Ilkka Taipale from Ramboll for conducting the measurements and the initial analysis of research data.

REFERENCES

Bergström, A., Åström, H. & Magnusson, R 2003. Friction Measurement on Cycleways Using a Portable Friction Tester. Journal of Cold Regions Engineering, 17, 1, 37–57.

EN13036-4 (2003). European Standard EN 13036-4 Road and airfield surface characteristics—Test methods—Part 4: Method for measurement of slip/skid resistance of a surface—The pendulum test. *British Standards.*

Finnish Pavement Technology Advisory Council 2000. *Finnish Asphalt Specifications* 2000, Helsinki: Edita Ltd.

Wallman, C. & Åström, H. 2001. Friction Measurement Methods and Correlation between Road Friction and Traffic Safety. VTI Meddelande 911A.

Advanced Testing and Characterization of Bituminous Materials – Loizos, Partl, Scarpas & Al-Qadi (eds)
© 2009 Taylor & Francis Group, London, ISBN 978-0-415-55854-9

Combined experimental and numerical analysis of moisture infiltration in the modified Lottman test

N. Kringos & A. Scarpas
Delft University of Technology, Delft, The Netherlands

H. Azari
AASHTO Materials Reference Laboratory, Gaithersburg, USA

ABSTRACT: The modified Lottman test method is frequently used for the evaluation of moisture susceptibility of asphalt concrete mixtures. Unfortunately, the test is known to be very variable and sometimes provides erroneous results. In this paper the various variables which are introduced in the T 283 test procedure due to moisture conditioning procedure are investigated via micro-scale finite element analyses. For the finite element meshes, X-Ray tomography scans are made of two gyratory and Marshall compacted mixtures. These mixtures are computationally analyzed for their outside and inside pore-space distribution, the moisture infiltration is simulated via finite element analyses and the resulting moisture fronts are discussed. From the research presented in this paper it can be seen that the two different compactions and geometries can result in entirely different moisture concentrations inside the specimen. This can have a significant impact on the variability of the test results.

1 INTRODUCTION

1.1 *Modified lottman test*

The modified Lottman (AASHTO T 283, 2007) test method is frequently used for the evaluation of moisture susceptibility of asphalt concrete mixtures. Despite its popularity, the test is known to be rather variable and to sometimes even provide erroneous results. Within the NCHRP 9–26A project, precision estimates of the test are being developed by determining the allowable difference between test results that are measured in one laboratory and the allowable difference between test results measured in different laboratories. For this purpose, the AASHTO Materials Reference Laboratory (AMRL) is collecting Tensile Strength Ratio (TSR) data from over 60 different laboratories on two mixtures with expected different levels of moisture susceptibility. Based on the laboratory results, repeatability and reproducibility statistics of the TSR results are being made.

Even though this statistical evidence will give a clear indication of the variability of the test, it will not give any insight into the reasons of the possible discrepancies of the test, nor gives any direction towards its improvement. Therefore, to develop a more fundamental understanding of the results of the precision estimates and possible solutions towards an improvement, finite element analyses are made with the Computer Aided Pavement Analyses finite element system, CAPA-3D, with the integrated RoAM (Raveling of Asphaltic Mixes) package (Scarpas 2005, Kringos 2007, 2008a–c). In the finite element analyses, various micro-scale finite element meshes are made, to represent the investigated mixtures. To simulate the moisture infiltration into the mix components, the finite element meshes are exposed to the same moisture conditioning and temperature cycling as in the laboratory test, followed by the mechanical loading to simulate the material response. For the finite element meshes, X-Ray tomography scans are made of the representative samples of the mixtures. For the accurate mechanical computational analyses, several material parameters of the individual components must first be determined and are discussed further on in the paper.

As a first step in the project, in this paper, focus is placed on identifying the important variables of the moisture conditioning procedure in the T 283 test, which could contribute to the statistical variations. From the assembled X-Ray tomography scans, the distribution of the pore-space within the samples is analyzed in detail, the possible misleading conclusions from comparing dry versus partially saturated samples are discussed, the moisture infiltration pattern within the samples is analyzed via finite element analyses and the necessity of additional mechanical tests in order to accurately simulate the mechanical response of the samples is discussed. First, in the following, the reported complains from highway agency and previous experimental studies about challenges that have so far been encountered with the test are summarized and the selected materials for the NCHRP study are discussed.

1.2 *Background of the test protocol*

The AASHTO T 283 test method is the result of several alteration to the original Lottman test in an attempt to improve its reliability (NCHRP Project 4-08(03) and NCHRP Project 10–17 (Lottman 1978, Tunicliff and Root 1982). The basic concept of the test is to compare the indirect tensile strength of dry samples and samples exposed to saturation, freezing, and thawing. The method is used for testing samples prepared as part of the mixture design process, as part of the plant control process and for cores taken from the pavement. The indirect tensile strength test is conducted on the dry and conditioned specimens according to ASTM D 6931 (2007). In addition to visual observation for stripping, the ratio of average tensile strength of the conditioned and dry specimens is reported as the tensile strength ratio of the average conditioned tensile strength over the the average dry strength of the sample. For the laboratory mixed-laboratory compacted specimens a minimum TSR of 0.80 is recommended for correlation with field performance (Kennedy et al. 1983, Solaimanian et al. 2003).

1.3 *Reported shortcomings of the test*

Although AASHTO T 283 is still the most widely used method for determining HMA moisture susceptibility, highway agencies have reported several shortcomings of the method. One of the major complains about the test is that the test does not always correctly predict moisture sensitivity of the mixtures as it has been observed in the field. Mixtures that performed well in the field have exhibited unexpectedly low TSR values and poor performing mixtures have indicated unexpectedly high TSR values (Solaimanian et al. 2007). The research by Epps et al. (2000) which included five different mixtures from various states indicated that the sensitivity of the mixtures to moisture damage, as described by the state highway agencies, did not satisfactorily match the observed T 283 behavior of a number of mixtures in the study.

Another frequently made complaint with regard to the test is the disagreement of the test results between 100 mm (4") and 150 mm (6") in diameter specimens. In a survey of 89 agencies compiled by AMRL it was reported by a number of state DOT's that 100 mm (4") Marshall specimens indicate better agreement with the field performance than 150 mm (6") gyratory specimens. However, Epps et al. have shown that 150 mm (6") gyratory specimens provide less variable results than 100 mm (4") Marshall Specimens.

The other complaint about the AASHTO T 283 test method is regarding the conditioning of the test. It has been stated that the duration and severity of saturation and moisture conditioning does not always promote the stripping of the mastic. Choubane et al. (2000) has suggested saturation levels above 90% and multiple freeze-thaw cycles in order to promote stripping. They found that degrees of saturation of 55% versus 80% would result in significantly different tensile strength of the mixtures. In addition, Kandhal and Rickards (2002) showed that in four different case studies of stripping in asphalt pavements, the asphalt pavement was nearly 100% saturated with water, which is much higher than the saturation level that is recommended in AASHTO T 283.

An additional reported complaint about the T 283 test is the mode of mechanical testing of the specimens. Kandhal and Rickards have argued that a cyclic load which can simulate the pumping action of traffic load is a better test than loading the samples with a constant rate.

Finally, a last complaint about the test that is often reported by state DOT engineers is that the test is very time-consuming. Several state highway agencies follow a shortened version of AASHTO T 283 test method, which might provide different findings than if all steps of the test are followed (Aschenbrener et al. 1995).

In this paper a theoretical and computational analyses is given of the moisture infiltration in the chosen mixtures in the NCHRP 9–26 project and a discussion regarding the structural nature of the test is given, which both address some of the complaints regarding repeatability and comparison between laboratory results and the field. Toward the end of the paper some additional comments are made with regard to the general reported complaints about the test, as summarized in the above. But first, in the following, a description of the chosen materials and some preliminary test data for the NCHRP study is given.

2 MATERIAL TESTING

2.1 *Selection of asphalt mixture components*

Since the level of moisture susceptibility of HMA is the main aspect to be determined from the AASHTO T 283, mixtures with varying levels of moisture susceptibility were selected in this project. Two aggregates with generally believed low and high moisture sensitivity were obtained for the study. The moisture sensitive aggregate is a sandstone (keystone, KST) from Maryland. Use of this aggregate without anti-stripping agent was banned by Maryland State Highway for pavement construction. The less moisture susceptible aggregate is a limestone (LMST) from a quarry in Pennsylvania. This aggregate has shown good performance both in the field and in laboratory as indicated in NCHRP 9-34 study (Solaimanian 2007). To keep the number of variables to a minimum, the same unmodified asphalt binder with performance grade of 64–22 was selected for use with both aggregates. To better control the variables of the test, a similar aggregate—asphalt system with nominal maximum aggregate size of 12.5 mm was used for the two mixtures. The mastic of the sandstone and the limestone mixture consists of 5.4% (by aggregate weight) sandstone and limestone dust, respectively, passing the #200 sieve and 5.2% (by mix weight) of asphalt binder.

Several purposes are intended for the experimental portion of the study. In addition to evaluating the performance of the two mixtures, the effect of compaction and specimen size on the test results is also investigated. For this purpose, 100 mm (4") Marshall and 150 mm (6") Superpave gyratory specimens were compacted and tested for each mixture. A total of 24 specimens were mixed, cured, compacted, conditioned, and tested. This included six- 4" Marshall Sandstone, six- 6" gyratory sandstone, six- 4" Marshall limestone, and six- 6" gyratory limestone. Two additional mixtures from each material were also prepared for the theoretical specific gravity measurements.

Several volumetric measurements were conducted on the compacted specimens. One set of measurements included the bulk specific gravity measurement according to AASHTO T 166. This was done firstly, to ensure that each specimen satisfies the air void requirement of 7 ± 0.5 and secondly, to be able to sort the specimens into two groups with similar average air voids.

2.2 *X-Ray tomography scans*

Following the fabrication, specimens were scanned using X-Ray computed tomography system of Federal Highway Administration at Turner-Fairbank Highway Research Center (TFHRC). The X-Ray system at TFHRC has a 420 keV X-Ray source and a 512 pixel $\times$ 1 mm linear array detector. The X-Ray computed tomography (XCT) scanning of the specimens was done continuously in 0.8 mm intervals for the entire depth of the specimens. The resolution of the images of 4" specimens is 0.2 mm (each millimeter is represented by 5 pixels) and the resolution of 6" specimens is 0.33 mm (each millimeter is represented by 3 pixels).

The images clearly show the three phases of asphalt concrete material: aggregates, mastic, and air. Since intensity of each pixel is proportional to object density, air voids with the lowest density are black while the solids vary from dark to light gray depending on relative densities.

The intensity differences in the image are sufficient to clearly distinguish the aggregates from the mastic.

The X-Ray images are used for quantifying the air void distribution of the compacted samples and for creating finite element meshes for the modeling of moisture infiltration in 4" Marshall and 6" gyratory specimens using the CAPA 3-D finite element program and will be used for the micro-scale mechanical finite element.

2.3 *Test results*

The TSR testing of the two mixtures was conducted at TFHRC. Following the T 283 test method procedure, the three dry samples, from each mixture, were kept at room temperature for 24 hours and were placed in 25°C water bath for additional 2 hours prior to tensile strength test. The conditioned specimens, prior to tensile strength test, were subjected to partial vacuum to reach a saturation of 70% to 80%, then placed for 16 hours at –18°C in a freezer. After this they were exposed for 24 hours in a water bath at 60°C, and additionally, 2 hours in a water bath at 25°C to reach the testing temperature.

The results of the tests on dry and wet specimens are shown in Table 2. Both the Marshall and the gyratory compacted specimens of the sandstone mixture, which was expected to be moisture susceptible, passed the test with very high wet/dry tensile strength ratio (TSR). The average TSR of the Marshall compacted specimens was 0.91 and the average TSR of the gyratory compacted specimen was 0.95. No visual stripping was observed for any of the sandstone specimens.

The results of the TSR test on the mixtures with the limestone aggregate are also shown in Table 2. Since the limestone has performed well in both field and laboratory, it was anticipated for these mixtures to have a rather high TSR values. Following this expectation, the gyratory specimens' TSR reached the rather high value of 1.06, stating more or less that the conditioning of the specimens had no effect on the tensile strength of the material. The TSR value of the Marshall compacted specimens was, however, unexpectedly low with a TSR of 0.82. The Marshall compacted samples also showed a significant amount of visual stripping. These results indicate that the previously expressed concerns regarding the precision and applicability of the T 283 procedure are valid and cause for a further investigation with regard to the fundamental reasons. For this reason, in the following sections of the paper, detailed analyses are given of the possible influences of the moisture conditioning procedure, the variable distribution of the inside and outside porosity of the specimens and the structural nature of the test.

3 SPECIMEN POROSITY

3.1 *Inside and outside porosity*

In AASHTO T 283-03, section 9.4, it is recommended to use T 166, Method A, for determining the bulk specific gravity (BSG) of the specimen. The problem with this procedure for the calculation of the air voids in the specimen is, that most air voids which are in direct contact with the 'outside' are not taken into account. This means that, even though it is aimed in the T 283 procedure to group specimens with the same air void percentage, the specimens may very well end up with different moisture conditioning because of a varying 'outside' porosity, Figure 1. A larger outside porosity, or: instantaneous contact surface of water with the specimen, may therefore results into a more severe moisture conditioning in the water bath, even when the inside porosity is the same.

So, following the T 283 procedure, only the inside porosity is measured. To quantify the inside and outside porosity, the X-Ray scans of all the specimens are assembled into the three dimensional representations, whereby the size of the smallest (voxel) element is 0.2 mm × 0.2 mm × 1.0 mm. From the X-Ray scan assembly, both the inside and outside porosity of the tested specimens is calculated, in which a perfect cylindrical shape of the specimen is assumed. From the calculated inside and outside porosities it can be found that the target

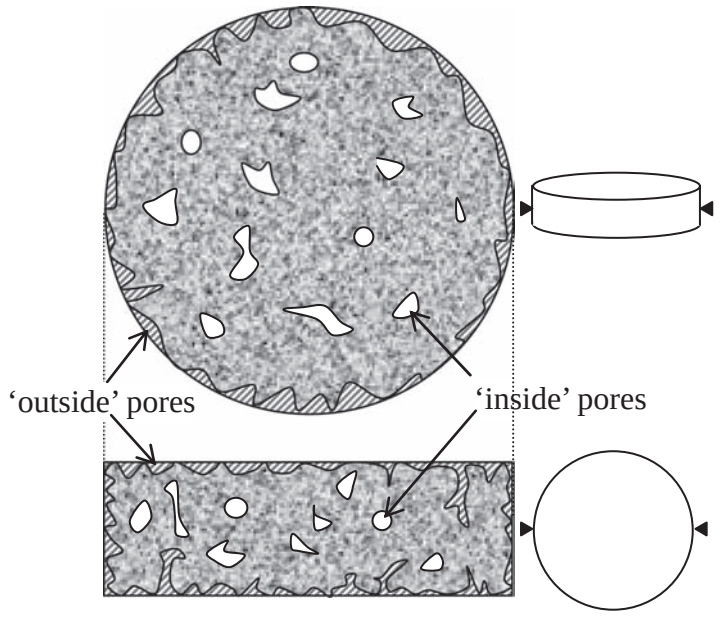

Figure 1. Schematic of inside and outside pore-space.

(inside) porosity of 7% ± 0.5 was reasonably well met. The measured values of the inside porosity in the laboratory are, on average, 1.8% lower than the values computed from the X-Ray scans, which can probably be contributed to in-accuracies in the laboratory measurements and/or the processing of the X-Ray scans. Adding the outside porosity to the total porosity measure, it is found that the gyratory specimens have an additional 23% and the Marshall have an additional 45% of pore space. This indicated that the Marshall specimens may have relatively more access to moisture during conditioning times and could therefore reach higher moisture concentrations. Even though the targeted saturated (inside) pore space should be a constant between the specimens, from the above, it can be seen that the total porosity may vary between the samples.

3.2 *Vacuum induced cracking*

The measured initially absorbed water percentages are compared with the outside connected pore space, Table 1. The third column in the table is showing the difference between the initially absorbed (i.e. before the vacuum) water and the pore space which is directly connected with the water bath. Assuming that all the outside pore space is filled with water, this difference can be seen as the outside 'roughness' of the sample, in comparison with a perfect cylinder, Figure 1. It could therefore be concluded that the investigated gyratory compacted samples give, on average, 0.4% imperfection and the Marshall compacted samples give, on average, 1.9% imperfection to the cylindrical shape.

In the case of a perfectly cylindrical specimen, this difference would indicate the pore space which is, in principal, in direct contact with the water bath, but cannot be initially filled with water due to the small pore-size. This would mean that the gyratory compacted specimens have, on average, 1.6% air voids available for direct saturation. For the Marshall compacted specimens this would be, on average, 3.3%. The test protocol, however, dictates a saturation level of 70–80% of mixtures with a targeted air void of 7% ± 0.5. This comes down to a water absorption level of 4.6–6.0%. Therefore, the applied vacuum suction must induce some micro cracking inside the sample to enable the necessary additional pore space. This induced micro-cracking can be an important factor which contributes to the variability of the test.

Table 1. Comparison initial absorption and outside connected porosity.

	Initial absorption %	Outside porosity %	Difference
KS_GYR	1.2	1.7	0.5
KS_MAR	1.2	3.2	2.0
LMS_GYR	1.2	1.4	0.2
LMS_MAR	1.6	3.3	1.7

Another important variable which could influence the moisture distribution within the sample, is the distribution of the inside pore space. To have a better idea on the variability of this distribution of the specimens, in the following section the distribution of the pore-space is quantified.

3.3 *Distribution of inside pore-space*

Since in the indirect tensile test, the tensile fracture area is located in the center of the specimen, the actual location of the infiltrated water is quite important. It could, for instance, be possible that, due to a clustering of the pore space on the outside of the specimens, most moisture damage is occurring away from the tensile area and is therefore not detected. To quantify the distribution of the pore space, the assembled X-Ray scans are divided into 8 parts (Azari 2005). To quantify the distribution of the possible moisture infiltration through the macro-pores of the mix, for each 1/8 specimen, a calculation is made of the connected outside air voids and the inside air voids.

From the analyses it was found that the Marshall compacted specimens have a rather high percentage of outside pore-space. The gyratory compacted specimens showed a higher porosity on the 'top' and a lower porosity on the 'bottom' of the specimens. This would indicate that one side of the specimen is more moisture conditioned than the other side. From the inside porosity distribution it can be seen that the gyratory compaction creates a rather well distributed pore-space, with a maximum variation of 2.5% from the mean.

Furthermore, the Marshall compacted specimens also showed an overall higher porosity on the 'top' and a lower porosity on the 'bottom' of the specimens, even though the porosities seem to be less dispersed than with the gyratory specimens. From the inside porosity distribution it can be seen that the Marshall compaction creates a less dispersed inside pore-space and tends to create clusters of air-voids. This could indicate a very asymmetric moisture front inside the Marshall compacted specimens which could lead to unexpected bad or unexpected good behavior of the specimens.

4 MOISTURE INFILTRATION SIMULATION

4.1 *Finite element analyses*

From the above analyses it can be seen that there seems to be quite some variation in the pore space distribution of the gyratory and Marshall compacted specimens. This would indicate that, even if 70–80% saturation is achieved in all specimens, the actual moisture conditioning of the specimens can be very different from case to case.

To visualize this moisture infiltration inside the specimens and to incorporate the effect of the different sizes of the gyratory and Marshall compacted specimens, in this section a finite element analyses is shown of the moisture infiltration in the specimen, made with the RoAM/CAPA-3D software (Kringos and Scarpas 2005, Kringos et al. 2008a–c). In Figure 2 the moisture infiltration front inside the gyratory compacted LMS specimen is shown. From the moisture front development in the mid-plane of the cylinder, Figure 2(c), it can be seen that the moisture distributes itself relatively uniform over the specimen. This is in agreement with

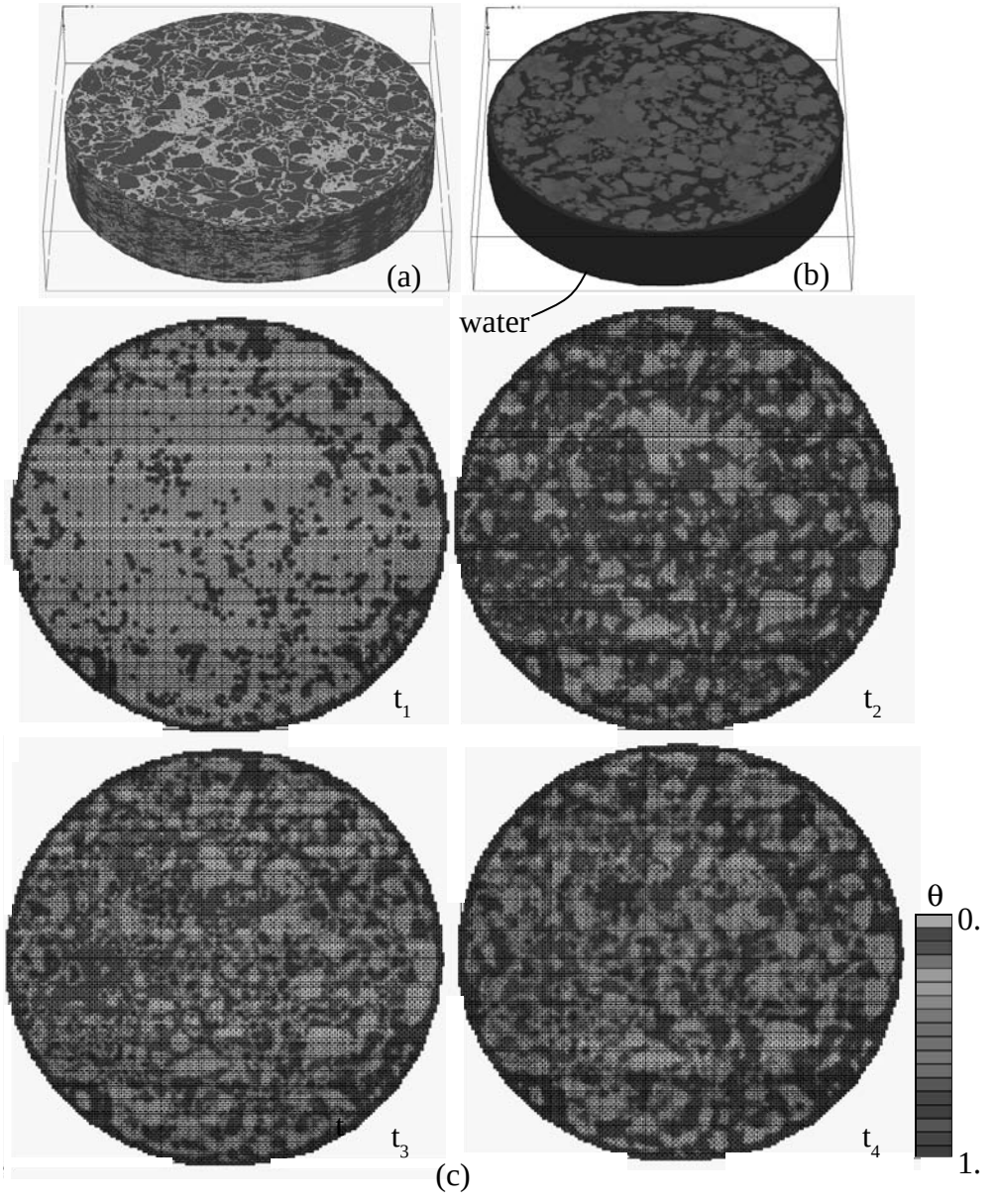

Figure 2. Finite element infiltration in Gyratory compacted LMS specimen (a) finite element mesh (b) moisture conditioning (c) moisture infiltration in mid-plane.

the earlier observations of the pore space distribution in gyratory specimens. The gyratory compacted KST specimen showed a similar moisture infiltration pattern. From the finite element pictures of the mid-plane of the Marshall compacted LMS specimen, it can be seen that a relatively large amount of moisture reaches the center of the core. In this case, the observed clustering seems to concentrate itself in the center of the specimen, which could explain why the Marshall compacted LMS specimens had an unexpected bad response.

In Figure 3 the finite element simulation of the Marshall compacted KST specimen is shown. From the analyses pictures of the mid-plane of the specimen it becomes clear that a very asymmetric moisture infiltration is created in the specimen. This would indicate that the material properties of these specimens are degrading asymmetrically and this will certainly contribute to problems with the repeatability of the test and the observed failure.

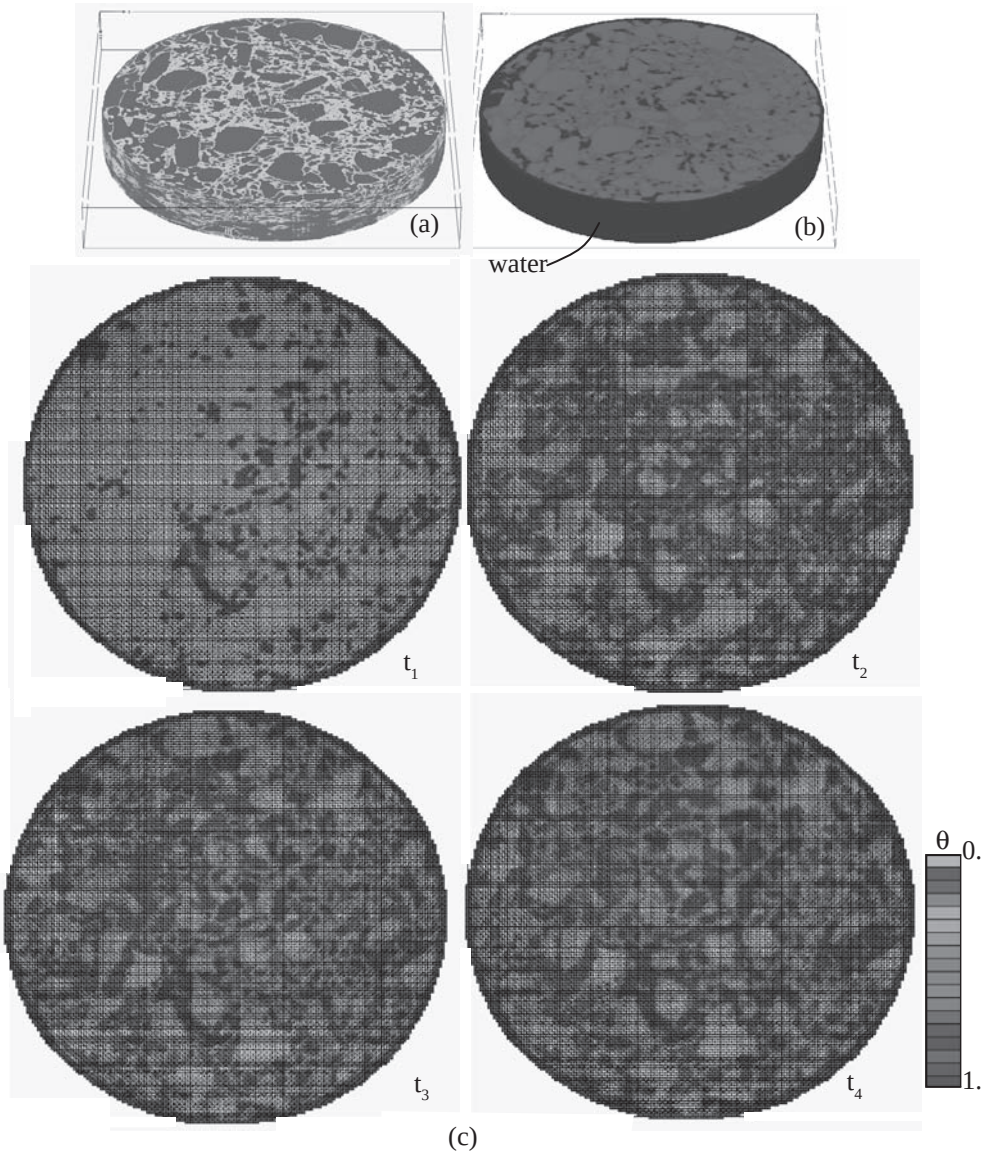

Figure 3. Finite element infiltration in Marshall compacted KST specimen (a) finite element mesh (b) moisture conditioning (c) moisture infiltration in mid-plane.

From the simulated moisture patterns it becomes clear that the TSR test specimens are exposed to large variations of the moisture conditioning of the samples, even when the moisture conditioning protocol is kept the same. This means that, depending on the distribution of the inside pore-space, the added 'moisture accessibility' of the specimen due to increased outside-porosity, and the connectivity of the inside pores within the sample, large differences can be expected when comparing the results of the TSR test.

To make this conclusion, however, on a more quantitative basis, rather than a qualitative one as done in the above, the mechanical properties of the individual mix components (mastic, stones and mastic-stone bond) and their susceptibility to moisture must be determined. In the following, a brief outline is given of the mechanics of the TSR test and the difficulties involved in making a judgment, simply on the basis of the overall specimen response.

5 CONCLUSIONS AND RECOMMENDATIONS

One of the documented complaints about the T 283 test is that the experienced field moisture sensitivity does not always correlate well with the test results. From the analytical and computational analyses performed in this paper it has been discussed that the moisture concentration levels of the various test samples are not necessarily comparable, nor do the samples themselves have a uniform moisture field inside the material.

These variations in the moisture conditioning of the samples can already partly explain some of the variability which is experienced with the test. It also contributes to the discrepancy between the laboratory moisture conditioning and the moisture conditions in the field. The time-frame over which the moisture can actually infiltrate within the material components, is a crucial factor in this. Even though it is aimed to create similar levels of mix saturation between the laboratory test specimens and the field, it should be kept in mind that the actual weakening of the asphalt mixture comes when the moisture starts infiltrating inside the mix components. This moisture infiltration process will be mainly concentration gradient driven, and will take longer than a pressure driven process. The time frame of moisture conditioning is therefore crucial, and the T 283 test protocol is certainly lacking with this respect.

The other moisture induced damage phenomena which can contribute to damage in the pavement are the mechanical and physical manifestations of the 'pumping action' which a (partially) saturated pavement experiences under mechanical loading. In addition to added mechanical stresses inside the material, which may cause added damage, these high water pressures may cause an erosion effect of the mastic, which contributes to the mechanical degradation of the mastic and the progressively increased moisture susceptibility (Kringos et al. 2009). The T 283 is not including these pumping action related moisture induced damage phenomena in the test. This means, for instance, that a mixture which is highly susceptible to mastic erosion may perform well in the T 283, but would have bad results in the pavement, when exposed to pumping action.

Two important aspect of the T 283 protocol are the vacuum suction and the freezing of the sample. As was shown in the paper, the vacuum suction must be inducing micro-cracking within the sample, which is introducing another variable to the test which can contribute to its inconsistency. For the freezing aspect of the test it has been suggested in the past that this would simulate a combination of the aging of the material and the cycling loading and/or pumping action as it would occur in practice. From a materials point of view, ageing of the material entails a physical change of its characteristics, which embrittles the material making it thus more susceptible to cracking. From a mechanical point of view, the added stresses inside the mix which are caused by the volumetric expansion when the water turns to ice and the embrittlement of the material at such low temperature will certainly induce damage inside the mixture. This damage is, however, different in nature than the long term effect of cycling loading, in time ageing and erosion of the mastic due to pumping action. This could be an additional reason for differences between the laboratory and the field.

Finally, it should be kept in mind that the state of stress which the sample is tested for is highly dependent on the geometry of the sample. So it would make perfect sense that by testing another geometry (such as Marshall versus gyratory), another (structural) result will be found. Likewise, the state of stress which is created in the indirect tension test is of course not similar to the actual stress development in a pavement. Therefore, from a mechanics point of view, the differences between the laboratory and the field make perfect sense.

In the next phase of this project, the developed micro-scale finite element meshes will be used for a simulation of the mechanical response. For this, several mechanical tests will be performed in the coming year.

ACKNOWLEDGEMENTS

The authors gratefully acknowledge the financial support of the NCHRP 9-26A panel in the context of which this research was performed and the support of the Turner-Fairbank

Highway Research Center in the testing of the samples and making the X-Ray system available for scanning of the specimens.

REFERENCES

AASHTO Standard Specifications for Transportation Materials and Methods of Sampling and Testing (Part 2—Tests) (2007). Twenty-Seventh Edition, American Association of State Highway and Transportation Officials, Washington, DC.

American Society for Testing and Materials (2007). Annual Book of ASTM Standards, Volume 04.03, West Conshohocken, PA.

Aschenbrener, T., McGennis, R.B. and Terrel, R.L. (1995). "Comparison of Several Moisture Susceptibility Tests to Pavement of Known Field Performance." Journal of the Association of Asphalt Paving Technologists, pp. 163–208.

Azari, H. (2005). "Effect of Aggregate Inhomogeneity on Mechanical Properties of Asphalt Mixtures," Ph.D. Dissertation, University of Maryland, College Park, MD, http://www.lib.umd.edu/drum/handle/1903/3148.

Choubane, B., Page, G.C. et al. (2000). "Effects of Water Saturation Level on Resistance of Compacted Hot-Mix Asphalt Samples to Moisture-Induced Damage." Transportation Research Record 1723: 97–106. Transportation Research Board, National Research Council, Washington, DC.

Epps, J.A., Sebaaly, P.E. Penaranda, J. Maher, M.R. McCann, M.B., and Hand, A.J. (2000). NCHRP Report 444: Compatibility of a Test for Moisture-Induced Damage with Superpave Volumetric Mix Design. Transportation Research Board, National Research Council, Washington, DC.

Kandhal, P. and Rickards, I. (2002). "Premature Failure of Asphalt Overlays from Stripping: Case Histories." Asphalt Paving Technology 70: 301–351.

Kennedy, T.W, Roberts, F.L., and Lee, K.W. (1983). "Evaluation of Moisture Effects on Asphalt Concrete Mixtures," Transportation Research Record 911, Transportation Research Board, National Research Council, Washington DC, pp. 134–143.

Kringos, N., and Scarpas, A. (2005), Ravelling of asphaltic mixes: Computational identification of controlling parameters, Transportation Research Record: Journal of the Transportation Research Board, No. 1929, Bituminous Paving Mixtures pp. 79–87.

Kringos, N., Modeling of Combined Physical-Mechanical Moisture Induced Damage in Asphaltic Mixes, PhD dissertation, Delft University of Technology, ISBN 978-90-9021765-9, 2007.

Kringos, N., Scarpas, A., and Bondt de, A. (2008a), Determination of Moisture Susceptibility of Mastic-Stone Bond Strength and Comparison to Thermodynamical Properties, Journal of the Association of Asphalt Paving Technologists, Vol. 77.

Kringos, N., Scarpas, A., and Selvadurai, A.P.S. (2008b) Modeling of combined physical-mechanical moisture induced damage in asphaltic mixes, Part 1: governing processes and formulations, International Journal for Pavement Engineering, Vol. 2.

Kringos, N., Scarpas, A., Copeland, A. and Youtcheff, J. (2008c),'Modeling of combined physical-mechanical moisture induced damage in asphaltic mixes- Part 2: moisture susceptibility parameters', International Journal for Pavement Engineering, 9, pp. 129–151.

Kringos, N., Scarpas, A., and Selvadurai, A.P.S. (2009), 'Simulation of Mastic Erosion from Open-Graded Asphalt Mixes Using a Hybrid Lagrangian-Eulerian Finite Element Approach', Computer Methods and Engineering Science, Vol.741, no. 1, pp. 1–13.

Lottman, R.P. (1978). "Predicting Moisture-Induced Damage to Asphaltic Concrete." NCHRP Report 192, Transportation Research Board, National Research Council, Washington, DC.

Scarpas, A., CAPA-3D: A Mechanics Based Computational Platform for Pavement Engineering, ISBN 90-9019040-6, 2005.

Solaimanian, M., Bonaquist, R. and Tandon,V. (2007)."Improved conditioning and Testing Procedures for HMA Moisture Susceptibility." NCHRP Report 589, Transportation Research Board, National Research Council, Washington, DC.

Solaimanian, M., Harvey, J. et al. (2003). "Test Methods to Predict Moisture Sensitivity of Hot-Mix Asphalt Pavements." Moisture Sensitivity of Asphalt Pavements: A National Seminar, San Diego, CA, Transportation Research Board.

Tunnicliff, D.G. and Root, R.E. (1982). "Antistripping Additives in Asphalt Concrete—State-of-the-Art." Proceedings, Association of Asphalt Paving Technologists, Vol. 51, 1982, pp. 265–293.

Advanced Testing and Characterization of Bituminous Materials – Loizos, Partl, Scarpas & Al-Qadi (eds)
© 2009 Taylor & Francis Group, London, ISBN 978-0-415-55854-9

Assessment of moisture effect on open graded mixes using water sensitivity and Cántabro after immersion tests

B. Rubio & R. Jiménez
Centro de Estudios del Transporte del CEDEX, Madrid, España

F. Pérez & A. Martínez
Universidad Politécnica de Cataluña, Barcelona, España

ABSTRACT: In Spain, water damage on the cohesion of porous asphalt (PA) and asphalt concrete for very thin layers (BBTM mixtures with a void content over 12%) was assessed using the Cántabro after immersion test (NLT-352).

European Standards for bituminous mixtures (EN 13108) have gone into effect requiring us to assess water damage through Water Sensitivity testing (EN 12697-12, 2003). This represents an important change in how to evaluate PA and BBTM water resistance. Accordingly, new requirements must be set and included in the Spanish Highway Technical Specifications (PG-3).

In order to assess and compare both methods, a series of bituminous mixtures have been prepared with several types of aggregates and fillers, and with different percentages of conventional and polymer modified bitumen.

Both methods allow the assessment of water effect. Cántabro test is more sensitive for the evaluation of moisture damage on open bituminous mixtures. A significant correlation between Cántabro and sensitivity tests was found, allowing us to establish new specifications in line with the European Standards.

1 BACKGROUND

European standards for hot bituminous mixtures are basically collected in two series of standards: EN 13108 and EN 12697. The objective of EN 13108 Standards is to define the requirements criteria of the different bituminous mixtures, as well as the evaluation of conformity (Initial Type Testing and Factory Production Control), while the aim of EN 12697 is to collect the different testing methods.

These standards were drawn up because of the European Commission Mandate (89/106/CEE Construction Products Directive) and, consequently, are mandatory harmonized standards. They have gone into effect since March 2008.

The need of harmonizing the characteristics of the bituminous mixtures used in all the European countries, each one of them with their own orography, climatic conditions, traffic loading, etc., resulted in a wide and open set of specifications as a unique frame of reference. Although these specifications are expected to be applied to different technologies, every country must define each of the specified characteristics. The testing methods were also tried to be unified and, in many cases, it will be possible to choose among several compaction and testing procedures.

Accordingly, Spain, as the rest of the EU countries, had to review its own standards and specifications, and adapt them in order to be in accordance with the harmonized standards. This task led to the definition of the specifications limits for the mandatory characteristics, the selection of the optional characteristics (among the whole), and the setting of the specimen production procedures as well as the testing method for the optional characteristics.

From this analysis of the European Standards for bituminous mixtures it was considered that some part of the Spanish Standards had to be adapted regarding both testing procedures

and their corresponding specifications. One of these procedures was the water sensitivity test, described in EN 12697-12 (2003).

The procedure used in Spain to evaluate cohesion loss in dense mixtures caused by water effect is NLT-162 Standard (NLT – 162/00, 2000). This test assesses water effect through compressive resistance before and after water immersion. For open gap-graded mixtures (air void content higher than 12%) Cántabro test after immersion is used, according to NLT-352 (NLT – 352/86, 1986).

Given the great differences between European water sensitivity test and Cántabro after immersion test, this paper presents the results of a study about water resistance for a series of porous mixtures and asphalt concrete for very thin layers (open gap-graded mixtures) using both tests. The variables for these mixtures were set basically the filler type and the bitumen content, in order to analyse different responses to water effect for comparing both methods. Subsequently, open mixtures prepared with different aggregates and bitumens were tested with the aim of correlating both methods and proposing a specification for these type of mixtures, so frequently used in Spain as wearing courses.

2 MATERIALS

The following materials were used:

Bitumens: a 50–70 penetration grade bitumen and a polymer modified bitumen (PMB 45/80-60) were used for the bituminous mixtures preparation. Both bitumens are commonly used in Spain.

Aggregates: the aggregates were crushed stone and gravel from Madrid and Catalonia. Three types of coarse aggregates were used: siliceous aggregate, from Velilla de San Antonio (Madrid), porphyritic aggregate from Aldeavieja (Ávila), and granite from Berta (Barcelona). As fine aggregate, in addition to the sources mentioned before, two calcareous sands from El Hoyon (Madrid) and from Foj Barcelona were used.

Mineral filler: there were three mineral filler: cement, calcareous filler and hygrophilous plastic kaoline.

Antistripping dope: in order to improve adhesion between asphalt binder and aggregate in presence of moisture, an amine type dope was used.

Bituminous mixtures: the above materials were used to prepare different mixture designs, all of which fitted to the gradations of porous asphalts (PA) and concrete asphalt for very thin layers—open gap-graded bituminous mixtures - (BBTM) usually employed in Spain. These gradations are shown in figures 1 and 2.

3 RESULTS AND DISCUSSION

To deal with this study and considering the different compaction procedures for the specimens to determine water sensitivity resistance, firstly it was necessary to select the more appropriate procedure and compaction energy, so as to get a similar bulk density to what is expected in the field. Then, all the mixtures were tested using the European water sensitivity and Cántabro after immersion tests. With the aim of analysing a correlation between both methods and to determine the threshold for the indirect tensile strength ratio (ITSR) for these Spanish open mixtures, different types of aggregates, fillers, bitumens, etc., were used.

3.1 *Selection of the compaction procedure for the specimens*

Water sensitivity test (EN 12697-12, 2003) allows the compaction of specimens by several procedures: impact compactor (EN 12697-30, 2007), gyratory compactor (EN 12697-31), vibratory compactor (EN 12697-32) and slab compactor (EN 12697-33). It is also possible to test cores taken from a bituminous layer. However, compaction energy must be selected in order to get a density or an air voids content corresponding to what is expected in the field.

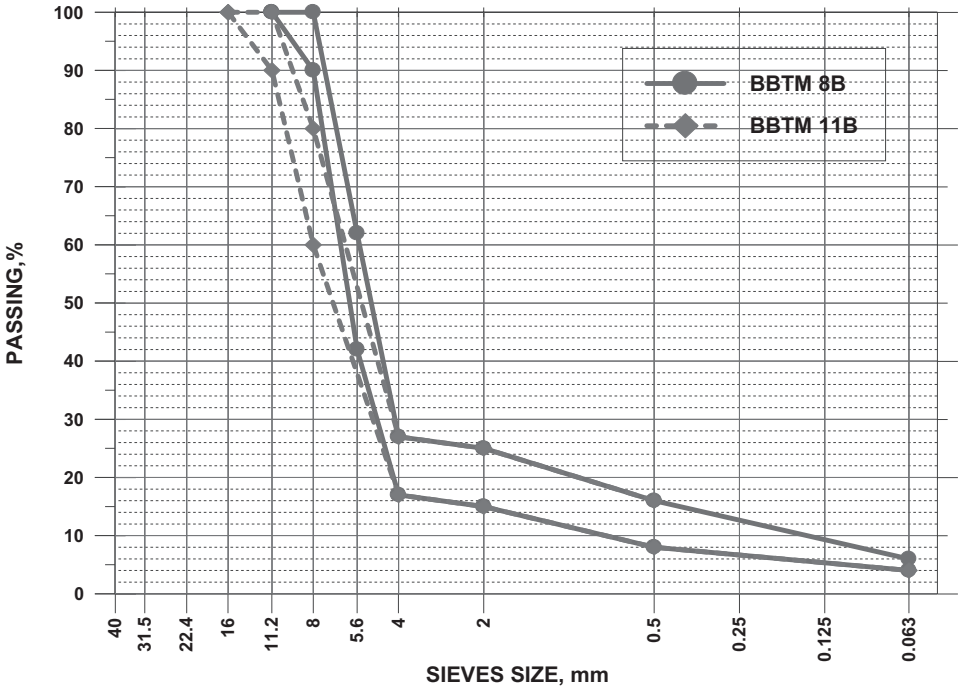

Figure 1. Gradation criteria for BBTM8B and BBTM11B mixtures.

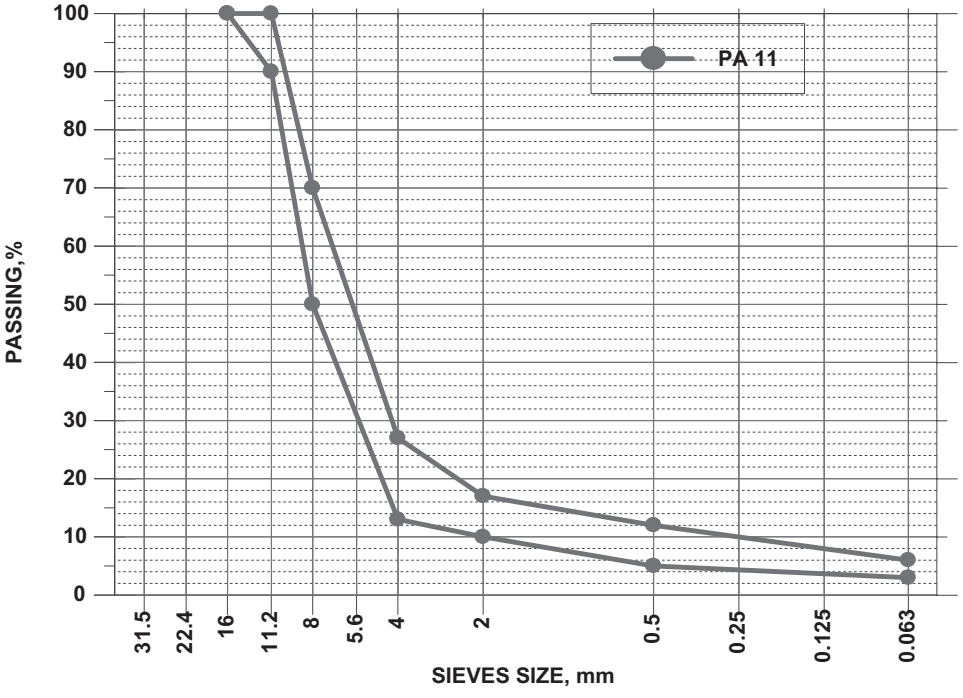

Figure 2. Gradation criteria for PA11 mixtures.

Impact compaction (Marshall hammer) was finally selected from the four options because of the vast experience with this method in Spain and also with the use of Marshall density as a reference to assess the compaction level obtained in the field.

For the determination of the necessary energy level to reach the field density, Marshall specimens were prepared according to EN 12697-30 (2007) with 50 and 25 blows per face.

Table 1 shows the different mixtures studied. Aggregates nature nature, bitumen type and content, filler type and dope percentage are also quoted.

The results presented in figure 3 show compaction percentage of the standard Marshall density for the mixtures indicated in table 1.

For porous and gap-graded mixtures, the Spanish Highway Technical Specifications (PG-3) (5–6) requires that voids content can not differ in more than two percent (± 2%) from the percentage obtained in the job mix formula. For these types of mixes this is equivalent to 97–98% of Marshall density in 50 blows compacted specimens. As a consequence, it is concluded that specimens must be compacted with Marshall compactor applying 50 blows per face, in order to achieve similar density to that obtained after the laying and compaction of the mixture.

With the objective of assessing the effect of compaction level on water sensitivity test specimens compacted with 25 and 50 blows per face were tested. The results obtained were plotted in figures 4 to 9 and compared. The results of Cántabro after immersion test were also included in these figures.

Table 1. PA and BBTM mixtures composition.

Reference	Coarse aggregate	Fine aggregate	Bitumen type	Bitumen content (%)	Filler type	Dope (%)
PA12-1	Siliceous	Calcareous	50/70	4.5	–	–
PA12-2	Siliceous	Calcareous	50/70	4.5	Cement	–
PA12-3	Siliceous	Calcareous	PMB 45/80-60	4.5	Cement	–
PA12-4	Siliceous	Calcareous	PMB 45/80-60	4.5	Cement	0.3
PA12-5	Siliceous	Calcareous	PMB 45/80-60	5	Cement	–
BBTM8B-1	Porphyritic	Calcareous	50/70	5	Cement	–
BBTM8B-2	Porphyritic	Calcareous	PMB 45/80-60	5.5	Cement	–
BBTM11-1	Porphyritic	Calcareous	50/70	5	Cement	–
BBTM11-2	Porphyritic	Calcareous	PMB 45/80-60	5	Cement	–

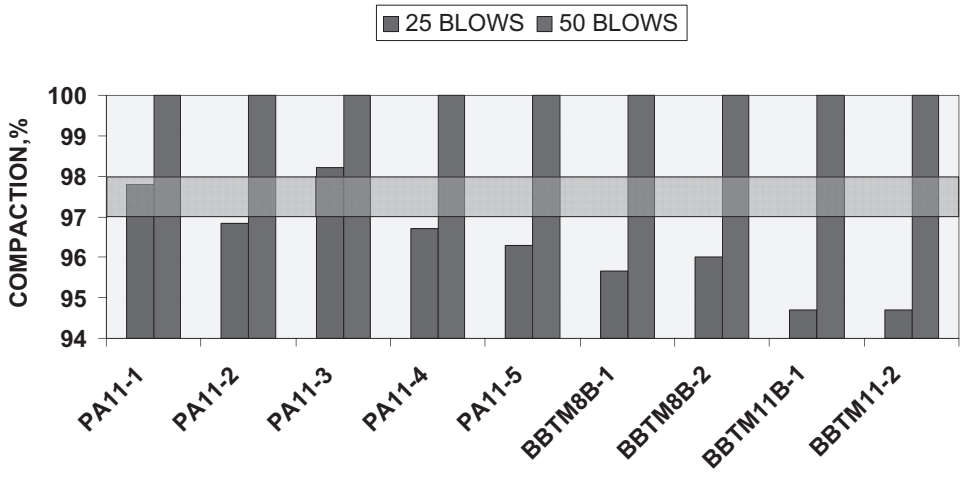

Figure 3. Compaction level obtained for PA and BBTM mixtures.

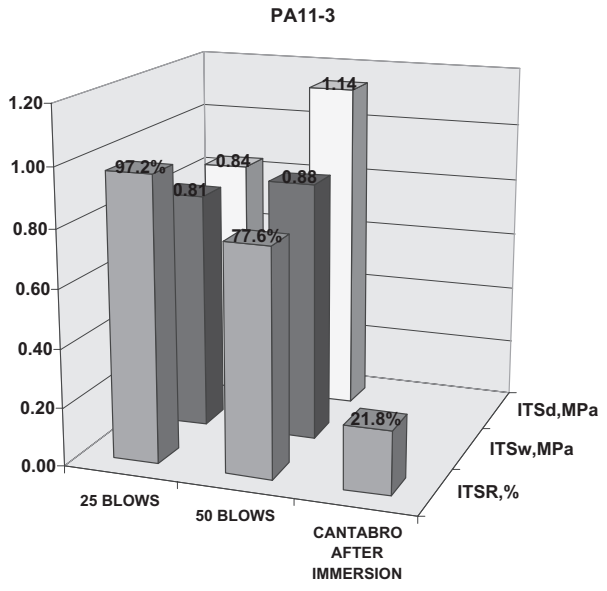

Figure 4. Water effect on mixture PA11-3.

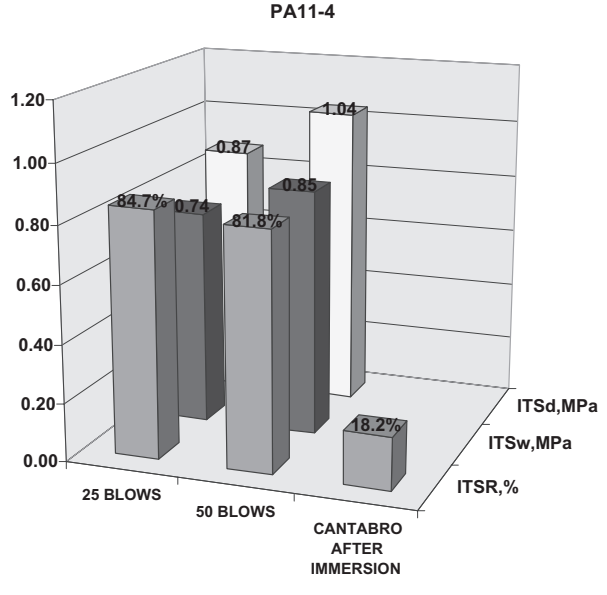

Figure 5. Water effect on mixture PA11-4.

From these results it is concluded that, in water sensitivity tests, indirect tensile strength increases when the compaction level increases, for both dry and wet specimens. However, there is no clear increasing trend for the ITSR with the compaction level increase. For this reason and considering that water sensitivity test result is expressed as a ratio between two strengths (ITSR), the 50-blow compaction proposed is valid since compaction level does not seem to significantly affect the test result.

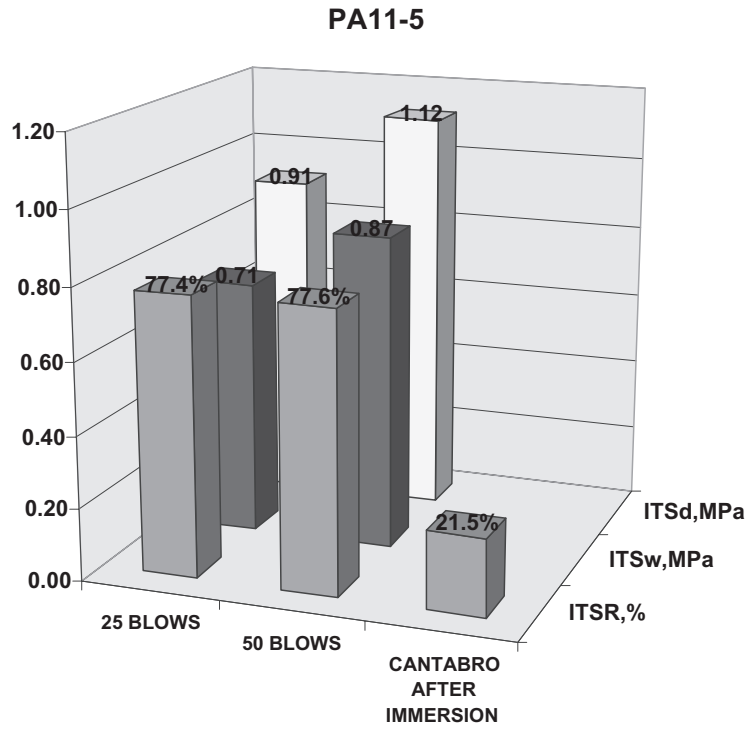

Figure 6. Water effect on mixture PA11-5.

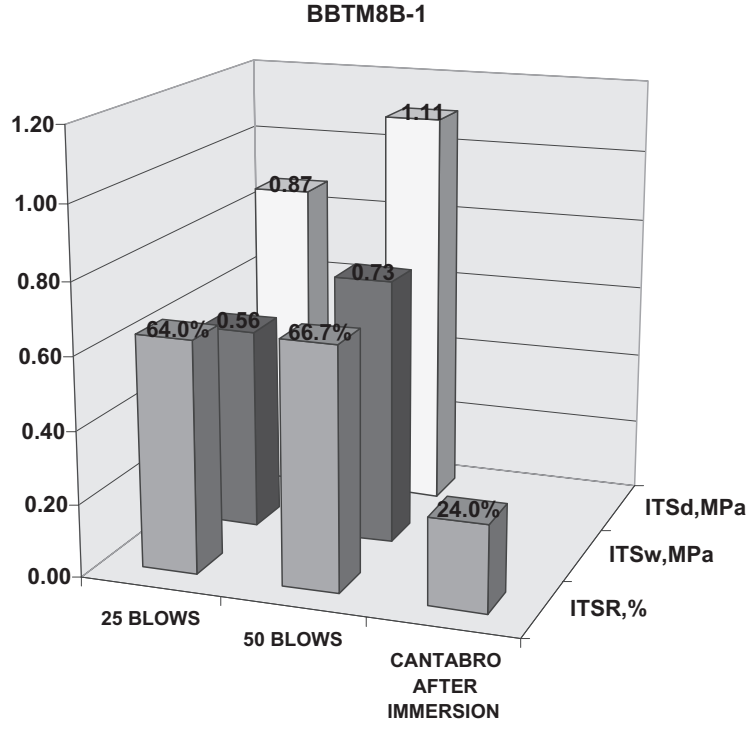

Figure 7. Water effect on mixture BBTM8B-1.

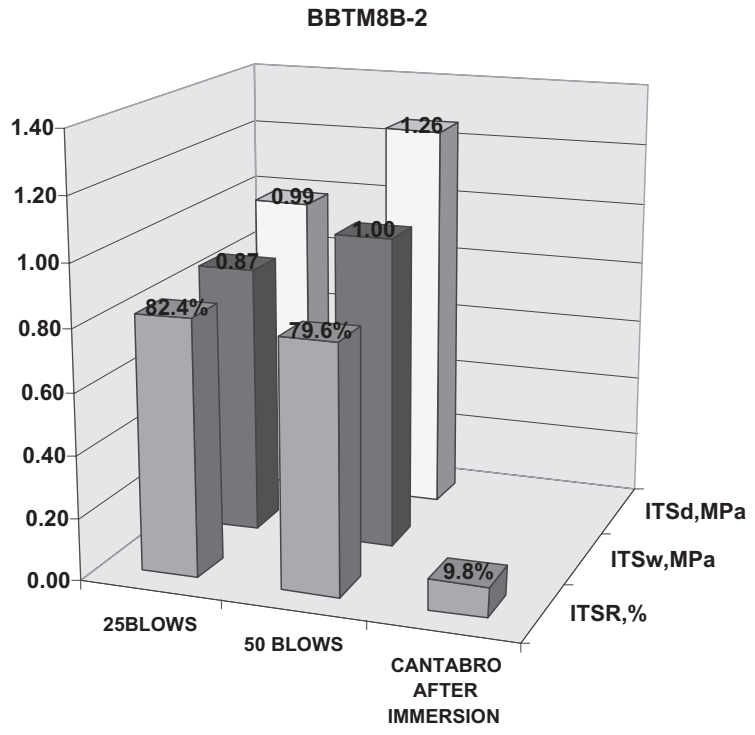

Figure 8. Water effect on mixture BBTM8B-2.

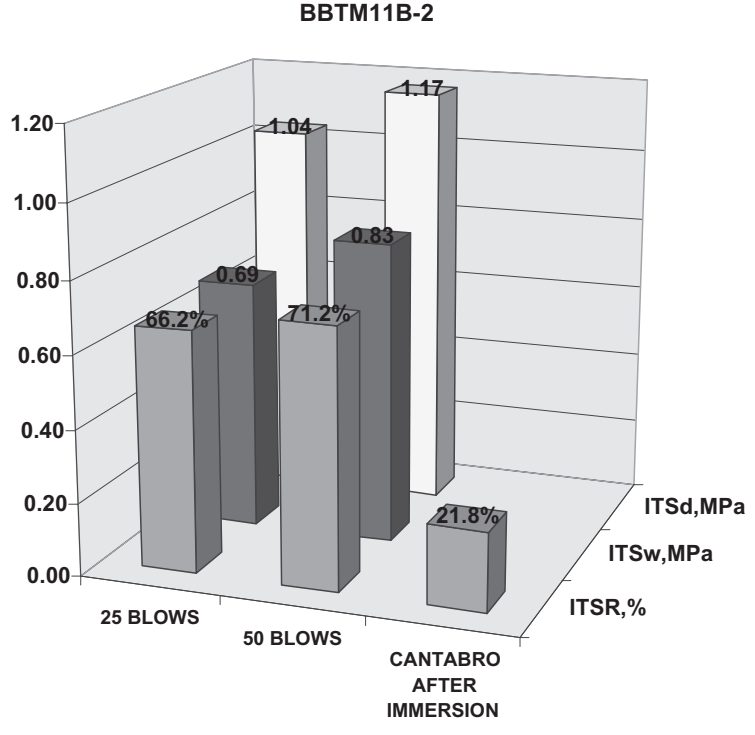

Figure 9. Water effect on mixture BBTM11B-2.

3.2 *Assessment of water effect through water sensitivity and Cántabro after immersion tests*

Once the compaction method and conditions were determined, a series of specimens of porous asphalt (PA) and gap-graded mixtures (BBTM) were manufactured with granite coarse aggregate, calcareous fine aggregate and different percentages of bitumen. Two different fillers have been used: calcareous dust, which is commonly used in Spain, and hygrophilous plastic kaoline. Water sensitivity and Cántabro after immersion tests have been used to measure the effects of water on the different mixtures behaviour. Table 2 shows the characteristics of the tested mixtures.

Test results are shown in table 3 and are plotted in figures 10 and 11.

The results show for both tests that water damage resistance increases when bitumen content does. Filler quality is the most influential factor in both tests. A slightly higher water resistance in BBTM than in PA was observed, being the later ones the mixtures with the higher voids content.

Table 2. PA and BBTM mixtures composition.

Reference	Coarse aggregate	Fine aggregate	Bitumen type	Bitumen content (%)	Filler type
PA12-6	Granite	Calcareous	50/70	4	Calcareous
PA12-7	Granite	Calcareous	50/70	5	Calcareous
PA12-8	Granite	Calcareous	50/70	6	Calcareous
PA12-9	Granite	Granite	50/70	4	Plastic kaoline
PA12-10	Granite	Granite	50/70	5	Plastic kaoline
PA12-11	Granite	Granite	50/70	6	Plastic kaoline
BBTM11B-3	Granite	Calcareous	50/70	4	Calcareous
BBTM11B-4	Granite	Calcareous	50/70	5	Calcareous
BBTM11B-5	Granite	Calcareous	50/70	6	Calcareous
BBTM11B-6	Granite	Granite	50/70	4	Plastic kaoline
BBTM11B-7	Granite	Granite	50/70	5	Plastic kaoline
BBTM11B-8	Granite	Granite	50/70	6	Plastic kaoline

Table 3. Test results of PA and BBTM mixtures.

Reference	Bitumen type	Bitumen content (%)	Filler type	ITSR (%)	Cántabro after immersion (%)
PA11-6	50/70	4	Calcareous	60.6	82.0
PA11-7	50/70	5	Calcareous	75.2	45.8
PA11-8	50/70	6	Calcareous	89.1	21.2
PA11-9	50/70	4	Plastic kaoline	48.7	96.6
PA11-10	50/70	5	Plastic kaoline	66.7	72.4
PA11-11	50/70	6	Plastic kaoline	80.7	28.5
BBTM11B-3	50/70	4	Calcareous	60.4	49.5
BBTM11B-4	50/70	5	Calcareous	86.9	22.3
BBTM11B-5	50/70	6	Calcareous	87.6	10.9
BBTM11B-6	50/70	4	Plastic kaoline	43.3	95.8
BBTM11B-7	50/70	5	Plastic kaoline	58.3	55.4
BBTM11B-8	50/70	6	Plastic kaoline	87.0	16.5

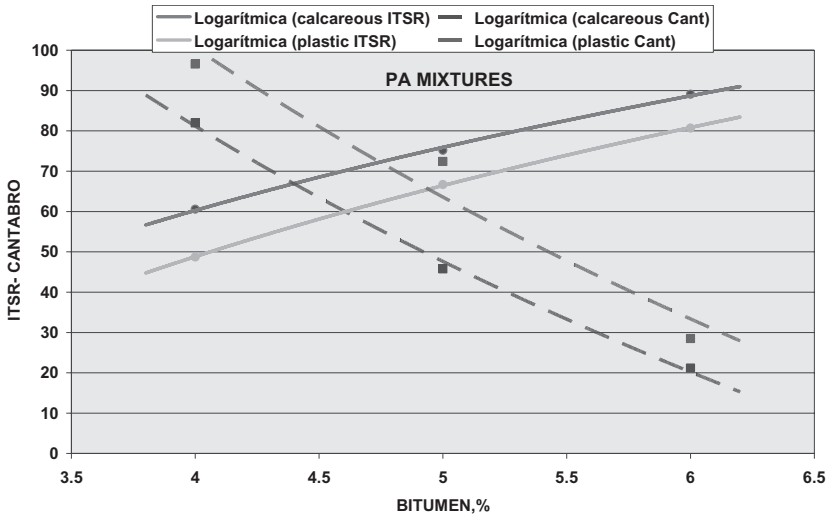

Figure 10. Variation of water sensitivity and Cántabro tests with the filler type and the bitumen content. PA mixtures.

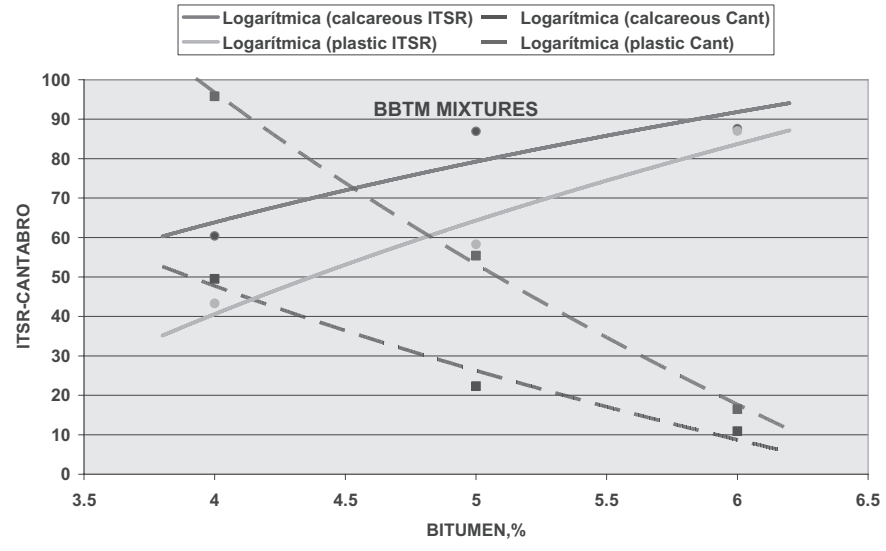

Figure 11. Variation of water sensitivity and Cántabro tests with the filler type and the bitumen content. BBTM mixtures.

Nevertheless, Cántabro losses vary considerably with the bitumen content and the filler type. Cantabro losses range between 10 and 97%, while ITSR varies in an interval from 43 to 87%. These results show that Cántabro test is more sensitive for the assessment of water damage in open bituminous mixtures.

3.3 *Correlation between both tests*

A correlation between water sensitivity and Cántabro after immersion tests was done, with the aim of determining the threshold for the European method. So, using the results from

table 4, Cántabro after immersion losses were plotted against ITSR obtained through water sensitivity test, as can be seen in figure 12.

These results show that there is a relatively high correlation ($R^2 = 0.77$) between Cántabro after immersion losses and ITSR. The maximum values of Cántabro after immersion losses required in the Spanish Highway Technical Specifications (PG-3) to assess water effect in BBTM and PA, are 25% and 35%, respectively. According to the regression line obtained in figure 12, these requirements are equivalent to an ITSR of 82% and 77% approximately.

Table 4. Test results of all PA and BBTM mixtures.

Reference	Bitumen type	Bitumen content (%)	Filler type	Dope (%)	ITSR (%)	Cántabro after immersion (%)
PA11-1	50/70	4.5	–	–	58.5	90.0
PA11-2	50/70	4.5	Cement	–	65.9	65.1
PA11-3	PMB 45/80-60	4.5	Cement	–	77.6	21.8
PA11-4	PMB 45/80-60	4.5	Cement	0.3	81.8	18.2
PA11-5	PMB 45/80-60	5	Cement	–	77.6	21.5
PA11-6	50/70	4	Calcareous	–	60.6	82.0
PA11-7	50/70	5	Calcareous	–	75.2	45.8
PA11-8	50/70	6	Calcareous	–	89.1	21.2
PA11-9	50/70	4	Plastic kaoline	–	48.7	96.6
PA11-10	50/70	5	Plastic kaoline	–	66.7	72.4
PA11-11	50/70	6	Plastic kaoline	–	80.7	28.5
BBTM8B-1	50/70	5	Cement	–	66.7	24.0
BBTM8B-2	PMB 45/80-60	5.5	Cement	–	79.6	9.8
BBTM11B-1	50/70	5	Cement	–	68.1	52.6
BBTM11B-2	PMB 45/80-60	5	Cement	–	71.2	21.8
BBTM11B-3	50/70	4	Calcareous	–	60.4	49.5
BBTM11B-4	50/70	5	Calcareous	–	86.9	22.3
BBTM11B-5	50/70	6	Calcareous	–	87.6	10.9
BBTM11B-6	50/70	4	Plastic kaoline	–	43.3	95.8
BBTM11B-7	50/70	5	Plastic kaoline	–	58.3	55.4
BBTM11B-8	50/70	6	Plastic kaoline	–	87.0	16.5

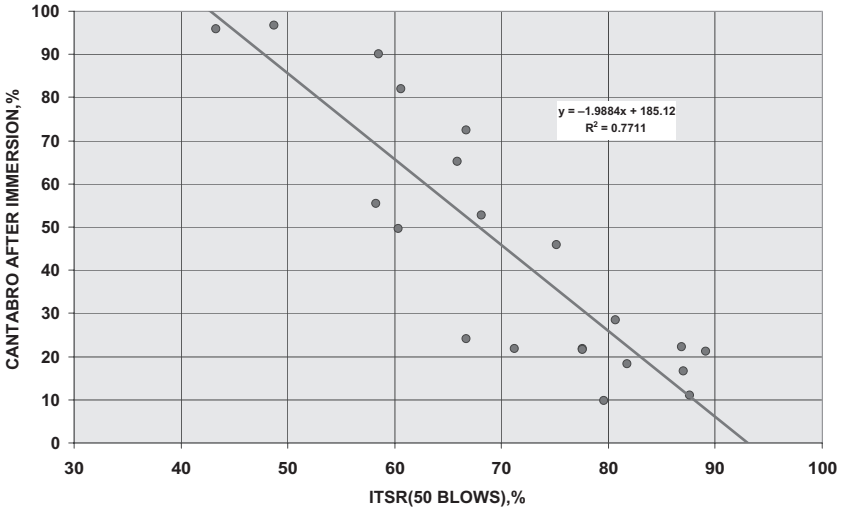

Figure 12. Correlation between water sensitivity and Cántabro tests.

Considering that PA and BBTM are the mixtures for wearing courses most frequently used in roads with high heavy-vehicle traffic (traffic intensity ranging from more than 4000 to 800 heavy vehicles per day) and the high voids content in these mixtures, a minimum 90% of ITSR for BBTM and 85% for PA was proposed. This threshold is necessary to ensure a good performance in presence of moisture, although in some cases the use of dopes to improve adhesion is required to fulfill this minimum requirement. The additional cost of adding between 1 and 3 kg of additive per ton of bitumen does not mean a significant increase in the cost of polymer modified bituminous mixture.

4 CONCLUSIONS

According to the results of this study aimed to compare water sensitivity and Cántabro after immersion tests, the following conclusions can be drawn:

- Marshall method has been considered as the more appropriate compaction procedure to manufacture the specimens for assessing water sensitivity. In order to reach the values of the field bulk density the specimens must be compacted by 50 blows per face.
- Experimental results obtained through water sensitivity test show that both dry and wet indirect tensile strength increase with the compaction level. However, there is no clear trend of the ITSR percentage increase when the compaction level rises, as dry and wet (after immersion) indirect tensile strengths show.
- The ITSR in this water sensitivity test decreases when bitumen content drops and hygrophilous filler is used. Nevertheless, ITSR variations are lower than Cántabro losses, thus showing the greater sensitivity of Cántabro test to assess the behaviour of mixtures in presence of moisture.
- Considering the specific characteristic of these mixtures, the obtained regression lines allow to propose a minimum value for ITSR, namely, 90% for BBTM and 85% for PA.
- The proposed requirements should be confirmed with those obtained by producers doing the CE marking of their mixtures, although these suggested values should be considered definitive once the mixtures behaviour is evaluated at full scale.

ACKNOWLEDGEMENTS

The authors would like to acknowledge the funding support from the Dirección General de Carreteras del Ministerio de Fomento, as well as thank to Mr. A. Viñuales, H. Muñoz and E. Corrochano for their cooperation at the experimental stage of this study.

REFERENCES

EN 12697-12, 2003. Bituminous mixtures—Test methods for hot mix asphalt—Part 12: Determination of the water sensitivity of bituminous specimens. European Committee for Standardization.

EN 12697-30, 2007. Bituminous mixtures—Test methods for hot mix asphalt—Part 30: Specimen preparation, impact compactor. European Committee for Standardization.

Mezclas bituminosas en caliente 2004. Artículo 542, Pliego de Prescripciones Técnicas Generales para Obras de Carreteras y Puentes, PG-3, Orden FOM/891/2004, Ministerio de Fomento.

Mezclas bituminosas discontinuas en caliente para capas de rodadura 2004. Artículo 543, Pliego de Prescripciones Técnicas Generales para Obras de Carreteras y Puentes, PG-3, Orden FOM/891/2004, Ministerio de Fomento.

NLT-162/00, 2000. Efecto del agua sobre la cohesión de las mezclas bituminosas compactadas (Ensayo de inmersión-compresión)" Normas NLT I.- Ensayos de carreteras, CEDEX.

NLT-352/86, 1986. Caracterización de mezclas bituminosas abiertas por medio del ensayo cántabro de pérdida por desgaste, Normas NLT I.- Ensayos de carreteras, CEDEX.

Advanced Testing and Characterization of Bituminous Materials –
Loizos, Partl, Scarpas & Al-Qadi (eds)
© 2009 Taylor & Francis Group, London, ISBN 978-0-415-55854-9

Moisture damage on bituminous stabilized materials using a MIST device

M.E. Twagira & K.J. Jenkins
University of Stellenbosch, South Africa

ABSTRACT: Several laboratory procedures for the determination of moisture sensitivity of pavement materials are used globally. However, current methods of saturation followed by mechanical evaluation after conditioning, yield both variable and unreliable residual strength ratios when compared with retained stiffness test results. This paper presents a new developed simple device, called moisture induction simulation test (MIST) to assess moisture-induced damage based upon cyclic pulsing of water, at pressure, into a triaxial specimen. The study investigates different saturation levels with experimental determination of stiffness ratio (Mr) and shear parameters (c and φ) of bitumen stabilized materials (BSMs) i.e. with foamed bitumen or emulsion binder. Mix compositions of aggregate blends with and without RAP, with different bitumen binder types and the influence of additional active filler (cement or lime) are investigated. The rating of moisture induced damage by MIST device on BSMs is discussed. Test results are validated with the known laboratory model mobile load simulator (MMLS3) device. The study found that the accelerated moisture induction process using the MIST device has potential for use as a tool to condition BSMs specimens. The use of static triaxial mechanical testing to determine moisture damage in terms of the residual cohesion at maximum saturation levels shows better ranking of mixture in term of moisture damage than, for example, a tensile strength retained (TSR) test. The validation of MIST device test results with laboratory MMLS3 device shows agreeable ranking of BSMs.

1 INTRODUCTION

Durability of BSMs depends on, amongst other factors, resistance to moisture-induced damage. This is due to thin film of bitumen binder dispersed in BSMs with only partial coating of large aggregates, lower binder content in the mix relative to HMA, the presence of moisture in the mix and high air void contents. The consequences of moisture damage on BSMs in the field have been reported. Chen et al. (2006) reports failure on full-depth recycling (FDR) foamed asphalt in Highway 82 Texas, Ramanujan and Jones (2007) failure of FDR foamed asphalt in Cunningham Highway in Australia, and Fu et al. (2007) reported failure of FDR foamed asphalt in California. According to Fu *et al*. all reported failures resulted from poor drainage and infiltration/suction of subgrade moisture to the BSMs layer. Similar distress due to suction of seepage ditch water, patched water table and unpaved shoulder has been modelled by Birgisson and Bryon (2003). The saturated condition of BSMs layer slightly above optimum moisture content (OMC) resulted to severe alligator cracking and rutting of the surfacing layer. Several laboratory procedures have been applied for the identification of BSMs with unacceptably high moisture sensitivity (Birgisson et al. 2003, De Beer 1989, Jenkins 2000 & Long et al. 2003). Generally, these procedures stem from early findings of the Asphalt Institute (1992), where the moisture conditioning for mix assessment was carried out using vacuum saturation of the compacted and cured specimen, in order to accelerate any possible moisture damage. The conditioned and unconditioned specimens are then compared in terms of retained strength, e.g. TSR obtained after Indirect Tensile strength (ITS), or from Unconfined Compressive Strength (UCS) or Indirect Tension Test (ITT). Although

this approach provides an empirical measure of moisture damage, it yields both variable and unreliable ratio in comparison with retained stiffness test results.

The new laboratory-based testing procedure and analysis protocol for the evaluation of moisture damage, considered more representatives of field conditions, was developed at Stellenbosch University. Although the laboratory simulation cannot be an exact replication of mechanisms that manifest in service, it should represent the fundamental or key failure mechanism for the BSMs, unlike previous, over-simplified procedures.At the same time, a simplified, reliable, and cost effective procedure is required for both research and classification testing of moisture susceptibility. In this study a testing and evaluation framework was based on the new MIST device that was developed. The moisture conditioning and mechanical testing (short dynamic and static tests) were applied for determining the level of moisture damage in the BSMs. The influence of saturation levels on stiffness ratio (Mr) and shear parameters (c and φ) were investigated. These parameters are critical for the performance prediction of the BSMs. Several types of aggregate blends, with and without RAP, with foamed bitumen or bitumen emulsion binders, were investigated. The rating of the severity of moisture related damage on the selected mixes, using the MIST test is discussed and validation of MIST test results with a laboratory MMLS3 (APT) device is presented. The influence and effect of the addition of active filler (cement or lime) in the selected mixes was also investigated.

2 EXPERIMENTAL PROGRAM

2.1 *Materials*

Two selected materials types were used in this study, i.e. reclaimed asphalt pavement, Hornfels-RAP, and crushed virgin Quartzites (G4)[1]. The grading of the aggregates has maximum aggregate size of 19 mm and percent passing 0.075 mm of 10% and 6% respectively. Selected materials were stabilized in the laboratory with either foamed bitumen or bitumen emulsion binder. Two percent (2%) net bitumen content was applied on both Hornfels-RAP and Quartzite materials. The addition of 0% or 1% active filler (i.e. cement or lime) was also applied on the selected materials. The constitution of tested mixes led into 12 mixes. Table 3 shows the matrix of the tested mixes.

2.2 *MIST device conditioning and testing*

MIST device was developed to evaluate the effect of moisture damage in the BSMs, while simulating the field pulsing conditions applied due to load repetitions. The essence of developing MIST conditioning procedure is to ensure repeatability and reproducibility of moisture damage for testing. Similar test procedures can be adopted for screening moisture susceptibility of other pavement materials such as hot mix asphalt (HMA) and cement treated materials (CTM), however testing parameters for fluid saturation would require

Table 1. Constituted mix type and testing matrix.

	Aggregates type	
Binder type	Hornfels-RAP + 2% net bitumen*	Quartzite + 2% net bitumen*
A—Emulsion	Mix 1: 0% active filler	Mix 7: 0% active filler
	Mix 2: 1% cement	Mix 8: 1% cement
	Mix 3: 1% lime	Mix 9: 1% lime
B—Foamed bitumen	Mix 4: 0% active filler	Mix 10: 0% active filler
	Mix 5: 1% cement	Mix 11: 1% cement
	Mix 6: 1% lime	Mix 12: 1% lime

*Net bitumen is residual binder after evaporation of water on foamed bitumen and bitumen emulsion.

[1]G4 is South African classification system of crushed or natural gravel (TRH14, 1985).

re-evaluation. The MIST testing procedure has the following major subsystems: 1) fluid saturation subsystem by pulsing moisture into triaxial specimen. 2) loading sub-system using material testing system (MTS) .

2.2.1 *Fluid conditioning*

Six triaxial specimens (250 mm × 150 mm) were prepared for each mix. Preparation of tri-axial specimens is done by compacting 50 mm layers in a mould of 150 mm diameter, using BOSCH® vibratory hammer. Compacted specimens are cured in draft oven at 30ºC for 20 hours followed by 40ºC sealed in a thin plastic bag for 72 hours (Jenkins et al. 2008). After compaction and curing, the specimens are grouped into a set of two, with approximately equal void content (P_a). The void contents are calculated after determining the specimen bulk relative density (BRD) and mix maximum theoretical relative density (Rice). The first set comprises three specimens for wet conditioning and static (monotonic) test, and the second set comprise three for dry (un-conditioning) static (monotonic) test.

The test variables of the MIST device are set at 0.54 sec load time, and 1.40 sec rest period. The pulsing water pressure is set at 140 kPa. The study on hydrodynamic force on seal surface conducted in New Zealand (2005) indicates that a vehicle travelling at 80 km/h can create hydraulic pressure under the seal with a magnitude of 140 kPa. Fluid conditioning for the MIST is done in triaxial cell after placing and assembling the specimen as shown in Figure 1.The conditioning variables were selected and related to the test setting of the MMLS3 scaled accelerated pavement tester (APT) device, where BSMs were tested further. After MMLS3 trials the test variables appeared to be agreeable as the ranking of the BMSs concurred with that of the MIST device, this validating the latter's procedure.

After MIST conditioning, the following specimen volumetric properties are determined. Volume of air voids (V_a) in specimen [cm^3],

$$V_a = \frac{P_a \times E}{100} \tag{1}$$

Volume of water absorbed (V_w) in specimen [cm^3],

$$V_w = B - A \tag{2}$$

Degree of saturation (S_r) in specimen [%],

$$S_r = \frac{V_w}{V_a} \times 100 \tag{3}$$

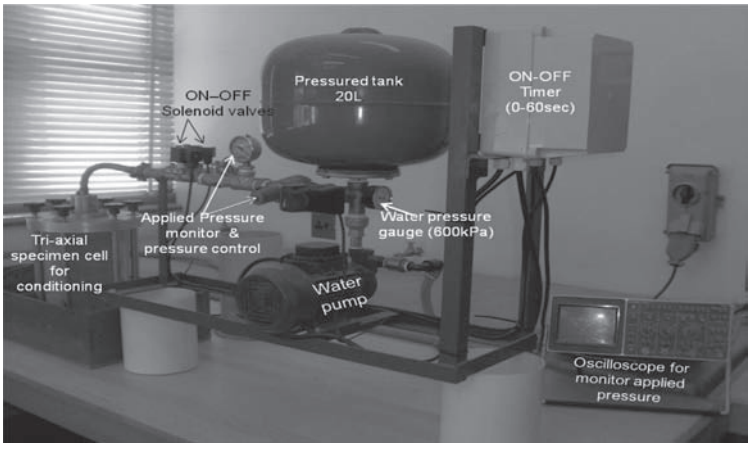

Figure 1. MIST device features and conditioning set-up.

where B = weight of saturated-surface dry specimen [g]; A = weight of dry specimen in air [g]; P_a = air void content in specimen [%]; E = volume of specimen [cm^3].

The degree of saturation should be at least 80% for accurate screening of the BSMs.

2.2.2 *Determination of retained cohesion and residual stiffness ratio*

Mechanical testing follows the MIST conditioning. Mechanical triaxial testing is performed using the MTS, see Figure 2, to determine the shear parameters (c and φ) and stiffness properties (Mr). The detailed testing procedure is performed in accordance with the procedure developed by Stellenbosch University (2005). One set of three specimens with predetermined height and approximately equal void content is tested using static (monotonic) loading at 50 kPa, 100 kPa, and 200 kPa confining pressures. Another set of three specimens is tested unconditioned at 50 kPa, 100 kPa, and 200 kPa confinements. The applied rate of loading is 2.1 mm/min. Retained cohesion ratio is calculated as follows:

$$Retained\,Cohesion,\ (RC) = \frac{Cohesion\ of\ wet\ mix, (CoW)}{Cohesion\ of\ dry\ mix, (CoD)} \times 100 \tag{4}$$

where, cohesion of wet and dry mix calculated from Mohr Coulomb cycle as per Equation 5.

$$\sigma_{1f} = \frac{1+\sin\varphi}{1-\sin\varphi}\sigma_3 + \frac{2.C.\cos\varphi}{1-\sin\varphi} \tag{5}$$

where, σ_{1f} = Maximum principal stress at failure [kPa], σ_3 = confining pressure [kPa], φ = internal angle of friction of the mix [deg], C = cohesion of the mix [kPa].

One set on six specimens grouped in section 2.2.2 above are tested using short dynamic (resilient) loading. The short dynamic test is non-destructive test. Therefore, it is performed on specimens prior to monotonic testing. The short dynamic (resilient) test is performed in accordance with the procedure developed in Stellenbosch University (2005). Conditioned and unconditioned sets of specimens are tested at a Stress Ratio of 10% and confinement pressure of 50 kPa at ambient temperature (25ºC). The lower values of stress ratio and confinement pressure were selected to minimize the effect of pore water pressure in the conditioned specimens. Three external LVDTs are mounted on the triaxial cell to measure recovered displacement.

After the application of 5000 load cycles, the specimen is conditioned in the MIST device at different saturation levels, i.e. 50%, 80% and 100% then the Resilient Modulus determined. For un-conditioned specimens, the dry Resilient Modulus is determined after application of 5000 load cycles. After Resilient Modulus tests, static (monotonic) tests are carried out on the same specimen at a confining pressure of 100 kPa to determine the shear properties (c and φ) of the conditioned and unconditioned sets of specimens. Residual Modulus ratio is calculated as follows:

$$Residual\ Modulus, (RM) = \frac{Resilient\ Modulus\ at\ S_r(100\%)}{Resilient\ Modulus\ of\ dry\ mix} \times 100 \tag{6}$$

where, S_r = Degree of saturation [%], Dry mix = Mix at equilibrium moisture content.

Ranking of mixtures in term of moisture damage severity is determined from the calculated ratios. The BSMs with high ratio show good resistance to moisture damage and BSMs with lower ratio shows poor resistance to moisture damage. A ratio in between can be ranked as medium to good or medium to poor. These ranking results on BSMs are then validated with laboratory MMLS3 which is setup at corresponding variables of 1.4 kN axial load, 420 kPa tyre pressure and full speed of 7200 wheel loads/hr. These variables are equivalent to light truck, hence minimal damage on BSMs and possible extended test duration. In addition to these variables a thin vinite layer was introduced at the interface of tyre and BSMs surface for the same purpose of minimizing tyre damage during wet trafficking. Illustrative MMLS3 test set-up is indicated in Figure 3 below.

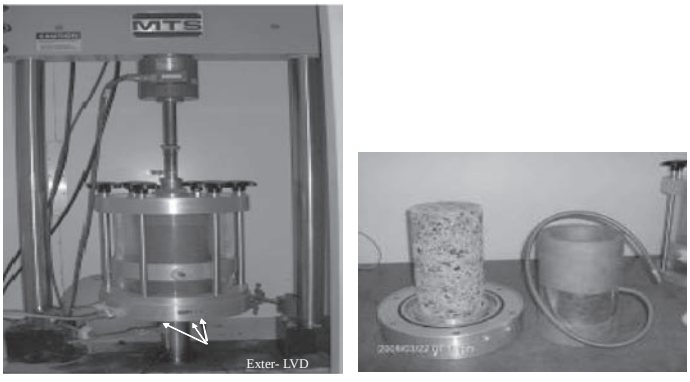

Figure 2. MTS loading system and triaxial specimen membrane fitting.

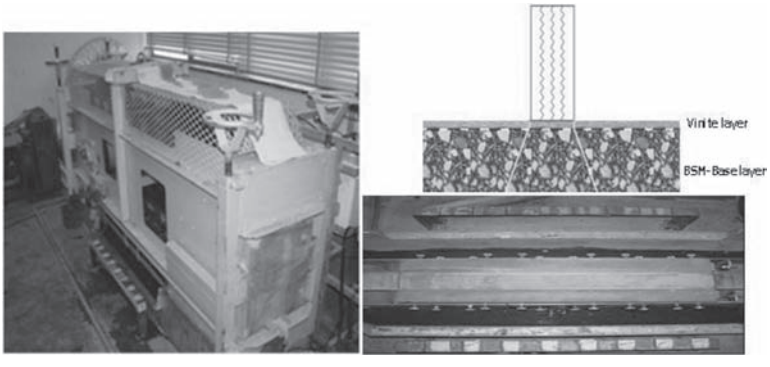

Figure 3. Illustration of MMLS3 test set-up including details of vinte installation.

3 RESULTS AND DISCUSSION

The particle inter-lock, particle type, and binder content determine the steady state saturation level of the BSMs. The mixes with high void contents show higher damage due to access of moisture during pulsing time. Table 2 shows the pulsing time and void content to achieve steady saturation level. The saturation level can be related to the OMC of the mixes. From the results in Table 2, it is evident that moisture susceptible mixes show early damage during saturation. BSMs produced from Quartzites had lower moisture contents at saturation before damage occurred. The causes of damage are; firstly higher void content and secondly, low cohesion and adhesion of binder to mix. These factors contribute significantly to the serious erosion during pulsing of water pressure into specimen.

The steady state of saturation in this study was determined by checking that there is no change in bulk mass on specimen on consecutive numbers of pulsing cycles (i.e. prohibiting more moisture ingress in a specimen) or where severe damage occurred on specimen. Aggregate type also contributes to the saturation level. Quartzitic aggregate particles show less ability to retain moisture. Although some of the Quartzites mixes are less moisture susceptible, but their steady saturation level is less than the OMC, see Table 2 and Figure 3. This is attributed to the glassy type of particles, which are resistant to moisture absorption. For the Hornfels-RAP aggregate types, the retention of moisture was approximately at OMC for both moisture susceptible mixes and less moisture susceptible mixes. OMC of BSMs is estimate to be 80% steady saturation level.

Table 2. MIST conditioning time and related retained cohesion and residual stiffness on different BSMs.

BSM-foam and BSM-emulsion	Pulsing time [min]	Rice density [Kg/m^3]	Bulk relative density [Kg/m^3]	Voids content [%]	Saturation level relative to % OMC	Steady saturation level [%]	Retained cohesion ratio [%]	Residual modulus ratio [%]
H+0C-F	1.1	2590	2177	16.0	73	73	–*	–
H+1C-F	3.6	2593	2332	13.5	102	90	–	62
H+1L-F	3.2	2592	2241	14.0	109	99	–	100
Q+0C-F	1.3	2572	2149	16.5	48	48	30.7	52
Q+1C-F	1.6	2573	2196	14.6	62	62	66.0	68
Q+1L-F	1.6	2561	2198	14.5	61	61	68.4	90
H+1C-E	9.7	2577	2215	14.0	114	100	74.1	79
H+1L-E	6.5	2694	2237	13.0	112	100	62.2	76
Q+0C-E	1.3	2540	2139	15.8	60	60	–	53
Q+1C-E	9.7	2516	2201	12.5	78	78	72.3	76
Q+1L-E	5.5	2584	2273	12.0	87	87	81.8	71

*(–) Incomplete results.
H = Hornfels; Q = Quartzite; L = Lime; C = Cement; F = Foam; E = Emulsion.

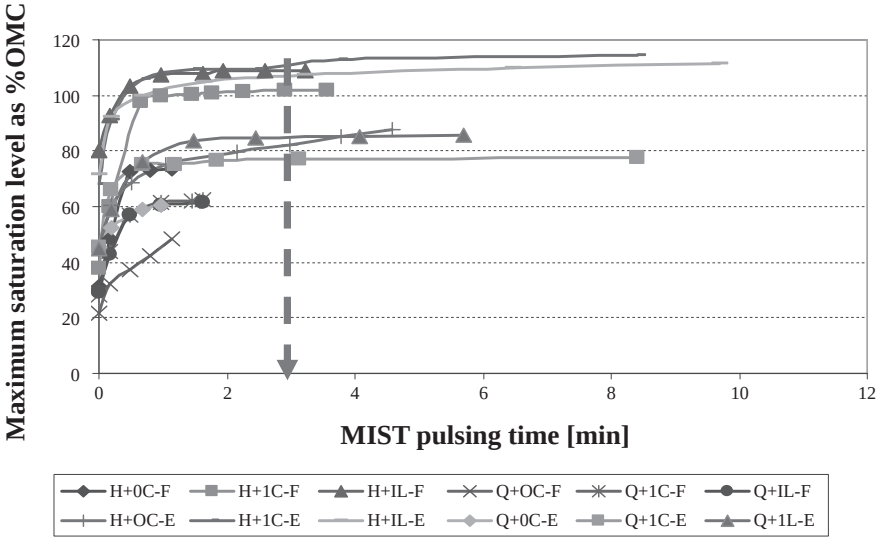

Figure 4. Saturation level after MIST conditioning on different BSMs.

From Figure 3, it is certain that most BSMs will attain steady state moisture saturation after 3.2 minutes of pulsing time or 100 pulsing cycles. Although saturation graphs begin to plateau after 2 minutes of pulsing time, this could be regarded as threshold for the highly moisture susceptible mixes, because high spalling from specimen occurs and signs of severe damage is observed. However to ensure reliable screening of BSM moisture susceptibility a threshold of 3.2 minutes of pulsing time or 100 pulsing cycles was identified. BSMs that cannot withstand the threshold are regarded highly susceptible to moisture damage. Therefore, their selection in the mix design needs proper consideration; while BSMs, which can withstand the threshold value, justify selection in the mix design.

The difference in MIST pulsing cycles (time) on BSMs, relates well with the residual cohesion determined by static and dynamic triaxial tests, see Table 2 & Figure 4. The BSMs that withstand higher number of pulsing cycles show high residual cohesion. While the BSM-mixes that withstand lower pulsing cycles show lower cohesion values. The influence and effect of the addition of active filler (cement or lime) is apparent in Figure 4. BSMs with the addition of active filler show higher moisture resistance, compared to mixes without additional of active filler.

By using the MIST threshold values, the following ranking criteria Table 3 are proposed for the BSMs mix design in relation to moisture damage. The classification of three different types of Bitumen Stabilized Materials is consistent with the new guidelines currently being developed in South Africa, where BSM1 will be able to withstand the highest levels of traffic.

Figure 5 shows the comparison of BSM-foam and BSM-emulsion stiffness reduction due to ingress of moisture in the mix. The ingress of moisture in BSM-foam has more effect on stiffness reduction than BSM-emulsion. However, the addition of active filler in the BSM-emulsion has significant contribution to its stiffness retention even after the ingress of water. Some interesting behaviour is noted with addition of lime to the BSM-foam and BSM-emulsion. The anti-stripping behaviour of lime causes an increase in Resilient Modulus as saturation levels of the mixes increase. However, the effect on stiffness reduction occurs at high saturation levels, above the OMC of the mixes. Although this does not apply to all of the mixes with lime, it is a phenomenon that needs to be recognised, when either cement or lime is selected for the BSM mix design.

The use of MIST devices has provided some insight on the failure behaviour of BSM with the ingress of water. The residual cohesion and retained modulus determined after MIST saturation yield results that are consistent with mechanical performance of BSM mixes under different moisture conditions.

Table 3. Recommended retain cohesion after MIST conditioning.

MIST pulsing cycle [no.]	MIST pulsing time [min]	Equivalent residual cohesion percentage [%]	Possible equivalent design material
100	3.2	≥75	BSM 1
		≥60	BSM 2
		≥50	BSM 3

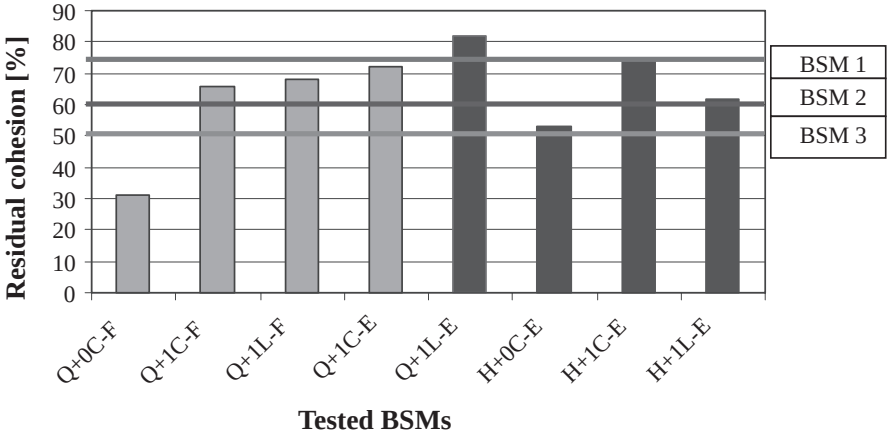

Figure 5. Retained cohesion of different BSMs and proposed limits.

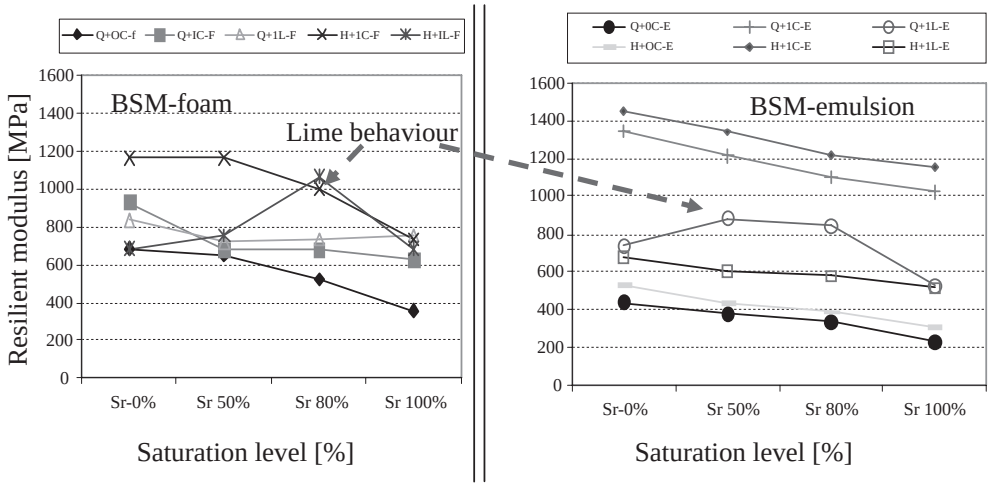

Figure 6. Resilient modulus versus saturation level of BSM-foam and BSM-emulsion.

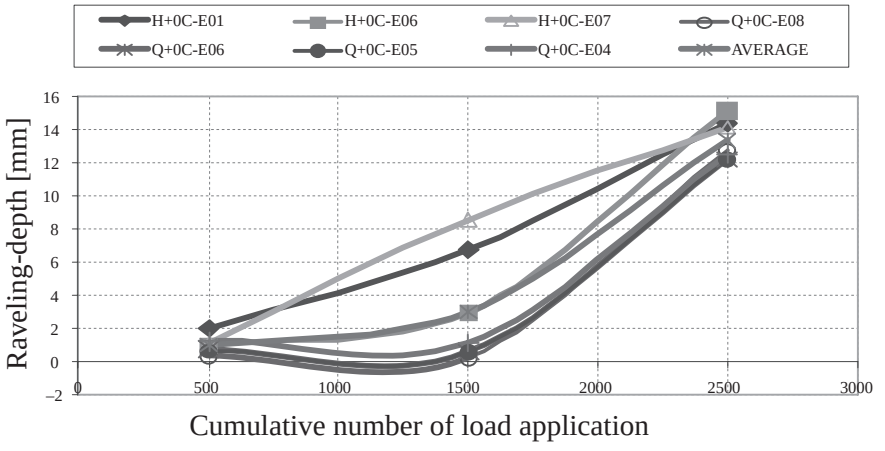

Figure 7. Cumulative ravelling-depth of BSM-emulsion (Quartzite & Hornfels) with no active filler, tested at 25ºC, 1.8 kN, 420 kPa and 7200 w/hr.

The representivity of the performance of BSMs conditioned in the MIST device could not be verified without a correlation test. The selection of MMSL3 scaled accelerated pavement testing device, for correlation tests, takes into account its known performance and ability to simulate field conditions. A similar testing matrix to Table 1for BSMs was prepared for the MMLS3 testing. Sample preparation and testing protocol for MMLS3 test is adequately reported elsewhere (Ebels et al. 2004). Wet and dry trafficking was carried-out to determine the residual tensile strength. The residual tensile strength was determined by carrying out ITS tests. However, ITS tests provide inconsistent results.

In order to find more meaningful relationships, ravelling depth (RvD) determined during MMLS3 wet trafficking was correlated to MIST Residual Cohesion (RC) ratio. Figure 6 presents the cumulative ravelling depth of the BSM-emulsion (Quartzites and Hornfels) without addition of active filler. The mixes were trafficked in wet conditions at 25ºC with MMLS3 axle loads of 1.8 kN, tyre pressures of 420 kPa and trafficking speed of 7200 wheel loads per hour. The average cumulative ravelling depth was 13 mm after 2500 load applications. These results show that BSM-emulsion without active filler is susceptible to moisture damage. Similar

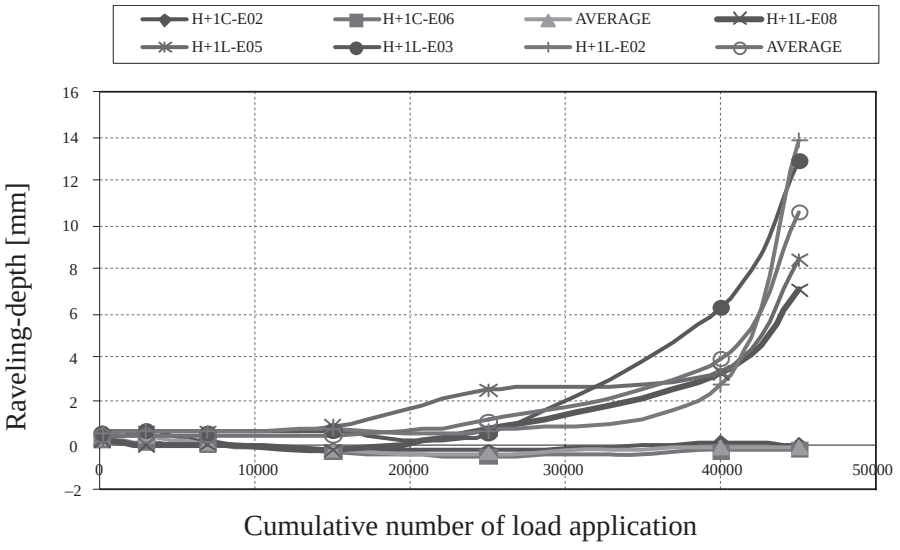

Figure 8. Cumulative ravelling-depth of BSM-emulsion (Hornfels) with 1% cement or lime, tested at 25°C, 1.8 kN, 420 kPa and 7200 w/hr.

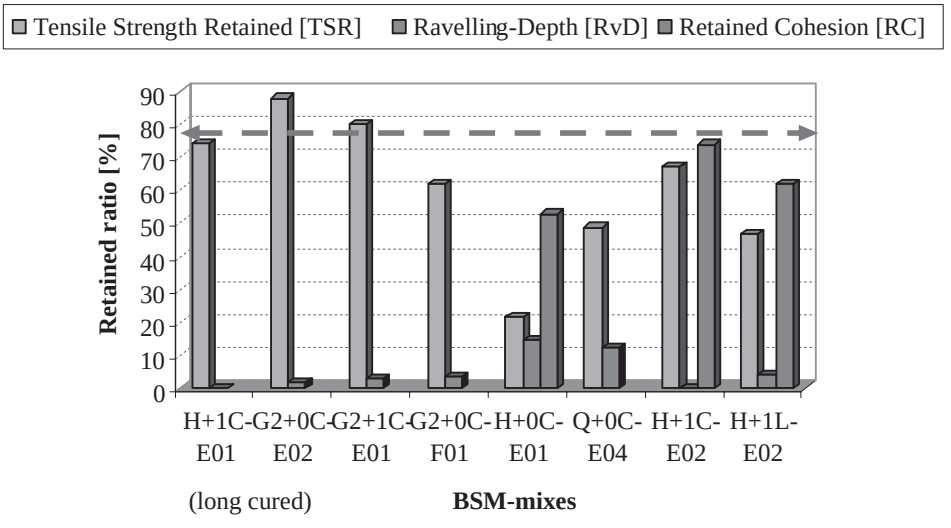

Figure 9. The correlation between TSR, RC and RvD on moisture susceptibility of BSMs.

conclusions were drawn from the residual cohesion ratios determined on MIST saturation and static dynamic test.

The effect of moisture damage during MMLS3 wet trafficking resulted in ravelling (loss of aggregates). No significant edge-heaving occurs in the wheel path, instead, the moisture ingress destroys the cohesion properties of the mixes, and hence aggregate particles become loose. The loss of cohesion and adhesion on the mixes causes spalling of coarse and fine aggregates during traffic loading. The negative values recorded in one briquette Figure 7 shows a sign of initial heaving prior to ravelling of the materials, though this is not a predominant characteristic with other briquettes.

The BSMs with known moisture susceptibility were trafficked first, followed by less moisture susceptible BSMs. Figure 8 presents the cumulative ravelling depth of the BSM-emulsion (Hornfels) with addition of 1% cement or lime. The MMLS3 wet trafficking on BSM-emulsion (Hornfels) with active filler, used test conditions similar to those applied on BSM-emulsion without active filler stated above. The average cumulative ravelling depth of 0.6 mm after 45000 load applications occurred on cement mix; whilst, an average of 10 mm ravelling depth after 45000 load applications occurred on lime mix. These results show that BSM-emulsion with the addition of cement is less susceptible to moisture damage relative to similar mix with addition of lime. Similar conclusions were drawn for the residual cohesion ratios determined on MIST saturation and static dynamic test.

In conclusion, the MMLS3 ravelling depth on wet trafficking of the BSM-emulsion shows good correlation with MIST and short dynamic tests. More testing is underway to be able to correlate ravelling with retained cohesion for each mix in the test matrix.

The comparison in Figure 9 superimposes TSR values, ravelling depths (RvD) from MMLS3 tests as well as Retained Cohesion (RC) ratios. Ranking of BSMs using these test results highlights the empirical nature of the TSR in measuring moisture related resistance of BSMs. TSR ranking criteria show inconsistencies with the other results. Reasonable comparison is obtained from MMLS3 tests and triaxial tests in terms of moisture sensitivity of BSMs. However, only limited results are available at present although more research is in progress.

4 CONCLUSIONS

The performance and fundamental characteristics of BSMs associated with moisture damage have been studied using the MIST device conditioning method, and validated using a known laboratory scaled APT device (MMLS3). Based on the data of the study, the following conclusions are drawn:

- The determined inter-particle voids in the BSM-foam and BSM-emulsion show a range of values of 12% to 17%. BSM-foam shows relatively higher inter-particle voids than BSM-emulsion for the aggregates in question and the same compaction energy.
- The aggregate type, in this case either Hornfels or Quartzites, has no particular affect on differences in voids content of BSMs. However, there is clear increase in the voids content of BSMs without active filler compared to BSMs with the addition of active filler (i.e. lime or cement).
- The MIST conditioning correlated well to moisture susceptibility of the BSMs. It is evident from the results that moisture susceptible mixes show severe damage upon saturation. BSMs with Quartzite aggregates had lower saturation moisture contents before damage occurred. The causes of severe damage are: firstly higher void content and secondly, low cohesion and adhesion of binder to mix. These factors contribute significantly to the serious damage during pulsing of water pressure into the specimen.
- The difference in MIST pulsing cycles (time) on BSMs, relates well to the residual cohesion determined by static dynamic triaxial test. The BSMs that withstand higher number of pulsing cycles show high residual cohesion. While the BSM-mixes that withstand lower pulsing cycles show less cohesion strength.
- From MIST conditioning, it can be seen that most BSMs attain steady-state saturation after 3.2 minutes pulsing time (100 pulsing cycles). Therefore, 3.2 minutes pulsing time or 100 pulsing cycles is threshold to screening of the BSMs. BSMs which can't withstand the threshold are regarded as highly susceptible to moisture damage. Therefore, the selection of such a BSM in the mix design requires proper consideration. While BSMs, which can withstand the threshold value, justify acceptable selection in the mix design.
- The MMLS3 ravelling depth on wet trafficking of the BSM-emulsion shows good correlation with MIST and short dynamic tests. More testing is underway to be able to correlate ravelling versus retained cohesion on each mix on the test matrix.

ACKNOWLEDGMENTS

The Author, wish to acknowledge SABITA and Gauteng Department of Transport and Public works South Africa, for sponsoring this research work.

REFERENCES

Asphalt Institute, 1992. A basic asphalt emulsion manual. Manual Series No 19: 87Second Edition. Lexington, USA.

Birgisson, B., Roque, R. & Page, G.C. 2003. Evaluation of the water damage using Hot Mix Asphalt fracture mechanics. Association of Asphalt Paving Technologists AAPT Volume 72, Kentucky.

Birgisson, B. & Byron E.R. 2003. Improving performance through consideration of terrain conditions (Soils, Drainage, and Climate). Transport Research Record 1819: 369–377.

Chen, D.H. Bilyeu, J. Scullion, T. Nazaria, S. & Chiu, C.T. 2006. Failure Investigation of a Foamed-Asphalt Highway Project. *Journal of Infrastructure Systems*: 33–40.

CSRA, Committee of State Road Authorities. 1985. Guidelines for road construction materials, Technical Recommendations for Highways (TRH) 14, Department of Transport, Pretoria, South Africa.

De Beer, M. 1989. Aspects of erodibility of lightly cementitious materials. Pretoria Division of Roads and Transport Technology. CSIR Research Report DPVT 39, Pretoria.

Ebels L-J, Jenkins K. & Sadzik E, 2004, Investigation into the Correlation of the MMLS3 and HVS Devices, CD-Rom Proceedings Second International APT Conference, Minneapolis, USA.

Fu, P. Harvey, J.T. Jones, D.J. & Bukhari S.A. 2007. Dry and soaked laboratory test for foamed asphalt mixes. Accepted for publication in Transport Research record.

Jenkins, K.J. 2000. Mix design considerations for cold and Half-warm bituminous mixes with emphasis on foamed bitumen. PhD Dissertation, University of Stellenbosch, South Africa.

Jekins, K.J. Ebels L.J, Twagira, M.E. Kelfkens, R.W.C Moloto, P.K. & Mulusa, W.K. 2008. Updating bituminous stabilized materials guidelines. Mix design technical report, Sellenbosch University. South Africa.

Land Transport New Zealand. 2005. The waterproofiness of first coat seal. Research report Style Guide. New Zealand: 35.

Long, F.M. & Ventura, D.F.C. 2003. Laboratory testing for the HVS Sections on the N7 (TR11/1). CSIR Transportek, Contract Report CR-2003/56. Pretoria, South Africa.

Ramanujam, J.M. & Jones. J.D. 2007. Characterization of Foamed-Bitumen Stabilization. International Journal of Pavement Engineering: 111–122.

Stellenbosch University, 2005. Performance Models of BSMs-Dynamic triaxial testing. Stellenbosch University, Stellenbosch, Institute of Transport Technology, (ITT) Technical Report. South Africa.

Advanced Testing and Characterization of Bituminous Materials – Loizos, Partl, Scarpas & Al-Qadi (eds)
© 2009 Taylor & Francis Group, London, ISBN 978-0-415-55854-9

Determination of gradual reduction of the flexible pavement bearing capacity

G. Fodor, C. Capitanu & T.C. Damian
Search Corporation, Bucharest, Romania

ABSTRACT: To knew the way of time decreasing under traffic loading of the pavements bearing capacity is extremely important to their design. This process has been studied in Romania by means of recurrent pavement deformability tests, accompanied by visual survey of the pavement distress condition.

The paper gives the results of some studies performed on a road section under traffic, for a 2 years period of time, which enabled assessment of pavement deformability increase as a result of diminution of the moduli of elasticity of the road layer materials.

Appreciations are made in paper both about the way the climatic factors influence the subgrade bearing capacity, and about the ageing process of the bituminous mix.

Knowledge of the way of reduction with time of the pavements bearing allows the pavement engineers to take into account this process for the period elapsed between the field study stage and the road rehabilitation stage.

1 INTRODUCTION

Gradual reduction of the pavement bearing capacity is extremely important to the road designers in our country. Alteration with time of the bearing capacity of a road is due to variation of the dynamic moduli of elasticity of the subgrade and road layer materials. In case of the subgrade, the modulus of elasticity is determined by its moisture, of which variation depends on the hydrological regime of the road. For the bituminous layers, variation of the modulus of elasticity shows the result of two antagonistic processes: the bitumen ageing and the micro-cracking of the layer, under traffic loading. In order to clear up the process, studies have been performed on the road network, consisting in recurrent tests of the bearing capacity, correlated with the pavement distress condition.

The paper presents the results of the study performed on 8 km road section located on the national road 2. This road, rated as European Road 85, assures connection between Bucharest km 0 + 000 and the north of the country, at border with Ukraine, km 482 + 230.

2 DESCRIPTION OF THE STUDIED ROAD SECTION

The studied road section is located on DN2, km 342 + 000 – 350 + 000. The road is at the ground level or in cutting earthwork. Existence of some non-waterproofed ditches and with inadequate operation placed it, in conformity with Romanian stipulations (STAS 1709/2-90), in a hydrological regime which allows high seasonal variations of the subgrade moisture (unfavorable hydrological regime type 2b). The pavement is flexible, being made up of bituminous layers with variable thickness, laid over granular material layers.

The frost depth in the area where the road is located is high, being of 100 cm (STAS1709/1-90). The frost—thaw process takes place into the subgrade, which consists of clayey silt—silty clay soils, very sensitive to frost.

The design traffic in cumulative number of equivalent standard axle loads of 115 kN is 1.69 million for a design period of 10 years. According to Romanian technical norms (Norm AND 584, 2002), the traffic is classified as "Very heavy".

3 PAVEMENT TESTS

The following pavement tests have been performed:

- *Pavement drilling cores*, in order to establish the structure of the existing pavement. On the road section under study 14 drilling cores have been performed in October 2003, finding the following:
  - The bituminous layers have variable thickness, between 10 cm and 22 cm, showing no adhesion at different interfaces and being friable at the bottom. The first about 4 cm of bituminous mix was recycled in the year 2003;
  - The sub-base consists of unbound granular materials, generally silted up, with variable thickness, ranged between 21 cm and 45 cm;
  - The subgrade consists prevalently of silty clay, type P5 and clayey silt soils, type P4, according to the geotechnical studies, soils rated as "very sensitive" at action of the frost-thaw phenomenon;
- *Pavement survey of the distress condition*, Assessment of the pavement distress condition (Instructions CD 155, 2001), in autumn of 2003, spring of 2004 and spring of 2005 has emphasized the following:
  - During 2003 (the year of overlay recycling) the road surface was without damages. The damage index was 0, what assessed as "Very good" the distress condition of the road surface at level of 2003;
  - In spring of 2004, the wearing course was damaged on about 12% of surface. The distress index was of 5.8%, what assessed as "Good" the distress condition of the road surface in spring of 2004;
  - In spring of 2005, the wearing course was damaged on about 80% of surface. The damage index was of 40.8%, what assessed as "Poor" the distress condition of the road surface in spring of 2005.

As the prevalent damages in spring of the year 2005 were alligator crackings, we think the main reason of their appearance was action of the frost—thaw phenomenon.

- *Deflection tests* with the aim of assessment of the pavement deformability. The tests have been performed with the falling weight deflectometer type Dynatest, (technical Instructions concerning utilization of the Dynatest FWD Deflectometer for pavement investigation), in station points located at 200 m apart one each other, in three stages:
  - 2003, in autumn;
  - 2004, in spring;
  - 2005, in spring.

The contact pressure and the deflection basins are stored for three drops at every station point, the data obtained from the last drop being used, the first two having only the role to assure a better contact between the loading plate and the pavement surface.

4 RESULTS OBTAINED

4.1 *Remarks about measured deflections*

From the deflection basins measured at every station point, the following data have been kept for judging: the central deflection, d_1, in μm, the deflection measured by the last sensor at a distance of 1.8 m of the loading plate, d_9, in μm, and the value of indicator (d_1–d_4), in μm, difference of deflection between sensors 4 and 1, respectively the difference between deflection measured at a distance of 45 cm of the loading plate and central deflection, for the last drop. The values of the measured deflection correspond to the reference temperature of 20°C. We specify that parameter $d_{1,20}$ expresses the pavement deformability and this deflection is influenced of about 60%–80% by the subgrade rigidity, d_9 expresses the subgrade quality and the

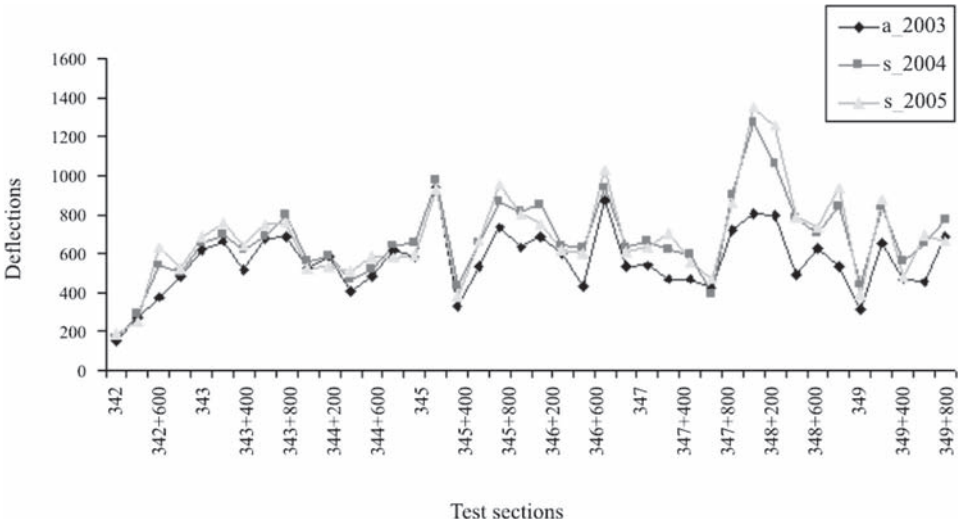

Figure 1. Values of $d_{1,20}$ during three test stages.

Table 1. The mean values of the deflections and percentage alterations.

Parameter	Autumn 2003		Spring 2004		Spring 2005
Mean value, d_9, μm	64		73		68
Mean value, d_1, μm	573		689		698
Variation, d_9, %		14.6		–7.3	
Variation, d_1, %		20.2		1.4	

parameter d_1–d_4 expresses the rigidity of the bituminous layers (Capitanu, 2006). Deflections measured in the three test stages are shown in figure 1.

Table 1 gives the mean values of the parameters $d_{1,20}$ and d_9, for the three periods of tests and percentage alterations for the road section under study.

Figure 2 gives the variation with time of the mean value of the deflection $d_{1,20}$.
From examination of the table 1 and figure 2, the following can be noticed:

– In spring of 2004, the pavement deflection had an increase of 20.2% given the deflection measured in autumn of 2003, in circumstances of increasing of the last sensor deflection with 14.6% (a loss of the subgrade bearing capacity);
– In spring of 2005, the pavement bearing capacity had a slow diminution (deflection higher with only 1.4% given in spring of 2004) in circumstances of carrying on of the design traffic for the period 2004–2005 by the road section under study. This situation is due mainly to improvement of the hydrological conditions (deflection at the last sensor being lower than in 2004, with 7.3%).

The deflection variations depend on a high degree on hydrological fluctuations of the pavement.

Based on the deflections measured in the three stages and the pavement structure, the moduli of elasticity of the road layer materials have been determined, inclusively the subgrade modulus, by means of ELMOD program (ELMOD User's Manual), (Capitanu 2000). Table 2 gives these data.

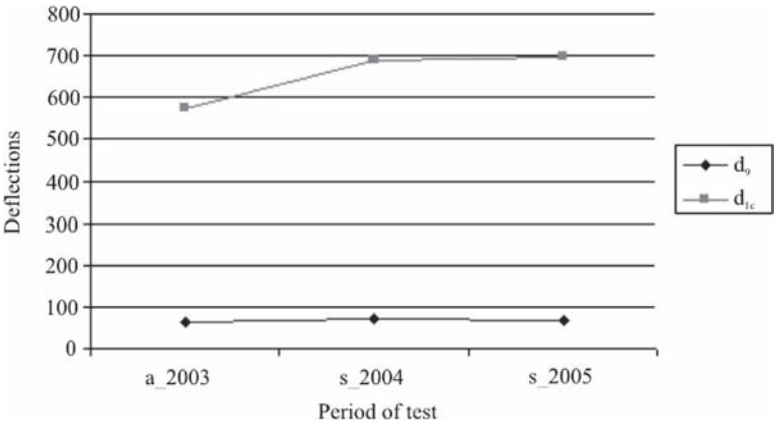

Figure 2. Mean values of the measured deflections.

Table 2. The mean values of the moduli of elasticity of the road layer materials and seasonal variations.

Parameter	Autumn 2003	Spring 2004	Spring 2005
Mean value, $E_{1,20}$ (asphalt mixture), MPa	2383	2333	2041
Mean value, E_2 (granular material), MPa	230	193	196
Mean value, E_3 (subgrade)	82	69	70
Variation of E_1, %		–2.1	–12.5
Variation of E_2, %		–16.1	1.6
Variation of E_3, %		–15.9	1.4

From examination of table 2, the following can be noticed:

- The modulus of the asphalt mixture, $E_{1,20}$, corresponding to the reference temperature of 20°C, was in spring of 2004, 2.1% lower than the modulus determined in autumn of 2003. In spring of 2005, this is 12.5% lower than the modulus determined in spring of 2004;
- The modulus of the subgrade, E_3, was in spring of 2004, 15.9% lower than that determined in autumn of 2003 and is approximately the same in spring of 2005 with that in spring of 2004. This situation is due to the similar seasonal variations of the hydrological conditions during the two test stages: spring 2004 and spring 2005;
- the modulus of the granular material has the same seasonal variation as that of the subgrade, because this depends on the subgrade modulus, with the relationship developed by Dormon & Metcalf (Ullidtz, 1998), thus:

$$E_2/E_3 = (h_2/35.75)^{0.45} \quad (1)$$

where h_2 is the thickness of the granular material layer, in mm.

4.2 *Determination of the bearing capacity reduction and the distress curve*

Knowledge of the mechanism of gradual reduction of the pavement bearing capacity is crucial for pavement designers because, as a rule, the rehabilitation solutions for a road are established within the pre-feasibility studies and between elaboration of studies and rehabilitation works there is usually a period of 2–3 years, time during which the road is damaged under traffic loading and hydrological conditions.

Processing of the deformability test results after one year elapsed, namely in the spring of years 2004 and 2005 allowed to establish the following relationship:

$$d_{2005}^{spring} = -12.058099 + 1.127014\, d_{2004}^{spring} - 11.379420 \Delta d_9,\ \eta = 0.975 \quad (2)$$

where $\Delta d_9 = d_9^{2004} - d_9^{2005}$

This relationship allows to stand out the influence of the variation of the subgrade bearing on the road deformation.

For $\Delta d_9 = 0$, (the subgrade bearing capacity remains unchanged) table 3 and figure 3 show the annual increase of pavement deformation (value, $d_{1,20}^{2005}$ and percentage), for usual deflection values assigned to the year 2004, $d_{1,20}^{2004}$.

From the above mentioned, the following appreciations results concerning the annual increase of the pavement deformation, in circumstances of an annual traffic of 0.169 million standard axles of 115 kN:

- Percentages of the pavement bearing capacity reduction range between 6.5% and 11.5%, varying with the deflection;
- The diminution is smaller for pavements with low values of deflections (adequate bearing capacity) and higher for pavement with high values of deflections (reduced bearing capacity).

Table 3. Annual increase of pavement deformation.

$d_{1,20}^{2004}$, μm	200	400	600	800	1000
$d_{1,20}^{2005}$, μm	213	439	664	890	1115
increase, %	6.5	9.8	10.7	11.3	11.5

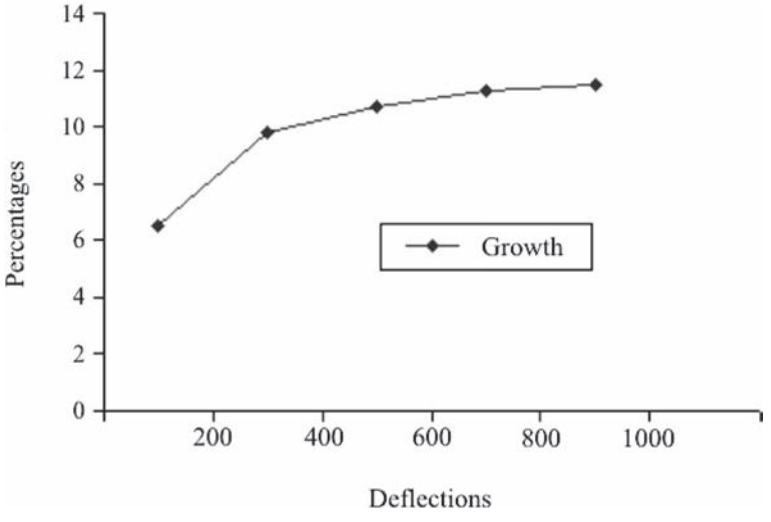

Figure 3. Annual increase of the pavement deformation.

In the same hydrological circumstance, a very heavy traffic (0.169 million standard axles yearly) has as result the annual increase of the pavement deformation with about 10%.

5 AGEING FACTOR OF THE ASPHALT MIXTURE

Another significant correlation was established through processing of some data of the deflection basins measured in spring of 2004 and spring of 2005. These data is: variation of the deflection $d_{1,20}$, $\Delta d_{1,20} = d_{1,20}{}^{2004} - d_{1,20}{}^{2005}$, variation of the parameter $(d_1 - d_4)$, $\Delta(d_1 - d_4) = (d_1 - d_4)(d_1 - d_4)^{2005}$, considered to express rigidity variation of the bituminous layers and variation of the parameter d_9, $\Delta d_9 = d_9^{2004} - d_9^{2005}$, which express variation of the subgrade bearing capacity.

This correlation has the following form:

$$\Delta d_{1,20} = 0.850176 + 1.046016 \times \Delta(d_1 - d_4) - 4.073247 \times \Delta d_9 \quad \eta = 0.937 \tag{3}$$

For $\Delta d_9 = 0$, respectively the same bearing capacity of the subgrade, it results:

$$\Delta d_{1,20} = 0.850176 + 1.046016 \times \Delta(d_1 - d_4) \tag{4}$$

Another parameter of the deflection basin which can be correlated to the stiffness of the bituminous layers is the angle formed by the segment AB and the horizontal line (A and B are the ordinates of the central deflection d_1 and deflection d_4 at the distance of 0.45 m apart the loading plate) and it is noted with α, in conformity with figure 4.

Alteration of this angle from one test stage to another shows variation of the bituminous layers stiffness, both under traffic loading and action of the climatic factors.

The relationship (4) becomes:

$$\Delta d_{1,20} = 0.850176 + 470707 \times \Delta tg\alpha \tag{5}$$

here, $tg\alpha\ (d_1 - d_4)/0.450{\times}10^6$, where $0.450{\times}10^6$ represents the distance from the center of the loading plate to the sensor 4, in μm.

The value $\Delta tg\alpha$ is considered as *ageing factor* of the asphalt mixture.

For the same hydrological condition, the annual growth of the deflection of 200 μm with 6.5%, of the deflection of 600 μm with 10.7%, of the deflection of 1000 μm with 11.5% (according to table 3), determines the values of ageing factor as follows (table 4):

The following results about ageing factor of the asphalt mixture:

– Action of the annual traffic (0.169 million standard axles of 115 kN), under influence of the climatic factors on the road under study leads to ageing of the asphalt mixture, which leads to diminution of the asphalt mixture stiffness;

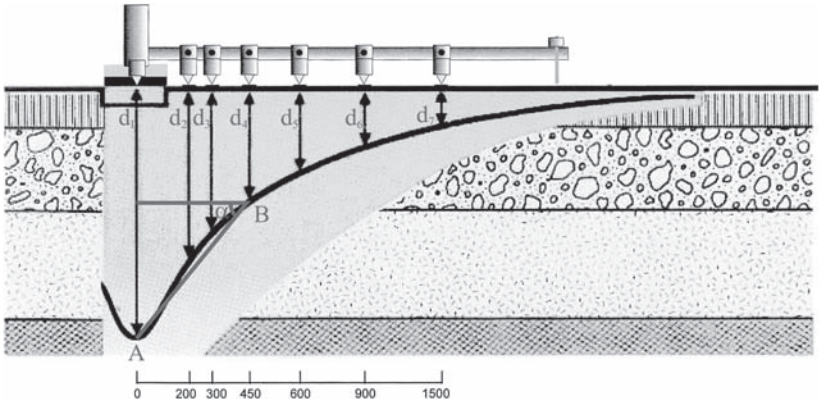

Figure 4. Ageing factor of the asphalt mixture.

Table 4. Values of ageing factor of the asphalt mixture.

Stage	Spring 2004	Spring 2005	Spring 2004	Spring 2005	Spring 2004	Spring 2005
$d_{1,20}$	200 μm	213 μm	600 μm	642 μm	1000 μm	1115 μm
$\Delta tg\alpha$	26×106		134×106		243×106	
$\Delta\alpha$, degrees	0.001		0.008		0.014	

– Variation of the angle α shows the modification of the shape of the deflection basin. Variation of this parameter is as higher as the pavement has lower bearing capacity.

6 CONCLUSIONS

A road bearing capacity is changing during its operation, both as result of traffic loading and due to the influence of climatic factors.

In the circumstances of an annual traffic of 0.169 million standard axles of 115 kN, the road section with flexible pavement located on DN 2 km 342 + 000 – km 450 + 000 shows an increase of 20.2% of the deformability since autumn of 2003 up to the spring of 2004, as a result of worsening of the hydrological condition during the winter 2003/2004. In spring of 2005, the pavement deformability shows an insignificant increase given that of spring 2004, under circumstances of improvement of the subgrade bearing capacity.

The seasonal variation of the pavement deformation represents both the effect of the alteration of the hydrological condition and of the very heavy vehicles traffic. Under the same hydrological condition, a very heavy traffic (0.169 million standard axles yearly) has as consequence the annual increase of the pavement deformation with about 10%. The modulus of the asphalt mixture, corresponding to the reference temperature of 20°C, was in spring of 2005, 12.5% lower than the modulus determined in spring of 2004. The paper allowed to define the ageing factor of the asphalt mixture, which establish the alteration with time of the shape of deflection basin as aresult of stiffness variation of the asphalt mixture.

Knowledge of the way of yearly reduction of the pavements bearing capacity is of great importance to designers, because, as a rule, between performance of the studies and fulfillment of the rehabilitation works there is a period of 2 … 3 years, during which the bearing capacity of the studied road is getting reduced. Determination of the optimum rehabilitation solutions imposes taking into account this variation with time of the road bearing capacity.

REFERENCES

Capitanu, C. 2000. Design of pavement strengthening on base of FWD tests, held within of short term courses of specialization. Technical University of Civil Engineering of Bucharest.

Capitanu, C. 2006. Studies of bearing capacity on the road network by nondestructive tests. Paper for doctor's degree Technical University of Civil Engineering of Bucharest.

ELMOD User's Manual Instructions CD 155, 2001. Technical Departmental Instructions concerning determination of the technical condition of the surfaced roads.

Norm AND 584, 2002. Norm for determination of the design traffic for road design from view point of the bearing capacity and of the traffic capacity.

STAS 1709/1-90 Action of the frost—thaw phenomenon at road works. Frost depth in the pavement system. Design stipulations.

STAS 1709/2-90 Action of the frost—thaw phenomenon at road works. Prevention and remedial of the frost—thaw damages. Technical stipulations.

Technical Instructions concerning utilization of the Dynatest FWD Deflectometer for pavement investigation.

Ullidtz, P. 1998. Modelling Flexible Pavement Response and Performance. Technical University of Denmark.

Advanced Testing and Characterization of Bituminous Materials –
Loizos, Partl, Scarpas & Al-Qadi (eds)
© 2009 Taylor & Francis Group, London, ISBN 978-0-415-55854-9

Testing of low temperature behaviour of asphalt mixtures in bending creep test

M. Pszczoła & J. Judycki
Gdansk University of Technology, Poland

ABSTRACT: The paper presents a method of bending beam test and its importance for evaluation of asphalt mixtures behaviour at low temperatures. Two types of asphalt mixtures: asphalt concrete AC with normal paving grade bitumen and stone mastic asphalt SMA with SBS-modified bitumen were tested. Long-term oven ageing (LTOA) test was also used in the laboratory according to SHRP procedure. The Burgers model was applied and rheological parameters of asphalt mixtures were determined in range of temperature from –10ºC to 10ºC. It has been found that the theoretical Burgers model fits well the experimental data obtained from the creep test. The testing method of bending beam under constant load was relatively simple and easy to use. The paper presents the method of testing, numerical results and analysis of data.

1 INTRODUCTION

The low temperature cracks formed in the asphalt wearing courses accelerate weather and traffic related deterioration of pavement. While lowering the overall strength of pavement these cracks have a negative effect on the fatigue life of pavement. Low-temperature cracking is a distress directly related with the stiffness of asphalt mixtures, which in low temperatures become brittle and susceptible to cracking. With the increasing stiffness the thermal tensile stresses in asphalt wearing course also increase and when they exceed the tensile strength, a crack is formed. For this reason low temperature properties are a crucial parameter of asphalt mixtures. These properties may be determined in bending test. It simulates the real conditions where the pavement is exposed to both low temperature and wheel loading. The bending creep test allows for determination of rheological parameters of tested specimens (Di Benedetto et al. 2004, 2007, Judycki 1990).

2 TESTING PROCEDURE

2.1 *Testing equipment*

The creep of specimens has been determined on a test stand prepared for bending test (Schmalz et al. 1990). Before the test, calibration of the loading force was carried out to determine the actual loads applied on the specimens. The test set-up included temperature chamber in which the specimens were subjected to temperatures below the freezing point.

The specimens were rectangular in shape of 50 × 50 × 300 mm in size. The specimens were compacted with a small manual roller and conditioned in the temperature chamber at the test temperature for at least 12 hours (for test temperatures of –10ºC, –5ºC and 0ºC) and at least 6 hours (for test temperatures of +10ºC and +20ºC). One series consisted of 3–4 uniform specimens.

The test set-up is schematically represented by a simple beam with a point load applied in the middle of the span. Bending load was applied for 1 hour (3,600 s) followed by 1 hour (3,600 s) unloading cycle. The strains on the beam underside were recorded both during loading and unloading, i.e. through 7,200 seconds.

The level of loading force depended on the testing temperature according to the rule that the generated stresses should not exceed half of the tensile strength in bending of a particular asphalt mixture. The loading diagram is presented in Fig. 1.

The tensile stresses in the bottom fibres of beam midsection have been calculated as follows:

$$\sigma_0 = \frac{M}{W} = 1{,}5\frac{Fl}{bh^2} \tag{1}$$

where:

σ_0 – tensile stress in the midsection bottom fibres under a constant load F, MPa,

M – bending moment, $M = \frac{Fl}{4}$,

W – section modulus, $W = \frac{bh^2}{6}$,

F – constant load applied at the beam mid-section,

l – span between supports, l = 260 mm,

b – beam width, [mm], as measured, average of 50 mm,

h – beam depth, [mm], as measured, average of 50 mm.

Displacement at the beam underside was measured with LVDT inductive transducer mounted in steel grips defining the measurement base. The steel grips were fixed to the specimen with epoxy glue.

The strain of beams under a constant load was calculated as follows:

$$\varepsilon = \frac{p}{e} \cdot \frac{c}{c+a} \tag{2}$$

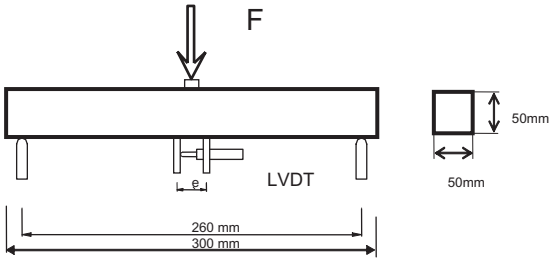

Figure 1. Testing assembly in bending creep test.

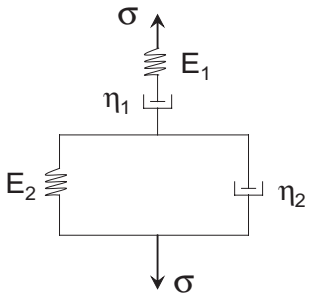

Figure 2. Schematic representation of Burgers model.

where:

ε – strain along measurement base e at the time t,
p – displacement of LVDT transducer under load F [mm].
e – measurement base [mm],
c – half of beam depth [mm],
a – distance between the beam underside and the LVDT axis [mm].

2.2 *Theoretical model*

The Burgers linear-viscoelastic model was employed to establish the rheological properties of the tested asphalt mixtures (Pszczola & Judycki 2003, Pszczoła 2006). This theoretical model was appropriate over narrow range of temperature used during the test. Over a wide range of temperature more appropriate could be the 2S2P1D model (Olard & Di Benedetto 2003). The basic configuration of the model used is presented in Fig. 2.

For proper recording of results a software program has been developed, which enabled recording of creep curve $\varepsilon(t)$ (relationship between strain ε under a constant load and during time t) and determination of the following rheological parameters:

- E-moduli: E_1 and E_2,
- viscosity coefficients: η_1, η_2, and
- stress relaxation time λ_2,

The program uses the creep curve $\varepsilon(t)$, approximating the test results with the theoretical relationship describing the Burgers model.

In the constant load test (creep test) the stress $\sigma(t)$ is either:

- σ_0 – for loading time $0 \le t \le t_0$, where t_0 is the time at the moment of unloading,
- 0 – for unloading time $t > t_0$.

The following equations describe the creep curve in the Burgers model:

- for loading time $0 \le t \le t_0$, while $\sigma_0 = \text{const}$.

$$\varepsilon(t) = \sigma_0 \left\{ \frac{1}{E_1} + \frac{t}{\eta_1} + \frac{1}{E_2}\left[1 - \exp\left(-\frac{t}{\lambda_2} \right) \right] \right\} \tag{3}$$

- for unloading time $t > t_0$, while $\sigma_0 = 0$

$$\varepsilon(t) = \sigma_0 \left\{ \frac{t_0}{\eta_1} + \frac{1}{E_2} \exp\left(-\frac{t}{\lambda_2} \right) \left[\exp\left(\frac{t_0}{\lambda_2} \right) - 1 \right] \right\} \tag{4}$$

where:

$\varepsilon(t)$ – strain,
σ_0 – constant stress under constant load, MPa,
E_1 and E_2 – E-moduli: E_1 – instantaneous elastic modulus, E_2 – retarded elastic modulus, MPa,
η_1 and η_2 – viscosity coefficients: η_1 – steady flow viscosity, η_2 – elastic delay viscosity and $\eta_2 = E_2 \cdot \lambda_2$, *MPa·s*,
λ_2 – stress relaxation time, s.

The Burgers model shows immediate elastic strain $\varepsilon_1 = \sigma_0/E_1$, retarded elastic strain $\varepsilon_2 = \sigma_0/E_2$ and viscous flow at a rate of σ_0/η_1. The first two strain types are recoverable, while viscous flow is non-recoverable. Removing of load is followed by immediate recovery of strains of σ_0/E_1. The permanent strains in long-term relaxation are calculated as follows: $\varepsilon_2 = \sigma_0 \cdot t_0/\eta_1$.

2.3 *Algorithm for determination of rheological parameters*

The indices of creep curve were established on the basis of files containing 7,200 records (measurement points) obtained from a single measurement. The data were recorded at 1 sec. intervals. The file contained the strains measured in the two respective phases: loading and unloading, as a function of time. The following equation has been established to describe the initial part of the creep curve, i.e. within the time span t (0, t_0):

$$\varepsilon(t) = A + Bt + C \cdot (1 - e^{-t/D}) \tag{5}$$

Equation (5) was established on the basis of Burgers model equation (3). The values of A, B, C and D constants were established on the basis of the experimental creep curves. The process of fitting the theoretical Burgers curve to the experimental creep curves consisted of two steps: first the values of A, B, C and D were established and then optimised by application of the least squares method.

When the values of A, B, C and D had been established on the basis of the above assumptions, optimisation was carried out to fit as closely as possible the theoretical curve based on equation (5) to the experimental creep curve.

The resulting equation (5) defines the relationship between the strain as a function of time and the five parameters which depend on the equation parameters. These equation parameters are adjusted with the non-linear least squares method (equation 6), using the experimental data described by the function $\varepsilon(t_i)$.

$$\Delta = \sqrt{\sum (\varepsilon(t_i) - f(A, B, C, D, t_i))} \Rightarrow \min \tag{6}$$

where:

$\varepsilon(t_i)$ – set of experimental data,

$f(A, B, C, D, t_i)$ – function, as in equation (5),

Optimisation was carried out first for D, then for C and finally for B. This sequence was related to the gradients of the respective parameters. The procedure was repeated until the assumed accuracy δ was attained. The target error δ was determined in the range: 0.01–0.001.

The numerically determined values of theoretical strain curve were used to determine the rheological parameters (parameters of the basic elements of rheological model).

2.4 *Types of asphalt mixtures*

Laboratory tests were carried out on two types of asphalt mixtures: 0/12.8 mm asphalt concrete (AC) with unmodified bitumen D50 and 0/9.6 mm stone mastic asphalt (SMA) with SBS modified bitumen DE80B. These mixtures are commonly used for production of wearing courses of asphalt pavements. The testing was carried out also to examine the effect of long-term ageing simulated under laboratory conditions on the rheological parameters of asphalt mixtures.

The specimens were taken from two coating plants. This has allowed for the effect of short-term ageing during production of asphalt mixtures. Such procedure had a significant effect on the research results, as the short-term ageing and other processes during coating affect the low-temperature resistance of asphalt mixtures.

Grading of the tested asphalt mixtures is presented in Table 1.

Table 1. Grading of the tested mixtures.

Type of mixture	Percent passing sieve, mm												Bitumen content
	12.5	10	8	6.3	4	2	0.85	0.42	0.3	0.18	0.15	0.075	
AC	100	93.1	77.0	66.1	52.0	40.1	27.1	20.6	17.9	13.9	12.2	7.9	5.6
SMA	100	91.3	67.9	45.9	31.8	20.5	15.1	12.8	11.8	10.4	9.8	8.3	6.2

2.5 *Long-term oven ageing in laboratory conditions*

The process of long-term oven ageing (LTOA) in laboratory conditions simulated the service life ageing of pavement. It has a significant effect on the properties of asphalt mixtures, as it increases the stiffness of asphalt mixture (Bell et al. 1994). The low-temperature resistance is affected in particular and early low-temperature cracking may occur. Long-term oven ageing was simulated according to SHRP procedure, which consisted of the following steps:

- conditioning of specimens in forced-air oven on perforated trays for 120 hours ± 0.5 hour at temperature + 85ºC ± 1ºC;
- on completion of ageing the specimens were taken out and left to cool down at temperature 25ºC.

3 TEST RESULTS

Table 2 presents the average values of the rheological properties of asphalt concrete—original and after long-term ageing.

The above results have demonstrated a definite effect of temperature on all the tested rheological properties of asphalt concrete. The lower are the temperatures, the higher are the values of immediate and retarded elastic moduli and viscosity coefficients. This is indicative of stiffening of asphalt concrete in low temperatures. The greatest increase was observed for steady flow viscosity η_1, which increased 100 times between +20ºC and –10ºC. The relationships between the rheological parameters and the temperature were approximately linear on a semi-logarithmic scale (this concerns in particular E_1 and η_1).

The longest stress relaxation time for asphalt concrete was noted at –10ºC. This is indicative of worse dissipation of stresses under low temperatures. As the temperature increased the stress relaxation time was shortened, which means faster and easier dissipation of stresses in the course of pavement.

Table 3 presents the average values of rheological properties of SMA—original and after long-term oven ageing.

Table 2. Average values of rheological properties of asphalt concrete – original and after long-term oven ageing.

		E-modulus		Viscosity coefficient		
Temperature [ºC]	Stress MPa	Immediate E_1 [MPa]	Retarded E_2 [MPa]	Steady flow η_1 [MPa·s]	Elastic delay η_2 [MPa·s]	Relaxation time λ_1 [s]
1	*2*	*3*	*4*	*5*	*6*	*7*
Original						
+20	0.27	390	74	2.7×10^5	5.7×10^4	681
+10	0.9	1852	665	1.1×10^6	3.1×10^5	607
0	2.37	3646	1110	4.6×10^6	3.2×10^5	1265
–5	2.23	6915	2047	1.1×10^7	5.2×10^5	1598
–10	2.46	10501	3013	3.05×10^7	7.8×10^5	2919
After long-term oven ageing						
+20	0.275	1292	434	7.1×10^5	1.3×10^5	554
+10	0.94	2542	708	3.0×10^6	3.9×10^5	1190
0	2.41	5184	2165	4.8×10^6	1.1×10^6	926
–5	2.75	9640	2565	3.8×10^7	8.0×10^5	3950
–10	2.25	10402	3884	3.5×10^7	1.0×10^6	3327

Table 3. Average values of rheological properties of SMA—original and after long-term oven ageing

Temperature [°C]	Stress MPa	E-modulus		Viscosity coefficient		Relaxation time λ_1 [s]
		Immediate E_1 [MPa]	Retarded E_2 [MPa]	Steady flow η_1 [MPa·s]	Elastic delay η_2 [MPa·s]	
1	*2*	*3*	*4*	*5*	*1*	*2*
Original						
+10	0.53	1270	164	5.4×10^5	9.8×10^4	422
0	2.44	5401	1441	2.5×10^6	3.3×10^5	465
–5	2.35	7846	1479	1.3×10^7	6.5×10^5	1666
–10	2.27	11500	2680	2.4×10^7	7.3×10^5	2104
After long-term ageing						
+10	0.51	1340	210	6.4×10^5	1.3×10^5	476
0	2.38	7297	1245	5.7×10^6	4.6×10^5	845
–5	2.30	10401	2151	1.5×10^7	6.1×10^5	1564
–10	2.33	16614	3327	3.3×10^7	9.4×10^5	1992

(*) – due to high susceptibility of SMA to deformation at temperature +20°C the temperature range was limited to +10°C to –10°C.

The above relationships between rheological properties and temperature for SMA are similar to asphalt concrete.

For the stress relaxation time non-linearity has been noted. This may be caused by greater non-uniformity of SMA, as compared to asphalt concrete.

Both the original and long-term oven aged specimens have shown a definite effect of decreasing temperature on increase of the rheological properties of SMA. Moreover, at 0°C a slight bent has been noted on the curve of E-modulus and viscosity coefficient.

4 EFFECT OF LONG-TERM OVEN AGEINING ON THE RHEOLOGICAL PROPERITES OF ASPHALT MIXTURES

Fig. 3 compares the rheological properties of asphalt concrete AC—original and after long-term oven ageing.

In order to clearly demonstrate the effect of long-term oven ageing on the rheological properties the ageing index *AI* was determined to indicate the degree of change in the rheological properties as a result of ageing. For all the tested properties the *AI* index is calculated as follows:

$$AI = \frac{values\ of\ (E_1, E_2, \eta_1, \eta_1, \lambda_2) \quad after\ ageing}{values\ of\ (E_1, E_2, \eta_1, \eta_1, \lambda_2) \quad before\ ageing} \tag{7}$$

Any values higher than one signify the effect of ageing on the analysed rheological properties. The values of ageing index are presented in the table below.

Fig. 3 compares the rheological properties of SMA—original and after long-term oven ageing.

The values of ageing index for SMA are presented in Table 5.

The effect of long-term oven ageing LTOA proved to be significant both for asphalt concrete and SMA. According to the graphs (Fig. 3 and Fig. 4) the rheological properties are higher after LTOA. This means that long-term oven ageing increases the stiffness of the tested

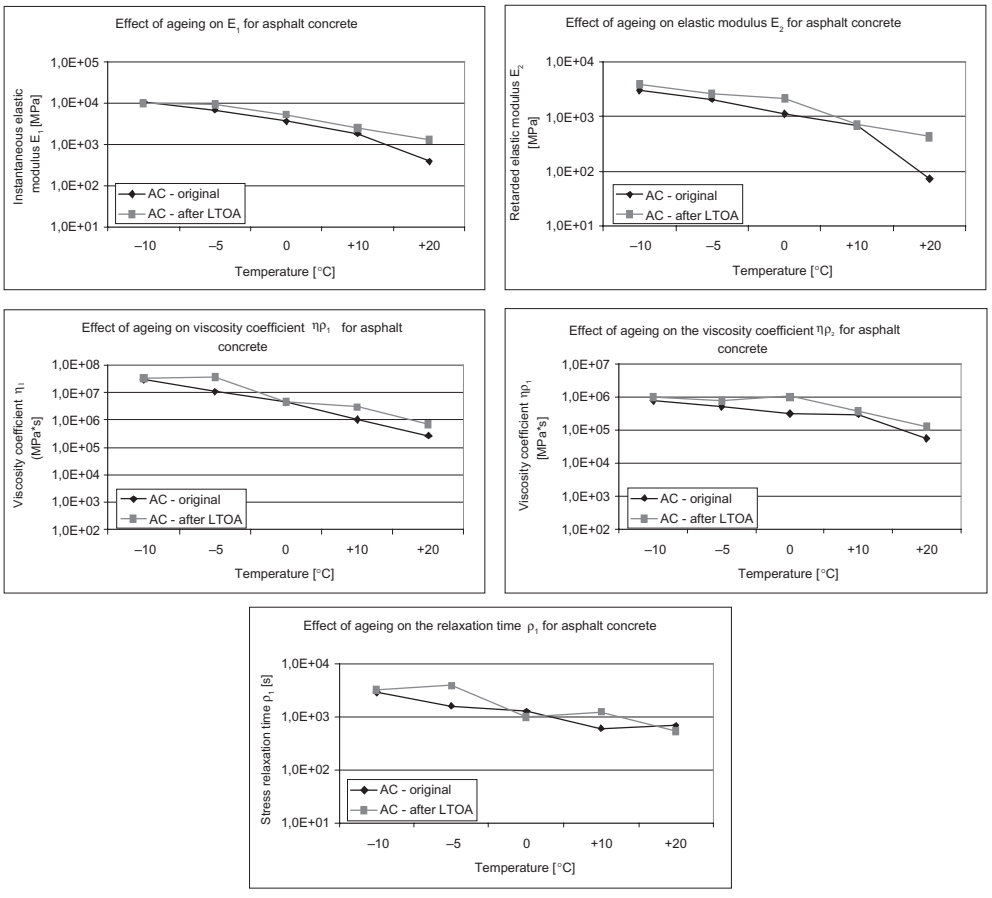

Figure 3. The effect of long-term oven ageing on the rheological properties of asphalt concrete.

Table 4. Values of ageing index for asphalt concrete.

Rheological property	Temperature [^{0}C]				
	–10	–5	0	+10	+20
E_1	0.99	1.39	1.42	1.37	3.31
E_2	1.29	1.25	1.95	1.06	5.86
η_1	1.13	3.47	1.05	2.83	2.65
η_2	1.30	1.54	3.35	1.26	2.38
λ_2	0.99	1.18	1.73	1.15	0.41

materials both in terms of elasticity and viscosity. In most cases the ageing index assumes values higher than 1 which signifies change of the properties due to ageing.

5 RHEOLOGICAL PROPERTIES DEPENDING ON MIXTURE TYPE

The rheological properties depending on mixture type are presented on the graphs in Fig. 5.

The effect of mixture composition on the rheological properties determined during the creep test showed better properties of SMA mixture in comparison with asphalt concrete

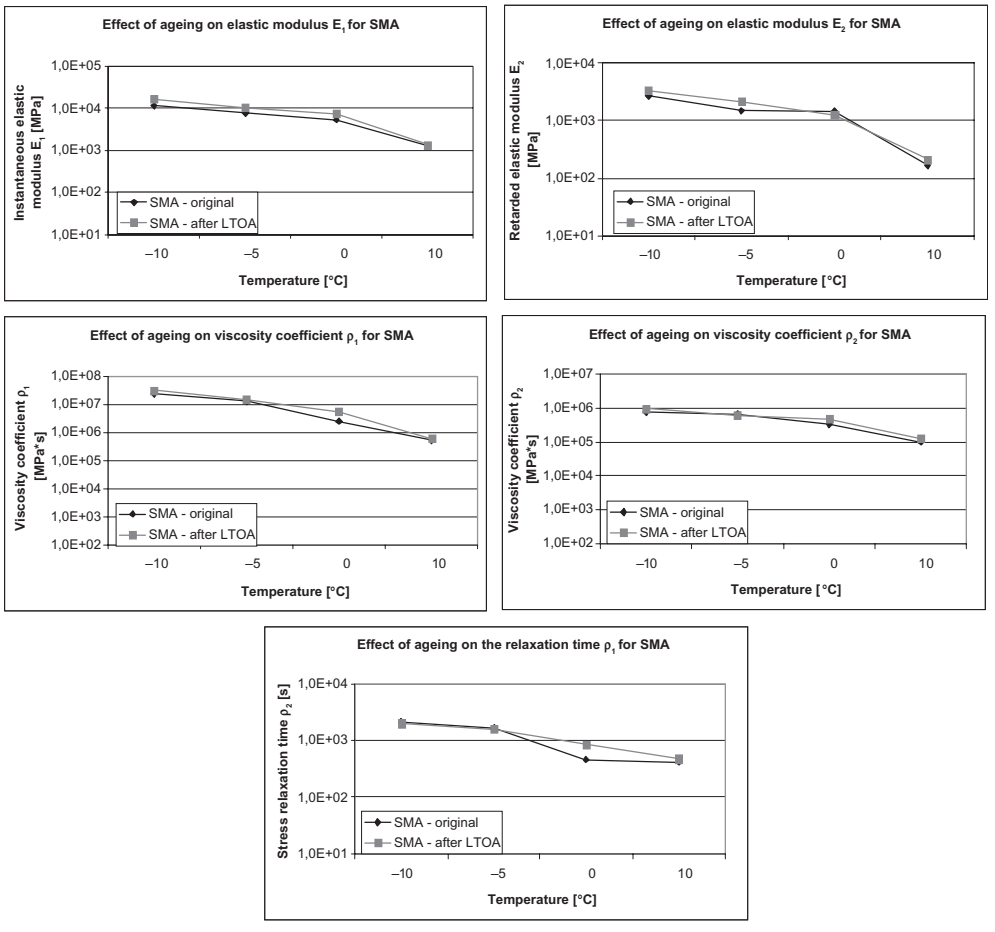

Figure 4. The effect of long-term oven ageing on the rheological properties of SMA.

Table 5. Values of ageing index AI for SMA.

Rheological property	Temperature [^{0}C]			
	–10	–5	0	+10
E_1	1.44	1.33	1.35	1.05
E_2	1.24	1.45	0.86	1.28
η_1	1.37	1.17	2.30	1.20
η_2	1.29	0.94	1.39	1.29
η_2	1.08	0.73	1.47	0.97

when exposed to low temperatures. The reason was the SBS-modified bitumen which was added to SMA mixture and significantly decreased the stiffness of SMA mixture.

6 CONCLUSIONS

The method used in the present research which analyses the long-term creep of beam-shaped specimens under constant load enables proper evaluation of rheological properties: elasticity,

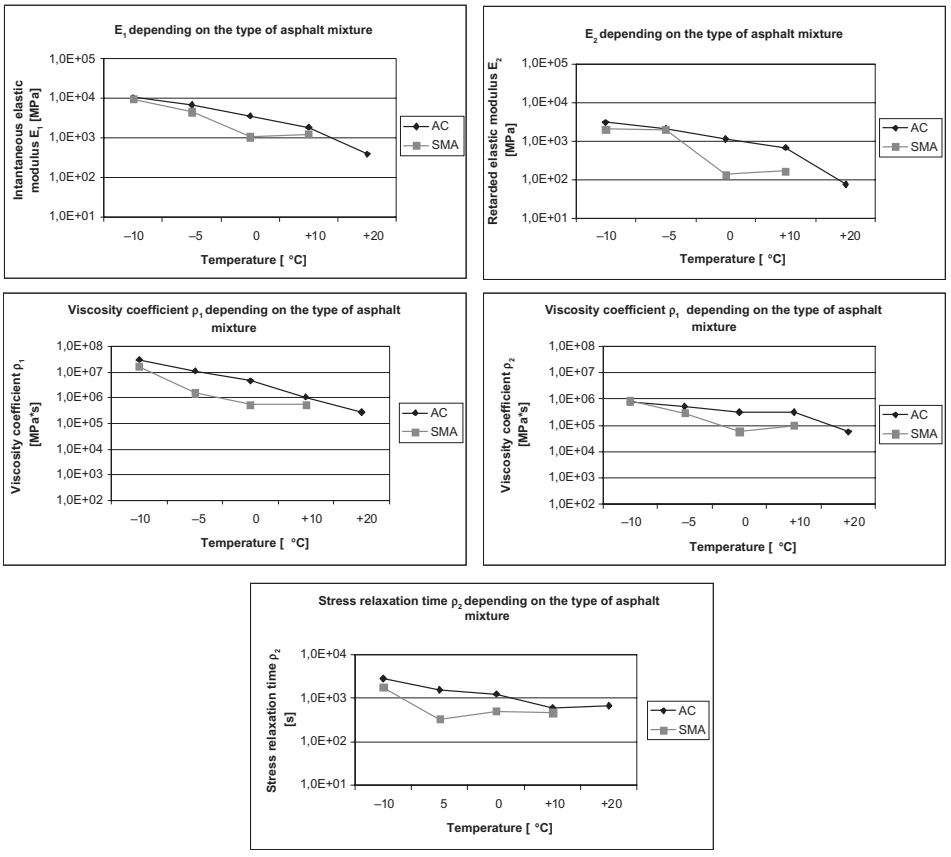

Figure 5. Rheological properties depending on the type of asphalt mixture.

viscosity and relaxation of stresses in asphalt mixtures. This enables a more accurate evaluation of the low temperature performance of asphalt mixtures.

Among the numerous rheological models the simple Burgers model was chosen, as it is quite accurate in representing the performance of asphalts in constant-load creep test. The experimental data were to a large extent consistent with the theoretical description of the model in the narrow range of temperature from –10ºC to +20ºC.

The test results showed a definite effect of temperature on all the analysed rheological properties of both asphalt concrete and SMA. Lowering of temperature increased the values of elastic modulus and viscosity coefficient, which is indicative of stiffening of the tested mixtures.

Lowering of temperature resulted in longer relaxation time which slows down the relaxation of thermal stresses caused by low temperatures.

The laboratory simulated long-term oven ageing showed significant changes in rheological properties of asphalt mixtures subjected to such long-term ageing process. The ageing index was determined, which showed a definite increase in the values of elastic modulus and viscosity coefficient in the aged specimens, as compared to the original ones at most temperatures. However, the effect of long-term ageing was not so definite for stress relaxation time. Therefore, we can conclude that ageing had a significant effect in long-term loading tests and had no effect in short-term loading tests.

The effect of mixture composition on the rheological properties determined during the creep test showed better properties of SMA mixture in comparison with asphalt concrete when exposed to low temperatures.

REFERENCES

Bell C.A., AbWahab Y., Christi M.E. & Sosnovske D. 1994. *Selection of laboratory aging procedures for asphalt concrete-aggregate mixtures*. Report No. SHRP-A-383. Strategic Highway Research Program, National Research Council, Washington DC.

Di Benedetto H., Olard F. Sauzeat C. *Linear viscoelastic behaviour of bituminous materials: from binders to mixes.* International Journal of Road Materials and Pavement Design, Vol. 5/2004, pp. 163–202.

Di Benedetto H., Mondher N., Sauzeat C. & Olard F. *Three—dimensional thermo-viscoplastic behaviour of bituminous materials. The DBN model.* International Journal of Road Materials and Pavement Design, Vol. 2/2007, pp. 285–315.

Judycki J. 1990. *Bending test of asphalt concrete mixtures under static loading*. IV International RILEM Symposium.

Olard F. & Di Benedetto H. 2003. *General 2S2P1D model and relation between the linear viscoelastic behaviours of bituminous binders and mixes.* International Journal of Road Materials and Pavement Design, Vol. 2/2003, pp. 185–224.

Pszczola M. & Judycki J. 2003. *Testing of rheological properties of asphalt concrete mixes at creep under bending at low temperatures*. IX International Conference *Durable and safe road pavements*.

Pszczoła M. 2006. *Low temperature cracking of asphalt concrete layers of pavements.* Ph.D thesis, Gdansk University of Technology, Gdansk.

Schmalz M., Letsch R. & Plannerer M. 1990. *Investigation on high and low temperature behaviour of asphalt concrete by static and dynamic creep tests*. IV International RILEM Symposium.

Advanced Testing and Characterization of Bituminous Materials – Loizos, Partl, Scarpas & Al-Qadi (eds)
© 2009 Taylor & Francis Group, London, ISBN 978-0-415-55854-9

Effect of beam size on the creep stiffness of asphalt mixtures at low temperatures

R. Velásquez, M. Marasteanu, M. Turos & J. Labuz
Department of Civil Engineering, University of Minnesota, Minneapolis, Minnesota, USA

ABSTRACT: Creep stiffness of asphalt mixtures is an essential property used to estimate the susceptibility to low-temperature cracking of asphalt pavements. Currently, creep stiffness is obtained by performing indirect tension creep tests on 150 mm (6 in.) cylindrical asphalt mixture specimens. A simpler test method, in which small mixture specimens are tested, has been recently proposed. The main obstacle in using this test method is the use of small size specimens and that the volume of material tested may not be representative. This paper addresses this critical issue by performing three point bending creep tests on beams of different sizes ($6.25 \times 12.5 \times 100$ mm, $12.5 \times 25 \times 200$ mm, and $18.75 \times 37.5 \times 300$ mm). The creep stiffness of 10 asphalt mixtures were determined at three low pavement service temperature levels: high temperature level (PG low limit + 22°C), intermediate temperature level (PG low limit + 10°C), and low temperature level (PG low limit –2°C). Visual inspection and statistical analysis of the experimental results indicate that the creep stiffness of asphalt mixtures can be obtained by testing small beam specimens at test temperatures in the vicinity of the component binder PG low limit.

1 INTRODUCTION

The current Superpave specifications for low temperature cracking are based on strength and creep tests performed on asphalt binder and asphalt mixture specimens. For asphalt mixtures, the Indirect Tension Test (IDT) is used to perform strength and creep tests on cylindrical specimens loaded in compression along the diameter, according to AASHTO T22-02 (2005). IDT testing equipment is expensive and requires time consuming calibration procedures. The size of the IDT specimen limits the use of this test to investigate variation of asphalt pavement properties with depth.

Previous research performed at the University of Minnesota (Zofka et al. 2005, Zofka et al. 2006, Zofka 2007 and Zofka et al. 2008) indicated that the Bending Beam Rheometer (BBR), currently used in the Performance Grading (PG) of asphalt binders, could be used to test thin asphalt mixture beams to obtain reliable measurements of creep compliance. There are significant advantages of using the BBR compared to the IDT:

- The BBR has a reasonable price and most agencies and laboratories already have it as part of the asphalt binder grading requirements.
- The BBR has a well documented history of good performance, user-friendly calibration verification, and the test procedure is very simple and has high repeatability.

In addition, testing of thin mixture beams can provide critical information related to surface aging and compaction effects on the mechanical properties of asphalt mixtures at different layer depths, and can also be used to assess the effective properties of the binder in asphalt mixture containing reclaimed asphalt pavement (RAP) (Zofka et al. 2005).

The use of small beams to estimate the properties of the actual asphalt pavement poses, however, a significant problem: the volume of material tested may not be representative, especially when the asphalt mixtures contain aggregates that are larger than the smallest dimension of the beam. The critical issue of the representative volume element of asphalt mixtures

has received little attention in the past. Very few studies are available in the literature, and only for intermediate and high temperature properties.

Weissman et al. (1999) performed finite element (FE) simulations to study the representative volume element (RVE) of asphalt mixtures subjected to triaxial loading and simple shear at room temperatures. The authors suggested that at low temperatures, where the discrepancy between aggregate and mastic moduli was significantly smaller, the RVE was smaller compared to RVE at intermediate and high temperatures. Romero & Masad (2001) investigated the RVE of asphalt mixtures with x-ray imaging and shear tests. It was found from laboratory testing that a stiffer binder diminishes the aggregate size influence on the variability of the response.

This paper presents a portion of the experimental work performed as part of a more comprehensive study that investigates the RVE of asphalt mixtures with respect to the low temperature creep stiffness.

2 MATERIALS AND TEST PROCEDURE

A total of 10 laboratory mixtures were tested in this study. The laboratory mixtures were prepared with four different asphalt binder grades, and two types of aggregate, limestone and granite. They were compacted to 4% air voids using a linear kneading compactor and following the Superpave mix design procedure for traffic level of 3,000,000 to less than 30,000,000 ESAL's (medium to high traffic). The mixing and compaction temperatures were 155°C and 135°C, respectively. Table 1 shows the 10 asphalt mixtures tested in this study.

Low temperature three point bending creep tests were performed on specimens with three different sizes: 6.25 × 12.5 × 100 mm (1x), 12.5 × 25 × 200 mm (2x), and 18.75 × 37.5 × 300 mm (3x). Additionally, the effect of temperature on the representative volume element was studied by performing bending creep tests at three temperatures: high temperature (HT) level (PG low limit +22°C), intermediate temperature (IT) level (PG low limit + 10°C), and low temperature (LT) level (PG low limit –2°C).

First, the slab compacted mixtures were cut into six 3x beams (Figure 1). Tests were performed at the three temperature levels HT, IT, and LT: three replicates were tested at HT and LT and six replicates were tested at IT.

The test for 3x and 2x beams were conducted using a MTS 810 servo hydraulic testing machine. A special support manufactured in house was used to hold the beam and to measure mid span deflection and deformation of the beam at both ends of the support, as shown in Figure 2. The ends can be adjusted to different span lengths. The beam deflections were measured using Epsilon extensometers with 38 mm gage length and ±1 mm range.

After testing was finished, the 3x beams were cut into 2x beams using a water-cooled diamond saw. Bending tests were performed on the 2x beams using the test setup for 3x beams. After testing was completed, the 2x beams were cut into 1x beams the size of BBR specimens and tested in the BBR device.

Table 1. Laboratory mixtures description.

PG binder	Modification	Aggregate
58-34	SBS	Granite
58-34	SBS	Limestone
58-28	Unmodified	Granite
58-28	Unmodified	Limestone
64-34	Elvaloy	Granite
64-34	Elvaloy	Limestone
64-28	Unmodified	Granite
64-28	Unmodified	Limestone
64-28	SBS	Granite
64-28	SBS	Limestone

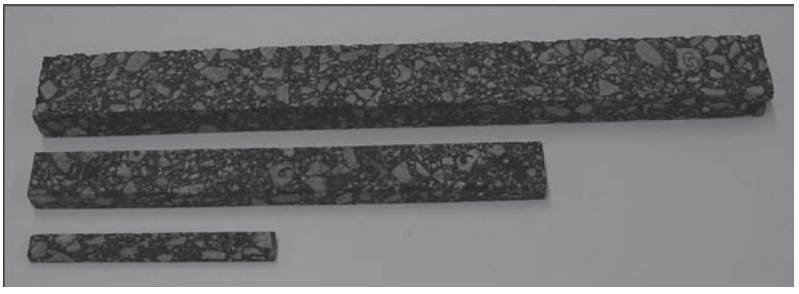

Figure 1. 1x, 2x, and 3x asphalt mixture beam specimens.

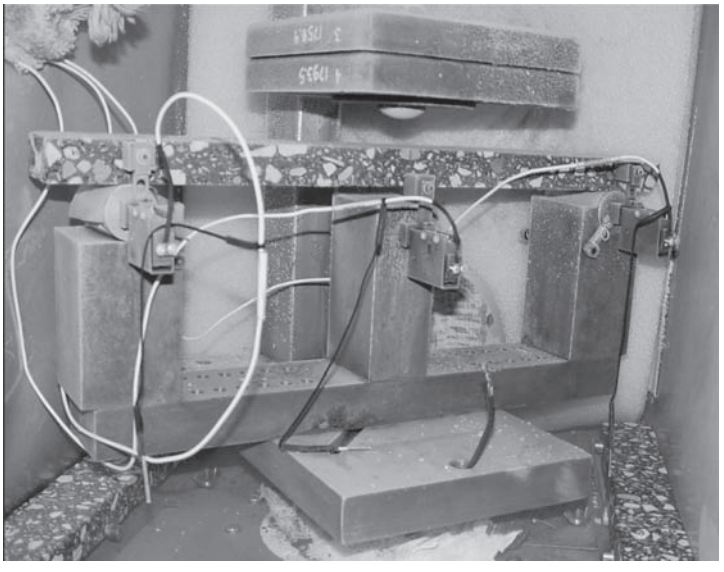

Figure 2. 2x and 3x mixture beam test setup.

To eliminate the creep from the weight of the 2x and 3x beams, the deflection measured was considered as the sum of the deflection due to the load applied at the mid span and the deflection due to a uniformly distributed load equivalent to the weight of the beam. For the 1x beams, the weight of the beam is counter balanced by the buoyancy forces in the BBR ethanol bath.

3 RESULTS

A total of 360 tests were performed on the three different size beams at three temperatures. The creep stiffness as function of time was calculated using Bernoulli-Euler beam theory and the correspondence principle. For each asphalt mixture and temperature level, the average creep stiffness was calculated.

Figures 3 to 7 show the creep stiffness curves for the ten asphalt mixtures tested. Visual inspection of the creep stiffness average curves indicates that, at intermediate temperature, the effect of the beam size seems to be negligible.

At low temperature the size of the beam appear to influence the creep stiffness. This effect is further investigated using statistical tools in the next section. It is important to note that, during testing of the 2x and 3x beams at LT, the formation of layers of ice on the supports

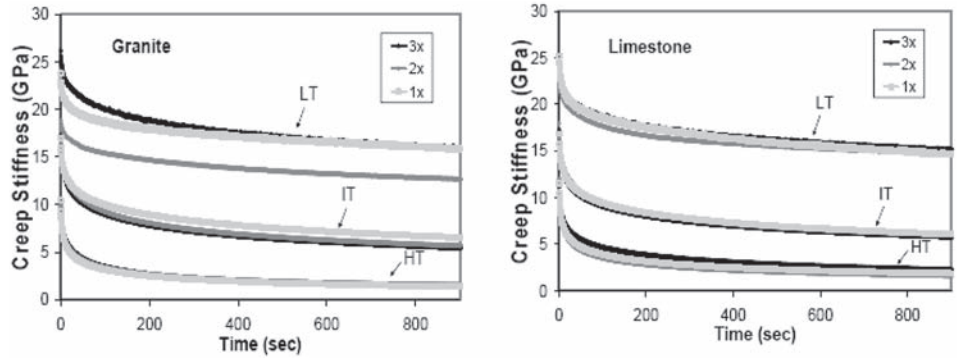

Figure 3. Test results for PG 58-34 mixtures.

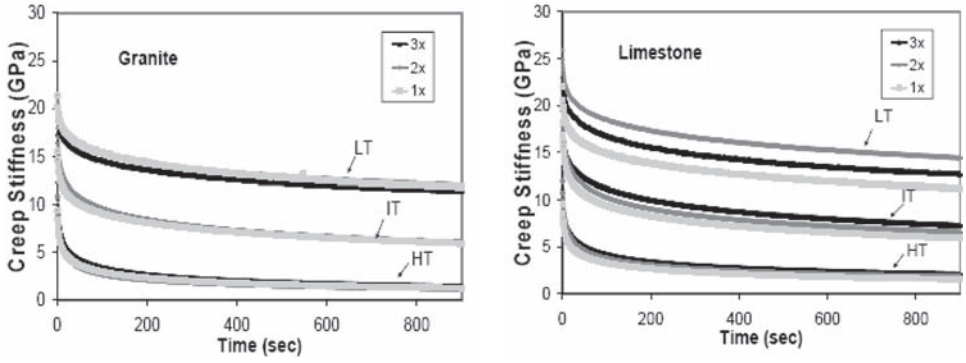

Figure 4. Test results for PG 58-28 mixtures.

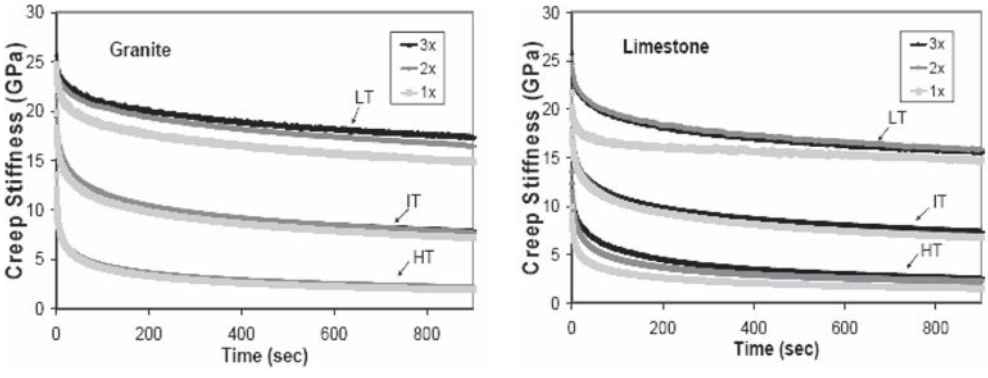

Figure 5. Test results for PG 64-34 mixtures.

and around the extensometers was observed. This may have influenced the deflection readings since the deflection values are very small at LT and the level of error in measurements is higher compared to the other higher temperature levels.

At the high temperature level, for some of the mixtures, the creep stiffness curves are slightly different as well. This observation may indicate that the mismatch between the

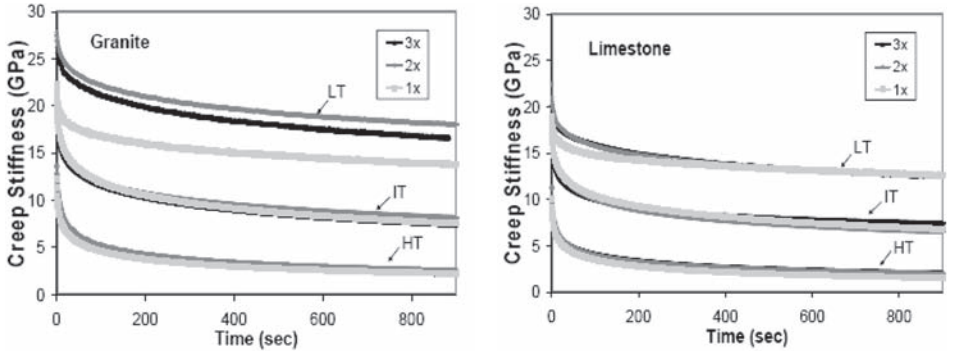

Figure 6. Test results for unmodified PG 64-28 mixtures.

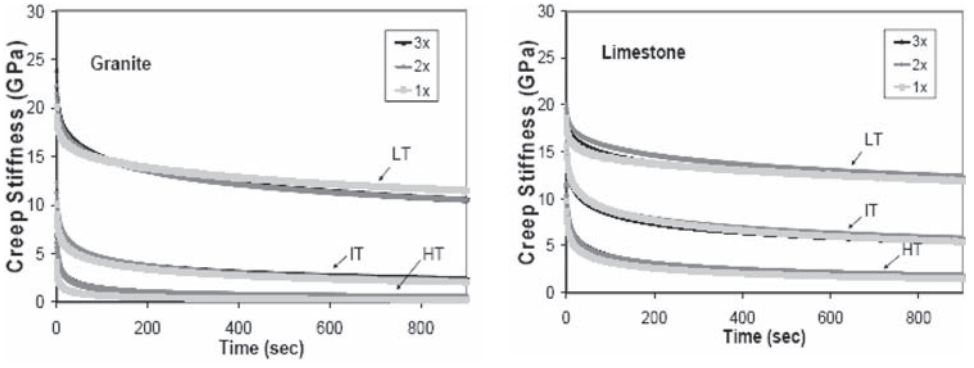

Figure 7. Test results for modified PG 64-28 mixtures.

Table 2. Variables definition for statistical analysis.

Variable	Type/Description
Binder PG	Factors (dummy): PG 58-34, PG 58-28, PG 64-34, PG 64-28
Binder modification	0 – unmodified; 1 – modified
Aggregate Type	0 – granite; 1 – limestone
Beam size	1–1x beams; 2–2x beams; 3–3x beams
Time	8, 15, 30, 60, 120 and 240 sec

mechanical properties of aggregates and the binder (mastic) starts to affect the results, and the response of the mixtures becomes dependent on the size and distribution of the aggregate particles.

4 STATISTICAL ANALYSIS

To investigate the influence of parameters such as the size of the specimen, PG of the binder, aggregate type, loading time and temperature on the creep stiffness of asphalt mixtures, correlation matrices were calculated and analyses of variance (ANOVA) were performed using the creep stiffness as response variable and size, time, temperature, binder type, and aggregate as the independent parameters. A linear relation was assumed between response variable and the predictors. To reduce calculations, only the creep stiffness values at 8, 15, 30, 60, 120 and 240 seconds were used in the analysis. Table 2 shows how the variables were treated in the statistical analysis.

First, the analysis considers all test results obtained at the three temperatures. Then, separate analyses are performed for each of the three temperature levels to avoid including errors that may occur in another temperature level such as the formation of ice at the LT.

4.1 *All temperatures*

Correlation factors for the results at all temperatures are presented in Table 3. Correlation factors more than $2/n^{0.5}$ (rule of thumb in statistics), where n is the number of sample points, indicates high linear correlation between the parameters. For the data set used in this analysis, correlations larger than 0.046 (n = 1902) are significant and presented in bold.

Significant correlation is observed between the interaction of size and time variables and the creep stiffness: as time and size increases, the creep stiffness decreases. As expected, significant correlation is observed between test temperature and creep stiffness. Negligible correlation is observed between creep stiffness and size of specimens. No correlation is observed between aggregate type and modification of the binder and the creep stiffness.

The results of ANOVA are presented in Table 4. For a significance level of 5%, the variables with p-values smaller than 0.05 are significant and are presented in bold.

The parameters that are significant in the linear regression are: size, the factors from PG 64-34 and PG 64-28 binders, aggregate type, temperature and time. Forward selection and backward elimination analysis on the regression model indicates that size does not change the residuals sum squares (RSS) of the model significantly. The significance of the size observed in the ANOVA may be caused by the interaction with other terms in the regression since the correlation between the creep stiffness and the size is not significant. The positive coefficients for PG 64-34 and PG 64-28 indicate that mixtures prepared with these binders are stiffer than the mixtures prepared with PG 58-34. The large negative coefficient for aggregate type indicates that mixtures with granite have significantly higher creep stiffness than mixtures with limestone. As indicated by the large t-values in Table 4, the variables that contain most of the information for the prediction of creep stiffness are temperature and time. As expected, when time and temperature increases, the creep stiffness of the mixture decreases.

Table 3. Correlation factors for all temperatures.

	Creep stiffness
Aggregate	–0.044
Modification	–0.011
Size	0.042
Size * Aggregate	–0.022
Size * Time	**–0.214**
Temperature	**–0.853**
Time	**–0.259**

Table 4. ANOVA for all temperatures.

Variable	Estimate	Std. Error	t-value	p-value
Constant	1642.10	324.93	5.05	**0**
Size	517.81	113.16	4.58	**0**
Size * Aggregate	–100.32	124.03	–0.81	0.4187
Size * Time	–0.97	0.74	–1.31	0.1913
Binder[58-28]	–386.72	222.88	–1.74	0.0829
Binder[64-34]	1300.94	152.69	8.52	**0**
Binder[64-28]	907.03	158.26	5.73	**0**
Modification	88.59	98.22	0.90	0.3672
Aggregate	–3120.94	287.30	–10.86	**0**
Temperature	–561.55	5.53	–101.52	**0**
Time	–16.48	1.59	–10.36	**0**

The parameters in the regression that do not significantly contribute to the prediction of creep stiffness are the interaction terms between size, aggregate and time and the modification of the binder. No significant difference is observed between the creep stiffness of mixtures prepared with PG 58-28 and with PG 58-34 (the reference level for binder PG in this analysis).

4.2 *High temperature level (PG low limit + 22˚C)*

Table 5 presents the correlation factors when only the high temperature level data is used. Correlations larger than 0.088 (n = 516) are significant and are presented in bold.

A significant positive correlation is observed between the size of the beam and the creep stiffness. Larger beam specimens have larger creep stiffness compared to smaller beams. It is also observed that specimens prepared with limestone are stiffer than specimens with granite. High positive correlation between the interaction of size and aggregate and stiffness is observed, indicating that mixtures prepared with limestone are stiffer when the size increases.

ANOVA results are presented in Table 6. The variables that contain important information for the prediction of creep stiffness are: binder modification, size, interaction of size and aggregate, binder type, and time. From the high negative coefficient for binder modification, the mixtures prepared with unmodified binder are stiffer than mixtures prepared with modified binder. At this temperature level, each PG binder has significantly different creep stiffness curves as indicated by the *p*-values and the coefficients estimates in the ANOVA. Mixtures prepared with PG 58-34, PG 64-28, and PG 64-34 have higher creep stiffness than mixtures with PG 58-28 (the reference level for binder PG in this analysis). As expected, time is significant and its estimate indicates that as time increases, the creep stiffness decreases. The aggregate type and the interaction of size and time do not provide significant information for the prediction of the creep stiffness in the assumed linear model.

Table 5. Correlation factors for high temperature level.

	Creep stiffness
Aggregate	**0.158**
Modification	–0.081
Size	**0.163**
Size * Aggregate	**0.235**
Size * Time	**–0.523**
Time	**–0.649**

Table 6. ANOVA for high temperature level.

Variable	Estimate	Std. Error	t-value	p-value
Constant	4753.42	252.50	18.83	**0**
Aggregate	–292.34	268.46	–1.09	0.2767
Modification	–2198.67	164.57	–13.36	**0**
Size	311.09	107.88	2.88	**0.0041**
Size * Aggregate	478.97	124.90	3.84	**0.0001**
Size * Time	–1.31	0.77	–1.71	0.0880
Binder[64-28]	1084.92	162.06	6.70	**0**
Binder[58-34]	2562.60	229.04	11.19	**0**
Binder[64-34]	3317.50	227.47	14.58	**0**
Time	–13.08	1.65	–7.92	**0**

4.3 *Intermediate temperature level (PG low limit + 10˚C)*

The correlation factors for the intermediate temperature are presented in Table 7. Correlations larger than 0.068 (n = 864) are significant and are presented in bold.

The results indicate that size does not have an effect on the creep stiffness at the intermediate temperature level. This is indicated by the high *p*-value in the ANOVA presented in Table 8.

The parameters that provide significant explanatory information for creep stiffness are: binder modification, binder PG, and time. Mixtures prepared with unmodified binder are stiffer than mixtures prepared with modified binder. Mixtures prepared with PG 58-34, PG 64-28, and PG 64-34 have higher creep stiffness than mixtures with PG 58-28 (reference level).

The high *p*-values observed for the interaction terms indicate that they do not provide significant information for the prediction of creep stiffness. The high correlation observed for the interaction term between size and time is due to the explanatory information carried by time. As observed in the ANOVA, when time is independently included in the linear regression then the interaction term between size and time becomes not significant.

4.4 *Low temperature level (PG low limit – 2˚C)*

The correlation factors for the low temperature level are presented in Table 9. Correlation factors larger than 0.088 (n = 522) are significant and are presented in bold.

Contrary to what is expected at very low temperatures, the size of beam has a significant effect on the creep stiffness of the asphalt mixtures. Most likely, this is due to the difficulties associated with measuring the creep stiffness at very low temperatures of the 2x and 3x beams in the MTS. The small deflection values measured at this temperature increase the variability of the measured creep stiffness and, combined with the formation of layers of ice on the supports and around the extensometers, may produce the size effect observed in the analysis.

Table 7. Correlation factors for intermediate temperature level.

	Creep stiffness
Aggregate	0.037
Modification	–0.211
Size	–0.004
Size * Aggregate	0.045
Size * Time	**–0.488**
Time	**–0.560**

Table 8. ANOVA for intermediate temperature level.

Variable	Estimate	Std. Error	t-value	p-value
Constant	12905.50	346.80	37.21	**0**
Aggregate	78.87	358.16	0.22	0.8258
Modified	–4196.73	214.26	–19.59	**0**
Size	–108.69	147.34	–0.74	0.4609
Size * Aggregate	171.09	167.60	1.02	0.3076
Size * Time	–0.04	1.03	–0.04	0.9703
Binder[64-28]	1068.76	216.07	4.95	**0**
Binder[58-34]	3706.56	303.57	12.21	**0**
Binder[64-34]	5552.45	307.72	18.04	**0**
Time	–20.95	2.19	–9.55	**0**

Table 9. Correlation factors for low temperature level.

	Creep stiffness
Aggregate	**–0.136**
Modified	0.067
Size	**0.227**
Size * Aggregate	–0.043
Size * Time	**–0.280**
Time	**–0.396**

Table 10. ANOVA for low temperature level.

Variable	Estimate	Std. Error	t-value	p-value
Constant	16682.20	564.07	29.58	**0**
Aggregate	–661.92	606.35	–1.09	0.2755
Modification	–2964.93	368.78	–8.04	**0**
Size	1144.53	243.19	4.71	**0**
Size * Aggregate	–134.53	285.61	–0.47	0.6378
Size * Time	–2.19	1.76	–1.25	0.2123
Binder[64-28]	1655.54	369.44	4.48	**0**
Binder[58-34]	4926.49	518.08	9.51	**0**
Binder[64-34]	5918.43	518.08	11.42	**0**
Time	–12.43	3.73	–3.33	**0.0009**

High negative correlation is observed between aggregate type and creep stiffness, indicating that mixtures prepared with granite are stiffer than mixtures with limestone. However, if a linear model is assumed to explain the creep stiffness of the mixtures then, the information provided by the aggregate is not significant as indicated by the high *p*-value in the ANOVA presented in Table 10. Time is significant as expected. It is important to note the reduction of the effect of loading time on the creep stiffness as the temperature decreases: –0.396 for LT, –0.560 for IT, and –0.649 for HT, respectively, which is expected.

The variables that are significant in the linear regression are: size, binder modification, binder type, and time. At this temperature, mixtures prepared with PG 64-34, PG 64-28, and PG 58-34 are stiffer than mixtures prepared with PG 58-28 (reference level). The large negative coefficient for binder modification indicates that mixtures with unmodified binder have significantly higher creep stiffness than mixtures with modified binder. The interaction terms of size and aggregate, and size and time do not provide significant information for the explanation of the creep stiffness.

5 CONCLUSIONS

The following important conclusions could be drawn from this experimental study:

- Creep stiffness of asphalt mixtures at low pavement service temperatures can be obtained by testing small beams. As the temperatures decreases, the mismatch between the stiffness of aggregates and of the binder (mastic) diminishes and the creep stiffness of asphalt mixture becomes less dependent on the size and distribution of aggregate particles.
- The analysis of the test results obtained at three temperature levels, high (HT), intemediate (IT), and low (LT) indicate that the effect of the beam size on the creep stiffness is negligible only at IT (PG low limit + 10°C).
- At HT (PG low limit + 22°C), the difference between the stiffness of the aggregates and the asphalt binder (mastic) starts to become significant and the mechanical response of the mixture becomes dependent on the size of the aggregates.

- At LT (PG low limit – 2°C), contrary to expectations, the size of the beam appears to be a significant factor with respect to mixtures creep stiffness. It is hypothesized that the small deflection values measured at this temperature, which increase the variability of the measured creep stiffness, combined with the formation of layers of ice on the supports and around the extensometers, may produce the size effect observed in the analysis.

ACKNOWLEDGEMENTS

The support provided by NCHRP-IDEA 133 is gratefully acknowledged. The results and opinions presented do not necessarily reflect those of the sponsoring agencies.

REFERENCES

American Association of State Highway and Transportation Officials (AASHTO) Standard T 322-03, 2005. Determining the Creep Compliance and Strength of Hot-Mix Asphalt (HMA) Using the Indirect Tensile Test Device, *Standard Specifications for Transportation Materials and Methods of Sampling and Testing*, 25th Edition.

Romero P., Masad E. 2001. Relationship between the representative volume element and mechanical properties of asphalt concrete, *Journal of Materials in Civil Engineering*, vol. 13(1): 77–84.

Weissman S.L., Sackman J.L., Harvey J., Long F. 1999. Selection of laboratory test specimen dimension for permanent deformation of asphalt concrete pavements, Transportation Research Board Annual Meeting.

Zofka, A., Marasteanu, M., Li, X., Clyne, T., McGraw, J. 2005. Simple method to obtain asphalt binders low temperature properties from asphalt mixtures properties, *Journal of the Association of Asphalt Paving Technologists*, Vol. 80: 255–282.

Zofka, A., Marasteanu, M., Turos, M. 2006. Investigation of Asphalt Mixture Creep Behavior Using Thin Beam Specimens, *Proceedings of the International Conference FGM IX, Multiscale and Functionally Graded Materials* , Honolulu, October 15–18: 718–723.

Zofka, A. 2007. Investigation of asphalt concrete creep behavior using 3-point bending test. Ph.D. dissertation, University of Minnesota.

Zofka, A., Marasteanu, M., Turos, M. 2008. Determination of Asphalt Mixture Creep Compliance at Low Temperatures Using Thin Beams Specimens. *CD Proceedings of the 87th Annual Meeting of the Transportation Research Board*, Paper No. 08-2361.

Zofka, A., Marasteanu, M., Turos, M. 2008. Investigation of asphalt mixture creep compliance at low temperatures", *Road Materials and Pavement Design*, Vol. 9: 269–286.

Advanced Testing and Characterization of Bituminous Materials – Loizos, Partl, Scarpas & Al-Qadi (eds)
© 2009 Taylor & Francis Group, London, ISBN 978-0-415-55854-9

Assessment of water sensitivity of asphalt rubber mixtures for wearing course

F.A. Batista & M.L. Antunes
Laboratorio Nacional de Engenharia Civil, Lisboa, Portugal

P. Fonseca
RECIPAV, Cartaxo, Portugal

ABSTRACT: To assess the water sensitivity of asphalt rubber mixtures an experimental study was carried out, in which different types of gap-graded mixtures applied in wearing courses were used. The experimental study compares the results obtained by the test method traditionally used in Portugal - the American army standard MIL-STD-620A—method 104 - with those obtained through the EN 12697-12:2008-method A. The application of the European standard leads to lower values of retained resistance than those obtained with the American army standard and allows for a better distinction of the behavior of different mixtures. This paper presents the main results achieved so far, and contributes for the achievement of reference values for water sensitivity of gap-graded asphalt rubber mixtures determined according to the European standard EN 12697-12:2008—method A.

1 INTRODUCTION

In Portugal, asphalt mixtures produced with bitumen modified with a high percentage of rubber (bitumen-rubber) are used in paving works since 1999. During these years, several studies have been developed by the Portuguese National Laboratory of Civil Engineering (LNEC) in order to characterize the performance of this type of mixtures (Antunes *et al.* 2000, 2003, 2006, Batista *et al.* 2008, Miranda *et al.* 2008). The present paper refers in particular to the evaluation of water sensitivity of asphalt rubber mixtures for application in wearing courses.

In Portugal, before the introduction of European standards, the minimum values required for water sensitivity of asphalt mixtures were established based on the American army standard MIL-STD-620A—method 104 (CRD-C 652-95).

In the present context of the European standards, in particular the EN 12697-12:2008, it is necessary to establish reference values to be obtained in tests performed according to this European standard. Indeed, there are significant differences between the test methods of the MIL-STD-620A and the EN 12697-12 standards, which may lead to very distinct results of the water sensitivity for a given mixture.

This paper reports an experimental study carried out in order to assess the water sensitivity of asphalt rubber mixtures in which different types of gap-graded mixtures were used.

The experimental study compares the results obtained with the test method traditionally used in Portugal with those obtained through the European standard EN 12697-12—method A, in which the effect of saturation and accelerated water conditioning on the indirect tensile strength of cylindrical specimens of bituminous mixtures is determined. One conclusion is that the application of the European standard leads to lower values of water resistance than those obtained with the American standard and allows a better distinction of the behavior of different mixtures.

This paper presents the main results achieved, and gives a contribution for establishing reference values for water sensitivity of gap-graded asphalt rubber mixtures determined according to the European standard EN 12697-12—method A.

2 EVALUATION OF WATER SENSITIVITY

In general the assessment of water sensitivity of bituminous mixtures is performed by determining the mechanical strength of two groups of bituminous mixtures test specimens with identical characteristics, which are previously submitted to different conditioning concerning to the detrimental effect of water (Airey & Choi, 2002). The ratio between the average resistance of the set of specimens submitted to more severe conditioning and the one in less severe conditioning provides an "index of retained strength", which is used as an indicator of water sensitivity.

A brief description of the MIL - STD - 620A and EN 12697-12 test methods is presented in the following sections.

2.1 *Test method 104 of the MIL - STD - 620A standard*

In order to assess water susceptibility of bituminous mixtures it has been of common practice in Portugal to use a test method based on the American standard MIL - STD - 620A. According to this test method, the reduction of Marshall stability of bituminous mixtures specimens caused by immersion in water for a prescribed period is measured.

With this purpose, the bituminous mix with the given composition is manufactured and a minimum of 8 Marshall test specimens of 101.6 mm in diameter and about 63.5 mm in height are prepared. These specimens are divided into two groups with approximately the same average bulk density.

The first group is immersed in water at 60ºC for 30 minutes (for 20 to 40 minutes according to the method 100 of the military standard (CRD-C 649-95)), and then the Marshall stability for each specimen is determined and the average value (F_1) is calculated.

The second group is conditioned for 24 h in a water bath at 60°C, after which the Marshall stability for each specimen is determined and the average value (F_2) is calculated.

Based on the results for the average Marshall stabilities, the Index of Retained Stability (IRS) is estimated as follows (Equation 1):

$$IRS = \frac{F_2}{F_1} \times 100 \quad (1)$$

2.2 *Test method A of the EN12697-12:2008 standard*

The evaluation of sensitivity to water of bituminous mixtures recommended in the method A of the EN 12697-12: 2008 is based on the comparison between the average values of indirect tensile strength (determined in accordance with the EN 12697-23) of two groups of cylindrical samples previously conditioned in different conditions.

In this case, 3 cylindrical test specimens are prepared for each group, whose dimensions are defined taking into account the dimension of the maximum aggregate. For mixtures with maximum aggregate size not exceeding 22 mm, specimens with a (100 ± 3) mm in diameter can be used, which means that test specimens are similar to those used in the previous method, compacted by the impact compactor, according to the EN 12697-30.

The test specimens are also be divided into two subsets having approximately the same average bulk density, as well as a similar average length. In this case, the difference between the average bulk densities of the two subsets is limited to a maximum of 30 kg/m^3 for the and the difference between the average lengths is limited to 5 mm. It is also established that the test specimens must be of the same age (prepared within one week), and have a curing time of 16 h to 24 h.

The first subset of specimens (dry specimens) is stored in air at (20 ± 5)°C. The second group (wet specimens) is firstly submitted to a vacuum (absolute pressure (6.7 ± 0.3) kPa) in water at (20 ± 5)ºC in order to ensure that water penetrates adequately in the pores of the test specimens, after which they are stored in a water bath at (40 ± 1)°C, for a period of 68 to 72 h. The volume of specimens from the wet subset must be checked after the application

of vacuum. Any specimen that has suffered an increase of more than 2% in volume must be rejected.

After conditioning, the indirect tensile strength of each specimen is determined, at a test temperature in the range of 5°C to 25ºC. The EN 12697-12 standard includes a note which recommends that a test temperature of 25°C should be selected to obtain the maximum influence from binder adhesion and to minimize influence from broken aggregates in the break line surface. Nevertheless, the EN 13108-20 standard establishes a temperature of 15°C for the initial type testing of CE marked bituminous mixtures.

Based on the ratio between the average indirect tensile strength of water conditioned specimens (ITS_w) and dry specimens (ITS_d), the ITSR value, in percent, is calculated according the formula (Equation 2):

$$ITSR = \frac{ITS_w}{ITS_d} \times 100 \tag{2}$$

2.3 *Features related to the implementation of the method A of the EN12697-12 standard*

Earlier experiences developed at LNEC with the EN 12697-12 test method A have shown that its application presents some difficulties, mainly concerning the application of vacuum to the wet subset of test specimens. The first results obtained for ITSR using EN 12697-12 test method A, showed a relatively high dispersion, with values which were much lower than those expected considering the type of mixtures tested. This type of problems were attributed to the application of vacuum to the wet specimens.

Taking into consideration the experience gained so far, it is recommended that the following steps are strictly followed in the application of vacuum (Fig. 1):

- Place the wet subset of specimens in the vacuum container (pycnometer) filled with distilled water at (20 ± 5)°C up to a level at least 20 mm above the top of the test specimen;
- Apply a vacuum to obtain an absolute pressure of (6.7 ± 0.3) kPa within (10 ± 1) min. It is very important to reduce the pressure gradually to avoid any damage. For this, the pressure should be reduced in steps between the atmospheric pressure (≈101.3 kPa at sea level) and the target value in steps, which can be achieved monitoring the duration of each step with a stopwatch.
- Keep the vacuum during (30 ± 5) minutes.
- Allow pressure to grow slowly till the atmospheric pressure.
- Leave the specimens immersed for a further period of (30 ± 5) minutes.

Figure 1. Vacuum being applied to the wet subset of test specimens.

3 WATER SENSITIVITY OF ASPHALT RUBBER MIXTURES

In order to assess water sensitivity of gap-graded asphalt rubber mixtures, two mixtures were produced using the same bitumen rubber binder produced with a 35/50 grade virgin bitumen and two different gap-graded mixtures: one produced with granite and another with crushed gravel. Table 1 identifies the tested mixtures.

The characteristics of the materials used in the production of the AR mixtures are described in the following paragraphs.

3.1 *Bitumen rubber binder*

The binder used for the production of the asphalt rubber mixtures, usually known as "bitumen-rubber" (BR) was obtained through the *in-situ* modification of a virgin bitumen with crumb rubber though the so-called "wet process".

Presently, there is a wide range of bitumen rubber binders in the Portuguese market, such as *in situ* manufactured binders with high content of crumb rubber and *ex situ* manufactured binders with lower contents of crumb rubber.

This paper refers specifically to AR mixtures produced with bitumen rubber containing more than 18% of crumb rubber, known as "modified bitumen with high content of crumb rubber", and produced with a 35/50 penetration grade bitumen. Table 2 presents the main properties of the BR used in this study.

3.2 *Aggregates*

The mixtures tested in this study were gap-graded mixtures produced with 0/12.5 mm aggregates of two different natures: granite and crushed gravel.

Table 3 presents the composition of the aggregates used in the production of the referred AR mixtures, and Figure 1 represents the corresponding grading.

3.3 *Experimental programme*

This study comprised AR water sensitivity assessment through the MIL - STD - 620A and the EN 12697-12 standards. In the last case, the indirect tensile tests were conducted at

Table 1. Tested asphalt rubber mixtures identification.

AR mixtures identification	GG-gravel-BR	GG-granite-BR
Aggregate nature	Crushed gravel	Granite
Binder characteristics	82% B35/50 + 18% rubber	82% B35/50 + 18% rubber
Binder content	8.5%	8.5%

Table 2. Rubber modified bitumen (18% to 22% of rubber) properties.

Bitumen rubber binder	Viscosity at 175ºC* (20 rpm) EN 13302:2003	Penetration at 25ºC (100 g, 5 s) EN 1426:1999	Softening point (ring and ball method) EN 1427:1999
	Pa.s	0.1 mm	ºC
Rubber modified 35/50 grade bitumen	2500 to 4500	15 to 30	≥68

*Determined using a Brookfield apparatus with thermosel and a SC4 - 27 spindle.

Table 3. Aggregates compositions.

AR mixtures identification	Fraction dimension	Fraction percentage
GG-gravel-BR	10/16 fraction	15%
	4/10 fraction	53%
	0/6 fraction	30%
	Commercial filler	2%
GG-granite-BR	10/15 fraction	23%
	6/10 fraction	58%
	0/5 fraction	17%
	Commercial filler	2%

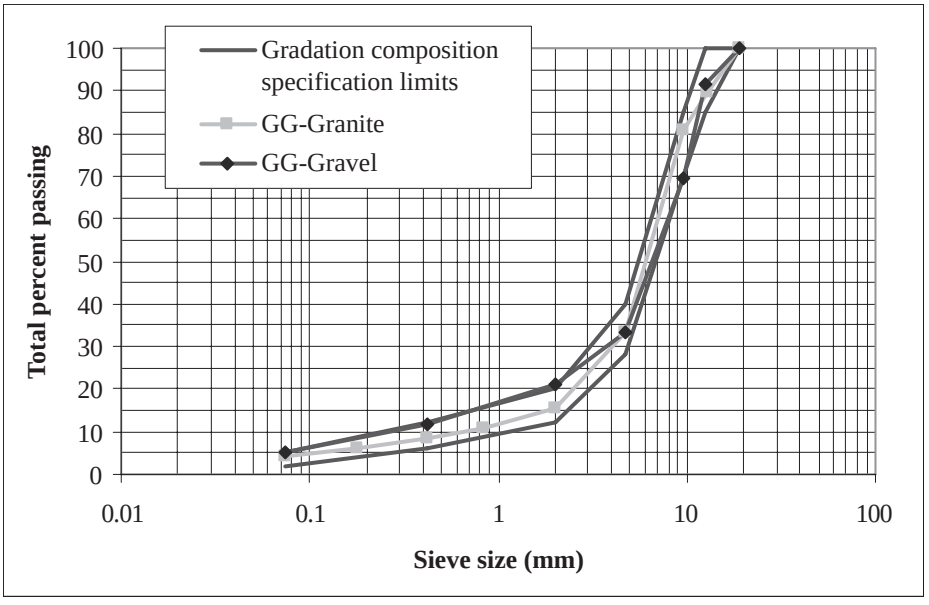

Figure 2. Aggregates gradation.

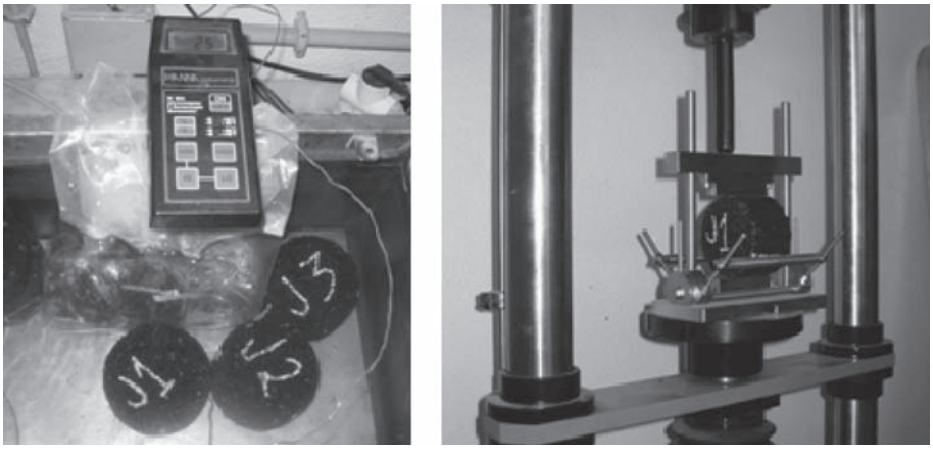

Figure 3. Snapshots of the test method A of the EN 12697 - 12:2008.

Table 4. Results of the water sensitivity tests (MIL - STD - 620A—method 104).

AR mixtures identification	Average air voids content (%)	Water sensitivity test		
		Property	Specimens 30 min. immersed in water at 60ºC	Specimens 24 h immersed in water at 60ºC
GG-gravel-BR	2.8	Average bulk density (kg/m^3)	2278	2283
		Average Marshall stability (kN)	13.3	13.2
		IRS (%)	99	
GG-granite-BR	4.6	Average bulk density (kg/m^3)	2202	2199
		Average Marshall stability (kN)	11.8	11.3
		IRS (%)	96	

Table 5. Results of the water sensitivity tests (EN 12697-12: 2008—method A).

AR mixtures identification	Average air voids content (%)	Water sensitivity test		
		Property	Specimens conditioned 3 days at 20ºC	Specimens submitted to vacuum and immersed in water at 40ºC for ≈ 70 h
GG-gravel-BR	2,5	Average bulk density (kg/m^3)	2286	2285
		Average indirect tensile strength (kPa)	1157	777
		ITSR (%)	67	
GG-granite-BR	3,8	Average bulk density (kg/m^3)	2221	2222
		Average indirect tensile strength (kPa)	990	847
		ITSR (%)	86	

temperature of 25ºC taking into account the benefits outlined in the EN 12697-12 for the selection of this test temperature. In both cases, Marshall specimens were prepared using a impact compaction (EN 12697-30) with an energy level of 2×75 blows.

Figure 3 illustrates two aspects of the application of method A recommended by EN 12697-12.

Tables 4 and 5 present respectively, the results obtained in the water sensitivity tests performed according to MIL - STD - 620A and European standard.

Figure 4 summarizes the retained strength obtained for the two different mixtures tested according to the referred test methods.

From the results presented it can be noticed that:

- The application of U.S. military standard (MIL-STD-620A) leads to very high values of retained strength, providing virtually the same results for both mixtures;

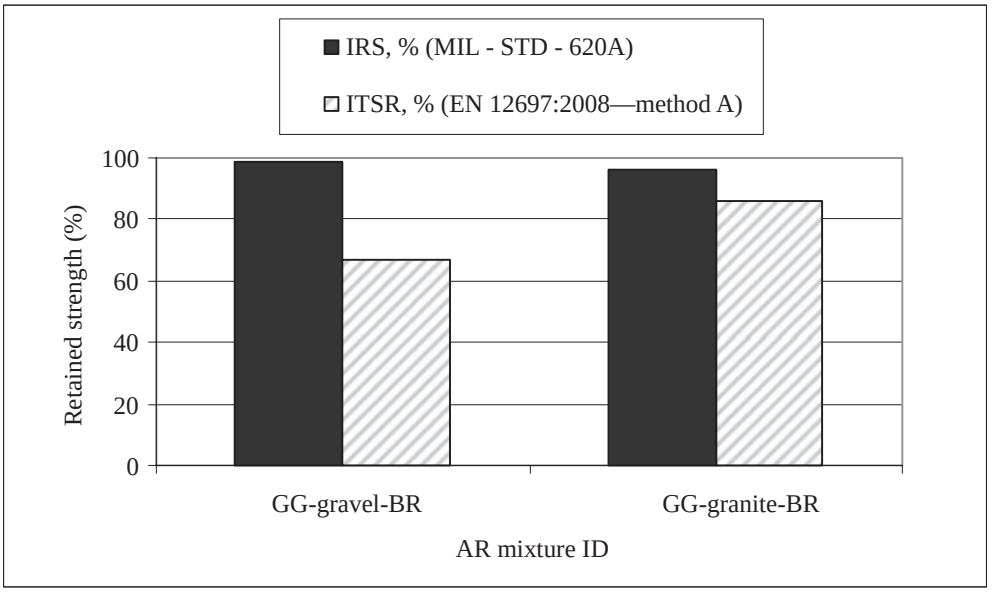

Figure 4. Variation of retained strength obtained using different test methods (MIL - STD - 620A standard versus EN 12697-12:2008—method A).

- These values were reduced when the water sensitivity tests were performed according to the European standard (EN 12697-12:2008—method A);
- The European standard provides a better distinction between the behaviour of the referred mixtures in the presence of water: as expected, the gravel AR mixture presented lower values for the retained strength (ITSR values).

4 FINAL REMARKS

This paper presented the first experiments undertook at LNEC in order to evaluate the water sensitivity of bituminous mixtures with a high percentage of rubber, according to the European standard EN 12697-12.

The experimental study compares the results obtained through the test method traditionally used in Portugal with those obtained through the European standard EN 12697-12. The application of the European standard leads, in general, to lower values of retained resistance when compared with those obtained with the US military standard and allows for a better distinction between mixtures produced with different aggregates.

There have been, however, some difficulties with the implementation of the European test method, especially during application of the vacuum to the immersed specimens. This paper presents some recommendations to overcome these difficulties.

REFERENCES

Airey, G.D. & Choi, Y.-K. 2002. State of the art report on moisture sensitivity test methods for bituminous pavement materials. *International Journal of Road Materials and Pavement Design,* 3 (4):355–372.

Antunes, M.L.; Batista, F.A.; Eusébio, I.; Costa, M.S. & Miranda, C.V. 2000. Characterization of asphalt rubber mixtures for pavement rehabilitation projects in Portugal. *Proc. of the "Asphalt Rubber 2000", Vilamoura, Portugal, 14-17 November 2000*:285–307.

Antunes, M.L.; Domingos, P.; Eusébio, I. & Costa, M.S. 2003. Studies concerning the use of Asphalt Rubber in Portugal. *Proc. of the "Asphalt Rubber 2003", Brasília, Brasil, 1–4 December 2003*:195–210.

Antunes, M.L.; Batista, F.A. & Fonseca, P. 2006. Asphalt rubber mixtures in Portugal: practical application and performance. *Proc. of the "Asphalt Rubber 2006", Palm Springs, California, USA, 25–27 October 2006*, p.14.

Batista, F.A.; Antunes, M.L.; Miranda, H. & Fonseca, P. 2008. Fatigue resistance of asphalt rubber mixtures. *Proc. of the TRA2008 - Transport Research Arena Europe 2008 conference, Ljubljana, Slovenia, 21–24 April 2008*.

CRD-C 649-95—Standard Test Method for Unit Weight, Marshall Stability, and Flow of Bituminous Mixtures (Formerly MIL-STD-620A, Method 100, 13 January 1996), *Construction Criteria Base - Handbook for Concrete and Cement, Whole Building Design Guide*, http://www.wbdg.org/, 2008.

CRD-C 652-95—"Standard Test Method for Measurement of Reduction in Marshall Stability of Bituminous Mixtures Caused by Immersion in Water" (Formerly MIL-STD-620A, Method 104, 13 January 1966), *Construction Criteria Base - Handbook for Concrete and Cement, Whole Building Design Guide*, http://www.wbdg.org/, 2008.

EN 12697-12:2008—European standard EN 12697 - Bituminous mixtures—Test methods for hot mix asphalt. Part 12 - Determination of the water sensitivity of bituminous specimens.

EN 12697-23:2003—European standard EN 12697 - Bituminous mixtures—Test methods for hot mix asphalt. Part 23 - Determination of the indirect tensile strength of bituminous specimens.

EN 12697-30:2004 + A1:2007—European standard EN 12697 - Bituminous mixtures—Test methods for hot mix asphalt. Part 30 - Specimen preparation by impact compactor.

EN 13108-20:2006—European standard EN 13108 - Bituminous mixtures—Material specifications. Part 20: Type testing.

Miranda, H.; Batista, F.A.; Neves, J.; Antunes, M.L. & Fonseca, P. 2008. Asphalt Rubber Mixtures in Portugal: Fatigue Resistance. *Proc. of the "3rd European Conference on Pavement and Asset Management", Coimbra, Portugal, 7–9 July 2008*, CD-ROM.

Advanced Testing and Characterization of Bituminous Materials – Loizos, Partl, Scarpas & Al-Qadi (eds)
© 2009 Taylor & Francis Group, London, ISBN 978-0-415-55854-9

Development of a laboratory bituminous mixtures ageing protocol

C. de la Roche
Laboratoire Central des Ponts et Chaussées, Nantes, France

M. Van de Ven
Delft University of Technology, Delft, The Netherlands

W. Van den bergh
Artesis Hogeschool Antwerpen, Antwerpen, Belgium

T. Gabet
Laboratoire Central des Ponts et Chaussées, Nantes, France

V. Dubois
Laboratoire Central des Ponts et Chaussées, Nantes, France/PRES Université Lille Nord de France—LAMTI, Béthune, France

J. Grenfell
Nottingham Transportation Engineering Centre, University of Nottingham, UK

L. Porot
Shell Bitumen, France

ABSTRACT: The RILEM TC-ATB-TG5, in charge of "recycling of bituminous materials" has decided to develop a laboratory procedure with the aim of reproducing the ageing of bituminous materials until the end of their service life (milled product). This procedure will help to assess the recyclability of mixtures and will allow Recycled Asphalt Pavement (RAP) production in the laboratory in a realistic way. The ageing of bituminous materials is mainly linked to the ageing of the binder and is normally separated into short and long-term ageing:

– The short-term ageing simulating ageing caused by the manufacture of the material in the mixing plant, transport and paving, especially the necessity to increase the binder temperature up to 160–190°C according to the type of binder and material to be manufactured.
– The long-term ageing simulating the influence of the climatic conditions and traffic loading on ageing during service life.

In the framework of an LCPC fatigue carousel experiment, a bituminous material with a 35/50 pure bitumen was laid in January 2008. Loose mix and components (aggregates, bitumen) of the mix have been sampled to carry out a laboratory ageing round robin test, organised between the labs of the RILEM group. Also, on the fatigue carousel, coring will be carried out at several intervals to follow the evolution of the material.

In this paper, a state of the art regarding the existing methodologies for the laboratory ageing of bituminous materials is presented as well as the round Robin test, including the tested ageing procedures and the tests chosen to validate these procedures according to the field site data. The first results are discussed with the focus on distribution analysis.

1 INTRODUCTION

Due to the trend to fulfil sustainable development requirements, the fact that access to easy to extract oil is over and the price increase and well as the shortage of good quality aggregates,

recycling of asphalt pavement is a very important activity. In this context, the recycling of Reclaimed Asphalt Pavement (RAP) is becoming a major concern for road owners, contractors and material suppliers. The development is to increase the percentages of RAP in new asphalt mixtures. In order to predict and improve the knowledge of the potential to recycle old bituminous materials and the influence of their use on the performance of new bituminous materials, specific laboratory tests have to be developed.

In the framework of the RILEM Technical Committee ATB—Advanced Testing of Bituminous Materials—Task Group 5 (TG5) "recycling of bituminous materials" focuses on the main issues regarding this subject. In addition to a European survey of the use of RAP (Planche, 2008), TG5 has decided to focus on the possibility to study recyclability of mixtures and RAP production in the laboratory. In order to achieve this goal, a laboratory procedure has been developed, aiming at reproducing in the laboratory the ageing of bituminous materials until the end of their service life (milled product).

After a literature review on existing ageing procedures for bituminous materials in the laboratory, the paper presents the testing protocol chosen after preliminary tests performed by LCPC. The organisation of a round robin test aiming at evaluating the relevance of the test procedure is described. The round robin tests are still running but the first results are presented and analysed in the paper.

2 DEVELOPMENT OF A MIXTURE AGEING PROTOCOL

2.1 *Literature review*

Previous studies have been carried out to define a laboratory procedure that can predict the future ageing of asphalt mixtures (Porot et al, 2008).

The SHRP programme A383 (Bell, 1994) has defined a laboratory ageing procedure for asphalt mixtures. The AASHTO R30-2 method is based on that procedure and it consists of:

- A short-term ageing step in which the loose mixture is aged in a forced-draft oven for four hours at 135°C. This represents an average level; in reality, mixtures may undergo very little ageing or considerably more ageing.
- A long-term ageing step in which compacted-mixture specimens are aged in an oven for 5 days at 85°C.

The process can be accelerated to two days by using 100°C, but the NCHRP A383 (Bell, 1994) report stresses that this could lead to specimen damage. This method is still a subject for research. The limitations of the protocol are related to the correlation with field data and in the differentiation by mixture type and thickness (Raghavendra et al, 2006).

In Japan, research has also been conducted to clarify the effect of ageing for asphalt concrete. A compacted sample was aged in an oven at 70°C for specified periods (Hachiya et al, 2003). In Europe, the University of Nottingham has developed a specific test called Saturation Ageing Tensile Stiffness (SATS) to assess the ageing and moisture sensitivity of asphalt mixtures (Airey et al, 2005).

However, all these methods use compacted samples. To produce materials for further use "as RAP", compacted samples must be reheated to become loose materials. This is one of the reasons why these methods have to be refined for the purpose of future recycling studies.

In 2006 a first experimental test for a Belgian ageing method for loose mixes was conducted by Artesis Hogeschool (Van den bergh et al, 2008, 2009). Several asphalt mixtures were aged in an air-ventilated oven during a short-term ageing period (3 hours at 130°C) and a long-term ageing period at 90°C. The binders extracted from the aged mix were tested with DSR, penetration, softening point and FTIR. The results indicated that ageing still proceeds in rheological and chemical terms after 7 days.

In addition, previous work done in this area has shown that the correlation with field data is extremely difficult; such correlation depends on the location of the road, sun exposure, climate, mixture type and void contents.

2.2 *Choice of experimental conditions*

Based on the previous literature review, a test protocol has been chosen. This method must be easy to implement and representative enough for practice. The protocol consists of heating a bituminous mixture in an oven, in order to oxidise the material. A loose mixture is used to allow obtaining more homogeneous aged materials. The size of the samples to be aged has been well defined in terms of height and surface to limit size effects during the oxidation process. UV ageing during service life has not been considered as it only affects a very thin skin of the surface layer (Wu et al, 2008) (Durrieu et al, 2007). A classical heating oven is used.

The ageing protocol has been divided in short and long term protocols after manufacturing (heating and mixing), in order to simulate ageing due to transportation and laying, and ageing on site during service life:

– For short-term ageing, loose mixture is aged in an oven for 4 hours at 135°C.
– For long-term ageing, loose mixture is aged in an oven for 9 days at 85°C.

The effect of ageing on the bituminous mixture is assessed through measurements on the recovered binder at different steps of the protocol. The results are compared to the classical ageing tests performed on the binder itself. Empirical rheological (penetration and softening point), fundamental rheological (complex modulus, phase angle) and chemical (oxidation levels) characteristics are investigated. In the future, it is planned to compare these results to the in situ material properties after long-term ageing on site.

In order to completely define this protocol and check its feasibility, preliminary tests have been performed at LCPC (§2.4).

2.3 *Material tested*

In January 2008, an experiment was carried out on the LCPC test track, see Figure 1. A 60 mm thick layer of a "0–10 mm" BBSG (medium coarse asphalt) was laid. This material is usually chosen in France as a wearing course material. The mix composition is given in Table 1. Loose mix (750 kg) has been sampled in the paver (see Figure 2) and aggregates and binder have been sampled (2950 kg) from the mix plant according to the mix composition in Table 1. Homogenisation of aggregates was necessary to make homogeneous samples for each lab.

Table 1. Components and characteristics of the material tested.

Component		Proportions
0–2 mm	Quarry Brefauchet	34%
2–6.3 mm	Quarry Brefauchet	16%
5.6–11.2 mm	Quarry Brefauchet	49%
Fillers		1%
Pure binder 35/50		5.7% (external percentage)

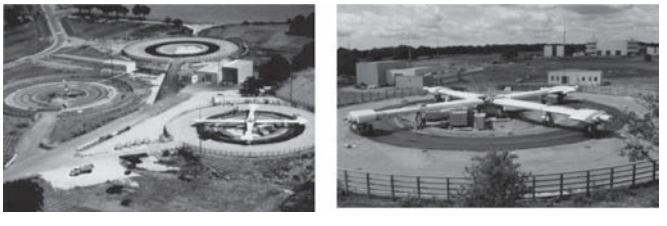

Figure 1. LCPC fatigue carrousel.

2.4 *LCPC preliminary tests*

Three research steps linked to the laboratory manufacturing or to the laboratory ageing procedure have been carried out.

As a first step, rheological properties of the pure binder after the binder laboratory ageing tests and recovered bitumen from plant samples are compared to evaluate the representativeness of laboratory ageing tests.

As a second step, the influence of the manufacturing temperature is studied. This was done because temperature measurements of the loose mix in the lorry at the arrival on the site were between 180 and 185°C. These values are 20°C higher than the temperature specified in the European standard EN 13108. This part aims to fix the laboratory manufacturing temperature for the round Robin test with all the partners and to verify the influence of the short term ageing.

Finally, in-situ, materials can be stirred during the manufacturing and the laying. The stirring induces a large air exposure to the material which can increase oxidation of the binder. So the third preliminary step aims to study the influence of stirring on the rheological test results, in working out a specific laboratory ageing of the material with stirring of material several times during the ageing process. Another objective of this step is to follow the evolution of the rheological properties of binder and to optimise the long term ageing protocol.

For each step and mode of manufacturing or ageing, recovered binder is characterised with penetration (EN 1426), softening point (EN 1427) and asphaltene content (LCPC protocol). Dynamic Shear Rheometry (EN 14770) has also been carried out on the binders of step 2 and step 3.

2.4.1 *Comparison between binders aged in the laboratory and binder recovered from the plant mix*

Table 2 presents the results of the investigations on the virgin binder, before and after ageing tests as well as binder recovered from the paver mix samples. From the results of the three tests it can be concluded that recovered binder is more aged than the bitumen after RTFOT. The overheating of the mix during the manufacturing could be the reason for this. The second step has been carried out to verify the influence of the manufacturing temperature, in the laboratory.

Figure 2. Sampling of loose mix.

Table 2. Results on binders aged in the laboratory and binder recovered from the plant mix.

Description	Penetration	Softening point	Asphaltene content
	[10^{-4}m]	[°C]	(%)
35–50 grade bitumen	43	54	14.2
Bitumen after RTFOT	29	59.6	16.4
after RTFOT and PAV	15.1	66.8	Not measured
Bitumen recovered*	20	62.8	18

*From the loose mix sampled from the paver during the road construction (see Figure 2).

2.4.2 *The Effect of manufacturing temperature and short-term ageing on the binder characteristics*

The influence of two different manufacturing temperatures combined with short-term ageing is studied and compared to the rheological properties of the recovered bitumen from the field sample (Table 3). Two manufacturing temperatures (165 and 185°C) with and without following short-term aging have been tested (Table 3). These results show that with short-term ageing, there is no influence of the manufacturing temperature. The mix after short-term ageing is close to the one sampled in the paver. So it is no problem to choose the manufacturing temperature from the standard (165°C) for laboratory mixing.

2.4.3 *Effect of stirring on ageing in laboratory*

This third step aimed to evaluate the influence of the stirring during the ageing procedure. Materials are manufactured with an identical laboratory procedure at 165°C, and are separated in two batches A and B. Each batch is aged according to the short-term ageing procedure. Then materials are placed in an oven at 85°C for nine days for long-term ageing.

For batch A, the material in the box is stirred after each sampling (after short-term ageing, at 2 days, 5 days, 7 days and 9 days). For batch B, no stirring is carried out during the long-term ageing. After each sampling, the residual material was kept at the original thickness of 0.05 m. One operator has performed all the extractions and one operator has tested all the samples for each type of measurement.

The results are shown in Table 4.

The ageing evolution is steady in both cases. Table 4 shows that the recovered binder without stirring seems to be a little more aged than the binder recovered from stirred materials. According

Table 3. Effect of manufacturing temperature and short-term ageing on the recovered binder properties.

Laboratory mixing temperature	Laboratory short term aging	Penetration	Softening point	Asphaltene content
°C	135°C, 4 hours	1/10e mm	°C	%
165	No	31	58	16.8
165	Yes	20	64.8	18.9
185	No	28	59.6	17.5
185	Yes	19	64.4	18.6
Binder recovered from plant mix	–	*20*	*62.8*	*18*

Table 4. The Effect of stirring on ageing.

		Penetration	Softening point	Asphaltene content
Description	Sampling	1/10e mm	(°C)	(%)
	After 135°C 4 h	22	62.6	15.8
With stirring	Batch A – J+2	21	64.0	19.9
	Batch A – J+5	17	66.0	20.0
	Batch A – J+7	16	66.8	20.0
	Batch A – J+9	15	68.0	20.1
Without stirring	Batch B – J+2	20	64.2	19.9
	Batch B – J+5	17	66.8	20.8
	Batch B – J+7	16	67.6	21.7
	Batch B – J+9	15	69.0	21.6

to the complex modulus results, with stirring, results are more homogeneous compared to the samples without stirring, after the first step of the long-term ageing. For the last steps of the long-term ageing, results are similar.

Based on these results and experience of researchers, it was decided to keep the stirring process in the final protocol.

3 SET UP OF ROUND ROBIN TEST

3.1 *Experimental program*

The final mixture ageing protocol chosen for the round robin test takes into account three steps which have to be consistent for all laboratories: the production of the mixture, the ageing of the mixture and the binder extraction and recovery. This last step is necessary only to evaluate the binder ageing in the developing phase of the ageing procedure but will not be required after the approval of the protocol.

Two types of materials are tested in each laboratory in order to make a comparison between laboratory and plant manufacturing.

– Batch 1 (36 kg lab-produced mix) is mixed with a target temperature of 165°C
– Batch 3 (36 kg plant mix), is reheated at 110°C for four hours in closed buckets. It was assumed that this reheating has no influence on the ageing of the material.

A batch 2, similar to batch 1 is also available, but it was decided to use it afterwards if necessary to improve the test protocol.

After production a short-term ageing and subsequently a long-term ageing is conducted. For this, the asphalt mixture is placed into two boxes each with a surface of 0.15 m², e.g. a box of 0.3 m × 0.3 m and a height of 0.08 m; each box contains 15 kg of mixture.

Two samples of 3 kg noted a and b (each from one box) are taken after each step: after production, after short-term ageing and after 2, 5, 7 and 9 days of long-term aging. From all

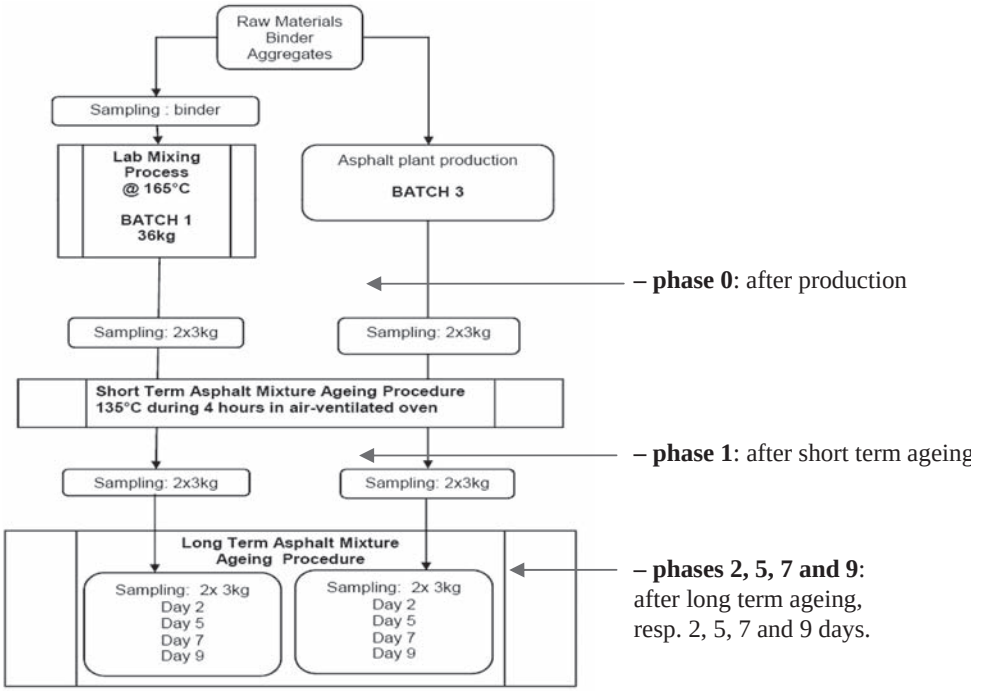

Figure 3. Final mixture ageing protocol, with associated phases.

Table 5. List of the participating laboratories (alphabetical order).

Acronym	Country
Aggregate industries	UK
AHA	Belgium
Delft University	Netherlands
Danish Road Institute	Denmark
EMPA	Switzerland
ISBS	Germany
LCPC	France
LRPC-Aix	France
NTEC	United Kingdom
University of Parma	Italy
Repsol	Spain
SINTEF	Norway
TOTAL	France

these samples, the binder is extracted and recovered for further analysis. Penetration, softening point, DSR frequency sweeps and FTIR tests are conducted. After each sampling, the wooden boundary of the box is moved in order to keep the height of the loose mixture constant at 0.08 m during the whole ageing process.

The protocols for short and long-term ageing are as follows:

– For the short term ageing process, the mix is placed in an air-draft ventilated oven for 4 hours at 135°C. Each hour the material is stirred for 1 minute and placed back into the oven. This stirring action is only for homogenisation.
– For the long-term ageing, the short-term aged mixture is placed in an air ventilated oven at 85°C for 9 days. After 2, 5, 7 and 9 days the mixture is stirred before sampling.

The flow chart displayed in Figure 3 presents the steps of the tests.

For convenience, the results for each step of the ageing process will be numbered in the paper according to the phase numbers indicated in Figure 3.

Besides ageing of loose asphalt mixture, the binder which is used in the asphalt mixture is also aged according to two ageing procedures: 1) RTFOT and PAV and 2) RCAT short-term and long-term ageing. These aged binders are also evaluated with penetration, softening point, DSR and FTIR.

3.2 *Participating laboratories*

The list of the 12 participating laboratories is presented in Table 5, as an acronym in alphabetical order. The loose material from the plant as well as the constituents have been sent from LCPC to the participating laboratories in November 2008.

4 FIRST RESULTS

The round robin test was still running at the time of the writing of the paper. 7 of the 12 participating laboratories have reported part of their results. However some trends can already be drawn from the available results. The complete analysis of the round robin will be published in a following paper.

4.1 *Penetration and softening point*

Seven participants have performed penetration and softening point tests for Batch 1 corresponding to laboratory manufacture. In Figure 4a and 4b, an overview is given of the mean results of the penetration and softening point tests for Batch 1. The results are expressed in relative values normalised at 1 for phase 0 corresponding to sampling after

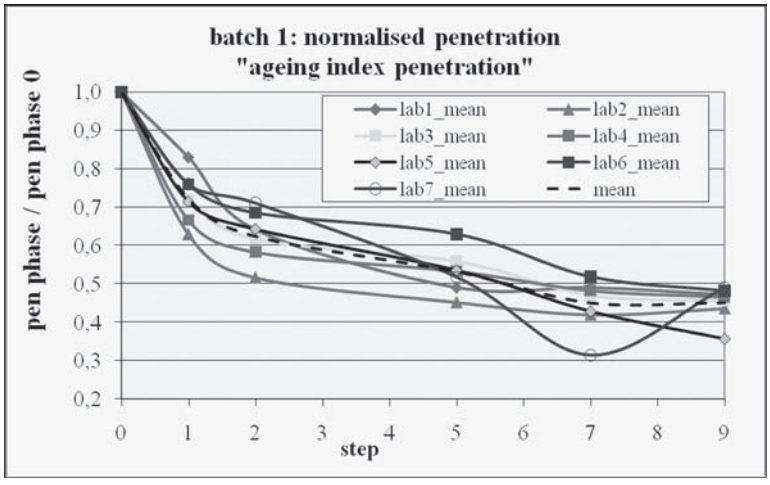

Figure 4a. Penetration relative evolution for the 9 phases of the ageing test (batch 1–laboratory manufacturing).

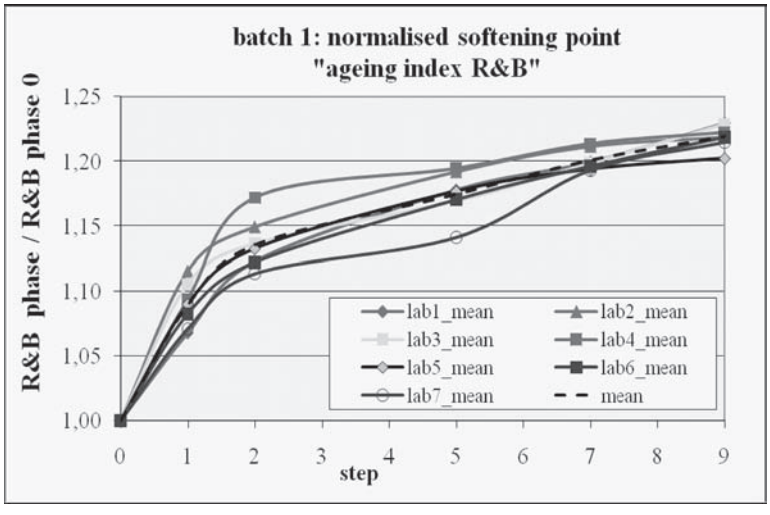

Figure 4b. Softening Point relative evolution for the 9 phases of the ageing test (batch 1–laboratory manufacturing).

manufacturing; the mean results are calculated as the mean values of samples a and b of each step. Laboratory 5 has done the tests on sample "a" only. In general, the results show a good reproducibility of the ageing test and recovery knowing that besides the recovery and extraction, the production and ageing of the mix is encompassed. The differences between the results are a parallel shift-factor throughout the ageing test.

For the penetration (expressed in 1/10 mm) the span at phase 0 is 12.2 and at phase 9 this is 9.1 for all individual results and respectively 10.7 and 5.5 for the mean values (mean of samples a and b).

For the softening points, the results can be considered in the light of the R-value giving the reproducibility limit of the softening point test according to the European standard for binder extraction and recovery: 3.7°C. The mean value in this analysis is the mean value of

all samples, knowing that the R-value in this case also integrates the variance of production and ageing processes between all labs. In general, the results show a good reproducibility (better than for penetration) of the ageing test, recovery and softening point measurement. The differences between the results are a parallel shift-factor throughout the ageing test. For the softening point the span at phase 0 is 2.8°C and at phase 9 this is 4.7°C for all individual results and respectively 2.5 and 3°C for the mean results.

For Batch 3 (Figure 5a and 5b), at the moment of writing the paper three labs had sent their results for further analysis of the penetration and two for the softening point (lab 7 has not sent results for phase 0, so a normalization for softening point is not possible). Therefore the absolute values are given in Figures 5a and 5b.

The absolute difference between Lab 3 and 7 at phase 0 shows the reproducibility for extraction, recovery and the penetration test for two labs.

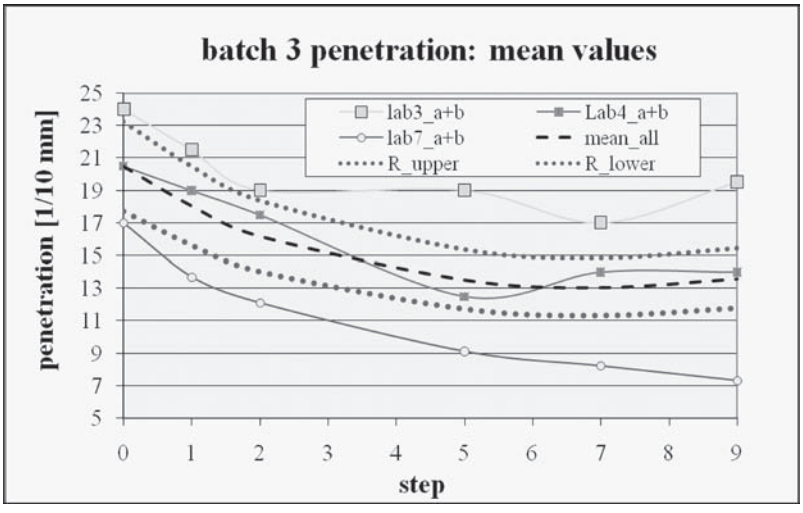

Figure 5a. Penetration values for the 9 phases of the ageing test (batch 3–plant manufacturing).

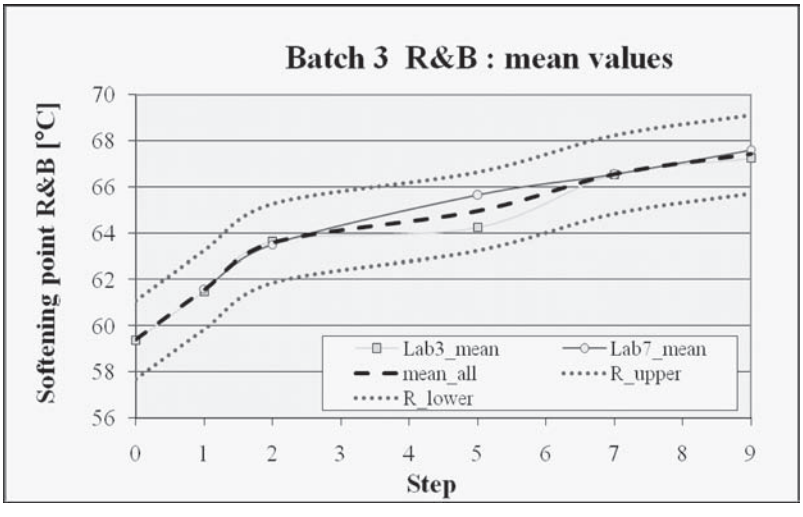

Figure 5b. Softening Points values for the 9 phases of the ageing test (batch 3–plant manufacturing).

Two labs have also tested penetration and softening point on the virgin binder. In the table 6 below the virgin binder characteristics are compared to phase 0 (after production) and phase 1 (after short term ageing). Both steps are in the same order of ageing.

At this point of the project with the received data, some preliminary conclusions can be drawn: even after 9 days the penetration value and softening point of the aged samples indicate that the binder still ages from a rheological point of view although the rate of this ageing decreases. The reproducibility of the ageing test is fulfilling regarding the R-values knowing that the deviations in the results described above are the sum of the deviations for mixing, ageing, the recovery procedure and the penetration test or softening point.

4.2 *Complex modulus*

Dynamic shear rheometers (DSRs) were used to assess the rheology of the recovered binder. The first parameter looked at to compare binder data from different conditions was G* at 25°C and 0.4 Hz. Frequency sweeps have also been performed in order to draw master curves but they will not be discussed in this paper.

4.2.1 *Ageing tests on binder itself*

As well as looking at the recovered binder from the mixing and ageing process, the virgin binder, virgin binder aged using the Rolling Thin Film Oven Test (RTFOT), virgin binder aged using the Rolling Thin Film Oven Test (RTFOT) followed by 20 hours at 100°C in a Pressure Ageing Vessel (PAV) and virgin binder aged for 25 hours at 100°C in a Pressure Ageing Vessel (PAV) were also looked at. The corresponding results are presented in Table 7.

4.2.2 *Results of mix ageing*

Figure 6 shows the effect of ageing steps on the G* of Batch 1. The results again follow a similar trend to the ageing of the virgin binder, with the phase angle decreasing with ageing step. Figure 7 shows the effect of ageing steps on the G* of Batch 3. Again it can be seen that the G* increases with ageing step from approximately 2×10^6 Pa after mixing to 3×10^6 Pa after short term ageing. It then increases to 3.5×10^6 Pa, 4.75×10^6 Pa, 5.3×10^6 Pa and 5.3×0^6 Pa after 2, 5, 7 and 9 days respectively.

Looking at the comparison of the average G* values and average Phase Angle values for the 2 batches (Figure 8) it can be seen that the lab mix is roughly one time step behind the plant

Table 6. Results of ageing tests on virgin binders. Penetration and softening point.

	Lab 5 pen (1/10 mm)	R&B (°C)	Lab 6 pen (1/10 mm)	R&B (°C)
Virgin binder	35	54.1	36	54.2
Phase 0, batch 1	28	58.8	27	58.1
Phase 1, batch 1	20	64.1	20.5	62.9

Table 7. Results of ageing tests on virgin binders. G ∗ 25°C, 0.4 Hz.

	Virgin binder	After RTFOT	RTFOT + PAV 20 hrs	PAV 25 hrs
G ∗ 25°C, 0.4 Hz (Pa)	7.61×10^5	1.50×10^6	3.30×10^6	3.43×10^6
δ (°)	68.5	61.7	52.8	55.0

G* decreases by half with consecutive ageing. It has to be noted that as expected the effect of RTFOT + PAV at 100°C for 20 hours is equivalent to the one of PAV for 25 hours for both G* and phase angle.

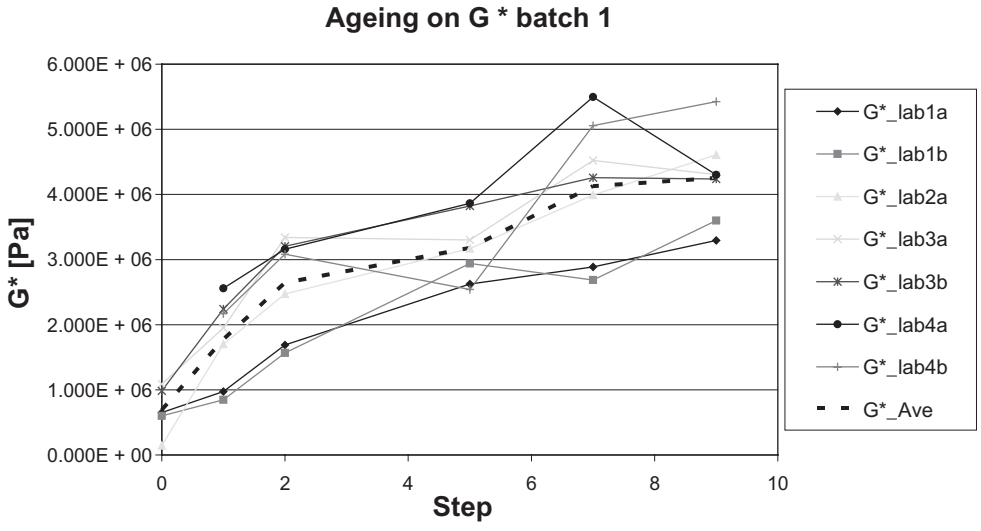

Figure 6. The effect of ageing step on the G* of Batch 1 on Complex Modulus at 0.4 Hz at 25°C.

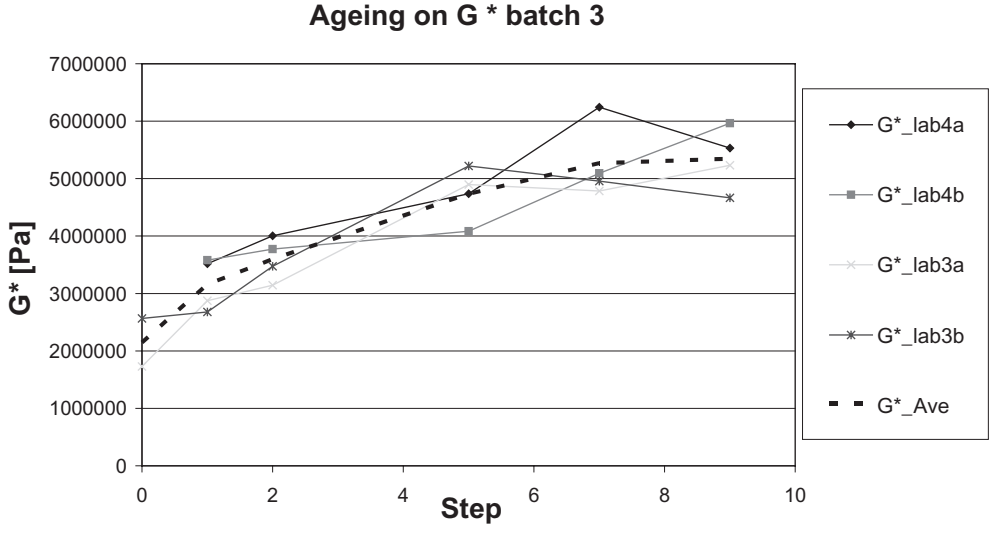

Figure 7. The effect of ageing step on the G* of Batch 3 on Complex Modulus at 0.4 Hz at 25°C.

mix in terms of its ageing. The G* values after mixing for the plant mix are approximately the same as the lab mix after short term ageing and after short term ageing the plant mix values are approximately the same as the lab mix after 2 days ageing etc.

These results are consistent with the ones obtained for penetration and softening point.

4.3 *Infra red spectroscopy*

FTIR (Fourier Transform InfraRed spectroscopy) tests have been carried out at each step of the ageing procedure. From a chemical point of view, ageing can be quantified by the

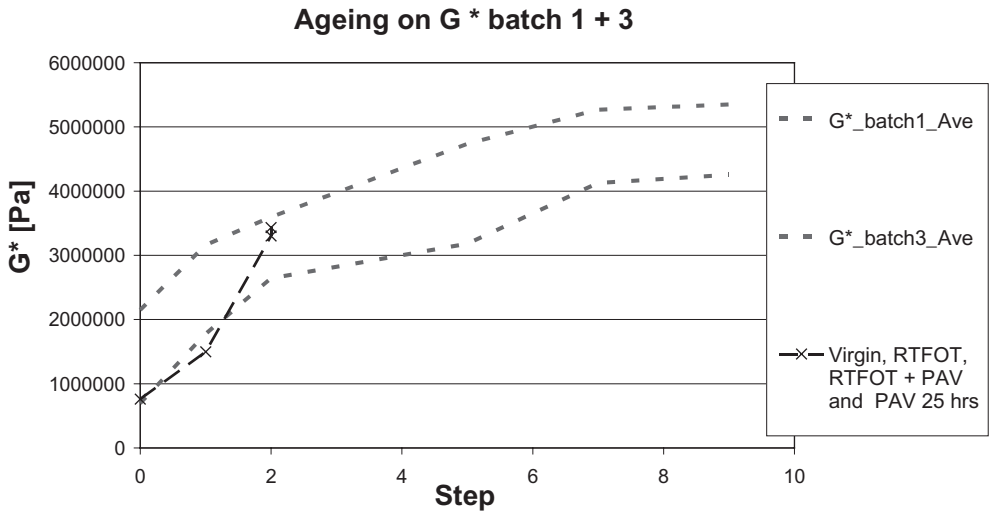

Figure 8. The effect of ageing step on the G* of Batches 1 and 3 on complex modulus at 0.4 Hz at 25°C.

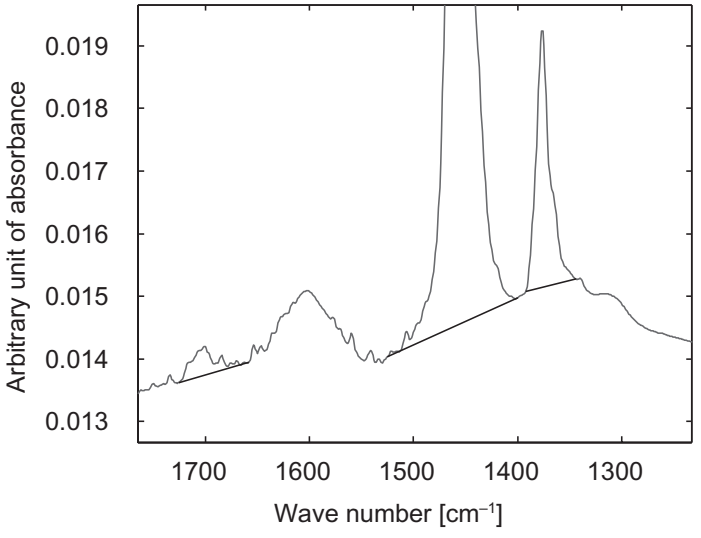

Figure 9. Example of spectrum resulting from FTIR analysis. Black lines define areas used to calculate carbonyl and sulfoxide indexes.

evolution of oxidation inside the bitumen. According to a method (Mouillet, 2009) developed at LCPC for analysing FTIR results (Lamontagne et al, 2001), the evolution of carbonyl and sulfoxide indices are assumed to well represent the evolution of oxidation inside bitumen. In this paper, only the results related to the carbonyl index (Ico) are presented. On Figure 9, an example of spectrum resulting from FTIR analysis is presented. Black lines on the spectrum delimit the areas used to define carbonyl index:

$$Ico = \frac{Area\ around\ 1700\ cm^{-1}}{Area\ around\ 1460\ cm^{-1} + Area\ around\ 1375\ cm^{-1}}$$

Presently, results of 3 laboratories are available for batch 1(laboratory mix). For the laboratory n°09, FTIR tests have been repeated 5 times at each step and for each sample, in order to assess test repeatability.

4.3.1 *Results of lab n°09, repeatability*

Results of lab n°09 are presented in Figure 10, with the Ico index as a function of the ageing protocol steps. An increase of the Ico index can be seen until step 7, which shows an oxidation of the material, as expected. Between step 7 and step 9, the decrease is hard to explain and needs further study. RTFOT and PAV tests have been performed on the virgin binder. Results are also presented in Figure 9, arbitrarily and respectively placed at step 0.5 and 1.5, in order to be compared to the results of the ageing tests. It seems that the ageing protocol results in more ageing of the recovered bitumen than the classical RTFOT and PAV tests only on bitumen. It can be seen that the repeatability is good, according to the small margin of error around the mean value.

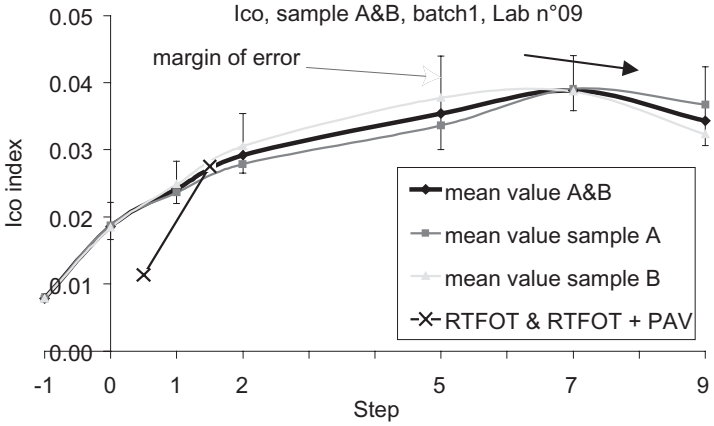

Figure 10. Evolution of Ico during the ageing test. Results of lab 09.

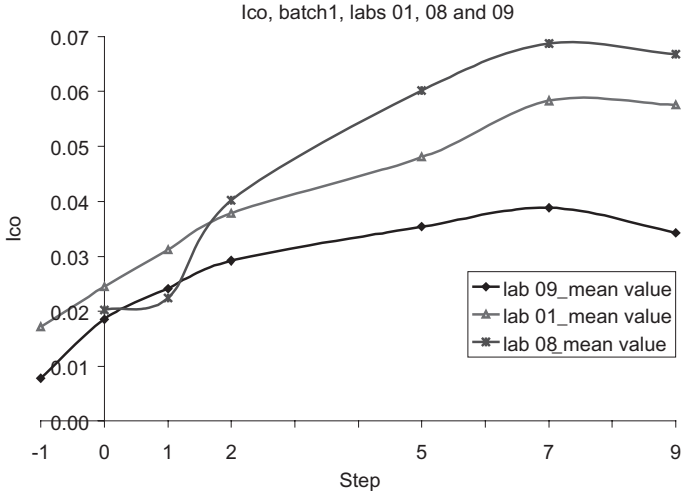

Figure 11. Evolution of Ico during the ageing test. Results of labs 01, 08 & 09.

4.3.2 *Comparison between results of lab n°01, 08 and 09*

In Figure 11, the results of the 3 labs are presented. An increase of Ico index can be noticed for the 3 labs, but the increase seems to be greater for laboratory 08. Laboratories 01 and 09 show similar behaviour despite the offset at step –1, for the virgin binders. We can note that a difference of results for the virgin binders is an issue which will have to be explained. For all the labs, a decrease between step 7 and step 9 can be noticed. The reasons are still to be discovered.

5 PRELIMINARY CONCLUSIONS AND PERSPECTIVES

In order to forecast and improve the knowledge about the recyclability potential of old bituminous materials and the influence of their use on the performance of new bituminous materials, specific laboratory tests have to be developed.

In the framework of the RILEM Technical Committee ATB—Advanced Testing of Bituminous Materials—Task Group 5, devoted to "recycling of bituminous materials" has decided to focus on recyclability of mixtures and RAP production in laboratory.

In order to achieve this goal, a laboratory procedure has been developed, aiming at reproducing the ageing of bituminous materials until the end of the service life in the laboratory.

Based on literature review, the ageing protocol has been divided in short and long-term protocols after the manufacturing, in order to simulate the two following phases of ageing: transportation and laying, and ageing on site once the road is constructed.

- For short-term ageing, loose mixture is aged in the oven for 4 hours at 135°C.
- For long-term ageing, loose mixture is aged in an oven for 9 days at 85°C.

The effect of ageing on the bituminous mixture is assessed through the evolution of the recovered binder at different steps of the protocol in comparison to the classical ageing tests performed on the binder itself.

The first results coming from a round robin test including 12 participating laboratories show that the ageing of the plant mix is similar to the ageing of the mix manufactured in the laboratory and subjected to the short-term ageing protocol, for all the indicators tested (penetration, ring and ball, DSR and FTIR).

The mix subjected to long-term ageing evolves until the 9 days of the protocol and seems to lead to a more aged binder compared to the classical ageing tests on binders.

Even if the results obtained show some scatter between the different laboratories, the results are quite consistent in terms of evolution and the scatter is not high taking into account that the results obtained on recovered binders include the reproducibility of the ageing protocol, the recovery procedure as well as the binder test itself.

The results presented are preliminary results and they will be completed and further analysed with the continuation of TG5 work and especially with the comparison to the actual ageing of the bituminous mix on site.

ACKNOWLEDGEMENTS

The authors greatly thank all the participating laboratories which produced these first results as well as the members of RILEM TC—ATB–TG5 for their comments on these results. Special thanks to Tanoe Porquet from LCPC who performed all the preliminary tests.

REFERENCES

AASHTO R30-2 Mixture Conditioning of Hot-Mix Asphalt (HMA).

Airey G., Choi Y.K., Collop A., Moore A. and Elliot R.C. 2005. Combined Laboratory Ageing/Moisture Sensitivity Assessment of High Modulus Base Asphalt Mixtures—Journal of AAPT—Vol. 75.

Bell C.A. 1994—NCHRP A383, Selection of Laboratory Aging Procedures for Asphalt-Aggregate Mixtures.

Durrieu F., Farcas F. and Mouillet V. (2007) The influence of UV ageing of SBS modified bitumen: comparison between laboratory and on site ageing. Fuel, vol 86, p. 1446–1451.
Hachiya Y., Nomura K. and Shen J. 2003. Accelerated Aging Tests for Asphalt Concretes– 6th RILEM Symposium PTEBM, Zurich.
Lamontagne J., Dumas P., Mouillet V. and Kister J. Comparison by Fourier Transform InfraRed (FTIR) Spectroscopy of different ageing techniques: Application to road bitumen. Fuel, vol 81, p. 483–488.
Mouillet V., Farcas F., Battaglia V., Besson S., Petiteau C. and Le Cunff F. (2009) Identification and quantification of bituminous binder's oxygenated species. Analysis by Fourier Transform InfraRed spectroscopy. LCPC Testing method n°69, to be published.
Planche J.P. 2008. European survey on the use of RAP. Proceeding of ISAP, Asphalt and Environnement conference, Zurich, pp. 3–18.
Porot L. and Bobrisow L. (2008). Laboratory mixture ageing protocol for RAP production. Proceedings of the 4th Eurasphalt & Eurobitume Congress, Copenhagen, 21–23 May.
Raghavendra S., Zapata C., Mirza W., Houston W. and Witczack M. 2006. Verification of the Rate of Asphalt Mix Aging Simulated by AASHTO PP2-99 Protocol by– TRB Meeting Washington DC.
Van den bergh, W. and van de Ven, M. (2008) "Asphaltgranulate: Experiences in Flandres, Belgium (in Dutch), Infradagen Nederland 2008, Delft, The Netherlands.
Van den bergh, W. (2009) "The development of an artificially aged asphalt mixture (in Dutch): AAAM; Artificial Aged Asphalt Mixture", Belgian Road Congres, Gent, Belgium.
Van den bergh, W. "Study concerning the Influence of Reclaimed Asphalt Pavement on the Durability of Asphalt Mixtures and the Healing Factor in particular", doctoral research program TU Delft.
Wu S., Pang L., Mo L., Qiu J., Zhu G. and Xiao Y. (2008). UV and thermal aging of pure bitumen—Comparison between Laboratory simulation and natural exposure aging. Road Materials and Pavement Design, Special issue EATA, Vol 9.

3. Hot bituminous mixtures characterization and design

Advanced Testing and Characterization of Bituminous Materials – Loizos, Partl, Scarpas & Al-Qadi (eds)
© 2009 Taylor & Francis Group, London, ISBN 978-0-415-55854-9

Optimum loading speed for deformation strength test of bitumen mixtures

Sung Hyun Baek, Jin C. Kim, Young S. Doh & Kwang W. Kim
Department of Regional Infrastructures Engineering, Kangwon National University, Chun Cheon, Republic of Korea

ABSTRACT: A series of studies were performed for developing a new test protocol and for characterizing the deformation strength, designated as S_D, which was found to have relatively high correlations with wheel tracking and APA results ($R^2 > 0.8$ on the average) at 60°C. In the test, the peak load (P) and vertical deformation (y) at the peak load point were obtained and S_D is then calculated by the equation of $S_D = 0.32P/(10+\sqrt{20y-y^2})^2$. Since rutting is known to be induced more severely by slow-moving vehicles, it is necessary to investigate the slower loading speed than 50 mm/min, by which Marshall Stability and indirect tensile strength tests are performed, is needed to be investigated. Therefore, S_D test was performed by loading speeds of 10, 30, 50 and 70 mm/min to select optimum loading speed which showed the highest correlation with WT results. From regression analysis results between S_D and WT, the 30 mm/min was found to show the highest correlation.

1 INTRODUCTIONS

A few test methods are available for measuring strength property of hot-mix asphalt (HMA) concretes in static mode. However, those HMA properties are known to have a little correlation with rut resistance of asphalt materials (Li X 2001, Witzack et al. 2002). Several studies were made on this issue to recommend the simple performance test (SPT) for rut estimation of bitumen mixtures (Witzack et al. 2002, Hafez 1997, Kaloush 2001). Their recommendations are not acknowledged as legitimate procedures due to lack of correlation with field rut performance. Rather, the rut potential is evaluated by repeated loading tests, such as wheel tracking (WT) (Brown, S.F. & Gibb, J.M. 1996), asphalt pavement analyzer (APA) (Kandhal & Cooley 2003), dynamic-load creep (DLC) (Zhu & Fwa 2005) and in a larger scale, accelerated loading facility (Bonaquist et al. 1998). Though, these are well-established techniques, equipments are expensive and some procedures are rather complex to follow. Therefore, there is a need for developing a simple strength test method that can measure an engineering property of HMA for estimating rut resistance in laboratory (Kim et al. 2002, Kim et al. 2004a, Doh et al. 2007, Kim et al. 2004b, Kim et al. 2008, Park et al. 2007).

A strength test method was developed in static mode so the property represented the strength against deformation, or the deformation strength, and designated as "S_D" of the HMA. The S_D test has been initiated using the loading speed of 50 mm/min which is used in the static indirect tensile strength test and Marshall Stability test. However, since rutting is known to be more severely induced by slowly-moving vehicles, the S_D value obtained by lower loading speed might represent rut potential better. Therefore, different loading speeds were applied and each S_D test result was compared with WT result for correlation analysis. The objective of this study was to find an optimum loading speed by which the S_D value had the highest correlation with WT result.

1.1 *Deformation strength*

When a wheel, which has a circular imprint, is standing on asphalt pavement, mainly the circular spot will suffer stress and the immediate surrounding body acts as a confining barrier of shear movement for deformation. Since the bearing strength of the limited area is the resistance against deformation of the spot, therefore, instead of applying load to the whole cross sectional area, a load application to the limited area was adopted for S_D test. However, because the imprint of the wheel is not flat, a round edge loading head (rod) was used to create a dimple on the surface of asphalt concrete at 60°C. In this sense, the resistance against this dimple is not simply bearing strength, but is called deformation strength.

Figure 1 (a) shows a 2-D illustration of the S_D test, by which the loading head contacts the mixture in a dimple shape resembling a bowl. The depth of this bowl is y at the peak load P as shown in a load-deformation curve obtained from a test in Figure 1 (b). To estimate rut resistance, S_D was calculated by dividing P by the dimple area projected to the surface or $A = \pi(D - 2r + 2x)^2/4$. The loading head (rod) diameter (D) and radius (r) of edge round were found to be important variables in sensitivity analysis of S_D and optimum values of D and r were determined as 40 mm and 10 mm, respectively (Kim et al. 2008, Park et al. 2007). Since x is a function of r and y, and D = 40 and r = 10, the A becomes $\pi[D - 2(r - \sqrt{2ry - y^2})]^2/4 = \pi[10 + \sqrt{20y - y^2}]^2$ making,

$$S_D = \frac{0.32P}{\left[10 + \sqrt{20y - y^2}\right]^2} \tag{1}$$

where, S_D = deformation strength in pressure unit (MPa), P = maximum load (N) at failure, y = vertical deformation (mm) for y < r. For y ≥ r, then y = r = 10.

Correlation analyses of S_D with WT, APA and dynamic-load creep (DLC) were performed for dense-graded bitumen mixtures. At more than 20 sites in queuing lane of traffic signal on the street, the rut depth of pavement in both wheel paths was measured and a core was taken from the mid lane of the same site. Using S_D values measured on field cores, correlation analysis was also performed between the field rut depth and S_D. R^2 values were found to be ranged from 0.71 to 0.95, indicating the S_D is an excellent engineering property for rut potential estimation of bitumen mixtures (Kim et al. 2004a, Doh et al. 2007, Kim et al. 2008, Park et al. 2007). The repeatability of S_D test results in terms of R^2 was 0.8069 and that of WT was 0.8172 (Kim et al. 2008). The S_D is adopted as one of the criteria in Korean HMA mix design and the test is designated as "Kim Test," details of which are given in elsewhere (Kim et al. 2002, Kim et al. 2004a, Doh et al. 2007, Kim et al. 2004b, Kim et al. 2008, Park et al. 2007, Interim guide for hot asphalt mix design procedures 2008).

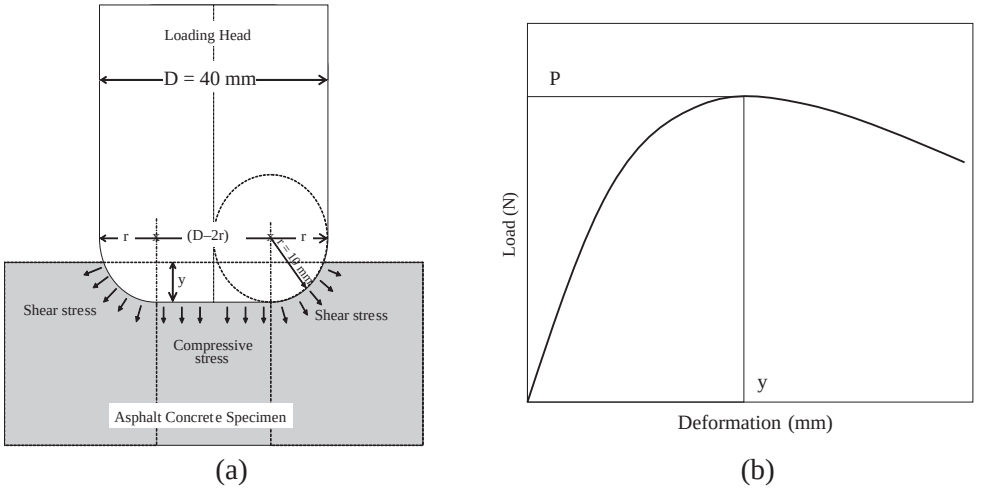

Figure 1. Illustration of (a) S_D test and (b) load-deformation curve.

2 EXPERIMENTAL PROGRAM

2.1 *Materials*

The base bitumen with a 60–80 penetration grade (or PG64-22) was used as a binder for mixture preparation. The base bitumen was modified using a crumb rubber modifier (CRM), recycled low-density polyethylene (RLDPE) and a styrene-butadiene-styrene (SBS). The contents and designation of each modified binder are given in Table 1. Two aggregate sources, gneiss (A) and granite (B), were used in two maximum sizes, 19 mm and 13 mm, for each source (Table 1). Screenings for each aggregate source and limestone powder were used as fine aggregate and mineral filler, respectively, for dense gradations (Figure 2).

2.2 *Test procedures*

The optimum bitumen content (OBC) for each mixture was determined by the mix-design method established by Korea Ministry of Homeland and Maritime Affairs (Interim guide… 2008). The 75 gyrations were applied for compaction of 100 mm diameter specimens to satisfy following mix-design specifications; 4% of air void, 70%–85% of void filled with asphalt (VFA), minimum S_D of 3.2 MPa, and 14% and 13% of void in mineral aggregate (VMA) for 13 mm and 19 mm, respectively. A 50 mm/min loading speed was applied for mix-design S_D test. A total of 16 mixes were made using 2 aggregates, 2 gradations and 4 binders for S_D and WT tests.

To find the S_D which might represent rut potential better, S_D test was performed using four loading speeds; 10, 30, 50 and 70 mm/min. For each mixture, 12 specimens were made at air void of 4 ± 0.5% and randomly divided into four groups for each speed test. The specimen was submerged into the 60°C water for 30 minutes and then placed in the apparatus for applying static load precisely at the center of the specimen (Figure 3). The loading head face was cleaned using a kerosene-wet towel every time. A load and deformation curve (Figure 1) was obtained and the P and y at P were read from the curve for each specimen.

Table 1. Designation and description of materials.

Designation	Description
AP5	Base Pen. 60–80 binder without any modifier (Control)
R10	Modified binder with 10% CRM by wt. of total binder
RL6R5	Modified binder with 6% RLDPE and 5% CRM by wt. of total binder
SBS	Modified binder with unknown content of SBS for commercial PG76-22
13 and 19	Maximum coarse aggregate size 13: 13 mm and 19: 19 mm
A, B	Aggregate A: gneiss and B: granite

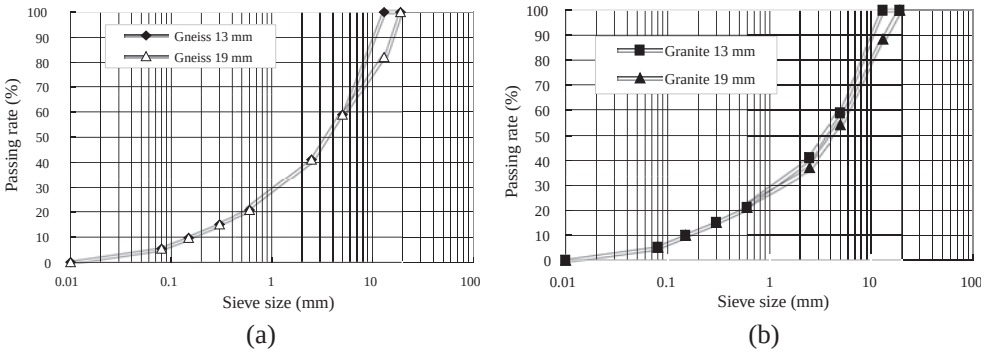

Figure 2. Gradation curves of (a) gneiss and (b) granite.

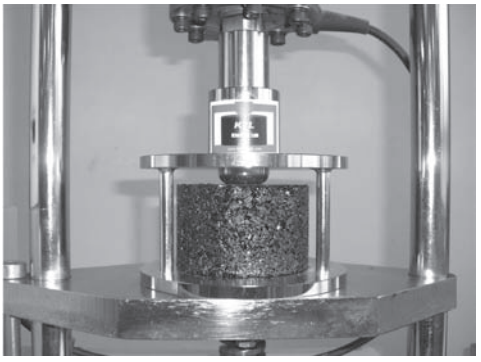

Figure 3. S_D test setup in a loading frame.

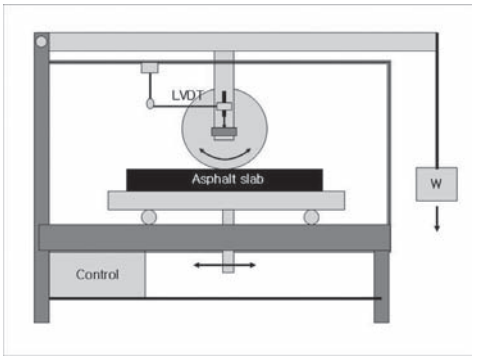

Figure 4. Schematic illustration of wheel tracker.

Table 2. Physical properties of 16 mixtures.

		Aggregate source A				Aggregate source B			
Agg. size	Designation	OBC (%)	Air void (%)	VMA (%)	VFA (%)	OBC (%)	Air void (%)	VMA (%)	VFA (%)
13 mm	A13AP5	5.3	4.55	16.63	76.62	5.5	3.94	16.59	76.25
	A13R10	6.0	4.44	17.97	75.29	5.8	3.79	16.98	77.68
	A13RL6R5	6.1	3.89	17.73	78.05	6.1	3.72	17.60	78.86
	A13SBS	5.3	4.07	16.19	74.84	5.4	4.21	16.54	74.55
19 mm	A19AP	4.8	4.05	15.14	73.28	5.0	3.79	16.08	76.45
	A19R10	5.3	4.42	16.55	73.27	5.6	4.05	17.00	76.19
	A19RL6R5	5.4	3.89	17.73	78.05	5.2	4.48	16.68	73.16
	A19SBS	4.7	4.07	16.19	74.84	4.6	4.09	14.86	72.51

It is widely held hypothesis that the WT is a reasonable rut prediction tool for bitumen mixtures. The wheel tracker used in this study, among many types, consisted of a steel wheel (200 mm in diameter and 50 mm in width), applying contact pressure of 689.4 kPa (100 psi), rolling on top of a slab specimen on the base plate moving with a 200 mm stroke back and forth (Figure 4). The WT test was repeated twice at the speed of 40 cycles/min for 3,600 cycles in 90 minutes at 60°C and average value of final rut depth at 3,600 cycles was used for correlation analysis with the mean of three S_D test data. A slab specimen (305 × 305 × 62 mm) was prepared at OBC using roller-press compactor and air void was checked first. If air void is out of 4 ± 0.5%, the slab was discarded and made again before being cut into two pieces for two WT tests.

3 RESULTS AND DISCUSSIONS

The optimum bitumen content, air void, VMA and VFA values for 16 mixtures are shown in Table 2. Rut depth of each bitumen mixture was measured by the WT method described above. But the S_D of each bitumen mixture was measured by four different loading speeds. It was found that the higher the loading speed, the higher the S_D value. Regression analysis was performed using WT rut depth as dependent variable and S_D as independent variable for each loading speed. The correlations of rut depth of WT with S_D are shown in Figures 5 and 6.

The R^2 value of each loading speed in four figures is summarized in Table 3. The loading speed showing the highest R^2 was found to be 30 mm/min. The mean R^2 was increased with the speed increase from 10 mm/min to 30 mm/min, and then decreased after the peak value at 30 mm/min.

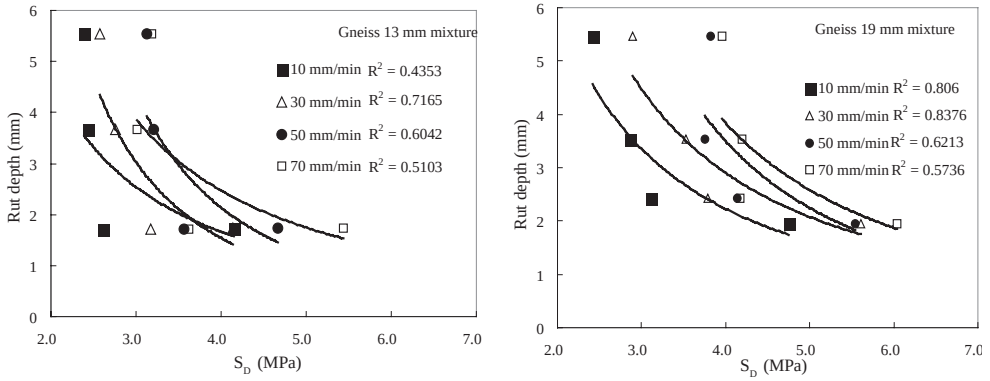

Figure 5. Correlation of WT rut depth with S_D by loading speed (a) gneiss 13 mm and (b) gneiss 19 mm.

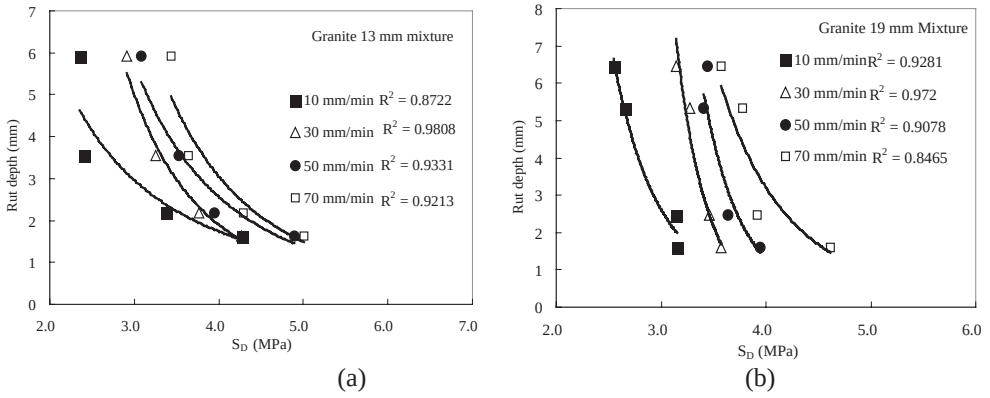

Figure 6. Correlation of WT rut depth with S_D by loading speed (a) granite 13 mm and (b) granite 19 mm.

Table 3. Summary of R^2 values by mixture and loading speed.

	Loading speed (mm/min)			
Mixtures	10	30	50	70
A (gneiss) 13	0.4353	0.7165	0.6042	0.5103
A (gneiss) 19	0.8060	0.8376	0.6213	0.5736
B (granite) 13	0.8722	0.9808	0.9331	0.9213
B (granite) 19	0.9281	0.9720	0.9078	0.8465
Mean	0.7604	0.8767	0.7666	0.7129

Using the four mean R^2 values for four loading speeds in Table 3, a regression analysis was carried out, as shown in Figure 7, to find the best loading speed showing the highest R^2 value. The loading speed showing the highest R^2 with WT rut depth was found to be 30.2 mm/min from the regression curve equation in Figure 7. Therefore, deleting the decimal number in 30.2, the loading speed of 30 mm/min was suggested as the optimum loading speed for S_D test.

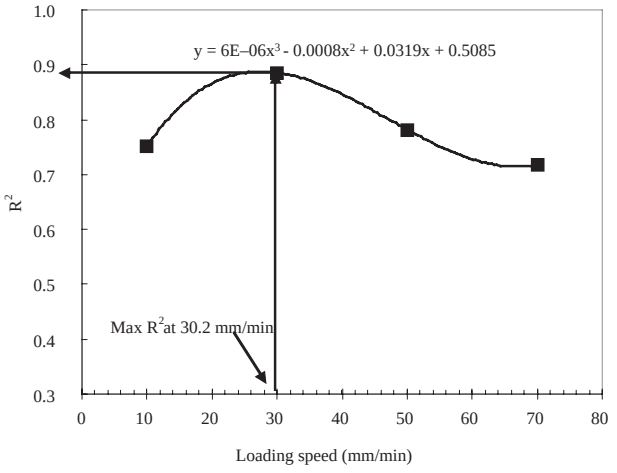

Figure 7. Regression curve of mean R^2 and the optimum speed at peak R^2 from the regression model.

4 CONCLUSIONS

It was found that the slower the loading speed, the lower the S_D value, showing a trend of increase with the loading speed increase. This is due to the effect of stress relaxation at the lower loading speed at high temperature. Therefore, the loading speed was found to be an important variable in S_D test. In the regression analyses of the rut depth of wheel tracking (WT) test with S_D, the R^2 was improved with the loading speed increase from 10 mm/min to 30 mm/min, and then decreased thereafter with the speed further increase. The loading speed showing the highest R^2 was found to be 30 mm/min, and this value was confirmed by regression analysis. Therefore, it was suggested as the standard loading speed of the S_D test. It is concluded that the loading speed of 30 mm/min is the optimum for estimation of rut resistance of HMA by the S_D test at 60°C.

ACKNOWLEDGEMENT

This study was made possible by the fund of Korea Ministry of Homeland and Maritime Affairs, using facilities of Institute for Advanced Construction Materials in Kangwon National University.

REFERENCES

Bonaquist, B., Sherwood, J.A. & Stuart, K.D. 1998. Accelerated pavement testing at the Federal Highway Administration pavement testing facility. *Journal of the Association of Asphalt Paving Technologists* 67.

Brown, S.F. & Gibb, J.M. 1996. Validation of experiments for permanent deformation testing of bituminous mixtures. *Journal of the Association of Asphalt Paving Technologists* 65: 255-299.

Doh, Y.S., Yun, K.K., Amirkhanian, S.N. & Kim, K.W. 2007. Framework for developing static strength test for measuring deformation resistance of asphalt concrete mixtures. *Construction and Building Materials* 21(12).

Hafez, I. 1997. Development of a simplified asphalt mix stability procedure for use in Superpave volumetric mix design. Ph.D. Dissertation, University of Maryland, College Park, MD.

Interim guide for hot-mix asphalt mix design procedures. 2008. Ministry of Homeland and Maritime Affairs, Republic of Korea.

Kaloush, K.E. 2001. Simple performance test for permanent deformation of asphalt mixtures. Ph.D. Dissertation, Arizona State University, Tuscan, AZ.

Kandhal, P.S. & Cooley, L.A, 2003. Accelerated laboratory rutting tests: evaluation of the asphalt pavement analyzer. *NCHRP Report 508*, TRB, Washington, D.C.

Kim, K.W., Lee, M.S., Kim, J.Y. & Lee, S.J. 2002. New experimental technique for estimating high-temperature deformation resistance of asphalt concrete. *Journal of Advanced Mineral Aggregate Composites* 7.

Kim, K.W., Doh, Y.S. & Amirkhanian, S.N. 2004. Feasibility of deformation strength for estimation of rut resistance of asphalt concrete. *Road Materials and Pavement Design, Vol. 5, No. 3*.

Kim, K.W., Choi, S.J., Lee, G.H., & Doh, Y.S. 2004. Correlation analysis of deformation strength and rut resistance of asphalt concretes at different temperature. *Journal of Korean Society of Civil Engineers* 24 No. 5D:743-748.

Kim, H.H., Park, N.W., Doh, Y.S., K. Ahn, Lee, S.J., Amrikhanian, S.N. & Kim, K.W, 2008. Rutting Estimation of Asphalt Pavement Mixtures using Deformation Strength. *Paper presented at 2008 European Asphalt Technology Association Meeting*, Lyon, France.

Kim, K.W. et al. 2008. Development of a test method for estimating high-temperature deformation resistance of asphalt concrete. *Final Report to Korea Institute of Construction and Transportation Technology Evaluation and Planning*, Kangwon National University.

Li X. 2001. Estimation of permanent deformation using volumetric and strength properties of asphalt mixture. Ph.D. Dissertation, Kangwon National University, Chun Cheon, Korea.

Park, N.W., Kim, H.H., Baek, S.H., Kim, K.W. & Doh, Y.S. 2007. Correlation of Deformation Strength (SD) with Lab Data and Field Rutting Data of Asphalt Pavements. *UKC Conference*, Washington, DC, USA.

Witzack, M., Kaloush, K. & Quintus, H. 2002. Pursuit of the simple performance test for asphalt mixture rutting. *Journal of the Association of Asphalt Paving Technologists* 71. AAPT.

Zhu, L.Y. & Fwa, T.F. 2005. Rutting potential evaluation of asphalt mixtures by dynamic load creep test. *Proceedings, 5th ICPT*.

Advanced Testing and Characterization of Bituminous Materials – Loizos, Partl, Scarpas & Al-Qadi (eds)
© 2009 Taylor & Francis Group, London, ISBN 978-0-415-55854-9

Enhanced algorithms for the derivation of material parameters from triaxial cyclic compression tests on asphalt specimen

Karl Kappl & Ronald Blab
Institute for Road Construction & Maintenance, Vienna University of Technology, Vienna, Austria

ABSTRACT: Material parameters, i.e. complex modulus E^* and phase lag φ as a function of temperature and test frequency of asphalt mixtures, from cyclic material tests on asphalt specimens are fundamental input parameters for material characterization in mix design and numerical calculations of pavement distress. Mostly, these material parameters are calculated by means of a "black box" software supplied by the machine manufacturer on the basis of simple "peak finding" methods. However, it can be proven, that the used post-processing algorithm to interpret measurement data of cyclic tests is crucial on the accuracy of the calculated material parameters. Simple "peak finding methods", where the machine data are used without diligent post processing, are not suitable for the calculation of complex modulus or phase lag, because of potential errors. The paper gives a brief survey of various mathematical methods for the determination of complex modulus E^* and phase lag φ calculated from various cyclic tests with sinusoidal loads. Furthermore, an enhanced approach is presented that allows the identification of differences in the evolution of material parameters during loading and unloading phases of individual load cycles.

1 INTRODUCTION

One of the most important and at the same time most sensitive subjects in materials research is the analysis of test data. Special caution is advisable in analyzing the outcome of cyclic tests in which high frequencies are applied (sinusoidal, cosinusoidal or haversinusoidal loading at $f > 1$ Hz), as the material parameters derived from the test data analyzed (complex modulus E^* and phase lag φ in viscous materials) are extremely sensitive to the analysis method used. These material parameters represent an important input in pavement design and finite element models used in projecting pavement performance (e.g. depth of rutting or fatigue resistance). They are usually determined by means of so-called "black-box" software supplied by machine manufacturers on the basis of simple "peak finding" methods (direct use of maximum/minimum points derived from raw test data). The use of "unfiltered raw data" includes the risk of producing inaccurate material parameters, as the "raw data", because of the data capturing method used, come with a certain "filter noise". Depending on the method used for analysis, this noise[1] has a greater or lesser impact on complex modulus or phase lag.

2 ANALYZING METHODS AND TECHNIQUES

The correct determination of material parameters of hot mixed asphalt HMA like i.e. complex modulus E^* or phase lag ϕ obtained from dynamic or cyclic material tests became more and more important. The complex modulus E^* is defined as the ratio of the maximum

[1]Noise as a physical phenomenon, namely measurable fluctuations in current or voltage, was first described by Walter Schottky in 1918. When these fluctuations are made audible through amplification, a typical noise is obtained after which the phenomenon was named. Meanwhile, the term "noise" is being used in a much more general sense (quoted from WIKIPEDIA).

applied stresses σ divided by the maximum resulting strains ε of the tested material. The phase lag ϕ (phase angle) is obtained by determining the time lag between stress and strain signal and multipliying with the angular frequency of the conducted test.

The question as to whether it is necessary at all to use algorithms for determining dynamic material parameters is easy to answer: any electrical signal, whether used for measuring or for machine control purposes, that is captured and recorded digitally by computer is subject to a certain "noise" that is caused by various factors. One important factor in the production of filter noise is the way in which signals are transmitted by means of various physical media, currently primarily electric current. Before transmission, raw data are converted to make them fit for transport via the medium selected. This may be done in analogue or digital mode and involves sampling of data, their transformation into discrete values, and their final transport by means of electric pulses. The production and processing of a measuring signal can be described as follows: A sensor is used to pick up the signals that are often quite weak (in the range of a few millivolts). The signals are then amplified for further processing. The track/sample hold amplifier samples the amplified analogue signal at certain time intervals. A time-continuous signal is thus transformed into a time-discrete signal (see Figure 1). This signal can be processed by the digital signal processor. For a variety of reasons, the analogue-to-digital transformation process also produces noise, which finally becomes part of the digitised signal. Sources and causes of such noise are, for example, resistance noise ("Nyquist noise", shot noise or thermal noise), tube hiss, contact noise at interfaces between electric conductors/semi-conductors or quantisation noise occurring in the conversion of analogue signals to digital (Wendemuth 2005).

Figure 2 illustrates this noise once again using the example of a signal from force measurements made during dynamic materials testing. The force signal measured over a time period

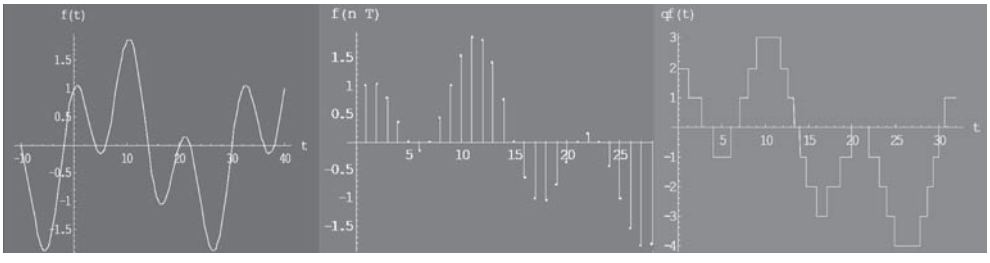

Figure 1. Idealized scheme of converting an analog, measuring signal (left) into digital one (right) by means of signal sampling (middle) [Wendemuth 2005].

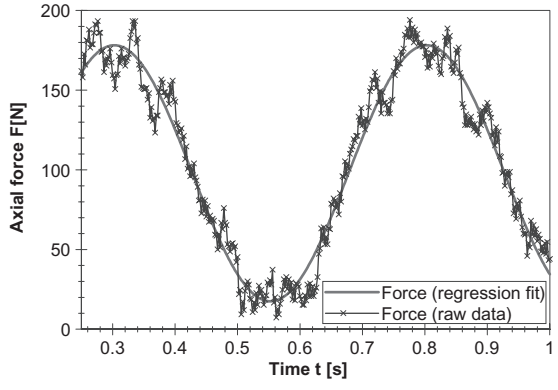

Figure 2. Schematic representation of a sinusoidal force signal afflicted by signal (electronic) noise (black line) and the mathematically fitted, sinusoidal regression function (gray line).

is represented by three sine waves. As can easily be seen from the diagram, the force signal measured includes a large amount of noise and thus substantial fluctuations in amplitude. These fluctuations in amplitude caused by filter noise ultimately have significant effects on the calculation of the dynamic material parameters. Therefore, a simple method has to be found for eliminating or reducing this noise without affecting or changing the signals in their time domains. The methods most frequently used are briefly discussed in the following chapter.

2.1 *State of the art*

Pellinen summarized in (Pellinen et al. 2003) the most commonly used post processing analysis techniques. These techniques comprise two different steps: first of all test machine "raw" data have to be filtered (smoothing) before complex modulus and phase angel could be determined (parameter estimation algorithms). Pellinen compared various analysis methods to determine dynamic modulus (amplitudes of waveforms) and phaselag (time shift), which are in detail:

- 2-step methods applied over a certain number of cycles, in which raw data from the test are first smoothed by means of suitable algorithms. Then the wave amplitudes and phase lags are determined by means of linear regression (A and B in Figure 3).
- Localized multiple linear regression analyses with peak peaking (taking only one point = the maximum of all localized points of a have sine wave) for the determination of wave amplitudes and phase lags from wave maxima and minima in the raw data ("peak finding method"; C and D in Figure 3).
- Use of wave maxima and minima without previous smoothing of raw data (E and F in Figure 3).
- Sinusoidal regression over a certain number of cycles (G in Figure 3).
- Various combinations of these analysis methods.

The results of a statistical analysis of the material parameters E^* and φ determined by means of these algorithms in a comparative test are represented graphically in Figure 3. In these Black diagrams, phase lag is plotted against the dynamic modulus E^*.
In summary, (Pellinen et al. 2003) arrived at the following conclusions:

- The analysis method used has a material influence on the outcome of the calculated dynamic material parameters, with the impact on the magnitude of dynamic modulus E^* being less than on phase lag φ.

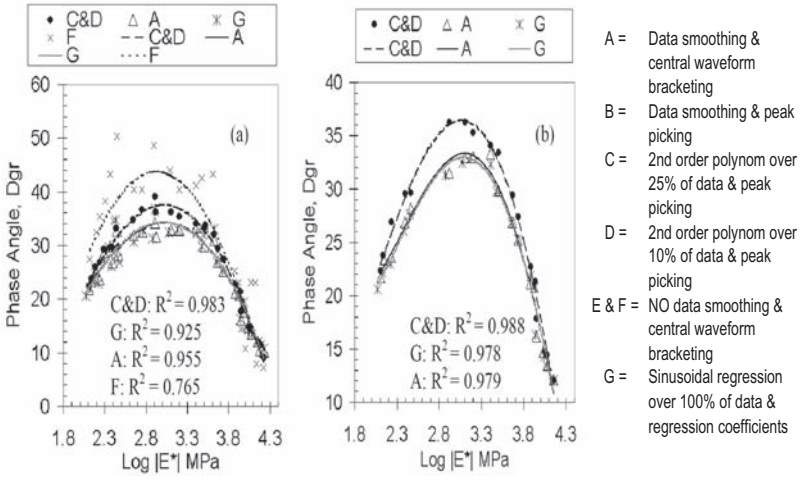

Figure 3. Schematic representation of a sinusoidal force signal afflicted by signal (electronic) noise (black line) and the mathematically fitted, sinusoidal regression function (gray line).

- Use of wave maxima and minima without previous smoothing of raw data results in the least fit between data measured and material parameters.
- Smoothing of the raw data obtained from the test apparatus followed by multiple linear regression analyses (e.g. using polynoms or power functions) over a certain range of cycles provides the best fit.
- Sinusoidal or cosinusoidal regression over a certain number of cycles provides the best fit of all regression analyses compared.
- In cyclic tests in which plastic deformation occurs, the use of additional function terms in the regression functions is indispensable, however.

2.2 *Enhanced regression approach*

As previously mentioned, sine and cosine functions are a suitable approach to regression analysis of data obtained from cyclic testing. It must be pointed out, however, that in certain tests, in which the material changes due to cracking or permanent deformation (such as fatigue testing or rutting tests), additional function terms are necessary in order to obtain good fit between the data measured and the mathematical regression functions. The most simple approach is the sine function with a constant term:

$$f(t,a_1,a_2,a_3) = a_1 + a_2 \cdot \sin(2\pi \cdot f \cdot t + a_3) \tag{1}$$

where $f(t)$ [–] stands for the regression function of the analyzed signal, a_1, a_2 and a_3 [–] are the regression coefficients, f [Hz] stands for the test frequency and t [s] for the time. The coefficient a_1 represents the offset, a_2 the amplitude and a_3 the phase lag from a sinusoidal signal.

Using this simple basis function (hereinafter called "simple sine function"), the data recorded (as shown, for example, in Figure 4 for axial stress σ_{ax} and axial strain ε_{ax}) are to be "approximated" as closely as possible. The quality of this fit is measured by the coefficient of determination[2] R^2.

As clearly illustrated by Figure 4, however, the simple sine function often fails to provide a good regression to the points measured, particularly when one of the signals fails to produce a constant line (as in the example of the triaxial cyclic compression test TCCT, see Figure 4, and the aim is to analyze several cycles e.g. 3 cycles such as in Figure 4). The differences between the axial strain data measured and the line fitted by means of the simple sine function are too big (see Figure 4), primarily because this function does not permit any "tilting" to take into account the non-linear nature of the permanent strains. Especially in triaxial cyclic compression tests, in which cyclical loading is performed to produce permanent deformation, the resulting axial or radial strains no longer oscillate around a horizontal base line but along a non-linear deformation curve.

To determine the regression parameters of sinusoidal deformation reactions not running in parallel with the x-axis, a simple sine function with an additional linear term ($a_4\,t$) is therefore used as a next step:

$$f(t,a_1,a_2,a_3,a_4) = a_1 + a_2 \cdot \sin(2\pi \cdot f \cdot t + a_3) + a_4 t \tag{2}$$

The result of this new regression function is illustrated in Figure 5. In contrast to the simple sine function, the approximated sine waves of the axial deformations are no longer

[2]The coefficient of determination R^2 of this non-linear regression is calculated in the following manner according to (Sachs 1989):

$$B_{nL} = r_{nL}{}^2 = r^2 = R^2 = 1 - \frac{A}{Q_y};\; A = \sum_{i=1}^{n}(y_i - y)^2;\; Q_y = \sum_{i=1}^{n}(y_1)^2 - \frac{1}{n}\left(\sum_{i=1}^{n} y_1\right)^2$$ with A being the sum of the squares of distance of the measured values y_i from the regression values $\hat{y}$ with Q_y being the covariance.

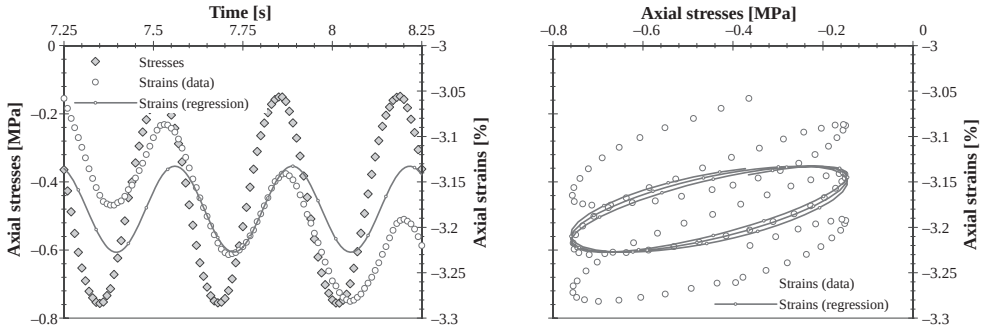

Figure 4. Triaxial cyclic compression test (TCCT) data from axial loading σ_{ax} and the resulting strain ε_{ax} and the mathematical approximation function—simple sine function—plotted against time (left) and as stress-strain diagram (right) (Kappl 2007).

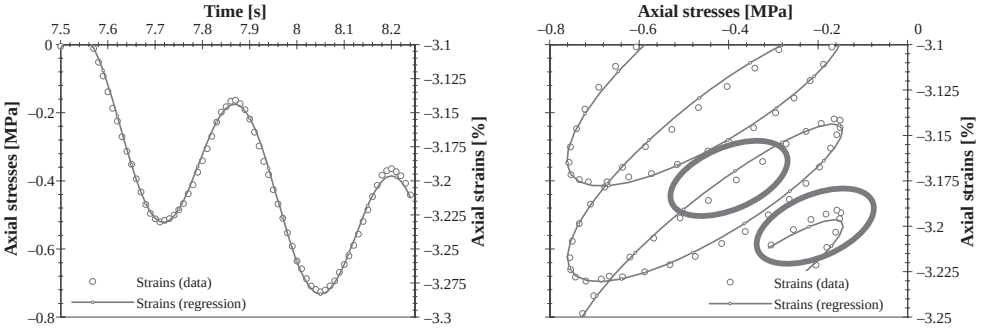

Figure 5. Triaxial cyclic compression test (TCCT) data from axial loading σ_{ax} and the resulting strain ε_{ax} and the mathematical approximation function—sine function + linear term—plotted against time (left; y-axis with stresses, left axis, and strains right axis) and as stress-strain diagram (right; y-axis with strains on right axis) (Kappl 2007).

horizontal but slanting downwards linearly, reflecting more accurately the actual positions of the points measured (see red lines in Figure 5).

This function appears more appropriate for TCCT tests than the simple sine function. A closer look at the stress-strain diagram in Figure 5 (right half) reveals, however, that this sine function with a linear term does not fit sufficiently the points recorded, particularly in the vertex points of the ellipsis. The shape of the ellipsis in the stress-strain diagram that is typical of an "undeformed" sine wave (= shape of ideal mathematical sine wave) does not exactly fit the measuring points (see marking in Figure 5).

For this reason, the sine function with the linear term was extended by adding a second sine term having double the frequency ($4\pi f$) of the first sine portion ($2\pi f$). This "extended sine function" is discussed in more detail below. This function reads:

$$f(t,a_1,a_2,a_3,a_4,a_5,a_6) = a_1 + a_2 \sin(2\pi ft + a_3) + a_4 t + a_5 \sin(4\pi ft + a_6) \quad (3)$$

with a_1 = offset (displacement of ordinate) of the base wave, a_2 = amplitude of base wave, a_3 = phase angle, a_4 = linear term, a_5 = amplitude of the harmonic wave, a_6 = phase angle of harmonic wave, f = frequency in [Hz] and t_i the time i at which a data point was recorded.

As Figure 6 shows, the data measured can be modelled with much greater accuracy when the extended sine function is used. Better fit is obvious in particular at the turning points of the sine waves (see marking in right-hand diagram in Figure 6).

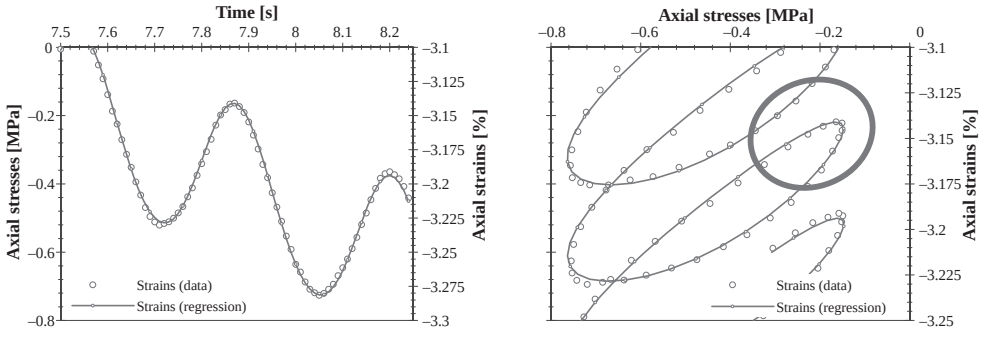

Figure 6. Differences between the data measured and the values obtained from regression analysis using the extended sine function (double sine function and linear term) for 2 cycles (Kappl 2007).

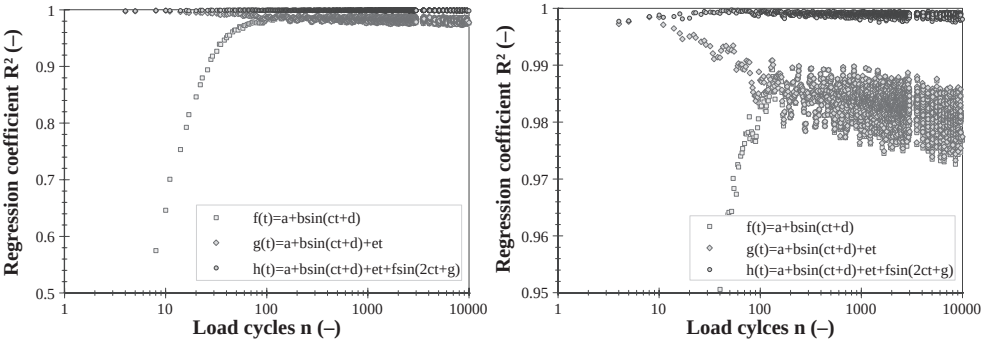

Figure 7. Comparison of coefficient of determination R^2 of the three regression functions for axial deformation after the first 10000 load cycles on a simple logarithmic scale (left diagram = overview; right diagram zoomed in between 0.95 and 1.00 on y-axis) (Kappl 2007).

2.3 *Comparative assessment of different regression functions on the base of triaxial cyclic compression test data*

Figure 7 compares the "quality of fit" of the three regression functions for axial deformation using the TCCT test as an example. As can be seen, the coefficient of determination R^2 of the simple sine function according to equation (1) is below 0.95 during the first 100 load cycles. During the first 10 load cycles, R^2 is even lower than 0.5. It is only later, at the beginning of the secondary creep phase, that R^2 exceeds the level of 0.95. The sine function with the linear term according to equation (2), on the other hand, has very good fit initially, during the first load cycles, but then loses some of its quality (R^2 around 0.98). The regression function with the dual sine according to (3) boasts a very high and constant R^2 throughout the entire test. Here, R^2 was on the average 0.995 or higher.

2.4 *Differences in material parameters E* and phase lag in triaxial cyclic tests based on the enhanced regression function*

Finally, further special characteristics in material response are discussed by reference to the triaxial cyclic tests (TCCT). As Figure 4 shows, the sine function with the linear term (2) does not produce a particularly good fit to the data measured (shown in left diagram of Figure 8 as black circles). Differences are still identifiable in the areas around the maximum and minimum (marked in Figure 8 by red arrows).

In addition, as can be seen from the diagram, this regression function provides a relatively good fit to the mathematical sine function when the test specimen is loaded. On loading, the axial deformation of the test specimen closely follows the projected loading curve of the hydraulic piston. On unloading, the fit is no longer satisfactory, however. Here, the test specimen has to provide the energy for "re-deformation" (recovery) alone. As the material of the test specimen (asphalt) is already highly viscous at the TCCT test temperatures (as a rule, $T = 40$ and 50°C), the recovery takes place at a slower pace. This is clearly apparent from Figure 8: the data measured (shown as black circles) show a certain time lag (graphically displaced to the left) compared with the mathematical sine regression function (broken red line).

These differences between loading and unloading are even more visible in the left diagram of Figure 8. This diagram plots axial stresses against axial strains. The individual sine waves are shown as hystereses. It can be seen that when the test specimen is loaded and the sensors are exposed to responses from both the apparatus and the material, the hystereses are "dented" (cf. arrow in the loading portion of the wave in Figure 8). All points measured are within the "sine function hysteresis". On unloading, on the other hand, when the sensors measure only the response of the material, the hysteresis is "drawn out". In addition, it can be seen from Figure 8, that the points measured in the vortexes of the hysteresis are not located precisely on the y_2 curve of the sine function with the linear term. In the top right of the hystereses in Figure 8 (see marking), the data measured are scattered more widely than on the opposite side (bottom left of diagram). This is also clearly noticeable (see markings "wide" and "small").

When using the extended sine function according to equation (3), approximation to the data measured is much better, both around the vertex and during loading and unloading phases. The changes in material response during loading and unloading phases described above ultimately also have an impact on the dynamic material parameters E^* and φ. Thus, for example, Figure 11 shows complex modulus E^*, E_1, E_2 (real and imaginary parts of dynamic modulus E^*) and the axial phase angle φ_{ax} of stone mastic asphalt SMA 11 PmB 45/80-65, S1, G1 containing diabase as aggregate. Strikingly, the dynamic material parameters change in these diagrams with increasing number of load cycles. This phenomenon can be illustrated very clearly, especially for the phase angle φ_{ax}. Figure 11 shows E^* and φ_{ax} plotted against the number of load cycles, with the phase angles determined, on the one hand, between the stress and strain peaks (named $\varphi_{ax\text{-}Max\text{-}Max}$) and between the lows (named $\varphi_{ax\text{-}Min\text{-}Min}$). These key points are shown graphically in Figure 9 and Figure 10 for two different stress and strain waves. It is clearly evident that the phase angle $\varphi_{ax\text{-}Min\text{-}Min}$ is produced by the imposition of loads—in the subject case in TCCT tests by axial loading applied by the loading piston—while the phase angle $\varphi_{ax\text{-}Max\text{-}Max}$ reflects the response of the material of the asphalt test specimen upon unloading. At this time, the sensor is not exposed to any impacts from the apparatus. This

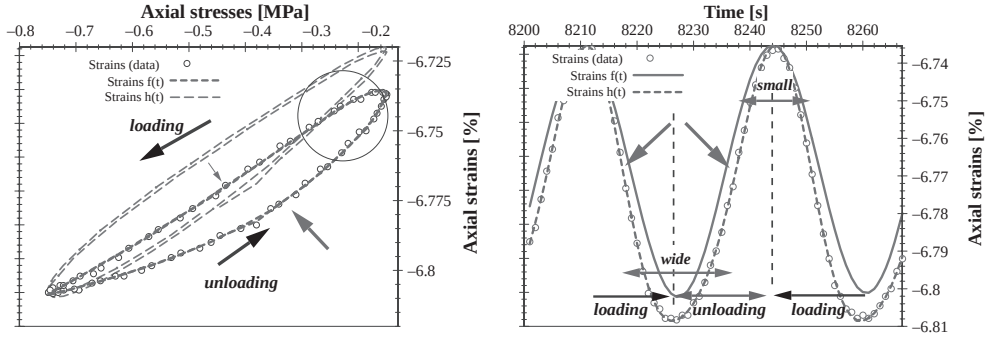

Figure 8. Simple sine function (sine term plus linear term; gray line) versus extended sine function (second sine term with double frequency and linear term; blue line) derived from axial test specimen deformations (Kappl 2007).

angle thus represents the "unadulterated" response of the material during unloading of the test specimen.

To illustrate this phenomenon, Figure 9 shows the phase lag angle between the "Max-Max" and "Min-Min" points at the beginning of the test (at the 40th load cycle). One can clearly see that the axial phase angle $\varphi_{ax\text{-}Max\text{-}Max}$ is smaller than $\varphi_{ax\text{-}Min\text{-}Min}$ between the "Min-Min" points. In Figure 10, the same material parameters are shown graphically at the end of

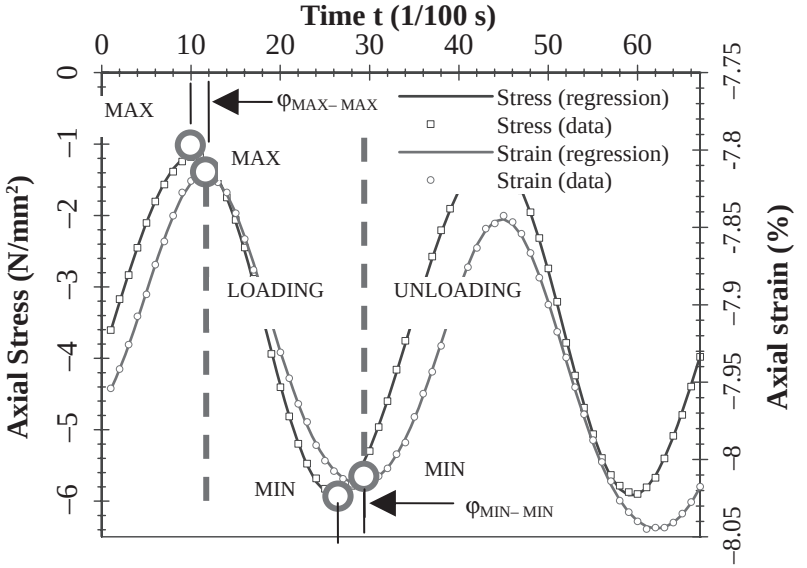

Figure 9. Axial strains and stresses at maximum and minimum wave points in the loading and unloading phases at the beginning of the test (40th load cycle) (Kappl 2007).

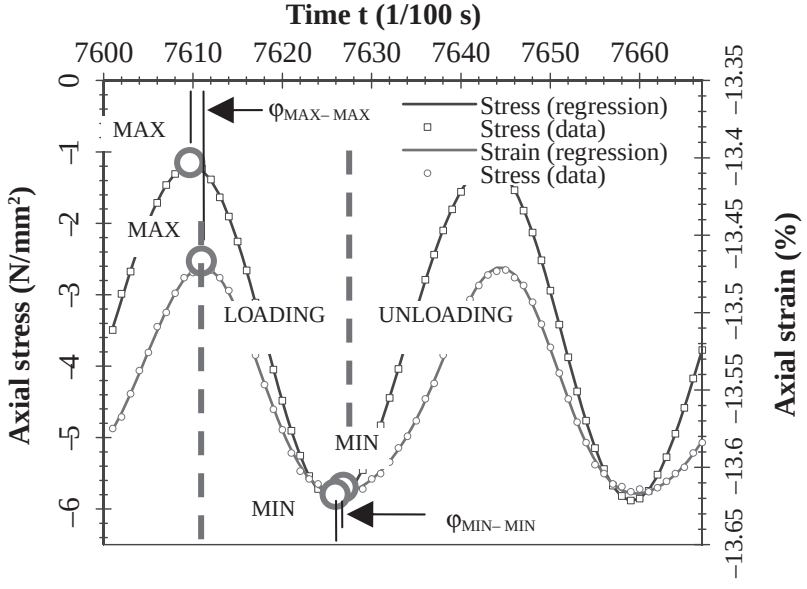

Figure 10. Axial strains and stresses at maximum and minimum wave points in the loading and unloading phases at the end of the test (25000th load cycle) (Kappl 2007).

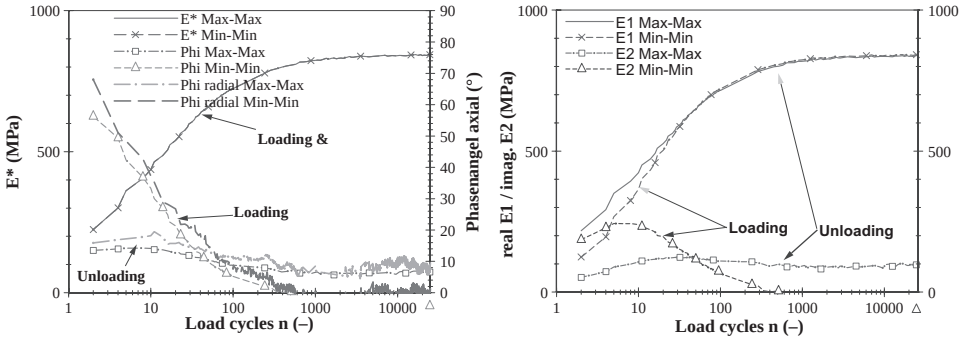

Figure 11. Dynamic modulus E^*, the axial and radial phase angles between wave maxima and minima (left) and the real and imaginary parts E_1 and E_2 for SMA 11 PmB 45/80-64, S1, G1 diabase (simple logarithmic scale on abscissa) (Kappl 2007).

the test, after 25000 load cycles. Here one can clearly see that the axial phase angle $\varphi_{ax\text{-}Min\text{-}Min}$ has become much smaller after exposure to the loading piston.

These effects may be explained by changes in the structure or displacements of particles in the asphalt test specimen, which may lead to the formation of "mineral skeleton pillars" in the cylindrical test specimen. As is known from soil engineering, aggregates (rock), when laterally constrained as in the case of triaxial tests, react elastically to impacts from outside (also see (Huschek 1977)). This is reflected by the reduction in the phase angle towards "more elastics values" during TCCT tests.

With dynamic modulus E^*, on the other hand, as shown in Figure 11, there is no big difference between the dynamic modulus $E^*_{Max\text{-}Max}$ (unloading) derived from the peak values and $E^*_{Min\text{-}Min}$ (loading) derived from the minimum points of the waves. The two material parameters are almost the same.

It is striking that as the loading time (number of load cycles) increases, the dynamic modulus rises up to a limit value. This means that a constant modulus E^* is reached after an initial phase of stresses and strains (about 100 load cycles). This would be in line with reports by Francken (e.g. (Francken 1977)), who uses a constant "plasticity modulus" for his permanent deformation model (BRRC model).

3 CONCLUSIONS

In summary, the following phenomena were observed during triaxial cyclic testing in the dynamic material parameters of the test specimen calculated by means of the extended sine function:

- In the primary creep phase (initial phase) of the TCCT tests, the dynamic material parameters change significantly. During the first 100 to 200 load cycles, the dynamic modulus E^* and its elastic part E_1 rise degressively as loading time increases, up to an almost constant limit value.
- The viscous part E_2 increases slightly during the first loading cycles but subsequently decreases again to a constant limit value. Here, it must be differentiated between the viscous modulus determined between the maximum (unloading; reaction of material) and minimum (during the loading phase) data points: The values found in the unloading phase $E_{2\text{-}Max\text{-}Max}$ are almost constant and linear, while the $E_{2\text{-}Min\text{-}Min}$ values produced by loading initially increase in a slightly degressive manner and then (after the initial phase) fall degressively to a limit value.
- The axial phase angles decrease disproportionately in the primary creep phase and then remain almost constant. A difference exists also in the phase angles between stresses and strains between $\varphi_{ax\text{-}Max\text{-}Max}$ (during unloading) and $\varphi_{ax\text{-}Min\text{-}Min}$ (during loading), as both

parameters develop differently: The $\varphi_{ax\text{-}Min\text{-}Min}$ quickly fall from very high levels (high viscosity) to low values (high elasticity), while $\varphi_{ax\text{-}Max\text{-}Max}$ (in the unloading phases) remain constant over the loading time, with smaller phase angles.
- These phenomena had not been detected and analysed previously by the analysis software used, which did not contain the regression algorithms required for this purpose. It is, however, specifically this "evolution" of the dynamic material parameters that may have a critical impact on the outcome of projections or model calculations. It should be studied in more detail in the future.

ACKNOWLEDGEMENTS

The authors' sincere thanks go to those who have made the evaluation of this mathematical algorithm possible: Mr. Walter Fusseis, who formulated mathematical functions for this algorithm. Cordial thanks are also due to Mr. Michael Wistuba and Mr. Markus Spiegl, who in numerous talks contributed their ideas and constructive criticism and were significantly involved in the development of this analytical method.

REFERENCES

EN 12697-25 (2004). Asphalt—Test methods for hot mix asphalt—Part 25: Cyclic compression test. Co-mité européen de normalisation CEN, Brussels, 2004-12-01.

EN 12697-26 (2005). Asphalt—Test methods for hot mix asphalt—Part 26: Stiffness. Comité européen de normalisation CEN, Brussels, 2004-10-01.

Francken Louis (1977): *Permanent deformation law of bituminous road mixes in repeated triaxial compression.* Proceedings of the 4th international conference on structural design of asphalt pavements, Vol. 1, Ann Arbor, 1977.

Huschek S. (1977): *Interpretation der Ergebnisse aus Kriechversuchen mit Asphaltprobekörpern.* Colloquium 77 zur plastischen Verformbarkeit von Asphaltmischungen, Mitteilung 37 der ETH Zürich, November 1977.

Kappl Karl (2007): *Bewertung und Modellierung des Verformungsverhaltens von Asphalten mit Hilfe von zyklischen Triaxialprüfungen.* Dissertation am Institut für Straßenbau und Straßenerhaltung, TU Wien, Wien, 2007.

Pellinen Terri & Crockford B. (2003): *Comparison of analysis techniques to obtain modulus and phase angle from sinusoidal test data.* 6th RILEM Symposium PTEBM'03, Zurich, Conference Proceedings RILEM, 2003.

Sachs Ludwig (1989): *Angewandte Statistik.* Berlin [u.a.], Springer, 1989.

Wendemuth A, Andelice E & Barth S. (2005): *Grundlagen der digitalen Signalverarbeitung.* Berlin [u.a.], Springer, 2005.

Advanced Testing and Characterization of Bituminous Materials –
Loizos, Partl, Scarpas & Al-Qadi (eds)
© 2009 Taylor & Francis Group, London, ISBN 978-0-415-55854-9

Reliability and suitability for standardization of methods for HMA density measurements: Experimental investigation on transverse vs longitudinal variations

F.G. Praticò, R. Ammendola & A. Moro
DIMET Department, Mediterranea University, Reggio Calabria, Italy

ABSTRACT: Lower density zones can occur at longitudinal joints. On the other hand, cores extraction is time-consuming and subjected to technical and operator errors. Consequently, a challenge is the use of electromagnetic sensors. In the light of above facts, the main objectives and scopes have been confined into the analysis of the reliability and suitability for standardization of high-speed devices. In particular the potential for detecting density non-conformities especially in joints area has been investigated. In-lab and on-site experiments were designed and performed. Different measurement methods (vacuum sealing method, portable non-nuclear devices, dimensional) have been used. In the factorial plan, longitudinal versus transverse variability has been considered. On the basis of the data analyses, it was possible to perform a tentative evaluation of the reliability and of the suitability for standardization of the specific test methods. The obtained data provided information and indications for specific recommendations and for practical applications.

1 INTRODUCTION

Lower density zones at the longitudinal joints affect pavement ultimate performance, expected life and life cycle cost.

Joint construction process is affected by many factors (AA.VV. 2004, Sebaaly et al. 2005a, Sebaaly et al. 2005b, Rao et al. 2007, Praticò et al. 2008a, Praticò et al. 2008b): paving technique, joint features, compaction strategy, etc. Visual inspection (surface defects) and joint density measurements are needed in order to estimate density levels and to assess if requirements are fulfilled.

On the other hand, cores extraction is time-consuming and subjected to technical and operator errors and, as a consequence, a challenge is the use of electromagnetic sensors, which do not require penetrating probes to perform the measurement. Though many progresses have been done (AASHTO TP 68 2004, ASTM D7113 2005, AA.VV. 2006), reliability and suitability for standardization of such methods still need experimental and theoretical investigations and studies. In the light of above facts, the main objectives and scopes have been confined into the analysis of the reliability and suitability for standardization of high-speed devices. In particular the potential for detecting density non-conformities especially in joints area has been investigated. In-lab and on-site experiments were designed and performed. Different measurement methods (vacuum sealing method, portable non-nuclear devices, dimensional) have been used. In the factorial plan of experiments, longitudinal versus transverse variability has been considered. In the next section the design of experiments is described, while section three deals with results and analyses.

2 EXPERIMENTAL PLAN

In order to pursue the above-mentioned objectives, an experimental plan has been designed. After the laydown and compaction of the Cold Lane (CL), the laydown and compaction of

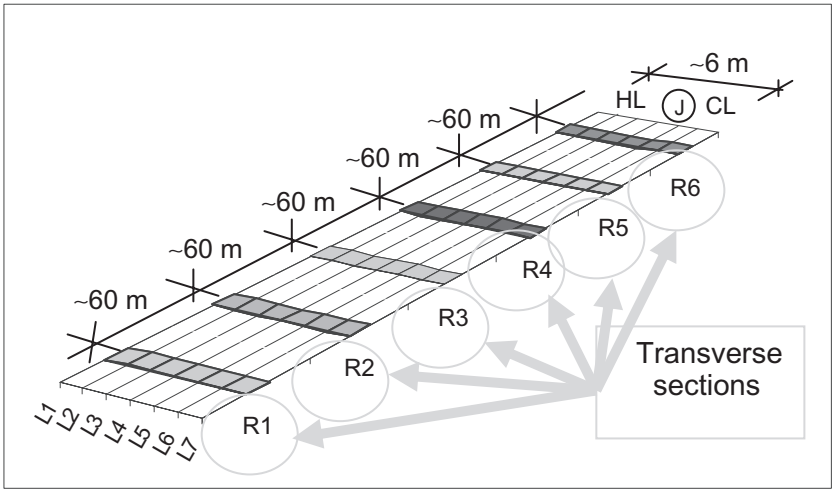

Figure 1. Longitudinal (L1, …, L7) and transverse, (R1, …, R6) sections.

the Hot Lane (HL) has been carried out. In this phase rolling from the hot side with overlapping onto the cold lane by about 150 mm has been carried out. After the construction of the (CL) and (HL), in-site and in-lab (on the extracted cores) measurements have been performed in the intersections ij between the longitudinal sections L_i (i = 1, …, 7) and the transverse sections R_j (j = 1, …, 6) as in figure 1.

In-site, the parameter P, density estimated through a non-nuclear portable device, has been measured.

On the extracted cores, the following parameters have been determined:

b (%) = asphalt binder content as a percentage of aggregate weight (B.U. CNR n.38/73; ASTM 6307; EN 12697-1: 2006);

G = aggregate gradation (B.U. CNR n. 4/53; EN 12697-2: 2008);

γ_g = aggregate apparent specific gravity (B.U. CNR n. 63/78; AASHTO T85: 2004);

G_{mbcor} = mix bulk specific gravity according to ASTM D6752; ASTM D6857;

G_{mbAO} = mix bulk specific gravity after opening (ASTM D6752; ASTM D6857);

n_{eff} = mix effective porosity (ASTM D6752; ASTM D6857);

G_{mbDIM} = mix bulk specific gravity according to AASHTO T269.

The effective porosity (n_{eff}) has been calculated from G_{mb} and G_{mbAO}: $n_{eff} = (G_{mbAO} \cdot \gamma_w - G_{mb} \cdot \gamma_w) \cdot (G_{mbAO} \cdot \gamma_w)^{-1}$, γ_W = water density.

The following main sources of variance have been considered for the given plan of experiments: i) Random distribution of actual values; ii) Construction; iii) Test procedures.

It is important to remark that three procedures have been considered for the determination of the bulk specific gravity: G_{mbdim}, G_{mbcor}, P.

In the case of the indicator P, the following main sources of variance have been taken into account (and therefore controlled): moisture, aggregate type, temperature, Nominal Maximum Aggregate Size, layer thickness.

Note that, as is well-known, G_{mb} is dimensionless, while P can be expressed in g/cm^3. Anyhow, all the results can be easily interpreted in terms of g/cm^3 ($G_{mb} \cdot \gamma_w$), i.e. density.

3 RESULTS

Results are summarized in figures 2 to 33 and tables 1 and 2.

Figures 2 to 7 refer to the transverse variation of G_{mbcor} (for each section R_j), while figures 8 to 13 refer to G_{mbdim} and figures 14 to 19 refer to P. Figures 20 to 26 show the regressions of P and G_{mbdim} as a function of G_{mbcor} along the transverse sections (R1 to R6).

It is important to point out previously that density curves are expected to present (from left, shoulder, to right, joint, see figure 3):

1. an initial domain (I), within the Hot Lane (HL), in which the first derivative is positive and there is an increase of density up to a given value;
2. a second domain (II), within the Hot Lane, in which the first derivative is substantially null and the density is constant;
3. a third domain (III), across the joint (J), in which the first derivative is negative and the density decreases;
4. a fourth domain (IV), on the right of the longitudinal joint (J), in which the first derivative is expected to be positive;
5. a fifth domain (V), quite stationary, as the second one.

Figure 3 shows, in the same plot, both the shape of the expected density plot and the obtained results (transverse section R2). The above-mentioned domains (I to V) are there represented. It is possible to observe that sections R2 (figures 3, 9, 15), R3 (figures 4, 10, 16), R4 (figures 5, 11, 17), R5 (figures 6, 12, 18) present the expected increase of density on the right of the joint, while in the remaining cases (R1, R6) there is not the expected increase. This fact could be due to the difference between the two lanes (HL vs. CL), constructed in different days, temperature and humidity conditions. Moreover, the same hypothesis of homogeneity of the HMA (Hot Mix Asphalt) could be too "strong" if compared to the expected range of variations.

As far as figures 20 to 26 are concerned (in which the circles refer to the measures carried out just on the joint, J), it is possible to observe that all the linear regressions P vs. G_{mbcor} show first derivatives always positive (in the range 0.1 ~ 0.9), while the constants range from 0.1 up to 1.6. It is important to focus that when all the points are considered (see figure 20), the R-square coefficient decreases from 0.3 ~ 0.8 mm to 0.3 (see also table 1). This fact could be due to a sort of section-specificity.

If this information is related to the strong differences observed in terms of water content among the different transverse sections, it is possible to refer the above-mentioned specificity to a peculiar range of water content.

On the other side, by referring to the linear regressions in which the explanatory variable is always G_{mbcor}, while the response (dependent) variable is G_{mbDIM} (always in figures 20 to 26), the slope results always positive (in the range 0.4 ~ 1.9), while the intercept ranges from –1.9 up to 0.8. R-square values range from 0.3 up to 1.0 and are in general higher than the ones obtained when the response variable is P. More importantly, the average R-square of the single sections results 0.57 for P vs. 0.72 for G_{mbDIM} (see also table 1, column "Average"). Now, if these values are compared with the R-square values obtained for all the sections (see figure 20 and table 1), it is possible to point out that for P-correlations there is a transition from 0.57 (average R-square) for transverse sections to 0.26 (all the sections), with a ratio of 0.5 (=0.26/0.57), while for G_{mbDIM} correlations there is a transition from 0.72 to 0.75, where the ratio is 1.0. This asymmetry (decrease for P vs. stationarity for G_{mbDIM}) could strengthen the above-mentioned hypothesis of section—specificity of P measures.

Figures 27 to 33 summarize the results obtained for points having the same distance from the shoulder but placed in different transverse sections. In particular, these figures refer to P vs. G_{mbcor} and G_{mbDIM} vs. G_{mbcor} correlations.

As far as the response variable P is considered, the slope ranges from –0.1 up to 0.9, while the intercepts vary from 0.2 up to 2.2. R-square values are quite low and range from 0.0 up to 0.8 with an average value of 0.3 (see also table 2). When all the points are considered R-square is again 0.3 (see figure 20) and consequently the ratio "average on all" is $0.3/0.3 \cong 0.98$ (cfr. table 2 last column). As for G_{mbDIM} correlations, the slope ranges from 1.0 up to 2.2, while the intercepts vary from –2.5 up to –0.1. R-square values range from 0.6 up to 0.9, with an average value of 0.72 (see table 2) and a ratio of 1.04. Also these results agree with the above-mentioned hypothesis of (transverse) section-specificity.

Tables 1 and 2 offer a resumé of R-square values and correlation significance. Note that in tables 1 and 2 the adjusted R-square has been reported. Adjusted R^2 is a modification of

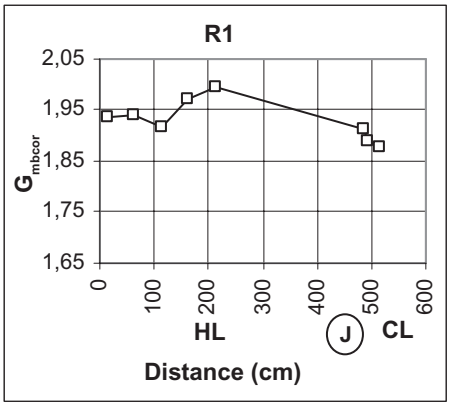

Figure 2. G_{mbcor} vs. Distance (R1).

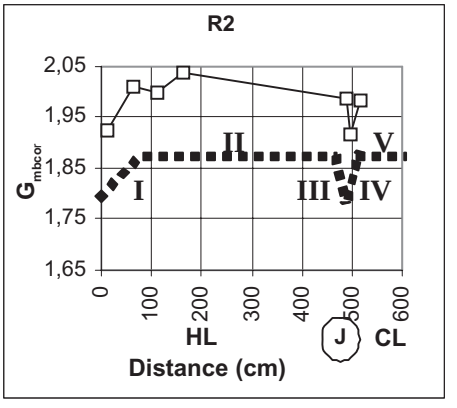

Figure 3. G_{mbcor} vs. Distance (R2).

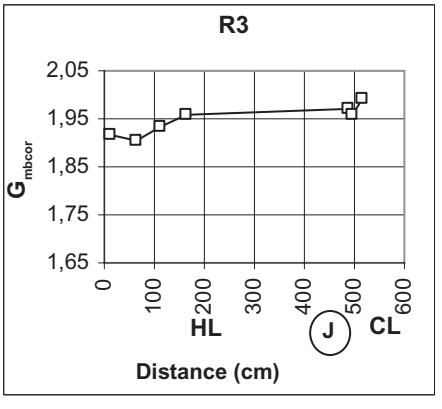

Figure 4. G_{mbcor} vs. Distance (R3).

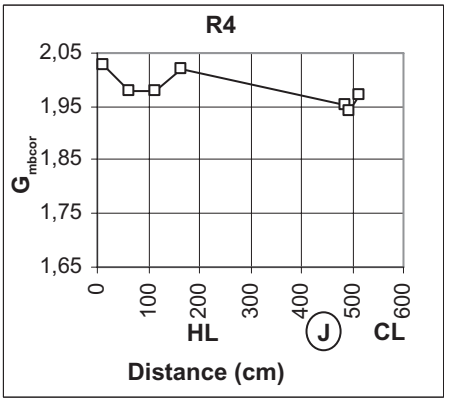

Figure 5. G_{mbcor} vs. Distance (R4).

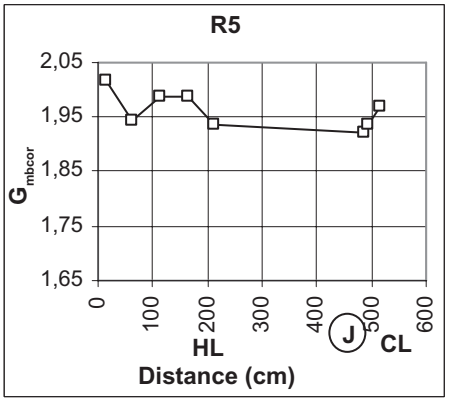

Figure 6. G_{mbcor} vs. Distance (R5).

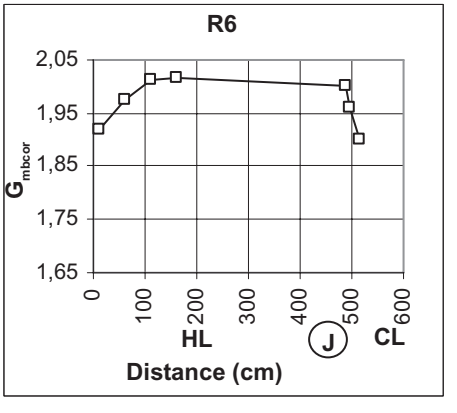

Figure 7. G_{mbcor} vs. Distance (R6).

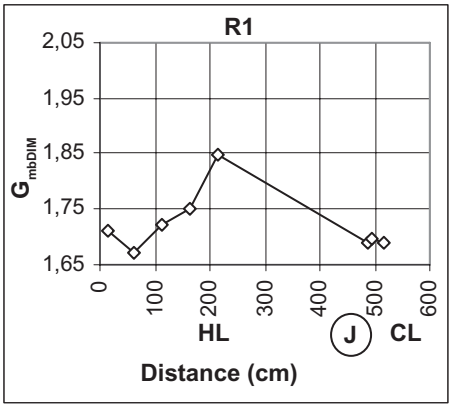

Figure 8. G_{mbDIM} vs. Distance (R1).

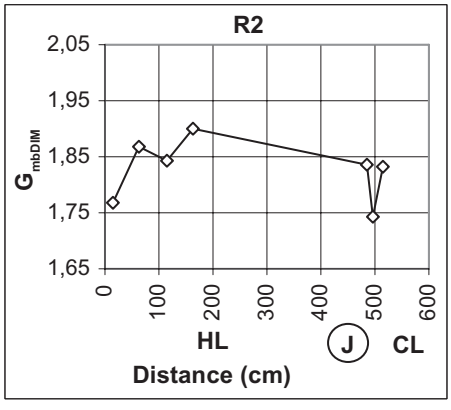

Figure 9. G_{mbDIM} vs. Distance (R2).

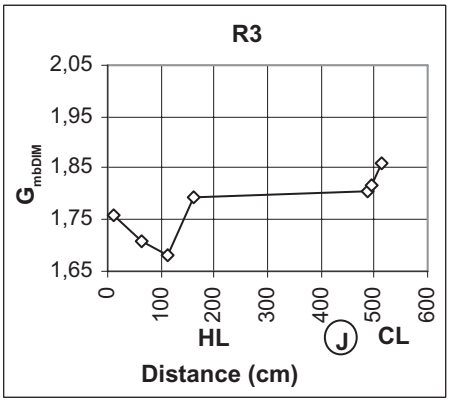

Figure 10. G_{mbDIM} vs. Distance (R3).

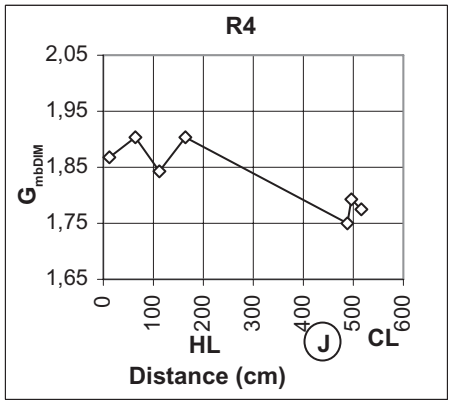

Figure 11. G_{mbDIM} vs. Distance (R4).

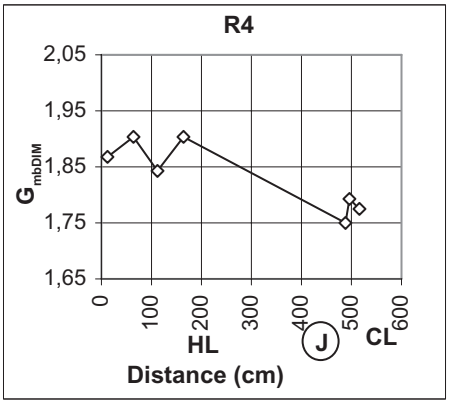

Figure 12. G_{mbDIM} vs. Distance (R5).

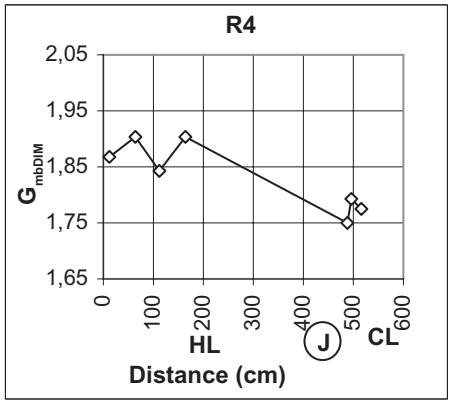

Figure 13. G_{mbDIM} vs. Distance (R6).

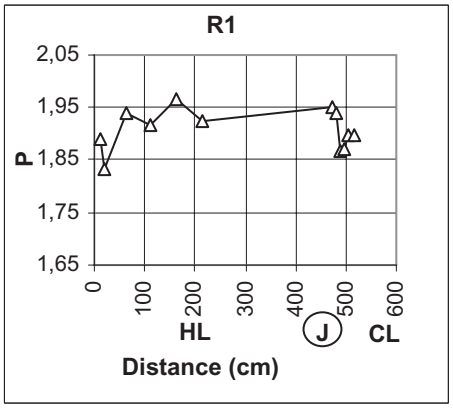

Figure 14. P vs. distance (R1).

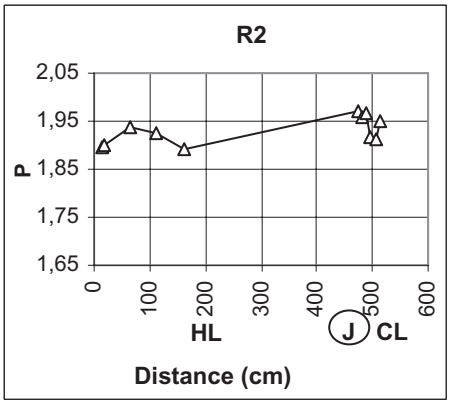

Figure 15. P vs. distance (R2).

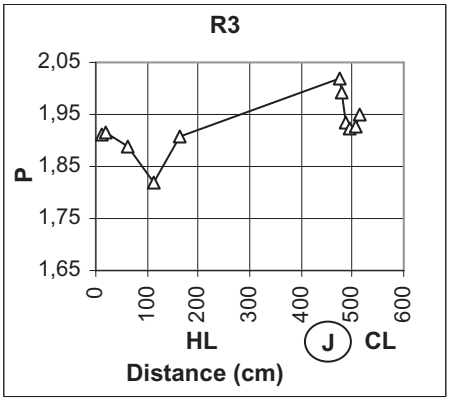

Figure 16. P vs. distance (R3).

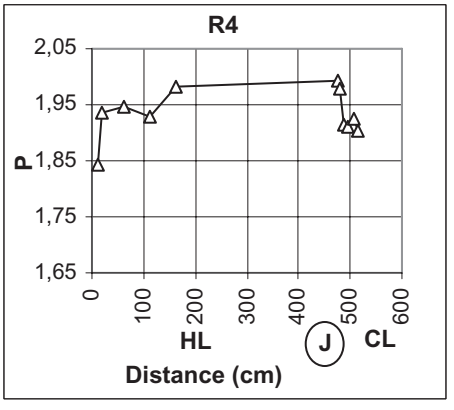

Figure 17. P vs. distance (R4).

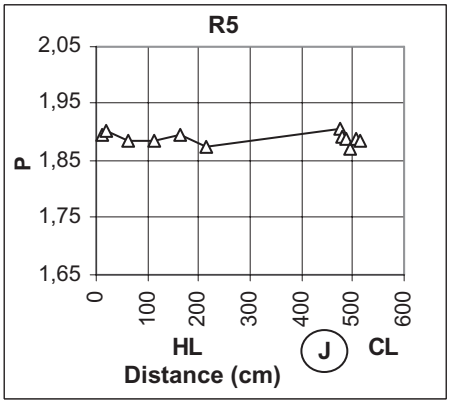

Figure 18. P vs. Distance (R5).

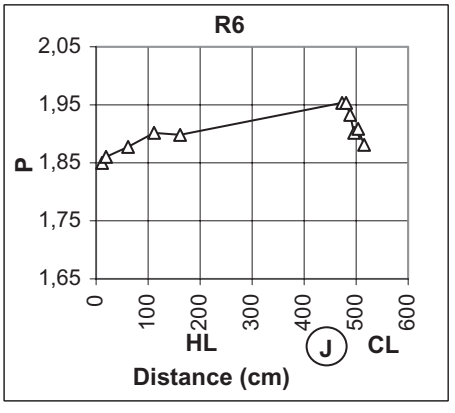

Figure 19. P vs. distance (R6).

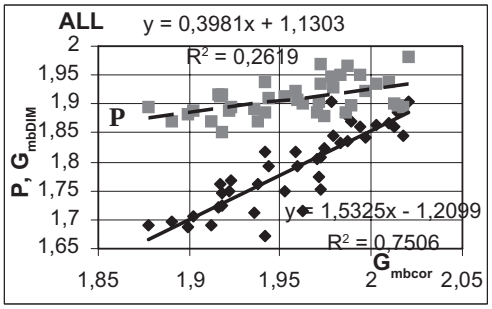

Figure 20. P, G_{mbDIM} vs. G_{mbcor} (ALL).

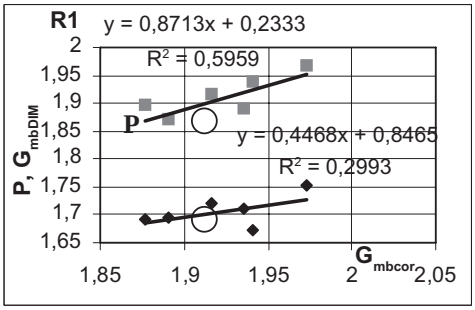

Figure 21. P, G_{mbDIM} vs. G_{mbcor} (R1).

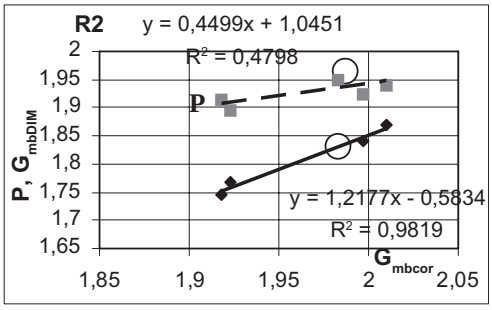

Figure 22. P, G_{mbDIM} vs. G_{mbcor} (R2).

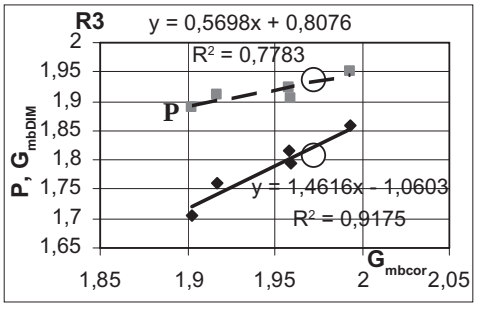

Figure 23. P, G_{mbDIM} vs. G_{mbcor} (R3).

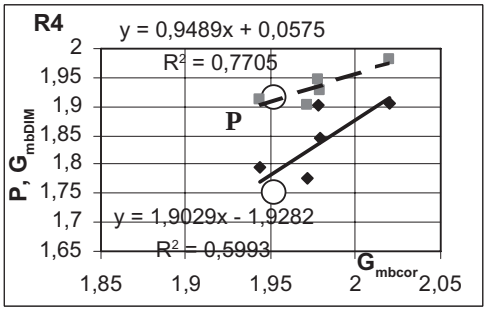

Figure 24. P, G_{mbDIM} vs. G_{mbcor} (R4).

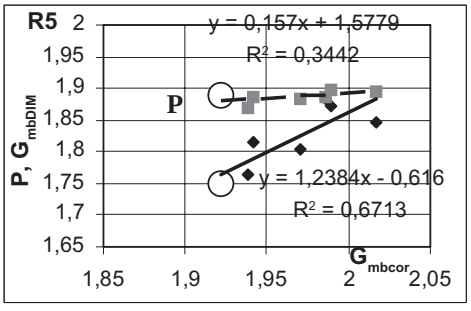

Figure 25. P, G_{mbDIM} vs. G_{mbcor} (R5).

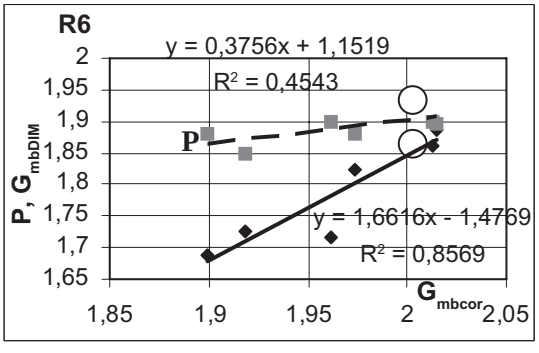

Figure 26. P, G_{mbDIM} vs. G_{mbcor} (R6).

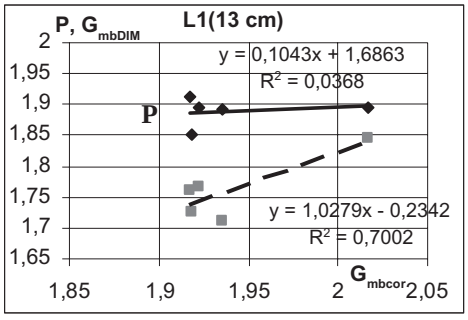

Figure 27. P, G_{mbDIM} vs. G_{mbcor} (L1).

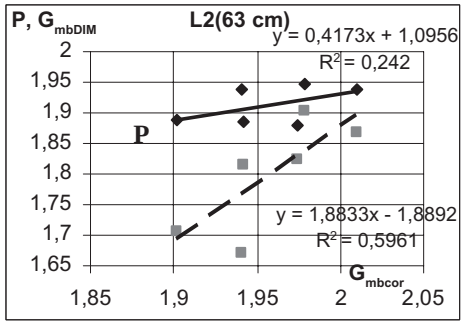

Figure 28. P, G_{mbDIM} vs. G_{mbcor} (L2).

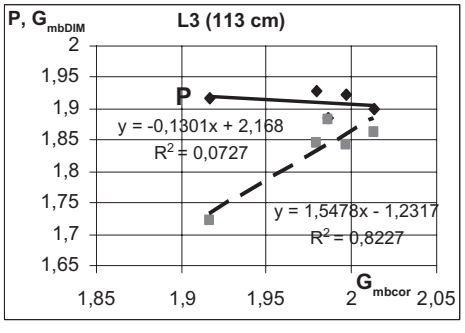

Figure 29. P, G_{mbDIM} vs. G_{mbcor} (L3).

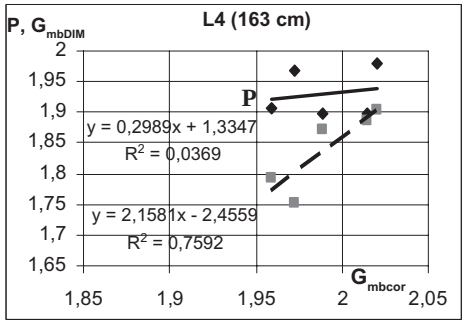

Figure 30. P, G_{mbDIM} vs. G_{mbcor} (L4).

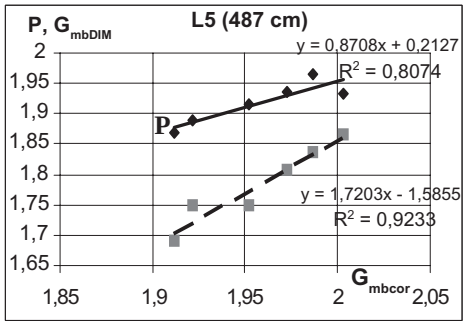

Figure 31. P, G_{mbDIM} vs. G_{mbcor} (L5).

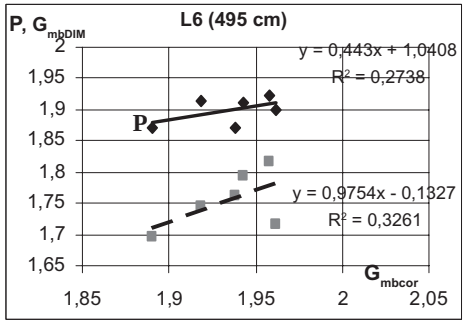

Figure 32. P, G_{mbDIM} vs. G_{mbcor} (L6).

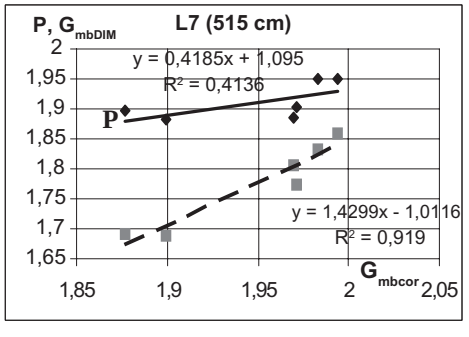

Figure 33. P, G_{mbDIM} vs. G_{mbcor} (L7).

R-square that adjusts for the number of explanatory terms (i.e. independent variables or regressors, *r*) and for the size of the sample (*n*) in a model. More importantly, Unlike R^2, the adjusted R^2 increases only if the new term improves the model more than it would be expected by chance. Note that due to the structure of the algorithm, the adjusted R^2 could result negative, but it will always be less than or equal to R^2. The adjusted R^2 is defined as:

$$R^2_{adj} = 1 - \left(1 - R^2\right)\frac{n-1}{n-r-1} \tag{1}$$

where *r* is the total number of regressors (but not counting the constant term) in the linear model (in our case $r = 1$), and *n* is sample size. Note that R_{adj}-square values result significantly lower than the corresponding *R*-square values, especially for some of the longitudinal sections (L1, L7). By referring to the level of significance of correlations (all the mixes, p-values), summarized in tables 1 and 2, it represents the probability of making the "wrong decision", i.e. a decision to reject the null hypothesis (the two variables are not correlated) when the null hypothesis is actually true (Type I error, or "false positive determination"). As a consequence, the smaller the p-value, the more significant the result is said to be. Traditionally, either the 0.05 level or the 0.01 level are used, although the choice of levels is quite subjective. It is confirmed that:

a) the "P vs. G_{mbcor}" correlations are often significant (at a 5% level of significance) for the single transverse section (Rj), while, for the longitudinal sections (Li), such correlations are usually low significant;
b) on the contrary, the "G_{mbDIM} vs. G_{mbcor}" correlations are often significant (at a 5% level of significance) both for the transverse and the longitudinal sections.

Table 1. R-square values and correlation significance.

		R1	R2	R3	R4	R5	R6	ALL	Average	Ratio
R^2	$P\text{-}G_{mbcor}$	0,60	0,48	0,78	0,77	0,34	0,45	0,26	0,57	0,46
R^2adj	$P\text{-}G_{mbcor}$	0,52	0,35	0,72	0,71	0,21	0,35	0,24	0,48	0,51
p	$P\text{-}G_{mbcor}$	0,030	**0,103**	0,010	0,011	**0,149**	**0,081**	0,001	**0,064**	
R^2	$G_{mbDIM}\text{-}G_{mbcor}$	0,30	0,98	0,92	0,60	0,67	0,86	0,75	0,72	1,04
R^2adj	$G_{mbDIM}\text{-}G_{mbcor}$	0,16	0,98	0,90	0,50	0,72	0,88	0,74	0,69	1,08
p	$G_{mbDIM}\text{-}G_{mbcor}$	**0,187**	0,000	0,001	0,050	0,015	0,001	0,000	0,042	

Table 2. R-square values and correlation significance.

		L1	L2	L3	L4	L5	L6	L7	ALL	Average	Ratio
R^2	$P\text{-}G_{mbcor}$	0,04	0,24	0,07	0,04	0,81	0,27	0,41	0,26	0,27	0,98
R^2adj	$P\text{-}G_{mbcor}$	–	0,05	–	–	0,76	0,09	0,26	0,24	0,29	0,83
p	$P\text{-}G_{mbcor}$	0,749	0,302	0,650	0,748	0,006	0,265	0,147	0,001	0,409	
R^2	$G_{mbDIM}\text{-}G_{mbcor}$	0,70	0,60	0,82	0,76	0,92	0,33	0,91	0,75	0,72	1,04
R^2adj	$G_{mbDIM}\text{-}G_{mbcor}$	0,60	0,49	0,76	0,68	0,90	0,16	0,89	0,74	0,64	1,16
p	$G_{mbDIM}\text{-}G_{mbcor}$	0,046	0,052	0,014	0,027	0,000	**0,214**	0,001	0,000	0,050	

4 CONCLUSIONS

In the light of the above facts the following observations may be drawn:

- variations due to material and construction greatly affect the collected data base and a greater number of points and a more symmetric plan of experiments results necessary;

- transverse variability reflects the presence of the longitudinal joint (in five cases on six), while, on the contrary, longitudinal variability doesn't present any recurrent gap;
- the bias among the three different methodologies for the determination of densities is quite evident. The minimum value is usually given by the dimensional method (G_{mb}), the maximum by the vacuum sealing method (G_{mbcor});
- by referring to the reliability and suitability for standardization of non-nuclear portable densimeter, the analyses showed that, for P, it is very plausible an effect of section-specificity, probably due to the role that humidity plays in the measurements carried out by the portable non nuclear densimeter and to the different distance among transverse and longitudinal points; this occurrence has been analysed from many points of view and R-square values and correlation significance confirmed the assessment; on the other hand, several phenomena confirm that the hypothesis of homogeneity of HMA properties still remains a complex topic.

Future research will include the consideration of the clustered measures of P (5 measures for each point) and a greater number of points for section.

REFERENCES

AA.VV., 2004. TRB of the National Academies, National Cooperative Highway Research Program, Quality characteristics for use with performance-related specifications for hot mix asphalt. Research Result Digest 291.

AA.VV., 2006. TRB Circular Number E-C105. Transportation Research Board, General Issues in Asphalt Technology Committee, Factors Affecting Compaction of Asphalt Pavements. September.

AASHTO TP 68. 2004. Standard Method of Test for Density of In-Place Hot-Mix Asphalt (HMA) Pavement by Electronic Surface Contact Devices.

ASTM D7113. 2005. Standard Test Method for Density of Bituminous Paving Mixtures in Place by the Electromagnetic Surface Contact Methods.

Praticò, F.G., Moro, A. & Ammendola, R. 2008b. New and old technologies fort the determination of density of HMAs. *3rd European pavement and asset management conference*, Coimbra, Portugal.

Praticò, F.G., Moro A., Ammendola, R. & Dattola, V., 2008a. A study on the reliability of new technologies for High-speed measurement of longitudinal joints density in HMA. *First International Conference on Transport Infrastructure (ICTI 2008)*, Beijing, China.

Rao,C., Von Quintus, H.L. & Schmitt R. 2007. Calibration of Non-nuclear Density Gauge Data for Accurate In-Place Density Prediction. Session 596. *86th TRB annual meeting*, Washington D.C., January.

Sebaaly, P.E., Barrantes, J.C. & Fernandez, G., 2005a. Development of a joint density specification: phase II: evaluation of test sections. Nevada Department of Transportation, Carson City, NV, USA.

Sebaaly P.E., Barrantes J.C., Fernandez G. & Loria L., 2005b. Development of a joint density specification: phase II: evaluation of 2004 and 2005 test sections. Nevada Department of Transportation, Carson City, NV, USA, December.

Advanced Testing and Characterization of Bituminous Materials –
Loizos, Partl, Scarpas & Al-Qadi (eds)
© 2009 Taylor & Francis Group, London, ISBN 978-0-415-55854-9

Research on coordinating deformation between Fiber Bragg Grating strain sensor and asphalt mixture

Dong Zejiao, Tian Gengliang & Tan Yiqiu
School of Transportation Science & Engineering, Harbin Institute of Technology, Harbin, P.R.China

ABSTRACT: Research on coordinating deformation between Fiber Bragg Grating (FBG) strain sensor and asphalt mixture is of a great importance on the application of FBG strain sensors in asphalt pavement. As a result, evaluation of coordinating deformation between them was discussed in this paper. At first, the viscoelastic characterization of asphalt mixture was performed through uniaxial creep test with dynamic repetitive loading. Then, a 3D finite element model for asphalt mixture beam with FBG strain sensor embedded using ABAQUS software was established to analyze the stress and strain redistribution close to the location of embedded sensor due to the existing of high-modulus FBG sensor, and the effect of sensor modulus on the strain and stress fields of asphalt mixture was also discussed. The result indicates that the existence of high-modulus sensor results in the redistribution of stress and strain fields, but it doesn't limit plastic deformation development of asphalt mixture; the stress and strain fields are more sensitive to the modulus of inserted sensor, with the decrease of sensor modulus, the influence decreases gradually. Finally, the influence curve of sensor modulus on strain field was obtained, and proposed to modify the measured data from FBG strain sensor.

1 INTRODUCTION

Frequent premature failure of asphalt pavement has excited many investigations to study the behavior of asphalt pavement subjected to vehicular loading and environmental conditions. The FBG sensor has some advantages compared to the conventional sensors like resistance strain gauge or vibrating wire sensor, such as good long-term durability, high reliability, high resistance to corrosion, high anti-electromagnetism, high reusability, good stability and high precision, etc. As a result, the development and application of FBG sensors for pavement monitoring is spreading rapidly (Eckroth 1999, Miller 2000, Cosentino et al. 2003, Wang et al. 2006, Galal et al. 2007). However, there is a discrepancy between the in-situ measured data and the analytically calculated data. One of the primary reasons is the worse coordination working between FBG sensors and asphalt mixture as there is a significant difference between asphalt mixture with elastic modulus of 1.0 ~ 2.0 GPa and currently available FBG sensors with elastic modulus of 50 ~ 70 GPa (Jinsheng 2007, Gengliang 2007). This huge difference of elastic modulus tends to change the strain and stress patterns in the vicinity of sensors, which can greatly affect the reliability of the measurements made by FBG strain sensors (Zafar et al. 2005). Whereas, this paper presents the evaluation of coordination deformation between FBG sensor and asphalt mixture through a comparison of strain and stress field between with and without sensors inserted into the asphalt mixture beam. What's more, the influence of sensor modulus on the result was also discussed.

2 COORDINATING DEFORMATION TEST DESIGN

Using the series of LFRP (Long Fiber Reinforced Plastic) FBG sensor and SFRP (Short Fiber Reinforced Plastic) FBG sensor developed by Harbin Institute of Technology (Wang, 2007),

the parameters of these sensors are listed in Table 1. The sample of LFRP and SFRP FBG sensors are shown in Figure 1.

Considering the mechanical state of asphalt mixture is clear in pure tension or compression mode, a four-point bending beam with FBG strain sensors embedded was designed. The specimen is 400 mm long, 100 mm wide and 100 mm deep, and the loading mode is Four-point bending. The LFRP FBG strain sensor (used to measure horizontal strain on site) was laid at the bottom of the beam where is the tension zone in the four-point bending test, while SFRP FBG strain sensor (used to measure vertical strain on site) was laid at the top of the beam where is the compression zone in the test.

The reason for such design is that there is no shear stress but in a pure tension or compression state at that zone. The offset from the center of strain sensor to the bottom or top of beam is set to 15 mm. The location of FBG strain sensor and loading mode are presented in Figure 2.

Table 1. The technical indexes of the LFRP and SFRP.

	Diameter	Length	Elastic modulus	Measurement range
Technical index	mm	mm	GPa	με
The LFRP	4	70	50	±5000
The SFRP	6	20	50	±5000

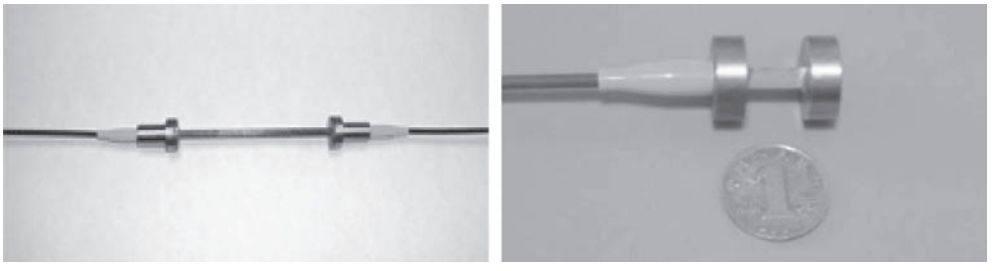

Figure 1. LFRP FBG strain sensor (left) and SFRP FBG strain sensor (right).

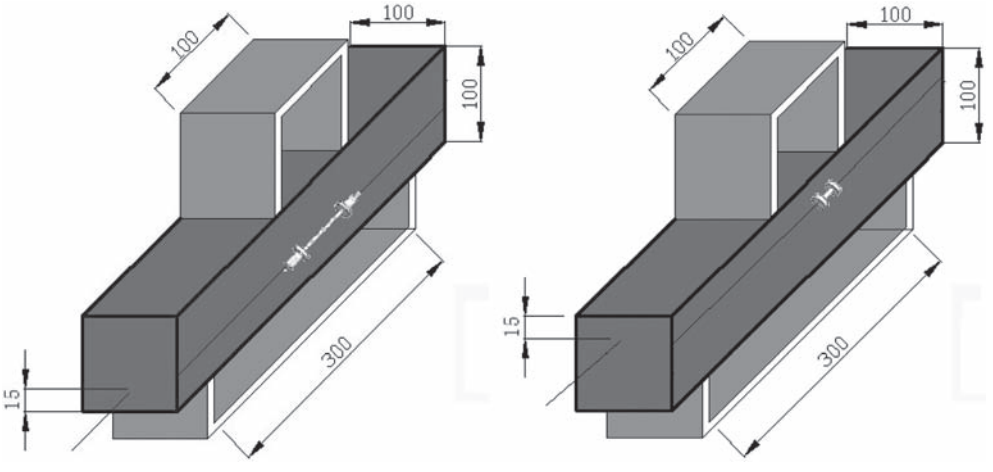

Figure 2. Four-point bending beam with embedded LFRP FBG strain sensors (left) and SFRP FBG strain sensors (right) (unit: mm).

3 MATERIAL CHARACTERIZATION

The characterization of asphalt mixture is defined by uniaxial creep test with repetitive loading, following the test procedure of Test Method for Repeated Load Testing of Asphalt Concrete Mixtures in Uniaxial Compression in NCHRP Report 465. Material Test System 810 is used to perform the test. The sample is 150 mm with a diameter of 101.6 mm. Three testing temperatures are chosen at 30°C, 40°C and 50°C, respectively. The load is applied for duration of 0.1-second with a rest period of 0.9-second. The rest period has a load equivalent to the seating load, as shown in Figure 3. The test is performed without confinement.

Here, we use Drucker-Prager/Creep model in ABAQUS to describe the result of uniaxial creep test, and the parameters A, n and m of the model can be obtained through parameters fitting of creep curve. The creep law uses "time hardening" function as follows:

$$\dot{\bar{\varepsilon}}^{cr} = A\bar{\sigma}_{eq}^{n} t^{m} \tag{1}$$

where $\dot{\bar{\varepsilon}}^{cr}$ denotes the equivalent creep strain rate; $\bar{\sigma}_{eq}^{n}$ represents von Mises equivalent creep stress; t is the total time; A, n and m is the creep parameters of asphalt mixture in ABAQUS. The plastic yield of asphalt mixture obeys the linear Drucker-Prager yield criterion. Here the angle of friction β assumed to be 30°, and 0° for the dilatancy angle Ψ and 1.0 for the flow stress ratio K.

From the curve of total strain vs. time of asphalt mixture, we can find the elastic part and the inelastic part easily. Taking 50°C result as an example, we can easily get the critical point for the elastic part in the curve, as shown in Figure 4. After removing the elastic part from the total strain, the curve of the creep strain vs. time can be got. Then we can get parameters A, n and m according to the data fitting, taking the result at 50°C as an example, as shown in Figure 5, in which, the red line is the fitting line, the blue ones are the prediction band, the light blue lines are the confidence band, and the green one is the residual error line. In the same way, we can get the parameters A, n and m under different temperatures, presented in Table 2.

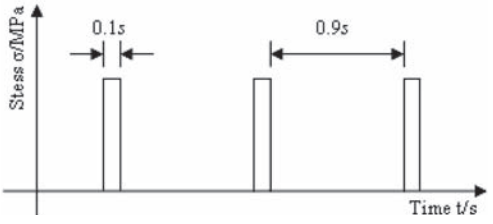

Figure 3. The schematic diagram of repeated load.

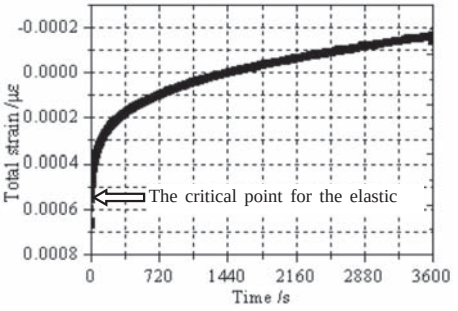

Figure 4. Total strain vs. time at 50°c.

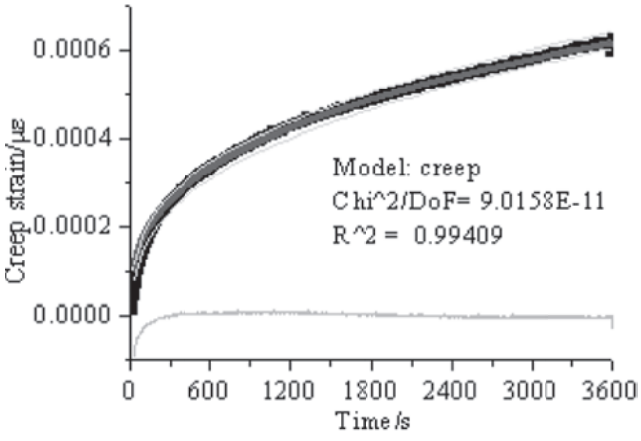

Figure 5. Nonlinear fitting to the creep curve at 50°C.

Table 2. Creep parameters of asphalt mixture Drucker-Prager/ Creep model.

Parameters	0°C	20°C	30°C	40°C	50°C
A	1.8E-5	4.1E-5	3.9E-5	7.8E-5	6.0E-5
n	0.948	0.812	0.787	0.728	1.037
m	–0.690	–0.806	–0.927	–0.726	–0.646

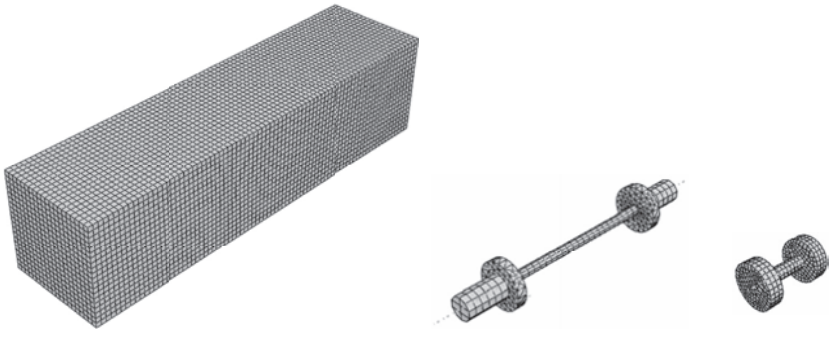

Figure 6. The meshing of asphalt mixture beam and FBG sensors.

4 FINITE ELEMENT MODELING

ABAQUS software was used to simulate the coordination deformation between FBG sensor and asphalt mixture. A three dimensional model for the beam with LFRP or SFRP sensor embedded using the real size were built. The interaction between FBG sensor and asphalt mixture was simulated with friction contact defined with a penalty function in ABAQUS, in which the Friction Coefficient was assumed to be 0.7.

Eight-node hexahedron quadratic reduced-integration element (C3D8R) was chosen for the element type of beam, while FBG sensor embedded in asphalt mixture was simulated with eight–node hexahedron incompatible element (C3D8I). Both anchor sides of FBG sensor were meshed with Free grid, while modify quadratic Tet element (C3D10M) was used. The final meshing of asphalt mixture beam and FBG sensor are shown in Figure 6.

5 RESULTS AND DISCUSSION

First, the comparison about the stress and strain distribution of asphalt mixture beam with and without FBG sensor embedded was performed to analyze the influence of sensor insertion. Here, asphalt mixture beam with LFRP FBG sensor embedded is defined as Case 1, while asphalt mixture beam with SFRP FBG sensor is name as Case 2 and asphalt mixture beam without any sensor as Case 3. Then, the influence of FBG modulus on the stress and strain distribution of asphalt mixture beam was also discussed.

5.1 *Comparision among case 1, case 2 and case 3*

5.1.1 *Horizontal stress, S_{33}*

The contours of horizontal stress on the center section in the transverse direction of asphalt mixture beam are shown in Figures 7, and the horizontal stress distribution along vertical central axis of beam is shown in Figure 8.

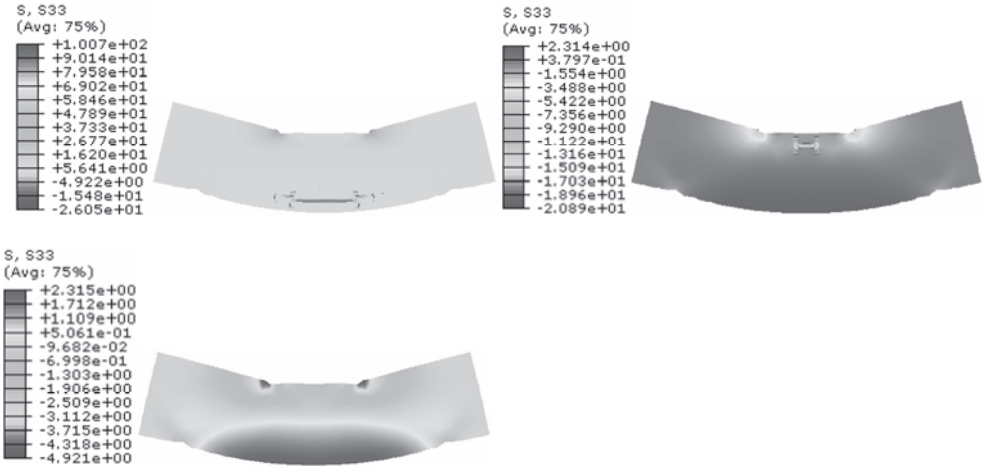

Figure 7. Horizontal stress contours, Case 1 (left top); Case 2 (right top); Case 3 (left bottom).

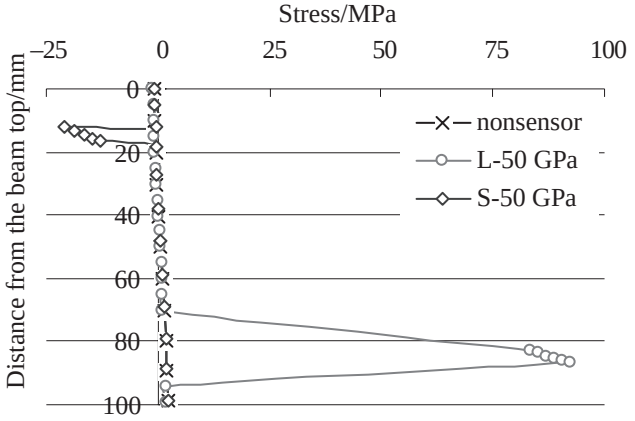

Figure 8. Horizontal stress distribution along the vertical central axis of beam.

As can be seen from Case 3 of Figure 7, the maximum horizontal tension stress occurs at the bottom of asphalt mixture beam and the maximum horizontal compression stress occurs at the top of beam, which accords with the mechanical characteristics of four-point bending beam. Comparatively speaking, As is shown in Case 1 and Case 2, there is stress concentration phenomenon at the position of FBG sensor due to the obvious change of modulus, which can also be seen clearly from Figure 8, That is to say, that the existence of high modulus FBG has significant effect on stress distribution, which results in the stress redistribution. It is concluded that this disturbance by the insertion of sensor should be evaluated before the measurement on site.

5.1.2 *Horizontal strain, E_{33}*

The contours of horizontal strain on the center section in the transverse direction of asphalt mixture beam are shown in Figures 9, and the horizontal strain distribution along vertical central axis of beam is shown in Figure 10.

As can be seen from Case 3 of Figure 9, the maximum horizontal tension strain occurs at the bottom of asphalt mixture beam and the maximum horizontal compression strain occurs at the top of beam, which also accords with the mechanical characteristics of four-point bending beam. Comparatively speaking, As is shown in Case 1 and Case 2, there is strain variation at the position of FBG sensor due to the change of material modulus. It can be

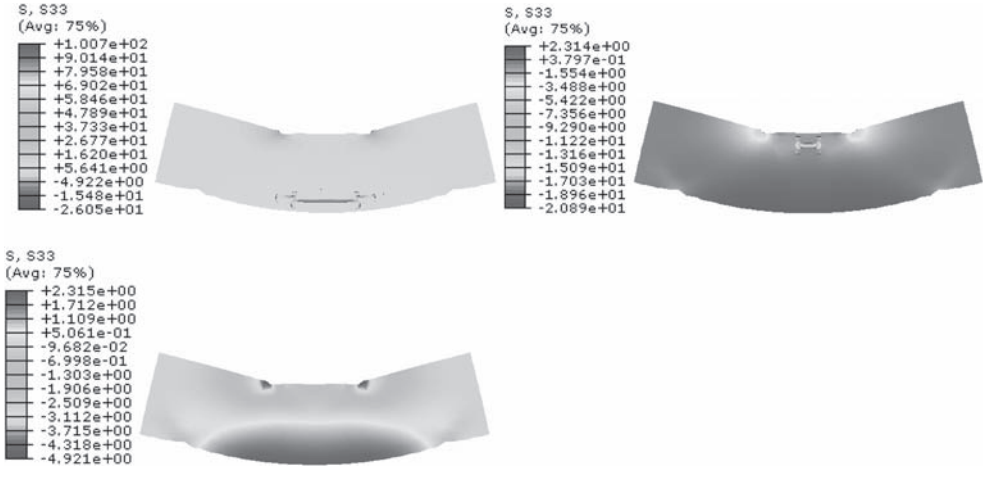

Figure 9. Horizontal strain contours, Case 1 (left top); Case 2 (right top); Case 3 (left bottom).

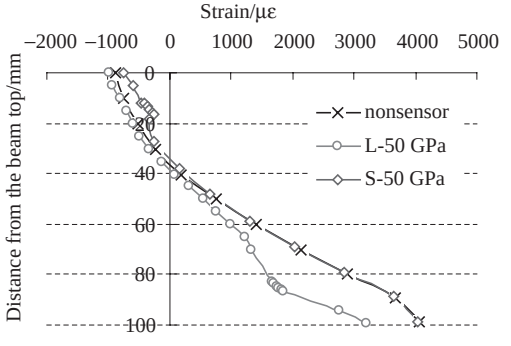

Figure 10. Horizontal strain distribution along the vertical central axis of beam.

seen from Figure 10 that the horizontal strain decreases at the position of FBG sensor, while the influence due to the insertion of sensor doesn't extend to the distal end of the beam. It is seen that the existence of FBG sensor with high modulus makes the strain near it less than the actual value.

5.1.3 *Plastic deformation, PEEQ*

In ABAQUS, the equivalent plastic strain PEEQ is a scalar used to represent the inelastic deformation of material. If this variable is larger than zero, it means that the material has already yielded. Through using dialog box "Contour Plot Option" and setting the minimum value of the contour to a small amount of the equivalent plastic strain, the region with elastic characteristics can be represented with the deep grey in ABAQUS/CAE, as shown in Figure 11. From the chart, we can see that the yield regions in different cases are similar. Although the high-modulus sensor has a protective function to its neighbor region on the deformation, it does not affect the plastic deformation distribution of beam due to its small volume fraction compared with the whole beam. The results are shown in Figure 11.

5.2 *Influence of sensor's modulus*

Changing the modulus of sensor from 50 GPa to 30 GPa, then 10 GPa, and comparing the stress and stain distribution around it, we can obtain the sensitivity of modulus on the stress and strain distribution. The horizontal stress S_{33} and strain E_{33} distribution along the vertical central axis of asphalt mixture beam for case 1 and case 2 are shown in Figure 12, 13, 14 and 15.

5.2.1 *Horizontal stress S_{33} along the vertical central axis of beam*

It can be seen that from Figure 12 and 13, the stress concentration around FBG sensor decreases with the decrease of sensor modulus rapidly as the modulus of sensor drops from 50 GPa to 30 GPa and then 10 GPa. In case 1, i.e. beam with LFRP FBG sensor embedded, the maximum horizontal tension stress on the top of sensor decreases from 92.4 MPa to 64.6 MPa, then 26.6 MPa, eventually reduces 71.2%; In case 2, the maximum horizontal compression stress on the top of FBG sensor decreases from 20.9 MPa to15.2 MPa, then 6.8 MPa, eventually reduces 67.5%. It is concluded that the stress field is sensitive to the change of sensor modulus, with the descrease of sensor modulus, the influence on the result falls off.

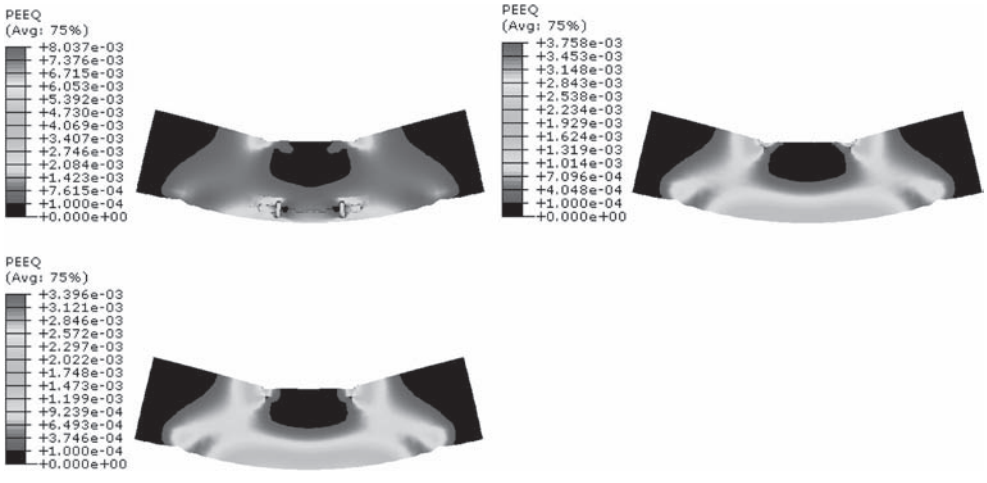

Figure 11. Plastic deformation contours, Case 1 (left top); Case 2 (right top); Case 3 (left bottom).

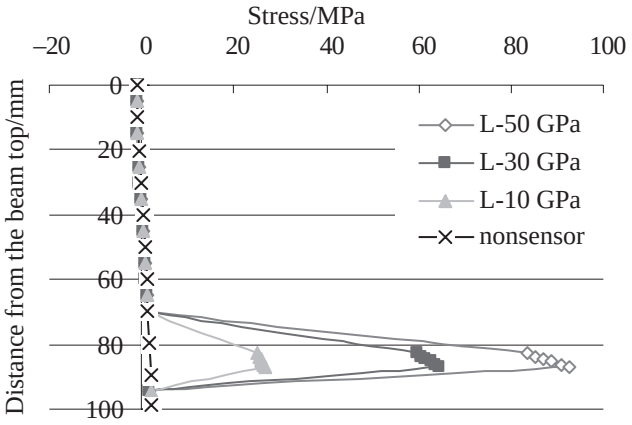

Figure 12. Horizontal stress variation with the change of sensor moduls in Case 1.

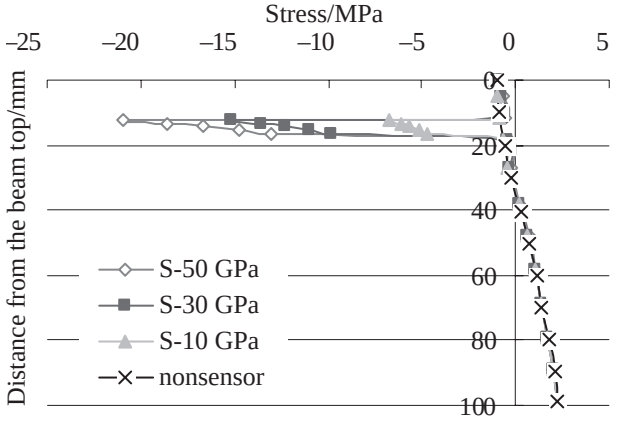

Figure 13. Horizontal stress variation with the change of sensor moduls in Case 2.

5.2.2 *Horizontal strain E_{33} along the vertical central axis of beam*

As is shown in Figure 14 and 15, the strain increases gradually around FBG sensor with the decrease of sensor modulus as the modulus of sensor deceases from 50 GPa to 30 GPa, and then 10 GPa. In case 1, the maximum horizontal tension strain on the top of FBG sensor increases from 1856 με to 2165 με, then 2686 με, eventually increase 44.7%; In case 2, the maximum horizontal compression strain on the top of FBG sensor increases from 411 με to 497 με, then 666 με, eventually reduces 62.0%. It is concluded that the strain field is also sensitive to the change of modulus, with the decrease of sensor modulus, the influence on the strain result drops.

In a word, we can modify the measured strain value according to the variation rules of sensor modulus. That's to say, the influence curve of strain under different sensor modulus can be used to calibrate the measured result. On the other hand, from the result shown here, we should try to reduce FBG sensor modulus to that of asphalt mixture as possible as it can.

6 SUMMARY AND CONCLUSIONS

This paper firstly presents the design of Four-point bending beam with FBG sensor embedded to evaluate the coordinating deformation between FBG strain sensor and asphalt mixture, then perform the viscoelastic characterization of asphalt mixture which were used for the three dimensional finite element simulation, the preliminary conclusions may be summarized:

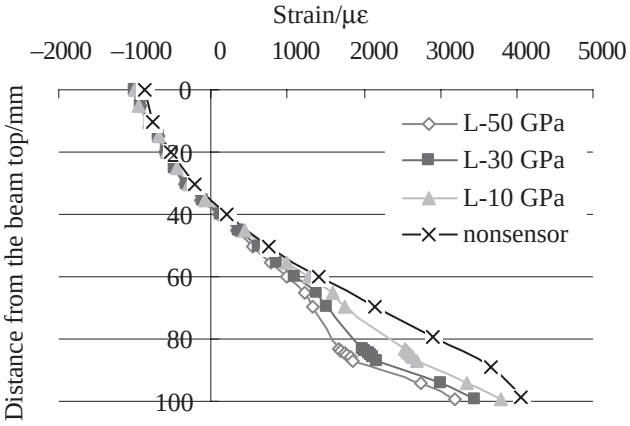

Figure 14. Horizontal strain variation with the change of sensor moduls in Case 1.

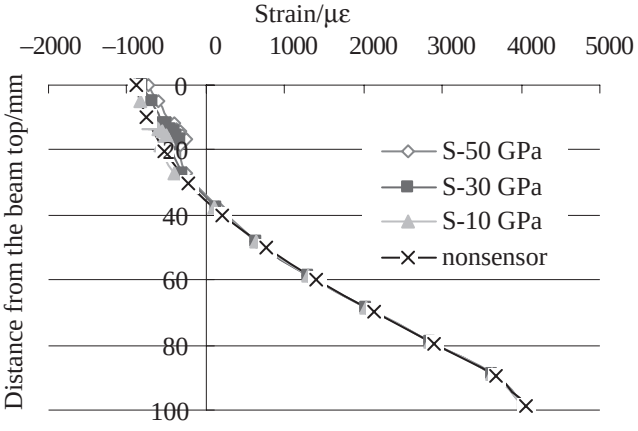

Figure 15. Horizontal strain variation with the change of sensor moduls in Case 2.

1. The existence of high-modulus sensor makes stress and strain around the sensor redistributing, resulting in a lower strain value than the real value compared with asphalt mixture beam without sensor;
2. Although the high-modulus sensor has a protective function to its neighbor region on the deformation, it do not affect the plastic deformation distribution of beam due to its small volume fraction compared with the whole beam;
3. The stress and strain fields were more sensitive to the sensor modulus, with the decrease of sensor modulus, the influence on the strain or stress result drops obviously;
4. We can obtain the influence curve of strain under different sensor modulus, which can be used to calibrate the measured result from FBG sensor. Simultaneously, we should try to reduce FBG sensor modulus to that of asphalt mixture as possible as it can.

REFERENCES

Cosentino, Paul J., Eckroth, Wulf von & Grossman Barry, G. 2003. Analysis of Fiber Optic Traffic Sensors in flexible pavements, *Journal of Transportation Engineering* 129(5): 549–557.

Eckroth, Wulf von 1999. Development and modeling of embedded Fiber-Optic Traffic Sensors, Doctoral dissertation of Florida Institute of Technology.

Galal, Khaled, Sharp, Stephen R. & Elfino, Mohamed, K. 2007. Fiber-optic sensors strain measurements under an asphalt layer during and after construction. *Transportation Research Board Annual Meeting 2007,* Paper #07-1712.

Gengliang, Tian 2007. Research on the coordination distortion performance between asphalt mixture and Optical Fiber Grating Sensor, Outstanding Bachelor Thesis of Harbin Institute of Technology.

Jinsheng, Li 2007. Development and performance of asphalt pavement strain sensors based on FBG technology, Master Thesis of Harbin Institute of Technology.

Miller, Craig E. 2000. Development of a fiber optic pavement subgrade strain measurement system, Doctoral dissertation of University of Maryland.

WANG Jian-Neng, TANG Jaw-Luen & CHANG Hsiang-Ping 2006. Fiber Bragg grating sensors for use in pavement structural strain-temperature monitoring. *Smart Structures and Materials 2006: Sensors and Smart Structures Technologies for Civil, Mechanical*, *and Aerospace Systems*, Proc. of SPIE Vol. 6174.

Wang, Hezhe 2007. Research on FBG Sensors for practical infrastructures and their application in the measurement of highway road, Master Thesis of Harbin Institute of Technology.

Zafar, R., Nassar, W. & Elbella A. 2005. Interaction between pavement instrumentation and hot-mix-asphalt in flexible pavements. *Emirates Journal for Engineering Research* 10(1): 49–55.

Advanced Testing and Characterization of Bituminous Materials –
Loizos, Partl, Scarpas & Al-Qadi (eds)
© 2009 Taylor & Francis Group, London, ISBN 978-0-415-55854-9

Influence of treatments on the surface characteristics of aggregate

D.Q. van Lent, A.A.A. Molenaar & M.F.C. van de Ven
Delft University of Technology, Delft, The Netherlands

ABSTRACT: Adhesion between bituminous mortar and aggregate particles is a key issue controlling the durability of open graded asphalt mixtures like porous asphalt concrete. For that reason, adhesion tests are important. In many adhesion tests however it is necessary to prepare stone samples of a specific size and shape such that they fit in the testing set up. Preparations of the stone samples could imply treatments like sawing and sandblasting. These treatments might change the surface characteristics of the stone samples, which could have an effect on the results obtained from the laboratory tests. In this paper the surface characteristics of two stone types are presented after receiving several surface treatments. Investigated treatments are for instance sawing and sandblasting. From the results presented in this paper it is concluded that some treatments used for preparations of stone samples for the laboratory experiments are affecting specific surface characteristics of the stone samples.

1 INSTRODUCTION

1.1 *General*

For reasons of traffic noise reduction the Dutch primary road-network is extensively surfaced with Porous Asphalt Concrete (PAC). Additional advantage of PAC is the significant reduction of splash and spray in wet weather conditions. However, the service life of PAC is much lower than the service life of dense asphalt concrete. The surface life of PAC is limited by the development of raveling of the surface. Raveling may cause a reduction of driving comfort to the road users, a decrease of traffic safety and a strong increase of traffic noise. The Road and Hydraulic Engineering Institute of the Dutch Ministry of Transport, has started research into raveling of PAC. As part of this research the Delft University of Technology developed a mechanistic design tool for the prediction of the lifetime of PAC. This tool is called Lifetime Optimization Tool (LOT).

In the LOT research program (Huurman et al. 2007) a characterization is made of the mechanical behavior of the adhesive zone between the aggregate particles and the bitumen with filler (mortar). Also the bituminous mortar in PAC mixtures was tested. Several mechanical tests were conducted on mortar and stone-bitumen specimen. To avoid scale effects it was decided to perform the tests at a similar scale as in practice, i.e. the scale of individual aggregates. It was considered of great importance to get the size of the aggregate specimens as used in the test program as constant as possible. To get similar sized samples with similar surface properties, the aggregates received all kinds of treatments.

Stone column specimens are used in Dynamic Mechanical Analyzer (DMA) and Dynamic Shear Rheometer (DSR) fatigue tests to give insight into adhesive zone fatigue behavior. In principle, circular column specimens with a 6.7 mm diameter are used. Between two stone columns a 15 μm interface binder layer is assembled (Fig. 1).

To obtain the stone columns some stone treatments were performed. First slices of about 10 mm thickness were sawn from boulders of Bestone and Greywacke of approximately 5 kg. The sawn surfaces of the slices are sandblasted to get a more reproducible surface

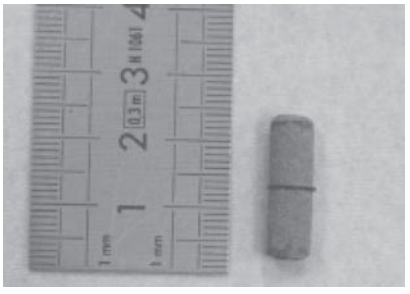

Figure 1. Stone column specimen with a 15 μm interface binder layer for use in DSR (Khedoe & Moraal 2007).

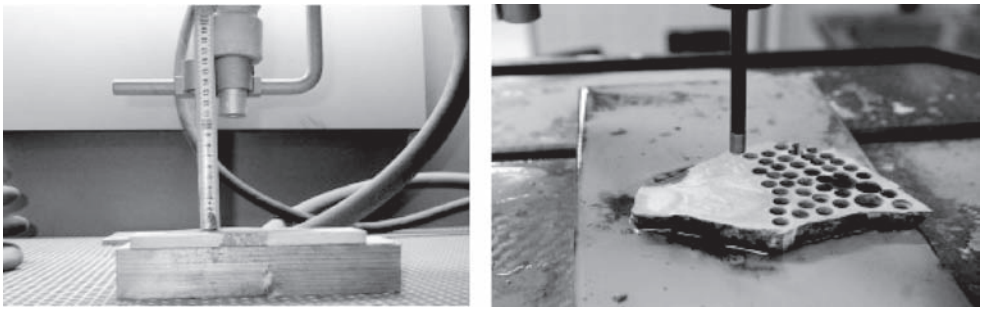

Figure 2. Sandblasting of slice (left) and drilling of the columns from a sandblasted slice (Khedoe & Moraal 2007).

(Fig. 2, left). The small columns were drilled from the sandblasted slices using a column drill (Fig. 2, right). To remove grease from the sawing and drilling process the stone columns were boiled in de-mineralized water for 15 minutes.

1.2 *Research question*

The effect of treatments like sawing and sandblasting on the result of tests to characterize the adhesive zone is unknown. The question arises how the surface characteristics of the stone samples were affected by the different treatments and how the surface characteristics of the stone samples in the laboratory relate to the same characteristics of stones used by contractors in asphalt concrete mixtures.

Therefore in this study the stone characteristics affecting bitumen-aggregate adhesion were investigated. Especially the effects of the surface treatments, used in the LOT research program on these stone characteristics were investigated. The results of this exploring study gave an insight in the aggregate characteristics affecting the bitumen-aggregate adhesion as well as an insight into the effects of the different treatments on the surface characteristics.

2 EXPERIMENTAL PROGRAM

2.1 *Method*

A literature review (van Lent 2008) showed that the chemical composition of the aggregates has a strong influence on adhesion. Chemical elements at the surface do not only affect the

Table 1. Aggregate properties affecting adhesion and their evaluation methods.

Aggregate Surface Property		Evaluation Method
Roughness	Macro roughness	Stereo microscope
	Meso roughness	Confocal microscope
	Micro roughness	Electron microscope
Specific surface area		Stereo microscope, confocal microscope
Porosity		Mercury intrusion
Chemical composition		Electron microscope, X-Ray fluorescence spectrometer
Acidity		pH meter
Surface free energy		Sessile drop method

Figure 3. From left to right: sawn columns, sandblasted columns, 4/8 aggregates.

Arrhenius acidity of the aggregate, but the surface free energy is affected as well. Geometry has, especially according to the mechanical adhesion theory, an important influence on the adhesive bond between bitumen and aggregate. Shape, angularity, size and roughness all determine this geometry and have their effect on the specific surface area of the stones, which is an important parameter for adhesion. According to the mechanical adhesion theory, also the porosity and the pore size distribution are affecting the adhesion with the bitumen (Bagampadde et al. 2001, Hefer & Little 2005).

In this paper the aggregate properties affecting the bitumen-aggregate adhesion are investigated. From the literature study (van Lent 2008) the aggregate properties influencing the bitumen-aggregate adhesion were retrieved and are given in Table 1.

2.2 *Materials*

In the LOT research program two different aggregate types are analyzed, being Greywacke and Bestone. A number of treatments are carried out on the stones. Some stone samples are sandblasted, some are only drilled and some are both drilled and sandblasted. Examples of some samples are given in Figure 3.

In order to allow comparisons to be made, also real aggregate particles of Greywacke and Bestone as used in asphalt mixtures are obtained. These Greywacke and Bestone aggregate particles have a sieve size of 4/8 mm.

3 EXPERIMENTAL RESULTS

It was not possible to present all the test results in this paper. For complete test results and background information reference is made to (van Lent 2008). In this chapter the analyses and discussion of the most important results are given.

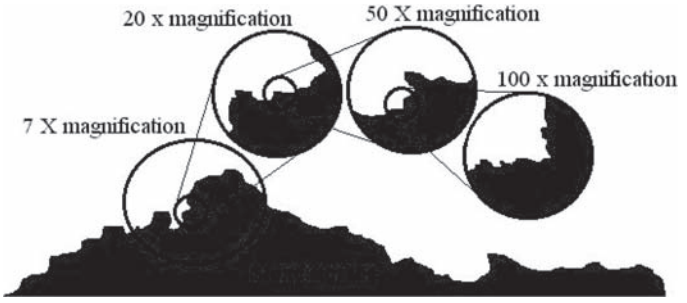

Figure 4. Stone surface roughness at different magnifications.

3.1 *Roughness*

To compare the roughness of the stones it is important to keep in mind that a unique roughness number of a surface doesn't exist, because roughness can for instance be defined at macro-, meso- and micro levels. Therefore the roughness of the stones is viewed at different levels of magnification. The magnification has a strong correlation with the representativeness of the measured roughness for the same type of stones (Fig. 4).

Figure 4. Stone surface roughness at different magnifications.

The roughness of the stones is measured at a magnification of 7 (macro level), 20, 50 (meso level) and a magnification of 100 (micro level). The roughness is measured by means of microscopes and from these measurements the roughness parameters Pa and Pq are calculated (Peekstok 2001). The Pa value is the sum of the deviations of the measured local points to the average peak height:

$$Pa = \frac{1}{n_x}\sum_{i=1}^{n_x}\left|z(i)-\bar{z}\right|$$

where $z(i)$ = local peak height of the sample at the ith measurement; $\bar{z}$ = average peak height; n_x = number of measurements on the length x.

The Pq value is the root-mean square value of the measured local points:

$$Pq = \sqrt{\frac{\sum_{i=1}^{n_x}\left|z(i)-\bar{z}\right|^2}{n_x}}$$

where $z(i)$ = local peak height of the sample at the ith measurement; $\bar{z}$ = average peak height; n_x = number of measurements on the length x.

The roughness parameters measured at a magnification of 7, 20 and 50 are given in Table 2. The results show that the 4/8 aggregates of both the Greywacke and the Bestone have a higher measured roughness than the sawn samples at these magnifications. This is an indication that sawing results in a less rough surface. In the same way it is found that the samples of both the Greywacke and the Bestone have a lower roughness than the same slices after sandblasting. So this sandblasting results in an increase in roughness. This increased roughness is still less than the surface roughness of the 4/8 aggregates. Table 2 shows that the roughness parameters aren't constant over the different magnifications. This is better shown at the micro level.

At a magnification of 100, environmental scanning electron microscope (ESEM) pictures show no clear visual difference in roughness of the surface of the Greywacke sandblasted samples and the sawn samples. Over the entire surface of the samples areas with lower and higher roughness are found. Also for the Bestone sawn and sandblasted samples it is

Table 2. Roughness parameters of the stone samples.

	Pa [µm] 7X	Pq [µm] 7X	Pa [µm] 20X	Stdev	Pq [µm] 20X	Stdev	Pa [µm] 50X	Stdev	Pq [µm] 50X	Stdev
Greywacke sawn	48.41	56.69	3.79	0.59	5.14	0.81	3.81	0.21	5.02	0.25
Greywacke sandblasted	50.67	59.47	4.99	1.01	6.85	1.06	5.15	0.77	7.00	0.74
Greywacke 4/8 aggregate	287	372	20.82	3.33	25.16	3.30	11.29	5.65	13.41	6.43
Bestone sawn	48.12	56.49	5.21	0.75	7.26	1.02	4.58	0.52	6.25	0.71
Bestone sandblasted	49.07	58.51	6.63	1.50	8.57	1.98	7.45	2.56	9.60	2.81
Bestone 4/8 aggregate	233	311	29.04	12.45	35.32	14.90	20.91	6.01	26.36	7.38

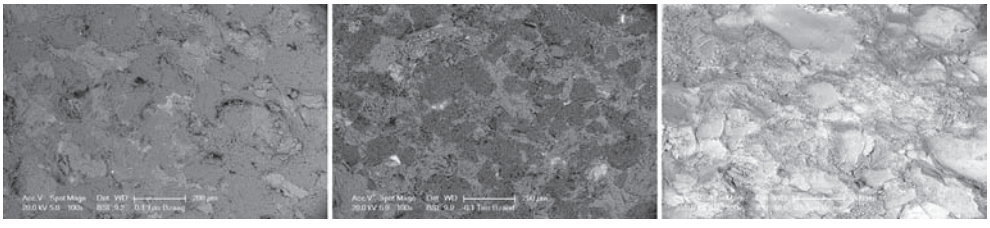

Figure 5. Surface of a Bestone sawn sample (left), a Bestone sandblasted sample (middle) and a Bestone 4/8 aggregate (right).

difficult to differentiate visually the micro roughness. All the Bestone sawn (Fig. 5, left) and sandblasted (Fig. 5, middle) samples show especially areas with a high roughness on their surfaces.

Again no clear indication is found that sandblasting of the samples results in a difference in the micro roughness. The visual difference of the micro roughness between the Bestone 4/8 aggregates and the sawn and sandblasted samples is larger than the difference between the Greywacke 4/8 aggregates and the Greywacke sawn and sandblasted samples. The Bestone 4/8 aggregates (Fig. 5, right) show on their surface more areas with a relative low roughness compared to the sandblasted and sawn columns. At some areas the number of areas with a relative low roughness is dominant.

The measurements of the micro roughness on the pictures are quantified by using the wavelet method (Masad 2003). The averaged results per stone sample are given in Table 3.

The quantitative results of the Greywacke pictures give a more clear distinction between the micro roughness of the differently treated samples. On the sandblasted Greywacke samples more areas with fine texture (77%) are found than on the Greywacke sawed samples (73%). More coarse texture areas are found on the sawn samples (7%) than on the sandblasted columns. This indicates that sandblasting of the Greywacke samples results in more areas of fine texture and thus micro roughness is added. Comparing the quantitative results of the Greywacke samples to the Greywacke 4/8 aggregates results in the observation that the 4/8 aggregates have less areas with fine texture and more areas with coarse texture than both sawed and sandblasted samples. So in contrast to the macro and meso roughness, the Greywacke sawed samples have more fine texture at micro level than the Greywacke 4/8 aggregates. With sandblasting additional fine texture is added to the Greywacke samples.

As mentioned above, a difference in micro roughness between the Bestone samples and the Bestone 4/8 aggregates is detected by means of the electron microscope pictures. This finding is contradicted by the quantitative analyses. According to the quantitative analyses, the Bestone sawed samples and the Bestone 4/8 aggregates have an equal percentage of areas

Table 3. Texture distribution on the pictures analysed using the wavelet method.

	Fine texture [areas]	Medium texture [areas]	Coarse texture [areas]	Fine texture [%]	Medium texture [%]	Coarse texture [%]
Greywacke sawn	456	129	43	73	21	7
Greywacke sandblasted	460	98	36	77	17	6
Greywacke 4/8 aggregate	448	137	58	70	21	9
Bestone sawn	397	152	173	56	21	23
Bestone sandblasted	820	219	152	68	19	13
Bestone 4/8 aggregate	481	208	171	56	24	20

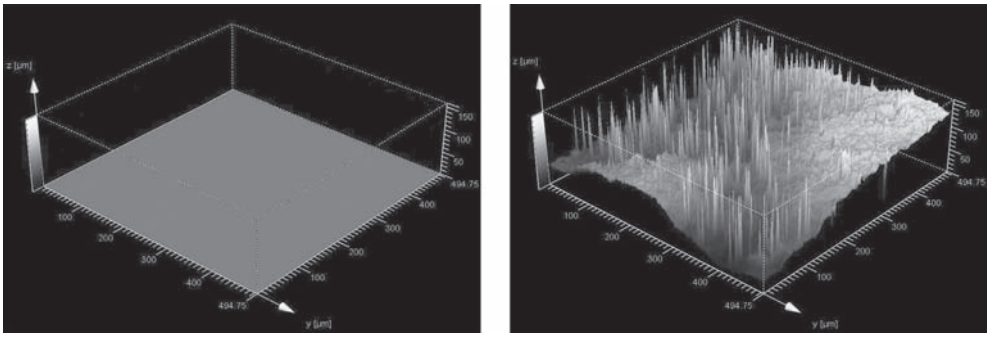

Figure 6. A total flat area has the same values for the evaluated area (axes) and the measured area (orange area) (left). A stone surface has an SSA larger than 1 m^2/m^2 (right).

with fine texture. It is found, similar to the Greywacke samples, that by sandblasting the sawed Bestone columns, micro texture is added to the samples. The quantitative results show a shift from medium and coarse texture at the Bestone sawed samples to the fine texture at the Bestone sandblasted samples.

The difference between the visual inspection of the microscope pictures and the quantification of the roughness of the same pictures using the wavelet method shows nicely the main point of attention for performing roughness measurements of aggregates. As mentioned before the roughness of aggregates is dependent on the magnification and the roughness index used for the measurement of the roughness. This means that roughness measured at different magnification can't be compared. It also shows that for a characterization it isn't sufficient to measure the roughness of aggregates at only one magnification.

3.2 *Specific surface area*

The specific surface area is determined by means of a stereo microscope and a confocal microscope. If an area with specific dimensions on stones is evaluated, the measured surface area is larger than the evaluated area, because of the roughness (Fig. 6). By dividing the measured surface area by the dimensions of the evaluated area a measure for the specific surface area (SSA) is obtained in [m^2/m^2].

The measured ratios between the measured surface area and the evaluated area are presented in Table 4.

The results show that at all magnifications this measured specific surface area of the 4/8 aggregates of both the Greywacke and Bestone is larger than that of the sandblasted and

Table 4. Measured specific surface area of the stone samples.

	SSA [mm/mm] 7X	SSA [µm²/µm²] 20X	Stdev	SSA [µm²/µm²] 50X	Stdev
Greywacke sawn	1.002	1.70	0.04	3.03	0.08
Greywacke sandblasted	1.006	1.86	0.19	3.41	0.24
Greywacke 4/8 aggregate	1.167	2.92	0.13	4.02	1.21
Bestone sawn	1.007	2.09	0.35	3.11	0.06
Bestone sandblasted	1.020	2.26	0.30	3.51	0.29
Bestone 4/8 aggregate	1.093	2.86	0.57	5.82	0.94

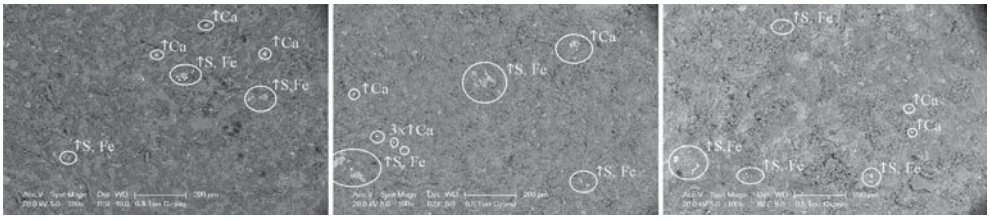

Figure 7. ESEM pictures of the surface of a Greywacke sawn sample (left), a Greywacke sandblasted sample (middle) and a Greywacke 4/8 aggregate (right).

sawn columns. At all magnifications the sandblasted columns have a larger specific surface area than the sawn columns. This indicates that, for both the Greywacke and the Bestone columns, sandblasting results in an increase of the specific surface area. This increased specific surface area of the sandblasted columns is however found to be less than the specific surface area of the 4/8 aggregates of both Greywacke and Bestone, at magnifications of 7, 20 and 50.

It is important to notice that the measured specific surface area of all samples increases with increasing magnification. An explanation for this could be that with increasing magnifications one obtains a better representation of the real surface. The problem however is that at higher magnifications the measurements become less representative, because a smaller area is measured. It is not expected that the real values could be measured using whatever microscope magnification, because of the unknown errors and the increasing values of the measured specific surface area. Therefore it is suggested to use other methods to measure the specific surface area of stone samples.

3.3 *Porosity*

No significant differences were found between the aggregate samples. Also between Bestone and Greywacke no significant differences were found.

3.4 *Chemical composition*

The ESEM chemical analysis of the surface of the samples didn't show a clear distinction between the different Greywacke samples. On all Greywacke samples the same concentrated elements were found (Fig. 7). The remaining area showed a high content of silica.

However for Bestone, a difference in concentrated elements on the surface was found between the 4/8 aggregates and the Bestone sawn and sandblasted samples, because no concentrated elements were found on the surface of the 4/8 aggregates (Fig. 8). Between the Bestone sawn samples and the Bestone sandblasted samples no clear distinction is visible.

It should be noticed that stones in general have a very heterogeneous character and that the elements found on the surface are influenced by a large number of uncontrollable external factors. In this particular case the ESEM chemical analyses gave no evidence that sandblasting and sawing have influenced the individual elements visible on the surface of the Greywacke samples. The differences in result between the Bestone 4/8 aggregates and the Bestone sawn samples can't directly be related with the treatments. A possibility is for instance that dust is present on the 4/8 aggregates.

To quantify the chemical composition of the stones an X-Ray Fluorescence Spectrometer (XRF) is used. These chemical analyses of the Greywacke samples (Table 5) show no effect of the surface treatments on the chemical composition. The silica content is almost constant over the Greywacke samples. The expectation that due to sandblasting more silica is present on the sandblasted columns is not likely. The oxides contents like, aluminum oxide (Al_2O_3), potassium oxide (K_2O), magnesium oxide (MgO), sodium oxide (Na_2O) and iron oxide (Fe_3O_2), show relative small differences between the sawn and sandblasted samples.

The quantitative XRF chemical analyses of the Bestone samples (Table 5) also show no effect of the surface treatments on the chemical composition. The oxides contents like, aluminum

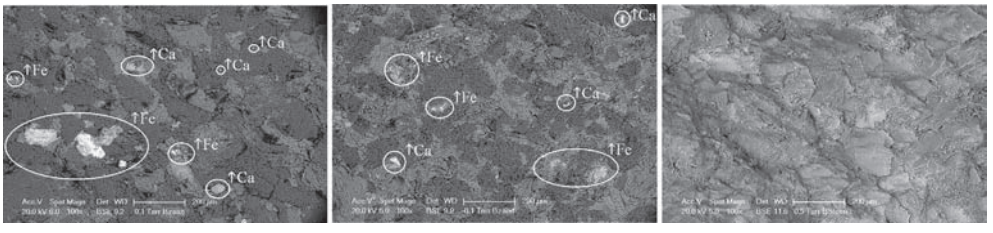

Figure 8. ESEM pictures of the surface of a Bestone sawn sample (left), a Bestone sandblasted sample (middle) and a Bestone 4/8 aggregate (right).

Table 5. XRF analyses of the stone samples in mass percentages.

	Greywacke sawn	Greywacke sandblasted	Greywacke 4/8 aggregate	Greywacke 4/8 aggregate cleaned	Bestone sawn	Bestone sandblasted	Bestone 4/8 aggregate	Bestone 4/8 aggregate cleaned
SiO_2	54.18	54.03	53.04	49.23	60.88	53.19	63.20	63.20
CaO	5.11	5.10	11.48	14.57	9.21	10.41	6.64	6.39
Al_2O_3	18.86	18.96	11.96	10.24	10.26	8.75	11.28	11.38
K_2O	4.29	4.30	2.16	1.76	2.11	1.84	2.23	2.28
MgO	3.31	3.30	2.31	1.97	1.77	1.42	2.32	2.29
Na_2O	0.552	0.529	0.840	0.795	2.04	1.80	2.06	2.02
Fe_2O_3	7.35	7.35	4.69	4.01	2.67	2.29	3.48	3.50
S	0.241	0.249	0.306	0.310	0.000	0.000	0.000	0.000
P_2O_5	0.083	0.083	0.068	0.061	0.123	0.094	0.126	0.131
TiO_2	0.920	0.900	0.661	0.583	0.402	0.365	0.460	0.497
V_2O_5	0.027	0.027	0.015	0.014	0.006	0.008	0.009	0.008
Cr_2O_3	0.032	0.039	0.063	0.041	0.051	0.051	0.060	0.052
MnO	0.091	0.086	0.108	0.115	0.057	0.070	0.057	0.580
NiO	0.074	0.088	0.166	0.088	0.155	0.164	0.194	0.147
BaO	0.122	0.114	0.077	0.071	0.092	0.096	0.106	0.110

oxide (Al_2O_3), potassium oxide (K_2O), magnesium oxide (MgO), sodium oxide (Na_2O) and iron oxide (Fe_3O_2), show relative small differences between the sawn and sandblasted samples.

3.5 *Acidity*

No significant differences were found between the aggregate samples. The acidity of the stone samples immersed in water is measured to be about pH 8.

3.6 *Surface free energy*

The surface free energy of the stones is measured by means of the Sessile Drop Method (Little & Bashin 2006). In this method small droplets of probe liquids are made on the surface of the stone samples and then the angle of the droplets with the surface are recorded by a camera (Fig. 9).

The Young-Dupré equation relates the contact angle of a probe liquid on ideal flat surfaces to the work of adhesion:

$$W^a = -\Delta G_{12}^a = \gamma_{lv} \cdot (1 + \cos\theta_{sl})$$

where W^a = work of adhesion; ΔG_{12} = change of Gibbs free energy per unit area; γ_{lv} = interfacial energy between liquid and vapour; and θ_{sl} = contact angle between solid and liquid.

The interfacial energy between liquid and vapour is related to the surface free energy of the liquid and the equilibrium spreading pressure.

$$\gamma_{lv} = \gamma_l - \pi_{elv}$$

where γ_{lv} = interfacial energy between liquid and vapour; γ_l = surface free energy of liquid; and π_{elv} = equilibrium spreading pressure of liquid in the saturated vapour of liquid.

It is common practice to neglect the contribution of the spreading pressure in surface free energy measurements by means of the Sessile Drop Method. This results in the next equation:

$$W^a \approx \gamma_l \cdot (1 + \cos\theta_{sl})$$

where W^a = work of adhesion; γ_{lv} = interfacial energy between liquid and vapour; γ_l = surface free energy of liquid; and θ_{sl} = contact angle between solid and liquid.

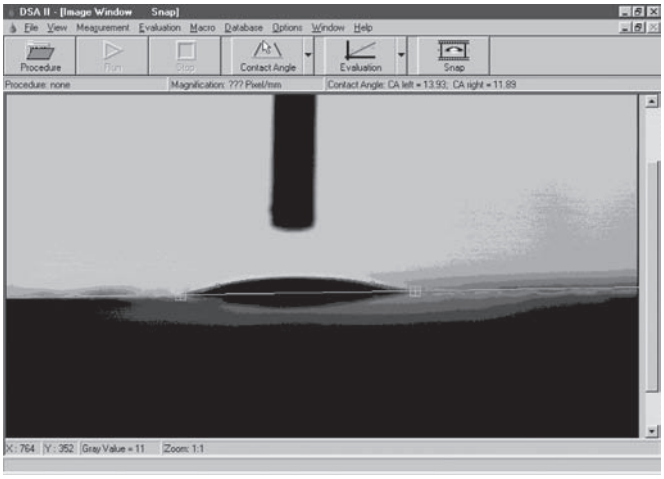

Figure 9. Computer recording of water droplet on the surface of a Bestone sandblasted sample.

Table 6. Surface free energy components of the different stone samples in [mJ/m²].

	γ_s^{TOT}	Stdev	γ_s^{LW}	Stdev	γ_s^{AB}	Stdev	γ_s^+	Stdev	γ_s^-	Stdev
Greywacke sawn	55.52	4.11	49.11	0.62	6.41	3.72	0.23	0.27	45.53	2.35
Greywacke sandblasted*MIN	63.71	0.42	50.53	0.09	13.18	0.36	0.95	0.06	45.57	0.55
Greywacke 4/8 aggregate*MIN	66.98	N.D.	50.66	N.D.	16.32	N.D.	1.53	N.D.	43.54	N.D.
Greywacke 4/8 aggregate cleaned*MIN	67.04	N.D.	50.78	N.D.	16.26	N.D.	1.52	N.D.	43.47	N.D.
Bestone sawn	56.34	7.92	46.10	2.74	10.24	6.71	0.53	0.76	49.08	13.09
Bestone sandblasted	60.05	3.80	48.49	0.22	11.56	3.72	0.68	0.41	48.98	2.98
Bestone 4/8 aggregate*MIN	66.58	N.D.	50.40	N.D.	16.18	N.D.	1.49	N.D.	43.94	N.D.
Bestone 4/8 aggregate cleaned*MIN	66.93	N.D.	50.75	N.D.	16.18	N.D.	1.50	N.D.	43.64	N.D.

*MIN value is minimum value, at least one not stable droplet of a reference liquid. N.D. not determined.

The van Oss, Good and Chaudhury theory is used to relate the derived work of adhesion to surface free energy of the stone samples (van Oss et al. 1988). This means that the total surface free energy (γ_s^{TOT}) of the stones is composed in a non-polar surface free energy component (γ_s^{LW}) and a polar surface free energy component (γ_s^{AB}). The polar surface free energy component is composed from a Lewis acid (γ_s^+) and a Lewis base (γ_s^-) component.

$$\gamma_l(1+\cos\theta_{sl}) = 2\left(\sqrt{\gamma_l^{LW}\cdot\gamma_s^{LW}} + \sqrt{\gamma_l^-\cdot\gamma_s^+} + \sqrt{\gamma_l^+\cdot\gamma_s^-}\right)$$

where γ_l = total surface free energy of liquid; θ_{sl} = contact angle between solid and liquid; γ_l^{LW} = free energy of Lifshitz-van der Waals forces of liquid; γ_s^{LW} = free energy of Lifshitz-van der Waals forces of solid; γ_l = contribution of Lewis base of liquid; γ_s^+ = contribution of Lewis acid of solid; γ_l^+ = contribution of Lewis acid of liquid; and γ_s^- = contribution of Lewis base of solid.

The results show that the sawn samples have a lower measured surface free energy than the sandblasted stone samples. Table 6 also shows that for some stone samples only a minimum value was measured. This means that those samples have at least one non-stable droplet of a used probe liquid (distilled water, diiodomethane and glycerol). A non-stable droplet keeps spreading over the surface of the stone. This occurs when the surface free energy of the probe liquid is smaller than the surface free energy of the stone surface ($\gamma_l < \gamma_s$). A non-stable droplet is taken into account as 0°. This means that the surface free energy of the surface might be larger than calculated. Because for all 4/8 aggregates only a minimum value for the surface free energy was found, the Sessile Drop Method isn't suitable for these surface free energy measurements of stone surfaces.

4 CONCLUSIONS

From the test results the following conclusions were drawn:

a. It was shown that sawing and sandblasting influences the roughness of the stone samples.
b. The specific surface area increases when the sawn stone samples are sandblasted. However the specific surface area of the 4/8 aggregates is larger than the specific surface area of both the sawn and sandblasted stone samples.

c. No indication is found that the porosity, the chemical composition and the pH acidity of the stone samples are affected by any of the treatments.
d. Sandblasting of the stone samples increases the measured surface free energy of the sawn stone samples.
e. From the results of this research it is concluded that the treatments used for preparations of the stone samples for the laboratory experiments have influenced specific surface characteristics of the stone samples which have an effect on the stone-bitumen adhesion.

REFERENCES

Bagampadde, U., Isacsson, U. & Kiggundu, B.M. 2001. Fundamentals of stripping in bituminous pavements. State of the Art. *Research Report ISSN 1650-867X*. Division of Highway Engineering. Royal Institute of Technology, Stockholm, Sweden.

Hefer, A. & Little, D. 2005. Adhesion in bitumen-aggregate systems and quantification of the effects of water on the adhesive bond. *Report ICAR/505-1*. Texas Transportation Institute. Texas A&M University, College Station, Texas, USA.

Huurman, M. 2007. Lifetime Optimization Tool, LOT, the Kernel. *Report 7-07-170-1*. Delft University of Technology, Delft, NL, 2007.

Huurman, M. & Mo, L.T. 2007. Lifetime Optimization Tool, fatigue in mortar and adhesive zones. Measurements, test interpretation and determination of model parameters. *Report 7-07-170-2*. Delft University of Technology, Delft, NL, 2007.

Huurman, M. & Woldekidan, M.F. 2007. Mortar response. Measurements, test interpretation and determination of model parameters. *Report 7-07-170-3*. Delft University of Technology, Delft, NL, 2007.

Khedoe, R.N. & Moraal, J. 2007. Sample preparation and laboratory testing for the Lifetime Optimisation Tool research program. *Report 7-07-170-4*. Delft University of Technology, Delft, NL, 2007.

Little, D. & Bashin, A. 2006. Using surface energy measurements to select materials for asphalt pavement. *Final report for NCHRP project 9–37*. Web-only document 104. Transportation Research Board, Washington, D.C., 2006.

Masad, E. 2003.The development of a computer controlled image analysis system for measuring aggregate shape properties. *NCHRP-IDEA Project 77 Final Report*. Transportation Research Board, Washington, D.C., 2003.

Peekstok, E.R. 2001. Application of laser scanning confocal microscope in metal research (in Dutch). *Materialen & Processen*, November/December 2001, pp. 24–30.

van Lent, D.Q. 2008. Aggregate characterisation in relation to bitumen-aggregate adhesion. *M.Sc. thesis*. Delft University of Technology, Delft, NL, 2008.

van Oss, C.J., Chaudhury, M.K. & Good, R.J. 1988. Interfacial Lifshitz-van der Waals and polar interactions in macroscopic systems. *Chemical Reviews*, 88, 1988, pp. 927–941.

Advanced Testing and Characterization of Bituminous Materials – Loizos, Partl, Scarpas & Al-Qadi (eds)
© 2009 Taylor & Francis Group, London, ISBN 978-0-415-55854-9

Mix design of grouted porous asphalt concrete for wearing course layers

M. la Agostinacchio
Polytechnic of Milan, Italy

D. Ciampa & S. Olita
University of Basilicata, Italy

ABSTRACT: A road is a multi-layer load-bearing structure, whose mechanical behavior depends on the design and arrangement of the layers. Asphalt surfaced pavements require resurfacing every 10 to 15 years and traditional repairs don't last at long.

Recent advances in pavement design suggest the use of a combi-layer (grouted porous asphalt) instead of the traditional asphalt concrete for the wearing-course in case of heavy or low-speed channellized traffic. With the aim to provide a guidance pertaining to combi-layers design, the Authors developed a research program for evaluating the performance of mixtures of asphalt concrete filled with cement mortar, produced using a soft modified bitumen and calcareous aggregates, adopting different particle size distributions.

Traditional tests (Marshall and Indirect Tensile Strength tests) were executed on the grouted mixtures in order to evaluate the performance varying different parameters, referring to the curing of the samples (1, 7, 28 days) and to the testing temperature (25, 45, 60, 70°C).

Moreover, the mechanical characterization was assessed by triaxial tests performed with an original apparatus (UNIBAS-M.P.T.), patented in Italy, achieving interesting results. In particular, the usefulness of the device for the evaluation of the structural response of the road pavements was shown on the basis of the rupture domains obtained analyzing the mixtures.

1 INTRODUCTION

In semi-flexible pavements (SFPs) the upper layer is an open grade asphalt filled with a cement mortar. This technology combines the benefits of asphalt (jointless surfaces) and concrete pavements (high strength and durability): in particular, the semi-flexible wearing-course doesn't show the plastic flows of the flexible pavements and reduces the main problem of the joints, i.e. the developing of cracks due to thermal stresses. The use of a grouted asphalt concrete (GAC) is suitable in applications where particular requirements of load bearing capacity and durability must be fulfilled (Da Rios et al. 2007), for example on docks, airports, goods terminals and for heavy or low-speed channellized traffic roads pavements, both in case of rehabilitations and new costructions.

The materials choice and their percentage of use, as well as the curing procedure, influence the performance of the mixtures. With the aim to furnish suggestions pertaining to semi-flexible wearing-course layers design, so as to produce an improvement of the performance values, the Authors present the results of a mix design study on grouted asphalt concretes, taking into account as variables the curing time after the filling of the specimens with the grout and the testing temperature.

Starting from the adoption of two different particle size distributions, cylindrical and cubic specimens were prepared; in particular cubic specimens were subjected to triaxial tests by the UNIBAS-M.P.T. device, carrying out the ruptures domains. The performance increment due to the use of the mortar was evaluated comparing the results of GCAs testing the same mixtures not filled with the grout.

2 MATERIALS AND MIXTURES DESIGN

The experimental analysis was performed at the Roads Constructions Laboratory of the University of Basilicata (Potenza, Italy). The mix design was defined so as to allow a correct penetration of the grout in the porous asphalt skeleton and achieving the required performance values.

2.1 *Aggregates and particle size distributions*

The optimal grading curve and the particle size of the aggregates were defined so as to obtain a voids percentage—20 ÷ 30% in this case—able to receive the mortar and to ensure an adequate number of contact points among the aggregates. Two asphalt mix—designed A and B—are considered in the paper. They are characterized by different particle size distributions: mixed for A (Table 1) and monogranular for B (Table 2). The material was selected on the basis of their availability on the Basilicata territory, in order to limit the transportation costs, making recourse to limestone, slaked lime for the filler in particular. The adoption of aggregates with a L.A. coefficient of 23% (UNI EN 1097-2:2008) assesses the possibility to take into account materials not usually used for high performance mixtures.

Table 1. Mix A: Particle size distribution.

Series ASTM	Passing (%)	Cumulative retained (%)	Retained (%)	Weight per kg (g)
3/4	100	0	0	0
1/2	80	20	20	200
1/4	30	70	50	500
# 4	20	80	10	100
# 10	14	86	6	60
# 20	10	90	4	40
# 200	5	95	5	50
Filler	–	–	5	50

$\gamma_{aggregate}$ = 2.65 g/cm^3.
Filler = hydrated lime 5%.
Bitumen = 50–70 (modified with polymers).
Bitumen percentage on the aggregate weight = 5%.

Table 2. Mix B: Particle size distribution.

Series ASTM	Passing (%)	Cumulative retained (%)	Retained (%)	Weight per kg (g)
3/8	100	0	0	0
1/4	20	80	80	800
# 10	7	93	13	130
Filler	–	–	7	70

$\gamma_{aggregate}$ = 2.65 g/cm^3.
Filler = hydrated lime 7%.
Bitumen = 50–70 (modified with polymers).
Bitumen percentage on the aggregate weight = 4.5%.

2.2 *Adoption of the grout type*

The performance of the grouted asphalt concretes is greatly influenced by the penetration capacity of the mortar. A powdered expanding cement binder with special additives produced by MAPEI Group, known as STABILCEM®, was adopted. This product, usually used for filling cavities and fissures, within internally porous concrete, rock and brickwork (www.mapei.it 2008), is added with water to obtain a slurry with controlled-shrinkage.

The quantity of the product, the mixing time and the water percentage were established so as to obtain a fluid and homogeneous mixture, characterized by high compressive strength at early ages and a time setting of 5 hours.

3 THE EXPERIMENTAL ANALYSIS: METHODOLOGY AND OBJECTS

Referring to the mix A and B, the tested samples were OPEN GRADE (without mortar) and grouted asphalt (GAC) concretes. The mechanical behavior of the mixtures and the performance increment due to the adding of the grout were evaluated by traditional tests—Marshall (UNI EN 12697-34:2004) and Indirect Tensile Strength (UNI EN 12697-23:2006) tests—varying the testing temperature (25, 45, 60, 70°C). Moreover, the influence of the curing time on the mechanical properties of GCAs was analyzed. The simplified ruptured domains of the grouted asphalt concretes were achieved using the UNIBAS-M.P.T. device (Agostinacchio et al. 2002).

3.1 *Compaction method and manufacturing of the samples*

The compaction method was defined on the basis of previous studies so as to guarantee a residual voids percentage of 20% at least and ensuring a correct penetration of the grout. The porosity values of the investigated mixtures were measured varying the blows applied by the Marshall Compactor (UNI EN 12697-34:2004), verifying the correspondence with the required percentage (≥ 20%). Applying 20 blows to the specimens, the achieved residual voids percentages were 20% for the Mix A and 25% for the Mix B.

Cylindrical and cubic samples were prepared. The manufacturing of the GCAs was accomplished using the same moulds set up for the open grade asphalt concretes, sealing a base. The filling with the grout was made by two steps. In the first, the grout penetration occurred for gravity through the interconnected voids by straining of the product on the free base of the sample in the mould. In the second step, after a time setting of five hours, the specimens were extracted from the dies and bathed in the mortar, so as to obtain a complete saturation and soaking the superficial voids. Once accomplished the process, the samples were tested valuating the mechanical properties of the mixtures at curing times of 1, 7 and 28 days.

3.2 *Indirect Tensile Strength and Marshall Tests: Evaluation of the GCAs performance with respect to the curing time*

In order to establish the performance of the mixtures varying the curing time, the Marshall and the Indirect Tensile Strength tests were took into account. For each age, four nominally identical specimens were tested, reporting the results as mean values. The performance increment was evaluated comparing the resistance values of the GACs at 1, 7, 28 days, referring to the results achieved testing the OPEN GRADE samples. The output are shown in Tables 3, 4 (Mix A), 5 and 6 (Mix B).

Tables 3–6 show the remarkable improvement of the performance values—tensile resistance, Marshall stiffness—due to the curing time increasing. Modelling the relationship between the tensile resistance σ_t and the logarithm of the age t of the grouted samples by a linear regression equation:

$$\sigma_t = a \cdot \ln(t) + b \tag{1}$$

and finding the derivative with respect to the age logarithm:

$$\frac{d\sigma_t}{d\ln(t)} = a \tag{2}$$

the curing speed is expressed by the angular coefficient *a*. Output show the gradient was 0.16 N/(mm^2 ln(days)) for both considered mixtures; moreover the constant term *b*, which is the short-term resistance, as pretty much the same for A and B, i.e. 1.153 N/mm^2 for the Mix A and 1.196 N/mm^2 for the Mix B. These results allow to assess that resistance initial increment and curing speed are fundamentally connected to the grout characteristics.

Table 3. Indirect Tensile Strength test: resistance increments (Mix A).

	Indirect Tensile Resistance	Increment	Age
Samples	(N/mm^2)	(%)	(days)
4	0.873	–	Open Grade
4	1.135	30	1
4	1.523	74	7
4	1.685	93	28

Table 4. Marshall test: stiffness increment (Mix A).

	Stability	Flow index	Stiffness	Stiffness Increment	Age
Samples	(kN)	(mm)	(kN/mm)	(%)	(days)
4	6.38	4.6	1.39	–	Open Grade
4	13.53	7.1	1.91	37	1
4	15.29	5.8	2.64	90	7
4	18.92	6.0	3.15	127	28

Table 5. Indirect Tensile Strength test: resistance increments (Mix B).

	Indirect Tensile Resistance	Increment	Age
Samples	(N/mm^2)	(%)	(days)
4	0.737	–	Open Grade
4	1.181	60	1
4	1.548	110	7
4	1.713	132	28

Table 6. Marshall test: stiffness increment (Mix B).

	Stability	Flow index	Stiffness	Stiffness increment	Age
Samples	(kN)	(mm)	(kN/mm)	(%)	(days)
4	4.48	3.0	1.49	–	Open Grade
4	15.22	4.9	3.11	109	1
4	21.99	5.8	3.79	154	7
4	24.50	6.0	4.08	174	28

3.3 *Indirect Tensile Strength and Marshall Tests: Evaluation of the GACs performance with respect to the temperature*

The evaluation of the mixtures resistance with respect to the testing temperature was performed adopting for the GACs a curing time of 7 days. For each temperature, four samples of each mixture (A, B) were tested, reporting the results as mean values. The mechanical behaviour of the OPEN GRADE was evaluated also.

The output of the experimental analysis referring to the Indirect Tensile Strength tests at 25, 45 and 60°C are shown in Table 7 (Mix A) and 8 (Mix B). The thermal susceptibility of the mixtures was obtained plotting the tensile resistance versus the testing temperatures (see Fig. 1).

The experimental analysis shows the resistance values decrease with the increment of the temperature, because of the viscoelastic component of the asphalt concrete. Supposing a relationship between the tensile resistance and the temperature logarithm and modelling it by a regression linear equation, by analogy with the thesis of the Paragraph 3.2—see equations (1) and (2)—the angular coefficient of the line expresses the tensile resistance variability with respect to the referring temperature, i.e. the thermal susceptibility of the mixture.

In detail, as the temperature increases, the resistance decreases and the reduction gradient is less than 1.00 N/mm^2/log(°C), except for the grouted asphalt concretes, that have a thermal susceptibility slightly higher than the OPEN GRADE characterized by the same design mix.

The good performance of the GAC versus the OPEN GRADE is assessed by the values of the *b* parameter also (see Fig. 1). Moreover, referring to the porous mixtures, as the temperature assumes higher values than 25°C, the resistance is influenced by the bituminous component, which produces a low cohesion and adhesion because of the temperature increment.

Referring to GACs, the different voids percentage, due to the particle size distribution of the mixtures, produced a lack of ductility in the grouted samples characterized by the Mix B. In fact, referring to the Ductility Index of the GACs—angle formed by the vertical line and

Table 7. Indirect Tensile Strength test: tensile resistance values (Mix A).

Samples	Type	Age (days)	Tensile resistance (N/mm^2)	Increment (%)	Temperature (°C)
4			0.885	–	25
4	Open grade	–	0.254	–	45
4			0.063	–	60
4			1.340	51	25
4	GAC	7	0.492	94	45
4			0.221	251	60

Table 8. Indirect Tensile Strength test: tensile resistance values (Mix B).

Samples	Type	Age (days)	Tensile resistance (N/mm^2)	Increment (%)	Temperature (°C)
4			0.700	–	25
4	Open grade	–	0.245	–	45
4			0.065	–	60
4			1.349	93	25
4	GAC	7	0.510	108	45
4			0.334	414	60

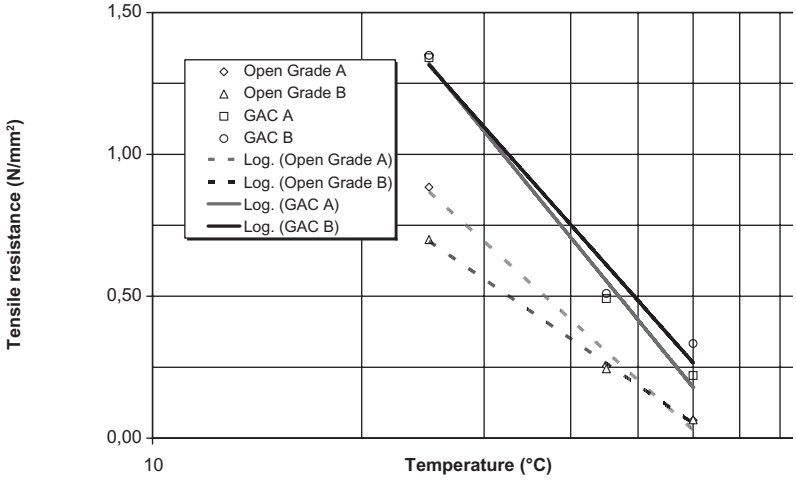

Figure 1. Tensile resistance versus testing temperature (25, 45 and 60°C).

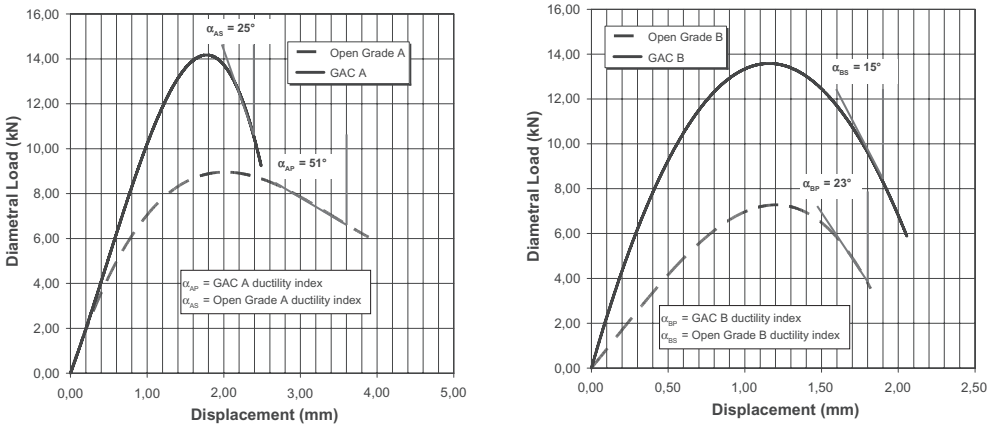

Figure 2. Ductility Index (T = 25°C).

Table 9. Marshall test: report of the results referring to a curing time of 7 days (Mix A).

Samples	Type	Stability (kN)	Stability increment (%)	Flow index (mm)	Stiffness (kN/mm)	Stiffness increment (%)	Temperature (°C)
4		9.08	–	5.6	1.62	–	50
4	Open grade	6.24	–	4.7	1.33	–	60
4		4.54	–	3.5	1.30	–	70
4		22.29	145	6.2	3.59	122	50
4	GAC	16.07	157	5.4	2.97	123	60
4		13.98	208	6.2	2.25	73	70

the descending branch of the stress-strain curve after the peak value (see Fig. 2)—in case of the Indirect Tensile Strength tests at 25°C, it can be seen the A type is characterized by an index higher than that one of the Mix B. This means an highest tensile resistance but, on the other hand, a greater frailty level in case of adoption of the Mix B.

Table 10. Marshall test: report of the results referring to a curing time of 7 days (Mix B).

Samples	Type	Stability (kN)	Stability increment (%)	Flow index (mm)	Stiffness (kN/mm)	Stiffness increment (%)	Temperature (°C)
4		8.15	–	2.8	2.91	–	50
4	Open grade	4.15	–	2.7	1.54	–	60
4		3.00	–	2.0	1.50	–	70
4		32.18	295	5.0	6.44	121	50
4	GAC	22.44	441	4.4	5.10	231	60
4		20.82	594	4.8	4.34	189	70

The comparison among the results achieved testing porous mixtures put on evidence that the filling of the specimens with grout causes a decreasing of the Ductility Index, i.e. a lack of ductility, due to the resistance increment.

In addition to the Indirect Tensile Strength tests, the samples were subjected to Marshall testing at 50°, 60° and 70°C, taking into account a curing time of 7 days for the GACs.

For each temperature, four samples of each mixture (A, B) were tested, reporting the results as mean values. The mechanical behaviour of the OPEN GRADE was evaluated also. The results are shown in the Tables 9 (Mix A) and 10 (Mix B).

4 UNIBAS-M.P.T. DEVICE: DEFINITION OF THE RUPTURE DOMAINS

The definition of the yield/rupture domains is very important for assessing the performance of the materials, which can be subjected to every stress state. Specifically, the UNIBAS-M.P.T. device permits to estimate the performance of asphalt concretes referring to the stresses which usually occurred during the pavement service life. The domains definition is obtained by a theoretical-experimental process widely described and tested in previous studies (Agostinacchio et al. 1997, Agostinacchio et al. 2002).

The laboratory tests were those able to characterize greatly the deviatoric response of the investigated material, i.e. the pseudo-tensile ($\alpha = 1$), pseudo-shear ($\alpha = 0$) and pseudo-compression ($\alpha = -0,5$) (Agostinacchio et al. 2002, Agostinacchio et al. 2004). For each sample was defined the Rupture Function, finding the stress-strain characteristics referring to the material collapse. For sake of brevity, the mathematic formulation is omitted; however, the experimental results obtained by the triaxial tests, accomplished through the UNIBAS-M.P.T. apparatus, are resumed below (see Table 11 and Figure 3).

Results are referred to a testing temperature of 25°C; the adopted methodology is usually used by the Authors to define the simplified conservative rupture domains. The rupture deviatoric stress values are shown in Table 11. The diagrams plotted in Figure 3 represent the rupture functions on the deviatoric plane, at a constant value of the mean confinement stress.

Referring to the GCAs, the compression ($\alpha = -0.5$) resistance values of the two mixtures were comparable (Table 11), although the Mix A was characterized by a mixed particle size distribution, because of the superior mortar quantity in the Mix B. Moreover, it can be seen that the grouting process caused a resistance increment—referring to the corresponding OPEN GRADE—of the 74% for the Mix B, greater than the increasing of the 27% exhibited by the Mix A.

Referring to the tensile ($\alpha = 1$) and the shear ($\alpha = 0$) response, the rupture deviatoric stresses (Table 11) carried out testing the OPEN GRADE evidence the best behaviour of the Mix A at low hydrostatic pressures; however this performance increment is reduced grouting the samples.

Table 11. UNIBAS-M.P.T. test: rupture deviatoric stress of the mixtures.

	Mix A (Open Grade)	Mix A (GAC)	Mix B (Open Grade)	Mix B (GAC)
α	(N/mm²)	(N/mm²)	(N/mm²)	(N/mm²)
1	2.082 (*)	3.144 (*)	1.704 (*)	3.164 (*)
	4.892 (**)	6.234 (**)	6.902 (**)	8.536 (**)
0	5.273 (*)	7.502 (*)	4.245 (*)	6.501 (*)
–0.5	8.810 (*)	11.189 (*)	6.682 (*)	11.627 (*)

(*) Rupture deviatoric stress at a mean hydrostatic stress of 7.026 N/mm².
(**) Rupture deviatoric stress at a mean hydrostatic stress of 9.776 N/mm².

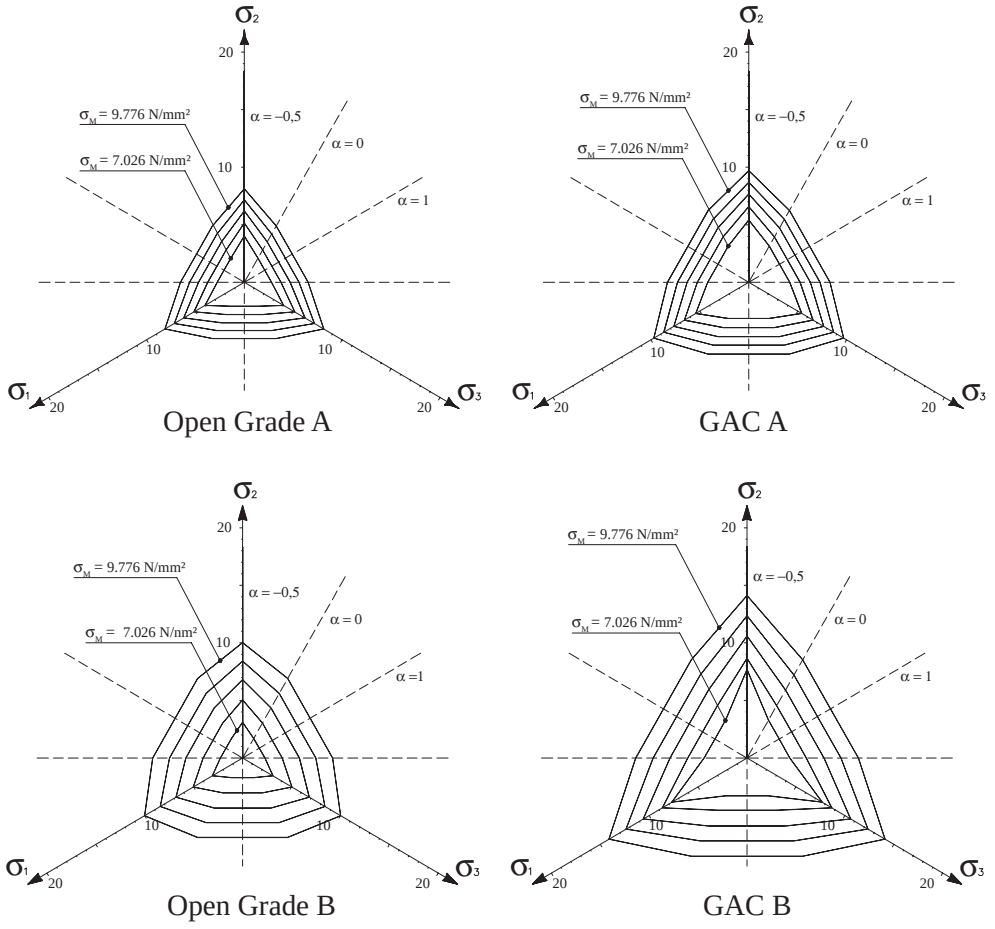

Figure 3. Rupture Functions diagrams on the deviatoric plane, referring to a constant mean stress value (T = 25°C).

5 CONCLUSIONS

This paper presents a significant study on mix design and on evaluation of mechanical properties of the grouted asphalt concretes (GAC). The mixtures were carried out adopting two different particle size distributions, monogranular for the Mix B and mixed for

the Mix A. Both porous asphalt and grouted concretes were tested. In detail, the mechanical characteristics were obtained by the following tests:

– Marshall test (UNI EN 12697-34:2004);
– Indirect Tensile Strength test (UNI EN 12697-23:2006);
– Triaxial tests by the UNIBAS-M.P.T. device.

The influence of the grout on the mechanical properties of the mixtures was investigated. The compaction method of the samples was defined so as to guarantee a residual voids percentage of 20% at least and ensuring a correct penetration of the mortar. At first, the resistance increment of the GCA—referring to the OPEN GRADE—varying the curing time (1, 7 and 28 days) was estimated. Results show the tensile resistance and the Marshall stiffness values increase with the curing time: in particular, the initial increment of resistance and the curing speed are essentially connected to the properties of the mortar used for filling the voids of the asphalt mixtures. Moreover, referring to the GACs, the Mix B exhibits a performance values in terms of Marshall stability and stiffness higher than the Mix A; the performance values in terms of tensile resistance are almost comparable.

The evaluation of the resistance of the GCA characterized by an age of 7 days, obtained varying the testing temperature, was accomplished by the definition of the Ductility Index, i.e. the angle formed by the vertical line and the descending branch of the stress-strain curve—plotted on the basis of the Indirect Tensile Strength tests—after the peak value. The experimental output show, as the temperature increases, the thermal susceptibility of the grouted asphalt concretes becomes slightly greater than the porous mixtures. Anyway, the highest values of the tensile resistance and of Marshall stiffness values were carried out testing the GACs.

Finally, the rupture domains of mixtures were defined by the use of the UNIBAS-M.P.T. apparatus. In particular, referring to the grouted samples, comparable values of compression resistance were obtained for both the mixtures, although the Mix A was characterized by a mixed particle size distribution. Moreover, the grouting process produced a resistance increment—referring to the corresponding OPEN GRADE—for the Mix B, greater than the increasing exhibited by the Mix A. Referring to the tensile and the shear response, the rupture deviatoric stresses carried out testing the OPEN GRADE evidence the best behaviour of the Mix A at low hydrostatic pressures; however this performance increment is reduced grouting the samples.

Anyway, triaxial tests assess the high performance of the GAC versus the porous asphalt and the usefulness of the UNIBAS-M.P.T. device for the evaluation of the structural response of the road pavements.

REFERENCES

Agostinacchio M., Bernetti R. & Diomedi M. 1997. "*Experimental investigation on asphalt strength loaded along three mutual orthogonal directions at different temperatures*", Proceedings of the fifth international RILEM symposium MTBM, Lyon '97, France, 14–16 May 1997.

Agostinacchio M., Diomedi M., Olita S. & Ciampa, D. 2002. "*Ottimizzazione del Protocollo di prova M.P.T. e proposta di domini conservativi semplificati per il calcolo razionale delle pavimentazioni stradali*", Atti del 1° Convegno Internazionale S.I.I.V. (Società Italiana Infrastrutture Viarie): Functional adjustement of road networks—volume 2: Materiali nella sovrastruttura stradale—Università degli Studi di Parma, Facoltà di Ingegneria, Parma 30–31 Ottobre 2002.

Agostinacchio M., Diomedi M., Olita S. & Ciampa D. 2004. "*UNIBAS M.P.T. triaxial apparatus: from the prototype planning to a consolidated test methodology*", 4as Jornadas Internacionales del Asfalto, Cartagena de Indias (Colombia), 16–20 Agosto 2004.

Da Rios, G., Agostinacchio, M.la & Fiori, F. 2007. *"Service Life Prediction Of Pavements Characterized By Open Grade Filled With Cement Mortar",* 5th International Conference on Maintenance and Rehabilitation of Pavements and Technological Control (MAIREPAV5), Park City, August 8–10 2007.

Web site 2008. www.mapei.it, 2008.

Advanced Testing and Characterization of Bituminous Materials –
Loizos, Partl, Scarpas & Al-Qadi (eds)
© 2009 Taylor & Francis Group, London, ISBN 978-0-415-55854-9

"Liquefaction" of asphalt caused by cyclic loading, as a potential reason of extreme rutting

Gajári György
H-TPA Ltd (member of STRABAG AG)., Budapest, Hungary

Frohmut Wellner
Institute of Town and Road Building, Technical University of Dresden, Dresden, Germany

Ivo Herle
Institute of Geotechnical Engineering, Technical University of Dresden, Dresden, Germany

ABSTRACT: The frictional resistance of compacted asphalt might diminish as a result of cyclic anisotropic loading, if the pores of the asphalt are sufficiently saturated with binder material. The authors introduce the term of liquefaction, describe the mode of adding the binder material in order to avoid the reduction of effective stresses and the resulting extreme rutting. A material model, known from soil mechanics, is introduced, which is suitable for describing the mechanical behaviour of high temperature asphalt.

1 INTRODUCTION

Triaxial compression tests with static cell pressure and the application of axial load, that is varied in sinusoid fashion, were already performed in the seventies by Francken (Francken, 1977). Similar tests are being made now at the Technical University of Dresden, where the cell pressure is varied also in a cyclic manner (Leutner & Wellner 2007). The results indicate that the cumulated (permanent) deformations increase with the increasing deviator stress (Francken, 1977, Leutner & Wellner 2007). The results are being used for establishing material models, which in turn will be incorporated in dimensioning algorithm, and in the procedure used for estimating the residual life (Leutner & Wellner 2007).

Considerations related to the components of the asphalt material, the mineral skeleton and the bitumen, have given rise to the idea that the mechanical behaviour of the high temperature asphalt could be conveniently described by a soil model, where the pores are filled only partially (Gajári, 2008). The basic methodology to be considered includes the established results of soil mechanics. Models based on large number of test results are available for describing monotonously increasing loading (Schofield & Wroth 1968, von Wolffersdorff 1995), as well as for describing the cyclic loading (Niemunis & Herle 1997, Wichtmann et al. 2004, Wichtmann 2005).

As part of the studies made for a Ph.D. thesis at the Technical University of Dresden we studied the phenomenon of bitumen pressure increase as a possible reason of rutting, based on one of the existing models of soil mechanics. As a result of long cyclic loading the phenomenon may occur in case of small deviator loads, as well as in case of highly compacted asphalt. The phenomenon is a result of an excess pressure in the pore liquid, caused by cyclic shear. At the same time, effective stresses between the mineral particles decrease. This leads to the diminished resistance to deformation, and consequently to the development of ruts. This contribution presents selected results of this research.

2 RESULTS OF EXPERIMENTS WITH ASPHALT MADE OF GRANULATE MATERIAL

The experimental results described below support the picture established about the mechanical behaviour of the high temperature asphalt that is subjected to cyclic loading.

2.1 *Static triaxial compression tests*

At the Technical University of Dresden we performed quasi-static triaxial tests with velocity control (displacement rate: 0.02 mm/s) and with a constant cell pressure (0.05, 0.13 and 0.4 MPa). The ratio (q/p) of shear stress ($q = \sigma_1 - \sigma_3$) and mean pressure ($p = (\sigma_1 + 2\sigma_3)/3$) decreased with increasing cell pressure, while the initial void ratio was kept constant (e = 0.2).

It could be seen after the experiment that all three specimen had became looser. The extent of loosening was the highest when the cell pressure was the lowest, and it was the lowest when the cell pressure was the highest. In summary, the behaviour corresponds to the theory of Critical State Soil Mechanics (CSSM) (Schofield & Wroth 1968). The specimen shown here had exhibited dilatancy behaviour at the particular stress conditions.

2.2 *The "optimum" bitumen content*

Experiences indicate that the risk of rutting increases with the increasing binder material component. On the other hand, however, there should be an "optimum" binder material content in terms of the ability to compact the asphalt, based on the analogy with the Proctor testing.

It is reasonable to assume that there is a correlation between the ability of compacting and the rut depth depending on the binding material content. A more detailed explanation of this relationship will be provided later based on the results of cyclic shearing.

Actually, we present a correlation between the "optimum" bitumen content, as determined with specimen compacted with gyratory compactor, and the rut depth measured at the rutting test performed in the laboratory. The results can be seen in the next four diagrams for asphalt grades AC-12 and SMA-11.

The highest compactness could be reached with a gyratory compactor speed of 233 rpm The bitumen was not squeezed out from specimen that have bitumen content exceeding

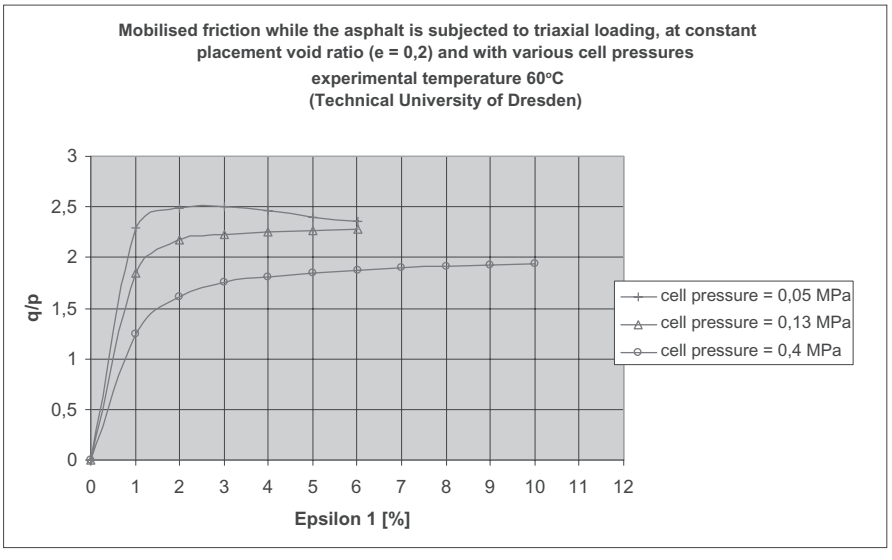

Figure 1. Triaxial compression of AC-12 asphalt at 60°C.

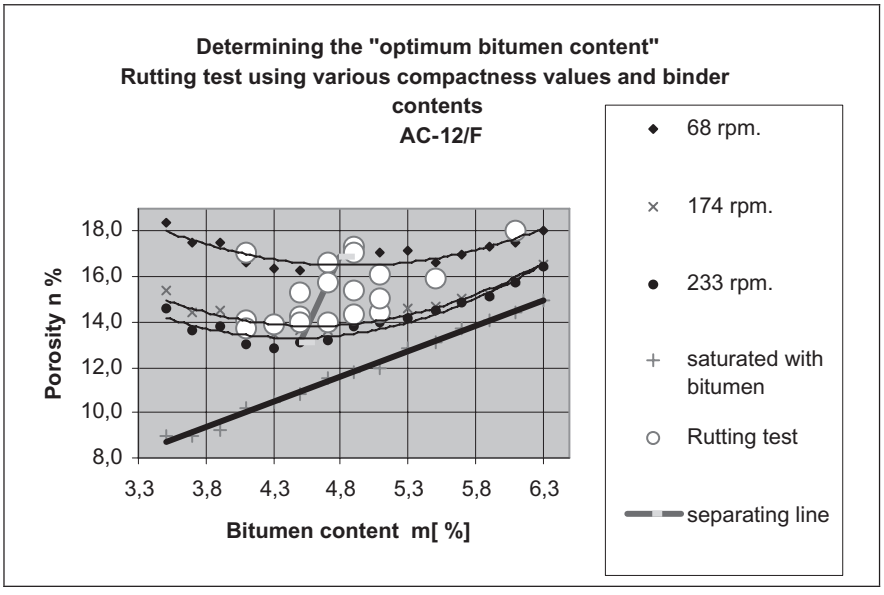

Figure 2. Determining the optimum bitumen content of asphalt mix AC-12.

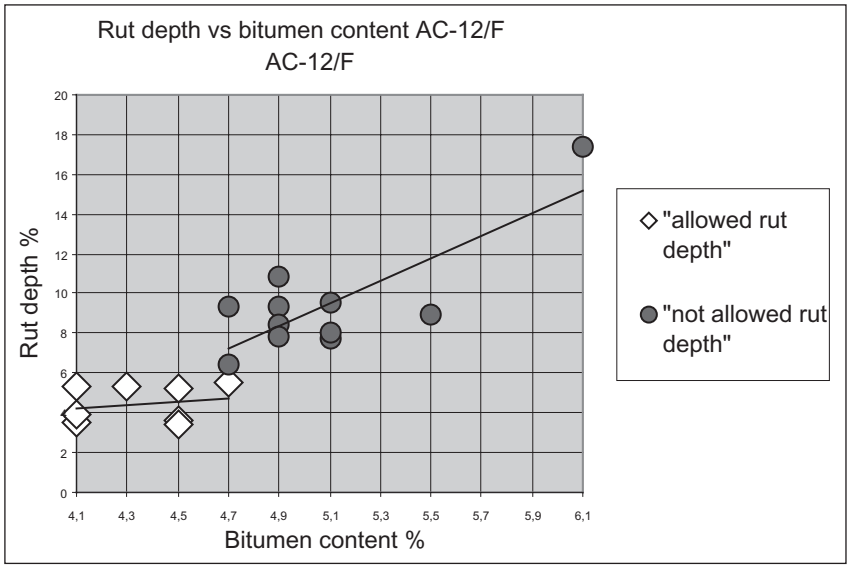

Figure 3. Determining the relationship between optimum bitumen content and rut depth of asphalt mix AC-12.

4.3–4.7% by mass, because of the viscosity. In this way the compacting of these specimen was hindered by the bitumen content. As can be seen in the diagram, the porosity of the mineral skeleton increased with bitumen content higher than that. From now on we use the terms "dry side" where the value of bitumen content is less than optimum, and "wet side" where the value is over the optimum (not to confuse with the similar terms used within CSSM).

It can be seen in the above diagram, that rut depth exceeding the allowed value always occurs at the "wet side".

The next two diagrams show similar results regarding asphalt grade SMA-11.

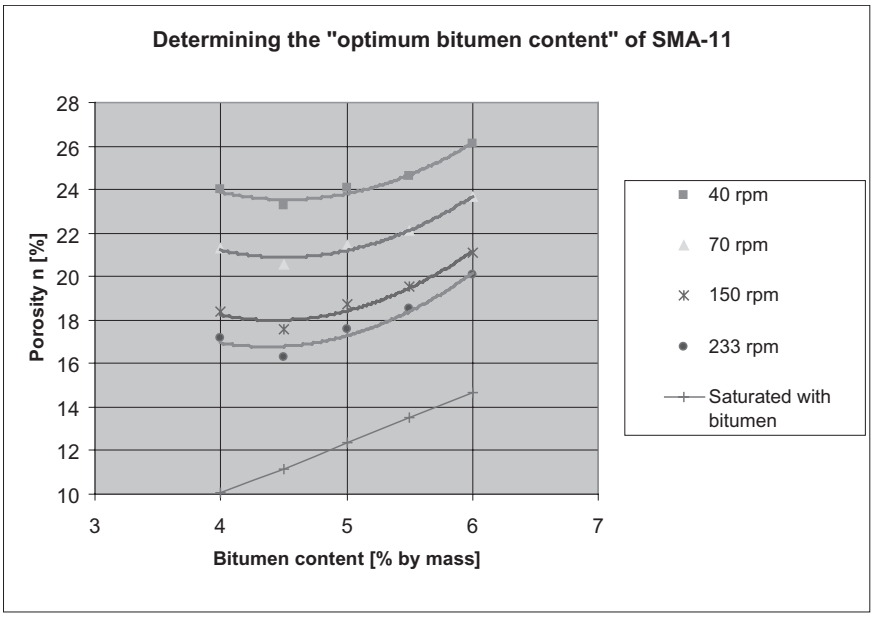

Figure 4. Determining the optimum bitumen content of asphalt mix SMA-11.

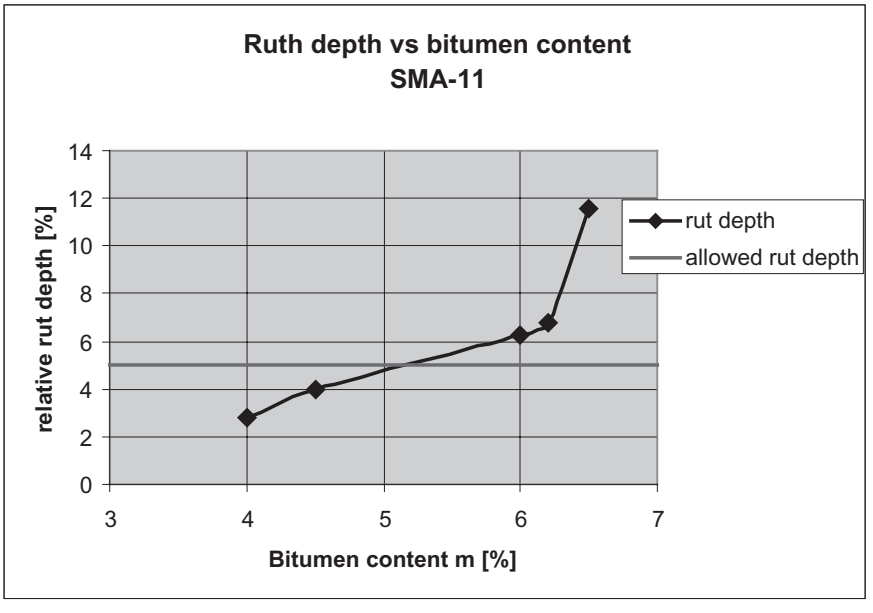

Figure 5. Relationship between bitumen content of asphalt SMA-11 and the rut depth.

2.3 *Operating principle of gyratory compactor as a simple shearing device*

For characterising the mechanical behaviour of asphalt it is necessary to take the effect of cyclic loading. The load-dependent maximum compactness can be reached with constant cyclic shear, while the pressure in normal direction is kept constant (Herle, 1997) (Fig. 6). This condition cannot be reached in case of static compression.

The gyratory compactors used in the laboratory work according to this principle too (Fig. 7).

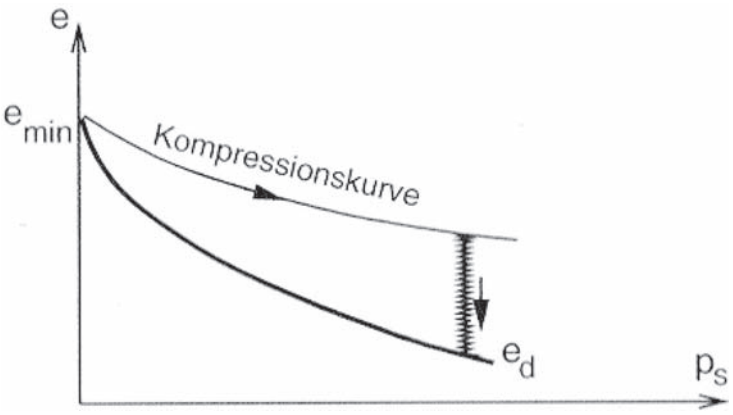

Figure 6. Reaching the highest load-dependent compacted condition by means of cyclic shearing (Herle, 1997).

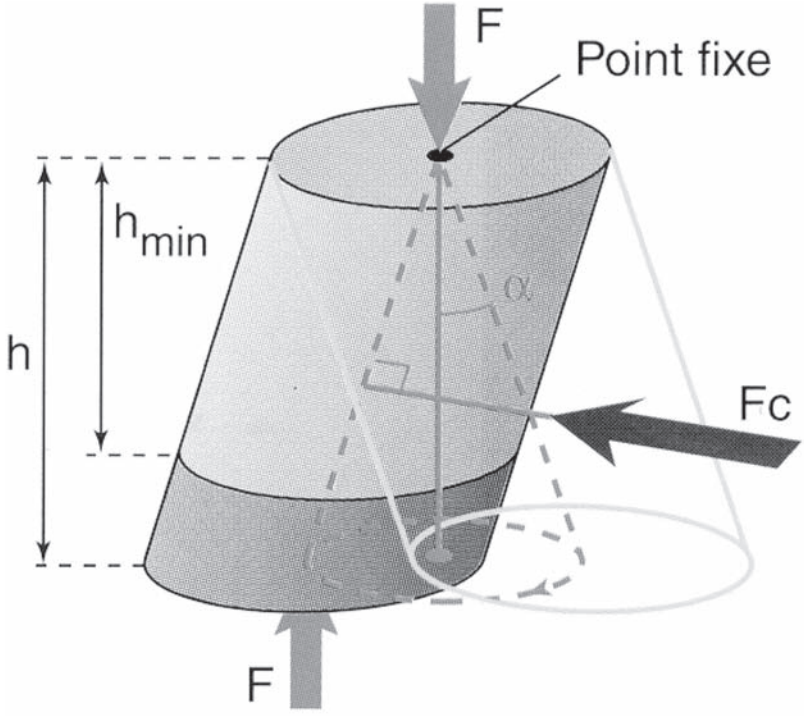

Figure 7. Operating principle of the gyratory compactor (LCPC product range, 2000/2001, Paris).

It is important to ensure very low deformation amplitudes. Large deformations would cause loosening and not compacting, according to CSSM. A bitumen outflow from the specimen can be observed if the mixture to be compacted contains too much bitumen.

2.4 *The phenomenon of liquefaction produced on oil holding mineral skeleton in rut testing equipment type LCPC*

We performed laboratory tests with the mineral skeleton of mix grade AC-12 with various liquid contents in order to reveal the effect of cyclic shear on the rutting. For making the observation easier we used engine oil instead of bitumen.

Figure 8. Hard specimen compacted at the "dry side" after rutting test (placement void ratio e = 0.18; 60 000 wheel passes).

Figure 9. Rutting of the specimen compacted at the "wet side" after a mere 2000 wheel passes (placement void ratio e = 0.18).

Figure 10. A "soft" consistency of the specimen compacted at the "wet side" after the rutting test (placement void ratio e = 0.18).

The preliminary compaction of the specimen was high, void ratio was e ~ 0.18 in both cases. At the "dry side" the compacted specimen did not exhibit tendency to develop ruts even after 60 000 passings of wheel. After removing the specimen, we observed a "hard" consistency of the material (Fig. 8). When the oil content of the specimen exceeded the optimum value, the specimen survived only 2000 passes of the wheel (Fig. 9). The specimen after removal exhibited a "soft" consistency. The liquid from the pores was pressed out to the vertical surfaces, where the liquid has flown down (Fig. 10). The softening of the specimen can be explained as the result of excess pressure occurring in the pore liquid. This excess pore pressure squeezes the liquid onto the surface of the specimen. This phenomen is related to cyclic anisotropic load exerted by the rolling wheel. As extreme case, the liquefaction is defined for vanishing effective stresses between the mineral particles due to the pore pressure (Niemunis & Herle 1997).

In case of the specimen treated with gyratory compactor the same phenomenon can be observed, if the specimen is prepared at the "wet side".

In terms of the mechanical response, both testing methods, namely the treatment with gyratory compactor and the rutting experiment, are similar. For this reason the observed correlation between them is justified.

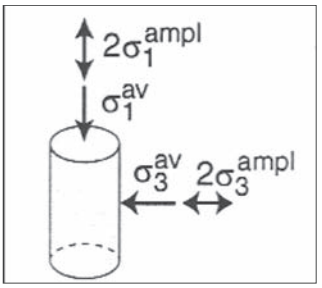

Figure 11. Load controll cyclic triaxial cell (Wichtmann et al. 2004).

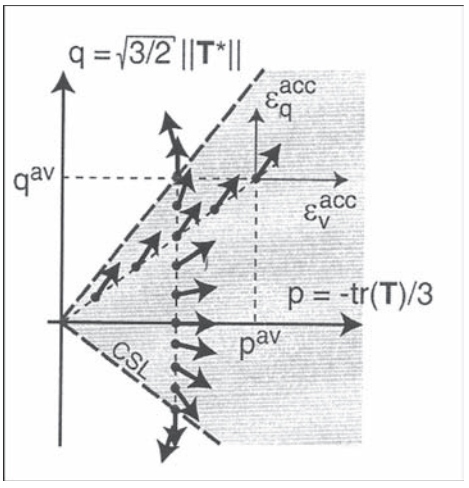

Figure 12. The measured cyclic flow direction (Wichtmann et al. 2005).

3 RESULTS OF CYCLIC LOAD TESTS PERFORMED WITH SOIL SAMPLES

Results of numerous experiments were published on cohesionless soil samples (Wichtmann et al. 2004, Wichtmann et al. 2005). In these experiments the triaxial cell was used, as well as the "multiple axis simple shear cell", which is essentially identical to the gyrator compactor.

It can be seen in Figure 11, that the cyclic loading consists of a static or average load, and an oscillating load. The static part is marked with "av" referring to the English term "average". The varying part is designated with "ampl" (amplitude).

The rate of accumulated strain is a function of the cyclic flow direction **m** (unit tensor) and 6 scalar multipliers (Wichtmann et al. 2004, Wichtmann et al. 2005):

$$\mathrm{D}^{\mathrm{acc}} = \mathrm{m}\ f_{ampl}\ \dot{f}_N\ f_p\ f_Y\ f_e\ f_\pi\ .$$

The cyclic flow direction follows from the static (average) part of the stress state, as can be seen in Figure 12. In case of axially symmetric triaxial test the stress state can be characterised by two stress parameters of CSSM, i.e. the mean pressure p and deviatoric stress q. The cyclic flow direction is a vector, wich can be defined with volumetric accumulated strain ε_v^{acc} and the deviatoric accumulated strain ε_q^{acc}. If stress is isotropic, then the accumulated strain corresponds to merely a volume change (compaction), as can be observed Figure 12. However, in pure shearing, corresponding to the critical condition of CSSM, is only a change of deviatoric strain (modification of shape).

The scalar multipliers represent the effects of the following parameters:

amplitude of strain
cyclic history
isotropic pressure
deviatoric stress
void ratio (compactness), and
change of flow direction.

In accordance with the results of tests performed with asphalt, the intensity of accumulation of strain increases with increasing deviatoric stress. There are, however, a number of futher factors to be considered, which influence the accumulation of deformation, and which are important in the field of road building.

The direction of the cyclic flow can be obtained either with the Cam Clay model of CSSM, or with the model introduced below (Wichtmann et al. 2004, Wichtmann et al. 2005).

4 THE KARLSRUHE HYPOPLASTIC MATERIAL MODEL

After a necessary extension of the model by including the "intergranular strain" (Niemunis & Herle 1997), it is possible to describe changes of the material state in case of monotonously increasing load, as well of cyclic load (Niemunis & Herle 1997).

In the hypoplastic material model the elastic and plastic strains are not distinguished. As a result, it is not necessary to use some common tools of the "classical" theory of plasticity, such as yield condition (von Wollfersdorff, 1995).

In general form the description is made with tensors. The basic version of model shown here was established by von Wolffersdorff (von Wollfersdorff, 1995). The simplified formula shown below is valid only for axially symmetric conditions (Herle, 2000).

$$\overset{\bullet}{T}_j = \frac{f_S}{\overset{\frown}{T}_1{}^2 + 2\overset{\frown}{T}_2{}^2}\left[D_j + a^2(\overset{\frown}{T}_1 D_1 + 2\overset{\frown}{T}_2 D_2)\overset{\frown}{T}_j + f_d \frac{a}{3}(6\overset{\frown}{T}_j - 1)\sqrt{D_1{}^2 + 2D_2{}^2} \right]$$

The rate of principal stress $\overset{\bullet}{T}_j$ is a function of the rate of principal strain D_j. The meaning of the further symbols is as follows:

$\overset{\frown}{T}_j = T_j/(T_1 + 2T_2)$, where: $T_1 < T_2 = T_3 \quad (T_{ij} = 0, \quad for \quad i \neq j)$ the principal stress components (pressure < 0);

$a = \frac{\sqrt{3}(3 - \sin\varphi_c)}{2\sqrt{2}\sin\varphi_c}$ this expression is determined by the "critical friction angle" φ_c (CSSM);

$$f_d = \left(\frac{e - e_d}{e_c - e_d} \right)^{\alpha},$$

where:

e: actual void ratio,
e_c: the pressure dependent "critical" void ratio (CSSM),
e_d: the pressure dependent minimum void ratio.

The following relationship is valid here: $\frac{e_i}{e_{i0}} = \frac{e_c}{e_{c0}} = \frac{e_d}{e_{d0}} = \exp\left[-\left(\frac{3p_s}{h_s} \right)^n \right]$, where mean pressure is $p_s = -(T_1 + 2T_2)/3$;

The meaning of the symbols of the equation is as follows:
e_i: the pressure dependent maximum void ratio,
e_{i0}: the maximum void ratio at zero pressure,
$e_{c0}(= e_{max})$: the "critical void ratio" at zero pressure (CSSM),
$e_{d0}(= e_{min})$: the minimum void ratio at zero pressure,

$$f_s = \frac{1 + e_i}{e_i}\left(\frac{e_i}{e} \right)^{\beta} \frac{h_s}{n}\left(\frac{3p_s}{h_s} \right)^{1-n}\left[3 + a^2 - a\sqrt{3}\left(\frac{e_{i0} - e_{d0}}{e_{c0} - e_{d0}} \right)^{\alpha} \right]^{-1},$$

where:
h_s: the granular hardness,
n: exponent of the compression law,
α: exponent related to pressure-dependent relative density
β: stiffness exponent.
For this reason, the following material constants are to be determined before using the material model: φ_c, h_s, n, e_{i0}, e_{c0}, e_{d0}, α, β.

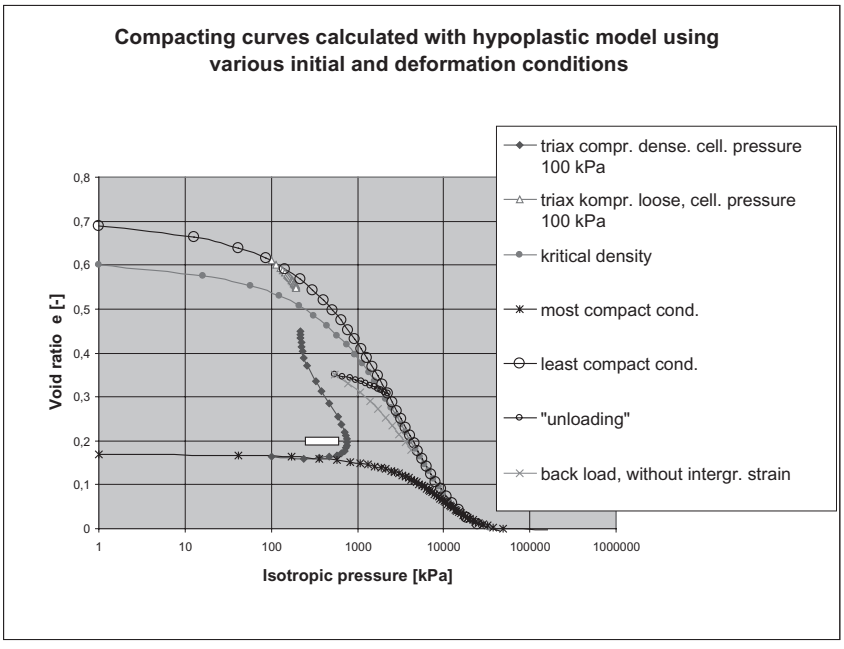

Figure 13. Compression curves calculated with the hypoplastic material model.

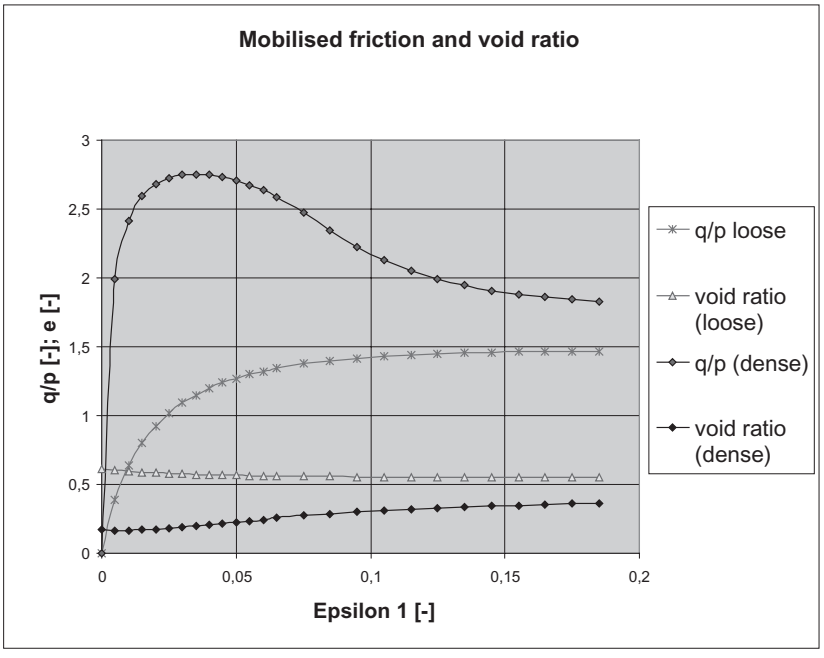

Figure 14. Behaviour of loose and dense materials in the triaxial compression test.

The material model can be characterised as follows:

The condition of the granular material is determined by the compactness (e) and effective stresses (T_j).

The model describes the evolution of effective stresses between the solid particles.

The model is independent of the deformation velocity.

Based on calculations with the basic hypoplastic model, some further properties of the model are shown in Figures 13 and 14.

Starting from the loose state at isotropic pressure (Figure 13), a specimen is compressed in axial direction at constant cell pressure (100 kPa). The curve of triaxial compression (Figure 13) approaches asymptotically the curve of critical density/compactness (CSSM), the specimen is getting compacted. At the same time, the axial stress and the mobilised friction increases in a monotonous manner (q/p), while the void ratio decreases (Figure 14). For the same initial stress condition, a specimen in the most dense/compacted state (Figure 13), becomes loose after a slight initial compaction, while the pressure increases (Figure 13). The loosening process continues and the values of mobilised friction and pressure reach their maximum values (Figure 14). Finally stress and void ratio tend to the critical state (CSSM) in the same way as in case of the loose specimen.

An isotropic unloading, starting from isotropic stress, can be seen in Figure 13. The numeric simulation of the unloading phase captoures the observed behaviour. The same cannot be said about the reloading phase, because the calculated compaction rate is too high. The basic version of the model is not suitable for calculating the cyclic behaviour which is important in case of rutting. This deficiency of the basic model was eliminated by Niemunis and Herle with the introduction of "intergranular strain" (Niemunis & Herle 1997). The extension includes a definition of further 5 material parameters. In Figure 13 a small light rectangle indicates the asphalt state after after its compaction into the pavement structure. It emphasizes the impact of cyclic loading with a high number of cycles. For an initially compacted material, a monotonously increasing load (according to CSSM) would produce loosening, and not a further increase of compaction.

The material parameters of the basic hypoplastic model are shown in Table 1 according to Herle (Herle, 1997).

The critical friction angle of the mineral skeleton and the critical void ratio can be determined by measuring the angle of repose and using a standardised procedure of soil mechanics for e_{max}. However, these methods cannot be used for asphalt because of the adhesive (cohesion) effect of the binding material.

The parameters related to the hypoplastic material law are include in Table 2. They were determined for pure mineral skeleton, as well as for the mineral skeleton containing oil or

Table 1. The experimental programme serving for the determination of material parameters for the basic hypoplastic model monotonous loading.

Compacting by means of Gyrator	Compacting by means of oedometer	Triaxial compression without drainage	Triaxial compression with drainage
e_{d0} Void ration of the most compact condition	h_s Granulate hardness	φ_c Critical friction angle (CSSM)	α Exponent expressing the compacting effect on shear resistance
	n Exponent of the compression law	e_{c0} Void ratio of critical condition (CSSM)	
	β stiffness exponent	e_{i0} ($e_{i0} \sim 1{,}15 \times e_{c0}$) Void ratio of the least compact condition	

Table 2. Material constants of the basic hypoplastic model.

	φ_c [°]	h_s [MPa]	n -	e_{d0} -	e_{c0} -	e_{i0} -	α -	β -
Pure mineral skeleton	37	50	0,6	0,27	0,6	0,69	0,2–0,3	1,4–1,9
Mineral skeleton containing oil	37	22	0,53	0,17	0,6	0,69	0,14	1,2–1,6
Mineral skeleton containing bitumen	*35–37*	*22*	*0,53*	0,15	*0,6*	*0,69*	*0,14*	*1,2–2,0*

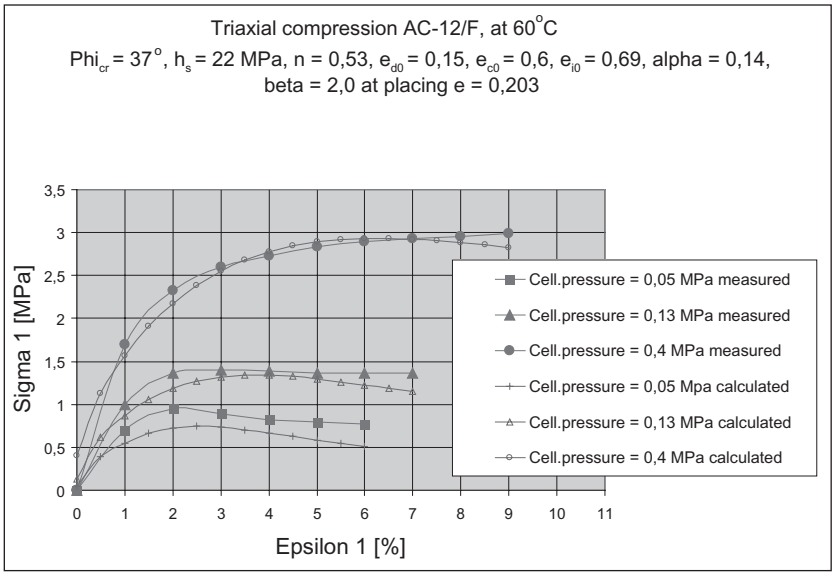

Figure 15. Measured and calculated axial principal stress in case of triaxial compression.

bitumen. Certain parameters that could not be determined for the asphalt are replaced with parameters that were determined for the other two mixtures.

The material model formulation for the axially symmetric state can be easily programm for a PC. In this way it is possible to numerically simulate the triaxial and oedometric compression experiments. The monotonous, quasi-static triaxial experiments were simulated with the parameters shown in Table 2. The measured and calculated loading curves are shown in Figure 15.

As it was mentioned above, the introduced basic model had to be extended for the cyclic case. Viscous forces caused by the bitumen and partial saturation of pores were not taken into account.

5 NUMERICAL EXAMPLE

The numerical example below demonstrates the possibilities of the introduced model.

The numerical example was calculated with help of the basic model with the parameters determined for the mineral skeleton of asphalt AC-12. As we emphasised above, the basic model is not suitable for simulating the cyclic loading. The extension with the intergranular

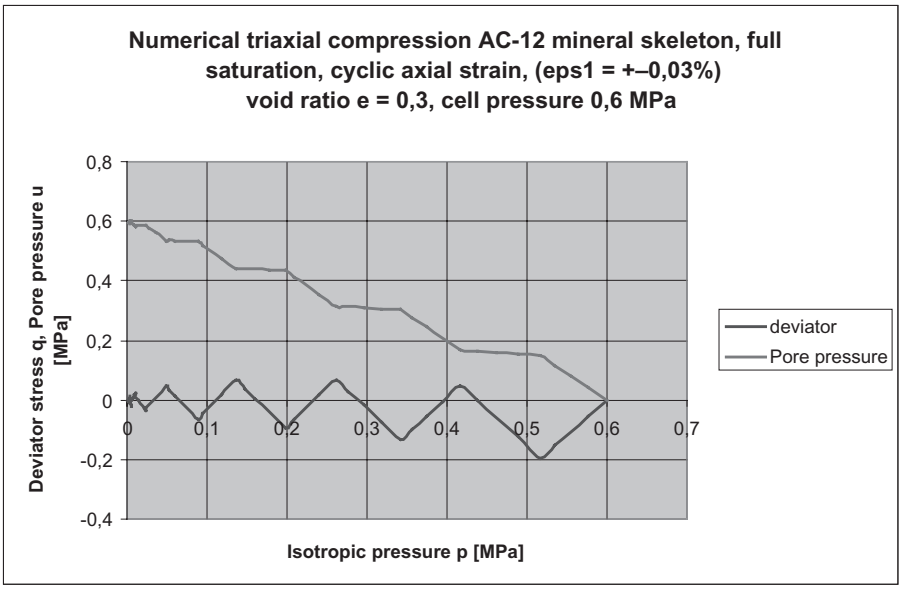

Figure 16. Cyclic axial undrained loading of asphalt AC-12 in triaxial cell.

strain, however, changes only the unloading and reloading stiffness of the model, thus the basic model is still capable of capturing the phenomenon of liquefaction.

In the initial condition an isotropic effective pressure is applied:

$$p' = 0{,}6 \text{ MPa}.$$

The deviatoric stress and pore pressure are equal zero. The pores are assumed to be fully saturated. The triaxial test is carried out without drainage (without liquid flow), i.e. the liquid cannot leave the pores. As a result, the deformation of the specimen takes place with constant volume.

During the experiment, a piston is moving the top plane of the specimen up and down producing a cyclic axial strain of:

$$\varepsilon_1 = \pm 0{,}03\%$$

while no permanent displacement occurrs. Although no substantial change in specimen shape could be observed from outside, the stress state had changed substantially. The mean effective pressure decreased to zero, while the pressure of the pore liquid increased to:

$$u = 0{,}6 \text{ MPa}.$$

The deviatoric stress, and in turn the mobilised friction approached zero. It means that the resistance to deformation became also zero. This condition is typical for liquids, that is why one uses the term "liquefaction".

Applying the extended hypoplastic model with intergranular strains, only the number of cycles necessary to produce liquefaction increases.

The calculation further neglects the compressibility of pores when the liquid contains air bubbles. In this case, the pore pressure increases more slowly, but the liquefaction is still possible.

As a summary: the liquefaction occurs for cyclic loading without drainage (no liquid flow), even for very small amplitudes of deviatoric stress.

6 PRACTICAL ASPECTS OF DESIGNING NEW ASPHALT

Figure 17 summarises the results of all triaxial experiments conducted within the research project.

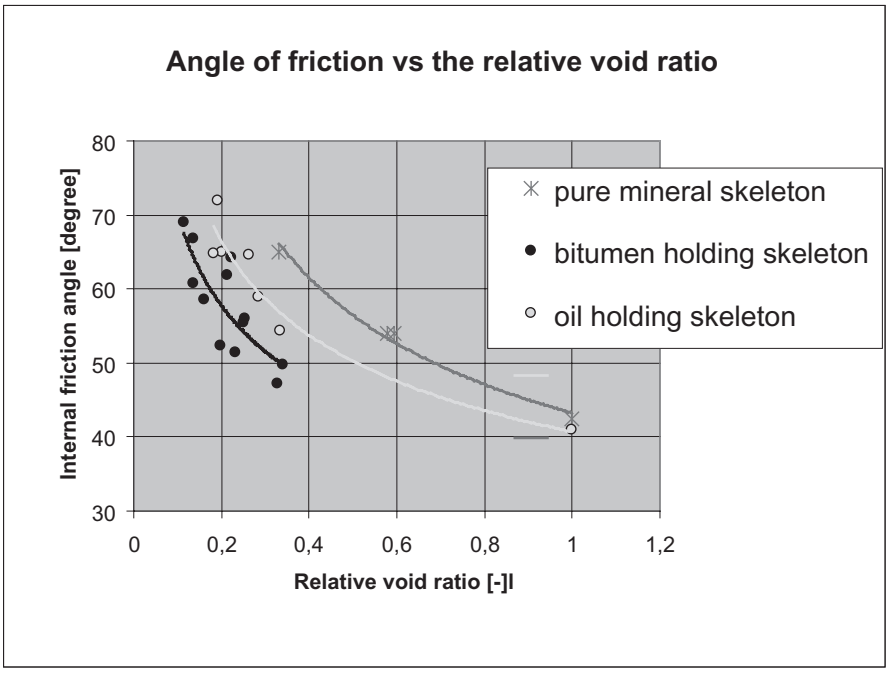

Figure 17. The angle of friction as function of the relative void ratio (AC-12).

In the diagram the internal friction angle is depicted as a function of the relative void ratio

$$\left(e_r = \frac{e - e_d}{e_c - e_d} \right).$$

The significance of the asphalt compactness becomes evident from here. The value of the relative void ratio is zero in the most compact state, and it is equal one in the critical state (CSSM).

The objective is to develop highly compacted asphalts. In order to achive this, the binding material has to be added in an appropirate amount. An optimum binding content may not be exceeded, since a high overall density can produce excess pore liquid pressures and thus increase the risk of liquefaction.

The "optimum bitumen content" introduced here, and the method used for its determination, can play a key role in planning of the new mixtures. For this reason it is submitted for consideration as an international patent as well.

REFERENCES

Francken L. 1977. Permanent deformation law of bituminous road mixes in repeated triaxial compression. Proceedings of the 4th international conference on structural design of asphalt pavements, Vol. 1, Ann Arbor.

Gajári Gy. 2008. Anwendung der Bodenmechanik in der Forschung des Straßenbauasphalts. Kolloquium anläßlich des 75. Geburtstages von Prof. i.R.Dr.rer.nat.habil. Dr.h.c. Wolfgang Förster, 16. Mai 2008. Veröffentlichungen des Institutes für Geotechnik der TU Bergakademie Freiberg, Heft 2008–2, S163–174.

Herle I. 1997. Hypoplastizität und Granulometrie einfacher Korngerüste, Veröffentlichungen des Institutes für Bodenmechanik und Felsmechanik der Universität Fridericiana in Karlsruhe.

Herle I. 2000. Granulometric limits of hypoplastic models, Task quaterly 4 No 3: 389–408.
Leutner, R. & Wellner, F. 2007. Prognose der Lebensdauer von Asphaltbefestigungen auf der Grundlage struktureller Eigenschaften. Straße und Autobahn 5. 2007. S241–250.
Niemunis A. & Herle I. 1997. Hypoplastic model for cohesionsless soils with elastic strain range, Mechanics of cohesive-frictional materials, Vol. 2: 279–299.
Schofield, A. & Wroth P. 1968. Critical State Soil Mechanics, McGRAW-HILL. London.
von Wolffersdorff P.-A. 1995. Hypoplastisches Stoffgesetz für granulare Materialien mit einer plastischen Fließbedingung für kritische Zustände, 5. Oktober 1995, Institut für Bodenmechanik und Felsmechanik der Universität Fridericiana in Karlsruhe.
Wichtmann, T. Niemunis, A. & Triantafyllidis T. 2004. Setzungsakkumulation in nichtbindigen Böden unter hochzyklischer Belastung. Bautechnik 82, Heft 1, S. 18–27.
Wichtmann, T. Niemunis, A. & Triantafyllidis T. 2005. FE-Prognose der Setzung von Flachgründungen auf Sand unter zyklischer Belastung. Bautechnik 82, Heft 12. S. 902–911.

Advanced Testing and Characterization of Bituminous Materials – Loizos, Partl, Scarpas & Al-Qadi (eds)
© 2009 Taylor & Francis Group, London, ISBN 978-0-415-55854-9

Experimental investigation on the dynamic properties of asphalt concrete using filler with waste hydrated lime

M. Arabani, H.R. Joodi & V. Shakeri
Civil Engineering Department, University of Guilan, Rasht, I.R. Iran

ABSTRACT: This paper focuses on the investigation of the dynamic properties of asphalt concrete using mineral fillers with waste hydrated lime. The ability of hydrated lime to improve the fatigue and rutting resistance of hot mix asphalt (HMA), has led to observed improvements in the field performance of lime-treated HMA pavements, and significant decreases in maintain and repair costs of highways network. The asphalt concretes, made of waste hydrated lime, and ordinary asphalt concrete, evaluated through their fundamental dynamic properties such as fatigue resistance, rutting depth, resilient modulus and permanent deformation. The experimental results showed that improvement the application of waste hydrated lime as mineral filler improves the permanent deformation, stiffness and fatigue endurance of asphalt concrete. It was also determined that the mixtures with waste hydrated lime showed higher resistance against rutting than conventional asphalt concrete.

1 INTRODUCTION

Bituminous paving mixtures are used as surface or base layers in a pavement structure to distribute stresses caused by loading and to protect the underlying unbound layers from the effects of water. To adequately perform both of these functions over the pavement design life, the mixture must also withstand the effects of air and water, resist permanent deformation, and resist cracking caused by loading and the environment. Numerous factors and associated properties affect a bituminous mixture's ability to meet these structural requirements (Tayebali et al. 1994; Roque et al. 2000; Arabani et al. 2006a). In the late 1970s, a number of premature asphalt pavement failures occurred in the south eastern and western United States. Stripping was identified as a major problem, but its rather sudden appearance has never been fully explained. Many researches were done around the world on use of hydrated lime (Little et al. 2006; Do et al. 2006). The major types of premature distress included rutting or permanent deformation in the wheel paths, bleeding in selected areas of the pavement, and alligator cracking. Millions of dollars of rehabilitation were necessary and research efforts were initiated to solve this problem. Most of the distresses which occur during the pavement service life are different types of cracks and rutting. Rutting is defined as surface deformation under the wheel paths. It stems from the permanent deformation in any of the pavement layers or the subgrade. There are two main types of rutting. The first one is rutting in asphalt layer, and the other is rutting in subgrade or base. Asphalt pavement rutting can be caused by insufficient pavement structural support allowing excessive stress to be transferred to the subgrade (structural rutting); however, the most common type of rutting is 'instability' rutting caused by the plastic movement of the asphalt mix under heavy, often slow moving loading (Chen et al. 2004; Uzarowski et al. 2006).

Most of rutting in today's pavements is due to the permanent deformation in the asphalt layer. Rutting is considered to be one of the important distresses in the pavement since significant rutting can lead to major structural failures and hydroplaning potentials. Since the cost of rehabilitation and reconstruction of these distresses is high, the prevention of rutting

and cracking would be more logical and beneficial. Mechanical properties of HMA mixtures play a major role in pavement design, analysis, and performance. They govern the relationships between traffic loads and pavement responses and the long term performance of pavement structures under the combined action of traffic and environment. Typical mechanical properties of HMA mixtures include the modulus as a function of temperature and loading rate, and fatigue and rutting performance relationships (Little et al. 2006).

Because hydrated lime had been used by states prior to the 1970s, several states (including Georgia, Nevada, Texas, Virginia, and Utah) began using lime to solve their water susceptibility problems. Lime has become a popular anti strip agent in the United States. Not only does the addition of lime provide anti stripping benefits, but it also acts as a mineral filler to stiffen the asphalt binder and HMA; Improves resistance to fracture growth (i.e., improves fracture toughness) at low temperatures and alters the plastic properties of clay fines to improve moisture stability and durability. The filler effect of the lime in the asphalt reduces the potential of asphalt to deform at high temperatures, especially during its early life when it is most susceptible to rutting. The hydrated lime filler actually stiffens the asphalt film and reinforces it. Furthermore, the lime makes the HMA less sensitive to moisture effects by improving the aggregate-asphalt bond. This synergistically improves rut resistance. As the HMA ages due to oxidation, hydrated lime reduces not only the rate of oxidation but also the harm created by the products of oxidation. This effect keeps the asphalt from hardening excessively and from becoming highly susceptible to cracking (through fatigue and low temperature (thermal cracking). Synergistically, the filler effect of the hydrated lime dispersed in the asphalt improves fracture resistance and further improves cracking resistance. Therefore it's probable that the use of hydrated lime will affect the mechanical properties of HMA (National Lime Association 2001).

In this research an attempt has been made to test the effects of using hydrated lime as a filler to increase the stiffness and creep resistance and fatigue life of the HMA.

2 EXPERIMENTAL

2.1 *Materials*

2.1.1 *Bitumen*

The bitumen used in this research is the 60/70 bitumen of Isfahan refinery center (Arabani et al. 2006b). Its properties are listed in table 1.

2.1.2 *Aggregates*

In this research two types of particle size of aggregate are used. The particle size of type 1 & 2 are listed in table 2. The design gradation is known as the topka and binder, respectively. All aggregates which have been used in this research are crushed aggregates.

Table 1. Properties of bitumen used.

	Lose weight	Deflagration	Plasticity index	Flow	Penetration grade	Density
Purity grade	(%)	0°C	(cm)	0°C	mm/10	25°C
99	0.75	262	112	51	66	1.02

Table 2. Gradation of used aggregate.

Sieving size (mm)	25	19	12.5	9.5	4.75	2.36	0.3	0.075
Topka's P.P (%)	–	100	95	–	59	43	13	6
Binder's P.P (%)	100	95	–	68	50	36	12	5

2.1.3 *Lime*

In highway engineering, lime is used both in pavement (HMA) and also in subgrade. Hydrated lime is made by adding water into the quicklime. Actually the hydrated lime is the product of chemical reaction between quicklime and water. It has a gray to white color. It is usually used to improve soil properties, resistance to moisture damages and to strengthen the resistance to permanent deformation. The physical and chemical properties of lime for use in HMA, is stated in AASHTO-M303 standard. The hydrated lime with high calcium rate, is more being used. The properties of this type of lime are given in table 3.

2.2 *Specimens preparation*

In order to determine the optimum percent of bitumen in asphaltic specimens with topka and binder aggregate gradation, some pretest specimens were prepared for marshal test (ASTM 2002). The marshal test results showed that bitumen percent of 5.5% is the optimum percent for binder aggregate gradation, and 6.5% is optimum for topka aggregate gradation. So these percents were used to make specimens with binder and topka aggregate gradation. Also specimens which were prepared to be tested were produced by 3 different percent of lime: 1%, 1.5% and 2% of bitumen weight. The specimens prepared for this research, have the diameter of 100 mm and the height of 70 and 40 mm respectively for stiffness modulus test and fatigue test (ASTM 2002; Arabani et al. 2006c).

These specimens carry under the stiffness modulus, creep and fatigue test. All tests were based on ASTM-D4123 and ASTM-D1074 standards. Various methods are being used to add hydrated lime to HMA. They range, for example, from adding dry lime to the drum mixer at the point of asphalt binder entry, to adding dry lime to damp aggregate followed by "marination" for several days (Little et al. 2006).

In this research, the "dry lime on damp aggregate" method was used. This method requires an equal distribution of lime on aggregates. It involves spreading lime powder onto the aggregate that has been wet to approximately 2 to 3% over its saturated surface dry (SSD) condition. In order for the chemical reaction to be done and the mixture to be processed, after mixing the lime with damp aggregates, the mixture must be kept for a certain period of time. Therefore the aggregates will be covered by hydrated lime, and it will spread through out the mixture equally. That part of hydrated lime which is not adhered to aggregates will remain through mixture and will improve the whole mixture and bitumen's properties. If quicklime remains un hydrated in the HMA, it will change to $Ca(OH)_2$ when it comes into contact with water during the service life of the pavement. This reaction (i.e., changing from CaO to $Ca(OH)_2$) is expansive and will create a volume change in the HMA and losses in strength and performance. Therefore, care must be taken when mixing them (Little et al. 2006).

2.3 *Methodology*

All tests are performed by the NAT (Nottingham asphalt tester) device. This test device is capable of performing dynamic tests on standard specimen, under different temperature condition (Cooper 1993). In this research 3 kind of tests were performed on the specimens, which are "Indirect stiffness modulus test" (ITSM), "Creep test" and "Indirect tensile fatigue test" (ITFT) (Cooper & Brown, 1989).

Table 3. Properties of lime.

Minimum weight percent of Calcium hydroxide $Ca(OH)_2$	90%
Maximum weight percent of lime	7%
Maximum weight percent of water	3%
Maximum weight percent of aggregate on sieve #30	12%
Maximum weight percent of aggregate on sieve #200	2%

2.3.1 *Indirect tensile stiffness modulus (ITSM) test*

This method measures the elastic stiffness of design mix specimens which have been laboratory prepared or taken from the pavement. The specimen is placed in a jig and loaded along the vertical diametral plane, which generates indirect horizontal tensile stresses within the specimen.

Measurement of the resulting horizontal deformation is carried out via two displacement transducers allowing the elastic stiffness of the specimen to be calculated by the UTM5-P software.

The tensile strength in the specimen is defined as equation 1:

$$S_T = \frac{2P_{ult}}{\pi t D} \tag{1}$$

where: S_T, is the tensile strength; P_{ult}, is load level; D, is diameter of specimen; t, is thickness of specimen (ASTM 2002; Chen & Liao 2002; Arabani et al. 2007).

Results can be outputted in a graphical form. The indirect tensile stiffness modulus test (ITSM) is a non-destructive method of measuring the stiffness modulus of asphaltic paving materials of the selected horizontal deformation. It can be seen that during loading on the specimens the deformation is increased and during unloading portion, the deformation is decreased but the speed of decreasing in unloading portion is more than the rest period. By increasing the number of load cycles, the plastic deformation is increased too (Haghi et al. 2005).

The measurement of the resulting horizontal deformation is carried out via two displacement transducers allowing the elastic stiffness of the specimen. The stiffness modulus measured in the second test is often lower than that measured in the first test. This is more evident with materials that have lower stiffness or while testing at higher temperatures. The difference is probably due to the fact that, in the second test, the LVDT probes are touching the specimen where, in the first test, loads were applied. The material is probably still recovering. It has been found that, if the second test is carried out 20 minutes or more after the first, any difference is reduced (Arabani et al. 2006b; Cooper, K. 1993).

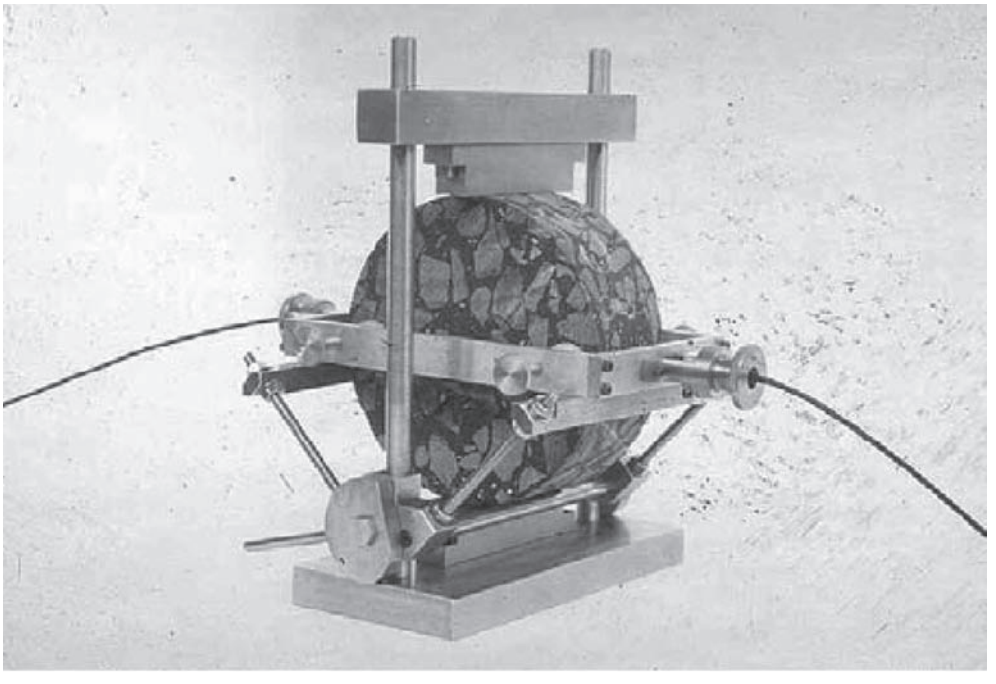

Figure 1. Indirect tensile testing mode—The Nottingham asphalt tester arrangement.

2.3.2 *Creep test*

Creep compliance testing is non-destructive in that the load is controlled so that the upper linear-elastic boundary of the HMA (typically 500 microstrain) is not exceeded, therefore each specimen can be tested at several temperatures. However, the load must be great enough to cause sufficient horizontal deformation (≥0.00125 mm based on a 38 mm gauge length). During the loading period, vertical and horizontal deformations are measured on the two sawn, parallel faces of the specimen using four extensometers, two per face (Richardson et al. 2008).

In this experimental work, specimens were tested with diameter of 100 mm and the height of 70 mm for creep test. The specimens that were used in creep test, are kept in an environmentally protected (enclosed area not subjected to the natural elements) storage area at temperatures between 5 and 24°C (FHWA 2001).

2.3.3 *Indirect tensile fatigue test (ITFT)*

Indirect Tensile Fatigue Test could easily be carried out in the newly developed Nottingham Asphalt Tester (NAT), the brainchild of Keith Cooper (Cooper and Brown, 1989). The indirect tensile fatigue test is a simple and effective method which is widely being used and can characterize the fatigue behavior of the mixture. The specimens were subjected to a sinusoidal oscillating axial loading in tension. ITFT test can be performed in two different ways: loading with constant stress, and loading with constant strain (Haghi et al. 2006; Huang, 1993). In the first method, by increase of pulses number, the strains will also increase. And in the constant strain method, by increase of pulses number, the stress will be decreased. For thick pavements the first method is used. In this method, failure will occur more quickly. The specimens which have been made for this research are known as thick. Thus in this research, the constant stress method was used. Fatigue and tensile stress relation can be calculated by performing this test.

3 RESULTS AND DISCUSSION

The variation of stiffness modulus of asphaltic specimens by 2 type gradations with different contents of hydrated lime is shown in figure 2. According to figure 2 increase of hydrated lime to topic filler is significantly increasing the stiffness modulus of asphalt specimens of both 2 type gradations. Additional of bitumen viscosity by increase of hydrate lime cause that adhesion and roughness between aggregate is increased. This is mainly caused to the fact that the stiffness modulus of asphaltic samples increased. When the percentage of hydrate

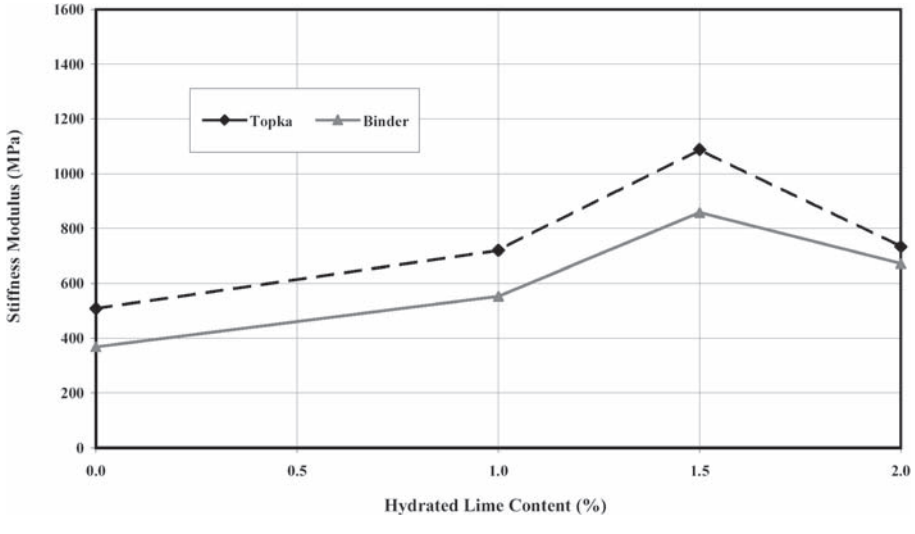

Figure 2. Stiffness modulus vs. Hydrated lime content.

lime is increased, the bitumen viscosity reaches to a limit that can not assemble necessary adhesion in asphalt specimens. So with additional hydrate lime, measure of stiffness modulus can be decreased gently. This trend can be observed in any 2 type gradations.

The effects of temperature changes on stiffness modulus of asphaltic samples with 2 type gradations are drawn in figures 3 and 4.

According to figures 3 & 4 the addition-reduction trend of measure of stiffness modulus for the given temperatures is constant. These measures in lime percentage of 1.5% have reached to maximum value. According to figures 3 and 4 it can be observed that with additional of temperature, measure of stiffness modulus of asphaltic specimens decreases. This reduction occurs because of the high sensitivity of bitumen content into changes of temperature. This high sensitivity appears on stiffness modulus of specimens of asphalt. Influence of temperature on asphaltic specimens conforms of same trend. With additional of temperature, reduction trend of stiffness modulus

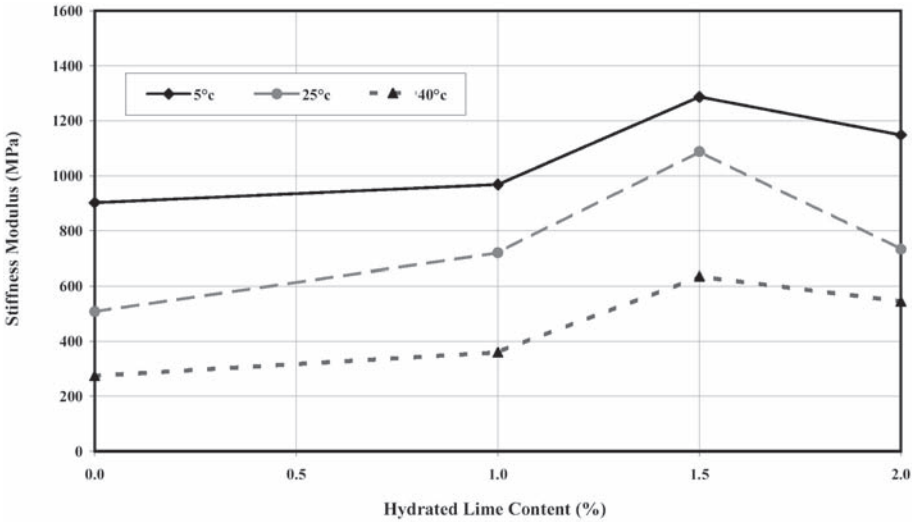

Figure 3. Effects of temperature on stiffness modulus of asphaltic samples with Topka gradation.

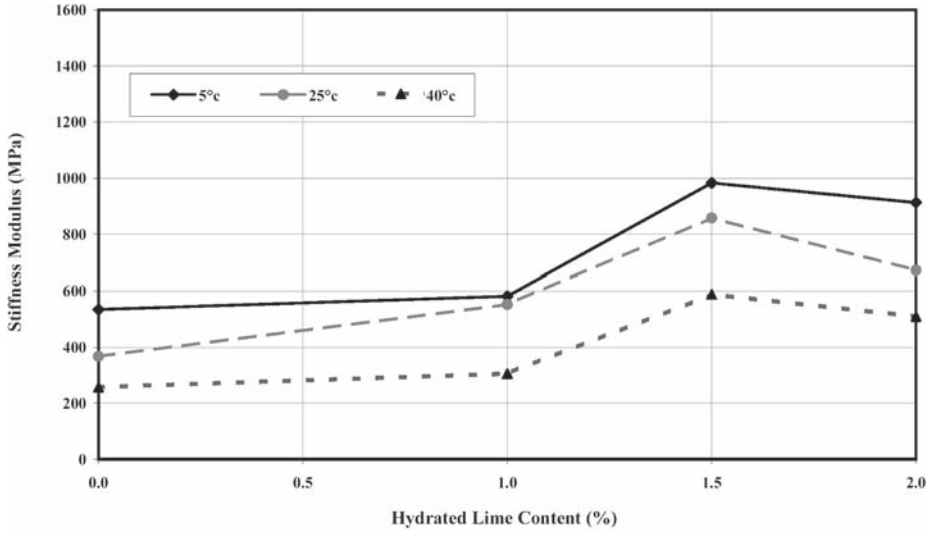

Figure 4. Effects of temperature on stiffness modulus of asphaltic samples with Binder gradation.

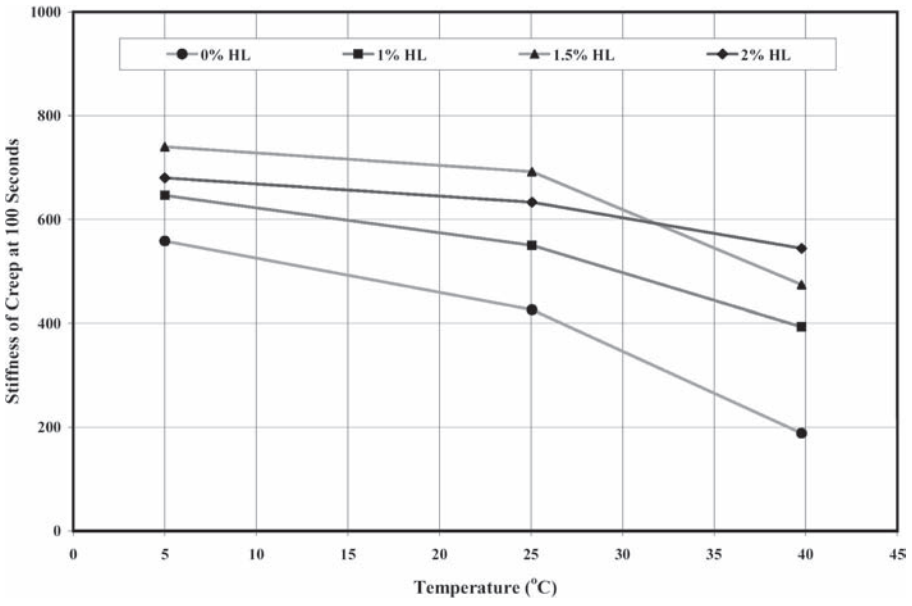

Figure 5. Stiffness of Creep vs. Temperature in specimen with Topka gradation.

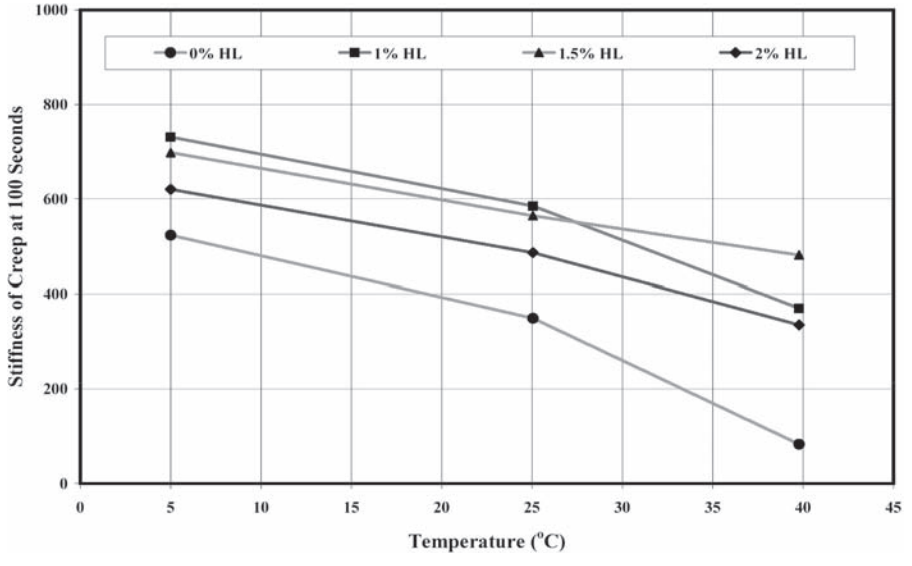

Figure 6. Stiffness of Creep vs. Temperature in specimen with Binder gradation.

value has rather rate. This rate in instance of specimens of asphalt inclusive less hydrate lime is low and increases gently with reduction of percentage of hydrate lime to side zero.

The variation of stiffness of creep in asphaltic specimens inclusive different percentages of hydrate lime versus changes of temperature is shown in figure 5. The reduction trend of stiffness of creep in relation to additional of temperature in specimens with gradation of topka conforms almost of the addition-reduction trend of measure of stiffness modulus of asphaltic specimens. However, this trend changes particular in more percentage of

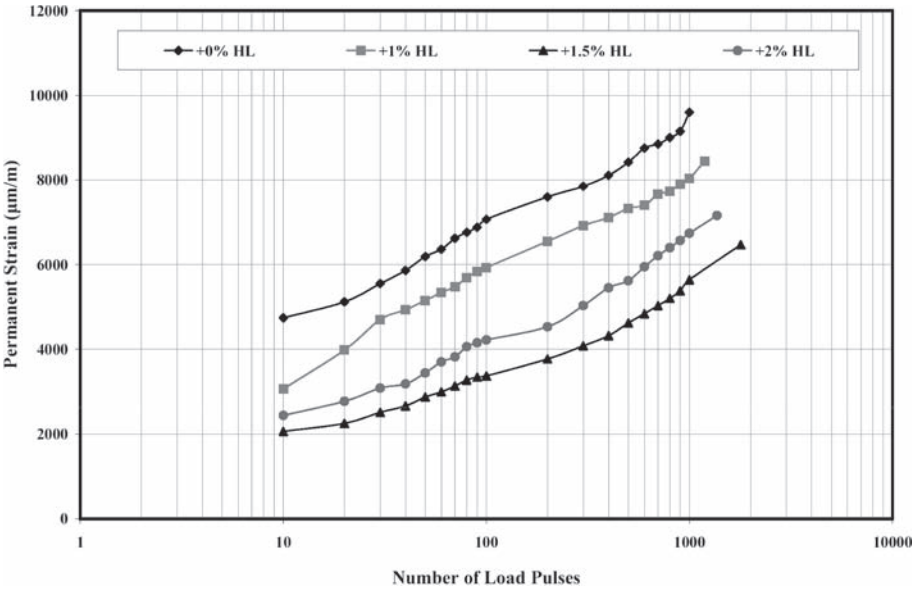

Figure 7. Permanent strain vs. Number of load pulse in specimen with Topka gradation.

hydrated lime. With additional of percentage of hydrated lime in specimens with topka gradation that optimum bitumen percentage is 6.5%. Influence of bitumen on slip properties are due to the fact that stiffness of creep of specimens of asphalt gently increases. This influence is obvious in higher percentages because of more sensitivity of bitumen content.

Reduction trend toward specimens of asphalt with gradation of binder is shown in figure 6. In these specimens also with change of temperature, stiffness of creep decreased. According to figure 6, reduction rate on effect of temperature changes in stiffness of creep in simple asphalt is far more of asphalt inclusive hydrated lime. The creep stiffness of specimens inclusive more hydrated lime is more of simple specimens. Use of less percentage of bitumen in specimens with gradation of binder, result to the decrease of the required optimum hydrated lime in these specimens. Increase of asphalt viscosity because of increase of hydrated lime result to the fact that aggregates slip on overlying decrease. Soften of bitumen in effect of temperature resulted to the control of measure of creep in the asphalt pavements.

The permanent strains versus the number of load pulse in asphaltic specimens with topka gradation are shown in figure 7. With application of loading cycles, permanent deformations of specimens of asphalt gently increase. But this ascendant trend is not same in all of percentages of hydrated lime content. The permanent deformation in simple asphalt under initial load pulse is about toward permanent deformations of asphalt inclusive hydrated lime under ultimate load pulse. More strain in specimens of asphalt is because of less hydrated lime due to less viscosity. With repeat of loading adhesion between aggregates and bitumen content decrease and aggregate slide on overlying. However, these deformations accomplish in micro scale, but must attend that number of loading cycles in this tests were confined and in actual qualification increase perhaps than 1000 equal.

According to figure 7, number of cycles for failure in specimens with different percentages of hydrated lime is not same. So can be observed with reach of hydrated lime content to optimum value in specimens with topka gradation, tenability of these specimens versus cycles loading is increased by additional rate. Also in instances was getting to 2 equal of normal condition. The permanent strains versus number of load pulse in asphaltic specimens with binder gradation are shown in figure 8.

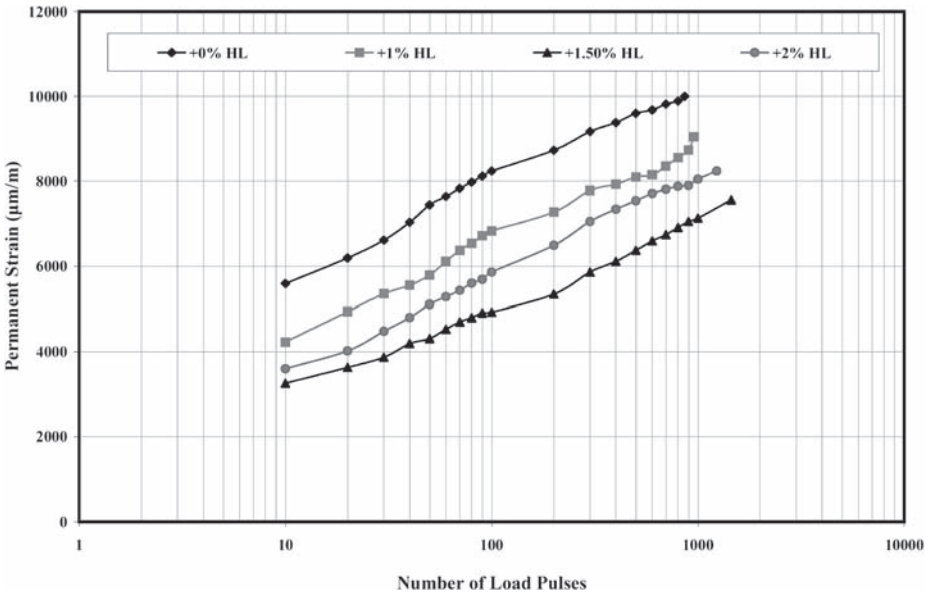

Figure 8. Permanent strain vs. number of load pulse in specimen with binder gradation.

Similar of specimens with topka gradation, in these specimens also measure of permanent strain decrease with get of hydrated lime up to optimum of 1.5%. Texture of more coarse aggregate of specimens by gradation of binder increase possible of aggregates slip on overlying and as permanent strain increase in those. The addition-reduction trend of permanent strain to state is that permanent deformations of specimens of asphalt by percentage reduction of hydrated lime content increase by more speed. So additional of hydrated lime content will have less negative effect on permanent strain of asphaltic specimens.

4 CONCLUSION

Use of hydrated lime to title filler by effect on viscosity property of bitumen and asphalt can significantly recuperate dynamic properties of asphalt mixtures. The results of lab tests on asphaltic specimens inclusive different percentages of hydrated lime by 2 gradations of topka and binder, have shown that hydrated lime with attention to particular properties have been recuperated dynamic properties of asphalt mixtures like stiffness modulus, stiffness of creep and fatigue life. The following result obtained from this research:

- The stiffness modulus and rigidity of asphaltic samples with additional of hydrated lime increased. Therefore, asphalt pavement with added hydrated lime will have greater service life, if they perform in correct manner.
- The cracks which are created by different causes might decrease, by adding hydrated lime. Form the experimental results it's seen that adding hydrated lime, increases the fatigue life.
- Permanent deformation and cracks due to fatigue can be reduced by adding hydrated lime into the HMA. Also, hydrated lime stabilizes the pavement. Because of this, it can be used as an anti-strip in pavements.

Due to these reasons, hydrated lime can improve mechanical and structural properties of bituminous mixture.

REFERENCES

Arabani, M. & Ferdosi, B. 2006a. *Evaluation of Semi Circular Bending test as a new method for determination of tensile strength of HMA mixtures*. 3rd international conference in civil engineering in Iran.

Arabani, M., Haghi, A.K., Mirabdolazimi, S.M. & Haghgoo, M. 2006b. *Increment of Stiffness Modulus in Asphaltic Pavement by Additional of Waste Tire Thread Mesh.* International Seminar on Asphalt Pavement Maintenance Technologies, ISSA World Congress. Beijing, China.

Arabani, M., Haghi, A.K., Mirabdolazimi, S.M. & Haghgoo, M. 2007. *Dynamic effects of waste tire thread mesh reinforcement on the asphaltic pavement characters*. Advanced Characterization of Pavement and Soil Engineerig Materials, Taylor & Francis Group. Athens, Greece.

Arabani, M. & T. Kheiry, P. 2006c. *A new method for determination Stiffness modulus of HMA mixtures*. ISSA world congress and International seminar on Asphalt pavement maintenance in China.

ASTM D. 1559. 2002a. *Standard Test Method for Marshal Ttest*. Annual Book of ASTM Standards, Vol. 04.03, American Society for Testing and Materials. West Conshohocken.

ASTM D. 4123. 2002b. *Standard Test Method for indirect tension for Resilient Modulus of Bituminous Mixtures*. American Society for Testing and Materials. West Conshohocken.

Chen, J.S. & Liao, M.C. 2002. Evaluation of internal resistance in hot mix asphalt concrete. *Construction and Bilding Materials*. 16 (6). pp. 313–319.

Chen, J.S., Lin, C.H., Stein, E. & Hothan, J. 2004. Development of a Mechanistic-Empirical Model to Characterize Rutting in Flexible Pavements. *Journal of Material in Civil Engineering*. V130, 519–525.

Cooper, K.E. & Brown S.F. 1989. *Developement of a simple apparatus for measurement of the mechanical properties of asphalt mixes*. proc. Eurobitumen Symp. in Madrid: 494–498.

Cooper, K. 1993. *Nottingham asphalt tester manual*. Cooper research Technology Limited. Nottingham: England.

Do, H.S., Mun, H.S. & Keun, R.S. 2006. *A study on engineering characteristics of asphalt concrete using filler with recycled waste lime.* A Korea Institute of Construction Technology. 2311.

Federal Highway Administration. 2001. *Test Method for Determining the creep Compliance Resilient Modulus and Strength of Asphalt Material Using the Indirect Tensile Test Device*. FHWA, Protocol P07. Version 1.1.

Haghi, A.K., Arabani, M. & Shakeri, M. 2006. Fracture Mechanics and Fatigue Cracks Reduction of Polymeric Asphalt Pavement. *Key Engineering Materials*. Trans Tech Publication. Vol 324–325. pp. 1277–1280. Swizerland.

Haghi, A.K., Arabani, M., Shakeri, M., Mirabdolazimi, S.M. & Haghgoo, M. 2005. *A Study on the Effect of Polymers on the Reduction of Fatigue Cracking in the Asphalt Pavement.* 7th International Fracture Conference. University of Kocaeli, Kocaeli, Turkey.

Huang Y.H. 1993. *Pavement analysis and design*. Prentice HALL, University of kentucky, USA.

Little, D.N., Epps, J.A. & Sebaaly, P.E. 2006. *The Benefits of Hydrated lime in Hot Mix Asphalt*. National Lime Association.

Richardson, D.N. & Lusher, S.M. 2008. *Determination of Creep Compliance and Tensile Strength of Hot-Mix Asphalt for Wearing Courses in Missouri*. Missouri Department of Transportation Organizational Results. Report No.: OR08–18.

Roque, R., Kim, Y., Harvey, J. & Epps, A. 2000. *Structural requirements for bitumen paving mixtures.* Transportation Research Board.

Tayebali, A., Tsai, B. & Monismith, C. 1994. *Stiffness of asphalt-aggregate mixes. Berkeley University of California.* national academy of science.

Uzarowski, L., Maher, M. & Prilesky, H. 2006. *The Use of Simple Performance Tests in the Development of Rutting Resistant Criteria for Asphalt Mixes in Canada Stage1*. Annual Conference of the Transportation Association of Canada. Charlottetown, Prince Edward Island.

Advanced Testing and Characterization of Bituminous Materials – Loizos, Partl, Scarpas & Al-Qadi (eds)
© 2009 Taylor & Francis Group, London, ISBN 978-0-415-55854-9

Monitoring and designing of wearing courses for orthotropic steel decks throughout the five-point bending test

A. Houel
CETE de Lyon, LRPC de Lyon, Bron cedex, France

T.L. N'Guyen & L. Arnaud
Université de Lyon, Lyon, Ecole Nationale des Travaux Publics de l'Etat, Département Génie Civil et Bâtiment, Vaulx-en-Velin cedex, France

ABSTRACT: The paper deals with methodology to monitor and design bituminous mixes for orthotropic steel decks. This methodology is based on two experimental tests: complex modulus test on cylindrical specimen and the five-point bending test (Arnaud & Houel 2007). In this paper, three different bituminous concrete mixes are tested and compared to an ultra high performance concrete (UHPC) pavement. Non-destructive tests based on ultrasonic waves propagation ensure the continuous evaluation of damage of the wearing courses. It is shown that this methodology enables to characterize and follow up continuously the mechanical evolution of the material throughout fatigue solicitations. Clear differences are observed between the different bituminous mixes. Finally, the UHPC contribute mechanically to reduce the stress level in steel decks whereas it is not the case for the bituminous mixes.

1 INTRODUCTION

On the one hand, the design of bituminous layers is a great importance when durability of wearing courses and the structure below this layer, both roads and bridges. Also, fatigue tests are performed in laboratory to selection the better bituminous mixture. On the other hand, an appropriate instrumentation gives a continuous follow-up of mechanical characteristics of the material at each instant throughout fatigue tests.

Thus in laboratory it is possible to evaluate the residual life of bituminous concrete and as a consequence the durability of the wearing course.

This subject is of interest for orthotropic steel decks since steel plates are very flexible and bituminous surfacing applied to such supports are submitted to very high levels of strain.

To answer to this issue, we have developed at the ENTPE laboratory two different associated tests on two specimens since 2003:

- Tests on cylindrical cores: it makes it possible to characterize mechanically bituminous material thanks to the complex modulus test and fatigue tests. It is also possible to obtain thermal intrinsic parameters of the material.
- Tests on representative specimen of steel orthotropic decks with the composite steel plate plus wearing course (eventually interface layer). The standard test in France is the five-point bending test (FPBT), a fatigue test performed at two temperatures –10°C and +10°C.

In the first part of this paper, different tested bituminous mixes and the particular case of wearing course which is an ultra high performance concrete (UHPC) pavement are presented. Then, tests on cylindrical cores—geometry, tests, results—are described. Moreover, the paper will deal with the five-point bending test—principle, test conditions, results—and compare the different solutions of wearing courses. Finally, new progress in these experimental studies will be summarized.

2 EXPERIMENTAL PROGRAM

Three bituminous concrete formulations are presented in this paper. They are characterized by a unique granulometry but are distinguished by different binders:

- a classic bituminous concrete with 7% polymer-modified binder (F2),
- a bituminous concrete with 7% pure binder (F3), and
- a bituminous concrete with 7% special polymer-modified binder called Styrelf and commercialized by Total (F4).

These mixes were tested on cylindrical cores and orthotropic specimen. We have also tested the bituminous mixture laid on the Millau viaduct (F1) on orthotropic specimen. This special mixture was developed by Eiffage TP (Héritier et al. 2005).

Moreover, a very different kind of wearing course on an orthotropic specimen has been tested: a 35 mm-thick UHPC pavement.

Finally, a key point is underlined: non-destructive testing has been developed to follow-up mechanical characteristics of the material. The principle of this method is used for both devices. This test consists in transmitting a wave with a first transducer and receiving this wave that propagate throughout the considered medium. Two kinds of ultrasonic waves are studied: P-waves or compression waves, and S-waves or shear waves. Two pairs of P-wave transducers are used to scan different excitation frequencies, and one pair of S-wave transducers is also positioned and senses the center part of the bituminous concrete layer. From the recorded signals, the below parameters are followed throughout fatigue tests (Fig. 1):

- the arrival time, which enables to know the wave velocity and by an inverse analysis the complex modulus of the bituminous concrete,
- the maximum amplitude of ultrasonic waves, and
- the Fast Fourier Transform of received signal.

Few precautions must be taken into account: an appropriate excitation frequency needs to be chosen carefully to avoid diffraction, scattering and so high attenuation because of the heterogeneity of bituminous concrete and the limited size of specimens. As a consequence, the wavelength should be larger than the grain size (10 mm) (Van Hauwaert 1998, Houel 2004, Arnaud & Houel 2007). Moreover, wave velocities depend on temperature. So, temperature effects must be analyzed before choosing adequate excitation frequencies. Characteristics of wave propagation are presented in Table 1.

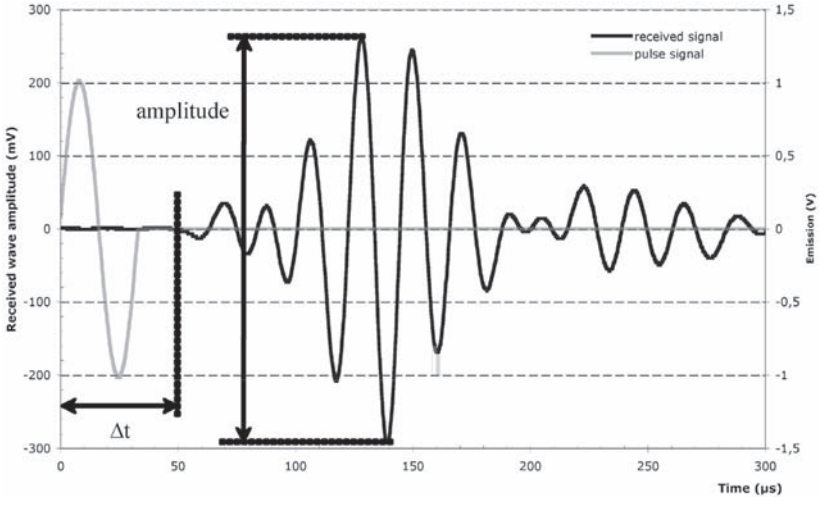

Figure 1. Emitted and received signals of P-wave propagation, determination of time delay and damping (Houel & Arnaud 2007).

Table 1. Wave velocities, frequency excitations of transducers and wavelengths used and measured at the beginning of fatigue tests.

Wave velocity and wavelength		Temperature –10°C	Temperature +10°C
P-wave (50 kHz)	Cp	4000 m/s	3600 m/s
	λ	7 cm	6 cm
S-wave (10 kHz)	Cs	2100 m/s	1800 m/s
	λ	15 cm	20 cm

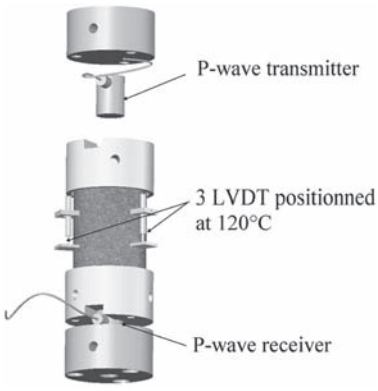

Figure 2. Experimental device for all the tests on cylindrical cores.

3 CYLINDRICAL TESTS

3.1 *Principle*

Different homogeneous tests have been developed on bituminous concrete cylindrical cores. Firstly the modulus complex test is performed on each bituminous concrete mixture. Throughout this test, specimens are submitted to different various temperatures. So, thanks to the follow-up of material's inside and surface temperatures it enables to determinate thermal intrinsic parameters such as thermal conductivity and heat capacity. Secondly we have developed on the same specimen with the same instrumentation as previous tests a fatigue test. The idea is to put a representative volume through the same level of stress as in the upper part where cracks appear throughout the FPBT that will be presented in the next part.

The dimensions of a cylindrical specimen are 78.5 mm in diameter and 188 mm high. It makes it possible to locate the rupture of the sample in the center part by creating a notch around the specimen in the range of the displacement sensors to avoid the breaking in the glue. Each specimen is stuck by its ends on a metallic support on which a P-wave transducer is positioned in contact with the bituminous concrete (Fig. 2). Axial strains are measured at the center of the sample by means of three extensometers ±5.0 mm $\Delta l = 50$ mm) or strain gauges (only if there is no notch), positioned at 120° around the specimen. These measurements enable the evaluation of the complex modulus of the bituminous concrete at each temperature and load frequency. Radial strains are measured thanks to strain gauges bonded transversally at the surface of specimens. Their monitoring makes it possible the evolution of Poisson's ratio and show that this parameter is not constant but depends on temperature and load frequency. As regards the fatigue test on cylindrical cores, the bituminous mixes were maintained on cylindrical specimens at –10°C and +10°C. The same kind of load was applied as on the FPBT, i.e. a sine load at 4 Hz and the same level of stress obtained at the beginning of the FPBT.

3.2 *Results*

Three bituminous mixtures—F2, F3, F4—are characterized from complex modulus tests. The Millau viaduct bituminous mixture was tested by Eiffage TP (Héritier et al. 2005). These tests are common and help plotting bituminous concrete modulus as a function of temperature and load frequency called mastercurve. Nevertheless, our device adds non-destructive tests by ultrasonic propagation. The results are presented in Houel (2008). Figure 3 shows the important results of these works. It proves that the bituminous concrete mastercurve is completed by P-wave propagation's analysis. These tests themselves complete and are repeatable.

Moreover, thanks to radial strain gauges, it is possible to follow up Poisson's ratio that depends on frequency and temperature solicitations (Fig. 4).

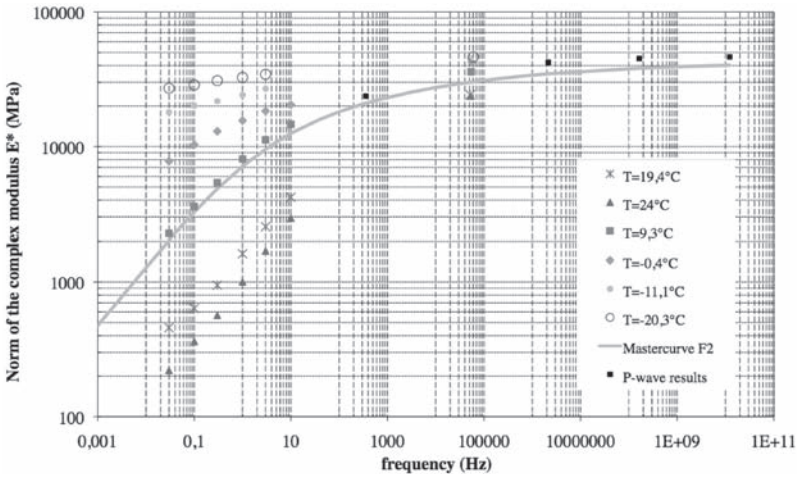

Figure 3. Example of bituminous concrete mastercurve from "classic" instrumentation and P-wave propagation by inverse analysis representing the norm of complex modulus at a reference temperature (+10°C) as a function of reduced frequency (F3 mix).

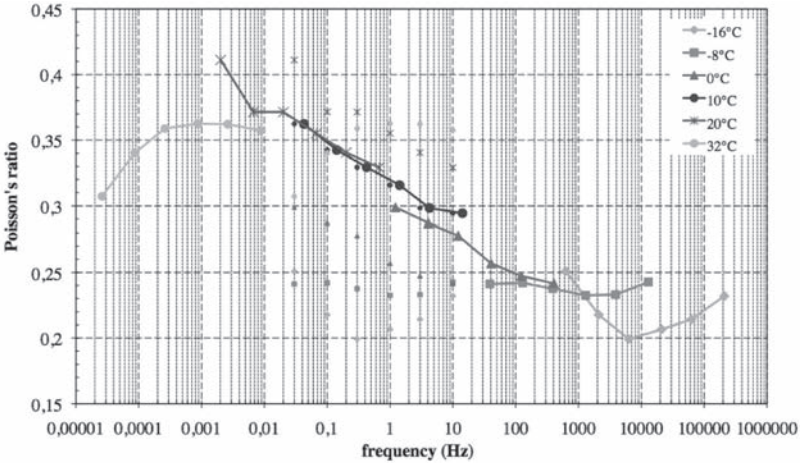

Figure 4. Example of bituminous concrete Poisson's ratio from radial strain gauges representing the norm of this mechanical characteristic at a reference temperature (+10°C) as a function of reduced frequency (F3 mix).

With exactly the same instrumentation as used on complex modulus tests, fatigue tests at +10°C and –10°C are performed. Figure 5 shows fatigue results at +10°C for these three bituminous concrete mixtures. They help choosing the better bituminous concrete that will be tested on non-homogenous test: the five-point bending test.

4 THE FIVE-POINT BENDING TEST

The design of the wearing course on orthotropic steel decks is very different as compared to the design on roads or the other bridges because of different effects: the softness of the steel plate of the deck and the stiffeners that create stress concentrations in the composite. Many recent bridges especially when large spans are needed use this design of structure. This is the

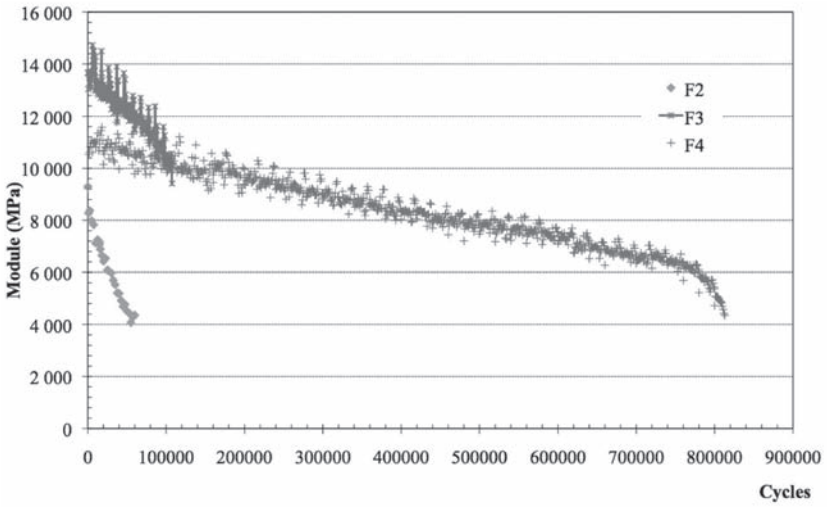

Figure 5. Experimental shapes of norm of complex modulus throughout the fatigue tests at +10°C performed on three bituminous concrete (F2, F3 and F4).

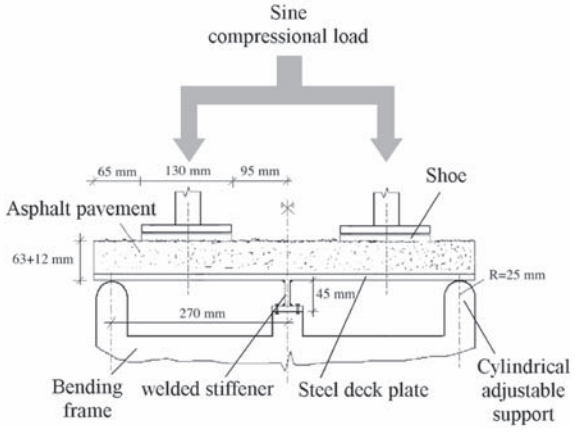

Figure 6. Experimental device of the FPBT (Laajili 2003).

case in Europe (the Millau viaduct in France for example), in North America or in Asia, where many bridges were built in these last years.

4.1 *Principle (AFNOR 2006, Arnaud & Houel 2006)*

The FPBT consists in testing a sample reproducing the area located on either side of an orthotropic plate longitudinal stiffener. This is the area where the largest strains are generated because of traffic, and therefore where the most important fatigue damage in the bituminous concrete layer is observed. This test is a fatigue test over several millions cycles.

Samples are constituted generally with three main materials:

- a 12 or 14 mm-thick steel plate reinforced at the center with a welded stiffener,
- a 3 mm-thick sealing sheet, and
- the wearing course, whose thickness is variable.

Each sample is held in its center on a rigid frame and is loaded using the device as presented in Figure 6. The steel plate is embedding in the center, and its two extremities rest on

two simple supports that are adjustable in order to correct the flatness defects of the steel plate. Above the bituminous concrete layer, the beam sets to apply the sine compression load. The load is composed by compression sine cycles at a frequency of 4 Hz (Hameau et al. 1981). The amplitude of the maximal load is determined during a calibration phase so as to take into account the mechanical role of the steel plate in the sample. This load, applied to the steel plate without any bituminous concrete layer, corresponds to a stress of 120 MPa at right angles to the weld. Of course, the effort depends on the thickness of the steel plate. For example, for calibrated 12 mm-thick plates, the maximal effort equals the load when a strain of 625 μm/m are observed at right angles to the weld, that is to say 32 kN in compression. Thus, the sine load, applied to the sample with the bituminous concrete layer, ranges in between the maximal effort and 10% of this load. A counter measures the number of applied load cycles. Based on the French bituminous concrete mix standardization, for each coating, one sample is tested at –10°C, and another at +10°C which is very often the critical case, thanks to a heat-regulated chamber.

According to the requirements, a bituminous concrete mix is considered "good" when no damage can be observed at –10°C after 1 million cycles, and at +10°C after 2 million cycles. No damage means that no crack was generated and observed with the soapy water. But there is no requirement for the mechanical evolution and the breaking threshold of the material. That is why a special instrumentation based on ultrasonic wave propagation is investigated.

4.2 *Instrumentation*

Two strain gauges are pasted on the two side faces the closest of the top face as possible in order to monitor the evolving strains of the bituminous concrete layer where cracks are likely to appear (Fig. 7). However, their installation is a delicate and difficult task, and it is possible that their breaking does not exactly account for crack appearance because of the glue. That is why two different displacement sensors, type LVDT (Linear Variable Differential Transformer) are positioned on the upper face of the sample at the center. Both accuracy and a large detection area are ensured: a first sensor (LVDT 1: ±2.5 mm and $\Delta l = 60$ mm) is certain to have a measurement zone where cracks are likely to appear, and a second (LVDT 2: ±1.0 mm and $\Delta l = 30$ mm) senses the displacements more precisely.

Moreover several temperature sensors are positioned in the chamber and one at the center on the upper face of the wearing course.

Finally wave transducers are placed in the central area on the side faces in order to continuously monitor the bituminous concrete pavement modulus where the material is submitted to tensile stress and thus where cracks are likely to appear.

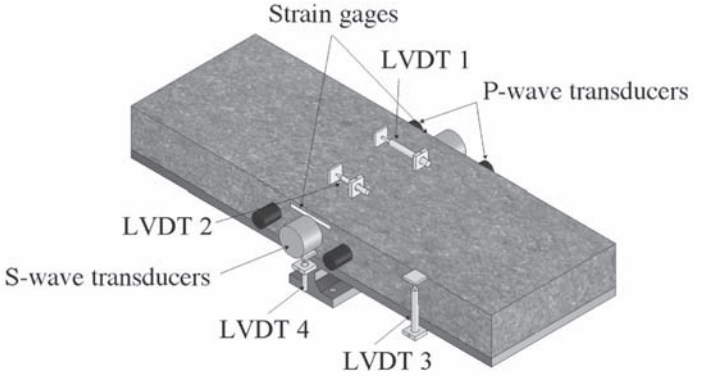

Figure 7. Locations of sensors on specimens for the FPBT: strain gauges, displacement sensors (LVDT 1 and LVDT 2), and wave propagation transducers (Houel 2008).

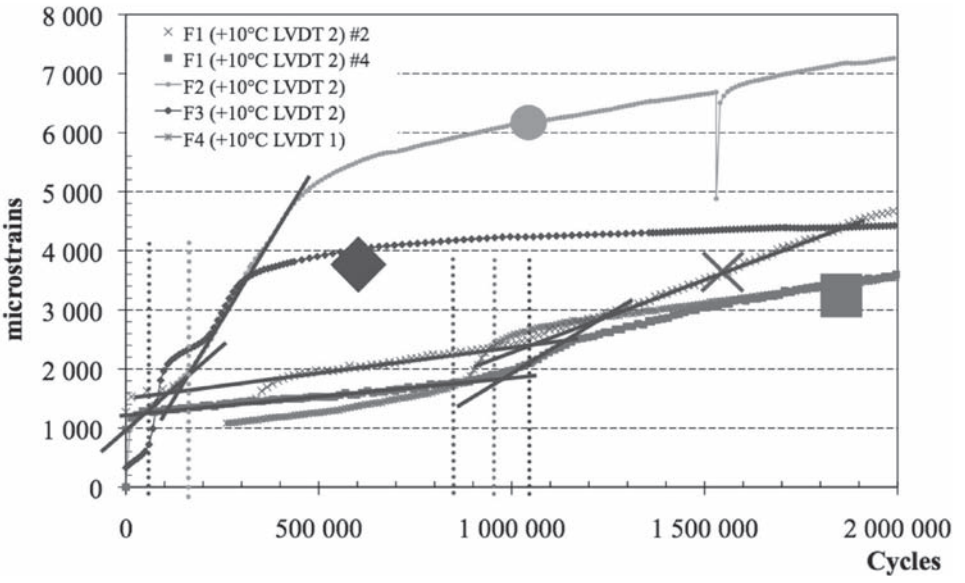

Figure 8. Experimental shapes of strain amplitudes throughout the FPBT measured by LVDT 2 on the upper face of specimens at +10°C (Houel & Arnaud 2008b).

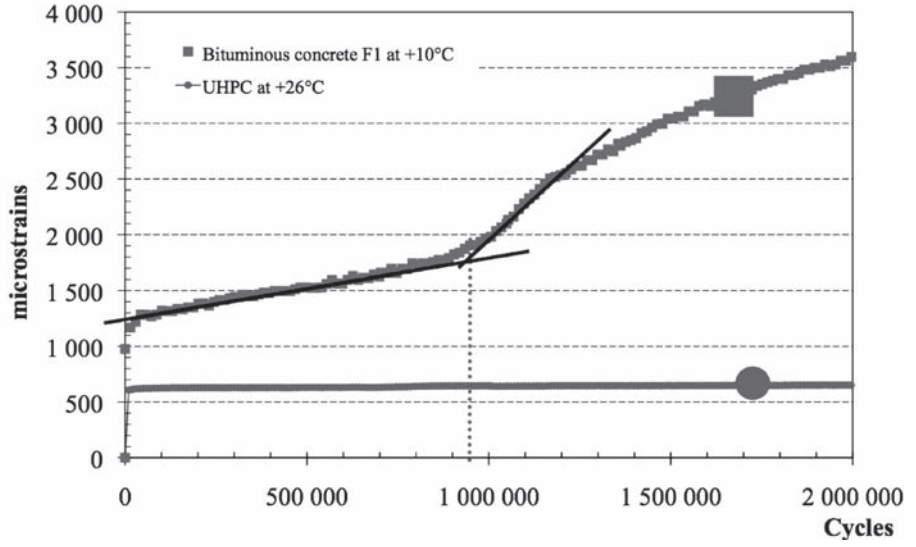

Figure 9. Experimental shapes of strain amplitudes throughout the FPBT measured by LVDT 2 on both wearing courses (bituminous concrete mix F1 and UHPC).

4.3 *Results*

Maximal and minimal strains are monitored throughout the fatigue test. As expected, both bituminous concrete mixtures show that strain amplitudes are greater at +10°C than –10°C (Fig. 8) (Houel 2008). The main differences between the four bituminous mixtures are observed:

– As far as the Millau viaduct bituminous concrete mixture, we firstly observed that amplitudes increase during the test until approximately 1,000,000 cycles, then a sudden variation of slopes is recorded from the most accurate sensor.

– As regards the bituminous concrete mixtures F2, F3 and F4 throughout both fatigue tests at –10°C and +10°C, amplitudes corresponding to one load cycle increase quickly at the beginning of the test, then a sudden and strong increase appears, and finally strain amplitudes do not increase any more but are relatively constant (Somda 2007, Houel 2008, N'Guyen 2008).

So, as regards the fatigue behavior and the appearance of cracks, the special bituminous concrete mixture F1 has a stronger resistance to cracking than the others.

In each case, variations are determined by linear regression, and the intersection of two straight lines defines the cycle number when cracks appear on the upper side of the bituminous concrete layer. This experimental set up is very sensitive to the appearance of cracks initiated from the top face of the bituminous concrete layer.

Figure 9 compares results for the UHPC wearing course and the bituminous concrete layer. We clearly observed that strain amplitudes are dramatically lower for UHPC layer whereas its thickness is half the one of bituminous layers. This important result proves that the UHPC layer supports a large part of the mechanical load and as a consequence leads to strain decrease in the steel plate. Thus, this results in new designing and this UHPC wearing course could improve durability of such steel structures.

Table 2 sums up crack detection results from displacement measurements. Hence, displacement evolution shows a sudden and significant variation in the strain amplitudes during the

Table 2. Number of cycles when crack is detected (Fig. 8).

	Temperature	
Wearing course layer	–10°C	+10°C
BC mix F1	900,000	950,000
(Millau viaduct BC)	1,200,000	1,050,000
BC mix F2	–	200,000
BC mix F3	200,000	100,000
BC mix F4	1,000,000	850,000
UHPC	no crack at ambient temperature	

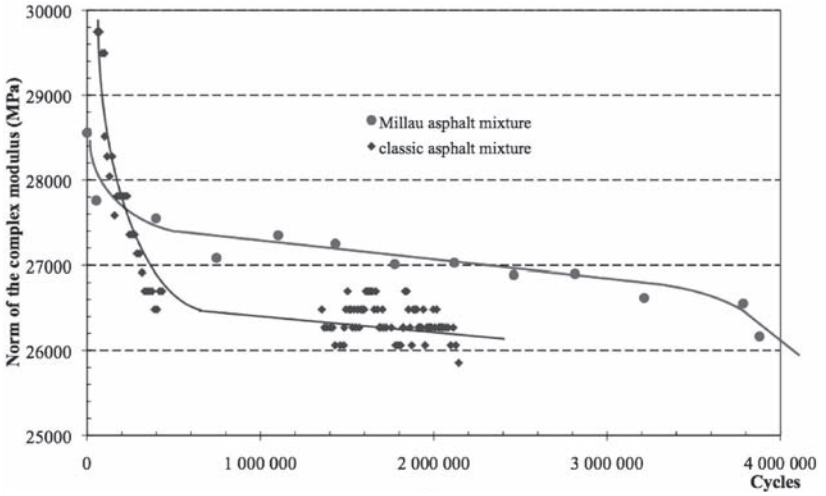

Figure 10. Norm of the complex modulus calculated from P-wave velocities and their damping by inverse analysis throughout the FPBT performed on two bituminous mixtures at +10°C (Houel & Arnaud 2008a, b).

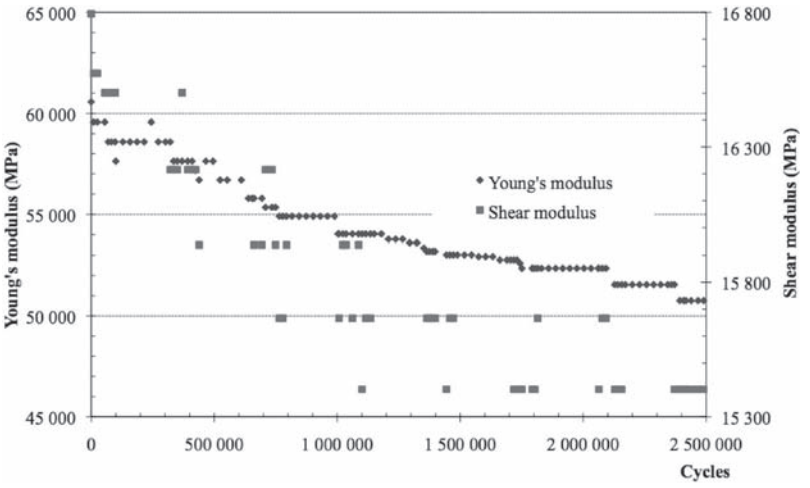

Figure 11. Young's modulus throughout the FPBT on UHPC layer at ambient temperature (N'Guyen 2008).

test that proves the appearance of fatigue cracks in the sensed zone for the bituminous concrete. Besides, tests based on ultrasonic wave propagation will confirm this method. Results are consistent for the same bituminous mixture.

An example of such results in Figures 10 and 11 shows the mechanical evolution of the bituminous concrete or UHPC layer through the results of the evolving modulus from P-wave and S-wave transducers throughout the FPBT. P-wave and S-wave velocities and their amplitude decrease clearly as the number of load cycles increases. Then signals stabilize before significant amplitudes decrease.

For the Millau viaduct bituminous concrete mixture (F1), the calculated modulus is about 28,500 MPa at the beginning, and decreases to 27,400 MPa after 800,000 cycles. Then, it stabilizes until 3 million cycles before significant decreases. This last stage reveals the appearance of cracks that are created and propagated as far as the middle of the thickness of the bituminous concrete pavement. In the second case, the decrease appears throughout the two hundred thousand first cycles like results from LVDT measurements, decreasing from 30,000 MPa to 26,500 MPa.

Therefore, wave propagation is an efficient way to compare and to monitor the evolutive behavior of different wearing courses at each instant of the FPBT, and helps damage curve plotting.

5 CONCLUSIONS

A special design is necessary for wearing courses on steel orthotropic deck, because it is subjected to very severe strains due to vehicle traffic and flexibility of steel structure.

In this paper, a methodology is presented and applied to various wearing courses. This is based on two devices with different geometries.

Fatigue tests on cylindrical cores are homogeneous and lead to characterize material: the viscoelastic mastercurve is plotted for three bituminous mixtures and fatigue solicitations lead to define time-dependant properties of the mix. This is a great importance for a future modeling. Moreover, the FPBT in laboratory is representative of solicitations applied on wearing courses on steel orthotropic decks. An accurate instrumentation is defined in this paper and makes it possible to obtain a continuous follow-up of mechanical evolutive characteristics of the wearing course throughout the fatigue test. This test constitutes an indispensable step for the design of wearing course on steel orthotropic bridges.

ACKNOWLEDGMENTS

The authors wish to thank the ANR (French acronym for "National Research Agency") French project "Orthoplus" for its support in this study.

REFERENCES

AFNOR 2006. Méthodes d'essai sur banc de fatigue en flexion sous moment négatif. Détermination de la résistance en fatigue d'une étanchéité/roulement sur tôle métallique, Essais relatifs aux chaussées—Produits d'étanchéité pour ouvrages d'art, French standard method (NF P 98-286). [In French]

Arnaud L. & Houel A. 2006. Fatigue damage and cracking of asphalt pavement on orthotropic steel bridge deck, *Transportation Research Board Annual meeting Compendium of Papers CD-ROM*, Washington D.C.

Arnaud L. & Houel A. 2007. Fatigue damage of asphalt pavement on an orthotropic bridge deck: mechanical monitoring with ultrasonic wave propagation. *International Journal of Road Materials and Pavement Design* 8-3.

Hameau G., Puch C. & Ajour A.-M. 1981. Comportement à la fatigue en flexion sous moment négatif, *Bulletin de liaison des Ponts et Chaussées* 111. [In French]

Héritier B., Olard F., Saubot M. & Krafft S. 2005. Design of a specific bituminous surfacing for orthotropic steel bridge decks: application to the Millau viaduct, *7th Symposium on Bearing Capacity of Roads, Railways and Airfields*, Trondheim, Norway.

Houel A. 2004. Comportement à la fatigue et fissuration mécanique des enrobés bitumineux sur dalle orthotrope, Master in Civil Engineering. Ecole doctorale MEGA-ENTPE, France. [In French]

Houel A. & Arnaud L. 2007. Damage characterization of asphalt concrete specimens by ultrasonic P and S-wave propagation in laboratory. *Advanced Characterization of Pavement and Soil Engineering Materials*. London: Loizos, Scarpas & Al-Qadi eds. Taylor & Francis Group.

Houel A. & Arnaud L. 2008a. A five-point bending test for asphalt cracking on steel plates, *Proceedings of the International RILEM Symposium*, Chicago.

Houel A. & Arnaud L. 2008b. The five-point bending test: a way to the dimensioning of the asphalt layer on steel orthotropic decks, *International Orthotropic Bridge Conference*, Sacramento.

Houel A. 2008. Endommagement et fissuration mécanique des enrobés bitumineux sur dalle orthotrope. Ph. D. Ecole doctorale MEGA-ENTPE, Lyon, France. [In French]

Laajili H. 2003. Caractérisation des enrobés bitumineux comme couche de roulement sur tabliers d'ouvrage d'art métallique, Master in Civil Engineering, Ecole doctorale MEGA-ENTPE, France. [In French]

N'Guyen T.L. 2008. Revêtements de dalle de pont métallique orthotrope, comparaison d'essais à la fatigue entre béton bitumineux et BFUP, Master in Civil Engineering, ENTPE, France. [In French]

Somda A.R. 2007. Revêtement de tablier de pont métallique: caractérisation et dimensionnement lors d'essai de fatigue, Master in Civil Engineering, ENTPE, France. [In French]

Hauwaert A.V., Thimus J.-F. & Delannay F. 1998. Use of ultrasonics to follow crack growth. *Ultrasonics* 36: 209–217.

Advanced Testing and Characterization of Bituminous Materials – Loizos, Partl, Scarpas & Al-Qadi (eds)
© 2009 Taylor & Francis Group, London, ISBN 978-0-415-55854-9

Evaluation of modified bitumen, High Modulus Asphalt Concrete and steel mesh as materials for road upgrading

M. Tušar
National Institute of Chemistry, Ljubljana, Slovenia

M. Ravnikar Turk
Slovenian National Civil Engineering and Building Institute, Ljubljana, Slovenia

W. Bańkowski
IBDiM (Road and Bridge Research Institute, Warsaw, Poland

L.G. Wiman & B. Kalman
VTI (The Swedish National Road and Transport Research Institute), Linkoping, Sweden

ABSTRACT: Within the framework of the SPENS project (Sustainable Pavements for European New Member States) WP 4 (Work Package 4), materials and pavement layers appropriate for road upgrading, considering the conditions in New Member States will be evaluated. Modified bitumen as asphalt binders and high modulus asphalt mixtures are more and more popular in road construction, but insufficient information is available on the actual performance of these mixtures. Within Task 1 (Investigation of the Performance of the Conventional and Polymer Modified Bitumen) the objective is to find performance based binder criteria founded on correlations between binder tests and critical asphalt performance tests. Within this objective we will test already suggested performance based binder criteria and try to find new or better criteria for those asphalt properties, where good and solid correlations has not yet been found. With sound performance based binder criteria the choice of binder for a particular application is simplified. Task 2 deals with studies of High Modulus Asphalt Concrete (HMAC) as technical solution providing improved durability of road asphalt pavement with possibility to reduce the pavement thickness and road construction costs. Further during the pavement service, well-designed pavement requires less maintenance operations, thus giving the reduction of maintenance cost. Accelerated load test was performed with Heavy Vehicle Simulator on pavement structure with HMAC. In Task 3 the effect of different layer thicknesses and strengthening treatments in the pavement structure were evaluated with the HVS-Nordic.

1 INTRODUCTION

The New Member States have mainly focused on the construction of new motorways, while less money has been available for the improvement of the existing roads. However at the same time there is a strong need for new, sustainable road pavement materials, with a high bearing capacity, in all of the EU countries. It is anticipated that maintenance costs in the New Member States could be lowered significantly by introducing better techniques and improving the prevailing procedures, which are used to deal with the assessment of road conditions and maintenance planning for road upgrading. Increasing traffic volumes and loads mean that wider roads, with a higher bearing capacity and better pavement durability, are needed. The reinforcing of pavements by means of geosynthetics, steel meshes or glass grids could prolong the service life of pavements by reducing deterioration. This type of strengthening has not yet been widely used in the New Member States, and the behaviour of such reinforced roads needs to be carefully investigated. The best practice still needs to be developed.

Chemically-modified bitumen, as asphalt binders, is used more and more in road construction, but not much information is available about the actual performance of these materials. A reliable correlation between the laboratory and in-situ performance of mixtures with modified bitumen has not yet been established. This knowledge is necessary for the evaluation of the behaviour or appropriateness of these materials in different climatic and environmental conditions. Pavements in the continental climate of the Central and Eastern European Countries need to be able to withstand large fluctuations between winter and summer temperatures.

2 ACTIVITIES IN TASKS AS PART OF WP 4

2.1 *Task 4.1 investigation of the performance of the conventional and polymer modified bitumen*

To upgrade roads in NMS to perform better with respect to traffic load, climatic variations environmental impact and cost efficiency, involves using new or improved materials and construction methods. Polymers and other additives used to modify bitumen are used in many places to improve asphalt mixtures. New and improved types of polymers for bitumen modification reach the market all the time. Formula based construction methods and traditional binder testing methods are not suitable for dealing with the complexity associated with polymer modified bitumen and asphalt mixtures made of these binders.

Upgraded roads should be constructed by using asphalt mixtures with better performance compared to conventional asphalt mixtures. Different asphalt layers in a road construction are subjected to different types of stresses and stress levels. The performance of the layers should be optimised accordingly. The most obvious performance related properties of asphalt mixtures are wear resistance, stiffness, resistance to plastic deformation, resistance to fatigue and durability (water sensitivity and ageing). All of these properties are to very large extent influenced by the properties of the binder and the binder aggregate interaction (Nicholls, 2006).

Binder test methods should guide the pavement engineer in selecting the most efficient binder for a certain type of aggregate and type of asphalt layer. The traditional bitumen test methods have been shown numerous times to be inadequate for evaluating modified bitumen. A combination of fundamental binder test methods, e.g. the complex shear modulus measured with DSR and methods characterizing the binder during severe stress have been suggested to be asphalt mixture performance related (Maccarone, 1995). Such performance related binder test methods will help the pavement engineers in the NMS and also in EU-15 to select the most cost efficient binder for the given traffic load, available aggregate and climatic conditions at the site.

The task has focused on selecting the most efficient combinations of binder test methods for predicting asphalt mixture performance. The testing program have include three different asphalt mixtures whose performance have been characterized by wheel tracking tests, TSRST, stiffness at different temperatures, water sensitivity and Marshall stiffness.

Seven binders, three conventional bitumen ranging from 70/100 to 20/30 in penetration and four polymer modified binders with softening points ranging from 45 to 70°C were chosen to ensure a wide range in binder properties. The binders denoted A-G were: A, a B85 bitumen modified with 1.5% Elvaloy; B, a 20/30 conventional binder; C, a 25/55 -60 polymer modified binder; D, a 50/90 -65 polymer modified bitumen; E, a 25/55 -55 polymer modified bitumen; F, a 70/100 conventional binder and G, a 50/70 conventional binder.

The binders have been characterized with a range fundamental test methods as well as traditional test methods and the results will be compared and correlated to the results from the asphalt mixture testing program.

The task will accomplish

- Recommendations for the choice of performance related binder tests
- Recommendations for selecting binder properties for different types of asphalt mixtures based on the performance related binder tests

Three types of mix gradations were chosen, an asphalt concrete mix (AC), a stone mastic asphalt mix (SMA), and a porous asphalt mix (PA). The AC were made both with basalt aggregate and a limestone aggregate while the other mixes were only made with basalt aggregate. The four types of mixes allow us to check whether or not the performance related connections between the binder tests and the asphalt mix tests are mix specific or of more general nature.

The task will increase the awareness of the benefits and drawbacks of different types of bitumen modification. The task will be beneficial for rapid upgrade of the infrastructure in NMS by introducing performance related test methods. These test methods are necessary for promoting innovation and cost efficiency in the upgrading process.

All tests, binder as well as asphalt mix tests, were performed according to current European norms unless otherwise stated. The force ductility test and elastic recovery test were only done on the polymer modified binders.

Table 1. A selection of binder and asphalt mixture properties.

Binder								
Test ↓	Unit ↓	A	B	C	D	E	F	G
Penetration	dmm	82	30	29	68	44	74	54
Penetration mod. I	dmm	147	43	42	104	66	141	88
Softening point	°C	47.6	62.2	67.6	71.2	66.8	49.6	54.8
Fraass Break Point	°C	–17.5	–9.5	–10	–12	–14	–19.5	–18.5
Kinematic viscosity	mm^2/s	599	1370	2234	713	2055	416	596
Dynamic viscosity	Pa s	271	2697	5184	1405	5029	181	528
Penetration/RTFOT	dmm	53	23	25	44	32	51	41
Soft. point/RTFOT	°C	53.4	68.4	73.6	75.4	75.2	56.2	60.8
Dyn. visc./RTFOT	Pa s	666	7819	15758	1902	8886	825	2373
Elastic recovery	%	46		74	99	89		
Deformation energy II	J/cm^2	2.2		12.6	4.3	9.1		
Deformation energy III	J/cm^2	0.1		1.8	2.2	3.6		
Cone Plate viscosity IV	Pa s	227	2022	3219	1407	2624	141	460
Cone Plate viscosity V	Pa s	0.219	0.587	0.734	0.286	0.691	0.133	0.176
Ekviviscous temp. VI	°C	145	162	167	151	168	138	144
Coaxial cyl. visk. VII	Pa s	1.69	4.74	6.93	1.89	5.42	1.08	1.97
Coaxial cyl. visk. VIII	Pa s	0.43	0.80	1.26	0.42	1.17	0.21	0.38
Asphalt test on SMA/basalts								
Wheel tracking rut	mm	2.45	1.86	1.53	1.54	1.33	2.48	1.98
IT-CY stiffness, 15°C	MPa	1657	4413	4031	2174	3218	1369	2279
Asphalt test on AC/basalts								
IT-CY stiffness, 15°C	MPa	1974	4163	4121	2171	2823	1696	3043
Asphalt test on AC/limestone								
IT-CY stiffness, 15°C	MPa	2494	9132	5297	4320	4572	2225	4934
Asphalt test on PA/basalts								
IT-CY stiffness, 15°C	MPa	838	2670	2889	1435	1975	969	1987

I: Penetration at 35°C with total weight of 50 g; II: At 10°C and speed 50 mm/min; III: At 25°C and speed 50 mm/min; IV: At 60°C; V: At 150°C; VI: According to ASTM D 1559 (2382); VII: At 120°C; VIII: At 150°C.

Table 2. Correlation coefficient, r2, in linear regression between of binder test results and test results from asphalt mixture tests.

	Asphalt mix test			
Binder test ↓	SMA/wheel tracking	AC(basalts)/stiff.	AC(limest.)/stiff.	PA(basalts)/stiff.
Penetration	0.43	0.88	0.67	0.97
Penetration mod. I	0.58	0.87	0.70	0.96
Softening point	0.90	0.23	0.22	0.37
Fraass Break Point	0.5	0.55	0.55	0.57
Kinematic viscosity	0.57	0.50	0.19	0.58
Dynamic viscosity	0.66	0.44	0.18	0.56
Penetration/RTFOT	0.53	0.89	0.72	0.94
Soft. point/RTFOT	0.94	0.25	0.23	0.40
Dyn. visc./RTFOT	0.44	0.67	0.25	0.75
Elastic recovery	0.47	0.00	0.03	0.00
Deformation energy II	0.48	0.93	0.78	0.97
Deformation energy III	0.86	0.08	0.50	0.23
Cone Plate viscosity IV	0.72	0.54	0.30	0.66
Cone Plate viscosity V	0.57	0.57	0.34	0.63
Ekviviscous temp. VI	0.68	0.54	0.36	0.61
Coaxial cyl. visk. VII	0.50	0.67	0.32	0.73
Coaxial cyl. visk. VIII	0.55	0.51	0.20	0.58

See table 1 for notes.

In table 1, a selection of binder and asphalt mix tests are presented. The asphalt test results were fitted with linear regression to the results of the binder tests. The regression coefficients for these correlations are presented in table 2.

The number of binder tested is limited so the data can essentially be used to corroborate or contradict proposed correlations made in other studies.

From table 2 it seems to be a fairly good correlation between the wheel tracking rut depth and the softening point even though the there are four polymer modified binders in the study. These results are in contrast with the conclusion drawn in the BitVal report (Nicholls, 2006), but in line with the current European specification for polymer modified bitumen.

The stiffness modulus correlates fairly well with penetration tests, but the proportionality constants are different for different mixes (data not shown). The data in table 2 suggest that the deformation energy measured at 10°C could be a candidate for a performance related test vis à vis the stiffness modulus of asphalt mixes, but the data is very limited.

2.2 *Task 4.2 material recommendations and performance-based requirements for high modulus asphalt mixtures and flexible pavement design*

The aim of this task is to develop a concept of high modulus asphalt mixtures (Format, 2005) for the implementation in the Central and Eastern European countries. It is obvious that the technology transfer has to take into account local climatic conditions as well as the availability of materials and equipment, both for the road construction and for laboratory testing. The following countries are interested in implementation of High Modulus Asphalt Concrete: Poland, Slovenia, Croatia, Serbia, Sweden and Estonia.

The first point of the task is preparation of initial recommendations for High Modulus Asphalt Concrete (HMAC) in different countries. Poland has experiences with this type of mix and the test in real scale will be performed in Poland. Recommendations for Poland have been already prepared. This will be adopted taking into account climate, materials and test methods for countries that are interested in implementation of HMAC (Slovenia, Serbia, Sweden, Croatia, and Estonia). Climate analysis consists of evaluation

Table 3. T_{EFF} in different countries.

		MAAT, °C	ha, cm	MAPT, °C	T_{EFF}, °C
Serbia	Beograd	11,5	10,0	16,8	10,7
		11,5	22,5	16,3	10,4
Croatia	Plitvice	9,1	8,0	14,0	8,5
		9,1	20,0	13,6	8,2
	Gospic	9,5	8,0	14,5	8,9
		9,5	20,0	14,1	8,6
	Varazdin	11,0	8,0	16,3	10,3
		11,0	20,0	15,8	10,0
	Zagreb	11,7	8,0	17,1	11,0
		11,7	20,0	16,6	10,6
	Knin	13,3	8,0	19,0	12,5
		13,3	20,0	18,5	12,1
	Rijeka	14,6	8,0	20,6	13,8
		14,6	20,0	20,0	13,3
	Senj	15,4	8,0	21,6	14,6
		15,4	20,0	20,9	14,0
	Hvar	16,9	8,0	23,4	16,0
		16,9	20,0	22,6	15,4
Slovenia	Ljubljana	9,0	8,0	13,9	8,4
		9,0	20,0	13,5	8,1
	Koper	12	8,0	17,5	11,3
		12	20,0	17,0	10,9
Sweden	Stockholm	6,6	12,0	10,2	5,5
		6,6	18,0	10,1	5,4
	Gothenburg	7,1	12,0	10,7	5,9
		7,1	18,0	10,7	5,8
	Malmoe	7,9	12,0	11,6	6,6
		7,9	180	11,5	6,5

of effective temperature for fatigue (TEFF) and PG temperatures for different layers. TEFF temperature in Table 3 was calculated on the basis of mean annual air temperature (MAAT) and thickness of typical flexible pavement structures with use of two equations (Deacon et al.):

$$MAPT = MAAT \cdot \left[1 + \left(\frac{1}{Z+4}\right)\right] - \frac{34}{Z+4} + 6$$
$$T_{EFF} = 0{,}8 \cdot (MAPT) - 2{,}7 \quad (1)$$

where:
MAPT – mean annual pavement temperature at depth Z, ˚F
Z – depth equal to 1/3 of asphalt layer thickness, inches.

Calculations were done in each case for two different thicknesses of asphalt layers (ha), which represent low and heavy traffic pavements.

Next part of climate analysis includes evaluation of PG temperatures. PG (Performance Grade) is SUPERPAVE classification system for binders that take into account conditions (climate and traffic) under which it is used.

Asphalt binder is characterised by PG x–y, where:
x – maximum pavement temperature T (max),
y – minimum pavement temperature T (min).

Examples of results of calculations are shown in Table 4.

Preparations of HMAC guidelines are continued in the next few months. Polish recommendations were implemented and verified in laboratory. Laboratory tests on materials were done and several HMAC were designed. It covered three binders: 20/30, DE30B

Table 4. Evaluation of PG for binder course (heavy traffic).

		d, mm	T(max), °C	Td(min), °C	PG(x–y)
Serbia	Beograd	100,0	49,0	–10,8	52–16
Croatia	Plitvice	75,0	41,7	–17,3	40–22
	Gospic	75,0	39,9	–21,6	40–22
	Varazdin	75,0	41,5	–17,4	40–22
	Zagreb	75,0	41,6	–13,5	40–16
	Knin	75,0	43,7	–9,5	46–10
	Rijeka	75,0	43,5	–4,0	46–4
	Senj	75,0	44,6	–5,5	46–10
	Hvar	75,0	45,1	–1,0	46–4
Slovenia	Ljubljana	80,0	45,9	–21,1	52–22
	Koper	80,0	46,1	–21,1	52–22
Sweden	Stockholm	65,0	35,6	–18,6	40–22
	Gothenburg	65,0	37,3	–16,6	40–22
	Malmoe	65,0	36,5	–14,6	40–16

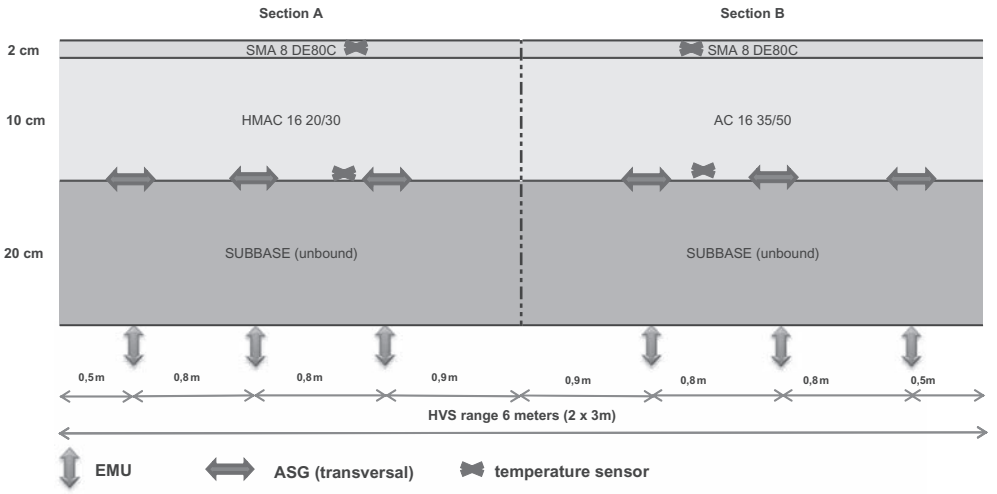

Figure 1. Test sections in poland (Pruszków).

(polymer modified), MG10/20 (multigrade) and five types of aggregates (basalt, granite, limestone, boulder, steel slag). The results of performance tests (fatigue, stiffness, rutting) indicate suitability of different binders and aggregates of different type, quality and origin (Sybilski et al. 2008).

Test sections were located in Pruszków—near Warsaw and construction works was done by STRABAG in October 2007. Test section was divided into two halves of the same layer thickness, but with two different mixes for base course: asphalt concrete (AC) and HMAC. It allows direct evaluation of an influence of HMAC on pavement durability.

Pavements were equipped with two kinds of sensors: strain gauges at the bottom of asphalt layers and vertical strain at the top of subgrade.

HVS was used in Poland for the second time (Blab et al.). Both times HVS test was performed at constant temperature of 10°C with use of single wheel (60 kN, 800 kPa). Wheel was moving on 6 meters path at speed of 10–12 km/h. Each day response measurements (strain in asphalt layers and in subgrade) were done together with rut profile evaluations. After 190 000 cycles deterioration of pavement was very small and it was decided to change wheel load to 80 kN. Test was stopped after 300 000 cycles.

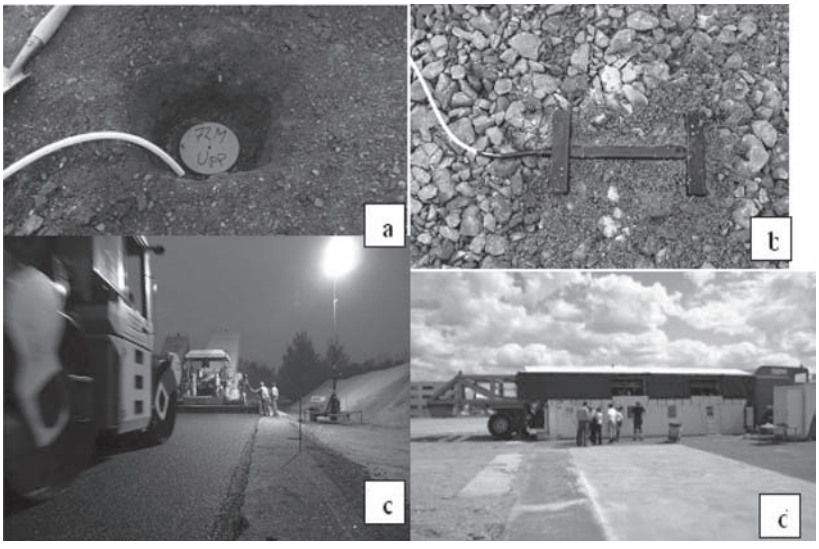

Figure 2. Placing of sensors in the subgrade; Xb—Transversal strain gauges; Xc—Compaction of wearing course; Xd—HVS on the test section in Pruszków.

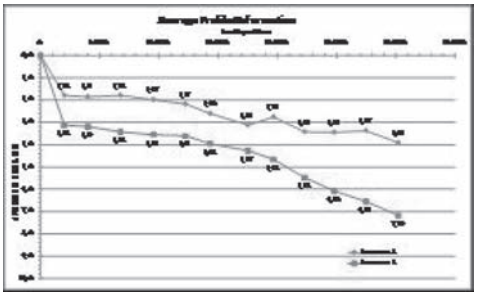

Figure 3. Evolution of profile deformation.

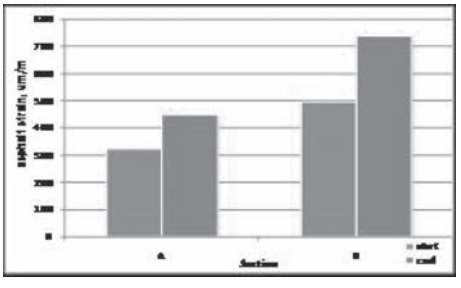

Figure 4. Comparison of strains at the bottom of asphalt layers at the beginning and at the end of the HVS test.

HVS tests are accompanied by field tests (Falling Weight Deflectometer, Ground Penetration Radar) and a number of laboratory tests. A few dozen of slabs and cores were cut from the pavement. Laboratory test program consists of evaluation of composition (binder content, grading, air voids), resistance to rutting, stiffness and fatigue. Laboratory tests were finished in December 2008 and final analyses are in progress. Laboratory results of the tests done on bituminous specimen cut from pavement do not show any damage if loaded and not laded areas are compared. It is opposite to HVS measurement that show increase of profile deformation (figure 3) and increase of strains at the bottom of asphalt layers (figure 4). Unexpected laboratory test results can be explained by healing of asphalt layers. Specimen were cut after 6 weeks after completion of HVS test and increase of pavement temperature (hot summer, direct sun operation) could cause closing of fatigue microcracks. General comparison of results indicates better performance of the structure with high modulus asphalt concrete. Final conclusions will be drawn after complete analysis. It should be also noted that thickness of the structures was smaller than it is typically used for this level of traffic (about 700 000 axles of 60 kN) and both structures stood this loading.

2.3 *Task 4.3 upgrading of asphalt macadam and light asphalt pavements to the bearing capacity level needed by EU*

For assessing the pavement bearing capacity, deflections of road pavement under a dynamic loading was measured with Dynatest Falling Weight Deflectometer (FWD). Surface unevenness was tested with ZAG-VP (ZAG Longitudinal Profilometer).

Accelerated load test (ALT) was performed on selected field trial with Heavy Vehicle Simulator, HVS-Nordic (Wiman, 2006). This cost-effective facility is convenient to investigate the effect of different strengthening treatments on existing pavements.

Field trials in Slovenia were prepared by DDC and ZAG. There were 3 meetings in Slovenia where 10 potential test fields were selected. Test field presented in figures 5, 6 and 7 were selected as the most proper for SPENS test fields. They are new road construction and not upgrade of low volume roads, as was planed. Advantage of new road construction comparing to a low volume roads is that they are more uniform. On subbase ground from crumble and clay, base gravel from sandy gravel (Pos) was built in. Thickness of base gravel was up to 60 cm. Unbound base layer (NNP) had thickness 20 to 25 cm. Uncrushed gravel with grain size 0 to 32 mm was used. The effect of unbound layers was almost uniform on all test fields (Odermatt, 2004). With different thickness of asphalt layers we can get a data for equivalence factors that will be used in WP 2. From results of test on fields 5 and 6 effect of steel mesh will also be evaluated, so we can get data about effect of reinforcement on bearing capacity of the road (Philajamäki, 2002). The producer of reinforcement suggested that we should put the steel mesh between the asphalt concrete layers and the crushed stone base layer.

Full-scale accelerated load testing was performed on these 6 test fields in Slovenia (Wiman, 2008). The test wheel runs in total 8 m and 6 m of these with constant speed. The test structures were instrumented in a proper way with strain gauges and inductive coils (deformation measurement). From this instrumentation it is possible to get response data at different load conditions e.g. wheel load, tire pressure etc. This was done before, during and after the main test. The main test for each test field lasted for 2 weeks and the machine was running day and night 7 days a week with interruptions only for daily service. During the main test cross profile measurements were carried out for calculation of rut depth propagation on the surface. It has been decided that the pavement temperature shall be kept constant at 20°C and the wheel load will be 60 kN at the beginning of the tests and then increased if necessary. The loading was

Table 5. Altogether thickness of asphalt layers.

Number test filed /measuring position	Thickness cm
1/1	6,2
1/2	5,7
1/3	7,1
2/1	9,6
2/2	10,6
2/3	11,1

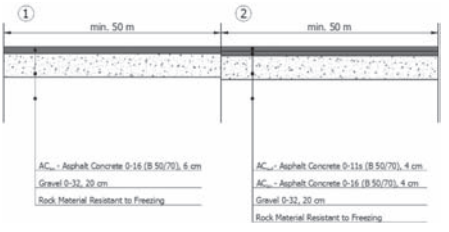

Figure 5. Test fields 1 and 2.

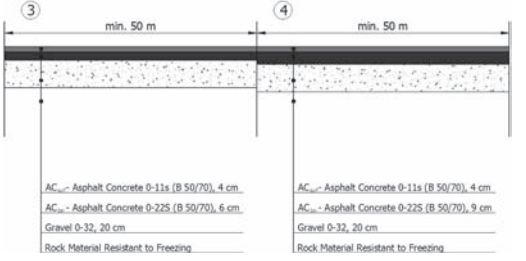

Figure 6. Test fields 3 and 4.

in both directions and with a chosen lateral wander. We have preliminary results for test fields 1 and 2. Deformation measurement in gravel is presented in figure 8 and in figure 9 is presented rut depth propagation on the surface of pavement. It can bee seen that results match.

The cores were bored from asphalt pavement after the HVS testing. The actual thicknesses of asphalt are presented in table 5. From Table 5 and figure 9 we can see that on test filed 1 there is clear dependence of thickness of asphalt layers on depth of permanent deformation, but on test field 2 all permanent deformations are the same and do not depend on thickness. From these data we can conclude there is some limit to which it is reasonable to go with thickens of asphalt pavement. Of course the limit depends on quantity of layer beneath the asphalt pavement and on the applied loads.

3 CONCLUSION

The WP 4 will contribute to standards indirectly. Test results will provide technical background for the relevant standardization committees.

The aim of the research work is also widening of the implementation of the existing EU standards in the New Member States. The results of tests performed according to the EU standards could be compared to the national specified tests, formerly used in the New Member States. A by-product of the project could be the preparation of recommendations for laboratory or field tests, as well as methodologies to reduce deviations in standardized and commonly used procedures.

The field trials with accelerated load tests on different road upgrading layers will lead to innovative road upgrading techniques. Systematically planed laboratory tests on different

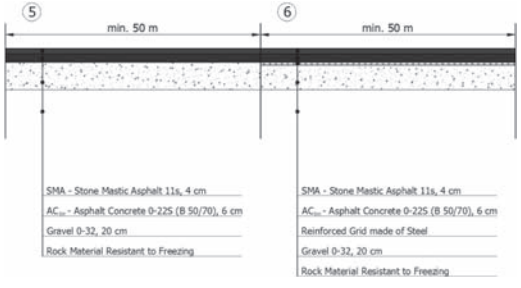

Figure 7. Test fields 5 and 6.

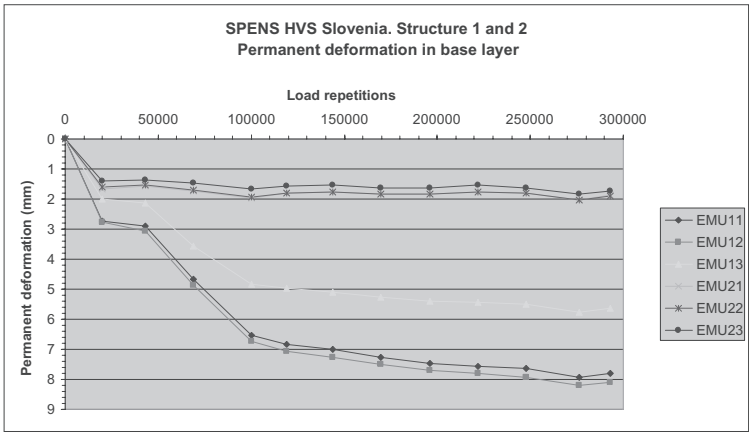

Figure 8. Propagation of permanent deflection in unbound gravel layer.

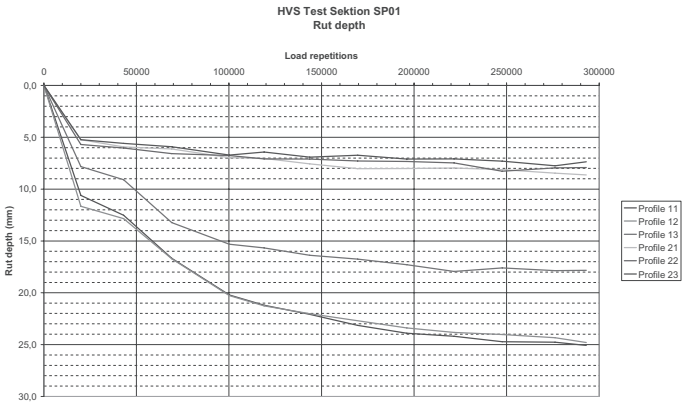

Figure 9. Propagation of permanent deformation (Rutting) on surface of test filed 1 and 2.

modified bitumen and asphalt mixes containing such bitumen will deepen existing knowledge about performance-related laboratory tests. In the field of high modulus asphalt mixes, the goal is not only the transfer of technology, but also the further development of similar materials.

REFERENCES

Blab R., Litzka J. & Girkinger P. 2002. *Verification of Pavement Structure Design on A2 Toll Motorway in Poland using Heavy Vehicle Simulator HVS NORDIC Mark IV.* Expertise for A2-Baudevelopment, Poznan, Poland.

Deacon J.A., Coplatz J.S., Tayebali A.A. & Monismith C.L. 2005. Temperature Considerations in Asphalt-Aggregate Mixture Analysis and Design, Transportation Research Record 1454.

Format: Final Technical Report, http://ec.europa.eu/transport/roadsafety_ library/publications/format_ final_report.pdf, 31.3.

Maccarone, S., Holleran, G. & Gnanaseelan, G.P. 1995. Rheological properties of polymer modified binders and relationship to performance. The rheology of bituminous binders, Eurobitume Rheology Workshop, Brussels.

Nicholls: BitVal—Analysis of Available Data for Validation of Bitumen Tests, http://bitval.fehrl.org/fileadmin/bitval/BitVal_final_report.pdf, 2006.

Odermatt N., Wiman L.G., Arm M. & Magnusson R. 2004. *Deformation of Unbound Pavement Materials—Heavy Vehicle Simulator and Cyclic Load Triaxial Test,* 2nd International Conference on Accelerated Pavement Testing, Minneapolis, Minnesota.

Philajamäki, J., Wiman, L.G. & Gustafson, K. 2002. *Full Scale Accelerated Tests,* REFLEX Final Report T4:02, EU Brite/Euram III RTD Programme Sybilski, D., Bańkowski, W., Maliszewski, M., Maliszewska, D., Mularzuk R. 2008. Evaluation of local and low quality aggregates in High Modulus Asphalt Concrete. Ljubljana, TRA.

Wiman, L.G., 2006. *Accelerated Load Testing of Pavements—HVS Nordic tests* at VTI *Sweden 2003–2004*. VTI report 544A, Swedish National Road and Transport Research Institute, Linköping, Sweden.

Wiman, L.G., 2008. Accelerated Load Testing of Roads—An Example of Trans-nationally Used Testing Equipment, Transport Research Arena Europe 2008.

Advanced Testing and Characterization of Bituminous Materials –
Loizos, Partl, Scarpas & Al-Qadi (eds)
© 2009 Taylor & Francis Group, London, ISBN 978-0-415-55854-9

Theoretical investigation of the stress distribution in a Bimodular IDT specimen

S. Katicha & G. Flintsch
Virginia Tech Transportation Institute, Blacksburg

ABSTRACT: It has been observed by a number of researchers that hot-mix asphalt (HMA) can exhibit different material properties in tension and compression. The indirect tension (IDT) test is used to determine HMA properties at low temperatures (creep compliance) or low to high temperatures (resilient modulus). Analysis of IDT test results is performed using linear elastic theory which is not adequate to account for possible differences between tensile and compressive HMA properties. In this paper, the stress distribution in a bimodular IDT specimen is determined based on the Ambartsumyan model for different compressive to tensile modulus ratios. Results show that tensile stresses throughout the specimen decrease with increasing modulus ratio while compressive stresses increase near the loading diameter and decrease away from the loading diameter with respect to the traditional solution.

1 INTRODUCTION

The difference between tensile and compressive properties of hot-mix asphalt (HMA) is well documented (Hargett & Johnson 1961, Monismith & Secor 1962, Secor & Monismith 1965, Kallas 1970, Kennedy et al. 1977, Lytton et al. 1993, Christensen & Bonaquist 2004). This difference is temperature dependent (Von Quintus et al. 1982, Bonaquist et al. 1986, Khanal & Mamlouk 1995). In this paper, the stress distribution in the indirect tension (IDT) specimen assuming different tensile and compressive moduli is determined. The effect of such an analysis on the interpretation of IDT test results can be found in (Katicha 2007, Katicha et al. 2008).

Materials that exhibit different tensile and compressive properties are referred to as bimodular materials (Tabaddor 1979, Curnier et al. 1995). Early investigation of bimodular materials go back to Sain-Venant (1864) and Timoshenko (1933). The extension of bimodular material response from the uniaxial state of stress to 2- and 3-dimensional cases started with the works of Ambartsumyan and his collaborators (Ambartsumyan 1965, Ambartsumyan & Khachartryan 1969) and was then pursued by a number of other authors (Shapiro 1966, Novak & Bert 1968, Green & Mkrtichian 1977, Spence & Mkrtichian 1977, Bert 1977, Jones 1977, Tabaddor 1979, Vjayakumar & Rao 1987, Sacco & Reddy 1992, and Curnier et al. 1995).

Curnier et al. (1995) remarked that some studies confused bimodular material behavior with anisotropy. To avoid such confusions, stress-strain relations are written in invariant forms (Tabaddor 1979, Shapiro 1966, Curnier et al. 1995). Two main approaches developed by Ambartsumyan (1965) and Curnier et al. (1995), have been proposed to develop the constitutive relationship of bimodular material. These are briefly presented in the following section.

2 CONSTITUTIVE MODELS

The main difficulty in modeling bimodular material response is to determine the criteria for modulus selection (tensile or compressive) in a multiaxial state of stress. While different approaches have been proposed, all have in common that the criteria should depend on invariants under change of reference axis. These are mainly the first second and third stress invariant

(I_1, I_2, I_3), and the principal stresses (σ_1, σ_2, σ_3). Two methods that have been proposed are presented in this paper; these are the conewise linear elastic model which is based on the first stress invariant, I_1, and the Ambartsumyan model which is based on the principle stresses.

2.1 *Conewise linear elastic model*

The conewise linear elastic model was developed by Curnier et al. (1995) for the general case of non-linear anisotropic materials. For the case of a linear isotropic material, the strain-stress and stress-strain relations written in tensor form are (Curnier et al. 1995):

$$\varepsilon_{ij} = \frac{1+\nu(\sigma_{kk})}{E(\sigma_{kk})}\sigma_{kl} - \frac{\nu(\sigma_{kk})}{E(\sigma_{kk})}\sigma_{kk}\delta_{ij} \tag{1}$$

$$\sigma_{ij} = \lambda(\varepsilon_{kk})\varepsilon_{kk}\delta_{ij} + 2G\varepsilon_{kl} \tag{2}$$

where, E = Young's modulus, v = Poisson's ratio, λ = bulk Lamé constant, G = shear modulus, δ_{ij} = Kronecker delta. Note that because the summation convention applies to repeated indices, $\sigma_{kk} = I_1$. Continuity of the shear modulus requires:

$$2G = \frac{E_c}{1+\nu_c} = \frac{E_t}{1+\nu_t} \tag{3}$$

In the IDT specimen, Hondros' stress distribution results in the first stress invariant to be negative (compressive) throughout the specimen and, therefore, the behavior of the conewise linear elastic material is the same as the behavior of a single modulus specimen with the modulus taken as the compressive modulus.

2.2 *Ambartsumyan model*

Ambartsumyan first expressed the stress-strain relation of a bimodular material under uniaxial loading as follows:

$$\varepsilon = \left[\frac{1}{E_t}U(\sigma) + \frac{1}{E_c}U(-\sigma)\right]\sigma \tag{4}$$

where,

$$U(\sigma) = \begin{cases} 0 & if \quad \sigma < 0 \\ 1 & if \quad \sigma > 0 \end{cases}$$

To expand this expression to 3-dimensional cases, certain restrictions to ensure agreement with the postulates of continuum mechanics are imposed. As stated by Tabaddor (1979) these restrictions are:

1. The modulus of bimodular materials is a step function of the stress or strain state. It should be able to assume two different values depending on the sign of the argument.
2. The constitutive equations should reduce to those of classical elastic materials in the stress states of all tension or all compression.
3. The constitutive equations should be in agreement with postulates of continuum mechanics.
4. There exists a strain energy function which assumes different forms depending on the multiaxial stress state. The symmetry of the compliances follows from the existence of the strain energy function.
5. The bimodular coefficients must satisfy certain inequalities for the strain energy to be positive definite.

The stress-strain relation in the three-dimensional case can be expressed similarly to the expression in Equation 1 in tonsorial form as follows:

$$\varepsilon_{ij} = S_{ijkl}\sigma_{kl} \tag{5}$$

where, $S_{ijkl} = S^t_{ijkl}U\left[f(\sigma)\right] + S^c_{ijkl}U\left[-f(\sigma)\right]$, S_{ijkl} = compliance, S^t_{ijkl} = tensile compliance, and S^c_{ijkl} = compressive compliance. One model for f proposed by Ambartsumyan (1965) is to take the function equal to the principal stress as follows:

$$f(\sigma) = \sigma_p \tag{6}$$

where, σ_p = principal stress (σ_1, σ_2 or σ_3). This means that the appropriate compliance values in each of the principal stress directions are selected based on the sign of the principal stress. For a 2-dimensional plane stress condition, the stress-strain relationship expressed in the coordinates of the principal stress directions is therefore written as follows:

$$\varepsilon_1 = \frac{1}{E_1}\sigma_1 - \frac{\nu_2}{E_2}\sigma_2 \tag{7}$$

$$\varepsilon_2 = \frac{1}{E_2}\sigma_2 - \frac{\nu_1}{E_1}\sigma_1 \tag{8}$$

where, the indices 1 and 2 refer to the principal stress directions. The modulus and Poisson's ratio are selected in accordance with the sign of the corresponding principle stress. For example for the case of $\sigma_1 > 0$ (tension) and $\sigma_2 < 0$ (Compression), the equations become:

$$\varepsilon_1 = \frac{1}{E_t}\sigma_1 - \frac{\nu_c}{E_c}\sigma_2 \tag{9}$$

$$\varepsilon_2 = \frac{1}{E_c}\sigma_2 - \frac{\nu_t}{E_t}\sigma_1 \tag{10}$$

where t is a subscript indicating tension and c is a subscript indicating compression. In the case where the principal stresses are either compressive or tensile, the equations reduce to that of a single modulus material with either the tensile or compressive modulus. Although Equations 10 and 11 suggest that four material constants need to be determined, the symmetry of the compliance matrix (condition 4) expressed in Equation 12 ensures that only three are independent (Tabaddor, 1979).

$$\frac{\nu_t}{E_t} = \frac{\nu_c}{E_c} \tag{11}$$

2.3 *Plane stress constitutive equation*

Because for the IDT specimen, the conewise linear elastic model for bimodular materials predicts the same behavior as a single modulus material, the stress strain relationships developed in this section are based on the Ambartsumyan model. The stress strain relationships are developed for an arbitrary reference frame (x–y). Denote by σ_2, the smaller principal stress, by σ_1 the larger principal stress, and by θ the angle measured from the x-axis to the principal stress direction σ_1. The stresses in the x and y directions can be determined from the principal state of stress according to the stress transformation formulae as:

$$\sigma_{xx} = \sigma_1 \cos^2\theta + \sigma_2 \sin^2\theta \tag{12}$$

$$\sigma_{yy} = \sigma_2 \cos^2\theta + \sigma_1 \sin^2\theta \tag{13}$$

$$\sigma_{xy} = -\sigma_1 \sin\theta\cos\theta + \sigma_2 \sin\theta\cos\theta \tag{14}$$

If we assume that the principal stress and principal strain directions coincide, the strains can be transformed according to the following equations:

$$\varepsilon_{xx} = \varepsilon_1 \cos^2\theta + \varepsilon_2 \sin^2\theta \tag{15}$$

$$\varepsilon_{yy} = \varepsilon_2 \cos^2\theta + \varepsilon_1 \sin^2\theta \tag{16}$$

$$\varepsilon_{xy} = -\varepsilon_1 \sin\theta\cos\theta + \varepsilon_2 \sin\theta\cos\theta \tag{17}$$

Substituting Equation 7 and Equation 8 into Equations 15 through 17 and using the stress transformation formulae (Equations 12 to 14), the strain-stress relationship can be expressed as:

$$\varepsilon_{xx} = \frac{1}{E_1}\sigma_{xx} - \frac{\nu_2}{E_2}\sigma_{yy} + \frac{E_1 - E_2}{E_1 E_2}\sigma_2 \sin^2\theta \tag{18}$$

$$\varepsilon_{yy} = \frac{1}{E_2}\sigma_{yy} - \frac{\nu_1}{E_1}\sigma_{yy} + \frac{E_2 - E_1}{E_1 E_2}\sigma_1 \sin^2\theta \tag{19}$$

The relationship between the shear stress and shear strain can be obtained using a similar approach:

$$\varepsilon_{xy} = \left[\frac{\sigma_{xx} + \sigma_{yy}}{2\sqrt{\left(\sigma_{xx} - \sigma_{yy}\right)^2 + 4\sigma_{xy}^2}} \left(\frac{1}{E_1} - \frac{1}{E_2} \right) + \frac{1}{2}\left(\frac{1}{E_1} + \frac{1}{E_2} \right) - \frac{\nu_1}{E_1} \right] \sigma_{xy} \tag{20}$$

If the principal stresses are all positive or negative, Equations 18, 19 and 20 reduce to the case of a single modulus material. Using the 2-dimensional (plane stress) stress-strain relationship of the bimodular material, the stress distribution in the IDT specimen can be obtained by solving the equations of continuum mechanics.

3 IDT BIMODULAR SOLUTION PROCEDURE

3.1 *Formulation*

Finding the stress distribution in a solid subjected to external loads is mathematically posed as a boundary value problem (BVP). The BVP can be expressed in terms of partial differential equations or integral equations. It is often very difficult, if not impossible, to obtain the exact analytic solution to the BVP and the problem is often solved using one of the different numerical methods that are available to obtain an approximate solution which can be quite satisfactory.

In this approach, a system of equations comprised of the equilibrium equations, the strain compatibility equations, and the imposed boundary conditions is solved. For 2-dimensional problems, neglecting body forces, these equations can be mathematically expressed as follows (Washizu, 1982):

$$\frac{\partial \sigma_{xx}}{\partial x} + \frac{\partial \sigma_{xy}}{\partial y} = 0 \tag{21}$$

$$\frac{\partial \sigma_{yy}}{\partial y} + \frac{\partial \sigma_{xy}}{\partial x} = 0 \tag{22}$$

$$\frac{\partial^2 \varepsilon_{xx}}{\partial y^2} + \frac{\partial^2 \varepsilon_{yy}}{\partial x^2} - \frac{\partial^2 \varepsilon_{xy}}{\partial x \partial y} = 0 \tag{23}$$

Subject to the boundary conditions,

$$\begin{aligned} \sigma_{xx} l + \sigma_{xy} m &= \bar{t}_x \\ \sigma_{xy} l + \sigma_{yy} m &= \bar{t}_y \end{aligned} \quad \text{on } C_1 \tag{24}$$

$$\begin{aligned} u_x &= \bar{u}_x \\ u_y &= \bar{u}_y \end{aligned} \quad \text{on } C_2 \tag{25}$$

where, l, m = direction cosines, $\bar{t}$ = prescribed tractions, $\bar{u}$ = prescribed displacements, C_1 = part of the boundary where tractions are prescribed, and C_2 = part of the boundary where displacements are prescribed

To solve for the stress field, the equilibrium Equations 21 and 22 can be satisfied by expressing the stresses in terms of the Airy stress function $F(x,y)$ such that

$$\sigma_{xx} = \frac{\partial^2 F(x,y)}{\partial y^2}, \quad \sigma_{yy} = \frac{\partial^2 F(x,y)}{\partial x^2}, \quad \sigma_{xy} = -\frac{\partial^2 F(x,y)}{\partial x \partial y} \tag{26}$$

The strains can be expressed in terms of the stresses and therefore the Airy stress function through the constitutive stress-strain relationship. The problem then reduces to finding the Airy stress function that satisfies Equation 23 subject to the boundary conditions in Equations 24 and 25. As it is analytically difficult to determine the exact stress function, an alternative is to express it as a sum of a function $F_0(x,y)$ that satisfies the boundary conditions, and a linear combination of basis functions $F_i(x,y)$ whose tractions vanish at the boundaries as follows:

$$F(x,y) = F_0(x,y) + \sum_{i=1}^{n} a_i F_i(x,y) \tag{27}$$

The conditions for the tractions of the basis functions to vanish at the boundaries can be expressed as follows (Washizu, 1982):

$$F_i(x,y) = 0, \quad \frac{\partial F_i(x,y)}{\partial x} = 0, \quad \frac{\partial F_i(x,y)}{\partial y} = 0 \quad \text{on } C \tag{28}$$

The coefficients a_i of the basis functions are determined using one of the methods of weighted residuals of which the Galerkin method (which is the method of choice for the finite element method (FEM) formulation) and some of the meshless methods (element free Galerkin method and meshless local Petrov-Galerkin method) are most often used. This comes down to finding the solution for the following n integral equations:

$$\iint_S \left(\frac{\partial^2 \varepsilon_{xx}}{\partial y^2} + \frac{\partial^2 \varepsilon_{yy}}{\partial x^2} - \frac{\partial^2 \varepsilon_{xy}}{\partial x \partial y} \right) F_i(x,y)\, dx dy = 0 \tag{29}$$

Solving the system of n equations in the n unknowns represented in Equation 29 is fairly easy; the most difficult part of the problem is to determine the appropriate functions $F_0(x,y)$ and $F_i(x,y)$.

3.2 *Stress function*

Since the boundary conditions for the bimodular IDT specimen are the same as the boundary conditions for the IDT specimen of a single modulus material, $F_0(x,y)$ can be taken as the stress function of either Hertz's or Hondros' solution. The stress distribution is therefore obtained from Equation 30 as follows:

$$\begin{aligned}
\sigma_{xx}(x,y) &= \sigma^0_{xx}(x,y) + \sum_{i=1}^{n} a_i \frac{\partial^2 F_i(x,y)}{\partial y^2} \\
\sigma_{yy}(x,y) &= \sigma^0_{yy}(x,y) + \sum_{i=1}^{n} a_i \frac{\partial^2 F_i(x,y)}{\partial x^2} \\
\sigma_{xy}(x,y) &= \sigma^0_{xy}(x,y) - \sum_{i=1}^{n} a_i \frac{\partial^2 F_i(x,y)}{\partial x \partial y}
\end{aligned} \tag{30}$$

where, σ^0_{xx}, σ^0_{yy}, σ^0_{xy} = stresses obtained from the solution of a single modulus material (Hondros, 1959).

The basis functions $F_i(x,y)$ are taken as orthogonal polynomials on the unit disk to improve the numerical computations. Early investigation of the IDT stress distribution in the bimodular material suggest that the stresses at the specimen boundary are equal to the stresses at the boundary of a single modulus IDT specimen which are equal to zero. Therefore, in our calculations, we will assume that the stresses in the bimodular material at the specimen boundary are equal to the stresses in the single modulus material to increase the numerical solution's rate of convergence. The basis functions for an IDT specimen of unit radius are therefore expressed in the following form:

$$F_i(x,y) = \left(1 - x^2 - y^2\right)^3 P_i(x,y) \tag{31}$$

where,

$P_i(x,y)$ = polynomial basis.

Note that the obtained basis is complete in the space of continuous and infinitely differentiable functions that vanish along with their first and second derivatives on the boundary of the unit disk B^2: = $[(x,y) : x^2 + y^2 = 1]$. A basis of polynomials that are orthogonal with respect to the weight function of Equation 32 is presented in Equation 33 (Dunkl and Xu, 2001).

$$W_\mu(x,y) = \left(1 - x^2 - y^2\right)^{\mu - 1/2} \quad \mu \geq 1/2 \tag{32}$$

$$P^n_k(x,y) = C^{k+\mu+1/2}_{n-k}(x)\left(1 - x^2\right)^{\frac{k}{2}} C^\mu_k\left(\frac{y}{\sqrt{1 - x^2}}\right) \tag{33}$$

where C^λ_n are the Gegenbauer polynomials which are orthogonal with respect to $(1 - x^2)^{\lambda - 1/2}$ on [–1, 1].

4 RESULTS

4.1 *Iterative solution procedure*

As presented in the derivation of the constitutive equations of the Ambartsumyan material, the stress-strain constitutive relationship is a function of the principal stresses' values and directions, which are not known a priori. The stress distribution was therefore obtained through an iterative procedure. In the first iteration, the stress distribution is calculated with principal stresses obtained from Hondros' solution. In subsequent iterations, the principal stresses are updated to the values obtained at the previous iteration. The procedure is

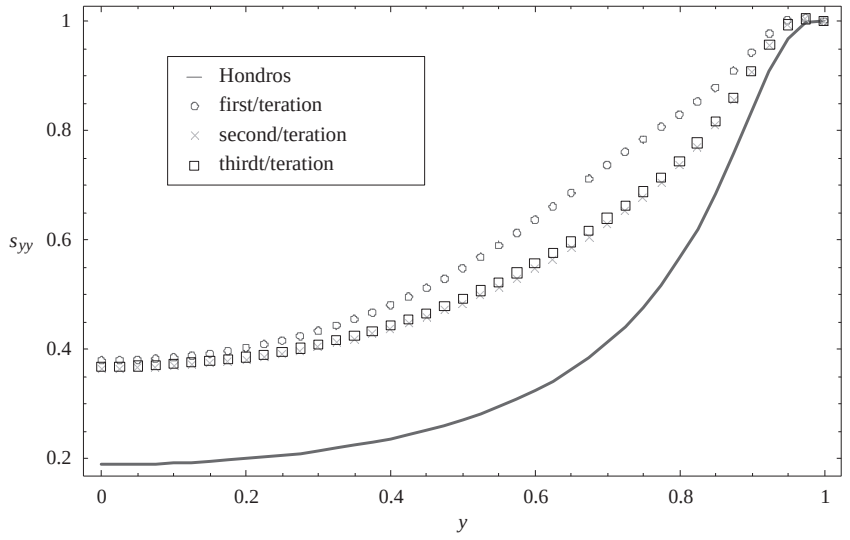

Figure 1. Vertical stress along the vertical diameter.

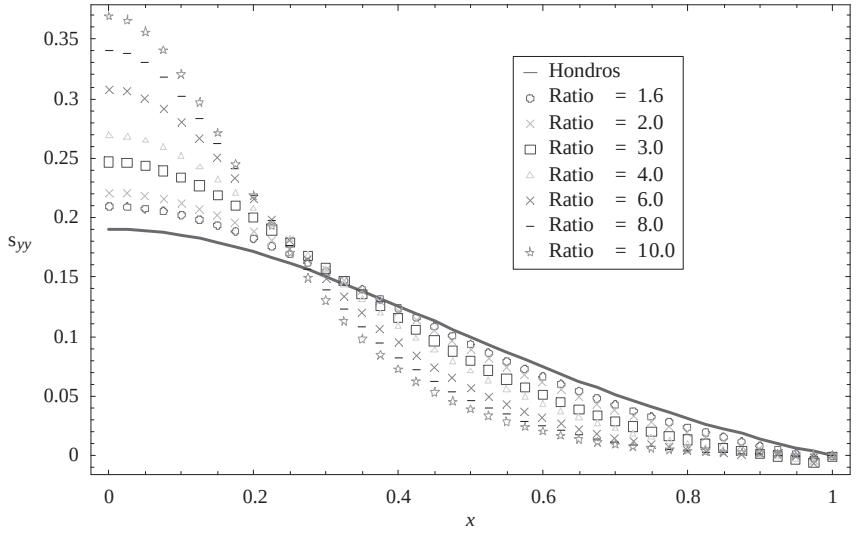

Figure 2. Vertical stress along the horizontal diameter.

repeated until acceptable convergence is achieved. In general, the number of iterations to achieve convergence increases as the modulus ratio increases. It was found that three iterations were sufficient to achieve convergence as shown in Figure 1 for the vertical stress along the vertical diameter.

4.2 *Solution for different modulus ratio*

This section presents the results of the calculation of the stress distribution in an Ambartsumyan bimodular IDT specimen for different compressive to tensile modulus ratios. The numerical input values were $p = 1$, $\alpha = 0.1$, $P = p$, $\alpha = 0.1$, $R = 1$. The problem is independent of the modulus (it only depends on the modulus ratio) or Poisson's ratio, and therefore

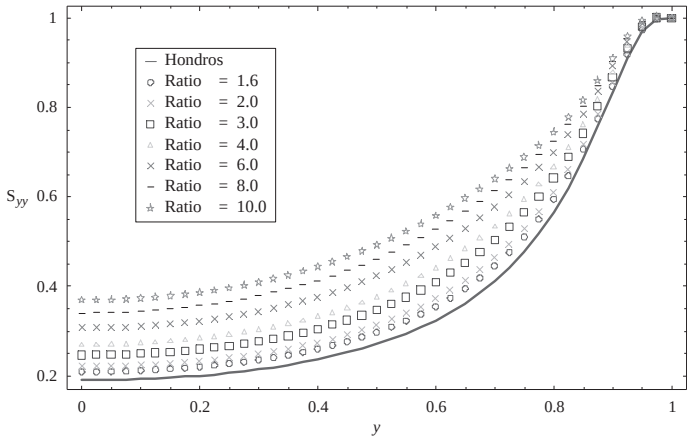

Figure 3. Vertical stress along the vertical diameter.

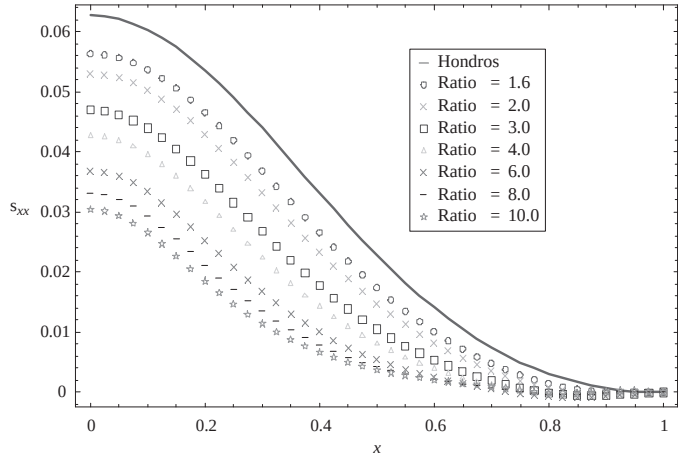

Figure 4. Horizontal stress along the horizontal diameter.

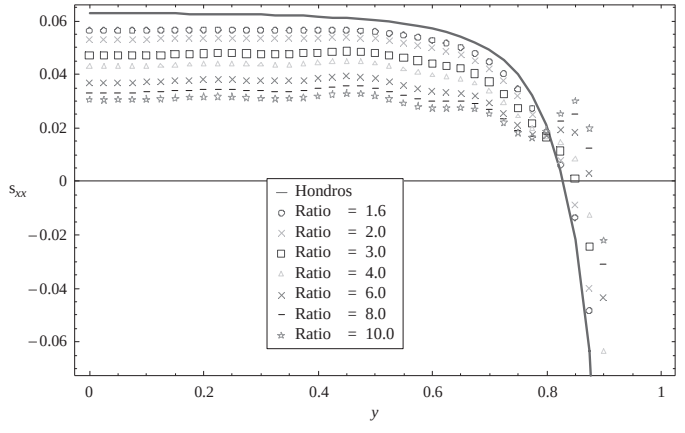

Figure 5. Horizontal stress along the vertical diameter.

no values for these parameters are needed to obtain the stress distribution. Modulus and Poisson's ratio values are, however, needed to determine the strain.

The results are presented in Figures 2–5. As expected, the compressive vertical stress σ_{yy} in the center of the specimen increased and the tensile horizontal stress at the same location decreased as the modulus ratio increased. Compared to Hondros' solution, the vertical stress distribution along the horizontal axis increased near the center of the specimen and up to a certain distance, then decreased all the way to the edges of the specimen so that to maintain equilibrium conditions, the area under the stress distribution is the same. To verify equilibrium, the area under the vertical stress distribution curve was numerically calculated for all modulus ratios using the trapezoidal rule. All the areas were found to equal the area obtained from Hondros' solution, which is equal to half the applied load, within 0.06% error. The distance where the transition from increasing stress to decreasing stress occurs depends on the compressive-to-tensile modulus ratio.

5 CONCLUSION

This paper presented a continuum-based approach to determine the bimodular stress distribution in the IDT specimen. The approach followed was to satisfy the equilibrium equation and determine the coefficients of basis functions of the stress function expansion to reduce the error of the strain compatibility equation. This approach was selected because the boundary conditions are easily satisfied by incorporating Hondros' stress distribution as part of the solution. The results obtained show that:

1. Tensile stresses throughout the specimen decrease as the compressive to tensile modulus increases.
2. Compressive stresses near the vertical diameter (loading diameter) increase as the compressive to tensile modulus increases.
3. Compressive stresses away from the vertical diameter decrease as the compressive to tensile modulus increases. This shows that with relatively small tensile modulus compared to the compressive modulus, the ability of the material to distribute stresses throughout the specimen and away from the loading diameter is reduced (i.e. stresses are concentrated along the loading diameter).

The bimodular behavior of HMA results from the fact that it is a composite material comprising of aggregates and binder (plus air voids). Therefore, the continuum approach presented in this paper is an approximation of the discrete behavior that causes different response in tension and compression. The next step to validate the presented continuum approximation would be to determine the response of the IDT specimen using a discontinuum based approach such as the discrete element method (DEM).

REFERENCES

Ambartsumyan, S.A., (1965), "The axisymmetric problem of circular cylindrical shell made of materials with different stiffness in tension and compression," *Izv. Akad. Nauk. SSR Mekh.* 4, 77–85.

Ambartsumyan, S.A., and Khachartryan, A.A., (1969) "Basic equations and relations of the different modulus theory of elasticity of an anisotropic body," *Mechanics of Solids*, 4, 48-56.

Bert, C.W.(1977) "Model for fibrous composites with different properties in tension and compression" *J. of Eng. Mat. And Tech*. 99, 344–349.

Christensen, D.W., and Bonaquist, R.F., (2004) "Evaluation of indirect tensile test (IDT) procedures for low-temperature performance of hot mix asphalt," NCHRP Report 530.

Curnier, A., He, Q., and Zysset, P., (1995) "Conewise linear elastic materials," *Journal of Elasticity* 37, 1–38.

Dunkl, C.F., and Xu, Y., (2001) *Orthogonal polynomials of several variables*, Cambridge University Press.

Green, A.E., and Mkrtichian, J.Z., (1977) "Elastic solids with different moduli in tension and compression" *Journal of elasticity*. 7, 369–386.

Hargett, E.R., and Johnson, E.E., (1961) "Strength properties of bituminous concrete tested in tension and compression," *Highway Research Record*, 40, 430–440.

Hondros, G., (1959) "Evaluation of Poisson's ratio and modulus of materials of low tensile resistance by the Brazilian (indirect tension) test with particular reference to concrete," *Australian Journal of Applied Science*, 10, 243–268.

Jones, R.M., (1977) "Stress-strain relations for materials with different moduli in tension and compression" *AIAA Journal*. 15, 16–23.

Kallas, B.F., (1970) "Dynamic modulus of asphalt concrete in tension and tension compression," *Journal of the Association of Asphalt Paving Technologists*, 39, 1–23.

Katicha, S.W., (2007) *Analysis of hot-mix asphalt (HMA) linear viscoelastic and bimodular properties using uniaxial compression and indirect tension (IDT) tests*, PhD dissertation, Virginia Polytechnic Institute and State University, Blacksburg VA.

Kennedy, T.W., Haas, R., (1977) "Smith, P., Kennepohl, G.A., and Hignel, E.T., Engineering evaluation of sulfur-asphalt mixtures," *Transportation Research Record*, 659, 12–17.

Khanal, P.P., and Mamlouk, M.S., (1995) "Tensile versus compressive moduli of asphalt concrete," *Transportation Research Record*, 1492, 144–150.

Lytton, R.L., Uzan, J., Fernando, E.G., Roque, R., Hiltunen, D., and Stoffels, S.M., (1993) *Development and Validation of Performance Prediction Models and Specifications for Asphalt Binders and Paving Mixes*, Strategic Highway Research Program (SHRP-A-357), National Research Council, Washington, DC.

Monosmith, C.L., and Secor, K.E., (1962) "Viscoelastic behavior of asphalt concrete pavements," *Proceedings of the International Conference on the Structural Design of Asphalt Pavements*, Ann Arbor, Michigan, 476–498.

Novak, R.C., and Bert, C.W., (1968) "Theoretical and experimental basis for more precise elastic properties of epoxy" Journal of Composite Materials, 2, 506–508.

Sacco, E., and Reddy, J.N., (1992) "A constitutive model for bimodular materials with an application to plate bending" *Journal of Applied Mechanics*, 59, no. 1, 220–221.

Secor, K.E., and Monismith, C.L., (1965) "Viscoelastic response of asphalt paving slabs under creep loading," *Highway Research Record*, 67, 84–97.

Shapiro, G.S., (1966) "Deformation of bodies with different tension and compression stiffnesses" *Mechanics of Solids*, 1, 85–86.

Spence, D.A., and Mkrtichian, J.Z., (1977) "The Boussinesq problem for a material with different moduli in tension and compression" *Journal of Mechanics and Applied Mathematics*, 30, 449-466.

Tabaddor, F., (1979) "A survey of constitutive equations of bimodular elastic materials," *ASME Conference on Mechanics of Bimodular Materials*, 1–15.

Underwood, S., Heidari, A.H., Guddati, M., and Kim, Y.R., (2005) "Experimental investigation of anisotropy in asphalt concrete," *Proceedings of the transportation research board*, CD-ROM.

Vjayakumar, K., and Rao, K.P., (1987) "Stress-strain relations for composites with different stiffnessses in tension and compression" *Comp. Mech*. 2, 167–175.

Von Quintus, H.L., Rauhut, J., and Kennedy T., (1982) "Comparisons of asphalt concrete stiffness as measured by various testing techniques," *Journal of the Association of Asphalt Paving Technologists*, 51, 35–49.

Washizu, K., (1982) *Variational methods in elasticity and plasticity*, Pergamon Press Ltd, Oxford.

Advanced Testing and Characterization of Bituminous Materials –
Loizos, Partl, Scarpas & Al-Qadi (eds)
© 2009 Taylor & Francis Group, London, ISBN 978-0-415-55854-9

Investigation of Alkali-Silica Reaction in asphalt mixtures exposed to potassium acetate deicing solution

A.K. Apeagyei, L.J. Struble & W.G. Buttlar
University of Illinois at Urbana-Champaign Urbana, Illinois, USA

ABSTRACT: When certain aggregates containing silica react with a highly alkaline solution, an alkali-silica gel may form, e.g., 'Alkali-Silica Reaction (ASR)'. This gel may subsequently expand in the presence of moisture, causing wide-spread cracking in structures composed of these materials. Although the mechanisms and manifestation of ASR in portland cement concrete pavements and structures has been extensively documented over the past several decades, the possibility of ASR formation in asphalt concrete mixtures has received little attention until recently. In this study, asphalt mixtures were tested to determine whether alkali-silica reaction occurs in asphalt containing reactive aggregate and calcium hydroxide when exposed to potassium acetate deicing solution. Two aggregates: ottawa sand (non-reactive aggregate) and fused silica (reactive aggregate) were investigated. Various soaking solutions were studied, including: water, sodium hydroxide solution, and potassium acetate solution saturated with calcium hydroxide. Samples were conditioned at 80°C for 7 days. Compelling evidence of alkali-silica reaction in mixtures containing the fused silica was observed, including: 1) gel formation in mixtures conditioned in the potassium acetate plus calcium hydroxide solution; 2) expansion and surface cracking in mixtures conditioned in the sodium hydroxide solution, and; 3) decreased fracture energy of mixtures conditioned in a sodium hydroxide or potassium acetate plus calcium hydroxide solution. Additional testing and field validation is still needed to fully understand the practical implications of ASR formation in asphalt mixtures and, if needed, to develop appropriate material specifications to avoid problems associated with ASR formation.

1 INTRODUCTION

This paper presents results of tests conducted to investigate the possibility of alkali-silica reaction (ASR) in asphalt mixtures containing reactive aggregate exposed to potassium acetate deicing solution. Mixtures were tested using a portland cement mortar bar test (ASTM 1260-07) and an asphalt concrete fracture energy test (ASTM D7313-07b).

Alkali-silica reaction occurs in portland cement concrete when certain aggregates containing silica react with a highly alkaline solution. The reaction results in the formation of an alkali-silica gel, which may expand in the presence of moisture and cause expansion and cracking of concrete. The alkaline solution is usually produced during hydration of portland cement with high alkali content (sodium and potassium). Alkali-silica reaction is widely acknowledged as an important mechanism for distress development in portland cement concrete pavements.

Potassium acetate (KAc) deicers have been approved for use on US airfields since the early 1990s. The deicer is a very concentrated aqueous solution, about 6 M. A recent study (Ai and Struble 2008) showed the pH of a typical potassium acetate deicing solution to be about 10; however, when mixed with calcium hydroxide the pH increased to more than 14. The solution has been shown to trigger alkali-silica reaction in portland cement concretes made using reactive aggregates.

Concerns have also being raised about the possible occurrence of ASR in asphalt concrete pavements. Potassium acetate deicers are used extensively on asphalt airfield pavements.

Thus, if the asphalt pavement contains reactive aggregate and some source of hydroxide ions, such as calcium hydroxide that is commonly used as an anti-stripping admixture in asphalt, then ASR is conceivable. The objective of this study was to determine whether such a reaction is possible in asphalt.

ASTM C1260-07 is the standard test method for evaluating ASR in Portland cement concrete. The test involves immersing a mortar bar in 1-M NaOH solution maintained at 80°C for at least one week and measuring expansion of the bar. A bar extension after 16 days of 0.1% or more indicates possible deleterious ASR reaction.

Few studies have been conducted to study the effect of deicing chemicals in asphalt pavements (Farha et al. 2002, Hassan et al. 2002, Alatyppö and Valtonen 2007, AAT 2007). Most of these studies used versions of AASHTO T283, a standard test method for evaluating moisture damage in asphalt mixtures. Expansion caused by ASR was not evaluated in these studies.

Farha et al. (2002) studied the effect of four deicing solutions on airfield asphalt concrete. Asphalt cores from existing airfield pavements were immersed in solutions including urea, sodium formate, potassium acetate, sodium acetate, and distilled water. They were subjected to 15 freeze-thaw cycles (freezing temperature –20ºC to –40ºC) followed by 40 wet-dry cycles at 40ºC. Damage caused by the various deicers were evaluated using weight loss, tensile strength, elastic modulus, penetration of recovered asphalt binder, and gradation of recovered aggregates. The results of the study indicated that the deicers caused no significant changes in tensile strength, elastic modulus, binder penetration, and aggregate gradation.

Alatyppö and Valtonen (2007) reported on a study of damage in several Scandinavia airports that recently started using acetates and formates as airfield deicers. The study involved both laboratory and field testing. Tests comprised various conditioning methods including boiling of binders and mixtures. The effect of the deicing solutions on the asphalt binder was evaluated using gas chromatography and indicated no significant changes occurred as a result of the deicers. Tensile strength of the asphalt mixtures was not significantly affected by the deicers.

Preliminary results of an on-going study sponsored by Airfield Asphalt Pavement Technology Program (AAPTP) suggest that acetate and formate deicers may produce damage on hot-mix asphalt pavements (AAT 2007). The study used an ultrasonic horn test, a modification of AASHTO T-283 and a long-term durability test they developed. During the ultrasonic test, pit depths were measured with an ultrasonic horn placed on vacuum saturated compacted asphalt samples that were heated at 60ºC for 24 hours. The results indicated no statistically significant difference in pit depth between the various deicers. Using the modified AASHTO T-283 test, it was found that tensile strength ratio was effective in distinguishing damage in some aggregates but not in others. The study also indicated softer binders are more susceptible to damage than harder ones. Measurement of weight loss of aggregates measured in the study indicated that damage caused to asphalt mixtures by deicing solutions is not related to aggregate degradation.

The key objective of this study was to determine whether ASR can occur in asphalt pavement mixtures treated with potassium acetate deicer. The study was limited to laboratory prepared asphalt mixtures. Samples were conditioned according to the standard ASTM C 1260, but using immersion in NaOH or potassium acetate plus calcium hydroxide. It should be noted that to control stripping in asphalt concrete pavements, 1–2% hydrated lime by weight of mix is sometimes added to wet aggregate (moisture content 3%) during hot-mix asphalt production. In addition to expansion testing, fracture energy testing was conducted on treated and untreated samples as a way to assess the effect of the deicing solution on the mode I fracture resistance of the mixture.

2 EXPERIMENTAL PROCEDURE

An experimental design was developed, which consisted of four conditioning methods (NaOH solution, KAc solution plus $Ca(OH)_2$, distilled water, and dry) and two sands (fused

silica glass, known to be reactive, and ottawa sand, known to be non reactive). A single asphalt mixture was used. More details on the experimental methods used are provided in the following sections.

2.1 *Materials*

The conditioning solutions were selected to provide control solutions, one that would produce ASR and one that would not produce ASR, and to explore whether potassium acetate deicing solution would produce ASR. The sodium hydroxide solution was used as a control to produce ASR. This is the solution used in the standard test ASTM C 1260. The 1-M solution was prepared using reagent grade sodium hydroxide (NaOH) pellets from Fisher Scientific. Distilled water and air drying were used as control cases where ASR was not expected to be produced. Finally, a potassium acetate deicing solution was used to determine whether it can cause ASR in asphalt concrete. This solution was obtained from CRYOTEC Deicing Technology (Cryotec E36 Liquid Runway Deicer). According to the manufacturers, the pH of this deicer is 11. Past work has shown that very high pH (>13.8) is essential for ASR, and past work at the University of Illinois has shown that the deicing solutions generally carry a high pH only when there is a significant source of hydroxide ions present. Calcium hydroxide [$Ca(OH)_2$], obtained from Fisher Scientific, was therefore added to the potassium acetate deicing solution at a saturation level to enable ASR.

The standard mortar bar test for evaluating ASR in portland cement concrete is performed at a temperature of 80°C. Typical asphalt binders used in Illinois may be too soft to be conditioned at 80°C without damaging the specimen. Therefore a PG 82-22 performance-graded asphalt binder was selected. A PG 82-22 binder can be employed in the field where pavement temperatures ranging from –22°C to 82°C are expected. The performance-graded polymer-modified asphalt PG 82-22 was supplied by SemMaterials, Tulsa, OK. The same asphalt binder content of 8% by weight of total mix was used in all of the fine-graded asphalt mixtures.

A 4.75 mm nominal maximum sized aggregate gradation was used in all of the mixtures, which represents a fine-grained mixture. The gradation is similar to Illinois Department of Transportation (IDOT) gradation for interlayer pavement used to control reflective cracking, containing manufactured sand, natural sand and mineral filler. This fine mix was chosen because it was felt it contained similar levels of "mortar" (asphalt mastic) as the cement mortar used in ASTM 1260-07 For this study, the natural sand components of the IDOT mix were replaced with either ottawa sand (to produce a non reactive mix) or fused silica glass (to produce a reactive mix). A blend of 80.4% by weight manufactured sand (IDOT designation FM-20), 18.1% by weight ottawa sand, and 1.5% mineral filler was used. The blend for the fused silica mix was a mixture of 80.4% FM-20, 18.1% fused silica, and 1.5% mineral filler. Table 1 provides the gradations of the final blends. Fused Silica (CAS # 60676-86-0) was obtained from a local supplier (C-E Minerals). Ottawa sand (CAS # 14808-60-7) is a standard graded (ASTM C778) and was obtained from US Silica.

2.2 *Preparation of compacted asphalt mixtures*

Mixing of hot asphalt and hot blended aggregate was performed at 185ºC while compaction was carried out at 155ºC. Initially, twenty-four mixtures were compacted in a SUPERPAVE gyratory compactor, while two mixtures were kept uncompacted for maximum specific gravity determination. An IPC (Industrial Process Company) SUPERPAVE Gyratory Compactor was used.

To ensure consistent air voids levels, all the samples were compacted to the same height, 130 mm, in the standard 150 mm diameter compaction mold. After compaction, mixture volumetrics including air void levels and percent absorption were determined. The maximum specific gravities of the mixtures were determined as 2.337 and 2.399 for fused silica and ottawa sand mixtures, respectively. Table 2 provides a summary of the mixture volumetric properties.

Table 1. Gradations of ottawa sand and fused silica used.

	Passing (%)	
Sieve Size	Ottawa sand blend	Fused silica blend
9.5 mm	100.0	100.0
4.75 mm (No. 4)	99.2	99.2
2.36 mm (No. 8)	76.8	63.3
1.18 mm (No. 16)	51.8	38.3
0.60 mm (No. 30)	36.3	23.2
0.30 mm (No. 50)	15.5	13.7
0.15 mm (No. 100)	8.1	7.7
0.075 mm (No. 200)	6.5	6.3

Table 2. Air void and water absorption (AASHTO T166) for ottawa sand and fused silica mixtures.

Aggregate	Specimen ID	Air voids (%)	Water absorption (%)
Fused silica	FS1	4.60	0.12
	FS2	6.90	0.19
	FS3	6.80	0.25
	FS4	4.50	0.19
	FS5	5.10	0.16
	FS6	4.30	0.10
Ottawa sand	OS1	7.30	0.96
	OS2	8.80	1.26
	OS3	7.00	0.63
	OS4	6.80	0.74
	OS5	6.90	0.64
	OS6	7.80	1.00

Interestingly, compacted mixtures containing Fused Silica appear to show significantly lower levels of water absorption (0.17%) compared with the Ottawa sand mix (0.87%). Inspection of Table 1 shows the ottawa sand blend is finer than the fused silica. Since the only difference between the two blends are ottawa sand and fused silica, any differences in air voids content and water absorption could be attributed to the constituents of ottawa sand (>99% quartz) and fused silica (>99% silica).

2.3 *Conditioning*

Soon after determining the bulk specific gravities and water absorption of the compacted specimens, two 150 mm diameter by 50 mm thick specimens were cut from each 150 mm diameter by 130 mm thick gyratory compacted mixture to produce 24 samples. A carbide-tipped water-cooled saw was used to fabricate the beam and disk-shaped compact tension test samples. The 24 cut samples were then subjected to the various conditioning regimes listed in Table 3. Specimens were conditioned in 1-M NaOH solution to study expansion potential of the mixtures.

The conditioning procedure followed a version of the standard test method for potential alkali reactivity of aggregates (ASTM C 1260-07). Samples conditioned in KAc + $Ca(OH)_2$ solution were vacuum saturated, immersed in solution, and stored in an oven for 7 days at 80ºC. The samples treated with NaOH were not vacuum-treated before storing because the containers used for vacuum saturation were constructed of aluminum, which may not be compatible for use with the NaOH solution. But they were also stored in an oven for 7 days at 80°C. Samples conditioned in water were also vacuum saturated, immersed, and stored

Table 3. Experimental design for specimen conditioning.

Asphalt binder	Aggregate	Treatment NaOH	KAc + $Ca(OH)_2$	Water	Dry
PG 82-22	Fused silica	3	3	3	3
	Ottawa sand	3	3	3	3

in an oven for 7 days at 80°C. The dry samples were simply air dried and stored at room temperature.

2.4 *Expansion*

Three cylindrical specimens of the fused silica mixture conditioned in 1-M NaOH solution for 7 days at 80°C were tested for expansion. The cylindrical specimens measured 150 mm in diameter and 50 mm in thickness. Three block specimens of the fused silica mixture conditioned in 1-M NaOH solution for 7 days at 80°C were also tested for expansion. These blocks measured about 80 mm in length, 50 mm in depth, and 25 mm in thickness. In both cases, the length in each dimension was measured using a Vernier caliper.

2.5 *DC(T) fracture energy testing*

After conditioning, specimens were prepared for the DC(T) fracture energy testing according to standard procedures. Fabrication of DC(T) fracture test specimens involved drilling 1-inch holes to accommodate loading pins and cutting starter notches. Details of DC(T) fracture energy test sample preparation are provided elsewhere (Wagoner et al. 2005, ASTM D7313-07b).

Specimens were tested in the DC(T) fracture energy test (Fig. 1).

Three replicates were tested in each group except the ottawa sand mix, for which six replicates were tested. Samples were conditioned in a cooling chamber for at least three hours before testing began. The test was run using crack mouth opening displacement (CMOD) control. A CMOD loading rate of 1 mm/min and a testing temperature of 0ºC were used for all DC(T) fracture tests. Samples were conditioned in the cooling chamber for at least three hours before testing, but no more than six hours. An Instron Model 8500 loading frame was used to apply the load. Loads were applied through loading pins shown in Figure 1. Load was measured by a load cell attached to the loading frame. CMOD was measured using an

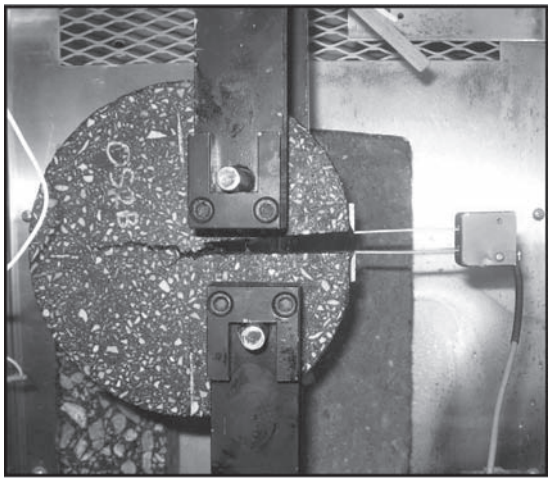

Figure 1. Typical DC(T) fracture energy test-setup.

Epsilon 3541-0020-250-ST clip-on gage. The displacement also provided feed-back for the control loop, which is critical for provide stable behavior during the post peak load testing phase, following ASTM D7313-07b.

3 RESULTS AND DISCUSSION

3.1 *Specimen appearance*

Fused silica mixes subjected to 7-day conditioning at 80ºC in potassium acetate solution saturated with calcium hydroxide showed the formation of a significant amount of gel-like substance on the mix surface (Fig. 2). No gel was observed on the inside of the specimens (fracture surfaces) after they were tested in fracture. No gel formation was observed in the case of the ottawa sand mixes (Fig. 2). It was also noticed that the gel deposits were limited to the surface of the fused silica mixes as shown in Figure 3. Another observation was that in the absence of calcium hydroxide, the KAc solution alone did not result in formation of gel in the fused silica mixtures. Also no gels formed when fused silica mixtures were kept

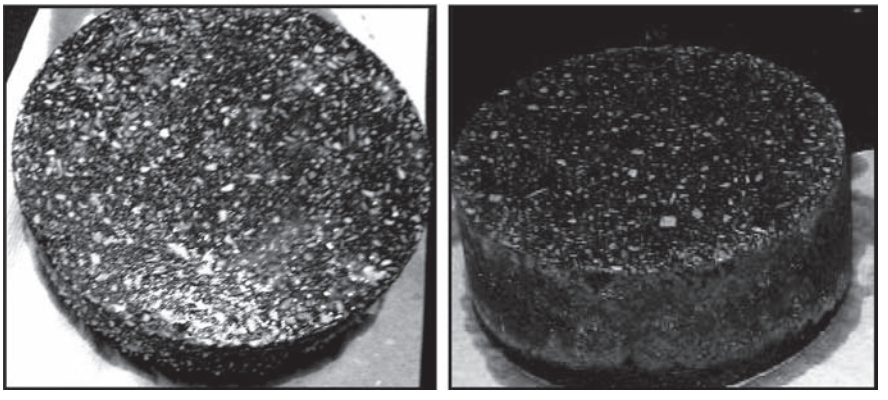

Figure 2. Outside surface of specimens conditioned in potassium acetate solution saturated with calcium hydroxide, showing gel formation for the fused silica mix (left) and no visible gel formation for the Ottawa sand mix (right).

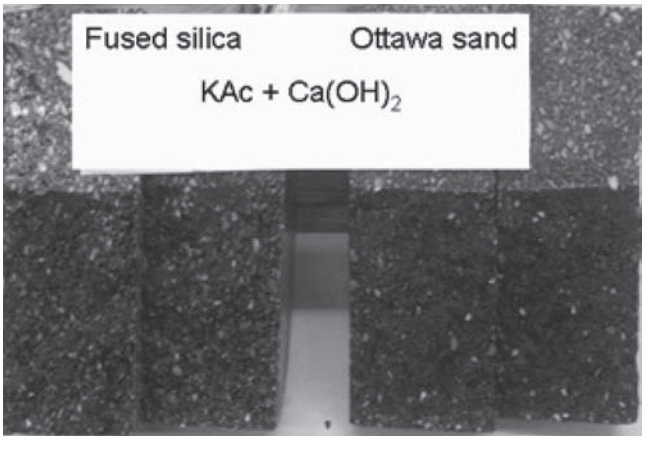

Figure 3. Fracture surfaces of specimens conditioned in potassium acetate solution saturated with calcium hydroxide, showing no gel formation on either the fused silica mix (left) or the ottawa sand mix (right).

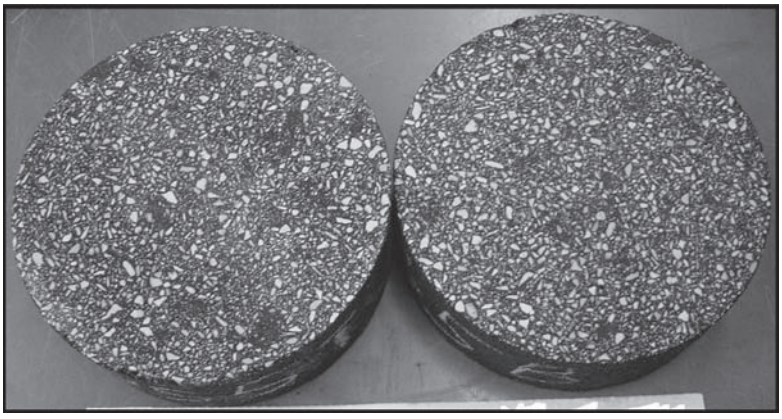

Figure 4. Ottawa sand mix conditioned in NaOH for 7 days at 80ºC, showing no gel formation, expansion or cracking.

in KAc + $Ca(OH)_2$ solution at room temperature for two weeks. Noticeable expansion was observed in the fused silica mix subjected to 7-day conditioning at 80°C in NaOH solution. Also tensile-like cracks (penetrating about 6.25 mm) appeared to have propagated across the surface of the specimens from the top downward. The "expansive cracks" were observed only on the top surface of the fused silica specimens but not on the underside, where the sample is constrained from movement. No visible cracks were found in the ottawa sand mix, shown in Figure 4. Since the only major difference between the specimens that were conditioned in the NaOH solution is the aggregate type (non-reactive ottawa sand versus reactive fused silica), it is reasonable to attribute the expansion and cracking to ASR. Similar expansion and cracking were observed in rectangular blocks of fused silica mixtures conditioned for 7 days in NaOH solution at 80°C. The surfaces of both the ottawa sand mix and the fused silica mix after conditioning in distilled water at 80°C for 7 days were free of any noticeable gel formation or cracks. The surfaces of both the ottawa sand mix and the fused silica mix not conditioned were similarly free of any noticeable gel formation or cracks.

3.2 *Expansion*

The IDT fused silica specimens conditioned in NaOH for 7 days at 80ºC showed considerable expansion. Specimen thickness increased on average 4.2% during conditioning. This is substantially higher than the 0.2% expansion threshold that indicates a deleterious level of ASR in portland cement concrete (PCC) subjected to similar conditioning (ASTM C1260-07) but for 16 days.

Because of the relatively higher levels of expansion observed in the asphalt specimens, three additional fused silica mix specimens were prepared in the form of rectangular blocks and conditioned for seven days in 1-M NaOH solution at 80ºC. After conditioning, the specimens showed visible surface cracks (Fig. 5). Dimensions of the three blocks measured before and after the NaOH conditioning are given in Table 4, and expansion values in length, width, and thickness are given in Figure 6. The highest expansion, 5.45 percent, was in the thickness direction. The fact that expansion in the thickness (vertical) direction was higher than in the length and width (horizontal) directions may be significant. For asphalt mixtures at elevated temperatures, the expansion in the length and width direction could possibly be attributed to plastic flow under gravitational forces. However, the vertical (upward) expansion measured in the blocks confirmed the earlier expansion measured in the cylindrical specimens and further supports the hypothesis that significant ASR-type expansion can occur in asphalt mixtures.

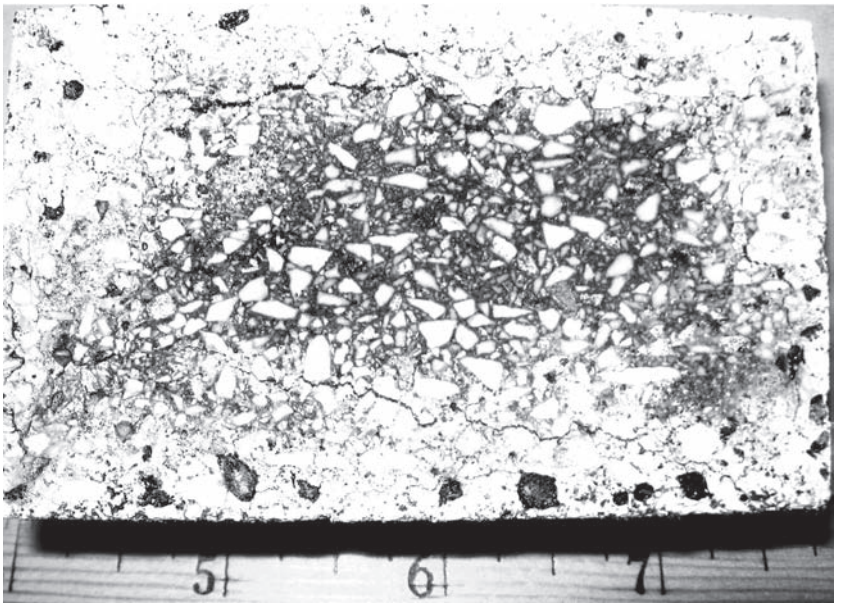

Figure 5. Blocks of fused silica mix after 7-day conditioning in 1N NaOH at 80ºC.

Table 4. Effect of conditioning in 1-M NaOH solution at 80ºC for 7 days on dimensions of blocks prepared from fused silica mixes (dimensions in mm).

	Before treatment			After treatment		
Sample ID	Length	Width	Thickness	Length	Width	Thickness
1	79.0	49.5	25.1	80.3	50.8	26.6
2	80.4	49.6	26.2	82.0	50.8	27.3
3	78.8	49.3	25.7	80.5	50.8	27.2

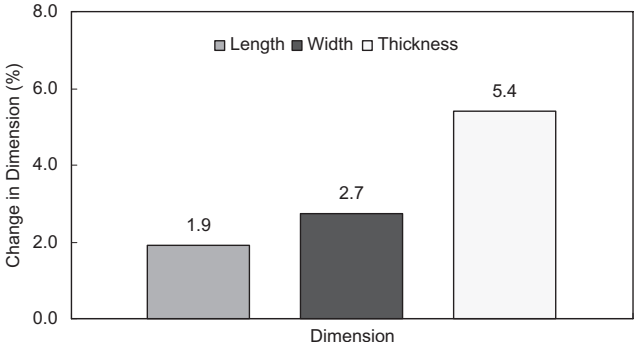

Figure 6. Expansion of blocks of fused silica mix after 7-day conditioning in 1-M NaOH solution at 80ºC.

3.3 *Fracture*

Measurements of applied load and crack-mouth opening displacement (CMOD) were used to compute fracture energy, G_f, following the ASTM D7313-07b standard. Fracture energy

was calculated as the area under the load-CMOD curve (A_f.) normalized by the fractured surface. Figure 7 shows load versus CMOD data for ottawa sand mixes tested in the dry state and conditioned in the calcium hydroxide saturated potassium acetate solution. Similar peak loads and fracture energy values were observed in both the conditioned and dry samples.

Figure 8 shows load versus CMOD for fused silica mixes conditioned in potassium acetate solution saturated with calcium hydroxide. Compared to the ottawa sand mixes, the fused silica mixes showed substantial differences between dry and conditioned specimens. For instance, peak load dropped from about 4 kN in the dry state to about 2 kN in the conditioned state. Examination of Figure 7 suggests potassium acetate saturated with calcium hydroxide has negligible effect on the ottawa sand blends. The significant differences between the dry and conditioned fused silica plots suggest to potassium acetate saturated with calcium hydroxide could be reactive in asphalt mixtures.

Figure 9 provides a comparison of the effect of water conditioning on load versus CMOD curves for ottawa sand mix and fused silica mixtures. Water appears to affect the ottawa sand mix more than either the NaOH solution or the KAc with calcium hydroxide solution.

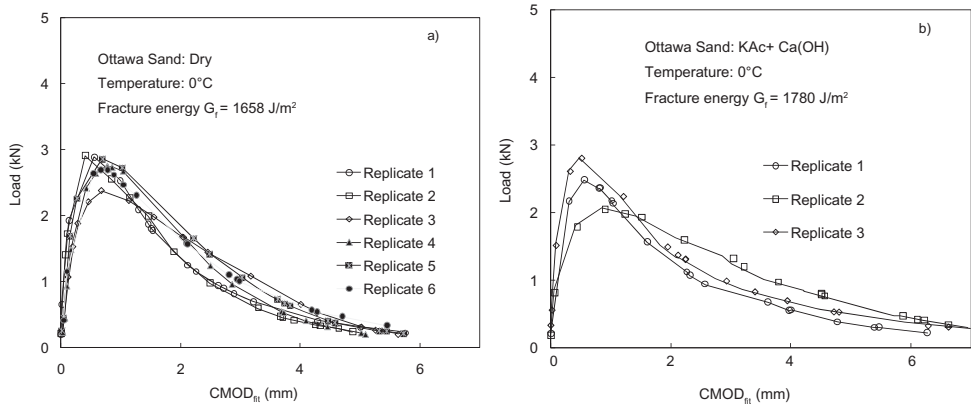

Figure 7. Load versus CMOD for ottawa sand mix (a) tested dry and (b) conditioned in KAc and $Ca(OH)_2$ at 80ºC for 7 days.

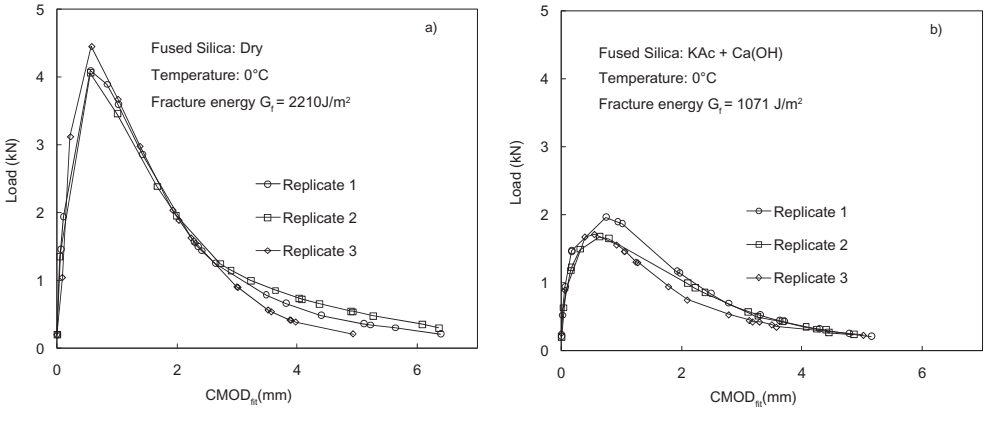

Figure 8. Load versus CMOD for fused silica mix (a) tested dry and (b) conditioned in KAc + $Ca(OH)_2$ at 80ºC for 7 days.

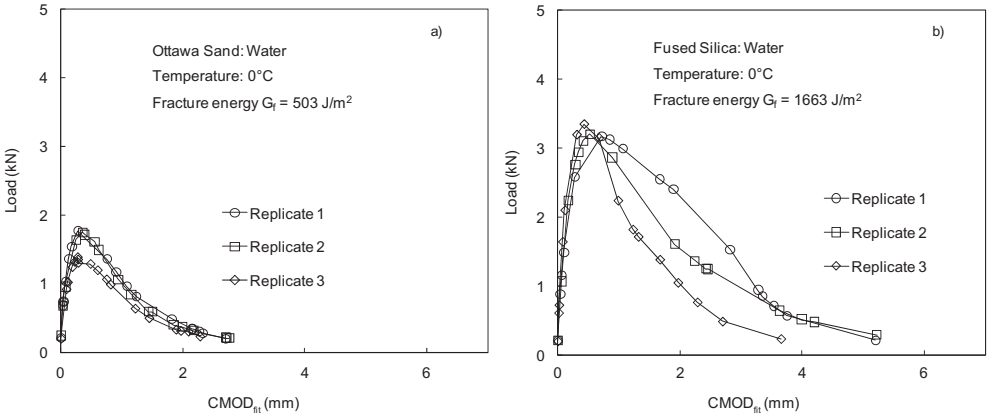

Figure 9. Effect of water conditioning on load versus CMOD curves: (a) ottawa sand (b) fused Silica.

Table 5. DC(T) fracture energy measured at 0ºC for mixtures tested.

Aggregate	Treatment	No. of replicates	Fracture energy (J/m^2)	COV (%)
Ottawa sand	Dry	6	1658	8
	Water	3	536	16
	NaOH	3	1214	26
	KAc + $Ca(OH)_2$	3	1960	15
Fused silica	Dry	3	2210	6
	Water	3	1797	22
	NaOH	3	959	12
	KAc + $Ca(OH)_2$	3	1106	8

As noted in Table 3, the ottawa sand mixes had significantly higher water absorption than the corresponding fused silica mixes. Figure 10 allows a comparison of load versus CMOD plots for the two mixtures considered in this study for the various conditioning treatments. Fracture energy obtained from the DC(T) fracture test are summarized in Table 5. The mean fracture energy values obtained for the unconditioned ottawa sand was 1559 J/m^2 and for the unconditioned fused silica mixes was 2210 J/m^2. These results were comparable to asphalt mixtures with similar gradations and binder contents. Wagoner (2006) obtained mean fracture energy value of 1794 J/m^2 for DC(T) fracture tests of 4.75-mm nominal maximum-sized polymer-modified asphalt mixtures tested at 0ºC. The coefficient of variation (COV) obtained in this study is also within levels reported by Wagoner (2006), which ranged from 3 to 28%.

The fact that some of the COV values were towards the high side of the range reported by Wagoner might be indicative of the damaged state of the mixtures. Both of the 'dry' mixtures had low COV values.

Statistical analysis was performed using commercial statistical software to investigate if the treatment regimes resulted in statistically significant difference in the measured fracture energy. The analysis of variance results indicated that fracture energy obtained for the fused silica mixtures were significantly higher than those of the ottawa sand mixture ($p < 0.001$). The higher fracture energy values could be the effect of the coarser and rougher surfaces of the fused silica particles. About 75% by weight of the fused silica used had particles larger than 2.36 mm but smaller than 4.75 mm. Only 2.5% of the Ottawa sand had dimensions larger than 0.6 mm and smaller than 4.75 mm. The results of the statistical analysis using the least significant difference method (t-test) are summarized in Table 6. It can be seen that

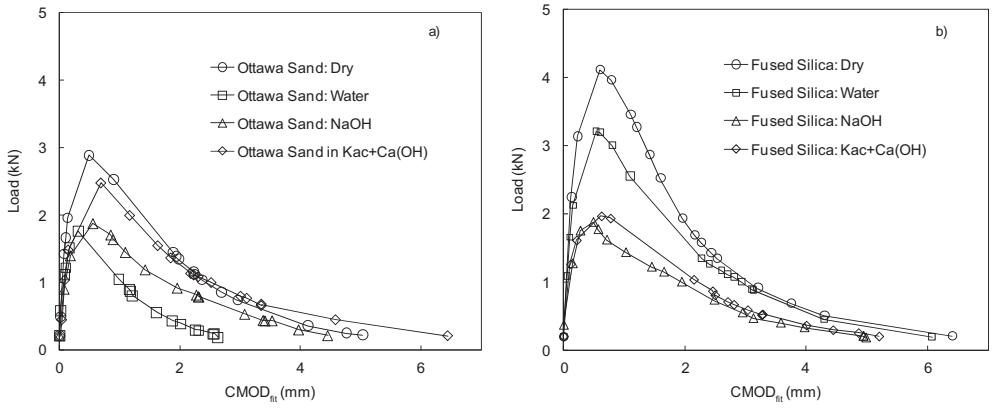

Figure 10. Typical ranking of load versus CMOD curves for (a) ottawa sand (b) fused silica.

Table 6. Statistical analysis of DC(T) fracture energy test results.*

t-Grouping	Fracture energy (J/m^2)	N	Mixture type	Treatment
A	2210	3	Fused Silica	Dry
B	1779	3	Ottawa Sand	KAc + Ca(OH)$_2$
B	1663	3	Fused Silica	Water
B	1658	6	Ottawa Sand	Dry
C	1071	3	Fused Silica	KAc + Ca(OH)$_2$
C	960	3	Ottawa Sand	NaOH
C	920	3	Fused Silica	NaOH
D	503	3	Ottawa Sand	Water

mixtures containing fused silica tested in the dry condition had significantly higher fracture energy than all the other mixtures. For fused silica mixtures, the effect of potassium acetate plus Ca(OH)$_2$ treatment on fracture energy was not significantly different from the effect of NaOH. For ottawa sand mixtures, there was no significant difference in fracture energy between the treatment with potassium acetate solution plus Ca(OH)$_2$ and the treatment with NaOH. It appears no ASR damage occurred in the ottawa sand mixtures conditioned in KAc and Ca(OH)$_2$. On the other hand, it appears that some ASR damage occurred in both ottawa sand mixtures and fused silica mixtures conditioned in NaOH.

To evaluate the effect of the various conditioning methods on fracture energy of fused silica and ottawa sand mixtures, a fracture energy ratio (FER) was used, which is a parameter roughly analogous to the tensile strength ratio used to evaluate moisture damage in asphalt mixtures (AASHTO T283). The fracture energy ratio is the ratio between the fracture energy of a conditioned mixture to the fracture energy of the dry, control mixture. The (FER) was used to evaluate moisture damage in antioxidant-modified asphalt mixtures in the laboratory by Apeagyei et al. (2006). Higher values of FER may indicate lower damage levels. Computed fracture energy ratios of 96% or less was correlated with moisture damage for asphalt mixture subjected to one freeze-thaw cycle in the laboratory Apeagyei et al. (2006).

Figure 11 shows a comparison of the FER for ottawa sand mixtures and fused silica mixtures. The worst performance was observed in the ottawa sand mixtures, where the water conditioning resulted in about 70% drop in fracture energy. As noted earlier (Table 3), water absorption in the ottawa sand mixtures was an order of magnitude higher than in the fused silica mixtures. The high water absorption rate in ottawa sand mixtures may account for the drastic drop in fracture energy seen in this study. However, conditioning in KAc plus

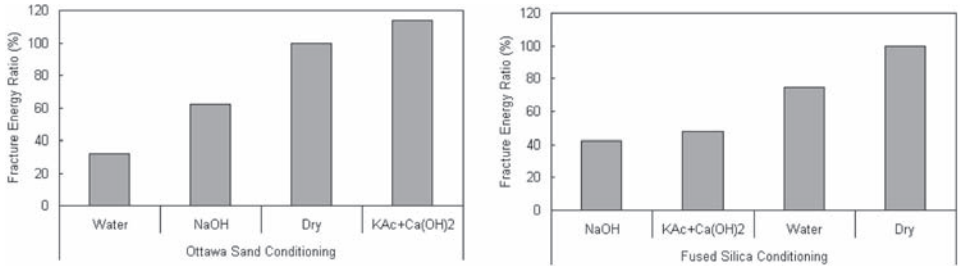

Figure 11. Fracture energy ratios for ottawa sand and fused silica mixtures.

$Ca(OH)_2$ solution did not result in a significant decrease in fracture energy for the ottawa sand mixtures. This result was expected since Ottawa sand is not reactive and damage due to ASR is not expected. Conditioning in NaOH solution and in KAc plus $Ca(OH)_2$ resulted in comparable ratios for fused silica mixtures. The mean FER for fused silica mixtures conditioned with NaOH solution was 42%, not significantly different than mean FER for fused silica mixtures conditioned in KAc plus $Ca(OH)_2$ solution (48%). The results may indicate that the level of reaction in fused silica mixtures was similar in KAc plus $Ca(OH)_2$ solution and in NaOH solution were similar and could in fact be ASR.

4 SUMMARY AND CONCLUSIONS

Two asphalt mixtures containing reactive and non-reactive aggregates were studied in the laboratory to investigate ASR occurrence in asphalt mixtures. Ottawa sand was used as the non-reactive aggregate while fused silica was selected as reactive aggregates. The mixtures used were all fine mixtures containing 8% PG 82-22 by weight of total mix asphalt binder with gradation similar to IDOT 4.75 mm nominal max mixtures. Four treatment solutions (Dry, Water, NaOH and KAc + $Ca(OH)_2$) were used for conditioning the mixtures to simulate ASR. To perform the conditioning, at least three replicates samples were submerged in each solution and kept in a forced-draft oven maintained at a temperature of 80ºC for seven days. Air dried samples were used for experimental control.

Two possible signs of ASR occurrence were observed in mixtures containing the reactive aggregates: significant gel formation occurred in mixtures conditioned in KAc + $Ca(OH)_2$ solution, and expansion and surface cracking occurred in mixtures that were conditioned in NaOH solution.

In general fracture energy of all the mixture except ottawa sand conditioned in KAc + $Ca(OH)_2$, decreased significantly after conditioning. For the ottawa sand mixture, a significant decrease in fracture energy was observed when conditioned in water, which strongly suggests that moisture damage occurred. For the fused silica mixture, no statistically significant difference in reduction of fracture energy was observed between specimens conditioned in NaOH solution and specimens conditioned in KAc + $Ca(OH)_2$ solution. The results may indicate similar reaction occurs in both solutions and, combined with visual examination of gel formation, indicates the occurrence of ASR. The results indicate that ASR may occur in asphalt mixtures exposed to potassium acetate deicing solution when the mixture contains reactive aggregate and calcium hydroxide. The results of the study warrant further investigation of ASR in asphalt mixtures.

REFERENCES

Ai, L. and Struble, L. (2008), *pH of Potassium Acetate Deicing Solution*. OMP Technical Note 36.

Advanced Asphalt Technologies AAT (2007). *Effect of Deicing Chemicals on HMA Airfield Pavements. AAPTP Project 05–03, http://www.aaptp.us/Report.Interim.05–03.pdf*

Alatyppö, V. and J. Valtonen (2007). *Experience on the Effects of De-icing Chemicals on Bituminous Airfield Runways in Finland. FAA Worldwide Airport Technology Transfer Conference.* Atlantic City, NJ.

American Society for Testing and Materials (2007). *Standard Test Method for Potential Alkali Reactivity of Aggregates (Mortar-Bar Method)*. ASTM C1260-07.

American Society for Testing and Materials (2007). *Standard Test Method for Determining Fracture Energy of Asphalt-Aggregate Mixtures Using the Disk-Shaped Compact Tension Geometry*. ASTM D7313-07.

Apeagyei, A.K., Buttlar, W.G. and B.J. Dempsey (2006). Moisture Damage Evaluation of Asphalt Mixtures using AASHTO T283 and DC(T) Fracture Test. *Proceedings of the 10th International Conference on Asphalt Pavements, International Society of Asphalt Pavement.* Quebec, Canada.

Farha, M.H., Hassan, Y., Abd El Halid, A.O., Razaqpur, A.G., El-Desouky, A. and Mostafa A. (2002). *Effects of New Deicing Alternatives on Airfield Asphalt Concrete Pavements*, *2002.* Federal Aviation Administration Technology Transfer Conference.

Hassan, Y., Abd El Halid, A.O., Razaqpur, A.G., Bekheet, W. and M.H. Farha M.H. (2002). Effects of Runway Deicers on Pavement Materials and Mixes: Comparison with Road Salt. *Journal of Transportation Engineering.* ASCE.

Wagoner, M.P., Buttlar, W.G. Paulino, G.H. and Blankenship P. (2005). Investigation of the Fracture Resistance of Hot-Mix Asphalt Concrete Using a Disk-Shaped Compact Tension Test. *Transportation Research Record 1929 Transportation Research Board, Washington, D.C*:183–192.

Wagoner, M.P., Buttlar, W.G. and Paulino G.H. (2005). Disk-Shaped Compact Tension Test for Asphalt Concrete Fracture. *Experimental Mechanics, Society for Experimental Mechanics, Inc.* 45(3): 270–277.

Wagoner, M.P. (2006). Fracture tests for bituminous-aggregate mixtures: Laboratory and field investigations. *Ph.D. dissertation, University of Illinois at Urbana-Champaign, Urbana, IL*: 74.

Advanced Testing and Characterization of Bituminous Materials – Loizos, Partl, Scarpas & Al-Qadi (eds)
© 2009 Taylor & Francis Group, London, ISBN 978-0-415-55854-9

Laboratory tests used in Cuba as low financial resources country for the evaluation of the mechanical properties of the asphalt mix

Rosa Herrera de la Rosa
Technical Centre for Development of Construction Materials, Havana City, Cuba

ABSTRACT: Marshall Method is the only standard test used in Cuba for design and evaluation of the asphalt mix properties. In spite of its numerous known limitations, as well as the advances in mix design in the world, the economic conditions of our country, have not allowed us the acquisition of the new equipment required for the mix design. The work exposes our development of solutions based in other laboratory test for complementing Marshall Method without big investments to give the necessary information of the behavior of the mixture in service. For the evaluation of the mechanical properties of the asphalt mix and their design, we use three equipment of common use in laboratories of construction materials, those are: a 50 kN Marshall press, a 400 kN compression hydraulic press of and Los Angeles Machine, with the incorporation of the Wheel Tracking Machine made in our Center according to the spanish specifications. The methodology of application of this combination of test for hot mix asphalt design is shown detailed with an example, based fundamentally in the execution of additional test to an interval of asphalts determined by Marshall Method from a diagram of bars, for finally determine the optimum asphalt content with bigger precision.The paper also exposes the need to correlate our methodology of laboratory test with the world advanced techniques for characterization of asphalt mixtures.

1 INTRODUCTION

Through the years, the several limitations, present in the Marshall method like making and tests of specimens for their extrapolation to real operation conditions of the roads, have been verified all over the world. On the other hand, the last solutions for project and design of the asphalt mix are mostly related to the behaviour of the mixture in the pavement, and a novel test technology is required.

However, the economic conditions of our country have made impossible the acquisition of new equipment required for design of mixtures. Therefore, in our country is essential to search for individual solutions based in the use of other laboratory tests which serve as a complement to the Marshall Test without big investments, and they should be able to provide the necessary information in order to value the behaviour of the mixture in service.

This paper presents the methodology of laboratory test for the asphalt mix design used in the Technical Centre for Development of Construction Materials (Herrera 2005, Cuban Standard NC261 2005, Herrera 2006). It includes the international experiences as well as the obtained results from national experience and researches.

2 AVAILABLE TEST TECHNIQUES

For evaluation and design of the mechanical properties of asphalt mix, we use three common equipment in laboratories of construction materials in Cuba, that is, a 50 kN Marshall press, a 400 kN compression hydraulic press and Los Angeles abrasion machine, with the incorporation of a Wheel Tracking Machine made in our Centre according to the Spanish specifications.

2.1 *Marshall*

Invented by Bruce Marshall and developed and improved by the U.S Corps of Engineers, through extensive research and correlation studies (The Asphalt Institute Manual 1984). The Marshall Test procedures were standardized by ASTM and applied to laboratory design of hot and could asphalt mix paving, but with aggregate of maximum size 25.4 mm or less (ASTM D 6926-04, ASTM D 6927-06).

The procedure starts with the preparation of test specimens of 64 mm height × 102 mm diameter impact-compacted in a Marshall Compaction Hammer. It has a mass of 4.74 kg in free fall from a height of 457 mm, and it is necessary to compact the test specimens 50 or 75 times per each side.

We prepare a number of 6 specimen for the two principal features of the Marshall Method, density-voids analysis and stability-flow (3 for each one).The test is made at 25 and 60 centigrade grades for cold or hot mixtures respectively.

Rigidity (kN/mm) is indicative of the toughness of the mixture, and it is determined as the quotient of the stability and the deformation reached by the Marshall test specimen.

2.2 *Diametrical compression test*

The diametrical compression test, also known as Brazilian test, is a simple procedure successfully used in Belgium and Latin American countries. The ASTM and the European standard have standardized this test (ASTM D 6931-07, UNE-EN 12697-23:2003). The traction test is made in an indirect way on cylindrical test specimens (Marshall). The test applies a diametrical load to speed of constant deformation up to their breakage determining the break load and the deformation associated to it.

This Test also allows studying the properties related to the elastic-viscous nature of asphalt mix based on the temperature. The test temperature may be varied between –10 and + 45 Celsius grades, and the standardized conditions are as follows:

Test temperature	Immersion time	Deformation speed
–10°C	24 hours	0.30 + –0.1 mm/seg
+25°C	6 hours	0.85 + –0.1 mm/seg (Marshall)
+45°C	6 hours	0.85 + –0.1 mm/seg (Marshall)

Photograph 1. Marshall press and thermostatic bath.

The calculation expression is as follows:

$$RT = \frac{2P}{\pi HD} \tag{1}$$

where:

RT: strength to indirect traction, Kgf/cm^2
P: break loads, Kgf
H: average height of the test specimen, cm
D: average diameter of the test specimen, cm
Dv: vertical deformation, mm
Dh: horizontal deformation, mm
Dv/d: unit vertical deformation.

In Cuba, the average maximum temperatures of the pavement at 20 mm of the surface are 25°C in winter and 51°C in summer. In our country, this test use the Marshall press with an addition built in our Centre. The temperature range is between 25 to 60°C. Also, this test is used to study the effect of water on asphalt mixtures with measurement of the loss of the strength after their immersion over several days and comparing with the results reached at the same age with dry specimens.

2.3 *Simper compression*

It is one of the first tests with good theoretical foundations that were standardized for the study of construction materials, and it can be used in conjunction with other mixture physical properties, contributing to the overall mixture characterization.

The main inconvenience is the standardized method of compression can produce important degradations of the mineral skeleton in some types of aggregates. Its biggest application is in the study on the effect of water on compacted bituminous mixtures.

For the elaboration and test of the specimens, we studied two procedures: the old Soviet Union method (CSN 736160:81) used in East Europe countries and some Asian and ASTM standard (ASTM D 1074-02).

In our centre, 3 cylindrical test specimens were made like in the old Soviet method, with a height equal to the diameter which varies in 3 sizes 50.5; 71.4 and 101.0 mm, according to the aggregate maximum nominal size of 8 mm; 19 mm and 25 mm respectively. The test specimens are compressed under low static pressure of 30 MPa during 3 minutes. The test can be

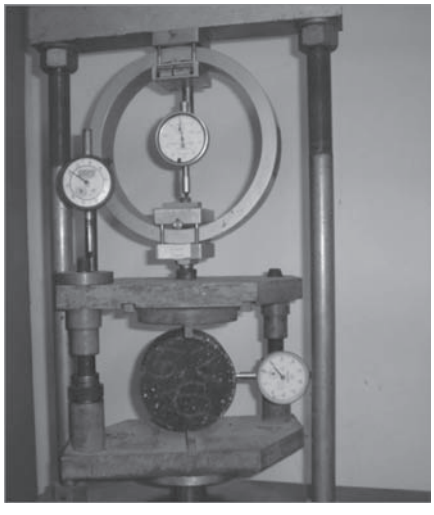

Photograph 2. Press Marshall with an addition built in our centre.

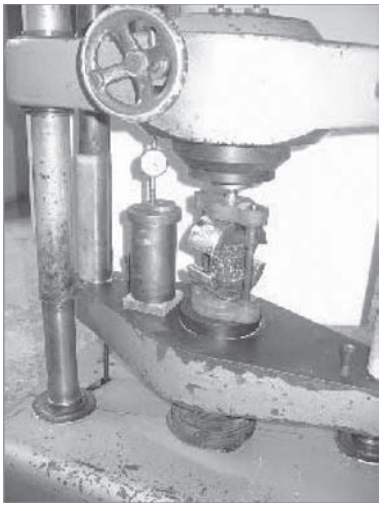

Photograph 3. Simple compression test with 400 kN compression hydraulic press.

carried out from 20°C to 50°C, after maintaining the test specimen in water during 2 hours at the test temperature. The load is applied to speed of constant deformation of 3 mm/min, up to the break.

It is calculated as follows:

$$R = \frac{P}{A} \tag{2}$$

R: compression strength, Kgf/cm^2

P: break loads, Kgf

To: Area of the base of the test specimen, cm^2.

This test method is used as an indicator of the susceptibility to moisture of compacted bituminous mixtures, testing the dry specimen and after being submerged in water for several days. The conserved strength should be bigger than 75% (ASTM D 1075-07, EN 12697-12 2003, Cuban Regulatory RC 3000-1984).

2.4 *Sheering strength*

Considering that the resistance to the permanent deformations (rutting) of the asphalt mixtures is given by their shear resistance, and it depends on the cohesion and the internal friction of the material, different test methods have been developed. One of them was that proposed by the Superior Institute of Engineering of Sofia, Bulgaria (Asenov Todorov 1970) that is used in our country for their simple equipment and operability.

This method uses test specimens of same dimensions than the compression strength ones. The test specimens are elaborated and tested in a similar way at 50°C.

The following parameters are determined:

$$R_{CD} = \frac{P}{2A} \tag{3}$$

R_{CD}: direct shear resistance, Kgf/cm^2

P: break loads, Kgf

A: Area of the test specimen base, cm^2

$$\sin\phi = \frac{1-2R_{CD}}{R} \tag{4}$$

Photograph 4. Sheering strength test with 400 kN compression hydraulic press with an addition built in our centre.

$$\cos\phi = \sqrt{1-\sin^2\phi} \tag{5}$$

$$C = \frac{R_{CD}}{\cos\phi} \tag{6}$$

$$R_{CM} = C(1+\sin\phi) \tag{7}$$

$\emptyset$: = Angle of internal friction among stone-on-stone, grades
R: = compression strength, Kgf
C: Cohesion of the mixture, Kgf/cm^2
R_{CM}: mixture shear resistance, Kgf/cm^2.

2.5 *Cantabrian*

The Cantabrian Test is a standard procedure to know the resistance to degradation of Compacted Bituminous Mixtures using Los Angeles Machine. It was conceived in 1984 by Miguel A. Calzada Pérez to characterize the open graded asphalt mix and later on, this test was developed by Rodrigo Miro of the Catalonia Polytechnic University in 1994 to characterize the asphalt binder for their employment in roads and pavements. In The Technical Center of Construction Materials was developed a statistics study of the result of the Cantabrian Test in dense graded hot asphalt concrete to obtain a admissible value for dense grade mix. (Herrera de la Rosa, 1995).

This test allows us to evaluate indirectly its cohesion and resistance to disintegration of the mixture that is submitted to the effects suction and abrasive of traffic. It also evaluates the function of the asphalt binder in the mixtures properties such as cohesion, adhesiveness, thermal susceptibility and durability when it is carried out at different temperatures and after their immersion in water.

Three test specimens are elaborate by the Marshall method, keeping them over 6 hours at room temperature, and the mass is determined. Later on, they were introduced in the drum of Los Angeles Machine without the abrasive load of the balls. The drum was rotated to the same standardized speed of 30.3 rpm during 300 turns. In the end, the test specimen is taken out and it is weighed again (NLT352 1986).

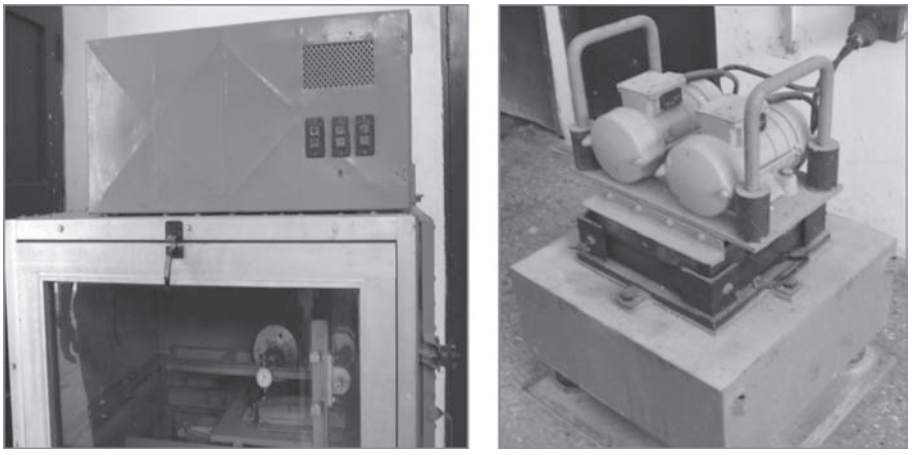

Photograph 5. Wheel tracking machine and vibrate compression unit.

The result of waste loss is calculated by the following expression:

$$P = \frac{P_1 - P_2}{P_1} * 100 \tag{8}$$

where:

P: Value of the lost by waste, %
P_1: Initial mass of the test specimen, g
P_2: Final mass of the test specimen, g.

2.6 *Wheel tracking machine*

Rutting is the most frequent damage of the pavements in Cuba. The necessity to introduce a dynamic type test and simple execution that allows evaluating the asphalt mix performance to the plastic deformations in the most reliable way. It seems evident if it is considered that we only had the flow Marshall to evaluate this property.

The equipment is made of three independent parts: vibrate compression unit of test specimen of 15 × 30 cm, the wheel tracking machine and acclimatized box.

The wheel tracking machine test determines the resistance to the mix plastic deformation, by measurement of the print that produces a loaded wheel in specific temperature and pressure conditions. The time of the test is two hours and the readings of deformation are taken at different time intervals and a curve is plotted. The deformation speed is specified in the last 15 min of the test (EN 12697-22 2003).

3 METHODOLOGY FOR THE APPLICATION OF THE TESTS IN THE DESIGN OF HOT ASPHALT MIXES

The methodology for the application of the tests is as follows:

1. Determination of optimum asphalt range by diagrams of bars using the Marshall Method.
2. With the asphalt range obtained previously, it made a test specimen for the available complementary tests.
3. From the result of the complementary tests using diagrams of bars, it can specify the optimum asphalt content in the asphalt mix design.

3.1 *Example of application*

Let assume that the data shown in table 1 represents Marshall Test results on a dense graded asphalt concrete mix to be used for heavy traffic category. Prepare a graphical plot of these values as it is shown in Figure 1 to obtain the adjusted values of each parameter. With the adjusted values of density, air voids and voids in mineral aggregates are calculated.

From the adjusted values, proceed to determine which asphalt ranges fulfill the requirements of the Marshall Design criteria of standard specification for each parameter (See table 3) (Cuban Standard NC253 2005). For example, stability is greater than 9 KN in whole asphalt range tested, from 4.5 to 6.5%. The deformation fulfills the criteria from 2 mm to 4 mm between the asphalt contents of 4.5% and 5.9%. These ranges are represented in a diagram of bars as it is shown in Figure 2.

Once the optimum asphalt range is obtained according to Marshall method, we proceed to carry out the complementary tests that will define with more precision the optimum asphalt content. For this purpose, specimen tests are elaborated for each complementary test within the previously established range by varying the asphalt content in 0.3%.

If the data obtained for the complementary tests are those shown in Table 4.

Table 1. Results obtained from the Marshall test (example).

Average bulk specific gravity = 2.5 y Asphalt absorption = 1.7					
Average values					
% asphalt	Stability (kN)	Flow (mm)	Density (g/cm^3)	Air voids (%)	Voids in mineral aggregates (%)
4.5	10	2	2.27	5.3	13.3
5	12.5	2.8	2.28	4.5	13.0
5.5	16	3.5	2.3	4.0	13.3
6	14.3	4	2.28	3.5	14.1
6.5	11.8	5.2	2.26	3.1	15.5

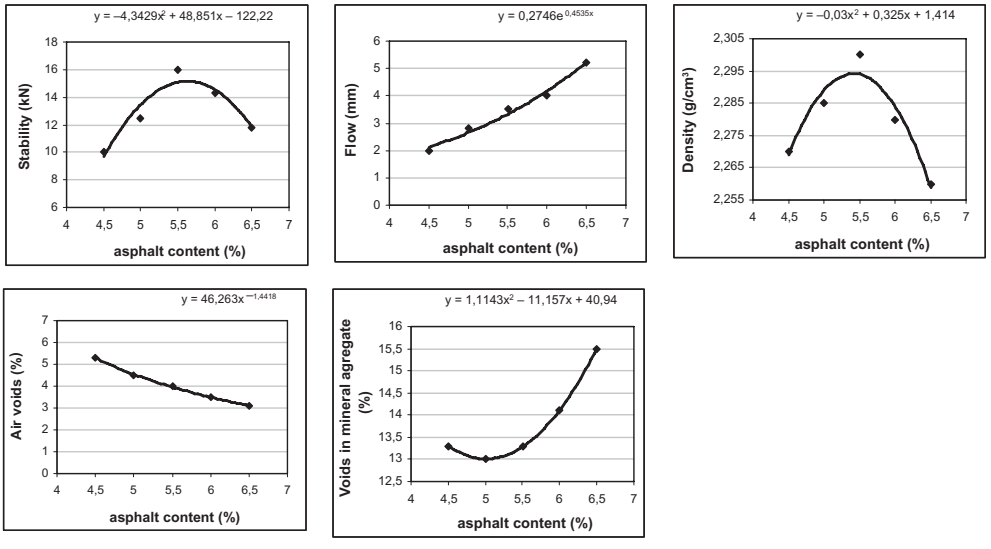

Figure 1. Marshall method test property curves.

Table 2. Marshall method test adjusted values.

% asphalt	Stability (kN)	Flow (mm)	Density (g/cm^3)	Air voids (%)	Voids in mineral aggregates (%)
4.5	9.7	2.1	2.269	5.3	13.3
5	13.5	2.7	2.289	4.5	13.0
5.5	15.1	3.3	2.294	4.0	13.3
6	14.5	4.2	2.284	3.5	14.1
6.5	11.8	5.2	2.259	3.1	15.5

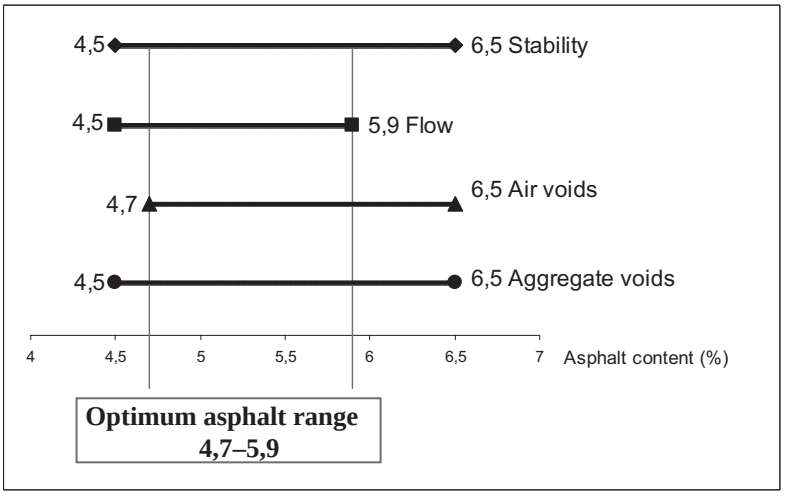

Figure 2. Schematic representation of the asphalt ranges performance in each parameter.

According to Wheel Tracking Machine test the asphalt contents 5.6 and 5.9 are eliminated because they are in the limit and over the specified maximum value (PG-3 art.542 2000), respectively. In immersion—compression test, asphalt contents greater than 5.3 are discarded because the conserved strength starts to diminish from that point on (Cuban Regulatory RC3000 1984). The indirect traction of the mixture has a good performance for 5.0 and 5.3 asphalt contents while in the Cantabrian test, 4.7 asphalt content is discarded (Herrera de la Rosa 2005). Then, the ranges of asphalts for each test are represented in a diagram of bars as it is shown in Figure 3 to determine the final optimum asphalt.

4 CONCLUSIONS

The project and design of the asphalt mix constitutes an aspect of national relevance as long as it has a great incidence in the durability of the roads and their level of service.

The methodology developed in Cuba takes the experience from SUPERPAVE and European procedures, in such way of achieving a bigger adaptation between the laboratory conditions and the real conditions of the mixtures in service.

In spite of our economic limitations, it is very important to keep the efforts aimed at introducing into the country, new criteria developed in the world for mixtures design, such as compactor gyratory for making the standard test specimen, the binder aging laboratory process, the elastic modules of the bituminous mixtures, among others.

Table 3. Results of the complementary tests.

Tests	Specification	% asphalt 4.7	5.0	5.3	5.6	5.9
Wheel Tracking Machine (deformation speed, μ_c/min)	20 max.	2	6	13	20	33
Immersion–Compression (conserved strength, %)	75 min.	55.8	79.3	93.0	81.0	74.4
Indirect traction (kg/cm^2)	2,0 min.	1.04	2.19	2.08	1.9	1.8
Cantabrian (% loss)	4,5 max.	6.4	3.1	1.9	1.5	1.0

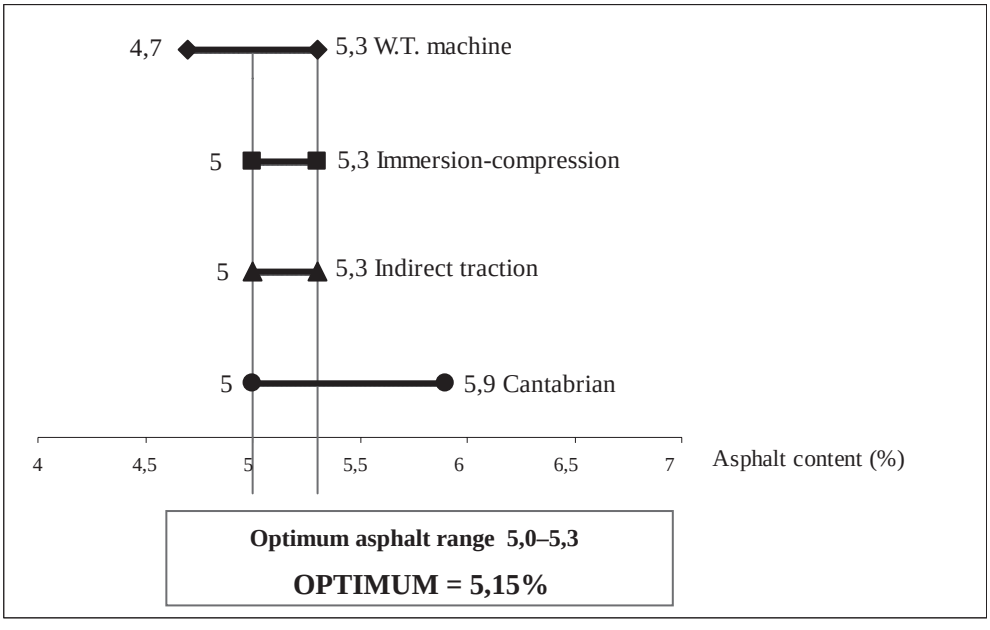

Figure 3. Schematic representation of the asphalt ranges performance in each test.

To accomplish that purpose, we need to correlate our methodology of laboratory test with the advanced technique of characterization of asphalt mix used in the world, from a partnership of collaboration among our countries, being convinced of usefulness of these purpose for the development of the asphalt mix design in low financial resources countries like Cuba.

REFERENCES

ASTM Standard Book. 2007. ASTM D 6926-04 Standard Practices for Preparation of Bituminous Specimens Using Marshall Apparatus. Volume 04.03.

ASTM Standard Book. 2007. ASTM D 6927-06 Standard Test Method for Marshall Stability and Flow of Bituminous Mixtures. Volume 04.03.

ASTM Standard Book. 2007. ASTM D 6931-07 Standard Test Method for Indirect Tensile (IDT) Strength of Bituminous Mixtures. Volume 04.03.

ASTM Standard Book. 2007. ASTM D 1074-02. Test Method for Compressive Strength of Bituminous Mixtures. Volume 04.03.

ASTM Standard Book. 2007. ASTM D 1075-07. Standard test method for effect of water on compressive strength of compacted bituminous mixtures. Volume 04.03.

Asenov Todorov. I. 1970. Method for project of hot asphalt concrete. Doctor´s degree Thesis. Superior Institute of Engineering of Sofia. Bulgaria.
Bulgarian Regulation. 1981. CSN 736160:81 Standard Method for simple compression.
Cuban Regulation. 1984. RC 3000-84 Hot asphalt concrete. Determination of stability loss by water immersion.
Cuban Standard NC 261. 2005. Determination of optimum asphalt content using the Marshall Apparatus.
Cuban Standard NC 253. 2005 Highway—Bituminous Materials—Hot Asphalt Concrete—Quality Specifications.
European Standard. 2003. UNE-EN 12697-23:2003. Bituminous mixtures. Test methods for hot mix asphalt Part 23. Determination of the indirect tensile strength of bituminous specimen.
European Standard. 2003. EN 12697-12:2003. Bituminous mixtures—Test methods for hot mix asphalt—Part 12: Determination of the water sensitivity of bituminous specimens.
European Standard. 2003. EN 12697-22:2003. Bituminous mixtures—Test methods for hot mix asphalt—Part 22: Wheel tracking.
Herrera de la Rosa, R. 1995. Statistics study of the result of the Cantabrian Test in dense graded hot asphalt concrete.Research report of Technical Center of Construction Materials.
Herrera de la Rosa, R. 2005. Hot asphalt mix design in Cuba by a complemented Marshall Methods. San José, Costa Rica, XIII CILA.
Herrera de la Rosa, R. 2006. Tendency new of hot asphalt mix design in Cuba using a complemented Marshall Methods. Havana City. Cuba. III Civil Engineer International Journey in Cuba & IV International Congress of Transport Infrastructure.
Spanish Regulation. 1986. NLT 352/86 Characterization of the open bituminous mixtures by The Cantabrian test.
Spanish Regulation. 1992. PG-3. General Technical Regulation of Spanish.
The Asphalt Institute Manual. 1984. Mix Design methods for asphalt concrete and other hot mix types. Chapter III. Marshall Method of design. Series N_0. 2 (MS-2).

Advanced Testing and Characterization of Bituminous Materials – Loizos, Partl, Scarpas & Al-Qadi (eds)
© 2009 Taylor & Francis Group, London, ISBN 978-0-415-55854-9

Polypropylene fiber modification of asphalt by using mechanical and optical means

S. Tapkın, Ş. Özcan, M. Tuncan & A. Tuncan
Anadolu University, Civil Engineering Department, Eskişehir, Turkey

ABSTRACT: In this study, first of all, the physical and chemical effects of polypropylene fiber modification on bitumen samples were investigated. Then, the amount of "optimum" polypropylene fibers was determined. In order to determine this value, first, static creep tests and Marshall tests were carried out and then, digital images of the modified binders under fluorescence microscopy were examined. The addition of the polypropylene fibers into the asphalt mixture enhances the mixture properties in a very favorable manner. The decrease of the accumulated strains at the end of the static creep tests correspond to approximately 60%. The initial and final creep stiffness values have increased by 129% and 149% correspondingly. Besides, the polypropylene modification ends up with a 30% economy from bitumen which deserves attention. Finally the optimal polypropylene addition amount was determined as 5.5% by weight of aggregate based on the static creep, Marshall tests and stereo microscopy analyses.

1 INTRODUCTION

Rutting is a very important problem in today's pavement engineering. To address rutting problem in flexible pavements, pavement engineers have developed some methodologies namely called as "bitumen modification". The most popular bitumen modification technique is polymer modification. Novel binders with improved rheological characteristics are continuously being developed by different scientists up to date (Airey 2002, 2003). The best known form of this bituminous binder improvement is by means of polymer modification, traditionally used to improve the temperature susceptibility of bitumen by increasing binder stiffness at high service temperatures and reducing the stiffness at low service temperatures (Airey 2004).

There are numerous studies carried by different researchers about polypropylene (PP) fiber modification in the literature (Maurer and Malasheskie 1989, Brown et al. 1990, Jenq et al. 1993, Simpson and Kamyar 1994, Ohio Department of Transportation 1998, Cleven 2000, Shao-Peng et al. 2006).

Tapkın (2008) has proven that the addition of PP fibers into the asphalt concrete in a dry basis (mixing the aggregate and bitumen first and then adding up PP fibers into the mixture) will alter the mechanical behavior of the mixture in a pronounced manner. Tapkın et al. (2009) have also worked on the addition of PP fibers to the asphalt concrete on a wet basis (mixing PP fibers and bitumen first and then adding aggregate to the modified bitumen). By carrying out repeated load creep tests under different loading patterns, they have shown that the lives of the PP fiber modified asphalt specimens under repeated creep loading at different loading patterns increased by 5–12 times vs. control specimens, which is a very significant improvement.

The static creep test has been used to estimate the rutting potential of dense bituminous mixtures. Up to date, widespread studies utilizing the static creep test as a basis of predicting permanent deformations have been conducted. It has been claimed by the previous researchers that the creep test must be performed at relatively low stress levels (less than 206.9 kPa) and low temperature (less than 40°C); otherwise the sample fails prematurely (Hills 1973,

Van de Loo 1974). The test conditions consist of a static axial stress of 100 kPa being applied to a specimen for a period of 1 hour at a temperature of 40°C (Zurich 1977). This test is in fact an inexpensive and an easy test to carry out but the ability of the test to predict performance is questionable (Özcan 2008). In-place asphalt mixtures are typically exposed to truck tire pressures of approximately 120 psi (828 kPa) and maximum temperatures of 140°F (60°C) or higher (Roberts et al. 1996). Therefore, the conditions of this test do not closely simulate in-place conditions (Roberts et al. 1996, Özcan 2008).

The starting point of this study was this main drawback of the static creep tests that have been carried out worldwide up to date (Özcan 2008). During the first static creep tests that have been carried out by applying 100 kPa axial stress to the specimens at 40°C, the performance prediction was really very questionable. Therefore a completely different loading pattern and testing temperature was adopted all throughout the studies that have been carried out. Also, the optimum PP amount that has to be added into the mixture by the percentage of aggregate has been determined for a dense bituminous by utilizing static creep, Marshall tests and stereo microscopy analyses which differ a lot in many respects from the similar studies carried out up to date (Maurer and Malasheskie 1989, Brown et al. 1990, Jenq et al. 1993, Simpson and Kamyar 1994, Ohio Department of Transportation 1998, Cleven 2000, Shao-Peng et al. 2006).

2 MARSHALL DESIGN

2.1 *Preparation of the marshall specimens*

The standard bitumen was modified in the laboratory with M-03 (multifilament, 3 mm long) PP fibers in a wet basis. Marshall stability and flow tests were carried out and the Universal Testing Machine was used to perform static creep tests. In addition stereo microscopy techniques were used in order to determine the optimum PP amount.

2.2 *Material properties*

In the conducted tests, continuous aggregate gradation has been used to fit the gradation limits for wearing course Type 2 (Highway Technical Specifications 2006). 50/70 penetration bitumen and calcareous type crushed stone were used. Physical properties of the control bitumen, coarse, fine aggregates and the mixture gradation and gradation limits are given in Tables 1 to 4. The apparent specific gravity of filler is 2.785.

2.3 *PP fiber modification*

Base bitumen was modified by PP fibers in a wet basis. The PP fibers were premixed with bitumen using a standard mixer at 500 revolutions per minute for two hours. The mixing temperature was around 165–170°C (Chen and Lin 2005). Only M-03 type fibers were used to modify the bitumen samples according to the workability criteria (Tapkın et al. 2009). Starting with 0.5‰ M-03 type fibers by weight of aggregate, and increasing by 0.5‰ up to 7.0‰, were premixed with bitumen and were used for preparation of standard Marshall specimens (Özcan 2008). The physical properties of the PP fiber based bitumen samples with 0.5–7.0‰ fiber content are given in Table 5.

Table 1. Physical properties of the reference bitumen.

Property	Test value	Standard
Penetration at 25°C, 1/10 mm	55.4	ASTM D 5-97
Penetration Index	–1.2	–
Loss on heating, %	0.0572	ASTM D 6-80
Ductility at 25°C, cm	>100	ASTM D 113-99
Softening point, °C	48.0	ASTM D 36-95
Specific gravity at 25°C	1.022	ASTM D 70-76
Flash point, °C	327	ASTM D 92-02
Fire point, °C	376	ASTM D 92-02

Table 2. Physical properties of coarse aggregates.

Property	Test value	Standard
Bulk specific gravity	2.705	ASTM C 127-04
Saturated surface dry specific gravity	2.714	ASTM C 127-04
Apparent specific gravity	2.729	ASTM C 127-04
Water absorption, %	0.322	ASTM C 127-04
Los Angeles abrasion coefficient (%)	30	ASTM C-131

Table 3. Physical properties of fine aggregates.

Property	Test value	Standard
Bulk specific gravity	2.685	ASTM C 128-04
Saturated surface dry specific gravity	2.717	ASTM C 128-04
Apparent specific gravity	2.776	ASTM C 128-04
Water absorption, %	1.236	ASTM C 128-04

Table 4. Type 2 wearing course gradation.

Sieve size, mm	Gradation limits, %	Passing, %
12.7	100	100
9.52	80–100	90
4.76	55–72	63.5
2.00	36–53	44.5
0.42	16-28	22
0.177	8–16	12
0.074	4–10	7
Pan	–	–

Table 5. Physical properties of control and PP modified samples in different percentages.

PP ‰	Specific gravity	Penetration (dmm)	Softening point (°C)	Ductility (cm)	Loss on heating (%)	Flash point (°C)	Fire point (°C)
0.0	1.022	55.4	48.00	109	0.0572	327	376
0.5	1.021	51.4	48.65	112	0.0346	322	370
1.0	1.020	49.4	49.70	126	0.0325	318	367
1.5	1.018	48.6	50.35	139	0.0316	313	364
2.0	1.017	47.4	51.30	148	0.0278	308	357
2.5	1.016	46.4	51.65	+150	0.0254	299	347
3.0	1.015	45.5	52.05	+150	0.0250	292	345
3.5	1.014	44.8	52.65	+150	0.0208	290	340
4.0	1.013	43.8	53.15	+150	0.0188	289	338
4.5	1.011	42.5	53.70	+150	0.0176	280	335
5.0	1.010	42.0	54.70	+150	0.0163	269	320
5.5	1.009	41.6	55.25	+150	0.0142	260	305
6.0	1.008	41.2	56.15	+150	0.0128	250	296
6.5	1.007	40.4	56.80	+150	0.0115	239	281
7.0	1.005	40.1	57.45	+150	0.0099	220	263

The figures in Table 5 show the positive effect of PP modification to the physico-chemical properties of unmodified bitumen clearly.

Physical properties of the PP fibers used in the study can be found in relevant literature (Tapkın 2008).

2.4 *Proportioning of the bituminous mixtures*

To determine the optimum bitumen content, the bitumen contents corresponding to the mixtures with maximal stability and unit weight, 4% air voids and 70% voids filled with asphalt, were found and averaged according to the acting standards (Highway Technical Specifications 2006). Mainly, two different Marshall designs were carried out. In the first design, the optimum bitumen content was found as 5%. Second design was ended with an optimum bitumen content of 4.96%. Therefore the optimum bitumen content of the unmodified specimens has been taken as 5.0% for research purposes. In both of these designs, bitumen samples were exposed to 170°C heating for 2 hours to resemble the same ageing conditions with PP modified bitumen samples.

3 TESTS FOR THE DETERMINATON OF OPTIMAL PP CONTENT

3.1 *Static creep tests*

The conditions of the static creep tests, starting from seventies and carried up to date, do not closely simulate in-place conditions (Roberts et al. 1996, Özcan 2008). Because of this fact, in this study, first of all, the test temperature has been chosen as 50°C to resemble the real in-situ conditions. Static axial stress of 100 kPa was applied to the specimens as a preloading for 10 minutes and after on, 500 kPa of loading was applied to the specimens for 1 hour to simulate the in-place conditions in a realistic manner. In order to validate this preloading time of 10 minutes, preloading times of 0 to 10 minutes, increasing one by one, has been applied to standard Marshall specimens prepared at optimum bitumen content. All of these specimens were subjected to the same loading regime. It has been verified that 10 minutes of preloading can be accepted as the optimum preloading time (Özcan 2008).

Starting with control specimens, Marshall specimens have been fabricated at the optimum bitumen content with changing PP contents of 0.5‰ to 7.0‰ by aggregate weight with 0.5 ‰ increments. For each PP content, a total of 6 specimens have been prepared. Therefore, in the end, a total of 84 modified specimens have been tested under the static creep test conditions stated above. In order to give a sample for the accumulated strain versus time graphs of the specimens subjected to creep loading, 6.0‰ modified specimens' curves are given below in Fig. 1.

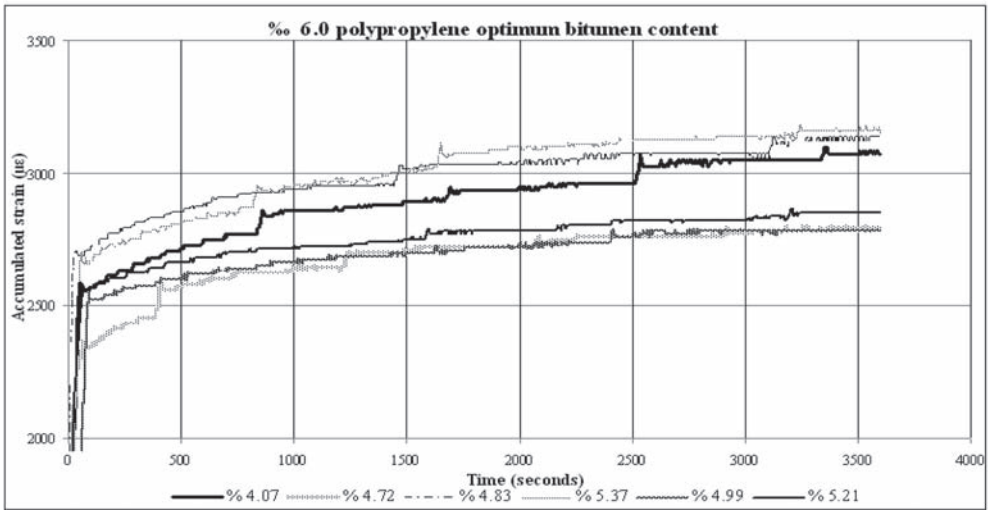

Figure 1. Accumulated strain versus time graphs for 6.0‰ PP modified specimens.

To identify the whole picture of the specimens with different amounts of PP modification, another figure is presented (Fig. 2.). The values stated in Fig. 2. are the average values of the accumulated strains at the end of the static creep tests (Özcan 2008). It can be clearly seen that the accumulated strains at the end of 1 hour of static loading decreases in a noticeable manner due to the addition of PP fibers. Another interesting point is, after 6‰ of PP addition with respect to the total weight of aggregate, the accumulated strains start to increase again. This is a perfect notification to be able to determine the optimal PP amount of the designated mixture.

The initial and final creep stiffness values for the 15 different sets of specimens are drawn correspondingly in Figs. 3 and 4. In these graphs, it can again be clearly seen that 5.5‰ of PP modification is an optimal amount.

One can easily notice form Figs. 2, 3 and 4 that the addition of PP enhances the mixture properties in a very favorable manner. For example, the control specimens have a final

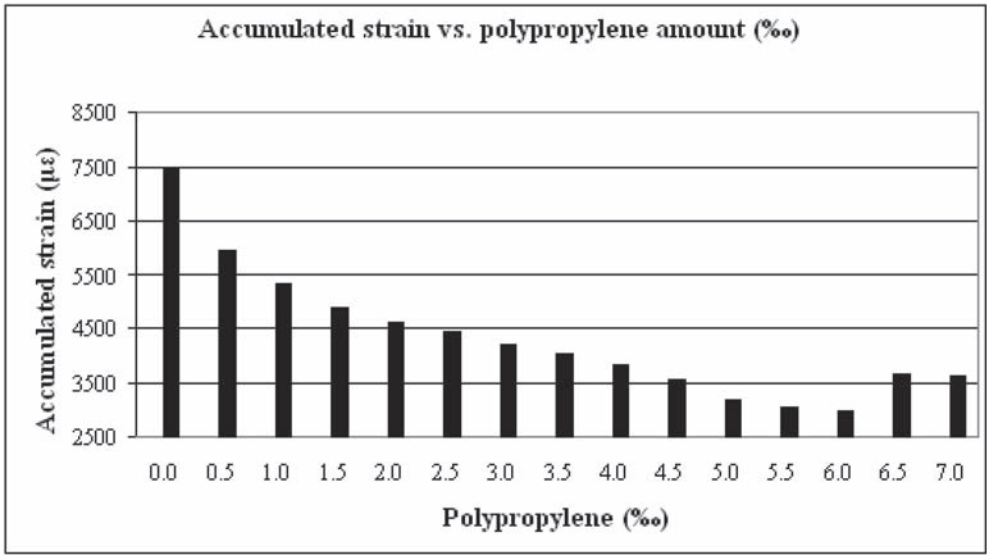

Figure 2. Accumulated strain values for 15 sets of specimens at the end of static creep tests.

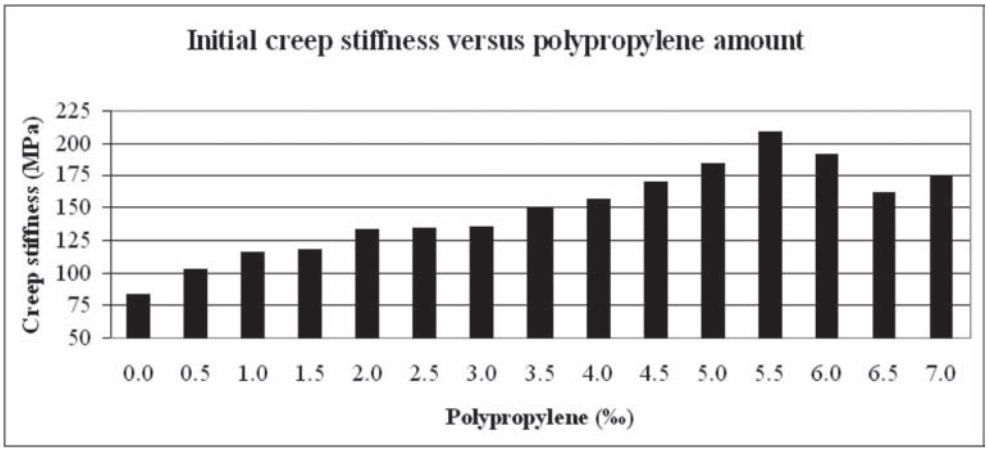

Figure 3. Initial creep stiffness values for 15 sets of specimens at the end of static creep tests.

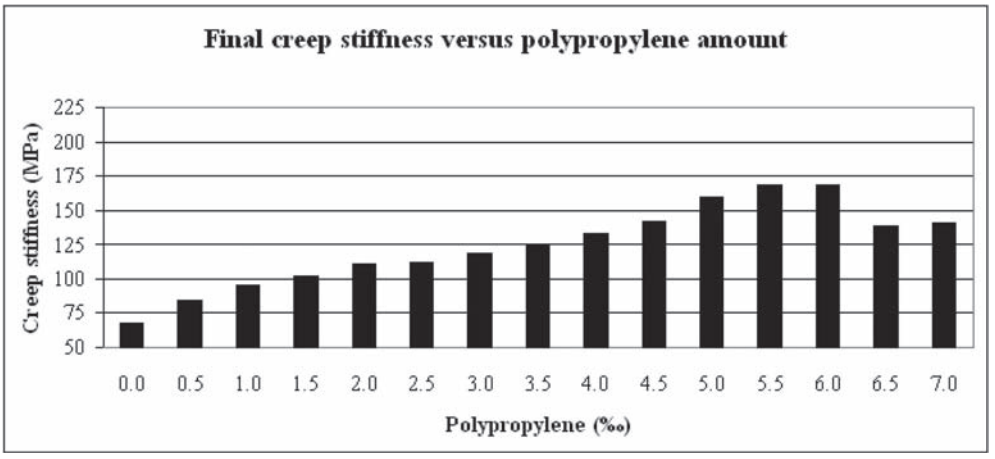

Figure 4. Final creep stiffness values for 15 sets of specimens at the end of static creep tests.

Table 6. The average physical and mechanical values obtained for 15 sets of specimens.

PP (‰)	Unit weight (kg/m³)	Air voids (%)	VMA (%)	Vf (%)	Stability (kg)	Flow (mm)	MQ (kg/mm)
0.0	2465	3.443	14.919	76.990	1294.355	3.463	376.899
0.5	2462	3.569	15.029	76.337	1355.712	3.416	400.559
1.0	2459	3.665	15.114	75.828	1378.510	3.408	405.166
1.5	2452	3.949	15.365	74.449	1391.292	3.388	411.593
2.0	2446	4.195	15.581	73.148	1453.083	3.233	463.103
2.5	2437	4.526	15.873	71.555	1500.593	3.081	490.412
3.0	2432	4.707	16.033	70.710	1542.140	2.982	523.329
3.5	2430	4.818	16.131	70.188	1626.905	2.826	588.954
4.0	2419	5.237	16.500	68.340	1703.500	2.788	618.161
4.5	2406	5.761	16.961	66.112	1837.763	2.748	680.879
5.0	2402	5.895	17.080	65.546	1971.715	2.628	755.850
5.5	2394	6.214	17.360	64.261	1917.643	2.678	724.647
6.0	2414	5.443	16.681	67.429	1989.972	2.984	682.360
6.5	2416	5.359	16.607	68.804	2113.038	3.169	678.393
7.0	2421	5.138	16.412	68.760	2186.930	3.211	683.755

accumulated strain value of 7433.89 με. On the other hand, the 6‰ PP modified specimens have a final accumulated strain value of 2964.50 με. This corresponds to a decrease of approximately 60% and deserves attention. On the other hand, the initial and final stiffness (creep stiffness) values are 83.46 and 67.99 MPa respectively for control specimens. When the 6‰ PP modified specimens are investigated, these values are 191.65 and 169.15 MPa respectively. These values correspond to an increase of 129% in the initial and 149% in the final creep stiffness values and must be highlighted (Özcan 2008).

3.2 *Marshall stability and flow tests*

Marshall stability and flow tests were performed with 90 more specimens. To find the optimal PP amount different tests have been carried out and averaged accordingly for the 15 sets of specimens. These values are stated in Table 6.

It can be visualized from Table 6 that the unit weight values drop by 2.9% until 5.5‰ PP amount is reached and after this point on, tends to increase again. The air voids increase by 80% until 5.5‰ PP amount. The voids in mineral aggregate values increase by 16.4% up to 5.5% addition of PP and start to decrease from this point on. Voids filled with asphalt values show a similar trend (16.5% decrease) up to 5.5‰ PP addition. The average stability values of the control specimens increase up to 70% when 7‰ PP modification is done. This is a dramatic increase when viewed from the pavement engineering point of view. The tendency of flow values are similar (23% decrease). Finally, Marshall Quotient values increase by 92%. At the end of the Marshall designs, the physical and mechanical properties of the 15 sets of specimens show the optimal PP addition of 5.5‰ in a perfect manner.

3.3 *Stereo microscopy techniques*

Stereo microscopy has been used to investigate the morphology of the various polymer modified bitumen samples by investigating the state of dispersion of the polymer within the base bitumen as well as to characterize the nature of the continuous and discontinuous phase. Stereo microscopy is based on the principle that polymers swell due to the absorption of some of the constituents of the base bitumen and due to the fluorescence effect in ultraviolet light (Airey 2002).

PP modified bitumen samples were investigated at room temperature under stereo microscope at a magnification level of 40x. Digital images were captured for 30 sets of specimens (duplicate specimens for all percentages). The images for different modification levels are given below through Figs. 5 to 8.

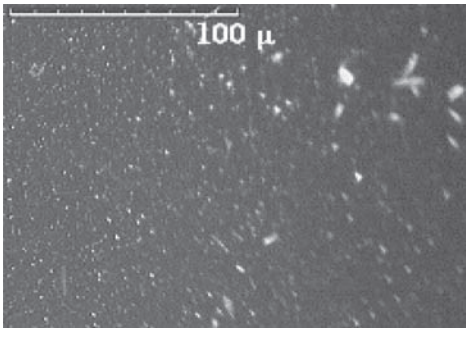

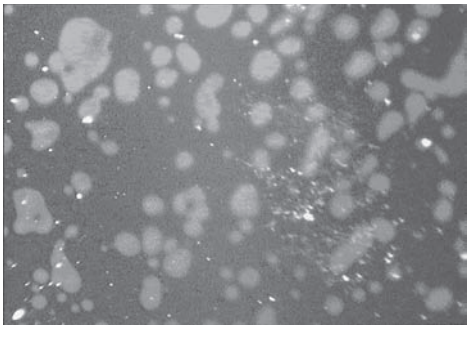

Figures 5 and 6. The stereo microscope image for control specimens with micron bar and 3.5‰ PP modified specimens (left to right).

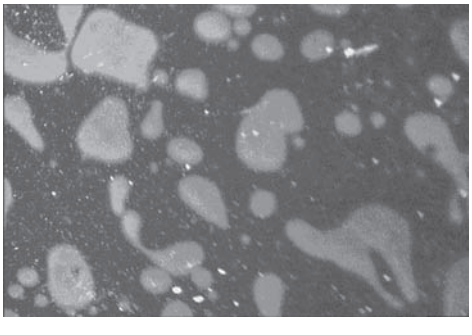

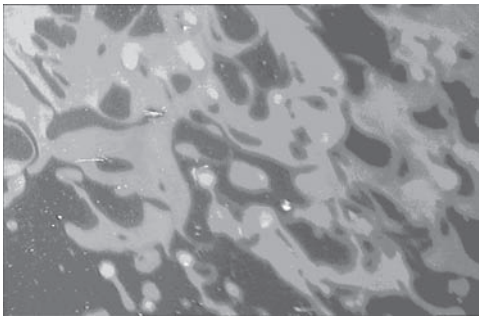

Figures 7 and 8. The stereo microscope image for 5.5‰ and 7.0‰ PP modified specimens (left to right).

When Fig. 6 is examined, it can be seen that the PP particles are distributed in a regular pattern in the bitumen phase. One can visualize that the PP particles tend to become as the dominant phase in Fig. 7. Finally, Fig. 8 shows that the PP particles have formed an irregular phase and bitumen is somehow scattered in between PP particles. This can further be explained by percolation theory (Özcan 2008).

In the light of the stereo microscope investigations, once more, it can be easily concluded that 5.5‰ PP modification is the optimal value.

4 DETERMINATION OF THE OPTIMUM BITUMEN CONTENT OF SPECIMENS PREPARED WITH OPTIMAL PP

Optimum bitumen content has been determined as 5.38% for the modified specimens. This value is only 7.6% more than the optimum bitumen content of the control specimens. Because of the swelling property of PP, more bitumen is needed to prepare same kind of specimens. Therefore for economic analysis, the optimum-optimal bitumen content can be taken as 5.0%.

4.1 *Economical analysis*

With the optimum-optimal bitumen content, new sets of Marshall specimens have been fabricated and static creep and Marshall stability and flow tests were again applied to these specimens. To investigate the economical concerns, 4 different sets of specimens with 3.5%, 4.0%, 4.5% and 5.0% were prepared (6 specimens for each content) and subjected to static creep tests again with the same loading pattern and temperature. To have better insight to the problem, for the six different curves, the values at each time interval were averaged accordingly and a single set of curves was drawn once more with the final accumulated strains shown in the corresponding graphs. An example of this study is given in Fig. 9.

As can be seen from Fig. 9, the permanent accumulated strain is measured as 3055.17 με for specimens prepared with 5.0% bitumen content. This value is only 5.20% less than the accumulated strain of specimens with 3.5% bitumen. Again, this value is 1.36% less than the

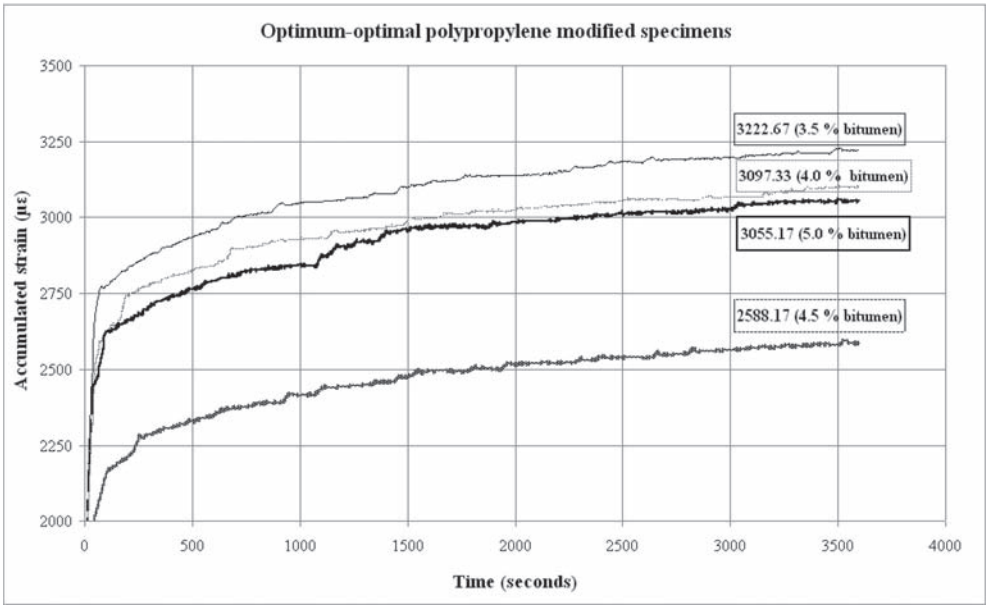

Figure 9. Average accumulated strain versus time graphs for optimum-optimal PP modified specimens.

accumulated strain of specimens with 4.0% bitumen. Besides this value is 18% higher than the accumulated strain of specimens with 4.5% bitumen. In the first glance, it can be said that, the specimens prepared with 4.5% bitumen behave in a very favorable manner when compared to specimens of 5.0%. But in this case, the economy from bitumen is only 10%. So the attention must be focused on the specimens with bitumen content of 3.5%. These specimens, when viewed from the physical properties, have 43% less average air voids contents, 2.7% less average specific gravity values, 5.75% less average voids in mineral aggregate values and finally 53% less voids filled with asphalt values (Özcan 2008). But they behave in a very similar fashion under static creep tests when compared to specimens prepared with 5.0% bitumen content. This really deserves great attention. 3.5% specimens are lighter, having more voids and having much less bitumen than 5.0% specimens. This is really a giant step to the way ahead to new generation of paving products. Altogether, there is an economy of "30%" from bitumen. This is really very important. Altogether the extra cost of using PP fibers as a modifier is only 9.3% (for research purposes only with no addition of technology and know-how of course) but this cost is becoming far more smaller when the dependency to imported expensive modifiers and the know-how being sold besides them. This is a very important item for developing countries.

Marshall test results for specimens prepared with optimal PP amount for economical analysis are given in the relevant literature (Özcan 2008). The physical and mechanical properties of the specimens prepared with 3.5% bitumen content compared with 5.0% bitumen content specimens are as follows: they are lighter, have more air voids and have less bitumen in their structures. Also the Marshall Quotient values are approximately 17% higher than the 5.0% bitumen samples. In the light of these facts, it can be concluded that 3.5% bitumen specimens can be utilized in the designs in a very favorable way.

5 CONCLUSIONS AND RECOMMENDATIONS

The performance characteristics, such as specific gravity, loss on heating, ductility, softening point and penetration of the fiber modified bitumen samples was greatly improved as compared to control specimens. The addition of the PP fibers into the asphalt mixture enhances the mixture properties in a very favorable manner.

Based on the static creep, Marshall tests and stereo microscopy analyses that were carried out with M-03 type PP fiber reinforced specimens, the optimal PP addition amount was determined as 5.5‰.

The physical and mechanical properties of the specimens prepared with 3.5% bitumen content compared with 5.0% bitumen content specimens are as follows: they are lighter, have more air voids and have less bitumen in their structures. Also the Marshall Quotient values are approximately 17% higher than the 5.0% bitumen samples. In the light of these facts, it can be concluded that 3.5% bitumen specimens can be utilized in the designs in a very favorable way. This new generation of high performance paving products can be an attractive solution for the flushing and bleeding problems and rutting phenomena observed especially in very hot climatic environments. Altogether, there is an economy of "30%" from bitumen. This is really very important. Altogether the extra cost of using PP fibers as a modifier is only 9.3% but this cost is becoming far more smaller when the dependency to imported expensive modifiers and the know-how being sold besides them. This is a very important item for developing countries like Turkey.

First of all, the benefits of the PP fiber modification should be evaluated for Superpave mixture designs and Superpave performance tests. Especially Superpave gyratory compactors should be used in preparation of 100 mm diameter specimens and similar mechanical tests should be carried out on these specimens. The static creep tests can be carried out on the PP fiber modified specimens at temperatures above or below 50°C and different loading patterns. Also, PP fiber reinforcement of the bitumen can be examined by the aid of atomic force microscopy. Further, the thin asphalt mixture films can be examined under scanning electron microscopes to be able to identify the bonding patterns of PP with bitumen and

aggregate. Finally, a prospective study may focus on the behavior of the PP modified asphalt specimens at lower temperatures below zero.

REFERENCES

Airey, G.D. 2002. Rheological evaluation of ethylene vinyl acetate polymer modified bitumens. Construction and Building Materials 16(8), 473–487.

Airey, G.D. 2003. Rheological properties of styrene butadiene styrene modified road bitumens. Fuel 82(14), 1709–1719.

Airey, G.D. 2004. Fundamental binder and practical mixture evaluation of polymer modified bituminous materials. The International Journal of Pavement Engineering, 5(3), 137–151.

Brown, S.F., Rowlett, R.D. and Boucher, J.L. 1990. Asphalt modification. Proceedings of the Conference on US SHRP Highway Research Program: Sharing the Benefits, ICE, 181–203.

Chen, J-S. and Lin, K-Y. 2005. Mechanism and behavior of bitumen strength reinforcement using fibers. Journal of Materials Science, 40, 87–95.

Cleven, M.A. 2000. Investigation of the properties of carbon fiber modified asphalt mixtures. M.S Thesis in Civil Engineering. Michigan Technological University, Michigan.

General Directorate of Highways. 2006. Highway Technical Specifications, Item No. 170/2. General Directorate of Highways, Ankara, Turkey.

Hills, J.F. 1973. The Creep of Asphalt Concrete Mixes. Journal of The Institute of Petroleum.

ITEM 400HS. 1998. Standard specification for Asphalt concrete-high Stress using polypropylene fibers, Ohio Department of Transportation, Construction and Materials Specifications, Ohio, USA.

Jenq, Y.S., Chwen-Jang, L. and Pei L. 1993. Analysis of crack resistance of asphalt concrete overlays. A fracture mechanics approach. Transportation Research Record n 1388, pp. 160–166.

Maurer, D.A. and Malasheskie, G. 1989. Field performance of fabrics and fibers to retard reflective cracking, Transportation Research Record n 1248, pp. 13–23.

Özcan, Ş. 2008. The Investigation of the Effect of Polypropylene Fiber Addition to the Static Creep Behavior of Bituminous Mixtures. MS. Thesis. Anadolu University, Civil Engineering Department, Eskişehir, Turkey (in Turkish).

Recommendation for the Performance of Unconfined Static Creep Test in Asphalt Specimens. 1977. Proceedings of the International Symposium on Plastic Deformability of Bituminous Mixes, pp. 335–359, Zurich.

Roberts, F.L., Kandhal, P.S. Brown, E.R., Lee, D.Y. and Kennedy, T.W. 1996. Hot Mix Asphalt Materials, Mixture Design, and Construction. NAPA Education Foundation, Second Edition.

Shao-Peng, W., Gang, L., Lian-Tong, M., Zheng, C. and Qun-Shan, Y. 2006. Effect of fiber types on relevant properties of porous asphalt, Transactions of Nonferrous Metals Society of China, Volume 16, n suppl. 1, 791–795.

Simpson, A.L. and Kamyar C.M. 1994. Case study of modified bituminous mixtures: Somerset, Kentucky, Proceedings of the Third Materials Engineering Conference 804, ASCE pp. 88–96.

Tapkın, S. 2008. The effect of polypropylene fibers on asphalt performance. Building and Environment,43,1065–1071.

Tapkın, S., Uşar, Ü., Tuncan, A. and Tuncan, M. 2009. Repeated Creep Behavior of Polypropylene Fiber-Reinforced Bituminous Mixtures. Journal of Transportation Engineering, ASCE, 135(4), 240–249.

Van de Loo, P.J. 1974. Creep Testing, a Simple Tool to Judge Asphalt Mix Stability. Proceeding of the Association of Asphalt Paving Technologists, Volume 43.

Advanced Testing and Characterization of Bituminous Materials – Loizos, Partl, Scarpas & Al-Qadi (eds)
© 2009 Taylor & Francis Group, London, ISBN 978-0-415-55854-9

Evaluation of Petroleum-Contaminated Soil effect on the properties of hot-mix asphalt concrete using dynamic modulus |E*| and indirect tensile tests

Hossam F. Hassan
College of Engineering, Sultan Qaboos University, Oman (On leave from Cairo University)

ABSTRACT: Petroleum-Contaminated Soil (PCS) can result from leaking oil spills on clean soils, or soils surrounding petroleum refineries and crude oil wells. In Oman, Petroleum Development Oman (PDO) generates approximately 50,000 tons/year of petroleum-contaminated soil (PCS) and faces a real challenge to safely dispose of these quantities. This paper presents the results of using PCS as an fine aggregate substitute in Hot Mix Asphalt concrete (HMA) with a percentage up to 40%, by total aggregate weight. Environmental assessment was performed by analyzing the raw contaminated soil for heavy metals, and hydrocarbons. The Marshall mix design method was used to prepare and test the mixes. As a simple performance test, the dynamic modulus (|E*|) test was conducted on 4 by 8 inches samples prepared at optimum asphalt contents for mixes containing different percentage of PCS. The test was conducted at different temperatures up to 60°C and frequencies 0.1, 0.5, 1, 5, 10, and 16 Hz. Master curves were developed from the testing results. The mixes at optimum asphalt content were evaluated for moisture susceptibility using the indirect tensile strength. The results indicated that the criteria for a surface mixture according to Oman's specifications can be met, with the exception of VMA, with up to 15% of contaminated soil. The tensile strength ratio (TSR) criteria can also be met. The (|E*|) master curves results indicated that the addition of PCS produces mixes that are more susceptible to rutting.

1 INTRODUCTION

Oil spills, leaks, and other releases of petroleum products often result in the contamination of soils and may penetrate down to the groundwater causing serious contamination problems. Petroleum-Contaminated Soil (PCS) is typically a mixture of sand, silt, clay and petroleum products (Meegoda et al. 1993).

Several studies have attempted to use PCS in hot mix asphalt concrete (HMA). In Massachusetts, negotiations with the Massachusetts Department of Environmental Quality and Engineering (DEQE) resulted in allowing the use of contaminated soils containing 3% of oil, gasoline or kerosene and allowing up to 5% contaminated soil replacement for aggregate to produce a good quality HMA (Czarnecki 1998).

Meegoda & Muller (1993) investigated the incorporation of Petroleum-Contaminated Soil (PCS) into HMA in New Jersey and found that it was possible to include up to 35% PCS in the mix. The mixes were evaluated for stability using the Marshall method and durability using the tensile strength ratio for conditioned and unconditioned specimens. Conditioning was done by wet-dry and freeze-thaw cycles. The stability results for PCS compared with control mixes indicated a much better paving material, while the durability was found to be the same as the control mix. The leachability tests showed neither significant concentrations nor significant increase in concentrations with time.

The user experience with the Superpave mix design method and the problems associated with the original SHRP Superpave performance models (Levels 2 and 3) demonstrated the need for a simple performance test (SPT). NCHRP project 9–19 undertook the evaluation of several existing test methods as potential SPT. The results from these tests were correlated

with actual performance field data form MnRoads, WES Track, and FHWA Accelerated Loading Facility (ALF). A total of 33 test parameters were investigated. The results indicated that the dynamic modulus ($E^*/\sin\varphi$) among two other test parameters correlates well (R^2 of 0.9) with the field data (Witczak et al. 2002).

The dynamic modulus |E*| of HMA is one of the fundamental inputs in the mechanistic-empirical (M-E) pavement design guide developed in NCHRP Project 1–37A. Tran & Hall (2006) conducted a study for determining laboratory-measured dynamic modulus for use in the M-E design guide. The study focused on evaluating different testing protocols, and recommended testing two replicates with four measurement instruments for conducting the dynamic modulus test.

Daniel & Lachance (2004) examined the effect of different Recycled Asphalt Pavements (RAP) percentages on the complex modulus and creep compliance of asphalt concrete. The study found that the addition of 15% RAP increased the stiffness but decreased the creep compliance. This indicated that the mixture containing RAP will be more resistant to permanent deformation and less resistant to fatigue and thermal cracking in the field. Further addition of RAP did not follow the expected trends.

Mohammad et al. (2006) conducted a study to evaluate the permanent deformation of six mixes based on laboratory tests including the dynamic modulus. One of the main conclusions of the study was that the predicted rut depth from the 2002 M-E pavement design software followed the same trend found in the |E*| test results at high temperature.

Sebaaly et al. (2007) investigated the effect of hydrated lime and a liquid anistrip agent on the mechanical properties of and Idaho HMA mixture. |E*| in compression was one of the used tests. The study indicated that both dry and moisture-conditioned lime mixture can be considered less susceptible to rutting based on their higher compression modulus at various frequencies compared with the evaluated liquid antistrip agent.

Clyne et al. (2003) conducted a study on four different mixes to determine the complex modulus |E*| and the master curves and to compare the modulus values with the results of the 2000 predictive equations. The master curves for two of the four mixes agreed with the Witczak's predictive equations reasonable well.

This paper investigates the effect of using PCS in hot mix asphalt concrete with a percentage up to 40% by aggregate weight on the dynamic modulus (|E*|) and indirect tensile strength properties.

2 MATERIAL PHYSICAL PROPERTIES

The materials used in this study consisted of four aggregates and mineral filler in addition to a petroleum-contaminated soil (PCS). The mix was composed of 20 mm and 10 mm coarse aggregate sizes. The sand sizes were 3–5 mm and 0–3 mm. The contaminated soil was obtained from the Fahud treatment area in northern Oman. The grain size distribution and specific gravity for the aggregate and contaminated soil were determined.

Figure 1 shows the gradation of the aggregate, PCS and mineral filler. The PCS gradation indicates that 95% of the soil sample falls in the range between 4.75 and 0.075 mm, which is mainly the range for sands. The bulk specific gravities of the soil were 2.13. The liquid limit

Table 1. Aggregate specific gravity and absorption.

	Aggregate size (mm)				
Sieve size (mm)	20	10	3–5	0–3	Mineral filler
Bulk specific gravity	2.812	2.805	2.795	2.790	–
Apparent specific gravity	2.848	2.845	2.834	2.833	2.750
Absorption (%)	0.45	0.5	0.45	0.5	–

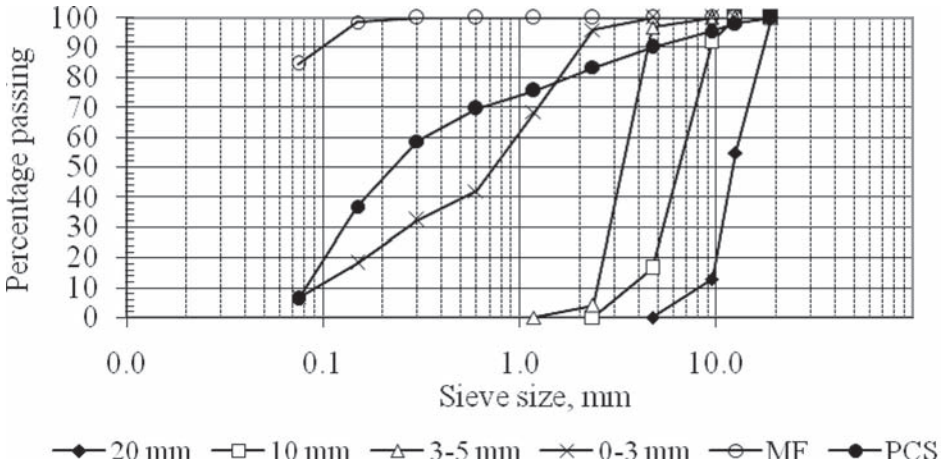

Figure 1. Aggregate and PCS gradation.

Table 2. Volatile organic compounds (VOC), non-halogenated VOC, and semi-volatile organic compounds (SVOC) tested for in the extract.

Bis (2-chloroethyl) ether	3-nitroaniline	1,2,4-trichlorobenzene	Dibutyl phthalate
2-chlorophenol	Acenaphthene	Naphthalene	Fluroanthene
1,2-dichlorobenzene	Dibenzofuran	4-chloroaniline	Pyrene
1,3-dichlorobenzene	2,4 dinitrotoluene	Hexachlorobutadine	Benzyl butyl phthalate
1,4-dichlorobenzene	Diethyl phthalate	4-chloro-3-methylphenol	Benz [a] anthracene
2-methylphenol	Fluorene	2-methylnaphthalene	Chrysene
4-methylphenol	4-chlorophenyl phenyl ether	Hexachlorocyclo pentadine	Bis (2-ethylhexyl) phthalate
Hexachloroethane	4-nitroaniline	2,4,6-trichlorophenol	di-n-octyl phthalate
Nitrobenzene	Azobenzene	2,4,6-trichlorophenol	Benzo [b] fluoranthene
Isophorone	4-bromophenyl phenyl ether	2-chloronaphtalene	Benzo [k] fluoranthene
2-nitophenol	Hexachlorobenzene	2-nitroanelene	Benzo [a] pyrene
2,4-dimethylphenol	Phenanthrene	Dimethyl phthalate	Indeno [1,2,3-cd] pyrene
Bis (2-chloroethomethane)	Anthracene	2,6 dinitrotoluene	Dibenz [a,h] antharacene
2,4-dichlorophenol	Carbazole	Acenaphthylene	Benzo [ghi] perylene

was found to be 21% and the plastic limit was NP (non-plastic). The soil was classified as poorly-graded sand (SP) according to the Unified Soil Classification System (USCS) system. The specific gravity of the aggregate and mineral filler is shown in Table 1.

3 ENVIRONMENTAL ASSESSMENT OF PCS

The gravimetric method USEPA 9071B (1998) was used in this study for separating water, oil and solids in the PCS sample and hence estimating the moisture, hydrocarbons and total heavy metals. Trichloroethylene was used as the extraction solvent.

The TPH concentration was found to be 68,000 mg/kg (6.8%), by dry weight of the soil. Concentrations of specific volatile organic compounds (VOC), non-halogenated VOC, and semi-volatile organic compounds (SVOC) listed by USEPA were measured using the GC/MS. Table 2 shows a list of hydrocarbons tested for in the extract. The results of concentrations indicated low undetectable levels.

Table 3 presents the total heavy metal content for the petroleum-contaminated soil. Table 3 shows that it contains a relatively high concentrations of nickel (Ni), followed by relatively

Table 3. Total heavy metal contents in PCS.

Heavy metal	Cd	Ni	Pb	Cr	V	Cu	Zn
Metal content (mg/kg)	<1.0	184.25	11.905	52	2.96	15.4	27.6

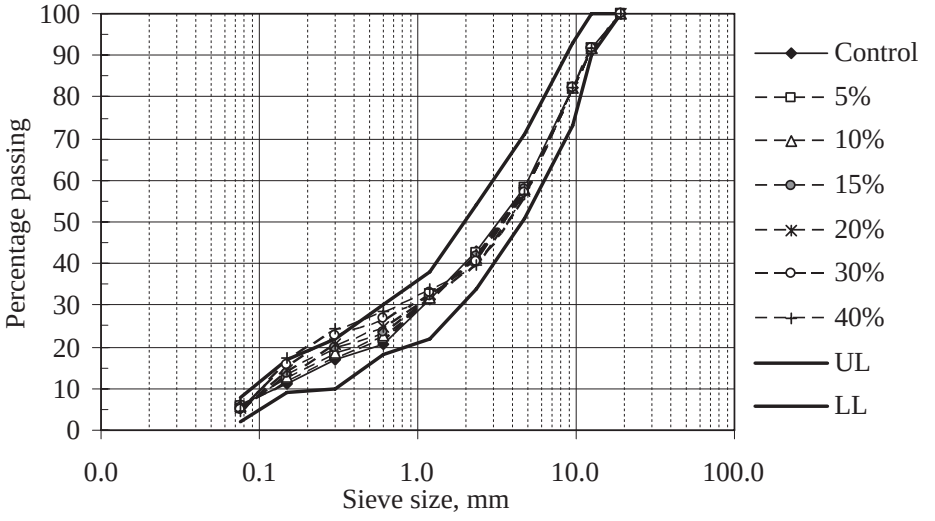

Figure 2. Blend gradation for different PCS mixes.

lower concentrations of chromium (Cr), zink (Zn), copper (Cu), lead (Pb), and vanadium (V) in decreasing order. The high concentrations of nickel can be attributed to the composition of natural soil, as some natural soils are known to be rich in certain metals such as nickel (USDA 2001).

4 MIX DEISGN

Different mixes were prepared by replacing the 0–3 mm fine aggregate by PCS with different percentages. The resulting percentages of PCS were 0 (control), 5, 10, 15, 20, 30, and 40%, by total aggregate weight. The used binder was penetration grade 60–70 asphalt cement. The control mix was designed to meet the Oman specification for wearing course class B (DGR 1994). The aggregate and PCS blend gradations as well as the specification limits for a class B wearing course according to Oman's specifications are shown in Figure 2.

The mix design was performed according to Marshall mix design method. The trial range of asphalt content was 3.5 to 5.5%, by total weight of the mix, in 0.5% increments. The evaluated mix properties were stability (failure load), flow (corresponding deformation), bulk specific gravity (BSG), air voids (AV), voids in mineral aggregate (VMA) and voids filled with bitumen (VFA).

The selection of the optimum asphalt content was based on satisfying the air voids, and flow limits, and maximizing the stability value. Following this procedure, the obtained optimum asphalt cement content (AC) is shown in Table 4, together with the Marshall mix criteria at the optimum asphalt content. For PCS, up to 15% of contaminated soil replacement can be made while meeting the Omani specifications. An exception would be the VMA which is lower than the minimum limit. However, when compared with the Asphalt Institute specification, higher percentage of replacement (up to 40% PCS) can be used in mixes for medium or light traffic surface or base course layers.

Table 4. Optimum asphalt content for different PCS mixes.

OCS (%)	AC (%)	Binder[a] (%)	Stability (kN)	Flow (mm)	BSG	AV (%)	VMA (%)	VFA (%)
0 (control)	4.1	4.1	20.0	3.01	2.484	5.5	15.1	63.7
5	3.5	3.8	24.3	2.63	2.510	5.3	13.1	58.8
10	3.5	4.2	24.3	2.63	2.539	3.5	11.7	69.9
15	3.5	4.5	13.8	2.95	2.539	3.7	11.5	67.7
20	3.5	4.9	10.4	3.39	2.530	4.4	11.4	70.0
30	3.5	5.5	6.2	3.44	2.460	6.8	13.3	48.1
40	3.5	6.2	4.7	3.80	2.402	9.4	14.6	35.7
Spec.[b]	3.5–5.5	–	14, min	2–4	–	3.5–5.5	15, min	63–75
AI[c]–light	–	–	3.3, min	2–4.5	–	3–5	Variable[d]	70–80
AI[c]–medium	–	–	5.3, min	2–4	–	3–5	Variable[d]	65–78
AI[c]–heavy	–	–	8.0, min	2–3.5	–	3–5	Variable[d]	65–75

[a]Asphalt cement and oil; [b]Oman wearing course class B; [c]Asphalt Institute (1995) traffic level; [d]varies according to the design air voids (from 13% to 15% for % AV from 3 to 5%).

5 DYNAMIC MODULUS

5.1 *Sample preparation*

Samples of 4 inches in diameter by 8 inches in height were prepared using static compaction with a 4000 kN compression machine, according to ASTM D 1074. Testing of the samples was performed according to AASHTO TP62-03 using an MTS 810 system. The bulk specific gravity of the resulting samples were within a range of 95.5 to 102% of that achieved at optimum asphalt content for different PCS percentages. The samples were tested at 0.1, 0.5, 1, 5, 10 and 16 Hz frequency and at 25, 30, 40, 50, and 60°C. The environmental chamber was fabricated in-house and equipped with a digital thermostat and a datalogger to verify the conditioning and testing temperature of the samples.

To determine when the specimen has reached testing temperature (equilibrium), a dummy specimen was placed inside the environmental chamber and a thermistor was mounted at the center. The temperature of the chamber is set at the desired testing temperature, and the temperature of both the chamber and the dummy sample were monitored using the data acquisition system. The measured data indicated that the equilibrium was reached after 4–5 hours.

The vertical displacement was measured using two extensometers. Figure 3 shows a sample before testing. Sulphur capping was used on both faces of the sample to provide plane surfaces. The extensometers were mounted between two rings fixed at a gauge length of 100 mm. Two fixed strips extend from the rings to the surface of the sample. Another strip moves with a tightening screw to be in contact with the sample surface. All three strips have an inner surface radius of 4 inch. The rings were fixed on the sample using three removable guiding rods. Once the rings were fixed, the extensometers were vertically aligned on opposite sides of the sample, and the guiding rods removed.

5.2 *Test results*

Figure 4 shows the average |E*| results of two samples at 5 Hz, as an example, at different temperatures. The figure indicates, as expected, that the modulus decreases as the testing temperature increases. With the exception of 5% PCS, the addition of PCS to the mix decreases the modulus progressively from 10 to 40% PCS. It is to be noted that the 5% PCS mix has a binder content of 3.8% while for the control mix and other PCS percentages, the binder content is 4.1% and higher. This could be a contributing factor to the higher stiffness of the 5% PCS mix.

The dynamic modulus master curves were developed based on the fact that the mechanical behavior of the mixes is viscoelastic and is therefore dependant on temperature and time of

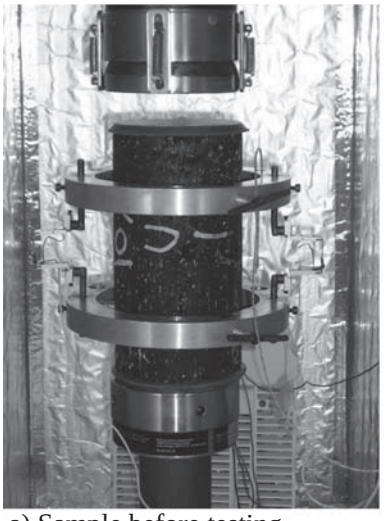

a) Sample before testing

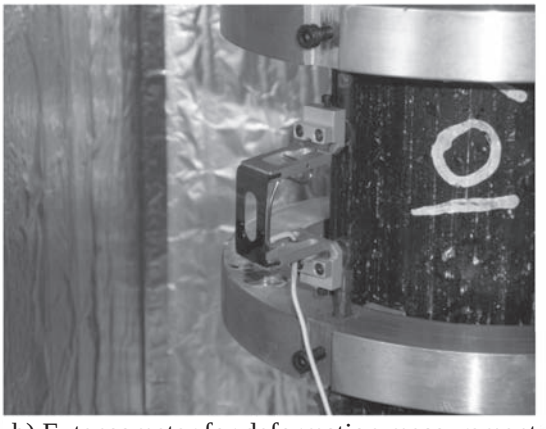

b) Extensometer for deformation measurement

Figure 3. Dynamic modulus test setup.

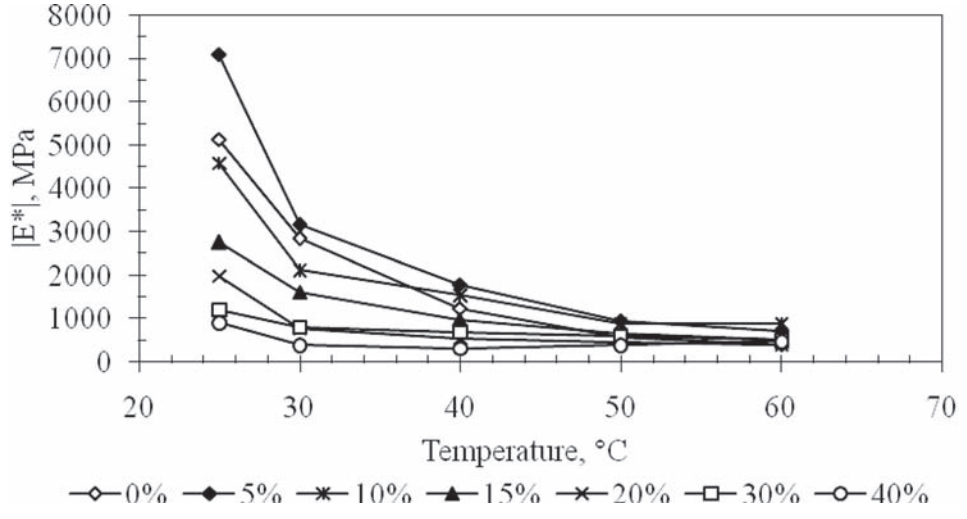

Figure 4. Dynamic modulus test result at 5 Hz.

loading or frequency. Data collected at different temperatures are shifted relative to the time of loading and the data is aligned to form a single curve (Timothy et al., 2003). Master curves are constructed from the test data fitting a sigmoidal function (Pellinen & Witczak 2002). The data is fitted to the following equation using the Marquardt-Levenberg algorithm for non-linear best fit equation. SigmaPlot program was used to perform the regression analysis.

$$\log|E^*| = \delta + \frac{\alpha}{1 + e^{\beta - \gamma(\log(f) + S_T)}} \quad (1)$$

where Log $|E^*|$ = log of dynamic modulus; δ = minimum modulus value; α = span of modulus; values, β, γ = shape factors; f = frequency; S_T = shift factor according to temperature. The regression analysis resulted in an R^2 in the range of 0.89 to 0.99 for different mixes.

Table 5. Model fit parameters.

Parameter	0%	5%	10%	15%	20%	30%	40%
α	1.3207	1.357	0.895	1.293	1.0994	0.9084	0.8098
β	–1.1387	–0.7847	–1.1857	–0.4177	–0.5364	–0.2179	–1
δ	–0.4373	–0.323	–0.3071	–0.6154	–0.6023	–0.5486	–0.7645
γ	1	1.3306	2.0627	1.0646	1.5198	1	1.4115

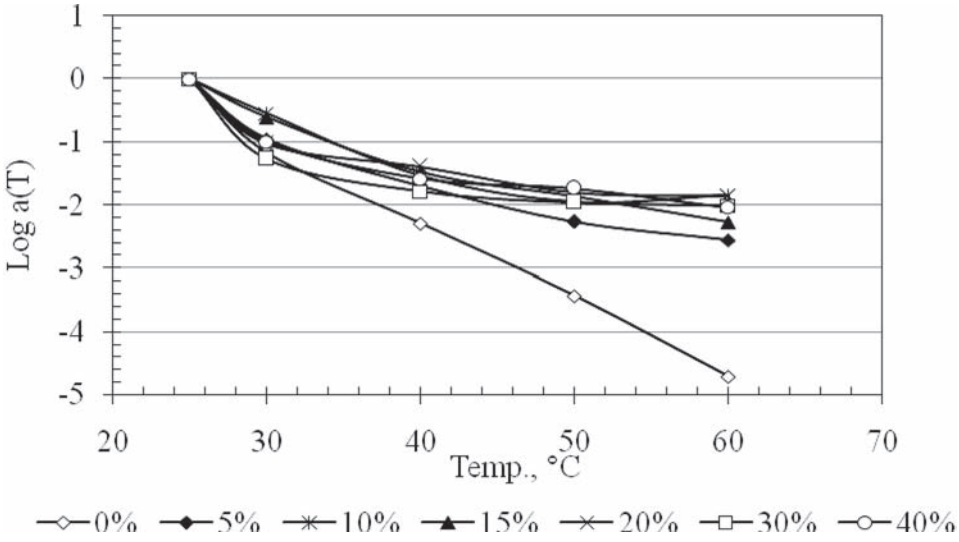

Figure 5. Shift factors versus temperature for different mixes.

The model fit parameters are shown in Table 5. Figure 5 shows that similar shift factors were obtained for PCS mixes (5% and above). The factors follow a smooth trend in the form of a second-order polynomial with respect to temperature with an R^2 in the range of 0.92 to 0.99.

The resulting |E*| master curves for a reference temperature of 25°C are shown in Figure 6. The curves indicate the expected increase in modulus value with the increase in frequency of loading. Furthermore, the results of the fitted curves, in general, are consistent with the measured data, as the modulus decreases through all the range of frequencies when PCS content is increased in the mix. Again, the 5% PCS mix shows a higher modulus at loading frequencies higher than 1 Hz. The low frequency behavior of the material is representative of that at slow or standing traffic or high temperature, which are critical conditions for permanent deformations. The trend shown by the dynamic modulus master curves indicates that the addition of PCS produces mixes with less resistance to rutting.

6 INDIRECT TENSILE TEST

The moisture susceptibility of the mixtures at optimum asphalt content was evaluated using the AAHTO T283 test. The result of this test is the indirect tensile strength (S_t) and tensile strength ratio (TSR). For each mix, two sets of three specimens each were prepared. One set was tested at 25°C and the other set (conditioned) was subjected to one cycle of freezing and thawing then tested at 25°C.

Figure 7 shows the average indirect tensile strength (S_t) for three specimens for both dry and wet sets at optimum asphalt content for each PCS percentage (left axis). The results

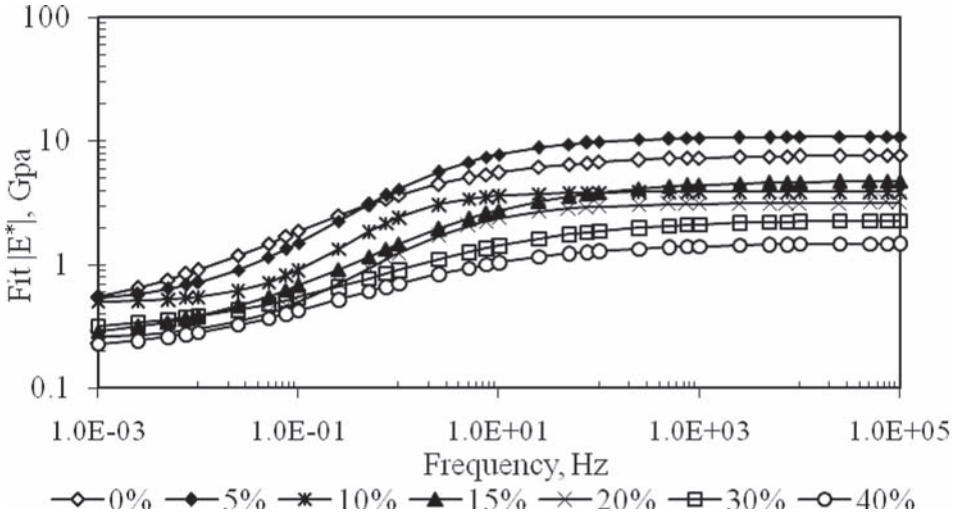

Figure 6. Dynamic modulus master curves.

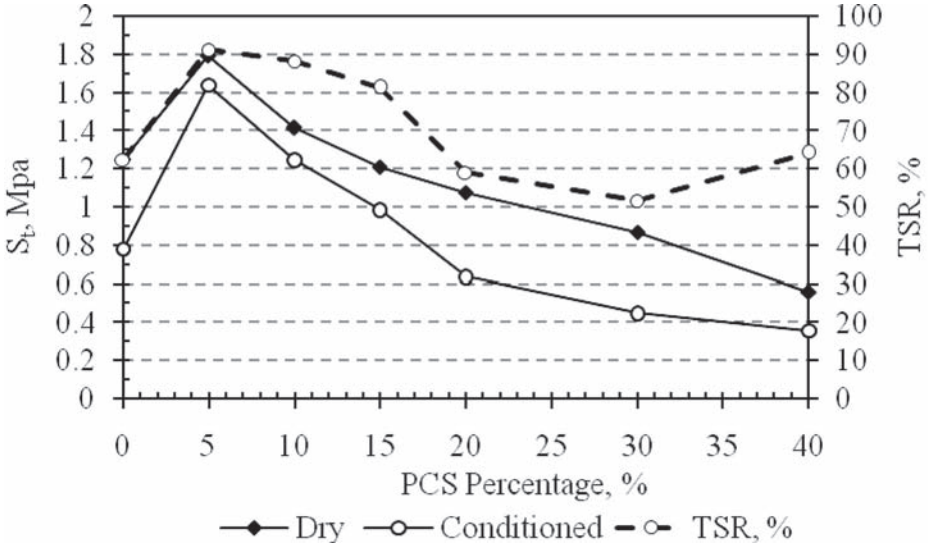

Figure 7. Indirect tensile strength and TSR test results.

indicate an increase in IDT for the 5% PCS which is consistent with the stability and |E*| results. At higher percentages of PCS, a gradual decrease is noticed. The tensile strength ratio (TSR) is shown on the right axis. The results indicate that the ratio remains above 80% (normal acceptance criteria) for PCS contents up to 15%. TSR values in the range of 59 to 64% are obtained with higher PCS contents.

7 CONCLUSIONS

This paper investigated the mechanical properties of hot mix asphalt concrete containing petroleum-contaminated soil up to 40% by aggregate weight. The mix design criteria for a surface mixture according to Oman's specifications can be met, with the exception of VMA, with up to 15% of contaminated soil.

The dynamic modulus increased with the increase in frequency and decrease in temperature. In general, it decreased as the percentage of contaminated soil was increased. The (|E*|) master curves results indicated that the addition of PCS produces mixes more susceptible to rutting. The shift factors obtained from the fitting of the modulus results indicated a smooth trend versus temperature. The results were similar for mixes containing 5% or more PCS. The tensile strength results were consistent by indicating generally a decrease in tensile strength as the PCS content increases. The tensile strength ratio criteria is satisfied for the mixes containing up to 15% PCS.

Further investigations need to done in predicting permanent deformation, fatigue and thermal cracking for the mixes containing different percentages of contaminated soil.

REFERENCES

American Association of State Highway and Transportation Officials. AASHTO T283-89. Standard Method of Test for Resistance of Compacted Bituminous Mixture to Moisture Induced Damage. Washington D.C.

American Association of State Highway and Transportation Officials. AASHTO TP62-03. Standard Method of Test for Determining Dynamic Modulus of Hot-Mix Asphalt Concrete Mixtures. Washington D.C.

American Society for Testing and Materials (ASTM). ASTM D 1074-96. Standard Test Method for Compressive strength of Bituminous Mixtures.

ARA, Inc., ERES Consultants Division. 2004. *Guide for Mechanistic-Empirical Design of New and Rehabilitated Pavement structures. NCHRP Report 1-37A.* Transportation Research Board, National Research Council. Washington, D.C.

Asphalt Institute. 1995. Mix Design Method for Asphalt Concrete and Other Hot Mix Types. Asphalt Institute Manual Series 2, Sixth Edition.

Clyne, T.R., Li. X., Marasteanu, M.O. & Skok, E.L. 2003. Dynamic and Resilient Modulus of Mn/DOT Asphalt Mixtures. Minnesota DOT Research Report Final Report 2003–09.

Czarnecki, R.C. 1998. Making Use of Contaminated Soil. *Civil Engineering* 58(12): 72–74.

Daniel, J.S. & Lachance, A. 2005. Mechanistic and Volumetric Properties of Asphalt Mixtures Containing Recycled Asphalt Pavement. *Transportation Research Record* 1929:28–36.

Directorate General of Roads (DGR). 1994. General Specifications for Roads. Ministry of Transport and Communications. Directorate General of Roads. Sultanate of Oman.

Meegoda, J.N. & Muller, R.T. 1993. Petroleum Contaminated Soils in Highway Construction. In *Recovery and Effective Reuse of Discarded Materials and By-Products for Construction of Highway Facilities*: 4-83–4-95. Denver, Colorado.

Mohammad, L.N., Wu, Z. & Obuareddy S. 2006. Permanent Deformation Analysis of Hot-Mix Asphalt Mixtures with Simple Performance Tests and 2002 M-E Pavement Design Software. *Transportation Research Record* 1970: 133–142.

Sebaaly, P.E., Little, D., Hajj, E.Y. & Bhasin, A. 2007. Impact of Lime and Liquid Antistrip Agents on Preperties of Idaho Hot-Mix Asphalt Mixture. *Transportation Research Record* 1998: 65–74.

Timothy, R.C., Xinjun, L., Mihai, O.M. & Eugene, L.S. 2003. *Dynamic and Resilient Modulus of Mn/DOT Asphalt Mixtures*. Research Report 2003–09. Minnesota Department of Transportation. Research Services. St.Paul, Minnesota.

Tran, N.H. & Hall, K.D. 2006. Evaluation of Testing Protocols for Dynamic Modulus of Hot-Mix Asphalt. *Transportation Research Record* 1970: 126–132.

United States Department of Agriculture (USDA). 2001. *National Program Annual Report on Soil Resource Management*. Agriculture Research Service.

US EPA. 1998. *N-Hexane Extractable Material (HEM) for Sludge, Sediment, and Solid Samples, Office of Water Method 9071B.* United States Environmental Protection Agency.

Witczak, M.W., Kaloush, K., Pellinen, T., El-Basyouny, M. & Von Quintus, H. 2002. *Simple Performance Test for Superpave Mix Design, NCHRP Report 465.* Transportation Research Board, National Research Council. Washington, D.C.

Advanced Testing and Characterization of Bituminous Materials –
Loizos, Partl, Scarpas & Al-Qadi (eds)
© 2009 Taylor & Francis Group, London, ISBN 978-0-415-55854-9

Overview of the LOT meso mechanical research into porous asphalt raveling

M. Huurman
Delft University of Technology, Delft, The Netherlands

L. Mo[1,2]
[1]*Delft University of Technology, Delft, The Netherlands*
[2]*Wuhan University of Technology, Wuhan, P.R. China*

M.F. Woldekidan, R.N. Khedoe & J. Moraal
Delft University of Technology, Delft, The Netherlands

ABSTRACT: More than 70% of Dutch primary road network is surfaced with PA (Porous Asphalt Concrete). Raveling is in most cases by far decisive for PA service life.

This paper gives a summarized overview of the development and validation of a mechanistic Lifetime Optimization Tool for PA, LOT. LOT is based on meso scale modeling, i.e. the scale of stone chippings. The paper discusses a laboratory research into the behavior of the mixture components. The forces acting on individual surface stones during tire passages are also discussed. Finally FE models of the PA mixture's structural geometry are discussed.

At the end of the paper the above is brought together to form LOT. For validation purposes full-scale raveling tests on four mixtures were done. For each mixture LOT calculations are compared to real PA performance. This validation indicates a very strong correlation between LOT and full-scale PA raveling performance.

1 INTRODUCTION

PA (Porous Asphalt Concrete) is the standard surfacing material for the Dutch primary road network. More than 70% of this network is surfaced with PA. This is mainly due to the advantages that follow from PA application, i.e. reduced traffic noise and no splash and spray in wet weather conditions.

Raveling, the loss of stone from the road surface, is in most cases by far determinative for PA service life and directly related to PA performance and not much dependant on the structural design of the pavement. Since the introduction of PA in the Netherlands in the mid 1980s empirical research increased the service life of PA on slow lanes from approximately 6 years to an average of 10 years today. In the previous decade, however, the steady growth of PA service life came to a stand still. For this reason the DVS (Centre for Transport and Navigation of the Dutch Ministry of Transport, Public Works and Water Management) started a 5 year research into PA raveling in 2002. The Delft University of Technology, DUT, is involved in meso scale mechanistic modeling of asphaltic materials since the early 2000s (Huurman *et al*., 2003; Huurman *et al*., 2004; Milne *et al*., 2004). On the basis of this work the DUT suggested to make use of meso scale modeling to obtain insight into the in-mixture phenomena that play a role in raveling. The plan to develop LOT was accepted by the DVS and in 2006 the DUT was commissioned to execute her plans.

The LOT program aims for the development of a meso scale mechanistic tool that gives insight into in-mixture phenomena taking place during tire passages. Use is made of Finite Element (FE) models. The chosen approach requires information and modeling of; the PA mixture geometry, the PA mortar response, the load signals on individual surface stones, PA mortar fatigue behavior and finally the fatigue behavior of the PA stone-mortar adhesive

zone. To quantify the effects of aging and water ingress, the properties of aged material components and retained specimens are also investigated.

This paper gives a summarized overview of the LOT project and briefly discusses all mentioned modeling issues. At the end of the paper LOT is validated using full scale tests done at the STUVA tests centre in Germany (van Hinthem 2007; ISAC 2007). For more detailed information reference is made to www.vbk.tudelft.nl where most LOT reports are available on-line.

2 MIXTURE DESIGN STRATEGY

Three basic insights form the basis of the LOT mixture design strategy:

1. Pavements and pavement materials have a life expectancy that is larger than 10^5 load cycles in any realistic case. The damage that accumulates in a single load cycle is thus very small and negligible in structural response calculations for mechanistic design purposes.
2. The response of any structure depends on three pillars, i.e. 1) structural geometry, 2) loading and 3) material behavior. (Boundary conditions translate into 1 or 2)
3. By respecting the three pillars phenomenological laboratory research may be brought up one level of scale by structural modeling, i.e. mixture performance follows from mixture component behavior provided that mixture structural models are available.

On the basis of these insights a simple and effective design strategy was chosen for LOT. In this strategy PA is modeled as a structure on the scale of individual stone chippings. Due to the choice of scale three material components are defined, i.e. mortar, stone and stone-mortar adhesive zones. Insight into material component properties (mortar response and mortar & adhesive zone fatigue) is obtained by means of phenomenological laboratory research. Combined with insights into surface contact stresses this information is input for a PA structural model. The outputs of this model are, amongst others, stress and strain signals. These signals, combined with knowledge of component damage development, allow the determination of PA service life. LOT is discussed in more detail elsewhere (Huurman, 2008).

3 PA STRUCTURAL MODEL

3.1 *Three models*

Three types of models have been developed, i.e. 2D-idealised, 3D-idealised and 2D-photo, see Figure 1. Use is made of the ABAQUS FE platform and combined the models give complete insight into in-mixture phenomena. The 2D-idealised model is most practical and foreseen to serve as *THE* mixture design tool in practice. By comparison of the 2D- and 3D-idealised models the effects of 2D modeling become known. Similar the effects of the idealized geometry are obtained by comparing the 2D-idealised and 2D- photo models. Adhesive zones are present in all models. These zones are 10 μm thick and only visible in blow-ups, see Figure 1.

3.2 *Idealized geometry*

The most important assumptions implemented to generate the idealized structural geometry on the basis of real mixture properties are the following. The size of the perfect spheres in the idealized models equals the average particle size (on basis of mass grading percentages) in the stone fraction (d > 2 mm) of the mixture of interest. The thickness of the mortar film surrounding the spheres is determined on the basis of volumetrics. The distance between stone particles is determined by assuming hexagonal packing while respecting the void ratio in the represented PA mixture. Finally the geometry of the mortar film in the contact area is adjusted so that the distance between stone particles is properly reflected in the idealized models. Hereto it is assumed that mortar is squished away from the contact area to form a filled surrounding the contact area. Figure 2 indicates that the fillet volume, V_2, is made equal to the volume of squished away mortar, V_1. The dimensions of the fillet are computed on the basis of 3D spheres.

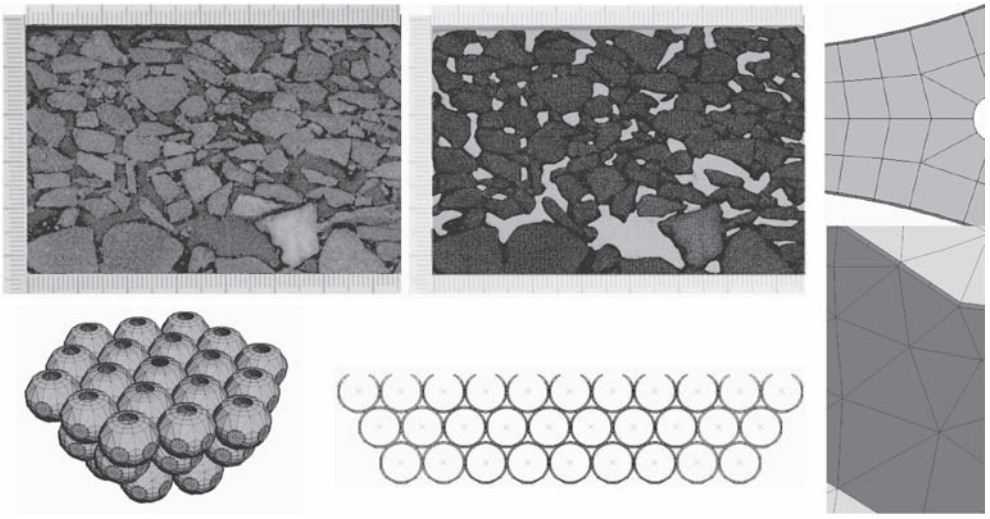

Figure 1. Three types of FE models in LOT; 3D-idealized (left bottom), 2D-idealized (mid bottom) and 2D-photo model with original photo (top). Impressions of modeled adhesive zones in blow-ups (right).

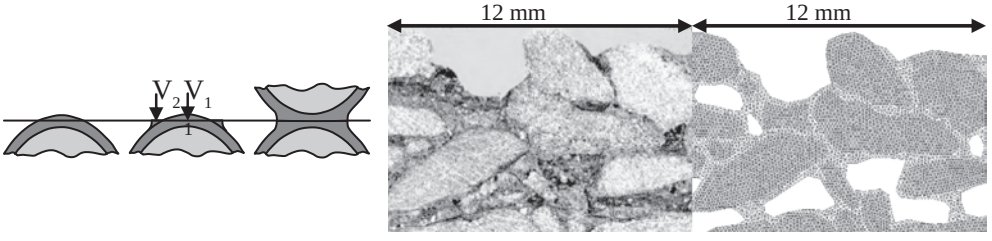

Figure 2. Left: fillets form around the contact areas so that $V_1 = V_2$ in a 3D world. Right: Detail of photo and detail of derived model (right).

3.3 *Photo model geometry*

The geometry of the photo models is copied from photos of real PA cross-sections. Use is made of photos of in-service PA made by the Danish Road Institute (Nielsen 2006) and of photos of the PA mixtures in the validation tests discussed at the end of the paper (Huurman 2008). For the transformation of photo to structural model first the outlines of voids and stones are defined by human action. Due to clogging material in the voids of in-service PA the transfer of photo to structural model is not 100% objective for in-service PA. This is illustrated in Figure 2 which gives a detail of a typical photo model and related photo of in-service PA.

4 MATERIAL COMPONENT BEHAVIOUR

4.1 *Involved materials*

The LOT laboratory test program considered mortar consisting of; Cariphalte XS SBS modified bitumen, Wigro 60 limestone filler with 25wt% hydrated lime and sand <0.5 mm. Two types of stone were considered; Bestone and Greywacke. The four PA mixtures involved in the full-scale validation test, see section 6, are produced using the exact same raw materials as tested. To obtain insight into the effects of aging both Short Term Aged, STA (1½ hour in oven at mixing temperature) and Long Term Aged, LTA (1000 hour protocol involving

air, UV, temperature and moisture, Hagos 2008) materials were tested. The effects of water ingress were tested by submerging specimens to water under vacuum for 1 hour.

All specimens are on a scale that equals the scale of their PA application, i.e. relevant specimen dimensions vary from approximately 3 mm to 6 mm. In the LOT philosophy the treatment (aging or water subjection) of materials may modify their mechanical properties, so leading to a new type of (modified) material.

Paper size does not allow to discus test program in detail, reference is made Huurman (2008) and Khedoe *et al*., (2007). Hereafter an overview of the test program is discussed.

4.2 *Mortar response*

In a 2-term Prony series constitutive model is applied for mortar response.

$$E(t) = E_0 \cdot \left(1 - \alpha_1 \cdot \left(1 - \exp\left(\frac{-t}{t_1}\right)\right) - \alpha_2 \cdot \left(1 - \exp\left(\frac{-t}{t_2}\right)\right)\right) \tag{1}$$

where; $E(t)$ = Time dependant stiffness [MPa]; E_0 = Instantaneous stiffness [MPa]; α_1, α_2 = stiffness reduction parameters [–]; t = time [s]; t_1, t_2 = time constants [s].

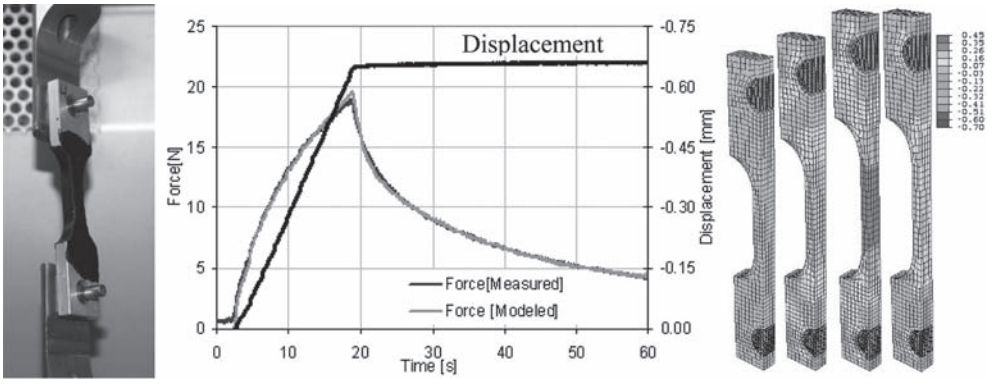

Figure 3. DTT relaxation test, results and back calculation and model of the test.

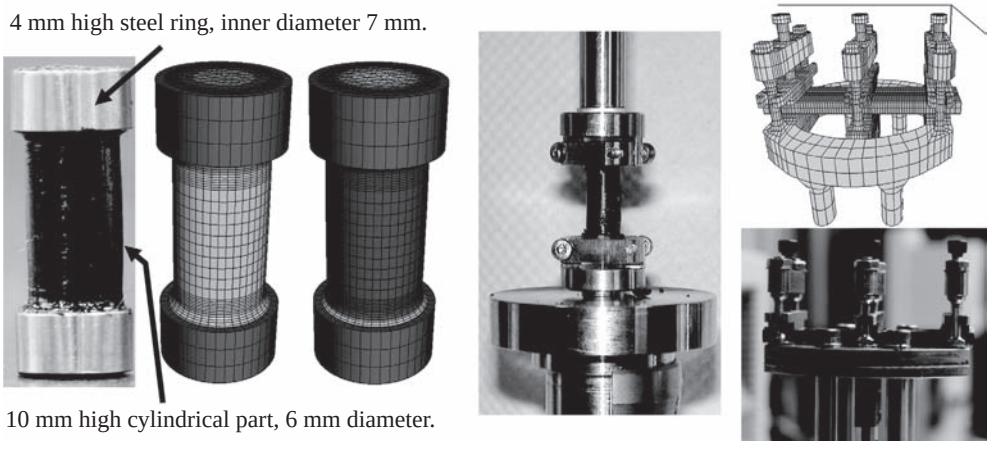

Figure 4. From left to right; specimens for DSR G* and DMA uniaxial E* testing, FE modeling of DMA uniaxial E* tests, specimen mounted in DSR and DMA dual cantilever E* test model and photo.

The five stiffness parameters (E_0, α_1, α_2, t_1 and t_2) can be determined accurately by utilization of a relaxation Direct Tension Test (DTT). Such tests are done on bone shaped mortar specimens, see Figure 3. In total 125 DTTs were done (56 STA; 17 retained STA and 52 LTA) at temperatures ranging from –10 to 20^{0}C. The elongation rate varied from 0.001 to 300 mm/min.

Figure 3 gives typical DTT relaxation test data. The figure indicates that the 2-term Prony series model is very capable in describing the response. It is noted that a FE model of the DTT is used to help interpret the measured data. This model takes the test geometry into account, so that the measured response can be related solely to material behavior. To generalize the DTT relaxation test data a total of 10 frequency sweep tests were done on STA, STA retained, LTA and LTA retained specimens. Three types of frequency sweep tests were done; 6x Dynamic Shear Rheometer, DSR G* test, 2x Dynamic Material Analyzer, DMA dual cantilever E* test, 2x Dynamic Material Analyzer, DMA uniaxial E* test. For the DSR G* and DMA uniaxial E* measurements use was made 20 mm high mortar columns with a 6 mm diameter. This test was specially designed for LOT. An impression of the involved tests is given in figure 4.

Figure 4 indicates that FE models are again used to compensate for geometrical issues so allowing relating the measured response to material behavior solemnly. Combined the tests resulted in the following:

- The VE 2-term Prony series parameters of STA, STA retained, LTA and LTA retained mortar are known over a wide range of temperatures and frequencies. This allows for PA mixture simulations on meso scale, i.e. LOT simulations.
- Water ingress has no significant effect on mortar response behavior.
- The response behavior of mortar changes due to aging.

For a more detailed discussion of the mortar response measurements and parameter determination reference is made to (Khedoe *et al.*, 2007; Huurman *et al.*, 2007a).

4.3 *Adhesive zone response*

An estimate of the 10 μm thick adhesive zone stiffness is made by consideration of the mortar E* and G* (see section 4.2) by application of the following equations.

$$k_n = E^*/0.01\,\text{mm} \quad \text{and} \quad k_s = G^*/0.01\,\text{mm} \tag{2 and 3}$$

where; k_n= adhesive zone normal stiffness [MPa/mm]; k_s= shear stiffness [MPa/mm].

4.4 *Mortar fatigue*

DSR mortar fatigue tests have been done on mortar column specimens shown in Figure 4. In total 78 DSR shear fatigue tests were performed on STA, STA retained, LTA and LTA retained specimens. Tests were performed at 10 and 40 Hz at temperatures of 0 and 10^{0}C in torque controlled mode. In the fatigue tests the specimens are subjected to oscillatory torque while measuring both rotational deformation and phase lag. Failure is indicated by a smooth but sudden increase of both deformation and phase lag.

The fatigue data was best described by a model that relates the mortar fatigue life to the energy dissipated in the initial cycles. The model is given by Equation 4. To allow regression on the total data set the model parameters n and W_0 are linearly related to temperature.

$$N_f = \left(W_0/W_{\text{initial}}\right)^n \tag{4}$$

where; n = material constant [-]; W_0 = reference energy [MPa]; W_{initial} = Dissipated energy per cycle in initial phase [MPa].

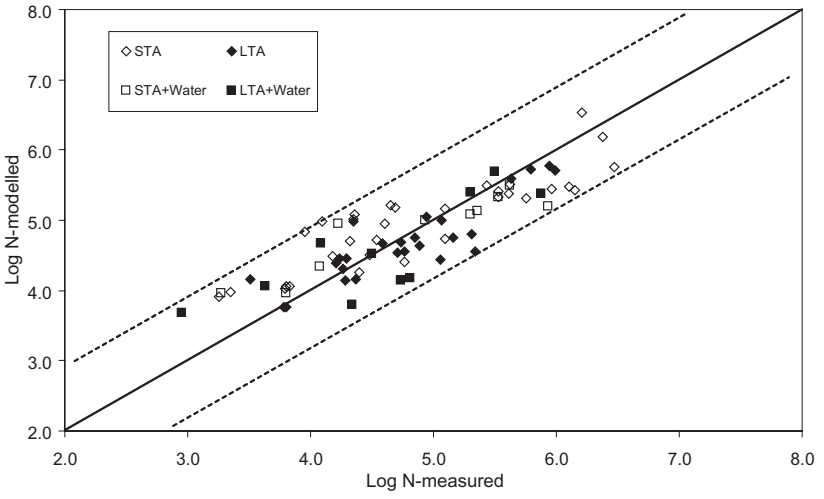

Figure 5. Indication of fit between measured data and the dissipated energy fatigue model.

The obtained fit of the model is visualized in Figure 5, indicating a good fit. The mortar fatigue tests resulted in the following:

- The fatigue properties of STA, STA retained, LTA and LTA retained mortar are known at relevant temperatures. Allowing determination of the fatigue life of mortar bridges on the basis of in-mixture stress-strain signals, i.e. interpretation of LOT simulation results.
- The fatigue behavior of STA mortar differs strongly from the behavior of LTA mortar.
- A much smaller difference is observed between water retained specimens and specimens that were not subjected to water.

Reference is made to (Khedoe *et al.*, 2007; Huurman *et al.*, 2007b) for more detailed information about testing and parameter determination.

4.5 *Adhesive zone damage*

Initial adhesive zone damage tests were developed at the Wuhan University of Technology (Mo *et al.,* 2006; Mo *et al.,* 2007) and further optimized during the LOT project. A good impression of the damage development in the stone-bitumen adhesive zone is obtained by performing destructive force controlled DSR and DMA tests on specimens that consist of two stone columns "glued" together by a thin bitumen film, see Figure 6. Specimen preparation is beyond the scope of this paper and discussed elsewhere (Khedoe *et al.*, 2007; Huurman *et al.*, 2007b). Here it stated that the thickness of the bitumen film between the stone columns is set to 15 μm.

Tests are done on STA, LTA, STA retained and LTA retained specimens. Two types of stone are involved, Bestone and Greywacke. A total of 95 destructive DSR tests are executed. In these tests a sinusoidal torque with a frequency of 10 Hz is applied to the specimen. In the DMA two types of tests are performed. In total 55 dynamic DMA tests were performed in which a 10 Hz haversine tension signal is applied. Also 16 static DMA tests were performed. In these later tests a constant tensile stress is applied to the stone columns.

Each of the tests was prolonged until fracture of the stone column specimens. Results of the tests were described by the equations below. Complete failure is indicated when D reaches the value of 1. Tests were done at temperatures ranging from -10^0C to 20^0C. To allow regression on the total data set the model parameters ϕ, n_0 and W_0 are linearly related to temperature.

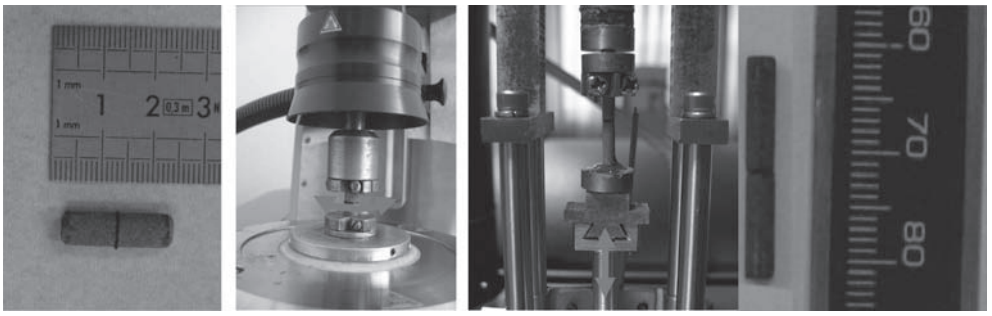

Figure 6. Stone column specimens for DSR (left) and DMA (right). Specimens mounted in machines and indication of loading DSR (mid left), DMA (mid right).

$$\dot{D} = \left(\frac{\sigma_{et}}{\sigma_0} \right)^{n_0} \quad \text{for } \sigma_{et} > 0, \quad \dot{D} = 0 \quad \text{for } \sigma_{et} \leq 0 \quad \text{with} \quad \sigma_{et} = \sigma_n + \tau / \tan\phi \qquad (5)$$

where; $\dot{D}$ = Rate of damage accumulation [–/s]; σ_{et} = equivalent tensile stress, i.e. tensile stress in the case of zero shear [MPa]; σ_n = adhesive zone normal stress [Pa]; τ = adhesive zone shear stress [MPa]; ϕ = friction angle [degr.]; n_0 = model parameter [-]; σ_0 = reference stress [MPa].

Figure 7 gives a visual impression of the obtained model fit. The adhesive zone damage tests resulted in the following:

- The damage properties of STA, STA retained, LTA and LTA retained adhesive zones are known for relevant temperatures for both Bestone and Greaywacke. This allows for the determination of the service life of adhesive zones on the basis of in-mixture stress signals, i.e. interpretation of LOT simulation results.
- With aging the performance of adhesive zones improves.
- Water ingress reduces the strength of adhesive zones, however, effects remain limited.

Reference is made to (Khedoe *et al.*, 2007; Huurman *et al.*, 2007b) for more detailed information about testing and parameter determination.

4.6 *Stone behavior*

In LOT stone chippings are modeled rigidly, no damage can develop in the modeled stones.

5 PA SURFACE LOAD MODEL

The PA surface load model was first developed to load models of surfacing seals (Huurman *et al.*, 2003; Huurman *et al.*, 2004). The model is based on contact pressure measurement data reported in literature (de Beer *et al.*, 1997; Groenendijk, 1998). On the basis of these measurements force signals for individual surface stones are derived, see Figure 8. As shown, surface stones are loaded by vertical, transversal and longitudinal forces during a tire passage. Close observation if figure 8 indicates a difference in the longitudinal load signal introduced by the first and second tire. This is because the first wheel is un-driven, while the second wheel is driven.

6 VALIDATION OF LOT

6.1 *Full scale test*

Validation tests should be as realistic as possible and take place in a controlled environment. The circular Accelerated Pavement Test, APT, at STUVA in Cologne, Germany (van Hithem,

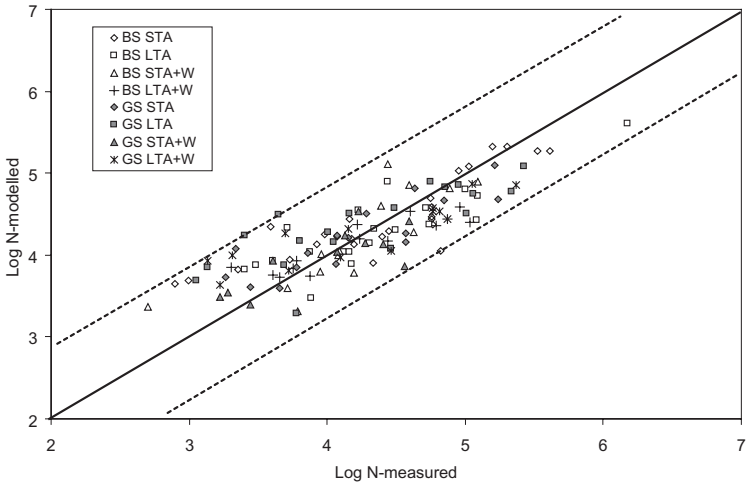

Figure 7. Impression of the adhesive zone damage model; combined DSR dynamic, DMA dynamic and DMA static data.

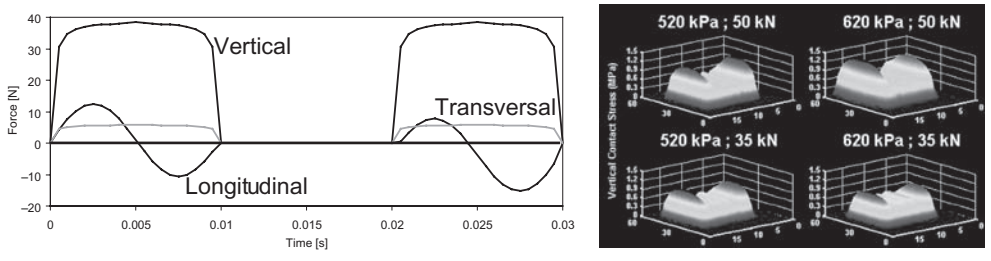

Figure 8. Example of applied load signals (left) and measurements by de Beer (1997) (right).

Figure 9. Left to right; test slab construction by using regular road building equipment, retrieval of test slabs, view on STUVA's APT.

Table 1. Top layer mixture composition.

Mixture	A	B	C	D
Aggregate	Greywacke	Greywacke	Bestone	Bestone
Bitumen content	6.3%	5.2%	6.6%	5.4%
Void content (desired/achieved)	20%/24.9%	26%/27.4%	20%/21.6%	26%/25.0%

2007; ISAC, 2007) fulfilled all demands for LOT validation. It is an indoor APT allowing for a constant and controlled pavement temperature of 10^0C. It has a circular track, allowing a realistic speed of 80 km/h and introducing some additional shear so enhancing the development of raveling. The APT machine allows for the application of real loads, i.e. a 50 kN wheel load applied via a Goodyear 425/65R22.5 G286A 165KL TL super singe tire inflated to 850 kPa.

STUVA's APT has a 10 m diameter, i.e. the test section has a total length of about 31.5 m. The test section consists of 16 parallelograms. Ordinary road building equipment was used to construct the test sections, see Figure 9. Four double layer PA mixtures were tested. In all cases the lower layer consisted of PA 11/16 mm with a void content of 18.8% and 4.2% bitumen. Variations were in the PA 4/8 mm top layer, see Table 1. All involved mixtures were produced form the material components (raw materials) involved in the discussed laboratory test program.

To eliminate dynamical effects the founding base of the APT was leveled with great care in advance of the test. Simulations by the University of Eindhoven indicated that tire load fluctuations due to dynamical effects remained within limits (Lopez *et al.*, 2007).

6.2 *Results and validation*

A total of 700,000 wheel load applications have been applied. Laser texture measurements by the German Bundesanstalt für Strassenwesen (BASt) gave detailed pictures of the surface texture, see Figure 10. From these measurements the Integral der Differenzen or integral of differences can be computed (ISAC 2007) which is an objective measure for raveling damage.

The raveling damage was also assessed by detailed inspection of the PA surface at the STUVA APT by a certified Dutch visual inspector. The results of this visual inspection were expressed in a score. Figure 10 gives an impression of the similarity between raveling damage assessed per texture measurement and per visual inspection.

The surface load applied by the 50 kN wheels that travel the circular track in the STUVA APT is complex. From other research (Lopez *et al.* 2007) it is known that an increased shear stress in the order of 0.3 MPa is generated as a result of the circular wheel path. An additional shear surface loading was therefore applied in the validation calculations. The material component properties applied in the validation simulations followed directly from the discussed laboratory research.

LOT was firstly validated on the basis of 2D-idealised models generated on the basis of mixture design inputs. The results of this validation were so promising that it was decided to extend the project. Four tested parallelograms were brought to the Delft University of Technology for two purposes. The first was to verify that the mortar in the tested mixtures is indeed the same as the mortar in the LOT laboratory research. Hereto additional laboratory

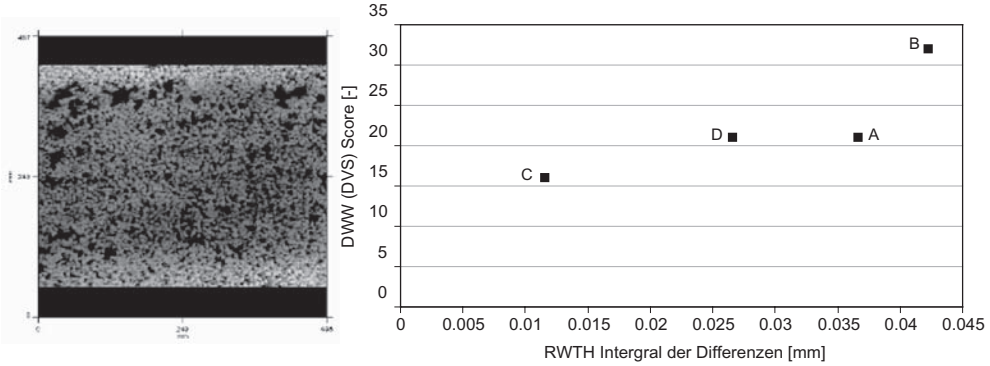

Figure 10. Laser texture measurement by BASt and comparison between raveling damage as per texture measurement (horizontal axis) and as per visual inspection (vertical axis), letters indicate the mixtures.

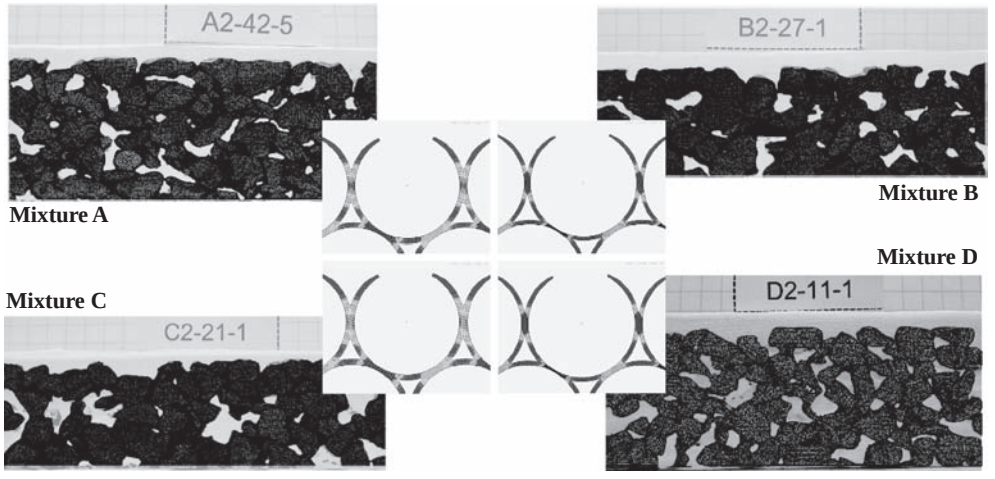

Figure 11. Impression of the geometry of the 2D-idealised models generated to validate LOT on the basis of the STUVA APT test (centre) and photo models of the in situ mixtures (out side).

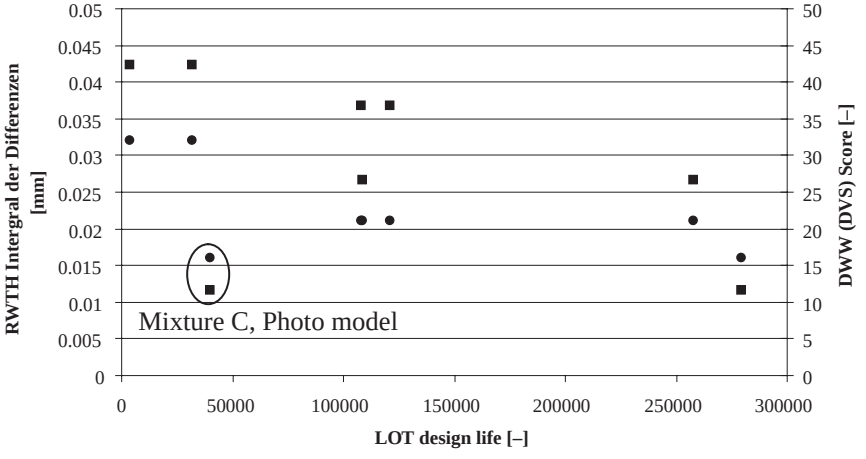

Figure 12. Graphical impression of the validation results.

tests were done on mortar retrieved from the slabs. Secondly the slabs were used to construct 2D photo models of the in situ mixtures tested in Germany.

It was shown that the mortar in the validation test has the same mechanical behavior as the mortar in the LOT laboratory research. And, photo models of the in situ mixtures were made. Figure 11 gives an impression of these photo models. Close observation of Figure 11 shows that the photo models are plotted over the photo's used to generate them.

A visual impression of the validation results is given in Figure 12. This figure gives the LOT determined life expectancy on the horizontal axis plotted against raveling damage in the STUVA tests on the vertical axes. Circular markers are used for damage determined via visual inspection and plotted against the right vertical axis. Damage determined from texture scans is plotted against the left vertical axis by rectangular markers. It is noted that the figure indicates the results of validation on the basis of the 2D idealized models as per mixture design and validation on the basis of the photo models of the in situ mixtures.

In a perfect world raveling damage determined by visual inspection would be the same as damage detected by texture measurements, so that the circular markers would fall over

the rectangular markers. Furthermore the more damage accumulated during the APT test the shorter the mixture service life. Combined this would lead to data points sitting on the diagonal from the upper left to lower right corner of figure 12.

As shown by Figure 12 most data points are fairly close to the described diagonal, indicating the validity of LOT. This is especially true when one appreciates the difference between visual inspection and texture measurements. As indicated, however, results obtained by the photo model of mixture C do not follow the general trend. The reason for this is unknown; however the most obvious explanation is that a weak spot in mixture C was used to come to the mixture C photo model.

7 CONCLUSIONS

The following conclusions have been drawn on the basis of the LOT project.

- It is possible to make use of meso scale mechanics to get insight into asphalt concrete mixture behavior and performance.
- Tests required to obtain the mechanical properties of various mixture components are feasible and available.
- Insight into the tire surface loading with ample detail is available from other research and literature.
- LOT model predictions are in good agreement with observed PA performance, indication that the chosen approach is not only feasible but also in good agreement with real material performance.
- The Accelerated Pavement Test at STUVA was an excellent way to validate LOT.
- In the STUVA APT non mechanical effects such as the effects of water ingress, chemical attack, aging, etc. are absent. The development of raveling in that test thus indicates that raveling may be introduced by the sole effects of repeated mechanical action, i.e. fatigue.
- Meso scale mechanics will enable performance based design of composite road building materials in the near future. It is shown that a meso scale mechanistic mixture design approach gives insight into in-mixture phenomena taking place during tire passages. On the basis of these insights the structure of, and raw materials used in a mixture may be optimized to obtain better performance, i.e. mechanistic performance based mixture design.

ACKNOWLEDGEMENT

The DVS is acknowledged for funding the project and for their trust in involved researchers. Wuhan University of Technology, Eindhoven University of Technology, STUVA, Heijmans, BASt, ISAC and RWTH Aachen are acknowledged for their kind cooperation with the Delft University of Technology.

REFERENCES

Beer M., C. Fisher, & F. Jooste, "Determination of pneumatic tyre/pavement interface contact stresses under moving loads and some effects on pavements with thin asphalt surfacing layers", *8th international conference on asphalt pavements*, Seattle, USA, ISAP, 1997.

Groenendijk J., "Accelerated Testing and Surface Cracking of Asphaltic Concrete Pavements", *PhD Thesis, Delft University of Technology*, The Netherlands, 1998.

Hinthem P. van, "LOT-rundlaufanlage, Construction and transport of asphalt plates (In Dutch: Vervaardiging en transport asfaltproefplaten)", *Heijmans infra*, The Netherlands, 2007.

Hagos E.T., "The Effect of Aging on Binder Properties of Porous Asphalt Concrete", *PhD Thesis, Delft University of Technology*, The Netherlands, 2008.

Huurman M., T. Scarpas, C. Kasbergen, & T. Milne, "Development of a structural FEM for Road Surfacing Seals", *International Conference on Computational & Experimental Engineering & Sciences (ICCES '03)*, Corfu, Greece, 2003.

Huurman M., M. van de Ven. Ven, & C. Kasbergen, "Material modelling on aggregate scale? Road to the future (in Dutch: Materiaalmodellering op korrelniveau? Weg naar de toekomst)", *CROW wegbouwkundige Werkdagen*, Ede, The Netherlands, 2004.

Huurman M., & M. Woldekidan, "LOT, Mortar response; measurements, test interpretation and determination of model parameters", *Delft University of technology, Laboratory of Road and Railway engineering, Report 7-07-170-3*, The Netherlands, 2007a.

Huurman M., L. Mo, "Lifetime Optimisation Tool, Fatigue in mortar and adhesive zones; measurements, test interpretation and determination of model parameters", *Delft University of Technology, Laboratory of Road and Railway engineering, Report 7-07-170-2*, The Netherlands, 2007b.

Huurman M., "Lifetime Optimisation Tool, LOT, Main Report", *Report 7-07-170-1, Delft University of Technology*, the Netherlands, 2008.

ISAC, Institut für Straßenwesen Aachen; RWTH Rheinisch Westfälische Hochschule Aachen, "Lifetime Optimisation Tool (LOT), Schlussbericht, (in German)", Aachen, Germany, 2007.

Khedoe R., & J. Moraal, "Sample preparation and laboratory testing for the LOT research program", *Delft University of Technology, Laboratory of Road and Railway engineering, Report 7-07-170-4*, The Netherlands, 2007.

Lopez A., R. Steen, "Prediction of Tyre/Road Contact Stress Distributions", *Report DCT 2007.106, Dynamics and Control Group, Eindhoven University of Technology,* Eindhoven, The Netherlands, 2007.

Milne T., M. Huurman, C. Kasbergen, A. Scarpas, "Prototype Behavioural FEM Model for Road Surfacing Seals", *International Conference on Computational & Experimental Engineering & Sciences (ICCES '04)*, Madeira, Portugal, 2004.

Mo L., S. Wu, M. Huurman, A. Molenaar, & T. Cao, "Damage accumulation model for monotonic and dynamic shear fracture of asphalt-stone adhesion", *Theoretical and Applied Fracture Mechanics, 46, 140–147*, 2006.

Mo L., M. Huurman, S. Wu, & A. Molenaar, "Finite-element analysis and experimental study on tensile fatigue behaviour of bitumen—stone adhesion", *Fatigue & Fracture of Engineering Materials and Structures, 30, 823–831,* 2007.

Nielsen C., "Ravelling of porous pavements, Experimental procedures", *Danish Road Institute*, Hedehusene, Denmark, 2006.

Advanced Testing and Characterization of Bituminous Materials – Loizos, Partl, Scarpas & Al-Qadi (eds)
© 2009 Taylor & Francis Group, London, ISBN 978-0-415-55854-9

Monitoring the introduction of Enrobé à Module Élevé class 2 onto UK roads

R.C. Elliott, R. Perera & A. Hunter
Scott Wilson Limited, Chilwell, Nottingham, UK

J.C. Nicholls & N.B. Meite
Transport Research Laboratory, Wokingham, UK

D. James
Highways Agency, Dorking, UK

ABSTRACT: Over the last decade there has been a general trend in the UK to use progressively stiffer base materials, due to their expected 'long life' performance. However, recent concerns over the durability of these materials have led to the introduction of high modulus asphalt with higher binder content, known as Enrobé à Module Élevé class 2 (EME2). Although the performance of EME2 has been documented in France, there is little UK experience of the material, in particular relating to its 'buildability' and durability. Therefore, the early sites with EME2 in the UK are being monitored in order to ensure that the anticipated benefits are actually being achieved. This work includes a review of the mixture design; obtaining data on the laying and compaction temperatures and weather conditions, incorporating any comments from the Contractor's Construction Report; undertaking an assessment of the material performance, including mixture design data, site data and the relevant specification requirements and, in some cases; undertaking annual Falling Weight Deflectometer (FWD) testing and subsequent back analysis. The testing programme established to monitor the construction and performance of EME2 sites in a consistent manner was designed to be reactive in that, if a pavement starts to exhibit a certain mode of damage, it is realigned to focus on that problem. The assessment of EME2 will help to contribute to the longer life of road materials, with better value for money, reduced need for maintenance and improved sustainability. Any extension of the life of asphalt roads will increase the time intervals between maintenance, with benefits to the road user in terms of reduced congestion, and improved safety. The results from several sites (predominantly inlays) have shown the actual performance achieved on site by a range of contractors with this base material. Overall, the objective is to support the Highways Agency in its intention to achieve wider use of EME2 for base and binder course layers on its road network.

1 INTRODUCTION

The Highways Agency is re-investigating the potential advantages of using high modulus asphalt materials on UK pavements despite the unsatisfactory experience of the initial use during the mid to late 1990s (Sanders & Nunn 2005). The re-investigation has been prompted based on the continued success the French have experienced with these materials.

The failure in the UK in the use of these materials was identified as being mainly due to the use of too low binder contents, inappropriate aggregate gradation and a failure to realise the materials specific compaction and laying requirements.

The re-introduction is mainly based on the high modulus asphalt material referred to as class 2 Enrobé à Module Élevé (EME2) in France, where it was developed (Sanders & Nunn 2005). The intention was to translate the French specification as exactly as possible

into a UK context, including requirements for Richness modulus, Duriez test and large-size wheel-tracker. Given the past experience in the UK, the relative success of the pilot projects is of high importance to the Highways Agency. As a result of this history, there is a need to carefully monitor and evaluate the performance of this newly formulated high modulus asphalt to ensure that the anticipated benefits shown by the French are being achieved in the UK.

2 METHODOLOGY FOR MONITORING

A framework has been developed to facilitate a consistent review of the different sites. The following elements are commented on:

- A review of the mixture design.
- Laying and compaction temperatures and weather conditions, incorporating any comments from the Contractor's Construction Report.
- An assessment of the material performance, including mixture design data, site data and the relevant specification requirements.
- In some cases detailed visual inspections undertaken from the hard shoulder (including video footage).
- In some cases Falling Weight Deflectometer (FWD) testing and subsequent back analysis, including evaluation against the criteria in HD29/94 (The Highways Agency 1994) where appropriate.

It was originally anticipated that the EME2 sites would be monitored on an annual basis, so that data from future years would augment the data already obtained. The testing programme was designed to be reactive so that, if the pavement started to exhibit a certain mode of damage, the testing programme and evaluation could be realigned to focus on the problem. In the event, limited repeat visits were made to sites because of budget limitations.

The key objective of this work was to provide an overview of workmanship, performance and potential serviceability of EME2 manufactured and laid on construction projects in the UK. To this end, reporting was based on the following detailed data:

- Mixture volumetrics and composition (grading, binder content, richness modulus).
- Binder properties (penetration, softening point).
- Laying/compaction temperatures and weather conditions.
- Performance data (mixture stiffness (Indirect Tensile Stiffness Modulus (ITSM) (British Standards Institution 1993)), deformation resistance (Vacuum Repeated Load Axial Test (VRLAT) (Nunn et al. 1997) or wheel track testing (WTT) using the large size device (Comite European de Normalisation 2003)), Percentage Refusal Density (PRD)).
- Interfacial bond performance (visual assessment and/or Leutner Shear tests).
- FWD back calculated stiffness of the EME2 layer, where possible.
- Site comments.

In the following sections, not all the data collected on the sites are given in full or even summary due to limitations of space. All of the sites are heavily trafficked, with design traffic for the three motorway sites being 80 msa (to give a "long-life" design).

3 SITE A

A section of two lane dual carriageway was laid with proprietary binder course and surface course materials in September 1998. The proprietary binder course material was a version of EME2 that was developed in France when a modified version of EME1 was being used by others in the UK. As such, this site is believed to be the earliest use of EME2 in the UK. The construction was limited to the nearside lane of one carriageway and had required the planing of a 900 m stretch of material prior to laying the binder course material. The surface course was applied over a greater length of the lane.

The site was visited in May 2007, when it was assessed visually as *Acceptable*. Although the visual condition is that of the surface course and not the binder course, the cracking was all in the offside lane with none on the nearside lane where the proprietary binder course had been laid.

Eight 100 mm diameter cores were extracted from the site in May 2007 and the binder course tested for stiffness (ITSM) at 20°C to give results having considerable scatter, ranging from 1.7 GPa to 6.4 GPa with an average of 4.9 GPa. An FWD survey was also carried out at the same time, which confirmed this variable performance. However, the precise construction details for this site, and its subsequent history, are unknown, making the drawing of clear conclusions difficult.

4 SITE B

The site forms part of a motorway contract that was initially constructed using a high modulus asphalt (HMB15) and completed in 2000. The high modulus asphalt developed significant cracking and structural problems in some areas soon after construction.

In December 2005, the surface course and 90 mm of the binder course were planed out on two 200 m sections and replaced with 0/14 mm EME2. One section (Area 1) had a granular sub-base and the other section (Area 2) had a capping layer consisting of lime stabilised soil; the granular sub-base section could therefore act as a control to isolate the effect of the lime capping layer.

The 0/14 mm EME2 was designed to NF P 98 140 (L'Association Français de Normalisation 1999) with limestone aggregate, limestone filler and 10/20 grade bitumen as the constituent materials. A proprietary bond coat was applied to the surface of the EME2, followed by a proprietary thin surface course using 0/14 mm nominal size aggregate and polymer-modified bitumen; some of the key data are summarised in Tables 1 and 2.

Laying and compaction temperature were an issue on this site; indeed, it was suggested that the initial compaction temperature could be lowered to avoid the occurrence of 'fatting up'. Meanwhile, the thermal imaging camera (TIC) temperatures, which were consistently lower than those recorded using thermocouple thermometers, indicated that the roller's steel drum had a dramatic effect in cooling the surface of the EME2 material. This difference was probably due to the temperature gradient which occurs between the surface (recorded by the TIC) and the core of the mat.

The air voids content achieved on site was extremely low (approximately 1%), but well within the requirement (Sanders, P.J. & Nunn, M.E. 2005) of less than 6.0%, which suggests that the material will be relatively impermeable and was readily compacted (but possibly prone to rutting, see below). The ITSM results showed that the stiffness achieved was satisfactory (average 6.2 GPa) as both areas achieved values greater than the required 5.5 GPa

Table 1. Design and site mixture characteristics, Site B.

Property	Design	Results Area 1	Results Area 2	0/14 EME2 Specification	Remarks
Gradation	Generally within EME2 specification range				6.3mm sieve result was lower than that of design target
Binder content (%)	**5.3**	5.6	5.8	≥ 5.4	
Richness modulus, K	3.42	3.43	3.46	≥ 3.4	
Penetration (0.1mm)	16	-	-	10 - 20	
Softening point (°C)	70.8	-	-	63 - 73 target ≤ 71	No site data
Water sensitivity (%) [7]	0.92	-	-	≥ 0.75	
Laboratory WTT % rut depth @ 60°C @ 30,000 cycles	5.3	-	-	≤ 7.5	
Laying temperature (°C)	-	**173**	**177**	150 - 170	Could be the cause for 'fatting up' in Area 2
Temperature after compaction (°C)	-	**138**	**133**	≥ 140	Specification is for substantial compaction completion temperature

Table 2. Design and site mixture characteristics, Site B.

Property	Design	Results Area 1	Results Area 2	0/14 EME2 Specification	Remarks
Air voids content (%)	4.9	**0.8**	**1.1**	≤ 6.0	Low - could affect permanent deformation performance
ITSM stiffness (GPa)	-	5.94	6.41	≥ 5.5	
Deformation resistance (VRLAT) Strain (%)	-	**2.12**	**1.97**	-	*SHW* Clause NG952, Class 1 ≤ 1.5 & Class 2 ≤ 1
Strain rate (με/cycle)	-	**1.87**	**2.22**	-	*SHW* Clause NG952, Class 1 ≤ 1 & Class 2 ≤ 0.7
Leutner peak shear stress (MPa)	-	1.46	1.06	-	Adopted criterion: peak shear stress ≥ 1
Bond between layers of 300mm diameter Cores	-	50% debonded	50% debonded	good bond	Due to torque from coring equipment
Bond between layers of 150mm diameter Cores	-	50% debonded	50% debonded	good bond	Debonding unexplained
FWD back analysed stiffness (MPa)	-		satisfactory	-	-

(Sanders, P.J. & Nunn, M.E. 2005). However, the VRLAT test results indicated that the EME2 core specimens from both areas failed to comply with the requirements for strain and strain rate by a significant margin. The low air voids content may be a detrimental factor with respect to permanent deformation performance. This divergence highlights a possible area for concern.

Wheel-tracking tests conducted on two specimens, manufactured to conform to the trial design, indicated an average proportional rut depth of 5.3% after 30,000 cycles, less than the specified limit of 7.5%, despite being greater than the 3.3% achieved during the mixture design procedure. The apparent difference in permanent deformation resistance observed between the VRLAT and wheel-tracking tests may be due to the difference in air voids content (VRLAT specimens' average of 1%, wheel-tracking specimens' average of 3.9%) and/or the method of specimen preparation (VRLAT specimens were from site whilst wheel-tracking specimens were laboratory manufactured).

The Leutner shear test results indicated that a strong bond existed between the EME2 and high modulus base (HMB15) material based on the assumption that a minimum shear strength value of 1 MPa is considered appropriate. However, these results did not correlate fully with visual observations indicating some lack of bond between layers.

The 50th percentile stiffness modulus at 20°C was calculated from back analysis of the FWD data (collected in February 2006) as 10 GPa for Area 1 and 16 GPa for Area 2. The high stiffnesses encountered in Area 2 were presumably due to the stabilised capping layer. Retesting in January 2008 revealed that the FWD back analysed stiffness results indicated an increase in EME2 stiffness in the intervening two years. Traffic ranged from 25–29 msa in 2006, increasing to 35–40 msa in 2008. The design traffic for the pavement was 80 msa.

A pre-construction site inspection describing the deterioration of the road and a post-construction site inspection were undertaken. The post-construction site inspection revealed no visible defects.

5 SITE C

A length of 2130 m of EME2 was laid in lane 1 of one carriageway of a major motorway in February 2006. The inlay construction operation involved planing the surface course and 70 mm of the binder course and replacing it with a 65 mm layer of 0/14 mm EME2 and a surface course. The 0/14 mm EME2 was designed to NF P 98 140 (L'Association Français de Normalisation 1999).

With component materials of Mountsorrel aggregate, 2% filler and 10/20 grade bitumen. Additional material used consisted of a surface layer and bond coat. Key data are summarized in Tables 3, 4 and 5.

Table 3. Design and site mixture characteristics, Site C.

Property	Design	Results Trial	0/14 EME2 Specification	Remarks
Gradation	Generally within EME2 specification range			Grading @ 0.063mm sieve = 9.0% (specification range 5 - 9%)
Binder content	5.6	5.33	≥ 5.4	Satisfactory - when applying the 0.3% allowed tolerance
Water sensitivity (%) [7]	0.86		≥ 0.75	
Laboratory WTT % rut depth @ 60°C @ 30,000 cycles	3.8		≤ 7.5	
Laying and compaction temperature (°C)		No data		

Table 4. Site mixture characteristics, Site C.

Property	Trial Results	0/14 EME2 specification	Remarks
Overall (mean) air voids content (%)	4.2	≤ 6.0	Variable data set
Air voids content at wheel-tracks (%)	4.4	≤ 6.0	
Air voids content middle of mat (%)	2.2	≤ 6.0	Low - could affect permanent deformation performance
Air voids content near unrestrained edge (%)	7.8	≤ 7.0	High air voids content
Air voids content near restrained edge (%)	3.0	≤ 7.0	Low air voids content
Refusal density (PRD) (%)	98.4		Indicates mixture readily compactable

Table 5. Site mixture characteristics, Site C.

Property	Trial Results	0/14 EME2 specification	Remarks
ITSM stiffness (GPa)	7.5	≥ 5.5	
Deformation resistance (VRLAT) strain (%)	0.7	-	*SHW* Clause NG952, Class 1 ≤ 1.5 & Class 2 ≤ 1
Deformation resistance (VRLAT) strain rate (με/cycle)	0.7	-	SHW Clause NG952, Class 1 ≤ 1 & Class 2 ≤ 0.7
Leutner peak shear stress (MPa)	0.98	-	Adopted criterion: peak shear stress ≥1
Bond between layers of 300 mm diameter cores	100% bonded	good bond	
Bond between layers of 150 mm diameter cores	96% bonded	good bond	
FWD back analysed stiffness (MPa)	satisfactory		

Compositional analysis undertaken on site sample materials indicated that the binder content and aggregate gradation were generally within the required tolerances. However, there were concerns regarding the richness modulus, K, due to the relatively high fines content and relatively low binder content. Also, the penetration and softening point values (not quoted here) had a wider range than would normally be expected, although it was suspected that this variability was due to problems with the test method rather than the source bitumen.

The average air voids content (determined from site cores) would be considered low (mean 4.2%). However, cores taken from close proximity to the unrestrained edge had much higher air voids content (mean 7.8%), thus failing to meet the requirement of ≤7% near joints (≤6% elsewhere in the mat).

Visual inspection of the cores suggested that the bond requirement between the EME2 and the underlying layer had been met with 46 out of the 48 cores remaining intact and all six of the 300 mm diameter cores remaining intact. The average peak shear stress of the cores tested using the Leutner test method was approximately 1 MPa.

The FWD back analysis modeled the road construction as a three layer construction:

– 65 mm upper asphalt layer (surface course and EME2)
– 265 mm lower asphalt layer
– Foundation layer

Table 5.2 of HD 29/94 (The Highways Agency 1994) states that "No attempt shall be made to model any layers less than 75 mm thick in a single layer". However, because the performance of the EME2 is of principal interest, it was modeled as a 65 mm thick layer; the resulting correlations achieved from the back analysis were deemed acceptable (representing an improvement over treating the asphalt as a single entity of 330 mm layer thickness). The FWD back analysis for the EME2 layer calculated a 50th percentile stiffness modulus of 11.5 GPa at 20°C. HD 29/94 (The Highways Agency 1994) states the following regarding correlation between FWD and ITSM: "As an approximate guide, ITSM values at 20°C should be multiplied by 1.5 to allow comparison with FWD derived bituminous layer stiffnesses at 20°C", with which the ITSM and FWD back analysis stiffness moduli are consistent. The design stiffness modulus for EME2 provided in HD 26/06 (The Highways Agency 2006) for use in analytical design is 8 GPa, taking into account factors such as deterioration and gain in stiffness over time.

6 SITE D

In March 2006, 480 m of the nearside lane of one carriageway of a major motorway was planed out and replaced with 0/14 and 0/20 EME2 mixtures at a target nominal compacted thickness of 90 mm and 110 mm, respectively. The two EME2 mixtures met the requirements of the UK specification for EME2. The underlying material is thought to be a 28 mm dense bitumen macadam (DBM). A proprietary bond coat was sprayed onto the surface of the newly laid EME2 material. The vertical joints were also painted with hot bitumen. The

Table 6. Design mixture characteristics, Site D.

Property	Design results 0/14mm	Design results 0/20mm	0/14-0/20 EME2 specification
Target binder content (%)	5.7	5.3	≥ 5.4; ≥ 5.2
Richness modulus (K)	3.61	3.45	≥ 3.4
Air voids content (%)	4.4	3.3	≤ 6.0
Water sensitivity (%), [7]	0.89	0.89	≥ 0.75
Laboratory WTT % rut depth @ 60°C @ 30,000 cycles	2.6	2.6	≤ 7.5
Fatigue properties @ 10°C, 25_{Hz} ($\mu\varepsilon/10^6$ cycles)	N/A*	157	≥ 130

* Because richness modulus, K, is >3.6.

Table 7. Site mixture characteristics, Site D.

Property	Trial results 0/14mm	Trial results 0/20mm	0/14-0/20 EME2 specification	Remarks
Gradation	All within construction tolerances			
Binder content (%)	5.3	5.0	≥ 5.4; ≥ 5.2	Satisfactory - when applying the 0.3% allowed tolerance
Penetration (0.1mm)	7	13	10 - 20	0/14 value considered very low for 0/14 EME2 mixture
Softening point (°C)	86.8	77.2	63 - 73 target ≤ 71	Considered high

Table 8. Site mixture characteristics, Site D.

Property	Trial results 0/14mm	Trial results 0/20mm	0/14-0/20 EME2 specification	Remarks
Delivery temperature (°C)	180	182	150 - 170	High Specification is for laying temperature
Compaction temperature (°C)	166	173	≥ 140	
Air voids content (%)	6.2	5.3	≤ 6.0	Values variable
Air voids content near joints (%)	8.9	7.8	≤ 7.0	High
ITSM stiffness (GPa)	6.6	7.7	≥ 5.5	
Deformation resistance	No site information			
Bond between layers		well bonded	good bond	

surface course consisted of a proprietary 0/14 surface course mixture, laid at a thickness of 35 mm; the design and site mixture results are summarized in Tables 6, 7 and 8 below.

The aggregate gradation of the two mixtures at the design and pilot stage met the specification. The target binder contents for the 0/14 and 0/20 EME2 mixtures (5.7% and 5.3%, respectively) were higher than those achieved in production (5.3% and 5.0%, respectively). However the resultant mixture was within specification, when taking into account the production limits specified (≤0.3% below, ≤0.6% above).

Both the delivery and rolling temperatures indicated that the temperatures achieved were on the higher side of the specification. However, there is no indication to show that these temperatures caused any undue problem, with the rolling temperature of 0/14 EME2 having actually fallen to 130°C near completion in some areas, whereas the specification states that "compaction must be substantially completed before the temperature falls below 140°C". The weather conditions during the laying of both sections (0/14 and 0/20 EME2 mixtures) were favourable with dry conditions prevailing throughout the work.

The air voids content of both mixtures at the design stage meet the specification of being less than 6%. However, the air voids content of the cores from both pilots indicated variability. In addition, the air voids contents from cores taken close to the joints averaged 8.4%, which exceeds the maximum allowable of 7% at joints. The degree of compaction achieved on this site was significantly less than that on Sites B and C.

Fatigue testing was conducted only on the 0/20 EME2 mixture because its richness modulus, K, of 3.45 was below the 3.6 that is required to avoid fatigue testing. The fatigue result showed that the mixture met the required fatigue criterion satisfactorily.

Visual observations during the material laying process indicated that the EME2 material was very mobile "and still relatively mobile near completion of rolling at around 130°C and/or just below". Visual inspection of the cores indicated that the bond requirement of having a good bond between layers and vertical interfaces were met, possibly assisted by the surface course being laid whilst the EME2 layer was still 'warm'. However, minor surface deformation was reported in the cooling EME2 layer due to the compaction plant and delivery wagons.

7 SITE E

6,500 t of 0/14 mm EME2 were laid on a single two-lane carriageway. This site had shops and houses on either side so that the work had to be undertaken over several weekends in August 2006. The design of the mixture was supported by a 300 t trial undertaken at a quarry in June 2006. Key design and site mixture data are summarized in Tables 9, 10 and 11 below.

8 SITE F

In April 2007, two locations on the eastbound carriageway of a new pavement being built on a major trunk road in the east of England was constructed using 0/14 mm EME2. The scheme involved the upgrading of single carriageway to dual carriageway.

Table 9. Design and site mixture characteristics, Site E.

Property	Trial results		0/14 EME2 specification	Remarks
	Design	Trial		
Gradation	All mean values within EME2 specification range			
Binder content (%)	-	5.1	≥ 5.4	Satisfactory - when applying the 0.3% allowed tolerance
Penetration (0.1mm)	20	-	10 - 20	
Softening point (°C)	67	-	63 - 73 target ≤ 71	
Mixing temperature (°C)	-	187 range 172 - 197	150 - 170	Specification is for laying temperature

Table 10. Site mixture characteristics, Site E.

Property	Trial results	0/14 EME2 specification	Remarks
Overall air voids content (%)	3.8 range 1.3 - 8.0	≤ 6.0	Variable data set
Air voids content - nearside wheel-track (%)	2.9	≤ 6.0	On the low side
Air voids content - offside wheel-track (%)	3.3	≤ 6.0	
Air voids content - 150mm from nearside edge (%)	4.7	≤ 7.0	
Air voids content - 25 to 50mm from outside edge (%)	4.4	≤ 7.0	

Table 11. Site mixture characteristics, Site E.

Property	Trial results	0/14 EME2 specification	Remarks
Overall ITSM stiffness (GPa)	7.0 range 4.6 - 14.5	≥ 5.5	Variable data set
ITSM stiffness - nearside wheel-track (GPa)	7.1	≥ 5.5	
ITSM stiffness - offside wheel-track (GPa)	7.0	≥ 5.5	
ITSM stiffness - 150 mm from nearside edge (GPa)	6.8	≥ 5.5	
ITSM stiffness - 25 to 50 mm from outside edge (GPa)	7.1	≥ 5.5	
Bond between layers	Apparent uneven bond coat application	good bond	Bonding between layers could be expected to be variable

Table 12. Site mixture characteristics, Site F.

Property	Trial results		0/14 EME2 specification	Remarks
	Area 1	Area 2		
Gradation	Majority within construction tolerances			Two 6.3 mm sieve and one 0.063 mm sieve results were lower than that of design target
Binder content (%)	5.37	5.67	≥ 5.4	Satisfactory - when applying the 0.3% allowed tolerance
Richness modulus, K	3.43	3.56	≥ 3.4	
Penetration (0.1mm)	11.5	10.3	10 - 20	Considered low
Softening point (°C)	76.3	80.9	63 - 73 target ≤ 71	Considered high

Table 13. Site mixture characteristics, Site F.

Property	Trial results		0/14 EME2 specification	Remarks
	Area 1	Area 2		
Laying temperature (°C)	**178**	**176**	150 - 170	Considered high
Compaction temperature (°C)	153	152	≥ 140	
Air voids content (%)	**2.8**	4.3	≤ 6.0	Values variable
Air voids content near joints (%)	4.3	**7.4**	≤ 7.0	Values variable
Refusal density (PRD) (%)	97.8	97.6		Indicates mixture readily compactable
ITSM stiffness (GPa)	8.1	8.7	≥ 5.5	

Table 14. Site mixture characteristics, Site F.

Property	Trial results		0/14 EME2 specification	Remarks
	Area 1	Area 2		
Deformation resistance (VRLAT) strain (%)	0.9	0.6		*SHW* Clause NG952, Class 1 ≤ 1.5 & Class 2 ≤ 1
Deformation resistance strain rate (με/cycle)	0.5	0.7		*SHW* Clause NG952, Class 1 ≤ 1 & Class 2 ≤ 0.7
Leutner peak shear stress (MPa)		0.73		Adopted criterion: peak shear stress ≥ 1
Bond between layers of 300 mm diameter cores		100% bonded	good bond	
Bond between layers of 150 mm diameter cores		100% bonded	good bond	

Table 15. Plant and site mixture characteristics, Site G.

Property	Trial results		0/14 EME2 specification	Remarks
	Plant	Trial		
Gradation	All values within EME2 specification range			
Binder content (%)	5.3	5.1	≥ 5.4	*Satisfactory - when applying the 0.3% allowed tolerance*
Discharge temperature (°C)	-	183 range 165 - 206	150 - 170	Specification is for laying temperature
Pre-rolling temperature (°C)	-	174 range 145 - 202	150-170	Specification is for laying temperature
Rolling completion temperature (°C)	-	158 range 128 - 188	≥ 140	Generally satisfactory with few lower than 140°C ('substantial compaction completion temperature)

Table 16. Site mixture characteristics, Site G.

Property	Trial results	0/14 EME2 specification	Remarks
Overall air voids content (%)	2.0 range 1.2 - 3.2	≤ 6.0	Generally low - could affect permanent deformation performance
Air voids content - nearside wheel-track (%)	1.7	≤ 6.0	
Air voids content - offside wheel-track (%)	2.3	≤ 6.0	
Overall ITSM stiffness (GPa)	7.7 range 6.35 - 9.22	≥ 5.5	
ITSM stiffness - nearside wheel-track (GPa)	7.5	≥ 5.5	
ITSM stiffness - offside wheel-track (GPa)	7.8	≥ 5.5	

All of the design mixtures complied with the UK EME2 specifications and a summary of the main site results is reproduced in Tables 12, 13 and 14 below.

9 SITE G

Inlay construction using 0/14 mm EME2 was carried out at one location on the southbound carriageway of a major trunk road in the South of England in January and February 2007. The EME2 design was the same as that used for Site E and a summary of the key results is reproduced in Tables 15 and 16 below.

10 CONCLUSION

A framework has been established for monitoring EME2 sites in order to store construction and performance data in a consistent manner. Information relating to several sites (predominantly inlays) has been recorded in this framework and a review of the data obtained to date has been undertaken. The overall objective is to support the Highways Agency in its intention for wider use of EME2 for base and binder course layers on its road network.

Several points of interest are revealed by a review of the data presented in this paper:

- Recovered binder properties were generally variable:
  - Penetration was in some instances on the low side;
  - Softening point was in some instances on the high side.
- The laying temperatures were generally above the specification range, and there was a difficulty being within the specification limits for both mixing and laying temperature.
- Air voids were:
  - Generally on the low side (away from joints), which could potentially affect deformation resistance;
  - Generally on the high side (near joints).

  Compaction techniques may require review/guidance in the light of the air voids being achieved.
- Grading and binder content tolerances require review, since high fines and low binder content reduces richness modulus (K).
- Lack of suitable specification criteria for some parameters, for example, interfacial bond.

Since this work was carried out, substantial revisions have taken place to Volume 1 of the Manual of Contract Documents for Highways Works, MCHW1 (The Highways Agency 2008). These revisions include a new Clause 930 entitled 'EME2 Base and Binder Course Asphalt Concrete', which has introduced a number of changes to the specification for EME2 in the UK. Significantly, these changes include:

- Removal of the requirement for a laying temperature. Temperature is now controlled by a requirement for material to be delivered to site to enable laying with a minimum paver-out temperature of 140°C, and for compaction to be substantially completed before the temperature falls below 120°C.
- Changes to the air void criteria at locations "centered 100 mm from the final joint position at any unsupported edge", to be less than or equal to 8%. The requirement for air void content in the body of the material (assessed in alternate wheel-tracks) remains at less than or equal to 6%.

Other changes introduced in MCHW1 include a documented test method for determining interfacial bond (Clause 954, 'Method for Laboratory Determination of Interface Properties Using the Modified Leutner Shear Test') and the transfer of the requirements for deformation resistance from MCHW Clause 952/NG952 to PD 6691 (British Standards Institution 2007), but for wheel tracking only. While the changes that have been introduced are sensible and broadly reflect practical experience, it will be important to continue to closely monitor the compaction being achieved on EME2 sites, particularly in view of the changes to laying and compaction temperatures.

ACKNOWLEDGEMENTS

The work described in this paper was carried out by Scott Wilson Limited and TRL Limited (Infrastructure Division) on behalf of the Highways Agency. This paper is published with the permission of the Chief Executives of all the organisations, whose support is gratefully acknowledged.

REFERENCES

British Standards Institution *Method for determination of the indirect tensile stiffness modulus of bituminous mixture*, DD 213: 1993, British Standards Institution, London, UK.

British Standards Institution, *Guidance on the use of BS EN 13108 Bituminous mixtures—Material specifications* BSi, PD 6691: 2007.

Comité Européen de Normalisation *Bituminous mixtures—Test methods—Part 22: Wheel tracking*, EN 12697-22: 2003.

L'Association Français de Normalisation *Couches d'assise: Enrobés à Module Élevé*, NF P 98 140, L'Association Français de Normalisation, La Défense, Paris, France, 1999.

L'Association Française de Normalisation *Essais relatifs aux chaussées—Essai Duriez sur mélanges hydrocarbonés à chaud*, NF P 98-251-1, L'Association Français de Normalisation, La Défense, Paris, France.

Nunn, M.E., Brown, A.J. & Lawrence, D. 1997. Repeated load axial test with vacuum confinement—Test procedure, TRL paper PA 3287/97, Wokingham, UK.

Sanders, P.J., & Nunn, M.E 2005. The application of Enrobé à Module Élevé in flexible pavements. TRL Report 636, Transport Research Laboratory, Wokingham, UK.

The Highways Agency 1994. Scottish Executive, Welsh Assembly Government and The Department for Regional Development Northern Ireland *Structural assessment methods*, HD 29/94, Volume 7, Section 3, Part 2, Design Manual for Roads and Bridges, The Stationery Office, London, UK.

The Highways Agency 2006. Scottish Executive, Welsh Assembly Government and The Department for Regional Development Northern Ireland *Pavement design*, HD 26/06, Volume 7, Section 2, Part 3, Design Manual for Roads and Bridges, The Stationery Office, London, UK.

The Highways Agency 2008. *Specification for Highway Works*, Volume 1, Manual of Contract Documents for Highway Works, August 2008. London, UK: The Stationery Office.

Advanced Testing and Characterization of Bituminous Materials –
Loizos, Partl, Scarpas & Al-Qadi (eds)
© 2009 Taylor & Francis Group, London, ISBN 978-0-415-55854-9

On the fracture properties of epoxy asphalt mixture with SCB test

Xianhua Chen
School of Transportation School, Southeast University, Nanjing, China

Hongtao Li
Headquarters of Yangtze River Bridges in Jiangsu, Nanjing, China

Zhendong Qian
School of Transportation School, Southeast University, Nanjing, China

ABSTRACT: The fracture properties of the thermo-setting materials of epoxy asphalt mixture were evaluated based on J-integral concept and ultimate strength. The results were compared to that of HMA with thermo-plastic binder materials. Totally 60 specimens cored from SGC with different notches were tested with SCB test under a temperature of −10°C and 20°C. IDT test was adopted to compare the capability of SCB test in characterizing tensile strength of epoxy asphalt. The experimental results reveals that epoxy asphalt mixture has a super higher resistance of fracture at low temperature than thermo-plastic HMA due to its super high tensile strength and flexibility, and the influences of temperature on the fracture resistance of EAM is not as significant as that of thermo-plastic HMA. Good repeatability of SCB test results indicates the capability of the SCB test to be useful for measuring the fracture toughness of epoxy asphalt mixture.

Keywords: epoxy asphalt concrete; tensile strength; critical *J*-integral; semi-circular bending

1 INTRODUCTION

Fracture resistance has been one of the most important requirements for asphalt pavements. Various pavement distresses are related to the fracture properties of the asphalt layer, including longitudinal cracking, thermal cracking, and reflective cracking. The fracture resistance of asphalt materials significantly influences the service life of asphalt pavements and consequently the maintenance and management of the pavement network. One of the most powerful tools to study the fracture properties of engineering materials is to incorporate fracture mechanics tools in HMA characterization. There are two approaches to a fracture analysis, one is the stress intensity approach, the other is energy approach. The specimen geometry used in fracture test on HMA can be categorized into two groups: (1) single edge or double edge notched beam with convenient specimen preparation; (2) cylindrical specimen prepared with gyratory compactor, such as Modified Superpave Indirect Tensile test (IDT), Semi-Circular Bending (SCB) test, and Disc-shaped Compact Tension Test (DCT). Due to the easier specimen preparation, capability to elasto-plastic fracture mechanics concept, and easy test set-up procedure with common fracture toughness testing apparatus, cylindrical specimens were widely used in asphalt mixtures fracture investigations.

In recent years, SCB test has drawn more and more attention since it was introduced to the asphalt community by the Europeans and South African researchers (Krans et al. 1996, Van de Ven & Smit 1997, Molenaar et al. 2002). The semi-circular test was originally used to characterize the fracture resistance in rock mechanics (Chong & Kuruppu, 1984, Lim et al. 1993). It has been used to characterize the tensile strength properties by Van de Ven and Smit

(1997) and fatigue resistance properties by Kran et al. (1996) in HMA mixtures. Mull et al. (2002) have been using SCB test on notched specimens to evaluate the fracture resistance of asphalt mixtures through the *J*-integral. Simple geometry of specimen, little machining operations, application of compressive loads rather than the tensile loads, ability of conducting the fracture toughness tests in the full range from pure mode I to pure mode II, easy test set-up procedure with common fracture toughness testing apparatus, simple data requirement from test procedure, and the ability to prepare specimens from typical rock cores, are the major advantages of the SCB specimen. And a numerical solution is available for the fracture toughness obtained with this configuration.

Asphalt surfacing on orthotropic steel bridge decks is a special type of asphalt pavement. The fracture resistance is one of the most important requirements for pavement on steel orthotropic bridge decks (Chen 2006 & Huang 2006). Only a few materials can meet these requirements, among which is epoxy asphalt mixture (EAM). EAM is a polymer concrete that is composed of a slow curing, epoxy asphalt binder mixed together with standard asphalt concrete aggregates in the pug mill of an asphalt plant. The epoxy asphalt binder is a two-phase chemical system in which the continuous phase is an acid cured epoxy and the discontinuous phase is a mixture of specialized asphalts, which makes the mixture's performance different with traditional HMA. Epoxy asphalt mixture has recently been used extensively in China as asphalt surfacing materials for orthotropic steel bridge deck applications due to its perfect performance in 2nd Nanjing Yangtze Bridge. Considerable laboratory tests and field performance histories have revealed that the cured EAM has extremely high temperature stability and strength, excellent fatigue and anti-bleeding properties, and superior rutting resistance (Huang et al. 2001). Currently, there are only a few researches conducted to investigate the fracture resistance of asphalt materials and the fracture performance of asphalt pavements on steel bridge decks, but there has very little experience with EAM. It becomes therefore a top priority to conduct a comprehensive research to evaluate the fracture resistance of EAM on well documented fracture test methods, develop a constitutive material model and incorporate the model into a realistic deck pavement model that takes into account the entire pavement system for designing EAM on steel bridge decks with improved the low temperature fracture resistance. This paper presents a part of a comprehensive research effort to evaluate the fracture properties of epoxy asphalt mixture for orthotropic steel decks of Sutong Bridge—the largest cable bridge around the world. The scope of this study included conducting SCB tests at 20ºC and −10ºC, which are resulted from 3 notched depths (12-, 18- and 24-mm) × 5 duplicates for each mixture. As previous effort of the comparison of IDT and SCB test are based on thermo-plastic HMA, 20 IDT tests on EAM were conducted to compare the results with 20 SCB tests.

2 FRACTURE PARAMETERS OBTAINED FROM SCB TEST

2.1 *Tensile strength*

The stress field in a SCB specimen was previously studied by Van de Ven & Smit (1997) and Molenaar et al. (2002). The SCB horizontal stress measurements at the bottom edge of the specimen, were computed by means of an equation based on the three point bending moment formula for linear elastic materials, adapted, by means of a finite element study (based on the theory of rate dependent consistent plasticity) conducted by Molenaar, to asphalt mixtures:

$$\sigma_h = 4.8\frac{P_{\max}}{Dt} \tag{1}$$

where σ_h is tensile stress at the central bottom area of the specimens (MPa), P is the peak load of the specimen (N), D is the diameter of the specimen (mm), and t is the thickness (mm).

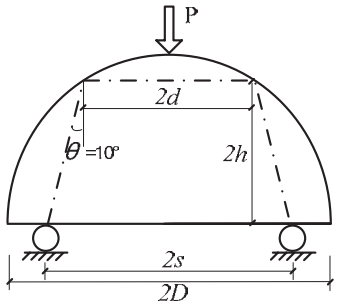

Figure 1. The definition of h in equation 2 (according to Huang, 2005).

Huang (2005) has given an approximate solution based on elasticity theory with a few assumptions and simplification, shown in Figure 2. The maximum tensile stress occurs at the middle point of the lower surface of the semi-cylindrical specimen, and the expression of is:

$$\sigma_h = -\frac{2q\beta h\sin(\beta l/2)\sin h(\beta h)\cos h(\beta h)}{\beta^2 h^2 - \cos h^2(\beta h)\sin h^2(\beta h)} \tag{2}$$

where q was obtained by equating the total sum of the distributed normal stress to the concentrated load (P) and it was found to be $q = \pi P/(2lt)$, $\beta = \pi/l$, $l = s + d$, and the definition of h is shown in Figure 1.

It must be noted that equations (1) and (2) are valid only if the distance between the supports is equal to 0.8 D. According to the test results, the value calculated by equation (2) is 1.2 times that of the results of equation (1). Thus only equation (1) will be choose for calculate tensile strength of SCB specimen as its simple form.

In order to evaluate the applications of SCB test to Epoxy asphalt concrete, Indirect Tensile Strength Test was also conducted in laboratory. According to ASTM D4123, IDT test specimen is loaded to failure at a 50.8 mm/min (2 inch/min) deformation rate. The load and deformations were continuously recorded and indirect tensile strength and strain were computed as follows:

$$\sigma_T = \frac{2P_{\max}}{\pi Dt} \tag{3}$$

2.2 *The critical J-integral*

The evaluation of ultimate strength and elastic modulus can only reveal the behavior of a homogeneous material with no inherent defects. HMA as a heterogeneous materials do not fit this description. The *J*-integral concept is thought to be more appropriate to describe the fracture resistance of asphalt mixtures (Little & Mahmoub 1985, Abdulshafi & Majidzadeh 1985, Dongre et al. 1989, Bhurke et al. 1997 & Mull et al. 2002). The definition of the critical *J*-Integral is as presented in equation (4):

$$J_c = -\left(\frac{1}{b}\right)\frac{dU}{da} \tag{4}$$

The utilization of the semi-circular specimen to determine the critical value of the *J*-integral intended to use only two notch depths. On this basis, Equation 4 can be written as (Mull et al. 2002):

$$J_c = \left(\frac{U_1}{b_1} - \frac{U_2}{b_2}\right)\frac{1}{a_2 - a_1} \tag{5}$$

where J_c, the critical J-integral; U_1, U_2, the strain energy values, calculated using the data from the beginning of the notched SCB beam test loading until the load reached the maximum value, b_1, b_2, thicknesses of the specimens with notch depths of a_1 and a_2, respectively.

It should be noted the utilization of the SCB specimen to determine the critical value of the J-integral intended to use only two notch depths. In the current study, however, three target notch depths were used. This will increase the accuracy of the value of J_c for EAM.

3 LABORATORY EXPERIMENTS

3.1 *Materials*

3.1.1 *Aggregates*

Both coarse (>2.36 mm) and fine (2.36 mm to 0.075 mm) aggregate is crushed basaltic, with Los Angeles abrading value 12.1%, polishing value 51, crushed value 9.6%, absorption 0.2% and compression strength 138 MPa. Percentage of crushed particles is 100. Percentage of flat and elongation particles is less than 2. Bulk specific gravity is 2.995.

The mineral filler (<0.075 mm) is calcareous, with low hydrophilic co-efficiency and moisture content, passing rate over 95%, specific gravity of 2.75.

Table 1. Part A (epoxy resin) for binder.

		Specification	
Property	Test results	Requirements	Test methods
Viscosity @ 23ºC. Poise	1.4	100 to 150	ASTM D 445
Epoxide equivalent weight	188	185 to 192	ASTM D 1652
Color, Gardner. max.	2	Max. 4	ASTM D 1544
Moisture content. % max.	0.02	Max 0.05	ASTM D 1744
Flash point, COC. ºC, min.	230	min. 200	ASTM D 92
Specific Gravity @ 23ºC.	1.17	1.16–1.17	ASTM D 1475
Appearance.	Transparent amber	Transparent amber	visual

Table 2. Part B (blend of asphalt and cure agent) for binder.

		Specification	
Proerty	Test results	Requirements	Test methods
Viscosity @ 100ºC. cP	212	Min. 140	Brookfield
Specific Gravity @ 23ºC	1.00	0.98 to 1.02	ASTM D 1475
Color, Gardner. max.	0.01	Black	Visual
Acid Value, mg KOH/g.	55	40 to 60	ASTM D 664
Flash point, COC. ºC, min.	235	min. 200	ASTM D 92

Table 3. Parts A and B combined and cured.

		Specification	
Property	Test results	Requirements	Test methods
Weight Ratio, Parts A/B	100/585	100/585	
Tensile Strength @ 23°C, MPa	2.8	Min. 1.5	ASTM D 638
Elongation at break @ 23°C, %	250	Min. 200	ASTM D 638
Viscosity increase to 1000cP @ 121°C, Minute	70	Min. 50	ASTM D 445
Thermal-set Property @ 300°C.	not melt	Shall not melt	visual

3.1.2 *Epoxy asphalt binder*

Use Epoxy Asphalt Type V as the binder for epoxy asphalt concrete is provided by the Headquarter of Sutong Bridges, both of which shall conform to the following specifications:

3.2 *Mixture design*

The Marshall mix design procedure was employed to design EAM. The mixture should be kept at a temperature of 121°C for 4 hours to assure fully cure. The aggregate gradation specification and the blended gradation in the experiment are listed in Table 4. The optimum binder content was 6.5%. Basic properties of the mixture are listed in Table 5.

3.3 *SCB Specimen geometry and preparation*

As previous research reveals that the fracture toughness of SCB specimen has been obtained independent of the specimen size(Molenaar et al.), a specimen geometry of 100 mm in diameter and 30 mm in thickness is selected. The SCB specimens were obtained from SGC cylindrical specimens of 150 mm in diameter and 200 mm in height.

The mixture was compacted with SGC to obtain a target air void content of 2.5%. The compaction temperature was 121°C and the number of gyrations used was 100. The mixture was aged in a 121°C for 35 minutes before compacted. The mixture should be kept at a temperature of 121°C for 4 hours to assure fully cure.

The SCB specimens were obtained from cured SGC cylindrical specimens. Each cylindrical SGC specimen was firstly drilled with the core of 100 mm in diameter, and then sliced

Table 4. Aggregate gradation and specification.

	Passing percentage, %					
Sieve	1/2”	3/8”	No.4	No.8	No.30	No.200
Specification	100	95~100	65~85	50~70	28~40	7~14
Blend gradation	100	97.5	74.5	59.6	33.6	10.4

Table 5. The basic properties of cured epoxy asphalt mixture.

		Specification	
Properties	Test results	Requirements	Test methods
Specific bulk gravity	2.562		
Void, %	2.2	Max. 3.0	T0705-2000
VFA, %	87	70 to 90	
Marshall stability @60°C, kN	58.5	Min. 40	T0709-2000
Flow value @60°C, 0.1 mm	35	20 to 5	

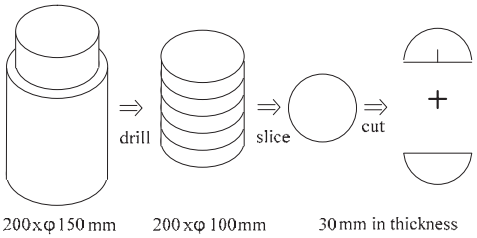

Figure 2. Sample preparation for SCB test.

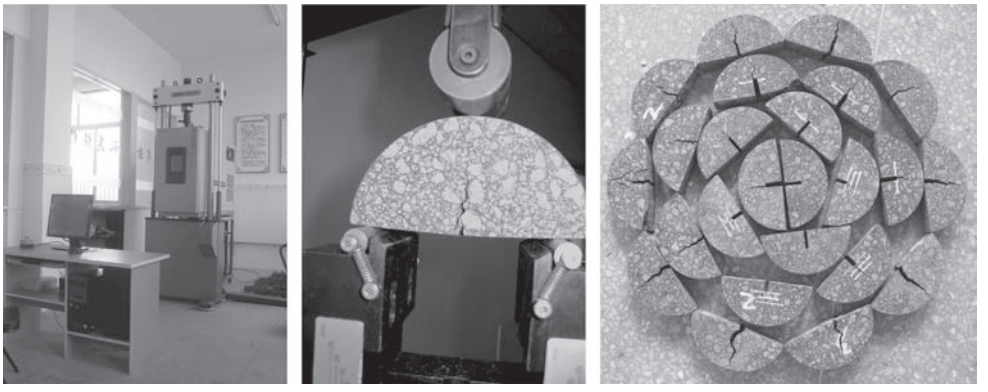

Figure 3. Test setup and some tested specimen.

into five plates of 30 mm thickness. Each plate was cut in half and a vertical notch was made along the symmetrical axis of the semi-circular specimen. The length of the notch varied from 12 mm to 25 mm and the width is 0.4 mm to 0.6 mm. Therefore, ten SCB specimens can be cut from a SGC cylindrical specimen, half is notched and half is un-notched, as shown in Figure 2. IDT specimen of 100 mm in diameter and 63.6 mm in thickness are also obtained from SGC cylindrical specimens.

3.4 *Test setup and instrumentation*

The SCB test is similar to the three-point bending beam test except for the specimen geometry: semi-circular instead of a rectangular beam. The SCB specimen is supported symmetrically with a fixed span of 80 mm by two rollers. A loading roller is used to load the SCB specimen on the top of the semi-circle.

3.5 *Testing procedure*

As the world-wide reported cracking in deck pavement is intimately related to high tensile stresses that develop at normal and low temperatures, test temperature of −10°C and 20°C were selected according to temperature estimation of deck pavement on Sutong Bridge. The specimens were tested using a universal testing system with a PowerTest automation package. The temperature of −10°C is controlled by an environmental chamber. For the temperature of 20°C, an air conditioner is used. Before being placed into the environmental chamber the specimens were stored and dried at room temperature overnight after being cut from the SGC cylindrical specimens. The specimens were then kept in the chamber for 4 hours at the desired temperature before test. A small seating load is firstly applied to the specimen to assure the contact between the loading roller and the specimen. And then the SCB loads monotonically a 100 mm diameter semi-circular specimen to failure applying a constant stroke of 50 mm/min and 1 mm/min for the un-notched and notched SCB specimen respectively. The load and displacement were measured and recorded by the PowerTest package.

4 RESULTS AND DISCUSSION

4.1 *Tensile strength*

The averaged tensile strength of semi-circular bending test and indirect tensile test are listed in table 6. The tensile strength with SCB test is about 1.4–1.7 times that of IDT test. The tensile strength from SCB and IDT test were different due to their different stress states under

Table 6. Comparison of SCB and IDT test results.

	Tensile strength (MPa)		Cov(%)		Ratio (SCB/IDT)		
Temperature	SCB	IDT	SCB	IDT	EAM	Huang	Van de Ven
–10°C	34.19	24.58	5.3	14.5	1.4		
20°C	11.04	6.43	1.4	7.6	1.7	3.2–4.1	4.4

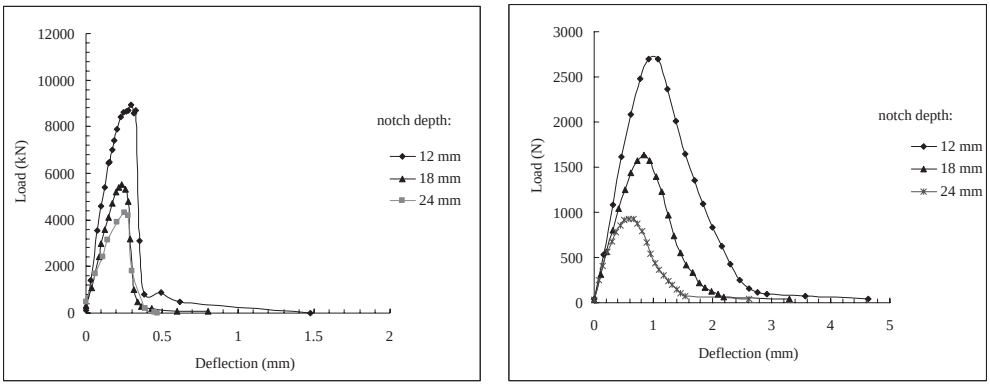

a) –10 Degree C b) 20 Degree C

Figure 4. Load-deflection behavior of epoxy asphalt concrete in SCB test.

loading. In IDT test, a biaxial state of stress exists and the maximum horizontal tensile stress at the center of the IDT specimen is one third of the vertical compressive stress at the same point. In SCB test, the specimen starts with a pure tensile flexural failure, which reflects a relatively "true" tensile strength of the mixture. SCB test could be used to characterize the tensile strength of asphalt mixtures with good repeatability, which makes it a potentially simple performance test for epoxy asphalt concrete mixtures. Huang reported the ratio of SCB to IDT is 3.2–4.1 with the test results of PG grade binder HMA at 25°C, and the tensile strength in IDT. Larger elastic modulus and stiffness of EAM may attribute to a lower ratio of SCB/IDT than that of traditional HMA. As geometry has also a significant effect on the results of the SCB test, further laboratory tests on SCB specimen of different sizes are desirable for EAM to obtain a optimum geometry.

4.2 *Load deflection behavior of notched specimen*

The load-deflection behaviors of notched specimens under different temperatures, with different notch depths are shown in figure 4. These curves represent the average values for 3–5 samples tested from each mixture at each notch depth. The relationships presented in figure 4(a) are tested at –10°C, and figure 4(b) are at 20°C. It can be seen from figure 5(a) that the initial load-deflection response is almost linear, for all specimens at various notch depths. A brittle response is observed immediately before the maximum sustainable load is reached. This is the case for all notch depths tested for the mixture. The crack then propagated rapidly from the notch tip after the maximum load was reached, and the fracture occurred in the Mode I-opening mode. The load-deflection curve decayed sharply. There is no significance of the deflection. At 20°C, there is a small increase in nonlinearity after the first linear portion of the load deflection curve. The decaying load-deflection curve after the maximum load was more slowly than that at –10°C. And there is also significant difference in the deflection relative to the maximum load, a visible increase in the deflection at the maximum load for the epoxy asphalt mixture. It is also noticed that this specimen gives reproducible results. That is

specimens always fracture along a similar path and the load-displacement curves as discussed earlier are within 10% of each other based on twice the standard deviation.

Figure 5 presents the results of ultimate bearing capacity along unit thickness as a function of the ration of notch depth/thickness for SCB tests at –10 to 20°C. The averaged value is used for un-notched SCB samples. The comparison is meaningful as the specimens are of the same size. It can be seen from Figure 5 that the ultimate bearing capacity decreases with notch depth and the influence of notch depth on bearing capacity at –10°C is larger than at 20°C, and at –10°C was about 3 times that of 20°C.

4.3 *Fracture resistance, Jc*

In order to obtain the critical value of the fracture resistance, the area under the loading portion of the load deflection curves, up to the maximum load, was measured from the curves as presented in figure 6. These values were then plotted as a function of notch depth as shown in figure. 7. It can be observed that the repeatability of the test is reasonable. As can be seen the relationship between the total strain energy to failure U and the notch depth at test temperatures are very linear. The correlation coefficients for the two straight lines are 0.99, and 0.94 for the temperature of –10°C and 20°C respectively.

The slope of the lines presented in figure. 6, is the critical fracture resistance, J_c, as obtained from Equation 2 instead of Equation 3. These values are given in Table 7 with comparison of other HMA. As can be seen, the J_c of EAC at 20°C is about 15% higher than at –10°C, however, the fracture resistance of EAC at –10°C has a value of J_c which is 6 times that of the sand asphalt mixture, while J_c at 20°C is nearly 3 times that of AC-20. The higher fracture resistance of the epoxy asphalt mixture is attributed to the chemical reactive resin modified binder, which has caused the mixture to become stronger in tensile strength and more resistant to crack tip separation.

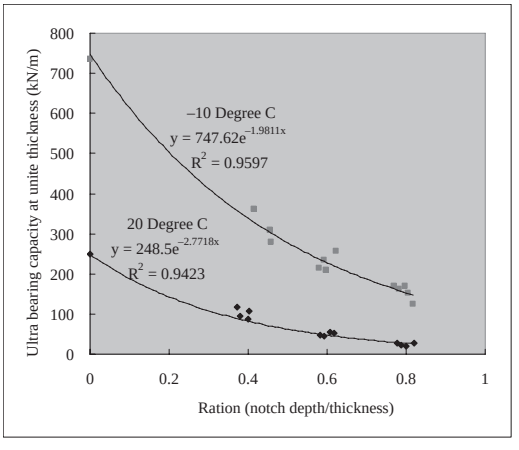

Figure 5. The ultimate bearing capacity at unit thickness as a function of the ratio of notch depth/thickness.

Table 7. The fracture toughness of epoxy asphalt concrete.

	EAC		AC-5 + 5% SEBS	AC-20
Temperature	J_c (kJ/m^2)	R^2	J_c (kJ/m^2)	J_c (kJ/m^2)
–10°C	2.60	0.99	0.42 (Mull, 2002)	–
20°C	2.92	0.94	–	1.03 (Mull, 2002)

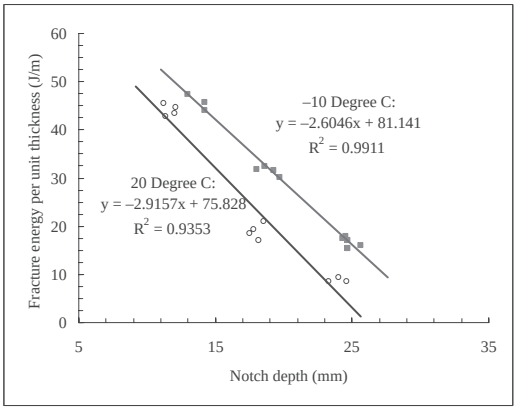

Figure 6. The fracture energy per unit thickness for EAC as a function of notch depth.

5 CONCLUSION

Static fracture toughness tests of epoxy asphalt mixture were performed using the semi-circular bending test. A number of conclusions can be drawn from the experimental results.

1. Epoxy asphalt mixture has a super higher resistance of fracture at low temperature than thermo-plastic HMA due to its super high tensile strength and flexibility. The temperature influences on the fracture resistance of EAM is not as significant as that of thermo-plastic HMA.
2. The changes of load-deflection behavior and critical fracture resistance with temperature indicate a change in mixture behavior from brittle to ductile behavior, revealing the capability to elasto-plastic fracture mechanics concept to characterize the fracture properties of EAM.
3. Good repeatability of SCB test results indicate the geometry of SCB specimen adopted in this research is suitable for EAM.

In general, the SCB test specimen has been shown to be useful for measuring the fracture toughness of epoxy asphalt mixture. Further works is desirable to explore the influences of fracture resistances of epoxy asphalt, develop a constitutive material model and incorporate the model into mixture and structural design for the pavement on steel bridge decks.

REFERENCES

Abdulshafi, A.A. & Majidzadeh, K. 1985. *J*-integral and cyclic plasticity approach to fatigue and fracture of asphalt mixtures. *TRB 64th Annual Meeting*: *January, 1985*, Washington DC.

Bhurke, A.S., Shin, E.E. & Drzal, L.T. 1997. Fracture morphology and fracture toughness measurement of polymer modified asphalt concrete. *TRB 76th Annual Meeting*, *12–16, January, 1997*, Washington DC.

Chen, X.H. 2006. *Fatigue characteristics of deck pavement based on composite beam test*, Nanjing: Transportation College of Southeast University, (in Chinese).

Chong, K.P. & Kuruppu, M.D. 1984. New specimen for fracture toughness determination for rock and other materials, *Int J Fract* 26: 59–62.

Dongre, R., Sharme, M.B. & Anderson, D.A. 1989. Development of fracture criterion for asphalt mixes at low temperatures. *Transportation Research Record 1228*: 94–105.

Huang, B.S., Shu, X. & Tang, Y.J. 2005. Comparison of semi-circular bending and indirect tensile strength tests for HMA mixtures. *GSP 130 Advances in Pavement Engineering, Proceedings of Sessions of the Geo-Frontiers 2005 Congress, 24–26, January, 2005*, Austin, Texas.

Huang, W. 2006. *Theory and method of deck paving design for long-span bridges*. Beijing: China Construction Industry Press, (in Chinese).

Huang, W., Yang, J., Cheng, G. Wang, X. & Wang, J.J. 2001, *Application of EAC for the orthotropic steel decks of 2nd Nanjing Bridge(Final report)*, Nanjing: Transportation College of Southeast University, (in Chinese).

Krans, R.L., Tolman, F. & Van de Ven, M.F.C. 1996. Semi-Circular Bending Test: A practical crack growth test using asphalt concrete cores. *Reflective Cracking in Pavements, Design and Performance of Overlay Systems, Proceedings of the 3rd International RILEM Conference*, *2–4, October, 1996*, Maastricht, The Netherlands.

Lim, I.L., Johnston, I.W. & Choi, S.K. 1993. Stress intensity factors for semi-circular specimen under three-point bending, *Eng Fract Mech* 44 (3): 363–382.

Molenaar, A.A.A. Scarpas, A., Liu, X. & Erkens, G. 2002. Semi-circular bending test; Simple but useful? *J Assoc Asphalt Technol* 71: 794–815.

Mull, M.A., Stuart, K. & Yehia, A. 2002. Fracture resistance characterization of chemically modified crumb rubber asphalt pavement, *Journal of Materials Science* 37: 557–566.

Little, D. & Mahmoub, K. 1985. Engineering properties of first generation plasticized sulfur binders and low temperature fracture Evaluation of plasticized sulfur paving mixtures. *TRB 64th Annual Meeting*, *January, 1985*, Washington DC.

Van de Ven, M.F.C. & Smit, A. 1997. Possibilities of a Semi-Circular Bending Test, *8th International Conference on Asphalt Pavements*, *10–14, August, 1997*, Seattle: University of Washington.

Advanced Testing and Characterization of Bituminous Materials –
Loizos, Partl, Scarpas & Al-Qadi (eds)
© 2009 Taylor & Francis Group, London, ISBN 978-0-415-55854-9

Viscoelastic response of asphalt-aggregate mixes to transient confining conditions

E. Levenberg
North Central Superpave Center, Purdue University, West Lafayette, Indiana

J. Uzan
Faculty of Civil and Environmental Engineering, Technion, Haifa, Israel

ABSTRACT: An asphalt-aggregate mix is subjected to creep and recovery sequences under isotropic compression mode in the triaxial apparatus. Duration of creep periods ranged between a few seconds to one minute, separated by half an hour of recovery intervals. Resulting strains are partitioned into viscoelastic (VE) and viscoplastic (VP) components with the study focusing on the nonlinear nature of the VE component. The VP response is represented using the classical strain hardening formulation; the VE response is represented using a linear formulation but with applied pressures replaced by 'effective VE pressures'. The ratio between applied and effective VE pressures at any moment during the test is defined as 'relative VE stiffness' and denoted as C^{ve}. The evolution of C^{ve} is exposed through direct analysis of the test data with minimal assumptions. Under the short creep periods it is shown that C^{ve} decreases in value from the very beginning of pressure application and increases during the following recovery intervals. Under the longer creep periods opposite trends appears, with C^{ve} raising after the initial drop and decreasing during the following recovery intervals. A conceptual breakdown into underlying causes is proposed for the seemingly erratic behavior of C^{ve} towards the development of a constitutive model.

1 INTRODUCTION

Asphalt-aggregate mixes (AAMs) exhibit a time-dependent response to load that is both viscoelastic (VE) and viscoplastic (VP). Under sustained loads, both strain parts creep at a decreasing rate; after complete unloading, the VE part can recover in full (i.e., VE solid behavior) while the VP part is deactivated and cannot recover. A nonlinear constitutive treatment is considered necessary to adequately represent these components (Uzan 1996). Within a pavement system, AAMs experience transient multiaxial stress states as a result of moving vehicles. However, the mechanical characterization of these materials had been traditionally limited to uniaxial conditions (Lai & Anderson 1973, Lai & Hufferd 1976, Abdulshafi 1983, Sides et al. 1985, Partl & Rösli 1985). In an effort to account for the three-dimensional state of stress, more recent investigations were carried out under superposed confining stresses (Kim et al. 1997, Pellinen & Witczak 2002, Gibson et al. 2003a, Collop et al. 2003, Uzan 2003, Sotil et al. 2004) in which pressures are applied first and the uniaxial testing commences only after 'equilibrium' is reached (i.e., after all deformation-rates vanish). In actuality though, the confining stresses are typically removed faster than the time required to achieve this 'equilibrium' state. Residual stresses may buildup in between axle passes due to the overall time-dependent response of the pavement system; however, these are expected to be small. Hence, the changes that take place in the material soon after pressure application are themselves relevant for mechanical characterization.

In the present paper the response to transient confinement conditions is studied. A material specimen is subjected to creep and recovery sequences under isotropic compression mode in the triaxial apparatus. The resulting strain history is analyzed assuming an overall VE–VP

behavior. The focus herein is on the nonlinear response of the VE component. To enable a reliable partitioning of the total deformation experimental attention is placed on fast unloading after each creep period and on relatively long recovery intervals (e.g., Levenberg & Uzan 2007). The investigation is limited to one AAM type and one (constant) temperature level; it is part of a larger study devoted to the development of a multiaxial VE–VP model for AAMs including nonlinear effects such as damage and healing (Levenberg 2006).

2 TESTING

One laboratory experiment is described hereafter, consisting of several creep and recovery sequences in isotropic compression mode under constant temperature conditions. The test specimen was prepared form a dense-graded AAM made of crushed limestone aggregates (12.5 mm nominal maximum size) and an AC-30 binder. The loose mix was designed according to the Marshall methodology with a 50-blow compactive effort (Asphalt Institute, 1997). The specimen was fabricated into a cylindrical shape, 200 mm tall and 100 mm in diameter, having 5% voids; this was accomplished using a combination of vibratory and static compaction equipment. It is important to note that the preparation method produced a transversally-isotropic specimen with the axis of material symmetry coinciding with the axis of the cylinder.

Testing was performed in a triaxial apparatus using a two-axis servo-hydraulic system. The first axis controls a piston that acts vertically on the test specimen; the second axis controls a piston that pressurizes the cell with fluid. For this purpose a relatively low (kinematic) viscosity silicone oil (~0.1 stokes) was used. The specimen was isolated from the cell-oil by a latex sleeve. Its underside was lightly glued to the triaxial cell using RTV silicon adhesive while the top remained free, completely disconnected from the vertical piston. The triaxial cell itself was placed inside an environmental chamber set to provide a constant temperature level of 30°C. A pressure transducer was positioned close to the specimen at mid height (penetrating the side of the triaxial cell).

All deformation measurements were done locally utilizing linear variable displacement transducers (LVDTs). Four LVDTs, each spanning 100 mm, were used for measuring axial strains. These were attached vertically to the middle part of the specimen at right-angles. Four additional LVDTs were mounted horizontally, with their tips in constant contact with the specimen via a spring mechanism; these were used for measuring radial strains. Subsequently, all reported axial and radial strains are averages of the individual readings in each direction.

The triaxial cell was first filled from the bottom up with the silicone oil. A valve extruding from the top plate of the cell, placed outside of the environmental chamber, was used for overflow control. As the cell was being filled, the valve remained open allowing all the entrapped air to exit. Once the cell was full the environmental chamber was closed and set to the target temperature. At this configuration the system was monitored for many hours until all gauge readings stabilized. Thereafter, the top valve was closed so the test could begin. Confining stresses were applied by gradually moving the second axis piston in position-controlled mode to pressurize the cell-oil. Removal of stresses was also done in position-controlled mode by quickly reversing the piston travel; at the same time the top valve was manually opened to impose atmospheric conditions. The combination of valve opening and position-controlled instructions of the testing equipment were timed such that cell-oil pressures decreased in fractions of a second (~150 milliseconds) to atmospheric conditions with no overshooting to negative values (i.e., suction). From this point on, the top valve remained open forcing atmospheric conditions inside the cell for the entire duration of the recovery interval. The valve was closed just before initiating a new creep interval.

Figure 1 presents the applied pressure history during the test and the resulting axial and radial strains. Strains are shown on the left ordinate and applied stresses are shown on the right ordinate; the abscissa represents (physical) test time. As is customary for geomaterials, a positive sign indicates compression and a negative sign indicates tension (of either stress or strain). Eight creep cycles can be seen, with peak magnitudes (and durations) generally

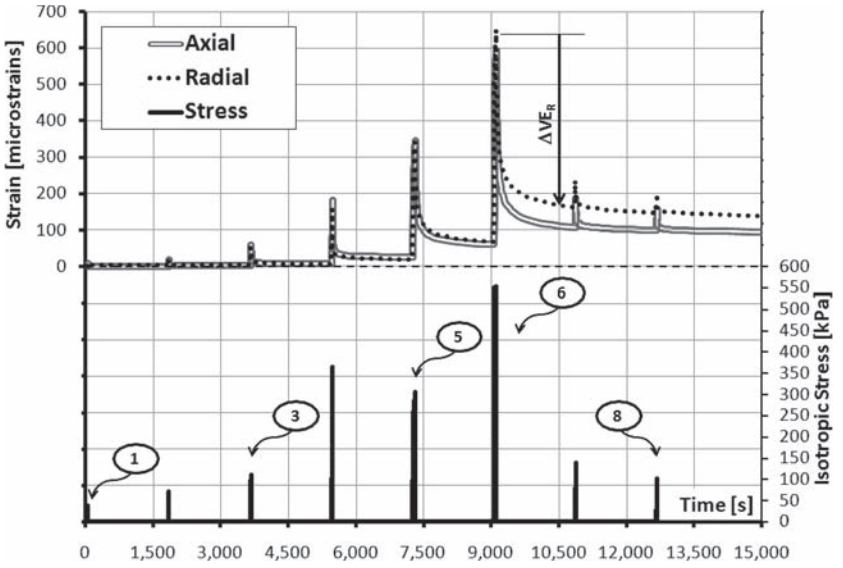

Figure 1. Applied pressure history and resulting strain response in the isotropic compression test.

increasing during the first six cycles and then decreasing in the final two. During creep cycles 5 and 6 the loading increased gradually towards the peak for about 10 seconds, then maintained at a constant level more or less for additional 50 seconds, and then completely and quickly removed. During all other creep intervals (i.e., cycles 1–4 and 7–8) the loading shape was approximately triangular; increasing gradually to peak pressure for several seconds and then decreasing rapidly to atmospheric conditions (see also Fig. 3). The first three creep cycles generated very small strain responses, with total amplitude changes of about 9, 18, and 58 microstrains respectively (axial direction). The peak strain response in the entire test was 645 microstrains, obtained during cycle 6 in the radial direction; the corresponding (peak) axial strain level was 600 microstrains. The first seven recovery periods (following creep cycles 1–7) were each 1,800 seconds (0.5 hours) in duration; after creep cycle 8 the material was allowed to recover for 30,000 seconds (~8.3 hours). The total test time was 44,000 seconds (~12.1 hours) of which only 15,000 seconds (4.2 hours) are shown in the figure. It should be noted that the rest intervals after creep cycles 1–3 and also after creep cycle 8 were long enough to allow full recovery of VE strains. This fact helped to better partition the measured strains into VE and VP components. Over the entire test, the total level of accumulated axial VP strain was 88 microstrains; the corresponding radial VP strain level was 128 microstrains.

3 ANALYSIS

Analysis of the test results was geared towards exposing the nonlinear nature of the VE component. As a preliminary step, the recovered strains in the axial and radial directions, obtained in unloaded conditions only (i.e., during recovery intervals), were cross-plotted. The resulting chart is shown in Figure 2, in which the recovered strains are denoted as ΔVE on the axis titles. For a given recovery interval, ΔVE at time t is defined as the difference between the strain level reached immediately after complete unloading (from a previous creep cycle) and the strain level at time t. As an example, ΔVE in the radial direction (denoted by a subscript R) is illustrated in Figure 1 for t = 10,500 seconds (i.e., during the recovery interval following creep cycle 6). It is important to note that ΔVE purely represents (part of) the VE strain response because the VP component is inactive under zero loads. As shown in Figure 2 using a dashed oblique line, an approximate linear relation is obtained with a slope

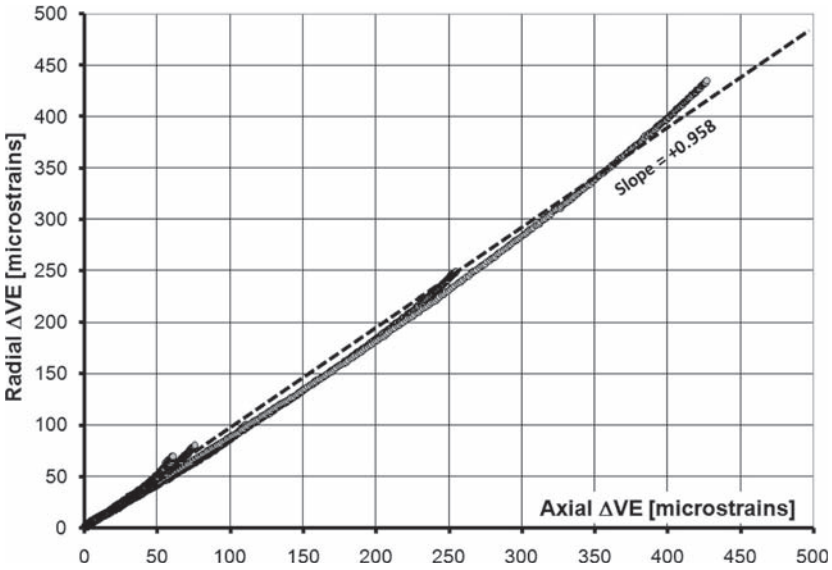

Figure 2. Cross plot of recovered strains in the axial and radial directions (based on Figure 1 data).

equal to 0.958. This finding means that a unique constant of proportionality may be used to relate axial and radial VE strains (not just ΔVE), at least for the range of strain levels included in the test. It also means that nonlinear VE effects may be assumed isotropic in nature given that the material's symmetry was not significantly altered; this conclusion was also shown to hold for AAMs exposed to pre-peak uniaxial stress conditions (Levenberg & Uzan 2007). When peak conditions are approached nonlinear VE effects may be accompanied by symmetry changes, as was found in Park & Schapery (1997) and in Ha & Schapery (1998) for particle-filled rubber.

The following multiaxial VE constitutive formulation (summation convention applies) is deemed appropriate, as it complies with the above findings and discussion for AAMs under pre-peak conditions:

$$\varepsilon_i^{ve}(t) = P_{ij}^{ve} \cdot \int_{\tau=0}^{\tau=t} D(t-\tau) \cdot d\tilde{\sigma}_j^{ve}(\tau) \qquad (i,j = 1..6) \tag{1}$$

$$\tilde{\sigma}_j^{ve}(t) = \frac{\sigma_j(t)}{C^{ve}(t)} \qquad (j = 1..6) \tag{2}$$

in which single index notation is used with ε_i^{ve} =VE strain tensor; P_{ij}^{ve} = unitless 6×6 tensor of engineering constants representing VE symmetry; $D(t)$ = uniaxial linear VE creep compliance; t = physical time; τ = time-like integration variable; $\tilde{\sigma}_j^{ve}$ = effective VE stress tensor; σ_j = applied stress tensor; and C^{ve} = relative VE stiffness (unitless). Equation 1 is nonlinear because applied stresses are replaced by effective VE stresses. Note that one scalar time function $D(t)$ is used to control the deformation in all directions. C^{ve} in equation 2 is a positive scalar entity that links the effective and applied stresses and embodies all nonlinear VE behavior. For a linear material the relative VE stiffness equals unity at all times; in the nonlinear case it equals unity only in the pristine state and may change thereafter. Decrease in C^{ve} under load is commonly referred to as 'damage' (e.g., Kim & Little 1990, Park et al. 1996, Lee & Kim 1998a, Chehab 2002, Chehab et al. 2003, Gibson et al. 2003b, Uzan 2005, Gibson 2006); increase in C^{ve} during recovery intervals may be referred to as 'healing' (e.g., Kim et al. 1990, 1994, 1997, Lee & Kim 1998b, Si et al. 2002); and increase in C^{ve} under compressive loads is referred to as 'stiffening' (Levenberg 2006, Levenberg & Uzan 2009). Note that changes

in C^{ve} do not influence the material's symmetry (characterized by P_{ij}^{ve}), complying with the assumption that nonlinear VE effects are isotropic in nature.

Equation 1 simplifies considerably for the test conditions described in the previous section because $\sigma_4 = \sigma_5 = \sigma_6 = 0$ and $\sigma_2 = \sigma_3$; accordingly, the P_{ij}^{ve} tensor for transversely-isotropic material reduces to (Graham & Houlsby 1983, Lings et al. 2000, Schapery 2002):

$$P_{ij}^{ve} = \begin{bmatrix} 1.0 & 2\cdot \mathrm{B} \\ \mathrm{B} & \mathrm{C}+\mathrm{D} \end{bmatrix} \quad (i,j = 1..2) \tag{3}$$

in which B = radial-to-axial VE strain ratio (analogous to Poisson's ratio in linear elasticity); and C + D = effect of radial stresses on the resulting radial strains (relative to the effect of axial stresses on the resulting axial strains). The indices 1 and 2 in P_{ij}^{ve} refer to the axial (vertical) and radial (horizontal) directions respectively. Additionally, since isotropic conditions are considered, with $\sigma_5 = \sigma_6 = p$, the following expressions are obtained from equations 1, 2 and 3:

$$\varepsilon_1^{ve}(t) = \left[1.0 + (2\cdot \mathrm{B})\right] \cdot \int_{\tau=0}^{\tau=t} D(t-\tau)\cdot d\tilde{p}^{ve}(\tau) \tag{4}$$

$$\varepsilon_2^{ve}(t) = \left[\mathrm{B} + (\mathrm{C}+\mathrm{D})\right] \cdot \int_{\tau=0}^{\tau=t} D(t-\tau)\cdot d\tilde{p}^{ve}(\tau) \tag{5}$$

$$\tilde{p}^{ve}(t) = \frac{p(t)}{C^{ve}(t)} \tag{6}$$

where P = applied pressure; and $\tilde{p}^{ve}$ = effective VE pressure. For later use, equation 4 is also written in 'reversed' form as follows:

$$\tilde{p}^{ve}(t) = \left[1.0 + (2\cdot \mathrm{B})\right]^{-1} \cdot \int_{\tau=0}^{\tau=t} E(t-\tau)\cdot d[\varepsilon_1(\tau) - \varepsilon_1^{vp}(\tau)] \tag{7}$$

in which $E(t)$ = uniaxial linear VE relaxation modulus, related to $D(t)$ by the convolution integral (e.g., Lockett 1972); ε_1 = axial strain in the test (measured entity); and ε_1^{vp} = axial VP strain component (calculated entity). Note that $\varepsilon_1 - \varepsilon_1^{vp}$ equals the axial VE strain component ε_1^{ve} .

The most desirable method for investigating nonlinear VE response is to expose the evolution of C^{ve} directly from the test data with minimal assumptions on material behavior. To accomplish this, analysis of the test measurements was performed according to the following steps. First, an error term was defined to quantify the ability of a VE–VP model to match the measured axial strains ε_1. Second, the axial VP component was represented using a classical strain-hardening formulation:

$$\varepsilon_1^{vp}(t) = \int_{\tau=0}^{\tau=t} \frac{K\cdot[p(\tau)]^n \cdot d\tau}{[q(\tau)]^m} \quad \text{with } \dot{q}(t) = \dot{\varepsilon}_1^{vp}(t) \tag{8}$$

where q = strain hardening parameter; K, n, m = positive model constants; q_0 = initial hardening level; and the 'overdot' indicates a derivative taken with respect to time. Additionally, it was assumed that the linear creep compliance has a sigmoid shape in a log-log scale (Smith, 1971):

$$D(t) = D_\infty + \frac{D_0 - D_\infty}{1 + (t/\tau_D)^{n_D}} \tag{9}$$

in which D_0, D_∞, τ_D, n_D = constants. τ_D has units of time identical to t or τ and n_D is unitless; D_∞ and D_0 are the long-time and the instantaneous values of the creep compliance respectively

with units reciprocal to stress. Third, the numerical values of the constants in equations 8 and 9 were assumed and the uniaxial relaxation modulus $E(t)$ concurrently calculated from $D(t)$. The interconversion was performed using a Prony (exponential) series representation of both the source and target functions (Mead 1994, Park & Schapery 1999). Fourth, the resulting $E(t)$ and ε_1^{vp} (from equation 8) were used in equation 7 to calculate the effective VE pressure $\tilde{p}^{ve}$ throughout the test. This was done with B = –0.375 based on a separate analysis of a uniaxial experiment performed on the same specimen (Levenberg 2006). Fifth, $\tilde{p}^{ve}$ and $D(t)$ were then used in equation 4 to calculate the axial VE strain component ε_1^{vp}. Finally, the sum $\varepsilon_1^{ve} + \varepsilon_1^{vp}$ was compared with ε_1 to evaluate the error term defined in the first step. At this point the entire procedure was repeated with a new set of parameters until a close fit of the data was achieved. For this purpose a gradient decent optimization algorithm was applied to minimize the error term (Fylstra et al. 1998); activated under the condition that C^{ve} equals unity in the very initial part of the test but otherwise unrestricted.

4 RESULTS AND DISCUSSION

Figure 3 presents the resulting changes in C^{ve} with values in the range of 0 to 1.3 depicted on the left ordinate. The abscissa represents cumulative time under pressure instead of total test time; this is done in order to save space because C^{ve} cannot be observed when the material is unloaded since both the applied pressure p and subsequently the effective VE pressure $\tilde{p}^{ve}$ vanish. The outcome is seen to be 'noisy', especially for the small strain cycles 1–3 and 7–8, because direct use of test data was made in the calculations (applied pressures in equation 6 and measured strains in equation 7). Also shown in this figure, on the right ordinate, are the applied confining stresses; from which the loading shape during the creep sequences can be clearly observed.

Figure 3 demonstrates that C^{ve} was changing under load throughout the experiment (i.e., effective VE pressures differed from applied pressures), which indicates that the response was in effect nonlinear. Comparison of C^{ve} levels just before and immediately after recovery intervals indicate that relative VE stiffness also changed during rest periods (path of change could not be observed and hence not shown). At the very beginning of the test (i.e., $t = 0$) C^{ve} equals unity; during the first creep cycle C^{ve} drops from 1.0 to 0.85; after the rest interval between cycles 1 and 2 C^{ve} reverted back to unity. In cycle 2, C^{ve} drops from 1.0 to 0.82; after the rest interval between cycles 2 and 3, C^{ve} reverts again back to unity. In the third creep cycle, C^{ve} drops from 1.0 to a minimum level of about 0.81; during the following recovery interval (between cycles 3 and 4), C^{ve} is regained to a level of about 0.97.

A different behavior compared to the one described above may be observed under creep cycles 4, 5 and 6. In cycle 4, C^{ve} first drops from an initial level of 0.97 to a minimum of 0.79 but then begins to slightly increase (up to 0.82); during the recovery interval between cycles 4 and 5, C^{ve} increases further to about 0.90. In cycle 5, C^{ve} first drops from 0.90 to a minimum of 0.70 and then begins to steadily raise under the slight increasing applied confining stresses to about 1.05; during the recovery interval between cycles 5 and 6, C^{ve} does not increase in value (as in the previous rest periods), but drops to a level of about 0.82. In cycle 6, C^{ve} drops from the initial level of 0.82 to a minimum of 0.66; it then begins to steadily increase up to about 1.25. Note that this increase takes place under constant applied pressure level of about 550 kPa. After the rest interval between cycles 6 and 7, C^{ve} decreases (again) to about 0.88. In cycle 7, in which the loading intensity was much lower compared to the two preceding cycles 5 and 6, C^{ve} is seen to drop from an initial level of 0.88 to a minimum of about 0.62; a value that is lower than the minimum obtained in the preceding cycles (i.e., 0.70 and 0.66 respectively); during the recovery interval between cycles 7 and 8, C^{ve} increases (similar to the case of cycles 1–4) to about 0.91. Under creep cycle 8, C^{ve} drops from 0.91 to about 0.65; subsequent changes in C^{ve} during the following recovery interval cannot be observed as no more pressure sequences were applied.

The behavior of C^{ve} described above seems complex and erratic. In an attempt to simplify matters, a conceptual breakdown of the overall behavior into underlying causes is hereby

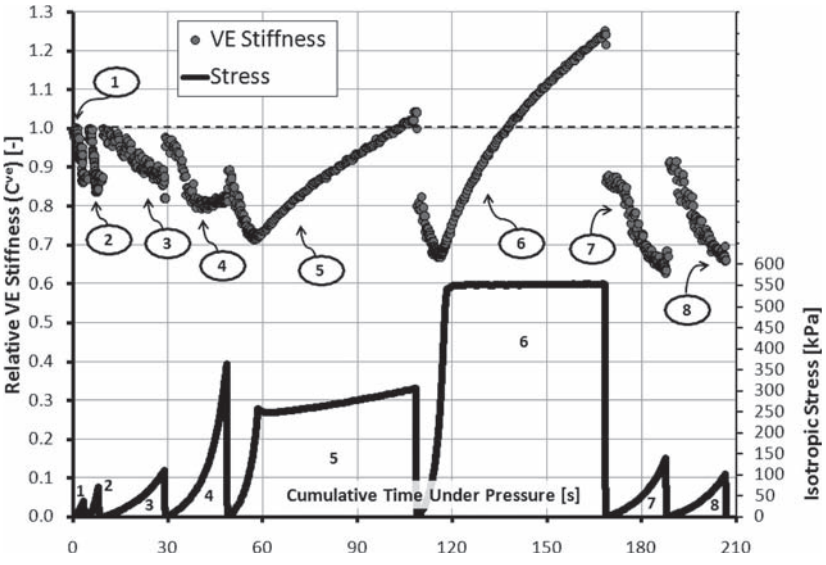

Figure 3. Evolution of C^{ve} under pressure (circular markers) and applied confining stress history (solid lines).

offered. Accordingly, the relative VE stiffness is understood to reflect the combined effect of three separate and 'competing' mechanisms: (i) damage, i.e., decrease in C^{ve} under loading; (ii) healing, i.e., increase in C^{ve} during recovery intervals; and (iii) stiffening, i.e., increase in C^{ve} under compressive conditions. Developing this conceptual viewpoint into a constitutive theory can be achieved by separating C^{ve} multiplicatively as follows (Levenberg & Uzan 2009):

$$C^{ve} = C_1(S_1) \cdot C_2(S_2) \cdot C_3(S_3) \tag{10}$$

in which with C_1 is responsible for simulating short-lasting (reversible) damage under load and subsequent healing during recovery intervals; C_2 accounts for reversible stiffening under compressive conditions; and C_3 is responsible for generating load related long-lasting (or quasi-permanent) damage. S_k (k = 1.3) are three independent (unitless) internal state variables, each introduced to control the corresponding C_k. Initially all S_k's equal zero and under any type of loading each exhibits time-dependent changes (rate of change not necessarily identical). During recovery intervals, both S_1 and S_2 gradually revert back toward zero while S_3 remains constant. Regardless of the applied stress mode, S_1 is always positive; for the loading history considered herein S_2 and S_3 take on positive values (in other cases they may become negative). The resulting C_k's are always positive.

Figure 4 schematically illustrates the expected behavior of each of the C_k's versus their corresponding S_k's. The three C_k's are depicted on the left ordinate with values in the range of 0.0 to 2.0; the S_k's are depicted on the abscissa with values in the range of 0.0 to 0.0005 (these numbers are inconsequential for the following discussion). As can be seen, when all the S_k's are zero each of the C_k's equal unity; this represents the conditions at the initial part of the experiment before loading is applied while the material is in pristine state (for which C^{ve} is unity). As the material is placed under confining pressure all S_k's begin to increase in value. Initially, this results in a rapid decrease in C_1, a small increase in C_2 and a small decrease in C_3. Hence, the overall level of C^{ve} first decreases. If the material is unloaded at this point and allowed to recover, both S_1 and S_2 will revert to zero; this will drive C^{ve} to take the value of C_3 which is not much different from unity. Referring to Figure 3, this behavior represents the observed drops in C^{ve} at the beginning of each creep cycle and also the return of C^{ve} to a level close to unity at the beginning cycles 2, 3 and 4.

Alternatively, if the confining pressure is not removed, then the S_k's increase further; this causes additional decrease in both C_1 and C_3 and an increase in C_2. Hence, after the initial

drop in C^{ve} an opposite trend should appear (i.e., increase) due to the dominance of C_2 in equation 10. Referring to Figure 3, this behavior is clearly seen in cycles 4–6. If the material is unloaded at this point, both C_1 and C_2 revert back to unity (or equivalently S_1 and S_2 revert back to zero), and the overall level of C^{ve} either increases or decreases towards the value of C_3. In Figure 3 the former case is seen to occur between cycles 4 and 5 (C^{ve} increased during recovery); the latter case is seen to occur between cycles 5 and 6 and also between cycles 6 and 7 (C^{ve} decreased during recovery). Note that because S_3 is not allowed to decrease during recovery intervals, the level of C_3 can only decrease in the course of the experiment; this characteristic is what makes it possible to simulate the decreasing minimum levels of C^{ve} in cycles 4, 5 and 6 (from Fig. 3 they are 0.79, 0.70 and 0.66 respectively).

Equations for computing the three S_k's are proposed in Levenberg (2006) and also in Levenberg & Uzan (2009). In general terms this is done using VE strain invariants to represent S_1 and S_2 while VP strain invariants are used for representing S_3. The outcome is an implicit multiaxial nonlinear VE formulation which, along with a VP model, can adequately capture and reproduce the strain response of AAMs under complex three-dimensional stress histories (pre-peak conditions).

5 SUMMARY AND CONCLUSIONS

An asphalt-aggregate mix was subjected to several creep and recovery sequences under isotropic compression mode in the triaxial apparatus. Duration of creep periods ranged between a few seconds up to one minute, separated by half an hour of recovery intervals (the final recovery interval was more than eight hours long). Corresponding peak strains ranged between a few microstrains up to about 0.65 millistrains.

Assuming an overall VE–VP response, analysis of the test results was geared towards exposing the nonlinear nature of the VE component. For this purpose the VP part was represented using the classical strain hardening formulation and the VE part was treated as nonlinear, using a linear model with applied pressures replaced by 'effective VE pressures'. To facilitate a reliable decomposition of the measured strains attention was placed in the experimental program on fast unloading after each creep cycle and on executing long recovery sequences while maintaining true zero (atmospheric) conditions inside the triaxial cell regardless of any mechanical or electrical drift in the system components.

The ratio between applied and effective VE pressures at any moment during the test was defined as 'relative VE stiffness' and denoted by C^{ve}. Consequently, C^{ve} is a unitless positive scalar entity that embodies all VE nonlinearities. For a linear VE material C^{ve} equals unity at all times; in the nonlinear case it equals unity only in the pristine state and changes thereafter according to the loading history.

The evolution of C^{ve} in the course of the experiment was exposed by means of direct analysis of the test data with minimal assumptions on material behavior. This was achieved by simultaneous application of both creep and relaxation formulations while retaining their interrelationship through the convolution integral. Under the short creep periods it was demonstrated that C^{ve} decreased in value from the very beginning of pressure application and later increased during the following recovery intervals. Under the longer creep periods opposite trends appeared, with C^{ve} increasing after the initial drop and later decreasing (instead of increasing) during the following recovery intervals.

A conceptual breakdown of the overall behavior into underlying causes was offered as an essential first step towards the development of a constitutive model. Accordingly, the relative VE stiffness was understood to reflect the combined effect of three separate and 'competing' mechanisms: (i) damage, i.e., decrease in C^{ve} under loading; (ii) healing, i.e., increase in C^{ve} during recovery intervals; and (iii) stiffening, i.e., increase in C^{ve} under compressive conditions.

Based on the aforementioned findings it is concluded that uniaxial tests conducted under sustained levels of confinement are missing an essential characterization ingredient. Results from such tests are conducted after the specimen attains 'equilibrium' with each new pressure

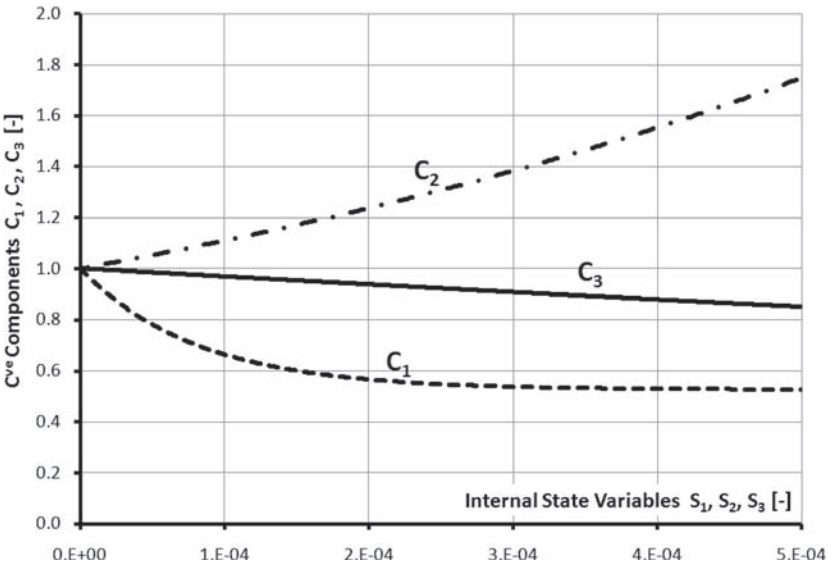

Figure 4. Schematic illustration of the shape of the nonlinear VE functions $C_1(S_1)$, $C_2(S_2)$ and $C_3(S_3)$.

level. Hence, the results will only apply to extremely slow loading conditions in which the transition between equilibrium states is of no interest. To be able to quantify a realistic response to transient confining stresses, characterization tests should focus on the path of transition between the equilibrium states. The testing procedure and analysis method described and employed herein were shown to be very well suited for the task.

REFERENCES

Abdulshafi, A.A. 1983. Viscoelastic/plastic characterization, rutting and fatigue of flexible pavements. *Ph.D. Dissertation*. Ohio State University.

Asphalt Institute. 1997. Mix design methods for asphalt concrete and other hot-mix types. *Manual Series 2 (sixth ed.)*. Lexington. Kentucky.

Chehab, G.R. 2002. Characterization of asphalt concrete in tension using a viscoelastoplastic model. *Ph.D. Dissertation*. North Carolina State University.

Chehab, G.R., Kim, Y.R., Schapery, R.A., Witczak, M.W. & Bonaquist, R. 2003. Characterization of asphalt concrete in uniaxial tension using a viscoelastoplastic model. *Journal of the Association of Asphalt Paving Technologists* 72: 326–370.

Collop, A.C., Scarpas, A., Kasbergen, C. & de Bondt, A. 2003. Development and finite element implementation of stress-dependent elastoviscoplastic constitutive model with damage for asphalt. *Transportation Research Record* 1832: 96–104.

Fylstra, D., Lasdon, L., Watson, J. & Waren, A. 1998. Design and use of the Microsoft Excel solver. *Interfaces* 28(5): 29–55.

Gibson, N.H. 2006. A viscoelastoplastic continuum damage model for the compressive behavior of asphalt concrete. *Ph.D. Dissertation*. University of Maryland at College Park.

Gibson, N.H., Schwartz, C.W., Schapery, R.A. & Witczak, M.W. 2003a. Confining pressure effects on viscoelasticity and damage in asphalt concrete. *16th ASCE engineering mechanics conference*. University of Washington. Seattle.

Gibson, N.H., Schwartz, C.W., Schapery, R.A. & Witczak, M.W. 2003b. Viscoelastic, viscoplastic, and damage modeling of asphalt concrete in unconfined compression. *Transportation Research Record* 1860: 3–15.

Graham, J. & Houlsby, G.T. 1983. Anisotropic elasticity of natural clay. *Géotechnique* 33(2): 165–180.

Ha, K. & Schapery, R.A. 1998. A three-dimensional viscoelastic constitutive model for particulate composites with growing damage and its experimental validation. *International Journal of Solids and Structures* 35(26–27): 3497–3517.

Kim, J.R., Drescher, A. & Newcomb, D.E. 1997. Rate sensitivity of asphalt concrete in triaxial compression. *Journal of Materials in Civil Engineering* 9(2): 76–84.
Kim, Y.R., Lee, H.J. & Little, D.N. 1997. Fatigue characterization of asphalt concrete using viscoelasticity and continuum damage theory. *Journal of the Association of Asphalt Paving Technologists* 66: 520–569.
Kim, Y.R. & Little, D.N. 1990. One-dimensional constitutive modeling of asphalt concrete. *Journal of Engineering Mechanics* 116 (4): 751–772.
Kim, Y.R., Little, D.N. & Benson, F.C. 1990. Chemical and mechanical evaluation on healing mechanism of asphalt concrete. *Journal of the Association of Asphalt Paving Technologists* 59: 240–275.
Kim, Y.R., Whitmoyer, S.L. & Little, D.N. 1994. Healing in asphalt concrete pavements: is it real? *Transportation Research Record* 1454: 89–96.
Lai, J.S. & Anderson, D. 1973. Irrecoverable and recoverable nonlinear viscoelastic properties of asphalt concrete. *Highway Research Record* 468: 73–88.
Lai, J.S. & Hufferd, W.L. 1976. Predicting permanent deformation of asphalt concrete from creep tests. *Transportation Research Record* 616: 41–43.
Lee, H.J. & Kim, Y.R. 1998a. A viscoelastic constitutive model for asphalt concrete under cyclic loading. *Journal of Engineering Mechanics* 124(1): 32–40.
Lee, H.J. & Kim, Y.R. 1998b. A viscoelastic continuum damage model of asphalt concrete with healing. *Journal of Engineering Mechanics* 124 (1): 1224–1232.
Levenberg, E. 2006. Constitutive modeling of asphalt-aggregate mixes with damage and healing. *Ph.D. Dissertation*. Technion. Haifa. Israel.
Levenberg, E. & Uzan, J. 2007. Uniqueness of the viscoelastic time-function for asphalt-aggregate mixes. In Loizos, A., Scarpas, A. & Al-qadi, I.L. (eds.), *Advanced Characterization of Pavements and Soil Engineering Materials* 1: 35–48; *Proc. Intern. Conf., Athens, 20–22 June 2007*. Greece.
Levenberg, E. & Uzan, J. 2009. Multiaxial viscoelastic response and modeling of asphalt-aggregate mixes with damage and healing. *Mechanics of Materials*. Submitted.
Lings, M.L., Pennington, D.S. & Nash, F.T. 2000. Anisotropic stiffness parameters and their measurement in a stiff natural clay. *Géotechnique* 50(2): 109–125.
Locket, F.J. 1972. Nonlinear viscoelastic solids. Academic Press Inc. (London) Ltd.
Mead, D.W. 1994. Numerical interconversion of linear viscoelastic material functions. *Journal of Rheology* 38(6): 1769–1795.
Park, S.W., Kim, Y.R. & Schapery, R.A. 1996. A viscoelastic continuum damage model and its application to uniaxial behavior of asphalt concrete. *Mechanics of Materials* 24: 241–255.
Park, S.W. & Schapery, R.A. 1997. A viscoelastic constitutive model for particulate composites with growing damage. *International Journal of Solids and Structures* 34(8): 931–947.
Park, S.W. & Schapery, R.A. 1999. Methods of interconversion between linear viscoelastic material functions. Part I—a numerical method based on Prony series. *International Journal of Solids and Structures* 36(11): 1653–1675.
Partl, M. & Rösli, A. 1985. An approximation of uniaxial creep during alternating tension-compression step loading at constant temperature. *International Journal of Solids and Structures* 21(3): 235–244.
Pellinen, T.K. & Witczak, M.W. 2002. Stress dependent master curve construction for dynamic (complex) modulus. *Journal of the Association of Asphalt Paving Technologists* 71: 281–309.
Schapery, R.A. 2002. Homogenized constitutive equations for linear visco-elastic unidirectional composites with growing transverse cracks. *Mechanics of Time-Dependent Materials* 6: 101–131.
Si, Z., Little, D.N. & Lytton, R.L. 2002. Evaluation of fatigue healing effect of asphalt concrete by pseudostiffness. *Transportation Research Record* 1789: 73–79.
Sides, A., Uzan, J. & Perl, M. 1985. A comprehensive visco-elastoplastic characterization of sand-asphalt under compression and tension cycle loading. *Journal of Testing and Evaluation* 13(1): 49–59.
Smith, T.L. 1971. Empirical equations for representing viscoelastic functions and for deriving spectra. *Journal of Polymer Science* 35(Part C: viscoelastic relaxation of polymers): 39–50.
Sotil, A., Kaloush, K.E. & Witczak, M.W. 2004. Reduced confined dynamic modulus testing protocol for asphalt mixtures. *Transportation Research Record* 1891: 153–162.
Uzan, J. 1996. Asphalt concrete characterization for pavement performance prediction. *Journal of the Association of Asphalt Pavement Technologists* 65: 573–607.
Uzan, J. 2003. Characterization of asphalt concrete materials for permanent deformation. *International Journal of Pavement Engineering* 4(2): 77–86.
Uzan, J. 2005. Viscoelastic-viscoplastic model with damage for asphalt concrete. *Journal of Materials in Civil Engineering* 17(5): 528–534.

Advanced Testing and Characterization of Bituminous Materials – Loizos, Partl, Scarpas & Al-Qadi (eds)
© 2009 Taylor & Francis Group, London, ISBN 978-0-415-55854-9

Evaluation of creep compliance of rubberized asphalt in compare with conventional hot mix asphalt

M. Arabani
Civil Engineering Department, University of Guilan, Rasht, I.R. Iran

S.M. Mirabdolazimi
Department of Chemistry, Iran University of Science & Technology, Tehran, I.R. Iran

ABSTRACT: Creep properties of bituminous mixture are very important to predict rutting depth in flexible pavement structures due to traffic loading. Rutting has been recognized as a problem in flexible pavements, and with the advent of high tire pressure and heavier wheel loads, permanent deformation potential in hot mix asphalt (HMA) layers has increased. Because of distresses due to permanent deformations, a good deal of budget is annually being expensed for repair and rehabilitation of asphaltic pavements. In this research, the effect of crumb rubber on creep performance of modified asphalt mixtures is studied. The results indicate that the performance of rubberized asphalt has good accuracy in comparison with conventional HMA.

1 INTRODUCTION

1.1 *Rubberized asphalt*

The waste materials can broadly be categorized as follows: (a) industrial wastes such as cellulose wastes, wood lignin, bottom ash and fly ash; (b) municipal/domestic wastes such as incinerator residue, scrap rubber, waste glass and roofing shingles; and (c) mining wastes such as coal mine refuse (Kandhal 1992).

About 285 million tires are discarded every year in the United States. Of these, about 55 million are rethreaded or reused, and about 42 million are diverted to various alternative uses such as combustion for generating power and additive to HMA mixes (Arabani et al. 2006).

Several states have enacted legislation to regulate the scrap tire problem. At the national level, Section 1038 of the Inter modal Surface Transportation Efficiency Act of 1991 specifically addresses the study and use of the scrap rubber by the highway industry (Kandhal 1992). Crumb rubber obtained from tires can either be ambient ground (grinding at room temperature or above) or cryogenically ground (grinding below embitterment temperature, liquid nitrogen is often used). Ambient ground crumb rubber has a sponge-like surface. Due to very high surface area this rubber reacts with asphalt cement reasonably fast. Cryogenically ground rubber usually has undesirable particle morphology. This process produces a clean flat surface which, in turn, reduces the reaction rate with hot asphalt cement. Cryogenically ground rubber also gives lower elastic recovery compared to the ambient ground rubber (Roberts et al. 1989).

The use of crumb rubber to modify asphalt cement has been developed over the past 25 years. Since the waste material will replace and/or modify the properties of HMA, it will affect the engineering properties (such as strength and durability) (Haghi et al. 2005).

Therefore, the HMA containing the waste material must be reevaluated thoroughly and carefully both in the laboratory and the field (Kandhal 1992). For the past several years, several researchers have concluded that the rubberized asphalt mixes can be helpful in reducing the overlay thickness (Holleran & Van 2000; Haghi et al. 2005) and its reflective cracking

(Cano et al. 1989; Esch 1982; Choubane et al. 1999; Haghi et al. 2005). Another research also indicated that these mixtures have a high resistance to rutting and fatigue cracking (Way 2003), in addition to protecting the environment and saving resources (e.g., landfill spaces). In 1960, Charles McDonald became the first engineer to use tire rubber in asphalt mixtures to improve pavements in the United States; since then, many experimental studies and field test sections have been constructed and tested. The mixing of crumb rubber with conventional binders results in an improvement in the resistance to rutting, fatigue cracking and thermal cracking (Way 2003; Sebaaly et al. 2003). (Antunes et al. 2003) pointed out; however, that the stiffness of the asphalt rubber being somewhat lower than the values generally obtained from the conventional asphalt mixture at test temperature.

1.2 *Creep compliance and rutting depth*

There are five major asphalt pavement distresses that may lead to loss of performance: fatigue cracking; rutting; thermal cracking; friction; and moisture susceptibility. Asphalt pavement rutting is one of the most common and destructive pavement distresses observed on Canadian roads (Fig. 1), particularly at intersections in the urban environment.

Asphalt pavement rutting can be caused by insufficient pavement structural support allowing excessive stress to be transferred to the sub grade (structural rutting); however, the most common type of rutting is 'instability' rutting caused by the plastic movement of the asphalt mix under heavy, often slow moving loading. The cost of asphalt pavement rutting repairs can be very high and disruptive on traffic operations. A reliable, accelerated laboratory performance test to evaluate the rutting resistance of asphalt mixes is considered necessary. It would be beneficial for use in verifying mix designs, for pavement failure investigations and for evaluating new materials (Chen et al. 2004; Uzarowski et al. 2006).

American Association of State Highway and Transportation Officials (AASHTO) new "Mechanistic-Empirical Pavement Design Guide" (AASHTO 2002) includes a procedure for predicting asphalt pavement permanent deformation (rutting).

In AASHTO 2002 rutting is predicted using the following model:

$$\frac{\varepsilon_p}{\varepsilon_r} = \beta_{r_1} 10^{k_1} T^{k_2 \beta_{r_2}} N^{k_3 \beta_{r_3}} \tag{1}$$

where: ε_p is accumulated plastic strain at N repetitions, ε_r is resilient strain of the asphalt material as a function of mix, N is number of load repetitions, T is temperature (°F), K_i are non-linear regression coefficients β_{r_i} and are calibration factors.

Figure 1. Asphalt pavement rutting due to heavy loads.

A joint research study was undertaken to develop rutting resistance criteria for Superpave and other asphalt mixes. The ultimate objective of that study was to develop rutting resistance criteria for accelerated laboratory testing. Based on the results of the entire study, recommendations will be developed for the rutting resistance criteria. However, as the study has not been completed, it is too early to provide any recommendations for the criteria (Uzarowski et al. 2006).

Improved understanding of rutting resistance of a rubberized asphalt concrete (RAC) pavement that contains reclaimed asphalt pavement (RAP) is important to stimulating the use of rubberized asphalt mixtures. Rubberized asphalt has been used successfully in improving the mechanical characteristics, such as rutting resistance, of hot mix asphalt mixture around the country and the world (Xiao et al. 2005).

However, the incorporation of asphalt concrete materials containing crumb rubber has not been investigated in great detail. In this experimental work the influence of temperature gradation on creep compliance under dynamic load conditions is investigated. Also the trend of permanent deformations verses stiffness of creep at 100 seconds in simple and rubberized asphalt specimen is determined. The aim of this research was to investigate the creep compliance of the rubberized asphalt mixtures through a laboratory testing program.

2 EXPERIMENTAL

2.1 *Materials*

2.1.1 *Aggregates*

The aggregate gradation (MPORG 2003) that used in this research is shown in Table 1.

2.1.2 *Bitumen*

In this experimental investigation, a neat bitumen 60/70-penetration grade from Isfahan mineral oil refinery was used (Arabani et al. 2007). Bitumen properties were shown in Table 2.

2.1.3 *Crumb rubber*

Crumb rubber is primarily used in HMA mixes by two processes:

2.1.3.1 Wet process (Asphalt-Rubber)

The wet process blends the crumb rubber with the asphalt cement prior to incorporating the binder into the project. The modified binder is commonly called "asphalt-rubber." Generally, 18–26 percent crumb rubber by weight of asphalt cement is reacted with asphalt cement at 190 to 218°C for 1 to 2 hours. The blend is formulated at elevated temperatures to promote potential chemical and physical bonding of the two constituents. The first technology which applied the "wet process" is called the "McDonald Process." This process is also used for constructing

Table 1. Gradation of used aggregate.

Sieving size (mm)	25	19	12.5	9.5	4.75	2.36	0.3	0.075
Topka's P.P (%)	–	100	95	–	59	43	13	6
Binder's P.P (%)	100	95	–	68	50	36	12	5

Table 2. Properties of bitumen used.

	Lose weight	Deflagration	Plasticity index	Flow	Penetration grade	Density
Purity grade	(%)	0°C	(cm)	0°C	mm/10	25°C
99	0.75	262	112	51	66	1.02

Table 3. Chemical composition of crumb rubbers used in this study (haghi et al. 2005).

Material	Synthetic rubber	Carbon block	Calcium car borate	Ash
Weight %	30	10	50	10

Table 4. Gradation of used crumb rubber.

Sieving size (mm)	6.4	4.75	2.36	1.18
Crumb rubber's P.P (%)	100	55	38	21

stress absorbing membrane and stress absorbing membrane interlayer, and manufacturing crack sealers. SAM is a seal coat which uses asphalt-rubber as a binder. When SAM is placed as an interlayer it is called SAMI (Kandhal & Cooley 2002; Haghi et al. 2005).

2.1.3.2 Dry process (Rubber-Modified Mix)

This process mixes the crumb rubber with aggregate before incorporating the asphalt cement. About 3–5 percent of coarse rubber particles (1.6–6.4 mm) by weight of aggregate are generally used. The natural aggregate is usually gap-graded to accommodate the rubber particles as aggregate. The amount of crumb rubber used in the dry process can be 2–4 times that used in the wet process (Arabani & Khodabakhshi 2006).

The first application of the "dry process" in the United States is called the "PlusRide Process." It has been claimed that ice debonds easily from the pavement surface consisting of rubber-modified mixture because of higher than usual resiliency of the mix (Haghi et al. 2005).

A chemical properties of crumb rubber used in this research are shown in Table 3. The crumb rubber gradation that used in this experimental work is shown in Table 4.

2.2 *Samples preparation*

Standard laboratory tests for this research were used, namely, Marshall Test (ASTM D1559- 89) and dynamic creep test performed according to the Shell procedure. Testing was conducted using the standard Marshall Apparatus. Creep test was done at temperature of 25°C (Arabani et al. 2007). The binder content of 4.5 to 6.5% is used for all different mixtures. In this research dry process mixes the crumb rubber with aggregate before incorporating the asphalt cement.

2.3 *Methodology*

2.3.1 *Creep test procedure*

In this experimental work, specimens were tested with diameter of 100 mm and the height of 70 mm for creep test. The Specimens that were used in the creep test are kept in an environmentally protected (enclosed area not subjected to the natural elements) storage area at temperatures between 5 and 24°C (40 and 75°F) (Arabani et al. 2006).

The tensile creep compliance is determined by applying a static compressive load of fixed magnitude along the diametric axis of a cylindrical specimen. The resulting horizontal and vertical deformations measured near the center of the specimen are used to calculate tensile creep compliance as a function of time (FHWA 2001).

3 RESULT AND DISCUSSION

The variation of Stiffness of creep at 100 seconds verses different percentage of bitumen content of rubberized asphalt specimens are shown in Figure 3. According to this figure, specimens with two gradations type of topka and binder in two simple case and rubberized standed under the creep compliance test.

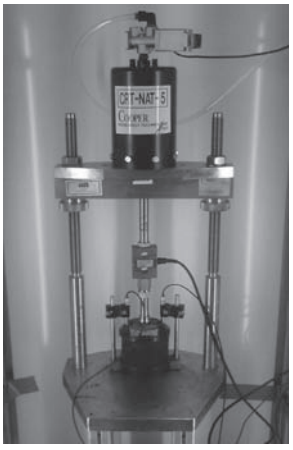

Figure 2. Creep compliance test equipment.

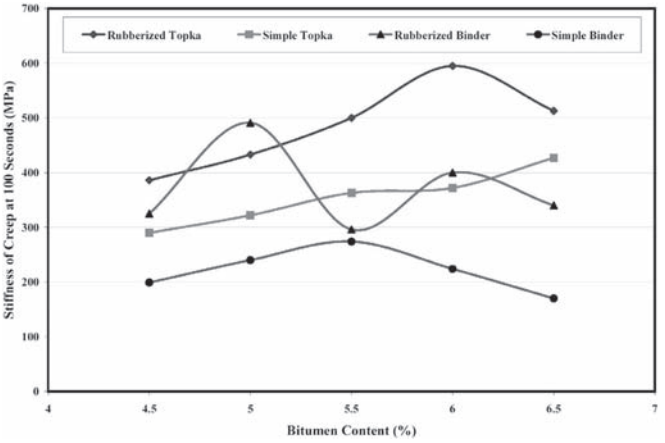

Figure 3. Stiffness of creep at 100 seconds vs. bitumen content.

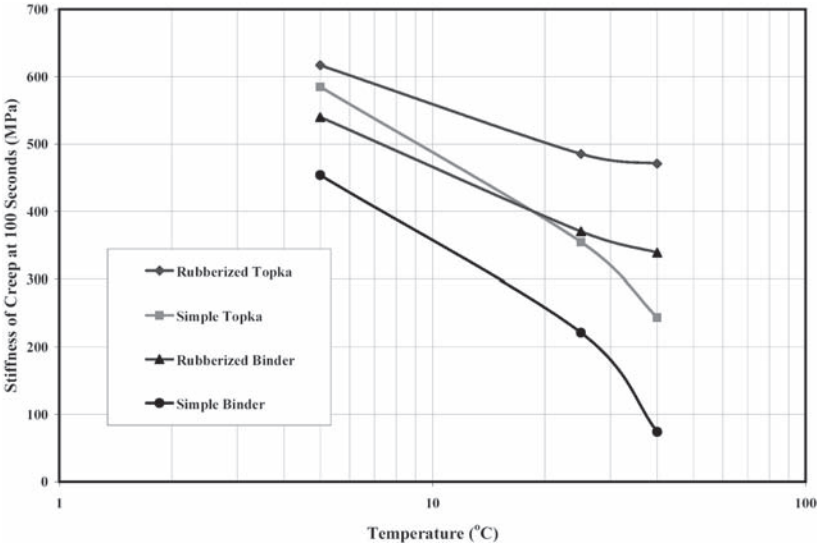

Figure 4. Stiffness of creep at 100 seconds vs. temperature.

As it can be seen that rubberized asphalt specimens in any two gradations type of topka and binder have more stiffness against creep phenomenon, however that measure additional trend of stiffness of creep in rubberized asphalt specimens is not same in different percentages of bitumen content. Results are shown that use of rubber in asphalt significantly decreases measure of bitumen content in asphalt specimens.

Increase of crumb rubber in rubberized asphalt specimens cause that samples by fuller texture is engendered, and this object will increase measure of stiffness of creep in samples inclusive waste crumb rubber.

The variation of stiffness of creep at 100 seconds verses temperature changes are shown in figure 4. According to this figure, rubberized asphalt specimens had the less sensitivity against temperature itself.

Variations of temperature has a less influence on rubber and this material in high temperature start to soften. But the influence of temperature on bitumen content is very high. This act cause that simple specimens are shown itself more sensitivity against temperature

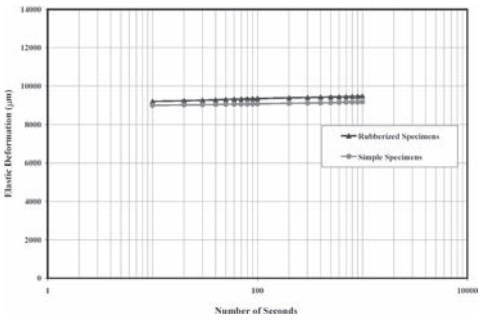

Figure 5. Elastic deformation vs. number of seconds.

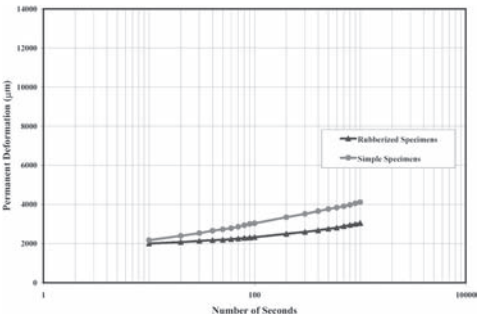

Figure 6. Permanent deformation vs. number of seconds.

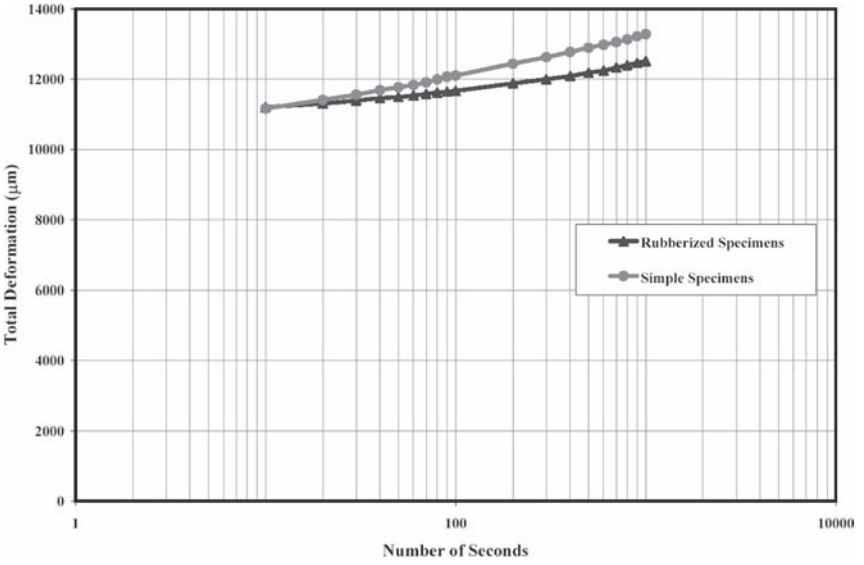

Figure 7. Total deformation vs. number of seconds.

changes. As at upper temperature, rubberized asphalt specimens with binder gradation have showed more stiffness of creep in comparison with simple specimens with topka gradation. The reduction trend of stiffness of creep is showing that rubberized asphalt can bear more temperature gradations than simple asphalt specimens.

The elastic, permanent and total deformations of asphaltic samples verses time are shown in figures 5, 6 and 7.

According to figure 5, elastic deformations of rubberized asphalt specimens are high in comparison with simple specimens. This object return to more flexible property of rubber against induction stress. Texture wrought of aggregate and crumb rubber in rubberized asphalt specimens in comparison with texture wrought of aggregate in simple specimens cause that rubberized asphalt are shown more flexible against inductive loads. This flexible properties cause that measure of permanent deformations of rubberized asphalt decrease in comparison with simple asphaltis specimens.

According to figure 6, permanent deformations of simple asphaltic specimens increase by more rates. Total deformations of asphaltic specimens inclusive topka gradation are shown in figure 7. Fuller texture and flexible up in rubberized asphalt specimens cause that this samples support more deformation against induction load.

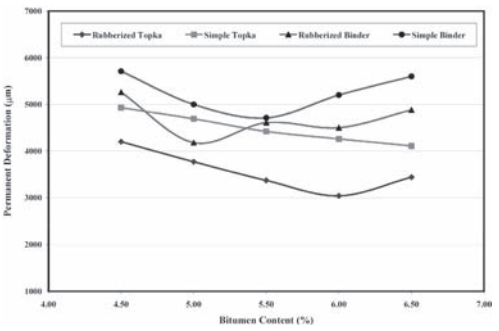

Figure 8. Permanent deformation vs. bitumen content.

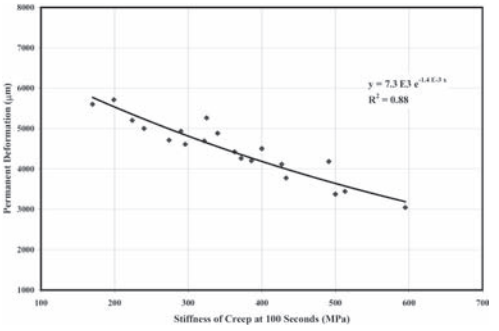

Figure 9. Permanent deformation vs. stiffness of creep at 100 seconds.

The variation of permanent deformations verses different percentage of bitumen content in simple and rubberized asphalt specimen with 2 gradations type of topka and binder are shown in figure 8.

It can be seen that the permanent deformations in rubberized asphalt specimens decrease in comparison with simple asphalt specimens. This trend in measure of permanent deformations with different percentages of bitumen content is not same. By attention results are denoted that measure of optimum bitumen in rubberized asphaltic specimens significantly decreases. Than side in some of instances is observed that rubberized asphaltic specimens with binder gradation in comparison to simple asphaltic specimen with topka gradation have showed the less permanent deformation itself.

The permanent deformations verses stiffness of creep at 100 seconds in simple and rubberized asphalt specimen is drawn in figure 9.

Sake get manner of asphaltic pavement against the creep phenomenon, stiffness of creep of rubberized specimen and simple specimen against those permanent deformations are drowned any which to shape aside with inductive loads. As it can be seen that reduction trend of permanent deformation with more stiffness of creep in rubberized asphalt specimen resume by more rate. Regression coefficient gets of the lab. tests results show that in rubberized asphalt specimens, measure of permanent deformation except measure of stiffness of creep depend to factors such as type and flexible of rubberized content and measure of use this waste substance in asphaltic specimens.

4 CONCLUSION

As it was mentioned earlier, the objective of this research was to advance understanding of the creep compliance via laboratory and computational studies and to convey the obtained results in a form that can be utilized for the prediction of rutting depth in flexible pavements. For materials engineers, the rutting models founded on basic principles in mechanics provide relationships between material properties (chemical or mechanical) and models parameters, which can be used for selection or design of more creep compliance binders or mixtures. The flowing reasons cause the improvement of rutting depth and creep compliance in rubberized asphalt specimen:

1) Increase of crumb rubber in rubberized asphalt specimens cause that samples by fuller texture is engendered, and this object will increase measure of stiffness of creep in rubberized asphalt specimens.
2) The less influence of temperature gradations on rubber that in up temperature start to soften, cause that rubberized asphalt specimens are shown itself less sensitivity against temperature gradations.
3) Flexible properties of rubber against induction stress cause that measure of permanent deformations of rubberized specimens decrease in comparison with simple specimens.

4) Trend of permanent deformations verses stiffness of creep at 100 seconds show that in rubberized asphalt specimens, measure of permanent deformation except measure of stiffness of creep depend to factors such as type and flexible of rubberized content and measure of use this waste substance in asphaltic specimens.

The overall conclusion of this research indicates that the addition of crumb rubber can have a positive effect on rutting depth.

REFERENCES

Antunes, M.L., Domingos, P., Eusebio, M. & Sa da Costa, M. 2003. *Studies Concerning the Use of Asphalt Rubber in Portugal.* Proceedings of the Asphalt Rubber 2003 Conference, Brasilia, Brazil, 195–210.

American Association of State Highway and Transportation Officials (AASHTO). 2002. *Procedure for predicting asphalt pavement permanent deformation (rutting)*. AASHTO Designation.

Arabani, M., Haghi, A.K., Mirabdolazimi, S.M. & Haghgoo, M. 2007. *Dynamic effects of waste tire thread mesh reinforcement on the asphaltic pavement characters Dynamic*. Advanced Characterization of Pavement and Soil Engineerig Materials, Taylor & Francis Group. Athens, Greece.

Arabani, M. & Khodabakhshi, M. 2006. *Utilization of Aromatic oil in Rubberized Asphalt Mixture.* International Seminar on Asphalt Pavement Maintenance Technologies, ISSA World Congress. Beijing, China.

Arabani, M., Sade, M.S. & Nickqalbpour, M. 2006. *The Effect of Aromatic oil in Rubberized Asphalt Mixture at Low Temperature.* International Seminar on Asphalt Pavement Maintenance Technologies, ISSA World Congress. Beijing, China.

Cano, J.O. & Charania E. 1989. *The Phoenix Experiences Using Asphalt-Rubber Proceedings*. National Seminar on Asphalt-Rubber, Kansas City Missouri.

Chen, J.S., Lin, C.H., Stein, E. & Hothan, J. 2004. Development of a Mechanistic-Empirical Model to Characterize Rutting in Flexible Pavements. *Journal of Material in Civil Engineering*. V130, 519–525.

Choubane, B., Sholar, G.A., Musselman, J.A. & Page, G.C. 1999. *A Ten-year Performance Evaluation of Asphalt-Rubber Surface Mixes.* Transportation Research Record CD, Washington, DC.

Esch, D.C. 1982. *Construction and Benefits of Rubber Modified Asphalt Pavements.* Transportation Research Record No. 860, TRB, National Research Council, Washington, DC.

FHWA. 2001. *Test Method for Determining the creep Compliance Resilient Modulus and Strength of Asphalt Material Using the Indirect Tensile Test Device*. FHWA, Protocol P07. Version 1.1.

Haghi, A.K., Arabani, M., Shakeri, M., Haj jafari, M. & Mobasher, B. 2005. *Strength Modification of Asphalt Pavement Using Waste Tires.* 7th International Fracture Conference. University of Kocaeli, Kocaeli, Turkey.

Holleran, G. & Van, K.J. 2000. *Asphalt Rubber Concrete Leads to Cost Effective Pavement Rehabilitation Reduced Thickness.* Synopses for 1st International Conference World of Pavement Sydney, Australia.

Kandhal, P.S. 1992. *WASTE MATERIALS IN HOT MIX ASPHALT—AN OVERVIEW*. Presented at the ASTM Meeting in Miami, Florida, December 8, 1992. National Center for Asphalt Technology. NCAT Report 92–06. Auburn University, Alabama.

Kandhal, P.S. & Cooley, L.A. 2002. Evaluation of Permanent Deformation of Asphalt Mixtures Using Loaded Wheel Tester. *Journal of the Association of Asphalt Paving Technologists*, V71, 739–753.

MPORG. 2003. *Road General Technical Specification. Management and Planning Organization Office of the Deputy for Technical Affairs Bureau of Technical Criteria and Specification*. Tehran, Iran.

Roberts, F.L., Kandhal, P.S., Brown, E.R. & Dunning, R.L. 1989. *Investigation and Evaluation of Ground Tire Rubber in Hot Mix Asphalt*. NCAT Report 89–3.

Sebaaly, P.E., Bazi, G., Weitzel D., Coulson, M.A. & Bush D. 2003. *Long Term Performance of Crumb Rubber Mixtures in Nevada*. Proceedings of the Asphalt Rubber 2003 Conference, Brasilia, Brazil, 111–126.

Uzarowski, L., Maher, M. & Prilesky, H. 2006. *The Use of Simple Performance Tests in the Development of Rutting Resistant Criteria for Asphalt Mixes in Canada Stage 1.* Annual Conference of the Transportation Association of Canada. Charlottetown, Prince Edward Island.

Way, G.B. 2003. *The Rubber Pavements Association, Technical Advisory Board Leading the Way in Asphalt Rubber Research*. Proceedings of the Asphalt Rubber 2003 Conference, Brasilia, Brazil, 17–33.

Xiao, F., Amirkhanian, A. & Juang, C.H. 2005. *Rutting Resistance of Rubberized Asphalt Concrete Pavements Containing Reclaimed Asphalt Pavement Mixtures*. ASCE Journal of Materials in Civil Engineering. MT/2005/023143.

Advanced Testing and Characterization of Bituminous Materials – Loizos, Partl, Scarpas & Al-Qadi (eds)
© 2009 Taylor & Francis Group, London, ISBN 978-0-415-55854-9

Characterizing volumetric deformation behavior of naturally occurring bituminous sand materials

J.K. Anochie-Boateng
CSIR, Pretoria, South Africa

E. Tutumluer
University of Illinois at Urbana-Champaign, Urbana, USA

ABSTRACT: Oil sand materials are natural bituminous sand deposits that are rich in bitumen or asphalt content to the extent that oil can be extracted from these deposits. The presence of high viscous bitumen content in the oil sand composition makes these materials problematic for field operations of off-road haul trucks and shovels. In this paper, volumetric deformation and bulk modulus properties are determined for three oil sand samples with bitumen contents of 8.5%, 13.3% and 14.5% by weight, using a newly proposed hydrostatic compression test procedure. The test procedure applies field loading conditions of off-road construction and mining equipment to closely simulate the volumetric deformation and stiffness behavior of oil sand materials. Based on the test results, bulk modulus properties were characterized as a function of the applied hydrostatic stress for individual oil sand samples. When the entire test data were combined, nonlinear bulk modulus models were successfully developed to account for applied hydrostatic stress states, test temperatures, and bitumen contents for the three oil sand materials. Results from the bulk modulus models show that oil sands are influenced by temperature due to the bitumen contents. The anticipated use of developed bulk stress models should provide essential guidelines for predicting volumetric deformation behavior of oil sand materials in the field.

1 INTRODUCTION

Oil sand is a generic name given to natural deposits of bituminous sand materials that are mined for crude oil production. The world's largest oil sand deposits are found in the Alberta Province of Canada. The significantly high bitumen content in the oil sand composition, which typically ranges from 8% to 15% by weight, makes these naturally occurring sands problematic for routine operations of construction and mining equipment during the warm spring and summer months. Field studies have indicated that the considerable amount of bitumen in the oil sands, high applied loads from mining equipment and seasonal changes in temperature are major factors that control the modulus and deformation behavior of oil sands (Joseph 2002).

To date, no comprehensive laboratory testing has been found to discuss the individual effects of these factors on bulk modulus of oil sand materials. Instead, research on oil sands has traditionally been focused on obtaining laboratory stress-strain test data to describe shear strength and the Young's modulus properties of oil sands (Dusseault & Morgenstern 1978, Agar et al. 1987, Samieh & Wong 1997, Wong 1999). Based on the data collected in these studies, confining stress, peak stress or strain, friction angle and cohesion are the material properties used for modeling the strength and stiffness behavior. Bulk modulus is an important material property that describes the resistance to volume change when an element of soil is subjected to hydrostatic loading. To properly characterize the volumetric deformation and stiffness behavior of oil sands, it is important to take into account its temperature dependent behavior and the bitumen content under hydrostatic loading conditions.

This paper mainly focuses on characterizing the volumetric deformation and stiffness behavior of three types of oil sand materials with bitumen contents 8.5%, 13.3% and 14.5% by weight using a newly proposed hydrostatic compression test procedure. The test procedure considers field loading characteristics of off-road construction and mining haul trucks and shovels. The deformation properties obtained from the laboratory testing program were used to determine bulk moduli at varying hydrostatic stress states, and two test temperatures of 20ºC and 30ºC. The test results were used to develop bulk modulus characterization models as a function of applied hydrostatic stresses for the individual oil sand samples. Based on the all the test data, a unified bulk modulus model is also developed for the three oil sand materials to include bitumen content and temperature variables in the predictive equations.

2 HYDROSTATIC COMPRESSION TESTING PROGRAM

2.1 *Oil sand materials and properties*

The oil sand materials used in this study were obtained from Suncor Energy, Inc. and Syncrude Canada Ltd. oil sand mines in Canada. Suncor Energy (SE), Inc. provided two types of low and high grades with respect to the bitumen contents, whereas Syncrude Canada Ltd. provided one sample of the Aurora (AU) high grade oil sand. The oil sand materials were initially tested for bitumen and water contents using AASHTO T 308 and AASHTO T 265 test procedures, respectively. The bitumen contents were found to be 8.5%, 13.3% and 14.5% for the SE low grade, SE high grade and AU high grade, respectively; and the water contents were 1.4%, 3.2% and 2.2%, respectively. Accordingly, the Suncor Energy high and low grades samples were designated as SE-09 and SE-14, respectively, and the Aurora high grade was designated as AU-14.

All the three oil sand samples were uniformly graded fine to medium sands with the smallest to largest size particles ranging from 0.6 mm to 2.36 mm and the fines contents, i.e., passing No. 200 sieve or 0.075 mm, ranging from 7% to 15%. The typical bulk densities achieved in gyratory compactors for SE-09 and SE-14 were 2,000 kg/m^3 at 100 gyrations and 2,050 kg/m^3 at 40 gyrations, respectively. The density achieved for AU-14 was 2,050 kg/m^3 at 25 gyrations. These achieved densities obtained for the 150 mm in diameter by 150 mm high cylindrical specimens prepared were very close to field density values reported by Joseph (2005). Figure 1 shows gyratory compacted specimens for one of the oil sand samples.

Figure 1. Gyratory compacted oil sand specimens.

2.2 *Laboratory test procedure and testing performed*

The loading characteristics of off-road large capacity construction and mining equipment dictate field loading stress states and therefore directly influence the volumetric deformation and stiffness behavior of oil sands in the field. For instance, Joseph (2005) noted from field studies that a Caterpillar 797B off-road haul truck could produce vertical stresses of about 800 kPa with confining stresses ranging between 250 and 300 kPa. He also observed that the P&H 4100 type BOSS shovels generated a static ground loading of up to 220 kPa, and could induce a ground confinement of about 70 kPa (Joseph 2005). Moreover Joseph (2005) reported that at ambient temperature of 28ºC oil sand materials in the field became soft and problematic to mining equipment.

The newly proposed hydrostatic compression test procedure for oil sands is based on the field loading characteristics of the haul trucks, shovels and other mining equipment. Hydrostatic loading stresses ranging from 41.4 kPa to as high as 276 kPa are applied on the oil sand samples at two temperatures, 20 degrees Celsius and 30 degrees Celsius, to account for spring and summer temperatures, respectively. In this study, an innovative advanced triaxial testing device, the University of Illinois FastCell (UI-FastCell) integrated with Universal Testing Machine (UTM) loading device at the Advanced Transportation Research and Engineering Laboratory (ATREL), was used for applying hydrostatic stresses on the specimen. Figure 2 shows the UI-FastCell test setup for asphalt and granular materials testing at ATREL. The UI-FastCell offers unique capabilities in laboratory material characterization including measurement of on sample vertical and radial displacements, and a bladder type horizontal confinement chamber with a built-in membrane which can be inflated to apply hydrostatic stresses to simulate high field loading conditions on granular and bituminous materials in the laboratory (Tutumluer & Seyhan 1999).

During laboratory testing, gyratory compacted oil sand specimens were subjected to a sequence of different applied hydrostatic stresses of 41.4, 69.0, 138.0, and 276.0 kPa. Specimens were loaded from zero stress conditions to these individual hydrostatic stresses, unloaded

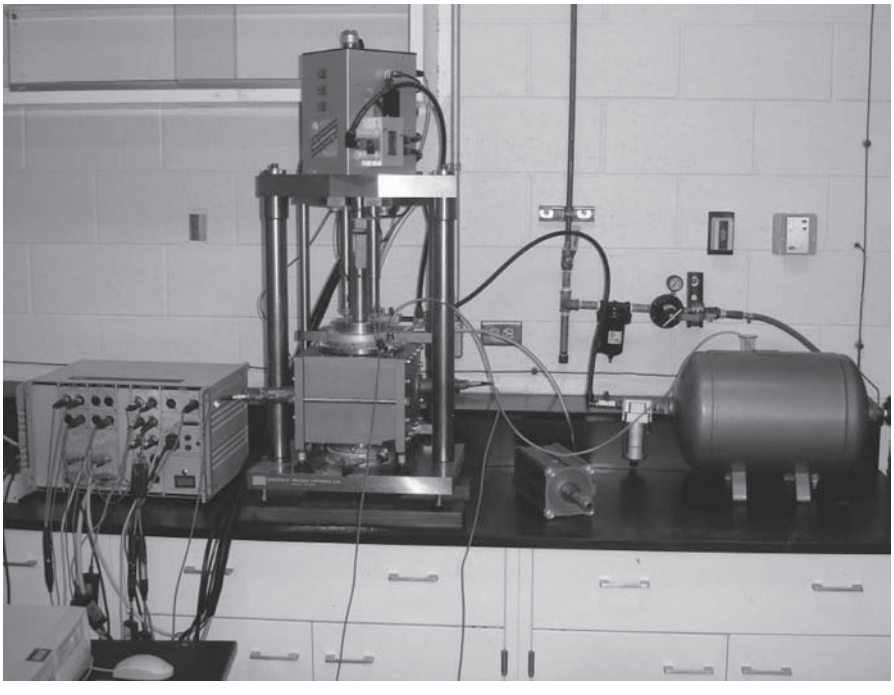

Figure 2. UI-FastCell triaxial test setup used in hydrostatic loading of oil sand materials.

to zero, and then, reloaded to the next stress state unti; the maximum hydrostatic stress of 276 kPa was reached. A pulsed wave shape with 60-second loading and 60-second unloading was applied on the test specimens. The axial static loading was controlled by the vertical load cell, and the radial loading was measured by a pressure transducer. Both axial and radial deformations were measured by two symmetrical linear variable displacement transducers (LVDTs) for each load cycle and the corresponding axial and radial strains (ε_1 and ε_3) were computed for the test specimens. Two replicate tests were performed for each type of oil sand material, i.e., SE-09, SE-14, and AU-14, with bitumen contents of 8.5%, 13.3% and 14.5%, respectively, to establish the full laboratory test matrix. Overall, 12 tests were conducted on the three oil sand samples at two temperatures, 20 degrees Celsius and 30 degrees Celsius.

3 ANALYSES OF TEST RESULTS

The applied hydrostatic (isotropic) stresses and measured volumetric strains obtained from hydrostatic compression tests were used to calculate bulk modulus of the oil sand samples. Previous research studies have indicated that by graphing the applied isotropic compression stresses against volumetric strains, a nonlinear trend was characterized for the volumetric deformation behavior for soils (Terzaghi & Peck 1967, Vesic & Clough 1968, Quabain et al. 2003). Vesic & Clough (1968) suggested that soil's elastic properties could conveniently be obtained from such a nonlinear curve by drawing straight line approximations that linearly relate increments of both the isotropic stresses and volumetric strains. In this study, the straight line approximation concept was used for analyzing the results of the oil sand tests. The bulk moduli (K) of the oil sand samples were calculated from the ratio of the incremental hydrostatic stress ($\Delta\sigma$) to the incremental volumetric strain ($\Delta\varepsilon_v$). Equation 1 defines the bulk modulus of the tested samples:

$$K = \frac{\Delta\sigma_1 + \Delta\sigma_2 + \Delta\sigma_3}{\Delta\varepsilon_v} = \frac{\Delta\sigma}{\Delta\varepsilon_v} \tag{1}$$

where the volumetric strain ε_v is computed from the axial strain ε_1 and the radial strain ε_3 as $\varepsilon_v = \varepsilon_1 + 2\varepsilon_3$, and for triaxial compression tests, hydrostatic stress is given by $\sigma = \sigma_1 = \sigma_2 = \sigma_3$.

A total of 270 stress-strain data sets were obtained from testing one oil sand specimen. Each data set represents an average value from two replicate specimens. Thus, about 540 data points were analyzed for each oil sand sample at the two test temperatures. Figures 3 and 4 show the variations of hydrostatic stresses with volumetric strains determined for the three oil sand samples at 20ºC and at 30ºC, respectively. Note that each point in these figures represents an average of 270 stress-strain data points. A polynomial regression curve was fit to the individual data sets of the three oil sand samples, i.e., SE-09, SE-14 and AU-14 at the two test temperatures, and the straight line approximation method was used to obtain the incremental hydrostatic stresses and the corresponding volumetric strains. The bulk modulus was then computed at each hydrostatic loading stress using Equation 1.

Tables 1 and 2 list the test results for all the oil sand samples at 20ºC and 30ºC, respectively. As expected, higher bulk modulus values were obtained at 20ºC than at 30ºC for all the oil sand samples. The SE-09 sample gives the highest bulk moduli while AU-14 sample gives the lowest values. At 20ºC, the difference in magnitude between the average bulk modulus of SE-09 and AU-14 samples is 1.61 MPa, i.e., about 26% difference; and the difference between SE-09 and SE-14 is 0.78 MPa, representing about 12.5%. Similar trends in bulk moduli at 20ºC are observed for the samples at 30ºC. That is, the SE-09 sample has the highest bulk modulus values whereas AU-14 sample has the lowest bulk moduli. It is interesting to note that the magnitude of the bulk moduli of SE-14 and AU-14 samples were comparable at the two test temperatures. The average bulk modulus of SE-14 at 20ºC is about 1.2 times greater than the bulk modulus of AU-14 compared to about 1.3 times at 30ºC. The amount of bitumen content appears to be a major factor that influenced the overall stiffness of the oil sand materials. Again, the AU-14 sample with the highest bitumen content of 14.5% has

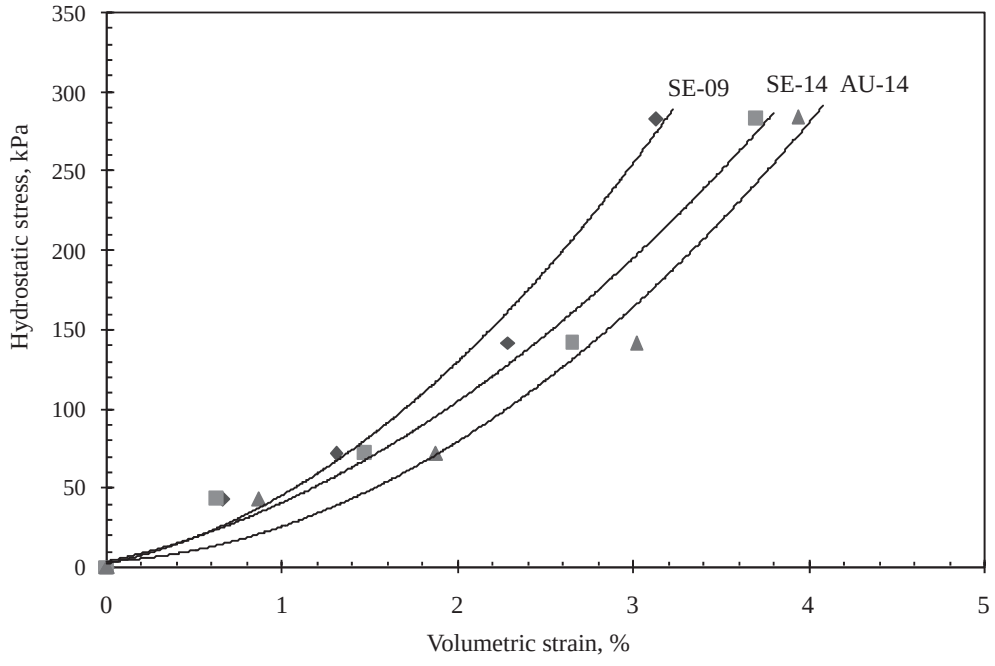

Figure 3. Variations of hydrostatic stresses with volumetric strains for the oil sands at 20ºC.

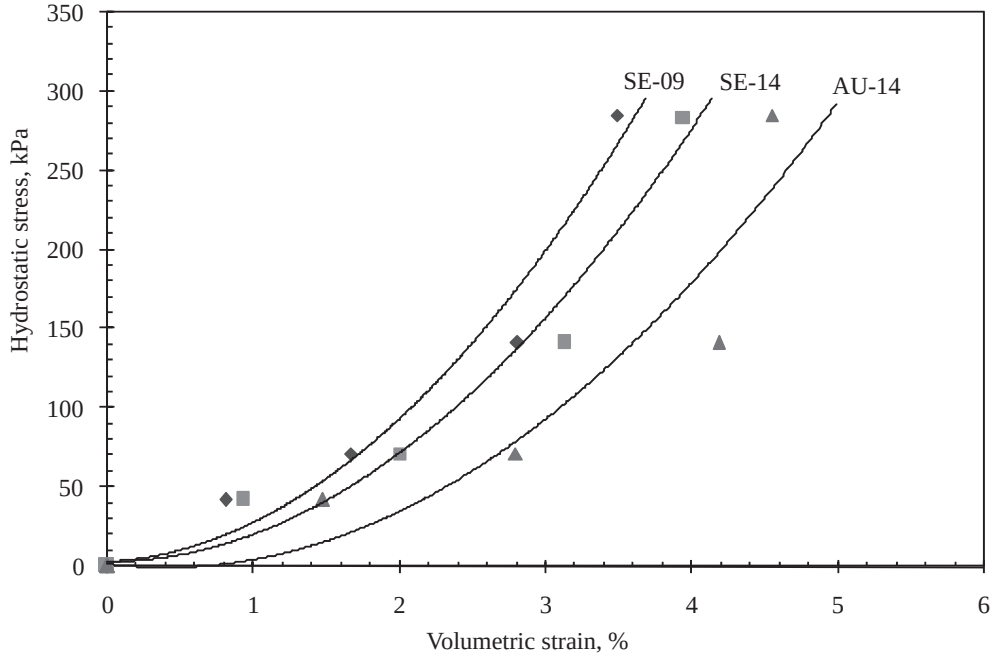

Figure 4. Variations of hydrostatic stresses with volumetric strains for the oil sands at 30ºC.

Table 1. Test results for oil sand samples at 20ºC.

	SE-09		SE-14		AU-14	
Δσ (kPa)	$\Delta\varepsilon_v$ (%)	K (MPa)	$\Delta\varepsilon_v$ (%)	K (MPa)	$\Delta\varepsilon_v$ (%)	K (MPa)
41.4	0.88	4.70	1.02	4.06	1.40	2.96
69.0	1.35	5.11	1.52	4.54	1.90	3.63
138.0	2.10	6.57	2.43	5.68	2.78	4.96
276.0	3.18	8.68	3.60	7.67	3.90	7.08

Δσ is hydrostatic stress increment; $\Delta\varepsilon_v$ is volumetric strain increment; K is bulk modulus.

Table 2. Test results for oil sand samples at 30ºC.

	SE-09		SE-14		AU-14	
Δσ (kPa)	$\Delta\varepsilon_v$ (%)	K (MPa)	$\Delta\varepsilon_v$ (%)	K (MPa)	$\Delta\varepsilon_v$ (%)	K (MPa)
41.4	1.30	3.18	1.50	2.76	2.18	1.90
69.0	1.65	4.18	1.95	3.54	2.60	2.65
138.0	2.30	6.00	2.80	4.93	3.70	3.73
276.0	3.58	7.71	4.00	6.90	4.90	5.63

Δσ is hydrostatic stress increment; $\Delta\varepsilon_v$ is volumetric strain increment; K is bulk modulus.

the lowest bulk moduli, whereas the SE-09 sample with low bitumen content of 8.5% has the highest bulk moduli.

4 STATISTICAL ANALYSES AND MODEL DEVELOPMENT

Statistical regression analyses were performed on the oil sand test results to develop relationships based on power functions for each oil sand sample at 20ºC and at 30ºC. Figures 5 and 6 show these relationships obtained between bulk moduli and hydrostatic stresses at 20ºC and at 30ºC, respectively, and the resulting power functions of hydrostatic stress for the three oil sand samples. The significantly high correlation coefficients ($R^2 > 0.97$) for all the three oil sand materials indicate that strong correlations existed between bulk modulus and hydrostatic stress for all the oil sand samples tested at the two temperatures.

Bulk modulus of soils and other geomaterials have been successfully used as material constitutive stress-strain properties for numerical analyses such as the finite element analysis. Since the overall objective in this study was to develop practical predictive equations to estimate field volumetric deformation and stiffness behavior of the oil sand materials, the stress-strain data sets obtained from the laboratory testing program were used to develop bulk modulus characterization models to include the loading conditions. A close examination of physical properties of the three oil sands, such as particle size distribution, density, and water content with the assumption of similar bitumen properties suggested that the individual databases of the three oil sand materials could also be combined for analysis. The R-square selection method in the SAS statistical analysis software was first used to ascertain which independent variables were potential candidates for the models. It was found that bulk modulus strongly depended on the hydrostatic compression stress (σ), temperature (T) and bitumen content (w_b). Based on the results, three models were selected to study the volumetric stiffness of oil sand materials. Among other mathematical forms including linear, nonlinear, and hyperbolic, the power function was the most suitable with the correlation coefficients for modeling bulk moduli of the oil sand materials.

Table 3 lists the generalized bulk modulus models developed using the combined test data and gives the model parameters obtained from the SAS stepwise multiple regression analyses.

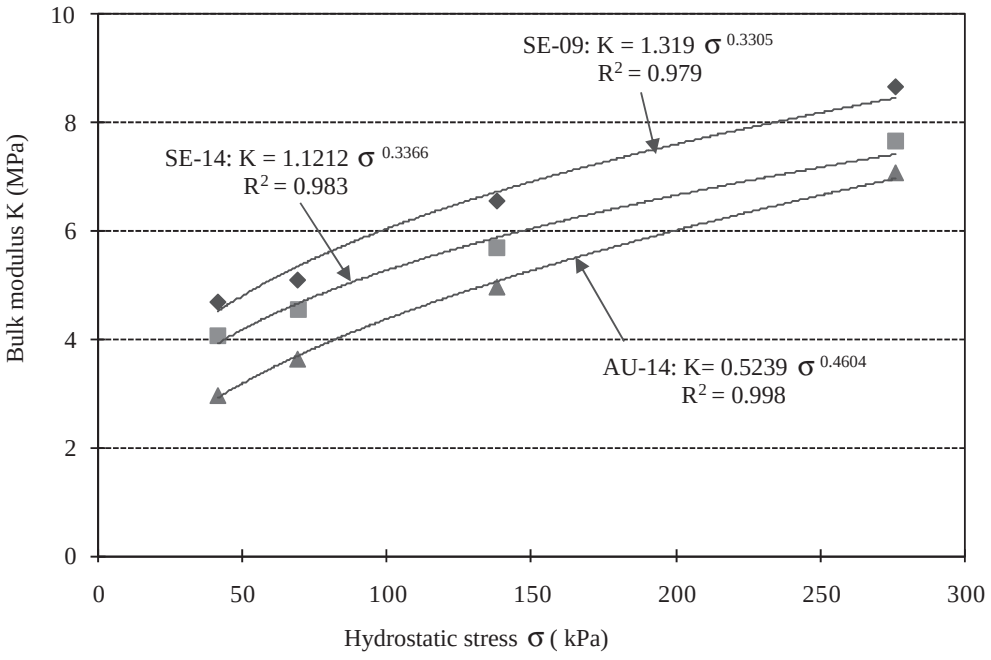

Figure 5. Bulk modulus and hydrostatic stress relationships for oil sands at 20ºC.

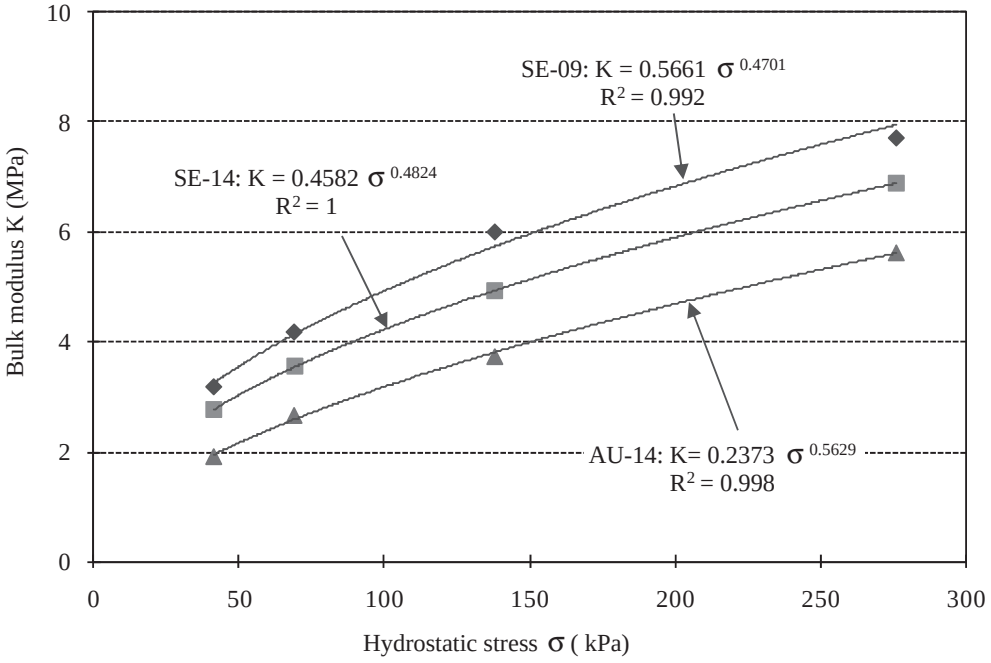

Figure 6. Bulk modulus and hydrostatic stress relationships for oil sands at 30ºC.

Table 3. Bulk modulus characterization models for combined oil sand data.

Model 1: $K = A * \sigma^{k_1}$
Model 2: $K = A * \sigma^{k_1} T^{k_2}$
Model 3: $K = A * \sigma^{k_1} w_b^{k_2} T^{k_3}$

	Model Parameters					
Model	log A	k_1	k_2	k_3	R^2	*RMSE*
1	–0.2204	0.4406			***0.690***	*0.096*
2	0.4068	0.4406	–0.5853		***0.821***	*0.075*
3	1.2494	0.4406	–0.5853	–0.6066	***0.926***	*0.049*

σ is hydrostatic stress; T is temperature in degrees Celcius; and w_b is bitumen content.

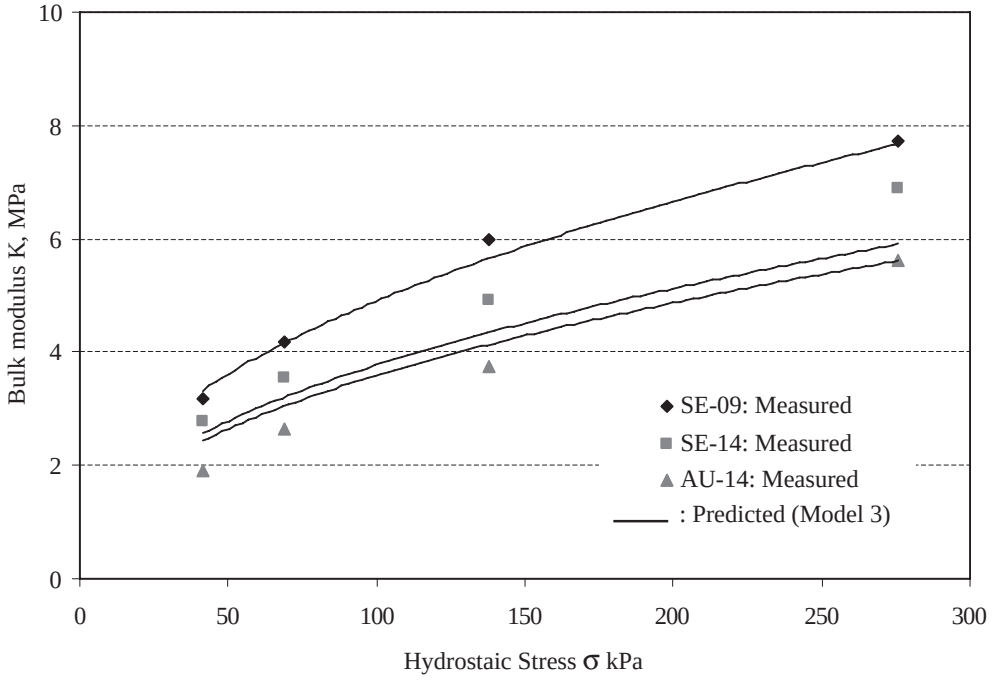

Figure 7. Bulk modulus model 3 performances for oil sand samples at 20ºC.

Note that improved models are obtained when temperature (T) and bitumen content (w_b) are included in model 1 although the change in coefficient of correlation (R^2) observed in models 2 and 3 indicates high dependency of bulk modulus on hydrostatic stress. As mentioned earlier, confining stress and shear strength properties have commonly been used to model the elastic modulus of oil sand materials. However, a comprehensive but yet practical model should account for the effects of temperature and bitumen content in the oil sand. High R^2 values obtained for models 2 and 3 indicate that temperature and bitumen content had predominant roles in predicting bulk modulus of oil sand materials. Recall that temperature and bitumen content are important factors that affect field loading behavior of oil sand materials. Model 3 can be proposed for routine use in the estimation field volumetric stiffness or bulk modulus of oil sands.

Next, model 3, which is represented by Equation 2, was used to fit into the individual oil sand test data at 20ºC and at 30ºC. There is a very good fit overall, for all the three oil sand test data at the two test temperatures (see Figures 7 and 8). Therefore, model 3 can be

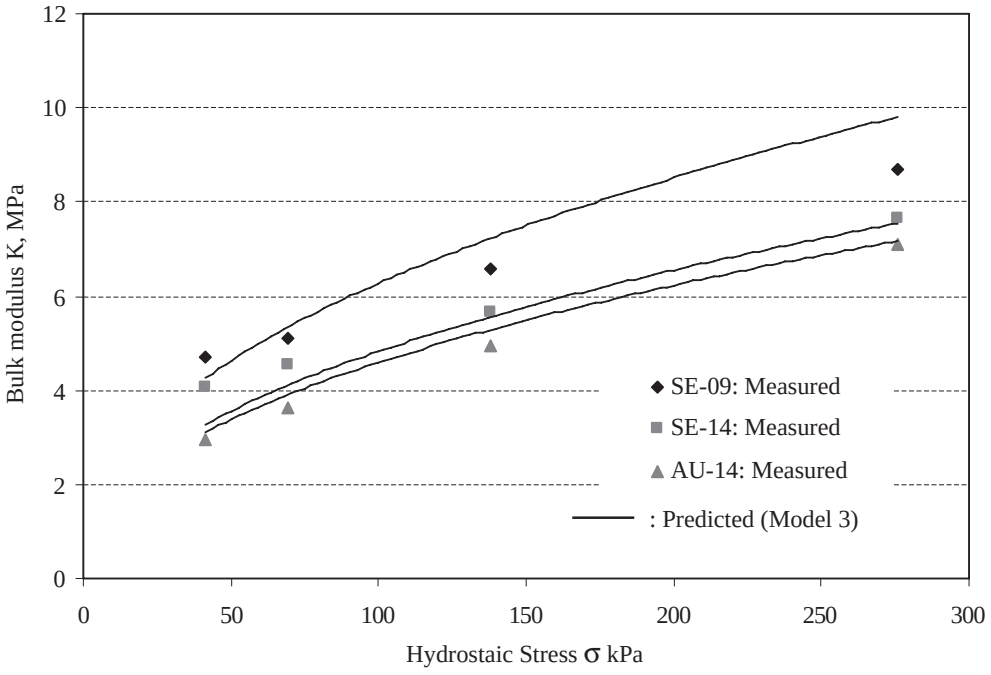

Figure 8. Bulk modulus model 3 performances for oil sand samples at 30ºC.

used for future studies on bulk modulus characterization of oil sand materials. Note that the coefficient representing parameter A in model 3 is proportional to the bulk modulus. Therefore, the value of A should be positive since the bulk modulus cannot be negative. However, parameters k_2 and k_3 in model 3 should be negative since increasing bitumen content and temperature would result in softening of the bituminous sand materials.

$$K = 17.78\ \sigma^{0.44}\ w_b^{-0.59}\ T^{-0.61} \tag{2}$$

5 SUMMARY AND CONCLUSIONS

The typical 8% to 15% by weight of bitumen or asphalt content in oil sands makes these naturally occurring sands problematic for routine operations of off-road construction and mining haul trucks and shovels. Field studies have shown that oil sands with high bitumen contents experience deformation and stiffness problems during the warm spring and summer months. However, the volumetric deformation and stiffness behavior of oil sand materials has not been characterized in the laboratory. In this paper, hydrostatic triaxial compression tests were performed in the laboratory to develop bulk modulus models to predict field volumetric deformation and stiffness behavior of oil sand materials.

A newly proposed hydrostatic loading test procedure was used to conduct tests on three types of oil sands with bitumen contents of 8.5%, 13.3% and 14.5% by weight. The test procedure applies low to high hydrostatic (isotropic) stress levels on the specimens at two test temperatures to closely simulate the field loading behavior of the oil sand materials under construction and mining haul trucks and shovels. Bitumen content appears to be a major material property that influenced the overall stiffness of the oil sand materials. The AU-14 sample with bitumen content of 14.5% had the lowest bulk moduli, whereas the SE-09 sample with 8.5% bitumen content gave the highest bulk moduli at the two test temperatures. Also, bulk moduli of the SE-14 sample having a bitumen content of 13.3% were higher than bulk moduli of the AU-14 sample although the average differences in the moduli of the two samples at 20ºC and 30ºC were comparable.

Based on the test results, bulk modulus characterization models in the form of power functions of the applied hydrostatic stress were established for the oil sand materials using individual test data. A generalized bulk modulus model also developed by combining all the test data from the three oil sands successfully accounted for the applied hydrostatic stress states, test temperatures, and sample bitumen contents. High correlation coefficients obtained for the developed models implied that the models would perform well in the field and could provide essential guidelines for estimating field volumetric deformation and stiffness behavior of oil sand materials.

REFERENCES

Agar, J.G., Morgenstern, N.R. and Scott, J.D. 1987. Shear strength and stress-strain behavior of Athabasca oil sand at elevated temperatures and pressures. *Canadian Geotechnical Journal*, Vol. 24: 1–10.

Dusseault, M.B. & Morgenstern, N.R. 1978b. Shear strength of Athabasca oil sands. *Canadian Geotechnical Journal*, Vol. 15: 216–238.

Joseph, T.G. 2002. OsEIP: The oil sands-equipment interactions program. *CIM Bulletin,* Vol. 95 (1064): 58–61.

Joseph, T.G. 2005. Physical, static and inferred dynamic loaded properties of oil sand. *Final Progress Report, Phases I, II, & III,* submitted to Caterpillar, Inc.

Quabin, B.S., Kaliakin, V.N., and Martin, J.P. 2003. Variable bulk modulus constitutive model for sand. *Journal of Geotechnical and Geoenvironmental Engineering*, 158–162.

Samieh, A.M. and Wong R.C.K. 1997. Deformation of Athabasca oil sand in triaxial compression tests at low effective stresses under varying boundary conditions. *Canadian Geotechnical Journal*, Vol. 34: 985–990.

AASHTO Standard specifications for transportation materials and methods of sampling and testing, 2000. 20th Edition, AASHTO, Washington D.C.

Terzaghi, K. and Peck, R.B. 1967. *Soil mechanics in engineering practice, 2nd ed.* Wiley, New York.

Tutumluer, E. and Seyhan, U. 1999. Laboratory determination of anisotropic aggregate resilient moduli using a new innovative test device. Transportation Research Record: *Journal of Transportation Research Board*, No. 1687, National Research Council, Washington D.C. 13–21.

Vesic, A.B. and Clough, G.W. 1968. Behavior of granular material under high stresses. *Journal of the Soil Mechanics and Foundation Division*, Vol. 3 (94): 661–668.

Wong, R.C.K. 1999. Mobilized strength components of Athabasca oil sand in triaxial compression. *Canadian Geotechnical Journal*, Vol. 36: 718–735.

Advanced Testing and Characterization of Bituminous Materials – Loizos, Partl, Scarpas & Al-Qadi (eds)
© 2009 Taylor & Francis Group, London, ISBN 978-0-415-55854-9

Alternative materials for asphalt mixture—steel slags

E. Diaconu & Ş.M. Lazăr
Technical University of Civil Engineering Bucharest, Bucharest, Romania

ABSTRACT: In Romania, steel slags sorts over than 8 mm have nowadays a relatively good market in the roads construction field as base and subbase courses. There is a limited market demand for 0–8 mm steel slag sort, but this sort can reach about 35% in double crushed slags. This paper presents the results of the laboratory tests performed in order to increase the capitalization level of steel slags sorts below 8 mm, by substitution of crushed stone in asphalt mixtures.

1 SUBSTITUTES OF CRUSHED STONE IN ASPHALT MIXTURES

1.1 *Steel slag and natural materials characteristics*

Crushed stone is the strength natural component in asphalt mixtures. Steel slag can substitute crushed stone but must be done with care because it contains free calcium oxide and/or free magnesium oxide in a significant percent. These mineral components absorb water and so, in time, conducing to damages of the road.

For the execution of the base layers of bituminous mixtures with aggregates of steel slag are imposed additional requirements for resistance to decomposition, resistance that can be fulfilled only if slags are properly cooled and uplift in the processing action.

Table 1 comparatively shows the characteristics of steel slag and of crushed and river stones (own measurements). We can see that some characteristics of steel slag are even better than those natural compounds (adhesivity to bitumen, polish index, resistence to compression).

For this reason we have performed laboratory experiments on HRA type (hot rolled asphalt) mixtures (base courses), in order to increase the capitalization level of steel slags sorts below 8 mm, by substitution of crushed stone in asphalt mixtures.

1.2 *0–8 mm steel slag sort chemical composition*

In Table 2 we present the chemical composition of 0–8 mm steel slag sort which was tested in our experiments.

Table 1. The characteristics of steel slag and natural aggregates.

Characteristics	Steel slag	Crushed stone	River stone
Apparent density, kg/m^3	3300–3500	2500–2700	2600
Water absorbtion, %	0.7–1.0	<0.5	<0.5
Shape index, %	<10	<10	<10
Breaking level, %	13–17	17	21
Wear (LA machine), %	18–22	18–24	21
Resistance to compression, N/mm^2	320–350	260	250
Resistance to frost-defrost, %	<0.5	<0.5	<1
Adhesivity to bitumen, %	>90	>80	>80
Polish index (PSV), %	58–61	48	45

Table 2. The chemical composition of 0–8 mm steel slag sort.

Component	%
CaO	40.10 ± 2
SiO_2	17.80 ± 2
FeO	12.92 ± 2
Fe_2O_3	6.58 ± 2
Fe_{met}	6.55 ± 2
MnO	6.52 ± 2
MgO	6.32 ± 2
P_2O_5	1.13 ± 0.5
S	0.46 ± 0.2
Al_2O_3	2.04 ± 1
C	0.45 ± 0.2
CaO_{free}	1.5 ± 0.2

Table 3. Grading analysis for steel slag in double crushed state.

Sort, mm	%
0–4	20–22
4–8	11–15
8–16	32–35
16–25	13–16
25–30	15–18

Table 4. Marshall stability (allowable minimum: 4.5 kN).

Steel slag, %	Marshall stability, kN
0	7.88
20	9.99
50	12.24
100	8.63

Table 5. Flow index (allowable range: 1.5–4.5 mm).

Steel slag, %	Flow index, mm
0	3.08
20	3.33
50	2.75
100	3.78

1.3 *The grading analysis of double crushed steel slag*

The grading analysis for steel slag in double crushed state (stipulated state by the standards of roads construction and asphalt mixtures production field) is presented in Table 3.

On the base of data from table 3 it is thought that double crushed steel slag is largely finer (0–8 mm sort reach even 35%).

All the sorts over 8 mm have nowadays a relatively good market in the field of roads construction in Romania and Europe (Diaconu & Lazăr, 2003; Koller, 1997; Zăman et al., 2006; and Diaconu et al., 2007). There is a limited market demand as concerns the use of sort 0–8 mm, which should be used widely for asphalt mixtures production.

2 HRA TYPE (HOT ROLLED ASPHALT) MIXTURE WITH STEEL SLAG

HRA type (hot rolled asphalt) mixtures are prescribed for base courses, which have the following mechanical characteristics: minimum 4.5 kN Marshall stability and 1.5–4.5 mm flow index.

- For the recipe determining, in the first stage of the study were made witness specimens with a binder percent of 4.5%. In the second stage were made and tested samples for three recipes with steel slag sort of 0–8 mm, as a replacement of similar sorts, in various proportions:

– D recipe with 20% of steel slag sort 0–8 mm;
– E recipe with 50% of steel slag sort 0–8 mm;
– F recipe with 100% of steel slag sort 0–8 mm.

The results of these tests concerning Marshall characteristics are presented in Table 4, Table 5 and Figures 1 and 2.

- We can observe that all obtained results are in the allowable range but for the percentage of 100% of steel slag sort 0–8 mm the samples do not present stability; the bitumen is insufficient and the samples break.

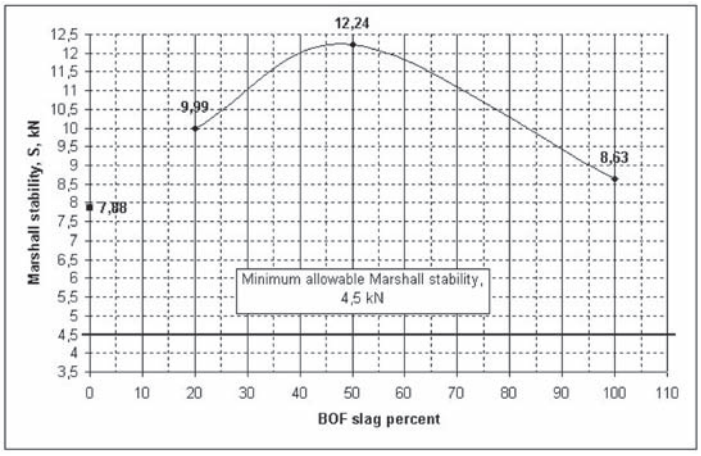

Figure 1. Marshall stability.

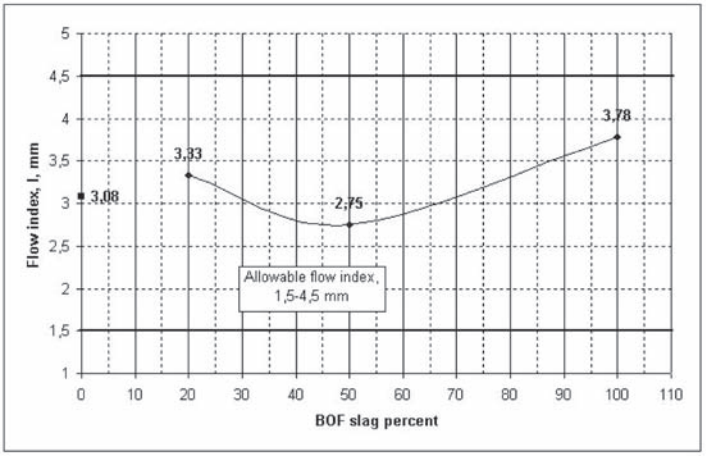

Figure 2. Flow index.

Because every mineral particle (crushed stone or slag) requires coverage with an bitumen film, so a high amount of fine compound needs a high amount of bitumen. Moreover, slag particles have a high porosity and so a high amount of bitumen is absorbed on the particle surfaces.

To improve the behaviour of bituminous mixture samples of 100% steel slag sort of 0–8 mm, next has pursued the determination of the optimal percentage of bitumen (Fig. 3 and 4).

From this analysis it results the optimal rate of bitumen of 5%, which can be used in asphalt mixtures with steel slag sort of 0–8 mm into a 100% proportion, as a substitute for natural sand and 4–8 mm crushed stone sort.

- The air voids of asphalt mixtures (VMA) and water absorption (Abs) were determined for samples with and without steel slag sort of 0–8 mm for 4.5% bitumen, as well as for those with 5% bitumen and slag steel sort of 0–8 mm into a 100% proportion (Figure 5 and Figure 6).
- In the final the Marshall characteristics were checked after 25 cycles of frost-thaw (Figure 7 and Figure 8).

For the samples of recipes D, E and F, after the 25 cycles of frost-thaw, the stability decreases by 40%, and flow index increases by 15%.

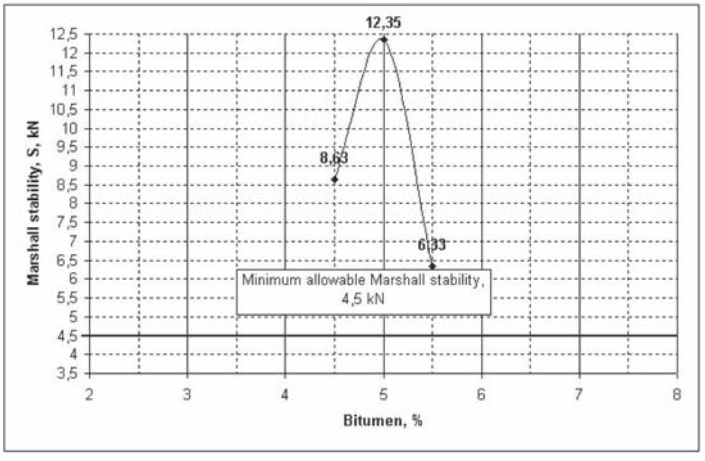

Figure 3. Marshall stability.

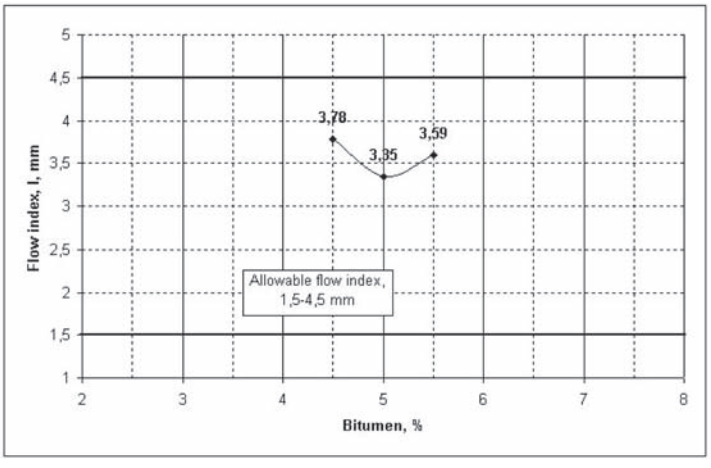

Figure 4. Flow index.

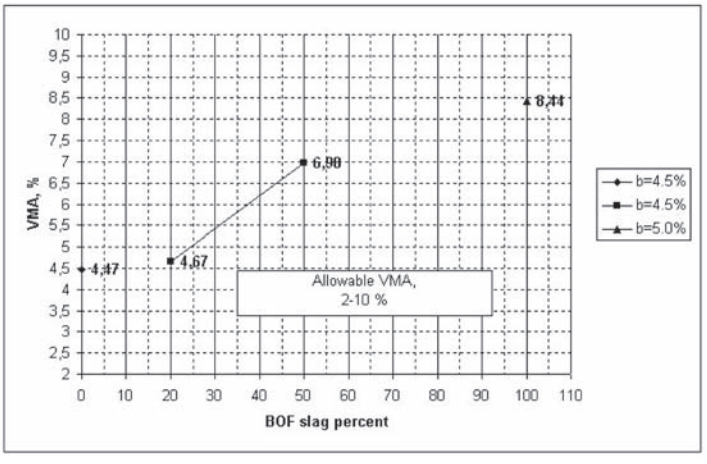

Figure 5. Air voids of asphalt mixtures.

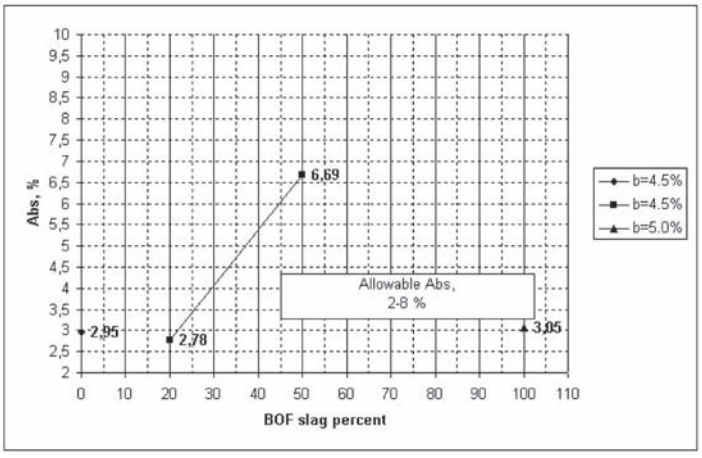

Figure 6. Water absorption.

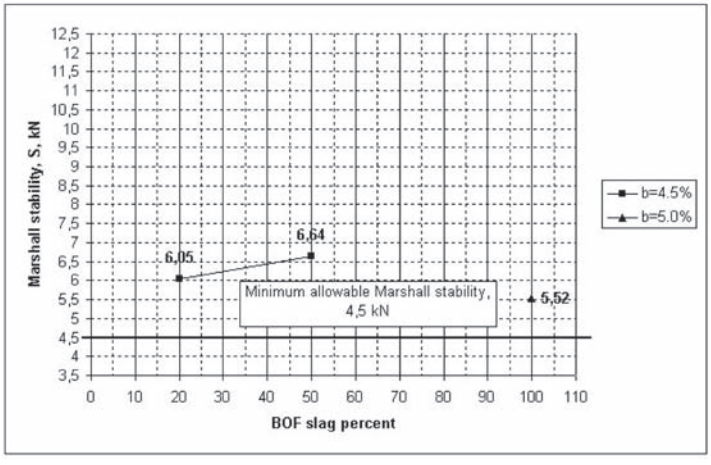

Figure 7. Marshall stability.

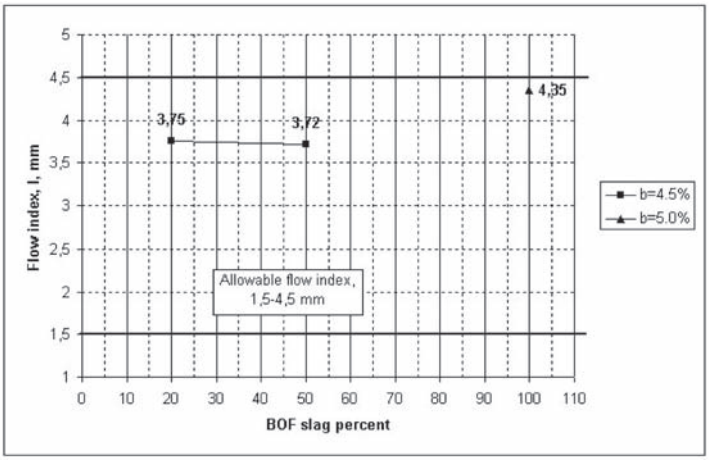

Figure 8. Flow index.

For samples that have in composition the steel slag sort 0–8 mm of 100% proportion, after 25 cycles of frost-thaw, the stability decreases by 25%, and flow index increases by 18%, For all samples, the results are included in prescriptions rules in force.

3 CONCLUSIONS

Capitalization's tests of 0–8 mm steel slag sort as a substitute for crushed stone in HRA (hot rolled asphalt) mixture have shown that slag can be used at least 50% in this mixture.

In the process of mixing with bitumen, steel slag have similar behavior to crushed stone, but in order to totally replace the crushed stone with steel slag, the amount of bitumen must be about 10% higher.

Because the results of the performed tests are encouraging, in the future we intend to conduct dynamic tests to see also the fatigue behaviour of the asphalt mixtures with steel slag.

REFERENCES

Diaconu, E. & Lazăr, Ş.M. 2003. Posibilitatea utilizării zgurei de oţelărie la alcătuirea mixturilor asfaltice pentru stratul de bază, Simpozionul "Infrastructuri eficiente pentru transporturile terestre", *Zilele Academice Timişene, Ediţia a VIII-a,* Timişoara, 22–23 mai.

Koller, O. 1997. *Slag, dust and debris from an oxigen steel plant—substances of value*, EOSC Taranto.

Zăman, Fl. Iorga, Ghe. Hritac, M. Diaconu, E. Lazăr, Ş.M. Burlacu, A. & Predescu, C. 2006. Solutions to capitalization of steel plant slags. Stage and perspectives in Romania, *5th European Oxygen Steelmaking Conference (EOSC)*, organized by The Steel Institute VDEh, Aachen, Germania, 26–28 june.

Diaconu, E. Burlacu, A. & Lazăr, Ş.M. 2007. Utilizarea zgurei de oţelărie în compoziţia mixturilor asfaltice, *Lucrările celei de a III-a Sesiuni Ştiinţifice Construcţii—Instalaţii "CIB 2007"*, organizate de Universitatea Transilvania din Braşov, Facultatea de Construcţii şi CANAM STEEL România, Braşov, 15–16 noiembrie, Editura Universităţii Transilvania Braşov.

Advanced Testing and Characterization of Bituminous Materials –
Loizos, Partl, Scarpas & Al-Qadi (eds)
© 2009 Taylor & Francis Group, London, ISBN 978-0-415-55854-9

Evaluation on the shear performance of asphalt mixture through triaxial shear test

Yang Jun, Zhu Haoran & Chen Zhiwei
School of Transportation, Southeast University, Nanjing, P.R China

ABSTRACT: As one of the primary distresses of asphalt pavement on highways, rutting is caused by the shear flow of asphalt concrete, which makes the study of the shear strength of asphalt mixtures is urgent and meaningful. This paper carries out a study on the shear properties of asphalt mixtures through Triaxial Shear Test and Triaxial Repeated Load Test. Also, the relationship between different shear strength indexes is discussed. What's more, rutting index is also reviewed. The results show that such factors as gradation type, asphalt content, asphalt properties and temperature have a notable influence on the shear strength of the asphalt mixtures. Shear strength decreases in an exponential manner along with the increase of loading passes, and the correlation between shear strength index and rutting index also shows itself a well-fitted logarithmic function.

1 INTRODUCTION

As one of the premature failures of asphalt pavement, rutting happens more often than before with the increase of traffic nowadays. Many studies conclude that the most part of rutting is caused by shear deformation of asphalt concrete. Patterson found that rutting happens as long as the shear stress exceeds the shear strength of asphalt concrete or there is enough creep deformation accumulated (Patterson, 1987). According to Eisenmann and Hilmer, rutting is caused by the flow of asphalt concrete (Eisenmann & Hilmer, 1987). Report of SHRP-A.318 indicated that the mechanism of rutting is the shear deformation of asphalt concrete (1991). In Simpson's research, it was found that the unstable transverse deformation mainly leads to rutting, the densification degree of which is quite small (Simpson, 1999). Accelerated testing on asphalt pavement with Heavy Vehicle System (HVS) by Harvey showed that the sidewise upheaval along the wheel track is obvious but if the rutting is just caused by densification, upheaval will not happen (Harvey, 2000). Both the study from AASHTO test road and round tracking test of Shell Company revealed that although densification of asphalt concrete mainly accounted for rutting at the initial stage after open to traffic, shear deformation of asphalt layer dominated the rutting developing subsequently. Wael Bekheet et al stated that through reviewing the former studies, it was considered that rutting mainly occurs in asphalt layer if the base course was of enough strength, and its mechanism was the shear deformation of asphalt concrete (Wael 2002, Kaloush, 2002). The round tracking test at Southeast University revealed that the deformation caused by shear flow accounts for more than 80% of the total rut depth (Yang, 2005).

It is obvious that densification and shear deformation are the two formation mechanisms of rutting, of which the latter one represents the deforming behavior of asphalt pavement on most occasions. In such a phase the volumetric decrease of asphalt concrete under wheel tracking equals nearly to the volumetric increase of the upheaval at the side of wheel tracking, which is mainly caused by the plastic flow deformation of asphalt concrete as a result of the excessive stress.

Given all discussed above, performance of shear resistance should be a significant point to address in road design; however, it's a pity that that shear resistance performance has been seldom considered in road design. For example, in "Specification for design of highway

asphalt pavement" of China (JTG D50-2006), it is specified that "intermediate and bottom layers should be rutting resistant, shearing resistant, dense and waterproof", and that "some measures should be taken for asphalt pavement with rigid base to strengthen the combination of the asphalt layer and rigid base, and enhance the shear strength of asphalt mixture", however, "determination of shear strength, allowable shear stress and other issues should be confirmed in further study, so till now these could not be included in this specification".

In view of this situation, triaxial shear test was adopted to evaluate the shear performance of asphalt mixtures with the expectation of improving the rutting resistance of asphalt pavement to update the pavement design specification.

2 TEST METHOD

As a classic test method, triaxial shear test can simulate the 3D stress state conforming to the actual state of in-situ pavement, from which the shear parameters, stress-strain properties, compressive strength and damage energy can be obtained. In this paper, this test method is chosen.

Advanced universal testing machine (UTM) is adopted as the test equipment, shown in Figure 1. During testing, samples were put in the pressure chamber with confining pressure imposed through high-pressure liquid, so that the samples were subjected to isotropic stress; afterwards, the loading cell imposed axial pressure on these samples, which brought deviation in the axial stress. With a certain rate of axial load during testing, axial deviation stress increased gradually at first before it reached its peak, and when it declined, the shear failure of specimen occurred.

The tests were conducted under different confining pressures and the corresponding axial peak stresses and a series of stress Mohr-circles of limit equilibrium were recorded.The envelope shows that the material comply with the law of the shear strength of Coulomb equation, and then the shear parameters Cohesion c and Internal Friction Angle φ were obtained, shown in Figure 2.

Asphalt mixture is visco-elastic-plastic, the shear strength of which is closely related to its deformation rate. With reference to the research project abroad (Kamil, 2001), loading rate of 1.27 mm/min (0.05 inch/min) was set, and the shear tests were conducted respectively at three levels of confining pressure of 0 kPa, 138 kPa, 276 kPa (0, 20, 40 psi) at the temperature of 60°C. Meanwhile, 25°C, the room temperature and 40°C, the high temperature were also selected in order to evaluate the influence of temperature on the shear strength as a reference. Cylinder specimens with the height of 150 mm and the diameter of 100 mm were prepared from gyratory compression machine.

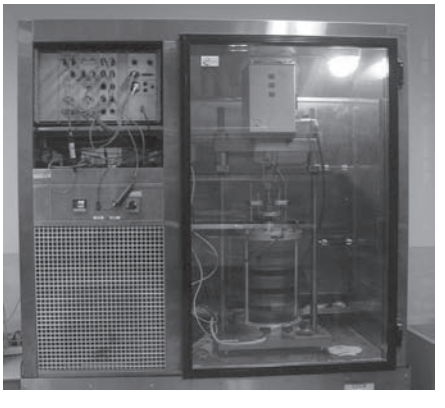

Figure 1. Test equipment UTM.

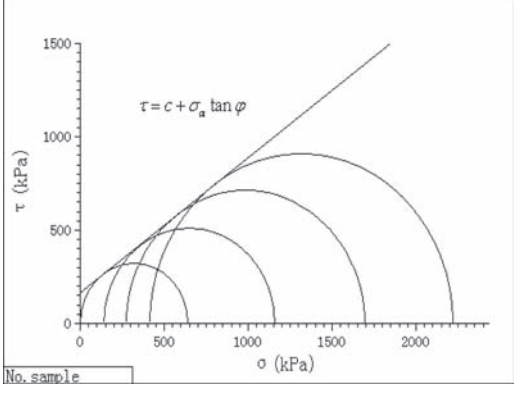

Figure 2. Mohr-Coulomb envelope curve.

3 RAW MATERIAL AND GRADATION DESIGN

In this paper, four types of asphalt mixtures AC13, SMA13, PA13 and Sup13 which are commonly used in the top layer in China were selected for the study objectives; basalt aggregates and limestone filler were also chosen. All the raw materials meet the national technical requirements.

SBS modified asphalt was used as binder. In order to evaluate the influence of asphalt properties, ordinary heavy-traffic asphalt AH-70 and high-viscosity modified asphalt were also selected for comparison. Their properties are shown in Table 1.

All the gradations of asphalt mixtures are shown in Figure 3.

All the asphalt contents and void contents of mixtures are shown in Table 2.

Table 1. Properties of asphalt.

Properties	AH-70	SBS Modified	High-viscosity modified
Penetration at 25ºC (0.1 mm)	65.5	58.5	37.8
Penetration Index	0.51	1.32	1.11
Ductility at 15ºC (cm)	93.5	100.5	81.7
Softening point (R&B) (ºC)	53.1	65.7	92.5
Viscosity at 60ºC (Pa.s)	206.4	2017.1	76,635.6
Specific gravity at 25ºC	1.005	0.993	1.036
Elastic recovery at 25ºC (%)	8	91.3	96.8
TFOT at 163ºC (5 h)			
TFOT mass loss (%)	–0.133	0.055	0.014
Softening point (R&B) (ºC)	55.8	65.9	87.3
Ductility at 15ºC (cm)	4.3	24.1	29
Viscosity at 60ºC (Pa.s)	262.8	2462.8	15,768.7

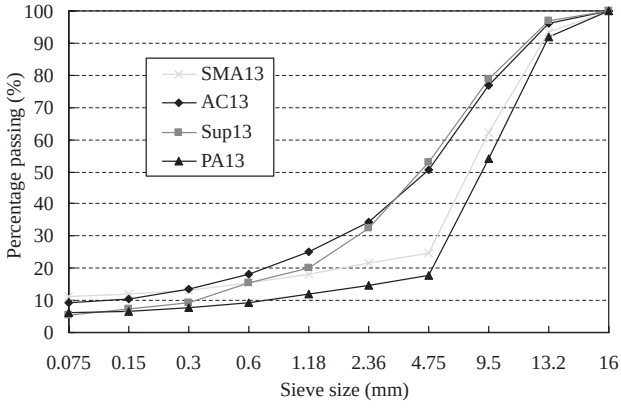

Figure 3. Gradation curves of asphalt mixtures.

Table 2. Optimal Asphalt-aggregate ratio and designed void.

Type	SMA13	AC13	Sup13	PA13
Optimal Asphalt-aggregate ratio (%)	6.0	5.6	5.0	5.15
Void content (%)	4	4	4	20

Table 3. Cohesion and internal friction angle of different gradation types.

Shear parameters	AC13	Sup13	SMA13	PA13
Cohesion c (kPa)	207.52	212.9	197.68	51.71
Internal friction angle φ (°)	33.3	37.52	39.47	29.71

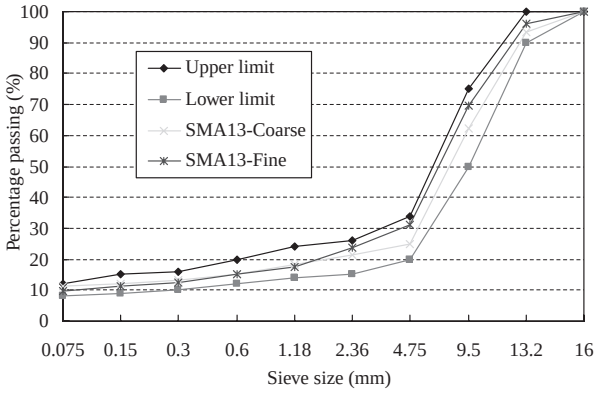

Figure 4. Gradation curves of SMA13.

4 SHEAR STRENGTH OF MIXTURE

Shear strength is contributed by cohesion and internal friction angle. In order to find out the feature of shear index c, φ of the asphalt mixture, the paper studies the shear properties of asphalt mixture on some influencing factors such as gradation type, gradation, asphalt content, asphalt properties and temperature etc.

4.1 *The influence of gradation type*

In order to investigate the shear properties of asphalt mixture of different gradation types, four kinds of mixture were selected as following: traditional asphalt concrete of "suspension-dense" structure AC13, stone mastic asphalt of "framework-dense" SMA13, porous asphalt mixture of "skeleton-void" PA13 and Sup13 of Superpave. The aggregates were basalt and the binder was SBS modified asphalt. The results of shear strength index obtained are shown as Table 3.

From the results it is found that the cohesion of "suspension-dense" structure AC and Sup are slightly larger than that of "framework-dense" structure SMA and "skeleton-void" structure. PA shows a much smaller cohesion than the others. The reason lies in that there is more fine aggregate and mineral filler in dense structure and they form viscous asphalt mastic which always has a larger cohesion. Meanwhile, the internal friction angle decreases due to the lubrication effect by the asphalt mastic in mixture. So as for internal friction angle, framework dense structure SMA is the largest; Sup is the second; the third is the skeleton dense type. In the experiments described in this paper, skeleton-void structure does not have large internal friction angle as most thought before. Instead, it has the smallest internal friction angle which may be ascribed to the property of asphalt binder. The strength characteristics of skeleton-void structure require further researches.

4.2 *The influence of gradation*

In the same type of asphalt mixture, the performance will be different with different gradation. In order to investigate the influence of gradation, two kinds of grading curve of SMA13 mixture has been designed. The gradation curves are shown in Figure 4.

Table 4. Cohesion and internal friction angle of coarse gradation and fine gradation of SMA.

Type	c (kPa)	φ (°)
SMA13-coarse	197.68	39.47
SMA13-fine	204.38	38.58

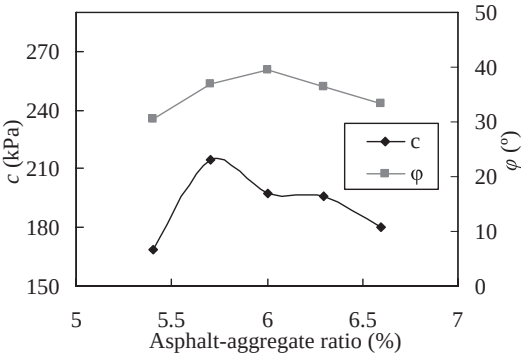

Figure 5. The influence of asphalt content.

As the properties of asphalt and aggregate did not change, the shear behavior of different gradations was compared. The test results are shown in Table 4.

From the results it is found that the friction angle of coarse-gradation mixture is slightly bigger than that of fine-gradation, while the cohesion is right the opposite, which is the result of the presence of fine-gradation. It also validates that triaxial shear test can be used to distinguish different gradation in a very sensitive manner.

4.3 *The influence of asphalt content*

In order to investigate the influence of asphalt content on mixture performance, five types of asphalt-aggregate ratio at an interval of 0.3% are chosen to design SMA13 mixture. The properties of asphalt and aggregate kept unchanged and the testing result is shown in Figure 5.

From the results, it is found that internal friction angle is the largest at the optimal asphalt content, and it decreases significantly as the asphalt content varies. Proper asphalt content offers effective cohesion in aggregates, making the aggregate structure interlocked tightly together and increasing internal friction angle. Insufficient asphalt content will decrease the internal friction angle. Meanwhile, if asphalt content is excessive that free asphalt is in place which lubricates, interlocking force in aggregates will decrease and the internal friction angle will also be reduced.

When a small content of asphalt is used, it can not form the structure of the asphalt film to bond aggregate particles. With the amount of asphalt increasing, the structured-asphalt is gradually formed so that the surface of the aggregate is wrapped and the cohesion between the asphalt and aggregate builds up with the increase of asphalt content. When the content of asphalt is sufficient to form thin films to bond aggregate particles at the surface, asphalt mastic has the best cohesion. With the amount of asphalt further increasing, the mineral aggregates are gradually pushed away to give way for free asphalt which induces the decrease of cohesion of asphalt mastic. Cohesion reaches its peak at the content of asphalt little smaller than the optimum asphalt-aggregate ratio, which ends up with the largest shear

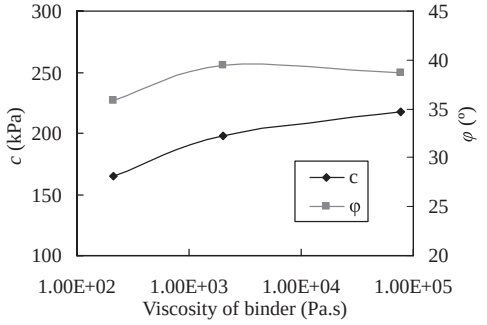

Figure 6. The influence of asphalt properties.

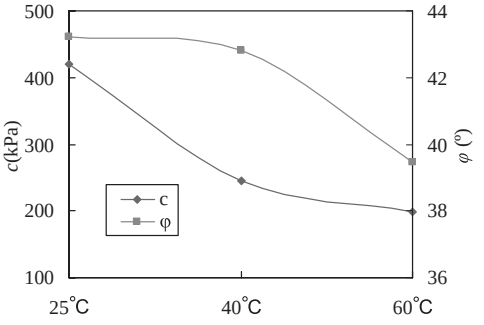

Figure 7. The influence of test temperature.

strength possible. So in the actual pavement, rutting resistance of pavement can be enhanced by reducing the amount of asphalt and increasing compaction power to ensure the degree of compaction and the interlocked-denseness at the optimum asphalt-aggregate ratio.

4.4 *The influence of asphalt properties*

In order to investigate the influence of asphalt properties on mixture performance, this paper selected ordinary heavy-traffic asphalt AH-70, SBS modified asphalt and high viscosity modified asphalt to design SMA13 mixture. The properties of the binders are shown in Table 2 and the properties of aggregate remains unchanged.

To evaluate the high temperature stability of asphalt pavement, the viscosity index of asphalt at 60°C is regarded important to be used as heat-resistance index of asphalt in summer. This paper compares the influence of the viscosity index at 60°C on mixture shear index, as showed in Figure 6.

Figure 6 shows that cohesion and internal friction angle of mixture using modified asphalt are improved significantly, especially after using high viscosity modified asphalt when the cohesion has increased more than 32 percent. When mixture is subjected to shearing load, the viscosity of asphalt behaves as the resistance of shear, so high viscosity asphalt enables mixture of larger viscosity to acquire higher shear strength.

The viscosity of binder material also has considerable influence on internal friction angle. Binder with a certain viscosity makes the aggregates interlock closer, so internal friction angle of modified asphalt mixture is bigger. But the effect of interlock comes mainly from the aggregate itself which can not increase infinitely.When the viscosity of the asphalt reaches a certain value, the internal friction angle will no longer increases. Thus the high viscosity asphalt and SBS modified asphalt exhibits the same internal friction angle. So it can be said that asphalt and aggregate is interdependent. Without good asphalt, good gradation can not provide stronger strength and vice versa. In a word, shear strength increases significantly as the viscosity of asphalt increases.

4.5 *The influence of temperature*

Asphalt is a material with high sensitivity to temperature. Its viscosity decreases significantly as the temperature rises, while the shear strength of the mixture decreases accordingly. SMA13 mixture was chosen to test the change of its shear strength characteristics in three temperature levels from normal to high. Figure 7 illustrates the change.

Figure 7 shows that both the cohesive force and the internal friction angle decrease as the temperature rises. This is because the increase of the temperature causes the decrease of the binder's viscosity which leads to the reduction of the shear strength. The internal friction angle decreases slightly, only a drop of four degrees, the cohesive force decreases more than a half. To sum up, the shear strength of the mix decreases apparently as the temperature rises.

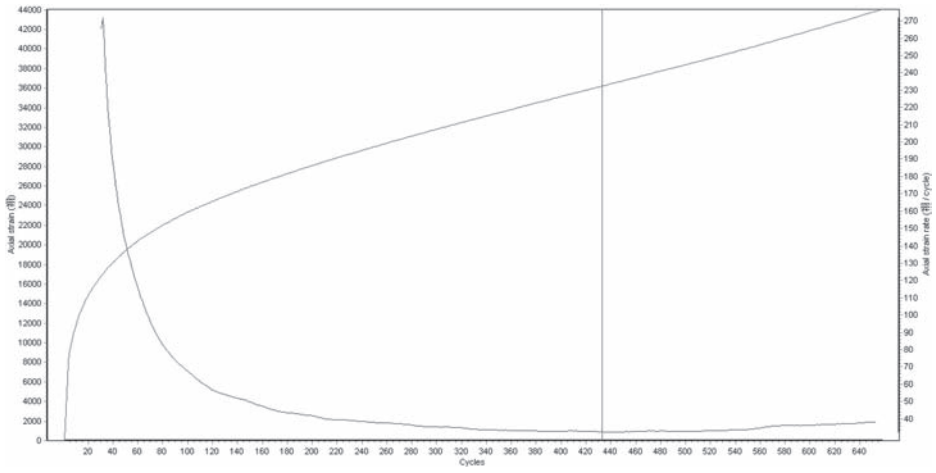

Figure 8. Asphalt mixture deformation with repeated loading number.

5 THE EFFECTS OF SHEAR FATIGUE

The real pavement will probably survive after a single time shear load; instead the damage of pavement is due to repeated traffic load. In other words, the shear fatigue should be to blame for the damage from mechanical view. The impact of repeated traffic load on pavement is simulated by the tri-axial repeated loading test in the SPT (simple performance test), which is a dynamic tri-axial loading test. In the test, loading on the specimen is actually repeated shearing due to the deviatoric stress (σ_d) between the axial stress and the confining pressure. So, actually it is a process of shear fatigue for the tri-axial loading test.

Figure 8 shows a typical rule that how the deformation of the asphalt mix develops under the repeated loading. In the figure, the rising curve shows how the axial strain develops to the repeated loading, and the falling curve depicts how the varying rate of the strain (strain change per loading cycle) develops. The varying rate of the strain at the vertical line reaches the minimum, which represents that after certain cycles of repeated loading, the specimen arrives at the phase of shear failure, and the load number is deemed as the critical cycles. In the dynamic tri-axial loading test, the dynamic shear stress with the amplitude of $\sigma_d/2$ on the particular plane ($\alpha = 45°$) when the specimen fails is usually called as the dynamic failure strength of the specimen, and the curve showing the relationship between the dynamic failure strength and the failure time is called as the dynamic strength curve (Liu, 2002).

SMA13 mixture is chosen as the subject to study the effects of shear fatigue on the strength. The load is semi-sinusoidal wave shape with 0.1 s loading and 0.9 s rest, with confining pressure 0, 138 KPa at 60°C. Figure 9 shows the dynamic strength curve of the SMA13 mixture, showing how the shear strength develops to the loading number, which is the effect of the shear fatigue.

Figure 9 demonstrates that the shear strength of the mixture decreases in power function as the loading cycles increases. Under the repeated shearing traffic load in realistic pavement, the strength of asphalt concrete decreases which may cause failure due to shear fatigue showing as rutting.

6 RELATIONSHIP BETWEEN THE PARAMETERS OF SHEAR STRENGTH AND RUTTING

As for the four mixtures used in this paper, the relationship between the parameters of shear strength and rutting was studied. Figure 10 shows the relationship between the shear strength parameters and the rut depth after 10,000 load cycles using Hamburg Wheel Tracking test.

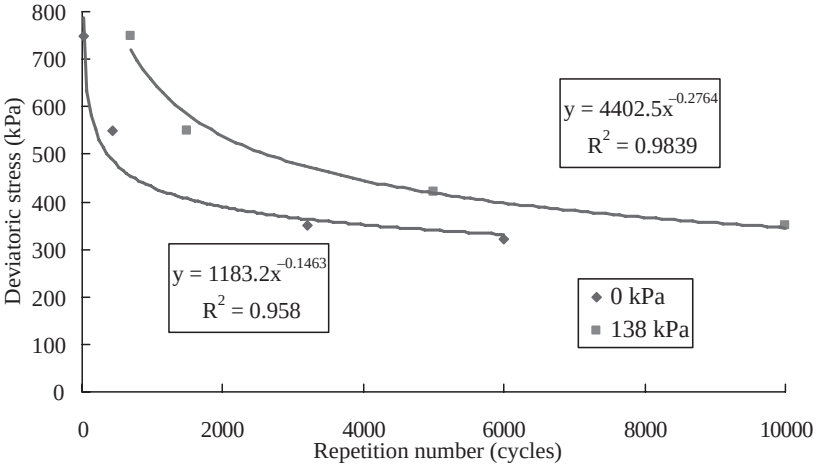

Figure 9. Dynamic strength curves of asphalt mixture.

Table 5. Relativity grade.

Criterion	R^2	S_e/S_y
Excellent	>0.90	<0.35
Good	0.70–0.89	0.36–0.55
Fair	0.40–0.69	0.56–0.75
Poor	0.20–0.39	0.76–0.90
Very Poor	<0.19	>0.90

It is clear that a well fitted logarithmic relationship between them is found with a relative coefficient $R^2 = 0.8315$ and a standard error ratio $S_e/S_y = 0.503$. According to the classification method of the NCHRP (Tab. 5) (2002), correlation of the relationship is good which also means shearing deformation is a main reason for rutting.

7 CONCLUSION

In this paper, the shearing performance of asphalt mixture was studied through triaxial shear test, and the following conclusions can be achieved:

1. Cohesion of "suspension-dense" structure mixture is bigger than that of "framework-dense" structure mixture and both are much bigger than that of "skeleton-void" structure mixture. However, the internal friction angle of "framework-dense" mixture is the biggest and that of "suspension-dense" mixture follows. The internal friction angle of the "skeleton-void" mixture is not very big, which does not agree with the thought held before, so further studies are needed to explore its strength characteristics. Mixture with a coarser gradation has a bigger internal friction angle, and mixture with a finer gradation has a bigger cohesion force.
2. The internal friction angle reaches the peak at the designed optimal asphalt content, while the cohesion force proves itself best at a relatively smaller content. As the viscosity of the asphalt increases, the cohesion force grows while the internal friction angle rises at first and finally stabilizes. High viscosity asphalt and "skeleton-void" structure are recommended here to increase the shear strength of the asphalt mixture at a high temperature. As the temperature rises, both the cohesion force and the internal friction angle decrease, and the internal friction angle declines to a little degree while the cohesion force declines much.

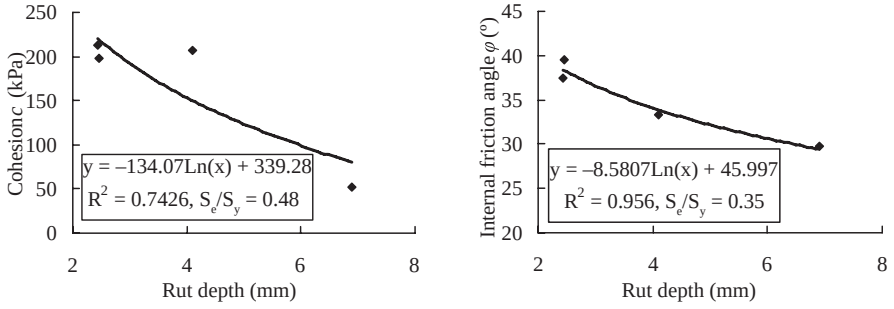

(a) Relationy between cohesion and rut depths (b) Relation between internal friction angle and rut depths

Figure 10. Relation between shear strength index and rut depth.

3. The shear strength of the mixture decreases in a power function as the loading cycles increases, so under the repeated shearing traffic load in realistic pavement, the strength of asphalt concrete decreases which may cause failure due to shear fatigue showing as rutting.
4. The parameters of shear strength and rut depth turn out to be a well fitted logarithmic relationship, and the correlation of the relationship is quite well, which proves that shearing flow deformation is a main reason for rutting.

REFERENCES

Eisenmann, J. & Hilmer, A. 1987. Influence of wheel load and inflation pressure on the rutting effect at asphalt-pavement-experiments and theoretical investigations. *6th international conference on the structural design of asphalt pavements*: 392–403. Ann Arbor: University of Michigan.

Harvey, J.T. & Popescu, L. 2000. Rutting of Caltrans asphalt concrete and asphalt-rubber hot mix under different wheels, tire and temperature-Accelerated Pavement Testing evaluation. Berkeley: Pavement Research Center, Institute of Transportation Studies, University of California.

JTG (D50-2006). 2006. *Specifications for Design of Highway Asphalt Pavement*. Beijing: People's Communication Press.

Kaloush, K.E. & Witczak, M.W.T. 2002. Tertiary flow characteristics of asphalt mixtures. *AAPT* 71: 248–280.

Kamil, E.K. 2001. Simple performance test for permanent deformation of asphalt mixtures [PhD thesis]. Arizona: Arizona State University.

Liu, C.Y. 2002. *Soil mechanics*[M]. Beijing: China Railway Press.

NCHRP. 2002. Simple performance test for Superpave mix design. *NCHRP Report 465*: 19–20. Transportation Research Board.

Paterson, W.D.O. 1987. *Road deterioration and maintenance effect: Models for planning and management standard series, the highway design and maintenance standard series*. Baltimore: Published for the World Bank, the John Hopkins University Press.

SHRP. 1991. Permanent Deformation of Asphalt-Aggregate Mixes. *Report SHRP-A-318*. Washington, D.C.: Strategic Highway Research Program.

Simpson, A. 1999. Characterization of transverse profile. *Annual Meeting of the Transportation Research Board*. Washington, D.C.: National Research Council.

Wael, B. 2002. Investigations of in-situ shear properties of asphalt pavement [PhD thesis]. Ottawa: Carleton University.

Yang, J. 2005. Report for Circular Road Test on the rutting resistance of asphalt pavement[R]. Nanjing: School of Transportation, Southeast University.

Advanced Testing and Characterization of Bituminous Materials –
Loizos, Partl, Scarpas & Al-Qadi (eds)
© 2009 Taylor & Francis Group, London, ISBN 978-0-415-55854-9

Development of a Dog-Bone Direct Tension Test (DBDT) for asphalt concrete

C. Koh, G. Lopp & R. Roque
University of Florida, Gainesville, Florida, USA

ABSTRACT: A new Dog-Bone Direct Tension Test (DBDT), and associated data reduction and interpretation procedures were developed, evaluated and proposed for obtaining fracture properties, stiffness and cracking performance of asphalt mixture. The DBDT provides advantages including the fact that the failure plane is known a priori and stress concentrations near the loading heads have a minimal effect on test results. Furthermore, DBDT specimens can be produced by simply coring each side of gyratory compacted specimens or field cores. A dual cylinder loading system was also developed to evenly load the specimen and reduce eccentric loading. 3-D finite element analysis was conducted to develop correction factors for stresses and strains to determine properties accurately using the testing system proposed. Properties obtained from the DBDT test for a reference material agreed well with published properties for that material. Results of tests on asphalt mixtures were also reasonable and consistent with expectations.

1 INTRODUCTION

1.1 *Background*

It is well recognized that load-related top-down cracking, which initiates at the surface of the pavement and propagates downward, commonly occurs in HMA pavements. This phenomenon has been reported to occur in many parts of the United States (Myers et al., 1998; Uhlmeyer et al., 2000; Myers et al., 2001; Schorsch et al., 2003; Kim, 2005) as well as in Europe (Monlenaar, 1984; Dauzats & Rampal., 1987; Gerritsen et al., 1987; Nunn, 1998; De Freitas et al., 2005), Japan (Matsuno & Nishizawa, 1992; Komoriya et al., 2001; Uchida et al., 2002) and other countries (Wambura et al., 1999; Raju et al., 2008). This mode of failure, however, cannot be explained by traditional fatigue mechanisms used to explain fatigue cracking that initiates at the bottom of the pavement.

For years, many researchers have made efforts to identify fundamental mechanisms that may lead to top-down cracking initiation and propagation. Myers et al. (1998) identified that this mode of distress may be caused by high surface tensile stresses due to non-uniform contact stress between the ribs of radial truck tires and the surface of the asphalt layer combined with thermal stresses. More recently, Myers et al. (2001) found that surface initiated longitudinal cracking occurs primarily under critical conditions and that temperature gradients have a strong effect on the development of stresses, which are not considered in traditional fatigue approaches. Kim (2005) concluded that although top-down cracking performance in Florida was most strongly affected by traffic loading, thermal effects can also affect performance. However, the mechanisms as well as the conditions which make the pavement susceptible to crack growth with respect to porous surface mixtures have not yet been clearly identified.

It might be obvious that there is a fundamentally close relationship between top-down cracking and properties of surface materials since surface mixtures are directly exposed to the surface tensile stress induced by both traffic loading and environmental conditions. However, studies on top-down cracking have not included the effect of surface course mixtures. Porous friction course (PFC) mixtures have been commonly used elsewhere throughout the world. In Florida, the top pavement layer often consists of a thin Open Graded Friction Course

(OGFC) designed to quickly remove the surface water during rain events. The performance of these porous surface mixtures are certainly more severely affected by environmental exposure issues than dense graded mixtures. They are directly exposed to UV radiation, intense heat and due to their inherent higher air void content, they are prone to oxidation, environmental leaching and are more susceptible to sudden dramatic temperature changes from rainfall. These combined effects most likely cause accelerated asphalt binder hardening. Recently, there has been a growing recognition that these surface mixtures may be the "first front" in resisting top-down cracking. Myers et al. (1998) concluded that more fracture resistant asphalt mixtures are needed to prevent top-down cracking. However, tensile properties of open-graded mixtures cannot be easily measured using existing test methods (e.g. Superpave IDT), primarily because of their thin and open-graded nature. Therefore, in order to acquire more insight into the crack behavior of open-graded mixtures, a practical and reliable system for evaluating the fracture resistance is needed.

1.2 *Objectives*

The objectives of this study were as follows:

- Evaluate the need for direct tension test particularly for open-graded mixtures and top-down cracking.
- Develop a dog-bone direct tension test and associated component and data interpretation methods for evaluating tensile properties of open-graded mixtures.
- Optimize specimen geometry in order to take full advantage of the dog-bone direct tension test.
- Perform 3-D FEM analysis of the dog-bone direct tension test to establish correction factors needed to accurately obtain the properties of asphalt mixtures.
- Investigate the feasibility and accuracy of proposed system for determining the tensile properties of open-graded mixtures and asphalt mixtures in general.

2 DEVELOPMENT OF A DOG-BONE DIRECT TENSION TEST (DBDT)

2.1 *Overview*

Determination of tensile properties are critical for evaluating top-down cracking mechanisms, since the cracks appear to develop mostly in opening mode, fracture mode I (Myers, 2000), indicating that tension is at least partially, if not predominantly responsible for the development of cracks. There are currently several tests which are being used to measure the tensile properties of asphalt mixture in the laboratory: Superpave IDT (Roque & Buttlar, 1992; Roque et al., 1997), semi-circular beam test (Li & Marastreanu, 2004; Huang & Shu, 2005), hollow cylinder test (Buttlar et al., 1999; Buttlar et al., 2004), and uniaxial direct tension test (Bolzan & Huber, 1993, Kim et al., 2002). Each of these testing modes offers advantages and disadvantages from the standpoint of practicality as well as their ability to provide accurate damage and fracture properties. Even though a complete discussion of all these methods is beyond the scope of this paper, an overview of the Superpave IDT and uniaxial direct tension tests is appropriate.

Currently, Superpave IDT test is widely used to evaluate the tensile properties of dense graded asphalt mixtures. Superpave IDT best represents a biaxial state of stress at the bottom of the asphalt layer. A key advantage of the Superpave IDT over the other testing systems is that the failure plane is known a priori; it is almost always along the vertical diametral plane (Roque & Buttlar, 1992). From a practical point of view, the test is relatively simple in nature using compressive loads through loading strips. One disadvantage of the Superpave IDT is that test results are more difficult to analyze. Also, tensile response depends strongly on Poisson's ratio. In addition, local failure can occur due to shear fracture under the loading strips at higher temperatures, particularly in open-graded mixtures. These problems are exacerbated for thin specimens (e.g., thin wearing courses). Based on the authors' experience using

the Superpave IDT test on open-graded mixtures, surface air void content and structure can have an effect on the test results at relatively higher test temperatures. Similar problems can be expected with SMA mixtures.

The typical uniaxial direct tension test for asphalt mixtures developed during the first SHRP program uses a cylindrical specimen that is bonded to end caps of the same or slightly larger diameter. In theory, the uniaxial direct tension test benefits from the uniform stress and strain fields in the middle of the specimen, but in practice, evaluation of asphalt mixtures is difficult due to the many detrimental effects associated with this method. Bolzan & Huber (1993) summarized the following disadvantages:

- Stress concentration near the ends of the samples has been observed in many experiments.
- Sample failure can occur due to misalignment.
- Sample preparation requires a long time and a skilled operator/technician.
- The failure plane is presumed to occur at the center of the specimen perpendicular to the vertical axis, but in practice, it may occur at any locations over the specimens.
- This test has had some difficulty in obtaining repeatability.

Therefore, it is necessary to develop a test method and system which reduces and improves the disadvantages of the uniaxial direct tension tests and, at the same time, meets the following requirements: a direct tension mode test, which can be performed on gyratory compacted specimens or field cores, can test samples of various thickness (thin or thick), and can be used on all mixture types (dense-graded, open-graded).

A Dog-Bone Direct Tension test (DBDT) was determined to meet these requirements. The DBDT provides some potential advantages including the fact that the failure plane is known a priori, which means failure limits can be measured directly on the failure plane. Due to DBDT specimen geometry, stress concentrations near the ends of specimen are less critical, and the location where failure is likely to occur is maximized. The DBDT specimens can be produced by simply coring opposing sides from slices or disks obtained from cylindrical laboratory samples or field cores. Development and evaluation efforts for the DBDT are described in the following sections.

2.2 *Development of a Dog-Bone Direct Tension Test (DBDT)*

Two dimensional finite element analysis was conducted to optimize the specimen geometry. Coring radius (r) and coring overlap (x) were the variables used for analysis as presented in Figure 1.

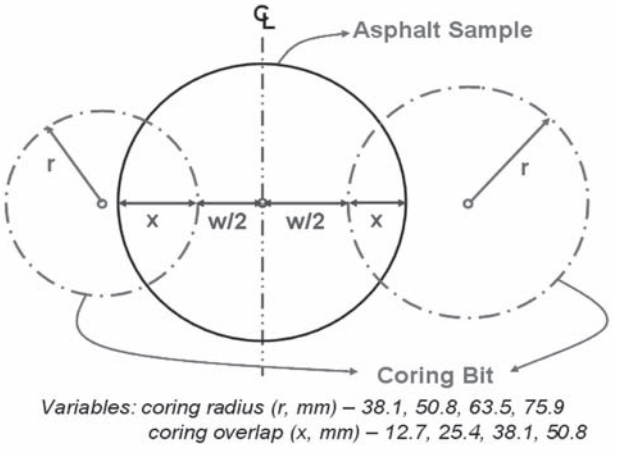

Figure 1. Coring radius (r) and coring overlap (x).

Based on the predicted stress distributions for two-inch wide specimens, a coring radius of 75.9 mm and a coring overlap of 50.8 mm produced centerline stresses that were reasonably uniform and considerably greater than stresses near the loading heads (headline). Analysis results for this case are summarized in Table 1. This final specimen geometry results in a large enough cross-section for testing without sacrificing the integrity of the mixture. As indicated in this table, a significant stress difference between the centerline and the headline of the specimen was observed. The stress concentration at the centerline should cause the specimen to break in this region, thereby compensating for any density gradients in gyratory compacted specimens as previously exposed by researchers (Harvey et al., 1991; Shashidhar, 1998). The percent difference in the computed stress along the centerline is around 30%. However, this 30% increase in stress between the outer edge and center of the specimen is about the same as that observed for Superpave IDT specimens from which material properties have been determined successfully (Roque & Buttlar, 1992). The key to success is to have the gages directly on the planes of maximum stress. Therefore, as can be seen in Figure 2, measurements are obtained in the center of edges of the specimen as well as on the specimen faces.

After exhaustive analysis and discussion, a DBDT prototype system was proposed, designed and built as shown in Figure 2. The complete system is composed of several pieces, including a specimen coring jig, a dual cylinder tensile load equalizer, specimen loading heads, strain gage sensors and attachment kits, and a PC controlled servo-hydraulic load frame with an integrally mounted environmental chamber. Loading heads were machined from 6061-T6 aluminum with V-grooved specimen contact surfaces to increase the bonding

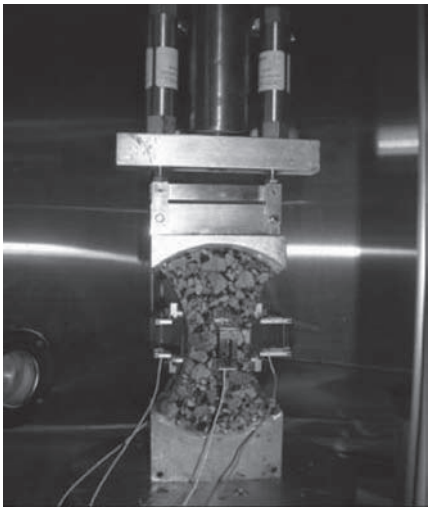

Figure 2. Dog-bone direct tension test prototype.

Table 1. Analysis results for determining DBDT sample geometry.

Various coring overlaps with fixed coring radius (75.9 mm)				
Coring overlap (mm)	12.7	25.4	38.1	50.8
% Difference of stress on centerline (%)	20.39	27.04	28.02	31.31
Stress difference between centerline and headline (%)	20.14	20.26	26.62	43.17
Various coring radii with fixed coring overlap (50.8 mm)				
Coring radius (mm)	38.1	50.8	63.5	75.9
% Difference of stress on centerline (%)	61.17	46.42	37.39	31.31
Stress difference between centerline and headline (%)	50.59	48.54	45.91	43.17

strength between the loading heads and the specimens. Four extensometers or strain gages are used to measure the on-specimen deformations. Two of the sensors are placed on the center of faces and the other two are placed on the center of curved edges. Results of detailed 3-D FEM analysis will be discussed in the next section.

A load equalization system consisting of two interactive hydraulic cylinders was conceived and designed to minimize eccentric loading that can induce premature failure near the loading heads. The upper chambers of both cylinders are filled and plumbed together, and the lower piston chambers are similarly plumbed. Therefore, as one piston goes up, the other piston comes down. In essence, if one side of the specimen starts to fail, the complete load is not transferred to the other side of the specimen. The piston rises moving hydraulic fluid to the other cylinder thereby reducing the load on the non-failing side until the load equalizes and then continues to equalize until failure. This takes place very quickly and extra low friction (ELF) seals were secured and incorporated inside each cylinder to reduce the effects of seal friction on load uniformity.

3 3-D FINITE ELEMENT ANALYSIS TO EVALUATE STRESSES AND STRAINS

Three-dimensional finite element analysis was conducted to analyze stress and strain of a 150 mm diameter specimen with the proposed system. The commercial computer program ADINA was used for analysis (ADINA, 2005). To simplify analysis and for time savings, symmetry was taken advantage of in all three dimensions. Therefore, only one eighth of the specimen was analyzed without sacrificing any accuracy or information. Figure 3 shows 3D FEM mesh for the specimen and its coordinates. The analysis was conducted assuming an asphalt modulus of 400,000 psi, while varying Poisson's ratio, the center width and thickness of the specimen. The 3-D FEM analysis indicated that corrections need to be applied to accurately and reliably determine the properties with proposed measurement system.

3.1 *Stress analysis*

Stress at the center of a specimen of uniform cross-section can simply be calculated as applied load divided by cross-sectional area. For illustrative purposes, results of the 3-D FEM analysis presented in Figure 4 indicate that stress distribution of the DBDT specimen

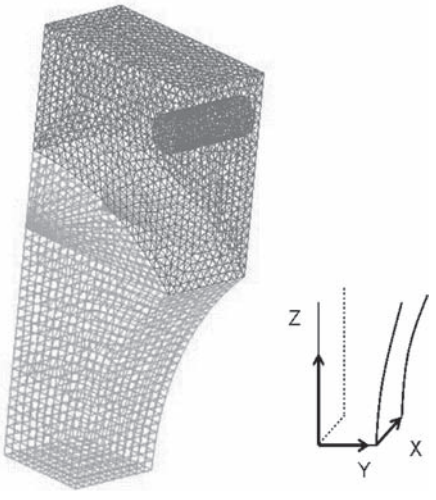

Figure 3. 3-D FEM mesh and coordinates.

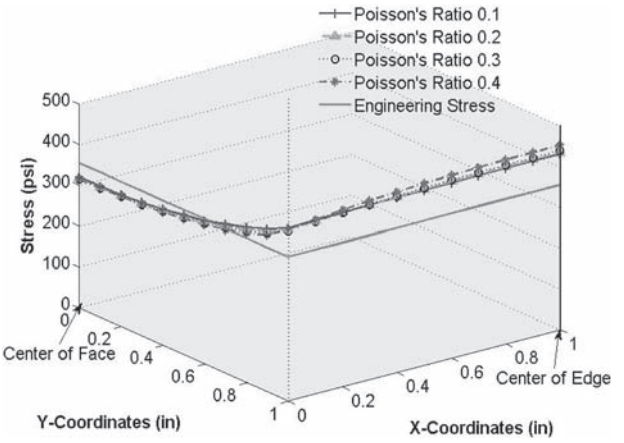

Figure 4. Stress distribution at the center of DBDT specimen. (50.8 mm thickness with 50.8 mm width).

having a 2 inch thickness and a 2 inch width varies from the center of the face to the center of the edge. The tensile stresses vary along the axis of symmetry and reach a maximum at the edge of the specimen.

According to this analysis, tensile failure will initiate at the edge of the specimen. An important finding is that stress distributions do not significantly depend on the Poisson's ratio. Based on multiple 3-D finite element analyses performed with a range of variables, stress correction factors were developed to adjust the stress obtained with the proposed DBDT testing system. The corrected point stresses on the face and edge can be calculated using the following Equations 1.

$$\sigma_{face_c} = \frac{P}{A_c} C_{\sigma f} \tag{1.a}$$

$$\sigma_{edge_c} = \frac{P}{A_c} C_{\sigma e} \tag{1.b}$$

$$C_{\sigma f} = -0.0198t - 0.0158w + 0.9607 \tag{1.c}$$

$$C_{\sigma e} = 0.0177t + 0.0901w + 1.0346 \tag{1.d}$$

where, σ_{face_c} = stress on face corrected, σ_{edge_c} = stress on edge corrected, P = applied load (kg), A_c = area at the center of a specimen (mm^2), $C_{\sigma f}$ = stress correction factor on face, $C_{\sigma e}$ = stress correction factor on edge, t = thickness of a specimen (mm), w = width at the center of a specimen (mm).

3.2 *Strain analysis*

The strain values obtained from the DBDT test are based on the point-to-point displacements measured by the finite length extensometers and are better represented by the average of the strain distributions between gage points as expressed by Equation 2.

$$\varepsilon_{face_a} = \frac{1}{GL} \int_{-GL/2}^{GL/2} f_1(x) dx \tag{2.a}$$

$$\varepsilon_{edge_a} = \frac{1}{GL} \int_{-GL/2}^{GL/2} f_2(x) dx \tag{2.b}$$

where, ε_{face_a} = average strain between two gage points on face, ε_{edge_a} = average strain between two gage points on edge, GL = gage length (mm) = distance over which vertical deformations are obtained.

Since only the average strain can be measured with a finite length gage, strain correction factors were developed to convert the average strain determined from the extensometer to a vertical point strain at the center of a specimen's face and edge. Figure 5 and 6 present the strain distributions between gage points on the face and edge. It is also pointed out that these are independent of Poisson's ratio. The strain is corrected using following Equations 3.

$$\varepsilon_{face_p} = \varepsilon_{face_c} = \varepsilon_{face_a} C_{\varepsilon f} \tag{3.a}$$

$$\varepsilon_{edge_p} = \varepsilon_{edge_a} C_{\varepsilon e} \tag{3.b}$$

$$C_{\varepsilon f} = -0.0028t - 0.00178w + 1.0545 \tag{3.c}$$

$$C_{\varepsilon e} = 0.0039t - 0.0015t^2 - 0.009w + 1.0770 \tag{3.d}$$

where, $\varepsilon_{face_p} = \varepsilon_{face_c}$ = corrected vertical point strain at the center of a specimen's face, ε_{edge_p} = corrected vertical point strain at the center of a specimen's edge, $C_{\varepsilon f}$ = strain correction factors on face, $C_{\varepsilon e}$ = strain correction factors on edge, t and w as previously defined.

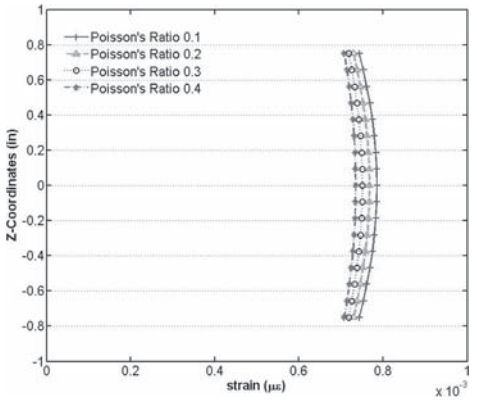

Figure 5. Strain distribution on face (50.8 mm thickness with 50.8 mm width).

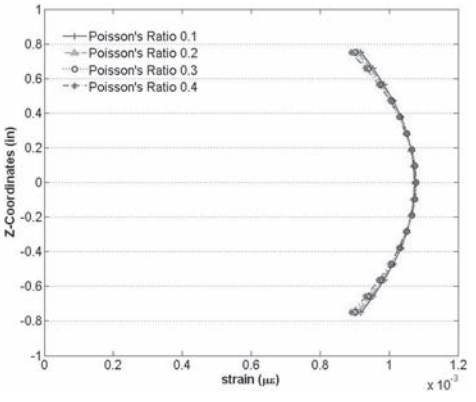

Figure 6. Strain distribution on edge (50.8 mm thickness with 50.8 mm width).

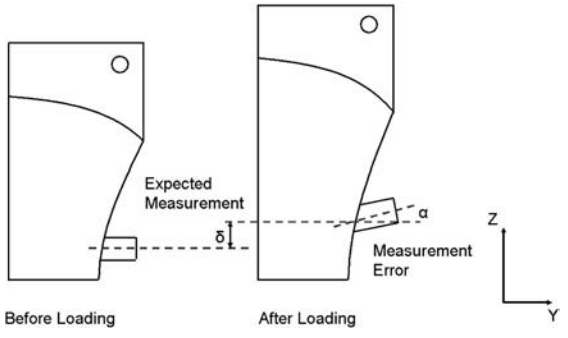

Figure 7. Rotational effect.

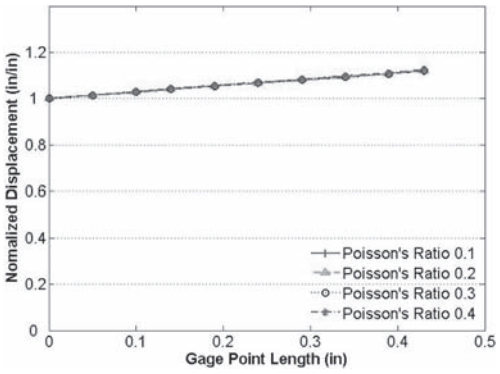

Figure 8. Normalized displacement along gage point on edge (50.8 mm thickness with 50.8 mm width).

3.3 *Rotational effect on edge*

Figure 7 shows how rotational effects of the gage points can influence the deformation measurements at the edges. According to the analysis, it was found that the rotational effects are significant, but not affected by Poisson's ratio, thickness or width of specimen.

Figure 8 presents the effect of Poisson's ratio for a 50.8 mm thick specimen with a 50.8 mm width. This shows a normalized deformation along the length of the gage point, where the contact surface between specimen and the gage point is given a value of 1. A single correction factor can be applied in all cases as long as gage point length is known as shown in Equation 4.

$$\varepsilon_{edge_d} = \varepsilon_{edge_a} C_{de} \tag{4}$$

where, ε_{edge_d} = corrected strain for rotation effect on the edge, C_{de} = displacement correction factors for the edge = 0.81, ε_{edge_a} as previously defined.

Therefore, a corrected point strain on the edge can be obtained using a combination of Equations 3.b and 4.

$$\varepsilon_{edge_c} = \varepsilon_{edge_a} C_{\varepsilon e} C_{de} \tag{5}$$

where, ε_{edge_c} = corrected strain for rotation effect on the edge, all other variables as previously defined.

4 PRELIMINARY EVALUATION WITH THE PROPOSED SYSTEM

4.1 *Preliminary test on delrin specimen*

Preliminary tests were performed using the DBDT prototype to investigate the feasibility and accuracy of this system for determining the tensile properties of asphalt mixtures and to validate the developed correction factors. Delrin plastic specimen was fabricated for calibration purposes. Published material specifications for Delrin report a modulus of 3.1 GPa. A resilient modulus test was performed on the Delrin DBDT specimen to determine the material modulus. The specimen was loaded using a repeated haversine waveform lasting 0.1 seconds, followed by a 0.9 second rest period. Results from the test presented in Figure 9 clearly show that before applying the correction factors, moduli on the edges and on the faces are significantly different and do not agree with the modulus reported by the manufacturer. However, after stress, strain and rotation correction factors are applied, modulus values as calculated from the edge and face deformations approach or equal the manufacturer reported value of 3.1 GPa. This result appears to indicate that these correction factors allow stress and strain to be accurately determined from the proposed DBDT system.

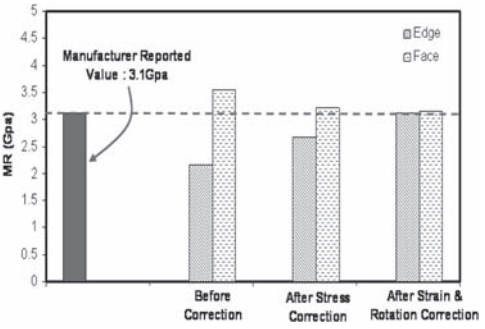

Figure 9. Resilient modulus of Delrin specimen.

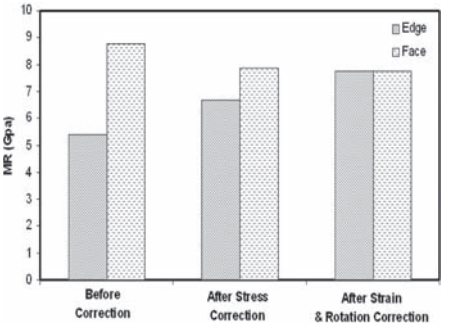

Figure 10. Resilient modulus of OGFC mixture.

4.2 *Preliminary test on OGFC asphalt mixture*

4.2.1 *Sample preparation and test methods*

Open-graded asphalt mixtures were prepared with granite aggregate and asphalt rubber binder (ARB-12). A Superpave Gyratory Compactor (SGC) set to 50 gyrations was used for mixture compaction as suggested by researchers (Mallick et al., 2000; Varadhan, 2004) to meet specified air void content. The compacted specimens were cut into 2 two-inch thick test specimens. After cutting, each side of the test specimens was cored to make dog-bone specimen using a specially designed coring fixture. To increase the effectiveness of the bonding interface, the top and bottom of the test specimens are coarsely sanded to remove the asphalt film. The test samples are then bonded to the loading heads using simple alignment bars in order to obtain proper alignment. All bonding was performed on a machinist granite block to provide a flat reference surface.

Resilient modulus, creep compliance and strength test were performed at 5°C on the DBDT open-graded asphalt mixture specimens. The resilient modulus test was performed using the same procedure described earlier. The creep test was conducted by applying a static load for 1000 seconds. The strength test was performed by applying a constant rate of displacement (50.8 mm) until the specimen failed.

4.2.2 *Evaluation of test results*

Resilient modulus test results are presented in Figure 10, which shows that almost the same modulus values were obtained from the face and the edge measurements once the correction factors were applied. Figure 11 shows 1000 second creep compliance curves for both on-face and on-edge measurements. As can be seen from this Figure, these two plots are almost identical, having similar creep parameters. These modulus and creep values are reasonable and consistent with those measured for similar material at this temperature using the Superpave IDT.

For the strength test, the key issue is to detect the instant of fracture to determine the true tensile strength of the mixture. As mentioned previously, fracture should occur on either edge first or on both edges simultaneously in this DBDT testing system. It was determined that the instant of failure can be detected by examining the difference between the average face deformations and each edge deformation, since failure first occurs at the location where the rate of deformation increases. The following failure limits were determined for the OGFC mixture at 5°C using this approach: tensile strength = 2.22 Mpa, failure strain = 537.53 με, fracture energy 0.72 kJ/m^3.

Once again, results appear to be reasonable and consistent with expectations. As expected, the fracture energy value for the open-graded mixtures was significantly lower than values for dense-graded Superpave mixtures produced with the same binder grade, which typically exceed 1.0 kJ/m^3. Figure 12 shows a specimen after the strength test.

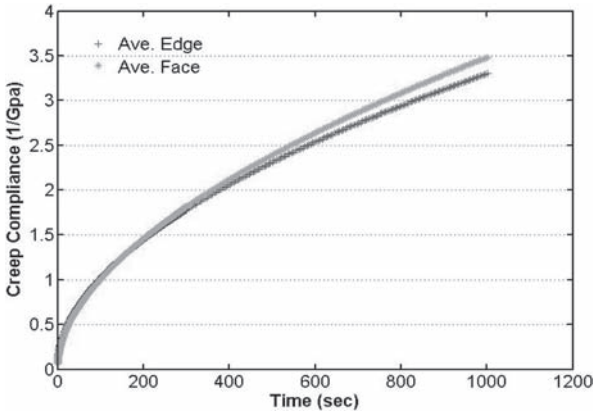

Figure 11. Creep compliance test results.

Figure 12. Specimen after strength test.

The specimen broke at the center of the specimen as expected. The test analysis to date seems to indicate that the DBDT test system with validated correction factors can accurately measure tensile damage and fracture properties of open-graded asphalt mixture and asphalt mixture in general.

5 SUMMARY AND CONCLUSION

In this paper, a new direct tension test, the Dog-Bone Direct Tension test (DBDT), was developed and proposed. The primary impetus for development was the need for a test suitable for evaluating tensile properties of open-graded mixtures. The following conclusions can be drawn from this work:

– The DBDT direct tension test provides a favorable method for obtaining tensile properties of open-graded asphalt mixture and asphalt mixture in general. The DBDT has the advantage that the failure plane, which is at the center of a specimen, is known a priori. Thus, failure limits can be more accurately determined from measurements directly on the failure plane with less propensity for failure due to eccentricity end effects than in specimens of uniform cross-section.

– Correction factors based on finite element analysis allow stress and strain to be accurately determined using simple equations from extensometers measurements obtained on the faces and edges of the DBDT specimens.
– The accuracy of the DBDT was verified with a Delrin specimen of known modulus. Tests on OGFC mixtures have shown promising results.
– Tensile properties from the DBDT system will allow for evaluation of the effect of open graded friction course on top-down cracking performance. Additional experimentation is recommended to validate the accuracy and precision of the DBDT.

REFERENCES

ADINA R & D INC. 2005. *User's Manual-Version 8.3*. Watertown, MA.

Bolzan, P.E. & Huber, G. 1993. *Direct Tension Test Experiments*. SHRP-A-641, Strategic Highway Research Program, National Research Council. Washington, D.C.

Buttlar, W.G., Al-Khateeb, G.G. & Bozkurt, D. 1999. Development of a Hollow Cylinder Tensile Tester to Obtain Mechanical Properties of Bituminous Paving Mixtures. *Journal of the Association of Asphalt Paving Technologists* Vol. 68: 369–403.

Buttlar, W.G., Wagoner, M.P., You, Z. & Brovold, S.T. 2004. Simplifying the Hollow Cylinder Tensile Test Procedure through Volume-Based Strain. *Journal of the Association of Asphalt Paving Technologists* Vol. 73: 367–400.

Dauzats, M. & Rampal, A. 1987. Mechanism of Surface Cracking in Wearing Courses. *6th International Conference Structural Design of Asphalt Pavements; The University of Michigan, Ann Arbor, MI.* 232–247.

De Freitas, E.F., Pereira, P., Picado-Santos, L. & Papagiannakis, A.T. 2005. Effect of Construction Quality, Temperature and Rutting on Initiation of Top-Down Cracking. *In Transportation Research Record: Journal of the Transportation Research Board, No. 1929, Transportation Research Board of the National Academies,* Washington, D.C. 174–182.

Gerritsen, A.H., van Gurp, C.A.P.M., van der Heide, J.P.J., Molenaar, A.A.A. & Pronk, A.C. 1987. Prediction and Prevention of Surface Cracking in Asphaltic Pavements. *6th International Conference Structural Design of Asphalt Pavements; The University of Michigan, Ann Arbor, MI.* 378–391.

Harvey, J., Sousa, J.B., Deacon, J.A. & Monismith, C.L. 1991. Effects of Sample Preparation and Air-Void Measurement on Asphalt Concrete Properties *In Transportation Research Record: Journal of the Transportation Research Board, No. 1317, Transportation Research Board of the National Academies,* Washington, D.C. 61–67.

Huang, B. & Shu, X. 2005. Laboratory Evaluation of Semi-Circular Bending Tensile Strength Test for HMA Mixtures. *Transportation Research Board*, Washington, D.C.

Kim, J. 2005. *Accurate Determination of Dissipated Creep Strain Energy and Its Effect on Load- and Temperature-Induced Cracking of Asphalt Pavement; Ph.D. Dissertation.* University of Florida, Gainesville, FL.

Kim, Y.R., Daniel, J.S. & Wen, H. 2002. *Fatigue Performance Evaluation of WesTrack Asphalt Mixtures Using Viscoelastic Continuum Damage Approach; Final Report of North Carolina Department of Transportation.* North Carolina State University, Raleigh, NC.

Komoriya, K., Yoshida, T. & Nitta, H. 2001. WA-DA-CHI-WA-RE Surface Longitudinal Cracks on Asphalt Concrete Pavement. *Transportation Research Board*, Washington D.C.

Li, X. & Marasteanu, M. 2004. Evaluation of the Low Temperature Fracture Resistance of Asphalt Mixtures Using the Semi Circular Bend Test. *Journal of the Association of Asphalt Paving Technologists* Vol. 73: 401–426.

Mallick, R.B., Kandhal, P.S., Cooley, L.A. Jr. & Watson, D.E. 2000. Design, Construction, and Performance of New Generation Open Graded Friction Courses. *Journal of the Association of Asphalt Paving Technologists* Vol. 69: 391–422.

Matsuno, S. & Nishizawa, T. 1992. Mechanism of Longitudinal Surface Cracking in Asphalt Pavement. *7th International Conference on Asphalt Pavements*. University of Nottingham, UK. Vol. 2: 277–291.

Molenaar, A.A.A. 1984. Fatigue and Reflective Cracking due to Traffic. *Journal of the Association of Asphalt Paving Technologists* Vol. 53: 440–474.

Myers, L.A., Roque, R. & Birgisson B. 2001. Propagation Mechanisms for Surface-Initiated Longitudinal Wheel Path Cracks. *In Transportation Research Record: Journal of the Transportation Research Board, No. 1778, Transportation Research Board of the National Academies,* Washington, D.C. 113–122.

Myers, L.A., Roque, R. & Ruth, B.E. 1998. Mechanisms of Surface-Initiated Longitudinal Wheel Path Cracks in High-Type Bituminous Pavements. *Journal of the Association of Asphalt Paving Technologists* Vol. 67: 401–432.

Nunn, M. 1998. Design of Long-Life Roads for Heavy Traffic. *Industry Conference, Australian Asphalt Pavement Association*, Surfers Paradise, Queensland, Australia.

Raju, S., Kumar, S.S., Reddy, K.S., Bose, S. & Pandey, B.B. 2008. Analysis of Top-Down Cracking Behavior of Asphalt Pavements. *Transportation Research Board,* Washington D.C.

Roque, R. & Buttlar, W.G. 1992. The Development of a Measurement and Analysis System to Accurately Determine Asphalt Concrete Properties Using the Indirect Tensile Mode. *Journal of the Association of Asphalt Paving Technologists* Vol. 61: 304–332.

Roque, R., Buttlar, W.G., Ruth, B.E., Tia, M., Dickson, S.W. & Reid, B. 1997. *Evaluation of SHRP Indirect Tension Tester to Mitigate Cracking in Asphalt Pavements and Overlays; Final Report of Florida Department of Transportation*. University of Florida, Gainesville, FL.

Schorsch, M., Chang, C. & Baladi G.Y. 2003. Effects of Segregation on the Initiation and Propagation of Top-Down Cracks. *Transportation Research Board*, Washington D.C.

Shashidhar, N. 1998. X-Ray Tomography of Asphalt Concrete. *Transportation Research Board*, Washington D.C.

Uchida, K., Kurokawa, T., Himeno, K. & Nishizawa, T. 2002. Healing Characteristics of Asphalt Mixture under High Temperature Conditions. *9th International Conference on Asphalt Pavements*. Copenhagen.

Uhlmeyer, J.S., Willoughby, K., Pierce, L.M. & Mahoney, J.P. 2000. Top-Down Cracking in Washington State Asphalt Concrete Wearing Courses. *In Transportation Research Record: Journal of the Transportation Research Board, No. 1730, Transportation Research Board of the National Academies,* Washington, D.C. 110–116.

Varadhan, A. 2004. *Evaluation of Open Graded and Bonded Friction Course for Florida; Master's Thesis*. University of Florida, Gainesville, FL.

Wambura, J.H., Mania, J. & Smith, H.R. 1999. Kenya Bituminous Materials Study. *In Transportation Research Record: Journal of the Transportation Research Board, No. 1681, Transportation Research Board of the National Academies,* Washington, D.C. 129–137.

Advanced Testing and Characterization of Bituminous Materials –
Loizos, Partl, Scarpas & Al-Qadi (eds)
© 2009 Taylor & Francis Group, London, ISBN 978-0-415-55854-9

Evaluation of performance grading parameters for crumb rubber modified asphalt binders and mixtures

N. Tabatabaee, H.A. Tabatabaee, M.R. Sabouri & P. Teymourpour
Department of Civil Engineering, Sharif University of Technology, Tehran, Iran

ABSTRACT: This study examined Crumb Rubber Modified (CRM) binders produced by mixing different percentages of crumb rubber with PG58-22 and compared them with PG64-22 and PG64-16 binders. Superpave performance grading was used to determine the performance grade of these modified binders. The modified and unmodified binders were then used to make asphalt concrete specimens. These specimens showed an increase in indirect tensile strength and in Marshall stability with the use of CRM binders. The laboratory performance of the specimens were tested and compared. Rutting susceptibility, selected as indicative of the high temperature performance of the mixes, was compared by conducting an unconfined static creep test at high temperature. Intermediate temperature performances were compared by determining the absorbed energy during the indirect tensile strength test at two temperatures. The results were used to evaluate the suitability of the Superpave performance grading procedure in predicting the performance of CRM binders.

1 BACKGROUND

Modification of asphalt binders is a common way of improving binder characteristics and performance. The use of crumb rubber as an asphalt binder modifier has received more attention because of its cost efficiency and environmental benefits. These binders are produced by mixing a percentage of crumb rubber with asphalt cement at an elevated temperature. In practice, a wide range of mixing temperatures and mixing times along with an array of crumb rubber types have been used with varying degrees of success.

From 1987 through 1993, the Strategic Highway Research Program (SHRP) carried out a major research program to develop the Superpave performance-based specifications and test methods for asphalt binders as well as similar tests and a mix design practice for HMA mixes (Bahia et al. 2001a). The specifications were believed to be "blind to source" and thus suitable for all binders, regardless of source, type and modification. However, the SHRP asphalt research was carried out almost exclusively with unmodified asphalt binders, so the applicability of the Superpave specifications and test methods to modified binders was not validated.

Soon after the introduction of the Superpave performance grading specification, a few studies were carried out on the effect of crumb rubber modifier on the parameters measured using the Superpave protocol (Bahia et al. 1995, Madapati et al. 1995). The high temperature performance grade for crumb rubber rose significantly. However, there was little positive effect on the low temperature performance grade. In these studies, the Superpave protocol was presumed to be valid for modified binders and, thus, no mixture tests were conducted for comparison.

Further studies and practice have shown that modified asphalt binders graded according to Superpave performance grading specifications show marked improvement in selected performance characteristics compared with unmodified asphalt binders. However, users and producers of modified asphalt binders remain concerned that the current specification and test methods do not fully measure the performance enhancement contributed by modification (Bahia et al. 2001a).

NCHRP Project 9–10 recommended changes to Superpave performance grading specifications and supporting test methods to fully characterize modified asphalt binders and validate those recommendations through laboratory performance testing of modified hot mix asphalt (HMA) (Bahia et al. 2001a). It was found that the current Superpave performance grading specification does not adequately characterize the performance of modified asphalt binders; typically, the binders' potential performance is underestimated. Many common modifiers were investigated, but the project concentrated on polymer modified binders and thus crumb rubber modifier was excluded from the scope of the project. (Kim et al. 2001) carried out a study on crumb rubber modified (CRM) binders using methods developed as part of the NCHRP 9–10 project, but the suitability of current Superpave protocols for crumb rubber modified binders was not discussed.

More countries are taking advantage of CRM pavements (Lee et al. 2007), thus determining the applicability of the Superpave performance grading specification to CRM binders is of great importance. It was for this purpose that the present study was carried out. Several unmodified binders and binders modified with various percentages of crumb rubber were selected. The binders were graded and analyzed according to Superpave performance grading specifications. Asphalt mixture specimens were then fabricated using the binders tested. These specimens were subjected to performance related tests at high, intermediate and low temperatures. The suitability of the Superpave performance grading protocol was evaluated by the comparison of the results of the mixture tests with the performance grading parameters derived during the Superpave binder tests.

2 MATERIALS AND METHODS

PG 58-22, PG 64-22 and PG 64-16 asphalt binders were selected for use in this study. They are identified as binders A, B and C, respectively. Different percentages of crumb rubber modifier were added to the binders. The crumb rubber was produced using an ambient grinding process. The rubber particle gradation was relatively coarse, with 12% remaining on the number 30 sieve and 80% remaining on the number 50 sieve.

The PG 58-22 binder (A) was modified by adding 3%, 6%, 9%, 12% and 15% crumb rubber. These are identified as A3%, A6%, A9%, A12% and A15%, respectively. Unmodified PG 58-22 (A), PG 64-22 (B) and PG 64-16 (C) binders were also tested for comparison with modified binder characteristics.

A densely graded aggregate gradation was selected for this study. A nominal maximum size of 12.5 mm was selected and the gradation was set to meet the ASTM D3515 and the Superpave gradation criteria for dense gradation. To compensate for the expansive effect of the crumb rubber, a gradation curve on the coarse side was used, as shown in Figure 1.

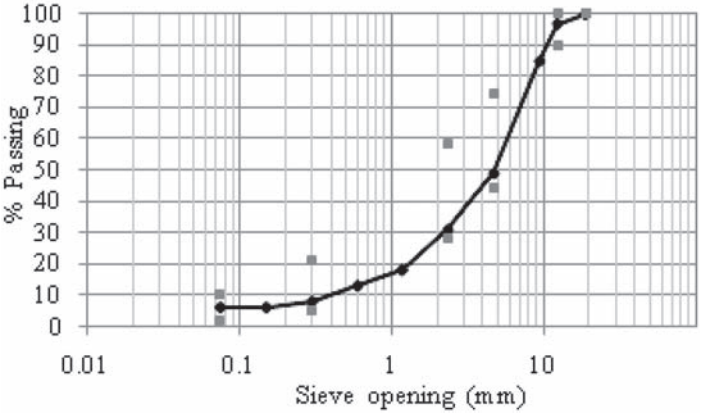

Figure 1. Aggregate gradation curve (12.5 mm nominal maximum size).

2.1 *Binder and mixture fabrication*

The crumb rubber was added to the PG 58-22 binder slowly over 5 min while being mixed at 350 rpm. Mixing time was then 60 min at 165°C.

Cylindrical asphalt concrete specimens of two thicknesses were made. The diameter of all specimens was 100 mm, with thicknesses of 63 and 100 mm. An optimum binder content of 6.2% total weight of the mixture was determined for binders A, B and C. For binders A3%, A6%, A9%, A12% and A15%, optimum binder contents of 6.5, 6.8, 7.1, 7.4 and 7.8 percent total weight of mixture were used. The Marshall mix design method was used to determine the optimum binder content for a target air void volume of 4 ± 1%. The binder and the aggregate were blended at 165°C and compacted using a standard Marshall hammer.

3 TESTING PROCEDURE

3.1 *Binder testing*

Rotational viscosity was measured at three temperatures (105, 135 and 165°C) and complex shear modulus (G*) and phase angle (δ) were measured at temperatures ranging between 7°C and 88°C using a dynamic shear rheometer (DSR). Creep stiffness (S) and creep rate (m-value) were measured at low temperatures (–18 to –6°C) using a bending beam rheometer (BBR). Standard procedure as recommended by Superpave performance grading specifications (AASHTO MP1) were followed except for DSR measurement, where the gap between the testing plates was increased to 2.0 mm to comply with gap to maximum particle size ratio requirements (Bahia et al. 1995 & Troy et al. 1996).

3.2 *Mixture testing*

The indirect tensile strength test, Marshall stability test and unconfined static creep test were carried out on the specimens as described below.

3.2.1 *Indirect tensile strength test*

This test was carried out on 100 mm diameter, 63 mm thick specimens using a 100 kN Dartek Universal Testing Machine. The two test settings were 30°C at a 0.85 mm/s crosshead displacement rate and 5°C at a 0.085 mm/s displacement rate. Vertical displacement and indirect tensile strength were recorded for each specimen.

3.2.2 *Marshall stability test*

The standard Marshall test was conducted on the 100 mm diameter, 63 mm thick specimens. These were placed in a 60°C bath for 30 to 40 min, after which the Marshall stability and flow were determined at a 50 mm/min (0.85 mm/s) displacement rate.

3.2.3 *Unconfined static creep test*

The unconfined creep test was used to rank the mixtures by rut susceptibility. The test was performed in a temperature-controlled chamber at a constant temperature of 42 ± 1°C, on specimens 100 mm in diameter and 100 mm in height. The test consisted of a 2 min preloading at 0.01 MPa as a conditioning stress. Constant loading stress of 0.1 MPa was applied during the test for 1 h loading, followed by 1 h of unloading (Ahmedzade & Yilmaz 2008). The strains after the loading and unloading stages were measured and the permanent strain for each mixture was calculated.

4 BINDER CHARACTERIZATION

Superpave performance grading specification response parameters were used to evaluate the effects of the percentage of crumb rubber modifier on asphalt properties. These parameters were rotational viscosity at temperatures of mixing and compaction as a measure of workability; G*/sinδ at high pavement temperatures as a measure of binder ability to resist rutting

at corresponding service temperatures; G*·sinδ at intermediate pavement temperatures as a measure of binder ability to resist fatigue cracking at corresponding service temperatures; and S and m-value at low temperatures as measures of binder ability to withstand thermal cracking (Bahia & Anderson 1995).

4.1 *G* and δ*

The G* and δ parameters were measured for all binders at a range of temperatures and aging conditions in accordance with the Superpave performance grading criteria. It was observed that increasing the crumb rubber content increased G* significantly and decreased δ, leading to a more elastic binder behavior.

It can be seen from Figure 2 that G*/sinδ increased as the rubber content increased. According to the Superpave performance grading specification, the observed trend indicates a significant increase in rutting resistance up to a temperature of 82°C, where this parameter reaches its limiting value of 1.0 kPa.

G*·sinδ decreased as the percentage of crumb rubber increased, as demonstrated in Figure 3. Lower values of G*·sinδ are taken to relate to higher resistance of the binder to fatigue cracking at intermediate temperatures (Bahia & Anderson 1995).

4.2 *Creep stiffness and m-value*

In a study conducted by several agencies (Hansen & Anderton 1993), low temperature performance tests were carried out on binders and mixtures modified with crumb rubber. The results showed a decrease in the resilient modulus of mixtures made with crumb rubber modified binders at low temperatures, as well as a greater stress relaxation ability that decreased the failure temperature in the constrained specimen tensile stress test. It was concluded that crumb rubber modification could decrease thermal cracking susceptibility and improve low temperature performance.

Evidence supporting these results was observed in the results of the BBR tests conducted in this study. Figure 4 shows the variation of S(60) (creep stiffness 60 sec after loading initiation) with rubber content for asphalt A. The data shown indicates that the reduction in S(60) is a linear function of rubber content, as has been noted by other researchers (Bahia et al. 1995).

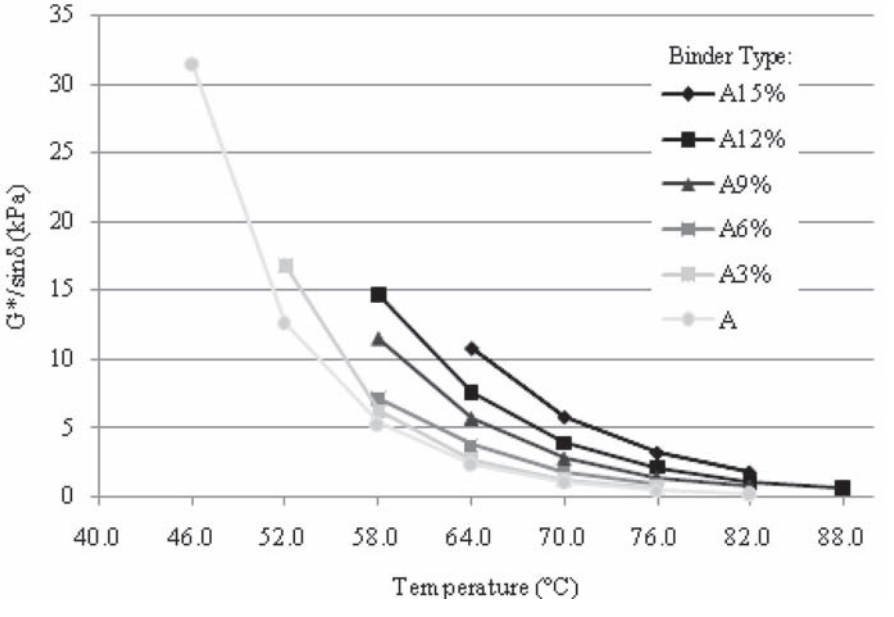

Figure 2. Variation of G*/sinδ with temperature.

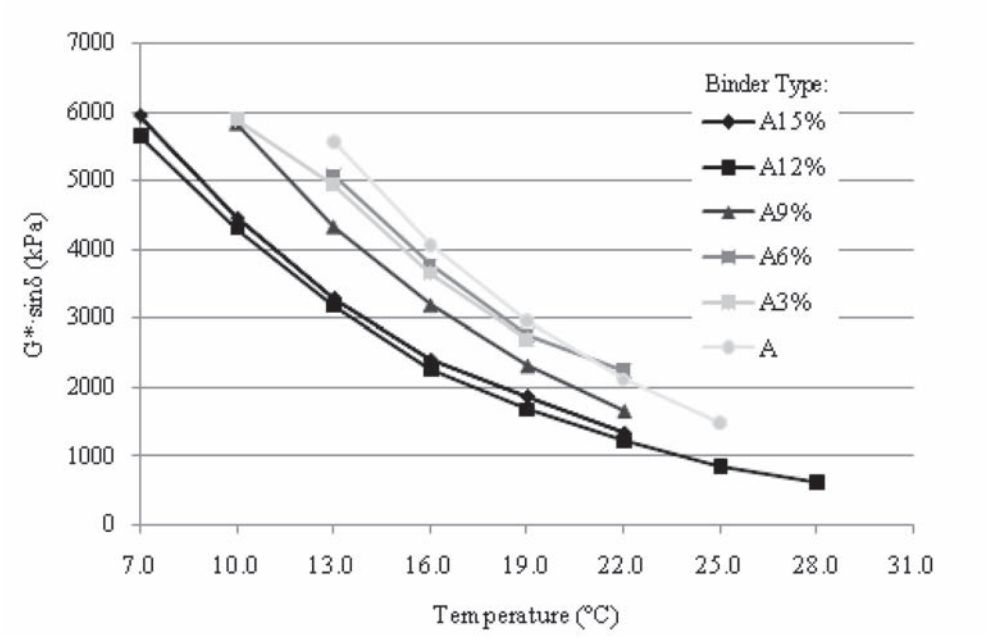

Figure 3. Variation of G*·sinδ with temperature.

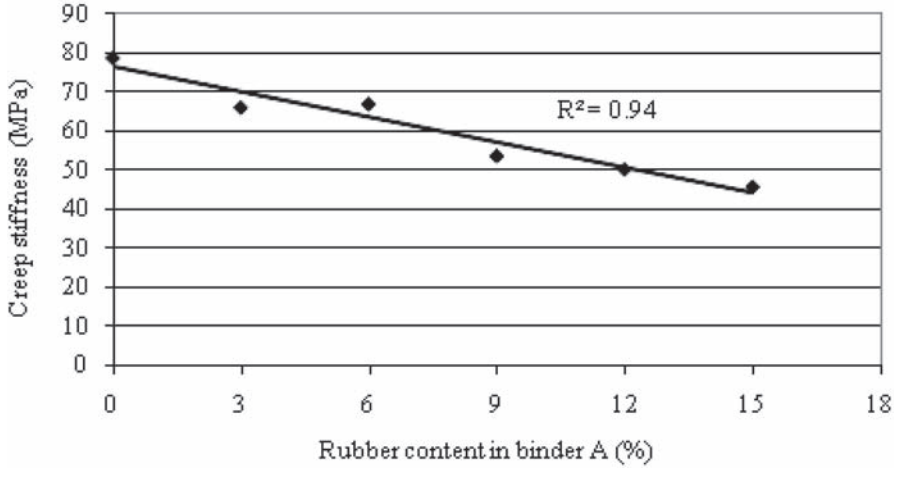

Figure 4. Creep stiffness by percent crumb rubber for asphalt A at −12°C.

Analysis shows that increasing the rubber content from 3% to 15% caused a 37% decrease in the creep stiffness of the binder, but not enough improvement in the m-value at the low temperatures to cause a grade change. Since the m-value was the controlling parameter for the low temperature grade, the significant reduction of stiffness did not change the low temperature performance grade according to the current Superpave protocol.

4.3 *Performance grade*

Table 1 shows the performance grade determined for each of the modified binders. In this paper, the temperature at which the Superpave performance grading criteria is met is referred

Table 1. Performance grade of the binders.

Binder	Rubber content %	Performance grade	True PG temperature	
			High °C	Intermediate °C
A	0	PG 58–22	63.4	14.9
A3%	3	PG 70–22	71.6	13.4
A6%	6	PG 70–22	73.9	12.8
A9%	9	PG 76–22	79.0	11.5
A12%	12	PG 82–22	84.0	8.5
A15%	15	PG 82–22	85.0	8.7

to as the "true performance grade" of the binder. Binder performance improves as the high temperature performance grade (HT) increases, and/or the intermediate (IT) and low temperature performance grades (LT) decrease. It can be seen that the addition of crumb rubber improved the high and intermediate performance grades. The low temperature grade remained unchanged as the rubber content increased.

5 RESULTS AND DISCUSSION

In the following sections the results of laboratory tests on mixtures conducted at high and intermediate temperatures are discussed and compared with the results of the Superpave binder tests presented in the previous sections. It should be noted that the most important parameter in assessing the performance of a mixture is its field performance. Although the ability of laboratory tests to accurately predict this performance is in some instances questionable, field testing was beyond the scope of this study.

5.1 *High temperature performance grade*

One of the most popular tests for evaluating rutting susceptibility is the unconfined static creep test. In this test the permanent deformation is the maximum (total) deformation minus the amount of recovery after the load is removed. When comparing mixtures, it is this permanent deformation that is important for estimating performance (Roberts et al. 1996). Since the rutting is caused by plastic shear deformation of asphalt pavement under traffic loading, rutting potential is best evaluated using this parameter (Kim & Sargand 2003).

Figure 5 shows the amount of permanent deformation occurring in the unconfined static creep test. The results show a decrease in both the amount of permanent deformation and the percent of permanent deformation of total (permanent plus recoverable) deformation as rubber content increases. This agrees with the results obtained by Hanson & Anderton (1993). They observed an improvement in the permanent deformation performance of crumb rubber modified mixtures compared to mixtures made with unmodified binders when tested with the unconfined static creep procedure, as well as in the triaxial confined repeated load compressive creep test at 40°C.

The Marshall stability test was performed on the specimens to measure the strength of the asphalt mixture. The Marshall quotient, the ratio of Marshall stability to flow, also known as the Marshall stiffness index, is an empirical stiffness value used to evaluate the quality of asphalt mixtures. The higher the value is, the stiffer the material is. Hence, the mixture is more likely to resist permanent deformation (Roberts et al. 1996).

Figure 6 shows the results of the Marshall test. An increase in Marshall stability and flow was observed as the rubber content increased. The results of the Marshall quotient calculations for the specimens are shown in Figure 7. It was observed that the Marshall quotient increased as the rubber content increased, suggesting lower susceptibility for permanent deformation. This agrees with the results of the unconfined static creep test. Previous studies by the author showed a decrease in Marshall stability with increasing the rubber content

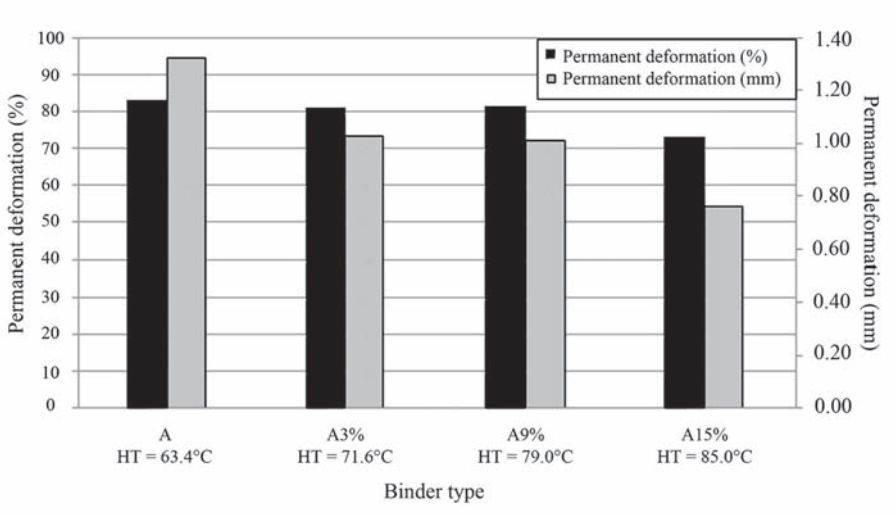

Figure 5. Permanent deformation at different rubber contents.

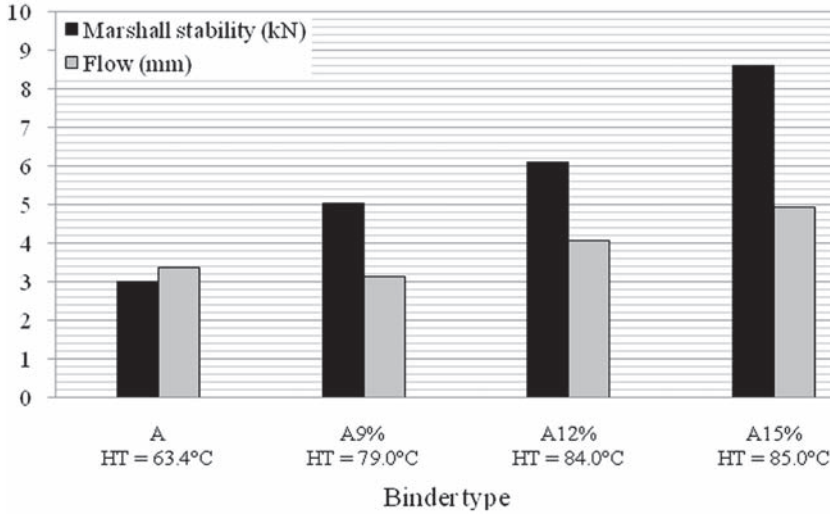

Figure 6. Marshall stability and flow number at different rubber contents.

(Tabatabaee & Bohlouli, 1997). It is postulated that the aggregate displacement caused by the increased film thickness of the CRM binder is responsible for this behavior. Thus, a relatively coarse aggregate gradation was used in this study to minimize this effect, resulting in an increase in Marshall stability as the rubber content increased.

As can be seen in Figure 5, as the rubber content increased, the true high temperature performance grade also increased, indicating an improvement in rutting resistance. This agrees with the results of the unconfined static creep test and the Marshall quotient as shown in Figures 5 and 7.

5.2 *Intermediate temperature performance grade*

It can be seen from Figure 3 that the introduction of a higher dose of crumb rubber into the binder has lowered the temperature at which $G^* \cdot \sin\delta$ has reached the 5000 kPa maximum

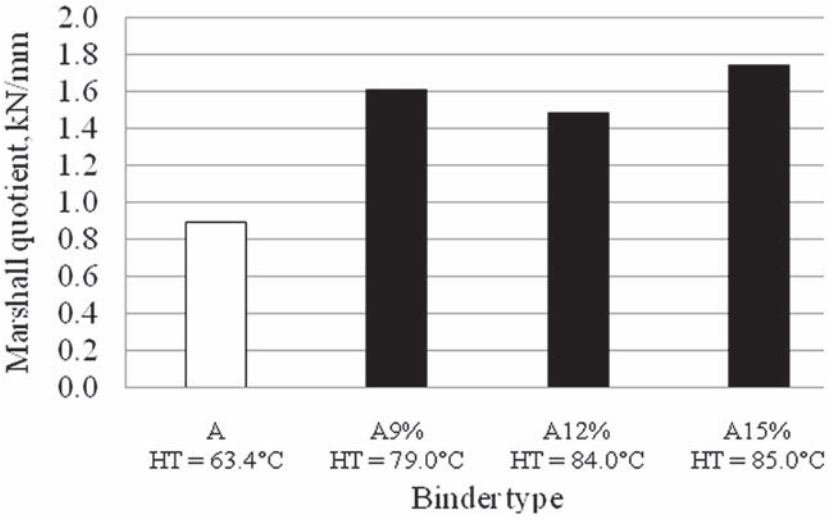

Figure 7. Marshall quotient at different rubber contents.

allowable value, because of the higher G*·sinδ at lower intermediate temperature grades where fatigue cracking is prevalent. This means that the binder has become more flexible at lower intermediate temperatures and more fatigue resistant.

To compare the performance of the modified and unmodified binders at intermediate temperatures, indirect tensile strength testing was carried out at 5 and 30°C. These temperatures are the two extreme ends of the observed intermediate temperature range in the binders tested. The results were plotted with their corresponding intermediate temperature performance grades for different binders, as shown in Figure 8. It was observed that the addition of 3% rubber caused a 42% increase in the indirect tensile strength at 30°C and a 30% increase at 5°C. As the rubber content increased from 3% to 15%, little variation was observed in the tensile strength at both test temperatures.

The more energy a pavement can absorb as it deflects before cracking, the lower the likelihood of fatigue cracking or other damage to occur (Roberts et al. 1996). Tests performed on field cores taken from the WesTrack test track sections showed that the amount of absorbed energy up to the point of failure (fracture energy) calculated from the results of the IDT strength test is an excellent indicator of the resistance of a mixture to fatigue cracking (Kim & Wen, 2002). The study showed that the results of the IDT strength test relate well with the actual field performance of a mixture, thus this test was selected to investigate the intermediate temperature performance (fatigue resistance) of mixtures in the present study. Figure 9 compares the amount of absorbed energy up to the point of failure for the indirect tensile strength tests.

Figure 3 shows that increasing rubber content causes a significant reduction in G*·sinδ, which is taken to signify an improvement in the fatigue performance. It may be observed from Figure 9 that the addition of 3% crumb rubber to binder A increased the absorbed energy by 32% and 14% for the tests conducted at 30 and 5°C, respectively. Further increasing the rubber content to 15% doubled the energy absorption at 30°C and caused a 37% increase in energy absorption when tested at 5°C.

However, although the intermediate temperature for binder A is less than binders B and C, the introduction of crumb rubber into binder A further improves (reduces) the intermediate temperature. This trend is not seen in the unmodified mixture's absorbed energy during the indirect tensile test, as is apparent from the sudden drop in energy absorption from binder B to binder A. This suggests that G*·sinδ is not a good fatigue performance indicator. Bahia et al. (2001) also questioned the validity of using G*·sinδ as an indicator of fatigue performance.

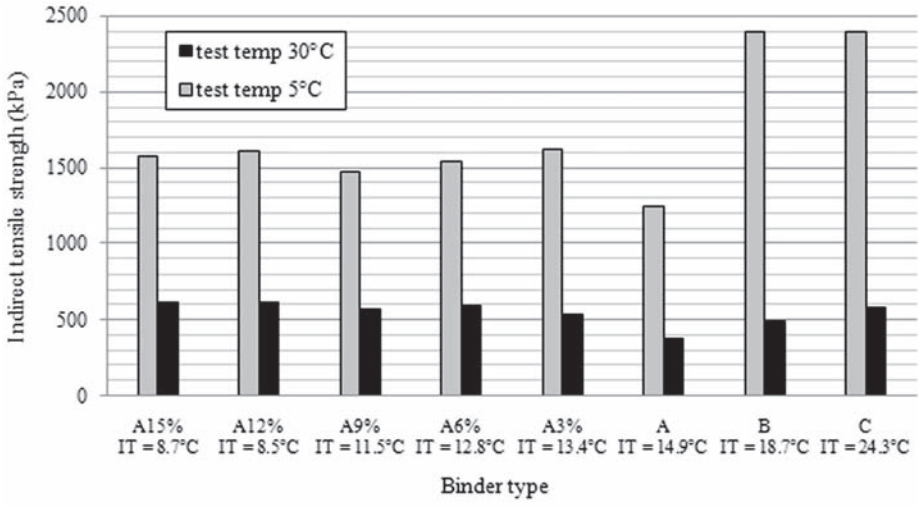

Figure 8. Variation in indirect tensile strength with different binders.

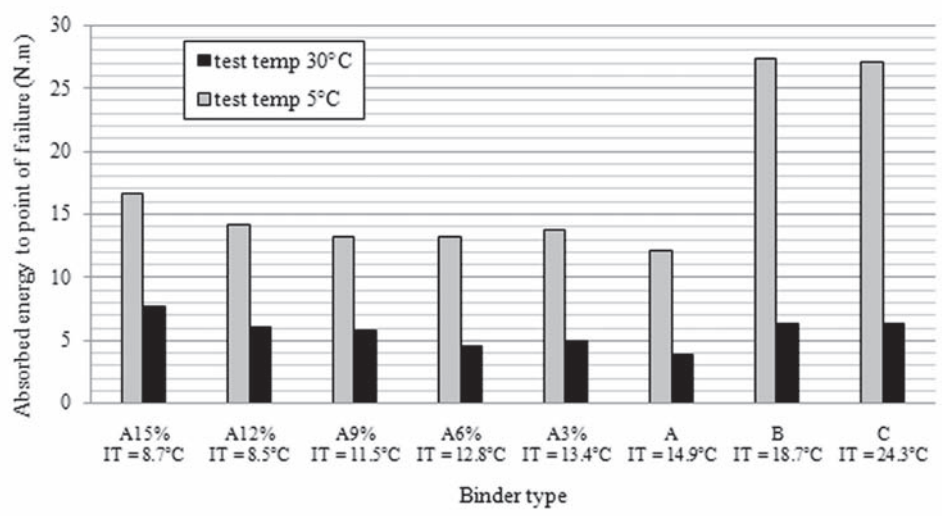

Figure 9. Absorbed energy to failure in indirect tensile strength tests.

6 FINDINGS AND CONCLUSIONS

Based on the test results and the analysis presented, the main findings of this study are:

1. Characterizing the studied binders in accordance to the Superpave performance grading specification showed that crumb rubber modification increased the high temperature performance grade while reducing the intermediate temperature grade. Both changes are favorable.
2. Crumb rubber modification caused a significant reduction in binder stiffness at low temperature. The effect of crumb rubber modification could not be seen using the Superpave performance grading criteria. Some revision in the criteria may be required.

3. The results of the unconfined static creep test showed that crumb rubber modified binders are more resistant to permanent deformation compared to unmodified base binders. Higher rubber content results in greater recovery of deformation during unloading.
4. Increasing the rubber content of the binder caused an increase in the Marshall stability and flow of the specimens.
5. Crumb rubber modified mixtures had higher energy absorption before failure during the indirect tensile strength test at both 30 and 5°C. This could lead to better resistance to both fatigue and low temperature cracking.
6. Tensile strength values measured in the indirect tensile test were unaffected by the change in binder rubber content. This was true regardless of the test temperature.
7. The change in the Superpave performance grade for high temperatures as the rubber content increased seemed to correctly reflect the behavior observed in the laboratory performance tests.
8. The intermediate temperature performance grade trend for the crumb rubber modified binders followed the observed behavior in energy absorption of the mixture in the indirect tensile test, but did not correctly reflect the decreasing energy absorption for the unmodified binders.

REFERENCES

Ahmedzade, P. & Yilmaz, M. 2008. Effect of polyester resin additive on the properties of asphalt binders and mixtures. *Const. and Build. Mater.* 22: 481–486.

Bahia, H.U. & Anderson, D.A. 1995. Strategic Highway Research Program binder rheological parameters: background and comparison with conventional properties. *Transportation Research Record 1488.* Washington, D.C.: National Research Council: 32–39.

Bahia, H.U., Davies, R. & Martinez, V. 1995. Recycling of scrap tires and plastic waste in modification of asphalt binders. In B.K. Lall & D.L. Jones, Jr. (eds.): *Transportation congress; Proc. conf., San Diego, October 22–26, 1995*. Reston, VA: ASCE Publications.

Bahia, H.U., Hanson, D.H., Zeng, M., Zhai, H., Khatri, M.A. & Anderson, R.M. 2001a. *Characterization of Modified Asphalt Binders in Superpave Mix Design.* NCHRP Report 459. Washington, DC: National Academy Press.

Bahia, H.U., Zhai, H., Zeng, M., Hu, Y. & Turner, P. 2001b. Development of binder specification parameters based on characterization of damage behavior. *Asphalt Paving Technology* 70: 442–470.

Hanson, K.R. & Anderton, G. 1993. A laboratory evaluation of recycled tire rubber in hot mix asphalt paving systems. In H.F. Waller (ed.) *Use of Waste Materials in Hot-Mix Asphalt*, ASTM STP 1193, Philadelphia: American Society for Testing and Materials.

Kim, S., Loh, S., Zhai, H. & Bahia, Hu. 2001. Advanced characterization of crumb rubber modified asphalts using protocols developed for complex binders. *Transportation Research Record 1767.* Washington, D.C.: National Research Council: 15–24.

Kim, S. & Sargand, S.M. 2003. Performance evaluation of polymer modified Superpave mixes using laboratory tests and accelerated pavement load facility. Presented at *82nd Transportation Research Board Annual Meeting, January 12–16, 2003;* http://www.ltrc.lsu.edu/TRB_82/TRB2003–001855.pdf.

Kim, Y.R. & Wen, H. 2002. Fracture energy from indirect tension testing. *Asphalt Paving Technology* 71: 779–793.

Lee, S.J., Amirkhanian, S., Putman, B. & Kim, K.W. 2007. Laboratory investigation of volumetric and rutting properties of CRM asphalt mixtures due to compaction conditions. *Transportation Research Board 86th Annual Meeting.* Paper #07-1888. Washington, D.C.: National Research Council.

Madapati, R.R., Lee, K.W. & Franco C.A., 1995. Evaluation of crumb rubber in asphalt. In B.K. Lall & D.L. Jones, Jr. (eds.): *Transportation congress; Proc. conf., San Diego, October 22–26, 1995*. Reston, VA: ASCE Publications.

Roberts, F.L., Kandhal, P.S., Brown, E.R., Lee, E.R. & Kennedy, T.W. 1996. *Hot Mix Asphalt Materials, Mixture Design, and Construction* (2nd ed.). Maryland: NAPA Research and Education Foundation.

Tabatabaee, N. & Bohlouli, S. 1997. Laboratory investigation of rubberized asphalt mixture characteristics. *4th international conference on civil engineering; Proc. conf., Tehran, Iran, May 4–6, 1997* (in Farsi).

Troy, K., Sebaaly, P.E. & Epps J.A. 1996. Evaluation systems for crumb rubber modified binders and mixtures. *Transportation Research Record 1530.* Washington, D.C.: National Research Council: 3–10.

4. Warm and cold bituminous mixtures characterization

Advanced Testing and Characterization of Bituminous Materials – Loizos, Partl, Scarpas & Al-Qadi (eds)
© 2009 Taylor & Francis Group, London, ISBN 978-0-415-55854-9

Design method for cold and warm emulsion mixtures based on links between laboratory and field

J.P. Serfass
USIRF, France

X. Carbonneau
COLAS, France

B. Eckmann
EUROVIA, France

J.P. Triquigneaux
EIFFAGE TP, France

ABSTRACT: There is evidence that the design methods for hot mixtures do not properly account for the specificities of cold emulsion mixtures. A cooperative research project has been launched in order to adequately characterize and design emulsion mixtures, either cold or warm. The approach is end-performance-oriented and therefore includes establishing relations between laboratory results and in-place behaviour.

Seven construction sites were selected, 4 with grave-emulsion, 3 with emulsion-asphalt-concrete. The materials were thoroughly evaluated and the sites are monitored since "point zero". The monitoring includes condition assessment, dry (air-cooled) coring and sampling, in situ deflection, water content, density and stiffness modulus measurements.

The fresh mixture workability has a great influence on the success of the paving operations (smooth spreading, absence of lumps, etc). Tests have been conducted using the Nynas festing facility. They have shown the influence of the aggregate internal friction, bitumen and water contents, as well as the emulsion breaking parameters. The most appropriate procedures for mixing and moulding the specimens have been defined.

Testing with Gyratory Shear Compactor appears to be an adequate method for comparing mixtures and optimizing a composition as regards its compactability. However, such tests do not provide a prediction of in-place density, which depends on local factors like substrate stiffness.

The procedure for moulding specimens for compressive tests has been modified: the moulding pressure has been reduced so that realistic densities are obtained.

A parallel has been made between accelerated curing in the laboratory and field curing, the main property evaluated being the stiffness modulus. The results show that, as regards mix stiffness, 14 days at 35°C can be assumed to correspond to 1 to 3 years in the field. The concomitant ageing of the bitumen has been assessed, and the evolution observed after accelerated curing in the laboratory is compared with the hardening that takes place in the field.

Bituminous emulsion mixtures have in many respects, a specific behaviour due to the presence of water, the chemical reactions between the minerals and the emulsifier, the microporous texture of the fresh binder (Serfass 2002a), (Serfass 2002b). Moreover, the mixture properties evolve considerably over time, due to curing and consolidation (Eckmann et al. 2004), (Triquigneaux & Brosseaud 2002). A cooperative research program has therefore been launched by the Union of the french road contractors (USIRF), in order to define a mix design method appropriate for emulsion mixtures.

Keywords: Design method—Emulsion mixtures—End-performance—Curing

1 TESTING PROGRAM

The basic principle of the approach is to establish links between site behaviour and laboratory results, so as to finalize an end-performance design method. For this purpose, seven field sections have been monitored and the materials properties were thoroughly investigated in the laboratory, including their evolution over curing periods.

The program encompasses two types of emulsion mixtures: grave-emulsion (GE) and emulsion asphalt concrete (EAC). Three reference sections of GE were laid in 2004 and have been monitored since. One test section of GE studied and constructed in 1997 has also been monitored. In parallel, three sections of EAC (one laid in 2004, the others in 2005) have also been followed.

Each mixture was subjected to extensive laboratory evaluation, comprising the following tests: mechanical mixing, rating of the coating percentage, workability, compactability, accelerated curing, compressive strength, water sensitivity, rutting, and stiffness modulus. In addition, the bitumen was extracted after certain curing periods and the characterized. Due to lack of space in the present paper, only the properties printed in bold above are presented and discussed hereafter (as well as the bitumen characteristics).

Site monitoring includes core sampling (dry process with air cooling), water content, density and modulus measurements, bitumen extraction and characterization.

2 WORKABILITY

The workability of cold mixtures depends on a number of factors: aggregate internal friction, water content, bitumen consistency and, above all, the breaking behaviour of the emulsion. As from the end of mixing, the material's workability varies in time. There is therefore a delay of workability, after which the mixture will be difficult, if not impossible, to place and compact.

2.1 *Description of the equipment and test procedure*

Mixture workability can be assessed using the Nynas facility. The basic principle of the test is to measure the maximum force developed when a given mass of the loose mixture is subjected to a shearing effort. The facility (figure 1) is similar to a shear box, as used in soil mechanics.

Immediately after mixing, the loose material (about 11 kg) is moulded into a rectangular box and trimmed to a height of 100 mm. Two opposite half walls (50 mm high) are then removed so as to allow the volume above the median horizontal plane to be pushed at a

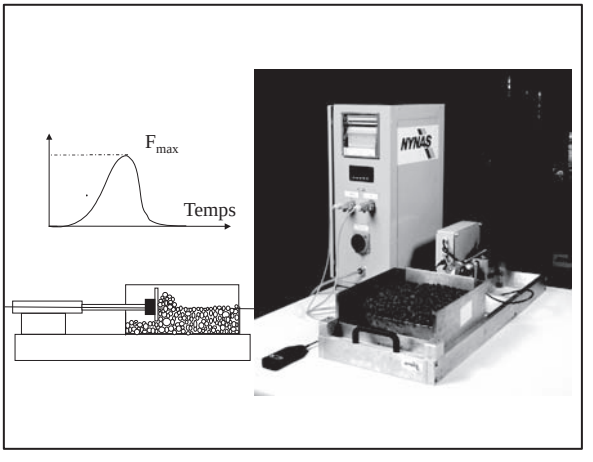

Figure 1. Workability test using the nynas facility.

constant speed of 1 cm/s over a 220 mm length (this speed is close to that of a paver in action). The force exerted is recorded over time. Its peak value, called "cohesive strength", is an indicator for the mixture workability. Several such boxes are prepared in advance and stored in an oven for variable lengths of time under controlled temperature and hygrometry. This allows to determine the evolution of cohesion over storage time and as a function of climatic conditions (Delfosse et al. 2002).

2.2 *Workability observed in the field. Correlation with laboratory results*

Grave-emulsions have practically never shown any workability problem in situ. Such good workability is attributed, in particular, to the fact that, in grave-emulsions, the bitumen is fixed preferably over the finer aggregate fraction. The resulting material thus contains a very rich mortar, in which the coarser aggregates are embedded, the rich mortar providing flexibility and workability.

In contrast, emulsion asphalt concrete mixtures have a much more uniform bitumen coating over all granular fractions and could be, in some cases, prone to workability problems. As regards the three EAC's chosen in the present project, they were laid and compacted without any difficulty, thanks to various know-how applied, i.e. emulsion formula, sequential coating or aggregate precoating.

In general, the feedback from the field shows that mixtures having a cohesive strength lower than 250 Newton are satisfactory as regards workability.

2.3 *Sample moulding procedure*

One important issue is the method of preparation of the sample that will be subjected to the workability test. Two procedures can be followed.

The first, referred to as "standard", comprises the following steps: mixing, dumping the fresh mixture into a small heap, keeping it for some time, loading it up to the upper part of a rectangular steel shaft on two horizontal half doors, opening the doors, thus making the material fall into the mould placed at the bottom of the shaft (falling height 1 m). This "standard" procedure is supposed to simulate the following real-life operation: stockpiling, loading, hauling, dumping from the truck, placing (as pushed by grader blade or finisher augers).

The second, referred to as "modified", consists in discharging the fresh mixture directly from the mixer into the mould. This procedure corresponds to the direct loading from the manufacturing plant into a haul truck.

The "standard" procedure closely replicates the most common method used in the field, but it has the disadvantage of requiring several manual handling operations, with the inherent risk of deviation. The "modified" procedure has the advantage of being simple and fully mechanized, but it corresponds to a method not frequently used in the field. Moreover, it is practicable only with horizontal twin-shaft laboratory mixers.

Whatever the procedure used, it is of the utmost importance to respect, in the laboratory, the lengths of time that the construction operations are likely to take, or to evaluate their effects on the mixture cohesion, so as to define practical guidelines to ensure sufficient workability.

3 COMPACTABILITY

3.1 *Gyratory shear compactor tests*

The compaction test on both GE and EAC were performed using LCPC Gyratory Shear Compactor (GSC) Mark 1 or 2. The first GSC tests were aimed at determining the optimum moisture content for each mixture, the type of emulsion most suitable for the given aggregate having been previously chosen according to local experience. GSC densification tests were then carried out at optimum moisture content, the results of which are shown in tables 1 and 2 below.

Table 1. Air voids in grave-emulsion (%)—GSC tests and field monitoring.

Reference section		RD 437	RD 10	RD 79	RN 126
GE thickness (mm)—average (range)		50	75 (60–100)	70 (50–100)	90 (80–120)
	V 10	22.3	23.2	25.4	23.9
Gyratory	V 50	16.9	16.9	19.2	18.4
Shear Compactor	V 100	15.0	14.9	17.0	16.5
V_x = air voids at x gyrations	V 200	13.4	13.2	15.3	15.0
	Immediate	13.1	20.0		17.0
In-place	Short term		21.1 (6 months)	17.0 (14 months)	14.5 (6 months)
voids	Middle term	12.7 (22 months)	19.0 (27 months)	17.1 (25 months)	
(average)	Long term	–	–	–	14.5 (7 years)

3.2 *Field compaction*

3.2.1 *Grave-emulsion sections*

The air voids measured on core samples taken at different ages, using a gamma –ray bench, are given in table 1.

All field densities were measured on core samples, using a nuclear gauge (gamma-ray bench), except for one set which was measured in-place, using a Troxler facility. The results obtained with the latter (portable device) are not always in line with those obtained in the lab, with the gamma-ray bench.

The GE compaction was carried out as follows:

- RD 437 1 vibrating roller VT2 (4 passes) + 1 pneumatic-tyred roller (3 t/wheel –6 passes)
- RD 10 1 VT2 (2 to 4 passes) + 1 pneumatic-tyred roller (3 t/wheel –12 passes)
- RD 79 1 compound steel-wheel/pneumatic roller (4 passes flat + 5 passes vibrating)
- RN 126 1 vibrating roller (16 passes) + 1 pneumatic-tyred roller (3 t/wheel –20 passes)

The compaction energy was practically the same on RD 437 and RD 79. It was higher on RN 10, because of the weaker substrate and much higher on RN 126, which is a major highway. The analysis of the compaction results shows the major influence of the existing pavement stiffness. Indeed, on RD 437, the GE was placed on a strong pavement (characteristic deflection $m + 2\sigma \sim 30.10^{-2}$ mm) and low air voids were immediately reached. On the contrary, the RD 10 pavement was extremely flexible (characteristic deflection in the region of $300 \cdot 10^{-2}$ mm), making the compaction partly ineffective, hence initial air voids over 20%. It can be seen that, in the laboratory, the densification curves of both GE are almost identical.

Comparing the two GE's of RD 79 and RN 126 also shows similar GSC densification curves, whereas the in-place voids are significantly different. The lower air voids of RN 126 result from higher compacting energy and heavier traffic (the characteristic deflection levels are identical on both roads: $\sim 120 \cdot 10^{-2}$ mm).

3.2.2 *Emulsion asphalt concrete sections*

The air voids measured on core samples and those recorded during the GSC tests are shown in table 2.

As for the GE's, no relationship can be established between any given level of air voids in GSC samples and short or middle-term site voids.

3.2.3 *Evolution of in-place air voids*

Grave-emulsion: On RD 437, a high degree of compaction was reached during construction, thanks of the stiff substrate. Virtually no further densification has occurred afterwards. On RN 126, the "final" percentage of air voids was attained after only 6 months, due to the

Table 2. Air voids in emulsion asphalt concrete (%)—GSC tests and field monitoring.

Reference section		RD 15	RD 60	RD 21—2004	RD 21—2005
EAC—average thickness (mm)		45	60	35+	35+
	V 10	24.5	25.7	24.2	23.9
Gyratory	V 50	18.7	19.7	18.6	18.2
Shear	V 100	16.7	17.5	16.8	16.2
Compactor					
V_x = air voids at x gyrations	V 200	15.0	15.5	14.4	14.5
In-place voids	Very short term	21.1 (3 months)	19.5 (2 months)	18.1 (18 months)	16.9 (4 months)
(average)	Middle term	20.0 (16 months)	19.8 (16 months)	12.9 (33 months)	13.2 (21 months)
	ditto				

combination of a hot summer immediately after the GE was placed and heavy traffic. On the two other sections, the densification is very limited or nil (the traffic is light).

Emulsion asphalt concrete: The voids have remained high on RD 15 and RD 60. A marked densification has taken place on both subsections of RD 21, thanks to the presence of a small amount of fluxing oil in the bitumen, which facilitates the mixture densification under light traffic.

3.2.4 *Recommended use of the GSC*

The Gyratory Shear Compactor test does not allow to predict the field density. Indeed, the stiffness (or reaction) modulus of the underlying layer has a major influence on the mixture densification. Other local factors, such as traffic and climate, may also have a strong impact. Nevertheless, the GSC remains a very useful tool for comparing and optimizing mixture formulas in terms of aggregate gradation, binder and moisture contents.

4 COMPRESSIVE STRENGTH—WATER SENSITIVITY

4.1 *Duriez compression tests*

The NF P 98-251 french standard (Duriez test for asphalt mixtures) has long been used for emulsion mixtures. In its initial version, it embodies the same static moulding procedure as for hot mixtures, that is a moulding force of 60 or 120 kN (depending on aggregate maximum size and mould dimensions) applied for 5 minutes. This procedure gives high densities, largely above those likely to be reached in situ, e.g. 9.5 to 12% for GE's and 10.5 to 14% for EAC's, to be compared to the figures in tables 1 and 2. Such high compaction degrees are due to the long static moulding time, which produces the same effect as high temperature.

Research and site experiments have led to modify the moulding procedure, dividing by 3 the moulding force (20 or 40 kN). The modified procedure gives realistic densities; of the same order as those obtained in the field, i.e. 14 to 17% for GE's and 16 to 21% for EAC's (see tables). The standard has then been supplemented accordingly. However, it is emphasized that the field air voids always depend an local factors, such as the substrate stiffness, and that the Duriez test alone in not sufficient for their prediction.

4.2 *Water sensitivity*

Duriez specimens were immersed for 7 days in water at 18°C after varied moulding and curing procedures:

A: 14 days in air 18°C–50% RH (standard moulding force);
B: 14 days in air 18°C–50% RH (reduced moulding force);
C: 14 days in air 35°C–20% RH (reduced moulding force).

The water sensitivity is characterized by the ratio compressive strength after immersion (r) over compressive strength "dry" (R). The results show that the ratio r/R is only slightly reduced (0 to 10%) when the moulding force is divided by 3. In contrast, it significantly increases after curing 14 days at 35°C. It can therefore be concluded that water sensitivity depends more on the coating quality (binder consistency and bond with the mineral aggregate) than on the percentage of air voids.

5 STIFFNESS MODULUS

A number of stiffness modulus measurements have been carried out. Two test procedures were used:

- complex modulus, the cylindrical specimen being subjected to sinusoidal compression (Carbonneau et al. 2005).
- indirect tensile modulus, with diametral pulse loads applied to a cylindrical specimen (Olard et al. 2005).

The reference modulus considered is the value at either 15°C–10 Hz or 15°C–124 ms. However, on fragile mixtures (not fully consolidated, high voids), the indirect tensile modulus had to be measured at 15°C–20 ms or 10°C–124 ms.

When trying to link laboratory study results and field results, a key point is the air voids content. In order to compare design and field modulus, it is essential to allow for the considerable effect of air voids on the mix rigidity 6. To this end, the modulus values obtained on lab-made specimens were "converted" or "adjusted" as explained below. Based on the experience gained in other research and design, the following "adjustments" have been made:

- Modulus (15°C–10 Hz) = modulus (10°C–124 ms)
- Modulus (10 or 15°C–20 ms) = 1.7 modulus (10 or 15°C–124 ms)
- One point (%) of air voids → 200 MPa at 15°C
- One point (%) of air voids → 350 MPa at 10°C
- Decrease in modulus between 10 and 15°C : as from numerous data available.

Field modulus was measured on samples obtained by dry, air-cooling coring. For the sake of clarity, all the moduli below are expressed in values at 15°C–124 ms.

5.1 *Grave-emulsion*

On the grave-emulsion of RD 79, accelerated curing at 35°C–20% RH was continued for 90 days (figure 2). The specimens subjected to curing were GSC-moulded and had therefore a large volume, which may be one cause of the moderate hardening observed.

Table 3. Grave-emulsion RD 437 and RD 10—Modulus measurements.

	Laboratory study			Field monitoring		
Site	Air voids	Standard curing 14 days–18°C–50% RH	Accelerated curing 14 days–35°C–20% RH	Air voids	Age	Modulus
RD 437	15% 13% 11%	1,200 MPa 1,250 MPa 1,450 MPa	1,600 MPa 1,800 MPa 1,950 MPa	12,7% (11.9–13.2)	22 months–2 summers	1,800 MPa
RD 10	12–13% *19%**	2,050 MPa ~1,200 MPa*	3,300 MPa ~2,000 MPa*	21,7% 19,3%	6 months–ε summer 27 months–2 summers	1,150 MPa 2,400 MPa

Much higher moduli were measured on field samples cored from RD79: 3,450 MPa after 14 months (1 summer) and 4,200 MPa after 25 months (2 summers), both for 17% voids. These values are unusually high for GE in the middle term. It was also observed that, for this particular GE, the laboratory accelerated curing has caused less bitumen hardening than site curing (effect of the specimen's volume?). This point is being investigated. On RN 126, samples were cored 82 months (7 summers) after construction. An average modulus of 5,500 Mpa was measured with air voids close to 14.5%. This result is in line with those obtained elsewhere on grave-emulsions in the long term (7 to 10 years).

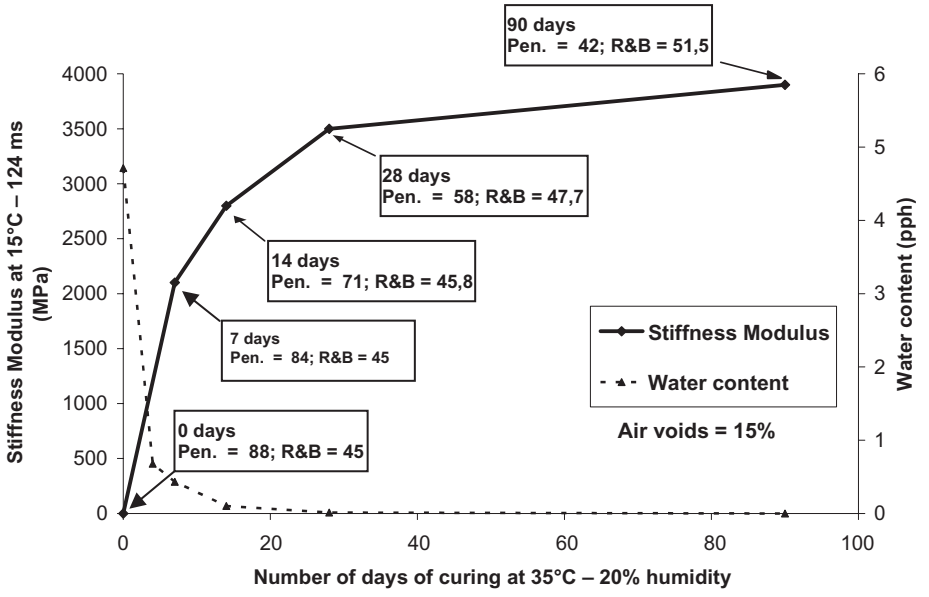

Figure 2. Grave-emulsion RD 79—Stiffness Modulus-Accelerated curing.

Table 4. Emulsion asphalt concrete—Modulus measurements.

	Laboratory study			Field monitoring		
Site	Air voids	Standard curing 14 days–18°C–50% RH	Accelerated curing 14 days–35°C–20% RH	Air voids	Age	Modulus
RD 15	22,5% *12,5%**	1,600 MPa *~2,200 MPa**		21,2% 19,5%	16 months–2 summers	2,300 MPa 2,400 MPa
RD 60	18%		1,750 MPa	20,7% 19,0%	16 months–2 summers	2,300 MPa 2,200 MPa
RD 21 2004				18,1% 12,9%	18 months–2 summers 33 months–3 summers	2,400 MPa 3,100 MPa
RD 21 2005	14%		1,100 MPa (60 days–35°C –20% RH)	16,9% 13,2%	4 months–no summer 21 months–1 summer	n.s. 1,100 MPa

The above results confirm the major influence of the air voids on the stiffness modulus. In the field, the number of summers appears to be the principal factor of mixture curing. In the laboratory, accelerated curing at 35°C–20% RH appears to be suitable for predicting the actual site curing, 14 days corresponding roughly to 2 summers. The standard procedure (14 days–18°C–50% RH) provides an approximation of the fresh mixture stiffness (Carbonneau et al. 2002), (Serfass et al. 2004).

5.2 *Emulsion asphalt concrete*

The EAC of RD 21 contained some fluxing oil, which softens the mixture in its early stage, hence facilitating its densification over time and under light traffic, as shown in table. Again, the number of summers appears to be a key factor for the field curing. In parallel, a specific research is under way to define the suitable curing procedure for mixtures containing a fluxing agent.

6 BINDER EVOLUTION

The bitumen was extracted from the cores taken at different ages and characterized by its penetration and Ring and Ball softening temperature (R&B).

Contrary to a generally a accepted idea, there is evidence of steady, pronounced in-place hardening of the bitumen in grave-emulsion (figure 3).

This can be attributed to the comparatively high air voids and, most probably, to the uneven distribution of the bitumen over the different granular fractions. Indeed, as the bitumen goes preferably in the mortar fraction, the film thickness on coarse aggregate is very thin, hence its tendency to age rapidly. The probable difference in hardening between the coarse and fine fraction should be further investigated.

There is also evidence of the retarding effect of top sealing the grave-emulsion. Indeed, the GE of RD 437 was covered with a thin hot mix 12 months after construction; its binder has remained softer than those of the uncovered GE's. On RN 126, the difference between the unsealed and sealed sections is obvious (the latter received a microsurfacing 1 year after completion).

The hardening of the binder of emulsion asphalt concrete appears to be much less pronounced than that of GE, e.g.:

– RD 15: initial: 83 dmm–46.0°C 16 months: 49 dmm–52.2°C
– RD 60: initial: 86 dmm–44.2°C 16 months: 53 dmm–48.2°C

Table 5. Grave-emulsion—Characteristics of the binder at different ages.

RD 437	Age	Initial			22 months
	Pen at 25°C (dmm)	76			40
	R&B (°C)	46.5			52.6
RD 10	Age	Initial	6 months	13 months	27 months
	Pen at 25°C (dmm)	85	45	36	26
	R&B (°C)	46.4	52.8	55.2	56.4
RD 79	Age	Initial	2 months	14 months	25 months
	Pen at 25°C (dmm)	88	58	34	23
	R&B (°C)	45.0	51.2	52.2	56.7
RN 126	Age	Initial		7 years-sealed	7 years-unsealed
	Pen at 25°C (dmm)	82		14	7
	R&B (°C)	46.0		65.0	75.0

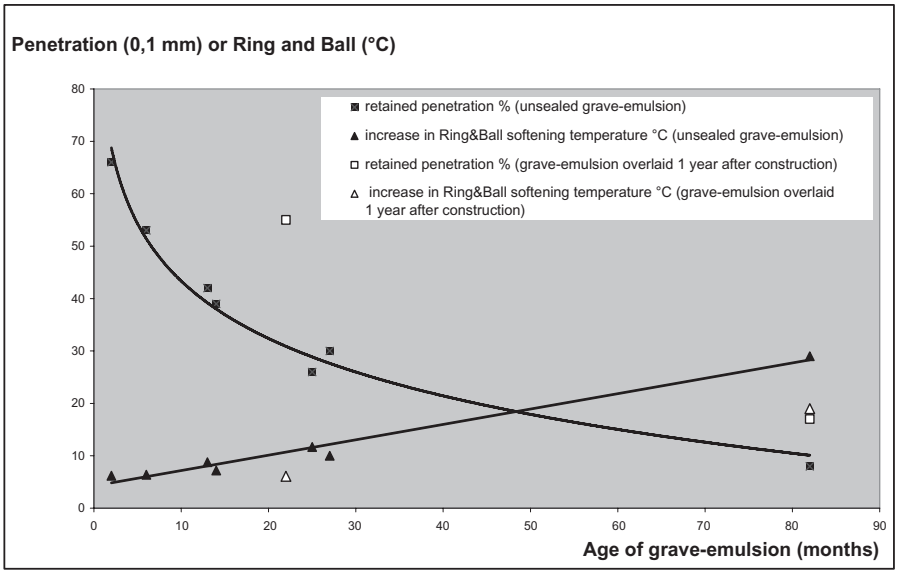

Figure 3. Grave-emulsion-Bitumen characteristics over time.

However, no conclusion can be drawn to date, as research on this issue is not completed. It is pointed out that some questions remain unanswered at this stage. One is how much of the hardening takes place during the emulsifying and mixing phases. Another question is the impact of the extraction on the bitumen characteristics. On the other hand, some tests have shown a difference between the effects of accelerated curing in the laboratory and those of field aging. All these issues are being investigated.

7 SITE CONDITIONS

It is remarkable that, despite the bitumen hardening, none of the sections monitored exhibits any cracking, nor any ravelling (no rutting either, logically). The only beginning of deterioration is some fine cracking, widely spaced, affecting the unsealed sub-section of RN 126, 7 years after construction. The main part of this section, which was covered with a microsurfacing one year after it was placed, is in perfect condition.

More generally, it should be borne mind that the overall site performance of emulsion mixtures similar to those investigated here is fully satisfactory. Grave—emulsions have behaved as flexible materials over long service life periods. Emulsion asphalt concrete mixtures have been used for wearing courses since 1992, with no sign of any deterioration.

8 CONCLUSION

The design method specific to emulsion mixtures is being gradually supplemented and adjusted. Links between laboratory and site are being established, as part of and—performance approach (Serfass et al. 2006). The present research has confirmed the satisfactory field behaviour of both grave-emulsion and emulsion asphalt concrete mixtures. The project has been extended, as a new joint project has recently started, for which contractors and state engineers are cooperating.

REFERENCES

Carbonneau, X, Henrat, J.P, Letaudin, F. & Poirier, J.E. 2002. *Mechanical characteristics of emulsion cold mixes.* RGRA n°807, June 2002.

Carbonneau, X, Yvinec, B, Legal, Y. & Poirier, J.E. 2005. *Mesure du module en compression diamétrale*. RGRA n°836, February 2005.

Delfosse, F, Pierre, M.L, Quinton, C. & Eckmann, B. 2002. Bituminous emulsion for cold mixes: the Nynas workability test. *3rd World Congress on Emulsions*. Lyon, September 2002.

Eckmann, B, Delfosse, F. & Conan, J. 2004. Cold bituminous mixtures for surface Courses. *3rd Eurobitume and Eurasphalt Congress*. Vienna, May 2004.

Olard, F, Noel, F. & Loup, F. 2005. *Mesure du module en compression diamétrale des enrobés bitumineux.*. RGRA n°844, November 2005.

Serfass, J.P. 2002a. Emulsion cold mixes: for a new design method. *Revue Générale des Routes et Aérodromes.* RGRAn°808. July–August 2002.

Serfass, J.P. 2002b. Emulsion cold mixes. Specific features and a new design method. *3rd World Congress on Emulsions. Symposium on emulsion-based cold mixes*. Lyon, September 2002.

Serfass, J.P, Henrat, J.P. & Carbonneau, X. 2004. Evaluation of cold mixes performance in the short and long term. *3rd Eurasphalt and Eurobitume Congress*. Vienna, May 2004.

Serfass, J.P, Carbonneau, X, Eckmann, B. & Triquigneaux, J.P. 2006. From laboratory to full-scale worksite: predicting the behaviour of materials treated with bitumen emulsion. *4th World Congress on Emulsions.* Lyon, October 2006.

Triquigneaux, J.P. & Brosseaud, Y. 2002. Méthodologie d'étude et de caractérisation des graves-émulsion structurantes. *Bilan de la recherche commune. Direction des Routes/USIRF.* RGRA n°808, August 2002.

Advanced Testing and Characterization of Bituminous Materials – Loizos, Partl, Scarpas & Al-Qadi (eds)
© 2009 Taylor & Francis Group, London, ISBN 978-0-415-55854-9

Fundamental property evaluation of styrene monomer modified warm-mix asphalt concrete

Ilho La, Min Y. Ryu, H.H. Kim, Kyongae Ahn, Young S. Doh & Kwang W. Kim
Department of Regional Infrastructures Engineering, Kangwon National University, Chun Cheon, Republic of Korea,

ABSTRACT: Recently, many warm-mix asphalt (WMA) mixtures are produced at approximately 120°C, which is 40°C lower than normal HMA processing temperature. This heat reduction is considered as a big achievement in asphalt paving industry. They used normal asphalt binders and WMA additives to make the mixes less at warm temperatures. However, this paper deals with a different WMA concept by using a styrene monomer (SM) for melting down the asphalt, making liquid asphalt beforehand. The objective of this study is to make the SM-modified WMA mixtures at 95°C, which is more than 60°C reduction of HMA temperature, and show strength properties of WMA concrete, as a new asphalt technology, in comparison with normal HMA mixes at 160°C or higher. The 6% of SM was selected as the optimum content at which the mix was blended well using a normal lab mixer and compacted well by gyratory and roller-press compactors at 95°C. Various property test results of the 6% SM-modified bitumen mixture were similar to those of conventional bitumen mixtures. Therefore, it was possible to use SM-modified bitumen for WMA production at much lower temperature than normal WMA.

1 INTRODUCTIONS

If asphalt mixture can be produced using lower heat without quality loss, corresponding advantage will be not only just energy saving, but also reduced emissions, fumes, odors and cost reduction. Therefore, processing asphalt mixture by lower heat is a major issue in the asphalt paving industry, making a less hot-mix or warm-mix asphalt (WMA) mixture. The Sasol wax, Aspha-min zeoliet, Evotherm emulsion, etc are currently available additive materials for producing low-emission WMA mixtures (Cervarch 2003, Kuennen 2004, McKenzie 2006).

Since the asphalt changes its characteristics by the temperature, the workability of asphalt-aggregate mixture will be poor if the processing temperature is drop 20°C or more from 160°C. Hot temperature ensures that the aggregate is completely dry so the asphalt will be able to coat the aggregate in addition to making sure that the hot-mix asphalt (HMA) has a suitable workability. To produce the normal HMA at 160°C or higher, in general, the aggregate and bitumen is heated at least 10°C or 15°C higher than 160°C to cover loss of heat during the process. Therefore, securing high temperature above a certain level is an important factor in controlling quality of HMA pavement.

The WMA uses additives for reducing stiffness of binder at approximately 110°C–130°C, which is approximately 30°C–50°C lower than conventional HMA processing temperature. However, this paper deals with a different warm mix concept by using a monomer for making liquid asphalt beforehand. A styrene monomer (SM) was used for dissolving the bitumen at 90°C and aggregates were heated at 110°C. The objective of this study is to make the SM-modified WMA mixtures at 100°C or lower, which is more than 60°C reduction of HMA, and to evaluate engineering properties of WMA concrete.

2 MATERIALS AND METHODS

The AP-5 (penetration grading of 60–80 at 25°C) was used as the base bitumen and for conventional HMA for control. The material used for liquidizing base asphalt by pre-mixing is a styrene monomer (SM). The SM is a colorless oily liquid with an aromatic odor. It is used in making polystyrene plastics, protective coatings, polyesters, resins, and as a chemical intermediate. The SM-modified bitumen was prepared by slowly adding 6, 7 and 8% by weight of total binder into the heated base asphalt at 90°C, while stirring binder by a homogenizer. The AIBN (azobisisobutyronitrile: $C_8H_{12}N_4$), which is a compound, often used as a foamer in plastics and rubber and as radical initiator, was used as initiator of SM polymerization.

A polymer-modified asphalt (PG76-22) was used for comparison purpose. The PG76-22 binder, which is commercially available in Korea, is known to be modified using an SBS and the content of it is unknown. The PG76-22 mixture was produced in the laboratory at 175°C, while the conventional HMA mixture using AP-5 was produced in the laboratory at 160°C.

A source (Gneiss) of 13 mm and 19 mm aggregates was used for dense-graded asphalt mixtures. Screenings of the same source and a limestone powder were used as fine aggregate and mineral filler, respectively. The 100 mm diameter specimen was prepared by using 100 gyration of a Superpave gyratory compactor (SGC) based on the specification of the Ministry of Homeland and Maritime Affairs, Korea (Interim guide… 2008). The aggregate, which was heated at 110°C for over four hours for eliminating moisture, was mixed with SM-modified binders to produce warm-mix asphalt (WMA) mixtures at approximately 95°C. The optimum binder content (OBC) was determined by following criteria; 4% of air void, 70%–85% of voids field with asphalt (VFA), the highest deformation strength (S_D), and 14% and 13% of void in mineral aggregate (VMA) for 13 mm and 19 mm, respectively.

The deformation strength (S_D) was measured for each mixture at 60°C. It is known to have a good correlation with rut potential of bitumen mixtures, even though it is measured by a static loading. The R^2 values were greater than 0.75 in the regression of S_D with well-known rut test results, such as wheel tracking (WT) and asphalt pavement analyzer (APA) tests (Kim et al. 2004, 2006, Doh et al. 2007, Park et al. 2007a, Kim et al. 2008). The repeatability of S_D test results in terms of R^2 was 0.8069 and that of WT was 0.8172 (Kim et al 2008). S_D is adopted as one property in Korea mix design criteria, explained previously (Interim guide… 2008).

The S_D test uses a loading head which simulates a static tire making a circular imprint on the pavement (Figure 1). The deformation process consists of an initial consolidation and steady depression which is leading to shear movement. Cracks are then initiated at peak load and propagated at tangential direction as a sign of failure. Therefore, it is an engineering property representing a static strength against vertical compressive and shear deformation of asphalt concrete at high temperature.

Figure 2 illustrates the bottom edge of loading head being pushed down into asphalt mixture at the depth of y. When it is pressed down into the asphalt mixture, the diameter ($D–2r + 2x$) and the cross section area [$A= \pi(D–2r + 2x)^2/4$] at depth y change as a function of y. The "A" is the projected cross section area of contact to the surface when the loading head is down at depth of y from the specimen surface. The maximum load (P) and the deformation (y) at maximum load point together with the diameter (D) and edge curvature radius (r) of loading head were the variables of the strength. The D and r were determined as 40 mm and 10 mm, respectively, by later studies (Kim et al. 2004, 2006, Doh et al. 2007). From the load-deformation curve, the P, and y were read and used for calculation of S_D by Equation (1). The test is designated as "Kim Test" and briefly introduced in this paper and details are given in elsewhere (Kim et al. 2002, 2003, 2004a, 2004b, 2005, 2008, Doh et al. 2007).

$$S_D = \frac{0.32\,P}{[10 + \sqrt{20y - y^2}\,)]^2} \tag{1}$$

in which, S_D = deformation strength in pressure unit (MPa), P = maximum load (N) at failure, y = vertical deformation (mm) for $y \le r$. If $y \ge r$, then $y = r$.

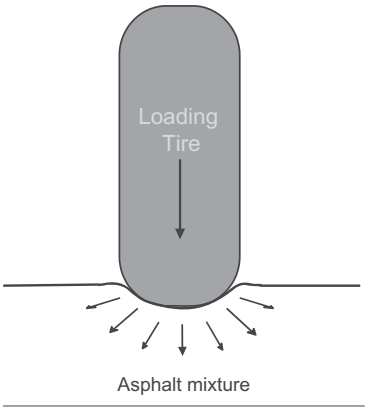

Figure 1. Tire depression on pavement surface.

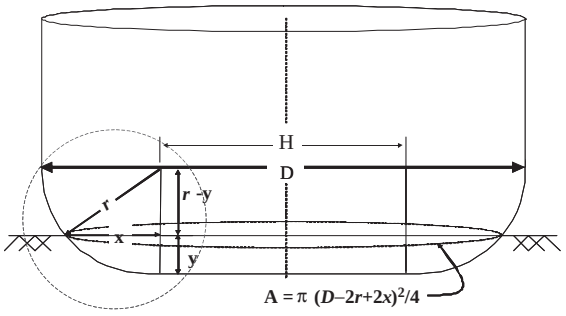

Figure 2. Details of loading head edge.

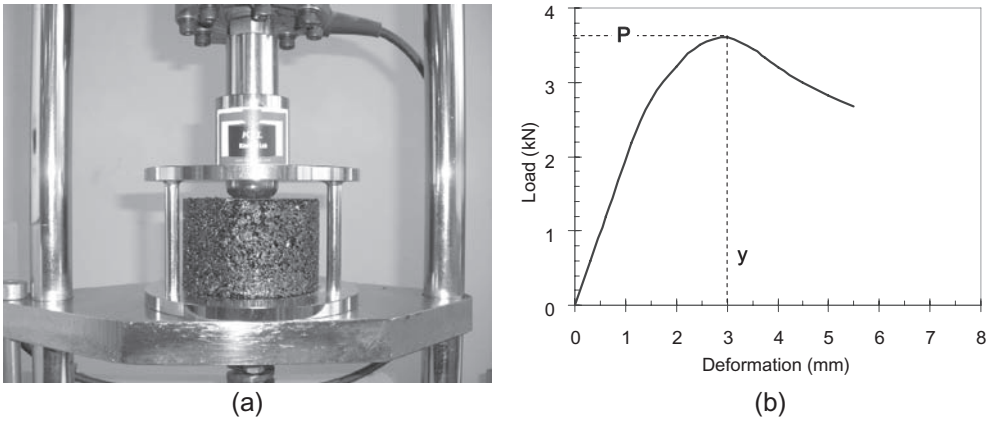

Figure 3. Illustration of (a) S_D test setup and (b) a load-deformation curve.

Figures 3 (a) and (b) show the S_D test setup and a load-deformation curve from the test, respectively. Once the specimen is prepared at the air void of 4% ± 0.5%, it is submerged into the 60°C water for 30 minutes before applying a vertical static load through the loading head at the top center of the specimen at the speed of 30 mm/min. The strength calculated by Equation (1) is defined as the strength measured against the static vertical deformation. Due to the variable y in the denominator of Equation (1), using this equation results in that the lower the deformation (y), the stronger the S_D, under the same load (P).

Wheel tracking test was performed at 60°C on the selected SM WMA, and its result was compared with those of conventional HMA and PG76-22 mixtures. A slab specimen (30.5 cm × 30.5 cm × 6.2 cm) was prepared at OBC using a roller-press compactor, with target air voids of 4% ± 0.5%. Once a slab was made, physical properties were measured. If the air void was out of 4% ± 0.5% range, the specimen was discarded and made again. It was then kept at 25°C for 24 hours before being cut into two pieces for WT test twice. The diameter and width of steel wheel were 200 mm and 50 mm, respectively. The bottom plate, on which a slab is fixed, moves 200 mm distance back and forth at the speed of 40 cycle/min or 80 pass/min. The depth of rut was measured using an LVDT and recorded from the start to end for 90 minutes.

The indirect tensile strength (ITS) was also tested at 25°C with the loading speed of 50 mm/min. Marshall Stability was also measured for each mixture at 60°C.

3 RESULTS AND DISCUSSIONS

The binder modified by 6, 7 and 8% of styrene monomer (SM) was a thick viscous material at ambient temperature (25°C), but became a soft liquid at 90°C. An initiator, AIBN, was added into the SM modified binder-aggregate mixture in three contents, 0, 0.5 and 1.0% by weight of styrene, when blended in a mixer. The mixture was blended for one minute by a lab mixer and stored for one hour for simulating short-term aging in the oven which is kept at 95°C. Following one hour storing, the mixture was compacted using a Superpave gyratory compactor (SGC) for making the 100 mm diameter specimen for S_D test. The binder contents determined were 5.4% and 4.8% for 13 mm and 19 mm aggregate, respectively.

The specimen was kept at room temperature for one day before measuring physical properties, such as densities, air void, VFA and VMA, and then kept another day in an environmental chamber at 25°C before strength test. The SM-modified mixture was well blended by a normal laboratory mixer and workable for process and compaction in the laboratory at 95°C. If air voids of any specimen was out of 4% ± 0.5% range, the specimen was discarded and made again.

Figure 4 shows S_D of SM-modified warm-mix asphalt (WMA) concretes by various treatments. The control mixtures (the solid black bars at 0% SM and 0% AIBN in each aggregate size in the figure) are conventional bitumen (pen. 60–80) concretes prepared at 160°C. The other mixtures are SM-modified WMA concretes prepared at 95°C.

From this result, it was shown that three levels of SM contents did not make any significant difference in S_D values, indicating the 6% is high enough content for liquidizing the normal bitumen for blending with aggregates at 95°C. This is a half of the MMA (methyl methacrylate) content, which was previously selected for another WMA study (Park et al 2007b). It was also shown that the mixture without AIBN (0%) showed the highest S_D values throughout the test, showing no AIBN effect for improving strength, probably due to inhibition effect of asphalt. The AIBN initiates polymerization of SM well if it is added into pure SM. But since SM is blended into asphalt, the polymerization of SM seems to be inhibited by the asphalt.

The S_D values of the 6% SM without AIBN were comparable to those of conventional bitumen mixtures (control) in two aggregate sizes. Therefore, the 6% of SM without AIBN (0%)

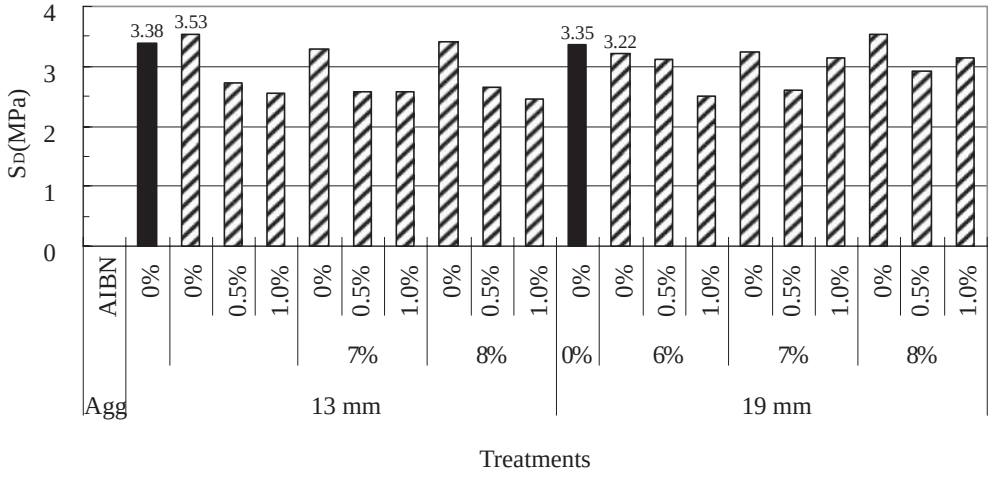

Figure 4. Comparison of S_D by styrene monomer (SM) and initiator (AIBN) contents for two-size gneiss aggregate-bitumen mixtures.

was selected as optimum warm-mix bitumen combination for later study. Since the S_D values of the controls and SM 6%-modified warm-mix asphalt (SM6-WMA) concretes were similar level in both 13 mm and 19 mm, it is an important finding that the bitumen mixture could be produced at 95°C by adding 6% of SM without strength loss. Since this temperature level is 65°C lower than the normal HMA processing temperature, more engineering properties of the SM6-WMA mixtures, Marshall Stability, indirect tensile strength and wheel tracking (WT) resistance were investigated in comparison with HMA mixtures.

In Table 1, comparing OBC values which were determined by respective mix design for each aggregate and binder combination, the SM6-WMA mixtures do not need higher binder content than normal bitumen mixes even though it is processed at 95°C. The Marshall Stability of SM6-WMA concrete satisfied the mixture stability of 7.5 kN, the requirement for all road class pavements by the MS-2 of the Asphalt Institute. The S_D satisfied the requirement of 3.2 MPa for the secondary class (general) road, given by Korean mix design guide (Interim guide 2008). The S_D of PG76-22 satisfied the requirements of 4.25 MPa for the first class (arterial) road.

Indirect tensile strength (ITS) value of asphalt concrete is an index of the property representing resistance against cracking. ITS seems to be a little lower than those of HMA mixtures, but strong enough for minimum requirement for normal asphalt pavement concretes (Kim 1988, Hot-mix… 2007). Since this study is an initial stage, the water susceptibility of SM WMA mixture was not evaluated in this ITS test.

In the property comparison, the WMA concrete revealed comparable mixture properties with normal HMA concrete, but lower than those of PG76-22. Since S_D and WT results showed high correlation, it was expected the SM6-WMA should have weaker rut resistance than PG76-22 mixture. The WT test was performed for more relative comparison of rut resistance evaluation. Figure 5 shows WT test results in rut depth-cycle curves for five asphalt concretes.

The final rut depths of 13 mm WMA [SM-WMA (13)] was similar to that of normal HMA [AP-5(13)], but much higher than that of PG76-22 (13) mixtures. It can be carefully said that the SM6-WMA 13 mm mixture can be used in place of conventional asphalt mixture even though it is prepared at warm temperature, i.e., 95°C. However, in comparison with a PMA mixture, the SM6-WMA is obviously lower quality material which needs improvements in rut and tensile strength resistance.

4 SUMMARY AND CONCLUSION

The asphalt was liquidized at 90°C by using 6% of styrene monomer (SM) and it was mixed with aggregates, which were heated at 105°C, to produce SM 6% modified warm-mix asphalt (SM6-WMA) concrete at 95°C. The mixture was well blended using a normal laboratory mixer and well compacted using a gyratory and roller-press compactors.

The engineering property evaluation showed that SM6-WMA concrete was similar to those of normal hot-mix asphalt (HMA) concrete, showing satisfactory deformation strength (S_D), Marshall Stability and indirect tensile strength for requirements of normal asphalt pavements.

Table 1. Comparison of three properties (gneiss aggregate mixtures).

Max agg. size (mm)	Material	OBC (%)	Mean air void (%)	Marshall Stability (kN)	Indirect tensile strength (kPa)	SD (MPa)
13	Normal HMA concrete	5.3	3.82	8.38	712	3.375
	SM6-WMA concrete	5.4	4.01	8.49	614	3.526
	PG76-22 concrete	5.3	4.15	10.22	1080	4.500
19	Normal HMA concrete	4.8	3.68	9.04	685	3.354
	SM6-WMA concrete	4.8	3.89	7.96	620	3.217
	PG76-22 concrete	4.8	4.08	11.73	1107	5.076

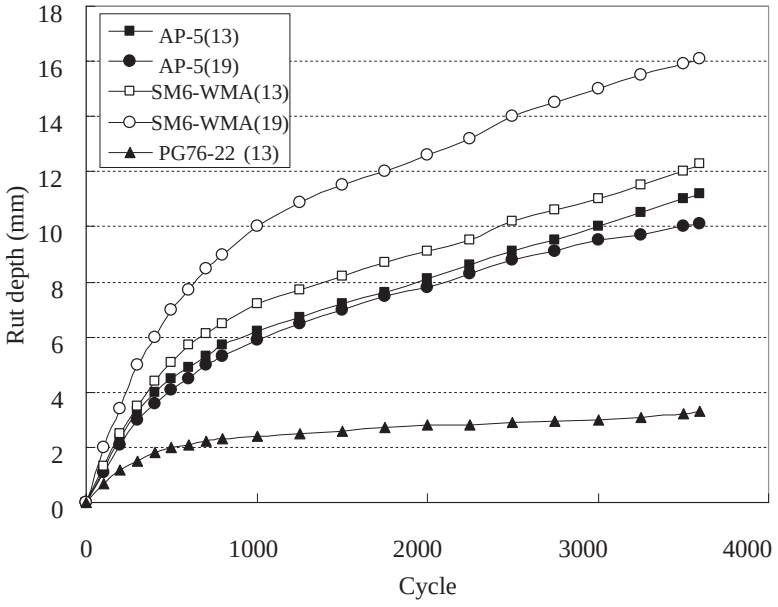

Figure 5. Results of wheel tracking tests.

Wheel tracking test result was also similar to normal HMA for 13 mm aggregate mixes, but weaker for 19 mm mixes. Therefore, it is tentatively concluded, based on this limited study, that the new bitumen mixture, which has comparable strength to conventional HMA mixture, can be produced at 95°C by adding 6% of SM.

Even tough this is initial stage of study for liquidizing asphalt using SM for WMA, a good possibility was found from using SM as a chemical intermediate. However, for more practical application, other base asphalt binders, some additives for strengthening binder and other SM brands need to be used with other sources of aggregates. The long-term performance, water susceptibility, effect of moisture content in aggregate and low-temperature property should also be evaluated in the future study.

ACKNOWLEDGEMENT

This study was supported by the Ministry of Homelands and Maritime Affairs, Korea, and performed using the facilities of the Institute for Advanced Construction Materials, Kangwon National University.

REFERENCES

Cervarch, M.B. 2003. Cooling down the mix. *Hot Mix Asphalt Technology.*

Doh, Y.S., Yun, K.K., Amirkhanian, S.N. and Kim, K.W. 2007. Framework for developing static strength test for measuring deformation resistance of asphalt concrete mixtures. *Construction and Building Materials, 21(12).*

Interim guide for hot-mix asphalt mix design procedures. 2008. Ministry of Homeland and Maritime Affairs, Republic of Korea.

Kim, K.W. 1998. Determination of critical tensile strength for bituminous concrete surface course. Ph.D. Dissertation, Clemson University.

Kim, K.W., Doh, Y.D. and Amirkhanian, S.N. 2004. Feasibility of deformation strength for estimation of rut resistance of asphalt concrete. *Road Materials and Pavement Design*, *5(3)*: 303–322.

Kim, B.I., Lee, M.S. and Kim, K.W. Mar. 2006. Methodology for developing HMA mix design taking into account performance-related mechanics properties. *Journal of Korean Society of Road Engineers, 8(1)*: 15–23.

Kim, K.W., Doh, Y.S., Ahn, K.A., Baek, S.H., Park, N.W., Kim, H.H., Kim, J.C. La, I.H. and Amirkhanian, S.N. 2008. Development of a test method for estimating high-temperature deformation resistance of asphalt concrete. *Final Report to Korea Institute of Construction and Transportation Technology Evaluation and Planning*, Kangwon National University.

Kim, H.H., Park, N.W., Doh, Y.S., K. Ahn, Lee, S.J. and Amrikhanian, S.N., Kim, K.W. 2008. Rutting Estimation of Asphalt Pavement Mixtures using Deformation Strength. *Paper presented at 2008. European Asphalt.*

Kuennen, T. 2004. Road Science: Warm mixes are a hot topic. *Better Road*: 30–41.

Mckenzie, P. 2006. Taking a closer look at warm mix. *Better Road*: 64–69.

Park, N.W., Kim, H.H., Baek, S.H., Kim, K.W. and Doh, Y.S. 2007a. Correlation of deformation strength (S_D) with lab data and field rutting data of asphalt pavements. *UKC Conference*, Washington, DC, USA.

Park, N.W., Jung, J.H. Cho, B.J. and Kim, K.W. 2007b. Fundamental Characteristics of Monomer-modified Warm-mix Asphalt Concretes. *ICPIC Proceedings*, Ed. by Yeon: 685–690.

Hot-Mix Asphalt Material Properties. 2007. SCDOT Designation: SC-M-402 (06/07).

Advanced Testing and Characterization of Bituminous Materials – Loizos, Partl, Scarpas & Al-Qadi (eds)
© 2009 Taylor & Francis Group, London, ISBN 978-0-415-55854-9

An evaluation of use of synthetic waxes in warm mix asphalt

F. Cardone, V. Pannunzio & A. Virgili
Università Politecnica delle Marche, Ancona, Italy

S. Barbati
Politecnico di Torino, Torino, Italy

ABSTRACT: The preservation and protection of both natural and workspace environment are two of the main objectives that also concern the field of road engineering. As such, there is an ever increasing use of new pro-environmental techniques and materials. One of these innovative processes includes warm mix asphalt (WMA).

Such asphalt mixtures, compared with traditional hot mix asphalt (HMA), need lower mixing and compaction temperatures, allowing lower CO_2 and fume emission, reducing energy consumption and operative benefits.

In this context the present experimental study was conducted to evaluate the workability and mechanical performance of WMA by adding synthetic waxes. Three different asphalt mixtures were selected, the first was a traditional mix, as reference material, while the other were two mixes modified with synthetic long carbon chain wax.

The experimental investigation consisted of a compaction grade study by different laboratory compaction techniques and of dynamic tests to evaluate the mechanical response of WMA compared to HMA.

1 INTRODUCTION

In last decades attempts to develop new processes and products capable of reducing the mixing, laying and compaction temperatures are not new for researchers and industries in the road engineering field. At the same time, the great importance of temperature control has been well known in order to warrant an effective coating of the aggregate by the binder so that a material with high performance can be manufactured. Therefore, reduction in production and application temperature, without sacrificing the mechanical properties and durability of materials has become the main target to reach.

Lower mixing, laying and compaction temperature for asphalt concrete contributes significantly to reducing energy consumption, greenhouse gas emissions and fumes. Moreover, it can allow longer haul distances, if the mix is produced at normal operating temperatures, longer construction season and less traffic closing time after compaction. Reduction in fuel energy consumption represent significant cost savings, considering problems connected with energy supply which concerns all developed countries. A decrease in both visible and not-visible emissions, guarantees to better protect both natural and workspace environment and allows social benefits when we consider the problems connected with air pollution. Furthermore, lower emissions may allow asphalt plants to be sited in non-attainment areas, where there are strict air pollution regulations, allowing shorter haul distances which improve production and shorten the construction period, thus reducing the delays associated with traffic congestion (Hurley & Prowell 2006a).

In this direction, where the preservation and protection of both natural and workspace environment are requested, the so-called "Warm Mix Asphalt" (WMA) processes seem to be the most suitable road construction technique. At the moment, the known WMA techniques can be divided into two main groups. The first group uses additives to modify the fluidity

of asphalt and the second group is based on the foaming of binder (Bonola & De Ferrariis 2006). Both techniques are able to reduce the binder viscosity at a fixed temperature. This allows the aggregate to be coated completely by the binder at lower mixing temperature and also allows the asphalt mixtures to be more workable at lower compaction temperature than traditional HMA. Some of the current processes available in the market are the following: Sasobit® or Asphaltan B®, (waxes or waxes with high molecular weight hydrocarbon), Asphamin® (synthetic zeolite), WMA-Foam® (a system with two binder component) and the emulsion Evotherm® (Hurley & Prowell 2006b).

In the first "warm" technologies research phase the possibility to use organic soluble substances that are able to modify the rheological characteristics of the binder with temperature was studied. Paraffin or crystalline waxes had more success. They work through the temporary reversible changing of the physical state (melting—crystallization) (McKay et al. 1995).

The second warm technique uses the binder foaming process. It combine a pre-heated binder at 180°C with small amounts of cold water. In this phase, the water is transformed into steam and favours the rapid expansion of bitumen in a large amount of small bubbles. The foam increases the specific surface of bitumen and reduces a lot its viscosity allowing intimate coating when it is mixed with cold and wet aggregates. Therefore, this technique allows to obtain energy benefits coming from reducing the heating temperature of aggregates before mixing. Moreover, the presence of residual moisture in aggregates, not completely dried, helps the laying and compaction of asphalt mixtures at lower temperatures (Olard et al. 2007).

As far as the use of crystalline waxes is concern the synthetic waxes produced by the Fisher-Tropsch (FT) process seems to be the most well known. In short, the synthetic waxes, produced from coal gasification by FT process, is a fine crystalline having a carbon chain length ranging from C_{45} to C_{100} plus with a melting point ranging from 90 to 100°C. It is contrary to macrocrystalline bituminous paraffin which has a carbon chain length ranging from C_{25} to C_{50} with a melting point ranging from 45 to 70°C. The longer carbon chains in the FT wax lead to a higher melting point and the smaller structure reduces brittleness at low temperatures as compared to bitumen paraffin waxes (Edwards & Isacsson 2005).

These FT synthetic waxes can be considered as a "binder flow improver" because at temperatures higher than 120–130°C they tends to lower the dynamic viscosity of asphalt binder. This results in a decrease in mixing temperature, guaranteeing a complete coating aggregates and a decrease in lay down and compaction temperature without penalizing the workability of asphalt mixtures. Moreover, at temperature below their melting point the synthetic waxes forms a crystalline structure in the binder which improves the stiffness of asphalt mixtures even at higher executive temperatures (Butz et al. 2000). The content of the wax ranges from 0.8% of the weight of the bitumen to 3%, which represent the maximum value in order to avoid susceptibility problems at high temperatures.

This is the context in which this research work is placed. It forms part of a research project in progress at the Università Politecnica delle Marche on WMA techniques. The experimental study focused mainly on the evaluation of the workability and mechanical performance of WMA with synthetic waxes in order to evaluate their potentialities of use.

2 MAIN GOALS

The main objective of the present work was to investigate and compare the warm mix asphalt (WMA) made with synthetic wax with respect to their volumetric and mechanical properties with the traditional hot mix asphalt (HMA). To this end the experimental investigation was divided into two distinct phases.

The first part of the research work deals with a compactability study on asphalt mixtures performed by using three different laboratory compaction equipments, in order to define which of these techniques is more suitable to highlight the higher compaction capacity of WMA as compared to HMA at prefixed temperatures.

The second part of the research work was based on a mechanical characterization of studied mixtures aimed to make a performance comparison between WMA and HMA. In particular, the testing program consisted of stiffness modulus tests, indirect tensile fatigue tests and

permanent deformation potential tests. Moreover, further mechanical tests were performed to evaluate the moisture susceptibility of WMA compared to HMA.

3 LABORATORY EXPERIMENTAL PROGRAM

In order to reach the main goals mentioned above and, hence, to verify the applicability of WMA made with synthetic waxes an experimental project, which is part of a wider research program still in progress, was carried out at the Road Materials Laboratory of the Università Politecnica delle Marche, Ancona, Italy.

In this chapter all laboratory activities, divided in section, were reported and described.

3.1 *Materials*

Three different types of binders were used to produce asphalt mixtures: a traditional 70/100 pen binder, named A used as control binder, and two plain binders modified with synthetic wax, named B and C respectively.

Binder B is a traditional binder 70/100 pen modified directly in plant with H50®, a refined production of synthetic waxes with a high number of carbon atoms (>100) which allows a sensible variation in the melting and crystallization point of the binder. This wax was used in the proportion of 3% of the binder weight.

Binder C was obtained through the modification of a traditional binder 70/100 pen with Sasobit®, a fine crystalline long-chain aliphatic hydrocarbon made from coal gasification by using the Fischer-Tropsch (FT) method. The modification was done in the laboratory by adding Sasobit® in the proportion of 3% of the binder weight, as recommended by the producer, at 160°C and mixing it by using a portable mechanical mixer with high shear rate for about 30 minutes.

In the experimental project a typical gradation curve, conformed to Italian Technical Specification for binder course hot mix asphalt concrete ($Ø_{max}$ = 15 mm) was considered. Limestone aggregates and an asphalt content equal to 4.5% was used to produce all asphalt mixtures. The three different asphalt mixtures were named as follows: mix MA made with binder A, mix MB made with binder B and mix MC made with binder C. The mixing temperature was approximately 10°C above the compaction temperature and each sample was conditioned for two-three hours at its corresponding compaction temperature before compacting.

3.2 *Testing program*

3.2.1 *Binder viscosity test*

The first phase of laboratory investigation involved viscosity measurements in order to evaluate the high temperature behavior of the selected asphalt binders. The dynamic viscosity tests were performed by means of a viscosimeter Brookfield (spindle SC4-21) at different temperatures (80–160°C) in accordance with UNI EN 13302 "Determination of viscosity of bitumen using a rotating spindle apparatus". These preliminary tests were useful to evaluate the possible difference in viscosity behavior due to the addition of synthetic waxes to the binders.

3.2.2 *Densification and air voids content*

The test samples of the asphalt mixture were produced to evaluate the ability of the mix to be compacted over a range of temperature. In particular, three different laboratory compaction equipment were considered to produce asphalt concrete specimens in order to evaluate their effects on the compactability of the mixtures. The first compaction technique was based on the use of Marshall Hammer, in accordance with UNI EN 12697-30 "Test methods for hot mix asphalt: Specimen preparation by impact compactor". The second compaction method used was a Shear Gyratory Compactor (SGC), in accordance with UNI EN 12697-31 "Test methods for hot mix asphalt: Specimen preparation by gyratory compactor". A constant pressure of 600 kPa, a rotation speed of 30 rpm and an inclination angle of 1.25° were

considered as test parameters. Moreover, 100 gyrations were set to compact each mixture. The last compaction method considered was the Roller Compactor, in accordance with UNI EN 12697-33 "Test methods for hot mix asphalt: Specimen prepared by roller compactor". This equipment allows to compact the asphalt mixture in slabs (300 mm × 300 mm) by setting prefixed values of compaction pressure and number of passing. Finally, for each asphalt concrete slab five cylindrical specimens, with standard dimension, were obtained by coring.

Each asphalt mixture was compacted at three compaction temperature, 100, 120 and 140°C respectively. Finally, an air voids content control, that conformed to UNI EN 12697-8 "Test methods for hot mix asphalt: Determination of void characteristics of bituminous specimens", was performed on each sample in order to evaluate the compaction grade of the investigated asphalt mixture. Once the air void level was determined, the samples were used to perform the mechanical characterization of each mix.

3.2.3 *Mechanical test*

The mechanical properties of the three asphalt mixtures were carried out primarily by means of the Nottingham Asphalt Tester (NAT). This equipment allowed to perform dynamic tests in order to characterize the asphalt mixtures in terms of indirect stiffness modulus, indirect tensile fatigue life and permanent axial deformation resistance. Before testing each selected sample was conditioned at the test temperature for 14–16 hours. In particular, stiffness modulus and fatigue tests were conducted at 20°C, while creep tests were conducted at 30°C. Since stiffness modulus is a non-destructive test, all set of samples after this test were submitted to an indirect tensile fatigue test or to a permanent axial deformation test.

Moreover, additional mechanical tests were carried out to evaluate the potential for water susceptibility of the mixtures made with waxes as compared to the reference mix. For each mixture, a set of six samples were compacted by a shear gyratory compactor at a prefixed air void content and then submitted to indirect tensile strength test.

4 TEST RESULTS AND DISCUSSION

4.1 *Viscosity test*

The first laboratory investigation was to perform viscosity tests of selected binders in order to verify the effect of wax addition on dynamic viscosity.

Figure 1 shows the plot of viscosity versus temperature for 70/100 pen binder compared to the 70/100 pen binder modified with H50® and Sasobit® wax respectively.

It is possible to note that binder C, compared to the traditional binder (binder A), reports a visible decrease in viscosity at temperatures higher than 80°C and a gap of about 10–15°C can be estimated to obtain the same viscosity. Finally, binder B shows an apparent increase in viscosity at temperatures less than 120°C but shows a viscosity trend similar to that of binder C at higher temperatures. This effect on viscosity, due to the addition of wax, guarantees an efficient coating of aggregates by the binder and a good workability of asphalt mixture also at lower temperatures than the traditional ones.

4.2 *Compactability*

As mentioned earlier, three laboratory compaction techniques were used to better understand the compaction grade of the selected asphalt mixtures at several temperatures. The following figures show the experimental results obtained. For each compaction method the compactability of asphalt mixtures is evaluated in terms of air void content.

Figure 2 reports the results obtained by using the Marshall method.

From figure 2 it is possible to note that, for each asphalt mixture, the compaction increases with an increase in compaction temperature. This is due to the decrease in the viscosity of the binders with the temperature that results in an increase in workability of the asphalt mixtures.

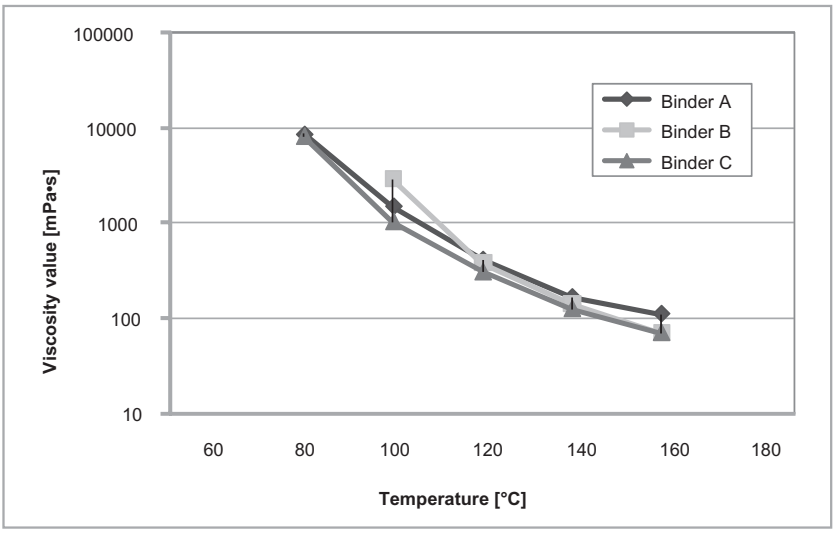

Figure 1. Dynamic viscosity by means of Brookfield apparatus.

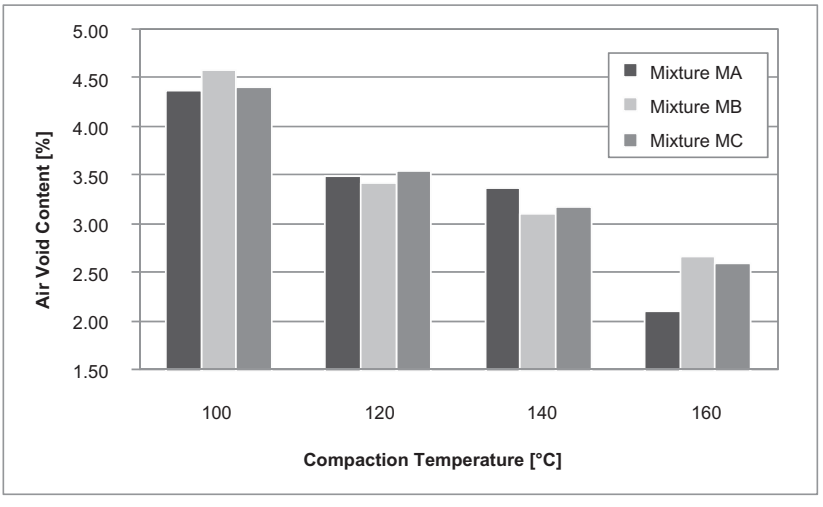

Figure 2. Air void content by means of the Marshall apparatus.

Moreover, it can easily be noted that no significant difference in compaction at all compaction temperature can be seen among the investigated asphalt mixtures. This would mean that the addition of synthetic waxes, Sasobit® and H50®, does not affect the compaction of asphalt mixture by means of Marshall method. This probably depends on the high compaction energy transferred by hammer that tends to uniform the compaction of asphalt mixture hiding the possible effects of added waxes.

Figure 3 reports the densification results by using Shear Gyratory Compactor.

Data results show that the positive effect of waxes on the compaction grade of asphalt mixtures, estimable at about 1%, is evident only at middle-high temperature and such a result tends to disappear with the decrease in temperature. In fact, at low temperatures no improvement in the compaction of modified asphalt mixtures as compared to the traditional asphalt mixture is seen. Therefore, the operational benefit to lower compaction temperatures by using warm asphalt has not checked. Moreover, it is possible to see that for each mix the air void

content decreases from 100°C to 140°C but tend to increase at higher temperatures and at this temperature it seems that the traditional mix shows better compaction than the modified mixtures. This opposing result confirms what is found in literature, according to which SGC is not very sensitive to temperature changes (Bahia & Hanson 2000, Huner & Brown 2001) and therefore it would not seem the best laboratory technique to evaluate the effect of waxes on the compaction of asphalt mixture.

Finally, Figure 4 shows the densification results of each asphalt mixture by using the Roller Compactor.

In this case the attention was focused only on a range of temperature below 140°C because it was important to understand how the investigated WMA works at lower compaction temperatures than the one that is commonly used. First of all, it is important to note that the air voids content decreases with the increase in temperature, even if there are no marked differences. From the observation of results it can also be seen that the addition of wax to mix MB and MC improves their compaction as compared to the traditional HMA and this

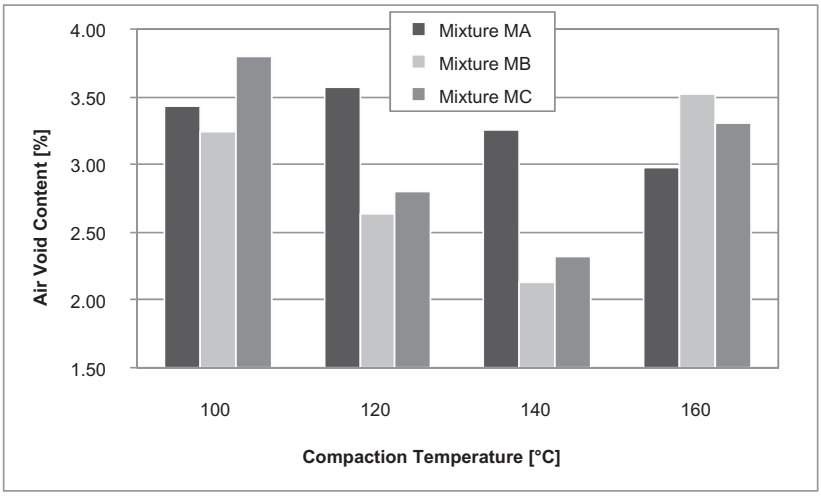

Figure 3. Air voids content by means of SGC apparatus.

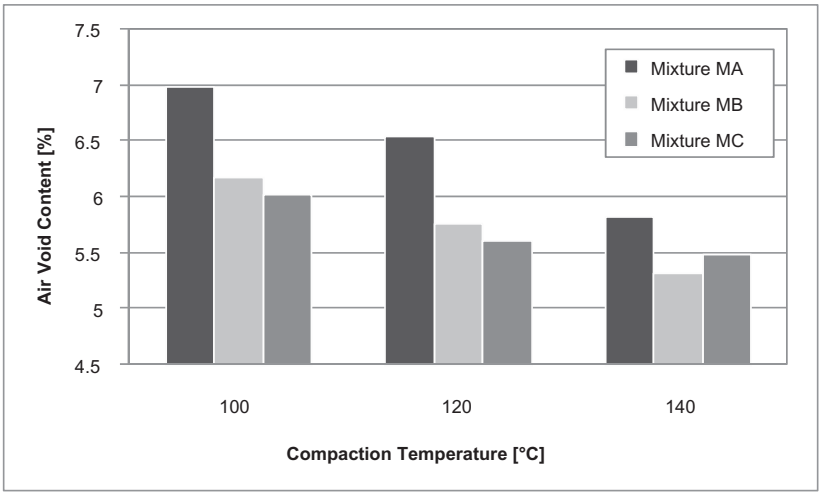

Figure 4. Air voids content by means of Roller Compactor apparatus.

difference is more evident at lower compaction temperatures. This difference can be estimated at about 1% and allows to estimate that the compaction grade of traditional asphalt mixture at 130–140°C can be obtained by WMA at a compaction temperature less than about 30°C. This double result allows to affirm that Roller Compactor can be considered to be an efficient compaction method, as on the one hand it allows to show the changes in compaction due to changes in temperature and on the other it allows to evaluate the potentialities of WMA in terms of a better workability in opposition to Marshall Hammer and Shear Gyratory Compactor.

In the light of these results, only the asphalt mixture samples produced by Roller Compactor were tested in the second phase of experimental investigation.

4.3 *Mechanical properties*

As reported above stiffness modulus, indirect tensile fatigue and permanent axial deformation test and finally indirect tensile strength test for water sensitivity were carried out to compare the different mixtures studied in terms of mechanical response. All mechanical tests were carried out on samples drilled from asphalt concrete slabs obtained by Roller Compactor and five cylindrical (Ø = 100 mm) samples were cored for each slab.

4.3.1 *Stiffness modulus*

The stiffness modulus tests were carried out at 20°C in accordance with UNI EN 12697-26 "Test methods for hot mix asphalt: Stiffness". In particular, a rise time of 124 ms and a pulse repetition of 3.0 s were used. The analysis of stiffness properties was extended to all asphalt mixture and all samples obtained at three different compaction temperatures (100, 120 and 140°C). The stiffness modulus results are shown in Figure 5 and the average of six measurements for each mixture and compaction temperature is reported.

The figure clearly shows a common trend of the mixtures to have an increase in stiffness modulus with the increase in compaction temperatures. This depends on the fact that high temperature guarantees best workability which allows to reach high compaction levels resulting in an improvement in stiffness properties. In fact, the mixtures compacted at the lower temperatures (100°C) reported lower stiffness properties due to the higher air void content.

If figures 4 and 5 are compared, it is possible to note that, for all studied mixtures, the stiffness modulus trend is related to the densification trend. This means that if a mixture is

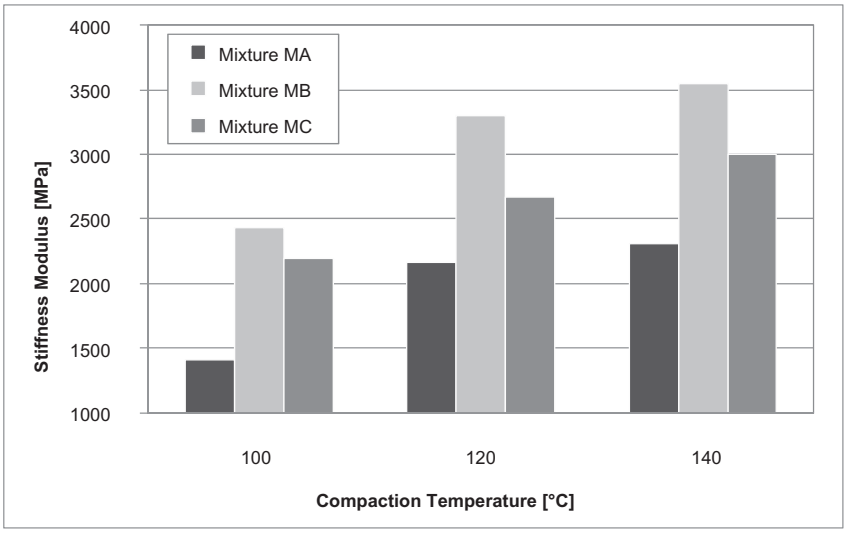

Figure 5. Stiffness modulus results.

characterized by a lower air void content it shows a better mechanical performance in terms of stiffness modulus. However, it is important to note that the increase in stiffness is also due to the increase in mixing temperature. In fact, the mixing temperature was always 10°C higher than the compaction temperature. Therefore the high mixing temperature ensured better particle coating which made the interparticle bonder stronger.

An interesting result is that the mixtures (MB and MC) modified with wax and compacted at low temperature (100°C) showed similar stiffness properties as those of the traditional mixture compacted at high temperature (140°C). This would mean that WMA is able to ensure good mechanical performance in terms of stiffness even when it is mixed and compacted at temperature that is lower than traditional temperature.

Moreover, comparing MB and MC, it can be seen that even if the two mixtures reported very similar compaction grade at each compaction temperature, they showed a sensible difference in terms of stiffness modulus. This behavior could be related to the nature of the binder and, hence, to the kind of synthetic waxes used to modify the binders. Probably, the crystallization process effects of H50® wax at 20°C ensures stronger interparticle bonds than Sasobit® wax.

In general, from the observation of the results, it can be noted that the addition of synthetic waxes significantly improves the stiffness of the traditional mix asphalt for each compaction temperature. This result mainly depends on the crystallization of the synthetic waxes which confer to the mixtures an higher stiffness at ordinary temperature.

4.3.2 *Indirect tensile fatigue*

The indirect tensile fatigue test (ITFT) were carried out in a controlled stress mode according to BSi 2nd DD ABF "Method for the determination of the fatigue characteristics of bituminous mixtures using indirect tensile fatigue". Particularly, a rise time of 124 ms and a temperature of 20°C were adopted as test conditions.

Table 1. Parameters of linear regression analysis.

Mixtures	a	b	R^2
MA	486.18	–0.126	0.88
MB	383.67	–0.104	0.99
MC	305.86	–0.084	0.82

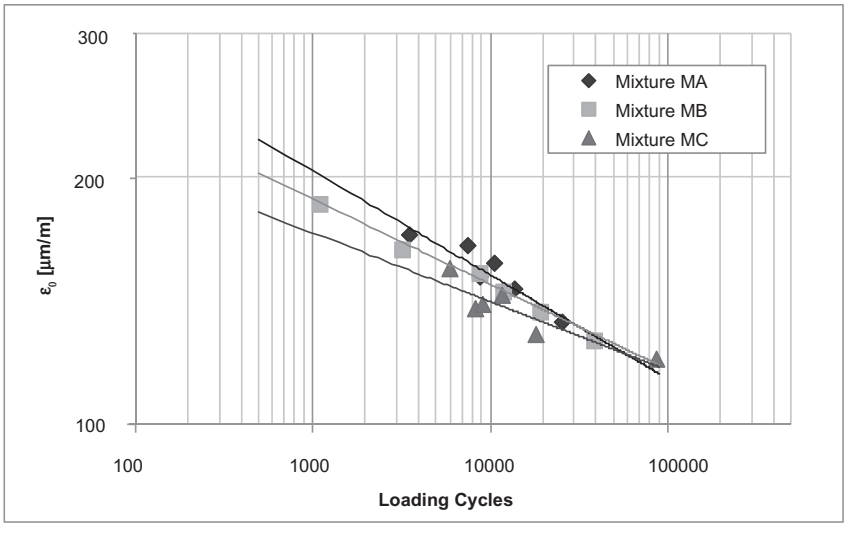

Figure 6. ITFT study results.

For each mixture six samples, already submitted to the stiffness modulus test, were tested at different stress levels, depending on the stiffness of the sample, and the number of loading cycles were registered.

In order to obtain the classical fatigue law $\varepsilon = a(N_f)^b$ the maximum tensile strain (ε_o) and the number of cycles at failure (N_f) were taken into account. In particular the number of cycles corresponding to the inflection point of the curve permanent deformation-cycles as fatigue failure criterion were considered.

Table 1 summarizes the linear regression parameters of the fatigue laws for each mixture.

Finally, Figure 6 below shows the fatigue response of the investigated mixtures.

From the analysis of Table 1, the high regression coefficient values ($R^2 > 0.8$) show that the chosen classical fatigue law well describes the fatigue behavior of warm mixes asphalt too and therefore this analytical fatigue model as comparison criterion can be considered.

From Figure 6 it can be noted that at low strain level all fatigue regression lines tends to converge. This allows to affirm that the different mixtures showed very similar fatigue response in terms of cycles to failure. On the contrary, at higher strain level, a difference in fatigue behavior among the mixtures can be noted. In particular, the mixtures MB and MC showed lower fatigue performance than reference mixture MA.

This different mechanical response could depend on the presence of synthetic waxes and, in particular, on their capacity to confer to the asphalt mixtures, (mixtures MB and MC) higher stiffness than the traditional mixture (MA) as verified through the analysis of the stiffness properties. In fact, the presence of wax in the asphalt mixture does not produce much ductile intergranular bonds, that as a result are not able to accumulate a high permanent strain level due to the applied repeated load. Therefore, this aspect results in a premature fatigue failure as showed in the experimental results.

4.3.3 *Permanent deformation*

Permanent deformation resistance was evaluated by using a Dynamic Creep Test. This mechanical test was performed, according to BSi DD 226:1996 "Method for determining resistance to permanent deformation of bituminous mixtures subject to unconfined dynamic loading", at 30°C on samples already submitted to the stiffness modulus test.

For each mixture four samples were tested and for each sample axial permanent deformation along the loading cycles was monitored. The four samples were selected to be characterized by a similar air void content.

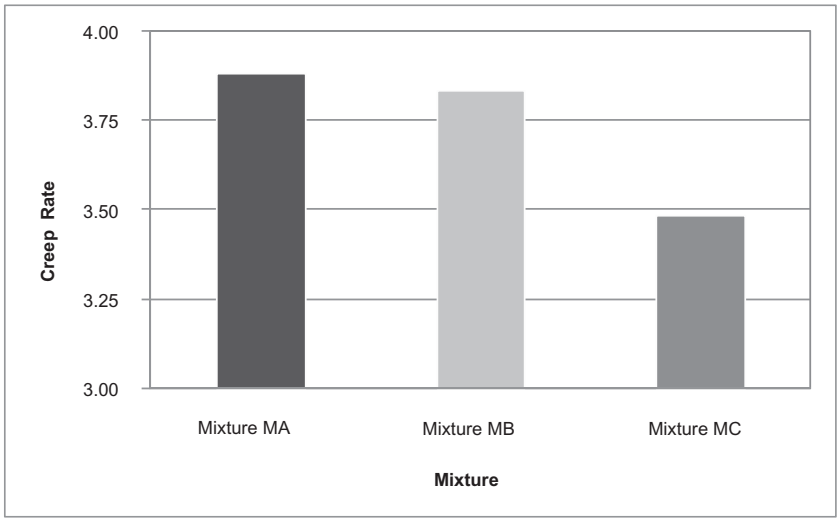

Figure 7. Creep rate values.

Finally, the asphalt mixtures were compared in terms of creep rate, which was defined as the rate between the difference of the cumulative axial strain registered at 1800 and 1200 load applications and the difference between the number of the corresponding repetitive load applications. Figure 7 shows the creep rate results; in particular. For each studied mixture the creep rate as average of four samples was considered.

Figure 7 shows very clearly that MC achieved the lowest creep rate, while MA and MB gave more or less the same response. It would seem that the addition of Sasobit® increases the rutting resistance, while the addition of H50® does not affect this response. This result can be considered conflicting but it is sufficient to state that in any case the addition of synthetic waxes does not penalize permanent deformation resistance of traditional asphalt mixture.

4.3.4 *Water sensitivity*

As mentioned before, additional tests were considered in order to evaluate the effect of the addition of wax on the water susceptibility of asphalt mixtures. These tests were performed in accordance with UNI EN 12697-12 "Determination of water sensitivity of bituminous specimens" and the set of samples was produced by using the Shear Gyratory Compactor at a prefixed air void content.

For a first set of samples 150°C mixing temperature and 140°C compaction temperature were used. In order to verify the possible influence of the mixing temperature on mixtures MB and MC a second series of samples were mixed at 120°C and compacted at the same air voids content. Three of them were submitted to an indirect tensile test after wet conditioning, while the remaining three were submitted to an indirect tensile test in dry condition and for both of them an indirect tensile strength was evaluated. Finally, for each set of samples the indirect tensile strength ratio (ITSR) was calculated. In particular, mixtures MA and MB showed ITSR values greater than 0.9, while mixture MC showed ITSR values greater than 0.8.

Figures 8 and 9 show the indirect tensile strengths of each mixture related to the two mixing temperatures.

In both figures it can be noted that the investigated mixtures reported very similar ITS values, both in dry and in wet conditions. Hence, it could be affirmed that the addition of synthetic waxes does not appreciably affect the failure strength of hot mix asphalt. Moreover, it can be easily seen that all samples after wet conditioning show a slight decrease in ITS. These results could be due to the slight lower air voids content checked for wet samples rather

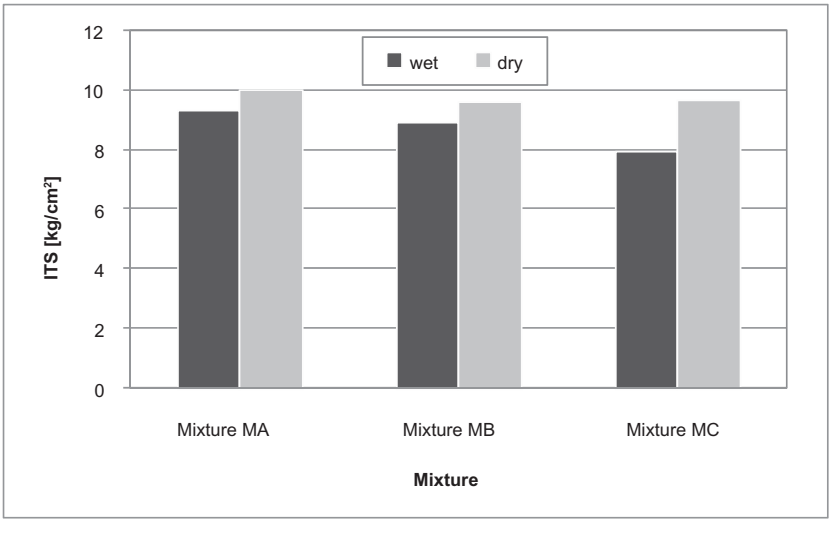

Figure 8. ITS results at 150°C–140°C, as mixing and compaction temperatures respectively.

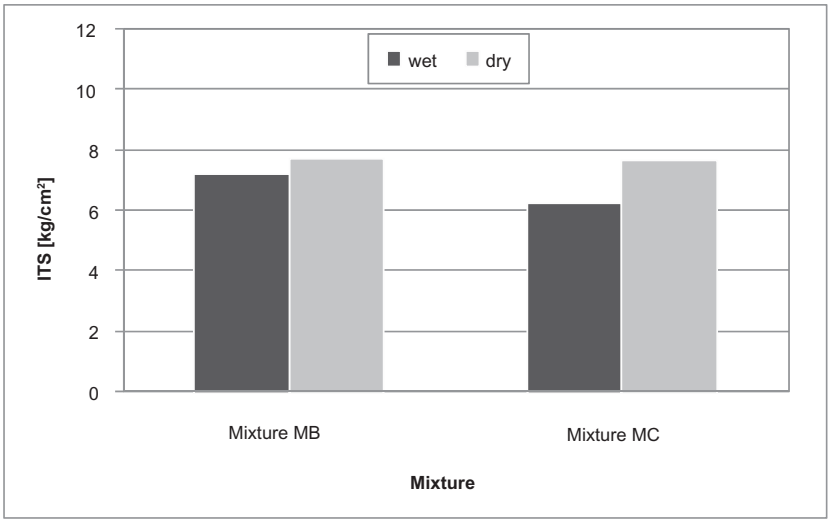

Figure 9. ITS results at 120°C–110°C, as mixing and compaction temperatures respectively.

than to the possible water sensitivity. In fact, the ITSR values calculated were very close to unity and this means that the presence of water does not affect the performance of asphalt mixtures. As these results were also found for mixtures MB and MC, it is possible to state that the addition of synthetic waxes does not even affect the water sensitivity of traditional mix asphalt.

Moreover, from Figures 8 and 9 it can be seen that mixtures MB and MC mixed at 120°C achieved a decrease in ITS as compared with those mixed at 150°C but no significant difference in ITS between the dry and wet condition can be noted. These double results mean that the decrease in the performance of asphalt mixture is only due to the lower mixing temperature only and not to the addition of synthetic waxes. This is due to the fact that the binder at lower temperatures is able to completely cover the aggregates less. This does not allow to obtain high cohesive and adhesive forces binder-aggregate, in order to ensure to the mixture good mechanical properties.

5 CONCLUSIONS

In the present research work the authors' main objective was to investigate the volumetric and mechanical properties of Warm Mix Asphalt, in order to evaluate its potentialities and limits as compared with traditional hot mix asphalt. The investigation was conducted by analyzing a reference hot mix asphalt and two warm mix asphalts made with two different types of synthetic waxes. The experimental program was divided into two sections. The first section aimed at investigating densification properties, while the second one aimed to evaluate possible lack of mechanical behaviour due to the presence of synthetic waxes.

The densification study, based on the use of three different laboratory compaction techniques, was carried out in order to understand which type of compaction method is more effective to evaluate the differences in workability between traditional HMA and WMA by adding synthetic waxes. Results showed that Roller Compactor can be considered an efficient compaction method, as on the one hand it allows to show the changes in compaction due to changes in temperature and on the other it allows to evaluate the potentialities of WMA in terms of better workability as opposed to the Marshall Hammer and Shear Gyratory Compactor. The addition of synthetic waxes improved the compactability of asphalt mixture. This improvement can be estimated on average at about 0.9–1% and for WMA this means

compaction temperature lower than about 20–30°C to obtain the same compaction grade of hot asphalt mixture compacted at ordinary temperatures. Therefore, these results highlight the importance of finding a right laboratory procedure and equipment to evaluate the potentialities and limitations of a non traditional material.

Performance characterization investigated the main mechanical properties of hot mix asphalt, such as stiffness and fatigue properties, permanent deformation resistance and moisture susceptibility. As regards the stiffness modulus it was ascertained that the addition of the synthetic waxes does not affect but rather confers to the mixtures higher stiffness properties than traditional mixes. This apparently satisfactory mechanical characteristic was however a limit for the fatigue response of the WMA. In fact, results showed that the addition of waxes decreased fatigue resistance and this may be related to the less ductile behavior of the mixture due to the presence of wax. A better response was verified in terms of permanent deformation resistance, where the results allowed to affirm that the addition of waxes does not certainly affect its rutting potential. In particular, it seems that the use of Sasobit® wax improves rutting resistance.

With respect to water sensitivity results show that the addition of synthetic waxes does not increase the potential for moisture damage. Moreover, lower mixing temperature results in a decrease in ITS but no significant difference in ITS between the dry and wet condition can be noted. This result confirms that the presence of wax does not affect the water sensitivity of hot mix asphalt.

Finally, considering overall results, is possible to state that by adding synthetic waxes when compared with traditional HMA, WMA showed higher tendency to compaction, even if the choice for a proper laboratory compaction technique is fundamental in order to evaluate the effectiveness of synthetic waxes on compaction. Moreover, the WMA showed mechanical responses comparable with those of the traditional asphalt mixture.

REFERENCES

Bahia, H.U. & Hanson, D.I. A project NCHRP 9–10 Superpave Protocols for Modified Asphalt Binders. *Draft Topical Report (Task 9), Prepared for National Cooperative Highway Research Program, Transportation Research Board,* National Research Council, May 2000.

Bonola, M. & De Ferrariis, L. 2006. Low energy bituminous mixes: the state of the art. *Rassegna del bitume n. 54/06, speciale Asphaltica 2006.*

Butz et al. 2000. Modifikation von Strassenbitumen mit Fischer-Tropsch-Paraffin. *Bitumen, Heft 3, 2000* (language: German).

Edwards Y., Isacsson, U. 2005. Wax in Bitumen. *Road Materials and Pavement Design (International Journal)* Volume 6 (3)/2006.

Huner, M.H. & Brown E.R. Effects of Re-Heating and Compaction Temperature on Hot Mix Asphalt Technology. *NCAT Report No. 01–04, National Center for Asphalt Technology*, Auburn, AL, 2001.

Hurley, G.C. & Prowell, B.D. 2006a. Evaluation of Sasobit® for use in warm mix asphalt. *NCAT Report 05–06. National Center for Asphalt Technology*, Auburn, AL.

Hurley, G.C. & Prowell, B.D. 2006b. Evaluation of Potential Processes for Use in Warm Mix Asphalt. *AAPT Annual Meeting 2006, Savannah, Georgia, 27–29 March 2006*.

Italian Technical Specification for binder course hot mix asphalt concrete. *Ministero delle Infrastrutture e dei Trasporti, Capitolato Speciale d'Appalto Tipo per Lavori Stradali,* Art. 4—Formazione di strati in conglomerato bituminoso a caldo tradizionale con o senza riciclato.

McKay J.F. et al. 1995. Isolation of waxes from asphalts and the influence of waxes on asphalt rheological properties. *Division of Petroleum Chemistry American Chemical Society 210th National Meeting, August 20–25, 1995. Chicago.*

Olard, F., Antoine, J.-P., Héritier, B., Romanier, A. & Martineau, Y. 2007. LEA® (Low Energy Asphalt): A new generation of asphalt mixture. *Advanced Characterization of Pavement and Soil Engineering Materials*—Loizos, Scarpas & Al-Qadi (eds). © 2007 Taylor & Francis Group, London, ISBN 978-0-415-44882-6.

Advanced Testing and Characterization of Bituminous Materials – Loizos, Partl, Scarpas & Al-Qadi (eds)
© 2009 Taylor & Francis Group, London, ISBN 978-0-415-55854-9

Study of the mechanical behaviour of gravel-emulsions using triaxial tests

P. Hornych, V. Gaudefroy & J.L. Geffard
Laboratoire Central des Ponts et Chaussées, Nantes, France

S. Goyer
Laboratoire Régional des Ponts et Chaussées, St-Brieuc, France

ABSTRACT: This paper presents a study of the cyclic behaviour of a gravel emulsion, from an experimental pavement, using repeated load triaxial tests, developed for unbound granular materials. The material has been tested in three conditions: the gravel emulsion at early age and after a period of curing of 14 days at 35°C, and the granular material without bitumen emulsion. The study included monotonic triaxial tests, to determine the resistance to failure, and cyclic tests, to determine the resilient (elastic) behaviour. The results show that qualitatively, the behaviour of the gravel emulsion is similar to that of unbound granular materials, with a strongly non linear (stress dependent) resilient behaviour and a low resistance to rutting. A non linear elastic model is proposed to describe the resilient behaviour of the gravel emulsion. Finally, the laboratory results are compared with moduli measured in situ, using FWD tests.

1 INTRODUCTION

Gravel-emulsions (GE) treated with bitumen emulsion are cold mixes with a high potential for development, as safe and environmentally friendly road materials. They are mainly used for construction or rehabilitation of low to medium traffic roads. Gravel-emulsions are characterized by a large evolution of their mechanical behaviour with time, due to the progressive drying and hardening of the bitumen emulsion. Due to their low stiffness, compared with hot mix asphalt materials, gravel emulsions are difficult to characterize using classical mechanical tests for hot mix bituminous materials, such as two point bending complex modulus tests.

In this research, an attempt was made to characterize gravel-emulsions using cyclic triaxial tests, similar to those used for unbound granular materials (UGMs). These tests, where a confining pressure is applied, are well suited for testing of granular materials with a low cohesion. The tests have been performed with a triaxial apparatus for UGMs, at ambient temperature (close to 20°C). The test programme included tests on the gravel emulsion at young age and after a period of curing of 14 days at 35°C, and also tests on the granular material without emulsion. At the end of the study, some additional tests have been performed at LRPC Saint-Brieuc, with a temperature controlled triaxial cell, to evaluate the sensitivity of the behaviour to temperature.

2 THE CYCLIC TRIAXIAL TEST

2.1 *Test principle*

The cyclic load triaxial test is widely used to study the mechanical behaviour of unbound granular materials for pavements and subgrade soils (Balay et al. 1998). The principle of the test is recalled on figure 1. The test is performed on a cylindrical specimen, placed in a cell, and submitted to a confining pressure (or lateral stress) σ_3 and a vertical stress σ_1. In this study,

tests with a Variable Confining Pressure (VCP), where both the axial load and the confining pressure are cycled, in phase, have been used. VCP tests simulate more closely in situ loading conditions than tests with a constant confining pressure. These tests can be used to study both the resilient (or elastic) behaviour and the permanent deformations of unbound materials.

2.2 *Triaxial apparatus*

The apparatus used in this study is shown on figure 2. The specimens have a diameter of 160 mm, and height of 320 mm. A hydraulic actuator is used to apply the cyclic axial load. The triaxial cell is filled with water and a servo-pneumatic system is used to apply the constant or cyclic cell pressure. The load signals are sinusoidal and the maximum loading frequency is 10 Hz with a constant cell pressure and 2 Hz with a cyclic cell pressure. The triaxial cell is equipped with an internal load cell, for the measurement of the axial load. the specimen is instrumented with Hall effect displacement transducers, measuring the axial and radial strains (see figure 2).

3 MATERIAL AND EXPERIMENTAL PROGRAMME

3.1 *Characteristics of the gravel-emulsion*

The gravel-emulsion tested in this study comes from an experimental pavement section, built on a rural road, RD 44, near Rennes, in France. The pavement section has been instrumented,

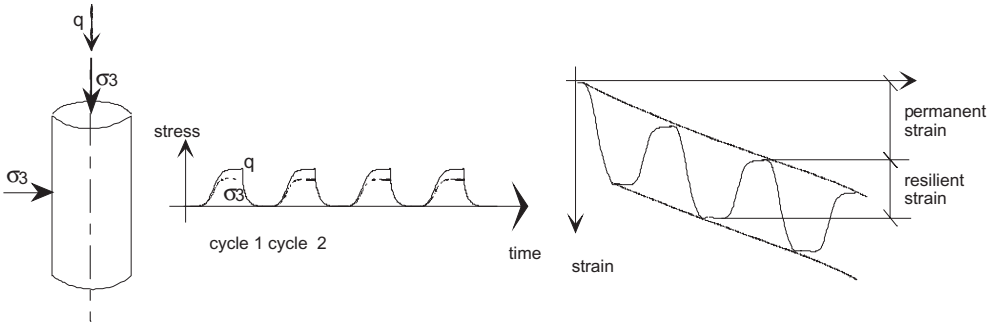

Figure 1. Principle of the cyclic triaxial tests.

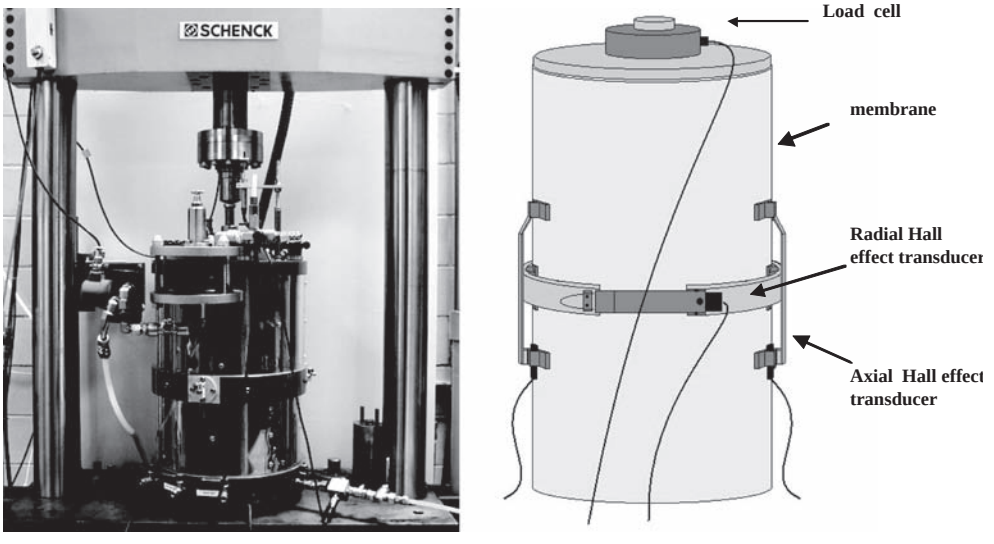

Figure 2. View of the LCPC cyclic load triaxial apparatus, and instrumented specimen.

and it will be monitored during about three years. The objective of the project is to characterize the behaviour of the material both in the laboratory and on site, using different test methods. The main characteristics of the gravel-emulsion are summarized in table 1.

3.2 *Preparation of test specimens*

The test specimens have been compacted using a vibrocompression method, used for the compaction of unbound granular materials, and cement-treated materials. The specimen is compacted in one layer, by applying simultaneously a vertical load and a horizontal vibration. This method is fast (less than 45 seconds) and produces homogeneous densities.

The specimens have been compacted at a void content of 15%, and tested in two conditions: at young age (after conservation for 24 h in a closed PVC mould), and after a period of curing of 14 days, at 35°C and 20% RH, which aim was to simulate the long term behaviour of the material on site. After compaction, the water content of the gravel-emulsion was close to 5% (due to a loss of water during compaction), and it decreased to about 2% after curing. The specimens were tested at these water contents (unsaturated), and in drained conditions.

3.3 *Test programme*

The test programme is summarized in table 2. The objective of the study was to compare the mechanical properties of three materials:

– the gravel-emulsion (GE) prepared in the laboratory.
– the gravel emulsion from the experimental pavement (sampled during the construction).
– The unbound granular material (UGM) without emulsion.

The test programme included monotonic triaxial tests, and resilient behaviour tests, used to study the elastic behaviour. On the gravel emulsion from lab, resilient behaviour tests have been performed at young age and after curing. The gravel emulsion from site has been tested only after curing. A detailed presentation of all the test results has been made by Goyer (2008).

Table 1. Characteristics of the gravel emulsion.

Aggregates	Grading	Percent emulsion	Water content	Bitumen	Residual bitumen content	Void content
Le Pilet (0/2; 2/4 fractions) Gué Morin (4/10; 10/14) origin: Hornfels	0/14 mm	6.7%	7%	Pen. 86 R&B 46°C	4.02%	15%

Table 2. Triaxial test programme.

Material	Tests
Unbound granular material (UGM)	3 monotonic shear tests 2 resilient behaviour tests
Gravel emulsion (GE) from lab	2 monotonic shear tests (at young age) 3 resilient behaviour tests (at young age) 2 resilient behaviour test (after curing)
Gravel emulsion (GE) from site	3 monotonic shear tests (at young age) 2 resilient behaviour tests (after curing)

4 MONOTONIC TRIAXIAL TESTS

The procedure of the monotonic tests consists in applying a constant confining pressure to the specimen, and then a constant vertical displacement rate (1 mm/minute) until failure (until a peak is obtained on the axial strain- deviatoric stress curve). An example of monotonic stress strain curves obtained on the gravel emulsion (from site) is shown on figure 3. Three monotonic tests, with different confining pressures, have been performed on each material. The results have been used to determine the failure line of each material, in the p, q stress space, (with $p = (\sigma_1 + 2\sigma_3)/3$ mean stress and $q = \sigma_1 - \sigma_3$ deviatoric stress) (see figure 4).

For each material, figure 4 gives the parameters m and s of the failure line in the p, q stress space (equation $q = m.p + s$), and the corresponding Mohr-Coulomb parameters ϕ (friction angle) and c (cohesion). The results show that the unbound granular material has a higher resistance to failure than the gravel emulsion, at young age. Therefore, it seems that the emulsion reduces the friction between the aggregates, and thus the resistance to failure of the material.

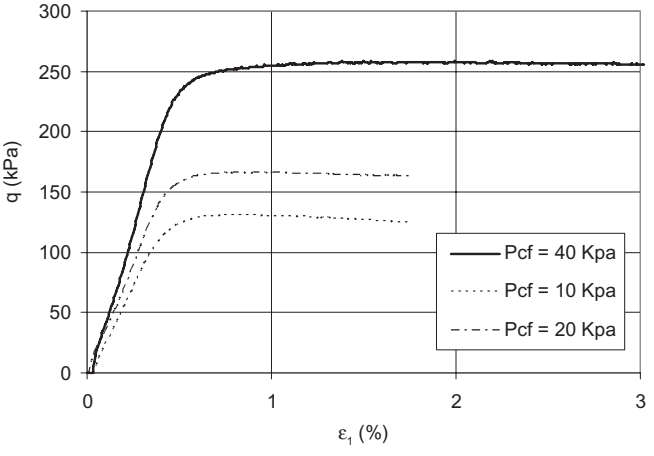

Figure 3. Stress-strain curves of monotonic triaxial tests on the gravel emulsion from site.

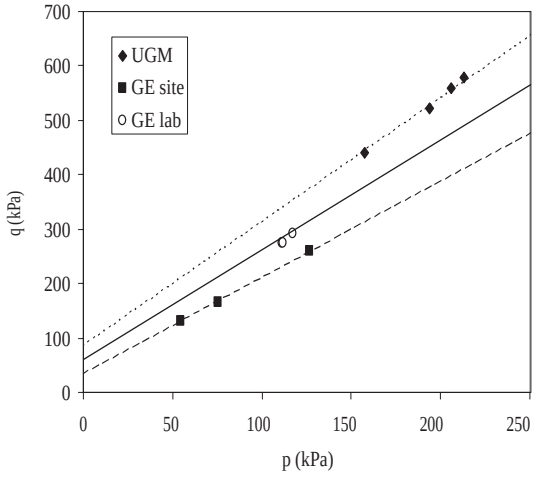

	Unbound granular material	Gravel emulsion (lab)	Gravel emulsion (site)
m	2.34	2.00	1.76
s (kPa)	63	61.8	34.7
ϕ (°)	54.4	48.6	42.9
s (kPa)	54.9	35	18.3

Figure 4. Comparison of the failure lines of the 3 materials.

5 RESILIENT BEHAVIOUR TESTS

5.1 *Results of the conditioning phase*

The resilient behaviour tests are used to determine the elastic or resilient behaviour of the material. The test procedure adopted in this work, proposed by El Abd (2006), includes two phases: first a cyclic conditioning, with a high stress level, which objective is to stabilise the permanent deformations occurring during the first load cycles; then, a series of short loadings (about 100 cycles each), following different stress paths, which are used to characterize the resilient behaviour, for different stress levels.

The main objective of the conditioning is to stabilize the permanent strains of the material, and reach a practically elastic behaviour. The permanent deformations measured during this conditioning also give an indication of the resistance to rutting of the material. Figure 5 shows permanent axial strains ε_1^p measured during the conditioning, for the UGM, and the gravel emulsion. For the same loading, the gravel emulsion presents much larger permanent strains than the UGM. After 20000 cycles, ε_1^p varies between 30 and 40.10^{-4} for the UGM, and is about 10 times higher for the gravel-emulsion at young age. After curing, ε_1^p decreases only by about 20%. Again, this indicates that the emulsion tends to reduce the friction of the material, and thus the resistance to rutting. The curing procedure does not modify significantly this behaviour.

5.2 *Study and modelling of the resilient behaviour*

The second phase of the tests is used to study the resilient behaviour of the materials, for different stress levels. This phase comprises 19 different cyclic load sequences, with different stress levels, and stress ratios q/p varying between 0 and 2 (see figure 6). Each sequence is applied during 200 cycles, at a frequency of 2 Hz. The stress levels correspond to typical stresses obtained in a pavement base course, under the application of a 130 kN axle load.

The resilient axial strains ε_1^r and resilient radial strains ε_3^r obtained for each load level are defined as the strains obtained during the unloading phase of the cycle:

$$\varepsilon_1^r = \varepsilon_1^{max} - \varepsilon_1^{min} \text{ and } \varepsilon_3^r = \varepsilon_3^{max} - \varepsilon_3^{min} \quad (1) \text{ and } (2)$$

where ε^{max} represents the maximum strains during the load cycle, and ε^{min} the strains at the end of the load cycle.

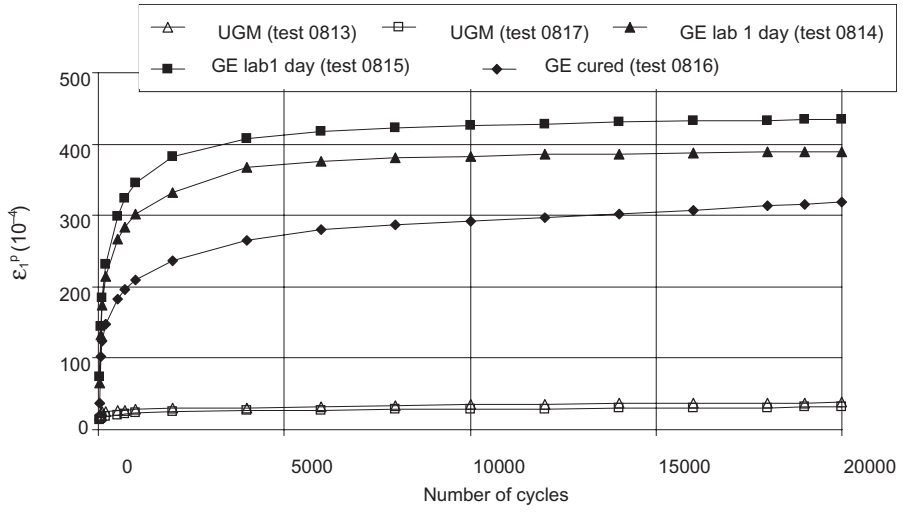

Figure 5. Permanent deformations of the materials during the cyclic conditioning.

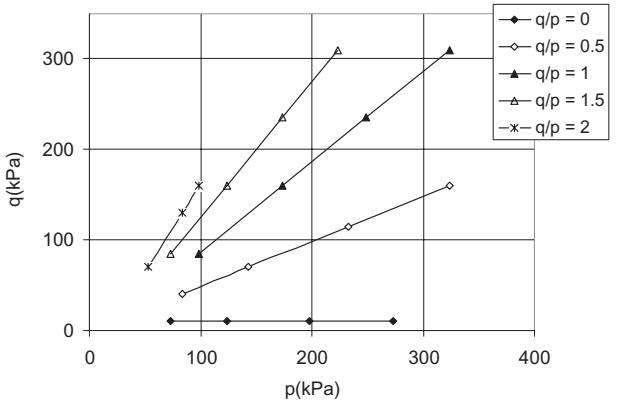

Figure 6. Cyclic stress paths applied for the study of the resilient behaviour.

For unbound granular materials, research carried out at LCPC has shown that the resilient behaviour is well described by a non linear elastic model proposed by Boyce (1980), and then modified by Hornych et al. (1998), to take into account anisotropy observed on many materials. The Boyce model is expressed in terms of Bulk Modulus, *K,* and Shear Modulus, *G,* with:

$$K = \frac{p}{\varepsilon_v} \quad \text{and} \quad G = \frac{q}{3\varepsilon_q} \qquad \text{(3) and (4)}$$

with: *p:* mean normal stress, *q:* deviator stress;
ε_v: volumetric strain, $\varepsilon_v = \varepsilon_1 2\varepsilon_3$, ε_p: shear strain, $\varepsilon_p = \frac{2}{3}(\varepsilon_1 - \varepsilon_3)$

The values of K and G are stress dependent according to the following relationships:

$$K = K_a \left(\frac{p}{p_a}\right)^{1-n} \Bigg/ \left(1 - \beta\left(\frac{q}{p}\right)^2\right) \quad \text{and} \quad G = G_a \cdot \left(\frac{p}{p_a}\right)^{1-n} \qquad \text{(5) and (6)}$$

with: $$\beta = (1-n)\frac{K_a}{6G_a} \qquad (7)$$

K_a, G_a, n: parameters of model; p_a: constant equal to 100 kPa.

To introduce anisotropy in the model, Hornych et al. (1998) proposed to multiply the principal stress, σ_1 by a coefficient of anisotropy γ. This leads to the equations:

$$\varepsilon_v{}^* = \frac{1}{K_a}\frac{p^{*n}}{p_a{}^{n-1}}\left[1 + \frac{(n-1)K_a}{6G_a}\left(\frac{q^*}{p^*}\right)^2\right] \quad \text{and} \quad \varepsilon_q{}^* = \frac{1}{3G_a}\frac{p^{*n}}{p_a{}^{n\text{-}1}}\frac{q^*}{p^*} \qquad \text{(8) and (9)}$$

with: $$p^* = (\gamma\sigma_1 + 2\sigma_3)/3 \quad \text{and} \quad q^* = \gamma\sigma_1 - \sigma_3$$

$$\varepsilon_v{}^* = \varepsilon_1/\gamma + 2\varepsilon_3 \quad \text{and} \quad \varepsilon_q{}^* = \frac{2}{3}(\varepsilon_1/\gamma - \varepsilon_3)$$

Figure 7 shows an example of results of a resilient behaviour test on the gravel emulsion (from lab). The figure presents the variations of the resilient volumetric strains ε_v and resilient

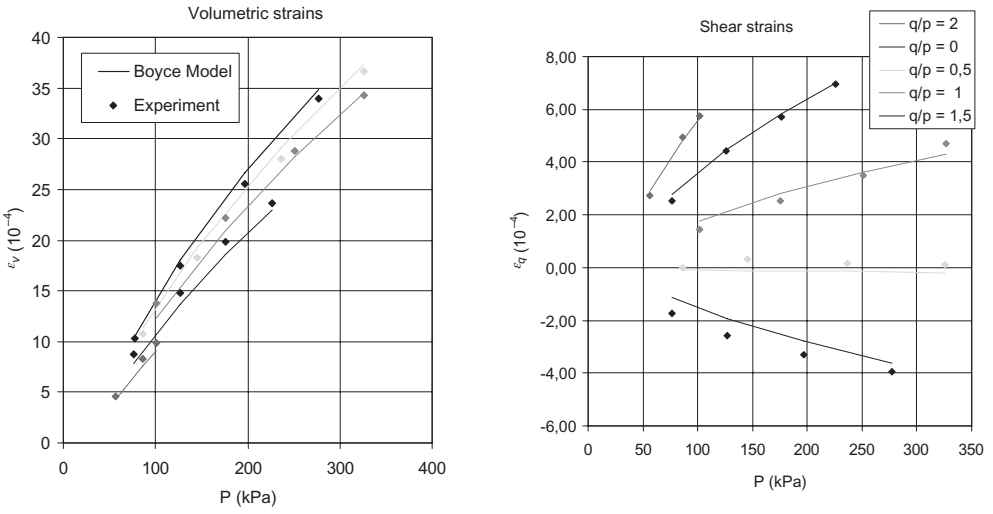

Figure 7. Example of results of a resilient behaviour test on the gravel emulsion at young age.

Table 3. Values of Boyce model parameters obtained for the tests on the 3 materials.

Material	***Test***	**W%**	**Temp.°C**	**Ka MPa**	**Ga MPa**	**n**	**γ**	**ρ**
UGM	*08–13*	5.2		31.70	81.40	0.37	1.03	0.758
UGM	*08–17*	5.2		36.58	57.87	0.49	0.92	0.682
GE lab	*08–14*	5.0	23	37.83	60.17	*0.57*	0.88	0.875
GE lab	*08–15*	5.3	23	34.32	52.80	0.57	0.78	0.903
GE lab	*08–203*	4.5	20	34.9	54.2	0.41	0.79	0.829
GE lab cured	*08–16*	4.4	26.5	15.98	57.91	0.28	0.76	0.749
GE lab cured	*08–197*	3.9	20	23.1	67.4	0.27	1.00	0.664
GE site cured	*08–19*	1.9	24	16.10	58.37	0.28	0.76	0.679
GE site cured	*08–20*	2.0	25	26.09	63.25	0.42	0.76	0.669

shear strains ε_q, as a function of the mean stress p, for different stress ratios q/p. The results show that the behaviour of the gravel emulsion is strongly non linear:

– ε_v increases with the mean stress p, and decreases when the stress ratio q/p increases;
– ε_q increases when p increases, and also when q/p increases. For the isotropic loading ($q/p = 0$), $\varepsilon_q = 2/3\ (\varepsilon_1 - \varepsilon_3)$ is negative, which indicates that the behaviour is anisotropic ($\varepsilon_3 > \varepsilon_1$ for an isotropic loading).

This behaviour is very similar, qualitatively, to that of unbound granular materials. For this reason, it was decided to use the anisotropic Boyce to describe this behaviour. Good predictions of the experimental results were obtained with this model for all the tests (see the example of figure 7). The values of the model parameters obtained for all the tests are summarized in table 3. The last parameter ρ, is a coefficient of adjustment of the model (varying between 0 and 1). The fit is considered satisfactory when $\rho > 0.6$.

The results of table 3 show that the Boyce model parameters of the UGM and of the gravel-emulsion (at young age and after curing) are of the same order of magnitude. The main difference concerns the parameter of anisotropy γ, which is close to 1 for the UGM, (isotropic behaviour), and around 0.8 for the gravel emulsion (anisotropic behaviour). This value corresponds to a ratio between the vertical modulus E_v and the horizontal modulus E_h equal to $E_v/E_h = 1/\gamma^2 \approx 1{,}56$. For the gravel emulsion, the curing

procedure does not seem to modify fundamentally the behaviour. The exponent n is lower on the cured material (about 0.3), indicating an even more non-linear behaviour than at young age. The parameter K_a, related to volumetric strains, also decreases slightly after curing.

6 INFLUENCE OF TEST PARAMETERS ON THE RESILIENT BEHAVIOUR

6.1 *Influence of material parameters*

To allow simple comparisons of the performance of the 3 tested materials, values of vertical young modulus E_v have been calculated for all the tests, for 2 different stress levels, to account for the non linear behaviour. The mean values of E_v obtained for each material, for the low stress level (p = 75 kPa, q = 150 kPa) and the high level (p = q = 300 kPa) are shown on figure 8. The results show that:

- For both stress levels, the elastic moduli of the unbound granular material are about 20 to 30% higher than those of the gravel emulsion.
- Concerning the gravel-emulsion, there is no significant effect of the curing procedure (depending on the stress level, the modulus of the cured material is slightly lower or higher than that of the material at young age). This result is important; in the field, experience shows that the aging and drying of the gravel emulsion lead to a significant increase of mechanical properties at long term (typically after one year). The accelerated curing procedure (14 days at 35°C), does not seem to have the same effect.

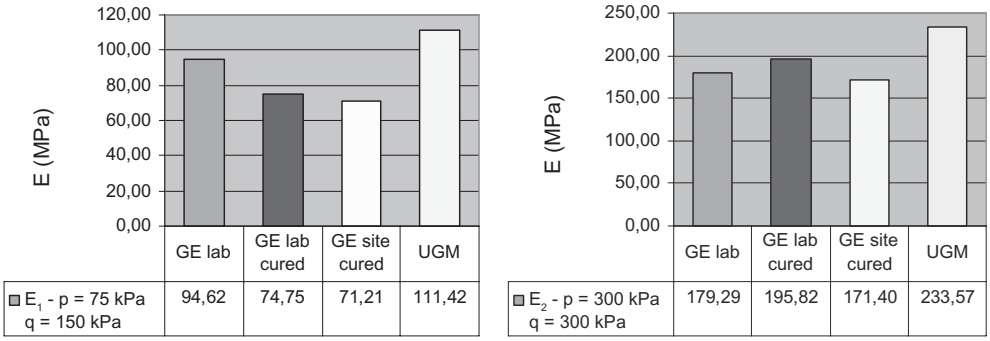

Figure 8. Mean values of elastic modulus E_v obtained for the different materials, for two stress levels.

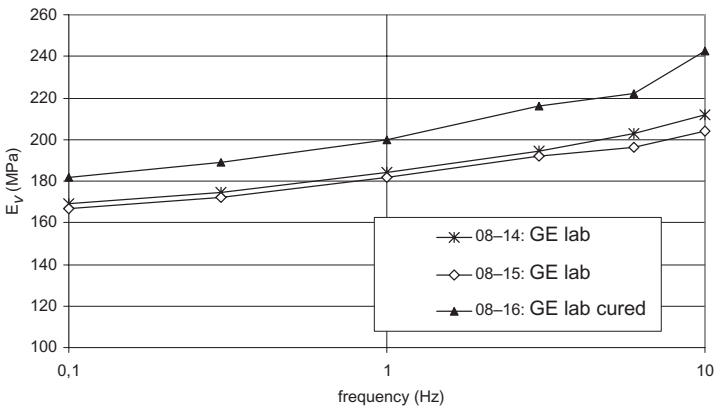

Figure 9. Influence of the loading frequency on the elastic modulus E_v of the gravel emulsion from lab.

– The elastic moduli of the gravel emulsion from site are close to those of the material prepared in lab (slightly lower).

6.2 *Influence of temperature and loading frequency*

The previous resilient behaviour tests have been performed using tests procedures developed for UGMs, with constant frequency and temperature. At the end of the study, some additional tests have been performed to evaluate the sensitivity of the gravel emulsion to these parameters:

At LCPC, at the end of tests 08-14 and 08-15 (gravel emulsion from lab, at young age), and 08-16 (gravel emulsion from lab cured 14 days), additional loadings have been performed, to determine the response of the material for 6 frequencies, varying between 0.1 Hz and 10 Hz. These loadings were performed with a constant confining pressure $\sigma_3 = 20$ kPa, and with a cyclic axial stress $\Delta\sigma_1 = 150$ kPa. Values of vertical elastic modulus E_v obtained for these variable frequencies are shown on figure 9. The sensitivity to frequency is limited: when the frequency is multiplied by 10, the modulus increases by about 10%. The trend is similar for the tests at young age and after curing.

Finally, two triaxial tests have been performed at LRPC Saint Brieuc, using a triaxial apparatus equipped with a temperature control system (temperature range 0 to 40°C). The specimen size, and the procedure of preparation of the specimens were the same as at LCPC. Two preliminary tests have been performed on the gravel-emulsion from lab, as follows:

– Conditioning (20000 cycles) at 10°C, and resilient behaviour test at 10°C, following the same procedure as at LCPC (fig. 6).
– Conditioning (5000 cycles) at 20°C and resilient behaviour test at 20°C.
– Conditioning (5000 cycles) at 30°C and resilient behaviour test at 30°C.

Values of vertical elastic modulus E_v calculated for the 3 temperatures, for 2 stress levels, are presented on figure 10. The results indicate a significant sensitivity to temperature, when the temperature increases from 10°C to 30°C, the modulus decreases by about 50%.

7 COMPARSION OF THE LABORATORY RESULTS WITH FIELD BEHAVIOUR

As mentioned previously, the gravel emulsion tested in this study has been used for an experimental pavement section, built on road RD44, near Rennes, in France. This project consisted in the reinforcement of an old pavement by a 12 cm thick layer of gravel emulsion, over a length of 300 m. The layer was put in place on July 3rd 2008. As part of the monitoring of the experimental section, FWD measurements have been made before the construction, on the old pavement, and 1 week after the construction. The results of these FWD tests have been used to evaluate the in situ moduli of the gravel-emulsion.

The analysis of the FWD results has been performed with the Software ALIZE, which is based on a multi-layer linear elastic model. The calculations have been made in two steps: first, the moduli of the layers of the old pavement have been back-calculated from the tests on the old pavement. In a second step, the measurements on the reinforced pavement have been used to determine the moduli of the gravel-emulsion layer. All the FWD measurements have been made at a temperature of 20°C (+/– 1°C), with a 300 mm diameter plate, and a 71 kN Load. Due to variations of the profile of the old pavement (thickness of the layers and subgrade), two different pavement structures (noted S1 and S2), with different thicknesses, have been considered for the back-calculations.

The results of the back-analysis of the FWD measurements are summarized in table 4. For each structure, table 4 gives, for each layer, a range of value of modulus, taking into account the scatter of the FWD measurements (mean deflection basin, and mean +/–1 standard deviation σ). The values of elastic modulus of the gravel-emulsion obtained on the two sections are very similar, with mean values of 566 MPa and 552 MPa, and a range of variation of about +/– 20%.

To compare the in situ moduli with the laboratory values, it is necessary to take into account the stress levels in the FWD tests. A linear elastic calculation, with the ALIZE software,

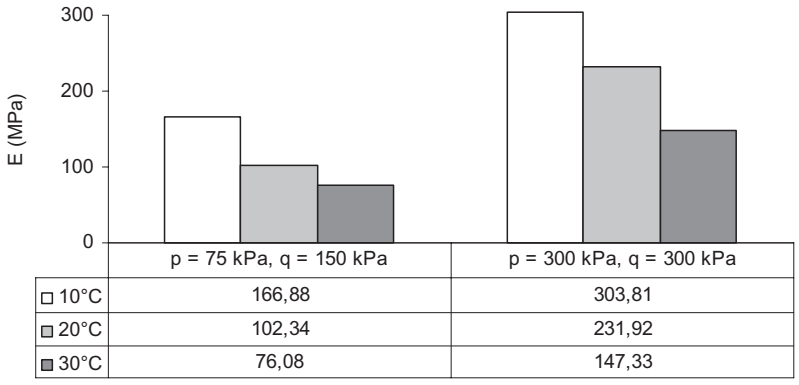

Figure 10. Values of elastic modulus of the gravel emulsion from lab (after curing) for 3 temperatures.

Table 4. Elastic moduli of the layers of the experimental pavement (back-calculated from FWD tests, at 20°).

Structure 1					Structure 2				
Material	Thickness cm	E_1 MPa	E mean MPa	E_2 MPa	Material	Thickness cm	E_1 MPa	E mean MPa	E_2 MPa
GE	12	536	566	592	GE	11	658	552	471
BC(1)	7	5500	5500	5500	BC(1)	10	4940	4050	3520
UGM(2)	42	354	289	242	UGM(2)	25	200	221	227
Subgrade	40	33	29	26	Subgrade	35	18	15	13

(1) BC: Bituminous concrete; (2) UGM: Unbound granular material.

indicates that in the FWD test, at mid-depth in the gravel-emulsion layer, the maximum stress levels are around $p \approx 500$ kPa and q/p ≈ 1. For this stress level, the values of vertical elastic modulus are the following:

- For the gravel emulsion from lab, at young age: $E_v = 200$ to 230 MPa
- For the gravel emulsion from lab, after curing: $E_v = 230$ to 300 MPa
- For the gravel emulsion from site after curing: 230 to 245 MPa

In conclusion, this first simple evaluation indicates that the elastic moduli measured in the field (one week after placement) are about 2 times higher than the laboratory values. Additional studies are planned to explain the origin of theses differences, which can be due to the differences in the compaction and curing of the material in laboratory and on site, and also to differences in the loading conditions of the two types of tests (stress level, frequency...).

8 CONCLUSIONS

This paper presents the first results of the study of a gravel-emulsion material, from an experimental pavement, using cyclic triaxial tests. The tests have been performed on the gravel emulsion at young age and after a curing procedure, and on the granular material without emulsion. Resistance to failure, resilient (elastic) behaviour and resistance to permanent deformations have been studied. Tests have been performed at a temperature of 20°C (except two last tests, with 3 different temperature levels)

The study shows that at 20°C, the gravel emulsion presents, at young age, a lower resistance to failure than the granular material without emulsion, and also a lower resistance to

permanent deformations. It seems, therefore, that at young age, the emulsion acts as a lubricant and reduces the shear strength of the material.

The resilient behaviour of the gravel emulsion (at 20°C) is, qualitatively, very similar to that of unbound granular materials and can be described using the same non linear elastic model (modified Boyce model). At young age, the gravel emulsion presents low elastic moduli, ranging from about 100 to 200 MPa, for the experimental stress levels. These values are slightly lower than those of the unbound granular material. The influence of the loading frequency on the resilient behaviour is low (10% increase of the modulus when the frequency is multiplied by 10). The sensitivity to temperature is more important, and will be studied more in detail.

A more surprising result is the low influence of the curing procedure on the mechanical properties of the gravel-emulsion. The resistance to failure and elastic moduli increase slightly after curing, but remain lower than those of the unbound granular material. This seems to indicate that the procedure used (14 days of curing at 35°C and 20% R.H.) does not reproduce adequately the long term conditions in the pavement. In comparison, typical in situ moduli of gravel emulsions, in pavements, after several months of service, range from 1000 to 3000 MPa (at 15°C), well above the values measured in this study. Therefore, further work is needed to develop a more realistic curing procedure.

Finally, this research confirms the interest of the cyclic triaxial test, for determining the mechanical properties of gravel-emulsions, which present a relatively low stiffness. The work will be continued on the same material, to study in particular the influence of temperature, more realistic curing procedures and different mix compositions on its behaviour.

REFERENCES

Balay, J., Gomes Correia, A., Hornych, P., Jouve, P. & Paute, J.L. 1998. Etude expérimentale et modélisation du comportement mécanique des graves non traitées et des sols supports de chaussées, *Bulletin de Liaison des LPC* n° 216, pp. 3–18.

Boyce, J.R. 1980. A non linear model for the elastic behaviour of granular materials under repeated loading, *Int. Symposium on Soils under Cyclic and Transient Loading*, Swansea, U.K. pp. 285–294.

El Abd, A. 2006. Prédiction des déformations permanentes des chaussées à assises non traitées. PhD Thesis, University of Bordeaux 1, France.

Hornych, P., Kazai, A. & Piau, J.M. 1998. Study of the resilient behaviour of unbound granular materials, *proc. 5th Conference on Bearing Capacity of Roads and Airfields*, Trondheim, Norway, July 1998.

Goyer, S. 2008. Etude des performances mécaniques de graves émulsions au moyen d'essais triaxiaux cycliques, *Master of Science*, Ecole Centrale de Nantes, France.

Advanced Testing and Characterization of Bituminous Materials – Loizos, Partl, Scarpas & Al-Qadi (eds)
© 2009 Taylor & Francis Group, London, ISBN 978-0-415-55854-9

Laboratory performance-based assessment of half-warm mix asphalts with high recycling rate by means of the factorial experiment design approach

F. Olard & E. Beduneau
Research & Development Department, EIFFAGE Travaux Publics, France

N. Seignez, S. Dupriet & D. Bonneau
Ciry Central Laboratory, EIFFAGE Travaux Publics, France

ABSTRACT: Nowadays, the criterion of materials—and cost—savings without sacrificing performance is systematically taken into account by building owners, prime contractors, asphalt producers and road contractors. In-plant reclaiming of asphalt pavement (RAP) at strong rate is more and more often used within the framework of rehabilitation or maintenance roadworks. The maximum RAP content percentage is generally between 30% and 50% according to the considered asphalt plant equipment limitations and to the national specifications. Nevertheless, new kinds of asphalt plants enable the use of RAP content up to 70% whatever the production temperature (hot-mix or warm-mix asphalt). This study, realized in the Ciry-Salsogne research centre of EIFFAGE Travaux Publics, aimed at determining the influence of the mix composition on the performance-based properties of half-warm mix asphalts, produced in laboratory at approximately 95°C following the innovative proprietary low energy asphalt technique labeled LEA®. By means of the factorial experiment design approach, this study highlights the influence of the bitumen pen grade (10/20, 35/50 and 50/70), the RAP content (30%, 50% and 70%) and the vegetable additive content used in the LEA process (0.2%, 0.6% and 1%). Many laboratory tests were conducted so as to determine the mechanical performances of LEA mixes, including the French gyratory shear compacting press, the Duriez test (evaluation of the water resistance) and the stiffness modulus. This laboratory characterization shows that very high recycling rates (from 30% to 70%) can be used in half-warm mix asphalts as a cheap and efficient way to minimize environmental impacts.

1 INTRODUCTION

With the threat of oil shortage and price increase, the lack of good quality aggregates, and the general conscience on environmental issues, both low-energy asphalt production and recycling of asphalt pavement are getting more and more attention.

As regards the low-energy solutions, they are categorized in warm and half-warm, depending on whether their production temperature is above or below 100°C. This paper focuses on the recent LEA® half-warm technique which is currently used on almost 40 plants mainly in Europe (Romier 2004, 2006, Olard 2007a, 2007b, 2007c, 2008, Prowell 2007, Sauzeat 2008) and the USA (Harder 2008). 250,000 tons have been realized over the past few years, demonstrating the feasibility of lowering the operating temperatures, the energy consumption and the fumes emissions (Gaudefroy 2008). More details on this technology are given in section 2.

Insofar as recycling is concerned, a tremendous number of publications can be found on the effect of RAP content on the mechanical performances of asphalt mixtures. However, the maximum RAP percentage is generally between 30% and 50% according to the considered asphalt plant equipment limitations and to the national specifications. Thus, this study focused on using a higher than usually used percentage of RAP—up to 70%—in asphalt base courses. Background of the recycling in Europe in particular is briefly given in section 3.

2 DESCRIPTION OF THE INNOVATIVE LEA® HALF-WARM MIX PROCESS

The originality of the LEA process lies in the ability of hot anhydric bitumen to foam or to emulsify when in contact with the residual aggregate moisture just below the water vaporization point at 100°C, therefore allowing coating at lower temperatures. Owing to the dispersed water (liquid or steam) inside bitumen, the spontaneous volume expansion of bitumen (see Figure 1a) leads to a thicker binder film around aggregate (from the mixing and coating stage in plant to the paving and compaction stage at job site); it thus fosters good mix workability. Some specific additives may be used to improve the foaming and coating ability of the binder. As displayed in Figures 1 & 2, different possible sequential drying and coating processes can be used in relation to the mix formula and to the asphalt plant configuration:

- LEA 1: the drying stage only affects a first part of the aggregates, then coated by the whole bitumen. The remaining cold and wet part is then added. All the constitutive elements of the mix are then mixed (Figure 1b), or
- LEA 2: the drying stage only affects a first part of the aggregates, which is then mixed, before the coating stage, to the remaining moist part (Figure 2a), or
- LEA 3: all the aggregates are partially dried, then coated by the hot bitumen (Figure 2b).

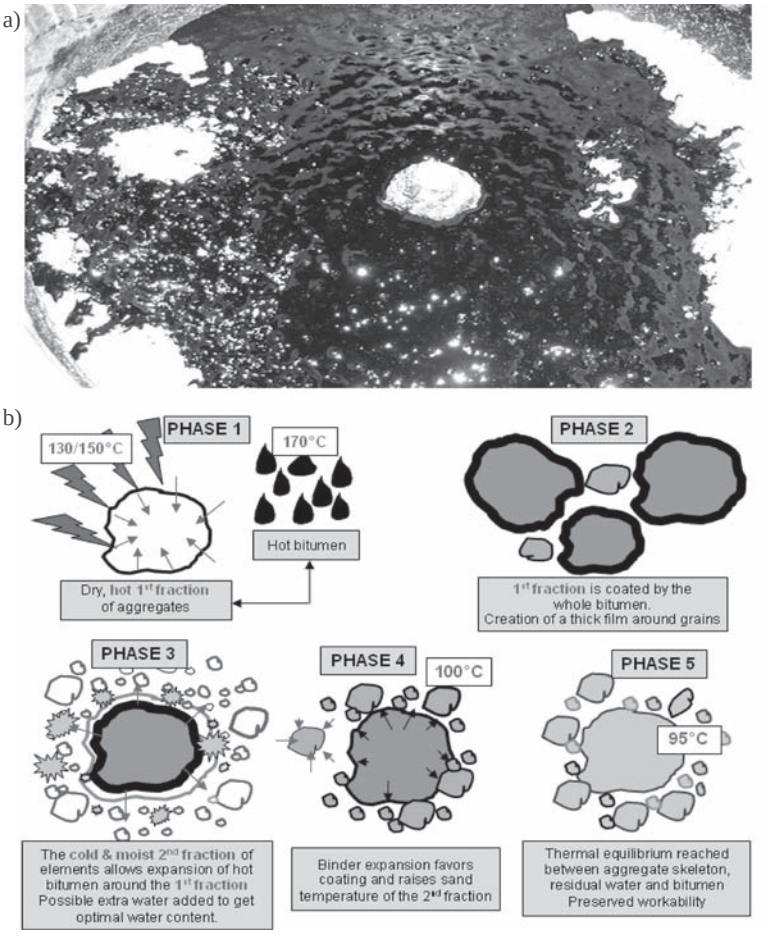

Figure 1. a) Binder expansion in a lab mixer; b) LEA® process diagram with pre-coating (Olard 2007c).

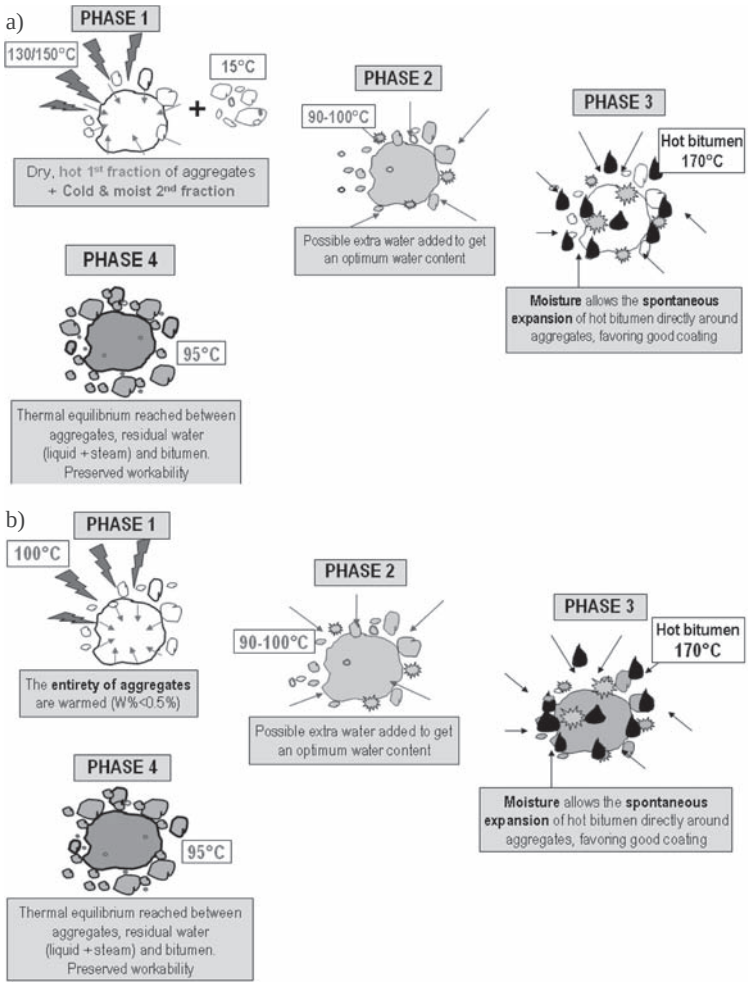

Figure 2. LEA® without pre-coating: a) drying of a first part of the aggregates which is then mixed, before coating, to the remaining part which has retained its initial humidity; b) partial drying of all the aggregates (allowing a fraction of the initial humidity to remain) prior to coating (Olard 2007c).

3 SOME KEY FIGURES ABOUT ASPHALT RECYCLING IN EUROPE

With the threat of oil shortage and related price increase, the lack of good quality aggregates, and the general conscience on environmental issues, recycling of asphalt pavement is getting more and more attention. Table 1 gives some key figures regarding recycling in the European asphalt industry. A comparison between the data obtained in 2002 and 2005, is proposed to illustrate the increasing use of RAP in the hot-mix production in most countries. These data have been established by the European Asphalt Pavement Association (EAPA 2002, 2005).

Table 2 which is drawn from a recent European survey on the use of RAP (Planche 2008), reports on the techniques used, giving the maximum RAP content authorized, according to the related layer in the new pavement, and to the technique used for mixing with fresh materials. As a matter of fact, these values are based upon field experience of the performance of asphalt pavements built with RAP. Yet, there is little information available about the effect of such high RAP contents on the mechanical properties of the resulting mixtures. Thus, it becomes an important priority to study and determine the effects that various types and percentages of RAP have on combined asphalt binders (RAP binder and virgin binder) and mixture properties.

Table 1. Shift in the use of RAP in some European countries between 2002 & 2005 (EAPA 2002, 2005).

	2002			2005		
Country	Available Materials (T)	% used in warm recycling	% of the new hotmix production that contains RAP	Available Materials (T)	% used in warm recycling	% of the new hotmix production that contains RAP
Belgium	1 500 000	29	31	1 500 000	40	36
Denmark	237 000	54	36	218 000	83	48
France	5 000 000	10–45	>15	6 500 000	13	<10
Germany	15 000 000	80	20	14 000 000	82	≈60
Italy	13 000 000	15	5	14 000 000	18	7
Netherlands	3 500 000	60–70	60–65	3 000 000	75	63
Norway	471 000	19	7	409 000	23	10
Poland	750 000	15–30	0,5	1 080 000	4	0,1
Sweden	900 000	15	20	750 000	40	25

Table 2. Recycling techniques (Planche 2008).

Country	Hot technique	Max RAP content in base/binder course	Max RAP content in wearing course	Cold technique
Belgium	Mainly	50% binder coming from RAP if homogeneous RAP; 20% binder coming from RAP if heterogeneous RAP		
Czech Republic		25 to 40% when fresh bitumen pen 30 to 70; 60% for softer grade	No	Foamed bitumen; Emulsions & Cement
France	Mainly	15% with no testing; 30% in drum dryers; 50% in double drums	10% max (no testing)	Emulsions
Germany	Mainly	20% in binder course; Up to 100% in base	20%	Emulsions or foams; Recommended for tar contaminated RAP
Italy	Mainly	Never above 50%; usually below 30%	No, except for special wearing course (<20%)	Mainly emulsions but foam increase; Higher % RAP allowed
Netherlands	Mainly	50%	50% in some cases	No
Denmark	Mainly	5 to 10% with no testing		
Spain	Mainly	5 to 10% with no testing; 10 to 50% on layers <15 cm	5 to 10% (no testing)	Slowly increasing; Emulsions; 100% RAP allowed in base courses (only if RAP made of more than 90% bituminous materials)
Switzerland	Mainly	70% in sub-base; 60% in base layer; 30% in binder course	30% in surface layer for secondary roads	Slowly increasing; Foamed bitumen
United Kingdom	Usual limit to 30% RAP	10% with no testing; 50% permitted with testing	10% with no testing	Bitumen foam with cement or lime as adhesion agent; 100% allowed in base

4 OBJECTIVES OF THE STUDY

The study presented herein, carried out at the EIFFAGE Travaux Publics lab in Ciry (France), aimed at determining the influence of the RAP content (%), the fresh binder penetration (1/10 mm) and the vegetable additive content (%) on the mechanical properties of the half-warm mix asphalt LEA, compared to the traditional HMA acting as a reference material. Many tests were conducted including the French gyratory shear compacting press, the Duriez test (evaluation of the water resistance) and the measurement of the stiffness modulus.

5 EXPERIMENTAL SECTION

5.1 *Materials*

The chosen grading formula is a dense high-modulus asphalt 0/20 (French Enrobé à Module Elevé "EME"), used as base course. The virgin limestone aggregates come from the North of France (French Haut-Lieu quarry in Avesnes/Helpes). The RAP aggregates come from the milling of the A43 highway near Chambéry (French Alps), the content and penetration of the recovered aged binder being respectively 5.53% and 13 1/10 mm.

Besides, three fresh pen grade bitumens of naphtenic nature were studied, the acidic nature of which allowing a rather good adhesion to the limestone aggregates. Oleoflux®, a vegetable fluxant (from sunflower), is the binder additive used in this study, acting as both a workability enhancer for LEA production at 95°C and also a rejuvenator of RAP aged binder.

An initial water content of 1.7% (before partial vaporization due to the foaming phenomenon) was used for the manufacture of each LEA mixture at 95°C.

5.2 *Description of tests used*

The following performances of LEAs and corresponding HMAs were determined in lab:

- Compacting ability, measured from the French gyratory shear compacting press PCG ("Presse à Cisaillement Giratoire", Fig. 4a) following the requirements of standard

Figure 3. Mixer used for the manufacturing of LEA® high-modulus mixtures (95°C) and corresponding HMAs (160–180°C) at the EIFFAGE Travaux Publics research centre in Ciry-Salsogne (France).

NF P 98 252. The test gives a good idea of the density values observed on the job site, according to course thickness, for HMAs. This compulsory test is thus run first. Yet, for LEAs, the results are somewhat optimistic compared to the in-situ density values.

- Water resistance, measured from the Duriez test (see standard NF P 98-251-1) which consists of unconfined direct compression test on two sets of cylindrical samples, one set after conditioning in water. If the ratio of the results (the so-called "r/R" ratio) after and before conditioning is above a certain value, the material is acceptable. The r/R ratio is the French counterpart of the ITSR (Indirect Tensile Strength Ratio) value.
- Complex stiffness modulus at 15°C–10 Hz, NF EN 12697-26 (Fig. 4b).

5.3 *Factorial experimental design*

The three studied factors are the RAP content (%), the virgin bitumen penetration (1/10 mm) and the vegetable additive content (%). Each factor has three levels:

– RAP percentage: 30, 50, 70%
– bitumen penetration: 17.9 (10/20 grade), 39.5 (35/50 grade), 61.1 (50/70 grade) 1/10 mm
– vegetable additive content (by weight of the total combined bitumen): 0.2, 0.6, 1%

The complete experimental design of this study corresponds to 3^3 possible combinations (three factors with three levels) of asphalt formulas. A specific reduced factorial experimental design optimized with 13 experiments (Box-Benken matrix), reported in Figure 5 and Table 3, enables to calculate the effects of the different factors on the properties of LEA mixtures.

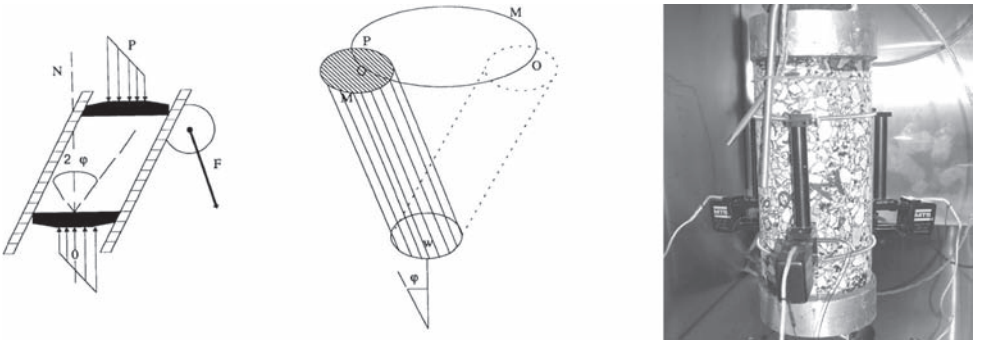

Figure 4. a) Principle of compacting with the gyratory shear compacting press, b) Complex modulus test.

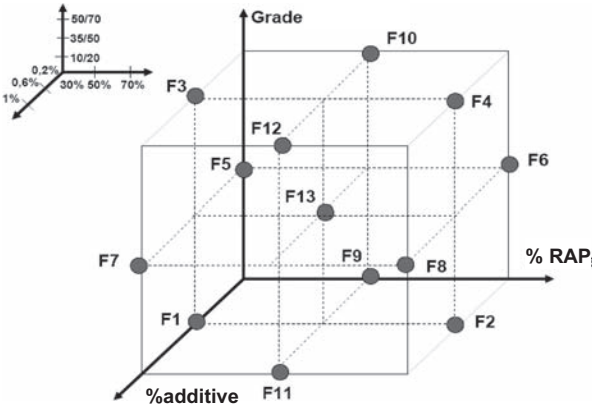

Figure 5. Spatial repartition of the 13 tested asphalt formulas in the experimental domain.

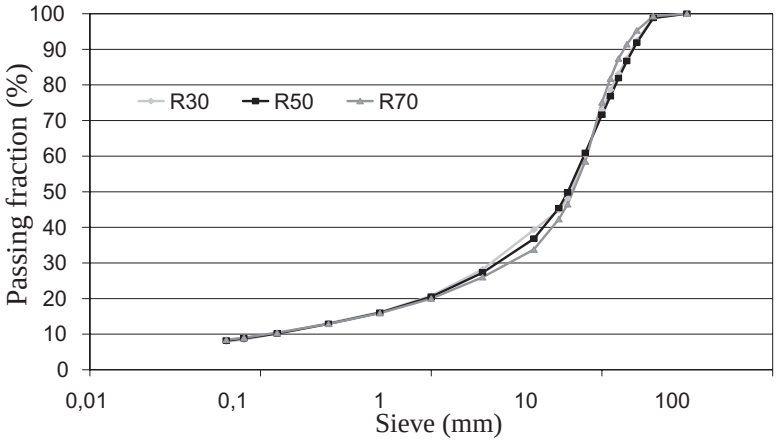

Figure 6. Similar grading for the three asphalt formulas at respectively 30%, 50% and 70% of RAP.

Table 3. Results of Duriez tests, shear compacting press and complex modulus obtained for each formula.

		Total Binder		Duriez Test		PCG	Modulus
N°	Formula RAP/ grade/additive	Calculated pen[(1)]	% voids	R (MPa)	Moisture res.	% voids at 120 gyrations	E* 15°C–10 Hz at 3.1% voids[(2)]
Specifications of NF P 98–140					>0,75	3%–6%	>14000
01	30% 10/20 0,6%	16.3	4.1	16.43	0.82	2.8	11 786
02	70% 10/20 0,6%	14.8	5.5	15.55	0.81	8.9	11 797
03	30% 50/70 0,6%	38.4	3.4	10.71	0.94	1.8	6 855
04	70% 50/70 0,6%	23.4	6.1	11.84	0.87	7.7	8 217
05	30% 35/50 0,2%	30.0	4.0	13.93	0.92	2.5	11 435
06	70% 35/50 0,2%	20.8	8.0	10.50	0.78	8.6	12 483
07	30% 35/50 1,0%	30.0	3.1	11.55	0.89	2.3	10 098
08	70% 35/50 1,0%	20.8	7.7	9.53	0.84	7.8	11 700
09	50% 10/20 0,2%	15.3	5.3	18.82	0.87	4.1	17 924
10	50% 50/70 0,2%	28.2	5.5	13.07	0.84	6.6	15 549
11	50% 10/20 1,0%	15.3	5.7	16.09	0.84	5.0	15 912
12	50% 50/70 1,0%	28.2	4.9	12.04	0.94	6.7	13 174
13	50% 35/50 0,6%	23.7	5.7	13.38	0.91	5.3	14 178

[(1)] without taking into account the additive content.
[(2)] calculated at an equi-density of 3.1% thanks to the Francken method (1977).

6 RESULTS AND DISCUSSIONS

Table 3 gives the results of the 13-experiment Box-Benken factorial experimental design, enabling to calculate the effects of the 3 different factors on the properties of the studied high-modulus LEA mixtures.

Figure 7 displays the results of compacting ability (% voids at the shear compacting press) and moisture resistance (Duriez ratio) according to the RAP percentage, the fresh

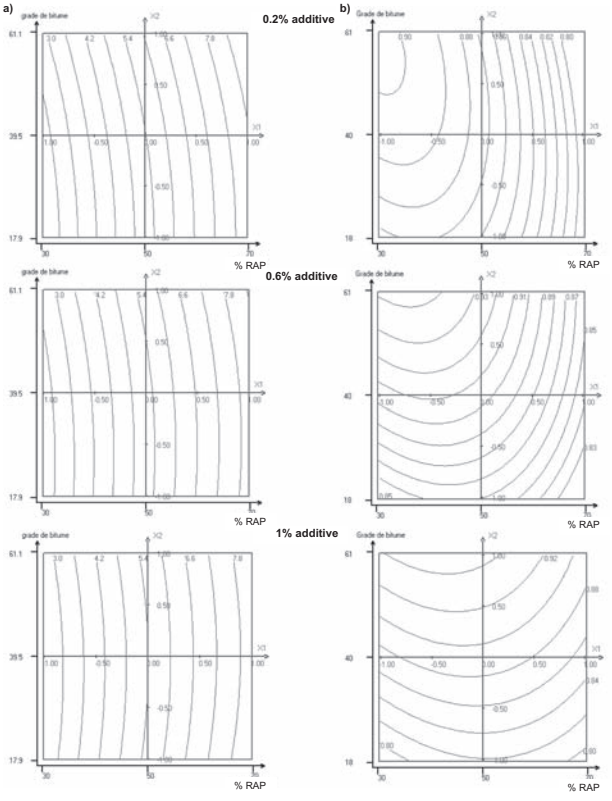

Figure 7. Results of a) compacting ability (% voids at the shear compacting press) & b) moisture resistance (Duriez ratio) according to the RAP percentage, the fresh binder penetration and the additive content.

binder penetration and the additive content, whereas Figure 8 shows the stiffness modulus results.

Figure 7 evidences the main following results for the studied high-modulus low energy asphalt:

– as regards the % voids obtained at the shear compacting press, the higher the RAP content (in the range 30–70%), the more difficult the mix compaction. Both the fresh binder grade and the Oleoflux® additive content seem to have little influence on the compaction ability.
– regarding the Duriez ratio, the softer the bitumen, the better the moisture resistance. The higher the RAP content (ranging from 30 to 70%), the worse the moisture resistance.

Figure 8 illustrates the possible design of a high-modulus low energy asphalt when considering the corresponding French specifications where the minimum value required is 14,000 MPa. In the case of this study with 0.2% of vegetable additive content, for a RAP content ranging from 40% to 60%, a fresh bitumen penetration ranging from 18 to 61 1/10mm is indeed satisfying.

7 CONCLUSIONS

This study aimed at determining the influence of the mix composition on the performance-based properties of half-warm mix asphalts. The considered half-warm mix asphalts were

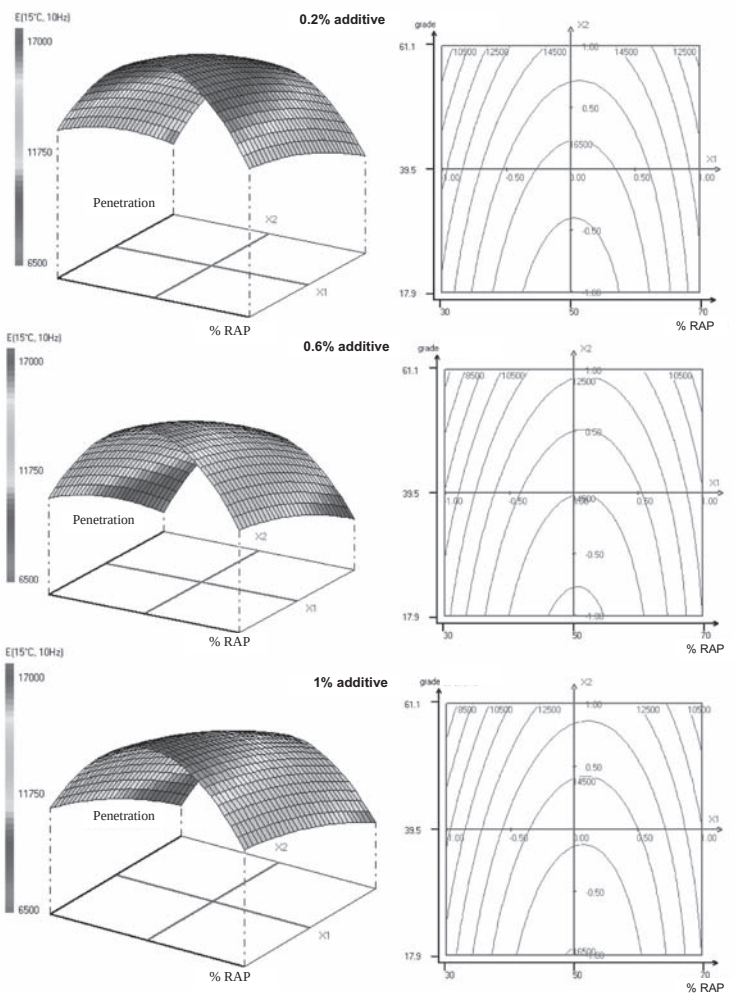

Figure 8. Evolution of the complex modulus at 15°C–10 Hz according to the RAP percentage, the fresh binder penetration and the additive content.

produced in lab at 95°C following the innovative proprietary low energy asphalt technique labeled LEA®. By means of the factorial experiment design approach, this study highlights the influence of the bitumen pen grade (10/20, 35/50 and 50/70), the RAP content (30%, 50% and 70%) and the vegetable additive content used in the LEA process (0.2%, 0.6% and 1%).

The main following conclusions can be drawn in the case of this study:

– As regards the % voids obtained at the shear compacting press, the higher the RAP content (in the range 30–70%), the more difficult the mix compaction. Both the fresh binder grade and the Oleoflux® additive content seem to have little influence on the compaction ability.
– Regarding the Duriez ratio (evaluation of the water resistance), the softer the bitumen, the better the moisture resistance. Besides, the higher the RAP content (ranging from 30 to 70%), the worse the moisture resistance.
– For a RAP content ranging from 40 to 60% and for a fresh bitumen penetration ranging from 18 to 61 1/10 mm, the measured stiffness modulus at 15°C–10 Hz is above 14,000 MPa. The design of a high-modulus low energy asphalt is thus possible according to the European specifications and in particular to the French one, even with a very high rate of RAP.

Further work in laboratory, focused in particular on fatigue and low temperature performances, is from then on planned.

Far beyond this specific study, the results of which are very encouraging, half-warm mix asphalts seem to have the potential to allow lower mixing and placing temperature for the production of hot mix asphalt and to use high RAP mixtures as well.

REFERENCES

EAPA, 2002. Asphalt in figures, leaflet distributed by the *European Asphalt Pavement Association*.

EAPA, 2005. Asphalt in figures, leaflet distributed by the *European Asphalt Pavement Association*.

Gaudefroy, V., Olard, F., de la Roche, C., Antoine, J.P. & Beduneau, E., 2008. Laboratory investigations on the Total Organic Compounds emissions of half-warm mix asphalt technology versus traditional hot mix asphalt, *ISAP Congress on Asphalt Pavements and Environment*. Zurich.

Harder, G., LeGoff, Y., Loustau, A., Martineau, Y., Héritier, B. & Romier, A., 2008. Energy and environmental benefits of warm and half-warm asphalt mix: quantitative approach. *87th TRB Annual Meeting*. Washington, D.C.

Olard, F., Le Noan, C. & Romier, A., 2007a. Low energy asphalt technique LEA for minimizing impacts from asphalt plants to road works, RGRA Special Issue, *European Roads review* N°10.

Olard F., Antoine, J.P. Heritier, B. Romier A. & Y. Martineau., 2007b. LEA (Low Energy Asphalt): a New Generation of Half-Warm Asphalt Mixtures. *International Conference on Advanced Characterization of Pavement and Soil Engineering Materials*, Athens.

Olard, F., Le Noan, C. & Romier, A., 2007c. Innovative low energy asphalt technique for minimizing impacts from asphalt plants to road works, *AIPCR (World Road Association) Congress*, Paris. AIPCR Sustainable Development Prize 2007.

Olard, F., Le Noan, C.Beduneau, E. & Romier, A., 2008. Low energy asphalt for sustainable road construction, 4th Eurobitume & Eurasphalt Congress, Copenhagen.

Planche, J-P. 2008. European survey on the use of RAP, *Proceedings of the International ISAP Symposium*, 18th–20th August, 2008 Zurich, Switzerland: 140–149.

Prowell, B.D., 2007. The international technology scanning program report on Warm Mix Asphalt, Report from the US Department of Transportation, Federal Highway Administration, consulted July 2008 from the internet website http://international.fhwa.dot.gov/pubs/wma/summary.cfm.

Romier, A., Audéon, M., David, J. & Martineau, Y. 2004. Low energy asphalt (LEA) with performance of hot mix asphalt (HMA). *European Roads Review*, special issue RGRA 2-2004.

Romier, A., Audéon, M., David, J., Martineau, Y. & Olard., F. 2006. Low-energy asphalt (LEA) with the performance of hot-mix asphalt, *85th Annual Meeting of the Transportation Research Board. Published in the Journal of the TRB, Transportation Research Record* N°1962.

Sauzéat, C., Di Benedetto, H., Olard, F. & Nguyen, M.L., 2008. Fatigue behaviour of half-warm mix asphalts, *Proceedings of the ISAP Congress on Asphalt Pavements and Environment*, Zurich.

Advanced Testing and Characterization of Bituminous Materials –
Loizos, Partl, Scarpas & Al-Qadi (eds)
© 2009 Taylor & Francis Group, London, ISBN 978-0-415-55854-9

Evaluation of the rheological behaviour of Warm Mix Asphalt (WMA) modified binders

H.M.R.D. Silva, J.R.M. Oliveira & E.J. Peralta
University of Minho, Guimarães, Portugal

C.I.G. Ferreira
Construções Gabriel A.S. Couto S.A., Vila Nova de Famalicão, Portugal

ABSTRACT: Several processes and products are available to produce warm mix asphalt (WMA). The use of those may reduce the mixing and compaction temperatures in relation to hot mix asphalt (HMA), ensuring a good performance of the pavement. Lower plant mixing temperatures mean reduction in fuel consumption and lower emissions, what may contribute to diminish odours and health problems. A laboratory study on the properties of the modified binders (using two commercial WMA additives—Sasobit® and Cecabase®) was carried out through conventional (penetration, softening point), dynamic viscosity and rheology (DSR) tests, in order to establish the optimum additive content. Stripping of binder from the aggregates is a reported problem in WMA. Thus, the affinity of the modified binders was assessed without encountering significant problems. It was also observed that only Sasobit® alters the viscosity of the binder. A maximum temperature reduction of 15°C was achieved using 4% of Sasobit® with a softer binder.

1 INTRODUCTION

Nowadays one of the most important challenges for our society is the necessary reduction in the consumption of fuel, with the corresponding reduction in the emission of greenhouse gases (GHG). For the production of bituminous mixtures, several new technologies have been developed, and increasingly applied, in order to reduce the temperature of production and application on site of the mixtures. Generally, these technologies refer to the production of WMA which can be developed for all types of bituminous mixtures, including dense, continuously and gap-graded mixtures, applied in different thicknesses and in roads with different traffic levels.

In the present study, the potential of one of the techniques of WMA is analysed, comprising the modification of the binder, by the use of additives, in order to reduce the viscosity and to ensure adequate conditions of mixture and compaction at temperatures slightly above 100°C. Thus, a study of the properties of the modified binder was initially carried out for two commercial additives (Sasobit® and Cecabase®), by adding different quantities of each and determining their influence on the properties of the resulting binder.

This study is part of an ongoing project where the performance of two WMA mixtures will be compared with the performance of a traditional mixture of similar composition. Presently, only the results of the binder properties and their affinity to the aggregates are available and presented in the following sections.

2 LITERATURE REVIEW ON WARM MIX ASPHALT

Reducing the environmental impacts caused by the industrial activities is a basic condition to adapt the new circumstances of development to the present requests of sustainability.

The emissions resulting from the production of Hot Mix Asphalts (HMA) can vary significantly depending on the materials selected, equipment or production modes.

The life cycle of a road pavement can be divided into four stages: (i) the manufacturing of materials used for its construction; (ii) the construction of the pavement itself; (iii) the maintenance/rehabilitation of its condition; (iv) the demolition or recycling of the pavement. According to Park et al. (2003), the environmental load of each of these stages can be estimated by applying an environmental emissions factor related to the source of the energy consumed. These authors also refer that most of the energy is consumed in the manufacturing stage of construction materials (and consequently most of the emissions are produced in that stage).

In this context, innumerable potential benefits in the use of WMA has legitimated its emergent development, especially if considering the lower amount of energy necessary for the production of the mixtures, what implies significant reduction in the GHG emission values. Typical expected reductions are 30 to 40 percent for CO_2 and sulphur dioxide (SO_2), 50 percent for volatile organic compounds (VOC), 10 to 30 percent for carbon monoxide (CO), 60 to 70 percent for nitrous oxides (NOx) and 20 to 25 percent for dust. Likewise savings that can reach 35% in the amount of fuel consumed in the burner devices for warming the aggregates are an important argument. On the other hand, in what respects to the application of the mixture on site, its lower production temperature allows for the compaction of the mixture at a lower temperature, without compromising the desired densities of the resulting layers. The reduction in the exposition to fumes by the workers is another important advantage of this type of mixtures, with values 30 to 50% lower in relation to those released by conventional mixtures (D'Angelo et al., 2008).

Warm mix asphalts also allow longer haul distances, a longer construction season and minimized oxidative hardening, since the mixes are produced closer to the operating temperatures. Several processes have been developed with the objective of reducing the temperature of production and compaction of bituminous mixtures, apparently without compromising their performance. However, the use of lower compaction temperatures when producing warm asphalt may increase the potential for moisture damage (Hurley and Prowell, 2006).

For the WMA mixtures to be accepted in the national and international market, it is essential that the performance of those mixtures can be compared to that of the conventional HMA mixtures and that the environmental benefits and the reduction in energy consumption can compensate the slightly higher costs of the WMA mixtures (due to the cost of the additives).

3 BINDER PRODUCTION AND CHARACTERISATION

3.1 *Original binders and additives used*

In the present study, three paving grade bitumens and two additives were used with the objective of determining the most appropriate binder constitution for the production of a Warm Mix Asphalt adapted to the Portuguese conditions.

The three paving grade bitumens used are a B35/50, a B50/70 and a B100/150 pen bitumen (classified according to the European Standard EN 12591). For the "modification" of these bitumens, two commercial additives, known as "Cecabase®" and "Sasobit®", were used in controlled amounts in order to determine their influence on the final binder properties.

Cecabase® is an additive containing surface active agents that, when mixed with asphalt, allows a reduction on the road surface application temperature of about 50°C with no effect on performance of the material. Compared to the classical paving process, the use of this additive reduces energy consumption by 20 to 50%, depending on the process, and considerably reduces dust emission (CECA, 2008). According to the producers, the incorporation of this additive in the production of bituminous mixtures (2 to 4 kg per tonne of asphalt binder) enables the application temperature to be reduced to 120°C and, at the same time, it enables the WMA layer to retain the same properties as a classical layer with HMA produced at 160–180°C.

Sasobit® is a Fischer-Tropsch (F-T) or synthetic wax that is created during the coal gasification process and that has been used as a compaction aid and a temperature reducer. The Sasobit® process incorporates a low melting point organic additive that chemically

changes the temperature-viscosity curve of the binder (Button et al., 2007). Sasobit® melts at approximately 100°C and significantly reduces the viscosity of the base bitumen. It increases the asphalt resistance to deformation throughout the operating temperature range without affecting the low temperature properties of the mixture, which are determined by the characteristics of the base bitumen (Sasol, 2008). Sasobit® is completely soluble in bitumen at temperatures above 115°C. It forms a homogeneous solution with base bitumen on stirring reducing remarkably its viscosity. This also enables mixing and reducing by 10–30°C the handling temperatures of the asphalt (Sasol Wax GmbH, 2004). According to Hurley and Prowell (2005), Sasobit® has shown to improve the compactability of mixtures in both the shear gyratory compactor and vibratory compactor. Statistics indicated an overall reduction in air voids. Improved compaction was noted at temperatures as low as 190°F (88°C). The addition of Sasobit® does not affect the resilient modulus of an asphalt mix nor does it increase the rutting potential of asphalt mixtures.

3.2 *Production of the "modified" binders*

Thirteen samples of modified binders were prepared in the laboratory for a thorough characterisation (penetration, softening point, dynamic viscosity and rheology). These samples comprised the addition of three percentages of each additive to the B35/50 and the B50/70 bitumens and one percentage (4%) of Sasobit® to the B100/150 bitumen. Based on the recommendations of the additive producers, 2, 3 and 4% of Sasobit® and 0.2, 0.3 and 0.4% of Cecabase® were added to the two conventional bitumens.

In order to determine the optimum additive content, several tests were carried out on the resulting binders as explained in the following sections.

The modified binders were obtained by mixing each bitumen with the additive for a period of five minutes at a temperature of 130°C.

3.3 *Basic characterization of the binders*

In order to classify the binders used in this study, a basic characterisation was performed in accordance with the EN 12591 standard. This included the tests of penetration at 25°C (following the EN 1426 standard) and of softening point (also known as Ring & Ball

Table 1. Results obtained for the penetration at 25°C and softening point of the binders.

Bitumen	Additive type	Amount %	Pen (dmm)	Δ_{Pen} (dmm)	Δ_{Pen} (%)	R&B (ºC)	$\Delta_{R\&B}$ (ºC)	$\Delta_{R\&B}$ (%)
B35/50	None		41.3	0.0	0%	56.7	0.0	0%
	Sasobit®	2	32.0	–9.3	–22%	72.6	16.0	28%
		3	33.1	–8.2	–20%	81.5	24.9	44%
		4	28.6	–12.6	–31%	91.9	35.3	62%
	Cecabase®	0.2	44.9	3.6	9%	55.8	–0.9	–2%
		0.3	41.8	0.5	1%	55.4	–1.3	–2%
		0.4	43.0	1.7	4%	55.4	–1.3	–2%
B50/70	None		58.9	0.0	0%	51.6	0.0	0%
	Sasobit®	2	45.2	–13.7	–23%	69.7	18.1	35%
		3	41.4	–17.5	–30%	81.5	29.9	58%
		4	36.6	–22.3	–38%	87.5	36.0	70%
	Cecabase®	0.2	61.1	2.3	4%	51.1	–0.4	–1%
		0.3	63.6	4.8	8%	50.6	–1.0	–2%
		0.4	63.6	4.8	8%	50.1	–1.5	–3%
B100/150	None		143.4	0.0	0%	44.3	0.0	0%
	Sasobit®	4	68.4	–75.1	–52%	87.0	42.8	97%

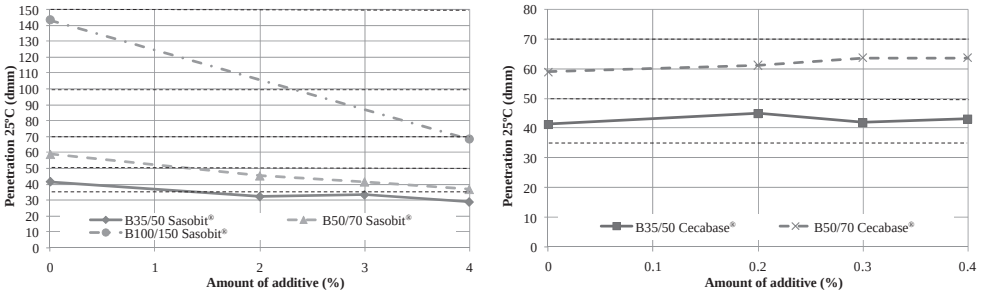

Figure 1. Evolution of the penetration value of the binders with the amount of additive.

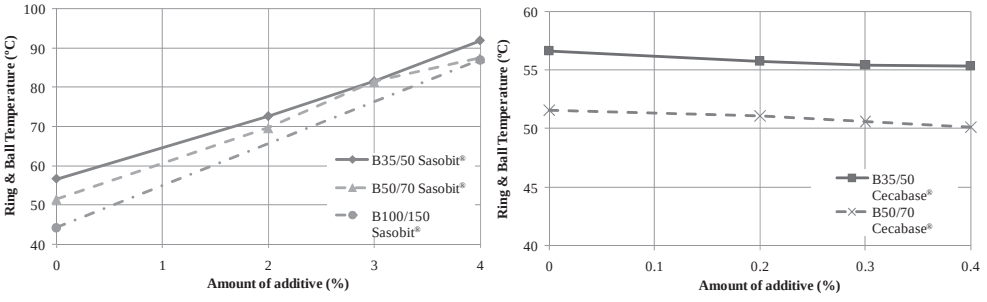

Figure 2. Evolution of the softening point of the binders with the amount of additive.

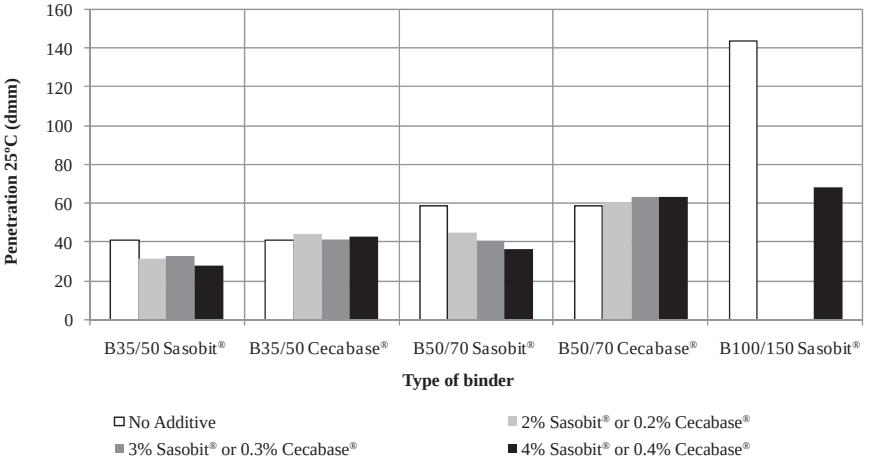

Figure 3. Influence of the amount and type of additive on the penetration value of the binders.

temperature, R&B, according to the EN 1427 standard). The results obtained for the paving grade bitumens and for those obtained by the addition of a certain amount of additive are summarised in Table 1.

The results presented in Table 1 are graphically illustrated in Figures 1 to 5. In Figures 1 and 2, the evolution of the values of penetration at 25°C and softening point with the amount of additive used in each paving grade bitumen (B35/50, B50/70 and B100/150) can be observed. For the latter, only the addition of 4% Sasobit® was considered.

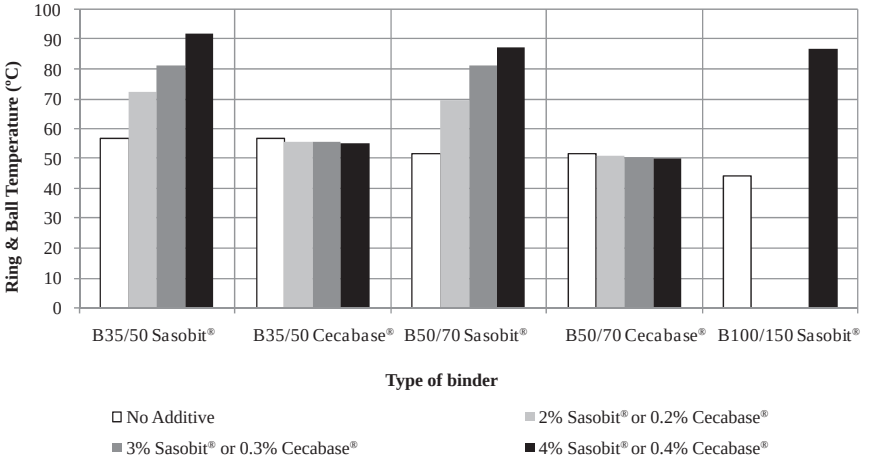

Figure 4. Influence of the amount and type of additive on the softening point of the binders.

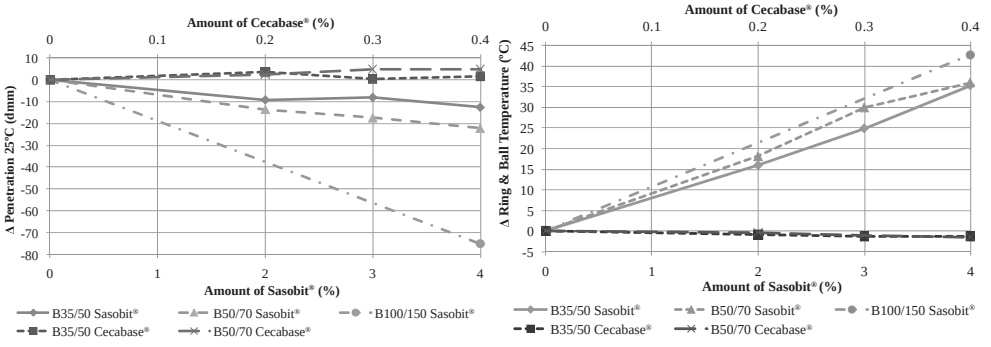

Figure 5. Variation observed in the values of penetration and softening point of the binders.

As can be seen from Figures 1 and 2, the addition of up to 0.4% of Cecabase® to the original bitumens does not change their classification (their penetration and R&B temperature is barely altered) while the addition of Sasobit® significantly modifies their properties (they can be classified as hard binder types, changing the penetration grade). This is easily observed, for example, from the addition of 4% Sasobit® to the 100/150 pen bitumen. Its classification changed to a 50/70 pen bitumen (2 grades difference) in terms of penetration at 25°C and to a much harder bitumen in terms of softening point (87°C, while a normal 20/30 pen bitumen has a softening point between 55 and 63°C). This is depicted in Figures 3 and 4, where the influence of the amount of additive in the properties of the binders is illustrated.

Figure 5 shows the variation of the values of penetration and softening point obtained for the studied binders. In this figure, it is clear that Cecabase® has negligible influence on the properties of the "modified" binders while Sasobit® has a great influence on the mentioned properties.

3.4 *Dynamic viscosity of the binders in the rotating spindle apparatus*

In order to evaluate the properties of the several binders at higher temperatures (100 to 170°C) in which the bituminous mixtures are mixed and applied, their dynamic viscosity was accessed using a rotating spindle apparatus (according to the EN 13302 standard). The typical temperature of a coaxial viscometer using a rotating spindle apparatus is ranged from 50 to 250°C.

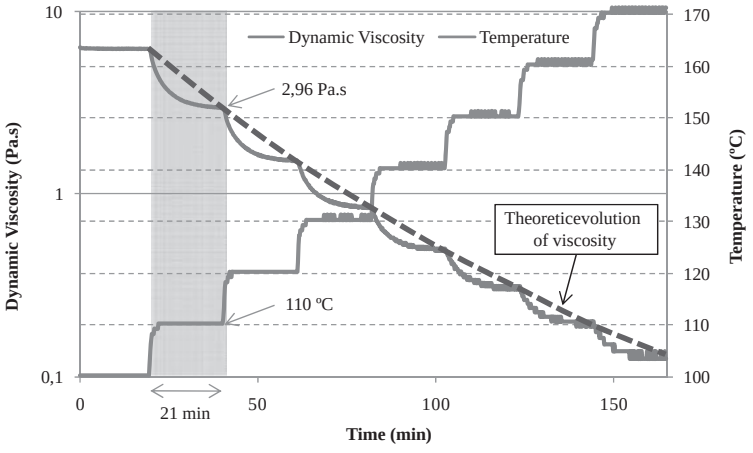

Figure 6. Method used to assess the viscosity at different temperatures in a rotating spindle apparatus.

During the test, the torque (relative resistance of the spindle to rotation) applied to a spindle rotating in a special sample container enclosing the binder measured its dynamic viscosity. According to EN 13302, after setting the test temperature and lowering the spindle into the binder, the system temperature should equilibrate after 15 to 30 min (lab practice showed that the usual equilibrium time is 18 min). Then, at least three readings were taken during the next 3 min for each evaluated temperature. The dynamic viscosity at each temperature is the arithmetic mean of the three readings taken between the 18th and 21st min of the test.

Figure 6 summarizes the method used to evaluate the dynamic viscosity of the binders at different temperatures, where the shaded area exemplifies the determination of the dynamic viscosity (2.96 Pa.s) at a temperature of 110°C. The dashed line would represent the theoretical evolution of dynamic viscosity if the test temperature had been increased gradually from 110 to 170°C. It can also be observed that the viscosity reached an equilibrium value, at every test temperature, just about after 21 min (18 plus 3 min), as stated previously.

The theoretical evolution of the dynamic viscosity of the several binders with the test temperature is the final result of the tests carried out to analyse the optimum amount of additive, both Sasobit® and Cecabase®, necessary to mix and apply the WMA at lower temperatures.

The evolution of the dynamic viscosity with the temperature for different types of paving grade bitumens (B35/50, B50/70 and B100/150), before and after their modification with WMA additives, can be observed in Figures 7 and 8 respectively, for the Sasobit® and Cecabase® modified binders. Although other amounts of additive were used to modify the bitumen, only some values are presented (2 and 4%) to demonstrate the evolution of the viscosity when different quantities of Sasobit® are used. For the Cecabase® modified binders, only the maximum addition of 0.4% is presented, in order to make the figures clearer.

Figure 7 shows that the addition of Sasobit® reduces the dynamic viscosity of the binder at production and application temperatures. Even though one of the objectives of using Sasobit® in WMAs is to reduce application temperatures, changes observed at these temperatures are lower than those observed at in service conditions (penetration and R&B). After analysing the temperatures at the limit equal-viscosity line for mixing (0.2 Pa.s), it can be concluded that the addition of 2% of Sasobit® allows reducing 2 to 4°C in comparison with the neat bitumens, while the binders modified with 4% Sasobit® presented higher reductions (7 to 9°C).

A 50/70 pen binder modified with 4% of Sasobit® can be considered as a 35/50 bitumen at operating conditions (based on the penetration and R&B results and on EN 12591), as

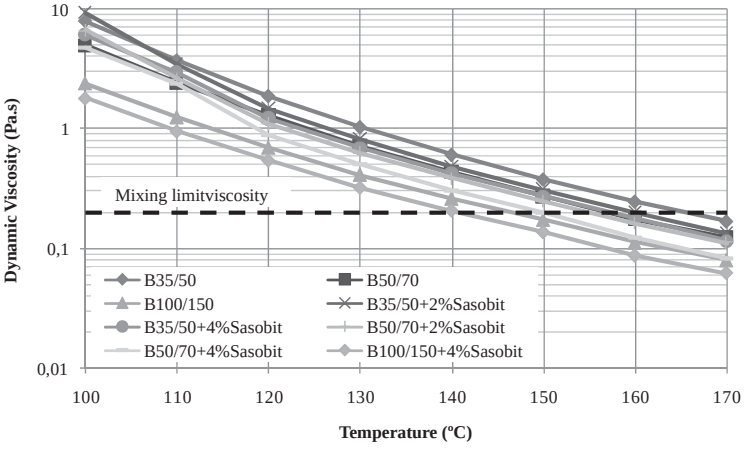

Figure 7. Dynamic viscosity of the Sasobit® modified binders (rotating spindle apparatus).

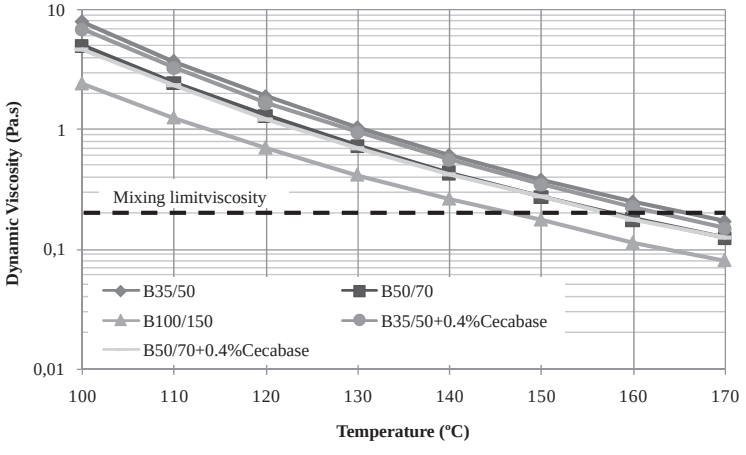

Figure 8. Dynamic viscosity of the Cecabase® modified binders (rotating spindle apparatus).

well as a 100/150 pen binder modified with 4% of Sasobit® can be considered as a 50/70 bitumen. When analysing the reduction of the mixing temperature at the equal-viscosity line of 0.2 Pa.s for these "equivalent" binders, a reduction of 15 to 17°C can be observed. Based on the main objective of WMA mixtures, it was concluded that the maximum temperature reduction was achieved using 4% of Sasobit® with softer bitumens (50/70 or 100/150), and thus these binders were further characterized through rheological testing (as presented in the following section).

Figure 8 shows that the addition of up to 0.4% of Cecabase® to the original bitumen barely changes its dynamic viscosity at the typical application temperatures. In fact, a minor reduction of viscosity can be observed (only in the 35/50 pen bitumen) after the addition of 0.4% of Cecabase® that allows a reduction of only 2°C in the equal-viscosity line of 0.2 Pa.s. Cecabase® additive does not change the binder properties (penetration, R&B temperature and viscosity) at the studied temperatures, and so the rheology of this modified binder will not be further characterized. In fact, Cecabase® is a chemical additive that acts as a surface active agent, improving the mixing workability at lower temperatures. The selection of the optimum amount of Cecabase® additive must result from further studies carried out on WMA mixtures.

4 RHEOLOGICAL CHARACTERISATION OF THE MODIFIED BINDERS

4.1 *Methodology used*

In order to determine the changes of the binders due to the addition of Sasobit®, three bitumens (35/50, 50/70 and 100/150), three modified binders (50/70 with 2 and 4% of Sasobit® and 100/150 with 4% of Sasobit®) and the Sasobit® additive were tested in a Dynamic Shear Rheometer (DSR) capable of measuring the rheology of these materials (EN 14770 standard).

Measurement of the rheological properties of the binders was carried out in a rotational DSR with parallel plate sample geometries of 40 mm and 1 mm gap (with manual gap compensation at each test temperature). The rheometer was set up to test in an oscillatory mode so as to guarantee a dynamic response from the specimen, ensuring that the specimen was tested in the linear region over the temperature (25 to 170°C) and frequency range selected (0.1 to 10 Hz). Thus, preliminary tests were carried out at different temperatures and frequencies in order to select stress values at which the binders are in the linear range (properties must not differ by more than 5 % of their value over the stress range chosen). Based on this preliminary study, the stress values selected to carry out the DSR tests varied between 1000 Pa at 25°C and 3 Pa at 170°C.

The DSR tests began at the lowest selected temperature, starting at the lowest frequency and proceeding to the highest. After the completion of each test temperature, it was possible to proceed to the next temperature at a rate not beyond 5°C per minute. During the test, the selected oscillatory shear stress is applied to the specimen and the resulting shear strain is measured.

4.2 *Results obtained*

The final results of the test involved determining the norm of the complex shear modulus (|G*|—ratio between peak stress and peak strain) and the phase angle (δ—phase difference between stress and strain) of the binders over a range of test frequencies and test temperatures. These results are presented in Figure 9 for bitumen 50/70 (before and after adding 4% of Sasobit®) and for pure Sasobit® additive so as to exemplify the rheological changes verified due to the use of this additive. Other result obtained from the DSR test is the dynamic viscosity of the material, which is presented in Figure 10 for an original bitumen, a modified binder and the Sasobit®.

The complex shear modulus of Sasobit® is very high (1 MPa), constant and independent of the frequency before its congealing temperature (102°C), behaving essentially as an elastic solid material. Slightly above that temperature the complex modulus decreases very quickly and Sasobit® becomes a liquid material with some residual viscoelasticity that is much more directly frequency dependent. The dynamic viscosity of Sasobit® has an evolution similar to its complex modulus, except for its variation with the frequency before 102°C.

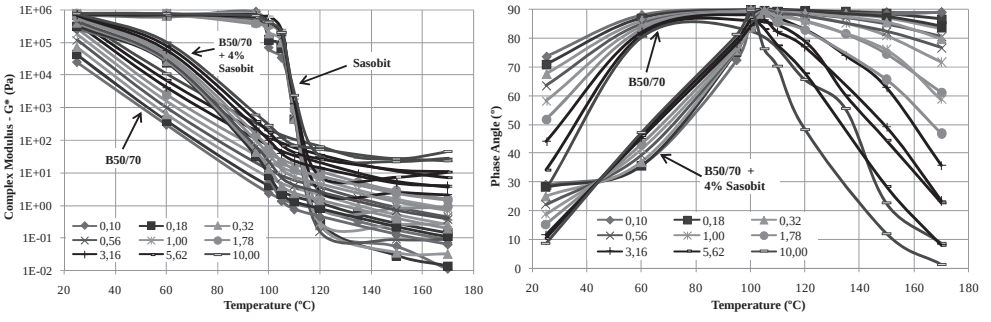

Figure 9. Rheology of a Sasobit® modified binder at different temperatures and frequencies (DSR).

It was noticed that at lower temperatures, usually below 100°C (while the materials have viscoelastic behaviour and have not yet become liquid), all the tested materials presented higher viscosities for lower frequencies, the opposite occurring at higher temperatures.

The complex modulus of the studied binders significantly changes for different test temperatures and frequencies. At 25°C the complex modulus of the original bitumen is slightly lower than that of Sasobit® (being almost equal at 10 Hz, but quite lower at 0.1 Hz). This difference increases for higher operating temperatures (between 50 and 90°C), which justifies the great raise of the R&B temperature of the binders modified with Sasobit®. Above 115°C the original bitumen has a complex modulus only slightly higher than that of Sasobit®, being this difference insufficient to allow a great reduction of the WMAs production temperature (the necessary reduction of temperature only occurs when using a softer binder to produce the modified binder). The dynamic viscosity of the original bitumen barely varies for different test frequencies, but the phase angle is very dependent on the frequency (being the behaviour more elastic for higher frequencies). It was observed that the bitumen has a viscoelastic behaviour at operating temperatures (25 to 60°C), then it mainly presents a viscous behaviour with a residual elasticity (60 to 100°C) and finally it behaves like a liquid, with a decrease of the phase angle due to reduction of the viscous modulus into residual values similar to the elastic modulus.

The rheology of the binder modified with Sasobit® is based essentially on the behaviour of the original bitumen, which is modified by Sasobit® mainly at temperatures between

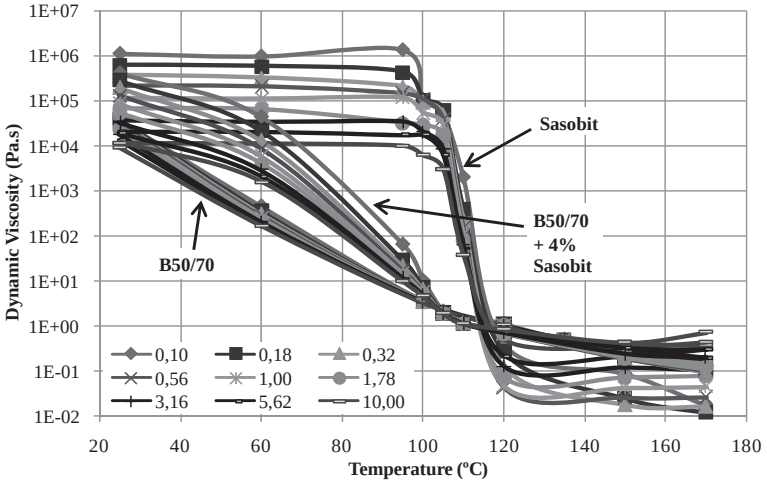

Figure 10. Viscosity of a Sasobit® modified binder at different temperatures and frequencies (DSR).

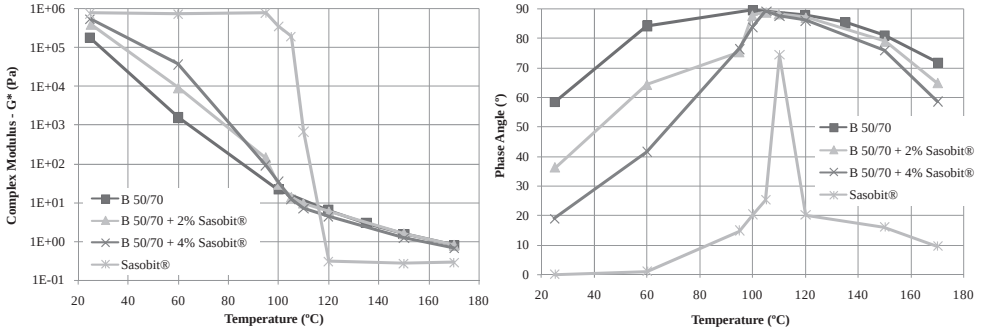

Figure 11. Influence of the Sasobit® content in the rheological properties of the binder (DSR).

25 and 100°C. In fact, for those temperatures (and especially for temperatures near the R&B softening point) the modified binder greatly increases its complex modulus and dynamic viscosity. The presence of Sasobit® in the modified binder increases its elasticity, reducing the phase angle values and restraining the purely viscous behaviour at temperatures above 100°C. At higher temperatures (WMA production) only small differences of behaviour were noticed between the modified binder and the original bitumen.

In order to ease the analysis of the rheology results, a reference frequency of 1 Hz was selected to compare the different materials tested using DSR. Thus, Figure 11 shows the comparison of the rheological properties (complex modulus and phase angle) of the original bitumen 50/70, the modified binders produced with this bitumen (with 2 and 4% additive) and the pure Sasobit® additive.

It was observed that Sasobit® is essentially an elastic material (lower phase angles), except at temperatures near its congealing point (102°C). Even when this additive becomes liquid, the elastic part of its complex modulus prevails. In contrast, the original bitumen presents essentially a viscous behaviour at 1 Hz over the evaluated temperatures. Modifying the original bitumen with Sasobit® mainly increases the elastic part of the complex modulus in direct proportion to the amount of additive used, which is essentially observed at operating temperatures (25 to 80°C). The reduction of the complex modulus and phase angle at application temperatures (above 120°C) is a central objective of WMA additives, but only a minor decrease is obtained by comparing bitumens before and after Sasobit® modification. Thus, the highest quantity of Sasobit® (4%) studied should be used in the modified binder in order to ensure a major decrease of the complex modulus, maximizing the decrease of WMA application temperatures.

Previously, it was observed that a 50/70 pen bitumen modified with 4% of Sasobit® can be considered as a 35/50 binder at in service conditions, as well as a 100/150 pen bitumen

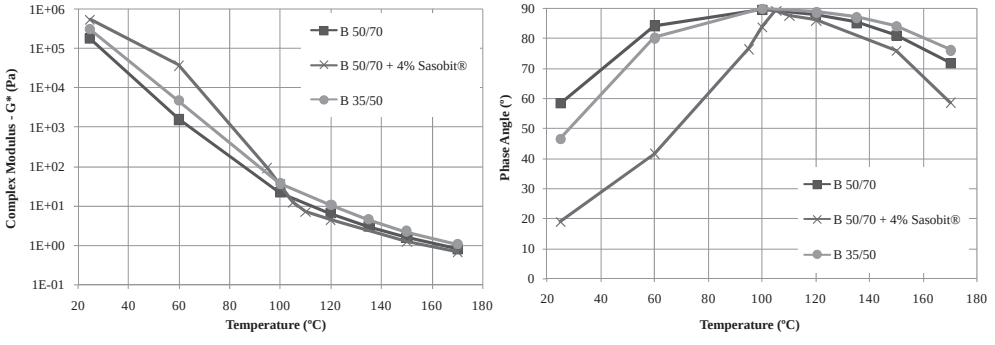

Figure 12. Rheological properties of a 35/50 bitumen vs a 50/70 Sasobit® modified binder (DSR).

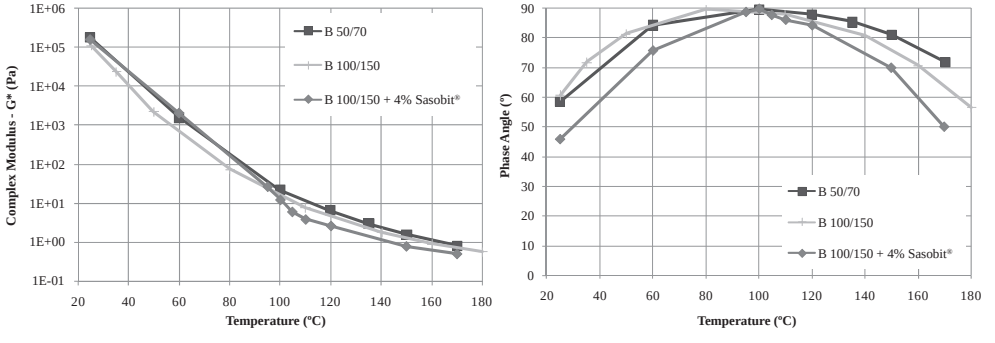

Figure 13. Rheological properties of a 50/70 bitumen vs a 100/150 Sasobit® modified binder (DSR).

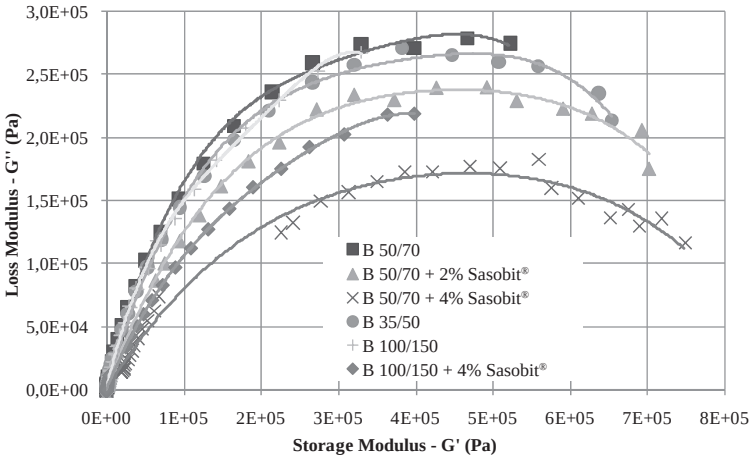

Figure 14. Cole-Cole plot of the studied binders based on their rheological properties (DSR).

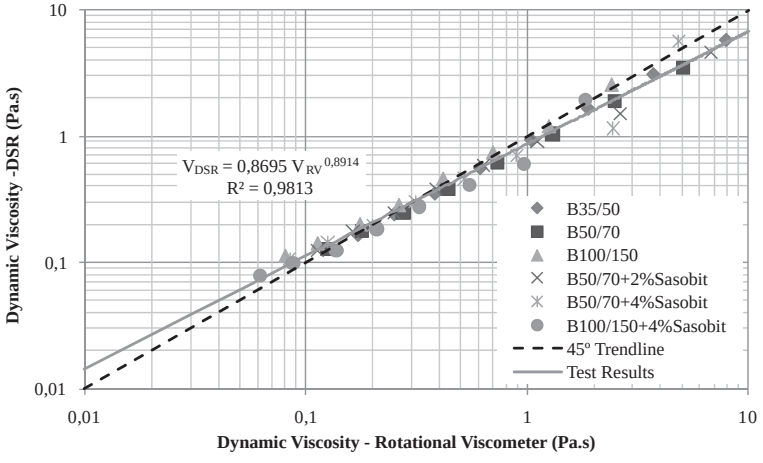

Figure 15. Relation between the viscosities measured in the rotating spindle apparatus and in the DSR.

modified with 4% of Sasobit® can be considered as a 50/70 binder. The comparison between the rheological properties (complex modulus and phase angle) of these binders is presented in Figures 12 and 13, respectively for the 50/70 and 100/150 modified binders (4% of Sasobit®).

The complex modulus results confirm that the modified binders using softer bitumens have similar or even higher modulus than harder original bitumens, being thus possible to obtain a major reduction of the application temperature of the WMA mixtures and upholding operating properties comparable to the HMA mixtures. Moreover, it was observed that the Sasobit® modified binders, even being produced with softer bitumens, still have a higher elastic modulus (lower phase angle) in comparison with that of harder original bitumens. Soenen et al. (2008) reached similar conclusions for several wax modified binders.

The real part of the complex shear modulus |G*| is G' (storage modulus) and it is associated with the elastic part of the material behaviour. The imaginary part of the complex shear modulus is G" (loss modulus) and it is associated with the viscous part of the material behaviour. The Cole-Cole plot of the loss modulus vs the storage modulus of the different binders is illustrated in Figure 14, so as to evaluate the influence of the Sasobit® additive in the viscoelastic rheological behaviour of the binders at operating temperatures. It was observed that the viscoelastic behaviour is greatly influenced by the amount of Sasobit® added to the

original bitumens, with a visible reduction of the viscous behaviour and a significant increase in the elastic behaviour of the modified binders. Although the maximum values of |G*| of the neat bitumens (35/50, 50/70 and 100/150) are distinct, it was observed that the relation between their loss and storage moduli (related with their viscoelastic behaviour) is similar. This typical behaviour of the neat bitumens is truly changed into a more elastic behaviour after Sasobit® modification.

4.3 *Comparison with dynamic viscosity results of the rotating spindle apparatus*

One of the methodologies used in the present study for determining the dynamic viscosity of the binders at different temperatures is very simple (rotating spindle apparatus) and do not demand a very expensive equipment to carry out the tests (like DSR). However, reference to such an approach was not found in the literature and, therefore, a comparison with a traditional methodology was necessary to assess whether it could be used more often to study the evolution of binder viscosity with temperature. The results obtained in both test types, for the conventional and the Sasobit® modified binders, are plotted together in Figure 15. The points situated on the 45º (dashed) line show similar results for both types of test. In fact, a good correlation between most of the points obtained can be observed, what indicates that if a DSR is not available the new methodology may be used in the future. Nevertheless, it was noticed that for temperatures below 120°C the rotational viscometer presents viscosities slightly higher than the DSR, occurring the opposite at temperatures above 160°C.

5 ASSESSMENT OF THE AFFINITY BETWEEN AGGREGATES AND BINDERS

In order to assess whether the use of the studied additives in the modification of the conventional binders would contribute to an increase in the water sensitivity of the final mixtures, a procedure indicated in the EN 12697-11 standard, regarding the affinity between aggregates and binders, was used. In this test, the aggregate used was obtained from a quarry next to a site where a trial was to be made, later in this project. Therefore, it was not possible to analyse the influence of using a different aggregate on the water sensitivity of the mixture. Thus, the results are significantly affected by the aggregate used, as it can be observed in Figure 16.

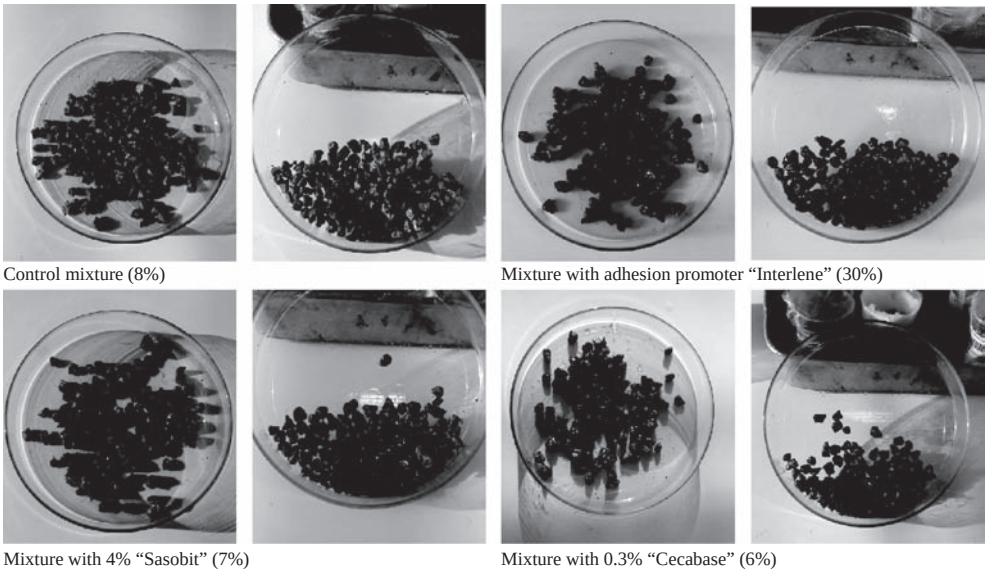

Figure 16. Results of the affinity tests obtained from the studied binders.

In fact, only 8% of the aggregate surface was covered by bitumen for the conventional mixture produced with 5% of a 50/70 pen bitumen. An adhesion promoter additive ("Interlene") was therefore used to enhance the behaviour of the mixture, resulting in an increase of the aggregate surface covered by bitumen from 8 to 30%. The results of the "modified" binders (with the amount suggested by the previous results and the producers recommendations, i.e. 4% Sasobit® and 0.3% Cecabase®) were not significantly affected (7 and 6% of the aggregate surface covered by binder, respectively) in comparison with the control mixture.

6 CONCLUSIONS

This paper presents the preliminary results of an ongoing project where the use of binder additives to reduce the temperature of the production and application of bituminous mixtures is being assessed. This project will involve the evaluation of the reduction in GHG emissions of two WMAs in comparison to a conventional HMA and the assessment of their mechanical properties. The results obtained up to the present date allow drawing the following conclusions:

- the modified binders did not show significant problems of affinity to the aggregate studied, in comparison with the conventional binder;
- it was also observed that only Sasobit® changes the viscosity of the binder;
- the Sasobit® additive mainly increases the elastic part of the complex modulus proportionally to the amount of additive used;
- the Sasobit® additive essentially modifies the bitumen rheological properties at operating temperatures (between 25 and 80°C);
- a maximum temperature reduction of 15°C was achieved using 4% of Sasobit® with a softer binder;
- a good correlation was found between the dynamic viscosity results obtained with the DSR and the Rotating Spindle Viscometer at different temperatures.

REFERENCES

Button, J.W., Estakhri, C. and Wimsatt A. 2007. *A Synthesis of Warm-Mix Asphalt*. Texas Transportation Institute and Federal Highway Administration. Report 0-5597-1. Texas.

CECA 2008. *Green Road Formulation—Warm Mix Asphalt—Cecabase RT.* Ceca, Arkema Group. <http://www.cecachemicals.com/sites/ceca/en/business/bitumen_additives/warm_coated_material/warm_coated_material.page> (Accessed on 4Nov08).

D'Angelo, J., Harm, E., Bartoszek, J., Baumgardner, G., Corrigan, M., Cowsert, J., Harman, T., Jamshidi, M., Jones, W., Newcomb, D., Prowell, B., Sines, R. and Yeaton, B. 2008. *Warm-Mix Asphalt: European Practice*. Federal Highway Administration, U.S. Department of Transportation, American Association of State Highway and Transportation Officials, National Cooperative Highway Research Program, Report no. FHWA-PL-08-007. Alexandria.

Hurley, G.C. and Prowell, B.D. 2005. *Evaluation of Sasobit® for use in Warm Mix Asphalt*. National Center for Asphalt Technology, Auburn University, NCAT Report 05–06. Auburn.

Hurley, G.C. and Prowell, B.D. 2006. Evaluation of Potential Processes for Use in Warm Mix Asphalt. *Journal of the Association of Asphalt Paving Technologists*, Vol. 75: 41–90.

Park, K., Hwang, Y., Seo, S. and Seo, H. 2003. Quantitative Assessment of Environmental Impacts on the Life Cycle of Highways. *Journal of Construction Engineering and Management*, American Society of Civil Engineers. Vol. 129 (1): 25-31.

Sasol Wax GmbH 2004. *The Bitumen Additive for Highly Stable Easily Compactible Asphalts.* Sasobit® Product Information 124. Sasol Wax GmbH. Hamburg.

Sasol 2008. *Sasobit Technology.* Sasol Wax. <http://www.sasolwax.com/Sasobit_Technology.html> (Accessed on 4Nov08).

Soenen, H., Tanghe, T., Redelius, P., de Visscher, J., Vervaecke, F. and Vanelstraete, A. (2008). A Laboratory Study on the Use of Waxes to Reduce Paving Temperatures. 4th Eurasphalt & Eurobitume Congress. Copenhagen.

Advanced Testing and Characterization of Bituminous Materials – Loizos, Partl, Scarpas & Al-Qadi (eds)
© 2009 Taylor & Francis Group, London, ISBN 978-0-415-55854-9

Author index

AI A1-Hadidy 227
Agostinacchio, M. 1131
Ahn, K. 619
Allen, B. 185
Ammendola, R. 367, 1151, 1247
Angelone, S. 917
Anochie-Boateng, J.K. 550
Antunes, M.L. 323
Apeagyei, A.K. 463
Arabani, M. 423, 551
Arnaud, L. 433
Artamendi, I. 185
Ayan, V. 1160
Azari, H. 261

Baek, S.H. 349
Balay, J.-M. 725
Baldo, N. 879
Bańkowski, W. 443, 1221
Barbati, S. 627
Batista, F.A. 323
Baumgardner, G. 81
Beckedahl, H.J. 33, 1269
Beduneau, E. 651
Bennert, T. 1279
Besamusca, J. 133
Blab, R. 357
Blasl, A. 899
Bocci, M. 1113
Bodin, D. 725, 773
Bonneau, D. 651
Botella, R. 707
Braham, A. 699, 785
Brar, H. 1279
Breysse, D. 725
Burlacu, A. 795
Buttlar, W. 699, 785
Buttlar, W.G. 463, 827

Canestrari, F. 1181
Capitanu, C. 295
Carbonneau, X. 609, 889, 1211
Cardone, F. 627, 1113
Cardoso de Lima, D. 1289
Carter, A. 1091
Chailleux, E. 773, 1221
Charmot, S. 1123
Chen, X. 531
Chen, Z. 575
Ciampa, D. 399
Cocurullo, A. 761
Collings, D.C. 1161
Currie, M. 251

Damian, T.C. 295
Dattola, V. 13
de la Roche, C. 331, 773
De Visscher, J. 1009, 1201
Di Benedetto, H. 69
Diaconu, E. 569
Dicu, M. 693, 795
Diomedi, M. 1131
Doh, Y.S. 349, 619
Dreessen, S. 971
Dubois, V. 331
Duif, C.P. 143
Dupriet, S. 651
Durand, G. 61, 195

Eckmann, B. 609
El Ayadi, A. 1049
Elliott, R.C. 519

Fakhri, M. 681
Fanouillet, L. 61
Farokhi, M. 681
Feng, D. 205
Ferreira, C.I.G. 661
Ferrotti, G. 1181
Flintsch, G. 453
Fodor, G. 295
Fonseca, P. 323
Freitag, S. 949

Gabet, T. 331
Gajewski, M. 1221
Gallet, T. 69
Gardel, V. 971
Garg, N. 1279
Gaudefroy, V. 639
Gauthier, G. 69, 1221
Geffard, J.L. 639
Gengliang, T. 377
Ghorbel, E. 849
Goldbaum, J. 1265
Goyer, S. 639
Grenfell, J. 331
Grilli, A. 1113
Guddati, M.N. 817
Gueit, C. 61, 195
György, G. 409

Hadad, Ah. 1257
Haddadi, S. 849
Hagos, E.T. 173
Hase, M. 23
Hassan, H.F. 497
Hassan, M.M. 961
Herle, I. 409
Herrera de la Rosa, R. 477
Hornych, P. 639
Hou, E.T. 859
Houel, A. 433
Hunter, A. 519
Huurman, M. 507, 749
Hyzl, P. 909

Jamek, M. 807
James, D. 519
Janssen, S. 33
Jenkins, K.J. 239, 283, 1161
Jiménez, R. 271
Joodi, H.R. 423
Judycki, J. 303

Kalman, B. 443
Kappl, K. 357
Kasbergen, C. 879
Katicha, S. 453
Kayser, S. 215
Kazatchkov, I.B. 93, 989
Khalid, H.A. 961

Khavandi, A. 1169
Khedoe, R.N. 507
Kheiry, P.T. 681
Kias, E.M. 735
Kim, H. 827
Kim, H.H. 619
Kim, J.C. 349
Kim, K.W. 349, 619
Kim, Y.R. 817, 859
Koh, C. 585
Kringos, N. 123, 143, 261, 839, 879

la Agostinacchio, M. 399
La, I. 619
Labuz, J. 313
Lazăr, Ş.M. 569
Le Gal, Y. 1211
Legal, Y. 889
Leguern, M. 773
Leuridan, A. 1201
Levenberg, E. 541
Li, H. 531
Liu, X. 939
Livneh, M. 1235
Lobază, M. 693
Loizos, A. 1081
Lopp, G. 585
Lu, X. 151, 1181
Lugmayr, R. 807

Machado, A.V. 109
Malkoç, G. 53
Manthos, E. 1019
Marasteanu, M. 313
Martínez, A. 271
Martinez, F. 917
Mat Zin, H. 1143
Meite, N.B. 519
Merbouh, M. 725
Meunier, M. 1091
Michalica, P. 93
Millien, A. 1181
Mirabdolazimi, S.M. 551
Mo, L. 507
Mohd Yazip, M. 1143
Molenaar, A.A.A. 133, 173, 387
Mollenhauer, K. 715
Mondschein, P. 869, 1101
Moraal, J. 507
Moriceau, L. 725
Moro, A. 367, 1151, 1247
Murali Krishnan, J. 999

N'Guyen, T.L. 433
Nafisah, A.A. 1143
Nicholls, J.C. 519
Nielsen, E. 99
Nikolaides, A. 1019
Nikzad Gharehaghaji, A. 1169

Oelkers, C. 23
Oeser, M. 949
Olard, F. 651
Olita, S. 399, 1131
Oliveira, J.R.M. 661
Özcan, Ş. 487

Pais, J.C. 109
Pannunzio, V. 627
Pap, I. 981
Papavasiliou, V. 1081
Paradis, M. 1091
Partl, M.N. 3, 827, 1181, 1191
Pasetto, M. 879
Pauli, T. 123, 143, 1130
Pellinen, T. 251, 1282
Peralta, E.J. 109, 661
Perera, R. 519
Pérez, F. 271, 707
Perraton, D. 1091
Peterson, C. 785
Petit, C. 1049, 1181
Ph. du Bus de Warnaffe 1201
Phelipot-Mardelle, A. 1181
Phillips, P. 185
Piber, H. 1191, 1181
Picoux, B. 1049
Piérard, N. 163, 1201
Planche, J.P. 971
Poirier, J.E. 61
Porot, L. 331
Praticò, F.G. 13, 367, 1151, 1235
Pronk, A.C. 749, 749
Prusenko, Y. 1039
Pszczoła, M. 303

Qian, Z. 531
Quigniot, S. 889

Raab, C. 3, 1181
Răcănel, C. 795
Ravnikar Turk, M. 443
Redelius, P. 151
Riedl, S. 1059
Robert, M. 195
Robertson, R. 123
Romanescu, C. 795
Romero, P. 1123
Roque, R. 585
Rowe, G. 43, 81
Rubio, B. 271
Ryu, M.Y. 619

Sabouri, M.R. 597
Saleh, F. 1257
Santagata, F.A. 1113
Saoula, S. 849
Savadatti, S. 817
Scarpas, A. 123, 143, 261, 830, 879, 939
Schelkens, E. 1201
Schitter, G. 143
Schmets, A.J.M. 143
Schmidt, C. 1265
Scullion, T. 927
Sebaaly, P.E. 1071
Seignez, N. 651
Serfass, J.P. 609
Shafabakhsh, Gh. 1257
Shakeri, V. 423
Sharrock, M. 81
Shuler, S. 1265
Siddharthan, R.V. 1071
Silva, H.M.R.D. 109, 661
Sivapatham, P. 33, 1269
Smiljanic, M. 981
Soenen, H. 151, 1221
Stastna, J. 93, 989
Stehlik, D. 909
Struble, L.J. 463
Surlea, C. 795
Sybilski, D. 1221

Tabatabaee, H.A. 597
Tabatabaee, N. 597
Tapkin, S. 487
Tarefder, R.A. 735
Tatic, U. 981
Teymourpour, P. 597
Thirunavukkarasu, S. 817
Thushara, V.T. 999
Triquigneaux, J.P. 609
Tschegg, E.K. 807
Tuncan, A. 487
Tuncan, M. 487
Turos, M. 313

Tušar, M. 443
Tutumluer, E. 559
Twagira, M.E. 239, 283

Underwood, B.S. 817, 859
Uzan, J. 541

Valdés, G. 707
Valentin, J. 869, 1101
Valle de Souza, A.C. 1289
Valtonen, J. 251
Van de Ven, M. 331
van de Ven, M.F.C. 133, 173, 387, 1029
Van den bergh, W. 331
van Lent, D.Q. 387
Van Rompu, J. 69
Vanelstraete, A. 163, 1009
Vansteenkiste, S. 1201
Varaus, M. 909
Velásquez, R. 313
Vignard, N. 773
Virgili, A. 627
Volovyk, O. 1039
Voskuilen, J.L.M. 1029

Wagoner, M.P. 827
Walubita, L.F. 927
Wang, D. 205
Wasage, T.L.J. 989
Weise, C. 899
Wellner, F. 215, 409
Wiman, L.G. 443
Wistuba, M. 715
Woldekidan, M.F. 507

Yang, J. 575
Yi, J. 205
Yi-qiu Tan 227
Yiqiu, T. 377

Zanzotto, L. 93, 989
Zdralek, P. 909
Zejiao, D. 377
Zhdanyuk, K. 1039
Zhdanyuk, V. 1039
Zhu, H. 575
Zulakmal, S. 1143

ADVANCED TESTING AND CHARACTERIZATION OF BITUMINOUS MATERIALS

PROCEEDINGS OF THE 7TH INTERNATIONAL RILEM SYMPOSIUM ATCBM09 ON ADVANCED TESTING AND CHARACTERIZATION OF BITUMINOUS MATERIALS, RHODES, GREECE, 27–29 MAY 2009

Advanced Testing and Characterization of Bituminous Materials

Editors

Andreas Loizos
National Technical University of Athens, Athens, Greece

Manfred N. Partl
EMPA, Chair of RILEM TC 206-ATB, Switzerland

Tom Scarpas
Delft University of Technology, Delft, The Netherlands

Imad L. Al-Qadi
University of Illinois at Urbana Champaign, Urbana, Illinois, USA

VOLUME II

CRC Press
Taylor & Francis Group
Boca Raton London New York Leiden

CRC Press is an imprint of the
Taylor & Francis Group, an **informa** business

A BALKEMA BOOK

CRC Press/Balkema is an imprint of the Taylor & Francis Group, an informa business

© 2009 Taylor & Francis Group, London, UK

Typeset by Vikatan Publishing Solutions (P) Ltd., Chennai, India
Printed and bound in Great Britain by Antony Rowe (A CPI-group Company), Chippenham, Wiltshire

All rights reserved. No part of this publication or the information contained herein may be reproduced, stored in a retrieval system, or transmitted in any form or by any means, electronic, mechanical, by photocopying, recording or otherwise, without written prior permission from the publisher.

Although all care is taken to ensure integrity and the quality of this publication and the information herein, no responsibility is assumed by the publishers nor the author for any damage to the property or persons as a result of operation or use of this publication and/or the information contained herein.

Published by: CRC Press/Balkema
P.O. Box 447, 2300 AK Leiden, The Netherlands
e-mail: Pub.NL@taylorandfrancis.com
www.crcpress.com – www.taylorandfrancis.co.uk – www.balkema.nl

ISBN: 978-0-415-55854-9 (set of 2 volumes + CD-ROM)
ISBN: 978-0-415-55856-3 (vol 1)
ISBN: 978-0-415-55857-0 (vol 2)
ISBN: 978-0-203-8674-88 (e-book)

Advanced Testing and Characterization of Bituminous Materials – Loizos, Partl, Scarpas & Al-Qadi (eds)
© 2009 Taylor & Francis Group, London, ISBN 978-0-415-55854-9

Table of contents

Preface XIII

Organization XV

VOLUME I

1. Evaluation of binder properties

Laboratory study on interlayer bonding using cationic tack coats 3
C. Raab & M.N. Partl

Factors affecting recovered asphalt binder properties: A theoretical and experimental study 13
F.G. Praticò & V. Dattola

Influence of low temperature behaviour of PmB on life cycle 23
M. Hase & C. Oelkers

Influence of granular polymer additives on the asphalt quality 33
P. Sivapatham, H.J. Beckedahl & S. Janssen

Phase angle determination and interrelationships within bituminous materials 43
G. Rowe

Evaluation of initial road performance correlating with different tests of binders 53
G. Malkoç

Laboratory study of environmental performance of binders by headspace gas chromatography 61
J.E. Poirier, C. Gueit, L. Fanouillet & G. Durand

New fatigue test on bituminous binders and mastics using an annular shear rheometer prototype and waves propagation 69
J. Van Rompu, H. Di Benedetto, G. Gauthier & T. Gallet

Functional forms for master curve analysis of bituminous materials 81
G. Rowe, G. Baumgardner & M. Sharrock

Linear viscoelastic spectra of asphalt binders from DSR and BBR 93
I.B. Kazatchkov, P. Michalica, J. Stastna & L. Zanzotto

Principal component analysis of rheological and hardening data from bituminous binders 99
E. Nielsen

Rheological and functional evaluation of the interactions between bitumen and rubber 109
E.J. Peralta, H.M.R.D. Silva, J.C. Pais & A.V. Machado

A thermodynamic approach to healing in bitumen 123
N. Kringos, A. Scarpas, T. Pauli & R. Robertson

Nanoclay for binder modification of asphalt mixtures 133
M.F.C. van de Ven , A.A.A. Molenaar & J. Besamusca

First-principles investigation of the multiple phases in bituminous materials: The case of asphaltene stacking 143
A.J.M. Schmets, N. Kringos, A. Scarpas, C.P. Duif, G. Schitter & T. Pauli

The morphology of SBS modified bitumen in binders and in asphalt mix 151
H. Soenen, X. Lu & P. Redelius

2. Testing and modeling the influence of climate and ageing effects

Developing a test method for the accelerated ageing of bituminous mixtures in the laboratory 163
N. Piérard & A. Vanelstraete

Chemical characterization of laboratory and field bitumen aging in Porous Asphalt Concrete 173
E.T. Hagos, A.A.A. Molenaar & M.F.C. van de Ven

Influence of temperature and aging on laboratory fatigue performance of asphalt mixtures 185
I. Artamendi, B. Allen & P. Phillips

Aging of SBS polymer in hot and cold bituminous coatings. Relationship between microstructure and performances: Low temperature and cohesion properties 195
C. Gueit, M. Robert & G. Durand

Impact of freeze-thaw cycles on the performance of asphalt mixture based permeability 205
J. Yi, D. Feng & D. Wang

Formulation of authoritative temperature gradients for an analytical design process of flexible pavements using statistical techniques 215
S. Kayser & F. Wellner

Performance evaluation of prepared gelled hot sealant in cold climates 227
AI A1-Hadidy & Yi-qiu Tan

Age hardening behaviour of bituminous stabilized materials 239
M.E. Twagira & K.J. Jenkins

Investigation of friction properties of various road surfaces affecting road safety 251
T. Pellinen, M. Currie & J. Valtonen

Combined experimental and numerical analysis of moisture infiltration in the modified Lottman test 261
N. Kringos, A. Scarpas & H. Azari

Assessment of moisture effect on open graded mixes using water sensitivity and Cántabro after immersion tests 271
B. Rubio, R. Jiménez, F. Pérez & A. Martínez

Moisture damage on bituminous stabilized materials using a MIST device 283
M.E. Twagira & K.J. Jenkins

Determination of gradual reduction of the flexible pavement bearing capacity 295
G. Fodor, C. Capitanu & T.C. Damian

Testing of low temperature behaviour of asphalt mixtures in bending creep test 303
M. Pszczoła & J. Judycki

Effect of beam size on the creep stiffness of asphalt mixtures at low temperatures 313
R. Velásquez, M. Marasteanu, M. Turos & J. Labuz

Assessment of water sensitivity of asphalt rubber mixtures for wearing course 323
F.A. Batista, M.L. Antunes & P. Fonseca

Development of a laboratory bituminous mixtures ageing protocol 331
C. de la Roche, M. Van de Ven, W. Van den bergh, T. Gabet, V. Dubois, J. Grenfell & L. Porot

3. *Hot bituminous mixtures characterization and design*

Optimum loading speed for deformation strength test of bitumen mixtures 349
S.H. Baek, J.C. Kim, Y.S. Doh & K.W. Kim

Enhanced algorithms for the derivation of material parameters from triaxial cyclic compression tests on asphalt specimen 357
K. Kappl & R. Blab

Reliability and suitability for standardization of methods for HMA density measurements: Experimental investigation on transverse vs longitudinal variations 367
F.G. Praticò, R. Ammendola & A. Moro

Research on coordinating deformation between Fiber Bragg Grating strain sensor and asphalt mixture 377
D. Zejiao, T. Gengliang & T. Yiqiu

Influence of treatments on the surface characteristics of aggregate 387
D.Q. van Lent, A.A.A. Molenaar & M.F.C. van de Ven

Mix design of grouted porous asphalt concrete for wearing course layers 399
M. la Agostinacchio, D. Ciampa & S. Olita

"Liquefaction" of asphalt caused by cyclic loading, as a potential reason of extreme rutting 409
G. György, F. Wellner & I. Herle

Experimental investigation on the dynamic properties of asphalt concrete using filler with waste hydrated lime 423
M. Arabani, H.R. Joodi & V. Shakeri

Monitoring and designing of wearing courses for orthotropic steel decks throughout the five-point bending test 433
A. Houel, T.L. N'Guyen & L. Arnaud

Evaluation of modified bitumen, High Modulus Asphalt Concrete and steel mesh as materials for road upgrading 443
M. Tušar, M. Ravnikar Turk, W. Bańkowski, L.G. Wiman & B. Kalman

Theoretical investigation of the stress distribution in a Bimodular IDT specimen 453
S. Katicha & G. Flintsch

Investigation of Alkali-Silica Reaction in asphalt mixtures exposed to potassium acetate deicing solution 463
A.K. Apeagyei, L.J. Struble & W.G. Buttlar

Laboratory tests used in Cuba as low financial resources country for the evaluation of the mechanical properties of the asphalt mix 477
R. Herrera de la Rosa

Polypropylene fiber modification of asphalt by using mechanical and optical means 487
S. Tapkın, Ş. Özcan, M. Tuncan & A. Tuncan

Evaluation of Petroleum-Contaminated Soil effect on the properties of hot-mix asphalt concrete using dynamic modulus |E*| and indirect tensile tests 497
H.F. Hassan

Overview of the LOT meso mechanical research into porous asphalt raveling 507
M. Huurman, L. Mo, M.F. Woldekidan, R.N. Khedoe & J. Moraal

Monitoring the introduction of Enrobé à Module Élevé class 2 onto UK roads 519
R.C. Elliott, R. Perera, A. Hunter, J.C. Nicholls, N.B. Meite & D. James

On the fracture properties of epoxy asphalt mixture with SCB test 531
X. Chen, H. Li & Z. Qian

Viscoelastic response of asphalt-aggregate mixes to transient confining conditions 541
E. Levenberg & J. Uzan

Evaluation of creep compliance of rubberized asphalt in compare with conventional hot mix asphalt 551
M. Arabani & S.M. Mirabdolazimi

Characterizing volumetric deformation behavior of naturally occurring bituminous sand materials 559
J.K. Anochie-Boateng & E. Tutumluer

Alternative materials for asphalt mixture—steel slags 569
E. Diaconu & Ş.M. Lazăr

Evaluation on the shear performance of asphalt mixture through triaxial shear test 575
J. Yang, H. Zhu & Z. Chen

Development of a Dog-Bone Direct Tension Test (DBDT) for asphalt concrete 585
C. Koh, G. Lopp & R. Roque

Evaluation of performance grading parameters for crumb rubber modified asphalt binders and mixtures 597
N. Tabatabaee, H.A. Tabatabaee, M.R. Sabouri & P. Teymourpour

4. Warm and cold bituminous mixtures characterization

Design method for cold and warm emulsion mixtures based on links between laboratory and field 609
J.P. Serfass, X. Carbonneau, B. Eckmann & J.P. Triquigneaux

Fundamental property evaluation of styrene monomer modified warm-mix asphalt concrete 619
I. La, M.Y. Ryu, H.H. Kim, K. Ahn, Y.S. Doh & K.W. Kim

An evaluation of use of synthetic waxes in warm mix asphalt 627
F. Cardone, V. Pannunzio, A. Virgili & S. Barbati

Study of the mechanical behaviour of gravel-emulsions using triaxial tests 639
P. Hornych, V. Gaudefroy, J.L. Geffard & S. Goyer

Laboratory performance-based assessment of half-warm mix asphalts with high recycling rate by means of the factorial experiment design approach 651
F. Olard, E. Beduneau, N. Seignez, S. Dupriet & D. Bonneau

Evaluation of the rheological behaviour of Warm Mix Asphalt (WMA) modified binders 661
H.M.R.D. Silva, J.R.M. Oliveira, E.J. Peralta & C.I.G. Ferreira

Author index 675

VOLUME II

5. Cracking in bituminous pavement materials

Modeling of Top-Down Cracking (TDC) propagation in asphalt concrete pavements using fracture mechanics theory 681
M. Fakhri, M. Farokhi & P.T. Kheiry

The cracking device with temperature control for the laboratory identification of the road material performance 693
M. Dicu & M. Lobază

Mode II cracking in asphalt concrete 699
A. Braham & W. Buttlar

Experimental study on resistance to cracking of bituminous mixtures using the Fénix test 707
F. Pérez, R. Botella & G. Valdés

Fatigue effects in uniaxial cyclic tensile stress test: The link between stiffness decrease and accumulation of irreversible strain 715
K. Mollenhauer & M. Wistuba

Experimental study of the waveform shape effect on asphalt mixes fatigue 725
D. Bodin, J.-M. Balay, M. Merbouh, D. Breysse & L. Moriceau

Experimental investigation of crack propagation in asphalt concrete 735
R.A. Tarefder & E.M. Kias

Theoretical analysis of the 4 point bending test 749
M. Huurman & A.C. Pronk

Investigation of the PH model as a prediction tool in fatigue bending tests with rest periods 761
A.C. Pronk & A. Cocurullo

Fatigue behaviour of bitumen in tension-compression loading mode: Rheological analysis and comparison with mix fatigue 773
E. Chailleux, D. Bodin, C. de La Roche, M. Leguern & N. Vignard

Mixed-mode cracking in asphalt concrete 785
A. Braham, C. Peterson & W. Buttlar

Fatigue lines for asphalt mixtures used in wearing course 795
C. Răcănel, C. Romanescu, M. Dicu, A. Burlacu & C. Surlea

Mechanism of fatigue crack growth and fracture behavior in bituminous roads 807
R. Lugmayr, M. Jamek & E.K. Tschegg

Simplified fatigue performance modeling of ALF pavements using VECD+3-D Finite Element Modeling 817
B.S. Underwood, Y.R. Kim, S. Savadatti, S. Thirunavukkarasu & M.N. Guddati

Size effect investigation on fracturing of asphalt concrete using the cohesive softening Discrete Element Model 827
H. Kim, M.N. Partl, M.P. Wagoner & W.G. Buttlar

6. Fundamental laboratory test methods and models

On the importance of performing accurate material characterization tests for bituminous materials 839
N. Kringos & A. Scarpas

Prediction of rutting risk of bituminous concrete using complex modulus 849
K. Ait Mokhtar, E. Ghorbel, S. Saoula & S. Haddadi

Application of simplified VECD modeling to the fatigue life prediction of asphalt concrete mixtures 859
B.S. Underwood, E.T. Hou & Y.R. Kim

Experimental observation of asphalt mix characteristics in the range of low temperatures 869
P. Mondschein & J. Valentin

Calibration and validation of a visco-elasto-plastic constitutive model for bituminous conglomerates 879
N. Baldo, M. Pasetto, N. Kringos, C. Kasbergen & A. Scarpas

Modulus measurement: European standardisation possibilities 889
X. Carbonneau, Y. Legal & S. Quigniot

The influence of the specimen shape on the results of the uniaxial tensile test 899
C. Weise & A. Blasl

Experience with triaxial loading systems for the testing of road construction materials 909
P. Hyzl, D. Stehlik, M. Varaus & P. Zdralek

The estimation of the dynamic modulus of asphalt mixture from creep test results 917
F. Martinez & S. Angelone

Application of a balanced mix-design concept to thin asphalt overlay mixes: Minimizing rutting and reflective-cracking 927
L.F. Walubita & T. Scullion

3D finite element modeling of polymer modified asphalt base course mixes 939
X. Liu & A. Scarpas

Neural networks in rheology: Theory and application 949
M. Oeser & S. Freitag

7. Test methods and models for permanent deformation

Permanent deformation behaviour of bituminous mixtures containing incinerator bottom ash aggregates under uniaxial testing conditions 961
M.M. Hassan & H.A. Khalid

A new performance related test method for rutting prediction: MSCRT 971
S. Dreessen, J.P. Planche & V. Gardel

Effect of binder type on the permanent deformation resistance of asphalt mix at different temperatures 981
M. Smiljanic, I. Pap & U. Tatic

Rutting evaluation of asphalt binders and mixes 989
T.L.J. Wasage, I.B. Kazatchkov, J. Stastna & L. Zanzotto

An integrated approach to modeling rutting of flexible pavements 999
V.T. Thushara & J. Murali Krishnan

Equiviscous temperature based on Low Shear Viscosity: Evaluation as binder indicator for rutting and critical discussion of the test procedure 1009
J. De Visscher & A. Vanelstraete

The effect of volumetric properties of asphalt concrete mixture to wheel track rutting with respect to EN and BS rutting test methods 1019
A. Nikolaides & E. Manthos

Rutting resistance of SMA determined with triaxial and wheel-tracking tests 1029
J.L.M. Voskuilen & M.F.C. van de Ven

Rut resistance of asphalt concretes of different aggregate gradation 1039
K. Zhdanyuk, O. Volovyk, V. Zhdanyuk & Y. Prusenko

8. Field methods for structural behavior assessment

Damage identification in flexible pavements using FWD technique 1049
A. El Ayadi, B. Picoux & C. Petit

Dynamic approach for the evaluation of the load carrying capacity and stability of flexible pavements with the Falling Weight Deflectometer 1059
S. Riedl

Behavior of asphalt pavements subjected to non-standard heavy vehicles 1071
P.E. Sebaaly & R.V. Siddharthan

Field behavior of foamed bitumen pavement material 1081
V. Papavasiliou & A. Loizos

Evaluation of cracking in overlays in Quebec: A case study 1091
A. Carter, D. Perraton, M. Meunier & M. Paradis

9. Recycling of bituminous pavement materials

Utilization of aggregate production waste filler in cold recycling mix optimization 1101
J. Valentin & P. Mondschein

Rehabilitation of an Italian highway by Cold In-Place Recycling techniques 1113
F.A. Santagata, M. Bocci, A. Grilli & F. Cardone

Fracture energy evaluation of Cold In-Place Recycling mixtures 1123
S. Charmot & P. Romero

The use of marginal materials in road constructions: Proposal of an eco-compatible section 1131
M. Agostinacchio, M. Diomedi & S. Olita

Influence of active filler, curing time, and moisture content on the strength properties of emulsion and foamed bitumen stabilized mix 1143
S. Zulakmal, A.A. Nafisah, M. Mohd Yazip & H. Mat Zin

An experimental study on the recycling of powder extinguishers into bituminous mixtures 1151
F.G. Praticò, A. Moro & R. Ammendola

Key characteristics of materials stabilised with foamed bitumen 1161
D.C. Collings & K.J. Jenkins

In-plant asphalt cold recycling in rehabilitation of Babaei expressway project 1169
V. Ayan, A. Khavandi, A. Nikzad Gharehaghaji

10. Synthesis of international coordinated research initiatives

RILEM interlaboratory test on interlayer bonding of asphalt pavements 1181
H. Piber, F. Canestrari, G. Ferrotti, X. Lu, A. Millien, M.N. Partl, C. Petit, A. Phelipot-Mardelé & C. Raab

RILEM interlaboratory test on pavement performance prediction and evaluation 1191
H. Piber, M.N. Partl & C. Raab

New tests for polymer-modified binders: Results of a Belgian round robin test 1201
J. De Visscher, S. Vansteenkiste, A. Leuridan, N. Piérard, E. Schelkens & Ph. du Bus de Warnaffe

Comparative test on indirect tension modulus test 1211
X. Carbonneau & Y. Le Gal

Binder fatigue properties and the results of the Rilem Round Robin Test 1221
D. Sybilski, M. Gajewski, W. Bańkowski, H. Soenen, E. Chailleux & G. Gauthier

11. Other topics

Skid-resistance capability of two newly resurfaced runways in Israel 1235
M. Livneh

Chemical spill tolerance of hot mix asphalts: New research and gaps identification 1247
F.G. Praticò, R. Ammendola & A. Moro

Result of numerical analysis of efficacy geogrids on reinforced pavements' vertical and horizontal deformations 1257
F. Saleh, Gh. Shafabakhsh & Ah. Hadad

Life cycle costs of typical asphalt pavement rehabilitation techniques in Colorado USA 1265
S. Shuler, C. Schmidt & J. Goldbaum

Performance oriented payment adjustment for flexible pavements 1269
P. Sivapatham & H.J. Beckedahl

Performance of hot mix asphalt surface under high tire pressure aircraft landing gear configuration at the FAA National Airport Pavement Test Facility 1279
N. Garg, T. Bennert & H. Brar

Quantification of the highway costs as a function of the road traffic and speed 1289
A.C. Valle de Souza & D. Cardoso de Lima

Author index 1299

Advanced Testing and Characterization of Bituminous Materials –
Loizos, Partl, Scarpas & Al-Qadi (eds)
© 2009 Taylor & Francis Group, London, ISBN 978-0-415-55854-9

Preface

Bituminous materials are used to build durable roads that sustain diverse environmental conditions. However, due to their complexity and a global shortage of these materials, the design and technical development of bituminous materials has become challenging. The *International Union for Testing and Research Laboratories for Materials and Structures* RILEM has contributed to this challenging task for the past several years through Technical Committees that focus on the characterization and performance of bituminous binders and mixtures. These Committees provide a platform for researchers from all over the world to share their expertise, develop recommendations on testing and evaluation approaches and publish state-of-the-art reports and papers in the RILEM *Journal of Materials and Structures* as well as other journals and conferences.

The *7th International RILEM Symposium on Advanced Testing and Characterization of Bituminous Materials* ATCBM09 is under the auspices of the RILEM TC 206-ATB. The ATCBM09 RILEM Symposium aims to provide an international forum for the exchange of ideas, information, and knowledge amongst experts involved in the development and implementation of specifications for the experimental characterization, design, utilization and evaluation of binders and bituminous mixes.

Currently, the committee, chaired by Manfred N. Partl of EMPA, Switzerland, comprises 50 experts from 20 countries. The committee focuses on fundamental and performance testing of binders and asphaltic mixtures. The committee is composed of five Task Groups:

- *TG 1 Binders* (Convener: Dariusz Sybilski, IBDiM, Poland): Focused on evaluating *bin*der properties with respect to durability relevant distress accumulation, *performance*, and application.
- *TG 2 Mixture design and compaction* (Convener: Hussain Bahia, University of Wisconsin, USA): Focused on the evaluation of laboratory compaction methods and models with respect to field compaction.
- *TG 3 Mechanical testing of mixtures* (Convener: H. Di Benedetto, ENTPE, France): Focused on the evaluation of existing test methods and models for different types of mixtures considering topics such as permanent deformation, micromechanics, and size effects.
- *TG 4 Pavement performance prediction evaluation* (Convener: Herald Piber, Bautechnik Carinthia, Austria, followed by Francesco Canestrari, Univ delle Marche, Italy): Focused on the evaluation of test methods to assess structural behavior such as interlayer bond and pavement performance prediction evaluation.
- *TG 5 Recycling* (Convener: Chantal De La Roche, LCPC, France): Focused on the evaluation of reclaimed asphalt pavements and hot-mix recycling.

This Symposium represents the seventh in a series of RILEM Symposia on characterization, performance testing, and evaluation of bituminous binders and mixtures. In chronological order, the previous symposia convened at the following locations: 1st 1968 Dresden, 2nd 1975 Budapest, 3rd 1983 Belgrade, 4th 1990 Budapest, 5th 1997 Lyon, 6th 2003 Zürich, 7th 2009 Rhodes.

All submitted contributions were subjected to an exhaustive refereed peer review procedure by at least three reviewers and the Editors. On the basis of their recommendations, the papers that contributed to the symposium subject and met the goals and the objectives of the Symposium were selected for inclusion in the Proceedings.

The accepted contributions indicate that many researchers from the academia, industry, and governmental agencies are currently utilizing advanced experimental and computational techniques to better understand the behavior of binders and bituminous mixtures and their role in the design and performance of complex pavement systems. The Proceedings clearly show that modern experimental material characterization techniques, sophisticated constitutive modeling, and innovative design provide the appropriate tools for pavement performance prediction. This ultimately would lead to the development and implementation of truly "mechanistic" pavement design methodologies.

The Editors would like to thank the reviewers and the Scientific Committee for their thorough and timely review of the papers. Special thanks also are extended to the Organizing Committee for their management of the Symposium.

The Editors

Andreas Loizos
Manfred Partl
Tom Scarpas
Imad Al-Qadi

Rhodes, May 2009

Advanced Testing and Characterization of Bituminous Materials – Loizos, Partl, Scarpas & Al-Qadi (eds)
© 2009 Taylor & Francis Group, London, ISBN 978-0-415-55854-9

Organization

Chairmen

Andreas Loizos	National Technical University of Athens, Greece
Manfred Partl	EMPA, Chair of RILEM TC 206-ATB, Switzerland
Tom Scarpas	Delft University of Technology, The Netherlands
Imad Al-Qadi	University of Illinois at Urbana-Champaign, USA

Scientific Committee

Chairmen: A. Loizos, M. Partl

G. Airey, UK
M. Ayala Canales, Spain
H. Azari,USA
H. U. Bahia, USA
W. Bankowski, Poland
R. Blab, Austria
D. Bodin, France
W. Buttlar, USA
F. Canestrari, Italy
C. Celauro, Italy
A. Chabot, France
E. Chailleux, France
J.S. Chen, Taiwan
A. Collop, UK
J. D'Angelo, USA
M. Darter, USA
C. De la Roche, France
H. Di Benedetto, France
B.J. Dongo-Engeland, Norway
R. Dongre, USA
G. Doré, Canada
B. Eckmann, Belgium
S. Erkens, The Netherlands
A.C. Freire, Portugal
G. Gauthier, France
M. Greenfield, USA
R. Gubler, Switzerland
T. Harman, USA
J. Harvey, USA
G. Huber, USA
M. Hugener, Switzerland
U. Isacsson, Sweden
I. Ishai, Israel
K. Jenkins, South Africa
K. Kaloush, USA
H.A. Khalid, UK
R. Kim, USA
G. King, USA
B. Koenders, France
N. Kringos, The Netherlands
D. Little, USA
H. Litzka, Austria
X. Lu, Sweden
B. Lytton, USA
J. Maeck, Belgium
M. Marasteanu, USA
E. Masad, USA
L. Mohammed, USA
A.A. Molenaar, The Netherlands
J. Nodes, USA
M. Oeser, Australia
J.C. Pais, Portugal
T. Pauli, USA;
D. Perraton, Canada
K. Petros, USA
H. Piber, Austria
J.P. Planche, France
J.E. Poirier, France
L. Porot, France
C. Raab, Switzerland
R. Robertson, USA
R. Roque, USA
G.M. Rowe, USA
S. Said, Sweden
M. Saleh, New Zealand
E. Santagata, Italy
C. Schwartz, USA
P. Sebaaly, USA

M. Smiljanic, Serbia
H. Soenen, Belgium
J.M.B. Sou sa, Portugal
D. Sybilski, Poland
G. Tebaldi, Italy
S. Toth, Hungary
M. Van de Ven, The Netherlands
A. Vanelstraete, Belgium
H. Von Quintus, USA
L.B. Wang, USA
M.W. Witczak, USA
J. Youtcheff, USA
M. Zaman, USA
L. Zanzotto, Canada

5. *Cracking in bituminous pavement materials*

Advanced Testing and Characterization of Bituminous Materials – Loizos, Partl, Scarpas & Al-Qadi (eds)
© 2009 Taylor & Francis Group, London, ISBN 978-0-415-55854-9

Modeling of Top-Down Cracking (TDC) propagation in asphalt concrete pavements using fracture mechanics theory

M. Fakhri, M. Farokhi & P.T. Kheiry
K.N. Toosi University of Technology, Department of Civil Engineering, Tehran, Iran

ABSTRACT: Fatigue is defined as the failure phenomena caused by repeated loading even though the stress due to the loading is less than ultimate strength of the material. Fatigue cracking in asphalt concrete layer is divided into two groups regarding to the place of crack initiation and the type of crack propagation. The first group is the cracks which is initiated in the bottom of asphalt layer and propagates upward. This type of cracking is produced in the asphalt layer with less than 16 mm thickness. The second type of cracking which is produced in thick asphalt layer is initiated in surface area then propagates downward which is called Top-Down Cracking. The second type of cracking is investigated less compared to the first one. One type of analysis and studying fatigue cracking is fracture mechanics approach in which the failure in asphalt mixture is related to number of repeated loading. In this study the fracture mechanics approach was implemented to understand the effective parameters in propagation of top-down cracking. As well as developing a model to interpret the crack propagation in pavement also some graphs were produced for different types of material and loading which gives the length of cracks versus the number of repeated loading.

1 INTRODUCTION

Top-down cracking has become an asphalt surface course distress of growing concern that must be dealt with during the design, construction, maintenance, and resurfacing of long-life asphalt pavements. The surface course is designed for heavy vehicle loadings and general traffic conditions in terms of rutting, resistance, durability, noise levels, smoothness, and frictional characteristics. The impact of top-down cracking on the life-cycle performance of asphalt pavements, and its complexity, is now widely recognized and the subject of considerable applied asphalt technology and improved pavement design research (Paterson 1987, Myers et al. 1998, Newcomb 2002, Uhlmeyers et al. 2000, Baladi et al. 2002, Witczak & El-Basyouny 2004, Emery 2006). The conventional studies in pavement performance modeling are focused mostly on classical fatigue cracking initiated at the bottom of the asphalt concrete layer. Longitudinal surface cracks are predominantly parallel to the asphalt concrete pavement centerline and located in the vicinity of the wheel paths. At the Minnesota road research facility, Mn/ROAD, longitudinal cracks have been observed to form perpendicular to the edge of the transverse cracks in the wheel paths, and then propagate away from the transverse cracks until they eventually meet and form one continuous crack the entire length of the pavement cell. Several researchers have concluded that the conventional approach to analyzing pavement distress cannot explain surface-initiated top-down cracking, and have proposed various hypotheses in an attempt to explain this phenomenon. One of the most widely accepted hypotheses is that surface cracking is wheel-induced cracking. This implies that the problem should be addressed in terms of contact mechanics, since the tire properties and geometry affect the induced stresses. Most importantly, there is a significant effect from the tire treads. The available analytical tools for pavement design and performance evaluation are based on the assumption of uniform pressure distributions exerted on the pavement surface by tires. Furthermore, the continuity of lateral strains in a multilayered pavement

Figure 1. Schematics of TDC in an asphalt concrete specimen.

system is assumed. Recent research (Holewinski et al. 2007, Perret 2002, Bensalam et al. 2000, Pottinger & McIntyre 1999, Seitz & Hussmann 1971, DeBeer 1997, Perdomo & Nokes 1993, Pottinger 1992) on the nature of near-surface stress distribution has shown that significant tangential (frictional) forces can be imparted to the pavement surface by truck tires. Estimates of the magnitude of these forces suggest that they may be sufficient to cause large tensile/shear stresses and localized failure near the pavement surface resulting in top-down propagating cracking. Site observations of flexible pavements' distress in various countries indicate frequent occurrence of longitudinal (top-down) cracking in the top asphalt concrete (AC) layer. Figure 1 shows a schematic of TDC in an asphalt concrete specimen.

Analytic and numerical studies of multilayer elastic systems subject to wheel loads have linked longitudinal cracking to surface tensile stresses. However, due to the complexity of tire/pavement interaction resulting from tire geometry and loading conditions, the accurate and fully representative distribution of surface stresses remains partly unknown. Recent trends emphasize incorporating mechanistic/empirical methods into the design of flexible pavements. These methods require the knowledge of the values of the horizontal tensile stress or strain at the bottom of the asphalt concrete (AC) layer and the vertical stress or strain in the base layer. Theoretical analyses of continuous flexible pavement systems have been presented by several researchers (Collop & Cebon 1995, Gerritsen 1987, Jacobs 1992, Molenaar 1984, Myers 1998). Generic computer codes such as ABAQUS, or specialized computational modules such as CIRCLY, BISAR, and ILLIPAVE, provide valuable tools for stress, strain, or displacement calculations. In contrast to the analysis of discontinuous rigid pavements with cracks or joints, limited references describe the effect of cracks on the behavior of flexible pavements. It can be concluded from the literature that the causes of TDC could be categorized into four classes: I) three dimensional tire-pavement interaction, II) frictional forces, III) thermal gradient and IV) segregation.

In this study the fracture mechanics approach was implemented to understand the effective parameters in propagation of top-down cracking. As well as developing a model to interpret the crack propagation in pavement also some graphs were produced for different types of material and loading which gives the length of cracks versus the number of repeated loading.

2 PAVEMENTS CRACKING MECHANISM

2.1 *Crack growth modes*

The basic difference between cracked pavement segments could be well represented by stress intensity factor. In other words, K is a factor indicating the measure of stress near

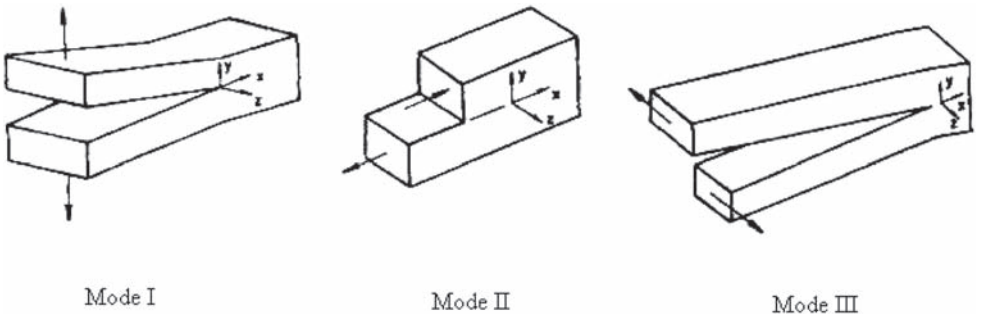

Figure 2. Three fundamental crack edges displacement modes.

the vicinity of a cracked area. Stress intensity factors K_I, K_{II}, and K_{III} are related to three fundamental surface crack displacement modes. These three modes are shown in Figure 2. In the tensile or opening mode, Mode I, the crack edges opens in two reverse directions parallel to the Y-axis shown in Figure 2. In the slipping or in plane shear mode, mode II, the crack edges slip along the X-axis without opening apart. And finally in case of the Mode III, the two surfaces of the crack edges slip along the Z-axis as illustrated by Figure 2 (Ekrami 2003, farrahi 1997).

It seems necessary to present some additional explanations about the different modes mentioned above. In case of the mode I, the crack would initiate as a result of the temperature differences, expansion, and contraction. Then it would grow as a result of the passing traffic loading and the corresponding bending in the asphalt concrete (AC) layer. The crack initiation and growth for mode II would be as a result of traffic loading induced shear forces. Mode III cracks would also be initiated as a result of tangential surface forces between tire and pavement and then propagates through the layer. Based on the literature it can be seen that cracking phenomenon is affected by particular state of stress and strain. It could also be recognized that the cracks developed in the form of modes I and II are the most observed ones.

2.2 *Crack propagation principles*

After conducting several tests on engineering materials, Paris and Erdogon expressed that the rate of crack propagation would be presented as a function of stress intensity factor and the parameters related to the characteristics of the material as presented in Equation 1:

$$\frac{dc}{dN} = AK^n \tag{1}$$

where dc/dN indicates the rate of the crack length growth per each loading cycle, K is the stress intensity factor, the terms A and n are the material related constants which could be determined from the experimental tests. For asphalt concrete, the latter parameters are mainly depended on bitumen content, VMA, filler content, bitumen type, testing temperature. The values for n and A would be determined in the laboratory tests, e.g. beam loading, however there are some simple equations to avoid conducting time consuming tests. For Example Equations 2 and 3 which thave been developed by Lytton are presented as follows:

$$n = 2 \times \frac{1}{m} \tag{2}$$

$$n = 1.558 - 0.4011 \log A \tag{3}$$

where m is the slope of the elastic modulus versus the loading time on logarithmic scales. Integrating the equation 1 would result into the number load repetitions which make the crack propagate from the length C_0 to C_1 as illustrated in the Equation 4:

$$N = \int_{C_0}^{C_1} \frac{dc}{A(K_{(c)})^n} \tag{4}$$

It can be recognized from Equation 4 that in order to calculate the above integral the first step is to determine the stress intensity factor as a function of crack length. Several methods are available among which Finite Element Method's (FEM) results provide more precision. Therefore in this study FEM is employed to calculate the K value. The scope of this study was to investigate crack propagation mechanism through the depth of asphalt concrete layer. In this case, a two-dimensional finite element model was employed. The 2D and 4 nodes solid elements were selecte d as are in common use for the modeling purpose and researches. For the simulation purpose, loading and the boundary conditions were carefully chosen in such a way that provide the most conformant conditions to the actual ones. Regarding to the stress concentration at the vicinity of the crack vertex, the number of the finite elements and the nodes must be increased. Consequently, this would result in a greater computation time; therefore the trial and error method was used to determine the optimum mesh dimension. In order to reduce the computation time while preserving the accuracy, the ABAQUS developed model was subdivided into different parts and appropriate mesh size was employed for each one. The model dimension was selected to completely accommodate the cross section of the wheel considering its lateral movements due to the nature of analyses. The structural system of the pavement was assumed to be four-layered linear elastic and fully bonded consisting of: a) asphalt concrete layer with variable thicknesses of 10 cm, 20 cm, and 25 cm, b) .30 cm base course, and c) 2.5 m embankment layers.

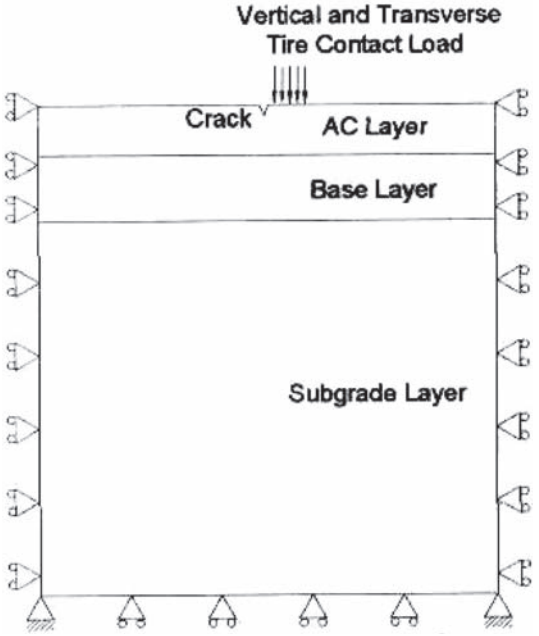

Figure 3. Schematic of the developed 2D model.

Table 1. Properties of the material used in the model.

	Asphalt (1)	Asphalt (2)	Base (1)	Base (2)	Embankment layers
Material type	Elastic	Elastic	Elastic	Elastic	Elastic
Elastic modulus (MPa)	5500	8275	140	300	100
Poisson's ratio	0.35	0.35	0.4	0.4	0.45
Fracture parameters	A	3.82E-6			
	n	3.79			

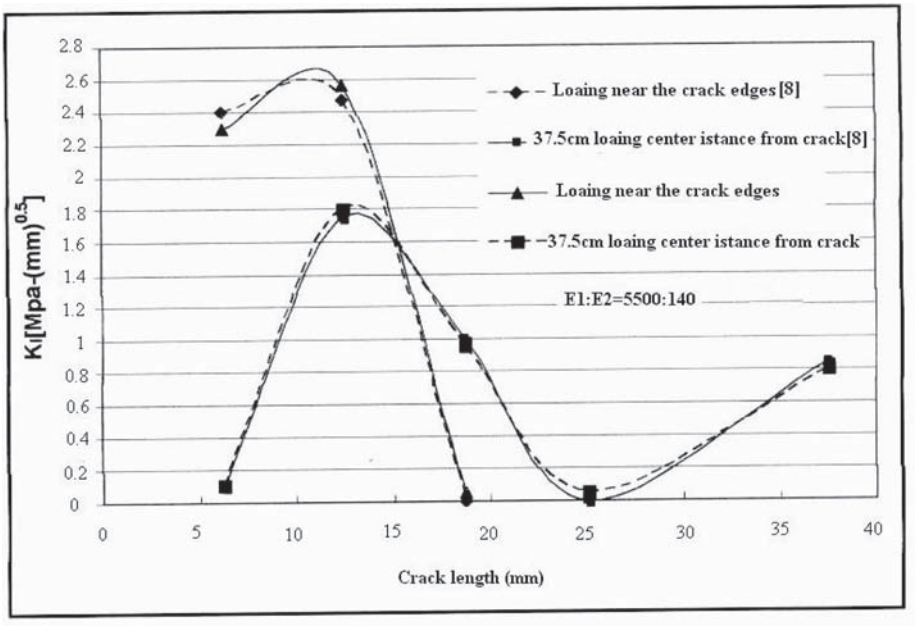

Figure 4. Load position effect on the stress values about the crack (the [8] after the series name in the figure refers to the results presented by Myers & Roque).

2.3 *Boundary conditions and material properties*

All the 2D developed models consist of a fixed bottom, the subgrade layer, and rollers along the sides to prevent any horizontal displacement. The continuum nodes surrounding the two vertical sides of the model were fixed against horizontal displacement however the vertical deformation of the pavement structure was provided. Schematic of the developed model is presented by Figure 3.

Employing the linear elastic method for analyzing the cracked section, the elastic properties of material, i.e. Poisson's ratio and elastic modulus, were employed according to the values illustrated in Table 1. The values of the parameters n and A in Paris law, which is used for determination of the number of load repetition, was concluded from the Florida Department of Transportation based on the assumed elastic modulus for asphalt concrete in the present study.

3 RESULTS AND DISCUSSION

3.1 *Model results for loading position and the stress*

Analyses were executed on the model to investigate the effect of the loading position on the stress values near the vicinity of the crack vertex. Therefore, four different cases of the

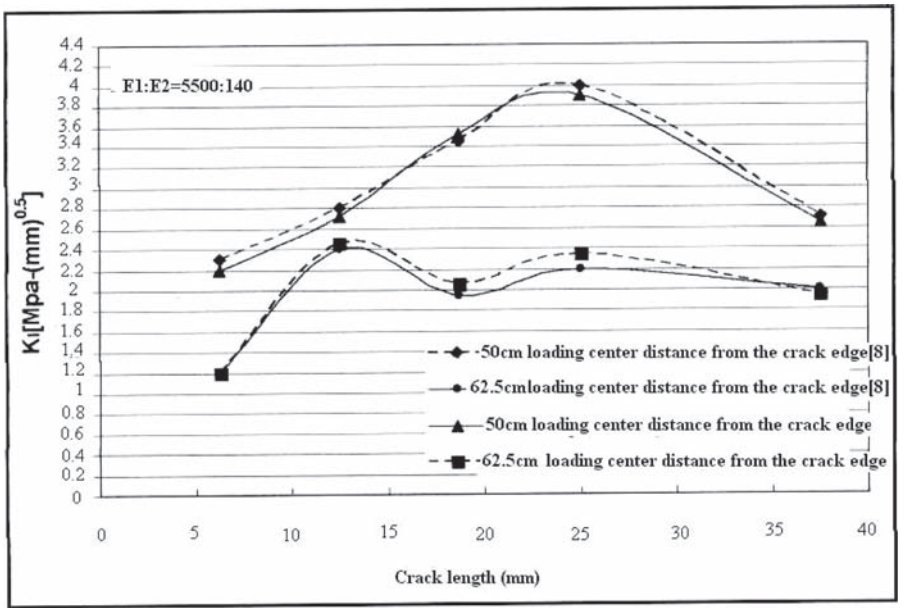

Figure 5. Effect of loading position on the stress values adjacent to crack vertex.

loading position were evaluated. For one of the cases the loading position was assumed to be properly adjacent to the cracked area and for the three others the loading center was located 37.5 cm, 50 cm, and 62.5 cm from the crack. For this purpose a thickness of 20 cm was assigned to the asphalt concrete layer. Variations in the stress intensity factor for Mode I (K_1) versus crack length are presented in Figure 4 and Figure 5. To investigate the validation of the developed model, other researchers' results (Myers & Roque 2002) are also presented in these Figures. As it could be concluded from Figures 4 and 5, applying appropriate dimensions for the model and the finite elements in this study, the results are considerably in good agreement with those presented by Myers et al. In this figures, it should be noted that the thickness of the asphalt concrete layer was considered to be 20 cm and the parameters E1 and E2 are the elastic modulus for Asphalt concrete and base layer, respectively.

3.2 *Layer thickness and elastic modulus ratio*

Model analyses were conducted to investigate the effect of asphalt concrete layer thickness on the stress magnitude near the vicinity of the crack. For this purpose, three different thicknesses of 10 cm, 20 cm, and 25 cm were considered in the model. Variations in the stress intensity factor for Mode I (K_1) versus crack length are presented in Figure 6 for each of these thicknesses. The results for 10 cm and 20 cm thicknesses were also compared with those obtained by other researchers. As indicated by Figure 6, thick AC layer presents less stress intensity factor.

In order to study the effect of the elastic modulus ratio between AC layer and the base, four different ratios were assumed and model analyses were executed for each of them. Brief results are illustrated in Figure 7. It can be seen from Figure 7 that as the elastic modulus ratios increase the corresponding stress intensity factor, K_1, increases. It should be noted that the AC layer thickness was assumed to be 10 cm and the loading center was applied 62.5 cm from the crack edge. It could be also observed that after a determinate crack length, say 25 mm in this case, the stress intensity factor would start to decrease.

3.3 *Temperature differences in the AC layer and the stress magnitude*

In order to evaluate the effect of temperature differences on the developed model, two different cases were studied. In the first case, thermal diffusion through the thickness of AC layer was assumed to be uniform. In the second case, the pavement surface was supposed to warm up considerably in a short period of time. An example for the latter case would be the early hours after sunrise. For both cases the loading center lies 75 cm along the crack. For each case Stress intensity factor Variations for Mode I, (K_I), versus crack length were presented in Figure 8.

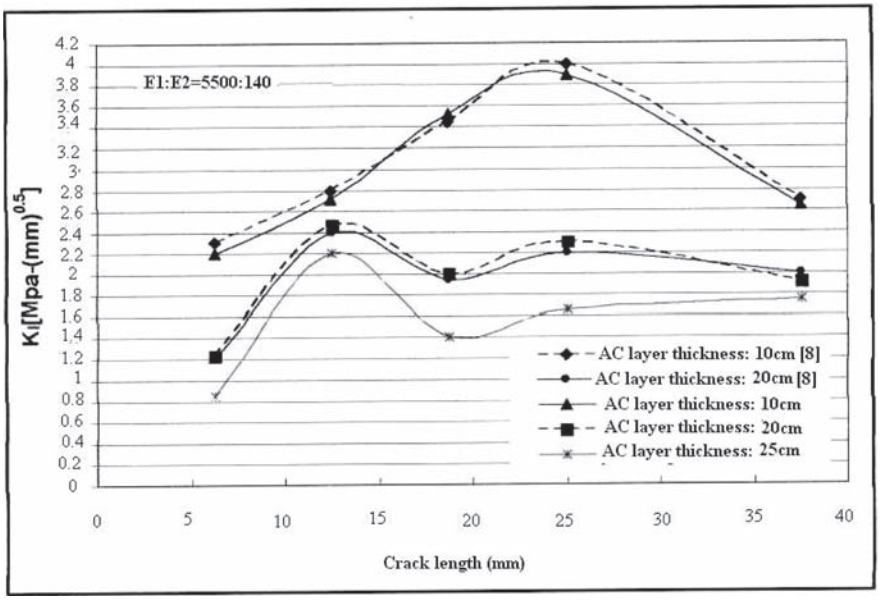

Figure 6. Effect of AC layer thickness on the stress values adjacent to crack.

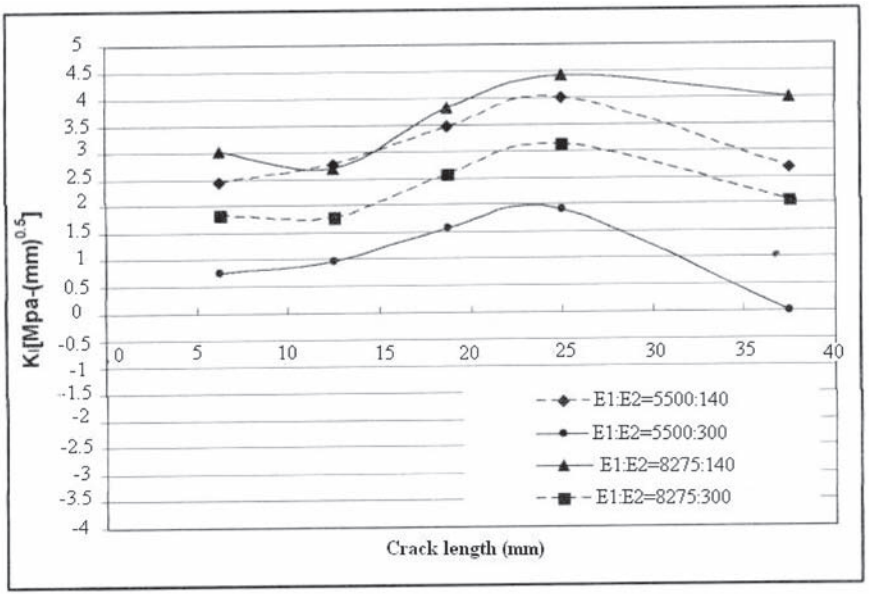

Figure 7. Effect of the elastic modulus ratio between AC and base layer.

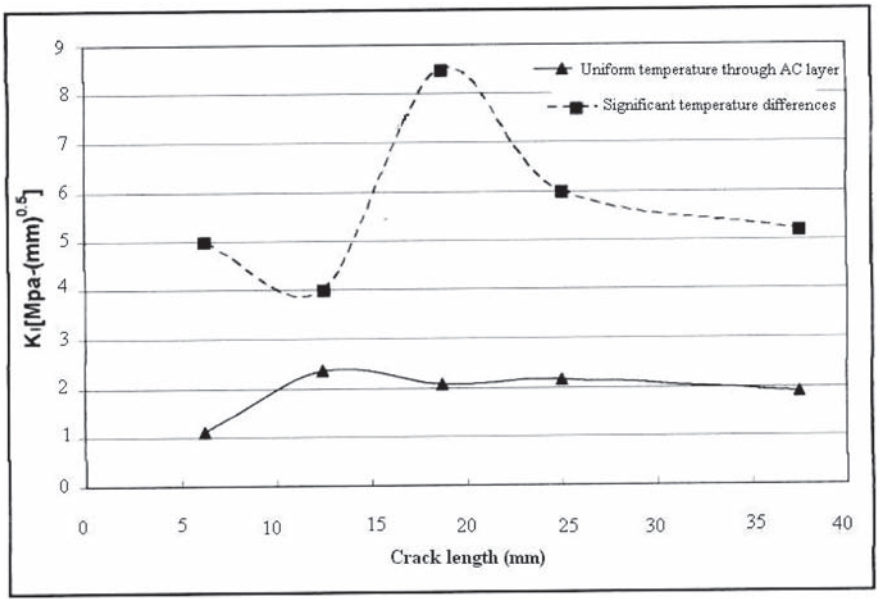

Figure 8. Thermal gradient and the stress values adjacent to the crack.

As it could be observed from Figure 8, the thermal gradient in depth of the AC layer would result in a significant increment of stress intensity factor.

3.4 *Determination of K_{II} and the equivalent K*

For each of the analyses the stress intensity factor for mode II, K_{II}, was also calculated. The K_{II} values are predominantly less than K_I values, about 0.1 times, and as the loading center position distance from the crack increases K_{II} value increases. The equivalent K factor for mode I and mode II was also calculated; however subsequently it will be shown that for the purpose of calculating the number of load repetition its effect is negligible. Figure 9 shows variation in stress intensity factor for Mode II (K_{II}) versus crack length for two different elastic modulus ratios. The results were also compared to those of the other researchers (Myers & Roque 2002). It can be concluded from Figure 9 that as the crack length increases the stress intensity factor continuously increases. As a matter of fact that the cracking mechanism is a combination of both modes I and II it would be necessary to calculate an equivalent K, therefore the Paris crack propagation law could be applied. The following equation could be employed to calculate the equivalent K:

$$K = \sqrt{JE} \tag{5}$$

Integral value of J could be calculated from Equation 6 as follows:

$$J = \frac{(K_I^2 + K_{II}^2)(1-\upsilon^2)}{E} \tag{6}$$

where υ is the Poisson ratio, and E is the elastic modulus. Considering the equation mentioned above, the first step to calculate the equivalent K is to determine the K_I and K_{II} value as functions of crack length. For this purpose polynomial functions were generated. Based on these functions the equivalent K values would be calculated from Equations 5 and 6. Brief results are illustrated in Table 2. The term x in the table represents the crack length in mm.

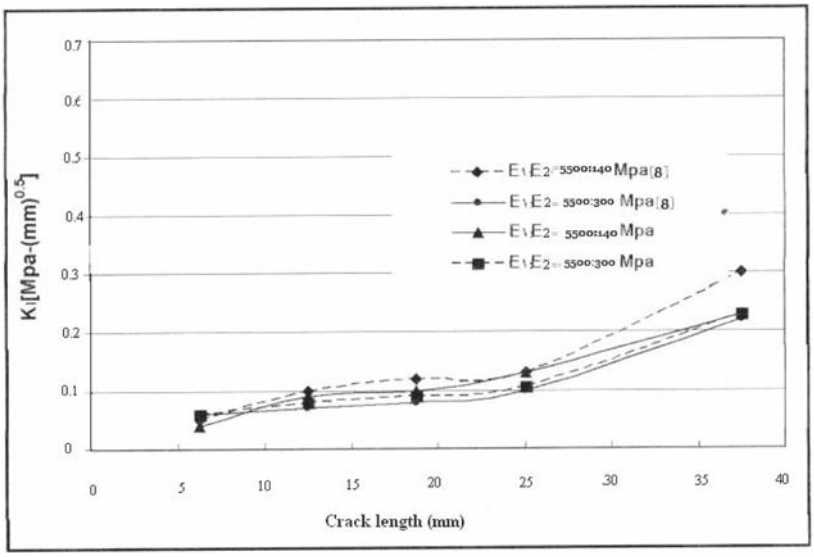

Figure 9. Determination of K_{II} for different elastic modulus ratios.

Table 2. Determination of K values for different crack length.

Row	AC elastic modulus (MPa)	Base elastic modulus (MPa)	AC layer thickness (cm)	Loading center distance from crack (cm)	Equivalent K as a function of crack length [MPa-mm 0.5]
1	5500	140	20	37.5	$K = (-4\times10^{-5}x^4 + 0.0042x^3 - 0.1505x^2 + 2.094x - 8.06)(1-\upsilon^2)$
2	5500	140	20	50	$K = (2\times10^{-6}x^4 + 0.0001x^3 - 0.0143x^2 + 0.305x - 0.53)(1-\upsilon^2)$
3	5500	140	20	62.5	$K = (-7\times10^{-5}x^4 + 0.0062x^3 - 0.183x^2 + 2.201x - 6.782)(1-\upsilon^2)$
4	5500	140	20	75	$K = (-5\times10^{-5}x^4 + 0.0046x^3 - 0.139x^2 + 1.716x - 5.14)(1-\upsilon^2)$
5	5500	140	25	62.5	$K = (-9\times10^{-5}x^4 + 0.0078x^3 - 0.2315x^2 + 2.76x - 9.12)(1-\upsilon^2)$

3.5 *Number of load repetitions for crack growth*

After determination of the equivalent K in the previous section, the next step is to calculate the number of load repetition required for the crack growth from 6 mm to 38 mm as presented in the Equation 6. In order to determine the corresponding N value from Equation 6, the integral was calculated by means of Simpson's method for each intervals of 12.5–6.25, 18.75–12.5, 25–18.75, and 37.5–25 mm. Following to the cases presented in Table 2, the corresponding

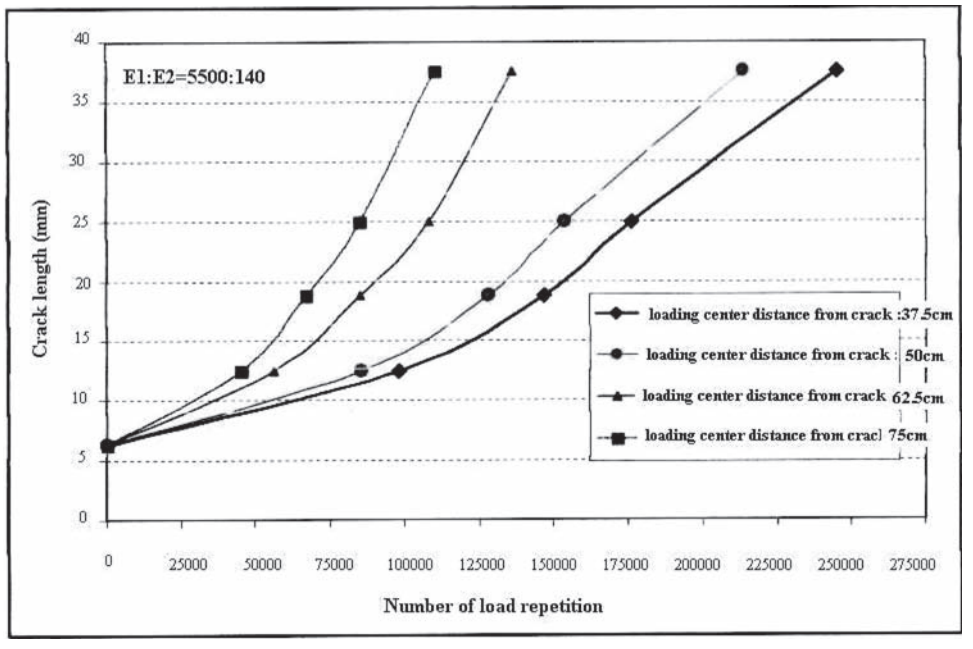

Figure 10. Number of load repetitions versus crack length (20 cm AC layer).

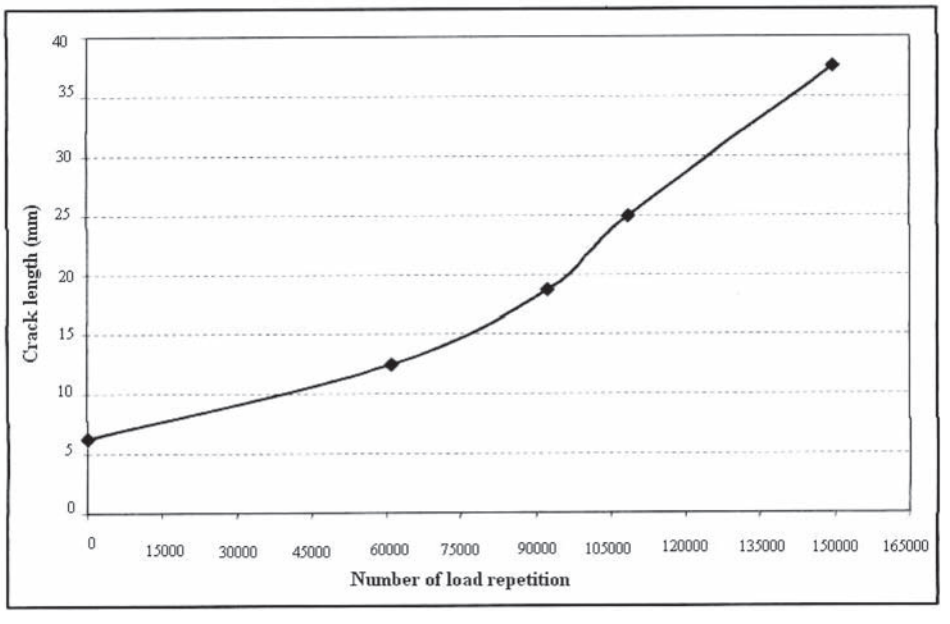

Figure 11. Number of load repetitions versus crack length (25 cm AC layer).

load repetitions were calculated and presented in Figures 10 and 11. It can be concluded from the Figures that as crack length grows the number of load repetition required to resume the crack growth process decreases. In other words the rate of crack growth would significantly increase as the crack length increases. Figure 10 shows the number of load repetition versus crack length for a 20 cm thickness of AC layer, and Figure 11 shows that of a 25 cm AC layer. In Figure 11, the loading center position is 62.5 cm away from the crack.

4 CONCLUSION

The aim of the present study was to investigate the top-down cracking propagation in asphalt concrete pavements and the related parameters. As a result of this study the following conclusions could be drawn:

- It was observed from the results that as the distance between applied load and the primarily initiated crack increases, the stress intensity factors for mode I and II consequently increases. The maximum ratio of K_{II} to K_I was recognized to reach 0.1.
- The difference between the elastic modulus of base and AC layers significantly increases the K_I, on the other hand greater elastic modulus of the AC layer would speed up the crack propagation phenomenon.
- Thermal gradient through the AC layer plays an important role in variation of stress intensity factors.
- As a result of the considerable difference between the K_I and K_{II} it could be concluded that the TDC propagation outside the wheel path would occur under tensile fracture mode (mode I), and the shear fracture mechanism would be negligible.
- As illustrated in the present study, the top-down cracking potential increases as the thickness of asphalt concrete layer increases. Therefore, applying several overlay layers in order to maintain TDC distress would facilitate the crack growth and propagation. As a result, it would be suggested to employ the mill and replace method instead.

REFERENCES

Baladi, G.Y., Schorsch, M. & Svasdisant, T. 2002. Determining the causes of Top-Down Cracking in bituminous pavements. MDOT-PRCE-MSU-2003-110, Michigan State University: East Lansing.

Bensalem, A., Brown, A.J., Nunn, M.E., Merrill, D.B. & Lloyd, W.G. 2000. Finite Element Modeling of fully flexible pavement: surface cracking and wheel interaction, *Proc. of the 2nd International Symposium on 3D Finite Element for Pavement Analysis, Design, and Research*: 103–113.

Collop, A. & Cebon, D. 1995. A theoretical analysis of fatigue cracking in flexible pavements, *Proc. of the Institution of Mechanical Engineers*, Part C, vol. 209(5): 345–361.

DeBeer, M., Fisher, C. & Jooste, F.J. 1997. Determination of pneumatic tyre/pavement interface contacts stresses under moving loads and some effects on pavements with thin asphalt surfacing layers, *Proc. of the 8th International Conference on Asphalt Pavements*, vol. 1: 179–227.

Ekrami, A.K. 2003. *Fracture mechanics and deformation of engineering materials*, Sharif University of Technology Publication: Tehran.

Emery, J. 2006. Evaluation and mitigation of asphalt pavement Top-Down Cracking, Assessment and Rehabilitation of the Condition of Materials Session of the *Annual Conference of the Transportation Association of Canada*, Charlottetown: Prince Edward Island.

Farrahi, Gh. 1997. *Fracture mechanics*. Bou-Ali-Sina University Publication.

Gerritsen, A., Gurp, C.V., van der Heide, J., Molenaar, A. & Pronk, A. 1987. Prediction and prevention of surface cracking in asphaltic pavements. *Proc. of the 6th International Conference on Structural Design of Asphalt Pavements*: 378–392.

Holewinski, J., Soon, S., Drescher, A. & Stolarski, H. 2007. Investigation of factors related to surface initiated cracks in flexible pavements. Minnesota Department of Transportation MN/RC–2003–07.

Jacobs, M.M.J., de Bondt, A. Molenaar, A.A.A. & Hopman, P. 1992. Cracking in asphalt concrete pavements, *Proceedings of the 7th International Conference on Asphalt Pavements*, vol. 1: 89–105.

Molenaar, A.A.A. 1984. Fatigue and reflection cracking due to traffic loads, *Proc. of the Association of Asphalt Paving Technologists*, vol. 53: 440–474.

Myers LA, Roque, R. & Ruth, BE. 1998. Mechanisms of surface-initiated longitudinal wheel path cracks in high type bituminous pavements. *Proc. of Association of Asphalt Paving Technologists*: 401–432.

Myers, L.A. & Roque, R. 2002. Evaluation of top-down cracking in thick asphalt pavements and the implications for pavement design, *TRB committee on general Issues in asphalt Technology*: 79–88.

Newcomb, D. 2002. Perpetual pavements, a synthesis. Asphalt Pavement Alliance, APA101: Latham.

Paterson, W. 1987. Road deterioration and maintenance effects. Johns Hopkins University Press: Baltimore.

Perdomo, D. & Nokes, B. 1993. Theoretical analysis of the effects of wide-base tires on flexible pavement using CIRCLY, *Transportation Research Board (TRB)*, National Research Council, Washington D.C.: 108–119.

Perret, J. 2002. The Effect of loading conditions on pavement response calculated using a linear-elastic model. *Proc. of the 3rd International Symposium on 3D Finite Element for Pavement Analysis, Design and Research:* 283–303.

Pottinger, M.G. 1992. The three-dimensional contact patch stress field of solid and pneumatic tires, *Tire Science and Technology, TSTCA*, vol. 20(1): pp. 3–32.

Pottinger, M.G. & McIntyre, J.E. 1999. Effects of suspension alignment and modest cornering on the footprint behavior of performance tires and heavy duty radial tires, *Tire Science and Technology, TSTCA,* vol. 27(3): 128–160.

Seitz, N. & Hussmann, A.W. 1971. Forces and displacements in contact area of free rolling tires, *Society of Automotive Engineers*: 1–7.

Uhlmeyer, J.S., Willoughby, K., Pierce, L.M., & Mahoney J.P. 2000. Top-Down Cracking in Washington State asphalt concrete wearing course. *Transportation Research Record*: 110–1730.

Witczak M.W. & El-Basyouny, M.M., 2004. Calibration of fatigue cracking models for flexible pavements. Guide for Mechanistic-Empirical Design, Appendix IT-1, *National Cooperative Highway Research Program*, Washington, D.C.

Advanced Testing and Characterization of Bituminous Materials – Loizos, Partl, Scarpas & Al-Qadi (eds)
© 2009 Taylor & Francis Group, London, ISBN 978-0-415-55854-9

The cracking device with temperature control for the laboratory identification of the road material performance

M. Dicu & M. Lobază
Technical University of Civil Engineering, Faculty of Railroads, Roads and Bridges, Bucharest, Romania

ABSTRACT: The cracking device with temperature control was conceived in the road laboratory of the Technical University of Civil Engineering, Bucharest, Romania, to identify in accelerated rate the road material performance. The method consists in testing the material performance through cracking comparison, controlling the temperature. It simulates the dynamic effect of the traffic on the bituminous layer, and the different weather (through season temperature).

1 INTRODUCTION

Obtaining quick data concerning the rate of the exploitation performances for a road material using low scale simulation models, tasted in the laboratory, was and continue to be a main concern for the specialists in the field.

The research carried out within a CEEX (2006–2008) project at the Roads Laboratory of the Bucharest Technical University of Civil Engineering aimed to achieve a cracking device able to test geometrically reduced specimen slabs.

For these reasons, several laboratory tests were made in order to simulate the behavior of asphalted road in service. The tests were made using loaded slab specimen prepared in the laboratory in order to determine the fracture behavior of asphalted road structure due to variation of weathering and to the geographical conditions of Romania.

Quick information regarding the fatigue behavior of the road layer assimilated to the lab specimen is another working hypothesis of the cracking device.

2 GENERAL DESCRIPTION

Quick data obtained in accelerated conditions concerning the exploitation performances of the road materials with bituminous binder alongside with loading hypotheses using some performance coefficients are the main targets for specialists as well as for the decision staff working in the field of road transport infrastructure.

Laboratory tests acquired by behavior simulation of a road in use that were produced on samples of slabs prepared in labs ascertain the choice of the optimal formulas for asphalted structure. The cracking device elaborated within a CEEX project at the Road Laboratory of Bucharest Technical University of Civil Engineering is a device able to do such laboratory tests, which continue other complex researches meant to choose the optimal formula for the asphalted structure.

The procedure consist in the determination of the fracture behavior of the asphaltic road structure, in steps of dynamic load and in accelerated conditions, obtained by increasing the test load at predetermined time.

Figure 1 represents the testing methodology related to well-known methods, such as the fracture static test (σ_{rs}) and stress failure (σ_{rs}). The accelerated breaking at fatigue test σ_{ra} (after the crack is propagated in the thickness of the asphalt mixture layer). A shorter time

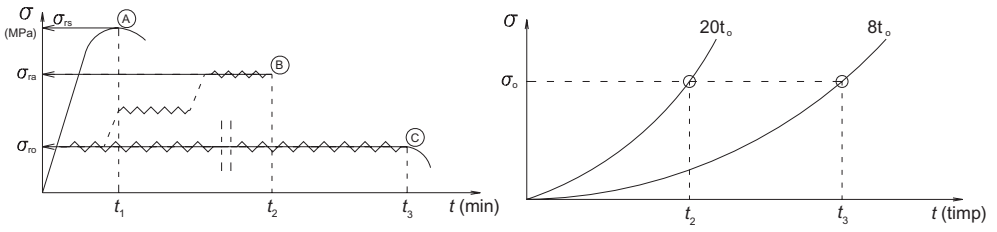

Figure 1. The procedure for the fracture behaviour.

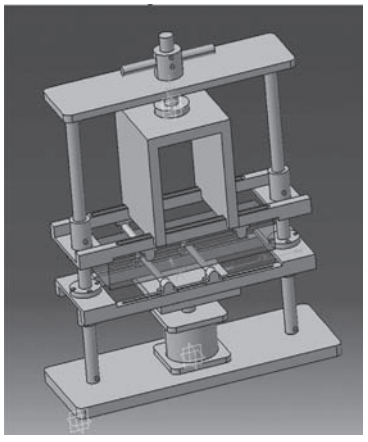

Figure 2a. "A" component: Mechanical system for the test specimen.

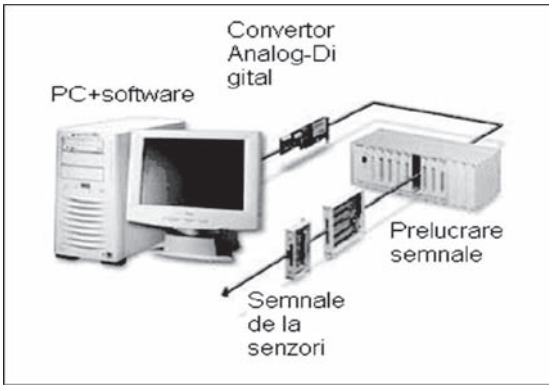

Figure 2b. "B" component: Data acquisition system.

opposing to the repeated stress failure is got, and it represents a characteristic equivalent to the dynamic test.

It reveals that the necessary time to obtain the repeated stress failure phenomenon, and the analysis of the crack propagation in the thickness of the asphalt mixture layer sample allows the rapid identification of the tested materials characteristics.

To obtain the accelerated failure phenomenon, using different formulas using lab prepared specimen, we increase the predetermined loading strain, assimilating exceptionally enhanced traffic. The neccessary time for the asphalt mixture layer to crack is reduced ($t_2 < t_3$), according to the known theory (to cause in a shorter time repeated stress failure σ_0, when the load is higher).

3 THE MAIN COMPONENTS OF THE CRACKING DEVICE

The cracking device has two components:

The constructive scheme of the "A" component is presented in figure 3.

The device records video data (processed by the equipment soft) for the failure phenomenon. The processed data are: *the vertical strain* (*d*) (deflection) of the specimen and the number of cycles when the cracking starts and amplifies (n_c).

4 THE RESULT INTERPRETATION

The result interpretation, through the performance factors (C_p), on the road materials which suffer structural changes (the influence of the altered or additive bitumen and the presence of

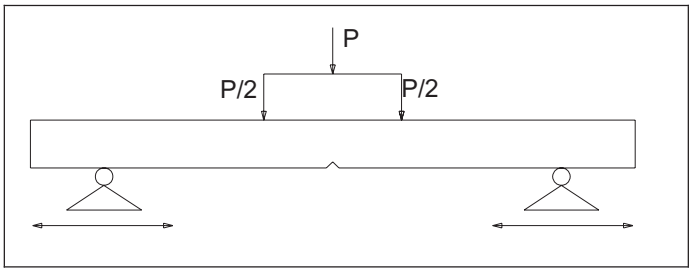

Figure 3. The constructive scheme of the "A" component.

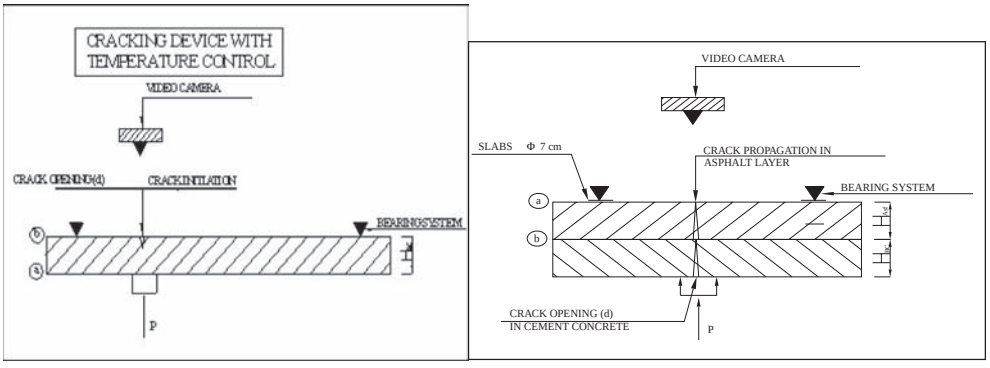

Figure 4. The constructive scheme of the "B" component.

an antifracture geocomposite), can be narrowed to the test deformation ratio before fracture (C_p), and to the stress cycles before fracture (C_p).

Actually, the two performance coefficients represent the specimen behavior image when subjected to permanent strain (practically obtained at extreme levels of strain (d = 30 mm), opposing to the admissible strain of the asphalt (d_{adm} = 1.2 mm) and the working time image, represented by the number of cycles when the material fracture occurs.

Using the cracking device, We have obtained the vertical strain d_1 and a number of cycles N_{c1} for the first specimen, and d_2 and N_{c2} for the second specimen.

The performance coefficient, C_p (%) can be calculated as followes:

$$c_{pd} = \frac{d_2 - d_1}{d_2} \quad \text{for} \quad \text{vertical strain,}$$

$$co = \frac{N_{c_2} - N_{c_1}}{N_{c_2}} \quad \text{for} \quad \text{lifetime.}$$

5 CASE STUDIES

Case studies regarding the performance of the asphaltic mixtures with geotextiles, through tests conducted with the cracking device

It can be made the same interpretations types dependent on the structural composition, when analyzing the cracks propagation from the pre-fractured pavement concrete in the asphaltic layers.

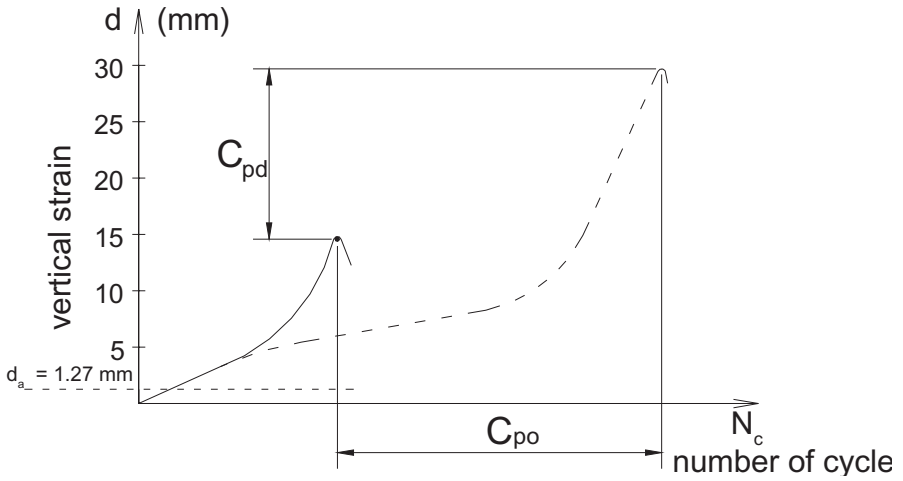

Figure 5. Identification procedures for the performance coefficients.

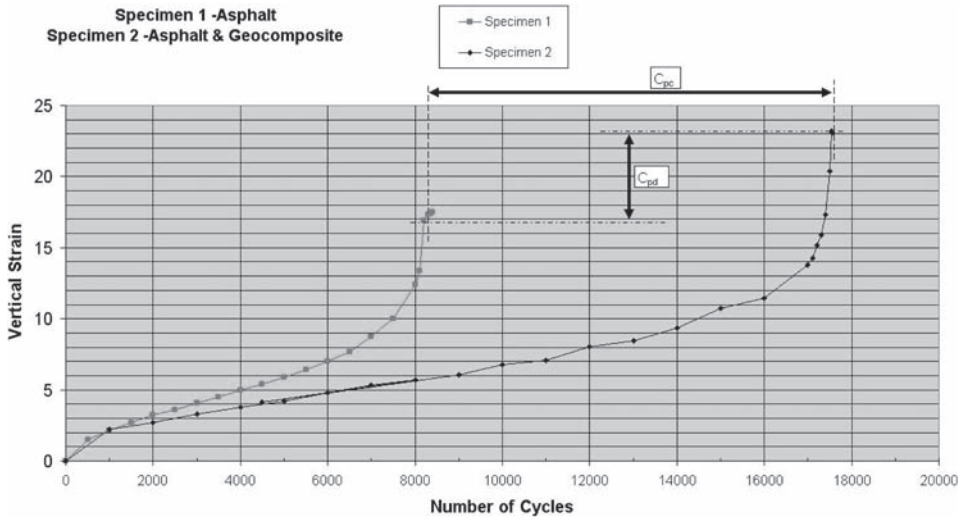

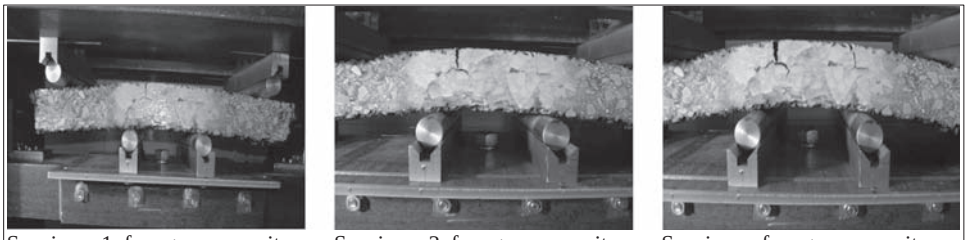

Specimen 1, free geocomposit–fissured (F)

Specimen 2, free geocomposit–cracked (C)

Specimen, free geocomposit–fractured (R)

Figure 6. The performance of the asphaltic mixtures with geocomposite.

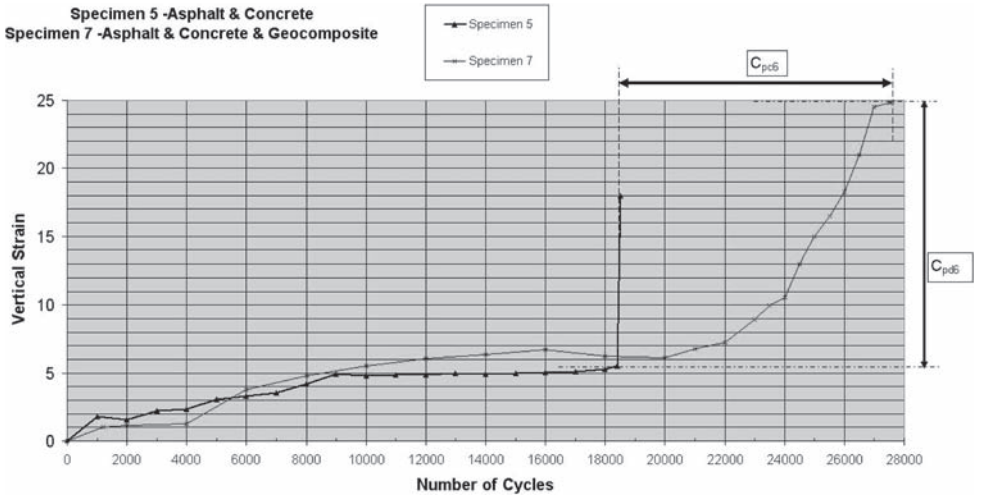

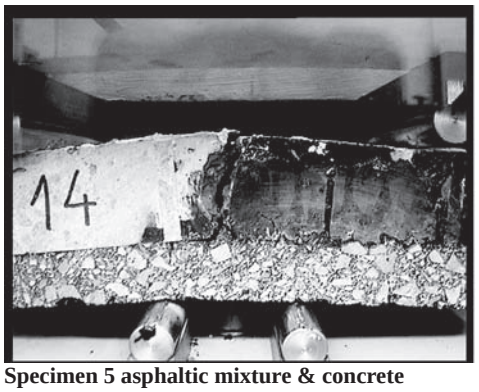

Specimen 5 asphaltic mixture & concrete

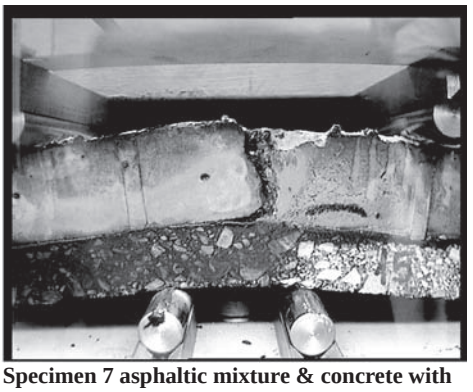

Specimen 7 asphaltic mixture & concrete with geocomposit

Figure 7. The performance of concrete and asphaltic mixtures with geocomposit.

In this case, we analized the cracking behaviour of the asphaltic mixture, reinforced with geocomposit, opposed to the cracking phenomenon of the specimen without geocomposit (P1).

The result for the asphaltic mixture, reinforced, was an increase in number of cycles when the rupture appears (R), $N_{c2} > N_{c1}$, where:

N_{c1} = number of cycles when the specimen is entirely cracked specimen is without geocomposit,

N_{c2} = number of cycles when the specimen is entirely cracked specimen is reinforced with geocomposit.

Studies through performance coefficients were made using mixed specimens (pre-cracked concrete, protected with a layer of asphaltic mixtures).

6 CONCLUSIONS

- The Analysis of asphalt layers related to the fatigue phenomenon due to the evolution of the process of cracking during the exploitation under traffic is an important necessity of present times. The increase of road traffic and of the loads on wheels of goods vehicles lead to permanent roads structure cracks.

- The foreseeing of the exploitation behavior of roads asphalt coating, through lab phenomenologic modeling, is a top priority in the research of the field.
- The experimental modeling through laboratory observations allows a qualitative and a rapid interpretation of the cracks through the comparison of behaviors at cracks of several of material recipes analyzed in laboratories with classical tested methods.
- The interpretation is done using indices of performance able to give adjacent information to optimal recipes studied in the laboratory.

The foreseeing of cracking behaviour through laboratory tests in accelerated conditions similar to those influencing the specimen of slabs and of their testing using the cracking device which was the main objective of the present research. Thus the relation target-result is obtained through the recording of images with crack propagation in road structure and the percentage quantification of performances to the optimal recipe obtained in laboratory.

Similar tests were published in the volume of the VI International Conference "RILEM, Chicago,USA, 2008, As follows: PAVAMENT CRACKING", (Khalid & Artamendi 2008, Mohammad et al. 2008, Perraton et al. 2008).

REFERENCES

Contract CEEX. Metodă de testare complexă a straturilor rutiere compozite şi a materialelor componente, în vederea evaluării şi certificării conform normelor europene. 2006–2008, Technical University of Civil Engineering, Bucharest.

Khalid, H.A. & Artamendi, I. University of Liverpool, U.K. 2008. Pavement Cracking. VI RILEM Symposium. *Measurement and effective evaluation of crack growth in asphalt mixtures.* Chicago USA.

Mohammad, L.N., Kalou, M.D., Lousianna State University & Saadeh, S. California State University, USA 2008. Pavement Cracking. VI RILEM Symposium. *Evaluation of fracture properties of hot mix asphalt.* Chicago USA.

Perraton, D., Guissi, G. Ecole de tehnologie superieure, Quebec, Pierre, P. & Dore, G. Universite Laval, Canada 2008. Pavement Cracking. VI RILEM Symposium. *A new laboratory test for reflective cracking in mode I and/or mode II.* Chicago USA.

Advanced Testing and Characterization of Bituminous Materials –
Loizos, Partl, Scarpas & Al-Qadi (eds)
© 2009 Taylor & Francis Group, London, ISBN 978-0-415-55854-9

Mode II cracking in asphalt concrete

A. Braham & W. Buttlar
University of Illinois at Urbana-Champaign, Urbana, Illinois, USA

ABSTRACT: While application of fracture mechanics principles in pavement mechanics is steadily gaining popularity, very little work has been devoted to experimental characterization of shearing-type (Mode II) fracture. Researchers at the University of Illinois at Urbana-Champaign have developed a Mode II fracture test, based on work from TU Delft, which captures Mode II fracture work from the point of crack initiation. This study outlines the development of the aforementioned Mode II test, including a thorough literature review, challenges faced, and solutions to obstacles. Two testing configurations were examined and compared to determine the most practical, yet informative configuration. Load-Line Displacement control and Crack Tip Sliding Displacement control testing setups were developed and compared. It was determined that Load-Line Displacement control provided more stable crack propagation, more reliable results, and easier test control. Data was analyzed to distinguish the concepts of crack initiation and propagation in an effort to understand the mechanisms behind the crack's behavior. In contrast to Mode I cracking, Mode II cracking appeared to transform from an initiating crack, to a propagating crack, to sliding surfaces in a very short time period; there is no graduate propagation to observe. Finally, initial data was analyzed and compared to existing literature to validate the accuracy of the test.

1 INTRODUCTION

1.1 *Background*

Fracture mechanics is a powerful research tool, which can be used to describe crack initiation and crack propagation in asphalt concrete pavements. Many researchers have explored Mode I fracture behavior of asphalt concrete through multiple tests, including the Disk-Shaped Compact Tension, the Single-Edge Notch Beam, and the Semi-Circular Bend. However, Mode I cracking tests only capture properties associated with an opening-type crack. While this type of crack does occur in the field, particularly as a result of thermal cycling, there are other important types of cracking as well. Little attention has been given to experimental characterization of Mode II, shear-type cracking, which may be caused by heavy vehicular loads. This paper will investigate Mode II cracking at lower temperatures.

1.2 *Objectives*

This research reviewed various techniques of Mode II fracture testing that are used in engineering materials. The most promising configuration, based on equipment availability at the University of Illinois, was the four-point beam configuration with two notches. This configuration was analyzed with one asphalt concrete mixture. Fracture work from Crack Tip Sliding Displacement (CTSD) and Load-Line Displacement (LLD) was captured and analyzed. Lessons learned were recorded, and future improvements were outlined and discussed.

2 MODE II TEST CONFIGURATIONS

There are several configurations in many engineering materials used to measure Mode II fracture properties. Four different configurations discussed herein are: double-edge notched,

shear box, Arcan, and four-point shear. All of these configurations were used to find the stress-intensity factor (K_{II}), the shear stress, or the shear stiffness. While these parameters were not of direct interest, the following approaches guided the final determination of the test configuration for determining the Mode II fracture work.

2.1 *Double-edge notched*

Reinhardt *et al.* (2000) used a double edge notched specimens to measure Mode II fracture toughness K_{IIc} of concrete as seen in Figure 1. Here, a compressive load is applied on the right half of the specimen, which creates regions of shear at the tips of each notch.

2.2 *Shear box*

Rao *et al.* (2003) found that pure shear loading applied on a pre-existing crack did not guarantee the development of Mode II fracture, therefore, Mode II fracture is not necessarily the same as fracture generated under pure shear loading. The shear box testing method (Figure 2) was adopted for measuring K_{IIC} of rock because it created favorable conditions for Mode II fracture. They found that clear Mode II fracture occurred between an alpha of 65 and 75°. For brittle materials, Mode I fracture toughness was usually smaller than Mode II, therefore, Mode I fracture usually occurred.

2.3 *Arcan*

Richard (1981) determined K_{IIc} values using a simple compact shape with pure shear loading over large areas of undisturbed specimen. This testing configuration eventually became known as the Arcan configuration. Richard studied pure shear loading at crack tips with a simple fabrication technique and a simple loading frame. Lo *et al.* (2003) used specimens adapted from Richard's study with an extended ligament. They compared their Mode II fracture toughness results to Banks-Sills and Arcan (1986). The loading fixture and specimen are displayed in Figure 3. Two commonly (but not precise) criteria of comparison, K_I/K_{II} or normalized Mode II stress intensity factor (K'_{II}), were investigated. In this study, the absolute value of K_I/K_{II} was minimized and K'_{II} was maximized.

2.4 *Four-point shear*

In asphalt concrete, there has been limited work performed on Mode II fracture. Delft University of Technology (Bondt 1999, Erkens 2002, Medani 2006) studied Mode II fracture

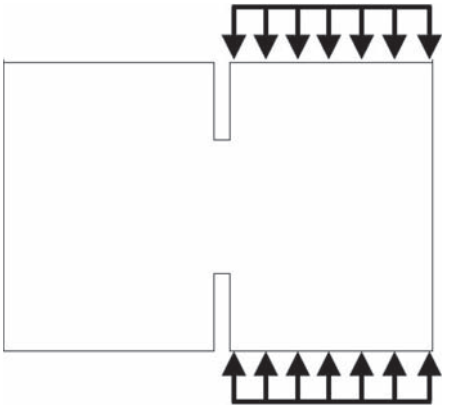

Figure 1. Double-edge notched mode II.

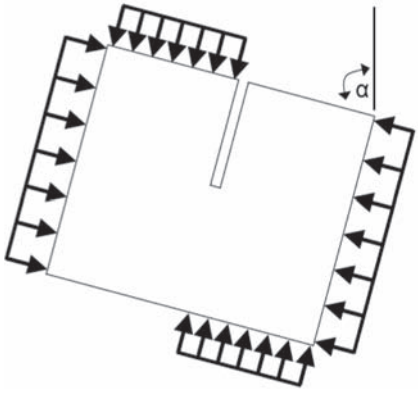

Figure 2. Shear box.

behavior with a four-point shear test. Bondt used a monotonic crack shear test at a load-line constant displacement of 51 mm/min. He determined the shear stress and stiffness during testing. Erkens examined various temperatures, strain rate, and confinement pressures for the four point shear setup. She also used load-line displacement and recorded the shear stress. Finally, Medani looked at the interfacial properties between asphalt and a membrane. He ran tests under load-line displacement and measured shear stress and stiffness. The research at Delft thoroughly investigated the four-point shear setup, but only measured shear stresses and did not measure Mode II fracture work.

Based on the available equipment at the University of Illinois and a review of existing literature, a four-point shear setup was selected.

3 TESTING CONFIGURATION

3.1 *Initial test set-up*

The University of Illinois at Urbana-Champaign utilizes a servo-hydraulic Instron testing load frame, with a temperature controlled chamber. The first round of testing was performed at –10°C with a 12.5 mm limestone aggregate mixture, compacted to 4% air voids with an unmodified PG58-28 binder. The testing samples were 100 mm tall, 75 mm thick, and 165 mm wide, with 12.5 mm notches at the top and bottom of the sample. Figure 5 shows the sample in the testing fixture.

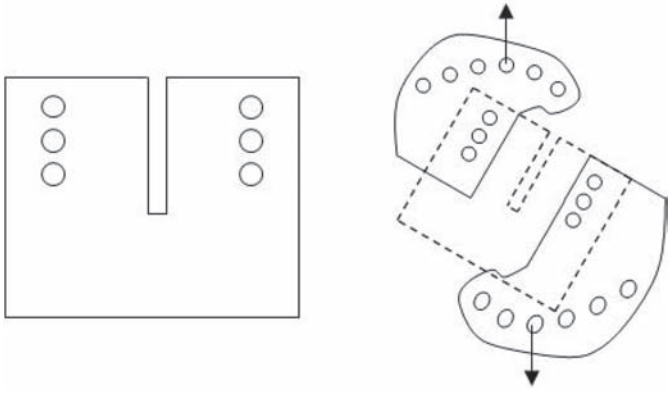

Figure 3. Arcan configuration (specimen on left, fixtures with specimens on right).

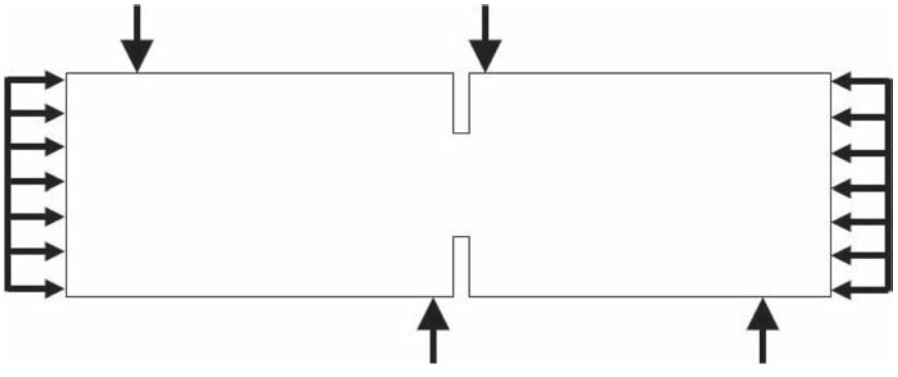

Figure 4. Four point shear setup at Tu Delft.

The first tests were run under Load-Line Displacement, with a constant displacement of 5 mm/min. Next, samples were run under a constant Crack Tip Sliding Displacement (CTSD) of 0.7 mm/min. This was achieved by placing gage points on the left and right of the notch, and orienting a clip gage so that it opened vertically. This measured the crack sliding. Figure 6 shows an example plot from this test.

In Figure 6, two distinct regions can be seen. Before the initial peak load, there is the crack initiation region. After the crack initiates, there is a decrease in load. However, a sliding friction develops and the load begins to increase again. Since the primary interest here is crack initiation, the sliding friction is not investigated at this point. In order to quantify the crack initiation, the fracture work was found by taking the area under the Load/CTSD curve and

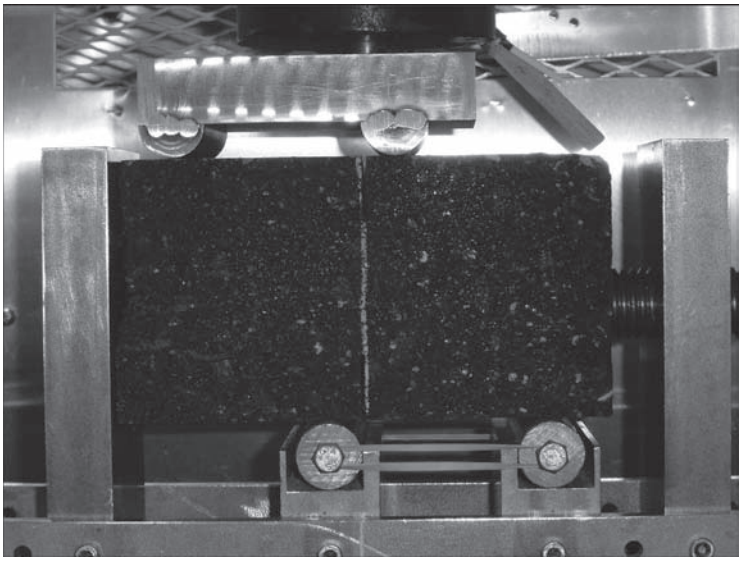

Figure 5. Initial Mode II test set-up.

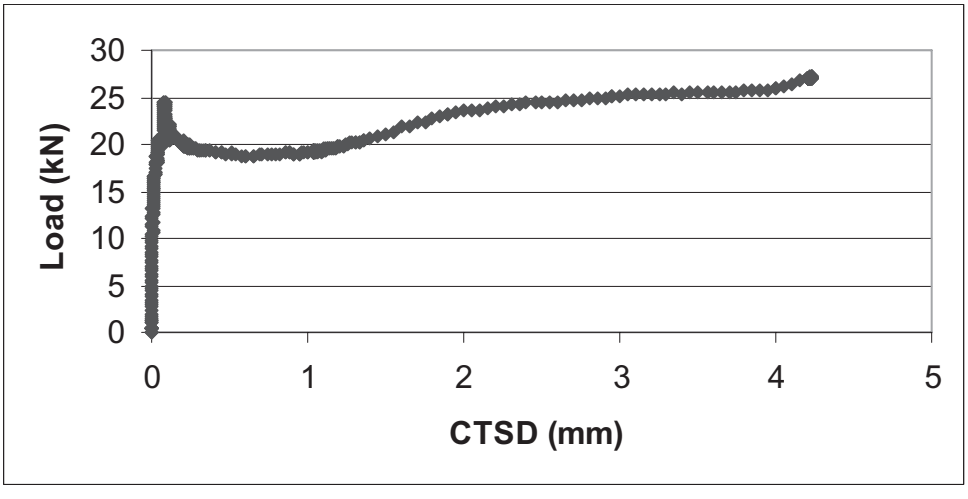

Figure 6. Load vs. CTSD curve for initial Mode II test set-up.

dividing it by the fracture face area. For the sample in Figure 6, the fracture work for crack initiation was 457 J/m^2.

However, with peak vertical loads of almost 25 kN, this setup created huge horizontal forces as well. In fact, the horizontal forces were so large that the fixtures were deformed during the test. Therefore, a smaller testing set-up was developed.

3.2 *Final test set-up*

In order to reduce the horizontal forces on the equipment, the sample size was reduced in order to decrease the fracture ligament area. This was accomplished by reducing the height of the specimen, so the samples were 50 mm tall, 75 mm thick, and 165 mm wide. With the reduced height, the notch length also had to be reduced, to 8 mm on the top on bottom of the specimen, creating a fracture ligament length of approximately 34 mm. The second round of testing was performed at three test temperatures, –30, –18, and –6°C with a mixture from Cell 03 at Minnesota Road Research Project (MnROAD). These temperatures were utilized in order to capture a wide range of low temperature properties, as the low temperature binder grade of the mixture was equivalent to a PGXX-28 binder. Therefore, the testing temperature was 2°C below the low temperature binder grade, 10°C higher (the same as the Bending Beam Rheometer temperature), and 22°C higher. MnROAD Cell 03 utilized a 12.5 mm NMAS crushed gravel/granite mixture, with a 120/150 binder. Figure 7 shows the final test set-up.

Tests were run under both Load-Line Displacement and a Crack Tip Sliding Displacement. The Load-Line Displacement, or LLD, was run with a constant head displacement of 5.0 mm/min. The Crack Tip Sliding Displacement, or CTSD, was run at a constant opening of 0.7 mm/min. These rates were chosen in order to match the rates used in the Single-Edge Notch Beam [SE(B)] test. Although beyond the scope of this study, Mode I and Mixed-Mode fracture properties were collected on the mixtures investigated in this study and will be used for numerical simulations of cracks under multiaxial stress states.

Figure 8 shows the test results for the mixture at –6°C using LLD control. Figure 8 only shows the crack initiation portion of the test since, as discussed above, the crack sliding portion of the test will be ignored at this time. In comparison to the initial test set-up, the peak load is slightly lower, which is expected as the test specimen is a smaller size. However, the test results using CTSD control are a bit steeper, as seen in Figure 9. This indicates that the load increases more quickly during CTSD control, which could decrease the precision of the test.

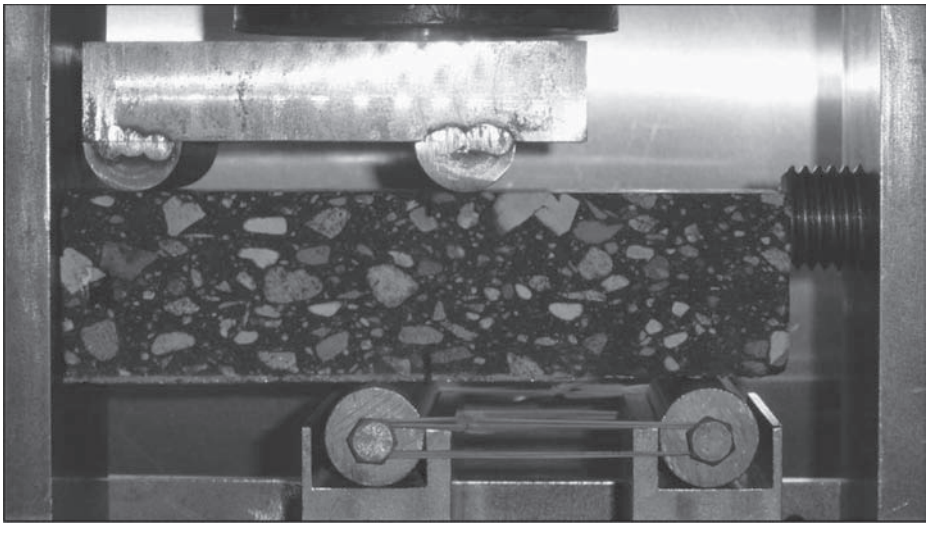

Figure 7. Final Mode II test set-up.

The fracture work for the crack initiation, which is calculated by taking the area under the Load/CTSD curve and dividing by the area of the fracture face, is summarized in Figure 10. Each of the three temperatures had three replicates, for a total of nine tests for both CTSD control and LLD control.

The results in Figure 10 were a strong influence in choosing Load-Line Displacement control in future work. Not only was LLD easier to control during testing (it provided a more stable test), but the test results are in line with expectations. As the temperature increases, fracture work is expected to increase, as mixtures become less brittle and more ductile.

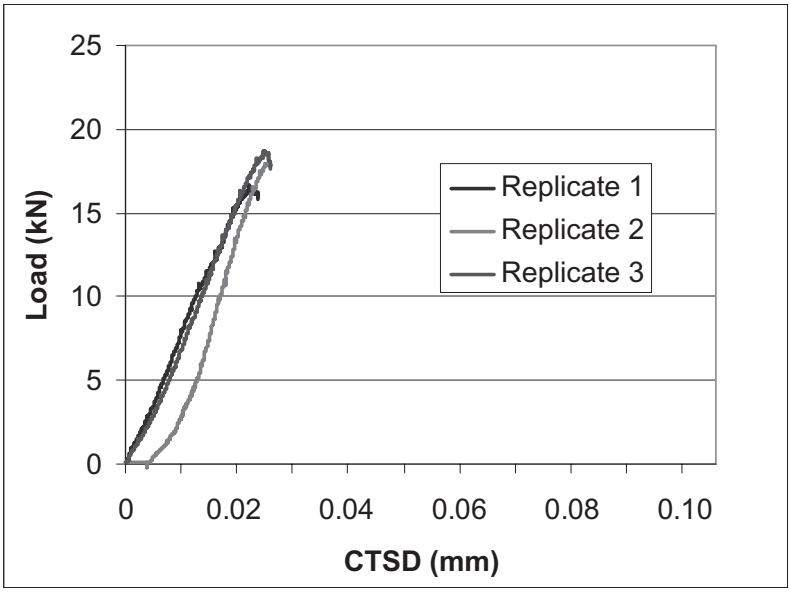

Figure 8. Load-Line Displacement control curves.

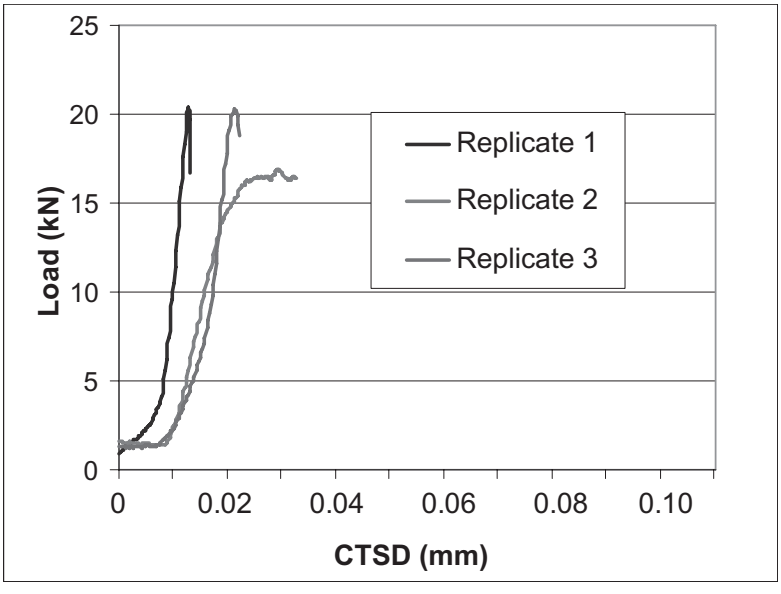

Figure 9. Crack-Tip Sliding Displacement control curves.

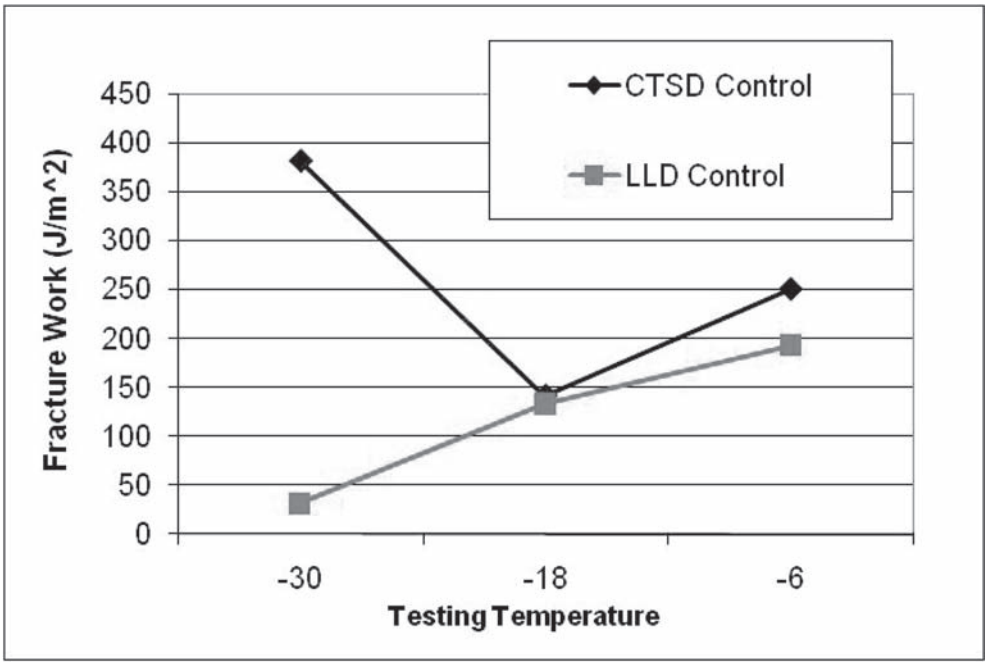

Figure 10. Comparison of crack-tip sliding displacement control versus Load-Line Displacement control at three temperatures.

A more ductile mix is expected to fail with a higher cohesiveness, which will increase the fracture work. In Figure 9, the trend of increasing fracture work is met with the LLD control, while the CTSD control is not as straight forward. This could be attributed to the very large amount of work needed to initiate the crack. If the test is controlled with a constant sliding displacement, the crack needs to initiate very quickly, thus perhaps giving an artificially high number. In any case, Load-Line Displacement control was found to be more appropriate for this test configuration.

4 CONCLUSIONS AND RECOMMENDATIONS

Four testing configurations for Mode II fracture energy were reviewed: double-edge notched, shear box, Arcan, and four-point shear. From this review, the four-point shear configuration was chosen for further study. After two iterations of the test set-up, the following conclusions were made:

- The behavior of Mode II Load/CMOD curves is much different than Mode I. Instead of the typical increase in load, followed by a clean softening curve as seen in typical Mode I tests, Mode II tests produced a very quick increase in load followed by a relatively constant load for the remaining of the test. Instead of the softening characteristics seen in Mode I, Mode II fracture tests appear to transition into a sliding friction test.
- By just investigating the initial increases in load, or the crack initiation, Load Line Displacement control appears to be a better test control versus Crack Tip Sliding Displacement for this asphalt mixture across multiple temperatures.
- As temperature increases, the Mode II fracture work increased, as expected.

There are several steps that need to be taken in order to more understand Mode II fracture properties of asphalt concrete. First, more mixtures need to be investigated, as this work only looked at a single mixture. By testing more mixtures, a clearer picture of the test's repeatability

and reproduction will be found. Second, the test set-up should be reevaluated, as the true CTSD should be measured at a point 45° from the center of the tip of the notch, whereas herein they were measured right at the tip of the crack. Finally, the behavior of material after the peak load is complex and not well understood at this time.

REFERENCES

Banks-Sills, L. & Arcan, M. 1986. Fracture Mechanics: Seventeenth Volume, ASTM-STP 905, American Society for Testing and Materials, Philadelphia 1986: 347–363.

De Bondt, A.H. 1999. Anti-Reflective Cracking Design of (Reinforced) Asphaltic Overlays. Delft University of Technology, PhD Dissertation.

Erkens, S.M. 2002. "Asphalt Concrete Response (ACRe)—Determination, Modeling, and Prediction," Delft University of Technology, PhD Dissertation.

Lo., K.W., Gong, Y.B., Tamilselvan, T. & Lai, M.O. A Proposed Specimen for K11C Testing. *International Journal of Fracture* 124, 2003: 127–137.

Medani, T.O. 2006. Design Principles of Surfacing on Orthotropic Steel Bridge Decks. Delft University of Technology, PhD Dissertation.

Rao, Q., Sun, Z., Stephansson, O., Li, C. & Stillborg, B. Shear fracture (Mode II) of Brittle Rock. *International Journal of Rock Mechanics and Mining Sciences* 40, 2003: 355–375.

Richard, H.A. A New Compact Shear Specimen. *International Journal of Fracture* 17, 1981: R105–107.

Reinhardt, H.W. & Xu, S. 2000. A Practical Testing Approach to Determine Mode II Fracture Energy G11f for Concrete. *International Journal of Fracture* 105, 2000: 107–125.

Advanced Testing and Characterization of Bituminous Materials – Loizos, Partl, Scarpas & Al-Qadi (eds)
© 2009 Taylor & Francis Group, London, ISBN 978-0-415-55854-9

Experimental study on resistance to cracking of bituminous mixtures using the Fénix test

F. Pérez & R. Botella
Universidad Politécnica de Cataluña, Barcelona, España

G. Valdés
Universidad de La Frontera, Temuco, Chile

ABSTRACT: The Road Research Laboratory of the Technical University of Catalonia (UPC) has developed a new tensile test called Fénix test. The objective of this test is to evaluate bituminous mixture crack behaviour. It is a simple procedure and has a low cost set up. The aim of this paper is to present Fénix test as a procedure to determine crack resistance through calculation of dissipated energy during the process. Test procedure and data analysis are shown for different types of mixtures. Variables studied were load application velocity, aging, binder type, binder content, test temperature and compaction temperature. As a result, authors found out that Fénix test is an effective procedure to determine mechanical properties regarding cracking resistance of bituminous mixtures.

1 INTRODUCTION

Cracking is one of the main causes of bituminous pavement distress; therefore it is necessary to understand its behaviour. However mixture complex rheological properties cause this cracking behaviour difficult to analyze. These properties change with temperature and load application velocity, among other things.

Nowadays, scientific community is using fracture mechanics concepts on quasi-brittle materials to understand cracking behaviour of bituminous mixtures, some of them by means of analytical models and others through experimental studies. These experimental studies try to simulate crack initiation and propagation. (Li et al. 2008)

Literature search returned three tests which main target is to determine fracture properties of bituminous mixtures (Figure 1). The Single-edge notched beam, SE(B), has been used in several studies with this purpose. Test set up and sample geometry provide an adequate mode I fracture. However, it is not possible to apply the test to field cores, due to sample shape (Wagoner et al. 2005). The Semi-Circular Bending test, SCB, has been used in several studies too, (Molenaar et al. 2002, Mull et al. 2002, Li et al. 2008). Samples shape make the test suitable to field cores and laboratory specimens, and test set up is simple, but the crack propagation with the SCB geometry creates an arching effect with high compressive stress as the crack approaches the top edge (Wagoner et al. 2005). The Disk-shaped Compact Tension test, DC(T), has a standard fracture test configuration in ASTM D 7313-07. It also has a bigger sample fracture area which benefits tests results. On the other hand, during the sample fabrication it is possible debilitate the area around the loading points, plus it is difficult to carry out the test at temperatures above 10ºC.

Following this research line, the Road Research Laboratory of the Technical University of Catalonia has developed a new test to evaluate bituminous mixtures cracking resistance.

This test provides dissipated energy in test process, which is a combination of dissipated creep energy and fracture energy (Li et al. 2008). Dissipated energy evaluation is a way to

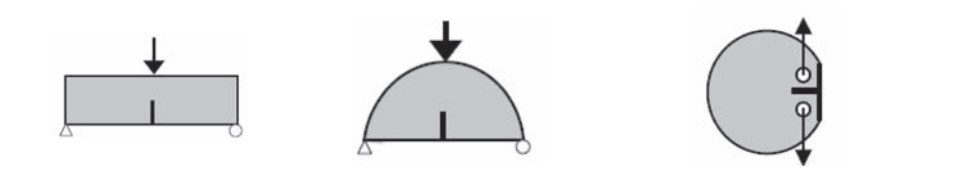

SE(B)	SCB	DC(T)
Single-edge notched beam	Semicircular bend	Disk-shaped compact tension

Figure 1. Different specimen fracture geometries.

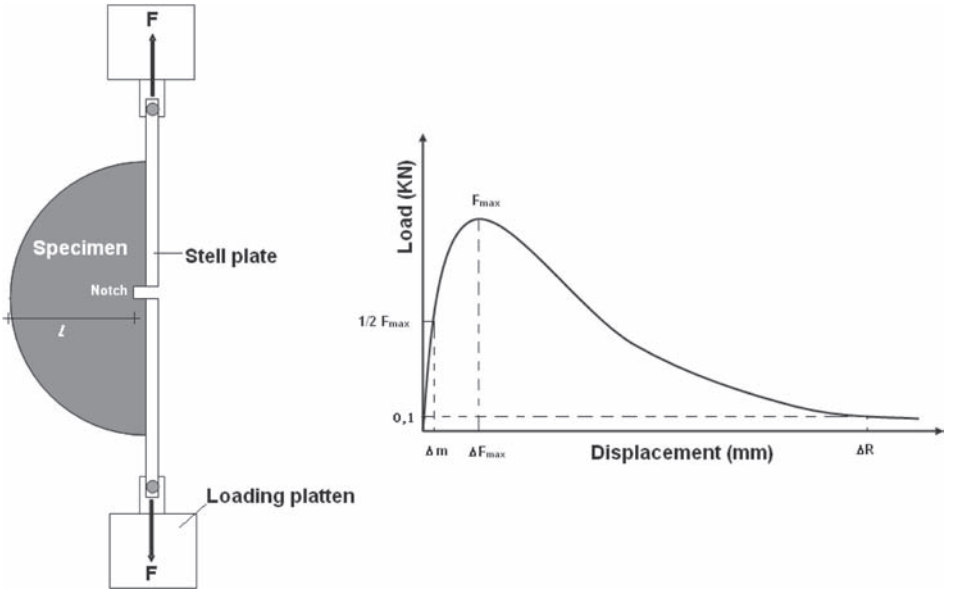

Figure 2. Fénix test and typical load vs. displacement output curve.

measure the cracking resistance of bituminous mixtures. This test has been called Fénix and its set up is shown in Figure 2.

2 FÉNIX TEST PROCEDURE

Fénix test is a traction test applied to a half cylindrical sample with a 6 mm depth notch, placed in the middle of the flat side of the specimen (Figure 2). This sample is fabricated through Marshall or gyratory-compactor procedures. Two steel plates are fixed on the flat side separated by the notch. Steel plates are attached to the loading platten, allowing plates to rotate around fixing points once test has begun. Test is carried out under controlled displacement conditions. Displacement velocity is established at 1 mm/min. Temperature is chosen according to the environmental conditions that have to be reproduced.

Load and displacement data are recorded along the test. Dissipated energy during the test, G_D, can be obtained using Equation (1).

$$G_D = \frac{W_D}{h \cdot l} \tag{1}$$

where G_D = dissipated energy during the test, J/m^2; W_D = dissipated work during the test, area under load-displacement curve, KN-mm; h = specimen thickness, m; l = initial ligament length, m.

Other parameters like peak load, F_{max}, displacement at peak load, ΔF_{max}, break displacement, ΔR, can be determined from load-displacement curve (Figure 2). Tensile stiffness index, I_{RT} can be obtained, by means of Equation (2).

$$I_{RT} = \frac{\frac{1}{2} \cdot F_{\max}}{\Delta_m} \tag{2}$$

where I_{RT} = tensile stiffness index, KN/mm; F_{max} = peak load, KN; Δ_m = displacement before peak load to ½ F_{max}, mm.

3 EXPERIMENTAL STUDY

The experimental study carried out consisted in calibrate Fénix test through sensitivity analysis for different variables:

- Loading rate
- Mixture aging (SHRP protocol)
- Binder type
- Binder content
- Test temperature
- Mixture compaction temperature

Fénix samples have been fabricated following Marshall Procedure. Mixtures analysed have been S-12, S-20 and G-20 according to Spanish specifications. Loading rate (0.1, 1 and 10 mm/min) and aging (SHRP protocol) have been studied using S-12 mixtures, while types of binder, test temperature (–10ºC, 5ºC and 20ºC) and compaction temperature (120ºC, 135ºC and 155ºC) have been evaluated using S-20 mixtures. Finally G-20 mixtures have been used to evaluate binder content and test temperature (again –10ºC, 5ºC and 20ºC). Three Marshall samples have been tested for each variable studied.

All mixtures have been fabricated using limestone aggregates and different types of binders. Aggregate gradations are shown in Table 1.

The bitumen used in S-12 mixtures has been B60/70 and content has been 5%. S-20 mixtures have been fabricated using B60/70, B40/50, B13/22 and polymer modified bitumen

Table 1. Aggregate gradations mixtures S-12, S-20 y G-20.

Sieve size (mm)	S-12 Percent passing	S-20 Percent passing	G-20 Percent passing
25	100	100	100
20	100	87.5	75
12.5	87.5	71.5	55
8	67.5	58	40
4	42.5	42.5	25
2	31	31	19
0.5	16	16	10
0.25	11	11	7
0.125	7.5	7.5	6
0.063	5	5	5

Table 2. Characteristics of bitumen.

Bitumen characteristics	Unit	Spanish standard (NLT)	B-13/22	B-40/50	B-60/70	BM-3c
Original bitumen						
Penetration (25ºC; 100 g; 5 s)	0.1 mm	124	17	43	64	58
Penetration index		181	0.1	–0.2	–0.2	2.8
Softening point	ºC	125	67.3	55.9	51.7	67.4
Frass brittle point	ºC	182	–5	–12	–17	–20
Ductility at 25ºC	cm	126	15	>100	>100	–
Dynamic viscosity 60ºC	(Pa.s)	–	4551	651	367	–
Dynamic viscosity 135ºC	(Pa.s)	–	1.92	0.72	0.56	2.37
Rolling thin film oven residue						
Mass loss	%	186	0.35	0.4	0.5	0.6
Penetration (25ºC; 100 g; 5 s)	% p.o.	124	10	23	32	40
Softening point increase	ºC	–	7.5	9.5	9.6	3.7
Ductility at 25ºC	cm	126	7	18	50	–

BM3c, all of them with a 4.3% binder content. Likewise, G-20 mixtures have been fabricated using B60/70 and B40/50 with three different binder contents, 3.5%, 4.5% and 5.5%. Binder properties are shown in Table 2.

4 EXPERIMENTAL RESULTS

Figure 3 shows load-displacement curves obtained in tests carried out at different loading rates and 20ºC test temperature. Aged and non-aged mixtures curves are shown. Aging has been applied following SHRP procedure (Kandhal & Chakraborty 1996). It consisted in 4 days period at 80ºC in a forced air oven. Both aged and non-aged mixtures have showed that dissipated energy and stiffness increase with loading rate at 20ºC. Aged samples have shown more fragile behaviour as their break displacements have been lower at higher loading rates. 0.1 mm/min loading rate at 20ºC has proved to be not adequate as peak load values have not achieved significant magnitude, for non-aged conventional bituminous mixtures. Finally 1 mm/min loading rate has been chosen to carry out the rest of tests.

All mixtures have shown similar response to test temperature variation. At –10ºC, mixtures have shown brittle behaviour with high peak load and low break displacement. At 20ºC, more ductile behaviour has been observed, higher breaking displacement, Δ_R, and lower peak load, F_{max}, and stiffness, I_{RT}. At 5ºC, an intermediate behaviour has been observed. As an example, figure 4 shows S-20 mixtures with B40/50 binder behaviour at different test temperatures. Only B-13/22 and B-60/70 have shown a different trend in peak load and breaking displacement, respectively. Mechanical parameters obtained in all evaluated types of binder are shown in table 3.

Figure 5 shows dissipated energy vs. test temperature for all types of binder studied. The polymer modified binder BM3c has obtained the highest value of dissipated energy, G_D, at all test temperatures showing the best cracking resistance. B60/70, B40/50, and BM3c have achieved their relative maximum value of dissipated energy at 5ºC. B13/22 has showed its highest dissipated energy at 20ºC due to its low penetration.

Figure 6 shows dissipated energy vs. test temperature for three different bitumen contents. At –10ºC and 5ºC the higher the binder content the higher the dissipated energy and the higher the cracking resistance. Mixture parameters obtained in bitumen content analysis at three different test temperatures are shown in table 4.

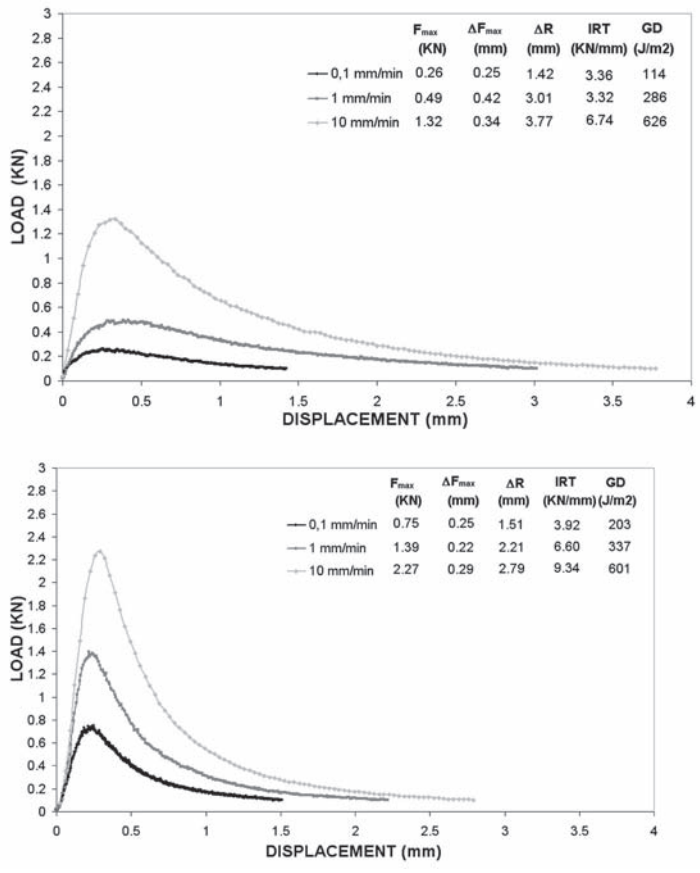

Figure 3. Influence of load application velocity in mixture S-12 non-aged (left) and aged (right), Fénix test at 20ºC.

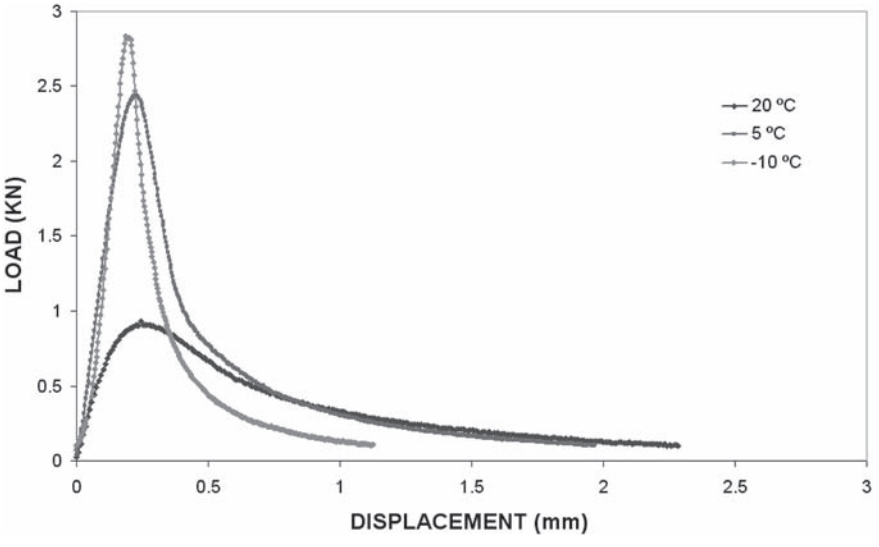

Figure 4. Fénix test at different temperatures, S-20 mixture with B-40/50.

Table 3. S-20 mixture results. variables: test temperature and bitumen type.

Bitumen	Temperature (ºC)	Peak load F_{max} (KN)	Displacement peak load ΔF_{max} (mm)	Break displacement ΔR (mm)	Tension stiffness index I_{RT} (KN/mm)	Dissipated energy in fracture process G_D (J/m^2)
B-13/22	20	1.44	0.24	2.79	9.25	472
	5	3.32	0.22	1.46	14.62	310
	–10	2.83	0.18	0.98	14.67	229
B-40/50	20	0.93	0.25	2.28	7.07	319
	5	2.44	0.21	1.96	12.78	430
	–10	2.83	0.19	1.12	12.27	281
B-60/70	20	0.58	0.25	2.15	7.02	225
	5	1.90	0.24	3.03	11.37	603
	–10	2.58	0.18	1.44	13.80	304
BM-3c	20	0.76	0.36	4.20	4.39	529
	5	1.94	0.27	3.73	10.83	698
	–10	3.29	0.22	1.46	15.30	356

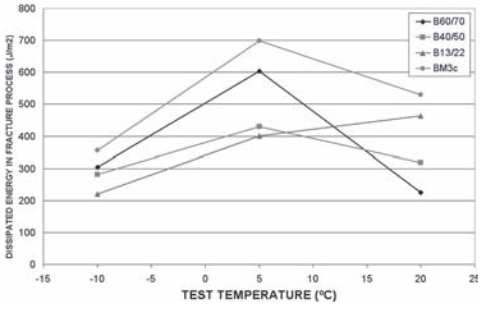

Figure 5. Dissipated energy in during the test at different test temperatures and for different bitumen types.

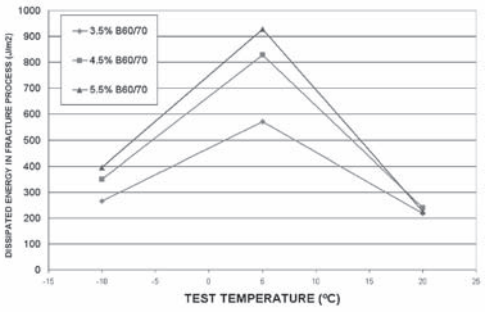

Figure 6. Dissipated energy in during the test at different test temperatures, for different bitumen contents.

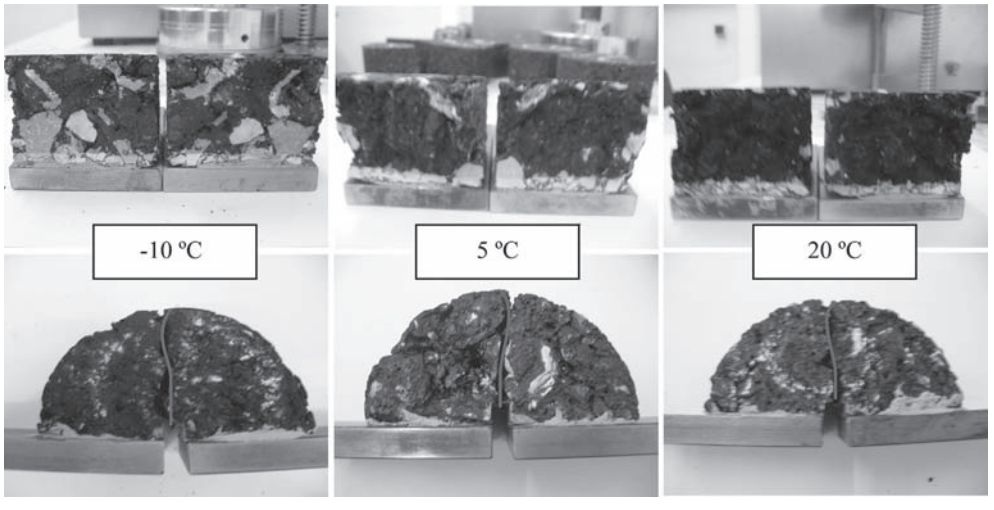

Figure 7. Typical fracture surfaces for mixture G-20 at different test temperatures.

Table 4. G-20 mixture results. Variables: test temperature and bitumen content.

Bitumens	Bitumen content %	Temperature (ºC)	Peak load F_{max} (KN)	Displacement peak load ΔF_{max} (mm)	Break displacement ΔR (mm)	Tension stiffness index I_{RT} (KN/mm)	Dissipated energy in fracture process G_D (J/m²)
B-40/50	3.5	20	0.84	0.31	2.58	5.11	344
		5	2.10	0.25	2.89	10.03	465
		–10	2.34	0.19	1.98	10.90	249
	4.5	20	0.82	0.39	3.06	4.54	407
		5	1.71	0.30	3.18	9.12	617
		–10	2.39	0.19	2.66	12.05	386
	5.5	20	0.75	0.34	3.54	4.53	431
		5	1.93	0.30	5.03	8.56	890
		–10	2.32	0.17	1.96	12.09	341
B-60/70	3.5	20	0.47	0.32	2.51	3.08	217
		5	1.90	0.23	3.20	9.90	571
		–10	2.38	0.16	1.80	12.33	265
	4.5	20	0.39	0.32	2.93	2.94	240
		5	1.99	0.30	4.92	9.54	829
		–10	2.11	0.16	1.91	11.51	348
	5.5	20	0.35	0.43	2.96	2.42	225
		5	1.74	0.33	5.51	6.87	928
		–10	2.36	0.21	1.97	9.74	395

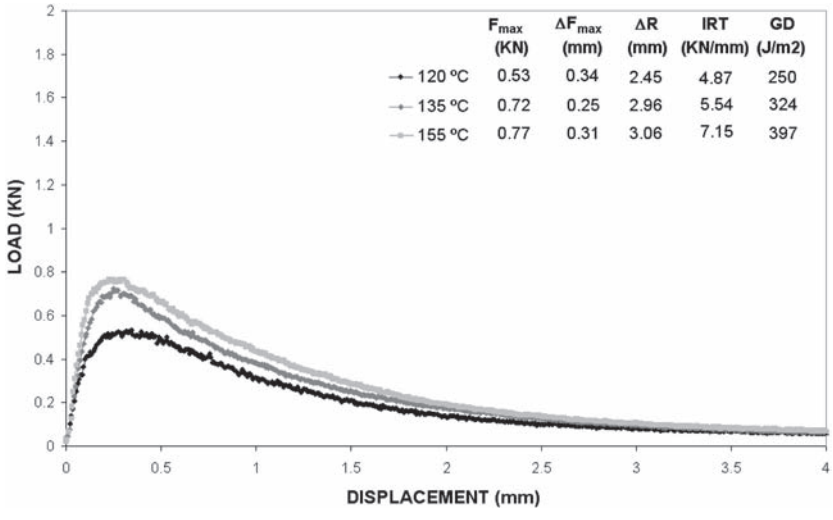

Figure 8. Fénix test 20ºC for different compaction temperatures, mixture S-20.

Figure 7 shows test temperature influence in fracture surfaces and cracks shape. At low temperature, –10ºC, fracture surface shows that crack crosses through bituminous mastic and large size aggregates, leaving those located on crack's path fractured. At intermediate temperatures, 5ºC, crack grows following bituminous mastic and fracturing only some of the large size aggregates. Finally, at 20ºC fracture takes place only in bituminous mastic.

Load vs. displacement curves belonging to different compaction temperatures are shown in figure 8. As can be seen from the graph, compaction temperature plays an important role

in cracking resistance. Dissipated energy and peak load decrease 37% and 31%, respectively, as compaction temperature drops from 155ºC to 120ºC.

Fénix test repeatability has been evaluated through coefficient of variation (COV) obtained from the results. COV average values have been 15% and 8.5% for dissipated energy and peak load respectively. Based on COV values for dissipated energy the test has a good repeatability compared with SE(B) (3–18%), DC(T)(4–25%) and SCB (15–34%) (Wagoner et al. 2005).

5 SUMMARY AND CONCLUSIONS

This paper presents the development of a simple test to determine cracking resistance in bituminous mixtures, through the calculation of dissipated energy during the test. Fénix test has a simple experimental procedure and can be applied to laboratory specimens (Marshall or gyratory compactor), and field cores. In order to validate the test and to verify its sensitivity, different test conditions and different bituminous mixtures have been evaluated in an experimental study.

Taking into account the results obtained, the main conclusions of this paper are:

- Fénix test has proved to be a good procedure to characterize cracking behaviour of bituminous mixtures due to its sensitivity and repeatability to test variables such as:
  - Loading rate.
  - Mixture aging (SHRP protocol).
  - Binder type.
  - Binder content.
  - Test temperature.
  - Mixture compaction temperature.
- It can be applied at a wide range of test temperatures.
- It is possible to analysed mixture behaviour after achieving peak load (softening area).

ACKNOWLEDGEMENTS

Authors would like to thank the support received from Centro para el Desarrollo Tecnológico e Industrial (CDTI) in the development of Proyecto FÉNIX.

REFERENCES

Kandhal P. & Chakraborty S. 1996. Effect of Asphalt Film Thickness on Short and Long Term Aging of Asphalt Paving Mixtures. National Center for Paving Technology. USA:T RB.

Li X., Braham A., Marasteanu M., Buttlar W. & Williams R. 2008. Effect of Factors Affecting Fracture Energy of Asphalt Concrete at Low Temperature. *Third EATA conference 2008*, European Asphalt Technology Association: 397–416.

Molenaar A., Scarpas A., Liu X. & Erkens S. 2002. Semi-Circular Bending Test; Simple but Useful? Journal of the Association of Asphalt Paving Technologists: 71, 795–815.

Mull M., Stuart K. & Yehia, A. 2002. Fracture Resistance Characterization of Chemically Modified Crumb Rubber Asphalt Pavement. Journal of Materials Science: 37, 557–566.

Wagoner M., Buttlar W. & Paulino G. 2005. Disk-shaped Compact Tension Test for Asphalt Concrete Fracture, Experimental Mechanics, 45(3): 270–277.

Advanced Testing and Characterization of Bituminous Materials – Loizos, Partl, Scarpas & Al-Qadi (eds)
© 2009 Taylor & Francis Group, London, ISBN 978-0-415-55854-9

Fatigue effects in uniaxial cyclic tensile stress test: The link between stiffness decrease and accumulation of irreversible strain

K. Mollenhauer & M. Wistuba
Braunschweig Pavement Engineering Centre (ISBS), Technische Universität Braunschweig, Germany

ABSTRACT: The uniaxial cyclic tensile stress test was developed to simulate the loading of asphalt surface courses due to low temperatures which is characterized by the combination of dynamic traffic loads and horizontal cryogenic tension stress due to prohibited thermal shrinkage. In this force-controlled cyclic test a prismatic asphalt specimen is loaded uniaxially until the total failure.

The force-controlled loading during this test generates a strain response, consisting of a visco-elastic and a visco-plastic strain reaction. The visco-plastic strain curve shows a specific shape comparably to a creep curve. Due to material deterioration, the creep curve is characterized by an inflexion point.

This study discusses a possible link between the decrease in stiffness modulus and the accumulation of visco-plastic strains. It is shown that the number of load impulses until specimen failure correlates with the slope of stiffness decrease. By application of a well-proven fatigue theory, which assumes the accumulation of micro-cracks in the specimen, it succeeds to simulate the course of visco-plastic strain by applying the Burger's model in combination with a deterioration function, which is drawn from the measured visco-elastic response.

1 INTRODUCTION

1.1 *Scope of this study*

In consequence of repeated loading, strength and stiffness modulus of hot mix asphalt materials decrease progressively. This phenomenon is generally attributed to material fatigue. Various test methods have been introduced to study fatigue behaviour of asphalt materials, considering diverse loading conditions such as bending, uniaxial, tensile splitting, triaxial, or shear stress (see, e.g. Di Benedetto et al., 2004).

The uniaxial cyclic tensile stress test (UCTST)—as discussed in this study—is a cyclic stress-controlled fatigue test on asphalt specimens of prismatic shape. The test mode was first introduced by Arand et al. (1984, 1996) to simulate the loading conditions which occur at low temperatures in surface asphalt courses. At the beginning of the test, the specimen is loaded by a static tensile stress, which is then super-imposed by a sinusoidal tensile stress signal until the specimen fails in consequence of macroscopic fracture. Advantageously, due to the elongated specimen shape and the uniaxial loading configuration the stress distribution within the specimen cross-section and within the predominant parts of its total length can be assumed as homogeneous, i.e. that the stress and strain amplitude do not vary from one point of the sample to another.

However, due to the viscous properties of asphalt materials and the persistent tensile stress during the test the visco-elastic strain response is superposed by a visco-plastic strain response. This phenomenon has to be considered for the interpretation of fatigue behaviour.

In this study, the question is raised, if there are links between the various effects which can be observed during uniaxial cyclic tensile stress tests. Based on extensive laboratory investigations (also discussed in Mollenhauer, 2008), the deteriorating process is attributed—on the

one hand—to the 'classical' fatigue damage that is initiated and spread in the material in the form of a diffuse micro crack network and provokes a change in the macroscopic rigidity. On the other hand, emphasis is put on the analysis of artefact damage that results from the repeated tensile excitation and the accumulation of irreversible strain and plastic creep deformations.

1.2 *Deterioration effects in cyclic fatigue tests*

In force-controlled cyclic fatigue tests, the course of the strain response as registered in function of the applied number of load cycles is generally used to derive key parameters to describe the fatigue phenomenon. From the applied stress amplitude σ_a and the registered strain amplitude ε_a, the stiffness modulus $|E| = \sigma_a/\varepsilon_a$ is derived, and the time lag between the stress signal and the strain signal is considered as the phase angle φ.

The classical fatigue criterion is defined in a controlled-force/stress test, when the elastic strain has increased to the double of its initial value. This corresponds to the number of load cycles ($N_{f/50}$) when the stiffness modulus has decreased to half of its initial value, as specified in the European standard for fatigue testing (EN 12697-24). However, as regards a force-controlled fatigue test at low test temperature, the specimen usually fails before a 50% stiffness reduction is stated. Other failure criteria are therefore applied alternatively, which can be applied independently from test temperature conditions. Van Dijk (1975) introduced the theory of dissipated energy for the evaluation of fatigue effects in asphalt materials. Following this approach, the energy dissipated during a load cycle $W_{dis,n}$ can be calculated from the stiffness modulus and the phase angle. The number of load cycles to failure (N_{Makro}) is determined according to Hopman et al. (1989) as soon as macro-cracking is supposed to be initiated. This is represented by a distinct change in dissipated energy course ($W_{dis,n}$), either determined in a N-$W_{dis,n}$-diagram, or in a diagram where the energy ratio (ER) is calculated from the product $N \cdot |E^*|$ of the number of load cycles and the stiffness modulus, and is plotted against the number of load cycles (Figure 1). At the beginning of the deterioration process a quasi-linear reduction in stiffness dE/dn is given, as it is usually observed in swelling tensile tests and therefore assumed for computational fatigue modeling (see, e.g. Bodin et al., 2003; Di Benedetto et al., 2004; Aschenbrenner, 2006).

In order to evaluate the effect of load variation on the fatigue resistance, multiple fatigue tests are performed at different stress amplitudes, and finally, the number of load cycles until fatigue is plotted against the applied load for all tests performed. A regression line (called Wöhler line) is drawn, indicating the fatigue life duration in function of the applied load amplitude. Based on the Wöhler line, the number of load cycles to fatigue can be estimated from Equation 1, where the regression factor K_1 and the exponent K_2 are experimentally derived

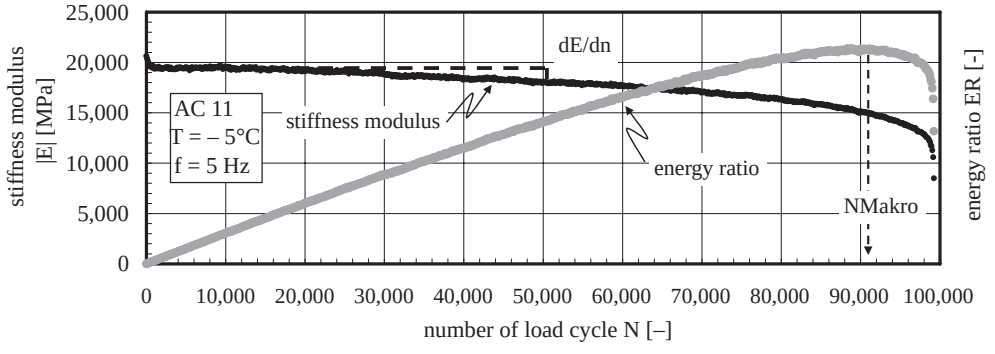

Figure 1. Example for the stiffness modulus |E*| and energy ratio ER during a uniaxial cyclic tensile stress & evaluation of N_{Makro} and the slope of stiffness decrease dE/dn.

material constants. This fatigue function is used as an indicator for the pavement's durability (Saal & Pell, 1960).

$$N_{Makro} = K_1 \cdot \Delta\sigma^{K_2} \quad (1)$$

2 LABORATORY TEST PROGRAM

2.1 *Tested material*

In the framework of this study a hot mix asphalt material AC 11, as often used as a wearing course material in Europe, was subjected to uniaxial cyclic tensile stress tests (UCTST). Main compositional characteristics of this material are summarised in Table 1.

2.2 *Test procedure*

The test procedure operated in this study is the uniaxial cyclic tensile stress test (UCTST) which is a homogeneous fatigue test conducted at low temperatures. The prismatic asphalt specimen is loaded with a sinusoidal tensile stress at a constant temperature. For this purpose, the specimen is glued to steel adapters. After joining it with the load device at +20°C, it is cooled down to test temperature without applying any load. During the cyclic loading, the force is generated by a hydraulic valve and measured in a load cell. The deformation of the specimen is detected by LVDT, which enables the analysis of the strain signal. The test ends as soon as the specimen fractures.

Because the test as performed in this study is intended to simulate the fatigue behaviour of asphalt surface materials at low temperature conditions (Arand, 1987), the test is usually

Table 1. Material properties of the hot mix asphalt AC 11 investigated in this study.

maximum aggregate density [kg/m³]		2,698
grading [mass-%]	<0.09 mm	9.5%
	>0,09 mm & <2.0 mm	37.5%
	>2.0 mm	53.0%
content of crushed aggregate		$C_{90/1}$
binder type		50/70
softening point Ring & Ball [°C]		52
binder content [mass-%]		6.0
maximum density [kg/m³]		2,476
mean void content of specimens [vol-%]		

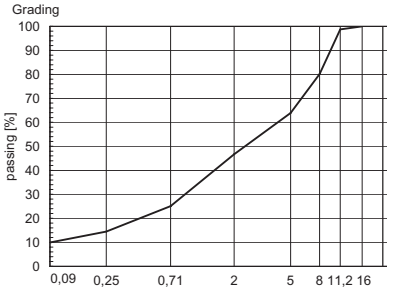

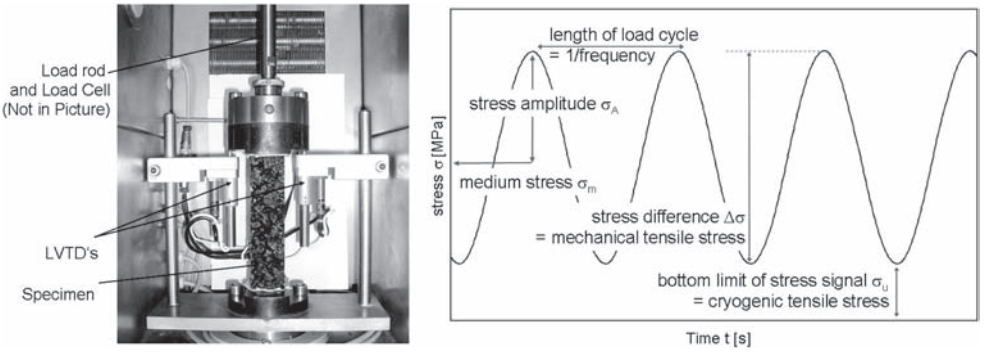

Figure 2. Test equipment and principle of the uniaxial cyclic tensile stress test (UCTST).

conducted at temperatures in the range of −15°C to +10°C. The stress amplitude moves between prescribed constant tensile stress limits, where the bottom stress limit is correlated to the material loading due to cryogenic stress, whereas the upper stress limit corresponds to the superimposed mechanical traffic loading (Figure 2). Prior to the UCTST, the cryogenic stress due to prohibited thermal shrinkage is determined by conducting a Thermal Stress Restrained Specimen Test (TSRST) on the asphalt specimen with a constant temperature decrease ($\Delta T = -10$ K/h). In the UCTST the bottom stress limit is kept constant for each test temperature, the super-imposed stress difference $\Delta\sigma$ is varied in at least three stages (Leutner et al. 2007).

3 INFLUENCE OF TEST FREQUENCY ON THE FATIGUE PERFORMANCE

3.1 *Test results*

The influence of stress signal's frequency on the fatigue performance during a UCTST was analysed by Mollenhauer (2008), based on an extensive experimental program including various asphalt materials (see also Mollenhauer & Lorenzl, 2008). From this analysis it was concluded, that the number of load cycles until fatigue failure is independently from the test frequency, but depends solely on the test duration. This observation is exemplarily shown in figure 3 for the asphalt wearing course material AC 11: The number of endured load cycles at 10 Hz is about the double of the corresponding number at 5 Hz, and about the triple of the corresponding number at 3 Hz. Consequently, if the time until macro-crack-initiation N_{Makro} is drawn versus the applied stress difference, it is stated, that all test results gained at varied frequencies can be represented by one single time-fatigue curve which can further be represented by one single frequency-independent fatigue function, reading

$$t(N_{Makro}) = L_1 \cdot \Delta\sigma^{L_2}, \tag{2}$$

where $t(N_{Makro})$ is the test duration until crack initiation, and L_1 and L_2 are the parameters of the fatigue function.

In analogy to these findings, frequency-independency can also be assumed for the course of the stiffness modulus, as well as for the course of the accumulated plastics strains. Figure 4 shows the course of the stiffness modulus at a temperature of +5°C for a frequency

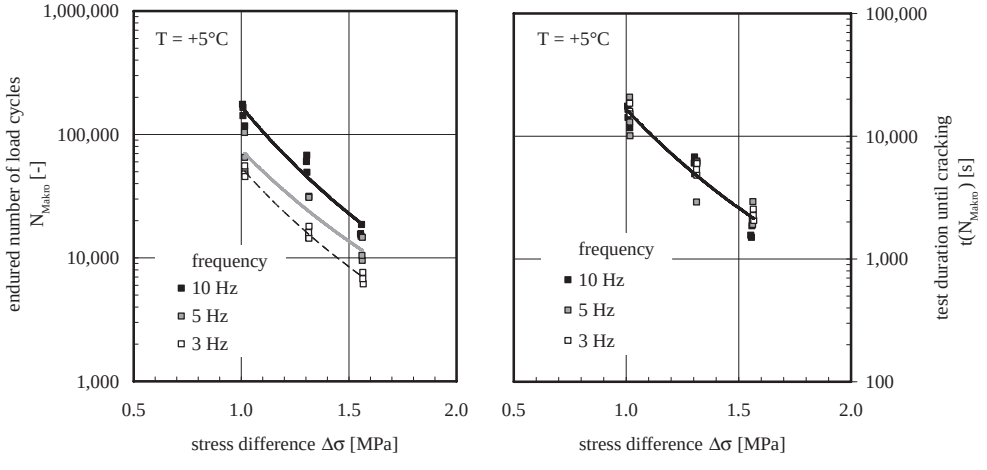

Figure 3. Wöhler lines and the influence of the test frequency on the number of endured load cycles (left); same results but plotted over the test duration until crack initiation leading to a single fatigue line (right).

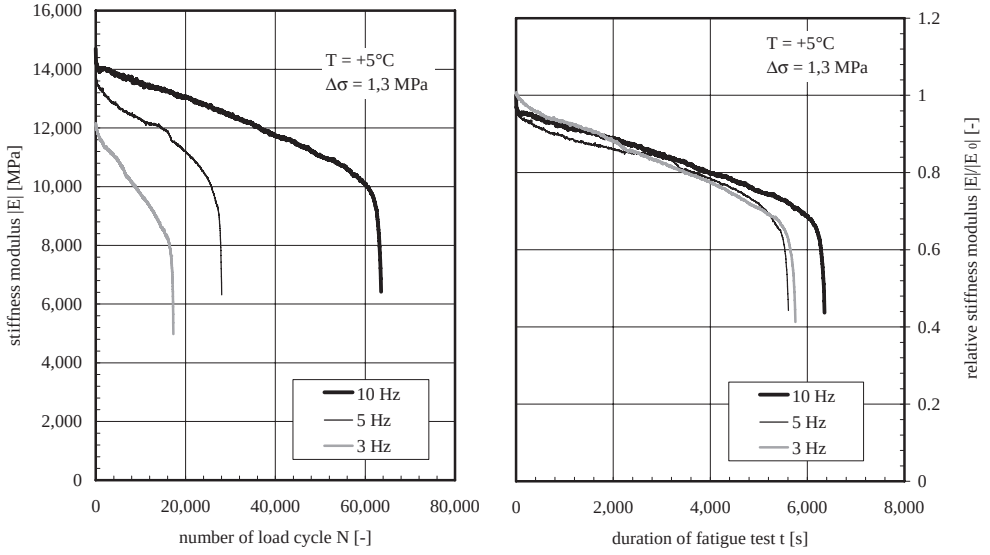

Figure 4. Course of the stiffness modulus |E| versus the number of load cycles N (left) and course of the relative stiffness modulus $|E|/|E_0|$ versus test duration t [s] (right).

of 3, 5, and 10 Hz (left), as well as the time-dependent but frequency-indifferent reduction of the relative stiffness modulus (right). As the stiffness modulus of the visco-elastic asphalt varies in function of the applied frequency, the stiffness modulus is plotted as 'relative' stiffness modulus, normalised by its initial value.

As represented by figure 5, an similar result is obtained for the course of the accumulated visco-plastic strain.

It may be assumed that the found independency of fatigue test results on the applied frequency may be extended to other frequencies (than 3, 5 and 10 Hz) by means of intra- and extrapolation techniques. This has to be proved in future studies.

3.2 *Discussion*

The stress signal of two different tests with same stress amplitude but varied frequencies are plotted versus the test duration (time) in figure 6 (left). The area below the sinusoidal plot of the stress signal may be interpreted as the energy introduced into the asphalt specimen in the course of the test. For the medium stress $\sigma_m = \sigma_u + \Delta\sigma/2$ corresponding to the sinusoidal stress signal, exactly the same area is found in the grey-colored area below the constant medium stress σ_m. Hence, it can be concluded, that the grey-colored area is always the same, independently from the test frequency applied. Moreover, the obtained creep curve is expected to be independent from the applied frequency. This should also be valid for a frequency of 0 Hz, i.e. a static creep test with a constant load, if any material effects due to the cyclic-dynamic excitation of the asphalt specimen are neglected.

For verification of this theory, the course of the accumulated visco-plastic strain as measured in UCTST is compared to the course of the creep curve as obtained from static tensile creep tests at a constant stress-level of σ_m (representing a frequency of 0 Hz).

Static creep tests (also called retardation tests) were conducted at varied static stresses and temperatures on prismatic specimens (for details see Wellner et al., 2007). Following the technique presented by Arand et al. (1997), the measured creep curves were used to back calculate the model parameters of a Burger's model. As the rheological model parameters E_1, E_2, λ_1 and λ_2 are both temperature-dependent and stress-dependent, tests were carried out at three

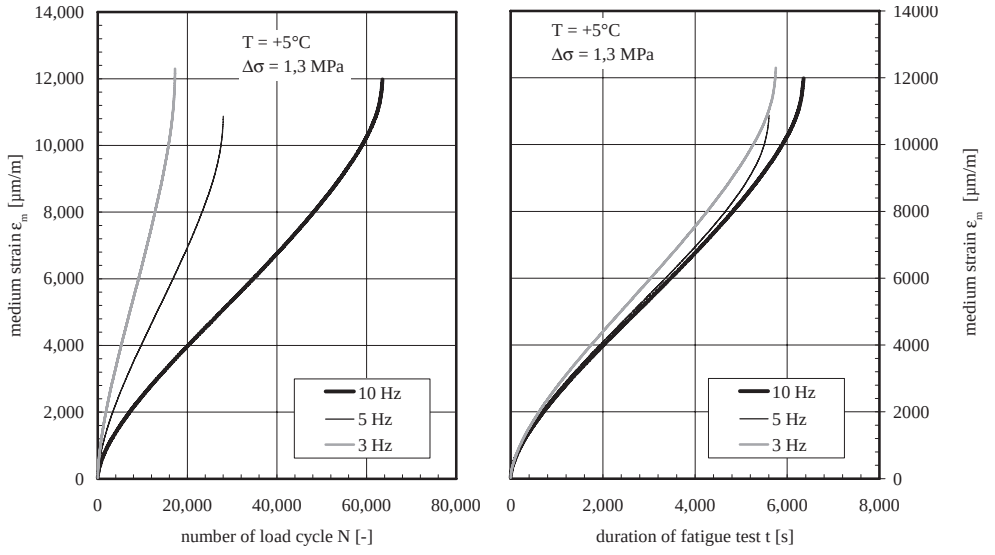

Figure 5. Course of the accumulated visco-plastic strain (medium strain ε_m) versus the number of load cycles N (left) and versus the test duration t [s] (right).

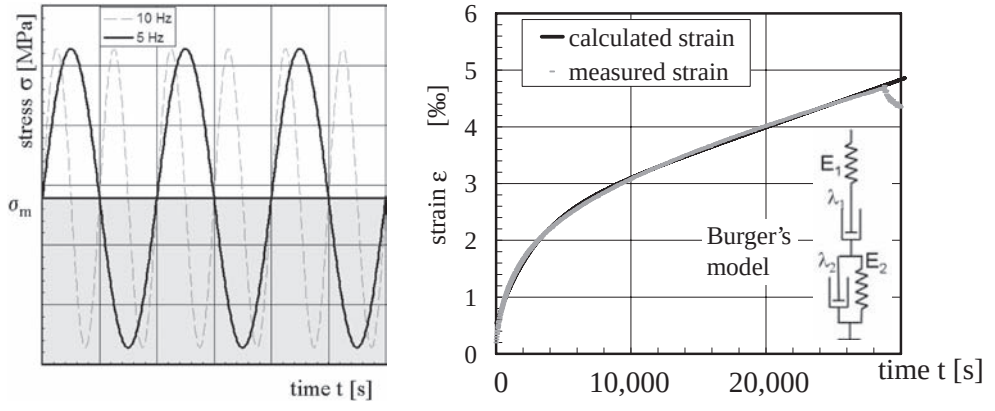

Figure 6. Stress signal versus time for two different frequencies (left); accumulated strain in creep test (right).

different stress-levels at various test temperatures. The course of the creep strains caused by a constant stress σ_m can then be calculated by use of Equation 3. For calculating the rheological model parameters i (E_1, E_2, λ_1 and λ_2) Equation 4 is used iteratively. The regression factors a_i and b_i, which describe the stress-dependency of the model parameters, are gained in a total number of 9 creep tests at each temperature.

$$\varepsilon_{creep}(t) = \frac{\sigma_m}{E_1} + t \cdot \frac{\sigma_m}{\lambda_1} + \frac{\sigma_m}{E_2}\left(1 - e^{-\frac{E_2}{\lambda_2} \cdot t}\right) \tag{3}$$

$$\{E_1, E_2, \lambda_1, \lambda\} = 10^{a_i^{(T)+b_1(T)\cdot\sigma_m}} \tag{4}$$

The creep curve as results from static testing and application of Burger's model can finally be compared to the accumulated visco-plastic strain measured in the UCTST at various frequencies. As can be seen in figure 7, in the beginning of the test the creep strains calculated from static tests are similar to the plastic strains stated in cyclic tests at varied frequencies. However, with increasing time, the static creep curve underestimates the cyclic curves significantly. This deviation is attributed to the neglecting of any effects from material deterioration within the rheological model.

In order to improve the model, consideration of material deterioration is needed. The stress acting on the asphalt specimen results from the quotient of the force F and the supporting area A of the specimen's cross-section. During the fatigue test, stiffness decreases due to micro-crack growth inside the specimen. In consequence, the area capable to support the force is reduced. As the testing device controls the applied force F only, the decrease in the specimen's supporting cross-section actually causes an increase of the stress acting on the un-cracked parts of the specimen. The stress increase is answered by a strain increase. Therefore, the slope of the accumulated visco-plastic strain increases and an inception point is observed, whereas the increasing visco-elastic response results in the observed stiffness decrease.

To calculate the increasing stress, the measured stiffness reduction can be used as an indicator of the crack growth. The resulting stress $\sigma_{det}(t)$ at the time t due to deterioration is calculated from

$$\sigma_{det}(t) = \sigma_0 \cdot \frac{E_0}{E(t)} \tag{5}$$

where σ_{det} is called the deteriorated stress, σ_0 and E_0 are the stress and the stiffness modulus at the beginning of the test, and E(t) is the stiffness modulus measured at the time t. In figure 8, the stress calculation is presented exemplarily.

As the stress-change during the test is known, the Burger's model can be used to estimate the resulting strain from the deteriorated stress σ_{det}. For considering the change of the Burger's model parameters in every time step j, the strain response is calculated from

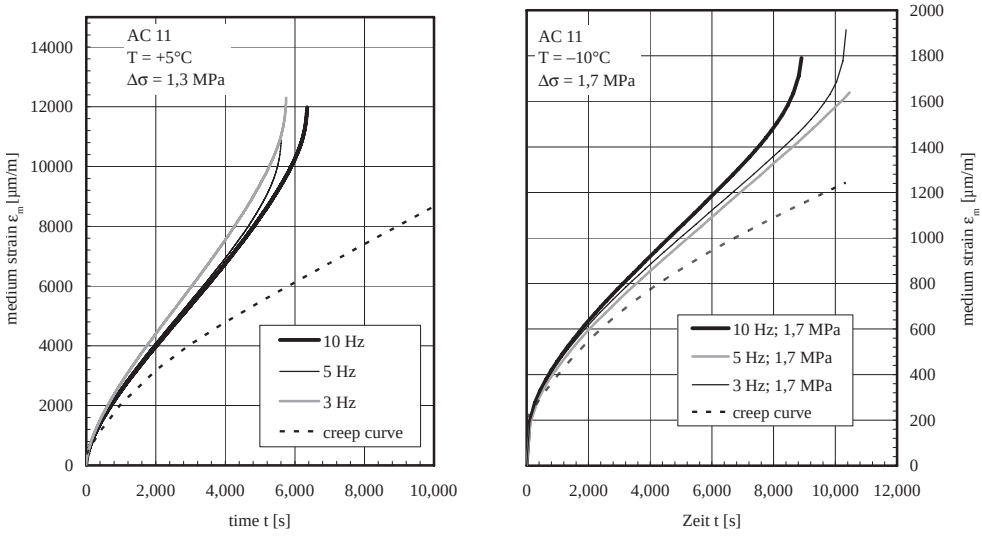

Figure 7. Vscio-plastic strains ε_m measured in UCTST, and creep curves calculated from static tests for a test temperature of 5°C (left), and 10°C (right).

$$\varepsilon_i = \frac{\sigma_{det,j}}{E_{1,j}} + \left(\varepsilon_{\lambda_1,j-1} + \frac{\sigma_{det,j}}{\lambda_{1,j}} \cdot dt \right) + \left(\varepsilon_{VE,j-1} + \left(\frac{\sigma_{det,j}}{\lambda_{2,j}} - \frac{E_{2,j}}{\lambda_{2,j}} \cdot \varepsilon_{VE,j-1} \right) \cdot dt \right) \quad (6)$$

where $\sigma_{det,j}$ is the resulting stress in the time interval j, $\varepsilon_{\lambda_1}, j-1$ is the viscous strain due to the solitaire viscosity λ_1 after time interval j–1, dt is the length of the time interval and $\varepsilon_{VE,j-1}$ is the visco-elastic strain of the parallel coupled elements E_2 and λ_2 after the time interval j–1.

In figure 9, the results using Equation 6 are illustrated, as obtained for the same loading conditions represented in figure 7. This time, the calculated strain signal corresponds

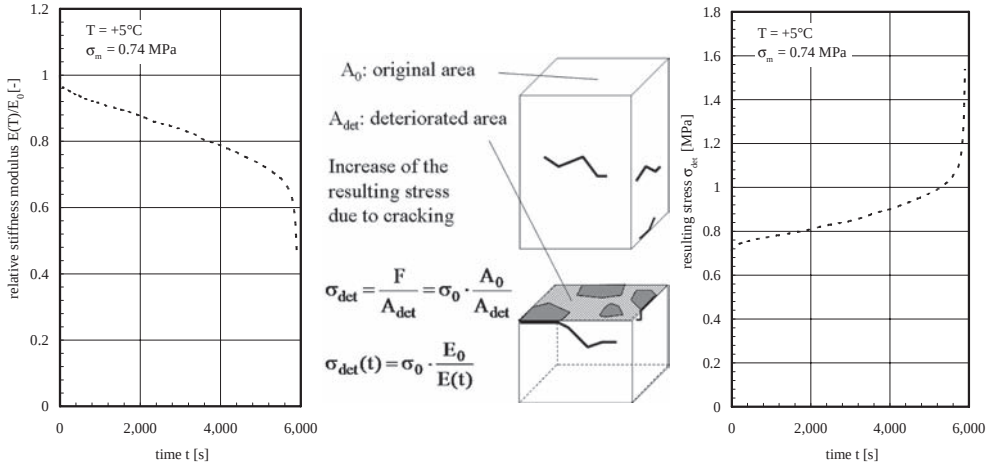

Figure 8. Stress calculation considering fatigue deterioration: Course of the stiffness decrease, estimation of the deteriorated supporting area, and calculation of the resulting stress.

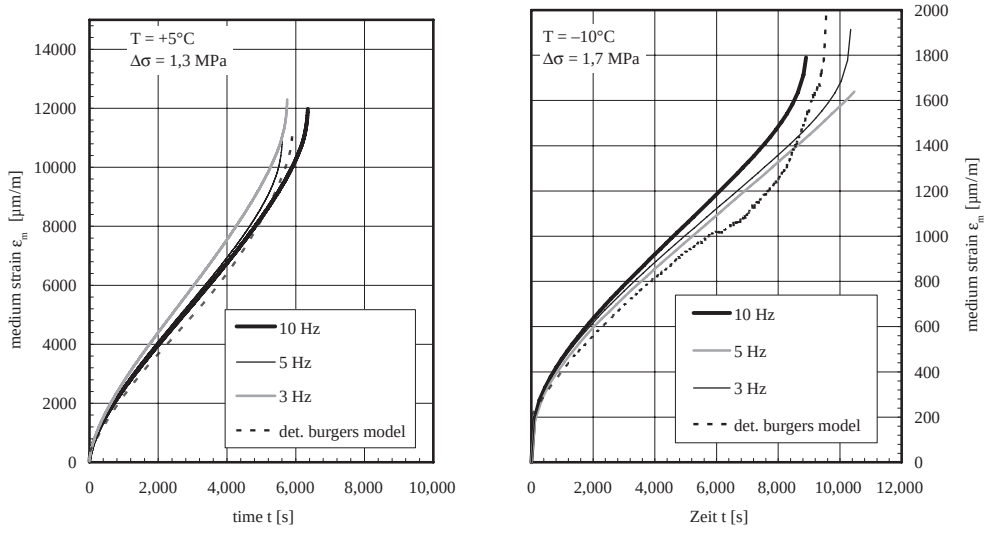

Figure 9. Comparison of irreversible strain measured in cyclic tests to strains calculated by means of the Burger's model under the consideration of material deterioration.

reasonably well to the measured accumulated visco-plastic strain. As the calculation procedure is based on the course of the stiffness reduction and in this way on the measured visco-elastic strain, it can be concluded, that these two strain responses are strongly linked to another.

4 CONCLUSIONS

The analysis of test data obtained from uniaxial cyclic tensile stress tests, from static creep tests and from rheological modeling using Burger's model leads to the following conclusions:

- Various effects that occur during cyclic asphalt testing are subsumed under the term fatigue deterioration, and these effects are strongly linked to another:
  - the number of endured load cycles until macroscopic fracture,
  - the particular course of stiffness decrease and
  - the course of accumulated visco-plastic strain.
- All observed fatigue deterioration effects show a frequency-indifferent behavior when the test duration is used as basis for data interpretation.
- In addition to cracking and the decrease in the stiffness modulus the development of accumulated visco-plastic strains is an effect attributed to fatigue phenomenon. The accumulation of visco-plastic strains can be modeled by applying Burger's model. It is assumed, that in the course of the fatigue test the increasing amount of micro-cracks provokes a reduction of the supporting specimen cross-section and in this manner an increase of the resulting stress. Based on the results from rheological modeling, it is concluded, that all degradation effects originate in a unique fatigue process, which is interpreted as crack growth.
- The uniaxial cyclic tensile stress test is a practical tool and well suited for the investigation of fatigue performance of asphalt materials.

ACKNOWLEDGEMENT

This investigational study is based on fatigue tests which have been performed in a research project generously funded by the German Federal Ministry of Education and Research (see Wellner et al., 2007). The authors want to thank their colleagues at the Braunschweig Pavement Engineering Centre (ISBS) involved in the laboratory work, and Holger Lorenzl, Peter Renken, and Stephan Büchler for fruitful comments as regards the interpretation of test results.

REFERENCES

Arand, W. 1987. Influence of bitumen hardness on the fatigue behaviour of asphalt pavement of different thickness due to bearing capacity of subbase, traffic loading and temperature. *Proceedings* of the *VI. International Conference on the Structural Design of Asphalt pavements, Ann Arbor/USA 1987.* Volume I, pp. 65–71.

Arand, W., Rubach, C. und v.d.Decken, S. 1996. Grundlegende Untersuchungen über den Einfluss der Zusammensetzung auf die Ermüdungsbeständigkeit von Walzasphalten mittels systematischer Variation kompositioneller Merkmale zur Schaffung quantitativer Bewertungsmaßstäbe. *Bundesministerium für Verkehr, Bau und Wohnungswesen, Forschung Straßenbau und Straßenverkehrstechnik; Heft 717.* Bonn, Germany.

Arand, W., Steinhoff, G., Eulitz, J. und Milbradt, H. 1984. Verhalten von Asphalten bei tiefen Temperaturen, Entwicklung und Erprobung eines Prüfverfahrens. *Bundesministerium für Verkehr, Bau und Wohnungswesen, Forschung Straßenbau und Straßenverkehrstechnik, Heft 407*, Bonn-Bad Godesberg, Germany.

Arand, W., Sörensen, A. und Büchler, S. 1997. Ermittlung der Zugviskositäten von Asphalten mittels Retardations- und Relaxationsversuchen. *Bundesministerium für Verkehr, Bau und Wohnungswesen, Forschung Straßenbau und Straßenverkehrstechnik; Heft 753*. Bonn.

Aschenbrenner, L. 2006. Mehrkomponenten-Modell zur Beschreibung des Deformationsverhaltens von Asphalt. *Schriftenreihe des Instituts für Statik der TU Braunschweig, Nr. 103*. Braunschweig.

Di Benedetto, H., de La Roche, C., Baaj, H., Pronk, A. and Lundström, R. 2004. Fatigue of bituminous mixtures. *Materials and Structures, Vol. 37, April 2004*, pp. 202–216.

Bodin, D., de la Roche, C. and Piau, J., Pijaudier-Cabot, G. 2003. Prediction of the Intrinsic Damage During Bituminous Mixes Fatigue Tests. *6th Rilem Symposium PTEBM'03, Zürich,* pp. 380–386.

Hopman, P., Kunst, P. and Pronk, A. 1989. A Renewed Interpretation Model for Fatigue Measurement. Verification of Miner's Rule. *4th Eurobitume Symposium, Madrid. 4–6 October 1989*; Vol. 1, pp. 557–561.

Leutner, R., Lorenzl, H., Schmoeckel, K., Donath, J., Bald, S., Grätz, B., Riedl, S., Möller, B., Oeser, M., Wellner, F., Werkmeister, S., Leykauf, G. und Simon, C. 2007. Stoffmodelle zur Voraussage des Verformungswiderstandes und Ermüdungsverhaltens von Asphaltbefestigungen. *Berichte der Bundesanstalt für Straßenwesen, Heft S 45*, Berg. Gladbach.

Mollenhauer, K. and Lorenzl, H. 2008. Testing of fatigue and deformation properties in uniaxial tension tests. *4th Eurasphalt & Eurobitume Congress, 21–23 May 2008*, Copenhague.

Mollenhauer, K. 2008. Dimensionierungsrelevante Prognose des Ermüdungsverhaltens von Asphalt mittels einaxialer Zug-Schwellversuche. PhD-Thesis. TU Braunschweig, http://www.digibib.tu-bs.de/?docid=00023217.

Saal, R. & Pell, P. Fatigue of bituminous mixes. *Kolloid-Zeitschrift Band 171, 1/1960*, pp. 61–71.

Van Dijk, W. 1975. Practical fatigue characterization of bituminous mixes. *Annual meeting of the Association of Asphalt Paving Technologists, Phoenix.*

Wellner, F., Weise, C., Leutner, R., Oeser, M., Jähnig, J., Lorenzl, H., Schindler, K., Mollenhauer, K., Zander, U. und Rabe, R. 2007. Nachhaltiger Straßenbau: Bemessungsmodell zur Förderung der Innovations- und Wettbewerbsfähigkeit kleiner und mittelständischer Straßenbauunternehmen. *Schlussbericht*; Dresden.

Advanced Testing and Characterization of Bituminous Materials – Loizos, Partl, Scarpas & Al-Qadi (eds)
© 2009 Taylor & Francis Group, London, ISBN 978-0-415-55854-9

Experimental study of the waveform shape effect on asphalt mixes fatigue

D. Bodin & J.-M. Balay
Laboratoire Central des Pont et Chaussées, France

M. Merbouh & D. Breysse
Université Bordeaux, France

L. Moriceau
Laboratoire Régional des Ponts et Chaussées de Bordeaux, France

ABSTRACT: The classical way of assessing fatigue performance of bituminous materials is to study the loss of stiffness during constant amplitude sinusoidal loading test performed in laboratory. This kind of signal is different from the signal induced by traffic load in real pavement. The temperature, frequency, rest periods and shape of the waveform may affect the results of the fatigue test, and therefore the results of pavement thicknesses computation based on fatigue performances. The study presented in this paper focuses on the influence of the shape of the periodic signal, by comparing the fatigue performances derived from classical sinusoidal signal; to those resulting from more realistic signal as it can be measured by strain gauges in full-scale pavement structures. Some multi-peak signals are studied modeling the effect of two axles loading. The main parameter studied is the decrease of the load between the two loading peaks within one cycle. The Wöhler curves of the different multi-peak test results are compared to the classical sinusoidal loading.

The study clearly shows that, for same loading amplitude, the two peaks signals are less damaging than the classical sinusoidal loading. Moreover, loading (or unloading) rate effect within the signals appears to affect fatigue life. Analytical analysis of signal aggressiveness is then proposed to take into account the signal shape complexity.

Therefore the effect of the frequency is also explored showing fatigue life reduction with the increase of frequency. This last point confirms the increase of damage with the frequency and opens future prospects.

Keywords: fatigue, bituminous mixes, wave shape, traffic aggressiveness, mechanistic pavement design

1 INTRODUCTION

For mechanistic pavement design, the evaluation of fatigue performances of bituminous materials is needed. The classical way of assessing fatigue resistance of asphalt mixes is to realize laboratory fatigue test and study the number of cycles leading to failure during constant amplitude sinusoidal loading. This kind of loadings is known to be different from the real loadings in the pavement. The temperature, frequency, rest periods shape of the waveform may affect the result (Rao Tangella et al. 1990). In the pavement design approaches, a reference single axle load is generally considered. The multi-axle effects are taken into account by considering the addition of the elementary strains profile due to each axle (LCPC-SETRA, 1994). Fatigue verification only considers the maximal local tensile strains at peaks, but not the complete signal. In airport pavements, the magnitude of loading can be very high when compared to road pavements, and the effect of the exact shape may also have to be considered. In particular, in the framework of the current modernization of the airfield design method,

the 4-axle and 6-axle landing gear configuration of the new large aircraft (Airbus 380 or Boeing 777) necessitate a better understanding of the fatigue behavior of asphalt materials under complex cyclic loading (Balay, 2008).

The shape of waveform of the loading during fatigue is known to affect the asphalt mixtures fatigue life (Raithby and Sterling, 1972). Force controlled tests under triangular, sinusoidal, and square waves had respectively lead to a fatigue life ratio of 1.45, 1.00 and 0.42 compared to the reference classical sinusoidal loading. In that study the square signal appears more damaging compare to the sinusoidal signal. For signals of the same period and same peak value, these experimental results clearly shows the influence of the time duration at the maximal loading value which is maximal for the square wave, minimal for triangular wave and intermediate for sinusoidal wave.

From an analytical point of view, Wöhler-Miner rule and alternative analytical approach (Stéfani, 1983) exists to take into account from the wave shape defining the relative aggressiveness of a wave shape compare to classical sinusoidal ones. These approaches will also be explored in the study as first interpretation formulas.

Firstly the experimental approach is presented and fatigue lines for different wave shapes are presented. Aggressiveness of the signal is defined and compared for all the tested loadings. Then analytical aggressiveness formulas are evaluated to interpret the data. Before conclusion the influence of the frequency of sinusoidal loadings is also presented.

2 EXPERIMENTAL APPROACH

2.1 *Fatigue device*

The fatigue campaign has been done at the Laboratoire Régional des Ponts et Chaussées in Bordeaux-France (Merbouh et al. 2007). Fatigue tests are bending tests on trapezoidal cantilever beams according the EN Standard (EN 12697-24). The trapezoidal specimens are tested in fatigue under periodical cyclic loadings. The machine used (Figure 1) has been adapted to use a numerical generator which allows imposing any signal on the specimen (Data Physic generator DP 550). The vibrator applies a force (F_{max} = 12 daN), which is adjusted by the generator to obtain the expected displacement. The picture (Figure 1) presents four specimens tested together which is used for classical sinusoidal loadings. In case of complex loadings only one specimen is tested.

As presented upper, the system is controlled to respect a given displacement at the top of the specimen. The loading has been chosen alternatively in tension and compression to avoid the creep of the specimen during the fatigue tests. The excitation signal is numerically

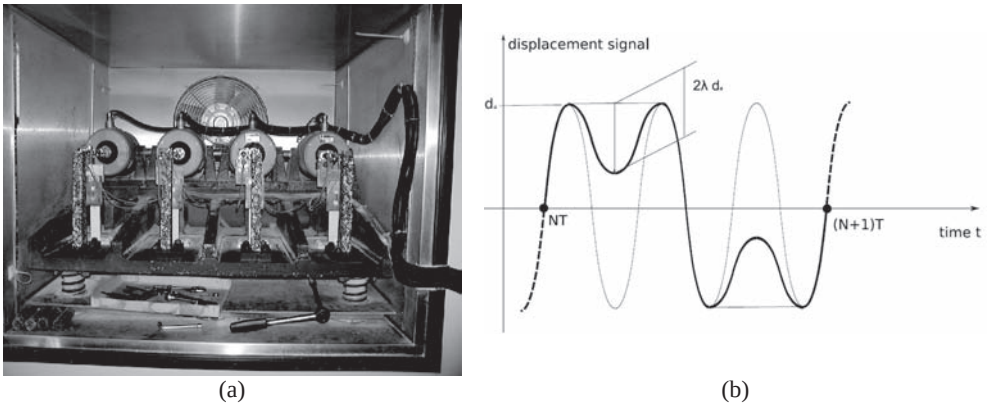

(a) (b)

Figure 1. (a) Experimental device, (b) displacement signal applied to the specimen: illustration of the λ parameter.

generated with different wave forms. On the figure 1(a), the parameter λ allows to adjust the decrease of the loading between two peaks. When $\lambda = 0$ there is no decrease of the load between the two peaks. When $\lambda = 1$ the signal is fully reversed between the peaks. Then the signal is equivalent to a sinusoidal loading (Figure 1). This sinusoidal signal has a frequency three times greater than the multipeak signals.

The generator used to drive the signal does not provide a strictly continuous signal, except for classical sinusoidal loading. It has to impose the signal by pulses. Each pulse is a serie of cycles. Their duration is T_f ($T_f = 12$ s ie 300 sinusoidal cycles at 25 Hz or 100 multipeak cycles at 8.3 Hz). Between each pulse a small rest period T_r ($T_r = 0.5$ s–4% of T_f) is imposed by the system. Another experimental bias has also been noticed at the beginning and the end of the pulse. A few cycles could have amplitudes (10%) higher or lower than the aimed value. To verify that these transient regimes have not too much influence on the fatigue results, two set of samples have been tested under a 25 Hz sinusoidal loadings, without and with pulses to check that their effect remains negligible (Figure 2).

According Figure 2, we can conclude that the micro rest periods applied by the system can be assumed negligible compare to the intrinsic fatigue tests scatter. It is specifically true for short fatigue life's tests treated in this paper.

2.2 *Material and experimental campaign*

The material used for this campaign has been widely studied in fatigue in past LCPC (Laboratoire Central des Ponts et Chaussées) and international RILEM research committee projects (Di Benedetto et al. 2004). It is a 0/6 mm (Diorite) continuously-graded dense asphalt concrete normally used for surface layer. The binder is a pure binder 50/70 and the binder content is 6.85%. The theoretical compacity of the mix is 95%. The composition is more detailed in Table 1.

The specimen are sawn from slabs (400 × 600 × 120 mm) manufactured with a rolling compactor according the standard (EN 12697-33). Then trapezoidal specimens are sawn to perform mechanical tests as complex modulus (EN 12697-26) and fatigue. The complex modulus of the mix is around 8000 MPa at (20°C–25 Hz) and 11000 at (10°C–10 Hz). Fatigue tests of the following campaign are performed at 20°C, and at different strain levels. Their range has been fixed to reach fatigue lifes between 10^4 and 10^5 loading cycles. This range of fatigue life is more representative of airfield pavements. They are higher than classical ones compared to levels to reach one million of cycles usually aimed to define the ε_6 value leading to a fatigue life of 10^6 cycles (EN 12697-24).

Multi peak signal are compared to classical sinusoidal approaches. The experimental investigations are focused, on the influence of the decrease between the two peaks. This is numerically controlled by the λ parameter (Figure 1b).

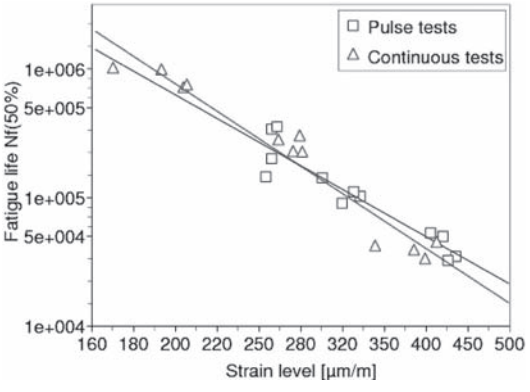

Figure 2. Influence of the micro-rest period T_r on the fatigue life evaluation.

Table 1. Grading curve and composition of the tested material.

Grading								Binder	
Sieve	0.08	0.315	1	2	4	6.3	8	Type	50/70
% passing	11.8	22.6	39	59.5	70.2	97	100	Content %	6.4

Table 2. Signal characteristics: type, periods and number of wheel passes per period.

Type of signal	Period of the signal T_s	Number of wheel n_w
Sinusoidal $f = 8.33$ Hz	0.12	1
$\lambda = 0.$	0.12	1
$\lambda = 0.25$	0.12	2
$\lambda = 0.50$	0.12	2
$\lambda = 0.75$	0.12	2
$\lambda = 1.0$	0.12	3

2.3 *Fatigue line analysis*

The fatigue performance is defined as the loading level amplitude ε_5 leading to a specimen failure for 10^5 cycles. The specimen failure is assumed to be reached for N cycles which correspond to a decrease of half of its initial stiffness. A linear interpolation of experimental data ($N - \varepsilon_a$) in a log-log diagram (Eq. 1) defines ε_5 and the slope p (Eq. 1).

$$N = 10^5 \left(\frac{\varepsilon_a}{\varepsilon_5} \right)^p \tag{1}$$

2.4 *Signal aggressiveness definition*

We define $s(t)$ a general form of a periodic signal defined on its period $[0, T_s]$ with equal values at its boundaries. A specimen submitted to a loading obtained by periodic extension of the s signal to $\Re^+$ will break at a time in the interval $[(N_r - 1)T_s, N_T T_s]$. The number of period (cycles) N_T is called "fatigue life". From its value, we defined the aggressiveness G_T of the signal s by

$$G_T = \frac{1}{N_T} \tag{2}$$

Nevertheless if we consider the number of peak N_p for $\lambda = 0.25$ to 1 the number of peak is two or three times the number of period N_T. Then two separate analysis could be done. Firstly, the number of signal's period which leads to failure N_F, are counted using the test time divided by the period T_S of the signal. Secondly, for pavement analysis, the representation of the number of wheel to failure is made assuming that function of its shape each elementary signal represents a certain number of wheel passes n_w per period assuming that each peak is related to one wheel (Table 2).

Then, equation 1 can be rewritten in terms of wheel passes. During a given fatigue life, if N_T is the number of periods, the number of wheel passes is then $N_w = N_T n_w$. In terms of wheel passes the aggressiveness is defined as

$$G_w = \frac{1}{N_T \, n_w} \tag{3}$$

Next section presents experimental results of fatigue tests performed using the different wave types.

3 EXPERIMENTAL RESULTS

All the fatigue tests are performed under displacement controlled conditions ie the displacement applied at the top of the tested specimen is driven according the signal shape given Figure 1. Different loading amplitudes are used to obtain fatigue lifes between 10^4 and 5 10^5 cycles (equivalent here to loading period). For different signal shapes the study focuses on the comparison of testing configurations. Results are presented in terms of fatigue lines and their two parameters ε_5 and the slope p defined equation 1. The period of the signals is kept constant, for all the used waves, and fixed at $T_s = 0.12$ s ($f = 8.33$ Hz).

3.1 *Influence of* λ

The effect of the decrease between the two peaks is presented by a λ parametric study. Four different values of λ have been used (see figure 1b). From, λ = 0 for the flat peak signal to λ = 1.00 for the signal equivalent to three cycles at 25 Hz, λ = 0.25, 0.5 and 0.75 differs from the depth of the decrease between the two peaks. Results are presented below. Table 3 gives all the details about fatigue lines parameters. Figure 3 shows the fatigue lines and the influence of λ on ε_5.

In the range from 0 to 0.75, λ has no significant effect. Both ε_5 and p are in the same range. For λ = 1.0 the fatigue lifes decrease. These signals appear more damaging than the other configurations. That physically means that the amount of decrease between the two peaks of the signal as no significant effect on the specimen's fatigue lifes until the signal is totally symmetrical.

3.2 *Comparison of the shape at same frequency*

At same frequency, comparison between the sinusoidal loading at 8.3 Hz and the multi-peak signal for λ equal to zero allows to focus on the effect of the duration of the peak zone of

Table 3. Fatigue lines parameters for different values of the shape parameter lambda (λ = 0, 0.25, 0.5, 0.75, 1.00).

Shape parameter	Nb. tests	Slope	Value	ε_5 [μm/m] 95% confidence interval
λ = 0	12	–4.29 ± 1.36	323	[256, 406]
λ = 0.25	12	–4.76 ± 0.90	324	[277, 319]
λ = 0.50	12	–4.26 ± 1.43	319	[232, 437]
λ = 0.75	12	–4.79 ± 1.89	321	[232, 447]
λ = 1	12	–3.61 ± 0.94	243	[170, 349]

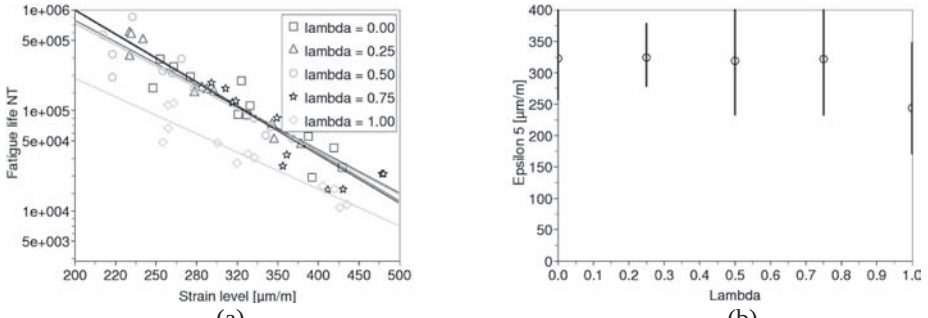

Figure 3. Influence of the shape parameter lambda (λ = 0, 0.25, 0.5, 0.75, 1.): (a) fatigue lines, (b) ε_5 values.

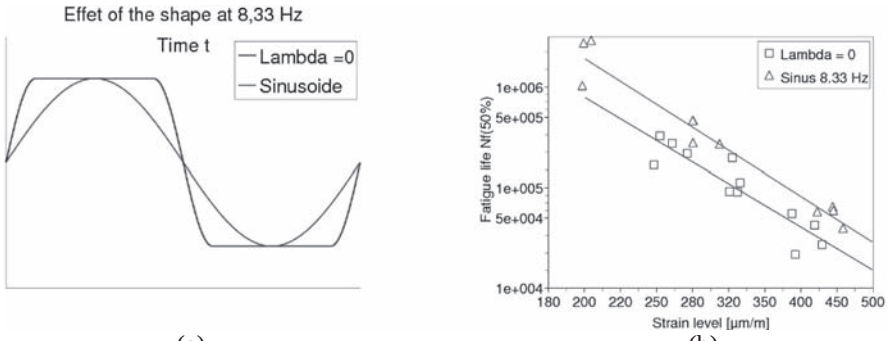

Figure 4. Influence of peak time duration (a) signals, (b) fatigue lines.

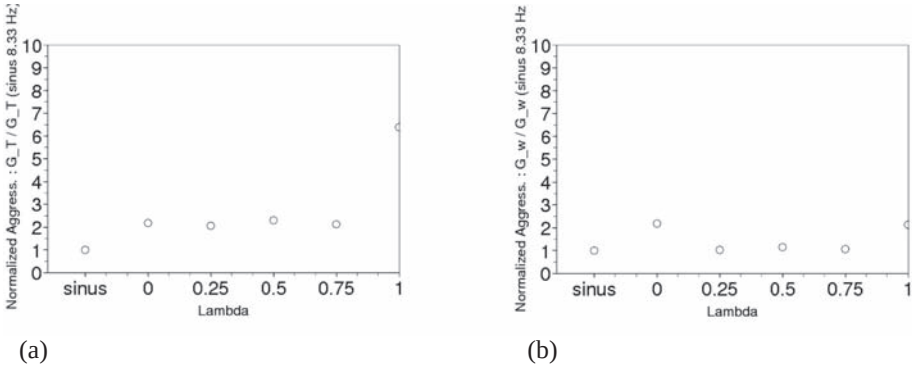

Figure 5. Experimental aggressiveness of the five different signals at frequency 8.33 Hz (sinusoidal, $\lambda = 0, 0.25, 0.5, 0.75, 1.$) (a) Aggressiveness related to signal's period (b) Aggressiveness related to wheel passes numbers.

the signal. The last one as no decrease between the two peaks. Each half cycle contains a sinusoidal growth a flap peak at the maximal value followed by a sinusoidal decrease.

Comparison between the $\lambda = 0$ signal and the sinusoidal loading of the same frequency ($f = 8.3$ Hz) shows that the signal $\lambda = 0$ leads to shorter fatigue life at the same loading amplitude (Figure 4b). Qualitatively, longer is the peak duration shorter is the fatigue life. In the present study, the ranking is identical to the comparison of fatigue life ratio obtained for the square and triangular signal vs the sinusoidal one (Raithby and Sterling, 1972).

3.3 *Aggressiveness of signal's period and equivalent wheel passes*

For the five studied signals ie sinusoidal at 8.33 Hz, and the four signals linked to the four values of $\lambda = 0$ to 1. Results of experimental aggressiveness (see §2.4) are presented figure (5). For the two plots, the values are normalized by the value obtained for the reference sinusoidal loading, leading to a relative aggressiveness of 1 for the sinusoidal wave at 8.33 Hz.

First, figure 5a, the aggressiveness of the signal is presented as a function of loading period (G_T, equation 2). It appears that the multi-peaks signals except $\lambda = 1$ leads to the same aggressiveness approximately two times greater than the sinusoidal signal at the same frequency (ie 8.33 Hz). The totally reversed signal $\lambda = 1$ shows 3 times higher values.

However, if we consider the equivalent number of wheel passes for each elementary signal (Table 2) the aggressiveness G_w (equation 3), the values are more related to the effect of an

Table 4. Fatigue lines parameters for different values of the signal frequency.

Signal type	Nb. tests	Slope	Value	ε_5 [μm/m] 95% confidence interval
Multi-peak ($\lambda = 0$)	12	-4.29 ± 1.36	323	[256, 406]
Sinus ($f = 8.3$ Hz)	11	-4.57 ± 0.75	380	[297, 488]

elementary wheel within a multi-axle load modeled in the lab. For this last analysis, the sinusoidal (8.33 Hz) and the three multi-peak signals ($\lambda = 0.25$, 0.5 and 0.75) are very similar. With this laboratory approach, the sinus 8.33 Hz signal equivalent to one wheel has the same aggressiveness to more complex signals which model two wheel passes in terms of wheel passes. The aggressiveness, of the signal $\lambda = 0$ (one wheel passes with flat peak) is approximately two times greater. The wheel aggressiveness of the $\lambda = 1$ (one wheel passes at higher speed equivalent to 25 Hz) is also in the same range.

4 ANALYTICAL APPROACH OF SIGNAL AGGRESSIVENESS

Existing fatigue damage analysis used for material based approach or for pavement design analysis can be explored in terms of multi-peak damage effect. The comparison with the previous theoretical approaches will be focused on Wöhler-Miner cumulative rules through a damage model and also an alternative mathematical aggressiveness relation. Then results are analyzed and compared to experimental results.

4.1 *Continuum fatigue damage model*

Using a continuous fatigue damage model for asphalt (Bodin et al. 2004) the effect expected with the multi peak signal can be estimated. In this model the damage growth is only driven by the strains induced by tension. The damage rate by cycle is integrated analytically (Eq. 4)

$$\begin{aligned}\frac{dD}{dN} &= f(D)\frac{1}{\beta+1}\left[\underbrace{\varepsilon_a^{\beta+1}}_{\text{first peak}} + \underbrace{\varepsilon_a^{\beta+1}\left(1-<1-2\lambda>^{\beta+1}\right)}_{\text{second peak}} + \underbrace{\varepsilon_a^{\beta+1}<2\lambda-1>^{\beta+1}}_{\text{third peak}}\right] \\ &= f(D)\frac{\varepsilon_a^{\beta+1}}{\beta+1}\left[2-<1-2\lambda>^{\beta+1}+<2\lambda-1>^{\beta+1}\right]\end{aligned} \tag{4}$$

$$\text{with } <x> = \frac{1}{2}(x+|x|)$$

For a fixed fatigue life criterion the effective ε_5 value for a given number of period

$$\varepsilon_5 = \varepsilon_5^{(0)}\left(2-<1-2\lambda>^{\beta+1}+<2\lambda-1>^{\beta+1}\right)^{-\frac{1}{\beta+1}} \tag{5}$$

where $\varepsilon_5^{(0)}$ is the classical strain value for sinusoidal single peak signal.

These expressions are identical to the classical Wöhler-Miner analytical expression for fatigue and the relative aggressiveness parameter can be directly deduced

$$\frac{G_T}{G_T^{(0)}} = \left(2-<1-2\lambda>^{\beta+1}+<2\lambda-1>^{\beta+1}\right) \tag{6}$$

4.2 *Mathematical aggressiveness factor*

A mathematical expression of this aggressiveness term had been proposed (Stéfani, 1983) to model the experimental evidences obtained by Raithby and Sterling, (1972).

$$G = K\,V(< s >)\ \frac{\int_0^T < s(t) >^m dt}{\int_0^T < s(t) > dt} \tag{7}$$

where V is the global signal variation over the cycle (sum of the absolute values of the signal on its increasing and decreasing intervals). The aggressiveness has some essential theoretical properties

- If the period of the signal contains n more elementary signal s then the relative aggressiveness of the resulting signal will be multiplied by n what should be respected by such aggressiveness term.
- For signals proportional to an elementary one, a fatigue line exists. Its slope is $p = -m$ and Miner law is verified.
- This definition is not affected by homothetic changes along the time axis (elastic case).

The two first properties are in accordance with experimental evidences on asphaltic materialls. Further work is needed to take into account frequency effect on similar shape signal as it can be observed with viscoelastic material as asphalt concrete. For elementary signals (triangle, sinusoidal, and square) at same frequency the analytical expression (Eq. 7) are qualitatively in accordance with the results obtained by Raithby and Sterling, (1972).

Then the application of these two analytical approaches is performed on the signals applied in the lab. The m exponent is related to the fatigue line slope and is fixed at 4 according the mean values obtained in Tables 3 and 4.

4.3 *Comparison with experimental aggressiveness factor*

In this section the aggressiveness G_T (Eq. 2) of signals of same period duration are compared. Experimental results presented (§3) are compared to the two previous analytical approaches are plotted Figure 6.

The application of analytical aggressiveness formulas shows a good qualitative agreement with experimental data. However, quantitatively, the calculated aggressiveness underestimate the experimental ones. The difference aggressiveness for the $\lambda = 1$ signal clearly shows the need of rate effect implementation in aggressiveness formula. The period also includes

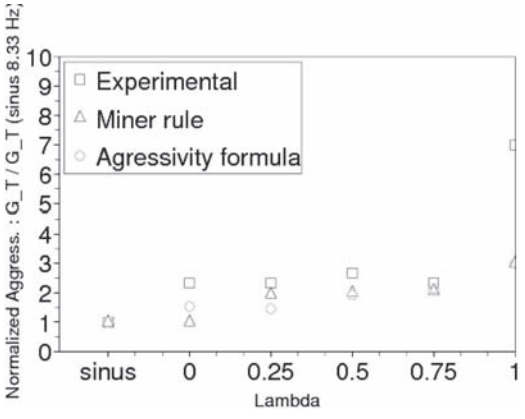

Figure 6. Comparison of experimental aggressiveness with analytical expressions.

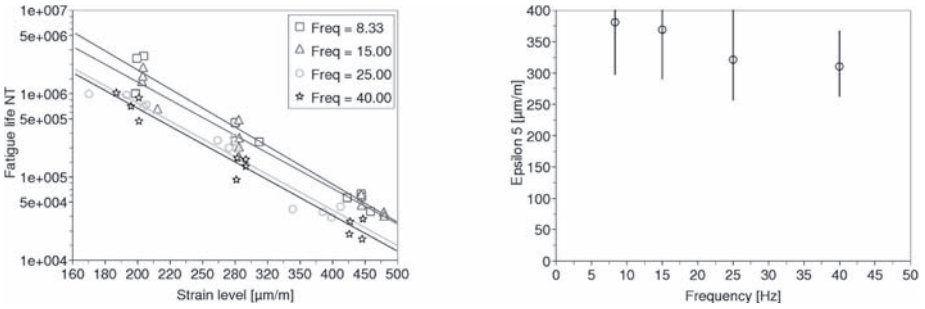

Figure 7. Influence of the loading frequency (f = 8.33, 15, 25, 40 Hz): (a) fatigue lines, (b) ε_5 values.

Table 5. Fatigue lines parameters for different values of the signal frequency.

Frequency	Nb. tests	Slope	Value	ε_5 [µm/m] 95% confidence interval
8.3	11	–4.57 ± 0.75	380	[297, 488]
15	12	–4.26 ± 0.66	369	[290, 470]
25	12	–4.26 ± 0.73	321	[256, 402]
40	12	–4.28 ± 0.54	310	[262, 368]

three elementary cycles compared to the 8.33 Hz. In that case, analytical formulas leads to a relative aggressiveness of three compared to six for experimental measures.

For $\lambda = 0$ the use of equation 6 shows the interest of the integration of the signal (or a function of the signal) over the period compared to the Wöhler-Miner formula which only integrates the peak values.

In this application, it appears relevant to integrate the rate effects in the aggressiveness expression. So, in addition to the multi-peak signals investigations, the effect of the test frequency has been studied, with sinusoidal tests, to confirm this last remark.

5 LOADING FREQUENCY EFFECT

A specific campaign has been performed on the studied material with sinusoidal tests. Four frequencies had been tested (f = 8.33, 15, 25 and 40 Hz). Experimental results shows a decrease of the fatigue lifes with the increase of frequency (figure 7).

Results plotted Figure 7 and gathered Table 5 exhibit an effect of the loading frequency on fatigue behavior. The decrease of ε_5 with the frequency is correlated with a more damaging effect of the loading with the increase of the frequency. These results are consistent with previous works on the frequency.

6 CONCLUSION

This novel approach for pavement material characterization is focused of the waveform shape on the fatigue response during two points bending laboratory fatigue tests on trapezoidal specimen. A parametric study of the decrease of loading between two-peaks signal has been done. The effect of the frequency at same shape has also been investigated as a parallel study. The main observations are: An increase of the peak duration of a single signal induces a decrease of fatigue life. For sinusoidal loading an increase of the loading frequency leads a decrease of the fatigue life. These two points are consistent with previous results cited in literature.

For two-peaks signals, the decrease between the two peaks does not have significant effect on the fatigue behavior. However, in this parametric study, it has been difficult to separate the two parameters quoted before, which are loading rate and time spent at maximal loading value.

Using two analytical aggressiveness approaches leads to a qualitative agreement with experimental trend. Quantitatively, the aggressiveness of the signals appears underestimated. However some interesting points have to be underlined. A relevant aggressiveness formula should take into account the shape of the signal trough an integration over the period and not only the peak values and the dependency of the behavior on the signal frequency.

These first encouraging results will be deeper investigated during a current research project focused on multi-axle effects on fatigue cracking. The research is based on the three following topics: loading measurements on LCPC Accelerated Pavement Testing facilities, material characterization using the method initiated in this paper, and the consequences for mechanical design of bituminous pavements.

ACKNOWLEDGMENTS

The work reported is part of a collaboration project between the French technical department of civil aviation (STAC) and LCPC. Experimental investigations were conducted at the regional laboratory (LRPC) in Bordeaux—France. The authors would like to thank Christian Stéfani from LCPC for the fruitful discussions and support.

REFERENCES

Balay, J.M. 2008. Dimensionnement des chaussées aéroportuaires et chaussées routières à assises non traitées—Structural design of airport and highway pavements with untreated bases, Revue Générale de Routes, n°864, fév. 2008.

Bodin, D., Pijaudier-Cabot G., de La Roche, C., Piau, J.M. & Chabot, A. 2004. Continuum Damage Approach to Asphalt Concrete Fatigue Modeling, Journal of Engineering Mechanics (ASCE) 130 (6): 700–708.

CEN, EN 12697-24. Bituminous mixtures—Tests methods for hot mix asphalt—Part 24: Resistance to fatigue. European standard, July 2004.

CEN, EN 12697-26. Bituminous mixtures—Test methods for hot mix asphalt—Part 26: Stiffness. European standard, July 2004.

Di Benedetto, H., de La Roche C., Baaj, H. Pronk, A. & Lundstrom, R. 2004. Fatigue of bituminous mixtures Materials And Structures, 37, 202–216.

LCPC-SETRA, French design manual for pavement structures, 1994, Technical guide, Ministère des l'Equipement des Transports et du Logement—France, (English version 1997).

Merbouh, M., Breysse, D. Moriceau, L. & Laradi, N. 2007, Comportement en fatigue des enrobés de chaussées aéronautiques sous actions de grande intensité. Actes des Rencontres de l'Association Universitaire de Génie Civil (AUGC)—Bordeaux—23–25 mai (in French).

Rao, Tangella, S.C.S., Craus, J., Deacon, J.A. & Monismith C.L. 1990, Summary report on fatigue response of asphalt mixture TM-UCB-A-003A-89-3. Strategic Highway Research Program—Project A-003. University of California—Berkeley, California. February 1990.

Raithby, K.D. & Sterling, A.B. 1972. *Some Effects of Loading History on the Performance of Rolled Asphalt*, TRRL-LR 496, Crowthorne, England.

Stéfani, C. 1983. Fatigue sous sollicitation périodique complexe, Internal Note, LCPC.

Advanced Testing and Characterization of Bituminous Materials –
Loizos, Partl, Scarpas & Al-Qadi (eds)
© 2009 Taylor & Francis Group, London, ISBN 978-0-415-55854-9

Experimental investigation of crack propagation in asphalt concrete

R.A. Tarefder & E.M. Kias
University of New Mexico, Albuquerque, NM, USA

ABSTRACT: This study evaluates cracking in asphalt concrete. Semi-circular notched asphalt concrete specimens are fractured in the laboratory using a strain-based load in three point bending. Crack opening displacement (COD) data is captured in real-time along the length of the crack using linear variable displacement transducers (LVDTs). Several parameters derived from the laboratory data are used to characterize the mix cracking in terms of resistance to crack initiation and crack propagation in dry and wet conditioned samples. These parameters are the crack initiation load, the ultimate load, the slope of the crack propagation curve, and crack velocity. The effects of mix type, air voids, and moisture conditioning on these parameters are evaluated. It is shown that wet samples can carry a higher ultimate load than the dry samples. Wet samples tend to show higher load decrease (higher slope) during crack propagation than the dry samples. Mix type and void ratio have very little effect on the crack velocity, although wet samples have slower cracks than dry samples.

1 INTRODUCTION

Cracking is considered to be one of the major distress of asphalt pavements. Cracks decrease the structural capacity of the pavement and increase the maintenance cost. Crack provides pathways for water and aggressive agents that greatly accelerate the deterioration process. Hence, understanding how a crack initiates and propagates in HMA is paramount for controlling cracks and mitigating deterioration in asphalt pavement structures. Several factors such as mix aggregate gradation, mix air voids, and wet/dry conditions can affect cracking in asphalt concrete (Roque et al. 2001, Li & Metcalf 2002). In this study, three different Superpave mixes are tested under wet and dry conditions. In essence, this study employs a laboratory procedure to initiate a crack at the notch tip within an asphalt concrete sample and capture its propagation in real-time. Recently, a several studies have evaluated tensile strength of Hot Mix Asphalt (HMA) using a semi-circular notched sample under three point bending load (Van de Ven et al. 1997, Molennar et al. 2002, Li & Marasteanu 2004). Some of the researchers have reported that the semi-circular bending test produces more repeatable results that the traditional indirect tension tests (Huang et al. 2005, Zhang et al. 2001, Roque et al. 1999). To this end, this study evaluated cracking in notched-semicircular asphalt concrete samples under wet and dry conditions. Most importantly, this study measures the crack initiation and crack velocity using Linear Variable Displacement Transducers (LVDTs) at different locations on the asphalt concrete sample while under loading. This study is different from previous study in terms of real-time measurement of crack initiation and propagation through the asphalt concrete samples, and evaluation of dry/wet conditions on crack initiation and propagation parameters.

2 OBJECTIVES AND SCOPE

The objectives of this study are to:

- Capture and analyze the crack path in asphalt concrete samples in the laboratory.
- Develop a methodology for determining crack velocity (v) using LVDTs at different locations on the surface of an asphalt concrete sample.

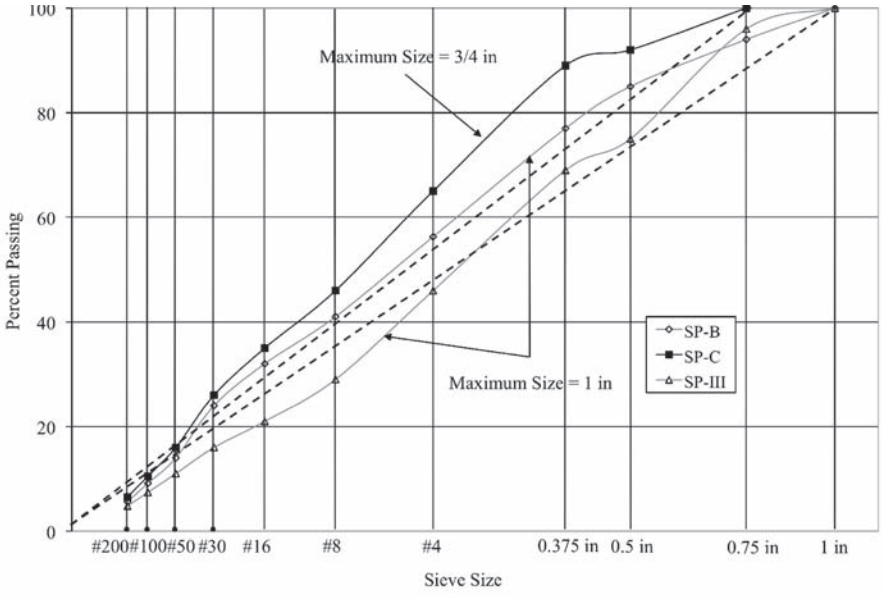

Figure 1. Aggregate gradation for Superpave mixes SP-B, SP-C and SP-III.

- Examine the effects of air voids, moisture, and aggregate gradation on crack initiation and propagation in asphalt concrete samples using the following parameters: the crack opening displacement at ultimate load (COD_{ult}), the crack initiation load (P_{int}), ultimate load (P_{ult}), the slope of the crack propagation curve (θ), and the crack velocity (v).

3 MIX DESCRIPTION

The Superpave mixes were collected from a local plant in cooperation with the New Mexico Department of Transportation. Mixes were selected to cover both fine and coarse mixes used in the state of New Mexico. The maximum aggregate size for these mixes are shown in Figure 1, which is a 0.45 power gradation chart. The maximum aggregate size in a mix has an impact on the overall gradation of a mix. The maximum aggregate size in an aggregate gradation is defined as the smallest sieve size through which 100 percent of the aggregate passes through. It is shown in Figure 1 that mix SP-C has a smaller maximum aggregate size than mixes SP-B and SP-III. Mix gradations that plot above the maximum density line tend to be fine mixes, while gradations below the maximum density line tend to be coarse mixes. The maximum density lines for maximum aggregate sizes of 3/4 in. and 1 in. are plotted in Figure 1. SP-C has a maximum aggregate size of 3/4 in. where as mixes SP-B and SP-III have a maximum aggregate size of 1 in. Mixes that plot above the maximum density line are generally fine mixes while mixes that plot below the maximum density line are generally coarse mixes. Superpave mixes SP-B and SP-C plot above their respective maximum density lines and mix SP-III plots below its respective density line. Therefore, mix SP-III is a coarse mix and mixes SP-B and SP-C are fine mixes. Of the fine mixes, SP-B is coarser than SP-C.

4 SAMPLE PREPARATION AND TEST MATRIX

Each of the mixes is compacted into 6 in. diameter cylinders by a Superpave gyratory compactor using a 600 kPa (87,02 psi) vertical pressure (AASHTO T 312 2002). Sample height

(a) Gyratory Sample (b) Sliced Sample (c) Notched Samples

Figure 2. Notched sample preparation steps.

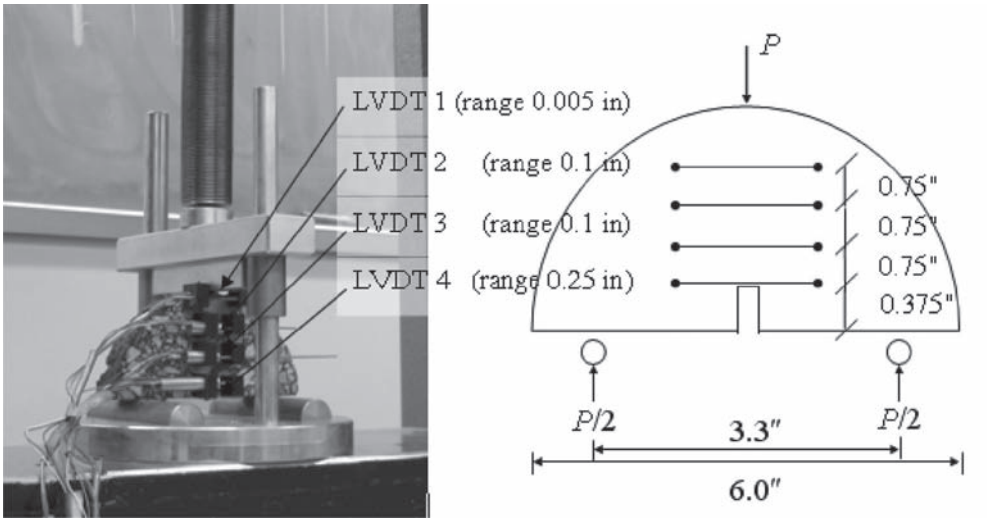

Figure 3. Sample loading configuration and LVDT placement.

is kept to about 5.0 in. (12.7 cm). Next, using a water cooled laboratory saw, two one-inch thick discs are sliced from the center of each cylinder in an attempt to acquire samples with uniform air voids. Finally the discs are halved and notched in the center of the flat edge with 3/8 in. (9.525 mm) deep slits using a laboratory saw of 1/8 in. (3.175 mm) blade thickness. Figures 2(a)–(c) show the compacted asphalt concrete cylinder, sliced discs, and notched samples, respectively.

This study aims to characterize the cracking in asphalt concrete of differing air void ratio and moisture condition. Therefore, six samples for each mix were prepared with varying void ratios and moisture condition. Two samples are prepared at a low air void ratio (≤ 4% air voids), two samples at a medium air void ratio (4% ≤ air voids ≤ 7%) and two samples at a high air void ratio (≥7% air voids) (ASTM D 2726 1996). One sample for each void ratio range is subjected to moisture conditioning by standard method AASHTO T-283 and one sample is kept dry and undamaged by moisture (AASHTO T 283 2002).

5 LABORATORY TESTING

The loading configuration for the notched sample is shown in Figure 3. It can be seen that four LVDTs are mounted 0.75 in. (19.05 mm) above one another beginning at the notch tip in order to measure horizontal displacement at different locations on the sample. Because

the horizontal displacement tended to diminish toward the upper portion of the sample the LVDTs are ordered in decreasing range from the bottom edge of the sample to the top loading point. The ranges of the LVDTs are 0.25 in. (6.35 mm), 0.1 in. (2.54 mm), 0.1 in., and 0.005 in. (0.127 mm), respectively.

The sample is loaded vertically at a constant strain rate of 0.01 in/min (0.254 mm/min). This loading rate is determined based on trials at different rates. It is found that a rate of 0.01 in/min is optimal in inhibiting cracking at the supports while inducing cracking at the notch tip. The LVDTs are mounted using epoxy and connected to the Labview Data Acquisition (DAQ) system. The LVDTs are mounted around a narrow region above the notch point so as to detect only the strain and crack opening displacement directly associated with crack initiation and propagation. The wet samples are allowed to surface dry to promote sufficient adhesion to the LVDT mounting blocks. Samples are loaded until the sample shows a finite crack or fracture.

6 LABORATORY PARAMETERS

Figure 4 is the load versus horizontal displacement data for four LVDTs for a sample of mix SP-B. The load versus horizontal displacement curve in Figure 4 is divided into two portions: the crack initiation phase and the crack propagation phase. The portion of the loading curve beginning at the onset of loading up to the crack initiation point is the crack initiation phase of the cracking process. In this phase micro cracks and micro voids are formed without reduction in loading. The crack becomes visible at the crack initiation load (P_{int}), which is defined as the crack initiation point. This value is determined by laboratory observation. Any increase in the horizontal displacement after crack initiation is considered actual crack width, or crack opening displacement. The sample continues to sustain increasing load as the crack propagates through the sample. The sample attains ultimate load (P_{ult}) at maximum point of the load versus displacement curve. After which, the load starts to decrease as the COD increases. A finite crack is visible in all samples when LVDT 4 measures a COD value of 0.035 in. after the COD value at ultimate load. In this study fracture is defined when

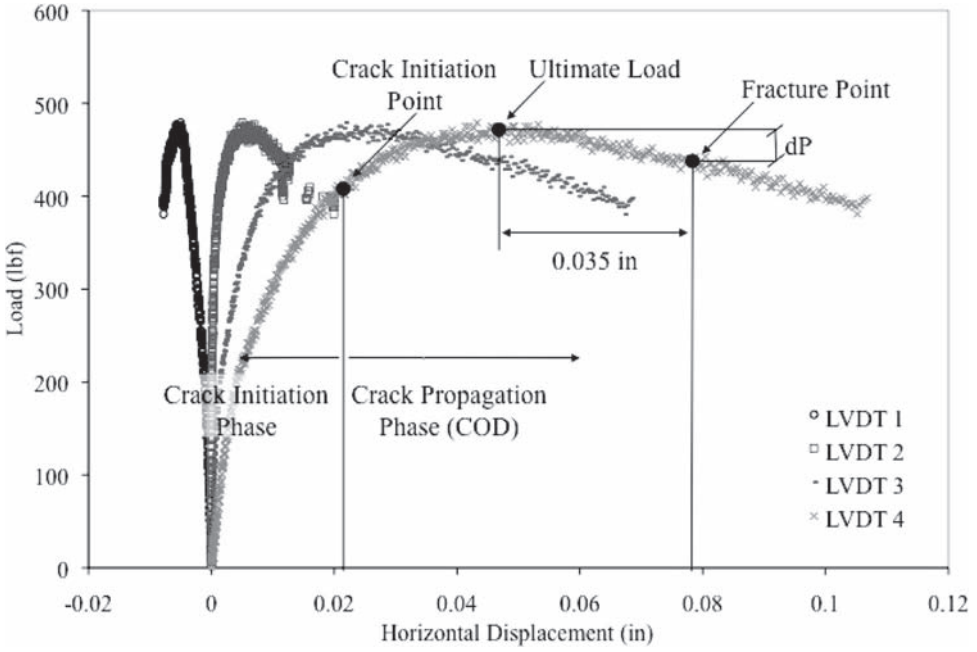

Figure 4. Load versus horizontal displacement data for three samples of SP-B.

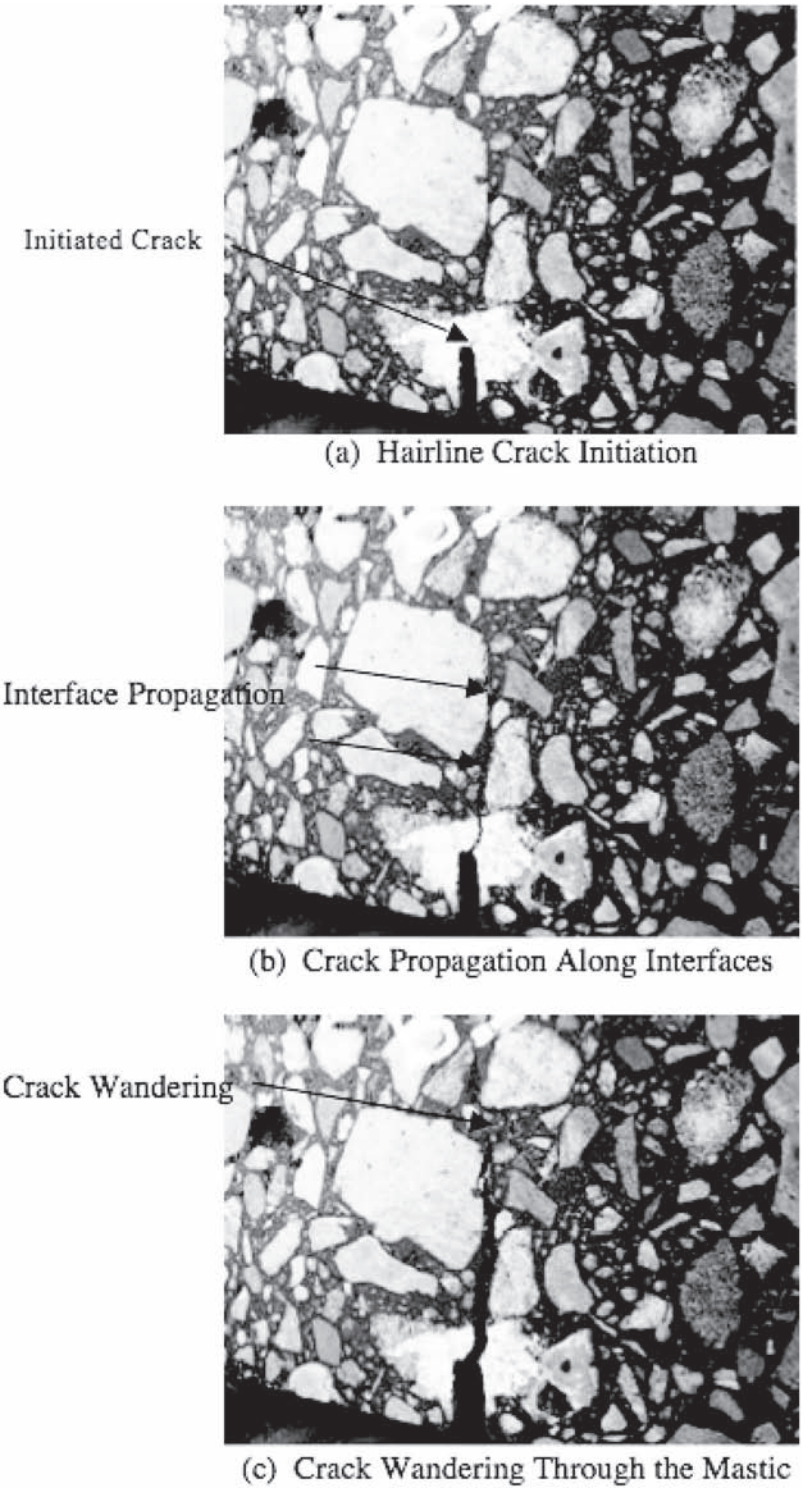

Figure 5. Crack propagation stills from video footage of testing.

the COD value reaches 0.035 in. past the COD at ultimate load. From laboratory observation, the authors discovered that in some of the samples, if testing continued 0.035 in beyond COD_{ult} several cracks occur in the sample. This makes it extremely difficult to capture the middle crack width, which is the main objective of this study.

While Pint can be used as a measure of crack initiation and Pult indicates the overall strength of the sample, the difference between the ultimate load and the crack initiation load (P_{ult}–P_{int}) is used to characterize a sample's resistance to failure to cracking. For example, a sample that can withstand 50 lbf additional load after crack initiation as opposed to 20 lbf additional load has a higher strength in the presence of cracking.

Two parameters are used to characterize propagation: the crack velocity (v) and the slope of the crack propagation curve (θ). The crack velocity is defined in a later section of this paper. The slope of the crack propagation curve (θ), is the change in load for a COD value of 0.035 in. past the COD at ultimate load. In summary, one parameter (P_{int}) is used to characterize crack initiation, one parameter (P_{ult}) is used to characterize a sample's strength, and two parameters (θ and v) are used to characterize crack propagation while varying mix type and moisture condition.

7 CRACK PATH IN ASPHALT CONCRETE

Figure 5 shows a typical crack propagation path as observed in the laboratory. Crack propagation is shown in Figure 5 by use of three still shots from a video taken during testing of a mix SP-B sample. In Figure 5(a), the crack initiates at the notch tip. The chalk around the notch tip helps to make this crack initiation more visible so as to accurately note the time and load of crack initiation by a single test operator. Figure 5(b) shows the common occurrence of crack propagation along aggregate-mastic interfaces. In addition, Figure 5(b) shows that one aggregate-mastic interface becomes less preferable for crack propagation, the crack path will transfer quickly to another interface. Abrupt transfer of a crack between aggregate-mastic interfaces demonstrates the crack's preference for propagation along an interface. In Figure 5(c), the crack is shown to propagate in a staggered path due to the lack of a conveniently located interface. This crack wandering shows that cracking in the mastic occurs without a defined pathway.

8 DETERMINATION OF CRACK VELOCITY

Figure 6 shows three different regions along the crack propagation path: the compression region, the tensile deformation region, and the crack widening region. The compression region in the sample denotes locations where the LVDT has recorded negative horizontal displacement values. The tensile deformation region in the sample is located where no crack is present (below the horizontal line where COD = 0.015 in. but positive values are recorded by the LVDTs. The crack widening region is above the horizontal line passing through the COD at the crack initiation point. From Figure 6, it is evident that there is not linear relationship between crack widening and crack growth. Crack velocity is calculated using COD and time data. In this section, the method of determining crack velocity is described. In Figure 6, half of the horizontal displacement is

plotted as a function of distance from the notch tip. Each line is plotted using four data points, one from each LVDT at a given time. Each line represents a different time at an interval 20-seconds. The total time of crack propagation (220 seconds) is spanned by 20-second intervals.

Crack velocity is defined as the crack length (Δl) divided by the time elapsed from crack initiation ($l = 0$) to a certain crack length (l_t). As a first step, half of the COD value at LVDT 4 at the crack initiation point is determined. So, when this horizontal value is measured by LVDT 3, the crack is considered to have traveled the length (Δl) from LVDT 4 to LVDT 3. In Figure 6, a horizontal line is drawn through the horizontal displacement value (0.015 in.) at LVDT 4 corresponding to crack initiation, COD = 0 in. The intersection of this horizontal line with any one of the other lines is considered as the location of the crack tip at that time

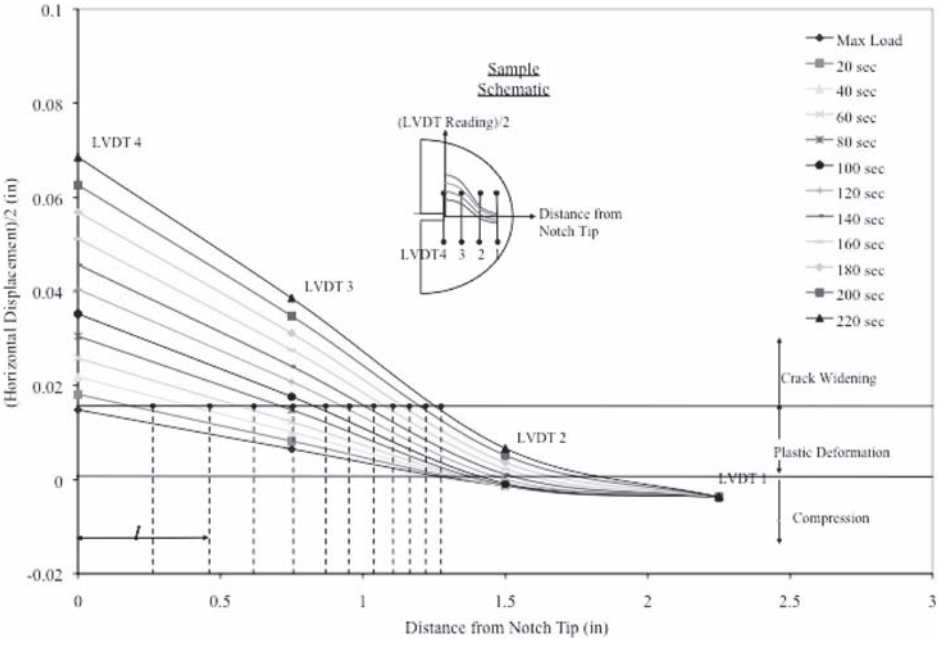

Figure 6. LVDT reading vs. distance from notch tip at 20 sec intervals.

interval. The horizontal distance of such intersection points are noted as the distance from the notch tip or the distance traveled by the crack. Crack velocity is determined from this distance at different time intervals.

The vertical dotted lines are plotted in Figure 6 to show the progressive distance traveled by the crack tip at equal time intervals. It is clear from the decreasing spacing between the dotted lines that as the crack travels from the notch tip to the top of the sample the velocity of the crack decreases. The crack velocity is examined in this study in the form of instantaneous crack velocity. The instantaneous crack velocity is calculated by dividing the distance the crack travels during a twenty second interval by twenty seconds.

In the following section the effect of varying mix type, air void ratio, and moisture condition are evaluated using the above defined parameters.

9 RESULTS AND DISCUSSION

9.1 *Effect of air voids on P_{ult}, P_{int}, and v*

Figures 7(a) and 7(b) are scatter plots of the ultimate load (P_{ult}) and the crack initiation load (P_{int}) versus air voids for each sample tested in this study. A second order trend line is fit to the data in each plot. The equation for the trend line and the coefficient of variation is displayed on each plot. Similar plots can be made for the only the wet and dry samples respectively for the ultimate load and the crack initiation load. The equations for the trend lines and the R^2 values for these plots are listed in Table 1. The coefficient of variation (R^2), is significantly less than unity for each plot, although the R^2 for the wet samples only is near 0.5 for both P_{ult} *and* P_{utl}. Even though 0.5 is not indicative of a clear relationship the consistently larger R^2 value for wet samples hints at that air void ratio is more influential on the ultimate load and crack initiation load than on dry samples.

Figure 8(a) shows the crack velocity versus the crack length in mix SP-B for three dry samples of varying void ratio and three wet samples of varying void ratio. It can be seen from the plot in that the samples of low and medium air void ratios show similar trends in crack velocity. The velocity starts highest at an initial value of about 3.25 in/min for the wet samples

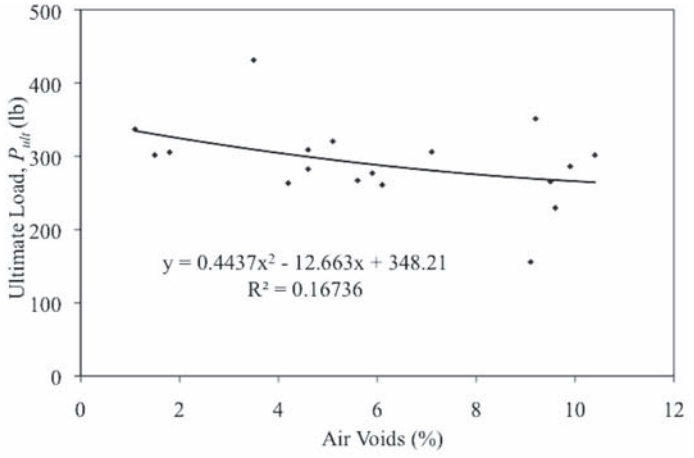

(a) Ultimate load vs. percent air voids

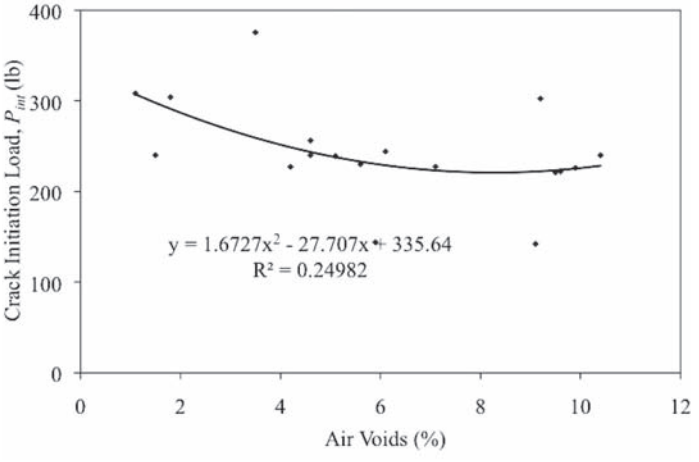

(b) Crack initiation load vs. percent air voids

Figure 7. Ultimate load and crack initiation load versus air void percentage.

Table 1. Cracking and loading parameters for each sample.

Sample	Ultimate Load, P_{ult}	Crack Initiation Load, P_{int}
Wet and Dry	$y = 0.4437x^2 - 12.663x + 348.21$	$y = 1.6727x^2 - 27.707x + 335.64$
	$R^2 = 0.1674$	$R^2 = 0.2498$
Dry	$y = 0.2967x^2 - 6.7651x + 306.62$	$y = 0.0679x^2 - 5.2799x + 271.71$
	$R^2 = 0.1146$	$R^2 = 0.1516$
Wet	$y = 3.8656x^2 - 55.134x + 453.41$	$y = 1.264x^2 - 30.332x + 354.54$
	$R^2 = 0.4717$	$R^2 = 0.4823$

and about 5.25 in/min for the dry samples, and then decreases at similar slope until the end of the test. The samples with the highest void ratio exhibit higher initial crack velocity. The crack velocity in the high air voids samples appears to be most erratic. It is possible that the increased amount of air voids in a sample leads to an increase in crack velocity by providing a crack pathway that requires less actual fracture of material.

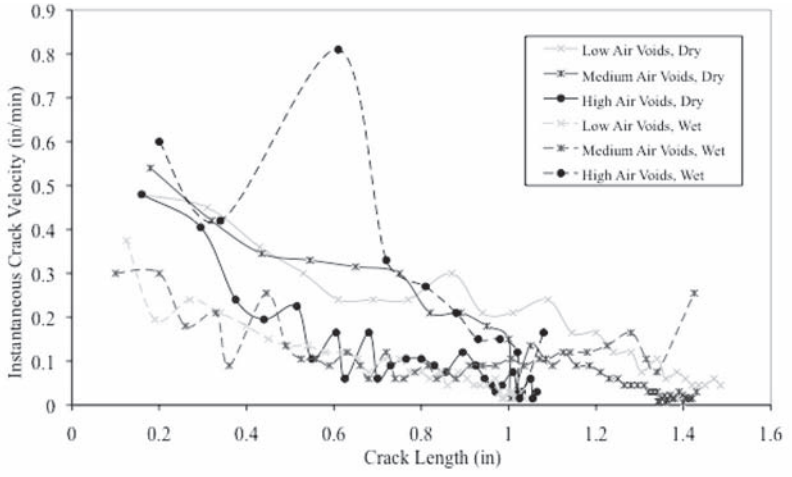

(a) Effect of air voids on crack velocity

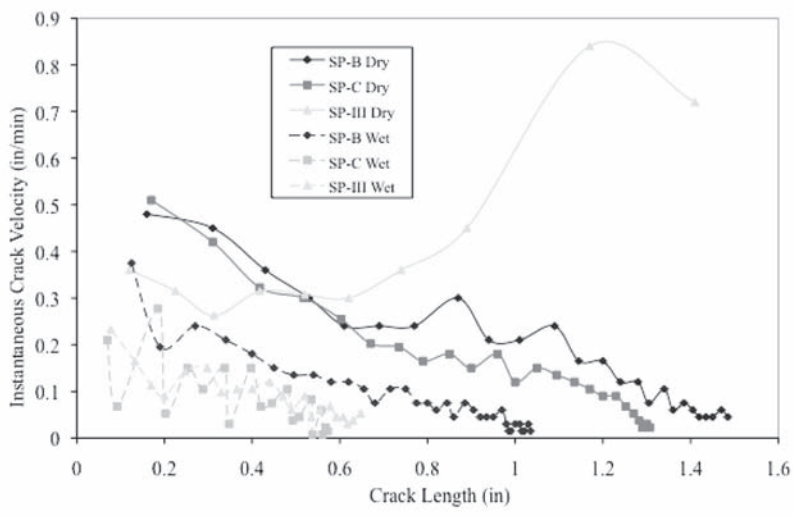

(b) Effect of mix type on crack velocity

Figure 8. Crack velocity versus crack length.

It can be seen clearly in both Figures 8(a) and 8(b) that wet samples generally exhibit slower cracks. The moisture damage process softens a sample, creating more ductility that allows for greater amounts of bending before fracture.

9.2 *Effect of moisture on COD_{ult}, P_{ult}, P_{int}, and v*

Figure 9 is a bar chart that shows the average crack opening displacement at ultimate load for all dry and wet samples of each mix type evaluated in this study. The COD at ultimate load (COD_{ult}) is an indication of the amount of cracking necessary to induce failure in a sample. Figure 9 indicates that, in general, wet samples experience higher COD at ultimate load than dry samples. The average COD for the dry samples of all mix types is 0.021 in. and the average COD for the wet samples of all mix types is 0.035 in. So, the moisture damage process facilitates the widening of cracks up to the point of ultimate load.

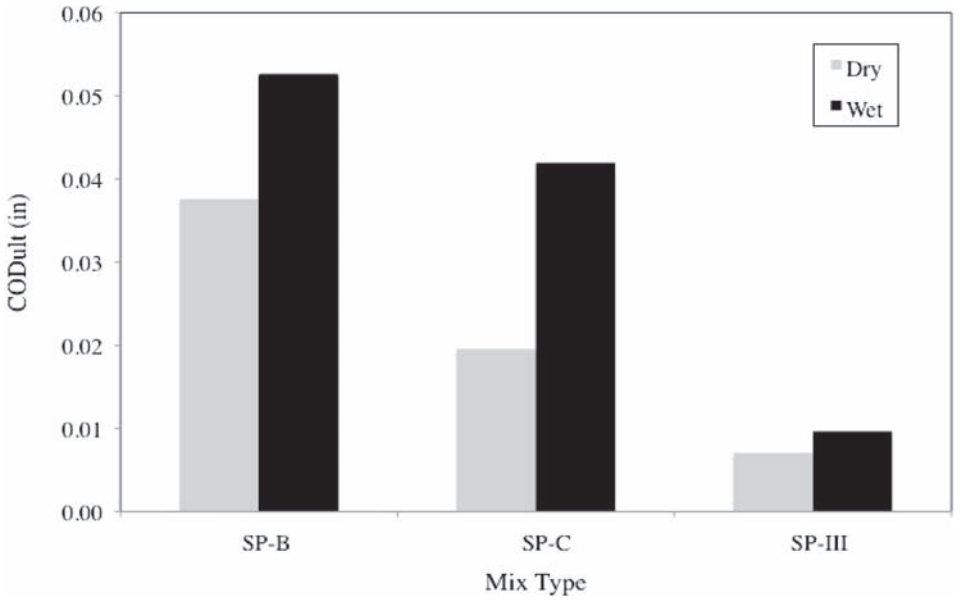

Figure 9. Crack opening displacement at ultimate load for dry and wet samples of each mix.

Figures 10(a) and 10(b) show the average ultimate load and average crack initiation load for wet and dry samples of each mix type. Figure 10(a) shows that the crack initiation load for dry samples in mixes SP-B and SP-C, while the crack initiation load in mix SP-III is higher for wet samples. This trend indicates that dry samples will take more load before crack initiation. This is expected since moisture is known to damage asphalt concrete. From Figure 10(b), the ultimate load for the wet samples is higher than or comparable to the ultimate load for dry samples.

The average of the ultimate load for the wet samples is 302 lb, while the ultimate load for the dry samples is 282 lb. The moisture damage in asphalt concrete results in increased ductility. The ductility in the sample allows for higher levels of strain. When the sample is strained the sample hardens as the air voids close. This effect is known as strain hardening.

Table 2 has a list of values for the difference between the ultimate load and the crack initiation load (P_{ult}–P_{int}). It can be seen from these load difference values that the values for wet samples are consistently higher than those for the dry samples. This trend indicates that after cracks have initiated in asphalt concrete, wet samples will withstand failure better than dry samples. This could be because wet samples are less brittle than dry samples.

9.3 *Effect of Gradation on P_{int}, P_{ult}, v, and θ*

Figures 10(a) and 10(b) show the average P_{int} and P_{ult} for wet and dry samples of each mix type. For the average crack initiation load, it can be seen in Figure 10(a) that mix SP-III generally has the highest average crack initiation load while mixes SP-B and SP-B. Distinct differences between mix SP-III from mixes SP-B and SP-C are the stiffer binder contained in mix SP-III and the high percentage of coarse aggregate. Any of these two mix characteristics could be contributing to the observed trend.

Now consider the average ultimate load for each mix type in figure 10(b). There is a general trend of increasing ultimate and crack initiation load with SP-B being the lowest in load, and SP-III being the highest. This is explainable because mix SP-III is a coarse mix that is expected to withstand larger loads. Of the two finer mixes; SP-B and SP-C, SP-B contains a higher percentage of coarse aggregate and therefore more interface along which a crack can continuously propagate.

Figure 8(a) shows the crack velocity for wet and dry samples of the three different mixes tested in this study. The crack velocity reveals no clear trend between aggregate gradation and

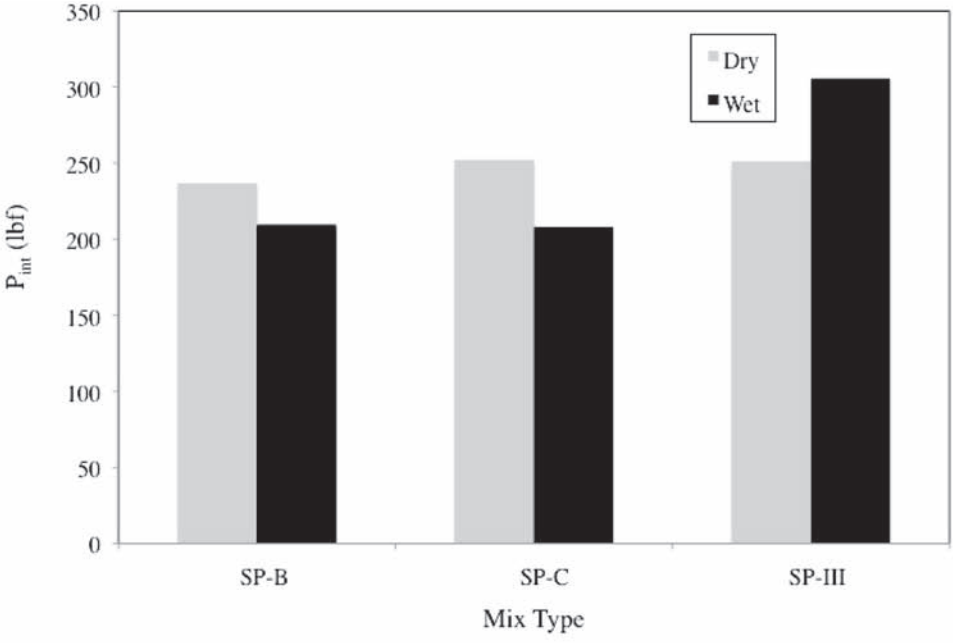

(a) Crack initiation load

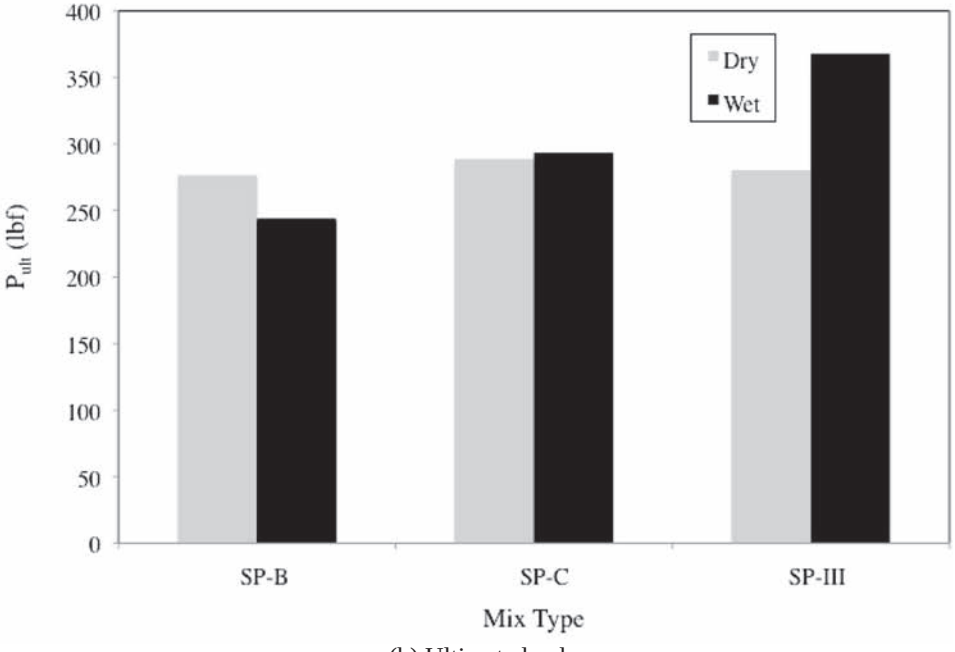

(b) Ultimate load

Figure 10. Average crack initiation and ultimate loads for dry and wet samples.

Table 2. Cracking and loading parameters for each sample.

		e	Moisture	*COD*	P_{ult} (*lbf*)	P_{init} (*lbf*)	P_{ult}–P_{int}
SP-B	e < 4	4.6	DRY	0.084	283	240	43
		4.6	WET	0.053	309	256	53
	4 < e < 7	6.1	DRY	0.012	261	244	17
		5.6	WET	0.065	267	230	37
	e > 7	9.9	DRY	0.016	286	226	60
		9.1	WET	0.040	156	142	14
SP-C	e < 4	1.1	DRY	0.017	337	308	29
		1.5	WET	0.028	302	240	61
	4 < e < 7	4.2	DRY	0.028	263	227	36
		5.9	WET	0.069	277	144	133
	e > 7	9.5	DRY	0.014	266	221	45
		10.4	WET	0.028	301	240	61
SP-III	e < 4	1.8	DRY	0.002	306	304	2
		3.5	WET	0.009	432	375	56
	4 < e < 7	7.1	DRY	0.013	306	227	79
		5.1	WET	0.009	321	239	82
	e > 7	9.6	DRY	0.007	229	222	7
		9.2	WET	0.011	351	302	49

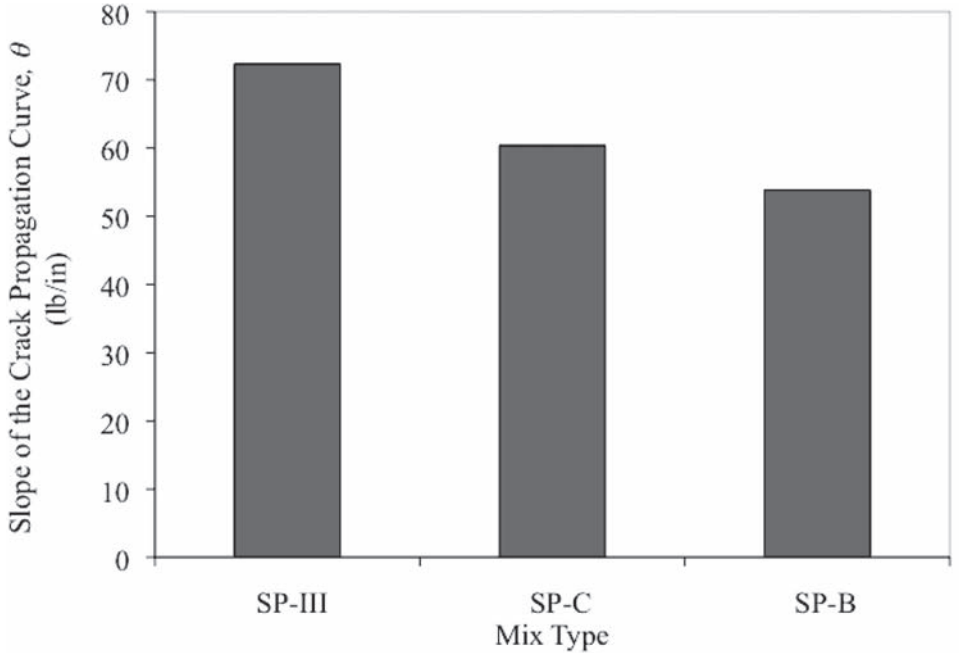

Figure 11. Average slope of the crack propagation curve for each Superpave mix type.

cracking. One might expect that crack velocity be highest in coarser samples due to interface cracking.

Figure 11 shows the average slope of the crack propagation curve for each mix type. Mix SP-III has the largest slope of the three mixes and mix SP-B has the smallest slope. The slope of the crack propagation curve (θ) is a measure of the sample's resilience to cracking damage as the crack width increases. In that respect, the coarse mix has the least resistance

to cracking damage. Preferred cracking along aggregate-mastic interfaces may indicate that the bond along the interface is weaker than that inside the mastic or aggregate. The large load decrease observed in mix SP-III can then be explained by realizing that mix SP-III is a coarse mix with large continuous interfaces along which cracks can propagate. These quasi-continuous crack path—ways facilitate extensive crack propagation and therefore high structural damage that leads to a decrease in load carrying capacity.

One might suspect that if coarse aggregate present in a mix leads to a large load decrease then mix SP-B should exhibit a larger load decrease than mix SP-C. The average value of load decrease for mix SP-C is somewhat misleading because one value is extremely high, while the remaining values are generally under 20 lb. If the outlying value for SP-C is overlooked, the average load decrease decreases to 34 lb. This hierarchy of load decrease well supports the interface cracking hypothesis.

10 CONCLUDING REMARKS

In this study, different semi-circular notched asphalt concrete samples are subjected to continuously increasing static load. The resulting crack path and crack width are captured using LVDTs as a function of time and distance from the notch. Based on the analysis of laboratory data the following conclusions are made:

- It is shown that cracks tend to propagate along aggregate-mastic interfaces.
- No clear trend in cracking due to air voids is evident based on the range of air voids included in this study.
- Cracks are wider at ultimate load in wet samples than in dry samples. Also, cracks propagate more slowly in wet samples. In addition, wet samples tend to resist failure after crack initiation better than dry samples as shown by higher P_{ult} and P_{ult}–P_{int} values.
- The coarse mix in this study failed at higher loads than the fine mixes. Mixes with more coarse aggregate allow for continuous crack propagation along aggregate-mastic interfaces, leading to steeper unloading curves after the ultimate load.
- A methodology for determining crack velocity in notched semi-circular asphalt concrete samples using LVDTs is developed.

ACKNOWLEDGEMENTS

This project is a part of the study funded by the National Science Foundation (NSF) through prestigious CAREER program. NSF grant number: 0644047 and Program: Infrastructure Materials & Structural Mechanics. Thanks to Mr. Robert Meyers, Materials Bureau Chief and Mr. Parveez Anwar, State Asphalt Engineer, of New Mexico Department of Transportation for their advice during the project.

REFERENCES

AASHTO T 283. 2002. Resistance of Compacted Asphalt Concrete to Moisture-Induced Damage *American Association of State Highway and Transportation Officials* (AASHTO), Washington D.C.

AASHTO T 312. 2000. Standard Procedure for Preparing and Determining the Density of Hot Mix Asphalt (HMA) Specimens by Means of the SHRP Gyratory Compactor. In *American Association of State Highway and Transportation Officials* (AASHTO), Washington D.C.

ASTM D-2726. 1996. Standard Test Method for Bulk Specific Gravity and Density of Non—Absorptive Compacted 1 Bituminous Mixtures. *Annual Book of ASTM Standards*, Vol. 04.03, Philadelphia, PA.

Huang, B., Shu, X., Zuo, G. 2005. Laboratory Evaluation of Semi-Circular Bending Tensile Strength Test for HMA Mixtures. In *Proceedings of the Geo-Congress 2005 Conference.*

Li, X., and Marasteanu. M. 2004. Evaluation of Low Temperature fracture Resistance of Asphalt Mixture Using the Semi-Circular Bend Test. In *Journal of the Association of Asphalt Paving Technologists*, Vol. 73: 401–426.

Li, Y. and Metcalf, J.B. 2002. Crack Initiation Model From Asphalt Slab Tests. *Journal of Materials in Civil Engineering,* Vol. 14(4): 303–310.

Molennar, A., Scarpas, A., Liu, X, and Erkens, G. 2002. Semi Circular Test; Simple but Useful. In *Journal of the Association of Asphalt Paving Technologists*, Vol. 71.

Roque, R., Birgisson, B., Sangpetngam, B., and Zhang, Z. 2001. Hot Mix Asphalt Fracture Mechanics : A Fundamental Crack Growth Law for Asphalt Mixtures. *Journal of the Association of Asphalt Paving Technologist*, Vol. 70, 816–827.

Roque, R., Zhang, Z. and Sankar, B. 1999. Determination of Crack Growth Rate Parameters of Asphalt Mixtures Using the Superpave IDT. *Journal of the Association of Asphalt Paving Technologists*, Vol. 68, 404-433.

Van de Ven, M., de Fortier Smit, A. and Krans. R. 1997. Possibilities of a Semi-Circular Bending Test. In *Proceedings of the Eighth International Conference of Asphalt Pavements*, Vol. 2: 939–950, Seattle, WA.

Zhang, Z., Roque, R. and Birgisson, B. 2001. Evaluation of Laboratory Measured Crack Growth Rate for Asphalt Mixtures, *Transportation Research Record,* 1767, 67–75.

Advanced Testing and Characterization of Bituminous Materials –
Loizos, Partl, Scarpas & Al-Qadi (eds)
© 2009 Taylor & Francis Group, London, ISBN 978-0-415-55854-9

Theoretical analysis of the 4 point bending test

M. Huurman & A.C. Pronk
Delft University of Technology Delft, The Netherlands

ABSTRACT: Practical solutions describing the behavior of a slender beam in pure bending can be found in many text books and international standards. These solutions form the basis of four point bending test analyses. The effects of overhanging beam ends, system damping and moving masses next to the weight of the beam can be included in the solution. However, beam deformation due to shear is often neglected or ignored in the procedures. Also the solutions describe a highly idealized beam in bending.

The paper deals with the analytical solution for the shear force which is of interest for calibration procedures. Next to the analytical approach (AA), finite element (FE) modeling of a more realistic bending beam is discussed.

An overview of the differences between a 3D FE simulation and the AA modeling is given and strong conclusions with respect to modeling of four point bending beams are drawn.

1 INTRODUCTION

In the structural design of (flexible) pavements the stiffness moduli of involved asphalt concrete layers play an important role. The four point bending test (4PB) is one of several methods available for stiffness determination. The 4PB is one of the few methods which have been included in the CEN standards for the characterization of stiffness and fatigue properties for pavement materials.

4PB data interpretation is based on the theoretical bending of a slender beam. The deduced formulas in this analytical approach (AA) describe a beam in nonexistent ideal equipment that fully meets all boundary requirements. Effects of extra moving masses, system damping and overhanging beam ends can be included in the analytical approach. However many physical, geometrical and mechanical aspects of the beam and the equipment cannot be described with AA modeling. This is mainly because the AA model is 1D and basically describes the behavior of a line (no cross section, no width, no height) with flexural stiffness excited by external forces or displacements. It is clear that this 1D line strongly differs from a real 3D beam. Furthermore it should be noticed that the evolution of the complex stiffness modulus, as occurring in a fatigue test cannot be taken into account.

The authors recognize the importance of the 4PB and aim for better models of this test. The interpretation of 4PB data would highly benefit from the availability of such models that need to consider the real 4PB set-up and not an idealized version. It is believed that the required models can only be obtained by utilization of some finite element (FE) tool.

Hereafter a comparison between AA and FE modeling of an idealized 4PB is discussed. The aim of the comparison is threefold.

– Prove the accuracy of FE modeling.
– Prove that boundary conditions affect beam deflection.
– Prove that shear deformation affects beam deflection.

2 THE REAL TEST

Figure 1 gives an overview of some 4PB equipments. By close observation it is noted that the equipments follow different paths trying to meet obliged boundary conditions. The machine

of the TU Delft tries to meet boundary conditions by combination of rotational bearings and rods. In the IBDIM equipment tries to meet the boundary conditions by application of both sliding and rotational bearing. The machines at DWW and Vienna try meeting boundary conditions by application of steel rods in the clamps that act as bearings.

Secondly it is noted different clamping systems exist. The upper devices have a separate rotating frame in which the beams are clamped by servo motors. The lower two devices make use of a small clamping frame glued to the beam. The clamping force is applied to this frame through steel rods that act as bearings. The total system is clamped by tightening nuts with predefined torque.

Thirdly differences in measuring the beam deflection exist. In the upper equipments measure the relative deflection by the use of a reference 'bridge' resting on the beam. The lower equipments measure absolute deflection.

Although only four 4PB set-ups have been discussed the authors believe that it is fair to say that many types of 4PB set-ups exist and that these set-ups may vary fundamentally in the way boundary conditions are met, deflections are measured and beams are clamped. The authors believe that each of the set-ups will have their own peculiarities and that they all differ from the idealized 4PB considered in the AA models applied to analyze test data.

Given the above it is highly unlikely that a single model of an idealized beam is fully suitable for describing all available 4PBs. The authors therefore believe that utilization of more realistic 4PB models will help harmonize 4PB results. Furthermore, more realistic models would make the 4PB a real research tests that can be utilized for the development of accurate fatigue damage models that incorporate stiffness degradation (Pronk 2000).

3 IDEALISED SYSTEM

3.1 *General*

The response of any structure to mechanical loading depends on the trinity GLM of: 1) Geometry (including the spatial boundary conditions), 2) Load (including the time boundary

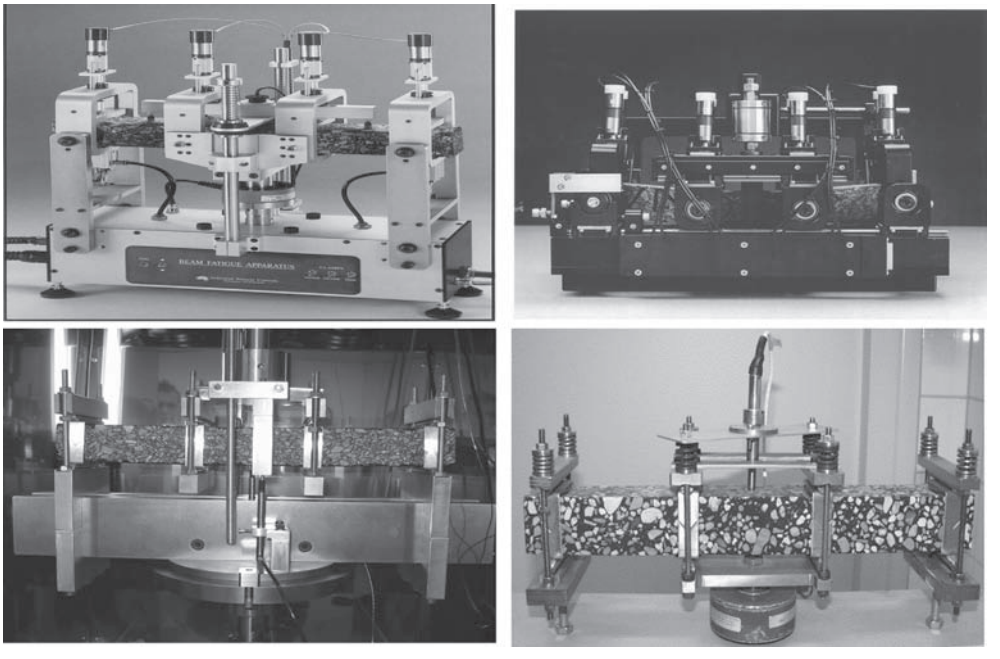

Figure 1. Pictures of existing 4PB equipments. Top row: 4PB at TU Delft & 4PB at IBDIM in Warsaw, second row: Modified "DWW" concept at University of Vienna & DWW concept.

conditions) and 3) Material. In section 2 of this paper some of these aspects with respect to existing 4PBs were discussed. In the sections hereafter the idealized 4PB is analyzed by AA and FE models.

3.2 *Geometry*

For the equipments at use at the Road & Hydraulic Engineering Institute, several Dutch consultants and the University of Vienna the following dimensions for the beam are valid. The total length L_{tot} of the beam is 450 mm. The effective length L of the system is 400 mm and the inner clamps are placed 130 mm from each. This is slightly different from the ASTM standards in which all spans should have the same lengths; in this case it would be 133.3 mm. However, the differences in deflections are very small (Pronk 1996). The width b and height h of the beam are both 50 mm. This leads to an h over L ratio of 1/8. Therefore the contribution of the shear forces to the deflection remains small and is in the order of 4%.

The spatial boundary conditions are that the bending moments and shear forces at both ends of the beam have to be zero and that no vertical displacement is possible at the outer clamps. Furthermore, all clamps should rotate freely and should be free to move horizontally. In order to obtain stability the horizontal movements of one clamp are constrained.

In the calculations discussed hereafter it is assumed that the weight of the moving inner clamps and other parts combined lead to a moving mass of 5 kg.

3.3 *Load*

In the calculations the system is loaded by 0.1 mm vertical excitement of the inner clamps. In dynamic calculations the load frequency is 10 Hz.

3.4 *Material*

In the linear elastic calculations the material has a stiffness of 3000 MPa and a Poisson's ratio of 0.35. The same values have been adopted for the viscous-elastic calculations using a phase lag of 30°. The beam is considered homogenous and isotropic with a constant (complex) stiffness modulus. The specific density of the beam was set at 2400 kg/m^3.

4 IDEALISED, STATIC LINEAR ELASTIC CALCULATIONS

4.1 *1D analytical modeling*

The analytical approach is based on the theory for bending of a slender beam. This approach is 1D, e.g. the resistance to bending is brought to a single line in space via the factor EI, see equation 1. In the analytical approach it is possible to formulate two separate differential equations for the deformation due to shear and the deformation due to pure bending (Timoshenko 1921, Timoshenko 1922, Pronk 1996). Although these equations contain many terms it is allowed to neglect the influences of most terms for the circumstances used in 4PB testing on asphalt beams. The neglect of these terms leads to equations 1 and 2 which are used in this paper.

$$E.I.\frac{\partial^4}{\partial x^4}V_b(x,t)+\rho.b.h.\frac{\partial^2}{\partial t^2}V_b(x,t)=Q(x,t) \tag{1}$$

$$G.\Psi\{b,h\}.\frac{\partial^2}{\partial x^2}V_s(x,t)=-Q(x,t) \tag{2}$$

where E = stiffness modulus [Pa]; I = bending beam moment [m^4]; x = distance along the beam [m]; ρ = beam density [kg/m^3]; b = width of beam [m]; h = height of beam [m]; t = time [s]; V_b = deflection due to pure bending [m]; Q = discrete point load distribution [N/m]; G = shear modulus [Pa]; $\Psi\{b, h\}$ = function for distorted cross section of beam during bending [m^2] and V_s = deflection due to shear force [m].

The solution follows from the development of a series of sine's (equation 3) that combined describe the beam deflection V_b in pure bending while explaining the discrete point loads Q at the supports by taking into account beam stiffness EI.

$$Q(x,t) = \frac{2F_0}{L_{tot}} \sum_{n=1}^{\infty} \left[\begin{array}{c} \left\{ \mathrm{Sin}\left((2n-1)\pi \frac{A+\Delta}{L_{tot}} \right) - \mathrm{Sin}\left((2n-1)\pi \frac{\Delta}{L_{tot}} \right) \right\} \times \\ \times \mathrm{Sin}\left((2n-1)\pi \frac{x}{L_{tot}} \right) \end{array} \right] \mathrm{Sin}(\omega t) \qquad (3)$$

where F_0 = force [N]; A = mid span between the two inner supports [m]; ω = circular frequency [rad/s]; L_{tot} = total length of the beam [m]; $\Delta = (L_{tot} - L)/2$ = overhanging beam end L = length of beam between the outer supports [m].

For the calculation of the shear deflection V_s a development in cosines is required[1]. By adopting proper solutions of the homogeneous differential equations it is possible to fulfill all boundary requirements. Detailed information on the approach and assumptions are given in reference (Pronk, 2007). The effects of moving masses (clamps and other parts of the equipment), system damping and overhanging beam ends can be included in the equations (Pronk 2002a; Pronk 2002b).

In equation 2 an "unknown" function $\Psi(b, h)$, that represents the stiffness of the beam against shear forces is present. Several expressions can be found in the literature, they all form the product of a parameter times the beam cross section surface $b.h$ (Yildirim 2005). The most common expression is the product of a constant α times $b.h$: $\psi\{b, h\} = \alpha.b.h$. In literature a value of 2/3 = 0.67 is sometimes adopted for the constant α (Uflyand 1948, Butcher, van Loon 1995). More often α is assigned a value close to 0.85, e.g. $\alpha = 5/6$ which is confirmed by FE calculations (Cowper 1966). For that reason in this project α is taken equal to 0.85.

For the static case the ratio of V_s over V_b is given by equation 4 if the mid span is equal to 1/3 of the effective beam length L.

$$\frac{V_s\{L_{tot}/2\}}{V_b\{L_{tot}/2\}} = \frac{36(1+\mu)}{23}.\alpha\left[\frac{h}{L}\right]^2 \qquad (4)$$

This ratio varies from 3 to 6% for the geometrical dimensions of beams used in practice for testing asphaltic mixes.

4.2 *Finite element method*

4.2.1 *1D modeling*

As mentioned AA models of the 4PB are 1D. The length of the beam is physically represented in such models. The width and the height of the beam are not represented and only used to determine the beam's resistance to bending and shear. This implies AA models basically exist of lines in space that do have resistance against deformation, but lack physical volume. As a result the beam material is not physically modeled and can thus not make contact with foreign objects like clamps.

Within many FE packages 1D beam elements are available that basically act according to the same theories as applied in AA models. Beam elements have no height and width, and the physical height and width of the beam are used only to determine the element's resistance to deformation (and mass when required).

[1]Of course a development into a series of sine's is also possible but will lead to a very slowly convergent series (Pronk 2007).

Two calculation sets are made on the basis of beam elements. In the first set the contribution of shear deformation is made negligible by application of a very high shear modulus $G = 9.10^9$ MPa (case 1D-G). In the second set of calculations a realistic shear modulus G of 1111,1 MPa is applied (case 1D-E). Comparison of 1D-G and 1D-E results for different h/L ratios supported the choice of 0,85 for the shear parameter α. Use is made of quadratic 3-node beam elements. In the calculations the mesh has been step wise refined.

4.2.2 *2D modeling*

In the 2D FE simulations the beam becomes more real in the sense that it now obtains its true physical height. The width of the beam is neglected by assuming a situation of plane stress, i.e. transversal stresses remain absent. A direct result of this more realistic representation is that the beam now physically needs to be grabbed in order to excite it. This of course will introduce larger stresses and strains at the locations where the beam is excited and constrained. To investigate the effects hereof two variations are taken into account.

1-point load: In these simulations the action of the outer clamps is represented by constraining the vertical movements of a single point (node) sitting on the central axis of the model. The action of the inner clamps is mimicked by enforcing prescribed vertical displacements on single nodes on the central axis of the model.

2-point load: Similar to the above the action of the clamps is now mimicked by restraining the movements of nodes at the beam upper and lower surface.

Figure 2 gives an impression of the vertical stress throughout the beam. As indicated by the figure larger vertical compressive and tensile stresses develop in the direct vicinity of the nodes that are constrained, i.e. at locations were the beam is grabbed. In the 2D simulations use is made of quadratic 8-node 2D elements.

4.2.3 *3D modeling*

In 3D FE simulations the modeled beam becomes a copy of the physical beam with a distinct length, height and width. Again the beam has to be grabbed in order to excite it. In the 3D simulation the action of the clamps is translated into prescribed vertical nodal displacements at the clamp positions. Similar to the 2D simulations this implies that larger vertical stresses are locally introduced. Figure 4 gives an indication hereof.

Figure 4 indicates that the vertical stress introduced at locations of the outer clamps is uniform over the width of the beam. At the location of the inner clamps the distribution over the width is not uniform. At these latter locations significantly smaller stresses are introduced at the edges of the beam.

The described phenomenon may be explained by effects of the Poisson's ratio in combination with a bending moment. In the longitudinal direction the bending moment lengthens the material at the top and compresses the material at the bottom of the beam. Due to the effects of the Poisson's ratio this generates the desire of the material to change the shape of its cross section. However, at location where nodes follow a prescribed vertical displacement of 0.1 mm the material is restrained to freely change the shape of its cross section. As a result hereof a non-uniform distribution of vertical stress emerges. The previous may be understood by observing figure 5 which gives a detail of the area of one of the inner clamps. Deformations are exaggerated by a factor of 4000.

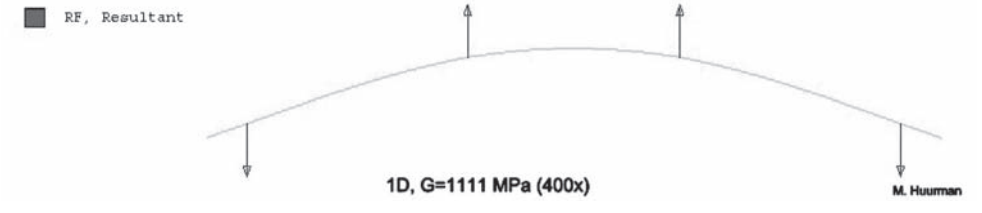

Figure 2. ABAQUS view on obtained results. Indication of model deflection and reaction forces.

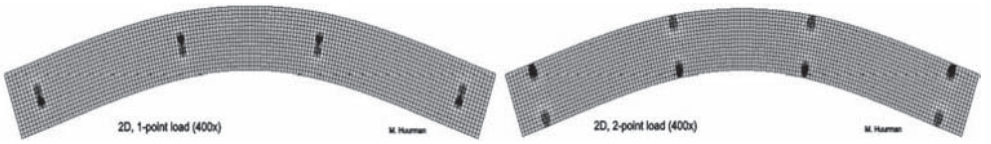

Figure 3. Indication of vertical stress. Left: 2D, 1-point load, Right: 2D, 2-point load.

The described phenomenon is also present in real beams where clamps limit the beams freedom to change cross section shape. In the 3D models use is made of quadratic 20-node brick elements.

4.3 *Conclusions*

Table 1 gives a summary of the calculations that are made. The table presents a comparison between (1D) AA calculations and various FE calculations for the total deflection and strain amplitude ε_{mid} at $L_{tot}/2$. The table furthermore gives an impression of the effects of mesh refinement.
From table 1 various conclusions can be drawn.

- The effects of mesh refinement are absent in the 1D FE calculations. From this observation it is concluded that accurate results only require a limited number of elements over the length of the beam.
- In the 2D and 3D calculations the effects of mesh refinement are limited but clearly present. These calculations all show a decrease in force with increasing mesh refinement. This is a direct result of the constraints that act on the models. By constraining individual points infinite high stresses would be introduced in the real world. Such infinite high stresses cannot develop in the FE model since nodal forces are spread over an area that is dependent on the element size. Due to this the constraints very locally lead to higher stresses with increasing mesh refinement. This effectively reduces the stiffness of the system resulting in a decrease in required force with increasing mesh refinement.
- Given the previous it is concluded that the 4PB test may well be modeled by application of 56 quadratic elements over the length of the beam. Application of more elements will not lead to better results especially in the case where a more realistic representation of the clamps will lead to a more representative introduction of stress due to beam constraints.
- The differences between AA and FE modeling remains very limited, compare calculations 1D-G and 1D-E.
- Physical clamping of the idealized beam in the 2D and 3D cases introduces differences compared to the 1D case that may add-up to almost 1%.
- It is shown that deformations introduced by shear reduce the force required for obtaining a deflection ($V_b + V_s$) of 0.1 mm at the inner clamps with 6.6 N, i.e. 4.3%.

5 IDEALISED, DYNAMIC LINEAR ELASTIC

In the calculations discussed in this chapter the beam is excited with a frequency of 10 Hz as prescribed in the European test standards for stiffness measurements of bituminous mixtures.

5.1 *Analytical*

It is possible to include the mass of the beam, extra moving masses, system damping and overhanging beam ends in AA models. The moving masses will result in forces that act on the inner clamps similar to machine applied forces F. Therefore they are developed in the same way as the force distribution $Q\{x, t\}$. If the inertia force due to the moving mass acts at a different location on the beam it is still possible to use a slightly modified series development (Pronk 2007). The same yields for the system damping which also can be seen as a "force" (Pronk 2002b).

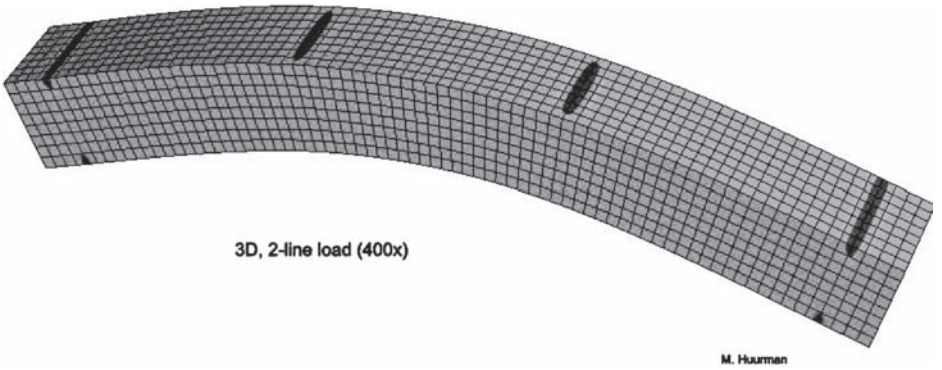

Figure 4. Indication of the vertical stress introduced at the locations of the clamps.

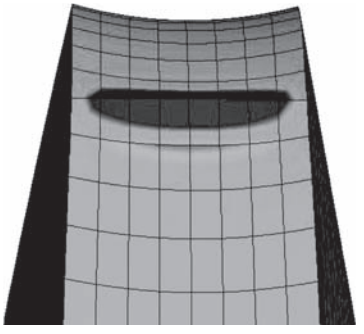

Figure 5. Detail of the clamping area modeled by nodes with prescribed displacements.

In the dynamic linear elastic AA model the beam mass (2400 kg/m^3) and the moving masses (5 kg) are considered. For comparison with FE calculations the force determined by the FE model is taken as input in the AA models.

5.2 *Finite element calculations*

The dynamic linear elastic FE calculations are performed in time domain. In these calculations the amplitude of excitement at the inner clamps is slowly increased to 0.1 mm so that the model may reach its periodic steady state in a stable manner. In the FE calculations the time step was varied. It was shown that a time step of 0.0025 s or less guaranties accurate results. In all models no less than 56 quadratic elements over the length of the beam are present. For convenience and to show the accuracy of the calculations a surplus of digits is given in the tables.

5.3 *Conclusions*

In almost all calculations the phase lag between force and deformation remained nil. In two cases a very small phase lag was observed, i.e. $\varphi < 0.02^0$. It is believed that these minor phase lags are due to numerical inaccuracy in calculation data processing.

From table 2 it is learned that the differences between FE modeling and AA modeling remains very limited, i.e. <1‰ in case 1D-G and <1.4‰ in case 1D-E. Furthermore it is shown that deformations introduced by shear reduce the force required for obtaining a deflection of 0.1 mm at the inner clamps with 6.6 N, i.e. 4.3%.

Table 2 also indicates that the difference between the 3D-2L model, which is considered the most accurate idealized representation of a real 4PB test, and other models (1D-E, 2D-1P and 2D-2P) may be as large as 1.3%.

It can also be concluded that terms which are ignored for the derivation of equations 1 and 2 can really be ignored.

Table 1. Summary of FEM & AA calculations (In 1D-G calculations only deflection V_b is present).

	FE modeling						AA modeling		
	Elements in length [–]	Elements in b & h [–]	F [N]	$V_b + V_s$ surface [mm]	$V_b + V_s$ centre [mm]	ε_{mid} [μm/m]	F [N]	$V_b + V_s$ centre [mm]	ε_{mid} [μm/m]
1D-G	28	–	155.88	–	0.11423	168.39	155.88	0.11423	168.35
1D-G	56	–	155.88	–	0.11423	168.39			
1D-G	113	–	155.88	–	0.11423	168.34			
1D-G	149	–	155.88	–	0.11423	168.39			
1D-E	28	–	149.23	–	0.11362	161.16	149.23	0.11361	161.17
1D-E	56	–	149.23	–	0.11362	161.16			
1D-E	113	–	149.23	–	0.11362	161.18			
1D-E	149	–	149.23	–	0.11362	161.21			
2D-1P	28	4	148.00	0.11258	0.11328	159.84	These calculations cannot be made by AA modeling		
2D-1P	56	6	147.81	0.11250	0.11319	159.63			
2D-1P	113	12	147.52	0.11237	0.11307	159.32			
2D-1P	149	16	147.40	0.11233	0.11302	159.19			
2D-2P	28	4	149.83	0.11336	0.11406	161.79	These calculations cannot be made by AA modeling		
2D-2P	56	6	149.61	0.11326	0.11396	161.58			
2D-2P	113	12	149.28	0.11312	0.11382	161.22			
2D-2P	149	16	149.14	0.11306	0.11377	161.08			
3D-2L	28	4	150.15	0.11318	0.11389	162.13	These calculations cannot be made by AA modeling		
3D-2L	56	6	149.92	0.11309	0.11380	161.90			
3D-2L	76	8	149.78	0.11303	0.11374	161.75			

case 1D-G = 1D FE model with very high shear modulus G, i.e. no shear deformation;
case 1D-E = 1D FE model with real and finite shear modulus G;
case 2D-1P = 2D FE model with excited /restrained nodes on beam centre line;
case 2D-2P = 2D FE model with excited /restrained nodes on beam top and bottom surface;
case 3D-2L = 3D FE model with excited /restrained nodes on beam top and bottom surface.

Table 2. Summary of dynamic linear elastic calculations.

	FE modeling				AA modeling		
	$V_b + V_s$ clamps [mm]	$V_b + V_s$ centre [mm]	ε_{mid} [μm/m]	F [N]	$V_b + V_s$ clamps [mm]	$V_b + V_s$ centre [mm]	ε_{mid} [μm/m]
1D-G	0.100	0.11405	168.118	154.9938	0.099927	0.11411	167.943
1D-E	0.100	0.11345	160.976	148.3594	0.099877	0.11349	160.755
2D-1P	0.100	0.11233	159.425	146.9611	These calculations cannot be made by AA modeling		
2D-2P	0.100	0.11309	161.363	148.7505			
3D-2L	0.100	0.11309	161.678	148.8788			

6 IDEALSED, DYNAMIC LINEAR VISCO-ELASTIC

In the calculations discussed in this chapter the beam is excited at a frequency of 10 Hz as prescribed in the European test standards for stiffness measurements of bituminous mixtures.

6.1 *Analytic*

The difference in the analytical approach compared to the calculations discussed in paragraph 5.1 is the viscous elastic stiffness modulus for the beam, complex modulus of 3000 MPa and a 30° phase lag. Although it is possible to take a separate viscous elastic character for the Poisson ratio but this is not done in this project.

6.2 *Finite element calculations*

It is not possible to define a visco-elastic 1D FE calculation, therefore only the cases 2D-1P, 2D-2P and 3D-2L are discussed. In these simulations the Prony series model was applied for representing the visco-elastic behavior of the beam. Parameters were chosen such that the material has a complex stiffness of 3 GPa and a 30° phase lag at a frequency of 10 Hz. The constitutive equation is described by the relaxation modulus (equation 5):

$$S_{mix}(t) = 3825.6\ \text{MPa} * \left(1 - 0.8 * \left(1 - e^{\left(- \frac{t}{0.0194483} \right)} \right) \right) \tag{5}$$

In all cases the beam was modeled by at least 56 quadratic elements over the length. The time step was 0.0025 and the amplitude of excitement was again slowly increased.

6.3 *Conclusions*

Table 3 summarizes the dynamic visco-elastic calculations. From the table it is concluded that both AA and FE modeling indicate that the system phase lag is larger than the material phase lag. This is due to the effects of moving masses. However, differences between the two approaches clearly exist.

It is further more observed that differences between beam deformation (U_{clamps}, U_{mid} and e_{mid}) explained by AA modeling and FE modeling remain limited <1.1%. These differences do not so much follow from differences in the type of analysis but depend much more in differences in the represented physical reality (2D-1P, 2D-2P and 3D-2L modeling versus 1D-E modeling). Overall the comparison between FE modeling and AA modeling is good.

Table 3. Summary of dynamic linear visco elastic calculations.

	FE modeling					AA modeling			
	$V_b + V_s$ clamps [mm]	$V_b + V_s$ centre [mm]	ε_{mid} [μm/m]	φ [°]	F[N]	$V_b + V_s$ clamps [mm]	$V_b + V_s$ centre [mm]	ε_{mid} [μm/m]	φ [°]
1D-E	These calculations cannot be made by FE modeling				147.07646	0.098949	0.112436	159.2569	30.137
1D-E					148.86620	0.100154	0.113804	161.1949	30.137
1D-E					149.04206	0.100272	0.113939	161.3853	30.137
2D-1P	0.100	0.112328	159.424296	30.046	147.07646	These calculations cannot be made by AA modeling			
2D-2P	0.100	0.113087	161.362134	30.045	148.86620				
3D-2L	0.100	0.113094	161.677530	30.095	149.04206				

7 BACK CALCULATION OF 3D FINITE ELEMENT CALCULATIONS

The 4PB test is primarily used for the determination of the (complex) stiffness modulus of a material. The test procedure is based on applying a pre-set sinusoidal force at a pre-set frequency and measuring the deflection at a certain point and the phase lag between the force signal and the deflection signal. The back calculation procedure of the stiffness is based on a (modified) first order approximation of the analytical solution (first term of an infinite fast decreasing series) for the deflection due to pure bending. It should be noted that in all standards (known to the authors) the effect of the shear deflection is ignored.

The previous has shown that shear deformation reduces the system stiffness. Neglecting shear deformation thus leads to a reduction of measured beam stiffness. On the basis of the discussed calculations it is concluded that this leads to a back calculated S_{mix} of 2.89 GPa instead of 3 GPa. The same is true for the determination of the strain. The procedure for the calculation of this parameter is based on a geometrical relationship with the deflection V_b due to pure bending. However, in practice the sum of the deflection due to bending and shear is measured. Ignoring the shear deflection Vs will lead to an overestimation of around 7 μm/m for the examples in this paper and represents an systematic error of 7/161 = 4.3%. A final remark should be made on the (modified) first order approximation used in the back calculation procedures. The obtained back calculated values are very close to the actual values as long as the applied frequency is much lesser than the (first) Eigen frequency of the 4PB device. This is true for most devices of which the first resonance frequency is above 100 Hz. However, when beams are tested which are much heavier (dimensions 600 * 100 * 100 mm^3) the Eigen frequency will drop.

8 FUTURE WORK

The calculations indicate that the need of grabbing (clamping) the beam introduces extra system stiffness. This is a result of the local lack of freedom for the beam to change its cross section shape. By use of the calculations the magnitude of the introduce error is estimated to be 0.45%.

It is noted that this error due to an increase in system stiffness is valid for the idealized beam that fully complies to boundary conditions. It should be clear that the introduction of additional stiffness in real 4PB's can only be larger, see figure 1. As an example it is stated that the effects of real clamps with some finite dimensions will be larger than the effects of prescribing nodal displacements over a row of nodes. Also is should be clear that none of the 4PBs in figure 1 will fully comply with obliged boundary conditions. Again this can only introduce additional system stiffness.

For further investigation into 4PB behavior and also to serve as a basis for research into damage development the authors, given time, plan to proceed with 3D modeling of existing 4PB equipment. Figure 6 gives an example of some preliminary work done by the authors.

9 CONCLUSIONS

1. Neglecting the deflection due to shear will result in introduction of an error of 3–6% in the back calculated strains and stiffness moduli.
2. For practical purposes all discussed models are very suitable. It is strongly advised to take shear deformation into account.
3. According to the FE calculations the coefficient α for the deformation of the cross section of the beam will be approximately 0.85. This value is in accordance with values like 5/6 = 0.833 found in literature. The sometimes used value of 2/3 = 0.667 is not in line with calculations.
4. It is clearly shown that only 1D FE calculations are fully equal to AA calculations as used in the standard.
5. In the more realistic 2D and 3D FE simulations the beam has to be grabbed to deflect it. This introduces stress concentrations near the supports.
6. 3D FE simulations indicate that some system stiffness is introduced by clamping the beam. The effects hereof in an idealized situation remain limited, approximately 0.45%.

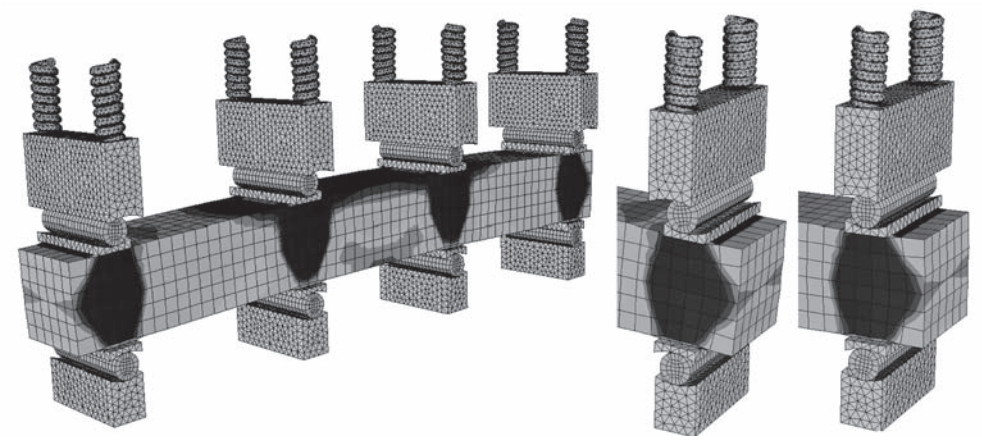

Figure 6. Left: overview of preliminary model of beam clamped in real set-up. Right: detail of movement in clamping system with steel rods, which introduce a minor moment.

7. Fundamental differences in complying with boundary conditions, beam clamping and measuring deflections, are observed between existing 4PB equipment.
8. Since no real 4PB tests complies with the idealized situation the additional system stiffness introduced by a real set-up can only be larger than 0.45% and differ from machine to machine. Realistic modeling of 4PBs may thus help harmonizing available equipment.

REFERENCES

Butcher M, van Loon H. 1995. Materials Technology Research and Development Program: Fatigue Characteristics of Local Asphalt Materials, Department of Transport, MTRD Report no. 17-1.

Cowper G.R. 1966, The shear coefficient in Timoshenko's beam theory, *Journal of Applied Mechanics* 33: 335–340.

Pronk, A.C. 1996. Theory of the four point dynamic bending test Part I: General Theory, P-DWW-96-008, Delft.

Pronk, A.C. 2000. Partial healing model - Curve fitting, W-DWW-2000-047,Delft.

Pronk, A.C. 2002a. Theory of the four point dynamic bending test Part II: Influences of 1. Overhanging beam ends & 2. Extra moving masses, DWW-2002-083, Delft.

Pronk, A.C. 2002b. Theory of the four point dynamic bending test Part III: Influences of system losses, DWW-2002-084, Delft.

Pronk, A.C. 2007. Theory of the four point dynamic bending test Part IV: Pure bending & Shear deformation, Proc. 1st European 4PB workshop, Delft.

Timoshenko, S.P. 1921. On the correction for shear of the differential equation for transverse vibration of prismatic bars, *Philosophical Magazine* 41: 744–746.

Timoshenko, S.P. 1922. On the transverse vibration of bars of uniform cross section, Philosophical Magazine 43: 121–131.

Uflyand Y.S. 1948. The propagation of waves in the transverse vibrations of bars and plates, Prikladnaia Mathematika Mekhanica 12: 287–300.

Yildirim, V. 2005. Vibration behaviour of composite beams with rectangular sections considering the different shear correction factors, Vibration Problems ICOVP: 531–536.

Advanced Testing and Characterization of Bituminous Materials –
Loizos, Partl, Scarpas & Al-Qadi (eds)
© 2009 Taylor & Francis Group, London, ISBN 978-0-415-55854-9

Investigation of the PH model as a prediction tool in fatigue bending tests with rest periods

A.C. Pronk
Delft University of Technology, Delft, The Netherlands

A. Cocurullo
University of Bologna, Bologna, Italy

ABSTRACT: The PH model (Partial Healing) is an excellent tool for describing the evolution of the complex stiffness modulus (modulus and phase lag) in continuous Four Point Bending tests (4PB). Parameters of the model obtained from 4PB tests can even be used in the prediction of the evolution of the complex stiffness modulus in uni-axial push-pull tests (Pronk 2005). Based on the parameters obtained from continuous fatigue tests in controlled deflection mode, predictions are made for the evolution of the complex stiffness modulus in bending tests with rest periods. The load—rest period was 40,000 (39,280)–400,000 (392,800) cycles at a frequency of 5 Hz. The strain amplitude was around 160 micro strains. After each load period and before the next load period started, the (beam) stiffness was also measured acoustically with an ultrasonic device. Although the ratio of rest and load period is rather high and after each load period the stiffness modulus recovered a bit, hardly any elongation in the life time was noticed. This was in accordance with the prediction using the PH model of which the parameters were based on fitting the first two load periods. The predictions based on a fit of the continuous fatigue tests for the same mix were less good.

1 INTRODUCTION

The Partial Healing (PH) model describes the evolutions of the loss and storage modulus during a bending test with the aid of two integral equations (Pronk 2000). These integrals represent the reversible (healing) and irreversible damage increase during loading. The target of this project is the investigation of the PH model as a tool for the prediction of the evolution of the complex stiffness modulus in a 4PB discontinuous fatigue test using the parameters determined in a continuous fatigue test. If the predictions are reasonable this will be very beneficially since, due to the big test time, discontinuous tests are very expensive. Moreover the parameters for the PH model do not have to be determined using the whole continuous fatigue test till failure. One "handicap" is the conflict with the traditional definition for the fatigue life Nf,50. In the present form the PH model describes the evolution up to 60–80% of the initial stiffness modulus (Nf,50 corresponds to 50%), which correspond to the fatigue life N1 which is based on a change in the dissipated energy per cycle (Hopman 1989). In contrast with other models (Kim 1997), the PH model is in essence a material model in stead of a 'beam' model. Nevertheless it can be successfully applied for describing the evolution of the weighed stiffness modulus for the beam. This weighed stiffness modulus is back calculated from the measured deflection assuming a homogenous distribution of the material stiffness modulus throughout the whole beam (Pronk 1996a). According to the authors, implementation of the PH model in finite element simulation will give more insight in the applicability of this model and can maybe clarify or explain the large differences in the traditional fatigue lives measured in geometrical different bending equipments using the same asphalt mix. In this paper the scope is focused on the applicability of the PH model in predicting the evolution in the weighed (back calculated) stiffness modulus in discontinuous fatigue tests.

2 THEORY

2.1 *General*

The PH model describes the evolution of the complex stiffness modulus (loss and storage modulus) due to reversible and irreversible damages in a fatigue (bending) test. Because these damages are unknown it is proposed that they are related to the dissipated energy per cycle which is a reasonable assumption (Pronk 1990). The PH model is based on two equations:

$$\text{Loss modulus } S_{mix}\,\text{Sin}(\varphi) = F\{t\} = F_0 - \int_0^t \left[F\{\tau\}(\alpha_1 e^{-\beta(t-\tau)} + \gamma_1) \right] d\tau \tag{1}$$

$$\text{Storage modulus } S_{mix}\,\text{Cos}(\varphi) = G\{t\} = G_0 - \int_0^t \left[F\{\tau\}(\alpha_2 e^{-\beta(t-\tau)} + \gamma_2) \right] d\tau \tag{2}$$

The parameters α_1, α_2, γ_1, γ_2 and β are the products of material constants times the squared occurring strain (ε^2). The values α and γ depend also on the applied frequency.

It should be marked that although the function $F\{\tau\}$ under the integral is in the formulation equal to the loss modulus, it is related (based on) to the dissipated energy per cycle (Pronk 2001, Pronk 2005). The solutions of these two equations are given by equations 3 and 4:

$$F\{t\} = F_0\, e^{-Bt}[\text{Cos}h\{Ct\} + D\text{Sin}h\{Ct\}] \tag{3}$$

$$G\{t\} = G_0 - F_0\left[\frac{\alpha^2}{C} e^{-Bt}\text{Sin}h\{Ct\} + \frac{\gamma_2}{\gamma_1}\left(1 - e^{-Bt}\left[\text{Cos}h\{Ct\} + E\,\text{Sin}h\{Ct\}\right]\right)\right] \tag{4}$$

where $B = \dfrac{\alpha_1 + \beta + \gamma_1}{2}$, $C = \sqrt{(B^2 - \beta\gamma_1)} \rightarrow \beta\gamma_1 = B^2 - C^2$, $D = (\beta - B)/C$ and $E = (B - \gamma_1)/C$.

2.2 *First load and rest period*

Because during a rest period no energy will be dissipated, the function $F\{\tau\}$ in the integral equals zero during the time of the rest period. When after a time t_1 no loading is applied (rest period) equation 5 is valid for the loss modulus.

$$F\{t\} = F_0 - e^{-\beta t}\int_0^{t_1} \alpha_1 F\{\tau\} e^{+\beta\tau} d\tau - \int_0^{t_1} \gamma_1 F\{\tau\}\, d\tau \tag{5}$$

The second term in the right hand of equation 5 represents the reversible damage and the third term the non recoverable (irreversible) damage P_{L1}. The index indicates the number of the load-rest period. The irreversible damage P_{L1} is given by equation 6.

$$\textit{Irreversible damage} = P_{L1} = \gamma_1 \int_0^{t_1} F\{\tau\}\, d\tau \tag{6}$$

The irreversible damage is, as expected, equal to the accumulation of the permanent damage in the load period. The reversible damage is given by equation 7.

$$\textit{Reversible damage} = \int_0^{t_1} \alpha_1 F\{\tau\} e^{-\beta(t-\tau)} d\tau = e^{-\beta(t-t_1)} \int_0^{t_1} \alpha_1 F\{\tau\} e^{-\beta(t_1-\tau)} d\tau = e^{-\beta(t-t_1)} R_{L1} \tag{7}$$

Due to the exponential time function the reversible damage at the end of the load period ($t = t_1$) will vanish in time. The evolution of the loss modulus during the rest period is described by equation 8.

$$F\{t\} = F_0 - R_{L1}\, e^{-\beta(t-t_1)} - P_{L1} \quad for \quad t \geq t_1 \tag{8}$$

Introducing the rest time $\Delta t_R = t_2 - t_1$ the loss modzulus $F\{t\}$ at $t = t_2$ when the second load period starts is given by equation 9.

$$F\{t_2\} = F_0 - R_{L1}\, e^{-\beta(t_2-t_1)} - P_{L1} = F_0 - R_{L1}\, e^{-\beta\Delta t_R} - P_{L1} \tag{9}$$

On the interval $t_1 < t < t_2$ the storage modulus is given by equation 10.

$$G\{t\} = G_0 - \int_0^{t_1} \alpha_2\, F\{\tau\}\, e^{-\beta(t-\tau)}\, d\tau - \int_0^{t_1} \gamma_2\, F\{\tau\}\, d\tau \tag{10}$$

This equation is similar to the equation for the loss modulus. Introducing the permanent damage P_{S1} and the reversible damage at the end of the load period, the following expressions (11 to 13) are obtained for the evolution of the storage modulus during the rest period and at the start of the following load period.

$$P_{S1} = \gamma_2 \int_0^{t_1} F\{\tau\} d\tau \quad \& \quad R_{L1} = \int_0^{t_1} \alpha_2 F\{\tau\}\, e^{-\beta(t_1-\tau)} d\tau \tag{11}$$

$$G\{t\} = G_0 - R_{S1}\, e^{-\beta(t-t_1)} - P_{S1} \quad for \quad t \geq t_1 \tag{12}$$

$$G\{t_2\} = G_0 - R_{S1}\, e^{-\beta(t_2-t_1)} - P_{S1} = G_0 - R_{S1}\, e^{-\beta\Delta t_R} - P_{S1} \tag{13}$$

2.3 *Solution during the second load period*

After the first rest period a second load period starts at $t = t_2$ and will end at $t = t_2 + t_1 = t_2 + \Delta t_L$. The evolutions of the loss modulus and the storage modulus are given by equations 14 and 15.

$$F\{t\} = F\{t_2\} - \int_{t_2}^{t} \left[F\{\tau\} \left(\alpha_1\, e^{-\beta(t-\tau)} + \gamma_1 \right) \right] d\tau \quad for \;\; t_2 < t < t_2 + \Delta t_L \tag{14}$$

$$G\{t\} = G\{t_2\} - \int_{t_2}^{t} \left[F\{\tau\} \left(\alpha_2\, e^{-\beta(t-\tau)} + \gamma_2 \right) \right] d\tau \quad for \;\; t_2 < t < t_2 + \Delta t_L \tag{15}$$

By moving the origin of the time scale to $t = t_2$ the same equations are obtained as for the first load period ($t^* = t - t_2$) as indicated by equations 16 and 17.

$$F\{t^*\} = F_0^* - \int_0^{t^*} \left[F\{\tau\} \left(\alpha_1\, e^{-\beta(t^*-\tau)} + \gamma_1 \right) \right] d\tau \quad for \;\; 0 < t^* < \Delta t_L (= t_1) \tag{16}$$

$$G\{t^*\} = G_0^* - \int_0^{t^*} \left[F\{\tau\} \cdot \left(\alpha_2\, e^{-\beta(t^*-\tau)} + \gamma_2 \right) \right] \cdot d\tau \quad for \;\; 0 < t^* < \Delta t_L \tag{17}$$

The only differences are the start values for the loss modulus $F\{t\}$ and the storage modulus $G\{t\}$ at the beginning of the (second) load period. Therefore the same solutions with shifted time scales can be used for all following load and rest periods.

3 MATERIALS, TEST CONDITIONS & PROCESSING DATA

The 4PB equipment at the Delft University of Technology uses a pneumatic plunger which limits the frequency range. The tests were carried out in controlled deflection mode with a frequency of 5 Hz and at room temperature (20°C). The geometrical dimension of the bending frame is according to the ASTM configuration (total span 357 mm and mid span 119 mm). The dimensions of the asphalt beams were 450 * 50 * 50 mm^3.

The mix was a Stone Asphalt Concrete (STAB) 0/22 with 4,5% bitumen on (4,3% in) according to Marshall mix design procedure. Other properties are given in table 1. The beams were sawn from slabs which were compacted according to EN-12697-35. More details are given in (vdVen 2006).

For the back calculation[1] of the stiffness modulus and phase lag the effects of extra moving masses and overhanging beam ends were not taken into account but these effects can be ignored in view of the goal of this project. Three continuous tests with a strain level of 160 micro strains were carried out. This choice was based on the results obtained in tests on different 4PB equipment (vdVen 2006).

The fatigue life N1 is determined as the number of cycles at which the ratio of the dissipated energy in cycle N and the accumulated dissipated energy deviates from a straight line as indicated in figure 1 (Hopman 1989). This point N1 is usually around 60 to 80% of the initial stiffness modulus.

Table 1. Material properties of the beams which are tested.

Plate-Beam	Test	Density EN 12697 [kg/m^3]	Air void EN [%]	Mass beam [kg]
3024-13	Continuous	2387	4.8	2.47
3025-04	Continuous	2375	5.2	2.59
3026-01	Continuous	2375	5.2	2.60
3026-02	Discontinuous	2386	4.8	2.70
3026-03	Discontinuous	2392	4.5	2.60
3026-04	Discontinuous	2386	4.8	2.62

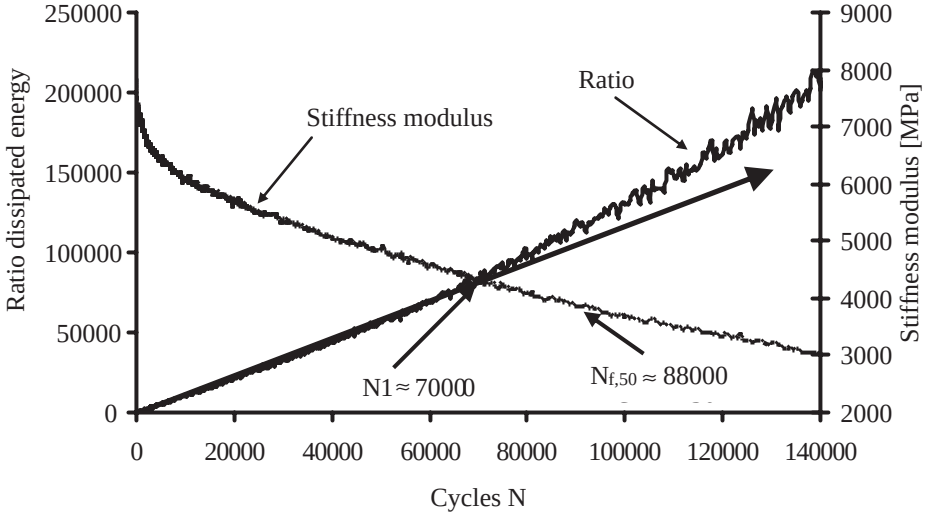

Figure 1. The complex stiffness modulus and the ratio of dissipated energy as a function of the number of cycles N for beam 3024-13.

[1]In the back calculation processing a homogenous stiffness distribution along the beam is assumed.

4 MEASUREMENTS

4.1 *Continuous tests*

The three beams were tested at room temperature (20°C). The back calculated strain during the test varied from 159 to 163 micro strains with a mean value of 161 micro strains. The fatigue lives N1 determined in the continuous tests are given in table 2.

Commonly the ratio $N1/N_{f,50}$ varies from 0.6 to 0.8. However, in these tests the range is larger, from 0.5 to 1.1.

4.2 *Discontinuous tests.*

The traditional discontinuous test used for healing experiments is build up out of one load cycle followed by M cycles in which no load is applied. To apply a pure single sinusoidal load signal is difficult and the response will also not have a pure single sinusoidal form. In practice a sequence of a 'burst' of N load cycles is applied followed by a rest period of M times N cycles. The ratio M between rest cycles and load cycles is set to 10 which is a common value used in healing experiments. The number N should of course be lower than the fatigue life N1. Due to practical circumstances N was set to 40,000 cycles. So, three discontinuous tests were carried out in which a load-rest sequence was applied of 40,000 cycles with a strain amplitude of 160 micro strain followed by a rest period of 80,000 s (= 400,000 cycles). In view of the rather long load period it was already possible to determine the parameters of the PH model in the discontinuous tests using the evolution of the stiffness modulus in the 1st load period. However, the target of this project is to use the parameters determined in the continuous tests.

4.3 *Ultrasonic tests*

Next to the 4PB measurements, the stiffness modulus in the discontinuous test was also measured using the Ultrasonic Pulse Velocity (UPV) device. The UPV device is one of the non-destructive techniques available and commonly used for the assessment of concrete structures according to the European standard (EN12504-4 2004). This test has been also performed for fatigue life and thDe healing estimation of bituminous mixtures in previous research (Abo-Qudais 2005). The measurements were carried out at the end of a load period, during the rest period and at the end of a rest period. The obtained stiffness modulus with this method is related to the stiffness behavior of the asphalt mix at high frequencies. Consequently it has been possible to relate the initial and the final stiffness modulus (4PB) evaluated for every load period to the respective dynamic modulus (UPV) determined at high frequencies. Furthermore, from the ultrasonic measurements carried out during the rest periods, it was found that the "4PB-UPV modulus" relationship might be used for assessing the stiffness behaviour of the asphalt mix also during the rest times, giving an indication of the healing in stiffness.

4.3.1 *Testing apparatus and equipment*

The apparatus consists of an electrical pulse generator, two transducers, an amplification system and an electronic timing device for measuring the travel time of ultrasonic longitudinal wave pulses. By holding the transducers in contact with the surface of the material being tested, a pulse of longitudinal vibrations is sent by the transmitting transducer

Table 2. Fatigue lives N1 for the three beams used in the continuous tests.

Plate-Beam	Test	Fatigue life N1 [kcycles]	Fatigue life $N_{f,50}$ [kcycles]
3024-13	Continuous	70	88
3025-04	Continuous	80	71
3026-01	Continuous	50	93

through the material and then, it is detected by a receiving transducer. The time interval taken for the pulse to travel from the transmitter to the receiver is defined as the travel time (or transit time).

In order to achieve adequate acoustic coupling between the material being tested and the transducers faces, a coupling medium, such as kaolin-glycerol paste has to be used.

All the measurements were performed by placing the beams on a foam rubber base support since this permitted to avoid any influence of other materials on the results.

4.3.2 *Test method*

According to the European standard (EN12504-4 2004) and according also to previous research (Abo-Qudais 2005), the direct transmission arrangement was chosen since it gives more accurate information about the propagation time. For direct transmission the path length can be considered as the distance measured from centre to centre of the transducers faces. The pulse velocity V was calculated as V = L/T [m/s] where L = path length [m] and T = travel time [s].

4.3.3 *Dynamic modulus of elasticity*

The dynamic modulus of elasticity E (UPV modulus) was determined from the UPV assessment as follows (Lavooi 1997):

$$E = v^2 Q \frac{(1+v)(1-2v)}{1-v} \tag{3}$$

where: E = "Young's modulus" [Pa], Q = density [kg/ m^3] and v = Poisson's ratio (0.35).

Table 3. PH model parameters fitted on the three continuous fatigue tests.

α_1 [1/s]	α_2 [1/s]	γ_1 [1/s]	γ_2 [1/s]	β [1/s]
192	1120	62	129	52,500

Table 4. Initial stiffness modulus and phase lag at cycle 1 determined by fitting.

Beam	3024-13	3025-04	3026-01
Smix (N = 1) [MPa]	7443	6809	7250
φ (N = 1) [o]	29.5	31.0	30.8

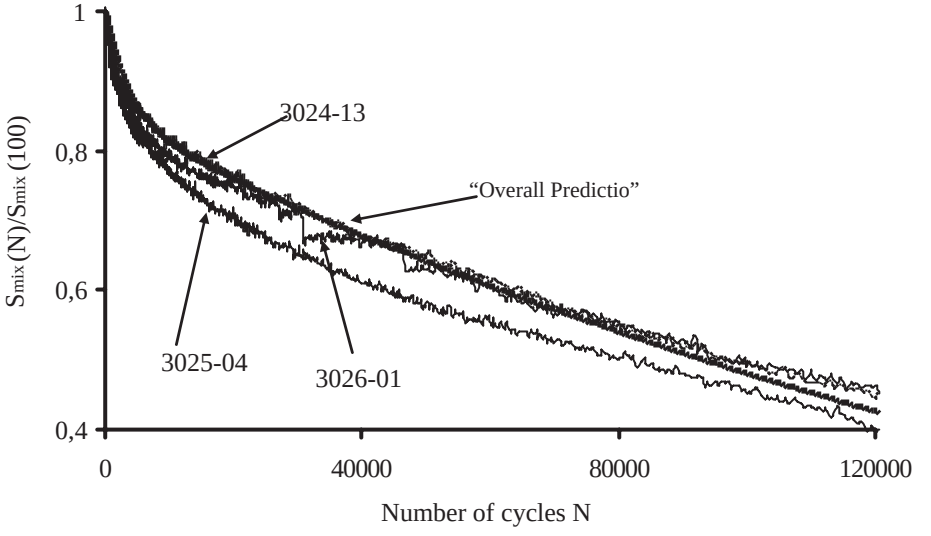

Figure 2. Standardized evolutions of the stiffness moduli for three beams and the mean fitted evolution as a function of the applied cycles.

5 RESULTS

5.1 *Continuous tests*

The goal of this project was to investigate if healing of the complex stiffness modulus in discontinuous tests could be predicted by the PH model using parameter values which were determined in continuous tests. The measured evolutions of the standardized stiffness moduli are given in figure 2 together with the mean 'prediction' (fitting) according to the PH model. The values for the parameters were determined in a fitting procedure using all three measurements and are given in table 3. These values are used in prediction of the evolutions of the complex moduli in the discontinuous tests. The initial stiffness moduli and phase lags which were determined in this fitting process are given in table 4. As can be seen in figure 2 the overall fitting for the stiffness modulus is fair but not excellent (beam 3025-04).

5.2 *Discontinuous tests and predictions*

The measured evolutions of the stiffness moduli and the predicted evolutions are given in figures 3 to 5.

The results presented in figures 3 to 5 show that the prediction of the stiffness modulus evolution is reasonable but not real satisfactorily. The measured "initial" stiffness modulus at the second and following load periods is much higher than the predicted increase and also the predicted decrease rate in the start of a loading period is lower than the measured rate. In paragraph 6 a plausible explanation will be presented for this phenomenon. Nevertheless, the resemblance is fair and indicates the potential of the PH model.

5.3 *Fitting of PH model directly on discontinuous tests*

In paragraph 5.2 the prediction was made using values for the PH model parameters which were established as mean values found in the fitting process on continuous tests. Due to the large number of cycles in the load periods in the discontinuous tests it is already possible to estimate the parameters of the PH model using data of the first load period only. The prediction based on these values for the evolution of the stiffness modulus in the second and following load periods was fair but not so good (figure 6).

As expected the fit for the first load period is excellent. However, the same deviations for the following load periods occur as in the case with the 'prediction' using a mean fitted curve based on the continuous tests.

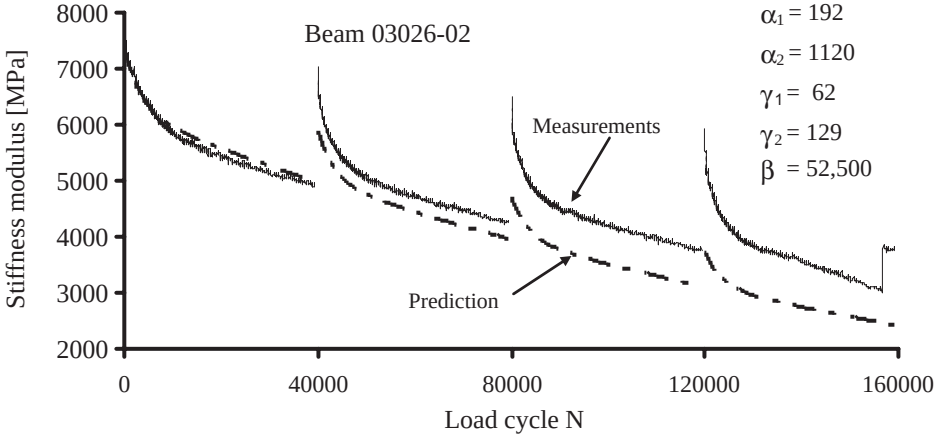

Figure 3. Measured and predicted evolutions of the stiffness modulus for beam 03026-02 using mean parameter values determined from the fitting on the continuous tests.

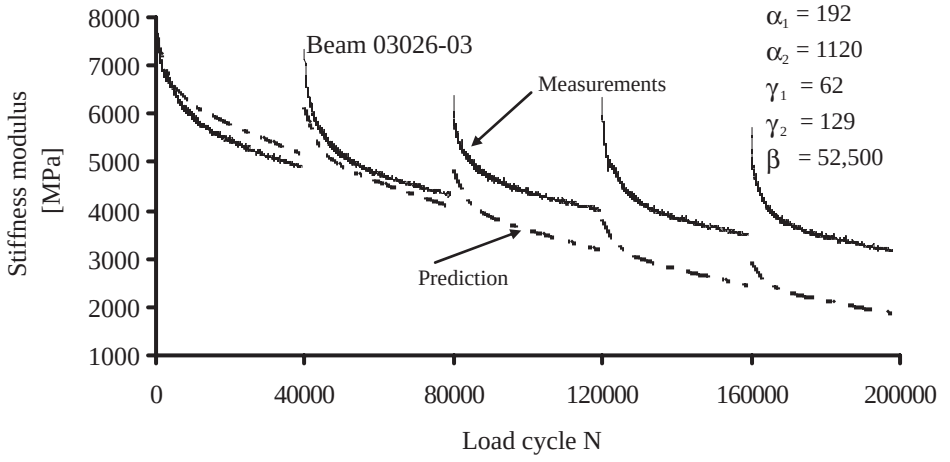

Figure 4. Measured and predicted evolutions of the stiffness modulus for beam 03026-03 using mean parameter values determined from the fitting on the continuous tests.

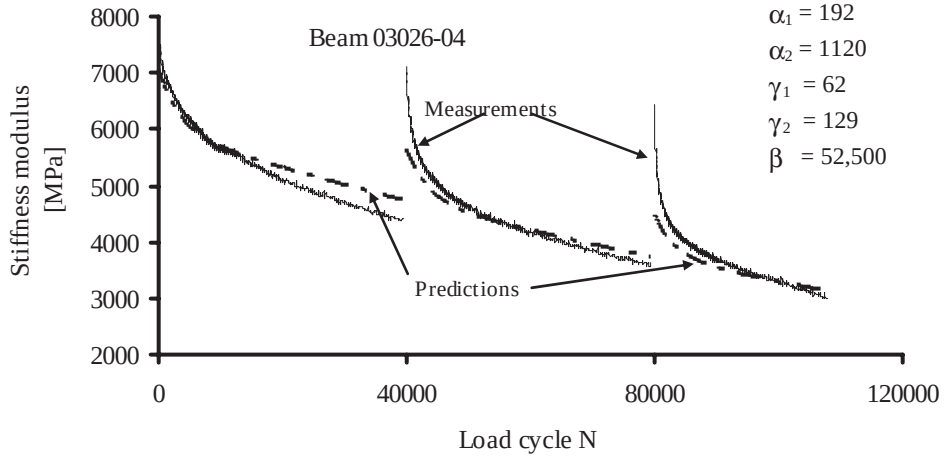

Figure 5. Measured and predicted evolutions of the stiffness modulus for beam 03026-04 using mean parameter values determined from the fitting on the continuous tests.

Table 5. PH model parameters fitted on the first and second load period for beam 3026-02.

α_1 [1/s]	α_2 [1/s]	γ_1 [1/s]	γ_2 [1/s]	β [1/s]
385	1105	50	91	37,500

When the second load period was added in the fitting for the determination of the parameters (see table 5) the prediction for the third and fourth period improved a lot (figures 7 and 8).

The only deviation which remains is the lower calculated "initial" stiffness moduli at the 2nd, 3rd and 4th load period.

5.3 *Ultrasonic tests*

The results of the UPV measurements are in given figure 9. Due to the frequency dependency of the stiffness modulus, the UPV and 4PB results for the stiffness are different. The 4PB

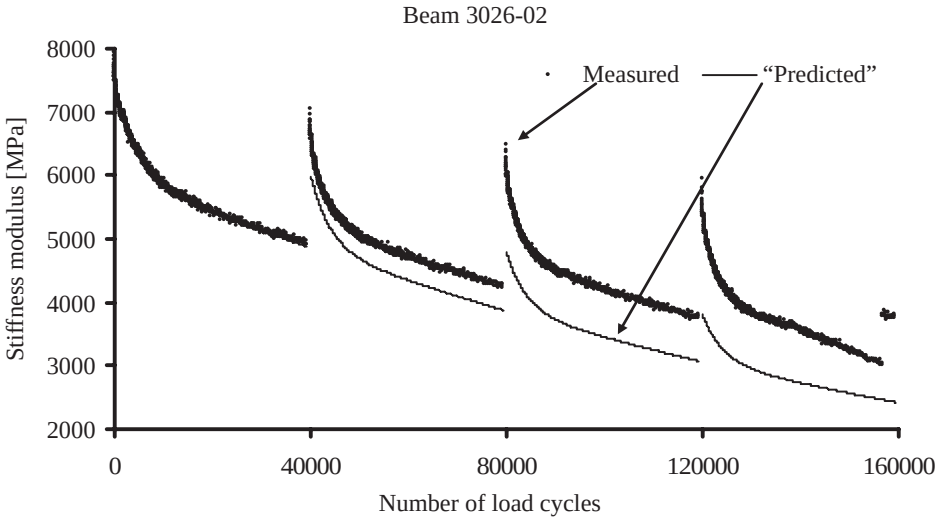

Figure 6. Comparison between measured and "predicted" values using the parameters determined on the first load period only.

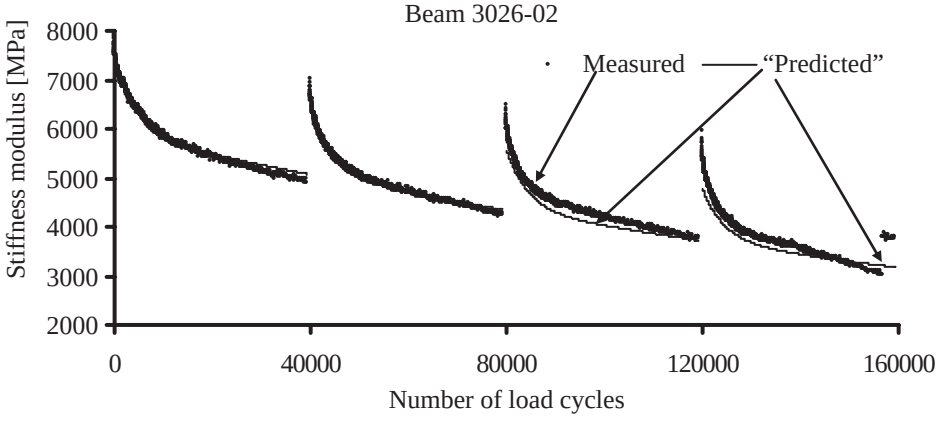

Figure 7. Comparison between measured and "predicted" stiffness moduli using the figures of table 5.

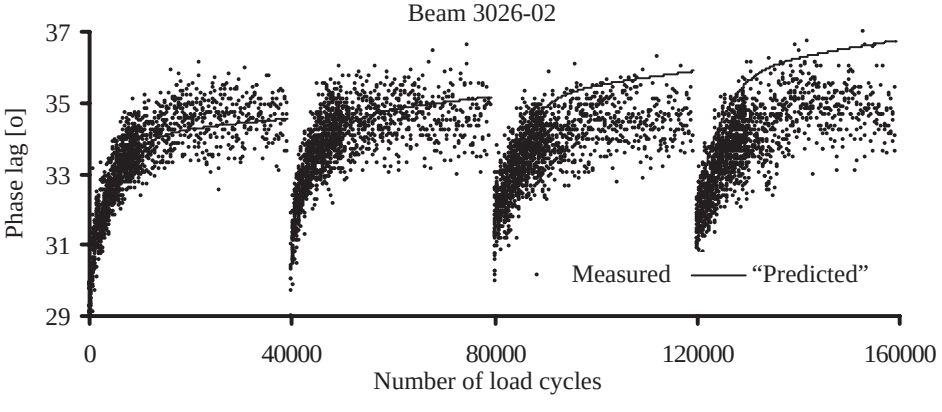

Figure 8. Comparison between measured and "predicted" phase lags using the figures of table 5.

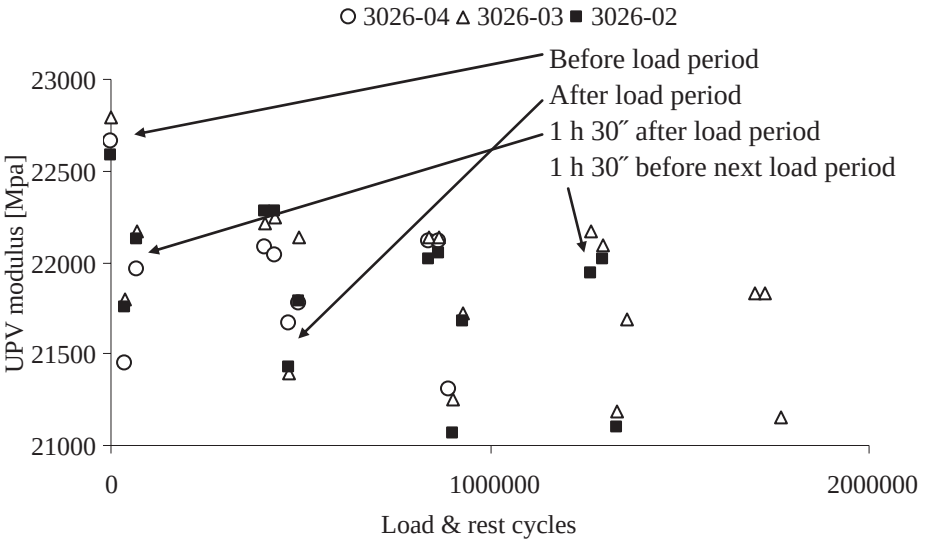

Figure 9. UPV stiffness moduli for the beams as a function of 'time' (in cycles).

stiffness modulus is measured at 5 Hz and the UPV result represents a stiffness modulus at around 50 kHz. Nevertheless there is a good relationship between both stiffness modulus measurements in the beginning and the end of a load period (figure 10).

The relationship between 4PB and UPV modulus, as depicted in figure 10, has a very high correlation (R2 = 0.96). This good correlation, obtained from measurements carried out only at the beginning and at the end of each set of load cycles, indicates that there could be a reasonable relationship between 4PB stiffness modulus and UPV measurements also during the applied rest times. This result is of great interest, since during the rest periods it is not possible to assess the 4PB stiffness modulus if no load is applied (therefore if no displacement is measured).

The results obtained from the UPV measurements conducting during the rest time (1 hour and 30 minutes before and after each load period), illustrated in figure 9, show very clearly the behavior of the beams during a discontinuous test. After the stiffness modulus decrease in the load period, a large partial stiffness recovery is observed just in the beginning of the rest period. During the remainig part of the rest period the recovery is small. Further investigation is needed in order to confirm these first findings. A more frequent set of UPV measurements might be adopted in order to define the whole stiffness recovery evolution during the rest period of a healing test.

6 DISCUSSIONS

The predictions for discontinuous tests based on interpretation of continuous tests with the PH model are fair but not as good as hoped. The form is good but the initial recovery is not as high as it should be. A possible explanation might be the temperature increase which phenomenon is not included in the PH model. The viscous elastic dissipated energy is transformed into heat. As a consequence the temperature will increase and the stiffness modulus will decrease. Although this effect is only 1–2°C in 4PB tests with forced convection cooling, the initial drop in stiffness modulus might be several hundred MPa. The determination of the PH parameters is very sensitive for the evolution of the complex stiffness modulus in the initial phase. Based on earlier findings (Pronk 1996b) it takes at least 1000 cycles or more before a kind of temperature balance is found. This implicates that for fitting the data in the continuous tests at least the first 1000 cycles should be ignored. The calculated initial stiffness modulus will be lower than the measured value and represents an 'initial' value for a one to two degrees lower temperature.

Another observation is that no significant increase in fatigue life (in terms of stiffness modulus recovery) is obtained. This is indicated by the fact that the evolutions in the stiffness

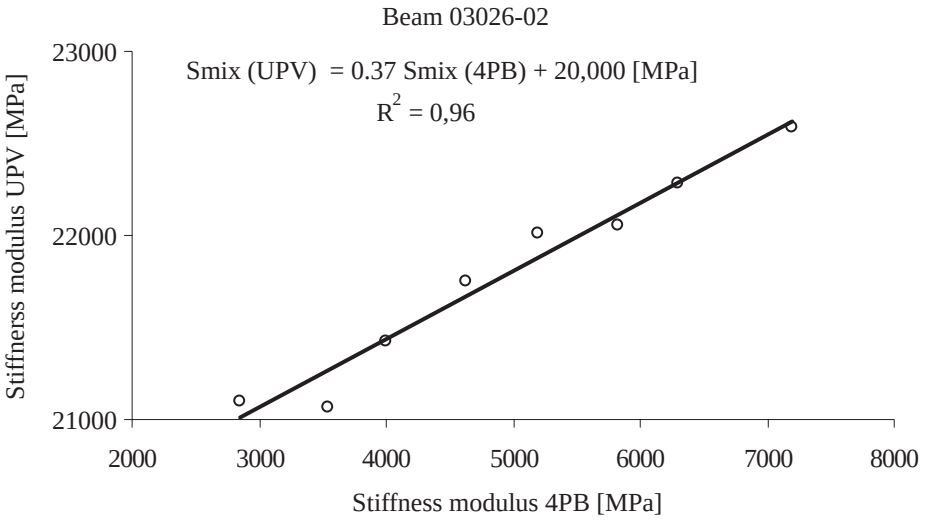

Figure 10. Comparison between 4PB and UPV modulus evolutions for beam 03026-02 at the beginning and the end of a load period.

modulus for the second and following load periods are in one line with the evolution in the first load period (see figure 3). In the author's view this is an indication that recovery in stiffness modulus is not equal or similar to recovery in fatigue life or better fatigue strength. Mark the change in stiffness modulus in the 4th load period for beam 3026-02 (figure 7). This takes place around 140,000 load cycles which is much more than Nf, 50 in the continuous tests. Further investigation is needed in order to explain this phenomenon.

Another explanation is that equilibrium is reached very fast in the load period for the reversible damage. The reversible damage in one cycle is compensated by the 'healing' of reversible damages of former cycles. Therefore the remaining reversible damage at the end of a load period is very fast 'healed'. So, the same figures would have been obtained if instead of 400,000 rest cycles only e.g. 15,000 rest cycles were applied. The slope of the stiffness modulus curve in the load period will be dominated very fast by the irreversible damage per cycle. These observations also indicate that only the ratio of applied load cycles and rest cycles will not be enough to determine the healing in a healing test. For this special mix it seems worthwhile to repeat the healing test with a load period of 5000 load cycles instead of 40,000 load cycles.

7 RECOMMENDATIONS

The PH model describes the evolution in stiffness moduli and phase lag in continuous tests very well. The prediction capacity of the PH model in discontinuous tests is not yet 100%. Based on the measurements of the first load period only, the decrease in the stiffness modulus for the following load periods is overestimated. But when the model parameters are determined from a fit on the evolutions in the first and second load period, the comparisons between measured and "predicted" values in the third and fourth load period are very reasonable. Therefore it is recommended to investigate the applicability of a healing protocol in which only two load periods are applied. If the prediction for the evolution of the complex modulus in the following load periods is good (as in this project), a good alternative measure method for the traditional time consuming healing protocol can be established.

The traditional fatigue life is defined as the number of cycles at which the stiffness modulus has decreased to half its initial value (Nf, 50). Although at the end of the first load period the stiffness modulus is above this figure, it is recommended to decrease the number of cycles in the load period in order to obtain at least 6 load periods before Nf,50 is reached.

Although not described in this paper, taking into account the fact that the PH model is in principle a material model, it can be shown by analytical calculations that the fatigue life definition N1 (based on a 'sharp' change in dissipated energy per cycle) corresponds very well with the moment at which the storage modulus at the top and bottom in the mid span of the beam becomes zero. Therefore fatigue tests with strain gages for measuring strain and controlling of the measure process (controlled strain mode instead of the traditional controlled deflection mode) is recommended.

It is not really proven by these preliminary tests that the PH model covers all reversible fatigue damages. In the PH model a real concrete rest period is not needed for restoring reversible fatigue damage from former load periods. Fatigue tests with pseudo rest periods in which a small strain is applied are recommended for obtaining an answer.

8 CONCLUSIONS

Although the prediction capacity of the PH model for stiffness modulus healing in discontinuous tests using results from continuous tests is not 100%, it is shown that the PH model can describe the evolution in the complex stiffness modulus for a discontinuous fatigue test very well. Based on the fitting for the first two load periods, the prediction for the evolutions in the following periods is quite good.

It is observed that a nearly complete recovery in the reversible damage does not guarantee an elongation of the fatigue life. It's recommended to make distinction between stiffness recovery and fatigue strength recovery.

In contrast with other healing models, the PH model calculates and predicts the evolution of the complex modulus, thus both stiffness modulus and phase lag.

The observed recovery is in line with UPV measurements. In spite of the high stiffness moduli determined with UPV devices (high frequency) it seems possible to correlate the measured values to the 4PB values (low frequency). The UPV test has the potential to be a very usefully test for determine the stiffness modulus during rest periods.

REFERENCES

Abo-Qudais S.A. & Suleiman A. 2005. Monitoring fatigue damage and crack healing by ultrasound wave velocity, *Non-destructive Testing and Evaluation* 20 (2): 125–145.

Hopman P.C., Kunst P.A.J.C. & Pronk A.C. 1989. A Renewed Interpretation Method for Fatigue Measurements—Verification of Miner's Rule, *Proceedings 4th Eurobitume Symposium*, Madrid, Spain.

Kim Y.R., Lee H-Y., Kim Y. & Little D.N. 1997. Mechanistic Evaluation of Fatigue Damage Growth and Healing of Asphalt Concrete, *Proceedings 8th International Conference on Asphalt Pave ments,* Seattle, United States of America.

Lavooi R.E. 1997. Koolteervrije Kunstof Slijtlagen: Eindrapportage bepaling van de elastische eigenschappen, Report W-DWW-97-015, Delft, The Netherlands.

Pronk A.C. & Hopman P.C. 1990. Energy Dissipation: The Leading Factor of Fatigue, *Proceedings The United States Strategic Highway Research Program: Sharing the Benefits,* London, England.

Pronk A.C. 1996a. Theory of the four point dynamic bending test Part I, Report: P-DWW-96-008, Delft, The Netherlands.

Pronk A.C. 1996b. Temperature Increase in an Asphalt Beam during Fatigue—Theory and Practice, *Proceedings Road Research Workshop,* Ede, The Netherlands.

Pronk A.C. 2000. Partial Healing Model—Curve Fitting, Report W-DWW-2000-047, Delft, The Netherlands.

Pronk, A.C. 2001. Partial Healing in Fatigue Tests on Asphalt Specimens, *International Journal Road Materials and Pavement Design* 4 (4).

Pronk A.C. 2005. Partial Healing, A new approach for the damage process during fatigue testing of asphalt specimen, *American Society Civil Engineering,* Baton Rouge, United States of America.

Van der Ven M.F.C., Voskuilen J.L.M. & Gubler R. 2006. Comparison Mechanical Properties determined with Co-axial Shear Test and Four Point Bending Test *Proceedings 10th International Conference on Asphalt Pavements.* Ontario, Canada.

Advanced Testing and Characterization of Bituminous Materials – Loizos, Partl, Scarpas & Al-Qadi (eds)
© 2009 Taylor & Francis Group, London, ISBN 978-0-415-55854-9

Fatigue behaviour of bitumen in tension-compression loading mode: Rheological analysis and comparison with mix fatigue

E. Chailleux, D. Bodin, C. de La Roche, M. Leguern & N. Vignard
LCPC, France

ABSTRACT: Considering that most of time, cracks in bituminous mixes occur inside the binder/mastic film, it can be assumed that fatigue properties of the bitumen itself could give accurate information on the fatigue behaviour of mixes. It has been already demonstrated that a strong link exists between bitumen and mixes fatigue properties. From these previous studies, it is clear that when the same composition is used, mixes can be ranked as the corresponding binders. Whereas numerous studies have been conducted on shear fatigue properties using Dynamic shear Rheometer (DSR), only a few data obtained with other modes of loading are available.Knowing that mixes are tested in mode I crack opening, it seems interesting to test binders under the same fracture mode. For these reasons, the present study focuses on the design of a tension-compression fatigue test as well as the interpretation of the first results taking into account the rheological phenomena occurring during the test.

The paper describes the design and the preparation of the "diabolo" shaped used samples. Fatigue test results from three binders are given and compared to the corresponding mixes results. Then, a particular attention is drawn on the phase angle versus stiffness (black diagram) during the fatigue experiments.

Keywords: fatigue, bituminous mixes, bitumen

1 INTRODUCTION

Bituminous pavement design is generally based on material fatigue criterion associated with the calculation of a multilayer structure response. The tensile strain at the bottom of each base layer is computed using an elastic multilayer structure calculation. To be acceptable, its value has to remain below a threshold value depending on the material fatigue behaviour. However, laboratory fatigue tests on mixes are time and money consuming. In the damage process, bituminous binder is strongly involved. Assessing binder fatigue properties could reduce time for binder selection. On a more fundamental point of view, it could help to understand the role of the bitumen in the mixture fatigue behaviour.

Relationship between binder and mix fatigue properties has been already established (Gauthier 2004) (Soenen 2003). These studies show that when mixture composition is constant, a clear trend exists between binders and mixes fatigue lifetime. Like in other numerous works dealing with binder or mastic fatigue properties (Bahia 1999, Anderson 2001, Bonnetti 2002, Martono 2007, Delaporte 2008) a shear mode of loading has been used. Knowing that most of the time, fatigue properties of bituminous mixes are carried out in mode I, it seems interesting to understand the binder fatigue properties under the same mode of loading. Only a few data exist regarding tension compression fatigue properties of bituminous binder. In a recent paper (Airey 2004) results from uniaxial and shear mode of loading are compared. A large scatter of fatigue data generated by both shear and uniaxial mode of loading is underlined.

The present paper focuses on the development and the interpretation of a new tension-compression fatigue test carried out on bitumen. In the first part, geometry and protocol are presented. A finite element modelling is used to optimize specimen size using strain field

in the sample. Typical results are then given and compared to the mix fatigue properties. Finally, a special attention is drawn on the bitumen rheological behaviour during fatigue in tension-compression.

This work is a side project of the RILEM group TC 206 ATB TG1 dealing with the development of a fatigue test using Dynamic Shear Rheometer (Sybiliski 2009).

D	Displacement amplitude (μm)
F	Force (N)
S	Cross-section of the sample
CA	Abscissa along the diabolo free edge (mm)
T	Temperature (°C)
F	Frequency of the sinusoidal loading (Hz)
$\nu = \lvert\nu^*\rvert$	Poisson's ratio
K*	Complex stiffness (N/m)
E*	Complex modulus (Pa)
E	Young modulus (Pa)
δ	Phase angle (°)
K	Stiffness (N/m)
α	Geometric factor $E = \alpha K$ and $\lvert E^*\rvert = \alpha \lvert K^*\rvert$
$\varepsilon = \varepsilon_{vv}^{max}$	Strain applied in the more loaded area of the diabolo specimen
N	Number of cycles
N_f	Number of cycles at failure
T	Temperature (°C)

1 BINDER FATIGUE TEST DESCRIPTION

1.1 *Design of the sample shape*

It is necessary to design the sample shape in order that the cracking zone develops in the bitumen itself. The uniform strain state of a cylindrical specimen in tension compression would have allowed determining more easily an intrinsic material fatigue property. However, an experimental problem has been experienced with cylindrical specimens. Indeed, in these cases, adhesive fractures between bitumen and steel had occurred. Hence, the

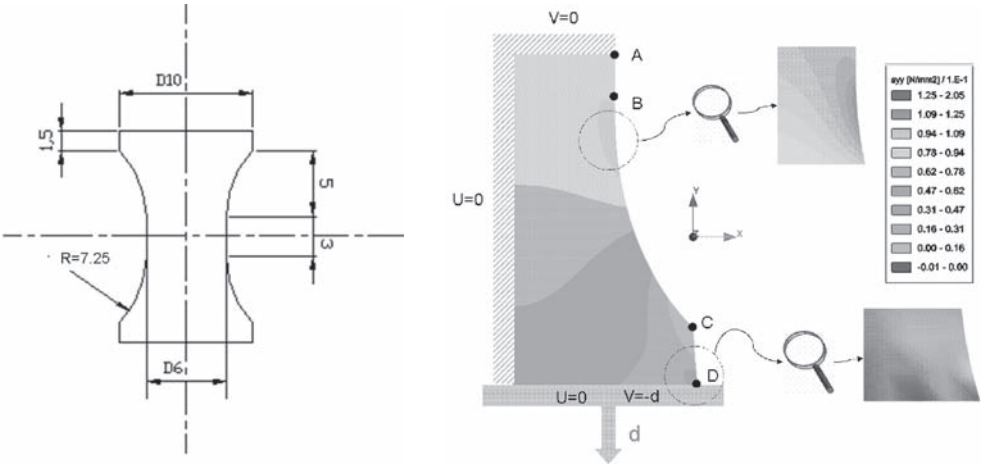

Figure 1. (a) Dimensions of the diabolo specimen (mm). (b) Stress state of the diabolo specimen in tension-compression loading mode. Finite-element output.

measured damage was not only the consequence of the bitumen fatigue behaviour, but also the consequence of the inter-phase degradation (glue/bitumen in this case). This problem was overcome by choosing geometry where the cracking zone is controlled. "Diabolo" shaped specimen is often used to assess fatigue or monotonic properties of polymers (Saintier 2006, Castagnet 2007) and also used for tension-compression in mixtures (Aguirre 1981). The diabolo sample chosen for this study is designed to give an uniaxial stress state under tension and to allow concentrating stresses in the material itself. Indeed, as it can be seen on the figure 1(a), the central part of the diabolo is cylindrical and the curvature radius is chosen in order that the shoulder is tangent to the cylinder edge.

1.2 *Size determination and stress state analysis*

Diabolo specimen is designed with the help of the finite element (FE) code Cesar-LCPC© . Only a quarter of the sample is modelled considering the symmetry axis (see figure 1(b)). Calculus is performed using linear mechanics in axisymmetric stress state. Poisson's ratio is determined from the viscoelastic model proposed by Di-Benedetto and al (Di Benedetto 2007) established for a pure 50/70 bitumen. In the experimental condition used in this study, T =10°C and f = 10 Hz, Poisson's ratio is found to be equal to 0.4945. The bitumen appears to be close to the incompressibility state. Mesh dependency is evaluated (see figure 2(a)). Stability of the solution (tension strain) is reached as soon as the mesh size is less or equal to 0.1 mm (mesh size is taken homogeneous all over the sample).

The length of the cylindrical part is chosen in order to be able to impose strain up to 1% according to the displacement capability of the TC device (Metravib Viscoanalysor). Moreover, the curvature radius is optimized to give the best possible strain homogeneity in the median zone (see dimensions of the specimen on figure 1(a)). Nevertheless, the finite element output (figure 2) shows that a stress concentration is localized at the shoulders (near the point B) on the free edge. This effect can not be observed with the simple analytical calculus $\varepsilon_{yy} = F_y/(E.S)$. So, non-linear effect and crack should be initiated in this zone. It has to be noted that FE calculus gives the more loaded zone on a very small area around the point D. This stress concentration is due to the Poisson's effect associated with the geometrical discontinuity between the sample and the boundary conditions. No distress mechanisms were experienced in this zone during the experiments. The angle considered in the finite element calculus at the point D appears not to be reproduced in the actual bitumen sample. Indeed, a smoother discontinuity is observed (due to imperfection of the sample and interface between glue and bitumen) which leads to a stress concentration decrease at this point.

Strain along the free edge (ABCD path visible on the figure 1(b)) of the diabolo is calculated and plotted on the figure 2(b). Maximum strain is found at the abscissa 1.9013 mm. The relation between this maximum strain and the amplitude of the displacement gives:

$$\varepsilon_{yy}^{\max} = 0.01036 \times d \tag{1}$$

(With ε_{yy} in % and d in µm)

Moreover the geometric factor can de deduced from the stiffness calculated with EF model and gives:

$$E = 384.8 \times K \tag{2}$$

(With E in N/m² and K n/m)

In the linear domain according to elastic-viscoelastic convolution principle, the norm of the complex modulus can be determined from the norm of complex stiffness: $|E^*| = \alpha |K^*|$. It has to be noted that this principle is only true when mechanical properties are homogeneous all over the sample. As soon as the modulus decreases due to a damage or heating process in a non homogenous way, the calculated |E*| is not strictly founded.

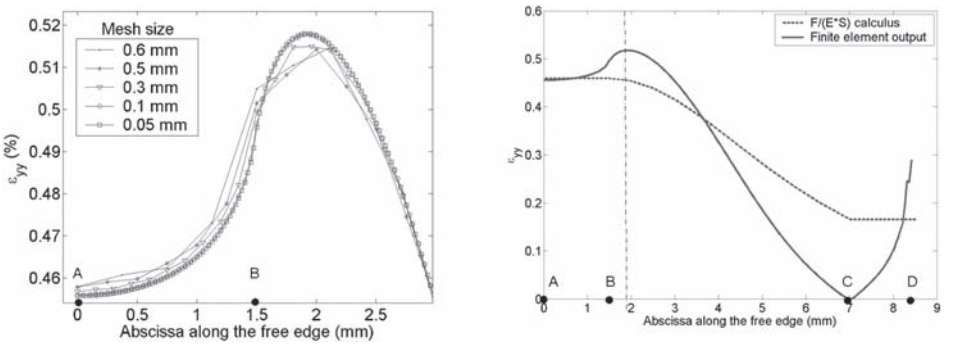

(a) (b)

Figure 2. (a) Strain in the yy direction along the maximum loaded zone according to mesh size. (b) Strain in the yy direction along the free edge ABCD (see figure 1(b)) calculated by finite element and using the analytical calculus F/(E.S).

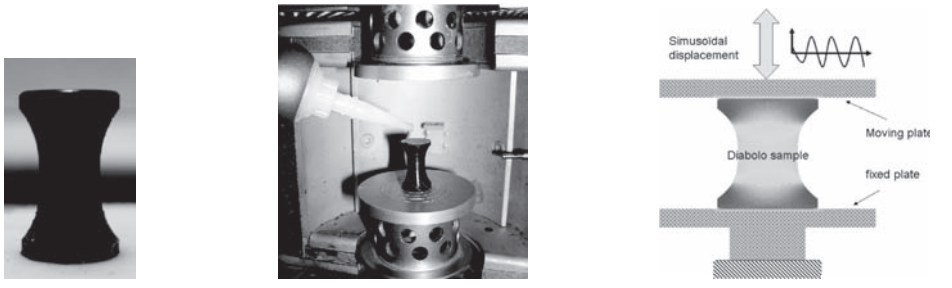

(a) (b) (c)

Figure 3. (a) Diabolo specimen after demoulding. (b) Diabolo specimen glued on the Metravib viscoanalysor plate. (b) Schematic view of the sample loaded in alternative tension compression mode.

1.3 *Preparation of the samples*

The samples are manufactured by pouring hot bitumen (160°C) in a silicon mould. When the room temperature is reached and in order to have a perfectly flat surface, the upper part is strimmed using a hot knife. Sample is then stored in the mould at low temperature (–10°C) until it is tested. As soon as the sample is demoulded (see figure 3(a)), it is glued on the two parallel plates using Cyanoacrylate (see figure 3(b)).

1.4 *Experimental protocol*

The sinusoidal tension compression tests are performed using a Viscoanalysor METRAVIB in displacement control mode. This device applies an oscillating linear mode of loading. The figure 3(c) shows a schematic view of the sample loaded in tension compression between the two moving plates of the viscoanalysor. The viscoanalysor can be driven by software especially designed to perform fatigue experiment (Multidyn). The main interest of this tool is the possibility to apply the wanted sinusoidal signal at the first cycle (after a learning phase where the PID parameters are determined for one experimental condition).

The test is divided into two steps. The first step, called "conditioning time", consists in applying sinusoidal loading in the small strain domain (d = 5 µm; $\varepsilon_{yy}^{\max} = 0.052\%$) during 30 min. This time appears to be sufficient to reach the test temperature. Then, test begins in the large strain domain (d = [20 µm–70 µm]; $\varepsilon_{yy}^{\max} = [0.207\% - 0.725\%]$) until the sample breaks. Stiffness and phase angle are recorded according to the number of cycles. All the tests are performed at 10°C and 10 Hz.

2 EXPERIMENTAL RESULTS

2.1 *Materials*

2.1.1 *Binders*

Tension-Compression fatigue tests are performed on three binders B1, B2 and B3. These binders have the same mechanical behavior at 10°C and 10 Hz. However, their physico-chemical structure looks different (see table 1), especially regarding asphaltene and cristalisable fraction contents. Binder B1 and B2 are pure binders whereas Binder B3 is polymer modified one.

2.1.2 *Mixtures*

Three types of mixtures, M1, M2 and M3 were manufactured respectively with the binders B1, B2 and B3. The bituminous mix is a 0/6 BBC (French standard NF 98-133), with a binder content of 6.88%. The grading curve of the mix is given in table 2. This is a continuous graded mix, made of aggregate from "La Noubleau" quarry (microdiorite). The filler came from "Airvault quarry (limestone)". This mix composition was chosen in order to consider the sample homogeneous in comparison to the sample size used for mechanical test. As a consequence, repeatability of the fatigue test with this composition is known to be better, what allows to study the binder effect.

Aggregates and binders are mixed in laboratory (EN 12697-35) and compacted with a LCPC slab compactor EN 12697-33). Complex modulus measurements are performed on these materials using a two point bending test on trapezoidal samples (EN 12697-26 Annex A). At 10°C, 10 Hz, mechanical properties of the mix are close to each other as it can be seen on the table 3.

Table 1. Physico-chemical properties of the binders.

	B1	B2	B3
Binder type	50/70 Pure	50/70 Pure	PmB
Asphaltènes content (%) (Insoluble in n-heptane)	12,4	17,8	17,8
Cristalizable fraction (%) (by DSC)	2,23	0,1	2,64
|E*| (MPa) (10°C, 10 Hz)	50.4	49.0	50.2
δ(°) (10°C, 10 Hz)	37.2	37.6	34.8

Table 2. Grading curve of the asphalt mixes.

Sieve (mm)	0,06	0,125	0,25	0,500	1,00	2,00	3,15	4,000	5,0	6
% Passing	10,9	14,7	20,1	28,2	39,9	59,9	66,4	69,6	81,1	95,6

Table 3. Mechanical properties of the mixture at 10°C, 10 Hz.

	Binder	|E*| (MPa) (10°C, 10 HZ)	Phase angle (°) (10°C, 10 HZ)	% void
Mixture M1	B1	13741	13.4°	3.6
Mixture M2	B2	12941	15.3°	3,2
Mixture M3	B3	14162	12.4°	3,4

2.2 *Qualitative description of a binder fatigue test in TC*

Records of the stiffness during the sinusoidal loading show classical fatigue behaviour of bituminous material (see the example on binder B1 in figure 4(a)). Just after the conditioning time, a rapid decrease of the stiffness is observed (phase 1), followed by a slow damaging process (phase 2). At the end of the fatigue process, a dramatic sharp decrease of the stiffness is due to the specimen failure (phase 3). It is generally assumed that phase 2 corresponds to micro-cracks onset whereas phase 3 is linked to macro-craks propagation. Physical meaning of the phase 1 is still under discussion. It could be attributed partially to self-heating of the material or thixotropic behaviour. What is interesting to note is the phase angle variation during the fatigue test. During both first phases, phase angle increases as the stiffness decreases, showing a liquefaction phenomenon. On the other hand, a phase angle maximum occurs during the phase 3 followed by a rapid decrease. A similar phase angle variation according to fatigue phases of bituminous mixture has been also observed (Gauthier 2004). The micro and macro cracks onsets can't explain phase angle variation since only the stiffness of the sample should be affected. The physical meaning of this phenomenon will be discussed in the followings part.

Figure 4(b) shows that crack in the diabolo specimen occurs at the shoulder what is in accordance to the finite element analysis.

Fatigue performance evaluation consists in performing cyclic tests at different amplitudes. As expected, lifetime is reduced when higher strains are used (figure 5). The stiffness decrease of the phase 1 is also strain dependent. However, it could be seen on the enlarge view of the first phase (figure 5(b)) that the stiffness measured during the first cycle at high strains ($\varepsilon = 0.39, 0.52, 0.73\%$) is equal to the stiffness determined at low strain during the conditioning time ($\varepsilon = 0.05\%$). As a consequence, it appears that non-linearity with strain doesn't exist at the early beginning under high strain loading. This phenomenon occurs with cycle repetition and depends on the input energy. Following this observation, it could be intuited that the physical phenomenon responsible for the non-linearity with strain or stress level and the stiffness decrease during fatigue first phase are the same. Hence, non-linearity evaluation in tension-compression mode should make sense only if the number of cycles is given in addition to the applied stress or strain level.

2.3 *Comparison of fatigue criteria*

The fatigue properties of the mixes M1, M2 and M3 are determined according to the standard EN 12697 using two points bending on trapezoidal samples. Tests are carried out in strain

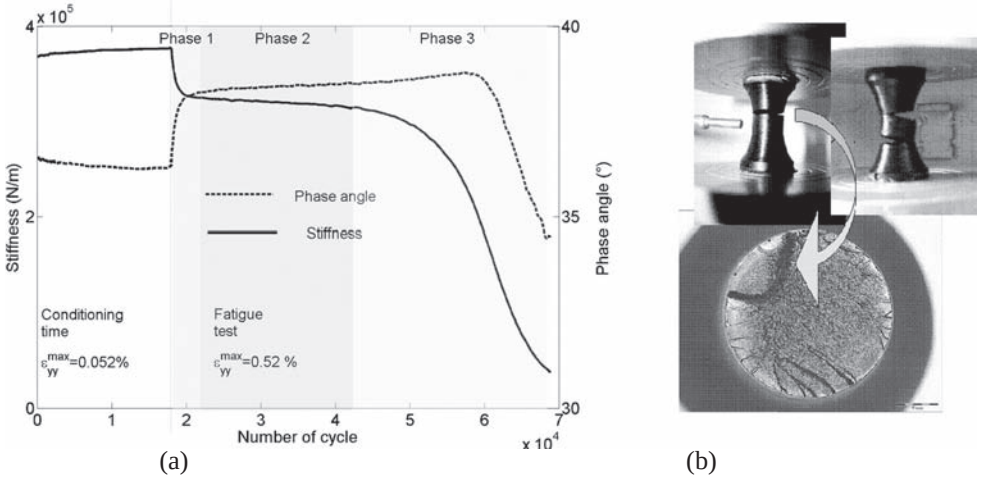

Figure 4. (a) Stiffness and phase angle, of the binder B1, plotted versus the number of cycles during the conditioning time at low strain and during the fatigue test at 0.52% strain. (b) Picture of the diabolo sample at the end of the fatigue test.

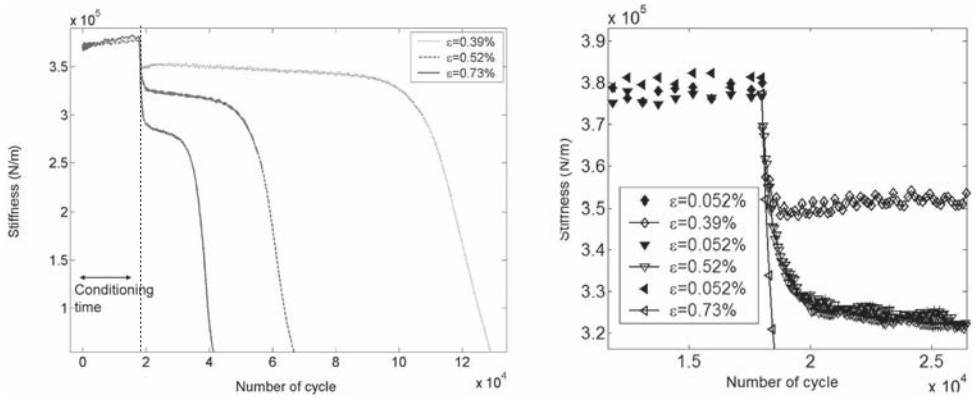

(a) (b)

Figure 5. (a) Stiffness of the binder B1 during conditioning time in the small strain domain and during fatigue tests performed at $\varepsilon = 0.73\%$, 0.52% and 0.39%. (b) enlarge view of the passage between conditioning time in the small strain domain and the beginning of the fatigue tests at higher loading level.

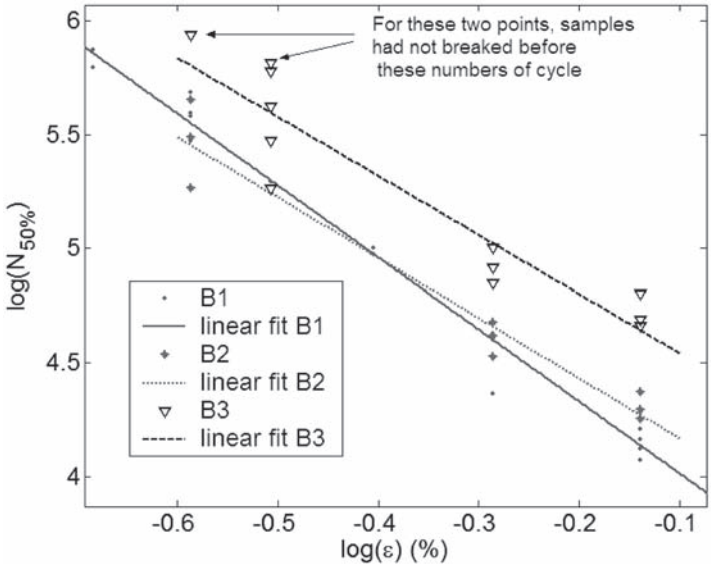

Figure 6. Fatigue line (Wohlër curve) of the binders B1, B2 and B3.

controlled mode. Considering the usual scatter of these fatigue tests, a minimum of six samples, for each strain level are used.

Fatigue life for both binder and mixture is defined as the number of cycles which corresponds to 50% decrease of the initial stiffness modulus. The fatigue tests are performed at least at three strain levels. The lowest strain is chosen in order that the life duration is close to one million cycles. Test conditions for binder and mix are the same: T = 10°C and f = 10 Hz.

Figure 6 shows the Wohlër curve of the three binders. Binders B1 and B2 appear to have an equivalent behavior in fatigue whereas binder B3 shows a larger lifetime whatever the applied strain. Concerning the tests on the binder B3, two points on the graph don't correspond to totally damaged samples. Indeed, experimental problem has

been encountered and these tests were stopped prematurely. Nevertheless, when the experiments have been stopped, the samples did not reach half of the initial stiffness. It is so necessary to add these points in order to not underestimate the fatigue life at low strain. So, for binder B3, slope of the fatigue line and strain for $N = 10^6$ represent a minimum of the real value.

In the table 4, results from binders and mixes are compared regarding the slope of the fatigue line and ε_6 (strain corresponding to $N_f = 10^6$ cycles). Considering the accuracy of the measurements, it is not possible to distinguish, neither the binders B1 and B2, neither

Table 4. Results of binders and mixes fatigue tests.

Materials	ε_6 (ε for $N_f = 10^6$)	Slope	Number of samples tested
B1	0.186% Min = 0.174%, Max = 0.200%	–3.15 ± 0.20	20
B2	0.161% Min = 0.127%, Max = 0.203%	–2.64 ± 0.44	9
B3	>0.217% Min = ? Max= ?	> – 2.59	10 broken 2 not broken
M1	0.0152% Min 0.0149%, Max 0.0155%	–5.23 ± 0,03	18
M2	0.0159% Min = 0.0152%, Max = 0.0166%	–6.43 ± 1,1	18
M3	0.0196% Min = 0.0187, Max = 0.0207%	–6.3 ± 0,95	18

the corresponding mixes M1 and M2. For both, binder B3 and mix M3, ε_6 criteria appear to be higher than ε_6 determined for binders B1, B2, and mixes M1 and M2.

The ranking, according to the fatigue criterion ε_6, is then the same for binders loaded in tension compression, and for mixes loaded in two points bending mode. Moreover, the ratio between ε_6 (binder) and ε_6 (mix) is, in each case, close to 10 (this ratio has to be verified for the binder B3). This ratio has to be compared to those found by Soenen (Soenen 2003) and Gauthier (Gauthier 2004). In both cases, shear loading mode for binders were used. Soenen found a ε_6 ratio close to 50 (binder and mix tests were performed at equistiffness). Gauthier found ε_6 ratio between 70 and 100 (in this case, mix fatigue test were performed in tension compression on cylinder at 10°C). These ratios have to be interpreted with care because the strain for shear test could have been taken as shear angle (distortion γ) or shear strain ($\varepsilon = \gamma/2$).

2.4 *Description in black diagram*

In this section, we focuses on the stiffness and phase angle changes during the fatigue test. It can be seen on figure 4(a) that the rheological behaviour of the diabolo sample during the fatigue experiment is evolving. During first phases, phase angle and stiffness appear to be linked whereas this relationship seems to be more complicated during the third phase. The voids and cracks created by the damage process can't explain alone this rheological behaviour since they should only affect the rigidity. Other phenomena like heating or thixotropy have to be considered in order to explain the phase angle variation. To discriminate between the real damage process and the others phenomena, Black curve representation can be useful. Indeed, for simple rheological material, the relationship between phase angle and norm of complex modulus is unique (for one modulus value, there is only one phase angle value (Rammond 2003)). Structural effect at the molecular scale, like ageing, can be observed in Black representation. One can imagine

that micro-structural damage occurring during the fatigue process should also be visible (de La Roche 1996, Di Benedetto 2004).

On figure 7, phase angle is plotted according to stiffness during a fatigue test and compared to the bitumen Black curve. This example is given for the binder B1 but the followings remarks can also be done for binder B2 and B3. Contrary to classical Black view, stiffness is plotted instead of norm of the complex modulus. Indeed, strain is not homogeneous in the diabolo specimen. As soon as conditions for non-linear behaviour are reached, elastic/viscoelastic convolution principle can't be applied. As a consequence, intrinsic modulus can't be calculated directly from the measured stiffness.

Nevetheless, figure 7 shows that the relationship between angle and stiffness during the phase 1 and the beginning of phase 2 follows the Black curve measured in the small strain domain. The gap between the two curves, at the beginning of the test, has to be attributed to experimental variability since the measurements have not been performed on the same samples.

Phase 2, is associated to a small variation of the rheological properties. However, this variation appears to be a transition and represent the larger number of cycles. At the end of the phase 2, the relationship between angle and stiffness stops to follow the initial Black curve. It has to be noted that, like it has been observed by others authors (de La Roche 1996, Di Benedetto 2004, Delaporte 2008), the angle and stiffness variations during the first phase is similar to a liquefaction phenomenon due to temperature. For the experiment performed at 0.52%, phase 1 is similar to temperature increase of 1.4°C (determined in first approximation by interpolation between points measured at 10°C and 12°C). It could be assumed that the damage process occurs actually at the end of the second phase. The moment when this cracking phenomenon has an effect on the sample mechanical properties could be detected precisely using the Black representation. Figure 8 shows also that the higher is the strain the more pronounced the liquefaction phenomenon. The energy given to the samples by mechanical loading is responsible for the first stiffness decrease during fatigue test.

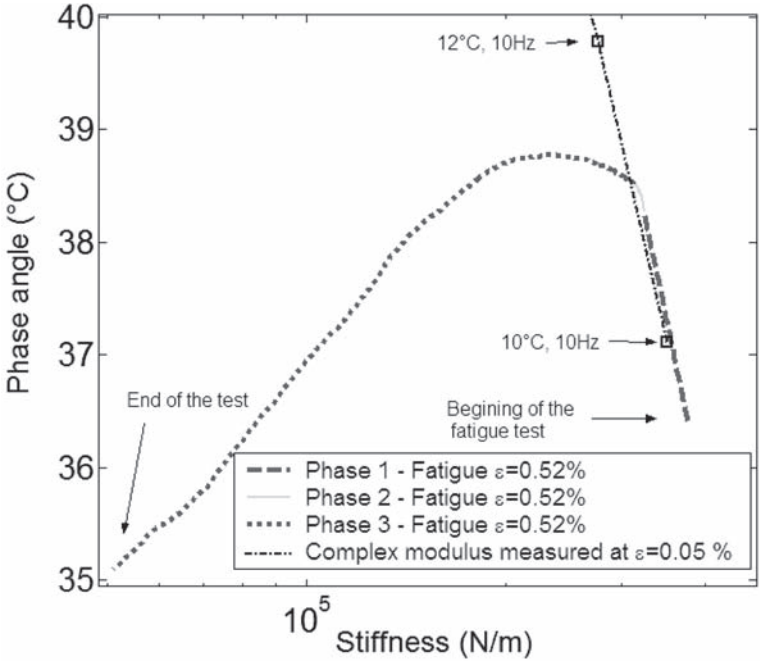

Figure 7. Phase angle versus stiffness during a fatigue test performed at ε = 0.52% (intermediate level) compared to the black curve measured in the small strain domain (binder B1).

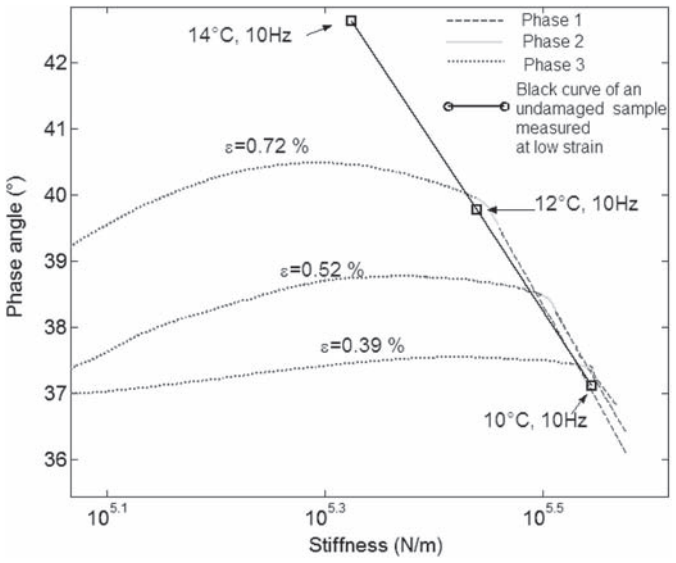

Figure 8. Phase angle versus stiffness of the binder B1 during fatigue tests performed at 0.72%, 0.52% and 0.39% strain level compared to measurements in the small strain domain (black curve).

3 CONCLUSION

A fatigue test has been developed to assess fatigue properties of bituminous binder in tension-compression. Sample shape has been designed with the help of a finite element analysis to be as close as possible to an uniaxial mode of loading. Experimental results show that diabolo shaped specimen allows crack to develop in the material itself. Strains are not homogeneous in this type of specimen. The level and coordinates of the maximum strain are so determined with the finite element calculus.

Three binders have been tested using this new test. As it is classically observed for asphalt mixtures, the decrease of the stiffness during the fatigue test, performed in tension compression, can be divided into three phases. A first one which could be attributed to self heating or thixotropy, a second phase where microcracks are developing and a third phase linked to the onset of macrocracks. A careful attention has been drawn on the first beginning of the phase 1. It appears that non linearity with strain is not instantaneous and depends on the number of cycles which is applied on the binder. Indeed, stiffness measured in tension compression in the small strain domain is the same as the stiffness measured at the first cycle at a larger strain level. It seems that non linearity in tension compression and the decrease of the stiffness during phase 1 are intimately linked. Moreover, when rheological data, stiffness and phase angle recorded during the fatigue test, are plotted in a Black diagram, phase 1 appears to follow the initial black curve measured in the viscoelastic linear domain. Hence, fatigue data in Black diagram show that the phase 1 is equivalent to a liquefaction phenomenon whatever the strain level. Further works are planned to understand the physical origin of this liquefaction: temperature increase and/or physical desctructuration. On the other hand, it is interesting to note that rheological data stops to follow the initial black curve during the phase 2. This point could be attributed to the real onset of the damage process.

On a more practical view, ranking of the three binders regarding fatigue lifetime is similar to the corresponding mixes test in two points bending mode. Other binders and mixes will be tested in the frame of the RILEM TC 206 ATB TG1 to confirm these results.

REFERENCES

Airey, G., et al. 2004. A comparison of bitumen/mastic fatigue data from different test methods. Proceedings of the Fifth Rilem conference on cracking in pavements. Limoges.

Aguirre, Morot, de La Taille, Doan Tu Ho, Bargiacchi, Smadja, Udron, Guay, & Roncin, 1981. Etude comparée des essais de module complexe et de résistance à la fatigue des enrobés bitumineux. Bulletin de Liaison des laboratoires des ponts et chaussées, N°116, pp. 33–34 [French].

Anderson D.A., Le Hir, Y, Marasteanu, M, Planche, J-P, Martin, D & Gauthier, G. 2001. Evaluation of fatigue criteria for asphalt binders. Transportation Research Record 1766, Paper N°. 01–3298.

Bahia, H, Zhai, H, Bonnetti, K & Kose, S. 1999. Non-linear viscoelastic and fatigue properties of asphalt binders, AAPT proceedings, Vol 68.

Bonnetti, K.S., Nam, K & Bahia, H.U. 2002. Measuring and defining fatigue behaviour of asphalt binders. TRB 2002 Annual Meeting CD-ROM.

Castagnet, S & Deburk, Y. 2007. Relative influence of microstructure and macroscopic triaxiality on cavitation damge in a semi-crystalline polymer, Materials science and engeneering A, 448: 56–66.

Delaporte, B, Rompu, J.V., Di Benedetto, H., Chaverot P. & Gauthier G. 2009. New procedure to evaluate fatigue of bituminous mastics using an annular shear rheometer prototype. Proceedings of Cracking in pavement, RILEM conference, Chicago.

De La Roche Saint André 1996. Module de rigidité et comportement en fatigue des enrobés bitumineux. Expérimentation et nouvelles perspectives d'analyse. Phd Thesis [French].

Di Benedetto, H, de La Roche, C, Baaj, H, Pronk, A & Lundström, R. 2004. Fatigue of bituminous mixtures, Materials and Structures Vol 37: 202–216.

Di Benedetto, H, Delaporte, B & Sauzéat, C. 2007. Three-dimensional linear behaviour of bituminous materials: experiments and modelling. *International journal of geomechanics ASCE*: 149–157 – March/April.

Gauthier, G, Le Hir, Y & Planche, J-P. 2004 Fatigue of bituminous binders and mixes: analysis and correlations using a new intrinsic approach. Proceedings of Euraphalt & Eurobitume: 1842–1853, Vienna, 2004.

Martono, W, Bahia, H.U. & D'angelo, J. 2007. J. Effect of testing geometry on measuring fatigue of asphalt binders and mastics. *Journal of materials in civil engineering*.

Rammond, G & Such, C. 2003. Le module complexe des liants bitumineux. Etudes et recherches des Laboratoires des Ponts et Chaussées.

Soenen, H, De La Roche, C & Redelius, P. 2003. Fatigue behaviour of bituminous materials: from binders to mixes. Road material and pavement design, vol 4, Issue 1: 7–27.

Sybiliski, D, Gajewsk, M, Soenen, H, Chailleux, E & Gauthier, G. 2009. Binder Fatigue Properties and the Results of the Rilem Round Robin Test, proceeding of the TC 206 ATB RILEM conference, Rhodos.

Saintier, N, Cailletaud, G & Piques, R. 2006. Crack initiation and propagation under multiaxial fatigue in a natural rubber. International journal of fatigue, 28: 61–72.

Advanced Testing and Characterization of Bituminous Materials –
Loizos, Partl, Scarpas & Al-Qadi (eds)
© 2009 Taylor & Francis Group, London, ISBN 978-0-415-55854-9

Mixed-mode cracking in asphalt concrete

A. Braham, C. Peterson & W. Buttlar
University of Illinois at Urbana-Champaign, Urbana, Illinois, USA

ABSTRACT: Cracking occurs in many different forms in asphalt concrete pavements. With a combination of an opening crack (such as thermal cracking) and a sliding crack (such as reflective cracking) Mixed-Mode cracking occurs. This research will include a comprehensive literature review into different testing configurations of various materials for Mixed-Mode cracking. It will also include initial data results of Mixed-Mode crack initiation in asphalt concrete using a Single-Edge Notch Beam with an offset notch. The beam span is approximately 330 mm long and offset notches were placed approximately 25, 50, 75, 100, and 125 mm from the center of the span. Similar to previous findings reported in the literature on other quasi-brittle materials, cracks did not initiate or propagate from notches offset at either 100 or 125 mm. Instead the crack formed directly underneath the loading head, away from the notch but at the location of maximum bending moment. There was a general trend of increase in Crack Tip Sliding Displacement, and a general trend of decrease in Crack Mouth Opening Displacement, as the notch moved further from the center, which was the expected trend. Recommendations for an improved measurement system based upon study findings will be described.

1 INTRODUCTION

1.1 *Background*

Cracking occurs in many different forms in asphalt concrete pavements. Thermal, fatigue, and reflective cracking are all common. Thermal cracking is generally considered a Mode I type crack, or a pure opening crack. Research in asphalt pavements has indicated that fracture mechanics is a plausible tool in characterizing and analyzing Mode I crack initiation and propagation. However, with the introduction of a wheel load, Mode I is not found isolated in the field. With a wheel load, a combination of Mode I and Mode II cracking usually occurs. Mode II cracking is a shearing crack, or a sliding crack, and often occurs as a wheel passes over an overlay with an existing joint. The joint below the overlay can deflect, causing a vertical sliding of the overlay. The combination of Mode I and Mode II cracking is called Mixed-Mode cracking (Anderson, 2005).

In order to investigate these and other mechanisms, a full-scale test was developed at the Advanced Transportation Research and Engineering Laboratory (ATREL) at the University of Illinois. This test included four different pavement configurations using three different asphalt concrete mixtures. In addition to the typical mixture characterization (creep compliance, tensile strength, dynamic modulus, Mode I fracture energy), the three asphalt concrete mixture's Mixed-Mode fracture properties were also investigated. This paper will review one asphalt concrete mixture's characterization and will report on lessons learned and improvements to be implemented in future testing of the other two mixtures.

1.2 *Objectives*

There were three primary objectives to this research:

- Explore various Mixed-Mode fracture testing configurations that are used in engineering materials

- Determine fracture energy, from Crack Mouth Opening Displacement (CMOD), Crack Tip Opening Displacement (CTOD), and Crack Tip Sliding Displacement (CTSD) with one asphalt mixture, using the Single-Edge Notch Beam with an offset notch
- Discuss lessons learned and future improvements

2 MIXED-MODE TESTING CONFIUGRATIONS

There are several existing Mixed-Mode testing configurations. In the fields of metal, plastic, rock, and Portland Cement Concrete, extensive testing has been performed. However, three configurations seemed to be used in a higher frequency, the Brazilian Disk with an angled interior notch, the Compact Tension Shear, and the Single-Edge Notch Beam with an offset notch. These three configurations are reviewed below.

2.1 *Brazilian disk with angled interior notch*

The first configuration reviewed is a Brazilian Disk with an angled interior notch, as seen in Figure 1. Shetty *et al.* (1987) investigated Mixed-Mode fracture of soda-lime glass. Krishnan et al. (1998) studied fracture toughness tests under Mode I, Mode II, and Mixed-Mode loading. They used the straight-edge Brazilian disk (SENBD) specimens. By angling notch in the middle of the specimen they were able to capture a range of Mixed-Modality. The tests were run on a soft, weakly-cemented, porous, natural Antler sandstone. Khan *et al.* (2000) used Brazilian disk specimens under diametrical compression for Mixed-Mode fracture toughness of a limestone rock. The fracture toughness increased with increase of diameter but had no significant variation with a varied notch length. The test did not significantly vary with a changed notch type (chevron vs. straight) either. Al-Shayea *et al.* (2000) also used the straight notched Brazilian disk under diametrical compression to investigate the fracture toughness of limestone rock.

2.2 *Compact tension shear*

The second testing configuration reviewed is the Compact Tension Shear. This configuration involves a compact tension specimen that is placed in a special fixture that can rotate in order to obtain several levels of mode-mixity. Hallbäck's (1997) goal was to investigate

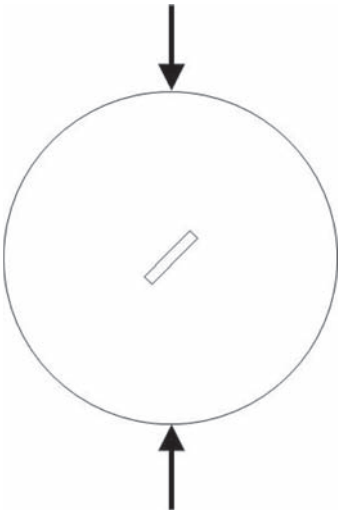

Figure 1. Brazilian disk with angled interior notch.

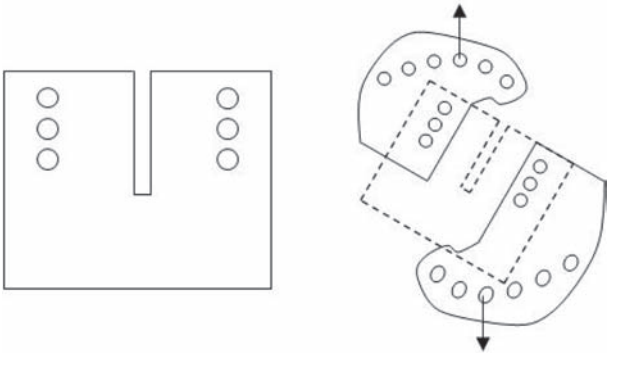

Figure 2. Compact tension shear sample (left) and fixtures (right).

implications of local crack tip processes on macroscopic mixed-mode fracture behavior of high strength steel using Arcan specimen and compact-tension-shear setups. The specimens were fatigued under mode I loading. This arraignment allowed for a range of Mixed-Mode levels and hypothetically provided a pure Mode II test. Figure 2 shows a Compact Tension Shear set-up.

Using the Compact Tension Shear test setup, Lin *et al.* (2003) found Mode I and Mode II stress intensities for initial straight cracks and subsequent kinked cracks assessed by method of caustics using geometrically equivalent specimens of polymethyl methacrylate (PMMA). The angle of formation had value of 72° for pure Mode II loading and 70.5° for max hoop tension. The crack initiation toughness in pure Mode II loading was less than the toughness in Mode I loading because there was no transformation zone shielding, where shielding occurs when the crack-tip stress intensity is less than the applied stress intensity. Saito *et al.* (2004) found that creep crack growth rates under combined Mode I and Mode II loadings could be correlated with a single effective stress intensity factor K_{Ieff}, which is based on a combined mode fracture envelope using the compact tension shear test. They found that a crack tends to grow normal to applied load with plastic opening and shearing displacements of crack tip and that the value of crack tip opening angle increases as component of Mode II increases.

2.3 *Single-edge notch beam with offset notch*

There has been much work done with the Single-Edge Notch Beam [SE(B)] with an offset notch, especially in the field of Portland Cement Concrete, as beam testing is very popular in this field. Figure 6 shows a schematic of the SE(B) configuration. Gdoutos *et al.* (1987) looked at shifting the notch from the center to the edge, and observed the behavior of K_I and K_{II}, as seen in Figure 3. On a beam that was 20 cm long, the K_I was at a maximum when the notch was located directly under the loading head, or an offset of zero, while K_{II} reached a maximum when the offset was approximately 5 cm, or when the notch was halfway between the middle of the specimen and the edge of the sample. Similarly, Fett (1991) looked at the stress distribution of samples when offsetting the notch on a beam specimen.

Jenq *et al.* (1988) looked at crack initiation angles, final failure path, and crack instability. In addition, they defined and explored important fracture parameters such as Crack Tip Displacement (CTD), Crack Tip Opening Displacement (CTOD), and Crack Tip Sliding Displacement (CTSD) as shown in Figure 4. Similarly, the Crack Mouth Displacement

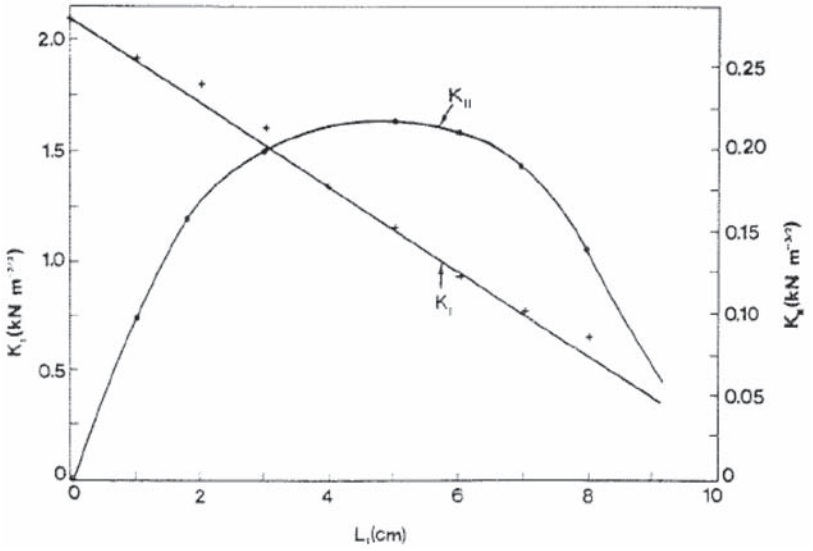

Figure 3. SE(B) K_I and K_{II} behavior with an offset notch (from Gdoutos *et al.*, 1987).

(CMD) was the vector sum of Crack Mouth Opening Displacement (CMOD) and Crack Mouth Sliding Displacement (CMSD).

While these tests have all been run in materials other than asphalt concrete, testing has been done at the University of Illinois exploring Mixed-Mode properties of asphalt concrete.

2.4 *Mixed-mode testing of asphalt concrete*

Two testing configurations have been explored in Mixed-Mode testing of asphalt concrete: the Semi-Circular Bend [SC(B)] and the Single-Edge Notch Beam [SE(B)]. TU Delft has looked into angling the notch at the bottom of a SC(B) test in order to obtain Mixed-Mode properties (Molenaar et al., 2002). However, since the SE(B) has already been tested at the University of Illinois, this test set-up was followed. Wagoner *et al.* (2005a, 2005b) developed the use of the SE(B) to test fracture properties of asphalt concrete, and off-set the notch in order to obtain Mixed-Mode properties. Wagoner tested one mixture using an offset notch, first with a 65 mm offset notch, then with three levels of offset. They found that as the notch became further offset, a point was reached when the crack no longer propagated from the notch, but from the bottom of the SE(B) sample, where no notch was located. This critical notch location occurred between 82–90 mm from the center of the beam. This value is in good agreement with the research in Portland Cement Concrete (Jenq *et al.* [1988]), which found the region of center failure versus notch failure occurred near 100 mm. Fracture energy was calculated from finding the area under the load versus CMOD curve. One of the recommendations from Wagoner's work was to measure both the CTOD and the CTSD. This theoretically captures both the Mode I and Mode II fracture energies.

This study will explore one asphalt concrete mixture with a range of offset notches (approximately 25, 50, 75, 100, and 125 mm from the center of the span), as studied through the measurement of CMOD, the CTOD, and the CTSD on beams tested in three-point bending.

3 TEST RESULTS

For this study, one mixture was investigated. The mixture was a 9.75 mm Nominal Maximum Aggregate Size (NMAS) mixture with a PG64-22 binder. Samples were compacted using a slab compactor designed and built at the University of Illinois. Figure 5 shows the beam compactor with the mold and the compaction mold.

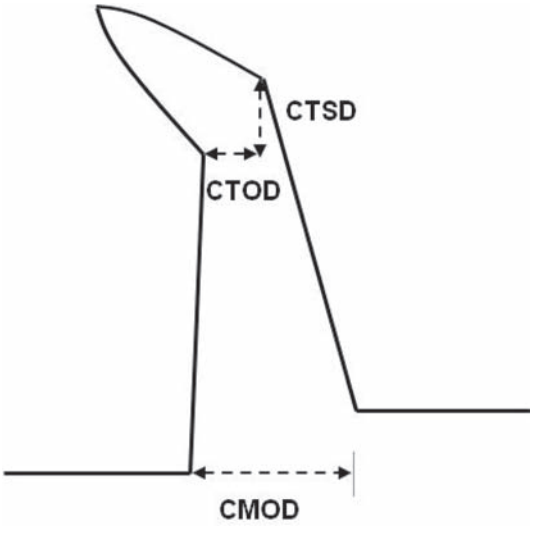

Figure 4. Fracture parameters.

Air voids were targeted at 4 percent. The beams were compacted and trimmed on the top and the bottom so the final specimen dimensions were 378 mm wide by 100 mm tall by 75 mm deep. The trimmed faces provided a smooth surface for the supports on the bottom of the beam and for the loading head on top of the beam. In the Mode I testing configuration for the SE(B), the 19 mm deep notch is placed directly underneath the loading head, as seen in Figure 6.

In Figure 6, the CMOD gage would be placed at the bottom of the notch, between the two arrows. However, since the CMOD, CTOD, and CTSD needed to be measured for this study, extra gage points allowing for proper gage orientation needed to be included.

3.1 *Gage configuration*

In Figure 6, the gage points for the CTOD gage can be seen on the front of the specimen, just next to the top of the notch. The CTSD gage points are located in a similar position, oriented in a vertical direction. In this manner, the CTOD was captured from the front of the specimen, while the CTSD was capture on the back of the specimen. Figure 7 shows a schematic of the gage points on the front and back of the SE(B).

The global fracture energy was still captured using a CMOD gage on the crack mouth. Therefore, for each sample, three displacements were captured: CMOD, CTOD, and CTSD.

3.2 *Test results*

One mixture was used in evaluating the SE(B) configuration with an offset notch, with the CMOD, CTOD, and CTSD captured on each sample. The tests were run at –12°C, under

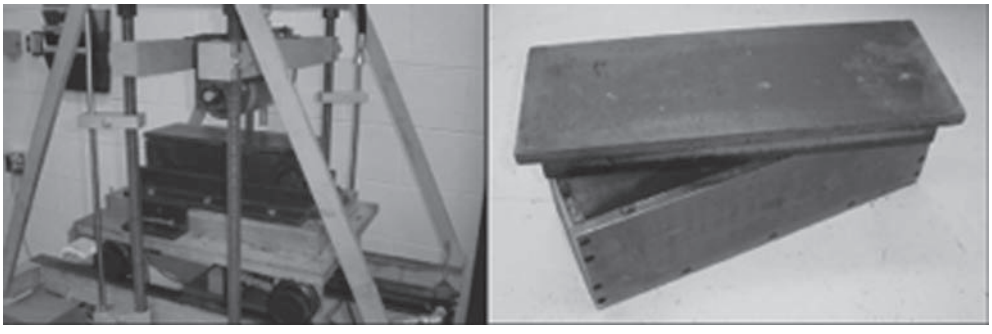

Figure 5. Beam compactor with mold (left) and compaction mold (right).

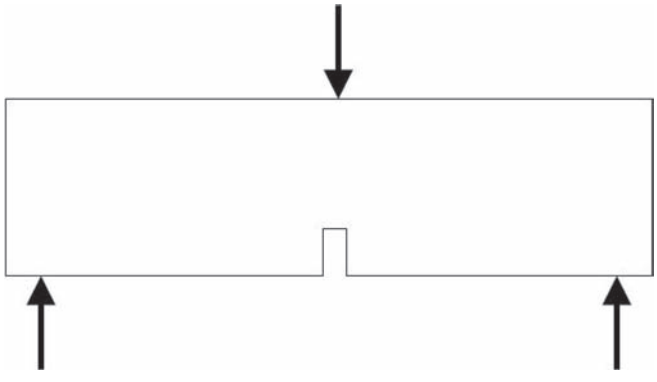

Figure 6. Single edge notch beam in mode I testing configuration.

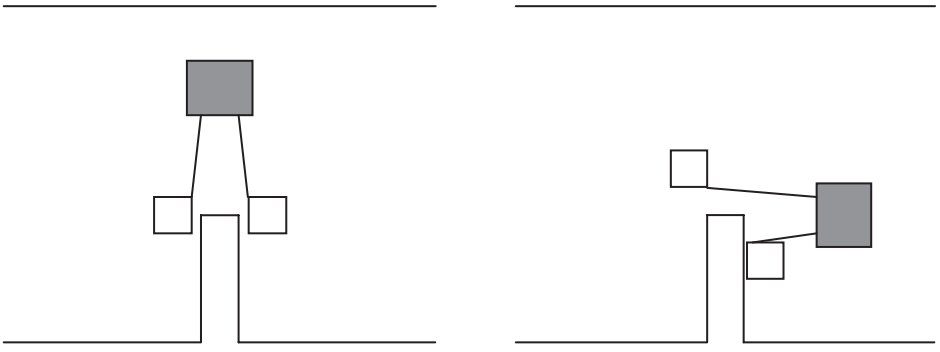

Figure 7. CTOD gage and gage points on the left; CTSD gage and gage points on the right (not to scale).

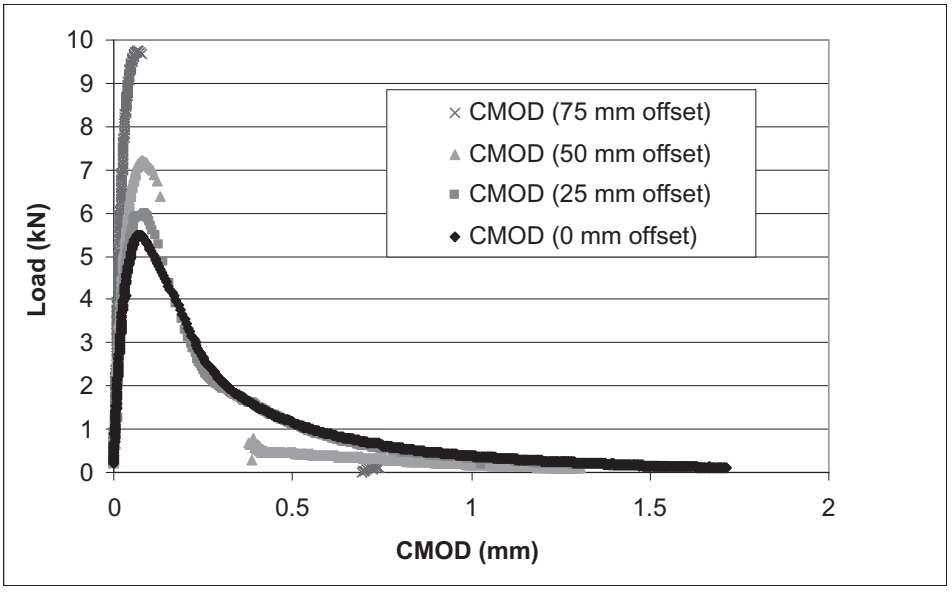

Figure 8. Example load vs. CMOD curves.

Load-Line Displacement control, at a rate of 5 mm/min. Figures 8–10 show the full load versus crack displacement curves, for all three measured crack displacements. As the notch offset from center increased, the peak load increased. For the CMOD, the softening curve shifted downward and to the left. From the curves, it appears that the peak load increases as the notch moves further from the center, while the softening curve for the CMOD and CTOD shifts down and to the left. With a notch offset of greater than 25 mm, the CMOD and CTOD curves lose their softening tail. One explanation is that Mode II fracture energy does not include softening. Therefore, when the Mode II component is increased, the softening characteristics decrease.

In Figures 8–10, it is worth noting that a break occurs in the curves as the offset increases. This occurs because as the Mode II influence increases, the softening characteristics decrease. After the crack initiation, there is very little crack propagation.

Since the softening curve decreased in significance as the notch was offset, the fracture energy was measured only up to crack propagation, or where the macro-crack began. This fracture energy will be referred to as fracture work, since the concept of energy includes softening characteristics. Even though fracture energy could be calculated for some of the

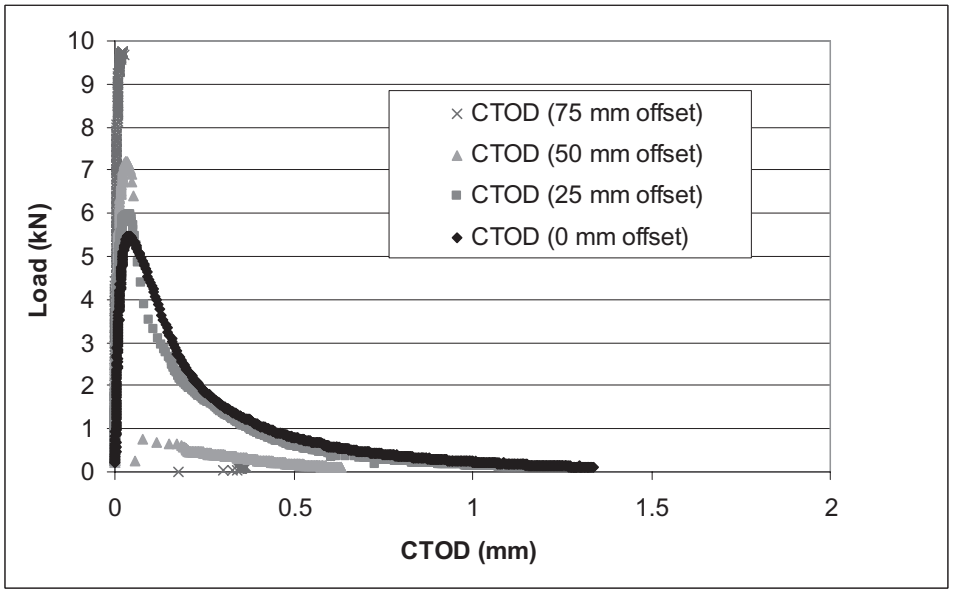

Figure 9. Example load vs. CTOD curves.

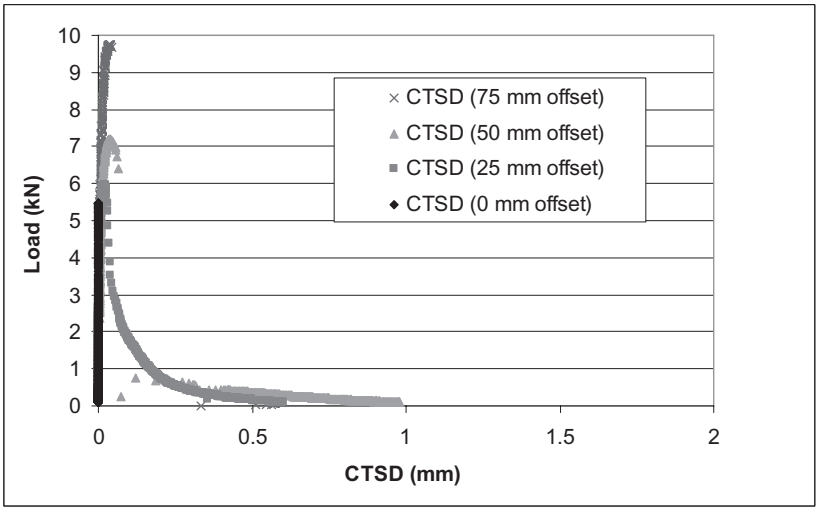

Figure 10. Example load vs. CTSD curves.

notch offset specimens, all specimen's fracture work was calculated until the point of crack initiation so that all sets of data could be fairly compared to each other. Based on previous research, the macro-crack began just past the peak load, at approximately 95% of the peak load (Wagoner *et al.*, 2005a). Therefore, the fracture work was found by taking the area under the load/crack displacement curves from the beginning of the test, through the peak load, to 95% of the peak load. Preliminary results of the Mixed-Mode test are found in Table 1, with each notch offset representing three replicates.

At 102 and 127 mm, the stresses in the bottom of the beam exceeded the tensile strength of the specimen. These stresses were also higher than the stresses that developed at the notch, but the stresses at the notch were not high enough to begin crack propagation. There may

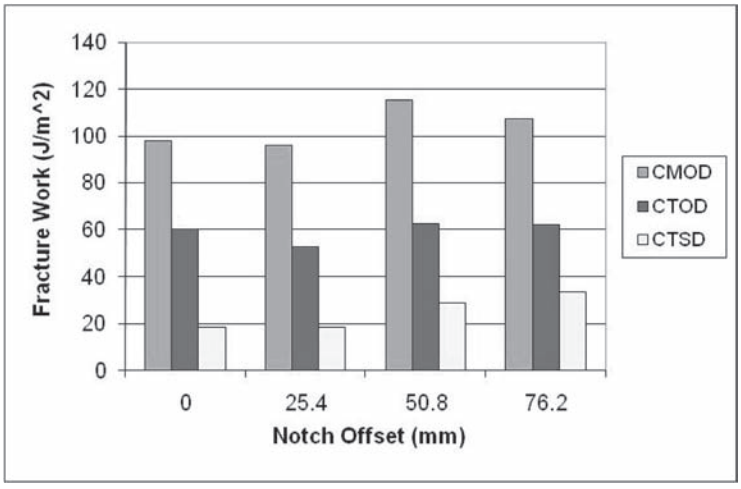

Figure 11. Mixed-mode testing of asphalt concrete.

Table 1. Mixed-mode testing of asphalt concrete.

Notch offset (mm)	Peak load (kN)	Fracture work (J/m^2)		
		CMOD	CTOD	CTSD
Zero	5.81	98.0	59.9	18.6
25.4	5.95	95.9	52.4	18.6
50.8	7.21	115.3	62.2	28.7
76.2	9.35	107.2	61.9	33.5
101.6	10.61	Broke in middle		
127.0	10.50	Broke in middle		

have been damage at the notch, but a macro-crack did not form. In Figure 11, a summary of the Mixed-Mode data is provided.

It can be seen that there is a general increase of fracture work as the notch moves further from the center. In addition, the CTSD is increasing as the notch moves to the side. This indicates, as expected, an increase of Mode II fracture work as the notch is offset.

4 CONCLUSIONS AND RECOMMENDATIONS

There are several promising testing configurations to capture Mixed-Mode fracture properties of asphalt concrete in the laboratory, including the Brazilian Disk with an angled interior notch, the Compact Tension Shear, and the Single-Edge Notch Beam with an offset notch. Based on laboratory equipment available and prior work, the Single-Edge Notch Beam with an offset notch was chosen to further investigate Mixed-Mode properties of a single asphalt mixture. Important findings include:

- Unlike previous research, the Crack Mouth Opening Displacement (CMOD), Crack Tip Opening Displacement (CTOD), and Crack Tip Sliding Displacement (CTSD) were captured.

- Increasing the notch offset tended to shift the softening curve down and to the left, while increasing the peak load. However, when the notch offset was greater than 100 mm, the specimen broke at the middle of the specimen instead of at the notch.
- For this one asphalt mixture, the CMOD fracture work increased as the notch moved further from the center, as did the CTSD. This indicates, as expected, an increase of Mode II fracture work as the notch is offset.

There are several steps that need to be taken in order to more understand Mixed-Mode properties of asphalt concrete. First, more mixtures need to be investigated, as this work only looked at one mixture. Second, understanding the complex relationship between CMOD, CTOD, and CTSD fracture energy and fracture work needs to be evaluated. More literature in other materials should be reviewed in order to determine how these fracture properties are evaluated. Also important is the influence of the softening curve. Since crack propagation is not considered in this study, the impact of neglecting this should be understood. Changing the test from monotonic loading to a dynamic loading could decrease this issue. Finally, the test set-up should be reevaluated, as the true CTOD and CTSD should be measured at a point 45° from the center of the tip of the notch, whereas here they were measured right at the crack tip of the notch. This shift in measurement could change the results shown in Figure 11.

REFERENCES

Al-Shayea, N.A., Khan, K. & Abduljauwad, S.N. 2000. Effects of Confining Pressure and Temperature on Mixed-Mode (I–II) Fracture Toughness of a Limestone Rock, *International Journal of Rock Mechanics and Mining Sciences* 37: 629–643.

Anderson, T.L. 2005. Fracture Mechanics, Fundamentals and Applications, Third Edition, Taylor and Francis, CRC Press.

Fett, T. 1991. Mixed-Mode Stress Intensity Factors for Three-Point Bending Bars, *International Journal of Fracture* 48 (R57–R74).

Gdoutos, E.E. & Zacharopoulos, D.A. 1987. Mixed-Mode Crack Growth in Plates Under Three-Point Bending, Experimental Mechanics 27(4): 366–369.

Hallbäck, N. 1997. Mixed-Mode I/II Fracture Behaviour of a High Strength Steel. *International Journal of Fracture* 87: 363–388.

Jenq Y.S. & Shah S.P. 1988. Mixed-Mode Fracture of Concrete. *International Journal of Fracture* 38: 123–142.

Khan, K. & Al-Shayea, N.A. 2000. Effect of Specimen Geometry and Testing Method on Mixed-Mode I-II Fracture Toughness of a Limestone Rock from Saudi Arabia. Rock Mechanics and Rock Engineering 33(3): 179–206.

Krishnan, G.R., Zhao, X.L., Zaman, M. & Roegiers, J.C. 1998. Fracture Toughness of a Soft Sandstone. *International Journal of Rock Mechanics and Mineral Science* 35(6): 695–710.

Lin, G.Y. & Shetty, D.K. 2003. Transformation zones, crack shielding, and crack-growth resistance of Ce-TZP/alumina composite in mode II and combined mode II and mode I loading. Engineering Fracture Mechanics 70: 2569–2585.

Molenaar, A.A. Scarpas, A.A., Liu, X. & Erkens, S.M.J.G. 2002. Semi-Circular Bend Test: Simple but Useful? *Journal of the Association of Asphalt Paving Technologists* 71: 795–815.

Saito, Y. & Yoda, M. 2004. Fracture Toughness and Creep Crack Growth in Polypropylene Under Combined Modes I and II Loading. *International Journal of Fracture* 127: L161–L166.

Shetty D.K., Rosenfield A.R. & Duckworth W.H. 1987. Mixed-mode fracture in biaxial stress state: application of the diametral compression (Brazilian Disk) Test. Engineering Fracture Mechanics 26: 825–839.

Wagoner, M.P., Buttlar, W.G. & Paulino, G.H. 2005a. Development of a Single-Edge Notched Beam Test for Asphalt Concrete Mixtures, *Journal of Testing and Evaluation* 33(6): 452–460.

Wagoner, M.P., Buttlar, W.G. & Paulino, G.H. 2005b. Development of a Single-Edge Notched Beam Test for the Study of Asphalt Concrete Fracture. Geotechnical Special Publication No. 130: *Advances in Pavement Engineering, Proceedings of Sessions of the GeoFrontiers 2005* Congress, Austin, TX.

Advanced Testing and Characterization of Bituminous Materials – Loizos, Partl, Scarpas & Al-Qadi (eds)
© 2009 Taylor & Francis Group, London, ISBN 978-0-415-55854-9

Fatigue lines for asphalt mixtures used in wearing course

C. Răcănel, C. Romanescu, M. Dicu, A. Burlacu & C. Surlea
Technical University of Civil Engineering, Bucharest, Romania

ABSTRACT: The degradations of pavement structures—consisting in cracks in the asphalt layers—that resulted from repeated load of bituminous layers are very important. Therefore, it is necessary that the bituminous material to be studied and tested in the laboratory, with the aim to minimize the effects of fatigue during service. In laboratory, the fatigue is simulated by two types of controlled load can be applied: constant stress and constant deformation. Among the tests for fatigue performed at constant strain recommended by the European norms testing, the four point bending test can be found that is usefull. This paper has the purpose to present the results obtained on Romanian asphalt mixtures from the wearing course, using this type of fatigue testing, with the equipment recently acquired by the Roads Laboratory of the Technical University of Civil Engineering Bucharest.

1 INTRODUCTION

Fatigue is defined as a failure phenomenon under repeated or fluctuant effort, having a maximum value, generally smaller than the tension resistance of material (Di Benedetto et al.1997); (Huang et al. 1993); (The Shell Bitumen Handbook.1990); (Bitumes et enrobés bitumineux. 1971); (COST 333. 1999). Figure 1 shows the tension stress that occures to the bottom of the bituminous layers and that leads to tensions strain.

The vertical compression stress acts on aggregate skeleton and the tension strain acts on bituminous mastic. Figure 2 shows the stress and strain variation at the top and the bottom of bituminous layers pack when a wheel passes.

So, the fatigue appears and develops because of repeated tension strains coming from traffic loads that determine the tension stresses from pavement. Although the maximum value of these tension strains is situated at the bottom of the bituminous layers, there are tension stresses and strains at the top of bituminous layers, not in the load axis (under the wheel track) but outside of the wheel track.

Because of repeated loads, there are initiated cracks and propagated in the layer at the same time with traffic intensification, finally leading at fatigue failure of the pavement.

These degradations of pavement structures that resulted from repeated load of bituminous layers are very important. Therefore, it is necessary that the bituminous material to be studied and tested in the laboratory, with the aim to minimize the effects of fatigue during service.

The changing of normal and shear efforts versus time, under the action of a given traffic load, is illustrated in Figure 3.

In order to obtain these effects, the real state of stresses and strains in a pavement structure for repeated loads is simulated in laboratory. In the fatigue study of asphalt mixtures, two types of controlled load can be applied: constant (controlled) stress and constant (controlled) deformation.

Under constant stress testing, the effort remains constant, but the deformation increases with the number of applied loads, while under the constant deformation test the deformation is maintained constant and the effort decreases with the number of applied loads.

The first type of test has the advantage that failure comes faster and can be easily defined, while for the constant deformation testing an arbitrary failure criteria is frequently used.

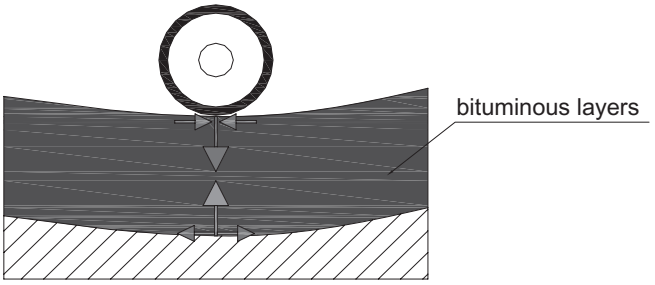

Figure 1. Tension stress and strain in bituminous layers.

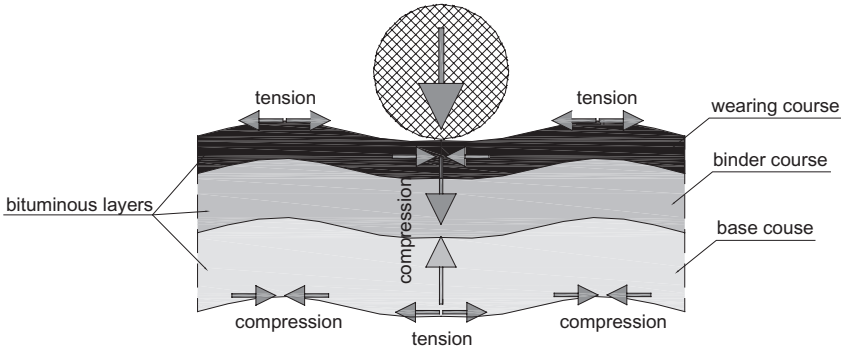

Figure 2. Stress and strain variation in a bituminous layers pack.

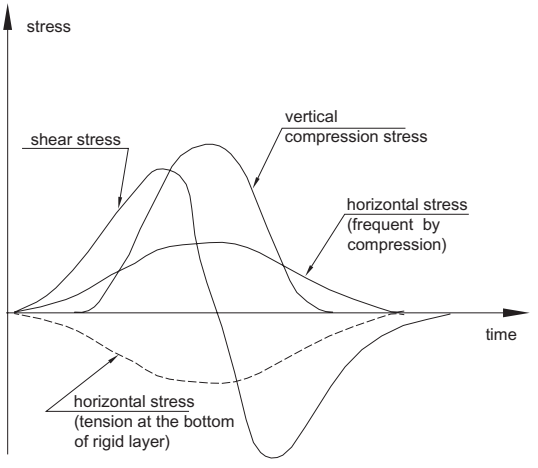

Figure 3. Changing of stress under a mobile load passing (The Shell Bitumen Handbook.1990).

It is known that (Doan. 1977):

– thin asphalt layers (<6 cm) are submitted to a constant strain;
– thick asphalt layers (>15 cm) are submitted to a constant stress.

Consequently, the behavior of asphalt concrete—like BA16, BAR16, MASF16 asphalt concrete type from Romanian standards (SR EN 174.2002)—from wearing course (with

4 cm thickness) at a fatigue test under constant strain, not under constant stress, should be studied.

To determine the asphalt mixtures stiffness and to evaluate the asphalt mixtures fatigue behavior, European norms, which are adopted in our country, require carrying out some appropriate laboratory testing. Among the tests recommended by the European norms, the four point bending test can be found that is performed at constant strain (controlled) in time, on prismatic asphalt mixture samples made in the laboratory, using the roller compactor (SR EN 12697/24 .2005); (SR EN 12697/26.2005).

This test is made on prismatic asphalt mixture samples submitted under a sinusoidal load. The prismatic beam is subjected to four-point periodic bending with free rotation and translation at all load and reaction points. During the test, the load required to bend the sample, the deflection and the phase angle can be measured as a function of time. The test is considered finished when the force reaches half of its initial value (Figs 4, 5).

The asphalt mixtures are viscoelastic materials; their viscoelastic behavior is mainly determined by the presence of bituminous binder. The properties of the materials with hydro carbonated binder depend on temperature and rate of applied loading. When a sinusoidal stress is applied on a certain sample of asphalt mixture, the resulting strain comes with a delay because of the phase angle, δ (Fig. 5).

Thus, it will be established the fatigue behavior of this asphalt mixtures taking into account the climate conditions and the mixture composition. Because of the climate conditions of our country, that are characterized by both high values of temperature during the summer and low values during the winter, the mixture must be designed to have a good behavior at both high temperatures and low temperatures.

This paper has the purpose to present the results obtained on Romanian asphalt mixtures from the wearing course, using this type of fatigue testing, with the equipment recently acquired by the Roads Laboratory of the Technical University of Civil Engineering Bucharest.

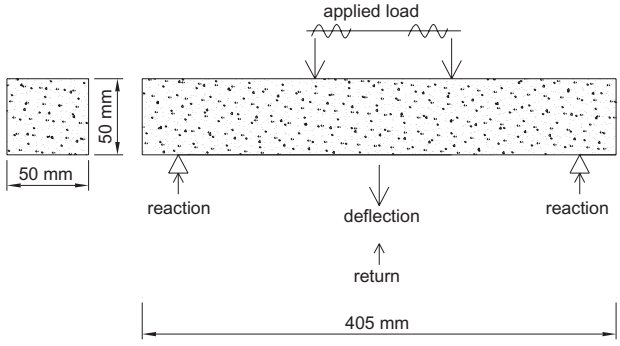

Figure 4. The four points bending test.

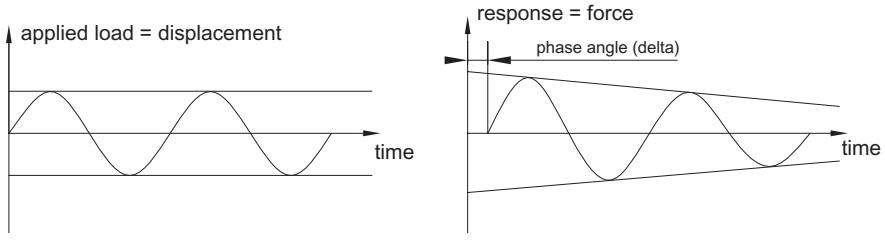

Figure 5. The load and response in the case of fatigue apparatus for four points bending test.

2 LABORATORY TEST, USED MATERIALS AND ASPHALT MIXTURE RECIPES

Asphalt mixture samples of the beam type were obtained by sawing at required dimensions (50 × 50 × 405 mm) from slabs compacted in laboratory with the roller compactor (SR EN 12697/33.2003), Figure 6. The compaction conditions were the following, from table 1.

The prismatic samples have been tested at four points bending apparatus (Fig. 7) under constant deflection, sinusoidal applied, having 30 Hz frequency. The test temperatures were 30°C and 20°C, according to European norms (SR EN 13108/20.2005), climate conditions of our country and taking into account the weather changes in temperature by it's increasing.

This study was carried out in Roads Laboratory of Faculty of Railways, Roads and Bridges (Technical University of Civil Engineering of Bucharest) on three types of asphalt mixtures frequently used in our country: a classic asphalt mixture, BA16 type, a rugged asphalt mixture, BAR16 type and an asphalt mixture with fiber, MASF16 type.

The aggregates used to prepare the asphalt mixture were of Turcoaia and the filler, of Basarabi. It was used a bitumen of Romania, Arpechim D 60/80. The fiber from MASF16 mixture was Topcel.

The grading curves and grading zones for the studied asphalt mixtures are shown in Figure 8, 9 and 10 and the asphalt mixtures recipes are presented in table 2. Figure 11 shows a comparison between asphalt mixture grading curves. It can be noticed that the grading curves of BA16 and BAR16 are very close to each other, especially because of asphalt mixtures grading zones stipulated in Romanian norms (SR EN 174.2002) and particularly because of aggregate type grading zone. Table 3 shows it required percentages for aggregates mixture and filler by 100% aggregates (SR EN 174.2002).

Figure 6. Roller compactor for asphalt mixture samples.

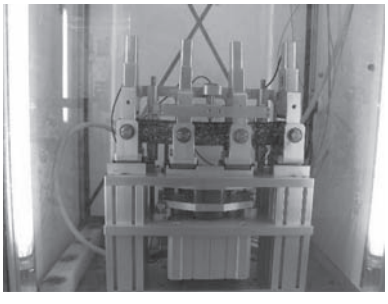

Figure 7. Four points bending apparatus for asphalt mixtures fatigue testing.

Table 1. The compaction conditions used for roller compactor.

Applied Pressure, bar	Number of passes
P1 = 2.4	2
P2 = 2.6	25
P3 = 3.25	20
P4 = 6.75	15

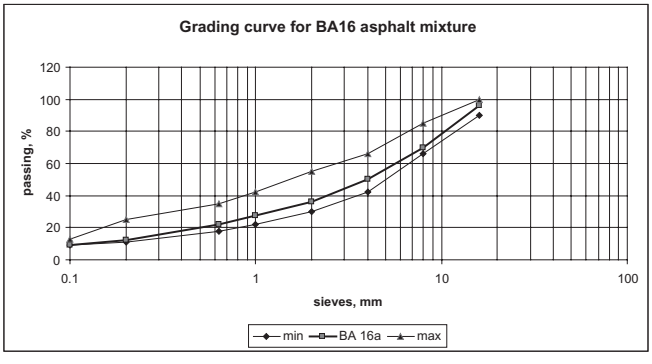

Figure 8. Grading curve and grading zone for BA16 asphalt mixture.

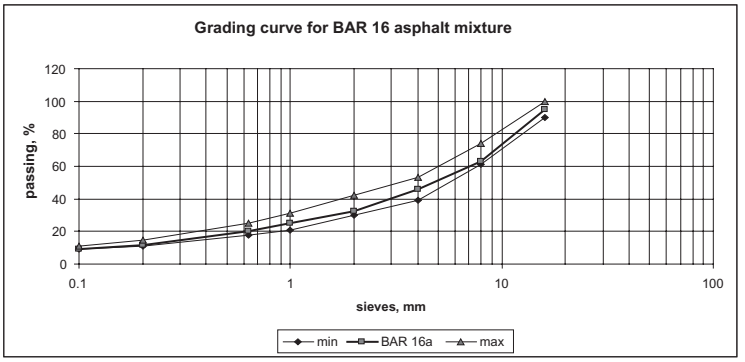

Figure 9. Grading curve and grading zone for BAR16 asphalt mixture.

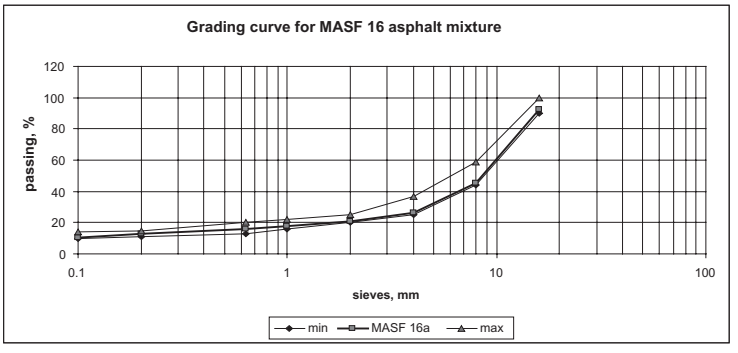

Figure 10. Grading curve and grading zone for MASF16 asphalt mixture.

Table 2. The recipes of the used asphalt mixtures.

Mixture	% Crashed rock 8/16	4/8	0/4	% Filler	% Fiber by mixture	% Bitumen by mixture
BA16	28	23	38	11	–	5.75
BAR16	35	20	34	11	–	5.60
MASF16	53	22	12	13	0.6	6.50

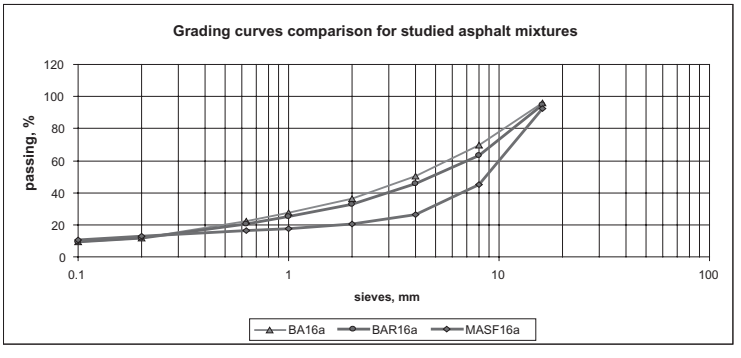

Figure 11. Grading curves comparison for studied asphalt mixtures.

Table 3. The required percentages for aggregates mixture and filler by 100% aggregates.

Mixture	% Filler	% Crashed rock >4 mm in size	% Crashed rock 0 … 4 mm in size
BA16	9 … 13	34 … 58	difference till 100%
BAR16	9 … 11	47 … 61	
MASF16	10 … 14	63 … 75	

3 EXPERIMENTAL RESULTS

In order to reach the goal of this paper, the prismatic samples were tested at three levels of strain, with a minimum of six repetitions per level, according to european norms (SR EN 12697/24.2005); (SR EN 12697/26.2005), SR EN 13108/20.2005). In table 4 and 5 the values of imposed strain, the number of cycles corresponding to the fatigue resistance, the values of stiffness modulus and phase angle of the studied asphalt mixture are presented.

From the above tables, there can be noticed the values of stiffness modulus depending on strain level of test. The stiffness modulus decreases with the increase of strain level only for

Table 4. Number of cycles, stiffness modulus and phase angle values for asphalt mixtures studied in certain testing conditions (T = 30°C).

Asphalt mixture type	Frequency [Hz]	Temperature [°C]	Strain [10^{-6}]	Number of cycles	Stiffness [MPa]		Phase angle [^{0}]		Stress [kPa]	
					initial	final	initial	final	initial	final
BA16	30	30	250	84941780	2895	1420	56	57	1099	575
	30	30	350	3247506	4779	2414	40	52	1135	607
	30	30	400	868989	3558	1782	44	59	1186	631
BAR 16	30	30	300	13945517	3099	1546	47	46	884	464
	30	30	350	2056250	4355	2205	33	59	1461	778
	30	30	400	216192	3909	1959	46	58	1484	783
MASF 16	30	30	300	950620	8575	4289	31	45	2445	1290
	30	30	350	163704	3943	1974	39	55	1312	692
	30	30	400	38975	3604	1785	39	58	1367	720

Table 5. Number of cycles, stiffness modulus and phase angle values for asphalt mixtures studied in certain testing conditions (T = 20°C).

Asphalt mixture type	Frequency [Hz]	Temperature [°C]	Strain [10^{-6}]	Number of cycles	Stiffness [MPa]		Phase angle [°]		Stress [kPa]	
					initial	final	initial	final	initial	final
BA16	30	20	200	3325299	6795	5360	26	35	1296	1073
	30	20	300	242500	7318	3935	30	39	2098	1191
	30	20	400	59920	8376	4180	27	41	3186	1671
BAR 16	30	20	250	476224	9779	4880	24	29	2328	1222
	30	20	280	202653	9818	4940	21	34	2622	1387
	30	20	300	59989	10115	5022	26	32	2881	1520
MASF 16	30	20	200	295686	12779	8570	13	17	2431	1737
	30	20	250	75363	11115	5535	14	26	2634	1388
	30	20	300	43270	10784	5361	18	25	3075	1611

MASF 16 asphalt mixture, as it must happen. Unfortunately, this does not occure for the other two mixtures, maybe because of too low strain level considered in the beginning of the test. More samples and studies have to be performed in this case.

The results obtained from laboratory test are represented graphically, from the mixture type point of view, in Figures 12–17.

Based on what was presented, the fatigue lines can be drawn up by considering in the abscissa, in logarithmic scale, the number of applied cycles and in ordinate line, in logarithmic scale, the initial strain applied (Figs 18–22).

The fatigue lines are useful to estimate the service life corresponding to a certain level of strain.

In table 6 the values for slope of fatigue line and initial strain corresponding with a fatigue life of 10^6 cycles are presented.

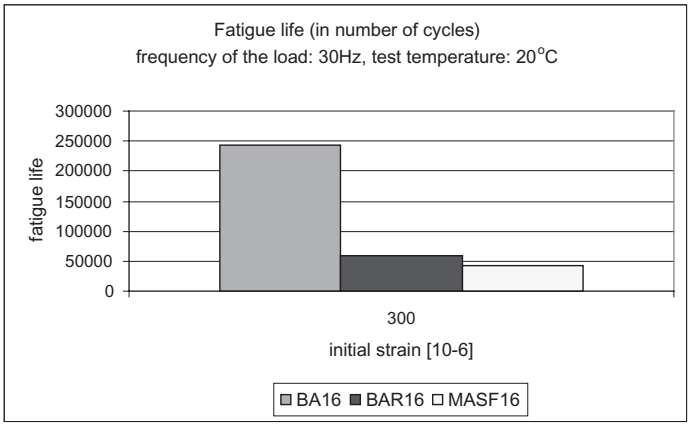

Figure 12. Fatigue life for different asphalt mixtures (T = 20°C).

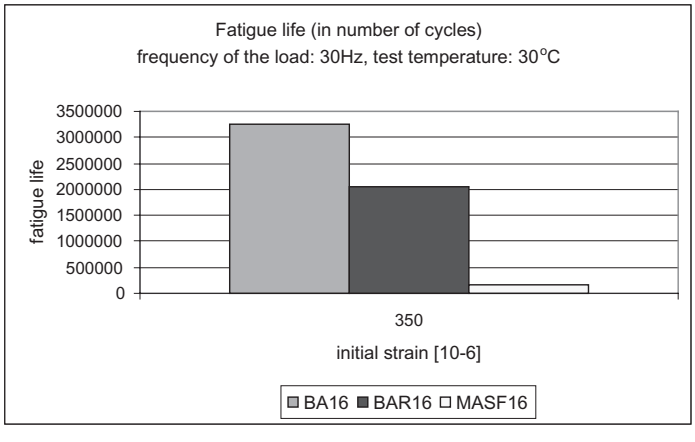

Figure 13. Fatigue life for different asphalt mixtures (T = 30°C).

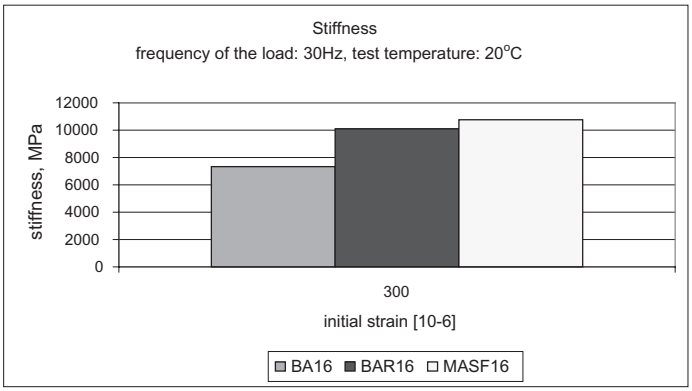

Figure 14. Stiffness modulus for different asphalt mixtures (T = 20°C).

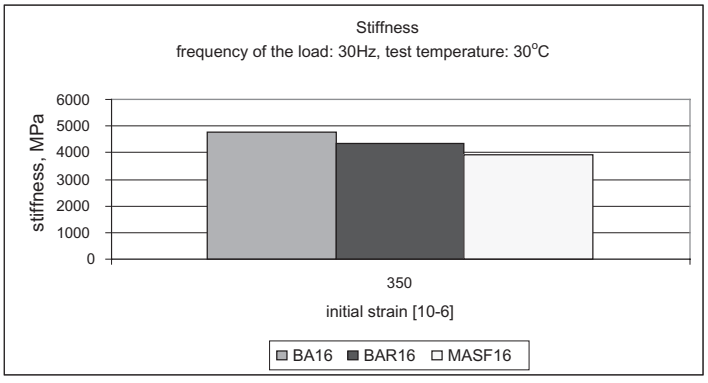

Figure 15. Stiffness modulus for different asphalt mixtures (T = 30°C).

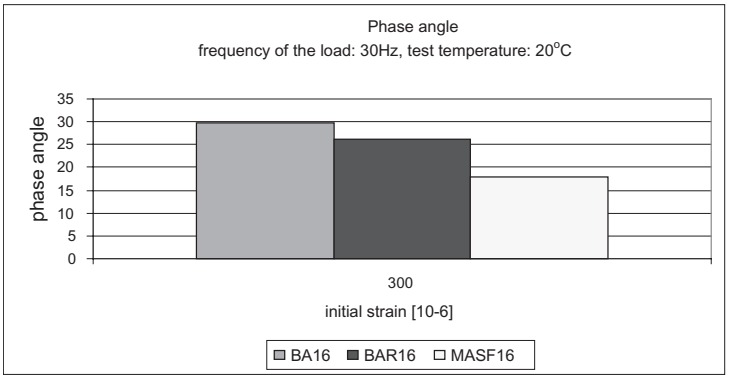

Figure 16. Phase angle for different asphalt mixtures (T = 20°C).

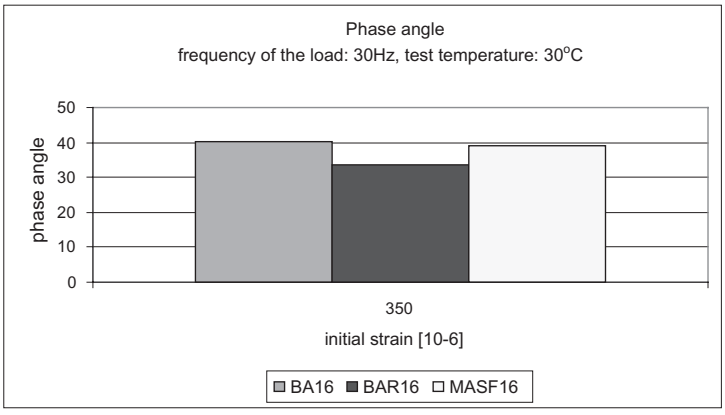

Figure 17. Phase angle for different asphalt mixtures (T = 30°C).

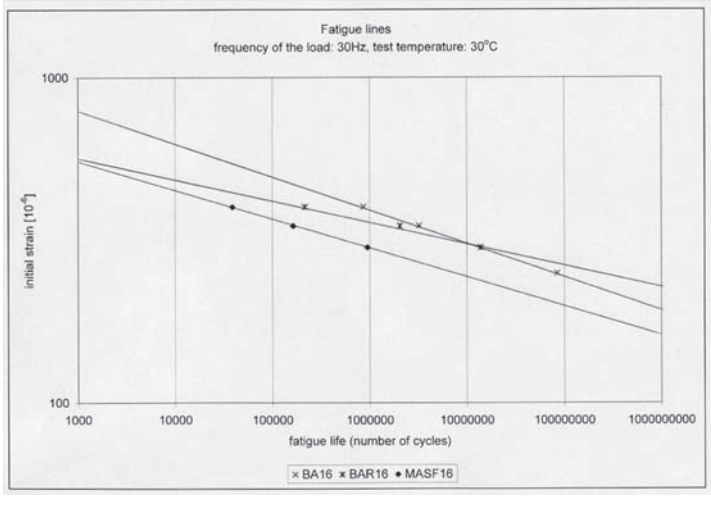

Figure 18. Fatigue lines, temperature: 30°C—asphalt mixture type influence.

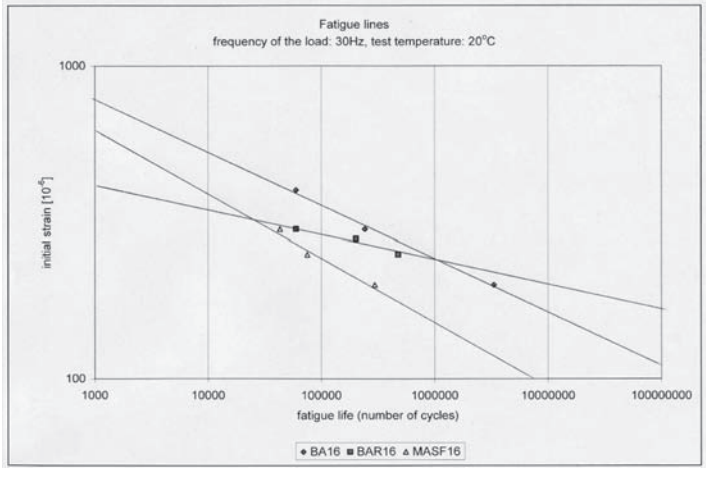

Figure 19. Fatigue lines, temperature: 20°C—asphalt mixture type influence.

Table 6. Slope of fatigue line and initial strain values for asphalt mixtures.

Asphalt mixture type	Frequency [Hz]	Temperature [°C]	Slope of fatigue line %	Initial strain for 10^6 cycles
BA16	30	30	35	400
BAR16	30	30	22	370
MASF16	30	30	27	300
BA16	30	20	57	220
BAR16	30	20	30	210
MASF16	30	20	72	50

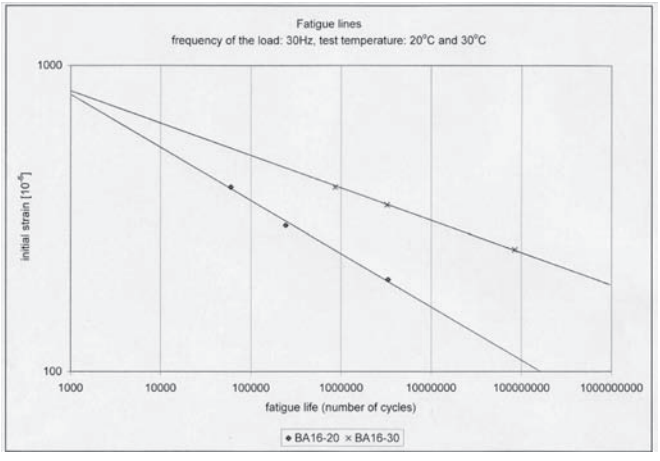

Figure 20. Fatigue lines, BA16 asphalt mixture—temperature influence.

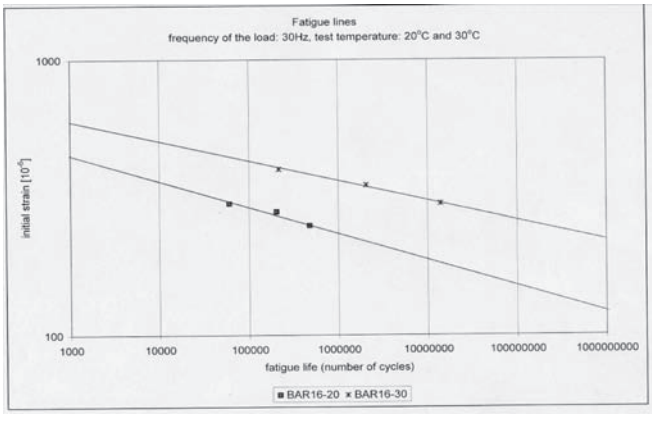

Figure 21. Fatigue lines, BAR16 asphalt mixture—temperature influence.

4 CONCLUSIONS

The conclusions that result from this study are presented bellow.

For the 4 point bending tests performed at 30 Hz frequency BA16 mixture presents fatigue life and phase angle values higher for both two test temperature used, compared to BAR16 mixture and MASF16 mixture (level of initial strain: 300 and 350).

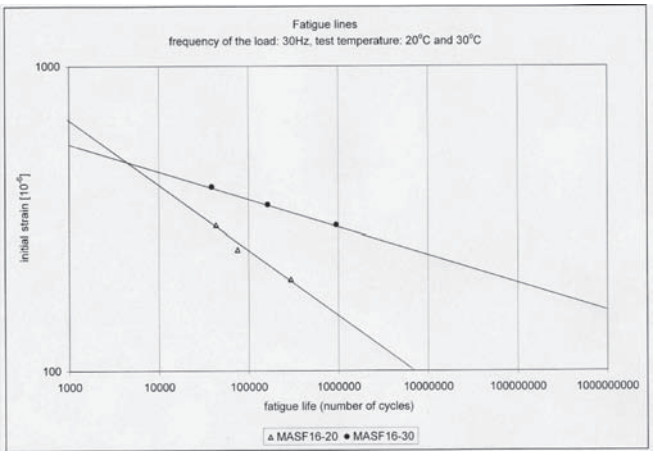

Figure 22. Fatigue lines, MASF16 asphalt mixture—temperature influence.

At 20°C test temperature MASF16 provides stiffness modulus higher than the other mixtures (level of initial strain: 300). At 30°C test temperature BAR16 provides stiffness modulus higher then the other mixtures (level of initial strain: 400).

For MASF 16 asphalt mixture the stiffness modulus decreases with the increase of strain level. The stiffness modulus increases with the decrease of temperature for the same strain level.

By comparing the fatigue lines it results that MASF16 mixture conducts faster to breaking than BA16 and BAR16 mixtures, so the number of applied cycles to fatigue is smaller, regardless of the asphalt mixture type, for 20°C test temperature. For 30°C test temperature BA16 mixture conducts faster to breaking than BAR16 and MASF16 mixtures; this results by comparing the slope of fatigue lines. For 10^6 applied load cycles at a level of initial strain can be obtained differently according to the asphalt mixture type: MASF16 asphalt mixture provides values of initial strain smaller with 25% than the BA16 mixture and with 19% than the BAR16 mixture, for 30°C test temperature; MASF16 asphalt mixture provides values of initial strain smaller with 77% than the BA16 mixture and with 76% than the BAR16 mixture, for 20°C test temperature; an increase of 10°C temperature conducts to a decrease of initial strain of 45% for BA16 mixture, 43% for BAR16 and 83% for MASF16 mixture.

It is necessary to perform more tests with this kind of equipment, in order to establish stiffness modulus and fatigue lines for different asphalt mixtures to obtain better results.

REFERENCES

Di Benedetto, H., De La Roche, C., Francken, L. 1997. Fatigue of Bituminous Mixtures: Different Approaches and RILEM Interlaboratory Tests, Mechanical Tests for Bituminous Materials, *RILEM*.

Huang, Yang. H. Inc., 1993. Pavement Analysis and Design. Ed. Prentice-Hall.

SR EN 174—2002. Road works. Hot bituminous rolled pavements. Requirements for quality.

SR EN 12697/33—2003. Bituminous mixtures—Test methods for hot mix asphalt—Part 33: Specimen prepared by roller compactor.

SR EN 12697/24—2005. Bituminous mixtures—Test methods for hot mix asphalt—Part 24: Resistance to fatigue.

SR EN 12697/26—2005. Bituminous mixtures—Test methods for hot mix asphalt—Part 26: Stiffness.

SR EN 13108/20—2005. Bituminous mixtures—Material specifications—Part 20: Type testing.

x x x. 1990. The Shell Bitumen Handbook. Ed. Shell Limited Co.

x x x. Nov., 1971. Bitumes et enrobés bitumineux. Journées d'information: Paris: 16–17.

x x x. COST 333.1999. Development of New Bituminous Pavement Design Method. Transport Research: Luxembourg.

Advanced Testing and Characterization of Bituminous Materials – Loizos, Partl, Scarpas & Al-Qadi (eds)
© 2009 Taylor & Francis Group, London, ISBN 978-0-415-55854-9

Mechanism of fatigue crack growth and fracture behavior in bituminous roads

R. Lugmayr
TenCate Geosynthetics, Linz, Austria

M. Jamek & E.K. Tschegg
Vienna University of Technology, Vienna, Austria

ABSTRACT: Durability and lifetime prediction of asphalt roads can only be obtained by fatigue tests. A correlation between fracture and fatigue behavior has not been verified yet enough. This paper reports a study of fatigue crack properties of asphalt interfaces by means of the wedge splitting test after Tschegg. Instead of beams and the 3- or 4-point bending beam test, drilling cores and the wedge splitting method is used for analyzing the fatigue crack properties of asphalt interfaces. The asphalt base layer surface has been prepared in two ways, fresh and sandblasted, before spreading the top layer. Due to temperature dependency of material properties the tests have been performed in a climate chamber at –10° to +10°C. The challenge of determining the crack length was solved optically in a qualified sense. The results show that the wedge splitting method according to Tschegg is a practicable and reproducible way for fatigue testing of asphalt interfaces.

1 INTRODUCTION

Cracks in pavements cause massive maintenance costs for road authorities. The exchange of asphalt layers is time consuming and may lead to problems in traffic infrastructure.

On one hand cracks are generated by overloads.—This kind of cracks can be simulated by fracture tests. On the other hand cracks originate in the long term run by fatigue and fatigue crack growths. Fatigue is the most frequent cause of cracks. Fatigue characterization of asphalt-aggregate mixtures and interfaces is an important but difficult issue of material design in road construction, but the major factor for accurate lifetime prediction. Knowing the fatigue behavior of asphalt and asphalt interfaces would help distinguish between long-lasting and short-dated products. Overall, preventing crack growth is the most efficient way in order to reduce maintenance costs. Therefore materials research will be the crucial point for improving road lifetime.

Years ago the pull-out test was the common and well known method to determine mechanical fracture properties of road construction materials. Nowadays better techniques have been developed to describe fracture and fatigue behavior of these materials more accurate.

Known testing procedures to characterize fatigue crack growth behavior of asphalt (mode I) are the three-point- and four-point-bending tests. A lot of fatigue testing was carried out, but unfortunately only a few papers are available in this field (Ramsamooj, 1980). Publications of fatigue tests of asphalt interfaces in mode I are not known by the authors yet.

Drawbacks of the bending test are the big specimen size and the difficult handling because of heavy self weight. Ramsamooj (Ramsamooj, 1980) stated to support the beams during fatigue crack growth measuring by an elastic solid to prevent them from breaking by its own weight. In addition, cutting beams directly out of the road is more or less impossible. So specimens can only be prepared in laboratory. Another disadvantage concerns the way of keeping constant environment properties during fatigue testing. This can only be achieved by building a climate chamber among the beam and the testing machine. These drawbacks however, make the bending test difficult and expensive in practically use.

To study fatigue crack growth behaviour of asphalt and asphalt interfaces, it is not enough, to know its properties at room temperature and higher (Ramsamooj, 1980) (16°C–35°C), but in a temperature range from –10°C to +10°C. In this range, the properties change dramatically from brittle and tough to ductile and weak. In (Tschegg et al. 1995, Tschegg 1999), it is shown that below –10°C and above +10°C no relevant changes in fracture behaviour occur. In order to ensure these conditions during fatigue testing, a climate chamber is essential.

A suitable method with compact specimens for determining fatigue life is desirable to overcome the disadvantages of the bending test. The wedge splitting method according to Tschegg (Tschegg, 1986) does use compact specimens but was usually applied only for fracture tests not fatigue crack growth tests yet. (Tschegg, 2008) was the first attempt to use the wedge splitting method successfully for fatigue crack growth testing on asphalt and asphalt interfaces. In this work the knowledge from (Tschegg, 2008) should be extended to asphalt interfaces with several surface treatments.

The specimens shape for the wedge splitting test are drilling cores, which can be taken either directly from the field or produced at laboratory. Each specimen can be handled by one person without utilities. A climate chamber was also built in a very compact way.

Lifetime calculations on the basis of previously published calculation models lead to results which sometimes fit to practical observations (Lee et al. 2000) and sometimes do not thoroughly be consistent (Ramsamooj, 1999). As part of the international conference "Reflective Cracking Pavements in 1996" in Maastricht this situation was particularly highlighted and remarked as an unsolved problem in the "Concluding remarks".

One explanation for the discrepancy could be that not all influences on the life of bituminous roads are known. For instance, the phenomenon of asphalt healing in warmer seasons, or healing of micro- and macroscopic material damage (such as micro-or macrocracks) under the influence of traffic loads at high temperatures in bituminous roads. Only a comprehensive knowledge of all relevant factors would make it possible to fix deviations between experimental and calculated data for lifetime prediction. The results of this work should help other scientists determining mathematical factors for healing more precisely.

1.1 *Main aim of this research*

This paper will show, that stable crack growth in asphalt interfaces during fatigue testing is possible by means of the wedge splitting test after Tschegg. Furthermore it will prove that the wedge splitting method for fatigue crack growth tests is able to generate results between asphalt systems with different prepared base-layer surfaces and different specimen temperatures.

A new optical method for analysing crack propagation rate, introduced in (Tschegg et al. 2008) will help determining crack growth progress and extend experience with this technique. The fatigue results from this paper can also help to improve models of fatigue life prediction, especially to get more information referring healing factors influencing road lifetime.

2 WEDGE SPLITTING METHOD AFTER TSCHEGG

Initially developed for fracture tests (Tschegg, 1986) the wedge splitting test after Tschegg is now used the first time for fatigue crack growth testing of asphalt interfaces as well. The principle of this method is shown in Figure 1. Besides other shapes like cylinders and beams (Tschegg, 1991), which would be also possible for this method, rectangular solids have been chosen as geometry for this testing series. These cuboids were cut out of drilling cores, so that the interfaces between base- and top-layers were in the middle of the specimen. A symmetrical groove on top of the sample can either be prepared by cutting or which is more common by gluing stone cuboids onto (Fig. 5). To assure crack initiation at interface, a so called "starter notch" has to be cut at the bottom of the groove. From here, the crack starts to grow along the interface down to the ground of the sample driven by load.

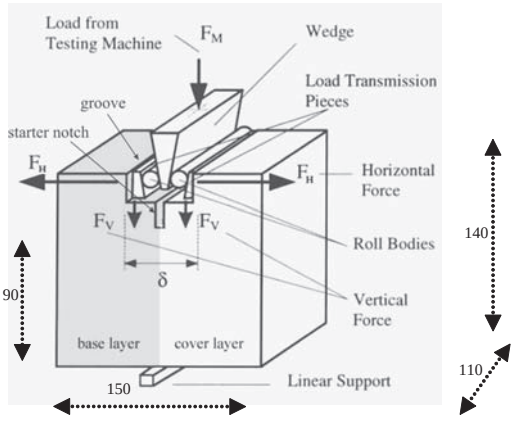

Figure 1. Wedge splitting method after Tschegg (1986) (Tschegg, 1986).

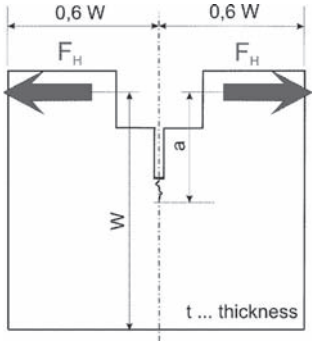

Figure 2. Profile dimensions according to (Murakami et al. 1987).

Therefore a vertical compressive force, F_M, generated by a pull-push-testing machine is transformed to a horizontal force F_H by a wedge and transmitted to the groove of the specimen by load transmission pieces. To minimize friction, roll bodies are used for the load transmission. Splitting of the sample is caused by this horizontal force component F_H which can be calculated easily from the equation $F_H = F_M/(2\mathrm{tg}(\alpha/2))$, where α is the angle of the wedge. If slim wedges (α = 5–12°) are used, the vertical force component F_V is small in comparison with the horizontal force F_H and stabilizes the crack to propagate within the area between the starter notch and the linear support.

2.1 *Evaluation of results*

The Stress-Intensity-Factor concept is used in fracture mechanics to predict the stress state near the tip of a crack caused by load. It is applicable to homogeneous elastic materials.

The assumptions of Linear Elastic Fracture Mechanics do not fit for asphalt at temperatures above 0°C. Below 0°C the fracture mechanic behaviour of asphalt assimilates to linear elastic behaviour. In order to compare experimental results within a temperature range of –10°C to +10°C, it makes sense to use the K-concept not only the J-integral for +10°C too, even if the process zone is large in scale of crack length.

The magnitude of K depends on sample geometry, the size and location of the crack, the magnitude and the modal distribution of loads on the material. From (Murakami et al. 1987) the already calculated geometry factor for compact tension specimen has been adopted to the wedge splitting specimen which has more or less the same (Fig. 2).

$$K_I = \frac{F_H}{t \cdot \sqrt{W}} \cdot f_I(\alpha) \tag{1}$$

$$\alpha = \frac{a}{W} \tag{2}$$

$$f_I(\alpha) = \frac{(2+\alpha)\cdot(0{,}886+4{,}64\cdot\alpha-13{,}32\cdot\alpha^2+14{,}72\cdot\alpha^3-5{,}6\cdot\alpha^4)}{(\sqrt{1-\alpha})^3} \tag{3}$$

K_I …… stress intensity factor [MPa*m^(1/2)]
F_H ….. Splitting load [N]
t …… specimen depth [m]

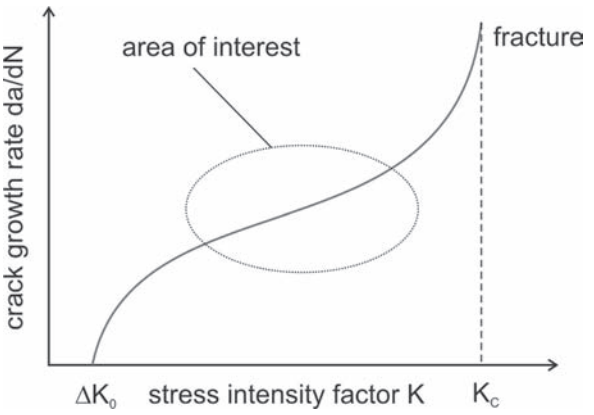

Figure 3. Paris-Law.

a …… distance load application line to crack tip [m]
W …… distance load application line to ground of sample [m]
f_1 …… geometry factor [1]

For Evaluation of results equation 1 to 3 have been used to describe Paris-Law at the area of interest (Fig. 3).

2.2 *Materials, specimens, shape and size*

In order to allow comparison of fatigue crack growth properties, laboratory samples with different asphalt interface systems have been prepared. Base and top layers were made of the same material BTI/16 (B100, M = 5%, Vol = 12%, flow-value 3.3 mm, according to (Österreichische Forschungsgesellschaft, 1986)), whereas the base layer surface was on one hand sandblasted and on the other fresh.

Between the two layers a polymer modified bitumen HB 60 K/PM-adhesive (ÖNORM B 3503, 1992) was applied in both cases.

At the beginning plates have been fabricated consisted of the two asphalt systems as described. Afterwards cores have been drilled out of these composite plates, the specimens were stored for 1 year and finally the cores were cut by a diamond saw to get cubes with dimensions shown in Figure 1.

2.3 *Determination of crack length*

The major technical challenge to determine the fatigue crack progress is to measure the crack length. From literature procedures with ink (Liang & Zhou 1997) are known, but they may not be suitable for permanent crack growth observing. The ink-method can only be applied when fatigue testing is stopped and will not allow continue testing afterwards.

An ideal way of measuring should give the possibility of continuous crack length determination without influencing the sample or the fatigue process. An electrical and an optical procedure (Tschegg et al. 2008) have been developed for this project to determine crack tip positions.

Jacobs (Jacobs, 1995) determined the crack length at fracture and fatigue by using the electrical crack length measuring method in (Tschegg et al. 2008). A net of thin conductors (wire) was applied onto the specimen and recorded the length of the crack immediately when the conductor broke. The net of conductors were destroyed after each test and could not be used for further testing.

A similar system was used in this paper. On front of the sample eight thin (about 3 mm wide) conductor paths are sprayed onto the asphalt surface. Therefore an electrical conducting spray

with graphite particles, cobalt or silver was used. Each path should be isolated from the others. This could be managed by using a pattern covering the non conducting areas while spraying.

During fatigue testing of the specimen, each conductor path is an independent electric circuit, driven by an external power supply (Fig. 4). Fatigue testing causes crack growth and crack opening displacement. The latter is responsible for cutting the conductor paths and therewith the electric circuits step by step. Splitting power circles increase voltage to idle voltage at power supply. This jump can be detected automatically and is correlated to the location of the crack tip. That is why the locations of the conductor paths have to be known. In Figure 5 is shown an already tested sample.

After numerous initially thought successful tests of this method it became obvious, that it may fail at low temperatures. At +10°C the crack opening is sufficient enough to cut the conductor paths, whereas at temperatures like 0°C or –10°C, the crack opening is too small to influence them. That means cracks grow beyond electrical circuits without influencing them. Already optically visible cracks do not lead to resistance change of crossed conductor path. The conducting material sprayed onto may be too plastic for detecting hairline cracks. Therefore it can be stated, that the electric measurement method is too insensitive for crack growth detection which goes together with small crack opening. Subsequently, the electrical measurement method was replaced by an improved method, the optical crack length measuring method.

The optical method for crack length determination is accomplished by evaluation of photos of the specimen front, taken by a camera, positioned outside the climate chamber (Fig. 6) and capturing the sample through the window of the chamber.

The sample front is prepared with a white, high reflective paint, which is additionally marked with a grid-pattern. The pattern has the function of a scale indicator on the photos for later evaluation. During crack growth the crack tip appears black and can be noticed continuously because of the high black-white contrast. Photos are taken every minute and saved by webcam software on a computer. Each photo goes together with a time stamp, which allows calculation of crack growth rate at any time (Fig. 7).

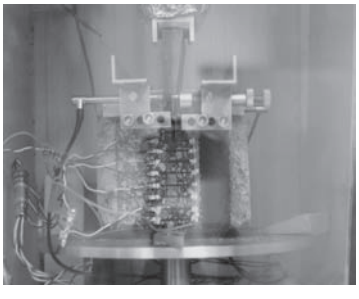

Figure 4. Electrical measurement method for determining crack length at the climate chamber.

Figure 5. Tested specimen.

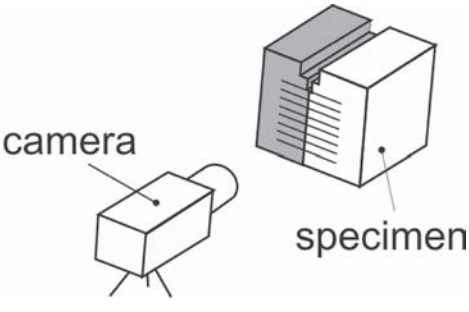

Figure 6. Camera observing specimen front.

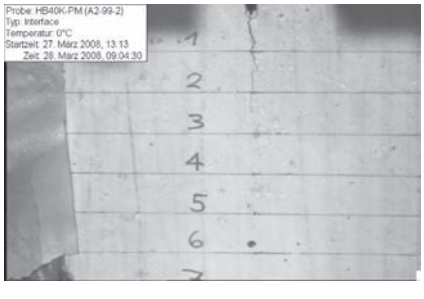

Figure 7. Video image during crack growth.

3 TEST CONDITION AND EQUIPEMENT

Testing was performed with a hydraulic fatigue testing machine made by Carl Schenck AG with a load capacity of 40 kN. The loading altered sinusoidal at a frequency of 2 Hz. The maximum load amplitude was also altered during each single test depending on the crack growth velocity. Usually one test was finished within 24 hours, when the crack had run to the bottom of the sample. Therefore the maximum load has to be adopted every few hours either to accelerate or to reduce crack growth velocity. The absolute maximum splitting-force-amplitude did not exceed 2500 N.

The frequency of 2 Hz gave the material enough time for relaxation and was chosen due to pretests, which showed no changes in results at lower frequencies than 2 Hz.

All tests were performed in a climate chamber built in the testing machine with a temperature control accuracy of ±0.5°C. The testing temperatures of the specimen were –10°C, 0°C and +10°C. Prior to testing, the samples had been stored in a refrigerator for more than two days. Three identical specimens of each asphalt interface system and for each testing temperature have been tested in order to provide enough data for statistical evaluation.

In addition to the hydraulic fatigue testing machine, a black/white video camera from Mintron Enterprise Co., Ltd. and a PC TV card from Pinnacle Systems were used for photo recording. Inductive transducers made by Hottinger Baldwin Messtechnik GmbH (Fig. 4) were set into the assembly to measure the crack mouth opening displacement. All signals of numerous temperature sensors, force, transducers are amplified and read by a data acquisition card from National Instruments, who is also the manufacturer of measurement software DasyLab, which records all data and controls the pre-storage chamber and the main climate chamber.

A climate chamber (–30°C to +40°C) was designed and built into the existing hydraulic fatigue testing machine (Fig. 8). The main parts of the chamber are a welded steel frame and polystyrene walls with a thickness of 5 cm. At the front of the chamber a window was built to make specimen exchange easily. At the left side of the chamber two nozzles and a fan enables energy transfer with air from a cold reservoir to the climate chamber and back. The chamber is therefore passive, fed by a reservoir from outside.

The cold "reservoir" is represented by a refrigerator (Fig. 9). Together with the climate chamber and two heat transfer tubes the reservoir builds a closed circuit. This circuit is forced controlled by means of a fan which pumps cold air from the reservoir into the chamber. The "warm" air from the chamber is thereby transmitted back to the reservoir.

4 RESULTS AND DISCUSSION

The results show that the wedge splitting test together with the optical crack length determination is a convenient method to distinguish fatigue lives between different specimen temperatures and different types of asphalt interfaces.

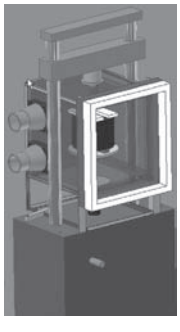

Figure 8. Design drawing of a climate chamber integrated in the fatigue testing machine.

Figure 9. Climate chamber fed from cooling reservoir.

4.1 *Fatigue crack growth behavior of asphalt interfaces*

The crack growth rates for asphalt interfaces at +10°C are higher than for interfaces at 0°C. Second, the fatigue live span of asphalt interfaces with sandblasted surfaces is shorter than with fresh surfaces (Fig. 10). This last statement is valid for temperatures of +10° and 0°C, whereas for 0°C the differences become small. Asphalt interfaces at –10°C will be tested in a next step. In (Tschegg et al., 2008) were comparable asphalt layers at –10°C to +10°C tested and resulted in similar Paris-curves like in Figure 10.

The Paris-Curves show at 0°C a higher resistance against fatigue crack growth than at +10°C. The fresh and sandblasted surface result at 0°C in a similar resistance against fatigue crack growth. At +10°C the sandblasted is less than at fresh surface condition. The expected life time of a road under the tested condition prefer fresh surface at 0°C compared to sandblasted surface at +10°C.

Beyond these results a lot of questions appeared like for instance the reason of scattering of data points caused by a non linear crack growth line.

4.2 *Deviation from linear crack growth line*

If fatigue crack growth is stopped on purpose before the crack tip has reached the ground of the specimen and the undamaged "rest" is broken by force, two areas at fracture surface can be distinguished (Tschegg et al., 2008). A fatigue area and fracture area (Fig. 11). For metals these areas could be identified permanently, whereas for asphalt the differences vanish after a few minutes at room temperature. The photo shown in Figure 11 was taken instantly after splitting the sample completely allowing discerning fatigue from fracture area.

The border between these two areas is not linear as it should be ideally. Due to this fact, there is always an error when using the optical method for crack length determination, because this method can only evaluate crack growth at the edge of the sample but not for the inner parts.

Another reason for scattering of data points is a non constant crack growth rate generated by the influence of rough interface topology. Crack growth sticks at areas which need more

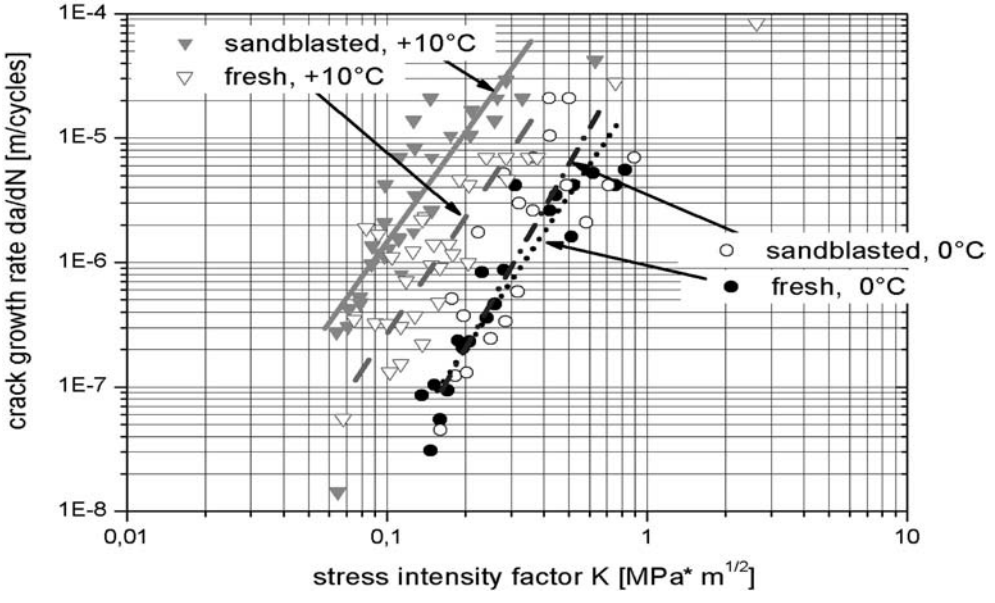

Figure 10. Fatigue crack growth properties of asphalt interfaces.

energy consumption than at others. Differences of energy consumption can be caused by the so called “bridging effect”.

4.3 *Bridging effect*

The bridging effect originates from the topology of the fracture surface. If this surface is smooth, no energy consuming interaction between the already broken parts is obtained. For asphalt interfaces, the aggregate from the top layer is pressed into the base layer by a road roller. Therefore the top and the base layer are interlocked up to a certain extend. In this case crack growth requires additional energy for either disconnecting the two layers or breaking the aggregate and pull out bitumen filaments. This process occurs almost completely behind the micro crack zone respectively behind the process zone (Fig. 12). In case of a small micro crack- and bridging zone the Linear Elastic Fracture Mechanics can be applied. Appear both zones huge to the crack length and to the size of the specimen other concepts should be used.

Another less explored effect which is also important for fatigue crack growth analysis is crack healing of asphalt layers.

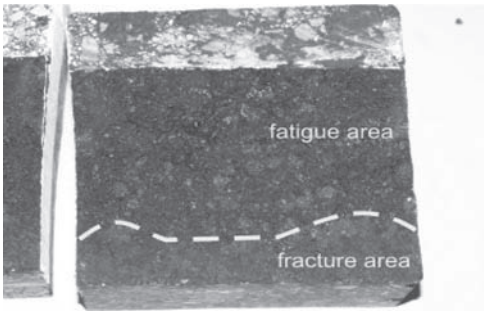

Figure 11. Fracture surface divided into two areas.

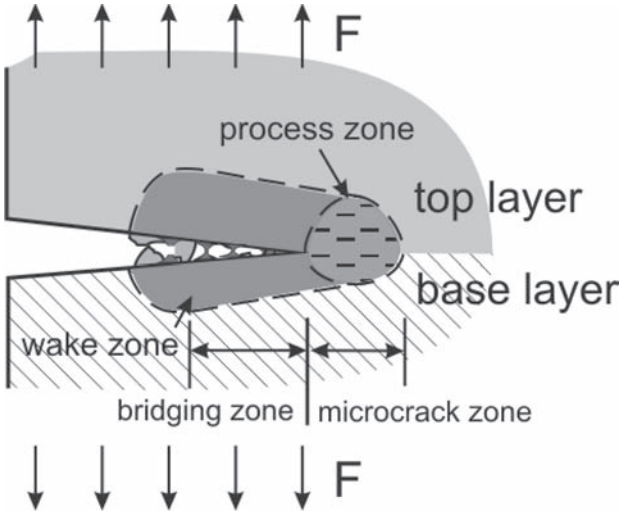

Figure 12. Crack process zone.

4.4 *Healing of asphalt layers*

Cracks in asphalt which appear in winter/spring season may heal during summer period. Healing is an inverse effect to crack growth. In summer asphalt has lower strength and thus crack initiation is easy. But also crack healing is present in summer whereas in winter/spring season the strength of asphalt is higher but crack healing is less.

By using the healing performance on reflective cracks in asphalt layers (BTI/16, B100 acc. (Österreichische Forschungsgesellschaft, 1986)) the crack growth behavior (notch tensile strength and specific fracture energy) was determined in (Tschegg et al. 2000). The healing cycle included the rupture at 0°C further 4 hours healing at +35°C followed by cooling down to 0°C and repeat the rupture behavior. The notch tensile strength (analogical to Adhesive bond strength) did not change after several healing actions. However the specific fracture energy (crack resistance) was reduced after each healing action (Tschegg et al. 2000). With regard to the fatigue crack propagation is it essential to analyse and evaluate the healing effect.

Until now only a few experimental (Wool 1995, Little et al. 1997, Little et al. 1999, Tschegg et al. 2000, Tschegg et al. 2001), numerical (Tschegg et al. 2001) and theoretical (Wool 1995) studies in the field of healing are available. No numerical theory yet bears this effect in mind, which can bring back up to 3 times more crack growth resistance than without temperature healing (Tschegg et al. 2001), depending on the type of asphalt and the healing temperature. In future at least at +10°C and above this effect must be taken into account.

Another interesting research field is the use of geosynthetic interlayer systems, laid between asphalt base and top layers. This application of Geosynthetics for road rehabilitation is growing substantially in Europe in the last years. In (Tschegg et al. 1998), the fracture behaviour of such geosynthetic systems has been tested. The wedge splitting method according Tschegg has proven to be sensitive enough to measure differences in base layer and surface treatment. The next step will be a research on fatigue crack growth behaviour using different geosynthetic interlayer systems and adhesives for asphalt road construction.

5 CONCLUSIONS

Up to the present, bending beam tests have been used to obtain fatigue behavior of asphalt layers. In this paper the wedge splitting method according Tschegg was applied successfully the first time for determining the fatigue crack growth properties of asphalt interfaces. The major challenge was observing crack growth state respectively to find the location of the crack tip and the crack length. An electrical approach was not successful, whereas an optical measurement procedure leads to sufficient results. Beyond all restrictions evaluating crack progress, the wedge splitting method managed to achieve feasible results for fatigue crack growth analysis at different temperatures and for different asphalt interface treatments. The described method is a step into future to provide important data for lifetime prediction of roads but certain phenomena like healing of cracks have to be taken into account in order to get efficient lifetime calculations based on theoretical models.

REFERENCES

Jacobs, M.M.J. 1995. Crack Growth in Asphaltic Mixes, Dissertation, Technical University Delft.

Lee, H.-J. Daniel, J.S. & Kim, Y.R. 2000. Continuum Damage Mechanics-Based Fatigue Model of Asphalt Concrete. *Journal of Materials in Civil Engineering* (May 2000).

Liang, R.Y. & Zhou, J., 1997. Prediction of fatigue life of asphalt concrete beams, Int. J. Fatigue 19 (2): 117–124.

Little, D.N., Lytton, R.L. & Williams, D. 1997. Propagation and Healing of Micro cracks in Asphalt Concrete and Their Contributions to Fatigue Asphalt Sc. Technology: 149–195.

Little, D.N., Lytton, R.L., Williams, D. & Kim, Y.R. 1999. An analysis of the Mechanism of Micro damage Healing based on the Application of Micromechanics First Principles of Fracture and Healing, Asphalt Paving Technology: 501–542.

Murakami, Y. et al. 1987. Stress Intensity Factors Handbook Vol. 1. Pergamon Press, ISBN-13: 978-0080348094.

ÖNORM B 3503 Standard 1992. Bitumenemulsionen für den Straßenbau—Anforderungen—Bitumen- und Polymerbitumenemulsionen für Haftbrücken.
Proceedings of the 3rd RILEM Conference (2–4. Oct. 1996), "Reflecting Cracking in Pavements—Design and Performance of overlay systems", ed. by Francken, L., Beuving, E., Molemaar, A.A.A., E & FN SPON, Maastricht, The Netherlands.
Österreichische Forschungsgesellschaft 1986. Bituminöse Tragschichten im Heißmischverfahren. FVS, Wien. RVS. 8.05.14.
Ramsamooj, D.V. 1980. Fatigue Cracking of Asphalt Pavements. Transportation Research Record 756.
Ramsamooj, D.V. 1991. Prediction of Fatigue Life of Asphalt Concrete Beams from Fracture Tests. American Society for Testing and Materials.
Ramsamooj, D.V. 1999. Prediction of Fatigue Performance of Asphalt Concrete Mixes. American Society for Testing and Materials.
Tschegg, E.K. 1986. Test method for the determination of fracture mechanics properties. Patent Specification No. A-233/86 390 328, Austrian Patent Office.
Prüfeinrichtung zur Ermittlung von bruchmechanischen Kennwerten sowie hiefür geeignete Prüfkörper, Österreichisches Patent AT-390328.
Tschegg, E.K., 1991. New Equipment for Fracture Tests on Concrete, Materials Testing (Materialprüfung), 33 (1991), p 338–342.
Tschegg, E.K., Kroyer, G., Tan, D-M., Litzka, J. & Stanzl-Tschegg, S. 1995. Charakterisierung der Brucheigenschaften von. Österreich. Bundesministerium für Wirtschaftliche Angelegenheiten, Bundesstraßenverwaltung, Wien, Straßenforschung 440.
Tschegg, E.K., Ehart, R.J.A., INGRUBER, M.M. (Sep./Oct.1998). Fracture Behavior of Geosynthetic Interlayers in Road Pavements. Journal of Transportation Engineering, ASCE.
Tschegg, E.K., 1999. Concept and Parameters to Characterize the Fracture Behaviour of Bituminous Materials and Layer Bonds EUROBITUME Workshop 99, Proc. "Performance Related Properties for Bituminous Binders, Kirchberg Luxembourg, Paper No. 009: 1–5.
Tschegg, E.K., Catharin A. & Stanzl-Tschegg, S.E., 2000. Healing Behaviour of Reflective Cracks, Fourth RILEM Conference, March 26–30, Ottawa.
Tschegg, E.K., Jamek, M. & Stanzl-Tschegg, S. 2001. Bruch- und Selbstheilungsverhalten von Asphalt und Asphaltverbunden. Ausmaß und Nutzen. Österreich, Bundesministerium für Verkehr, Innovation und Technologie, Bundesstraßenverwaltung, Wien, Straßenforschung 516.
Tschegg, E.K., Jamek, M. & Lugmayar, R. 2008. submitted. Fatigue Crack Growth in Asphalt and Asphalt Compounds. (by means of the wedge splitting method). *Journal of Transportation Engineering*, ASCE.
Wool, R.P. 1995. Polymer Interfaces, Structure and Strength, Hanser Publishers, Munich, Vienna, New York.

Advanced Testing and Characterization of Bituminous Materials – Loizos, Partl, Scarpas & Al-Qadi (eds)
© 2009 Taylor & Francis Group, London, ISBN 978-0-415-55854-9

Simplified fatigue performance modeling of ALF pavements using VECD+3-D Finite Element Modeling

B.S. Underwood, Y.R. Kim, S. Savadatti, S. Thirunavukkarasu & M.N. Guddati
North Carolina State University, Raleigh, North Carolina, USA

ABSTRACT: This paper presents results from a study that uses an in-house developed finite element analysis program, FEP++. In this work, the asphalt concrete layers are considered as linear viscoelastic and the unbound layers as linear elastic. The advantage of using this level of complexity is that it offers an improved representation of asphalt concrete pavements while using the same inputs that are required for the NCHRP 1-37A Mechanistic Empirical Pavement Design Guide. After using the finite element package to assess the impacts of wheel speed, temperature gradient, and material type on pavement response, attention turns towards an advanced mechanistic material model for predicting the fatigue response of asphalt concrete, i.e., the viscoelastic continuum damage (VECD) model. This model is characterized using mixtures from the Federal Highway Administration's Accelerated Load Facility (FHWA ALF) and is found to capture an underlying material property, the damage characteristic relationship. Finally, results from FEP++ simulations of the FHWA ALF pavements are combined, in a simplified modeling scheme, with the VECD model to predict the fatigue performance of these pavements.

1 INTRODUCTION

The current state of practice in pavement response and performance modeling includes layered elastic analysis and using empirical relationships with a predictive scheme, such as Miner's law (ARA 2004). These techniques have certain shortcomings regarding the accuracy of the response modeling and the appropriateness of universally applying the empirical relationships. Layered elastic analysis has been used for years as the standard for the analysis of asphalt concrete pavement systems. Its longevity, in light of the fact that asphalt concrete is known to be a viscoelastic material and that soils are known to be stress state-dependent, is a reflection of the simplicity of the analysis. Additionally, some may argue against more complicated analyses that use layered theories, based on the notion that these theories are inherently flawed due to their assumption of homogeneity and isotropy (Irwin 2002).

However, the fact is that true linear viscoelastic (LVE) characterization of asphalt concrete material is the future direction of the field, as evidenced by the inclusion of the dynamic modulus ($|E^*|$) in the current NCHRP 1-37A and 1-40A reviewed Mechanistic Empirical Pavement Design Guide (MEPDG), and the development of the Asphalt Material Performance Tester (AMPT) and protocols (Witczak et al. 2002, ARA 2004, NCHRP 1-40A 2006). Unfortunately, given the current state of computational power, analysis needs, and/or the willingness of the pavement engineering community to accept the MEPDG, the developers of the MEPDG utilized layered elastic analysis for the pavement response modeling platform. This mismatch in theory has complicated the existing analysis techniques and has raised considerable confusion regarding, for example, the definitions of frequency and time (Dongre et al. 2005, Underwood and Kim 2008, Al-Qadi et al. 2008).

Currently, state of the art pavement analysis includes the use of finite element-based response modeling. In its most complex form this analysis may account for the nonlinear soil response, imperfect bonding between layers in the pavement system, the viscoelastic nature of the asphalt concrete, and other mechanisms that contribute to the response of asphalt pavements (Kim and

Hanna 2001, Long and Monismith 2002, Yoo et al. 2006). Major material modeling efforts are also producing advanced models that mathematically consider key material characteristics beyond linear viscoelasticity, such as microcrack initiation, coalescence and propagation for fatigue and aggregate interlock, viscoplastic flow, and yield surface recovery for rutting (Erkens et al. 2003, Underwood et al. 2006). Together, these conceptual approaches may form the basis for the next generation of pavement design and analysis tools. Today, though, computational limitations and the need for rapid and routine design decisions make the full and consistent implementation of such approaches inefficient.

These limitations, however, should not undermine efforts to use certain components of these analysis techniques to aid engineers today. The purpose of this paper is to apply and report on an existing advanced response modeling approach, the finite element method. In addition to this first objective, it is also the purpose of this paper to show that an advanced material model can be combined with the outcomes of these response models in a simplified way to provide an accurate field performance prediction. The viscoelastic continuum damage (VECD) model is used for this purpose. The VECD model has been developed and refined over the last twenty years through multiple research efforts and has been shown to accurately describe the constitutive relationship for asphalt concrete subjected to fatigue (Kim and Little 1990, Lee and Kim 1998, Daniel and Kim 2002, Underwood et al. 2006).

2 MATERIALS

Four different mixtures from an ongoing study at the Federal Highway Administration's Accelerated Loading Facility (FHWA ALF) were used for this study. The aggregate structure for each of the mixtures is a coarse Superpave 12.5 mm blend. Specific details of these materials and the specimen fabrication protocols are given elsewhere (Underwood et al. 2006); here, it is only important to recognize that each of the four mixtures uses a different asphalt binder, as summarized in Table 1. The asphalt content for each mixture is 5.3% by total mix mass, and all experimental data were obtained from specimens having air voids between 3.5 and 4.5%.

3 PAVEMENT RESPONSE MODELING

To model the pavement response of the asphalt concrete pavement, a 3-D finite element model (FEM) has been utilized (Guddati et al. 1998). A characteristic of the software used in this study, which distinguishes it from software used in other efforts (Kim and Hanna 2001, Long and Monismith 2002, Yoo et al. 2006), is that it is part of an in-house developed environment and overcomes the need to use expensive commercial packages, such as ABAQUS or ANSYS. Details of the mesh, temperature, and load characteristics of this software package are beyond the scope of this paper, but are presented elsewhere (Underwood et al. 2009a). In short though the analysis simulates the pass of a tire or axle configuration over a pavement surface where the pavement is simulated using 3-D block elements. For this analysis dynamic effects are not considered. Materials far from the wheel load (vertically and horizontally) are simulated using special infinite elements. Temperature gradients are considered by assuming each layer of elements has a consistent temperature. Finally the element size is established based on a mesh sensitivity analysis to balance run-time and analytical accuracy.

Table 1. Relevant asphalt binder information.

Binder	Designation	Asphalt grade	Cont. asphalt grade
Unmodified	Control	PG 70-22	PG 72-23
Crumb rubber terminal blend	CRTB	PG 76-28	PG 79-28
Styrene-butadiene-styrene	SBS	PG 70-28	PG 74-28
Ethylene terpolymer	Terpolymer	PG 70-28	PG 74-31

The finite element package used in this analysis treats asphalt concrete layers as LVE and unbound paving materials as linear elastic. Although a more sophisticated analysis could be performed, it was decided that this level is acceptable because the necessary inputs are already part of the NCHRP 1-37A MEPDG characterization process.

The LVE properties of the asphalt concrete layers are represented by: 1) the Prony coefficients for the axial relaxation modulus, seen in Equation (1) ; 2) Poisson's ratio (assumed constant); and (3) the coefficients for the time-temperature shift factor function, seen in Equation (2).

$$E(t) = E_{\infty} + \sum_{m=1}^{m} E_m e^{-t/\rho_m} \tag{1}$$

where E_{∞} is the long time elastic modulus; E_m are the Prony coefficients that physically represent the individual spring stiffness values in the Wiechert mechanical model; and ρ_m are the characteristic relaxation times, generally assumed in the characterization procedure. It is possible, though not shown, to characterize Equation (1) using dynamic modulus and phase angle data.

$$\log a_T = \alpha_1 T^2 + \alpha_2 T + \alpha_3 \tag{2}$$

where a_T is the time-temperature shift factor at some temperature T, and α_1, α_2 and α_3 are fitting parameters.

These characteristic properties were assessed with laboratory mixed-laboratory compacted specimens using the AASHTO TP-62 protocol, with the modification that tension-compression instead of compression only loading was used. Experimental evidence demonstrates that there are no clear differences among the LVE moduli measured from multiple protocols, including tension-compression versus compression, only as long as the on-specimen strain magnitudes (peak-to-peak) are between 50–75 microstrains (Kim et al. 2004, Underwood et al. 2006).

Comparisons of the LVE characteristics of the mixtures in this study are shown in Figure 1 a–d where the replicate averaged dynamic modulus mastercurves for all mixtures are shown in both semi-log and log-log scales, the phase angle mastercurves are shown, and the time-temperature shift factor functions are shown. A thorough review of the differences and similarities of these materials

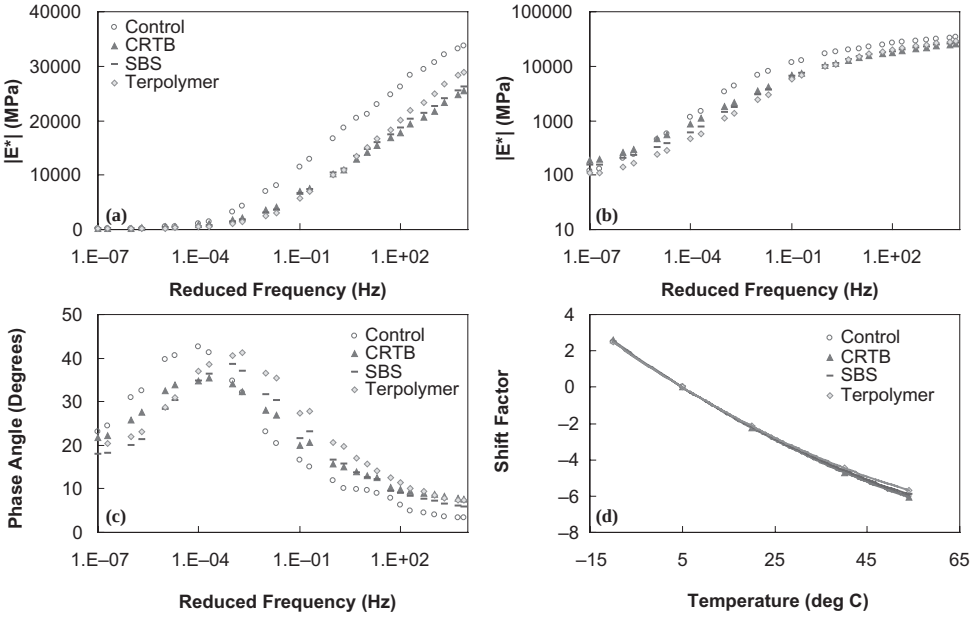

Figure 1. Linear viscoelastic characterization for Control, CR-TB, SBS and Terpolymer mixtures: a) dynamic modulus mastercurve in semi-log space, b) dynamic modulus mastercurve in log-log space, c) phase angle mastercurve, and d) time-temperature shift factor function.

along with the techniques used to extract the parameters in Equation (1) are given elsewhere (Underwood et al. 2006); however, a few key observations can be made with regard to this paper:

- The Control mixture shows a much higher stiffness at higher reduced frequencies (physically representing cooler temperatures and/or faster loading frequencies) than the modified mixtures.
- The modified mixtures show similar stiffness values from approximately 10,000 to 0.01 Hz. Below 0.01 Hz, the mixtures rank in terms of decreasing stiffness: 1) CR-TB, 2) SBS, and 3) Terpolymer.
- Although the Control mixture shows higher stiffness values at higher reduced frequencies, it either exhibits or tends to exhibit lower stiffness values than the modified mixtures at lower reduced frequencies (physically representing higher temperatures and/or slower loading frequencies).
- The Control mixture shows a higher degree of elasticity than the modified mixtures show at high reduced frequencies, but lower elasticity at lower reduced frequencies.

4 FEP++ FOR FATIGUE ASSESSMENT

4.1 *ALF experiment overview*

The current experiment at the FHWA ALF consists of 12 lanes of unmodified, polymer-modified, air-blown and fiber-reinforced asphalt concrete mixtures. Each lane is large enough to contain four different test sites, two for rutting, one for fatigue, and one currently unassigned. The fatigue test sites are instrumented with transverse and longitudinal strain gauges that are monitored, along with the surface crack length and area, at regular intervals during loading. For the purposes of this paper, the test lanes containing the Control, CRTB, SBS and Terpolymer mixtures are of primary importance because the materials in these lanes have been characterized by the research team.

Each of the test lanes considered consists of a 100 mm thick asphalt concrete layer resting on top of a 560 mm thick crushed aggregate base, which is, in turn, above an AASHTO A-4 subgrade. For these fatigue tests, the pavement is loaded with a 425/64R22.5 (super-single) tire moving at 17 km/hr (10.5 mph), with a load of 73.8 kN (16.6 kip), a contact pressure of 827 kPa (120 psi), and a temperature of 19°C (66.2°F). These same conditions are simulated in the FEP++ simulation. The site-specific base and subgrade moduli values, obtained from falling weight deflectometer (FWD) tests and summarized in Table 2, were used in the analysis due to inconsistencies in the constructed base materials across the test lanes (Qi et al. 2005 and 2008).

4.2 *Comparison of measured and predicted responses*

Strain measurements taken on the ALF pavements before any damage had accumulated were used to verify the FEP++ simulations and compare them to actual field conditions. For this purpose, only two of the four mixtures, Control and CRTB (Lanes 2 and 5), were used, and all valid and working strain gauges in these lanes were examined. Because the ALF test lane materials and the materials used in the laboratory have inherent and inevitable differences

Table 2. Base and subgrade moduli for the ALF pavement simulation.

ALF lane	Mixture	Base modulus MPa (ksi)	Subgrade modulus MPa (ksi)
2	Control	160 (23.2)	46 (6.7)
4	SBS	132 (19.1)	42 (6.1)
5	CRTB	105 (15.2)	37 (5.4)
6	Terpolymer	108 (15.7)	36 (5.2)

due to air voids, compaction techniques and internal structure, it is unfair to compare the measured and predicted responses directly. Instead, the measured and predicted responses have been normalized such that the magnitudes have a peak value of one. Note that for these simulations the load level is 62.0 kN (14.0 kip), because that is the load level that was used when the measurements were taken.

Comparing the measured values from the Control and CRTB lanes (Figure 2a and b), the CRTB mixture shows a more rapid increase and decrease in strains, an indication of greater elasticity and a reduced load spreading capacity (i.e., lower stiffness) in the CRTB mixture. As shown in Figure 2c and d, the simulations also predict these behaviors. Unlike the measured data, though, the simulations tend to show a more symmetric response from both pavements, particularly with regard to longitudinal strains.

It is believed that the primary reason for the discrepancies in the measured and predicted responses is due to errors in the treatment of the asphalt concrete and unbound layer bond. When viscoelastic and elastic media are assumed to be perfectly bound, as is the case in FEP++ analysis, the viscoelastic effects are dampened, and the analysis results may be more elastic than is the case in reality. This problem has been encountered by other researchers when modeling asphalt concrete pavements (Yoo et al. 2006, Korkiala-Tanttu 2003) and is overcome by including an interface model to account for incomplete bonding of the two layers. Because the purpose of this paper is to use as simple an analysis as possible, save computational time, and still capture the most important characteristics, this interface element, essentially a friction element, is omitted. This approach is deemed reasonable for this study, because the test lanes were similarly constructed and, thus, the true bonding between the layers should be consistent across lanes; likewise, the effect of ignoring this factor should also be consistent.

4.3 *Damage model for fatigue performance assessment*

The most fundamentally appropriate and accurate method for modeling fatigue cracking distress is to include the VECD model in the 3-D finite element code, thereby making the material response a function of pavement damage. However, this type of fully consistent approach is a time-consuming process. As an intermediate step, a simplified modeling

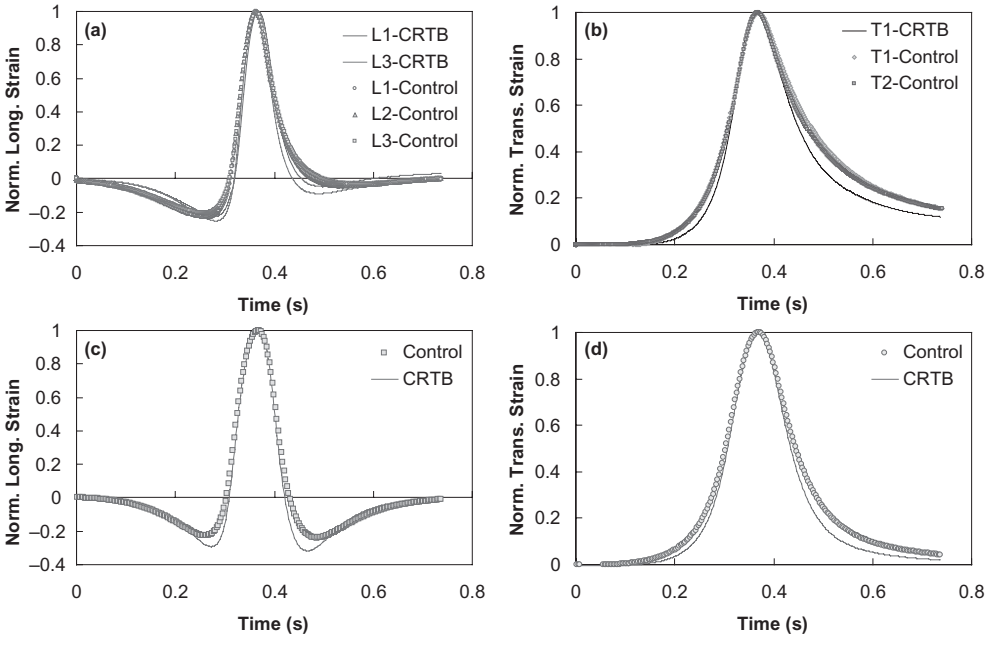

Figure 2. Comparison of strain responses in Control and CRTB ALF lanes: a) measured longitudinal strains, b) measured transverse strains, c) predicted longitudinal strains and d) predicted transverse strains.

scheme that uses the 3-D FEP++ simulations to model the pavement response and uses a new derivation of the VECD model to model the material deterioration has been applied. This modeling scheme is specialized for the case of a repeating loading history, defined by some amplitude and a time-dependent function, $f(\xi)$, and is capable of quickly predicting the fatigue response under such conditions. This new derivation is summarized in Equations (3)–(7). The details of this model have been presented elsewhere (Underwood et al. 2009b) and are not repeated here in the interest of brevity.

$$\sigma = \varepsilon^R * C(S);\ \sigma_0 = {\varepsilon_0}^R * |C^*|(S) \tag{3}$$

$$\varepsilon^R = \frac{1}{E_R}\int_0^{\xi} E(\xi-\tau)\frac{d(\varepsilon)}{d\tau}d\tau,\ {\varepsilon_0}^R = \varepsilon_0 * |S^*| \tag{4}$$

$$|S^*| = \frac{\max\left(\int_0^{\xi} E(\xi-\tau)\frac{d(\varepsilon_o f(\xi))}{d\tau}d\tau\right)}{\varepsilon_o} \tag{5}$$

$$|S^*| = \frac{\sigma_o}{\max\left(\int_0^{\xi} D(\xi-\tau)\frac{d(\sigma_o f(\xi))}{d\tau}d\tau\right)} \tag{6}$$

$$S_{i+1} = \begin{cases} S_i + \left(-\frac{1}{2}\left(\varepsilon^R\right)_i^2 \frac{\partial C}{\partial S}_i\right)^{\alpha} * (\Delta\xi)_i & \xi \le \xi_p \\ S_i + \left(-\frac{1}{2}\left(\varepsilon_0^R\right)^2 \frac{\partial |C^*|}{\partial S}\right)^{\alpha} * (\Delta\xi_p) * (R)^{\alpha+1} & \xi > \xi_p \end{cases} \tag{7}$$

$$R = \left(\frac{1}{\xi_f - \xi_i} * \int_{\xi_i}^{\xi_f} \left(f(\xi)\right)^{2\alpha} * d\xi\right)^{1/1+\alpha} \tag{8}$$

$$|C^*|(S) = C(S) = e^{aS^b} \tag{9}$$

where

ξ_p	=	the reduced pulse time of the loading pulse;
ε^R	=	transient pseudo strain, Equation (4);
${\varepsilon_0}^R$	=	cyclic pseudo strain amplitude, Equation (4);
C	=	pseudo stiffness;
C^*	=	cyclic pseudo stiffness assumed equal to pseudo stiffness;
ε_0	=	cyclic strain amplitude (only tension amplitude if loading is in tension and compression);
σ_0	=	cyclic stress amplitude (only tension amplitude if loading is tension and compression);
$\|\Sigma^*\|$	=	loading form-specific LVE stiffness function $\|E^*\|$ for continuous sinusoidal loading, Equation (5), or Equation (6);
S	=	internal state variable denoting damage;
R	=	form factor adjustment factor, Equation (8);
ξ_i	=	reduced time within loading cycle when tensile loading begins;
ξ_f	=	reduced time within loading cycle when tensile loading ends; and
$f(\xi)$	=	normalized time function found from loading type assumption or from external analysis, such as 3-D FEP++.

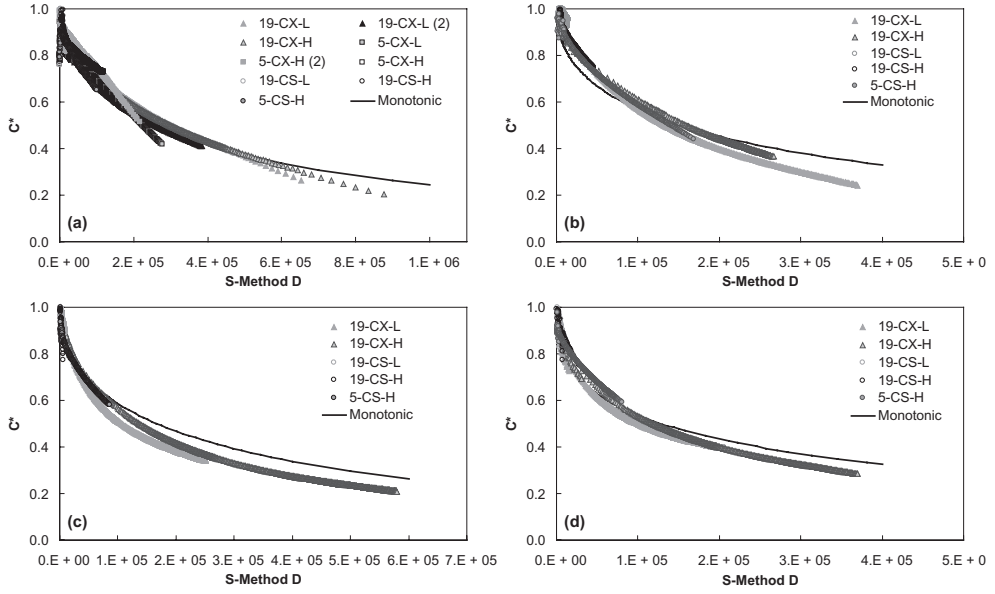

Figure 3. Use of simplified method for damage characterization for: a) Control, b) CRTB, c) SBS, and d) Terpolymer mixtures (legend titles are temperature-control-high level or low level).

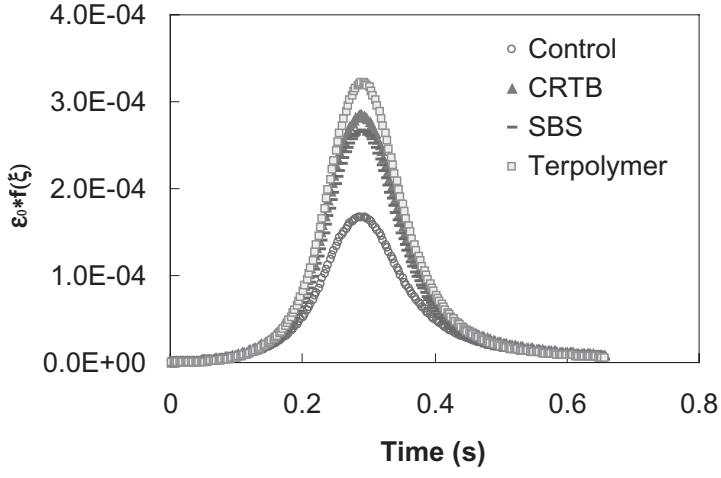

Figure 4. Loading function for each pavement structure.

This model has been proven to accurately capture a material-dependent underlying damage function, the C vs. S curve, that is responsible for the engineering behavior of asphalt concrete subjected to controlled stress (CS) and controlled crosshead (CX) fatigue tests as well as constant rate monotonic tension tests. This verification is shown in Figure 3 for the four ALF mixtures. Note that, following the findings of Lee and Kim (1998), α is defined to be 1 & 1/m for the constant rate and CX tests, and is 1/m for the CS tests. The details of the tests shown in Figure 3 are given elsewhere (Underwood et al. 2009b), but it should be understood that the tests represent a range of magnitudes, temperatures and control conditions.

4.3.1 *Performance prediction*

The first step in the performance prediction scheme is to predict the pavement response under a load history using the 3-D FEP++ software. For this paper, these conditions are those used

in the ALF experiment, discussed in the previous section. Results from this simulation are shown for each pavement in Figure 4. As expected, and based on the findings in Figure 1, the modified pavements show substantially higher strains than the control pavement (the reduced frequencies that loosely correspond to the ALF loading speed and test temperature are 0.1–0.01 Hz). To predict the field performance of these pavements, the strain histories shown in Figure 4 are assumed to repeat until failure and are used with Equations (3)–(7) to compute damage and pseudo stiffness as a function of load replications. Based on the experience of others (Daniel and Kim 2002, Underwood et al. 2006), failure is assumed to occur when the pseudo stiffness, C*, equals 0.25.

The results of the test simulations are shown for the available ALF pavements in the line-of-equality plots in Figure 5. Based on the results of Kutay et al. (2008), failure in the actual ALF pavements is defined as the cycle at which 20% of the lane has cracked. Note that in all of the simulations the modified pavements are predicted to provide better fatigue resistance in spite of the fact that the strain histories are greater in magnitude for these pavements than the control pavement. This situation occurs because: 1) the reduced stiffness also results in less pseudo strain, which from Equation (7) means that less energy is available for damage growth; and 2) each material has its own unique characteristic behavior that determines the influence of the available energy on damage growth.

In Figure 5 two scenarios are shown in the regression line analysis, one that includes Terpolymer and one that does not include Terpolymer. The reason that both are shown is that other researchers (Kutay et al. 2008) have noted certain problems relating to the distribution of hydrated lime throughout the Terpolymer test lane, which may have influenced the ALF test results.

The findings from Figure 5 are quite encouraging and provide some interesting insight. Comparisons are drawn between the continuum damage model failure point and surface crack density. These observed surface cracks are the result of initiated microcracks that have propagated and coalesced into some dominant macrocracks, which have then propagated to the surface. (Measurements at the ALF confirm that failure occurred due to bottom-up fatigue cracking.) Material in the continuum damage model fails due to coalescence of the microcracks into macrocracks. This point of failure is referred to as *localization* in the literature relating to the VECD model. However, the fact that the continuum model, which does not account for macrocrack propagation, shows a good relationship with the measured surface cracking suggests that the microcrack and macrocrack propagation behaviors are related. It is felt that extending the VECD model to fracture (i.e., continuum damage to fracture) is a natural evolution of the model. This belief is also based on the fact that the VECD model was originally derived based on fracture mechanics generalizations; thus, clear similarities exist in the formulations.

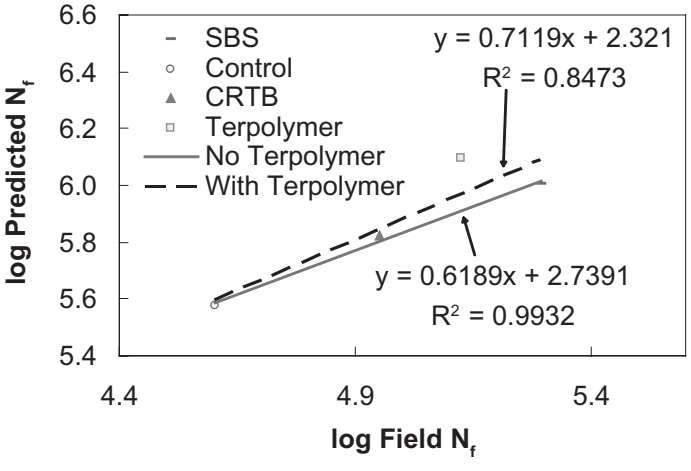

Figure 5. Comparison of measured and predicted cycles to failure in ALF experiment using the best fit function.

5 SUMMARY AND CONCLUSIONS

Layered elastic analysis and empirical material models form the basis for the current state of practice in asphalt concrete pavement analysis. These techniques are popular because they provide a level of analytical accuracy and can be performed relatively quickly using existing computational power. Although these techniques do provide a rational framework to analyze pavements, shortcomings exist with regard to the universality of the empirical material models and to the appropriateness of linear elasticity for paving materials. The future of asphalt concrete pavement analysis will involve more advanced structural analysis tools and mechanistic material models.

One such structural analysis technique is finite element modeling, which provides the user with the ultimate flexibility to include any number of mechanisms and/or processes in the analysis. A finite element code, FEP++, has been applied in this study to perform such an analysis. The advantage of this method over other similar finite element analyses is that it has been developed without the need for costly commercial packages, such as ABAQUS or ANSYS. Also, the model can use inputs currently available and necessary in the NCHRP 1-37A MEPDG.

Simulations of the FHWA ALF pavements were performed, and the results compared to the field-measured responses. In general, the trends are favorable; however, there is some discrepancy between the two strain histories, particularly with regard to the recovery portion. It is believed that this discrepancy is due to the interface condition between the asphalt concrete and base layers, as well as differences in laboratory and field materials.

An advanced mechanistic material fatigue model, the VECD model, is rigorously reformulated for rapid fatigue assessment and is combined with the outcomes of the ALF pavement simulations. This reformulation is necessary due to certain shortcomings in the rigor of earlier derivations and because it is cumbersome to use the non-simplified versions for fatigue simulations. The validity of this derivation is evident because this model unifies the results of CS, CX, and monotonic testing and supports earlier findings that the damage characteristic curve is a material property independent of temperature and test type. The initial pavement responses of the ALF pavements have been predicted using the laboratory characterization data and FEM simulations and then used with this simplified VECD model to predict the fatigue life. The fatigue life predicted using this procedure is found to agree well with the measured field response. Finally, the outcomes of these simulations are combined with the engineering reasonableness of continuum damage models to argue that such models may be extended to account for macrocrack propagation, i.e., continuum damage to fracture.

ACKNOWLEDGEMENTS

The authors would like to gratefully acknowledge the financial support from the Federal Highway Administration under projects FHWA DTFH61-05-RA-00108 and the pooled fund study TPF-5(019). The research team would like to offer special thanks to Nelson Gibson, Xicheng Qi, and Katherine Petros for generously providing ALF test results.

REFERENCES

Al-Qadi, I.L., W. Xie, and M.A. Elseifi. (2008). "Frequency Determination from Vehicular Loading Time Pulse to Predict Appropriate Complex Modulus in MEPDG." In Press. *Journal of the Association of Asphalt Paving Technologists*.

ARA, Inc. ERES Consultants. (2004). "Guide for Mechanistic-Empirical Design of New and Rehabilitated Pavement Structures." National Cooperative Highway Research Program. Transportation Research Board, National Research Council.

Daniel, J.S. and Kim, Y.R. (2002). "Development of a Simplified Fatigue Test and Analysis Procedure Using a Viscoelastic Continuum Damage Model." *Journal of the Association of Asphalt Paving Technologists*, Vol. 71, pp. 619–650.

Dongre, R.N., L.A. Myers, J.A. D'Angelo, C. Paugh and J. Gudimettla. (2005). "Field Evaluation of Witczak and Hirsch Models for Predicting Dynamic Modulus of Hot-Mix Asphalt." *Journal of the Association of Asphalt Paving Technologists*, Vol. 74, pp. 381–442.

Erkens, S.M., X. Liu, T. Scarpas, A.A.A. Molenaar. and J. Blaauwendraad. (2003). "Modeling of Asphalt Concrete–Numerical and Experimental Aspects, Recent Advances in Materials Characterization and Modeling of Pavement Systems." Geotechnical Special Publication No. 123, ASCE Reston, VA: pp. 160–177.

Guddati, M.N., Savadatti, S. and S. Thirunavukkarasu, (1998). "FEP++: A general purpose object-oriented finite element program for nonlinear dynamic analysis," North Carolina State University, Raleigh, 1998—current.

Irwin, L.H. (2002). "Backcalculation: An Overview and Perspective." FWD/Backanalysis Workshop. 6*th* International Conference on the Bearing Capacity of Roads, Railways and Airfields, Lisbon, Portugal.

Kim, Y.R. and D.N. Little. (1990). "One-Dimensional Constitutive Modeling of Asphalt Concrete." *ASCE Journal of Engineering Mechanics*, Vol. 116, No. 4, pp. 751–772.

Kim, Y.R. and A.N. Hanna. (2001). "Assessing Pavement Layer Condition Using Deflection Data: NCHRP 10–48." *Research Results Digest* No. 254. National Cooperative Highway Research Program. Transportation Research Board, National Research Council.

Kim, Y.R., Y. Seo, M. King and M. Momen. (2004). "Dynamic Modulus Testing of Asphalt Concrete in Indirect Tension Mode." *Transportation Research Record*. National Research Council. Washington, D.C., No. 1891, pp. 163–173.

Korkiala-Tanttu, L. (2003). "Modelling With Multilayer Programs; Modelling with VEROAD and NOAH." Cost 347 Mission 2 Report: Improvements in Pavement Research with Accelerated Load Testing, Short Term Scientific Mission at EPFL-LAVOC / Switzerland Analytical Pavement Response.

Kutay, M.E., N. Gibson and J. Youtcheff. (2008). "Conventional and Viscoelastic Continuum Damage (VECD) - Based Fatigue Analysis of Polymer Modified Asphalt Pavements." In Press. *Journal of the Association of Asphalt Paving Technologists*.

Lee, H.J. and Y.R. Kim. (1998). "A Uniaxial Viscoelastic Constitutive Model for Asphalt Concrete under Cyclic Loading." *ASCE Journal of Engineering Mechanics*, Vol. 124, No. 1, pp. 32–40.

Long, F. and C.L. Monismith. (2002). "Use of Nonlinear Viscoelastic Constitutive Model for Permanent Deformation in Asphalt Concrete Pavements." 3*rd* International Symposium of 3D Finite Elements for Pavement Analysis. Amsterdam, The Netherlands, pp. 91–110.

NCHRP 1-40A Project Team. (2006). "Independent Review of the Mechanistic-Empirical Pavement Design Guide and Software." *Research Results Digest* No. 307. National Cooperative Highway Research Program. Washington, D.C.

Qi. X., G. Al-Khateeb, T. Mitchell, K. Stuart and J. Youtcheff. (2005). "Determining Modified Asphalt Properties for the Superpave Specification: Report on the Construction of Pavements with Modified Asphalt Binders." Draft Report for Pooled Fund Study TPF-5(019). FHWA.

Qi, X., N. Gibson and J. Youtcheff. (2008). "Fatigue Cracking Characteristics of Accelerated Testing Pavements with Modified Binders." 6*th* RILEM International Conference on Cracking in Pavements. Chicago IL, USA.

Underwood, B.S., Y.R. Kim and M.N. Guddati. (2006). "Characterization and Performance Prediction of ALF Mixtures Using a Viscoelastoplastic Continuum Damage Model." *Journal of Association of Asphalt Paving Technologists*, Vol. 75, pp. 577–636.

Underwood, B.S. and Y.R. Kim. (2008). "Determination of the Appropriate Representative Elastic Modulus for Asphalt Concrete". In Press. *International Journal of Pavement Engineering*.

Underwood, B.S., Y.R. Kim, S. Savadatti, S. Thirunavukkarasu and M.N. Guddati. (2009a). "Response and Fatigue Performance Modeling of ALF Pavements Using 3-D Finite Element Analysis and a Simplified Viscoelastic Continuum Damage Model." In Press. *Journal of the Association of Asphalt Paving Technologists*.

Underwood, B.S., Y.R. Kim and M.N. Guddati. (2009b). "Use of Viscoelastic Continuum Damage Model for Asphalt Concrete Fatigue Predictions." In review. *International Journal of Pavement Engineering*.

Yoo, P.J., I.L. Al-Qadi, M.A. Elseifi and I. Janajreh. (2006). "Effect of Moving Wheel Load Amplitude and Interface Condition on Flexible Pavement Responses." 85*th* Annual Meeting of the Transportation Research Board. National Research Council, Washington, D.C.

Witczak M.W., K. Kaloush, T. Pellinen, M. El-Basyouny and H. Von-Quintus. (2002). "Simple Performance Test for Superpave Mix Design." NCHRP Report 465. National Cooperative Highway Research Program. Transportation Research Board, National Research Council.

Advanced Testing and Characterization of Bituminous Materials – Loizos, Partl, Scarpas & Al-Qadi (eds)
© 2009 Taylor & Francis Group, London, ISBN 978-0-415-55854-9

Size effect investigation on fracturing of asphalt concrete using the cohesive softening Discrete Element Model

H. Kim & M.N. Partl
Empa, Swiss Federal Laboratories for Materials Testing and Research, Dübendorf, Switzerland

M.P. Wagoner & W.G. Buttlar
University of Illinois at Urbana-Champaign, Illinois, USA

ABSTRACT: Cracking in asphalt concrete is one of the major causes of structural and functional deterioration of the pavement systems, particularly in cold climates. A clustered Discrete Element Method (DEM) was applied into the investigation of size effect on fracturing of asphalt concrete based on a disk-shaped compact tension (DC(T)) test. A bilinear cohesive softening model was implemented into the DEM framework to enable simulation of crack initiation and propagation in asphalt concrete. The influence of specimen size was investigated on the fracture of asphalt concrete using the homogeneous and heterogeneous DEM fracture models. The laboratory tests were conducted for specimen sizes of asphalt concrete varying from 100 mm to 450 mm in diameter. The DEM simulations were shown to compare favorably with experimental results and Bazant's size-effect law.

1 INTRODUCTION

The fracturing of asphalt concrete is a significant cause of premature pavement deterioration. Cracks at the pavement surface create a permanent maintenance liability, and those, which extend through the thickness of pavement, reduce structural capacity and greatly increase pavement permeability and the intrusion of moisture into the pavement foundation. There have been various efforts to investigate the fracture mechanism of asphalt concrete during the past several decades (Majidzadeh et al. 1971, Jacob et al. 1991, Jenq & Perng 1991). However, those fracture tests and numerical investigations were limited to a specific size range of the test specimen. Although the experimental and numerical results provided new insights towards the toughening mechanisms in the fracture of asphalt concrete, another area of interest is the influence of specimen size on the fracture behavior. This paper shows how the experimental fracture test and DEM fracture model are used to capture the dependency of specimen size. In the classical theories based on plasticity or limit analysis, the strength of geometrically similar structures are independent of the structure size. As already known, however, concrete structures and, in general, structures made of brittle or quasi-brittle materials do not follow this trend. The size effect is rigorously defined through a comparison of geometrically similar structures of different sizes. Based on the energy approach, Bazant (1984) developed a size-effect model that allows scaling for fracture energy. For example, a laboratory-sized specimen can be tested but large-scale fracture energy can be determined. Bazant used the phenomenon that, at very small sizes, a material will behave in a yield criterion, which is determined from classical mechanics. At the larger sizes, or if the material was brittle, linear elastic fracture mechanics (LEFM) is applicable. However, between these two sizes, the material behaves in a manner that lies somewhere between these two theories.

By testing different specimen sizes, but geometrically similar specimens, the fracture dependency of quasi-brittle material can be determined using the size-effect law. The equation that defines the size-effect law is:

$$\sigma_n = \frac{Bf_t}{\sqrt{1+\beta}} \tag{1}$$

where, σ_n is the nominal strength; f_t is the tensile strength; β is the brittleness number and is equal to d/d_0; d is the depth of the beam; and B and d_0 are empirical constants.

However, the influence of specimen size on fracture energy can be an issue in viscoelastic materials such as asphalt mixtures, polymers, etc. From the literature for Portland cement concrete (PCC) and test results from asphalt concrete (AC), properties such as tensile strength and fracture energy are specimen size dependent and require a scaling model in order to obtain a size-independent fracture property from laboratory tests.

2 EXPERIMENTAL TESTING

2.1 *Materials*

A Superpave® 9.5 mm NMAS mixture with a PG64-22 asphalt binder was used for DC(T) tests (Wagoner et al. 2005). The target gradation of mixture is shown in Table 1. The mixture was produced with a blend of three aggregate stockpiles, two of crushed dolomite limestone and one of natural sand. For asphalt mixtures compacted, asphalt binder contents were 5.25% and the targeted residual air void contents were 6.5%. The Superpave® indirect tension test (IDT) was used to determine the viscoelastic properties of the mixture and the indirect tensile strength (AASHTO T322-03 2004). The IDT test provided the creep compliance of the material at three temperatures (–20, –10, and 0°C). Time-temperature superposition principle was utilized to shift the creep data at the different temperature to a reference temperature to develop a master creep compliance curve. Figure 1. shows the master creep compliance curve for this material. The average indirect tensile strength of the mixture, measured at –10°C was 2.37 MPa.

Table 1. Material gradation curves.

Sieve size (mm)	12.5	9.5	4.75	2.36	1.18	0.6	0.3	0.15	0.075
Percentage by mass	100	99	77	49	24	15	10	7	6

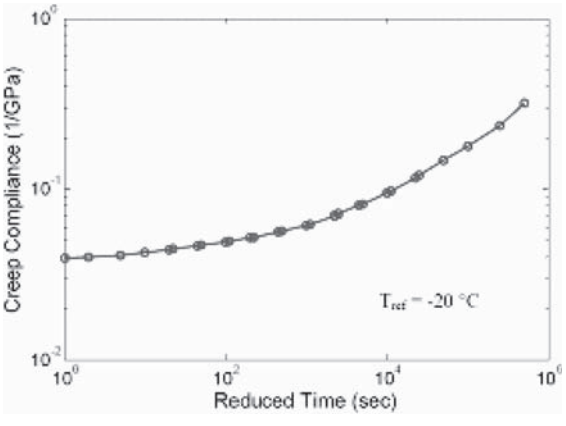

Figure 1. Master creep compliance curve for asphalt concrete.

2.2 *Fracture test*

A disk-shaped compact tension (DC(T)) specimen geometry was developed to investigate the fracture behavior of asphalt concrete and it has the ability to test cylindrical cores obtained from in-place asphalt concrete pavements and gyratory-compacted specimens fabricated during the asphalt concrete mixture design process for relevant fracture properties (Kim et al. 2008). Figure 2(a) shows the DC(T) test configuration inside a temperature chamber and a typical fractured specimen. The DC(T) test is loaded in tension through the loading holes and is conducted with a constant crack mouth opening displacement (CMOD) rate. The CMOD can be measured at the edge of the notched crack by a clip gauge. The standard specimen diameter is 150 mm and both cored hole diameters within the specimen are 25 mm. The width of the specimen (W) was 110 mm with the notch length (a) being 27.5 mm (a/W = 0.25). Therefore, the initial ligament length (W–a) was 82.5 mm. The thickness (t) of the specimen was 50 mm.

As shown in Figure 2(b), the limited size range of DC(T) fracture specimens were cored from the test pad built using standard asphalt paving equipment and procedures. DC(T) specimen with 450 mm diameter was not showed in Figure 2(b) although it was experimentally tested. A limitation was the current testing equipment used for fracture testing of asphalt concrete. Specifically, the temperature controlled environmental chamber would limit the maximum dimension to approximately 560 mm. The temperature chamber is crucial for testing asphalt concrete since the fracture properties are temperature dependent. Another limitation to specimen size was the ability to handle the specimen without incurring damage. For very large specimens, the self-weight of the specimen could induce deformations due to creep and introduce damage in the specimen. Therefore, the above limitations were taken into consideration to select the DC(T) geometry. The DC(T) specimen dimensions with varying diameters can be found in Table 2. Each specimen has the same thickness, 50 mm, to focus on the diametric size effects (i.e., ligament length). However, the thickness effect on fracturing of asphalt concrete should not be ignored and the scope is beyond this diametric size effect study.

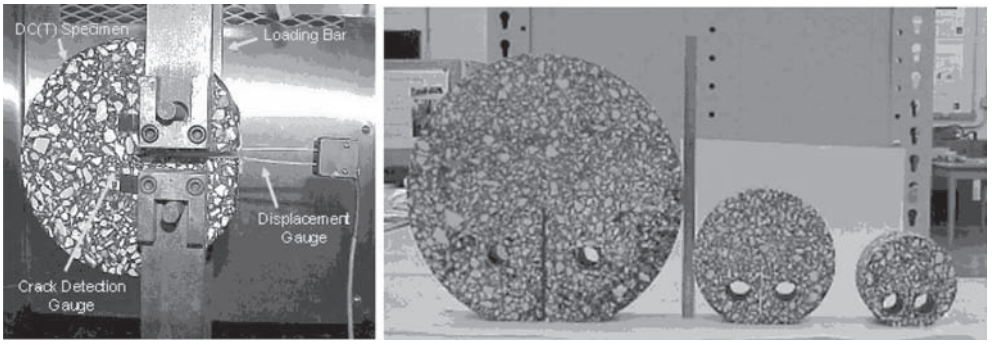

(a) Test set-up (b) DC(T) specimens (from left: 300,150, 100 mm)

Figure 2. DC(T) test setup and a typical fractured specimen.

Table 2. DC(T) specimen dimension for size effect analysis.

DC(T) Dimension (mm)				
D	100	150	300	450
W	73.3	110	216.3	330
a	18.3	27.5	54.1	82.5
d	16.7	25	49.2	75
C	23.3	35	68.8	105
Φ	35	35	35	35
t	50	50	50	50

The testing for all specimens was conducted at −10°C. The main purpose for using this temperature was to reduce the viscous response of the materials. The loading rate of the different sized specimens must be considered to ensure that the fracture energy comparison between the different sizes is valid. The reason for considering the loading rate is that fracture energy is dependent on the rate of loading. The crack mouth opening displacement (CMOD) was used as the measurement for closing the servo-hydraulic control loop. The standard CMOD rate for the DC(T) was 1 mm/min for the standard geometry. The loading rates for other specimen sizes are 0.667 mm/min for 100 mm, 2 mm/min for 300 mm, and 3 mm/min for 450 mm diameter specimen, respectively to make the CMOD rate constant.

3 NUMERICAL MODELING

3.1 *Constitutive law*

The discrete element method (DEM) originally developed by Cundall (1971) has proven to be a powerful and versatile numerical tool for modeling the behavior of granular and particulate systems, and also for studying the micromechanics of materials such as soil at the particle level. The DEM discretizes a material using rigid elements of simple shape that interact with neighboring elements according to interaction laws that are applied at points of contact. In this paper, discrete element modeling (DEM) is performed using the commercial software package, PFC-2D, which utilizes fixed-size and fixed-shape circular elements that can be used to approximate bulk material stress-strain behavior (ITASCA 2002).

The translational and rotational stiffnesses ([*K*]) of a particle relate increments of force and moment (Δf) to increments of displacement (δu) and rotation via the matrix relations:

$$\{\Delta f\} = [K]\{\delta u\} \tag{2}$$

The linear contact stiffness (K^n or K^s) is defined by the normal and shear particle stiffness k_n and k_s (force/displacement) of the two contacting entities (ball-to-ball or ball-to-wall) acting in series. Based on the strain energy density and Hooke's law, the relationship between the discrete element springs and the elastic properties of a plane strain conditions are given by (Morikawa et al. 1993).

$$K^n = \frac{E}{\sqrt{3}(1+\nu)(1-2\nu)} \tag{3}$$

$$K^s = \frac{E(1-4\nu)}{\sqrt{3}(1+\nu)(1-2\nu)} \tag{4}$$

Cohesive zone models (CZMs) have recently been used to simulate the fracture process in a number of material systems under a variety of loading conditions. In the fracture study of asphalt concrete discussed herein, the bilinear cohesive fracture model, as shown in Figure 3,

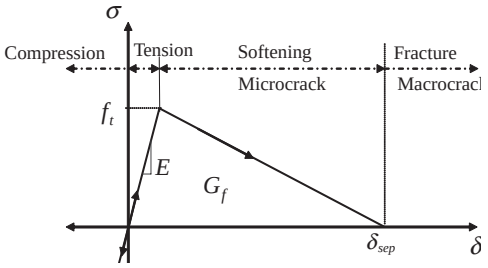

Figure 3. Cohesive fracture model.

was selected due to the effectiveness of assigning fracture parameters such as tensile strength (f_t) and fracture energy (G_f). The shape function of cohesive fracture model can be varied and it depends on the material behavior.

3.2 *DEM mesh*

By integrating of numerical simulation with size effect experiments, a better understanding of the fracture process in asphalt concrete and its relation to specimen size was obtained. Figure 4 shows the detail description of homogeneous fracture model with bulk viscoelastic contacts. The mechanical loadings with constant velocities were applied to numerical loading bars inside of specimen holes like in laboratory tests. The cohesive fracture contacts, which were represented by solid lines between particles, were inserted into the middle of specimen ligament and the viscoelastic contacts were assigned into the whole specimen area. The radius of circular elements used to approximate the material fracture behavior was 0.5 mm, which was smaller than the notched crack width, 2 mm. However, the "real" crack tip width can be smaller than the element size used here. The notched crack length was from 41.6 mm to 187.5 mm depending on the different specimen sizes.

Also, the details of heterogeneous DEM mesh can be found in Figure 2(b). Each aggregate is composed of various numbers of particle meshes, which depend on the aggregate size and shape. Based on an image processing procedure, the two-dimensional microstructure of asphalt specimen can be obtained and projected into DEM mesh. More details of image processing technique can be found in author's previous publication (Kim et al. 2008).

3.3 *Material parameters*

The fracture parameters, i.e., 3.56 MPa for tensile strength and 344 N/m for fracture energy, were determined by the indirect tensile test (IDT) and DC(T) fracture test at –10°C. Also, the viscoelastic properties were obtained from creep tests conducted at multiple temperatures, and shift factors are evaluated from shifting the compliance versus time curve at different temperatures in a log scale to establish a smooth and continuous curve. Interconversion of the time dependent creep compliance function yields a relaxation modulus given as

$$E(\xi) = \sum_{i=1}^{N+1} E_i (1 - e^{-\xi/\tau_i}) \tag{5}$$

where, $E(\xi)$ is a relaxation modulus at the reduced time of ξ, and E_i and τ_i are model constants for the master relaxation modulus curve.

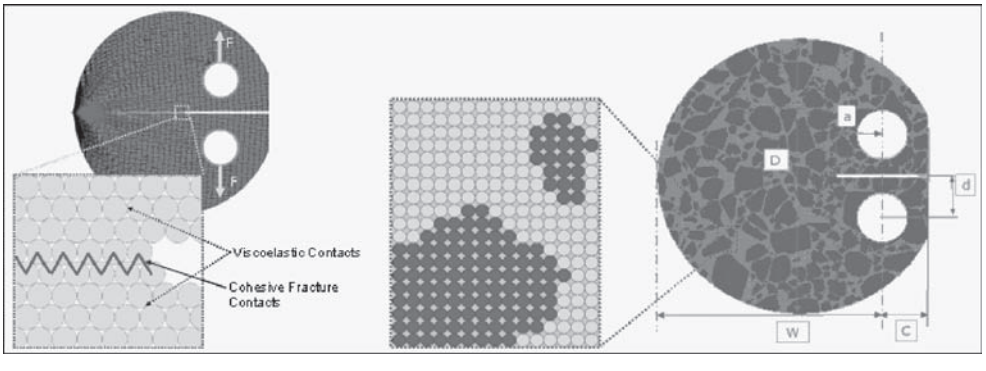

(a) Homogeneous model mesh (b) Heterogeneous model mesh

Figure 4. Description of homogeneous fracture model.

Table 3. Burger's model parameters.

Maxwell		
Stiffness (N/m)	Viscosity (Ns/m)	Poisson's ratio
9.260E+8	1.601E+12	0.25
Kelvin		
Stiffness (N/m)	Viscosity (Ns/m)	Poisson's ratio
4.995E+8	4.998E+10	0.25

For the viscoelastic simulation, Burger's model was inserted at each particle contact point. The determined relaxation modulus can be converted to the DEM contact stiffness based on Equation (3), Equation (4), and Equation (5) as shown in Table 3.

4 RESULTS AND COMPARISIONS

4.1 *Homogeneous fracture results*

Figure 5 presents the comparisons of global responses between experimental and numerical results for three different specimen sizes (100 mm, 150 mm, and 300 mm). Elastic and viscoelastic models were compared using force versus CMOD curves to investigate both elastic and viscoelastic model capabilities in the fracture prediction of asphalt concrete. The same fracture parameters were selected for fracture simulations with different specimen sizes. Same loading rates as in experimental tests were applied in the numerical simulations. The results show that the elastic simulations deviate far from the experimental results as the DC(T) specimen size increases. Larger specimen has greater amount of viscoelastic dissipated strain energy. Therefore, the effect of viscoelastic behavior is getting significant in the larger specimens.

Using Bazant's size effect law, the nominal strength versus the characteristic dimension was illustrated as shown in Figure 6. The nominal strength was calculated by dividing the peak load P with the ligament area. The characteristic dimension was selected as the depth, W, of the specimens. The depth was selected for determining the geometric factors required to determine the specific fracture energy (G_f). The size dependency of asphalt concrete on the nominal strength has a similar trend to that of Portland cement concrete. The results for the homogeneous DEM fracture model with bulk viscoelastic properties were found to agree with experimental results. For the homogeneous viscoelastic DEM model, the same material parameters for each set were used in the fracture simulations for all different specimen sizes to verify if DEM models can capture the specimen size dependency or not.

4.2 *Heterogeneous fracture results*

Using the high-resolution image technique, the coordination of microstructure in asphalt specimens was successfully obtained and projected into the DEM mesh to investigate various heterogeneous fracture behaviors. The bulk and fracture parameters were determined from modulus, strength, and fracture tests for each material (i.e., aggregate, mastic) and the interface parameters could be determined based on the known parameters and inverse analysis [Kim 2007]. The determined input parameters are shown in Table 4. As shown in Figure 7, DC(T) DEM specimens which capture the sand-size and larger aggregate features of 9.5 mm nominal maximum aggregate size (NMAS) mixtures could be obtained.

Although the homogeneous viscoelastic DEM fracture model can predict specimen size effect in quasi-brittle materials, it was desired to study size effect using a heterogeneous DEM fracture model. However, it was difficult to handle the microstructure of large size specimen using the image techniques employed in this study due to the limitation of image resolution

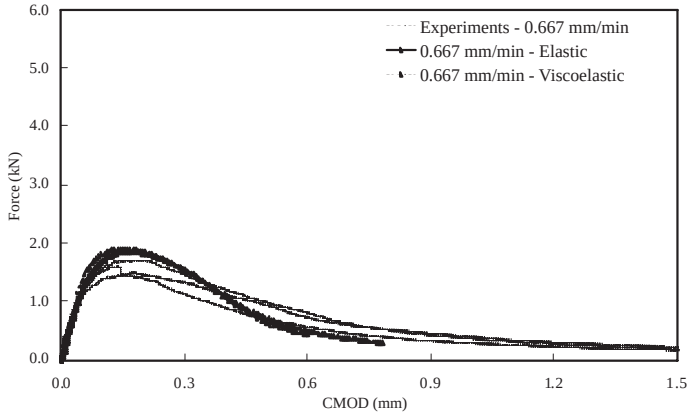

(a) 100 mm

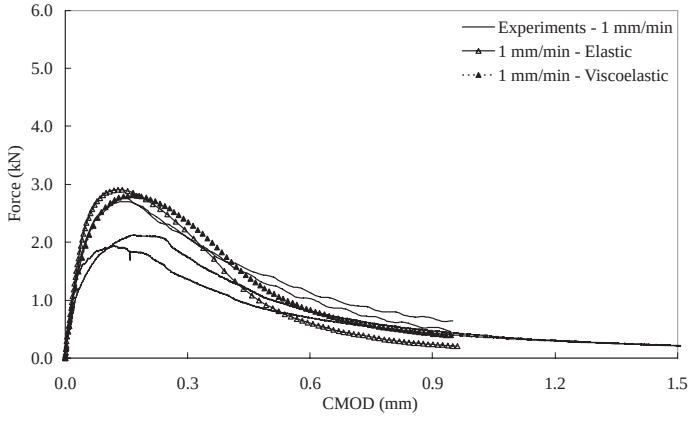

(b) 150 mm

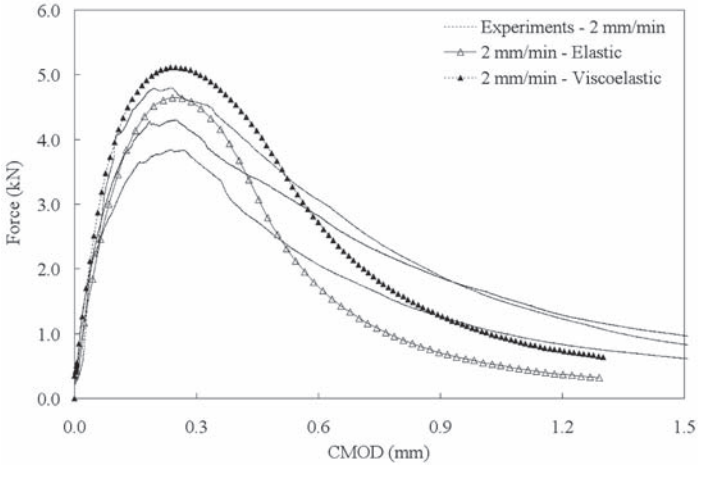

(c) 300 mm

Figure 5. Comparisons between homogeneous DC(T) fracture models and experimental tests.

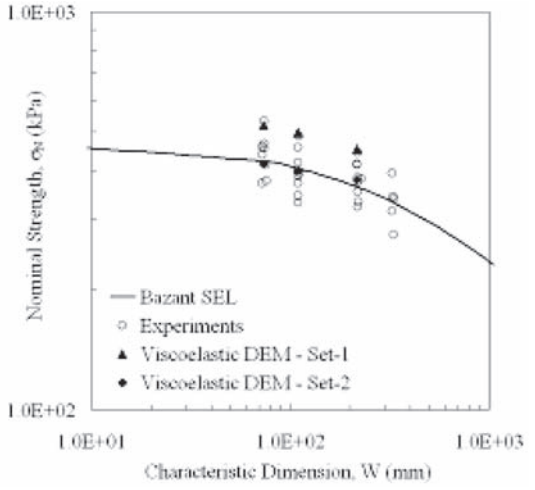

Figure 6. Nominal strength versus specimen size.

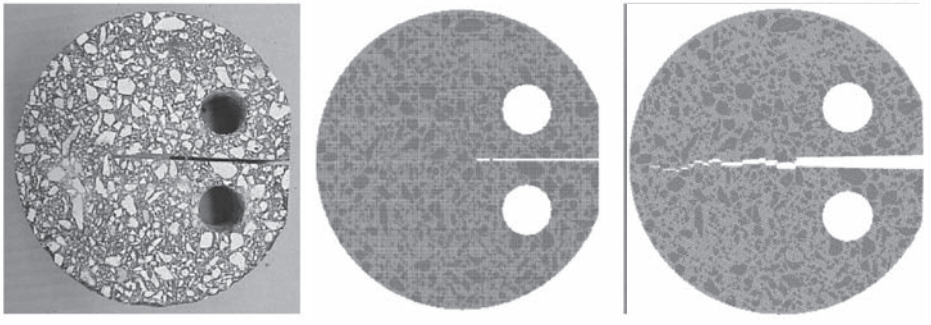

(a) Experimental specimen image (b) DEM specimen (c) Failed DEM specimen

Figure 7. Heterogeneous DEM model mesh and multi-phase material properties.

Table 4. Material parameters for heterogeneous DEM fracture model.

DC(T) at –10°C with PG64-22			Material properties	
Specimen size (mm)	Phase	Poisson's ratio	Young's modulus (GPa)	Tensile strength (MPa)
100, 150, 300	Aggregate	0.15	56.8	6.59
	Mastic	0.25	11.4	2.87
	Interface	0.25	11.4	2.61

and the large image size, which is computationally intensive to process. Figure 9 shows the global responses of heterogeneous fracture models compared with experimental results from 100 mm to 300 mm specimens. The heterogeneous fracture model has material properties calibrated based on the fracture energies obtained from experimental tests for different specimen sizes. The global response of heterogeneous fracture model with 100 mm diameter was slightly over-predicted as shown in Figure 9(a). Due to the small difference in the ligament length between 100 mm and 150 mm specimen, the response difference was not significant.

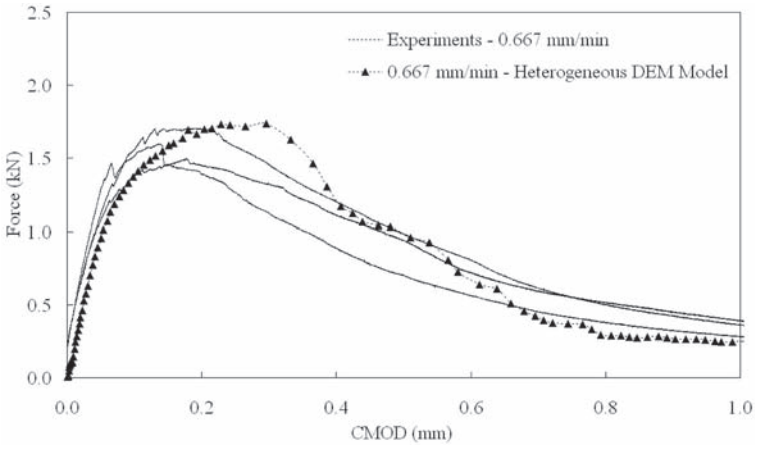

(a) D = 100 mm

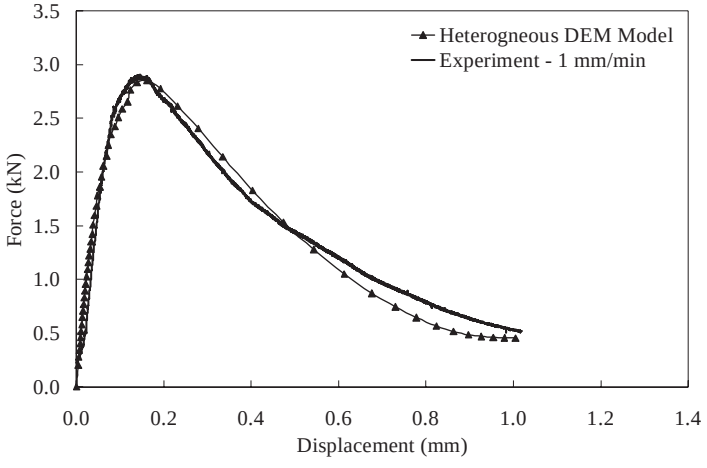

(b) D = 150 mm

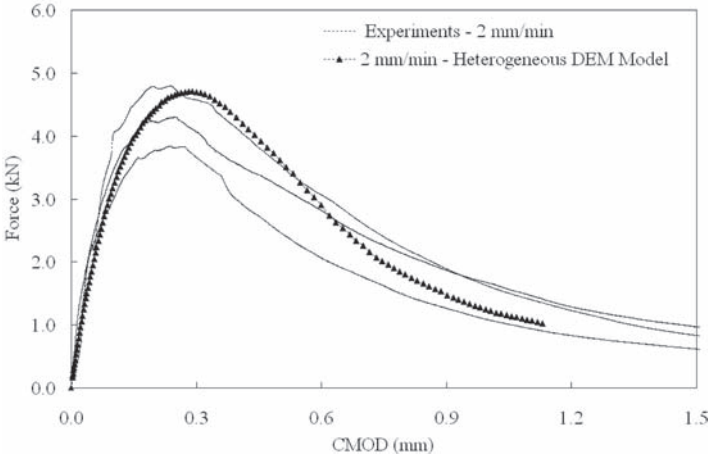

(c) D = 300 mm

Figure 9. Comparisons between heterogeneous DC(T) fracture models and experimental tests.

5 CONCLUSIONS

A micromechanical fracture modeling approach has been employed to investigate the specimen size effect and toughening mechanism in the fracture of asphalt concrete. Cohesive softening model was employed to analyze asphalt fracture behaviors based on the discrete element method. DC(T) fracture tests were conducted for different sizes of asphalt concrete varying from 100 mm to 450 mm diameter but the 450 mm specimen was not simulated with the DEM fracture model due to the limitation of the high computational time and the handling difficulty of specimen image. The fracture energies determined by experiments were varied for the different specimen sizes. Different size specimens were modeled and simulated using homogeneous DEM fracture models with bulk viscoelastic properties. The experimental and numerical specimen size dependency of asphalt concrete was compared with the size effect law, which was proposed by Bazant.

The bulk viscoelastic DEM fracture model with the same material properties could predict the size effect on the nominal strength of asphalt concrete based on two sets of material properties. By comparing with elastic and viscoelastic homogeneous DEM fracture models, it was shown that viscoelastic properties of asphalt concrete play an important role on the fracture behavior as the specimen size becomes larger. The heterogeneous fracture model for different specimen size could be implemented and applied for the investigation of size effects but the calibration procedure of material parameters is necessary based on experimental test data. The global fracture responses of heterogeneous DEM models were matched well with experimental fracture behaviors in the force versus CMOD curves. For the large size of DEM, the fast contact algorithm or simplified approach is much needed to investigate the fracture behavior of asphalt concrete. 3-D fracture analysis should be conducted to investigate more realistic fracture behavior and the specimen thickness effect on the fracture of asphalt concrete. However, the computational running time should be considered for both large size and three-dimensional fracture analyses and will be limited in size of the numerical simulation by current.

REFERENCES

AASHTO T322-03. 2004. Standard test method for determining the creep compliance and strength of hot mix asphalt (HMA) using the indirect tensile test device. *Standard Specifications for Transportation Materials and Methods of Sampling and Testing*, 24th Edition.

Bazant, Z.P. 1984. Size effect in blunt fracture: concrete, rock, metal. *ASCE Journal of Engineering Mechanics* 110: 518–535.

Cundall, P.A. 1971. A computer model for simulating progressive, large-scale movements in blocky rock systems. *Proceedings of the International Symposium of Rock Fracture*, Nancy, France.

ITASCA Inc. 2002. *PFC 2D Version 3.0*. Minneapolis, Minnesota 55415, USA.

Jacob, M.M., Hopman, P.C. and Molenaar, A.A.A. 1991. Application of fracture mechanics in principles to analyze cracking in asphalt concrete. *Journal of Asphalt Paving Technologists* 65: 1–39.

Jenq, Y. and Perng, J. 1991. Analysis of crack propagation in asphalt concrete using cohesive crack model. *Transportation Research Record* 1317: 90–99.

Kim, H. 2007. *Investigation of toughening mechanisms in the fracture of asphalt concrete using the clustered discrete element method*. Ph.D. Thesis, University of Illinois at Urbana-Champaign.

Kim, H., Wagoner, M.P. and Buttlar, W.G. 2008. Simulation of heterogeneous cohesive fracture model in asphalt concrete using discrete element method. *ASCE Journal of Materials in Civil Engineering* 20(8): 552–563.

Majidzadeh, K., Kauffmann, E.M. and Ramsamooj, D.V. 1971. Application of fracture mechanics in the analysis of pavement fatigue. *Journal of Asphalt Paving Technologists* 40: 227–246.

Morikawa, H., Sawamota, Y. and Kobayashi, N. 1993 Local fracture analysis of a reinforced concrete slab by the discrete element method. *Proceedings of the Second International Discrete Element Methods*, MIT Press, Cambridge, MA, USA.

Wagoner, M.P., Buttlar, W.G. and Paulino, G.H. 2005. Disk-shaped compact tension test for asphalt concrete fracture. *Experimental Mechanics* 45(3): 270–277.

6. Fundamental laboratory test methods and models

Advanced Testing and Characterization of Bituminous Materials – Loizos, Partl, Scarpas & Al-Qadi (eds)
© 2009 Taylor & Francis Group, London, ISBN 978-0-415-55854-9

On the importance of performing accurate material characterization tests for bituminous materials

N. Kringos & A. Scarpas
Delft University of Technology, Delft, The Netherlands

ABSTRACT: Selecting appropriate experiments to measure the important parameters that define the behavior of bituminous materials is far from a trivial task. In most cases, testing and modeling go hand-in-hand, and one should be confident that the selected experiment is capturing the important parameters. At different stages of the investigation, different tests may be required. This paper is addressing some of the important issues and defines the differences between structural and material tests. The introduction of moisture in asphalt characterization tests is becoming a topic of increased interest in recent years. Using the 'wrong' conditioning procedure could result in misleading conclusions about the moisture susceptibility of the tested mixtures, which could lead to unexpected failures in the field. This paper is discussing some of the issues of moisture conditioning. The challenges involved with rotational tests, which are often used by pavement engineers, and the need to measure the behavior of mastics rather than neat bitumen are also discussed.

1 INTRODUCTION

1.1 *Modeling and parameter determination*

Over the years, the pavement industry and asphalt researchers and engineers have developed many different laboratory experiments for the mechanical characterization of bituminous materials, Figure 1. The purpose of such tests can range from measurement of important material parameters, such as stiffness, tensile or compressive strength, to 'simply' comparing the response degradation of various mixtures after conditioning procedures, such as ageing or moisture infiltration.

The choice of the appropriate experiment(s) is, however, not a trivial task. It has to be clear, first of all, which parameters are being measured and how dependent they are on the

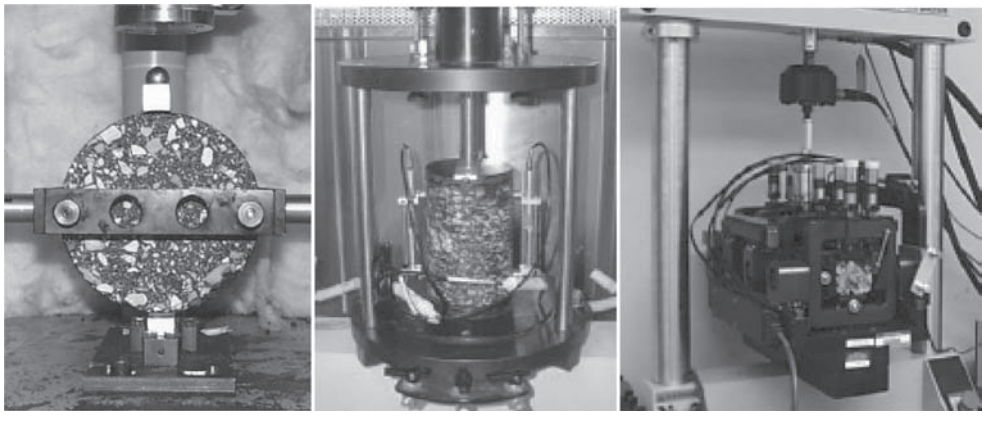

Figure 1. Many meso-scale asphalt mixture tests are nowadays available.

boundary conditions of the test and the mode and rate of loading. Given the limitations of simulating actual in-time pavement response in the laboratory, many researchers and engineers include modeling as part of their design and maintenance routine. The finite element method or other types of techniques are ideally suited to give insight into the long-term response of an integral pavement design, where one has to account for different layers of material, environmental conditions and billions of loading cycles. Using this approach, modeling and laboratory experiments go hand-in-hand and the choice of the appropriate experiments becomes an important aspect of the quality of the model predictions. It is important that the experiments capture the directionality and triaxiality of the material response and include, among others, its temperature and strain rate dependency. For both the model and the experimental component of this design and prediction process, it is important to keep a critical eye on the limitations of the outcome.

As an example of this, in Figure 2 the results of a compressive strength test are given. In the experiment, several cores where made of one type of asphalt mixture. All the cores had the same diameter D, but varied in height h. From the figure it can be seen from the square dots that depending on the height to diameter ratio h/D, different compressive strength was found for the asphaltic mixtures. Due to a bulging effect of the core, shorter cores showed a higher strength than the taller ones. Since the strength of the material is a unique parameter, given the same confinement, temperature and loading conditions, this is obviously an erroneous result. From this experiment [Erkens 2002] it became clear that, unless measures were taken to reduce the friction between the loading platen and the sample (the round dots), the structure of the sample starts interfering with the measurements. Since cores of asphalt mixture are made via various methods, such as gyratory or Marshall compaction, or are retained from the field, it is important to ensure that the geometry of the sample is not influencing the measured parameter.

Therefore, a distinction is made between structural and material tests. In a structural test, the geometry of the sample is influencing the results of the test. By changing the geometry, for example by increasing the height, and keeping the loading conditions equal, a different strength or stiffness will be measured. In a material test the sample is exposed to a uniform stress field which is giving a unique measurement of the material, under the given conditions. In model development, sometimes a material test is required and sometimes a structural test. In the following, this concept is discussed in further details.

1.2 *Material calibration and structural validation tests*

In Figure 3 an example of a finite element analysis of an indirect tension test made with CAPA-3D is shown. From the comparison of these finite element simulations with the

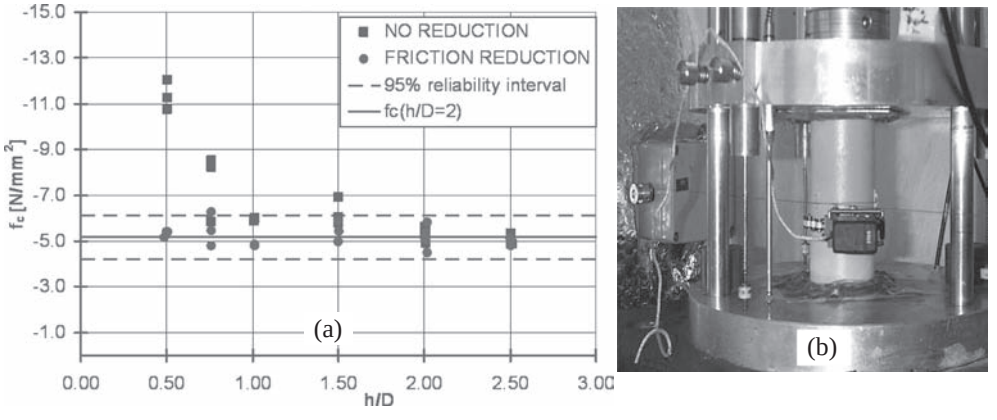

Figure 2. Variation in compressive strength depending on h/D ratio (a) data (b) test set-up (Erkens 2002).

laboratory test results, Figure 4, it can be seen that the analyses was able to capture the overall response of the specimen quite well. From the colors in the plots it can be clearly seen that the specimen is undergoing a complicated stress field during the test:

- At t_1 the specimen is building up tensile stresses in the center of the specimen and is starting to build up a compressive stress field on the top and bottom of the specimen, under the loading platen.
- At t_2 the specimen has not yet failed in tension in the middle, but is already showing considerable bulging on the top and bottom of the specimen due to the shear stresses developing there.
- At t_3 the specimen has failed, since it can no longer transfer tensile stresses in the middle of the sample, which can be seen from the white color in the legend and the large deformations of the finite elements in this area.

During the test, each location in the specimen experiences at all times a different stress and strain level and direction (tension in the middle and compression on the top and bottom) and continuously changing rates. By changing the size of the specimen, such as is done for Marshall and gyratory compacted specimens, the material will experience different stresses and strains inside the material. It is therefore, from a mechanical point of view, not surprising that a difference is found between the response of the Marshall and gyratory compacted specimens, when tested for example in an indirect tension test. The geometry of the sample is dictating such a complex state of stress inside the material, that it would be nearly impossible to use this test for model development.

In order to be able to actually simulate this (structural) test, as shown in Figure 3 and Figure 4, the asphalt mix must be tested for its tensile and compressive response under various strain rates. For this continuum analyses, triaxial direct tension and compression test were performed on the asphalt mixtures. These tests are considered to be 'material tests' and should be independent of their geometry. These individual tests are used to calibrate the model prediction of material response under tension and compression, with varying confinements and strain rates. Once the model is calibrated and capable of back-predicting the same test where the parameters came from, it becomes appropriate to perform a structural test. In the structural test, such as the bending beam or the indirect tensile test, a complex state of

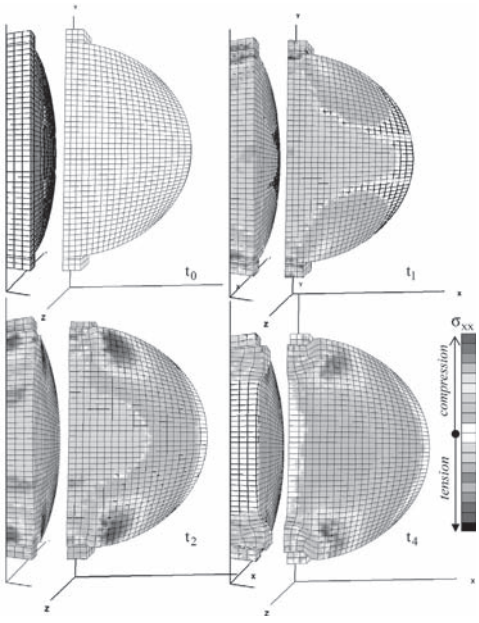

Figure 3. Finite element continuum analysis of TSR test (Scarpas 2004).

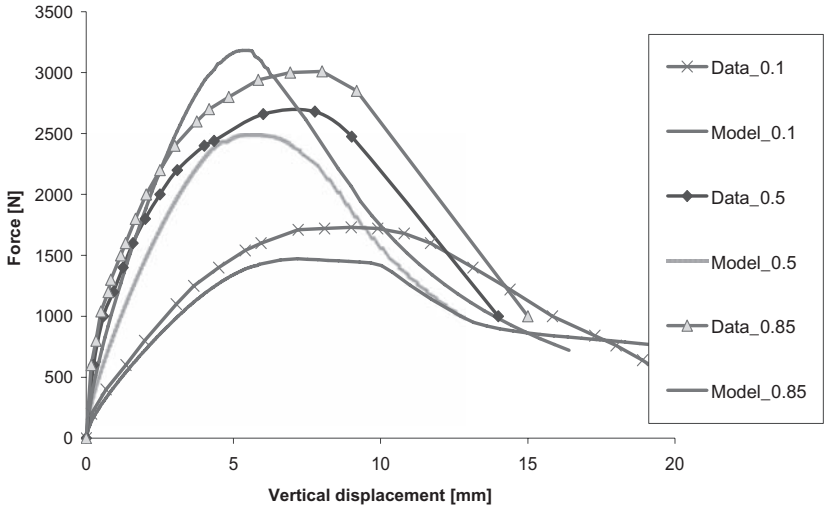

Figure 4. Comparison laboratory data and CAPA-3D simulation.

stress is created during the test, where the material is exposed to both compressive and tensile stresses. This test is ideally suited for the validation of the model, where now the model must be able to accurately predict the complex state of stress. Once this stage is completed satisfactory, the model can be used to predict the response of a pavement or a wheel-tracking test.

Therefore, different tests are appropriate in different stages of the model development. The material tests are important for the calibration, the structural tests are important for the validation of the model.

2 MOISTURE CONDITIONING

2.1 *Fully saturated versus dry*

In recent years, moisture induced damage has been acknowledged as one of the important failure mechanisms of asphaltic pavements. Many laboratory tests are therefore performed under dry and wet conditions to capture the moisture susceptibility of various asphaltic mixtures. In most moisture susceptibility tests which are used, such as the Modified Lottman test, it is common practice to prescribe (partially) saturated versus unsaturated moisture conditioning for the test samples. It is often suggested that, even though the moisture conditions in the test are not completely representative of the situation in the field, a 'worst case scenario' is being created and therefore, a conservative judgment can be made on the moisture susceptibility of the mixtures. Yet, by performing these moisture susceptibility tests under "dry" and "saturated" conditions, a number of implicit assumptions are being made, which may, in fact, give misleading results and erroneous conclusions. To demonstrate this, in the following a simple example is given for two mastics.

In a hypothetical test case, mastic (or asphalt mixture) A & B are tested for their strength during dry and "fully" saturated conditions. From the test results it is found that both mastics have a dry strength of 3 MPa. After fully saturating the samples with water, the strength of both mastics is tested again. It is found that mastic A has a reduction of 83% of its original–dry- strength and mastic B has a reduction of 50% of its original strength, Table 1.

Based on these result, most test protocols would lead to the conclusion that mastic B is "less moisture susceptible" than mastic A and would most likely be recommended to be used in pavements which are exposed to a wet climate.

This, however, could be a completely wrong conclusion, since there is an implicit assumption being made regarding a linear relation between loss of strength and moisture concentration,

Table 1. Hypothetical test data.

Material	Dry Strength	Saturated Strength
Mastic A	3 MPa	0.5 MPa
Mastic B	3 MPa	1.5 MPa

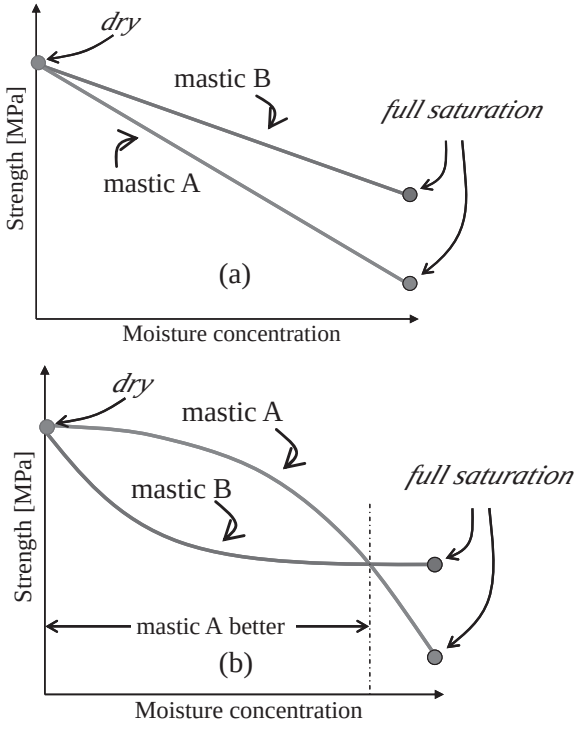

Figure 5. Strength versus moisture concentration (a) linearity assumption (b) possible reality.

Figure 5(a). Yet, if the same test was performed at different levels of moisture concentration (i.e. in between dry and fully saturated) it may be found that there is in fact a non-linear relationship between the material strength and the moisture concentration, Figure 5(b).

From Figure 5(b) it can be seen that this may mean that in reality it is mastic A which is less moisture susceptible for most moisture levels than moisture B and should be preferred. This is in complete contrast to the initial conclusion based only on the "dry" and "saturated" test data.

2.2 *Actual moisture levels in the pavement*

The determination of the (possible) non-linear relationship between strength reduction and moisture concentration may, however, still not be sufficient to judge which mastic should be used in the field, since the moisture concentration levels which are reached in the field are important and may be different for the two mastics.

For example, the mastics may never reach higher moisture concentration than 30 % of its maximum -fully saturated- uptake, Figure 6(a). In this case, mastic A has at all times an equal or higher strength than mastic B and should be preferred. It may, however, be possible that mastic A has a higher moisture absorption coefficient than mastic B. This means that, given the same availability of moisture, mastic A will reach higher moisture concentrations than mastic B, Figure 6(b). In this case, both mastics may have an equal strength range during the

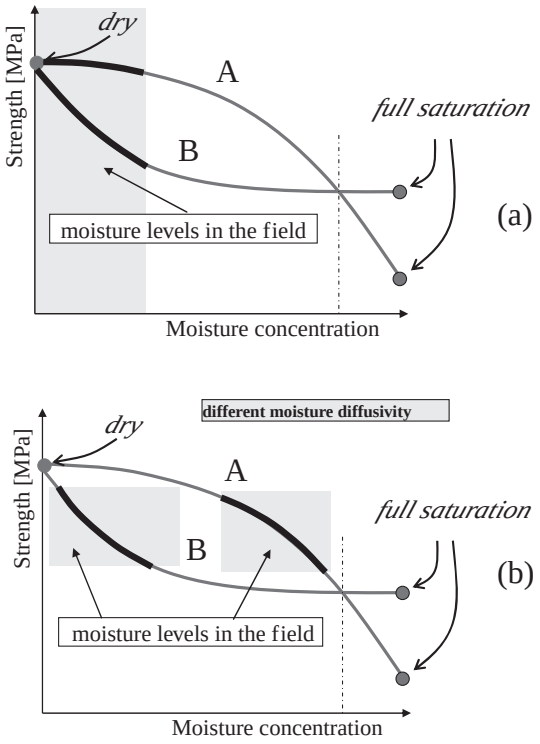

Figure 6. Moisture concentrations reached in the pavement. (a) Same mastic moisture diffusivity (b) different mastic moisture diffusivity.

service life of the pavement and either one could be chosen, based on the moisture susceptibility criterion.

2.3 *Time frame over which moisture becomes a problem*

An important aspect of the "moisture levels in the field" is the time-frame over which these levels are reached. A material which looses 99% of its initial strength at moisture concentration X seems dramatic. Yet, if it is also known that it would take a 100 years before this material will ever reach moisture concentration X, moisture induced damage may not necessarily become a problem in the pavement.

Therefore, a realistic quantification of the actual moisture concentrations reached over time inside the material is important and should always be taken into account. Moisture which is available in the macro-pores of the mixture may, in time, start penetrating inside the mix components (i.e. the mastic, the aggregate-mastic bond and the stones) via a gradient driven diffusion process (Kringos and Scarpas 2005, Kringos et al. 2008a, 2008b). As the moisture concentration inside these components increases, mechanical properties such as strength and stiffness degrade. Understandably, the time-frame of the problem is such, that it will be hard to accurately simulate the (often) slow moisture diffusion process as it happens in the pavement. Yet, it is possible to determine the most dominant material parameters which control these processes, and thus make a better in-time prediction of the moisture susceptibility of a mix.

There are several other processes which are relevant to the issue of moisture susceptibility, such as erosion and pumping action, which are often not or all at the same time taken into account in the moisture induced damage experiment. These other moisture induced damage phenomena are the mechanical and physical manifestations of the 'pumping action' which a

(partially) saturated pavement experiences under mechanical loading. In addition to added mechanical stresses inside the material, which may cause added damage, these high water pressures may cause an erosion effect of the mastic, which contributes to the mechanical degradation of the mastic and the progressively increased moisture susceptibility (Kringos and Scarpas 2005, Kringos et al. 2009). For example, the Modified Lottman test is not including these pumping action related moisture induced damage phenomena in the test. This means that a mixture which is highly susceptible to mastic erosion may perform well in the test, but would have bad results in the pavement, when exposed to pumping action. Similarly, other tests, such as the Hamburg wheel tracking test, is including many phenomena at the same time even though the timeframe of the moisture conditioning is too short to represent the actual pavement conditions.

2.4 *Separation of adhesive from cohesive failures*

In order to gain fundamental insight into the dominant parameters which control moisture induced damage, it is therefore crucial to design tests which enable the investigation of the individual processes, rather than have them occur at the same time. To include the influence of the degradation of the mechanical properties of an asphaltic mix as a function of moisture concentration, the graphs which were shown in Figure 5 must be determined for each asphalt mix component (mastic, stone and mastic-stone bond). From such analyses it will become clear which failure mechanism (e.g. adhesive or cohesive, Figure 7) may occur at what moisture concentration and which parameters are dominant for the failure of the specimens and the variability of the test results.

In Figure 7 a detail of a test is shown in which an aggregate-mastic bond is tested after various moisture conditioning times. From the graph it can be seen that for different moisture concentrations different failures can be expected. Therefore, similar to the uniform state of stress in material tests, moisture induced damage tests should have a uniform moisture concentration at the location of failure. If this is not the case, a mixed failure will be result: e.g. location I will fail in the mastic, location III will fail in the aggregate-mastic bond and location II is undetermined. This outcome will not lead to any fundamental insights nor will give any practical guidance for the improvement of the material. It is therefore crucial to control the moisture concentrations in the test and to focus of the measurement of a particular component.

3 TORSIONAL TESTS

Bituminous materials are known to be, among others, strain-rate dependent. Yet, quite frequently it is attempted to test them under a rotational state of stress. The concept being that the induced strains remain in the small-strain regime and therefore a linear interpretation of

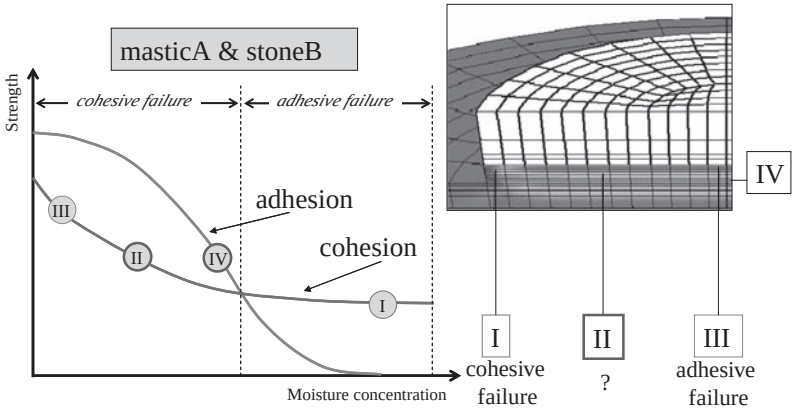

Figure 7. Cohesive and adhesive moisture susceptibility.

the outside measurements can be used. Similar to the challenges of testing a material under a non-uniform stress and/or non-uniform moisture concentration field discussed in the previous sections, testing under a non-uniform strain and strain-rate field would be complex. To illustrate this concept, in Figure 8 a finite element simulation of a modified shear-rheometer is shown.

From the changing colors in the pictures it can be seen that the shear stresses (and therefore the compressive and tensile stresses) which the material is generating under the torsional displacement are continuously changing. The center of the specimen is exposed to zero stresses at all times, but all the other locations in the material the stresses and strains (and their rates) are continuously changing. For a material which is strain rate and state-of-stress dependent, it would be very challenging to come up with any conclusions. The non-linear behavior of the material is of crucial importance in the field and can certainly not be captured from a tortional test.

4 MASTIC OR NEAT BITUMEN

A lot of the asphalt testing is focused on neat bitumen. I should, however, be taken into account that the actual material in pavement will never be a neat bitumen. And even though the assumption could be made that the material is a collection of neat bitumen, fillers, sand and larger aggregates, the concept that the bitumen itself is changed by the existence of the other components is not very far fetched. To illustrate the difference in response of the neat bitumen and a bitumen with mineral particles in it (i.e. a mastic), in Figure 9 a finite element analysis is shown of a constant strain rate tensile test on both materials.

The visco-elastic properties of the bitumen are kept constant in both analyses and the mineral particles in the mastic, Figure 9(b), are assumed elastic. From the analyses the stiffening

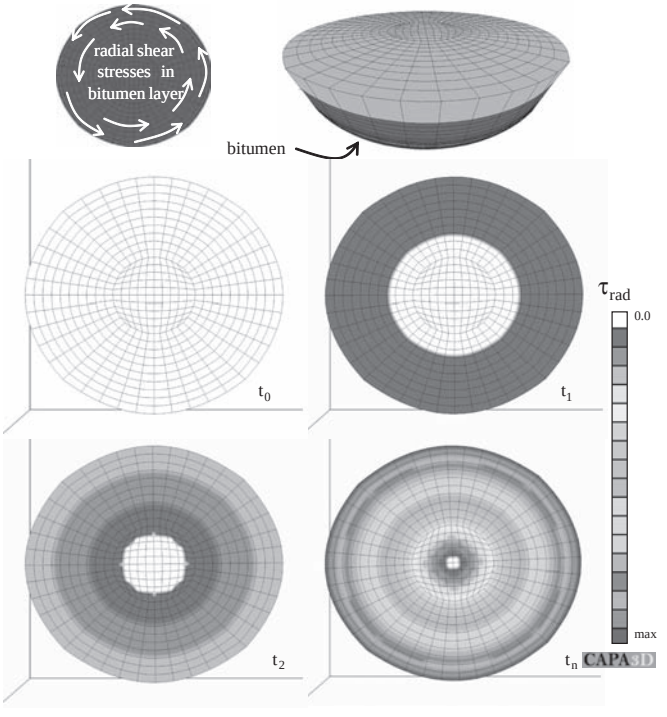

Figure 8. Radial shear stresses in a tortional test.

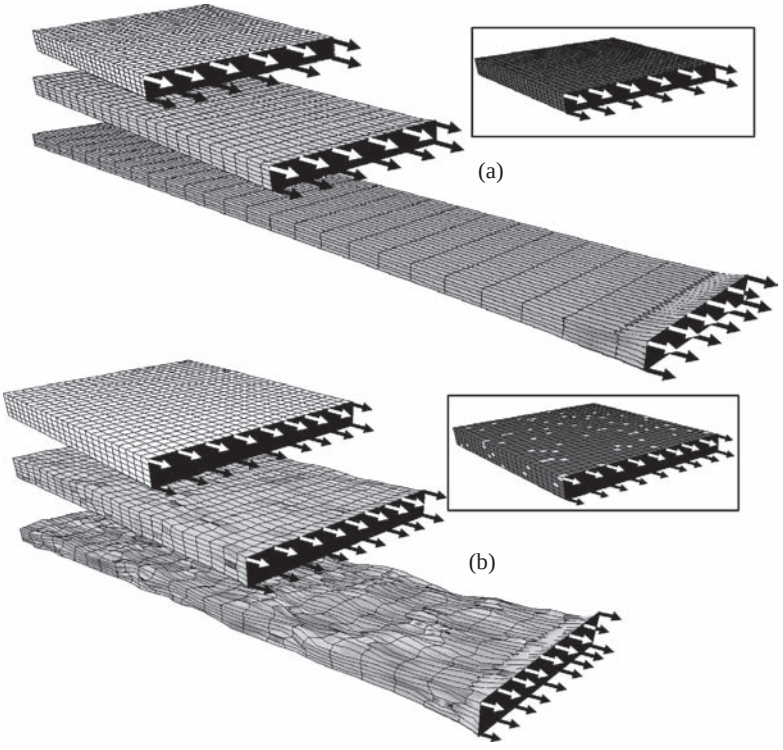

Figure 9. Stress development in a constant strain rate tension test simulation (a) bitumen (b) bitumen with fillers.

effect of the mineral particles becomes clear. Furthermore, the non-uniform stress development in the mastic becomes obvious and seems to originate from the interface zones between the particles and the bitumen. Therefore, given the same strain rate, significantly different stresses result in the two materials. It should therefore be kept in mind that testing the bitumen without the mineral fillers may not be sufficient to capture the resulting behavior in the pavement.

5 CONCLUSIONS AND RECOMMENDATIONS

In this paper several issues related to appropriate characterization of bituminous materials were discussed. It was shown that most experiments can be divided into material tests and structural tests and it is very important to realize which one to choose at what stage of the design process. Challenges in the moisture conditioning process of asphaltic mixtures were addressed and the importance of a uniform moisture field of known concentrations was emphasized. Some issues regarding non-linearity and strain rate dependency were illustrates via a simulation of a rotational test. Finally, the different response of neat bitumen and mastics were shown in a constant strain rate tensile test simulation.

Choosing the appropriate experiment to capture the asphalt mix response is not a trivial task. The issues discussed in this paper stimulate the awareness of the challenges which are often encountered but not always addressed properly or given sufficient thought. It is therefore recommended to avoid non-uniform fields inside the material, be it stresses, strains, moisture of temperatures, when looking for a fundamental material parameter or a calibration of a model. More complex states could be useful in experiments, once a certain level of fundamental information of the material response has been reached, or for the validation of a model.

REFERENCES

Erkens S.M.J.G., Asphalt Concrete Response—Determination, Modeling and Prediction, ISBN 90-407-2326-5, *Delft University Press*, 2002.

Scarpas A., *Keynote lecture: Modeling and Characterization of Cracking in Asphaltic Pavements*, 5th RILEM Conference on Cracking, 2004, Limoges, France.

Kringos N. and Scarpas A. (2005), Ravelling of asphaltic mixes: Computational identification of controlling parameters, Transportation Research Record: *Journal of the Transportation Research Board*, No. 1929, Bituminous Paving Mixtures pp. 79–87

Kringos N., Scarpas A, and Selvadurai A.P.S. (2008a), Modeling of combined physical-mechanical moisture induced damage in asphaltic mixes, Part 1: governing processes and formulations, *International Journal for Pavement Engineering*, Vol. 2.

Kringos N., Scarpas A., Copeland A. and Youtcheff J. (2008b),'Modeling of combined physical-mechanical moisture induced damage in asphaltic mixes- Part 2: moisture susceptibility parameters', *International Journal for Pavement Engineering*, 9, pp. 129–151.

Kringos N., Scarpas A. and Selvadurai A.P.S. (2009), 'Simulation of Mastic Erosion from Open-Graded Asphalt Mixes Using a Hybrid Lagrangian-Eulerian Finite Element Approach', *Computer Methods and Engineering Science*, Vol. 741, no. 1, pp. 1–13.

Advanced Testing and Characterization of Bituminous Materials – Loizos, Partl, Scarpas & Al-Qadi (eds)
© 2009 Taylor & Francis Group, London, ISBN 978-0-415-55854-9

Prediction of rutting risk of bituminous concrete using complex modulus

K. Ait Mokhtar
USTHB, FGC/LEEGO, Bab Ezzouar Algiers, Algeria

E. Ghorbel
University of Cergy-Pontoise, Neuville-sur-Oise, Cergy-Pontoise Cedex, France

S. Saoula & S. Haddadi
USTHB, FGC/LEEGO, Bab Ezzouar Algiers, Algeria

ABSTRACT: This work shows that adding polymers to asphalt binders improves the resistance of bituminous concrete to rutting and allows the design of surfacing layers with low thickness offering better performances and lower costs. The rheological behavior of three Algerian bitumens is studied. Experiments were carried out on pure asphalts characterized by different penetration classes (35/50; 50/70; 70/100). Black's diagram shows that 35/50 pen bitumen is less likely to form wheel ruts at hot weather. 35/50 pen bitumen is then modified by 3, 5 and 7% of Ethylene Acetate Vinyl (EVA) polymer to manufacture Hot Mix Asphalt Concrete with an optimum bitumen content estimated at 6%. Marshall tests show that the highest stiffness and the better permanent deformation are obtained for 3% of EVA content.

1 INTRODUCTION

The mechanical behavior of HMA mixtures is affected by the behavior of asphalt cement binders which are viscoelastic materials. Their response to external solicitations depends strongly on the loading conditions: the temperature and the frequency (Ait Mokhtar 1994, Airey & Rahimzadeh 2004, Martinez et al. 2008). The bitumen must be manageable at high temperatures and stiff at service temperatures in order to limit the creep of the coated layer and consequently the rutting phenomenon. Furthermore, it must be soft at low temperatures and resistant to fatigue cracking and thermal shrinkage.

Dynamic Rheometer instrumentations enable the characterization of rheological properties of asphalt binders by measuring the complex modulus and the phase angle for different temperatures and frequencies. The complex modulus is an indicator of the resistance of material to deformation when exposed to cyclic loading conditions while the phase angle characterizes the relative amount of the deformation recoverability. Several authors (Glita & Conan 1996, Ramond & Epinat 2000a, Ramond et al. 2000b, Olard 2003) show that the obtained results give information on:

- the thermal susceptibility (complex modulus and phase angle isochrones at a given frequency),
- the resistance to fatigue cracking at low temperatures (the loss modulus isochrones),
- the resistance to the thermal fatigue cracking (the phase angle isochrones),
- the resistance to the permanent deformations (the compliance isochrones).

For many decades, conventional bituminous materials have been used satisfactorily in most road applications. However, accelerating wear and tear caused by heavy traffic and severe climates as well as increasing demands for quieter and safer roads observed in these last years led to a need to enhance the material properties. Polymer modification offers one solution to improve the resistance to permanent deformation, fatigue life, thermal cracking, wear and ageing resistance of existing asphalt materials.

2 MATERIALS AND EXPERIMENTAL PROCEDURE

Used materials and experimental procedures in this study are following.

2.1 *Bitumen*

Three grades of conventional bitumen are investigated: B1 (35/50 pen), B2 (50/70 pen) and B3 (70/100 pen). The usual technological and structural characteristics of these bitumens are summarized in table 1.

The aged binders were evaluated by measuring the penetration at 25°C (Figure 1a) and the softening temperature (figure 1b).

2.2 *Experimental method*

The complex modulus has been determined by means of viscoanalysor METRAVIB with a sweep in frequencies (7.8 to 250 Hz) and in temperatures (–30°C/+70°C). The measurements have been carried out in tension/compression at low temperatures (Figure 2) and under annular shearing (coaxial cylinders) at high temperatures (T > 20°C). (Figure 3)

Before tension/compression rheological tests the bitumen is heated to 180°C for 30 minutes. The specimens are molded then stored in a refrigerator for 10 minutes before being introduced into the machine and tested. Before annular shear dynamic tests the binder is heated at 80°C for 10 minutes.

Complex Shear Modulus given by the annular shearing experiment is converted into tension/compression modulus using the relationship |E*| = 3|G*| based on the assumptions of incompressibility and isotropy of the pure bitumen (Olard 2003). It can be noticed that absolute shear modulus is defined as the ratio of the amplitude of the stress to the amplitude of the strain in forced oscillation: $|G^*| = \tau_0 / \gamma_0 = \sqrt{G'^2 + G''^2}$ with G' is the storage modulus, G'' the loss modulus and the phase angle Φ is calculated as follows: $\tan g(\Phi) = G''/G'$. Hence purely elastic material does not exhibit a phase angle while a pure viscous material shows a phase angle of 90°.

Table 1. The results of tests performed on bitumens.

Test	B1	B2	B3
Grade	35/50	50/70	70/100
Penetration (25°C, 1/10 mm) $Pen_{25°C}$	48	54	89
Softening point (°C) SP	52	48	44
Pfeiffer penetration Index (PI)	–0.79	–1.52	–1.43
Asphaltenes %	11.32	10.75	10.82

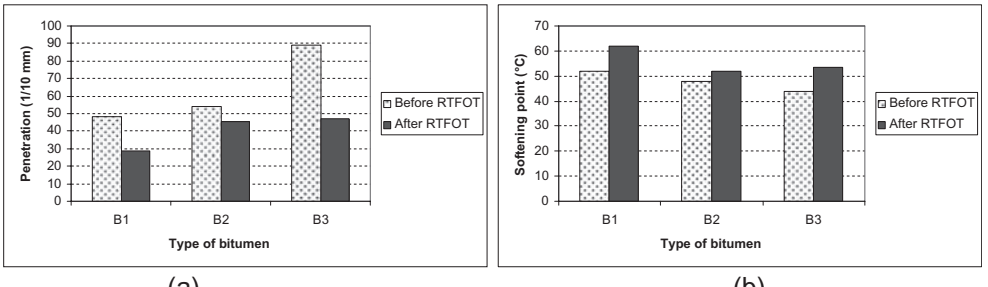

(a) (b)

Figure 1. Evolution of the penetration and softening temperature after RTFOT.

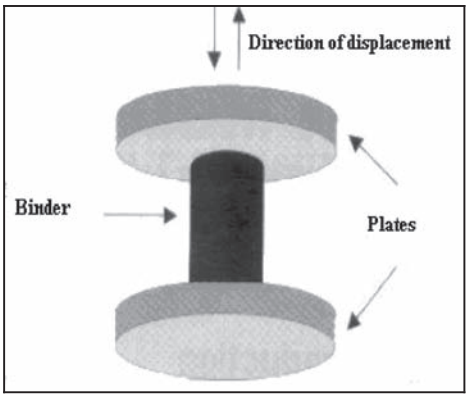

Figure 2. Beam of bitumen in tension/compression.

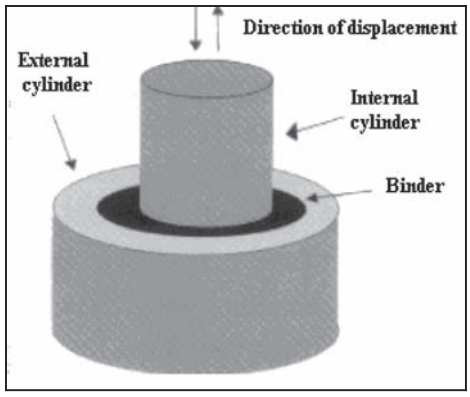

Figure 3. Beam of bitumen in annular shear.

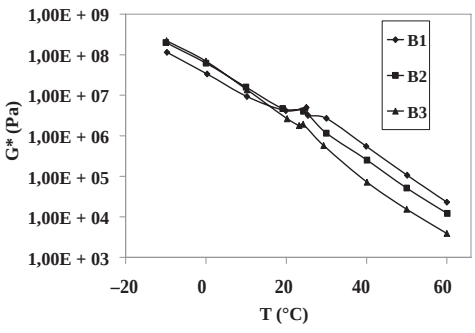

Figure 4. Absolute shear modulus isochrones.

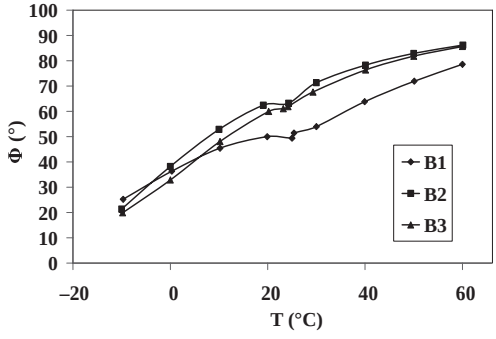

Figure 5. Phase angle isochrones.

Bitumen with higher storage modulus has greater ability to recover from deformation, and materials with higher loss modulus have greater ability to resist deformation at any prescribed frequency.

3 COMPLEX MODULUS RESULTS

The isochrones curves of the complex modulus for a frequency of 7.8 Hz are given in Figures 4 and 5.
It appears that:

- Phase angle which represents the immediate elastic and the delayed viscous responses of the binder increases with temperature for the three bitumens depending on the grade of bitumen. At high temperature, the phase angle is lower for B1 which means that bitumen B1 is more elastic and have more ability to able to recover its original shape after being deformed by a load than B2 and B3. At low temperatures the values of the phase angle of the three bitumens are close.
- The grade bitumen affects the rheological characteristics of the bitumen. The use of asphalt binders with low penetration numbers (called "hard" utilized for warm climates) leads essentially to an increase in consistency at high temperatures and a reduction of thermal susceptibility as it is observed by the analysis of the isochrones curves of the absolute modulus. Moreover it can be observed that the lower the penetration numbers, the stiffer the asphalt binder is and consequently its resistance to deformation.

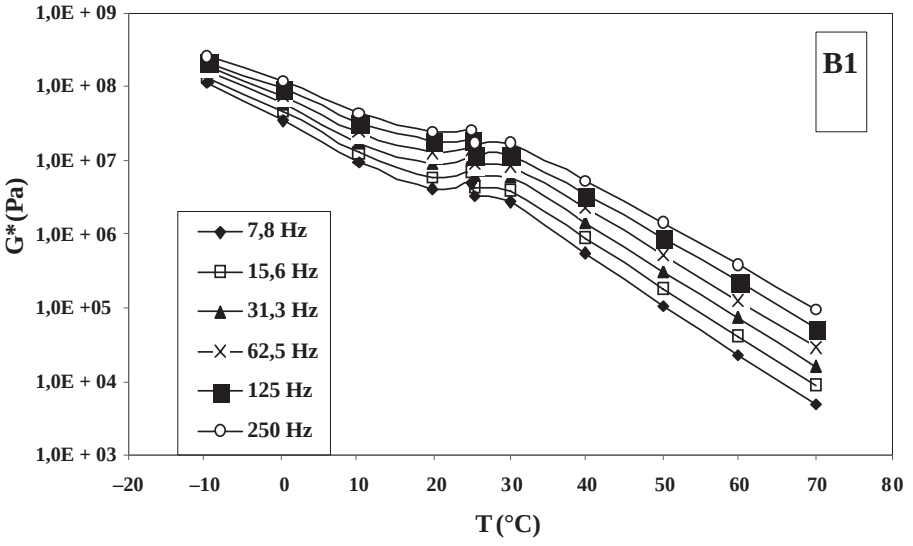

Figure 6. Influence of the frequency and temperature on |G*| for B1.

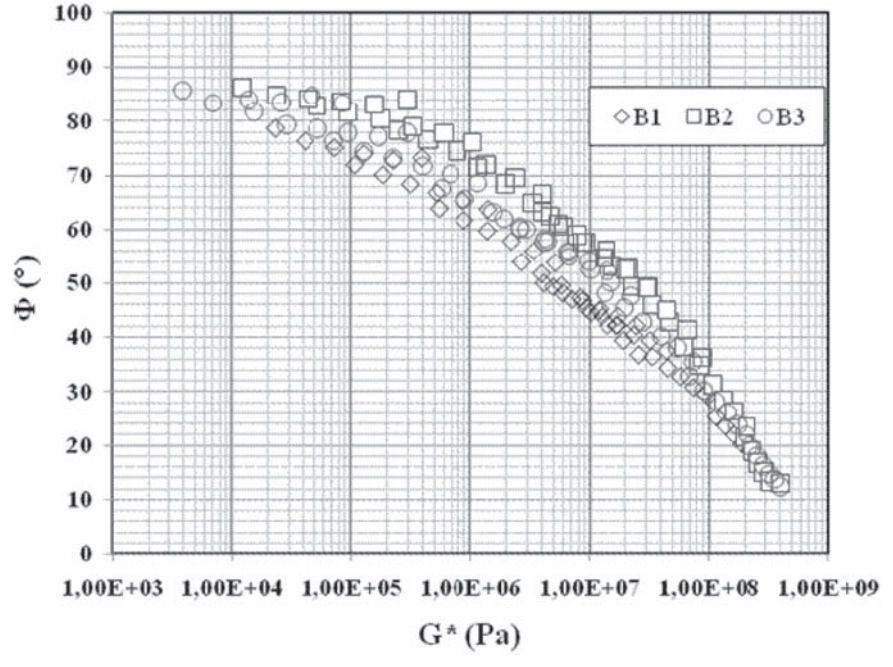

Figure 7. Black curves of three pen bitumens.

The influence of the frequency and temperature on the absolute shear modulus is illustrated for bitumen B1 in Figure 6. The same trend is observed for B2 and B3. For a given temperature, a difference in the absolute modulus at low and high frequencies is observed. Hence, the asphalt binder behaves differently at different traffic speeds (for example, a 10.0 Hz test frequency approximately corresponds to traffic at highway speeds). The higher frequencies which simulate high traffic speeds, the higher G* values are and therefore the more resistant to rutting the asphalt binder is.

Figure 7 correponds to the black curves of three pen bitumens (B1, B2, B2). It can be seen that the three bitumens are very structured because the black curves are non linear. Moreover, it appears that the binder with low penetration numbers (B1) is more resistant to rutting and fatigue cracking at high temperatures while the grade of bitumen has no influence on the properties of bitumen at low temperatures and high frequencies. As a matter of fact compared to B2 and B3, B1 exhibits lower values of phase angle and consequently the more elastic behavior allowing dissipating energy by rebounding and not by cracking. In the other hand, the complex modulus is not too stiff allowing deformation-then-rebounding rather than cracking.

4 PREDICTION OF THE RUTTING RISK

In what follows, the rutting risks of a bituminous concrete based on the results of the complex modulus tests are provided. For that, we have taken into account a band approximately 200 Km of the shore of the Mediterranean to the highlands. We can observe the climatic conditions following:

- The maximum temperatures of 40.0°C.
- Some minimum temperatures of –5°C.
- Some deviations between the day and night of 20°C.

However in reality, the black coating absorbs the solar rays, the maximum temperature at the surface of the road is much higher than the air temperature. An American study made in the context of SHRP (Strategic High Way Research Program) (Ramond & Epinat 2000a, Ramond et al. 2000b, Lee et al. 2004) showed that at the surface of the coating material, the maximum temperature was given by the following formula:

$$T_s - T_a = -0.00618L^2 + 0.2289L + 24.4 \quad (1)$$

where T_a and T_s: are respectively the temperature of air and of surface course of coating material and L the latitude in degrees.

The equation (1) was used in California in the US, but it is also adopted in Algeria because of similar weather conditions. By considering the latitude in Algeria in the order of 36° the surface temperature can be estimated using equation (2):

$$T_s - T_a = 24.6 \quad (2)$$

Hence the surface temperature is equal to

- the minimum air temperature for low-temperature analysis: $T_s = T_a = -5$°C
- the maximum temperature of surface T_s is approximately equal to 64.6°C.

The values of absolute modulus and the temperature T_s are determined by the mean of the modulus isochrones curves established for 7.8 Hz (Table 2).

It can be seen that the values of |G*| at T_s cannot be obtained for the bitumen B2 and B3 but the reference value of |G*| = 1,104 Pa is reached for a temperature of 61°C for the binder B2 and a temperature of 53°C for the binder B3.

Table 2. Complex modulus at 7.8 Hz for T_1 = 64.6°C.

Bitumen	B1	B2	B3
|G*|	1.1 10^4	Not measurable	Not measurable

Table 3. Parameters of structures of three binders R.

Bitumen	B1	B2	B3
R	2.42	1.91	2.19

This confirms that for the bitumen B1 there is no rutting risk while for the bitumen B2 and B3 the rutting risk is obvious.

The parameter of structure *R* who is an indicator of the thermal susceptibility of bitumens may be determined; the higher the value for *R*, the lower the temperature susceptibility of the bitumen. *R* is defined by the following formula:

$$R = \log \frac{|G^*_\infty|}{|G^*_{45}|} \tag{3}$$

where:

✓ $|G^*_\infty|$ is the limit of the modulus when the temperature tends toward very negative values and the frequency toward infinity. For all the binders, it is on the order of 3.10^9 Pa.

✓ $|G^*_{45}|$: is the modulus for which phase angle is to 45°.

It can be observed that the bitumen binder B1 is the less susceptible to temperature, when the bitumen B2 is the most susceptible to temperature. This confirms the results of Pfeiffer penetration index (PI). For that, we choose B1 binder for the modification by EVA polymer.

5 POLYMER MODIFIED BITUMINOUS

5.1 *Aggregates*

Crushed aggregates are used in this work. They are obtained from quarries located of Algeria. The Figure 8 shows the grading curves of the aggregates and sand. The chemical analysis shows that the sand is calcareous while the gravel contains an important proportion of silica and oxides. The physical proprieties are summarized in Table 4.

5.2 *Polymer EVA*

An ethylene vinyl acetate (EVA) copolymer is used as a modifier agent. EVA is a semi-crystalline copolymer containing 18% vinyl acetate with a melt index of 1.5 g/10 min and a specific gravity equal to 0.939 g/cm^3.

5.3 *Preparation of polymer modified bitumen*

Polymer modified bitumen is prepared using an agitator. Temperature control during mixing is achieved by means of thermocouple attached to the mixer. The machine was operated at a speed of 300 rpm (Saoula et al. 2008). The utilisation strategy must be coupled with

Table 4. Physical properties of aggregates.

Test	0/3	3/8	8/15
Los Angeles abrasion test (%)	/	13.96	14.09
Micro Deval test (%) Humid	/	17.65	13.56
Mry	/	5.80	2.18
Specific gravity	2.67	2.69	2.72

Table 5. Specification of algerian highway for wearing surface course.

Proprieties of Marshall specimens	Specification limits
Stability (kg)	Min. 800
Flow (mm)	2–4
Compactness (%)	Max. 97

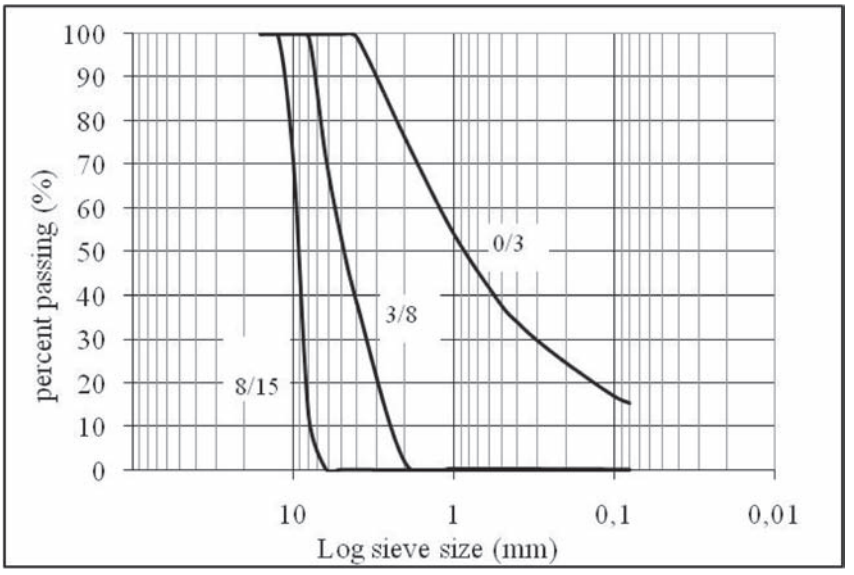

Figure 8. Grading curves of sand and gravels.

environmental energy considerations to use available materials most efficiently. Since the bitumen polymer mixing temperature and bitumen-polymer mixing time play a crucial role in determining the performances of polymer modified asphalt concrete. In this work, 500 g of bitumen was heated to fluid condition into a 1000 ml spherical flask. Upon reaching 175°C reweighed polymer amount was added to the bituminous material. Three contents of EVA copolymer by weight of unmodified bitumen are selected ranged from low polymer modification at 3% to higher degrees of modification at 5% and 7%. Mixing was then continued at 180°C for 4 hours.

5.4 *Bitumen concrete*

Bitumen concrete should be designed to meet the necessary criteria based to the specifications of Algerian highways (Haddadi et al. 2008). These criteria require carrying out some tests such Marshall Stability and flow test (Table 5). Marshall method (ASTM D1559) was used for determining optimal bitumen content for conventional and modified asphalt mixtures. Marshall test remains the most common method for quality control evaluations of asphalt rutting and it would not be easily abandoned by the road construction industry in favour of a new one. In this investigation, the hot mixtures asphalts were characterised through Marshall Test. The dimensions of the cylindrical specimens are 101.6 mm diameter by 63.5 mm height. The specimens were compacted by applying 50 blows on each side of the specimen at 150°C in accordance with ASTM D1559 then stored at ambient temperature for one day. Before performing Marshall Test, the compactness is measured after which, standard specimens were immersed in water at 60°C for 30 min and then loaded to failure at a constant rate of compression of 51 mm/min.

The Marshall stability value (in kg) corresponds to the maximum force recorded during test while the flow (in mm) is the deformation noted at the maximum force.

6 RESULTS AND DISCUSSION

6.1 *Compactness and residual voids of bitumen concrete*

The selected gradation for the control mix is 40% of sand 0/3, 20% of gravel 3/8, 40% of gravel 8/15 and 6% of bitumen ratio B1.

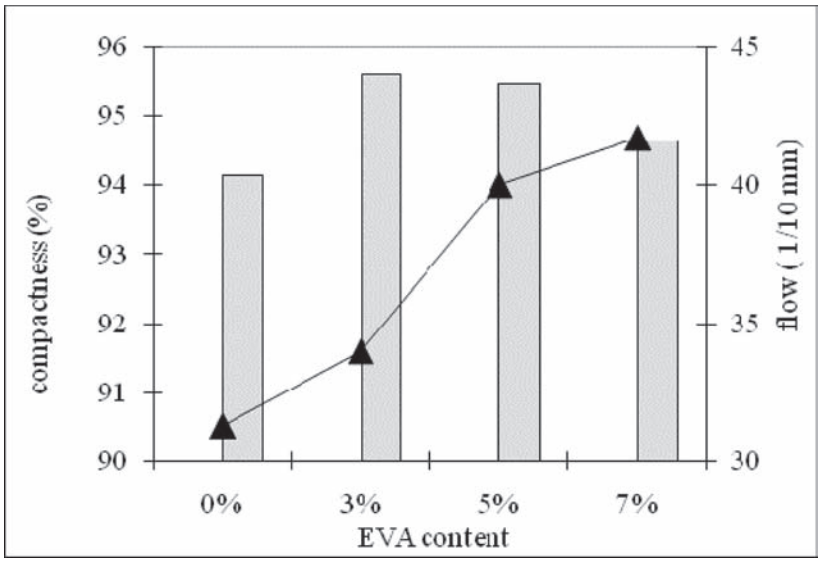

Figure 9. Marshall mix compactness and flow values of the different bitumen concrte mixtures versus the EVA content.

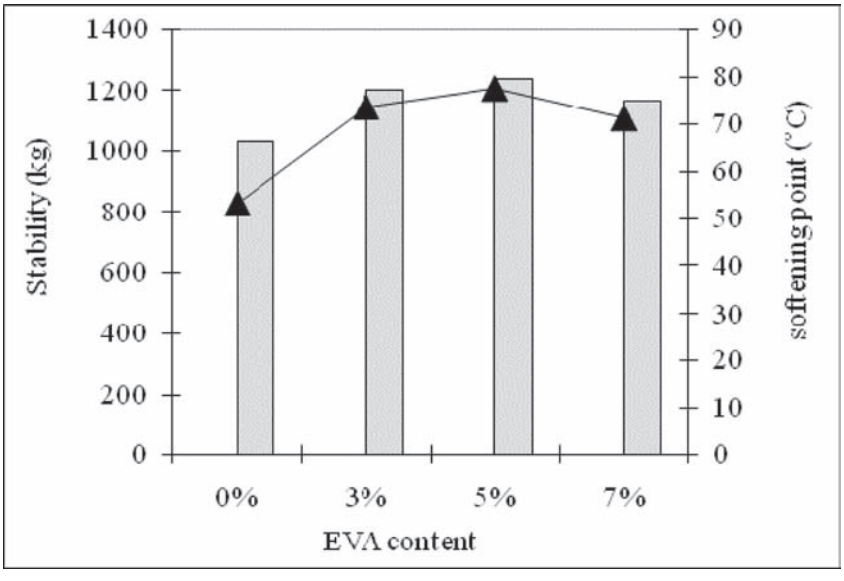

Figure 10. Stability and softening of bitumen concrete versus the EVA content.

The results on compactness are presented as follows in the figure 9.

It can be noticed that, although the modified bituminous concrete has greater compactness than that containing pure bitumen, the EVA does not seem to have a great effect on the covering compactness.

Indeed, the variation of compactness (and the residual voids) between the covering containing pure bitumen and those modified, is highly reliable and not gradual. It is very improbable

that the EVA could be the cause of this variation. The latter would be due to compactness and measurements methods' conditions.

6.2 *Stability of bitumen concrete*

The mixtures' stability is represented in the figure 10. The stability of the bituminous concrete increased for the three contents of EVA. However, a modification at 5% gives the greater stability followed by that of 3%.

These figures show that the EVA influences considerably the Marshall stability of the covering. Indeed, the modification within EVA brought a profit of stability.

6.3 *Flow of bitumen concrete*

The results on flowing variation are presented in the figure 9. The flowing increases progressively with the content in EVA, what gives, as one increases the polymer's content , more and more bituminous concrete tend to flow. However, the obtained flowing at 7% is the most important, doesn't satisfy the requirements. With 3% and 5%, the flowing increase is lower than 1mm, and its covering remain in the acceptable flowing standards.

Lastly, these figures show that the polymer confers to the covering a greater elasticity although, flowing tends to increase with EVA, the stability profit is such as the covering with the EVA will have a better resistance under heavy traffic. However, a modification at 3% gives more satisfactory overall performances: stability profit (16, 47%) and acceptable flow.

The figure 10 shows the variation of stability and softening point. It may be seen that the variation of bituminous mixtures stability follows that of the softening point. This can be explained in Marshall Test's conditions. Indeed, the covering is at the temperature of 60°C, which is in fact an extreme condition taking in consideration the softening point of bitumen and classical bituminous concretes. Thus, this condition hasn't a changing effect on the coverings with EVA. All softening temperatures of bitumen-EVA, being are about 70°C. What follows, in the same temperatures conditions. A better resistance to temperature and a greater stability for the covering with EVA are noted. In other words, it would have been more comparative to carry out the test on the mixtures with EVA at 70°C.

7 CONCLUSION

In view of the results presented above, it appears that at a given frequency, the 35/50 unmodified bitumen is the stiffest and its phase angle is the smallest. All experimental results enhance the fact that asphalt binders with low penetration numbers (called "hard") used for warm climates are more resistant to fatigue cracking, to rutting and show less thermal susceptibility.

Hot Mixture Asphalt concrete made with unmodified asphalts of 35/50 grade penetration and EVA modified are characterized through Marshall test. Results reveal that a modification at 3% of EVA had better results, since it makes possible to obtain a polymer-bitumen at the same time more hard and more viscous that of the pure one 35/50.

The modification by EVA has no significant effects on compactness and on the residual voids of the bituminous concrete, but improves the stability and increases the temperature ball and circle.

REFERENCES

Airey, G.D. & Rahimzadeh, B. 2004. Combined bituminous binder and mixture linear rheological properties. Construction and Building Materials 18: 535–548.

Ait Mokhtar, K. 1994. Influence de l'affinité liant hydrocarboné granulat sur les caractéristiques des mélanges hydrocarbonés. Magister Thesis, USTHB.

Glita, S. & Conan, J. 1996. Rheological analysis of 7 hard 10/20 bitumens. Eurasphalt & eurobitume congress.

Haddadi, S. Ghorbel, E. & Laradi, S. 2008. Effects of the manufacturing process on the performances of the bituminous binders modified with EVA; Const Build Mater 22: 1212–1219.
Lee, M-G. et al. 2004. Comparison of Results of SHRP and Conventional Binder Tests on Paving Asphalts. International Journal of Applied Science and Engineering 2, 3: 245–256.
Martinez, A. et al. 2008. Rheological modification of bitumens with new poly-functionalized furfural analogs. Fuel 87: 1148–1154.
Olard, F. 2003. Comportement thermomécanique des Enrobés bitumineux à basses températures, Relations entre les propriétés du liant et de l'enrobé. Doctoral Thesis, INSA de Lyon, p 221.
Ramond, G. & Epinat, M. 2000a. Contribution à l'élaboration d'un mode opératoire de mesure du module complexe des bitumes. Bitume actualité 101: 37–42.
Ramond, G. Laradi, N. & Pastor, M. 2000b. Caractéristiques des bitumes utilisés en Algérie. Bulletin des laboratoires des ponts et chaussées 225: 3–11.
Saoula, S. Ait Mokhtar, K. Haddadi, S. & Ghorbel, E. 2008. Improvent of the stability of modified bituminous binders within EVA; IJAER; 3/4: 575–584.

Advanced Testing and Characterization of Bituminous Materials –
Loizos, Partl, Scarpas & Al-Qadi (eds)
© 2009 Taylor & Francis Group, London, ISBN 978-0-415-55854-9

Application of simplified VECD modeling to the fatigue life prediction of asphalt concrete mixtures

B.S. Underwood, E.T. Hou & Y.R. Kim
North Carolina State University, Raleigh, North Carolina, USA

ABSTRACT: The use of continuum damage theories for modeling the fatigue performance of asphalt concrete has gained national attention in recent years. These theories ignore specific microscale behaviors and instead characterize a material based on its macroscale properties. A continuum damage model based on the extended elastic-viscoelastic correspondence principle with pseudo strains, the so-called *viscoelastic continuum damage* (VECD) model, is explored in this study. This model is rigorously reformatted for the purpose of predicting the fatigue test results under various load amplitudes and temperatures from monotonic test results at a single temperature. It is shown through this process that certain theoretical shortcomings are evident in other similar models, but that it is possible to correct these deficiencies. This process also has resulted in a modeling method that is capable of capturing the underlying material property, i.e., the damage characteristic curve, which is responsible for the responses of controlled stress, controlled crosshead strain, and constant-crosshead-rate monotonic tension tests. After applying an empirical failure criterion, it is found that the VECD model provides reasonable predictions for the fatigue life of an asphalt concrete mixture.

1 INTRODUCTION

Fatigue cracking in asphalt concrete pavements is a major form of pavement distress in the United States. Currently, no effective tests and analysis protocols exist that can be easily and quickly performed by field engineers. To properly understand and model fatigue cracking over the range of conditions encountered in the field, without performing a large number of experiments, requires a mechanistic model. This model should describe the material responses to repeated loading, particularly the phenomena of crack initiation, coalescence, and finally propagation. Existing empirical techniques often smear these mechanisms into a predictive scheme by developing power law relationships between some input parameter (stress or strain) and the number of cycles to failure (Deacon et al. 1995). Another technique that is gaining support in the asphalt community is the continuum damage model.

Continuum damage theories are advantageous for materials such as asphalt concrete because they focus on understanding and modeling a material using macroscale observations, i.e., the net effect of microstructural changes on observable properties. These theories contain two primary parameters, one to represent the material integrity and one to represent the microstructural changes (damage). Of these two parameters, damage is the more difficult to quantify and generally relies on macroscale measurements combined with rigorous theoretical considerations. One such theory, which is used for the work in this paper, is Schapery's thermodynamically-based work potential theory (Schapery 1987). Within this theory, damage is quantified using internal state variables (S_m) that may account for specific microstructural mechanisms. Other researchers have utilized elastic-based nonlocal continuum damage theories for this purpose (Bodin et al. 2004, Bazan and Pijaudier-Cabot 1989), and still others have assumed that the internal state variables are directly related to the strain history, both viscoelastic and viscoplastic, of the material (Uzan and Levenburg 2007).

The work of Kim and Little (1990) was the first to apply Schapery's nonlinear viscoelastic constitutive theory for materials with distributed damage to describe the behavior of sand asphalt under controlled strain cyclic loading. This effort was also the first in asphalt concrete modeling to use the correspondence principle with pseudo strains to remove material time effects. Later research using the so-called *viscoelastic continuum damage* (VECD) model shows that this theory can also describe the behavior of asphalt concrete under controlled stress, controlled strain cyclic loading and constant rate tension loading (Lee and Kim 1998a and b, Daniel and Kim 2002). A later discovery that the time-temperature superposition (t-TS) principle, developed from low strain dynamic modulus tests, also applies at high damage levels is equally significant (Chehab et al. 2002, Chehab et al. 2003). The most recent work applies these principles to mixtures tested at the Federal Highway Administration Accelerated Load Facility (FHWA ALF) in McLean, VA (Underwood et al. 2006), and successfully demonstrates the use of the modeling principles to both modified and unmodified asphalt concrete mixtures.

Independent efforts using pseudo strain-based models to predict the fatigue behavior of asphalt concrete have also shown positive results. Christensen and Bonaquist (2005) developed a version of a simplified mechanistic model that is based on the approach suggested by Kim et al. (2002) in which simplifications are made in the calculation of pseudo strain and in the idealization of the input conditions. Kutay and associates (2008) applied a form of the VECD model and showed that two different test protocols, controlled stress and controlled crosshead push-pull tests, yield the same damage characteristic relationship. These researchers also utilized the damage functions for different FHWA ALF mixtures to predict and rank the field performance. Although these research efforts have shown positive results, it is felt that they have certain faults that limit their application. This document clarifies and cements certain issues in these work potential/pseudo strain-based models to allow a more complete and accurate application for performance assessment.

The purpose of this paper is to describe the rigorously accurate simplified pseudo strain-based continuum damage model, which provides closure to issues raised in earlier derivations and includes certain key advantages over these other derivations. In the final section of this paper, the simplified fatigue model is used, along with an empirical failure criterion, to predict the fatigue performance of an asphalt concrete mixture.

2 MATERIALS

For the purposes of this study a single finely graded Superpave 9.5 mm NMSA mixture was utilized. The mixture consists of a standard PG 64–22 asphalt binder at a total content of 5.2% and granite aggregates. All specimens were compacted by the Superpave gyratory compactor and prepared for testing according to Kim and Chehab (2004). After obtaining specimens of the appropriate dimensions, air void measurements were taken via the core-lock method (tolerance of $5.75 \pm 0.25\%$), and specimens were stored until testing. To avoid any negative effects from material aging, specimens were sealed in plastic bags and stored in an unlit cabinet for no longer than two weeks before testing.

3 TEST METHODS

The fatigue test protocol used in this study is a controlled crosshead (CX) test (sometimes referred to as a controlled actuator displacement test). A sample of the input and stress-pseudo strain responses of these tests is shown in Figure 1. Because a true controlled strain test using cylindrical specimens is difficult to conduct and can damage equipment if improperly performed, the CX test protocol was utilized. Due to machine compliance issues, the actual on-specimen strain is significantly less than the programmed level, as shown in Figure 1a. Even though the on-specimen strains remain tensile, the stress and

pseudo strain both transition to a zero mean condition with only a slight amount of permanent pseudo strain growth, as shown in Figure 1b. Note that these tests result in a mixed mode of loading that is neither controlled stress nor controlled strain. Some researchers have proposed systems that allow users to perform true controlled strain testing of cylindrical specimens (Christensen and Bonaquist 2005). However, these researchers often do not allow the test to run to complete failure. In this study, the CX protocol tests are performed to complete failure. For this paper, *failure* is defined by the method suggested by Reese (1997), whereby the cycle at which the phase angle shows a sharp decrease is taken as N_f. A summary of the fatigue tests performed in this study and the naming conventions used are given in Table 1.

In addition to these fatigue tests, a constant crosshead rate tension (monotonic) test protocol (M) has been used. In these tests, the crosshead (or actuator) displaces at a constant rate

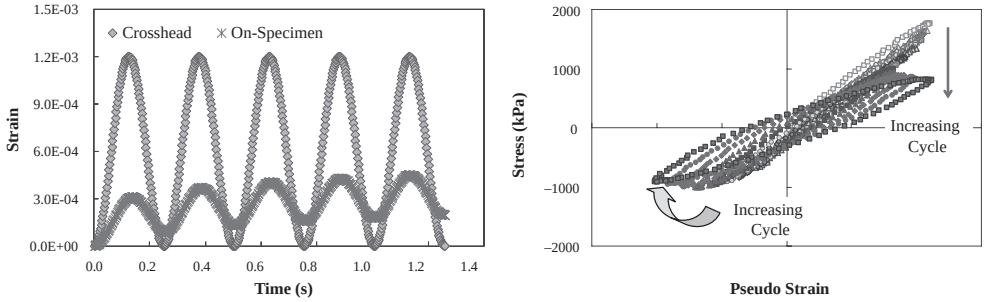

Figure 1. Typical input and responses for: a) CX (input vs. time) and b) CX (stress versus pseudo strain).

Table 1. Test summary.

Test type	Test designation	Rate (ε/s)	Initial level (με)	Frequency (Hz)	N_f
CX	27[a]-CX[b]-VH[c]	–	668	10	1640
CX	27-CX-VH2	–	638	10	430
CX	27-CX-H	–	437	10	18560
CX	27-CX-H2	–	520	10	810
CX	27-CX-L	–	303	10	91820
CX	27-CX-VL	–	225	10	198910
CX	27-CX-VL2	–	247	10	171670
CX	19-CX-VH	–	402	10	2672
CX	19-CX-H	–	240	10	46389
CX	19-CX-H2	–	332	10	12310
CX	19-CX-H3	–	425	10	3940
CX	19-CX-VL	–	190	10	311172
CX	5-CX-VH	–	213	10	1460
CX	5-CX-H	–	150	10	70136
CX	5-CX-H2	–	189	10	1150
CX	5-CX-L	–	126	10	145408
M	5-T1	5.0×10^{-5}	–	–	–
M	5-T2	3.0×10^{-5}	–	–	–
M	5-T3	2.2×10^{-5}	–	–	–

[a] Test temperature in degrees Celsius.
[b] Test protocol.
[c] Relative magnitude: H = high, L = low, VH = very high, VL = very low.

until the specimen fails. Due to the aforementioned machine compliance issues, this test does not produce a constant rate of on-specimen strain. The crosshead rates and temperatures used are also given in Table 1.

Finally, independent of these damage tests, low strain amplitude (approximately 60 $\mu\varepsilon$ peak-to-peak) tension-compression dynamic modulus tests have been performed at multiple temperatures and frequencies. The purpose of these tests is to establish the linear viscoelastic properties, $|E^*|_{LVE}$ and $E(t)$ (dynamic modulus in the linear viscoelastic range and relaxation modulus) of the material, independent of any damage or other nonlinear mechanisms.

All specimens were tested with a diameter of 75 mm and a height of 150 mm to mitigate to the extent possible any end effects. Additionally all tests were performed in an MTS closed loop servo-hydraulic machine. Temperature was controlled via an environmental chamber using liquid nitrogen cooling and circulated heating.

4 SIMPLIFIED MECHANICAL MODELING

The damage calculation equation from the rigorous mechanical modeling (Underwood et al. 2006) is given in discrete form by

$$dS_i = \left(-\frac{1}{2}(\varepsilon^R)_i^2 \Delta C_i \right)^{\alpha/1+\alpha} * (\Delta\xi)_i^{1/1+\alpha} \tag{1}$$

where the variables ε^R (pseudo strain), ΔC (change in pseudo stiffness), and $\Delta\xi$ (change in reduced time) are known at each time step, i, for the entire loading history.

To characterize or apply this model to cyclic data then requires the pseudo strain (Equation (2)), pseudo stiffness, and damage (S) to be calculated and tracked for the entire loading history. An average test with 30,000 cycles to failure and 100 data points per cycle (to gain good cycle pulse definition and avoid computational irregularities) would then require the analysis of 3,000,000 data points. Although this task is not impossible with modern computers, it is cumbersome even using advanced computational schemes. Further, experimental difficulties, such as data storage and electrical interference (noise and phase distortion), can lead to significant errors. Some researchers have suggested making idealizations of the loading history in order to compute pseudo strain (Daniel and Kim 2002). The advantage of this rigorous approach is that it provides a mostly accurate calculation of the pseudo strain magnitude and tracks any permanent pseudo strain during the test. The primary disadvantage of this approach is that it takes time to perform all of the necessary calculations. Others (Christensen and Bonaquist 2005, Kutay et al. 2008) have made an assumption of a steady-state response and greatly simplified the calculation of pseudo strain, cf. Equation (3). The disadvantages of this simplification are the potential errors in pseudo strain, particularly early in the test when the material state may change rapidly, as well as the inability to track any permanent pseudo strain that may evolve. The simplifications suggested in this paper are implemented to alleviate the shortcomings of each of these two basic approaches.

$$\varepsilon^R = \frac{1}{E_R}\int_0^{\xi} E(\xi - \tau)\frac{d(\varepsilon)}{d\tau}d\tau \tag{2}$$

$$\varepsilon_0{}^R = \frac{1}{E_R}\varepsilon_0 * |E^*|_{LVE} \tag{3}$$

$$\xi = \frac{t}{a_T} \tag{4}$$

where; E_R is the reference modulus used for dimensional compatibility (typically taken as 1), ε is the measured strain, $E(\xi)$ is the relaxation modulus, τ is the dummy integration variable,

ξ is the reduced time, a_T is the time-temperature shift factor at the temperature of interest, ε_0 is the strain amplitude, $|E^*|_{LVE}$ is the dynamic modulus in the linear viscoelastic range and ε_0^R is the pseudo strain amplitude.

4.1 *Defining alpha*

Through theoretical arguments that use the macrocracking phenomenon, the power, α, in Equation (1) is found to relate to linear viscoelastic time dependence (Schapery 1990). Motivated by earlier work on this subject (Lee and Kim 1998a and b, Daniel and Kim 2002, Chehab et al. 2003, Underwood et al. 2006), here the maximum absolute value of the log-log slope of the relaxation modulus, m, is taken to represent the linear viscoelastic response. According to Schapery's theory, if the material's fracture energy and failure stress are constant, then $\alpha = 1 + 1/m$, but if the fracture process zone size and fracture energy are constant, then $\alpha = 1/m$. Although different researchers have used differing α values, the general suggestion of Lee and Kim (1998a and b), which is that it is most appropriate to use $\alpha = 1/m$ for the pure tension controlled stress (CS) cyclic tests and $\alpha = 1 + 1/m$ for the CX tests, is adopted in this research. This approach is supported by the work of Daniel and Kim (2002) that uses the constant failure stress and energy criteria for the CX tests. It is also supported by the work of Kim and Chehab (2004) and Underwood et al. (2006) that use CS-type tests and $\alpha = 1/m$. For this study α is taken to be equal to $1 + 1/m$.

4.2 *Identification of tensile loading time*

Because fatigue is a tensile related distress, it is important to identify the actual time that a given cycle is under tensile loading. To determine this time for the tests used in this study, it is assumed that the following analytical function is descriptive of the stress history of any given cycle:

$$\frac{\sigma(\xi)}{\sigma_{0,ta}} = \left(\beta - \cos(\omega\xi)\right)\frac{1}{\beta+1}, \tag{5}$$

where $\sigma_{0,ta}$ is the tension stress amplitude, and ξ is reduced time and is used instead of physical time because of the positive verification of the t-TS principle at high damage levels (Chehab and Kim 2003, Underwood et al. 2006). The β term, defined by Equation (5), is a factor that allows direct quantification of the duration that a given stress history is tensile.

$$\beta_i = \frac{(\sigma_{peak})_i + (\sigma_{valley})_i}{\left|\sigma_{peak}\right|_i + \left|\sigma_{valley}\right|_i} \tag{6}$$

when $\beta = 1$, the entire stress (and therefore pseudo strain minus permanent pseudo strain) history for the given cycle is tensile; when $\beta = 0$, half of the history is tensile; and when $\beta = -1$, the entire history is compressive. None of the tests used in this study has $\beta = -1$. From Equation (5), the time during the load pulse at which tensile loading begins, ξ_i, and ends, ξ_f, for any given cycle is given by

$$\xi_i = \frac{\pi}{\omega} - \frac{\pi - \cos^{-1}(\beta)}{\omega} \text{ and} \tag{7}$$

$$\xi_f = \frac{\pi}{\omega} + \frac{\pi - \cos^{-1}(\beta)}{\omega}. \tag{8}$$

4.3 *Simplified VECD model*

All existing simplified VECD type models have one basic flaw in the rigor of their derivations, which is related to the fact that each of these models implicitly assumes that pseudo strain is some constant value within a cycle. This flaw is corrected by using a form adjustment factor, K_1, which is a rigorously defined parameter dependent on the time history of loading, $f(\xi)$, only. For the assumption that the damage growth within an individual cycle is small, it can be shown that the factor K_1 is given by:

$$K_1 = \frac{1}{\xi_f - \xi_i} * \int_{\xi_i}^{\xi_f} (f(\xi))^{2\alpha} * d\xi \tag{9}$$

The steady-state assumption made by other approaches is most inaccurate during the first loading path. This portion of the loading history is also important because it is used to define the specimen-to-specimen correction factor, I, and because damage growth in this first loading path can be substantial. For the simplified model proposed in this paper it is suggested that pseudo strain should be calculated piecewise, whereby for the first loading path the rigorous calculation is used, but for all other cycles the simplified calculation is used, i.e., Equation (9). As a result of the piecewise definition of pseudo strain, the pseudo stiffness is also piecewise, as defined in Equation (10).

$$\varepsilon^R = \begin{cases} \varepsilon^R = \dfrac{1}{E_R}\int_0^{\xi} E(\xi-\tau)\dfrac{d\varepsilon}{d\tau}d\tau & \xi \le \xi_p \\ (\varepsilon^R_{0.ta})_{\text{cycle } i} = \dfrac{1}{E_R} * \dfrac{\beta+1}{2}((\varepsilon_{0,pp})_i * |E^*|_{LVE}) & \xi > \xi_p \end{cases} \tag{10}$$

$$C = \begin{cases} C = \dfrac{\sigma}{\varepsilon^R \times I} & \xi \le \xi_p \\ C^* = \dfrac{\sigma_{0,ta}}{\varepsilon^R_{0,ta} I} & \xi > \xi_p \end{cases} \tag{11}$$

For a similar reason and because significant damage can occur along the first loading path, the rigorous calculation shown in Equation (1) is used. After this time, however, the simplified calculation method is used. For lack of a clearer term, this portion of the damage calculation is referred to as the *transient calculation* and the remaining calculations as the *cyclic calculations*, i.e.,

$$dS = \begin{cases} (dS_{\text{Transient}})_{\text{timestep } j} = \left(-\dfrac{I}{2}(\varepsilon^R)_i^2 \dfrac{\partial C}{\partial S}\right)^{\alpha} * (d\xi)_j & \xi \le \xi_{\text{p}} \\ (dS_{\text{Cyclic}})_{\text{cycle } i} = \left(-\dfrac{I}{2}(\varepsilon^R_{0.ta})_i^2 \dfrac{\partial C^*}{\partial S}\right)^{\alpha} * (\xi_p) * (\text{K}_1) & \xi > \xi_{\text{p}} \end{cases}. \tag{12}$$

4.4 *Model calibration*

To calibrate the VECD model, measurements of stress and pseudo strain obtained directly from cyclic fatigue tests could be used. However, for this paper characterization is performed using constant rate tension tests. The purpose of performing such characterization is to show the effect of using the simpler constant rate tests for fatigue performance assessment. These tests are conducted at conditions where mechanisms not related to viscoelastic damage, such as viscoplasticity, are negligible. The measured stresses and strains in these tests are used along with the processed dynamic modulus to compute I, ε^R, C, and ultimately, S.

Cross-plotting C and S for tests at multiple rates provides the damage characteristic curve shown in Figure 2 along with its analytical representation. Note that the rates for each of the tests shown are given in Table 1. The parameters of this function are ***a = –0.00108*** and ***b = 0.534***. Details regarding the process of finding damage characteristic curves from monotonic testing are given elsewhere (Underwood et al. 2006).

4.5 *Simulation failure criteria*

The simplified fatigue model does not account for changing time dependencies and, therefore, it is not possible to observe a sudden decrease of the phase angle, which is used to define failure in the measured tests, to define failure in the simulations. For this reason, an empirical observation of the mixtures from the FHWA ALF project and another material subjected to cyclic fatigue is used. The observation is shown in Figure 3 where the pseudo stiffness at failure is plotted against test temperature for multiple mixtures (both unmodified and polymer-modified).

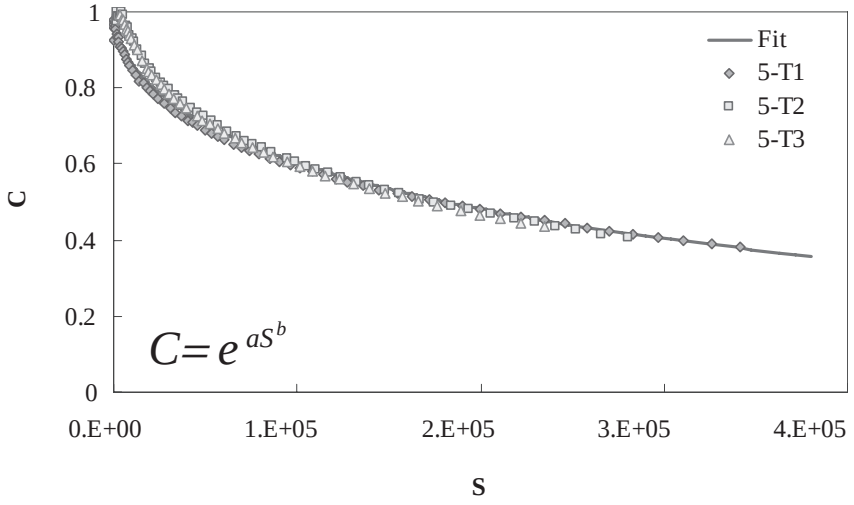

Figure 2. Damage characteristic relationship for study mixture.

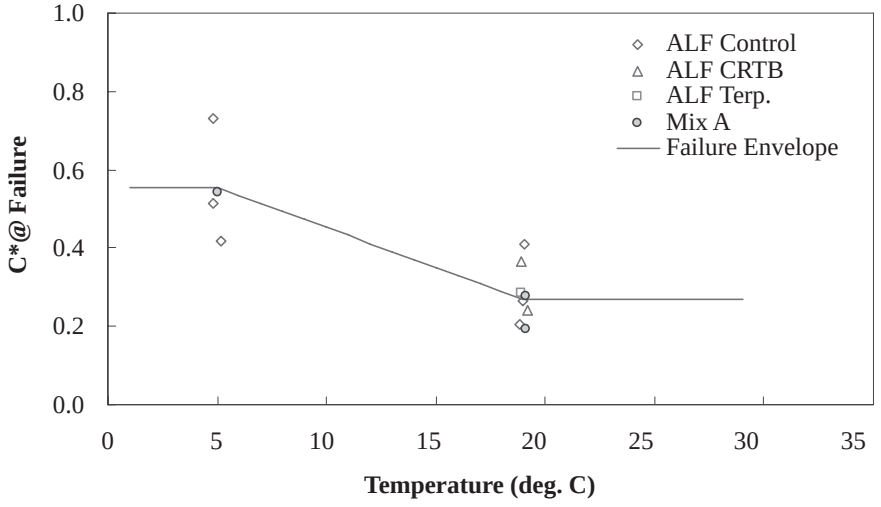

Figure 3. Calibration of simulation failure criteria.

It is found from Figure 3 that the pseudo stiffness at failure increases as the temperature decreases. Above approximately 19°C failure for the CX tests occurs at a pseudo stiffness of approximately 0.28, a value similar to that observed by Daniel and Kim (2002) for their tests, which were performed at 25°C. At 5°C and colder, failure tends to occur at a higher level of pseudo stiffness, approximately 0.55. It is believed that this effect is due to the higher initial stiffness of the materials at 5°C and the general increase in ductility at higher temperatures. For the purposes of this paper, a piecewise fitting function given in Equation (12) has been applied. Note that because calibration data are not available above 19°C or below 5°C, it is assumed that the failure pseudo stiffness neither increases nor decreases beyond this range. In addition a simple linear fit is applied between 5° and 19°C because it is the only function that can be supported with the available data. Efforts at calibrating the relationship between 5° and 19°C are part of ongoing efforts.

It is understood that this failure criterion is not completely ideal and contains certain shortcomings. In particular, substantial data scatter does exist in this relationship, however, the purpose here is to find some basic material behavior and then refine the relationship further as more experimental data is developed. The major advantage of this criterion though is that the modeled pseudo stiffness is known at every cycle, and it is easy to determine if the value is below some critical threshold. A more theoretically appropriate failure criterion is part of ongoing investigations.

$$C_f(CX) = \begin{cases} 0.553 & T \le 5 \\ -0.0196 * T + 0.651 & 19 > T > 5 \\ 0.279 & T \ge 19 \end{cases} \tag{13}$$

4.6 *Simulation results*

The predicted and measured pseudo stiffness values for a typical good prediction are shown in Figure 4, and results from a typical bad prediction are shown in Figure 5. Comparing the measured and predicted fatigue curves (Figure 6), it can be seen that the model does a reasonable job of predicting the failure envelopes at all temperatures. Note that the strain magnitude for these plots is somewhat arbitrarily selected at 100 cycles. There is a slight tendency to overestimate the fatigue life of the 27°C data, but with the exception of the lowest loading magnitude tests these expected maximum errors are approximately 30%. This percentage is in line with that reported elsewhere (Daniel and Kim 2002) and is considered adequate for fatigue life predictions. At the lowest loading magnitudes it is believed that other mechanisms, such as viscoplasticity, begin to affect the material response and performance. A framework for including these mechanisms has been established in other work that uses constant rate tension data (Underwood et al. 2006). However, the approach has not yet been applied to the cyclic data presented here.

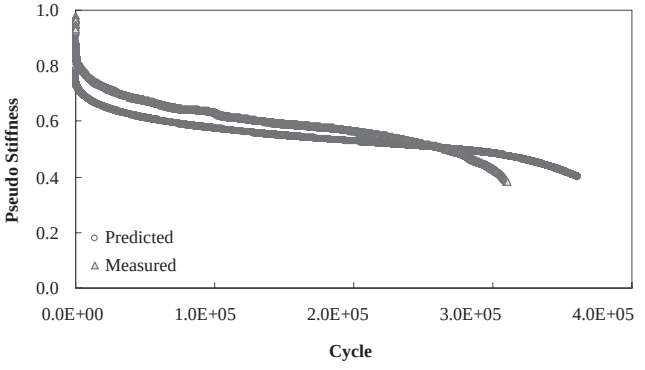

Figure 4. Typical good VECD model prediction (19-CX-VL).

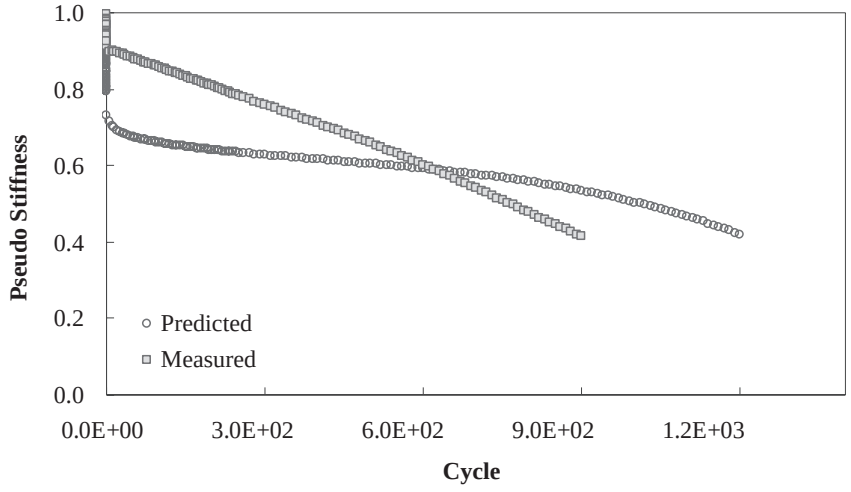

Figure 5. Typical bad VECD model prediction (5-CX-H2).

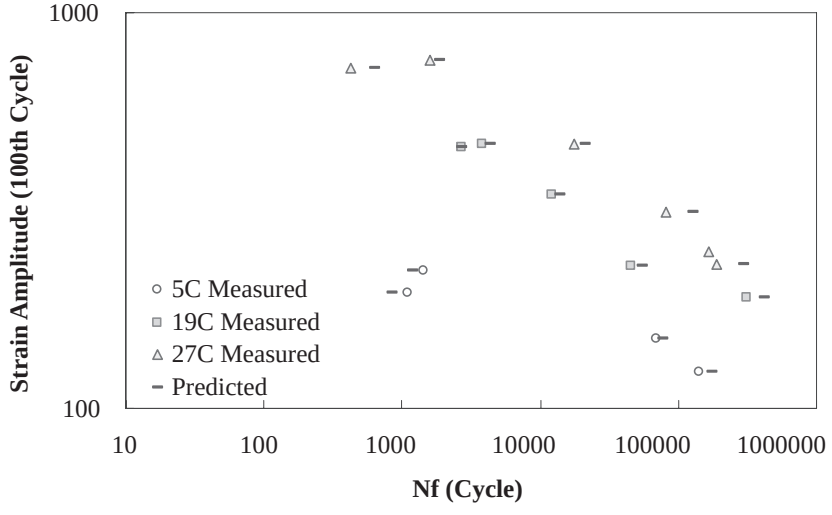

Figure 6. Comparison of measured and predicted fatigue failure envelopes.

5 SUMMARY AND CONCLUSIONS

A simplified form of the VECD model has been derived, characterized and verified using cyclic fatigue data at multiple temperatures and input magnitudes. The advantage of this simplified model over the full VECD model is that it can be applied to fatigue data quickly without the need to compute parameters at every time step. This simplified model also solves certain key flaws in the rigor and accuracy of existing simplified schemes. The model is verified by applying the function that is characterized from constant rate tension tests to fatigue tests. The effect of characterizing the function using cyclic data is not explored; however, the formulation is such that the task would be easy to perform. The ability to easily and rigorously characterize the model using cyclic fatigue data or constant rate data is considered a key advantage, because the newly released AMPT has load level limitations that may not allow the use of constant rate tension tests. Overall, the model shows expected trends

with regards to input magnitude and temperature, with typical fatigue life prediction errors ranging from 5–30%.

ACKNOWLEDGEMENTS

The authors would like to gratefully acknowledge the financial support from the Federal Highway Administration under projects FHWA DTFH61-05-RA-00108 and the pooled fund study TPF-5(019).

REFERENCES

Bazant, Z.P. and G. Pijaudier-Cabot. (1989). "Measurement of Characteristic Length of Nonlocal Continuum." *ASCE J. of Engineering Mechanics*, Vol. 115, No. 4, pp. 755–767.

Bodin, D., G. Pijaudier-Cabot, C. de La Roche, J.M. Piau and A. Chabot. (2004). "Continuum Damage Approach to Asphalt Concrete Fatigue Modeling." *ASCE J. of Engineering Mechanics*, Vol. 130, No. 6, pp. 700–708.

Chehab, G.R., Y.R. Kim, R.A. Schapery, M. Witczack, and R. Bonaquist. (2002). "Time-Temperature Superposition Principle for Asphalt Concrete Mixtures with Growing Damage in Tension State." *J. of the Association of Asphalt Paving Technologists*, Vol. 71: 559–593.

Chehab, G.R., Y.R. Kim, R.A. Schapery, M. Witczack, and R. Bonaquist. (2003). "Characterization of Asphalt Concrete in Uniaxial Tension Using a Viscoelastoplastic Model." *Journal of the Association of Asphalt Paving Technologists*, Vol. 72, pp. 315–355.

Christensen, D.W. and R. Bonaquist. (2005). "Practical Application of Continuum Damage Theory to Fatigue Phenomena in Asphalt Concrete Mixtures." *Journal of the Association of Asphalt Paving Technologists*, Vol. 74, pp. 963–1002.

Daniel J.S. and Y.R. Kim. (2002). "Development of a Simplified Fatigue Test and Analysis Procedure Using a Viscoelastic Continuum Damage Model." *J. of the Association of Asphalt Paving Technologists*, Vol. 71, pp. 619–650.

Deacon, J.A., A.A. Tayebali, G.M. Rowe, and C.L. Monismith. (1995). "Validation of SHRP A-003A Flexural Beam Fatigue Test." In *Engineering Properties of Asphalt Mixtures and the Relationship to Their Performance*. ASTM STP 1265, pp. 21–36.

Kim, Y.R. and D.N. Little. (1990). "One-Dimensional Constitutive Modeling of Asphalt Concrete." *ASCE J. of Engineering Mechanics*, Vol. 116, No. 4, pp. 751–772.

Kim, Y.R., D.N. Little, and R.R. Lytton. (2002). "Use of Dynamic Mechanical Analysis (DMA) to Evaluate the Fatigue and Healing Potential of Asphalt Binders in Sand Asphalt Mixtures." *J. of the Association of Asphalt Paving Technologists*, Vol. 71, pp. 176–206.

Kim, Y.R. and G.R. Chehab. (2004). *Development of Viscoelastoplastic Continuum Damage Model for Asphalt-Aggregate Mixtures*. Final Report to Arizona State University/NCHRP.

Kutay, M.E., N. Gibson, and J. Youtcheff. (2008). "Conventional and Viscoelastic Continuum Damage (VECD) Based Fatigue Analysis of Polymer Modified Asphalt Pavements." *J. of the Association of Asphalt Paving Technologists*, Vol. 77. In Press.

Lee, H.J. and Y.R. Kim. (1998a). "A Uniaxial Viscoelastic Constitutive Model for Asphalt Concrete under Cyclic Loading." *ASCE J. of Engineering Mechanics*, Vol. 124, No. 1, pp. 32–40.

Lee, H.J. and Y.R. Kim. (1998b). "A Viscoelastic Continuum Damage Model of Asphalt Concrete with Healing." *ASCE J. of Engineering Mechanics*, Vol. 124, No. 11, pp. 1224–1232.

Reese, R. (1997). "Properties of Aged Asphalt Binder Related to Asphalt Concrete Fatigue Life." *J. of the Association of Asphalt Paving Technologists*, Vol. 66, pp. 604–632.

Schapery, R A. (1987). "Deformation and Fracture Characterization of Inelastic Composite Materials using Potentials." *Polymer Engineering and Science*, Vol. 27, Issue 1, pp. 63–76.

Schapery, R.A. (1990). "A Theory of Mechanical Behavior of Elastic Media with Growing Damage and Other Changes in Structure." *J. of Mechanics of Physical Solids*, Vol. 38, pp. 215–253.

Underwood, B.S., Y.R. Kim, and M.N. Guddati. (2006). "Characterization and Performance Prediction of ALF Mixtures Using a Viscoelastoplastic Continuum Damage Model." *J. of the Association of Asphalt Paving Technologists*, Vol. 75, pp. 577–636.

Uzan, J. and E. Levenburg. (2007). "Advanced Testing and Characterization of Asphalt Concrete Materials in Tension." *ASCE International J. of Geomechanics*, Vol. 7, No. 2, pp. 158–165.

Advanced Testing and Characterization of Bituminous Materials – Loizos, Partl, Scarpas & Al-Qadi (eds)
© 2009 Taylor & Francis Group, London, ISBN 978-0-415-55854-9

Experimental observation of asphalt mix characteristics in the range of low temperatures

P. Mondschein & J. Valentin
Faculty of Civil Engineering, Czech Technical University, Prague, Czech Republic

ABSTRACT: Behavior of asphalt mixes and typical failures of the pavement structure, which are influenced by high or low temperatures, are most significantly influenced by the behavior of bituminous binder. The experimental method for assessment of asphalt mix characteristics at low temperatures has not been set in European standards yet, however a test method based on the experience of Prof. Arand is at the moment in preparation. Using this test method the specimen is exposed in a special chamber to decreasing temperature of the ambient environment without the possibility of shrinkage. In the Czech Republic the asphalt mix behavior in the range of low temperatures is so far observed and assessed using the approach of bending beam test at the zero temperature or even lower temperatures. A second test method, which is usually done in parallel on the same testing apparatus, is the relaxation test. The practical part of the paper addresses the testing, analysis and evaluation of low temperature characteristics for various HSM (high stiffness modulus) asphalt mixes as well as of asphalt mixes for SAL (stress absorbing layers).

1 INTRODUCTION

The mechanical-physical and rheological characteristics of asphalt mixes in the low temperatures domain, i.e. at temperatures below 0°C, are completely different from their characteristics at high temperatures in the summer. This differentiation in behavior is given by the properties of bituminous binders sensitive to temperature changes. As generally known the issue of asphalt pavement failures and their types are closely associated with the behavior of mixes at different temperatures.

The road network quality is particularly affected by the technical discipline during construction, the regularity of maintenance works, the traffic volumes and climatic conditions. In the context of the last mentioned factor it must be admitted that the Czech Republic is not fitted with the most favorable climatic conditions. These, however, are similar to the neighboring countries Germany and Austria where the road infrastructure quality is on a much higher level being affected by the above-mentioned factors in the same way. The extremes in air temperatures measured on the territory of the Czech Republic between 2004 and 2007 may serve as an example of these unfavorable climatic conditions. The maximum air temperature was measured in July 2006 (37.3°C), and the minimum temperature (–27.9°C) in January of the same year (Czech Meteorological Institute, 2007).

The facts above clearly imply that pavements must resist extreme temperatures below freezing, but also very high temperatures in summer months. These temperatures should not be confused with the temperatures in the road pavement construction, which are affected by the temperature characteristics of materials or the duration of temperature extremes etc. The typical failures of summer months are rutting, mix bulging, transverse and longitudinal unevenness etc. The failures characteristic of winter seasons, on the other hand, include the appearance of frost cracks, wearing course corrosion, potholes.

2 BEHAVIOR OF ASPHALT MIXES AT LOW TEMPERATURES

The solution to the problem of the behavior of asphalt mixes or bituminous binders depends both on the traffic load (volumes, duration, and time pattern) and the temperature as material characteristics of asphalt mixes and binders dramatically rely on the temperature of the surrounding environment. The dependences between the asphalt mix stiffness and temperature, the asphalt mix resistance to permanent deformations and the structural layer temperature etc. are notoriously known. On the other end of the temperature scale, at low temperatures, the mix becomes stiffer but, at the same time, more brittle.

The behavior of structural layers at low temperatures involves all layers. Each layer is subjected to specific stresses arising from the combinations of tensile and compressive forces acting under specific climatic conditions; these, in turn, from the temperature perspective, tend to decrease with the increasing depth. The issues related to structural pavement layers performance behavior, therefore, depend both on the function and the loading of structural layers. The values of the strength characteristics, like material characteristics, depend on temperature changes within materials. Experience shows (Wistuba, 2007) the growth of these strengths up to the highest values in a temperature range from –10°C to –5°C. Due to the embrittlement of the bitumen, however, the tensile bending strength successively falls again.

Figure 1 depicts the relationship between stress due to temperature changes in material and tensile bending strength in relation to temperature. The figure shows that the tensile bending strength grows with falling temperatures up to a certain maximum value, and successively, with a further temperature decrease, it goes down. The stress due to tensile forces in material grows with falling temperatures until the material tensile strength is exceeded and a temperature (frost) crack appears. This temperature is referred to as fracture or critical temperature. The

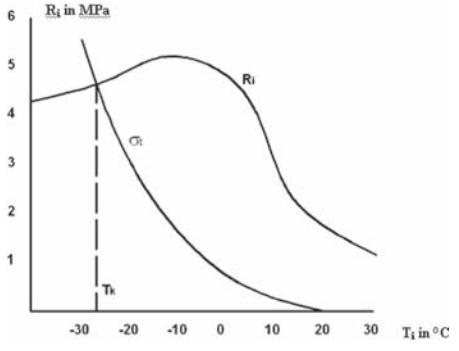

Figure 1. Relationship between stress due to temperature changes (T_i in °C) in material and tensile bending strength (R_i in MPa).

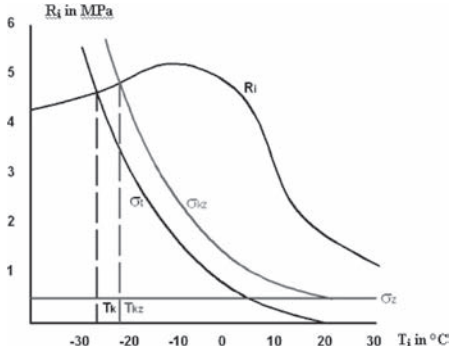

Figure 2. Relationship between stress due to temperature changes (T_i in °C) in material and loading and tensile bending strength (R_i in MPa).

frost crack formation theory is based on the presumption that cracking due to shrinkage occurs at the first exposure of the binder to critical conditions (Deme, 1999). In the case of superposition of the stress due to temperature with the stress due to loading (traffic), there is a shift in the so-called fracture temperature towards a value of 0°C as is shown in Figure 2.

The appearance and development of cracks at low temperatures, however, is a far more complex phenomenon than simply only road pavement cracking at reaching the critical temperature. A detailed monitoring of trial pavement sections in Canada (Deme, 1999) revealed that if the pavement is exposed to temperatures slightly milder than the critical temperature, it suffers from internal disintegration. It must also be taken into account that the stresses occurring in the pavement due to cooling are combined with the effects of traffic. Minimum critical temperatures usually occur at night or in early morning hours when there is minimum traffic, mainly in periods of heavy frosts when roads are hardly passable. Slightly higher temperatures, however, may occur for a longer time. They also make the combinations with traffic induced effects more realistic.

3 TESTING OF ASPHALT MIXES AT LOW TEMPERATURES

The behavior of asphalt mixes at low temperatures may principally be determined by several methods. The tests may be divided into static and dynamic.

The static tests for the determination of asphalt mix behavior at low temperatures are (Wistuba, 2007):

- thermal stress restrained specimen test (TSRST),
- uniaxial tensile-strength test (UTST),
- tube suction test (TST),
- creep test (CT),
- relaxation test (RT).

With regard to dynamic loading, the cyclic dynamic tensile test is known. Concerning the type of dynamic behavior, this test is similar to the stiffness modulus determined by the Nottingham Asphalt Tester (NAT) apparatus using the non-destructive indirect tensile test.

The complex characteristics of the behavior of asphalt mixes at low temperatures requires the combination of the results of all these tests where they are exposed to traffic loads and climatic effects.

Testing procedures may also be classified by the measurement principles as follows:

- thermal stress tests without shrinkage,
- thermal stress tests with shrinkage,
- relaxation tests,
- further testing procedures for the determination of mechanical-physical and functional characteristics performed at low temperatures, such as the ITS test or the stiffness modulus test in the NAT apparatus etc.

The monitoring of the characteristics of asphalt mixes and bituminous binders in the Czech Republic is guided by the following aspects:

- monitoring characteristics at low temperatures under Czech technical standards,
- monitoring characteristics at low temperatures under newly introduced CSN EN standards,
- monitoring characteristics at low temperatures using procedures included in technical specifications (TP or ZTP),
- monitoring characteristics at low temperatures using non-standardized procedures.

4 MEASUREMENT OF LOW TEMPERATURE CHARACTERISTICS IN CR

The term low temperature characteristics of asphalt mixes in the Czech Republic refers to the determination of the tensile bending strength of an asphalt mix at a temperature of 0°C or

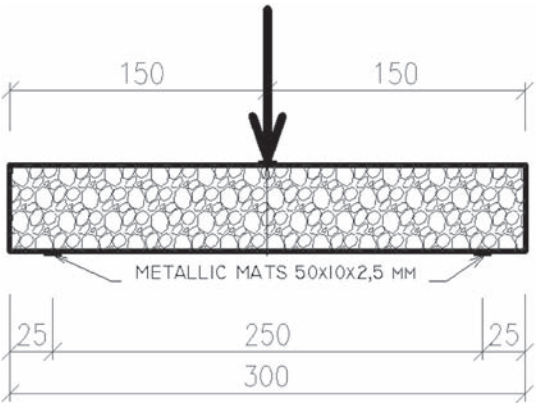

Figure 3. Loading diagram of the test specimen for relaxation and tensile bending strength tests.

lower, or a parameter describing a decrease in the stress input in a test specimen to a specified level at identical temperatures—the relaxation test.

It must be said that the principles of relaxation tests have been described in numerous sources (Eulitz, 1987). The test procedures performed on beams loaded by bending forces carried out by (Gauer, 1996) as well as other experience from literature testify to the fact that the relaxation behavior of asphalt is more complex than that corresponding to the simple two-parametric Maxwell model.

Low temperature characteristics are experimentally determined in the Czech Republic mainly for asphalt mixes of HSM and SAL type using two tests. It is the tensile bending strength test and the relaxation test. Both apply the same set of test apparatus and the same type of specimen (a beam with dimensions of $50 \times 50 \times 300$ mm). The test is carried out in a special air-conditioned bath at a temperature of 0×1°C. While measuring the tensile bending strength, the specimen is loaded until failure, where the maximum reached force (stress) and the corresponding deformation are recorded. An important factor strongly affecting the stress value is the loading speed. The resulting tensile bending strength R_i (MPa) is calculated from the equation:

$$R_i = \frac{3}{2}\frac{P \cdot l}{b \cdot h^2} \tag{1}$$

where P maximum force achieved (N),
l distance of the test specimen supports (mm),
b test specimen width (mm),
h test specimen height (mm).

Furthermore, this test serves for the evaluation of the tensile bending modulus of elasticity E (MPa) and the relative deformation ε_s.

The relaxation test runs in two phases. The first, preparatory phase serves for the determination of the maximum tensile bending strength. In this phase, the maximum loading speed should be applied to minimize the undesirable impact of relaxation effects. In the second phase, the specimen is loaded for a minimum time with a force amounting to ⅔ of the magnitude measured in the first step. From the start of loading, the decrease in stress (force) in relation to time under constant deformation is recorded. The tensile bending stresses $\sigma(t)$ at individual time periods are calculated from equation (2). The decrease in the relative relaxation stress is expressed in percent and obtained from the equation:

$$\sigma_r(t) = \frac{P_r(t)}{P_r(t_0)} \tag{2}$$

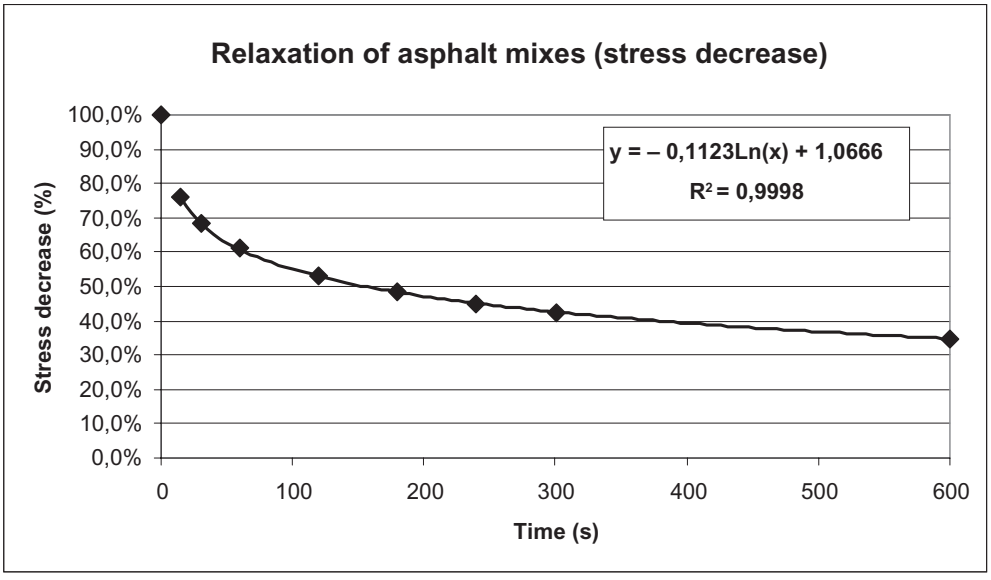

Figure 4. Relaxation graph showing the relationship between decrease in stress and time.

Relaxation specifies the time during which relative stress falls to a 50% or 30% or 15% value, and the time is expressed in seconds. It might be possible to describe the decrease in stress by a logarithmic function in equation (3):

$$y = -A \cdot \ln(x) + B \tag{3}$$

The correlation between measured values and calculated ones ranges within 0.96–0.99. The respective parameters A and B characterize the asphalt mix behavior in relation to the input stress level. More outstanding influence on this level can be seen by the parameter A, which determines the velocity of the input stress decrease.

Another apparatus also used in the Czech Republic is CYKLON 40. The measurement principle of low temperature characteristics of asphalt mixes in this apparatus (Kudrna et al., 2001) consists in the measurement of changes in the tensile stress inside the test specimen under gradual cooling with simultaneous prevention of its deformation. Tensile stresses in the test specimen grow as it is not allowed to naturally shrink with falling temperatures.

5 RESULTS OF LOW TEMPERATURE CHARACTERISTICS TESTING IN CR

5.1 *High stiffness modulus asphalt mixes*

The technology of asphalt mixes with a high stiffness modulus has been known and used worldwide and Europe-wide for a decade. In the Czech Republic, this technology has been regulated by Czech technical specifications TP 151 (Ministry of Transport, 2001). The main characteristics of these mixes and requirements set in TP 151 are summarized in Table 1. HSM mixes are designed for use in sub-bases and binder courses of roads with very heavy traffic loads. These modifications minimize the occurrence of permanent deformations and have a very good resistance to the effects of water. Due to their mechanical-physical and rheological characteristics (fatigue—service life) their application allows reducing the thickness of the above-mentioned structural layers. Preserving the same thicknesses of structural layers prolongs the favorable fatigue characteristics, while higher stiffness modules of HSM mixes extend the service life of the road pavement construction.

Table 1. Technical requirements for asphalt mixes of HSM type (according to TP 151).

Parameter	Value	Unit
Marshall stability	min. 14	kN
Marshall deformation	20–50	0.1 mm
Rut depth Y_3 (Y_s) after 10 000 travels	max. 1.3	mm
Rut depth increase between 20 000 and 10 000 travels	max. 0.22	mm
Stiffness modulus at 15°C	min. 9000	MPa
Decrease in stress to a 50% value at T 0°C - binder course	600	
- sub-base	1200	s
Tensile bending strength R_i	6	MPa

Table 2. Requirements for stress absorbing asphalt layers (SAL).

Parameter	Value	Unit
Minimum tensile bending strength ($R_{\pm 0°C}$)	0.8	MPa
Maximum modulus of deformation (E_s)	350	MPa
Decrease in relative stress after loading to a 50% value	60[1]	s
	15[2]	
Decrease in relative stress after loading to a 30% value	180[1]	s
	120[2]	
Residual stress after 10 minutes of the test run	15[1]	%
	15[2]	
Resistance to permanent deformation according to technical specifications TP 109 after 10 000 travels (y_3, y_s)	2.4[3]	mm
Rut depth increase between 10 000 and 15 000 travels (p_3, p_s)	0.40[3]	mm
Rut depth increase between 10 000 and 20 000 travels (p_3, p_s)	0.75[3]	mm

Note:
[1]bitumen with 160/220 penetration;
[2]modified bitumen including mixes with additives;
[3]thickness of testing specimen 50 mm, testing temperature 40°C.

Generally enhanced parameters of asphalt mixes of HSM type are caused by the use of harder bituminous binders or modified and multigrade bituminous binders. The second aspect affecting the behavior of HSM mixes is the aggregate skeleton composition. It must satisfy high demands concerning the narrow range of the aggregate grading curve.

5.2 *Stress absorbing asphalt layers (SAL)*

Stress absorbing asphalt layers (SSŽ, 2001) are able due to their favorable relaxation characteristics to absorb input stresses thus protecting asphalt surfacing, particularly the wearing course from the propagation of reflexive cracks from sub-base courses or preventing the propagation of failures from old layers into new multilayer constructions during repairs.

The stress absorbing asphalt layer (SAL) is mostly laid under binder courses or on hydraulically bound sub-base. It replaces the use of reinforcing elements and membranes, which work to prevent the propagation of reflexive cracks or exposed and construction joints, e.g. from granular material bound with cement into surfacing layers. Another potential application of the SAL technology is to dilate the rigid base of e.g. an old concrete pavement from asphalt-bound layers. The maximum grain size in these modifications is usually 8 mm. Soft bituminous binders 160/220 or modified bituminous binders 45/80-50, 45/80-55, 45/80-60, 60/105-45 or 60/105-70 (under CSN EN 14023) with high restored ductility values and good shape memory are used. Due to greater amounts of binders in the mix, bitumen carriers, like

Table 3. Relationship of selected properties from the tensile bending strength test on the amount and type of asphalt binder in mixes of HSM type.

Distilled bitumen 50/70			Modified bituminous binder		
Binder content (%)	Tensile bending strength (MPa)	Tensile bending modulus of elasticity (MPa)	Binder content (%)	Tensile bending strength (MPa)	Tensile bending modulus of elasticity (MPa)
4.2	4.35	830	4.2	5.79	790
4.4	4.77	1087	4.5	6.02	780
4.6	4.80	750	4.6	7.21	920

cellulose fibers, are recommended for use. The demands for mechanical-physical, rheological or low temperature characteristics are summarized in Table 2.

5.3 *Results of tensile bending strength*

In evaluating the tensile bending strength test, including the calculation of tensile bending modulus of elasticity it must be repeated that these parameters are specified only for mixes of HSM ($R_{0°Cmin}$ = 6 MPa) and SAL ($R_{0°Cmin}$ = 0,8 MPa and $E_{0°Cmax}$ = 350 MPa) type. For mixes of HSM type, this requirement results from stresses arising due to traffic loads and due to the layer shrinkage at low temperatures. Analogical values, however, should also be reached for coarse graded asphalt concrete AC22 or AC16) mixes in binder or sub-base layers if hard bitumen is used in them.

The total of 46 mixes have been evaluated in the last four years, of them AC22 (1), SMA (6), DBM (2), HSM (21), SAL (16). It was confirmed that the binder used in the mix has a significant effect on the resulting tensile bending strength values. In using modified bituminous binders, strength values by approx. 115% to 143% higher were achieved. TP 151 prefers the use of hard bituminous binders, modified or multigrade binder in HSM mixes. Related to HSM mixes developed e.g. in France the bitumen content required by Czech technical specifications might be lower. The use of these mixes allows reaching the required value of 6 MPa. The highest strength values were measured in the AC22 mix, which together with the results of the stiffness modules measured in the NAT confirms the fact that the HSM mix represents a subclass of AC22 or AC16 mixes. According to European standard, HSM mixes could be ranked among asphalt concretes—AC see CSN EN 13108-1 with the corresponding complementation of the values of National Appendix (NA) parameters of this standard.

The worst results were manifested by mixes of dense bituminous macadam (DBM) type. This technology is definitely suitable only for less traffic-loaded roads. Comparing HSM mixes by their grading composition, modifications with the maximum grain size of 16 mm seems to be more suitable. This is most probably caused by greater mix homogeneity and also by a greater contact interface in the critical cross-section, i.e. a greater amount of binder under stress.

The tensile bending strength is also affected by the amount of binder in the mix. Table 3 gives an overview of the tensile bending strength and tensile bending modulus in elasticity relationship to the amount and also type of bitumen. Mixes with greater bitumen content show higher tensile bending strength values.

SAL mixes confirm that the satisfaction of the requirement for the minimum tensile bending strength is very easy. Thanks to their high bitumen contents, smaller grain size and the resulting number of contact interfaces in the critical cross-section, dramatically higher strength values are reached than in HSM mixes. The grain size effect on the strength of mixes may be found in Table 4. The observation of the condition of the maximum tensile bending modulus of elasticity, however, is a more complicated issue. The SAL structural layer is required to display elastic behavior, it should be able to carry higher deformations and

Table 4. Overview of average tensile bending strength values in relation to mixes of SAL type and loading speed.

Mix type	Loading speed (mm.min^{-1})	Tensile bending strength (MPa)	Tensile bending modulus of elasticity (MPa)	Relative deformation (%)
SAL 0–11	1.25	6.10	418	178.8%
	3.12	5.78	300	194.1%
	6.25	9.52	1290	73.7%
	12.5	8.32	525	157.2%
	25	7.60	1390	54.8%
	50	9.20	1074	85.9%
SAL 0–5	50	8.20	1179	77.2%
SAL 0–8	1.25	6.76	510	143.0%
	50	10.72	1365	79.1%

Table 5. Relationship of selected characteristics from the tensile bending strength test on the amount and type of bitumen in mixes of SAL type.

Binder	Amount of binder (%)	Tensile bending strength (MPa)	Tensile bending modulus of elasticity (MPa)
Caribit 45	9.3%	5.89	440
Caribit 65		4.8	340
Olexobit 65	8.3%	7.48	710
	8.8%	6.58	490
Olexobit 65	8.1%	8.58	860
	9.0%	6.58	440
	9.3%	5.72	350

prevent crack propagation from sub-base layers. This demand may be met by using distilled soft bituminous binders or by using modified bituminous binders with higher penetration.

An example of the effect of the bitumen on both variables is reported in Table 5 which shows a decrease in the bending modulus of elasticity (more distinct "chewing gum" behavior) for higher bitumen content or lower penetration for selected test conditions. The relationship between the tensile bending strength value and the test specimen loading speed was not confirmed. The results indicate that the smaller the grain size used in the mix, the higher the difference between the strength values specified at a loading speed of 50 mm.min^{-1} and a loading speed of 1.25 mm.min^{-1} may be.

5.4 *Results of the relaxation test*

The relaxation test was performed on a total of 43 mixes. These were mixes of HSM (20), SAL (17), SMA (3), DBM (2) and AC22 (1) type. The requirements for the characteristics of the mixes are specified in technical specifications TP 151. For mixes of HSM type, there is a requirement according to TP151 for a decrease in input stress to a 50% value at 0°C in 600 seconds for binder courses and 1,200 seconds for sub-base layers. According to our knowledge these requirements have been defined in the Czech technical specifications based on the findings of Gauer (Gauer, 1996). For mixes of SAL type, a decrease in stress to a 50% value is prescribed after 60 seconds for an asphalt mix with bitumen pen 160/220 or after 15 seconds for mixes with modified bituminous binders, including mixes with additives. A decrease in stress to a 30% value should be reached in 180 or 120 seconds respectively. Residual stress after 10 minutes of the test must not exceed 15%. An overview of selected results is in Tables 6 to 9.

Table 6. Relaxation test results in relation to asphalt mix and bitumen type.

Mix type	Grain composition	Bitumen	Relaxation test A parameter	Relaxation test B parameter	Stress decrease to 50%
AC22	0–22	modified	0.847	–0.101	32
SMA	0–11	modified	0.836	–0.105	28
	0–11	non-mod.	0.816	–0.097	35
DBM	0–22	modified	0.925	–0.099	79
HSM	0–16	modified	0.975	–0.106	108
	0–16	non-mod.	0.893	–0.097	81
	0–22	modified	0.962	–0.109	121
	0–22	non-mod.	0.974	–0.113	82

Table 7. Relaxation test results for a mix of SAL type in relation to grading and bitumen used.

Mix type	Grain composition	Bitumen	Relaxation test A parameter	Relaxation test B parameter	Stress decrease to 50%
SAL	0–5	modified	0.522	–0.066	2
	0–5	non-mod.	0.735	–0.090	27
	0–8	modified	0.811	–0.103	23
	0–11	modified	0.748	–0.097	20

Table 8. Relaxation test results for a mix of HSM type in relation to the bitumen content.

Bitumen content 50/70 (%)	Stress decrease to 50% (s)
4.2	91
4.4	54
4.6	33

Table 9. Relaxation test results for a mix of SAL type in relation to the amount and type of the bitumen.

Bitumen	Bitumen content (%)	Residual stress (% after 10 minutes)	Stress decrease to 50% (s)	Stress decrease to 30% (s)
Caribit 45	9.3%	15.7	20.2	130
Caribit 65		14.0	10.8	100
Olexobit 65	8.3%	24.5	50.5	314
	8.8%	14.0	15.0	104
Olexobit 65	8.1%	23.0	35.5	260
	9.0%	16.0	18.6	126
	9.3%	13.9	13.6	95

The generalized results lead to the following conclusions:

– The demand for a decrease in stress for mixes of HSM type (or mixes with similar use in the pavement construction, i.e. AC22, AC16, DBM) is very easy to fulfill. None of the specimens has a problem in satisfying this condition. For specification reasons, however, the tested mix specimens did not apply significantly harder binders. Despite this, the required strength was reached with softer binders as well, although the values reached approached limit values.
– Mixes with a smaller grain size "release" stress more easily. This holds true for both mixes of HSM and SAL type; the differences recorded for the latter type, however, were much smaller.

– The amount and type of binder affects relaxation times, see Tables 8 and 9.
– The amount and type of binder affects residual stresses, see Table 9.

6 CONCLUSION

Due to their principle, the tensile bending strength test and the relaxation test represent simple test procedures, which, nevertheless, give a good account of the behavior of individual mixes, make good distinctions between the used binders, their amounts, and also react to the tested asphalt mix, i.e. its type and the maximum grain size used in the mix.

The tensile bending strength determined on HSM mixes showed, that this characteristic turns up with increasing bitumen content in the asphalt mix. If polymer modified binders are used the mixes reach even considerable higher strength values. For SAL asphalt mixes, which are characterized by high bitumen contents, it has been proven, that with increasing binder content the strain behavior of the mix is more influenced, i.e. higher content decreases the mix stiffness. In the case of both mix types higher bitumen contents usually result in shorter relaxation time periods.

The required parameters are set up in a reasonable way, with a single arguable exception: the value of the relaxation time for HSM mixes of 600 seconds for softer binders is a very easily reachable parameter. Despite the lower frequency of tested hard binders, i.e. 20/30 binders, it seems that this requirement is not strict enough for these binders either.

ACKNOWLEDGEMENTS

This paper was written with financial support from the Ministry of Education, Youth and Sport of the Czech Republic, project No. 1M0579.

REFERENCES

CSN EN 13108-1, Asphalt Mixes—Specifications for Materials—Part 1: Asphalt Concrete, National Appendix.

Czech Meteorological Institute 2008. http://www.chmi.cz/meteo/ok/infklim.html

Deme I.J. 1999. Relation between Bitumen Properties and Cracking of Canadian Pavements at Low Temperatures. In Eurasphalt & Eurobitumen, *Proceedings of E&E Congress 1999*, Paper No. 019. Brussels: Eurasphalt & Eurobitumen.

Eulitz, H.J. 1987. Kalteverhalten von Walkzasphalten. In Institut fur Strassenwesen TU Braunschweig (ed.) *Schriftenreihe Heft 7*. Braunschweig: TU Braunschweig.

Gauer, P. 1996. Relaxationverhalten von Asphalt bei tiefen Temperaturen. In Eurasphalt & Eurobitume, *Proceedings of E&E Congress 1996*, paper 4.061. Brussels: Eurasphalt & Eurobitumen.

Kudrna, J. & Hýzl, P. 2001. Apparatus for the Determination of Low Temperature Characteristics of Asphalt Layers, In SILMOS (ed.) *Proc. of the International Conference Asfaltové vozovky 2001*, pp. 350–353. České Budějovice: SILMOS.

Ministry of Transport and Communications 2001. Asphalt Mixes with High Stiffness Modulus (HSM), In SSŽ, PSVS, CTU Prague, TU Brno (eds.) *Technical Specifications TP151*, Prague: Ministry of Transport of the Czech Republic.

SSŽ 2001. Special Technical Conditions BIPLAST, Technical Conditions for the Stress Absorbing Asphalt Layer, Prague: SSŽ.

Wistuba, M.P. 2007. Testing of Asphalt Mixes in the Low Temperature Range, In SILMOS (ed.) *Proc. of the International Conference Asfaltové vozovky 2007*, České Budějovice: SILMOS.

Advanced Testing and Characterization of Bituminous Materials – Loizos, Partl, Scarpas & Al-Qadi (eds)
© 2009 Taylor & Francis Group, London, ISBN 978-0-415-55854-9

Calibration and validation of a visco-elasto-plastic constitutive model for bituminous conglomerates

N. Baldo & M. Pasetto
University of Padova, Padova, Italy

N. Kringos, C. Kasbergen & A. Scarpas
Delft University of Technology, Delft, The Netherlands

ABSTRACT: The paper presents and discusses the calibration and validation of a three-dimensional constitutive visco-elasto-plastic model developed for the analysis of the mechanical behaviour of bituminous mixes. The methodology, an inverse problem technique, uses a one-dimensional analytic formulation of the constitutive model and four different algorithms of non-linear constrained optimisation: the Conjugate Gradient, Montecarlo, Davidon-Fletcher-Powell and Simplex. On the basis of the creep recovery data obtained from an experiment in support of the model calibration, it was verified that the values of the constitutive parameters can be reliably identified, even starting from different initial guesses. A subsequent comparison between the experimental creep curves and numerical ones of the 3-D model demonstrated minimal shifts, confirming the robustness of the identification procedure for the parameters.

1 INTRODUCTION

In recent years, the scientific community in the roads sector has become increasingly interested in the development and numerical implementation of constitutive mechanistic models for bitumen mixes. The reason for this is the by now widespread awareness of the many advantages deriving from a reliable analysis of the tensio-deformational behaviour of the materials forming the bituminous layers of the pavement, such as a more rational sizing of the superstructure (Scarpas, 2004), which takes into consideration the main causes of deterioration (rutting, fatigue cracking, thermal cracking), and more efficient support for road maintenance planning, by being able to estimate the residual useful life of the pavement (Baldo, 2006).

In the computer modelling of bituminous conglomerates, the estimate of the constitutive parameters is a fundamental prior step for a reliable simulation of the mechanical behaviour of the materials and hence the pavements. The calibration process obviously becomes increasingly complex as the sophistication of the studied model increases.

This paper presents a calibration and validation procedure for a visco-elasto-plastic model developed by the Group of Mechanics of Structural Systems at Delft University of Technology (Scarpas, 2004), the two main characteristics of which are the energy based formulations and parallel workings of the elasto-plastic and visco-elastic components. As the determination of the parameters should always be based on a comparison between experimental and model (analytical and/or numerical) data, an appropriate laboratory investigation was developed, at the Experimental Road Laboratory of Padova University, in support of both the calibration and validation.

In the following, some more details of the energy based formulation of the computational model are given.

2 ENERGY BASED THREE DIMENSIONAL FORMULATION

2.1 *Hyper-elastic formulation*

A material filament defined by vector d**x** in the deformed current configuration is related by means of the *deformation gradient* tensor **F** to its undeformed (reference) configuration via the relation

$$d\mathbf{x} = \mathbf{F}\, d\mathbf{X} \tag{1}$$

If it is now assumed that the forces acting on the material element containing the filament are removed, the initial reference configuration will only be obtained if the material is elastic. In all other cases, another configuration will be obtained in which the original vector d**X** is mapped onto vector $d\mathbf{x}_r$ with the subscript r indicating the residual nature of deformation. The Helmholtz free energy ψ can be defined as a function of the deformation gradient **F** so that

$$\dot{\Psi} = \frac{\partial \Psi(\mathbf{F})}{\partial \mathbf{F}} : \dot{\mathbf{F}} \tag{2}$$

then, from the second law of thermodynamics, often referred to as the Clausius-Planck relation, for a non-dissipative material, the second Piola Kirchhoff stress tensor and the Cauchy stress tensor can be found as

$$\mathbf{S} = 2\frac{\partial \Psi}{\partial \mathbf{C}}; \quad \sigma = 2J^{-1}\mathbf{F}\frac{\partial \Psi}{\partial \mathbf{C}}\mathbf{F}^{\mathrm{T}} \tag{3}$$

Depending on the choice of the Free Energy function, the formulation of the stress tensor will change. It can be shown (Scarpas, 2004) that a general formulation of the Second Piola Kirchhoff stress tensor can be written as

$$\begin{aligned} \mathbf{S} &= 2\left[(\partial_{I_1}\Psi + I_1\partial_{I_2}\Psi)\mathbf{I} - \partial_{I_2}\Psi\,\mathbf{C} + I_3\partial_{I_3}\Psi\,\mathbf{C}^{-1} \right] \\ &= s_1\mathbf{I} + s_2\mathbf{C} + s_3\mathbf{C}^{-1} \end{aligned} \tag{4}$$

In (Kringos, Scarpas and Drescher 2008) a comparison is given between CAPA-3D and an analytical solution for a constant deformation test in tension and compression. From this reference it can be seen that a good comparison is found.

2.2 *Elasto-visco-plastic energy based formulation*

Consider now a loading/unloading cycle with residual configuration. Let $\mathbf{F}_e$ denote the deformation gradient relating the residual deformation configuration to the current configuration. Then, according to Eq. (1):

$$d\mathbf{x} = \mathbf{F}_e\, d\mathbf{x}_r \quad \mathbf{F} = \mathbf{F}_e\,\mathbf{F}_r \tag{5}$$

In which $\mathbf{F}_r$ denotes the deformation gradient relating the residual deformation configuration to the reference configuration. This process of decomposing the deformation gradient is known as the "*multiplicative decomposition*" of the deformation gradient to a residual deformation component and a component signifying the elastic unloading that the material must undergo from the configuration at time t to the residual configuration. The concept of multiplicative decomposition of the deformation gradient provides an elegant tool for description of the three dimensional response of elasto-visco-plastic material models consisting of elasto-plastic and visco-elastic components.

The deformation gradient of a material in which the elasto-plastic and the viscoelastic components act in parallel can be decomposed as

$$\mathbf{F} = \mathbf{F}_{\infty}\,\mathbf{F}_{p} \quad ; \quad \mathbf{F} = \mathbf{F}_{e}\,\mathbf{F}_{v} \tag{6}$$

in which $\mathbf{F}_{\infty}$ is the elastic component of the deformation gradient of the elasto-plastic element, $\mathbf{F}_{p}$ is the plastic component of the deformation gradient of the elasto-plastic element, $\mathbf{F}_{e}$ is the elastic component of the deformation gradient of the visco-elastic element and $\mathbf{F}_{v}$ is the viscous component of the deformation gradient of the visco-elastic element.

From this the right Cauchy-Green strain tensor $\mathbf{C}$ can be shown to be

$$\mathbf{C} = \mathbf{F}^{T}\,\mathbf{F} = \mathbf{F}_{v}^{T}\,\mathbf{C}_{e}\,\mathbf{F}_{v} = \mathbf{F}_{p}^{T}\,\mathbf{C}_{\infty}\,\mathbf{F}_{p} \tag{7}$$

with this, a definition has been derived to compute the total strain tensor of the material $\mathbf{C}$, based on either of the elastic strain tensors and the plastic or the viscous deformation gradient, respectively. The Helmholtz free energy function for a three dimensional model equivalent to the generalized model proposed in the above can be expressed as

$$\Psi = \Psi_{v}(\mathbf{C}_{e}) + \Psi_{p}(\mathbf{C}_{\infty}, \xi_{p}) \tag{8}$$

where ξ_{p} is a measure of the plastic deformation.

The Clausius-Planck local dissipation inequality and can be formulated as

$$\mathbf{S} : \tfrac{1}{2}\dot{\mathbf{C}} - \left[\frac{\partial \Psi_{v}}{\partial \mathbf{C}_{e}} : \dot{\mathbf{C}}_{e} \right] - \left[\frac{\partial \Psi_{p}}{\partial \mathbf{C}_{\infty}} : \dot{\mathbf{C}}_{\infty} + \frac{\partial \Psi_{p}}{\partial \xi_{p}}\,\dot{\xi}_{p} \right] \geq 0 \tag{9}$$

The above formulation give the general frame-work of the large-strain, energy based, CAPA-3D model which is utilized to simulate the behavior of asphaltic materials.

3 CALIBRATION AND VALIDATION OF THE VISCO-ELASTO-PLASTIC MODEL

The constitutive model described in Section 2, of general validity for materials with visco-elasto-plastic behaviour including bituminous conglomerates, was calibrated and then validated in the specific case of a Stone Mastic Asphalt (SMA) mix. As documented in Pasetto and Baldo (2008), SMA is a dense mix 0/11 (d/D) characterised by a discontinuous grading curve, with a filler—bitumen ratio of 1.7, containing 25% artificial inert and produced with 6% of hard modified bitumen.

Data relating to the SMA deformational response were elaborated, which were obtained from experiments conducted specifically for the model calibration. These were tests of static creep with free lateral expansion, conducted at a temperature of 40°C on cylindrical SMA specimens, 100 mm in diameter and 60 mm in height. Three load application times of 10 s, 20 s, 30 s were used, and a rest period for visco-elastic recovery set at 110 s, 100 s and 90 s respectively, for an overall test duration of 120 s. In order to obtain a sufficiently representative study of the deformational response of the mix, a set of three tension levels was chosen (100 kPa, 300 kPa, 500 kPa) for each of the three stress times (Pasetto and Baldo, 2007).

The experimental programme, for each loading level, can be summarised as follows:

$$\begin{aligned} &t \leq 0, && \sigma(t) = 0 \\ &0 < t < t_{1}, && \sigma(t) = \sigma_{0} = \text{const} \\ &t > t_{1}, && \sigma(t) = 0 \end{aligned} \tag{10}$$

where t_{1} indicates the moment of unloading and σ_{0} the value of the creep load applied.

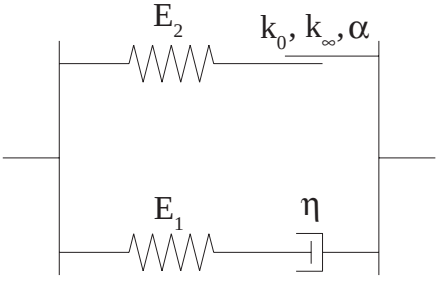

Figure 1. One-dimensional visco-elasto-plastic model.

3.1 *One-dimensional costitutive formulation*

Figure 1 represents the one-dimensional scheme of the simplified analytical model, derived from the 3-D one delineated in Section 2. It is composed of a Maxwell visco-elastic element, in parallel with an elasto-plastic element; the latter being characterised by an elastic spring, connected in series to a plastic slider, which presents non-linear hardening, with the yielding limit Y linked to the plastic strain ε_p by the equation:

$$Y = k_\infty + (k_0 - k_\infty)e^{-\alpha\varepsilon_p} \tag{11}$$

In Eq. (11), k_0 and k_∞ are the initial and asymptotic yielding limits respectively, while α is the exponent of the hardening law.

The constitutive parameters of the analytical model are therefore given by the viscosity η of the viscous dashpot, by Young's moduli E_1 and E_2 of the visco-elastic and elasto-plastic elements respectively, as well as the previously cited k_0, k_∞, and α, linked to the plastic slider.

For this type of model, the response to a static creep load results as being visco-elastic, as long as the tension in the elasto-plastic element is lower than the initial yielding limit. When, during the loading phase, the tension in the elasto-plastic element is above the initial yielding limit, the slider becomes active, leading to the development of irreversible plastic strains. The critical instant (t_{cr}) that delimits the two different mechanical behaviours can be determined with the following equation (Kringos, Drescher and Scarpas 2008 and Kringos, Kasbergen and Scarpas 2008):

$$t_{cr} = \frac{\eta(E_1 + E_2)}{E_1 E_2} \ln\left[\frac{\sigma_0 E_1}{(\sigma_0 - k_0)(E_1 + E_2)}\right] \tag{12}$$

So, for $t \le t_{cr}$, the response of the model is governed by the equation:

$$\frac{\eta}{E_1}\dot{\sigma} + \sigma = \frac{\eta(E_1 + E_2)}{E_1}\dot{\varepsilon} + E_2\varepsilon \tag{13}$$

which, in terms of total strains, leads to the equation:

$$\varepsilon(t) = \frac{\sigma_0}{E_2}\left[1 - \frac{E_1}{(E_1 + E_2)}e^{-\frac{E_1 E_2}{\eta(E_1 + E_2)}t}\right] \tag{14}$$

Vice versa, for $t_{cr} < t \le t_1$, the behavior of the model is defined by:

$$\frac{\eta}{E_1}\dot{\sigma}+\sigma=\eta\dot{\varepsilon}+\left[1-\frac{\alpha\dot{\varepsilon}\eta}{E_1}\right](k_0-k_\infty)e^{-\alpha\left(\varepsilon-\frac{k_0}{E_2}\right)}+k_\infty \tag{15}$$

that allows to write, in terms of strain rate:

$$\dot{\varepsilon}=\frac{\sigma_0-k_\infty-C}{\eta\left(1-\frac{\alpha}{E_1}C\right)} \tag{16}$$

where

$$C=(k_0-k_\infty)\exp\left(\frac{\alpha k_0}{E_2}\right)\exp(-\alpha\varepsilon) \tag{17}$$

When a backward Euler scheme is used, Eq. (16) can be written incrementally as:

$$\Delta\varepsilon_T=\frac{\sigma_0-k_\infty-C}{\eta\left(1-\frac{\alpha}{E_1}C\right)}\Delta t \tag{18}$$

Eq. (17), being an analytical approximation based on the result of the numerical integration, allows the following equation to be assumed for the total strain:

$$\varepsilon(t)=\varepsilon_0+(a-\varepsilon_0)\,(1-e^{-bt}) \tag{19}$$

where ε_0 is the total instantaneous strain developed by the material at the initial moment of stress, while a and b can be determined by the following equations:

$$a=-\frac{1}{\alpha}\ln\left(\frac{k_\infty-\sigma_0}{k_\infty-k_0}\right)+\frac{k_0}{E_2} \tag{20}$$

$$b=\frac{\sigma_0-k_\infty-C_0}{(a-\varepsilon_0)\eta\left(1-\frac{\alpha}{E_1}C_0\right)} \tag{21}$$

with

$$C_0=(k_0-k_\infty)\exp\left(\frac{\alpha k_0}{E_2}\right) \tag{22}$$

At the release, for $t > t_1$, the temporal evolution of the total strain is given by:

$$\begin{aligned}\varepsilon(t)=\varepsilon_0+(a-\varepsilon_0)(1-e^{-bt_1})-\frac{k_\infty}{E_2}-\frac{(k_0-k_\infty)}{E_2}e^{-\alpha\left(\varepsilon_0+(a-\varepsilon_0)\left(1-e^{-bt_1}\right)-\frac{k_0}{E_2}\right)}\\ -\frac{1}{E_2}\left\{\sigma_0-k_\infty-(k_0-k_\infty)e^{-\alpha\left(\varepsilon_0+(a-\varepsilon_0)\left(1-e^{-bt_1}\right)-\frac{k_0}{E_2}\right)}-\frac{\sigma_0E_1}{(E_1+E_2)}\right\}\\ \times e^{-\frac{E_1E_2}{\eta(E_1+E_2)}(t-t_1)}\end{aligned} \tag{23}$$

3.2 *Plastic strain curve*

The calibration procedure requires preliminary determination, for each stress level, of the Plastic Strain Curve (PSC), by interpolation of the experimental time-strain pairs of data, formed, for each creep test, by the time of application peak of the stress and the corresponding value of permanent strain (Figure 2).

The PSC was thus determined for each stress level and from this the value of the critical time, identified as the temporal instant when the PSC intercepts the temporal axis of the abscissa. The ordinate value corresponding to the critical time represents the total instantaneous strain ε_0 necessary for the calculation of the model's total strains according to Eq. (18). Table 1 reports the values of t_{cr} and corresponding ε_0 for each of the three stress levels investigated.

3.3 *Non linear optimization and analytical validation*

The calibration method is based on the inverse problem technique, i.e., on the identification of the set of values of the constitutive parameters that minimises the difference, in terms of least squares, between the experimental total strains and those of the model.

This consists of an iterative optimisation procedure of the objective function $f(\boldsymbol{x})$ defined by:

$$f(\boldsymbol{x}) = \sum_{i=1}^{N} \left(\varepsilon_i^{Exp} - \varepsilon_i^{Mod} \right)^2 \tag{24}$$

where ε_i^{Exp} and ε_i^{Mod} represent a pair of total strains, experimental and model respectively, corresponding to the same temporal instant i ; $\boldsymbol{x}$ is the vector of the constitutive parameters; N is the number of experimental observations. Eqs. (18), (22) were used for the calculation of ε_i^{Mod} in Eq. (24).

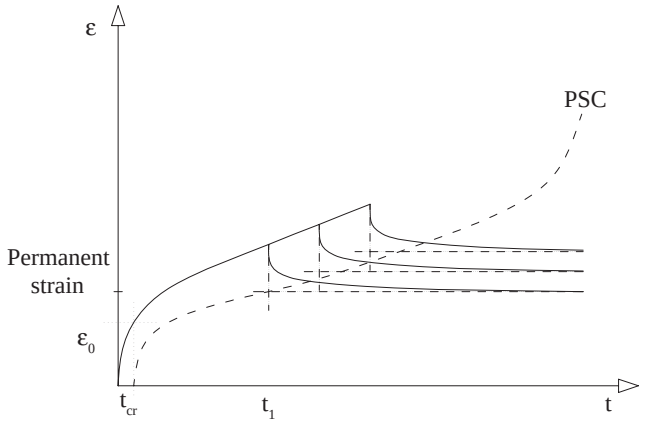

Figure 2. Creep curves and plastic strain curve.

Table 1. Critical times and initial total strains at different stress levels.

Stress level [kPa]	t_{cr} [s]	ε_0 [–]
100	0.636115	0.000739
300	0.079554	0.000953
500	0.001863	0.000973

For the minimising of the objective function $f(\boldsymbol{x})$, four different non-linear optimisation algorithms were used (Press et al, 1997): the Conjugate Gradient (CG), Simplex (S), Davidon-Fletcher-Powell (DFP) and Montecarlo (M). The iterative procedure stops when the preset tolerance is reached, yielding the final values of the constitutive parameters.

To avoid the algorithms identifying physically unacceptable values, the minimisation was developed within the ambits of constrained optimisation, defining specific acceptability ranges for each of the six variables in play. The values to be assigned to the constraints that delimit the space within which the algorithms search for the optimal solution, and which must be maintained reasonably ample, depend on the type of material being examined, as well as on the sensitivity of the model with respect to each specific constitutive parameter. A preliminary series of calibrations, in which the amplitude of the constraints range has been progressively reduced, was done in order to define the best suited space solutions domain.

The initial guess was determined, for each of the six variables, in correspondence to the average value of the relative acceptability range, so as not to influence the search direction towards the upper or lower constraints.

Of the nine available creep curves (three for each stress level), it was decided to use the fewest possible for the calibration of the model, so as to have a valid set of experimental data available for the subsequent validation. Consequently, only the creep curve of 100 kPa and 20 s of stress was used for the calibration, while the remaining eight made up the dataset for the validation.

Because neither the plastic slider nor the viscous dashpot are active at the moment of release ($t = t_1$), it is possible to estimate the total stiffness of the two elastic springs of the analytical model (E_{TOT}) from the experimental value of the total strain retrieved instantaneously ($\Delta\varepsilon$), according to the equation:

$$E_{TOT} = \left(E_1 + E_2\right) = \frac{\Delta\sigma}{\Delta\varepsilon} \tag{25}$$

where $\Delta\sigma$ represents the variation in tension recorded at the release.

In order to eliminate one variable from the set of parameters in the optimisation, $E_1 = E_{TOT} - E_2$ was defined; so, E_{TOT} being known from Eq. (25), of the two Young's moduli, only E_2 was identified through the optimisation algorithm.

The calibration procedure is now split into two phases: in the first one E_2 and η are identified, by means of the objective function minimization for the unloading time period, during which the material behaviour is visco-elastic and can be described by Eq. (22); the plastic constitutive parameters are "frozen" and therefore they are not optimized in this step. Then, in the second part of the calibration, assuming as constant the values just obtained for E_1, E_2, and η, the objective function is minimized during the loading phase, in which the material response is visco-elasto-plastic and can be described by Eq. (18), giving in this way the possibility to identify the values of k_0, k_∞, and α.

Table 2 presents the results obtained from the calibration, with the values of the constraints imposed and the initial guess used. The values estimated with the four algorithms are equal for E_1, E_2 and k_0, similar for η, while differences emerged for k_∞ and α.

Table 2. Initial guess, optimization constraints and parameters identification results.

Parameters		E_1 [MPa]	E_2 [MPa]	η [MPa·s]	k_0 [MPa]	k_0 [MPa]	α [–]
Initial guess		166.0000	105.0000	270.0000	0.0350	1.6000	27.0000
Algorithm	Simplex	176.0000	95.0000	290.0000	0.0300	2.6049	19.0003
	Montecarlo	176.0000	95.0000	289.9999	0.0300	1.8069	28.0081
	DFP	176.0000	95.0000	290.0000	0.0300	2.6050	19.0000
	CG	176.0000	95.0000	289.9999	0.0300	1.7930	27.9258
Constraints	min	–	95.0000	250.0000	0.0300	0.5000	19.0000
	max	–	115.0000	290.0000	0.0400	2.7000	35.0000

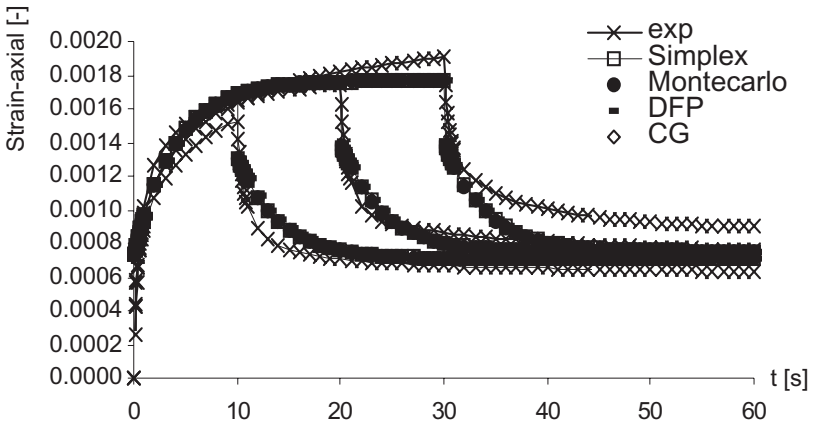

Figure 3. Experimental and analytical creep curves @ 100 kPa.

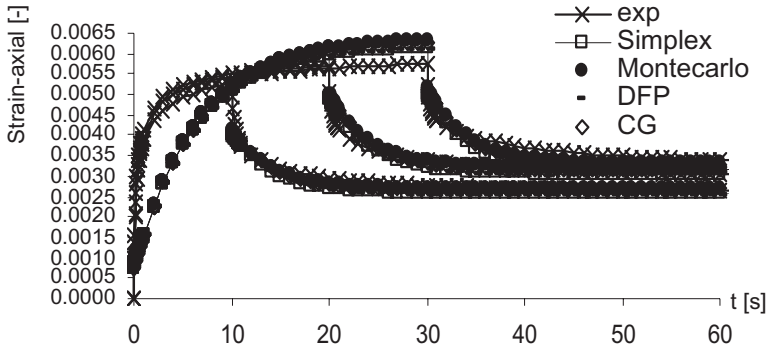

Figure 4. Experimental and analytical creep curves @ 300 kPa.

Further analyses with initial guesses other than that reported in Table 2 always led to the estimate of the same final values of the parameters, with only minor deviations.

The comparison between the experimental data of total strains and those computed with the analytical model, using the four sets of constitutive parameters identified in the optimisation, for both the calibration curve and those of validation, is proposed in Figures 3, 4 and 5, relative to the stress levels of 100 kPa, 300 kPa and 500 kPa respectively.

The curve of 100 kPa and 20 s used for the calibration shows the minimum shift of the model's from the experimental data; the four analytical curves, relative to the sets of parameters identified with the different optimisation algorithms, are more or less overlapping.

The shifts between the model's and corresponding experimental curves increase at increasing stress levels, and the differences between the four analytical solutions become more evident. In particular, Figure 5 shows that at 500 kPa it is possible to distinguish two different evolutionary trends of the total strain: one common to the Montecarlo and CG, the other similar for the DFP and Simplex.

The deviations between the experimental values and those of the analytical model, relating to both the peak and permanent strains, are obviously minimal for the calibration curve, but also remain reasonably limited for all the other curves used in the validation, never being above the threshold of 18%. The validation of the analytical model can therefore be considered satisfactory. Focusing attention on the permanent strains, which are linked to rutting phenomena of flexible pavements, the set of parameters optimised by the CG algorithm resulted as being preferable, since it led a lower underestimate of the permanent strains.

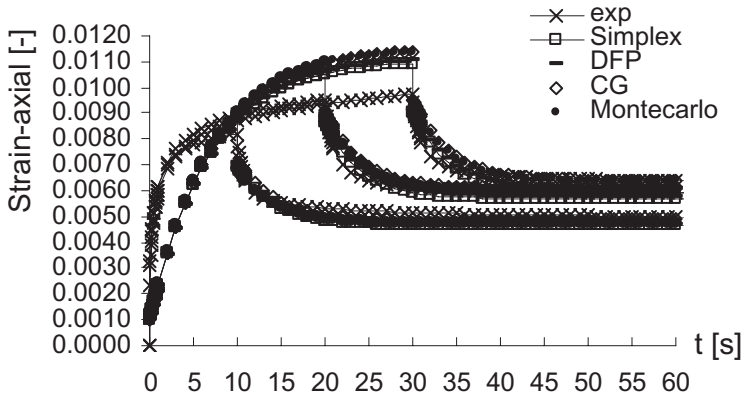

Figure 5. Experimental and analytical creep curves @ 500 kPa.

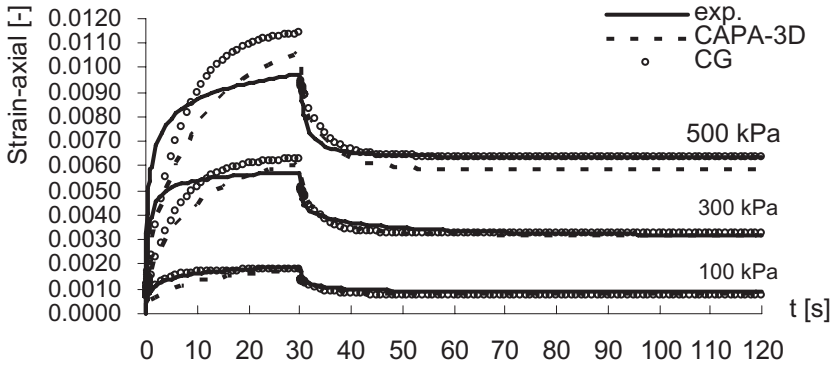

Figure 6. Experimental, analytical and numerical creep curves.

3.4 *Numerical validation with CAPA-3D*

The parameters estimated by the CG algorithm were subsequently compared with the analytical and numerical experimental curves obtained with the 3-D visco-elasto-plastic model implemented in CAPA-3D (Scarpas, 2000).

In the numerical model, the viscosity has a deviatoric component η_D, and a volumetric one η_V, linked by the equation:

$$\eta = \left(\frac{1}{3\eta_D} + \frac{1}{9\eta_V} \right)^{-1} \tag{26}$$

Given that the studied SMA mix is characterised by less than 3.5% of residual voids, the volumetric behaviour of the material was assumed to be uncompressible, setting an η_V of 10000 MPa·s; the value of η being known from the calibration (289.9999 MPa·s in the case of the set estimated by the CG), from Eq. (26), that of η_D resulted as being equal to 96.9792 MPa·s.

As regards Poisson's coefficient, a value from the literature of 0.35 was assumed in the CAPA 3-D model.

Figure 6 reports the creep curves relative to the 100 kPa, 300 kPa, 500 kPa stress levels and application time of 30 s; similar results have been obtained for the other two loading times.

The percentage deviations between the numerical and experimental data were a maximum of 11.51% for the permanent strains and 7.95% for the peak strains. The numerical validation with the CAPA-3D model can thus also be considered a success.

4 CLOSING REMARKS

The work presented in this paper deals with the determination of the material parameters that characterize an energy based, visco-elasto-plastic constitutive model, for bituminous materials.

The identification method is based on a specific experimental-analytical procedure developed ad hoc; it is splitted in two main phases, related with the unloading and loading parts of experimental creep recovery curves. The core of the calibration procedure is given by the one dimensional analytical version of the constitutive model, characterized by six material parameters, related to plasticity with non linear hardening and visco-elasticity.

The inverse problem is defined with the minimization of the function that characterizes the error between the experimental values and those obtained analytically with the constitutive model. In order to solve such constrained optimization problem, four different algorithms were used: the Conjugate Gradient, Simplex, Davidon-Fletcher-Powell and Montecarlo. All the solvers used have been fully capable of successfully determining material parameter sets; however, the parameters obtained are distinct.

The experimental-numerical validation has demonstrated that the 3-D constitutive model can interpret the fundamental aspects of the response of the asphalt concrete, in terms of both maximum and permanent strains, at different loading times and stress levels.

The model has been calibrated and validated on the basis of the deformational response of a particular Stone Mastic Asphalt, however the identification procedure has a more general applicability with the framework of the asphalt concrete.

REFERENCES

Baldo, N. 2007. Advanced constitutive modelling of bituminous materials by energetic approach: formulation, calibration and experimental evaluation. *Proceedings 4th International SIIV Congress, Palermo, 12–14 Settembre 2007*.

Kringos, N., Kasbergen C. and Scarpas A. (2008), Large strain benchmarks for CAPA-3D, *TU Delft progress report*, in preparation.

Kringos, N., Drescher A. and Scarpas (2008) A. On the Behavior of a Parallel Elasto-Visco-Plastic Model for Asphaltic Materials, Submitted for review to *Mechanics of Materials*.

Pasetto, M. & Baldo, N. 2007. A theoretical-experimental visco-elastic-plastic analysis of the Mastic Asphalt. *Proceedings International Conference on Advanced Characterisation of Pavement and Soil Engineering Materials, Athens, 20–22 June 2007*.

Pasetto, M. & Baldo, N. 2008. Performance comparative analysis of bituminous mixtures with Electric arc furnace steel slags: a laboratory evaluation. *Proceedings Rewas 2008 Global Symposium on Recycling, Waste Treatment and Clean Technology, Cancun, 12–15 October 2008*.

Press, W.H., Teukolsky, S.A., Vetterling, W.T., Flannery, B.P. 1997. *Numerical recipes in Fortran 77*, Cambridge University Press.

Scarpas, A. 2000. CAPA-3D Finite Element System Users Manual I, II, and III, *Delft University of Technology publication*.

Scarpas, A. 2004. *A Mechanics Based Computational Platform for Pavement Engineering*, TU Delft publication, ISBN 90-9019040-6.

Advanced Testing and Characterization of Bituminous Materials –
Loizos, Partl, Scarpas & Al-Qadi (eds)
© 2009 Taylor & Francis Group, London, ISBN 978-0-415-55854-9

Modulus measurement: European standardisation possibilities

Xavier Carbonneau, Yves Legal & Sébastien Quigniot
COLAS S.A, Scientific and Technical Campus, Magny les Hameaux cedex, France

ABSTRACT: The recent publication of EN standards has yielded five different recognized tests in EN 12697-26, which means that each of these tests only has small-scale experience and practice in a limited number of countries. Test conditions are specified in asphalt mix design EN 13108-20. There are significant differences in these test conditions, frequency between 8 and 10 Hz for cyclic loading, pulse loading of 124 ms or extrapolation to 0,02 s for loading time in direct tension, and a temperature test of 15 or 20°C. The cost of the equipment and the needed experience obviously means that only one test will be selected because it is difficult—and unnecessary—to purchase all the devices and to have skilled technicians able to conduct the entire range of tests. Nevertheless it is interesting for mix design specialists to be able to correlate results from different tests. It is important to be able to estimate which level of performances corresponds to a mix design that has already been evaluated with another test and to check coherence regarding fundamental requirements. This last point is even more important because the possibilities given in EN standards lead to significant differences in measured characteristics, with results that may vary for example between 6,000 and 10,000 MPa for the same mix. We present here modulus results obtained with 4 mechanical tests on two asphalt mixes, a BBSG (semi-coarse asphalt mix) and an EME (high modulus asphalt mix). We show also first results regarding correlation between four-point bending and direct tension tests. These data complete works previously published by the Colas Group on the diffusion of the law of simple correlations between the results of modulus tests. These two mixes are also characterised with the Simple Performance Test. This is a first comparison between results with the SPT and tests used in Europe.

1 INTRODUCTION

Over the last five years, European standardisation on mixes has yielded a large number of texts, on tests to be carried out (EN 12697 series), mix design (EN 13108-20) and bituminous mixtures (EN 13108 1 to 8). This normative framework allows a fundamental approach concerning mix design to be implemented, an important part of which is determining the modulus of the bituminous mixtures. But this initial standardisation of existing methods and practices on a European level has not culminated in a single testing method for a characteristic being selected. This situation is easily explained by constraints which are difficult to bear; countries having to abandon their experience, laboratory tools and specifications imposed. But there remain differences in values measured between the various tests existing on a European level. For those without a great deal of experience in the fundamental approach, the choice of a single testing method is not easy, with questions remaining virtually unanswered: which testing method, at what cost, what investments are required, for what result. Working on the assumption of a transfer of technology within the European Union, there could be difficulties concerning performances measured on the same mixture and complications for the organisation or administration charged with validating a proposal based on modulus performances. This is our modest contribution to shedding some light on this situation through results achieved on various bituminous mixtures, assessed using all the testing methods defined by European standardisation. We present rough correlations between

experimental results between four-point bending and tensile strength, which complete data already published, allowing an initial comparison of data from different measuring methods.

2 METHODOLOGY AND CHARACTERISED PRODUCTS

Comparisons of this kind have already been carried out but some of them were done long before European standardisation testing conditions were defined (Franken 1996). Others only show results for 4 of the possible testing methods, for example (Hauser 2007).

We have selected two bituminous mixtures, an EB 10 wearing 35/50 frequently implemented as a wearing course and an EB 14 Subbase 10/20 applied as a base layer, formulated, respectively, with bitumen classes 35/50 and 10/20. These two mixtures were chosen for a comparative test within the Colas Group on part of our inventory of diametral compression modulus measuring machines (Carbonneau 2009a). We have two mixtures, each presenting a significantly different level of performance. All test bodies are extracted from 600 × 400 plates, manufactured with an LCPC plate compactor, such as that shown in figure 1, except for characterised specimens under diametral compression.

In this way, for 4 of the testing methods presented here, we avoid any possible effects linked to the preparation mode of test bodies, high compaction gradients within samples or their orientation with regard to the compaction direction of the plate (Doubanneh 1995). As the tests were performed in 3 different laboratories in the Colas Group, 5 plates needed to be prepared. The plates were inspected for compaction after manufacture, as well as all the specimens extracted from them. The series of specimens used for diametral compression were moulded using a Gyropac type press for reasons of convenience (Carbonneau 2009a). It was proved that 100 mm diameter specimens manufactured in this way are uniformly compacted, eliminating the possibility of an error of measurement resulting from an anisotropy of the test bodies, such as a compaction gradient between the core and the surface of the sample (Carbonneau 2009b). The tests carried out (number of characterised samples, dimensions of the specimens, experimental measuring conditions) are recalled in table 1. As the equipment allowing the test to be carried out according to appendix D was only acquired during this measuring campaign, and after preparation of the plates selected for Simple Performance Test (SPT) testing presented afterwards, it was only possible to assess the EB 14 Subbase 10/20 using this method. The length selected for carrying out this measurement is slightly below the minimum value imposed by the testing standard, since we have a aspect ratio of 1.5 times the diameter, although the recommended minimum is 1.8.

The measuring conditions presented by the various tests differ, of course, by the possible measuring frequencies. It is difficult to exceed frequencies of 20 Hz with the four-point bending system. Complex bending modulus measurements on trapezoidal samples are possible

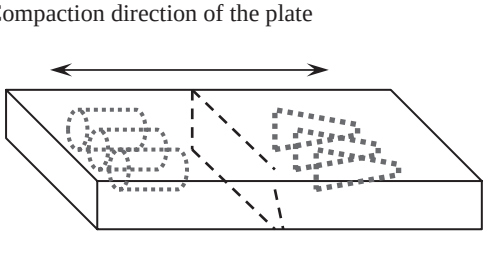

Figure 1. Cutting of specimens for specimen preparation.

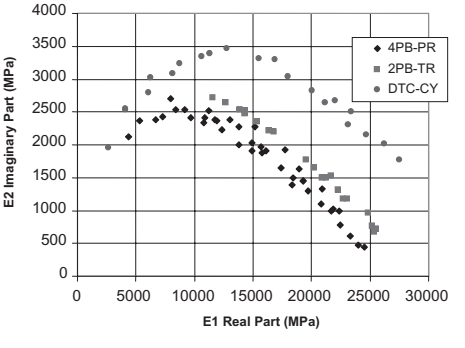

Figure 2. Cole-Cole representation of test results achieved on the EB 14 subbase 10/20, under bending on trapezoidal samples, under tension compression and four-point bending.

Table 1. Presentation of the various tests carried out.

	Test Standard EN 12697-26				
Test	Appendix A 2PB-TR	Appendix B 4 PB-PR	Appendix C IT-CY	Appendix D DTC-CY	Appendix E DT-CY
Shape of the specimens	Trapezoidal	Parallelepiped	Cylindrical	Cylindrical	Cylindrical
Dimensions (mm)	Th 25, h 250 Small base 25 Large base 56	50 × 50 × 400	ϕ100, h 40–50	ϕ80 h 120	ϕ80 h 200
Number	4	4	4	4	4
Machine	Vibrating pots	IPC bending bench	IPC UTM 14P	MTS press	MAER press
Measuring conditions	–10, 0, 5, 15, 20°C 5, 10, 20, 25 Hz	0, 5, 10, 15, 20°C 0, 1, 0, 2, 0, 5, 1, 2, 5, 10, 20 Hz	15, 20°C 124 ms	0, 10, 20, 26°C 0, 1, 0, 3,1, 3, 10 Hz	0,5, 10, 15°C 3,10,30, 100, 300 sec

up to 30 Hz but this type of equipment is limited to a low frequency. For direct tension, only 5 loading times are accessible. Finally, for the diametral compression modulus, possible loading pulse durations are relatively limited in the case of pneumatic equipment and only the duration defined in the testing standard, i.e. a 124 ms pulse, has been selected. With 3 of these testing methods we have, however, been able to establish modulus master curves for EB 10 wearing 35/50 (semi-coarse asphaltic concrete mix) and EB 14 subbase 10/20 (high modulus asphalt mix). As an example, figure 2 shows the graph of the result achieved for EB 14 Subbase.

3 RESULTS ACHIEVED

From this experimental data, we have also been able to establish, for both products, contractual modulus values defined by standard EN 13108-1. These are specified in table 2. There is also a reminder of the average void content of the batch used for each test.

In the case of diametral compression, this is the average experimental value determined during the test. For the tensile test, appendix E, this is the extrapolated value for a loading time of 0.02 s. For the tension compression test, the value has been drawn from the master curve, the same for the complex modulus.

This series of results clearly demonstrates the large variations which exist if comparisons are performed without an accurate knowledge of the different tests proposed by European standardisation. It is possible to affect categories of performance which are completely different, for example for the previous EB 14 subbase 10/20 S_{min} 11000 MPa or S_{min} 16000 MPa, if four-point bending or direct tension results are taken into account. This situation is particularly delicate if performances from different characterisation methods are compared. It is, therefore, indispensable to have theoretical equivalences or, at the very least, correlations which are sufficiently reliable to allow interpretation and comparison of data from different methods.

3.1 *Machine equivalence*

Over and above method comparison, it has also proved to be important to have concrete elements demonstrating equivalence between different machines, manufacturers always guaranteeing compliance with the testing method. It is an important job but rarely within the grasp of a single laboratory. This is because it is difficult and impossible to possess all types of equipment capable of carrying out testing. For diametral compression for pneumatic type machines, this verification has been carried out in a simplified way within the Colas Group and has led to very satisfactory

Table 2. Modulus values (in MPa) established with the various tests. The average void content for the specimens tested is recalled in brackets.

	Appendix A 2PB-TR	Appendix B 4PB-PR	Appendix C IT-CY	Appendix D DTC-CY	Appendix E DT-CY
Test	15°C 10 Hz	20°C 8 Hz	20°C 124 ms	15°C 10 Hz	15°C 0.02 s
EB 10 roll	9950 (7.8)	5810 (5.3)	5570 (6.5)	Not measured	10770 (5.2)
EB 14 subbase	15540 (4.9)	11810 (3.2)	12860 (3.2)	18700 (4)	17830 (3.9)

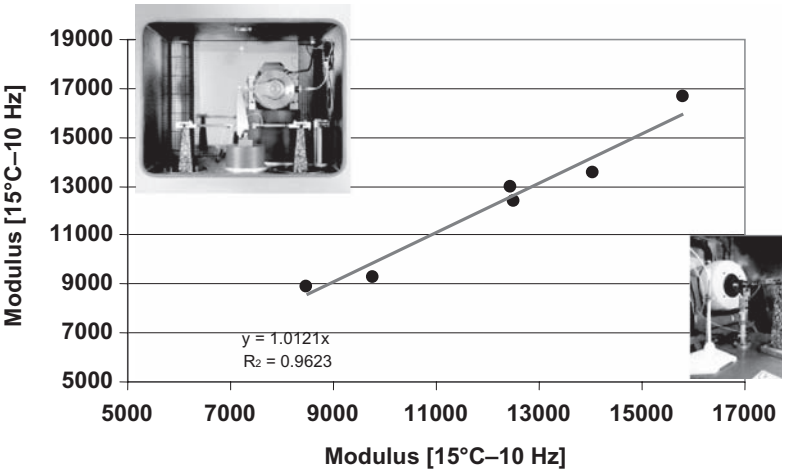

Figure 3. Correlations between the bending modulus value on trapezoidal samples measured on vibrating pots and the Cooper bending machine (eccentric type).

results. At the time of writing this publication, there have been numerous exchanges on four-point bending and a circular test on a reference aluminium specimen is in progress, organised by Ad Pronk (T.U. Delft). For the bending modulus on a trapezoidal specimen, a round robin test, carried out in 1999–2000, allowed the repeatability and reproducibility of the measurement to be determined. These have now been included in the testing standard. Figure 3, presenting the correlation between complex modulus results achieved with a vibrating pot type machine and a bending test machine on trapezoidal specimens, allows us to consider that the latest equipment to appear on the market achieves results equivalent to those of traditional machines. This verification remains, of course, limited as it only bears on a small number of mixtures, 6 different formulae, for which the specimens have all been prepared in a single laboratory before making up 2 batches of 4, tested at 15°C and 10 Hz on each machine. Nevertheless, on the modulus range spanned, from 8000 to 16000 MPa, the variation between results from two different machines has always been less than 900 MPa, at the limit of reproducibility determined for this test.

4 CORRELATIONS BETWEEN EN STANDARD TESTS

If it is accepted that there is equivalence between machines, there are still no studies of correlations between results from different tests. This remains a considerable piece of work in itself. This work was started more than ten years ago within the Colas Group, by a study comparing the direct tension modulus with the bending modulus on trapezoidal samples (Pellevoisin 1997). The equivalence between these two methods has since been confirmed in

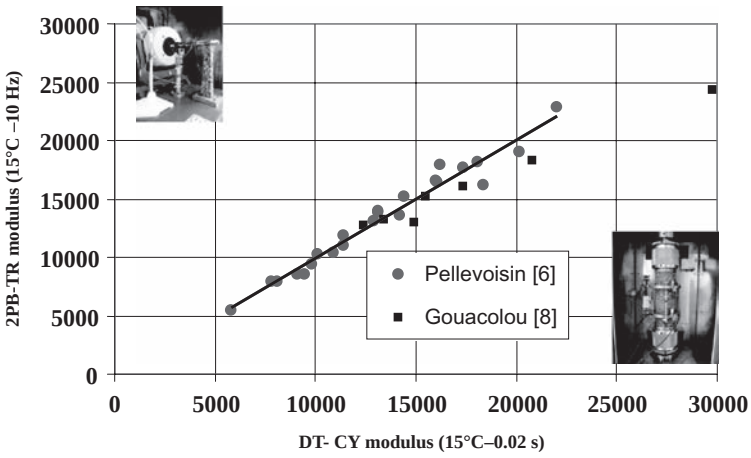

Figure 4. Experimental correlations already published between the direct tension modulus (15°C–0.02 s) and the bending modulus on trapezoidal samples (15°C–10 Hz).

a theoretical way (Di Benedetto 2005) and, on figure 4, we recall the first experimental data published, completed by other values from a similar study (Gouacolou 2000).

Numerous studies have also been carried out on diametral compression modulus measurement testing, particularly in France where it was relatively unknown (Carbonneau 2005), (Esh 2006). On figure 5, we recall the correlation proposed in 2005 from results drawn from 23 formulae (Carbonneau 2005). This correlation is established between the value determined by pulse loading under diametral compression at 15°C–124 ms and that measured under bending on trapezoidal specimens at 15°C–10 Hz. The first results were completed with data obtained within Colas during the 20 complementary formulation studies. The bending measurements on trapezoidal samples were all carried out at the Colas Group Scientific and Technical Campus, the diametral compression measurement results are from laboratories of our equipped subsidiaries, with some tests carried out on site samples.

Integration of all these experimental results to establish a new correlation does not significantly improve accuracy of the value which can be estimated for the complex bending modulus on trapezoidal specimens. This confirms the strength of the first correlation established, that we will keep for future reference. By applying this relationship to all 43 experimental results presented in figure 5, we can observe variations between estimated and measured values which always remain below the limit of reproducibility of the 2740 complex modulus test, except for two mixtures.

Over the last 3 years, we have also carried out several four-point bending modulus measurements on about 10 mixtures in order to complete this work. Parallel to this, we determined the direct tension modulus of these mixtures using the DT-CY, according to appendix E. In both cases the specimens were extracted from 600 × 400 plates and the results are always the average determined from assessing the 4 specimens. This data is shown in graph form in figure 6. For the direct tension modulus, this is the value extrapolated at 15°C–0.02 s and for four-point bending, we have selected the value at 20°C–8 Hz.

These results only constitute an initial rough correlation but already span a fairly large field in the modulus range. The various relationships drawn from the experimental correlations presented lead to the following relationships:

$$\begin{cases} E_{2PB\text{-}TR(15°C\text{–}10\,Hz)} = 0.989 \times E_{DTCY(15°C+0.02\,s)} + 15 \\ E_{2PB\text{-}TR(15°C\text{–}10\,Hz)} = 0.759 \times E_{IT\text{-}CY(15°C+124\,ms)} + 3680 \\ E_{DTCY(15°C+0.02\,s)} = 1.44 \times E_{4PB\text{-}PR(20°C\,8\,Hz)} + 2160 \end{cases}$$

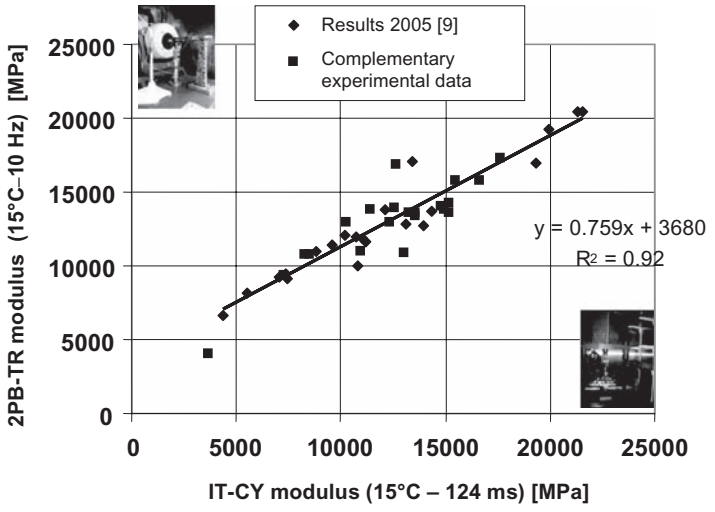

Figure 5. Correlation between the diametral compression modulus 15°C 124 ms and the bending modulus on trapezoidal specimens 15°C 10 Hz.

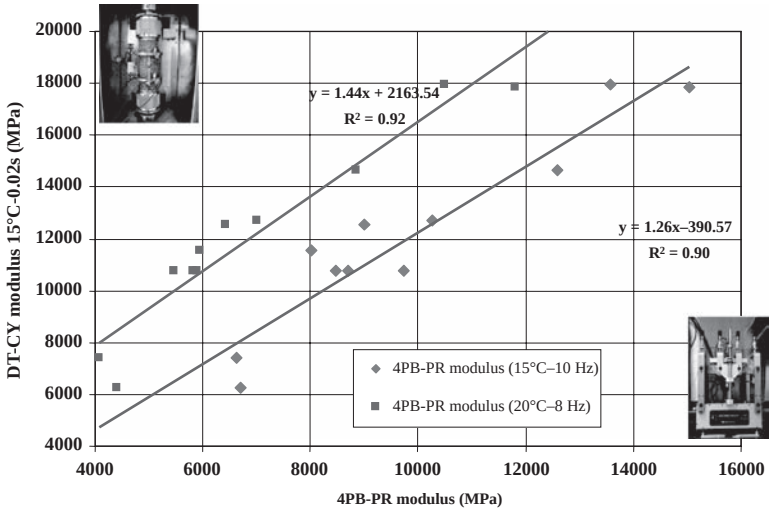

Figure 6. Experimental correlation between four-point bending and direct tension test results.

Unfortunately this set remains incomplete because, to this day, we do not have enough data for the tension compression test on cylindrical specimens. For the diametral compression test, the correlation has been established for a test temperature of 15°C, although the temperature finally selected for the European standard is 20°C. We have, however, applied it to the experimental data presented in table 1, for which we also possessed measurements at 15°C.

Starting from the experimental value measured in four-point bending for the two mixtures initially tested (data drawn from table 1) and applying the previous relationships, we arrive at estimated values for the modulus, given in table 3.

The estimation obtained in this way is very satisfactory in the case of the EB 10 wearing 35/50. In the case of the EB 14 subbase it remains, however, fairly approximate. The reproducibility of the modulus test must be retained, however, (2740 MPa for an average value of 15200) as well as the differences of compaction of the test bodies recorded in table 1. In the case of the EB 14 subbase, the value of the bending modulus on trapezoidal samples was achieved on specimens with a void content 1.7% greater than that of the characterised specimens under diametral compression. The variation is not so great for the EB 10 roll. 35/50 with, however, void content differences of the same order between tests. If this approach of calculation, attempting to estimate a diametral compression value at 15°C 124 ms from previous relationships is continued, we arrive, respectively, at values of 8887 MPa for the EB 10 roll. and 20146 for the EB 14 subbase. It is possible to recompare the estimated modulus values with the experimental data that we possess (Carbonneau 2009a). The difference between measured value and experimental result is specified in table 4.

The difference between the calculated and measured values is of the same order. In this approach the impact of a variation in compaction on the modulus value has not been taken into account, to free ourselves of this parameter. We are simply comparing a set of experimental values but, taking into account the reproducibility of the test, if we retain that determined for the bending test on a trapezoidal specimen, we still arrive at an initial indication of the modulus level that we can hope for with another test knowing the result.

5 SIMPLE PERFORMANCE TEST

Developing a more fundamental approach to the mix design of bituminous mixtures and the need to possess the modulus characteristic, has also led to a new test appearing in the USA, the Simple Performance Test. We have taken advantage of the testing program campaign already undertaken to complete our results with a measurement achieved on the two selected mixtures, using this test. The tests were performed on the SPT machine developed by IPC, at temperatures of 5, 10, 20 and 30°C, for strain frequencies between 0.1 and 25 Hz. An haversine loading is applied to cylindrical specimens. As the strain was applied without confining pressure, it is very close to that practised in tension compression on cylindrical specimens, DTC-CY appendix D of standard EN 12697-26. Extra plates were manufactured and sent to Nactech, a Colas Group laboratory located in North America possessing this equipment. Cylindrical test bodies with a diameter of 100 mm and thickness of 150 mm were extracted

Table 3. Estimation of the bending modulus from the four-point bending modulus and comparison between calculated values and experimental results.

	4PB-PR modulus 20°C–8 Hz	2PB-TR "estimated" modulus 15°C–10 Hz	2PB-TR modulus 15°C–10 Hz	Difference between calculated and measured
EB10 wearing 35/50	5810	10426	9950	476
EB14 base 10/20	11810	18971	15540	3430

Table 4. Estimation of the diametral compression modulus from the four-point bending modulus and comparison between calculated values and experimental results.

	4PB-PR modulus 20°C–8 Hz	IT-CY "estimated" modulus 15°C–124 ms	IT-CY modulus 15°C–124 ms	Difference between calculated and measured
EB10 wearing 35/50	5810	8887	8548	339
EB14 base 10/20	11810	20146	16663	3486

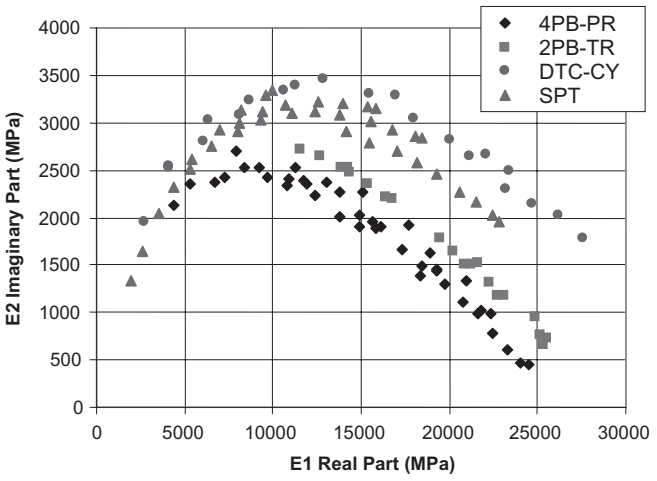

Figure 7. Cole-Cole representation of all the test results obtained on the EB 14 subbase 10/20 (2PB-TR, 4PB-PR, DTC-CY, and SPT).

from them. So specimens were not cored in bodies moulded with a superpave gyratory shear press, and their were not cured 4 hours at 135°C, as is it specified in AASHTO R30. 5 specimens were characterised for each surfacing material. This has allowed us to obtain experimental modulus values at 15°C–10 Hz of 12830 MPa for EB 10 roll. (average void content of 6%) and 17035 MPa for EB 14 Subbase (average void content of 5%). This data is slightly too high for the EB 10 roll. 35/50 and fairly close to the determined values for the EB14 subbase, whether under tension compression or direct tension. For information only, the experimental results achieved with the Simple Performance Test on the EB 14 Subbase 10/20 have been indicated in the Cole-Cole plane in figure 7.

6 CONCLUSION

This study clearly demonstrates the differences in results that can be achieved by applying conditions currently imposed by European standardisation. In the fundamental approach promoted in Europe, it is imperative to specify the method and test conditions practised with the modulus category attributed to the product.

In the same way, specimen manufacturing conditions and void contents are essential. The correlations proposed, even if they are not perfect, are a simple means of estimating the performance of a mixture through another modulus test.

ACKNOWLEDGEMENTS

The authors would like to thank J.P. Fort (NACTECH) and B. Tessier (SINTRA) for their contribution through SPT and tension compression testing.

REFERENCES

Carbonneau X. & Legal Y. 2009a, "*The diametral compression modulus measurement test*" submitted to RILEM.

Carbonneau X. & Perriot A. 2009b, "*Influence of anisotropy of specimens on results of indirect tensile stiffness modulus test*", submitted to RMPD.

Carbonneau X., Yvinec B., Legal Y. & Poirier J.E. 2005, "M*esure du module en compression diamétrale*", Revue Générale des routes et aérodromes, N° 836.

Di Benedetto H. & Corte J.F. 2005, "*Matériaux routiers bitumineux Tome 2, constitution et propriétés thermomécaniques des mélanges*", p 100. Edition Lavoisier.
Doubbaneh E. 1995, "*Comportement mécanique des enrobes bitumineux des petites aux grandes deformations*", doctoral thesis, INSA Lyon.
Esh M., Pouteau B., Yotte S. & Breysse D. 2006, "*Détermination du module des enrobés bitumineux par l'essai de compression diamétrale*" RGRA N° 853.
Francken L. 1996, "*Rilem Interlaboratory test on bituminous mixes in repeat loading—teaching and recommendations*", Eurasphalt Eurobitume congress.
Gouacolou H. & Mazé M. 2000, "*Enrobés à haut module élastique*", Eurasphalt Eurobitume Barcelone, p 269–275.
Hauser E. 2007, European 4pt bending workshop, TU Delft 8–9 March 2007.
Pellevoisin Ph. & Bense P. 1997, "*Loi de corrélation entre les différents procédés de mesure du module sur enrobés bitumineux*", Mechanical Test for Bituminous Materials, p 225–230, Lyon.

Advanced Testing and Characterization of Bituminous Materials – Loizos, Partl, Scarpas & Al-Qadi (eds)
© 2009 Taylor & Francis Group, London, ISBN 978-0-415-55854-9

The influence of the specimen shape on the results of the uniaxial tensile test

C. Weise & A. Blasl
Chair of Pavement Engineering, Dresden University of Technology, Germany

ABSTRACT: Material parameters can be determined using the uniaxial tensile test. The test results, e.g. the Young's modulus and the fatigue function can be used in the pavement design process. Therefore it is necessary to be aware of the influence of the specimen shape and size on the test results. The results of 3D FEM simulations and of laboratory tests (force controlled tests with a sinusoidal wave) are presented in this paper. Different sources of error are described and recommendations for performing uniaxial tensile tests are given.

1 INTRODUCTION

The test arrangement for the uniaxial tensile test can be used for different investigations, e.g. the determination of the elastic modulus (Young's modulus), fatigue behaviour or cryogenic stresses. Hence, it is important that the influence of the specimen shape and size is well known. Otherwise, inaccurate material parameters form the basis of the pavement design process. This may lead to an incorrect layer thickness.

A number of researchers have used uniaxial fatigue tests on cylindrical specimens as an alternative to flexural tests. Weissman et al. (Weissman, 1999) determined that the specimen height to diameter or width ratio should be considered. Hence, the stress and strain in the middle of a (cylindrical) specimen are as close as possible to a uniform distribution. Weissman et al. (Weissman, 1999) also explained that a larger height to diameter ratio is required for tensile tests to achieve the same accuracy (e.g. in calculating Young's modulus) as in compression tests because the steel end platens of the testing equipment are glued to the specimen.

Soltani et al. (Soltani, 2005) and Lundström et al. (Lundström, 2003) have described the use of cylindrical specimen and an on-sample measuring system. The uniformity of the applied strain and stress fields in the middle of the specimen is an essential advantage for the measuring system.

In Germany cylindrical specimens as well as an on-sample measuring system were previously not used for uniaxial tensile tests. Therefore it is necessary to demonstrate the differences and potential sources of error.

2 3D FEM SIMULATIONS OF THE STATE OF STRESS

The state of stress depends on the shape and size of the specimen. Until recently, specimens with a square cross-section and a length of 160 mm have been used in Germany. The width depends on the maximum aggregate size of the asphalt mix. Figure 1 shows the progression of the von Mises stress for specimens with square or circular cross-sections and a length of 160 mm. The von Mises stress σ_v can be calculated using Equation 1.

$$\sigma_V = \sqrt{\sigma_x^2 + \sigma_y^2 + \sigma_z^2 - \sigma_x\sigma_y - \sigma_x\sigma_z - \sigma_y\sigma_z + 3 \cdot (\tau_{xy}^2 + \tau_{xz}^2 + \tau_{yz}^2)} \quad (1)$$

where σ_i = principal stresses; τ_{ij} = shear stresses.

In the case of uniaxial stress or simple tension, $\sigma_x \neq 0$, $\sigma_y = \sigma_z = 0$, the von Mises criterion reduces to $\sigma_x = \sigma_V$. This relation does not hold for the performed uniaxial tensile tests because the specimen had to be glued to two adapters to apply the sinusoidal tensile force. Because of this, the transverse strain was interfered with in the area of the end planes. By using the von Mises stress it was possible to detect areas of maximum loading in the specimen.

The state of the von Mises stress in the specimens was calculated using the FE program ANSYS. Figure 1 shows that the highest stress was located in the four edges of the end plane of the square specimen. The state of stress in the specimen with the circular cross-section was more homogeneous, both in the end planes and also in the whole specimen.

Figure 3 gives the progressions of the state of stress in the three areas defined in Figure 2 for half of the specimens. FEM simulations were performed for specimens with different cross-sections. For the simulations, a load of 1 MPa was applied to the specimen. Table 1 gives a summary of the specimen dimensions chosen.

It is obvious that the stresses in the edge and the margin area of the end planes are nearly three times the applied reference stress of 1 MPa. Only at z ~ 40 mm, the von Mises stress is approximately 1 MPa.

Figure 4 provides evidence that the dimension of the area with a homogeneous and uniaxial stress depends on the shape of the specimen. The dotted lines delimit the area where the von Mises stress differs from the reference stress of 1 MPa by 0.05% at most.

Table 1. Specimen dimensions for the 3D FEM simulations.

Cross-section geometry	Width/Diameter [mm]	Cross-section surface [mm²]	Length [mm]
Circle	50	1963.5	
Circle	56.41	2500	160
Square	50	2500	

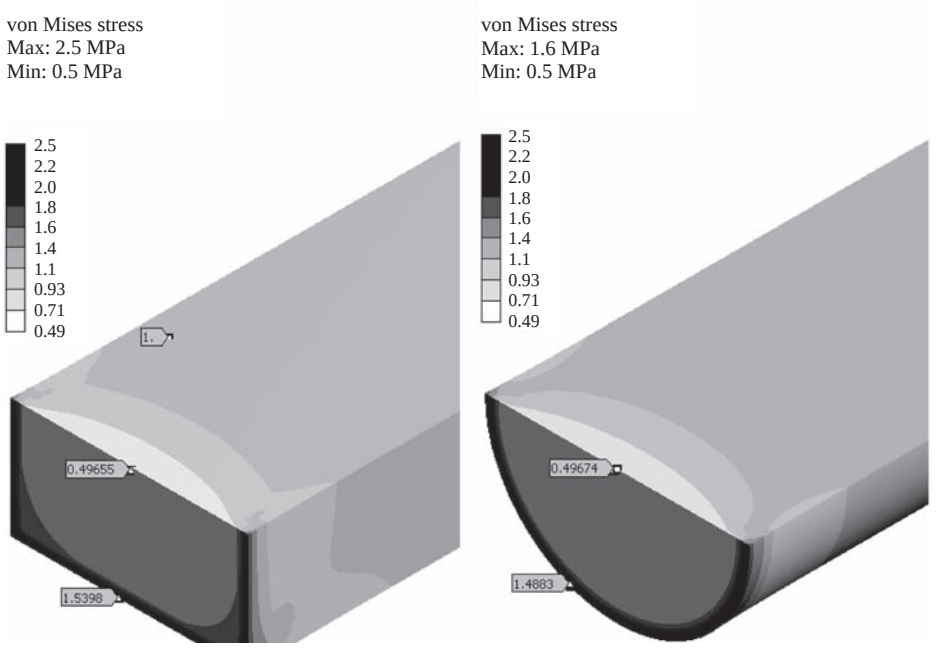

Figure 1. State of stress in specimen with square and circular cross-sections (Blasl, 2008).

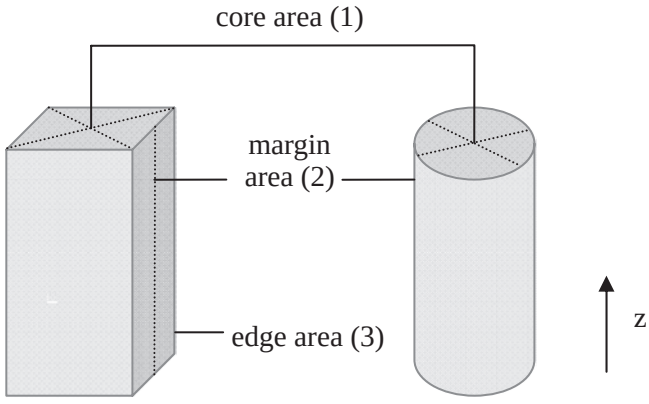

Figure 2. Position of the core, the margin and the edge area (Blasl, 2008).

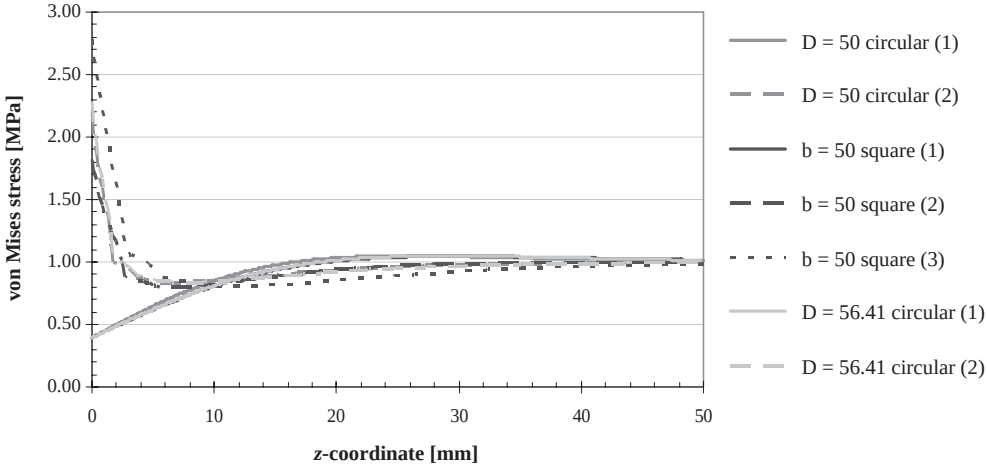

Figure 3. Progressions of the von Mises stress along the coordinate z for specimens with different cross-sections (Blasl, 2008).

It can be concluded from the FEM simulations and the figures that slender specimens with smaller and circular cross section surfaces are most suitable concerning a homogeneous state of stress. It can be derived from the simulations that the deformations within the tests should be measured in the area of the homogeneous and thus uniaxial stress.

3 LABORATORY INVESTIGATIONS

3.1 *Asphalt mixes*

Three different asphalt mixes were used in the laboratory investigations. Table 2 gives the parameters of the asphalt mixes. The mixes were regularly produced in different asphalt mixing plants. The asphalt mix design followed the German Guideline ZTV Asphalt (ZTV Asphalt-StB 2001) for the binder course and the Stone Mastics Asphalt and the ZTVT (ZTVT-StB 1995) for the asphalt base mix, respectively.

3.2 *Specimen geometries*

The investigations comprised two test series. The influence of the specimen geometry on the Young's modulus was determined in test series A. The shape of the cross-section and also the

length of the specimen was varied. In test series B the influence on the fatigue behaviour was determined for specimens with circular and square cross-sections. Table 3 lists all specimen shapes and sizes tested.

3.3 *Sample preparation*

For the uniaxial tensile test, specimen cores were taken from asphalt slabs that were produced using a laboratory roll segment compactor, on the one hand. On the other hand, prismatic specimens were cut out of the asphalt slabs. Afterwards, each specimen was cut to the exact length required. The specimens were ground to achieve coplanar surfaces. The specimens were

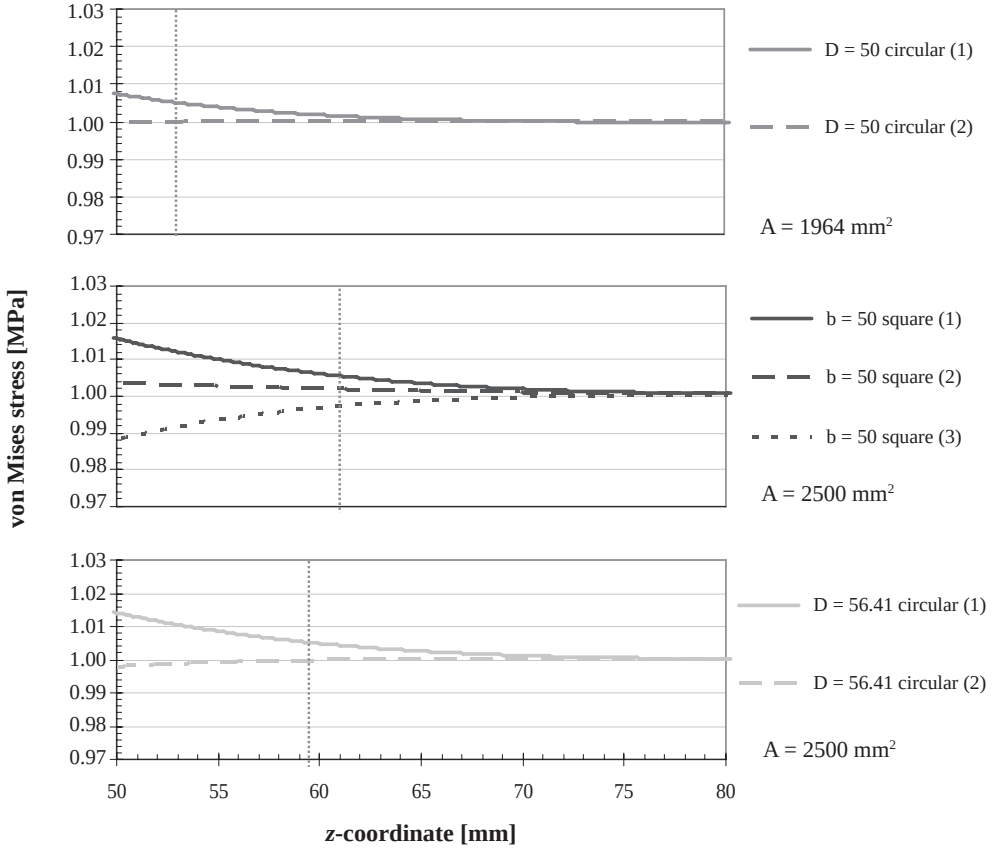

Figure 4. Progressions of the von Mises stress for z = 50 … 80 mm in the core, the margin and the edge area for specimens with different cross-sections.

Table 2. Asphalt mixes.

Mix [–]	Binder [–]	Bitumen content [%]	Max. aggregate size [mm]	Aggregate [–]
Stone Mastics Asphalt—SMA	PmB 45A*	6.5	11	Gabbro
Binder Course Asphalt—ABi	PmB 45A*	4.5	16	Moraine
Asphalt Base—AB	50/70	4.2	32	Crushed gravel

*Different manufacturers.

Table 3. Specimen geometries tested in test series A and B.

Test series	Specimen size width × depth × length [mm]	diameter × length [mm]	Asphalt mix		
			SMA	ABi	AB
A	35 × 35 × 160	35 × 160	✓	✓	
A	50 × 50 × 160	50 × 160	✓	✓	
A	65 × 65 × 160	65 × 160	✓	✓	✓
A	80 × 80 × 160	80 × 160	✓	✓	✓
A	100 × 100 × 160	100 × 160	✓	✓	✓
A	50 × 50 × 100		✓	✓	
A	50 × 50 × 130		✓	✓	
A	50 × 50 × 190		✓	✓	
A	50 × 50 × 220		✓	✓	
A	35 × 85 × 160		✓	✓	
A	85 × 35 × 160		✓	✓	
A	70 × 35 × 160		✓		
A	50 × 35 × 160		✓		
A	65 × 46 × 160		✓		
B	40 × 40 × 160	40 × 160	✓		
B	65 × 65 × 160	65 × 160	✓		

Table 4. Test conditions for test series A and B.

Test series	Asphalt mix	Test temperature [°C]	Loading frequency [Hz]	Lower stress [MPa]	Upper stress [MPa]
A	SMA	5	1, 5, 10	0.106	0.7/0.8/0.9
(Young's	ABi	5	1, 5, 10	0.078	0.7/0.8/0.9
modulus)	AB	5	1, 5, 10	0.058	0.5/0.6/0.7
B (fatigue)	SMA	5	10	0.106	1.0/1.3/1.6

cleaned and dehumidified at room temperature. Finally, the dimensions of each specimen and the bulk density values were checked.

For testing, the specimens were glued to two adapters using synthetic resin glue with a minimum cure time of 24 hours. Before testing, the temperature in the specimen must be consistent throughout. A tempering time of four hours was chosen.

3.4 *Conducted tests*

The uniaxial tensile tests described in this paper were performed at a testing temperature of +5°C in a temperature chamber. The specimens were loaded with their longitudinal axis aligned with the measuring device. Sinusoidal forces without cycling through zero were applied to the specimen. The vertical deformations of the specimen during the test were measured using LVDTs.

The temperature-induced stresses were defined as the lower stress levels for the uniaxial tensile tests. Loading frequencies of 10, 5 and 1 Hz were chosen for the determination of Young's modulus (series A). The fatigue tests (series B) were carried out at a loading frequency of 10 Hz. Table 4 summarises the stress conditions for both test series.

Multistage tests were conducted to determine Young's modulus. Each specimen was successively loaded with the three different stresses at the three loading frequencies. The number of cycles for the multistage tests was chosen depending on the loading frequency.

For 10 Hz, 1,000 load cycles were applied for each upper stress level. For 5 Hz, 500 and for 1 Hz only 100 load cycles were recorded. The sampling rate of 50 measured values per load cycle was constant for all three loading frequencies.

Figure 5 shows the testing device for uniaxial tensile tests. The vertical deformations are measured using two LVDTs. The adapters to which the specimen was glued were screwed on the leverage of the testing machine.

3.5 *Data interpretation*

Written examination interpreted the data using different tools to realise the sinusoidal regression for the vertical deformation and the applied force for each load cycle. Hence, it was possible to determine the progression of the Young's modulus value concerning the chosen test conditions (stress level and loading frequency) or during the whole fatigue test.

The number of load cycles until macro-cracking was determined using the method developed by Rowe (1993).

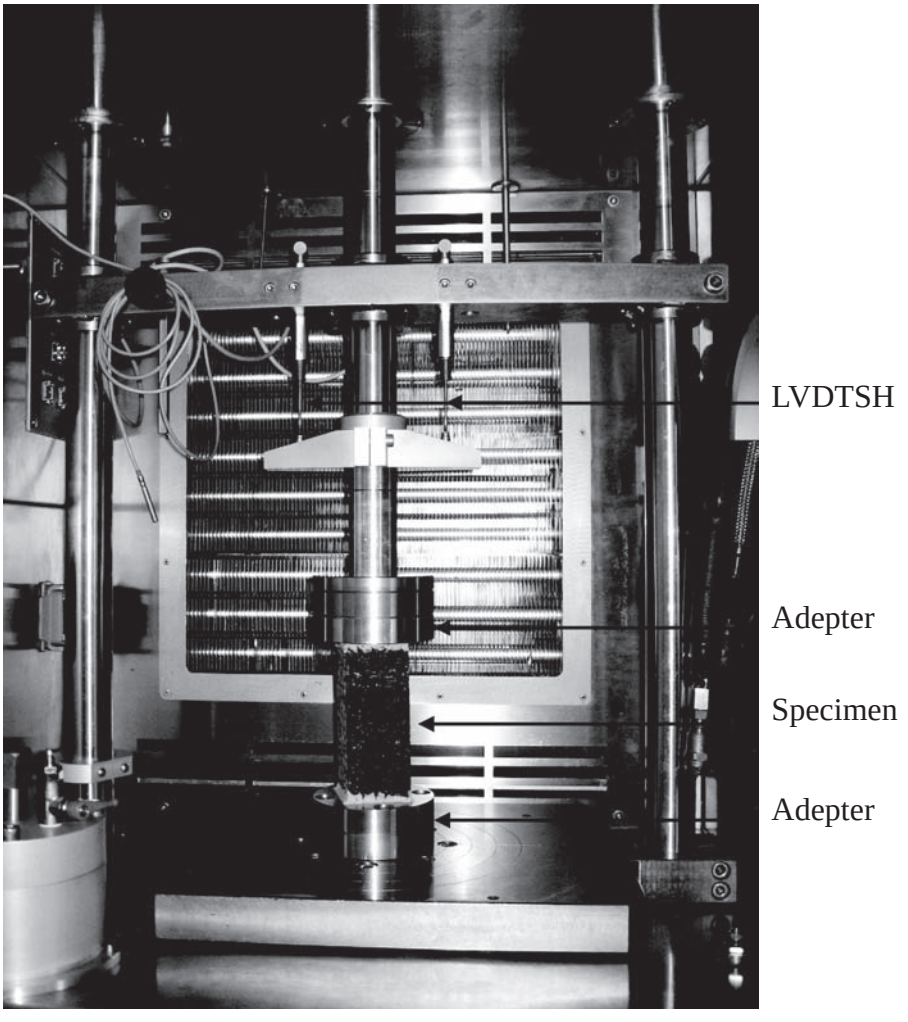

Figure 5. Testing device for uniaxial tensile tests.

4 TEST RESULTS AND DISCUSSION

The results of test series A indicated a clear dependence of the Young's modulus value on the cross-section and length of a specimen. Figure 6 shows the relation between the Young's modulus value and the cross-section area for the binder course asphalt. The lower Young's modulus values for specimens with larger cross-section areas are explained by the failure caused by the deformation of the adapters (see chapter 5).

Figure 7 shows the fatigue functions of the Stone Mastics Asphalt based on specimens with different cross-section areas and shapes. A steep slope was obtained for

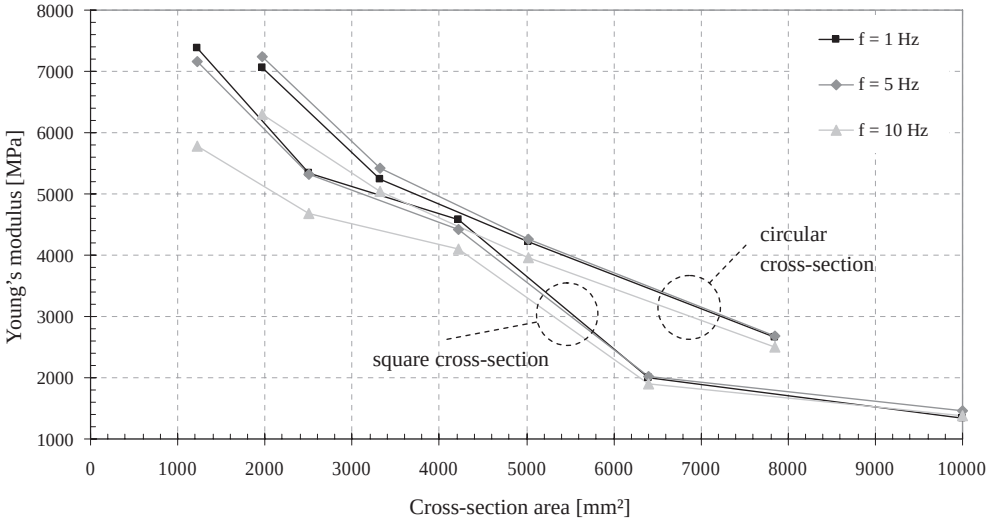

Figure 6. Relation between the Young's modulus value and cross-section area for the binder course asphalt (Blasl, 2008).

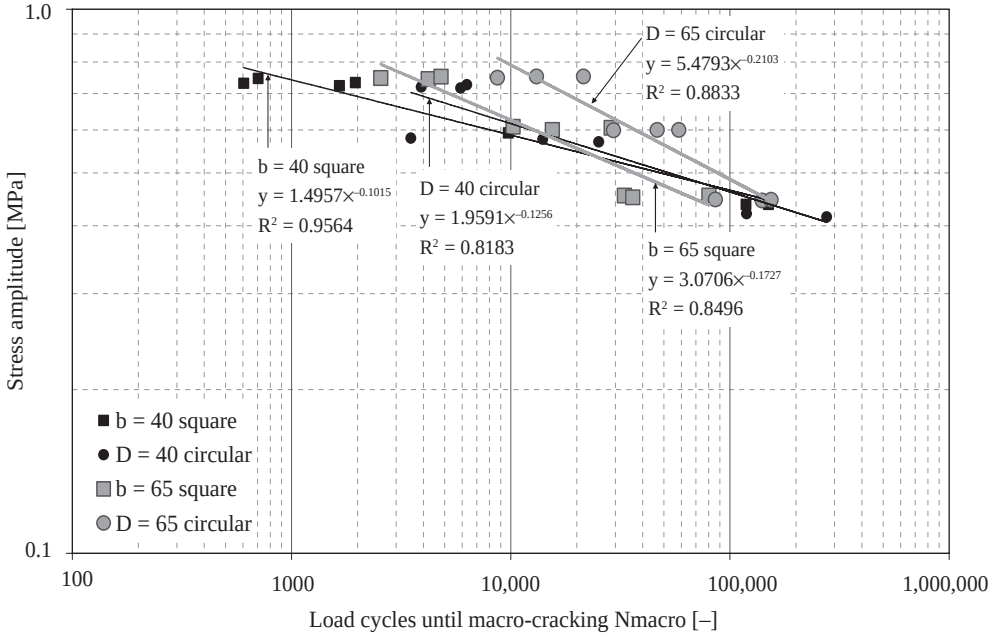

Figure 7. Comparison of fatigue functions for Stone Mastics Asphalt (Blasl, 2008).

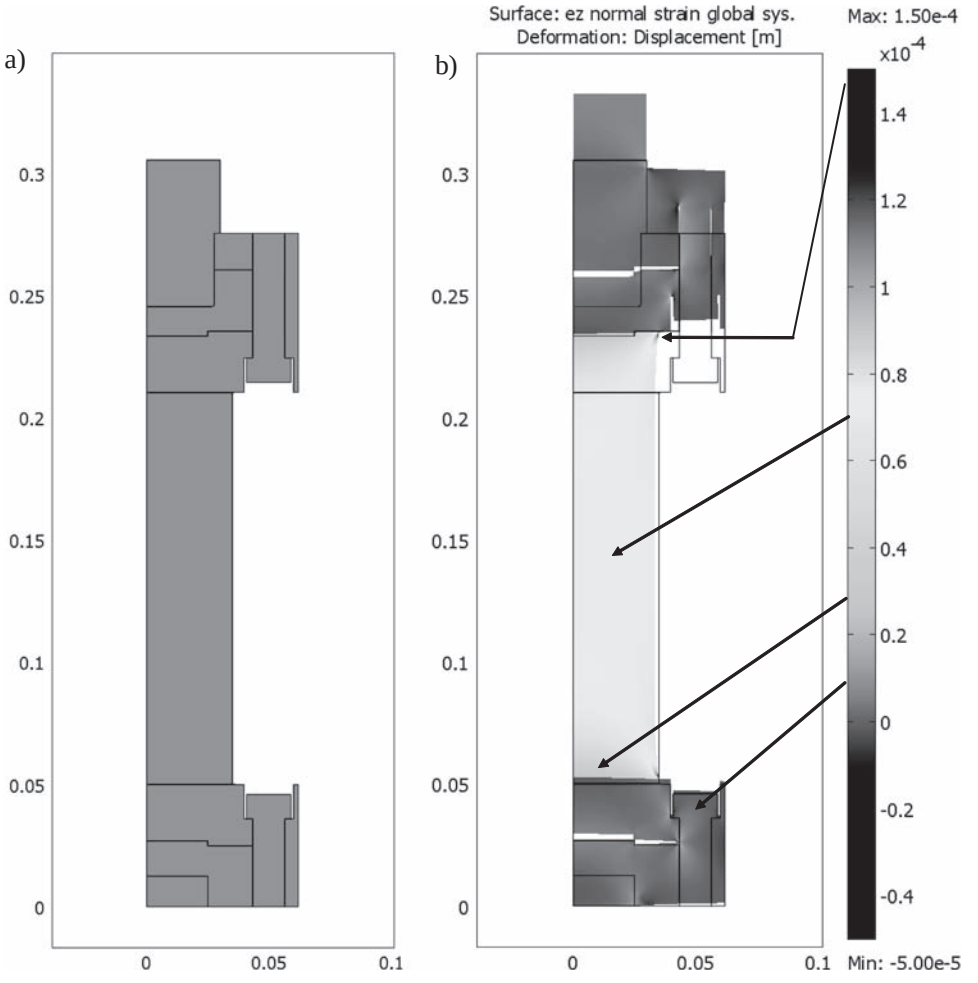

Figure 8. a) Rotationally symmetrical model of the testing device and the specimen; b) Deformation of the testing device and the specimen (inflation rate: 2000) (Blasl, 2008).

the fatigue functions of the larger specimens (circular and square). Additionally, the number of load cycles until macro-cracking was greater for circular specimens than for square ones.

5 ANALYSIS OF ERROR SOURCES

5.1 *Deformation of adapters*

Various factors influenced the results of the uniaxial tensile test. The deformation of the adapters used lead to a smaller Young's modulus value because of the arrangement of the LVDTs. The LVDTs measure the deformation of the specimen as well as the deformation of the adapters and a part of the leverage of the testing machine.

Figure 8 shows the model and the calculated deformation at an inflation rate of 2,000. The simulations were carried out using COMSOL. Significant deformations and also a gap between the different plates/adapters of the testing device can be obtained. This error source can be eliminated with a deformation measuring system that measured the deformation directly at the specimen.

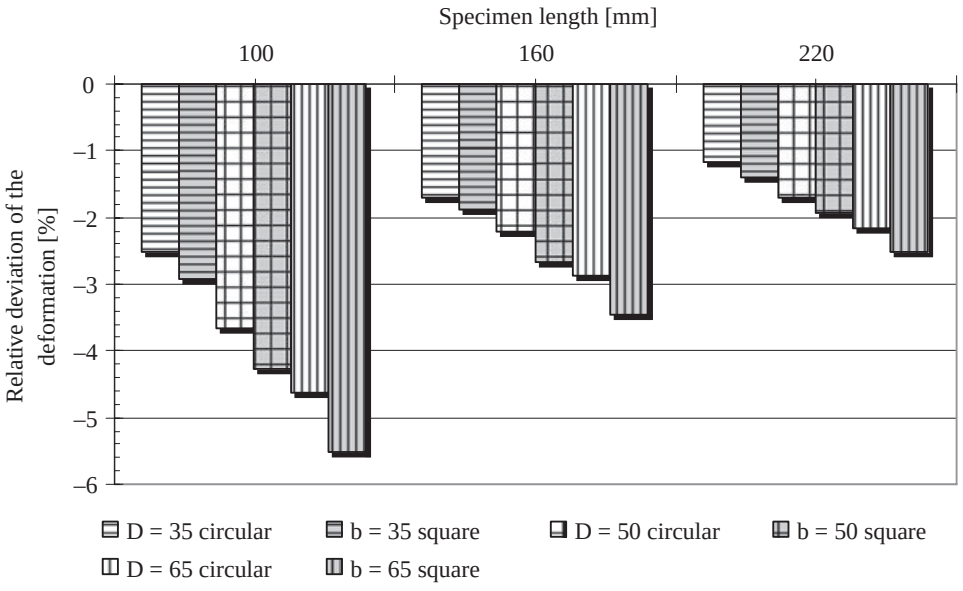

Figure 9. Relative deviation of the deformation determined using 3D FEM simulation (inhomogeneous state of stress) and Hooke (homogeneous state of stress) for different specimen shapes and lengths (Blasl, 2008).

5.2 *Effects of the inhomogeneous state of stress*

Because the specimen was glued to the two adapters the state of stress in the specimen was inhomogeneous. This lead to a lower deformation value when compared with the deformations that can be calculated using Hooke's law and expecting a homogeneous state of stress. Figure 9 shows the relative deviation of the deformation for different specimen shapes and lengths. The smallest relative deviation can be obtained for slender specimens with circular cross-sections. To avoid this error, the vertical deformation should be measured in the area with the homogeneous state of stress using a on-sample measuring system.

5.3 *Effects of oblique specimens*

Oblique specimens also cause an inhomogeneous state of stress during the installation of the specimen in the testing device. Due to the large stresses applied during installation, the specimen was damaged. The Young's modulus values and also the load cycles obtained until macro-cracking in a fatigue test were incorrect. Therefore it is necessary to check each specimen for coplanar surfaces.

6 CONCLUSIONS AND RECOMMENDATIONS

Several factors influenced the results of the uniaxial tensile tests. The state of stress was not homogeneous because the specimen was glued to two adapters to apply the tensile forces.

To avoid errors that occur during the uniaxial tensile tests, the vertical deformation should be measured directly on the specimen. As a result, the potential deformation of the adapters did not distort the test results. Additionally, the measuring system should be placed in the area of the homogeneous state of stress. The differences in the fatigue functions of the investigated specimen shapes can be explained by the state of stress in the specimen.

The differences in the relative deviation of the deformation between specimens with circular and square cross sections highlight that the height to diameter ratio should be as

large a possible considering the maximum aggregate size of the asphalt mixture. A height to diameter or width ratio of at least 3 is recommended. Weissman et al. (Weissman, 1999) suggested to use a specimen diameter of at least 125 mm and a height of 350 mm for an asphalt mixture with a maximum aggregate size of 19 mm. This is a height to diameter ratio of 2.8.

More research is necessary to verify the results of the FEM simulations. Additionally, the results of the uniaxial tensile test should be compared with the results of other test methods using a on-sample measuring system.

ACKNOWLEDGEMENT

The authors thank the German Research Foundation (DFG) for funding the research project.

REFERENCES

Ansys. Canonsburg. USA.

Blasl, A. 2008. Influence of the geometry of the specimen on the test result of the uniaxial tensile test (German: Einfluss der Probekörpergeometrie auf die Versuchsergebnisse im Einaxialen Zugschwellversuch). Diploma Thesis. Dresden. Germany.

Comsol, Multiphysics GmbH. Göttingen. Germany.

Lundstörm, R., Isacsson, U. & Ekblad, J. 2003. Investigation of Stiffness and Fatigue Properties of Asphalt Mixtures. Journal of Materials Science. 38: 4941–4949

Rowe, G. 1993. Performance of Asphalt Mixtures in the trapezoidal Fatigue Test. Proceedings of the Association of Asphalt Paving Technologists 62: 344–384.

Soltani, A. & Anderson, D.A. 2005. New Test Protocol to Measure Fatigue Damage in Asphalt Mixtures. Road Materials and Pavement Design Vol. 6, No. 4/200: 485–514.

Weissman, S.L., Harvey, J., Sackman, J.L. & Long, F. 1999. Selection of Laboratory Test Specimen Dimension for Permanent Deformation of Asphalt Concrete Pavements, Transportation Research Record No. 1681: 113–120.

ZTV Asphalt-StB 01. 2001. German Guideline for the creation of asphalt layers. FGSV. Köln. Germany.

ZTVT-StB 95. 1995. German Guideline for the creation of road bases. FGSV, Köln, Germany.

Advanced Testing and Characterization of Bituminous Materials –
Loizos, Partl, Scarpas & Al-Qadi (eds)
© 2009 Taylor & Francis Group, London, ISBN 978-0-415-55854-9

Experience with triaxial loading systems for the testing of road construction materials

P. Hyzl, D. Stehlik & M. Varaus
Brno University of Technology, Faculty of Civil Engineering, Department of Roads, Brno, Czech Republic

P. Zdralek
TPA ČR, s.r.o., Czech Republic

ABSTRACT: At the moment there are two cyclic triaxial loading systems for the testing of road construction materials under operation in the Czech Republic. Both equipments were constructed in the Road Laboratory of the Brno University of Technology, with in the frame of several research projects. The first one system is used for the evaluation of the susceptibility of asphalt mixtures to creation of permanent deformation according to the EN 12697-25. The second one is used for deriving of material characteristics of unbound and hydraulically bound base course road materials. The article evaluates and summarizes the experience with the above-mentioned testing equipments, it concentrates in detail on the influence of the applied stresses and frequencies on the test results. In the part devoted to the base course materials the evaluation is aimed at the measurement of design E-moduli and permanent deformations of recycled and secondary used materials from the building and industrial production and their use for the lower base courses. In the part dealing with the asphalt mixtures there are presented the arguments for the changes in the setup of testing conditions (particularly applied stresses) in EN 13108-20 Type testing.

1 INTRODUCTION

In addition to using the empirical design approach, the introduction of the new European standards for asphalt mixtures enables also to use the functional design approach. The functional tests should simulate the way of loading of compacted asphalt mixtures in the real road structure. The typical example of these functional tests is the triaxial test with cyclic loading according to EN 12697-25 for asphalt mixtures and according to EN 13286-7 for unbounded a bound base course materials. The principle of this test is the evaluation of the dynamical creep of test specimens by the three-axle-compression, where the cylindrical specimen is exposed to side-pressure, simulating the confinement of the real road, and simultaneously to the vertical cyclic loading, simulating loading by the traffic. The triaxial test according to EN 12697-25 is aimed at the testing of resistance of asphalt mixtures against creation the permanent deformation. The triaxial test according to EN 13286-7 is aimed at the testing of E-moduli and permanent deformation of unbound based materials.

2 TESTING EQUIPMENTS ACCORDING TO EN 12697-25 AND THE TESTS CARRIED OUT

At the moment there are only few states in Europe, in which the triaxial testing equipment is introduced. All equipments except for one use the hydraulic system with haversinusoidal loading. Only the triaxial test used at the Brno University of Technology uses as the only one the servopneumatic system with the cyclic time delayed loading (both loading systems and the triaxial chamber—see Figure 1; the complete triaxial testing device of the Brno University of Technology—see Figure 2). During the test the specimen is exposed to the

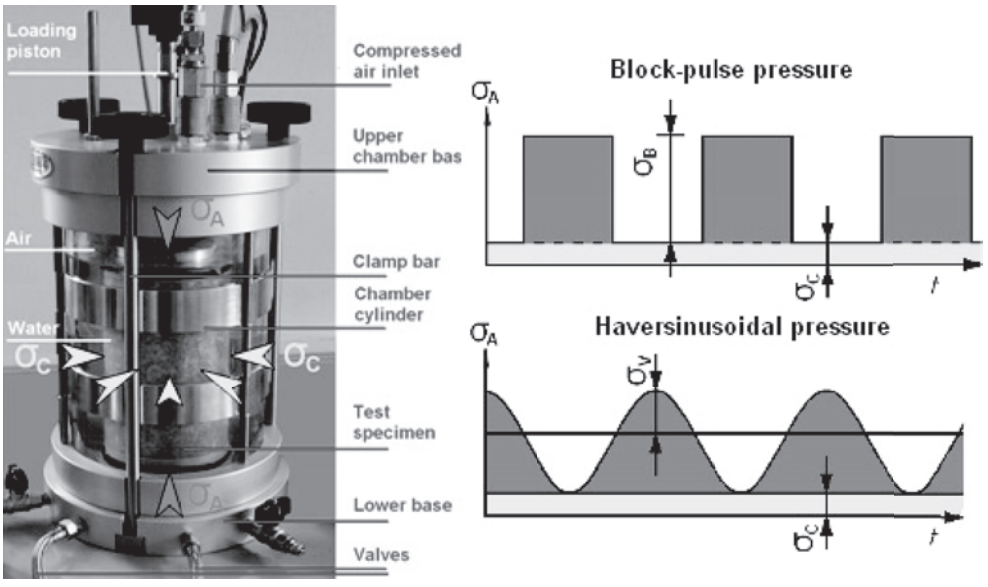

Figure 1. Detail of the triaxial chamber and illustration of the two possible ways of loading.

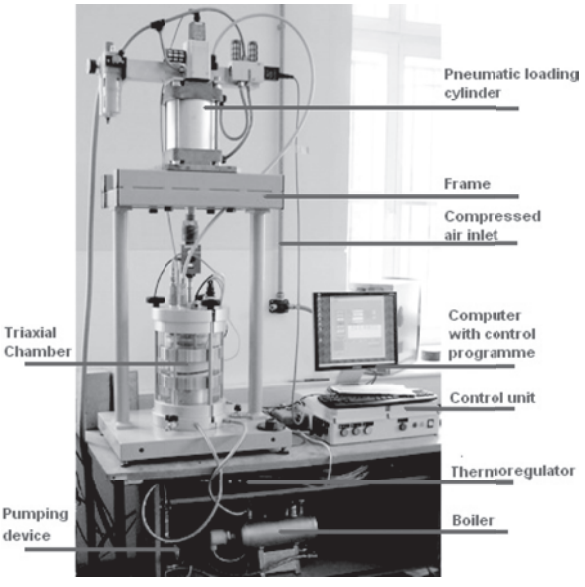

Figure 2. Complete triaxial testing device—Brno University of Technology.

constant loading cell confining pressure σ_C and axial cyclic pressure $\sigma_A(t)$—pulses with time delay and the pulse height $\sigma_B(t)$. The height of the test specimen is measured continuously and then the permanent deformation is defined as the deformation caused by the cumulative axial pressure after specified number of loading cycles. The boundary conditions for this test type are stated in the Table 1.

As the above described testing equipment is the only one in the Czech Republic, an effort was made to gain the first experience about this new way of rutting resistance measurement after its construction, namely to find out the basic problems with testing and evaluation. Then, after collection of a greater number of data, it is important to design the limiting

Table 1. Test conditions for the pneumatic loading system.

	Axial	pulses with time delay	Pulse height σ_B	100–750 kPa		
Loading	confining	constant	Pressure in the chamber σ_C	10–250 kPa	Frequency	1 s/1 s
Dimensions of test specimen		diameter 100 mm height 50 to 200 mm	Number of cycles	min. 10 000	Test temperature	25°C–70°C

Table 2. Matrix of the loading combinations.

Confining pressure (kPa)	Axial pressure (kPa)	Time loading/ unloading (ms)	Number of cycles
10	300		
10	450		
10	600		
50	300		
50	450		
50	600	1000/1000	10 000
100	300		
100	450		
100	600		
150	300		
150	450		
150	600		

Table 3. Asphalt mixture composition.

Asphalt mixture components	Aggregate skeleton fractions	Designation of the fraction	Name of the quarry	Content [%] in the asphalt mixture
Aggregate	Fraction 1	0/4	Štěpánov	10,4%
	Fraction 2	0/4	Jakubčovice	32,8%
	Fraction 3	4/8	Jakubčovice	19,8%
	Fraction 4	8/11	Jakubčovice	24,5%
	Filler	Lime stone	Měrotín	6,6%
Bitumen	Paving grade bit.	70/100		5,9%

parameters into the national annex of the standard CSN EN 13108-1 Asphalt concrete—functional approach, which was issued in the Czech Republic in 2008.

For this purpose the experimental measurements were carried out with the use of various combinations of the axial and confining loading cell pressures to investigate the influence of these pressures on the test results. The applied pressures, loading time/unloading and number of cycles are presented in the table 2. Another purpose for this research was to find out the influence of the pressure levels specified in the standard EN 13108-20 Type testing, chapter D.2.2 and their changes in the results.

2.1 *Composition of the tested asphalt mixtures*

For testing the asphalt mixtures ACO11-asphalt mixture was chosen and sampled at the mixing plant. This low-traffic asphalt mixture was tested because of its expected worse resistance against the creation of permanent deformation and thus more transparent results. From this mixture the test specimens were prepared according to the EN 12697-30 by the impact compactor (2×50 blows), which were afterwards trimmed on the height of 60 mm before testing.

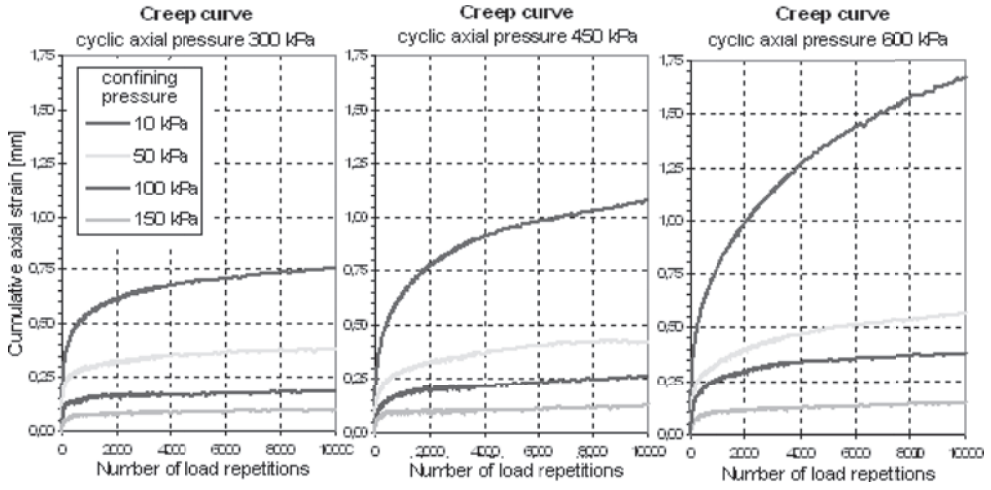

Figure 3. Permanent deformation diagrams.

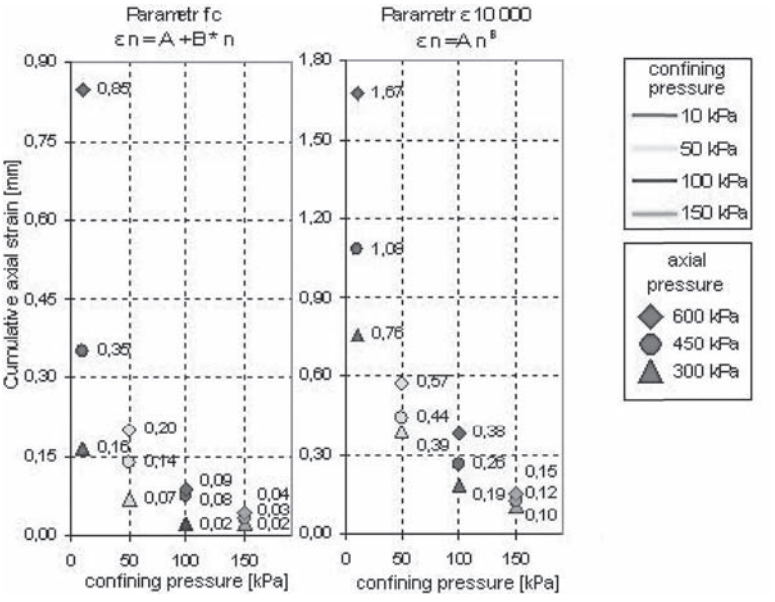

Figure 4. Dependence of permanent deformations on applied pressures, interval of evaluation 2 500 to 10 000 cycles.

2.2 *Measurement results*

It is possible to see very clearly from the results of the experimental measurements with various confining and axial loading pressures the influence off applied pressures on the testing results (figure 3, 4). The results correspond to the applied pressures. The greater the axial pressure is, the greater is the permanent deformation. The achieved results show, that at the confining pressure of 150 kPa demanded by the standard, very low permanent deformation were achieved even at high axial pressure of 600 kPa. The dependence of the deformation on the axial pressure is at high pressures rather linear, but the dependence on the confining pressure is approximately exponential. All results in the following diagrams represent the average of at least 3 test specimens in each condition.

Figure 5. Cyclic triaxial equipment by EN 13286-7 at TU Brno and destroyed testing specimens.

Table 4. Technical parameters of testing.

	Axial	Pulses with time delay	Pressure σ_A–σ_C	20–300 kPa		
Loading	Confining	Constant	Pressure in the chamber σ_C	20–150 kPa	Frequency	1 s/1 s
Dimensions of test specimen		diameter 100 mm height 200 mm	Number of conditioning cycles	20 000	Test temperature	20°C
			Number of loading cycles	29		

3 TESTING EQUIPMENT ACCORDING TO EN 13286-7

In the triaxial testing equipment according to the standard EN 13286-7 it is possible to carry out three types of tests: first, the measurement of elastic deformation, second, the measurement of plastic deformation and third, the multilevel test. The first two types can be operated at variable confining pressure (method A) or at the constant confining pressure (method B). The multilevel test is running only at constant confining pressure.

At the beginning of the year 2008 there were carried out as the first the comparative tests of the commonly used unbound base course materials of the categories G_A and G_C with secondary materials from the aggregate production and recycled demolition products of similar properties (grading, amount of fines). The testing equipment, on which the tests were carried out is in the following figure 5.

3.1 *Tested materials*

In case of the use of dump materials there were chosen 19 samples from quarries with the highest number of secondary waste. These materials were classified according to the particular tests. After the classification the best materials were used for some types of unbound base course mixtures and tested with further functional tests. The same classification procedure was employed for crushed materials from demolitions.

These materials were tested with the method B (constant confining pressure) at low stress levels, as these materials were intended to be used into the unbound base courses or upper part of the embankments. The measurements were carried out on compacted cylindrical specimens Ø100 mm and 200 mm height. As the granular mixtures with low amount of fines can cause difficulties at the stage of specimen preparation, the mostly used compaction method was the static or vibration method with the loading of 400 kg/cm^2.

4 CONCLUSIONS FOR THE TESTING ACCORDING TO EN 12697-25

4.1 *Influence of the confinement pressure*

In the laboratory conditions, neither any of the testing methods, nor the triaxial test according to the EN 12697-25 can cover the whole spectra of variable parameters and their combinations (time and magnitude of loading, way of loading, temperatures), which influences the creation of permanent deformations in the real pavement.

The functional testing with the triaxial test tries to simulate the real conditions. But even if there is the pressure acting from all sides onto the test specimen, it is actually only two-axial test ($\sigma_X = \sigma_Y \neq \sigma_Z$), where the σ_X and σ_Y are confining pressures of the same magnitude acting in the horizontal direction. In the real pavement the confining side pressures in the traffic direction and perpendicularly to the traffic direction are different ($\sigma_X \neq \sigma_Y \neq \sigma_Z$). The action of the stresses in the horizontal direction in the real pavement represents the figure 6. On the top of it there is a time delay between the axial and confining pressures, simulation of which the triaxial equipment is not able to provide. The demanded confining pressure of 150 kPa by the above-mentioned standard seems to be too high as we can see from the results in the figure 3 and 4, where the differences between the deformations at the axial pressures of 300, 450 or 600 kPa are very low.

4.2 *Testing conditions according to EN 12697-25*

EN 12697-25 enables to carry out the triaxial test in two basic ways: either with haversinusoidal axial loading or with cyclic pulses with time delay. Both methods differ not only in the shape of the loading curve, but also in the max. axial loading pressures, where according to the EN 13108-20 Type testing, there are the same confining pressures $\sigma_C = 150$ kPa for both methods, however there are different max. axial pressures. For haversinusoidal loading the max. axial pressure is 600 kPa, whereas for the block cyclic loading the maximal axial pressure is only 300 kPa. Another difference between these two variants of the triaxial test is the frequency. For the haversinusoidal loading the frequency is 3 Hz, i.e. 10 000 loading cycles last 55 minutes, whereas for the cyclic loading with time delay the frequency is 1 s/1 s = 0,5 Hz and the whole duration of the test takes 5½ hours.

4.3 *Expression of the results and evaluation*

In EN 12697-25 we can find the description of parameters, which characterize the resistance against the creation of the permanent deformation. The standard states two different ways of evaluation—either linear ($\varepsilon_n = B * n + A$, $fc = B * 10^4$) or exponential ($\varepsilon_n = A * n^B$). The linear

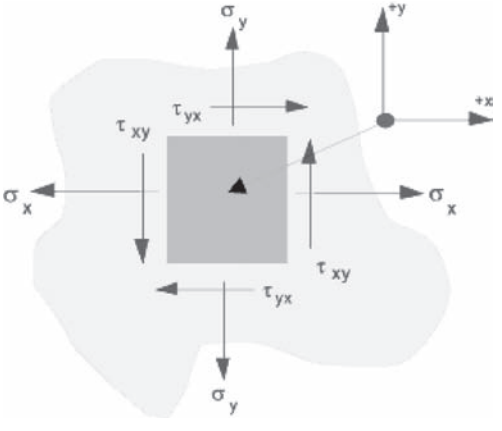

Figure 6. Stresses acting on the element in the horizontal direction.

description is not very accurate and the slope fc depends on the chosen interval of evaluation (figure 7).

The exponential way of evaluation is more accurate and is not very much dependent on the chosen interval of evaluation (figure 8). The parameter $\varepsilon_{10\,000}$ expresses the permanent deformation at the end of the measurement but does not cover the increment of permanent deformation.

Based on the carried out measurements according to the standard EN 12697-25 the authors of these article propose a few corrections for the evaluation.

In EN 13108-20 Type testing it is necessary to specify the way of evaluation of the results. To achieve more accurate parameters, which describe the development of permanent deformations,

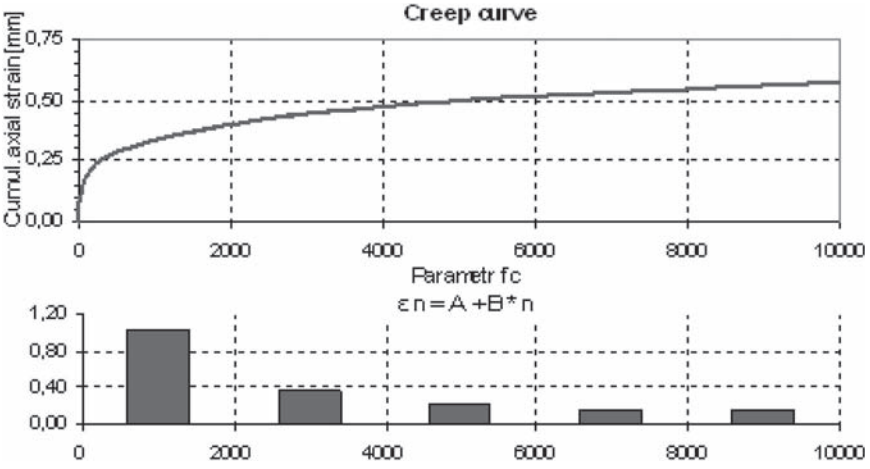

Figure 7. Parameter fc in dependence on the chosen interval of cycles (intervals 0–2000, 2000–4000, 4000–6000, 6000–8000, 8000–10 000).

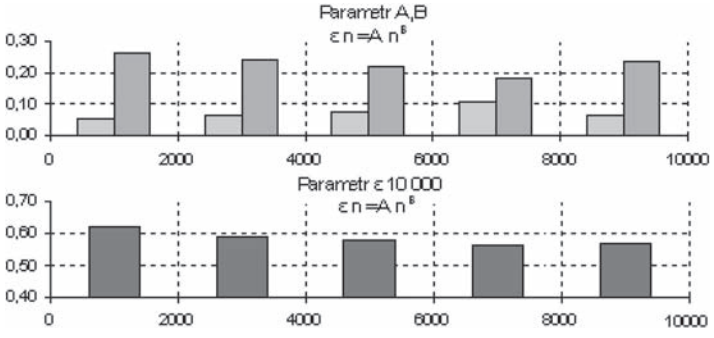

Figure 8. Parameters A, B and $\varepsilon_{10\,000}$ in dependence on the chosen interval of cycles.

Table 5. Suggested changes for EN 12697-25, EN 13108-20.

Parameter	EN 12697-25	EN 13108-20 for haversinusoidal loading	EN 13108-20 for loading with pulses	New suggestion
Evaluation interval	Does not exist			5000–10 000 cycles
Axial loading	–	σ_V(t) 300 kPa	σ_B(t) 300 kPa	σ_B(t) 600 kPa
Confining pressure		σ_C(t) 150 kPa		σ_C(t) 100 or 50 kPa,
Loading frequency	–	0,16 s/0, 16 s (3 Hz)	1 s/1 s	0,5 s/ 0,5 s (1 Hz)

Table 6. Demanded values for elasticity moduli in the design method in the Czech Republic.

Unbound mixture into the road base courses (CZE)	Minimal demanded values of elasticity moduli E_r according to Czech design method
Mechanically bound aggregate (MZK)	600 MPa
Crushed gravel (ŠD)	400 MPa
Mechanically bound soil (MZ)	150 MPa

it is necessary to specify the max. number of cycles and fix interval for evaluation. Further suggestion concerns the unification of the testing conditions for haversinusoidal loading and cyclic loading with time delay. The achieved results have shown, that there should be discussion on the value of the confining stress, as 150 kPa seems to be too high to distinguish the particular asphalt mixtures regarding the resistance against permanent deformations.

5 CONCLUSIONS FOR THE TESTING ACCORDING TO EN 13286-7

Based on the functional test according to EN 13286-7 the design elasticity module E_r for particular specimens for the secondary materials from aggregate production was found in the interval between 75–160 MPa and in case of demolition materials in the interval 120–350 MPa.

The intended use of the tested secondary products from the aggregate production and recycled materials from demolitions (after the verification by functional tests) is into the upper subgrade layer (active zone of embankments, where the reaction on traffic is expected) or in case of materials with adapted grading into the lower road base courses.

ACKNOWLEDGEMENT

The article was written with the support of the research projects of Czech Ministry of Transport CG712-043-910 “Management system of secondary materials for road structures in the Czech Republic”, further 1F45B/066/120 “Introduction of European standards concerning the material specifications for improvement of the road serviceability, lifetime and traffic safety” and research project of Czech Ministry of Education MSM 0021630519 “Progressive reliable and durable constructions”.

REFERENCES

EN 12697-25. Bituminous mixtures—test methods for hot mix asphalt—Part 25: *Cyclic compression test*.
EN 13108-20. Bituminous mixtures—Material specifications—Part 20: Type Testing.
EN 13286-7. Unbound and hydraulically bound mixtures—Part 7: *Cyclic load triaxial test methods for unbound mixtures*.

Advanced Testing and Characterization of Bituminous Materials –
Loizos, Partl, Scarpas & Al-Qadi (eds)
© 2009 Taylor & Francis Group, London, ISBN 978-0-415-55854-9

The estimation of the dynamic modulus of asphalt mixture from creep test results

F. Martinez & S. Angelone
Institute of Applied Mechanics and Structures, Road Laboratory, School of Engineering, University of Rosario, Rosario, Argentina

ABSTRACT: The dynamic modulus *Ed* is the main input material property of asphalt mixtures for the modern mechanistic-empirical flexible pavements design methods. The dynamic modulus is determined in laboratory by different procedures but in all cases, they require sophisticated equipment and well-trained personnel. This study experimentally analyzes the estimation of the dynamic modulus of asphalt mixtures from creep test results using much simpler testing equipment and by an interconversion procedure in order to validate it. The obtained results show that the procedure is very promising to estimate the dynamic modulus of bituminous mixes for practical applications.

1 INTRODUCTION

The dynamic modulus is the main input material property of asphalt mixtures for the modern mechanistic-empirical flexible pavements design methods. It determines the distribution of stress and strains into the pavement structure and also, it can be correlated with the rutting and fatigue cracking behaviour of the bituminous layers (NCHRP 2004). The dynamic modulus *Ed* is determined in laboratory by different procedures but in all cases, they require sophisticated equipment and well-trained personnel.

For practical purposes, the asphalt mixtures behave as linear viscoelastic materials and the applicability of linear viscoelastic theory has been tested by different researchers. Thus, it can be hypothesized that the dynamic modulus could be obtained from other stiffness measurements like the creep compliance using much simpler equipment. Several researchers have long-established the mathematical interrelationships between linear viscoelastic material functions (Park & Schapery 1999; Schapery & Park 1999; Park 2001; Oza et al. 2006; Sorvari and Malinen 2007).

This study experimentally analyzes the estimation of the dynamic modulus of asphalt mixtures from creep test results by an interconversion procedure in order to validate it.

A testing program was developed determining the creep compliance and the dynamic modulus of two different asphalt mixtures used as surface and base courses of asphalt pavements in Argentina, at different loading times or frequencies and temperatures.

The creep compliances master curves were fitted using Prony series and the adjusted parameters were used to calculate the complex compliance and finally, the dynamic modulus of both mixtures. The adjustment and the interconversion procedures were developed on spreadsheets in order to automate and to simplify them.

The measured and estimated dynamic modulus results were compared and discussed. In general, well agreement exists between these results showing that the procedures used in this investigation are promising to estimate the dynamic modulus of bituminous mixes for practical applications.

2 DEFINITIONS

The stiffness of the asphalt mixtures is a material response parameter that determines the strains and displacements pavement structure as it is loaded or unloaded. Historically, various

types of material parameters have been used for presenting the stiffness characteristics of asphalt mixtures. Among them, the dynamic modulus and the creep compliance are used to describe the viscoelastic properties of asphalt mixtures.

The dynamic modulus, *Ed* is defined as the relationship between the absolute value of the maximum (peak-to-peak) stress divided by the maximum recoverable (peak-to-peak) axial strain for a viscoelastic material subjected to a sinusoidal loading as:

$$Ed = \frac{\sigma_0}{\varepsilon_0} \tag{1}$$

with Ed = dynamic modulus; σ_0 = stress amplitude; and ε_0 = strain amplitude.

The creep compliance $D(t)$ is defined as the relationship between the time-dependant strains divided by the constant axial stress for a viscoelastic material subjected to a constant loading as:

$$D(t) = \frac{\varepsilon(t)}{\sigma_0} \tag{2}$$

with $D(t)$ = creep compliance; $\varepsilon(t)$ = time-dependant strain; and σ_0 = constant axial stress.

3 EXPERIMENTAL PROGRAM

3.1 *Materials*

Two typical asphalt concretes used in Argentina for surface or base courses were used in this study. Both mixtures have the same gradation and the same binder content with a 19-mm maximum nominal aggregate size but one of them, named ACC mix, was formulated using a conventional bitumen while the other, designed as ACM mix, was formulated using a SBS modified bitumen. The gradation of both mixtures is presented in Table 1 and the average volumetric properties of both mixtures are presented in Table 2.

The samples used in this study were laboratory compacted following the Marshall procedure in order to obtain an average air void content approximately equal to 4 percent as it is stated by the specifications used in Argentina for this type of mixtures.

3.2 *Testing procedures*

The Dynamic Modulus *Ed* was experimentally measured with the Indirect tension (IDT) mode with sinusoidal loadings following a procedure very similar as it was developed by Kim et al. 2004.

Assuming the plane stress state, the linear viscoelastic solution for the dynamic modulus of asphalt mixtures under the IDT mode results:

Table 1. Gradation of the mixtures.

Sieve size mm	Percent passing %
19	100.0
12.5	88.0
9.5	80.0
4.75	50.0
2.36	43.0
1.18	36.0
0.6	27.0
0.3	22.0
0.15	14.0
0.075	5.3

Table 2. Average volumetric mixture properties.

Asphalt mixture	Binder content % by volume	Air voids content %
ACC mix	13.66	4.1
ACM mix	13.64	3.9

$$Ed = \frac{P}{\Delta h \cdot h}\left(K_1 + \mu \cdot K_2\right) \tag{3}$$

where Ed = dynamic modulus; P = amplitude of the applied sinusoidal load; Δh = amplitude of the resulting horizontal deformation; h = thickness of specimen; K_1 and K_2 = coefficients depending on the specimen diameter and gauge length; and μ = Poisson's ratio.

Testing was performed using a servo-pneumatic machine, developed at the Road Laboratory of the University of Rosario, using a 5000 N load cell, which is capable of applying load over a range of frequencies ranging from 0.01 Hz to 5 Hz. A proportional valve controlled by the computer is used to generate the sinusoidal loadings at the required frequency. The test frame is enclosed into a temperature chamber. The temperature control system is able to achieve the required testing temperatures ranging from 0°C to 50°C. The data acquisition system was also developed at the Road Laboratory of the University of Rosario and is capable of measuring and recording data from three channels simultaneously: two for horizontal displacements and one for the load cell. A more detailed description of the testing equipment and the data analysis procedures were reported by Martínez & Angelone, 2006.

In order to increase the simplicity of the test, only horizontal deformations were measured.

From previous studies (Gschösser 2008), the Poisson's ratio was adopted as a function of the test temperature in the form:

$$\mu = a + b\,T \tag{4}$$

where μ = Poisson's ratio, T = test temperature; and a and b = regression constants.

The horizontal deformations were measured using LVDTs mounted on each of the specimen faces using a 50 mm gauge length. The applied load and the average horizontal deformation were calculated fitting sinusoidal functions to the measured experimental data.

For the adopted gauge length and for specimens with 100 mm diameter, the coefficients K_1 and K_2 result: $K_1 = 0.236$ and $K_2 = 0.777$. In this study, five temperatures (0, 10, 20, 30 and 40°C) and five frequencies (4, 2, 1, 0.5 and 0.25 Hz) were used.

Creep compliances were also determined with the Indirect tension (IDT) mode with constant loads and with the same experimental equipment used for the dynamic modulus determination.

The creep compliance as a function of time was calculated as:

$$D(t) = \frac{\Delta h(t) \cdot h}{P_0}\left(\frac{1}{K_1 + \mu \cdot K_2}\right) \tag{5}$$

with $D(t)$ = creep compliance as a function of time; $\Delta h(t)$ = resulting average horizontal deformation at time t; h = thickness of specimen; P_0 = constant applied load; K_1 and K_2 = coefficients depending on the specimen diameter and gauge length; and; μ = Poisson's ratio.

The horizontal deformations were measured using LVDTs mounted as in the determination of the dynamic modulus. The constant load was applied for a period of time of 600 seconds for the same five testing temperatures used for the dynamic modulus tests. At each temperature, the lowest load compatible with the capability of the data acquisition system was used in order to reduce the induced damage in the samples to the minimum. Two samples per mixture were used for the dynamic modulus tests and the creep tests.

4 OBTAINED RESULTS

4.1 *Dynamic modulus results*

Tables 3 presents the average dynamic modulus for both mixes.

As expected, under a constant loading frequency, the magnitude of the dynamic modulus decreases with an increase in temperature. Also is noticeable the influence of the SBS modified

Table 3. Average dynamic modulus results for the ACC mix.

Temperature °C	Frequency Hz	Dynamic modulus ACC mix MPa	ACM mix MPa
0	4	24995	18177
0	2	24005	17250
0	1	22910	16245
0	0.5	21711	15168
0	0.25	20410	14028
10	4	18568	13643
10	2	17071	12439
10	1	15516	11209
10	0.5	13930	9972
10	0.25	12340	8752
20	4	10861	8714
20	2	9355	7537
20	1	7936	6425
20	0.5	6630	5397
20	0.25	5458	4469
30	4	4805	4677
30	2	3869	3832
30	1	3080	3100
30	0.5	2428	2479
30	0.25	1901	1965
40	4	1754	2196
40	2	1367	1734
40	1	1065	1361
40	0.5	832	1065
40	0.25	654	834

bitumen producing lower values of the dynamic modulus at low temperatures and higher values of the dynamic modulus at higher temperatures. The measured data were used to construct an average master curve for the dynamic modulus at a reference temperature of 20°C and for each mixture. The used method was developed in the Excel spreadsheet in order to automate the procedure and to simplify it. The method consists of using nonlinear regression techniques to fit experimental data to a sigmoidal function and solving the shift factors, based on the Arrhenius equation, simultaneously with the coefficients of that function. The compared dynamic modulus master curves for the ACC mix and the ACM mix are presented in Figure 1.

4.2 *Creep compliance results*

Figures 2 and 3 show the average creep compliance results for the ACC mix and the ACM mix, respectively at the five different temperatures used in this study.

A master curve of the creep compliance was constructed for a reference temperature of 20°C for both mixes using an analogous procedure than the used for the dynamic modulus. A sigmoidal function was adjusted to fit experimental data by nonlinear regression techniques and also, solving the shift factors simultaneously with the coefficients of that function. The method was also developed in the Excel spreadsheet in order to obtain the master curve automatically. Figure 4 shows the adjusted creep compliance master curves for the ACC mix and the ACM mix.

Once the creep compliance master curves were constructed, Prony series models were fit to these curves.

This type of fitting is needed in order to convert the creep compliance into dynamic modulus data as will be explained in the next section. The model is:

$$D(tR) = D_0 + \sum_{i=1}^{n} D_i \left(1 - e^{-tR/T_i} \right) \tag{6}$$

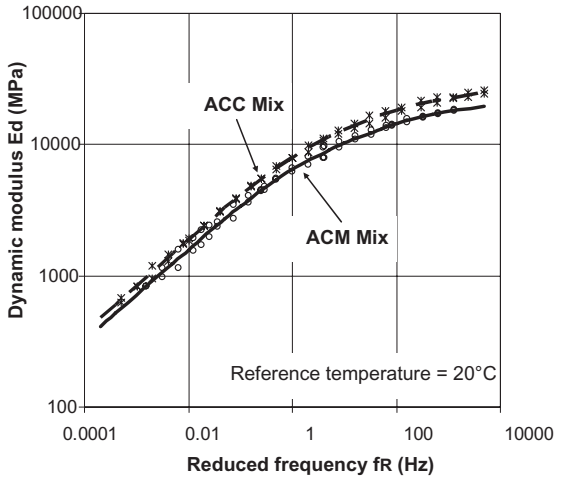

Figure 1. Dynamic modulus master curve for both mixtures.

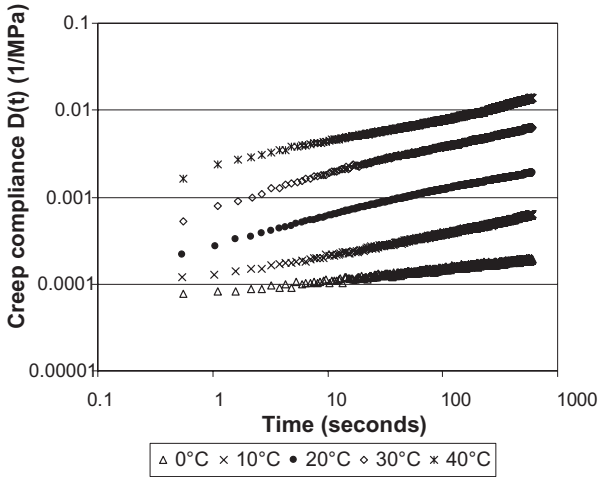

Figure 2. Creep compliance results for the ACC mix.

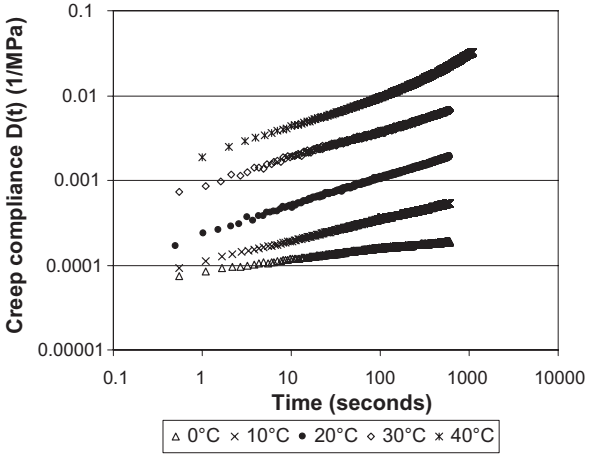

Figure 3. Creep compliance results for the ACM mix.

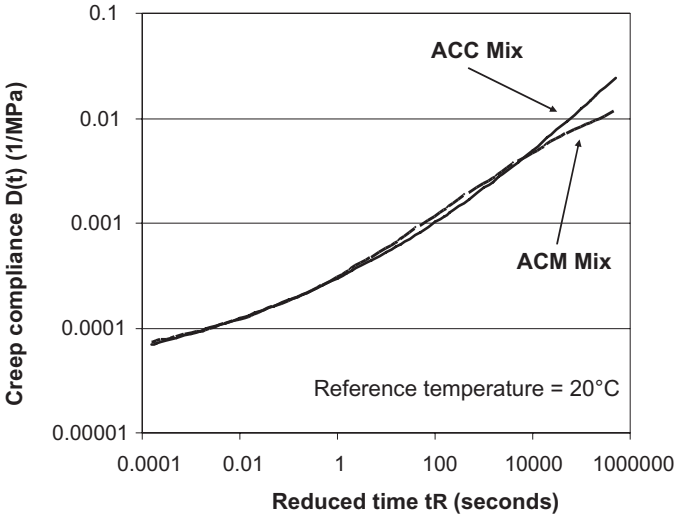

Figure 4. Creep compliance master curves for both mixtures.

Table 4. Calculated Prony series parameters.

Parameter	ACC mix	ACM mix
D_0	4.54E-05	5.74E-05
D_1	1.61E-05	1.24E-05
D_2	3.12E-05	2.88E-05
D_3	5.77E-05	5.80E-05
D_4	1.20E-04	1.43E-04
D_5	2.90E-04	3.61E-04
D_6	6.60E-04	8.19E-04
D_7	1.67E-03	1.73E-03
D_8	8.52E-03	4.41E-03
T_1	1.53E-05	2.88E-05
T_2	6.31E-04	1.03E-03
T_3	1.62E-02	2.77E-02
T_4	3.89E-01	5.87E-01
T_5	7.98E+00	1.04E+01
T_6	1.36E+02	1.54E+02
T_7	1.90E+03	1.83E+03
T_8	3.61E+04	2.49E+04

with $D(tR)$ = creep compliance at reduced time tR; D_0 = equilibrium creep compliance; D_i and T_i = Prony series parameters in 1/MPa and seconds, respectively; and n = number of terms in the series.

An eight-term Prony series was found to be suitable in order to obtain a very good fitting between the creep compliance master curves and the model for the range of reduced times resulting from the creep compliance master curves. Table 4 shows the calculated Prony series parameters for both mixtures.

5 ESTIMATION OF DYNAMIC MODULUS FROM CREEP COMPLIANCE

If the creep compliance is expressed as a Prony series in the time domain then the complex compliance in the angular frequency domain can be derived theoretically. The real and imaginary part of the complex compliance are given as:

$$D'(\omega) = D_0 + \sum_{i=1}^{n} \frac{D_i}{\omega^2 T_i^2 + 1} \tag{7}$$

$$D''(\omega) = D_0 + \sum_{i=1}^{n} \frac{\omega D_i T_i}{\omega^2 T_i^2 + 1} \tag{8}$$

where $D'(\omega)$ = real part of the complex compliance; $D''(\omega)$ = imaginary part of the complex compliance; and ω = angular frequency.

Thus, the complex compliance can be calculated as:

$$D^*(\omega) = \sqrt{D'(\omega)^2 + D''(\omega)^2} \tag{9}$$

The dynamic modulus can be calculated as the inverse of the complex compliance as:

$$Ed = \frac{1}{D^*(\omega)} \tag{10}$$

Following this procedure, the dynamic modulus of both mixtures was calculated from the creep compliance results. Figure 5 shows the comparison between the dynamic modulus master curve of experimentally measured dynamic modulus values and the dynamic modulus master curve of calculated values from the creep test results for the ACC mix. Figure 6 shows the same comparison for the ACM mix. For these comparisons, the angular frequency ω in rad/sec has been converted into reduced frequency in Hz as:

$$fR = \frac{\omega}{2 \cdot \pi} \tag{11}$$

In most cases, the calculated dynamic modulus was smaller than the measured one. In general, there are an acceptable agreement between measured dynamic modulus values and calculated values from creep test results with the same trends of variations.

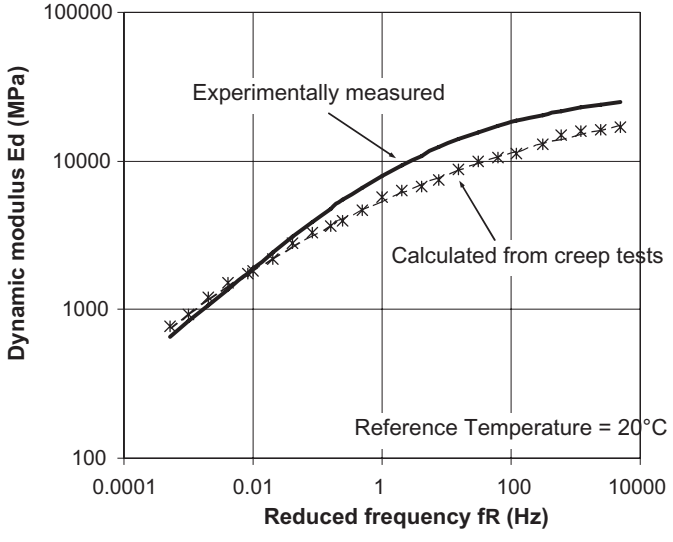

Figure 5. Comparison of dynamic modulus master curves for the ACC mix.

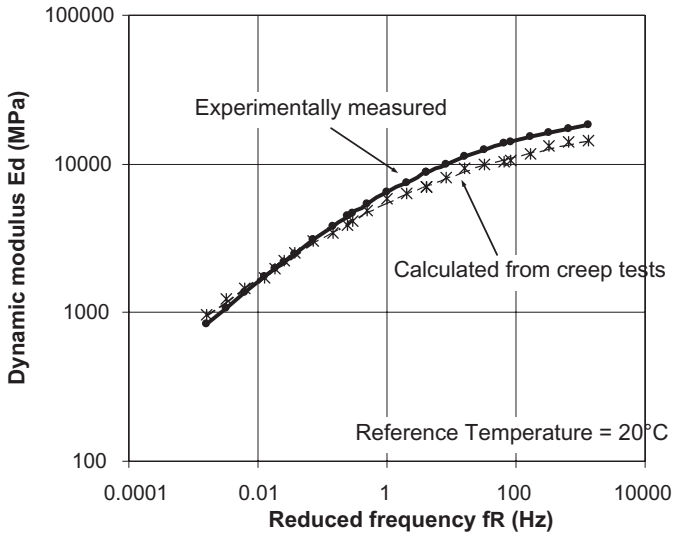

Figure 6. Comparison of dynamic modulus master curves for the ACM mix.

In these comparisons, the relative errors (the difference between the measured and calculated values divided by the measured dynamic modulus in absolute value) were lower than 38% for the ACC mix and 21% for the ACM mix. These errors are within the same orders of magnitude than others obtained from predictions of the dynamic modulus using predictive equations and models well accepted by the pavement community like the Witczak predictive equation or the Hirsch model (Andrei et al. 1999; Christensen et al. 2003; Kim et al. 2005; Schwartz 2005).

The comparison of measured and calculated dynamic modulus values is presented in Figure 7 (in logarithmic space) for the two mixtures considered in this study. In this Figure, the line of equality is also presented.

To evaluate the performance of the estimative capability of the analyzed procedure, the correlation of the measured and calculated values was assessed using goodness-of-fit statistics according to the subjective criteria proposed by Witczak et al. 2002, and shown in Table 5. The statistics include correlation coefficient, R^2 and Se/Sy (standard error of calculated values/standard deviation of measured values). Table 6 presents this evaluation for the ACC mix and the ACM mix compared in the arithmetic space and the logarithmic space.

The calculated values have an excellent correlation to the measured dynamic modulus values and the goodness-of-fit statistics show an excellent performance, according to the subjective criteria used.

Based on the obtained results, it could be concluded that when testing results are not available, reliable first order dynamic modulus estimates for mixtures typical to Argentina can be obtained using the conversion procedure from creep compliance results to dynamic modulus values considered in this study. The required equipment to perform the creep tests is simpler than the sophisticated equipment required performing the dynamic modulus testing. The procedure used in this study is very promising to estimate the dynamic modulus of asphalt mixtures for their application in mechanistic pavement design procedures.

6 CONCLUSIONS

An experimental study was carried out in order to analyze if the estimation of the dynamic modulus of asphalt mixtures from creep test results by an interconversion procedure could be validated.

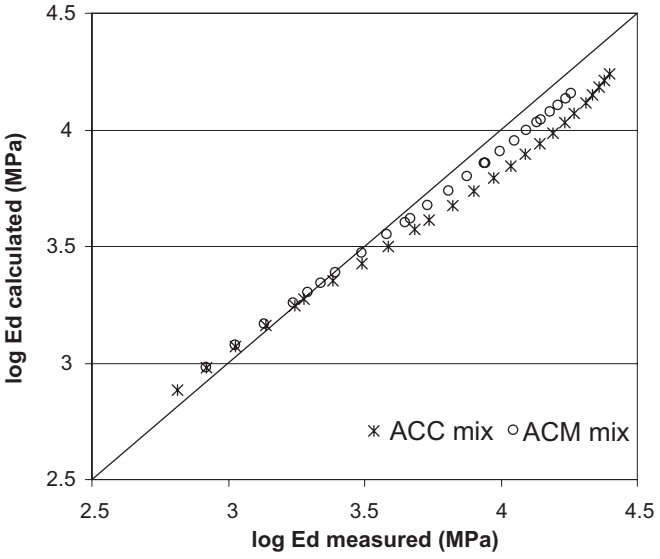

Figure 7. Comparison of measured and calculated dynamic modulus values (in logarithmic space).

Table 5. Criteria for goodness-of-fit statistical parameters.

Criteria	R^2	Se/Sy
Excellent	≤0.90	≤0.35
Good	0.70–0.89	0.36–0.55
Fair	0.40–0.69	0.56–0.75
Poor	0.20–0.39	0.76–0.89
Very poor	≤0.19	≤0.90

Table 6. Evaluation of the estimative procedure.

	Arithmetic space			Logarithmic space		
Procedure	R^2	Se/Sy	evaluation	R^2	Se/Sy	evaluation
ACC mix	0.99	0.05	Excellent/Excellent	0.99	0.06	Excellent/Excellent
ACM mix	0.99	0.02	Excellent/Excellent	0.99	0.02	Excellent/Excellent

A testing program was developed determining the creep compliance and the dynamic modulus of two different asphalt mixtures used as surface and base courses of asphalt pavements in Argentina, at different loading times or frequencies and temperatures. The creep compliance and dynamic modulus were measured at various temperatures and creep compliance master curves, and dynamic modulus master curves were constructed using Excel spreadsheets in order to simplify and automate the involved calculations.

Then, the creep compliance data were used to compute the dynamic modulus. In general, there are well agreement between measured dynamic modulus values and calculated values from creep test results. In most cases, the calculated dynamic modulus was smaller than the measured one. The relative errors between measured and calculated values are within the same orders of magnitude than others obtained from predictive equations and models well accepted by the pavement community.

Based on the obtained results, it could be concluded that when experimentally determined dynamic modulus results are not available, reliable first order estimates can be obtained using the conversion procedure used in this study. As the required equipment and testing protocol

to perform creep tests are simpler than those required for the dynamic modulus testing, the procedure used in this investigation is promising to estimate the stiffness properties of bituminous mixes for practical applications in mechanistic empirical pavement design procedures.

REFERENCES

Andrei, D., Witczak, M. and Mirza, W. 1999. Development of a revised predictive model for the dynamic (complex) modulus of asphalt mixtures. Design Guide for New & Rehabilitated Pavements. Appendix CC-4. NCHRP Project 1–37A National Research Council, Washington DC.

Christensen, D.W., Pellinen, T.K. and Bonaquist, R.F. 2003. Hirsch model for estimating the modulus of asphalt concrete. Journal of the Association of Asphalt Paving Technologists Volume 72.

Gschösser, F. 2008. Modeling the mechanical behaviour of asphalt mixtures. *Thesis for the degree of Civil Engineer*, Leopold Franzens University, Innsbruck.

Kim, Y.R., Seo, Y., King, M. and Momen, M. 2004. Dynamic modulus testing of asphalt concrete in indirect tension mode, *Transportation Research Record: Journal of the Transportation Research Board* 1891: 163–173.

Kim, Y.R., King, M. and Momen, M. 2005. Typical dynamic moduli values of hot mix asphalt in North Carolina and their prediction. 84th Annual Meeting of the Transportation Research Board. Paper No. 05-2568, Washington D.C.

Martínez, F. and Angelone, S. 2006. Un modelo para la descripcion del modulo dinamico de mezclas asfalticas. II Simposio Iberoamericano de Ingenieria de Pavimentos. Trabajo N° 12. Quito. (In Spanish)

NCHRP 2004. Design Guide for New & Rehabilitated Pavements (Final Report); Part 2- Design Inputs, Chapter 2 Material Characterization, 2.2.2 Input Characterization for the Asphalt Material Group; *NCHRP Project 1–37A*.

Oza, A., Vanderby, R. and Lakes, R. 2006. Generalized solution for predicting relaxation from creep in soft tissue: Application to ligament. *International Journal of Mechanical Sciences* 48: 662–673.

Park, S.W. and Schapery, R.A. 1999. Methods of interconversion between linear viscoelastic material functions. Part I—a numerical method based on Prony series. *International Journal of Solids and Structures* 36: 1653–1675.

Park, S.W. 2001. Analytical modeling of viscoelastic dampers for structural and vibration control. *International Journal of Solids and Structures.* 38: 8065–8092.

Schapery, R.A. and Park, S.W. 1999. Methods of interconversion between linear viscoelastic material functions. Part II—an approximate analytical method. *International Journal of Solids and Structures*. 36: 1677–1699.

Schwartz, C.W. 2005. Evaluation of the Witczak dynamic modulus prediction model. 84th Annual Meeting of the Transportation Research Board Paper No. 05–2112, Washington DC.

Sorvari, J. and Malinen, M. 2007. Numerical interconversion between linear viscoelastic material functions with regularization. *International Journal of Solids and Structures* 44: 1291–1303.

Witczak, M.W., Kaloush, K., Pellinen, T., El-Basyouny, M. and Von Quintus, H. 2002. Simple performance test for Superpave mix design. NCHRP Report 465. Transportation Research Board. Washington, DC.

Advanced Testing and Characterization of Bituminous Materials –
Loizos, Partl, Scarpas & Al-Qadi (eds)
© 2009 Taylor & Francis Group, London, ISBN 978-0-415-55854-9

Application of a balanced mix-design concept to thin asphalt overlay mixes: Minimizing rutting and reflective-cracking

Lubinda F. Walubita & Tom Scullion
Textas Transportation Institute (TTI), Texas A&M University System,
College Station, Texas, USA

ABSTRACT: In lieu of the traditional Superpave and Marshall mix-design methods which are predominantly volumetric- or stability-based, the objective of the work contained in this paper was to investigate in the laboratory, the applicability of a balanced HMA mix-design concept for designing thin overlay HMA mixes; that checks for both rutting-and reflective cracking-resistance, respectively. This proposed balanced HMA mix-design concept is based on selecting an optimum asphalt-binder content that simultaneously meets a prescribed laboratory rutting and reflection-cracking test criteria, respectively. In the study, the Hamburg wheel tracking test and the Overlay tester were utilized for characterizing the rutting resistance and reflective cracking resistance, respectively. Thus far, satisfactory laboratory test results have been obtained with fine-graded HMA mixes; predominantly composed of 9.5 mm NMAS high quality clean aggregates (such as granite) and stiff polymer-modified asphalt-binder content of over 7.0% (e.g., PG 76-22S); where NMAS stands for nominal maximum aggregate size.

1 INTRODUCTION

Thin asphalt overlays are non-structural preventative maintenance (PM) mixes used for the routine maintenance and rehabilitation of existing pavements. They are typically placed in thin layer lifts of about 25 mm thick. Traditionally, thin overlay application is primarily used to preserve pavements exhibiting surface distresses such as raveling, ageing, bleeding, minor cracking, minor disintegration, texture loss, skid resistance loss, etc. Candidate pavements for thin overlays should generally be structurally sound with no major structural defects such as rutting or fatigue cracking; otherwise a thicker overlay or reconstruction is recommended (Technical Bulletin 2002). Rutting greater than 6.25 mm should be sealed and any surface deformities greater than 12.5 mm should be filled up (but not over filled) prior to overlay placement. Equally, potholes should be sealed and patched up, respectively (Uhimeyer 2003).

1.1 *Thin HMA overlay application*

In general, thin hot-mix asphalt (HMA) overlays are considered as a cost-effective application of preserving and maintaining existing "structurally sufficient" pavements; applicable to both flexible HMA and rigid concrete pavements. Thin HMA overlays enhance pavement performance and extend the service life (up to 15 years) including functional characteristics such as improved user serviceability (i.e., improved smoothness, comfort, quite ride, etc), surface leveling up, skid resistance, noise reduction, water spray reduction, and conspicuity of the road markings and glare/reflections (Gilbert et al. 2004). Overlays also contribute to the improvement of the pavement strength and durability including impermeability properties; thus minimizing moisture damage and asphalt-binder oxidative ageing from water and air infiltration, respectively.

Furthermore, Overlays also improve the aesthetic appearance of the pavement surface (Cooley (Jr) et al. 2002). Thin HMA overlay applications on steel and concrete bridge decks has also been reported in the literature and is widely practiced in Europe; primarily as a

waterproofing and surfacing layer (Nichollas et al. 2002). According to Rosenberg (2000) and Nicholls et al. (2002), approximately 5% of the Danish bridges are paved with thin HMA surfacings.

1.2 *Thin HMA overlay mix-design characteristics*

Thin overlay HMA mixes that are place-able as a thin layer lift thickness of about 25 mm revolve around the 4.75 mm or 9.5 mm Nominal Maximum Aggregate Size (NMAS) fine-graded mixes. In general, the following mix-design characteristics are considered critical for the thin overlay HMA mixes:

- High quality gap-graded (fine) aggregates (such as granite or crushed gravel).
- Use of modified asphalt-binders with relatively high asphalt-binder contents (i.e., about 6.0% to 8.5%).
- Increased asphalt-binder film thickness (most literature recommend at least 10 to 12 microns [Pretorius et al. 2004, Kandhal et al. 1996, Cooley (Jr) et al. 1997]) for improved durability.
- High VMA and reduced air voids (i.e., high compaction target density of around 98%).
- Use of additives such as lime (about 0.5 to 1.5%).

Gap-grading ensures good stone-on-stone contact for an efficient load transfer mechanism that ultimately improves the rutting resistance of the mix. Additives such as anti-aging agents, anti-stripping agents (lime), and Silicon Dioxide may also be used to enhance durability, moisture damage resistance, skid resistance, and other functional characteristics.

According to the literature, HMA mixes that can be or have been used for thin overlay applications include stone mastic asphalt (SMA; 4.75, 9.5, or 12.5 mm NMAS), Superpave (4.75 or 9.5 mm NMAS), smoothseal (Ohio, USA), ultra-thin HMA (Michigan, USA), ultra-thin friction course (UTFC; South Africa), Novachip™, micro-surfacing, asphalt rubber (AR), and TxDOT Type D and F mixes (Texas, USA) (Technical Bulletin 2002, Gilbert et al. 2004, Cooley (Jr) et al. 2002, Oliver 1997, TxDOT 2004).

Others include the ultra-thin open-graded asphalt (UTOGA; Australia), thin asphalt concrete (TAC; Canada, UK), etc (Nichollas et al. 2000, Yeo 1997, Scott et al. 1990). All these mixes are place-able in layer lift thickness of about 25 mm thick or less. Different or special (agency-specific) mix-design methods including the modified Superpave and Marshall are used for designing these mixes while others like the Novachip™ and some micro-surfacings are proprietary.

1.3 *Thin HMA overlay mix property requirements*

To ensure durability and adequate performance, it is envisaged that the thin overlay HMA mixes should exhibit good stone-on-stone contact, contain premium high content asphalt-binders, and additives such as fibers and anti-stripping agents (e.g., lime). Relatively high asphalt-binder contents serve to simultaneously improve workability, cracking resistance, and durability. Fine high quality aggregates with good frictional properties are essential to ensure adequate skid resistance and durability characteristics.

Note that even with the fine-graded mixes such as with 9.5 mm NMAS aggregates (which are easily place-able in thinner layer lifts) it is possible to attain sufficient rutting resistance in the field. As pointed out by Newcomb et al. (2006), some of the HMA mix property characteristics to ensure sufficient rutting resistance are the internal friction provided by the aggregate interlock and the cohesiveness or stiffness of the asphalt-binder. Therefore, it is not so important that a mix contains larger or coarse aggregates as it is to having a good aggregate interlock and stone-on-stone contact.

Kandhal et al. (2002) have in fact shown that fine-graded mixes, with good aggregate interlock and stone-on-stone contact, may provide as much resistance to rutting as coarse-graded mixes. On the same basis, it is also arguable that sufficient field rutting resistance can be attained with a 25 mm thick HMA layer provided there is good aggregate interlock and

stone-on-stone contact within the HMA mix matrix. The use of high stiff PG graded asphalt-binders that are relatively less temperature sensitive also adds on to the rutting resistance characteristics of the mix. In any event, the exposure to the harshest environmental conditions and high temperatures (which also fluctuate considerably) may often dictate for the use of stiffer polymer modified asphalt-binders for surfacing mixes such as overlays.

1.4 *Life span of thin HMA overlays*

If well designed and constructed, thin HMA overlays can last between 8 to 15 years. However, a service life of up to 18 years has been reported for thin SMA overlays in Germany, where the SMA was first developed (Belin 1998). On a cost comparison basis, thin HMA overlays are on average about 11% to 40% cheaper than other conventional surface treatments (Gilbert et al. 2004, Pretorius et al. 2004). Additionally, their construction time is relatively shorter and they are generally open for all seasons placement, even at night provided the weather conditions permit satisfactory compaction. As observed by Cooley Jr. et al. (2002, 1997), thin HMA overlays also provide a very economical use for left-over manufactured screening stockpiles. Additionally, utilizing a thinner lift thickness generally allows for more project length to be covered with the same tonnage of HMA; thus being cost-effective.

2 STUDY OBJECTIVES AND SCOPE OF WORK

Worldwide, thin HMA overlays are gaining popularity as a cost-effective and less disruptive PM treatment. However, because thin HMA overlay surfacing is a relatively new PM application, particularly in the USA, standardized specifications and/or guidelines on thin overlay HMA mixes including mix-design methods are limited and most often are agency-specific and not elaborate or better still, are proprietary like the Novachip™. Hardly any thin overlay HMA mix-design specifications have been standardized for general application or use as reference guidelines.

In the USA, modified (agency-specific) Superpave mix-design methods are utilized in limited States including Alabama (NCAT), Arizona (asphalt rubber), Georgia, and Maryland. Like most of the countries outside of the USA, other States like Ohio (smoothseal) and Michigan (ultra-thin HMA) utilize the Marshall method; most often modified to their specific materials and environment (Pretorius et al. 2004, MDOT 2005). Texas utilizes the volumetric-based Superpave gyratory method for designing surface HMA mixes; with hardly any standardized mix-design methods specifically for thin overlay HMA mixes (TxDOT 2004).

Other countries like Australia (ultra-thin graded asphalt), Europe (e.g., France, Denmark, Germany [SMA], and the UK), South Africa (ultra-thin friction course), and New Zealand (SMA), where thin surfacings are extensively used, have over the years developed or adopted their own mix-design specifications; which are predominantly Marshall based (Cooley (Jr) 1997). However, these specifications are applicable only to their conditions and their thin HMA overlay applications are primarily used for texture and skid resistance restoration and bridge deck surfacings. Additionally, few if any, incorporate a balanced mix-design concept for checking both rutting and cracking resistance. Consequently, there is a need to formulate a mix-design method that at least takes into account both rutting and cracking (reflective). Note that reflective cracking is one of the major critical distresses associated with HMA overlays.

Based on the foregoing discussions, the objective of the work presented in this paper was to explore in the laboratory, the application of the balanced mix-design concept for designing thin overlay HMA mixes; that takes into account both rutting- and cracking-resistance, for fine-graded mixes, which are place-able in a layer lift thickness of about 25 mm or less. In the paper, the balanced HMA mix-design concept together with laboratory testing is described first followed by the proposed mix-design process. The materials and HMA mix characteristics are then presented followed by some laboratory demonstration examples with fine-graded Texas HMA mixes. This is followed by a discussion of the results, and finally a summary of findings and recommendations is presented to conclude the paper.

3 THE BALANCED MIX-DESIGN CONCEPT

Pioneered by Dr. F. Zhou, the concept of the balanced mix-design method is fundamentally centered on ensuring adequate rutting and cracking resistance for the HMA mixes (Zhou et al. 2006). The idea is to design a HMA mix that is at least both rutting-and cracking-resistant. With this concept, the design philosophy is based on designing and selecting an optimum asphalt-binder content (OAC) that simultaneously meets certain prescribed laboratory rutting and cracking requirements based on the Hamburg and Overlay tests, respectively. Both the Hamburg and Overlay tests are discussed in the subsequent text of this paper.

As documented elsewhere, Zhou et al. (2006) have demonstrated that most of the existing mix-design methods are empirical or insufficient in ensuring satisfactory HMA performance in the field. For instance, the current Texas HMA mix-design process uses the volumetric design method (volumetric requirements) to select the OAC and the Hamburg Wheel Tracking Test (HWTT) to ensure adequate rutting resistance and moisture-damage resistance of the proposed HMA mix. By contrast, cracking resistance evaluation is not yet part of the standard mix-design procedure. As a result, most of the Texas HMA pavements are today still more susceptible to cracking than rutting. In general, the Superpave process determines OAC based on volumetric requirements that may not be directly related to performance. Other empirical HMA mix-design methods such as the Hubbard-Field, Marshall, and Hveem also utilize volumetric properties and stability (rutting resistance) to determine the OAC (Zhou et al. 2006). Clearly, most of these methods do not sufficiently address other performance-related distresses such as cracking. By contrast, the proposed balanced HMA mix design method checks for both rutting and cracking resistance in the laboratory. This concept is schematically illustrated in Figure 1.

In Figure 1, the upper line graph represents the HWTT rut depth for different asphalt-binder contents. Rut depths below 12.5 mm are considered acceptable, i.e., $Rut_{HWTT} \leq 12.5$ mm. The lower line graph shows the performance in the Overlay Tester (cracking resistance). In this case, HMA mixes (dense-graded) which last over 300 load cycles to failure at 93% stress reduction are judged as acceptable, i.e., $N_{OT} \geq 300$.

Figure 1 clearly shows that as the asphalt-binder content increases, the rutting resistance decreases, but the cracking resistance improves. Conversely, the opposite result would be expected if the asphalt-binder content is decreased. A balanced design includes an asphalt-binder content in the zone of the asphalt-binder contents (i.e., the shaded region in Figure 1) in which the HMA mix simultaneously passes both the rutting ($Rut_{HWTT} \leq 12.5$ mm) and cracking

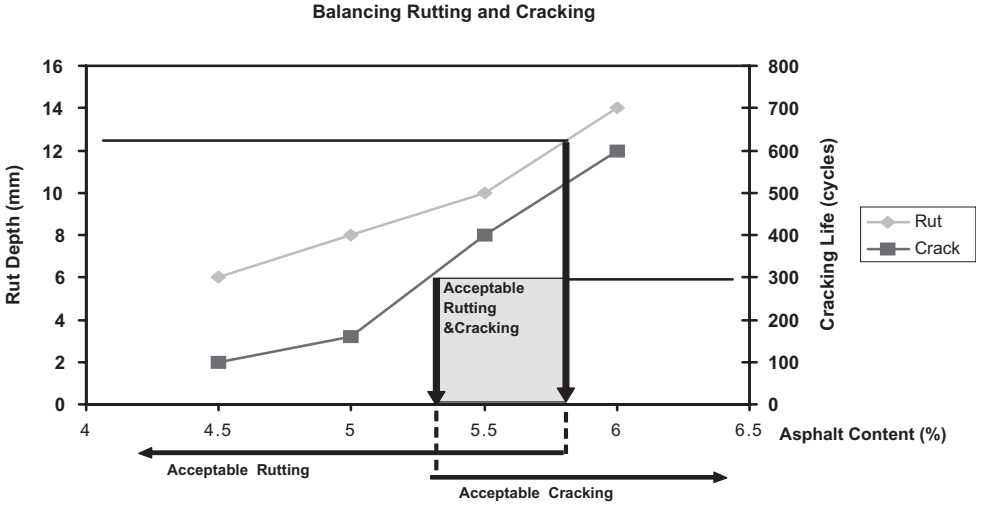

Figure 1. The balanced mix design concept (Zhou et al. 2006).

($N_{OT} \geq 300$.) requirements. For the purpose of this study however, the failure criterion for the Overlay Tester (OT) was conservatively revised to 750 load cycles for the thin overlay HMA mixes (i.e., $N_{OT} \geq 750$). This stringent requirement was viewed as necessary to ensure sufficient cracking resistance as one of the primary purposes of the thin overlays would be to seal underlying cracks and/or minimize reflective crack propagation.

Being the surface layer also means that these mixes would be subjected to the harshest environmental conditions such as oxidative ageing, which has a tendency to reduce the HMA cracking resistance. Inevitably and as will be seen later in this paper, this stringent requirement (i.e., $N_{OT} \geq 750$) calls for a high asphalt-binder content. Consequently, the following HWTT and OT failure criteria were utilized in this study:

- Hamburg: Rut $Depth_{HWTT} \leq 12.5$ mm under wet conditions at 50°C.
- Overlay: Number of load cycles to failure ≥ 750 (i.e., $N_{OT} \geq 750$) at 93% stress reduction at 25°C.

3.1 *The hamburg wheel tracking test (HWTT)*

The HWTT is a test device used for characterizing the rutting resistance of HMA mixes in the laboratory including stripping susceptibility assessment (moisture damage potential). The loading configuration consists of a repetitive passing load of 705 N at a wheel speed of 52 passes per minute and a test temperature of 50°C in a controlled water bath. The HWTT test specimens are 62.5 mm thick by 150 mm in diameter, with one trimmed edge; and can easily be sawn from lab molded specimens or field-extracted cores. Figure 2 shows the HWTT test set-up.

During HWTT testing, the measurable parameters include the applied load, temperature, number of load passes, and the rut depth. The HWTT terminal rutting failure criterion is 12.5 mm rut depth ($Rut_{HWTT} \leq 12.5$ mm) at 10,000 load passes for HMA mixes with PG 64-XX asphalt-binder; 15000 load passes for HMA mixes with PG 70-XX asphalt-binder; and 20,000 load passes for HMA mixes with PG 76-XX asphalt-binder, respectively (Zhou et al. 2006).

3.2 *The Overlay Tester (OT)*

The Overlay Tester (OT) is a simple performance test used for characterizing the reflection cracking potential of HMA mixes in the laboratory at an ambient (room) temperature of 25°C. The test loading configuration consists of a cyclic triangular displacement-controlled waveform at a maximum horizontal displacement of 0.63 mm and a loading rate of 10 s per cycle (5 s loading and 5 s unloading). The OT test specimens are 150 mm total length, 75 mm wide, and 38 mm thick that can be conveniently sawn by trimming a lab molded specimen, field-extracted core, or a field sawn slab. The OT test setup is shown in Figure 3 together with an example of a test specimen.

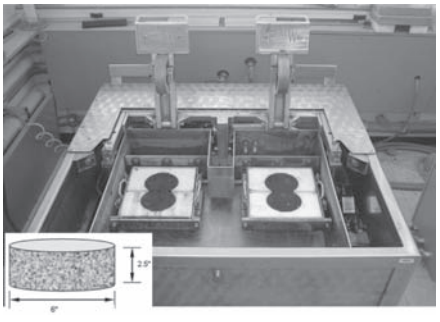

Figure 2. The Hamburg (HWTT) device and specimen setup.

Figure 3. The Overlay Tester (OT) and specimen setup.

During OT testing, the measurable parameters include the applied load (stress), opening displacement (fixed at 0.63 mm), time, the number of load cycles, and the test temperature. As mentioned previously, the OT terminal failure criteria was set at 750 load cycles for thin overlay HMA mixes. Full details of the HWTT and OT can be found elsewhere (Zhou et al. 2006).

4 THE PRPOPOSED THIN OVERLAY HMA MIX-DESIGN PROCEDURE

Within the frame work of the balanced HMA mix-design concept, the mix-design process and OAC selection criterion for thin overlay HMA mixes were formulated as follows:

Step 1: Aggregate sourcing and material-property characteristics

- Review locally available aggregate sources or otherwise import from foreign sources.
- Typically fine graded F rock is recommended. (i.e., 98–100% passing the 9.5 mm sieve and screening materials).
- Aggregates with low soundness value are desired, e.g., granite, crushed gravel, etc.
- High quality fine-graded aggregates with good skid resistance are desired.
- Perform wet sieve analysis prior to any aggregate batching to account for the dust content.

Step 2: Mold HMA specimens at 50 gyrations and 98% target density to determine the OAC

- With at least 3 trial asphalt-binder contents (6.5%, 7.0%, and 7.5% are preferred)
- For each proposed trial asphalt-binder content, determine the Rice density.
- For each trial asphalt-binder content, gyratory mold at least 2 HMA specimens of 150 mm diameter by 125 mm in height.
- Measure the HMA specimen density; target = 98% (to determine the OAC).
- Cut the molded samples to test in HWTT and OT tests for rutting-and cracking-resistance characterization, respectively.
- Select the OAC as the asphalt-binder content simultaneously meeting both the HWTT rutting and OT cracking criteria, i.e., Rut $Depth_{HWTT} \leq 12.5$ mm at 50°C and $N_{OT} \geq 750$ cycles at room temperature. A window of acceptable OAC will usually be determined.
- Preferably draw a graph as shown in Figure 1 to indicate the window of acceptable OAC.

Step 3: OAC verification

- Gyratory mold at least 2 separate HMA specimens at the balanced OAC and 93 ± 0.5% density.
- Then run the HWTT and OT tests to verify the balanced OAC.
- Select the balanced OAC as the design OAC or otherwise select a different OAC within the window of the acceptable balanced OAC determined from Step 2 till the balanced OAC is verified at 93 ± 0.5% density.

For the HWTT and OT tests, the HMA specimens are typically cut from the same gyratory molded sample; be it at 98 or 93 ± 0.5% density. This is to ensure some level of reasonably

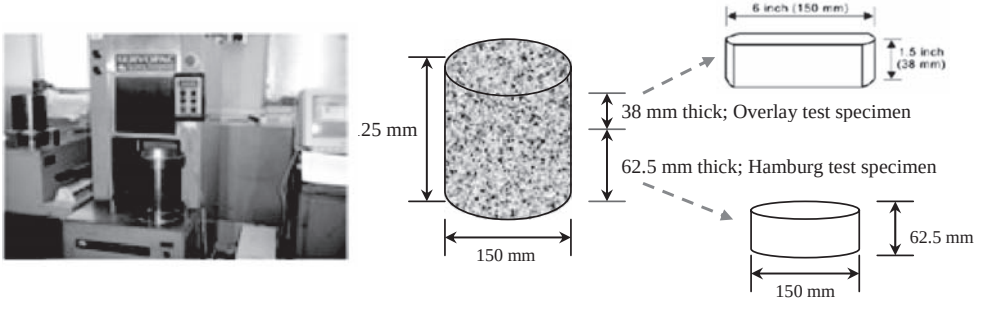

Figure 4. Gyratory molding and sawing of the HWTT and OT specimens.

acceptable consistency in homogeneity and air void uniformity for the test specimens. Figure 4 shows how the samples were gyratory molded and cut to produce HWTT and OT specimens, respectively.

However, one of the critical aspects during specimen sawing is to have parallel and smooth end surfaces for the OT test specimens. In particular, smooth end surfaces are necessary to allow for proper visual monitoring of the crack development during OT testing.

5 MATERIALS AND HMA MIXES

Stiff high PG asphalt-binder grades (mostly PG 76-22S modified with about 5% SBS) were utilized. As pointed out previously, stiff high PG asphalt-binders are relatively less temperature sensitive and therefore not very rut susceptible. Recent studies have also shown that mixes designed with polymer modified asphalt-binders are relatively less susceptible to oxidative ageing and therefore, not as much prone to age-related decline in cracking resistance over time (Walubita et al. 2007, Wisneski 1996). High asphalt-binder content of around 7.0% was utilized.

All the HMA mixes were 9.5 mm NMAS with high quality fine-graded aggregates having an LA abrasion and soundness values of less than 40 and 30, respectively, based on Texas standards (*11*). On average, the limits for the aggregate percent passing the No. 4 (4.75 mm) sieve was about 70% to 90%; larger NMAS mixes are unsuitable and difficulty for placement in layer lifts less than 25 mm thick. For the aggregate percent passing the No. 200 (0.075 mm) sieve, the maximum specification limit was 10% (basically ranging from 2% to 10%); this helps in addressing stability and durability issues (Cooley (Jr) 2002). Lime, on the order of about 1.0 to 1.5%, was also added in some instances to improve the moisture damage resistance properties of the mixes. To ensure good stone-on-stone contact, a high VMA of at least 15% was targeted.

Ten microns was arbitrarily used as the reference bench mark for the asphalt-binder film thickness (T_F) (Pretorius et al. 2004). Note that this T_F was calculated according to the equation expressed below:

$$T_F = 1000\left(\frac{V_{asp}}{SA \times W}\right) \tag{1}$$

where T_F = average binder film thickness in microns; V_{asp} = effective binder volume in liters; SA = aggregate surface area in m^2/kg; and W = aggregate weight in kg. According to Roberts et al. (1996), asphalt-binder film thickness is generally correlated with performance/durability and that thin asphalt-binder films are often more susceptible to oxidation (than thicker binder films) due to the ease of air infiltration into the compacted mix. Rapid asphalt-binder oxidation often results in a more brittle mix and consequently, a decreased resistance to cracking; which is undesirable. This is therefore very critical especially for thin surfacing mixes such as overlays that would be directly exposed to the harshest environmental conditions.

6 DEMONSTRATION EXAMPLES AND LABORATORY TEST RESULTS

In this section, both HMA mixes that were designed and those that were just evaluated using the balanced mix-design concept using the previously described procedure are presented. The HMA mix characteristics including laboratory test results are summarized in Tables 1 and 2 and Figure 5 (TxDOT 2007). An analysis and discussion of each mix is presented in the subsequent text.

6.1 *Vulcan-spicewood CAM mix*

This mix was designed based on the balanced mix-design procedure described in this paper. As evident in Table 2, the mix was satisfactorily verified at 93% density; passing both the laboratory Hamburg and Overlay test requirements, respectively. The laboratory results are shown in Figure 6.

Table 1. Aggregate blend characteristics.

Case study no.	Mix-design (TxDOT)	Aggregate type	Aggregate blend characteristics	Soundness value*	LA abrasion	Polish value	SAC	Source
1. Vulcan-Spicewood	CAM	Limestone (9.5 mm NMAS)	50% F-rock + 50% screenings	6	32	34	B	Vulcan Materials
2. BU 59 Lufkin	CAM	Granite (9.5 mm NMAS)	30% ⅛" NMAS rock + 69% screenings + 1% lime	3	8	24	A	Martin Marietta
3. NCAT	Type D Class A surfacing	Granite (9.5 mm NMAS)	25% D-rock + 35% F-rock + 40% screenings	**–	–	–	–	Jones Mill (AR)
4. US 82 Texakarna	Type F Hybrid	Sandstone (9.5 mm NMAS)	60% F-rock + 40% screenings	10	32	23	A	Martin Marietta

SAC = Surface aggregate classification for wet weather accident reduction program;
*In Texas, the Magnesium Sulfate Soundness test is used; **Data unavailable.

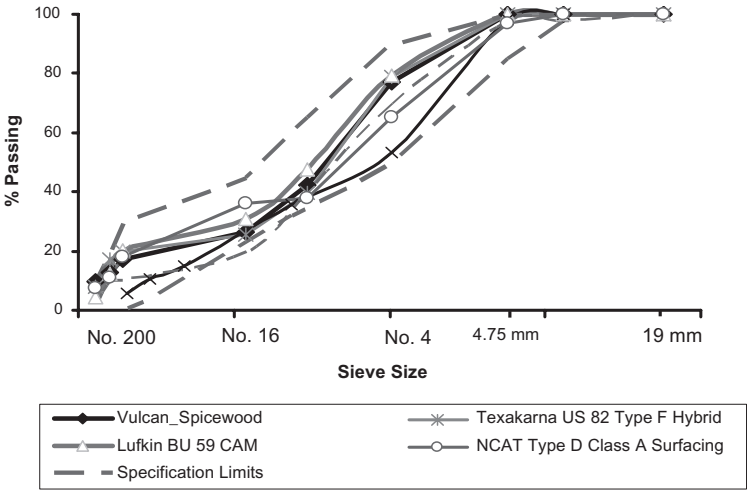

Figure 5. Aggregate gradations.

From Figure 6, the window of acceptable OAC based on the 50 gyrations at 98% density (mix-design) ranges approximately from 7% to 8.3%. This is a reasonable room for OAC selection flexibility. However, the TxDOT verification procedure at 93 ± 0.5% density was satisfactorily met at 7.8% OAC. So, 7.8% was selected as the design OAC for this mix. This mix will be placed on a US highway in the Austin District of Texas, USA. This will facilitate an opportunity to validate the mix-design as well as monitor performance.

6.2 *BU 59 lufkin CAM mix*

As evident in Table 2, this mix equally met all the balanced mix-design requirements at 8.3% OAC. The mix was placed as a 25 mm overlay to rejuvenate an existing pavement downtown in Lufkin (Texas, USA) on business BU 59 highway and is currently under performance

Table 2. Mix-Design characteristics and laboratory test results.

	Mix-design characteristics					Lab test results		
Case study no.	Mix type	Materials	Rice	VMA (AV)	T_F (Microns)	HWTT (mm)	OT (cycles)	Wet SN
1. Vulcan-Spicewood	TxDOT CAM	7.8% PG 76-22S + Limestone	2.418	23.9% (6.9%)	13.68	11.2	750 +	41
2. BU 59 Lufkin	TxDOT CAM	8.3% PG 76-22S + Granite	2.302	20.4% (7.0%)	15.05	7.81	900	44
3. NCAT	TxDOT Type D Class A surfacing	6.7% PG 76-22S + Granite	2.424	15.9% (6.9%)	16.60	3.77	900 +	53
4. US 82 Texakarna	TxDOT Type F Hybrid	7.8% PG 70-22S + Sandstone	2.289	18.8% (6.8%)	15.59	6.78	900 +	40

NMAS = nominal maximum aggregate size; VMA = voids in minerl aggregate; AV = air voids (target AV = 7 ± 0.5%).
T_F = asphalt-binder film thickness (reference bench mark: $T_F \geq 10$ microns).
HWTT = Hamburg wheel tracking test (pass criterion ≤ 12.5 mm rut depth); OT = Overlay tester (pass criterion ≥ 750 load cycles).
SN = skid resistance number based on the Bristih Pendulum (proposd pass criterion is wet SN ≥ 34).

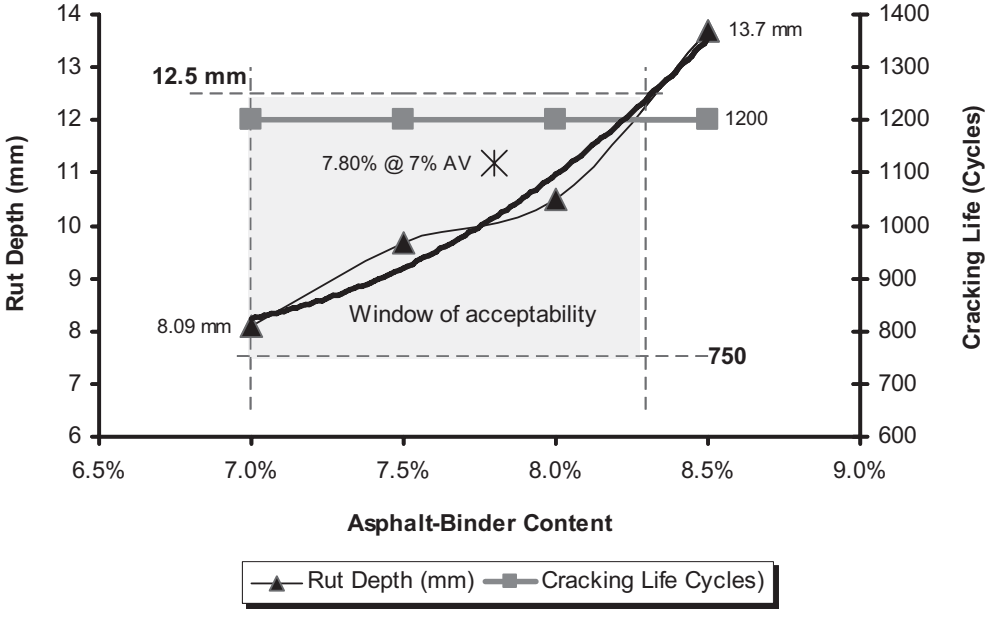

Figure 6. Hamburg-Overlay tests results for the vulcan-spicewood mix.

monitoring. The existing underlying pavement structure is jointed concrete with approximately 75 to 100 mm of existing HMA. Prior to overlay placement, load transfer measurements were conducted and the measured load transfer efficiency was judged as reasonable (>80%). As BU 59 is a high traffic volume city road with a low traffic speed of around 48 km/h to 64 km/h, it will provide an ideal framework to validate the mix-design. Because of the high volume and slow traffic, this will be a critically interesting project to watch out for possible rutting and wheel path bleeding problems.

6.3 *US 82 texakarna—type F hybrid mix*

This mix was initially designed by TxDOT and was used in an emergency work to overlay the severely raveling seal coat on the in-service business highway (US 82) in Texakarna (Texas). The overlay thickness was 25 mm placed over an approximately 1.0 km stretch of the 4-lane business US 82 highway in 2004.

This mix was incorporated in this study for evaluation and verification purpose only; of both the balanced mix-design concept and the initial TxDOT mix-design. Based on the laboratory test results in Table 2, the mix-design was satisfactorily verified at 93% density. As shown in Figure 7, satisfactory field performance has also been observed with this mix after over 2 years of service, with a measured field skid number of 36 (bald tire at 64 km/h). No rutting or reflection cracking has been observed at the time of writing this paper.

6.4 *NCAT type D—class A surfacing mix*

This mix was also included for evaluation and verification purposes, only. The mix was initially designed by TxDOT for accelerated performance-evaluation studies at the NCAT test track in Alabama (USA). The results in Table 2 indicate that the mix satisfactorily met the mix-design verification requirements at $93 \pm 0.5\%$ density. Note that the results in Table 2 are for the Type D plant-mix that was hauled from NCAT.

This mix was placed in a 75 mm layer thickness as the surfacing layer resting directly on a 25 mm rich asphalt bottom layer (RBL). Based on the NCAT preliminary field performance data after 3.0 million ESALs of trafficking, the following performance results have been reported; rut depth of about 9.1 mm (ARAN), about 1578 mm/km average IRI (international roughness index), and about 0.75 mm mean texture depth. Preliminary evidence suggests that the underlying RBL could be the source of this high rutting (9.1 mm). However, elaborate investigative studies are underway to ascertain the actual source of this rutting. Nonetheless, construction could be another probable cause. Although the extracted asphalt-binder content was higher than the design value (i.e., 7.3% versus 5.7% design), the field cores nonetheless passed both the Hamburg (7.31 mm) and Overlay (>750 load cycles) tests, respectively.

Figure 7. TxDOT type F hybrid overlay mix on US 82 (Texakarna, USA).

7 DISCUSSION

The results listed in Table 2 have shown that a balanced mix-design for ensuring adequate rutting and cracking resistance is attainable in the laboratory even for fine-graded 9.5 mm NMAS mixes albeit that field validation remains to be conducted. All the four designed/evaluated mixes were satisfactorily verified at 93 ± 0.5% density. Based on Table 2, the range of the design OAC meeting both the Hamburg (rut depth ≤ 12.5 mm and Overlay (N_{OT} ≥ 750 load cycles) laboratory test requirements is from 6.5% to about 8.5%. The mix VMA is relatively high; greater than 15%. This is essential for ensuring stone-on-stone contact in the mix matrix that is critical for providing the desired rutting resistance; i.e., all the mixes passed the Hamburg test.

The average computed asphalt-binder film thickness was 15.23 microns, which is higher than the 10 microns used as a reference benchmark. With the high asphalt-binder contents shown in Table 2, it was not unexpected that relatively higher T_Fs were obtained. Combined with the low in-situ target AV (about 2 to 3%), this high T_F also adds on to the improved impermeability characteristics of the mix.

On an experimental basis, the British Pendulum (BP) was utilized to measure the wet skid resistance of the molded mixes in the laboratory. This was achieved through testing, under wet conditions, of the test specimens prior to Hamburg testing. If a wet skid number (SN) of 34 is utilized as the threshold (i.e., SN ≥ 34), then all the SN results shown in Table 2 would be considered reasonable; indicating that all the mixes designed/evaluated have sufficient laboratory skid resistance.

8 SUMMARY AND RECOMMENDATIONS

The laboratory data presented in this paper have demonstrated that the balanced mix-design concept can be satisfactorily applied to fine-graded overlay HMA mixes; place-able in thin layer lifts about 25 mm thick or less. These results further provides evidence that the proposed thin overlay HMA mix-design procedure of 50 gyrations at 98% density is potentially promising and must be explored further. Provided that (1) high stiff PG graded asphalt-binders with a relatively high asphalt-binder content and (2) high quality fine-graded (preferably gap-graded) mixes with a high VMA and good stone-on-contact in the mix matrix are used, a balanced mix-design meeting both the Hamburg rutting and Overlay cracking requirements is attainable in the laboratory.

In general, 9.5 mm NMAS HMA mixes with high polymer modified asphalt-binder content of over 7.0% and high quality clean fine aggregates (typically the Granite Type F-rock + screenings) were found to sufficiently meet the proposed laboratory Hamburg rutting and Overlay cracking requirements, i.e., HWTT rut depth ≤12.5 mm and number of OT load cycles ≥750, respectively. However, the currently ongoing laboratory research with more mixes and field demonstration studies will lend further lend credence to the utilization of the balanced mix-design concept and the proposed thin overlay HMA mix-design procedure.

ACKNOWLEDGEMENTS AND DISCLAIMER

The authors are thankful to the Texas Department of Transportation (TxDOT) and the Federal Highway Administration (FHWA) for their support in funding this research study and all those who helped during the course of this research work. In particular, special thanks are due to Lee Gustavus, Tony Baborsa, Nick Sweet, Gautam Das, and Zachary L. Rolan for their help with laboratory work. Special thanks are also due to Mr. Geoffrey Simate Simate (Wits University) and Mr. Sihle Ndlovu (Siral Consulting Engineers Ltd) for their insightful editorial and technical comments on the paper.

The contents of this paper reflect the views of the authors who are responsible for the facts and accuracy of the data presented herein and do not necessarily reflect the official views or policies of any agency or institute. This paper does not constitute a standard, specification, nor is it intended for design, construction, bidding, or permit purposes. Trade names were used solely for information and not for product endorsement.

REFERENCES

Belin P. 1998. Stone Mastic Asphalt in Germany—The Asphalt Yearbook 1998. Stanwell: The Institute of Asphalt Technology.

Cooley (Jr), L.A., James, R.S., and Buchanan, M.S. 2002. "Development of Mix Design Criteria for 4.75 mm Mixes", NCAT Report 02-04. National Center for Asphalt Technology (NCAT), Auburn University, Alabama.

Cooley (Jr), L.A., and Brown, E.R. 2003. "Potential of Using Stone Matrix Asphalt (SMA) for Thin Overlays", NCAT Report 03-01. NCAT, Auburn University, Alabama.

Gilbert, T.M., Olivier, P.A., and Gale, N.E. 2004. "Ultra Thin Friction Course: Five Years on in South Africa". CAPSA, South Africa.

Kandhal, P.S., and Cooley, L.A. 2002. Coarse Versus Fine-Graded Mixtures: Comparative Evaluation of Resistance to Rutting. Report No. 02-02. National Center for Asphalt Technology, Auburn University, Auburn, Alabama.

Kandhal, P.S. and S. Chakraborty. 2005. Effect of Asphalt Film Thickness on Short- and Long-Term Aging of Asphalt Paving Mixtures, Transportation Research Board, 1535, 1996.

MDOT—Michigan Department of Transportation. "Guide Specification for HMA Ultra-Thin". Michigan.

Newcomb, D.E., and Hansen, K.R. 2006. Mix Type Selection for Perpetual Pavements. *CD-Proceedings: International Conference on Perpetual Pavements*. Columbus, Ohio, September 13–15.

Nicholls, J.C., Carswell, I., and Williams, J.T. 2002. "Durability of Thin Asphalt Surfacing Systems: Part 1 Initial Findings". Highway Agency, TRL Report TRL557, UK.

Oliver, J.W. H. 1997. Thin Bituminous Surfacings and desirable Road User Performance. Research Report ARR 325, ARRB Transport Research Ltd.

Pretorius, F.J., Wise, J.C., and Henderson, M. 2004. "Development of Application Differentiated Ultra-Thin Asphalt Friction Courses for Southern African Application". CAPSA, South Africa.

Roberts, F.L., Kandhal, P.S., Lee, D.Y., and Kennedy, T.W. 1996. Hot mix asphalt materials, mixture design, and construction. NAPA Research and Education Foundation, Lanham, Maryland, 187–189.

Rosenberg J. Thin Pavements with Synthetic Binder Used in Denmark. Nordic Road and Transport Research, Journal No. 2, 2000.

Scott, J., Chursinoff, R.W., and White, S. 1990. Performance of Thin Overlays in Saskatchewan. Quebec: Canadian Technical Asphalt Association, Polyscience Publications.

Technical Bulletin. 2002. Smoothseal (ODOT, SS 854, Fine Graded Polymer Asphalt Concrete), Overlays for Use as Preventive Maintenance Surface Treatments. Flexible Pavement Association of Ohio, Ohio (July 2002).

TxDOT. 2007. Online Manuals: ftp://ftp.dot.state.tx.us/pub/txdot-info/cmd/mpl/brsqc.pdf Accessed July 2007.

TxDOT. 2004. Texas Department of Transportation. *Standard Specifications for Construction and Maintenance of Highways, Streets, and Bridges*, Austin, Texas.

Uhlmeyer, J.S. 2003 "Tech Notes—The Use of NovaChip™ as a Surface Treatment". Washington State Department of Transportation (WSDOT) (June 2003).

Walubita, L.F., and A. Epps Martin. 2007. "Laboratory Fatigue Characterization of Asphalt Mixtures Using the Flexural Bending Beam Fatigue Test". *Proceedings*: *Athens 2007 International Conference: Advanced Characterization of Pavements and Soil Engineering Materials,* Athens, Greece (20–22 June 2007).

Wisneski, M.L., Chaffin, J.M., Davison, R.R., Bullin, J.A., and Glover, C.J. 1996. "Use of lime in recycling asphalt." *Transportation Research Record* 1535, Washington, D.C., 117–12.

Yeo, Rey. 1997. Bituminous and Concrete Surfacing Trial: Report on Performance Monitoring. Proceedings of 10th AAPA International Flexible Pavements Conference, Vol 1, paper 25. Perth (Australia).

Zhou, F., Hu, S., and T. Scullion. 2006. Integrated Asphalt (Overlay) Mix Design with Balancing Both Rutting and Cracking Requirements, Technical Report FHWA/TX-05/5123-1, TTI, College Station, Texas, US.

Zhou, F. and Scullion, T. 2005. Overlay Tester: A Rapid Performance Related Crack Resistance Test, Technical Report FHWA/TX-05/0-4467-2, TTI, College Station, US, p. 85.

Advanced Testing and Characterization of Bituminous Materials –
Loizos, Partl, Scarpas & Al-Qadi (eds)
© 2009 Taylor & Francis Group, London, ISBN 978-0-415-55854-9

3D finite element modeling of polymer modified asphalt base course mixes

X. Liu & A. Scarpas
Group of Mechanics of Structural Systems, Faculty of Civil Engineering and Geosciences, Delft University of Technology, Delft, The Netherlands

ABSTRACT: One of the primary goals of this investigation is the development of a material constitutive model capable of describing the non-linear response of SBS modified asphalt mixes in pavements with full depth modification. The parameters of the material constitutive model are obtained from mechanical data of base course asphalt mixes. The model has been verified and implemented into a 3D finite element system that enables the simulation of dynamic non-linear response of the pavement. In this contribution, the details of the material constitutive model and its use for describing the nonlinear behavior of the SBS modified base course mixes are presented. 3D Finite element analyses were run on two different pavement profiles with two different mixes (one is polymer modified mix and another is the non-modified reference mix) being subjected to moving wheel loads. The pavement structure containing polymer modified asphalt showed about four times less damage (accumulated plastic strain) than the non-modified reference mix. Also the effect of the polymer modified asphalt on the rut depth was significant. The results until date have shown that polymer modification can be an effective measure to extend pavement life.

1 GENERAL INTRODUCTION

An ideal asphaltic mix should be capable of maintaining its stiffness characteristics throughout the range of design temperatures. Unfortunately though, real mixes are not ideal and this is not what happens. Because of the temperature sensitivity of the bituminous binder, asphaltic mixes are stiff at low temperatures, prone to cracking and soft at high temperatures, prone to load induced inelastic deformations. Also, with time, the capacity of the binder to bond the aggregates is diminished and raveling occurs.

The use of polymer modified mixes has been found to be capable of (a) reducing the stiffness at low temperatures and, (b) increasing the stiffness at high temperatures. These advantages of polymer modification have widely been recognized for top layer modification in asphalt pavements. The use of polymer modification in base courses is however an area that has hardly been explored. A full-depth polymer modified pavement should bring advantages in terms of durability of the total pavement as well as the possibility to construct thinner pavements. Improving the performance of the traditionally non-modified base courses could lift the overall quality of the asphalt pavement to new levels and to an improved economy.

In previous phases of this study, experimental work done on SBS modified base course mixes showed that modifying the binder with polymers can give better mechanical performance than the reference base course mix without polymer modifiers.

The modification of hard bitumens typically used in base courses requires special SBS polymers to overcome compatibility and workability issues. The results obtained in the earlier phases have shown that these speciall selected polymers provided the largest performance increase.

The work presented in this paper is one part of the study to assess the performance of the special SBS polymer modified base courses. The study is still ongoing hence this paper describes the modeling work done so far.

One of the primary goals of the modeling part of this study is the development of a material constitutive model capable of describing the non-linear response of the SBS modified asphalt mixes. The parameters of the material constitutive model are obtained from mechanical test. The model has been verified and implemented into a 3D finite element system that enables the simulation of dynamic non-linear response of the pavement. This model will be used to evaluate the effects of the modified base courses.

In the first part of this paper, the details of the material constitutive model are presented and its use for describing the nonlinear behaviour of the modified base courses. This includes description of the flow surfaces and the general constitutive framework. Furthermore, a proposed procedure to determine the parameters of the material model is discussed using results of uniaxial monotonic compression and tension tests. Comparisons of model predictions and laboratory measurements at temperatures 20°C and at different deformation rates are presented.

The finite element system CAPA-3D developed at the Section of Structural Mechanics of TU Delft has been utilized as the numerical platform for this study. So far one polymer modified mix and the non-modified reference mix have been evaluated in two asphalt pavement thicknesses: 150 mm and 250 mm. The finite element simulation shows the importance of the damage distribution in the different mixes and different pavement structures Translated in terms of mix design, the results of the finite element analyses reveal the interrelation between the mix characteristics and pavement performance.

2 CONSTITUTIVE MODELLING

2.1 *Flow surface characteristics*

The material constitutive model, which is used to describe the response of the asphalt mixtures is based on the flow surface proposed originally by Desai (1980, 1986, 2001) and further developed by Scarpas (1997), Erkens (2002), Liu (2003) and Medani (2006) resulting in the Asphalt Concrete Response (ACRe) material model.

The chosen form of the surface is given by:

$$F = \frac{J_2}{p_a^2} - \left[-\alpha \cdot \left(\frac{I_1 + R}{p_a} \right)^n + \gamma \cdot \left(\frac{I_1 + R}{p_a} \right)^2 \right] = 0 \tag{1}$$

where I_1 is the first and J_2 is the second stress invariants respectively, p_a is the atmospheric pressure with units of stress, R represents the triaxial strength in tension. In 3D space, Equation (1) represents a closed surface, as shown in Figure 1. The value of the yield function F determines the response of the material to a state of stress. For $F < 0$, the state of stress is within the yield surface and the response of the material is elastic. For $F = 0$, the state of stress is on the yield surface and the response of the material is inelastic. States of stress outside the yield surface cannot exist.

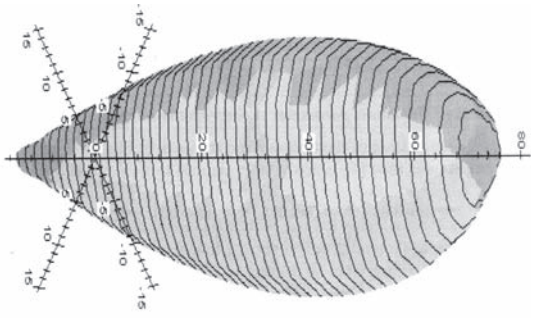

Figure 1. 3D representation of Desai response surface.

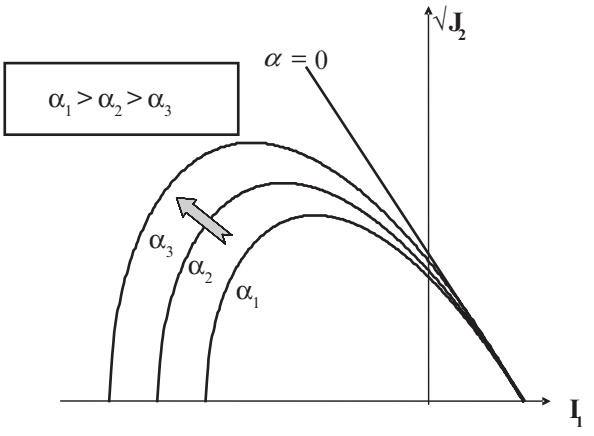

Figure 2. Parameter α determines the size of the response surface.

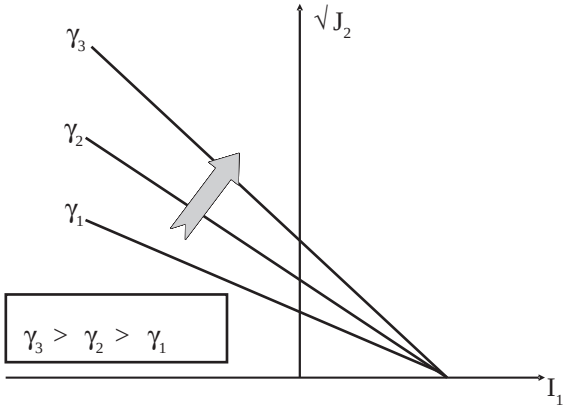

Figure 3. Influence of γ on the ultimate stress response flow surface.

The values of α control the size of the flow surface. It is typically defined as a function of deformation history. As α decreases, the size of the flow surface increases so this parameter controls the hardening of the material. When $\alpha = 0$, the ultimate stress response surface of the material is attained, Figure 2.

Parameter γ is related to the ultimate strength of the material. It denotes the slope of the ultimate stress response surface. As γ increases, the slope of the ultimate response surface increases, Figure 3.

2.2 *Simulation of hardening and softening behaviour*

In this investigation, the hardening and softening response have been emphasized on simulation of material compressive behaviour. Due to the differences in the response mechanism of a compressive and tensile test, The Hoffman response surface will be utilized for simulation of tensile response degradation on crack plane.

2.2.1 *Material hardening*

As discussed earlier, parameter α in the model controls the size of the flow surface. In the constitutive model it is postulated to be a function of the plastic deformation history. In the framework of this investigation, on the basis of laboratory tests for the mixture, the following

relationship was found between α and the effective plastic strain ξ over the range of test data:

$$\alpha = \frac{\alpha_0}{\xi_{\lim}}(\xi_{\lim} - \xi)\exp-(\kappa_\alpha \xi) \tag{2}$$

where α_0 is the α value that corresponds to the initiation of plasticity, $\xi_{\lim}$ is the value of the effective inelastic strain at peak stress and κ_α is a material hardening parameter. Non-linear curve fitting over the available data sets results to the expression of κ_α for the mixture:

$$\kappa_\alpha = \kappa_{\alpha_1}[1 - \exp(-(\beta_T \cdot \dot{\varepsilon})^{\kappa_{\alpha_2}})] \tag{3}$$

where T and $\dot{\varepsilon}$ are the temperature and strain rate respectively.

2.2.2 *Material softening*

An isotropic measure of the degradation response can be introduced into the model to simulate the softening response. This can be done by means of specifying the variation of the model parameter γ, after the initiation of the degradation response, as a decaying function of a monotonically increasing physical quantity (e.g. equivalent post fracture strain ξ^{pf}), strain rate $\dot{\varepsilon}$ and temperature T. The expression of γ is given by:

$$\gamma = \gamma_{\min} + (\gamma_{\max} - \gamma_{\min})\exp[-\eta_1(\xi^{pf})^{\eta_2}] \tag{4}$$

in which $\gamma_{\max}$ and $\gamma_{\min}$ are the value of γ at the point of peak stress and the point of complete annihilation of the material respectively. η_1 and η_2 are material constants.

2.2.3 *Cracking*

The tension softening model proposed by Scarpas and Blaauwendraad (1998) is used. This implies that for states of stress exceeding the magnitude of the fracture surface, a plane of cracking is introduced perpendicular to the principal tensile stress direction. On the crack plane a Hoffman response surface is specified to control the subsequent softening response. The following expression is proposed for the softening in tension:

$$\sigma_t = f_t \cdot e^{-k_t \xi^{pf}} \tag{5}$$

$$\kappa_t = \kappa_{t_1} \cdot (\beta_T \cdot \dot{\varepsilon})^{\kappa_{t_2}} \tag{6}$$

in which σ_t is the tensile stress, $\kappa_{\alpha i}$ (i = 1 – 2) are material constants.

2.3 *Parameter determination*

To determine the parameters of the material model using results of uni-axial monotonic compression and tension tests, a two-steps procedure has been applied. The first step is the setting of the framework and getting the mathematical formulations using the methodology proposed by Scarpas et al. (1997) and Liu (2003). The dependency of the material properties on strain rate and temperature, will be expressed using the unified model presented by Medani (2006). This model allows material parameters like tensile strength, fracture energy etc at a given temperature and strain rate to be estimated from the same parameters as determined at other temperature—strain rate combinations, using a time—temperature superposition principle. This allows definition of the flow surface at any given combination of strain rate and temperature.

In order to interpret the FEM simulation results, it is necessary to introduce the definition of damage. Damage is defined as the cumulative amount of plastic strain (ε^p) in the material. In mathematical terms, damage denoted as ξ can be defined as:

$$\xi = \sqrt{d\varepsilon_{ij}^p : d\varepsilon_{ij}^p} = \sqrt{d\varepsilon_{xx}^p \cdot d\varepsilon_{xx}^p + d\varepsilon_{yy}^p \cdot d\varepsilon_{yy}^p + d\varepsilon_{zz}^p \cdot d\varepsilon_{zz}^p + d\varepsilon_{xy}^p \cdot d\varepsilon_{xy}^p + d\varepsilon_{yz}^p \cdot d\varepsilon_{yz}^p + d\varepsilon_{xz}^p \cdot d\varepsilon_{xz}^p} \tag{7}$$

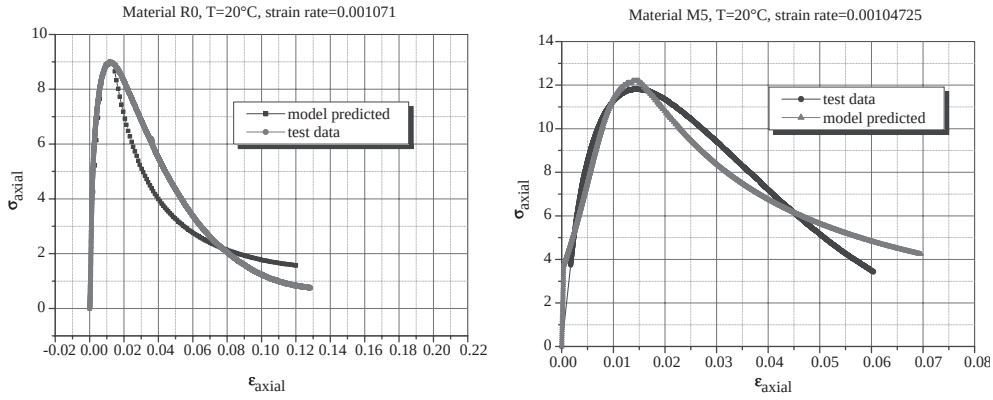

Figure 4. Numerical predictions and actual test data of compression test for non-modified reference mix (left) and polymer modified mix (right).

The total damage can be divided into volumetric and deviatoric (shear) components. The volumetric damage can further be subdivided into compressive volumetric deformation and dilatant tensile volumetric deformation.

This helps in understanding what kind of damage is developed. Compressive volumetric damage is associated with permanent deformation of the material (rutting). Dilantant volumetric damage is associated with cracking. Deviatoric damage is the result of tensile-compressive states of stress and can lead to Mode II associated cracking.

Both the capability of the model and the accuracy of the determination of the parameters can be examined by comparing the numerical predictions of the material response with the observed laboratory behaviour. The proposed constitutive model has been calibrated and verified with the test data. Figure 4 presents two comparisons of the numerical predictions with the results of monotonic compression tests. The left part of Figure 4 shows the model fit for the reference mixture (No. R0) while the right hand part of Figure 4 shows the model fit for a polymer modified mixture (No. M5). The model parameters utilized for each comparison are determined on the basis of the proposed constitutive model. It is observed that the numerical predictions obtained from the constitutive model show good agreement with the experimental results. Because of the complexity of performing the tension test in the laboratory, it is difficult to identify clearly the hardening and the softening regimes from the test data.

3 FINITE ELEMENT ANALYSES

3.1 *Numerical example 1*

Wheel tracking test has been widely utilized to evaluate rutting resistance of asphalt pavement structure because it reflects the cumulative permanent deformation in asphalt layers. Nevertheless, it is common knowledge that when wheel load is imposed on a pavement, a non-uniform displacement field develops giving rise to a multitude of triaxial states of stress. This induces the highly complex nonlinear inelastic characteristics of asphaltic concrete which are difficult to simulate. It is especially true when the loading involves multidimensional stress paths and their reversal. In order to understand the development of triaxial states of stress inside pavement when moving load is applied, in this numerical example, the linearelastic response of a pavement structure was investigated first by means of CAPA-3D. The dynamic analysis option was utilized to subject the model to moving wheel-loading.

The pavement profile was assumed to consist of three material layers, Figure 5. The bottom layer represents a layer of soil with a thickness of h3 = 15 m. The middle layer represents a sub-base material with a thickness of h2 = 0.3 m. The top-layer represents the asphalt

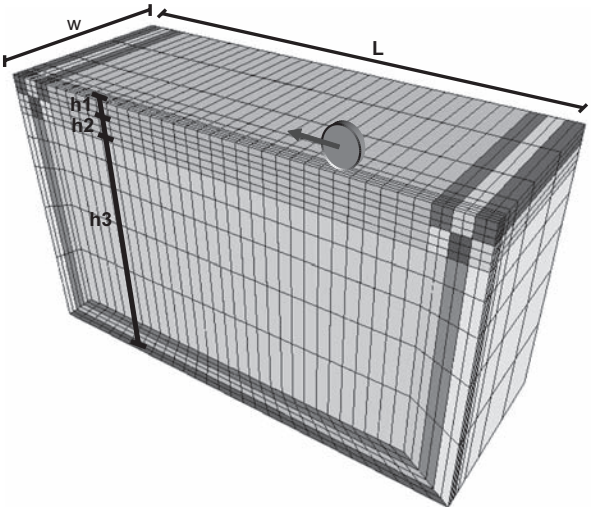

Figure 5. Finite element mesh for moving wheel-load analyses.

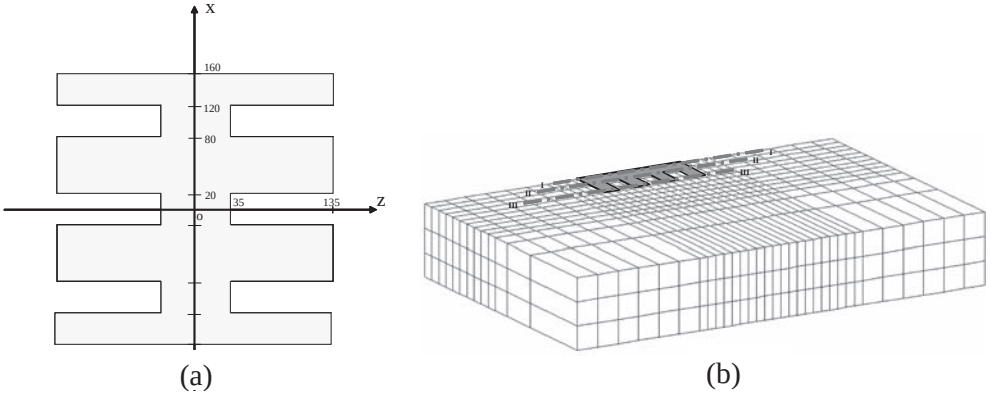

Figure 6. (a) Typical tire imprint; (b) Output locations.

layer with a thickness h1 = 0.15. The asphaltic concrete, the subgrade and the base layer are assumed to behave linear elastically. In order to reduce the dynamic wave reflection, layers of impendence element were introduced to the boundaries of the mesh. Because of symmetry, only a half of the pavement is modeled. The single moving wheel load with speed 60 km/h was applied on the top of the pavement. The axial loads 100kN with 0.8 MPa was considered. Uniform tire pressure and corresponding contact shape of the imprints were utilized in the FE models. Figure 6 (a) shows the simplified tire contact shape considered for analysis along with dimensions.

By means of FEM simulations, as shown in Figure 6 (b), the variations of stress state inside the pavement at three different locations are plotted in Figure 7 and 8.

It is observed that, when wheel load moves on the pavement, typically tension and compressive normal stresses are imposed on the asphalt material, see Figure 7 (a) and Figure 7 (b). The compressive normal stresses result to higher volumetric damage concentration in the vicinity of the wheel. The nature of volumetric damage in this region is compressive indicating the gradual development of permanent deformation (commonly classified as rutting). It can observed also that higher shear stress occurs in xy plane in front of wheel at section I-I (Figure 8 (a) and higher shear stress occurs in yz plane at section III-III, see Figure 7 (b).

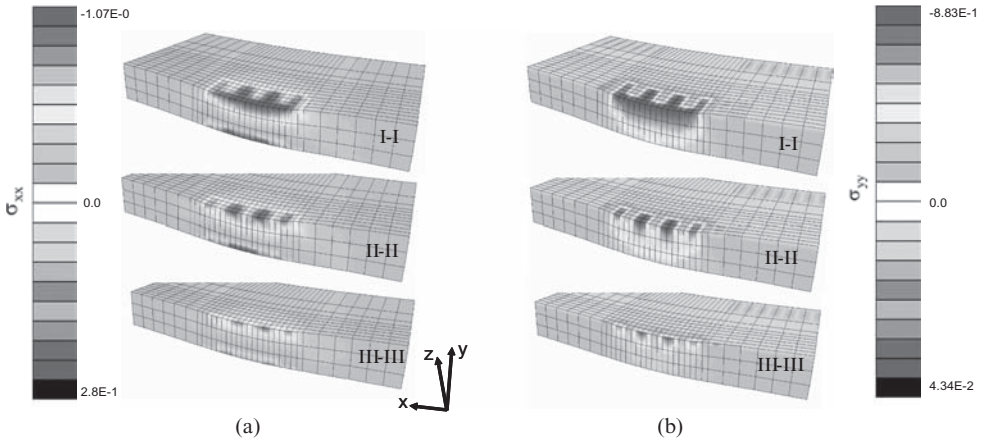

Figure 7. σ_{xx} and σ_{yy} stress distribution inside the pavement.

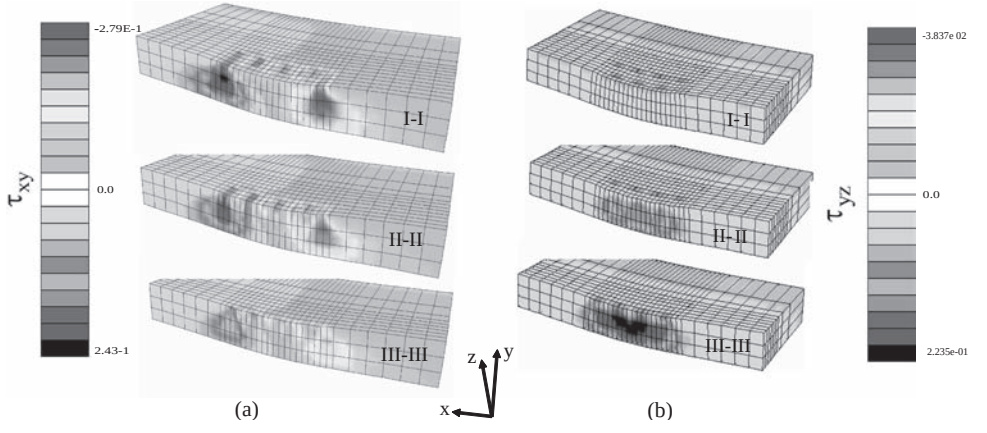

Figure 8. Shear stress τ_{xy} and τ_{yz} distribution inside the pavement.

Table 1.

	Asphalt concrete	Granular subbase	Subgrade
Young's modulus (MPa)	800	300	100
Poisson's ratio	0.35	0.35	0.35
Mass density (kg/m^3)	2300	2000	1500

It should be noted that section I-I stands for a material point directly underneath the center of wheel load and section III-III stands for a material point on the edge of the wheel load. During wheel movement, the direction of shear stress in xy and yz plane is changed continuously. The variation of the higher shear stress in combination with the normal stresses may result to principal stresses that may induce the initiation and gradual development of cracks near the surface of the pavement or near the edge of the wheel load. In next section it is shown that the crack location depends on also the characteristics of the pavement material. Table 1 shows the main material elasticity parameters.

3.2 *Numerical example 2*

Similar as previous example, the pavement profile was assumed to consist of three material layers, Figure 8. The top-layer represents the asphalt layer with nonlinear characteristics. The temperature of the asphalt mixture is assumed to be 20°C. The reference mixture (No. R0) has been compared with a polymer modified mixture (No. M5). In the finite element analyses, two different top layer thicknesses, h1 = 0.15 m and 0.25 m, were investigated. In this study the thicker (0.25 m) pavement with non-modified mixture (No. R0) has been compared with the thinner (0.15 m) pavement with modified mixture (No. M5).

Figure 9 show the different type of damages in the thicker pavement with non-modified and thinner pavement with modified mix after the 10000 traffic load cycles. It can be observed that, at the top of the asphalt layer, higher deviatoric damage can be identified in the vicinity of the edge of the moving wheel. Intense compressive volumetric damage is developed near the pavement surface under the moving wheel. The nature of volumetric damage in this region is compressive indicating the gradual development of permanent deformation (i.e. **rutting**). By comparing the magnitude of damage, it can be observed that pavements with modified mix (No. M5) demonstrate less damage accumulation than pavements with non-modified mix (No. R0), even with a 40% thickness reduction. A comparison between the two pavements clearly indicates the contribution of the modifier in reducing the degree of damage in the body of the pavement.

As was indicated in the previous section, the state of stress in the body of a pavement varies both, in time and space. This induces the highly complex crack development of asphaltic concrete. Figure 10 indicate the initiation of longitudinal cracking at the edge of the wheel as a combination of curvature reversal and deviatoric deformations. A comparison between the two pavements indicates the contribution of the modifier in reducing the degree of crack in the body of the pavement.

Fig. 11 shows the comparison of the surface rut between the two pavements after 10000 traffic load cycles. It can be observed that the maximum rut depth occurring in the thicker

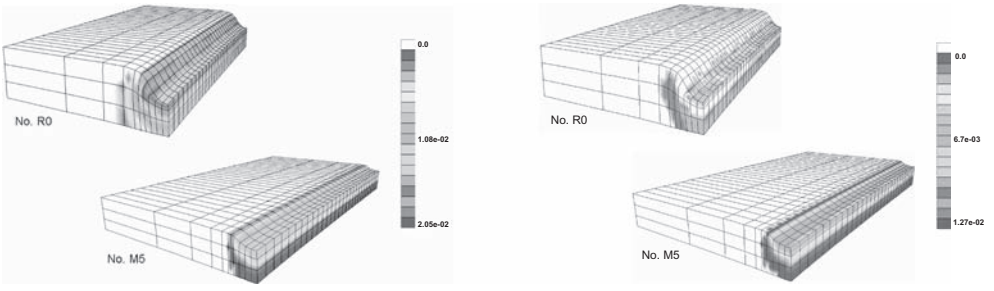

Figure 9. (a) deviatoric damage and (b) volumetric damage distribution inside the two pavements.

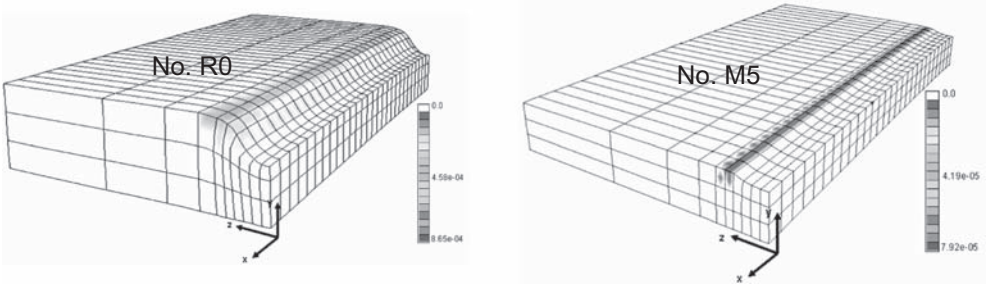

Figure 10. Crack development in the two pavements.

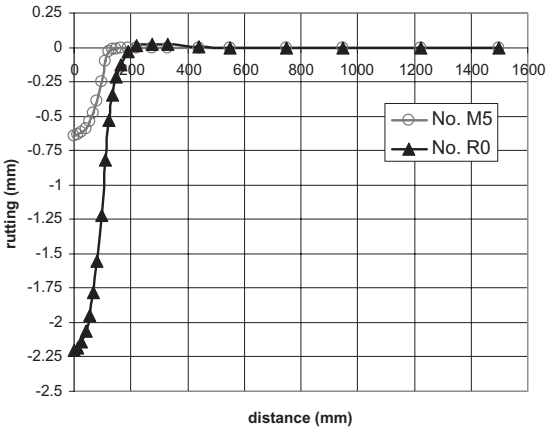

Figure 11. The rutting profile of pavements after 10000 cycles.

pavement with non-modified mix (No. R0) is almost 4 times higher than the thinner pavement with modified mix (No. M5).

4 CONCLUSIONS

The study of full depth modification has resulted in some interesting insights into the performance of non-modified and polymer-modified asphalt pavements. The concept of reducing the asphalt layer thickness in combination with an increased performance (less damage and rutting depth development) has been verified with finite element modelling and has proven to be feasible.

The CAPA-3D wheel tracking numerical simulations of the asphalt mixes have shown a much better performance of the SBS modified mixtures compared to the non-modified reference. The results showed distinct differences both in damage development (accumulated non-recoverable strain) and cracking development between the polymer modified and non-modified pavement. The polymer modified mix contained a tailor made SBS polymer, designed for application in hard base course binders. Even in a thinner pavement structure (150 mm asphalt) the SBS modified asphalt had up to 3 times less damage than a thicker (250 mm) non-modified pavement. Furthermore, the non-modified thicker pavement structure showed almost 4 times more permanent deformation than the SBS modified thin structure.

REFERENCES

Desai, C.S. 1980. A General Basis for Yield, Failure and Potential Functions in Plasticity. *International Journal of Numerical Analytical Methods in Geomechanics*, 4, pp. 377–387.

Desai, C.S., Somasundaram, S. and Frantziskois, G.N. 1986. A Hierarchical Approach for Constitutive Modelling of Geological Materials. *International Journal of Numerical Analytical Methods in Geomechanics,* 8, pp. 19–43.

Scarpas, A, Gurp, C.A.M.P. van, Al-Khoury, R.I.N. and Erkens, S.M.J.G. 1997. Finite Element Simulation of Damage Development in Asphalt Concrete Pavements. *8th International Conference on Asphalt Concrete Pavements,* Seattle, Washington, U.S.A.

Scarpas, A. and Blaauwendraad, J. 1998. Experimental Calibration of a Constitutive Model for Asphaltic Concrete. In: *proceeding of Euro-C Conference on the Computational Modelling of Concrete Structures*, Badgastein, Austria.

Desai, C.S. 2001. Mechanics of Materials and Interface: The Disturbed State Concept, CRC Press LLC, New York, U.S.A.

Erkens, S.M.J.G. 2002. Asphalt Concrete Response (ACRe), Determination, Modelling and Prediction. PhD. Thesis, Delft University of Technology, the Netherlands.
Liu, X. 2003. Numerical Modelling of Porous Media Response Under Static and Dynamic Load Conditions. PhD Thesis, Delft University of Technology, the Netherlands.
Medani, T.O. 2006. Design Principles of Surfacings on Orthotropic Steel Bridge Decks. PhD Thesis, Delft University of Technology, the Netherlands.

Advanced Testing and Characterization of Bituminous Materials –
Loizos, Partl, Scarpas & Al-Qadi (eds)
© 2009 Taylor & Francis Group, London, ISBN 978-0-415-55854-9

Neural networks in rheology: Theory and application

M. Oeser
The University of New South Wales, Sydney, Australia

S. Freitag
Technische Universität Dresden, Dresden, Germany

ABSTRACT: A neural network based concept for modeling the rheological behavior of asphalt is presented in this paper. The network is used to replace a special group of rheological elements that require the storage of the entire stress history during the analysis process. A strategy is developed that explains the design of more complex rheological models by combining neural networks with springs and other rheological elements. The new concept focuses on the creep and energy dissipation characteristics as well as on the special memory effects observed when asphalt is subjected to time varying loads. The networks are trained by means of data obtained from six different simulations using creep loads as well as cyclic loading. The network architecture as well as a complete set of network parameters is presented in this paper. A numerical validation of the network has been carried out and the network performance was tested.

1 INTRODUCTION

Rheological models are widely used to mathematically describe the behavior of materials that exhibit viscous deformation characteristics. The majority of these rheological models are based on time derivatives of integer order, e.g. NEWTON body, MAXWELL body, KELVIN body or BURGERS body. To determine the parameters of these rheological models creep tests are used. Creep-recovery tests usually consist of a loading phase followed by a phase without loading. The loading phase can be used to study the creep strain development while the phase without loading delivers information on the strain recovery. However, research has shown that it is not possible to match both phases (the creep strain development and the strain recovery) with only one set of parameters when time derivatives of integer order are used for the rheological formulation, see (Pellinen et al., 2007). A method to solve this problem has arisen with rheological models on the basis of time derivatives of real order. In this paper rheological models that are based on time derivatives of integer order are called conventional rheological models, while models based on real order time derivatives are referred to as fractional rheological models. A comprehensive foundation on fractional rheological modeling of visco-elastic materials is given in (Schmidt, 2003). The characteristic creep strain development and strain recovery behavior of fractional rheological elements is discussed in (Aschenbrenner, 2006) and (Oeser, et al. 2008). The mathematical basis for the fractional differential formulation is provided in (Diethelm, 2003) and (West et al., 2003).

In (Diethelm, 2003) it is also shown that fractional differential equations exhibit special time-history characteristics. These characteristics need to be considered when incorporating boundary conditions into the solution of the fractional differential equation, which is discussed in (Oeser et. al. 2008a). When modeling the behavior of viscous materials by means of fractional rheological elements, the development of strain at a certain point in time is not only influenced by the current strain state and the current stress rate, but also by the entire stress history. For an incremental solution this leads to a significant increase in the computational effort, as all stress states of all previous increments have to be available in order to determine the strain of the new increment. The computational effort increase linearly with the number of increments analyzed.

To overcome this problem the fractional creep functions have been approximated by a certain number of DIRICHLET-series in (Aschenbrenner, 2006). If DIRICHLET-series are used instead of fractional creep functions the influence of the strain history on the new strain increment can be lumped in one factor per series. However, for long load duration, the DIRICHLET-series and the fractional creep functions deviate from each other, as the DIRICHLET-series exhibit a strain limit while the fractional creep functions predict infinite strain for infinite loading time. There are a number of papers that have been published more or less recently, which contain attempts and strategies to reduce the computational effort associated with the aforementioned time-history effects of the fractional differential equation, e.g. (Padovan, 1987), (Podlubny, 1999), (Ford, 2001), (Schmidt et al., 2002) and (Aschenbrenner, 2006). The majority of these papers focus on the fading impact of previous strain states on the new strain increment with progressing time. In some of the papers mentioned above it is speculated that stress states with a certain distance in time can be neglected. This might or might not lead to accurate computational results. In any case, the strategies proposed in these papers require the definition of a "time horizon" that separates between a range in time where strain history does have impact on the new strain development and a range in time with no impact. To be sure about the appropriateness of the defined 'time horizon' the computation should be repeated using different 'time-horizon' positions.

In (Oeser et al. 2008a) an artificial neural network has been developed that represent the response of a fractional NEWTON body. There, it was shown that through the application of the network it was possible to overcome the aforementioned restrictions and numerical difficulties that are associated with the use of fractional rheological models. Furthermore, the computational time-need of the different approaches based on fractional rheological bodies was compared against the time need of the neural network approach. Thereby, it turned out that the neural network approach requires much less operations than the rheological approaches when large numbers of increments are analyzed. In the research that is presented here, the neural network that has been developed in (Oeser et. al. 2008a) will be used to capture the time dependent behavior of asphalt mixes. Thereby the network is connected to other networks and to springs to form more complex models. This method is similar to the "in series" and "in parallel" coupling of dashpots and springs that is frequently used when modeling the material behavior with conventional and fractional rheological bodies. To accomplish the goals of the research presented here, the following steps have been carried out: (A) in section two a neural network that represents a fractional dashpot is developed and trained, (B) the performance of the network is verified in section three, and (C) the network is coupled with other networks and springs in section four. The outcome of further performance and accuracy tests using loading schemes that have not been utilized for training purposes are also included in section three. Section five contains a summary.

2 NEURAL NETWORK

The artificial neural network concept is adapted from the structure and function of human brains. In (Haykin, 1999) and (Zell, 1996) various types of artificial neural networks are described. Nowadays, neural networks are used in many engineering applications, e.g. parameter identification, response surface approximation, long-term prediction, etc. The widely-used type in these applications is the multilayer perceptron network with feed forward architecture.

2.1 *Recurrent network architecture*

The strain response of materials like asphalt is characterized by a so called fading memory phenomenon. Fading memory phenomenon means that stress states (that have been applied to the material with a certain distance in time) gradually loose there impacts on the future material behavior. Fading memory is a special mode of time-history dependant behavior of materials. In most of the publications fading memory is referred to as the fading impact of previously imposed stresses on the future strain response of materials, while the declining

impact of previously imposed strain states is attributed to time-history effects. For linear material behavior time-history and fading memory are identical. It has been shown in (Oeser, et. al. 2008) that fading memory phenomena can be captured by means of the fractional rheological concept. However, using this concept requires the consideration of the whole chronology of the loading process as mentioned above.

In order to capture fading memory/time-history effects with neural networks a network-architecture with internal time representation is required. For this purpose a network with a special feedback structure can be used. Here, a partial recurrent structure is chosen. That is, the signal flow occurs in the forward direction through the network. The fading memory is realized by internal feedback connections. During the training process the output error is traced back in the backward direction.

In Figure 1 an example of a possible network structure is shown. The network consists of an input layer, three hidden layers and an output layer. The input neuron is fed with the stress $^{[n]}\sigma$ at a fixed point in time $^{[n]}t$. The transformation of the stress into an input signal $^{[n]}\sigma^{(1)}$ is performed using Equation (1) in which σ_{max} denotes the maximum stress for which the network shall be used.

$$^{[n]}\sigma^{(1)} = \frac{^{[n]}\sigma}{\sigma_{max}} \tag{1}$$

The output neuron yields an approximation of the memory stress $^{[n]}\sigma_h^{(M)}$. The strain response $^{[n]}\varepsilon^{(M)}$ can be obtained from Equation (2), where Δt is the time step, p and α are material parameters and Γ is the Gamma-function.

$$^{[n]}\varepsilon^{(M)} = \frac{\Delta t^{\alpha} \cdot \sigma_{max}}{p \cdot \Gamma(\alpha+2)} \cdot {}^{[n]}\sigma_h^{(M)} \tag{2}$$

Scope of the training process is to reduce the approximation error between the exact strains and the strains predicted through the neural network. If the network is meant to replace a particular rheological body as it was done in (Oeser et. al. 2008a) for a fractional dashpot, the exact strain are determined from the strain response of this body. However, neural networks can also be used to directly capture the results of material tests. In this case the exact strain would be obtained from the test results. This is not further examined in this paper, as the authors do not see the neural network as a substitute for a proper constitutive law, but as a mathematical tool that can replace fractional dashpots. There are two reasons for this attitude: (A) if the network only replaces the fractional dashpots in complex rheological models, than the other bodies like springs and sliders will remain inside the models. Springs and sliders are often linked to constitutive formulations that govern the three-dimensional strain development of rheological materials. These formulations would not be affected by the networks. And, (B) existing models that have already been calibrated and implemented into source-code of numerical analysis programs can easily be upgraded by means of the networks without influencing the response of those models, but improving their numerical characteristics and performance. The parameters p and α in Equation (2) are the viscosity and the order of the fractional derivative, see (Oeser, et. al. 2008). In (Olard et. al., 2003) and in other publications the fractional dashpots are called parabolic elements. Combinations of those parabolic elements with other rheological elements like springs and conventional dashpot were developed in (Olard et. al., 2003). These combinations are widely used and have been proven very effective and accurate. For some of these combinations of rheological elements similar numerical problems exists like the once mentioned above. The particular formulation that has been chosen for the research that is presented here also provides solutions to these problems.

In Figure 1 the architecture of a partial recurrent network is shown. It can be denoted as a hierarchical ELMAN Network, see (Zell, 1996). The internal feedback loops enable the consideration of the stress history for the determination of the new strain increment.

The neurons of the hidden layers as well as the output layer (filled circles in Figure 1) are connected to context neurons (blank circles in Figure 1), which are located in the previous layer. The context neurons send weighted signals to the hidden neurons. These signals are sent with a time delay. The signal processing in the neurons is realized with the aid of activation functions. The activation functions may be of various kinds. Herein, a nonlinear activation function is used for the hidden neurons. The output neuron converts their inputs with a linear activation function.

2.2 *Prognosis*

In Figure 2 the structure of a neuron, which is a part of the network shown in Figure 1, is displayed. Neuron (k) is a member of the network layer (m). In view of a general description the total number of synaptic connections (J), which corresponds to the number of hidden neurons in the previous layer (m-1), and the number of synaptic connections (I), which corresponds to the number of context neurons in the previous layer (m–1), are defined as variables.

The input signals $^{[n]}x_j^{(m-1)}$, which are the output signals of the hidden neurons of the previous layer (m–1), are multiplied by the synaptic weights $w_{kj}^{(m)}$ and lumped together in a summing junction. This yields to the first term in Equation (3). Additionally, a second term,

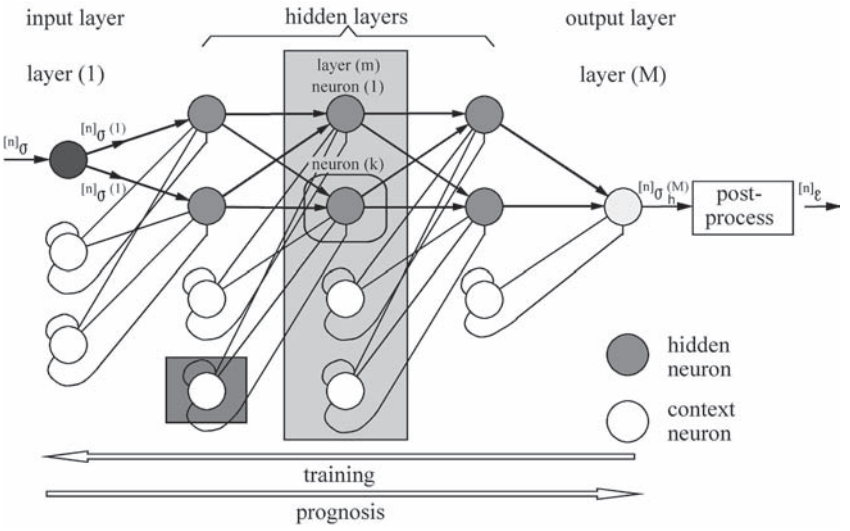

Figure 1. Architecture of a partial recurrent network.

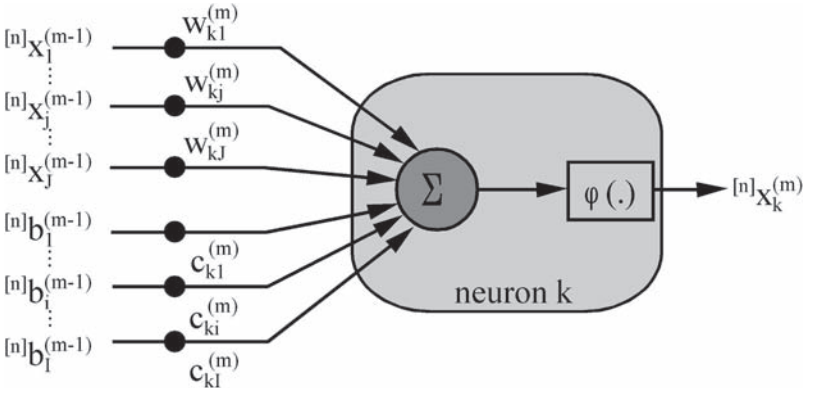

Figure 2. Construct of a neuron with synaptic connections.

which includes the history signals $^{[n]}b_i^{(m-1)}$ multiplied by the context weights $c_{ki}^{(m)}$, is added. Specifically, the signals are processed according to.

$$^{[n]}v_k^{(m)} = \sum_{j=1}^{J} w_{kj}^{(m)} \cdot {}^{[n]}x_j^{(m-1)} + \sum_{i=1}^{I} c_{ki}^{(m)} \cdot {}^{[n]}b_i^{(m-1)} \quad \text{for} \quad k = 1, 2, \ldots, K \tag{3}$$

K is the total number of neurons in layer (m). For the first time step (n = 1) no history is to be considered. That is, $^{[1]}b_i^{(m-1)} = 0$ for i = 1, 2, …, I. In this case the second term of Equation (3) is zero. In the following time steps (n > 1) the history signal $^{[n]}b_i^{(m-1)}$ is calculated with the previous (in time) output signals $^{[n-1]}x_j^{(m)}$ of the neurons in layer (m).

$$^{[n]}b_i^{(m-1)} = {}^{[n-1]}x_i^{(m)} \cdot \gamma_i^{(m-1)} + {}^{[n-1]}b_i^{(m-1)} \cdot \lambda_i^{(m-1)} \quad \text{for} \quad i = 1, 2, \ldots, I \tag{4}$$

In Figure 3 the construct of a context neuron is shown. The factors $\gamma_i^{(m-1)}$ in Equation (4) are the memory factors, which have to be chosen in the interval [0,1]. For $\gamma_i^{(m-1)} = 0$ no history is considered. If all memory factors in the partial recurrent network are zero, a typical feed forward network is obtained as a special case. For $\gamma_i^{(m-1)} \to 0$ the influence of the history on the new signal decreases. The factors $\gamma_i^{(m)}$, for m = 1, …, M–1 of the partial recurrent network are chosen randomly in the interval [0,1], and than kept constant throughout the training process. The factors $\gamma_i^{(m-1)}$ in Equation (4) are the feedback factors that are also chosen randomly in the interval [0,1], and remain unchanged during the training.

To produces the output signal $^{[n]}x_k^{(m)}$ of neuron (k) the result of Equation (3) $^{[n]}v_k^{(m)}$ is used as input value for the activation function $\phi(.)$, see Figure 2.

$$^{[n]}x_k^{(m)} = \varphi({}^{[n]}v_k^{(m)}) = a \cdot ar\sinh({}^{[n]}v_k^{(m)}) \tag{5}$$

Herein, a nonlinear activation function in the form of the area hyperbolic sine is used for the hidden neurons. The $\text{arsinh}(^{[n]}v_k^{(m)})$ is a sigmoide function, which does not exhibit a limit for $v \to \pm\infty$. If the neuron (k) is the output neuron, the activation function is linear:

$$^{[n]}x_k^{(M)} = \varphi({}^{[n]}v_k^{(M)}) = a \cdot {}^{[n]}v_k^{(M)} \tag{6}$$

Note that $^{[n]}x_k^{(M)}$ equals $^{[n]}\sigma_h^{(M)}$. The parameter a in Equation (5) and (6) is a scaling factor that needs to be chosen in dependence of the problem, see section five. In contrast to the memory factors $\gamma_i^{(m)}$ and the feedback factors $\lambda_i^{(m)}$, (that are randomly chosen and than kept constant) the weights $w_{kj}^{(m)}$ and the context weights $c_{kj}^{(m)}$ enable the neuron to be adjusted to particular conditions. This is realized in the training process.

2.3 *Network architecture and training (network preparation)*

The neural network used in (Oeser et al. 2008a) consists of one input neuron, two hidden layers and one output neuron. The first hidden layer possesses four neurons $J^{(2)} = 4$ and

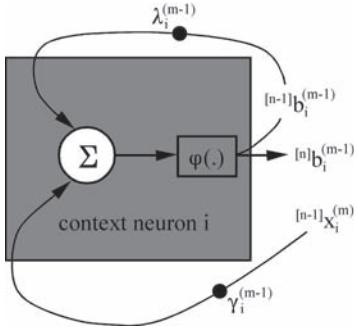

Figure 3. Construct of a context neuron with synaptic connections.

the second hidden layer consists of three neurons $J^{(3)} = 3$. The network structure may be summarized as [1,4,3,1] architecture. As mentioned in section two, each hidden neuron and the output neuron have one context neuron in the previous layer. That is, the total number of context neurons is 8. The training of the network was conducted with six different stress-time functions (u = 1, 2, …, 6, dashed lines in Figure (4), ${}^{[n]}_{u}\sigma$) considering creep as well as cyclic loading. The parameter a in Equation (5) and (6) was set to 0.75. The network training yielded the following weights, context weights, memory factors and feedback factors:

The approximation quality of the network is shown in Figure 4. It was found in (Oeser et. al. 2008a) that the network was capable of learning the training data with a very high accuracy.

3 NETWORK PERFORMANCE

The data prediction quality of the network was studied with the aid of four (g = 1, 2, 3, 4) stress input series that had not been used when training the network, (see Figure (5) dashed lines, ${}^{[n]}_{g}\sigma$). The outcome of this study is shown in Figure 5 by comparing ${}^{[n]}_{g}\sigma_h$ with ${}^{[n]}_{g}\sigma_h^{(M)}$. Again, a very high good fit between desired response and network prediction was achieved. In addition to the tests that are shown here, further performance tests were conducted in (Oeser et. al. 2008a). In all the tests it was found that the network predictions and the desired responses concur almost exactly.

With the network, the parameters given in Table 1 to 3 and with Equation (2) the strain response of fractional dashpots that are subjected to arbitrary load processes can be determined. Thereby, the storage of only eight internal variables is necessary. The model has been trained for a rheological behavior of order $\alpha = 0.25$. If α differs from 0.25 the training of additional artificial neural networks is necessary. For future research, the authors intend to introduce α as input value of the network by adding one more input neuron. Therewith, it will become possible to create networks that capture the entire spectrum of rhological behavior, which is characterized through $\alpha = [0, 1]$.

4 COUPLING OF RHEOLOGICAL ELEMENTS AND NETWORKS

4.1 *In-series coupling*

The coupling of the network with other elements like springs, conventional dashpots and/or sliders can be accomplished by adding the strain components of the single elements if "in series" coupling is investigated. Figure 6 demonstrates the approach for a fractional Maxwell element that consists of a spring and a fractional dashpot. The fractional dashpot

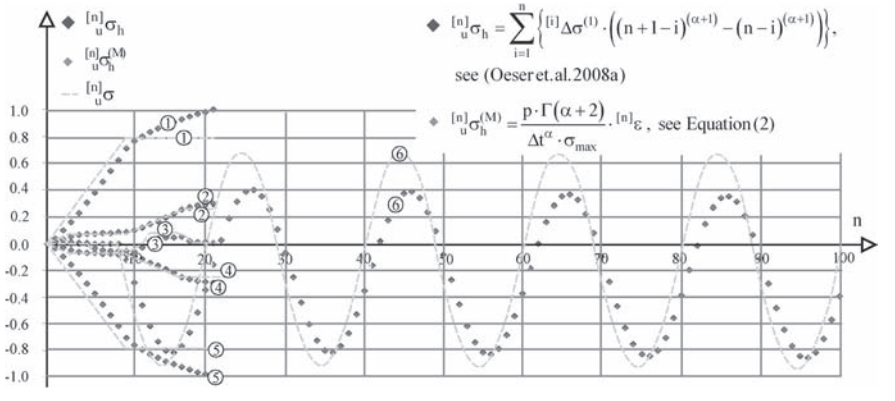

Figure 4. Desired response ${}^{[n]}_{u}\sigma_h$ and network prognosis ${}^{[n]}_{u}\sigma_h^{(M)}$—network training.

Table 1. Weights.

j	$w^{(2)}_{j^{(2)}1^{(1)}}$	$w^{(3)}_{1^{(3)}j^{(2)}}$	$w^{(3)}_{2^{(3)}j^{(2)}}$	$w^{(3)}_{3^{(3)}j^{(2)}}$	$w^{(4)}_{1^{(4)}j^{(3)}}$
1	0.41503	1.39928	0.84422	0.36649	2.47083
2	1.18464	–0.69190	0.46819	0.27021	1.24446
3	–0.70596	–0.79876	–0.04512	–0.18935	0.72403
4	0.09859	–0.30528	1.02783	0.70018	

Table 2. Context weights.

j	$c^{(2)}_{1^{(2)}j^{(2)}}$	$c^{(2)}_{2^{(2)}j^{(2)}}$	$c^{(2)}_{3^{(2)}j^{(2)}}$	$c^{(2)}_{4^{(2)}j^{(2)}}$	$c^{(3)}_{1^{(3)}j^{(3)}}$	$c^{(3)}_{2^{(3)}j^{(3)}}$	$c^{(3)}_{3^{(3)}j^{(3)}}$	$c^{(4)}_{1^{(4)}j^{(4)}}$
1	–0.07591	–0.34930	–0.03401	0.46056	0.00635	0.60712	0.47619	0.09893
2	0.08103	0.35399	0.32246	0.42950	–0.00605	–0.30638	0.16863	
3	–0.26667	–0.32004	–0.06083	0.16464	0.79990	0.32929	–0.28046	
4	–0.74897	–0.96929	–0.55943	0.34662				

Table 3. Memory factors and feedback factors.

j	$\gamma^{(1)}_{j^{(2)}}$	$\gamma^{(2)}_{j^{(3)}}$	$\gamma^{(3)}_{j^{(4)}}$	$\lambda^{(1)}_{j^{(2)}}$	$\lambda^{(2)}_{j^{(3)}}$	$\lambda^{(3)}_{j^{(4)}}$
1	0.33493	0.00808	0.27825	0.39499	0.22260	0.95869
2	0.36166	0.26433		0.46886	0.97551	
3	0.73974	0.48050		0.11525	0.73928	
4	0.16426			0.36161		

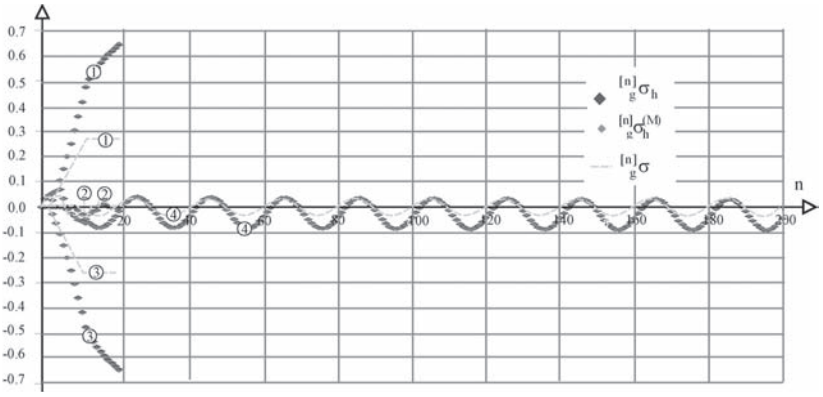

Figure 5. Desired response $^{[n]}_{g}\sigma_{h}$ and network prognosis $^{[n]}_{g}\sigma_{h}^{(M)}$—network verification.

is replaced by the neural network that has been discussed above. (The capitals ANN in Figure 6 stand for artificial neural network)

If the elements in Figure 6 are subjected to the stress $^{[n]}\sigma$, the neural network will yield the strain $^{[n]}\varepsilon^{(M)}$ while the spring will exhibits the strain $^{[n]}\varepsilon^{el}$. The network strain $^{[n]}\varepsilon^{(M)}$ can be determined with Equation (2) and the spring strain is calculated from Equation (7).

$$^{[n]}\varepsilon^{el} = \frac{^{[n]}\sigma}{E_0} \tag{7}$$

Following the small strain concept, the strain in the fractional Maxwell element $^{[n]}\varepsilon$ is obtained by adding the network strain and the spring strain. Note that the memory stress $^{[n]}\sigma_h^{(M)}$ is a function of the current stress $^{[n]}\sigma$ and all previous stresses $^{[n]}\sigma$ with i = 1, 2, …, n–1.

$$^{[n]}\varepsilon = \frac{^{[n]}\sigma}{E_0} + \frac{\Delta t^{\alpha} \cdot \sigma_{\max}}{p \cdot \Gamma(\alpha+2)} \cdot {}^{[n]}\sigma_h^{(M)} \tag{8}$$

In numerical analysis processes, incremental formulations are generally used rather than formulations based on total stress and total strain values. The mathematical operations in Equation (8) are than carried out using strain increments $^{[n]}\Delta\varepsilon$ and stress increments $^{[n]}\Delta\sigma$, $^{[n]}\Delta\sigma_h^{(M)}$.

$$^{[n]}\Delta\varepsilon = \frac{^{[n]}\Delta\sigma}{E_0} + \frac{\Delta t^{\alpha} \cdot \sigma_{\max}}{p \cdot \Gamma(\alpha+2)} \cdot {}^{[n]}\Delta\sigma_h^{(M)} \tag{9}$$

The stress increment $^{[n]}\Delta$ in Equation (9) depends on the stress $^{[n]}\sigma$ as well as on the total stress of the previous increment $^{[n-1]}\sigma$ and can be determined by means of Equation (10).

$$^{[n]}\Delta\sigma = \left[{}^{[n]}\sigma - {}^{[n-1]}\sigma \right] \tag{10}$$

The determination of the memory stress increment $^{[n]}\Delta_h^{(M)}$ at increment [n] can also be determined by subtracting the total memory stress $^{[n]}\sigma_h^{(M)}$ at [n–1] from the total memory stress $^{[n-1]}\sigma_h^{(M)}$ at [n].

$$^{[n]}\Delta\sigma_h^{(M)} = \left[{}^{[n]}\sigma_h^{(M)} - {}^{[n-1]}\sigma_h^{(M)} \right] \tag{11}$$

The total memory stresses $^{[n]}\sigma_h^{(M)}$ and $^{[n-1]}\sigma_h^{(M)}$ depend on all previous stress increments. However, this does not mean that all these stress increment must be kept in the memory as $^{[n]}\sigma_h^{(M)}$ and $^{[n-1]}\sigma_h^{(M)}$ are determined with the neural network and the use of the network only requires knowledge of the current total stress $^{[n]}\sigma$ and the history signals $^{[n]}b_i^{(m-1)}$, see section two.

4.2 *Parallel coupling*

Parallel-coupling of rheological elements can be accomplished by subjecting the elements to a defined strain $^{[n]}\varepsilon^{el}$ and adding the stresses of the individual elements. This is demonstrated by means of a fractional Kelvin element, (see. Figure 7 and Equation (12)).

$$^{[n]}\sigma = {}^{[n]}\sigma^{(SPRING)} + {}^{[n]}\sigma^{(ANN)} \tag{12}$$

The variable $^{[n]}\sigma^{(SPRING)}$ denotes the amount of stress that is transferred through the spring. The relationship between the stress in the spring $^{[n]}\sigma^{(SPRING)}$ and the stain $^{[n]}\varepsilon$ is given by Equation (13).

$$^{[n]}\sigma^{(SPRING)} = E_1 \cdot {}^{[n]}\varepsilon \tag{13}$$

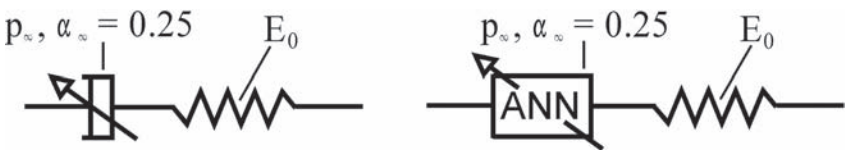

Figure 6. Fractional Maxwell element with fractional dashpot and artificial neural network.

The variable ${}^{[n]}\sigma^{(ANN)}$ represents the stress component in the artificial neural network. In order to derive a relationship between ${}^{[n]}\sigma^{(ANN)}$ and ${}^{[n]}\varepsilon$, two different solution methods can be proposed: (A), an inverse network is trained, using the stresses as training data and the strain as input values. However, this solution strategy requires two networks with two different approximation qualities when rheological elements are considered that consist of both Maxwell elements and Kelvin elements like the Burgers body. Therefore, this strategy is not further pursued. (B), A more sophisticated solution strategy arises from the special mathematical characteristics of the artificial neural network. This is, if the network is fed in increment [n] with the stress of the pervious increment [n–1] it yields the memory stress ${}^{[n]}\sigma_h^{*(M)}$ as well as the history signals ${}^{[n]}b_i^{*(m-1)}$. The strain response of the network (that is determined with Equation (2)) is than equivalent to a creep strain increment under a constant stress, (see. Figure 8). As this does not necessarily represent the true loading scenario in increment [n] (where the stress might well change) the previous history signals ${}^{[n-1]}b_i^{(m-1)}$ are not updated by ${}^{[n]}b_i^{*(m-1)}$ and only ${}^{[n]}\sigma_h^{*(M)}$ is kept in the memory. After that the increment is repeated with the true stress ${}^{[n]}\sigma^{(ANN)}$ and the true memory stress ${}^{[n]}\sigma_h^{(M)}$ as well as the true history signals history signals ${}^{[n]}b_i^{(m-1)}$ are determined. The true history signals are used to update the previous history signals, and by this, the network is prepare for the next increment [n+1]. The difference between the true history stress ${}^{[n]}\sigma_h^{(M)}$ and ${}^{[n]}\sigma_h^{*(M)}$ yields the stress increment ${}^{[n]}\Delta\sigma^{(ANN)}$, (see Figure 8 and Equation (14)).

$$ {}^{[n]}\Delta\sigma^{(ANN)} = \left({}^{[n]}\sigma_h^{(M)} - {}^{[n]}\sigma_h^{*(M)} \right) \cdot \sigma_{\max} \tag{14} $$

Equation (14) and Equation (2) are now used to develop a relationship that yields the strain increment of the network in the Kelvin element.

$$ {}^{[n]}\varepsilon = \frac{\Delta t^{\alpha}}{p \cdot \Gamma(\alpha+2)} \cdot {}^{[n]}\Delta\sigma^{(ANN)} + \frac{\Delta t^{\alpha} \cdot \sigma_{\max}}{p \cdot \Gamma(\alpha+2)} \cdot {}^{[n]}\sigma_h^{*(M)} \tag{15} $$

The variable ${}^{[n]}\sigma_h^{*(M)}$ only depends on known values, namely the stress increment up to and including increment [n-1]. Note: ${}^{[n]}\sigma_h^{*(M)}$ was determined by feeding the network at increment [n] with the stress ${}^{[n-1]}\sigma^{(ANN)}$. Finally, Equation (12) and Equation (13) are transformed into their incremental configuration, and rearranged with respect to ${}^{[n]}\Delta\sigma^{(ANN)}$.

$$ {}^{[n]}\Delta\sigma^{(ANN)} = {}^{[n]}\Delta\sigma - E_1 \cdot {}^{[n]}\Delta\varepsilon \tag{16} $$

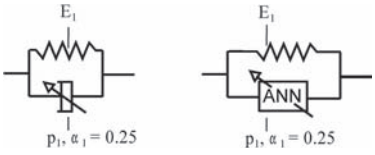

Figure 7. Fractional Kelvin element with fractional dashpot and artificial neural network.

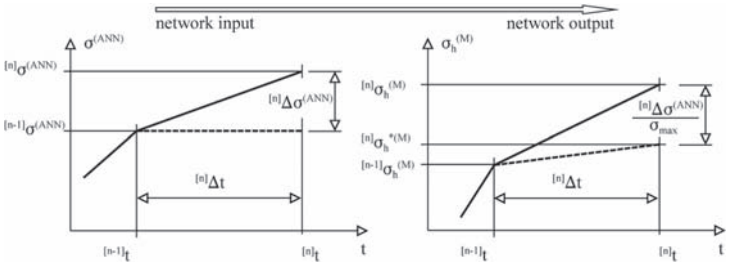

Figure 8. Artificial neural network input and output for fractional Kelvin element.

Equation (16) can now be used to replace ${}^{[n]}\Delta\sigma^{(\mathrm{ANN})}$ in Equation (15). Hence, the governing equation for the Kelvin body in incremental formulation is given through Equation (17).

$$ {}^{[n]}\Delta\varepsilon = \frac{1}{1+\dfrac{\Delta t^{\alpha}\cdot E_1}{p\cdot\Gamma(\alpha+2)}}\cdot\left(\frac{\Delta t^{\alpha}}{p\cdot\Gamma(\alpha+2)}\cdot{}^{[n]}\Delta\sigma+\frac{\Delta t^{\alpha}\cdot\sigma_{\max}}{p\cdot\Gamma(\alpha+2)}\cdot{}^{[n]}\sigma_h^{*(M)}-{}^{[n-1]}\varepsilon\right) \tag{17} $$

The coupling strategies that have been applied here can be extended to any combination of rheological bodies without any restrictions. This allows for a convenient way of adopting the networks to the modeling of materials with rheological behavior.

5 CONCLUSION

In this paper it has been shown that artificial neural networks can be used to replace fractional dashpots in rheological models. An artificial neural network with a recurrent structure was used to approximate the history stress of fractional dashpots under arbitrary load processes. The neural network required the storage of a number of internal variables only. This enabled a reduction of the numerical effort in contrast to the exact solution of the fractional differential equation where the whole stress chronology is to be stored. The network has been coupled to other rheological bodies and an efficient coupling strategy could be suggested. The network as well as the coupling strategy was formulated in a generic way, so that the approach can be applied to a wide spectrum of rheological models.

REFERENCES

Aschenbrenner L., 2006: *Mehrkomponenten-Modell zur Beschreibung des Deformationsverhaltens von Asphalt,* TU Braunschweig, PhD-Thesis.

Diethelm K., 2003: *Fractional differential equations, theory and numerical treatment*. TU Braunschweig, (lecture notes).

Ford N.J., 2001: *The Numerical Solution of Fractional Differential Equations; Speed versus Accuracy.* Numerical Algorithms 26, No. 4: 333–346.

Haykin S., 1999: *Neural Networks.* Prentice Hal, Upper Saddle River.

Oeser M. & Freitag S., 2008a: *Modelling of materials with fading memory using neural networks*. International Journal for Numerical Methods in Engineering, accepted.

Oeser M. & Pellinen T., Scarpas T., 2008: Kasbergen C. *Studies on creep and recovery of rheological bodies based upon conventional and fractional formulations and their application on asphalt mixture*, International Journal of Pavement Engineering**,** Vol. 9/5: 373–386**.**

Olard, F. & Di Benedetto, H., 2003: *General "2S2P1D" model and relation between the linear viscoelastic behaviours of bituminous binders and mixes*, Road Materials and Pavement Design, Vol. 4.

Padovan J., 1987: *Computational algorithms for FE Formulations involving fractional operators.* Computational Mechanics 2: 271–287.

Pellinen T., Oeser M. & Scarpas T., 2007: Kasbergen C. *Creep and recovery of linear and nonlinear rheological bodies*, In: Loizos A., Scarpas T., Al-Qadi I. (Ed.), *Proceeding of the International Conference on Advanced Characterization and Soil Eng. Materials*, Athens, Greece.

Podlubny I., 1999: *Fractional differential equations*. Academic Press, New York and London.

Schmidt A. & Gaul L., 2002: *Application of Fractional Calculus to Viscoelastically Damped Structures in the Finite Element Method*. In: Maia N.M.M., Montalvao e Silva J.M., Relogio Ribeiro A.M. (Editors), *Structural Dynamics Modelling (SDM)*, Madeira Island, Portugal.

Schmidt A., 2003: *Finite Elementformulierungen viskoelastischer Stoffgesetze mit fraktionalen Ableitungen*, UNI Stuttgrat, PhD-Thesis.

West B.J., Bologna M. & Grigolini P., 2003: *Physics of fractal operators*. New York: Springer.

Zell A., 1996: *Simulation Neuronaler Netze.*, Paris: Addison-Wesley, Bonn.

7. Test methods and models for permanent deformation

Advanced Testing and Characterization of Bituminous Materials – Loizos, Partl, Scarpas & Al-Qadi (eds)
© 2009 Taylor & Francis Group, London, ISBN 978-0-415-55854-9

Permanent deformation behaviour of bituminous mixtures containing incinerator bottom ash aggregates under uniaxial testing conditions

M.M. Hassan & H.A. Khalid
University of Liverpool, UK

ABSTRACT: The deformation behaviour of four bituminous mixtures, containing 0, 30, 60, and 80% IBAA content, was investigated over a wide range of strain rates, stresses and temperatures under uniaxial monotonic compression test conditions. Two types of uniaxial test were conducted: the constant strain rate test and the constant stress test. The steady state axial strain rates and stresses were interpreted and used to identify the monotonic permanent deformation behaviour of the four mixtures. The radial strain and, hence, dilation of the four mixes were also measured. The uniaxial permanent deformation behaviour of the mixtures was found to have the same form as the relevant binders, which was evaluated in a previous study. Results showed that the aggregate matrix acted as stiffener. The IBAA content was found to have a noticeable effect on the mixtures' permanent deformation behaviour. The uniaxial permanent deformation behaviour of the four mixes was modelled using the Modified Cross Model (MCM), which was found to capture the permanent deformation properties adequately.

1 INTRODUCTION

Incinerator Bottom Ash Aggregates (IBAA) are the most common waste material produced by burning municipal solid wastes in energy from waste plants. It was not uncommon to use IBAA for landfill. However, due to European Union restrictions imposed in 2004 on landfill sites, alternative usage has become necessary. One such alternative is using IBAA in asphalt for roads. Interest in IBAA started in the 1970s and declined in the 1980s then it picked up, again, from 1990 to be a common research field. IBAA Properties have been studied mechanically, physically and environmentally. These properties likened IBAA to lightweight aggregates. Numerous successful trials were conducted to study IBAA as a road construction material. Nevertheless, higher usage is still desirable.

In this paper, the permanent deformation behaviour of bituminous mixtures containing high level of IBAA was investigated. Bituminous mixtures containing 0, 30, 60, and 80% IBAA by weight, were studied. Two types of compressive uniaxial tests were conducted: the constant strain rate test and the constant stress (creep) test. Results were used to study the steady state permanent deformation behaviour of the tested mixtures.

2 BACKGROUND

Visual classification of IBAA fractions shows the presence of metals, slag, stone, ceramic, glass and organic materials. IBAA is a highly porous aggregate, which enhances its water absorption and, consequently, bitumen absorption. IBAA was reported to have high modulus values when it is in a compacted state (Hartlen & Elander 1986). The unit weight, mean Proctor density and optimum moisture content values of IBAA have confirmed its classification as lightweight aggregates (Eighmy et al. 1992). Moreover, It has been shown that its use as unbound

aggregate in road construction is safe environmentally (Bruder-Hubscher 2001). As a result, the use of IBAA in numerous road construction applications has been found promising.

Regarding IBAA's use in bituminous mixtures, a number of trials have been conducted. It was found that substitution of up to 20% IBAA for virgin aggregates resulted in mixtures with binder content 1.2% higher than the virgin aggregate mixtures (Ogunro et al. 2004). A second study (Vassiliadou & Amirkhanian 1999) showed that up to 30% substitution of natural aggregates with IBAA resulted in lower resilient modulus values. Moreover, using 32% IBAA has been suggested as satisfactory for use in a base layer in a lightly trafficked road pavement (Garrick & Chan 1993). High IBAA replacement has been attempted with success in the US, where 50% was used in a binder course asphalt mixture on a major road trial (Zhang et al. 1999). The afore-mentioned studies all seem to indicate encouraging experience worldwide related to the use of IBAA in pavement construction.

With regard to permanent deformation resistance of mixtures containing IBAA, there were mixed observations. On one hand, using 20% IBAA yielded mixtures having aggregate structures that are well developed to resist compaction and rutting (Ogunro et al. 2004). On the other hand, a study by Huang et al. (2006) showed an increase in the rutting resistance of asphalt mixtures with different IBAA contents used as fine aggregate replacement. Wheel tracking test results showed that rut depth increased with IBAA addition. This study concluded that the testing machine reached its maximum depth measurement ability when 75% IBAA was used. These mixed observations indicate the need for further studies on the response of bituminous mixtures with different IBAA levels to applied loading.

3 MATERIALS

Three materials were used in this study: limestone, IBAA and bitumen. Limestone from North Wales, UK was used to produce control bituminous mixtures. It was supplied in six sizes: 20, 14, 10, 6, 3 mm—dust and filler. IBAA from Teesside, UK was supplied in two sizes: 20–10 mm and 10 mm—down. The binder used was 100/150 Pen bitumen sourced from Venezuelan crude. These materials were utilised to produce hot bituminous mixtures containing 0, 30, 60, and 80% IBAA by weight. The composition and volumetric parameters of each mixture are shown in Table 1. The Optimum Binder Content was selected based on indirect tensile stiffness at 20°C and volumetric criteria relevant to UK binder course specifications (BSI 2005) and details of the mix design procedure were published elsewhere (Hassan & Khalid 2007).

4 EXPERIMENTAL PROGRAMME

Cylindrical samples of 67 mm diameter and 134 mm height were manufactured. Firstly, a laboratory roller compactor was used to produce 300 × 300 mm asphaltic slabs of 100 mm height. The slabs were compacted at four different pressures, namely 175, 275, 345 and 495 kPa. Each pressure was applied for 10 passes over each slab. The slabs were then cut into two halves. Each half was turned on its side and cored to produce cylinders of 67 mm diameter and 150 mm height. Each cylinder was then trimmed from both ends to 134 mm height.

Table 1. Mixture details.

Mix	Binder content (%)	IBAA content by weight (%)	Compacted density (g/cm^3)	Voids (%)	Stiffness (MPa)
OA	4.5	0 (control mix)	2.380	7.0	1480
AA	5.5	30	2.293	7.4	1805
BA	6.5	60	2.177	11	2138
AC	7.5	80	2.063	14	1700

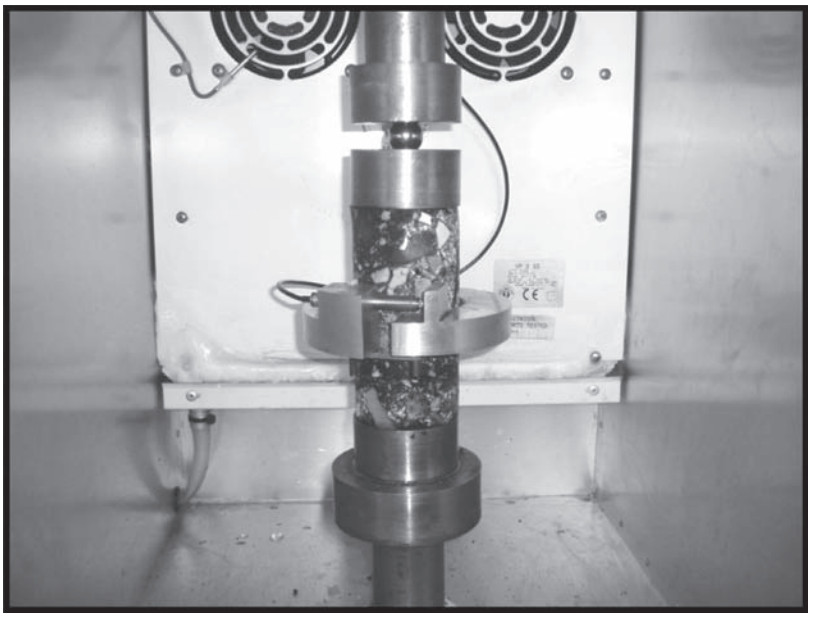

Figure 1. Sample instrumentation.

The compressive deformation behaviour of the mixtures was investigated over a wide range of strain rates, stresses, confinement pressure and temperatures under monotonic uniaxial compression test conditions. Two types of uniaxial test were conducted: constant strain rate and constant stress (creep) tests. The equipment arrangement for the uniaxial tests comprises a temperature controlled cabinet (–20 to 50°C) mounted on a loading frame, an axially mounted 10 tonne load cell, the sample and its instrumentation, and a linear variable deferential transducer (LVDT) with its conditioning box connected to a data logger.

In the constant strain rate tests, samples were tested at temperatures of 20 and 40°C. To ensure temperature uniformity with samples, they were conditioned in a temperature control cabinet at the test temperature, for at least 12 hrs preceding the test. Samples were then placed between two steel platens, which were smeared with silicon grease to reduce friction and a small pre-load was applied to take out any relaxation in the system. Specimens were then allowed to deform under a uniaxial compression stress. The compression machine was used to apply constant strain rate loads up to failure. For each strain rate, the stress-strain relationship was captured and recorded by a computer. The axial deformation of the specimens was measured via recording the cross-head movement, whereas the radial deformation of the specimens was measured using a LVDT. This LVDT was held in place using a circular collar, Fig. 1, which was glued to the specimens.

In constant stress (creep) tests, the same sample instrumentation as in the constant strain rate tests was used. Samples were tested at 5 and 20°C and the cross-head was allowed to apply a constant load over samples for 1800 sec. This time was found to be adequate for mixtures to reach steady state conditions. In each test, the axial and radial strains over time were recorded.

5 RESULTS AND DISCUSSION

5.1 *Constant strain rate test results*

For each strain rate, the stress-strain relationship was captured and recorded. For all mixtures, the relationship between stress and strain, both axial and radial, had the same

behavioural trend. This relationship consisted of three stages. In the first stage, the stress-strain relationship resembled a linear elastic behaviour. This stage was noticed over a narrow range of strains and was followed by a second stage in which the relationship exhibited an increase in the load, up to a peak value, which represents the steady state stress. This was followed by a descending softening part up to failure, shown in Fig. 2. For all mixtures, it was noticed, at any stress value, that the axial strain was higher than the radial strain. In addition the radial strain reached the steady state stage before the axial strain and starts to decrease while the axial strain is continue to increase up to a point after which the axial strain reaches the steady state stage and levels before starting to decrease. This was not the case at the early beginnings of the tests as both strains were almost identical. This may be attributed to the occurrence of pre-deformation compaction. The samples could have undergone a small amount of compaction, only in the vertical direction, before commencement of deformation. This compaction has been accompanied by a decrease in volume. This decrease has been followed by a volume increase when the internal cracks start to open in a phenomenon known as dilation (Erkens 2002).

The steady state stress corresponding to each strain rate was determined using a method proposed by Ward (1971). In this method, the maximum observed stress, at each strain rate as seen in Fig. 2, was defined as the steady state stress at that particular rate.

5.2 *Creep test results*

For all mixtures, axial and radial strains over time were recorded. Fig. 3 shows typical creep test results, from which it can be seen that a creep curve can be divided into two regions. In the first region, primary creep, the material underwent deformation at a high strain rate. In the second region, the strain rate was predominantly constant. This region was called the secondary creep region and its strain rate was adopted as the steady state strain rate corresponding to a particular value of applied compressive stress. A third region, not visible in Fig. 3 but appeared only in some tests, exhibited tertiary creep in which the strain rate increased significantly as the sample became progressively damaged.

In creep tests, the radial deformation behaviour, with respect to its rate of increase and initiation of dilation, was similar to that noticed in the constant strain rate test results.

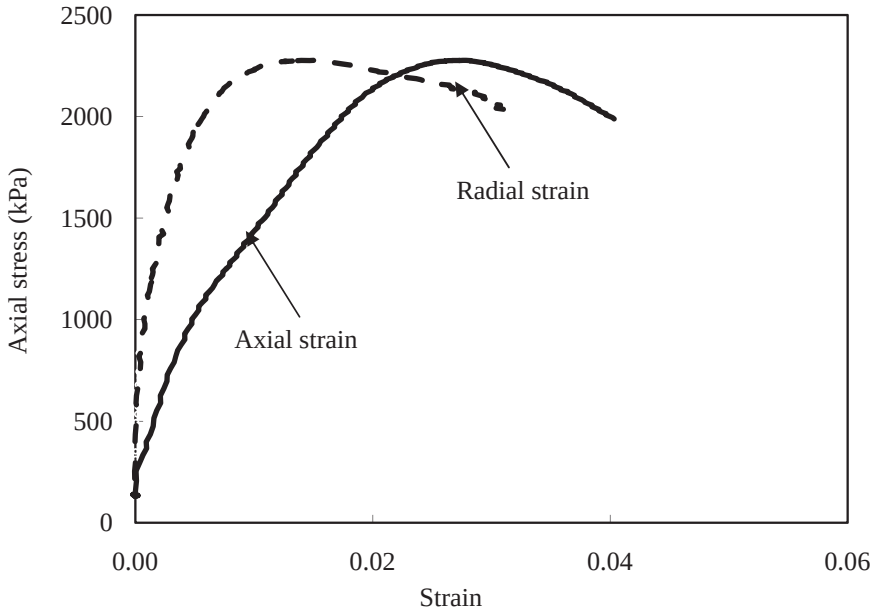

Figure 2. A typical uniaxial constant strain rate test result; mix AA at 0.001 1/s and 20°C.

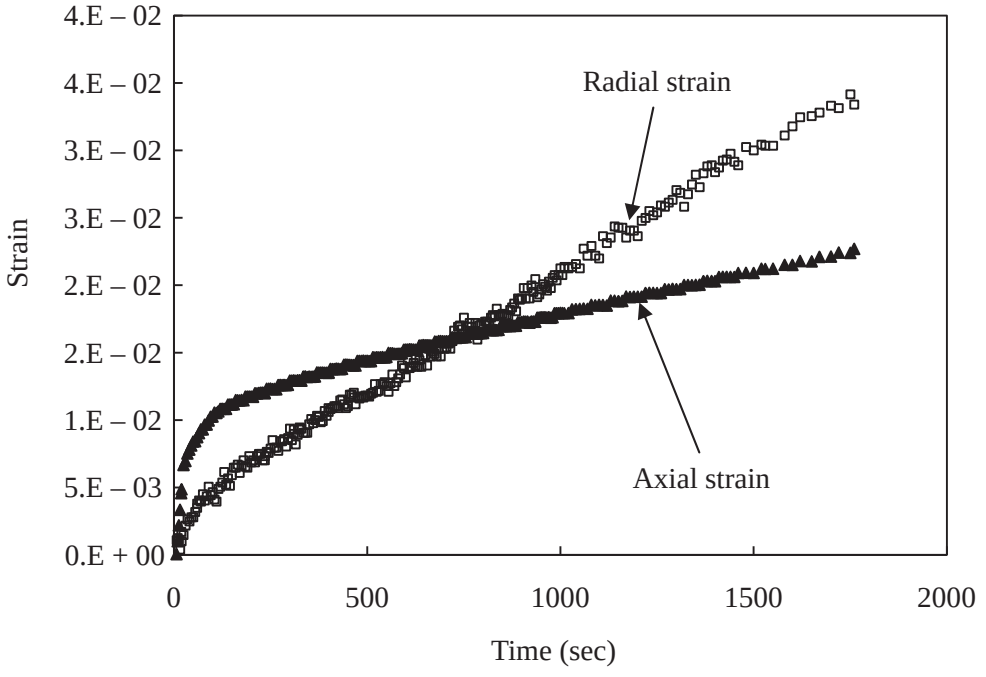

Figure 3. A typical creep test result; mix BA 2000 kPa and 5°C.

5.3 *Steady state deformation behaviour*

Steady state stresses were plotted against their corresponding steady state strain rates to produce steady state permanent deformation curves for mixtures at each test temperature. The experimental results were found to be adequately captured by a Modified Cross Model (MCM), which was firstly developed by Cross (1965) then modified by Cheung (1995) and Deshpand (1997). The MCM was used successfully, in numerous studies, to predict bituminous mixtures permanent deformation characteristics (Deshpand & Cebon 2000, Collop & Khanzada 2001, Ossa et al. 2004, Ossa et al. 2006).

$$\sigma = \frac{S\sigma_0 \dot{\varepsilon}}{\dot{\varepsilon}_p}\left[\frac{1}{1+(S\dot{\varepsilon}/\dot{\varepsilon}_p)^m}\right] \tag{1}$$

where: σ is the uniaxial stress, $\dot{\varepsilon}$ is the uniaxial strain rate, S is the stiffening factor, and σ_0, m, $\dot{\varepsilon}_p$ are material constants for mixtures.

Figs. 4 and 5 show examples for these steady state behaviour curves for mixes OA and BA under uniaxial test conditions. Mixes AA and CA exhibited the same shape relationships and their curves are not shown here to avoid repetitiveness. The MCM (presented in figures as solid lines) predicts that the steady state deformation behaviour of bituminous mixtures containing IBAA is linear at low stress levels, while at high stress levels the mixtures exhibit non linear power law viscous behaviour. This behaviour is similar to that of idealised asphalt mixtures (Deshpand & Cebon 2000) and of typical dense bitumen macadam and hot rolled asphalt mixes (Ossa et al. 2006).

Figs. 4 and 5 show that the steady state results, under uniaxial testing conditions, exhibit a very good agreement with binder modelling data published elsewhere (Hassan et al. 2008) and included in these figures. The mixtures' curves showed a shift from that of the binders. This shift is attributed to the stiffening effect of the aggregate matrix and the ageing of bitumen during mixing. The latter is due to the thin films of bitumen subjected to high temperatures during mixing which harden the binder. The aggregate matrix stiffening effect

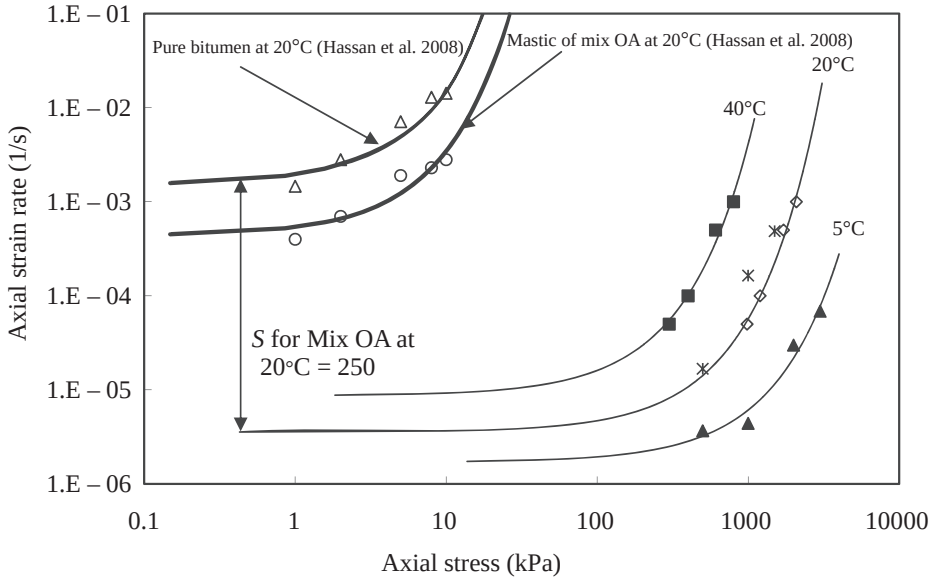

Figure 4. Steady state permanent deformation behaviour of mix OA.

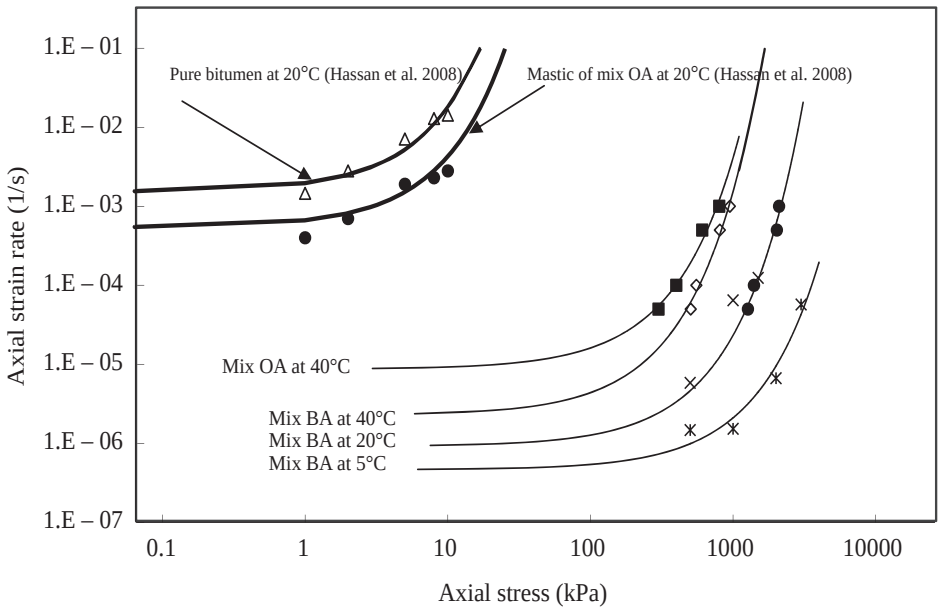

Figure 5. Steady state permanent deformation behaviour of mix BA.

can be expressed as stiffening factor, *S*, which can be determined experimentally, as shown in Fig. 4, and used for modelling purposes using the MCM. This stiffening factor was found to increase with IBAA content up to 60%, at all test temperatures. At 40°C, adding 30% IBAA led to 150% increase in *S*, compared to the control mix, while adding 60% IBAA increased *S* by 4 times. At 20°C, 30% IBAA led to 140% increase in *S* while 60% IBAA led to 400% increasing in *S*. The case at 5°C was similar: 30% IBAA increased *S* by 2 times and 60% IBAA increased it by 5 times. For 80% IBAA, *S* was at its highest value, 6600, at 5°C

and decreased with temperature increase: $S = 500$ and 250 at 20 and 40°C respectively. This may be attributed to the high binder content used in mix CA. A significant amount of this binder content was absorbed by IBAA resulting in high voids content, low adhesion properties and a thin bitumen film. Increasing the temperature led to softening the bitumen film and, consequently, a reduction in stiffness. Fig. 6 shows, as an example, the steady state deformation behaviour for the mixtures at 20°C. From the figure, it is clear that mixes AA and BA exhibited an increase in their deformation resistance compared to mix OA, the control mix. Mix CA, on the other hand, although showed an improved deformation resistance compared to mix OA, was less resistant compared to mix BA which contains lower IBAA content, as a result of the above-mentioned softening.

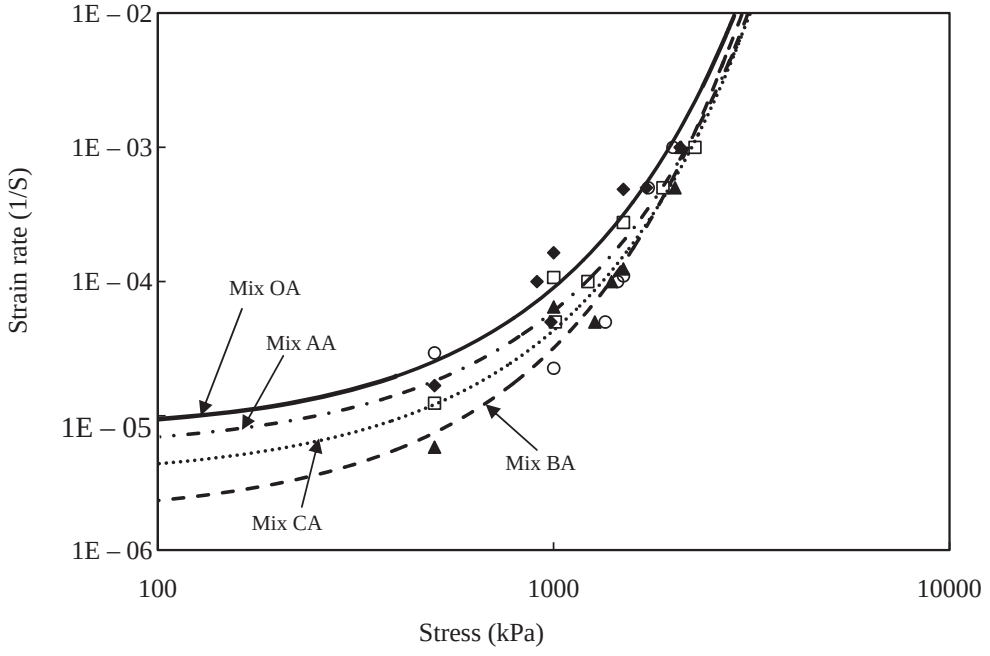

Figure 6. Effect of IBAA on rutting resistance at 20°C.

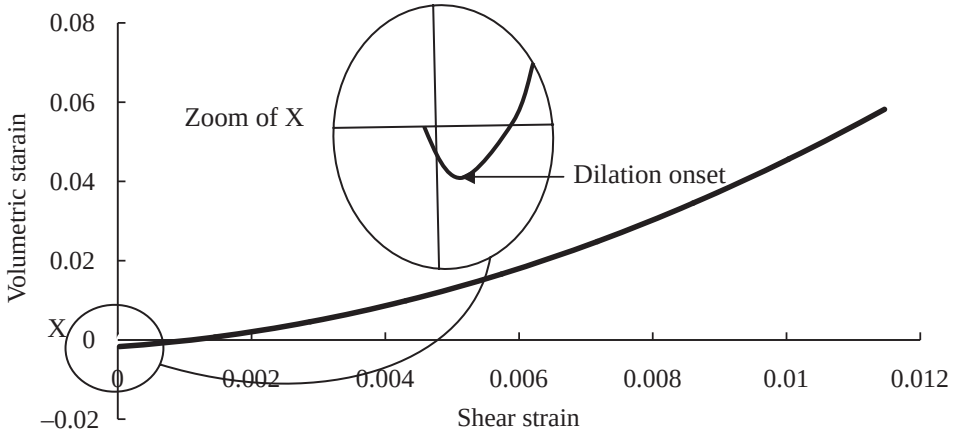

Figure 7. Volumetric strain behaviour (mix BA under 2000 kPa and 5°C).

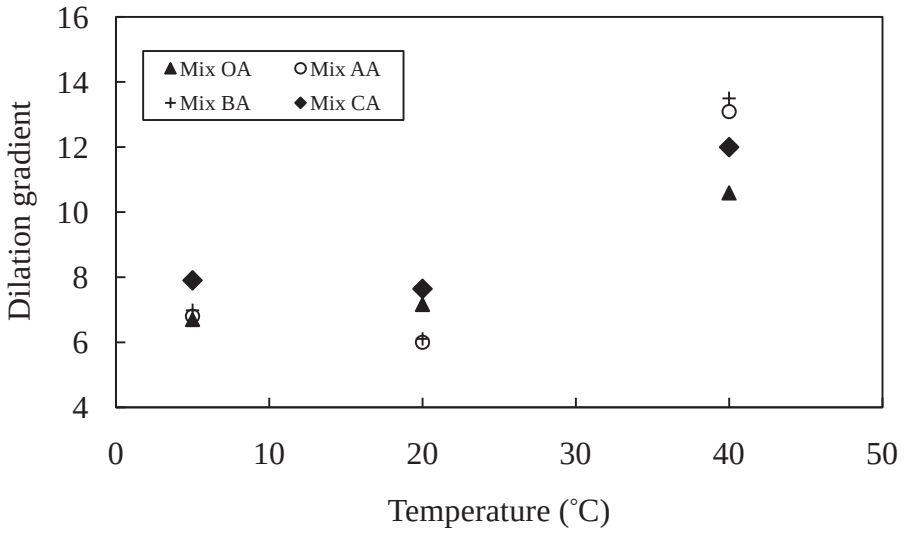

Figure 8. Dilation gradient as a function of test temperature.

5.4 *Volumetric deformation*

Studying the volumetric behaviour of the mixtures is important in understanding their deformation properties. To do so, the radial deformation of the samples was measured as explained earlier. Fig. 7 shows the variation of volumetric strain and the shear strain during a constant strain rate test under selected testing conditions; similar results were obtained from creep tests. It is obvious that, initially, the volumetric strain decreased due to densification up to a point, hence the initial sub-zero values, after which the volumetric strain increased almost linearly with shear strain. The trough point is referred to as the point of dilation onset (Erkens 2002, Muraya 2007). The slope of the linear part of the curve is referred to as the dilation gradient. The dilation gradient, shown in Fig. 8, was found to be independent of the applied stress for all tested mixtures. Dilation gradients at 5°C were observed to be very close to the values recorded at 20°C for unknown reasons. The mixtures exhibited higher dilation gradients at 40°C. This shows that more dilation occurred at higher temperatures.

6 CONCLUSIONS

The general findings from the results discussed in the preceding sections can be summarised as follows.

The monotonic uniaxial constant strain rate test is useful to study the steady state deformation behaviour of bituminous mixtures containing IBAA at high temperatures. At low temperatures, the uniaxial creep test is more desirable. Both tests can be used at 20°C. This steady state deformation behaviour was found to be well captured by the Modified Cross Model.

The Modified Cross Model predicted that the steady state deformation behaviour of bituminous mixtures containing IBAA is linear at low stress levels while at high stress levels the mixtures exhibit non linear power law viscous behaviour. The IBAA mixture deformation behaviour was similar to their respective binders with a stiffening factor resulting from the effect of aggregate matrix and ageing of bitumen during mixing. For all mixtures, the slope of the linear region of the volumetric against shear strain curve, referred to as the dilation gradient, was found to be independent of stress level and dependent on IBAA content and test temperature.

It was shown that IBAA content has a significant effect on mixture deformation behaviour. At low temperatures, the higher the IBAA content, up to 80% content level, the higher

the deformation resistance was of the bituminous mixture. At high temperatures, the same effect was noticed, up to 60% IBAA, except for mix CA at 80% IBAA. Based on these results, it can be proposed that IBAA can be used at up to 60% without risk of undergoing excessive permanent deformation.

ACKNOWLEDGMENT

The authors are indebted to Ballast Phoenix, Tarmac and Nynas Bitumen for their financial and technical support of the project. The authors are also grateful to the Egyptian government for the award of a study scholarship to pursue this research.

REFERENCES

Bruder-Hubscher, V., Leroy, F., Coughanowr, C. & Enguehard, F. 2001. Utilisation of bottom ash in road construction: evaluation of the environmental impact. *Waste Management and Research* 19(6): pp. 545–556.

BSI. 2005. Coated Macadam (Asphalt Concrete) for Roads and Other Paved Areas—Part 1: Specification for Constituent Materials and Mixtures, British institution*, BS 4987–1:2005.*

Cheung, C. 1995. *Mechanical behaviour of bitumens and bituminous mixes*. PhD thesis, Engineering Department, Cambridge University.

Collop, A. & Khanzada, S. 2001. Permanent deformation in idealized sand asphalt bituminous mixtures*. International Journal of Road Materials and Pavement Design* 2(1): pp. 7–28.

Cross, M. 1965. Rheology of non-newtonian fluids: a new flow equation for pseudoplastic systems*. Journal of Colloid Science* 20: pp. 417–437.

Deshpand, V. & Cebon, D. 2000. Uniaxial experiments on idealized asphalt mixes*. Journal of Materials in Civil Engineering* 12(3): pp. 262–271.

Deshpand, V. 1997. *Steady state deformation behaviour of bituminous mixes*. PhD thesis, Engineering Department, Cambridge University.

Eighmy, T., Grees, D., Zhang, X., Tarr, S. & Whitehead, I. 1992. Bottom ash utilization evaluation for the concord, New Hampshire waste-to-energy facility*. Environmental research interim report. University of New Hampshire.*

Erkens, S. 2002. *Asphalt Concrete Response*. PhD thesis, TU Delft.

Garrick, W. & Chan, K. 1993. Evaluation of domestic incinerator ash for use as aggregate in asphalt concrete*. Transportation Research Record* 1418: pp. 30–34.

Hartlen, J. & Elander, P. 1986. Residues from waste incineration—chemical and physical properties*.* Report no. SGI VARIA 172. *Swedish geotechnical institute, Linkoping, Sweden*.

Hassan, M.M. & Khalid, H.A. 2007. Incinerator Bottom Ash Aggregates in Bituminous Mixtures*. In Bituminous Mixtures and Pavements, Proceedings of the 4th International Conference*, Thessaloniki, pp. 489–498.

Hassan, M.M., Khalid, H.A. & Artamendi, I. 2008, Effect of Incinerator Bottom Ash Aggregates on Binders' Permanent Deformation Using a Dynamic Shear Rheometer. *In Asphalt Pavements and Environment, Proceedings of the ISAP International Symposium*, Zurich, pp. 43–51.

Huang, C., Chiu, C. Li. K. & Yang, W. 2006. Physical and Environmental Properties of Asphalt Mixtures Containing Incinerator Bottom Ash. *Journal of Hazardous Materials, B137*, pp. 1742–1749.

Muraya, P. 2007. *Permanent Deformation of Asphalt Mixtures*. PhD thesis, TU Delf.

Ogunro, V., Inyang, H., Young, D. & Oturkar, A. 2004. Gradation control of bottom ash aggregate in Superpave bituminous mixes*. Journal of Materials in Civil Engineering* pp. 604–613.

Ossa, E.A., Taherkhani, H. & Collop, A. 2006, Compressive behaviour of asphaltic mixtures*. Association of Asphalt Paving Technologists* pp. 620–655.

Ossa, E.A., Deshpand, V. & Cebon, D. 2004. Uniaxial monotonic and cyclic behaviour of bituminous mixes*.* CUED/C-MICROMECH/TR.95*. Cambridge University. Engineering department report.*

Vassiliadou, E. & Amirkhanian, S. 1999. Coal Ash Utilization in Asphalt Concrete Mixtures, *Journal of Materials in Civil Engineering*, pp. 295–301.

Ward, M. 1971. Review: the yield behaviour of polymers*. Journal of Material Science* 1071(6), pp. 1397–1417.

Zhang, X., Grees, D., Kaprinski, S. & Eighmy, T. 1999. Utilization of municipal solid waste combustion bottom ash as a paving material. *Transportation Research Record* 1652: pp. 257–263.

Advanced Testing and Characterization of Bituminous Materials – Loizos, Partl, Scarpas & Al-Qadi (eds)
© 2009 Taylor & Francis Group, London, ISBN 978-0-415-55854-9

A new performance related test method for rutting prediction: MSCRT

S. Dreessen
Total Centre de Recherche de Solaize, Solaize, France

J.P. Planche
Total Bitumen Département, Puteaux, France

V. Gardel
Université Claude Bernard Lyon I, Villeurbanne, France

ABSTRACT: The rheological measurements of binders have received considerable attention in the past several years as a predictor of the rutting potential of bituminous binders, particularly of modified binders.

The current binder characteristics G* and δ are measured in the linear range. But the rutting is the plastic deformation of an asphalt mix caused by heavy traffic loads under low speed. This is a high strain failure in the pavement and leads to a non-linear response. So multiple stress testing is needed to describe the binder properties in the non-linear range.

One of the promising candidates is the multiple stress creep recovery test (MSCRT) under current development in the USA. The MSCRT is measured in a dynamic shear rheometer at various stress levels.

This paper presents a study on the rutting resistance of several mixtures and the corresponding binders. Relations between the behavior of mixtures and binders are discussed through the use of the different analysis methods DSR (G*, δ), MSCRT and the French wheel-tracking test for the mixtures.

The influence of parameters, such as binder nature, penetration grade, nature and level of polymer modification are also discussed and related to the resistance performances of both binders and mixtures.

The non-recoverable creep compliance Jnr could be considered as a better alternative method to replace the G*/sin δ and/or R&B softening point for the prediction of the rutting due to better correlation to the French rutting test at 60°C . The value normalizes the strain response of the binder to stress which clearly shows the differences between different binders. It differentiates binders having penetrations, softening points or G*/sin δ in the same range.

1 INTRODUCTION

Rutting is one of the major defects in heavily loaded asphalt pavements. Therefore, one of the main objectives of binder specifications is to set up criterion limits that would prevent the use of binders not performing well against rutting.

In Europe, CEN binder specifications relies on the mainly the Ring and Ball softening point to address rutting.

In the USA, the Superpave bituminous binder specification is based on the values of G*/sin δ measured by the dynamic shear rheometer at the upper pavement temperature to warranty against rutting.

Due to the increased use of modified binders, limitations of these criteria have been identified. Neither one seem to be sufficient to predict the rutting behavior of modified asphalt mixtures only from the laboratory characterization on bituminous binders. This is due to

the fact that rutting is caused by an accumulation of irreversible deformation or permanent deformation in the pavement layers under repeated traffic load.[1,2,3]

Other tests have been suggested to provide a performance based test pertinent for all modification types at the upper grading temperature.[4,5] The repeated creep and recovery test has been proposed by different research teams.[6,7,8] Zero shear viscosity (ZSV)[9,10,11] has been developed mainly in Europe.

On the other hand, the multiple stress creep and recovery test (MSCRT) has been proposed as potential specification criteria by J. D'Angelo et al.[12,13] in the United States as a replacement for the existing high temperature binder test. MSCRT is based on repeated creep and recovery sequences, conducted at different stress levels.

This paper presents the behavior under this test of a wide variety of binders, modified and unmodified, in comparison with classical characteristics such as the ring and ball softening point. This article also aims to correlate these binder properties against rutting performances of mixes made out of those same binders; permanent deformation was assessed using the LCPC wheel tracking rut tester.

2 EXPERIMENTAL

2.1 *Materials*

2.1.1 *Bitumen*

The properties of the binders used in the current study are displayed in the following tables. A wide range of bitumens was used including pure and polymer modified. The properties include classical ones, penetration at 25°C (EN 1426) and ring and ball softening point (EN 1427) and rheological ones such as the SHRP Superpave binder criterion for rutting resistance G*/sin δ measured using a dynamic shear rheometer according to EN 14770. The tables also feature Jnr measured at three stress levels after RTFOT aging at 60°C. Jnr is one of the parameters obtained through MSCRT. Its meaning will be explained in section 2.2.1 hereafter.

The polymer modified binders A–G are commercial grades fabricated according to the Styrelf® crosslinking process[14]. The polymer content ranges from 2 to 5%. The experimental polymer modified binders have been produced with the 70/100 mentioned in table 1; the binder 70/100 + 3% SBS XL has been cross-linked in situ. The other two mixtures are physical blends.

The special grade is a Multigrade bitumen fabricated using a blend of refining bases, according to the Ornital® proprietary recipe[15]. It is used as a reference for a non-polymer modified anti-rutting binder.

2.1.2 *Asphalt mix*

The primary aggregate source used in the asphalt mix design was a diorite type from the quarry "La Noubleau". The materials were used to produce an optimized rut resistant asphalt concrete wearing course EB 10 according to the standard EN 13108-1 which fits into the third class with a rut depth less than 5%. The asphalt concrete was laboratory mixed according to EN 12697-35, and then compacted using a roller compactor (EN 12697-33) to produce slabs with the dimension of $500 \times 180 \times 100$ mm. Aggregate gradation and mix design volumetric properties are shown in figure 1.

2.2 *Testing procedures*

2.2.1 *MSCRT*

Since one of the purpose of this study is to evaluate MSCRT power to predict the binder impact on rutting resistance, the binders were first short term aged according to the European standard EN 12607-1 (RTFOT). The aged bitumens were then submitted to MSCRT carried out in a dynamic shear rheometer using a 25 mm parallel plate geometry with a 1 mm gap. The test was run at 60°C for a better comparison with French rutting test carried out at the exact same temperature, using a constant stress creep of 1 second duration followed by a zero stress recovery of 9 seconds duration. Complementary to the procedure described in AASHTO and ASTM[16,17] the test were performed at 11 stress levels from 25 to 26500 Pa.

Table 1. Pure binders.

Binder	Before RTFOT aging		After RTFOT aging			Jnr @ 60°C		
	R&B	Penetration	R&B	Penetration	G*/sin δ	100 Pa	12800 Pa	26500 Pa
70/100	45,0	76	47,2	64	2,3	0,055	0,24	0,33
35/50 A	51,0	41	58,0	28	14,3	0,049	0,06	0,08
35/50 B	53,6	37	58,4	25	21,3	0,047	0,105	0,25
35/50 C	52,4	37	58,0	29	9,5	0,043	0,057	0,093
35/50 D	50,8	41	56,2	24	56,2	0,05	0,136	0,21
20/30 A	58,7	23	65,6	14	38,7	0,0051	0,056	0,01
20/30 B	57,0	23	62,6	16	22,6	0,013	0,029	0,04

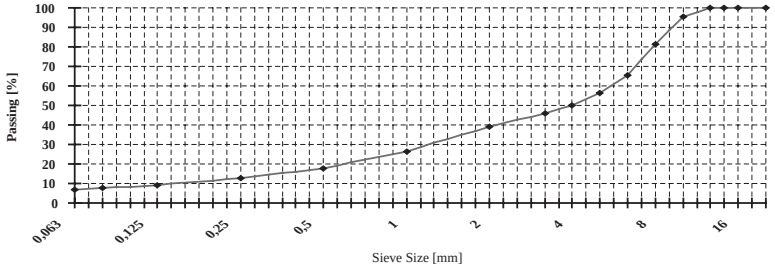

Sand 0/2 - La Noubleau [%]	37,0
Gran. 2/4 - La Noubleau [%]	10,0
Gran. 4/6 - La Noubleau [%]	12,0
Gran. 6/10 - La Noubleau [%]	39,0
Filler [%]	2,0
Binder content [ppc]	5,7
Gmix [g/cm^3]	2,62
Gagg [g/cm^3]	2,87
Air void content [%]	7,2

Figure 1. Aggregate gradation and mix design volumetric properties.

Table 2. Polymer modified binders.

Binder	Before RTFOT aging		After RTFOT aging			Jnr @ 60°C		
	R&B	Penetration	R&B	Penetration	G*/sin δ	100 Pa	12800 Pa	26500 Pa
70/100 + 3% SBS	58,2	41	62,0	35	10,5	0,072	0,029	0,055
70/100 + 3% SBS XL	63,6	36	68,0	29	13,9	0,088	0,028	0,046
70/100 + 3% EVA	62,0	28	66,0	21	19,7	0,013	0,024	0,028
PmB A	56,0	55	62,6	34	13,8	0,022	0,052	0,098
PmB B	55,0	58	60,8	38	35,6	0,027	0,049	0,066
PmB C	67,4	34	67,6	26	24,3	0,0041	0,013	0,024
PmB D	66,4	42	70,4	21	48	0,007	0,0103	0,0128
PmB E	67,2	28	72,2	17	29,3	0,0015	0,0028	0,0035
PmB F	71,2	26	75,0	14	53,8	0,0015	0,0021	0,0025
PmB G	65,4	25	70,7	22	19,8	0,0042	0,0066	0,0092

Table 3. Special binders.

Binder	Before RTFOT aging		After RTFOT aging			Jnr @ 60°C		
	R&B	Penetration	R&B	Penetration	G*/sin δ	100 Pa	12800 Pa	26500 Pa
10/20	64,6	14	74,0	10	12,5	0,0056	0,0064	0,0074
Special grade	61,0	35	66,6	27	40,6	0,0061	0,012	0,021

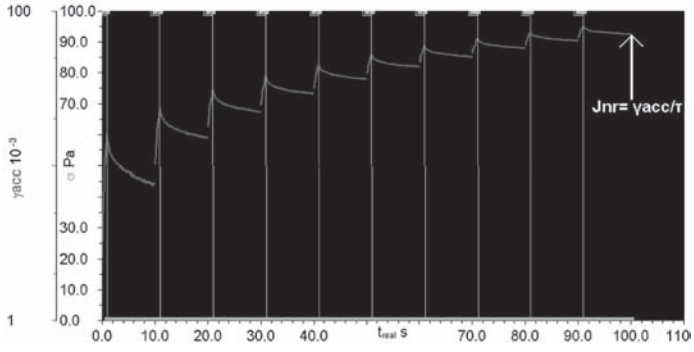

Figure 2. Plot of creep and recovery data for the determination of non-recoverable compliance Jnr at a stress of 100 Pa.

At each stress level ten cycles of creep and recovery were applied with no rest period, neither between those cycles nor between changes in stress levels.

Originally the percentage of recovery is calculated by equation (1),

$$R = \frac{\sum_{\varepsilon_r=1}^{10} \varepsilon_r (A,N)}{10}$$

A = Stress level either 100 or 3200 Pa
N = Number of cycles = 10
$\varepsilon_r = (\varepsilon_1 - \varepsilon_{10}) * 100/\varepsilon_1$
ε_1 = Adjusted strain value at the end of the creep portion = $\varepsilon_c - \varepsilon_0$ for each cycle
ε_{10} = Adjusted strain value at the end of recovery portion of each cycle
ε_c = strain value at the end of the creep portion of each cycle
ε_0 = initial strain value at the beginning of the creep portion cycle. (1)

But in this paper only the non-recoverable compliance Jnr, the non-recovered strain at the end of the recovery part of the test divided by the initial stress applied during the creep is used.[13,17] The value Jnr is calculated by equation (2) for each stress level:

$$Jnr = \gamma_u / \tau$$

γ_u = average non-recovered strain
τ = stress applied during creep (2)

As an example figure 2 shows one stress level of ten cycles of a polymer modified binder.

The higher the non recoverable compliance Jnr, the weaker the resistance to deformation induced by creep and recovery solicitation under different stress levels. High Jnr values are supposed to mean low resistance to permanent deformation.

2.2.2 *French wheel tracking test (EN 12697-22)*

Wheel tracking tests were run using the French LCPC rut tester according to the European standard EN 12697-22. The tests were run in a constant temperature air chamber at 60°C with rut depth profiles measured at 100, 300, 1000, 3000, 10000 and 30000 passes of a rubber tire with a load of 500 daN and frequency of 1 sec^{-1}. The result is expressed in %.

3 RESULTS AND DISCUSSION

3.1 *Binder results*

The multiple stress creep recovery test allows observing the stress depending behavior of the tested binders. The following figures show that at high stress level, normally above 3200 Pa the binder resistance to deformation starts to decrease as shown by a sharp increase in non recoverable compliance, whereas this binder compliance remains very constant at low stress level.

Increasing stress level, the binder sensitivity to stress becomes visible and the differences due to the binder origin or fabrication process in binder responses become more obvious.

The same tendency could be seen for the polymer modified binders but their Jnr values are much lower (below 0.1) and the binder sensitivity to stress even starts at higher stress level. The differentiation is more important at a stress level higher than 6400 Pa. This high stress level compared to the ones published elsewhere[12,13,16] could be explained by the testing temperature of 60°C. The ASTM test method[17] recommends testing at the SHRP high critical temperature, which is significantly higher and therefore leads to a softer binder more stress susceptible.

Figure 5 shows clearly the influence of the addition of polymers to primary binder. The three modified binders by SBS crosslinked or not, and EVA have similar dependencies on

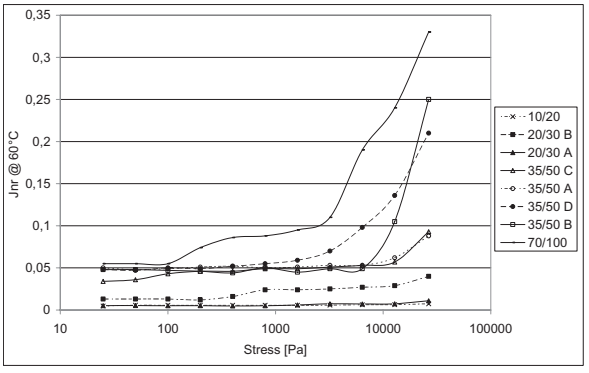

Figure 3. Jnr values at several stress levels for pure binders.

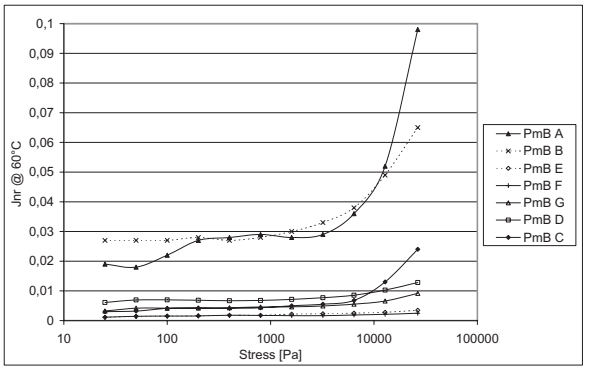

Figure 4. Jnr values at several stress levels for polymer modified binders.

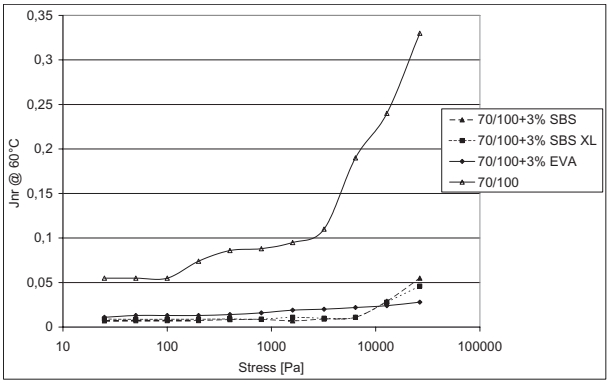

Figure 5. Influence of Jnr values due to polymer modification.

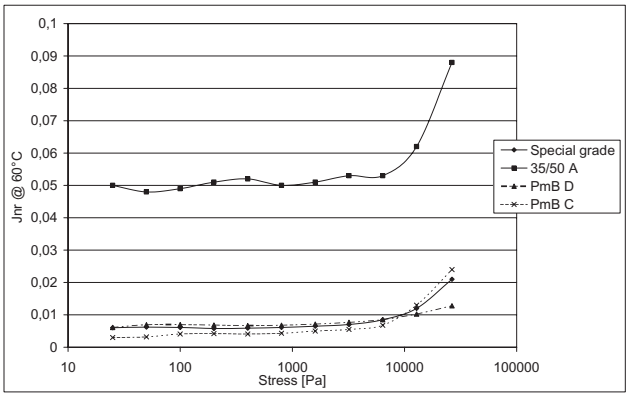

Figure 6. Comparison of several binders of same penetration range.

Table 4. Correlation coefficients R^2 of binder parameters with Jnr values at several stress levels.

Jnr at stress	Softening point	Penetration	G*/sinδ	G*	δ
26500	0,7459	0,4645	0,4511	0,5242	0,5698
12800	0,7824	0,5722	0,5508	0,6309	0,5717
6400	0,7727	0,5801	0,5801	0,6564	0,6005
3200	0,7722	0,5433	0,5919	0,6814	0,3756
1600	0,4293	0,4353	0,519	0,6178	0,1311
800	0,4756	0,4501	0,5388	0,635	0,1341
100	0,3444	0,3015	0,3804	0,46	0,0853

stress. The increase in the SBS modified binders Jnr values above 10000 cycles is not significant. Wider differentiation between PmB's would require testing at higher temperature as recommended in the ASTM protocol.

The comparison shows no significant difference between the Special grade, PmB C and PmB D until 6400 Pa stress application. At higher stress level, the more highly polymer modified binder has less stress susceptibility. Contrarily, the unmodified binder 35/50 A is constantly at a higher Jnr level so that it clearly differentiates from the modified and special binders.

Table 4 demonstrates that there is no correlation between Jnr values at several stress levels and the other widely used binder parameters like softening point, penetration, G*/sin δ, G* and the phase angle δ. In particular, no better correlation (R^2 coefficient) could be pointed out with the characteristics measured at the same 60°C temperature like G* and δ, than with softening point and penetration. The correlation coefficients are slightly better at higher stress.

3.2 *Results of correlation of binder performances and French rutting test*

For the evaluation of the correlation of binder properties measured by R&B Softening Point, Penetration, G*/sin δ and MSCRT after RTFOT aging and the rutting performances of an asphalt mix, 7 pure, 6 polymer modified and 2 special binders were taken into account.

First, only the highest stress level of the MSCRT (26500 Pa) was used.

In terms of classical testing the correlation coefficients confirm the much better prediction power of softening point (in a log scale) compared to penetration, to eliminate asphalt susceptible to permanent deformation. However, R^2 values indicate the correlation is only a trend (Fig. 7 and 8).

The correlation of the current used SHRP-criterion G*/sin δ and rutting parameter does not show any significance either.

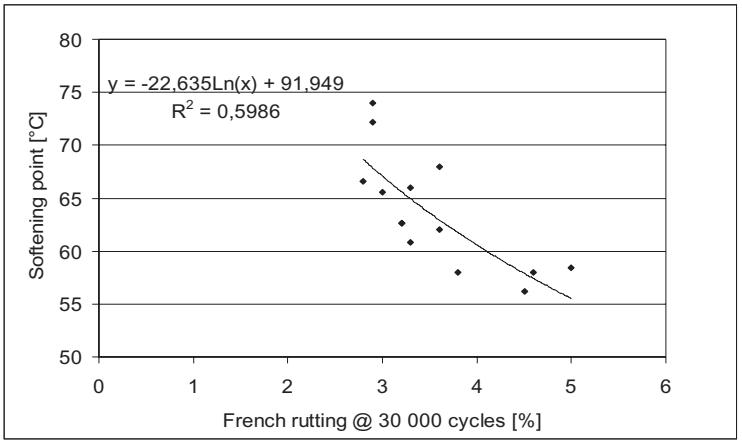

Figure 7. Correlation between softening point and French rutting.

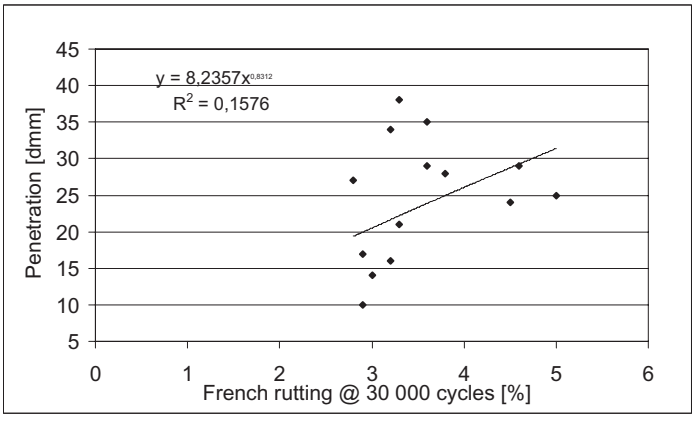

Figure 8. Correlation between penetration and French rutting.

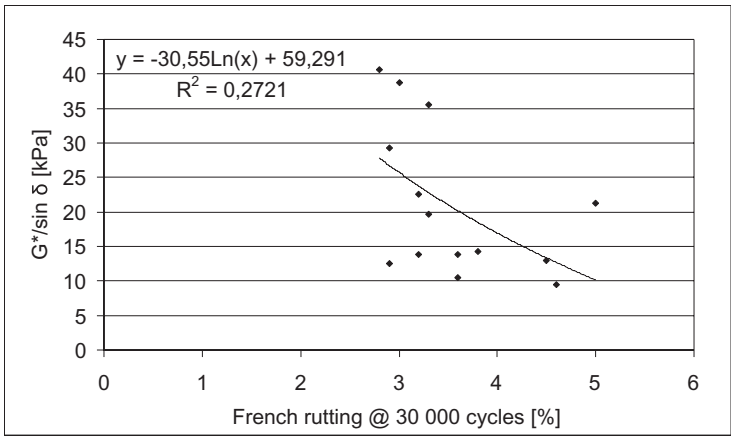

Figure 9. Correlation between G*/sin δ @ 60°C and rutting.

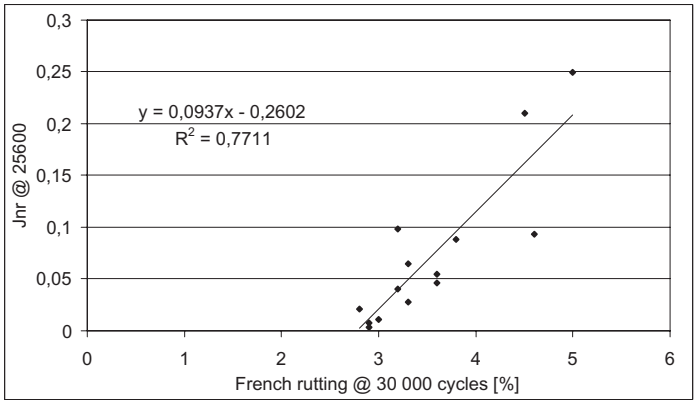

Figure 10. Correlation between Jnr at 26500 pa and rutting.

Table 5. Correlation coefficients of Jnr values at several stress levels and French rutting.

Jnr [Pa-1] \ Rut cycles	1000	3000	10000	30000
100	0,2186	0,1857	0,1074	0,3604
800	0,3642	0,3571	0,2756	0,3547
1600	0,3441	0,3468	0,2925	0,3028
3200	0,6350	0,6374	0,4916	0,4453
6400	0,8498	0,9025	0,8483	0,5674
12800	0,8787	0,9008	0,8050	0,7149
25600	0,8475	0,8059	0,6410	0,7711

The Jnr values at the stress level of 26500 Pa appears to linearly correlate far better to French rutting than the Superpave G*/sin δ criterion and the classical test method softening point (Fig. 10).

Looking deeper into the correlation coefficients, one can see in Table 5 that they are stress level related. Trends start to show up at 3200 Pa, whereas correlations are more pronounced at the higher stress values 6400 and 12800 Pa. There is also a dependency in the number

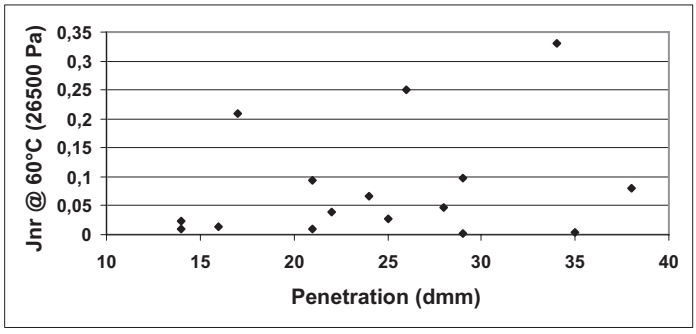

Figure 11. Differentiation by Jnr of binders with similar penetration.

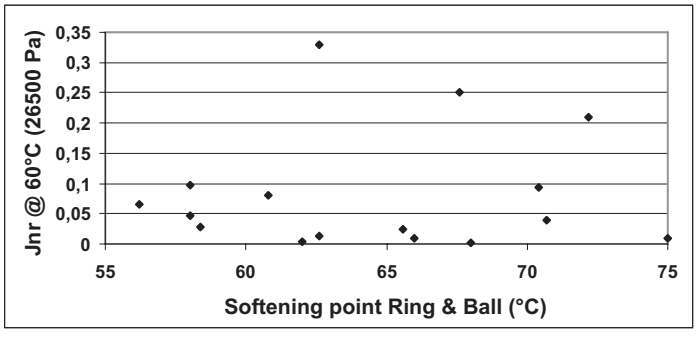

Figure 12. Differentiation by Jnr of binders with similar softening point.

of passes which can easily be explained by the fact that the soft binder 70/100 failed in the rut tester before 30000 cycles. Nearly all of the other asphalt mixes are characterized by a good resistance against permanent deformation so that they fulfill all the specification of an asphalt mix BBSG class 3; i.e. less than 5 mm rut depth at 30000 cycles.

Consequently, there is no correlation between Jnr and the classical parameters like R&B softening point or penetration. This is clearly shown on figures 11 and 12. Moreover, those figures demonstrate that binders having similar penetration or softening point can have very different Jnr. This latter parameter better differentiates binder properties.

4 CONCLUSIONS

The non-recoverable creep compliance Jnr could be considered as a better alternative method to replace the G*/sin δ and/or R&B softening point for the prediction of the rutting. The value normalizes the strain response of the binder to stress which clearly shows the differences between different binders. It clearly differentiates binders having penetrations, softening points or G*/sin δ in the same range. No correlation between the Jnr values at different stress levels and the measured binder properties softening point, penetration, G*, δ and G*/sin δ have been found.

The criterion Jnr can characterize modified as well as unmodified binders and gives better correlation to the French rutting test at 60°C than the current G*/sin δ value for the SHRP specifications and softening point and penetration for the classical testing.

It has to be mentioned that this study was only carried out at the temperature of 60°C to compare the resulting values with the French rut tester run at the same temperature. Possibly, due to this fixed temperature, higher stress levels are necessary to influence the binder resistance to deformation than in previous published papers 12, 13, 16, 17.

Out of this work, the proposed stresses to conduct MSCRT would be 100, 6400, 12800 and 25600 Pa.

Further development work would involve a wider range of binders and mixes, and binder testing at various temperatures to seek for even better binder differentiation, and evaluating the MSCRT method precision.

ACKNOWLEDGEMENTS

The authors would like to acknowledge the asphalt mix team of the TOTAL Research Center who contributed substantially to this work and John D'Angelo from FHWA in the USA for sharing practical information with us.

REFERENCES

[1] American Association of State Highway and Transportation Officials (AASHTO), Multiple Stress Creep Recovery Test of Asphalt Binder Using a Dynamic Shear Rheometer (MSCR), TP70-07, 2007.

[2] Anderson, D.A., Kennedy1993. T.W, Development of SHRP Binder Specification, *Journal of the Association of Asphalt Paving Technologies*, 62: 481–501.

[3] Bahia, H.U., Hanson, D.L., Zeng, M., Zhai, H., Khatri, M.A. & Anderson, R.M. 2001. Characterization of Modified Asphalt Binders in Superpave Mix Design, Report No. 459, National Coopérative Highway Research Program, National Academy Press, Washington, D.C.

[4] Bouldin, M.G., Dongre, R. & D'Angelo, J. 2001. Proposed Refinement of Superpave High-Temperature Specification Parameter for Performance-graded Binders, Transportation Research Record 1766.

[5] D'Angelo, J., Dongre, R., Reinke, G., Evaluation of Repeated Creep and Recovery Test Method as an Alternative to SHRP + Requirements for Polymer Modified Asphalt Binders, *Canadian Technical Asphalt Proceeding, November 2006,* Prince Edward Island.

[6] D'Angelo, J., Kluttz, Robert Q, Dongre, Raj, & Stephens Keith. 2007. Revision of the Superpave High Temperature Binder Specification: The Multiple Stress Creep Recovery Test, *Journal of The Association of Asphalt Paving Technologists* 76: 123, 2007.

[7] D'Angelo, J. & Dongre, R. 2002. Superpave binder specifications and their performance relationship to modified binders, Proceedings of Canadian Technical Asphalt Association: 91–103.

[8] Desmazes, C., Lecomte, M., Lesueur, D. & Phillips, M. 2000. A Protocol for Reliable Measurement of Zero-shear-viscosity in Order to Evaluate Anti-rutting Performance of Binders, Proceedings of 2″d Eurasphalt & Eurobitume Congress, Book 1: 203–211. Barcelona.

[9] Le Hir, Y., Anderson, D.A., Planche, J.P. & Martin, D. 2003. Rheological Characterization of Bituminous Binders to Predict Pavement Rutting, 6th RILEM Symposium PTEBM'O3: 117–123. Zurich.

[10] Marasteanu, M.O., Clyne, T., McGraw, J., Li, X., Velasquez, R. 2005. High Temperature Rheological Properties of Asphalt Binders, *Journal of the Transportation Research Board*, 1901: 52–59. TRB, Washington.

[11] Multiple Stress Creep Recovery Test of Asphalt Binder Using a Dynamic Shear Rheometer, Annual Book Of ASTM Standards, Designation D7405-08A,. 4.03(4), American Society For Testing And Materials, ASTM, West Conshohocken, PA.

[12] Phillips, M.C. & Robertus, C. 1996. Binder Rheology and Asphaltic Pavement Permanent Deformation, The Zero-shear Viscosity, lst Eurasphalt & Eurobitume Congress, Strasbourg.

[13] Reinke, G., Engber, S., Herlitzka, D., Tranberg, D. & Jorgenson, J. Utilization of Binder Stress Sensitivity to Investigate the Impact of Applied Load, Binder Type, and Aggregate Structure on the Rutting Behavior of Bituminous Mixtures, of the 4th Eurasphalt & Eurobitume Congress, Copenhagen.

[14] Sybilski, D., Zero-Shear Viscosity of Bituminous Binder and its Relation to Bituminous Mixtures Rutting Resistance, Transportation Research Record, 1535: 15–21.

[15] Brevet FR7639233.

[16] Technical data sheet Ornital® 40, TOTAL.

[17] Wasage, T.L.J., Reyes, M., Stastna, J. & Zanzotto, L. Creep Characteristics of Conventional, Oxydized, Polymer and Tire Crumb Rubber Modified Asphalt Binders and Mixtures, Proceedings of the 4th Eurasphalt & Eurobitume Congress, Copenhagen.

Advanced Testing and Characterization of Bituminous Materials –
Loizos, Partl, Scarpas & Al-Qadi (eds)
© 2009 Taylor & Francis Group, London, ISBN 978-0-415-55854-9

Effect of binder type on the permanent deformation resistance of asphalt mix at different temperatures

M. Smiljanic, I. Pap & U. Tatic
The Highway Institute, Belgrade, Serbia

ABSTRACT: The paper presents the results of measurements obtained under various temperatures regarding the resistance to permanent deformations of asphalt mix with 0/11 mm maximum nominal size using conventional bitumen B 50/70 penetration grade and Polymer-modified bitumen PmB 50/90 penetration grade. Testing was carried out using Nottingham Asphalt Tester, with cyclic vertical load and confined lateral expansion of the sample.The results thus obtained indicate that at 30°C asphalt mixtures with Polymer-modified bitumen show less resistance to permanent deformation in contrast to asphalt mixtures with conventional bitumen, while at higher temperatures (>40°C) an opposite effect was obtained due to influence of elastic characteristics of SBS-polymer. The results shown in this paper are part of project SPENS (Sustainable Pavements for European New Member States) financed by EC.

1 INTRODUCTION

For evaluating the performance based characteristics of asphalt mixtures using the resistance to permanent deformations as a performance indicator, the following tests are proposed:

- Wheel tracking test on a laboratory circular compactor is used to determine asphalt mix resistance to plastic deformation (ruts) depending on the number of wheel passes (up to 30 000 cycles) at the temperature of 45–600°C (EN 12697-22 Bituminous mixtures; test methods for hot mix asphalt; Part 22: Wheel tracking test).
- Resistance to permanent deformation should be determined with dynamic creep test with confine shear strain at 400°C for base course and 500°C for wearing course asphalt mixtures according to the EN 12697-25 (Bituminous mixtures; test methods for hot mix asphalt; Part 25: Cyclic compression test). Creep rate is also useful information for determination the resistance to permanent deformation in accordance with EN 13108-20:2006 (Type testing).

Performance based testing on asphalt mixture can be done with equipment such as Nottingham Asphalt Tester NAT, which exist in Serbia in the Highway Institute in Belgrade.

With NAT it is possible to measure dynamic resistance to permanent deformation in dynamic creep test. These tests can be done in temperature range between 30°C and 60°C and at frequency of 1 Hz.

The results shown in this paper are part of project SPENS (Sustainable Pavements for European New Member States) financed by EC.

2 DESIGN AND TESTING OF ASPHALT MIXTURE

The example of asphalt mixture testing regarding the type of asphalt concrete with maximum nominal aggregate size 11 mm (0/11 mm) with conventional B 50/70 penetration grade and polymer-modified bitumen PmB 50/90 penetration grade for the wearing course construction meant for heavy trafficked road transport facilities has been presented herewith.

Testing of asphalt mixture 0/11 for permanent deformations has been carried out in compliance with European Specifications EN 12697-25 (Bituminous mixtures, Testing

methods for hot-mix asphalt; Part 25; Dynamic creep test) (1) Nottingham Asphalt Tester (NAT-14) at various temperatures (300°C, 400°C and 500°C).

In order to carry out the testing of asphalt mixture 0/11, the following components have been utilized:

– carbonate filler,
– crushed silicate aggregate 0/2, 2/4, 4/8 and 8/11 m/m,
– bitumen B 50/70 and Polymer-bitumen PmB 50/90 from local production sources.

2.1 *Asphalt mixture composition with B 50/70, (PmB 50/90)*

Asphalt mixture composition 0/11 is presented in Table 1.

2.2 *Gradation of aggregate mixture 0/11*

Designed grading of aggregate mixture 0/11 is shown on both Table 2 and Figure 1.

2.3 *Volumetric properties of asphalt mixture 0/11*

Volumetric properties of asphalt mixtures 0/11 with conventional bitumen B 50/70 and Polymer-modified bitumen PmB 50/90 are presented in Table 3.

Table 1. Asphalt mixture composition with 5.8% B 50/70, (PmB 50/90).

Mix composition	Mineral mixture	Asphalt mixture
Filler	6.0	5.6
Silicate aggregate 0/2 mm	31.0	29.2
Silicate aggregate 2/4 mm	21.0	19.8
Silicate aggregate 4/8 mm	12.0	11.3
Silicate aggregate 8/11 mm	30.0	28.3
Binder, B 50/70, (PmB 50/90)	–	5.8
Total:	100,0	100.0

Table 2. Gradation of aggregate mixture 0/11, passage in % (m/m).

	0.09 mm	0.25 mm	0.71 mm	2.0 mm	4.0 mm	8.0 mm	11.2 mm	16.0 mm	22.4 mm
Designed	8.9	13.7	21.9	38.2	59.3	82.3	98.4	100	100
SRPS U.E4.014/90	3–11	8–18	16–30	31–48	49–65	75–87	97–100	100	100

Table 3. Volumetric properties of asphalt mixture 0/11.

Characteristics	Method	Test results		Criteria SRPS U.E4.014/90
		B 50/70	PmB 50/90	
Air voids in asphalt sample, % (v/v)	SRPS U.E4.014	5.0		4.5–5.5
Air voids in aggregate mixtures, filled with binder % (v/v)		72.7	72.8	66–78
Voids in mineral mixture, % (v/v)		18.3	18.4	–
Bulk density of asphalt sample, (kg/m^3)	SRPS U.M8.092	2318	2316	–
Maximum density of asphalt mixture, (kg/m^3)	SRPS U.M8.081	2441	2438	–

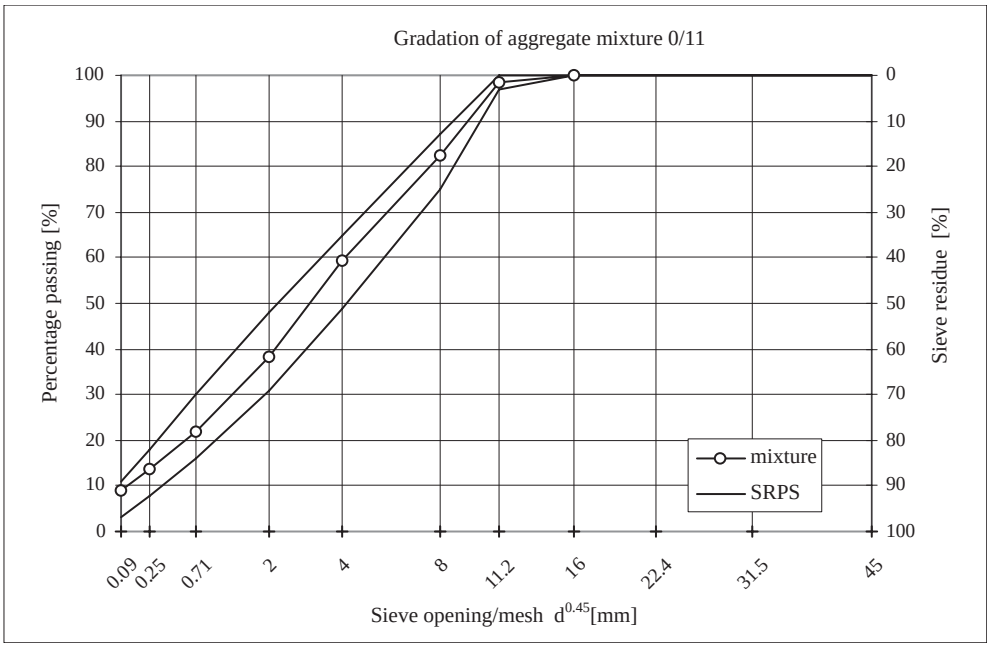

Figure 1. Gradation of aggregate mixture.

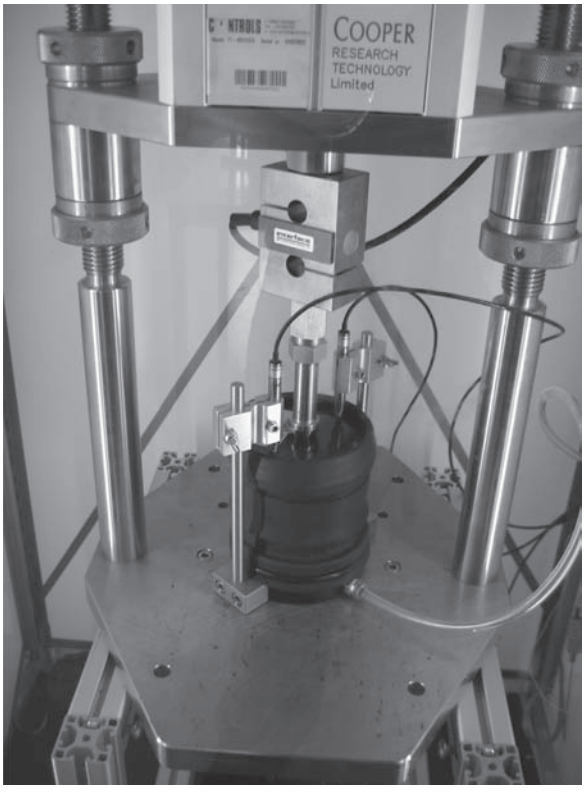

Figure 2. Permanent deformation test.

2.4 *Determination of the permanent deformation (ε) (VRLT—Vacuum Repeated Load Test)*

The resistance to permanent deformation is made under the dynamic test with confined horizontal radial strain according to the standard EN 12697-25 (Bituminous mixtures; test methods for hot mix asphalt; Part 25: Cyclic compression test), and condition:

– test temperature: 30 ± 0,5°C
– axial stress: 100 ± 2 kPa
– load period: 1 ± 10 ms
– unload period: 1 ± 10 ms
– cycles number: 1800
– confining stress: 50 kPa

The results of measurements are presented in form of graphs (figures 3, 4, 5, 6 & 7) which represent dependence of axial micro-strain (% mm/mm) versus number of vertical load cycles at different temperatures.

Resistance to permanent deformation of asphalt mixture depending on the type of binder and temperature utilized in the test is presented on Table 4.

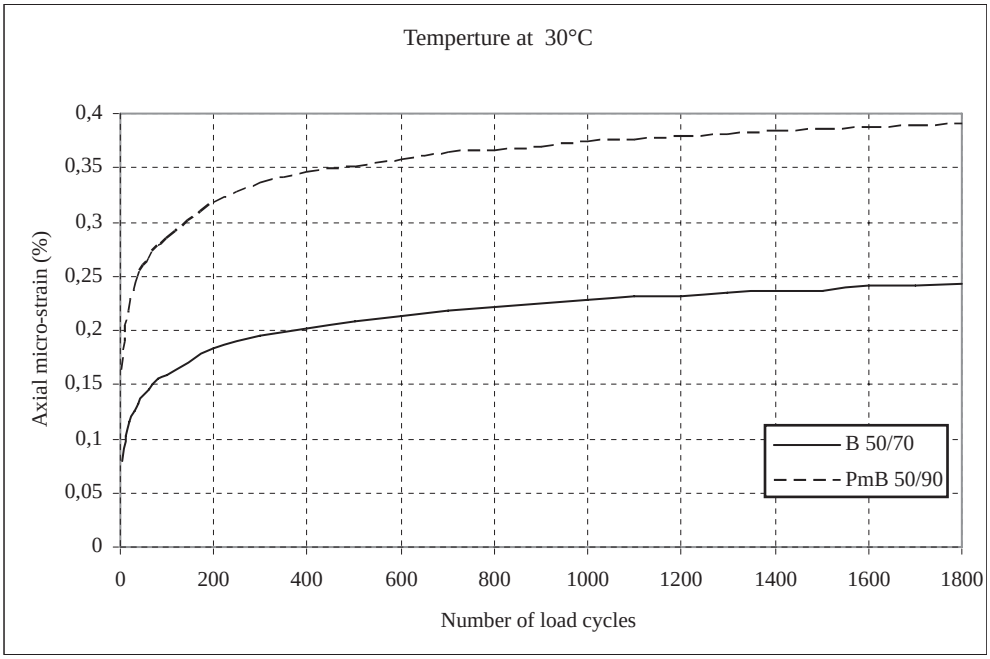

Figure 3. Chart of axial micro-strain of asphalt mixture depending on the type of bitumen at temperature 30°C.

Table 4. Resistance to permanent deformation of asphalt mixture.

Dynamic characteristics	T = 30°C		T = 40°C		T = 50°C	
	B 50/70	PmB 50/90	B 50/70	PmB 50/90	B 50/70	PmB 50/90
Percent of axial micro-strain ε_v (% mm/mm) after 1800 loading cycles	0,243	0,390	0,716	0,587	2,181	0,934

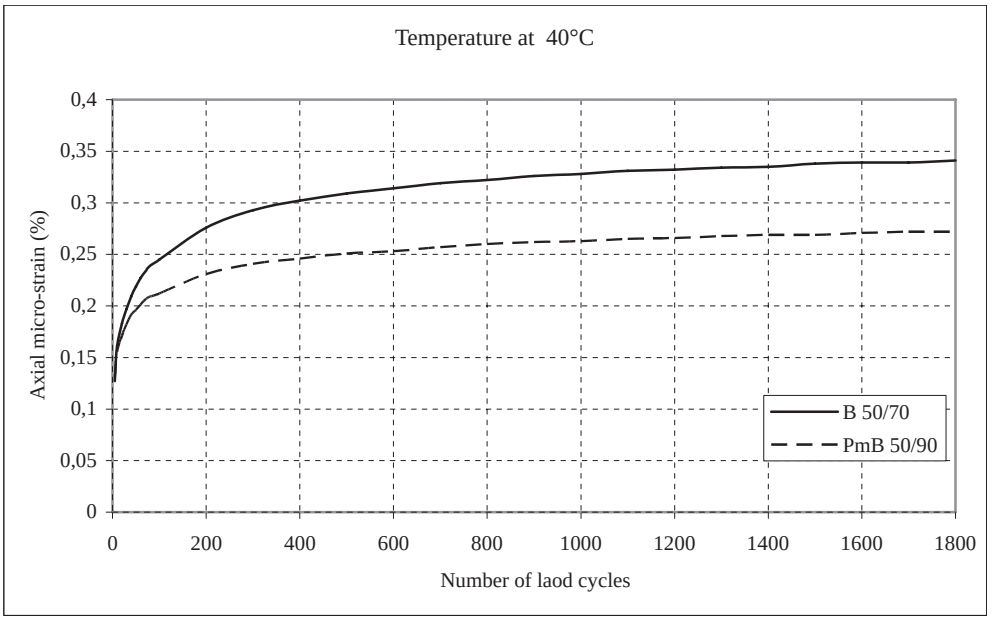

Figure 4. Chart of axial micro-strain of asphalt mixture depending on the type of bitumen at temperature 40°C.

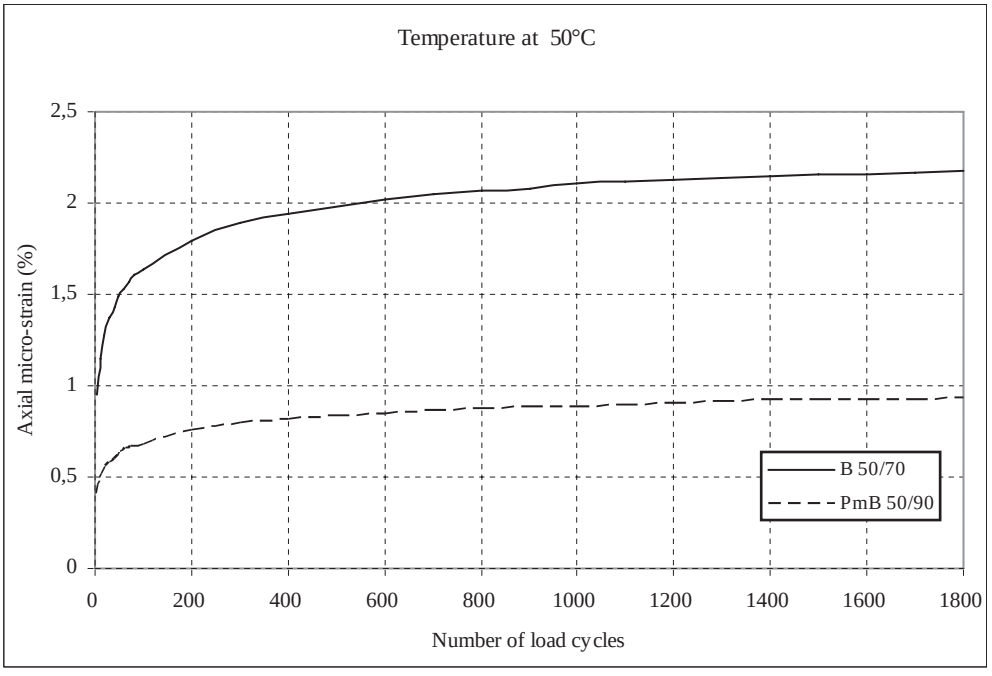

Figure 5. Chart of axial micro-strain of asphalt mixture depending on the type of bitumen at temperature 50°C.

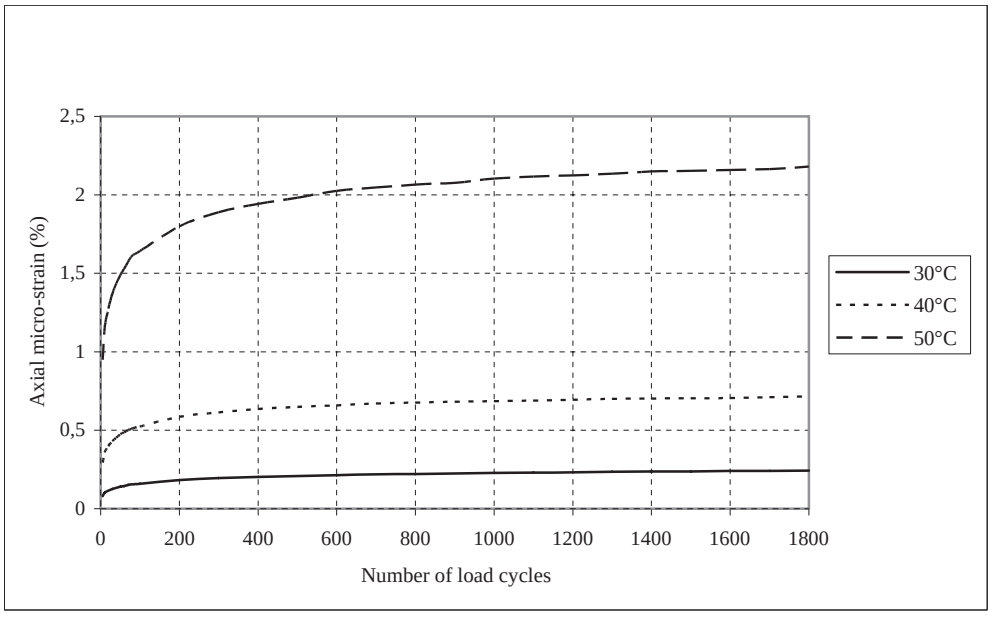

Figure 6. Chart of axial micro-strain of asphalt mixturewith bitumen B 50/70 as a function of temperature.

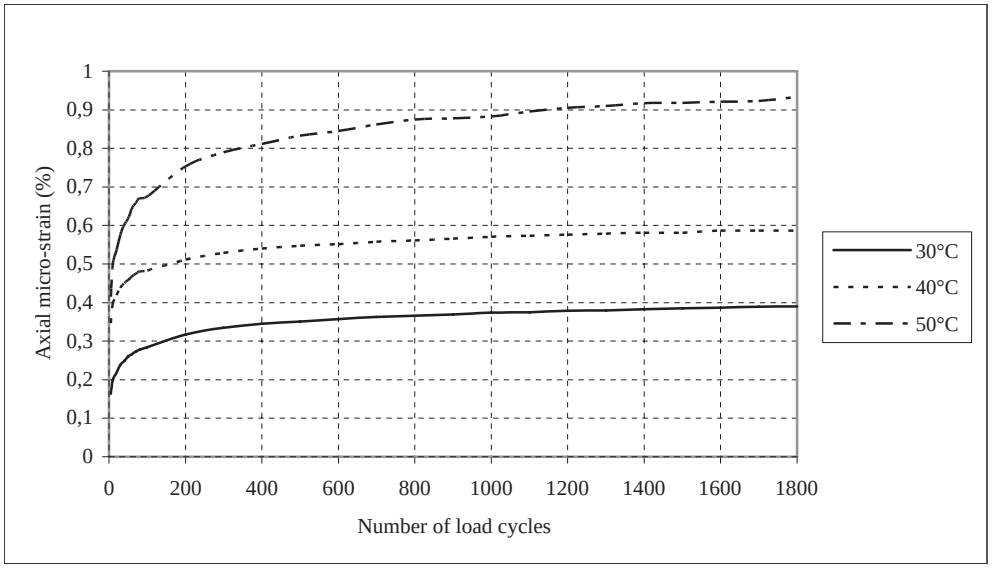

Figure 7. Chart of axial micro-strain of asphalt mixture withPolymer bitumen PmB 50/90 as a function of temperature.

3 PROPOSAL FOR PERFORMANCE BASED CRITERIA

Proposed criteria for dynamic characteristics of asphalt mixture tested with NAT depending on which binder are used PmB or standard bitumen (B 50/70) are given in Table 5.

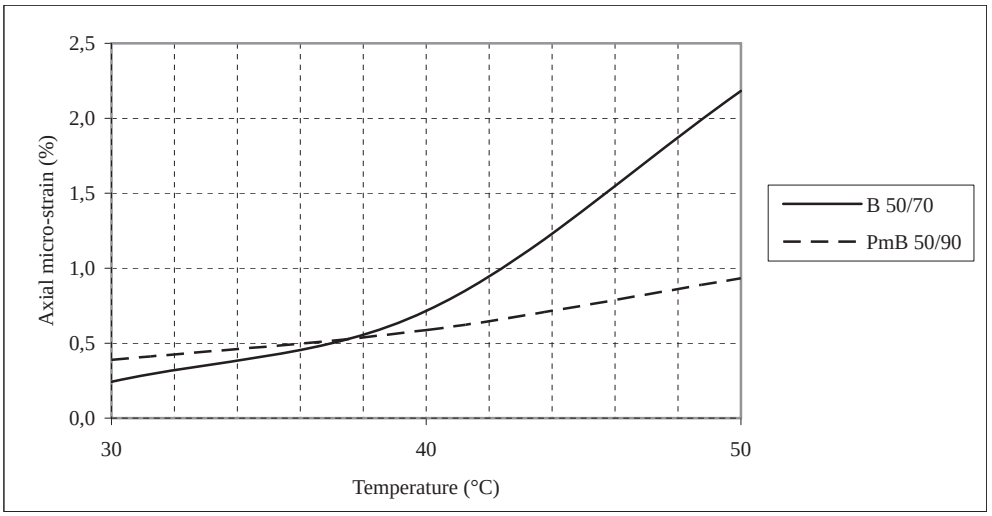

Figure 8. The accumulated strain as a function of temperature with B50/70 and PmB 50/90 after 1800 loading cycles.

Table 5. Proposed performance based criteria (NAT).

Dynamic characteristics	T = 30°C		T = 40°C		T = 50°C	
	B 50/70	PmB 50/90	B 50/70	PmB 50/90	B 50/70	PmB 50/90
Percent of axial micro-strain ε_v (% mm/mm) after 1800 loading cycles	<0,5	<1,0	<1,0	<1,0	<2,5	<1,5

4 CONCLUSION

Dynamic creep test at 30°C seems to be inappropriate for measurement of permanent deformation especially for asphalt mixtures with PmB, due to elastic deformation of SBS-polymer.

Resistance to permanent deformation for asphalt mixtures with SBS-Polymer modified Bitumen should be determined with dynamic creep test with confined lateral expansion at 40°C or even at 50°C for wearing course asphalt mixtures according to the EN 12697-25.

Analysing the results of axial micro-strain from VRLT at 30°C after 1800 cycles, following remarks can be made:

Test temperature of 30°C is not convenient especially for asphalt mixtures with PmB, because at lower temperatures elastic deformation of SBS-polymer is much higher than at higher temperatures. That's why it is better to use test temperature of 40°C or even 50°C for wearing course mixtures. The results from tests show higher accumulated strain with asphalt mixture with conventional bitumen B 50/70 than with the asphalt mixture with PmB 50/90 as a function of temperature. It is recommended determining the creep rate as a much accuracy value than axial micro-strain.

REFERENCE

EN 12697-25 (2005), Bituminous mixtures, Test methods for hot mix asphalt, Part 25: Cyclic compression test.

Advanced Testing and Characterization of Bituminous Materials –
Loizos, Partl, Scarpas & Al-Qadi (eds)
© 2009 Taylor & Francis Group, London, ISBN 978-0-415-55854-9

Rutting evaluation of asphalt binders and mixes

T.L.J. Wasage, I.B. Kazatchkov, J. Stastna & L. Zanzotto
Bituminous Materials Chair, University of Calgary, Canada

ABSTRACT: The main objectives of this research study were to identify the rut prone asphalt binders (conventional and modified) via the repeated creep and recovery test; and to check whether the measured accumulated strain can be related to the asphalt mixture performance. Creep and recovery testing, which is performed by multiple creep and recovery steps at various stress levels, has been a basic material test for polymers and variety of materials for many years. Federal Highway Administration (FHWA) has recently proposed a new test method called "Repeated Creep and Recovery Test (RCRT)" for asphalt binders to identify the rut susceptible asphalt binders. Furthermore, the National Cooperative Highway Research Program (NCHRP) project 9-19 study has proposed the use of tertiary flow parameter, Flow Number (FN) of cycles, from Repeated Load Permanent Deformation (RLPD) test as one of the Simple Performance Test (SPT) candidates for asphalt mixture testing. In this study several conventional and modified asphalt binders were tested according to the RCRT to identify the rut prone binders. The asphalt concrete mixes were prepared with the same asphalt binders and tested according to the RLPD tests. Since the mix design is the same, the major factor contributing towards rutting of asphalt concrete mixes could be traced to the asphalt binders which were the only component altered between the mixes. The test results suggested that the rut susceptible asphalt binders can be identified by RCRT.

1 INTRODUCTION

1.1 *Rutting in asphalt pavements*

One of the most important criteria in the mix design of asphalt paving mix is its ability to resist rutting. Rutting of asphalt pavements is caused by accumulation of irreversible deformation (permanent deformation) in any or all pavement layers under the repeated traffic loading. The permanent deformation mode of asphalt pavements can be resulted not only from traffic-associated causes but also from non-traffic-associated ones. This study focuses on traffic-induced (load-associated) deformation occurring within the asphalt paving layer itself. Rutting of asphalt paving layer under various loading conditions is the result of a series of complex internal processes. Some researchers (Finn 1967, Van de Loo 1974, Ameri-Gaznon 1989) stated that the concept of stability may be used to express the resistance of a mix to rutting in an actual pavement. Stability in general is a function of interparticle friction, cohesion of the asphalt, and resistance to displacement due to mass viscosity effects. Ameri-Gaznon summarized that rutting in an asphalt surfacing layer was due to three major causes: (a) viscous flow of the asphalt binder into the mineral aggregate voids, resulting in reduction in the thickness of aggregate coating and reduction in the relative distance between aggregate particles; (b) shearing displacements of aggregate coated with a thin film of asphalt binder; and (c) densification of the mixture due to a decrease in the air content. Many researchers (Hofstra & Klomp. 1972, Sousa et al. 1988, Collop 1995) observed that rutting occurred as a combination of densification (volume change) as well as shear deformation (without volume change), and the shear deformation rather than densification was the primary rutting mechanism.

The major portion of rutting occurs during the initial phase of loading. Initially the asphalt mix would be load-compacted and stiffened due to the rearrangement of particles

and expelling of air voids, accompanied by shear deformation. Shear deformation dominates after the initial densification phase. The irreversible deformation during the rutting process is strongly loading-time-dependent, primarily due to the viscous nature of the asphalt binder. Both densification and shear deformations were observed by Fwa T.F. & Tan S.A. 1992 experimentally in laboratory-accelerated wheel tracking tests. They concluded that densification would happen directly under the applied load. Lateral movements of aggregates were observed near the loaded area, and upward movements happened near the side of the loading area.

El Hussein, H.M. & Zhongqi, Y. 1994 separated the rutting process into three stages: strain hardening (volume change), shear flow and fracture failure. Based on his test results of repetitive uniaxial compression, he concluded that during the shear flow stage, the rate of accumulation of permanent axial strain was constant and was sensitive to the shear strength of asphalt mixture.

There exist different views regarding the distribution of rutting with depth. Hofstra, A. & Klomp, A. 1972 observed in their test track that permanent deformation in the asphaltic concrete layer was greatest near the load and gradually decreased with depth. This distribution of permanent strain with depth seems reasonable, as there should be more resistance to plastic flow with increasing depth below the wheel loading. Repeated load triaxial tests by McLean, D.B. & Monismith, C.L. 1974 indicated that the greatest amount of permanent deformation occurred at a depth of about 2 inches (50 mm) below the surface, at the point of occurrence of the largest value of stress difference. Research at the University of Waterloo (Morris & Haas 1974) suggested that nearly all of the permanent deformation in the asphalt layer occurred in the lower half of the layer as the result of lateral tensile stresses, which was in contradiction to the observations by Hofstra, A. & Klomp, A. 1972, and those by McLean, D.B. & Monismith, C.L. 1974. These differences in findings highlight the importance of the test procedure selection to simulate field conditions as closely as possible.

1.2 *Inadequacy of current high temperature binder and mix testing methods*

The Strategic Highway Research Program (SHRP) conducted a major research program from 1987 to 1993, to develop the Superpave performance-based specifications and test methods for asphalt binders and similar tests and a mix design practice for Hot Mix Asphalt (HMA) mixes. SHRP particularly suggested asphalt binder performance tests at high and low temperatures due to the important role of the asphalt binder in mixes. The American Association of State Highway and Transportation Officials (AASHTO) Superpave™ (Superpave) specification M-320 is the result of SHRP program and it is the most widely used asphalt binder specification in North America. However, the applicability of this specification in high temperature binder performance characterization of modified binders was questioned by many researchers (Anderson & Kennedy 1993, Bahia et al. 2001) as it was based on the study of unmodified asphalt binders. It was found that it underestimates the performance of the modified binders. For example, the currently used parameter in North America (AASHTO M30 2001) is $|G^*|/\sin\delta$ (= 1/J") ($\omega = 10$ rad/s) as the specification for high temperatures. Since the loss compliance J" measures the energy dissipated per cycle of sinusoidal deformations (Ferry J.D. 1980) it was assumed that a larger value of J" will lead to greater deformation in the binder. Consequently the pavement with such a binder will be more prone to rutting. This parameter, which was found to work well for unmodified asphalts, however does not give correct predictions for polymer-modified asphalts (Shenoy 2001, D'Angelo & Dongre 2002). Also the use of modified asphalt binders has grown tremendously in North America due to the increased stress on the highways from higher traffic volumes and heavier loads. Nowadays it is clear that a new approach has to be taken in order to characterize the performance of modified binders at high temperature. Recently, a new test called repeated creep and recovery test (RCRT) has been proposed by Bahia et al. 2001 and by Marasteanu et al. 2005 that measures fundamental properties of asphalt binders and can be used to identify the rutting potential of asphalt binders. This alternative test uses a sequence of shear creep and recovery experiments and is usually referred to as the dynamic creep. In its recent form

the dynamic creep test consists of a number of "cycles" of one second creep followed by nine seconds of recovery.

Furthermore as a part of the Superpave research program, the National Cooperative highway research Program (NCHRP) project 9-19 had a primary objective to recommend a simple performance test (SPT) to evaluate asphalt mix resistance to permanent deformation and fatigue cracking (NCHRP report 547, 2005). The outcome of the NCHRP project 9-19 study was the recommendation of the tertiary flow parameter, Flow number (FN) of cycles, from the repeated Load Permanent Deformation (RLPD) test as one of the SPT candidates. In this RLPD test, several thousand repetitions of load are applied and the accumulated permanent deformation is recorded as a function of number of load cycles over the full test period. This approach was employed by Monismith et al. in the mid 1970s using uniaxial compression tests. The researchers at the Arizona State University have suggested the unconfined deviator stress levels of 69, 138, 207 kPa (10, 20, 30 psi) and 10000 of loading and unloading cycles (Witczak et al. 2002). Brown and Cooper (Brown & Cooper 1984) used a range of various levels of confining pressure for their testing and suggested the stress level of 100 kPa (14.4 psi) as the confining pressure. However the test performance and the rutting prediction models are still under the research and in the development stage. Both these tests (RCRT and RLPD) are not fully understood yet. It is also necessary to understand the relationship between the quality of asphalt binder and the mixture performance, thus, the reasons for the hot mix asphalt concrete rutting potential can be identified as poor choice of non-bituminous components or asphalt binder quality.

2 EXPERIMENTAL DETAILS

2.1 *Materials*

2.1.1 *Asphalt binders*

Three different asphalt binders were used. Note that the asphalt binders are in the same high temperature performance grade (PG) category according to the Superpave binder specification.

- Base asphalt: Commercially available asphalt of 85-100 penetration grade characterized as PG64-25 (split grade) according to the Superpave binder specification, AASHTO M320. (Referred to as asphalt A).
- Oxidized asphalt: PG64-28 oxidized asphalt binder (referred to as asphalt B) was obtained by oxidation of softer asphalt from the same crude oil source as of asphalt A.
- Polymer-modified asphalt (PMA): Commercially available PG64-37 (referred to as asphalt C) and contained 4% (by weight) of a styrene-butadiene-styrene copolymer.

2.1.2 *Asphalt mixes*

The asphalt mixes were compacted using the same gradation, asphalt content (5.3%) and air voids (4%) according to the Superpave mix design. All three asphalt binders were used to prepare the mixes. All samples were compacted in a gyratory compactor, sawed and cored to the final dimensions of 100 mm in diameter and 150 mm in height.

Table 1. Superpave performance grading of the asphalt binders.

Designation	Description	Performance grade
Asphalt A	Base asphalt (penetration 85/100)	PG64-25
Asphalt B	Oxidized asphalt	PG64-28
Asphalt C	Polymer modified asphalt	PG64-37

2.2 *Test descriptions*

Two types of test machines were used in this work. A controlled stress rheometer, CVO-R (Malvern Instruments), was used for the asphalt binder samples; and the digital servo-hydraulic universal testing machines, UTM-25 and UTM-100 (IPC Global) were used for the asphalt mix samples.

The CVO-R is a rotational rheometer used to characterize the viscous and elastic behavior of bituminous materials. The creep and recovery tests were conducted at 40°C, 50°C and 60°C using the plate-plate geometry (diameter of 25 mm and gap of 1.5 mm). A set of one hundred cycles of repeated creep and recovery data was taken by the instrument, with a loading time of 1 second and unloading time of 9 seconds under a particular stress level. The studied stress level varies from 100 Pa to 5000 Pa.

The UTM-100 is a servo-hydraulic asphalt mix tester machine with a maximum load capacity of 100 kN. The unit includes an integrated control and data acquisition system (CDAS), in order to provide accurate force or displacement waveform generation and control and to enable automatic sequencing of test procedures. RPLD test was conducted and mixes were tested with the confining pressure of 69 kPa. An axial stress of 689 kPa was applied to test specimens. Unconfined testing was conducted with the varying load level from 69 kPa to 630 kPa.

3 TEST RESULTS

3.1 *Asphalt binders*

3.1.1 *Creep and recovery testing in asphalt binders*

In a creep and recovery experiment, the stress is increased from zero to a particular value in a short time period (almost instantly) and the strain is recorded as a function of time. Every shear creep experiment has several characteristic parameters. These are: the applied shear stress (τ), the test temperature (T), the total time of creep ($\bar{t}$) and if the recovery is followed, also the total time of recovery ($\bar{t}_r$). The first three parameters determine weather the performed creep test is in the linear or nonlinear domain. In an isothermal creep test the applied stress and the duration of the creep set the limit of a possible linear viscoelastic description of the test. In such a description the shear strain is a function of time only, ($\gamma(t)$). The shear compliance function, $J(t) = \gamma(t)/\tau$, can then be defined. In linear viscoelastic theory of materials the compliance function is determined via the retardation spectra $L(\Lambda)$. Analogously as with Maxwell model, the Voigt model (Ferry J.D. 1980) yields:

$$J(t) = J_g + \int_{-\infty}^{\infty} L(\Lambda)\left(1 - e^{-t/\Lambda}\right) d\ln\Lambda + t/\eta_0$$

where J_g represents an instantaneous (glassy) compliance and η_0 is zero shear viscosity.

In nonlinear regime, the shear strain function depends on time and the applied shear stress, τ. In linear viscoelastic theory, the temperature enters the picture via the time-temperature superposition principle, i.e. the time of creep is scaled by the horizontal shifting factor and the magnitude of creep function is scaled by a vertical shifting factor (often very close to 1), (Ferry 1980). In nonlinear regime the strain is generally a function of time, the applied shear stress and the temperature, $\gamma(t,\tau,\mathrm{T})$. It is not easy to determine the boundary between the two regimes even in a simple creep test and it is more complicated in the dynamic creep test. Dynamic creep test consists of applying a series of creep and recovery cycles. Creep and recovery cycle time, applied stress and the number of cycles are the free parameters to choose in this test. (D'Angelo & Dongre 2002). Figure 1 shows the total accumulation of compliance in one hundred cycles for all the materials. It is clear that the dynamic creep test can easily recognize the different asphalt binders even if they are characterized by the same high temperature, in the Superpave performance grading. One can easily recognize a different

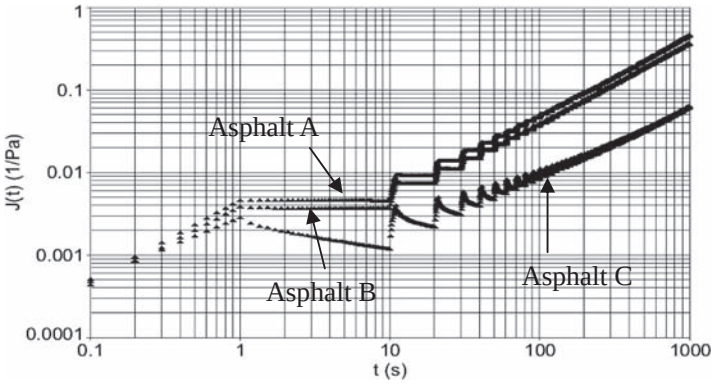

Figure 1. Accumulated compliance in asphalt A, B, and C. 100 cycles. Stress: 100 Pa, T = 60°C.

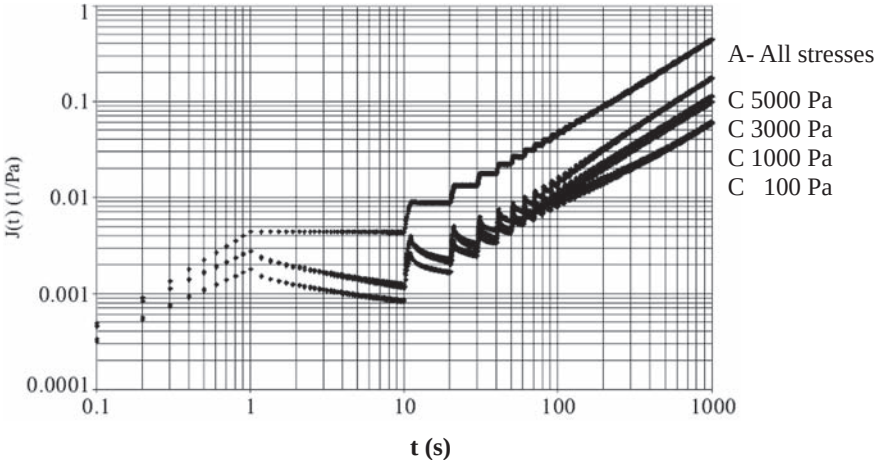

Figure 2. Accumulated compliance in asphalt A and C at different stresses. 100 cycles. Stresses: 5000 Pa to 100 Pa↓, T = 60°C.

character of $J(t)$ in the studied base and oxidized asphalt and in the modified asphalt. The first two samples (Asphalt A and B) exhibit almost no recovery in all one hundred cycles at 60°C for τ = 100 Pa. The difference between the conventional (or oxidized asphalts) and polymer modified binders is clearly seen. Generally the conventional binders (and oxidized binders) show very small recovery. The rates of increase of the accumulated compliance (or strain) are quite similar. Asphalt C exhibits a strong recovery in every cycle. The rates of increase of the accumulated compliance (or strain) depend now strongly on the used modifier and its concentration.

With increasing stress the accumulated compliance is increasing in conventional as well as in polymer modified samples. In conventional samples as in the oxidized sample the graphs of accumulated compliance at different stresses are almost parallel. That this is not the case for polymer modified samples is shown in Figure 2 where the asphalt A and C is portrayed at 60°C for different stresses (100 Pa to 5000 Pa). The shape of portrayed function $J(t)$ depends on stresses and temperatures in the dynamic creep test.

The base asphalt A reaches always the same final accumulated creep compliance (after 100 cycles) thus showing the independence of this function on the stress. This observation does not seem to apply to the modified materials where there is an increase in the final accumulated creep compliance as the shear stress increases. Hence multiple stress creep and

recovery test was conducted to understand the limiting stresses in viscoelastic region. In this experiment, same sample was loaded by a series of stresses. Stress was doubled after every ten cycles starting from 25 Pa up to 25600 Pa. A set of ten cycles of repeated creep and recovery data was taken for the particular stress level, with a loading time of 1 second and unloading time of 9 seconds. Figure 3 shows the recovered compliance J_r vs. stress for asphalts C. The recovered strain on the test was normalized by the applied stress to determine the compliance called J_r. Modified material exhibits uniform behavior at the lower stress levels. Testing temperature was also a governing parameter. At low testing temperature the material behave more uniform manner. As the stress level increases the non linear behavior of the materials appeared at the higher testing temperature. This test could be used to establish the limiting stress conditions.

3.2 *Asphalt mixes*

3.2.1 *Repeated load permanent deformation (RLPD)*

3.2.1.1 Unconfined testing

Figure 4 presents the accumulated permanent deformation in unconfined testing for mixes prepared with asphalts A, B and C. From this plot it can be seen that the RPLD test differentiates between mixes prepared with conventional and modified binders (same binder content) and same aggregate proportions and mixing conditions. The effect of the binder on the creep deformation of the mixes can also be seen. Modification of the binder by polymer did reduce the accumulated creep deformation of the mixes. It is also noted that the tertiary state was not achieved in the mix with polymer modified asphalt C with the loading condition and the temperature level used. Figures 5 and 6 shows the 10000 cycles of the repeated load permanent deformations for asphalt A and C respectively at 40°C for all the tested stresses. Tertiary flow occurred in the mixes prepared with asphalt A and B with lower loading levels compared to the mixes prepared with asphalt C. Flow numbers of the mixes prepared with asphalt A and B shown in Figure 4 are 5024 and 6656 respectively. Tertiary flow was not achieved in the mixes prepared with asphalt C with the loading of 138 kPa, indicating that the mix could be withstand for the higher loading conditions. This shows that although the asphalt binders

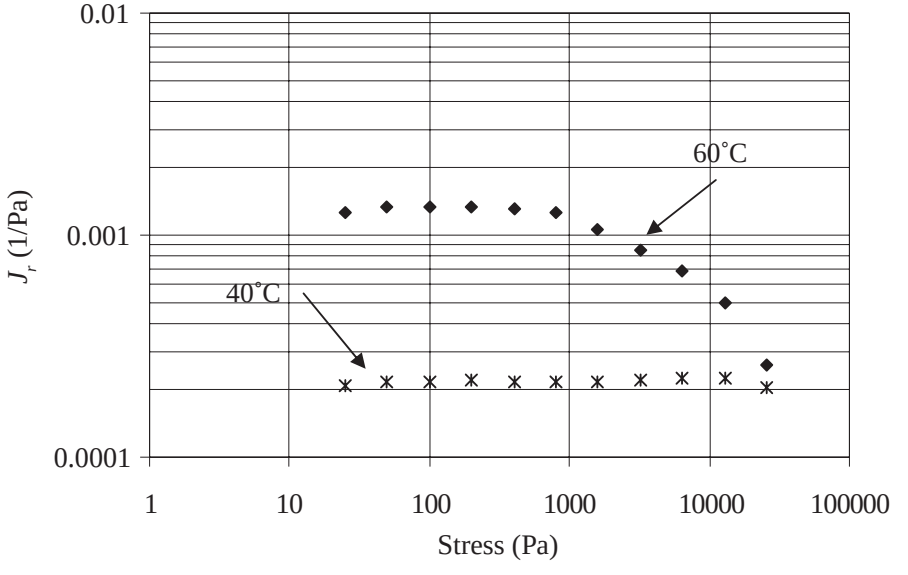

Figure 3. Effect of stress level on the compliance of asphalt C. T = 40°C and 60°C.
Note: J_r is the recovered strain of 10 cycles normalized by the applied stress.

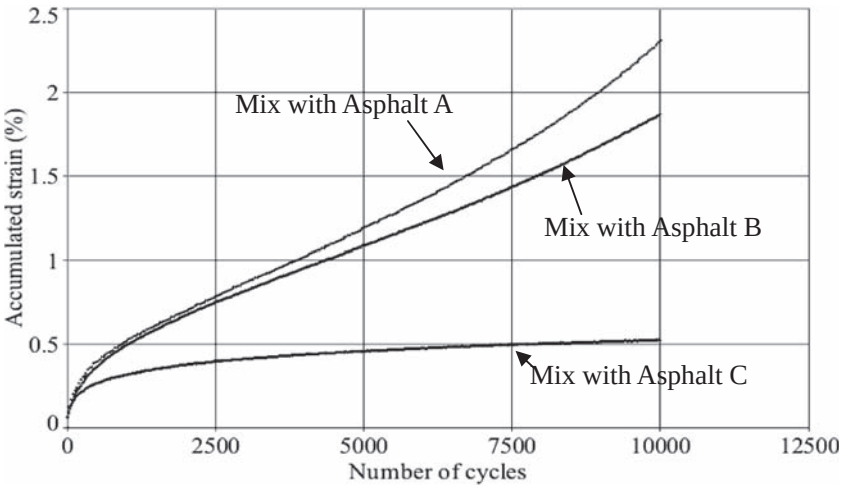

Figure 4. Accumulated strain in mixes prepared with asphalt A, B and C. T = 40°C. Load: 138 kPa. Loading type: Haversine pulse load.

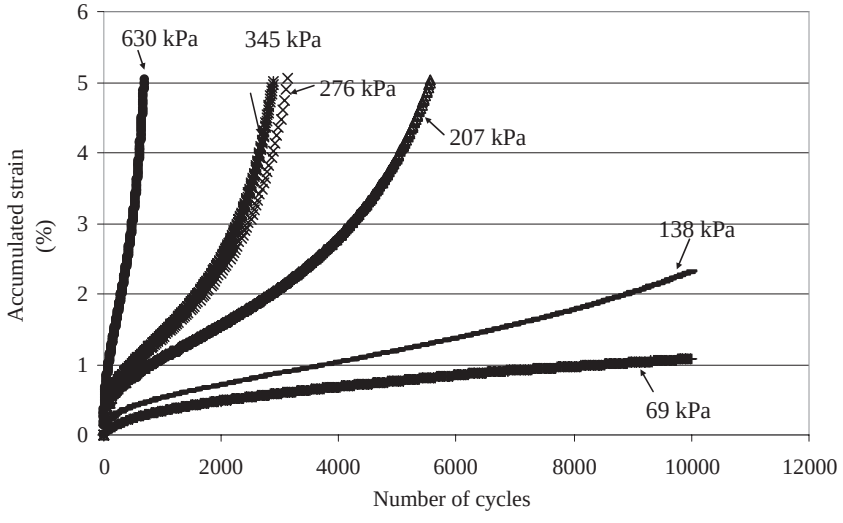

Figure 5. Accumulated strain in asphalt A. T = 40°C. Load: 69 to 630 kPa.

were characterized in the same PG category the mix behavior was different and RLPD test was able to characterize the mix performance.

3.2.1.2 Confined testing

Figure 7 presents the accumulated permanent deformation in confined testing for mixes prepared with asphalts B and C. It was observed that the mixes prepared with the conventional and oxidized binders are susceptible to failure with the lower number of cycles under the load level of 689 kPa and confining pressure of 69 kPa. However polymer modified asphalt was able to withstand this loading level with the 10000 loading cycles. Flow numbers for the mixes B and C shown in Figure 7 are 984 and 6434 respectively. RLPD test results shows that the asphalt mixes were consistent with the test results obtained for the asphalt binders from the RCRT testing highlighting the correlation between two test methods.

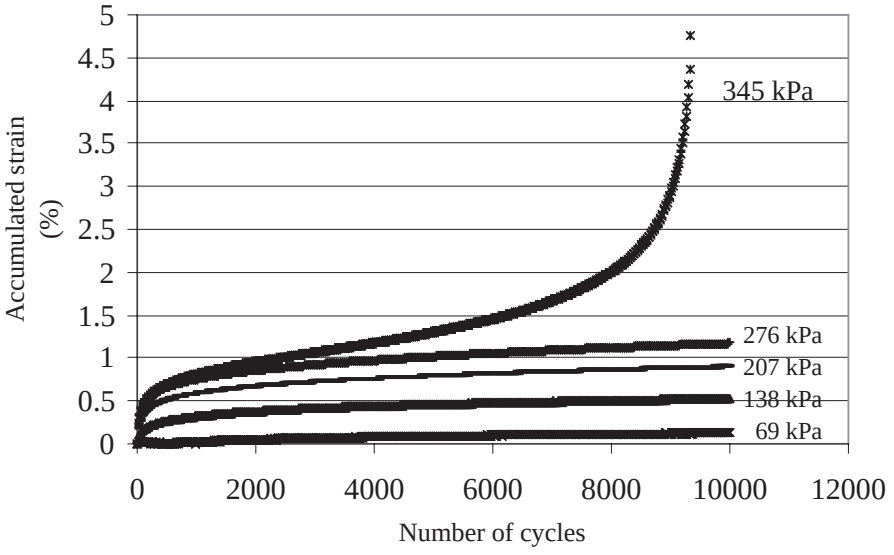

Figure 6. Accumulated strain in asphalt C. T = 40°C. Load: 69 to 345 kPa.

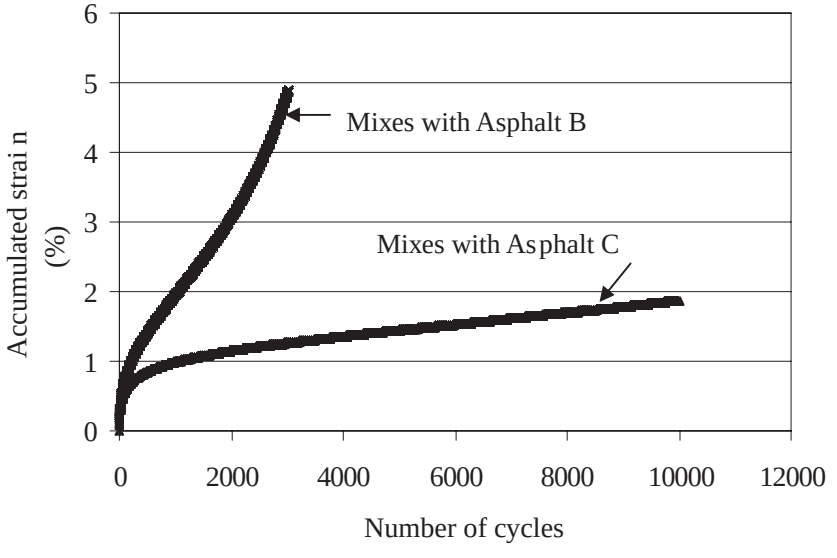

Figure 7. Accumulated strain in mixes prepared with asphalt B and C. T = 40°C. Load: 689 kPa. Confining pressure: 69 kPa. Loading type: Haversine pulse load.

4 CONCLUSIONS

Conventional, oxidized and polymer modified asphalts were studied in dynamic creep test. RCRT experiment in conventional asphalt showed that the magnitude of recovery in every cycle (up to 100 cycles) was very small. The situation was similar for the oxidized asphalt. However it was quite different for modified asphalts. The magnitude of recovery in individual cycles was much higher in these modified materials. The accumulated deformation was much smaller in polymer modified asphalt than in its base asphalts. The role of applied stress was very strong in asphalt modified by SBS polymer. In the studied base asphalt, the role of stress

seems to be week. It was observed that the "boundary" between linear and nonlinear behavior of accumulated compliance can depend not only on the material but also on time, applied stresses and temperatures. Further, for the set of asphalts studied, it was shown that the RCRT test can clearly distinguish the materials even if they have the same high temperature characteristics, given by the Superpave performance grading. Even if the parameter $|G^*|/\sin \delta$ might be useful for conventional asphalts, the dynamic creep test seems to be more effective in its ability to characterize the conventional as well as polymer modified asphalt binders. RPLD tests in asphalt mixes were more suitable to describe the high-temperature performance of asphalt mixes prepared with the same performance grade asphalt binders than single dynamic experiments. The dynamic creep test in asphalt mixes and binders, and the appropriate modeling of this test offer new elements for the laboratory evaluation of these materials.

ACKNOWLEDGEMENTS

The authors express their gratitude to the National Sciences and Engineering Research Council of Canada (NSERC) and to Husky Energy Inc. for their financial support of this work.

REFERENCES

American Association of State Highway and Transportation Officials, Standard Specification for Performance Graded Asphalt Binders M30, 2001.

Ameri-Gaznon, M. 1989. Permanent Deformation Potential in Asphalt Concrete Overlays over Portland Cement Concrete Pavements. Ph.D Thesis. Texas, A & M University.

Anderson, D.A. & Kennedy, T.W. 1993. Development of SHRP Binder Specification. *Journal of the Association of Asphalt Paving Technologies* 62: 481–501.

Bahia, H.U., Hanson, D.I., Zeng, M., Zhai, H., Khatri, M.A. & Anderson, R.M. 2001. Characterization of Modified Asphalt Binders in Superpave Mix Design. Report 459, National Cooperative Highway Research Program, *National Academy Press.* Washington, D.C.

Brown, S.F. & Cooper K.E. 1984. The Mechanical Properties of Bituminous Materials for Road Bases and Basecourses, Proceedings of Association of Asphalt Paving Technologists, Asphalt Paving Technology 53: 415–439.

Collop, A.C., Cebon, D. & Hardy, S.A. 1995. Viscoelastic Approach to Rutting in Flexible Pavements. *Journal of Transportation Engineering* 121(1): 82–92. January/February.

D'Angelo, J. & Dongre, R. 2002. Superpave Binder Specifications and Their Performance Relationship to Modified Binders. Proceedings of Canadian Technical Asphalt Association : 91–103.

El Hussein H. Mohamed & Zhongqi Yue. 1994. Criteria for Evaluation of Rutting Potential Based on Repetitive Uniaxial Compression Test. 73rd Annual Meeting of Transportation Research Record.

Ferry, J.D. 1980. Viscoelastic properties of polymers. John Wiley & Sons, Inc.

Finn, F.N. 1967. Factors Involved in the Design of Asphaltic Pavement Surfaces. The National Cooperative Highway Research Program (NCHRP) 39.

Fwa, T.F. & Tan, S.A. 1992. Laboratory Evaluation of Rutting Potential of Asphalt Mixtures. Effects of Aggregates and Mineral Fillers on Asphalt Mixture Performance, ASTM STP 1147, Richard C. Meininger, Editor, American Society for Testing and Materials, Philadelphia: 211–224.

Hofstra, A. & Klomp, A. 1972. Permanent Deformation of Flexible Pavements under Simulated Road Traffic Conditions. 3rd International Conference on the Structrural Design of Asphalt Pavements 1: 613–621.

Marasteanu, M.O., Clyne, T., McGraw, J., Li, X. & Velasquez, R. 2005. High-Temperature Rheological Properties of Asphalt Binders. Transportation Research Record: *Journal of the Transportation Research Board No. 1901*: 52–59. TRB, National Research Council, Washington, D.C.

McLean, D.B. & Monismith, C.L. 1974. Estimation of Permanent Deformation in Asphalt Concrete layers Due to Repeated Traffic Loading. Transportation Research Record 510: 14–30.

Morris, J. & Haas, R.C.G. 1974. Permanent Deformation in Asphalt Pavements can be Predicted. Association of Asphalt Paving Technologists, 43: 41–76.

National Cooperative Highway Research Program Report 547, 2005. Simple Performance Tests: Summary and Recommended Methods and Database, Transportation Research Board. Washington D.C.

Shenoy, A. 2001. Refinement of the Superpave Specification Parameter for Performance Grading of Apshalt. *Journal of Transportation Engineering*, American Society of Civil Engineers 127(5): 357–362.

Sousa, J.B., Lysmer, J., Chen, S.S. & Monismith, C.L. 1988. Dynamic Loads: Effects on the Performance of Asphalt Concrete Pavements. Transportation Research Record 1207: 145–168.
Van de Loo, P.J. 1974. Creep Test, A Simple Tool to Judge Asphalt Mix Stability. Proceeding, Association of Asphalt Paving Technologists, Vol. 43.
Witczak, M.W., Kaloush, K., El-Basyouny M. & Von Quintus H., 2002. Simple Performance Test for Superpave Mix Design, NCHRP Report 465, Transportation Research Board, National Research Council. Washington, D.C.

Advanced Testing and Characterization of Bituminous Materials – Loizos, Partl, Scarpas & Al-Qadi (eds)
© 2009 Taylor & Francis Group, London, ISBN 978-0-415-55854-9

An integrated approach to modeling rutting of flexible pavements

V.T. Thushara
Department of Civil Engineering, TKM College of Engineering, Kerala, India

J. Murali Krishnan
Department of Civil Engineering, Indian Institute of Technology Madras, India

ABSTRACT: Pavement rutting is caused by the accumulation of residual deformation in one or more of the pavement layers and in the subgrade. The application of repetitive wheel loads result in certain amount of residual and permanent strain in the pavement layers. With the passage of traffic this residual/permanent strain will accumulate and ultimately lead to significant failure by rutting. The rutting in the underlying layers will also contribute to the rutting characteristics of the layers above. Hence it is essential to use appropriate constitutive models for pavement materials and solution techniques which will capture these responses to simulate the actual behavior of pavement under traffic loading.

In this study, the asphalt layer is characterized by a linear viscoelastic material model, the granular layers by elastic-plastic model of the Drucker-Prager type and the sub-base as well as sub-grade by linearized elastic model. The pavement response when subjected to various traffic loading conditions is analyzed using the finite element package ABAQUS. In specific, the residual/permanent strain accumulations as well as the deformation at various component layers during traffic load repetitions are monitored. Different type of loading conditions and rest periods are applied on the pavement model. It is seen that the mechanical response of asphalt layer completely controls the mechanical response of all the other layers below in terms of response even during rest periods.

Keywords: Flexible pavement, Rutting, Finite Element Analysis, Viscoelastic, Drucker-Prager

1 INTRODUCTION

A flexible pavement is a complex structural system and its performance involves the interaction of large number of factors. Some of them include the materials used, the environmental conditions, traffic and loading conditions and the method of construction. A typical flexible pavement consists of an asphalt surfacing, a base, a sub-base and sub-grade. Pavement foundation can be broadly defined as one or more layers of compacted unbound granular material placed over the sub-grade soil (Brown 1996). Typically it consists of the sub-base and sub-grade. The mechanical behavior of each layer differs from each other. In reality, the asphaltic layer exhibits non-linear viscoelastic/viscoplastic behavior and this depends very much on time and temperature. The granular materials comprising the pavement foundation follow a nonlinear stress-strain behavior due to its pressure sensitive nature (Kim & Tutumluer 2006). In addition to these, the random traffic parameters such as vehicle speed, duration and intensity of loading, frequency of vehicle arrival, axle configuration etc., have to be considered while modeling the response of the pavement. The change in material character throughout the day as well as throughout the year due to changes in temperature and moisture content contributes to the complexity in modeling the stress-strain response of pavement layers.

Residual/permanent deformation occurring during repetitive wheel load application leads to pavement failure in the form of rutting. Rutting in flexible pavement materials is essentially

composed of two components: densification and plastic flow. Due to the particulate nature of the asphalt mixtures and granular materials, considerable amount of densification takes place. There is also permanent deformation due to shear failure of the material and this essentially results in the material flowing outward the wheel path. While the issues related to rutting in individual layers due to the constitutive response has been reasonably understood, the rutting in the pavement structural system due to the individual rutting of each layer has not been investigated in detail. A typical pavement will have at least four distinct layers. For the sake of discussion, one can visualize a scenario in which there is permanent deformation in the sub-grade layers. Due to this deformation, the layer above it is likely to lose its structural effectiveness. However, since rutting in an individual layer is essentially a local phenomenon, it is expected that this will result in the layer above the sub-grade exhibiting a deflected shape conforming to the rutting seen in the sub-grade layer. There is also a possibility of rutting in this layer in terms of densification and plastic flow. Hence, for this layer, there are two components of rutting, the first one is essentially due to the rutting in the individual layers and the second component is due to the "reflected component" of rutting from the layer below. This can propagate further to the top resulting in the topmost layer exhibiting the largest rutting.

In a layered structure with several layers having different material properties, one can assume that there is no slippage in the interface of the layers. This assumption will ensure that the rutting exhibited by the bottom layer will be reflected to the top layer. It is also necessary to assume that the reflected rutting to the top layer will not result in the imminent failure of that particular layer. Hence, when numerically solving this problem, one needs to take into account the rutting in the individual layers as well as the rutting in the layers due to the movement from underneath. Typically, one can solve this problem, by remapping the locations of the individual layers in proportion to the movement in the layers below. This involves development of numerical framework that takes into account the integrated response of each of the sub-system of pavement layers on the overall response of the pavement layers. For performance prediction, it is of great importance to know whether a given flexible pavement will experience progressive accumulation of permanent deformation till an acceptable level or not.

At the present time, no overall framework has been established to explain satisfactorily the mechanical behavior of pavement layers under the complex repeated loading. As far as pavement engineering is considered, theories were developed based on the assumption of material behavior to be linearized elastic. While elastic theory may be a reasonable approximation in the design of asphalt pavements under fast moving wheel loads, the effect of slow moving vehicles as well as parking loads cannot be considered by this approach. In addition, the accumulation of small deformations under repeated load cannot be accounted by linearized elastic layer theory. Recently theories based on some of the real life material behavior are suggested by many authors (Zhagoul & White 1993, Chazallon et al. 2006, Elsefi et al. 2006) and the predictions were closer with the field measurements. In this contest, it is thus desirable to look in to various material models and their relationship with the response of pavement.

The interesting questions related to the state of stress in a granular layer when overlain with a viscoelastic layer conditions have not been investigated in detail in the reviewed studies. This assumes special importance when one is analyzing the full pavement system for failures due to rutting. In this study, the pavement is modeled as a four layered structural system and analyzed using the finite element package ABAQUS for various traffic loading conditions. The asphalt layers are characterized by a viscoelastic material model, granular base by elastic-plastic material model and the sub-base and sub-grade by linearized elastic material models. The pavement response when subjected to various traffic loading conditions are analyzed.

2 LITERATURE REVIEW

Based on the analysis of surface profiles generated using different material behavior assumptions, Sousa et al. (1993), stated that there is a need to model nonlinear behaviors of hot mix

asphalt if realistic profiles are to be predicted. Creep models are used to characterize the rutting behavior of asphalt layers by many authors. Shakedown concept is used by Collins et al. (1993) to model the plastic strain accumulation in pavement granular layers. Simpson et al. (1995) suggested that one should be able to identify weak layers in a pavement structure on the basis of the shapes and dimensions of deformation at the pavement surface. From these study results it is inferred that to predict the rutting behavior of the flexible pavement the characteristic properties of the component layers as well as the deformation profile of each of the component layers has to be taken into account.

Due to the limitations of the current layer theories, most of the investigations have been carried out assuming either asphalt concrete to be linearized elastic in nature or using a surrogate elastic modulus such as dynamic modulus. However, the real behavior of asphaltic layer is time dependent at the stress level of interest. Elastic analysis of asphaltic layers cannot simulate permanent deformation or delayed recovery, a known characteristics of hot mix asphalt materials. Results of the analysis by Elseifi et al. (2006) indicated that the elastic theory grossly under predicts pavement responses to vehicular loading at intermediate and high temperatures, and the results of the finite element viscoelastic model were in better agreement with field measurements. Significant studies have been carried out by Monismith and Secor (1962), Papagiannakis and Taha (1996), Helwany et al. (1998), Siddharthan et al. (2005), White et al. (1997) and Mulungye et al. (2007), by considering the viscoelastic response of asphalt layers. The inelastic deformation of the pavement layers, to characterize rutting, was simulated by Kettil et al. (2007) by considering visco-plastic model for asphalt concrete.

Pavement foundation granular materials which are particulate in nature behaves as nonlinear and pressure dependent even at low traffic loads. The layer properties are not constants but are functions of the confinement pressure. Saad et al. (2005) studied the effect of elasto-plasticity of base and sub-grade on the dynamic response of pavement systems by considering granular base as elastic-plastic (Drucker-Prager) and the sub-grade as elastic-plastic strain hardening (Cam-Clay) materials. Chazallon et al. (2006) developed a simplified method for the finite element modeling of flexible pavement rut depth evolution with time based on the shakedown theory. Kettil et al. (2007) used a poroelastic material model to describe the elastic strain and Drucker-Prager model to describe the plastic strain as well as the strain hardening of the unbound granular layers. Studies by Helwany et al. (1998), White et al. (1997) and Sukumaran (2004) also considered the elastic-plastic behavior of granular layers and studies by Hadi and Bodhinayake (2003), Park and Lytton (2004), Kim and Tutumuler (2006) and Kuo and Huang (2006) considered the properties of pavement granular layers by the use of resilient modulus models. Collins et al. (1993) used the upper bound, kinematic shakedown theorem to obtain estimates of the critical shakedown load.

Most of the pavement analyses are conducted assuming that vehicles or test loads are static. In reality vehicles or test-loads can be static or moving. Markow (1988) proposed a quasi-static approach for modeling the pavement response under moving loads. Studies by Papagiannakis et al. (1992) and Helwany et al. (1998) indicated that the measured tensile strains at the bottom of the AC layer exhibited a large sensitivity to vehicle speed. Other significant studies by considering these aspects of loading were done by Zaghloul and White (1993), White et al. (1997), Sukumaran (2004), Elseifi et al. (2006).

Lots of the studies have focused on the characterization of each layer in order to account their contribution in the rut depth formation. Since the layers are acting together as a structural system, the response of one layer will contribute to the response of the total system. It is significant to look into the response of pavement system under complex traffic loading incorporating the interaction of response in each of the component layers as well as the system as a whole to predict pavement distresses. Appropriate constitutive response and their structural response have to be included in the analysis to focus in to the above issue.

3 FINITE ELEMENT MODEL

The pavement structure analyzed consists of 15 cm of asphalt surface layer, 25 cm of base layer, 30 cm of sub-base layer and sub-grade. The radius of the axi-symmetric section considered

is 5 m. A fixed boundary is given at the bottom constraining all the movements and hinged condition is given for the sides so as to restrain the horizontal deformation. Same nodes are at contact for the elements of adjacent layers, restraining the relative movement of the layers at the interface. A circular loading of 16 cm radius with uniform pressure of 650 kPa is applied. This uniform pressure is caused by 10.1 *t* axle load. A parametric study was done to select the mesh size so as to make a compromise between computational time and accuracy and finally a global mesh size of 0.02 m is adopted throughout the analyses. However for studying some minute aspects a global mesh size of 0.01 m is also used. Four noded quadrilateral elements of reduced integration are used for the whole 2D analyses (ABAQUS 2003).

3.1 *Constitutive models for pavement layers*

3.1.1 *Viscoelastic material model for asphalt layer*

Viscoelastic phenomena are characterized by the fact that the rate at which inelastic strains develop depends not only on the current state of stress and strain but, in general, on the full history of their development. Thus to determine the increment of inelastic strain over a given time interval, it is necessary to know the state of stress and strain at all preceding times. ABAQUS (2003) uses an integral equation model for the deviatoric stress and it is expressed in terms of relaxation modulus function which is defined by an idealized experiment in which at time, $t = 0$, the specimen is subjected to suddenly applied and constant strain, e_0 and stress response $s(t)$ is measured.

The material parameters required for the implementation of viscoelastic analysis is taken from the constant compressive load creep simulated data at 40°C of Kettil et al. (2007). One important aspect in capturing the precise pavement response due to the viscoelastic nature of asphalt layers is the accuracy of the model calibrated during very fast application of load. This involves the collection and use of creep data sensitive for very short time steps. The data of Kettil et al. (2007) is chosen due to the above fact. Prony Series expansion with 13 coefficients is used to define the linear viscoelastic fluid-like material. Comparison of normalized predicted creep data and test data is given in Figure 1.

3.1.2 *Elastic-plastic model for base layer*

The model to characterize pavement granular base should reflect some of the important characteristics of the granular materials such as elastic response at lower stress level and plastic response at higher stress level, elastic unloading as well as hardening of the material. The model should be computationally stable and the parameters should be easily measurable. The linearly hardening extension of the original Drucker-Prager model (Drucker and Prager, 1952) is able to meet the above requirements and hence used in this study to characterize the granular base of the modeled pavement system. The linear Drucker-Prager model used provides a circular section in the deviatoric plane, associated inelastic flow in the deviatoric plane, and separate dilation and friction angles (ABAQUS 2003).

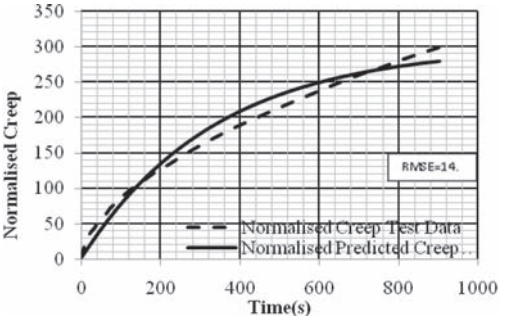

Figure 1. Comparison of creep test data and predicted model at 40°C for viscoelastic analysis (Kettil et al. 2007).

Table 1. Granular base drucker prager parameters used.

Material property	Value
Modulus of elasticity (kPa)	138000
Poisson's ratio	0.4
Angle of internal friction, degree	40
Dilation angle	40
Yield stress (kPa)	610
Absolute Plastic Strain at yield	0

Table 2. Elastic parameters for sub-base and sub-grade (Helwany et al. 1998).

Layer	Young's modulus (MPa)	Poisson's ratio
Sub-base	68.9	0.3
Sub-grade	50	0.3

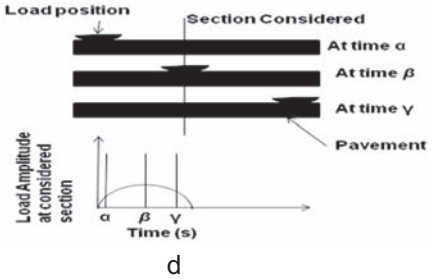

Figure 2. Schematic diagram of moving traffic loading.

The material parameters required for defining the linear Drucker-Prager material model for base course is taken from White et al. (1997). The parameters used are given in the Table 1.

3.1.3 *Linearized elastic model for sub-base and sub-grade*

Sub-base layer and sub-grade layer is modeled as linearized elastic layers, considering the fact that the stress in these layers will be considerably less than that in the surface layer and base layer, and will remain within the elastic regime. The material parameters required for the numerical implementation of linearised elastic models for sub-base and sub-grade is taken from the study of Helwany et al. (1998) and is tabulated in Table 2.

3.2 *Traffic loading*

Repeated haversine load with and without rest period, is applied in order to simulate the loading pattern of a moving load. The schematic diagram of the haversine loading is given in the Figure 2 and the mathematical expression is given in Equation 1.

$$\left(p(t) = \sum_{n=0}^{n=N} p_0 \sin^2 \omega t [H(t - n\Delta T) - H(t - n\Delta T - T_l)] \right) \tag{1}$$

where, $\Delta T = T_l + T_r$, T_l = time of one haversine load and T_r = rest period after a load wave, H = Heaviside step function, ω = angular frequency of the load wave and $n = n$th repetition.

When the load is at a considerable distance from a given point, the load above the point is zero or $p(t) = 0$. When the load is directly above the given point, the load intensity is p_0. The duration of load d depends on the vehicle speed s and the tyre radius a. A reasonable assumption is that the load has practically no effect when it is at a distance of 6 a from the point (Huang 2004).

$$d = \frac{12a}{s} \tag{2}$$

The effect of randomness of traffic is incorporated by giving traffic repetitions without rest period and with a rest period of 4 s and 0.8 s. The effect of speed of vehicles in the stress strain response of the pavement system is analyzed by giving haversine load periods of 6.28 s, 1 s and 0.2 s, which correspond to speeds of 1.1, 7 and 35 kilometer per hour respectively and thus capturing the effect of vehicles moving with different speeds.

4 RESULTS

4.1 *Comparison with elastic solution*

In this section, the simulations are shown for the case when the pavement is modeled as a four-layer elastic pavement, called herein after as Case-I. Another pavement section is considered in which only the top layer is considered as viscoelastic and all the remaining three layers are considered as linearized elastic, called herein after as Case-II. For case-I and case-II, same material parameters are assumed for all the elastic layers (layers two to four). These values are E = 500, 68.9 and 50 MPa. For case-I, the instantaneous elastic modulus values of the viscoelastic layer is assumed, which in the present case is 2000 MPa. For all the elastic cases, a Poisson's ratio of 0.3 is assumed. Figure 3 shows the residual strain formation after the removal of load in the viscoelastic case when cycles of haversine loading of 1 s and rest period of 4 s are given. In elastic analysis as soon as the load is removed the strain will come to zero, but in the viscoelastic analysis there will be still residual strain which will recover with time. Hence, the application of subsequent wheel load will cause the strain to get accumulated with the residual strain.

4.2 *Effect of loading pattern*

The effect of duration of loading on the stress-strain response of the pavement is analyzed for the case-II conditions. Sinusoidal load of 0.2 s as well as 1 s are applied with 4 s rest period and the strain values at the bottom of asphalt layer are plotted in Figure 4. It can be observed that the strain after 4 s of removal of single application of load is 52 microstrain for 1 s loading and is 9.5 microstrain for 0.2 s loading. With traffic repetitions, the unrecovered strain

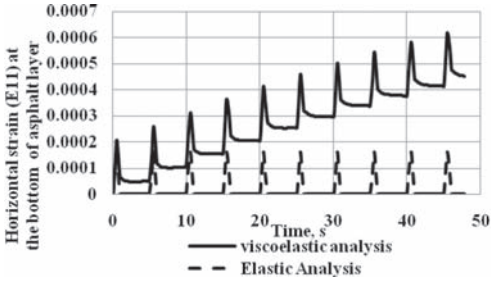

Figure 3. Comparison of elastic and viscoelastic analysis (case-I and case-II) haversine loading of 1 s and rest period of 4 s.

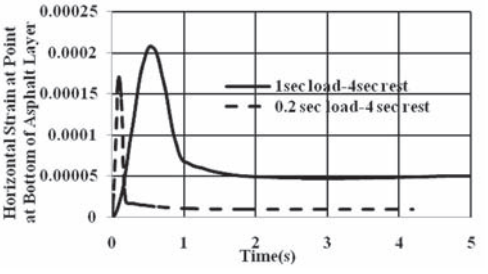

Figure 4. Effect of loading time in the horizontal strain at the bottom of asphalt layer (case-II).

due to the previous loading will get added up and the cumulative strain will significantly depend on the load duration.

The strain accumulation will also depend on the arrival pattern of vehicles. For various frequency of arrival of vehicles the total strain accumulated varies. When the rest period is less, i.e., when the frequency of arrival of vehicles is more the residual strain accumulation is significantly high. This effect is plotted in Figure 5. When the vehicle arrival is more without giving enough rest periods, the residual strain accumulation is much greater than when enough rest period is obtained.

4.3 *Influence of viscoelastic nature of surface layer on elastic response of the underlying layers*

The elastic granular layers are also affected by the viscoelastic behavior of the layer above. Due to the viscoelastic nature of the asphalt layer, even after the load is removed, there will be a time bound recovery of strain and relaxation of stresses. This will in turn affect the state of stress in the granular layers.

To illustrate this, two cases each for 0.2 s loading and 1 s loading are considered. The peak vertical strain values vs. number of repetitions at bottom of sub-grade are plotted in Figure 6. In the case-II, the strain values in the granular layers will keep on increasing in the initial load cycles and gradually it reaches a constant value due to the time effect during stress transfer when overlain by a viscoelastic layer. This effect in elastic granular layers will also depend on the duration and frequency of loading as in the case of viscoelastic asphalt layer which can be observed from the change in response for 0.2 s loading and 1 s loading. On the other hand, in the first case, when the granular layer is considered to be overlain by a linearized elastic layer, the strain in the granular layer will be constant despite the duration of loading and number of load repetitions.

4.4 *Plastic strain formulation in the base layer*

In this section, a third case (Case-III) is considered in which the top layer is viscoelastic, the second layer is elastic-plastic of the Drucker-Prager type and the remaining layers are considered linearlzied elastic. The plastic strain formulation in the base layer also depends on the characteristics properties of the layer above, the yielding and straining characteristics of the base layer as well as the loading pattern as shown in Figure 7. A haversine load of peak amplitude 1800 kPa is applied with period 6.28 s and 0.2 s. No plastic deformation is formed when the load period is 0.2 s where as plastic strain of magnitude 0.00145 is formed for 6.28 s load period. Another observation from the simulation results is that when 1500 kPa load is applied with elastic surface layer as well as with viscoelastic surface layer. An irrecoverable strain is observed in the second case where as no such strain is seen in the base layer which is overlain by an elastic surface layer (Figure 8). The point B is on the top of the base layer.

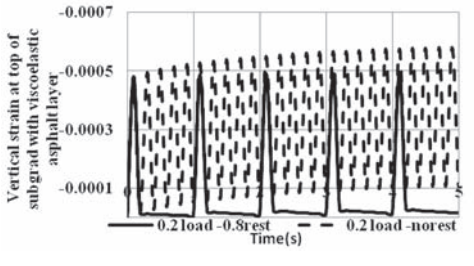

Figure 5. Haversine load application of period 0.2 s with and without rest period (case-II).

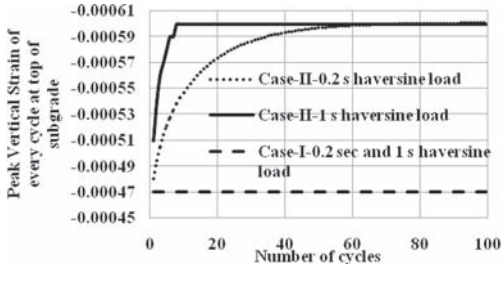

Figure 6. Effect of load repetitions in the vertical strain (E22) at the top of sub-grade.

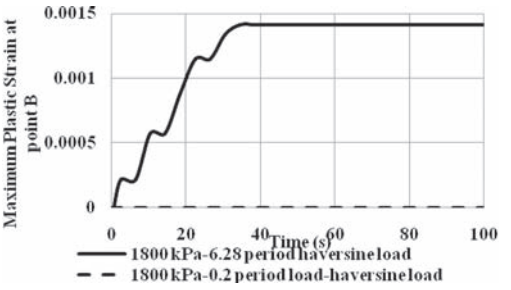

Figure 7. Effect of duration of loading in plastic strain formation.

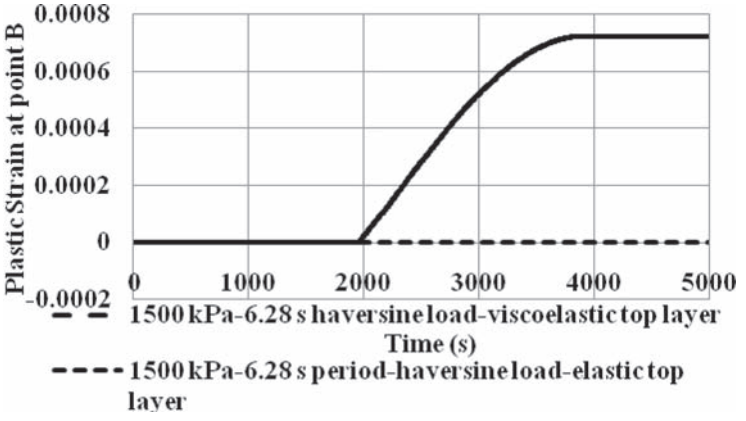

Figure 8. Comparison of plastic strain formation at base due to linear viscoelastic surface layer and elastic surface layer.

5 CONCLUSIONS

The entire pavement structure is analyzed with appropriate material models for different loading, material conditions and the critical stress as well as strain at various positions are monitored. The rutting of the pavement due to the plastic deformation in the base material as well as the structural deformation throughout the pavement structure is accounted in the analysis. The interplay of the mechanical response of various layers on the stress-strain response of these systems is also incorporated in this study. Calibration of material model as well as field validation provide road for further research in this area to use the results with full confidence in design procedure.

REFERENCES

ABAQUS user's manual-version 6.6. 2003. Hibbitt, Karlsson & Sorensen, Pawtucket, R.I.

Brown, S.F. 1996. Soil Mechanics in Pavement Engineering. *Geotechnique*. 46(3): 383–426.

Chazallon, C., Hornych, P. & Mouhoubi, S. 2006. Elastoplastic Model for the Long-Term Behavior Modeling of Unbound Granular Materials in Flexible Pavements. *International Journal of Geomechanics*, 6(4): 279–289.

Collins, I.F., Wang, A.P. & Saunders, I.R. 1993. Shakedown in layered pavements under moving surface loads. *International Journal for Numerical and Analytical Methods in Geomechanics*, 17: 165–174.

Drucker, D.C. & Prager, W. 1952. Soil mechanics and plastic analysis or limit design. *Quarterly of Applied Mechanics*, 10: 157–165.

Elseifi, M.A., Al-Qadi, I.L. & Yoo, P.J. 2006. Viscoelastic Modeling and Field Validation of Flexible Pavements. *Journal of Engineering Mechanics*, 132(20): 172–178.

Hadi, M.N.S. & Bodhinayake, B.C. 2003. Non-Linear Finite Element Analysis of Flexible Pavements. *Advances in Engineering Software*, 34: 657–662.
Helwany, S.H., Dyer, J. & Leidy, J. 1998. Finite-Element Analyses of Flexible Pavements. *Journal of Transportation Engineering,* 124(5): 491–499.
Huang, Y.H. 2004. Pavement Analysis and Design. Pearson Prentice Hall : USA.
Kettil, P., Lenhof, B., Runesson, K. & Wiberg, N.E. 2007. Simulation of inelastic deformation in road structures due to cyclic mechanical and thermal loads. *Computers and Structures*, 85: 59–70.
Kim, M. & Tutumluer, E. 2006. Effect of stress-dependent modulus and Poisson's ratio on structural responses in thin asphalt pavements. *Pavement Mechanics and Performance*, GSP 154: 29–36.
Kuo, C.M. & Huang, C.W. 2006 "Three-Dimensional Pavement Analysis with Non-linear Subgrade Materials." *Journal of Materials in Civil Engineering*, 18(4): 537–544.
Markow, M.J., Hedrick, J.K., Brademeyer, B.D. & Abbo, E. 1988. Analyzing the interaction between dynamic vehicle loads and highway pavements. *Transportation Research Record* 1196, Transportation Research Board, Washington, D.C.: 161–168.
Monismith, C.L. & Secor, K.E. 1962. Viscoelastic behavior of asphalt concrete pavements. International Conference on Structural Design of Asphalt Pavements.
Mulungye, R.M., Owende, P.M.O. & Mellon, K. 2007. Finite Element Modelling of Flexible Pavements on Soft Soil Subgrades. *Materials and Design*, 28: 739–756.
Papagiannakis, A.T. & Taha, R. 1996. Formulation For Viscoelastic Response of pavements Under Moving Dynamic Loads. *Journal of Transportation Engineering*, 122(2): 140–145.
Papagiannakis. A., Oancea, A., Ali, N., Chan, J. & Bergan, A.T. 1992. Application of ASTM E1049-85 in calculating load equivalence factors from in situ strains. *Transportation Research record* 1307: 82–89.
Park, S.W. & Lytton, R.L. 2004. Effect of stress-dependent modulus and Poisson's ratio on structural responses in thin asphalt pavements. *Journal of Transportation engineering*, 130(3): 387–394.
Saad, B., Mitri, H. & Poorooshasb, H. 2005. Three-dimensional Dynamic Analysis of flexible Conventional Pavement foundation. *Journal of Transportation Engineering*, 131(6): 460–469.
Siddharthan, R.V., Sebaaly, P.E., El-Desouky, M., Strand, D. & Huft, D. 2005. *Heavy Off-Road Vehicle Tire-Pavement Interactions and Response*, 131(3): 239–247.
Simpson, A.J., Daleiden, J.F. & Hadley, W.O. 1995. Rutting analysis from a di7erent perspective, *Transportation Research Record* 1473, Transportation Research Board—National Research Council, Washington, DC.
Sousa, J.B., Weissman, S.L., Sackman, J.L. & Monismith, C.L. 1993. Nonlinear elastic viscous with damage model to predict permanent deformation of asphalt concrete mixes, *Transportation Research Record 1384*, Transportation Research Board,National Research Council, Washington DC.
Sukumaran, B. 2004. Three Dimensional Finite Element Modeling of Flexible Pavements. *FAA worldwide Airport Technology Transfer Conference*, Atlantic City, New Jersey, USA.
White, T.D., Zaghloul, S.M., Anderton, G.L. & Smith, D.M. 1997. Pavement Analysis for Moving Aircraft Load. *Journal of Transportation Engineering*, 123(6): 436–446.
Zaghloul, S.M. & White, T.D. 1993. Use of a three-dimensional dynamic finite element program for analysis of flexible pavement. *Transportation Research Record*. 1388, National Research Council, Washington, D.C: 60–69.

Advanced Testing and Characterization of Bituminous Materials –
Loizos, Partl, Scarpas & Al-Qadi (eds)
© 2009 Taylor & Francis Group, London, ISBN 978-0-415-55854-9

Equiviscous temperature based on Low Shear Viscosity: Evaluation as binder indicator for rutting and critical discussion of the test procedure

J. De Visscher & A. Vanelstraete
Belgian Road Research Centre, Brussels, Belgium

ABSTRACT: This paper contributes to the development of a test method for the determination of a binder indicator for the rutting susceptibility of asphalt. Low shear viscosity, measured in oscillation mode in DSR, has been shown to correlate well with the permanent deformation of asphalt, in laboratory tests like the wheel tracking test and the cyclic triaxial compression tests. The task group of CEN TC336 WG1/TG1, responsible for the high temperature binder test methods, developed a new test procedure, published in document prCEN/TS_15324. The procedure leads to the determination of a temperature, at which the viscosity measured at very low shear rate is 2000 Pa.s (EVT: equiviscous temperature). The provisional document prCEN/TS_15324 provides the users with a common test procedure, to collect more data and experience with the method, before actually proposing it as a European standard test method. In this paper, this test procedure was used to measure the EVT of a series of 12 binders (pure bitumen, different types of PmBs, semi-blown bitumen and waxy bitumen). Recommendations on possible improvements of the test are given, which is another step forward towards a European standard test that satisfies the general need for a reliable binder indicator for rutting. Correlations with asphalt tests on mixes prepared with these binders were evaluated and compared to other indicators for rutting. This allowed to evaluate the equiviscous temperature as an indicator for rutting and to investigate whether this indicator actually improves the correlations with permanent deformation tests on asphalt.

1 INTRODUCTION

Experience in Europe and the USA has shown that binder properties, such as the Ring & Ball softening point or the high temperature rutting parameter of the Superpave system ($G^*/\sin\delta$ at $\omega = 10$ rad/sec), only show good correlations with rutting tests on asphalt mixtures in case of non-modified binders. The rutting resistance of PmBs is generally underestimated by these binder properties. The challenge is however to find a rutting indicator which works equally well for all types of binders.

Zero shear viscosity (ZSV) was proposed as an indicator more suitable for PmBs (Phillips & Robertus 1996). It has to be noted that, since the viscosity is measured at very low shear rate (but not zero), the name low shear viscosity (LSV) is more appropriate. The idea of using LSV as rutting indicator is that not only high temperature and traffic load are critical factors for rutting, but also traffic speed. Field experience has shown that very slow heavy traffic leads to a faster accumulation of permanent deformation. Some extensive laboratory studies, like the ARBIT study in Germany (Guericke 2000), confirmed this and showed good correlations between ZSV (or LSV) and asphalt rutting.

In the USA, another alternative binder indicator for rutting was proposed: the creep viscosity η_0 derived from repeated shear creep tests (RSCT) (NCHRP 2001). This test is interesting because the binder is subjected to cycles of loading, unloading and resting periods during which the binder can recover, similar to what can be expected on asphalt roads subjected to traffic.

Table 1. Overview of the binders and their conventional properties.

Binder type	Name	PEN (0.1 mm)	R&B (°C)
B35-50	B-1	47	49.5
B50-70	B-2	58	48.1
B70-100	B-3	89	45.2
Semi-blown	S-1	60	50.5
Semi-blown	S-2	20	62.4
Semi-blown	S-3	22	63.2
Wax	W-1	79	46.5
PmB 3.5% SBS	SBS-1	54	56.7
PmB 5% SBS	SBS-2	58	72.8
PmB 3.5% EVA	EVA-1	59	57.9
PmB 5% EVA	EVA-2	54	62.7
PmB with a polymer blend	po-bl	55	58.2

To find out which of these binder characteristics and which test conditions give the best indication of the rut resistance of asphalt mixtures, a test program was carried out by Nynas and BRRC on a set of 12 binders. The binder test results were correlated to asphalt tests carried out on mixtures prepared with these binders: Wheel tracking Test according to EN12697-22 (large device) and Cyclic Triaxial Compression Test according to EN12697-25. The outcome of this study was published in several papers (Soenen et al. 2005 & De Visscher et al. 2006).

The task group of CEN TC336 WG1/TG1, responsible for the high temperature binder test methods, prepared drafts for two test methods related to LSV: one method using a dynamic shear rheometer in oscillation mode (prCEN/TS_15324 2006) and the other one in creep mode (prCEN/TS_15325 2006). The task group also organised a Round Robin Test with 15 participating laboratories to evaluate the precision of the test methods, using a set of 5 binders (2 pure, 3 PmB). The repeatability and reproducibility, which were added to the drafts of the test methods, were quite satisfying for the method in oscillation mode, but far less for the creep test method.

The aim of the work described in this paper was to evaluate the oscillation test method of prCEN/TS_15324, by applying it to the same set of binders used in the previously mentioned study by Nynas and BRRC. An overview of these binders is seen in table 1. In this way, the results could be compared to the previously measured indicators for rutting, and correlated with the asphalt tests on the mixes prepared from these binders.

2 TEST PROCEDURE

2.1 *Brief description*

Low Shear Viscosity is defined in prCEN/TS_15324 as the dynamic viscosity at a shear stress or shear rate close to zero. Instead of measuring LSV at a fixed temperature, a procedure is developed to measure the temperature at which LSV has a fixed value. The procedure recommends a value of 2000 Pa.s. This temperature, called the equiviscous temperature EVT, can be interpreted as an indication of the temperature range in which rutting becomes critical, in other words: the higher EVT, the better the resistance to rutting.

The determination of EVT according to prCEN/TS_15324 is performed in two steps:

- The first step consists of a temperature sweep at a fixed low frequency f_1 (e.g. 0.01 Hz) and a low strain (e.g. 0.1 or 10%). The temperature at which the dynamic viscosity has a value of 2000 Pa.s (recommended value) is determined and called EVT1 (Fig. 1).
- In the second step, a frequency sweep is performed at the temperature EVT1. This frequency sweep goes down to lower frequency f_2 (e.g. 0.0001 Hz), so that the dynamic viscosity increases (Fig. 2). The dynamic viscosity increase ΔLSV is then used to determine a corresponding temperature interval ΔT, based on the curve measured in part 1 (Fig. 1).

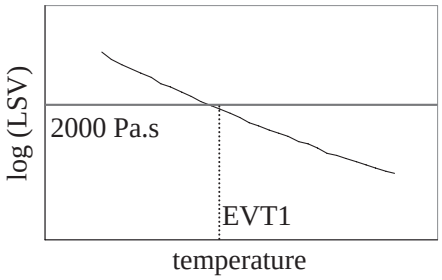

Figure 1. Test part 1—temperature sweep.

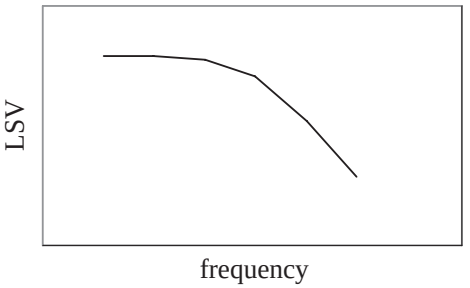

Figure 2. Test part 2—frequency sweep.

The sum of EVT1 and ΔT is called EVT2. EVT2 is in fact an estimation of the temperature at which a LSV of 2000 Pa.s would be measured, if the temperature sweep in test part 1 had been done at the lower frequency f_2 (a test that can not be performed in practice because of time limitations).

EVT2 is expected to be a better indicator for rutting than EVT1, since it based on the viscosity at lower frequency.

The test procedure is hereafter applied to two representative binders: the pure binder B-1 and the PmB SBS-1, with the aim to explain the test procedure in more detail, to discuss possible problems and to propose possible improvements.

2.2 *Application to B-1*

Figure 3 shows the temperature sweep from 40°C up to 70°C, at a frequency of 0.01 Hz. It is the average result of two measurements carried out on different samples. Following the test procedure, the data (log (LSV), T) shall be fitted by a linear equation (where a and b are positive constants):

$$\text{Log (LSV)} = -a * T(°C) + b \quad (1)$$

The result is shown as the dotted line in figure 3. Using the linear equation, the temperature EVT1 for LSV = 2000 Pa.s is determined as 52.3°C.

It can be seen in figure 3 that a linear fit of the data is not the most accurate fit and that the difference between measured data and fitted values depends on the temperature range. The exponential fit shown by the full line would result in a more accurate determination of EVT1: in this example 51.7°C instead of 52.3°C.

The second step of the test procedure is the frequency sweep, carried out at temperature EVT1, in this example 52.3°C. The test procedure recommends a sweep from 1 Hz down to 0.003 Hz (Fig. 4). The frequency sweep shown in figure 4 is the average of two measurements carried out on different samples. Note that, in this practical example, LSV is below 2000 Pa.s, while a value of 2000 Pa.s would be expected at a frequency of 0.01 Hz. This may be due to the fact that the frequency sweep is performed on different samples than the temperature sweep (reproducibility of test sample fabrication) or to the fact that the frequency sweep was carried out at a temperature above the more correct estimation of 51.7°C for EVT1.

Following the test procedure, the data (LSV, log (freq)) shall be fitted by a linear equation (where c and d are positive constants):

$$\text{LSV} = -c * \log(\text{freq}) + d \quad (2)$$

The result is the dotted line in figure 4. With this linear equation, LSV has to be extrapolated to a frequency close to zero (0.0001 Hz is recommended). This leads to a value of 2105 Pa.s.

Finally, the increase of LSV from 0.01 to 0.0001 Hz is used to determine the equivalent temperature variation ΔT, from the relation (log(LSV), T) determined in test part 1. This results in a value of 0.7°C.

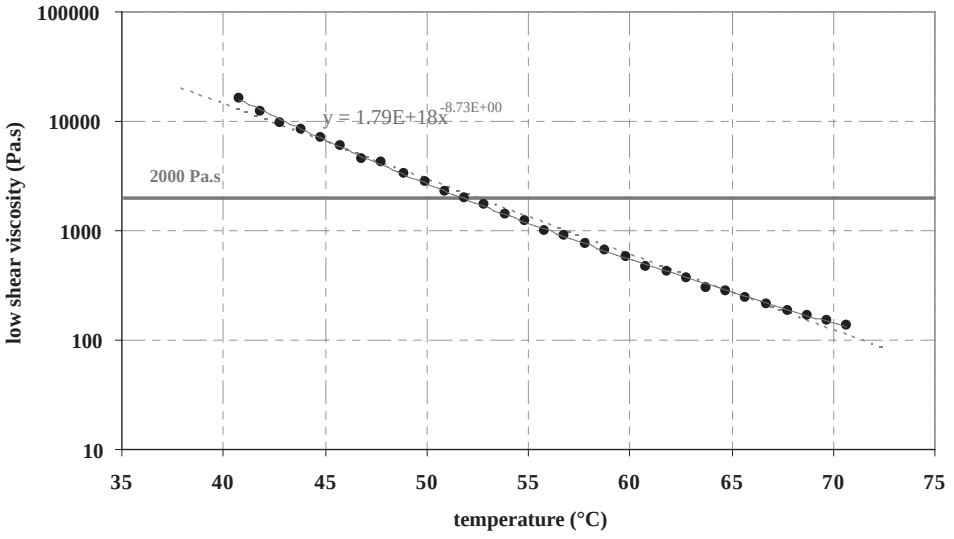

Figure 3. Temperature sweep for binder B-1.

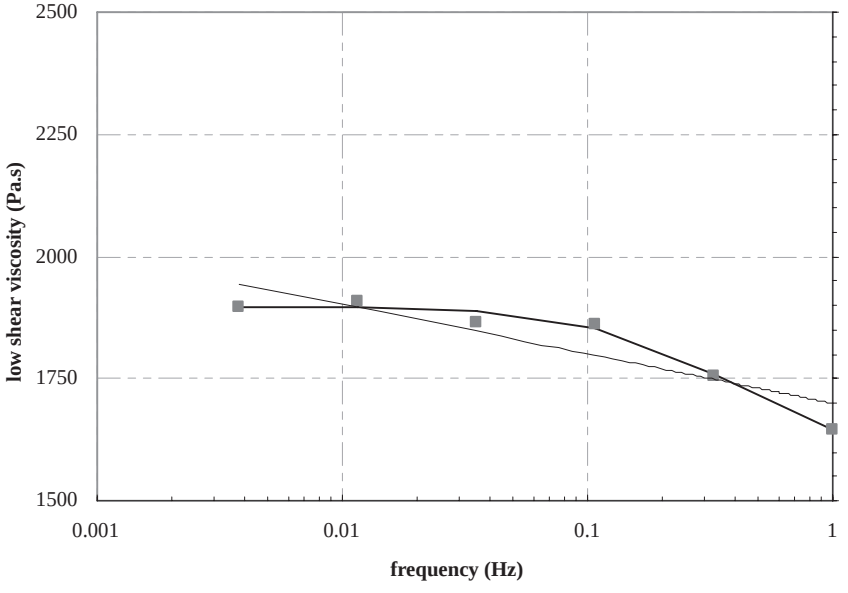

Figure 4. Frequency sweep for binder B-1.

In this practical example, it is clearly seen in figure 4 that a linear fit is not accurate and results in an overestimation of LSV in the range of low frequencies. A more correct estimation could be obtained by using a more appropriate function to fit the data. Such a function is given by the four-parameter Cross model, which describes the evolution of the dynamic viscosity as function of the circular frequency ω (= 2πf):

$$\eta(\omega) = \frac{\eta_0 - \eta_\infty}{1 + (K\omega)^m} + \eta_\infty \tag{3}$$

The full line in figure 4 is the data fit obtained with this function. The extrapolated value of LSV to 0.0001 Hz is now 1897 Pa.s instead of 2105 Pa.s. The increase of LSV from 0.01 to 0.0001 Hz is therefore practically zero, which corresponds to a temperature variation ΔT of 0.0°C.

This practical exercise shows that, by following the exact procedure described in prCEN/TS 15324, EVT2 is determined as 53.0°C (52.3 + 0.7). Using other and more accurate functions to fit the measured data would result in a lower value of 51.7°C (51.7 + 0.0).

2.3 *Application to SBS-1*

Figure 5 shows the temperature sweep, at a frequency of 0.01 Hz (mean of two measurements). Applying the linear fit to the data leads to EVT1 = 58.3°C, while the exponential fit leads to EVT1 = 57.6°C.

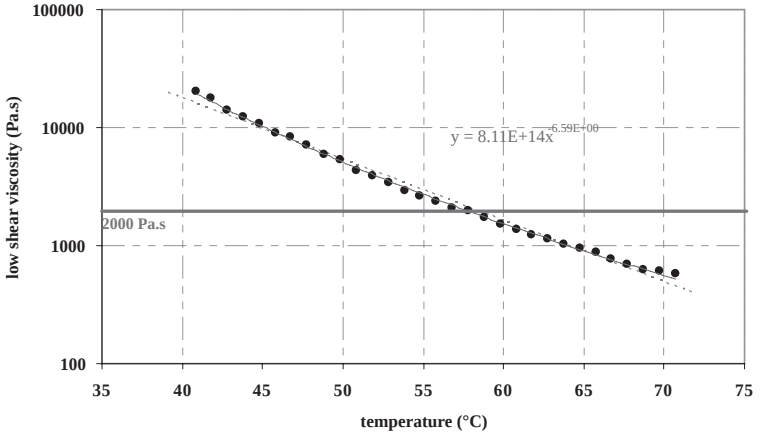

Figure 5. Temperature sweep for binder SBS-1.

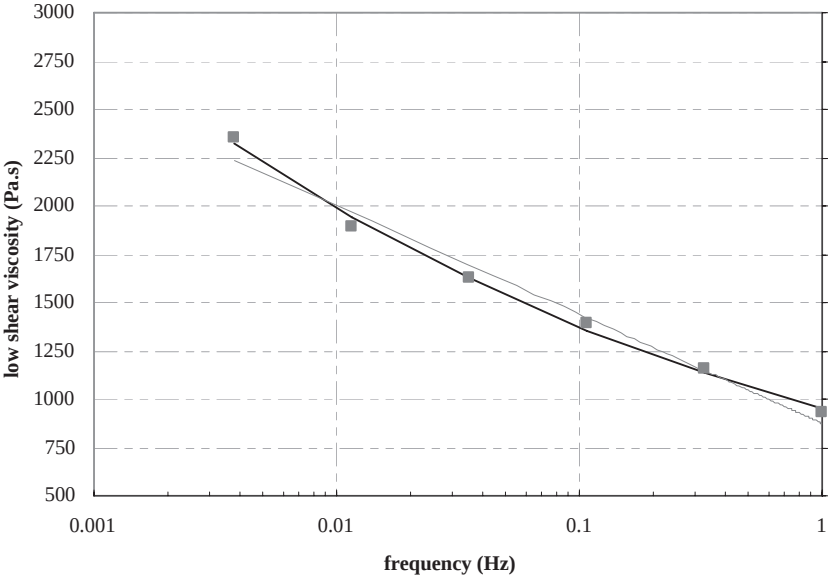

Figure 6. Frequency sweep for binder SBS-1.

The frequency sweep at a temperature of 58.3°C is shown in figure 6 (mean of two measurements). Compared to the frequency sweep of the binder B-1 in figure 4, which covers exactly the same frequency range, the viscosity shows a continuous increase when the frequency decreases. Consequently, extrapolation of LSV to a frequency of 0.0001 Hz using the linear data fit will now lead to an underestimation, compared to the extrapolation with the Cross model: LSV at 0.0001 Hz is estimated as 3133 Pa.s using the linear fit (dotted line) and 4145 Pa.s using the Cross model (full line). This corresponds to temperature variations ΔT of 3.7°C and 9.4°C respectively.

The conclusion is that, by following the exact procedure described in prCEN/TS153, EVT2 is determined as 62.0°C (58.3 + 3.7). Using other and more accurate functions to fit the measured data would results in a higher value of 67.0°C (57.6 + 9.4).

2.4 *Evaluation of the test procedure*

The two previous examples show the typical difference between a pure binder and a PmB in the test. In the frequency sweep in step 2, the viscosity curve of the pure binder is practically flat in the low frequency range, while the viscosity of the PmB continues to increase when the frequency goes down. Such behaviour is expected to correspond to a better resistance to permanent deformation at low frequency. EVT2 is thus significantly higher than EVT1 for the PmB, while EVT2 ≈ EVT1 for the pure binder. The second step could therefore have been omitted in case of the pure binder.

The main comments on the test procedure are related to the data fitting procedures, which are not sufficiently accurate. Because of this inaccuracy, the results of the curve fittings will also depend on the considered measurement range. Especially the fit of the frequency sweep by a linear function leads to large errors, as this fit is used to extrapolate the data far below the lower limit of the measured frequency range. A fit by the 4-parameter Cross model seems to be a good solution, since it fits equally well the data of the pure binder as the data of the PmB over a wide frequency range, despite of the very different behaviour of both types of binders in this test.

Another important comment is related to the test conditions (strain levels, temperatures and frequency ranges). Recommended values are given in the different notes of prCEN/TS_15324. It is important to stress that the result of the test will depend on the choice of most of these test conditions. Therefore, if test results would be compared or the results would be used for specification purposes, it is necessary to fix the test conditions exactly. Note that in this paper, all test results have been obtained by following exactly the recommendations given prCEN/TS_15324.

Table 2. EVT results.

		Linear data fits (prCEN/TS15324)			Improved data fits		
Binder	R&B °C	EVT1 °C	ΔT °C	EVT2 °C	EVT1 °C	ΔT °C	EVT2 °C
B-1	49.5	52.3	0.7	53.0	51.7	0.0	51.7
B-2	48.1	50.0	0.9	50.9	49.6	0.1	49.7
B-3	45.2	45.3	1.0	46.3	45.5	0.1	45.6
S-1	50.5	50.6	1.0	51.6	50.1	0.0	50.1
S-2	62.4	63.0	1.1	64.1	62.9	0.0	62.9
S-3	63.2	66.2	1.6	67.8	65.8	0.1	65.9
W-1	46.5	45.8	1.1	46.9	45.9	0.2	46.1
SBS-1	56.7	58.3	3.7	62.0	57.6	9.4	67.0
SBS-2	72.8	61.4	5.5	66.9	60.9	19.1	80.0
EVA-1	57.9	54.9	3.2	58.1	54.3	4.9	59.2
EVA-2	62.7	60.2	4.0	64.2	61.2	26.3	87.5
po-Bl	58.2	57.0	3.4	60.4	56.3	7.7	64.0

3 TEST RESULTS FOR THE OTHER BINDERS

Table 2 gives an overview of the equiviscous temperatures measured on the whole set of binders using the linear data fitting procedures of the test method in prCEN/TS 15324, and the proposed improved data fitting procedures.

The determination of EVT1 is lightly sensitive to the data fitting method, with a difference of less than 1.0°C. The results of ΔT and EVT2 on the other hand are very different depending on the curve fitting function. The use of the more accurate Cross model leads to $\Delta T \approx 0°C$ for all non-modified binders. This confirms the statement that the second step of the test procedure is not necessary for these binders. On the other hand, for the modified binders, the effect of the modification is clearly seen in ΔT.

4 CORRELATIONS WITH ASPHALT TESTS

Before considering the correlations with laboratory asphalt tests, a few remarks are necessary to emphasize that the correlation coefficients given hereafter shall be considered with due caution:

- The set of considered binders is still limited and, depending on the selection, the calculated correlation coefficients can vary.
- Both the binder tests and the asphalt tests are susceptible to measurement errors and the calculated correlations are very sensitive to these errors.
- Correlations with asphalt tests depend on the type of asphalt test and the test conditions used. Ideally, these test conditions should simulate as close as possible the real conditions on a road. In this study we consider two different types of asphalt tests: a wheel tracking test and a cyclic triaxial compression test.

The asphalt tests were made on an asphalt concrete mix typically used for top layers in Belgium (AC0/14-type 1). Three test plates were made per binder. Two plates were used to measure the rut depth in the wheel tracking device (large size, EN 12697-22), the third plate was cored to obtain five cylindrical test specimens for the cyclic triaxial compression tests (EN 12697-25, part B). The wheel tracking tests were carried out by Nynas, at a frequency of 1 cycle per second. The cyclic triaxial compression tests were done at the BRRC laboratory, at a test frequency of 1 cycle per second (haversine loading pulse of 400 ms, followed by a rest period of 600 ms). All asphalt tests were made at a temperature of 50°C.

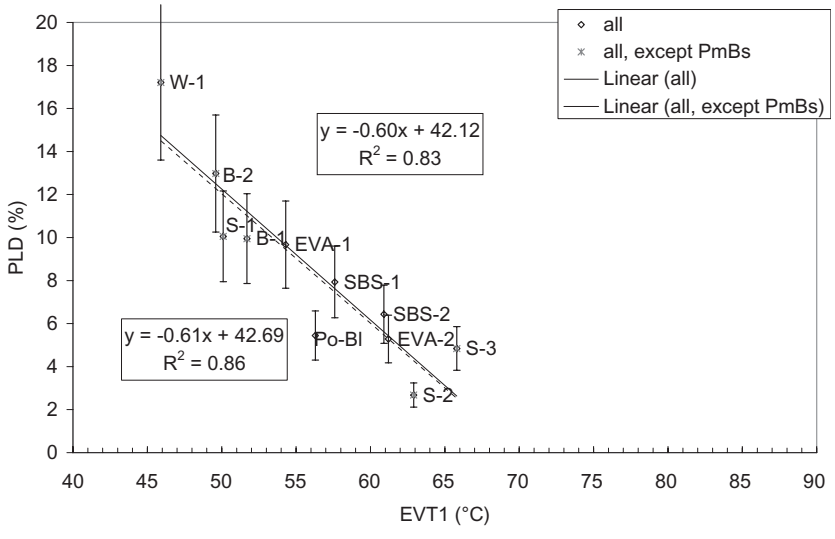

Figure 7. Proportional rut depth (after 30,0000 cycles) versus EVT1.

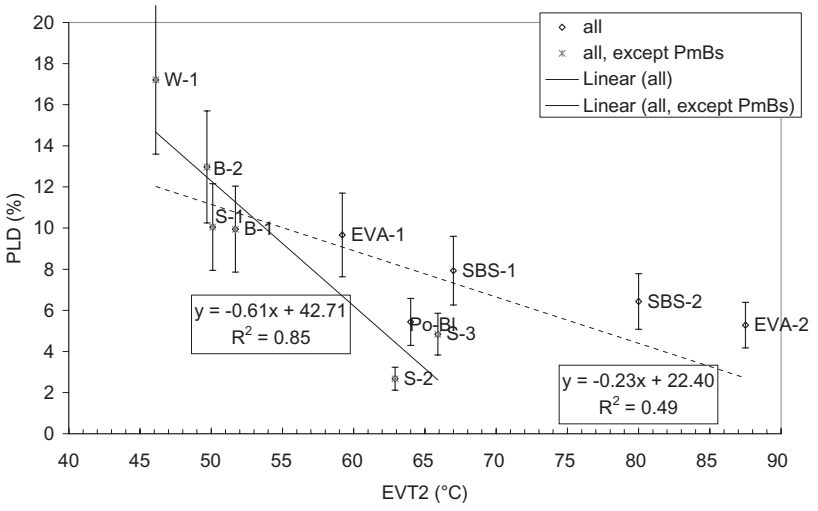

Figure 8. Proportional rut depth (after 30,0000 cycles) versus EVT2.

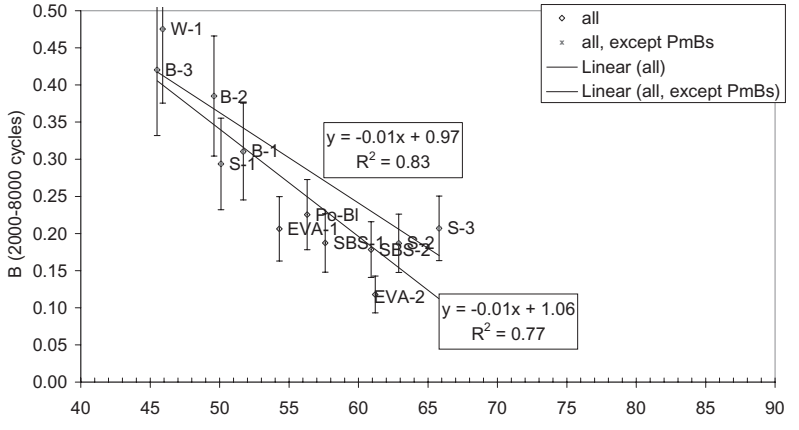

Figure 9. Slope of the accumulated strain curve of the triaxial compression test versus EVT1.

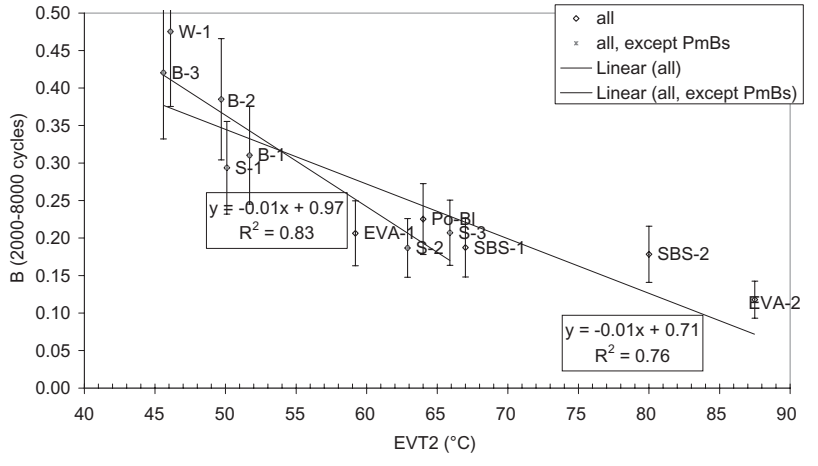

Figure 10. Slope of the accumulated strain curve of the triaxial compression test versus EVT2.

Figures 7 and 8 show the results of the wheel tracking tests (proportional rut depth, PLD in % after 30,000 cycles) versus EVT1 and EVT2 (calculated using the improved curve fitting methods). The correlation with EVT1 is just as good for the pure binders as for the PmBs (Fig. 7). Surprisingly, the correlation with EVT2 (Fig. 8) is much worse for the complete set of binders. As EVT2 is significantly higher for the PmBs, the data points all shift to the right, indicating a much better resistance to rutting. However, this outstanding behaviour is less significant in the results of the wheel tracking tests. EVT2 thus overestimates the rut resistance of PMBs in this wheel tracking test.

Figure 9 and 10 show the results of the cyclic triaxial compression test (slope B of the creep curve between 2,000 and 8,000 cycles) versus EVT1 and EVT2. As all the data points of the PmBs in figure 9 are below the regression line, EVT1 tends to underestimate the resistance to permanent deformation of these binders in the cyclic triaxial compression test. In the plot of EVT2 (Fig. 10), the data points of the PmBs are all shifted to the right and the other side of the regression line. EVT 2 thus tends to overestimate their rut resistance.

Finally, tables 3 and 4 compare the correlation coefficients of the previous data plots with the correlation coefficients that were found with other binder properties, for the same set of binders. All these binder properties were measured at a fixed temperature of 50°C.

The following observations can be made:

EVT2 does not correlate well with the wheel tracking results, as this binder characteristic overestimates the rut resistance of the PmBs. EVT1 on the other hand leads to a much better correlation. As expected, the correlation of EVT1, which is measured at 0.01 Hz, compares well with LSV, measured at 0.01 Hz and 50°C.

The correlation of EVT2 with the results of the cyclic triaxial compression test is somewhat better, since this test appears to simulate better the permanent deformation of asphalt under low frequency loading. This can be explained by the fact that the period of the loading pulse is longer than for example in the wheel tracking test, where the loading pulse in one point of the plate is very short due to the movement of the load. That is also the reason why the cyclic triaxial compression test correlates better with LSV at 10^{-3} Hz than at 10^{-2} Hz. If EVT2 were obtained by extrapolating the frequency sweep to 10^{-3} Hz instead of 10^{-4} Hz, the correlation would also be improved.

The main conclusion from these correlations is that EVT2 does not correlate as well as expected to the permanent deformation of the asphalt mixtures. EVT2 is too high for the case of the PMBs, because the related frequency (10^{-4} Hz) is too low.

Table 3. Comparison of correlation coefficients with wheel tracking test results.

Rut depth (wheel tracking test)									
	$T_{R\&B}$	LSV @ 10^{-3} Hz	LSV @ 10^{-2} Hz	LSV @ 1 Hz	η_0 (RSCT)	G*/sinδ @ 1.59 Hz	G*/sinδ @ 10^{-3} Hz	EVT2	EVT1
All, except PmBs	0.85	0.82	0.85	0.90	0.83	0.89	0.82	0.85	0.86
All binders	0.61	0.81	0.84	0.77	0.73	0.64	0.78	0.49	0.83

Table 4. Comparison of correlation coefficients with cyclic triaxial compression test results.

B (cyclic triaxial compression test)									
	$T_{R\&B}$	LSV @ 10^{-3} Hz	LSV @ 10^{-2} Hz	LSV @ 1 Hz	η_0 (RSCT)	G*/sinδ @ 1.59 Hz	G*/sinδ @ 10^{-3} Hz	EVT2	EVT1
All, except PmBs	0.83	0.81	0.84	0.88	0.82	0.88	0.81	0.83	0.83
All binders	0.72	0.81	0.72	0.51	0.87	0.46	0.80	0.77	0.76

It may be argued that by using the EVT2 data in table 2, as obtained with the linear data fits, the correlations would be better. That is correct, but the explanation is that two errors are made which partly compensate each other: the underestimation due to the inaccurate linear data fit of the frequency sweep function and the overestimation due to the too low frequency. Consequently, this is not a valid argument.

5 CONCLUSIONS

Applying the test procedure for measuring the equiviscous temperature EVT, as described in prCEN/TS_15324, to a series of 12 binders allowed for a practical evaluation of the test. The test was applicable to all binders, but the numerical curve fitting procedures prescribed by the test method can be more accurate. Better curve fitting functions were proposed, that resulted in a closer fit over a wider range and were consequently less susceptible to the considered measurement range.

The equiviscous temperatures EVT1 and EVT2 of the binder set were subsequently correlated with tests on an asphalt mix prepared with the various binders. EVT1 correlates well with the results from the wheel tracking tests, but EVT2 overestimates the rutting potential of the PmBs. While it was the intention to improve the correlation with asphalt rutting by estimating the EVT at a frequency as low as possible, it appears that the frequency is too low, compared to the loading frequency of the wheel tracking test according to EN12697-22 (large device).

The correlation of EVT2 with the results from the cyclic triaxial compression test (performed according to EN12697-25 at a frequency of 1 cycle per second) is better and equivalent to that found for EVT1. It could still be improved by estimating EVT2 at a frequency of for example 0.001 Hz instead of 0.0001 Hz.

The main conclusion is that the equiviscous temperature based on low shear viscosity may be a valuable binder indicator for rutting, but the frequency of 0.0001 Hz to which EVT2 is related seems to be too low. A frequency of 0.001 Hz or 0.01 Hz would lead to better correlations with asphalt tests. As EVT1 is related to a frequency of 0.01 Hz, it could even be considered to limit the test procedure to the determination of EVT1 for PmBs as well as for pure binders.

ACKNOWLEDGEMENTS

The authors wish to thank Philippe Peaureaux from BRRC and Hilde Soenen, Tine Tanghe and Per Redelius from Nynas, for their valuable contributions to the test programme.

REFERENCES

Cross, M. 1965. Rheology of non-Newtonian fluids: a new flow equation for pseudo-plastic systems. *J. of Colloid Science* 20: 417–437.

De Visscher, J., Vanelstraete, A., Soenen, H., Tanghe, T. & Redelius, P. 2006. Binder performance indicators for rutting: evaluation of experimental correlations with asphalt tests. *Proc. 10th International Conference on Asphalt Pavements* paper 81 *Quebec, 12–17 August 2006*.

Guericke, R. 2000. Results of ARBIT test programme 1998/99 involving 36 unmodified and modified bituminous binders on the German market. *Proc. 2nd Eurasphalte & Eurobitume Congress* paper n°0171*, Barcelona, 20–22 september 2000.*

NCHRP. 2001. Characterization of modified asphalt binders in Superpave Mix Design. *NCHRP report* 459.

Phillips, M. & Robertus, C. 1996. Binder rheology and asphaltic pavement permanent deformation: the zero-shear viscosity. *Proc. 1st Eurasphalte & Eurobitume Congress* paper n°5.134*, Strasbourg, 7–10 may 1996.*

prCEN/TS 15324. 2006. Bitumen and bituminous binders—Determination of equiviscous temperature based on Low Shear Viscosity using a Dynamic Shear Rheometer in low frequency oscillation mode.

Soenen, H., De Visscher, J., Tanghe, T., Vanelstraete, A. & Redelius, P. 2006. Selection of Binder Performance Indicators for Asphalt Rutting Based on Triaxial and Wheel tracking Tests. *Journal of the Association of Asphalt Paving Technologists* 75: 165–202.

Advanced Testing and Characterization of Bituminous Materials – Loizos, Partl, Scarpas & Al-Qadi (eds)
© 2009 Taylor & Francis Group, London, ISBN 978-0-415-55854-9

The effect of volumetric properties of asphalt concrete mixture to wheel track rutting with respect to EN and BS rutting test methods

A. Nikolaides
Department of Civil Engineering, Highway Engineering Laboratory, Aristotle University of Thessaloniki (AUTh), Thessaloniki, Greece

E. Manthos
Civil Engineer, Ph.D candidate

ABSTRACT: Permanent deformation of bituminous layers, due to axle loading increase and the undisputable global increase of average air temperature, has become the major type of pavement's distress in many countries. Each bituminous mixture to be used must have sufficient resistance to permanent or rutting deformation. Among other parameters, volumetric properties of the mixture are one of the major factors affecting the resistance to permanent deformation. The resistance to permanent deformation can be determined by the wheel tracking test. In this study, a dense asphalt concrete mixture (AC19) with 50/70 penetration grade bitumen was examined in terms of its resistance to permanent deformation by varying its volumetric properties. The wheel tracking test was carried out by two valid procedures as described in BS 598-110 and EN 12697-22. The volumetric properties of the mixture varied as a result of the binder content variation and the degree of compaction. The effect of testing temperature was also examined. Results showed that EN 2697-22 testing procedure detects better the effect of volumetric properties of asphalt concrete mixtures to their rutting performance. In terms of acceptability of mixture significant differences were found between the two testing procedures.

1 INTRODUCTION

Rutting of flexible pavements is a common type of distress, particularly in locations with heavy traffic loading and high in-service temperatures. Assuming that the subgrade and the overlying unbound layers have been adequately compacted and possess the required strength, rutting is caused by the permanent deformation of the bitumen bound courses, particularly the upper layers. The permanent deformation of the bitumen bound courses, which represents an accumulation of unrecoverable deformation that occurs each time a load is applied, is due to the intrinsic visco-elastic behaviour of the bituminous binder and/or to the low shear strength of the asphalt mixture. When the asphalt mixture possesses sufficient shear strength, rutting will occur after a long period of pavement service life. On the contrary, when the asphalt mixture possesses low shear strength, rutting will occur within a short period of time under construction.

The permanent deformation of an asphalt mixture can be improved by modifying the elastic behaviour of the bitumen binder (use of modified binders) and by increasing the shear strength of the mixture. The latter can be achieved by selecting an aggregate gradation that develops particle-to-particle contact and has a high degree of internal friction, or by using a stiffer bituminous binder.

However, the volumetric characteristics of the asphalt mixture, in particular the available voids, also affect its permanent deformation behaviour. Every time a load is applied, a minute displacement and rearrangement of the aggregate particles takes place. This displacement

and rearrangement is accommodated, to a certain extend within the available voids without causing any change in volume. If the asphalt mixture has insufficient voids, the displacement will cause a volumetric change and the mixture will deform rapidly.

In this study the performance of a dense asphalt concrete mixture in rutting behaviour was evaluated. In particular, the effect of binder increase and decrease, above and below the optimum binder content, respectively, was examined, as well as the degree of compaction. The binder content was such as to result in mixtures with 3% and 5% void content. As for the degree of compaction it was chosen to be 97% and 100% of the compacted density obtained at optimum binder content. The above simulates the case where binder content and degree of compaction get in situ extreme but permissible values in relation to mix design. The rutting performance of the AC19 mix was examined by carrying out the wheel tracking test according to BS 598-110 and EN 12697-22, described procedures. The reason for choosing both the BS and the EN, wheel tracking testing procedures was to determine whether both tests give comparative results.

2 MATERIALS

The materials used for the production of the dense 19 mm AC mixture consisted of 50/70 penetration grade bitumen and crushed limestone aggregate. The characteristic properties of the the aggregates and bitumen used are as shown in Table 1.

3 MIX DESIGN AND MARSHALL PROPERTIES

3.1 *Aggregate gradation*

The particle size distribution of the aggregates for the dense Asphalt Concrete mix with maximum nominal size 19 mm (AC-19), used in this study is as shown in Figure 1. In the same figure the upper and lower limits are shown as proposed by ASTM 3515. Similarly the restricted zone for AC-19 is also, shown as proposed by Asphalt Institute.

Figure 2 shows the aggregate gradation raised to the power 0.45 and the Fuller line for maximum density, together with restricted zone.

3.2 *Optimum binder content*

The optimum binder content of the asphalt mixture was determined by the Marshall method and found to be 4.75% by weight of mix. The volumetric properties of the mix at the optimum binder content are as shown in Table 2. In the same table Marshall properties of the mixtures having binder content +0.5% (rich mix) and –0.4% (lean mix) above and below, respectively, the optimum binder content, are also shown.

Table 1. Materials characteristic properties.

		Property			
Material	Fraction	PD: Kg/m^3	WA: %	LA: %	FI: %
Aggregate	12.5–25 mm	2699	0,2	29	20
	6.3–12.5 mm	2678	0,3	–	14
	2.36–12.5 mm	2619	0,8	–	–
	0–4.75 mm	2581	1,2		–
Bitumen		Penetration (EN 1426) : 66 Softening point (EN 1427) : 48 Penetration index: –1.1 Density: (EN ISO 3838): 1.030			

PD: Particle Density, EN 1097-6, WA: Water Absorption, EN 1097-6
LA: Los Angeles value, ASTM C131-06, FI: Flakiness Index, BS 812-105

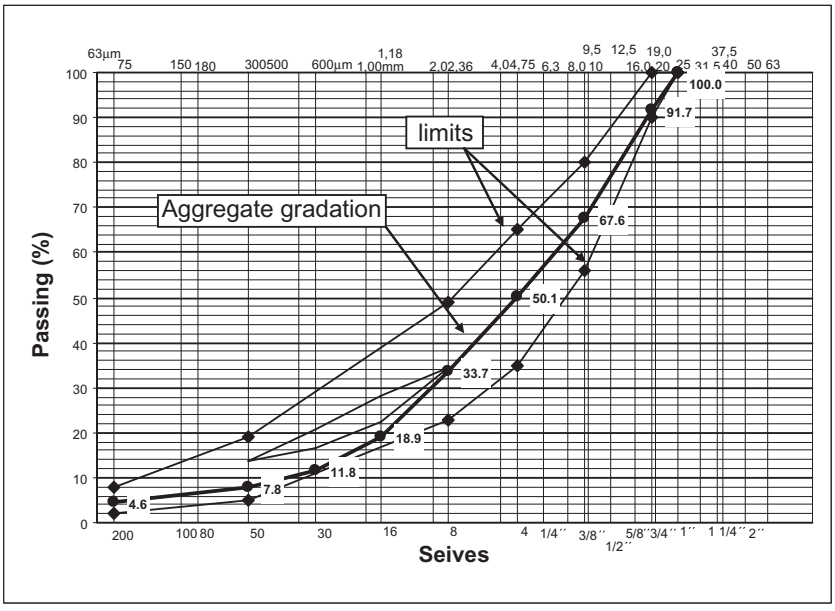

Figure 1. Aggregate gradation for the AC-19 mix used.

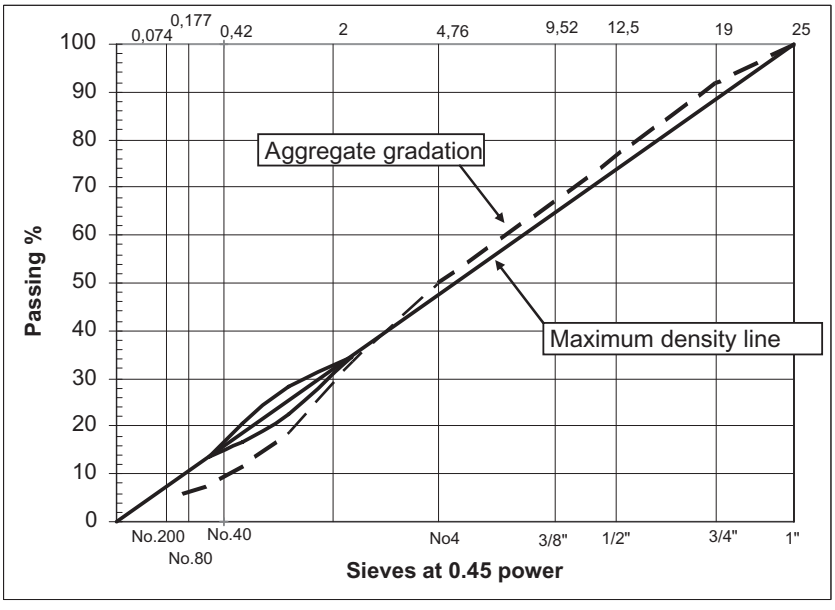

Figure 2. Aggregate gradation for the AC-19 and maximum density line.

4 PRODUCTION OF SLAB SPECIMENS AND WHEEL TRACKING TEST

4.1 *Production of slab specimens*

Slab specimens produced at the two binder contents mentioned previously, i.e +0.5 and –0.4 above and below the optimum content. These two mixtures will be notified from now on as AC-5.25 and AC-4.35.

Table 2. Volumetric properties of AC-19 mixes.

Binder content, per weight of mix, %	4.75	4.35	5.25
Air voids, %	4.2	5.1	3.0
Marshall stability, KN	8.9	9.0	9.2
Flow, mm	2.5	2.5	3.0
Voids in mineral aggregate, (VMA) %	14.4	14.3	14.5
Void filled with asphalt, (VFA) %	71.1	64.7	79.0
Bulk density of asphalt mix, (kg/m^3)	2366	2358	2377

Table 3. Principal differences between EN 12697-22 procedure B and BS 598-110.

Specification	BS 598-110	EN 12697-22 Procedure B (in air)
No. of samples	6	2
Conditioning time	4 h to 16 h	1 h
Conditioning passes	0 cycles	5 cycles
Frequency	21.0 ± 0.2 cycles/min	26.5 ± 1 cycles/min
Duration	45 min (= 945 cycles)	10000 cycles
Load	520 N	700 N
No. of measurement points	Single point	25 points
Measurements	Rut rate (mm/h)	Rut rate (mm/10^3 cycles)
	Rut depth (mm)	Proportional rut depth (%)
Slope measurement length	Final 15 min (= 315 cycles)	Final 5000 cycles

Sufficient numbers of slabs were compacted at 97% and 100% degree of compaction, with respect to the density at optimum binder content. The size of every slab was 305 mm in length by 305 mm in width. The thicknesses of the slabs were either 50 mm or 60 mm so to conform with the BS and EN requirements.

Compaction was carried out by a roller compactor with smooth steel roller according to EN 12697-33, see Photograph 1. In all cases compaction temperature was 140 ± 3°C. The total number of slab specimens produced in this study was 32. This number of slab specimens was derived by applying the requirements of BS and EN relevant specifications.

4.2 *Wheel tracking test conditions*

The conditions of the wheel tracking test were as prescribed in BS598-110 and EN 12697-22, Procedure B (in air). The test was performed, using a small size device with samples conditioned in air, see Photograph 2. Table 3 shows the principal differences between the BS 598-110 and EN 12697-22, Procedure B (in air) specifications. Wheel tracking test was carried out at 45°C and 60°C testing temperature.

5 TEST RESULTS

5.1 *Volumetric properties of slab specimens*

The volumetric properties of the slab specimens are as shown in Table 4. It must be noted that the values shown are the average of eight (8) specimens per type of mix.

5.2 *Permanent deformation characteristic properties*

The permanent deformation characteristic properties according to BS 598-110 are the wheel tracking rate and wheel tracking depth. Alternatively the permanent deformation

Table 4. Volumetric properties of the specimens tested.

Mixture	Degree of compaction	Bulk density (kg/m^3)	Voids (%)	VMA (%)	VFA (%)
AC-4.35	97%	2286	8.0	17.0	52.9
AC-5.25		2337	4.7	15.9	70.5
AC-4.35	100%	2360	5.1	14.3	64.8
AC-5.25		2379	3.0	14.4	79.3
Typical acceptable range	95%–97%		3.0-5.0	>12	65–75

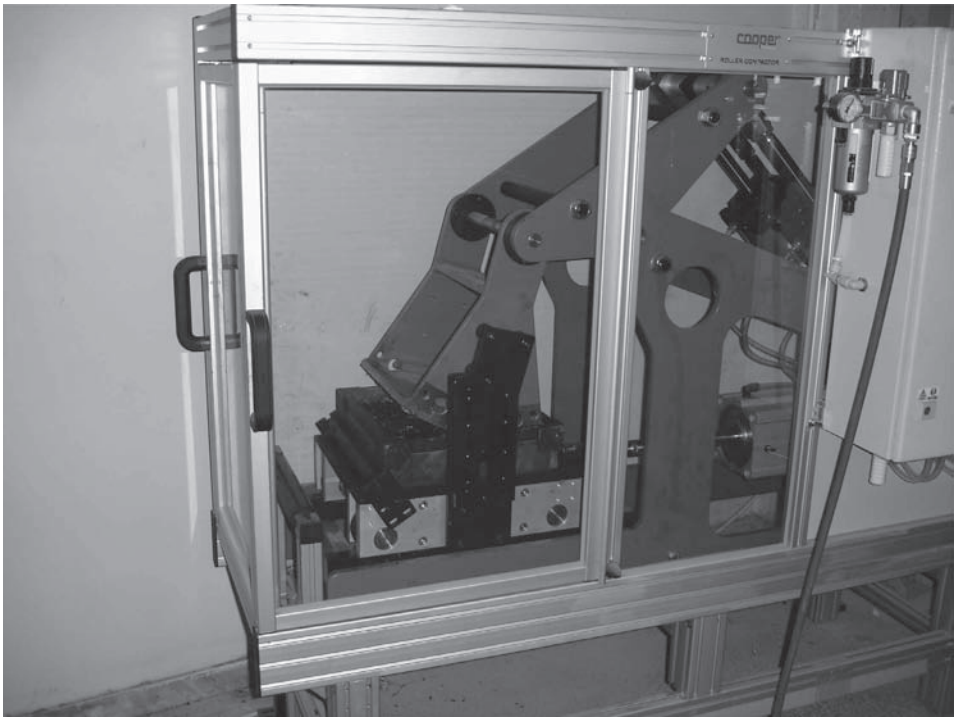

Photograph 1. Smooth steel roller compactor.

characteristic properties according to EN 12697-22, Procedure B (in air) are the wheel tracking slope and proportional rut depth.

The results obtained in this study in relation to permanent deformation characteristics, are as shown in Table 5 and 6, respectively.

6 DISCUSSION

6.1 *Results obtained by BS procedure*

Statistical analysis was carried out on the characteristic properties of permanent deformation in order to examine the significance of each factor involved. In the statistical analysis, the independent samples t-test method with 95% confidence level was used. Prior to this, the normal distribution of results was examined and verified (Kolmogorof-Smirnoff test).

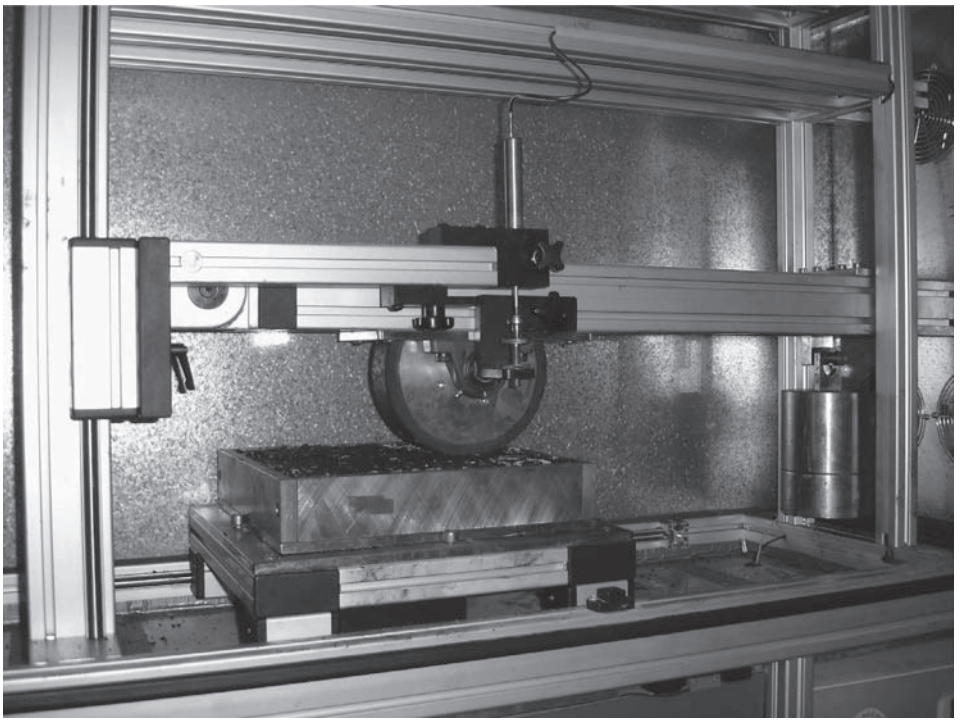

Photograph 2. Wheel tracking testing machine-small size device.

Table 5. Average wheel tracking rate and rut depth using the BS 598-110 specification.

Mixture	Degree of compaction	Wheel tracking rate: mm/h		Wheel tracking depth: mm	
		45°C	60°C	45°C	60°C
AC-4.35	97%	0.9	1.3	3.2	3.3
AC-5.25		1.1	1.4	3.4	4.1
AC-4.35	100%	0.5	0.8	2.2	2.0
AC-5.25		0.6	1.4	2.4	2.9

Table 6. Average wheel tracking rate and rut depth using the EN 12697-22 specification.

Mixture	Degree of compaction	Wheel tracking slope: mm/10^3 cycles		Rut depth: mm		Proportional rut depth: %	
		45°C	60°C	45°C	60°C	45°C	60°C
AC-4.35	97%	0.3	0.5	3.3	7.3	5.4	12.1
AC-5.25		0.4	0.7	3.6	9.4	5.9	15.6
AC-4.35	100%	0.1	0.3	2.6	6.7	4.4	11.1
AC-5.25		0.1	0.4	2.9	8.3	4.8	13.9

6.1.1 *The effect of binder content*

The effect of binder content on the wheel tracking results after statistical analysis, is as shown in Table 7.

As it can be seen, when the test was carried out at 45°C the effect of the binder variation was non significant in relation to the wheel tracking rate and rut depth, at either degree of

Table 7. Significance analysis of results with respect to binder content.

Mixture	Degree of compaction	Wheel tracking rate: mm/h		Wheel tracking depth: mm	
		45°C	60°C	45°C	60°C
AC-4.35 AC-5.25	97%	N.S	N.S	N.S	S
AC-4.35 AC-5.25	100%	N.S	S	N.S	S

S = Significant.
N.S = Non Significant.

Table 8. Significance analysis of results with respect to compaction degree.

Mixture	Degree of compaction	Wheel tracking rate: mm/h		Wheel tracking depth: mm	
		45°C	60°C	45°C	60°C
AC-4.35	97 % 100%	S	S	S	S
AC-5.25	97% 100%	S	N.S	S	S

S = Significant.
N.S = Non Significant.

Table 9. Significance analysis of results with respect to testing temperature.

Mixture	Degree of compaction	Wheel tracking rate: mm/h		Wheel tracking depth: mm	
		45°C	60°C	45°C	60°C
AC-4.35	97 %	N.S		N.S	
AC-5.25		N.S		S	
AC-4.35	100%	N.S		S	
AC-5.25		S		S	

S = Significant.
N.S = Non Significant.

compaction. When the test was carried out at elevated temperature of 60°C, the effect of binder content to both wheel tracking parameters was significant only at 100% of compaction.

6.1.2 *The effect of degree of compaction*

The effect of the degree of compaction on the wheel tracking results after statistical analysis is as shown in Table 8.

As it can be seen from Table 8, the effect of compaction to both wheel tracking parameters was significant for the lean mixtures irrespective of testing temperature. As for the rich mixtures the effect of compaction to both wheel tracking parameters is significant only when

test was carried out at 45°C. At 60°C testing temperature the degree of compaction affects significantly only the wheel tracking depth.

6.1.3 *The effect of temperature*

The effect of temperature on the wheel tracking results after statistical analysis, significance is as shown in Table 9.

As it can be seen from Table 9 the effect of temperature to both wheel tracking parameters was not significant for the lean mixes at 97% degree of compaction. On the contrary, the effect of temperature was significant to both wheel tracking rate and wheel tracking for the rich mixture at 100% of compaction. The effect of temperature is significant to the wheel tracking depth alone for the rich mixture at 97% degree of compaction as well as for the lean mixture at 100% degree of compaction.

6.2 *Results obtained by EN procedure*

Statistical analysis, similar to the one carried out on the results obtained by BS procedure was not possible due to small number of specimens. For this reason the discussion of the results obtained by the EN procedure will be based on the categorization of the asphalt concrete mixtures with respect to the wheel tracking slope and the proportional rut depth. These two parameters are used by EN 13108-1 to classify the asphalt concrete mixtures with respect to their rutting performance.

Based on the results shown in Table 6 the mixtures with respect to their wheel tracking parameters are classified as shown in Table 10.

6.2.1 *The effect of binder content*

When testing was carried out at 45°C the characterization of the mixtures in terms of wheel tracking slope and proportional rut depth category is almost unchanged, for a given degree of compaction. When testing is carried out at 60°C and for a given degree of compaction the wheel tracking slope category changes, while the proportional rut depth is higher than the highest category specified.

The above proves that the effect of the binder content is distinct when testing is carried out at 60°C, according to EN procedure.

6.2.2 *The effect of degree of compaction*

At 45°C testing temperature, the degree of compaction causes changes to the characteristic categories of wheel tracking slope and proportional rut depth. The changes caused are to the betterment of the permanent deformation behaviour. In other words, by increasing the degree of compaction both wheel tracking parameters are improved. Similar results were observed at elevated temperature of 60°C.

6.2.3 *The effect of degree of temperature*

By increasing the testing temperature both wheel tracking parameters increase noticeably.

Table 10. Categorization of mixtures according to EN-13108-1.

Mixture	Degree of compaction	Wheel tracking slope: mm/10³ cycles		Proportional rut depth: %	
		45°C	60°C	45°C	60°C
AC-4.35	97%	$WTS_{AIR\ 0.30}$	$WTS_{AIR\ 0.50}$	$PRD_{AIR\ 7.0}$	PRD> $PRD_{AIR\ 9.0}$
AC-5.25		$WTS_{AIR\ 0.40}$	$WTS_{AIR\ 0.80}$	$PRD_{AIR\ 7.0}$	PRD> $PRD_{AIR\ 9.0}$
AC-4.35	100%	$WTS_{AIR\ 0.10}$	$WTS_{AIR\ 0.30}$	$PRD_{AIR\ 5.0}$	PRD> $PRD_{AIR\ 9.0}$
AC-5.25		$WTS_{AIR\ 0.10}$	$WTS_{AIR\ 0.40}$	$PRD_{AIR\ 5.0}$	PRD> $PRD_{AIR\ 9.0}$

Table 11. Limiting wheel tracking requirements for site classifications.

Classification	Test temperature	Requirements when tested to BS 598-110	
No. description	°C	Max rut rate mm/h	Max rut depth mm
1. Moderate to heavily stressed sites requiring high rut resistance	45	2	4
2. Very heavily stressed sites requiring very high rut resistance	60	5	7
3. Other sites	No requirement	–	–

6.3 *Acceptability of mixes*

Generally, the purpose of running the wheel tracking test is to determine whether the design mix will have satisfactory rutting performance in situ.

Until now the only limiting values of wheel tracking properties for asphalt concrete mixtures when the test is carried out by a small device wheel tracking machine in air, are those proposed by Highways Agency. These values with respect to stressed sites are as shown in Table 11.

As far as the EN specifications, no limiting values have been yet proposed. The engineer has to specify out of his experience the required wheel tracking characteristics (wheel tracking slope and proportional rut depth) in terms of categories specified.

Therefore, the acceptability of the mixtures can only be judged by the results obtained by BS procedure.

Based on the results of this study, when wheel tracking test was carried out by BS procedure, all mixtures irrespective of binder content and degree of compaction (within the ranges used), are acceptable even for heavily stressed sites.

Looking at the results obtained by carrying out the test according to EN procedure, it can clearly be said that the behaviour of the mixtures in permanent deformation is distinct, as parameters vary.

As a general remark the lean and rich mixture, irrespective of degree of compaction, when tested at 60°C are classified outside the categories for maximum proportional rut depth. This can be translated as these mixtures been unacceptable for very heavily stressed sites.

7 CONCLUSIONS

Based on the results obtained in this study, for the asphalt concrete mixtures and the variables considered, the following useful conclusions can be drawn:

1. The effect of the volumetric properties of the mixtures, as varied in this study, to the permanent deformation behaviour, although significant in most cases did not affect the acceptability of the mixtures when tested by BS procedure and judged by Highways Agency requirements.
2. The same to the above conclusion is drawn when the test is carried out at 45°C or 60°C.
3. The effect of variation of the volumetric properties to rutting performance was clearly seen when testing was carried out at in accordance with EN 12697-22, Procedure B (in air).
4. The asphalt concrete mixtures with low void contents (rich mixtures), when tested in accordance with EN procedure, gave worse rutting performance than the mixtures with high void contents (lean mixtures).
5. The effect of over compaction to the rutting performance was apparent only when the test was carried out by EN procedure at 60°C.
6. Rutting performance of these asphalt concrete mixtures when judged by BS procedure may lead to erroneous results, if the existent limiting proposed values are used.

7. EN 12697-22, Procedure B (in air) testing procedure detects better the effect of volumetric properties of asphalt concrete mixtures to their rutting performance.
8. In review of the above, studies are urgently needed in order to determine limiting values on rutting parameters for asphalt concrete mixtures, when tested according to EN 12697-22. It is recommended to be determined not only per different stressed or traffic volume sites but also per temperature zone (North, Central, South Europe).

REFERENCES

Asphalt institute, Superpave Mix Design, Superpave Series No. 2 (SP-2), 3rd Edition.

ASTM C131-06, Test method for Resistance to degradation of small-size coarse aggregate by abrasion and impact in the Los Angeles machine.

ASTM 3515-01, Standard specification for Hot-mixed, Hot-laid bituminous paving mixtures.

BS 598-110: Sampling and examination of bituminous mixtures for roads and other paved areas-Part 110: Methods of test for the determination of wheel-tracking rate and depth.

BS 812-105: Testing aggregates, Part 105: Section 105.1, Flakiness index.

EN 1097-6: Tests for mechanical and physical properties of aggregates- Part 6: Determination of particle density and water absorption.

EN 1426: Bitumen and bituminous binders-Determination of needle penetration.

EN 1427: Bitumen and bituminous binders-Determination of softening point-Ring and Ball method.

EN ISO 3838, Crude petroleum and liquid or solid petroleum products—Determination of density or relative density—Capillary stoppered pycnometer and graduated bicapillaty pycnometer methods.

EN 12697-6: Bituminous mixtures—Test methods for hot mix asphalt-Part 6: Detrmination of bulk density of bituminous specimens.

EN 12697-8: Bituminous mixtures—Test methods for hot mix asphalt-Part 8: Determination of void characteristics of bituminous specimens.

EN 12697-22: Bituminous mixtures—Test methods for hot mix asphalt-Part 22: Wheel tracking.

EN 12697-33: Bituminous mixtures—Test methods for hot mix asphalt-Part 22: Specimen prepared by roller compactor

EN 13108-1: Bituminous mixtures-Material specifications-Part 1: Asphalt Concrete.

Highways Agency-MCHW -Volume 2-Notes for guidance on the specification for highway works-Series NG 900: road pavements-Bituminous bound materials, August 2008.

Advanced Testing and Characterization of Bituminous Materials –
Loizos, Partl, Scarpas & Al-Qadi (eds)
© 2009 Taylor & Francis Group, London, ISBN 978-0-415-55854-9

Rutting resistance of SMA determined with triaxial and wheel-tracking tests

Jan L.M. Voskuilen
Centre for Traffic and Navigation, Delft, The Netherlands

Martin F.C. van de Ven
Technical University Delft, The Netherlands

ABSTRACT: In the Netherlands a CROW working group has developed a new mix design for SMA based on a volumetric approach. A software program can calculate the realised void content in SMA with the following input data: mix composition, densities of the components, air voids content of the compacted stone skeleton. The theoretical voids content in SMA, based on filling the air voids in the stone skeleton with a volume of mortar, can be translated into the realised air voids content in SMA with a socalled shift factor. This shift factor takes into account the enlarging effect of air voids content of the stone skeleton in SMA due to the presence of mortar between the stones in SMA. In this way the desired SMA mixture can be calculated based on air voids content requirements. This mix design procedure has to be validated by compacting three SMA mixtures: one mixture with the calculated required air voids content and two mixtures with a stone content +/– 2,5 % the calculated stone content. Based on the realised air voids content in SMA and the stone content in SMA the required mixture can be chosen by interpolation.

To validate the new mix design procedure two mixtures from test sites were studied. To study the effect of filling the air voids content of the SMA stone skeleton with mortar on the resistance to rutting different variations of filling of those SMA mixtures were investigated with the wheel-tracking and triaxial test. For the mixture of each test site 5 different compositions were tested varying from strongly underfilled to strongly overfilled with mortar. The 5 different mix compositions were volumetrically kept constant. For one test site the normal crusher sand in the mixture was substituted by Scottish granite crusher sand and in the other case by fine natural sand. This was done to investigate the effect of the sand on the enlarging effect of the stone skeleton and on the resistance to permanent deformation. In this paper the results of wheel-tracking and triaxial tests on these mixtures are discussed.

1 INTRODUCTION

The Dutch CROW working group Implementation Volumetric Mix Design SMA (IVO-SMA) has developed a new volumetric mix design method, see Van de Ven & van Leest (2008). With new software using as input the data of grading, densities of components and air void contents of the compacted stone skeleton (HRS), SMA mixtures can be designed by calculation. The idea is based on filling the HRS of the stone skeleton in such a way with mortar volume that the SMA mixture will meet the target air void content (AV). The software takes into account the enlarging effect of the stone skeleton, the socalled shift factor. The cause of this enlarging effect of the stone skeleton (higher HRS in the stone skeleton in the mix) is that sand and/or filler grains are between the stones of the stone skeleton after compaction resulting in higher HRS of the stone skeleton. The shift factor translates the theoretical AV into the realised AV in a compacted SMA mixture.

The major parameter in the SMA mixture design is still the specified AV of the compacted SMA specimen. To investigate if the specified AV will lead to an optimal SMA mixture, rut tests were carried out on two SMA mixtures from test sites of the working group, by varying the mix composition from underfilled to overfilled with mortar. The idea was that with triaxial and/or wheel-tracking tests a turning point in the permanent deformation could be found between underfilled and overfilled SMA mixtures. This was based on the assumption that underfilled SMA mixtures would hardly deform due to the stable stone skeleton and that with increasing the filling of the stone skeleton with mortar a turning point could be found to more rutting sentive SMA mixture (no more stone-to-stone-skeleton).

The reason why in this project was chosen for two rutting tests is based on the experience of Van Dommelen & Houben (2004) and Surie et al. (2006) that the triaxial test probably does not predict the rut resistance of SMA always well.

The theoretical degree of filling of SMA can be calculated with the filling ratio (FRS) conform Voskuilen (2000). The FRS is defined as the ratio between the mortar volume and the HRS of the compacted stone skeleton. The enlarging effect of the stone skeleton in the realised SMA is not taken into account, so the real AV in SMA is higher than based on FRS calculations. An FRS value of 0 will theoretically result in an AV of 0% (in reality higher due to the enlarging effect of the stone skelton), the more negative the FRS, the higher the AV in SMA. A possitive FRS value results in an overfilled SMA and a theoretical AV content of 0%.

SMA is well known as a durable stable mixture. Due to the grain-to-grain contact of the stone skeleton the mixture has a high restistance to rutting and due to the high binder content the mixture SMA is very durable. The stone skeleton is realised if the mortar volume (sand + filler + drainage inhibitors + bitumen) is smaller than the available HRS in the stone skeleton. This is shown in figure 1.

For volumetric calculations, the HRS of the stone skeleton >2 mm is determined with gyratory compaction conform CROW (2003). With data of mix composition, material densities and HRS the filling ratio (FRS) is calculated as follows:

$$FRS = (((Vm\text{-}HRS)/HRS)) \times 100\%$$

in which:

FRS = filling ratio (ratio between mortar volume and volume of available air void content in the optimal compacted stone skeleton)
V_m = mortar volume (bitumen, drainage inhibitor, filler and sand)
HRS = air void in optimal compacted stone skeleton

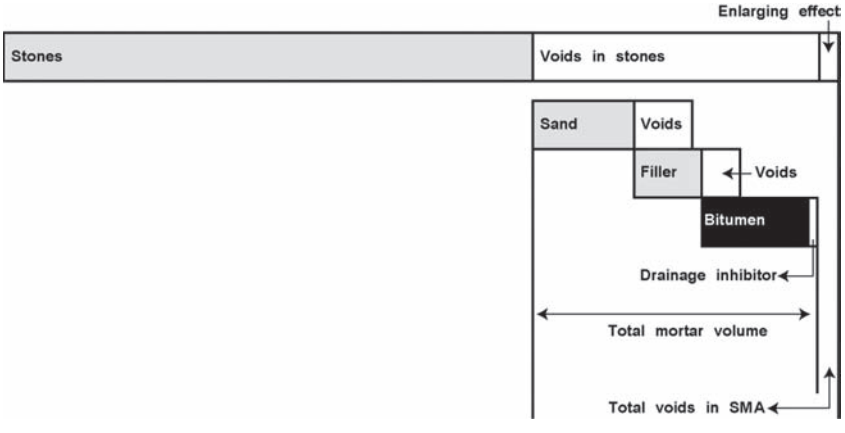

Figure 1. Schematic volumetric composition of SMA.

The FRS is used as a tool to calculate the mix composition of the investigated series SMA mixtures to obtain mixtures with the same volumetric mix composition, but consisting of other materials.

2 OBJECTIVE

The aim of this research work was to get answers to the three following questions:

Question 1. The current mix design is based on of the specified AV after lab compaction. Four SMA mixtures with constant bitumen content but with different coarse material contents are prepared with two times fifty Marshall blows. In those four mixtures the sand/filler ratio is kept constant and the sand/filler volume in the mortar changes dependent on the coarse material content; the more stone, the less sand/filler. The question is how the rutting resistance of those SMA mixtures with different mortar composition will be influenced.

The objective is to investigate what the effects of changes in mortar composition are on rutting resistance with underfilled SMA mixtures. (see figure 2).

Question 2. In Van de Ven & van Leest (2008) it was determined that the shift factor is dependent of the HRS value of the coarse material. With the help of the shift factor the theoretical AV in SMA, calculated with the HRS value, is converted into the realised AV in a compacted SMA specimen. Maybe the shift factor also can be influenced by de fineness and/or the quality of the sand. The objective of this research is to determine if the fineness and/or quality of the sand has influence on the enlarging effect of the stone skeleton with volumetricly equal mixtures.

Question 3. In Van Dommelen & Houben (2004) and Surie et al. (2006) it is questioned if the triaxial test can predict resistance to rutting of SMA mixtures. The objective of this research is to determine if SMA mixtures varying from underfilled to overfilled act the same in the triaxial and the wheel-tracking test (small device). To answer these three questions a combined research was carried out.

3 EXPERIMENTAL

To investigate if a turning point in the rutting resistance can be determined in the range of under to overfilled SMA mixtures, four series of SMA mixture are investigated with FRS values of –12, –4, +4, +12 and +20. The expectation was that the turning point would be around –4, because in CROW (2003) it was determined that an FRS value of –4 gives an AV of SMA of about 5% (= requirement of the SMA mixture for heavy trafficked roads). As basis of the research work two SMA mixtures were selected from the IVO-SMA test sites: SMA 11 mixture from the Ureterp test site and SMA 11 mixture from the Zeddam test site. The coarse material of the Ureterp SMA mixture was Bestone with a HRS value

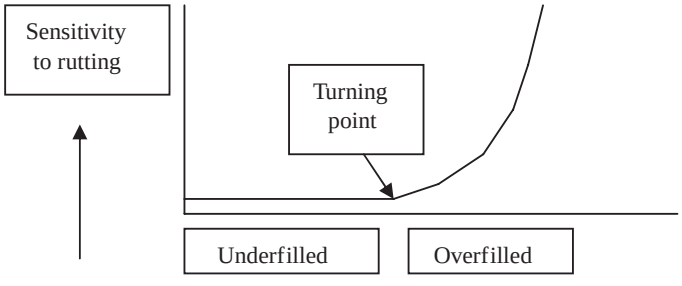

Figure 2. Hypothesis question 1.

of 38.4%, the coarse material of the Zeddam SMA mixture was Augit Porphyry with a HRS value of 40.9%.

The Ureterp SMA mixture was also used to investigate the influence of the sand. To investigate this separately from the standard Ureterp SMA also two 2 series SMA specimens were prepared with FRS values from –12 to +20, with the same materials as the standard Uretep SMA except the sand. Instead of moraine crusher sand as used in the standard Ureterp SMA in one case a fine natural sand was applied and in the other case Scottish granite crusher sand, with a lower resistance to crushing were used. Summarised mix compositions of the four groups are given in table 1.

All mixtures in the series have the same FRS values, the bitumen content is constant, the coarse material content decreases if the FRS value increases. Note that also the volume of sand and filler decreases when the FRS value increases. As a consequence of this the free bitumen contant decreases in the mortar when the FRS value increases resulting in a mortar that will become stiffer. In figure 3 the volumetric compositions are presented of mixtures

Table 1. Mix composition in mass percentages of the tested SMA mixtures.

Mix variation	FRS	–12	–4	4	12	20
Standard Ureterp mixture	**Ureterp SMA test site mix (moraine)**					
	Passing sieve 2 mm	25.1	27.4	29.6	31.6	33.4
	Passing sieve 0.063 mm	93.6	92.9	92.1	92.9	90.7
	Bitumen in mix	6.5	6.5	6.5	6.5	6.5
Sand fraction in Ureterp mixture replaced	**Ureterp SMA Scottish crusher sand**					
	Passing sieve 2 mm	25.1	27.4	29.6	31.5	33.4
	Passing sieve 0.063 mm	93.6	92.9	92.1	91.4	90.7
	Bitumen in mix	6.5	6.5	6.5	6.5	6.5
	Ureterp SMA natural sand					
	Passing sieve 2 mm	25.0	27.3	29.5	31.4	33.3
	Passing sieve 0.063 mm	93.7	92.9	92.1	91.5	90.7
	Bitumen	6.5	6.5	6.5	6.5	6.5
Standard Zeddam mixture	**Zeddam SMA test site mix**					
	Passing sieve 2 mm	27.2	30.1	32.4	34.3	36.4
	Passing sieve 0.063 mm	92.8	91.6	91.1	90.5	89.8
	Bitumen in mix	6.5	6.5	6.5	6.5	6.5

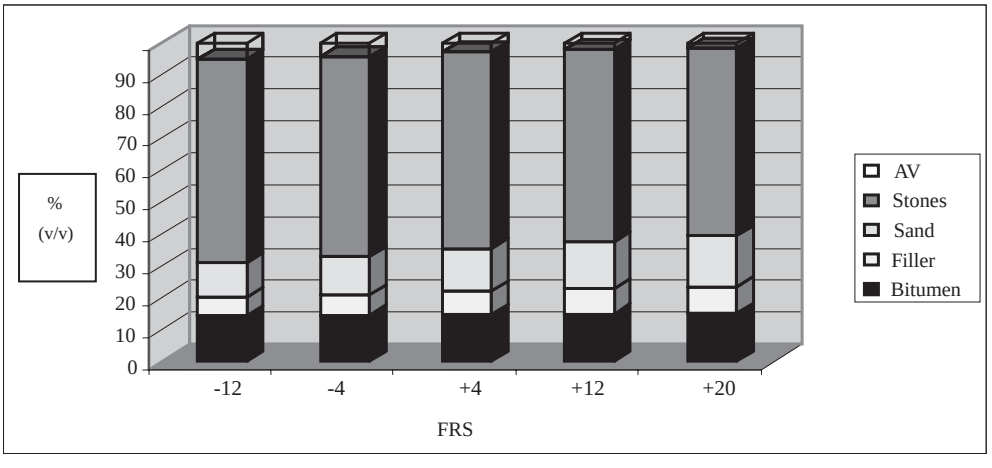

Figure 3. Volumetric composition of investigated SMA mixtures.

with FRS values varying from –12 to +20. These volumetric compositions are used for the FRS series of all four mixtures summarised in table 1.

3.1 *Specimen preparation*

To determine the reference density after compaction for all mixtures, first Marshall specimens were compacted with two times fifty blows. The asphalt was mixed conform EN 12697-35 with a laboratory mixer of 30 liter and compacted with a laboratory compactor conform FGSV (2003). The compacted slabs had a degree of compaction between 99 and 101% based on the target density determined with two times fifty Marshall blows.

3.2 *Determination of rutting resistance*

The resistance to permanent deformation of the SMA mixtures is determined with the triaxial and wheel-tracking test (small device), both conform the European norms EN-12697-25B and EN 12697-22. In Gharabaghy & Scharnigg (2006) and FGSV (2003) more background information is given about this research. The Technical University of Aachen has prepared the specimens for the rutting tests and carried out the research work.

4 RESULTS

4.1 *Air voids contents (AV) in SMA mixtures*

In figure 4 the AV of SMA is given of the Marshall compacted specimens of the Ureterp SMA specimens. The standard Ureterp test site mixture contains moraine crusher sand, and in the two other series specimens the moraine crusher sand is substituted by fine natural sand and Scottish granite crusher sand (table 1).

From figure 4 the following conclusions can be made:

- The Ureterp SMA has at FRS –4 a lower AV compared to earlier investigated SMA mixtures with the same FRS value.
- The fine natural sand has lower enlarging effect than both crusher sands. As a consequence of that the AV in SMA with fine natural sand is lower.
- Although overfilled SMA mixtures (positive FRS) theoretically should have an AV of 0%, AV's of these SMA's are between 1.2 to 3%. Possibly this is due to trapped air in the mortar. Based on experiences it is well known that SMA mixtures with such low air void content have a low rut resistance.
- SMA mixtures with different types of sand with FRS values of –12 have the same AV level. The sand type doesn't have influence on the realised AV content of SMA. The relatively low volume of mortar and the very bitumen rich mortar can explain this.

In table 2 the AV is given of the Marshall compacted SMA specimens of the Zeddam SMA mixture at FRS values of –12 to +20.

From table 2 it can be seen that positive FRS values can result in air void contents of 3.3 to 4.8% or higher, while the realised AV's in SMA theoretically on basis of filling the AV content of stones with mortar should be zero. This means that besides the enlarging effect of the stone skeleton also air must be trapped in the mortar. Because there is no real stone-to-stone contact, these mixtures can be sensitive to rutting.

Table 2. Results of AV of SMA Zeddam mixtures of FRS values from –12 to +20.

FRS	–12	–4	+4	+12	+20
Air void content in SMA (v/v%)	7.7	6.2	4.8	3.7	3.3

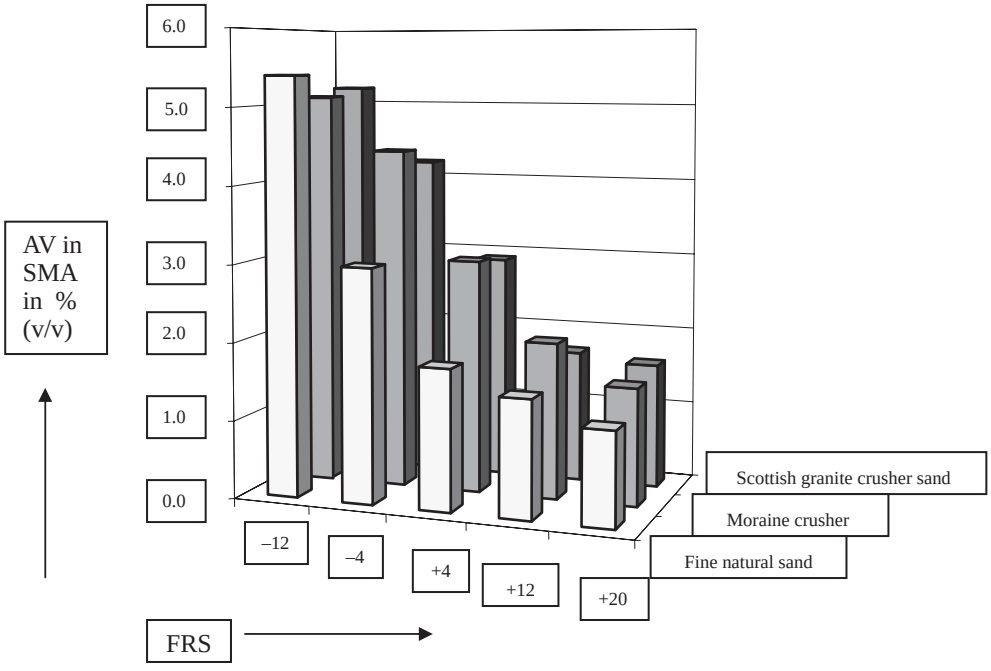

Figure 4. Air void contents versus FRS values of Ureterp SMA mixtures.

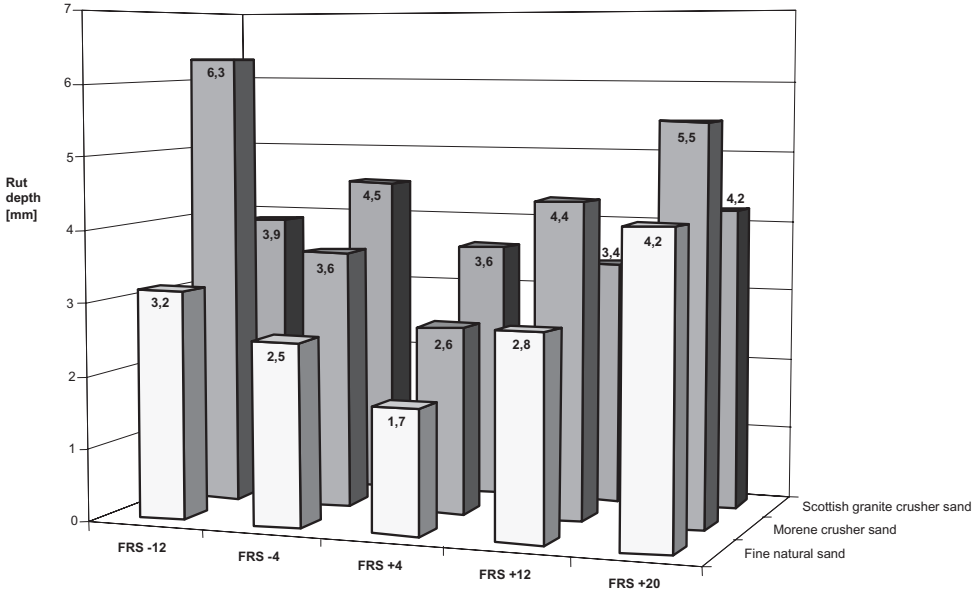

Figure 5. Results of the wheel-tracking tests of the Ureterp SMA mixtures (small device).

4.2 *Reseach into the turning point between under and overfilled SMA mixtures*

4.2.1 *Results of the wheel-tracking test (small device)*

In figures 5 and 6 results are given of the small wheel-tracking device for the Ureterp and Zeddam SMA mixtures.

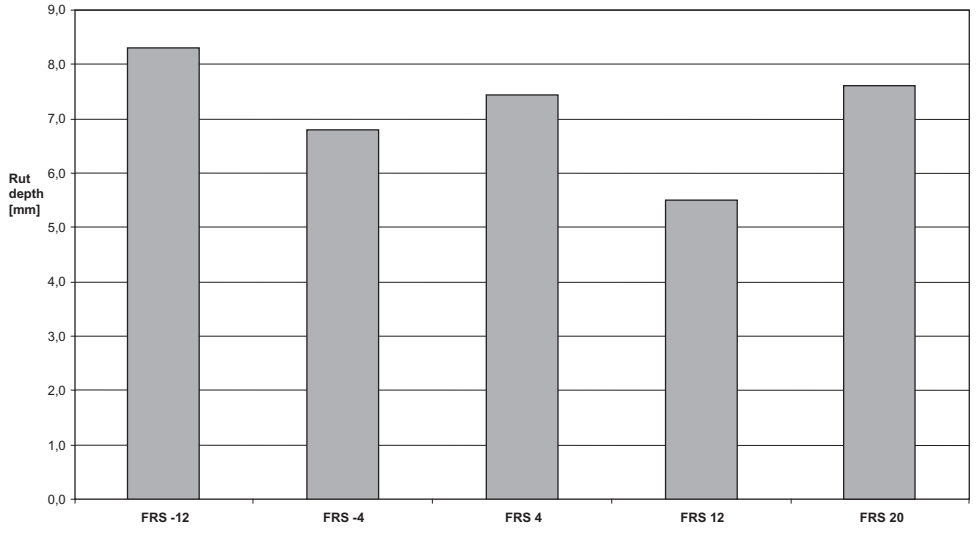

Figure 6. Results of the wheel-tracking test of the Zeddam SMA mixture (small device).

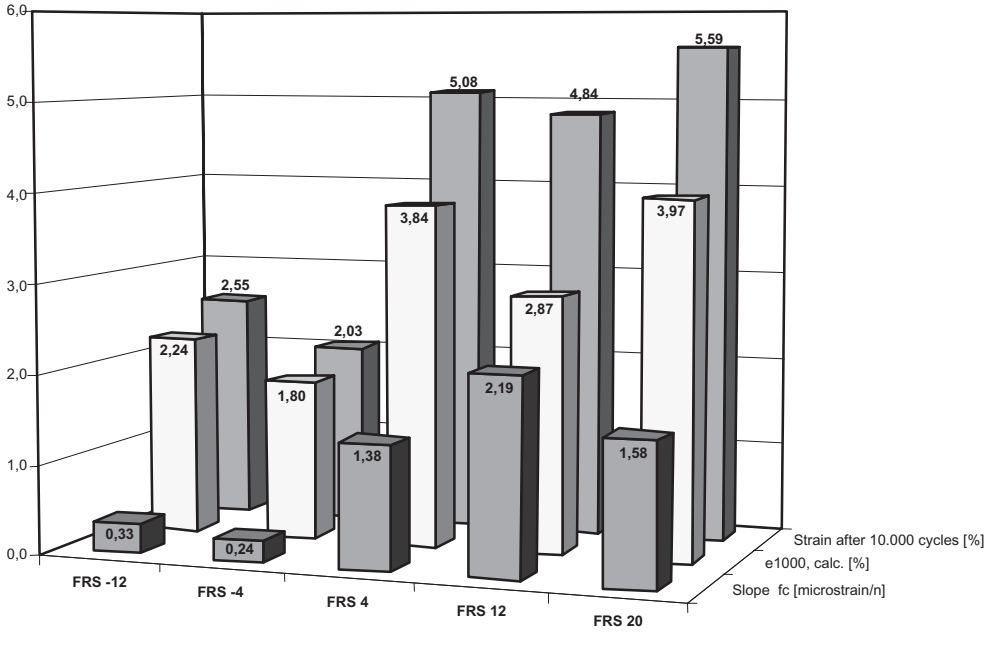

Figure 7. Results of the triaxial tests of the Ureterp SMA mixtures.

4.2.2 *Results of triaxial tests*

In figure 7 and 8 results are given of the traiaxial tests of the Ureterp SMA series and the Zeddam SMA mixture. Parameters used are strain after 1000 and 10000 cycles and the slope of the creep curve in the *steady state*, see Gharabaghy & Scharningg (2006).

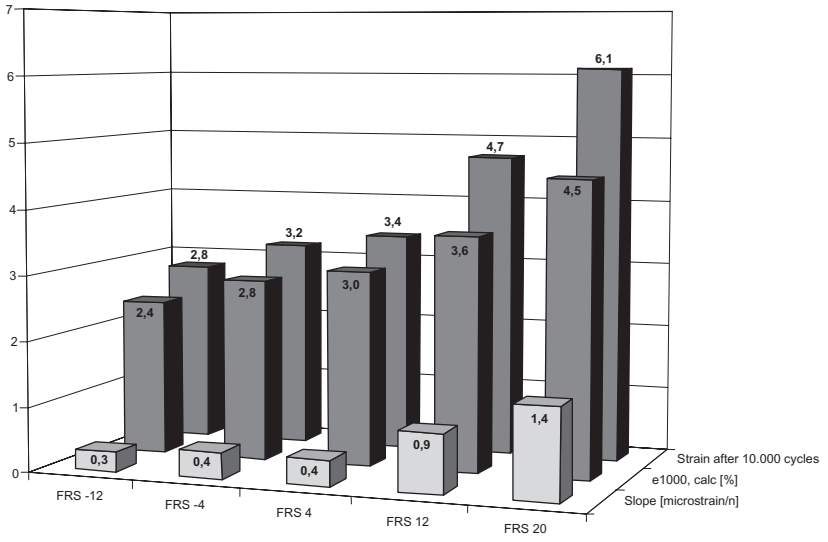

Figure 8. Results of the triaxial tests of the Zeddam SMA test site mixture.

5 DISCUSSION

5.1 *Air void content (AV) in the mix design*

The question to be asked is whether it is sufficient to design the SMA mix only on AV to guarantee a good rut resistance. This is very relevant, because during the Dutch mix design no mechanical tests are carried out to determine the rut resistance. The idea with SMA is that if at the used compaction level a mixture is underfilled and has sufficient AV, the mixture cannot get overfilled with mortar during service life and will have a good rut resistance due to the grain-to-grain contact of the stone skeleton.

The results of the wheel-tracking tests show that the Ureterp SMA test site mixtures with FRS values of –12 to –4 with air void contents from 6.3 to 3.6% still can be sensitive for rutting!

The triaxial test results show that the same Ureterp SMA mixtures have a good rutting resistance!! This can probably be explained by the continuous confinement of the specimen in this test, making it difficult to develop permanent deformation.

If SMA mixtures are designed with a high stone content (very negative FRS) with sufficient AV, these mixtures still can be sensitive for rutting if the mix composition is outsite the field of experience, for example by using alternative stones with a high HRS value. It is recommended to design SMA mixtures in the field of experiences with FRS values varying between approximately –6 to 0.

5.2 *Fixed bitumen percentage*

To ensure the durability the high bitumen content is kept constant during mix design, while the stone percentages vary of the investigated mixtures. As a consequence of this the composition of the mortar varies, because the mortar is compensated volumetrically by adding or deminishing sand/filler at the fixed bitumen content, by which the sand/filler ratio is kept constant (65/35). To give insight in the permissable deviations in mortar composition in table 3 a comparison is given of the mortar compositions of SMA and Porous Asphalt conform the Dutch national standard RAW 2005. The minimum and maximum tolerances of SMA 11 mortar are shown. Based on assumed densities of sand and filler of 2700 kg/m^3 and bitumen of 1020 kg/m^3 the ratios between volumes of the sand/filler mix and bitumen are given to show some insight in the allowed deviations. The same is done for the PA 16 mortar.

Table 3. Overview of mortar compositions of PA 16 and SMA 11.

	PA	SMA		
	Standard PA 16 mortar composition (mass %)	Standard SMA 11 mortar Composition (mass %)	Minimum tolerance SMA 11 mortar composition (mass %)	Maximum tolerance SMA 11 mortar composition (mass %)
Sand	10	15	10	20
Filler	4.5	8	6	10
bitumen	4.5	7	7	7
Volume ratio (sand+filler)/bitumen	1.22	1.24	0.86	1.62

Table 3 shows that the volume ratio for SMA is allowed to vary considerably. It is striking that the volume ratio between sand/filler and bitumen of PA and SMA are quit simular. Because of the gap between 2 and 6 mm, the air void content of 20% of PA is coarse divided. To keep the stone skeleton stable, a stable mortar is needed. Field experience have shown that the mortars of PA and SMA are stable and durable.

SMA mixtures with a high free bitumen content and with a low mortar volume ratio will cause a shorter service life. Wheel-tracking results show that those mixtures can't keep the stone skeleton stable, resulting in premature rutting.

Due to high stone percentages the mortar will consist of a relatively low amount of sand and filler. As a result of this the mortar will have a high free bitumen content. These mortars will be more unstable than the standard mortar composition.

Relatively low stone contents will result in mortars with a relative high amount of sand and filler. Due to that these mortars will have lower free bitumen content and will be stiffer than the standard mortar.

The differance in mortar composition in combination with high and low stone percentages will have influence on the bonding strengh of the stone skeleton and thus stability.

For the benefit of stability it should be considered to keep the mortar composition constant during mix design and to vary only the mortar volume. To ensure the durablity a requirement for minimum bitumen content in the mortar is recommended.

5.3 *Enlarging effect*

If realised AV contents of SMA mixtures with the same volumetric mix composition (theoretical same AV content) but prepared with coarse and fine natural sand it can be seen that the fineness of the sand has influence on the realised AV content of SMA. From this it can be concluded that the grading of the sand fraction has influence on the enlarging effect of the stone skeleton and so also on the shift factor. It is recommended to take into account this enlarging effect of the sand fraction if the shift factor is determined.

5.4 *Predictability of rut resistance tests*

The wheel-tracking tests give unexpected results. Especially SMA mixtures with very low negative FRS values and very high FRS values had the worst rutting resistance. Underfilled SMA mixtures (high stone %) with a strong overfilled mortar are more sensitive to rutting than SMA mixtures with a less overfilled mortar. Mixtures with FRS values of about +4 show the best rut resistance.

The triaxial results were as aspected; mixtures with a negative FRS have a good rut resistance and the more positive the FRS, the worse the rut resistance.

The results of the triaxial tests possibly differ from wheel-tracking tests because underfilled SMA mixtures with overfilled mortar can't develop permanent deformation due to

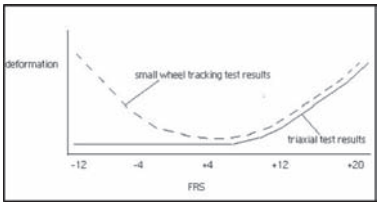

Figure 9. Trends from triaxial and small wheel-tracking tests.

the confinement. This is different in the wheel-tracking test, where the specimens have only temporary passive confinement.

On the A2 close to Maastricht premature rutting developed in SMA 11 four months after construction (rut depth up to 20 mm!). The contractor had to replace this layer in the guarantee period. From the emergency lane consisting of the same SMA mixture specimens were taken.

On these specimens the Technical University of Aachen did triaxial tests as well as wheel-tracking tests. From the triaxial tests, which were carried out with the same test conditions as the tests shown in figure 7 and 8, it can be seen that the strain after 10 000 load repetitions was 1.62% and the slope was 0.33 (micro strain/cycle) and the strain after 1000 load repetitions was 1.39%. From these results it can be concluded that the failed A2 SMA act excellent in the triaxial test.

The small wheel-tracking test had to be finished prematurely, because the test specimens were exceeding the maximal allowable deformation. From this it can be concluded that the A2 SMA acts very poor, which agrees with the field performance on the A2. Because it is only one test with one asphalt mix type the conclusion cannot be generalised, but it seems that the predictability for field performance of the small wheel-tracking device is better than that of the triaxial test.

The triaxial test as well as the small wheel-tracking test predicts the same trend for field rutting, if the SMA mixtures are overfilled. If the SMA mixtures are underfilled, but the mortar is overfilled, the small wheel-tracking test predicts well and the triaxial test not. The trend of the observations is schematically summarised in figure 9.

If the designed SMA mixtures consist of standard materials, the mix composition is within the field of experiences and the air void content and the bitumen content is sufficient, a good rutting resistance will be realised. If one moves outside the field of experience (for example high HRS of the coarse material), extra attention must be given to the mortar composition and probably extra mechanical testing is necessary.

REFERENCES

CROW publication 186, 2003. Volumetrische ontwerpmethode op basis van holle ruimte steenskelet en vullingsratio steenskelet (VRS).

FGSV 2003. Arbeitsanleitungen zur Prüfung von Asphalt (ALP A-StB) Teil 11: Herstellung von Asphaltprobeplatten im Laboratorium mit dem Walzsektor-Verdichtungsgerät (WSV); Forschungsgesellschaft fürr Strassen- und Verkehrswesen.

Gharabaghy, C. & Scharnigg, K. 2006. Vervormingsweerstand van SMA mengsel. Interpretation der Ergebnisse. ISAC RWTH.

LINTRACK-SMA verklaard. CROW Wegbouwkundige Werkdagen.

Surie, M., van Dommelen, A. & Voskuilen, J.L.M. 2006. Spoorvormingsgevoeligeheid.

Van de Ven, M.F.C. & van Leest, A. 2008. Mengselontwerp SMA, Eindverslag IVO-SMA. CROW Infradagen.

Van Dommelen, A. & Houben, L.J.M. 2004. Triaxiaalproef op asfalt maakt belofte nog niet waar, de proef op de som (en andersom). CROW Wegbouwkundige Werkdagen.

Voskuilen, J.L.M. 2000. Ideeën voor een volumetrische mengselontwerpmethode voor steenmastiekasfalt. CROW Wegbouwkundige Werkdagen.

Advanced Testing and Characterization of Bituminous Materials – Loizos, Partl, Scarpas & Al-Qadi (eds)
© 2009 Taylor & Francis Group, London, ISBN 978-0-415-55854-9

Rut resistance of asphalt concretes of different aggregate gradation

K. Zhdanyuk
State Scientific and Technical Center "Dorjakist", Kyiv, Ukraine

O. Volovyk & V. Zhdanyuk
Kharkiv National Automobile and Highway University, Kharkiv, Ukraine

Y. Prusenko
UKRDIPRODOR, Kyiv, Ukraine

ABSTRACT: Comparative research of resistance of hot dense asphalt concretes of different gradations to rutting within wide temperature range has been carried out. It has been established that increase of crushed stone content in compositions of fine-grained asphalt concretes results in increase of their resistance to plastic deformations in the form of ruts.

1 INTRODUCTION

In Ukraine while constructing wearing courses on urban streets and roads of common use (i.e. state and local roads, except urban, technological roads and roads on private territories) hot fine-graded asphalt mix is the most widely used material. Stone mastic asphalt is used on heavily trafficked highways, while sand asphalt concrete is used for paving sidewalks, bicycle lanes and footpaths.

Results of an asphalt wearing course survey on the road network of Ukraine indicate that asphalt pavement layers are often characterized by permanent deformations such as ruts in summer period of service at high ambient temperature. One of the reasons of the deformation accumulation is insufficient shear resistance of asphalt concretes in wearing courses. However National Standard of Ukraine "Asphalt mixes, road and airfield asphalt concrete. Specifications" contains no requirements for parameter of rut resistance. This does not allow the prediction of asphalt pavement resistance to permanent deformation accumulation (rutting) on the stage of asphalt mix design.

It is known that the most popular simulation method of asphalt pavement resistance to permanent deformation accumulation (rutting) is testing of asphalt concrete samples by means of special equipment called Rutting Testers (Uzarowski 2006) or Asphalt Pavement Analyzers (Stricland 2008). In Ukraine research of rut resistance of asphalt concretes with different aggregate gradation has not been carried out.

2 EXPERIMENTAL STUDY

The aim of the research is to perform comparative evaluation of rut resistance of hot dense asphalt concretes with different aggregate content within service temperature range as well as influence of bitumen modification by polymers on the magnitude of the parameter.

Fine-grained asphalt concrete mixes of A, B and V types, as well as sand asphalt concrete mixes of G type were accepted for the investigation. Asphalt concretes were prepared using petroleum road bitumen, characterized by penetration within 60 and 90 mm^{-1}, as well as polymer modified binder, characterized by penetration within 60 and 90 mm^{-1} and softening

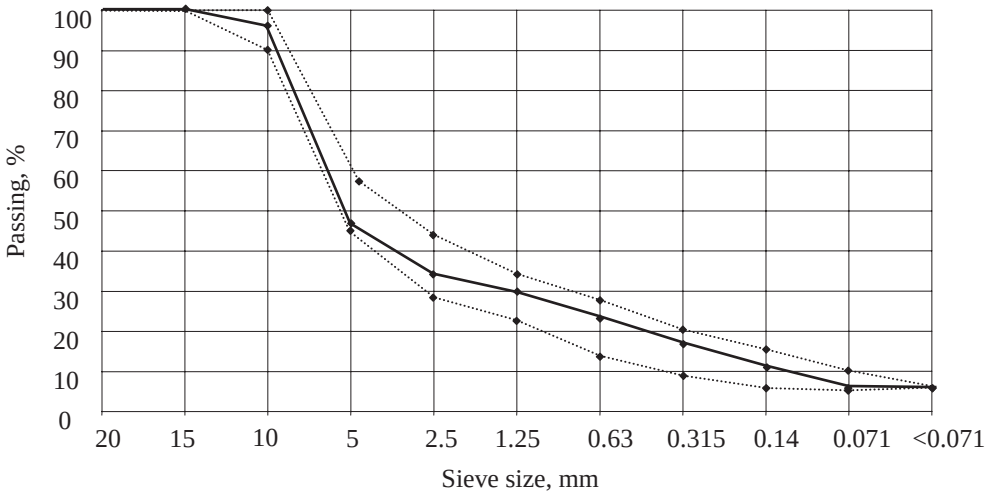

Figure 1. Aggregate gradation of dense fine-grained asphalt concrete of A type characterized by continuous gradation with maximum aggregate size 10 mm.

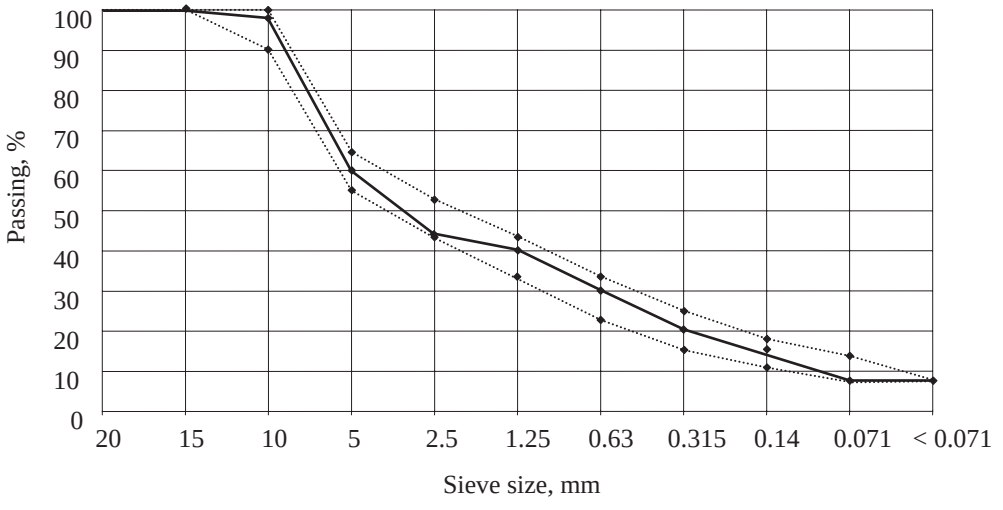

Figure 2. Aggregate gradation of dense fine-grained asphalt concrete of B type characterized by continuous gradation with maximum aggregate size 10 mm.

point of 52°C. By aggregate gradation (Figure 1–5) and parameters of physical and mechanical properties (Table 1) the asphalt concretes meet the requirements of National Standard.

Asphalt concrete testing was performed by means of wheel tester equipped with rubberized wheel (Zhdanyuk 2007) within the temperature range between 20°C to 65°C and 57.5 kN loading on the wheel.

Results of comparative experimental research of rut resistance of asphalt concretes of different aggregate gradation are shown in Figure 6.

Results of comparative experimental research of asphalt concrete resistance to accumulation of permanent deformations indicate that rut depth increases for all asphalt concretes used for research with the increase of wheel pass number. Rut depth of the asphalt concretes does not exceed 4 mm after up to 5000 wheel passes. Among fine-grained asphalt concretes minimum rut depth is appropriate to asphalt concrete with the highest crushed stone content (A type), and asphalt concrete with the smallest crushed

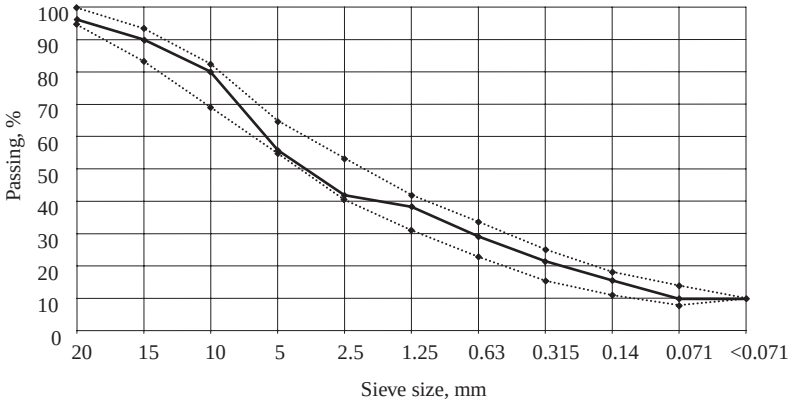

Figure 3. Aggregate gradation of dense fine-grained asphalt concrete of B type characterized by continuous gradation with maximum aggregate size 20 mm.

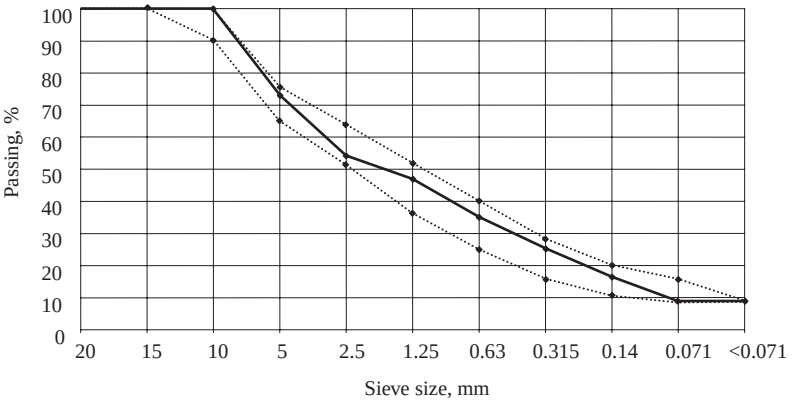

Figure 4. Aggregate gradation of dense fine-graded asphalt concrete of V type characterized by continuous gradation with maximum aggregate size 10 mm.

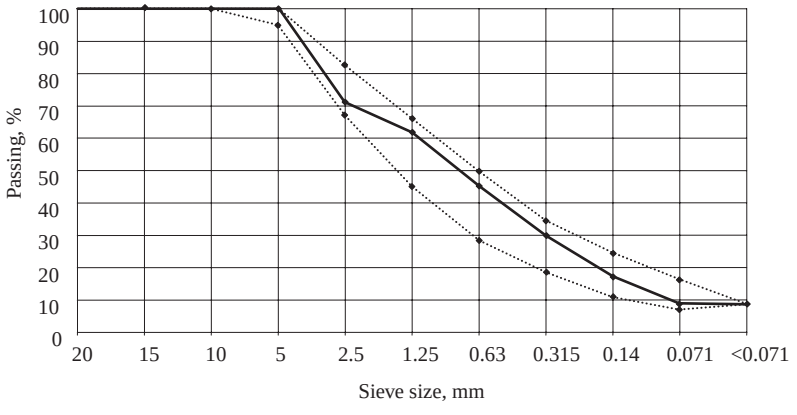

Figure 5. Gradation of dense sand asphalt concrete of G type characterized by continuous gradation.

Table 1. Physical and mechanical properties of asphalt concretes with maximum aggregate size 10 mm.

Property	Values for asphalt concrete			
	A type	B type	V type	G type
Water saturation, % by volume	2.5	3.3	1.7	2.7
Average density, kg/m^3	2376	2382	2398	2327
Swelling, % by volume	0	0.1	0	0
Uniaxial compression strength, MPa, at:				
0°C	8.0	7.9	9.5	9.0
20°C	3.2	4.0	4.0	4.3
50°C	0.70	1.25	1.26	1.28
Water resistance coefficient	0.91	1.00	0.95	0.91
Bitumen content, %	5.5	5.6	6.2	7.4
Crushed stone content, %	53	40	27	0

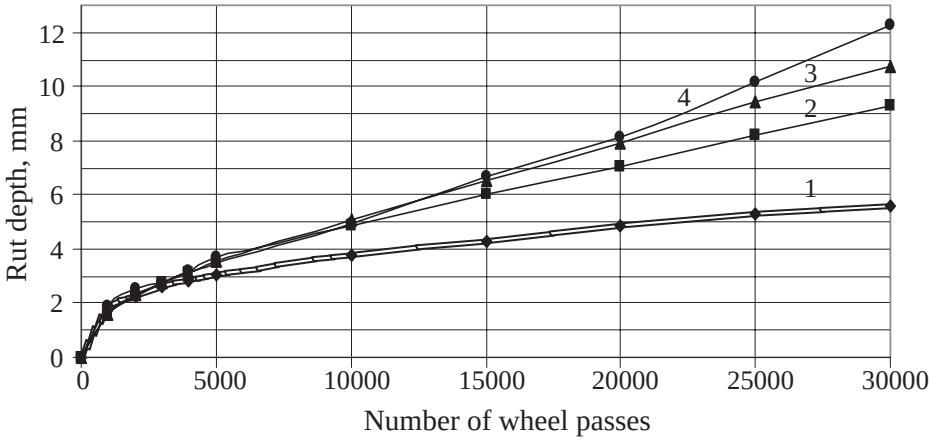

Figure 6. Rut depth versus number of wheel passes for asphalt concretes of different aggregate gradation at 50°C. Curve 1—A type asphalt concrete, 2—B type, 3—V type, 4—G type.

stone content (V type) is characterized by maximum rut depth. Sand asphalt concrete is characterized by the deepest rut in comparison with fine-grained asphalt concretes (Figure 7). After 25,000 wheel passes sand asphalt (G type) has twice as deep rut as fine-grained asphalt concrete of A type.

Experimental research results allow us to stumble at the objectivity of known statement that asphalt concretes with higher strength evaluated at uniaxial compression (at optimal bitumen content) are more shear resistant.

In order to evaluate the influence of bitumen content in asphalt concrete and temperature of the environment on rut formation process fine-grained asphalt concrete of B type of gradation shown in Figure 3, was chosen as the material most used for wearing courses in Ukraine. The research performed indicates that bitumen content deviation from optimal value has significant influence on both physico-mechanical properties and rut resistance of asphalt concretes (Figure 8–11).

Dependence of rut depth on bitumen content in asphalt concrete is characterized by absence of extremum as compared to uniaxial compressive strength. The same character has rut depth dependence on asphalt concrete test temperature (Figure 12).

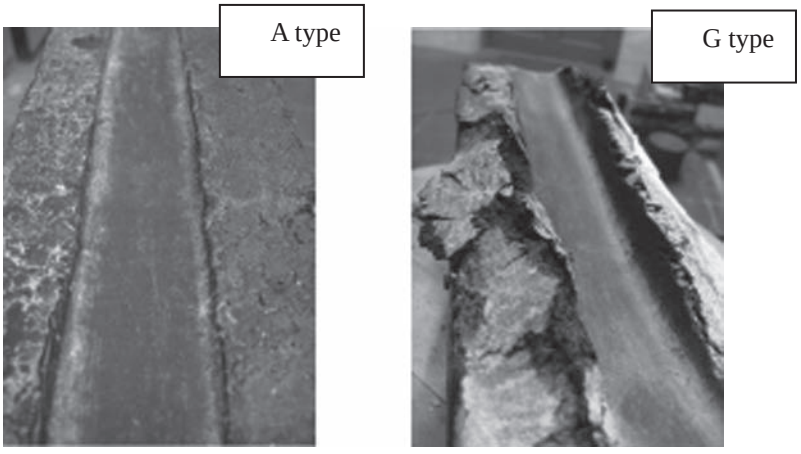

Figure 7. General view of asphalt concrete samples after 30,000 wheel passes.

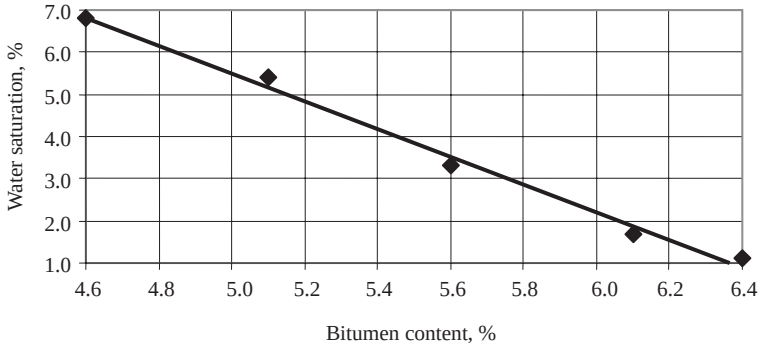

Figure 8. Dependence of water saturation of fine-grained asphalt concrete of B type on bitumen content.

Dependences shown indicate that temperature increase results in significant increase of rut depth. Thus, when increasing the temperature from 20°C to 50°C, rut depth increases up to 6 mm after 15,000 wheel passes. When further raising the temperature up to 65°C rut depth increases more intensively and reaches more that 20 mm.

Research results of influence of crushed stone size in fine-grained asphalt concrete of B type on rut formation process are shown in Figure 13. It is evident that the smaller the maximum size of crushed stone in fine-grained asphalt concrete of B type the less is rut depth.

Results of comparative research of polymer modified binder influence on rut formation process in fine-grained asphalt concrete of B type with maximum crushed stone size 10 mm are given in Figure 14.

The dependence indicate that addition of 3% low-molecular modifier Licomont BS 100 to petroleum road bitumen, characterized by penetration within 90 to 130 mm^{-1}, decreases intensity of rut depth increase in fine-grained asphalt concrete, prepared on it, almost by three times. Application of bitumen modified simultaneously with 1.5% low-molecular modifier Licomont BS 100 and 1.5% polymer Kraton D 1101 for asphalt concrete preparation, promotes further decrease of rut depth. Asphalt concrete prepared on bitumen modified with 3% thermoplastic elastomer Kraton D 1101 is characterized by the smallest rut depth in comparison with other asphalt concrete chosen for the research.

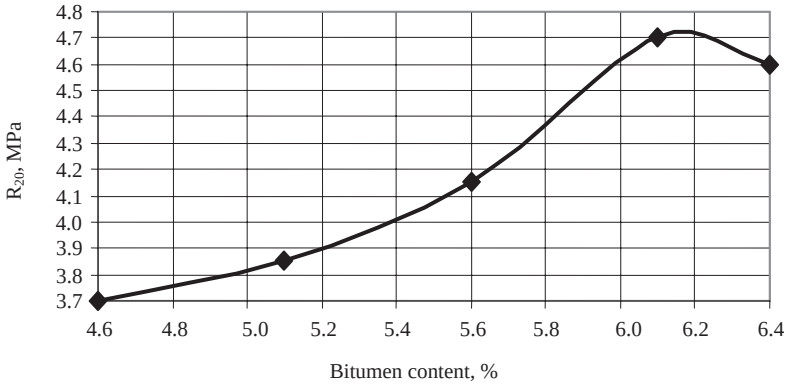

Figure 9. Dependence of compressive strength of fine-grained asphalt concrete of B type on bitumen content.

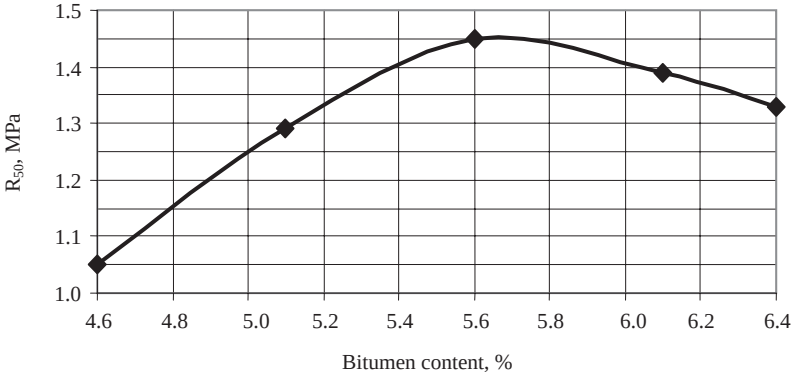

Figure 10. Dependence of compressive strength of fine-grained asphalt concrete of B type on bitumen content.

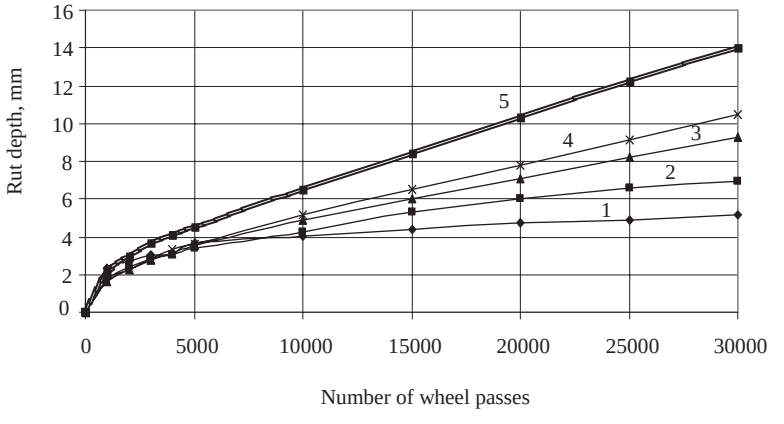

Figure 11. Rut depth versus number of wheel passes for asphalt concrete of B type at 50°C. Curve 1—bitumen content in asphalt concrete 4.6%; 2–5.1%; 3–5.6%; 4–6.1%; 5–6.4%.

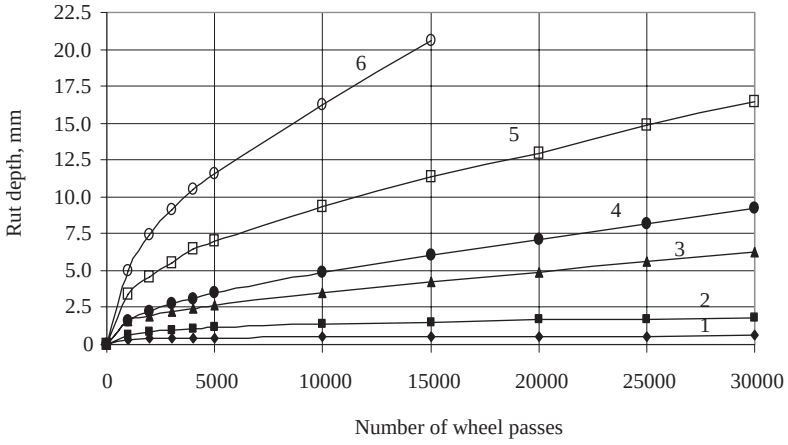

Figure 12. Rut depth versus number of wheel passes for fine-grained asphalt concrete of B type at different temperatures. Curve 1—test temperature 20°C; 2–35°C; 3–45°C; 4–50°C; 5–57°C; 6–65°C.

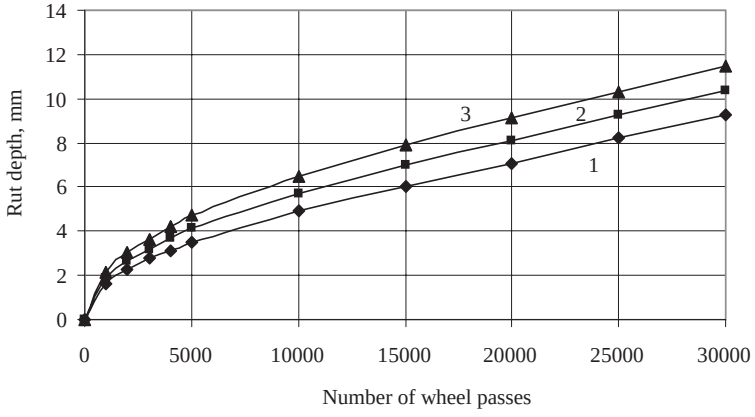

Figure 13. Rut depth versus number of wheel passes for fine-grained asphalt concrete of B type at 50°C. Curve: 1—asphalt concrete with maximal aggregate size 10 mm; 2–15 mm; 3–20 mm.

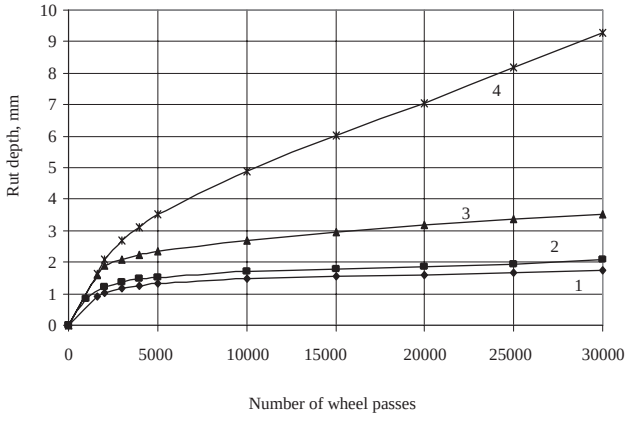

Figure 14. Dependence of rut depth on number of wheel passes for fine-grained asphalt concrete of B type at 50°C. Curve 1—asphalt concrete on bitumen modified with 3% Kraton D 1101; 2–1.5% Kraton D 1101 and 1.5% low-molecular modifier Licomont BS 100; 3–3% Licomont BS 100; 4–pure bitumen.

3 CONCLUSIONS

Analysis of experimental research results shows that the increase of crushed stone content in asphalt concrete and decrease of its size results in increase of their resistance to permanent deformations. Out of all asphalt concretes taken for the research, prepared on pure petroleum road bitumen, fine-grained asphalt concrete of A type is the most rut resistant and sand asphalt concrete turned out to be the least resistant material.

Shear resistance of asphalt concrete significantly decreases with the increase of bitumen content in asphalt concrete composition, number of wheel passes or temperature. Significant increase of rut resistance of asphalt concrete can be gained through utilization of bitumen modified with high-molecular polymer Kraton D 1101 of SBS type, low molecular modifier Licomont BS 100 as well as simultaneous application of the additives mentioned above.

REFERENCES

EN 12697-22:2003 Bituminous mixtures—Test methods for hot mix asphalt—Part 22: Wheel tracking.

OHD L-43. Method of Test for Determining Rutting Susceptibility Using the Asphalt Pavement Analyzer. p.12.

Stricland, D., Colang, J., Martin, M. & Deme, I. 2008. Performance properties of paving mixtures made with modified sulphur pellets. In M.N. Partl (ed.), *Asphalt Pavements and Environment; Proc. intern. symp.;* Zürich, 18–20 August 2008. Dübendorf: Empa.

Uzarowski, L., Maher, M., Prilesky, H., Tighe. S. & Rothenburg L. 2006. The Use of Dynamic Modulus and Creep Tests in the Development of Rutting Resistant Criteria for Asphalt Mixes in Canada. *Asphalt Pavements; Proc. intern. conf.*; Quebec, 12–17 August 2006. Quebec: ISAP.

Zhdanyuk, V.K., Masyuk, Y.A., Chugujenko, S.A. & Plugin, V.I. On the Evaluation of Resistance of Asphalt Pavements to Permanent Deformations. *Construction, reconstruction and Rehabilitation of Buildings of Municipal Economy; Proc. intern. conf.*; Kharkiv, 20–25 December 2007. Kharkiv: KhNAME. (In Russian).

8. Field methods for structural behavior assessment

Advanced Testing and Characterization of Bituminous Materials – Loizos, Partl, Scarpas & Al-Qadi (eds)
© 2009 Taylor & Francis Group, London, ISBN 978-0-415-55854-9

Damage identification in flexible pavements using FWD technique

A. El Ayadi, B. Picoux & C. Petit
GEMH Laboratory, Civil Engineering and Durability team, University of Limoges, Egletons, France

ABSTRACT: Several testing techniques exist for determining the bearing capacity of a flexible pavement. Among these techniques, the Falling Weight Deflectometer (FWD) is one of the operational in the pavement area. Using a backcalculation program, the FWD deflection data is often exploited to determine the pavement material properties and to evaluate the structural condition of flexible pavements. However, it will be interesting to use this technique for the detection and location of damage in damaged pavement as cracks and interface flaws seems to be interesting.

This paper includes a dynamic study of the mechanical behavior of safe and damaged flexible pavements using the FWD technique. A numerical finite element model is developed in order to verify the effectiveness of the methods proposed to detect damage from FWD data. Experimental results are driven from tests conducted on an Asphalt Pavement Testing (APT) section, in which we have constructed defects (interface flaws, cracks), to validate the numerical results.

Keywords: flexible pavement, non destructive testing, falling weight deflectometer, finite element method, dynamic analysis, damage.

1 INTRODUCTION

Road networks fulfil an important function in economic, social and cultural countries' development. In Europe, the road network represents approximately 250 000 kilometers of major roads and more than ten million kilometers of secondary roads. However, the deterioration against time of all these roads means an astronomical maintenance cost. Indeed, the prediction of the pavement life span and the accurate localization of its damage thus represent a major challenge given the maintenance cost of the French road network. Almost one million kilometers (with 7500 km of highways) represent 471 M€, meaning half of those on new structures.

The damage state of a flexible pavement is generally attributed to two factors which are environmental and traffic loading.

Pavements are subjected to moving traffic loads that are repetitive in nature. Each traffic load repetition causes a certain amount of damage to the pavement structure that gradually accumulates over time and can lead to the pavement failure. Thus, pavements are designed to perform for a certain life span before reaching an unacceptable degree of deterioration. However, the lack of tack coat or its damage has shown that the asphalt wearing course fatigues quickly and unduly reducing the pavement life span (Ziari 2007).

In addition to the aging asphalt, temperature variations generate stresses and deformations in the material due to thermal expansion or contraction and allow seed cracks which can propagate throughout the structure during thermal cycling. At low temperatures, the asphalt has a brittle behavior, therefore sensitive to cracking under the combined impact of climatic conditions and traffic loading. Moreover, water penetrating the pavement through cracks can cause damage in both warm and cold weather.

In this paper, we present a numerical model of a FWD tests on a healthy and damaged flexible pavement. First the FWD operating principle and the method used to analyze the FWD

test results are discussed. Then, we present the numerical model and a comparison between numerical and experimental results of an undamaged pavement. Finally, the methods used to detect and find defects location in damaged pavement are illustrated and their effectiveness discussed.

2 FALLING WEIGHT DEFLECTOMETER (FWD)

The falling weight deflectometer or FWD is a non-destructive control device used for the estimation of pavement materials properties, evaluation of its structural bearing capacity, and prediction of the future pavement performance. The aim of the testing (Figure 1) is to reproduce a dynamic impulse load which simulates heavy vehicle moving from 65 to 85 km/h, the standard load used for structural flexible pavement analysis is usually 30 to 50 kN. The pavement's response is estimated by measuring the deflection basin using 7 to 9 sensors.

The interpretation of FWD generated data leans on software systems called backcalculation programs (Burak 2006, Rada 1994) which can be used to obtain the in-situ resilient modulus of a pavement structure. The main existing programs are based on the static assumption, which uses only the maximum values of the FWD response history (deflection basin). This approach is very effective when the layers thickness are known, and their properties are mainly homogeneous in each layer.

There are three basic approaches to back-calculating elastic modulus of pavement structures:

- Method of Equivalent Thicknesses (ELMOD): the traditional Dynatest FWD model which uses the Boussinesq-Odemark method (Ullidtz 1998) to obtain the in-situ resilient modulus of each layer. This method is based on the assumption of the equivalent thickness by supposing that the strains within layers depends only on stiffness.
- The optimization method (MODULUS): A linear elastic program (numerical model) is used to generate a database of deflection basins by assuming different modulus ratios. A numerical optimisation (Burak 2006) method is employed so that computed deflection agrees with the measured one. The solution is defined as the optimum set of modulus ratios that minimizes the weighted sum of the difference between the measured and calculated deflections.
- The iterative method (MODCOMP): in this method a model based on multilayered elastic theory is used to calculate layers modulus from assumed modulus. An iterative procedure (Burak 2006) in which the elastic moduli of the layers are successively changed in order to fit the measured deflections.

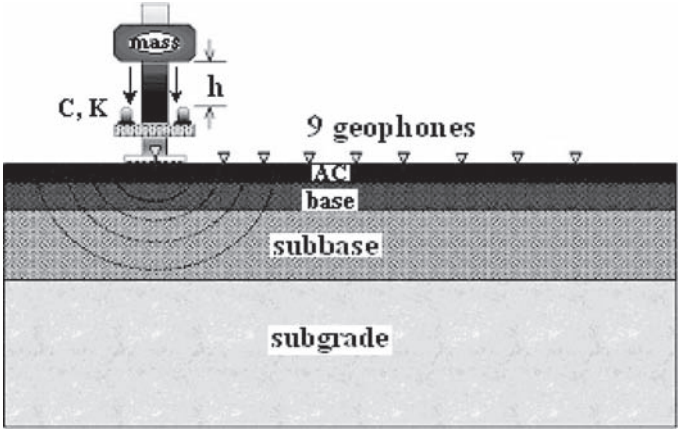

Figure 1. Description of the FWD testing.

3 NUMERICAL MODEL

The easiest model used to get the behavior of a pavement structure under dynamic loading is a combination of springs and dashpots. So the equation of motion can be expressed as

$$M\ddot{u}(t) + C\dot{u}(t) + Ku(t) = P(t) \quad (1)$$

where

M, C and K are the mass, damping coefficient and stiffness matrixes respectively;
$u(t)$, $\dot{u}(t)$ and $\ddot{u}(t)$ are the displacement, velocity and acceleration respectively;
$P(t)$ is the FWD impulsive loading.

The numerical simulation is implemented in the finite element code Castem which use the Newmark Central Finite Difference (CFD) algorithm (Combescure 2006) for solving dynamic equation. The CFD algorithm is one of the most widely used algorithms in structural dynamics because of the explicit scheme character and the resolution requires only one time step.

Throughout this study we assume that:

– the model ensure stresses and displacements continuity across the interfaces;
– the homogeneous layers have isotropic linear elastic behavior;
– small deformations.

3.1 *Modeling of a flexible pavement structure*

FWD test modeling using finite element method was one of the main objectives of this study. To simulate the multi-layered pavement structure, a 2D axisymmetric model is chosen. A very expansive mesh is adopted in order to comply with the semi-infinite soil (Figure 2). In order to get accurate fields, mesh densities are optimized. A high mesh density is close to the load area and gets increasingly coarse as we move toward the boundaries. The experimental load-time response is used as data in finite element model.

Absorbing boundaries (Combescure 2006, Darry 1992) were used at the boundaries so as to limit the size of the pavement structure mesh. These boundaries which are composed of viscous dampings aim at avoiding, as best as possible, the waves reflection on the mesh edge. In the finite element model, these dampings located at the model's borders dissipate energy and represent a transfer of energy to the semi-infinite part unrepresented in the model. The absorbing boundaries available in the computational codes allow radiation to infinity of compression and shearing waves affecting the normal border.

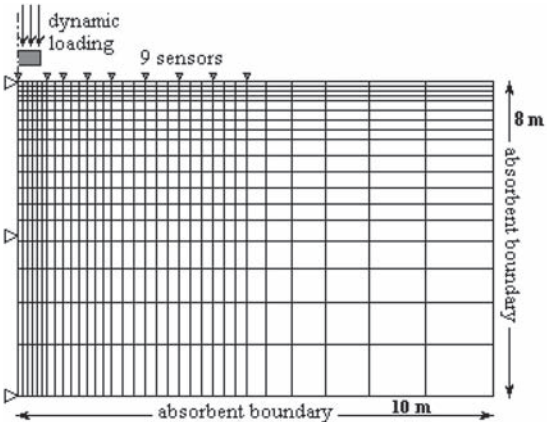

Figure 2. 2D axisymetric mesh of a flexible pavement structure.

3.2 *Numerical/experimental results of healthy pavement*

An experimental pavement of 70 m long and 10 m wide was constructed. The main originality is that defects have been constructed too (interface flaws, cracks,…). Temperature, humidity and pressure sensors have been located in the pavement structure. In this experimental pavement, three types of structures are tested:

- Type 1 (classical structure): AC layer (5 cm)/tack coat/gravel stabilised with bitumen-GB (8 cm)/unbounded granular material (30 cm)/soil-subgrade layer;
- Type 2 (more evolutionary structure properties): AC layer (5 cm)/gravel emulsion-GE (8 cm)/unbounded granular material (30 cm)/soil-subgrade layer;
- Type 3 (simple structure): AC layer (5 cm)/unbounded granular material (38 cm)/soil-subgrade layer.

The comparison applies only to in-situ testing results carried out on the pavements type 1 (4 layers) and type 3 (3 layers).

The effect of temperature variation on the resilient modulus of the asphalt-bound material can be easily determined from the table 1. Using a simple polynomial interpolation, we get the modulus evolution as a function of temperature.

$$E(BB) = -0.0059T^4 + 0.4914T^3 - 6.5947T^2 - 442.97T + 12018 \quad (2)$$

$$E(GB) = -0.0011T^4 + 0.2449T^3 - 2.0189T^2 - 737.82T + 20895 \quad (3)$$

where E: Young's modulus in MPa; T: Temperature in °C.

3.2.1 *Comparison of 3 layers structure*

In this comparison, properties of the pavement structure are given in table 2.

In order to compare experimental measurements and numerical simulations, first parameters1 were allocated to the pavement structure. In figure 3, we can see a good agreement between the two results close to loading area, but a great difference is observed with the third geophone. The numerical model used is based on a linear elastic approach, then it is obvious that the calculation of deflection will be wrong (as a result of the non-linearity of the subgrade). To modify this error and to get the same values as measured, we will allocate a small base modulus and a high subgrade modulus (Figure 3, parameters 2).

This phenomenon called compensating layer effect is operated by a MODCOMP back-calculation program (Loizos 2005). According to Per Ullidtz (Ullidtz 2005), if MODCOMP

Table 1. Asphalt-bound material modulus as a function of temperature (LCPC 1994).

T (°C)	–5	0	5	10	15	20	25	30
E_{BB} (MPa)	14000	12000	9800	7200	5300	3600	2100	1300
E_{GB} (MPa)	24500	20900	17200	13500	10200	7100	4600	2700

Table 2. Properties of the 3 layers pavement structure.

Layer	Modulus (MPa)	ν	Thickness (m)	ρ (kg/m^3)
AC	10400	0.35	0.05	2300
Base	120	0.35	0.38	2000
Subgrade	50	0.35	–	1600

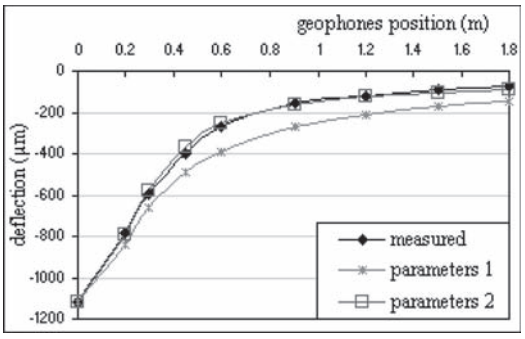

Parameters 1: base and AC layers modulus giving in table 2;
Parameters 2: E (base) = 80 MPa; E (subgrade) = 100 MPa.

Figure 3. Numerical/experimental comparison of deflection basins of the FWD testing.

Table 3. Properties of the 4 layers pavement structure.

Layer	Modulus (MPa)	ν	Thickness (m)	ρ (kg/m^3)
AC	10400	0.35	0.05	2300
Base (GB)	19600	0.35	0.08	2200
Subbase	120	0.35	0.3	2000
Subgrade	65	0.35	–	1600

is used in the linear elastic mode, it allocates a small base modulus and a high subgrade modulus in order to correct errors due to the exclusion of the nonlinear subgrade behavior. To explain this phenomenon, a parametric study previously conducted shows that deflections close to load area are strongly influenced by the base modulus and a little bit less by the subgrade modulus. But far from this area, the subgrade modulus has the greatest impact on the pavement response. So reducing the base modulus and greatly increasing the subgrade modulus, deflection close to load area reduced slightly while deflection far from this zone reduced sharply.

3.2.2 *Comparison of 4 layers structure*

The properties of the pavement structure are given in table 3.

The numerical fitting is good for the first two geophones but it is not for the third and others (Figure 4). The assignment of a high modulus to the subgrade layer and a small modulus to the subbase allows us to reduce this difference away from the load area. But in the middle area, the difference remains significant. To get the same results (numerical and experimental), the GB modulus should be reduced (Parameters 3). The approach followed confirms the findings of the 3 layers comparison (i.e. 3.2.1).

3.2.3 *Detection of the presence of a stiff layer*

Sometimes, numerical simulation enables us to explain phenomena observed during in-situ testing, which is true about a stiff layer detection. For most of deflection histories, the pavement continues to oscillate even after cancellation of the solicitation. These oscillations fade in a pseudo harmonic shape. Guzina (2002) has proved that these oscillations are caused by the reflection of transverse waves on a stiff layer located at a certain depth of pavement surface.

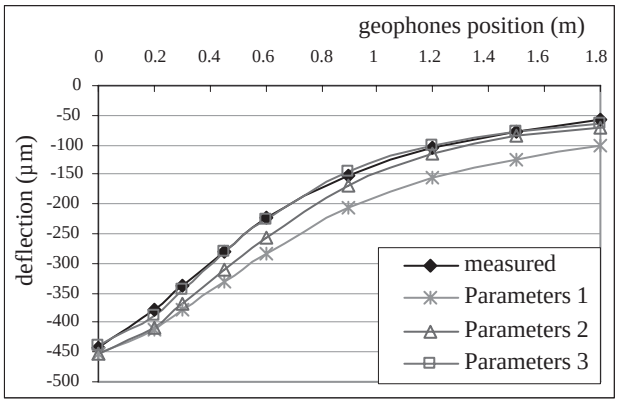

Parameters 1: Properties giving in table 3;
Parameters 2: E (subbase) = 40 MPa; E (subgrade) =120 MPa;
Parameters 3: E (GB) = 12000 MPa; E (subbase) = 60 MPa;
E (subgrade) = 130 MPa.

Figure 4. Numerical/experimental comparison of deflection basins.

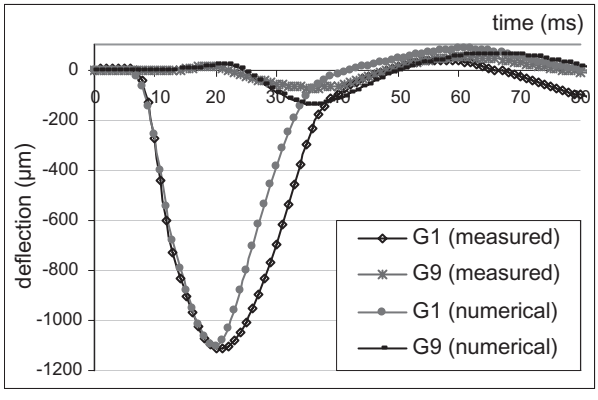

Figure 5. Pavement deflection with a stiff layer at 3 m from the pavement surface.

A structure of pavement with a stiff layer at different depths has been modelled to verify the hypothesis of its presence. The figure 5 shows that the modeling of the pavement with a stiff layer located at 3 m from the pavement surface allows to obtain the same form and amplitude of the measured deflection signal.

3.3 *Numerical/experimental results of damaged pavement (cracks and interface flaws)*

The modeling of the interface flaw can be done considering the interface state as slippery or by creating a thin interlayer with a weak modulus. This solution is the most commonly used to design the maintenance solution. However, carrying out the simulated interface flaws in the laboratory platform-testing was made with a sand layer which is spread on the base layer (GB). So, the interface flaws are modeled by a layer of 5 mm thick (Figure 6) and very weak Young's modulus (Young's modulus for the sand is 50 MPa).

Cracks were carried out on the experimental platform by a 5 mm saw stroke to a depth of 80 mm across the width of the base layer. Therefore, its modeling has been performed by a thin trench.

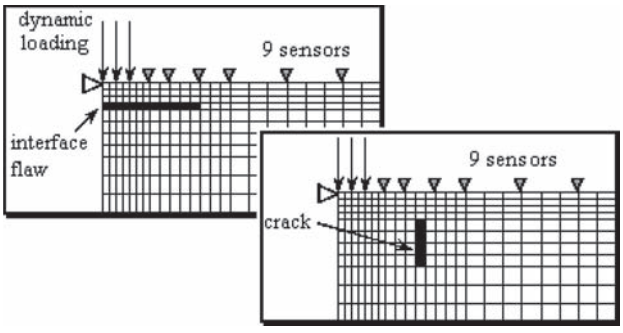

Figure 6. Modeling of interface flaw and crack.

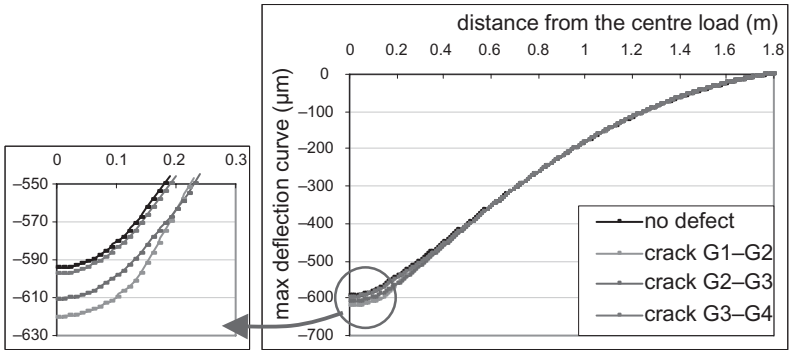

Figure 7. Maximum deflection curve: crack.

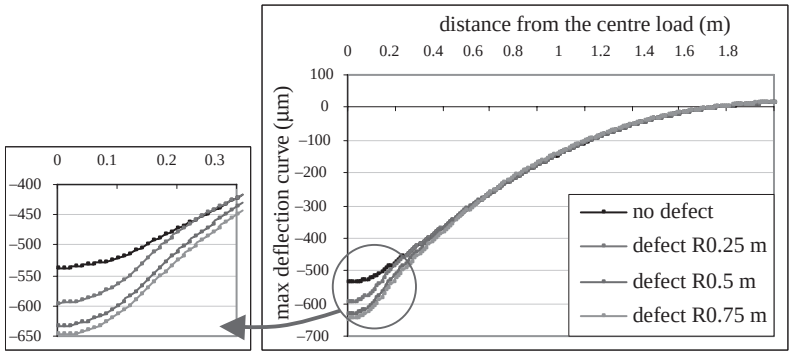

Figure 8. Maximum deflection curve: interface flaw.

3.3.1 *Numerical defects identification: maximum deflection curve*

Modeling results of a damaged pavement shows that the maximum deflection is more important in a cracked structure (Figure 7). However, the difference is significant if a crack is close to the loading area. In figure 7 we can see that 45 cm from the axis load, the crack has almost no influence on the maximum deflection of pavement.

In the case of interface flaw (Figure 8), the difference between safe and damaged pavement deflection is significant whatever the interface flaw size.

Theoretically, it is possible to find the presence of defects in a damaged pavement using deflection basin. However, the amplitude of deflections is not an appropriate indicator, as there may be other causes such as the temperature effect, the deterioration of pavement materials, etc.

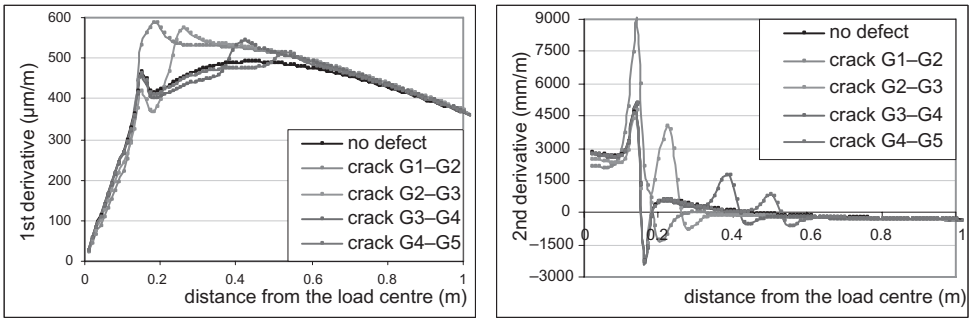

Figure 9. 1st and 2nd derivatives of the maximum deflection curve (crack case).

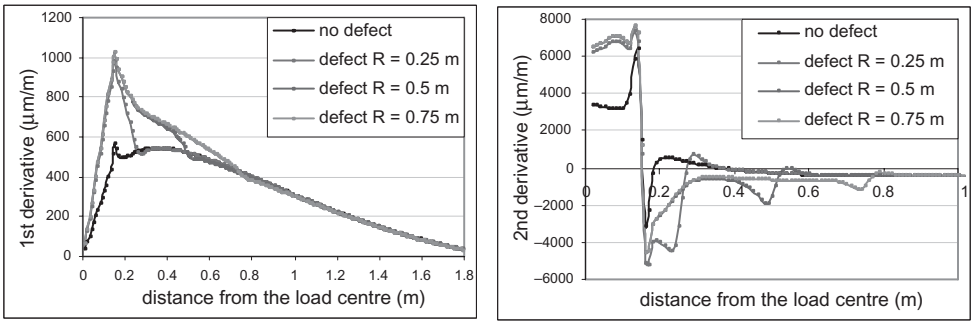

Figure 10. 1st and 2nd derivatives of the maximum deflection curve (interface flaw case).

3.3.2 *Numerical defects identification: 1st and 2nd derivatives*

In literature, radius of curvature is one of the most used indicators to identify the presence of a discontinuity in a pavement structure (Simonin 2006). In moving load case, this indicator can be approximated from the second derivative of the deflection curve following the expression:

$$R = \frac{1}{\partial^2 w(x)/\partial^2 x} \tag{4}$$

where $W(x)$ is the deflection curve measured at the load centre.

Based on Chea's works (Chea 2007), the first derivative function of the deflection curve can also be a good indicator of defect identification. In our case of a fixed load, instead of the deflection basin which is the only exploited part of the FWD data, we preferred to use the deflection curve of the pavement structure at the moment when the deflection under centre load is maximum (maximum deflection curve).

The first and second derivatives of maximum deflection curve provide better results allowing better exploitation of discontinuity effect on the pavement structure response and dynamic aspect of FWD data.

Figure 9 shows the effectiveness of the first and second derivatives of the maximum deflection curve to identify the presence of a crack in pavement structure. The first derivative allows to detect the presence of the crack by exploiting deflection curve discontinuity at the defect level. While the second derivative, in addition to defect detection, permits to locate it.

In figure 10, we can see that both of first and second derivatives allows to identify the presence of an interface flaw in pavement structure and, at the same time, to determine its expense.

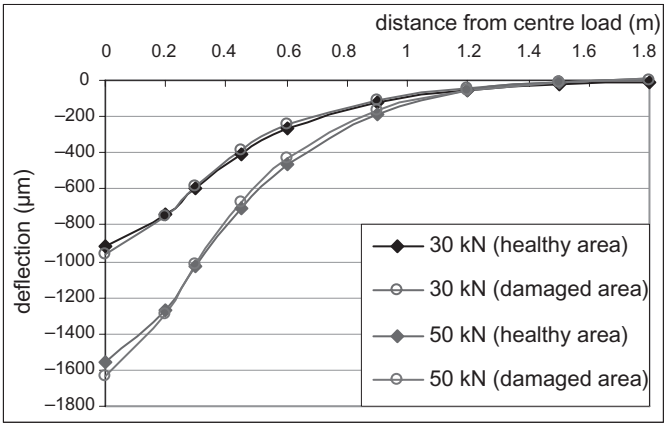

Figure 11. Maximum deflection curves of healthy and damaged pavement (crack).

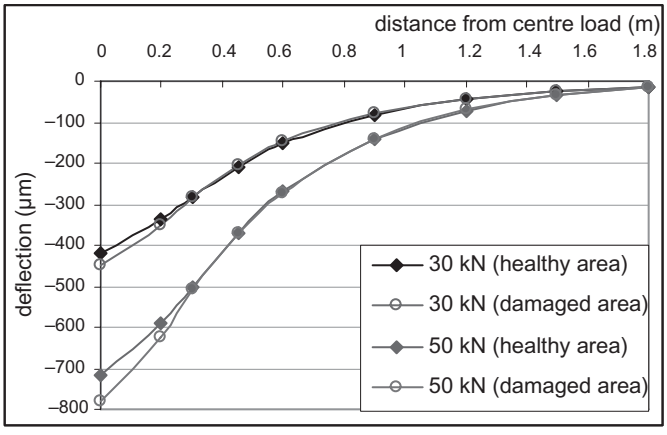

Figure 12. Maximum deflection curves of healthy and damaged pavement (interface flaw).

Comparing the two types of defects, we find that the interface flaw detection using the first and second derivatives gives more interesting results than the crack detection. This is mainly due to the remark made previously (i.e. 3.2.1) on the fact that cracks have little influence compared with interface flaws on pavement response with regard to deflection.

3.3.3 *Experimental results*

Figure 11 shows a comparison of experimental measurements between safe and damaged pavement. We can see that when a crack is located in the vicinity of the top geophones, the pavement surface deflection is more important compared to safe pavement case. More over, the defect can be detected and located by observing deflection curves close to the top geophones area where safe pavement deflection is more important than damaged pavement deflection.

Figure 12 is a comparison of experimental measurements between safe and damaged pavement, the defect concerns an interface flaw. We can see that pavement surface deflection is more important in damaged pavement. Moreover, we can get an idea on the defect expense by observing the zone of deflection when the two curves are separated. The zone when the two curves are merged represents the safe part of pavement.

The drawback to FWD that the whole load and sensors are fixed, so with only 9 points of measurement, it seems very difficult to use the first and second derivatives method to identify

the presence of discontinuity in a pavement structure. However, the derivative method may be experimentally interesting in the case of measuring device equipped with a mobile loading system or mobile sensors.

4 CONCLUSIONS

A finite element model was developed to study the flexible pavements behavior subjected to dynamic loading. The numerical simulation of FWD testing allows a better understanding of pavement response in terms of influence level of each layer, which makes possible an interpretation of backcalculation programs results and a verification of their effectiveness to evaluate the pavement material properties. Moreover, the numerical modeling allows us to explain phenomena observed during in-situ testing such as a stiff layer effect on deflection-time history.

The comparison between the experimental and numerical results shows the limits of a linear elastic model and proves the need to develop a more realistic model which takes into account the non-linear behavior of the soil and the viscous behavior of bituminous materials.

The criteria used to demonstrate the possibility to identify and locate defects on damaged flexible pavement are efficient using a numerical model. However, these criteria are difficult to exploit in practice. Relying on other existing methods like impact-echo method (Simonin 2006), frequency analysis of pavement response was made. However, as the FWD was mainly designed to determine pavement material properties, the results were disappointing.

REFERENCES

Burak Goktepe, A. and al. 2006. Advances in backcalculating the mechanical proprties of flexible pavements. Advances in Engineering Software 37: 421–431. (2006).

Chea, S. 2007. Contribution à l'auscultation structurelle des chausses mixtes: Détection de défauts d'interface à l'aide de la déflexion. Thèse de doctorat, INSA de Rennes, Décembre 2007.

Combescure, D. 2006. Eléments de dynamique des structure, Septembre 2006. Disponible sur: www.cast3m.cea.fr/cast3m/xmlpage.do?name=documentation.

Darry, S. Carlstone. 1992. Radiation damping in the mechanical oscillator. Proceedings of the Oklahoma Academy of Science, 72: 45–49.

Guzina, B.B. and Osburn, R.H. 2002. Effective Tool for Enhancing Elastostatic Pavement Diagnosis. In Transportation Research Record: Journal of the Transportation Research Board, No. 1806: 30–37TRB, National Research Council, Washington, D.C.

LCPC 1994. Guide technique "Conception et dimensionnement des structures de chaussées", LCPC-SETRA 1994.

Loizos, A. and Scarpas, A.T. 2005. Verification of falling weight deflectometer backanalysis using a dynamic finite elements simulation. *The International Journal of Pavement Engineering* 6(2): 115–123. June 2005.

Rada, G., Richter, C. and Jordahl, P. 1994. SHRP's Layer Moduli Backcalculation Procedure, Second Volume, STP 1198, American Society for Testing and Materials, Philadelphia, PA, December 1994.

Simonin, J.M. 2006. Contribution à l'étude de l'auscultation des chausses par méthodes d'impact mécanique pour la détection et la caractérisation des défauts d'interface. Thèse de doctorat, INS A de Rennes—LCPC Bouguenais, Décembre 2006.

Ullidtz, P. 1998. Modelling Flexible Pavement Response and Performance. ISBN-87-502-0805-5, Polyteknisk Forlag, Copenhagen.

Ullidtz Per. 2005. Note on: Verification of falling weight deflectometer backanalysis using a dynamic finite elements simulation by Andreas Loizos and A. (Tom) Scarpas. *International Journal of Pavement Engineering* 6(4): 295–297. December 2005.

Ziari, H. and Khabiri, M. 2007. Interface conditions influence on prediction of flexible pavement life. *Journal of Civil Engineering and Management*, 2007 Vol XIII, No 1: 71–76.

Advanced Testing and Characterization of Bituminous Materials – Loizos, Partl, Scarpas & Al-Qadi (eds)
© 2009 Taylor & Francis Group, London, ISBN 978-0-415-55854-9

Dynamic approach for the evaluation of the load carrying capacity and stability of flexible pavements with the Falling Weight Deflectometer

Steffen Riedl
University of Applied Science Erfurt, Germany

ABSTRACT: To evaluate the load carrying capacity of existing pavements the dynamic method of the Falling Weight Deflectometer (FWD) is often used. With this device, the traffic is simulated by a falling weight. The deflections invoked in the roadway are measured with up to nine geophones. During the measuring procedure the maximum deflection hollow, as well as the time dependent and force and deformation data ("Time History") are recorded. For evaluating the load carrying capacity out of the measured data currently static methods based on the maximum deflection hollow is used. In this paper, new procedures for a dynamic evaluation as well as interpretation of the time history data are presented.

1 INTRODUCTION

The preservation of the existing road network is one of the main tasks of the public road administration. This is on the one hand a result of a steady increase in traffic, combined with an increase in the permitted axle loads and on the other hand a result of increasing scarcity of budgets for road construction and maintenance activities. This fact is confirmed not only in the statistics of the Federal Statistical Office or automobile associations, but rather in a network, more and more suffering wear and substance and hence public fixed assets continue to lose value.

In the past, the design of road construction and the selection of appropriate maintenance activities are were carried out on the basis of experience. Today aspects like efficiency, economy, and environmental sustainability get more and more important. A great difficulty is to assess the existing substance of pavements and to propose a maintenance activity as well as to assess the tender in accordance with the German Building Contract Code VOB/A. In recent years, especially in the field of detection of surface features such as the evenness or the skid resistance large progress has been achieved enabling the possibility to evaluate the condition of a road surface with sufficient precision within the moving traffic. The measurement and evaluation of the load carrying capacity of existing pavements is however still a problem for most engineers. This is less of a lack of measurement methods than on different evaluation methods.

Almost all standard procedures are based on the principle of simulating the traffic statically. The resulting measured displacements, as well as the applied loads may be evaluated but only statically. Depending on the type of the investigated pavement different mechanical models are available which for different procedures are more or less suitable. Another problem is the enormous time required for most measurement methods, which can only give scattered information on the existing pavement performance. Therefore in addition cores are drilled which can be analyzed precisely in the laboratory. A drilling-core however, can also only give scattered information which may not be representative to assess the state of the entire pavement. Moreover, laboratory tests due to the constant controlled conditions can be carried out with a high precision, but they usually simulate the real situation only on a small scale and under idealized conditions.

2 STATE OF THE ART

2.1 *The falling weight deflectometer*

To record the deformation behavior of pavement structures different methods have been developed based on the principles of static or dynamic loading. As an example of static measurement methods the Benkelman Beam can be mentioned. These devices were described in detail in (Durth & Grätz 1995) and (Köhler 1995). For the dynamic measurement methods like the Lacroix, the Dynaflect or the Road rater should be mentioned which has been described in (Plehm 2005), or (Mamlouk 1985) Another dynamic device is the Falling Weight Deflectometer which is explained in more detail below. A comparison of these static and dynamic measurement methods was published for example in (Tholen et al. 1985), (Buseck 1989) and (Wolf 2004) and will not be explained further.

The Falling Weight Deflectometer is a measuring device for dynamic measurement of the load carrying capacity of pavements. The load is established by a weight which can be dropped from variable height on rubber buffers mounted on a circular plate. The resultant impulse is essentially depending on the weight of the mass, the drop height and the hardness of the rubber buffer. Depending on the type of road construction and used FWD, it is possible to achieve a force up to a maximum of about 250 kN. In Germany the procedure of measuring the load carrying capacity with the FWD is described in (APTRAG 2004). In Germany the Force of 50 kN representing a 10 t standard axle is used. The choice of rubber buffers with different hardness allows the adjustment of the duration of the impulse width. In the mentioned German paper (APTRAG 2004) an impulse width between 25 and 30 ms is proposed. The short-term loading invokes surface oscillations within the pavement. The vertical deformation velocities are recorded by (depending on the type of FWD by 7 to 9) Geophones placed at a bar at varying distance from the load centre. The first Geophone is fixed in the center of the load plate and records the deformation speed of the load centre. Besides the Geophone within the load center there is a load cell, which allows recording the force induced into the pavement. The temperatures of air, road surface as well as the temperature within a depth of 4 cm of the top layer are recorded additionally. Thus, for any measured point, the time dependent force and deflection values, the so called Time History is available in a recorded data file.

In a second file, the maximum value from the time dependent force and deflection data is extracted and stored together with the positioning of each Geophone. With this file, the maximum deflection hollow depending on the distance from the load centre is stored. Since the deflection maxima of the pavement surface at the individual positions of each Geophone is not set simultaneously, the deformation hollow cannot be considered as a snapshot of vibration. In Figure 1 the measuring principle of the FWD with several

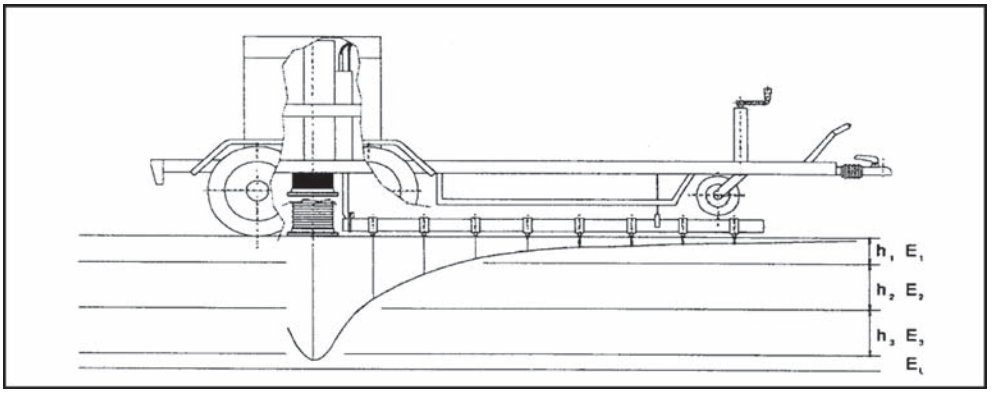

Figure 1. Falling Weight Deflectometer (FWD).

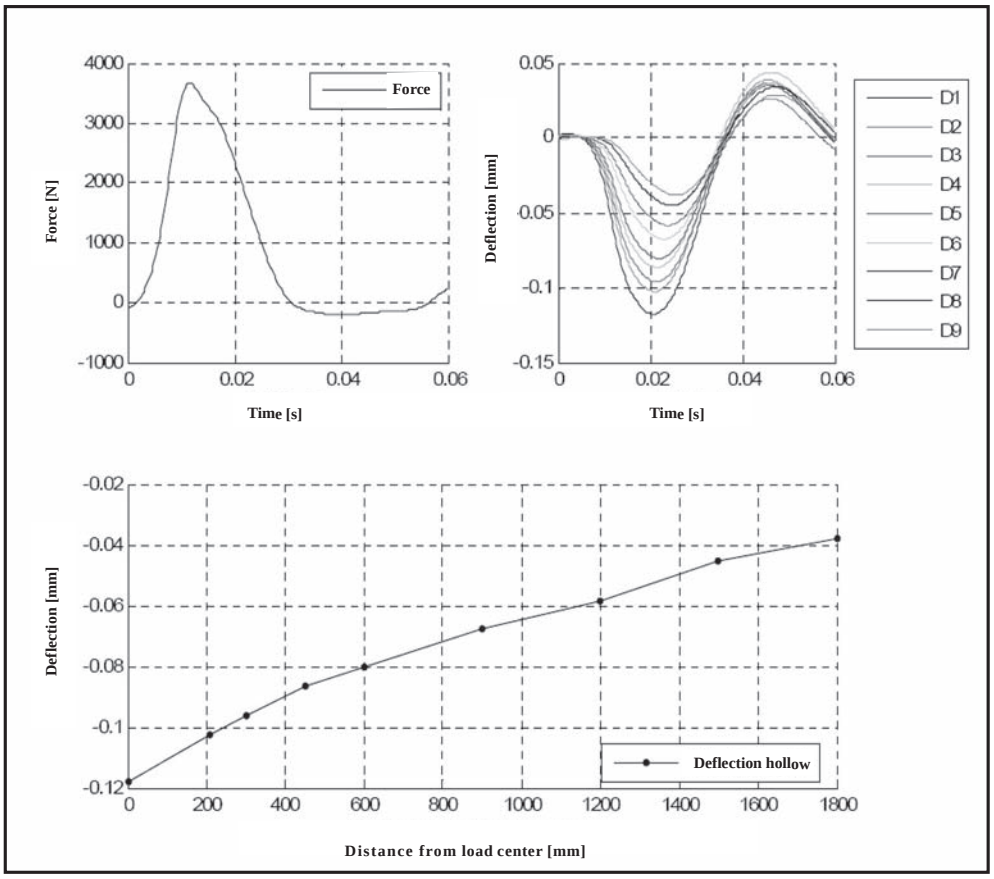

Figure 2. Top: Time-History data Bottom: maximum deflection hollow.

Geophones, as well as a qualitative deflection hollow can be seen. In Figure 2 the Time-History Data is presented on top and half of the resulting maximum deflection hollow can be seen below. The time differences of each maximum deflection can be seen clearly visible.

3 STATIC INTERPRETATION OF THE RECORDED FWD-DATA

The name refers to the static evaluation of the maximum deflection hollow. As already mentioned, the measured values of the maximum deflection hollow indicate time-independent values and therefore cannot be regarded as dynamic. With the measured deflection values characteristic values describing the load carrying capacity of roads can be back-calculated based on the following mechanical-models

– theory of the semi infinite space (single or double layered theory),
– multi-layer theory or
– plate theory.

Details of the different calculation models can be read in (Durth et al. 1995) or (Gerlach 1971) in detail. On the basis of the plate theory (Grätz 1999) developed a regression approach to identify mechanical properties and to evaluate characteristic values for the load carrying capacity of roads represented by the elastic length l and the layer modulus of the unbound

layers M_0. Therefore the integral equation for calculating the deformation on the surface according to (Shuo et al. 1998)

$$D_{(r)} = \frac{1}{M_0 \cdot l} \cdot Q \cdot H_w \tag{1}$$

D = Deflection at the distance r from the load center
M_0 = Layer-modulus of the unbound layers [N/mm²]
l = elastic length (load carrying capacity) of the whole construction [mm]

was simplified by a numeric solution of the value H_w.

$$H_w = \frac{2 \cdot l}{\pi \cdot r_0} \cdot \int_0^{\infty} \frac{J_0\left(\frac{r}{l} \cdot t\right) \cdot J_1\left(\frac{r_0}{l} \cdot t\right)}{t \cdot (1 + t^3)} dt \tag{2}$$

J_n = Bessel function n-th order
r_0 = Radius of the loading plate

J_0 and J_1 are Bessel functions, which can be solved by relevant table works (for example Bronstein 2001). The calculation of the characteristic values for the load carrying capacity is based on the mechanical model "plate on isotropic elastic semi infinite space" as presented in (Grätz 1999). In this consideration the semi infinite space consists of the unbound granular layers of the base cour se and the subbase whereas the plate consists of all bound layers. Investigations of (Grätz 1999) arose following regression approach

$$D_{(r)} = A \cdot (0{,}392948 \cdot e^{-0{,}398483 \cdot B \cdot r} + 0{,}0137024) \tag{3}$$

D(r) is a substitute for the maximum values of the deflection of each Geophone depending on their distance r from the load center. With the resulting parameters A and B the elastic length l and the layer modulus M_0 can be computed with the use of the maximum value of the induced force Q according to the following approach:

$$A = \frac{Q}{M_o \cdot l} \tag{4}$$

$$B = \frac{1}{l} \tag{5}$$

By applying this process (Grätz et al.) proposed the following "preliminary assessment map" based on numerous tests on different roads of the German construction class III according to the German guideline for the design of pavements RStO 01. So without the knowledge of any layer thickness the load carrying capacity of a measured pavement can be evaluated with this proposal (see Figure 3). This "preliminary assessment map" identifies four different characteristics of the load carrying capacity.

4 PROBLEM

In the methodology described above the maximum deflection hollow is the basis for the evaluation and analysis of the load carrying capacity. The recorded "Time-History" is still not considered in any assessment procedure. Therefore, the road measurement methodology can only be used to assess the load carrying capacity in a static sense and therefore only static loading can be considered. Aspects concerning the dynamic interpretation of the

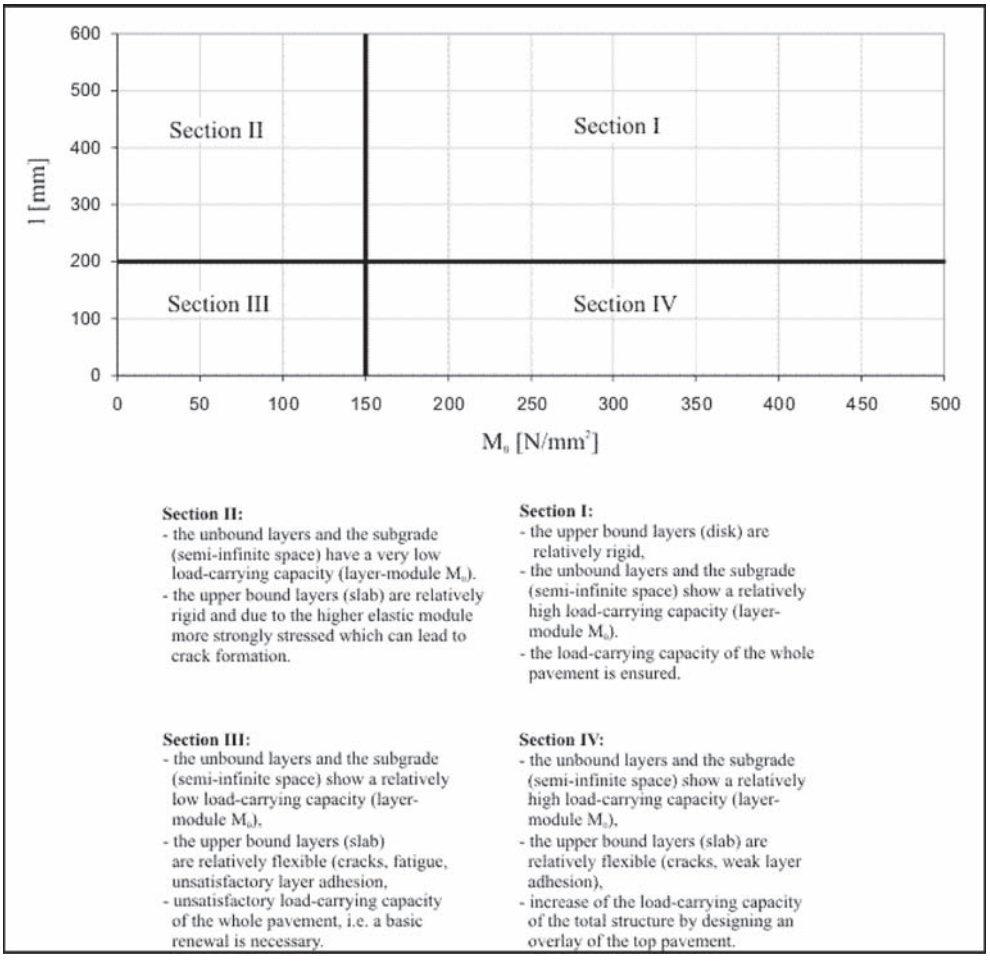

Figure 3. Preliminary assessment map for the interpretation of the characteristic values describing the load carrying capacity (Grätz et al.).

measurements by means of assessing speed or frequency dependent influences or by means of assessing the remaining performance of a structure is currently impossible.

5 DYNAMIC APPROACH

The procedure of measuring the load carrying capacity with the Falling Weight Deflectometers has already been interpreted as a single degree of freedom model and published by several researchers (e.g. Beckedahl et al. 1996). The equations of motion of this mechanical model can be established and solved by the use of differential equations (e.g. Al-Khoury et al. 2002). In comparison of these purely analytical results with the FWD measurement data, however, it is evident that the analytical approach mentioned above will not always be reconciled. Moreover, in practice it is often impossible to describe real systems mathematically or by idealized models in an exact way. Therefore, there is another way based on the signal theory to solve dynamic systems. This method uses measured excitation or deflection data represented by a discretization of the input and output signals during finite time intervals. In order to assess the characteristic transfer function which describes the transition from input to output signal, it is necessary to transform the sampled time series into the frequency domain.

This transformation is performed by using mathematic transformation algorithms like the Laplace or the Fourier transformation according to the following approach:

$$X_{(\omega)} = F\left[x_{(t)}\right] = \int_{-\infty}^{\infty} x_{(t)} \cdot e^{-i-2\pi\cdot\omega t} dt \tag{6}$$

By using the Fourier transformation the time dependent data is transformed into a complex function in the frequency domain. A back-transition rule is given mathematically by the inverse Fourier transformation. The transfer function of a vibrating system can therefore be described on the basis of sampled values as follows:

$$H_{(\omega)} = \frac{X_{(\omega)}}{F_{(\omega)}} \tag{7}$$

with X (ω) and F (ω) representing the Fourier-transformed input and output data. This approach describes the transfer function under ideal conditions. In practice, the recorded signals, however, very often are superimposed by interfering signals (noise). This interference can be taken into account by the evaluation of two additional variants of the transfer function. By averaging the cross power spectrum not correlated signals are suppressed. This technique was described in (Riedl 2006). In (Bald & Grätz, 1999) this dynamic approach was examined the first time. This attempt failed, however, because the 30 milliseconds span for data recording during the FWD-measurements was too short. This had the consequence that in the frequency range only three representative values of the transfer function could be found and therefore a detailed description of the mechanical transfer behavior was not possible.

One possible solution of this problem is the reconstruction of the FWD measurement system, with an extension of the recording time. This attempt was, however, excluded because of the double impact of the reflected falling weight. This second impact could affect the free vibration of the system and hence impose additional frequencies that could not be separated from the original signal. Another possibility is the enlargement of the accounting

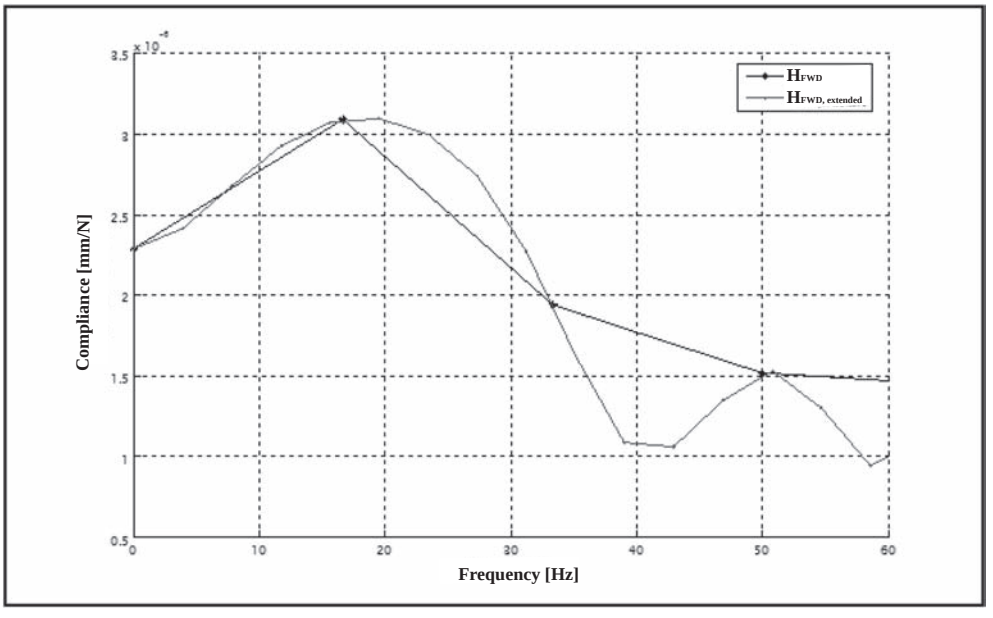

Figure 4. Transfer function of the original FWD-data and of the extended data (Riedl 2006).

data by fitting the measured data by mechanical vibration equations and thus extending the measured data synthetically.

Another variant of this methodology is the "zero-padding" which is often used in signal-engineering. With this method the measured data is extended by adding zeros. The zeros have no additional information on the actual measurement data and do not affect the frequency range. However, they increase the data density significantly. In Figure 4 the transfer function generated out of the original data as well as the transfer function resulting from the synthetical extension of the measured date is shown. It is apparent that the data density of the original transfer function is increased, but not distorted. It is also clear that the measured structure in a certain frequency (here about 20 Hz) reacted very lax (resonance frequency) and another smaller maximum can be detected at a higher frequency (50 Hz). These results confirm the observations of (Baum et al. 1965) due to extensive vibration measurements. Consequently, the maximum in the lower frequencies can be interpreted as the reaction of the entire structure, while the maximum in the upper frequency range represents the bound upper layers.

In Figure 5 the transfer functions of all Geophones are shown as a three-dimensional transfer function. By an implementation of the static methodology developed by (Grätz 1999) and described above it is possible to identify the mechanical parameters M_0 and l for each frequency. An exemplary result of this analysis is shown in Figure 6. It is clear that the characteristic mechanical values vary significantly with the frequency of excitation and therefore change the entire load carrying capacity of road constructions.

Another way of interpretation of the "Time-History" data is to display this data equivalent to hysteretic slopes. An example is shown in Figure 7 comparing the hysteretic slopes of FWD-measurements on an asphalt construction with that of a concrete structure, both invoked by a maximum force of 50 kN. Through the integration of the areas surrounded by the path of loading and unloading the different energy rates (e.g. the elastic and dissipated energy) of the measured impulse can be calculated. In Figure 7 it is evident, that the energy induced by the falling weight is implemented differently with varying road construction. The concrete

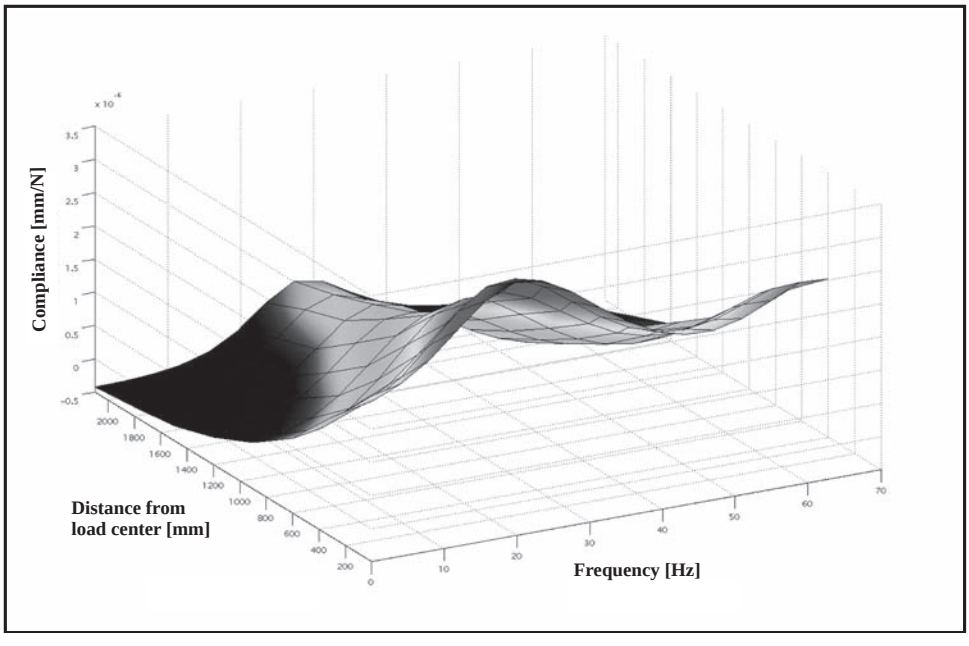

Figure 5. Preliminary assessment map for the interpretation of the characteristic values describing the load carrying capacity (Grätz et al.).

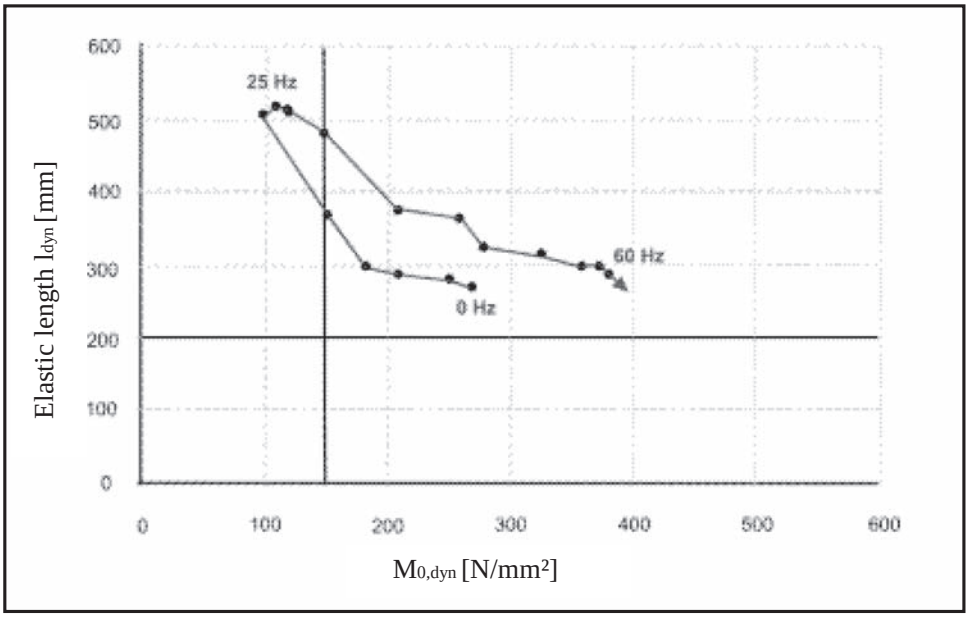

Figure 6. Preliminary assessment map for the interpretation of the characteristic values describing the load carrying capacity (Grätz et al.).

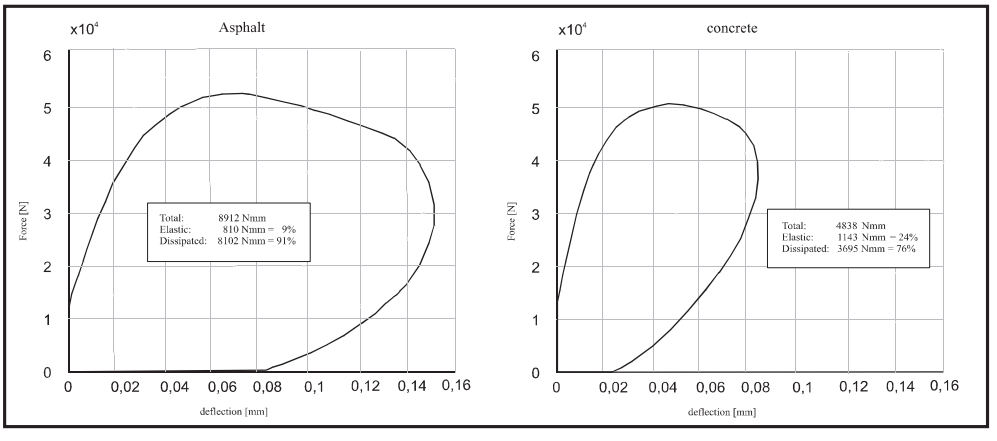

Figure 7. Hysteretic Slopes of an asphalt and concrete construction (Riedl 2006).

structure transfers 24% of the induced energy elastically while the asphalt construction transfers only 9% elastically and dissipates 91% of the induced energy.

6 FIRST APPLICATION OF THE NEW DYNAMIC METHODOLOGY

The previously described methodology developed by (Riedl 2006) was first examined at existing FWD data measured on a model-road at the German Federal Highway Research Institute. This data included different pavements according to the construction-classes SV, SV-line 2.1 as well as III and V in line with the German Guideline RStO 01. The results are shown in Figure 8. It is evident that the construction-classes can be differentiated clearly.

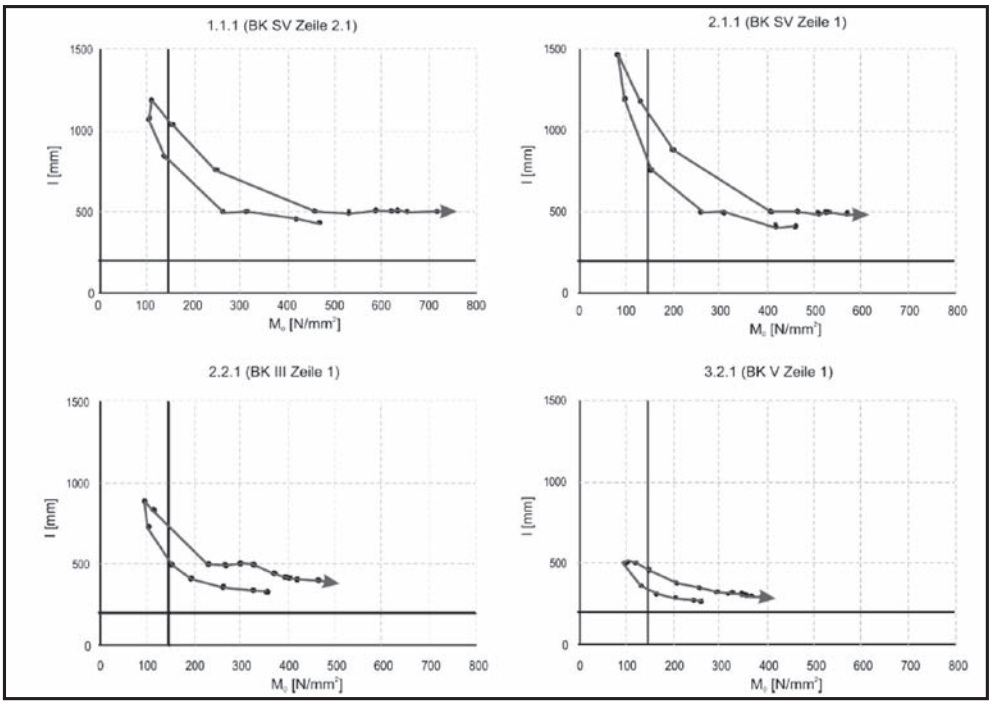

Figure 8. Dynamic interpretation of the load carrying capacity according to the preliminary assessment map (Riedl 2006).

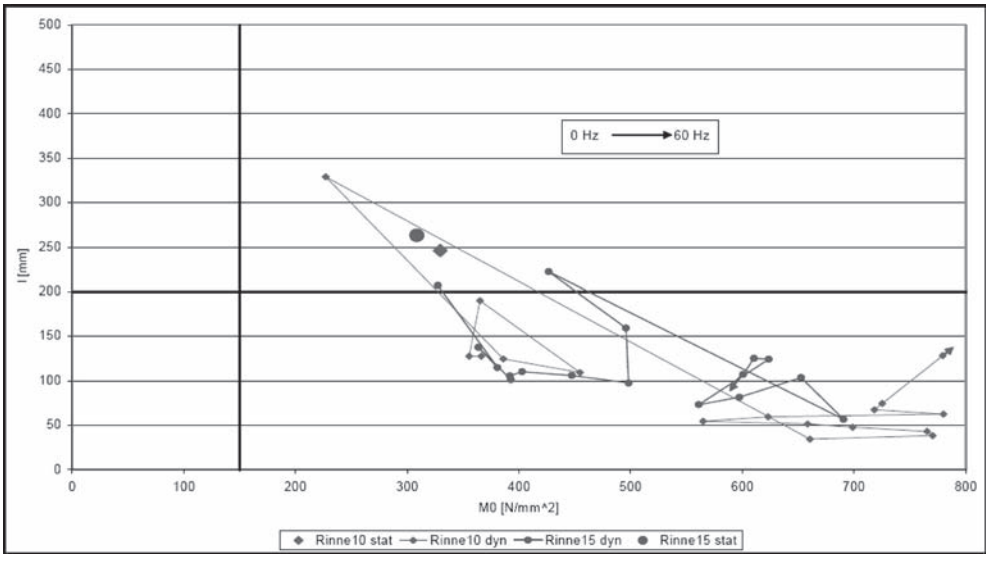

Figure 9. Comparison of the static and dynamic interpretation of the load carrying capacity according to the preliminary assessment map (Riedl 2006).

Also it can be noticed that the dynamic characteristic values representing the load carrying capacity (M0 an l) perform like slopes and change their values with varying frequency from the very good Sector-I of the preliminary evaluation chart to the Sector-II which describes the risk of reflection cracking through the upper bound layers.

As a further step the new methodology was performed on a fatigue asphalt construction to make a comparison with the static evaluation. Therefore was a bus stop was used which showed significant wheel-tracks. In the area of the bus-stop the busses travel in a 15 minutes rhythm.

The buses are approaching the bus-stop slowly, delay to the arrest and remain until the start for about 5–10 minutes. In Figure 9 the results of the static analysis of a measuring point are compared with the results of the dynamic analysis. The static analysis results in a very good load carrying capacity according to Sector-I of the evaluation chart. The dynamic values in particular show that the load carrying capacity of the bonded layers is reduced significantly which is equivalent to the visual appearance of the pavement. In addition, notice that the dynamic values no longer show slopes, but very dramatically change their position. This may be a proof for a fatigue or disturbed structure (in comparison to the model of a good pavement condition in Figure 8). This assumption was confirmed in (Riedl 2006) due to further measurements performed on pavements before and after maintenance activities.

7 OUTLOOK

As described in the chapters before it will be possible in future to supplement the static back-calculation of FWD-measurements with dynamic considerations. A first approach was confirmed in (Riedl 2006) on the basis of some representative examples. Whether the postulated methodology is suitable for further application, or can contribute to further research works remains to be answered. In addition to the present practice of static interpretation of FWD-measurements, an assessment chart for dynamic interpretation has to be evaluated based on further measurements in car of regarding the dynamic aspects of the load carrying capacity in the context of the present traffic. In particular, the energy considerations by (Riedl 2006) especially the considerations about the imaginary and the real parts as well as the phase angle of the complex transfer function has to be regarded in further research works for a possible correlation with factors affecting the stability of asphalt layers. However, further research and application in a widespread sense of increasing the data basis in context with the results of further surveillance observations are necessary. In (Riedl 2006) a further possibility was shown to simulate the reaction of a measured structure invoked by any loading with the use of the transfer function. Whether and how far this approach is suitable for a possible use in the context of a computational design of pavements has to be proved. This is also another approach to future research activities.

REFERENCES

Al-Khoury & Scarpas, 2002. Asphalt Complex Moduli determination via FWD test, *Publication of the 9th International Conference on Design of Asphalt Pavements in Copenhagen, Paper No. 09006*, 2002.

Aptrag, 2004. Arbeitspapier Tragfähigkeit Teil B2 "Falling Weight Deflectometer (FWD): Beschreibung, Messdurchführung" *Entwurf der Forschungsgesellschaft für Straßen- und Verkehrswesen*, September 2004.

Bald & Grätz, 1999. Einfluss der Temperatur, der Belastungsfrequenz und der Impulskraft beim Falling Weight Deflectometer (FWD) auf die Größe der effektiven Schicht-EModuli, *Schlussbericht zum FE 04.174*, November 1999.

Baum, Behr & Buseck, 1965. Die Reaktion von Straßen bei zeitabhängiger Belastung, *Teil 1 und 2 Wissenschaftliche Berichte der Bundesanstalt für Straßenbau Heft 4*, Ernst & Sohn Verlag, 1965.

Beckedahl, Hürtgen, Straube, Horz, Wolf, Klaas & Lengnick, 1996. Begleitende Forschung zur Einführung des Falling Weight Deflectometer (FWD) in der Bundesrepublik Deutschland, *Forschung Straßenbau und Straßenverkehrstechnik, Heft 733.*

Bronstein, 2001. *Taschenbuch der Mathematik, 5. überarbeitete und erweiterte Auflage* Verlag Harri Deutsch, 2001.

Buseck, 1989. Tragverhallten von Straßenkonstruktionen, *Forschung Straßenbau und Straßenverkehrstechnik, Heft 572*, 1989.

Durth & Grätz, 1995. Überprüfung praktischer Methoden zur Messung der Tragfähigkeit und Einschätzung der Restnutzungsdauer, insbesondere für Straßen auf dem Gebiet der neuen Bundesländer, *Schlussbericht zum FE 04.162 G92E, Anhang 1, Literaturstudie Teil 1 und Teil 2*, 1995.

Gerlach, 1971. Stand und Entwicklung von Bemessungsverfahren für Straßen- und Flugplatzbefestigungen, *Mitteilungen aus dem Institut für Baustoffkunde und Materialprüfwesen der Technischen Universität Hannover, Heft 18*, 1971.

Grätz, 1999. Möglichkeiten und Grenzen des Falling Weight Deflectometers, *FGSV-Tagung der Arbeitsgruppe 4, Fahrzeug und Fahrbahn in Celle*, 1999.

Grätz, Schellenberger, Wolf. Grundlagen für die Erstellung eines Bewertungshintergrundes für die mit dem Falling Weight Deflectometer (FWD) durchgeführten Tragfähigkeitsmessungen *Veröffentlichung in Vorbereitung.*

Köhler, 1995. Ein Beitrag zur Analyse und Bewertung des strukturellen Zustandes flexibler Fahrbahnbefestigungen, *Mitteilungen aus dem Fachgebiet Konstruktiver Straßenbau im Institut für Verkehrswirtschaft, Straßenwesen und Städtebau der Universität Hannover, Heft 18*, 1995.

Mamlouk, 1985. Use of Dynamic Analysis in Predicting Field Multilayer Pavement Moduli, *Transportation Research Record No. 1043*, 1985.

Plehm, 2005. Der Deflektograph „Lacroix" 12 Jahre im Dienst der Straßenbauverwaltung Brandenburgs, *Straße und Autobahn Heft 2/2005.*

Riedl, 2006. Rückrechnung dynamischer Tragfähigkeitswerte aus den Messdaten des Falling Weight Deflectometer; *Schriftenreihe des Instituts für Verkehr der Technischen Universität Darmstadt, Heft S8*, 2006.

Shuo, Fwa & Tan, 1998. Parameters Back-Calculation for Concrete Pavement with two Slab Layers, *Journal of Transportation Engineering* 124(6), November/December 1998.

Tholen, Sharma & Terrel, 1985. Comparison of Falling Weight Deflectometer with other Deflection Testing Devices, *Transportation Research Record No. 1007*, 1985.

Wolf, 2004. Bericht über die Vergleichsmessungen mit dem Benkelmann-Balken und dem FWD auf der *Sitzung des AK 4.8.2 „Tragfähigkeit",* September 2004.

Advanced Testing and Characterization of Bituminous Materials – Loizos, Partl, Scarpas & Al-Qadi (eds)
© 2009 Taylor & Francis Group, London, ISBN 978-0-415-55854-9

Behavior of asphalt pavements subjected to non-standard heavy vehicles

P.E. Sebaaly & R.V. Siddharthan
University of Nevada, Reno, Nevada, USA

ABSTRACT: Pavements are designed to carry traffic that conforms to legal axle loads. In recent years, the size and capacity of agricultural equipment have increased dramatically. As farm sizes have grown to maintain profitability, producers have moved to larger and heavier equipment. At the request of the agricultural industry, the South Dakota DOT (SDDOT) initiated research to determine whether heavy agricultural loads could be moved on state and local highways. Two asphalt pavement sections were instrumented with pressure cells in the base and subgrade, strain gauges at the bottom of the asphalt layer, and surface deflection gauges to measure critical pavement responses. Vehicles tested included two chemical applicators and a grain cart. The measured field data were used to validate the applicability of the 3D-MOVE pavement analysis model to predict the responses of flexible pavements subjected to non-standard loads such as agricultural equipment. Next, fatigue Load Equivalency Factors (LEF) were calculated to estimate the reduction in fatigue service life resulting from the increased levels of strains under heavy agricultural equipment. Through the use of three-dimensional dynamic analysis (3D-MOVE), it was possible to estimate LEFs, not only for the two pavement sections actually field-tested, but for the wide range of conditions describing the vast majority of highways in South Dakota. Depending on the load, axle configuration, and pavement characteristics, calculated LEFs ranged from 1 to 20 for the agricultural equipment. In general, all of the loaded agricultural equipments were significantly more damaging than the 80 kN single axle.

1 INTRODUCTION

The operation of agricultural equipment on highway pavements presents new challenges to the pavement engineering and management community. Equipment such as chemical applicators and grain carts has become larger and heavier, and is often supported by unconventional tire configurations, including low-pressure floatation tires and lugged tires. All such characteristics are unique to the off-road equipment and do not distribute the loads to the pavement surface as normal highway traffic vehicles would. Some of their characteristics could in fact cause less damage than normal highway traffic while other characteristics could cause more damage. It is usually not the individual characteristic but the combination of characteristics of a given vehicle that leads to more or less damage as compared to normal highway traffic. For example, the low tire inflation pressure of off-road equipment should be less damaging than the high tire pressure of normal highway traffic. But when the low tire pressure is coupled with heavier loads, certain tire designs, and low vehicle speed, it may become more damaging than higher tire inflation pressures.

Without knowledge of the effects of off-road equipment on typical state and local pavements, it is impossible to assess the financial impacts of its use, or to determine whether present regulations are too strict, too loose, or appropriate. Without the appropriate background analyses and justifications, the goodwill actions of a SHA to preserve the road system could be interpreted as an unjustifiable action toward a single group of road users who believe they are doing their fair share toward maintaining the road system.

2 OBJECTIVES

The overall objective of this research project was to evaluate the impact of agricultural equipment on flexible pavements (Sebaaly et al. 2002). The research used a combination of field testing and theoretical modeling of the pavement structure to evaluate its response to tires used on agricultural equipment under their respective speed and axle load levels. Field testing of typical pavement sections instrumented with sensors to measure critical pavement responses was used to validate the theoretical model, which was then used to cover other pavement, environmental, and material conditions.

3 BACKGROUND

A research study was conducted by the Center for Transportation Research and Education (CTRE) at the Iowa State University to evaluate the impact of agricultural equipment on Iowa's paved county roads (Fanous et al. 1999). In order to achieve this objective, the research evaluated the response of a flexible pavement under agricultural equipment using a combination of field instrumented pavement sections and theoretical analyses. One flexible pavement section with a 229 mm hot mixed asphalt layer (HMA) was instrumented and tested. The strain gauges in the flexible pavement were placed at the mid-depth of the HMA layer.

The report did not provide any specific conclusions or recommendations. However, if the data provided in the report were evaluated, it can be seen that for single axles on flexible pavements, the agricultural vehicles can be allowed up to 5,000–7,000 lb per single axle over the 20,000 lb/axle load limit of the semitrailer. In the case of dual-axle grain carts, the allowable load for the two axles ranges from 33,200 during spring to 44,500 during fall as compared to 20,000 lb/single axle on a semitrailer.

4 EXPERIMENTAL PROGRAM

The agricultural equipments that were evaluated in this study included: Terragator Model 8103 (three wheels), Terragator Model 8144 (four wheels), and Grain Cart (single axle) (Figure 1). Terragators are used to apply agricultural chemicals in the field. Grain carts are used to transport grain in the field from combines to trucks (Sebaaly et al. 2002).

In order to achieve the objective of this study, pavement sites were identified on clayey soil on U.S. Route US212 and on silty soil on State Route SD26 in South Dakota (Sebaaly et al. 2002). At each site, a thin flexible and a thick flexible pavements were identified for a total of 4 different sections at both locations. Each flexible pavement section was instrumented with the following:

- Four strain gauges at the bottom of the HMA layer
- One pressure cell at the middle of the crushed aggregate base (CAB) layer
- One pressure cell 4" below the top of the subgrade layer
- One single layer deflectometer
- Temperature sensors throughout the pavement depth

The sections on US212 were new construction, while the sections on SD26 consisted of an HMA overlay over an old flexible pavement. The instrumentations on US212 were installed during construction while the instrumentations on SD26 were retrofitted into the existing base and subgrade by excavating to the appropriate locations and installing the gauges prior to the overlay. Each section was 30 m long with 100 m transition between the sections on US212 and 120 m transition between the sections on SD26. All instrumentations were installed in the outer wheel path. One hundred percent of the pressure cells were operational throughout the entire testing program. The strain gauges experienced 85 percent survival rate throughout the testing program.

Field testing programs were conducted on September 14–15, 2000 (fall 2000) and April 4–5, 2001 (Spring 2001). Table 1 summarizes the conditions for the field testing programs. Each

Terragator 8103 Terragator 8144 Grain Cart

Figure 1. Agricultural equipments.

Table 1. Vehicle-load combinations tested in the field.

Vehicle	Condition	Speed (kph)	Tire pressure (kPa)	Nominal axle load (kN)	
				Fall 2000	Spring 2001
Single Axle Truck	Loaded	64	700	80	81
Terragator 8103	Empty	64	248	83	83
Terragator 8144	Empty	64	248	80	80
Terragator 8103	Loaded	64	248	147	151
Terragator 8144	Loaded	64	248	140	136
Single Axle Truck	Loaded	32	700	80	81
Grain Cart	Legal Load	32	110	93	93
Grain Cart	Over Legal	32	110	138	147

vehicle-load combination was driven at its normal operating speed for a minimum of five replicate runs. The single axle truck was tested at various time intervals during the day at speeds consistent with the agricultural equipment being tested at the time.

5 ANALYSIS OF FIELD DATA

The objective of this effort was to use the field measured data to validate the 3D-MOVE pavement analysis model for the use of predicting flexible pavement responses under agricultural equipment. The basic principles and theories of the 3D-MOVE model have been described in details in several publications (Siddharthan et al. 1998, 2000, 2002).

Field tests were conducted during the fall and spring seasons. In general, the fall season represents a warm HMA layer (average pavement temperature of 35°C) and a moist subgrade, while the spring season represents a cold HMA layer (average pavement temperature of 5°C) and a wet subgrade.

The field testing program collected the pavement response time histories under five replicate runs of each combination of test vehicle and load level (Table 1). In the case of pressure and deflection responses, the replicate data were examined for repeatability and the average of the most repeatable set of measurements was calculated and tagged for further analysis. The repeatability of the pressure and deflection measurements was excellent (coefficient of variations less than 5%). In the case of strains, however, combinations of vehicle wander and tire lugs resulted in a higher variability among individual runs. All four strain gauges were examined under each run and the maximum from all replicates was selected. This was because only the maximum computed strain responses were used in the comparisons described subsequently. Field data were analyzed under the following criteria: pressure less than 35 kPa, deflection less than 0.13 mm and strains less than 25 microns are below the accuracy of the gauges and also do not indicate a significant damage to pavements, and therefore not considered. In addition, whenever sensors showed unrealistic responses such as significant non-zero

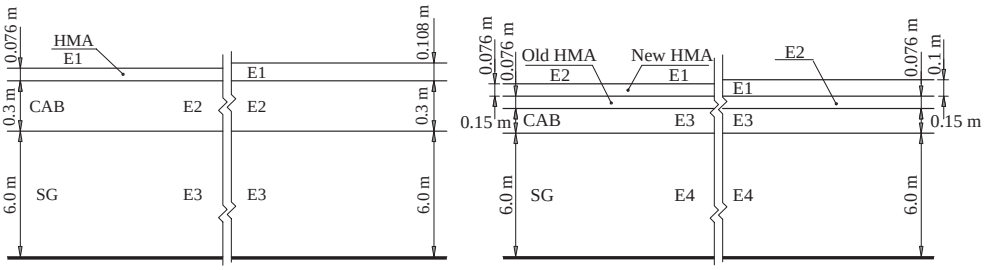

	Resilient Modulus MPa		
	E1	E2	E3
Fall 2000	689.5	172.4	55.2
Spring 2001	5143.5	172.4	33.1

(a) Thin and thick US212 pavement sections and properties

	Resilient Modulus MPa			
	E1	E2	E3	E4
Fall 2000	2413	2068	103	69
Spring 2001	13790	6894	103	69

(b) Thin and thick SD26 pavement sections and properties

Figure 2. Pavement structures and materials properties used in the validation process.

values after the vehicle travel, inconsistent and erratic changes etc., those responses were also not considered in the field verification reported below.

When dealing with field measurements, it should be recognized that the repeatability of the sensors, the interference of the embedded sensors within the pavement, change of pavement stiffness caused due to the installation of the sensors, wheel wander and the variations in the actual dynamic loading (vehicle bouncing) would contribute to the expected accuracy of the measured responses. In addition, filtering of noise from the time histories (zero-phase filtering) can also affect the measured response (Oppenheim and Shafer 1989). A careful review of each of those sources independently found that the compounded impact of the factors mentioned above on any response measured was estimated to be in the range of ± 30%. This level of uncertainty in the measurements has been subsequently taken into account in the verification of the applicability of the 3D-MOVE model in this study.

6 PAVEMENT STRUCTURES AND MATERIAL PROPERTIES

The pavement structures associated with US212 and SD26 pavement sections are shown in Figure 2. The resilient moduli of the pavement layers were obtained based on the field testing using Falling Weight Deflectometer (FWD). The FWD tests were carried out on each of the pavement section during the actual field testing. The pavement layer moduli backcalculated using FWD deflection measurements are also shown in Figure 2. It may be noted that the modulus of unbound layers at SD26 pavement sections are the same in both seasons and this observation was consistent with moisture measurements made from the field samples.

7 AGRICULTURAL EQUIPMENTS PAVEMENT CONTACT STRESS DISTRIBUTION

Conventional trucks use axles equipped with dual tires with a maximum load per axle of about 93 kN. When such loads are used the tire load is 23 kN/tire. On the other hand, when the agricultural equipment considered here are loaded, the load per tire is much higher. In the field testing program the loads per tire were as much as 74 and 69 kN for loaded terragator and grain cart, respectively. Since tire pressures on the agricultural equipments are much lower than conventional tire pressures, the contact areas of agricultural equipment are much wider. For example, the length of the gross contact area for the terragator was

found to be as much as four times higher. Furthermore, unlike conventional truck tires, the vehicle-pavement interaction of off-road vehicles occurs at the lugs that have different sizes, shapes and orientations. In the early stages of the validation effort, it became clear that the success of the 3D-MOVE prediction depends heavily on the realistic representation of the vehicle-pavement contact stress distribution. A thorough review of literature revealed no data on the contact stress distribution for the agricultural equipments tires used in the study.

In view of these observations, an iterative procedure was used to arrive at an approximate contact stress distribution for the agricultural equipments tires. This was accomplished by calibrating the computed (3D-MOVE) longitudinal pavement strain responses at the bottom of the asphalt concrete (AC) layers with those measured in the field. The procedure that was adopted involved two major steps: (1) determination of shape and extent of contact area and (2) evaluation of a "representative" contact pressure distribution. Specific details on the steps associated with this iterative procedure along with actual field data from the entire experimental program have been described in details in Sebaaly et al. 2002 and are omitted here due to space limitations. Figure 3 shows the results of the stress distribution calculations for the Grain Cart.

As shown in Table 1, the total pavement responses collected in the field testing include: response values for two test seasons (fall and spring), four pavements (thin and thick from US212 and SD26) and three vehicles (two types of terragators and grain cart) under empty and loaded conditions. All computed and measured pavement responses along with their ± 30% ranges are presented in Figures 4 through 7. Comparison between the computed and measured responses is generally good. Among all responses, the strain response match is the

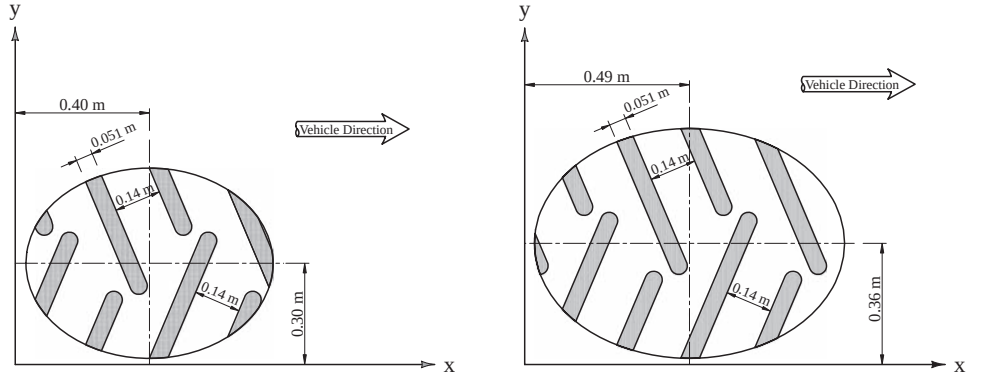

Layout of the developed foot print

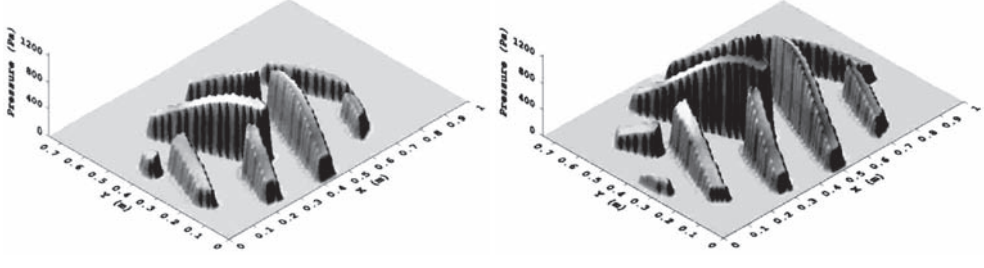

3-D vertical contact pressure distribution

Grain cart with legal load | Grain cart with over legal load

Figure 3. Estimated pressure distributions at the tire-pavement interface for the grain cart.

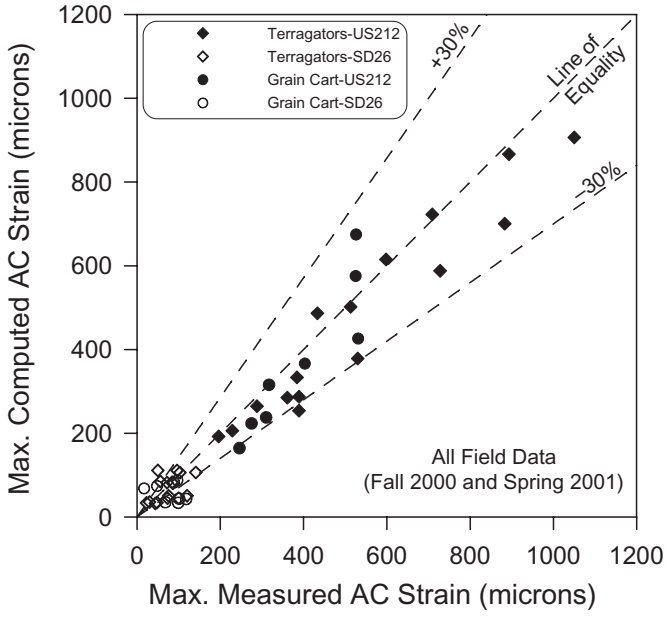

Figure 4. Comparison of measured and computed tensile strains at the bottom of the HMA layer.

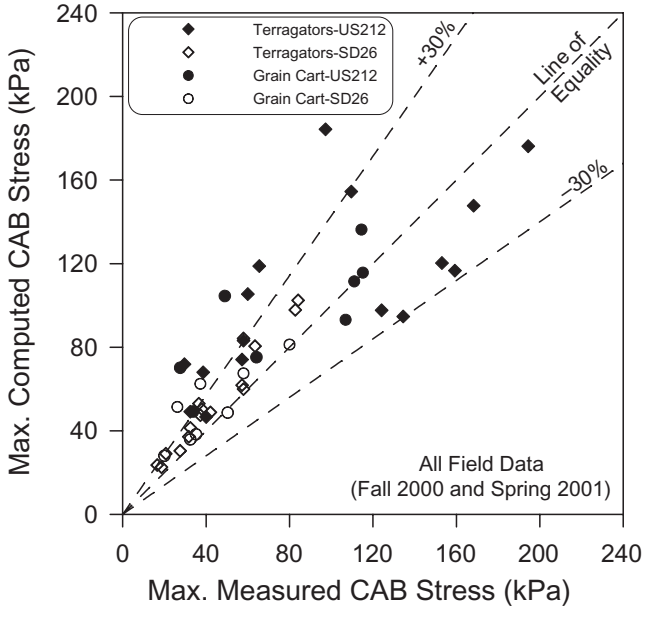

Figure 5. Comparison of measured and computed compressive stresses in the CAB.

best, while the surface deflection match is not very good. Given the fact that the calibration of pavement contact stress distribution was based on strain responses, this observation is not surprising. Relatively small magnitude of the measured surface deflections (0.3 to 1.6 mm) may have contributed to the lower correlation.

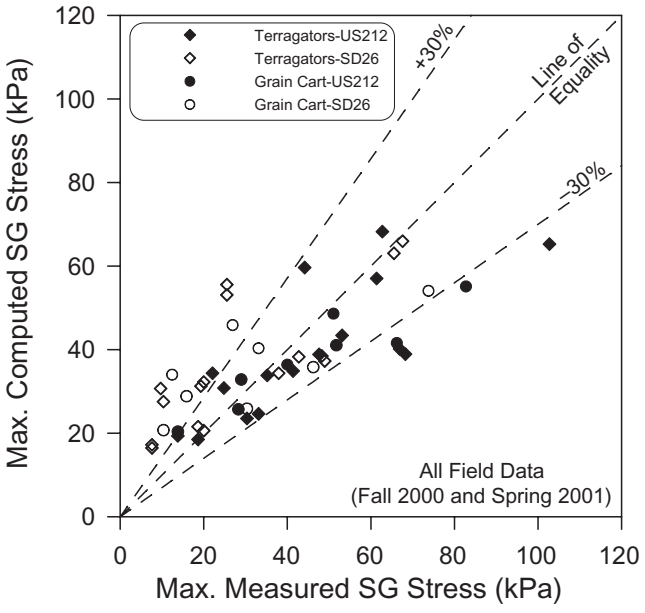

Figure 6. Comparison of measured and computed compressive stresses in the subgrade.

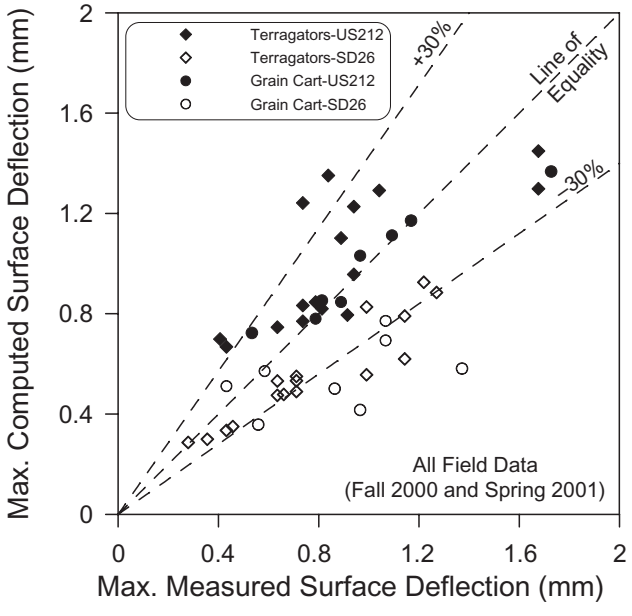

Figure 7. Comparison of measured and computed surface deflections.

8 IMPACT OF AGRICULTURAL EQUIPMENT BASED ON THEORETICAL MODELING

The objective of this effort was to expand the analysis of the impact of agricultural equipments to cover the wide range of pavement structures and soil types that are commonly encountered in South Dakota. Based on the available properties of typical South Dakota soil

deposits, it was recommended to group the soils types into four distinct classes. In order to cover a range of pavement structures, the following layer thicknesses were recommended:

- HMA Layer: 38, 75, 125, and 178 mm
- CAB Layer: 150 and 300 mm
- Subgrade: 4 classes

Recognizing that the properties of pavement materials change drastically at various seasons, each pavement structure within each soil class was assigned a set of four seasonal resilient modulus properties established based on available laboratory data from earlier SDDOT research efforts. The approach used to assess the impact of agricultural equipment on the identified flexible pavements consisted of the following steps:

- Use the 3D-MOVE model to calculate the strain response of the pavements under the loading conditions imparted by the Terragators and Grain Cart.
- Use the fatigue performance model that is being included in the AASHTO 2002 Mechanistic-Empirical Pavement Design Guide MEPDG (NCHRP 1-37A).
- Evaluate the fatigue LEFs for Terragators and Grain Cart.

Table 2. Fatigue load equivalency factors for the terragator agricultural equipment.

Soil class	Pavement	Terragator empty				Terragator loaded			
		Winter	Spring	Summer	Fall	Winter	Spring	Summer	Fall
1	38–150*	9.3	3.8	150	12.2	34.3	13.5	605	45.8
	38–300	11.8	4.8	110	15.9	42.4	15.8	424	58.0
	75–150	1.7	1.4	4.9	1.8	6.0	6.2	16.6	6.4
	75–300	1.8	1.4	5.7	1.9	5.6	5.4	17.1	5.9
	125–150	1.0	1.0	1.0	1.0	4.9	6.6	3.4	4.7
	125–300	0.9	1.0	0.9	0.9	4.0	5.6	2.4	3.8
	178–150	0.9	0.9	0.8	0.9	6.0	7.4	3.3	5.7
	178–300	0.9	0.9	0.7	0.8	5.0	6.6	2.1	4.7
2	38–150*	9.6	4.1	98.4	12.6	35.4	14.0	419	47.8
	38–300	11.5	4.8	82.9	15.1	42.1	15.9	338	56.5
	75–150	1.7	1.4	4.9	1.8	5.8	5.7	16.6	6.2
	75–300	1.8	1.4	5.3	1.9	5.5	5.2	16.9	5.9
	125–150	1.0	1.0	1.0	1.0	4.5	5.9	3.2	4.2
	125–300	0.9	1.0	0.9	0.9	3.9	5.3	2.5	3.6
	178–150	0.9	0.9	0.7	0.9	5.6	7.0	2.9	5.2
	178–300	0.9	0.9	0.6	0.8	4.8	6.4	2.1	4.4
3	38–150*	9.8	4.3	84.2	12.8	36.4	14.5	364	48.9
	38–300	11.4	4.8	74.3	14.8	41.9	15.9	310	55.9
	75–150	1.7	1.4	4.8	1.8	5.7	5.3	16.7	6.0
	75–300	1.8	1.4	5.2	1.9	55	5.0	16.9	5.9
	125–150	1.0	1.0	1.0	0.9	4.3	5.4	3.1	4.0
	125–300	0.9	1.0	0.9	0.9	3.8	5.0	2.5	3.5
	178–150	0.9	0.9	0.7	0.9	5.3	6.6	2.8	4.9
	178–300	0.9	0.9	0.6	0.8	4.7	6.2	2.0	4.3
4	38–150*	10.3	4.7	50.7	14.0	38.4	15.5	229	54.9
	38–300	11.2	4.9	51.0	13.9	41.6	16.0	228	54.2
	75–150	1.7	1.4	4.8	1.9	5.5	4.9	16.7	5.8
	75–300	1.8	1.4	4.8	1.9	5.4	4.8	16.8	5.8
	125–150	0.9	1.0	0.9	0.9	3.8	4.8	2.6	3.0
	125–300	0.9	1.0	0.9	0.9	3.6	4.6	2.6	3.1
	178–150	0.9	0.9	0.6	0.8	4.8	5.9	2.0	3.6
	178–300	0.8	0.9	0.6	0.8	4.4	5.8	2.0	3.7

*HMA = 38 mm, CAB = 150 mm.

Table 3. Fatigue load equivalency factors for the grain cart agricultural equipment.

Soil class	Pavement	Grain cart legal				Grain cart over legal			
		Winter	Spring	Summer	Fall	Winter	Spring	Summer	Fall
1	38–150*	7.8	2.4	240	11.1	24.0	7.2	799	34.6
	38–300	10.1	3.0	163	14.9	31.0	9.0	528	45.6
	75–150	0.8	0.7	3.0	0.9	2.4	2.5	8.6	2.6
	75–300	0.8	0.7	3.2	0.8	2.2	2.0	8.6	2.3
	125–150	0.5	0.7	0.4	0.5	1.8	2.7	1.1	1.8
	125–300	0.4	0.6	0.3	0.4	1.4	2.2	0.7	1.3
	178–150	0.6	0.7	0.3	0.5	2.3	3.3	1.0	2.2
	178–300	0.5	0.6	0.2	0.4	1.8	2.7	0.5	1.6
2	38–150*	8.1	2.5	157	11.7	25.0	7.6	532	36.5
	38–300	10.0	3.0	125	14.3	30.8	9.1	414	44.5
	75–150	0.8	0.7	3.0	0.8	2.3	2.1	8.7	2.5
	75–300	0.8	0.6	3.2	0.8	2.1	1.9	8.7	2.3
	125–150	0.5	0.6	0.3	0.4	1.6	2.3	1.0	1.5
	125–300	0.4	0.5	0.3	0.4	1.3	2.0	0.7	1.2
	178–150	0.5	0.7	0.3	0.5	2.0	2.9	0.9	1.8
	178–300	0.4	0.6	0.2	0.4	1.7	2.5	0.5	1.4
3	38–150*	8.3	2.7	134	12.0	25.9	8.0	454	37.6
	38–300	9.9	3.0	112	14.1	30.6	9.1	375	44.1
	75–150	0.8	0.6	3.0	0.8	2.2	2.0	8.7	2.4
	75–300	0.7	0.6	3.1	0.8	2.1	1.8	8.7	2.3
	125–150	0.4	0.6	0.3	0.4	1.5	2.0	1.0	1.4
	125–300	0.4	0.5	0.3	0.4	1.3	1.8	0.7	1.1
	178–150	0.5	0.6	0.3	0.4	1.9	2.6	0.8	1.6
	178–300	0.4	0.6	0.2	0.4	1.6	2.3	0.5	1.4
4	38–150*	8.9	2.9	76.9	13.6	27.7	8.8	264	43.3
	38–300	9.8	3.1	77.0	13.4	30.5	9.2	264	42.6
	75–150	0.7	0.6	3.0	0.8	2.1	1.8	8.8	2.3
	75–300	0.7	0.6	3.0	0.8	2.1	1.7	8.8	2.3
	125–150	0.4	0.5	0.3	0.3	1.3	1.7	0.8	0.9
	125–300	0.4	0.5	0.3	0.3	1.2	1.6	0.8	0.9
	178–150	0.4	0.6	0.2	0.3	1.6	2.2	0.5	1.0
	178–300	0.4	0.5	0.2	0.3	1.4	2.1	0.5	1.0

*HMA = 38 mm, CAB = 150 mm.

The fatigue performance that was recommended at the time of this research by the MEPDG takes the following form:

$$N_f = \beta \times (\varepsilon_t)^{-5} \quad (1)$$

The above equation indicates that the fatigue LEFs can be calculated as the ratio of the tensile strain at the bottom of the asphalt layer under a given vehicle-load level combination to the tensile strain under the 80 kN single axle truck, raised to the 5th power. Note that the material constant (β) cancels out since the LEF is based on the same pavement section. For example, the fatigue LEF for the Terragator 8144 loaded generating a strain of 893 microns on the US212 thin section during the fall season relative to the 80 kN single axle truck generating a strain of 733 microns, is:

$$\text{LEF (terragator loaded, fall)} = (893/733) \times 5 = 2.7$$

Similar process was used to evaluate the fatigue LEFs for all vehicle-load level combinations under various seasons for the four soil classes in South Dakota. The analysis of the Terragators 8103 and 8144 was combined since they both use the same tires and have similar axle loads. Tables 2 and 3 summarize the fatigue LEFs for the agricultural equipments that were evaluated in this program.

9 CONCLUSIONS

The analyses of the field data and the fatigue LEFs that were generated in this research lead to the following conclusions.

- Agricultural equipment exhibit unique stress distributions at the tire-pavement interface that are significantly different than the distributions under standard highway trucks.
- The 3D-MOVE model can effectively simulate the strain responses of flexible pavements under agricultural equipments. Therefore, the use of the 3D-MOVE model to predict the fatigue LEFs of agricultural equipments on flexible is warranted.
- Significant fatigue damage is caused on ultra-thin flexible pavements of 38 mm HMA over 150 mm and 300 mm CAB by all vehicles-load combinations during the summer season. The following observations can be made: a) One trip of the empty Terragator is equivalent to 51–150 trips of the 80 kN single axle truck, b) One trip of the loaded Terragator is equivalent to 230–605 trips of the 80 kN single axle truck, c) One trip of the legally loaded grain cart is equivalent to 77–240 trips of the 80 kN single axle truck and d) One trip of the grain cart over legal is equivalent to 264–799 trips of the 80 kN single axle truck.
- On flexible pavements that are not ultra-thin (HMA = 75 mm – 178 mm), the following observations can be made: a) One trip of the empty Terragator is equivalent to 1–3 trips of the 80 kN single axle truck, b) One trip of the loaded Terragator is equivalent to 2–20 trips of the 80 kN single axle truck, c) One trip of the legally loaded grain cart is equivalent to 1–5 trips of the 80kN single axle truck, and d) One trip of the grain cart over legal is equivalent to 1–20 trips of the 80 kN single axle truck.

REFERENCES

Fanous, F., Coree, B. & Wood, D., 1999. Response of Iowa Pavements to Heavy Agricultural Loads, CTRE at Iowa State University.

NCHRP 1-37A, Development of the 2002 Guide for the Design of New and Rehabilitated Pavement Structures. Transportation Research Board, National Research Council.

Oppenheim, A.V. & Shafer, R.W., 1989. Discrete-Time Signal Processing, Prentice-Hall Publishers, New York.

Sebaaly, P.E., Siddharthan, R.V., El-Desouky, M., Pirathapan, Y., Hitti, E. & Vivekanathan, Y., 2002. Effects of Off-Road Tires on Flexible and Granular Pavements, Final Report, South Dakota DOT.

Siddharthan, R.V., Yao, J. & Sebaaly, P.E., 1998. "Pavement strain from moving dynamic 3-D load distribution," in *Journal of Transportation Engineering*, Vol. 124(6), ASCE, Nov./Dec., pp. 557–566.

Siddharthan, R.V., Krishnamenon, N. & Sebaaly, P.E., 2000. "Pavement response evaluation using finite-layer approach," in *Transportation Research Record 1709*, TRB, National Research Council, Washington , D.C., pp. 43–49.

Siddharthan, R.V., El-Mously, M., Krishnamenon, N. & Sebaaly, P.E., 2002. "Validation of a pavement response model using full-scale field tests," in *Int. Journal of Pavement Engrg.*, Vol. 3(2), 2002, pp. 85–93.

Advanced Testing and Characterization of Bituminous Materials – Loizos, Partl, Scarpas & Al-Qadi (eds)
© 2009 Taylor & Francis Group, London, ISBN 978-0-415-55854-9

Field behavior of foamed bitumen pavement material

V. Papavasiliou
Laboratory of Highway Engineering (NTUA), Athens, Greece

A. Loizos
National Technical University of Athens (NTUA), Athens, Greece

ABSTRACT: In terms of an experimental study conducted by the Laboratory of Highway Engineering of the National Technical University of Athens (NTUA), recycled material stabilized with foamed bitumen was used as a base of a rehabilitated semi-rigid pavement of a heavily trafficked highway. This study focuses on the in-situ characterization of foamed bitumen pavement material, with six-year monitoring experience, using mainly Non Destructive Tests (NDTs), accomplished with advanced analysis tools. Preliminary analysis considering non-linear behavior of the material was also performed. According to the deflection analysis, no decrease of the stiffness of the recycled layer is shown at least 6 years of heavy traffic loading. It is worth mentioned, that foamed bitumen mix moduli obtained from different FWD load levels produce similar strain response analysis results (max horizontal tensile strain) in the body of the foamed bitumen pavement material.

1 INTRODUCTION

Foamed bitumen pavement materials have strong cohesive bonds and a relative high resilient modulus (compared with the untreated materials) as long as the cohesive bond is retained. This intact condition is maintained for a certain period of traffic loading and is referred in (Asphalt Academy 2002) as the "effective fatigue life phase", shown in Figure 1. Eventually, the cohesive bond is destroyed through the repeated flexing of the material under traffic loading to the point where the effective resilient modulus of the layer has decreased to a value comparable to that of an untreated granular material and the layer is referred to as being in an "equivalent granular state" (Fig. 1).

Research (Long & Theyse 2004) on the behavior of foamed bitumen pavement materials based also on Heavy Vehicle Simulator (HVS) tests showed that the resilient modulus (stiffness) of the treated base layer starts at a relatively high value and then decreases under the

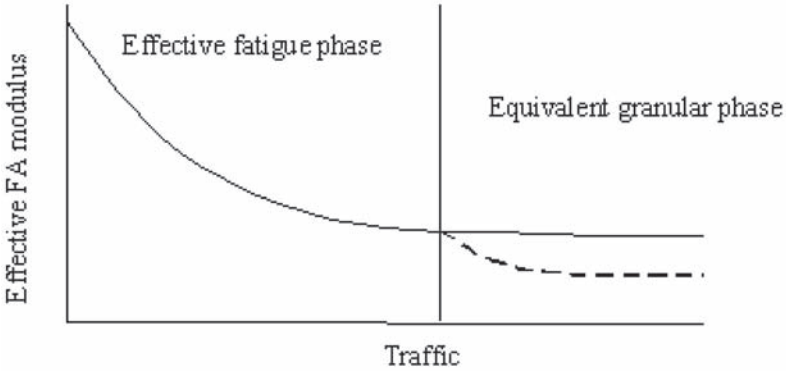

Figure 1. Behavior of pavements with foamed bitumen treated materials (Asphalt Academy 2002).

action of traffic until a constant resilient modulus or stiffness state is reached. The latest is a scientific interpretation replacing the term "equivalent granular state". This occurs relatively early in the life of the pavement, and can occur rapidly under heavy traffic loading. The load repetition from the initial state to the constant stiffness state doesn't mean that the material has experienced fatigue or is in cracked state at the end of the phase. The layer is also not in a terminal state at the end of the effective fatigue life. To ensure the end-condition of the material is not misunderstood, the phase is referred in the international literature as the 'constant stiffness phase'.

However, such advanced mechanical interpretation of the behavior of the foamed bitumen treated recycled mixes are still on a research basis and do not clearly indicate the precise way for the in situ behavior of the as build recycled mix. For this reason a respective field experiment in a major Greek heavy trafficked highway was undertaken by the Laboratory of Highway Engineering of the NTUA for the in-situ characterization of the foamed bitumen pavement material. Preliminary non-linear aspects were also investigated. In order to achieve this goal, a comprehensive research study was performed involving a six-year monitoring of the pavement performance using mainly non-destructive tests (NDTs). The main findings of the data analysis are presented and discussed in the present research work.

2 BACKGROUND

The semi-rigid pavement before rehabilitation comprised two layers of cement bound material (CBM), overlaid with an 8 cm asphalt concrete layer. In terms of an experimental study, cold in-place recycling (CIPR) using foamed bitumen and cement (Fig. 2) was applied for the rehabilitation of a severely cracked semi-rigid pavement test section.

Foamed bitumen mix (referred hereafter as FB) designs were undertaken to establish the application rates for foamed bitumen and active filler (cement), to achieve optimal strengths and to determine the strength characteristics for use in the structural design exercise on several different blends of material recovered from the test pits. These blends were treated with foamed bitumen using the appropriate laboratory unit and several briquettes were manufac-

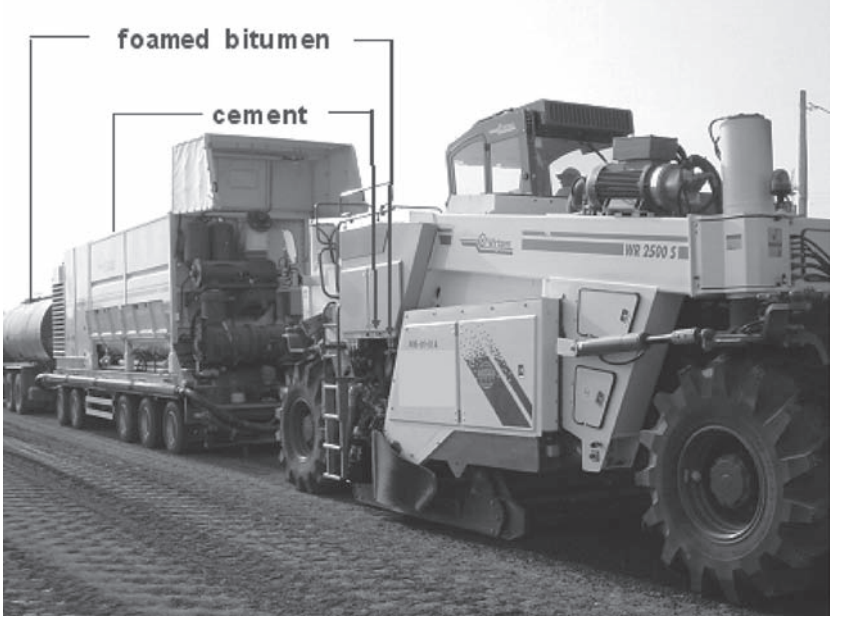

Figure 2. Implementation of the CIPR using foamed bitumen and cement.

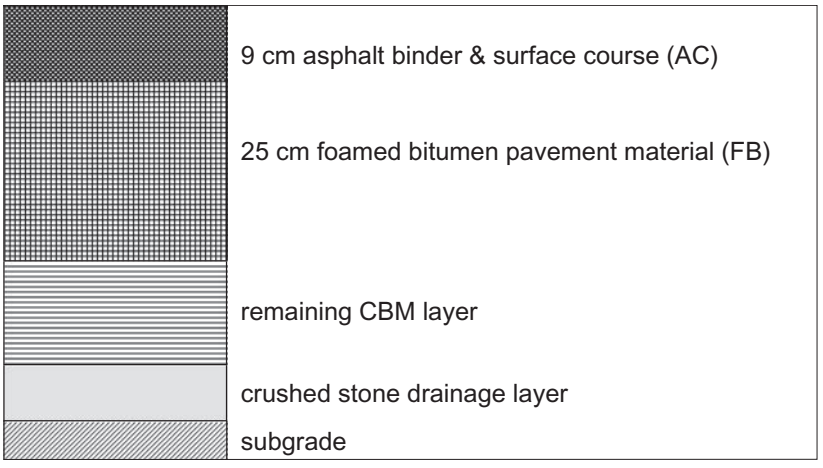

Figure 3. Recycled pavement structure.

tured for testing purposes to determine the indirect tensile strength (ITS), the unconfined compressive strength (UCS), the cohesion (c) and the angle of internal friction (Φ), as well as the determination of the indirect tensile stiffness modulus (ITSM). Details of the mix design can be found by Loizos et al. (2004).

Since milling machines produce few fines, it was decided to introduce 30% (by volume) natural fine sandy material (semi-rigid pavement) to blend with the recovered material, standard application rates (expressed as a percentage by mass of the recycled material) as stabilizing agent, 3.2% foamed bitumen (from 80/100 Pen grade bitumen) and 1% ordinary Portland cement as active filler. The decision to introduce 1% cement was based on improvement in the achieved soaked strengths.

An analytical rehabilitation design approach was used based both on national and international experience to estimate the structural capacity of each pavement configuration. According to the analytical design with a structural capacity requirement in excess of 10 million 13-ton axle-loads, the pavement structure is described by an asphalt concrete (AC) layer (9 cm thick) and a recycled (FB) layer (25 cm thick). The AC layer was constructed of two courses, a 5 cm binder course and a 4 cm final semi-open graded surface course using polymer modified asphalt. Figure 3 shows the pavement cross-section after the rehabilitation.

For analytical pavement design purposes the maximum stiffness modulus (AC and FB) was considered to be 3000 MPa, which is equal to the maximum expected (at the design stage) moduli of the recycled material (FB), as estimated from ITSM (ASTM 2004a) laboratory results on FB specimens.

3 EXPERIMENTAL WORK

3.1 *Deflection measurements*

During and after completion of the recycling works at the site of the field experiment a comprehensive FWD survey was undertaken, which comprised several monitoring levels in chronological order. The test section of the semi-rigid pavement was about 350 m long. In-situ non-destructive tests (NDTs) using the FWD were performed on two paths of the heavy-trafficked lane: the outer traffic wheel path (OWP) as well as the respective path in between (BWP). The different pavement monitoring levels were comprised of in-situ measurements on the surface of the recycled layer (FB), after the laying of the binder course and finally on the surface course 3 weeks after the rehabilitation work.

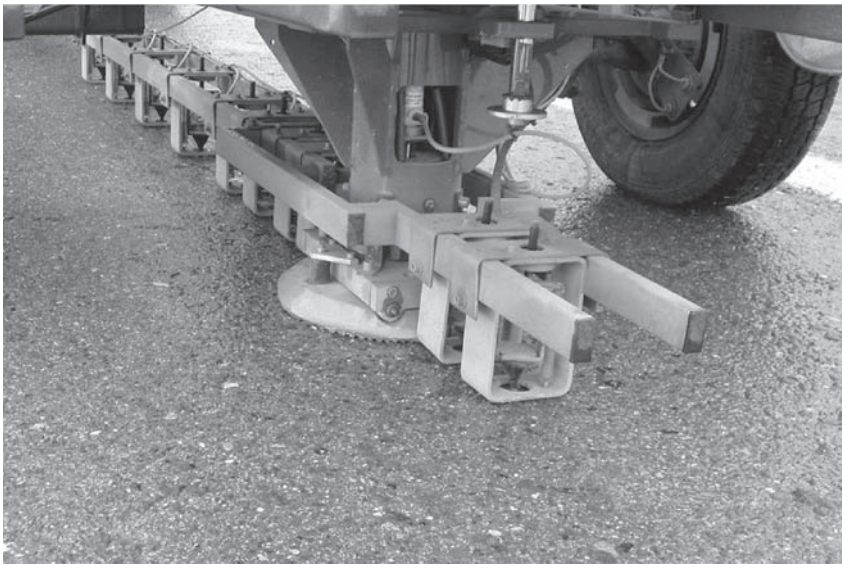

Figure 4. FWD measurements using 5 different load levels (40–75 kN).

The post-construction monitoring levels were comprised of measurements on the related paths on the surface course 6 months to about 6 years after construction, in order to investigate the recycled layer characteristics and the structural condition of the recycled pavement.

In order to examine the influence of the load applied on the deflection analysis results, not only the standard load used for the field (FWD) measurements 50 kN (pressure 700 kPa), but also different load levels were used: 40, 57.5, 65 and 75 kN to 75 kN (Fig. 4).

3.2 *Coring*

Several cores from the recycled layer were extracted at five specific test points along the test section, in accordance to a predetermined coring schedule set out at the beginning of the monitoring program. Cores were drilled along both the OWP as well as the BWP. It was not feasible to extract cores to the full depth of the recycled layer before curing of the material (about 6 months after construction), while coring during the construction stage was completely impossible. The cores were used for the estimation of the different layer (AC and FB) thicknesses for the purpose of the analysis.

3.3 *Ground penetrating radar*

The GPR system of the Laboratory of Highway Engineering of the NTUA (Geophysical Survey Systems Inc. 2002) was used for the analysis, with the aim to estimate the thickness of the remaining CBM layer beneath the recycled layer. These data are useful for the backanalysis procedure. The system used, is appropriate for the evaluation of the upper part of the pavement structure since it produces reliable information to an approximately 0.7 m penetration depth (Saarenketo 2002). The system follows the principles of (ASTM 2004b) and is supported by the appropriate software (RoadScanners 2001). In order to increase the accuracy of the thickness estimation, a 1 GHz air-coupled antenna and a 400 MHz ground couple antenna were used.

3.4 *Backanalysis*

A thorough field data analysis was performed including a backanalysis with the aim to verify the robustness of the newly built trial recycled pavement. The backanalysis was undertaken

using the latest metric version of the MODCOMP software (Irwin 2002). Considering the level of the subgrade, not at the bottom of the drainage layer (Fig. 4), but at the bottom of the CBM layer, the backanalysis model consisted of four layers

The backcalculation was performed at five test points, where detailed AC and FB cores' information was available. The GPR analysis enabled the estimation of the underneath the recycled layer remaining sublayer thickness. Thus a more reliable estimation of the FB modulus is achieved.

4 DATA ANALYSIS

4.1 *Backanalysis results*

The backcalculated recycled layer moduli (based on the standard FWD load of 50 kN) were corrected to 25°C according to ITSM tests results on laboratory produced FB specimens during the mix design (Loizos & Papavasiliou 2007). The backanalysis results (average values) are presented in Figure 5.

The average moduli obtained from the outer wheel path (OWP) were higher in comparison with the values from the relative between the two wheel paths (BWP). This fact is an indication of the inhomogeinity of the material and might be due to the absence of post compaction between the two paths.

During the first year an increase of the stiffness of the recycled material has been observed. This period is referred as "curing phase", shown in Figure 6. The in-situ estimated FB moduli 6 months after construction and hereafter were higher than the design value. It must be noted, that similar results were drawn also in previous research study (Loizos et al. 2006).

No decrease of the stiffness of the recycled layer is shown at least 6 years after the implementation of the rehabilitation, indicating that the recycled material has not reached yet the "stiffness reduction phase", shown in Figure 6. This comes to contrary with previous research (Long & Theyse 2004) on the behavior of foamed bitumen treated materials based on Heavy Vehicle Simulator (HVS) tests (Fig. 1).

4.2 *Backanalysis using different load levels*

Material characteristics for the foam bitumen treated material were determined through triaxial tests in the laboratory. The results showed stress dependency, similar to granular

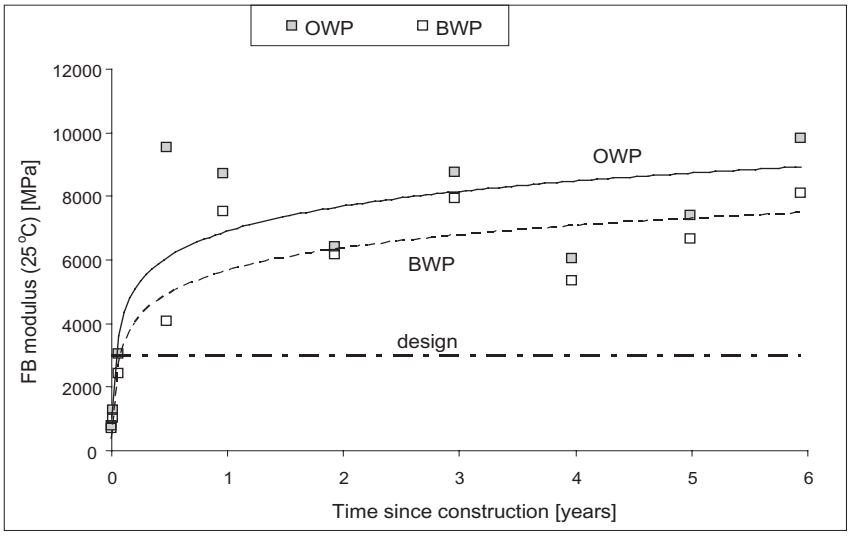

Figure 5. Backcalculated recycled layer moduli.

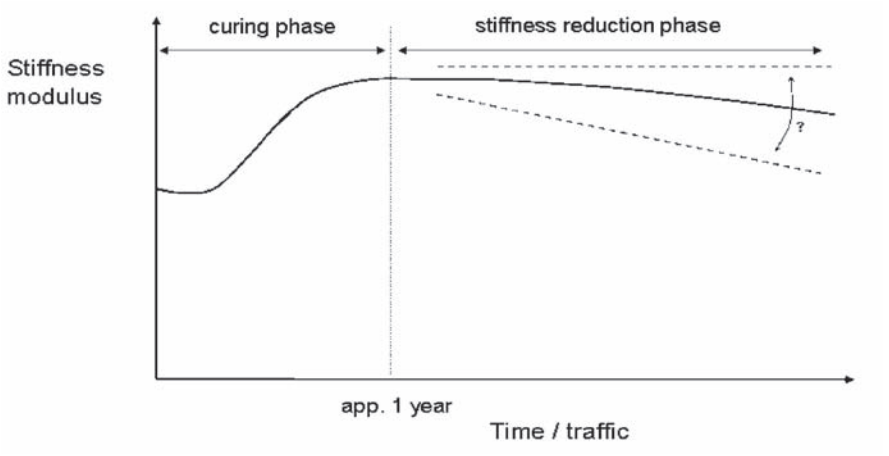

Figure 6. Behavior of foamed bitumen treated materials.

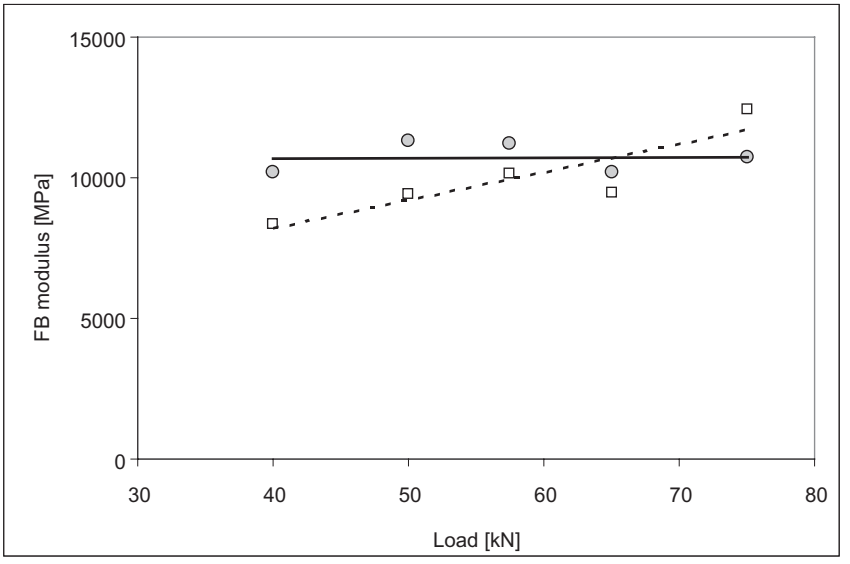

Figure 7. Backcalculated FB moduli for different load levels 6 years after construction.

materials (Jenkins et al. 2002). According to another research (Bredenhann & Jenkins 2004), different falling weight loads allow stress dependent models to be cost-effectively developed. Stress ratios in granular and foamed bitumen treated layers determined using stress dependent analyses of pavement structures incorporating these layers, should be used for pavement design.

In order to investigate the influence of the load applied on the backcalculated FB modulus, several FWD load levels were used, ranging from 40 kN to 75 kN. Results (average values of the test section) during the monitoring 6 years after construction are presented in Figure 7.

A reduction of the average backcalculated FB modulus was observed at the lower load level (40 kN), in comparison with the standard load of 50 kN on both the OWP and BWP. An increase of the backcalculated modulus at the upper load levels was observed on the BWP, indicating stress dependent behavior of the recycled material, while on the OWP no significant trend was observed.

4.3 *Strain response analysis*

The horizontal tensile strain (ε_r) at the bottom of the recycled layer, as well as at other characteristic locations within the recycled layer (e.g. top of the layer, ¼ distance from the top, mid-depth, ¾ distance from the top, see also Figure 8) were calculated, using multi-layer linear elastic analysis tools (BISAR, 1998). he load used for the calculations was 57.5, 65 and 75 kN single wheel with a 15 cm radius.

In order to investigate the influence of the load applied to the maximum horizontal tensile strain (max ε_r) in the body of the recycled layer, the strains were calculated in two ways: with moduli E_1, E_2, E_3 and E_4, backcalculated from deflections measured at FWD load equal to the load used for the strain response analysis (max ε_r (load) in Fig. 9) and moduli backcal-

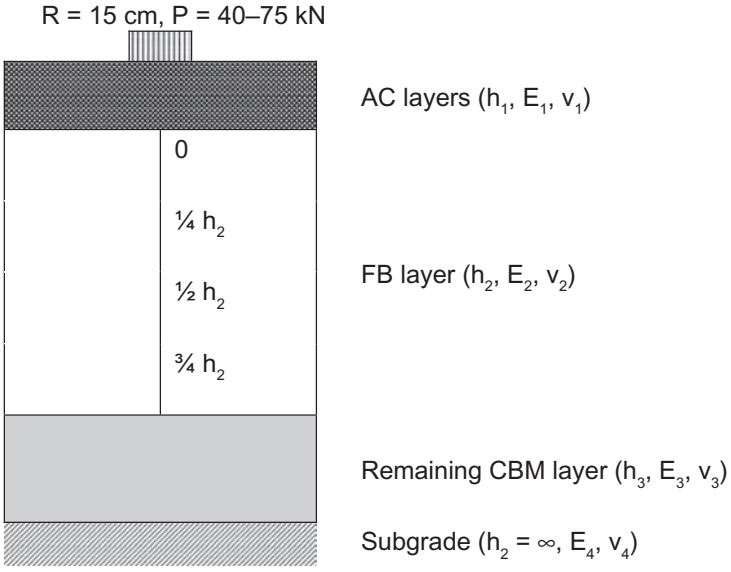

Figure 8. Pavement modeling for structural layer analysis.

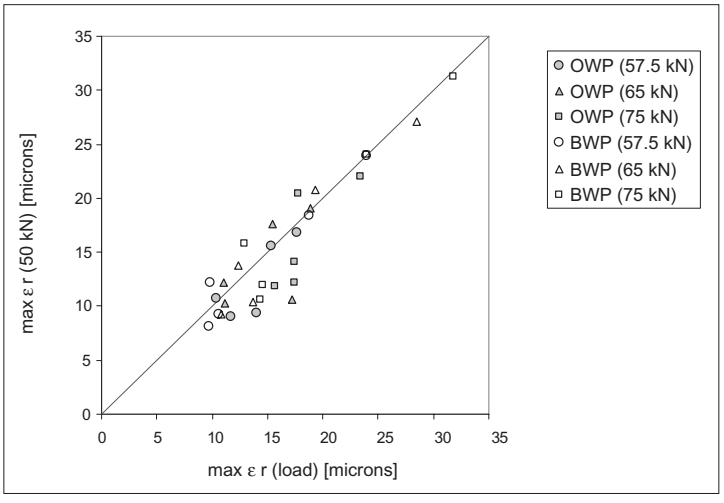

Figure 9. Strain response analysis comparative results.

culated from deflections measured at standard load of 50 kN (max ε_r (50 kN) in Fig. 9). The comparative results are presented in Figure 9.

According to the above mentioned comparative results, no significant different or trend to the calculated maximum horizontal tensile strain was observed when using higher loads, in comparison with the standard load level (50 kN). This is an indication, that moduli obtained from different FWD load levels produce similar strain response analysis results (max horizontal tensile strain) in the body of the recycled material.

It must be noted, that the calculated strains are influenced by uncertainties and assumptions of the load application (FWD vs. traffic), the backanalysis procedure and the linear strain response analysis. For this reason, the Laboratory of Highway Engineering of the NTUA undertook further investigation using in-situ instrumentation for direct strain measurements.

5 CONCLUSIONS

In the present research study an effort was made towards the in-situ characterization of the foamed bitumen pavement material. Preliminary non-linear aspects were also investigated. The aforementioned material was used for the purpose of the present experiment as a base of a rehabilitated semi-rigid pavement. The major findings and discussion points are the following:

The backcalculated moduli of the foamed bitumen pavement material 6 months after construction and hereafter are higher than the design value.

The average moduli obtained from the outer wheel path were higher in comparison with the values from the relative between the two wheel paths. This fact is an indication of the inhomogeinity of the material and might be due to the absence of post compaction between the two paths.

No decrease of the stiffness of the recycled layer is shown at least 6 years of heavy traffic loading.

Taking into account the backcalculated moduli from deflections measured at different load levels, an indication of stress dependent behavior of the foamed bitumen pavement material was observed on the inner wheel path. The expectation of non-linear behavior of the in-situ material has not clear proven through the field data analysis.

According to the strain response analysis, no significant different or trend to the calculated maximum horizontal tensile strain was observed when using higher FWD load levels, in comparison with the standard load level (50 kN). This is an indication, that moduli obtained from different FWD load levels produce similar strain response analysis results (max horizontal tensile strain) in the body of the foamed bitumen pavement material.

The Laboratory of Highway Engineering of the NTUA continues to undertake further research on the subject, including continuous monitoring of the field behavior of the foamed bitumen pavement material through detailed FWD data analysis. In-situ instrumentation for direct strain measurements is also ongoing.

ACKNOWLEDGMENTS

The authors would like to thank the Greek Ministry of Public Work, the Responsible Road Authority and the involved contractors for supporting the research work of this study. They would like also to express thanks to Professor Kim Jenkins (University of Stelenbosh) for providing valuable information.

REFERENCES

Asphalt Academy, 2002. The Design and Use of Foamed Bitumen Treated Materials, *Interim Technical Guideline 2*. 1st Ed., Pretoria.

ASTM D4123-82, 2004a. Standard Test Method for Indirect Tension Test for Resilient Modulus of Bituminous Mixtures, *American Society of Testing and Materials*. Pennsylvania.

ASTM D4748, 2004b. Standard Test Method for Determining the Thickness of Bound Pavement Layers Using Short-Pulse Radar, *Non-destructive Testing of Pavement Structures, American Society of Testing and Materials*, Pennsylvania.

Baltzer, S. & Jansen, J.M. 1994. Temperature Correction of Asphalt-Moduli for FWD-Measurements. *Proceedings, 4th International Conference on the Bearing Capacity of Roads and Airfields*: 7–25. University of Minneapolis, Minnesota.

BISAR. 1998. User Manual. *Bitumen Business Group*.

Bredenhann, S.J. & Collins, D. 2004. Determination of Stress-dependent Material Properties with the FWD for Use in the Structural Analysis of Pavements Using Finite Element Analysis Technique *Proceedings, 8th Conference on Asphalt Pavements for Southern Africa (CAPSA 04,)*: 633–650.

GSSI, 2002. RADAN for Windows NT (Version 4.0), *User's Manual*. Geophysical Survey Systems Inc., North Salem, New Hampshire.

Irwin, L.H. 2002. Back-Calculation Analysis, *Tutorial, 9th International Conference on Asphalt Pavements,* International Society for Asphalt Pavements (ISAP), Copenhagen Denmark.

Jenkins, K.J., Van de Ven, M.F.C., Molenaar, A.A.A. & de Groot, J.L.A. 2002. Performance Prediction of Cold Foamed Bitumen Mixes. *Proceedings, 9th International Conference on Asphalt Pavements*. Copenhagen Denmark.

Loizos, A., Collins, D. & Jenkins, K. 2004. Rehabilitation of a Major Greek Highway by Recycling/ Stabilizing with Foamed Bitumen. *Proceedings, 8th Conference on Asphalt Pavements for Southern Africa (CAPSA 04,)*: 119–126. Sun City.

Loizos, A. & Papavasiliou, V. 2007. In situ Characterization of Pavement Materials Stabilized with Foamed Asphalt and Cement. *Proceedings, International Conference on Advanced Characterization of Pavement and Soil Engineering Materials*: 875–882. Athens, Greece.

Loizos, A., Papavasiliou, V. & Plati, C. 2006. Evaluation of Cold-in-Place Recycling Using Foamed Asphalt. *Proceedings, International Conference on Asphalt Pavements ICAP*. Quebec, Canada.

Long, F., & Theyse, H. Mechanistic: Empirical Structural Design Models for Foamed and Emulsified Bitumen treated Materials. *Proceedings, 8th Conference on Asphalt Pavements for Southern Africa (CAPSA 04)*: 553–567. Sun City.

RoadScanners, 2001. Use of Ground Penetrating Radar in Relation with FWD. *Road Doctor Software, Version 1.1 User's Guide,* Rovaniemi, Finland.

Saarenketo, T. 2002. FWD/Backanalysis. *Workshop, Proceedings, 6th International Conference of the Bearing Capacity of Roads, Railways and Airfields (BCRA)*: 24–26. Lisbon, Portugal.

Advanced Testing and Characterization of Bituminous Materials –
Loizos, Partl, Scarpas & Al-Qadi (eds)
© 2009 Taylor & Francis Group, London, ISBN 978-0-415-55854-9

Evaluation of cracking in overlays in Quebec: A case study

A. Carter, D. Perraton & M. Meunier
École de technologie supérieure, Montreal, Canada

M. Paradis
Ministère des Transports du Québec, Québec, Canada

ABSTRACT: In 2002, a severely cracked highway was overlaid, in part, with a stone matrix asphalt (SMA) mix and a coarse mix with asbestos fiber (EGA) commonly used in Quebec. Before the paving operation, a complete mapping of the transversal and longitudinal cracking, both in and outside the wheel path, was done. The operation was repeated two years later in order to evaluate the capacity of those two mixes to slow the apparition of reflective cracking.

In this paper, the characteristics of the mixes (gradation, bitumen content, air voids, etc) and their properties (complex modulus, rutting resistance, TSRST results) are shown. It's also shown that both mixes have similar resistance to reflective cracking and that very few new cracks have appeared in the two years period.

1 INTRODUCTION

Stone Matrix Asphalt (SMA) mixes have been used in over 150 countries. In the early 1990's, the Quebec Ministry of Transportation (MTQ) tried its first SMA type mix with asbestos fiber. However, in mid 1990, the MTQ changed considerably its mix design methods (which is now volumetric) which results in the need to validate all the usual mixes, including SMA. The LUCREB (Laboratoire Universitaire sur les Chaussées, Routes et Enrobés Bitumineux) at the ÉTS (École de Technologie Supérieure) in Montreal was mandated by the MTQ to first, verify if the new mix design procedure was applicable to SMA and second to do a test section with a SMA. This report concentrates on the test section that was done after the laboratory work.

2 BACKGROUND

SMA mixes are Hot Mix Asphalt (HMA) mixes with a stone on stone contact and high binder content. Those mixes have many advantages:

- Good rutting resistance (Kennepohl & Davidson 1992);
- Increase of adherence due to a coarse surface texture (EAPA, 1998);
- Better low temperature cracking resistance due to a high binder content (Kennepohl & Davidson 1992);
- Less sensitive to aging also due to the high binder content (Kennepohl and Davidson, 1992).

In a study by Schmiedlin and Bischoff (2002), it was shown that SMA tends to minimize the reflective cracking compared to standard dense graded mixes. However, even if it's believed that SMA mixes have design life 25% superior to the design life of standard mixes (Watson, 2003), their cost is usually between 20% and 40% higher than a conventional mix.

3 OBJECTIVES

The main objectives of this research are:

- Fully characterize the two studied mixes, i.e. SMA-10 and EGA-10;
- Evaluate how those mixes resist to reflective cracking;
- Study if there is a relation between the characteristic that were evaluated and their resistance to reflective cracking.

4 LABORATORY WORK

The SMA and the EGA mixes were characterized at the LUCREB. The first step was to do the mix design with the volumetric method and the results are shown in Table 1.

After the mix design, both mixes were tested in rutting resistance, complex modulus and thermal cracking resistance.

4.1 *Rutting resistance*

The rutting resistance was measured with a French rut tester. In this device, two slabs, 500 mm in length, 180 mm wide and 50 mm thick are compacted with a MLPC (Matériel du Laboratoire des Ponts et Chaussées) Slab compactor to 5% air voids. A curing period of 48 hours at room temperature is needed before the rut test begins.

To measure the rutting resistance of the mixes, a rubber tire inflated to 6 bars rolls on the slabs at a frequency of 1 Hz while applying a load of 5000 N. According to the MTQ, for 50 mm a slab, the maximum rut depth is 10% at 10 000 cycles at 60°C. The percentage of the rut depth is calculated by dividing the measured rut depth by the slab thickness. Since SMA are known for their good rutting resistance, 30 000 cycles were used. The results are shown in Figure 1.

As it can be seen, the SMA performs much better than the EGA on the rutting test. Since this was expected, the rutting test was pursued up to 60 000 cycles for the SMA. But even at 60 000 cycles, the rut depth was at 9,4%, which is still under the 10% limit normally measured at 10 000 cycles.

Table 1. Characterization of the SMA-10 and EGA-10.

		EGA-10	SMA-10
Asbestos Fiber (%)		1,0	1,0
Bitumen Grade (PG)		58–28	58–28
% passing	14 mm	100	100
	10 mm	91	92
	5 mm	46	34
	2.5 mm	32	29
	1.25 mm	24	22
	630 µm	19	17
	315 µm	14	13
	160 µm	8	10
	80 µm	4,3	8,1
Characteristics	Bitumen content (%)	6,40	6,49
	V_{be} (volume of effective binder) (%)	14,3	13,5
	V_a (voids) (%)	1,5	2,1
	FBE (binder effective film thickness) (µm)	12,60	9,11
	G_{mb} (bulk specific gravity)	2,379	2,404
	G_{mm} (maximum specific gravity)	2,415	2,456

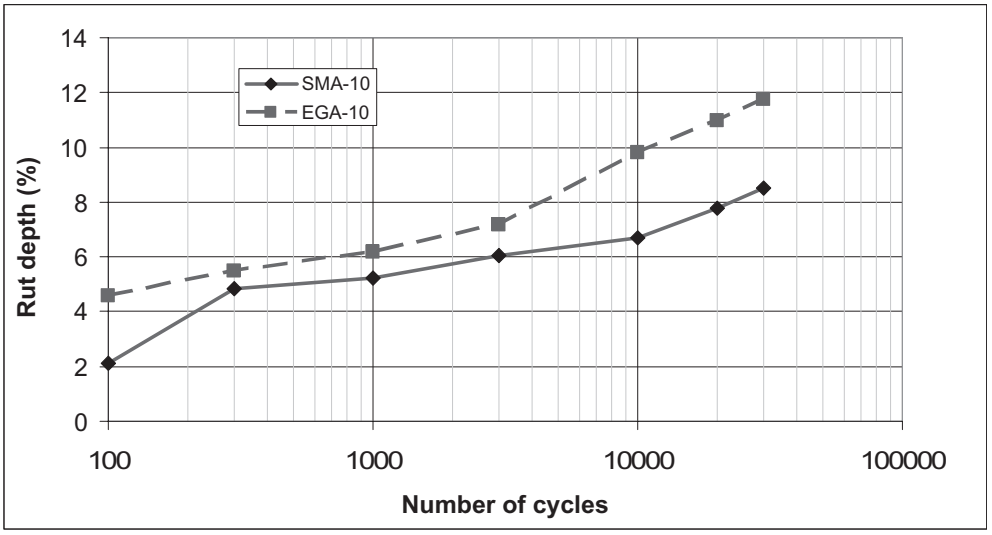

Figure 1. French Rut Tester Results for the SMA-10 and the EGA-10.

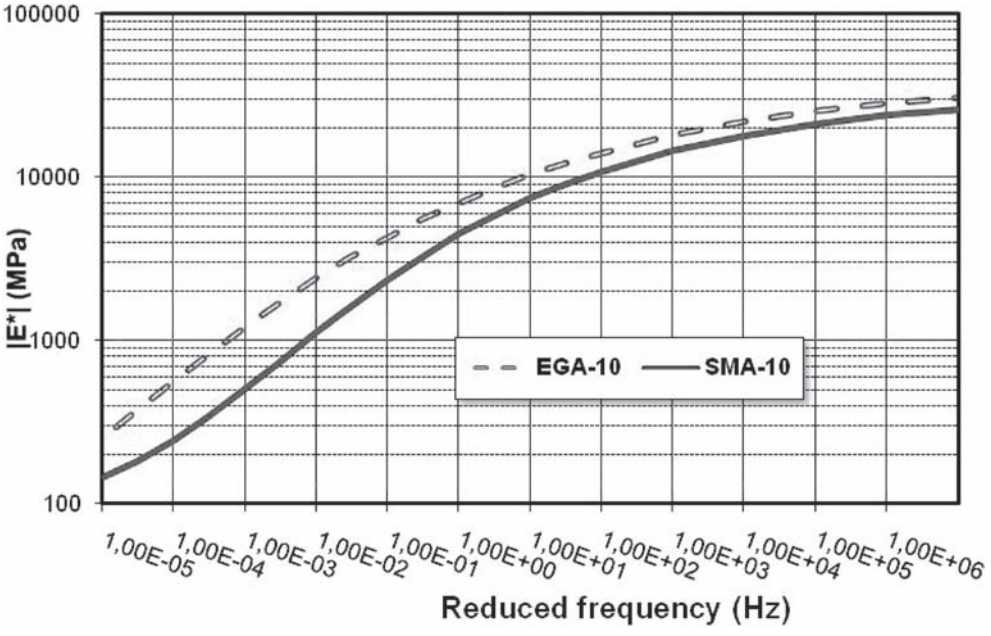

Figure 2. Master curves for the SMA-10 and the EGA-10 at 10°C.

4.2 *Complex modulus*

The complex modulus was measured with a sinusoidal tension-compression uni-axial test done on specimen of 80 mm in diameter and 120 mm in length. The test is performed at 35, 20, 10, 0, –10, –25 and –35°C and at 20, 10, 3, 1, 0,3, 0,1, 0,03 and 0,01 Hz. The results for both mixes are shown on Figure 2. Figure 2 shows the master curves at 10°C.

As shown on Figure 2, the modulus of both mixes are not far apart, but the EGA modulus is always higher; however, in a log-log graph, the difference is not great at high frequencies (colder temperature). On the other hand, if modulus at 10°C are compared at a precise temperature, it is easier to evaluate the differences in the modulus. Examples of the modulus are given in Table 2.

Table 2. Example of complex modulus values at different frequencies.

	Complex modulus (MPa)		
Frequency	EGA-10	SMA-10	Difference (%)
0,01	2 412	1 114	117
1,0	7 022	4 465	57
10,0	10 391	7 409	40
1000,0	18 243	14 446	26

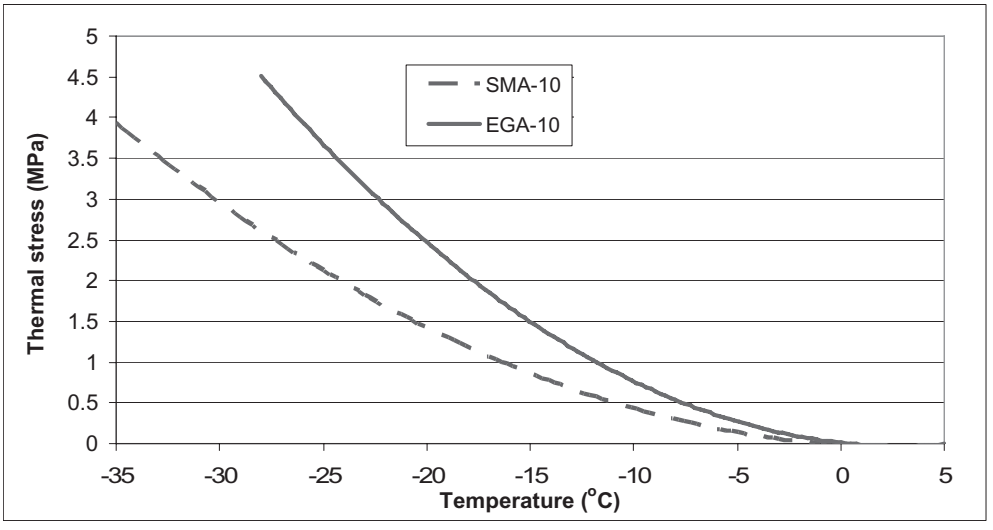

Figure 3. TSRST results for the SMA-10 and the EGA-10.

4.3 *Thermal cracking resistance*

The thermal cracking resistance was measured with the Thermal Stress Restrained Specimen Test (TSRST). In this test, a specimen of 60 mm in diameter and 250 mm in length is kept at constant length while the temperature is decreased at a rate of 10°C/hour until the specimen breaks. The results of this test are shown on Figure 3.

There is a big difference between the behavior of both mixes at cold temperature. The SMA fractures at lower temperature, but at a lower stress than the EGA. The slope of the stress vs temperature is a lot steeper for the EGA than for the SMA. This means that the EGA is more sensitive to temperature gradient than the SMA. That translates into a bigger stress gradient over the thickness of the HMA layer. Those results are a bit unexpected since both mix have the same binder grade and similar binder content. On the other hand, the higher air voids content of the SMA might be creating some kind of insulation which could, at least in part, explain the difference between the two curves.

5 TEST SECTIONS

The two test sections studied are located on highway 20 at Berthier-sur-Mer in the province of Quebec. Both sections of two lanes are 150 m long, and the thickness for both studied layers is 48 mm. It should be noted that both sections are built over the same pavement structure, withstand the same traffic and weather conditions. The first test section chosen for this project is a section of flexible pavement severely cracked; there was a bit over 787 m of cracking on the 150 m long section, which results in 610 mm/m^2 of cracks. 39% of

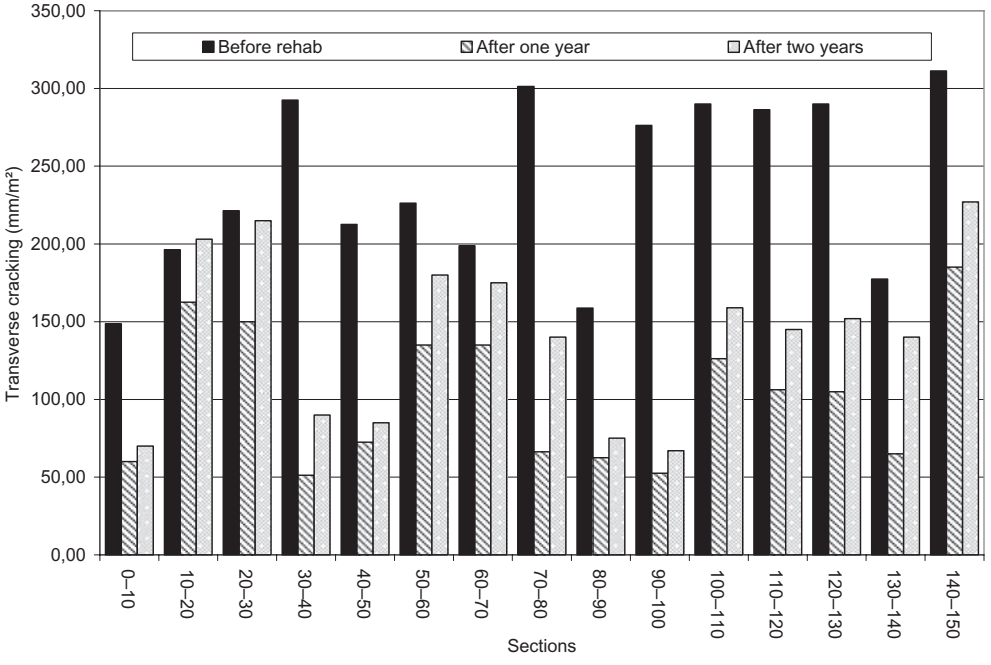

Figure 4. Transverse cracking for the SMA section.

those cracks were transverse cracking, 59% longitudinal cracking in the wheel path and 2% cracking outside the wheel path. The degradations were also noted on a second test section, the test section which will be overlaid with a EGA-10. This second 150 m section had similar cracking than the first one; 819 m of cracking (737 mm/m^2) in which 25% were transversal cracking, 56% longitudinal cracking in the wheel path and 19% longitudinal cracking outside the wheel path. In both sections, it seems that the cracks were fatigue cracks since they were located in the wheel paths.

The evaluation of the degradation was done again 1 year after the rehabilitation and two years after the rehabilitation. The results of the evaluation of the degradations are shown in Figures 4 to 9.

For both sections, the evaluation of the pavement degradations was done manually. To evaluate the effectiveness of both surface mixes to resist to reflective or new cracking, the evaluation was done on both sections one and two years after the paving operations. As shown on Figure 4 and 5, most of the transverse cracks reappeared on the SMA section after two years, which was not the case for the EGA section. This was not expected since transverse cracking is mostly thermal cracking and the SMA did performed better than the EGA in the thermal cracking test.

On Figures 6 and 7, it can be seen that the longitudinal cracking in the wheel path did not reappeared after two years for both sections. This was expected since the cracking in the wheel path is associated with fatigue, and two years is not enough to reach the fatigue limit of those mixes or to have the existing cracks reflect on the surface.

Finally, on Figures 8 and 9, it can be seen that the EGA section shows a lot more longitudinal cracking outside the wheel paths after two years than on the SMA section. However, in both cases, the cracking did not reach its initial level.

Since the mapping of the degradations was done precisely, it was possible to discern which crack was new and which one was reflective. On Figure 10, its shown that for both sections, the vast majority of the cracks are reflective and not new.

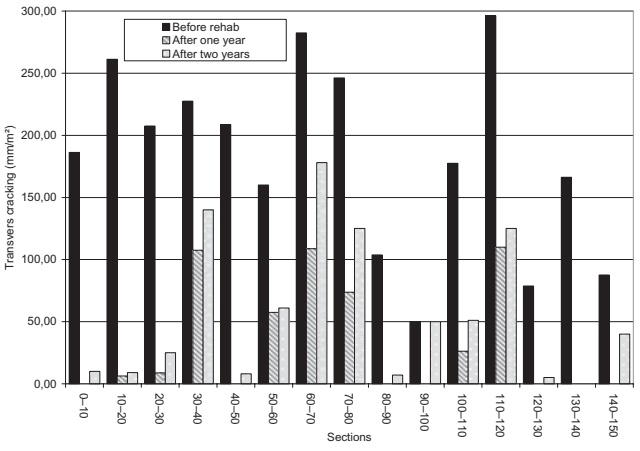

Figure 5. Transverse cracking for the EGA section.

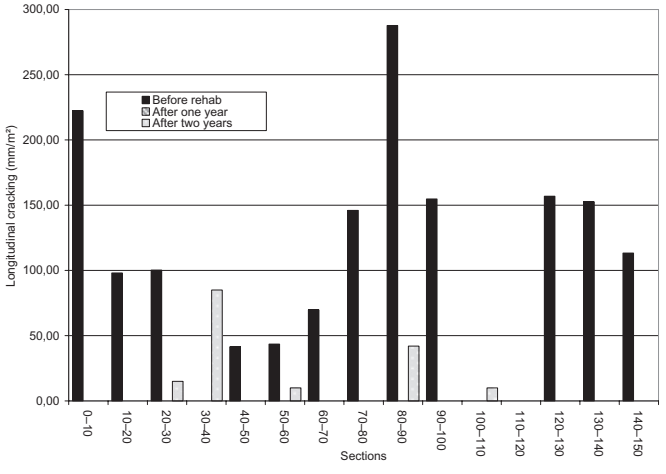

Figure 6. Longitudinal cracking in the wheel paths for the SMA section.

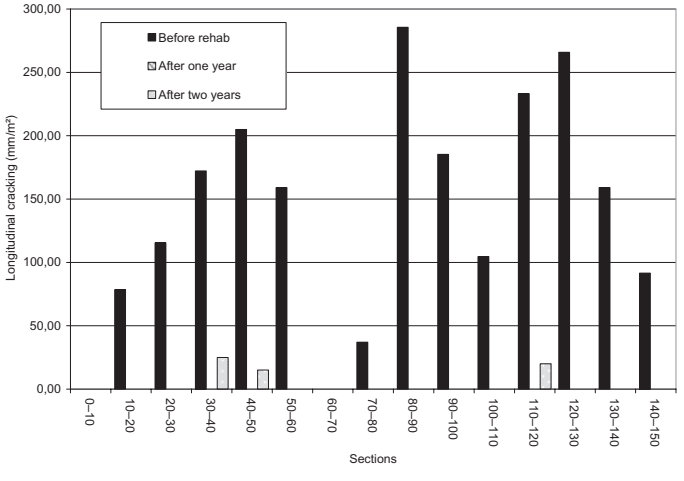

Figure 7. Longitudinal cracking in the wheel paths for the EGA section.

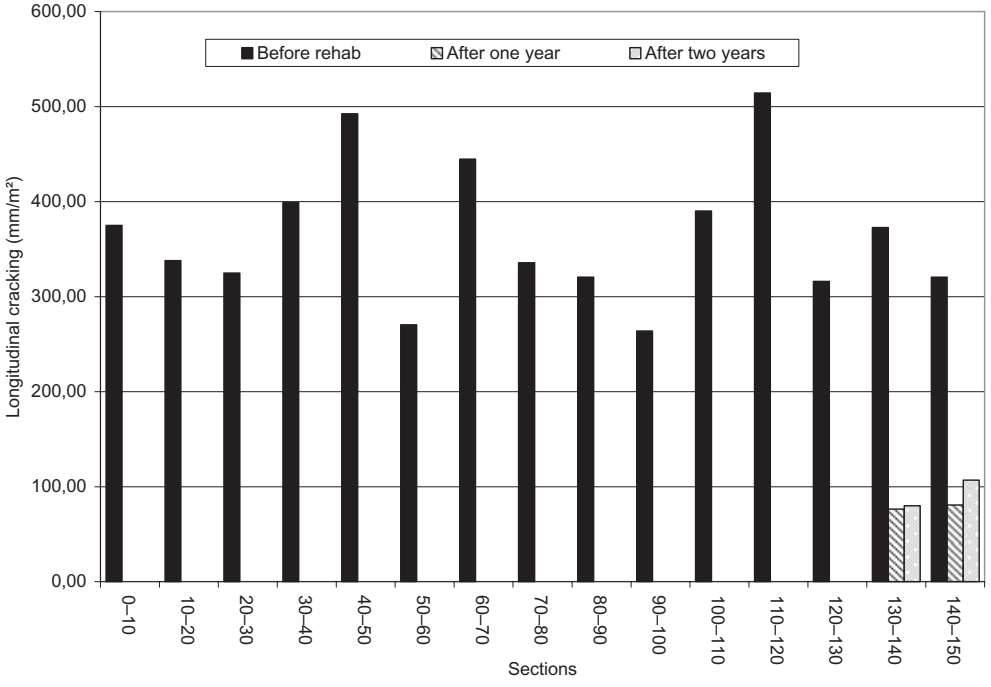

Figure 8. Longitudinal cracking outside the wheel paths for the SMA section.

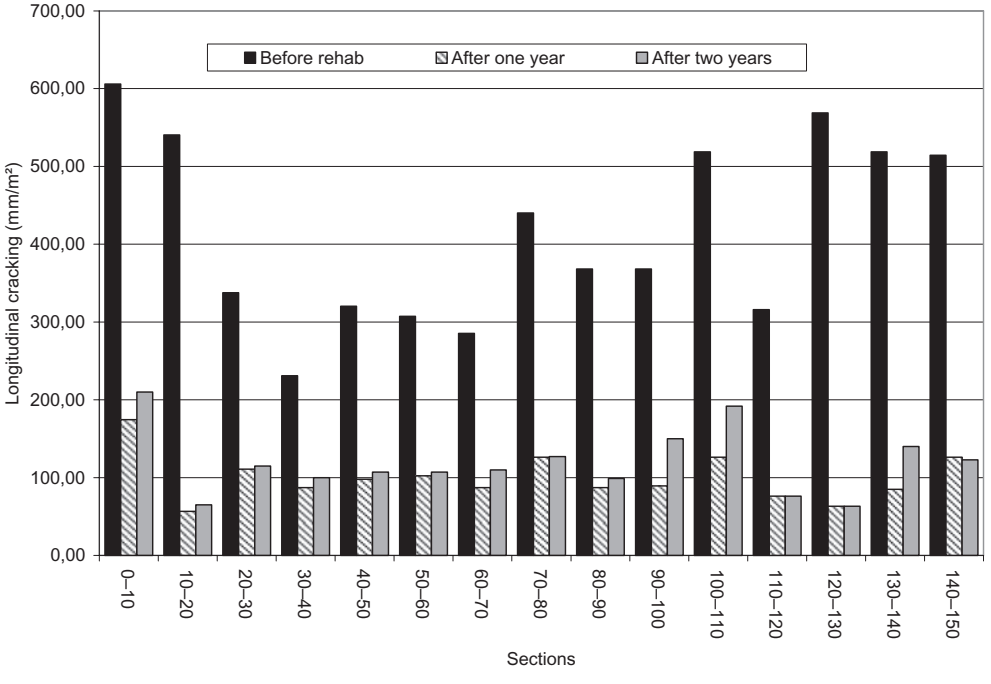

Figure 9. Longitudinal cracking outside the wheel paths for the EGA section.

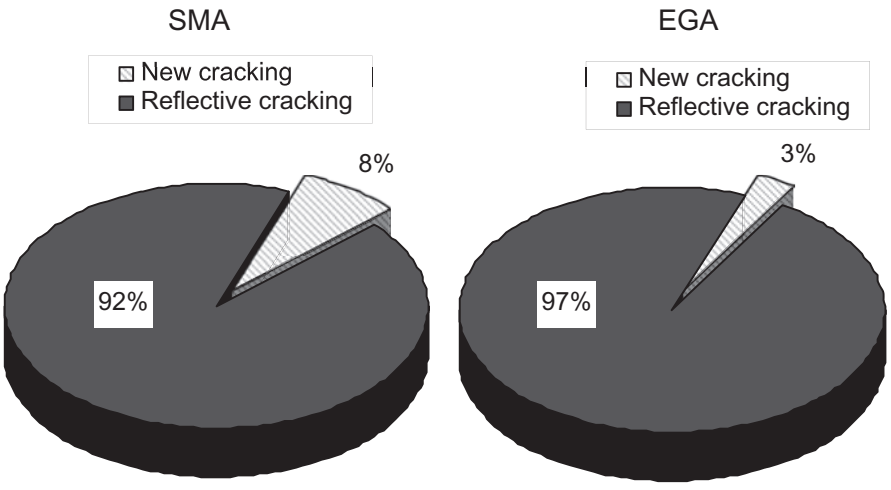

Figure 10. Comparison between new and reflective cracking.

6 CONCLUSION

Both the SMA-10 and the EGA-10 have shown good cracking resistance after two years. Unfortunately, with the results obtained in this study, it is not possible to say if the SMA performs better than the EGA. With our results, the only advantage of this SMA over the standard EGA is its rutting resistance.

One of the results that is puzzling us the most is the fact that there is more transverse cracks on the SMA surface than on the EGA surface. The SMA-10 did perform better than the EGA-10 on the TSRS test, but most of the transverse cracks are reflective cracks and not new thermal cracks. Tensile resistance tests as well as reflective cracking tests should be done with the two materials in order to get a better understanding of what happened. The reflective cracking resistance test that should be done for those mixes is the one developed by Perraton et al. (Perraton et al., 2008).

Finally, in order to verify the SMA reflective cracking resistance in comparison with a standard dense graded mix in the field, the mapping of the different degradations should be done every year for at least three more years.

REFERENCES

European Asphalt Pavement Association 1998. Heavy duty surfaces—The argument for SMA, EAPA, 40 pages.

Kennepohl, G.J. & Davidson, J.K. 1992. Introduction of stone matrix asphalts (SMA) in Ontario, Asphalt Paving Technologists, Vol. 61, South Carolina.

Perraton, D., Guissi, G., Pierre, P. & Doré, G. 2008. A new laboratory test for reflective cracking in mode I and/or in mode II, Pavment Cracking: Mechanisms, Modeling, Dtection, Testing and Case Histories, Proceeding of the 6th RILEM International Conference on Cracking in Pavements, 16–18 June, Chicago, USA.

Schmiedlin, R.B. & Bishoff, D.L. 2002. Stone matrix asphalt, the Wisconsin experience, WisDOT Highway Research Study #91–07, Final Report WI/SPR-02-02.

Watson, D.E. 2003. Updated review of stone matrix asphalt and Superpave projects, Transportation Research Record, No. 1832.

9. Recycling of bituminous pavement materials

Advanced Testing and Characterization of Bituminous Materials – Loizos, Partl, Scarpas & Al-Qadi (eds)
© 2009 Taylor & Francis Group, London, ISBN 978-0-415-55854-9

Utilization of aggregate production waste filler in cold recycling mix optimization

J. Valentin & P. Mondschein
Faculty of Civil Engineering, Czech Technical University, Prague, Czech Republic

ABSTRACT: Cold recycling techniques continue to become standard technology used for Czech roads rehabilitation. Generally combination of bituminous emulsion and cement or foamed bitumen and cement is applied. The portion of cement should be according to the technical specifications 3–5%. The reason for this fairly high content can be explained by the most frequent use of this technique in pavement structure—bearing capacity increase and sub-base improvement. On the other hand the industry of aggregate production is at the moment confronted with the issue of waste production. To achieve reasonable cut-downs it is necessary to find industrial utilization for waste products or by-products. One of such by-products might be waste filler—fine particles gained during washing and cleaning of crushed aggregates. During an ongoing research this material has been used in cold recycling mixes together with reclaimed asphalt (RAP). Results demonstrated on selected characteristics of cold recycling mix with both binder systems is discussed in the presented paper. The waste filler has been used as substitution of RAP as well as an partial alternative for cement. Especially in the second case important results have been reached improving the mix performance and reducing the content of valuable cement in the mix.

1 INTRODUCTION

Cold recycling technologies have become standard procedures in the Czech Republic; they are used more and more in asphalt pavement rehabilitation. At present, the cold recycling application in situ has been the most widely spread technique. The technological procedure is utilized both in recycling of layers up to 100 mm thick and in the form known as in-depth recycling up to a depth of 350 mm. The most frequent use is the application for a new sub-base layer where its characteristics allow for significant improvements in the bearing capacity of the pavement. At present, this is a major issue with repaired structures which results in significant degradation of the pavement. The utilization of cold recycling in the binder course or even in the wearing course has been rather rare so far. It has been restricted to less important roads with smaller loads of heavy loaded vehicles (up to 15 HLV/day). In such cases, the technical regulations (Ministry of Transport and Communications, 2007) always require the application of a suitable surface dressing, thin asphalt layer or slurry surfacing.
From the perspective of the binders employed, the combination of bitumen emulsion and cement has spread the most. A combination of foamed bitumen and cement has been used to a lesser degree. Purely bitumen stabilized courses are rather exceptional due to the aforementioned need of increasing the bearing capacity of the sub-base layer.

Since 2006, in co-operation with TARMAC CZ a.s., a partial research project has been running in the field of identification and experimental verification of options of finding a suitable use for waste fillers in an appropriate road construction technology; in this case it means cold recycling using both foamed bitumen and bituminous emulsion. The aim of the partial research project is defining the suitability of waste filler application in cold recycling mixes on one hand and partially substituting the effects of more costly cement with a by-product of aggregate production—waste filler. This is a product occurring during the

washing, cleaning and crushing of aggregates; from the point of view of aggregate producers, it is difficult to utilize and, in fact, used very little.

2 DESIGN OF EXPERIMENTAL MIXES

The experimental research was divided into two separate sets which differed in the combinations of binders used. The first set (A) which was analyzed in 2007, used a combination of foamed bitumen and cement; four laboratory mixes were designed. The other set (B) was analyzed in early 2008; it utilized slow-setting cationic bituminous emulsion and cement. In the case of this set, three mixes were designed. The composition of individual mixes including an indication of the ratio of reclaimed asphalt pavement material (RAP) to the waste filler is stated in Tables 1 and 2.

The reclaimed material used for the laboratory mixes consisting of a blend containing agglomerates of the milled asphalt mix and aggregate grains covered by bitumen film or bituminous plaster was taken from the Středokluky mixing plant (set A) and the Běchovice mixing plant (set B)—in both cases the plants belong to the construction company PSVS, a.s. In both cases, sorted and relatively fine material of grading 0–11 has been chosen. The RAP material was first subjected to a more detailed analysis of the filler content; grading sieve analysis was performed and the grading size curve was determined. Bitumen was extracted with the objective of defining its proportion in the reclaimed material. No more laboratory tests were performed in either case of the bitumen; therefore, the binder could not have been classified under ČSN EN 12 591 specifications. After the extraction, grading analysis was carried out again and the grading size curve was determined. In the case of waste filler which, as has been mentioned above, constitutes a by-product of crushed aggregate production, the material came from the Těškov quarry (TARMAC CZ, a.s.) with maximum grain size 0.09 mm.

Table 1. Cold recycling mix composition including reclaimed asphalt and foamed bitumen.

Mix (set A)		FC	FF	FCF1	FCF2
Binder		Bitumen foam + cement			
Reclaimed asphalt: waste filler ratio		100:0	80:20	80:20	90:10
Bitumen foam content	: %-m.	3.0	3.0	3.0	3.0
H_2O content	: %-m.	4.0	5.0	5.0	5.0
Cement content	: %-m.	3.0	–	2.0	2.0
Waste filler content	: %-m.	–	18.0	18.0	9.0
Reclaimed asphalt 0–11	: %-m.	90.0	74.0	72.0	81.0

Table 2. Cold recycling mix composition including reclaimed asphalt and bituminous emulsion.

Mix (set B)		REC1	REC2	REC3	REC4	REC5
Binder		Bituminous emulsion + cement				
Reclaimed asphalt : waste filler ratio		90:10	80:20	80:20	90:10	100:0
Bituminous emulsion content	: %-m.	2.5	2.5	2.5	2.5	2.5
H_2O content	: %-m.	5.0	5.0	5.0	5.5	5.1
Cement content	: %-m.	3.0	2.0	1.5	2.0	3.0
Waste filler content	: %-m.	9.0	18.1	18.2	9.0	–
Aggregates 0–2	: %-m.	–	–	–	18.0	–
Reclaimed asphalt 0–11	: %-m.	80.5	72.4	72.8	63.0	89.4

For the production of foamed bitumen, distilled bitumen with grading pen 160/220 (softening point R&B 36°C according to CSN EN 1427, penetration at 25°C with a value of 208 mm/10) was selected; it met the requirements of ČSN EN 12 591 specification. The foamed bitumen was produced using the Wirtgen WLB10 laboratory apparatus available to the accredited laboratory NIEVELT Labor Praha. The requirements for foamed bitumen as defined by technical specifications TP 112 (Ministry of Transport and Communications 2007) which require the determination of half-life ($t_{½}$) and the expansion ratio (ER). With respect to the general quality parameters of the present-day bituminous binders and the effect of provenience of crude oil on the chemical composition of the bitumen, a very short half-life has been recorded repeatedly in the manufacture of foamed bitumen. As has been stated in (Valentin et al., 2006), the cause of the phenomenon can be attributed to a higher proportion of oil fractions in the bitumen binder which are used in fluxing (diluting) of the initial harder binder to achieve a higher penetration value. Due to that, it is recommended either to use suitable additives which, from the practical point of view, constitute another economic requirement of the solution, or to reduce the time period between the process of production of the bitumen foam as such and its addition to the mix to 15 to 20 seconds maximum when preparing the foamed bitumen mix per se. In the event of a gap exceeding 15–20 seconds, larger clusters (agglomerates) of bitumen and fine particles occur which will not allow for binding larger grains of the initial reclaimed material mix; as a consequence, the foamed asphalt mix becomes less efficient, degraded and is more difficult for practical application. As a rule, such a requirement will not be critical in applying the in situ foamed asphalt mix technology. In the case of mixes produced in a mobile mixing plant, observance of the time limit depends on the set up of the production process as such.

In the case of bitumen emulsion, preference was given to an Austrian product, VIALIT RE60, which meets the requirements for cold recycling application. From the point of view of classification of the emulsion according to the valid ČSN EN 13808, it can be designated as C60 B6. In all cases, the cement used was Portland-slag cement II/B-S 32.5 R recommended for cold recycling mixes by Czech technical specifications (Ministry of Transport and Communications, 2007).

The optimum quantity of water was defined based on the procedure described e.g. in technical specifications TP162 (Ministry of Transport, 2007). The bituminous emulsion content and foamed bitumen content as well as the cement content respect the requirements specified in the technical conditions (Ministry of Transport, 2007). The proportion of reclaimed material to the waste filler was determined based on the analysis of the reclaimed asphalt material

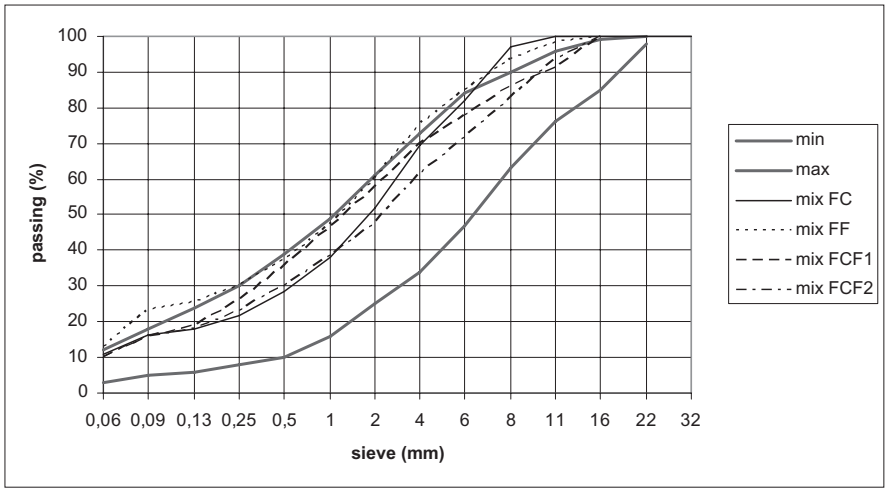

Figure 1. Foamed asphalt mixes gradation.

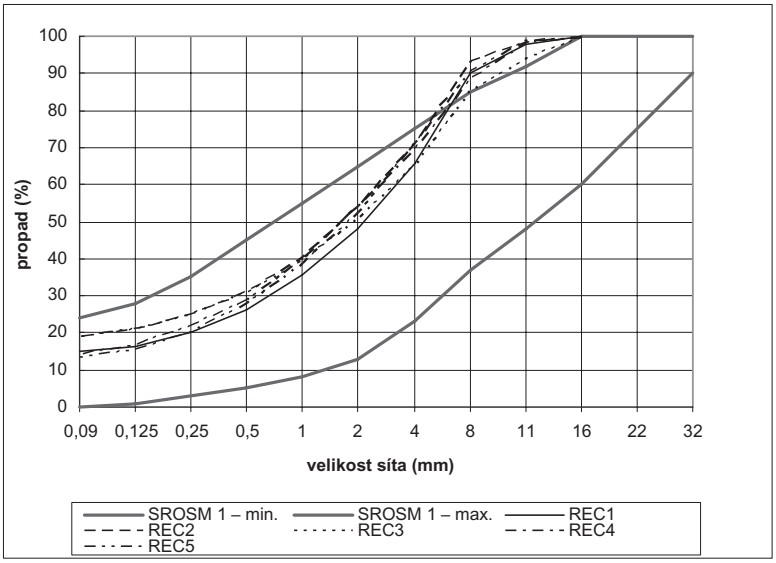

Figure 2. Cold recycling mixes gradation, bituminous emulsion + cement.

grading while attempting to increase the proportion of fine particles and achieve a lower void content and improved strength characteristics.

Mix gradations for observed and further tested mixes are shown in following two graphs. The domain of gradation as specified for foamed asphalt in Czech technical conditions TP126 and for cold recycling mixes where bituminous emulsion is used in TP162 is represented by bold minimum and maximum gradation curves. However the present technical condition specifies the domain of gradation only for coarse graded mixes 0–22 and more. Because the gradation of mixes described in this paper were designed as a 0–11 mix with higher contents of small-sized particles, the gradation curves do not completely fit in the most usable gradation domain.

3 PREPARATION OF TESTING SPECIMENS

From the point of view of testing specimen preparation, current technical conditions TP162 or TP112 prefer the method of preparing specimens using static compression. However, the experiment presented used impact compaction to prepare the specimens (standard procedure for Marshall specimen compaction). The compaction method of static compression (Ministry of Transport and Communications, 2007) is used to prepare primarily testing specimens with ø150 mm; the specimens are compacted by axial compressive force of 88.5 kN (this corresponds with pressure of 5.00 MPa). Where the force is exerted, due to the plastic and flexible behaviors of the cold recycling mix there is a decrease in the applied pressure; therefore, it is necessary to repeatedly increase the loading to the required value for instance in 30-second intervals until the pressure stops decreasing below a value approx. 5 kN lower than the compacting compressive force. According to the experience so far the final pressure is usually reached after 6 to 8 cycles depending on the humidity and character of cold recycling mix. In the research in question, the latter method utilized for hot asphalt mix cylindrical specimens compaction has been preferred; also due to the fact that the grading of reclaimed material used allowed to prepare test specimens with ø100 mm which were a determining factor from the perspective of the Nottingham Asphalt Tester (NAT) apparatus available to the Czech Technical University in Prague. This method prepares the test specimens similarly to common asphalt mixes, applying 2×50 blows.

4 EXPERMENT AND RESULTS ACHIEVED

The objective of the research presented in this paper was assessing the possibilities of suitable utilization of waste filler in combination with RAP material in cold recycling mixes. Several laboratory mixes were composed for the purpose and tests of physical, mechanical and selected rheological (functional) characteristics were performed. Out of those tests, the following text presents the results of void content, specific gravity of the compacted mix determined in accordance with the procedures defined e.g. by the technical specifications TP162, (Ministry of Transport and Communications, 2007). The results summarized separately for cold recycling mixes with foamed bitumen and bituminous emulsion are listed in Tables 3 and 4. Subsequently, Tables 5 and 6 summarize the results of indirect tensile strength (ITS) which is one of the determining quality criteria for cold recycling mixes not only in the Czech Republic but also in Germany or Austria. Both the values of ITS reached after 28 days curing and values of relative deformation and the computed values of elasticity modulus are listed. From the point of view of functional testing, the results of stiffness modulus determined by a non-destructive test of indirect tensile test were selected and are presented separately in Section 5.

Te following conclusions can be made based on the analysis of physical and mechanical characteristics of experimental cold recycling mixes with both binder systems:

– According to the valid Czech technical specifications TP162 (Ministry of Transport, 2007), the void content of individual mixes must fall within the range of 8–15%-vol. for use in the sub-base and 8–13%-vol. for use in the binder course. The requirement for sub-base layers was not met by mixes which did not consider the use of waste filler; to a certain degree, these can be interpreted as representatives of mixes most commonly used at present in practice—that is, a combination of bituminous emulsion or foamed bitumen, cement and reclaimed material. In the case of REC2–4 mixes, the requirement for a sub-base layer was met; this confirms the potential of utilizing waste filler as suitable accompanying filler in quantities up to 20% of the mix in total. Under technical specifications TP112, void content of foam bitumen mixes should not exceed the threshold value of 18%-vol. This condition was met by all foamed asphalt mixes designed. In general it has to be stated, that the results might be negatively influenced by the chosen laboratory specimen compaction method. Mixes were not designed as open graded, however results show higher air voids values even for mixes with higher content of added waste filler, which can be quite illogical.

Table 3. Summary of basic mechanical and physical characteristics of foamed asphalt mixes.

Mix			FC	FF	FCF1	FCF2
Bituminous binder content	:	%-m.	7.60	8.77	9.10	8.67
Passing, sieve 0,125 mm	:	%-m.	18.0	25.5	15.7	15.9
Passing, sieve 0,09 mm	:	%-m.	16.2	23.5	17.8	18.1
Specific gravity (compacted)	:	$g \cdot cm^{-3}$	2.021	2.047	2.068	2.018
Air voids	:	%-vol.	16.3	13.8	8.8	11.7

Table 4. Summary of basic mechanical and physical characteristics of cold recycling mixes with bituminous emulsion.

Mix			REC1	REC2	REC3	REC4	REC5
Bituminous binder content	:	%-w.	6.18	5.89	5.64	6.33	6.31
Passing, sieve 0,125 mm	:	%-w.	16.5	21.5	21.3	17.3	15.7
Passing, sieve 0,09 mm	:	%-w.	15.0	19.5	19.4	14.7	13.7
Spec. gravity (compacted)	:	$g \cdot cm^{-3}$	2.121	2.253	2.238	2.149	1.993
Air voids	:	%-vol.	14.5	9.2	13.3	12.7	16.3

Table 5. Indirect tensile test results for cold recycling mixes, binder—bitumen foam, 28 days curing at 5°C and with loading speed of 50 mm.min^{-1}.

Mix	Force of specimen rupture, $F_{28\ days}$ (kN)	Transverse deformation, $\Delta_{28\ days}$ (mm)	Indirect tensile strength, $ITS_{28\ days}$ (MPa)	Strain, $\varepsilon_{28\ days}$ (%)	Modulus of elasticity, $E_{28\ days}$ (MPa)
FC	5.94	2.48	0.53	5.12	20.60
FF	4.71	2.73	0.46	5.65	16.13
FCF1	6.27	1.94	0.60	4.02	29.89
FCF2	7.07	2.09	0.67	4.32	30.69

Table 6. Indirect tensile test results for cold recycling mixes, binder—bituminous emulsion, 28 days curing.

Mix	Force of specimen rupture, $F_{28\ days}$ (kN)	Transverse deformation, $\Delta_{28\ days}$ (mm)	Indirect tensile strength, $ITS_{28\ days}$ (MPa)	Strain, $\varepsilon_{28\ days}$ (%)	Modulus of elasticity, $E_{28\ days}$ (MPa)
REC1	9.85	1.50	1.02	3.08	65.63
REC2	7.61	1.65	0.85	3.39	52.05
REC3	5.83	1.76	0.63	3.62	34.28
REC4	5.91	1.91	0.65	3.92	32.83
REC5	5.65	3.19	0.51	6.58	15.54

– From the perspective of recommendations in particularly foreign sources, (e.g. Nielsen, 2008) for the maximum proportion of particles smaller than 0075 mm, all mixes designed meet the threshold value despite the addition of waste filler.
– According to technical specifications TP162 (Ministry of Transport, 2007), the independently stated results of the indirect tensile strength test constitute the determining quality criterion at present. The test was performed for all mixes assessed after at least 28 days of air curing. Besides an assessment of the results against the technical requirements, both the associated systems—foamed bitumen and bituminous emulsion—can be compared to each other. The results make it clear that from the perspective of this criterion, three out of the designed mixes do not meet the minimum required value of $ITS_{28\ days}$ 0.6 N · mm^{-2} (FC, FF and REC5). In both sets, these are primarily mixes representing the mix design commonly used at present. However, at the same time, it is necessary to add that the criterion is required from cold recycling mixes with grading 0–32 mm and the technical specifications do not distinguish mixes where the maximum grain size is less than 32 mm.
– With mixes that did not meet the criterion of minimum indirect tensile strength after 28 days of air curing, it is obvious that they show higher values of relative deformation; on the other hand, also a significantly lower value of elasticity modulus has been determined.
– Based on the learning in the field of indirect tensile strength testing, the researches proposed (Luxemburk et al., 2008) that any future innovation of technical specifications in the Czech Republic determines the indirect tensile strength criterion after 28 days air curing $ITS_{28\ days} \geq$ 0.5 N · mm^{-2} for foamed bitumen mixes instead of the currently used criterion $ITS_{28\ days} \geq$ 0.6 N · mm^{-2} which does not distinguish between cold recycling mixes utilizing bituminous emulsion from foamed asphalt mixes despite the fact that a number of foreign sources have proven differences in the behavior of both the systems in the past (e.g. Kweir et al., 2001). At the same time, with respect to the issue of stiffness modulus it is necessary to consider the suitability and applicability of the elasticity modulus criterion resulting from the indirect tensile strength test which has not been considered in Czech regulations at all so far.
– In the assessment of the effect of waste filler in cold recycling mixes, it is possible to declare a positive effect even in the case of indirect tensile strength; the comparison of REC1–REC2

mixes demonstrates the potential for partial substitution of hydraulic binder (cement) through the effect of the waste filler in the mix. The reduced quantity of cement in the mix due to the utilization of waste filler is also noticeable in the case of foamed asphalt mixes where FCF1 and FCF2 mixes achieve very good results in comparison to FC mix.
– The comparison of foamed asphalt mixes and bituminous emulsion cold recycling mixes confirmed the earlier findings; particularly those about a higher indirect tensile strength value of the cold recycling mixes using bituminous emulsion.

5 STIFFNESS MODULUS ASSESSMENT

The stiffness modulus of asphalt mixes acquired by repeated indirect tensile tension by the Nottingham Asphalt Tester (NAT) constitutes according to technical specifications TP170 a significant deformation characteristic used, together with the Poisson's ratio, in the process of road pavement construction design in the Czech Republic (Ministry of Transport and Communications, 2004). Generally, the stiffness modulus is defined as the ratio between the tension and the strain under a given temperature for which there is a particular value of Poisson's ratio, and characterizes material's ability to resist the effects of loading. The resistance to load increases with increasing stiffness modulus values.

Stiffness modulus values are determined based on a non-destructive repeated indirect tensile test which is regularly performed on Marshall specimen. Direct compressive stress transferred in the plane of vertical cross section of the specimen results in indirect tensile tension perpendicular to the direction of the load. Horizontal deformation is measured with LVDT sensors during the test. Generally, the stiffness modulus acquired by indirect tensile tension can be expressed by means of following equation:

$$S = \frac{F \cdot (\mu + 0{,}273)}{\Delta \cdot h} \tag{1}$$

where μ Poisson's ratio of the asphalt mix depending on the temperature of stiffness modulus definition,

Δ maximum horizontal deformation caused by the loading pulse (mm),
h average height of the test specimen (mm),
F maximum vertical load (N).

In the case of cold recycling mixes using RAP material and bituminous binder in the form of bitumen foam or bituminous emulsion, the mix is assumed to be close to asphalt mixes from the point of view of material characteristics and, therefore, similar values of the Poisson's ration can be applied as in the case of hot asphalt mixes.

Measurement of the stiffness modulus of an asphalt mix is in Czech Republic usually performed under temperatures of 15°C to 40°C with subsequent determination of the relative mix quality indicator which is the asphalt mix's thermal susceptibility. From the perspective of asphalt mix quality, it can be applied that the lower the thermal susceptibility indicator, the better quality of the mix in question. Generally, the thermal susceptibility can be defined by the ratio of stiffness modulus measured under the highest and lowest temperatures:

$$t_S = \frac{S_{\min}}{S_{\max}} \tag{2}$$

where $S_{\min}$ stiffness modulus of the asphalt mix obtained under the minimum testing temperature of 15°C,
$S_{\max}$ stiffness modulus of the asphalt mix obtained under the maximum testing temperature of 40°C.

In the case of cold recycling mixes, temperatures of 5°C, 15°C and 27°C were preferred. The reason is the fact that very low stiffness modulus values were obtained for a number of mixes under 27°C and any further increasing of the test temperature would probably reach

the measurability threshold. Moreover, the temperature of 5°C meets the requirements under the existing technical specifications where the indirect tensile strength is determined under this particular temperature. Due to this reason, an adjustment of the thermal susceptibility criterion has been proposed in the following form for cold recycling mixes:

$$t_{S,REC} = \frac{S_{5°C}}{S_{27°C}} \tag{3}$$

From the perspective of regressive analysis, based on the studies performed and assessment of the dependence of the stiffness modulus on temperature, it is possible to conclude that the trend for cold recycling mixes is best characterized by an exponential or linear regressive function. The exponential function which can be generally formulated as the following equation was more suitable for the course of the dependence of the stiffness modulus on the temperature for mixes described in this article; the statistical suitability of the exponential function an its general formulation should be further verified in ongoing research.

$$S = a_S \cdot e^{-b_S \cdot T} \tag{4}$$

where S stiffness modulus (MPa),
T temperature of stiffness modulus determination (°C),
a_S constant which determines the probable value of the stiffness modulus under temperature T = 0°C from the statistical point of view,
bs statistical thermal susceptibility constant.

In the case of analyzing the parameter of a statistically derived thermal susceptibility, defined by parameter b_S, it is possible to conclude that the mix achieves better quality with a lower value of the constant. Generally, it is also possible to state that the flatter the slope of the regressive curve the less susceptible the mix is to changes in temperature.

Stiffness measurements have been done for each mix and each mix on at least 4–5 different specimens. For mixes REC1-3 there were further replicate tests which had to verify the reproducibility of gained testing data. Achieved results have shown a variation coefficient between 8% and 25%. With respect to non-homogenous pattern of the reclaimed asphalt material such variation has been interpreted positive.

Based on the analysis of the experimental measurements performed for the laboratory designs of commonly applied cold recycling mixes modified with waste filler, the following conclusions can be made from the point of view of the stiffness modulus:

– If the value under 15°C is considered the determining criterion for the mutual comparison of mix quality from the point of view of the stiffness modulus, the characteristic (identically to the indirect tensile strength) demonstrates the difference between the systems using bituminous emulsion and foamed bitumen. While mixes FC and REC5 which represent a combination of bituminous binder, cement and RAP material, show more or less identical values, the foamed asphalt mixes where a part of the reclaimed material was substituted with waste filler demonstrated values on average 35% lower when compared to the values of cold recycling mixes with bituminous emulsion and waste filler.

Table 7. Stiffness modules for cold recycling mixes after 28 days air curing, binder—foamed bitumen.

Mix	Stiffness modulus (MPa) @ T°C			Thermal susceptibility $t_{S,REC}$	Statistical thermal susceptibility b_S
	5	15	27		
FC	3,800	2,750	1,950	1.95	0.0303
FF	3,250	1,600	950	3.42	0.0555
FCF1	8,050	6,400	5,900	1.36	0.0246
FCF2	6,650	4,800	3,850	1.73	0.0139

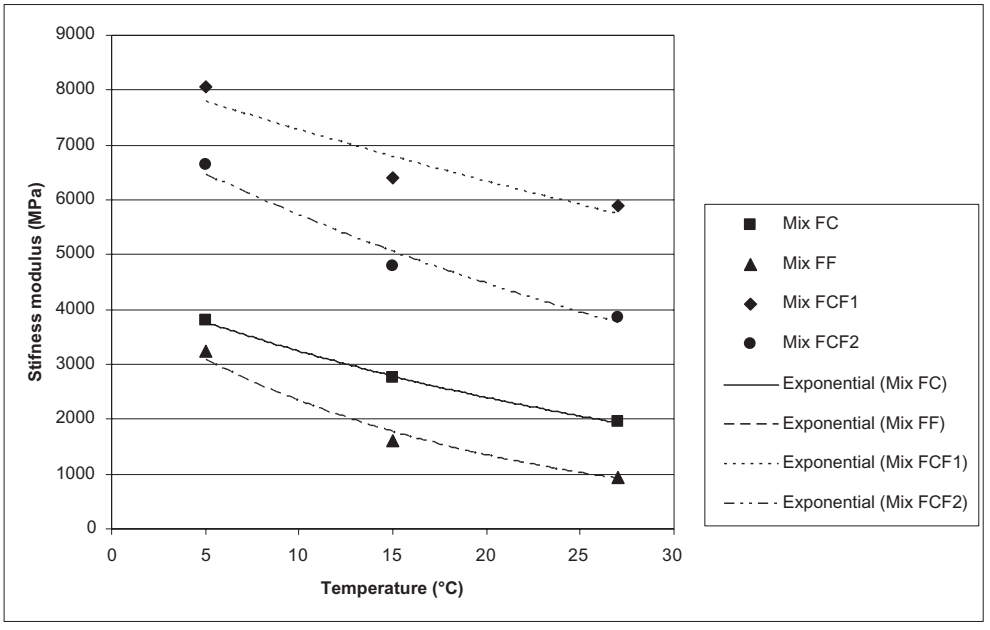

Figure 3. Stiffness modules for cold recycling mixes after 28 days air curing, binder—foamed bitumen.

Table 8. Stiffness modules for cold recycling mixes after 28 days air curing, binder—bituminous emulsion.

Mix	Stiffness modulus (MPa) @ T°C			Thermal susceptibility $t_{S,REC}$	Statistical thermal susceptibility b_S
	5	15	27		
REC1	9,100	8,300	5,900	1.54	0.0200
REC2	10,000	9,500	8,200	1.22	0.0091
REC3	8,400	7,900	6,700	1.25	0.0104
REC4	7,500	7,000	4,950	1.52	0.0192
REC5	4,200	2,850	1,650	2.55	0.0426

– The effect of the waste filler is obvious in both sets of mixes also from the point of view of thermal susceptibility, whether defined as a classic ratio indicator or calculated theoretically based on a simple regressive analysis. Here, the reduction of thermal susceptibility was approx. 20% in the case of foamed asphalt mixes; and even almost 50% in the case of cold recycling mixes with bituminous emulsion. The effect of bitumen content in both sets of experimental mixes regarding thermal susceptibility can be excepted, because of same RAP used for all mixes and same bituminous emulsion or foamed bitumen content used.
– If we compare the effect of waste filler separately for both the sets we can say that the foamed asphalt mixes, despite the proportion of cement reduced by 1%-m, achieved almost doubly improved stiffness modulus value (in relation to the test temperature of 15°C). The reason for such increase in stiffness might be caused by lower air void content and improved concurrence between the aggregate particles. Mineralogical skeleton is more compact.
– It has been demonstrated that reclaimed material can be effectively substituted by waste filler probably up to 20%—both systems show an increase in the stiffness modulus value when the proportion of waste filler is increased from 0% to 20%, any further increase is expected to result in a rather negative effect due to excessive proportions of fine particles in the mix. The results correspond quite well with both the void content values and

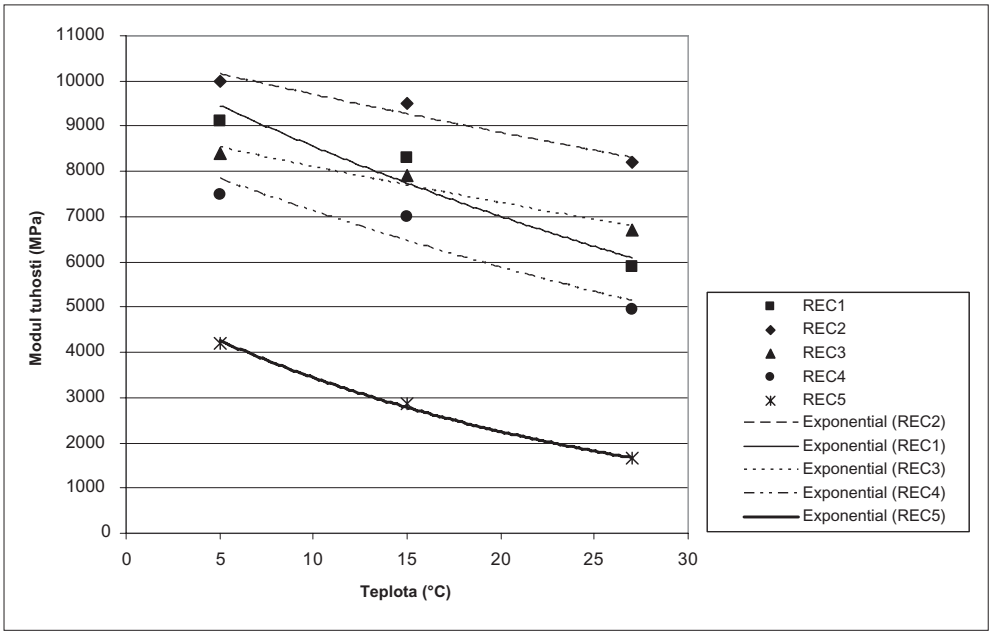

Figure 4. Stiffness modules (MPa) for cold recycling mixes after 28 days air curing, binder—bituminous emulsion.

indirect tensile strength. Even the result of comparing mixes REC3 and REC4 is rather interesting; the former mix only contains 1.5% cement and the proportion of RAP material to waste filler is 80:20 while the latter mix has 2.0% cement and a ratio of 90:10. The former mix achieves better values despite the lower cement content.

– The aforementioned positive effect of substituting a part of the reclaimed material by waste filler in the case of a foamed bitumen mix where the proportion of fine particles plays a very important role, results from a comparison of the FC mix to mixes FCF1 and FCF2. The stiffness of the mix improves significantly; moreover, a positive effect from the perspective of reduced thermal susceptibility was recorded as well. According to the results presented, stiffness modulus can be improved on average by 60–130% in comparison with the basic mix as used today while simultaneously reducing the proportion of cement by 1%-m. at the same time. This allows achieving two effects at the same time—increasing the stiffness modulus value which makes the foamed bitumen layer, particularly if used as a binder or sub-base layer, an absolutely new quality level, and limiting the proportion of valuable hydraulic binder (especially cement).
– The comparison of foamed asphalt mix and cold recycling mix with bituminous emulsion as binder confirms the conclusion stated in the final progress report of foamed asphalt mix design optimization (Luxemburk et al., 2008). Depending on the composition of the cold recycling mix, a mix applying bitumen foam system demonstrates a stiffness modulus value lower, on average, by 20–50%. The main reason is particularly the method of creating a binding effect in the mix. While all grains and particles are covered by bituminous emulsion upon mixing the individual ingredients of bituminous emulsion and all the ingredients subsequently adhere to each other after the emulsion has set and a thin asphalt film has been generated; in the case of bitumen foam, individual droplets of bitumen cover fine particles which subsequently ensure the adhesion of larger grains and filling of the voids with a plaster of bitumen foam and fine particles.

In the cited report (Luxemburk et al., 2008), based on the experimental results achieved for the temperature of 15°C which is determining from the point of view of the design method of road pavement multilayer structure under technical specifications TP170, the authors

proposed that the guiding minimum value of the stiffness modules considered for the application of cold recycling mixes in the pavement structural design, amount to 2500–3000 MPa for a standard cold recycling mix with a combination of bituminous binder and hydraulic binder; according to the authors, the values on the lower limit are particularly determining for foamed bitumen mixes what corresponds with the results presented in (Valentin et al., 2007). Based on the findings obtained from the experimental designs and assessment of mixes with partial substitution of the reclaimed material with simultaneous reduction of the total cement proportion due to waste filler application, this criterion could possibly be set more strictly to the level of 5,000–6,000 MPa while, again, the lower limit of the interval would apply to foamed asphalt mixes.

6 CONCLUSION

Cold recycling techniques are without question interesting solution for reuse of reclaimed material from existing pavements. At the same time they enable the utilization of other secondary materials as well. With respect to the importance of fine particles content in cold recycling mixes if bitumen foam or bituminous emulsion is used as binder allowing creation of effective binding mastic, the experimental activities and research of Civil Engineering Faculty, CTU Prague in this field focused in the last two years on the possibilities of waste filler utilization. As mentioned in this paper waste filler can by mainly identified as by-product of aggregate crushing.

While certain positive effect of waste filler was expected if used in cold recycling mixes, the so far reached results are significantly encouraging and achieved increase in values of some characteristics indicates the potential for utilization of this fine particle material. Significant improvement has been obtained for indirect tensile strength and stiffness. Results emphasized that the mastic in cold recycling mixes improves the cohesion and stiffness of the mix and at the same time enables very good decrease in voids content of the mix. In spite of relatively large number of experimentally designed mixes, it is necessary to validate current results by further laboratory testing with similar mixes as well as with more coarse-grained mixes. Another important issue will be the relationship between increased stiffness and susceptibility of cracking. Because cold recycling mixes are in Czech Republic used especially for the pavement sub-base or binder course fatigue testing will be most important. Simultaneously it will be necessary to verify experimental knowledge of improved mixes behavior by suitable in-situ trials.

ACKNOWLEDGEMENTS

This paper was supported by the research project of Ministry of Transport and Communications of the Czech Republic, No. CG712-043-910.

REFERENCES

Kweir, K. et al. 2001. Aspects influencing the performance of foamed bitumen stabilized aggregate mixtures. In Institute of Asphalt Technology (ed.), *The Asphalt Yearbook 2001*, pp. 27–34. Institute of Asphalt Technology: Stanwell.

Luxemburk, F. et al. 2008. Design Optimization of Foamed Asphalt Mixes and Assessment of Selected Rheologic Characteristics. In CTU Prague, *Final Research Project Report, project No. GACR 103/05/2055*, Prague: CTU Prague.

Ministry of Transport and Communications 2004. Design Manual for Road Pavements, In CTU Prague, TU Brno (eds.) *Technical Specifications TP170 (in Czech)*, Prague: Ministry of Transport of the Czech Republic.

Ministry of Transport and Communications 2007. Cold Foamed Asphalt Mixes., In IMOS Brno (ed.) *Technical Specifications 112* (revised edition, in Czech), Prague: Ministry of Transport of the Czech Republic.

Ministry of Transport and Communications 2007. TP 162 Cold In-Situ Recycling of Flexible Pavements Structural Layers with Bituminous Binders and Cement, In (ed.) *Technical Specifications 162* (revised edition, in Czech), Prague: Ministry of Transport of the Czech Republic.

Nielsen, N. et al. 2008. Full Depth Reclamation on Existing Asphalt Pavements, In: Eurasphalt & Eurobitumen, *Proceedings of 4th Euroasphalt & Eurobitume Congress 2008*, paper No. 403-002, Copenhagen: Eurasphalt & Eurobitumen.

Valentin, J. et al. 2006. Foamed Asphalt Mixes Used for Cold Recycling—Present Experience. In Faculty of Civil Engineering TU Bratislava (ed.) Proceedings of the Seminar *Reuse of structural materials for construction purposes (in Slovak)*: 117–122. Štrbské Pleso (SK): 2006.

Valentin, J. & Mondschein, P. 2007. Design Optimization of Foamed Asphalt—Czech Experience. In *Proceedings of Advanced Characterization of Pavement and Soil Engineering Materials*: 843-851. Athens: Balkena.

Advanced Testing and Characterization of Bituminous Materials – Loizos, Partl, Scarpas & Al-Qadi (eds)
© 2009 Taylor & Francis Group, London, ISBN 978-0-415-55854-9

Rehabilitation of an Italian highway by Cold In-Place Recycling techniques

F.A. Santagata, M. Bocci, A. Grilli & F. Cardone
Università Politecnica delle Marche, Ancona, Italy

ABSTRACT: In Cold In-Place Recycling (CIR), emulsion and foamed bitumen have currently used as the most common binders. However, there is a need to better understand the mechanical performance of these stabilized mixtures. This paper shows the results obtained from two trial sections in order to optimize the rehabilitation process of an Italian highway through CIR techniques for a subbase layer. The trial sections were built through two different stabilization techniques: cement-foamed bitumen and cement-emulsion treatment. Both applications considered recycled mixtures of 50% Reclaimed Asphalt Pavement (RAP) and 50% cementitious and granular milled materials, combining different contents of cement and bituminous binder. The experimental program provided the mechanical characterization in laboratory and *in-situ*. The result analysis allowed to evaluate and compare mechanical performance of stabilized-recycled materials and to highlight the practical application of the two stabilization techniques.

1 INTRODUCTION

This technical paper deals with the upgrading works of the Italian East Highway A14, linking the city of Bologna to the city of Taranto. In particular, the section of highway investigated is between Ancona Sud and Porto Sant'Elpidio, located in the Marche region.

Currently, the above mentioned highway is a four-lane dual carriageway facility. The old pavement structure consists of 300 mm of asphalt concrete, 200 mm of cement concrete and 200 mm of granular mixture.

In the last few years, the increase in heavy vehicle traffic has called for the widening of each carriageway to a three-lane facility.

In order to reduce the construction costs as well as the supply of natural aggregates, a Cold In-Place Recycling has been chosen as a rehabilitation technique for the subbase layer. In particular, the design provides stabilization with foamed bitumen of the subbase layer of the new slow lane, corresponding to the current emergency lane, and the new emergency lane. As an alternative solution stabilization with bituminous emulsion was suggested.

The main construction phases can be summarized as follows:

- widening of both carriageways;
- milling of asphalt layers and the cement-treated layer of the old emergency lane;
- stabilization of the recycled subbase layers;
- paving of asphalt layers (wearing, binder and base course).

In order to guarantee the required structural capacity, the new pavement structure consists of 290 mm asphalt concrete, and 300 mm of stabilized recycled subbase.

In order to select the cold recycling technique two distinct trial sections were built:

1. trial section stabilized with bituminous emulsion and cement;
2. trial section stabilized with foamed bitumen and cement.

The main aims of the trial sections were to select the optimal recycled mixture in terms of cement and bituminous binder content and to determine the working procedures from the milling of the old emergency lane to the construction of the new slow and emergency lanes. To that end the pavement performance analysis was developed by means of *in situ* and laboratory mechanical characterization of the treated mixtures.

2 PILOT PROJECT

Trial section n°1 and n°2 had a length of about 200 meters and width of about 7 meters and were built between design cross section 274 ÷ 268 and 244 ÷ 236, respectively.

2.1 *Trial section n° 1: cold recycling with bituminous emulsion*

The trial section n°1 had a length of about 200 meters and width of about 7 meters. On the basis of other research projects (Liebenberg 2003, Liebenberg & Visser, 2004) two cement contents (2.0 and 2.5%) and two bituminous emulsion contents (2.5 and 3.0%) were selected. From the combination of the two cement contents and two bituminous emulsion contents, four different recycled-stabilized mixtures were considered and laid on four different areas (about 100 × 3,5 m^2 for each area).

The recycled aggregate blend was recovered from the milling of the asphalt and cement base pavement layers of the old emergency lane. The sequence of the milling procedure was decided so as to obtain a recycled blend consisting of about 50% RAP and 50% cement-treated and granular material from the old pavement.

Finally, a cement type II/B-LL 32,5 R and a bituminous cationic emulsion (table 1) were selected.

2.2 *Trial section n° 2: cold recycling with foamed bitumen*

In this case, the stabilized subbase layer of the trial section was divided in six areas so that six different recycled-stabilized mixtures were studied.

Table 1. Characteristics of the cationic emulsion.

Emulsion characteristics	
Water content (EN 1428)	40%
pH value (EN 12850)	3
Application temperature	5 ÷ 80°C
Characteristic of the extracted bitumen	
Needle penetration (EN 1426)	70 dmm
Softening point (EN 1427)	50°C
Fraass breaking point (EN 12593)	–10°C

Table 2. Characteristics of the foamed bitumen.

Foamed bitumen characteristics	
Expansion ratio	15 ÷ 25
Half-life (secs)	15 ÷ 18
Application temperature	160 ÷ 190°C
Characteristics of the bitumen	
Needle penetration (EN 1426)	90 dmm
Softening point (EN 1427)	45°C
Dynamic viscosity (EN 13702)	0,13 Pa · s

On the basis of other research projects (Jenkins et al.1999, Jenkins 2000, Jenkins et al. 2007, Smith 1999, Loizos et al. 2004, Loizos 2007, Raffaelli 2004) three different cement contents (1.5 ÷ 1.75 ÷ 2%) and two foamed bitumen contents (2.5 and 3%) were considered. As for the trial section n°1, from the combination of the three cement contents and two bituminous emulsion contents, six different recycled-stabilized mixtures were considered and laid on six different areas.

Even in this case, the recycled blend consisted of about 50% RAP and 50% cement- treated and granular material from the old pavement. Finally, a cement type II/B-LL 32,5 R and a foamed bitumen (table 2) were selected.

2.3 *Construction sequence*

In order to obtain a recycled blend consisting of about 50% RAP and 50% cementitious and granular milled materials, an articulated milling sequence was undertaken involving the asphalt layers, the cement-treated layer and the upper part of the foundation layer of the old emergency lane.

The construction works of both trial sections can be summarized as follows:

- Step 1: widening and construction of the new embankment on which the emergency lane will be built. The top level of the embankment is 0.55 m below the surface level of the old asphalt pavement. In fact, the top of the binder course corresponds to the old pavement surface level;
- Step 2: milling of asphalt concrete to a depth of 0.05 m as from 9.50 m from the highway center line for the total width of the old emergency lane (3.50 m) and storing of the milled RAP on the top of the new embankment;
- Step 3: milling of asphalt concrete for a further 0.20 m (to a depth of 0.25 m) as from 9.75 m from highway center line. Note that the depth of 0.25 m corresponds to the top level of the new recycled-stabilized layer. Moreover, this second milling operation generates a stair (0.25 m wide and 0.05 m thick) required for the joint stagger of the new binder layer. Even in this case the recovered RAP was placed on the new embankment by the side of the old emergency lane so as to form a support for the milling machine for the next milling step;
- Step 4: milling of further 0.20 m (to a depth of 0.45 m) involving the remaining 0.05 m of the old asphalt concrete and 0.15 m of the old cement concrete. This milling operation starts from 10.15 m from the highway center line. Note, this milling operation generates another stair (0.40 m wide and 0.20 m thick) required as support for the wheel of the recycler. The milled materials were placed on the external side of the new embankment;
- Step 5: leveling of total milled materials by means of a grader and compaction to the required level using a vibrating smooth drum roller;
- Step 6: on the basis of fixed contents spreading of cement by means of a proper vehicle equipped with volumetric batchers. Subsequently, the recycler, coupled to a tank truck to carry the emulsion or hot bitumen and a tank truck to carry cold water to foam the bitumen, was used to stabilize a thickness of 0.30 m of the milled material to a depth of 0.55 m. Note that the stabilizing operation also involves the remaining 0.05 m of the cement concrete and 0.05 m of the granular foundation in the old emergency lane;
- Step 7: the treated material was compacted immediately behind the pulvimixer by a vibrating smooth drum roller before being shaped by a grader. Finally a 20 ton vibrating smooth drum roller and a 25 ton pneumatic-tyred roller were used to compact the stabilized subbase layer;
- Step 8: paving of asphalt layers. Note that the new binder level corresponds to the the surface level of the old asphalt pavement. This implies a superelevation of 0.04 m (wearing course) with respect to the old asphalt pavement.

3 PILOT SECTION EVALUATION

The evaluation phase involves the selection of the optimal binder contents by means of mechanical characterization of the subbase layer and the selection of the most reliable

technical process. The mechanical characterization was conducted through field and laboratory measurements by performing non-destructive and destructive tests. In particular, the *in-situ* non-destructive tests consisted of Falling Weight Deflectometer (FWD) measurements performed at different construction times. The laboratory investigation consisted of preliminary size gradation of recycled material to control its correspondence with the technical specification requirements and dynamic tests in order to measure the stiffness and fatigue performance of the recycled materials.

3.1 *Size gradation*

Size gradation of the recycled materials was checked on 15 kg samples taken from the new slow and emergency lane after the pulverizing and before the stabilizing procedures.

The figure 1 shows the size gradation of two samples. It is possible to note that the size gradation of these blends conforms to the technical specification. Moreover, a careful visual inspection of recycled materials allowed to check that the ratio between the RAP and crushed cemented materials was about 0,5 as expected.

3.2 *Specimen preparation*

Samples of 4.5 kg were compacted *in situ* by a mobile gyratory shear compactor (UNI EN 12697-33) at 180 revolutions in a mould of diameter 150 mm according to Italian Highway Specifications.

After one day curing, the central part of specimen with a height of 75 mm was taken out by means of double parallel cutting.

3.3 *Indirect tensile stiffness modulus*

The stiffness modulus tests were carried out by means of the Nottingham Asphalt Tester (NAT) in indirect tensile configuration. In particular, the stiffness modulus tests were performed in a strain mode with strain target of 2 μm, rise time of 124 μs and test temperature of 20°C. Since the material is tested in its quasi-elastic state, each specimen was tested at different curing times and respectively at 7, 14, 21 and 28 days in order to evaluate the increase in modulus due to the curing of cement.

Figures 2 and 3 show the average value of stiffness modulus for each type of mix treated with emulsion (trial section n°1) and foamed bitumen (trial section n°2) as a function of curing time, respectively.

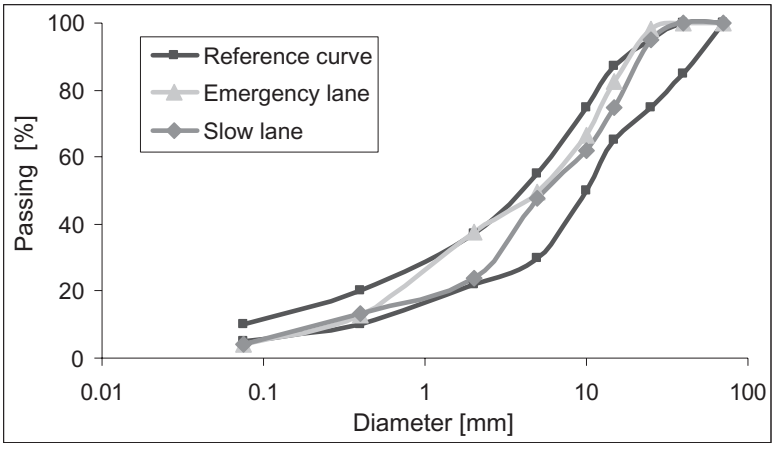

Figure 1. Recycled blend size gradation.

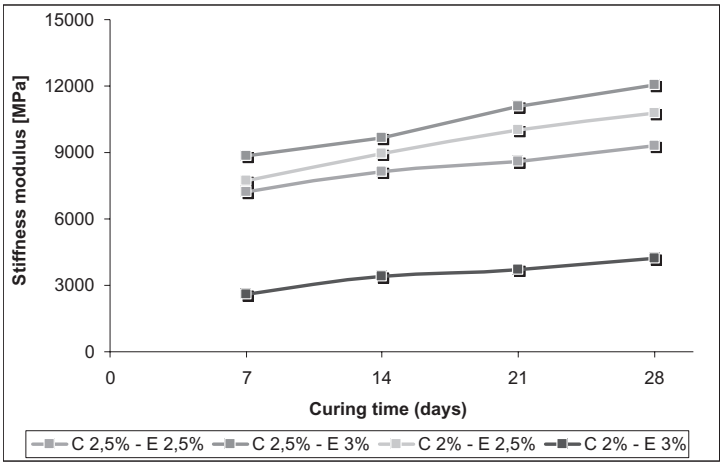

Figure 2. Stiffness modulus evolution for emulsion treated specimens (trial section n°1).

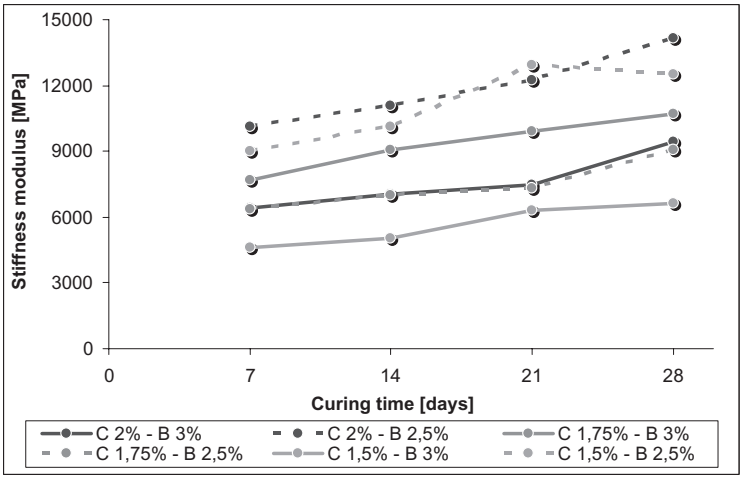

Figure 3. Stiffness modulus evolution for foamed bitumen treated specimens (trial section n°2).

From the analysis of results, it is possible to note that after 7 curing days all recycled samples showed high stiffness moduli ranging between about 2500 and 10000 MPa. Moreover, for all recycled samples the effect of the curing time resulted in a significant increase in modulus of about 40% with peaks of 60% after 28th day, satisfying the technical requirements.

Even though mixtures with high modulus values would better guarantee the respect of technical requirements, it is worth remarking that too high stiffness is not a synonym of durability and could lead to brittle behaviour, implying premature failure under repeated loading cycles. On the other hand, the use of bitumen in addition to the cement reduces the brittle behaviour of cement-treated material and confers the ductility which is typical of bituminous mixtures.

3.4 *Fatigue test*

Fatigue tests were carried out in indirect tensile configuration and in controlled stress mode by means of the NAT. Tests were performed on the specimens previously subjected to the

modulus test (curing time >28 days). Since the mechanical properties of these materials depend highly on the curing time, it was necessary to repeat the modulus test on each specimen before performing the fatigue test. Moreover, as is well-known, according to the elastic multi-layer theory, the stiffer the layer, the higher the tensile stress in the material. Therefore, the tensile stress applied was related to the stiffness of each specimen. In particular, each tensile stress was selected in order to induce a typical initial strain level ε_t for a highway foundation and evaluated in 50 microstrain.

According to the theory of elasticity for the indirect tensile configuration test, stress is related to strain as follows:

$$\sigma_t = \frac{S \cdot \varepsilon_t}{1000 \cdot (1 + 3 * \nu)} \tag{1}$$

where σ_t (kPa) is the applied tensile stress along the horizontal diameter, ε_t is the maximum tensile horizontal strain, S is the stiffness modulus and ν is Poisson's ratio assumed to be 0.3 for the material tested.

Finally, in order to investigate the fatigue properties of each type of mixture, the number of load pulse to the fracture was considered and compared.

While all series treated with foamed bitumen showed fracture at the end of the test, none of the series treated with emulsion showed any fracture in a reasonable time and compatible with laboratory needs. Therefore it can be preliminary asserted that the mixtures stabilized with emulsion showed higher fatigue performance. However, an initial strain level of 50 microstrain did not allow the effects of the different dosage of binders in emulsion-treated mixtures to be evaluated.

To assess the influence of different emulsion/cement dosages, a higher tensile stress, corresponding to ε_t of 60 microstrain, was selected in order to lead the mixtures to failure. Figure 4 summarizes the fatigue results for each type of recycled mixture and allows a direct comparison among of all the mixtures. It is important to remember that the strain level adopted to characterize the two types of mixtures was different (ε_t of 50 microstrain for foamed bitumen mixtures and ε_t of 60 microstrain for emulsion-treated mixtures).

From figure 4 it can be noticed that, at a fixed cement content, the recycled mixtures with the highest foamed bitumen content showed the highest fatigue resistance.

In the same way, at a fixed cement content, the recycled mixtures which were richest in emulsion showed fatigue resistance that was significantly higher than those with a lower emulsion dosage.

These findings confirm the importance of ductile and durable intergranular bonds, resulting from the bituminous binder, which are able to accumulate higher deformation without

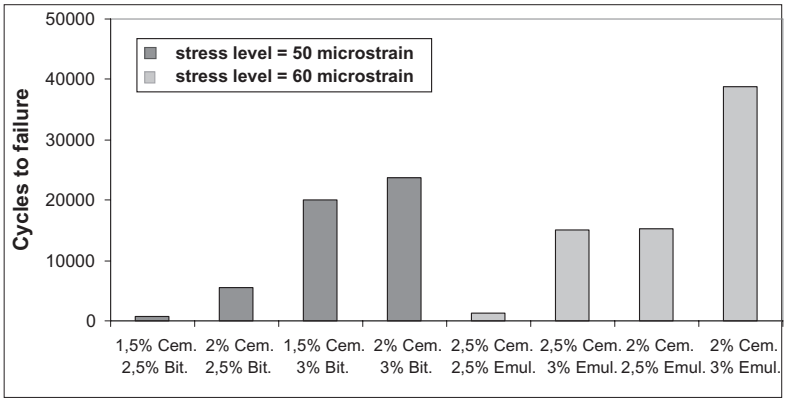

Figure 4. Fatigue results for specimens of both trial sections.

reaching premature fracture as opposed to the rigid and brittle bonds produced by cement. Therefore, it can be stated that the recycled mixture which guarantees the best fatigue performance is the mixture stabilized with 3% emulsion and 2% cement.

3.5 *Falling Weight Deflectometer test*

In order to verify the uniformity of the pavement construction technique and the pavement structural properties versus time, several FWD measurements were carried out on the two trial sections.

Two different series of FWD measurements were performed. In particular, the first one was carried out 3 weeks after the construction of the trial section stabilized with bituminous emulsion (trial section n°1) and 2 weeks after the construction of the trial section stabilized with foamed bitumen (trial section n°2), respectively. The second series were carried out 12 weeks after the first series measurements on both trial sections. This second series was carried out to conform with the Italian Technical Standards which require the elastic modulus to be checked after 90 days.

The FWD measurements of the first series were performed every 10 meters and the monitored temperature was 7.4°C.

As temperature dependent law for the elastic modulus, the following equation was adopted:

$$E_{ref} = \frac{E}{10^{a(T_{ref}^2 - T_{pav}^2)}} \tag{2}$$

where E_{ref} is the elastic modulus at reference temperature, E is the elastic modulus at test temperature from the back-calculation analysis, T_{ref} is the reference temperature, T_{pav} is the test temperature and a is an experimental parameter depending on the nature of the material.

To estimate the experimental parameter a on the basis of the effective influence of temperature on the investigated recycled material, ITSM tests were carried out on cylindrical specimens compacted *in-situ* after the stabilization activities on the above mentioned design trial sections. After a curing time of 28 days, ITSM tests were performed at three different temperatures, i.e. 5, 20 and 35°C. Through a least square regression between the measured and calculated modulus values, it was possible to find the parameter a equal to 0.000029. This value is lower than the one generally assumed for HMA (0,000050), confirming a lower temperature sensitivity of this kind of recycled materials.

Table 3 shows the elastic modulus values from back-calculation analysis related to the first series measurements at a reference temperature of 20°C for both trial sections. By considering the short past curing time, all series gave satisfactory results.

As previously mentioned, the second series of FWD tests was performed 12 weeks after the first series of FWD tests on both the trial sections. The FWD measurements were carried out only on the new slow lane because of technical problems.

The figures 5 and 6 show the elastic modulus of stabilized layers for the slow lanes in both trial sections considering different curing times.

From the figure 7, it can be seen that the emulsion stabilized mixtures already showed modulus values (about 3000 MPa) close to those required by technical standards after 3 weeks of treatment. Moreover, it is possible to evaluate an increase in modulus, due to the curing time, of more than 100% after 12 weeks.

On the contrary, from the figure 8, it is possible to note that, even though the foamed bitumen stabilized mixtures showed significant increases in modulus over time, they never guaranteed the minimum required value of 3000 MPa at 90 days.

It is important to add that both the analysis of laboratory results and the results from the FWD tests indicated that the emulsion stabilization technique, if compared with the foamed bitumen stabilization technique, showed in general a better mechanical performance. This result induced the design team to choose emulsion stabilization as provisional construction

Table 3. Elastic modulus values from back-calculation analysis related to the first series measurements.

	Mixture composition		Elastic modulus FWD–21 days		
	Cement	Emulsion	Subbase	Foundation	Subgrade
Lane	(%)	(%)	(MPa)	(MPa)	(MPa)
Slow lane	2,5	3	1866	455	209
	2,5	2,5	2607	537	207
Emergency lane	2	3	1287	529	265
	2	2,5	762	278	178
	Mixture composition		Elastic modulus FWD–14 days		
	Cement	Emulsion	Subbase	Foundation	Subgrade
Lane	(%)	(%)	(MPa)	(MPa)	(MPa)
Slow lane	2	3	1431	349	162
	2	2,5	1328	330	165
Emergency lane	1,75	3	2354	462	189
	1,75	2,5	2536	989	243
Emergency lane	1,5	3	2250	700	189
	1,5	2,5	2856	475	170

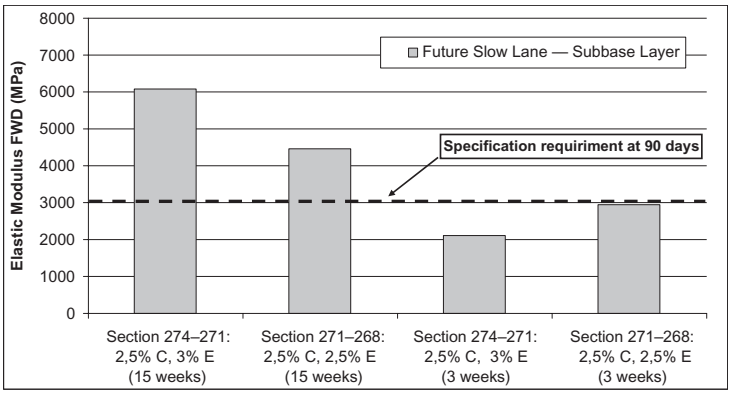

Figure 5. FWD measurements on future slow lane for the trial section n°1.

technique waiting for further confirmations. Therefore, in a provisional way and while waiting for the overall evaluation of results, it was decided to stabilize a further stretch of highway (design cross 347–291), adopting an emulsion content of 3% and a cement content of 2,5%.

In order to check the mechanical properties of these stabilized layers, and therefore to validate the choice, further FWD measurements were performed at different times.

The figures 7 and 8 show the results of elastic modulus of the emulsion-stabilized subbase (emulsion content 3% and cement content 2.5%) as a function of curing time at a reference temperature of 20°C for the emergency and slow lane, respectively.

In both figures, it is possible to note that the elastic modulus obtained was generally higher than or close to the threshold value required by technical specifications even if a shorter curing times had passed. This confirmed the result obtained from trial section n°1 and, in order to choose a non-stiff mixture with good fatigue performance, the design dosage was 2% cement content and 3% emulsion content.

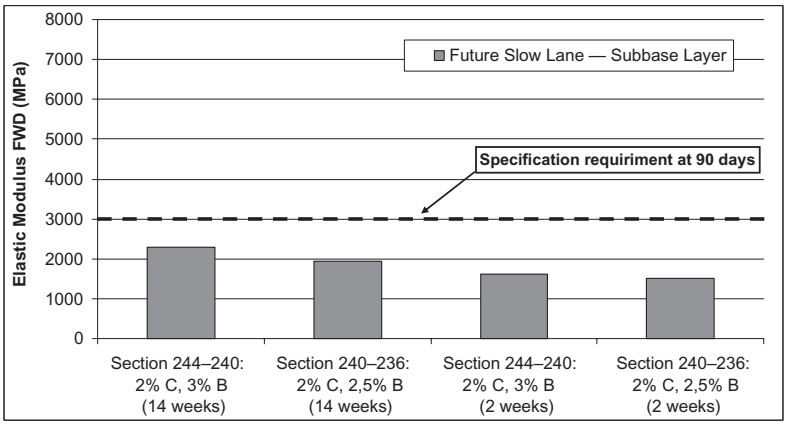

Figure 6. FWD measurements on future slow lane for the trial section n° 2.

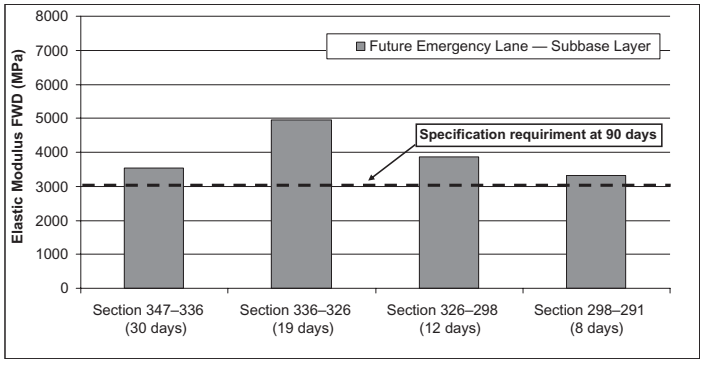

Figure 7. FWD measurements on future emergency lane for emulsion-stabilized subbase (emulsion content 3% and cement content 2.5%).

4 CONCLUSION

In this technical paper, the upgrading works and techniques used on an Italian Highway A14 have been described. In particular, the study focused on the attempt to verify the most efficient and suitable Cold In-Place Recycling rehabilitation technique. The emulsion treatment technique and the foamed bitumen treatment technique were both investigated in terms of mechanical performance and operational benefits throughout the construction phase. The experimental project involved two trial sections rehabilitated using the above mentioned Cold In Place Recycling techniques. The overall analysis of data results, obtained through *in-situ* and laboratory tests, led to the following findings:

– for proper bituminous binder dosages, the use of bituminous emulsion as an alternative to foamed bitumen allowed satisfactory performance to be guaranteed in terms of bearing capacity;
– on the basis of ITSM results, for both recycling treatment the stabilized-recycled mixtures characterized by high cement and low binder contents showed high stiffness moduli at 7 days. In order to avoid stabilized layers which are too stiff and therefore subject to premature failures, it would be appropriate to also take into account recycled mixture characterized by lower stiffness. Such a consideration indicates that the emulsion stabilized mixture with 3% emulsion and 2% cement is the most suitable;
– the fatigue results show better fatigue performance for the emulsion-treated recycled mixture compared with the foamed bitumen-treated mixture. In particular, it can be stated

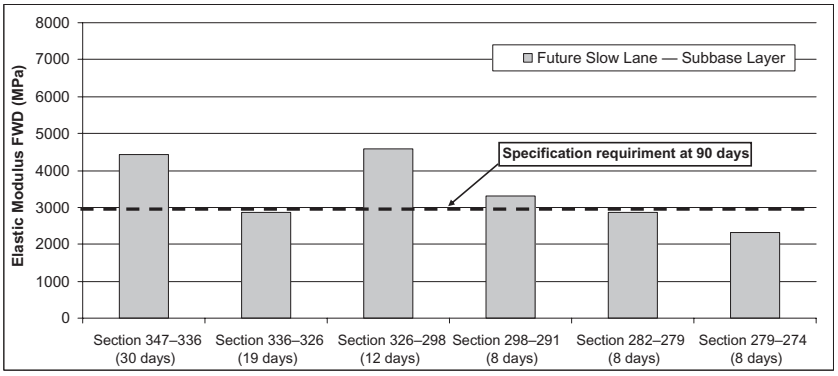

Figure 8. FWD measurements on future emergency lane for emulsion-stabilized subbase (emulsion content 3% and cement content 2.5%).

that the recycled mixture stabilized with the 3% emulsion and 2% cement guaranteed the best fatigue performance, as previously supposed;

– in confirmation of the laboratory findings, the FWD measurements allowed the emulsion stabilized-recycled mixtures to be evaluated as satisfactory because they guarantee the minimum specification requirements. In particular, because of the high stiffness moduli of stabilized-recycled layers of trial section due to the higher cement content (2,5%) it was considered proper to adopt the 3% emulsion and 2% cement as optimal dosages;

In addition to these performance advantages, the emulsion treatment proves to be a more suitable rehabilitation technique because of operational benefits obtained during the construction phase since:

– the emulsion treatment technique does not require the heating of bitumen and leads to more safety workplace;
– in the event of any delay in the work if the bitumen tank cools to under 160°C, it needs to be heated again at the mix-plant, causing operational complications. This does not happen with the emulsion treatment technique since good results have been reached even with emulsion at ambient temperature;
– during the first hours of application emulsion slows down the cement curing thereby guaranteeing a longer working time for compaction after the mixing by recycler.

REFERENCES

Jenkins K.J., Van de Ven M.F.C. & de Groot J.L.A. 1999. Characterization of foamed bitumen, 7th Conference on Asphalt Pavements for Southern Africa.

Jenkins K.J. 2000. Mix design considerations for cold and half-warm bituminous mixes with emphasis on foamed bitumen, PhD Dissertation, University of Stellenbosch.

Jenkins K.J., Long F.M. & Ebels L.J. 2007. Foamed bitumen mixes = shear performance?, International Journal of Pavement Engineering.

Liebenberg J.J.E. 2003. A structural design procedure for emulsion treated pavement layers, PhD dissertation, University of Pretoria.

Liebenberg J.J.E. & Visser A.T. 2004. Towards a mechanical structural design procedure for emulsion-treated base layers, Journal of the South African Institution of Civil Engineering.

Loizos A., Collings D. & Jenkins K. 2004. Rehabilitation of a major Greek highway by recycling/stabilizing with foamed bitumen, 8th Conference on Asphalt Pavements for Southern Africa.

Loizos A. 2007. In-situ characterization of foamed bitumen treated layer mixes for heavy-duty pavements, International Journal of Pavement Engineering.

Raffaelli D. 2004. Foamed asphalt base stabilization, Institute of Trasportation Studies, University of California Berkeley.

Smith W. 1999. Foamed bitumen stabilisation project—Warwick, QLD, Joint Transport South Australia/AustStab Seminar.

Advanced Testing and Characterization of Bituminous Materials – Loizos, Partl, Scarpas & Al-Qadi (eds)
© 2009 Taylor & Francis Group, London, ISBN 978-0-415-55854-9

Fracture energy evaluation of Cold In-Place Recycling mixtures

S. Charmot
SemMaterials, North Salt Lake, Utah, USA

P. Romero
University of Utah, Salt Lake City, Utah, USA

ABSTRACT: The fracture characteristics of Cold In-place Recycling (CIR) mixtures are discussed in this research on the basis of fracture energy measured according to ASTM D 7313-07: "*Standard Test Method for Determining Fracture Energy of Asphalt-Aggregate Mixtures Using the Disk-Shaped Compact Tension Geometry*". An experimental design was conducted in an effort to understand the variables that can impact the fracture energy of CIR mixtures measured at –20ºC. The following variables that materials designers have control over were investigated: two emulsion types, three emulsion contents and two additive conditions. The variables that significantly affected the fracture energy of CIR mixtures were emulsion type and emulsion content. As long as other critical mixtures properties are not adversely affected, an increase in emulsion content is expected to significantly improve the fracture resistance of CIR mixtures.

Keywords: cold recycling mixture, fracture energy, cracking, disk shape compact test, emulsion

1 OBJECTIVES AND APPROACH

Cold mix asphalt recycling is defined as a process in which reclaimed asphalt pavement (RAP) materials are combined with new asphalt and/or recycling agents to produce cold base mixtures without the addition of heat (ARRA 2001). An asphalt emulsion is often used as the recycling or bonding agent in the cold recycling process. As the name implies, Cold In-Place Recycling (CIR) is performed on site, thus providing potential savings in terms of energy requirements from heating the materials and transporting them to the site as shown in Figure 1. The use of CIR has increased over the last decade. Agencies have used Cold In-place Recycling (CIR) as a cost effective rehabilitation alternative to address either functional or structural pavement deficiencies (Maurer et al. 2007). In both cases the CIR performance is based on the ability of the mixture to resist cracking. It is therefore of great interest to materials engineers to better understand factors that may affect CIR cracking resistance in order to optimize such mixes.

The objectives of the study are to evaluate factors that can affect the fracture potential or cracking resistance of CIR mixtures measured in terms of facture energy according to ASTM D 7313-07: "Standard Test Method for Determining Fracture Energy of Asphalt-Aggregate Mixtures Using the Disk-Shaped Compact Tension Geometry". The emphasis of the paper is the evaluation of factors that are under the control of the materials engineers such as emulsion type, emulsion content and lime additive usage with the ultimate goal to optimize CIR crack resistance. An experimental design is presented to evaluate the effect of such factors on fracture energy.

Figure 1. Overview of the CIR train and process.

2 FRACTURE ENREGY DETERMINATION OF COLD MIXTURES

2.1 *Test selection*

Fracture energy has been selected in this study as the property most suited to evaluate the facture resistance of bituminous roadway mixtures. The disk-shaped compact tension DC(T) test can be utilized as a practical method to measure the fracture energy of asphalt concrete (Wagoner et al. 2005). The DC(T) test has the capability of evaluating cylindrical cores obtained from in-place asphalt concrete pavements or laboratory gyratory-compacted specimens and has been used to show that the fracture energy obtained with the DC(T) test can rank materials according to their expected resistance to fracture (Wagoner et al. 2005b, 2006). The fracture energy, G_f, can be computed using the following equation on the basis of the experimental set up shown in Figure 2 (ASTM D 7313 2007):

$$G_t = \frac{AREA}{B \times (w - a)} \tag{1}$$

where G_f = Fracture Energy (J/m^2), $AREA$ = Area under Load-CMOD curve, B = Specimen thickness (m), and ($w - a$) = Initial ligament length (m).

2.2 *CIR sample preparation for DC(T) fracture energy testing*

Sample preparation and design procedures have been established for this research project (Caltrans 2005). The CIR DC(T) sample preparation main steps are summarized below:

RAP belt samples are obtained from the CIR train and dried to a constant weight at a temperature no greater than 40°C.

Moisture is added at an amount expected to be introduced at the milling head (typically 1.5 to 2.5 percent) and additives, if any, are introduced in a similar manner as they will be added during field production.

Test specimens are mixed using a mechanical bucket mixer at ambient temperature.

For DC(T) testing, specimens are compacted immediately after mixing using a Superpave gyratory compactor (SGC) in a 150 mm mold at 1.25° exterior angle, 600 kPa ram pressure, and 30 gyrations.

Specimens are extruded from molds immediately after compaction and are then placed in a 60ºC forced draft oven to be cured to constant weight for no less than 16 hours and no more than 48 hours.

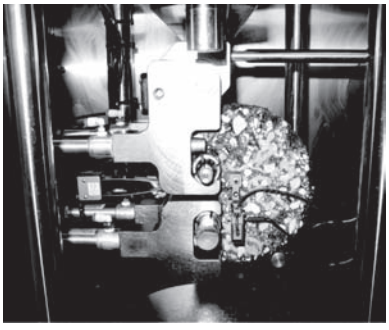

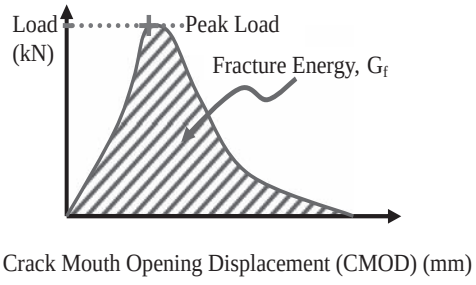

Figure 2. (a) Set up for DC(T) specimen testing (b) Experimental determination of fracture energy, G_f.

Table 1. Solventless Cold In-Place Recycling engineered emulsion (CIR EE).

Test	AASHTO test method	Test results	Minimum	Maximum
Residue, % by mass	T59	65.9	63	
Sieve, %	T59	0.02		0.3
Oil Distillate, % by volume of emulsion	T59	0.3		1
Tests on Residue from Distillation	T59			
Penetration, dmm at 25°C, 100 g, 5 sec	T49	107	75	125

The compacted specimens are sliced to obtain DC(T) specimens that are 50 mm thick.

Two holes are drilled to accommodate for the DC(T) loading fixtures. A starter notch and a flat surface are cut at the crack mouth to mount the Crack Mouth Opening Displacement (CMOD) clip-on gage.

3 CIR FRACTURE ENERGY EXPERIMENTAL DESIGN

3.1 *Experimental design and testing matrix*

A full factorial experimental design with fracture energy at –20ºC as the response variable for one RAP source on the basis of four replicates will evaluate the effect of the following variables: two emulsion types (solventless and solvent containing), three emulsion contents (Low, Medium, Superior), and two additive states (with Lime and without Lime).

According to ASTM D7313 section 7, a test temperature of 10ºC greater than the low temperature performance grade of the asphalt binder as defined in ASTM D6373 is suggested for the temperature at which to perform the fracture energy test. With asphalt concrete binder grades of PG64-34 or PG70-28 typically specified by the agencies in Utah a reference test temperature of –20ºC was selected for comparative testing purposes.

The emulsion types considered in this study were plant produced and commercially available grades with properties and specification requirements shown in Table 1 and 2.

Both CIR EE and CMS2s have been used successfully in CIR applications. Because of environmental restrictions due to the presence of solvents CMS2s is becoming less and less popular. Typical emulsion percentages by dry weight of RAP for CIR applications are 2.5% for CIR EE and 1.5% for CMS2s. CMS2s typically requires less emulsion than CIR EE because of the presence of solvent which "softens" the existing RAP binder. Using too much of CMS2s could result in rutting of the CIR under the action of the traffic loads. As shown in Table 1 and 2 the two emulsions are significantly different as indicated by their respective

Table 2. Solvent containing CMS2s emulsion.

Test	AASHTO test method	Test results	Minimum	Maximum
Saybolt Furol Seconds Viscosity at 50°C	T59	296	50	450
Sieve, %	T59	0.02		0.10
24 Hour Storage Stability, %	T59	0.0		1.0
Particle Charge	T59	Cationic	Cationic	
Oil Distillate, % by volume of emulsion	T59	6.0	5.0	15.0
Residue by Distillation, %	T59	66.0	60	
Tests on Residue from Distillation	T59			
Penetration, dmm at 25°C, 100 g., 5 sec	T49	237	100	250
Solubility in Trichloroethylene, %	T59	100	97.5	

Figure 3. Condition of State Highway 125 in Colorado with transverse cracking on the left lane before CIR on the right line.

penetration and oil distillate properties. Another factor of interest to CIR performance is the use of lime as an additive. Lime is often used in hot mix asphalt to improve the moisture resistance characteristics of the mixture (McCann et al. 2000). In the case of CIR, it can be added for early strength gains and moisture resistance benefits (Chemical Lime 1997). CMS2s is almost always used in conjunction with lime while CIR EE often does not require lime. An evaluation of the effect of lime onto fracture energy of CIR mixtures is warranted.

3.2 *RAP source*

RAP belt samples were obtained from a CIR project in Colorado that took place on State Highway 125 in August 2007. The 14.1 km project was located north of Cowdrey on the Colorado-Wyoming border. The project consisted of 89 mm of CIR to be followed by an asphalt concrete overlay. Some roadway sections had more recent asphalt concrete overlays, but much of the project was noticeably oxidized with extensive transverse cracking averaging

a crack every 4.1 m throughout the length of the roadway as presented in Figure 3. No lime was added to the CIR process and the CIR EE emulsion content used in the field was 2.5%. Field RAP belt samples before the addition of the emulsion were secured to conduct the experimental design. Gradation analysis was performed and all the experimental design samples were prepared to meet the average field RAP gradation.

3.3 *Experimental design results*

Analysis of variance (ANOVA) was used to investigate fracture energy as the dependent continuous variable and three independent discrete variables (emulsion type, emulsion content and use of Lime) (Johnson et al. 2002). The SPSS computer program was used to perform the three way-ANOVA analysis (SPSS 2008).

Table 3. Descriptive statistics CIR fracture energy measured at –20ºC in J/m^2.

Emulsion type	Emulsion content (*)	Lime (**)	Mean	Std. deviation	N
CIR EE	L (1.0%)	N	111.901	23.6810	4
		Y	88.396	2.1530	3
	M (2.5%) (***)	N	156.565	16.2279	4
		Y	168.100	47.6978	4
	S (4.0%)	N	207.093	44.6657	4
		Y	240.436	30.2577	4
CMS2S	L (0.5%)	N	155.533	31.8061	4
		Y	97.376	30.0500	3
	M (1.5%) (***)	N	190.674	36.4829	4
		Y	192.189	48.9493	4
	S (2.5%)	N	266.876	54.5961	4
		Y	213.096	50.2534	4

*L: Low, M: Medium, S: Superior.
**Y: Yes, N: No.
***This is considered the design value.

Table 4. Test of between subjects effects for fracture energy a as the continuous dependant variable.

Source	Type III sum of squares	df	Mean square	F	Sig.
Corrected model	122252.113(*)	11	11113.828	7.471	0.000
Intercept	1377072.895	1	1377072.895	925.691	0.000
Emulsion type	6480.430	1	6480.430	4.356	0.044
Emulsion content	103826.532	2	51913.266	34.897	0.000
Lime	2504.179	1	2504.179	1.683	0.203
Emulsion type* Emulsion content	363.557	2	181.778	0.122	0.885
Emulsion type* Lime	5485.093	1	5485.093	3.687	0.063
Emulsion content* Lime	4208.176	2	2104.088	1.414	0.257
Emulsion type* Emulsion content* Lime	3088.595	2	1544.297	1.038	0.365
Error	50578.961	34	1487.617		
Total	1622890.221	46			
Corrected total	172831.074	45			

*R Squared = 0.707 (Adjusted R Squared = 0.613).

Table 5. Test of between subjects effects for fracture energy as the continuous dependant variable excluding CMS2s without lime from the analysis.

Source	Type III sum of squares	df	Mean square	F	Sig.
Corrected model	84661.000(*)	8	10582.625	7.644	0.000
Intercept	839867.112	1	839867.112	606.685	0.000
Emulsion type	19.698	1	19.698	0.014	0.906
Emulsion content	67628.235	2	33814.117	24.426	0.000
Lime	288.472	1	288.472	0.208	0.652
Emulsion type* Emulsion content	2767.568	2	1383.784	1.000	0.382
Emulsion type* Lime	0.000	0	–	–	–
Emulsion content* Lime	3008.625	2	1504.312	1.087	0.353
Emulsion type* Emulsion content* Lime	0.000	0	–	–	–
Error	34608.862	25	1384.354		
Total	1079840.691	34			
Corrected total	119269.861	33			

*R Squared = 0.710 (Adjusted R Squared = 0.617).

Experimental results are summarized in Table 3. As shown in Table 4 the variables that significantly effect fracture energy, based on a 95% confidence interval, are emulsion type and emulsion content. The effect of emulsion content is more pronounced than emulsion type as indicated by the highest F value.

From a practical standpoint, CMS2s without lime is seldom used as lime is almost always required to meet minimum CIR mix strength and moisture resistance requirements when using a solvent containing emulsion such as CMS2s. Therefore, ANOVA analysis removing CMS2s without lime from the data pool was also performed. The results show that the only significant variable affecting fracture energy is emulsion content as shown in Table 5.

4 SUMMARY OF OBSERVATIONS

Fracture energy was selected in this study to evaluate the fracture resistance of CIR mixtures. Such property can be determined experimentally by applying ASTM D 7313-07: "*Standard Test Method for Determining Fracture Energy of Asphalt-Aggregate Mixtures Using the Disk-Shaped Compact Tension Geometry*" to CIR mixtures. Data from field samples and laboratory prepared samples was analyzed resulting in the following observations:

The variables significantly effecting fracture energy of CIR mixtures at –20ºC based on a 95% confidence interval are emulsion type and emulsion content.

Removing CMS2s without lime from the analysis as CIR with CMS2s almost always require the use of lime for strength and moisture resistance requirements the only significant variable affecting fracture energy was asphalt content

Fracture energy was positively influenced when raising emulsion content. An increase in emulsion content is therefore expected to improve the fracture resistance of CIR mixtures. There are, however, other practical reasons such as rutting concerns that have to be considered in order not to add too much emulsion that may cause adverse effects.

5 CONCLUSIONS

Based on the results obtained from this study the following conclusions can be drawn:

Factors that can be controlled by materials engineers during the CIR process include emulsion type, emulsion content and lime usage. An experimental design was conducted to

evaluate the effect of such factors on the fracture energy of CIR mixtures at –20ºC using actual project RAP belt samples. The results of an analysis of variance clearly demonstrated that emulsion content had a significant positive effect on fracture energy. Materials designers should therefore consider maximizing emulsion content in CIR mixtures in order to optimize fracture energy. Practical considerations should, however, be given when considering higher emulsion contents so as to not negatively affect rutting resistance.

Two significantly different emulsion types, solventless and solvent containing, as indicated by their oil distillate and penetration of the residue were purposely part of the experimental design. Emulsion type was initially determined to have a significant effect on fracture energy. Removing the solvent containing emulsion without lime from the analysis as CIR with this type of emulsion almost always require the use of lime for strength and moisture resistance requirements, the only significant variable affecting fracture energy was asphalt content.

Lime usage at 1.5% loading did not have a significant effect on the fracture energy of CIR mixtures and is therefore believed not to have a negative impact on the cracking related properties of CIR mixtures.

More research is needed to further expend the understanding of CIR crack resistance and provide highway designers with tools and guidelines necessary to maximize CIR performance. It is recommended to validate this research by testing field core and investigating the link between field performance and fracture energy of cold recycling mixtures.

ACKNOWLEDGEMENTS

The authors would like to acknowledge SemMaterials. Chad Wendell was instrumental in the fracture energy CIR sample preparation and testing. Wayne Felix and John Cheever who are Field Engineers dedicated to the successful construction of CIR projects need to be acknowledged for their efforts. Richard Steger and Dr. Jason Bausano provided valuable input.

REFERENCES

AASHTO T59-05. 2007. Testing Emulsified Asphalts. Standard Specification for Transportation materials. Methods of Sampling and Testing Part 2A: Tests. American Association of State Highway and Transportation Officials. Twenty Seventh Edition.

AASHTO T49-07. 2007. Penetration of Bituminous Materials. Testing Emulsified Asphalts. Standard Specification for Transportation materials. Methods of Sampling and Testing Part 2A: Tests. American Association of State Highway and Transportation Officials. Twenty Seventh Edition.

ARRA (Asphalt Recycling and Reclaiming Association). 2001. *Basic Asphalt Recycling Manual*.

ASTM D6373-99. 2006. Performance Graded Asphalt Binder. Section Four. Construction. Volume 04.03 Road and Paving Materials; Vehicle-Pavement Systems. American Society of Testing and Materials.

ASTM D7313-07. 2007. Standard Test Method for Determining Fracture Energy of Aggregate-Asphalt Mixtures Using the Disk-Shaped Compact Tension Geometry. American Society of Testing and Materials.

Caltrans Laboratory Procedure #8. 2005. Method of Test for Determining the Percent of Emulsified Recycling Agent to Use for Cold Recycling of Asphalt Concrete. Department of Transportation, Engineering Service Center, Office of Flexible Pavement Materials, Sacramento, California. http://www.dot.ca.gov/hq/esc/Translab/ofpm/pdf/LP_8.pdf

Chemical Lime Company. 1997. *The Advantages of Cold In-Place Recycling with Emulsified Asphalt and Hot Lime Slurry*. http://www.chemicallime.com/pdf/Cold_Downl_07.pdf

Johnson & Wichern. 2002. Applied Multivariate Statistics. Prentice and Hall. Fifth Edition.

Maurer, G., Bemanian S. & Polish P. 2007. Alternative Strategies for Rehabilitation of Low-Volume Roads in Nevada. *Transportation Research Record: Journal of the Transportation Research Board No 1989*, pp. 309–301, Transportation Research Board of the National Academies. Washington, D.C.

McCann, M., Sebaaly, P.E., & Epps, J.A. 2000. *Lime in Hot Mix Asphalt Pavements: A Synthesis of Information.* Pavements/Materials Program Report No. 1358-1, Department of Civil Engineering, University of Nevada, Reno.

SPSS Statistics Program. 2008. http://www.spss.com

Wagoner, M.P., Buttlar, W.G. & Paulino G.H. 2005. Disk-Shaped Compact Tension Test for Asphalt Concrete Fracture, *Experimental Mechanics*, Vol. 45 pp. 270–277.

Wagoner, M.P., Buttlar, W.G., Paulino, G.H. & Blankenship, P. 2005b. Investigation of the Fracture Resistance of Hot-Mix Asphalt Concrete Using a Disk-Shaped Compact Tension Test. *Transportation Research Record: Journal of the Transportation Research Board No. 1929*, pp. 183–192. Transportation Research Board of the National Academies, Washington, D.C.

Wagoner, M.P., Buttlar, W.G., Paulino, G.H. & Blankenship, P. 2006. Laboratory Testing Suite for Characterization of Asphalt Concrete Mixtures Obtained from Field Cores. *Journal of the Association of Asphalt Pavement Technologists.*

Advanced Testing and Characterization of Bituminous Materials –
Loizos, Partl, Scarpas & Al-Qadi (eds)
© 2009 Taylor & Francis Group, London, ISBN 978-0-415-55854-9

The use of marginal materials in road constructions: Proposal of an eco-compatible section

M. Agostinacchio, M. Diomedi & S. Olita
University of Basilicata, Potenza, Italy

ABSTRACT: In road constructions, Prescriptions have always imposed the use of precious materials, as high characteristics grounds and aggregates, in order to guarantee the requested efficiency and safety standards of the infrastructure. The increasingly more restrictive measures in mining, which is the consequence of a higher sensibility towards environmental issues, along with the increasing difficulty in finding quarry materials, pushed road technicians towards alternative resources, able to substitute the traditional ones. This study is focused on the possibility to use marginal materials in road constructions, with a look at materials belonging to demolition of civil engineering structures (C&D—Construction and Demolition waste—and RAP—Reclaimed Asphalt Pavement) and at blast furnace slag (EAF—Electric Arc Furnace slag and ladle slag). In particular, the intention is to define the optimal mix design of the mixtures to be used in road embankments, foundations, bases, binder and wearing courses, therefore getting to the design of an eco-compatible superelevated road section, thanks to the contemporaneous presence of C&D in the embankment, of RAP, C&D and ladle slag in the foundation, of EAF slag and ladle slag in the cement mixture of the base layer, of C&D and EAF slag in binder and of EAF slag in the wearing course.

1 INTRODUCTION

Plain and stabilised natural materials with high performances have always been used in road constructions in order to answer to the severe stresses due to commercial and industrial vehicles.

The wide national road network, with the inevitable decrease of efficiency standards, needs frequent ordinary and extraordinary maintenance interventions and therefore the use of significant quantities of adequate materials.

In addition, there is a require for a continuous and planned improvement of Italian road infrastructures, whose achievement needs further natural resources, in terms of high quality grounds and aggregates.

The continuous request for natural resources, in conjunction with the increase of waste materials produced by industries and civil constructions, induced the road researchers to study new technical solutions for the construction of the body and of the road pavement.

Moreover, an efficient reuse of materials implies an environmental and economical advantage; indeed, by limiting the extraction of natural aggregates which cannot be substituted, the mining activity is reduced and, as a consequence, there is a limited environmental impact belonging to waste material to be disposed off in damp and the opening of new quarries.

In order to validate the importance of this issue for the community, the Legislators of the most evolved countries have seriously considered this aspect in the last years, by issuing Laws on the different typologies of waste materials and their reuse.

The possible use of different waste materials should be considered case by case; moreover, as for the case of C&D materials, an appropriate selection might be necessary for the elimination of paper, plastic, wood and other impurities, as well as for the elimination of steel from concrete and for the chipping of the single elements so to reduce them to proper dimension.

The aim of this study is to verify and optimise the mixtures to be used in road embankments, foundations, bases, binder and wearing courses, through the use of reclaimed asphalt pavement (RAP), from the reclaiming of superficial layers of asphalt pavements, of civil C&D (Bocci et al. 2002, D'Andrea 2002) and steel industry slag called EAF and the finest ladle slag (Agostinacchio et al. 2005b, Porisiensi et al. 2005).

2 ITALIAN STANDARDS

By means of the Italian Decree D.Lgs. 5 February 1997, n. 22, requiring the approval of Parliament, called Ronchi, three European Standards were issued: on waste materials (91/156/CEE), on dangerous waste materials (91/689/CEE) and on packaging materials (94/62/CEE), imposing the respect of human health and of the environment in the activities of collecting and disposing of waste materials.

The Italian Ministerial Decree D.M. 5 February 1998 on "*Technical Standards for the reuse of non dangerous materials*" allowed to find out which are the non dangerous materials subjected to the simplified reuse procedures, as indicated in Artt. 31 and 33 of the Decree D.Lgs. n. 22/97.

Waste can be classified as urban or special, hazardous or not, and their different typologies, belonging to different production activities, are identified by CER codes (European Catalogue of Waste).

The European Commission Decision 2000/532/CE of 3/5/2000, which was modified with the Decisions 2001/118/CE, 2001/119/CE and 2001/573/CE arranged the new waste materials list, which all member States must comply with since 1/1/2002; non dangerous materials belonging to group 17 of CER "*C&D waste*" can be used in road constructions.

D.M. n. 203/2003 and the following 19/07/2005 Circular gave the operative norms in order to allow the Regions to adopt the adequate dispositions to be sure that public offices and societies used at least 30% of products obtained from recycling to satisfy their annual need of virgin materials, all these aspects being deepened and improved with D.Lgs. 152/2006 and D.M. 186/2006.

3 EXPERIMENTAL PHASE

The aim of the paper is the analysis of mixtures mainly made of marginal materials, which can be used in subgrade and in lower layers of road superstructures.

In order to build eco-compatible roads made of marginal or waste materials, some mixtures were examined by combining C&D, RAP and EAF slag, used as both granular mixture and bitumen and cement bound materials and ladle slag.

In doing so, after characterising waste with respect to UNI EN standards, the particle size derived from several mixtures was investigated, manufacturing some specimens to be tested in laboratory.

In particular, Proctor specimens (CNR 1978) were manufactured for the lower layers in order to determine the optimal water content (W_{opt}) of the mixes to be subjected to the CBR test (Californian Bearing Ratio), both in normal and saturated condition, while Marshall specimens were prepared for the binder in order to optimize the mix-design.

For mixtures with hydraulic binder, the mixture was subjected to ageing for two hours before compaction, afterwards all the CBR procedure was performed.

Moreover, in order to compare the different mixtures from the point of view of performances and to assess the influence of binder, ladle slag or cement, different mixtures of granular mixture cement or ladle slag bond have been tested.

3.1 *Description of the materials used*

The materials used during the investigation carried out at the Laboratory of Road Constructions of University of Basilicata are the following:

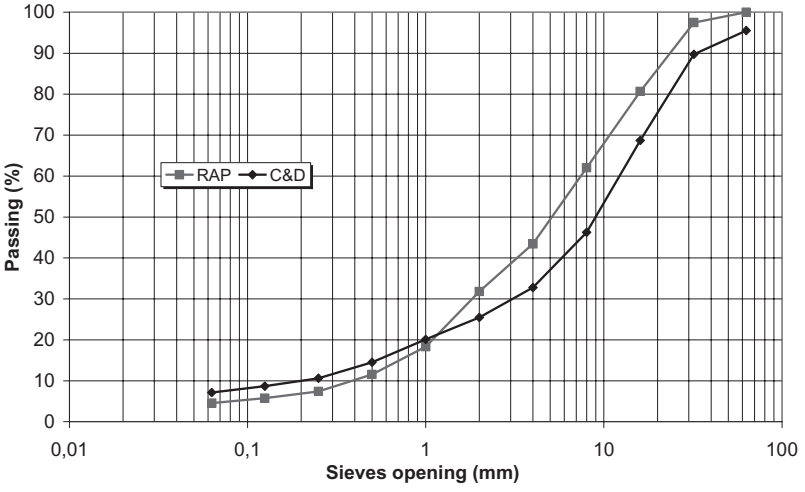

Figure 1. Particle size of original RAP and C&D.

- C&D: original construction and demolition material, coming directly from a construction site for the restoration of a public building of the city of Potenza, mainly made of bricks 17%, plaster 53%, ceramic 1% and concrete 20% and aggregates 9%. C&D with the particle size of Figure 1, has sand equivalent SE equal to 73, plasticity index PI = 0, mass density equal to 2.45–2.60 g/cm^3 and Los Angeles coefficient equal to 56 (complying with UNI EN 1097-2);
- RAP: original reclaimed asphalt concrete, taken from the milling of binder and wearing course of the road SS 658 Potenza-Melfi, made of 5% of bitumen and of silica aggregates. RAP SE is equal to 74, Los Angeles index to 20 and the particle size is the one described in Figure 1;
- EAF slag, defined in CER as steel industry slag (code 10 02 02), derived from the fusion of steel in electric arc furnaces, divided in three sizes sand-grit (0–4 mm), grit (4–8 mm), grit-fine-crushed stone (8–14 mm), with Los Angeles Coefficient equal to 13% and mass density equal to 3.4–3.9 g/cm^3;
- first use lime: coming from Pantano quarry in Pignola (PZ), with Los Angeles coefficient equal to 23 and mass density to 2.62 g/cm^3;
- first use silica from Salandra (MT), with Los Angeles coefficient equal to 18.5 and mass density equal to 2,70 g/cm^3;
- hydraulic binder: 325 Portland cement or ladle slag chemically made of SiO_2 (15–20%), Al_2O_3 (8–15%), CaO (55–65%), FexOy (1–5%) and MgO (3–8%);
- bituminous binder: 70/100 bitumen.

3.2 *Investigated mixtures*

Several mixtures for subgrade, foundation, base, binder and wearing course have been tested and investigated during the experimental phase; to keep the length of the paper to the minimum, only the most interesting ones are reported.

A special mention is due to the sole C&D mixture, classified GA85 according to UNI EN 13242:2004 Standards, for which, because of the high LA coefficient value, the evolution of the modified particle size before and after compaction was evaluated (AASHTO modified).

In fact, after compaction the material (Fig. 2) is finer, because of the chipping due to the laboratory hummer and to rollers on site.

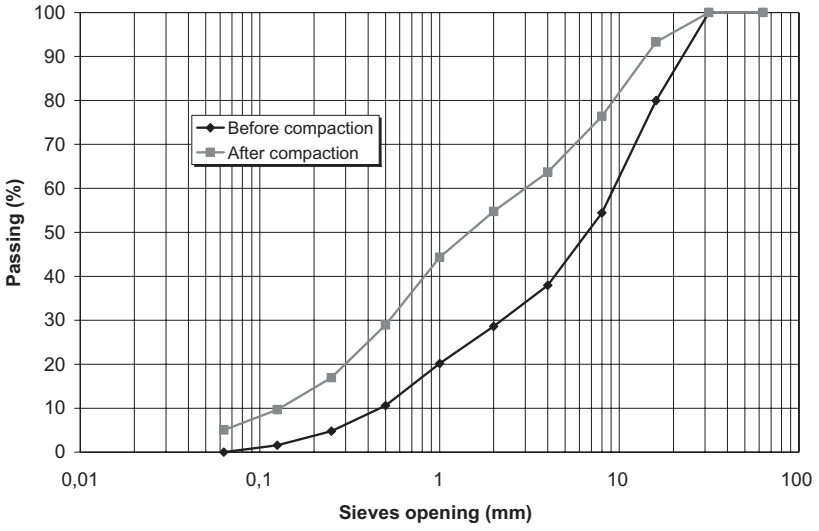

Figure 2. Evolution of the modified particle size before and after compaction.

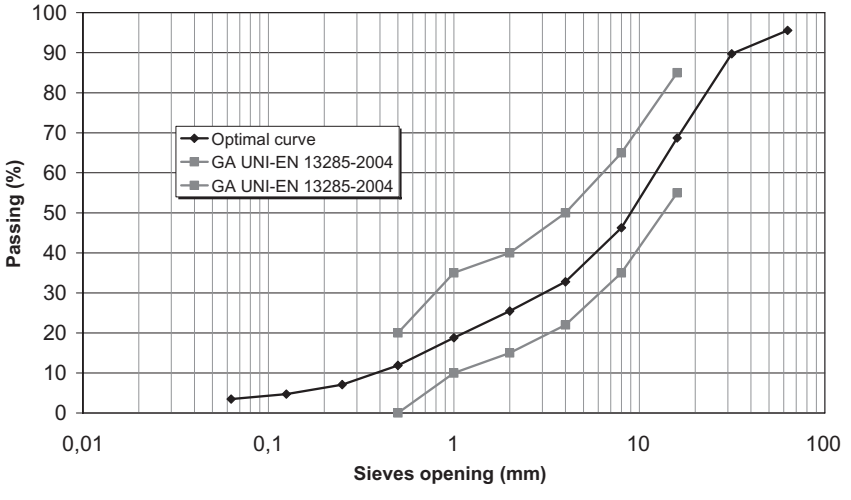

Figure 3. Optimal particle size curve of C&D and RAP.

3.2.1 *Subgrade mixtures with C&D and RAP*

A good subgrade mixture should be compacted, with a particle size continuous and similar to the Fuller one. In addition, the material should be lacking in clay and with good mechanical performances.

The examined C&D, which can be defined according to UNI EN as crushed aggregate, has a high crushing which negatively influences the use if not integrated by other materials, if acceptable performances are requested.

From this point of view, C&D has to be integrated with other materials as RAP, with respect to D.Lgs. 152/2006. More specifically, the particle size obtained with the available materials and which furnished the best bearing values, is the one closest to the GA particle size of the UNI EN 13285:2004 Standards (see Fig. 3).

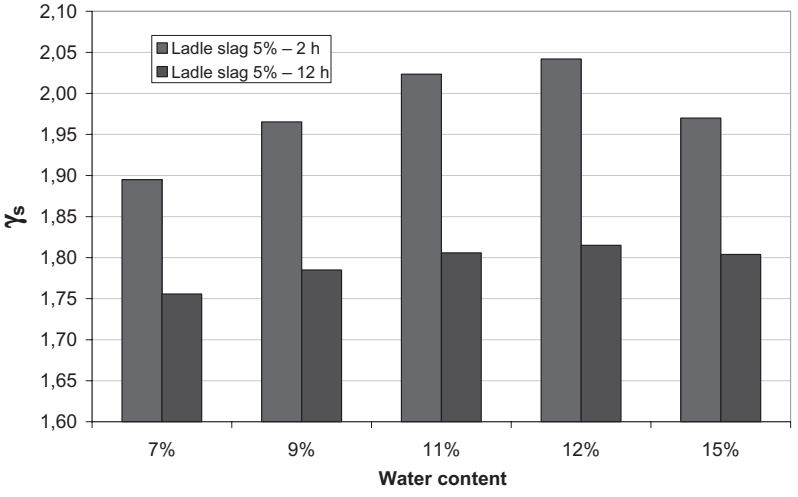

Figure 4. Proctor data of C&D mixtures specimen.

In fact, the mixture presented in the curve of Figure 3 and composed by C&D in 0–2 mm size and over 20 mm and by RAP within 2–20 mm, exhibited a CBR value equal to 50% with a water content W_{opt} equal to 9%.

3.2.2 *Subgrade mixtures with C&D and EAF slag*

Once the curve of Figure 3 was singled out in the investigation other mixtures for subgrade have been tested. The mixture made of C&D aggregates was integrated in the size 2–14 mm with EAF slag, whose use is mainly indicated for the superficial layers of the road pavement.

This mixture for the subgrade, made of C&D in the size 0–2 mm and larger than 15 mm and of EAF slag 2–14 mm, showed a CBR equal to 28% with an optimal water content W_{opt} equal to 4%.

3.2.3 *Mixtures for foundation courses in C&D stabilized with RAP and EAF slag and bound with ladle slag*

Granular mixture is generally used in foundation layers, whose correct particle size is fundamental for the realization of this layer, where the maximum diameter of the aggregate is generally equal to 71 mm or 30 mm depending on the referring particle size.

Once the particle size was singled out and the quality of each component was verified, the CBR index has been used as performance control parameter, which, as prescribed by Specification, in saturated conditions has to be higher than 30%.

C&D curve of Figure 3, with the appropriate qualitative corrections of the materials (RAP or EAF slag) and the use of a binder (ladle slag), has been used in the foundation layer.

Obviously the mechanical resistance of the mixture increases with the increase of the percentage of ladle slag since, keeping the optimal humidity invariable and equal to 11% and referring to a constant particle size (see Fig. 3), it was seen that the CBR index, measured immediately after compaction, varied within 40–84%, with ladle slag percentages varying 3–15% on the aggregate weight.

For bound mixtures, especially for the bearing capacity they have inside the layer, the thickening rate, which depends on compaction, is fundamental.

The investigation carried out, referring to the different seasoning times and binder percentages, showed that the highest thickening rate is obtained by compacting the mixture two hours after its preparation. In Figure 4 the details of Proctor specimens prepared with C&D mixtures treated with 5% of ladle slag and humidity varying within 7% and 15%, compacted after 2 or 12 hours, are reported.

Table 1. CBR index results.

After compaction seasoning (days)	Mixture R C&D + RAP + 5% ladle slag (%)	Mixture G C&D + RAP + 5% ladle slag (%)
0	72	84
4	94	110
7	122	140

The dry weight γ_s decreases with the increase of time and after 2 hours seasoning it is higher than 2 g/cm^3 and after 12 hours he does not get lower than 1.85 g/cm^3.

This is due to the formation of chemical bonds between C&D and ladle slag, which are difficult to break, especially in laboratory with the Proctor hammer, already few hours after the preparation of the mixture.

The curve chosen for the foundation layer showed experimentally that the optimal percentage of ladle slag is 5; therefore referring to the curve in Figure 3, using C&D swapped with RAP for 2–20 mm size and EAF slag for 2–14 mm, the performances of the mixture have been evaluated in terms of bearing capacity with the CBR index.

The mixture R "*C&D + RAP + ladle slag* 5%" with W_{opt} equal to 7%, tested with the CBR test with 0, 4 and 7 days seasoning after compaction, gave CBR indices respectively equal to 72%, 94% and 122% (see Tab.1).

The mixture G "*C&D + RAP + ladle slag* 5%" with W_{opt} equal to 4%, tested with the CBR test with 0, 4 and 7 days seasoning after compaction, gave CBR indices respectively equal to 84%, 110% and 140% (see Tab. 1).

The mixtures with EAF slag gave better results from the point of view of bearing capacity, compared to the RAP ones, with 15–20% difference: this is the proof of a better adhesion ladle slag—EAF slag, compared to ladle slag-RAP during binder hydration.

3.2.4 *Mixtures for base courses: cement mixtures with ladle slag*

The good results, obtained using ladle slag as binder in the mixtures, pushed the Authors to change Portland cement, normally used in cement mixtures, with ladle slag, in order to verify its behaviour and the possibility of using it.

For this reason, some mixtures referred to a previously analysed curve (Agostinacchio et al. 2005a) and reported in Figure 5, which lies inside the particle sizes of ANAS and Società Autostrade Specifications have been prepared.

Respecting laboratory tests and the manufacture procedures of cement mixtures, some specimens have been manufactured, and after 7 days seasoning in 90% humidity environment at 20°C, they have been subjected to both free lateral expansion compressive test and indirect tensile stress test.

Virgin lime (CV), RAP, 325 Portland concrete and ladle slag (S) were the materials employed for these mixtures.

The first mixture analyzed, called CVSiv_3,5, was that with 100% of virgin lime (Fig. 5) treated with 3.5% ladle slag, whose value was chosen considering the percentage of cement (3–5%) generally used in cement mixtures, in order to compare the mechanical performances of the mixture with the changes of the kind of binder.

The second mixture, bound with 3.5% Portland cement, was called CVPort_3,5.

CVSiv_3,5 exhibited free lateral expansion compressive strength R_c and indirect tensile stress resistance R_t, respectively equal to 1.15 N/mm^2 and 0.1 N/mm^2, while CVPort_3,5 was 5.6 N/mm^2 and 0.6 N/mm^2; it was, then, found that the values of CVSiv_3 do not comply with the minimum ones prescribed by the Specifications ($R_c = 3$ N/mm^2 and $R_t = 0.25$ N/mm^2).

In order to find out the ladle slag percentage needed to stay within minimum R_t and R_c, some other mixtures were manufactured with virgin lime and ladle slag, called CVSiv_15

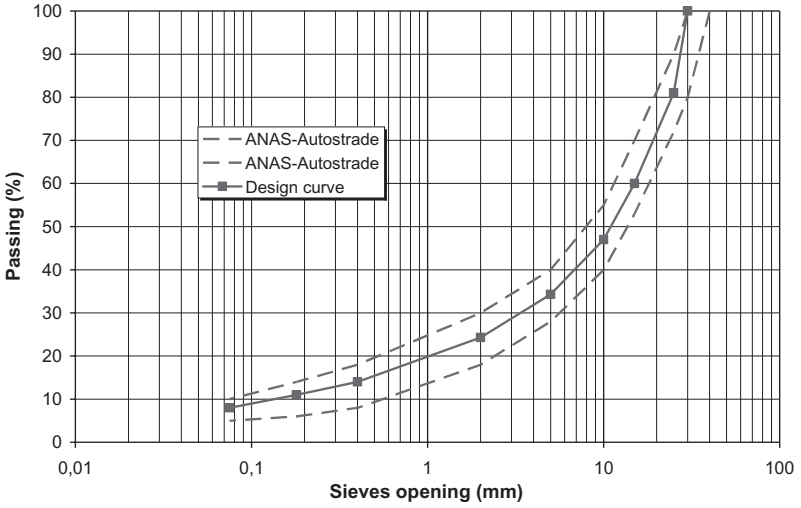

Figure 5. Design curve of base course and ANAS-Autostrade particle size.

Table 2. R_t and R_c results.

Mixture	R_t @ 7 days (N/mm^2)	R_c @ 7 days (N/mm^2)
CVSiv_3,5	0.1	1.15
CVSiv_6	0.15	1.87
CVSiv_15	0.4	3.40
CVSiv_20	0.5	4.40
CVPort_3,5	0.6	5.60
RAP + Siv_15	0.3	3.15
RAP + Siv_20	0.32	3.45
RAP + Port_3,5	0.35	3.85

and CVSiv_20, with 15% and 20% ladle slag, with R_c respectively equal to 3.40 N/mm^2 and 4.40 N/mm^2.

Therefore, after defining 15% and 20% of ladle slag, some RAP mixtures were prepared, called RAP + Siv_15 and RAP + Siv_20, which gave, after 7 days seasoning, R_c values respectively equal to 3.15 N/mm^2 and 3.45 N/mm^2 and R_t values respectively equal to 0.3 N/mm^2 and 0.32 N/mm^2.

Finally, in order to compare the results with previous studies (Agostinacchio et al. 2005a), the mixture called RAP + Port_3,5, was proposed again, confirming what expected.

3.2.5 *Mixtures for binder layers with C&D and EAF slag*

In case of mixtures bitumen bound the mix design was defined for the binder layer, using different typologies of silica aggregates (S), C&D and EAF slag (G). Once the ANAS Specification particle size was defined (see Fig. 6), several mixtures were prepared and, amongst them, mixture A with 80% S + 20% C&D, B with 70% S + 30% C&D, C with 32.50% S + 52.50% C&D + 15% G and D with 32.50% S + 45.30% C&D + 22.20% G were the best.

In all the mixtures silica was used for the size 2/0.075 (sand) and for the larger parts, part of silica was changed with C&D and/or EAF slag, respecting the above reported percentages.

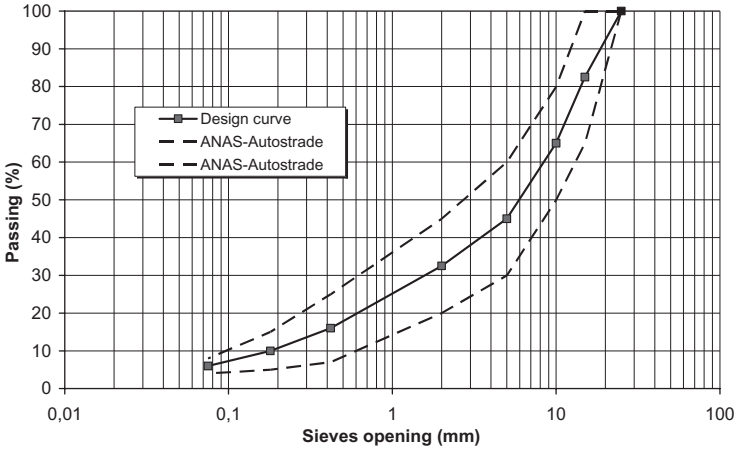

Figure 6. Design curve of binder course and ANAS-Autostrade particle size.

Table 3. Marshall and indirect tensile stress resistance results.

Mixture	Porosity %	Marshall stability kN	Sliding mm	Indirect tensile stress strength N/mm^2
A – (80% S + 20% C&D)	3.5	1.442	2.42	0.886
B – (70% S + 30% C&D)	3.9	1.512	1.90	0.891
C – (32.5% S + 52.5% C&D + 15% G)	3.5	2.393	2.95	1.122
D – (32.5% S + 45.3% C&D + 22.2% G)	6.0	1.549	2.56	0.868

Table 4. Wearing course aggregate and binder.

Sieves UNI N.	Passing %	Type
15	100	EAF slag
10	85	EAF slag
5	51	EAF slag
2	37	lime
0.42	18	lime
0.18	9	lime
0.075	6	lime

Hard or soft PMB 4.32%.

5–4.85% of bitumen on the aggregate weight, decreasing with the increase of the EAF slag quantity, was used in the mixtures.

All the previously reported mixtures from A to D gave good results in terms of Marshall stability and indirect tensile stress resistance, which allow their use for the binder layer (see Tab. 3). However, C is the mixture with the best results, with Marshall stability equal to 2.393 kN, 2.95 mm sliding and indirect tensile stress resistance equal to 1.122 N/mm^2.

3.2.6 *Mixtures for wearing courses with EAF slag*

In order to complete the road pavement package with eco-compatible construction, thus using waste materials in all the layers, the results of a previous investigation (Agostinacchio

et al., 2007) on a wearing course high modulus asphalt concrete, capable to guarantee a significant fatigue resistance in presence of heavy traffic, was used.

Briefly, the components of this closed mass asphalt concrete for wearing course are EAF slag, used instead of basalt, lime and 4.32% of hard or soft modified bitumen (see Tab. 4).

In particular, the tested mixtures, in presence of a porosity of 4.7–5.4%, furnished Marshall stability and indirect tensile stress resistance higher than, respectively, 2.600 kN and 1.3 N/mm^2.

3.2.7 *Economical analysis of the mixtures used*

At the end of the investigation an economical analysis of the mixtures used was performed.

The economical evaluation of a mix including marginal materials should take into account the use of natural resources, the cost of raw materials (aggregates, binder) and the mechanical performances.

Therefore, in doing so, the environmental issues, together with the mechanical performances, are more important than the mere monetary cost.

For this reason a "*synthetic evaluation index*" (I.V.S.) has been formulated to assess the efficacy of a marginal material and therefore its economical convenience. In particular I.V.S. arranged in this investigation is expressed by the following relation:

$$I.V.S. = f(V_{m1};\ V_{m2};\ \ldots\ ;\ V_{mn};V_{EC};\ V_{EC}) \tag{1}$$

For a statistical elaboration of the experimental data, a multiparameter regression was used represented by the following equation:

$$y = m_1 \cdot x_1 + m_2 \cdot x_2 + \cdots + m_n \cdot x_n + b \tag{2}$$

where:

- y = I.V.S.;
- x_i = values associated with the measured parameters;
- m_i = coefficients corresponding to each parameter;
- b = constant coefficient of the equation.

In order to make the previous equation applicable it was necessary to previously fix a variability range of I.V.S. as function of the parameters x_i relative to each mixture. For the purpose, a qualitative and quantitative analysis of the monitored data was performed, in order to highlight first of all the belonging classes to which assign the pre determined scores.

The division was made on the basis of what available in literature and Standards and the assessment of the economical and environmental data was performed with subjective evaluation of the resources and monetary consumption, referred to market prices. For example, the evaluation synthetic parameters of a cement mixture are:

- V_{m1} compressive failure tension;
- V_{m2} Los Angeles coefficient;
- V_{EC} environmental cost;
- V_{MC} monetary cost.

In particular, referring to environmental costs, in terms of non renewable environmental resources consumption, a high score was given to aggregates with a high "environmental consumption".

Monetary costs were defined looking at the data available from the Chamber of Commerce and/or the producing factories, with the hypothesis that the site is located in the centre of gravity of the aggregates production plants.

In order to give a synthetic evaluation of the validity of a material or an mixture, four classes were defined according to the achieved score (see Tab. 5).

As function of the mentioned categories and of the score assigned to the mixture, it was possible to define a synthetic assessment of the investigated mixtures. For example, limiting the survey for brevity only to some cement mixtures investigated, the synthetic assessment is reported in Table 6.

Table 5. Classes and score of mixtures.

Class	Score	Assessment
1	<20	Poor mixture
2	20–30	Average mixture
3	31–40	Good mixture
4	41–50	Excellent mixture

Table 6. Mixture synthetic assessment.

Mixture	Sum	Synthetic assessment
RAP + Siv_15	40.80	Excellent
RAP + Port_3,5	40.15	Excellent
RAP + cement 2,5%	39.15	Good
CVPort_3,5	28.65	Average
CVSiv_15	28.65	Average
CVSiv_20	30.00	Average

Table 6 shows that the best mixtures are those manufactured with recycled aggregates.

Generally speaking, all the marginal mixtures investigated have high I.V.S. values, filed within good and excellent, confirming that they can be used in road constructions from the technical and economical point of view.

4 CONCLUSIONS

This investigation faced the theme of recycling waste materials coming from demolition of civil engineering buildings and from steel industry; hence, several mixtures to be used in the construction of road pavements have been studied, using different components as C&D, RAP, electric arc furnace (EAF) slag and ladle slag.

In particular, some mixes to be used in the different layers of the road superstructure and in the subgrade were proposed; in fact, starting from the available C&D particle size and integrating it with 2–20 mm sizes of RAP, a good mixture was obtained which, compacted with $W_{opt} = 9\%$, showed a CBR index equal to 50%.

On the other hand, the same C&D curve, integrated with 2–14 mm EAF slag, gave a lower CBR, equal to 28%, in presence of optimal humidity of 4%, and this was the proof of the poor capacity of EAF slag to make good bonds with C&D in presence of water.

For the foundation layer different mixtures of waste materials bound with ladle slag were analysed, getting to the best performances given by the particle size of Figure 3 and 5% of ladle slag.

In particular, with C&D aggregates integrated with RAP, EAF slag and ladle slag both the mixture *R* (*C&D* + *RAP* + *ladle slag* 5%, where RAP plays the role of C&D for the sizes 2–20 mm) and the mixture G (*C&D* + *EAF slag* + *ladle slag* 5%, with EAF slag instead of C&D in the sizes 2–14 mm) were obtained.

R and G mixtures (see Tab. 1) gave positive results from the point of view of performances, the CBR index at 7 days being, respectively, 122% and 140%, showing for the mixture G values 15% higher than the corresponding R ones.

In the investigation the pre-compaction seasoning time parameter was evaluated: it has to be smaller than two hours, since higher times, because of ladle slag hydration, would bring to difficulties in compaction.

In fact, the same mixture compacted in laboratory after 12 hours seasoning showed 8% reduction of the dry weight γ_s compared to the value referred to 2 hours seasoning.

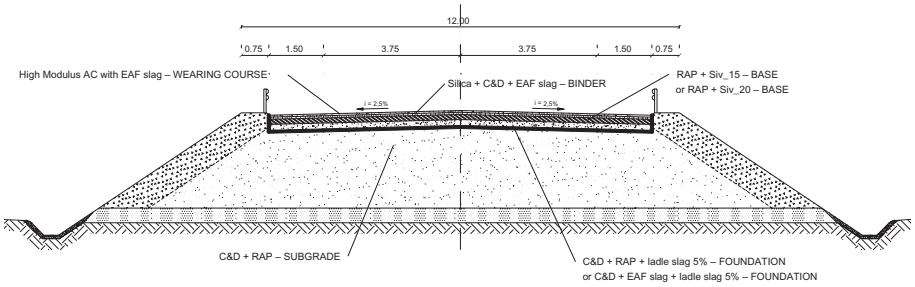

Figure 7. Eco-compatible road section.

Furthermore, in order to evaluate the behaviour of ladle slag compared to cement, and therefore its potential use in cement mixtures, some virgin lime mixes (CV) were prepared varying the ladle slag content, the particle size being illustrated in Figure 5.

In particular, mixtures with acceptable R_c e R_t values have been obtained only in case of 15% of ladle slag on the aggregate weight; an increase of such value up to 20% involved 25% and 8% increase of R_c e R_t, but the values obtained with Portland cement ($R_c = 0.6$ N/mm^2 and $R_t = 5.6$ N/mm^2) have not been achieved (see Tab. 2).

Moreover, with respect to the results obtained, the mixes RAP + Siv_15 e RAP + Siv_20, where the particle size complies with Figure 5, can be accepted for cement mixtures.

Furthermore, in order to have marginal materials in each layer of a road pavement, the two upper layers (binder and wearing course) were taken into account, considering for the latter the outcomes of a previous investigation (Agostinacchio 2007).

In particular, different mixtures made of EAF slag, C&D and silica have been analysed for the binder layer; for brevity, only the best ones have been included in Table 3, which gave Marshall stability values higher than 1.440 kN and direct tensile stress resistance higher than 0.868 N/mm^2.

For the wearing course a high modulus asphalt concrete analysed in a previous investigation (Agostinacchio et al. 2007) was used, where basalt is changed with EAF slag.

The mix-design of this mixture, which furnished excellent results from the physical and mechanical point of view, is reported in Table 4.

Finally, the results were validated by an economic analysis which, for the sake of brevity, is reported only with respect to cement mixture.

In conclusion, thanks to the positive outcomes of the investigation, the following eco-compatible road section made of waste materials can be proposed (see Fig. 7):

- C&D + RAP subgrade;
- C&D + RAP + ladle slag 5% or C&D + EAF slag + ladle slag 5% foundation;
- RAP + Siv_15 or RAP + Siv_20 base;
- Silica + C&D + EAF slag binder;
- High modulus asphalt concrete with EAF slag wearing course.

Being sure that there are positive environmental implications in the proposed solution, the Authors hope that a real scale investigation could be carried out shortly, in order to verify the expected results.

REFERENCES

Agostinacchio, M. & Diomedi, M. 2005a. *Mix Optimisation for Cement Mixtures Made of R.A.P. and C&D*, Proceedings of SIIV 2005—3rd International SIIV Congress—People, Land, Environment and Transport Infrastructures—Reliability and Development—Politecnico di Bari, Aula Magna, Via Re David 200. September 22–24. Bari.

Agostinacchio, M. & Olita S. 2005b. *Use of Marginal Materials in Road Constructions: Electric-Arc Furnace Slag*, Proceedings of SIIV 2005—3rd International SIIV Congress—People, Land, Environment

and Transport Infrastructures—Reliability and Development—Politecnico di Bari, Aula Magna, Via Re David 200. September 22–24. Bari. Italy.

Agostinacchio, M.la. Ciampa, D. & Diomedi, M. 2007. *Eletric arc furnace slag in high modulus asphalt concrete for wearing-course layer: mix design and mechanical properties evaluation*. Proceedings Volume I, pag. 499–508. 4th International Conference Bituminous Mixtures and Pavements. 19–20 April 2007. Thessaloniki. Greece.

Bocci, M., Cardone, F. & Colagrande S. 2002. *Impiego dei materiali di riciclo nella confezione dei misti cementati,* Atti del XII Convegno Internazionale SIIV: Riqualificazione *funzionale del sistema viario*, 30–31 Ottobre 2002. Parma. Italy.

C.N.R. B.U.- n. 69. 1978. "*Prova di costipamento di una terra*".

D'Andrea, A. 2002. *Caratteristiche degli aggregati riciclati: requisiti e prestazioni*, Convegno ISSI, 28 marzo 2002. Roma. Italy.

Porisiensi, S., Maschietto, M. & Grandesso P. 2005. Scorie di acciaieria: un nuovo aggregato ad elevate caratteristiche per conglomerati bituminosi speciali, *Rassegna del Bitume* n. 50, Italy.

Advanced Testing and Characterization of Bituminous Materials – Loizos, Partl, Scarpas & Al-Qadi (eds)
© 2009 Taylor & Francis Group, London, ISBN 978-0-415-55854-9

Influence of active filler, curing time, and moisture content on the strength properties of emulsion and foamed bitumen stabilized mix

Sufian, Zulakmal
Public Work Department, Kuala Lumpur, Malaysia

A. Aziz, Nafisah
Roadcare (M) Sdn. Bhd, Kuala Lumpur, Malaysia

Matori, Mohd Yazip & Hussain, Mat Zin
Kumpulan Ikram Sdn. Bhd., Selangor, Malaysia

ABSTRACT: Foamed bitumen and emulsion are common stabilizing agents used for recycled asphalt pavement construction. The strength of emulsion and foamed bitumen stabilized Reclaimed Asphalt Pavement (RAP) is influenced by factors such as filler content, moisture level and curing time. This paper describes the effect of ordinary Portland cement as active filler, curing time and moisture content on the strength properties of foamed bitumen and emulsion stabilized mix. Foamed bitumen and emulsion treated samples with different RAP proportions were tested for their strength properties at various active filler contents, curing time and moisture contents. It was found that the strength in terms of resilient modulus, Unconfined Compressive Strength (UCS) and Indirect Tensile Strength (ITS) values, increased with curing time and percentage of active filler. It was also found that the strength decreased as the RAP proportion increased. However in construction practice, it is possible to use 100% RAP to meet the desired strength, when an adequate amount of active filler is added.

1 INTRODUCTION

1.1 *Background*

The Cold-In-Place Recycling (CIPR) technique was first introduced in Malaysia around the mid 80's. Since then, the concept of recycling road pavements as an alternative rehabilitation measure has become popular and acceptable. The technique involves recycling of all the asphalt pavement section and a portion of the underlying materials with an addition of stabilizing agents to produce a stabilized base course. The advantages of the CIPR include cost savings of up to 40 percent over conventional techniques and the benefits associated with material recycling.

Research works elsewhere (Cooley, 2005) have shown that the performance of the recycled asphalt layer depends on the proportion of reclaimed asphalt pavement (RAP), types of stabilizing agents, and amount of active filler. For the purpose of this paper, active filler is referred to Ordinary Portland Cement (OPC) added to the recycled mixtures.

Although the CIPR technique is gaining acceptance as a cost effective solution in rehabilitating distressed pavement, very little local research has been carried out on its cost effectiveness, design, construction and long term performance. Subsequently, the Public Work Department (PWD) has embarked on a research program in this field, in collaboration with Kumpulan Ikram and Roadcare Sdn. Bhd. as the basis for the establishment of Malaysian Guidelines for CIPR Design and Construction.

1.2 *Objectives*

The objective of this paper is to highlight the effect of active filler, curing time and moisture content on the strength properties of foamed bitumen and emulsion treated mix, more specifically this paper attempts to answer some of the issues faced during:-

- Is active filler required in recycling works and how does it affect the strength of the recycled layer?
- If the active filler is required, how soon can the recycled pavement be opened to traffic at a minimum active filler?
- How does variation in the moisture content affect the strength of the recycled layer?

2 METHODOLOGY

2.1 *Experimental matrix and sample preparation*

In the study, foamed bitumen and emulsion treated samples with different proportions of RAP and crushed stone aggregates (CR) were tested for their strength properties at various active filler contents, curing time and moisture contents. Table 1 summarizes the experimental matrix used in the study involving five different RAP proportions which represent the possible combinations that may be encountered during construction. The test matrix is therefore designed to investigate the expected field performance for these different mixture compositions.

Samples for ITS and Resilient Modulus test (100 mm briquettes) were prepared in accordance to Marshall test method with modifications to the compaction temperature and curing procedures. Samples for UCS test (150 mm diameter) were prepared in accordance to Modified Proctor BS 1377.

In order to analyze the effect of active filler on the strength properties, samples were mixed at optimum moisture content (OMC) as determined by the modified Proctor test method (BS 1377) and dry cured for 3 days. To determine the curative period, which is the time taken for the samples to reach the required strength, the samples were dry cured for 1, 2, 3, 7 and

Table 1. Experimental matrix and sample quantities.

		Curing time (Day)					Moisture content (%)					Active filler (%)			
Aggregate proportion	Strength test	1	2	3	7	28	–30	–15	OMC	+15	+30	0	1	2	3
		Sample quantities													
100% RAP	UCS	3	3	3	3	3	3	3	3	3	3	3	3	3	3
	ITS	3	3	3	3	3	3	3	3	3	3	3	3	3	3
	R.Modulus	3	3	3	3	3	3	3	3	3	3	3	3	3	3
75% RAP + 25% CR	UCS	3	3	3	3	3	3	3	3	3	3	3	3	3	3
	ITS	3	3	3	3	3	3	3	3	3	3	3	3	3	3
	R.Modulus	3	3	3	3	3	3	3	3	3	3	3	3	3	3
50% RAP + 50% CR	UCS	3	3	3	3	3	3	3	3	3	3	3	3	3	3
	ITS	3	3	3	3	3	3	3	3	3	3	3	3	3	3
	R.Modulus	3	3	3	3	3	3	3	3	3	3	3	3	3	3
25% RAP + 75% CR	UCS	3	3	3	3	3	3	3	3	3	3	3	3	3	3
	ITS	3	3	3	3	3	3	3	3	3	3	3	3	3	3
	R.Modulus	3	3	3	3	3	3	3	3	3	3	3	3	3	3
100% CR	UCS	3	3	3	3	3	3	3	3	3	3	3	3	3	3
	ITS	3	3	3	3	3	3	3	3	3	3	3	3	3	3
	R.Modulus	3	3	3	3	3	3	3	3	3	3	3	3	3	3

Table 2. Material gradation, OMC, MDD, OBC.

Grading sieve size (mm)	Aggregate proportion (% Passing)				
	100% RAP	75% RAP + 25% CR	50% RAP + 50% CR	25% RAP + 75% CR	100% CR
50	100	100	100	100	100
37.5	100	99.5	99	98.5	97
20	93.8	89.5	85.5	82	78
10	71	69	66	63	60
5	45.3	45	45	45	45
2.36	26.4	28	29	31	32.11
0.425	2.2	7	9.5	12	13.71
0.075	0.4	3	4.5	5	6.91
OMC (%)	4.81	5.14	5.82	6.08	6.13
MDD (Mg/m^3)	1.879	2.024	2.161	2.281	2.253
OBC $_{\text{Foamed Bitumen}}$ (%)	1.5	3	3	3	3
OBC $_{\text{Emulsion}}$ (%)	4	4	6	6	6

28 days using 1% active filler being at OMC. To study the effect of varying moisture content on the strength properties, the active filler was set constant at 1% and samples were dry cured for 3 days.

2.2 *Description of materials*

Table 2 shows the gradation, Optimum Moisture Content (OMC), maximum dry density (MDD) and optimum binder content (OBC) of the samples for each RAP proportions. The gradation and composition of the samples represent typical values obtained from recycling projects throughout the country. Strength tests such as ITS, UCS and resilient modulus were carried out on each RAP proportion shown in Table 2 and the average result obtained from three samples for each proportion are reported. The test results would simulate the actual performance of the recycled layer.

From Table 2, it can be seen that the Optimum Moisture Content, increases as the RAP content decreases since more fluid is required to pack the aggregate to its maximum density due to the presence of higher percentage of fines. The OBCs were determined at the highest ITS values for each mix proportion. For foamed bitumen stabilized samples, the OBC was 1.5% for samples with 100% RAP and 3% for the other samples. For emulsion stabilized samples, the OBC was 4% for samples with 100% and 75% RAP and 6% for the other samples.

It was also observed that the recycled material (100% RAP) has less fines than the normal crushed aggregate which is due to the conglomeration of fines in the RAP binder.

3 RESULTS AND DISCUSSION

3.1 *Unconfined compressive strength (UCS) test*

3.1.1 *UCS vs. Curing time*

Both foamed bitumen and emulsion stabilized samples showed similar results. The UCS values increased with curing time depending on the percentage of RAP and type of stabilizing agent. There was a rapid increase in UCS within the first 5 days of curing for all samples, after which the increase was gradual. Generally it was observed that higher RAP proportion resulted in lower UCS values.

In the local construction practice, the UCS requirement for recycling works is specified at 0.7 MPa for a 7-day curing period (REAM, 2005). However, the protection and maintenance

period before overlaying with the asphaltic layer is only 2 days. For foamed stabilized samples, all samples achieved the required strength as early as 2 days except for the 100% RAP. At 100% RAP, the UCS value did not meet the minimum requirement of 0.7 MPa at 7 days, however, it was achievable at 28 days curing time. In order for the treated road to be opened for traffic after 2 days it is recommended that the maximum RAP content be set at 75%. It is worth noting that, samples with 0% to 50% RAP achieved the 0.7 MPa requirement as early as 1 day.

For emulsion stabilized samples, only the samples with 0%–25% RAP met the UCS requirement after 2 days. The 50% RAP sample reached the requirement at 3 days, whilst the 75% RAP achieved the required strength only at 12 days. The 100% RAP sample did not meet the required strength even after 28 days of curing.

These observations suggest that at 1% active filler, the time taken to open the treated road to traffic depends on the RAP proportions. Consequently, higher active filler content may be necessary to shorten the curing time in cases where it requires early opening to traffic.

3.1.2 *UCS vs. Active filler content*

For both foamed bitumen and emulsion treated samples that contained RAP, the required strength of 0.7 MPa could not be achieved without the inclusion of active filler. The results indicated that the active filler is vital in recycling works in Malaysia involving the use of RAP. It was also found that the UCS increases with the active filler content.

For foamed bitumen treated samples, except for 100% RAP, all other combinations of RAP satisfied the strength requirement when a minimum of 1% active filler was added. For the 100% RAP samples a minimum of 2% active filler was essential to attain the required strength.

For emulsion treated samples with 100% RAP, a minimum of 3% active filler was needed to achieve the required strength. Samples with 75% RAP required 1.5% active filler, whilst those with 50% RAP needed only 1% active filler.

3.1.3 *UCS vs. Moisture content*

UCS is also influenced by the moisture content which is critical for compaction. All foamed bitumen treated samples consistently showed the highest UCS values occurring at OMC. A similar trend was not observed for the emulsion treated samples where the highest UCS values did not necessarily occur at OMC. It was found that variations in moisture content within ±30% of OMC did not affect the UCS values significantly for both types of treatment. This confirms findings by other research works (Lee, 2003, Mohammad, 2003) that mixing can be done in the range of 65%–85% of the OMC. It is a common practice in Malaysia to lay and compact the foamed bitumen and emulsion treated layer at ±20% of OMC. The results also showed that UCS is a poor indicator of moisture sensitivity of treated samples. Similar conclusion has been suggested by M. Houston (Houston, 2004).

It was also observed that 0% RAP samples achieved higher UCS strength within the studied range of moisture content. This may be due to the presence of higher fines content in the crusher run which contributed to the strength.

The following graphs in Figure 1 summarize the results of the UCS tests.

3.2 *Indirect tensile strength (ITS) test*

3.2.1 *ITS vs. Curing time*

The ITS values were observed to increase with curing time. There was a rapid increase in ITS within the first 5 days of curing for all samples, after which the increase was gradual. For foamed bitumen treated samples, the 75% RAP and 100% RAP did not achieve the required value of 200 kPa at 3 days, whilst for the emulsion treated samples only 100% RAP did not achieve the required strength at 3 days. The results did not seem to indicate positive correlation between RAP proportions and ITS values. This was unexpected, as the authors anticipated the trend to be similar to that of the resilient modulus against curing time, since both testing methods investigate the shear parameters of the samples.

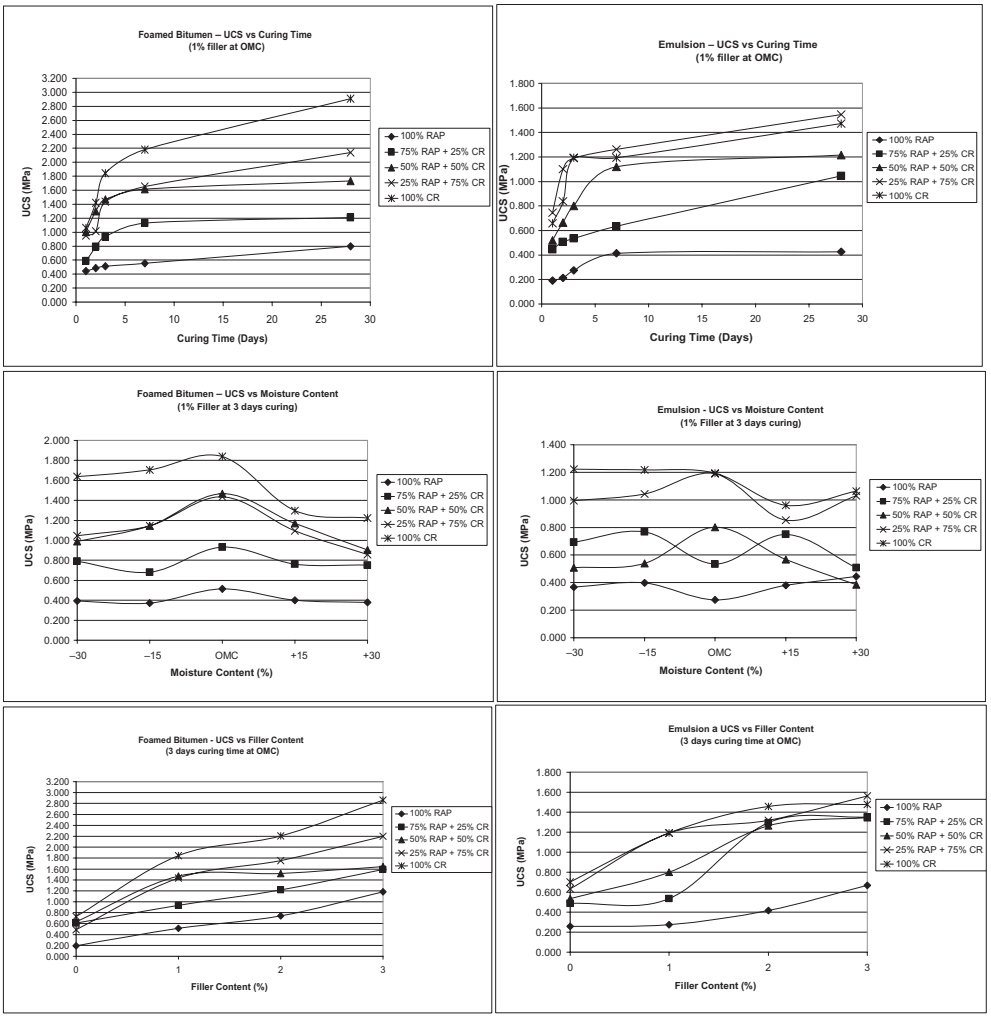

Figure 1. UCS test results.

3.2.2 *ITS vs. Active filler content*

Generally the ITS values increase with the amount of active filler. The minimum filler content to achieve the required 200 kPa varied for different RAP proportions and stabilizing agents. As an example for foamed bitumen treated samples, 1.5% of active filler content was sufficient for 100% RAP, whereas no filler was required for the 0% RAP. For emulsion treated samples, 1.5% of active filler was also sufficient for 100% RAP while a nominal amount of 0.3% active filler was required for the 25% RAP.

3.2.3 *ITS vs. Moisture content*

The ITS values are also influenced by moisture content. Similar to the UCS test, the maximum ITS was expected to occur at the OMC since the sample achieved the highest density at this moisture level. However, this was not reflected in the results. Except for the 50% RAP samples which achieved the maximum ITS values at the OMC, most of the other samples did not indicate a distinct maximum ITS value within the moisture content investigated.

For foamed bitumen treated samples with higher RAP content, variation in the moisture content did not affect ITS values significantly. However, for low RAP proportions of 25%

RAP and below, the ITS values increased when the moisture content decreased. For the emulsion treated samples, there was generally no specific pattern linking the ITS and the moisture content.

The following graphs in Figure 2 summarize the results of the ITS tests.

3.3 *Resilient modulus*

3.3.1 *Resilient modulus vs. Curing time*

There was a rapid increase in resilient modulus within the first 5 days of curing for all samples, after which the increase was gradual. It was also observed that the higher RAP proportion resulted in lower resilient modulus. For foamed bitumen and emulsion treated samples containing higher RAP proportion of 75% and 100% RAP, a longer curative period was required to achieve the required value of 2000 MPa. As an example, the foamed bitumen treated samples with 100% RAP needed 10 days, whilst the emulsion treated sample with 100% RAP could not achieve the required strength at 28 days. This suggests that higher active filler content shall be used to shorten the curative period in cases where it requires early opening to traffic.

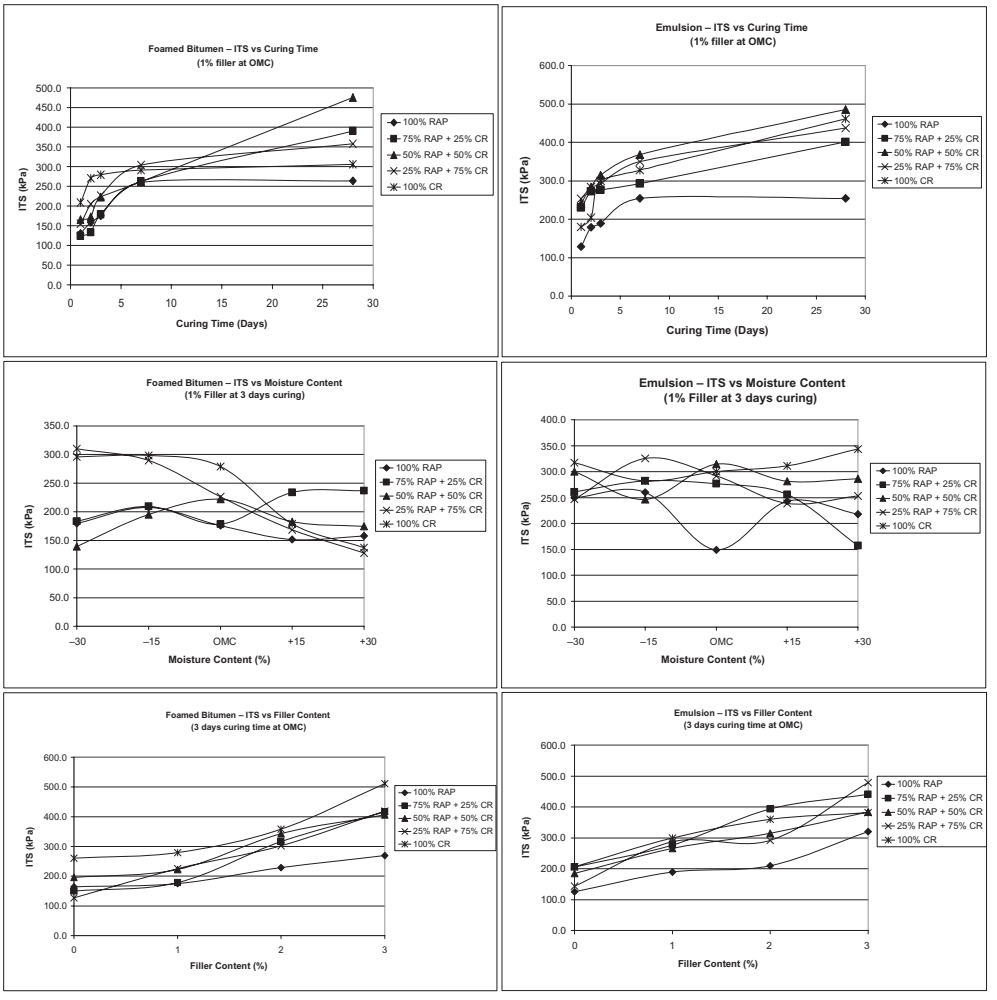

Figure 2. ITS test results.

3.3.2 *Resilient modulus vs. Active filler content*

The resilient modulus increases with an increase in active filler content. It was observed that for foamed bitumen treated samples with 75% and 100% RAP, a minimum of 1.5% active filler content was necessary to achieve the resilient modulus value of 2000 MPa at 3 days. This is in line with the construction practice in Malaysia of using 1.5% active filler for foamed bitumen recycled base.

For emulsion treated samples, it was found that more than 3% active filler may be required for 100% RAP to achieve the 2000 MPa resilient modulus at 3 days. For 75% RAP, 1.2% active filler was sufficient.

3.3.3 *Resilient modulus vs. Moisture content*

The variation of the moisture content did not affect the resilient modulus values of samples with high RAP content. For foamed bitumen treated samples with less RAP proportions, the modulus peak at certain moisture content. The results showed that at 1% active filler, samples with high RAP content of more than 50% did not meet the resilient modulus of 2000 MPa, a value normally assumed in pavement design. For samples with low RAP contents, the resilient modulus at their respective OMC could be as high as 6000 MPa. Therefore it is suggested that the seed values to be used in pavement design for RAP layer be based on the modulus of the corresponding RAP proportions.

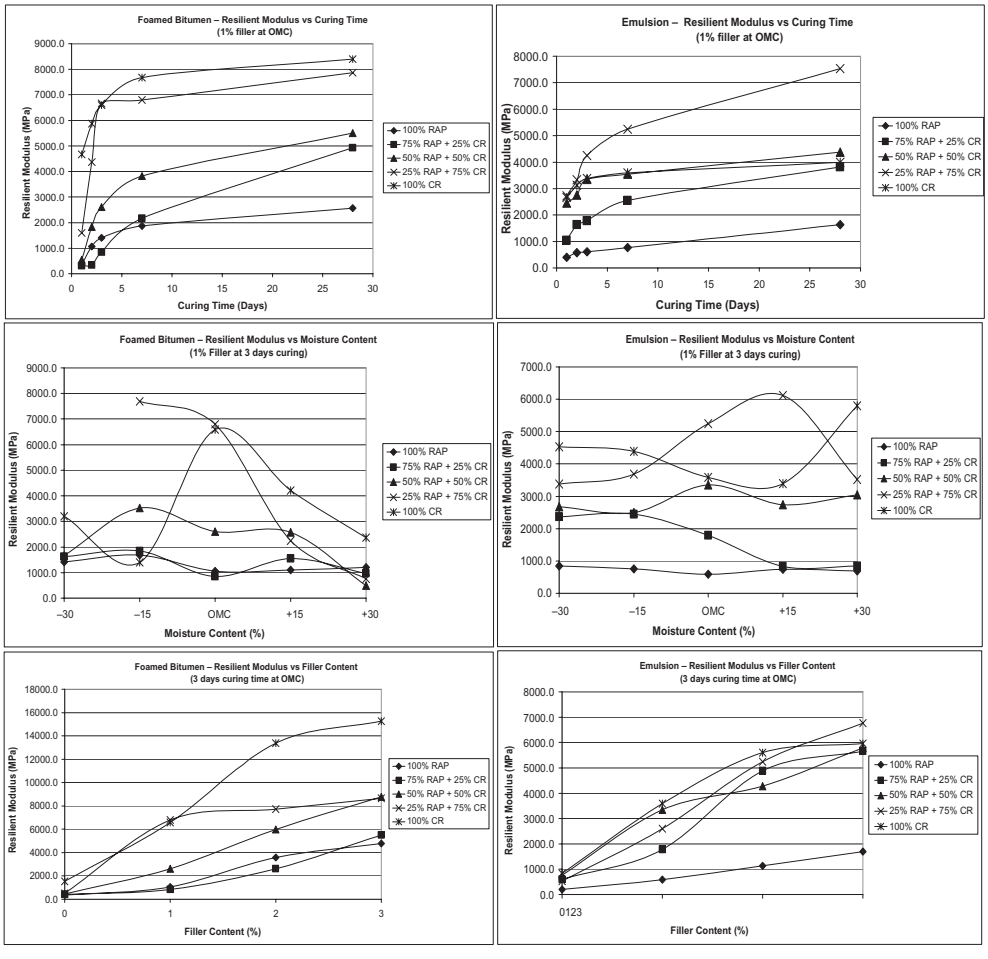

Figure 3. Resilient modulus test results.

For emulsion treated samples with 100% RAP, the resilient modulus was well below 2000 MPa within the studied moisture content. For the 75% RAP, the resilient modulus was higher than 2000 MPa at moisture content lower than OMC.

The following graphs in Figure 3 summarize the results of the resilient modulus tests.

4 CONCLUSION

Based on the study, active filler content, curing time, moisture content, and RAP proportions are contributing factors to the performance of recycled asphalt layers in the CIPR works utilizing foamed bitumen and emulsion as the stabilizing agents. It can be concluded that active filler is required in recycling works in Malaysia. At 1% active filler the curative period is 3 days provided the RAP proportion is not more than 50%. For 75% RAP, 1.5% active filler is recommended. For 100% RAP, the minimum active filler for CIPR with foamed bitumen and emulsion is 2% and 3% respectively. The effect of moisture content variation on foamed bitumen and emulsion treated samples with high RAP proportion is not significant. For low RAP proportion samples, higher ITS and resilient modulus values were recorded at lower moisture content.

REFERENCES

Cooley, A. Dane. 2005. *Effects Of Reclaimed Asphalt Pavement On Mechanical Properties Of Base Materials*. A thesis submitted to the faculty of Brigham Young University.

Lee, H.D & Yong, K.J. 2003. *Development of Mix Design Process for Cold In Place Rehabilitation Using Foamed Asphalt*. A report on Research Sponsored by Iowa Department of Transportation.

Mohammad L.N, Abu Farsakh M.Y, Wu Zhong & Abadie, C. 2003. *Louisiana Experience With Foamed Recycled Asphalt Pavement Base Materials*. 82th Transportation Research Board Annual Meeting. Washington DC.

Houston, M & Long, F. 2004. Correlation Between Different ITS and UCS Test Protocols for Foamed Bitumen Treated Materials. Proceedings of the 8th Conference on asphalt Pavements for Southern Africa (CAPSA '04), Sun City South Africa.

Road Engineering Association of Malaysia (REAM), 2005. *Specification For Cold In-Place Recycling*.

Advanced Testing and Characterization of Bituminous Materials –
Loizos, Partl, Scarpas & Al-Qadi (eds)
© 2009 Taylor & Francis Group, London, ISBN 978-0-415-55854-9

An experimental study on the recycling of powder extinguishers into bituminous mixtures

F.G. Praticò, A. Moro & R. Ammendola
DIMET Department, Mediterranea University, Reggio Calabria, Italy

ABSTRACT: Fire extinguishers should be maintained at regular intervals.

This includes a thorough examination and any necessary repairs, recharging or replacement. As a consequence, an important problem arises when such dry powers finish their usual life cycle.

In the light of the above facts, the idea was to recycle extinguisher dry powders into the road pavement. Therefore, a research project was undertaken and the main object of the study has been confined into the study of volumetrics, mechanical-chemical performance and environmental compatibility of bituminous mixes containing such powders.

Based upon the data collected, mechanical performance resulted sufficient, environmental compatibility satisfied European requirements, while fuel resistance resulted possibly increased. Finally, gaps and new research needs have been identified.

1 INTRODUCTION

As is well known, the ABC or Multi-Purpose dry chemical is a dry chemical extinguishing agent. It utilizes a specially fluidized and siliconized mono ammonium phosphate powder ($NH_4H_2PO_4$, 50–80% in weight). It insulates Class A fires by melting at approximately 180–200 degrees Celsius and coats the surface to which it is applied and breaks the chain reaction of Class B fires and is a non-conductor of electricity. The ABC type is filled with monoammonium phosphate, a yellow powder. Fire extinguishers should be maintained at regular intervals (at least once a year), or when specifically indicated by an inspection.

Maintenance is a "thorough check" of the extinguisher. It is intended to give maximum assurance that an extinguisher will operate effectively and safely. It includes a thorough examination and any necessary repair, recharging or replacement. As a consequence, problems arise when such dry powers finish their life cycle.

Therefore, a research project was undertaken and the main object of the study has been confined into the study of volumetrics, mechanical-chemical performance and environmental compatibility of bituminous mixes containing fire extinguisher agents (Mogawer, W.S et al., 2002; Brown, E.R., 2004; Cooley, L.A. Jr., 2002; Spellerberg, P. et al., 2004).

This paper presents the results of the study. Section 2 describes the experimental plan, while in section 3 results are analyzed and discussed.

2 EXPERIMENTAL PLAN

Following powder characterization (gradation, stiffening properties), three bituminous mixes has been considered, with different extinguisher powder contents. Experiences in laboratory and field tests for performance-oriented bituminous materials evaluation have been carried out. Gradation bands, asphalt binder content and quality, volumetric properties, mechanical resistance tests, environmental compatibility (elution) and fuel resistance have been specifically addressed. Results have been analyzed statistically in order to evaluate the effect of the extinguisher powder on the tested characteristics.

Three bituminous mixes (Binder Courses A_1, A_2, A_3), with different extinguisher powder contents, have been produced and tested (see Figure 1 and Table 1):

– Mix A_1 with 0% REP; Mix A_2 with 3% REP; Mix A_3 with 6% REP,

where REP stands for Reclaimed Extinguisher Powder.

The main phases of the experiments have been the following:

- design of experiments (3 mixes A_1, A_2, A_3, tests, timetable, see Table 1);
- delivering of the REP to the plant;
- production of the HMA according to the design;
- testing (on asphalt binder, on REP, on mixes).

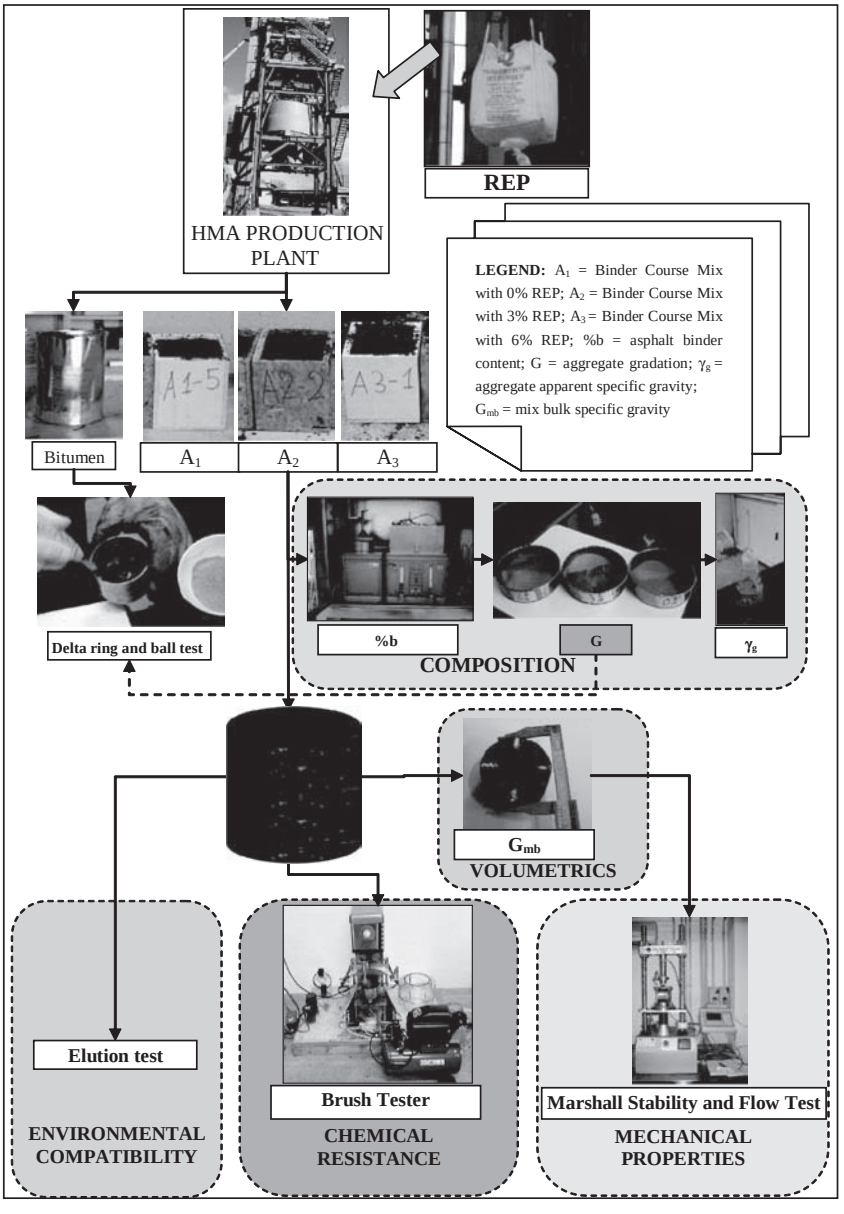

Figure 1. Experimental plan.

Table 1. Factorial plan of experiments.

	MIX A_1		MIX A_2		MIX A_3		
	Sieve (mm)	Passing (%)	Sieve (mm)	Passing (%)	Sieve (mm)	Passing (%)	
MIX DESIGN	40	100	40	100	40	100	Asphalt Content: 5%
	30	100	30	100	30	100	
	25	100	25	100	25	100	
	15	75	15	75	15	75	
	10	65	10	65	10	65	
	5	45	5	45	5	45	
	2	32	2	32	2	32	
	0,4	15	0,4	15	0,4	15	
	0.18	10	0.18	10	0.18	10	
	0.075	6 (0% REP)	0.075	6 (3% REP)	0.075	6 (6% REP)	

	Tested material	Property	Test	Standard
TESTS	asphalt binder and on asphalt binder and/or filler		Softening point	CNR BU n.35-1973; EN 1427: 2007
			Delta ring and ball test	EN 13179-1:2002; CNR N. 122/1988
			Penetration test	CNR BU n. 24-1971; EN 1426:2007
			Viscosity	ASTM D4402-02; EN 14896:2006
	MIX A_1 MIX A_2 MIX A_3	Composition	asphalt binder content as a percentage of aggregates	B.U. CNR n.38/73; EN 12697-1: 2006
			aggregate gradation	B.U. CNR n. 4/53; EN 12697-2:2008
			aggregate apparent specific gravity	B.U. CNR n. 63/78
			mix bulk specific gravities	EN 12697-6, ASTM D6752;
			mix effective porosity	ASTM D6752 ASTM D6857
		Mechanical Properties	Marshall Stability and Flow Test	EN 12697-34:2004; CNR BU 30/73);
		Fuel Resistance	Brush Test	EN 12697-43:2005
	MIX A_1 MIX A_3	Environmental compatibility	Elution test	UNI 10802:2004, EN UNI 12457-2/2004

Experiments have been planned and performed according to the following procedures and standards (see Table 1): 1) Volumetric tests: 1a) %b = asphalt binder content as a percentage of aggregates; 1b) G = aggregate gradation (P_{200} stands for percent passing to the 0.075 mm, n.200, sieve); 1c) γ_g = aggregate apparent specific gravity; 1d) G_{mb} = mix bulk specific gravities; 1e) n_{eff} = mix effective porosity; 2) Tests on asphalt binder and on asphalt binder and/or filler: 2a) Softening point (Ball and ring); 2b) Delta ring and ball test; 2c) Penetration test; 2d) Viscosity at 135°C, 160°C, 170°C; 3) Mechanical Properties: Marshall Stability and Flow Test; 4) Fuel Resistance: Brush tests in order to estimate *A*, *B* and *C*. These tests have been carried out through the new device Brush testeRC®; 5) Environmental compatibility: Elution test.

3 RESULTS

Figures 2 to 14 and Tables 2 to 4 summarize the obtained results. Figures 2 to 4 refer to HMA composition. These figures show that aggregate grading and composition parameters of the as-constructed HMA differ from that of the as-designed HMA.

In particular (Figure 4), as far as the filler content is concerned, it is important to point out that there is a mass "loss" of filler: it ranges from less than 1% up to 2% (on the total weight of the mix). More importantly, the higher the REP content, the higher the mass loss. More in detail, up to 22% of the filler mass has been "lost", due to one or a combination of these causes: a) mass loss after the weighting in the filler line; b) drying effect (loss of liquid content); c) sublimation (passage from the solid to the gas state); d) process variance.

By referring to asphalt binder content (Figure 4) it is possible to remark that the higher the REP content the lower the asphalt binder content (and the lower the filler content). This experimental evidence could depend on many causes, among which: a) a consequence of the reduced total filler content; b) differences in the specific surface of the REP when compared to traditional filler; c) changes at a microstructural level in terms of compatibility filler—bitumen; d) process variance. Moreover, Figure 4 shows a slight decrease in γ_g (apparent specific gravity of aggregates) due to the presence of REP.

Figure 5 shows the main characteristics of the asphalt binder used in the experiments.

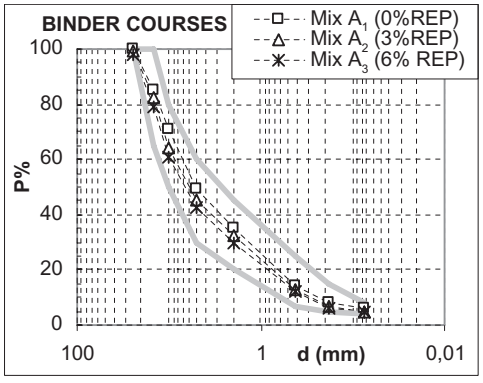

Figure 2. Aggregate gradations.

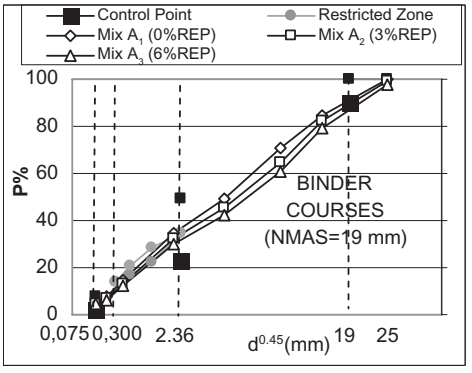

Figure 3. Aggregate gradations (*superpave* approach).

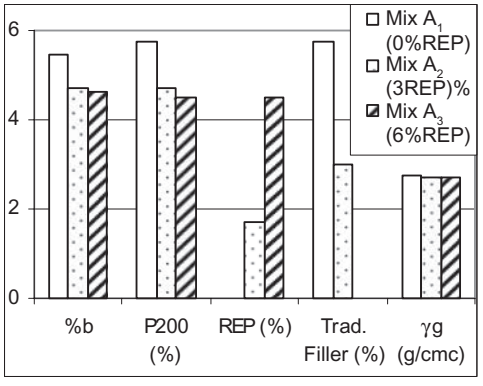

Figure 4. Composition.

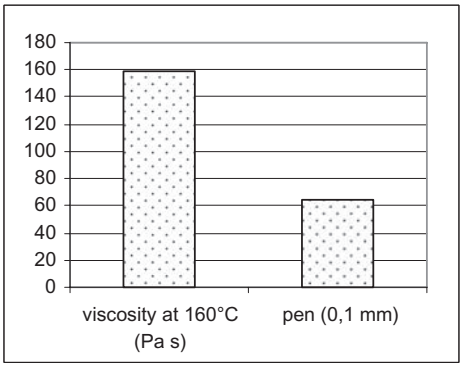

Figure 5. Bitumen viscosity and penetration.

As for delta ring and ball tests (Figure 6), no appreciable differences have been detected for the traditional filler vs. the REP one. The increase of the softening point (SP, °C) resulted for both the mixes (traditional filler + bitumen vs. REP + bitumen) around a 6°C.

Figure 7 illustrates the differences in volumetrics among the three classes of mixes. In particular the effective porosity ranged from 5% (REP = 0%) up to 8% (REP = 3%).

As for Marshall test (Figure 8) slight differences in terms of flow and stability have been detected. This fact could be related to the differences in filler content and/or asphalt binder content.

Figures 9 and 10 show that, for a given bulk specific gravity, the higher the REP percentage the higher the Marshall Stability and Stiffness (averages are shown).

Figures 11 to 14 refer to the chemical resistance of the studied mixes. *A* stands for mass loss *per* soaking (in diesel oil), while *B* refers to mass loss *per* brushing and *C* for mass loss *per* soaking & brushing. In particular, the parameter *A* is the loss of mass after soaking in fuel (diesel oil): $A = \Sigma_i A_i/3$, with $i = 1, 2, 3$ (specimens), $A_i = ((m_{1,i} - m_{2,i})/ m_{1,i}) \cdot 100$, $m_{1,i}$ = initial dry mass of the i-th specimen for soaking in fuel, in grams (g), $m_{2,i}$ = mass of the i-th dry test specimen after soaking in fuel, in grams (g).

The parameter *B* is the loss of mass after the brush test, where $B = \Sigma_i B_i/3$, with $i = 1, 2, 3$ (specimens), $B_i = ((m_{2,i} - m_{5,i})/ m_{2,i}) \cdot 100$, $m_{2,i}$ = mass of the i-th dry test specimen after soaking in fuel, in grams (g), $m_{5,i}$ = mass of the i-th test specimen after soaking and after 120 s of brushing, in grams (g). *C* is a descriptor able to combine the two different actions (soaking & brushing) and is defined as the mean value of the loss of mass of the specimens, where $C = \Sigma_i C_i/3$, with $i = 1, 2, 3$ (n° specimen), $C_i = ((m_{1,i} - m_{5,i})/ m_{1,i}) \cdot 100$.

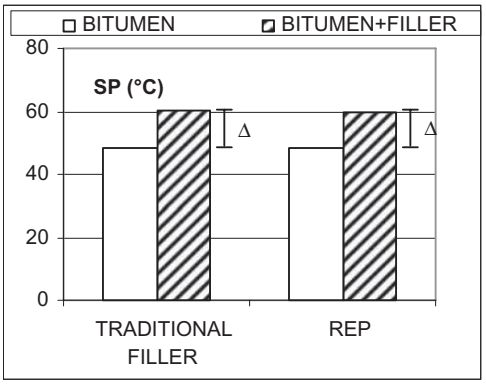

Figure 6. Delta ring and ball test.

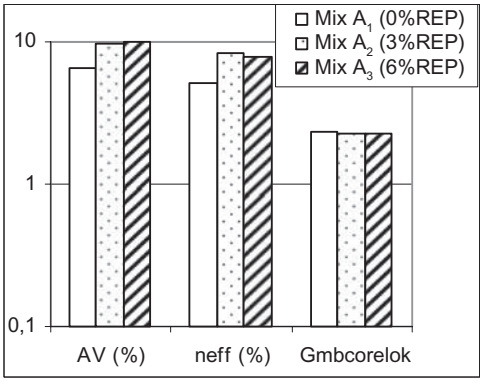

Figure 7. Volumetrics.

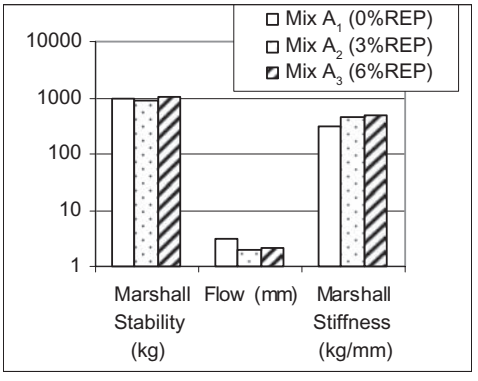

Figure 8. Marshall test.

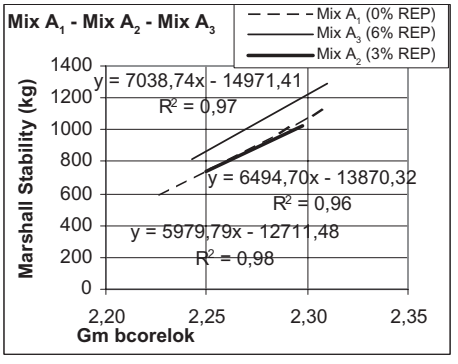

Figure 9. Marshall stability vs. gmb.

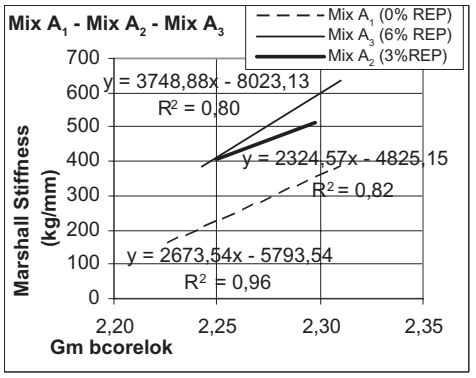

Figure 10. Marshall stiffness vs. gmb.

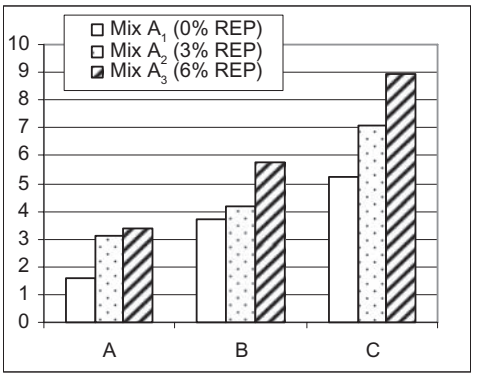

Figure 11. Chemical resistance (to diesel oil).

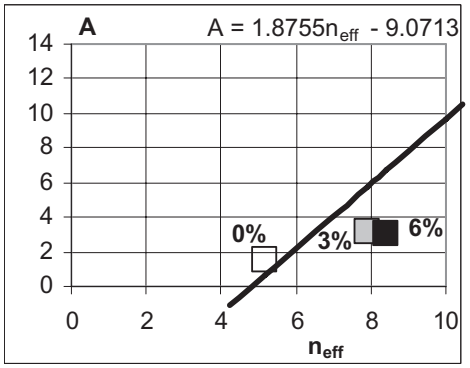

Figure 12. A vs. n_{eff}.

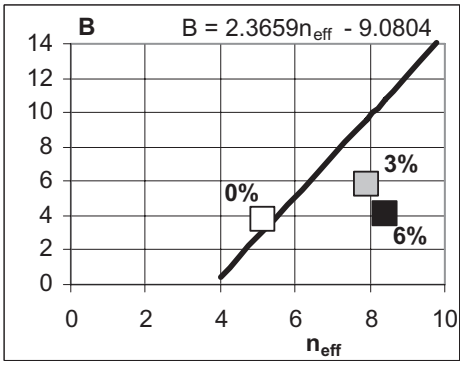

Figure 13. B vs. n_{eff}.

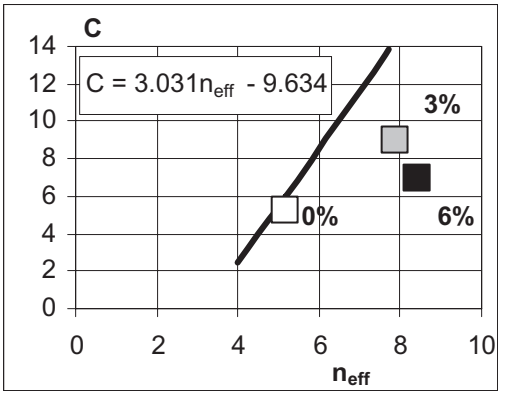

Figure 14. C vs. n_{eff}.

By observing these figures it is possible to observe that the higher the REP percentage the lower the chemical resistance (Figure 11). In figures 12 to 14 a comparison is showed between the obtained results and fitting curves derived from (Praticò et al., 2008). The fitting curves refer to *A*, *B* and *C* vs. n_{eff} correlations for mixes containing only mineral filler.

As far as the relationship between chemical resistance and effective porosity (n_{eff}) is examined, it is possible to point out that results are consistent with the fitting curves showed when

Table 2. Correlation matrix.

R	Marshall stability (kg)	Flow	Marshall stiffness (kg/mm)	$G_{mbdimensional}$	%b	P_{200} (%)	REP (%)	Trad. filler (%)	γ_g (g/cmc)
Marshall stability (kg)	1,00	–0,13	0,72	0,93	0,32	–0,32	0,11	–0,17	0,17
Flow	–0,13	1,00	–0,74	–0,02	0,68	0,86	–0,64	0,74	0,90
Marshall stiffness (kg/mm)	0,72	–0,74	1,00	0,58	–0,31	–0,79	0,52	–0,62	–0,49
$G_{mbdimensional}$	0,93	–0,02	0,58	1,00	0,43	–0,12	–0,18	0,11	0,31
%b	0,32	0,68	–0,31	0,43	1,00	0,49	–0,71	0,69	0,84
P_{200}	–0,32	0,86	–0,79	–0,12	0,49	1,00	–0,74	0,85	0,81
REP (%)	0,11	–0,64	0,52	–0,18	–0,71	–0,74	1,00	–0,98	–0,76
Trad. filler (%)	–0,17	0,74	–0,62	0,11	0,69	0,85	–0,98	1,00	0,81
γ_g (g/cmc)	0,17	0,90	–0,49	0,31	0,84	0,81	–0,76	0,81	1,00

Table 3. Correlation significance.

	Marshall stability (kg)	Flow	Marshall stiffness (kg/mm)	$G_{mbdimensional}$	%b	P_{200}(%)	REP (%)	Trad. filler (%)	γ_g (g/cmc)
Marshall stability (kg)	0,00	0,69	0,01	0,00	0,31	0,30	0,73	0,59	0,60
Flow	0,69	0,00	0,00	0,94	0,01	0,00	0,02	0,00	0,00
Marshall stiffness (kg/mm)	0,01	0,00	0,00	0,04	0,33	0,00	0,08	0,03	0,10
$G_{mbdimensional}$	0,00	0,94	0,04	0,00	0,16	0,71	0,56	0,72	0,32
%b	0,31	0,01	0,33	0,16	0,00	0,10	0,01	0,01	0,00
P_{200}	0,30	0,00	0,00	0,71	0,10	0,00	0,00	0,00	0,00
REP (%)	0,73	0,02	0,08	0,56	0,01	0,00	0,00	0,00	0,00
Trad. filler (%)	0,59	0,00	0,03	0,72	0,01	0,00	0,00	0,00	0,00
γ_g (g/cmc)	0,60	0,00	0,10	0,32	0,00	0,00	0,00	0,00	0,00

Table 4. Elution test.

Chemical parameters	Measure unit	Limit A	Limit B	Limit rivel	A_3	A_3 < limit A_1	A_3 < limit B_1	A_1	A_1 < limit A_3	A_1 < Limit B_1	A_1 < limit rivel?	A_3/A_1
Total dissolved solids	mg/l	6000	10000	5	530	TRUE	TRUE	29	TRUE	TRUE	TRUE	18,3
Cianydes	mg/l	0,5	5	0,01	0,01	TRUE	TRUE	0,1	TRUE	TRUE	FALSE	0,1
Chlorides	mg/l	1500	2500	0,5	4,2	TRUE	TRUE	1,4	TRUE	TRUE	TRUE	3,0
Fluorides	mg/l	15	50	0,5	0,5	TRUE	TRUE	0,5	TRUE	TRUE	FALSE	1,0
Sulphates	mg/l	2000	5000	0,5	189	TRUE	TRUE	0,9	TRUE	TRUE	TRUE	210,0
Dissolved organic carbon (DOC)	mg/l	80	100	1	2,8	TRUE	TRUE	1,2	TRUE	TRUE	TRUE	2,3
Total chromium	mg/l	1	7	0,0005	0,0005	TRUE	TRUE	0,0005	TRUE	TRUE	FALSE	1,0
Zinc	mg/l	5	20	0,0005	0,093	TRUE	TRUE	0,02	TRUE	TRUE	TRUE	4,7
Antimony	mg/l	0,07	0,5	0,0005	0,0005	TRUE	TRUE	0,0005	TRUE	TRUE	FALSE	1,0
Arsenic	mg/l	0,2	2,5	0,0005	0,0005	TRUE	TRUE	0,0005	TRUE	TRUE	FALSE	1,0
barium	mg/l	10	30	0,0005	0,0158	TRUE	TRUE	0,0115	TRUE	TRUE	TRUE	1,4
Cadmium	mg/l	0,02	0,2	0,0005	0,0005	TRUE	TRUE	0,0005	TRUE	TRUE	FALSE	1,0
Mercury	mg/l	0,005	0,05	0,0005	0,0005	TRUE	TRUE	0,0039	TRUE	TRUE	FALSE	0,1
Molybdenum	mg/l	1	3	0,0005	0,005	TRUE	TRUE	0,0005	TRUE	TRUE	TRUE	10,0
Nickel	mg/l	1	4	0,0005	0,0147	TRUE	TRUE	0,0005	TRUE	TRUE	TRUE	29,4

REP = 0%, while points are below the curves for REP = 3 ÷ 6%. This fact could mean that the loss in chemical resistance showed in figure 11 is due to the increase in effective porosity and not to the change of filler typology (from lime to REP).

More importantly, it seems that, at a given effective porosity, the higher the REP content the better the chemical resistance (see Figures 12 to 14).

Tables 2 and 3 summarize the above-mentioned results in terms of R values and correlation significance. The level of significance of correlations (all the mixes, p-values) is summarized in table 3.

The values reported in table 3 represent the probability of making the "wrong decision", i.e. a decision to reject the null hypothesis (the two variables are not correlated) when the null hypothesis is actually true (Type I error, or "false positive determination").

The smaller the p-value, the more significant the result is said to be.

Relationships and trends for %b, P_{200}, γ_g and Marshall flow result confirmed but more research is needed on these topics.

Table 4 summarizes tests on environmental compatibility according to the well-known concept of elution (appearance of chemicals from the column of a chromatograph).

The mixes A_1 (REP = 0%) and A_3 (REP = 6%) are compared. 15 chemical parameters are taken into account.

Results seem satisfactory, but due to the extreme relevance of the topic, this issue calls for further and extended research.

4 CONCLUSIONS

In the light of the obtained results the following conclusions may be drawn:

1) a phenomenon of mass loss of REP has been observed and some hypotheses have been formulated. More research is needed on this topic;
2) mechanical properties resulted substantially independent on REP content, though an increase of Marshall stability/stiffness (for a given specific gravity) and an increase of chemical resistance (for a given effective porosity) have been found. Also these issues call for further research;
3) another interesting issue is the increase of effective porosity for the mixes added with REP, probably related to the above mentioned mass loss of REP;
4) Environmental compatibility resulted satisfactory.

The following key-factors have been focused for future research:

a) Optimizing REP content (calibrating the process);
b) Checking for compaction issues;
c) Making a more robust experimental plan (on a statistical point of view).

Future research will aim to address some of the uncertainties arose during the experiments and in the analysis of the results. Many efforts will be oriented to the design of a new plan of experiments with more tests in order to achieve more reliable inferences.

REFERENCES

ASTM D4402-02: Standard test method for viscosity determinations of unfilled asphalts using the Brookfield thermosel apparatus.

Brown, E.R., Hainin, M.R., Cooley, A. & Hurley G. 2004. Relationship of Air Voids, Lift Thickness, and Permeability in Hot Mix Asphalt Pavements NCHRP Report 531, National Center for Asphalt Technology—Auburn University, Auburn, AL, Transportation Research Board, Washington, D.C.

CNR BU 30/73. Determinazione della stabilità e dello scorrimento di miscele di bitume e inerti lapidei a mezzo dell'apparecchio Marshall.

CNR BU n.24-1971. Norme per l'accettazione dei bitumi per usi Stradali. Metodi di prova: penetrazione.

CNR BU n.35-1973. Norme per l'accettazione dei bitumi per usi stradali. Metodi di prova: punto di rammollimento (Metodo palla e anello).
CNR N. 122/1988. Determinazione dell'influenza di un filler sul punto di rammollimento palla-anello di un legante idrocarburico.
Cooley, L.A.Jr., Prowell, B.D., Hainin, M.R., Buchanan, M.S. & Harrington, J.—Bulk specific gravity round-robin using the corelok vacuum sealing device—National Center for Asphalt Technology Report 02–11, FHWA-IF-02-044, November 2002.
EN 12697-34:2004. Metodi di prova per conglomerati bituminosi a caldo. Parte 34: Prova Marshall.
EN 12697-43:2005. Metodi di prova per conglomerati bituminosi a caldo—Parte 43: Resistenza al carburante.
EN 13179-1:2002 Tests for filler aggregate used in bituminous mixtures—Part 1: Delta ring and ball test.
EN 1426:2007: Bitumen and bituminous binders—Determination of needle penetration.
EN 1427:2007: Bitumen and bituminous binders—Determination of the softening point—Ring and Ball method.
EN 14896:2006: Bitumen and bituminous binders—Dynamic viscosity of bituminous emulsions, cutback and fluxed bituminous binders—Rotating spindle viscometer method.
Mogawer, W. S. et al. 2002. Evaluation of Permeability of Superpave Mixes Project No. NETC 00-2.
Praticò, F.G., & Ammendola, R. & Moro, A. 2008. Fuel resistance of HMAs: Theory and Experiments. *International Journal of Pavement Research and Technology, July 2008*, 1(3).
Spellerberg, P. and Savage D.—An investigation of the cause of variation in HMA Bulk Specific Gravity test results using non-absorptive aggregates—National Cooperative Highway Research Program Web Document 66 (Project 9–26 (Phase 2)), July 2004.
UNI 10802:2004. Rifiuti—Rifiuti liquidi, granulari, pastosi e fanghi—Campionamento manuale e preparazione ed analisi degli eluati.
UNI EN 12457-2/2004. Caratterizzazione dei rifiuti—Lisciviazione—Prova di conformità per la lisciviazione di rifiuti granulari e di fanghi
UNI EN 12697-6 : 2003. Bituminous mixtures. Test methods for hot mix asphalt. Determination of bulk density of bituminous specimens.

Advanced Testing and Characterization of Bituminous Materials – Loizos, Partl, Scarpas & Al-Qadi (eds)
© 2009 Taylor & Francis Group, London, ISBN 978-0-415-55854-9

Key characteristics of materials stabilised with foamed bitumen

D.C. Collings
Loudon International (A Division of PDNA), South Africa

K.J. Jenkins
University of Stellenbosch, South Africa

ABSTRACT: The first properly-engineered equipment for producing foamed bitumen was launched in Germany in 1996. Since then, foamed bitumen treatment has seen a remarkable increase in usage, worldwide. However, thirteen years later, there is much ignorance as to what a foamed bitumen treated material actually is, what it is not and, most importantly, the performance characteristics of such a material.

The way the bitumen disperses amongst the aggregate particles when treated at ambient temperatures dictates performance. Similar to a granular material that has been treated with bitumen emulsion, particle coating is confined to the smaller fractions leaving the larger ones untouched. Consequently, these materials are very different from conventional hot-mixed asphalt and cold mixes. Pavement layers constructed from bitumen stabilised materials therefore behave differently under applied loads.

The results of research carried out over the past decade, coupled with long-term pavement performance data are used to highlight the in-service behavioural characteristics of these materials and their failure mode. The development of design methodology (both mix- and pavement-design) is reviewed along with recent research programmes to obtain reliable indicators of performance. This includes the outline of a newly developed "intelligent Structural Number" approach to pavement design.

The publication on Bitumen Stabilised Materials that was recently released in South Africa is reviewed, focusing on material classification that is based on the characteristics of the pre-treated material, the inclusion of active filler and the type/application rate of bitumen used in the stabilisation process.

1 INTRODUCTION

A variety of in situ pavement materials have been successfully treated with bitumen emulsion for over thirty years, proving that such treatment is a cost-effective way of improving the strength, as well as reducing the detrimental effects of water. In addition, a pavement layer constructed from a bitumen stabilised material is relatively flexible compared to using cement to stabilise the same material. The inevitable shrinkage cracks associated with cement treatment are absent from a bitumen stabilised material. In South Africa, several pavements with bitumen treated base layers have provided service lives in excess of 20 years and are still performing well today (Long et al. 2007a).

There are currently two agents used for bitumen stabilisation, bitumen emulsion and foamed bitumen. One problem often experienced when stabilising in situ materials with bitumen emulsion, however, is material saturation during construction. Although most bitumen emulsions are comprised of 40% water suspending 60% bitumen droplets (by volume), they are 100% fluid. Applying 3% (by mass) of residual bitumen to achieve the required stabilisation implies that 5% fluid (bitumen emulsion) needs to be added to the material. Adding this amount of fluid to an in situ pavement material with a moisture content approaching the

optimum is often sufficient to cause saturation, thereby preventing the material from being compacted. Pore pressures that develop when compaction energy is applied to the material cause instability (the well-known heaving phenomenon), making it impossible to construct a pavement layer. This phenomenon tends to limit the use of bitumen emulsions for stabilisation.

In the mid-1950s, foamed bitumen was identified as an alternative bitumen stabilising agent. One of the primary attractions of using foamed bitumen in place of emulsion was the elimination of the added water with the bitumen. Foamed bitumen and bitumen emulsion have one common characteristic: both reduce the viscosity of the bitumen, allowing it to be mixed with cold moist materials that are encountered when recycling an existing pavement. Early laboratory test results indicated that foamed bitumen offered similar performance benefits as those achieved with bitumen emulsion, but without the compulsory addition of unwanted fluid (Twagira et al. 2006). An additional attraction was the lower cost of the bitumen stabilising agent.

Unlike bitumen emulsion that is manufactured under factory conditions using expensive chemicals (emulsifiers), foamed bitumen is produced by injecting a small amount of water into Penetration-grade bitumen at elevated temperatures (>160°C). Since the foaming state is short-lived, the foamed bitumen has to be produced on site in a purpose-built spraybar immediately before stabilising. However, whether it is introduced in an emulsified or foaming state, the end product is a bitumen stabilised material with similar characteristics that are discussed in the following section.

2 CHARACTERISTICS OF BITUMEN STABILISED MATERIALS (BSMS)

Unlike hot-mix asphalt, a material stabilised with bitumen is not black in appearance and does not have a sticky feel. This is because the larger aggregate particles are not coated with bitumen. The bitumen disperses amongst the finest particles only when the temperature of the aggregate is at normal summer temperatures (15°C to 25°C). The reason for such dispersion is different for bitumen emulsion and foamed bitumen. Being charged, the bitumen droplets in an emulsion are drawn to the smaller particles that exhibit the maximum opposite charge. Tiny bitumen particles produced when the foam bubbles burst have only sufficient heat energy to warm tiny aggregate particles sufficiently to permit adhesion. The resulting mix sees the bitumen confined to the fines fraction, or the mortar between coarse particles, as shown by the black spots in Figure 1 (Wirtgen, 2004). The colour of the material therefore only darkens slightly after treatment.

Regardless of whether bitumen emulsion or foamed bitumen is used, small amounts of active filler (cement or lime) are normally added in conjunction. In addition to improving the retained strength under saturated conditions, such active filler assists in dispersing the foamed bitumen particles by increasing the fines fraction for foamed bitumen, whilst it assists in extracting the water phase from a bitumen emulsion, causing separation (break). Research has,

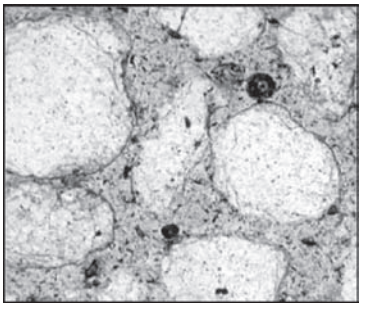

Figure 1. Bitumen dispersion.

however, shown that small amounts of active fillers (1% by mass of hydrated lime or cement) do more than assist the bitumen to disperse (foamed bitumen) or break out of the emulsified state. Adding or omitting the active filler can have a significant effect on the treated material's ability to maintain strength under saturated conditions (Jenkins et al. 2007).

2.1 *Primary characteristics*

BSMs are different from all other pavement materials, primarily due to the "spotty" nature of the bitumen dispersion that creates a non-continuously bound material. The following summarises the main features of these materials:

- the bitumen droplets are not joined to each other;
- when compacted, the cohesion of the material is increased by between 5 and 10 times without a significant reduction in the internal angle of friction;
- the material acquires significant flexural strength as a result of the visco-elastic properties of the dispersed bitumen;
- since the individual bitumen droplets are not interlinked and the coarser aggregate particles remain uncoated, the treated material reflects the granular characteristics of the untreated material. It is therefore stress dependent and not prone to cracking when subjected to tensile stresses (induced by applied or thermal forces);
- since the bitumen is dispersed only amongst the finer aggregate particles, they are encapsulated and immobilised. Such materials are not prone to pumping when load is applied under saturated conditions (Paige-Green et al. 2004 & Collings et al. 2008).

The effective stiffness of a layer of BSM in a pavement structure and its behaviour under load is a function of the parent material, the density of the material in the layer, the amount of bitumen added (and how well it is dispersed), active filler, temperature, moisture content and support characteristics (Asphalt Academy 2002 & Long et al. 2007b).

Although they are flexible and have a tensile strength, their mode of failure within a pavement structure as a consequence of repeated loading is permanent deformation. The shear properties of these materials are therefore of paramount importance.

BSMs are used for the construction of base or subbase layers. They are therefore always surfaced and protected from the direct effects of environmental and traffic forces. Under such conditions the bitumen droplets are protected from UV bombardment and the ageing effects of oxidation and high temperature. They can therefore be expected to retain their elastic properties for extended periods, especially the droplets located in the lower portion of thick layers where tensile stresses develop when the pavement structure is loaded.

2.2 *Fundamental performance properties of BSMs*

Structural design procedures anticipate fatigue cracking (bottom-up) as the failure mechanism for a continuously bound material (asphalt concrete and cement stabilised aggregates) caused by repeated load applications. Such repeated load applications cause unbound granular materials (graded crushed stone and natural gravels) to consolidate, or permanently deform as a consequence of the applied shear forces rearranging the individual particles relative to each other. When the confining pressures within the body of the material are insufficient to resist high levels of applied stress, lateral movement of the material occurs (shoving).

A non-continuously bound BSM behaves in a similar way to a granular material when subjected to load. However, it is the increase in cohesion as a result of the dispersed bitumen that allows these materials to withstand relatively high levels of stress before failing in shear and causing permanent deformation.

Recycled materials combine the influences of mineral aggregates, bituminous binders, active fillers and water to create complex visco-elasto-plastic material with anisotropic characteristics. The matrix of a BSM is "*neither fish nor fowl*" showing stress dependency similar to granular materials (see Figure 2) and dependency on frequency of loading similar to asphalt (see Figure 3).

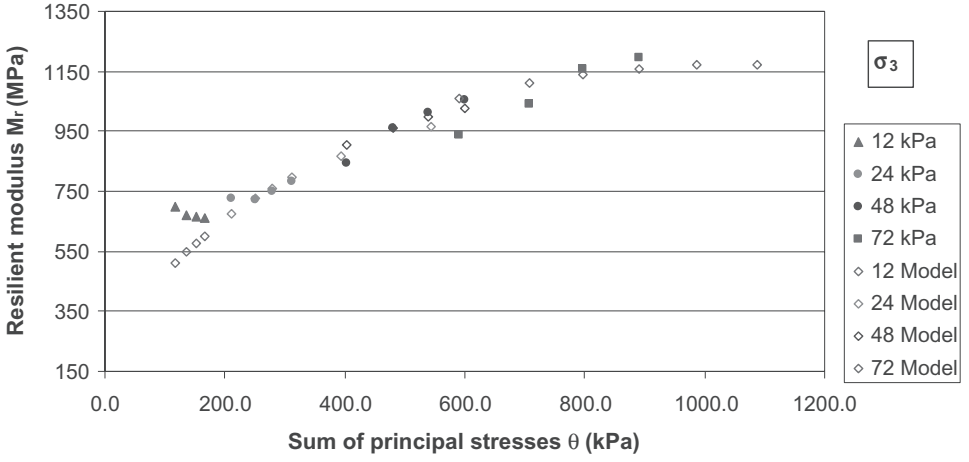

Figure 2. Resilient modulus of recycled mixed granulate with 2% foamed bitumen (Jenkins et al. 2002).

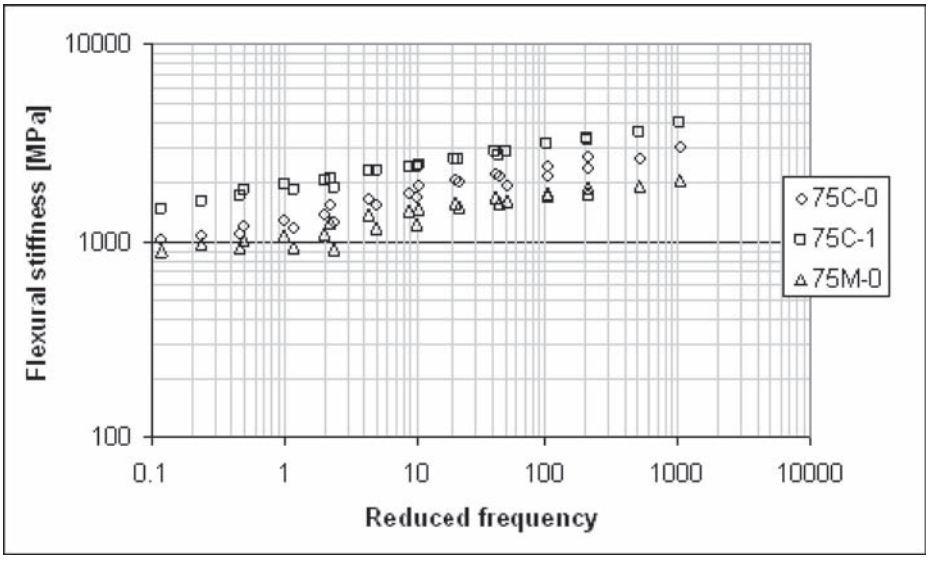

Figure 3. Flexural modulus of crushed limestone and RAP (reclaimed asphalt pavement) stabilised with emulsion, reference temperature 20ºc (Twagira et al. 2006).

Note: 75C-0 = 75% Crushed Limestone with 25% RAP, no cement.
75C-1 = 75% Crushed Limestone with 25% RAP, with 1% cement.
75M-0 = 75% RAP with 25% Crushed Limestone, no cement.

Gathering the available knowledge generated through research and laboratory testing begins to create a two dimensional matrix representing the link between material behaviour and the type and amount of binder, as shown in Figure 4. It assists in understanding the typical failure mechanisms of the cold recycled materials, including BSMs.

The modelling of BSMs needs to look beyond just the binders and must take cognisance of the moisture in the material. It is this added dimension that sets BSMs apart from HMA, and poses challenges for characterisation and design of cold recycled mixtures (BSMs). The initial knowledge gathered from laboratory testing and APT (Accelerated Pavement Testing) on

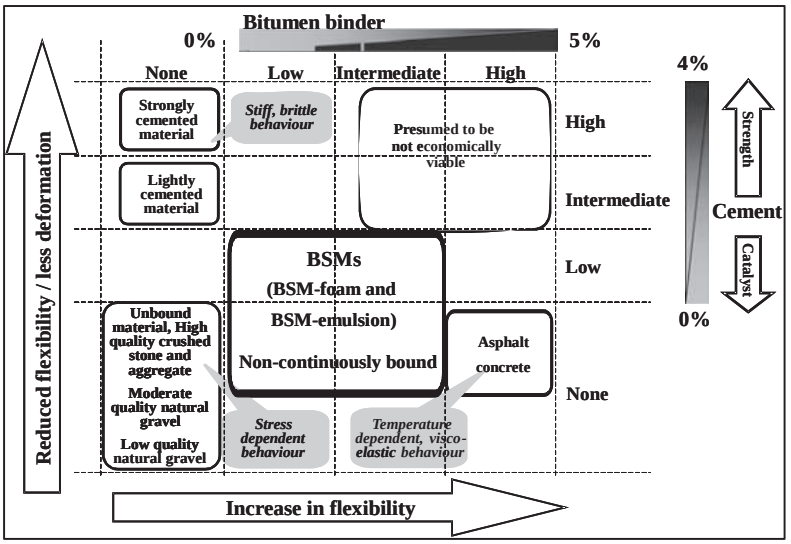

Figure 4. Matrix of bituminous and mineral binder influence on BSM behaviour after (Asphalt Academy, 2002).

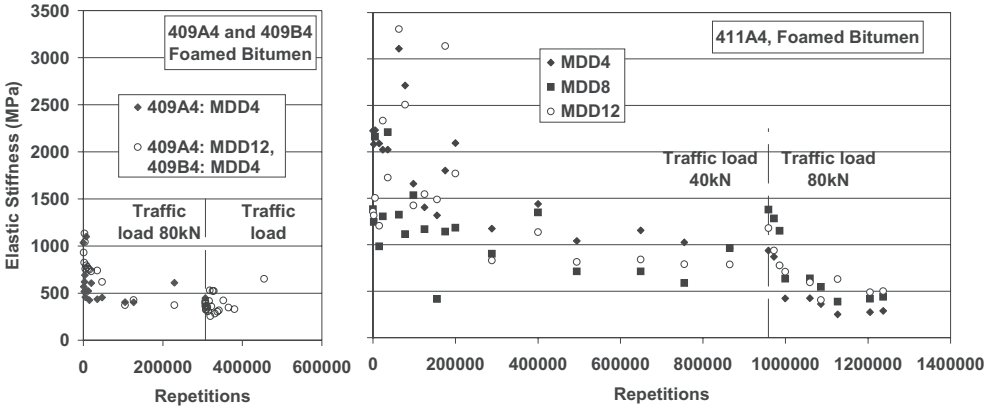

Figure 5. Change of resilient modulus of foamed BSM (2.3% Bitumen and 1% cement) with axle loading of heavy vehicle simulator (HVS) (Long et al. 2004).

BSMs pointed towards a reduction in stiffness of the material during short duration dynamic loading, as shown in Figure 5. However, numerous projects over the past 15 years have provided evidence of an increase in stiffness of the BSM layer with time, under traffic. An example is provided in Figure 6, where FWD deflection analyses on a Greek Highway recycled with foamed bitumen prior to the 2004 Athens Olympics, showed that the stiffness could continue to increase for up to 4 years after construction. Besides a small contribution from the cement, the predominant influence of stiffness accumulation is curing, i.e. moisture reduction in the BSM. This raises the question: how does one develop design tools to take account of the change in stiffness with time? This will be addressed under pavement design in Section 3.

In addition to understanding the behaviour of BSMs, is the need to develop the right tests to be able to critically analyse the mixes, specify them and carry out reliable quality control. The granular nature of BSMs with added bitumen of less than 4%, has led researchers to

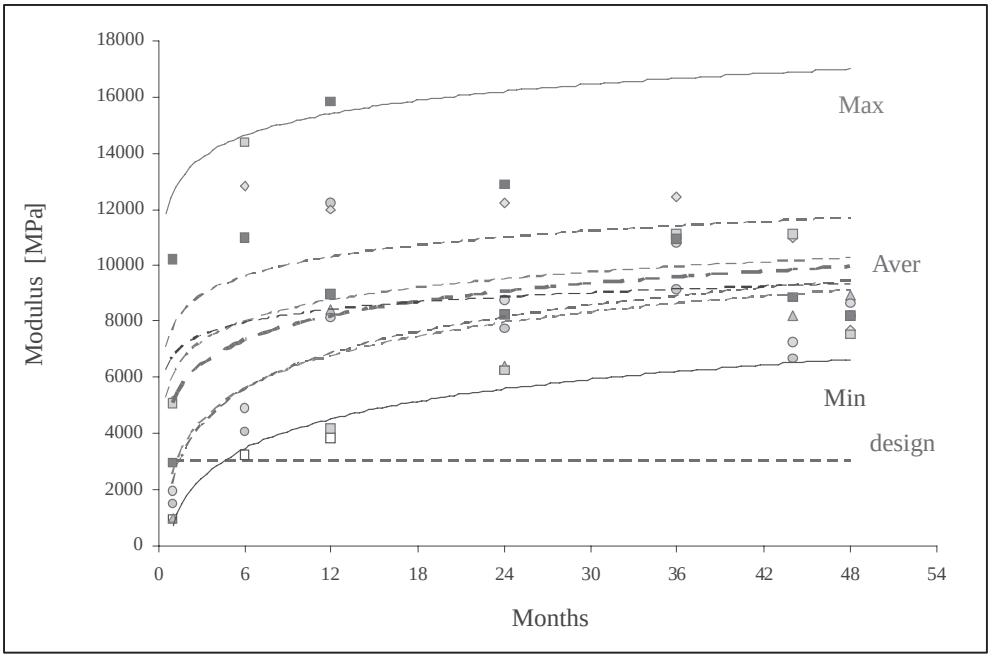

Figure 6. Evolution of resilient modulus from FWD back-analysis of foamed BSM (2.1% bitumen and 1% cement) on a Greek highway (Loizos et al. 2007).

use triaxial tests for the analysis of the shear parameters of the mixes and establish a link to performance. Back in 1974 (Shackel et al. 1974), triaxial tests were used to good effect to understand foamed BSMs. More recently, triaxial testing has become a standard testing procedure for analysing mix performance in terms of moisture sensitivity, durability and resistance to permanent deformation (Jenkins et al. 2008). In fact, the project to rewrite the South African Guidelines for BSMs (TG2) has undertaken 2 tasks under the mix design phase to improve the triaxial testing procedures:

- Task 1 includes the development of a standard research triaxial testing protocol so that research institutes in South Africa can provide interchangeable results.
- Task 2 focuses on the development of a "simple triaxial test" that would make this procedure more accessible to commercial laboratories.

The development of more appropriate triaxial testing procedures has created a need for improved laboratory compaction procedures of the specimens and accelerated curing protocols before testing. These issues, amongst others, are discussed in a separate paper at this conference.

Modelling of BSMs and in particular foamed BSMs, has reached the levels of sophistication where image analysis of Fracture Face Asphalt Coverage (FFAC) is being analysed and modelled at UC Davis (Fu et al. 2007) so that the imaging can provide insights into mix performance. This area is likely to develop further in the future.

3 STRUCTURAL CONTRIBUTION OF BSMS

Probably the greatest challenge in stabilising recycled materials in creating BSMs, is dealing with the variability. Jooste et al (2007) developed a classification system for pavement materials as part of the pavement design portion of TG2. This includes BSMs and takes account of relative certainty of test procedures and numbers of tests in a cumulative updating method.

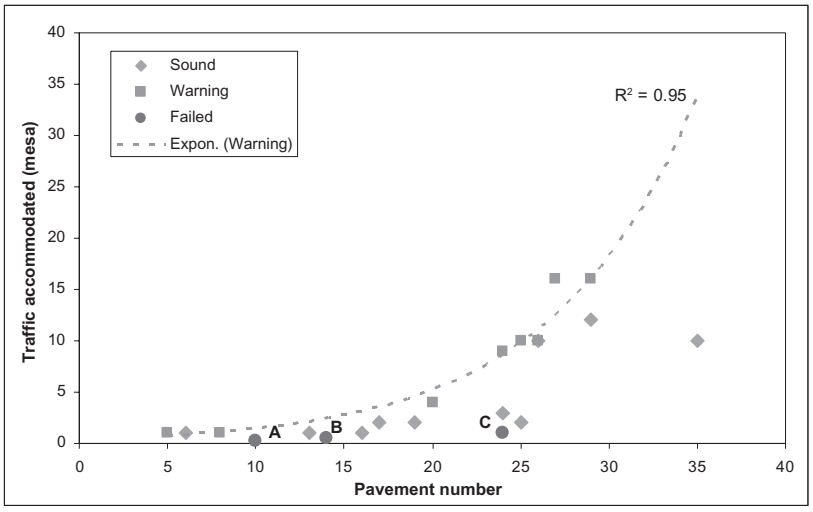

Figure 7. Pavement number design system based on a data set of 15 LTTP sections, and HVS sections with BSMs (Long et al. 2007b).

It provides an indication of the ultimate certainty of the classification of a material given all available information, which can be linked to a level of confidence. This method is discussed in a separate paper at the conference and highlights how the level of confidence in a material can be improved by increasing the number or quality of the classification tests.

The second major challenge associated with the design of pavements incorporating BSMs, is integrating the findings of laboratory, APT and LTPP data from research. As was noted with the stiffness versus time relationship of BSMs, the laboratory and APT trends are often divergent from the LTPP trends. Laboratory tests show that fatigue properties can be evaluated as a failure mechanism of these mixes; however, the increasing stiffness of the mix with time, as observed with LTPP sections, indicates to the contrary. Long et al (2007b) have developed a useful and realistic pavement design system (without a deformation or fatigue phase) using LTPP data collected from BSM pavements of more than 7 years old, based on information of the pavement condition. The system uses a Pavement Number approach, with some similarities to the AASHTO Structural Number, but incorporates modular ratio requirements and long term stiffness values linked to material classification, that ensures a realistic pavement balance. This is also discussed in a separate paper at the conference.

4 CLOSING REMARKS

In summary, BSMs possess some properties of granular materials and some of asphalt, namely stress-dependency and visco-elasticity respectively. Nevertheless, BSMs need to be prepared and analysed using test protocols that are suited to the specific behavioural characteristics of the materials.

In particular, the tests used in the mix design procedures for BSMs need to focus on the shear properties as a differentiator in the performance of these materials. Aspects such as laboratory-compaction and curing of specimens before testing require special attention. Research has shown the BSMs experience an increase in stiffness for several years after construction, and this phenomenon needs to be simulated in laboratory testing protocols.

Improved models for the structural design of BSM-foam and BSM-emulsion have been developed based on LTPP data. Pavements incorporating layers of BSM have sustained more than 30 million ESALs according to some of the data that has been collected. The structural design method uses an "intelligent structural number" type of approach, which includes modular ratios between layers to maintain a realistic pavement balance with regard to layer stiffness.

REFERENCES

Asphalt Academy 2002. Interim Technical Guideline (TG2). The Design and Use of Foamed Bitumen Treated Materials. ISBN 0-7988-5543-6. Pretoria, South Africa.

Collings, D.C. & Jenkins, K.J. 2008. Characteristics of Materials Stabilised with Foamed Bitumen. Eurobitume Conference, Copenhagen, Denmark.

Fu, P., Harvey, J.T., Jones, D. & Chao, Y. 2007. Understanding Internal Structure Characteristics of Foamed Asphalt Mixes with Fractured Face Image Analyses. Paper for consideration for IJPE International Journal of Pavement Engineering.

Jenkins, K.J., van de Ven, M.F.C., Molenaar, A.A.A. & de Groot J.L.A. 2002. Performance Prediction of Cold Foamed Bitumen Mixes. Ninth International Conference on Asphalt Pavements, Copenhagen, Denmark. p. 16.

Jenkins, K.J., Long, F.M., & Ebels, L.J., 2007. Foamed Bitumen Mixes = Shear Performance? *IJPE International Journal of Pavement Engineering. Volume 8 Number 2*.

Jenkins, K.J., Ebels, L.J., Twagira, E.T., Kelfkens, R.W.C., Moloto, P.K. & Mulusa, M.K. 2008. Updating Bituminous Stabilised Materials Guidelines—Mix Design Report Phase II. PaveEng report prepared for Sabita and GDPTRW.

Jooste, F.J., Long, F.M., & Hefer, A. 2007. A Method for Consistent Classification of Materials for Pavement Rehabilitation Design. Modelling and Analysis Systems report prepared for Sabita and GDPTRW.

Loizos, A. & Papavasiliou, V. 2007. In situ characterization of Pavement Materials Stabilised with Foamed Asphalt and Cement. International Conference on Advanced Characterisation of Pavement and Soil Engineering Materials ICACPSEM, Athens, Greece.

Long, F.M. & Theyse, H.L. 2004. Mechanistic Empirical Structural Design Models for Foamed and Emulsified Bitumen Treated Materials, Conference on Asphalt Pavements for Southern Africa CAPSA 2004, Sun City.

Long, F.M. & Jooste, F.J. 2007a. Summary of LTPP Emulsion and Foamed Bitumen Treated Sections. Technical memorandum compiled on behalf of SABITA and GDPTRW. Modelling and Analysis Systems, Cullinan, South Africa. (Gautrans report: CSIR/BE/ER/2007/0006/B).

Long, F.M. & Jooste, F.J. 2007b. A Materials Classification and Knowledge Based Structural Design Method for Pavements with Bituminous Stabilized Materials. Conference for Asphalt Pavements in Southern Africa CAPSA 2007, Gaberone, Botswana.

Paige-Green, P. & Ventura, D. 2004. Durability of Foamed Bitumen Treated Basalt Base Courses. Council for Scientific and Industrial Research, Transportek Division. Contract Report: CR-2004/08, Pretoria, South Africa.

Shackel, B., Makiuchi, K. & Derbyshire, J.R. 1974. The Response of Foamed Bitumen Stabilised Soil to Repeated Triaxial Loading. 7th ARRB Conference. 7(7): 74–89 1974. Australia.

Twagira, E.M., Jenkins, K.J. & Ebels, L.J. 2006. Characterisation of Fatigue Performance of Selected Cold Bituminous Mixes. International Conference on Asphalt Pavements ICAP, Quebec, Canada, pp. 1–10.

Wirtgen Cold Recycling Manual, 2nd Edition. 2004. ISBN 3-936215-05-7, Wirtgen GmbH, Windhagen, Germany.

Advanced Testing and Characterization of Bituminous Materials – Loizos, Partl, Scarpas & Al-Qadi (eds)
© 2009 Taylor & Francis Group, London, ISBN 978-0-415-55854-9

In-plant asphalt cold recycling in rehabilitation of Babaei expressway project

Vahid Ayan
Department of Civil, College of Technical, Islamic Azad University, Islamshahr Branch, Iran

Alireza Khavandi
Department of Civil, Zanjan University, Zanjan, Iran

Azam Nikzad Gharehaghaji
Colegio de Postgraduados, Institucion de Enseñanza e Invistigacion en Ciencias Agricolas, Canpos Montecillo, Mpio. De Texcoco, Edo. de México. México

ABSTRACT: Babaei express-way, length of 16 kilometers with three lines in every direction, is located in the north of Tehran. Investigation showed that the state of pavement is unsuitable and it was damaged very widely. On the other hand, there were longitudinal and transverse cracking and mostly alligator crack on the pavement layer. Our observation showed that the state of the lower layers of asphalt was fundamentally unsuitable; also there was a large quantity of clay seen in these layers. Under these circumstances, all of the asphalt was milled and the lower layers were improved. Then the cold recycled asphalt with cement and foamed bitumen was replaced. This study, tries to state the executive approach and the results of operations. It is necessary to notice that we have used a new experiment in Iran for asphalt recycling in addition to lime stabilization of the soil layer for heavy rehabilitation of Babaei express-way.

1 INTRODUCTION

Expressways are considered one of the vital infrastructures of a country. Since construction of an expressway imposes huge cost on an organization, its construction costs will be also high and Babaei expressway isn't exception. Babaei expressway, as one of the important and strategic expressways of the capital city, has primarily performance country road; however, it took also performance of urban road in course of time, thanks to construction of towns and organizations which were extended around it in addition to its initial duty to link the capital to the northern cities.

Maintenance of the expressway, in addition to conventional alternative maintenance which is carried out by related organizations, includes an extensive project which has been defined during recent several years and includes rehabilitation, heavy rehabilitation and reconstruction. Every one of these activities has been defined for different components of the expressway after extensive studied depending on the existing defects in different phase. It should be noted that besides these rehabilitation and reconstruction operations, constructional operations to expand the expressway, including added a divided lane to both direction and adding auxiliary lane as well as local accesses ways were undertaken. One of the phases of the project was studied in 2007 with three kilometer length which necessitated whole asphalt layer (surface, binder and black base) it is beneath soil layer improvement. This soil layer may include sub-base and sub-grade of the expressway. Studies and researches carried out by both the contractor and consultant of the project recommended substructure improvement through stabilization. Therefore, cold in-plant recycling method was chosen for sub-base layer for environmental reasons as well as the project being urban. Primary studies included

evaluation of pavement distresses and PCI and PSI indexes computing which resulted in thickness of cold mix layer computation. Determining job mix formula of cold in-plant recycling on the bases of reliable codes and standards, existing tests and the tests carried out was the next stage of the work. It should be noted that the construction operation was primarily defined for a section with nearly 3 km length of whole expressway in both directions which had more improper state compared to other sections of the project from superstructure and substructure point of view. This article deals with studies and constructional operation processes for given section.

2 CRITERIA AND REASONS OF CHOOSING COLD RECYCLING FOR BABAEI EXPRESSWAY REHABILITATION

Project choosing and its evaluation for successful execution of cold recycling have significant importance. This selection has been made by the project consultant, considering existing

Table 1. Factors effective in cold recycling capability.

Description	Results of studies
Type and quality of existing superstructure and substructure material	Pavement condition index(PCI) lesser than 50 in most points. Layers consist of uniform material with different thicknesses and lengths. (Fig. 1) Existing superstructure and Black base have suitable load bearing capacity and superstructure problems transferred to sub-base layer and sub-base on sub-grade. The rate of patching and rutting in pavement surface is relatively high. (Fig. 2) Intensity of cracks in surface of pavement is relatively high. However, all these cracks weren't extended in black base depth. Asphalted layers thickness is high. Considering one-sized graded asphalt milled material, there are a few new materials needed for recycling layer stability and modification. The moisture content of embankment layers material is uniformity.
Expressway geometric situation	Crossings and local accesses of the expressway, number of manholes and buried facilities of superstructure is low. Deflections of pavement layers is fixed and specified. Number of earthwork (cut and fill) along the project is low.

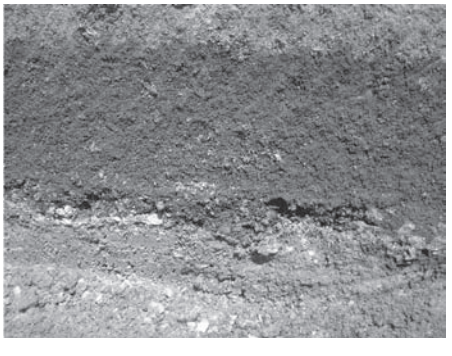

Figure 1. Pavement after milling.

Figure 2. Asphalt distresses.

superstructure and substructure state, while sample taking and testing asphalt layer, unbound layers and sub grade, and acknowledging road construction and maintenance records, past and present traffic figures, local and climate conditions of the region, drainage systems, access roads to the project area and finally, emphasizing on applying conventional procedures of technical and economical feasibility studies carried out for Babaie expressway rehabilitation on the basis of pavement life cycle costs. Results are given in Table 1.

2.1 *Evaluating pavement distresses*

2.1.1 *PCI index computing*

These studies did trough visual condition survey of pavement distresses for road pavement distresses evaluation. Distresses surveying planned so that the results to be suitable for pavement condition index (PCI). Distresses surveying and related computations are carried out according to PCI method as per standard (ASTM D6433-99). In this standard, 19 types of distresses and 3 severity per type defined, extension and severity of distresses were recorded in forms and then analyzed. (Al-Omari & Darter 1992). Number of evaluated sample units for the section under study in this paper in southern direction is 15 units and PCI index, 27 and quality is weak. For northern direction, sample units were evaluated in two sections number of which is 14 and 12 and their PCI index obtained 44 and 54 respectively and their quality were moderate.

2.1.2 *Distresses classification*

Different distresses including crack, pothole and settlement separately evaluated in southern and northern directions of Babaei expressway.

2.1.3 *Classification of causes of distresses*

In another analysis which has been carried out on evaluation data, causes of distresses have been classified in three general groups inclosing distresses due to loading, distresses due to climatic and local conditions and other distresses. The main cause of distresses in west-east direction is loading and climate and other factors are placed in following ranks (Fig. 3). For east-west direction, factors resulted from climatic conditions are the main cause of distresses and loading and other factors have less effect on distress occurrence (Fig. 4).

2.1.4 *Computing PSI*

Roughness data collected by RPS (Road Surface Profiler) were used for PSI index calculation. International Roughness Index (IRI) Roughness index calculated from data extracted from

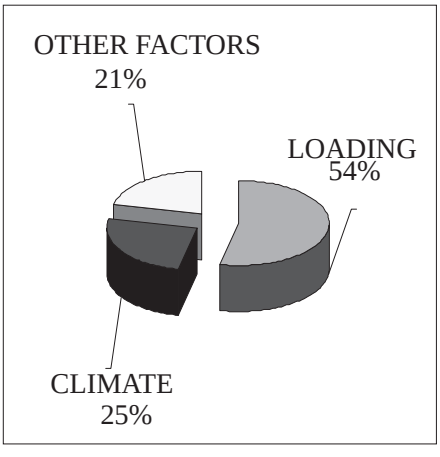

Figure 3. Cause of distress in west to east direction.

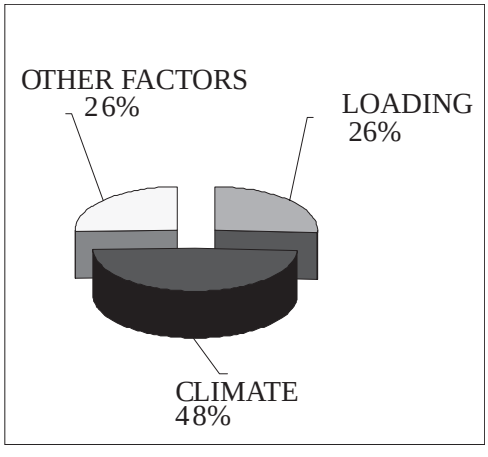

Figure 4. Cause of distress in east to west direction.

RSP by a mean move method which, in deed, a type of smoothness filter of data. In this study, PSI index have been computed using experimental relations (1) [Paterson 86] and (2) [Omari 92] (Al-Omari & Darter 1992).

$$PSI = 5 * e^{(-0.18*IRI)} \quad (1) \qquad PSI = 5 * e^{(0-0.26*IRI)} \quad (2)$$

where IRI: International Roughness Index (m/km) and PSI: Pavement Serviceability Index.

3 CRITERIA AND REASONS FOR CHOOSING COLD IN-PLANT RECYCLING

Cold in-plant recycling is one of the choices which it cannot be ignored in general recycling process. Particularly in conditions that more production, more accurate control and evaluation of reclaimed aggregate pavement, final cold asphalt mixture quality or using of mixtures in renewals or rehabilitations which pavement thickness increase or its reinforcement through new asphalt stabilized layers execution are considered.

Distresses studies on substructure and pavement of the expressway has shown that sub-base and, in some points, the expressway sub grade should be stabilized with hydrated lime and then its cants corrected. Substructure stabilization operation required that PAP should be removed from in-situ operation and should be remix in a central plant. Another reason for its omission was central refuge and landscape inside it which intensify water penetration from the refuge into substructure and pavement distresses. Therefore, a system should be adapted which cause integrated substructure and pavement and removing weak point between constructional areas. Low price of in-plant cold recycling machinery was another reason to choose this option.

4 COLD RECYCLING LAYERS

The results of calculations made on northern and southern directions are given below according to the studies already made:

4.1 *Pavement design for northern (east-west) direction*

CBR of unbound layer or soil under asphalt is averagely equal to 7. Since soil is sensitive against moisture and its stability is low, to improve plasticity properties and reduce its sensitivity against water, it was stabilized with lime which its CBR increased. The traffic design for analysis period of 15 years, 19,790,126 equivalent single axle load (ESAL) was computed. Considering the AASHTO we will have:

$Mr = 750\ kg/cm^3$	(Mr = Resilient modulus for sub grade.)
S0 = 35%	(S0 = overall standard deviation.)
R = 95%	(R = Reliability.)
PSI i = 4.5	(PSI i = Initial Pavement Serviceability Index.)
PSI t = 2.5	(PSI t = Final Pavement Serviceability Index.)

Therefore, required SN (structural number) will be 4.8. Given this, the layers thickness is chosen as follow:

- A 25 cm layer of cold recycling with foamed bitumen and cement (layer coefficient is 0.2)
- 12 cm binder layer in two layer of 6 cm (layer coefficient is 0.4)
- A layer of 4 cm of surface layer (layer coefficient is 0.4)

4.2 *Pavement design for southern (west-east) direction*

The design CBR (California Bearing Ratio) in this direction has been measured 29. The projected Traffic for critical line as per calculations made considering for analysis period of 15 years is 20,004,334 equivalent single axle load (ESAL). Considering:

S0 = 35%, R = 95%, PSI i = 4.5, PSI t = 2.5.

Therefore, required SN will be 4.8. Given this, the layers thickness is chosen as follow:

– A 25 cm layer of cold recycling with foamed bitumen and cement (layer coefficient is 0.2)
– 8 cm binder layer (layer coefficient is 0.4)
– A layer of 5 cm of surface layer (layer coefficient is 0.4).

5 THE PLAN OF COLD RECYCLING MIXED WITH FOAMED BITUMEN

To prepare and construct asphalt cold recovering layer, reference manual instructions of (2005, 2004, 2002 and www.WirtgenAmerica.com) have been used. Generally, specifications of the mixture under design have been defined on the basis of uniaxial compressive strength (UCS) and indirect tensile strength (ITS).

5.1 *Analyzing of RAP*

Test results show that nearly all samples in an area are identical and there have been seen no any considerable difference between the samples related to different areas of the route. According to the results obtained, values of aggregates passing from 2 mm sieve is variable between 16% to 22% which should be corrected to required values minimum of which is 25% as per (2005) and 18% as per (2002). In Fig. 5 the curve A shows RAP aggregate. In RAP aggregate, the value of aggregates passing from 0/075 mm sieve is low with reference to the required minimum, which is 3%–12% reference (2005) but is compatible with standard (2002) which has been defined 0%–7%.

5.2 *Natural and local sand analysis*

RAP aggregate gradation results show that sand (0–2 mm) is needed to compensate passing from 2 mm sieve aggregate deficiency. Unfortunately, no fine aggregate sands (0–2) are usually produced in Tehran as well as other parts of the country and (0–6 mm) and (0–4 mm) are the only sands existed. Sand gradation (0–4) is given in Fig. 5 as curve B. By composing local sand with 10%, 20% and 25% portions of RAP material, the quality of aggregate were analyzed. This gradation is given in Fig. 6. Test results show that by adding 25% sand (0–4 mm) to RAP, gradation is relatively improved, and however, it is tries to prepare sand with more filler.

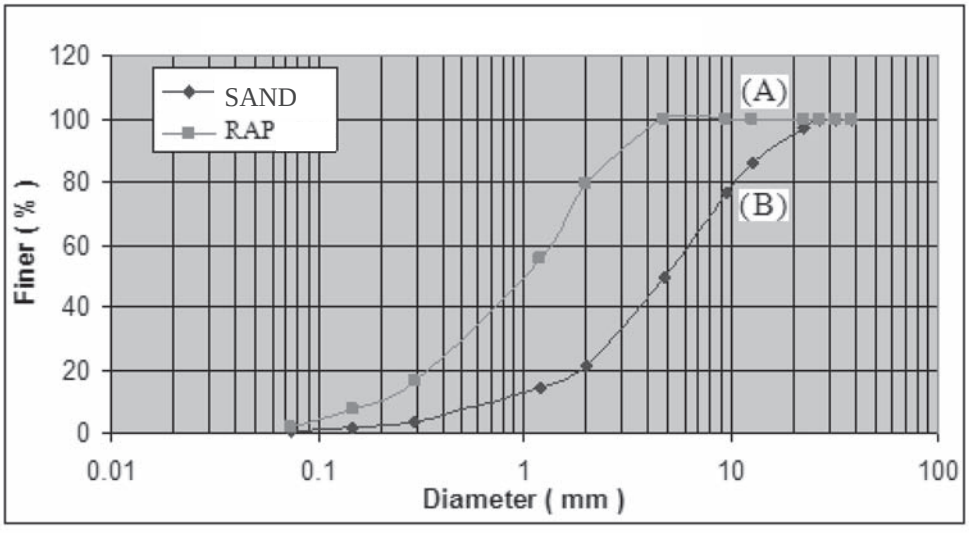

Figure 5. Gradation curve of RAP and sand.

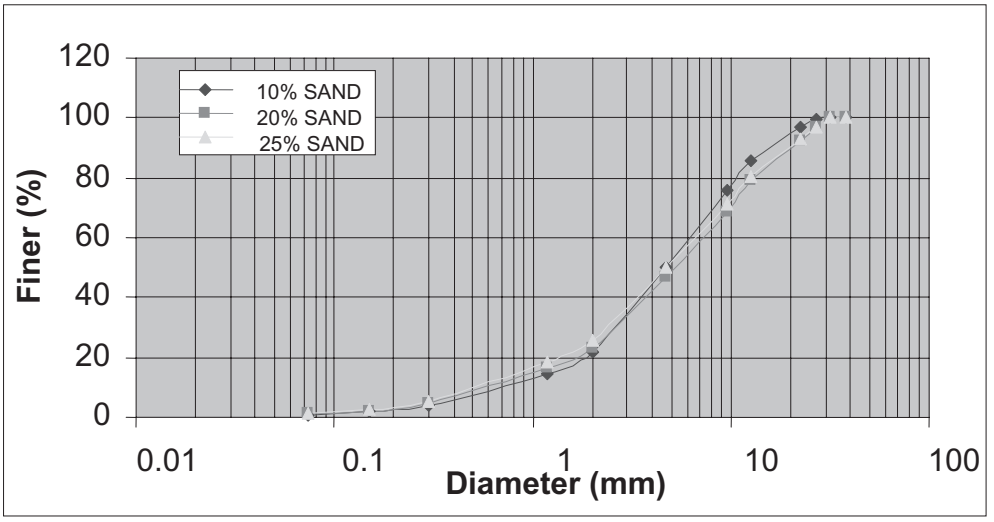

Figure 6. Gradation curve of adding sand to RAP.

5.3 *Active filler*

It should be noted that mastic mixture with is very suitable for mixing with foamed bitumen, since in foamed bitumen mixtures only fine aggregates have a chance to have complete bitumen film on them and, while, this opportunity isn't available for all aggregates, particularly for coarse aggregates.

Additionally, in items 8-1 and 8-2 it has been pointed out that the amount of filler (aggregates passed sieve 0.075 (No. 200) of RAP material is insufficient and added 25% sand (0–4 mm) to RAP has relatively been improved gradation. However, it hasn't reached justified limit in reference (2005). Therefore, we need for active fillers like cement or lime. Active fillers may be added to the mixture in order to reduce the moisture susceptibility, increased strength, stiffness and cohesion of bitumen to aggregates which finally results in increased rate of mixture filler too. When active filler is added to the mixture, the time between filler adding to the aggregates as well as foamed bitumen addition should be reached to the minimum both in laboratory and during recycling operation. Active filler reaction begins immediately after its contact with wet stone material surface and causes fine grained aggregates to stick together which finally results in bad dispersion of the binder through the aggregate and coating of aggregates. Tests showed that adding cement to RAP material as active filler, with 2 to %2.5 portions improves filler deficiency seriously. Fig. 7 shows RAP with %25 sand (0–4 mm) and %2.5 cement.

5.4 *Anti-stripping additive*

Since Babaei expressway is located within a damp and with relatively high raining rate and its drainage doesn't work properly, due existing of median and surrounded forests, bitumen anti-stripping chemical additive should be used for recycling. If aggregate has proper quality, using of only one percent active filler will be sufficient for this purpose. As will be mentioned in following paragraph, adding of 2.5 percent cement has been also covered this case.

5.5 *Foamed bitumen*

Road construction conventional foamed bitumen from 60–70 type were produced by adding 2–4 weight percent of bitumen, under 3bar pressure, bitumen temperature between

160–180ºC and by air blowing in expansion chamber of the device KMA 150. Foamed bitumen temperature during out letting from the tank was around 80–100ºC. The main parameters which were considered and tested in foamed bitumen production quality are:

– Bitumen temperature: foamed bitumen properties are improved by bitumen temperature increase.
– water content: generally foamed bitumen volume is related to the amount of water added to the hot bitumen which, of course, it should be noted that its half-life will be reduced.
– Bitumen compression: low compression causes low explosion as well as reduced half-life.

Generally, produced foamed bitumen with minimum expansion ratio of 10 times and half-life of minimum 10 seconds evaluated suitable.

5.6 *Results of recycling layer laboratory production*

In order to determine optimum cement and bitumen Indirect Tensile Strength (ITS) tests were performed during 7th day of recycling layer production. Samples were produced according to the manuals (2005) by adding 25% sand to RAP and in the forms of 2%, 2.5% and 3.5% bitumen while fixing 2 and 2.5 percent cement. The test results are given in table 2 and 3.

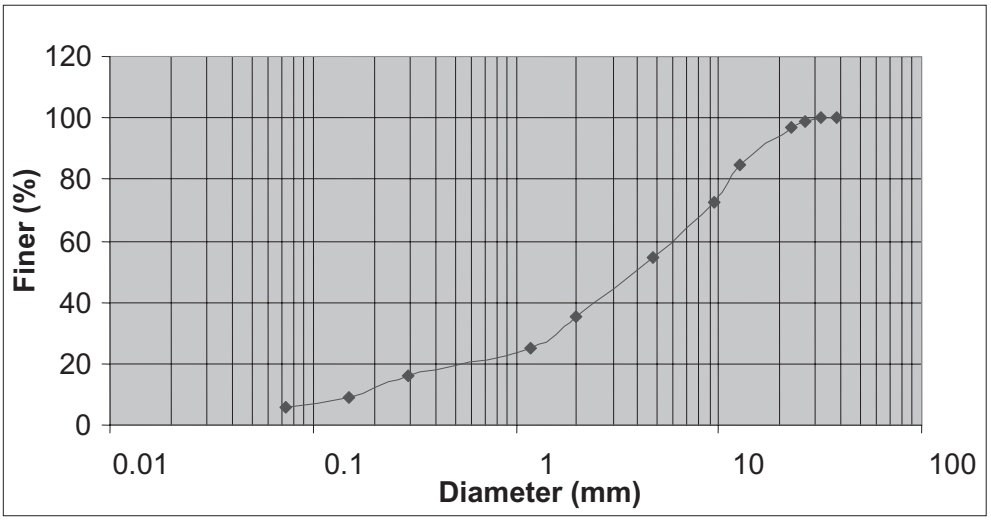

Figure 7. Gradation curve with (2.5% cement + 25% sand + RAP).

Table 2. Laboratory test results of recycling layer with 2% cement.

Sample production		Sand 25% + RAP 75%			Requirements
Cement content	%	2	2	2	–
Bitumen content	%	2.5	3	3.5	–
Water content	%	5	5	5	–
Dry density	gr/cm^3	2.072	2.057	2.060	–
Mix density	gr/cm^3	2.530	2.489	2.468	–
Air content	Vol.%	18	17.6	16.5	8–15 Vol.%
ITS in 7th day	N/mm^2	0.3	0.35	0.42	Acc. (2005) >0.50 N/mm^2 Acc.(2002) >020 N/mm^2

Table 3. Laboratory test results of recycling layer with 2.5% cement.

Sample production		Sand 25% + RAP 75%			Requirements
Cement content	%	2.5	2.5	2.5	–
Bitumen content	%	2.5	3	3.5	–
Water content	%	5	5	5	–
Dry density	gr/cm^3	2.076	2.069	2.103	–
Mix density	gr/cm^3	2.535	2.529	2.521	–
Air content	Vol.%	17.9	16.5	16.2	8–15 Vol.%
ITS in 7th day	N/mm^2	0.35	0.42	0.52	Acc. (2005) >0.50 N/mm^2 Acc. (2002) >020 N/mm^2

5.7 *Evaluation of laboratory test results*

Required ITS rate was obtained on the basis of reference (2005) for 2.5% cement and 3.5% bitumin. Since the value of ITS obtained for all samples on the basis of reference (2002), it was recommended that the rate of 2.5% cement and 3% bitumin to be considered as mix design. To prepare samples, given water content in mix design was considered 5%.

6 STAGES OF EXCUTING IN-PLANT COLD RECYCLING OPERATION

Stages of the project execution include followings, respectively:

– Asphalt milling and carrying to the workshop
– Regarding (add virgin aggregate)
– Cold recycling production with machine KMA150
– Placing and compaction
– Curing
– Surfacing.

6.1 *Asphalt milling and carrying to the workshop*

As can be seen from Figures 1, 8, asphalt layer and black base were milled by asphalt milling machine type Wirtgen W2100 and as a separate project, bed surface was stabilized with lime and its surface prepared for recycled asphalt placing in-plant. (www.WirtgenAmerica.com, www.Wirtgen.co.uk, www.Wirtgen.de).

Recycled material which usually were crushed during milling operation carried to the central workshop. Depot height was not exceeded 3 m in order to ovoid RAP adhesion to each other due to the material weight or environment temperature effect, moreover, road construction machinery weren't run on stored material, as far as possible. To minimize RAP adhesion to each other as well as to reduce ground water penetration into martial volume and finally top decrease their moisture content, coordination between milling and remixing of the material and their direct feeding to KMA machine were effective so that excessive accumulation RAP and their saving in workshop avoided.

6.2 *Re-grading (add virgin aggregate)*

RAP were regarding after carrying into the workshop and depot. First, the maximum RAP size limited to 35 mm (Fig. 8) which are used for some purposes such as repairing and improving access road as well as yard construction inside the workshop.

Then fine materials (0–4 mm sand) added to the material passed sieve 35 mm (25% of their weight) in the mixing process in order to rectify a deficiency in fines. In some cases even sand 0–2 mm with higher filler were added in limited amount and all mixing operation were carried

out uniformity before carrying to the machine KMA-150 (Fig. 8). (www.WirtgenAmerica.com, www.Wirtgen.co.uk, www.Wirtgen.de).

6.3 *In-plant cold recycling production by KMA-150*

After rectifying of gradation, rectified aggregates were poured inside KMA-150 machine by a loader and on the basis of aggregate weight, required amount of bitumen, cement as well as water were added to the mixer unit as per job mix formula (Fig. 8). Aggregates were mixed inside the mixer hemogenically and were loaded on trucks by KMA-150 feed belt and carried to along the track. (www.WirtgenAmerica.com, www.Wirtgen.co.uk, www.Wirtgen.de).

6.4 *Placing and compaction*

Cold asphalt recycled material were placed by a finisher and compacted by vibrating and static rollers after production. Cold recycled layer were placed in double 12.5 cm layers, every one of which were compacted first by 20 ton vibrating roller in 4 passes and then in 6 passes with 12 ton static rollers. Required level of compaction of the mixture for each layer is measured 98% maximum dry density with AASHTO method (Fig. 8).

6.5 *Curing*

In order to prevent cold recycling rapid drying and since construction operation was carried out during summer season, depending on environmental temperature , the recycled layer was water sprayed minimum 2 times per day (Fig. 8). This operation took one or two weeks.

6.6 *Surfacing*

Before surfacing consists of binder and surface layer on a cold recycled layer, existing distress, in any, eliminated and after quality control prime coat was carried out. After curing, residual water in compacted cold recycled layer measured. This water rate in 10 cm layer upper section should not exceed 50% optimum moisture which is computed by AASHTO T180 in laboratory. (Fig. 8). In Figure 8, the cycle of the machinery employed in in-plant cold recycling operation is illustrated.

7 QUALITY CONTROL TESTS

Quality Control tests with standard methods are very important in order to obtain the results which represent used material and in-plant operation in cold recycling process. For sample taking from used material and for testing, preparing a work plan for evaluating construction stages and discovering probable or necessary changes and improvements is highly valued. In addition to this controls, the cold recycling process needs presence of experienced and talented manpower which is obligatory to be observed. Quality control tests are:

– Recycling mixed gradation
– Foamed bitumen and cement laboratory tests

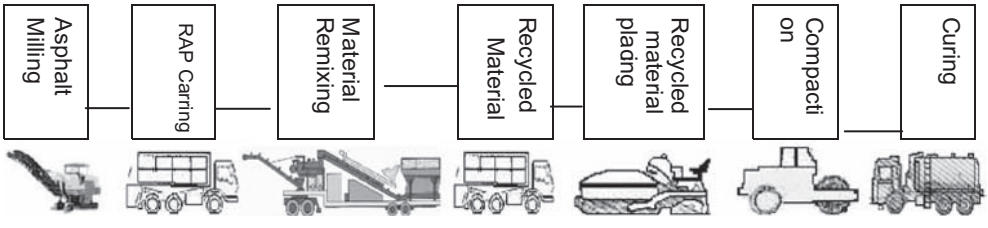

Figure 8. Operation process.

– Moisture content in mix and compaction process moisture content
– Tensile strength of mix
– Level of compaction
– Calibration of mixing devices and tools for recycling unit
– Measuring material temperature during mixing
– Measuring of placed recycled layer with finisher
– Asphalt surface monotony
– Lateral joints control and their overlapping
– Measuring the existing bitumen and recycling mixture bitumen.

8 CONCLUSIONS

The road rehabilitation by new machinery meets all objectives mentioned in item-3. These objectives included technical and economical aspects which they obtained results from quality control and tests carried out respecting technical objectives such as pavement quality and strength increase, defect elimination, operation and maintenance coasts reduction of the road can be estimated. On the other hand, saving in resources which can be include both material and energy and environment protection as well as accelerating construction operation due to material accessibility and application of modern machinery justified economy of the project. Clearly, heavy rehabilitation in this level will have a vital role in reducing conventional and alternative maintenance costs in future.

REFRENCES

Merkbalt für kaltrecycling in situ im straßenoberbau (M KRC). 2005. —Ausgabe.
Instandsetzung einer straße für schwerlastverkehr
FGSV—Arbeitspapier : *"Kaltrecycling mit Schaumbitumen"—Ergänzungen zum "Merkblatt für Kaltrecycling in situ im Straßenoberbau"*—(Entwurf 2004).
OBERBAVARBEITEN, Tragschichichten mit Bindemittel stabilisierten Tragchichten (ST–BZ) RVS85.05.13. 2002. Ausgabe.
www.WirtgenAmerica.com
www.Wirtgen.co.uk
www.Wirtgen.de
Al-Omari, B. and Darter, M.I. September 1992. *Relationship between IRI and PSR*, UILU-ENG-92-2013, Illinois Department of Transportation.

10. Synthesis of international coordinated research initiatives

Advanced Testing and Characterization of Bituminous Materials –
Loizos, Partl, Scarpas & Al-Qadi (eds)
© 2009 Taylor & Francis Group, London, ISBN 978-0-415-55854-9

RILEM interlaboratory test on interlayer bonding of asphalt pavements

H. Piber, F. Canestrari, G. Ferrotti, X. Lu, A. Millien, M.N. Partl, C. Petit, A. Phelipot-Mardelé & C. Raab
RILEM TC 206 ATB TG 4

ABSTRACT: The RILEM TG 4 organized an interlaboratory test in order to compare the different test procedures to assess the interlayer bonding properties of asphalt pavement. The pavement was composed of two layers. Three different interface conditions were chosen. The first pavement was laid without interface treatment and the others with two different types of emulsion. 14 laboratories from 11 countries participated in this study and carried out shear or torque tests on 1400 cores. The maximum shear or torque load and the corresponding displacement were measured and the shear or torque stress was calculated as a function of the following parameters: diameter, test temperature, test speed, stress applied normal to the interface and age of the specimen. This paper presents the results of this study in terms of precision and correlations regarding the parameters.

1 INTRODUCTION

Interlayer shear resistance has recently attracted increasing interest worldwide due to the fact of steadily increasing requirements on pavement performance properties in terms of bearing capacity and durability as well as new innovative developments regarding pavement materials and construction. However, test methods available for assessing interlayer shear resistance and their reliability are under much discussion. In particular interpretation of laboratory data in connection with data from real pavements are subject to uncertainties. So far, no general consensus exists regarding test methods, assessment criteria and international standardization. Hence, RILEM TC 206 ATB TG 4 organized an interlaboratory test on interlayer bonding considering three different interface conditions of asphalt concrete pavements. The test focused on the comparison of shear test procedures, test conditions, specimen geometries and devices that allow determining interlayer shear resistance in asphalt concrete.

The aim of this interlaboratory test was twofold:

Determine the repeatability and reproducibility of interlayer shear tests proposed by the majority of the different participants.

Determine correlations between different test procedures and evaluate the influence of different test conditions.

2 TRIAL SECTION

Samples were taken from a newly laid asphalt pavement near Ancona (Italy) in summer 2005, managed by the Università Politecnica delle Marche.

The trial section was 3.5 m wide and about 20 m long and composed of two layers. The lower layer had a thickness of 70 mm and consisted of an asphalt mixture type AC 16 base 70/100 (EN 13108-1). The upper layer was 30 mm thick and produced with an asphalt mixture type AC 11 surf 70/100 (EN 13108-1).

Three different interface conditions were chosen.

- Pavement 1: without treatment (not hot on hot!)
- Pavement 2: pre-coated with a polymer modified emulsion
- Pavement 3: pre-coated with a conventional cationic emulsion.

The two courses were laid by an asphalt finisher and compacted by a roller. The production of the three pavements was done consecutively in one single construction process. The application rate was about 150 g/m² of residual bitumen for both Pavement 2 and Pavement 3. Asphalt cores were taken following a well defined coring pattern with a clear documentation of the position of the cores (Figure 1). Each core was marked by a special code defining its location in the trial section. The cores had a nominal diameter of 100 mm or 150 mm. The direction of laying was marked and identical to the direction of testing.

3 TEST PROGRAM

3.1 *Participating laboratories*

The 14 laboratories participating on a voluntary basis are listed as follows:

- Amt der Kärntner Landesregierung—Bautechnik, Klagenfurt, Austria
- EMPA Dübendorf, Switzerland
- Institut für Straßenbau und Straßenerhaltung der TU Wien, Vienna, Austria
- Institut für Straßenwesen der TU Braunschweig, Braunschweig, Germany
- Laboratoire 3MsGC, Centre Universitaire de Génie Civil, Egletons, France
- National Centre for Asphalt Technology, Auburn, AL, U.S.A
- National Cheng Kung University, Department of Civil Engineering, Tainan, Taiwan
- NCPE University of Nottingham, Nottingham, UK
- Nynas AB, Nynäshamn, Sweden
- Nynas UK AB, South Wirral, UK
- Road and Bridge Research Institute, Jagiellonska, Poland
- Transport Research Centre of CEDEX, Madrid, Spain
- Università Politecnica delle Marche, Ancona, Italy
- University of California Pavement Research Centre, Richmond, CA, U.S.A.

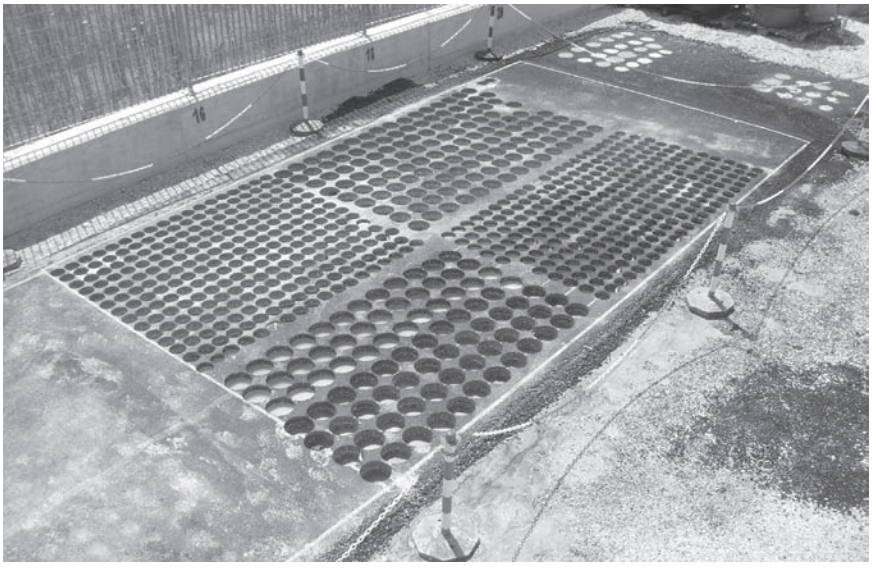

Figure 1. Trial section after taking 100 and 150 mm cores from Pavement 1.

3.2 *Test program*

The laboratories carried out shear or torque tests on a total of about 1400 cores. At each test condition 7 specimens were tested. The test conditions varied in terms of diameter, test temperature, test speed, stress applied normal to the interface and age of the samples. The maximum shear load or torque moment and the corresponding displacements were measured and the nominal maximum shear or torque shear stress were calculated. The test program is given in Table 1. In this paper only the results of the static shear test are reported.

3.3 *Shear test devices*

The shear tests were performed either in pure direct shear configuration (Figure 2) or direct shear configuration with normal stress (Figure 3).

4 PRECISION OF THE SHEAR TEST

The evaluation of the precision will give information about the quality of the data within each laboratory (repeatability standard deviation s_r) and among different laboratories (reproducibility standard deviation s_R). The statistical analysis was done according to ISO 5725-2—Accuracy (trueness and precision) of measurement methods and results—Part 2: Basic method for the determination of repeatability and reproducibility of a standard measurement method.

The results of the shear test were analyzed if more than three laboratories tested "identical" specimen under the same test conditions. In this part of the research program 539 specimens were tested without normal stress and evaluated.

- Diameter D = 100 mm, test speed v = 2,5 mm/min, temperatures T = 10°C, 20°C, 30°C,
- Diameter D = 100 mm, test speed v = 50 mm/min, temperature T = 20°C,
- Diameter D = 150 mm, test speed v = 50 mm/min, temperature T = 20°C, 30°C.

The study showed that the values s_r (repeatability standard deviation) and s_R (reproducibility standard deviation) are closely related to the mean values of the maximum nominal shear stress "τ" regardless of specimen diameter, test speed and temperature. Precision within

Table 1. Test Program; "x" in matrix denote test conditions; (v: test speed, σ_n: normal stress).

Unidirectional monotonic static shear test										
Diameter (mm)		150					100			
Temperature (°C)		10	20	25	30	40	10	20	30	40
σ_n (MPa)	v:									
	1.27 (mm/min)				x					
	12.7 (mm/min)				x					
0	2.5 (mm/min)				x		x	x	x	
	25 (mm/min)				x					
	50 (mm/min)	x	x	x	x	x	x	x	x	
	200 (mm/min)	x	x		x					
0.049	2.5 (mm/min)			x	x	x				
0.2	2.5 (mm/min)						x	x	x	
0.483	2.5 (mm/min)								x	x
0.6	2.5 (mm/min)						x	x	x	
Monotonic static torque test										
0	180°/min	x	x		x		x	x	x	
	600 N/min						x	x	x	
Unidirectional cyclic fatigue shear test										
	10 Hz		x							

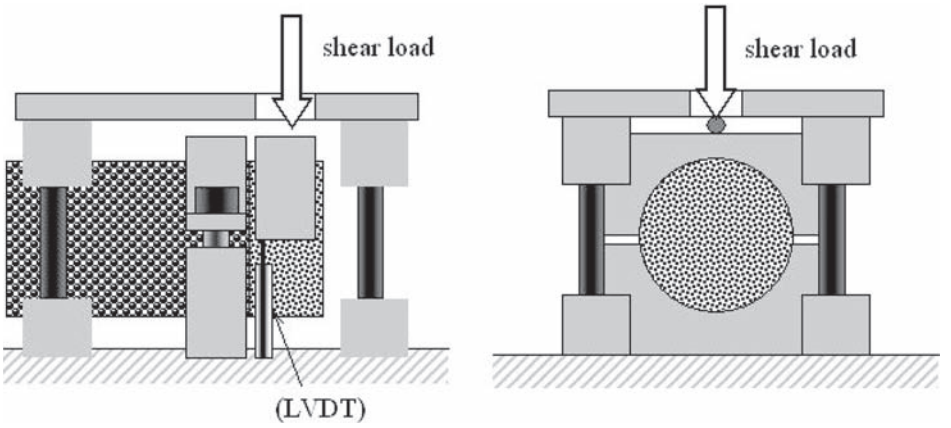

Figure 2. Pure direct shear device (Leutner).

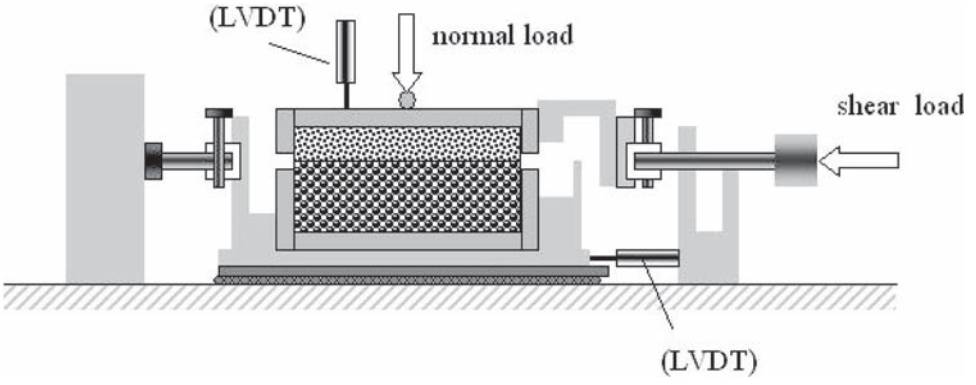

Figure 3. Direct shear device with normal load (ASTRA).

one laboratory is based on testing the "same" sample by the same technician with the same device. Since shear tests are destructive tests this condition was not fulfilled. Therefore the results of the shear test had to be checked with respect to their homogeneity within the trial section. Finally it was found that the precision of the shear test in case of absolutely homogeneous area of the trial section is:

– Repeatability standard deviation: $s_r = 0.05\ \bar{\tau}$ (MPa)
– Reproducibility standard deviation: $s_R = 0.12\ \bar{\tau}$ (MPa)

5 INFLUENCE OF TEST PARAMETERS ON SHEAR TEST RESULTS

5.1 *Influence of specimen diameter*

For the determination of the influence of specimen diameter nine pairs of values were available. The mean shear stress values for all three pavements tested at a speed of 50 mm/min and temperatures of 10°C, 20°C and 30°C were evaluated based on 616 cores. The evaluation showed that all shear stress values for all temperatures tested with cores of 150 mm diameter were lower than the results of the test carried out with 100 mm asphalt cores. The correlation is given by Equation 1 and the corresponding coefficients are listed in table 2.

$$\tau_{D=100\ \mathrm{mm}} = a \cdot \tau_{D=150\ \mathrm{mm}} \quad (1)$$

Table 2. Coefficient a and R^2 of the different pavements.

Pavement	a	R^2
1	1.07	0.86
2	1.13	0.99
3	1.16	0.94

It appears that the factor "a" depends on the interface condition. Moreover as expected the presence of emulsion mitigates the scatter of shear stress at the interface giving higher R^2 values for pavement 2 and 3. The linear regression for all samples has a coefficient of $R^2 = 0.970$. It was found that shear stress of 100 mm cores is about 14% higher than shear stress of 150 mm cores.

5.2 *Influence of the test speed*

Totally 77 cores were tested. The test speed used by the different laboratories for the shear tests ranged from 1.27 mm/min to 200 mm/min. In Figure 4, the shear stress results obtained for Pavement 3 considering five different test speeds are presented.

Figure 4 indicates in the speed range indicated a strong power function type of relationship with a high regression coefficient ($R^2 = 0.99$).

The other data were evaluated in a similar way and lead to the general equation for all temperatures and pavements (D = 150 mm).

$$\tau = 0.41 \cdot v^{0.22} \tag{2}$$

Again, the regression coefficient ($R^2 = 0.99$) is very high. Note that the exponent of the power function slightly changed as compared to Figure 4. Hence, if one shear stress value and its test speed are known shear stress can be calculated by Equation 3 for whatever test speed as follows.

$$\tau_{vx} = \tau_{v1} \cdot \left(\frac{v_x}{v_1}\right)^{0.22} \tag{3}$$

where:

τ_{v1} shear stress at test speed 1
v_1 test speed 1
τ_{vx} shear stress at test speed x
v_x test speed x

5.3 *The influence of normal stress*

In order to study the influence of nominal normal stress on the maximum shear stress, the results from one laboratory were considered. The results obtained for the three pavements and for three temperatures (10, 20 and 30°C) were analysed, for a total of 63 specimens (D = 100 mm, v = 2.5 mm/min).

Figure 5 allows the determination of two important contributions to the maximum shear stress: the cohesion and the friction. The cohesion is the value of τ_{max} when the normal load is not applied. Therefore the cohesion is represented by the x axis. The friction is given by the intercept of the straight lines in Figure 5. Further evaluations of the parameters of regression lines in Figure 5 show that these parameters were linearly dependent on the normal stress and lead to the Equation 4 as functions of a general value of σ_n.

$$\tau_{\sigma n} = (1 + 0.38 \cdot \sigma_n) \cdot \tau_{\sigma 0} + (0.74 \cdot \sigma_n) \tag{4}$$

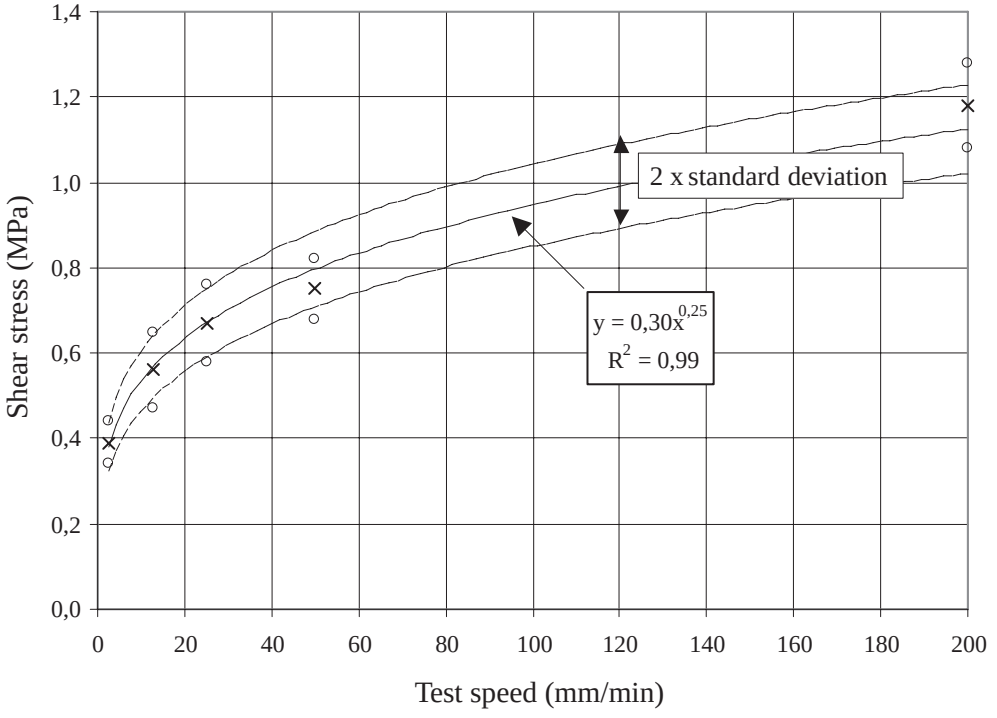

Figure 4. Correlation between test speeds and shear stress at 30°C and D = 150 mm for Pavement 3.

where:

$\tau_{\sigma n}$ shear stress with normal stress σ_n (MPa)
$\tau_{\sigma 0}$ shear stress without normal stress (MPa)
σ_n normal stress (MPa)

5.4 *Influence of the temperature*

In this investigation all laboratories carried out the tests at various temperatures. One laboratory used five temperatures (10°C, 20°C, 25°C, 30°C and 40°C). As an example the results of Pavement 2 are shown for D = 150 mm and v = 50 mm/min in Figure 6.

A relation between shear stress and temperatures was found as follows.

$$\tau_{T_x} = 10^{a \cdot T_x + b} \tag{5}$$

Table 3 presents the corresponding regression coefficient.

From these tests it appears that all pavements follow the same temperature dependency. The mean value of coefficient "a" is –0.023 (± 0.004).

The following figure 5 is an example for D = 100 mm and v = 50 mm/min and was produced by using these coefficients.

5.5 *Influence of the sample age*

The influence of the sample age in the absence of traffic was checked for Pavement 2. Tests were carried out by two laboratories. The results are shown in table 4.

The evaluations showed an increase of the shear stress. The fact that both laboratories found an increase of shear stress (up to 27%) shows the influence of sample age. However the amount of increase was different which is partly due to the fact that the testing conditions were not identical.

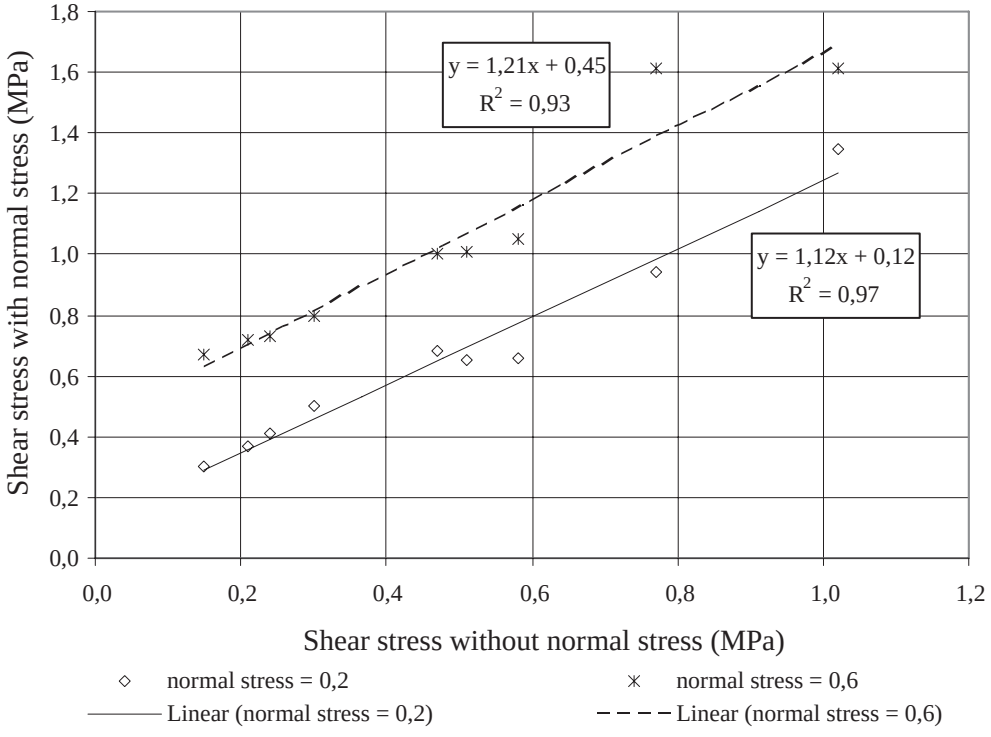

Figure 5. Correlation between shear stress with and without normal stress applied.

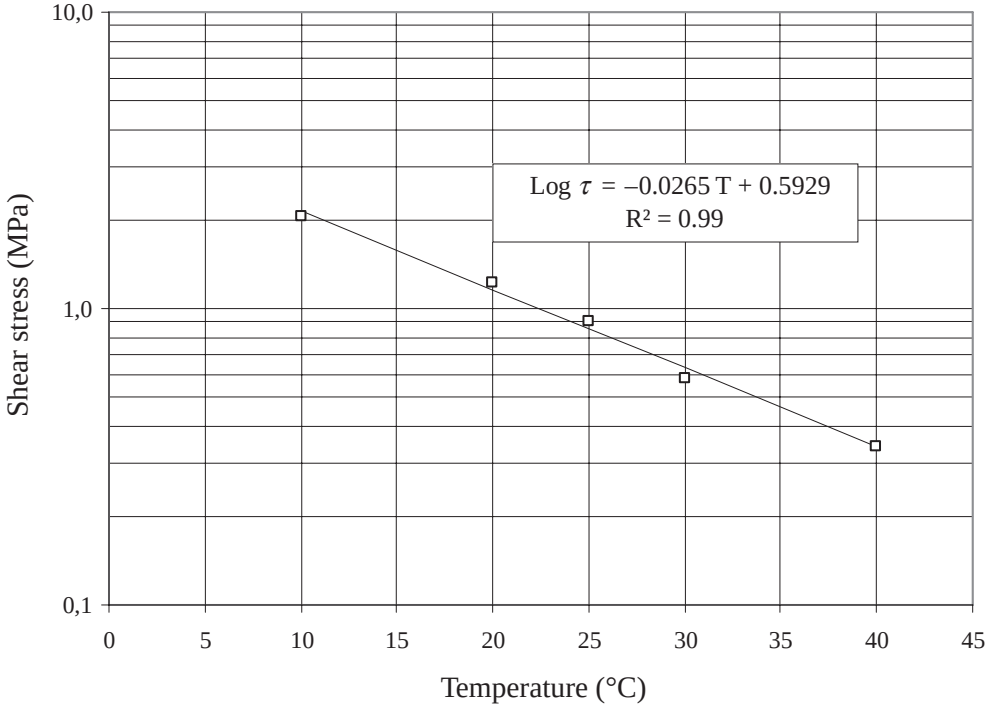

Figure 6. Correlation between shear stress without normal stress and temperatures for Pavement 2 D = 150 mm, v = 50 mm/min.

Table 3. Coefficient a and b for all pavements according to Equation 5.

		Pavement 1			Pavement 2			Pavement 3		
D	v	a	b	R^2	a	b	R^2	a	b	R^2
mm	mm/min	Shear test without normal stress								
100	2.5	–0.021	–0.013	1.00	–0.026	0.308	0.99	–0.023	0.334	0.99
100	50	–0.016	0.211	0.92	–0.025	0.612	1,00	–0.020	0.611	0.97
150	50	–0.026	0.369	0.94	–0.026	0.586	1.00	–0.026	0.638	0.99

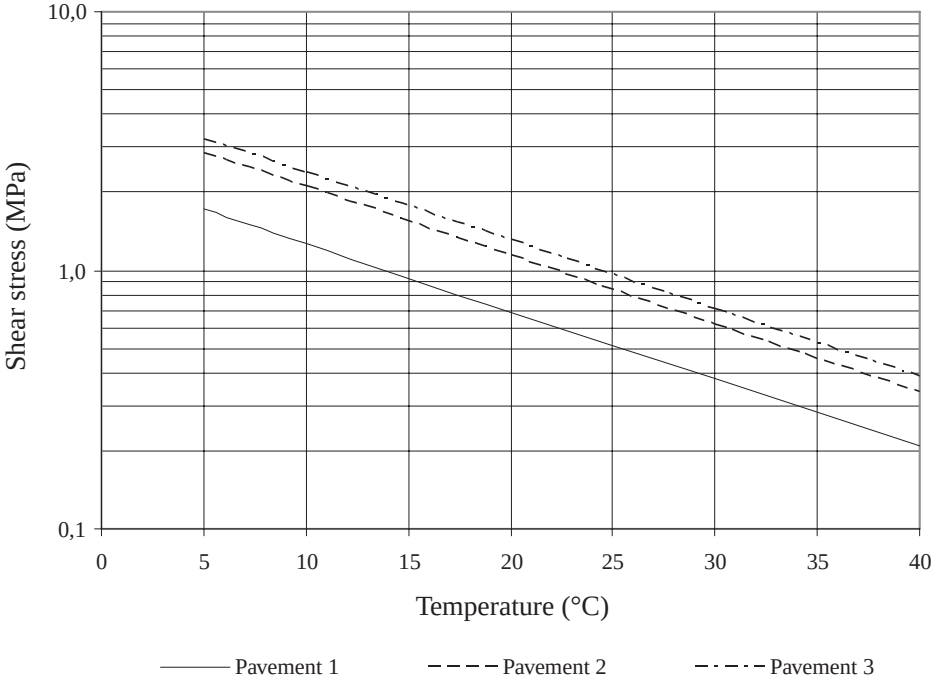

Figure 7. Shear test D = 150 mm, v = 50 mm/min.

6 CONCLUSION

This RILEM interlaboratory test program compares test methods for the assessment of interlayer bonding of asphalt pavements. The conclusions from this investigation can be summarized as follows.

- Generally good agreement exists between different unidirectional monotonic static shear tests.
- The reached precision of the different shear tests is satisfactory; it was found that the precision of the shear test in case of absolutely homogeneous area of the trial section is:
- Repeatability standard deviation: $s_r = 0.05\ \bar{\tau}$ (MPa)
- Reproducibility standard deviation: $s_R = 0.12\ \bar{\tau}$ (MPa)
- The influence of the temperature, the size of the specimen and the test speed could be mathematically evaluated and clear correlations could be found.
- As for the influence of the diameter, it was found that the shear stress values for all temperatures tested with cores of 150 mm diameter were lower than the results of the test carried out with 100 mm asphalt cores.

Table 4. Influence of the sample age on shear stress.

Laboratory	1		2	
Test conditions	D = 150 mm, v = 50 mm/min, normal stress = 0 MPa		D = 100 mm, v = 2.5 mm/min, normal stress = 0.2 MPa	
Test date	May 2006	November 2007	June 2006	November 2007
Temperature	Shear stress (MPa)			
10°C	2.03	2.49	0.95	1.09
20°C	1.23	1.59	0.68	0.68
30°C	0.58	0.98	0.37	0.44

- The presence of emulsion seems to mitigate the scatter of shear stress at the interface.
- A relationship was found that allows to estimate the influence of the test speed on shear stress.
- Friction parameter appeared to be approximately linearly dependent on normal stress. This was also true for the slope of the linear regression between shear stress with and without normal stress.
- Regardless of the interface conditions, the interlayer shear stress appears to follow the same temperature dependency.
- Within 18 months before first and second sampling, an increase of the shear stress with sample age was found.

REFERENCES

ALP A-StB part 4. 1999. Examination of interlayer bonding with the Leutner shear test. Germany.

ISO 5725-2. 2004. Accuracy (trueness and precision) of measurement methods and results—Part 2: Basic method for the determination of repeatability and reproducibility of a standard measurement method.

MCHW NG 954. 2004. Method for Laboratory Determination of Interface Properties using the Modified Leutner Shear test. UK.

ÖNORM B 3639-1. 1997. Asphalt for road construction and related purposes—testing—shear resistance in contact surfaces of asphalt layers. Austria.

Schweizer Norm 671961. 2000. Bituminöses Mischgut, Bestimmung des Schichtenverbunds (nach Leutner).

SG 3/01/221. 2005. Guidelines Document for the assessment and certification of thin surfacing systems for Highways. Appendix A. 3, Torque Bond Test (Draft), UK.

UNI/TS 11214. 2007. Caratterizzazione prestazionale a taglio delle interfacce—Metodo di prova ASTRA.

Advanced Testing and Characterization of Bituminous Materials –
Loizos, Partl, Scarpas & Al-Qadi (eds)
© 2009 Taylor & Francis Group, London, ISBN 978-0-415-55854-9

RILEM interlaboratory test on pavement performance prediction and evaluation

H. Piber, M.N. Partl & C. Raab
RILEM TC 206 ATB, TG 4

ABSTRACT: The former RILEM TC 182 PEB organized 1997 an international interlaboratory test on pavement performance, prediction and evaluation. The aim was to predict the expected damages after 10 years on the basis of traffic and climatic data. Two sections in Austria and Portugal were constructed and test samples were cut from the pavement and send to the different laboratories. 13 laboratories of 12 countries participated in the study and gave performance predictions according their own methods and standards. The report which summarizes the results in detail is available on the RILEM web site. RILEM TC 206 ATB TG 4 continued the long term observation. Unfortunately, only the Austrian section in Villach could be monitored as planned, since the Portuguese section had problems in the data supply. In 2007 the Austrian road administration stopped the observation of the test section in Villach. The paper summarises the actual road condition and compares it to the predicted performance.

1 INTRODUCTION

With increasing number of vehicles and axle loads on motorways the long term performance of asphalt pavements and its prediction are gaining more and more importance. Numerous long term projects in many countries have been established during recent years to monitor and evaluate pavement performance. In 1997 the former RILEM TC 182 PEB organized an international interlaboratory test on pavement performance prediction and evaluation with laboratories participating from around the world. For this purpose, two test sections, one in a moderate climate (Portugal) and another one in a climate with high summer and low winter temperatures (Austria), were constructed. Test slabs were cut from the pavement and samples send to different laboratories, which were asked to predict the damage for a ten years period (Partl & Piber 2001). The prediction was based on testing the distributed asphalt samples as well as the provided traffic and climate data. Each laboratory was asked to use its own methods and test procedures. Meanwhile the test sections were further monitored and eventually the predicted behavior was compared to the in situ performance. Since only one of the sections, the section in Villach (Carinthia), Austria, could be monitored over the whole observation period, the condition of this section after ten years trafficking was compared to the predicted performance.

2 TEST SECTION

The 100 m long test section was located at an altitude of 500 m above sea level on the motorway "Tauern Autobahn A 10" on the carriageway to Salzburg. The carriageway consisted of two 3.75 m wide lanes and a hard shoulder (emergency lane). The longitudinal gradient was 0.5%. and the cross fall was 3.4%. The motorway runs on an 8 m high embankment and follows a slight left bend with a radius 2500 m. There is a speed restriction of 100 km/h and a no passing zone for trucks. 1997 a base course (160 mm) and a wearing course (35 mm) were laid and the construction work finished (figure 1).

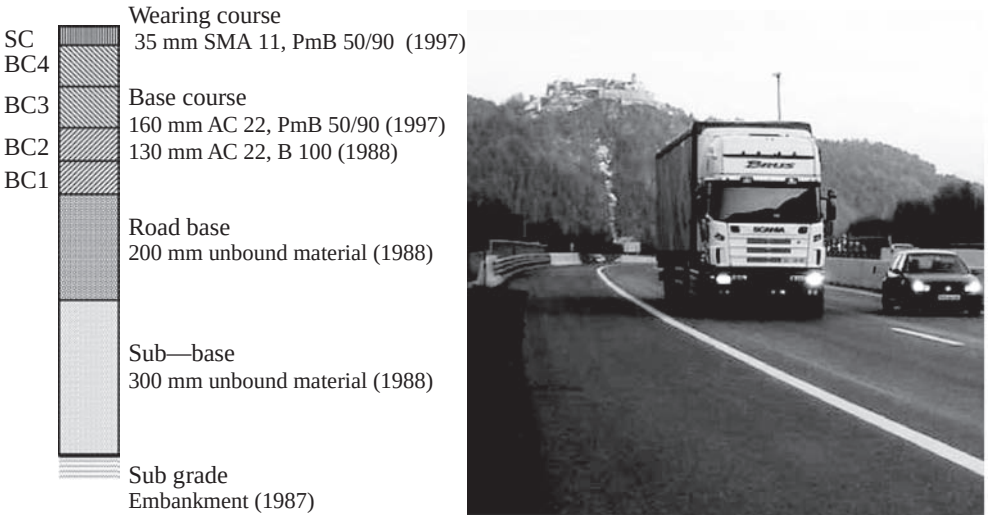

Figure 1. Pavement of the test section and year of construction.

3 LABORATORY TESTS AND PREDICTION

13 laboratories of 12 countries participated on a voluntary basis in this performance prediction. The laboratories received asphalt samples (250 × 550 × 325 mm) cut from the pavement for mechanical testing and evaluation. Additionally, information concerning climatic conditions (meteorological data), traffic census data including heavy traffic data and the annual growth rate of traffic were given.

All laboratories were asked to conduct their testing and evaluation based on their own national standards and methods. Their damage prediction for a 10 years period had to be characterized in terms of level of severeness A to D the following damage types: rutting, single cracking, net cracking and surface defects.

Since the laboratories tested the different layers either separately or as multilayer system and the test equipment and conditions differed considerably, the results of could not be compared in a direct way.

Table 1 shows the categorized performance prediction (A…C) by the participating laboratories:

Regarding the damage types "single cracks" "net cracks" and "surface defects" all laboratories came to the same conclusion that cracking was not expected to be a major issue and therefore these types of damage were categorized as "A". Concerning the damage type "rutting", on the other hand, the assessment is widely scattered. The detailed results of this project can be downloaded (Partl and Piber 2001) and were summarized later by Piber et al 2003.

4 FIELD MEASUREMENTS

4.1 *Surface characteristics*

The road administration of Carinthia (Austria) observed and monitored the test section continuously. After 10 years, the road surface showed neither single cracks nor net cracking or surface defects. Therefore, the class of damage was in all cases "A". This result was in a good agreement with the prediction by all laboratories.

Table 1. Result of the interlaboratory test; number of labs and performance prediction categories (A…D).

Type of damage											
Rutting[1] mm				Single cracks (Thermal cracking) m/100 m		Net cracks (fatigue cracking) % of 100 m²				Surface defects[2] % of 100 m²	
<5	5–10	10–20	≥20	<4	≥4	≥5	5–10	10–20	20	<2	≥2
A	B	C	D	A	B	A	B	C	D	A	B
Number of laboratories corresponding to the performance prediction categories											
5	3	4	0	4	0	9	0	0	0	2	0

[1]Rutting in surface course and deformation of each asphalt course. (max. depth and change of thickness)
[2]Loss of material and/or raveling.

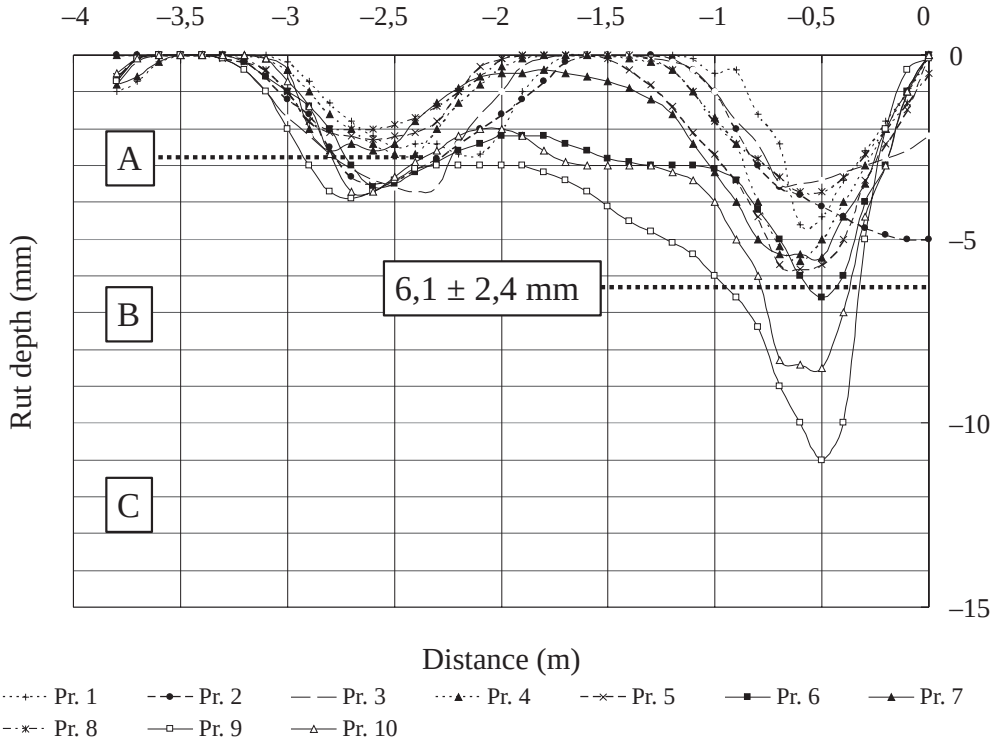

Figure 2. Rut depth measurement 2007.

To investigate rutting, 10 cross profiles were defined on the 100 m long section and the rut depth was measured annually. Already in the first year ruts were measurable in the right lane. As shown in figure 2, at the end of 2007 the average rut depth in the right wheel track of the right lane was 6.1 mm (±2.4 mm). With a rut depth of 5 mm rutting occurred mainly in the wearing course (SMA 11). While the bituminous base course was affected by 1 mm only. The actual rut depth after 10 years of trafficking was in accordance with the damage class "B", a prediction which was given by 3 of the 12 laboratories.

The development of the rut depth shown in figure 3 follows a potential curve. The equation 1 has a high regression ($R^2 = 0.99$).

$$RD = -0.2406 \cdot HV^{0.2113} \quad (1)$$

where:
RD = rut depth (mm)
HV = Number of heavy vehicles.

4.2 *Traffic census*

The traffic census 1995 had been the basis for the performance prediction. The AADT (Average Annual Daily Traffic) was 16.200 vehicles and the AADHT (Average Annual

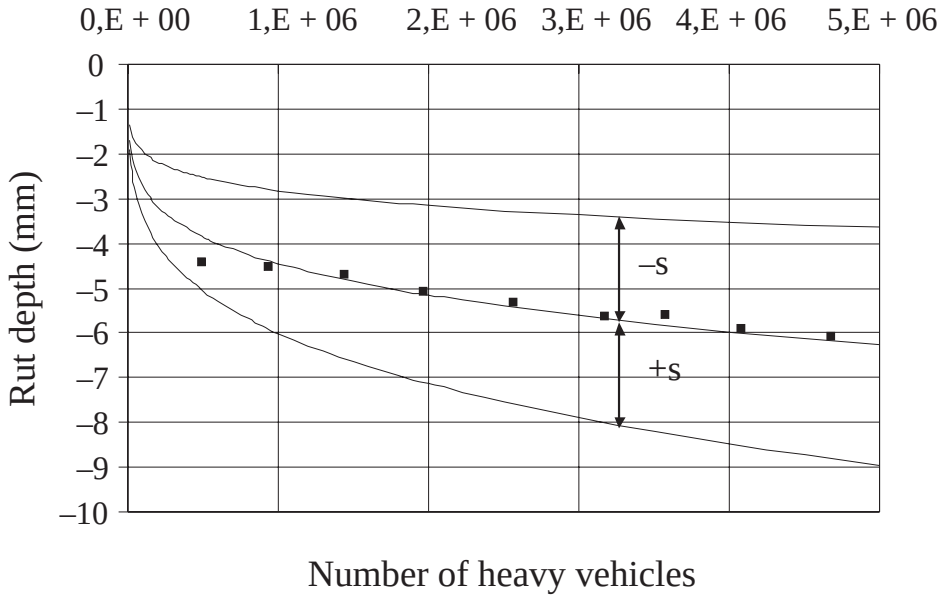

Figure 3. Development of the average rut depth.

Table 2. Composition of the heavy traffic permissible total weight and proportion.

Type	Number of axles	Total weight	Proportion 1996	Proportion 1998–2006
Truck	2	<18 t	17.1%	13.3%
Truck	3	<25 t	6.8%	4.6%
Truck	4	<32 t	1.1%	0.7%
Trailer truck	2 + 2	<36 t	8,2%	7.4%
Trailer truck	2 + 3	<38 t	11.3%	5.7%
Trailer truck	3 + 2	<38 t	9.5%	11.5%
Trailer truck	3 + 3	<38 t	1.1%	0.8%
Semi trailer truck	2 + 1	<36 t	0.1%	0.6%
Semi trailer truck	2 + 2	<38 t	2.2%	1.1%
Semi trailer truck	2 + 3	<38 t	40.6%	53.0%
Semi trailer truck	3 + 2	<38 t	1.3%	0.7%
Semi trailer truck	3 + 3	<38 t	0.7%	0.4%

Table 3. Axle load distribution and heavy vehicle type in percent on the "Tauern Autobahn A 10".

Axle load	T2	T3	T4	TT 2+2	TT 2+3	TT 3+2	TT 3+3	ST 2+1	ST 2+2	ST 2+3	ST 3+2	ST 3+3
<1 t	0,0	0,9	1,6	0,0	0,0	0,0	0,0	0,0	0,0	0,0	0,0	2,1
1–2 t	0,0	3,5	3,5	4,3	0,5	0,3	0,0	0,5	0,0	0,2	1,4	2,1
2–3 t	0,8	2,4	9,1	2,6	4,2	1,9	0,0	3,1	7,7	3,7	3,9	6,3
3–4 t	1,9	5,6	15,9	6,0	7,8	6,6	16,7	13,5	26,8	7,5	11,4	12,5
4–5 t	3,8	10,0	15,1	11,2	4,2	16,9	16,7	14,6	12,7	8,4	9,4	14,6
5–6 t	9,7	17,1	17,8	12,9	13,5	19,2	33,3	25,0	17,7	13,2	13,9	22,9
6–7 t	23,5	17,7	20,1	18,1	31,2	20,3	25,0	15,1	17,3	28,3	21,4	6,3
7–8 t	13,8	16,5	7,4	24,1	17,1	16,6	8,3	8,9	5,0	21,7	18,9	12,5
8–9 t	3,5	10,3	4,3	9,5	9,1	8,9	0,0	7,8	5,9	4,4	8,3	10,4
9–10 t	8,6	8,3	2,4	5,2	5,5	4,2	0,0	3,1	1,4	3,9	3,3	8,3
10–11 t	14,9	5,0	2,1	4,3	4,4	3,8	0,0	4,2	2,7	4,0	4,4	0,0
11–12 t	16,8	1,8	0,4	0,9	2,1	1,1	0,0	2,6	2,3	2,9	1,7	0,0
12–13 t	2,4	0,3	0,2	0,9	0,5	0,4	0,0	0,5	0,5	1,1	1,9	2,1
13–14 t	0,3	0,3	0,0	0,0	0,0	0,0	0,0	1,0	0,0	0,3	0,0	0,0
14–15 t	0,0	0,0	0,0	0,0	0,0	0,0	0,0	0,0	0,0	0,1	0,0	0,0
15–16 t	0,0	0,3	0,0	0,0	0,0	0,0	0,0	0,0	0,0	0,0	0,0	0,0

Daily Heavy Traffic) counted 2.350 trucks in both directions. The annual increase of the heavy traffic was 3%.

The traffic census occurred automatically. Until the end of 2006 a total of 4.70 millions trucks drove over the right lane of the test section, which met the predicted number of 4.76 millions trucks by 98.8%.

4.2.1 *Heavy traffic composition*

Heavy traffic composition changed in the last 10 years as depicted in table 2.

The increase of semi trailer trucks with five axles was significant. The total weight went up 3.5%. The total number of axles was with 22.7 millions about 3% higher than expected. The sum of 10 t ESALs in the right lane of the test section was 5.22 millions, whereas only 3.92 millions ESALs had been predicted.

4.2.2 *Axle load distribution*

The axle load distribution was provided by the Institute of road construction of the technical University of Vienna (ISTU Wien). In the frame of their research work, investigations of axle load distributions were carried out on Austrians motorways (table 3).

4.3 *Temperature data*

4.3.1 *Air temperature*

The climatic data were provided in terms of temperature data. For their performance prediction the laboratories obtained the monthly maximum, the average monthly maximum, monthly average, the average monthly minimum and monthly minimum temperature. The comparison in figure 4 shows that the average monthly temperatures of the last ten years were clearly higher than in the previous years. In summer the difference measured was +2°C.

The number of days with temperatures higher than 25°C with average 59 days was clearly higher than before 1996 where 46 days were counted. The evaluation according the SHRP (Strategic Highway Research Program) (SHRP-A-637, SHRP-A-645, SHRP-A-648 & Anderson 1999), showed similar results, as presented in table 4.

Table 4. Comparison of the SHRP temperatures.

	<1996	1998–2007
Mean value of the average maximum temperatures of the hottest 7-day period of a year	30.7 ± 1.8°C	32.0 ± 1.4°C
Mean value of the annual minimum temperature	–19.3 ± 1.4°C	–16.2 ± 1.8°C
Maximum Asphalt temperature 20 mm below surface (A_{MAX})	52.6°C	53.1°C
Minimum Asphalt temperature 20 mm below surface (A_{MIN})	–18.6°C	–16.7°C
Required "Performance Grade" of Bitumen	PG 58–22	PG 58–22

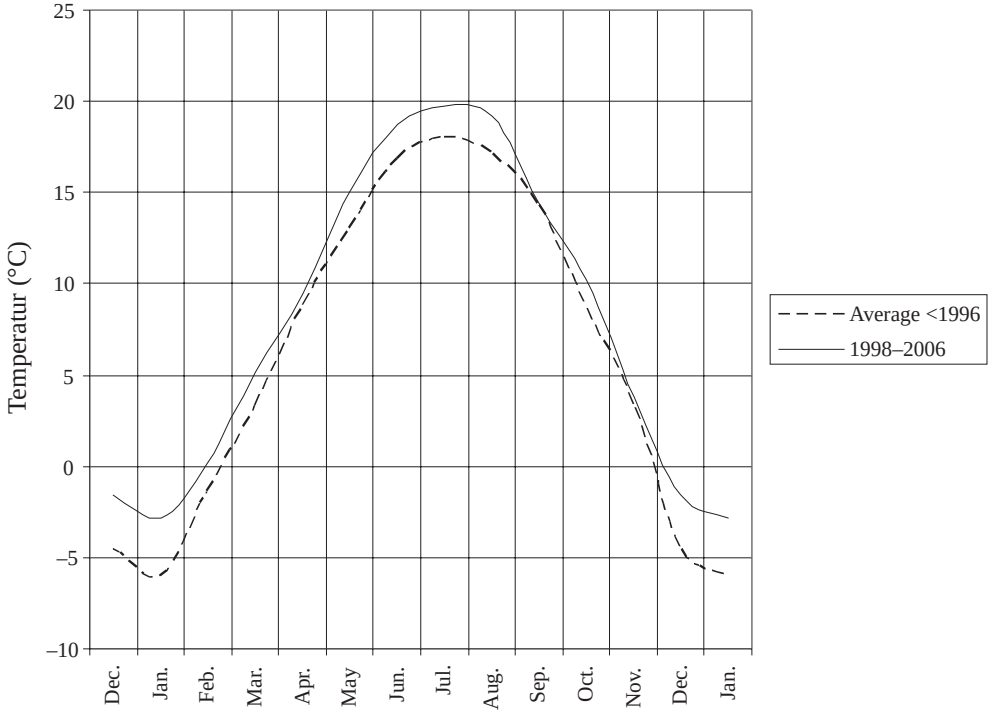

Figure 4. Comparison of the average monthly air temperature before 1996 and between 1998 and 2006.

4.3.2 *Pavement temperatures*

Temperature gauges were located in the asphalt pavement 25, 50, 80 and 180 mm below the surface. Temperatures were measured hourly. Figure 5 depicts the maximum temperatures in the courses measured between 1998 and 2007.

The maximum temperature in the wearing course (35 mm) was higher than 52°C. In the upper layer of the base course (80 mm) the maximum temperature achieved between 43 and 52°C and in the lower layer of the base course (80 mm) still 37 to 43°C was measured.

4.4 *Pavement temperatures and heavy traffic*

The previous evaluations showed that in reality the amount of heavy vehicles was slightly lower but the total loads in term of axles were higher than predicted. Due to climatic warming the summer temperatures proved to be higher than expected.

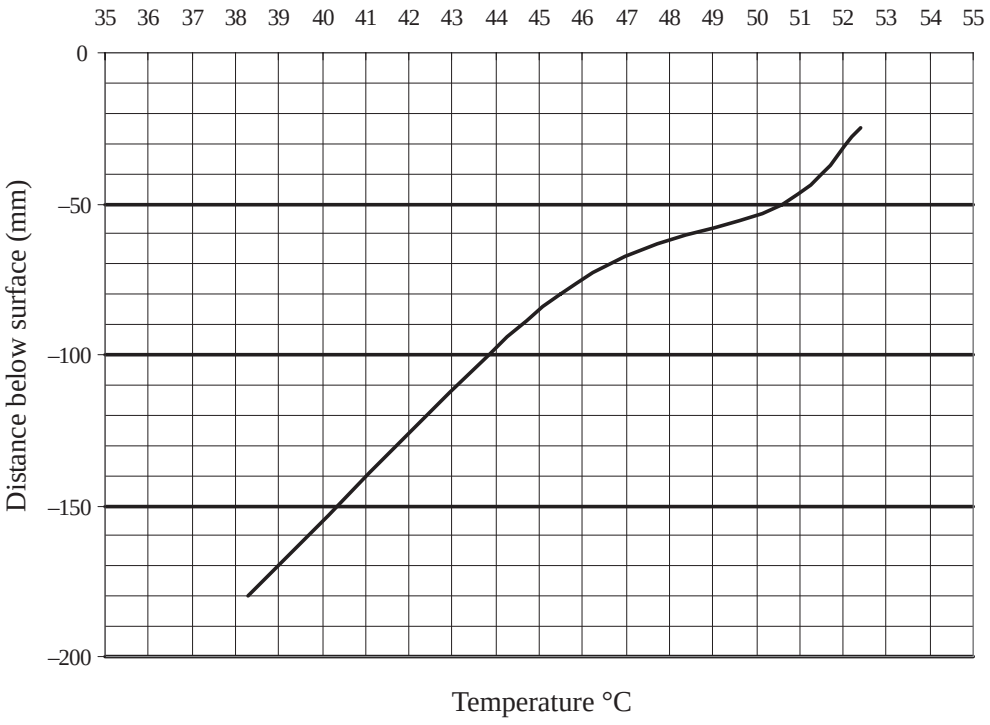

Figure 5. Maximum temperature in asphalt pavement.

The climate and traffic investigations were combined. Table 4 contains the combination of the temperature measurements in various depth below the surface and the census of heavy traffic at temperatures between 30 and 53°C.

The wheel loads were calculated from the axle loads in table 3. These wheel loads were combined with the proportion of heavy traffic (table 2) and in this way for each pavement layer the total number of wheel loads at specific layer temperatures (table 4) was determined. Figure 5 shows an example for the wearing course. Altogether, at temperatures higher than 30°C more than 3.2 million wheel loads drove over the test section. 1.0 million wheel loads were counted at temperatures higher than 40°C, 0.4 million at temperatures higher than 45°C and still 47.000 wheel loads passed at temperatures of more than 50°C. The majority of wheel loads (65%) ranged between 2.5 and 4 t, whereas wheel loads of more than 5 t were the exception (0.2%).

5 ASSESSEMENT OF THE LABORATORY TESTS

When looking at the monitoring results, rutting proved to be the most critical parameter for the long term performance. As predicted by all laboratories other damages such as single cracking, net cracking or surface defects were negligible. In the prediction of the rutting behavior the laboratories showed quite some differences. Six out of 12 laboratories derived the development of the rut depth from their rutting test method, while others based their prediction on the test result compared to the requirement of their national regulation or standard. All of these six laboratories used different test devices. Lab 1 used a static compression test (S–CO), lab 2 a cyclic compression test (C–CO), lab 6 a cyclic indirect tensile test (C–IT) and the labs 3, 4 and 5 conducted a wheel tracking test (WT–large device). In figure 7 the results for all six laboratories are shown:

Table 5. Temperatures in different depth below surface and number of heavy vehicles (1998–2006).

25 mm below surface		50 mm below surface		80 mm below surface		180 mm below surface	
T (°C)	Trucks	T (°C)	Trucks	T (°C)	Trucks	T (°C)	Trucks
54	0	54		54		54	
53	335	53		53		53	
52	1 601	52	0	52		52	
51	2 521	51	86	51		51	
50	6 320	50	475	50		50	
49	8 898	49	2 440	49		49	
48	13 861	48	5 325	48		48	
47	14 150	47	6 937	47	0	47	
46	18 542	46	13 476	46	315	46	
45	25 580	45	17 503	45	1 579	45	
44	25 521	44	20 486	44	4 792	44	
43	24 551	43	24 608	43	7 191	43	
42	30 728	42	32 922	42	15 174	42	
41	29 070	41	32 164	41	19 343	41	
40	34 180	40	34 694	40	23 111	40	0
39	33 092	39	32 060	39	28 751	39	305
38	35 890	38	26 045	38	33 869	38	1 270
37	39 771	37	37 667	37	37 197	37	5 166
36	43 462	36	40 872	36	40 460	36	10 161
35	49 793	35	51 818	35	51 001	35	21 393
34	47 790	34	52 439	34	53 827	34	35 937
33	52 808	33	54 123	33	68 019	33	55 757
32	52 722	32	59 390	32	66 500	32	62 511
31	70 460	31	73 739	31	83 496	31	81 591
30	65 585	30	79 805	30	89 250	30	97 557

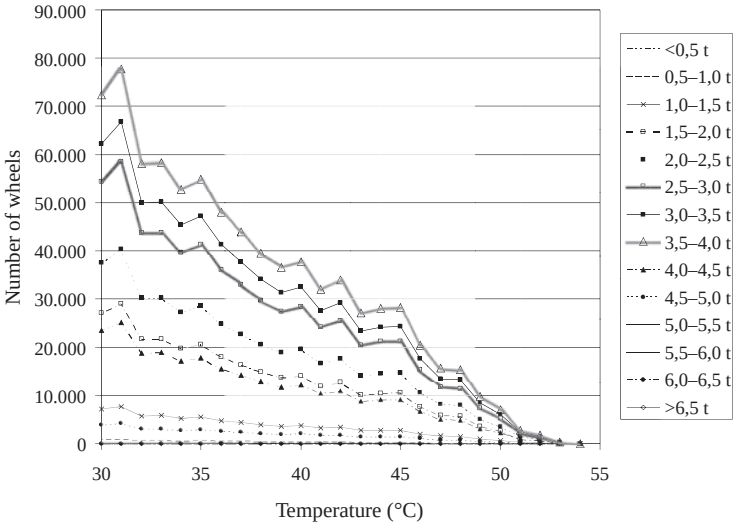

Figure 6. Number of wheel loads and temperature in the wearing course (–35 mm).

The in situ measured rut depth after 10 years monitoring was 6.1 mm ($\sigma \pm 2.4$ mm). Comparing this result with the laboratory prediction shows that the laboratories number 3, 4 and 5 came very close to this value. It is notable that the best predictions are based on the wheel tracking test (large devise). All three laboratories used a testing machine with a

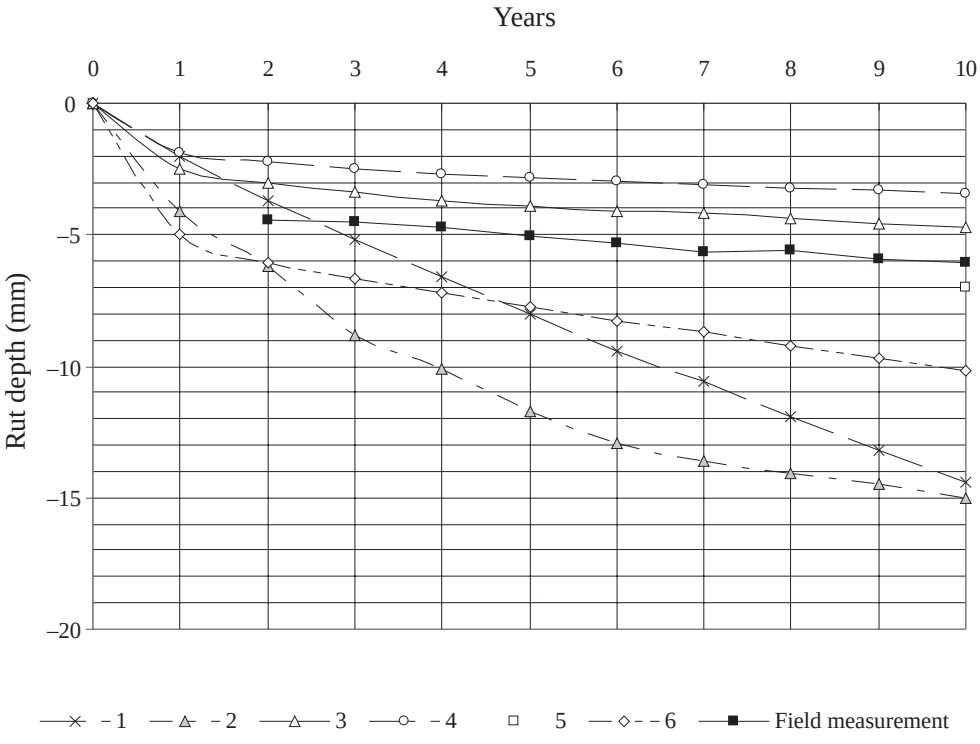

Figure 7. Calculated rutting; the figure indicated the number of the laboratory.

Table 6. Test and configuration.

Lab	Type of test	Sample size	Loading conditions	Test temperature	Test result
3	WT	l = 550 mm	L = 5 kN	40°C	SC + BC4 + BC3 + BC2
		w = 250 mm	p = 600 Pa		ε_{10000} = 1.24 mm,
		h = 250 mm	f = 0.6 Hz		ε_{40000} = 1.82 mm,
4	WT	l = 500 mm	L = 5 kN	35°C	SC: ε_{10000} = 6.3%,
		w = 180 mm	p = 600 Pa		BC4: ε_{10000} = 2.4%,
		h (SC) = 30 mm	f = 60 cycle/min	45°C	SC: ε_{10000} = 6.1%,
		h (BC4) = 100 mm			BC: ε_{10000} = 4.2%,
5	WT	l = 480 mm	L = 5 kN	38°C	SC + BC4: ε_{10000} = 1.4%,
		w = 160 mm	p = 600 Pa		BC4 + BC3: ε_{10000} = 1.0%,
		h = 100 mm	f = 1 Hz	60°C	SC + BC4: ε_{10000} = 13.6%,
					BC4 + BC3: ε_{10000} = 4.0%,

pneumatic tire (400 × 80 mm). However, the sample size varied. Some laboratories tested each course separately others tested the courses together. The test characterizations and results are represented in table 6.

6 CONCLUSIONS

The prediction of long term performance of asphalt pavements on motorways is still not an easy task. Test sections which have been established during recent years provided a good base for monitoring the pavement conditions under specified traffic and climate data. The RILEM

test section in Villach, Austria showed that in a middle European climate with high summer and low winter temperatures rutting proves to be one of the most likely damage cases.

Although traffic and temperature data can be collected and their development can be predicted quite precisely, it seems difficult to give damage predictions based on laboratory experiments and theoretical analysis as the variety of test methods and prediction models seems quite large.

Since rutting proved to be the most critical damage case, test devices to evaluate this parameter have attracted major focus. The interlaboratory study showed that the rutting behavior can best be estimated using large size wheel tracking tests with pneumatic tires.

The prediction of the maximum pavement temperature with help of SHRP equations was very precise.

Regarding the prediction of long term performance it seems important that uniform and standardized methods based on material characteristics and mechanical properties will be developed.

REFERENCES

Anderson, D. 1999. *SUPERPAVE Binder Test and Specification*. Eurobitume Workshop, Workshop Briefing, Luxembourg.

Partl, M.N. & Piber, H. (editors) 2001. *Pavement Performance Prediction and Evaluation (PPPE)*- Report of RILEM TC 152-PBM and 182-PEB, Report rep029, e-ISBN: 2912143683 download from www.rilem.net–Publications—Reports.

Piber, H. & Partl, M.N. 2003. *RILEM—Interlaboratory tests on performance prediction of pavement*. Proceedings of the 6th International RILEM Symposium, Zürich 2003.

SHRP-A-637. Analysis of the Integrated Model of Climatic Effects on Pavements.

SHRP-A-645. Asphalt Cements. A conceit Data Compilation.

SHRP-A-648. Weather Database for the SUPERPAVE Mix Design System.

Advanced Testing and Characterization of Bituminous Materials – Loizos, Partl, Scarpas & Al-Qadi (eds)
© 2009 Taylor & Francis Group, London, ISBN 978-0-415-55854-9

New tests for polymer-modified binders: Results of a Belgian round robin test

J. De Visscher, S.Vansteenkiste, A. Leuridan, N. Piérard & E. Schelkens
Belgian Road Research Centre, Brussels, Belgium

Ph. du Bus de Warnaffe
COPRO, Brussels, Belgium

ABSTRACT: An extensive Round Robin Test (RRT) was conducted in Belgium in the course of 2007, mainly to evaluate the reproducibility of the new performance-related tests for polymer-modified binders (DSR, BBR, EVT2). As heterogeneity of test samples might be related to polymer modification, pure road bitumen was included in the analysis as a reference. In addition, two polymer-modified binders were chosen, one of which was sampled from a tank with a so-called "high-shear mixer"; this type of mixer is deemed to ensure better homogeneity of the binder. In order to minimize the differences induced by sample preparation, additional instructions were sent to the participating laboratories, complementing the specifications in the relevant standard EN 12594 for sample preparation. Although the RRT was intended for the new tests for PmBs, conventional tests such as needle penetration and Ring & Ball softening point were included in the test program as well. This allowed drawing conclusions at a later stage as to whether a possible dispersion in the test results is due to differences between laboratory samples or inherent to the test itself. This paper presents the statistical analysis of the results and draws conclusions on the reproducibility of the test results among Belgian laboratories. The results from the RRT are compared to precision data from other sources (including the test standards themselves), where available. In addition, the detailed data on sample preparation and test conditions are analyzed in order to establish any relationships with deviating results. This RRT, therefore, makes a contribution to both the knowledge and the validation of the new European tests for bituminous binders, especially polymer-modified binders.

1 INTRODUCTION

In 2005, a small scale interlaboratory test was organized between a few Belgian laboratories to investigate the reproducibility of the new European test methods for polymer-modified binders (PmBs). These tests were limited to only one PmB and only four laboratories took part. The results indicated very poor reproducibility. This was not only the case for the new European performance-related tests, but also for conventional tests such as needle penetration and Ring & Ball softening point. The limited number of laboratories, the limited number of samples (only one) and missing information about sample preparation and precise test conditions unfortunately did not allow to explain the results or to draw any conclusions. Differences between samples, due to either the sampling procedure or the preparation of the test samples in the individual laboratories, was however suggested as one of the possible causes of the wide dispersion in the test results. The laboratories had been asked to follow the standard EN 12594 for preparing the test samples. However, this norm is not sufficiently precise on the heating procedure, while it is known that in case of PmBs, the thermal history of the samples has an important impact on the results of certain binder tests (Soenen et al. 2006).

To investigate this in more detail, a new RRT was organized on a more extensive basis. The following requirements were set:

– The number of laboratories shall be as large as possible
– At least two binders shall be considered: one pure binder and one PmB
– The procedure for sample preparation shall be described in more detail than in the standard EN 12594
– Information shall be acquired about sample preparation and the exact test conditions used by each participant

A total of 25 Belgian laboratories participated, although a much smaller number was equipped to perform the new European tests on PmBs. Nevertheless, all laboratories were invited to participate, since carrying out conventional tests like needle penetration and softening point was also useful for detecting any differences between laboratory samples.

In addition to the pure reference binder, two PmBs were chosen, one of which was sampled from a tank with a so-called "high-shear mixer"; this type of mixer is deemed to ensure better homogeneity of the binder. Table 1 gives an overview of the three binders and the corresponding code names which are used throughout this paper. The laboratory samples were all taken at the same time from the bitumen tanks and stored into securely closed one-liter cans. These cans were numbered and sent to the participating laboratories, together with the instructions.

The laboratories were asked to prepare the test samples from the laboratory samples in accordance with EN 12594. In addition, a new document was sent along in which the procedure was described and specified in more detail. This document was based partly on the 'Code of practice: manufacture, storage and handling of polymer-modified binders' of the Australian Asphalt Pavement Association (AAPA 2004) and partly on practical experience of the Belgian Road Research Centre. The aim of these additional instructions was to minimize as much as possible any differences between test results, induced by the sample preparation procedure and not by the actual test method. In particular, attention was paid to the temperature trajectory while handling samples and the mixing process used.

Finally, for every test, a checklist was added, which had to be filled out by the participating laboratories while doing the tests. These checklists provided more detailed information about the sample preparation and the used test conditions, which were used in the analysis of the RRT to explain possible anomalies in the test results.

It has to be reminded that the main goal of the RRT was to evaluate the reproducibility of the test methods, not the repeatability. Given the large number of tests that was considered,

Table 1. Overview of the tested binders.

Code	Binder type
B1	pure binder
BP1	PmB, from tank with high-shear mixer
BP2	PmB, from tank without high-shear mixer

Table 2. Overview of the test methods used in the RRT.

Binder property	Test procedure	# participants
Needle penetration	EN 1426	25
R&B Softening point	EN 1427	25
Complex modulus G* and phase angle δ (DSR)	EN 14770	7 (4 in case of BP2)
BBR	EN 14771	6 (5 in case of BP1; 3 in case of BP2)
Equiviscous temperature for low shear viscosity (EVT2)	prCEN/TS15324	4

it was not realistic to ask all participants to do also a number of repeated tests. Also, repeatability is generally known to be much better than the reproducibility of these tests.

2 OVERVIEW OF THE TEST METHODS

Table 2 gives an overview of the test methods included in the RRT and of which test results are discussed in this paper. The last column shows the number of results that were received. For the conventional test methods, the number of test results was sufficient to calculate a good estimate of the reproducibility. Unfortunately, for the less conventional and new test methods, the number of results was still limited.

3 RESULTS

3.1 *Needle penetration*

The results of the needle penetration (EN 1426) were analysed according to ISO 5725-2:1996. Compared to the previous interlaboratory tests on a PmB in 2005, the data showed less dispersion. The statistical Mandel and Grubbs' test were applied to detect the presence of doubtful or nonsensical values. Only a few such values were found as indicated in table 3; they were subsequently rejected before calculating the reproducibility.

It is worthwhile to notice that one nonsensical value in case of B1 and BP1 is directly related to a prolonged exposure of the sample to air before carrying out the measurement, resulting in an extremely low needle penetration value. Moreover, one laboratory with a nonsensical value for BP2 reported a very low temperature following the 2 hours heating procedure while applying no stirring of the sample. Therefore, it may be assumed that the nonsensical value is linked to the heterogeneity of the PmB sample.

Table 4 shows the reproducibility that was estimated from the RRT, in percent of the global mean for each binder, compared to the precision data given in the European test method. Although the reproducibility is much better than in the previous interlaboratory test, it is still

Table 3. Occurrence of doubtful or nonsensical values (needle penetration).

	# participants	# nonsensical values	# doubtful values
B1	25	3	1
BP1	25	1	2
BP2	25	2	0

Table 4. Reproducibility for needle penetration PEN (% of the global mean).

	B1	BP1	BP2	According to EN 1426:1999
Global mean (0.1 mm)	53.0	62.4	67.9	
Reproducibility "R" (=2.8*s_R)	12.2%	8.9%	9.0%	6%

Table 5. Reproducibility for Ring & Ball softening point $T_{R\&B}$ (°C).

	B1	BP1	BP2	According to EN 1427:1999
Global mean	49.7°C	60.9°C	50.9°C	2°C (for pure bitumen)
Reproducibility "R" (=2.8*s_R)	1.5°C	2.5°C	2.4°C	3.5°C (for PmB)

Table 6. Occurrence of doubtful or nonsensical values (R&B softening point).

	# participants	# nonsensical values	# doubtful values
B1	25	2	1
BP1	25	1	2
BP2	25	1	1

above the reproducibility limit given in the European standard EN 1426 (R = 6%). The conclusion is that we are not able at this moment to achieve this level of reproducibility, despite of the care that was taken in the preparation of the test samples. This observation is in agreement with conclusions drawn from a RRT recently conducted in Germany.

It is interesting to note that the precision data are even better for the PmBs than for the pure binder B1. Another interesting observation is that the reproducibility is just as good for BP2 as for BP1. This shows that all laboratory samples (cans) of the binder BP2 were comparable and that the initial concern about larger variations between laboratory samples taken from a tank without high-shear mixer was unnecessary.

3.2 *Ring & Ball softening point*

Table 5 shows the reproducibility data found in the RRT. The data were calculated again after rejection of doubtful and nonsensical values (table 6).

The reproducibility of the results is well within the reproducibility limit given in the European standard EN 1427. The precision is less for the PmBs than for the pure binder, which is usual for this test. The precision data in the standard test method EN 1427 thus also makes a distinction between both types of binders. Again, the reproducibility is as good for BP2 as for BP1.

It was noted that in the case of B1, the occurrence of the two nonsensical values was directly related to the excessive heating of the binder: up to 180°C where as a maximum of 135°C was proposed. Not surprisingly, the resulting R&B values exceeded largely the average value. In the case of BP1 and BP2 both nonsensical values were reported by the same laboratory. Based on the detailed information with respect to the heating procedure, it was doubtful if the minimal final temperature of 180°C within the binder sample was reached in both cases. Moreover, no stirring was applied while heating the sample.

3.3 *Dynamic shear rheometer (DSR)*

The complex modulus (G* and phase angle δ) was to be reported for two temperatures (25 and 52°C) and three frequencies (0.1, 1.6 and 10 Hz). The tests had to be repeated on two different samples, which also gave a rough estimate of the repeatability. The reproducibility was calculated on the mean values of each laboratory.

The statistical analysis of the results according to ISO 5725-2 revealed only one nonsensical value for the case of B1 at 25°C and 10 Hz. Even though it was not possible to find the cause of this nonsensical value in the checklist data, this result was eliminated before calculating the standard deviations. For BP2, the results of one laboratory at 52°C and 0.1 Hz were also eliminated because the repeatability was unacceptably large, although the mean value itself was not identified as nonsensical. Table 7 shows the estimates of the standard deviations under conditions of repeatability (sr) and reproducibility (sR). They are expressed in percent of the global mean values.

Typically for DSR measurements, the precision depends strongly on the range of the test temperature and frequency; the highest standard deviations are observed at the combination of low temperature and high frequency (25°C and 10 Hz). Also typical for DSR, the repeatability is much better than the reproducibility, which is explained by the influence of the test equipment on the results.

Table 7. Results of the statistical analysis of the DSR test data.

B1 (results from 7 laboratories)

T (°C)	f (Hz)	G* mean (kPa)	sr (%)	sR (%)	δ mean (°)	sr (%)	sR (%)
25	0.1	149	2.6	26	76.5	0.2	1.6
25	1.6	1347	2.7	16	64.0	0.5	7.7
25	10	3963*	3.9*	35*	55.6*	1.2*	15.4*
52	0.1	0.657	3.5	11	88.4	0.2	0.4
52	1.6	9.582	2.8	11	85.1	0.1	0.3
52	10	52.105	1.7	10	82.1	0.2	0.6

BP1 (results from 7 laboratories)

T (°C)	f (Hz)	G* mean (kPa)	sr (%)	sR (%)	δ mean (°)	sr (%)	sR (%)
25	0.1	83	2.2	13	67.0	0.5	1.5
25	1.6	734	1.5	14	64.1	0.9	4.8
25	10	2640	2.1	25	56.5	1.0	12.4
52	0.1	1.528	2.6	6	68.8	0.3	0.9
52	1.6	12.428	2.2	6	68.3	0.2	0.3
52	10	49.458	2.4	5	69.7	0.2	0.6

BP2 (results from 4 laboratories)

T (°C)	f (Hz)	G* mean (kPa)	sr (%)	sR (%)	δ mean (°)	sr (%)	sR (%)
25	0.1	79	2.3	11	70.4	0.2	1.3
25	1.6	711	6.9	9	67.7	0.3	3.5
25	10	3152	3.6	23	59.5	0.4	11.9
52	0.1	0.689*	1.5*	9*	84.5*	0.3*	1.2*
52	1.6	8.757	2.5	10	77.3	0.2	1.5
52	10	39.260	2.3	8	73.0	0.2	0.2

*Values calculated after elimination of one value.

Given the small number of participants, the calculated standard deviations can not be used as reliable estimates of the reproducibility of the test method. However, the values can be compared to the reproducibility data that followed from the RILEM round robin test, in which 18 laboratories took part (Sybilski et al. 2003). This RRT showed that the reproducibility standard deviation for most test conditions varies between 15 and 30% for G* and is smaller than 10% for the phase angle δ. Table 7 shows that the results from the Belgian RRT are indeed of the same order. For G*, the reproducibility was less good for the pure binder B1 at 25°C and 10 Hz (35%). For δ, the reproducibility was less good for all binders at 25°C and 10 Hz (>10%).

In France, the mirror group of WG1 of CEN/TC336 recently conducted a similar RRT focusing on the complex modulus (Eckmann et al. 2008). The conclusions were very similar: in general, the values given by the RILEM RRT were confirmed, except for some binder related cases.

In Belgium, the road authorities ask to report the complex modulus of the binder at a temperature of 52°C and a frequency of 1.6 Hz. For these test conditions, the reproducibility standard deviations are smaller (10 to 11% for G* and 1.5% for the phase angle).

3.4 *Bending beam rheometer (BBR)*

The bending beam rheometer is used to determine the following two critical temperatures:

- T for S(60 s) = 300 MPa: temperature at which the stiffness after 60 seconds attains a value of 300 MPa
- T for m(60 s) = 0.3: temperature at which the slope of the curve stiffness versus time after 60 seconds has a value of 0.3

To determine these critical temperatures, the BBR-test is done according to EN 14771, at 3 different temperatures. The critical temperatures are subsequently derived by interpolation of the test results as function of temperature.

For the RRT, it was asked to report both critical temperatures. The recommended temperatures for the execution of the BBR-test were –12, –18 and –24°C. The test had to be repeated on two different samples at each test temperature. The critical temperatures had to be derived from the mean values of S(60 s) en m(60 s). Six laboratories sent in results, as shown in table 8.

The reproducibility of the critical temperatures could be evaluated by analyzing the data according to ISO 5725-2. Applying the Mandel and Grubbs' test identified two nonsensical values: one for B1 and one for BP1 (see table 8). A more detailed analysis of the test data revealed some possible causes for the nonsensical value for B1. The laboratory performed the BRR-tests in a higher temperature range, so that the critical temperature was close to the lowest measurement temperature. It is also observed that this laboratory systematically produced critical temperatures higher than the mean. Finally, this laboratory did not do the repeated test (while the other laboratories did two to three repeated tests). For the nonsensical value for BP1, it is observed that this laboratory systematically produced the lowest critical temperature. This may be an indication of a systematic error in the temperature measurement of the BRR equipment.

Table 9 shows a summary of the statistical results after elimination of the nonsensical values. The standard deviations can be compared to the reproducibility data determined in the RILEM round robin test on BBR, conducted on four binders, in which 14 laboratories took part (Sybilski et al. 2003). The main conclusions of this RRT were:

Table 8. Overview of the critical temperatures derived from BBR-tests.

Laboratory number (coded):			1	2	3	4	5	6	mean	st.dev.
B1	T for S = 300 MPa	(°C)	–14.7	–14.6	–16.5	–15.9	–15.5	–16.3	–15.6	0.8
	T for m = 0.3	(°C)	–17.0	–15.9*	–18.4	–17.5	–17.7	–17.6	–17.3	0.8
BP1	T for S = 300 MPa	(°C)	/	–20.0	–20.8	–20.4	–19.7	–20.3	–20.2	0.4
	T for m = 0.3	(°C)	/	–21.4	–22.8*	–22.2	–21.5	–21.4	–21.9	0.6
BP2	T for S = 300 MPa	(°C)	/	–17.3	/	/	–17.3	–19.5	–18.0	1.3
	T for m = 0.3	(°C)	/	–17.9	/	/	–19.4	–19.7	–19.0	1.0

*Nonsensical values.

Table 9. Global means and reproducibility standard deviations for critical temperatures.

	T for S(60 s) = 300 MPa (°C)		T for m(60 s) = 0.3 (°C)	
	mean	st.dev.	mean	st.dev.
B1	–15.6	0.8	–17.6*	0.5*
BP1	–20.2	0.4	–21.6*	0.4*
BP2	–18.0	1.3	–19.0	1.0

*Values calculated after the elimination of nonsensical values.

– The reproducibility standard deviation was different from binder to binder, but it was not larger for the tested PmBs than for the pure bitumen
– T for S(60 s) = 300 MPa, the reproducibility standard deviation varied from 0.35 to 0.75°C
– T for m(60 s) = 0.3 varied from 0.6 to 1.35°C

The results of the Belgian RRT thus comply with the results from the RILEM RRT. Only for BP2, the standard deviation of the Belgian results is higher (only for T for S(60 s) = 300 MPa). It has to be reminded that for this binder, only three laboratories sent in results, so the estimation of the standard deviation can not be considered as very reliable.

The European test method EN 14771 also contains precision data, but these are given as the reproducibility R on the stiffness S and the slope m. To quantify the corresponding precision in terms of the critical temperatures, a graphical method was used as illustrated by figure 1. This figure shows measurement data for the pure binder B1. The dotted lines correspond to two times the reproducibility standard deviation according to EN 14771. At 300 MPa, this corresponds to 1.4°C in terms of temperature. The reproducibility standard deviation on the critical temperature is thus approximately half of this value, 0.7°C. Using the same technique for the slope also yields a value of 0.7°C for the critical temperature T for m (60 s).

Applying this technique also to the data for the other two binders, it was observed that the standard deviation on the critical temperatures is approximately the same for the three binders (from 0.65 to 0.75°C) Comparing the reproducibility standard deviations in table 9 to these values allows to conclude that the reproducibility of the Belgian test results also complies with the precision data given in EN 14771, except for BP2 for which the standard deviation was larger. It has to be recalled that for this particular binder, the standard deviation was calculated on the basis of results from only three laboratories, so it shall be considered as a very rough estimation of the reproducibility.

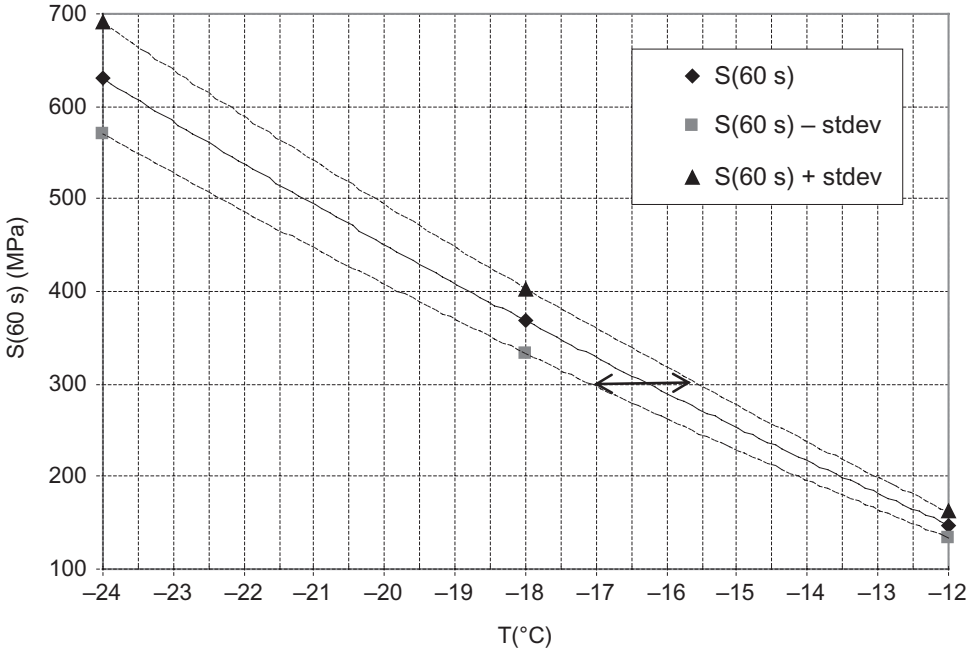

Figure 1. Graphical determination of the standard deviation of the critical temperature for S (60 s) = 300 MPa.

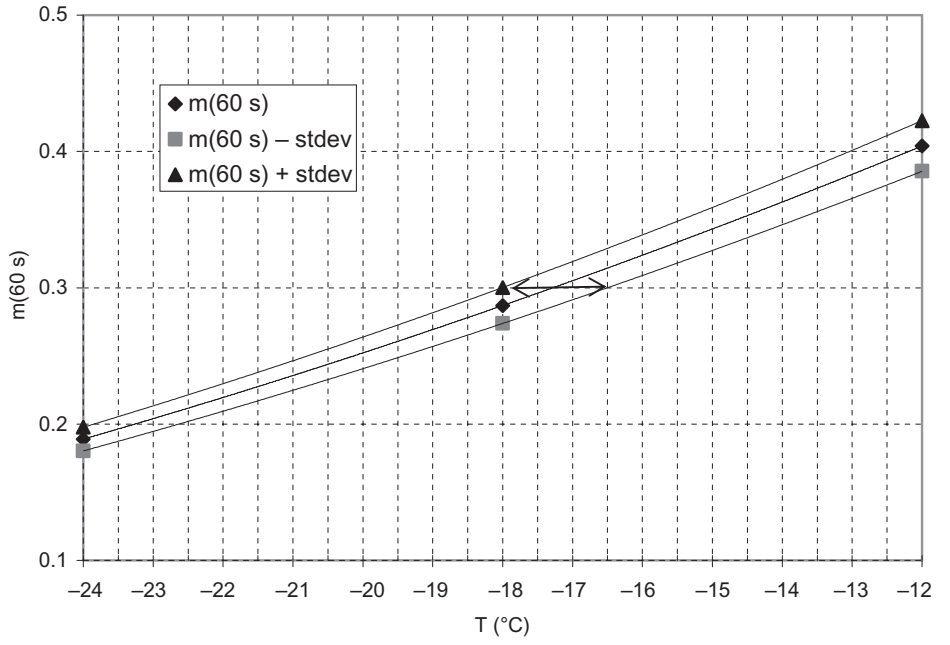

Figure 2. Graphical determination of the standard deviation of the critical temperature for m(60 s) = 0.3.

Table 10. Results RRT for EVT2 (°C).

	Laboratory					
	1	2	3	4	mean	st.dev.
B1	48.6	48.3	49.3	48.2	48.6	0.5
BP1	63.0	59.4	62.1	62.3	61.7	1.6
BP2	51.6	49.1	–	52.6	51.1	1.8

*Values calculated after the elimination of nonsensical values.

3.5 *Equiviscous temperature for low shear viscosity (EVT2)*

Only four laboratories performed these tests, according to the method described in prCEN/TS15324. The results, mean values and standard deviations are given in table 10. They can be compared to the precision data given in prCEN/TS15324, resulting from a European RRT organized by CEN TC336/WG1/TG1. In this RRT, 5 binders were tested by 15 laboratories. Depending on the binder, a reproducibility standard deviation was found between 1.0 to 2.5°C. The standard deviations found in this Belgian RRT are of the same order. It is also interesting to note that the reproducibility standard deviation of EVT2 is smaller than that of the R&B softening point.

4 CONCLUSIONS

The results of this Belgian Round Robin Test on binders delivered useful data for the evaluation of test procedures and test precision. A large number of laboratories (25) participated for the traditional binder tests of needle penetration and R&B softening point.

For the needle penetration, the main findings are as follows:

– Statistical analysis of the data by the Mandel and Grubbs' test indicated only few doubtful or nonsensical values.

– Most of the nonsensical values could be related to the impact of the temperature during sample preparation, which deviated from the instructions (excessive heating or prolonged exposure to air in case of pure binder, insufficient heating in case of PmBs).
– Surprisingly, the precision data are better in the case of PmBs in comparison with pure binder.
– The reproducibility of the RRT does not meet the criteria described in EN 1426, neither in the case of pure binder or polymer-modified binders. A revision of latter limits should be considered in the future.

The main findings for the R&B softening point measurements are:

– Statistical analysis of the data by the Mandel and Grubbs' test indicated only few doubtful or nonsensical values.
– Most of the nonsensical values could be related to the impact of the temperature during sample preparation, which deviated from the instructions.
– As anticipated, the precision is less in the case of PmBs than for the pure binder.
– The reproducibility of the results is well within the reproducibility limit given in the European standard EN 1427.

The results from these traditional tests allowed to draw conclusions regarding the homogeneity of the laboratory samples and the repeatability of the sample preparation procedure:

– The reproducibility of the test results is a good indication that the test samples were comparable, for the PmBs as well as for the pure binder.
– A possible influence of the high-shear mixer on the homogeneity of PmB test samples was not reflected in these test results. Of course, this is not a general conclusion, since it may depend on the type of PmB.

Probably, the additional instructions regarding the sample preparation had a positive effect on the reproducibility of the test data. As these instructions are relatively simple without any unnecessary complication of the procedure, it is recommended to follow them systematically.

A smaller number of laboratories participated for the new European test methods (DSR, BBR, EVT2). Consequently, the obtained standard deviations only gave a rough estimation of the reproducibilities. The following conclusions were drawn:

– For the complex modulus G* and phase angle δ, measured in DSR, the results agree with the reproducibility as assessed in the RILEM Round Robin Test. Only for the lowest temperature and highest frequency, the standard deviation was higher.
– For the critical temperatures T for S(60 s) = 300 MPa and T for m(60 s) = 0.3, measured in BBR, the results agree with the RILEM Round Robin Test and with the reproducibility as given in the European norm EN 14771.
– For EVT2, the results are in agreement with the reproducibility standard deviation as assessed in the Round Robin Test organized by CEN TC336/WG1/TG1.

REFERENCES

AAPA (Australian Asphalt Pavement Association), 2004. Code of Practice: Manufacture, Storage and Handling of Polymer-modified Binders, 1st Edition.

Soenen, H., De Visscher, J., Vanelstraete, A. & Redelius, P. 2006. Influence of thermal history on rheological properties of various bitumen. *Rheologica Acta* 45 (5):729–739.

Sybilski, D. & Vanelstraete, A. 2003. Precision of bituminous binder rheology tests in the 2nd RILEM round robin test. *Proc. of the 6th RILEM Symposium PTEBM'03*:74–80, Zurich, may 2003.

Eckmann, B., Nigen, S., Largeaud, S., Soenen, H., Lapalu, L., Mouillet, V., Chabert, D., Moglia, O., Chailleux, E., Descroix, P. & Perez-Lepe, A. 2008. Complex modulus of bituminous binders—Results of the Round Robin Test of the GE1 working group (France). *Proceedings of the 4th Eurasphalt & Eurobitume Congress 2008, Copenhagen*, may 2008.

Advanced Testing and Characterization of Bituminous Materials –
Loizos, Partl, Scarpas & Al-Qadi (eds)
© 2009 Taylor & Francis Group, London, ISBN 978-0-415-55854-9

Comparative test on indirect tension modulus test

X. Carbonneau & Y. Le Gal
COLAS S.A., Campus Scientifique et Technique, France

ABSTRACT: EN standardisation on asphalt concrete is now enforced in a number of European Countries. Test standards in the EN 12697 series define the methods used to measure mechanical characteristics of asphalt mixes. For a fundamental approach based on modulus and fatigue resistance measurements, frequency and temperature test conditions are specified in EN 13108-1. Because of the fact that there are several tests for each characteristic, comparisons are still necessary to correlate results. In addition, suppliers propose a variety of devices for each test, all of which are of course supposed to provide perfect compliance with the test standard. However, certain devices have been in use for over than ten years, long before the last standard was issued. Modifications in test conditions appeared during the final phases of the European test standardization process. Round robin tests are very expensive and time consuming, but they are necessary to compare laboratory findings when different devices are used to perform tests. For indirect tension modulus tests, only a few round robin tests were conducted in the past, and this was well before the final version of the existing standard. This paper presents a comparative test conducted in 6 laboratories of the Colas group with three different devices, from two suppliers. Two different asphalt mixes have been selected, a common asphalt concrete used for wearing courses and a High Modulus Asphalt (HMA) mix. Samples were made, controlled, and characterised in a single laboratory before they were sent to the participants. Results obtained show that devices provide very similar results, if samples are cautiously moulded and controlled. It is also possible, using correlations between results obtained with different modulus tests, to show that we are able to predict modulus in direct tension tests from indirect tension tests.

1 INTRODUCTION

In recent years, French road contractors have become increasingly interested in the indirect tension modulus measurement (Carbonneau et al. 2005, Olard et al. 2005, Esh et al. 2006). This is explained by its simplicity, its moderate cost compared to the two points bending test on trapezoidal samples, and the information it is able to provide, which is briefly reviewed here along with the inherent limits of the available equipment. It is thus essential to enhance our knowledge about the test and the extent to which it can be trusted, because our main experience is based on direct tension (DT-CY) and 2 point bending tests on trapezoidal samples (2PB-TR). The industry therefore set up a working group within the USIRF (Union of French Road Industry Associations). As such, this paper presents a series of results obtained as part of comparison tests within the Colas Group. Its aim was to increase our test knowledge, to demonstrate the equivalence between the available machines. We also wanted to check that this method can be successfully applied to characterised asphalt mixes, even HMA ones.

2 THE INDIRECT TENSION MODULUS TEST

The test described in the European standard EN 12697-26 annex C (IT-CY) measures resilient modulus, with the application of a pulsed load to the test specimens. To begin with, a series of 10 pre-loading operations is performed, then an initial measurement is made of the average modulus during 5 load applications, supplemented by another test after the specimen

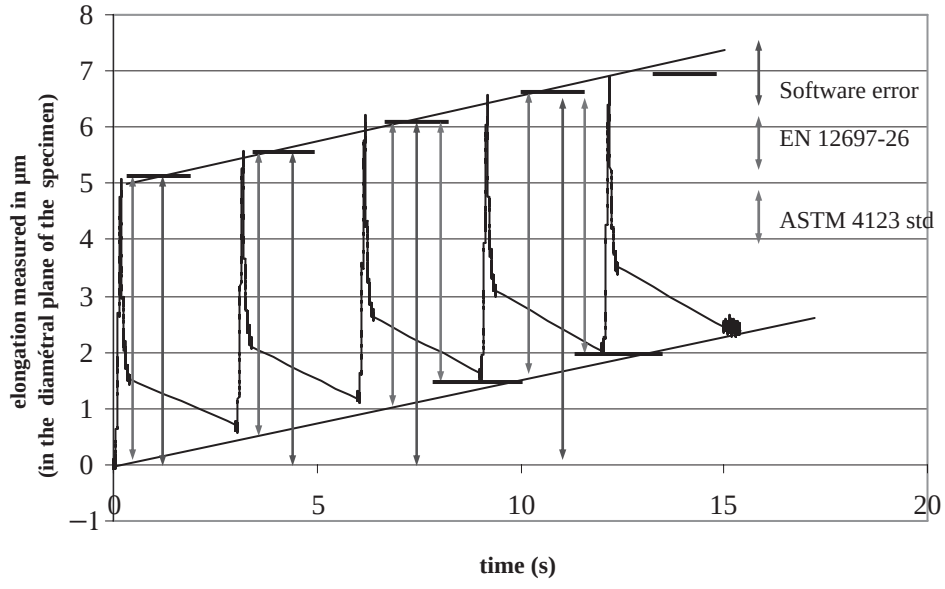

Figure 1. Correction of the anomalies in the equipment supplied by the manufacturers.

has been rotated 90 degrees. The test can be performed at different temperatures and with different loading times. However, pneumatic equipment currently on the market cannot produce very short loading times, typically of less than 30 ms. There are also difficulties in maintaining constant deformation when the pulse rise time is reduced from 124 ms, which is the duration specified in the test's standard to 90, 60 or even 30 ms. It is therefore difficult to establish how modulus varies with the loading time and thereby to obtain master curves. Another part of the European standard EN 13108-20 (June 2006) lays down the test conditions, specifying 20°C for the test temperature and 124 ± 4 ms for the rise time. This is the maximum recommended temperature for this test (Di Benedetto & Corte 2005). Using this temperature, the peak horizontal length variation defined in the standard can be reached, even on High Modulus asphalt, for 100 mm diameter samples, and even for 150 mm ones. This may still be difficult at 15°C. It is therefore necessary to use the temperature of 20°C in order to comply with the standards, while possibly performing a supplementary evaluation at 15°C, which is the temperature used for design and for which we already have correlations with a conventional complex modulus (2PB-TR) or direct tensile tests (DT-CY). Last, the strain which is considered when determining the modulus, more precisely the change in length as a function of the diameter, is not the same in the different published test standards. Therefore, some variations in the data used in the software available on existing devices could exist. As an example for the strain use for modulus calculation a British pneumatic device closely followed the specifications in the European standard, as shown in figure 1. However, an Australian device initially exhibited a minor data-processing anomaly, quickly corrected by the supplier. Recent devices should therefore, in principle, give results which are fairly similar, or at least comparisons between them will not suffer from problems due to data processing methods.

3 COMPARATIVE TEST

Determination of the precision of a measurement method is a fairly long operation which is detailed in the ISO 5725 1 to 5 series of standards. The more laboratories participate part, the more accurate the estimation of the standard deviations of repeatability and reproduceability is. The number of devices available in the Colas Group does not enable a fine statistical analysis of the results to achieve a high enough level of accuracy to fully satisfy all requirements

in the ISO 5725 standards. Neither is it the proper role of a contractor to establish quality criteria of this type for a test which has now gained acceptance at European level. Nevertheless, the procedure we have followed adds to the few published results as we have concentrated on high performance products such as high modulus asphalt (HMA), for which the modulus is an essential characteristic. This is important as the 1998 inter-comparison test carried out to measure the indirect tension modulus (Ulmgren et al. 1998), in which 14 laboratories took part (British, Danish, Norwegian and Swedish) in the framework of the TC 227 working group, involved fairly low performance asphalt mixes. The modulus was measured on two "Dense Graded Asphalt Concrete" mixes, with 0/16 and 0/22 gradings respectively at 20 and 10°C and provided an average value of 2,400 MPa for the first and 6,170 MPa for the second. The average value determined for an SMA was 4,770 MPa at 10°C. Moreover, these measurements were made on specimens of material that had been applied in situ. This test led to a repeatability result of between 12 and 15% and a reproduceability of between 15 and 22%.

4 MACHINES ASSESSED

The process described here had several goals: to identify and describe the test facilities at our disposal and verify that the different laboratories provide equivalent results. We therefore conducted a brief survey in order to list the available machines, the models, the version of the software, and the normal procedure for conducting measurements. Responses are presented in Table 1. Five laboratories took part, giving us a total of 6 different measurement machines, all pneumatic.

The three main types are shown in Photo 1. The oldest, known as UMATTA (Universal MATerial Testing Apparatus) does not strictly speaking meet the requirements of the test standard. It is nevertheless possible to apply the 10 pre-loading operations by repeating the 5 pre-loading operations that are initially programmed, following a previous British test standard (BS DDD 213, 1993). In addition, data processing applied the method described in the ASTM standard (ASTM 4123 – 82). This clearly shows the background work that had to be

Table 1. The evaluated machines.

Laboratory	Model	Supplier	Software	EN 12697-26
Laboratory 1 (M1)	UMATTA	IPC	Matta version 3 (June 94)	No
Laboratory 1 (M2)	UTM 14P	IPC	UTM 16 V2-02 (Jan. 06)	Yes
Laboratory 2	Nu tester	Cooper	ITSM French (06)	Yes
Laboratory 3	CRT NU 14	Cooper	ITSM (Nov. 05)	Yes
Laboratory 4	Nu 14	Cooper	TSMI (Sept. 03)	Yes
Laboratory 5	Nu 10	Cooper	Dec. 05	Yes

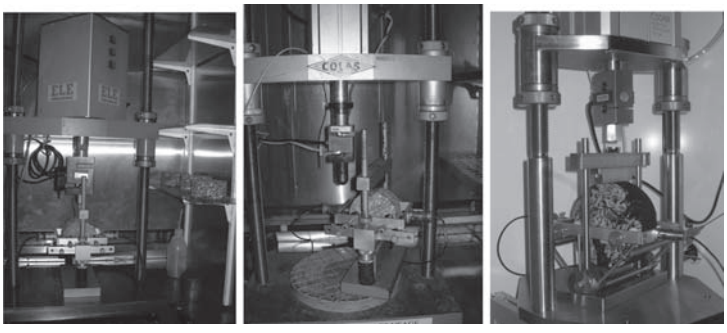

Photo 1. The different models of machine featuring in the comparative test.

conducted on these test methods and the machines on the market in order to conduct the tests, with a detailed evaluation of their operation. This was made even more difficult by the fact that the process began before the European test standards were published. This tended to make our contacts with the suppliers more difficult, as they did not wish to accept modifications of their software until the standard had been published in its final version. Fortunately, one of the manufacturers was a British company that was fully aware of this aspect and worked on the text that was adopted, which ultimately guaranteed that their machine would be absolutely compliant. The results given below nevertheless show that, in spite of the differences that have been identified, the value of the results obtained with the UMATTA machine are very close to the data output by machines which scrupulously comply with the standard.

5 TESTED MIXES AND TEST CONDITIONS

We decided not to restrict ourselves to a single mix, but used two products for our comparison: a semi-coarse asphalt concrete made with 0/10 aggregate from the La Noubleau quarry and a 35/50 pen bitumen, and a high modulus asphalt made with 0/14 aggregate supplied by CCM from the Wallers-Trélon quarry and hard 10/20 pen bitumen (Respectively EB 10 wearing course 35/50 and EB 14 base Course 10/20 according to EN 13108-1). We also decided to manufacture all the test specimens in the same laboratory which was asked to decide on the compositions to be tested and then check all the specimens before preparing the batches. This meant we had an accurate description of the different fractions of the two selected aggregates and the two bituminous binders used in these mixes. We thus retained the ability to manufacture additional quantities of mix to allow us to perform other tests in the standard EN 12697-26 in addition to the test specimens required for the intercomparison test. Table 2 provides a detailed description of the two mix designs. We thus have moduli of two significantly different levels. They allow us to evaluate the response levels of the machines on a product (the semi-coarse asphalt concrete) that has a relatively low modulus as this is not its essential characteristic, and a product with much better mechanical performance. The initial idea was

Table 2. Detailed composition of the studied mix designs.

	EB 10	EB 14
% passing a screen of (mm)		
20		
14		100
12		97
10	100	86
8	96	72
6.3	88	63
4	64	57
2	46	49
1	34	31
0.5	23	20
0.063	16	14
	7	7.6
Bitumen class	35/50	10/20
Binder content (%)	5.3	5.66
Richness modulus (k)	3.68	3.7
% voids with Gyropac 60 gyrations	9.2	
100 gyrations		3.5

Photo 2. Gyropac press used to make specimens.

Table 3. Characteristics of the 4 specimen batches supplied to each laboratory (average geometric density).

Product	ϕ (mm)	Lab 1 (M1)	Lab 1 (M2)	Lab 2	Lab 3	Lab 4	Lab 5
EB 10 WC	100	6.5	6.5	6.4	6.6	6.4	6.6
EB 14 BC	100	2.4	3.2	2.6	2.5	2.8	2.7

to demonstrate the ability of the machines to characterize the two types of mix in a satisfactory manner, or on the contrary, reveal their possible limitations.

6 PREPARING THE SPECIMENS

Thirty-two specimens with a diameter of 100 mm and a thickness of 50 mm, were therefore prepared for each of the materials. The specimens were moulded with a gyropac press, as shown in Photo 2. This solution guarantees fairly good reproduction of the moulding conditions, and makes the preparation of such a large number of specimens a considerably lighter task. All the specimens were individually measured in order to prepare "homogeneous" batches to be sent to each of the participating laboratories. Our criterion for creating these batches was for the average geometric voids contents to be very similar for all the laboratories. We therefore decided to characterize 4 specimens of each mix design in order to have a significant average value for each machine. The average voids content characteristics of the different batches are presented in Table 3.

In addition, before the specimens were sent to the laboratories, the modulus of all the moulded specimens was measured at 20°C–124 ms. Figure 2 shows the distribution of the results. The modulus values ranged from 2677 MPa for the semi-coarse asphalt concrete and 3929 MPa for the high modulus asphalt. Manufacture took place over a period of 4 weeks and the characterization of specimens continued for 4 weeks. After all the laboratories had received their specimens, measurements were conducted on specimens that had been conserved for a maximum of 6 months prior to testing.

7 RESULTS

The full set of results obtained is shown in Figure 3 for the EB 10 and Figure 4 for the EB 14. In the case of 4 of the laboratories and 5 of the machines, these results were the average value for the 4 specimens sent to them. Only one laboratory (No. 5) did not strictly comply with the programme that was initially planned, only conducting the measurements on 2 specimens at each temperature. The data were nevertheless used in this comparison. They were also used in Table 4, which also shows the range of measurements obtained in each laboratory for the tested population of specimens.

Beforehand, the results sent by each participant were checked, to ensure that they complied with the test conditions specified in the standard, namely a loading time of 124 ± 4 ms, a pulse repetition period of 3.0 ± 0.1 s, a peak horizontal strain of $5 \pm 2 \pm$ µm, and a small difference between the two sequences of measurements made for 5 consecutive pulses of between +10 and –20% of the initial value. This check confirms that it is possible to use pneumatic equipment when testing high modulus asphalt, when the test specimens have a diameter of 100 mm. It is nevertheless possible that in the case of particularly high performance mix designs the limitations of these machines will be reached for measurements at 15°C, although this temperature is not specified in the standard EN 13108-20.

Overall, these data elicit the following comments. First, the average results determined with the UMATTA machine differ little from the others, in spite of the difference in the way the measurements are processed and a minor difference in the strain used in the modulus calculation. With a sufficiently large population of specimens, as long as variations in the densities are low, these machines give satisfactory results. This is shown by the very low

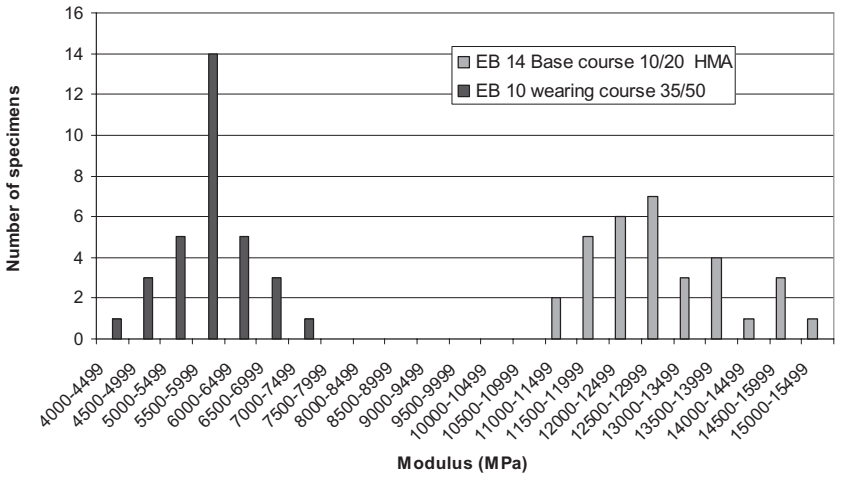

Figure 2. Distribution of the modulus values measured at 20°C on all the prepared specimens. (Measurements from Laboratory 1 Machine M2).

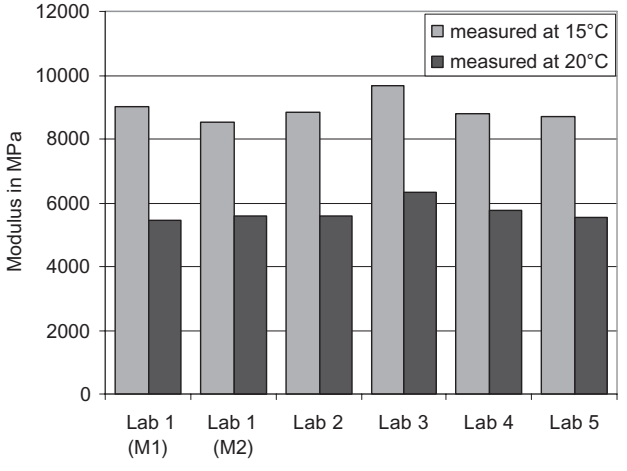

Figure 3. Modulus measurement results for the EB 10 wearing course 35/50.

impact of not removing this device when determining an average value for all the laboratories (See Table 4).

It can be seen in Figures 3 and 4 and in Table 4 which presents all the test conditions (products, temperatures), that all the results differ by less than 10% from the mean, except for the measurement at 20°C on the semi-coarse asphalt concrete (whatever the average value considered, with 5 or 6 machines). As we have mentioned above, these data are insufficient to allow us to precisely determine the repeatability and reproduceability of this test method. They nevertheless show the quality of the different machines. If we look at the range of the value measured individually for each specimen obtained by each laboratory at 15°C, i.e, under the conditions where the range is greatest, we can see from Table 4 that it remains below 1800 MPa for the semi-coarse asphalt concrete and that its value is 4534 MPa for the high modulus asphalt. These values are considerably lower than that determined beforehand by the laboratory that studied all 32 manufactured specimens. Only the range observed for the 4 measurements performed with the UMATTA machine (M1) remains slightly high.

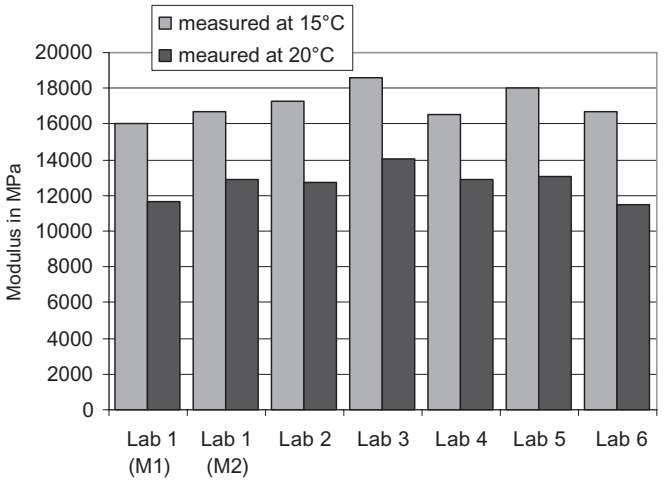

Figure 4. Modulus measurement results for the EB 14 Base course 10/20.

Table 4. Average value measured in each laboratory, and the range of values for each tested batch (in MPa).

Product	Temp. (°C)	Lab 1 (M1)	Lab 1 (M2)	Lab 2	Lab 3	Lab 4	Lab 5	Average 6 machines	Average 5 machines (without M1)
EB10 WC	15	9017	8548	8852	9678	8790	8705	8932	8915
	range	1774	987	975	726	1662	440	–	–
EB10 WC	20	5466	5568	5604	6340	5748	5549	5713	5762
	range	960	419	590	1193	1070	72	–	–
EB14 BC	15	16029	16663	17253	18580	16505	18010	17173	17402
	range	4534	2822	2926	1942	1405	1496	–	–
EB14 BC	20	11681	12861	12752	14046	12899	13080	12887	13128
	range	3107	1920	2697	1842	1263	1248	–	–

The range of average values measured by all the laboratories was 1130 MPa for the semi-coarse asphalt concrete and 2551 MPa for the high modulus asphalt at 15°C. For the record, we should bear in mind that the range of values for the different replicas during the comparative tests performed in France for the complex modulus varied between 2600 and 2800 MPa, with an average value of 15385 MPa at 15°C and 10 hz. Even although the objection can be raised that we have not replicated the measurement, and that a statistical interpretation is difficult because of the inadequate amount of data, the range obtained is obviously more than satisfactory.

We have also verified that the length of time taken to perform this test has no significant effect, and the fact that no date was fixed for making measurements for each laboratory does not lead to an increase in the disparities between results. As all the specimens had been tested at 20°C before being sent to the laboratories, we were able to compare the results of the measurements of the batch intended for laboratory 1, where all the specimens were prepared, with those taken from the initial measurement of the 32 test specimens for each product, conducted on the same machine (M2). The variation was 2.8% for the semi-coarse asphalt concrete, i.e. 157 MPa and 2.1%, i.e. 265 MPa for the high modulus asphalt, after 4 months conservation.

Once these results were obtained another lab invested in a modulus measurement device. A new batch of 4 specimens of EB14 BC was moulded, prepared with the same binder and same batch of aggregates as previous ones. Mean modulus values at 15°C and 20°C for the last lab taking part in this comparison were respectively 16173 MPa and 11524 MPa. At 15°C the range of measured values was 4763, and at 20°C it was 2641. The difference between the modulus value measured in this last lab and the previous mean value given in table 4 is roughly 6.5%. Therefore, our previous comments stand.

8 EFFECT OF TEMPERATURE

We also evaluated the difference in the moduli measured at 15 and 20°C. The ratio between these moduli is shown in Table 5. In addition, on other samples moulded with the same composition, modulus was measured with a direct tension test (DT-CY) and with four point bending (4PB-PR) respectively according to the annexes E and B of EN 12697-26. With the DT-CY test, and a loading time of 0.02 s, the ratio of moduli measured at 10 and 15°C is 0.7 for the semi-coarse asphalt concrete and 0.78 for the high modulus asphalt. Under 4 PB-PR test, the ratio between moduli measured at 10 Hz at 15 and 20°C was 0.7 for the semi-coarse asphalt concrete and 0.83 for the high modulus asphalt. It is clear that the ratios calculated with the results from the different laboratories reflect a variation in mechanical performance with temperature which is completely consistent with that obtained with other tests. This observation is very interesting, as it means it is possible to build on the experience that has already been gained when the test was performed at 15°C and to have a link with the conditions laid down in the EN standard and a temperature that we use more frequently for the complex modulus and direct tensile tests.

9 COMPARISON WITH OTHER MODULUS MEASUREMENT

Another part of this study was to compare the results obtained with indirect tension test to other measurement in direct tension (DT-CY) on the same two mixes. It was interesting for us as our main experience is based on DT-CY and 2PB-TR tests. Using the following equation we are able to estimate the complex modulus from a indirect tension test results

$$E_{(15°C - 10\ Hz)} = 0{,}759\ E_{(15°C - 124\ ms)} + 3680$$

It has already been published and validated for specimens with a diameter of 100 mm and a thickness of 40 mm (Carbonneau et al. 2005), we obtain the value pairs shown in Table 6.

Using this equation means we ignore the effect of thickness, as in the present case we worked with specimens that were 50 mm thick. But the two correlations that have already been published, for thicknesses of 25 and 40 mm, show a difference of 3.3% in the calculated modulus values, i.e. differences of between 200 and 600 MPa in the range between 6,000 and 16,000 MPa. The effect of specimen preparation conditions is also ignored in the calculation shown in Table 6. We have also assumed that there is an equivalence between the direct tensile modulus and the complex modulus, as has previously been shown experimentally (Pellevoisin & Bense 1997).

Table 5. Ratio between the modulus values measured at 20 and 15°C.

Produit	ϕ (mm)	Lab 1 (M1)	Lab 1 (M2)	Lab 2	Lab 3	Lab 4	Lab 5	Average
EB 10 WC	100	0.61	0.65	0.63	0.66	0.65	0.64	0.64
EB 14 BC	100	0.73	0.77	0.74	0.76	0.78	0.73	0.75

Table 6. Comparison between the estimated complex modulus values and the direct tensile modulus on the direct tension test.

EB 10 wearing course	Indirect tension modulus at 15°C and 124 ms	Estimated complex modulus at 15°C and 10 Hz	Direct tensile modulus At 15°C and 0,02 s	% difference between the estimated complex modulus values and the measured direct tension
Lab 1 (M1)	9017	10524		–2.3
Lab 1 (M2)	8548	10168		–5.6
Lab 2	8852	10399		–3.5
Lab 3	9678	11026	10770	+2.4
Lab 4	8790	10352		–3.9
Lab 5	8705	10287		–4.5
Average	8932	10459		–2.9
EB 14 Base course	Indirect tension modulus at 15°C and 124 ms	Estimated complex modulus at 15°C and 10 Hz	Direct tensile modulus At 15°C and 0,02 s	% difference between the estimated complex modulus values and the measured direct tension modulus
Lab 1 (M1)	16029	15846		–11.1
Lab 1 (M2)	16663	16327		–8.4
Lab 2	17253	16775		–5.9
Lab 3	18580	17782	17830	–0.3
Lab 4	16505	16207		–9.1
Lab 5	18010	17350		–2.7
Average	17173	16714		–6.3

Once these assumptions have been made, we can calculate the difference between the complex modulus and the single value measured with our direct tension test. For all the participating laboratories, the estimates are relatively close to the measured value, and always 10% lower except in the case of the UMATTA machines. It is also important to note that these estimates are all lower than the direct tension result, except for the modulus calculated for the semi-coarse asphalt concrete by laboratory 3. This method is therefore relatively conservative, and the values calculated by the proposed method seem slightly low, which gives an additional guarantee that the modulus has not been overestimated.

10 CONCLUSION

Overall, the results are particularly encouraging with regard to the faith we can place in the indirect tension modulus measurement test (IT-CY). As long as the conditions specified in the standard are complied with, it would seem possible to characterize products of all types working with test specimens with a diameter of 100 mm. This work should be continued in order to draw the maximum from this conclusion. Our needs in the area of characterization are constantly increasing as a result of our objective of evaluating the performance of our products by applying the fundamental approach specified in the standard EN 13108-1. Application of this test therefore needs to be extended, for example to enable us to accept mix designs that have been characterized with this test by our clients. The cost and time involved in performing direct tensile tests using the direct tension test DT-CY and the complex modulus test 2PB-TR which involve cutting trapezoidal specimens means we should take advantage of this alternative which gives a reliable result fairly rapidly and at low cost. This benefits the client who is able to obtain the information required to make a judgment about the proposed mix designs. At the very least, its application would seem to be possible for mix designs such as semi-coarse asphalt concrete where the modulus is not an

essential characteristic. But the quality of the results presented here shows that the test also seems perfectly suitable for the high practical levels that we have to comply with (categories defined in EN 13108-1: $S_{min\ 7000}$, $S_{min\ 9000}$, $S_{min\ 11000}$ and $S_{min\ 14000}$ MPa). For mixes with a "very high modulus" $S_{min\ 17000}$ and especially $S_{min\ 21000}$ MPa, it might be necessary to adjust the test. Lastly, even if the use of this approach is currently marginal, it also provides an opportunity for monitoring a product in situ.

ACKNOWLEDGEMENTS

The authors would like to give special thanks to V. Husson (Screg Est), A. Kavannagh (Colas Ireland), D. Goutebroze (Screg Sud est), Laszlo Oszetzky (Colas Hungary), P. Quandalle (Colas Nord Picardie).

REFERENCES

ASTM 4123–82 Standard test method for indirect tension Test for resilient modulus of bituminous mixtures.

BS DDD 213 1993. Method for determination of the indirect tensile stiffness modulus in bituminous mixtures. Final draft December 1006.

Carbonneau, X. Yvinec, Y., Legal, Y. & Poirier, J.E. 2005. Mesure du module en compression diamétrale *Revue Générale des Route et Aérodromes* (836): 52–59.

Di Benedetto, H. & Corte, J.F. 2005. *Matériaux routiers bitumineux Tome 2 Constitution et propriétés thermomécanique des mélanges*, traité MIM, Paris: Lavoisier.

Esh, M., Pouteau, B., Yotte, S. & Breysse, D. 2006. Détermination du module des enrobés bitumineux par l'essai de compression diamétrale. *Revue Générale des Route et Aérodromes* (853): 81–87.

Olard, F. Noel, F. & Loup, F. 2005. Mesure du module en compression diamétrale des enrobés bitumineux, *Revue Générale des Route et Aérodromes* (844).

Pellevoisin, P. & Bense, P., Lois de corrélation entre les différents procédés de mesures de modules sur enrobés bitumineux in *Mechanical Tests for Bituminous Materials*; *Proc. Fifth Intrn. Rilem Symposium, Lyon, 14–16 Mai 1997* p. 225–230. Rotterdam: Balkema.

Ulmgren, N. Olsson, K. & Thau, M. 1998. Mechanical Test of Bituminous Mixes. European Round Robin CEN: TC 2227 Work item pr EN 12697–26 , 6 Mai 1998.

Advanced Testing and Characterization of Bituminous Materials – Loizos, Partl, Scarpas & Al-Qadi (eds)
© 2009 Taylor & Francis Group, London, ISBN 978-0-415-55854-9

Binder fatigue properties and the results of the Rilem Round Robin Test

D. Sybilski, M. Gajewski & W. Bańkowski
Road and Bridge Research Institute (IBDM), Poland

H. Soenen
Nynas N.V., Belgium

E. Chailleux
Laboratoire Centrale des Ponts et Chaussées, France

G. Gauthier
Total, France

ABSTRACT: This paper presents the results of a round robin test (RRT) on binder fatigue, with data received from 11 participating laboratories. Most data were obtained with a Dynamic Shear Rheometer (DSR) equipment, one laboratory used a tension-compression test. In a first stage, the RRT consisted of three binders, two unmodified binders and one polymer modified binder. These three binders had almost the same stiffness level at the testing conditions, 10°C and 10 Hz. Fatigue tests were conducted at three strain levels, and each strain level was measured in three repeats. For each test it was asked to follow the small strain stiffness during an equilibration time of 30 minutes. A second stage of this RRT including two more binders is foreseen. The same three binders were also tested in two and in four point bending mix fatigue tests. The analysis was separated into two parts, in a first part the repeatability and reproducibility of the small strain equilibrium stiffness was evaluated and in a second part the fatigue data were analyzed. Small strain stiffness data showed that the repeatability and reproducibility of G* is still not very high, and possible reasons are under evaluation. The analysis of the fatigue data showed that the overall reproducibility was not good. But when all participants that did in some way not follow the preparation procedure or that had problems with recording, were excluded, it was found that for 6 of the participating laboratories the fatigue properties gave good repeatability and reproducibility levels, for the two unmodified binders in this study. Each laboratory could distinguish the better fatigue life of the polymer modified binder compared to the unmodified binders as was also confirmed by mixture tests. This shows that the binder behavior plays an important role in the fatigue behavior of the mix, and that a binder test should be able to evaluate this role. The binder fatigue test can be used as a surrogate test for mixture fatigue, implying considerable time savings in sample preparation, however the testing of the binders is still time consuming.

1 INTRODUCTION

In the last decade, binder fatigue tests have become common and are used to investigate the fatigue behavior of bituminous binders and mastics, to compare different binder types, and to investigate the role of the binder in mixture fatigue behavior (Bahia et al., 1999, Phillips, 1999, Soenen et al., 2004, Planche et al., 2003). The most common equipment for binder fatigue tests has definitely been the DSR plate-plate rheometer, although other test geometries have been proposed (Airey et al., 2004). In literature, data on repeatability and reproducibility of DSR stiffness levels are available, but up to now no data on the reproducibility of this type of fatigue testing have been published.

The purpose of this paper is to investigate the repeatability as well as the reproducibility of binder fatigue tests. A round robin tests (RRT) was set up within the TG1 of the ATB (advanced testing of bituminous materials) working group within the Rilem organization. The results of the first stage of this RRT are presented.

2 EXPERIMENTAL

2.1 *Samples*

2.1.1 *Binders*

For the first testing stage of the Rilem RRT, the investigations were limited to three bituminous binders. Two unmodified and one polymer modified binder were selected, the binders were supplied from different producers and differed in behavior in several physical tests. For example the black curves with different character are given in figure 1(a). It was also noted that binder A and C showed physical hardening at 10°C and 10 Hz (an isothermal increase in stiffness), while sample B did not show any hardening under these conditions.

In order to avoid the question of testing at an equi-stiffness level or at a constant temperature, the binders were selected to have the same stiffness level at 10°C and at 10 Hz (see table 1).

2.1.2 *Mixtures*

Three types of mixtures, MA, MB and MC were manufactured respectively with the binders A, B and C. The bituminous mix is a 0/6 BBC (French standard NF 98-133), with a binder content of 6,88%. The grading curve of the mix is given in table 2. This is a continuous graded mix, made of aggregate from "La Noubleau" quarry (microdiorite). The filler came from "Airvault" quarry (limestone). This mix composition was chosen in order to consider

Table 1. Overview of some physico-chemical properties of the binders.

	Binder A	Binder B	Binder C
Asphaltene content (%)			
(defined as insoluble part in n-heptane)	12,4	17,8	17,8
Crystalline fraction (%) (by DSC)	2,23	0,1	2,64
Tg (°C) (by DSC)	–23	–18,5	–25,1
|G*| (MPa) (10°C,10 Hz)			
(average data of RRT, will be discussed further)	48.3	47.7	53.6

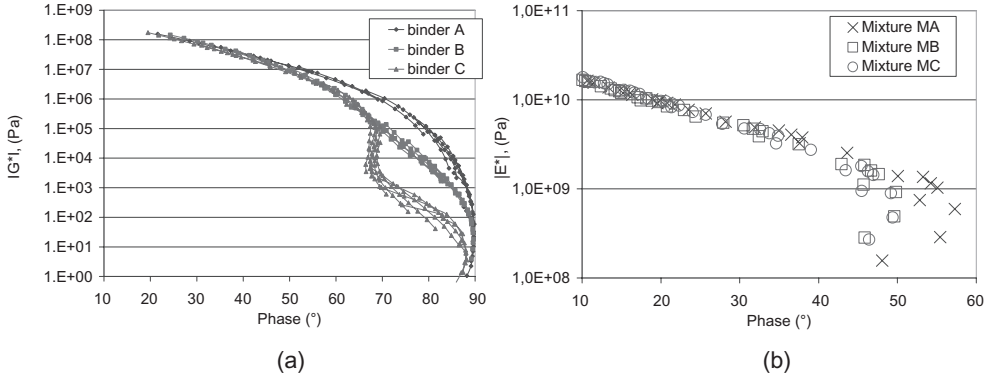

Figure 1. (a) Black curves of the three binders selected for the first phase testing. (b) Black curves of the three mixtures prepared with binder A, B and C.

Table 2. Grading curve of the asphalt mixes.

Sieve (mm)	0,06	0,125	0,25	0,500	1,00	2,00	3,15	4,000	5,0	6
% Passing	10,9	14,7	20,1	28,2	39,9	59,9	66,4	69,6	81,1	95,6

Table 3. Mechanical properties of the mixture at 10°C, 10 Hz.

	Binder	|E*| (MPa) (10°C, 10 Hz)	Phase angle (°), (10°C, 10 Hz)	% void	Std of |E*| (MPa)
Mixture MA	A	13741 (2PB) 12193 (4PB)	13.4° (2PB) 13.3° (4PB)	3.6	978 (4PB)
Mixture MB	B	12941 (2PB) 11606 (4PB)	15.3° (2PB) 15.4° (4PB)	3,2	703 (4PB)
Mixture MC	C	14162 (2PB) 12282 (4PB)	12.4° (2PB) 13.0° (4PB)	3,4	793 (4PB)

the sample homogeneous in comparison to the sample size used for mechanical test. As a consequence, repeatability of the fatigue test with this composition is known to be good, what allows to study the binder effect.

Aggregates and binders are mixed in the lab (NF EN 12697-35) and compacted with an LCPC plate compactor NF EN 12697-33). Complex modulus measurements are performed by two laboratories; LCPC in Nantes and IBDM in Warsaw, on these materials using respectively a two point bending (2PB) test on trapezoidal samples (NF EN 12697-26) and four point bending (4PB) on prismatic beams (PN-EN 12697-26). It can be noted in figure 1(b), that the visco-elastic behaviors of mixes, are quasi identical, contrary to rheological behaviors of the binders which are relatively different (especially at high temperature). At 10°C, 10 Hz, the mechanical properties of the mixes are closely related to each other as it can be seen in table 3. It can also be observed that results from 2PB and 4PB are very close to each other especially when phase angle is concerned. Stiffness from 2PB is 12–15% higher than for 4PB, but for both methods, taking into account the standard deviations it is impossible to rank the mixes according to their stiffness (the binders also have almost the same values of |G*|, cf. tab.1), what confirms that binders play a crucial role in the mechanical characteristics of the analyzed mixes.

2.2 *Binder fatigue tests*

Almost all participants used the 8 mm plate-plate DSR equipment, only one laboratory used a diabolo-shaped sample in a tension compression type of equipment. The DSR equipments that were used were all controlled stress rheometers, for example from Anton Paar: the MCR 501, the MCR 300, the MCR 301 and the UDS200, from Haake: the Rotovisco RT10 and the Mars II, and from Bohlin: the DSR II 50 and the Gemini 200.

The test procedure included a sample preparation description, and a silicon mold suited for the 8 mm plate-plate setup. The homogenization of the sample (heating times and temperature) and the loading of the sample in the rheometer (temperature at loading, trimming, cooling rate to the fatigue test temperature) were described. The equilibration period before starting the fatigue test, was set at 30 minutes, and a recording of the low strain stiffness and phase angle (also at 10°C & 10 Hz) during this equilibration period was asked. The fatigue testing had to be conducted at 10°C and at 10 Hz, in controlled strain mode, tests at three strain levels, 2.5%, 1.8% and 0.8%, were requested, and at each strain level three repeats had to be conducted. Samples were sent to 26 laboratories. But, due to the large amount of tests requested, a number of smaller control labs decided not to participate, and data were finally received from 11 labs.

2.3 *Mixture fatigue tests*

The fatigue properties of the mixes MA, MB and MC were measured by two laboratories, LCPC and IBDM, according to the standard EN 12697-24. Two modes of loading

were used: four points bending on rectangular beams, and two points bending on trapezoidal samples. Tests were carried out in strain controlled mode. Considering the usual scatter of these fatigue tests, a minimum of six samples, for each strain level was used. Fatigue life is defined as the number of cycles which corresponds to 50% decrease of the initial stiffness modulus. The fatigue tests are performed at three strain levels. The lowest strain is chosen in such way that the rupture time reaches one million cycles. The test conditions in the mixture tests were chosen to be the same as in the binder fatigue test: 10°C and 10 Hz.

3 RESULTS

3.1 *Binders: Low strain stiffness and phase angle*

In this section, low strain stiffness and phase angle, recorded during the equilibration is analyzed. Various repeats are available per sample and per laboratory, since testing at three strain levels and three repeats was required. Although in literature there exists a number of DSR low strain round robin reports, an overview of the results of this dataset is also presented.

In figure 2 & 3, the evolution of |G*| and phase angle in the equilibration period is shown for sample A (only one repeat). The strain is indicated, and based on literature data all these strains levels are inside the linear viscoelastic region (Airey et al., 2003). For lab-M, the only laboratory that did not use a plate-plate rheometer but a tension compression device, the |E*| data are divided by three to obtain |G*| values. Although statistical procedures do not find outliers, some problems become clear from figure 2 & 3: for lab-B, thermal equilibrium is not obtained within the 30 minutes period. The data from lab-T indicate a temperature problem, since |G*| values are slightly lower and phase angles are slightly higher. For lab-E, the stiffness seems to be rather low, while the phase angle is similar as for the other laboratories.

Many of the problems indicated at this RRT stage were reported to the labs, and in some of them, the problems are already solved. This is important because a second round is planned, with the aim to obtain better repeatability and reproducibility levels.

In table 4, statistics of the repeats within each of the respective laboratories are provided for binder A. COV refers to the coefficient of variation and is calculated as the average divided by the standard deviation, (multiplied by 100, if in percentage). The variation between the repeats, within a fixed laboratory is rather good, for stiffness as well as for the

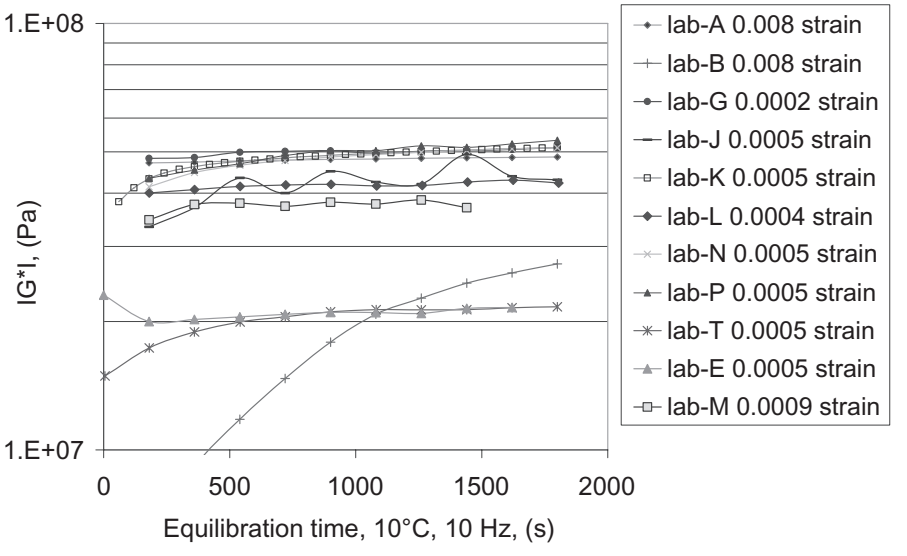

Figure 2. Evolution of the complex modulus norm during the equilibration period (binder A).

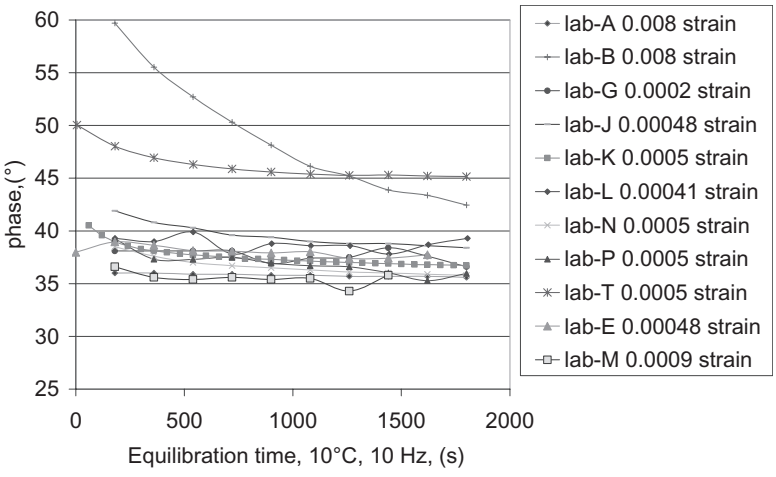

Figure 3. Evolution of phase angle during the equilibration period (binder A).

Table 4. Overview of average values of low strain |G*| and low strain phase angle (10 Hz, 10°C). Presented numbers refer to the average of all repeats measured within the respective laboratory. The number of repeats that was provided is indicated. Data relate to binder A only.

Lab	av.- |G*| (Pa)	cov%	av.-δ (°)	cov%	Nr. repeats	strain (%)	notes
Lab-A	4.85E+07	2.1	35.5	1.7	4	0.8	
Lab-B	2.39E+07	8.8	43.6	1.1	9	0.8	no thermal equilibrium
Lab-G	4.98E+07	3.8	37.3	1.9	9	0.02	
Lab-J	4.59E+07	8.2	38.4	1.8	9	0.048	
Lab-K	5.18E+07	3.5	36.4	1.0	9	0.05	
Lab-L	4.25E+07	7.1	38.3	2.2	9	0.041	
Lab-N	5.54E+07	6.7	34.8	2.6	9	0.05	
Lab-P	5.32E+07	4.3	37.0	5.2	9	0.05	
Lab-T	2.19E+07	7.1	44.7	2.5	9	0.05	
Lab-E	3.16E+07	18.6	35.8	4.6	9	0.048	
Lab-M	3.94E+07	4.6	35.3	1.3	8	0.09	|G*| derived from |E*|/3

Table 5. Overview of average values of low strain |G*| and low strain phase angle data, for all binders.

	All data		Excluding data from lab-B & T		Excluding data from lab-B, T & E	
	|G*| (Pa)	δ (°)	|G*| (Pa)	δ (°)	|G*| (Pa)	δ (°)
Binder A						
average	4.22E+07	37.9	4.64E+07	36.6	4.83E+07	36.6
Std dev	1.17E+07	3.3	7.55E+06	1.3	5.44E+06	1.3
cov %	27.7	8.7	16.3	3.5	11.3	3.7
Binder B						
average	4.28E+07	38.9	4.65E+07	38.0	4.77E+07	38.4
Std dev	1.07E+07	2.1	7.60E+06	1.2	7.20E+06	0.8
cov %	24.9	5.4	16.4	3.2	15.1	2.0
Binder C						
average	4.80E+07	34.1	5.20E+07	32.9	5.36E+07	33.2
Std dev	1.22E+07	2.9	9.19E+06	1.3	8.35E+06	1.2
cov %	25.3	8.5	17.7	4.1	15.6	3.5

phase angle. The behavior for binder B and binder C is not shown separately, since it was very similar to binder A. In table 5, statistics of the averages between the various laboratories are provided, for all three binders. Reproducibility levels are not binder specific and are not reduced when going from the unmodified to the modified binder. Since the sample loading and equilibration times were fixed, the presence of physical hardening (binder A & binder C) does not influence the reproducibility. However, it should be stressed that if data from all the laboratories are used, the overall reproducibility is not very high, even though in literature a lot of reports have been published, demonstrating the various factors that can influence the results.

The COV obtained in this study (when excluding two laboratories) is in agreement with the reproducibility level found in a recent round robin test (B Eckmann et al., 2008). The reproducibility is slightly less good compared to levels found in a previous Rilem round robin test, where COV levels were below 10% (after excluding outliers), (Sybilski et al., 2003).

3.2 *Binder fatigue tests*

A typical fatigue curve, including the equilibration period, is shown in figure 4, the fatigue strain levels are indicated. As expected, the modulus decreases, and this happens faster when the strain is higher. When evaluating the fatigue data of the different participants some remarks can be made, in addition to the deviations seen in the low strain stiffness and phase angle data:

- One laboratory did not record the equilibration period.
- For some tests (especially at high strains) the modulus dropped almost immediately when the fatigue test was started, these measurements were excluded from the analysis since this behavior is typical for an adhesive failure to one of the plates of the rheometer.
- For lab-G, the rheometer had problems recording the large number of data that are obtained in the fatigue test. At certain stages in the data, strain levels of zero, and modulus levels of $|G^*| > 10^{12}$ Pa were observed, these data were of course deleted from the analysis.
- In general it was observed that the strain levels were not exactly the ones that were requested and they also tend to increase slightly with testing time.

The fatigue life was evaluated using the number of cycles needed to reduce the low strain level stiffness |G*| to half its value. The result of this analysis for binder A, including all data, is given in figure 5. In order to compare the fatigue data, it was necessary to recalculate the fatigue life at certain strain levels or the strain level at a certain life time, since each laboratory

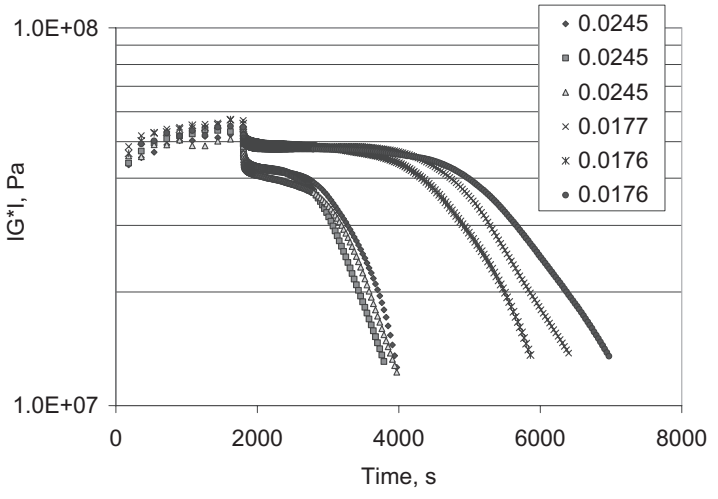

Figure 4. Example of a typical fatigue curve, at two strain levels, with the three repeats (Binder A).

used slightly different strain levels. In table 6, this statistical analysis is given, but only for laboratories without any deviations from the testing procedure. And data that were deviating in low strain stiffness levels were also not included in the fatigue analysis. And the data from lab-M, who used a diabolo shaped geometry, were also not included in table 6, since although stiffness is geometry independent, from figure 5 fatigue results seem to be geometry dependent.

In table 6 the reproducibility levels seem to be rather good for binder A tested in the 6 residual labs as long as calculations are done within the measurement range. Binder B and C were analyzed in the same way. Since binder B was very similar to binder A, only the outcome of the statistical analysis is given in table 7. Again the reproducibility level of binder B seems to be rather good.

The fatigue lines of binder C are shown in figure 6, while the statistical analysis is given in table 8. Binder C is quite different from the other two, its fatigue resistance is clearly higher, and therefore most participants did not get a failure at the lowest strain level. The reproducibility for

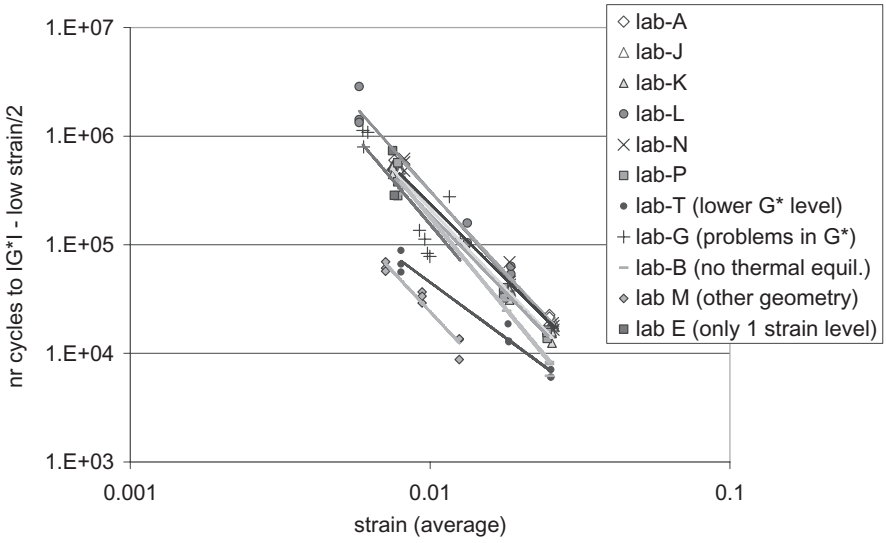

Figure 5. Fatigue lines, based on |G*| low strain level /2 for all data received, for binder A.

Table 6. Overview of trend lines based on the fatigue lines in figure 5, the strain levels for a certain fatigue life are calculated using the trend line. Data relate to values obtained for binder A.

Binder A	Trend line: log(lifetime) = log(intercept) + slope * log (strain)		Strain levels calculated from the trend lines for the lifetimes indicated in upper row:			
	Slope	intercept	1.00E+06	1.00E+05	1.00E+04	1.00E+03
Lab-A	–2.7864	0.6273	5.9E-03	1.4E-02	3.1E-02	7.1E-02
Lab-J	–2.7474	0.7599	5.9E-03	1.4E-02	3.2E-02	7.3E-02
Lab-K	–2.9179	0.3111	5.9E-03	1.3E-02	2.9E-02	6.3E-02
Lab-L	–3.1081	0.1907	6.9E-03	1.4E-02	3.0E-02	6.4E-02
Lab-N	–2.9922	0.3215	6.8E-03	1.5E-02	3.2E-02	6.8E-02
Lab-P	–2.8588	0.3651	5.6E-03	1.3E-02	2.8E-02	6.3E-02
Average	–2.9018	0.4293	6.2E-03	1.4E-02	3.0E-02	6.7E-02
Stdev	0.13	0.22	5.3E-04	8.1E-04	1.6E-03	4.5E-03
COV %	4.6		8.5	5.9	5.1	6.8

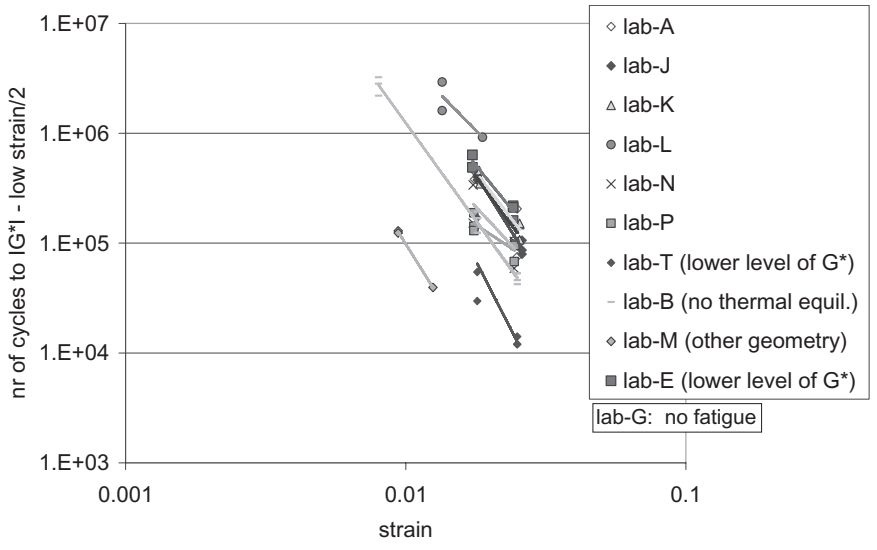

Figure 6. Fatigue lines, based on |G*| low strain level/2 for all data received for binder C.

Table 7. Overview of average fatigue life calculated using trend lines, the laboratories that were included are similar as the ones used in table 6. Data relate to values obtained for binder B.

Binder B	Trendline: log(lifetime) = log(intercept) + slope * log (strain)		Strain levels calculated from the trend lines for the lifetimes indicated in upper row:			
	Slope	intercept	1.00E+06	1.00E+05	1.00E+04	1.00E+03
Average	–2.9036	0.6213	6.8E-03	1.5E-02	3.3E-02	7.4E-02
Stdev	0.20	0.39	7.8E-04	1.1E-03	1.9E-03	6.3E-03
COV %	6.9		11.4	7.0	5.6	8.5

Table 8. Overview of trend lines based on the fatigue lines in figure 6, strain levels for a certain fatigue life are calculated using the trend line. Data relate to values obtained for binder C.

Binder C	Trend line: log(lifetime) = log(intercept) + slope * log (strain)		Strain levels calculated from the trend lines for the lifetimes indicated in upper row:			
	Slope	intercept	1.00E+06	1.00E+05	1.00E+04	1.00E+03
Lab-A	–3.4411	0.3807	7.0E-03	1.4E-02	2.7E-02	5.2E-02
Lab-J	–4.0472	0.0346	8.1E-03	1.4E-02	2.5E-02	4.5E-02
Lab-K	–3.2995	0.7387	6.9E-03	1.4E-02	2.8E-02	5.6E-02
Lab-L	–2.5918	30.953	7.5E-03	1.8E-02	4.4E-02	1.1E-01
Lab-N	–2.7441	3.3735	4.4E-03	1.0E-02	2.3E-02	5.4E-02
Lab-P	–1.6936	160.25	1.5E-03	5.7E-03	2.2E-02	8.7E-02
Lab-B	–3.5520	0.0978	5.6E-03	1.1E-02	2.0E-02	3.9E-02
Lab-E	–3.1319	1.6886	6.9E-03	1.4E-02	3.0E-02	6.2E-02
Lab-T	–4.9847	0.0001	6.2E-03	9.9E-03	1.6E-02	2.5E-02
average	–3.2762	21.9463	6.0E-03	1.2E-02	2.6E-02	5.9E-02
stdev	0.9283	52.8185	2.0E-03	3.6E-03	8.0E-03	2.5E-02
COV %	28.3		33.6	29.3	30.5	42.7

Table 9. Overview of repeatability levels of the binder fatigue test (3 repeats), data refer to binder A. Data in the last row related to 2PB mixture fatigue data.

COV (%)	High strain	Intermediate strain	Low strain
Lab-J	5.5	7.5	16.9
Lab-K	12.3	12.4	10.0
Lab-L	29.4	27.2	45.9
Lab-N	7.2	27.4	12.8
Lab-P	8.7	10.8	35.3
Mixture fatigue 2PB (6 repeats)	20	14	19

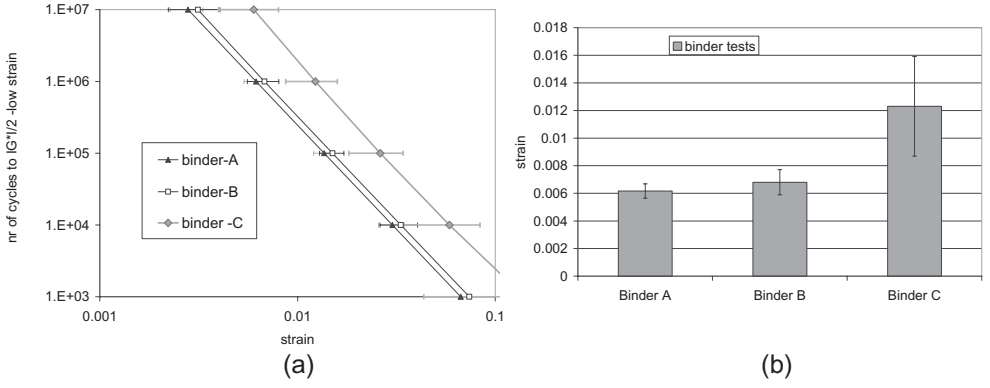

Figure 7a. Fatigue lines for the three binders based on average values using data from 6 laboratories, error bars are derived from the standard deviation. 7b. Values of ε_6 with confidence intervals.

binder C is considerably reduced. At this stage it is not clear whether the reduced reproducibility is related to the nature of the binder (polymer modified) or is due to the longer testing time.

The average values, presented in respectively tables 6, 7 & 8, are plotted in figure 7. The error bars are derived from the standard deviations also shown in tables 6, 7 & 8. Even though the error bars for binder C are large, it is still obvious that this binder is better in this fatigue test compared to the other two binders. The behavior of binder A and B with regard to fatigue testing can be considered as identical.

Finally the repeatability levels were also evaluated and some results are shown for binder A, in table 9. Table 9 shows that the repeatability levels are not very high, and tend to reduce if the fatigue life becomes longer. But they are still in the range of levels obtained in the mixture fatigue test, also indicated in table 9. Lab-L measured at lower strain levels compared to other participants, so this could explain why the values for this lab are different. The repeatability levels in binder tests are based on only three repeats, and since the levels are worse than the reproducibility levels, it may indicate that three repeats is not enough.

3.3 *Mixture fatigue tests*

Fatigue test results on the MA, MB and MC mixes are depicted in figure 8. Mix MC, whatever the procedure used (2PB or 4PB) shows clearly a better behavior in fatigue. Table 10 gives the fatigue criteria ε_6 according to the mixes and the fatigue procedure used. Mix MC has an ε_6 20% higher than the others. Mix MB seems to be slightly better than the mix MA, as was also found for binders (Figure 7). Nevertheless, the confidence intervals are too large to definitely rank these two mixes. It is interesting to note that the ε_6 given by 2PB and 4PB fatigue tests, are similar whereas the slope of the fatigue line seems to be "procedure dependent". It should be noted that this is in fact the second comparison tests and that the results

Table 10. Outcome of the two mixture fatigue tests.

Mix	Epsilon 6-2PB	Slope-2PB	Epsilon 6-4PB	Slope-4PB
MA	152 (min 149, max 155)	−5.23 ± 0,03	142 (min 134, max 151)	−5.25 ± 0,78
MB	159 (min 152, max 166)	−6.43 ± 1,10	154 (min 150, max 158)	−5.73 ± 0,53
MC	196 (min 187, max 207)	−6.3 ± 0,95	190 (min 174, max 208)	−4.99 ± 1,37

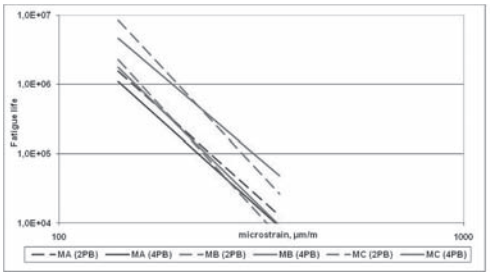

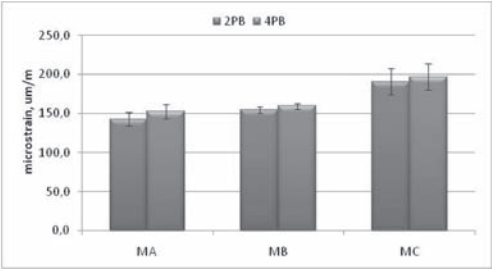

Figure 8a. Fatigue lines for the three mixes MA, MB and MC using the two fatigue test (2pts: two points bending, 4pts: four points bending). 8b. Values of ε_6 with confidence intervals for the mixes.

obtained previously by LCPC (2PB) and IBDM (4PB) were also very close [Di Benedetto et al., 2003].

4 DISCUSSION & CONCLUSIONS

For the low strain modulus and phase angle, at least two, or even three data sets, needed to be excluded from 11 participating laboratories to get reproducibility levels common for bitumen stiffness data. This means that about 20% of testing equipments still have problems. In this group of participants one problem could be related to a very slow equilibration, and another problem could be linked to an insufficient temperature control of the sample between the plates of the rheometer. This shows in general that for testing laboratories, there is a continuous need to participate in regular round robin tests, this is probably the best way to detect deviations in the testing device. These findings are also a message to the producers of rheometers, very often a reliable temperature calibration method is not provided, and a yearly recalibration of the temperature is often not included in their maintenance contracts.

Some preliminary conclusions are obtained with respect to the binder fatigue test: The results of binder fatigue tests of plain bitumen (binders A and B) present a reasonable reproducibility, after eliminating outliers. Results of 6 participants were included in the analysis. The repeatability levels for binder A and B were less good compared to the reproducibility levels, this is a strange finding and may indicate that three repeats per strain level are not enough. In mixture fatigue tests it is also common to use 6 repeats per strain level. The results of binder C are of low repeatability and reproducibility, but the fatigue life of this binder was much higher, and it seems to be more difficult to measure longer fatigue life. The geometry also seems to have an effect on the result, but up to now only 2 geometries were used, and one only in one lab.

The ranking achieved in binder fatigue tests is similar for each pair of binders compared (A, B, C) and is confirmed by mixture fatigue tests. However at this moment there are only three binders tested, and two of them have a very similar fatigue life so this conclusion needs to be evaluated with more binders showing different fatigue behavior. A second stage, including more samples has been initiated, but the testing is still ongoing.

Finally it can be noted that the binder fatigue test is not easy to perform and that the gain in testing time is limited, binder fatigue tests are also time consuming. But, there is no need

to make an asphalt mixture and influences from the mix type (binder content, void content, aggregate type, …) are not interfering in this fatigue phenomenon investigation. Therefore the proposed procedure has a value as a research tool, allowing to evaluate the role of the binder. This round robin also shows that it should be possible to use non-linear tests with the DSR, but to have tests with an exact strain value with controlled stress rheometers will be rather difficult.

ACKNOWLEDGEMENTS

The authors wish to acknowledge all the participating laboratories for their efforts in testing.

REFERENCES

Airey G.D., Rahimzadeh B., Collop A.C. 2003 Viscoelastic linearity limits for bituminous materials, 6th Rilem symposium PTEBM '03, Zurich.

Airey G.D., Thom N.H., Osman S., Huang H., Collop A.C. 2004, A comparison of bitumen/mastic fatigue data from different test methods, 5th Rilem Conference: Cracking in Pavements, May 5–7.

Bahia H., Zhai H., Bonnetti K., Kose S. 1999: Non-Linear Viscoelastic and Fatigue properties of Bitumen, Proc. of AAPT, Vol. 68.

Di Benedetto H., de La Roche C., Baaj H., Pronk A., Lundström R. 2003: "Fatigue of bituminous mixtures: different approaches and RILEM group contribution" 6th Rilem sym. PTEBM '03, Zurich.

Eckmann B., Chabert D., Moglia O., Largeaud S., Descroix P., Chailleux E., Mouillet V., Soenen H., Perez-Lepe A., Nigen-Chaidron S., Champion-Lapalu L. 2008. Complex modulus of bituminous binders results of the round robin test of the GE1 working group (France), E&E conference. Copenhagen.

Phillips M. 1999: Multi-Step Models for Fatigue and Healing, and Binder Properties Involved in Healing. Eurobitume Workshop: Performance Related Properties for Bituminous Binders, Luxemburg,

Planche J.-P., Anderson D.A., Gauthier G., Le Hir Y.M., Martin D. 2003.: Evaluation of fatigue properties of bituminous binders. 6th Rilem symposium PTEBM '03, Zurich.

Soenen H., de La Roche C., Redelius P., 2004 "predict mix fatigue tests from binder fatigue properties, measured with a DSR" E & Conference, Barcelona.

Sybilski D., Vanelstraete A. 2003. Precision of bituminous binder rheology tests in the 2nd Rilem round robin test. 6th Rilem symposium PTEBM '03, Zurich.

11. Other topics

Advanced Testing and Characterization of Bituminous Materials –
Loizos, Partl, Scarpas & Al-Qadi (eds)
© 2009 Taylor & Francis Group, London, ISBN 978-0-415-55854-9

Skid-resistance capability of two newly resurfaced runways in Israel

M. Livneh
Transportation Research Institute, Technion-Israel Institute of Technology, Haifa, Israel

ABSTRACT: Experience and research documents clearly demonstrate that airfield runways must provide adequate friction between an aircraft tire and a wet surface for safe operation during landing and in the event of a rejected take-off. Various aviation agencies specify limiting friction values for newly constructed surface layers and other limiting friction values for existing surfaces before initiating maintenance. For example, the American Federal Aviation Administration (FAA) specifies three friction-level classifications: minimum, maintenance planning and new construction. To alleviate skid-resistance problems, a major civilian runway in Israel was recently resurfaced. The conventional Israeli dense asphaltic mixture was used for this project. A GripTester revealed, however, only marginal skid-resistance properties just after the completion of the resurfacing. Thus it was essential to analyze the reasons that only marginal skid-resistance properties were obtained. The conclusions of this study were implemented recently in the design of a new dense asphaltic mixture for the resurfacing of a second major civilian runway in Israel. After the completion of the resurfacing of this second runway, skid-resistance measurements were again conducted with the GripTester apparatus. These measurements revealed more appropriate and almost fully satisfactory skid-resistance results, suggesting that future resurfacing projects should routinely implement the newer resurfacing practice.

1 INTRODUCTION

Experience and research documents clearly demonstrate that airfield runways must provide adequate friction between an aircraft tire and a wet surface for safe operation during landing and in the event of a rejected take-off. Various aviation agencies specify limiting friction values for newly constructed surface layers and other limiting friction values for existing surfaces before initiating maintenance. For example, the American Federal Aviation Administration (FAA, 2004) specifies three friction-level classifications: minimum, maintenance planning, and new construction (see Table 1).

The critical values given in Table 1 obviously relate to wet pavements. More specifically, these values are compared with measured values obtained by any of the continuous friction-measuring equipment (CFME) listed in Table 1. These measuring devices are equipped with a self-wetting system to simulate wet pavement surface by providing a uniform water depth of 1.0 mm in front of the friction-measuring tires.

The main concern of this paper is to deal with newly constructed surface layers in order to elaborate the factors that influence the acceptance of various asphaltic mixes for friction targets specified in the New Construction column in Table 1. In more detail, the objectives of this study are as follows:

- To summarize the properties of hot-mix asphalt mixtures that affect surface texture and thus lead to varying levels of skid resistance;
- To compare friction-measurement values recently obtained by a GripTester apparatus from two newly resurfaced runways at a major civilian airport in Israel;
- To suggest specific modifications to the construction specifications in order to improve the skid-resistance properties of newly constructed runway surfaces.

Table 1. Friction-level classification for runway pavement surfaces (FAA, 2004).

Continuous Friction Measuring Equipment (CFME)	Operating speed [kmh]	Minimum	Maintenance planning	New construction
Douglas Equipment Ltd. Mu	65	0.42	0.52	0.72
Meter	95	0.26	0.38	0.66
Dynatest Consulting, Inc.	65	0.50	0.60	0.82
Runway Friction Tester	95	0.41	0.54	0.72
Airport Equipment Co.	65	0.50	0.60	0.82
Skiddometer	95	0.34	0.47	0.74
Airport Surface Friction	65	0.50	0.60	0.82
Tester	95	0.34	0.47	0.74
Airport Technology USA	65	0.50	0.60	0.82
Safegate Friction Tester	95	0.34	0.47	0.74
Findlay, Irvine, Ltd.	65	0.43	0.53	0.74
GripTester Friction Meter	95	0.24	0.36	0.64
Intertech Engineering	65	0.48	0.57	0.76
Tatra FrictionTester	95	0.42	0.52	0.67
Norsemeter Runar	65	0.45	0.52	0.69
(Operated at fixed 16% slip)	95	0.32	0.42	0.63

Note that the same values in Table 1 are recommended by the International Civil Aviation Organization (ICAO, 1995) and by the American Air Force Civil Engineer Support Agency in determining the need for runway rubber removal (AFCESA, 2004).

The process of meeting the aforementioned three objectives will now be elaborated.

2 DESIGN OF HMA PAVEMENT MIXTURES

The surface texture of newly constructed hot-mix asphalt (HMA) pavements is usually quite smooth. This is due to the rolling done during construction to achieve the required compaction and density. Nevertheless, several methods are available to improve surface texture and friction in these pavements. One of these methods includes the implementation of a proper mix design.

In this matter, several factors are of relevance to the pavement designer in selecting the appropriate design mix for the hot-mix asphalt (HMA) pavement. These factors include the blending of aggregate sources, aggregate size and gradation, the relationship between aggregates and binder, and the construction methods to obtain the required surface properties, which must in turn meet other requirements.

In these factors, the aggregate size and gradation constitute easily-changed parameters for any given source of aggregates. In other words, the maximum size of the aggregates, as well as the mix gradation, may easily be varied by the pavement designer to produce the desired surface texture and adequate skid-resistance values. It is well known that for HMA pavement, the size and properties of the coarse aggregates are critical for a good macrotexture. Generally, the larger-size aggregates in HMA pavement mixtures provide greater skid-resistance than do the smaller ones.

At this juncture, it should be mentioned that runway surface texture has been a subject of intense investigation for the last twenty-five years. Two ranges have been identified that conveniently describe total surface texture microtexture and macrotexture (Agrawal, 1986). Microtexture consists of the fine, small-scale surface irregularities (less than 0.5 mm) found on individual aggregates, whereas macrotexture defines the coarse, large-scale irregularities of the whole runway surface. These irregularities have characteristic wavelengths in the range of 0.5 to 50 mm and amplitudes in the range of 0.2 to 20 mm; see Figure 1 (Cenek et al., 2000).

Obviously, a surface must have both macrotexture and microtexture to maintain adequate friction level during tire-runway contact. The macrotexture provides relief

channels for rapid expulsion of water from the runway contact area; this process can be characterized by bulk-water drainage effectiveness. The macrotexture provides the harshness or grittiness needed to penetrate the thin water film formed between the tire and the surface aggregate to permit adhesion to develop. In light of the above, microtexture tends to control the level of skid resistance at speeds below 60–70 kmh while macrotexture becomes more dominant at speeds above 90–100 kmh (Toan, 2005). This phenomenon is shown in Figure 2.

The two curves in Figure 2 refer to the constant surface state of a good microtexture. For the constant surface state of a poor microtexture, these two curves maintain the same curvatures but start from a lower level of friction coefficient.

Finally, designing asphalt mixtures for skid resistance, it is suggested, should rely on two measures: the Polished Stone Value (PSV) and the mixture-gradation type. Recently, a method has been developed for estimating (a) the macrotexture from the aggregate gradation and bitumen content and (b) the microtexture from the aggregate PSV (Sullivan, 2005). The influence of the bitumen grade seems to be secondary, but its over-content should be limited to avoid bleeding.

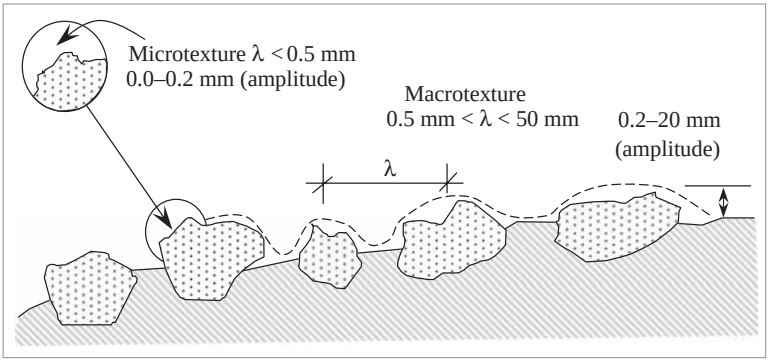

Figure 1. The components of surface texture.

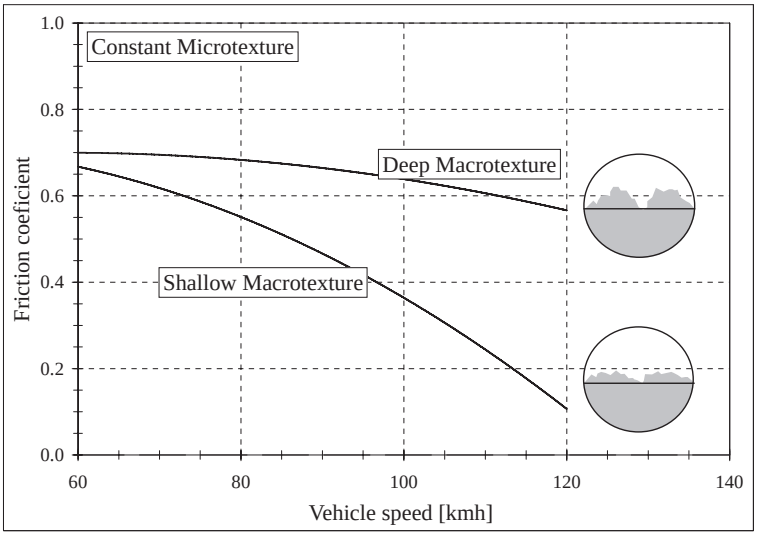

Figure 2. Schematic display of the effects of texture on friction.

3 THE GRIPTESTER AND TEXTURE

The Israel Airports Authority uses the GripTester to measure skid resistance. This apparatus, manufactured by Findlay Irvine Ltd in Scotland, consists of a small three-wheeled trailer (one measuring test wheel and two bogey drive wheels) weighing approximately 87 kg. It is a Continuous Friction Measuring Equipment (CFME) device that can be operated between speed ranges of 5 kmh, (generally in push mode) and up to 130 kmh when towed behind a vehicle. It is commonly used for friction measurements, allowing testing on roads, airfields, helipads, and footway surfaces, and can be used for monitoring road and airfield networks.

The GripTester is a fixed slippage device, with the measuring wheel fitted with a smooth ASTM standard tire that is geared to rotate at a proportionally different rate, thereby producing a 14.5% slip relative to the drive wheels. Two forces, the drag force induced on the slipping wheel and the vertical force, are monitored, and the calculated friction is logged on a computer file.

GripTester surveys are normally carried out on a wetted surface. Water can be supplied by an automatic pump system that applies a nominal specified depth of water under the slipping wheel, based upon the testing speed.

For the two operating speeds of Table 1 (65 and 95 kmh), the two comparative GripTester slip speeds were found to be rather low: $0.145 \times 65 = 9.4$ kmh and $0.145 \times 95 = 13.8$ kmh. Thus, for this type of testing, the influence of the surface macrotexture on the skid-resistance values is rather low. This can also be concluded from the following two PIARC equations taken from the International Friction Index (PIARC, 1995); see, also, ASTM E 1960–98-Standard Practice for Calculating the International Friction Index of a Pavement Surface:

$$FR_S = \frac{FR_{60}}{\exp\left(\frac{S-60}{S_P}\right)} \tag{1}$$

$$S_P = 11.6 - 113.6 \times T_X \tag{2}$$

where FR_S = friction measured by the equipment at the slip speed; S = slip speed in kmh; FR_{60} = friction value adjusted to 60 kmh; S_P = speed constant in kmh; and T_X = micrometer depth—MTD (i.e., Mean Texture Depth according to ASTM E 965-96, Re-approved 2001: Test Method for Measuring Pavement Macrotexture Using a Volumetric Technique; this method is known as the Sand Patch method). Note that the constant values of Equation 2 were also adopted from (Davis, 2001).

According to Equations 1 and 2, for a skid-resistance value of 1.0 at a slip speed of 0.0 kmh and for $T_X = 0.75$ mm, the increase of T_X to 1.0 mm augments the skid-resistance value by 4% only at a slip speed of 9.4 kmh (a GripTester operating speed of 65 kmh), or by 5% only at a slip speed of 13.8 kmh (GripTester operating speed of 95 kmh). For the same T_X changes, but when its initial value equals 0.5 mm (instead of 0.75 mm), the increase percentages are higher: 12% and 18%, respectively.

It should be noted here that similar conclusions can be derived from the equations developed by the Engineering Sciences Data Unit (ESDU) (Van Es et al., 2004). All together, these conclusions lead to the need for measuring macrotexture along with the GripTester skid-resistance measurements. And indeed, according to international regulations, the average surface-texture depth of a new surface should not be less than 1.0 mm (ICAO, 1995). However, as mentioned previously, the two comparative GripTester slip speeds for the two operating speeds of Table 1 are rather low, requiring mainly microtexture to assure the required skid-resistance values.

4 THE NEW RESURFACED 08-26 RUNWAY

To alleviate skid-resistance problems, a major civilian runway in Israel (the 08-26 Runway at Ben-Gurion International Airport) was recently resurfaced. The conventional Israeli dense

asphaltic mixture was used for this project. The gradation curves for this mixture are shown in Figure 3, together with the gradation limits for a Hot-Mix Asphalt surface and binder courses according to various specifications (Israeli, USCOE, and FAA). The Figure indicates that in order to increase macrotexture, the lower bounds of these gradations should be adhered to, and indeed this was followed in the recent surfacing project. However, the MTD measurements (Sand Patch method) showed somewhat insufficient values as reported in Table 2. The MTD values given in Table 2 indicate that serious heterogeneity (segregation) exists in the mixture surface. Furthermore, the very low value of 0.6 mm may be the result of fine practical spot-accumulations, which are sometimes coated with excessive bitumen content.

For this runway, a GripTester revealed only marginal skid-resistance properties just after the completion of the resurfacing activities. The results of these measurements are given in Figure 4. Again, a substantial scatter characterizes these results along the runway, especially along its perpendicular direction. It should also be noticed that the skid resistance in some spots descended even below the minimum target of 0.43.

As shown in Figure 4, scatter occurs because of the expected point-to-point variations on the pavement surface. The friction data, however, is relevant only when averaged over a distance of 100-150 m, which is commensurate with the speed of landing aircraft (around 250 kmh) even though spot measurements over 10 m are routinely taken (Toan, 2005; De Paiva, 2006). It should be mentioned that according to the FAA (FAA, 2004), newly constructed runway-pavement surfaces serving turbojet aircraft require an average wet-skid resistance value for each 150-m segment that is no less than the New Construction Level in Table 1.

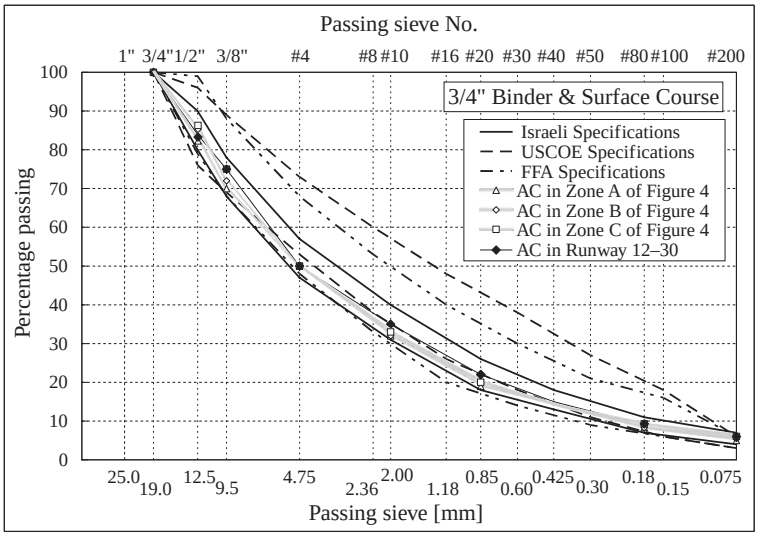

Figure 3. Gradation curves of the 08–26 and 12–30 mixtures and gradation limits for Hot-Mix Asphalt surface and binder courses according to various specifications.

Table 2. Measured macrotexture depth values (MTD) along an axis right of the centerline of the 08–26 runway.

Distance from 08 edge to 26 edge [m]	775	797	1013	1279	1451	1655	1910	2135	2355	2742
Macrotexture Depth [mm]	0.64	0.64	0.85	0.67	0.71	0.60	0.94	0.64	0.68	0.67

In the light of the above, Figure 5 shows the cumulative percentages of skid-resistance results from Figure 4 (operating speed of 65 kmh), averaged along consecutive 150-m sections. The Figure shows that most results are below the new construction target given in Table 1 (89%), but above the maintenance planning target given in the same table (80%).

In addition, Figure 6 shows the cumulative percentages of skid-resistance results for an operating speed of 95 kmh, averaged along consecutive 150-m sections. The Figure shows that more 95 kmh results than 65 kmh results are above the new construction target (25%),

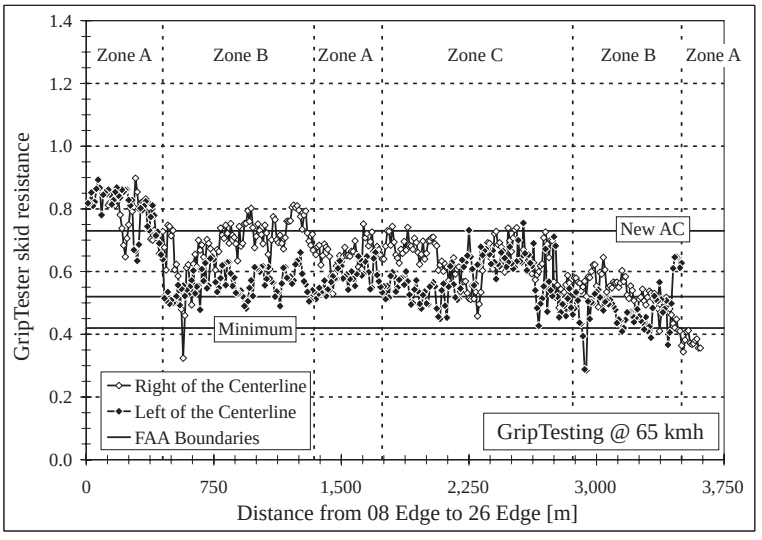

Figure 4. Longitudinal measurements (in 10-m increments) by GripTester at 65 kmh, of the 08–26 runway, after resurfacing completion.

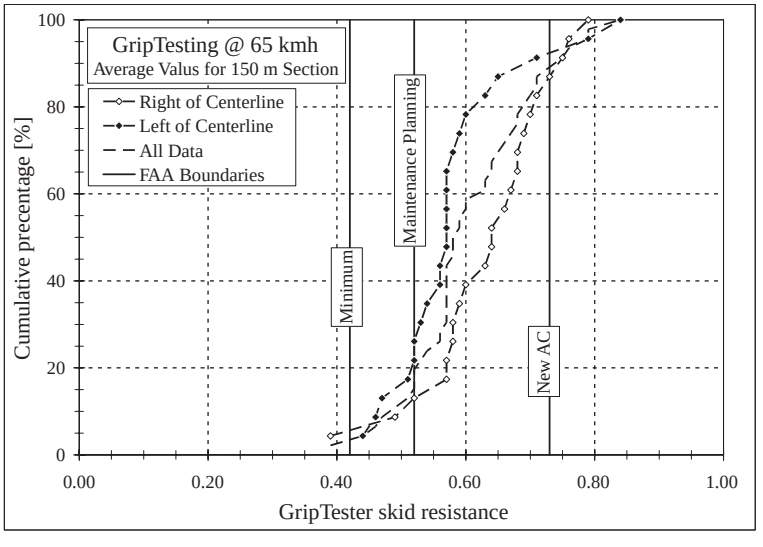

Figure 5. Cumulative percentage of skid-resistance results for the 08–26 runway (operating speed of 65 kmh): average values for a 150-m section.

and almost all of the former are above the maintance planning (95%). Thus, the 95-kmh measurements convey better skid-resistance behavior. This may lead to the conclusion that in contrast to the measured macrotexture values shown in Table 2, the real values, resulting from Figure 2, may be higher.

Additional information concerning the recent re-surfacing project is given in Figure 3. The three zones (A, B, & C) shown in this figure refer to three different contractors. It can be seen that the skid-resistance results are almost independent of the contractor type. Furthermore, Figure 3 depicts the gradation curves of the three zones, and Table 3 presents some aggregate and mixture properties. It can be concluded that the differences in the aforementioned properties are negligible, except perhaps for the bitumen percentage of 5.2% (Zone B).

5 THE NEWLY RESURFACED 12-30 RUNWAY

In the light of the 08-26 runway skid-resistance findings, it was decided that some modifications should be applied to the routine specifications that guided the design of the asphaltic mixtures used for re-surfacing this runway. These modifications included (a) raising the total laboratory density target (at the optimum bitumen content) from 2340 kg/m^3 to 2380 kg/m^3; (b) using PG68-10 bitumen instead of a softer-grade bitumen; (c) testing mixture gradation after its spreading; (d) tightening visual inspection for segregation, flushed surface, or over-fatty surface with too many fines; and (e) having a percentage void tolerance of ±0.75%.

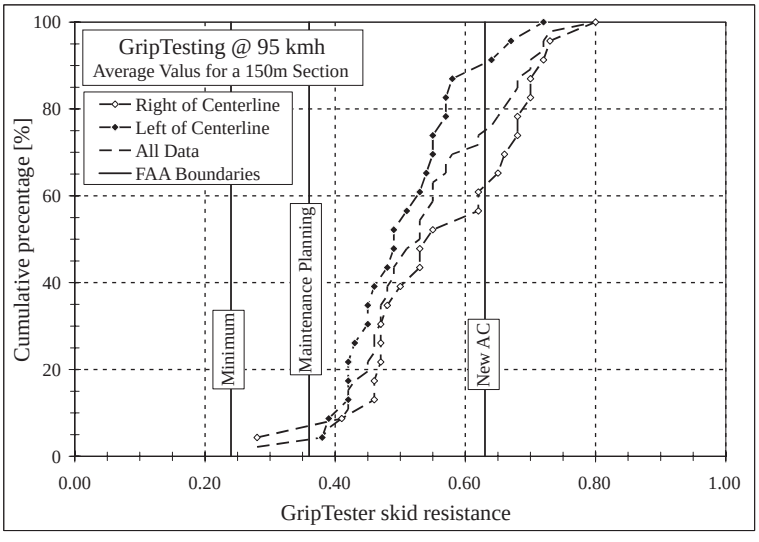

Figure 6. Cumulative percentage of skid-resistance results for the 08–26 runway (operating speed of 95 kmh): average value for a 150 m section.

Table 3. Aggregate and mixture properties for the three 08–26 runway zones.

Zone/Contractor	Los angeles abrasion [%]	Bitumen percentage [%]	Total laboratory density [kg/m^3]
A	20.4	4.7	2380
B	17.8	5.2	2360
C	18.9	4.8	2397

These modifications, which focused more on workmanship and quality control, did not include any change to a coarser aggregate gradation that may have been due to possible FOD occurrence or any change in type of rock (dolomite versus basalt), as the findings for the 08–26 runway skid-resistance measurements did not call for such change. Furthermore, the following properties were recorded for the new 12–30 asphaltic mixture: (a) aggregate Los Angeles abrasion value of 18.3%, (b) optimum bitumen content of 4.7%, and (c) gradation curve as given in Figure 3.

After the resurfacing of this second runway (the 12-30 runway) was completed, skid-resistance measurements were again conducted with the GripTester apparatus. These measurements, shown in Figure 7, revealed more appropriate skid-resistance results, suggesting that future resurfacing projects should routinely implement the recently applied resurfacing practice. Figure 7 also indicates that a lesser scatter characterizes the skid-resistance results along the runway, especially along its perpendicular direction; here, the skid resistance descended below the minimum target of 0.43 only at three spots.

Figure 8 shows the cumulative percentages of skid-resistance results for operating speed of 65 kmh averaged along consecutive 150 m sections. The figure shows that 25% of the results are above the new construction target and that all of them are above the maintenance planning. Thus, these 65 kmh measurements convey better skid-resistance behavior than did measurements with 10 m increments.

6 SOME ADDITIONAL NOTES

Several studies described in the technical literature report a period of low initial friction for a freshly laid AC surfacing owing to the residue of petroleum products and the bitumen coating on the aggregates. The residues are quickly lost because of either rain or evaporation (over a few weeks) on exposure to air, and the bitumen coating is rapidly worn away (after a few months). This type of behavior is shown in Figure 9. In this Figure, the increase in skid resistance over its initial value is about 25%.

The AC friction then remains relatively constant along the period, depending on the wear resistance of the aggregates (10–20 years). Aggregates with high polished-stone values will

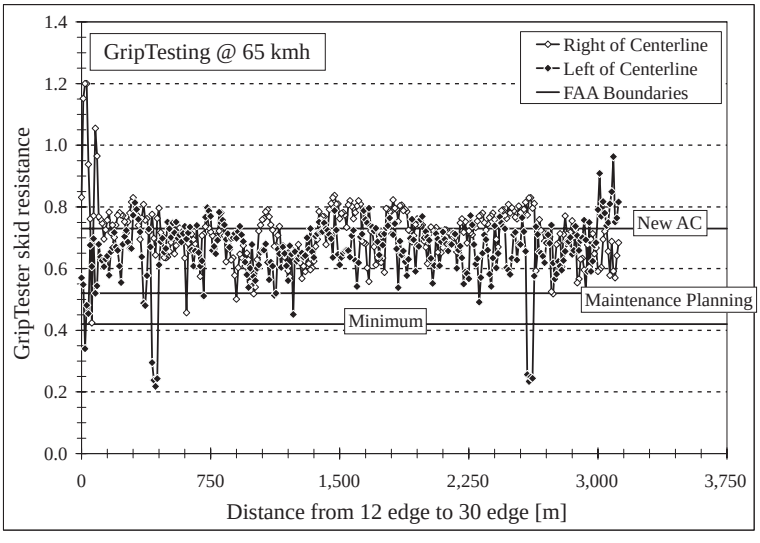

Figure 7. Longitudinal measurements (10 m increments) with GripTester at 65 kmh: 12–30 runway, after resurfacing completion.

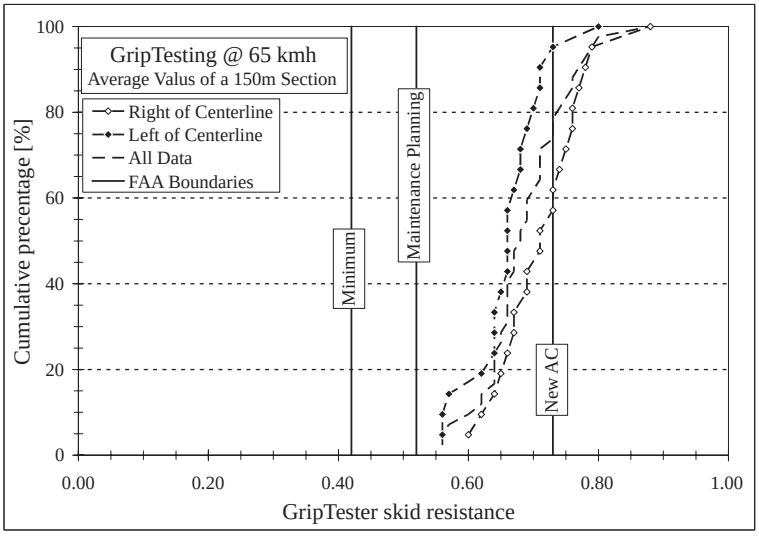

Figure 8. Cumulative percentage of skid-resistance results for the 12–30 runway (operating speed of 95 kmh): average value for a 150-m section.

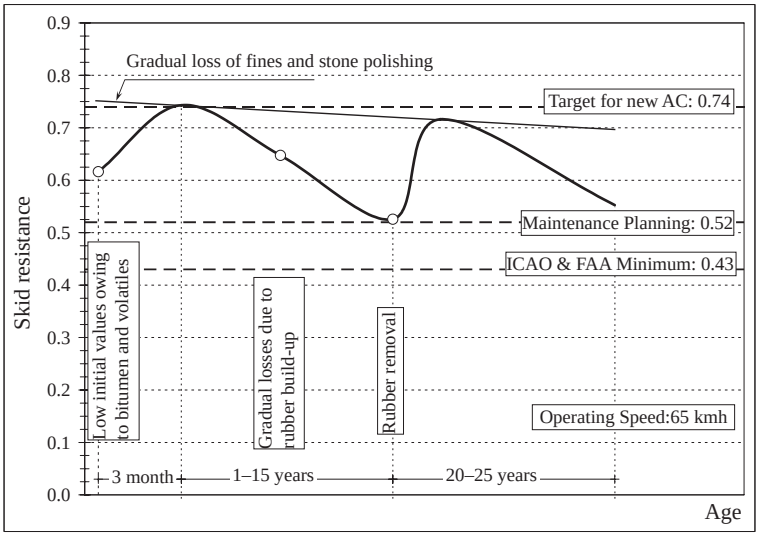

Figure 9. Variation in skid-resistance results with age for an asphaltic concrete using crushed stones (Toan, 2005).

tend to keep their operating friction characteristics longer (up to 25 years or more). However, AC in Israel tend not to last long enough for exposed stones to become worn smooth on runways; the life of the AC is limited by ageing and deterioration (i.e., embrittlement), loss of fine aggregates, and/or fatigue (10–15 years).

The same behavior of an increase in skid resistance with time elapsed since surfacing is very common with SMA mixtures; see Woodward et al., (2005) or Bastow et al., (2005). For these mixtures, the increase may be effective for the course of approximately 10 months.

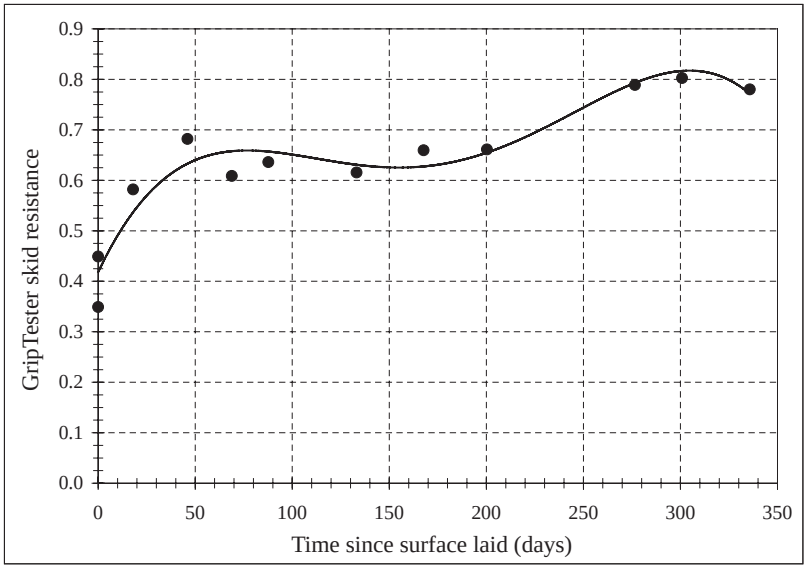

Figure 10. Change in GripTester skid resistance with time for a section of 14 mm SMA (Woodward et al., 2005).

If the increase seen in Figure 9 of 25% in the GripTester's skid resistance is taken into account in an analysis of the skid-resistance measurement of runway 12–30 (see Figures 7 and 8), it can be assumed that this runway fully complies with the new FAA or ICAO AC skid-resistance requirements.

Another factor that has to be considered when measuring skid-resistance values is the possible accumulation of dust and other types of contaminants on the runway surface during the period starting from the end of the construction day to the day-measuring. The mixture of these contaminants with the 1.0 mm film of sprayed water may create a somewhat muddy and slippery film, which will reduce skid-resistance values by about 12%, according to various sources. Thus, it is essential that prior to conducting skid-resistance measurements, it is necessary to wash the runway surface without any pressure jetting.

7 SUMMARY AND CONCLUSIONS

The importance of pavement skid resistance in terms of safety has been well established. Although the interaction of the tire and pavement interface is complex, skid resistance is known to be dependent not only on tire properties, but also on pavement texture properties (Davis, 2001).

The texture of the pavement surface is primarily a function of the type and gradation of the aggregates that are used in the mixture. Large, open-graded aggregates produce a high macrotexture value, which results in good skid resistance at high speeds. The microtexture of the pavement is a function of the type of aggregate that is used in the mixture. Microtexture has been shown to contribute to good skid resistance at low speeds.

After construction, some wearing of the aggregate surface occurs, thereby removing the initial asphalt film and exposing adequate microtexture. In addition to the aggregate properties, other HMA properties also affect the skid resistance of a pavement-wearing course. If the asphalt content of the mixture is high, bleeding will occur, which prevents aircraft tires from making adequate contact with the aggregates in the pavement surface.

In light of the above, it is not surprising that the main conclusion of this study is the necessity of avoiding any segregation, flushed surface, or over-fatty surface with too much fines;

these elements were avoided more with Ben-Gurion Airport's 12–30 runway more than with its 08–26 runway. Furthermore, for dolomite aggregates, it seems that the gradation utilized for the asphaltic concrete wearing course (Figure 3) is satisfactory when (a) the proper grade bitumen is chosen and its proper content is designed; (b) a higher bulk specific gravity (which affects the total laboratory density of the compacted asphaltic mixture at the optimum bitumen content) is assigned for the given type of aggregates.

Finally the measurements of skid-resistance values for the two runways suggest that future resurfacing projects should routinely implement the recently applied resurfacing practice used for the 12–30 runway. The skid-resistance measurements should also be carried out only after water cleaning of the pavement surface. These measurements should be re-run after six months of service.

ACKNOWLEDGMENTS

The results presented in this paper were obtained in the course of consulting projects that the author executed for the Israel Airports Authority, which also conducted the skid-resistance measurements, and thanks are therefore due it. The paper was prepared with the assistance of Mr. Arieh Aines, graphics editor of the Transportation Research Institute at the Technion, to whom thanks are also due.

REFERENCES

AFCESA. 2004. Determining the Need for Runway Rubber Removal. *Engineering Technical Letter* ETL 04-10, Air Force Civil Engineer Support Agency.

Agrawal, S.K. 1986. Braking Performance of Aircraft Tires. *Proceedings Aerospace Sciences* 23: 105-150.

Bastow, R., Webb, M., Roy, R. & Mitchell, J. 2005. An Investigation of the Skid Resistance of Stone Mastic Asphalt Laid on a Rural English County Road Network. *Proceedings of 2005 International Surface Friction Conference*, Christchurch, New Zealand.

Cenek, P.D., Jamieson, N.J. & Towler, J.I. 2000. *The Influence of Texture Depth on Skidding Resistance,* Unpublished paper, New Zealand.

Davis, R.M. 2001. *Comparison of Surface Characteristics of Hot-Mix Asphalt Pavement Surfaces and the Virginia Smart Road*. Master's thesis submitted to the Faculty of Civil and Environmental Engineering, Virginia Polytechnic Institute and State University.

De Paiva, C.E.L., Pestana, M.R.R. & Filho, S.R. 2006. The Rubber Accumulation in the Touchdown Zone, the Friction and the Roughness in the Safety of the Landing and Take-Off Operations. *Proceedings of the Second International Conference on Airports: Planning, Infrastructure, & Environment*, Sao Paulo, Brazil.

FAA. 2004. Measurement, Construction, and Maintenance of Skid-Resistance Airport Pavement Surfaces. *Advisory Circular* AC 150 5320-12C, Change 1, Federal Aviation Administration, Washington, DC.

ICAO. 1995. *International Standards and Recommended Practices, Aerodromes. Annex 14 to the Convention on International Civil Aviation*, Vol. 1, Aerodrome Design and Operation, 2nd Edition, International Civil Aviation Organization.

PIARC. 1995. *International PIARC Experiment to Compare and Harmonize Texture and Skid Resistance Measurements.* PIARC Report 01.04.T, PIARC (Permanent International Association of Road Congresses) Technical Committee on Surface Characteristics C.1.

Sullivan, B.W. 2005. Development of a Fundamental Skid Resistance Asphalt Mix Design Procedure. *Proceedings of 2005 International Surface Friction Conference*, Christchurch, New Zealand.

Toan, D.V. 2005. Runway Friction Performance in New Zealand. *Proceedings of 2005 International Surface Friction Conference*, Christchurch, New Zealand.

Van Es, G., Van Leest, A., Fafie, J., Van der Vegte, R., Van Dijk, H., Van Gurp, H. & Moeniel, M. 2004. Comparison of Self-Wetting Friction-Measuring Devices. *Proceedings of 2004 FAA Worldwide Airport Technology Transfer Conference*, Atlantic City, NJ.

Woodward, W.D.W., Woodside, A.R. & Jeille, J.H. 2005. Early and Mid-Life SMA Skid Resistance. *Proceedings of 2005 International Surface Friction Conference*, Christchurch, New Zealand.

Advanced Testing and Characterization of Bituminous Materials – Loizos, Partl, Scarpas & Al-Qadi (eds)
© 2009 Taylor & Francis Group, London, ISBN 978-0-415-55854-9

Chemical spill tolerance of hot mix asphalts: New research and gaps identification

F.G. Praticò, R. Ammendola & A. Moro
DIMET Department, Mediterranea University, Reggio Calabria, Italy

ABSTRACT: When fuels, or lubricants or Hazardous Materials (Hazmats) accidentally come into contact with asphalt pavements for a given period of time, under given load conditions, the asphalt binder is softened, leading to aggregate loss on the surface. This process depends on many parameters: mix effective porosity, diameter of the pores, quantity and type of fuel, course thickness, immersion time, asphalt binder characteristics, etc. This paper deals with models and strategies for the analysis of the consequences of hazmat releases on hot mix asphalts. A model has been formalized and experimentally validated through a new device, the Brush TesteRC®. Different mixes, in combination with various fuels, have been investigated. Advanced tests on volumetrics, asphalt binder characteristics and HMAs chemical tolerance have been carried out. Results demonstrated that asphalt binder properties and mix volumetrics can be the basis for the interpretation of the involved phenomena. The obtained results provided information and findings for practical benefit of the work.

1 INTRODUCTION

Hazardous materials (Hazmat), and in particular fuels, are a potential threat to road networks and airports. Infact, spillage (release) and propagation on road and airport infrastructures can be related to many classes of risks.

Surface friction, bearing properties, and therefore operational speeds, traffic and safety can be greatly affected in the short, middle and long term (Steernberg et al. 2000; Maarten et al. 2002; Van Rooijen et al. 2004; Praticò et al. 2008).

In the light of the above facts a model has been here formalized for interpreting soaking and brushing processes (next section). The model has been finally validated.

2 TOWARDS A GENERALISED MODEL

When a fuel spillage occurs, Hot Mix Asphalts (HMAs) result progressively damaged.

The resistance to shear stresses becomes consequently decreased. The standard EN12697-43: 2005 provides a test method for assessing HMA resistance to fuel. Both soaking (i.e. immersion in fuel and therefore extended action of the fuel) and shear (*per* brushing) actions are considered and two indicators (A and B) are defined (see figure 1).

A is the loss of mass after soaking in fuel (fig.1): $A = \sum_i A_i/3$, with $i = 1, 2, 3$ (specimens), $A_i = ((m_{1,i} - m_{2,i})/ m_{1,i})\cdot 100$, $m_{1,i}$ = initial dry mass of the i-th specimen for soaking in fuel, in grams (g), $m_{2,i}$ = mass of the i-th dry test specimen after soaking in fuel, in grams (g).

B is the loss of mass after the brush test (fig.1): where $B = \Sigma_i B_i/3$, with $i = 1, 2, 3$ (specimens), $B_i = ((m_{2,i} - m_{5,i})/ m_{2,i})\cdot 100$, $m_{2,i}$ = mass of the i-th dry test specimen after soaking in fuel, in grams (g), $m_{5,i}$ = mass of the i-th test specimen after soaking and after 120 s of brushing, in grams (g). C (fig.1), introduced by the Authors in order to have a descriptor able to combine the two different actions (soaking & brushing), is defined as the mean value of the loss of mass of the specimens, where $C = \Sigma_i C_i/3$, with $i = 1, 2, 3$ (n° specimen), $C_i = ((m_{1,i} - m_{5,i})/m_{1,i})\cdot 100$. In the light of the definitions above, figure 1 shows that, under the

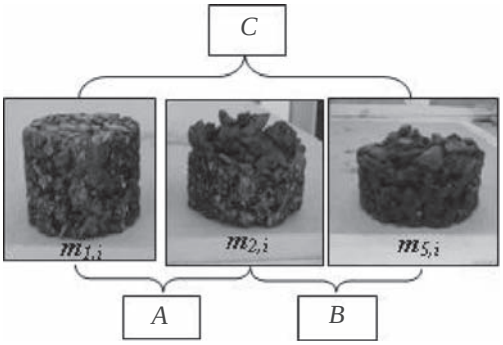

Figure 1. Indicators *A, B, C*.

given hypotheses, A takes into account for the transition from the mass $m_{1,i}$ to the mass $m_{2,i}$, while B refers to the transition from the mass $m_{2,i}$ to the mass $m_{5,i}$, and C relates to the complete process, i.e. from $m_{1,i}$ to $m_{5,i}$.

From a practical standpoint, it is important to point out that, as far as EN 12697-43: 2005 is considered, three classes of fuel resistance are defined:

1. good resistance to that fuel ($A \leq 5\%$, $B < 1\%$);
2. moderate resistance to that fuel ($A \leq 5\%$, $1\% \leq B \leq 5\%$);
3. poor resistance to that fuel ($A > 5\%$ or $B > 5\%$).

Three models have been formalized in order to obtain physical-based expressions for the parameters *A, B* and *C*. Below a generalization is proposed.

The models below described have been formalized in order to obtain physical-based expressions for the parameters *A*, *B* and *C*.

2.1 *Parameter A*

If a given mass of fuel is poured into a pavement, the starting mass M_0 (control sample or test specimen) decreases due to the loss of aggregates (AG) and asphalt binder (B_A), though small quantities (F) of fuel can remain entrapped in the specimen (Praticò et al., 2008):

$$M_d = M_0 - B_A + F - AG \cong M_0 - \Delta M \tag{1}$$

where M_d is the mass of the dry sample after hazmat percolation or soaking in the fuel.

From the equation (1) it is possible to derive the following expression

$$\frac{A_i}{100} = \left(\frac{4n_{eff}}{\phi^*} + \frac{2\alpha}{r} + \frac{1}{h} \right) \frac{\Delta_t}{a} \cdot \frac{\gamma_L}{\gamma_{cb}} \cong \left[\frac{4n_{eff}}{\phi^*} + E \right] \cdot \frac{G}{\gamma_{cb}} \tag{2}$$

Figure 2 summarizes the main factors involved in the theoretical model above described and the main phases of the experimental determination of the parameter A: 1. Soaking: the specimen is immersed in the fuel; 2. Checking for pH: the specimen is washed with water until the acidity of the water pH is (7.0 ± 0.5); 3. Weighting: after cleaning, the mass of the specimen is determined ($m_{2,i}$).

Symbols: n_{eff}: Effective porosity; ϕ^*: Reference diameter of the pores; α: Adimensional parameter ($0 \leq \alpha \leq 1$), $\alpha \cong h_1/h \cong 0{,}55$; h_1, h: Height of the fuel around the sample and sample height; r: Radius of the sample; Δt: Immersion time; $\Delta t = 72^h \pm 30$ min (polymer-modified bitumen) or $\Delta t = 24^h \pm 30$ min; γ_L; γ_{cb}: Specific gravity of the loss mass; specific gravity of the specimen; ΔV: Volume loss caused by hazmat

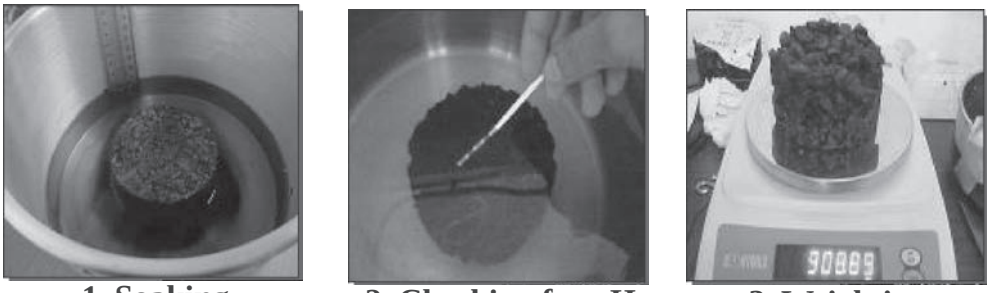

Figure 2. Procedure and main factors for modelling the parameter A.

percolation; S_{Te}: Total exposed Surface, expressed as $a \cdot \Delta V \cdot \Delta t^{-1}$. $E \cong [(2 \cdot 0.55 \cdot 2)/10.16 \text{ cm}] + [1/6.35 \text{ cm}] \cong 0.37 \text{ cm}^{-1}$; $G \cong (24^{h} \cdot \gamma_L)/a$; a: Parameter which takes into account asphalt binder, size and shape of the flow paths, fuel characteristics, etc; it has the dimensions of the reciprocal of a speed. $a = -log(pen_{pre}/pen_{post})$, where $post_{pen}$ is the penetration (0.1 mm) on the mix "fuel + asphalt binder", after 24 hours, at 25°C and pen_{pre} is the penetration (0.1 mm) on the pure asphalt binder (without fuel), at 25°C. Note that pen_{post} is expected to be greater than pen_{pre}.

On the basis of the structure of equation 2, in this paper, the existence of a critical effective porosity n_{CR} is assumed. As a consequence, it is:

$$A = \alpha_j (n_{eff} - n_{CR}) \cdot \xi_1 \tag{3}$$

where α_j depends on Bitumen vs. fuel compatibility, ξ_i depends on the type of chemical resistance involved, ($i = 1$, A, resistance to soaking; $i = 2$, B, resistance to brushing; $i = 3$, C, resistance to soaking and brushing).

2.2 *Parameter B*

For the determination of the parameter B, the specimen is brushed for a time Δt_B and the mass $m_{5,i}$ is determined. As far as B is concerned, it is possible to observe that the mass (M_d) of the sample after the soaking in the fuel and before the brush test is given by

$$M_d = h_d \cdot \pi \cdot r^2 \cdot G_{mb\dim} \cdot \gamma_W \tag{4}$$

where h_d = sample height before brush test; $G_{mb\dim}$ = bulk specific gravity (dimensional method); γ_W = water density; $A_S = \pi \cdot r^2$ (area of the sample); r = radius of the sample.

M_b, the mass of the sample after the brush test, can be expressed as:

$$M_b = h_b \cdot \pi \cdot r^2 \cdot G_{mb\dim} \cdot \gamma_W \tag{5}$$

where $M_b \le M_d$ and h_b is the sample height after brush test.

It results

$$B = \frac{\Delta M}{M} \cong \Delta t_B \cdot f_L \cdot \left(\log \frac{pen_{post}}{pen_{pre}} \right) \cdot (a + b \cdot n_{eff}). \tag{6}$$

In figure 3 two images of the Brush TesteRC® (designed and patented at the DIMET Department) are provided, and the main factors involved in the theoretical model are described.

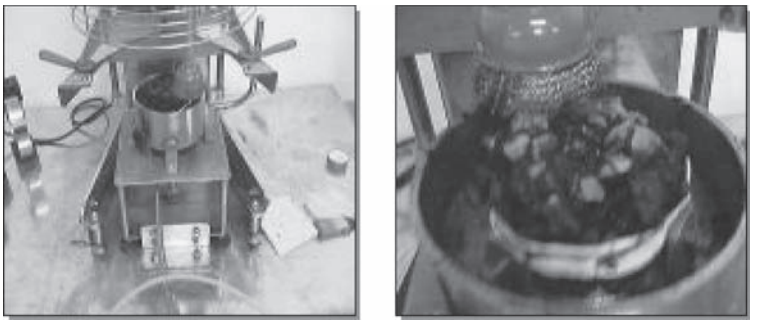

Brushing **Brushing (particular)**

Figure 3. Procedure and main factors for modelling the parameter *B*.

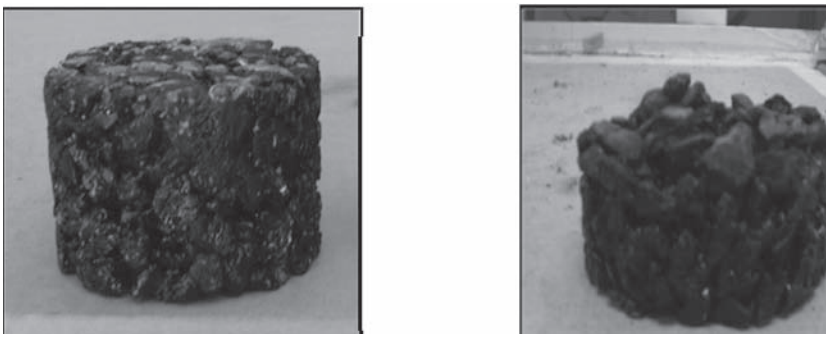

Figure 4. Marshall specimen before the soaking phase and after the brushing phase.

Δt_B is the Total brushing time (for example, 120 s); f_L is a coefficient which depends on dynamic conditions (pressure, speed of rotation, state of the brush).

In the light of the structure of equation 7, in this paper, the existence of a critical effective porosity n_{CR} is assumed also for the parameter *B*. As a consequence, it is:

$$B = \alpha_j (n_{eff} - n_{CR}) \cdot \xi_2 \tag{7}$$

where α_j depends on Bitumen vs. fuel compatibility, ξ_i depends on the type of chemical resistance involved, ($i = 1$, *A*, resistance soaking; $i = 2$, *B*, resistance to brushing; $i = 3$, *C*, resistance to soaking and brushing).

2.3 *Parameter C*

By referring to the parameter *C*, it is important to observe that, owing to the definition set out in section 2, it results:

$$C_i = A_i + (m_{2,i}/m_{1,i}) \cdot B_i \tag{8}$$

Due to the above-mentioned hypotheses, it is possible to write:

$$C = \alpha_j (n_{eff} - n_{CR}) \cdot \xi_3. \tag{9}$$

Figure 4 illustrates the i-th typical Marshall specimen before the soaking phase (mass $m_{1,i}$) and after the brushing phase (mass $m_{5,i}$).

2.4 *Parameter A, B, C*

In the light of the previous equations, the following generalised model can be proposed:

$$R_i = \alpha_j \cdot (n_{eff} - n_{effCR}) \cdot \xi_i \tag{10}$$

where R_i stands for A ($i = 1$), B ($i = 2$) or C ($i = 3$), α_j depends on Bitumen vs. fuel compatibility, ξ_i depends on the type of chemical resistance involved, ($i = 1$, A, resistance soaking; $i = 2$, B, resistance to brushing; $i = 3$, C, resistance to soaking and brushing).

3 EXPERIMENTAL PLAN

In order to perform the validation of the above described models, the following experiments have been planned:

- Volumetric tests. The following parameters have been determined: %b = asphalt binder content as a percentage of aggregates (ASTM 6307-05); G = aggregate gradation (EN 12697-2: 2008; ASTM D6913-04); NMAS = Nominal Maximum Aggregate Size; γ_g = aggregate apparent specific gravity (AASHTO T-85:2004); G_{mb} = mix bulk specific gravity (ASTM D6752; ASTM D6857); G_{mbAO} = mix bulk specific gravity after opening (ASTM D6752; ASTM D6857); n_{eff} = mix effective porosity (ASTM D6752; ASTM D6857);
- Brush tests in order to estimate A, B and C (EN 12697-43:2005), where A(%) is the mean value of the loss of mass after soaking in fuel, B(%) is mean value of the loss of mass after the brush test; C(%) is the mean value of the loss of mass of the specimens. Experiments have been carried out by using the new Brush TesteRC® (Praticò et al., 2008).

Three different fuel types (Diesel oil, $\gamma \cong 820 \sim 845$ Kg/m³; Jet A1, $\gamma \cong 797.6$ Kg/m³; Avion 100, $\gamma \cong 720.0$ Kg/m³), five different types of mixes (PEM-Porous European Mix, DGFC-Dense Graded Friction Course, SMA-Stone Mastic Asphalt, BIC-Binder Course, BAC-Base Course) have been considered. All the mixes had the same asphalt binder typology (B 70/90, i.e. with a penetration at 25°C between 7 mm and 9 mm). All the experiments have been carried out on Marshall specimens.

4 RESULTS

Figures 5 to 16 and tables 1 to 3 summarize the obtained results.

Figures 5 to 8 show that A increases when the effective porosity (n_{eff}) increases. More importantly, the first derivative of A ranges from 2 (when the fuel is Diesel oil and Jet fuel) up to 5 (when the fuel is AVion). The intercept on n_{eff} axis ranges from 1% (Jet) up to 5% (AVion – see table 1). R-square values range from 0.5 up to 0.9.

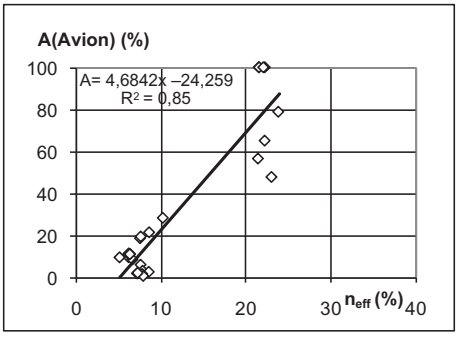

Figure 5. A(Avion) (%) vs. n_{eff} (%).

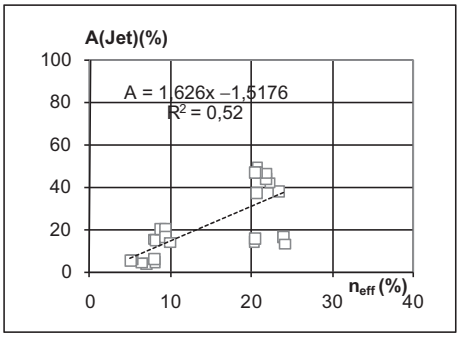

Figure 6. A(Jet) (%) vs. n_{eff} (%).

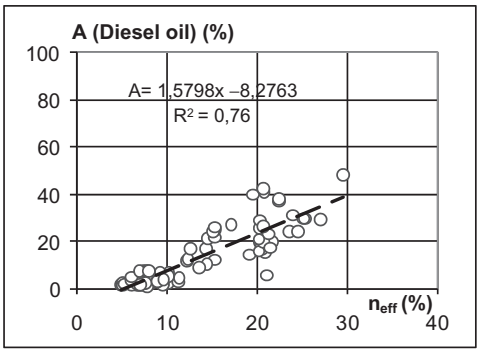

Figure 7. A(Diesel oil) (%) vs. n_{eff} (%).

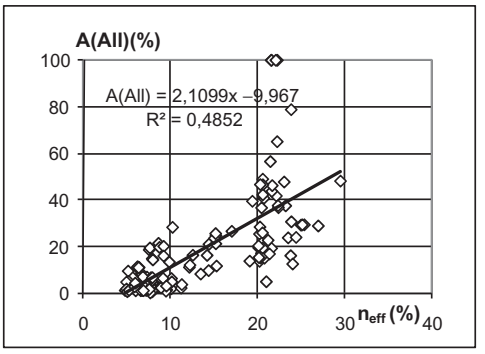

Figure 8. A(All) (%) vs. n_{eff} (%).

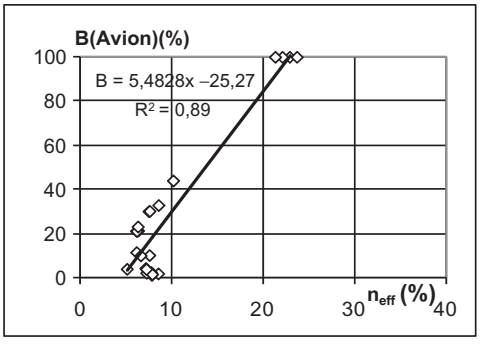

Figure 9. B(Avion) (%) vs. n_{eff} (%).

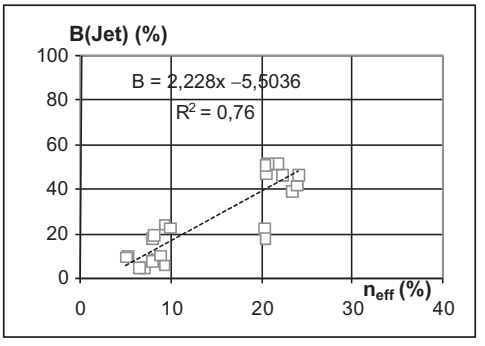

Figure 10. B(Jet) (%) vs. n_{eff} (%).

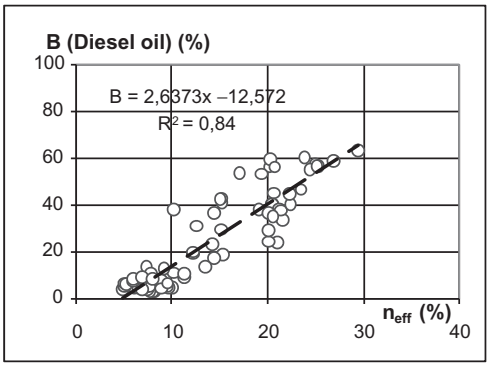

Figure 11. B(Diesel oil)(%) vs. n_{eff} (%).

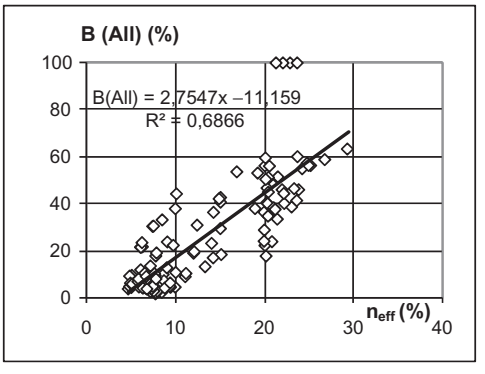

Figure 12. B(All) (%) vs. n_{eff} (%).

Figures 9 to 12 refer to B vs. n_{eff} correlations. The higher the effective porosity the higher the mass loss per brushing. The intercept on n_{eff} axis ranges from 3% up to 6% (see table 1), while the first derivative ranges from 2 to 5. From these figures it appears that Diesel oil and Jet fuel have a similar effect on HMA chemical resistance as far as the mass loss for brushing actions is considered. R-square values range from 0.7 up to 0.9.

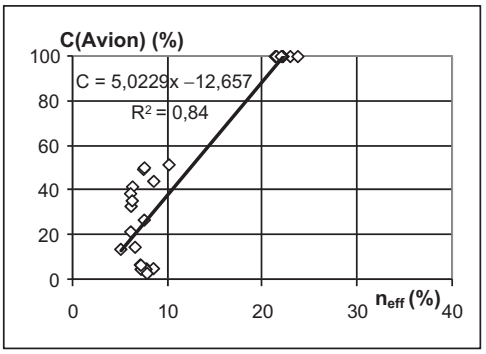

Figure 13. C(Avion) (%) vs. n_{eff}(%)

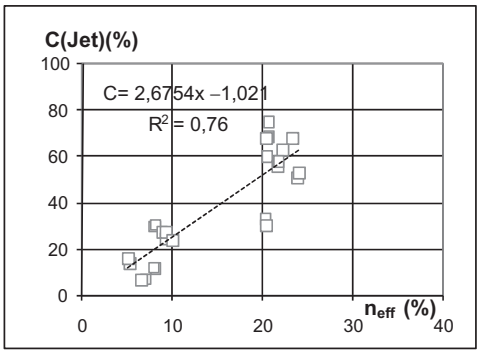

Figure 14. C(Jet)(%) vs. n_{eff}(%)

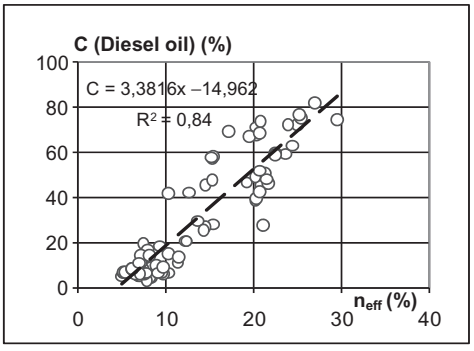

Figure 15. C(Diesel oil)(%) vs. n_{eff}(%).

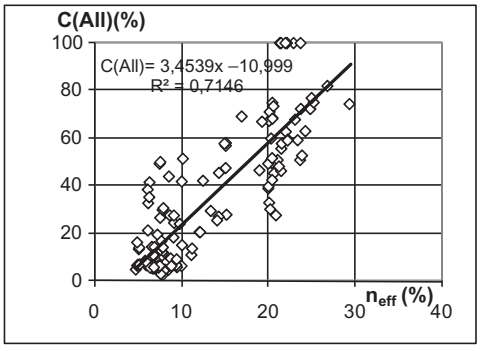

Figure 16. C(All)(%) vs. n_{eff}(%).

Table 1. a, b, R^2 for linear interpolating curves.

	b				a				– b/a				R^2			
y	**AV**	**J**	**D**	**ALL**	**AV**	**J**	**D**	**ALL**	**AV**	**J**	**D**	**ALL**	**AV**	**J**	**D**	**ALL**
A	–24	–1,5	–8	–10	5	1,7	2	2,10	5	0,9	4	3,2	0,85	0,52	0,76	0,48
B	–25	–5,5	–13	–11	5	2,2	2	2,75	5	2,5	6	3,6	0,89	0,76	0,84	0,68
C	–13	–1,0	–15	–11	5	2,6	3	3,45	2,5	0,4	5	5,2	0,84	0,76	0,84	0,71

Note: $y = a \cdot n_{eff} + b$, where y stands for *A, or B, or C. A, B, C*: indicators of chemical resistance.
AV: AVion100; J:Jet A1; D: Diesel oil; ALL: all the fuels.

Figures 13 to 16 show that an increase in effective porosity (n_{eff}) is related to an increase in mass loss per soaking and brushing. In this case the first derivatives range from 3 to 5 and the intercept on x axis ranges from 0.4 up to 5 c.a. R-square values are around 0.8.

Finally table 1 summarizes regression coefficients and R-square values.

It is possible to observe that:

1. the intercept with the x-axis (i.e. n_{eff}) represents the theoretical value which minimizes the mass losses and optimizes the chemical resistance. Due to practical and theoretical reasons, it should result $-b/a \geq 2$ ($N_{des} = 4\%$, $N_{max} \geq 2\%$);
2. under the hypothesis of $-b/a = n_{CR}$ the above introduced generalized model (equation 10) can be tested.

Table 2. Generalized model (eq. 10).

	$n_{CR} = 4$					
	AV		**J**		**D**	
	$\alpha \cdot \xi$	R^2	$\alpha \cdot \xi$	R^2	$\alpha \cdot \xi$	R^2
A	4,28	0,83	1,95	0,48	1,44	0,74
B	5,19	0,88	2,45	0,75	2,49	0,83
C	5,55	0,82	3,30	0,69	3,28	0,84

n_{CR}: critical effective porosity; α: coefficient which depends on Bitumen vs. fuel compatibility; ξ: coefficient which depends on the type of chemical resistance involved (to soaking or/and to brushing).

Table 3. Tentative values for the parameters in (eq. 10).

	Chemical resistance indicator			Couple Bitumen vs. fuel		
	A	*B*	*C*	B 70/90 vs. Avion	B 70/90 vs. Jet	B 70/90 vs. Diesel oil
Parameter	ξ_1	ξ_2	ξ_3	α_1	α_2	α_3
Value	1,5	1,9	2,2	2,7	1,4	1,3

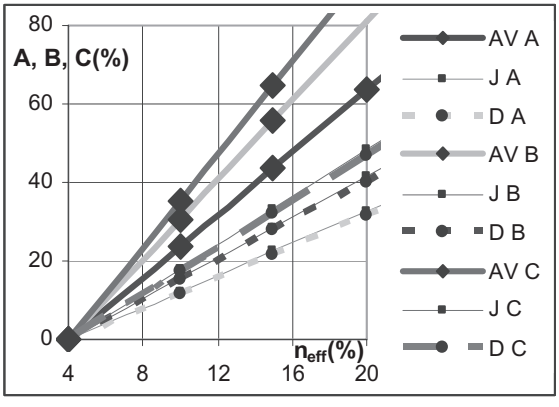

Figure 17. Generalised model.

Table 2 summarizes the results obtained through the generalized model (10), for $n_{CR} = 4$.

By solving the system of nine equations (of the type $\alpha_j \cdot \xi_i = \Delta_{ij}$, where Δ_{ij} are given in table 2), in six variables (α_j, ξ_i), the following tentative values of α_j and ξ_i can be derived (table 3).

Figure 17 offers a *resumé* of the application of equation 10 for the set of coefficients reported in table 3.

5 CONCLUSIONS

More experiments are needed in order to gain a better understanding of the phenomena analysed in this paper. Nonetheless, in the light of the obtained results the following main conclusions can be drawn.

HMA Chemical resistance depends mainly on mix effective porosity, quantity and type of fuel and asphalt binder characteristics.

Advanced tests on volumetrics, asphalt binder and fuels characteristics are so needed.

The effective porosity of the HMA (and, consequently, the air voids content) rule the process of soaking and weakening and it is able to explain a considerable part of the process variance. As a consequence, A, B, and C are greatly affected by the effective porosity of the mix and a suitable (and comparatively inexpensive) strategy is to design very dense mixes (e.g. DGFCs, Dense Graded Friction Courses).

On the other hand, it is important to remark that the chemical relationship between fuel and asphalt binder is of primary relevance. The generalised model here set out is an attempt to obtain a synthetic representation of all the processes as a result of just two main variables, that is to say effective porosity and bitumen vs. fuel compatibility.

Bitumen role still calls for further investigations and future research will be aimed at gaining a better understanding of the influence of asphalt binder properties on the effects, investigating on how they do relate to the physical properties of the soaked specimens.

REFERENCES

EN 12697-43: 2005. Bituminous mixtures—Test methods for hot mix asphalt—Part 43: Resistance to fuel.

EN 12697-2: 2008. Bituminous mixtures—Test methods for hot mix asphalt—Part 2: Determination of particle size distribution.

Maarten, J.M.J., Stet, M.J.A. & Molenaar, A.A.A. 2002. Decision model for the use of polymer modified binders in asphalt concrete for airfields, *FAA airport technology transfer conference,* Atlantic City, New Jersey, USA.

Praticò, F.G., Ammendola R. & Moro A. 2008. Fuel resistance of HMAs: theory and experiments. *International Journal of Pavement Research and Technology*, 1(3):100-106 - ISSN: 1997-1400.

Steernberg, K., Read, J.M. & Seive, A. 2000. Fuel resistance of asphalt pavements, *2nd Eurasphalt & Eurobitume Congress,* Barcelona, Spain.

Van Rooijen, R.C., De Bondt, A.H. & Corun Ronald L. 2004. Performance evaluation of jet fuel resistant polymer—modified asphalt for airport pavements, *FAA airport technology transfer conference,* Atlantic City, New Jersey, USA.

Advanced Testing and Characterization of Bituminous Materials –
Loizos, Partl, Scarpas & Al-Qadi (eds)
© 2009 Taylor & Francis Group, London, ISBN 978-0-415-55854-9

Result of numerical analysis of efficacy geogrids on reinforced pavements' vertical and horizontal deformations

Fatemeh Saleh
Master's Degree Program in Civil Engineering, Road and Traffic at Semnan Province

Gh. Shafabakhsh & Ah. Hadad
Faculty of Engineering of Semnan Province

ABSTRACT: The Pavement structure is a multi-layer system which is designed to distribute and transfer loads on the top of subgrade. The used materials and thickness of the pavement is designed aiming fulfilling two main objectives: 1- Decreasing the intensity of vertical pressure to a level suitable for subgrade, and 2- Reducing tensile stresses on the lower layer of the subgrade to lower than admissible tensile stress of subgrade to avoid tensile crakding on the top of this layer.

Vertical and horizontal strains are the main reasons of progressive cracking. This problem can be overcome using Geogrid. Geogrid are very efficient in controlling the vertical and horizontal strains.

This paper describes result of finite element studies that analyzed the behavior of reinforced asphalt pavement under monotonic loading. The Geogrid was modeled using a one-dimensional linear elastic bar element and the effects of the stiffness of Geogrid reinforcement and strength of subgrade foundation were also investigated.

This paper deals with the vertical and horizontal strain of pavement reinforced by Geogrids using Plaxis software.

The finite element procedure was validated by comparing the results of analysis with the results obtained from a series of other Software models.

Keywords: Geogrid, Traffic, Pavement, PLAXIS

1 INTRODUCTION

Nowadays, the new technologies have lead to the development of the science of construction of subgrade. Use of high quality materials and good operation of top subgrade layers, will result in a proper pavement load capacity.

Construction of subgrade is done with the objective of having a smooth and stable surface for vehicles roads and airport runways. Normally the ground can not tolerate stresses caused by the wheels of heavy vehicles such as trucks. So, the exerted loads will result in failure of subsoil.

If all standard rules are covered in designing and constructing of the subgrade layers, the pavement should not have any failure during its service life. But in many situations, some special conditions such as:

1. Number and type of passing vehicles
2. Weather conditions
3. Drainage conditions
4. Construction quality
5. Subsoil layer materials
6. Conditions and criteria of the road alignment
7. Maintenance

Will cause the inefficiency of pavements (Moghadasneghad, 2005).

All above causes express the need to investigate pavement considering similar loads to real situation, and reinforcing the layers if required. One of the ways to increase the resistance of pavement is use of reinforcements and Geosynthetics such as Geogrids and Deotextiles or a combination of them.

2 USED SOFTWARE

In this study for the purpose of investigations, numerical analysis and finite element methods are utilized for the pavement under real traffic loading conditions. The finite element method is an analytical method which concept have been used centuries ago (Athanasiu, 2000).

This method was first used in 1950's for investigation of complex structures and now is used in different branches of civil engineering and also other engineering fields such as electrical and mechnical engineering (Bauduin et al. 2000).

PLAXIS is one of numerical analysis software that uses finite element method to model and analyze geotechnical problems and is used for calculation of stability and analyzing strain and deformation of geotechnical structures. The software can be used to model elastic-plastic strains, static analysis, strength analysis, and underground waters problems.

It is also able to model the soil, structure element, soil-structure interactions and the analysis of very complex geotechnical structures.

Although a great number of test models result in similar behavior predicted by the application software, but nobody can claim a 100% correctness of the software. The most important item to get a correct result is a correct modeling of the structure, enough knowledge about different behaviors of soil and its limitations, a correct selection of parameters and a good engineering view of the user. In this study *PLAXIS* 8.0 is used or pavement analysis.

3 PLAN MODEL

The general specifications of the materials which are assumed in most patterns are tabulated in the following table. The used Geogrid is the Hatelite C Geogrid, produced by HUESKER Co. Geogrid specifications explain in table (1) and pavement layers specifications in table (2).

Figure 1. Shows the geometrical shape and the point where the pavement is investigated.

Table 1. Specifications of the used Geogrids.

Value	Unit	Standard	Item
Biaxial			Product type
100% polyester			Rare material
40 × 40	mm	–	Hole size
50	KN/m	EN-ISO10319	Tension strength vertical/horizontal
12	%	EN-ISO10319	Tension in maximum force vertical/horizontal
190	°C	ASTM D276	Melt-point

Table 2. Specifications of the used pavement layers.

υ	φ	Permeability factor a cm/day	C	E_{SB}	Material type
0.3	30°	0.001	210	31500 kg/cm^2	Asphalt
0.3	30°	0.1	20	1925 kg/cm^2	Base
0.3	30°	0.1	10	980 kg/cm^2	Subbase
0.35	35°	1	20	700 kg/cm^2	Subgrade

4 PROJECT STEPS

Minimum lifetime of pavement is 10 years in rural roads. In important roads in which usually after 10 years pavement deterioration requires maintenance coating, reinforcing Geogrids are useful. So used Geogrids in one and two layers pavement are applied in several possible positions:

1. On the top of base layer;
2. On the top of subbase layer;
3. On the top of subgrad layer;
4. On the top of base and subbase;
5. On the top of subbase and subgrad;
6. On the top of base and subgrad.

It should be noted that modeling 10 years period in PLAXIS was not feasible from modeling time point of view so we decided to investigat 2×10^6 *ESAL* traffic load during 5 years (1825 days).

Figure (2) shows the pavement failure under loading and significant deformation because no reinforcements are used and loading magnitude is very high. In reinforced pavements using Geogrid stability of pavement is increased and in the mean time total deformation is reduced. In pavement top layers are critical. Analysis results show that location of Geogrids in pavement layers are very important and can influence the stability of pavement. Therefore

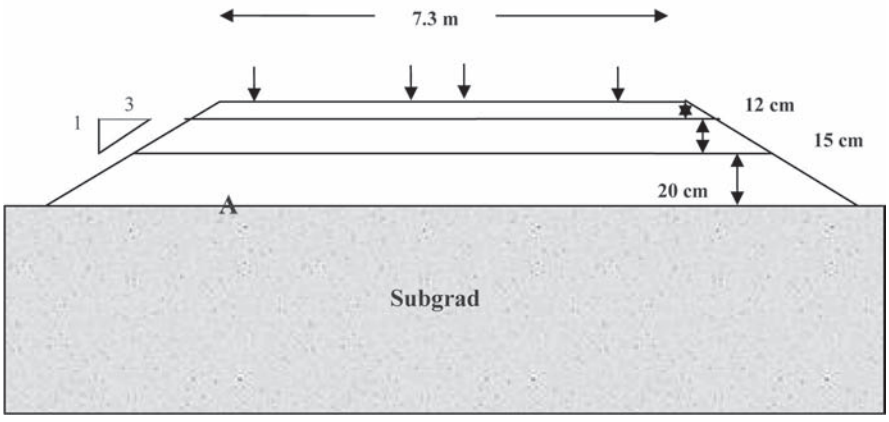

Figure 1. Geometrical model of pavement; the modeling and investigation is made on point A.

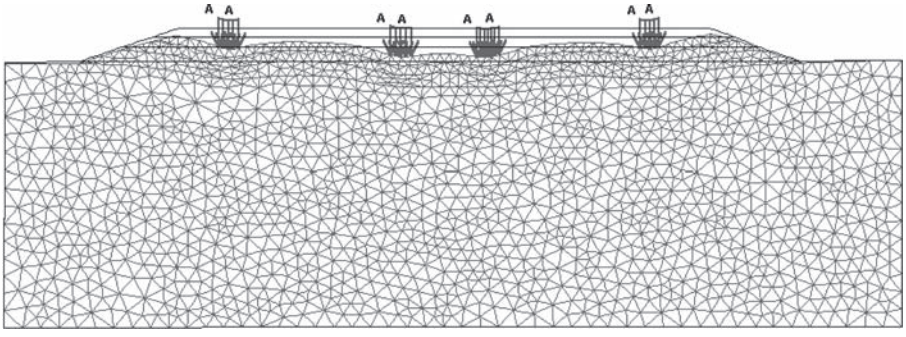

Figure 2. Sample pavement without of Geogrids.

several locations of reinforcement are investigated and it is concluded that locating Geogrids between main course and base layer has the optimum results.

3 meshing arrangements were evaluated in pavement during analysis in PLAXIS to obtain the predicted total stiffness in pavements.

Results of this study depict that strains and deformation in reinforced pavements (Geogrid reinforced pavements) are significantly lower than conventional pavement structures. Vertical deformation has great impact on settlement and formation of shrinking cracks. The significant decrease in the deformation in this model is very important. Although this is a case study but the results can be extended to some other applications. The results of analysis of different models are presented in the following tables:

Table 3. Deformation results in analysed pavement.

Deformation (cm)	
No Geogrid	4.166
Geogrid on subgrade	2.25
Geogrid on sub base layer	2.215
Georid on Base layer	1.9717
Geogrid on base and sub base	1.79
Geogrid on subgrad and sub base	2.056
Geogrid on base and subgrade	2.1536

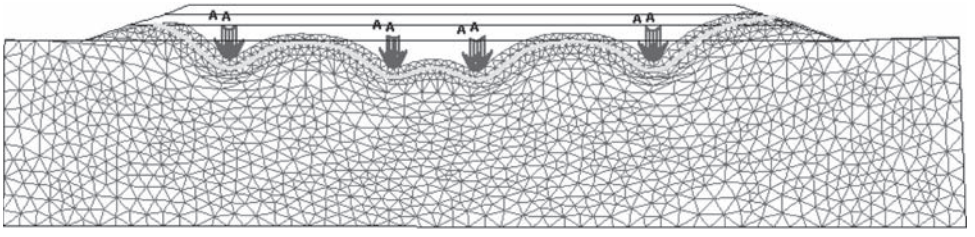

Figure 3. Model showing application of single layer Geogrid under main course of pavement.

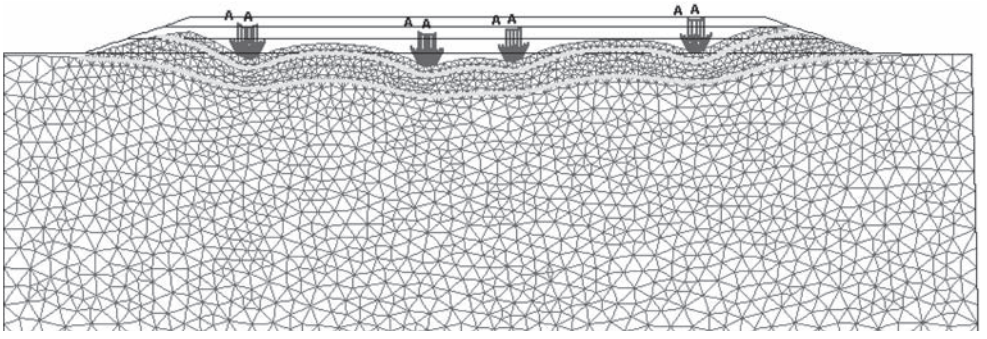

Figure 4. Model showing application of double layer Geogrid under main course and on the top of subgrade.

Vertical stresses in modeled pavements are different depending on the location of Geogrid layer. Considering the stress distribution characteristics of Geogrid layer, better performance of reinforced pavements comparing with traditional ones can be observed. Following tables show the results of analyzed stresses in all models.

But reinforced pavement using Geogrid have horizontal strain due to Geogrid movement relative to layers. This point is very critical and in designing of reinforced pavements this point should be taken into consideration.

As seen in figure 9, the pavement will experience different volume strains under different reinforcing approaches. Reinforced pavements with one layer of Geogrid results in less volomine strain but adding another Geogrid layer increases the horizontal strain of the pavement.

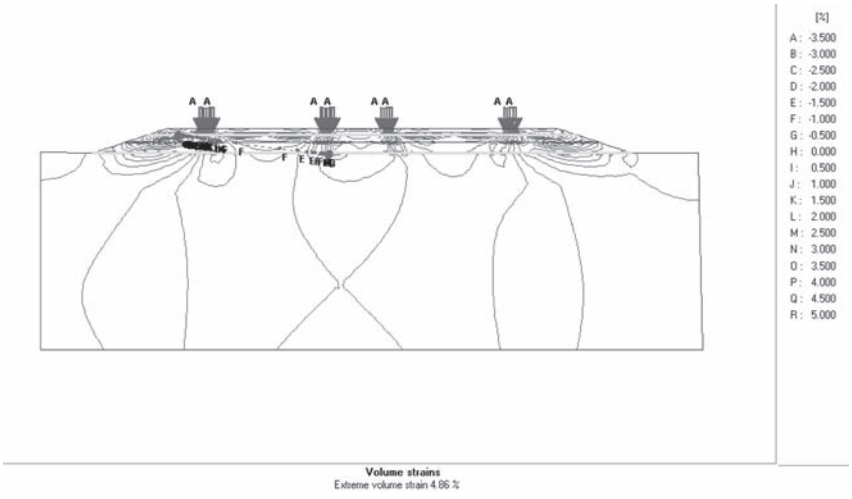

Figure 5. Volume strain contours of a pavement model with two Geogrid layers arrangement.

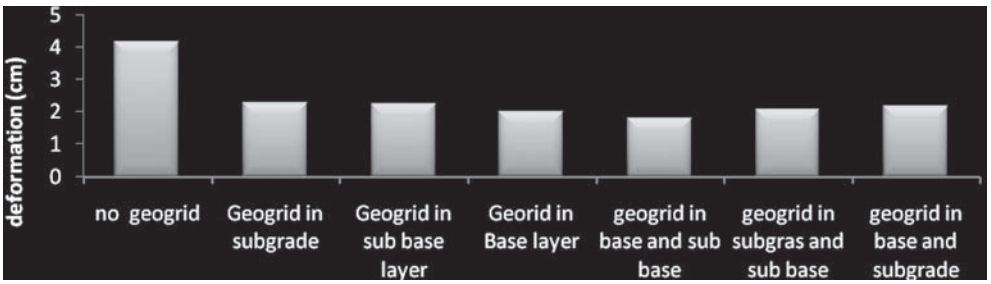

Figure 6. Summary results of vertical deformation of analysed pavements.

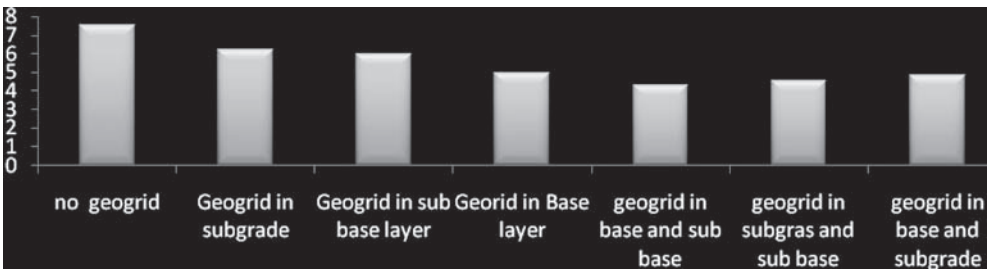

Figure 7. Summary results of volume strain in analysed models.

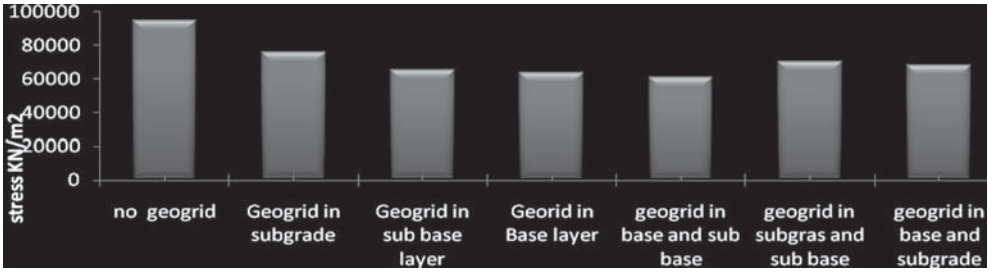

Figure 8. Magnitude of vertical stresses in different locations of Geogrid reinforcing layers..

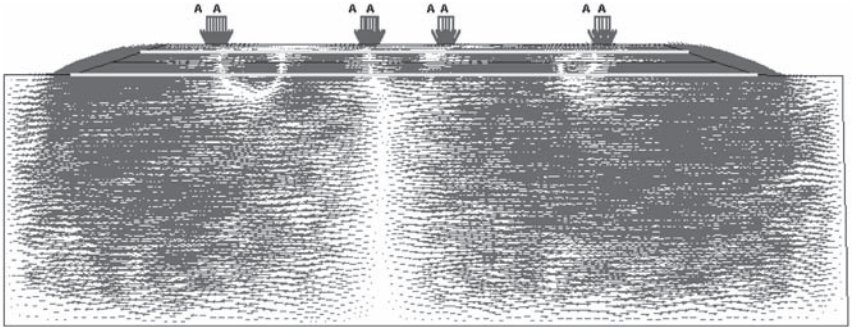

Figure 9. Direction of horizontal strain of pavement with two Geogrid layers.

Table 4. Result of volume strain (in % in square meter) in analysed pavements.

Volouminal strain (% in m^2)	
No Geogrid	7.55
Geogrid on subgrade	6.23
Geogrid on sub base layer	5.99
Georid on Base layer	4.93
Geogrid on base and sub base	4.27
Geogrid on subgrad and sub base	4.53
Geogrid on base and subgrade	4.86

Table 5. Results of vertical stress analysis depending on location of Geogrid layer.

Vertical stress (kN/m^2)	
No Geogrid	95000
Geogrid on subgrade	67000
Geogrid on sub base layer	65500
Georid on Base layer	63500
Geogrid on base and sub base	61000
Geogrid on subgrad and sub base	68000
Geogrid on base and subgrade	65000

5 CONCLUSION

Results of this study show that pavement will improve in strength with the application of reinforcing Geogrids. Decrease of the horizontal and vertical strains and deformations of pavement are very important. Although it should be noted that importance of vertical strains is more significant. But in many conditions, horizontal strains lead to Geogrid slip and increase of the movement between pavement layers, which require detailed investigations.

Use of PLAXIS helps us dealing with these problems. An important result of the investigation is that, although the increase of Geogrid layers increases pavement strength, but it increases horizontal strains as well. But for solving this problem, certain adhesive or prime coad in on both sides of Geogrid layers is useful.

REFERENCES

Use Geosynthetices in pavement layerse in decrease plate and stoppage crack in this, ministry of transportation in Iran, Dr. Moghadasneghad, 2005.

Proposal for an anisotropic, soft clay model to be incorporated infuture developments in PLAXIS, C. Athanasiu, NOTEBY AS, Oslo, Norway, 2000.

Back analysis of staged embankment failure; The case study Streefkerk, C.M. Bauduin" Besix, Brussels, Belgium", M. De Vos" Belgian Building Research Institute, Brussels, Belgium", P.A. Vermeer" Institut für Geotechnik, Stuttgart, Germany, 2000.

Advanced Testing and Characterization of Bituminous Materials – Loizos, Partl, Scarpas & Al-Qadi (eds)
© 2009 Taylor & Francis Group, London, ISBN 978-0-415-55854-9

Life cycle costs of typical asphalt pavement rehabilitation techniques in Colorado USA

Scott Shuler & Christopher Schmidt
Colorado State University, Ft. Collins, Colorado, USA

Jay Goldbaum
Colorado Department of Transportation, Denver, Colorado, USA

ABSTRACT: Rehabilitation of hot mix asphalt pavements costs approximately $600 million annually. The Colorado Department of Transportation maintains 28,000 lane miles of asphalt pavements. Of the many rehabilitation strategies employed to maintain this network, three strategies have been utilized most frequently. These strategies are: 1) overlays of 50 mm (2 inch) thickness, 2) 50 mm (2 inch) cold milling of the existing surface and 50 mm (2 inch) overlay, and 3) heater scarification and 50 mm (2 inch) overlay. This research was conducted to determine the life-cycle costs of these strategies. Projects were selected based on a ten-year design life, constructed between 1997 and 2001. There were 151 projects analyzed which met this criteria. Performance was judged based on smoothness, permanent deformation, and transverse, longitudinal and fatigue cracking over a six-year service period. Independent variables included asphalt binder type, traffic loading, aggregate gradation and climate. Results indicate significant differences with respect to rehabilitation method. The best performing method was cold milling and overlay and the poorest was heater scarification and overlay. However, heater scarification provided the lowest agency present value costs with cold milling and overlay providing the highest agency cost.

1 INTRODUCTION

Rehabilitation of asphalt pavements is done when pavement condition has been reduced to a level that exceeds the ability of preservation techniques to restore serviceability. The cost of rehabilitation varies based on damage severity and the rehabilitation method. In addition, the length of time the rehabilitation method is effective is dependent on the method used, pavement condition prior to rehabilitation, traffic, climate and materials.

This study provides an evaluation of the life-cycle cost of three common rehabilitation methods utilized to restore serviceability to hot mix asphalt pavements. It is believed that each of these rehabilitation methods performs differently depending on how and where the method is being utilized. However there has not been an extensive study examining the performance of each method, so relative performance and cost effectiveness of the strategies are not well understood. This research compares three common strategies based on a one-lane mile segment of hypothetical roadway in Colorado USA. Costs were obtained from the Colorado Department of Transportation Cost Data Book from 2007.

1.1 *Rehabilitation methods studied*

Two-Inch (50 mm) Overlay

This process includes a dense graded hot mix asphalt overlay applied directly over the existing asphalt pavement. The only preparation of the existing surface includes sweeping and tack coat.

Cold Planing and Overlay

Cold planing and overlay involves removing the top two inches (50 mm) of the existing pavement with a milling machine at ambient temperatures. The milled pavement surface is then swept, a tack coat applied and a two inch (50 mm) dense graded hot mix overlay is applied.

Heater Scarification and Overlay

Heater scarification and overlay begins with the process of heating the pavement with infrared or propane heaters, scarifying the heated pavement, and then spraying a rejuvenating agent on the scarified surface. The rejuvenating agent and the scarified asphalt pavement are mixed together and leveled using a screed. After this rejuvenated material is leveled and compacted a 2-inch (50 mm) hot mix asphalt surface is placed.

1.2 *Independent variables evaluated*

Independent variables evaluated for each of the rehabilitation strategies were:

a. PG Binder Temperature Range
b. Traffic Volume
c. Overlay Nominal Maximum Aggregate Size
d. Climate

PG Binder Temperature Range

Asphalt binders used in this study were graded according to the Superpave PG system. The projects were analyzed based on PG temperature range of greater than 90°C and less than 90°C.

Traffic Volume

The highways are split into three different traffic volumes based on 20 year, 18 kip equivalent single axle loads (ESALs):

- Low Traffic <0.3 million ESALs
- Moderate Traffic 0.3 to 11 million ESALs
- High Traffic >11 million ESALs

Overlay Nominal Maximum Aggregate Size

Two hot mix aggregate gradations were evaluated in this study. The 'S' gradation has a nominal maximum aggregate size of 25 mm (1 inch). The 'SX' gradation has a nominal maximum aggregate size of 19 mm (¾ inch).

Climates

Four different temperature regimes were evaluated: a very cool environment has an average seven day high air temperature of less than 27°C (81°F), a cool environment with a average high air temperature between 27–31°C (81–88°F), a moderate environment that has an average high air temperature between 31–36°C (88–97°F), and a hot environment that has an average high air temperature of greater than 36°C (97°F) (Shuler & Schmidt 2008).

1.3 *Performance evaluation*

Performance was judged based on the condition of the pavements over time with respect to each of the following criteria:

1. Smoothness
2. Rutting
3. Fatigue Cracking
4. Transverse Cracking
5. Longitudinal Cracking

2 LITERATURE REVIEW

A review of the literature did not reveal any studies specifically evaluating life-cycle costs of the three rehabilitation strategies presented here. However, many studies have been done to evaluate pavement performance over time including a Texas study (Chen et al. 2006) where reflective cracking of asphalt overlays on jointed concrete was done to evaluate six rehabilitation methods. Another study in Pennsylvania (Morian & Cumberledge 1997) evaluated techniques for selecting correct pavement rehabilitation strategies. They determined that understanding project history was most significant although assessment of traffic history, evaluation of materials used, general understanding of past construction practices, history of climate, and an understanding of the type of subgrade were also factors. A study for the Nevada Department of Transportation (Hand et al. 1999) developed a network optimization system to evaluate alternate rehabilitation techniques and then recommend the most efficient and cost effective technique for different sections of highway.

3 LIFE-CYCLE COST ANALYSIS

Performance data utilized in this study was obtained from the pavement management database of the Colorado Department of Transportation and reported by Shuler and Schmidt (Shuller & Schmidt 2008). In this study pavements were compared based on the independent variables discussed above and were separated based on construction between 1997 and 2001 which had at least six years of performance data to evaluate. This resulted in a total of 73 two inch (50 mm) overlays, 57 cold planing and overlay projects and 19 heater scarification projects for 149 total projects.

A life cycle cost analysis was conducted on each rehabilitation strategy with the help of the *Real Cost v2.2* software available from Federal Highway Administration (FHWA) (Life—Cycle analysis, 2004).

Common input for all of the rehabilitation strategies is shown in Table 1 below.

Rehabilitation and maintenance costs used in the analysis are shown in Table 2 and are based on previous analysis of the three rehabilitation strategies with respect to service life and maintenance intervals.

The values shown in Table 2 are based on a 1.6 km (1 mile) pavement 4 m (12 feet).

The analysis uses a 20 year period for comparison of the strategies based on the maintenance intervals and life expectancy of each strategy.

4 RESULTS

The analysis is capable of computing both user costs and agency costs using deterministic or probabilistic output. For space considerations only the deterministic output is shown in Table 3.

Table 1. Common input variables for life cycle cost analysis.

Average annual daily traffic (AADT) Year 0	42726
Single unit trucks, %	5
Combination trucks, %	10
Growth, %/yr	2.5
Speed, mph (kph)	65
Lanes	3
User cost cars, $/hr	11.5
User cost combination trucks, $/hr	21.5

Table 2. Construction and maintenance costs for each option.

Rehab	Tons	$/ton	Sq-yds	$/sq-yd	Maint, yrs	Life, yrs	Initial cost, $
2" Overlay	792	65	Na	Na	4	7	51,480
2" Mill Fill	792	65	7040	3	5	9	72,600
Heater Scarif	792	65	7040	2.5	5	6	69,100

Table 3. Life cycle cost analysis for three rehabilitation strategies.

	2 inch Overlay		2 inch Mill Fill		Heater scarification	
Total, $	Agency ($1000)	User ($1000)	Agency ($1000)	User ($1000)	Agency ($1000)	User ($1000)
Present value	137.00	10.47	147.67	12.58	199.80	18.17

The 2-inch (50 mm) overlay provides the lowest life cycle present cost to the agency over a 20 year analysis period. This is due to the approximate $20,000 per lane-mile discount over the next costly alternative at Year 0 with only a one year difference in service life and one year differnce maintenance interval.

The 2-inch (50 mm) overlay also provides the lowest life cycle present cost to the users over a 20 year analysis period. Heater scarification is the highest cost strategy due to the more frequent rehabilitations at six years and maintenance intervals.

5 CONCLUSIONS

1. The lowest life cycle agency cost for the three rehabilitation strategies studied was the 2-inch overlay. This method was also the lowest with respect to user cost.
2. The highest life cycle agency cost for the three strategies was the 2-inch (50 mm) heater scarification and overlay due to an initial cost only slightly lower than the 2-inch (50 mm) cold planing and overlay, shortest service life and more frequent maintenance intervals.

REFERENCES

Chen, D., Scullion, T. & Bilyeu, J. 2006. Lessons Learned on Jointed Concrete Pavement Rehabilitation Strategies in Texas. *Journal of Transportation Engineering*, 132(3): 257–265.

Morian, D. & Cumberledge, G. 1997. Techniques for selecting pavement rehabilitation strategies: Pennsylvania case studies. Transportation Research Record. *Journal of the Transportation Research Board*. 1568: 131–138.

Hand, A., Sebaaly, P. & Epps, J. 1999. Development of performance models based on department of transportation pavement management system data. Transportation Research Record. *Journal of the Transportation Research Board*. 1684: 215–222.

Shuler, S. & Schmidt, C. 2008. Performance Evaluation of Various HMA Rehabilitation Strategies, Colorado Department of Transportation, Final Report, August 2008.

Life-Cycle Cost Analysis 2004, *Real Cost v2.2 User Manual*, Federal Highway Administration, Office of Asset Management, May 2004.

Advanced Testing and Characterization of Bituminous Materials – Loizos, Partl, Scarpas & Al-Qadi (eds)
© 2009 Taylor & Francis Group, London, ISBN 978-0-415-55854-9

Performance oriented payment adjustment for flexible pavements

P. Sivapatham & H.J. Beckedahl
Pavement Research Centre, University of Wuppertal, Germany

ABSTRACT: According to German quality control and quality assurance specifications asphalt layers have to be compacted to a minimum compaction degree of k = 97%. In case of dropping below the minimum compaction degree the agreed unit price will be reduced. After German specifications, the payment adjustment takes the compaction degree into account without considering the compaction degree dependent asphalt quality and the sensitivity subjected to the binder used. On that account, in this paper a performance oriented calculation method for payment adjustment is recommended. According to this calculation model, the improvement of asphalt quality is rewarded with bonuses and the quality loss is punished with penalties. The asphalt quality is described by means of calculated lifetime with respect to compaction degree and binder used. To calculate adequate lifetime of asphalt, suitable analytical performance models have been used. As a result of this payment adjustment method, highest bonus and lowest penalty for asphalt with long lifetime and low maintenance costs, as well as the lowest bonus and highest penalty for asphalt with low lifetime and high maintenance costs have been determined.

1 INTRODUCTION

The paving quality of asphalt is the most important performance indicator of flexible pavements and its compliance will be checked by means of quality control and quality assurance. The contractor is fully responsible for paving quality. The client is responsible to ensure that the quality achieved is adequate to meet the specifications of the bid. In the case of dropping below the agreed paving quality, it is common practice that the agreed unit price will be reduced. One of the crucial indicators of the paving quality is the compaction degree of asphalt layers. According to the German quality control and quality assurance specifications ZTV Asphalt-StB 07 (ZTV Asphalt-StB 2007) for most asphalt layers a minimum compaction degree of k = 97% of Marshall Density is defined.

In the case of dropping below the agreed minimum compaction degree, the payment adjustment will be calculated in Germany after the equation 1.

$$A = 3 \times \frac{p^2}{100} \times EP \times F \tag{1}$$

A penalty (€)
p difference of in situ and agreed minimum compaction degree k (%)
EP agreed unit price [€/m²] or [€/t]
F construction area [m²] or paving mass [t]

In this calculation, the only indicator of paving quality is the compaction degree. The compaction degree dependent asphalt quality and its sensitivity against the binder used are currently not considered. The binder used has a significant influence on lifetime of asphalt pavements with similar mixture recipes (Beckedahl H.J. et al. 2008a). At middle and high service temperatures (≈t > 0°C), asphalt with a stiff and very elastic binder has an excellent performance and can normally bear higher loads compared to asphalt with a soft binder with low elasticity.

At low service temperatures (≈t < 0°C) asphalt with a very elastic and soft binder show normally better performance compared to asphalt with a stiff binder with low elasticity. These properties of binders can be modified, normally improved, by means of polymer additives. Thus, asphalt with polymer modified binder or asphalt with added polymers is able to transfer higher loads compared to conventional asphalt. The less the compaction degree, the lower is the number of contact points between the (bituminous covered) grains in the asphalt layer. Due to that, with decreasing compaction degree the contact stress between the (bituminous covered) grains will increase. Thus, a stiff asphalt pavement with high elastic properties will show different sensitivity (high resistance against rutting) compared to a soft asphalt pavement with high plastic properties particularly with decreasing compaction degree.

Decreasing compaction degree will cause always a quality loss. Thus, the quality loss shall be adjusted with penalty. Also an improvement of asphalt quality because of an improved asphalt mix and a high paving quality shall be rewarded with bonuses. Hence the payment shall be based on the asphalt performance quality in situ and not only by means of the achieved compaction degree as currently practiced. Taking this into consideration, in this paper a method is introduced to calculate a performance oriented payment adjustment with respect to asphalt performance quality in situ.

2 CALCULATION OF LIFETIME WITH RESPECT TO COMPACTION DEGREE

By means of analytical performance calculation models, the performance properties of asphalt pavement structures have been estimated with respect to the binder used and the compaction degree reached. The main asphalt pavement performance properties are resistance against permanent deformation, resistance against fatigue, low temperature behaviour, ageing, as well as adhesion between binder and aggregate. The classical pavement design criterion is the fatigue at the bottom of the asphalt base layer. But most important damages for flexible pavements are permanent deformation and cracking initiating at the surface (COST 333 1999). Generally the decisive criteria are subjected to deterioration mechanisms due to magnitude, frequency and configuration of loads, climatic effects and local conditions.

By means of development of performance properties the lifetime can be calculated. In this framework, to predict the lifetime of the asphalt base layer the classical design criterion resistance against fatigue has been taken into account. Lifetime of surface- and binder layers has been determined on base of calculated rut depths. Therefore mechanical properties of flexible pavement structures like strain (ε), stress (σ) and deformation (w) were calculated at critical locations by means of a pavement calculation model based on the elastic multi layer theory. Thereby the thicknesses of correspondent layers have been selected for heavy loaded pavements after the RStO 01. The development of fatigue behavior for asphalt base layers and of permanent deformation for surface- and binder layers were investigated by means of calculated mechanical properties (ε, σ, w) in combination with material parameters derived from laboratory test. Thereby three different binders (a conventional 50/70 pen bitumen, a polymer modified binder PmB 45A and a high polymer modified special binder PmB 25 H) have been used. Three different asphalt types (stone mastic asphalt 0/11 S for surface layer (SMA), asphalt concrete 0/16 S for asphalt binder layer (ABI) and asphalt concrete 0/22 CS for asphalt base layer (ABL) have been used to produce specimens with compaction degrees between k = 93% and k = 103%. For details of the laboratory test results with these specimens see (Beckedahl H.J. et al. 2008b).

In this paper the lifetime of four different asphalt pavements have been calculated with respect to different compaction degrees:

- Reference asphalt pavement (reference): SMA (50/70), ABI (PmB 45A) and ABL (50/70)
- Asphalt pavement with conventional bitumen (conventional): SMA (50/70), ABI (50/70) and ABL (50/70)
- Asphalt pavement with polymer modified binder (PmB 45A): SMA (PmB 45A), ABI (PmB 45A) and ABL (PmB 45A)
- Asphalt pavement with high polymer modified special binder (innovative): SMA (PmB 25 H), ABI (PmB 25 H) and ABL (PmB 25 H)

2.1 *Lifetime of asphalt surface and asphalt binder layer*

The most important deterioration type of asphalt surface and asphalt binder layers is permanent deformation. According to this, lifetime of surface- and binder layers with respect to the development of rut depth has been calculated. Rut depths can be calculated by means of many different models. In this work the development of rut depths are calculated on base of the VESYS method (COST 333 1999). The basic assumption of the VESYS method is that the accumulated permanent deformation $w_{pZ,k}(n)$ is a function of the number of load repetitions ***n***. Only heavy vehicles at high temperatures contribute permanent deformations to an important extend. Thus, relevant traffic loading or number of axle loads at decisive temperatures has to be taken into account during calculation. In this work the number of load cycles has been determined according to the statistic distribution of asphalt surface temperatures after RDO Asphalt 08 (RDO Asphalt 2008). As decisive asphalt surface temperature, which is responsible for the main permanent deformation, higher temperatures than 42.5°C were assumed. Thus 1.2% of design axle loads can be considered as relevant load cycles. 240 million ESAL (10-ton axle loads) has been taken into account for a lifetime of 30 years and these load cycles represent high loaded asphalt pavements. As design temperature for the surface layer the median value of 47.5°C has been considered. For the asphalt binder course and asphalt base course the design temperature has been calculated after the temperature gradient according to RDO Asphalt 08 (RDO Asphalt 2008).

The rut depth development with respect to the load cycles ***n*** is described in equation 2. The total deformation $w_{iZ,k}$ is calculated with respect to the resilient layer modulus. The influence of mix design, binder properties and compaction degree can be characterised by means of resilient modulus. The material constants μ_k and α_k are derived from wheel tracking test results. For details of the calculation see (Beckedahl H.J. et al. 2008a).

$$w_{pZ,k}(n) = w_{rZ,k}\ \mu_k\ n^{\alpha_k} \tag{2}$$

By means of this calculation method, rut depth developments have been calculated. The calculated rut depths are displayed against corresponding lifetime in Figures 1 to 4. The calculation results show significant effects with respect to the binders used and to the different compaction degrees ***k***. As expected, rut depths increase with decreasing compaction degree for any asphalt mix till a compaction degree of k = 101.5%. It is obvious that with decreasing compaction degree the rut depths of asphalt pavements with PmB 25 H increase to a much smaller extend compared to the other asphalt pavements. The conventional asphalt pavements with 50/70 show the highest rut depths.

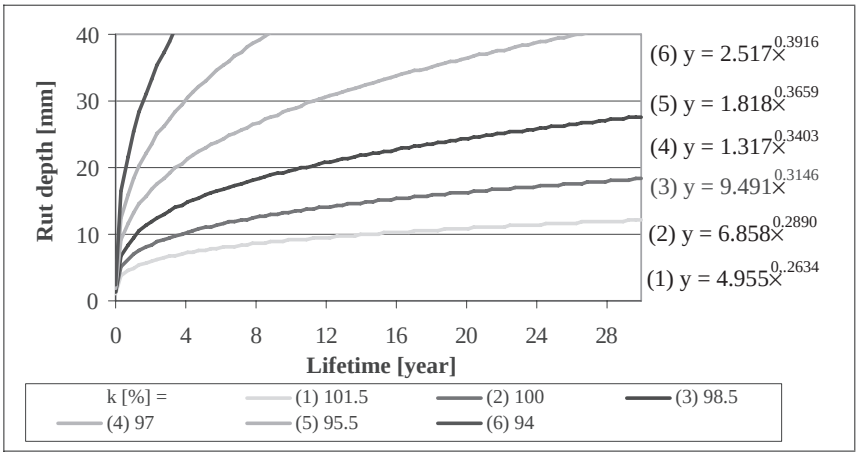

Figure 1. Development of rut depth, Reference (SMA + ABI).

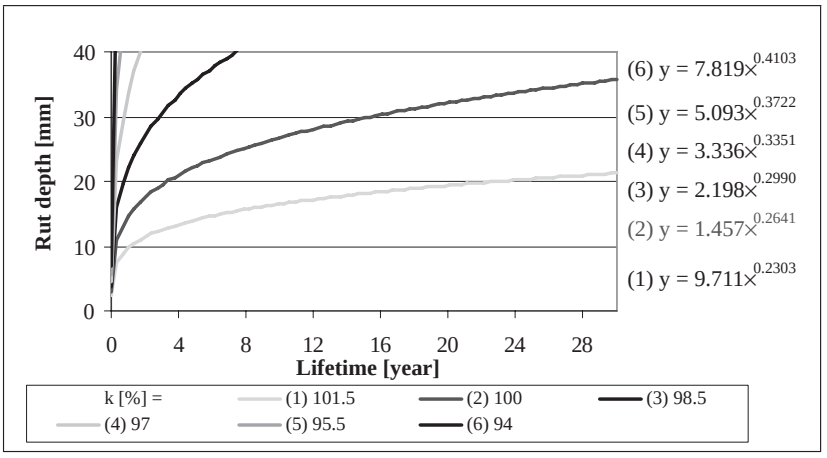

Figure 2. Development of rut depth, 50/70 (SMA + ABI).

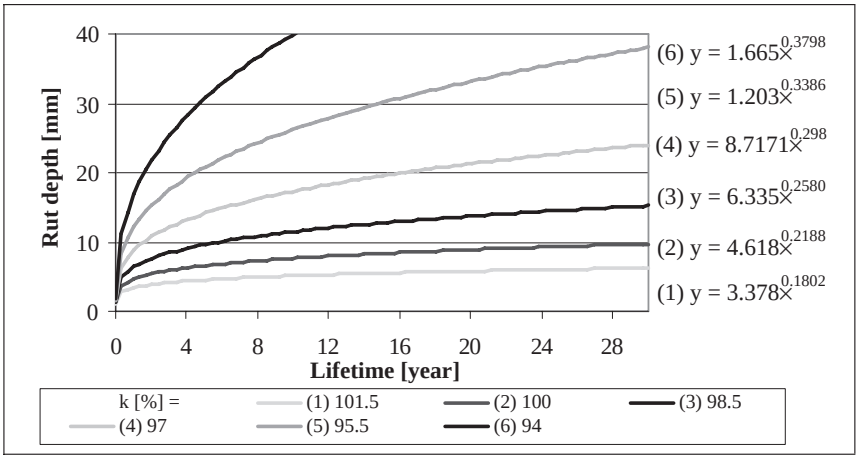

Figure 3. Development of rut depth, PmB 45A (SMA + ABI).

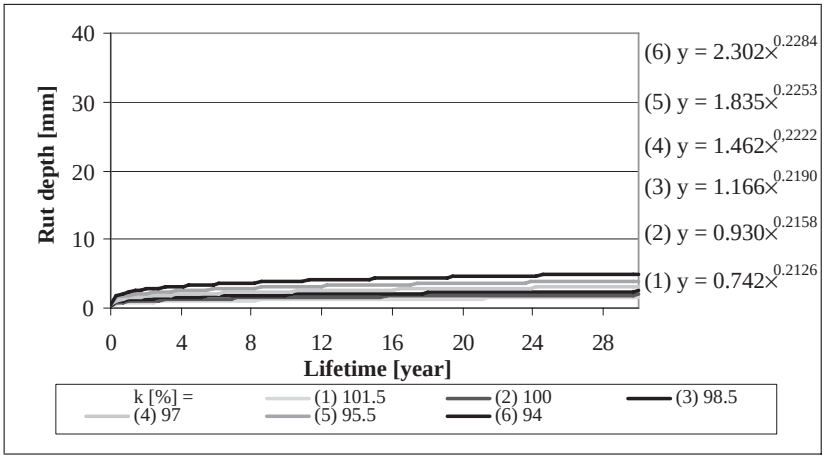

Figure 4. Development of rut depth, PmB 25 H (SMA + ABI).

After the pavement management system guidelines, a rut depth of 20 mm is deemed to be a critical value (AP Nr. 9/A1 2001). According to experience surface layers will be reconstructed, if the rut depth reaches 30. Hence a rut depth of 25 mm will be considered as a limit. Thus, the lifetime of pavement construction is limited if the rut depth reaches 25 mm. According to this prediction, the lifetime of surface- and binder layers can be calculated. The calculated rut depths show, that the reference pavement with a compaction degree of k = 97% will match the rutting limit after 8 years. The pavement with conventional bitumen and a compaction degree of k = 97% will reach the rutting limit during the first year. The innovative asphalt pavement PmB 25 H will not exceed the value of 10 mm within the design lifetime of 30 years, even at a compaction degree of k = 94%. The calculated rut depths indicate that the permanent deformation can be kept much smaller by using innovative asphalt instead of conventional or reference asphalt. According to these calculated results, a reconstruction of surface and/or binder layers for innovative pavement till a compaction degree of k = 94% and for polymer modified asphalt pavement PmB 45A till a compaction degree of k = 97% will not be necessary during the design period of 30 years. For surface layers the average period until reconstruction is 12 years and for asphalt binder layers 24 years.

2.2 *Asphalt base layer*

The fatigue behaviour plays worldwide an important role as a pavement design criterion. The strain at the bottom of the asphalt base layer is commonly the crucial criterion to fatigue failure and can be calculated by means of elastic multilayer theory taking into account temperature dependent resilient layer modules and relevant loads. Keeping other conditions constant, the strain at the bottom of the base layer is dependent on the resilient modules of the asphalt layers. The fatigue behaviour of asphalt base layer used can be described by means of equation (3).

$$\varepsilon = a\, N_f^{-b} \tag{3}$$

The fatigue equation (3) has been derived from the corresponding fatigue line (Woehler line) and describes the relationship between the number of load cycles until to failure (N_f) at the initial strain (ε). By means of the fatigue equation, the number of load cycle to failure (N_f) can be calculated with respect to calculated strain at the bottom of the asphalt base layer. In Figure 5, the calculated load cycles for four different asphalt pavements with respect to the compaction degree are listed. For the details of the fatigue line derived from the fatigue tests and resilient modules see (Beckedahl H.J. et al. 2008b).

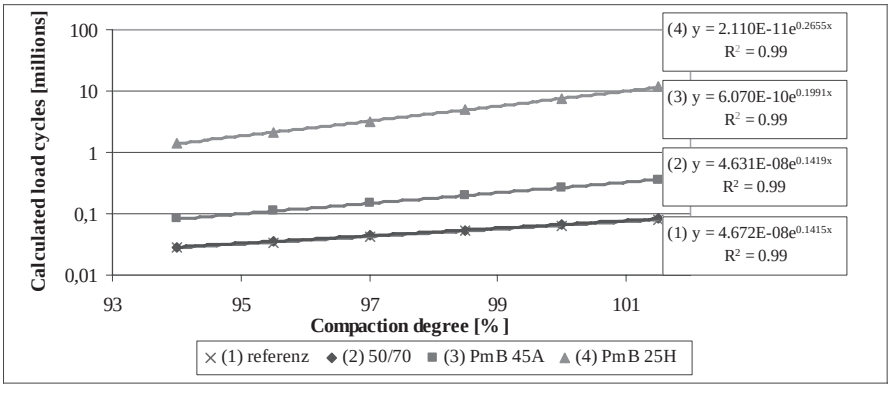

Figure 5. Calculated load cycles to failure N_f.

Comparisons of test results show significant differences in fatigue behaviour with respect to the binder used and the compaction degree. With decreasing compaction degree the number of load cycles until failure decrease for all asphalt variants tested. The innovative pavement PmB 25 H has an excellent fatigue resistance even at decreasing compaction degrees. The pavement PmB 25 H and PmB 45A with a compaction degree of k = 94% bears much more load cycles until failure compared to the reference pavement with a compaction degree of k = 100%, Figure 5. It should be mentioned, that the calculated load cycles until to failure (N_f) cannot be compared one to one to the load cycles in situ, because ageing and healing of asphalt as well as the 3-dimentional stress have not been considered. Thus, the load cycle in situ can be determined by multiplication of calculated load cycle with a shift factor of SF = 1500 (RDO Asphalt 2008).

3 PAYMENT ADJUSTMENT WITH RESPECT TO ASPHALT PAVING QUALITY AND ASPHALT USED

The binder used show a significant influence on the calculated compaction degree dependent lifetime. At decreasing compaction degree increasing rut depths and decreasing fatigue resistance have been calculated which indicates quality loss. A decrease of compaction degree influence asphalt mix behaviour with innovate binder (PmB 25 H) to a much lower extend than asphalt mixes with conventional binder. PmB 45 A shows also positive effects on asphalt pavements but the trend is much smaller compared to asphalt mixes with PmB 25 H. Using asphalt mixes with innovative binder (PmB 25 H) the destructive influence of falling below the minimum compaction degree is limited. According to this, with the use of innovative binder (PmB 25 H) the risk due to the variation in compaction degree and temperature can be reduced significantly. Thus, the payment adjustment for dropping below the minimum compaction degree shall be calculated with respect to the influence on asphalt performance.

Asphalt pavements with compaction degrees up to k = 101.5% of Marshall Density cause an improvement of asphalt performance whereas degrees higher than k = 101.5% of Marshall Density may cause deterioration of asphalt performance. That's why an over-compaction should be avoided. Hence, in this work asphalts till a compaction degree of k = 101.5% will be considered. The improvement of asphalt performance because of increasing compaction degree and/or asphalt used should be adjusted with bonuses. Decreasing compaction degree causes always a quality loss. The quality loss compared to the quality at minimum compaction degree is to adjust with penalty. Dropping below the minimum compaction degree should be avoided, because it causes always a quality loss and leads to excessive maintenance procedures. This will lead to a reduction of lifetime and will increase maintenance costs. Hence, falling below the minimum compaction degree should be considered by a variable, which is calculated with respect to the achieved compaction degree. As basis of payment adjustment, following indicator should be taken into account

- the calculated lifetime by means of laboratory tests and performance models compared to design lifetime,
- relation of the lifetime improvement or lifetime loss of asphalt pavement at paved compaction degree to the lifetime at minimum compaction degree,
- falling below the agreed minimum compaction degree with a compaction degree dependent variable.

3.1 *Payment adjustment for surface- and binder layer*

The payment adjustments for surface- and binder layers can be calculated by means of equation 4 and 5.

$$\text{bonus/penalty} = \tfrac{1}{2} * \ln\left(t_{\text{calculated}} - t_{\text{design}} + 1\right) + \tfrac{1}{2} * \ln\left(w_{k\,(\min)}/w_k\right) - e_p \qquad (4)$$
$$t_{\text{calculated}} > t_{\text{design}}$$

$$\text{penalty} = -\tfrac{1}{2} * \ln (t_{design} - t_{calculated} + 1) + \tfrac{1}{2} * \ln (w_{k\,(min)}/w_k) - e_p \quad (5)$$
$t_{calculated} < t_{design}$

bonus/penalty bonus/penalty (%) of agreed unit price [€/m²] or [€/t],
$t_{calculated}$ calculated lifetime (year),
t_{design} design lifetime (year),
$w_{k\,(min)}$ calculated rut depth at agreed minimum compaction degree (mm),
w_k calculated rut depth at achieved compaction degree (mm),
p difference of in situ and agreed minimum compaction degree (%), in case of dropping below the minimum compaction degree.

The design lifetime of asphalt layers is a requirement of the client and has to be mentioned in the bid. In this study, a lifetime of 12 years for surface layers is taken into account. The calculated lifetime, the calculated rut depth at agreed minimum compaction degree and at achieved compaction degree can be determined by means of corresponding equations from Figures 1–4. In consideration of these calculated values, the sum of corresponding indicator can be calculated (Table 1). The improvement of lifetime compared to design lifetime will be awarded with a bonus (marked with "+" in Table 1) and the deterioration of lifetime compared to design lifetime will be imposed with a penalty (marked with "–"in Table 1). The improvement with respect to compaction degree will be also awarded with a bonus. The quality loss with respect to dropping below the minimum compaction degree will lead to a penalty. In the case of dropping below the agreed minimum compaction degree, a variable ***p*** will be considered, which is calculated with respect to the achieved and the minimum compaction degree. The calculated variable for dropping below the minimum compaction degree increases rapidly with increasing variable ***p***. Thus, the value for dropping of the compaction degree will dominated the payment adjustment.

By means of adding the indicators, the amount of payment adjustment can be determined. The calculated payment adjustment (bonus and penalty) with corresponding curve are displayed in Figure 6. As expected, after matching the minimum compaction degree, the penalty rises in a progressive way with decreasing compaction degree. In case of over-compaction, the bonus curves show flat slopes.

In Germany, the asphalt pavement is to design according to the specification RStO 2001, ZTV Asphalt-StB 2001 and ZTV T-StB 2002 for a lifetime of 30 years. In these specification, the layer thicknesses, minimum compaction degree and mixture design are defined. Normally, the lifetime of surface layer average out twelve years, the binder layer 24 years and the asphalt base layer 30 years. Thus, the surface layer of reference variant has to bear a minimum lifetime of 12 years. The calculated lifetime of the reference variant with a compaction degree of k = 97% does not reach the minimum lifetime of twelve years. Hence, for

Table 1. Calculation of indicator (SMA and ABI).

	$\frac{1}{2} * \ln (t_{calculated} - t_{design} + 1); t_{calculated} > t_{design}$ $\frac{1}{2} * \ln (t_{design} - t_{calculated} + 1); t_{calculated} > t_{design}$				$\frac{1}{2} * \ln(W_{p97}/W_{p,k})$				
k [%]	Reference	50/70	PmB 45A	PmB 25 H	Reference	50/70	PmB 45A	PmB 25 H	e^p
101.5	+2.86	+1.56	+4.89	+8.24	+0.58	+0.76	+0.60	+0.35	
101.0	+2.65	+1.18	+4.58	+8.04	+0.52	+0.68	+0.56	+0.31	
100.0	+2.22	–0.69	+3.94	+7.64	+0.39	+0.51	+0.42	+0.23	
99.0	+1.74	–1.12	+3.30	+7.24	+0.26	+0.34	+0.28	+0.16	
98.0	+1.06	–1.22	+2.63	+6.84	+0.13	+0.17	+0.14	+0.08	
97.0	–0.75	–1.26	+1.89	+6.43	+0.00	0.00	0.00	0.00	0.00
96.0	–1.11	–1.27	0.66	+6.01	–0.13	–0.17	–0.14	–0.08	–2.72
95.0	–1.22	–1.28	–1.10	+5.59	–0.26	–0.34	–0.28	–0.16	–7.39
94.0	–1.25	–1.28	–1.24	+5.17	–0.39	–0.51	–0.42	–0.23	–20.09

The prefix plus distinguishes bonus and the prefix minus distinguishes penalty.

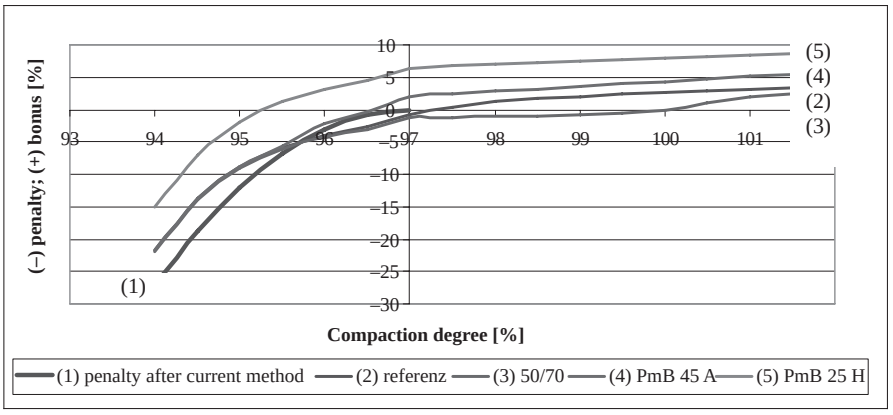

Figure 6. Payment adjustment for surface- and binder layers.

the reference asphalt with a compaction degree k > 97.5% a bonus and with a compaction degree < 97.5 a penalty will be determined. According to this, to fulfil the minimum lifetime of twelve years and to elude the penalty, the pavement construction with reference asphalt shall be paved with a compaction degree of k < 97.5%. The innovative asphalt variants PmB 25 H till a compaction degree of k = 94.0% show long life time than the average lifetime of 12 years. But this variant will be awarded till a compaction degree of k > 95.5%. With dropping below the compaction degree of k = 95.5%, a penalty will be calculated, although this variant shows a long lifetime than minimum lifetime of 12 years till a compaction degree of k = 94%. The penalty is caused by the parameter for dropping below the agreed minimum compaction degree, which is higher than the parameter for improvement of lifetime. Furthermore this variant will be imposed with lowest penalty compared to other variants. The conventional asphalt 50/70 with the lowest lifetime compared to other asphalt with similar compaction degree gets the lowest bonus and highest penalty. The modified asphalt PmB 45A with a compaction degree k > 96.8% will be awarded with a bonus and with dropping below this compaction degree the payment will be adjusted with a penalty.

For the reference asphalt with a compaction degree of k = 100 % the payment increases up to 3% of agreed unit price. For this 3% cost increase, an improvement of fivefold lifetime for surface- and binder layer has been determined. For the other surface- and binder asphalts similar performance improvements have been investigated. For the high quality asphalt PmB 25H with the agreed minimum compaction degree of k = 97% a bonus of 6.4% of agreed unit price has been calculated. Therefore a reconstruction of surface and binder layer within the design lifetime of 30 years will not be necessary. This shows, that the payment adjustment, recommended in this paper, results in high cost effectiveness for both client and contractor. By means of bonuses the contractor can compensate the increased costs caused by additional compaction and can plan from the beginning with more compaction than else. Furthermore the chance to dropping below the minimum compaction degree with additional compaction is much lower compared to tight calculated compaction. For the bonus the client gets high quality asphalt with low life cycle cost.

3.2 *Payment adjustment for asphalt base layer*

The payment for asphalt base layer will be calculated by means of equation 6 and 7.

$$\text{bonus/penalty} = \ln\left(t_{calculated} - t_{design} + 1\right) + \ln\left(N_{f,k}/N_{f,k\,(min)}\right) - e_p \qquad (6)$$
$$t_{calculated} > t_{design}$$

$$\text{penalty} = -\ln\left(t_{design} - t_{calculated} + 1\right) + \ln\left(N_{f,k}/N_{f,k\,(min)}\right) - e_p \qquad (7)$$
$$t_{calculated} < t_{design}$$

bonus/penalty bonus/penalty (%) of agreed unit price [€/m²] or [€/t],
$t_{calculated}$ calculated lifetime (year),
t_{design} design lifetime (year),
$N_{f,k\ (min)}$ calculated load cycle at agreed minimum compaction degree (mm),
$N_{f,k}$ calculated load cycle at achieved compaction degree in situ (mm),
p different of agreed minimum compaction degree and achieved compaction degree in situ, in case of dropping below the minimum compaction degree.

For asphalt base layer a design lifetime of 30 years is considered. It is assumed, that the reference asphalt with the compaction degree of k = 97% has a lifetime of 30 years. Thus, the load cycles to failure $N_{f,k}$ of the reference pavement at a compaction degree of k = 97% will be equal to a 30 year lifetime. Lifetime of other asphalt pavements with respect to different compaction degrees will be calculated proportional to load cycles $N_{f,k}$ of the reference pavement at a compaction degree of k = 97%. The load cycles $N_{f,k}$ can be calculated by means of regression equations from Figure 5 with respect to different compaction degrees. By means of such calculated lifetimes and load cycles to failure with respect to a specific compaction degree, the sum of the indicators can be calculated (Table 2). The calculated payment adjustment is displayed in Figure 7.

With respect to the calculated payment adjustment and the curve trend, it can be summarised, that the asphalt with long lifetime will have the highest bonus and lowest penalty

Table 2. Calculation of indicator (ABL).

	$\ln (t_{calculated} - t_{design} + 1);\ t_{calculated} > t_{design}$				$\ln (N_k/N_{k\ (min)})$				
	$-\ln (t_{design} - t_{calculated} + 1);\ t_{calculated} < t_{design}$				$\ln (N_k/N_{k\ (min)})$				
k [%]	Reference	50/70	PmB 45A	PmB 25 H	Reference	50/70	PmB 45A	PmB 25 H	e^p
101.5	+3.32	+3.39	+5.42	+8.92	+0.64	+0.64	+0.90	+1.19	
101.0	+3.17	+3.24	+5.31	+8.78	+0.57	+0.57	+0.80	+1.06	
100.0	+2.83	+2.91	+5.08	+8.52	+0.42	+0.43	+0.60	+0.80	
99.0	+2.38	+2.49	+4.84	+8.25	+0.28	+0.28	+0.40	+0.53	
98.0	+1.72	+1.89	+4.58	+7.98	+0.14	+0.14	+0.20	+0.27	
97.0	0.0	0.65	+4.32	+7.71	+0.00	+0.00	0.00	0.00	0
96.0	–1.60	–1.43	+4.03	+7.44	–0.14	–0.14	–0.20	–0.27	–2.72
95.0	–2.13	–2.04	+3.71	+7.17	–0.28	–0.28	–0.40	–0.53	–7.39
94.0	–2.43	–2.38	+3.34	+6.90	–0.42	–0.43	–0.60	–0.80	–20.1

The prefix plus distinguishes bonus and the prefix minus distinguishes penalty.

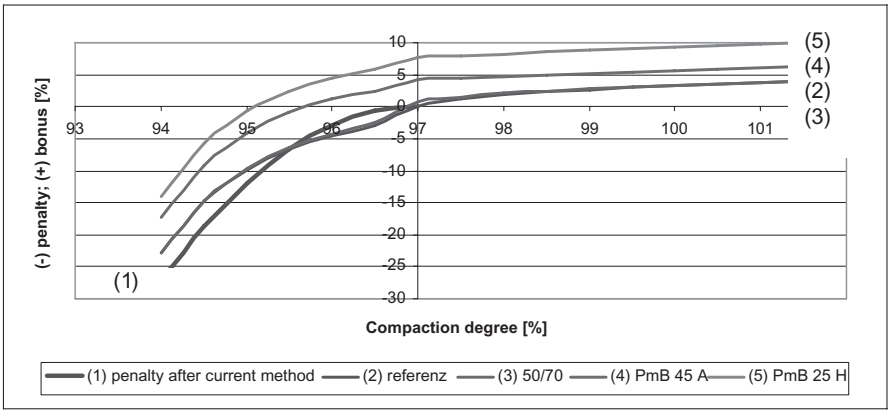

Figure 7. Payment adjustment for asphalt base layers.

compared to asphalt with low lifetime. In addition, in the case of dropping below the minimum compaction degree, asphalt with long lifetime can be awarded too, if the bonus for the improvement of lifetime is higher than the penalty for the dropping below the minimum compaction degree. A low quality asphalt with an over compaction degree compared to the agreed minimum compaction degree can be also punished with a penalty, if the paved asphalt the agreed lifetime will not achieve.

4 SUMMARY

A performance oriented calculation of payment adjustment will be recommended, so that in case of lifetime improvement compared to design lifetime a bonus and in the case of dropping below the minimum compaction degree a penalty can be calculated. Thereby the lifetime for four different asphalt pavement types with three different binders have been calculated by means of laboratory tests and analytical performance models. The lifetime of surface- and binder layers have been calculated with respect to the rutting development. The lifetime of asphalt base layers was calculated with respect to the fatigue failure. The calculation results show significant effects with respect to the binder used and to the different compaction degrees investigated. Asphalt with high quality binder shows a significant increase in lifetime and also a significant decrease of life cycle costs compared to asphalt with conventional binder. By means of this calculated results, highest bonus and lowest penalty for asphalt with long lifetime and lowest bonus and highest penalty for asphalt with low lifetime has been determined. It shows that the payment of paving quality for innovative asphalt with a long lifetime can be adjusted in a different manner than in case of using conventional asphalt with low lifetime.

REFERENCES

AP Nr. 9/A1 2001. Arbeitspapiere zur Systematik der Straßenerhaltung, Teil: Zustandserfassung und—bewertung der Fahrbahnoberflächen von Straßen (ZEB), Reihe A: Auswertung, Abschnitt A1: Zustandsbewertung, FGSV press, Cologne, Germany [Outline for systematical pavement maintenance, acquisition and evaluation of pavement condition].

Beckedahl, H.J. et al. 2008a. A Comparative Design of Asphalt Pavement with Innovative and Conventional binders, *ICTI 2008, International Conference on Transport Infrastructure*, *April 24–26 2008*. Beijing, China.

Beckedahl, H.J. et al. 2008b. Impacts of the Compaction Degree of Asphalt Mixes on the Asphalt Pavement Performance—Temperature Dependent Resilient Modules, Rutting and Fatigue, *4th Eurasphalt & Eurobitume Congress 2008, 21st to 23rd May 2008*. Copenhagen, Danmark.

COST 333 1999. Development of New Bituminous Pavement Design Method, Transport Research, European Commission, Luxembourg.

RDO Asphalt 2008. Richtlinien für die rechnerische Dimensionierung des Oberbaues von Verkehrsflächen mit Asphaltdecke, FGSV press (draft), Cologne, Germany [guidelines for analytical design of asphalt pavement construction].

RStO 2001. Richtlinien für die Standardisierung des Oberbaues von Verkehrsflaechen, FGSV Press, Cologne, Germany [guidelines for design of asphalt pavement construction].

ZTV Asphalt-StB: Zusätzliche Technische Vertragsbedingungen und Richtlinien für den Bau von Fahrbahndecken aus Asphalt, FGSV-Verlag, Cologne, Germany, 2001 [Additional terms of contract and guidelines for asphalt pavement construction].

Advanced Testing and Characterization of Bituminous Materials –
Loizos, Partl, Scarpas & Al-Qadi (eds)
© 2009 Taylor & Francis Group, London, ISBN 978-0-415-55854-9

Performance of hot mix asphalt surface under high tire pressure aircraft landing gear configuration at the FAA National Airport Pavement Test Facility

N. Garg
FAA Airport Technology R&D Branch, Atlantic City International Airport, NJ, USA

T. Bennert
Rutgers University, Center for Advanced Infrastructure and Transportation, New Brunswick, NJ, USA

H. Brar
SRA International Inc., Linwood, NJ, USA

ABSTRACT: During Construction Cycle 5 (CC5) at the Federal Aviation Administration (FAA) National Airport Pavement Test Facility (NAPTF), flexible pavement test items will undergo full-scale testing under 10- and 6-wheel landing gear configurations at high wheel loads (in excess of 55,000 lb (25 tonnes)) and tire pressures (in excess of 220 psi (1.52 MPa). The NAPTF is located at the FAA William J. Hughes Technical Center, Atlantic City International Airport, New Jersey, and is used to generate full-scale pavement response and performance data for development and verification of airport pavement design criteria. All the test items have 5-inch (127-mm) thick P-401 Hot Mix Asphalt (HMA) surface, 8-inch (203-mm) thick P-209 crushed stone aggregate base, and two different P-154 subbase thicknesses (34 and 38 inches (864 and 965 mm)). The HMA mix design was performed using the Marshall mix design procedure (as per FAA P-401 specification). During HMA surface construction, the mix was collected for laboratory testing. Cylindrical samples were prepared using a Marshall hammer, and a Superpave Gyratory Compactor. Cores from the paved HMA surface were extracted. The HMA was characterized using laboratory test results (including dynamic modulus tests, simple performance test/repeated load mode, rut resistance tests using asphalt pavement analyzer, etc.). The performance (rutting, surface cracking, and other distresses) of pavement test items under heavy gear loads and high tire pressure was regularly monitored. After the complete structural failure of pavement test items, cores from HMA surface will be extracted to study rutting experienced in the HMA layer. This paper summarizes the results from laboratory HMA characterization tests and observed pavement performance under accelerated full-scale traffic tests. The results from this study provide HMA performance data under high tire pressures.

1 INTRODUCTION

Hot Mix Asphalt (HMA) design for commercial airports in the United States of America is performed in accordance with guidelines set forth in the Federal Aviation Administration (FAA) Advisory Circular AC 150/5370-10C, "Standards for Specifying Construction of Airports," Item P-401—Plant Mix Bituminous Pavements (2007). A Marshall mix design criterion is used. For pavements designed for aircraft gross weights in excess of 60,000 lb (27.2 tonnes) and tire pressures exceeding 100 psi (0.69 MPa), a 75-blow mix is used. The FAA airport pavement thickness design standards, referenced in Chapter 7 of Advisory Circular AC 150/5320-6D, change 3, are implemented in the computer program LEDFAA. For new flexible or HMA overlay pavement design, the HMA modulus is fixed at 200,000 psi (1.38 GPa). Rutting in the HMA layer is not directly considered and the fatigue life of the pavement is assumed to be directly related to cracking initiated at the bottom of

the asphalt layer ("bottom-up") and is computed using the Heukelom and Klomp (1964) relationship. The same procedure will be followed in the new thickness design computer program FAARFIELD.

According to Roginski (2007), the trend in aircraft design is to produce aircraft with extended range capability, which results in high gross weight and tire pressures. The new generation aircraft such as Boeing 787 and Airbus 350 are anticipated to have tire pressures in excess of 220 psi (1.52 MPa). The effects of high tire pressure are localized and concentrated in the surface layers (HMA). This makes it imperative to study the effects of high tire pressures on the HMA surface and also develop HMA mix design procedures to produce mixes that can withstand these anticipated high tire pressures. The FAA has started two projects to achieve this objective. The first project is titled "Research and Testing to Establish Updated Specifications for FAA Airfield Quality Hot Mix Asphalt." The objective of this project is to establish specifications for designing asphalt mixes using the Superpave Gyratory Compactor (SGC) that provides performance equivalent to the specifications for the Marshall mix designs. The second project is the "HMA Design and Testing for High Pressure Aircraft Tires." The main objective of this project is to conduct research into the design of HMA to resist damage from high pressure aircraft tires.

During Construction Cycle 5 (CC5) at the FAA National Airport Pavement Test Facility (NAPTF), flexible pavement test items will undergo full-scale tests under 10- and 6-wheel landing gear configurations at high wheel loads (in excess of 55,000 lb (25 tonnes)) and tire pressures in excess of 220 psi (1.52 MPa). During HMA surface construction, mix samples were collected for laboratory testing. Cylindrical samples were prepared using the Marshall hammer and the SGC. Cores from the paved HMA surface were extracted. The HMA was characterized using laboratory test results. Tests included dynamic modulus tests, simple performance test/repeated load mode, rut resistance tests using asphalt pavement analyzer, etc. The performance (rutting, surface cracking, other distresses) of pavement test items under heavy gear loads and high tire pressure was regularly monitored. This paper summarizes the results from laboratory HMA characterization tests and observed pavement performance under accelerated full-scale traffic tests. Results from tests on samples compacted using the SGC are presented. Other tests results will be added once the tests are completed.

2 NATIONAL AIRPORT PAVEMENT TEST FACILITY

The FAA NAPTF is located at the FAA William J. Hughes Technical Center, Atlantic City International Airport, New Jersey. The primary objective of the tests is to generate full-scale

Figure 1. National airport pavement test facility.

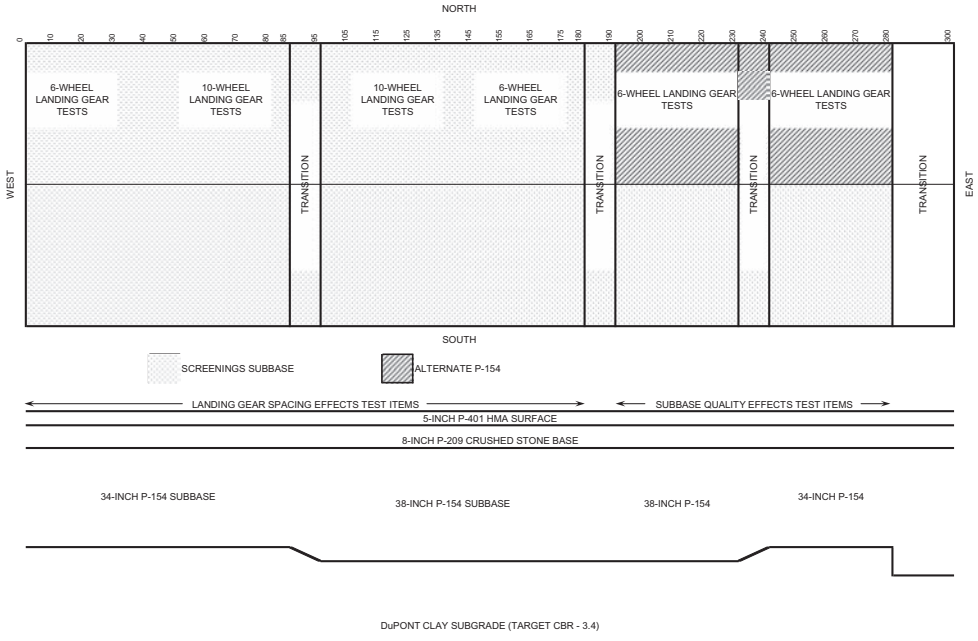

Figure 2. CC5 test item layout (1 inch = 25.4 mm).

Table 1. Job mix formula properties at optimum asphalt content.

Test property	Value
Compactive effort	75 Blows
Asphalt content	5.2%
Marshall stability	2402 lb (10.68 kN)
Flow value (0.01 inch)	10
Air voids	3.9%
Voids in mineral aggregate (VMA)	16.4%
Unit weight	155.8 lb/ft^3 (2496 kg/m^3)
Tensile strength ratio (ASTM D 4867)	87.1
Maximum theoretical specific gravity	2.598

pavement performance and response data for development and verification of airport pavement design criteria. It is a joint venture between the FAA and the Boeing Company, which became operational on April 12, 1999. The test facility consists of a 900-ft (274.3-m) long by 60-ft (18.3-m) wide test pavement area, embedded pavement instrumentation and a dynamic data acquisition system, environmental instrumentation and a static data acquisition system, and a test vehicle for loading the test pavement with up to 12 aircraft tires at wheel loads of up to 75,000 lb (334 kN). Figure 1 shows the NAPTF and the test vehicle.

The main objectives for CC5 were to study the effect of landing gear spacing and subbase quality on flexible pavement performance. Test item details (layout and layer thicknesses) are given in Figure 2.

The HMA mix design was performed using the Marshall mix design procedure following the FAA P-401 specification. The job mix formula properties at optimum asphalt content are shown in Table 1.

3 HMA CHARACTERIZATION

HMA characterization tests were conducted on loose mix sampled during the paving operation at the NAPTF. The loose mix was brought back to the Rutgers Asphalt Pavement Laboratory (RAPL) for compaction and testing. All samples were laboratory-aged according to AASHTO R30 prior to compaction. Samples were compacted to a target air void level of 5.0% ± 0.5%, which corresponded to the in situ air void levels recorded from extracted cores.

3.1 *Measured dynamic modulus*

Dynamic modulus tests were conducted to evaluate the time-temperature dependency of the HMA. The recommended procedure from NCHRP Report 614 (Bonaquist, 2008) was used. The data was collected at three temperatures: 39º, 68º, and 95ºF (4º, 20º, and 35ºC) using loading frequencies of 25, 10, 5, 1, 0.5, 0.1, and 0.01 Hz.

The dynamic modulus test results were used to construct a dynamic modulus master curve, shifted to 77ºF (25ºC), which represented the average in situ temperature of the asphalt layer. Figure 3 shows the resultant dynamic modulus master curve.

The benefit of constructing a dynamic modulus master curve is that the asphalt modulus can be determined at any loading frequency (speed) or temperature by simply "shifting" the curve using superposition principles of visco-elasticity theory (Pellinen et al., 2004). Loading frequencies were determined for the top and bottom of the HMA layer, based on wheel loads and tire pressures. The NAPTF load configurations (55,000 lb (25 tonnes) and 220 psi (1.52 MPa) tire pressure) create a contact area of 250 in^2 (0.16 m^2). Based on Figure 4 (ARA, 2004), 17.84 inches (0.45 m) is the effective length (contact diameter) at the surface of the HMA layer.

Assuming that the stress bulb migrates downward at a 45-degree angle and the HMA thickness is 5 inches (127 mm), the effective length at the bottom of the HMA is 27.84 inches (707 mm). Using the relationship shown in Figure 4 (ARA, 2004) and the general trafficking speed (2.5 mph (4 kmph)) at the NAPTF, the loading frequency at the surface is 2.47 Hz,

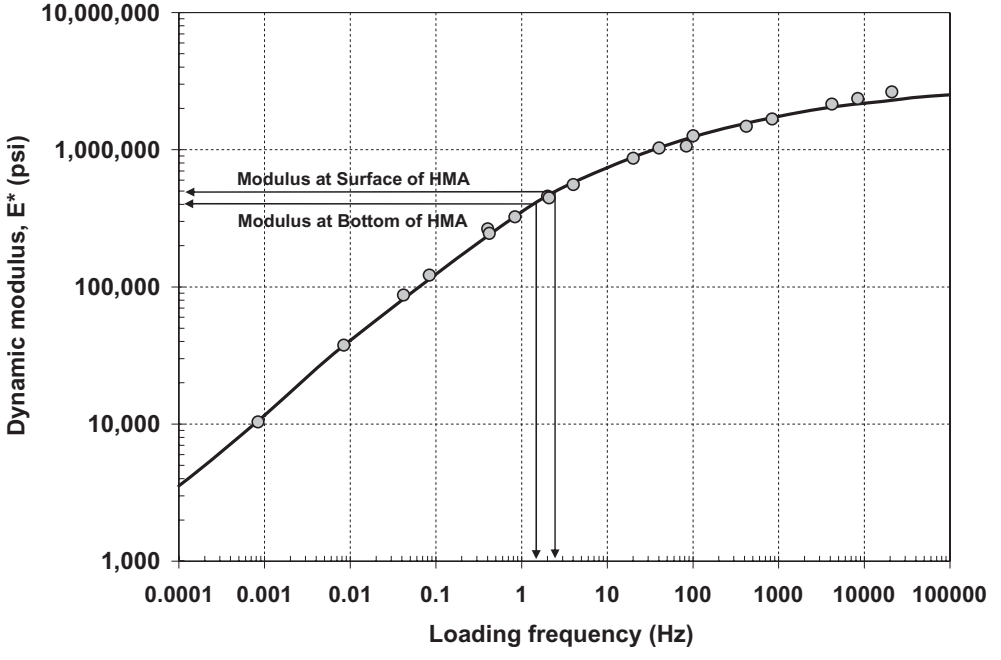

Figure 3. Dynamic modulus master curve of the HMA at the NAPTF (1 psi = 6.89 kPa).

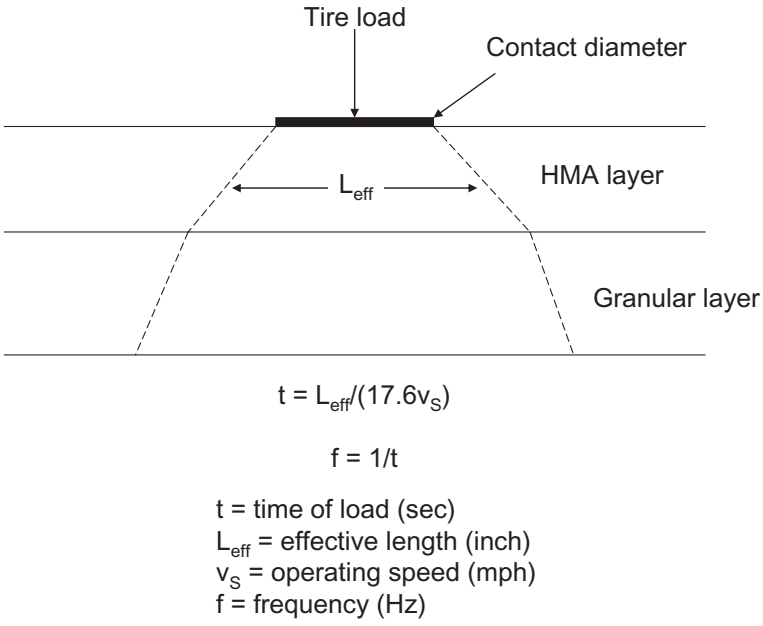

Figure 4. Effective length and loading frequency determination (adapted from ARA, 2004).

and the loading frequency at the bottom is 1.58 Hz. Utilizing the dynamic modulus master curve shown in Figure 3, these loading frequencies correspond to dynamic modulus values of 483,000 psi (3.33 GPa) (surface) and 416,000 psi (2.87 GPa) (bottom), respectively. Both modulus values are over two times the recommended design value (200,000 psi (1.38 GPa)) currently used in the LEDFAA software.

3.2 *Predicted dynamic modulus comparisons*

For most FAA design projects, it may be impractical to actually measure the dynamic modulus values since pavement designs are conducted far in advance of the contractor selection and construction. Therefore, using the dynamic modulus prediction equations may be a more viable solution if future FAA design procedures are to include Dynamic Modulus Master curves for the asphalt layer design modulus.

Two different dynamic modulus prediction methodologies were evaluated in this study: Witczak Prediction Equation (Andrei et al., 1999) and the Hirsch Model (Christensen et al., 2002). The Witczak Prediction Equation (WPE) utilizes aggregate gradation properties, mixture volumetrics (effective binder content by volume and air voids), and the asphalt binder viscosity properties to predict the dynamic modulus of asphalt mixtures. Meanwhile, the Hirsch Model utilizes the mixture's volumetric properties (voids in mineral aggregate (VMA) and voids filled with asphalt (VFA)) and the shear modulus (G*) properties of the asphalt binder tested at the identical temperatures and loading frequencies as the dynamic modulus test.

Dynamic modulus master curves were generated for both prediction methodologies and compared with the measured test results (Figure 5). The test results from Figure 5 show that a better correlation was found between the measured test results and the Hirsch model than with the WPE.

The measured and predicted results were further compared using the calculated loading speeds (frequencies) at the top and bottom of the HMA layer. The comparisons are shown in Table 2 and further show the Hirsch Model results are in better comparison to the measured test results.

Table 2. Predicted vs measured dynamic modulus results at in situ loading speeds.

Test method	Modulus at top of HMA (2.47 Hz), psi (GPa)	Modulus at bottom of HMA (1.58 Hz), psi (GPa)
Measured	483,255 (3.33)	415,964 (2.866)
WPE	526,028 (3.624)	479,912 (3.307)
Hirsch	471,640 (3.250)	413,322 (2.848)

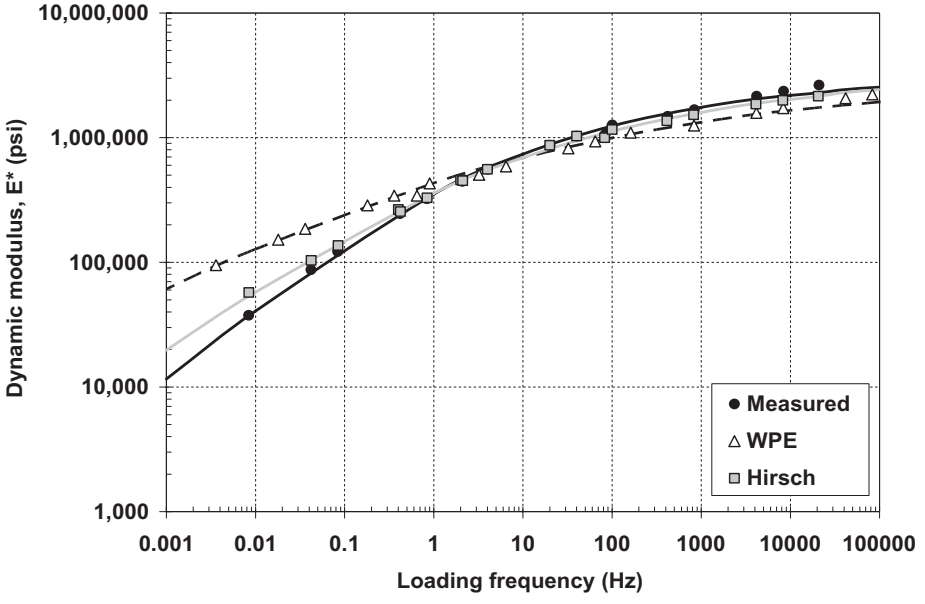

Figure 5. Comparisons of measured and predicted dynamic modulus (1 psi = 6.89 kPa).

3.3 *Flexural fatigue evaluation*

To evaluate the fatigue response of the HMA, the Flexural Beam Fatigue test was conducted in accordance with AASHTO T321. However, AASHTO T321 recommends that a haversine waveform be used, which would represent the general pavement response from a single wheel load (Figure 6a). A majority of the loading at the NAPTF is conducted using tandem and tridem wheel configurations, which results in very different asphalt strain gage response patterns (Figure 6b and 6c).

To represent the actual NAPTF pavement response (asphalt strain gage response) conditions, the applied tensile strain pulse for tandem and tridem gears were used in the Flexural Beam Fatigue test, along with the single axle response represented by a haversine waveform. The different waveform profiles matched those previously used by Carpenter and Jansen (1997). The test conditions during the fatigue test included:

– 77°F (25°C) test temperature (equivalent to measured in situ temperatures)
– 10 Hz loading frequency
– Variable applied waveforms

The test results of the fatigue analysis are shown in Figure 7. The results clearly show the dependence of the fatigue resistance on the type of applied waveform (i.e., axle gear configuration). Higher fatigue resistance was achieved during the single axle configuration, while the lowest fatigue resistance was achieved during the three-axle configuration. On average, the

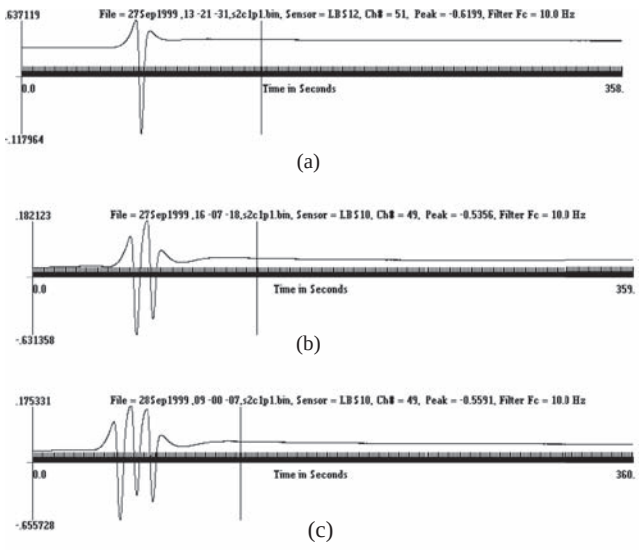

Figure 6. NAPTF asphalt strain gage response from a) single axle gear, b) 2 axle gear, and c) 3 axle gear (from Garg, et al., 2001).

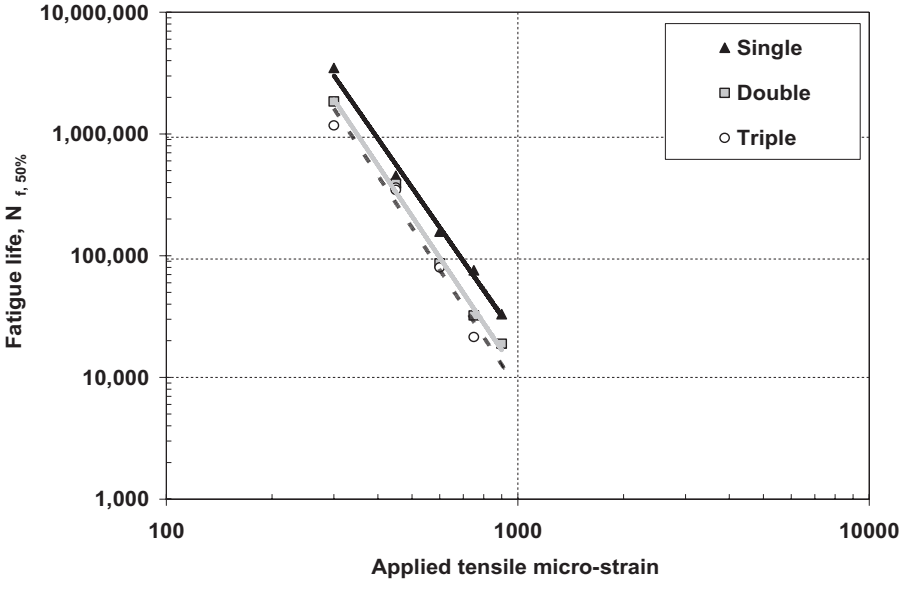

Figure 7. Flexural beam fatigue test results modeling different axle loading configurations.

two-axle configuration resulted in a 41.3% reduction in fatigue resistance compared to the single-axle configuration, whereas the three-axle configuration resulted in a 51.8% reduction in fatigue resistance compared to the single-axle configuration.

3.4 *Rutting evaluation (asphalt pavement analyzer)*

The rutting resistance of asphalt mixture was evaluated using the Asphalt Pavement Analyzer (APA) (AASHTO TP63) at two different test temperatures 77°F (25°C) and 148°F (64°C).

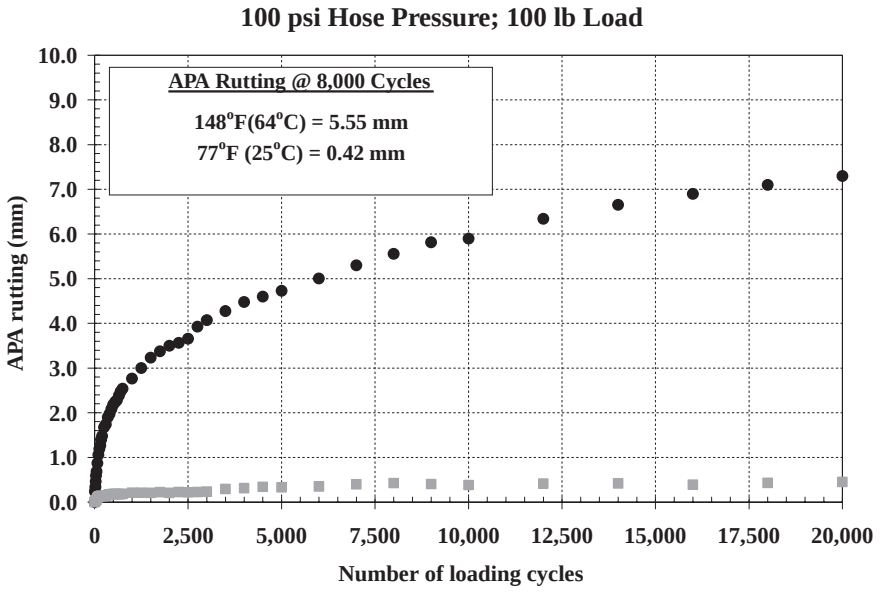

Figure 8. Results from APA tests (1 psi = 6.89 kPa).

The 77ºF (25ºC) test temperature was selected to correspond to the measured in situ test temperature while 64ºC (148ºF) is the commonly used test temperature in the APA. Although it is recognized that the loading conditions in the APA are more commonly associated with highway conditions, the main goal of the APA test was to evaluate the change in rutting response due to test temperature.

As the results in Figure 8 indicate, the change from 148ºF (64ºC) to 77ºF (25ºC) resulted in a 92.4% reduction in the asphalt mixture rutting. This corresponds to the general findings at the NAPTF where minimal to no rutting is commonly measured. To date, all measured rutting has been associated with permanent deformation in the subgrade and the unbound aggregate layers.

4 HMA PERFORMANCE UNDER TRAFFIC TESTS

Traffic tests were started on the test items north of centerline (as shown in Figure 2). The traffic tests were started with a 10-wheel gear configuration (center to center spacing of 114 inches (2.9 m) between the 6- and 4- wheel landing gears) and 6-wheel landing gear configuration (on the subbase quality effects test items), as shown in Figure 2. Wheel load was set at 50,000 lb (22.7 tonnes) for the landing gear spacing test items (both for the 10- and 6-wheel gear configurations), and 59,000 lb (26.8 tonnes) for the subbase quality effects test items (only the 6-wheel gear configuration was used). The landing gear configuration had dual and tandem spacing of 54 and 57 inches (1.21 and 1.45 m), respectively.

Trafficking started on August 14, 2008. A fixed wander pattern was applied to the traffic during the tests. The wander pattern consisted of 66 repetitions, 33 traveling east and 33 traveling west. The transverse position of the gears was changed only at the start of the eastward repetitions. The wander pattern was designed to simulate a normal distribution with standard deviation of 30.5 in. (775 mm) (equivalent to a taxiway distribution for design). The distribution of the transverse wheel positions is not random, but consists of nine equally spaced wheel paths at intervals of 10.25 in. (260 mm).

Traffic tests will continue until either structural failure occurs or it is estimated that failure is unlikely to occur within a reasonable number of passes at the applied load. The failure criterion is the presence of at least 1 inch (25.4 mm) of surface upheaval adjacent to the

traffic lane. This is the same as the criterion used by the U.S. Army Corps of Engineers in previous full-scale tests of flexible airport pavements and is indicative of shear failure in the subgrade. During the traffic tests, the test items were monitored through a combination of visual surveys and non-destructive testing, including periodic straightedge rut depth measurements, surface profile measurements, and heavy weight deflectometer measurements.

Due to a minimal amount of distress in the landing gear spacing test items, after about 8,000 passes, the applied wheel loads were increased from 50,000 lb (22.7 tonnes) to 58,000 lb (26.3 tonnes).

About 12,408 passes have been completed and traffic tests have been suspended due to the winter. Traffic tests will restart in the summer of 2009. There are no signs of any fatigue cracking. HMA cores (18 in number) were extracted from the trafficked and non-trafficked area for laboratory testing. No signs of any significant/measurable rutting were observed from the cores (from trafficked area). Dynamic modulus tests will be performed on the cores extracted from the test items.

5 SUMMARY/CONCLUSIONS

The main objectives for CC5 flexible test items were to study the effect of landing gear spacing and subbase quality on pavement performance. This paper presents the results from HMA characterization tests that included dynamic modulus tests, simple performance test/repeated load mode, and rut resistance tests using the asphalt pavement analyzer. The performance (rutting, surface cracking, and other distresses) of pavement test items under heavy gear loads and high tire pressure was regularly monitored. These tests were performed on samples compacted using a SGC at air voids representative of in situ conditions. The test results on cores obtained from the pavement test items will be added at a later stage once the tests are completed. The laboratory test results do not show any inherent weakness or problems in the mix design. The HMA layer has been performing well under heavy gear loads and high tire pressures. No signs of any significant rutting or fatigue failure were observed. The results from the study highlight the fact that HMA mix, designed following P-401 specifications, in general, would be rut resistant and is capable of handling heavy aircraft wheel loads and high tire pressures.

ACKNOWLEDGMENTS/DISCLAIMER

The work described in this paper was supported by the FAA Airport Technology Research and Development Branch, Manager, Dr. Satish K. Agrawal. The authors would like to thank Jeffrey Gagnon (Manager, Airport Pavements AJP-6312), Dr. Gordon Hayhoe (Manager, NAPTF), and Dr. David Brill for their comments and support during preparation of this paper. The contents of the paper reflect the views of the authors who are responsible for the facts and accuracy of the data presented within. The contents do not necessarily reflect the official views and policies of the FAA. The paper does not constitute a standard, specification, or regulation.

REFERENCES

Andrei, D., Witczak, M. & Mirza, M. 1999. Development of a revised predictive model for the dynamic (complex) modulus of asphalt mixtures. *NCHRP 1-37A Inter Team Report*, University of Maryland.

Applied Research Associates (ARA). 2004. Development of the 2002 guide for the design of new and rehabilitated pavement structures. *NCHRP 1-37A, Final Report*. National Research Council.

Bonaquist, R. 2008. Refining the Simple Performance Tester for Use in Routine Practice. *NCHRP Report 614.* National Cooperative Highway Research Program, NCHRP, Transportation Research Board, Washington, D.C.

Carpenter, S. & Jansen, M. 1997. Fatigue behavior under new aircraft loading conditions. *Proceedings, Aircraft/Pavement Technology: In the Midst of Change.* American Society of Civil Engineers, Seattle, Washington.

Christensen, D., Pellinen, T. & Bonaquist, R. 2002. Hirsch model for estimating the modulus of asphalt concrete. *Proceedings of the Association of Asphalt Paving Technologists*, Vol. 72.

Federal Aviation Administration, Office of Airport Safety and Standards. *Standards for Specifying Construction of Airports*. *Advisory Circular AC 150/5370-10C*, U.S. Department of Transportation, 2007 (also see http://www.faa.gov/arp/150acs.htm for updates).

Garg, N. & Hayhoe, G.F. 2001. Asphalt concrete strain responses at high loads and low speeds at the National Airport Pavement Test Facility (NAPTF). *Proceedings, 2001 Airfield Pavement Specialty Conference: Advancing Airfeld Pavements.* American Society of Civil Engineers. Chicago, IL, USA.

Heukelom, W. & Klomp, A.J.G. 1964. Road design and dynamic loading. *Proceedings, Association of Asphalt Paving Technologists*, Vol. 33.

Pellinen, T., Witczak, M.W. & Bonaquist, R. 2004. Asphalt mix master curve construction using sigmoidal fitting function with non-linear least squares optimization. *Recent Advances in Materials Characterization and Modeling of Pavement Systems, Geotechnical Special Publication No. 123.* American Society of Civil Engineering.

Roginski, M.J. 2007. Effects of aircraft tire pressures on flexible pavements. *Proceedings, Advanced Characterisation of Pavement and Soil Engineering Materials.* Athens, Greece.

Advanced Testing and Characterization of Bituminous Materials – Loizos, Partl, Scarpas & Al-Qadi (eds)
© 2009 Taylor & Francis Group, London, ISBN 978-0-415-55854-9

Quantification of the highway costs as a function of the road traffic and speed

A.C. Valle de Souza & D. Cardoso de Lima
Universidade Federal de Viçosa, Viçosa, MG, Brazil

ABSTRACT: An analysis of the maintenance and investment costs was carried out in order to contribute for the road traffic operation. Based on the concepts of resilience or deformability of the asphalt mixtures, the sensibility of the maintenance costs in some reference pavement structures in which the asphalt layer has different values for resilient modulus were analyzed. In the methodology under use, the variation in the loading time was taking into account in order to obtain the value of the resilient asphalt modulus, by simulating the variation of the vehicle speed in situ. The application of the capacity and service level concepts of TRB (Transportation Research Board) made possible to quantify the increment in the maintenance costs based on the decreased capacity in the transversal section of the highways. It is also presented the evolution of the maintenance costs due to highway traffic increase at different service levels.

1 INTRODUCTION AND OBJECTIVES

Aiming to contribute to the operation of the road traffic, this study presents an estimative analysis of both maintenance and investment costs of the bituminous mixtures in flexible pavements. It also presents some results obtained by Souza (1998).

For a better understanding about the behavior of an asphalt mixture, it is necessary to know the resilience concept and the parameter used in its evaluation, that is called as resilient modulus.

The resilient modulus (M_r) of a bituminous mixture is defined by Bernucci et al. (2006, p. 291) as the relationship between the tension stress (σ_t) repeatedly applied on the vertical diametrical plan at the cylindrical sample of bituminous mixture and the recoverable specific deformation (ε_t) corresponding to the applied tension at a temperature (T°C), for determined frequency and time of load application.

$$M_r = \frac{\sigma_t}{\varepsilon_t} \tag{1}$$

In this definition the resilient modulus of asphalt mixtures is obtained from the Brazilian tensile strength test as described by Motta and Medina (2005, p. 213).

The frequency is associated to the number of vehicle axes on a highway, and the loading time simulates vehicles speed. Taking into account that the resilient modulus value of the asphalt covering is a function of the characteristics of the mixture (Motta et al., 1992), of the environmental conditions, and of the loading application time or speed (Fernandes Jr., 1994), and that different asphalt layer thicknesses conducts to different cost estimations (MacDowell, 1976 and 1994), this work was conducted with the following objectives: a) to study the conservation costs as a function of different dynamic requirements of the pavement, that is to evaluate the effect of load application at variable speed levels; b) to present the evolution of the maintenance costs along the pavement service life based on the characteristics of traffic flow and capacity of the highway transversal section at different service

levels, as defined by HCM (Transportation Research Board—TRB, 2000); and c) to investigate the effect of bituminous mixtures grain size distribution on costs behavior.

2 METHODOLOGY

The methodology used to evaluate the effects of traffic speed on both maintenance and investment costs consisted of a cost sensibility analysis applied to reference structures consisting of three layer pavements. The resilient modulus values of the asphalt layers were estimated using formulas developed by Heukelon and Klomp (1964). Values of 1,200 kgf/cm^2 and 3,000 kgf/cm^2 were adopted, respectively, for the modulus of the road subgrade and base layer. The modulus of the surface layers were obtained via the mentioned formulas, for three types of bituminous mixtures, at 25°C and speed levels varying with the rigidity characteristics of the chosen asphalt (CAP-20).

The bituminous mixtures design encompassed the following grain size ranges: (i) Sample 1—mixture following the range C of the DNER's recommended grain size distribution (currently DNIT)[1]; (ii) Sample 2—mixture following the range B of the DNER's recommended grain size distribution; and (iii) Sample 3—mixture following the range V-A of the Asphalt Institute recommended grain size distribution. The Annex A presents information about the asphalt and the mixtures grain size distributions, as well as respective design indexes. Adopted traffic design data were as follows: (i) trucks percentage = 40%; (ii) TMD = 10,000 (daily average traffic assuming a geometric growth yearly rate of 4%; (iii) FV = 3,318 (average vehicle factor of commercial vehicles); (iv) f = 4 (lane numbers: two by direction); and (v) $N = 4{,}12 \times 10^7$ (number of equivalent single axle load (ESAL) determined using DNER's load equivalence factors (or USACE) for a 20-years project period.

Table 1 presents data from the pavements structure design performed through the software *Fepave* (Silva, 1995), at the speed level of 35 km/h (time of the standard loading corresponding to 0.10 s). The correspondence between speed and loading time was obtained for a 10 cm average depth from Figure 1.

Considering the thicknesses shown in Table 1, and the surface layer modulus corresponding to the design mixtures at different traffic speed levels, the reference pavements structural numbers were obtained. From these structural numbers together with the adopted traffic data previously reported, and applying the Methodology of the Modified Basic Cost (MacDowell, 1976 and 1994), it was possible to determine the forecast equations for the maintenance costs which are presented in Table 2. The Annex B details this Methodology, and the Annex C shows the limit-parameters considered in the previous design.

It is worth to emphasize that in the design of the thicknesses of the asphalt layers, the value of the resilient modulus of the surface layer regarding to 0.10 s loading time was always considered. The structural numbers used as input data for the application of the methodology above mentioned were obtained from the layer thickness previously calculated employing the modules values obtained at different levels of traffic speeds.

Table 1. Data from design of the reference pavement structures using the software Fepave[2].

Mixture type	Surface layer modulus (kgf/cm^2)	Surface layer thickeness (cm)	Base course thickness (cm) (Base modulus = 3,000 kgf/cm^2)	Subgrade modulus (kgf/cm^2)
Sample 1	22,344	11.0	15	
Sample 2	30,295	10.5		1,200
Sample 3	11,420	11.0		

[1]DNER: Brazilian Federal Road Agency currently named DNIT.
[2]Fepave—Software originally from Berkley that has been used in COPPE (UFRJ), to calculate stresses, deformation and displacement in pavement structures.

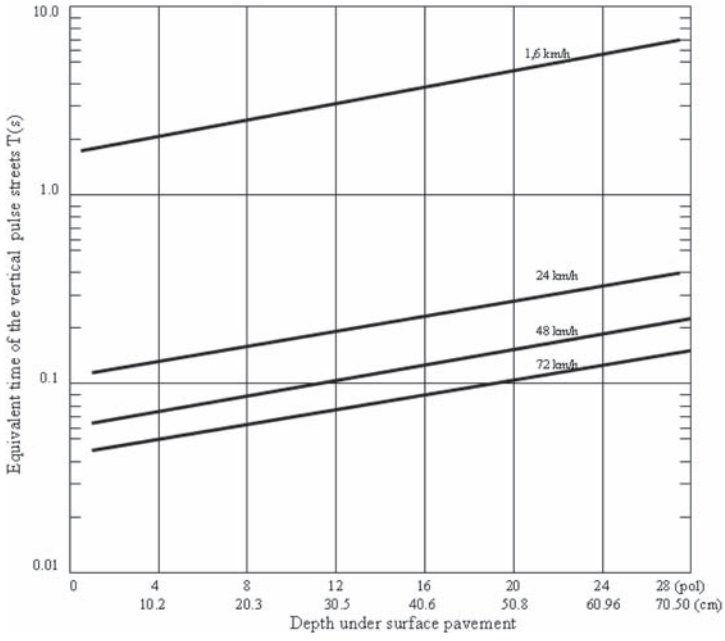

Figure 1. Pulse time for different depths and vehicle speeds in a Brazilian typical pavement structure. Source: Medina and Mota (1995).

Table 2. Conservation cost equations (US$/km/year) as a function of TMD (Average Daily Traffic) at different traffic speed levels.

Traffic speed (km/h)	Mixture type		
	Sample 1	Sample 2	Sample 3
90	11020 + 0.0255 TMD	10980 + 0.0126 TMD	11256 + 0.2089 TMD
85	11020 + 0.0255 TMD	10992 + 0.0132 TMD	11285 + 0.1170 TMD
80	11019 + 0.0458 TMD	10999 + 0.0160 TMD	11325 + 0.1253 TMD
64	11049 + 0.0492 TMD	11029 + 0.0292 TMD	11557 + 0.1793 TMD
48	11208 + 0.0939 TMD	11080 + 0.0514 TMD	12114 + 0.2817 TMD
35	11750 + 0.2207 TMD	11398 + 0.1476 TMD	13391 + 0.4403 TMD
7	11875 + 0.4613 TMD	11896 + 0.2462 TMD	14644 + 0.5588 TMD

Obs.: Values in US Dollars (reference: jan/2008).

It should be emphasized that the traffic speeds are the average speeds of the total traffic, as admitted by HCM (TRB, 1985), as well as it was adopted to work with this reference and not with the latest version of HCM (2000), because of the prevalent conditions of Brazilian roads.

When substituting the value adopted for the daily average traffic and considering its annual growth rate, as well as updating the annual values for the year "0" and accumulating the results, the conservation costs were obtained along the pavement service life and added to the investment cost, as shown in Table 3.

The investment costs of the structures presented in Table 3 were obtained using the unitary cost values supplied by the DER/RJ[3] and were applied to the pavement layer thicknesses

[3]DER/RJ—Brazilian State Road Agency from Rio de Janeiro.

Table 3. Pavements costs of maintenance and investment over 20 years, updated to year "0", in a hypothetical highway.

Traffic speed (km/h)	Maintenance costs + investment costs (US$/km)		
	Bituminous mixture type		
	Sample 1	Sample 2	Sample 3
90	302708.23	277639.50	286013.00
85	304523.20	278029.10	286013.00
80	306438.30	278278.10	289555.00
64	318790.08	281160.70	290500.00
48	343527.49	285638.20	300327.00
35	387704.63	306430.03	329272.00
7	423606.39	329895.55	364369.00

Obs.: Values in US$ dollars (reference: jan/2008).

shown in Table 1, as follows: (i) Mixture 1—US$ 75.86/m^3; (ii) Mixture 2—US$ 73.74/m^3; and (iii) Mixture 3—US$ 75.06/m^3. According to the same source, estimation of the pavement base crushed stone 15 cm thick layer at 5 km average transport distance was US$ 7.03/m^2.

In order to evaluate the effect of the speed on the costs, the Tukey test was applied to the Table 3 cost values. The result showed significant effect of the speed on the costs, at 5% significance level. However, this result is based on the assumption that all daily average traffic is flowing at the same speed level. Nevertheless, this premise is not real because the speed of the vehicles in a highway varies along the day as a function of its design characteristics, and traffic volume and composition, as shown in HCM (TRB, 1985). Thus, the analysis was deepened by the application of the concepts of capacity and service levels as described in HCM (1985).

3 APPLICATION AND RESULTS

The cost equations presented in Table 2 were useful to deepen the cost analysis, since they involved the capacity concepts and service levels of HCM (TRB, 1985) towards the association of the cost behavior with the capacity characteristics, in sections of the highway and their respective traffic volumes and speeds. Two capacity levels were assumed for the highway under study, as follows: (i) Section 1: 3125 PCE/h (passenger car equivalent)/h); and (ii) Section 2: 1818 PCE/h. The previous values were obtained, by considering a highway with four lanes (two by direction), and calculating its capacities according to HCM (TRB, 1985).

So, the value 3125 PCE/h is the highway capacity value assuming a transversal section in plane terrain and 40% trucks in the traffic flow, and the value 1818 PCE/h refers to a capacity assuming a transversal section of this highway in wavy terrain. In both cases, the value 3.60 m was admitted as the lanes width, besides the inexistence of lateral obstructions in the highway.

For each capacity level, the traffic operation hour numbers were determined at each service level (A, B, C, D and E) along a typical day of the highway operation, during some years of the highway service life. By integrating the traffic volumes along those hours, and substituting the values in the cost equations of the respective speed that characterizes each service level, it was possible to estimate the highway annual conservation cost by summing the different costs corresponding to the different service levels. This was accomplished by using the spreadsheets for each capacity level, type of mixture and year of the highway service life. Table 4 presents the values corresponding to year "0" and to year "16" of the highway service life. The cost values were updated for year "0" at a yearly rate of 11%.

To determine the operational hour numbers and the corresponding daily traffic volume for each service level in the highway sections, the model developed by MacDowell (1994),

Table 4. Costs for the sample 1 considering a section capacity of 3125 PCE/h.

Year numbers and daily average traffic (vehicle/day)	Characteristic speeds at the service levels A, B, C, D, E (Km/h)	Mixture resilent modules correspond-ing to each speed level (Kgf/cm^2)	Number of daily hours during which the traffic flows at each service level A, B, C, D and E (hours)	Daily volume of traffic flowing at each service level A, B, C, D and E (vehicle/day)	Annual parcel of the con-servation cost referring to the traffic flowed at levels A, B, C, D and E (US$/km)
	90	59333	19.32	1527.3	1722,16
0	85	56854	1.043	1139.1	1284,43
	80	54250	0.923	1407.8	1615,89
10000	64	45850	0.980	1896.9	2189,22
	48	36020	1.727	4028.1	4893,79
Total conservation cost (all levels) US $/km/year					11705,53
	90	59333	15.249	2861.7	691,60
16	85	56854	1.953	2134.4	515,83
	80	54250	1.729	2638.3	893,66
18729	64	45850	1.835	3552.3	893,66
	48	36020	3.234	7542.9	2056,09
Total conservation cost (all levels) US$/km/year					4815,90
Total conservation cost (in US $/km) during 17 years, by taking into account the Levels, speeds and modules updated for the year 0 US$/km.					**132029,41**

that was applied to the capacity studies of the Brazilian Régis Bittencourt highway was also applied in the present study. Following, it is presented a description of this model.

3.1 *Model for obtaining the highway hourly distribution curves of traffic*

For running the model, the capacity of the highway section and the daily average traffic must be supplied. The program constructs a histogram of the hourly traffic volumes (Va_j) that flows during 24 hours in a typical day (t_j) of traffic operation, as presented in Figure 2.

Thus, the traffic volumes corresponding to the operation at several service levels can be obtained by integrating the area under the histogram curve among the maximum volumes that characteres each service level, which are determined by the limit volumes/capacity defined by HCM (TRB, 1985). These volumes allow to obtaining the number of hours the highway will be operating at each level.

The logic of this model consists into an analogy with the probability distribution concept of a random variable. According to this, the random variable is the number of hours in a typical day, whereas the probabilities referring to this variable are the traffic volume flows that are represented by the area under the curve of the histogram as depicted in Figure 2. This modeling applied to the volumes measured in the Brazilian Régis Bittencourt highway allowed for adjustment of the probability density function, which is also assumed for the highway under study:

$$f(t_j) = \int_0^{23} vol\ e^{-\frac{1}{2}\left(\frac{t_j}{i}\right)^2} dt \qquad (2)$$

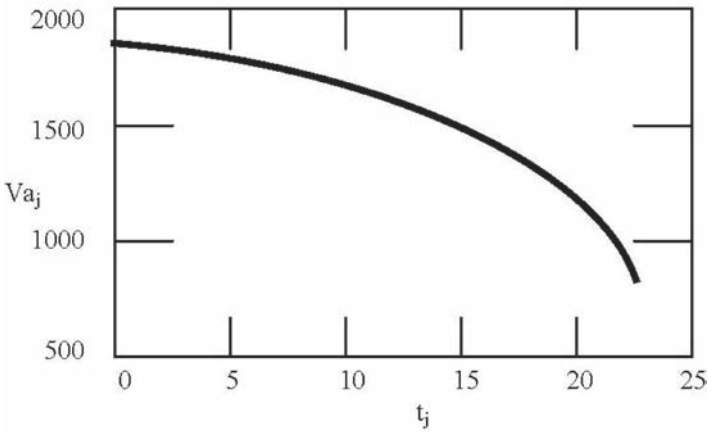

Figure 2. Distributional histogram of the highway hourly volumes of traffic during a typical day obtained through application of the MacDowell (1994) model.

where t_j = hour numbers of the day; *vol* = section capacity; and i = value to be calibrated for the conditions of the highway and obtained by the following equation:

$$\int_0^{23} vol\ e^{-\frac{1}{2}\left(\frac{t_j}{i}\right)^2} dt = TMD \tag{3}$$

3.1 *Results*

The previous model was applied for both capacity levels assumed, along 17 years of the highway service life. The results were applied to the cost equations of the three mixtures presented in Table 2. Considering that those equations supply the costs in US$/km/year as a function of the daily average traffic, as well as the model supplies a traffic volume related to a determined number of hours, there was a need for constructing datasheets, such as the one exemplified in Table 4 for the first 17 years of the highway service life. Accumulating the values of this datasheet, the costs corresponding to the several service levels of the highway annual traffic during those years were obtained. Table 5 presents the results.

4 CONCLUSIONS

Regarding the maintenance and the total pavement costs (Table 5), it was observed tendency to increase with the decrease in the highway transversal section capacity, which was

Table 5. Highway maintenance, investment and total costs during 17 years in a hypothetical highway considering three types of bituminous mixtures surface layer.

Mixture	Section	Capacity PCE/h	Maintenance US$/km	Investment US$/km	Total US$/km
Sample 1 (Range C)	1	3.125	132029,41	144125,6	276155,08
	2	1.818	133127,98	144125,6	277253,68
Sample 2 (Range B)	1	3.125	127113,30	138482,3	265474,91
	2	1.818	127648,45	138482,3	266131,00
Sample 3 (Range V-A)	1	3.125	158116,52	143300,4	301417,36
	2	1.818	161670,01	143300,4	304971,00

Obs.: Values in US dollars (reference: jan/2008).

more perceptible for sample 3 (finer grain size distribution), and less sensible for samples 1 (intermediate grain size distribution) and 2 (coarser grain size distribution).

Concerning to investment costs, the values shown in Table 5 were equal for both levels of the section capacity, because in spite of considering different transversal sections (one in plane land and the other one in wavy land) the costs presented refer to the pavement construction (base and surface layers).

The results showed that the maintenance cost of a highway increases when its section capacity decreases. This increment can be higher or lower depending upon the surface layer mixture characteristic and the traffic volume, which will determine the number of the operational hours at several service levels and their characteristic speeds. The cost increase would be higher if the reduction in the section capacity would lead to a higher value of the operational hour number at level F, which generates the highest costs, according to data from Tables 2 and 3.

However, the model under application shows restrictions relative to evaluation of this hour numbers. The lowest costs obtained for sample 2 are explained by the fact that the highest values have been found for higher resilient modulus, and this can lead to the simplified conclusion that as higher is the module, the better it will be.

On the other hand, the highway engineering also considers an other criteria for evaluating the performance of mixtures, such as the compatibleness of the module values among the different pavement layers, layers mechanical resistance to permanent deformation (whell paths), *in situ* aging, effects from complex loadings and others as composing an multi-criteria analysis. Therefore, it is suggested the inclusion of pavement "foreseen costs" as one of the evaluation criteria, that would be an important tool mainly in the case of the urban roads where speed reductions are more frequent because of traffic jams.

The foreseen costs could be estimated according to the methodology applied in the present study, evaluating the pavement degradation and service maintenance costs based on the PSI (Present Serviceability Index) and on the correlations with the resilient modulus via a structural number. The use of PSI turns possible to analyze the highway service loss capacity and to provide indication about the need for maintenance services or overlay of the pavement with a new asphalt layer, according to recommendation of MacDowell (1994), as well as allows for considering the pavement global behavior, although emphasizing the significant paper of the bituminous layers. The maintenence costs depend on the degradations suffered by the pavement. Though, if it is true that some of those degradations fundamentally depend on the superior layers performance, many others will depend on the behavior of the whole pavement structure, therefore depending from the structural design, the foreseen traffic and the prevalent climatic conditions.

It is also observed that, at the same level of the traffic volume, a higher level of traffic operational speed will result into lower costs (Table 3), leading to the conclusion that it is advantageous to provide the best possible conditions of the highway section capacity.

REFERENCES

Bernucci, L.B., Motta, L.M.G., Ceratti, J.A.P. & Soares, J.B. (2006). *Pavimentação asfáltica*: formação básica para engenheiros. Rio de Janeiro: Petrobrás, Abeda. 504 p.

Coelho, V. (1996). *Contribuição do estudo das deformações permanentes, nas condições do Brasil, em camadas de concreto asfáltico*. Tese de Doutorado E.E.S.C., São Paulo.

DNER-ME 43–64 (1964). *Ensaio Marshall para misturas betuminosas*. Departamento de Estradas e Rodagem, Rio de Janeiro.

Fernandez Jr. (1994). *Investigação dos efeitos das solicitações do tráfego sobre o desempenho do pavimento*. EESC-USP, São Paulo.

Heukelon, W. and Klomp, A.J.G. (1964). Road design and dynamic loading. *Proc. Association of Asfhalt Paving Technologisty*, v. 33.

Köstenberger, H. (1989). *Design of roadway surface course in Austria*. II Simpósio Internacional de Avaliação de Pavimentos e Projeto de Reforço—ABPv, Rio de Janeiro.

MacDowell, F.L.C. (1976). *Engenharia de transporte rodoviário—síntese das metodologias*. IPR/DNER, Rio de Janeiro. (Publ., 611).

MacDowell, F.L.C. (1994). *Modelo para estimativa de custo de conservação da Régis Bittencourt*. DNER/BID, Rio de Janeiro.
Medina, J. and Motta, L.M.G. (1995). Análise do pulso de carga em pavimentos. *Anais da XXIX Reunião Anual da ABPV*, ABPV, Cuiabá.
Medina, J. and Motta, L.M.G. (2005). *Mecânica dos pavimentos*. 2.ed. Rio de Janeiro. 570 p.
Motta, L.M.G. (1991). *Métodos de dimensionamento de pavimentos flexíveis, critério de confiabilidade e ensaios de cargas repetidas*. Tese de Doutorado, COPPE/UFRJ, Rio de Janeiro.
Motta, L.M.G., Medina, J., Cruz, A.M. & Viana, A.D. (1998). Aspectos do comportamento das misturas asfálticas. *Anais do XI Encontro de Asfalto*, IBP, Rio de Janeiro.
Silva, P.D.E.A. (1985). *Contribuição para o aperfeiçoamento do Programa Fepave 2 em estudos e projetos de pavimentação flexíveis*. COPPE/UFRJ, Rio de Janeiro.
Souza, A.C.V. (1998). *Custos de conservação de rodovias, velocidades de tráfego e módulos de resiliência de misturas asfálticas*. COPPE/UFRJ, Rio de Janeiro.
Transportation Research Board—TRB (1985). *Highway capacity manual*. 3.ed. National Research Council, Washington, D.C. (Special Report, 209).
Transportation Research Board—TRB (2000). *Highway capacity manual*. 4.ed. National Research Council, Washington, D.C. (Special Report, 209).

ANNEXES

Annex A—Characteristics of bituminous mixtures and asphalt of the samples 1, 2 and 3.

A.1. The Sample-1: grain size distributions of sample 1 and of DNER's C range.

Sieves	3/4"	1/2"	3/8"	n. 4	n. 10	n. 40	n. 80	n. 200
Superior limit of the C range	100	100	100	85	75	40	30	10
Mixture	100	90.7	84	65.7	45.5	21.5	13.9	6.5
Inferior limit of the C range	100	85	75	50	30	15	8	5

Obs.: DNER—Brazilian Federal Road Agency, Currently is named DNIT.

A.2. Sample-2: grain size distributions of sample 1 and of DNER's B range.

Sieves	3/4"	1/2"	3/8"	n. 4	n. 10	n. 40	n. 80	n. 200
Superior limit of the B range	100	–	80	60	45	32	20	8
Mixture	100	82.27	71	45.54	29.69	15.12	9.72	5.52
Inferior limit of the C range	100	–	45	28	20	10	8	3

A.3. Sample-3: grain size distributions of sample 1 and of the Asphalt Institute V-A range.

Sieves	3/4"	1/2"	3/8"	n. 4	n. 10	n. 40	n. 80	n. 200
Superior limit of the V-A range	100	100	100	85	75	40	30	10
Mixture	100	90.7	84	65.7	45.5	21.5	13.9	6.5
Inferior limit of the V-A range	100	85	75	50	30	15	8	5

A.4. Asphalt (CAP 20) characterization.

Penetration at 25°C, 100 g, 5 s (0,1 mm)	65
Absolute viscosity at 60°C	2192 (poise)
Saybolt-furol viscosity 135°C	198.8 s
Saybolt-furol viscosity 177°C	34.5 s

A.5. Physical indexes obtained from Marshall laboratory testing of bituminous mixtures using samples 1, 2 and 3.

Mixture	Ligand content	Void volumes
Sample 1	5.4%	4%
Sample 2	5.0%	3.2%
Sample 3	6.8%	4%

Annex B—Characteristics of the modified basic cost methodology

According to MacDowell (1976, 1994), this methodology should be applied at planning level, and it has been already applied on Brazilian road director-plans during certain time. It consists into analytical evaluation of the service forecasting quantitative for the maintenance of a highway along its service life, which are later multiplied by unitary costs of those services. In forecasting those quantitative, the AASHOT's concept of PSI (Present Serviceability Index), that appeared during the experiment by AASHOT road test.

By considering the PSI value equal to 5 at the initial year of a highway, its decrease along the years is calculated as a function of structural pavement number and of the qualitative traffic volume (axes equivalent to 80 KN).

The volume of the annual maintenence services can be calculated using the equations obtained during the mentioned study, that are the following ones:

$$\overline{RD} = -0.03PSI^2 + 0.09PSI + 0.32 \quad (4)$$

$$C + P = (0.3PSI^3 - 1.3PSI^2 - 6.2PSI + 29)^2 \quad (5)$$

for $PSI < 4.3$

$$C + P = 0 \quad (6)$$

for $PSI > 4.3$

where $\overline{RD}$ is the depth of the whell's path in inches; C refers to the cracks classified as 2 and 3 in feet^2/1000 feet^2; and R = repairs in feet^2/1000 feet^2.

The PSI decreases with pavement deterioration and also indicates the need for overlay when it reaches 2.5. Then, an average value is converted into annual cost and adopted as the PSI value. It is also a need for adopting an annual average value for the other conservation services such as the cleaning of the gutters, cuverts and the domain lane, as well as the erosion control by repairing the faults in slopes, substitution of the signalization and lane paintings.

The final product from the application of the methodology is an equation of costs as a function of TMD (daily average traffic) in US$/km/year, as shown in Table 2.

Annex C—Limit-Parameters in designing the pavement structures presented in table 1

The Fepave program was used in the design showed in Table 1. This program is useful to the calculation of both stresses and deformations in a transversal pavement section that occur due to the wheel load effect. The program requires the following factors as input data: the thicknesses of the different pavement layers and their respective resilient modulus, besides the "Poisson" coefficients. Then, it is possible to obtain a proposal for dimensioning each of the three structures presented in Table 1, by considering the following values as limits admitted for the project parameters:

a) for vertical stress on the subgrade

$$\sigma_{v\max} = \frac{0.006 \text{ dynamic modulus}}{1 + 0.7 \log N} \text{ (kgf/cm}^2\text{)} \quad (7)$$

where N is the equivalent whell loads to ESAL

b) for stress differences in the asphalt layer (horizontal stress less vertical stress)

b1) for module with 22,344 kgf/cm^2

$$N = 1.4 \cdot 10^5 (\Delta\sigma)^{-2.01} \quad (8)$$

b2) for module with 30.295 kgf/cm^2

$$N = 5.6 \cdot 10^5 (\Delta\sigma)^{-2.61} \quad (9)$$

b3) for module with 11.420 kgf/cm^2

$$N = 1.4 \cdot 10^5 (\Delta\sigma)^{-2.01} \quad (10)$$

In these equations, N is the number of the loading applications on asphaltic mixture samples that cause horizontal stresses less vertical ($\Delta\sigma$) in the specimen, therefore causing its rupture byfatigue. The equations were developed in COPPE/UFRJ by the Preussler, Pinto and Motta, and were mentioned by Motta (1994). Para those three cases, a shift factor equal to 10^4 was admitted according to the same source.

However, the study did not considered the permanent deformation in the asphalt layer, since the mixture design adopted the Marshall laboratory testing procedure (DNER-ME, 1964), as well as according to Coelho (1996) well-designed mixtures that take into account the climatic conditions do not show high premature permanent deformations.

Advanced Testing and Characterization of Bituminous Materials – Loizos, Partl, Scarpas & Al-Qadi (eds)
© 2009 Taylor & Francis Group, London, ISBN 978-0-415-55854-9

Author index

AI A1-Hadidy 227
Agostinacchio, M. 1131
Ahn, K. 619
Allen, B. 185
Ammendola, R. 367, 1151, 1247
Angelone, S. 917
Anochie-Boateng, J.K. 550
Antunes, M.L. 323
Apeagyei, A.K. 463
Arabani, M. 423, 551
Arnaud, L. 433
Artamendi, I. 185
Ayan, V. 1160
Azari, H. 261

Baek, S.H. 349
Balay, J.-M. 725
Baldo, N. 879
Bańkowski, W. 443, 1221
Barbati, S. 627
Batista, F.A. 323
Baumgardner, G. 81
Beckedahl, H.J. 33, 1269
Beduneau, E. 651
Bennert, T. 1279
Besamusca, J. 133
Blab, R. 357
Blasl, A. 899
Bocci, M. 1113
Bodin, D. 725, 773
Bonneau, D. 651
Botella, R. 707
Braham, A. 699, 785
Brar, H. 1279
Breysse, D. 725
Burlacu, A. 795
Buttlar, W. 699, 785
Buttlar, W.G. 463, 827

Canestrari, F. 1181
Capitanu, C. 295
Carbonneau, X. 609, 889, 1211
Cardone, F. 627, 1113
Cardoso de Lima, D. 1289
Carter, A. 1091
Chailleux, E. 773, 1221
Charmot, S. 1123
Chen, X. 531
Chen, Z. 575
Ciampa, D. 399
Cocurullo, A. 761
Collings, D.C. 1161
Currie, M. 251

Damian, T.C. 295
Dattola, V. 13
de la Roche, C. 331, 773
De Visscher, J. 1009, 1201
Di Benedetto, H. 69
Diaconu, E. 569
Dicu, M. 693, 795
Diomedi, M. 1131
Doh, Y.S. 349, 619
Dreessen, S. 971
Dubois, V. 331
Duif, C.P. 143
Dupriet, S. 651
Durand, G. 61, 195

Eckmann, B. 609
El Ayadi, A. 1049
Elliott, R.C. 519

Fakhri, M. 681
Fanouillet, L. 61
Farokhi, M. 681
Feng, D. 205
Ferreira, C.I.G. 661
Ferrotti, G. 1181
Flintsch, G. 453
Fodor, G. 295
Fonseca, P. 323
Freitag, S. 949

Gabet, T. 331
Gajewski, M. 1221
Gallet, T. 69
Gardel, V. 971
Garg, N. 1279
Gaudefroy, V. 639
Gauthier, G. 69, 1221
Geffard, J.L. 639
Gengliang, T. 377
Ghorbel, E. 849
Goldbaum, J. 1265
Goyer, S. 639
Grenfell, J. 331
Grilli, A. 1113
Guddati, M.N. 817
Gueit, C. 61, 195
György, G. 409

Hadad, Ah. 1257
Haddadi, S. 849
Hagos, E.T. 173
Hase, M. 23
Hassan, H.F. 497
Hassan, M.M. 961
Herle, I. 409
Herrera de la Rosa, R. 477
Hornych, P. 639
Hou, E.T. 859
Houel, A. 433
Hunter, A. 519
Huurman, M. 507, 749
Hyzl, P. 909

Jamek, M. 807
James, D. 519
Janssen, S. 33
Jenkins, K.J. 239, 283, 1161
Jiménez, R. 271
Joodi, H.R. 423
Judycki, J. 303

Kalman, B. 443
Kappl, K. 357
Kasbergen, C. 879
Katicha, S. 453
Kayser, S. 215
Kazatchkov, I.B. 93, 989
Khalid, H.A. 961

Khavandi, A. 1169
Khedoe, R.N. 507
Kheiry, P.T. 681
Kias, E.M. 735
Kim, H. 827
Kim, H.H. 619
Kim, J.C. 349
Kim, K.W. 349, 619
Kim, Y.R. 817, 859
Koh, C. 585
Kringos, N. 123, 143, 261, 839, 879

la Agostinacchio, M. 399
La, I. 619
Labuz, J. 313
Lazăr, Ş.M. 569
Le Gal, Y. 1211
Legal, Y. 889
Leguern, M. 773
Leuridan, A. 1201
Levenberg, E. 541
Li, H. 531
Liu, X. 939
Livneh, M. 1235
Lobază, M. 693
Loizos, A. 1081
Lopp, G. 585
Lu, X. 151, 1181
Lugmayr, R. 807

Machado, A.V. 109
Malkoç, G. 53
Manthos, E. 1019
Marasteanu, M. 313
Martínez, A. 271
Martinez, F. 917
Mat Zin, H. 1143
Meite, N.B. 519
Merbouh, M. 725
Meunier, M. 1091
Michalica, P. 93
Millien, A. 1181
Mirabdolazimi, S.M. 551
Mo, L. 507
Mohd Yazip, M. 1143
Molenaar, A.A.A. 133, 173, 387
Mollenhauer, K. 715
Mondschein, P. 869, 1101
Moraal, J. 507
Moriceau, L. 725
Moro, A. 367, 1151, 1247
Murali Krishnan, J. 999

N'Guyen, T.L. 433
Nafisah, A.A. 1143
Nicholls, J.C. 519
Nielsen, E. 99
Nikolaides, A. 1019
Nikzad Gharehaghaji, A. 1169

Oelkers, C. 23
Oeser, M. 949
Olard, F. 651
Olita, S. 399, 1131
Oliveira, J.R.M. 661
Özcan, Ş. 487

Pais, J.C. 109
Pannunzio, V. 627
Pap, I. 981
Papavasiliou, V. 1081
Paradis, M. 1091
Partl, M.N. 3, 827, 1181, 1191
Pasetto, M. 879
Pauli, T. 123, 143, 1130
Pellinen, T. 251, 1282
Peralta, E.J. 109, 661
Perera, R. 519
Pérez, F. 271, 707
Perraton, D. 1091
Peterson, C. 785
Petit, C. 1049, 1181
Ph. du Bus de Warnaffe 1201
Phelipot-Mardelle, A. 1181
Phillips, P. 185
Piber, H. 1191, 1181
Picoux, B. 1049
Piérard, N. 163, 1201
Planche, J.P. 971
Poirier, J.E. 61
Porot, L. 331
Praticò, F.G. 13, 367, 1151, 1235
Pronk, A.C. 749, 749
Prusenko, Y. 1039
Pszczoła, M. 303

Qian, Z. 531
Quigniot, S. 889

Raab, C. 3, 1181
Răcănel, C. 795
Ravnikar Turk, M. 443
Redelius, P. 151
Riedl, S. 1059
Robert, M. 195
Robertson, R. 123
Romanescu, C. 795
Romero, P. 1123
Roque, R. 585
Rowe, G. 43, 81
Rubio, B. 271
Ryu, M.Y. 619

Sabouri, M.R. 597
Saleh, F. 1257
Santagata, F.A. 1113
Saoula, S. 849
Savadatti, S. 817
Scarpas, A. 123, 143, 261, 830, 879, 939
Schelkens, E. 1201
Schitter, G. 143
Schmets, A.J.M. 143
Schmidt, C. 1265
Scullion, T. 927
Sebaaly, P.E. 1071
Seignez, N. 651
Serfass, J.P. 609
Shafabakhsh, Gh. 1257
Shakeri, V. 423
Sharrock, M. 81
Shuler, S. 1265
Siddharthan, R.V. 1071
Silva, H.M.R.D. 109, 661
Sivapatham, P. 33, 1269
Smiljanic, M. 981
Soenen, H. 151, 1221
Stastna, J. 93, 989
Stehlik, D. 909
Struble, L.J. 463
Surlea, C. 795
Sybilski, D. 1221

Tabatabaee, H.A. 597
Tabatabaee, N. 597
Tapkin, S. 487
Tarefder, R.A. 735
Tatic, U. 981
Teymourpour, P. 597
Thirunavukkarasu, S. 817
Thushara, V.T. 999
Triquigneaux, J.P. 609
Tschegg, E.K. 807
Tuncan, A. 487
Tuncan, M. 487
Turos, M. 313

Tušar, M. 443
Tutumluer, E. 559
Twagira, M.E. 239, 283

Underwood, B.S. 817, 859
Uzan, J. 541

Valdés, G. 707
Valentin, J. 869, 1101
Valle de Souza, A.C. 1289
Valtonen, J. 251
Van de Ven, M. 331
van de Ven, M.F.C. 133, 173, 387, 1029
Van den bergh, W. 331
van Lent, D.Q. 387
Van Rompu, J. 69
Vanelstraete, A. 163, 1009
Vansteenkiste, S. 1201
Varaus, M. 909
Velásquez, R. 313
Vignard, N. 773
Virgili, A. 627
Volovyk, O. 1039
Voskuilen, J.L.M. 1029

Wagoner, M.P. 827
Walubita, L.F. 927
Wang, D. 205
Wasage, T.L.J. 989
Weise, C. 899
Wellner, F. 215, 409
Wiman, L.G. 443
Wistuba, M. 715
Woldekidan, M.F. 507

Yang, J. 575
Yi, J. 205
Yi-qiu Tan 227
Yiqiu, T. 377

Zanzotto, L. 93, 989
Zdralek, P. 909
Zejiao, D. 377
Zhdanyuk, K. 1039
Zhdanyuk, V. 1039
Zhu, H. 575
Zulakmal, S. 1143

Bituminous materials are used to build durable roads that sustain diverse environmental conditions. However, due to their complexity and a global shortage of these materials, their design and technical development present several challenges. **Advanced Testing and Characterisation of Bituminous Materials** focuses on fundamental and performance testing of binders and asphaltic mixtures. Issues addressed in the volume include:

- Evaluation of binder properties with respect to durability relevant to distress accumulation and application
- Testing and modelling the influence of climate and ageing effects on performance
- Characterization and design of bituminous mixtures with respect to performance
- Evaluation of fundamental laboratory test methods and models for pavement performance prediction
- Laboratory compaction methods and models with respect to field compaction
- Test methods for the assessment of the structural behaviour and performance of pavements
- Investigation of pavement performance prediction and evaluation sections
- Testing, mix design and evaluation of recycled bituminous road materials
- Synthesis of international coordinated research initiatives for the development of performance related test methods and specifications

Advanced Testing and Characterisation of Bituminous Materials demonstrates that modern experimental material characterization techniques, sophisticated constitutive modeling, and innovative design provide appropriate tools for pavement performance prediction. The book is of interest to academics and engineers in pavement and road engineering.

CRC Press
Taylor & Francis Group
an **informa** business
www.crcpress.com

6000 Broken Sound Parkway, NW
Suite 300, Boca Raton, FL 33487
Schipholweg 107C
2316 XC Leiden, NL
2 Park Square, Milton Park
Abingdon, Oxon OX14 4RN, UK

RILEM

ISBN-13: 978-0-415-55854-9
9 780415 558549

an **informa** business